EANM'17

Annual Congress of the
European Association of Nuclear Medicine
October 21 – 25, 2017
Vienna, Austria

Abstracts

This supplement was not sponsored by outside commercial interests. It was funded entirely by the association's own resources

Dear colleagues, dear friends,

It is with great pleasure that the European Association of Nuclear Medicine welcomes you to its 30th Annual Congress in Vienna, Austria.

Over the 30 years since our first Congress, nuclear medicine has made significant strides. Overall usage of nuclear medicine procedures is expanding rapidly, and this trend is especially evident with respect to new imaging technologies. We can affirm that the revolution of tomographic hybrid imaging within the nuclear medicine landscape is now a matter of fact, spurred by evidence-based medicine. Our discipline's next step is the integration of genome-specific targeted theranostics, utilising in vivo whole-body assessment of tissue morphology, physiology and biochemistry. The ultimate goal is to design personalised, super-selective therapies and to identify more precise means of monitoring response to treatment in routine clinical practice.

The annual EANM Congress has become the world-leading meeting in nuclear medicine. In order to maintain the high level of excellence of our Congress, the 2017 meeting will build on the traditions that are highly appreciated by all attendees, with expansion of the newer features introduced by the former Congress Chair. A specific educational track, implemented in collaboration with the European School of Multimodality Imaging and Therapy, will include up-to-date Teaching Sessions, enriched by Pitfalls & Artefacts and Continuous Medical Education (CME) sessions. In all these "active learning" sessions, attendees will have the possibility to enhance their knowledge of multimodality imaging. With similar pedagogic intent, numerous multidisciplinary joint symposia organised by EANM Committees and our sister societies will offer an integrative approach to various topics relevant to the state of the art in our discipline. On the occasion of its 30th anniversary, our Congress will feature two new events (as well as a very big surprise). First, a panel display of the best regional posters will illustrate its global scope. Second, a specific Presidential Session will be dedicated to the best-ranked papers from the under-30s. Our young colleagues represent the future of our discipline and should begin to shape their knowledge in ways that will contribute to a brighter tomorrow for the whole nuclear medicine community!

All these learning sessions will not impact adversely on the predominant role of the entire Congress, which is to enable the presentation of oral papers and posters about the latest achievements in clinical nuclear medicine, science and technology. On the contrary, the Rapid Fire sessions, for example, will be enriched. The spirit of such sessions is to draw attention to the most highly rated abstracts in specific areas: a panel of top-level presentations is followed by extensive discussions, providing attendees with an integrated and coherent view on a wide variety of topics. Furthermore, featured oral sessions with one invited speaker in combination with "regular" presentations will broaden the perspectives on all topics. The now well-established tracks M2M – Molecule to Man (basic and translational science) and Do.MoRe (radionuclide therapy and dosimetry) will promote high-quality research through interaction between basic and translational clinical scientists and allow presentation of the latest achievements and developments in the fields of clinical molecular imaging and nuclear medicine therapy. During the plenary lectures, distinguished speakers will address state of the art science together with new developments in clinical and allied sciences, covering a broad range of topics with the goal of promoting the best possible care for our patients. At the end of the meeting, two eminent lecturers, Prof. Stefano Fanti from Bologna, Italy and Prof. Clemens Decristoforo from Innsbruck, Austria will present the traditional Highlights Lecture.

The Congress will take place in Vienna, Austria, where the EANM Executive Office is also based. The city – located in the heart of Europe, on the banks of the river Danube – is world famous for its imperial heritage, its cultural attractions and its culinary highlights. To quote the slogan of the city: Vienna awaits you!

For all these reasons, I cordially invite you to the EANM'17 Congress and to actively participate in our 30th anniversary. Meet and interact with friends and colleagues from all over the world, break away from the daily routine and enjoy Vienna's hospitality.

Francesco Giammarile,
EANM Congress Chair 2017-2019

Saturday, October 21, 2017

Time	Hall A,B,C	Meeting Room	Hall E1	Hall E2	Hall F2	Hall K1	Hall K2	Hall G1	Hall G2
09:00 - 09:30					**Pre-Symposium 1** Physics/Dosimetry	**Pre-Symposium 2** Oncology/ Radionuclide Therapy/EWALT	**Pre-Symposium 3** Dosimetry/ Radiation Protection	**Pre-Symposium 4** Neuroimaging/ Drug Development/ Radiopharmacy	**Pre-Symposium 5** Radiopharmacy
09:30 - 10:00					Monte Carlo Simulation / Image Reconstruction – Part I	Integrated Approach for the Diagnosis and Treatment of Primary Liver Tumors (HCC & CCC)	Clinical Introduction of New Radiotherapeutics: Challenges and Opportunities	Tau Imaging in Humans	Validation & Risk Assessment
10:00 - 10:30									
10:30 - 11:00									
11:00 - 11:30		**EANM Advisory Council Meeting**							
11:30 - 12:00									
12:00 - 12:30									
12:30 - 13:00									
13:00 - 13:30					**Pre-Symposium 6** Physics/Dosimetry	**Pre-Symposium 7** Oncology/ Radionuclide Therapy	**Pre-Symposium 8** Drug Development/ Neuroimaging	**Pre-Symposium 9** Translational Molecular Imaging & Therapy/ Radiopharmacy/ Drug Development	**Pre-Symposium 10** Cardiovascular/ Inflammation & Infection
13:30 - 14:00					Monte Carlo Simulation / Image Reconstruction – Part II	PET Imaging for Response Assessment of Immune Modulation and Therapy	The Contribution of Imaging in the Exploration of Autism		Role of Nuclear Medicine in the Detection of Infection of Cardiac Prosthesis or Devices
14:00 - 14:30		**EANM Delegates Assembly**						Bioorthogonal and Click Chemistry for Molecular Imaging	
14:30 - 15:00									
15:00 - 15:30									
15:30 - 16:00									
16:00 - 16:30			**EANM Members Assembly** (first call 16:00)						
16:30 - 17:00									
17:00 - 17:30									
17:30 - 18:00									
18:00 - 18:30									
19:30 - 20:30	**EANM Opening Ceremony**								

Sunday, October 22, 2017

Time	Hall A	Hall B	Hall C	Hall E1	Hall E2	Hall F1	Hall F2	Hall K	Hall G1	Hall G2	e-Posters
08:00 - 08:30	*101* **CME 1** Physics	*102* **Joint Symposium 1** Oncology/ESTRO	**Technologists' Opening**	*104* **Do.MoRe**	*105* **M2M**	*106* **Pitfalls & Artefacts 1 - ICC***		*108* **Committee Symposium 1**		*110* **Joint Symposium 16**	
08:30 - 09:00	Challenges and Solutions for MR-Based Attenuation Correction of PET	Molecular PET Imaging in Adaptive Radiotherapy: Focus on Current Trends, Challenges and Solutions	*103* **CTE 1** Technologists/ SNMMI	Radionuclide Therapy - Miscellaneous (RIT & Bone Palliation)	α-Therapy	Neuroimaging/ Physics/EFOMP		Inflammation & Infection/ Drug Development		Neuroimaging/JSNM	**e-Poster Walks**
09:00 - 09:30			Quality Control and Protocol Standardisation - Tech Guide Launch			Pitfalls and Artefacts in Visual vs. Quantitative Reading		68Ga-Tracers for Infection Imaging		Educating Referring Physicians and Recognising Their Needs	E-PW01, E-PW02, E-PW03
09:30 - 10:00											
10:00 - 10:30	*201* **Plenary 1 incl. Marie Curie Lecture**		*203* **IN HALL A**								
10:30 - 11:00	Theranostic Developments for Prostate Cancer		**Plenary 1 incl. Marie Curie Lecture** Theranostic Developments for Prostate Cancer								
11:00 - 11:30											
11:30 - 12:00	*301* **CME 2** Inflammation & Infection/ESVS	*302* **Joint Symposium 2** Radionuclide Therapy/ENETS	*303* **CTE 2** Interactive Technologists/EARL	*304* **Do.MoRe**	*305* **M2M**	*306* **Pitfalls & Artefacts 2 - ICC***	*307* **Clinical Oncology**		*309* **Do.MoRe - Featured**	*310* **Conventional & Specialised Nuclear Medicine**	
12:00 - 12:30	Vascular Graft Infection	Establishing a Position for PRRT in the Multidisciplinary Treatment of NETs	Technologist Role in Research and EARL Accreditation	Modeling & Radiobiology	Antibodies	Cardiovascular	We Want a New Drug		Photodynamic Therapy & Molecular Imaging – The Perfect Couple?	Benign Thyroid & Parathyroid Diseases	
12:30 - 13:00						Pitfalls and Artefacts with CZT Cameras					
13:00 - 14:30						**EANM Young Daily Forum**	**Industry Sponsored Symposium**	**Industry Sponsored Symposium**	**Industry Sponsored Symposium**		
14:30 - 15:00	*401* **CME 3** Cardiovascular	*402* **Joint Symposium 3** Thyroid/ETA-CRN	*403a* **Mini Course 1** Technologists	*404* **Do.MoRe**	*405* **M2M**	*406* **Teaching Session 1 - ICC***	*407* **Clinical Oncology**		*409* **Neurosciences**	*410* **Conventional & Specialised Nuclear Medicine**	
15:00 - 15:30	How to Perform Myocardial Perfusion Imaging According to EANM Recommendations	Update Thyroid Cancer Beyond I-131	Cardiology: Pitfalls & Artefacts	Radiopeptides for Therapy	New Targets	Applied Cross Sectional Anatomy and Correlative Imaging – Head and Neck	Rapid Fire Session Prostate		Imaging Amyloid and Amyloidogenesis	Pulmonology & Nephrourology	
15:30 - 16:00											
16:00 - 16:30			*403b* **Mini Course 2** Technologists/ Inflammation & Infection								
16:30 - 17:00	*501* **CME 4** Oncology	*502* **Joint Symposium 4** Dosimetry/Radiation Protection/ICRP/ICRU	Inflammation: Pitfalls & Artefacts	*504* **Do.MoRe**	*505* **M2M - Featured**	*506* **Teaching Session 2 - ICC***	*507* **Clinical Oncology**	*508* **Cardiovascular System**	*509* **Neurosciences**	*510* **Conventional & Specialised Nuclear Medicine**	
17:00 - 17:30	PET in Multiple Myeloma	Radiological Protection for Patients Receiving Radiopharmaceutical Therapy	*403c* **Mini Course 3** Technologists **Interactive**	SPECT Quantification	Combination Therapies	Applied Cross Sectional Anatomy and Correlative Imaging – Foot and Ankle	NET, a Classic!	Myocardial Function, Metabolism & Perfusion - From Preclinical to Clinical Practice	Imaging Neurotransmission Systems in Parkinson	Paediatrics	
17:30 - 18:00			Bone and Joint: Pitfalls & Artefacts								

Plenary Sessions | CME Sessions | Joint/Special/Committee Symposia | Technologist Sessions | Do.MoRe | M2M | Pitfalls & Artefacts / Teaching Sessions (*ICC = Interactive Clinical Cases) | Clinical Oncology Sessions | Cardiovascular System | Neurosciences | Conventional & Specialised Nuclear Medicine

Monday, October 23, 2017

	Hall A	Hall B	Hall C	Hall E1	Hall E2	Hall F1	Hall F2	Hall K	Hall G1	Hall G2	e-Posters
08:00 - 08:30 / 08:30 - 09:00 / 09:00 - 09:30	**601** **CME 5** Radiopharmacy/ Drug Development/ Radionuclide Therapy/ SNMMI — Theranostics and Companion Drugs (CME)	**602** **Joint Symposium 5** Cardiovascular/ESMI — Imaging Cardiac Remodelling	**603** **Technologists** Oral Presentations 1	**604** **Do.MoRe** PSMA Therapy	**605** **M2M** Optical/ Multimodality Imaging	**606** **Pitfalls & Artefacts 3 - ICC*** Oncology/ Inflammation & Infection/Bone & Joint — Pitfalls and Artefacts in Abdomen and Pelvis	**607** **Clinical Oncology** Rapid Fire Session — What's New? Texture Analysis and More!		**609** **Committee Symposium 2** Neuroimaging — PET/MR - Making it Clinical	**610** **Conventional & Specialised Nuclear Medicine** Musculoskeletal (Benign)	**e-Poster Walks** E-PW04, E-PW05, E-PW06, E-PW07, E-PW08
09:30 - 10:00											
10:00 - 10:30 / 10:30 - 11:00 / 11:00 - 11:30	**201** **Plenary 2** Hot Topics in Nuclear Cardiology!		**702** **IN HALL A** **Plenary 2** Hot Topics in Nuclear Cardiology!								
11:30 - 12:00 / 12:00 - 12:30 / 12:30 - 13:00	**801** **CME 6 - Interactive** Bone & Joint — Skeletal Scintigraphy Today - Accurate Diagnosis of Bone Disease with Therapeutic Impact (CME)	**802** **Joint Symposium 6** Cardiovascular/EACVI — Fast-Track Cardiac Imaging: Is There an Ideal One-Stop Shop?	**803** **Technologists** Oral Presentations 2	**804** **Do.MoRe - Featured** Harmonization of Hybrid Molecular Imaging	**805** **M2M** Peptides	**806** **Pitfalls & Artefacts 4 - ICC*** Paediatrics — Pitfalls and Artefacts - FDG-PET Imaging in Children	**807** **Clinical Oncology** Women's Only	**808** **Committee Symposium 3** Inflammation & Infection/ Neuroimaging — Neurological Autoimmune Disorders	**809** **Tomorrow's Experts Session** Best-Ranked Papers from the Under-30s		
13:00 - 14:30						**EANM Young Daily Forum**	**Industry Sponsored Symposium**	**Industry Sponsored Symposium**	**Industry Sponsored Symposium**		
14:30 - 15:00 / 15:00 - 15:30 / 15:30 - 16:00	**901** **CME 7** Radionuclide Therapy/Thyroid — Safety Aspects in Radionuclide Therapy (CME)	**902** **Symposium 7** Bone & Joint — Painful Hip Arthroplasty	**903** **CTE 3** Technologists — Prostate Imaging and Therapy	**904** **Committee Symposium 4 Do.MoRe** — Validation of Quantitative Imaging, Dosimetry & Estimates of Uncertainty	**905** **M2M** SPECT/CT & SPECT/MRI	**906** **Teaching Session 3 - ICC*** — Applied Cross Sectional Anatomy and Correlative Imaging – Spine	**907** **Clinical Oncology** It's in the Blood	**908** **Cardiovascular System** Cardiac Sarcoidosis & Amyloidosis	**909** **Neurosciences** Imaging Neurodegeneration in Alzheimer's Disease by TAU and FDG Imaging	**910** **Conventional & Specialised Nuclear Medicine** Infection & Inflammation	
16:00 - 16:30											
16:30 - 17:00 / 17:00 - 17:30 / 17:30 - 18:00	**1001** **CME 8** Radionuclide Therapy/ Radiopharmacy/ Dosimetry — Clinical Trial Design for Radionuclide Therapy (CME)	**1002** **Joint Symposium 8** Neuroimaging/EANO — High Grade Glioma	**1003** **CTE 4** Technologists/ CAMRT — Radionuclide Production	**1004** **Do.MoRe** Dosimetry in Thyroid Disease	**1005** **M2M** PET/CT	**1006** **Teaching Session 4 - ICC*** — Applied Cross Sectional Anatomy and Correlative Imaging – Abdomen & Pelvis	**1007** **Joint Symposium 18** Oncology/TBA — Treatment Landscape in Metastatic CRPC	**1008** **Cardiovascular System** Cardiac Sympathetic Innervation - 123I-mIBG & Arrhythmias		**1010** **Committee Symposium 5** Radiation Protection — CT-Optimisation of Hybrid Imaging	

Legend: Plenary Sessions · CME Sessions · Joint/Special/Committee Symposia · Technologist Sessions · Do.MoRe · M2M · Pitfalls & Artefacts / Teaching Sessions (*ICC = Interactive Clinical Cases) · Clinical Oncology Sessions · Cardiovascular System · Neurosciences · Conventional & Specialised Nuclear Medicine

Tuesday, October 24, 2017

	Hall A	Hall B	Hall C	Hall E1	Hall E2	Hall F1	Hall F2	Hall K	Hall G1	Hall G2	e-Posters
08:00 - 08:30 / 08:30 - 09:00 / 09:00 - 09:30	**1101** CME 9 Paediatrics/ Inflammation & Infection — FDG PET in Paediatric Infections	**1102** Joint Symposium 9 Physics/EFOMP — New Developments in CT Technology	**1103** Technologists — Technologist e-Poster Sessions 1, 2, 3, 4	**1104** Do.MoRe — Preclinical & Clinical Dosimetry	**1105** M2M — Automation & Production	**1106** Pitfalls & Artefacts 5 - ICC* Oncology — Pitfalls and Artefacts of PET in Neuroendocrine Tumours	**1107** Clinical Oncology — Cured or Not Cured?			**1110** Do.MoRe — Clinical Dosimetry for 90Y Radioembolization	**Technologist e-Poster Sessions** (08:00-09:30) E-TPW1, E-TPW2, E-TPW3, E-TPW4 **e-Poster Walks** (08:30-09:30) E-PW09, E-PW10, E-PW11, E-PW12
09:30 - 10:00											
10:00 - 10:30 / 10:30 - 11:00 / 11:00 - 11:30	**1201** Plenary 3 Radiobiology of Molecular Radiotherapy		**1203** IN HALL A Plenary 3 Radiobiology of Molecular Radiotherapy								
11:30 - 12:00 / 12:00 - 12:30 / 12:30 - 13:00	**1301** CME 10 Neuroimaging — Brain PET and SPECT in Dementia - Beyond Alzheimer's Disease	**1302** Joint Symposium 10 Thyroid/ESES/IFCC — Diagnosis and Treatment of Hyperthyroidism	**1303** Technologists — Oral Presentations 3	**1304** Do.MoRe — Radiation Protection	**1305** M2M — Prostate Cancer Targeting	**1306** Pitfalls & Artefacts 6 - ICC* Dosimetry — Pitfalls and Artefacts in Pre- and Post-Therapeutic Imaging	**1307** Clinical Oncology — Bad Brain	**1308** Cardiovascular System — Myocardial Perfusion PET - 13N-Ammonia and 15O-Water		**1310** Do.MoRe — Detector Technology	
13:00 - 14:30						EANM Young Daily Forum	Industry Sponsored Symposium	Industry Sponsored Symposium	Industry Sponsored Symposium		
14:30 - 15:00 / 15:00 - 15:30 / 15:30 - 16:00	**1401** CME 11 Paediatrics/ Oncology/ SIOPEN — SSR Imaging and Therapy in Children	**1402** Joint Symposium 11 Cardiovascular/EACVI — Quantification of Myocardial Blood Flow	**1403** CTE 5 Technologists — Gastrointestinal Imaging	**1404** Do.MoRe — Dosimetry/ Physics/AAPM — PET Auto-Segmentation: Review and Evaluation Strategies - Insights from AAPM Task Group No. 211	**1405** M2M — Nanoparticles	**1406** Teaching Session 5 - ICC* — Applied Cross Sectional Anatomy and Correlative Imaging – Cross Sectional CT and PETCT for the TNM Staging of Lung Cancer	**1407** Clinical Oncology Rapid Fire Session — Mix it Up, please!		**1409** Neurosciences Rapid Fire Session — Imaging Brain Physiology in Preclinical & Clinical Models	**1410** Do.MoRe — Thyroid Cancer - Clinical	
16:00 - 16:30											
16:30 - 17:00 / 17:00 - 17:30 / 17:30 - 18:00	**1501** CME 12 Translational Molecular Imaging & Therapy/ Oncology/Neuroimaging — 18F-DOPA and Radiolabelled Choline PET in Recurrent Glioblastoma	**1502** Joint Symposium 12 Oncology/EORTC — PET Criteria for Response Assessment: Quo vadis PERCIST?	**1503** CTE 6 Technologists/ Dosimetry — Imaging, Reconstruction and ROI Analysis Techniques for Dosimetry	**1504** Do.MoRe — Rapid Fire Session — Radionuclide Therapy, Miscellaneous	**1505** Joint Symposium 15 M2M/ESMI — Best of European Molecular Imaging Meeting - EMIM 2017	**1506** Teaching Session 6 - ICC* — Correlative Imaging for Nuclear Medicine Specialists: Interactive Live Radiology and Nuclear Medicine Quiz Using the Experior Medical System	**1507** Clinical Oncology — In the Air & Beyond	**1508** Cardiovascular System — Myocardial Perfusion SPECT: Quantification & Artificial Intelligence		**1510** Do.MoRe - Featured — PET/MRI	

Legend:
Plenary Sessions · CME Sessions · Joint/Special/Committee Symposia · Technologist Sessions · Do.MoRe · M2M · Pitfalls & Artefacts / Teaching Sessions (*ICC = Interactive Clinical Cases) · Clinical Oncology Sessions · Cardiovascular System · Neurosciences · Conventional & Specialised Nuclear Medicine

Wednesday, October 25, 2017

	Hall A	Hall B	Hall C	Hall E1	Hall E2	Hall F1	Hall F2	Hall K	Hall G1	Hall G2	e-Posters
08:00 - 08:30	**1601** CME 13 Dosimetry/ Radionuclide Therapy/ Radiation Protection Treatment Planning for Radionuclide Therapy, How Simple Can it Be? CME	**1602** Joint Symposium 13 Paediatrics/SNMMI Standartisation of Diuresis Renography in Children		**1604** Do.MoRe Image Reconstruction	**1605** M2M Radiolabelling Methods	**1606** Pitfalls & Artefacts 7 - ICC* Oncology Pitfalls and Artefacts in PSMA PET Reading	**1607** Clinical Oncology Anything Goes	**1608** Cardiovascular System Myocardial Perfusion PET - 82-Rubidium		**1610** Do.MoRe Dosimetry in Diagnostic Nuclear Medicine	
08:30 - 09:00											
09:00 - 09:30											
09:30 - 10:00											
10:00 - 10:30	**1701** CME 14 Dosimetry/ Radiation Protection/ Translational Molecular Imaging & Therapy Alpha Particle Dosimetry, Does High LET Lead to High RBE? CME	**1702** Joint Symposium 14 Oncology/ESSO Head & Neck Cancer	**1703** CTE 7 Interactive Technologists/ Paediatrics Practical and Technical Aspects of Paediatric Nuclear Medicine	**1704** Do.MoRe Molecular Imaging Artefacts & Corrections	**1705** M2M CNS/ Neurotransmission/ Brain Targets		**1707** Clinical Oncology PSMA - Saving Nuclear Medicine	**1708** Cardiovascular System Atherosclerotic Plaque Imaging			
10:30 - 11:00											
11:00 - 11:30											
11:30 - 12:00	**1801** Awards Ceremony (11:45 - 12:15) Plenary 4 Highlights Lecture (12:15 - 13:15) Closing Ceremony (13:15 - 13:20)		**1803** IN HALL A Awards Ceremony (11:45 - 12:15) Plenary 4 Highlights Lecture (12:15 - 13:15) Closing Ceremony (13:15 - 13:20)								
12:00 - 12:30											
12:30 - 13:00											
13:00 - 13:30											

Plenary Sessions ■ CME Sessions ■ Joint/Special/Committee Symposia ■ Technologist Sessions ■ Do.MoRe ■ M2M ■ Pitfalls & Artefacts / Teaching Sessions (*ICC = Interactive Clinical Cases) ■ Clinical Oncology Sessions ■ Cardiovascular System ■ Neurosciences ■ Conventional & Specialised Nuclear Medicine

Oral Sessions

PS1   Saturday, October 21, 2017, 09:00 - 12:00, Hall F2

Pre-Congress Symposium 1 - Monte Carlo Simulation / Image Reconstruction – Part I

PS01
SPECT/(CT) Quantitative Reconstruction Techniques
R. van Holen; Ghent University, Department of Electronics and Information Systems, Ghent, BELGIUM

PS02
Motion Detection and Correction in PET/CT and PET/MRI
K. Thielemans; University College London, UCL Hospital, Institute of Nuclear Medicine, London, UNITED KINGDOM.

PS05
Basics and Principles of 4D PET Image Reconstruction
A. Reader; King's College London, Biomedical Engineering Department, London, UNITED KINGDOM.

PS06
TOF Reconstruction Methods and Benefits for Clinical Imaging
J. Karp; University of Pennsylvania school of Arts and Sciences, Department of Radiology, Philadelphia, UNITED STATES OF AMERICA.

PS07
A Focus on MLAAPET Reconstruction
R. Boellaard; University of Groningen, Center for Medical Imaging, Groningen, NETHERLANDS.

PS2   Saturday, October 21, 2017, 09:00 - 12:00, Hall K1

Pre-Congress Symposium 2 - EANM/EWALT: Integrated Approach for the Diagnosis and Treatment of Primary Liver Tumours (HCC & CCC)

PS08
Pathological Diagnosis and Molecular Predictors in Primary Liver Tumours
L. Rubbia-Brandt; Hôpitaux Universitaires de Genève, Service de Pathologie Clinique, Geneva, SWITZERLAND.

PS09
Hepatologist Perspective on Primary Liver Tumours from Diagnosis to Prevention
Y. Kallis; Barts and the London School of Medicine and Dentistry, Queen Mary University London, London, UNITED KINGDOM..

PS10
Cross Sectional Imaging in HCC and CCC Including Novel MRI Techniques for Early Detection
M. Ronot; Department of Radiology, Beaujon Hospital, AP-HP, Paris, FRANCE

PS11
Molecular Imaging with FDG and Non-FDG PET Tracers
J.-N. Talbot; Hospital Tenon, AP-HP & Université P&M Curie, Paris, FRANCE.

PS13
Locoregional Treatment in Primary Liver Tumours
L. A. Solbiati; Department of Biomedical Sciences - Humanitas University, Milan, ITALY.

PS14
Innovative Surgical Approaches in HCC and CCC
G. Torzilli; Humanitas University, School of Medicine, Humanitas Research Hospital, IRCCS , Milan, ITALY.

PS15
Update on Oncological Management of Cholangiocarcinoma and HCC Including Novel Agent
N. Starling; The Royal Marsden , London, UNITED KINGDOM.

PS16
Role of Transarterial Radioembolisation in Primary Liver Tumours
S. Ezzedin; Universitätsklinikum des Saarlandes, Klinik für Nuklearmedizin, Homburg, GERMANY.

PS3   Saturday, October 21, 2017, 09:00 - 12:00, Hall K2

Pre-Congress Symposium 3 - Clinical Introduction of New Radiotherapeutics: Challenges and Opportunities

PS17
Introduction
G. Flux; Royal Marsden NHS Trust & Institute of Cancer Research, London, UNITED KINGDOM.

PS18
Phosphorous-32 Microparticles
A. Soman; Oncosil medical Ltd, Sydney, AUSTRALIA.

PS19
Holmium-166 Microspheres
F. Nijsen; Quirem Medical, Groningen, NETHERLANDS.

PS20
Y-90 Glass Microspheres
T. Mauxion; BTG, Nantes, FRANCE.

PS21
Alpha Therapy with Radium-223 and Thorium-227
J. Gay; Bayer Healthcare, Berlin, GERMANY.

PS23
Treatment of NHL with Lutetium-177 Labelled Anti-CD37 Antibodies
J. Dahle; Nordic Nanovector, Oslo, NORWAY.

PS24

Lutetium-177 Peptides and Antibodies

M. Mariani; Advanced Accelerator Applications, Saint-Genis-Pouilly, FRANCE.

PS25

Copper Isotopes for Imaging and Therapy

M. Harris; Clarity Pharmaceuticals, Sydney, AUSTRALIA.

PS4   **Saturday, October 21, 2017, 09:00 - 12:00, Hall G1**

Pre-Congress Symposium 4 - Tau Imaging in Humans

PS27

Tau Pathology in Tauopathies

G. Kovacs; Institute of Neurology, Medical University Vienna, Vienna, AUSTRIA.

PS28

Preclinical Pharmacokinetic Modelling: A Strategy to Select and Compare Tracers?

S. Krämer; ETH Zurich, Institute of Pharmaceutical Sciences, Zurich, SWITZERLAND.

PS29

Imaging Tau with 18F-THK5317

A. Nordberg; Center for Alzheimer Research, Karolinska Institutet, Stockholm, SWEDEN.

PS32

Imaging Tau with 18F-T807

B. van Berckel; VUMC, Amsterdam, NETHERLANDS.

PS33

Imaging Tau with 11C-PBB3 and its 18F Derivatives

M. Higuchi; National Institutes for Quantum and Radiological Science and Technology National Institute of Radiological Sciences, Chiba, JAPAN.

PS34

Tau as a Therapeutic Target

C. Wischik; School of Medicine, Medical Sciences and Nutrition, University of Aberdeen, Aberdeen, UNITED KINGDOM.

PS5   **Saturday, October 21, 2017, 09:00 - 12:00, Hall G2**

Pre-Congress Symposium 5 - Validation & Risk Assessment

PS36

Economic Impact of Qualification/Validation from Full GMP Perspective

R. Suchi; GE Healthcare Buchler GmbH & Co. KG, Braunschweig, GERMANY.

PS37

Validation of Analytical Methods

N. M. Gillings; Copenhagen University Hospital, Rigshospitalet, PET & Cyclotron Unit, Copenhagen, DENMARK.

PS38

Risk Assessment - How Much Validation is Needed?

V. Ferrari; The Grove Centre, QA department, Amersham, Buckinghamshire, UNITED KINGDOM.

PS41

Design, Qualification and Validation of a Cyclotron Facility: It's Fun! – Practical Example

L. Perk; Radboud University Medical Center, Radboud Translational Medicine, Nijmegen, NETHERLANDS.

PS42

Risk Assessment – Practical Example

P. Colombo; IBA Molecular Italy, San Gerardo dei Tintori Hospital, Monza, ITALY.

PS6   **Saturday, October 21, 2017, 13:00 - 16:00, Hall F2**

Pre-Congress Symposium 6 - Monte Carlo Simulation / Image Reconstruction – Part II

PS44

Short Introduction to the Principles of Monte Carlo Methods

D. Visvikis; CHU MORVAN, Bat 2 bis, U650 INSERM, LaTIM - I35, Brest, FRANCE.

PS45

Monte Carlo Simulation of PET Systems

S. Vandenberghe; Ghent University, Department of Electronics and information systems, Ghent, BELGIUM.

PS46

Monte Carlo Simulation of SPECT Systems

D. Sarrut; Léon Bérard cancer center, CREATIS, Lyon, FRANCE.

PS48

Quality Assurance of Nuclear Medicine Procedures Using Monte Carlo Simulated Images of Virtual Patients

M. Ljungberg; Lund University, Medical Radiation Physics, Lund, SWEDEN.

PS49

Full Monte Carlo Based Image Reconstruction – Are we there? Part 1

H. de Jong; University Medical Center Utrecht, Image Sciences Institute, Utrecht, NETHERLANDS.

PS50

Full Monte Carlo Based Image Reconstruction – Are we there? Part 2

M. Ljungberg; Lund University, Medical Radiation Physics, Lund, SWEDEN.

Pre-Congress Symposium 7 - PET Imaging for Response Assessment of Immune Modulation and Therapy

PS52

Introduction to Immune Modulation Therapy Focusing on PD1- anti PDL1 Checkpoint Inhibitors, CAR T-Cell Therapy and Vaccine Therapy

S. Lheureux; Princess Margaret Hospital, Toronto, CANADA.

PS53

Unmet Challenges and Clinical Needs for Assessing Response to Immunotherapy

C. Le Tourneau; Oncology Department Curie Institute, Paris, FRANCE.

PS54

Radiologic (CT) Aspects of Immune-Related Tumour Response Criteria and Patterns of Immune-Related Adverse Events in Patients Undergoing Immunotherapy

L. Umutlu; Radiology Department, University Hospital, Essen, GERMANY.

PS57

FDG PET Imaging for Response to Immune Modulating Therapies

E. Lopci; Istituto Clinico Humanitas IRCCS, Nuclear Medicine Department, Milano, ITALY.

PS58

Case Series: How to Identify Pseudo Progression and Immune Toxicities on FDG PET

R. Hicks; Cancer Imaging, Peter Mac Callum Cancer Institute, Melbourne, AUSTRALIA.

PS59

New Emerging PET Probes for Monitoring Immune Modulation Therapy

E. de Vries; University Medical Centre, Medical Oncology Department, Groningen, NETHERLANDS.

Pre-Congress Symposium 8 - The Contribution of Imaging in the Exploration of Autism

PS61

Needs in Biomarkers for Autism Spectrum Disorder

F. Bonnet-Brihaul; University Hospital of Tours, INSERM, Department of Child Psychiatry, Tours, FRANCE.

PS62

Social Brain and Autism

M. Zilbovicius; University René Descartes, INSERM, Hôpital Necker, Department of Pediatric Radiology, Paris, FRANCE.

PS63

What Can Bring MRI to Autism Exploration?

A. Retico; Istituto Nazionale di Fisica Nucleare, University of Pisa, Pisa, ITALY.

PS66

Neurotransmission Imaging in Autism

J. Borg; Karolinska Institutet, Centre for Psychiatric Research, Stockholm, SWEDEN.

PS67

New Targets and Future PET Radiotracers for Autism

A. Gee; King's College London, Division of Imaging Sciences, London, UNITED KINGDOM.

Pre-Congress Symposium 9 - Bioorthogonal and Click Chemistry for Molecular Imaging

PS69

The Basics of Click Chemistry

V. Bouvet; Memorial University of Newfoundland, Department of Radiology, St. John's, St. John's, CANADA.

PS70

Click Chemistry for Imaging of Glycoconjugates

V. Wittmann; Universitaet Konstanz, Konstanz, GERMANY.

PS73

Imaging and Therapy Agents Using Click Chemistry

M. Robillard; Tagworks Pharmaceuticals, Nijmegen, NETHERLANDS.

PS74

Pre-Targeted Imaging Using Click Chemistry

J. Knight; University of Oxford, Department of Oncology, Oxford, UNITED KINGDOM.

Pre-Congress Symposium 10 - Role of Nuclear Medicine in the Detection of Infection of Cardiac Prosthesis or Devices

PS76

Clinical Challenges in Establishing the Diagnosis Endocarditis

J. Ambrosioni; Hospital Clinic - IDIBAPS, University of Barcelona, Barcelona, SPAIN.

PS77

Role of Echocardiography in the Diagnosis of Endocarditis

R. Dulgheru; Department of Cardiology, University of Liège Hospital, GIGA-Cardiovascular Sciences, Liège, BELGIUM.

PS78

Role of White Blood Cell Scintigraphy in the Diagnosis of Endocarditis

P. Erba; Nuclear Medicine, Department of Translational Research and New Technology in Medicine, University of Pisa, Pisa, ITALY.

PS80

Role of FDG-PET Imaging in the Diagnosis of Endocarditis

F. Rouzet; Nuclear Medicine Department and Département Hospitalo Universitaire Fibrose Inflammation et Remodelage en Pathologies Cardiovasculaires, Bichat Claude Bernard Hospital, AP-HP, University of Paris VII, Paris, FRANCE.

PS81

Role of CTA and MRI in the Diagnosis of Endocarditis

G. Feuchtner; Department of Radiology, Innsbruck Medical University, Innsbruck, AUSTRIA.

PS82

Is There an Optimal Imaging Strategy for Patients Suspected for Endocarditis?

F. Hyafil; CHU Bichat, AP-HP, Nuclear Medicine, PARIS, FRANCE.

---

101   **Sunday, October 22, 2017, 08:00 - 09:30, Hall A**

CME 1 - Physics: Challenges and Solutions for MR-Based Attenuation Correction of PET

OP-001

Introduction to MR-Based AC

V. Schulz; University Hospital Aachen, Institute for Experimental Molecular Imaging, Dept. of Physics of Molecular Imaging, Aachen, GERMANY.

OP-002

MR Based Attenuation Correction for Brain

N. Burgos; University College London, Translational Imaging Group, London, UNITED KINGDOM.

OP-003

MR Based Attenuation Correction for the Body

G. Schramm; University of Leuven, Nuclear Medicine & Molecular Imaging, Leuven, BELGIUM.

---

102   **Sunday, October 22, 2017, 08:00 - 09:30, Hall B**

Joint Symposium 1 - EANM/ESTRO: Molecular PET Imaging in Adaptive Radiotherapy: Focus on Current Trends, Challenges and Solutions

OP-004

Prostate Cancer: The Radiation Oncologist's Point of View

W. Vogel; The Netherlands Cancer Institute - Antoni van Leeuwenhoek, Departments of Nuclear Medicine and Radiation Oncology, Amsterdam, NETHERLANDS.

OP-005

Prostate Cancer: The Nuclear Medicine Physician's Point of View

M. Picchio; IRCCS San Raffaele Scientific Institute, Nuclear Medicine Department, Milan, ITALY.

OP-006

Cervical Cancer: The Radiation Oncologist's Point of View

E. Troost; Universitätsklinikum Carl Gustav Carus, Department of Radiotherapy and Helmholtz-Zentrum Dresden-Rossendorf, Institute of Radiooncology-OncoRay, Dresden, GERMANY.

OP-007

Cervical Cancer: The Nuclear Medicine Physician's Point of View

J. A. Adam; Academic Medical Center Amsterdam, Department of Radiology and Nuclear Medicine , Amsterdam, NETHERLANDS.

---

103   **Sunday, October 22, 2017, 08:00 - 09:45, Hall C**

CTE 1 - Joint Session with SNMMI: Quality Control and Protocol Standardisation - Tech Guide Launch

OP-008

Welcome and Opening of the Technologist's Track

OP-009

Quality Control for PET Systems

C. Pestean; Dept. of Nuclear Medicine, "Ion Chiricuţă" Oncology Institute, Cluj-Napoca, ROMANIA.

OP-010

Optimisation of PET-CT – Acquisition & Reconstruction

D. M. York; Chattanooga State Community College , Chattanooga, UNITED STATES OF AMERICA.

OP-011

Radionuclide Dose Calibrator

A. Socan; Department of Nuclear Medicine; University Medical Center, Ljubljana, SLOVENIA.

---

104   **Sunday, October 22, 2017, 8:00 - 9:30, Hall E1**

Do.MoRe: Radionuclide Therapy - Miscellaneous (RIT & Bone Palliation)

OP-012

Pre-dosing with Lilotomab Prior to Antibody-Radionuclide Conjugate Therapy with ^{177}Lu-Lilotomab Satetraxetan Significantly Increases the Ratio of Tumour to Red Marrow Absorbed Dose in non-Hodgkin Lymphoma Patients

J. Blakkisrud[1], A. Løndalen[2], J. Dahle[3], A. C. Martinsen[4,1], H. Holte[5], A. Kolstad[5], C. Stokke[1,6]; [1]Department of Diagnostic Physics, Oslo University Hospital, Oslo, NORWAY, [2]Division of Radiology and Nuclear Medicine, Oslo University Hospital, Oslo, NORWAY, [3]Nordic Nanovector ASA, Oslo, NORWAY, [4]The Department of Physics,

University of Oslo, Oslo, NORWAY, [5]Department of Oncology, Radiumhospitalet, Oslo University Hospital, Oslo, NORWAY, [6]Oslo and Akershus University College of Applied Science, Oslo, NORWAY.

Introduction: ^{177}Lu-lilotomab satetraxetan is a novel anti-CD37 antibody radionuclide conjugate for treatment of non-Hodgkin lymphoma. Four different combinations of pre-dosing and pre-treatment have been investigated in the phase 1 study. All patients were pre-treated with different regimens of rituximab. Two arms included cold lilotomab pre-dosing (arm 1 and 4; 40 mg fixed and 100 mg/m^{2} BSA dosage respectively) and two did not (arm 2 and 3). Patients received either 10, 15 or 20 MBq ^{177}Lu-lilotomab satetraxetan per kg body weight. Previously, we have shown that absorbed red marrow (RM) doses were lower in arm 1 vs arm 2, and that haematological toxicity was more severe for patients receiving higher RM doses. The aim of this work was to compare the ratios of tumour to RM absorbed doses between arm 1, 4 and non-pre-dosed patients (arm 2 + 3). **Subjects and Methods:** A total of 16 patients were included for RM dosimetry, of these 14 were included for tumour dosimetry. A total of 35 tumour lesions were included, 1 to 5 from each patient (mode 3). RM and mean tumour absorbed doses per administered activity were determined from multiple SPECT/CT-images for each patient. Two-sided student-t-tests were used for all statistical analyses. **Results:** The mean RM absorbed doses were 0.83, 0.91 and 1.39 mGy/MBq for arm 1, 4 and non-pre-dosing arms 2+3, respectively. There was a significantly higher RM dose for non-pre-dosing compared to arm 1 (p = 0.04), and arm 4 (p = 0.05). Mean tumour absorbed doses were 1.62, 2.78 and 1.37 mGy/MBq for arm 1, 4 and non-pre-dosing respectively. Tumour doses were higher in arm 4 patients compared to patients without pre-dosing (p = 0.04). Tumour doses in arm 1 were not significantly higher compared to non-pre-dosing (p = 0.71). The mean tumour to RM absorbed dose ratios were 2.16, 3.93 and 1.07 for arm 1, 4 and non-pre-dosing respectively. Ratios were significantly higher in both arm 1 and 4 compared to non-pre-dosing (p = 0.05 and p = 0.04). No statistically significant difference between arm 1 and 4 was found for any parameters (p >= 0.12). **Conclusion:** Pre-dosing with lilotomab has a mitigating effect on red marrow absorbed dose for ^{177}Lu-lilotomab satetraxetan patients, and increased pre-dosing amounts was found correlated with a higher tumour dose. While the optimal amount of lilotomab is yet to be investigated, both pre-dosage levels significantly increased the tumour to RM absorbed dose ratio.

OP-013

Bi-213-anti-EGFR-MAb therapy of recurrent bladder cancer - a pilot study

K. Scheidhauer[1], C. Seidl[1], F. Bruchertseifer[2], C. Apostolidis[2], M. Autenrieth[1], F. Kurtz[1], T. Horn[1], M. Schwaiger[1], J. Gschwend[1], C. D'Alessandria[1], C. Pfob[1], R. Senekowitsch-Schmidtke[1], A. Morgenstern[2]; [1]Technische Universität München, München, GERMANY, [2]EC, JRC, Directorate for Nuclear Safety and Security, Karlsruhe, GERMANY.

Purpose/Introduction: Following transurethral resection of non-muscle-invasive bladder cancer (carcinoma in situ) and subsequent chemotherapy and treatment with Bacillus Calmette-Guérin (BCG), up to 40% of patients relapse within 5 years and need complete bladder excision. Therefore, new therapeutic strategies to combat tumor recurrence are needed. Because treatment of mice bearing intravesical human bladder cancer xenografts with Bi-213-anti-EGFR-MAb turned out highly efficient, the aim of this pilot study was to evaluate feasibility, safety and therapeutic efficacy of the α-emitter radioimmunoconjugate in recurrent bladder cancer patients. **Subjects & Methods:** The alpha-emitter Bi-213 was eluted from a Ac-225/Bi-213 generator system and coupled to the anti-EGFR-MAb (cetuximab, Merck, Germany) via the chelating agent CHX-A"-DTPA. 12 patients (10 m, 2 f) suffering from carcinoma in situ bladder cancer that had shown no response to BCG treatment were intravesically applied with 366-821 MBq (9.9 - 22.2 mCi) of Bi-213-anti-EGFR-MAb in 40 ml of PBS. Distribution of Bi-213-anti-EGFR-MAb was monitored by SPECT/CT. Treatment was terminated by emptying of the radioimmunoconjugate from the bladder up to 120 min after injection. Efficacy was evaluated via endoscopy and histology after eight weeks, and then six-monthly. Results: All patients (pts) showed excellent toleration of the treatment without any side effects. SPECT/CT monitoring clearly revealed location of the Bi-213-anti-EGFR-MAb immunoconjugate in the bladder. Treatment resulted in a documented complete eradication of tumor cells in three patients (CR is lasting 2.1 yrs, resp. 3.2 yrs, 1 pt with relapse after six months), PR in one patient and progressive tumor growth in eight patients. **Discussion/Conclusion:** Intravesical instillation of Bi-213-anti-EGFR-MAb is a promising, well tolerated therapeutic option for treatment of in situ bladder cancer after BCG failure and can help to avoid or postpone radical bladder surgery. A follow up study is planned to investigate further improvement of therapeutic efficacy through dose escalation and repeated treatments.

OP-014

Synfrizz : A first in Man study investigating the biodistribution, the safety and optimal recommended dose of a new radiolabeled monoclonal antibody targeting Frizzled homolog 10 (FZD10) in patients with relapsed or refractory non resectable synovial sarcomas

A. Giraudet[1], P. Cassier[1], G. Garin[1], J. Badel[1], S. Baconnier[1], D. Sarrut[2], D. Kryza[3], C. Iwao-Fukukawa[4], Y. Nakamura[5], A. Halty[6], D. Perol[1], J. Blay[1]; [1]Centre Léon Bérard, Lyon, FRANCE, [2]Créatis, Lyon, FRANCE, [3]UCBL1, Lyon, FRANCE, [4]OncoTherapy Science, Kawasaki City, JAPAN, [5]University of Tokyo, Tokyo, JAPAN, [6]Creatis, Lyon, FRANCE.

Introduction: Synovialosarcoma (SS) are rare tumors occurring predominantly in adolescents and young adults. Standard of care for relapsing SS is rarely curative and median survival is close to 12 months. OncoTherapy Science (Japan) has developed a monoclonal antibody (OTSA101) targeting the receptor frizzled-10 (FZD-10) highly expressed by SS but not present in normal tissues. When it was radiolabeled with ^{90}Y, tumor

shrinkage was observed in immunocompromised mice bearing FZD10-positive SS tumors, without significant toxicity. These preclinical data supported the clinical application of ^{90}Y-OTSA101 in a first in man phase I trial. **Subjects and Methods:** This study was conducted as a theranostic trial and included advanced SS patients resistant to standard treatments. In the first part, patients received 275 MBq of ^{111}In-OTSA101 in order to evaluate the in vivo bio-distribution and tumor uptake on repeated whole body and SPECT-CT acquisitions. In the second part, patients with significant tumors radiotracer uptake were randomized between 370 MBq (Arm A) and 1110 MBq (Arm B) of ^{90}Y-OTSA101. Patients' follow-up evaluated the safety and tumors response. 3D dosimetry with Monte Carlo simulations (GATE) was performed to evaluate normal tissues and selected tumor lesions absorbed dose (AD). **Results:** From January 2012 to June 2015, 20 pts (10 females, median age 43 years, [21-67]) with advanced SS were enrolled. Ten patients had sufficient tumor uptake to proceed to part 2 and 8 were randomized (Arm A: 3; Arm B: 5). Two patients were not randomized due to worsening PS. During part 2, the most common Grade ≥ 3 AEs were haematological, and were more common in Arm B. This was explained by 3D dosimetry as the bone marrow AD was closer to the MTD than in any other normal tissues (median, 0.09 cGy/MBq; [0.02–0.18] for a 2 Gy bone marrow MTD). One patient with SD after 12 weeks received a 2nd injection of 90Y-OTSA101, but experienced fatal hemoptysis afterwards. No objective response was observed explained by 3D dosimetry as the maximal tumor AD was 10 Gy (median, 0.25 cGy/MBq [01 to 0.82]). Best response was stable disease in 5/8 patients lasting up to 21 weeks for 1 patient. **Conclusion:** This first in human study shows that radioimmunotherapy targeting FZD10 is feasible and safe in metastatic SS patients. Tumor uptake was heterogeneous but sufficient to select 50% of pts for 90Y-OTSA101 treatment. 3D dosimetry results appeared to be correlated with side effects and tumors responses.

OP-015

Radioimmunotherapy with Panitumumab Modified with Metal Chelating Polymers (MCP) Labeled with ^{111}In and ^{177}Lu - A Novel Theranostic for Pancreatic Cancer

S. Aghevlian[1], D. Hedley[2], M. Winnik[3], R. Reilly[1,4,5]; [1]Department of Pharmaceutical Sciences, University of Toronto, Toronto, ON, CANADA, [2]Princess Margaret Cancer Centre, University Health Network, Toronto, ON, CANADA, [3]Department of Chemistry, University of Toronto, Toronto, ON, CANADA, [4]Toronto General Research Institute and Joint Department of Medical Imaging, University Health Network, Toronto, ON, CANADA, [5]Department of Medical Imaging, University of Toronto, Toronto, ON, CANADA.

Aim: Our aim was to study radioimmunotherapy (RIT) of pancreatic cancer (PnCa) using a novel theranostic agent composed of panitumumab (PmAb; anti-EGFR) conjugated to hydrazino nicotinamide metal chelating polymers (HyNic-MCP) harbouring 13 DOTA chelators for labeling with ^{111}In and ^{177}Lu, and 10 polyethyleneglycol (PEG) chains to minimize liver and spleen uptake. ^{111}In (t$_{1/2}$ = 2.8 d) emits γ-radiation [Eγ=171, 245

keV] enabling SPECT and subcellular range Auger electrons ideal for RIT of micrometastases. ^{177}Lu (t$_{1/2}$=6.7 days) is a β-emitter [Eβ(max)=0.2-0.5 MeV] suitable for treatment of millimeter sized tumours, that emits two γ-photons for SPECT imaging [Eγ=113, 208 keV]. Imaging may aid in selection of patients for RIT and estimating radiation doses to tumors and normal organs. **Methods:** The tumor-growth inhibitory effects of ^{111}In-MCP-PmAb were compared to ^{111}In-DOTA-PmAb in NOD/SCID mice engrafted s.c. with EGFR-positive PANC-1 human PnCa xenografts. For 70 days, every 3 weeks mice were injected i.v. with 10 μg (11 MBq) of ^{111}In-MCP-PmAb, ^{111}In-DOTA-PmAb, unlabeled PmAb or saline. Since NOD/SCID mice are radiation sensitive, RIT with ^{177}Lu-MCP-PmAb or ^{177}Lu-DOTA-PmAb was performed in NOD-Rag1(null)IL2rγ(null) (NRG) mice. NRG mice with PANC-1 tumours were injected i.v. with 10 μg (7 MBq) of ^{177}Lu-MCP-PmAb or ^{177}Lu-DOTA-PmAb every 6 weeks for 75 days. Tumor size was monitored and changes in body weight assessed every 2-3 days. A tumor growth index (TGI) was calculated by dividing the tumour volume at each time point by the initial volume. A body weight index (BWI) was similarly calculated. **Results:** The mean TGI (P-values compared to untreated mice) at 33 days in NOD/SCID mice treated with ^{111}In-MCP-PmAb, ^{111}In-DOTA-PmAb, PmAb and saline were 2.3±0.2 (p<0.001), 2.9±0.3 (p<0.001), 5.7±1.2 (p<0.001) and 18.6±3.5, respectively. The mean TGI at this time point in NRG mice treated with ^{177}Lu-MCP-PmAb, ^{177}Lu-DOTA-PmAb, PmAb and saline were 2.7±0.7 (p<0.01), 1.8±0.7 (p<0.001), 6.0±2.7 (p>0.05) and 5.8±0.9. No body weight loss was observed in any treatment groups. **Conclusions:** Both ^{111}In- or ^{177}Lu-MCP-PmAb or DOTA-PmAb decreased tumor growth compared to untreated mice. However, in a separate study, we found that MCP conjugation permits more robust and higher specific activity radiolabeling than DOTA-conjugated PmAb. Unlabeled PmAb was less effective than RIT at inhibiting tumor growth. The effectiveness of unlabeled PmAb for inhibiting tumor growth compared to untreated controls varied with the strain of mice used for tumor implantation. **Research Support:** Supported by the Canadian Cancer Society, Cancer Research Society, Centre for Pharmaceutical Oncology,and STARS21 strategic training program in radiation research.

OP-016

Radium-223-Dichloride in Castration-Resistant Metastatic Prostate Cancer: Therapy Assessment with 11C-choline PET/CT and Bone Scan

P. Ghedini[1], T. Graziani[1], E. Lodi Rizzini[1], G. Lima[1], I. Bossert[2], F. Ceci[1], G. Montini[1], C. Pettinato[3], F. Monari[4], V. Dionisi[5], A. Morganti[4], P. Castellucci[1], S. Fanti[1]; [1]Nuclear Medicine S. Orsola-Malpighi Hospital - University of Bologna, Bologna, ITALY, [2]Nuclear Medicine & Physics Unit, Fondazione Salvatore Maugeri, Pavia, ITALY, [3]Fisica Sanitaria - S. Orsola-Malpighi Hospital - University of Bologna, Bologna, ITALY, [4]U.O. Radioterapia - S. Orsola-Malpighi Hospital - University of Bologna, Bologna, ITALY, [5]U.O. Radioterapia - S. Orsola-Malpighi Hospital - University of Bologna, Bologna, ITALY, Bologna, ITALY.

Aim: our purpose was to evaluate Radium-223 therapy with [11C]Choline PET/CT and Bone Scan in patients with symptom-

atic bone metastases in castration-resistant prostate cancer (mCRPC). **Material and Methods:** we retrospectively enrolled 32 patients (age mean/range=72.4/58-88 years-old) by using these inclusion criteria: 1) mCRPC patients with symptomatic bone metastases 2) 6 subsequent cycle of Radium-223-Dichloride (55 kBq/kg); c) [11C]choline-PET/CT and Bone scan performed at baseline (BS1; PET1) and two months after the last cycle of radium223 (BS2; PET2). PSA, Alkaline phosphatase (ALP), and Hemoglobin (Hb) values were measured before (mean value=2.7 months) and after the end of therapy (mean value=2.8 months). BS2 and PET2 were reported by two nuclear medicine physicians as complete (CR), partial response (PR) or stable disease (SD). The appearance of a new lesion at BS2 or PET2 was reported as progression disease (PD). Follow-up (Clinical and radiological) was from 6 - to 18 months (mean 14.6 months). **Results:** the 56.3% (18/32) of patients were reported PR at PET2; 28.1% (9/32) showed a PD of bone metastasis; 9.4% (3/32) were in SD at PET2; 6.3% (2/32) were in CR at PET2. Considering the 18 patients with PR, CR or SD the 83% (15/18) showed increasing PSA-trend while considering the 9 patients with PD at PET2, the 77.7% (7/9) showed increasing PSA-trend. 100% of responders patients at imaging showed a significant decrease of ALP (mean reduction of 41.6%). 75% (22/32) of patients showed PR at BS2, 6.3% (2/32) CR, 25% (8/32) of patients showed PD at BS2: 1 PET2 in PD resulted CR at BS2; 3 PET2 in SD were PR at BS2; 1 PET2 in CR was PR at BS2. BS2 discordant results were confirmed with clinical and radiological follow up. Responders patients at imaging (PR/CR at BS2) showed a significantly better Overall Survival (OS) compared with non-responders (19.7 months vs 15.1). 46% of patients showed progression disease in visceral or lymph nodes at PET2. **Conclusion:** our preliminary results showed that Bone Scan is a more useful tool than [11C] Choline PET/CT in Radium 223 therapy assessment. However, Choline PET/CT is important to identify visceral or lymph nodes disease progression. Responders patients at Bone Scan seem to have better OS.

OP-017

Quantification of skeletal tumor burden on bone scintigraphy for prediction of overall survival in Radium-223 therapy

M. Ø. Fosbøl, P. M. Petersen, A. Kjaer, J. Mortensen; Rigshospitalet, Copenhagen, DENMARK.

Background: The role of bone scintigraphy in prediction and response assessment in Radium-223-dichloride (Ra-223) approved for metastatic castration-resistant prostate cancer (mCRPC) is not fully elucidated. The aim of this study was to investigate the predictive value of visual assessment of bone scintigraphy and automated quantification of skeletal tumor burden (Bone Scan Index) in mCRPC patients receiving Ra-223. **Methods:** National study of the Danish mCRPC patients who received ≥ 1 cycle of Ra-223 from March 2014 to October 2015 and who had a baseline bone scintigraphy available. Baseline bone scintigraphies were reviewed and graded according to extent of disease (EOD). Scintigraphic response to therapy after

three cycles and at end of therapy (EOT) was evaluated according to Prostate Cancer Working Group 2 (PCWG-2). All scintigraphies were analysed with the software EXINI Bone[BSI] Version 2 (EXINI Diagnostics, Lund, Sweden) to obtain Bone Scan Index (BSI). Primary outcome was overall survival (OS) from first cycle of Ra-223 to death of any cause. Parameters included in Cox regression analysis were: baseline BSI, visual grading of EOD, serum alkaline phosphatase (ALP), serum lactate dehydrogenase (LDH), serum PSA, opioid use and presence of lymph node metastases. **Results:** A total of 88 mCRPC patients were included. Baseline EOD showed 75% of patients (n=66) had > 20 metastases or superscan. Median baseline BSI was 5.0. Significant predictors of OS were baseline BSI (HR 1.042 per unit increase, p=0.035) and LDH (HR 1.02 per unit increase (U/l), p<0.001). Median OS for patients with BSI > 5 was 8.2 months vs. 15.0 months for BSI ≤ 5 (HR 2.65, p=0.001). BSI was stable or decreased during therapy in 44% (n=23) of patients who completed three cycles and in 59% (n=19) of patients after EOT. No association between changes in BSI during therapy and OS was found. Bone scintigraphy response according to PCWG from baseline to EOT showed stable disease in 38% (n=12), progression in 63% (n=20) and response was significantly associated with OS. Median OS for patients who progressed during therapy was 11.9 months (95% CI: 8.0-15.7), while median OS was not reached for patients with stable disease (HR 5.82, 95% CI: 1.31-25.9). **Conclusion:** Automated BSI is a promising biomarker for prediction of OS in mCRPC patients with advanced disease receiving Ra-223. Bone scintigraphy response according to PCWG-2 during Ra-223 therapy is associated with OS. Further studies are needed to evaluate the potential for BSI in response assessment.

OP-018

Radium-223 in Combination with Paclitaxel in Cancer Patients wiith Bone Metastases: Safety Results from an Open-Label, Multicenter Phase 1b Study

J. S. Lopez[1], R. Perets[2], S. Danson[3], H. Joensuu[4], A. Peer[2], S. J. Harris[1], F. Souza[5], B. Ploeger[6], K. M. C. Pereira[7], R. Geva[8]; [1]The Royal Marsden Hospital and The Institute of Cancer Research, Sutton, UNITED KINGDOM, [2]Rambam Health Care Campus, Haifa, ISRAEL, [3]Sheffield Experimental Cancer Medicine Centre, Weston Park Hospital, Sheffield, UNITED KINGDOM, [4]Helsinki University Hospital, Helsinki, FINLAND, [5]Bayer HealthCare Pharmaceuticals, Whippany, NJ, UNITED STATES OF AMERICA, [6]Bayer Pharma AG, Berlin, GERMANY, [7]Bayer Pharma AG, São Paulo, BRAZIL, [8]Tel Aviv Sourasky Medical Center, Tel Aviv, ISRAEL.

Aim: Concomitant radium-223 and chemotherapy is a potential option for cancer patients with bone metastases. Both therapies impact hematologic parameters, and myelosuppression risk during coadministration is unknown. This phase 1b study in cancer patients with bone metastases evaluated radium-223+paclitaxel safety and mode of interaction regarding myelosuppression. **Materials and Methods:** Eligible patients had a confirmed malignant solid tumor with ≥2 bone metastases and were candidates for paclitaxel. Treatment included 7 paclitaxel cycles (90

mg/m²/wk IV per local standard of care; 3 wk on/1wk off) + 6 radium223 cycles (55 kBq/kg IV; 1 injection every 4 wk, starting at paclitaxel cycle 2). The primary end point was percentage of patients with neutropenia and thrombocytopenia during treatment with radium223+paclitaxel (cycles 2, 3) versus paclitaxel alone (cycle 1). A previously developed dose-exposure-response model describing the time course of radium-223+paclitaxel-induced suppression of absolute neutrophil counts was used to evaluate radium-223+paclitaxel mode of interaction (additive or synergistic). **Results:** Of 22 enrolled patients, 15 were treated; 13 completed cycles 1-3 and were included in the pharmacodynamics analysis; 7 completed all 6 radium-223 cycles. Tumors in treated patients were breast (7 patients), prostate (4 patients), bladder (1 patient), non-small cell lung (1 patient), myxofibrosarcoma (1 patient), and neuroendocrine (1 patient). 7 patients received ≥3 prior chemotherapy treatments. Grade 3/4 treatment-emergent adverse events (TEAEs) occurred in 9 patients, grade 5 TEAEs in 2 patients (both associated with disease progression and unrelated to study treatment), and serious TEAEs in 6 patients. No patients discontinued treatment due to toxicity from the treatment combination. 13 patients had paclitaxel dose modifications (interruptions in 11 and reductions in 5); 5 patients had radium-223 dose modifications (all interruptions). Grade 3/4 TEAEs occurring in >10% of patients were neutropenia (40%), white blood cell count decreased (13%), and leukopenia (13%). In 13 patients who completed cycle 3, grade 3 neutropenia rates in cycles 2 and 3 were 31% and 8%, respectively, versus 23% in cycle 1; there were no cases of grade 4 neutropenia or grade 3/4 thrombocytopenia. The myelosuppression model showed an additive effect of radium-223 to paclitaxel-induced neutropenia, with an additional 10% average decrease in absolute neutrophil count versus paclitaxel alone. **Conclusion:** Radium-223 was well tolerated when combined with paclitaxel, with an additional 10% average decrease in neutrophil levels versus paclitaxel monotherapy, but no other significant additive toxicity. This combination should be explored further in patients with bone metastases.

OP-019

Analysis of Clinical parameters for the outcame prediction of mCRPC patients treated with [223]Ra-dichloride

V. Frantellizzi, G. A. Follacchio, S. Sollaku, J. Lazri, A. Farcomeni, M. Pacilio, M. Liberatore, F. Monteleone, G. De Vincentis; *Sapienza University of Rome, Rome, ITALY.*

Aim: Treatment with [223]Ra-dichloride in mCRPC patients is in use for several years with an increasing clinical experience. It has tried to find some parameters that may predict the prognosis of these patients. PSA and tALP have been extensively studied. Purpose of this study is to evaluate whether the Hemoglobin value associated with numbers of previous chemotherapeutic treatment can be assumed as a predictive tool for Overall Survival (OS). **Materials and Methods:** [223]Ra-dichloride (55 KBq/Kg IVq4w) was administered to 92 consecutive mCRPC symptomatic patients in our Nuclear Medicine Unit in 17 months. Baseline Hemoglobin value and number of systemic treatments prior [223]Ra were evaluated. Multivariate analysis were performed and a ROC curve was built. **Results:** 390 [223]Ra cycles were administered to 92 patients (mean age 73 years). Among 92 patients, 40 (43%) completed the 6 scheduled administrations, 27 patients (29%) discontinued [223]Ra treatment while 25 (27%) were still receiving [223]Ra therapy at the time of analysis. 44 patients were deceased while 22 were in follow-up. 46 (50%) patients had baseline Hemoglobin value higher than 12g/dl. 20 patients (22%) did not receive any treatment before [223]Ra administration, 30 patients (32%) received 1 treatment, 24 patients (26%) received 2 treatments, finally 18 patients (20%) received 3 or more systemic treatments prior [223]Ra. From the start of [223]Ra therapy the median follow-up time was 6 months (1-31). Patients with a baseline Hemoglobin value higher than 12g/dl and lesser of 2 previous chemotherapeutic treatment had a median OS of 10 months (95%CI 7-16 months). Baseline patients' Hemoglobin and number of treatment at multivariable analysis were significantly correlated with OS (HR=0.71, 95%CI 0.58-0.86, *p*<0.001). **Conclusions:** [223]Ra therapy is related to survival and the choice of parameters that improve the prognosis is a continuous challenge. The high Hemoglobin value before the onset of [223]Ra therapy and lower number of previous systemic therapies show a significantly increased survival due to the preserved bone marrow reserve that is crucial in these patients. We recommend, when it is possible, to start early [223]Ra therapy.

| 105 | Sunday, October 22, 2017, 08:00 - 09:30, Hall E2 |

M2M: α-Therapy

OP-020

Preclinical evaluation of astatinated nanobodies for targeted alpha therapy

Y. D. Dekempeneer[1,2], M. D'Huyvetter[1], E. Aneheim[3], C. Xavier[1], T. Lahoutte[1,4], T. Bäck[3], H. Jensen[5], V. Caveliers[1,4], S. Lindegren[3]; [1]Vrije Universiteit Brussel, Jette/ Brussel, BELGIUM, [2]Belgian Nuclear Research Center (SCK•CEN), Mol, BELGIUM, [3]Targeted Alpha Therapy group, University of Gothenburg, Gothenburg, SWEDEN, [4]Nuclear Medicine Department (UZBrussel), Jette/ Brussel, BELGIUM, [5]Cyclotron and PET Unit, Copenhagen, DENMARK.

The use of nanobodies (Nbs) as vehicles in targeted alpha therapy (TAT) has gained traction due to their excellent *in vivo* properties, high affinity and specificity and fast clearance kinetics. This study investigates a novel targeted therapy which combines the α-particle emitter Astatine-211 ([211]At) and the HER2-targeting 2Rs15d-Nb to selectively kill HER2^{+} metastases. To achieve astatinated 2Rs15d-Nbs, two different radiochemical methodologies were validated using 3 prosthetic groups. In the "random labeling method", the primary amines of lysines on the Nb are used as conjugation sites. The "site-specific labeling approach" aims at obtaining a homogeneous tracer population with a fixed conjugation. Here the prosthetic group is conjugated to the carboxyl-terminal cysteine of 2Rs15d-His6-Linker-Cys. The different conjugates were evaluated for their

binding specificity, immunoreactivity and degree of internalisation in HER2+ SKOV-3 cells. Moreover, *in vivo* evaluation in HER2+ SKOV-3 tumor xenografts gave us more insight in the biodistribution of the 3 different 211At-Nbs radioimmunoconjugates. 2Rs15d-Nb was randomly labeled with 211At via the prosthetic groups N-succinimidyl-3-(trimethylstannyl)benzoate (**m-eATE**) and N-succinimidyl3-[211At]astato-4-guanidino-methylbenzoate (**SGMAB**), while 2Rs15d-His6-Linker-Cys was site-specifically labeled using N-[2-(maleimido)ethyl]-3-(trimethylstannyl)benzamide (**MSB**). The immunoreactive fraction (IRF) was evaluated on HER2+ cells using the Lindmo assay. *In vivo* biodistribution of the 3 different 211At-Nbs was evaluated in HER2+-SKOV-3 tumor xenografts. Furthermore, *ex vivo* α-camera imaging was done on tumor, kidneys, stomach, lungs, spleen. Radioastatination of 2Rs15d-Nb using m-eATE resulted in a radiochemical yield (RCY) of 75,4% and a RP of 99,09%. The use of SGMAB resulted in a RCY of 31,02% and a RP of 98,44%. Finally, the site-specific labeling with MSB resulted in a RCY of 73% and a RP of 96,34%. The IRF of astatinated me-ATE-, SGMAB- and MSB-Nb was 51,3%, 65% and 78%, respectively. Furthermore, binding to HER2 could be blocked (p<0.0001) for the three different astatinated Nbs, confirming its specificity of binding. The tumor uptake of 211At-SGMAB-Nb was 8,86;5,18; 5,35; 0,94 % ID/g at 1, 3, 6 and 24 h, respectively. Except for the kidneys, rapid clearance of 211At-SGMAB-Nb from normal tissues was observed. Although higher activity levels were measured in stomach, lungs and spleen of m-eATE and MSB coupled Nbs. Based on this preclinical data, 211At-SGMAB-Nb is the preferred radioimmunoconjugate for targeting HER2-expressing malignancies, due to its superior labeling purity, IRF, binding specificity, internalization rate and biodistribution. Overall, the results are highly encouraging and suggest that 211At-labeled anti-HER2-Nbs requires further investigation and optimization.

OP-021

Locoregional alpha-RIT, a novel therapeutic option, against peritoneal metastasis of gastric cancer

H. K. Li[1,2,3], Y. Morokoshi[3], S. Hasegawa[3]; [1]Graduate School of Medical and Pharmaceutical Sciences, Chiba University, Chiba, JAPAN, [2]Research Fellow of Japan Society for the Promotion of Science, Tokyo, JAPAN, [3]National Institute of Radiological Sciences, QST, Japan, Chiba, JAPAN.

Objective: Gastric cancer is one of the main causes of cancer related death. It is curable at early stage, but it often being found at late stage with metastasis because of the asymptomatic. Patients with peritoneal metastasis of gastric cancer (PMGC) have extremely poor prognosis because no effective therapeutics has been established. About 20% of GC is reported as HER2-overexpressed (HER2+), and a humanized anti-HER2 monoclonal antibody, trastuzumab, has been clinically used for the treatment of HER2+ PMGC. Locoregional radioimmunotherapy (RIT) has huge advantage in targeting metastatic cancer existing inside of body cavities, such as PM, for delivering radioisotopes directly to the tumor. Alpha-emitter is getting higher attention for the application to RIT because its physical characteristics, high liner

energy transfer and short range, meet the conception of ideal RIT, providing higher damages to targeted tumor and limit damage to surround normal tissues. Astatine 211 (211At) is one of the attractive alpha-emitter for clinical use. The aim of this study is to establish an efficient alpha-RIT against HER2+ PMGC by evaluating the advantage and therapeutic efficacy of locoregional alpha-RIT with 211At-trastuzumab using preclinical mouse model. **Material and Methods:** 211At was produced via 209Bi(α,2n)211At reaction using cyclotron in NIRS and labeled to trastuzumab. PMGC mouse model was established by injecting luciferase labeled N87, HER2+ human GC cell line, into the abdominal cavity of SCID mice a week before the treatment. The biodistribution of 211At-trastuzumab in PMGC model mice with both intraperitoneal (i.p.) and intravenous (i.v.) injection were monitored up to 24 h post injection. Locoregional alpha-RIT was demonstrated by injecting 211At-trastuzumab (1 MBq) i.p. to PMGC model mice and monitored the tumor by in vivo bioluminescence images. PBS, intact trastuzumab and free 211At (1MBq) were also injected to mice as individual controls. The number of white blood cells (WBC) and bodyweight were monitored to check the side effects. **Results:** The biodistribution results referred faster and higher tumor accumulation of 211At-trastuzumab by i.p. compare to i.v. injection. The activity of 211At in blood was able to be reduced by i.p. injection. Locoregional alpha-RIT with 211At-trastuzumab effectively cured PMGC in vivo and significantly prolonged the survival of preclinical model mice compare to other controls. No significant leukopenia and bodyweight loss were observed. **Conclusions:** Our preclinical study suggested that locoregional alpha-RIT with 211At-trastuzumab could be a novel therapeutic option for HER2+ PMGC.

OP-022

Re-localization of 212Pb from 224Ra sources due to thoron (220Rn) diffusion

E. Napoli[1,2,3], S. Westrøm[1,2,3], T. B. Bønsdorff[3], Ø. S. Bruland[1,2,3], R. H. Larsen[4]; [1]University of Oslo, Oslo, NORWAY, [2]The Norwegian Radium Hospital, Oslo, NORWAY, [3]Oncoinvent AS, Oslo, NORWAY, [4]Sciencons AS, Oslo, NORWAY.

Aim: Alpha-particle-emitting radium nuclides have been the subject of considerable biomedical research due to their highly localized effect. Radium-224, with a convenient half-life of 3.6 days, has promising properties for use against micro-metastatic disease. The aim of this work was to investigate the radiation safety aspects with a focus on thoron (220Rn) diffusion from its parent nuclide 224Ra. Thoron diffusion was studied for 224Ra either as free cation in solution or bound to biocompatible calcium carbonate (CaCO3) microparticles. **Materials and Methods:** Radium-224 was extracted from 228Th immobilized on Actinide Resin in 1 M hydrochloric acid (HCl). The acid was evaporated and the residue reconstituted in 0.1 M HCl and subsequently neutralized with ammonium acetate. The CaCO3 microparticles were prepared by precipitation of the combination of sodium carbonate and calcium chloride solutions. Thereafter, the microparticles were radiolabeled by mixing with 224Ra solution at neutral pH. Re-localization of 212Pb, due to thoron escape from solu-

tions of free ^{224}Ra and ^{224}Ra-CaCO$_3$ microparticle suspensions, was studied in various experimental setups. The potential leakage of thoron was examined from frequently used containers such as: 1.5/5 ml Eppendorf tubes, 6 ml Chromacol head-space injection vials capped and crimped with a stopper and different size of syringes. In addition, the influence of liquid volume on thoron diffusion into air was studied from open vials. Due to its short physical half-life of 56 s, thoron diffusion into the air was evaluated by measuring its decay product ^{212}Pb, which has a longer half-life of 10.64 h. Gamma-counting was performed with the Hidex Automatic Gamma Counter (Turku, Finland). **Results:** The results indicate that free cationic ^{224}Ra solutions and ^{224}Ra-CaCO$_3$ microparticle suspensions can be used in a safe manner, without significant leakage of thoron, when contained in vials or syringes. The data shows that at very low volumes *i.e.* 10-100 μl, there is significant diffusion of thoron from free cationic ^{224}Ra solutions into air from open vials. Less diffusion from open vials was observed with ^{224}Ra-CaCO$_3$ suspensions. Diffusion from 10 μl volumes was between 70% and 95% less for ^{224}Ra-CaCO$_3$ in comparison with free cationic ^{224}Ra solutions. **Conclusion:** When considering the low expected activity level needed for a therapeutic dosing, the current work indicates that, with certain precautions, ^{224}Ra based biomedical products can be used in a safe manner for the hospital staff and patients.

OP-024

Novel Intracavitary α-Therapeutic Based on Calcium Carbonate Microparticles As Carriers for ^{224}Ra: Biodistribution and Toxicity in Mice

S. Westrøm[1,2,3], *T. B. Bønsdorff*[3], *M. M. Malenge*[3], *Ø. S. Bruland*[1,2,3], *R. H. Larsen*[4]; [1]*University of Oslo, Oslo, NORWAY,* [2]*The Norwegian Radium Hospital, Oslo University Hospital, Oslo, NORWAY,* [3]*Oncoinvent AS, Oslo, NORWAY,* [4]*Sciencons AS, Oslo, NORWAY.*

Aim: Peritoneal carcinomatosis occurs when cancer cells from a primary tumor in an adjacent organ migrate into the peritoneal cavity and cause micrometastases. Intraperitoneal radiation therapy with β-emitting ^{32}P-colloid was previously used in treatment of ovarian cancer. It was shown to be as effective as adjuvant cisplatin, but resulted in higher incidence of late bowel complications, most likely caused by the several millimeters range of ^{32}P-electrons. Our aim was to design an intracavitary treatment for peritoneal carcinomatosis with highly localized effect to minimize risk of irradiation of surrounding normal tissues. We have developed a novel therapeutic based on CaCO$_3$ microparticles as carriers for the α-emitter ^{224}Ra, a nuclide which emits four α-particles during its decay and has considerably shorter range than ^{32}P. Here, the preparation of the product is presented along with evaluation of tissue distribution and toxicity in mice. **Materials and Methods:** CaCO$_3$ microparticles with median diameters from 2-20 μm were prepared by spontaneous precipitation and radiolabeled by co-precipitation of ^{224}Ra on the particle surface. The labeling yield was determined and retention of ^{224}Ra on the microparticles was investigated *in vitro*. Biodistribution after intraperitoneal administration of the radiolabeled microparticles was studied in immunodeficient

athymic nude mice and compared with that of free ^{224}Ra. Toxicity of the ^{224}Ra-labeled CaCO$_3$ microparticles was evaluated in immunocompetent BALB/c mice. **Results:** Radiolabeling of the CaCO$_3$ microparticles was successful and resulted in high yield. Experiments also showed that ^{224}Ra was well retained on the microparticles for several days *in vitro*. Because of the bone-seeking capacity of ^{224}Ra, the stability of the radiolabeled particles *in vivo* could be determined from the uptake of ^{224}Ra in mice femurs. A fundamental shift in tissue radiation exposure was observed when free ^{224}Ra was compared with ^{224}Ra-labeled CaCO$_3$ microparticles. The femur uptake of ^{224}Ra was significantly reduced and radioactivity on intraperitoneal tissues and surfaces was substantially increased after administration of ^{224}Ra-labeled CaCO$_3$ microparticles. In immunocompetent mice, doses up to 1000 kBq/kg of ^{224}Ra-labeled microparticles were well-tolerated and no clinical signs of toxicity were observed. **Conclusion:** Efficient ^{224}Ra-labeling of the CaCO$_3$ microparticles was achieved with high retention of the radionuclide by the particles *in vitro*. The *in vivo* studies show that ^{224}Ra-labeled CaCO$_3$ microparticles could be safely administered in mice at therapeutically relevant doses and with a high degree of intraperitoneal retention. In conclusion, the novel α-emitting microparticles have properties that make them a promising new modality for intracavitary cancer therapy.

OP-025

A Novel Multi-Component Reaction for ^{211}At-Astatination: Providing new Tools for (pre)Targeted Alpha Therapy

C. Denk[1], *E. H. K. Aneheim*[2], *S. Lindegren*[2], *M. Herth*[3,4], *M. Wilkovitsch*[1], *H. Mikula*[1]; [1]*Vienna University of Technology, Vienna, AUSTRIA,* [2]*The Sahlgrenska Academy, University of Gothenburg, Gothenburg, SWEDEN,* [3]*Ringhospitalet, Copenhagen, DENMARK,* [4]*University of Copenhagen, Copenhagen, DENMARK.*

Purpose & Introduction: The α-emitter ^{211}At is a highly promising radionuclide for targeted alpha therapy (TAT). ^{211}At is the only α-emitter used in therapy that allows for covalent labeling, thus preventing the use of chelators. Although astatine is the rarest naturally occurring element, ^{211}At can be produced in medium energy cyclotrons. In general, astatinations are carried out utilizing stannyl-precursors and oxidative conditions. Due to the low abundance of this element, the chemistry of astatine is rather unexplored. The availability of other straight forward radio-astatination procedures would extend the variety of accessible ^{211}At-TAT agents, leading to more options in the treatment of malignant disease. **Methods & Results:** Within this contribution a novel methodology for introduction of ^{211}At into small molecules is presented. In this multi-component labeling reaction, an azide-moiety (**A**), an alkyne-moiety (**B**), and ^{211}At are combined using base and metal catalysis. The product formed consists of a 1,2,3-triazole (**T**) bearing both structural motifs (**A** and **B**) with the astatine located at the triazole system (**A**-**T**(^{211}At)-**B**). The reaction, which is unaffected by high starting activities, was optimized towards reaction time and radiochemical yield (RCY), finally providing >70% RCY within 10 min. The reaction is highly tolerant considering the structural motifs **A**

and **B**, as shown in a related study applying [125]I.[1] This allows high structural variation, enabling straight-forward tuning of pharmacokinetic properties. We chose to use biotin-azide as **A** and tetrazine-alkyne as **B**, giving rise to a [211]At-agent that is suitable for biotin/streptavidin or tetrazine/*trans*-cyclooctene (TCO) based labeling and pre-targeting studies. The structure of the product was verified by binding experiments to TCO and streptavidin modified beads. Stability of the astatine-triazole bond was investigated by incubation of formed [211]At-Beads in plasma for 300min, showing 88% intact substance. Stability was further increased to 99% by click-assembly of a PEG-corona to the bead, using the tetrazine moiety of this multifunctional agent. **Discussion & Conclusion:** To the best of our knowledge we have developed a new, high yielding, fast and versatile labeling system for astatine-211. Applying this chemistry, we prepared the first [211]At-labeled 1,2,4,5-tetrazine that furthermore bears a biotin motif. This agent is capable of binding to TCO and/or streptavidin in a highly efficient manner, providing a tool for pre-targeted alpha radiotherapy (pTAT) and macromolecule labeling. We are convinced that this new astatination-strategy is a step forward towards broader application of TAT by expanding the variety of [211]At based therapeutic agents. [1]Yan et.al *JACS*,2013

OP-026

Bismuth-213 labeled nanobodies as a new treatment approach in Targeted Alpha Therapy

Y. Dekempeneer, Jr.[1,2], *D. Maertens*[2], *M. Gysemans*[2], *T. Lahoutte*[1,3], *M. D'Huyvetter*[1], *T. Cardinaels*[2,4], *V. Caveliers*[1,3]; [1]*Vrije Universiteit Brussel, Jette/ Brussel, BELGIUM,* [2]*Belgian Nuclear Research Center (SCK•CEN), Mol, BELGIUM,* [3]*Department of Nuclear Medicine (UZBrussel), Jette/ Brussel, BELGIUM,* [4]*Department of Chemistry (KU Leuven), Leuven, BELGIUM.*

The use of nanobodies (Nbs) as vehicles in targeted alpha therapy (TAT) has gained traction due to their excellent in vivo properties, high affinity and specificity, fast diffusion and clearance kinetics. Moreover, Nbs show good tumor penetration due to their small size. The main strength of TAT is the potential to deliver a high level of ionizing radiation in a localized manner because of the short range of alpha particles in tissue. In combination with a tumor-seeking vehicle, TAT could specifically eliminate isolated cancer cells, while causing little damage to healthy cells. The aim of this study is to develop a novel molecular targeted therapy that combines the α-particle emitting radioisotope Bismuth-213 ([213]Bi) and the HER2-targeting 2Rs15d-Nb to selectively destroy HER2-positive metastases. From an onsite [229]Th source, the purified [225]Ac is loaded on a pre-packed column containing AG MP-50 cation exchange resin. In dilute acid, both [225]Ac and [213]Bi are efficiently adsorbed to this cation exchange resin due to their stable 3+ oxidation state. [213]Bi is selectively eluted from the cation exchange resin as anionic BiI_4^- / BiI_5^{2-} species. Chemical separation experiments were performed on non-radioactive solutions (were La was used as simulant for Ac) to develop a reliable Ac/Bi separation methodology which will then be applied on radioactive [225]Ac. Different bed volumes

and eluents concentrations were evaluated. Inductively-coupled plasma mass spectrometry (ICP-MS) was used to evaluate the performance of the separation methodology. The final goal is to produce high purity [213]Bi and minimize [225]Ac breakthrough. In a next step, [213]Bi-labeled HER2-targeting 2Rs15d-Nbs will be developed. Therefore, classical diethylenetriaminepentaacetic acid (DTPA) and 1,4,7,10-tetraazacyclododecane-N,N',N'',N'''-tetra-acetic acid (DOTA) derivatives will be used as bifunctional chelator, conjugated to tumor-targeting 2Rs15d-Nbs on one hand and complexing [213]Bi on the other hand. The different conjugates will be evaluated for their stability, binding specificity and immunoreactivity in HER2^{pos} SKOV-3 cells. Due to the 46 min half-life of [213]Bi, the [213]Bi labeling reaction and quality control of [213]Bi preparations must be performed in a very short time frame to avoid significant decay losses.

---

106 Sunday, October 22, 2017, 08:00 - 09:30, Hall F1

Pitfalls & Artefacts 1 (Interactive) - Neuroimaging/Physics/EFOMP: Pitfalls and Artefacts in Visual vs. Quantitative Reading

OP-027

Instrumentation Induced Artefacts in PET and SPECT
N. Belcari; University of Pisa, Pisa, ITALY

OP-028

Brain FDG PET
S. D. Morbelli; San Martino Hospital, Genoa, ITALY

OP-029

DAT SPECT
P. Payoux; Centre Hospitalier Universitaire Purpan, Toulouse, FRANCE

OP-030

Amyloid PET
J. Arbizu; Clinica Universidad de Navarra, University of Navarra, Pamplona, SPAIN

---

108 Sunday, October 22, 2017, 08:00 - 09:30, Hall K

Committee Symposium 1 - Inflammation & Infection/Drug Development: 68Ga-Tracers for Infection Imaging

OP-031

Advantages and Possibilities of 68Gallium Tracers
I. Velikyan; Uppsala University, Dep. of Medicinal Chemistry, Uppsala, SWEDEN.

OP-032

68Ga-Ubiquidicin
M. Sathekge; University of Pretoria and Steve Biko Academic Hospital, Dep. of Nuclear Medicine, Pretoria, SOUTH AFRICA.

OP-033
68Ga-Biotin
E. Lazzeri; Regional Center of Nuclear Medicine AOUP, Pisa, ITALY.

OP-034
68Ga-Citrate
C. Nanni; Policlinico S.Orsola-Malpighi, Department of Nuclear Medicine, Bologna, ITALY.

---

110   **Sunday, October 22, 2017, 08:00 - 09:30, Hall G2**

Joint Symposium 16 - EANM/JSNM: Educating Referring Physicians and Recognising Their Needs

OP-036
Increasing the Reliance of Referring Physicians on Nuclear Cardiology: A Cardiologist's Perspective
T. Chikamori; Department of Cardiology, Tokyo Medical University, Tokyo, JAPAN.

OP-037
The Role of PET for Selecting Surgical Candidates and Deciding a Mode of Surgery for Lung Cancer
K. Suzuki; Department of General Thoracic Surgery, Juntendo University School of Medicine, Tokyo, JAPAN.

OP-038
The Integration of Dementia Molecular Imaging into Clinical Management
V. Garibotto; Geneva University and Geneva University Hospitals, Geneva, SWITZERLAND.

201/203   **Sunday, October 22, 2017, 10:00 - 11:15, Hall A**

Plenary 1: Theranostic Developments for Prostate Cancer (incl. Marie Curie Lecture)

OP-040
Clinical Aspects
J. Walz; Institute Paoli-Calmettes, Dept. of Urology, Marseille, FRANCE.

OP-041
PSMA Imaging – Which Knife is the Sharpest?
K. Herrmann; Universitätsklinikum Würzburg, Nuclear Medicine, Würzburg, GERMANY.

OP-042
PSMA Labelled with Alfa-Emitters
U. Haberkorn; University Hospital Heidelberg, Department of Nuclear Medicine, Heidelberg, GERMANY.

---

301   **Sunday, October 22, 2017, 11:30 - 13:00, Hall A**

CME 2 - Inflammation & Infection/ESVS: Vascular Graft Infection

OP-043
Importance of Imaging Vascular Graft Infections in Clinical Practice
N. Chakfé; University Hospital of Strasbourg, Department of Vascular Surgery and Kidney Transplantation, Strasbourg, FRANCE.

OP-044
Radiological Possibilities in Vascular Graft Infections
L. Marques; Ev.-Luth. Diakonissenanstalt zu Flensburg In guten Händen, Flensburg, GERMANY.

OP-045
Nuclear Medicine Possibilities in Vascular Graft Infections
C. Lauri; "Sapienza" University, Osepdale S. Andrea, Nuclear Medicine Unit, Faculty of Medicine and Psychology, Dept. of Medical-Surgical Sciences and Translational Medicine, Rome, ITALY.

---

302   **Sunday, October 22, 2017, 11:30 - 13:00, Hall B**

Joint Symposium 2 - EANM/ENETS: Establishing a Position for PRRT in the Multidisciplinary Treatment of NETs

OP-046
Current Status of PRRT in the Post-NETTER1 Phase
L. Bodei; Memorial Sloan Kettering Cancer Center, New York, UNITED STATES OF AMERICA.

OP-047
Lessons from the Various Clinical Trials in NETs: Evidence-Based Results and Post-Hoc Analysis
M. Pavel; Campus Virchow-Klinikum Charité, Centrum 13, Berlin, GERMANY.

OP-048
Where does PRRT fit in?
D. O'Toole; Trinity College Dublin, the University of Dublin, St James's Hospital & National Centre for Neuroendocrine Tumours | St Vincent's University Hospital, Dublin, IRELAND.

---

303   **Sunday, October 22, 2017, 11:30 - 13:00, Hall C**

CTE 2 - Joint Session with EARL: Technologist Role in Research and EARL Accreditation

OP-049
Research Opportunities as a Nuclear Medicine Technologist
K. Pathmaraj; Austin Health Melbourne, Department of Molecular Imaging and Therapy, Melbourne, AUSTRALIA.

OP-050

EARL Accreditation Projects and Possible Evolution

R. Boellaard; University of Groningen, Center for Medical Imaging, Groningen, NETHERLANDS.

OP-051

Technologist Involvement in Accreditation and Future Directions

G. Testanera; Department of Nuclear Medicine, Barts Health NHS Trust, London, UNITED KINGDOM.

---

304   **Sunday, October 22, 2017, 11:30 - 13:00, Hall E1**

Do.MoRe: Modeling & Radiobiology

OP-053

DNA damage in blood leukocytes after internal in-vitro irradiation of blood with the α-emitter ^{223}Ra

S. Schumann[1], U. Eberlein[1], R. Muhtadi[2], M. Lassmann[1], H. Scherthan[2]; [1]University of Würzburg, Würzburg, GERMANY, [2]Bundeswehr Institute of Radiobiology affiliated to the University of Ulm, München, GERMANY.

Introduction: ^{223}Ra-dichloride is the first α-emitter that has been licensed for the treatment of metastatic castration-resistant prostate cancer. In this study we investigate radiation-induced DNA double strand break (DSB) formation by internal irradiation of blood leukocytes with ^{223}Ra using co-localizing foci of γ-H2AX and 53BP1 DNA damage biomarkers. The aim was to quantify the induction of DSBs and to correlate the results to the absorbed dose to the blood, thus generating an in-vitro calibration curve for ^{223}Ra. **Methods:** Blood samples from six healthy volunteers were split into 3.5 ml aliquots to which 1 ml of a ^{223}Ra solution was mixed followed by incubation at 37℃ on a roller-mixer for 1h. Additionally, corresponding baseline samples without radioactivity were prepared. The ^{223}Ra activity in each sample was chosen to result in absorbed doses to the blood up to 150 mGy and determined individually with a calibrated germanium detector. After leukocyte separation, fixation and two-color immunofluorescent staining, the number of the radiation-induced co-localizing γ-H2AX and 53BP1 foci were detected manually using a fluorescence microscope equipped with a red/green double band pass filter. The average absorbed dose rates to the blood per nuclear disintegration in 1 ml of blood were calculated for all nuclides of the decay chain under the assumption that the energy off all non-penetrating particles is deposited locally. **Results:** In contrast to β- and γ-emitters, α-particles do not generate distinct foci but tracks that consist of multiple foci representing complex DNA damage. The number of α-tracks in 100 cells was evaluated for 36 blood samples with absorbed doses ranging from 0 to 142 mGy. A linear regression showed a good correlation (r^2=0.94) between the number of α-tracks per 100 cells and the absorbed dose to the blood. The linearity is in agreement with our previously established calibration curves for distinct foci

generated by β-emitters. The number of foci per cell for small distinct foci assumed to be induced by β-particles was similar to the baseline values, which is in agreement with the low absorbed β-doses (~3.7% of the total absorbed dose). **Conclusion:** A linear relationship between the number of α-induced DNA damage tracks and the absorbed dose to the blood could be established. Since the individual foci in α-tracks cannot be resolved by conventional microscopy techniques, a direct comparison to DNA damage foci values obtained by γ- and β-emitter exposure is currently not possible.

OP-054

Involvement of cell cycle checkpoints in the therapeutic efficacy of ^{177}Lu-lilotomab in non-Hodgkin B-cell lymphoma

A. Pichard[1], A. Courteau[2], S. Marcatili[2], G. Cartron[3], I. Isabelle Navarro-Teulon[1], A. Repetto-Llamazares[4], H. Heyerdahl[4], M. Bardiès[2], J. Dahle[4], J. Pouget[1]; [1]IRCM/INSERMU1194, Montpellier, FRANCE, [2]Centre de Recherche en Cancérologie de Toulouse, Toulouse, FRANCE, [3]Centre Hospitalier Universitaire de Montpellier, Montpellier, FRANCE, [4]Nordic Nanovector ASA, Oslo, NORWAY.

Aims: To elucidate the mechanisms of action of radioimmunotherapy with ^{177}Lu-labeled lilotomab (Betalutin®) directed against the CD37 receptor on non-Hodgkin lymphoma (NHL) B-cells, we have developed a radiobiological approach that discriminates between the cytotoxic effects of unlabelled antibodies and of radiation. Comparison was done with ^{177}Lu-rituximab. **Materials and Methods:** *In vitro*, Ramos (Burkitt), DOHH2 (follicular) and Rec-1 (mantle) lymphoma cell lines were exposed for 18 hours to increasing activities (0—6 MBq/mL) of ^{177}Lu-rituximab, of ^{177}Lu-lilotomab, of the non-specific ^{177}Lu-cetuximab or to unlabelled mAbs (0-40μg/mL). A radiobiological model considering the contribution of cytotoxic effects of ^{177}Lu (radiation only) and of unlabelled antibody (mAb only) to the cytotoxicity of ^{177}Lu-mAbs was established. We next investigated in which B-cell NHL subtypes ^{177}Lu-lilotomab would be the most efficient and how biological (genetic background, cell cycle, apoptosis) and/or physical (tumour absorbed doses) parameters could affect the final therapeutic outcome. *In vivo*, mice bearing subcutaneous Ramos or DOHH2 tumour xenografts, were treated at MTA of ^{177}Lu-mAbs and tumour growth was monitored. Organ and tumour absorbed doses were determined according to MIRD formalism. **Results:** We showed in the three lymphoma cell lines that unlabelled rituximab was more cytotoxic than lilotomab. When antibodies were radiolabeled, ^{177}Lu-lilotomab was as cytotoxic as ^{177}Lu-rituximab in the radiosensitive DOHH2 cells, but not in the most radioresistant Ramos cells. The higher response to ^{177}Lu-lilotomab in DOHH2 cells than in Ramos cells was mainly mediated by lack of G2/M cell cycle arrest followed by strong induction of apoptosis in DOHH2 cells. Inhibition of signal pathways involved in cell cycle control radiosensitized Ramos cells. These results were supported by *in vivo* data. ^{177}Lu-lilotomab was as efficient as ^{177}Lu-rituximab in Ramos tumour xenograft models only if tumour absorbed radiation dose was increased over a certain

limit. Conversely, in DOHH2 tumour xenografts, ^{177}Lu-lilotomab was as efficient as ^{177}Lu-rituximab for similar absorbed radiation doses, although lilotomab was less efficient than rituximab. **Conclusion.** A radiobiological approach identified the parameters determining ^{177}Lu-lilotomab therapeutic efficacy in different subtypes of lymphoma.

OP-055

Internal exposure of [131]I - potential biomarkers and functional analysis for long-term effects in thyroid

M. Larsson[1], N. Rudqvist[1], J. Spetz[1], B. Langen[1], T. Parris[2], K. Helou[2], E. Forssell-Aronsson[1]; [1]Department of Radiation Physics, Institute of Clinical Sciences, Sahlgrenska Cancer Center, Sahlgrenska Academy, Gothenburg, SWEDEN, [2]Department of Oncology, Institute of Clinical Sciences, Sahlgrenska Cancer Center, Sahlgrenska Academy, Gothenburg, SWEDEN.

Aim: [131]I is a commonly used isotope in radiotherapy of different diseases, such as thyroid cancer and hyperthyroidism (^{131}I iodide), neuroblastoma, pheochromocytoma and paraganglioma (^{131}I-MIBG), and with ^{131}I-labelled monoclonal antibodies. However, there is a lack of knowledge of the long-term effects on thyroid tissue, after treatment with ^{131}I-containing radiopharmaceuticals. The aim of the present study was to identify biomarkers for long-term effects of ^{131}I exposure of the thyroid, related to thyroid function and cancer, using rats as a model system. **Materials and Methods:** Young male Sprague Dawley rats (5w) were i.v. injected with 0, 0.5, 5.0, 50 and 500 kBq [131]I ($D_{thyroid}$ = 0-10 Gy). The rats were killed 9 months after injection and thyroid and blood samples were collected. Microarray analysis (Agilent) was performed on RNA isolated from thyroid. Differentially expressed transcripts and associated GO-terms were identified using Nexus Expression 3.0. Proteins from thyroid and blood samples were analyzed by LC-MS/MS. For functional annotation of proteins, GO-term association was performed using DAVID bioinformatics research tool. Canonical pathway, function and diseases, and upstream regulation analysis was performed using Ingenuity Pathway Analysis (IPA) software. **Results:** The IPA and GO-term analyses showed a difference in biological effects dependent on dose and tissue type. In the IPA analysis, LC-MS/MS-data from thyroid samples had the most significant influence on both canonical pathways, biological functions and upstream regulators. Most of the significantly regulated canonical pathways were up-regulated and the majority were only present in one dose group, but NGF2-mediated oxidative stress response was present in three of the dose groups. In the biological functions and diseases analysis, an association with features regarding cell development and survival was seen. Only a few up-stream regulators were significantly regulated, including PPARG which was seen in all four test groups. PPARG is not found in normal thyroid and may indicated malfunction and potentially certain types of thyroid cancer. In the GO-term analysis, metabolism (nucleic acid-related response) showed the highest response to ^{131}I irradiation. On the other hand, little or no response to DNA integrity was seen. **Conclusion:** In conclusion, effects on thyroid function depend on the administrated dose and are not strictly proportional with dose. A potential thyroid function candidate marker is the up-stream regulator PPARG, but further tissue analysis is necessary to fully evaluate its potential as a cancer biomarker.

OP-056

Contribution of macro and micro-dosimetry in alphatherapy

N. Benabdallah[1], M. Bernardini[2], D. Franck[1], C. de Labriolle-Vaylet[3,4], W. Bolch[5], A. Desbrée[1]; [1]IRSN - Institute for Radiological Protection and Nuclear Safety, Fontenay aux Roses, FRANCE, [2]Georges Pompidou European Hospital, Paris, FRANCE, [3]UPMC, University of Paris 06 Biophysics, Paris, FRANCE, [4]Trousseau Hospital, Paris, FRANCE, [5]Department of Biomedical Engineering, University of Florida, Gainesville, FL, UNITED STATES OF AMERICA.

Purpose: In nuclear medicine, the injected activity needs to be personalized for each patient. For alpha-particle emitting radiopharmaceuticals, a personalized dosimetry is challenging because of the short range of alpha particles. The aim of this work was to develop tools to optimize patient-specific dosimetry in alphatherapy. To that aim, the study focuses on [223]Ra-dichloride (Xofigo®) used for the treatment of patients with castration-resistant prostate cancer metastasized to bones. **Methods:** First, quantitative imaging must be performed to characterize the macroscopic biodistribution of the radiopharmaceutical in the patient body. As SPECT imaging gives a better quantification than planar imaging, the possibility of quantitative SPECT imaging of [223]Ra was investigated for the first time. Several phantoms studies were performed in order to determine the best SPECT/CT imaging protocol, according to the MIRD Pamphlet No. 23. Then, as bone marrow is an organ at risk for these treatments, the dose to this region is needed. Current dose models do not account for energy or bone-site dependence as shown by alpha-particle absorbed fractions given in ICRP Publication 30. Using the most realistic voxelized model of the skeleton for adult male that describes the bones at a microscopic scale, developed by the University of Florida, and MCNP6 Monte Carlo code, the S-values to the two radiosensitive tissues, endosteum and red bone marrow, have been calculated for several source tissues such as the trabecular bone, the yellow marrow or the cortical bone. Furthermore, as the marrow cellularity is dependent of the age, the evolution of alpha absorbed fraction to the red bone marrow with the marrow cellularity was studied. Finally, the short range of alpha-particles relative to the typical scale of human organ dimensions can lead to a highly non-uniform irradiation of the target volume. The microdistribution of [223]Ra was investigated in skeletally mature mice and metastasis models, using autoradiography. **Results:** Quantification accuracies of approximately 4% for a 5.6mL sphere containing 20kBq/mL can be expected. This protocol has been implemented in a new clinical trial for treatment of patients with bone metastases in renal cell carcinoma. Differences, up to 50% when considering the trabecular bone surface as source and red bone marrow as target, were observed between our model and the ICRP Publi-

cation 30. The autoradiography images will be used to correlate absorbed dose to therapeutic response. **Conclusion:** This study investigates different aspects of the ^{223}Ra dosimetry and offers tools to optimize dosimetry for other alpha emitters.

OP-057

Monte-Carlo modelling of energy deposition within a realistic 3D model of follicular lymphoma

J. Bordes[1,2], S. Incerti[3,4], C. Rossi[1,2,5], J. Bordenave[1,2], C. Bezombes[1,2], M. Bardies[1,2], M. Bordage[1,2]; [1]Centre de Recherches en Cancérologie de Toulouse, Toulouse, FRANCE, [2]UMR 1037 Inserm/UPS, Toulouse, FRANCE, [3]Centre d'Etudes Nucléaires de Bordeaux-Gradignan, Gradignan, FRANCE, [4]CNRS / IN2P3 / Université de Bordeaux, Gradignan, FRANCE, [5]Service d'hématologie clinique, CHU le Bocage, Dijon, FRANCE.

Aim: Small-scale dosimetry modelling often considers spherical tumours and uniform source distributions. However, geometry and radiopharmaceutical distribution is known to impact energy deposition in targeted radionuclide therapy (Arnaud *et al.* NIMB 316:227-233 2016). In this study, we used an innovative 3D model of follicular lymphoma and rituximab distributions to model energy that would be imparted by different radioisotopes in a context of radioimmunotherapy (RIT). **Material and methods:** The starting point of this study is a 3D model of follicular lymphoma (Gravelle *et al.* Am J Pathol 184:282-95 2014), named Multicellular Aggregates of Lymphoma Cells (MALC). MALCs were incubated with rituximab, an anti-CD20 monoclonal antibody used in the treatment of non-Hodgkin lymphomas. Geometry, antibody location and concentration were extracted from single plan illumination microscopy. Assuming antibody labelling with Auger (^{111}In and ^{125}I) or β- (^{90}Y, ^{131}I and ^{177}Lu) emitters, we simulated energy deposition in MALCs using two Monte-Carlo codes. Interactions of low-energy electrons (Auger) were simulated using the Geant4-DNA toolkit with the CPA100 set of physics models recently validated from 10 eV to 250 keV (Bordage *et al.* Physica Medica 32:1833-1840 2016), whereas β- emitters were simulated using the Geant4 toolkit with the Livermore set of physics models, validated from 250 eV to 1 GeV. For each isotope, 10^6 decays were considered. **Results:** Rituximab was concentrated in the periphery of a 1 mm diameter MALC. For Auger emitters, energy deposition was mostly local, with 67% vs. 30% of voxels hit for ^{111}In vs. ^{125}I, respectively. In comparison, β- emitters deposited energy inside at least 96% of the MALC's voxels. Within the MALC, ^{111}In and ^{125}I deposited 22 and 19 keV/decay, whereas ^{131}I, ^{177}Lu and ^{90}Y deposited 83, 82 and 66 keV/decay, respectively. This results from β- emitters releasing more energy per decay than Auger emitters, but also from the relationship between radiation range and MALC geometry: for example, despite higher emitted energy, ^{90}Y deposits less energy per decay inside the MALC than the other ß emitters. **Conclusion:** This study combined realistic geometry and vector distribution with Monte-Carlo modelling of ionizing radiation interactions to evaluate the potential of several isotopes for NHL RIT. In the tested configuration, β- emitters delivered energy inside nearly all the voxels of the MALC. In terms of energy depos-

ited in the targets, ^{131}I and ^{177}Lu proved more effective than ^{90}Y. Future work will consider MALCs of different sizes and different antibody repartitions.

OP-058

Voxel-based multi-model fitting method for modelling time activity curves in SPECT images

D. Sarrut, Sr.[1], A. Halty[1], J. Badel[2], L. Ferrer[3], M. Bardies[4]; [1]CREATIS / CLB, Lyon, FRANCE, [2]CLB, Lyon, FRANCE, [3]ICO / CRCINA, Nantes, FRANCE, [4]CRCT, Toulouse, FRANCE.

Purpose: Estimating the biodistribution and the pharmacokinetics from time-sequence SPECT images on a per-voxel basis is useful for studying activity non-uniformity or computing absorbed dose distributions by convolution of voxel kernels or Monte-Carlo radiation transport. Current approaches are either region-based, thus assuming uniform activity within the region, or voxel-based but using the same fitting model for all voxels. **Methods:** We propose a voxel-based multi-model fitting method (VoMM) that estimates a fitting function for each voxel by automatically selecting the most appropriate model among a predetermined set with Akaike criteria. This approach can be used to compute the time integrated activity (TIA) for all voxels in the image. To control fitting optimization that may fail due to excessive image noise, an approximated version based on trapezoid integration, named restricted method, is also studied. From this comparison, the number of failed fittings within images was estimated and analyzed. Numerical experiments were used to quantify uncertainties and feasibility was demonstrated with real patient data. **Results:** Regarding numerical experiments, root mean square errors of TIA obtained with VoMM were similar to those obtained with bi-exponential fitting functions, and were lower (< 5 % vs > 10%) than with single model approaches that consider the same fitting function for all voxels. Failure rates were lower with VoMM and restricted approach than with single-model methods. On real clinical data, VoMM was able to fit 90% of the voxels and led to less failed fits than single-model approaches. On regions of interest (ROI) analysis, the difference between ROI-based and voxel-based TIA estimations was low, less than 4%. However, the computation of the mean residence time exhibited larger differences, up to 25%. **Conclusions:** The proposed voxel-based multi-model fitting method, VoMM, is feasible on patient data. VoMM leads to similar organ-based TIA estimations as conventional ROI-based method. However, for pharmacokinetics analysis, studies of spatial heterogeneity or voxel-based absorbed dose assessment, VoMM could be used preferentially as it prevents model overfitting.

OP-059

A Monte Carlo method to evaluate confidence intervals of time-integrated activity curve in molecular radiotherapy

B. Cassano[1], A. Napolitano[1], M. Longo[1], E. Genovese[1], S. Donatiello[1], T. Insero[1], E. Richetta[2], M. Pasquino[2], M. Stasi[2], M. Pacilio[3], V. Cannatà[1]; [1]Medical Physics Unit, Bambino Gesù Children's Hospital, Rome, ITALY, [2]Medical Physics Department, AO Ordine Mauriziano

di Torino, Turin, ITALY, [3]Medical Physics Department, Azienda Ospedaliera Universitaria Policlinico Umberto I, Rome, ITALY.

Purpose/Introduction: In molecular radiotherapy (MRT) calculating biokinetic parameters plays a crucial role to assess the absorbed dose to lesions or organs at risk. The assessment of the time-integrated activity curve is affected by fitting model, number of acquired points and sampling timing. The main purpose of this work was to introduce a methodology which is able to estimate error associated to Time-Integrated Activity Coefficient (TIAC) and mainly due to the uncertainty in fitting procedure. This method was applied to whole-body and blood biokinetic data of patients affected by metastatic differentiated thyroid cancer (mDTC) enrolled in two different Italian Hospitals. **Subjects & Methods:** The Monte Carlo method is implemented in matlab and relied on the generation of a large number of data-set based on root mean square error (RMSE) associated to the fit model. To compute the confidence intervals of the time-integrated activity coefficient, physical constraints on fit parameters were introduced. Biokinetic data (time acquisition window of about 50 hours) of 35 patients affected by mDTC and administered with two different radionuclides (^{123}I and ^{131}I) were analyzed, by fitting all data sets with a mono-exponential curve. Two classes of data sets were considered: Low Number of Points (LNP) and High Number of Points (HNP) time-activity data, consisting of 4 and 20 points respectively. As the confidence intervals of TIAC are not symmetric respect to the best-fit values, both upper and lower bandwidths were calculated. The correlation between RMSE and bandwidths was also investigated. **Results:** The bandwidths assessed ([mean lower, mean upper]) was [-14.3, +17.1]% for LNP and [-9.3, +10.6]% for HNP. The RMSE is demonstrated to be correlated to the bandwidths with two different power laws for LNP and HNP. For LNP the R^2 was 0.98 and 0.97 for lower and upper band respectively while for HNP the R^2 was 0.94 and 0.97 for lower and upper band. **Discussion/Conclusion:** The method is very simple to be implemented and it has the advantage of high flexibility when there is need to impose physical constraints to the fitting. As expected, the bandwidths decrease when considering data with a larger number of points. Moreover, having our data similar time window acquisition, the RMSE itself has been observed as a good predictor of the bandwidths as computed with the present method. The proposed method is also versatile and can be employed to calculate the confidence interval of time activity data, regardless instrumentation and administered radionuclides

OP-060

Validation of a voxel-dosimetry and radiobiology tool for patient specific peptide receptor radionuclide therapy

D. Finocchiaro[1,2], S. Berenato[3], E. Grassi[1], F. Fioroni[1], G. Castellani[2], N. Lanconelli[2], A. Versari[4], E. Spezi[3], M. Iori[1]; [1]Medical Physics Unit, Arcispedale Santa Maria Nuova-IRCCS, Reggio Emilia, ITALY, [2]Dept. of Physics, University of Bologna, Bologna, ITALY, [3]School of Engineering, Cardiff University, Cardiff, UNITED KINGDOM, [4]Nuclear Medicine Unit, Arcispedale Santa Maria Nuova-IRCCS, Reggio Emilia, ITALY.

Purpose: In this work VoxelMed2.0 (VM) , the voxel dosimetry tool developed at ASMN-IRCCS, is validated in a phantom and patient study, in comparison with Raydose (Monte Carlo based software, Cardiff University) and OLINDA. The aim is to assess the importance of estimating an accurate voxel level absorbed dose and biological effective dose (BED) for individualized therapy. **Subjects & Methods:** The phantom validation was performed with: a homogeneously 177Lu-filled cylindrical phantom (Jaszczak, Data Spectrum Corporation), an anthropomorphic phantom (Liqui-Phil™,The Phantom Laboratory) with organ shaped inserts (liver,spleen,pancreas,kidneys) and two cylindrical phantoms with in total 11 inserts different for shape and volume (toroidal 3,3,10ml; ellipsoidal 4,15,28ml; cylinder-like 28,29ml and pyramid-like 29,30,31ml). Every phantom was scanned once and the time-activity-curve obtained by 177Lu physical decay. For the clinical validation 50 patients were scanned 5 times, after a therapeutic administration of 177Lu. Images were acquired with a Siemens Symbia T2 SPECT-CT. The percentage difference (PD) between VoxelMed2.0 and either of the two reference software was evaluated for mean dose. Mean BED for patients and dose-volume histograms (DVH) of phantoms also were evaluated. **Results:** PDs for homogeneous phantom were: -12% VM vs OLINDA, and -5% VM vs Raydose. PDs (VM-Olinda/VM-Raydose) were: (-29%/-31%) toroid-3ml and (-23%/-16%) toroid-10ml. Mean PDs (VM-Olinda[SD]/VM-Raydose[SD]) for the other inserts: (-19%[2%]/-8%[20%]) ellipsoid, (-21%[0%]/3%[4%]) pyramid-like, (-21%[1%]/4%[8%]) cylinder-like. PD (VM-Olinda/VM-Raydose) for organ inserts were: -14%/-8% pancreas, -13%/-5% kidney, -12%/-6% spleen, -12%/-6% liver. Dose maps obtained by the two voxel-dosimetry software showed visually similar dose distributions, and DVH showed similar slopes. As regards patients VoxelMed2.0 was compared with OLINDA, obtaining mean PD [SD]: -12%[10%] kidney, -5%[11%] liver and -9%[9%] for spleen. Variance analysis provided statistical difference in the dose measured for kidney and for liver (p-value 0.006 and 0.012), while no statistical difference for spleen (p-value 0.268). Similar PD remains for the BED calculations. **Conclusions:** In phantoms we obtained different dose values for the three software, most likely because of the different method of calculation. In particular differences were more pronounced for irregular geometries of VOI (i.e. toroidal), while there is a best accordance for homogenous and anthropomorphic phantoms. In general we observed the best agreement between VoxelMed and Raydose, while greater difference in respect to OLINDA. For patients the variance analysis between VoxelMed and OLINDA doses showed that the two populations are significantly different in case of kidney and liver, even if further investigations is required. Work supported by EMPIR-MRTDosimetry project(15HLT06), co-funded by EU's Horizon-2020-programme.

---

305   Sunday, October 22, 2017, 11:30 - 13:00, Hall E2

M2M: Antibodies

OP-061

Immunotargeting of Galectin-3 in thyroid orthotopic tumor models opens new challenges for thyroid cancer imaging and biological characterization in vivo

C. D'Alessandria[1], F. De Rose[1], M. T. Kuhlmann[2], M. Braeuer[1], S. Reder[1], S. Braesh-Andersen[3], A. Bartolazzi[4], M. Schwaiger[1]; [1]Klinikum rechts der Isar - Technical University of Munich, Munich, GERMANY, [2]European Institute for Molecular Imaging (EIMI), University of Münster, Münster, GERMANY, [3]Mabtech AB Research Laboratory, Stockholm, SWEDEN, [4]Pathology Research Laboratory, Sant'Andrea Hospital, University Sapienza, Rome, ITALY.

Introduction: The preoperative characterization of thyroid nodules is challenging. Thyroid scintigraphy with radioiodine provides functional information (cold or hot nodules) based on radio-iodine uptake, but fails to distinguish among benign and malignant lesions. Galectine-3 is expressed in well-differentiated thyroid carcinomas but not in normal thyrocites or benign nodules. Herein, we aimed to demonstrate the specificity of Galectin-3 immuno-targeting compared to radio-iodine imaging in thyroid orthotopic tumor models, which mimic the human condition. **Methods:** FRO82-1 and CAL62 carcinoma cells were chosen and characterized for Gal-3 and sodium/iodide symporter (NIS) expression via WB and qPCR. A anti-Gal3 F(ab')$_2$ fragment was generated from a rat mAb via pepsin digestion, functionalized with DFO-NCS, labeled with ^{89}Zr and characterized for binding and immunoreactivity on 2D cell cultures. Iodine-125 internalization studies using both cell lines were also performed. Binding of ^{89}Zr-DFO-F(ab')$_2$ anti-Gal3 and iodine-125 accumulation were evaluated on tumor spheroids. Thyroid orthotopic murine model were established by inoculation of FRO82-1 and CAL62 cells into the left thyroid lobe of athymic nude mice, and tumor growth was monitored weekly via US imaging. Mice were imaged by PET/CT after i.v. injection with Iodine-124 and later with ^{89}Zr-DFO-F(ab')$_2$ anti-Gal3, followed by biodistribution studies and immunohistochemistry analysis for Gal-3 and NIS expression. **Results:** FRO82-1 and CAL62 carcinoma cells were invariably Galectin-3 positive, while being NIS+ and NIS- respectively. ^{89}Zr-DFO-F(ab')$_2$ anti-Gal3 showed high stability, high affinity to Gal3 (K_d ~0.5 nM) and immunoreactivity (>75%) on 2D cell cultures and specific binding on tumor spheroids. Iodine-125 was internalized by FRO82-1 cells while background accumulation was measured for CAL62 cells, both in 2D and spheroids. *In vivo* PET/CT imaging showed excellent image contrast for ^{89}Zr-DFO-F(ab')$_2$ anti-Gal3 and signal associated to the orthotopic-implanted tumors. Iodine-124 signal was visible for FRO82-1 tumors (NIS+) with only background signal for CAL62 tumors (NIS-). Biodistribution studies for ^{89}Zr-DFO-F(ab')$_2$ anti-Gal3 revealed higher uptake in tumor-bearing thyroid lobe and no uptake in the healthy thyroid, due to Gal-3 expression in tumor-bearing left lobes and absence in tumor-free right lobes. Differential accumulation of iodine-124 was measured based on NIS expression. **Conclusions:** Using thyroid orthotopic models, we reproduced the clinical situation with *hot* (FRO82-1) and *cold* (CAL62) nodules, based on radio-iodine uptake. Specific and selective accumulation of ^{89}Zr-DFO-F(ab')$_2$ anti-Gal3 even in absence of radioiodine uptake was demonstrated. Translation of this method in clinical setting promises to improve and change the management of patients bearing thyroid nodules allowing tumor biological characterization *in vivo*.

OP-062

Pretargeted radionuclide therapy of HER2-expressing SKOV-3 human xenografts using an Affibody molecule-based PNA-mediated pretargeting

M. Altai[1], K. Westerlund[2], M. Konijnenberg[3], B. Mitran[4], M. Oroujeni[1], M. de Jong[3], A. Eriksson-Karlström[2], A. Orlova[4], V. Tolmachev[1]; [1]Institute of Immunology, Genetics and Pathology, Uppsala, SWEDEN, [2]Division of Protein Technology, Royal Institute of Technology, Stockholm, SWEDEN, [3]Department of Nuclear Medicine and Radiology, Erasmus MC, Rotterdam, NETHERLANDS, [4]Division of Molecular Imaging, Uppsala, SWEDEN.

Aim: Targeting using radiometal-labelled affibody molecules is associated with high renal uptake and retention of radioactivity. Reducing kidney uptake of radioactivity by e.g. co-injecting Gelofusine or amino acids was inefficient. Pretargeting is a promising approach to overcome renal toxicity. We developed a pretargeting approach based on hybridization between two complementary peptide nucleic acids (PNAs). The primary targeting agent is $Z_{HER2:342}$-SR-HP1, an anti-HER2 affibody-PNA chimera containing HP1 PNA. The complementary PNA HP2 probe contains DOTA and can be labelled with a variety of radiometals. In the current study we optimized this pretargeting approach using ^{177}Lu and performed experimental therapy study. **Methods:** Tumour targeting of ^{177}Lu-HP2 was studied in mice bearing HER2-overexpressing SKOV-3 ovarian carcinoma xenografts preinjected with $Z_{HER2:342}$-SR-HP1 4, 8, or 16 h in advance. Dosimetry was evaluated and pre-clinical therapeutic study was assessed. **Results:** Tumour uptake of ^{177}Lu-HP2 (1 µg) 1h p.i. was 75-fold higher for the pretargeted (18.4±1 %ID/g) than the non-pretargeted group (0.23±0.08%ID/g). The tumour uptake of ^{177}Lu-HP2 (1 µg) 1h p.i. was 22±5, 21±3 and 18±1 %ID/g when mice were pre-injected with 50 µg $Z_{HER2:342}$-SR-HP1 at 4, 8 and 16 h respectively. Interestingly the kidney uptake decreased significantly from 16±6 %ID/g (when ^{177}Lu-HP2 was injected 4h p.i. of $Z_{HER2:342}$-SR-HP1) to 4±1 and 2.8±0.2 %ID/g (8 and 16 h post $Z_{HER2:342}$-SR-HP1 injection, respectively). The tumour-to-kidney ratio was the highest (ca.6), at 16 h post $Z_{HER2:342}$-SR-HP1 injection. ^{177}Lu-HP2 uptake in the tumour exceeded that in any other organ up to 216 h p.i. Estimated absorbed radiation doses (Gy/MBq) to the tumour per single treatment cycle was ca. 1.08 Gy/MBq, 5-fold higher than the kidney dose of 0.21 Gy/MBq. Mice (n=10/group) were treated weekly (for 6 weeks) with iv doses of (A) PBS, or (B) 100µg $Z_{HER2:342}$-SR-HP1, or (C) 3.5 µg, 16 MBq^{177}Lu-HP2, or (D) preinjected 100µg $Z_{HER2:342}$-SR-HP1 followed 16 h later by 3.5 µg, 16 MBq^{177}Lu-HP2 (corresponding to 6 x 17 Gy tumour dose). Group D demonstrated significant inhibition of tumour growth. The median survival was 37 d for A, 32 d for B, 37 d for C and 66 d for D. Treatment was not associated with the loss of body weight, which indicates its moderate toxicity at a kidney dose of 6 x 3.3 Gy. **Conclusion:** The use of affibody-based PNA-mediated pretargeting can deliver high dose to tumours while sparing kidneys. Experimental therapy studies showed clear improvement of survival in treatment group compared to control groups.

OP-063

Immuno-PET imaging for PD-L1 expression in non-small cell lung cancer xenograft

*D. Li, S. Cheng, S. Zou, D. Zhu, **X. Zhu**; Tongji Hospital, Tongji Medical College, Huazhong University of Science and Technology, Wuhan, CHINA.*

Programmed cell death protein-1 and programmed cell death ligand-1 (PD-1/PD-L1) axis, known as a main immune checkpoint inhibitory pathway, plays a critical role in cancer immunotherapy. Antibodies targeting the PD-1/PD-L1 pathway have shown durable tumor regression and improved patient survival in the treatment of a broad set of cancer subtypes, such as Hodgkin lymphoma, non-small cell lung cancer, melanoma, renal cell carcinoma, et al. Patients with tumors expressing PD-L1 are most likely to respond to anti-PD-1/PD-L1 treatment. The aim of this study is to develop a novel immune-PET technique to non-invasive determine and timely monitor tumor PD-L1 expression in vivo, which could help to select the patients who are most likely to benefit from anti-PD-1/PD-L1 treatment and evaluate the prognosis. **Methods**: KN035, an anti-PD-L1 heavy chain antibody selected from a large camel naïve phage display Nanobody library, was labeled with radionuclide 89Zr through conjugated to pisothiocyanatobenzyl-desferrioxamine (Df-Bz-NCS). The resulting probe, 89Zr-Df-KN035, was then evaluated by in vitro cell uptake and blocking studies using PD-L1 positive cell lines, human lung adenocarcinoma cell line A549. Next, serial immnuo-PET (at 1, 6, 24, 48, 72 and 120 h post-injection respectively, n=4) and biodistribution studies were performed in nude mice bearing A549 tumor xenografts to evaluate in vivo performance of 89Zr-Df-KN035. Furthermore, the mice were received 100 mg/kg of gefitinib by intragastric administration once a day for 21 days (n=6). After that, immnuo-PET was performed at 48 h post-injection of 89Zr-Df-KN035. **Results**: Serial immnuo-PET imaging revealed that A549 tumors xenografts were clearly visible from 24h to 120h after radiotracer injection, while markedly reduced accumulations of 89Zr-Df-KN035 were noticed in blocking group. Moreover, tumor uptakes of 89Zr-Df-KN035 decreased after gefitinib therapy, confirmed by the PD-L1 expression with IHC. **Conclusion**: 89Zr-Df-KN035 demonstrates promise for use as an immuno-PET agent to image tumor PD-L1 expression in living system, as well as monitor the change of tumor PD-L1 expression in real time after therapy, which might be helpful in selection of patients with NSCLC performing anti-PD-1/ anti-PD-L1 antibody therapy.

OP-064

SPECT imaging of carbonic anhydrase IX with 111In-girentuximab-F(ab')2 as radiotracer in head and neck xenografts

F. J. Huizing, B. A. W. Hoeben, S. Heskamp, J. Bussink, O. C. Boerman; Radboudumc, Nijmegen, NETHERLANDS.

Introduction: Tumor hypoxia is a major cause of radio- and chemoresistance in solid tumors. Carbonic anhydrase IX (CAIX) is an endogenous hypoxia-related marker strongly associated with poor outcome, which makes it an important prognostic and predictive marker. Assessment of CAIX expression may allow patient selection and monitoring for hypoxia- or CAIX-targeted treatment combined with radiotherapy. The aim of this study was to validate and optimize 111In-girentuximab-F(ab')$_2$ SPECT for imaging of CAIX expression in head and neck tumor models. **Methods:** The optimal timing and protein dose for imaging were determined in athymic nude mice with subcutaneous SCCNij153 xenografts (head and neck squamous cell carcinoma with high CAIX expression). SPECT/CT images were acquired of mice with SCCNij202 and SCCNij153 xenografts. The non-specific tumor-targeting property of 111In-girentuximab-F(ab')$_2$ was determined by blocking the specific uptake with co-injection of unlabeled G250 IgG. Tracer uptake was determined using SPECT/CT, ex vivo radioactivity counting and autoradiography of tumor sections. Spatial correlation between immunohistochemical staining of CAIX expression and tracer uptake on autoradiography was determined. **Results:** Optimal SPECT/CT images were obtained at 24 hours after injection of the tracer. A protein dose of 10 μg resulted in the highest tumor-to-blood ratio after 24 hours post-injection. Ex vivo measurements showed a tumor uptake of 3.0 ± 0.9 %ID/g, and a tumor-to-blood ratio of 31:1. Unlabeled G250 IgG markedly reduced tumor uptake to 1.1 ± 0.3 %ID/g. Immunohistochemistry and autoradiography images of tumor sections showed a distinct spatial correlation between localization of the tracer and CAIX expression. **Conclusion:** 111In-girentuximab-F(ab')$_2$ shows specific targeting of CAIX-expression in head and neck squamous cell carcinoma xenografts. For optimal pre-clinical imaging in mice, a tracer protein dose of 10 μg should be administrated 24 hours before scanning. These results indicate that 111In-girentuximab-F(ab')$_2$ is a promising tracer for imaging of hypoxia-induced CAIX expression. In ongoing studies we will assess the tracer's applicability for treatment selection and monitoring of hypoxia response to therapy.

OP-065

Ab-1881, An Anti-PDL1 Immune Checkpoint Inhibitor Serves as A Theranostic Agent for Cancer Immunotherapy

*M. Xu, Y. Han, **Z. Liu**; Peking University, Beijing, CHINA.*

Objective: Inhibiting PD-1/PD-L1 pathway using antiPD-1 or antiPD-L1 antibody has shown great success on cancer treatment. However, only 20~25% cancer patients exhibit positive response to PD-L1 immunotherapy. Though immunohistochemistry (IHC) is the gold standard for patient classification, a non-invasive method is highly favored for clinical diagnosis. Herein, we report a new antiPD-L1 monoclonal antibody (Ab1881), of which Copper-64 labelled derivative exhibited significantly different tumor uptake on PD-L1 positive and negative types of xenografts. In addition, the xenografts of high Ab1881 uptake demonstrated notable therapeutic efficacy, while the xenografts of low Ab1881 uptake kept growing rapidly till scarification, demonstrating a strong correlation between PET imaging and therapeutic efficacy. **Method:** Ab1881 was

conjugated with a bifunctional chelator 2-S-(4-Isothiocyanato-benzyl)-1,4,7-triazacyclononane-1,4,7-triacetic acid (p-SCN-Bn-NOTA) to give NOTA-Ab-1881. Copper-64 radiolabeling was conducted in sodium acetate buffer (pH=4), and quality control was performed by radio-HPLC equipped with size-exclusion column. The metabolic stability of ^{64}Cu-NOTA-Ab1881 was assessed under both *in vitro* and *in vivo* conditions. PET imaging and bio-distribution studies were performed in mice bearing MC38 (PDL1 positive) and 4T1 (PDL1 negative) xenografts on the left and right shoulder, respectively. Ab1881 treatment was performed 3 days a time, 0.25 mg for each therapy. **Result:** Cu-NOTA-Ab1881 and Ab1881 bound to PD-L1 with the binding affinity of 0.47 ± 0.12 nM and 0.92 ± 0.33 nM, respectively. ^{64}Cu-NOTA-Ab1881 exhibited 4.7 ± 2.1, 10.3 ± 3.2, 14.3 ± 4.1, 19.7 ± 3.7 %ID/g uptake in MC38 xenografts at 2.0, 4.0, 12.0, 24.0 hours post injection, respectively. Meanwhile, ^{64}Cu-NOTA-Ab1881 exhibited 3.7 ± 1.3, 4.3 ± 1.2, 5.3 ± 2.1, 6.8 ± 2.7 %ID/g uptake in 4T1 xenografts at 2.0, 4.0, 12.0, 24.0 hours post injection, respectively. The rest of radiotracer was excreted mainly through hepatobiliary system, and liver uptake reached to maximum at around 12 hours post injection, which is 17 ± 4.3%ID/g. In regards to treatment, xenografts of MC38 kept the same size if did not shrink at day 21 post therapy. In contrast, at day 21, xenografts of 4T1 were 12.7 ± 1.2 times larger than them of day 0. **Conclusion:** A Copper-64 labelled Ab1881 was reported that successfully distinguished PD-L1 positive and negative xenografts in mouse model with PET imaging. Moreover, Ab1881 also demonstrate impressive therapeutic efficacy, which is highly correlated to the tumor uptake of its radioactive derivative.

OP-066

Monitoring tumor PD-L1 expression with microSPECT/CT during radiotherapy

S. Heskamp, J. D. M. Molkenboer-Kuenen, G. W. Sandker, P. J. Wierstra, J. Bussink, O. C. Boerman; Radboud University Nijmegen Medical Centre, NIJMEGEN, NETHERLANDS.

Introduction: Programmed death-1 (PD-1) is expressed by T-cells and is a major co-inhibitory immune checkpoint. Its ligand PD-L1 is expressed on tumor cells. By upregulating PD-L1, tumors are capable of escaping immune recognition and attack. Clinical trials with anti-PD-1/PD-L1 immune checkpoint inhibitors (ICI) have shown impressive and durable antitumor activities. However, only a subgroup of patients benefit from these drugs. To use ICI more effectively, rational treatment combination strategies are warranted. Imaging of tumor PD-L1 expression during conventional anti-cancer treatment may aid in finding optimal treatment combination strategies. Here, we studied the potential of PD-L1 microSPECT/CT imaging to monitor changes in PD-L1 expression during radiotherapy. **Material and Methods:** Anti-murine PD-L1 antibody was radiolabeled with ^{111}In and in vitro binding was assessed using CT26 (low PD-L1), LLC1 (low PD-L1), and B16F1 (high PD-L1) tumor cells. Mice were injected s.c. with CT26, LLC1, or B16F1 cells in the right hind leg. Tumors were irradiated with a single dose of 10 Gy. Control mice were not irradiated. One day after irradi-

ation, mice received 25 MBq ^{111}In-labeled anti-PD-L1 antibody (30 μg), followed by microSPECT/CT imaging and ex vivo bio-distribution one day post injection. Tumors were stained for PD-L1 by immunohistochemistry. **Results:** ^{111}In-labeled anti-PD-L1 showed specific binding to CT26 (5.7 ± 0.5%), LLC1 (10.7 ± 0.3%), and B16F1 (26.8 ± 1.0%) cells in vitro. MicroSPECT/CT showed increased uptake of the radiolabeled anti-PD-L1 antibody in irradiated tumors versus non-irradiated CT26 tumors (23.4 ± 2.1 %ID/g versus 15.2 ± 2.7 %ID/g, p=0.003). In LLC1 and B16F1 tumors, the difference in tracer uptake between irradiated versus non-irradiated tumors was not significant (LLC1: 14.0 ± 1.7 versus 11.7 ± 2.5 %ID/g, B16F1 17.0 ± 0.2 versus 16.3 ± 3.4 %ID/g). Immunohistochemical staining showed that the increased tumor uptake in CT26 tumors was related to increased PD-L1 expression. **Conclusion:** These studies demonstrate that PD-L1 microSPECT/CT can be used to monitor the dynamic expression levels of PD-L1 in syngeneic murine tumor models during radiotherapy. This technique can potentially be used to monitor PD-L1 during conventional anti-cancer treatment to find optimal ICI treatment combination strategies.

OP-067

PET Imaging of Programmed Cell Death Protein 1 (PD-1) in a Humanized Mouse Model of Lung Cancer

W. Cai, D. Jiang, C. G. England, T. E. Barnhart; University of Wisconsin-Madison, Madison, WI, UNITED STATES.

Objectives: PET imaging of human programmed cell death protein 1 (PD-1) could have profound clinical utility in personalized/precision cancer immunotherapy. Therefore, this study investigates a novel radiotracer targeting PD-1 (^{89}Zr-Df-Nivolumab) for mapping the biodistribution of activated PD-1-expressing T-cells (which is expected to localize to the tumor) in a humanized murine model of lung cancer. **Methods:** Nivolumab (FDA-approved for PD-1 targeted cancer therapy) was conjugated to p-SCN-deferoxamine and radiolabeled with Zr-89 to form ^{89}Zr-Df-Nivolumab. Humanized tumor-bearing mice were created by first implanting one million A549 cells into 6-8 week-old non-obese diabetic severe combined immunodeficient (SCID) gamma (NSG) mice. Once the tumor reached 1-2 mm in diameter, mice were intravenously injected with human peripheral blood mononuclear cells (hPBMCs) to form PBL tumor-bearing mice. Two weeks after injection of hPB-MCs, mice were injected with ^{89}Zr-Df-Nivolumab for serial PET imaging. Region-of-interest (ROI) analyses of the images and ex vivo biodistribution studies were performed to determine tracer uptake in major organs/tissues and quantitative results were given as percentage injected dose per gram of tissue (%ID/g). Fluorescence immunohistochemistry was performed to assess the expression of PD-1 and CD3 (T-cell markers) in excised tissues. **Results:** The expression of human PD-1 was investigated in three groups by injection of ^{89}Zr-Df-Nivolumab, including humanized tumor-bearing mice (PBL-A549) and non-humanized tumor-bearing mice (NSG-A549). In PBL-A549 mice, tracer accumulation in the tumor was 6.93±1.21 and 9.85±2.74 %ID/g at 72 and 168 h post-injection. ^{89}Zr-Df-Nivolumab uptake in

the tumor of non-humanized NSG-A549 mice was significantly lower at 5.35±0.48 and 3.88±0.38 %ID/g at the same time points, suggesting that the accumulation was nonspecific due the significant decrease from 72 to 168 h. To further investigate human PD-1 specificity of [89]Zr-Df-Nivolumab, a nonspecific tracer ([89]Zr-Df-IgG) was injected into PBL-A549 mice. As expected, tumor uptake was low with the maximum signal of 3.08±0.40 %ID/g at 72 h post-injection. *Ex vivo* biodistribution validated these findings with PBL-A549 mice showing the highest tumor uptake. Confocal imaging of tissue sections revealed high CD3 and PD-1 expression in the tumor, spleen, and lung of PBL-A549 mice, indicative of PD-1-expressing T-cells. Minimal signal was found in the tissues from NSG-A549 mice. **Conclusion:** [89]Zr-Df-Nivolumab was successfully used to monitor the distribution of PD-1-expressing T-cells in humanized mouse models of lung cancer. This tracer holds great promise to aid in further understanding of immune checkpoint blockade therapy and the development of future PD-1-targeted imaging strategies.

OP-068a

Radiocobalt-labeled anti-HER1 affibody molecule DOTA-$Z_{EGFR:2377}$ for imaging of low HER1 expression in prostate cancer pre-clinical model

B. Mitran[1], J. Garousi[1], M. Rosestedt[1], E. Lindström[1], K. G. Andersson[2], S. Ståhl[2], J. Löfblom[2], V. Tolmachev[1], A. Orlova[1]; [1]Uppsala University, Uppsala, SWEDEN, [2]KTH-Royal Institute of Technology, Stockholm, SWEDEN.

Aim: Expression of human epidermal growth factor receptor type I (HER1) in prostate cancer (PCa) is associated with disease progression towards castration resistance. These receptors are potential targets for second line therapy in PCa and imaging of their expression might serve for patient stratification and therapy monitoring. Imaging of HER1 in PCa is however challenging due to the relatively low receptor expression and endogenous expression in many healthy organs (e.g. liver and intestinal walls). Earlier, we have demonstrated that imaging contrast could be improved by (i) optimization of injected protein dose and (ii) by extending the time between administration and imaging. Using of PET should further improve imaging sensitivity. The aim of this study was to prove the hypothesis that radiocobalt labeled affibody molecule DOTA-$Z_{EGFR:2377}$ could be used for imaging of low expression of HER1 in PCa. **Methods:** Cobalt-57 was used as a surrogate to positron emitter cobalt-55 (T1/2=17.5 h). Affinity and cellular processing of cobalt labeled affibody DOTA-$Z_{EGFR:2377}$ was studied using PCa cell line DU145 (2x10^{5} receptors/cell). The biodistribution pattern of [57]Co-DOTA-$Z_{EGFR:2377}$ in DU145 xenografted mice was compared (i) after the injection of 35 and 10 μg of conjugate and (ii) at 3, 7 and 24 h pi of 10 μg of conjugate. **Results:** Radiocobalt labeled affibody DOTA-$Z_{EGFR:2377}$ retained subnanomolar affinity to HER1. The strong binding to low HER1-expressing PCa cells is important because [57]Co-DOTA-$Z_{EGFR:2377}$ demonstrated a very low internalization rate. Binding of the radioconjugate to cells decreased in the presence of anti-HER1 therapeutic mAb cetuximab. In vivo radioactivity uptake in blood, lungs, intestines and tumors was 2-fold high-er for mice injected with 10 μg of radioconjugate compared to the 35 μg group. However, the uptake in liver increased only by 60% after the 10 μg injection and the uptake in muscles was not changed. With time, the release of radioactivity from tumors was slower than from healthy tissues with the exception of kidneys. Tumor-to-organ ratios (T/O) increased with time after administration and, at 24 h pi, T/O were 3.5±0.2 for blood, 2.2±0.5 for colon, 7±1 for muscle, and 4.0±0.7 for bones (relevant organs for PCa imaging). High contrast images of PCa xenografts were obtained despite low HER1 expression. **Conclusion:** Radiocobalt-labeled DOTA-$Z_{EGFR:2377}$ is a promising imaging agent for the detection and monitoring of HER1 expression in PCa.

OP-068b

Preclinical evaluation of a single-chain variable anti TEM-1 fragment labeled with ^{111}In and [152]Tb

F. Cicone[1,2], T. Denoël[1], D. Viertl[1], G. Jakka[3], M. Irving[3], S. Dunn[3], T. Stora[2,4], N. P. van der Meulen[5], C. Müller[5], C. Vermeulen[5], U. Köster[6], K. Johnston[4], S. Gnesin[1], N. Riggi[7], N. Schaefer[1], G. Coukos[2,3], J. O. Prior[1,2]; [1]Nuclear Medicine, CHUV, Lausanne, SWITZERLAND, [2]Marie Sklodowska-Curie Innovative Training Network MEDICIS-PROMED, CERN, Geneva, SWITZERLAND, [3]Ludwig Center for Cancer Research, Lausanne, SWITZERLAND, [4]ISOLDE/CERN, Geneva, SWITZERLAND, [5]Paul Scherrer Institut, Villigen-PSI, SWITZERLAND, [6]Institut Laue-Langevin, Grenoble, FRANCE, [7]Molecular Pathology, CHUV, Lausanne, SWITZERLAND.

Purpose: Tumor Endothelial Marker-1 (TEM-1) is a promising target for immunotherapy, being upregulated by tumor cells, tumor vasculature and tumor-associated microenvironment. Our purpose was to test in-vitro and in-vivo a single-chain variable fragment directed against TEM1 (scFv78-Fc) labeled with either ^{111}In or [152]Tb, a positron-emitting CERN-produced radionuclide. **Methods:** [152]Tb was produced by proton-induced spallation of tantalum targets followed by mass separation, and purified using cation exchange chromatography. A concentrated solution of scFv78-Fc in pH 9.0 buffer and 10 eq. of CHX-A''-DTPA chelator were conjugated by heating at 42°C for 1 h, and then purified with a 50 kDa filter. [111]In or [152]Tb were complexed by additional 1 h heating at 42°C. The maximum binding sites (B_{max}) of purified TEM1 antigen and equilibrium dissociation constant (K_d) were determined with Scatchard plot. Immunoreactivity (IR) was determined by Lindmo plot. Two human cell lines, RD-ES (Ewing Sarcoma) and SK-N-AS (Neuroblastoma) were xenografted in NOD-SCID common gamma KO female mice. TEM1 expression was confirmed by fluorescence-activated cell sorting; antigen positivity was additionally proven by immunohistochemistry in excised tumors. Biodistribution was assessed 5, 24 and 48 h after i.v. injection of 0.1 MBq ^{111}In-CHX-A''-DTPA-scFv78-Fc (0.2 μg). The non-tumor antigenic sink was evaluated by co-injecting different amounts of unlabeled scFv78-Fc (range 0.2 - 200 μg). Additionally, after validation of [152]Tb activity quantification with a NEMA NU4 phantom, tumor-bearing mice were injected with 7 MBq [152]Tb-CHX-A''-DTPA-scFv78-Fc for μPET imaging and dosimetry (μSPECT/PET/CT Albira, Bruker). **Results:** Radiolabeling yield was >80% for both [111]In- and [152]Tb-labeled products (iTLC).

99% pure products were obtained after ultrafiltration. B_{max} and K_d were between 2-6 nmol/mg antigen and between 2-8 nM, respectively. IR was retained after radiolabeling (>70%). TEM1 expression was higher in SK-N-AS than in RD-ES cells. The best tumor-to-non-target ratios were obtained by co-injecting 25 µg of unlabeled CHX-A''-DTPA-scFv78-Fc. 24-h percent of injected ^{111}In-CHX-A''-DTPA-scFv78-Fc activity/g varied in the range 8-16, 16-22 and 10-14 for tumor, liver and kidneys, respectively. Tumor-to-background ratios increased slightly between 24 and 48 hours (average 24-h and 48-h tumor-to-liver ratios were 0.55 and 0.64, respectively). µPET imaging of [152]Tb-CHX-A''-DTPA-scFv78-Fc gave results comparable to those of biodistribution, showing enhanced tumor uptake and similar tumor-to-liver ratios. **Conclusion:** The scFv78-Fc anti-TEM1 was successfully labeled with ^{111}In and [152]Tb. Final products showed specific binding and preserved immunoreactivity. Biodistribution and µPET imaging showed favorable tumor uptake in two human tumor cell lines. TEM1 has promise as a target for radiolabeled antibodies.

---

306 Sunday, October 22, 2017, 11:30 - 13:00, Hall F1

Pitfalls & Artefacts 2 (Interactive) - Cardiovascular: Pitfalls and Artefacts with CZT Cameras

OP-069

Acquisition (Detector pbs, Gating, Patient Movement, Quality Control)

O. Lairez; Rangueil University Hospital, Toulouse, FRANCE

OP-070

Image Analysis (Attenuation, Image Quality)

P. L. Jager; Department of Nuclear Medicine, Isala Hospital, Zwolle, NETHERLANDS.

OP-071

Signal Quantification (LVEF, Bulls Eye, Extent of Myocardial Perfusion Abnormality)

A. Gimelli; Fondazione Toscana Gabriele Monasterio, CNR, Pisa, ITALY

OP-072

Blood Pool Gated Acquisitions / Dual Isotope Acquisitions

A. Manrique; Centre Hospitalier Universitaire de Caen, Caen, France

---

307 Sunday, October 22, 2017, 11:30 - 12:45, Hall F2

Clinical Oncology: We want a New Drug

OP-073

Comparison study between 18F-Choline (FCH) and 68Ga-NODAGA-MJ9 (MJ9, Bombesin) PET-CT in prostate cancer initial staging

L. Haefliger[1], P. Mitsakis[1], T. Zilli[2], C. Pozzessere[1], J. Delage[3], H. Maecke[4], R. Mansi[4], R. Miralbell[2,5], N. Schaefer[1], J. Prior[1];

[1]Department of Nuclear Medicine, Lausanne University Hospital, Lausanne, SWITZERLAND, [2]Department of Radiation, Oncology, Geneva University Hospital, Geneva, SWITZERLAND, [3]Department of Pharmacy, Lausanne University Hospital, Lausanne, SWITZERLAND, [4]Department of Nuclear Medicine, University Hospital of Freiburg, Freiburg, GERMANY, [5]Institut Oncològic Teknon, Barcelona, SPAIN.

Purpose: To perform a one-to-one comparison of both ^{18}F-choline (FCH) and ^{68}Ga-NODAGA-MJ9 (MJ9) PET/CT in prostate cancer (PC) initial staging. **Material and Methods**: This prospective study included 15 Patients (age 71±6y [range 59-82y]) with histologically-proven prostate cancer with Gleason score 7±1 (6-9) and PSA 40±73 ng/ml (5.4-300 ng/ml). Initial staging PET/CT was performed both with FCH (200MBq) and MJ9 (200 MBq) 70 min p.i., within a period of 15 days (mean 1.5±3.5d, median 0d, range 0 to 13 day). Lesions were classified according to anatomical region (prostate primary lesion by lobe, lymph node and bone), and SUVmax was recorded in each location both for FCH and MJ9. **Results:** After this initial staging, 10 (66%) patients presented suspicious lymph nodes uptake for a total of 40 lymph nodes considered as metastatic (FCH 5.4±3.1 g/ml, MJ9 9.3± 8.9 g/ml). 2 patients (13%) presented bone metastasis with 4 lesions reported (FCH 9.5±4.7 g/ml, MJ9 4.6±3.6 g/ml). Primary prostate lesions uptake by lobe was inferior on FCH as compared to MJ9 (SUVmax 9.1±2.9 g/ml vs. 13.8±9.0 g/ml), but not significantly. In average, SUVmax, was 63% higher with MJ9 as compared to FCH in the prostate/lymph nodes, but lower for bone lesions (p=0.006). Compared to lymph node, FCH uptake was significantly higher in bone (p=0.048) and prostate (p=0.010), while MJ9 uptake was similar in all site. No significant correlation between FCH or MJ9 uptake and PSA, total Gleason score or age was found, except for higher MJ9 SUVmax in the prostate for higher Gleason score (p=0.003, test for trend). **Conclusion:** In initial prostate cancer staging, MJ9 uptake is significantly higher in the prostate and lymph nodes as compared to FCH, while FCH uptake was significantly higher than MJ9 in bone lesions. Our results show a potential interest for MJ9 in initial staging at the prostate and lymph node level.

OP-074

Clinical translation of bombesin antagonist based GRPR targeting PET radiotracer ^{68}Ga-NOTA-RM26

J. Zhang[1,2], G. Niu[2], X. Fan[3], L. Lang[2], H. Wu[4], J. Zang[1], G. Hou[1], F. Li[1], Z. Zhu[1], X. Chen[2]; [1]Department of Nuclear Medicine, Peking Union Medical College Hospital, Chinese Academy of Medical Sciences and Peking Union Medical College, Beijing, CHINA, [2]Laboratory of Molecular Imaging and Nanomedicine (LOMIN), National Institute of Biomedical Imaging and Bioengineering (NIBIB), National Institutes of Health (NIH), Bethesda, MD, UNITED STATES OF AMERICA, [3]Department of Urology, Peking Union Medical College Hospital, Chinese Academy of Medical Sciences and Peking Union Medical College, Beijing, CHINA, [4]Department of Pathology, Peking Union Medical College Hospital, Chinese Academy of Medical Sciences and Peking Union Medical College, Beijing, CHINA.

Purpose: This study aims to document the first-in-human application of a ^{68}Ga-labeled bombesin-antagonist peptide NOTA-RM26 that targets gastrin releasing peptide receptor (GRPR). We evaluated the safety, biodistribution, calculated the radiation dose, and assessed the clinical diagnostic value in tumors. **Methods:** a macrocyclic chelator, 1,4,7-triazacyclononane-N,N',N''-triacetic acid (NOTA) conjugated GRPR antagonist RM26 was synthesized and labeled with [68]Ga. After the study protocol was approved by the institute review board, five healthy volunteers (M 3, F 2, age range 32-54 y) were enrolled to validate the safety of ^{68}Ga-NOTA-RM26. A total of 36 cancer patients including 18 prostate cancer, 11 breast cancer and 7 glioma with written informed consent were recruited. For the healthy volunteers, after low-dose CT scan, 111-148 MBq of ^{68}Ga-NOTA-RM26 was injected intravenously, followed by serial whole-body PET acquisitions. The acquisition duration was 40 sec/bed position for the 5, 10 and 15 min time points, 2 min/bed position for the 30, 45 and 60 min time points. Dosimetry was calculated using the OLINDA/EXM software. All the patients underwent ^{68}Ga-NOTA-RM26 PET/CT. GRPR immunohistochemical staining of tumor samples against GRPR was performed and correlated with PET. **Results:** The whole labeling process of ^{68}Ga-NOTA-RM26 took about 30 min with a radiochemical purity of greater than 95%. The administration of ^{68}Ga-NOTA-RM26 was well tolerated by all subjects with no adverse symptoms being noticed or reported during the whole procedure and 2 weeks follow up demonstrating the safety. A patient would be exposed to a radiation dose of 2.70 mSv with an injected dose of 129.5 MBq. For the 18 patients with pathologically confirmed prostate cancer by needle biopsy, ^{68}Ga-NOTA-RM26 PET/CT showed positive findings in 12 patients, with tracer strongly localized in primary prostate-confined lesions with SUVmax (7.20 ± 2.06), 19 metastatic lymph nodes with SUVmax (4.98 ± 2.15) and 21 bone metastasis with SUVmax (6.03 ± 4.90), respectively. Moderate to high uptake of ^{68}Ga-NOTA-RM26 were demonstrated in 11 breast cancer. The immunohistochemical staining confirmed positive correlation between the SUVs and GRPR expression level. The SUVmax and SUVmean in glioma patients at 30 min were 1.51 ± 0.28 and 2.80 ± 0.73 and tumor-to-background ratios were 29.7 ± 10.9 and 16.4 ± 7.27, respectively. **Conclusion:** This study indicates the safety and efficiency of bombesin antagonist ^{68}Ga-NOTA-RM26. This novel GRPR targeting PET radiotracer showed significant value in cancer diagnosis. ^{68}Ga-NOTA-RM26 is expected to be an excellent imaging marker to evaluate GRPR expression and guide GRPR-targeted therapy.

OP-075

Correlation of Clinical GRP Receptor PET Imaging of Prostate Cancer to Receptor Expression Status

I. L. Bakker[1], G. J. L. H. van Leenders[1], M. Segbers[1], A. C. Fröberg[1], S. U. Dalm[1], J. Veenland[1], M. Konijnenberg[1], M. B. Busstra[1], J. F. Verzijlbergen[1], I. Schoots[1], E. de Blois[1], W. M. van Weerden[1], T. Maina[2], B. Nock[2], M. de Jong[1]; [1]Erasmus MC, Rotterdam, NETHERLANDS, [2]NCSR „Demokritos", Athens, GREECE.

Aim: Gastrin releasing peptide receptor (GRPr) targeted imaging can aid in detection of prostate cancer (PCa). However, information on tumor characteristics in correlation with clinical imaging results is still limited. Earlier we reported the potential of the diagnostic agent [68Ga]SB3 for imaging primary tumor in therapy-naive PCa patients. In this study we investigate the GRPr-expression in carcinoma lesions and normal prostate tissue in radical prostatectomy specimens. These results were correlated to [68Ga]SB3 uptake values. **Materials and Methods:** Ten therapy-naive patients with biopsy-proven PCa scheduled for curative prostatectomy were included in the study. [68Ga]SB3 (190±44 MBq, 40±5µg) was administered, followed by PET-CT imaging. PET uptake values were determined by SUV$_{max}$. Within two weeks after acquiring images, the patients underwent robot assisted radical prostatectomy. A four millimeter thick slice was immediately frozen to enable autoradiography. The remaining tissue was formalin-fixed cut into slices and paraffin-embedded. On each slice H&E staining was performed and evaluated by an expert pathologist to determine tumor localization and Gleason score (GS). In vitro autoradiography using the GRPr antagonist [111In]JMV4168 was performed on the frozen sections, GRPr expression was quantified in digital light units (DLUs). **Results:** [68Ga]SB3 PET-CT imaging visualized 13 lesions in 9 of the patients. A total of 19 tumor lesions were found in pathological evaluation of tissues of 10 patients. These lesions were classified as 9x GS6, 9x GS7 and 1x GS8. Six lesions were small, being only present in 1 slice. The frozen tissue showed tumor in 7 patients. One of these tumor lesions did not show any GRPr-expression; this was a sample from the [68Ga]SB3 PET negative patient, who showed a total of 4 lesions in pathological evaluation. The two other missed lesions were a small GS6 lesion and a GS8 lesion. GRPr-expressing tumor lesions showed significantly higher GRPr levels compared to sections with normal prostate tissue. SUV$_{max}$ uptake in tumor lesions on [68Ga]SB3 PET images showed a significant correlation to the GRPr expression levels. **Conclusion:** In this small patient group primary PCa visualization using [68Ga]SB3 PET was successful in 90% of patients. SUV$_{max}$ uptake levels showed a significant correlation with GRPr expression levels. The only [68Ga]SB3 PET negative patient had at least one GRPr negative tumor lesion.

OP-076

Imaging GRPr expression in metastatic castration resistant prostate cancer with ^{68}Ga-RM2 - A head-to-head comparison with ^{68}Ga-PSMA-11

V. Kramer[1,2], R. Fernandez[2], J. Ribbeck[1], R. Pruzzo[2], E. Hernandez-Behm[2], A. Haeger[2], B. Morales[2], H. Lavados[2], H. Amaral[1,2]; [1]Positronpharma SA, Santiago de Chile, CHILE, [2]Nuclear Medicine & PET/CT Fundación Arturo López Pérez, Santiago de Chile, CHILE.

Purpose/Introduction: Gastrin releasing peptide receptors (GRPr) are differentially overexpressed in different types of cancer including prostate cancer (PC). ^{68}Ga-RM2 is a selective PET tracer for GRPr and has shown high sensitivity for detecting primary PC and biochemical recurrent PC. ^{177}Lu-RM2 has been proposed as theranostic agent for radio ligand therapy (RLP) of advanced PC. The aim of this study is to evaluate GRPr expression in advanced metastatic castration resistant prostate cancer

(mCRPC) and to compare GRPr with PSMA expression as target for subsequent ^{177}Lu-RLT. **Subjects & methods:** We recruited 20 patients, diagnosed with mCRPC (mean age 68.0 ± 7.8 years), all with written consent and actual PSA values within one week prior to imaging (mean 496 ± 757; range 2.44-2980). All participants underwent a ^{68}Ga-PSMA-11 PET scan and a second PET scan with ^{68}Ga-RM2 within one week. Both PET studies were evaluated by overall biodistribution of the tracers and SUV_{max} and SUV_{mean} values in target lesions in prostate, soft tissue and bone. **Results:** ^{68}Ga-PSMA-11 PET was positive in all patients with mean SUV_{max} values of 34.9 ± 22.9 (range: 5.8-105.0) in target lesions. ^{68}Ga-RM2 PET was positive and able to detect GRPr expression in 18/20 patients with mean SUV_{max} values of 12.9 ± 10.8 (range: 1.4-37.8) in target lesions. ^{68}Ga-RM2 failed to detect tumor lesions in 2/20 patients and GRPr expression was significantly lower than PSMA expression in 16/20 patients. In 4/20 patients ^{68}Ga-RM2 and ^{68}Ga-PSMA showed similar distribution, SUVmax values and target expression. **Discussion/Conclusion:** GRPr expression in advanced mCRPC is significantly lower than PSMA expression and reduced in comparison to previously published data from primary and recurrent PC. Nevertheless RLT with ^{177}Lu-RM2 might be an alternative for patients with advanced mCRPC and low PSMA expression. As GRPr, and its endogen ligand GRP, show endocrine function and promote cell growth, PET imaging with ^{68}Ga-RM2 might also be a useful measure for disease prognosis.

OP-077

Imaging tumor biology with [89]Zr-cetuximab, ^{15}O-H$_2$O and ^{18}F-FDG PET/CT in patients with advanced colorectal cancer treated with cetuximab monotherapy

E. J. van Helden[1], O. S. Hoekstra[2], M. C. Huisman[2], E. Boon[3], S. C. van Es[4], G. A. M. S. van Dongen[2], D. J. Vugts[2], D. J. de Groot[4], R. Boellaard[2,5], C. M. L. van Herpen[3], E. G. E. de Vries[4], H. M. W. Verheul[1], C. W. Menke - van der Houven van Oordt[1]; [1]Department of Medical Oncology, VU University Medical Center, Cancer Center Amsterdam, Amsterdam, NETHERLANDS, [2]Department of Radiology and Nuclear Medicine, VU University Medical Center, Cancer Center Amsterdam, Amsterdam, NETHERLANDS, [3]Department of Medical Oncology, Radboud University Medical Center, Nijmegen, NETHERLANDS, [4]Department of Medical Oncology, University Medical Center Groningen, Groningen, NETHERLANDS, [5]Department of Radiology and Nuclear Medicine, University Medical Center Groningen, Groningen, NETHERLANDS.

Aim: In this multicenter study we evaluated [89]Zr-cetuximab PET/CT as predictive biomarker for treatment efficacy of cetuximab monotherapy in patients with RAS wild-type metastatic colorectal cancer (mCRC). Additionally, we evaluated if tumor perfusion on, ^{15}O-H$_2$O PET/CT, affects [89]Zr-cetuximab tumor accumulation. ^{18}F-FDG PET/CT was performed to identify (viable) tumor lesions. **Methods:** Patients with chemotherapy refractory, RAS wild-type, mCRC were treated with 500 mg/m^2 cetuximab 2-weekly (NCT02117466). Within 2 hours after the first cetuximab infusion, patients received 37 MBq [89]Zr-cetuximab (10mg) followed by PET/CT 6 days post-injection. Three independent nuclear physicians visually assessed tumor uptake. [89]Zr-cetuximab PET was classified as positive if there was visual uptake in ≥1 extra-hepatic lesion (≥2cm). In case of a negative [89]Zr-cetuximab PET, therapeutic cetuximab dose was escalated (750-1250 mg/m^2) and a second [89]Zr-cetuximab PET was performed. Tumor uptake and biodistribution were quantified and baseline blood levels of soluble EGFR (sEGFR) were measured. All patients underwent a baseline ^{18}F-FDG PET/CT and 10 patients underwent a dynamic ^{15}O-H$_2$O PET/CT. Clinical endpoints were treatment benefit (response or stable disease according to RECIST v1.1), progression-free survival (PFS) and overall survival (OS). **Results:** Twelve of 35 patients had a visually negative [89]Zr-cetuximab PET/CT. Dose escalation in eight patients did not result in visual tumor accumulation on a second [89]Zr-cetuximab PET/CT. Patients with visually positive or negative [89]Zr-cetuximab PET/CT had comparable treatment benefit (55% versus 75%, p= 0.24), PFS (median 4.4 versus 6.2 months, p= 0.35) and OS (median 9.1 versus 12.0 months, p= 0.36). In total, 129 lesions were quantified on [89]Zr-cetuximab PET/CT. SUV_{peak} of tumor lesions was comparable for patients with and without treatment benefit (2.7 versus 2.7; range 0.4-9.6). Percentage injected-dose [89]Zr-cetuximab in whole liver (potential sink organ due to high EGFR expression; median 25.3%, range 9.4-40.4%), other organs, and the blood pool (using Nadler's method, median 20.7%, range 8.9-30.5%) did not differ between patients with or without treatment benefit (p= 0.22 and p= 0.97). Tumor, blood and liver uptake were not affected by baseline plasma sEGFR concentrations. [89]Zr-cetuximab tumor uptake was positively correlated with tumor perfusion (p=0.011) on ^{15}O-H$_2$O PET/CT. Additionally, [89]Zr-cetuximab uptake was correlated with metabolic tumor activity (p<0.001), possibly due to the fact that EGFR overexpressing lesions have higher proliferation rates. **Conclusions:** [89]Zr-cetuximab PET/CT, as performed in this setting, does not predict treatment efficacy of cetuximab in patients with mCRC. [89]Zr-cetuximab uptake, perfusion and metabolic activity are positively correlated.

OP-078

A PET imaging study to investigate the biodistribution and clearance of an albumin binding domain antibody (AlbudAb™) in healthy subjects

K. Thorneloe[1], M. Bergstrom[2], L. Galinanes-Garcia[2], P. Galette[1], W. Al-Azzam[1], V. Vincent[1], D. Vugts[3], G. van Dongen[3], P. Elsinga[4], J. Wiegers[4], A. Glaudemans[4], J. Renaux[2], M. Cleveland[2], M. Davies[2], S. Zhang[1]; [1]GSK, King of Prussia, PA, UNITED STATES OF AMERICA, [2]GSK, Stevenage, UNITED KINGDOM, [3]VU University Medical Centre, Amsterdam, NETHERLANDS, [4]University Medical Center Groningen, Groningen, NETHERLANDS.

Aim: Conjugation or fusion to albumin-binding domain antibodies (AlbudAbs™) is a novel approach to extend the half-life and/or alter the distribution of biological and small molecule therapeutics. To more accurately predict and model the properties of therapeutic candidates attached to an AlbudAb in humans, we have studied the tissue distribution and elimination kinetics of unconjugated AlbudAb in healthy volunteers. **Methods**: The scaffold AlbudAb GSK3128349 was radiolabeled

with ^{89}Zirconium and a single 1 mg (~12.5 MBq) dose was intravenously administered to 8 healthy male subjects. The ^{89}Zr-GSK3128349 biodistribution was then followed for up to 7 days with 4 repeated whole body PET/CT scan sessions. PET signal intensities were measured in various organs. Blood samples were drawn at multiple time points to measure plasma PK by radio-detection and UHPLC-MS/MS analysis. **Results**: Administration of ^{89}Zr-GSK3128349 and the PET/CT procedures were well tolerated by subjects. The plasma PK profile was biexponential with a terminal half-life ($T_{1/2}$) of 18 days as measured by both radio-detection and UHPLC-MS/MS analysis. The PET images showed rapid tracer distribution primarily in the vasculature followed by gradual tissue uptake during the first 50-70 hours post dose in the kidneys, muscle and liver. SUV mean values ranged from ~9 in the kidneys and blood, to ~4 in liver and spleen, and 0.6 in skeletal muscle when averaged across all scan time points. In some organs, SUV remained constant while in other organs this decreased with time. The tissue-to-plasma ratio was in the range of 0.1-0.2 for most organs, but 0.025 for the brain suggesting limited blood-brain-barrier penetration. Muscle showed a prominent increase over time from 0.03 to 0.1 and kidney increased from 0.5 to 1.4. **Conclusions**: The ^{89}Zr-GSK3128349 biodistribution in healthy volunteers was successfully evaluated using a low level of radioactivity (~12.5 MBq). The data suggests a rapid binding of the AlbudAb to albumin with limited renal elimination, and a $T_{1/2}$ of 18 days. Similar plasma PK profiles by radio-PK and UHPLC-MS/MS suggest that the presence of ^{89}Zr did not affect the tissue distribution of the molecule. The unconjugated AlbudAb GSK3128349 biodistribution data in humans will form the base for a physiological-based PK model, which will be used to predict the biodistribution of future therapeutics linked to AlbudAbs. This information will enable the appropriate selection of targets in AlbudAb drug discovery efforts and aid in improving clinical study designs, particularly in dose selection and assessment of target engagement.

OP-079

A proof-of-concept study of ^{68}Ga-TATE-RGD PET/CT for duel-target imaging of somatostatin receptor and integrin $\alpha_v\beta_3$ to detect lung cancer and neuroendocrine tumor in a single scan

Y. Zheng[1,2], *H. Wang*[1], *X. Cui*[1], *L. Zhang*[1], *H. Tan*[2], *S. Yao*[1], *Z. Zhu*[1]; [1]*Peking Union Medical College Hospital, Beijing, CHINA,* [2]*China-Japan Friendship Hospital, Beijing, CHINA.*

Purpose: This study aims to document the first-in-human application of ^{68}Ga-TATE-RGD, a ^{68}Ga-labeled heterodimeric peptide targeting both somatostatin receptor and integrin $\alpha_v\beta_3$, in order to detect lung cancer and neuroendocrine tumors (NET) in a single PET/CT scan. **Methods:** TATE and RGD were connected with 1,4,7-triazacyclononane-N,N',N"-triacetic acid (NOTA) through 3 polyethyleneglycol (PEG$_4$) spacers (NOTA-3P$_4$-TATE-RGD). ^{68}Ga was labeled by conjugation with NOTA at 100°C for 10 min. The radiochemical purity was >99%. With IRB approval and written informed consent, 37 patients underwent ^{68}Ga-TATE-RGD PET/CT, including 18 patients with pathologically proved non-small cell lung cancer (NSCLC), 14 patients with small cell lung cancer (SCLC), and 5 patients with NET. The patients underwent PET/CT scans 40-60 min after intravenous injection of ^{68}Ga-TATE-RGD at a dosage of 1.85 MBq (0.05 mCi) per kilogram body weight. The NSCLC, SCLC and NET patients also accepted ^{68}Ga-TATE, ^{68}Ga-RGD, and ^{18}F-FDG PET/CT, respectively within 1 week for comparison. The maximum standardized uptake value (SUV) of the primary or prominent tumor (T) and the mean SUV of blood pool (B) were measured, and the T/B ratios were calculated for comparison of different tracer uptake in the same patients using the paired *t* test. **Results:** No side effect correlated with ^{68}Ga-TATE-RGD injection was found in the patients. The image quality of ^{68}Ga-TATE-RGD PET/CT was good. The kidneys and spleen showed the highest physiological uptake in the body. ^{68}Ga-TATE-RGD uptake was observed in all known lesions of NSCLC, SCLC and NET. In 18 patients with NSCLC (15 adenocarcinoma, 2 adenosquamous cell carcinoma and 1 squamous cell carcinoma), the T/B ratios of ^{68}Ga-TATE-RGD were 4.54 ± 3.00, significantly higher than those of ^{68}Ga-TATE (4.10 ± 2.83, *P*=0.0058). In 14 patients with SCLC, the T/B ratios of ^{68}Ga-TATE-RGD (6.06 ± 6.09) were significantly higher than those of ^{68}Ga-RGD (2.65 ± 1.19, *P*=0.0344). In 5 patients with NET (1 G1, 2 G2 and 1 G3 gastro-entero-pancreatic NET with multiple liver metastases and 1 thymus atypical carcinoid with multiple lymphatic metastases), the T/B ratios of ^{68}Ga-TATE-RGD were 19.79 ± 18.39, significantly higher than those of ^{18}F-FDG (2.72 ± 1.24, P=0.0187). The uptake difference was much prominent in the low grade NET. **Conclusion:** This proof-of-concept study preliminarily indicates the safety and efficacy of ^{68}Ga-TATE-RGD, a novel PET tracer targeting both somatostatin receptor and integrin $\alpha_v\beta_3$, with the possibility to detect NSCLC, SCLC, and NETs in a single PET scan using the same tracer.

---

309 | **Sunday, October 22, 2017, 11:30 - 12:45, Hall G1**

Do.MoRe - Featured: Photodynamic Therapy & Molecular Imaging – The Perfect Couple?

OP-079a

From Radionuclide Imaging to Photodynamic Therapy – Novel Prospects for Nuclear Medicine

M. Gotthardt; Radboud UMC, Nijmegen, NETHERLANDS.

OP-079b

Core-Satellite Nanomaterials for Multimodal Image-Guided Combination Cancer Therapy

W. Cai, S. Goel, T. E. Barnhart; University of Wisconsin-Madison, Madison, WI, UNITED STATES.

Objective: To develop a multifunctional nanoplatform integrating photothermal therapy (**PTT**) and photodynamic therapy (**PDT**) for tumor eradication under the guidance of fluorescence imaging (FL) and positron emission tomography (PET). **Methods:** Hollow mesoporous silica nanoparticles (HMSNs) were synthesized with surface -NH$_2$ groups. The hollow cavity

was loaded with Tetrakis(4-carboxyphenyl)porphyrin (TCPP, for PDT). Electrostatic adsorption was used to assemble positively-charged TCPP-loaded HMSN core ([TCPP]HMSN-NH$_2$) and negatively-charged citrate-stabilized CuS nanosatellites to form [TCPP]HMSN@nCuS core-satellite nanoconjugates (**CSNCs**), which was PEGylated. PTT (*via* CuS) and PDT (*via* TCPP) properties of CSNCs was studied by irradiation with near-infrared (NIR; 980 nm) and ultrared (660 nm) lasers respectively. CSNCs were intrinsically radiolabeled with ^{89}Zr (t$_{1/2}$=78.4 h) and serial PET and FL (*via* intrinsic FL of TCPP, ex/em: 640/720 nm) imaging were performed in 4T1 tumor-bearing mice. Combined PTT/PDT was performed in 4T1 tumors after single intratumoral injection of CSNCs, followed by laser irradiation (L$_{980}$ for 10 min and L$_{660}$ for 20 min) and tumor growth were monitored. **Results:** Transmission electron microscopy (TEM) indicated uniform morphology and excellent dispersity of the individual components as well as assembled CSNCs (~ 163 nm). High loading efficiency (~50%) of TCPP was observed, and calculations estimated ~8000 CuS nanosatellites per HMSN. CSNCs demonstrated high absorption in the ultrared and NIR windows and excellent PDT and PTT conversion efficiency upon laser irradiation *in vitro*. The oxophillic nature of ^{89}Zr and abundant -SiO$_2^-$ groups in HMSN were harnessed for chelator-free ^{89}Zr-labeling of CSNCs demonstrating excellent labeling yield (~80%) and serum radiostability. ^{89}Zr-labeled CSNCs also demonstrated Cerenkov Luminescence (CL) and Cerenkov Radiation Energy Transfer (CRET) *in vitro*. *In vivo* FL and PET showed rapid and persistent accumulation of CSNC-PEG in 4T1 tumors via enhanced permeability and retention (EPR) effect at 5.5±1.2, 5.2±1.4 and 5.0±1.0 %ID/g at 4, 24 and 48 h post-injection (p.i.). Single dose (5 mg/mL; 50 µL) of intratumorally injected CSNCs and dual-laser treatment demonstrated synergistic phototherapeutic effect in 4T1 tumor-bearing mice, with complete tumor remission and no relapse. Control groups receiving same dose of CSNCs but single-laser treatment (980nm or 660nm) showed initial tumor growth retardation up to day 7, which relapsed rapidly. Control cohorts receiving CSNC alone without laser irradiation or PBS (with and without laser irradiation) reached final relative tumor volumes of 8.1±1.6, 6.3±1.7 and 10.5±0.5, respectively, indicating negligible efficacy. **Conclusion:** A multifunctional core-satellite nanoconstruct is reported, integrating PET/FL/PDT/PTT into a single platform for image-guided synergistic cancer therapy.

OP-079c
Targeted Photodynamic Therapy in CEA Expressing Colorectal Tumor Xenografts

F. M. K. Elekonawo, D. Bos, O. C. Boerman, A. J. A. Bremers, J. H. W. de Wilt, M. Rijpkema; Radboudumc, Nijmegen, NETHERLANDS.

Introduction: Photodynamic therapy (PDT) relies on the combination of a photosensitizer and light of a specific wavelength, to create a toxic environment by formation of radical (oxygen) species. In oncology, tumor-targeted PDT might increase the efficacy of this technique by specific accumulation of the photosensitizer in tumor tissue. CEA is overexpressed in more than 90% of all colorectal cancers (CRC) and may serve as a target for

tumor-targeted PDT. Labetuzumab is a monoclonal humanized IgG with high affinity for CEACAM5, a cell surface glycoprotein that is member of the CEA family of proteins. Thus, using a labetuzumab-photosensitizer conjugate, tumor-targeted PDT for treatment of residual disease after incomplete resection of colorectal cancers might become feasible. **Purpose:** The aim of the current study is to evaluate the efficacy of tumor-targeted PDT in colorectal tumor xenografts, using labetuzumab-IRDye700DX. **Methods:** CEA-expressing cell lines LoVo, LS174T, SW1222, GW39 and HT29 were evaluated. First, cells were plated into transparent 24 well-plates and subsequently incubated with different concentrations and labetuzumab:IRDye700DX substitution ratios of 1, 2 and 4. Then, cells were washed and irradiated with different intensities (5-300 W/cm^2) of NIR light using a LED light source at 690nm. Post-therapeutic cell viability was analyzed with the ATP dependent *Celltiter Glo® Luminescent Cell Viability Assay*. Optimal labetuzumab:IRDye700DX substitution ratio and irradiation time and intensity were tested in a mouse model. Tumor growth was monitored for 8 weeks post irradiation. **Results:** All CEA-expressing cell lines were evaluated for susceptibility for tumor-targeted PDT in vitro. Post-therapeutic cell viability levels ranged from 20-90% and were dependent on the labetuzumab:IRDye700DX substitution ratio, conjugate concentration, irradiation time and intensity, and cell type. In vitro, LoVo and GW39 were more susceptible to tumor-targeted PDT than the other cell lines. The first in vivo studies are currently underway. **Discussion and Conclusion:** CEA-targeted PDT is feasible and leads to cell death in vitro. As expected, more light and higher conjugate concentrations resulted in a larger effects. Levels of CEA expression did not directly correlate with the observed effects on cell viability. This suggests that other factors, e.g. CEA availability on the cellular membrane surface and/or differences in cellular regulation of protective mechanisms could play a role in the efficacy of tumor-targeted PDT using labetuzumab-700DX. Also, an immune response to PDT is suggested to play a crucial role in the successful treatment, which is currently investigated in vivo.

OP-079d
Photodynamic therapy in rheumatoid arthritis; targeting the activated fibroblasts

D. N. Dorst[1], M. Buitinga[1], M. Brom[1], D. Bos[1], A. Freimoser[2], C. Klein[2], B. Walgreen[1], M. I. Koenders[1], M. Gotthardt[1]; [1]Radboud umc, Nijmegen, NETHERLANDS, [2]Roche Pharmaceutical Research and Early Development, Zurich, AUSTRIA.

Introduction: Rheumatoid arthritis (RA) is a chronic, inflammatory disease of the synovial joints. However, not all patients respond to conventional therapy while others lose response, warranting alternatives. Activated synovial fibroblasts, expressing the fibroblast activation protein (FAP), play an important role in developing and sustaining joint inflammation. Here, we investigated the potential of a novel FAP-targeting photodynamic therapy (PDT) to selectively induce cell death in activated fibroblasts. **Methods:** DTPA-28H1-IRDye700DX was prepared with two substitution ratios (SR) of 700DX (1.2 and 3). All *in vitro*

assays were performed with 3T3 cells, stably transfected with FAP. The immunoreactive fraction (IRF) was determined using the Lindmo assay. For PDT, cells were incubated with various concentrations of DTPA-28H1-IRDye700DX or a nonspecific antibody-700DX conjugate for 4 hours and exposed to varying LED doses. Cell viability was measured using the cell titer glo assay. For biodistribution studies, DTPA-28H1-IRdye700DX and DTPA-28H1 were labelled with ^{111}In and injected (0.4 MBq ^{111}In labelled to 50 μg Ab) in healthy C57BL/6 mice. **Results:** The IRF of [111]In-28H1-700DX (SR1.2: 94.7%, SR3: 116.8%) was comparable to that of [111]In-28H1 (91.4% (1)), indicating that conjugating 28H1 with 700DX did not affect the immunoreactivity of the antibody. To assess the effect of SR on PDT efficacy, we applied PDT to 3T3-FAP cells. 13.7 J/cm^2 LED exposure of 3T3-FAP cells incubated with 6.67 pM 28H1-700DX significantly reduced cell viability (SR1.2: 89.24%+/-3.67, SR3: 89.27%+/-2.48 compared to control (p<0.001)). No cell death was observed when cells were incubated with the control 700DX-conjugate. Conjugating the antibody to 700DX changed the *in vivo* biodistribution of the antibody, with a higher accumulation of the labelled compound in the liver (High SR :129.43 +/- 14.00 %ID/g, DTPA-only: 5.32 +/- 1.17 %ID/g (p<0.001)). Conversely, the concentration of the tracer in the blood decreased (High SR: 1.73 +/- 0.08 %ID/g , DTPA-only: 18.75 +/- 3.21 %ID/g(p<0.001)). Accumulation in the spleen, pancreas and bone marrow were also higher in the 700DX conjugated groups. **Conclusion:** We have demonstrated target-specific cell death using 28H1-700DX PDT indicating that PDT may be a promising new tool in treating RA. Conjugation of the anti-FAP antibody 28H1 with the photosensitizer 700DX did not affect the IRF. We demonstrated that higher 700DX SR resulted in faster liver clearance of the antibody. Future research will further elucidate the applicability of the conjugate for PDT in animal models of RA. **References** 1) Terry SY[1], et al. J Nucl Med. 2016 Mar;57(3):467-72.

OP-079e

Photodynamic treatment of rheumatoid arthritis by liposomal targeting of macrophages

M. Boss[1], M. Buitinga[1], D. N. Dorst[1], B. Walgreen[1], L. van Bloois[2], M. Brom[1], G. Storm[2], M. I. Koenders[1], M. Gotthardt[1]; [1]Radboud University Medical Center, Nijmegen, NETHERLANDS, [2]Utrecht University, Utrecht, NETHERLANDS.

Introduction: Rheumatoid arthritis (RA) is a chronic, progressive inflammatory disease of the synovial joints. While immunosuppressive therapy is the treatment of choice, some patients do not respond or loose response over time to this treatment. Research into alternative treatment options is therefore of importance. Resident macrophages in the arthritic joint are attractive therapeutic targets, since there is a central pathogenic role for macrophages in RA. Macrophages are numerous in the inflamed synovial membrane and at the bone-pannus junction. They contribute considerably to inflammation and joint destruction both in the acute and chronic phase of the disease. Macrophages in the arthritic joints can be targeted with liposomes, which will accumulate in these joints as a result of higher blood perfusion and vascular leakage. After accumulation in the joints, the liposomes will be phagocytosed by resident macrophages. Here we tested the feasibility of inducing cell death in macrophages by photodynamic therapy (PDT) using liposomes labelled with the photosensitizer 700DX. **Methods:** To assess the effect of PDT *in vitro*, RAW 264.7 cells were incubated for 24 hours with various concentrations of PEGylated liposomes containing 200ug/ml of the photosensitizer IRdye 700DX and control liposomes without the photosensitizer. After removing unbound liposomes, the cells were exposed to near-infrared (NIR) LED light at various intensities (ranging from 19.0 - 95.1 J/cm^2). Cell viability was assessed using a cell titer glow assay. **Results:** Incubation of the cells with concentrations of IRdye 700DX containing liposomes or control liposomes as high as 4 μg/ml did not cause cellular toxicity. After incubation with IRdye 700DX containing liposomes, NIR light exposure reduced cell viability in a dose-dependent manner. At 19.0 J/cm^2, ~50% cell viability remained. Cell viability was reduced to ~5% at 38.0 J/cm^2, while cells incubated with the control liposomes remained 100% viable at light doses as high as 95.1 J/cm^2. **Conclusion:** These data show the feasibility of introducing cell death in macrophages by photodynamic therapy with liposomal IRdye 700DX in a light-dose dependent manner. This indicates that targeting of macrophages by PDT could be a promising new method for therapy of RA. Further studies are ongoing to assess the effectiveness of this therapeutic method *in vivo* in murine models of RA.

---

310   **Sunday, October 22, 2017, 11:30 - 13:00, Hall G2**

Conventional & Specialised Nuclear Medicine: Benign Thyroid & Parathyroid Diseases

OP-080

18F-Choline PET-CT in assessment of primary hyperparathyroidism comparing with 99mTc-Sestamibi or 99mTc-Tetrofosmin SPECT-CT: How differentiate parathyroid hyperplasia from adenoma?

C. Pirich[1], L. Hehenwarter[1], L. Imamovic[2], G. Rendl[1], O. Tsybrovskyy[3], D. Hackl[4], F. Fitz[2], W. Langsteger[2], M. Beheshti[2,1]; [1]Nuclear Medicine & Endocrinology, Medical University of Salzburg, Salzburg, AUSTRIA, [2]PET-CT Center Linz, St. Vincent's Hospital, Linz, AUSTRIA, [3]Clinical Pathology, St. Vincent's Hospital, Linz, AUSTRIA, [4]General Surgery, St. Vincent's Hospital, Linz, AUSTRIA.

Aim: In this prospective study, we evaluated the accuracy of ^{18}F-Choline (FCH) PET-CT comparing with ^{99m}Tc-Sestamibi (MIBI) or ^{99m}Tc-tetrofosmin (TETRO) SPECT-CT for preoperative detection of parathyroid adenoma in patients with primary hyperparathyroidism. Furthermore, we assess the value of semi-quantitative parameters in differentiation between parathyroid hyperplasia from adenoma. **Methods:** Both FCH PET-CT and MIBI/TETRO SPECT-CT were performed in 100 consecutive patients with biochemical evidence of primary hyperparathyroidism. At least one abnormal FCH and MIBI/TETRO focus corresponding to a parathyroid gland or ectopic parathyroid tissue

in each imaging modality was considered as positive finding. In 76 patients with positive findings in at least one imaging modality, surgical exploration was performed and the results were related to histopathologic findings as the standard of truth. In 24 patients, no surgery was performed: 18 patients with positive imaging findings refused it or have been at increased general risk of surgery and 6 patients with negative imaging. **Results:** All patients showed biochemical evidence of primary hyperparathyroidism with a mean serum calcium level of 2.78 ± 0.34 mmol/l and parathormone (PTH) level of 196.5 ± 236.4 pg/ml. The results of study were analyzed in 76 patients with verified histopathology and 3 patients with negative imaging findings. Three of 6 patients with negative imaging showed normalized PTH and serum Ca levels in 3 and 6 month laboratory follow-up which was considered as "true negative". In patient-based analysis, FCH PET-CT was able to detect parathyroid adenoma in 96% of patients (76/79) while ^{99m}TC-Sestamibi SPECT-CT was positive in only 67% of patients (53/79). In a lesion-based analysis, FCH PET-CT showed a sensitivity of 93% comparing with 63% in ^{99m}TC-Sestamibi SPECT-CT. Semi-quantitative analysis by means of SUVmax showed significantly higher FCH uptake in parathyroid adenomas vs. hyperplasia [7.18 (±3.42) vs. 4.98 (±0.90); p<0.001]. Among analyzed parameters such as PTH, Ca and size and weight of parathyroid adenomas, size was significantly difference in patients with negative ^{99m}TC-Sestamibi SPECT-CT and positive FCH PET-CT [mean size (mm):17.8 ± 7.2 vs. 13.0 ± 6.7, respectively; p=0.02]. **Conclusion:** In this prospective study, FCH PET-CT showed promising results to be a potential functional imaging modality - clearly superior to MIBI or TETRO SPECT-CT - especially in the detection and localization of small parathyroid adenoma in patients with primary hyperparathyroidism. SUVmax was siginifically higher in parathyroid adenoma than in hyperplasia.

OP-081

Quantitative Washout Rate of ^{99m}Tc-Sestamibi in Parathyroid and Thyroid Tissues Assessed Using Quantitative SPECT-CT

J. Gardner, B. Ziebarth, S. Bazarjani, S. Razavi, R. Klein, L. S. Zuckier, W. Zeng; The Ottawa Hospital, Ottawa, ON, CANADA.

Introduction: Dual phase parathyroid scintigraphy is a well-established procedure for preoperative localization of parathyroid adenomas. Although discrimination of parathyroid adenomas has been postulated as occurring due to more-rapid washout of ^{99m}Tc-Sestamibi (MIBI) from thyroid than from parathyroid adenomas, there are limited quantitative data reported in the literature to support this hypothesis. In our center, in addition to planar images, we obtain early SPECT-CT and 2-hour delayed SPECT imaging for anatomic localization. The aim of this study was to employ quantitative methods to derive tissue MIBI washout rates from our SPECT data. **Materials and Methods :** We retrospectively studied 125 consecutive patients (age: 62.2±13.8, F:M=100:25) accrued over 10 months. Lab values (mean±SD) were tabulated for PTH (28.5±54.1 pmol/L), calcium (2.60±0.45 mmol/L), TSH (2.61±2.20 mIU/L), T4 (12.18±2.52 pmol/L) and T3

(4.54±0.74 pmol/L). Early CT scans were co-registered with delayed SPECT using a previously validated manual method. Early and late SPECT-CT images were reconstructed using attenuation, scatter, and resolution recovery correction and quantified in Standard Uptake Value (SUV) units (HERMES HybridRecon). Maximum SUV (SUV$_{max}$) were measured on all image sets. Thyroid lobes were considered measurable if they are found clearly separated from parathyroid adenoma and if patients were not receiving exogenous thyroid hormone. Washout rates for normal thyroid tissue and parathyroid adenomas were calculated using early and late SUV$_{max}$. **Results:** Of the 125 patients imaged, 59 adenomas were successfully localized in 58 patients (1 patient with 2 adenomas) and these patients were subject to analysis below. There was an overall significant difference in PTH levels between the patients with and without localizable parathyroid adenomas (47.5± 90.2 pmol/L vs. 18.6± 19.3 pmol/L, p=0.03). SUV$_{max}$ was higher in parathyroid adenomas than in measurable thyroid lobes on both early (7.23 ± 4.59 vs. 4.56 ± 1.43, p<0.001) and late (4.46 ± 3.53 vs. 2.02 ± 0.77, p<0.001) images. Mean washout rates (%/hour) from parathyroid adenomas was slower than that of the thyroid lobes in patients positive for parathyroid adenoma (21.8% ± 9.6% vs. 32.1% ± 11.2%, p<0.001). **Conclusion:** Quantitative SPECT-CT analysis revealed higher absolute SUV values in parathyroid adenomas versus thyroid tissue, as well as a statistically higher rate of MIBI washout from the thyroid tissue. Our data therefore support the hypothesis that discrimination of parathyroid adenomas on dual-phase studies occurs, at least in part, due to the more-rapid washout of ^{99m}Tc-Sestamibi (MIBI) from thyroid than from parathyroid tissue.

OP-082

A Type of Uptake in Dual-phase ^{99m} Tc-Sestamibi SPECT/CT Parathyroid Scintigraphy & a Level of Parathormone Might Indicate a Histopathology Diagnosis in Patients with Primary Hyperparathyroidism-Experience of One Centre

M. H. Listewnik, H. Piwowarska-Bilska, K. Safranow, M. Ostrowski, J. Iwanowski, M. Chosia, A. Borowiecki, M. Laszczyńska, M. Kurnatowicz, B. Birkenfeld; Pomeranian Medical University in Szczecin, Szczecin, POLAND.

Introduction/purpose: This prospectively designed study aimed to assess the concordance between abnormal results of preoperative dual-phase ^{99m}Tc-Sestamibi SPECT/CT parathyroid scintigraphy, histopathology (HP), biochemical parameters in patients operated on for primary hyperparathyroidism (pHPT). **Subject & Methods:** In 181 among 242 patients with suspicion of pPHP abnormal result were found. Three types of ^{99m}Tc-Sestamibi uptake: I-lack in an early (thyroid) phase (EP) and presence in a delayed (parathyroid) phase (DP); II-presence in EP and DP;III-presence in EP and lack in DP were distinguished. Patients with more than one lesion were excluded to obtain the subgroup "one lesion and one parathormone (PTH) result" (n=137). Among 181 patients with abnormal result, 40 (mean age 58.7 years) patients had surgery. In surgery group 45 from 46 lesions indicated on ^{99m}Tc-SestamibiSPECT/CT basis were removed and

sent for HP. According to the rule "one lesion and one PTH result" 37 from 45 removed lesions were further analyzed PTH was analyzed in relation to three types of[99m]Tc-Sestamibi uptake. Additionally, in the surgery group HP was examined in relation to PTH in types of ^{99m}Tc-Sestamibi uptake. **Results:** Type I of uptake presented 18.3% (n=25) lesions, type II 70.8% (n=97) and type III 10.9% (n=15). A significant difference between PTH plasma concentration in relation to three types of tracer uptake was found (p=0.002). PTH level in type II was significantly higher than in type I and III (p=0.002 and 0.023, respectively). In the surgery group 37 (80.4%) lesions in EP and 44 (95.6%) in DP showed abnormal uptake in ^{99m}Tc-SestamibiSPECT/CT. On the basis of HP results as true positive were established: parathyroid adenoma (n=20; 44.5%), parathyroid hyperplasia (n=11; 24.5%), parathyroid cancer (n=2; 4.4%) and normal parathyroid gland (n=4; 8.9%). As false positive: lymph nodes (n=2; 4.4%) and thyroid gland (n=6; 13.3%). Positive predictive value of the method was 82.2%. In the surgery group PTH was significantly higher for type II of uptake than for type I (p=0.039). In patients with type II uptake, PTH concentration was significantly higher in adenoma than in hyperplasia subgroup (p=0.01). **Discussion/Conclusion:** (1) In SPECT/CT parathyroid scintigraphy ^{99m}Tc-Sestamibi uptake is generally visible both in thyroid and parathyroid phase (2) In patients with type II of uptake higher PTH concentration might distinguish parathyroid adenoma from parathyroid hyperplasia. This study was supported by a grant from budget resources for science in the years 2010-2015 as research project No. N N402 463339.

OP-083

Comparison of F-18 Choline PET/CT with Tc-99m MIBI and USG for Detection of Parathyroid Adenomas in Patients with Elevated Parathyroid Hormone Levels: Preliminary Results

L. Uslu-Beşli[1], K. Sönmezoğlu[1], E. Kaymak Akgün[1], S. Teksöz[2], E. Karayel[1], H. Pehlivanoğlu[1], M. Ocak[3], T. Öztürk[4], S. Sağer[1], L. Kabasakal[1], Y. Bükey[2]; [1]Istanbul University Cerrahpaşa Medical Faculty Department of Nuclear Medicine, Istanbul, TURKEY, [2]Istanbul University Cerrahpaşa Medical Faculty Department of General Surgery, Istanbul, TURKEY, [3]Istanbul University Pharmacy Faculty Department of Pharmaceutical Technology, Istanbul, TURKEY, [4]Istanbul University Cerrahpaşa Medical Faculty Department of Pathology, Istanbul, TURKEY.

Purpose: In patients with elevated parathyroid hormone(PTH) levels, conventional imaging modalities including ultrasonography(USG) and parathyroid scintigraphy with Tc-99m MIBI(MIBI) are used for detection of suspected parathyroid adenomas. However, both modalities could be negative despite persistent hyperparathyroidism. F-18 Choline(FCH) PET has recently been suggested to be a better alternative for detection of parathyroid adenomas. The aim of our study is to compare the diagnostic accuracy of FCH-PET with conventional imaging modalities for detection of parathyroid adenomas. **Subjects and Methods:** Among 130 adult patients with primary or secondary hyperparathyroidism that have been prospectively enrolled in our

on-going study, 93 patients with postoperative histopathological confirmation or follow-up biochemical results were included in our comparison. FCH-PET/CT, MIBI dual-phase imaging and USG were performed to all patients. Mean 8,8±2,4 mCi(325±88,8 MBq) FCH was applied iv and dual-time PET/CT imaging was performed 15min and 45min after FCH administration. Gold standard was postoperative histopathology in patients that have undergone parathyroidectomy operation, and follow-up serum PTH, calcium, phosphate and vitamin-D levels in patients with negative imaging results. **Results:** Total 61 patients underwent surgery, resulting in parathyroid adenoma in 54, neoplasia in 3 and hyperplasia in 3 patients. In one patient parathyroid tissue was not found in the pathology specimen. FCH-PET could successfully localize 95,1% of the hyperfunctioning parathyroid glands among operated patients. It was false negative(FN) in 3,3% and false positive(FP) in 1,6% of patients. Sensitivity and positive predictive value(PPV) of FCH-PET are 96,7% and 98,3%, respectively. MIBI could detect only 48,3% of the lesions and missed 50%. USG was positive in 50% of the lesions and missed 48,1%. Sensitivity of MIBI and USG remained 49,2% and 51,0%, respectively. Total 32 patients were followed without surgery and PTH levels decreased in 9 patients, remaining high in 23 patients. FCH was positive in 52,2%(12/23) of patients with persistent hyperparathyroidemia, whereas MIBI and USG was positive in 17,4%(4/23) and 8,7%(2/23), respectively. Out of 30 patients, that were negative with both MIBI and USG, 15 were FCH positive and adenoma was confirmed with histopathology in 10 patients, whereas PTH level remained high in 5 patients, who could not be operated. **Conclusion:** FCH-PET is an effective imaging tool with higher sensitivity compared to conventional imaging modalities for detection of hyperfunctioning parathyroid glands. It should be used especially in cases with persistent hyperparathyroidism despite negative MIBI and USG results. Acknowledgements: This work was supported by Istanbul University Scientific Research Projects (project-no:24412).

OP-084

Impact of F18-Fluorocholine PET/CT in the pre-surgical work up of primary hyperparathyroidism

S. Grimaldi[1], J. Young[2], P. Kamenicky[2], D. Hartl[1], M. Terroir[1], S. Leboulleux[1], E. Baudin[1], M. Schlumberger[1], D. Deandreis[1,3]; [1]Institut Gustave Roussy, Villejuif, FRANCE, [2]Hôpital de Bicêtre, Le Kremlin-Bicêtre, FRANCE, [3]Università degli Studi, Torino, ITALY.

Introduction: Pre-surgical localization of hyper-functioning parathyroid gland in patients with primary hyperparathyroidism (HPT) is crucial, but it can be difficult in case of multi-glandular disease, small adenomas, and relapse after previous surgery. Due to promising results in previous studies, the aim of our study was to evaluate the added value to standard work up of F18-Fluorocholine (FCH) PET/CT in this pre-surgical setting. **Patients and Methods:** We evaluated 27 consecutive patients with primary HPT that underwent Tc99mMIBI scintigraphy, neck US and FCH PET/CT (median age 58 years; 19 F, 8 M). FCH PET/CT was added to standard work up in patients with (i) non-conclusive/ negative pre-surgical localization with MIBI scintigraphy and US

(n=20); (ii) relapse of previously surgically treated primary HPT or clinical suspicion of multiple gland disease for HPT familiar forms (n=7). Sensitivity (Se), specificity (Sp), positive predictive value (PPV) and negative predictive value (NPV) of FCH PET/CT were calculated in a per gland analysis. Histological findings and postoperative biochemical resolution of HPT were considered as the gold standard. **Results:** FCH PET/CT was positive in 24/27 patients. Finally 21/27 patients underwent surgery with a total of 27 resected lesions. Despite a positive FCH PET/CT six patients did not undergo surgery because of comorbidities, refusal and/or stable calcium level. Nineteen/21 patients (90%) had a biochemical resolution of HPT after surgery. Histological examination of 27 resected lesions found adenomas (n=14), hyperplastic glands (n=11) and hyper-functioning glands with normal histological appearance (n=2). In two patients HPT persisted after surgery and at least one lesion was localized neither at imaging nor at the surgical exploration. FCH PET/CT successfully localized 22/29 hyper-functioning glands (per gland Se 76%; PPV 85%, Sp 93%; NPV 88%). FCH PET/CT correctly identified 13/17 lesions in patients with a single lesion (Se 76%, PPV 76%, Sp 92%; NPV 92%) and 9/12 hyper-functioning glands in patients with multiple gland disease (Se 75%, PPV 100%, Sp 100%; NPV 57%). In particular in patients with previous neck surgery FCH PET/CT was able to localize all sites of recurrence (10/10 lesions). **Conclusion:** FCH PET/CT is a promising imaging modality in the pre-surgical localization of hyper-functioning parathyroid glands especially as a second line examination in patients with non-conclusive pre-surgical localization with MIBI scintigraphy and neck US and/or an additional method in those patients in which standard work up performance is known to be limited (in particular in case of disease relapse).

OP-085

Factors Associated with the Occurrence of Graves' Orbitopathy after Radioiodine Therapy in Patients with Graves' disease

S. Gaberscek[1,2], D. Šfiligoj[1], K. Zaletel[1], E. Pirnat[1], P. Jaki Mekjavić[3,2];
[1]Department of Nuclear Medicine, University Medical Centre Ljubljana, Ljubljana, SLOVENIA, [2]Faculty of Medicine, University of Ljubljana, Ljubljana, SLOVENIA, [3]University Eye Hospital, University Medical Centre Ljubljana, Ljubljana, SLOVENIA.

Purpose: In patients with Graves' disease (GD) Graves' orbitopathy (GO) may occur or worsen after therapy with radioactive iodine 131 (RAI). Several factors have been proposed to be associated with the worsening of GO after RAI. The aim of our study was to retrospectively establish factors associated with the occurrence of GO after RAI in patients without GO immediately before RAI. **Subjects and Methods:** In this retrospective study we reviewed medical records of all patients who were first diagnosed with GD between January 2005 and December 2009 and later treated with RAI. Out of 724 patients, 552 patients (427 women and 125 men) did not have GO immediately before RAI. The state of GO was followed for 12 months after RAI therapy. We evaluated the role of sex, age, smoking, duration of treatment with antithyroid drugs, level of TSH receptor antibodies before RAI, presence of GO at the first examination of GD, and number of doses of RAI. **Results:** Out of 552 patients, 529 patients (407 women and 122 men) remained without GO after RAI, while in 23 patients (20 women, 3 men), GO occurred after RAI. Between the two groups we found no difference with respect to sex (p=0.261). Patients without GO after RAI did not differ from patients with GO after RAI with respect to age (median, 46 and 43 years, respectively, p=0.113). We found no statistically significant differences between patients without GO after RAI and patients with the occurrence of GO after RAI with respect to smoking, duration of treatment with antithyroid drugs, and level of TSH receptor antibodies (p=0.380, p=0.379, p=0.875, respectively). Patients with the occurrence of GO after RAI had significantly more frequently GO at the first examination than patients without GO after RAI (13% and 3.8%, respectively, p=0.030). The first dose of RAI was effective in 504 (91.3%) GD patients, while the second and the third dose of RAI were required in 48 (8.7%) and 3 (0.5%) patients respectively. In patients treated with the second and third dose of RAI, GO occurred significantly more frequently than in patients treated with a single dose of RAI (p=0.008 and p<0.001, respectively). **Conclusion:** Patients with GO at presentation of GD have a higher risk of developing GO after RAI. Our results reveal the importance of a sufficiently high first dose of RAI since additional doses of RAI increase the likelihood of the occurrence of GO.

OP-086

Factors Associated with the Duration of Graves' Orbitopathy Activity in Patients with Graves' disease

S. Gaberscek[1,2], D. Šfiligoj[1], K. Zaletel[1], E. Pirnat[1], P. Jaki Mekjavič[3,2];
[1]Department of Nuclear Medicine, University Medical Centre Ljubljana, Ljubljana, SLOVENIA, [2]Faculty of Medicine, University of Ljubljana, Ljubljana, SLOVENIA, [3]University Eye Hospital, University Medical Centre Ljubljana, Ljubljana, SLOVENIA.

Objective: Radioiodine (RAI) is a safe and effective definitive treatment of Graves' disease (GD). However, in patients with concomitant active Graves' orbitopathy (GO), special caution is usually recommended. Glucocorticoids are used to prevent worsening of GO after RAI. The duration of GO activity in patients treated with RAI is not precisely established. Our aim was to evaluate factors associated with the duration of GO activity. **Subjects and Methods:** In this retrospective study we reviewed medical records of all patients who were first diagnosed with GD between January 2005 and December 2009 and later treated with RAI. Out of 724 patients, 154 patients had mild or moderate-to-severe active GO. Immediately after RAI, all but two patients received glucocorticoids in various regimens. The course of GO was followed until GO became inactive. We evaluated the role of age, duration of treatment with antithyroid drugs, and the role of the timespan until RAI. **Results:** The median age of 124 women and 30 men with the active GO was 45 years (range, 16-75 years). The median duration of GO activity was 8 months (range, 2-24 months). The median duration of the treatment with antithyroid drugs was 7 months (range, 0-22 months). We found no significant correla-

tion between the age, the duration of treatment with antithyroid drugs and the duration of GO activity (R=0.087, p=0.283; R=0.019, p=0.817, respectively). The median timespan until RAI was 7 months (range, 1-48 months). The duration of GD activity was significantly shorter in patients who received RAI therapy up to 6 months after GD occurrence than in patients who received RAI later (median, 7 and 10 months, respectively, p=0.032). We found a significantly positive correlation between the timespan until RAI and the duration of GO activity (R=0.206, p=0.010). Furthermore, with multiple regression analysis, the timespan until RAI was significantly associated with the duration of GO activity (beta=0.198, p=0.014), while age and duration of treatment with antithyroid drugs did not show such association (beta=0.016, p=0.847; beta=0.041, p=0.624, respectively). **Conclusions:** Our results reveal the beneficial effect of the timely RAI therapy on the course of GO, since the shorter the time until RAI therapy the shorter the duration of GO activity. It seems that in patients with active GO "the sooner the better" principle as regards RAI therapy should be considered.

| YDF1 | Sunday, October 22, 2017, 13:00 - 14:30, Hall F1 |

EANM Young Daily Forum 1: Presentation Skills Workshop

R. Sheppard; Somerset, UNITED KINGDOM.

| 401 | Sunday, October 22, 2017, 14:30 - 16:00, Hall A |

CME 3 - Cardiovascular: How to Perform Myocardial Perfusion Imaging According to EANM Recommendations

OP-087
Stress Test
O. Lindner; Institut für Radiologie, Nuklearmedizin und Molekulare Bildgebung, Herz- und Diabeteszentrum NRW, Bad Oeynhausen, GERMANY.

OP-088
Injected Doses and Tracers
J. Bucerius; Department of Nuclear Medicine, Maastricht University Medical Center (MUMC+), Maastrich, NETHERLANDS.

OP-089
Image Analysis
A. Scholtens; Department of Nuclear Medicine, Meander Medical Center, Amersfoort, NETHERLANDS.

OP-090
Reporting
E. Trägårdh; Department of Clinical Sciences, Clinical Physiology and Nuclear Medicine Unit, Lund University, Skåne University Hospital, Malmö, SWEDEN.

| 402 | Sunday, October 22, 2017, 14:30 - 16:00, Hall B |

Joint Symposium 3 - EANM/ETA-CRN: Update Thyroid Cancer Beyond I-131

OP-091
I-131 Refractory Differentiated Thyroid Cancer
M. Kreissl; Klinik für Radiologie und Nuklearmedizin, Universitätsklinikum Magdeburg A.ö.R., Otto-von-Guericke Universität, Magdeburg, GERMANY.

OP-092
Medullary Thyroid Cancer
L. Giovanella; Oncology Institute of Southern Switzerland, Nuclear Medicine and PET Centre, Bellinzona, SWITZERLAND.

OP-093
Anaplastic Thyroid Cancer
L. Fugazzola; University of Milan, Department of Endocrinology, Milan, ITALY.

| 403a | Sunday, October 22, 2017, 14:30 - 15:30, Hall C |

Mini Course 1: Cardiology - Pitfalls & Artefacts

OP-094
Common Artefacts in Nuclear Cardiology Imaging
A. Ghilardi; Nuclear Medicine DPT and Medical Physics DPT, ASST Papa Giovanni XXIII, Bergamo, ITALY.

OP-095
Artefacts and Image Interpretation
A. Flotats; Universitat Autònoma de Barcelona, Consultant, Nuclear Medicine Department, Hospital de la Santa Creu i Sant Pau, Barcelona, SPAIN.

| 403b | Sunday, October 22, 2017, 15:45 - 16:45, Hall C |

Mini Course 2: Inflammation and Infection - Pitfalls & Artefacts

OP-096
Pitfalls and Artefacts in Infection and Inflammation Imaging: Labelled Leukocytes
E. Lazzeri; Regional Center of Nuclear Medicine AOUP, Pisa, ITALY.

OP-097
Pitfalls in FDG-PET Imaging of Infection and Inflammation
A. Glaudemans; University of Groningen, Groningen, NETHERLANDS.

| 403c | Sunday, October 22, 2017, 17:00 - 18:00, Hall C |

Mini Course 3 (Interactive): Bone and Joint - Pitfalls and Artefacts

OP-098
Bone and Joint – Pitfalls and Artefacts
W. Grootjans; Leiden University Medical Centre, Radiology and Nuclear Medicine Department, Leiden, NETHERLANDS.

Do.MoRe: Radiopeptides for Therapy

OP-099

177 Lu-Dota-octreotate therapy in advanced Gastrointestinal Neuroendocrine tumors: outcomes after 5 years follow up

M. Sansovini[1], I. Grassi[2], S. Severi[1], A. Ianniello[1], S. Nicolini[1], M. Celli[1], E. Amadori[3], V. Di Iorio[4], M. Monti[5], E. Scarpi[5], A. Bongiovanni[6], A. Lambertini[7], C. Grana[8], G. Paganelli[1]; [1]Nuclear Medicine and Radiometabolic Unit, IRST-Istituto Scientifico Romagnolo per lo Studio e la Cura dei Tumori (IRST) IRCCS, Meldola (FC), ITALY, [2]Nuclear Medicine Unit, Faenza Hospital, Romagna Local Health Service, Faenza (RA), ITALY, [3]Radiology Unit, IRST-Istituto Scientifico Romagnolo per lo Studio e la Cura dei Tumori (IRST) IRCCS, Meldola (FC), ITALY, [4]Oncology Pharmacy, IRST-Istituto Scientifico Romagnolo per lo Studio e la Cura dei Tumori (IRST) IRCCS, Meldola (FC), ITALY, [5]Unit of Biostatistics and Clinical Trials, IRST-Istituto Scientifico Romagnolo per lo Studio e la Cura dei Tumori (IRST) IRCCS, Meldola (FC), ITALY, [6]Osteoncology and Rare Tumors Center, IRST-Istituto Scientifico Romagnolo per lo Studio e la Cura dei Tumori (IRST) IRCCS, Meldola (FC), ITALY, [7]Nuclear Medicine, Azienda Ospedaliero-Universitaria di Bologna, Bologna (Bo), ITALY, [8]Division of Nuclear Medicine, European Institute of Oncology Milan (IEO), Milan (MI), ITALY.

Background and Aim: We already reported activity and safety of 177Lu-dotatate (Lu-PRRT) at different dosages in patients with metastatic progressive GI-NETs. A minimal effective PRRT activity was determined and prognostic factors such as the presence of FDG avid lesions was addressed. Here we report the five year follow up (FU) and the role of hepatic involvement in advanced GI NET patients treated with of Lu-PRRT. **Patients and Method:** The study was prospective, phase II, open label and disease-oriented. Every 6 to 8 weeks, all patients received 3.7 GBq or 5.5 GBq of 177Lu-DOTATATE each cycles repeated 5 times (Total Activity 18.5 GBq or 27.5 GBq according to the presence of toxicity risks). **Results:** 43 patients (28M and 15 F) were evaluable and were monitored for a median period of 67 months (range 12.6-96.3). All patients had PET 68Ga-dotapeptide/octreoscan positive in documented lesions. Median PFS of patients who received reduced activity (RA) was 55.6 mo (29.8-69.0) while median PFS of patients treated with full activity (FA) was 52.7 mo (23.3-69.0; p=0.999). Median OS was 82.0 mo (55.6-nr, p=0.4) in patients who received FA and has not been reached in those treated with RA. FDG PET imaging was available in 33/43 patients (77 %). When no FDG uptake was present at tumor site median PFS was 60.1 mo (36.8-nr), while PFS was 29.8 mo in FDG positive patients (9.0-69.0, p=0.05). In 19 patients (44.2%) with less than 6 liver metastases, PFS was 55.6 mo (18.0-nr), while in 18 pts (41.9%) with more than 6 hepatic lesions was 30.4 mo (14.3-36.8, p=0.01). Neither hematological nor renal grade 3-4 toxicity was noticed in both groups. **Conclusion:** After 5 years of FU, Lu-PRRT proves to be a safe and effective therapeutic option in advanced GI NET. Important prognostic factors are the presence of FDG avid lesions and hepatic involvement regardless total activity injected.

OP-100

Update: Edmonton Lu-177 Protocol (Induction and Maintenance Regimen) Improves Progression Free Survival (PFS) in Patients with Advanced Neuroendocrine Tumours (NETs)

A. J. B. McEwan[1], M. Wieler[1], D. Murray[1], M. B. Sawyer[1], D. Morrish[1], B. A. Schaitel[2], L. D. Schrader[2], T. McMullen[1]; [1]University of Alberta, Edmonton, AB, CANADA, [2]Cross Cancer Institute, Alberta Health Services, Edmonton, AB, CANADA.

Introduction: The Edmonton LuTATE Protocol (ELP) - a PRRT protocol of induction (4 cycles of up to 6.11 GBq every 10 - 14 weeks) and long-term maintenance treatment (up to 8 cycles of up to 4.07 GBq /cycle every 5.5 - 10 months) - is an effective therapeutic option for patients with advanced gastrointestinal and pancreatic NETs (GEPNETs). We hypothesize ELP improves outcomes, and is effective and safe for these patients. We evaluated toxicity and PFS in a GEPNET cohort in a 2nd interim analysis of ELP. **Subjects & Methods:** A subset of 170 participants of the 195 enrolled in the Edmonton LuTATE Protocol had PNETs (n=49), GNETs (n= 103), or presumptive GNETs (n=18). Of these 170 participants, 22 had 1-2 cycles, 42 had 3-4 cycles, 40 had 5-6 cycles, 29 had 7-8 cycles, 26 had 9-10 and 11 had 11-12 cycles. Cumulative mean administered dose was 6.53 ± 2.52 GBq (1-2 cycles), 17.03 ± 2.84 GBq (3-4 cycles), 23.96 ± 4.40 (5-6 cycles), 30.18 ± 4.47 GBq (7-8 cycles), 38.38 ± 4.05 GBq (9-10 cycles) and 48.92 ± 5.77 GBq (11-12 cycles). Doses were modified by a defined algorithm for age, metastatic burden and renal function. **Results:** 124 patients remain on treatment and 46 have stopped treatment: 1 is surgically confirmed disease free (after 4 cycles); 3 have no clinical evidence of disease; 24 have discontinued due to biochemical, anatomic or symptomatic progression between cycles (after 1-2 cycles, n=5; after 3-4, n=3, after 5-6; n=3, after 7-8; n=5, after 9-10; n=6, after 11-12, n=2); and 18 died (after 1-2 cycles, n=6; after 3-4, n=2, after 5-6; n=5, after 7-8; n=3, after 9-10; n=2). Mean time from first treatment: 11.0 weeks -1-2 cycles; 31.8 weeks - 3-4 cycles; 18.6 months - 5-6 cycles; 7-8 cycles - 30.8 months; 47.4 months - 9-10 cycles; and 62.5 months - 11-12 cycles. A Kaplan-Meier survival curve shows median PFS is ~55.7 months. Transient Grade 2 renal toxicity was seen in 16% of patients; transient Grade 3 haematological toxicity was seen in 15% of patients; no Grade 4 toxicity was observed. **Conclusion:** These data support our hypothesis that Edmonton LuTATE Protocol improves PFS in patients with GEPNETS, and supports the hypothesis of low dose hypersensitivity as the mechanism of action for PRRT in GEPNETS. This regimen is more effective than literature reported treatment regimens; in this cohort, median PFS is ~55.7 months

OP-101

Improvement of PFS and OS after salvage therapy with 177-Lu[Dota0,Tyr3]octreotate in patients with gastroenteropancreatic and bronchial neuroendocrine tumours - the Rotterdam cohort

W. A. van der Zwan[1], T. Brabander[1], B. L. K. Kam[1], J. J. M. Teunissen[1], E. P. Krenning[2], D. J. K. Kwekkeboom[1], W. W. de Herder[1]; [1]Erasmus

MC, Rotterdam, NETHERLANDS, ²Cyclotron BV, Rotterdam, NETHERLANDS.

Aim: Peptide receptor radionuclide therapy (PRRT) with 177-Lu[Dota⁰,Tyr³]octreotate is an effective treatment option for patients with metastasized and/or inoperable neuroendocrine tumours. We evaluated the efficacy and toxicity of salvage therapy with PRRT in a large group of patients with a long follow-up. **Materials and Methods:** Dutch patients with gastroenteropancreatic or bronchial neuroendocrine tumours were selected for re-(re)-treatment if they had had benefit from initial therapy and suffered from renewed progressive disease. Benefit is defined as objective response of at least a partial response according RECIST 1.1 or conversion of progressive disease into stable disease. The cohort underwent salvage therapy between October 2003 and October 2015, with follow-up up to and including December 2016. The intended cumulative dose for re-(re)-treatment was 14.8 GBq (400mCi) divided over two administrations. The total intended cumulative dose per patient for the initial treatment was 29.6 GBq (800mCi), for re-treatment 44.4 GBq (1200mCi) and for re-re-treatment 59.2 GBq (1600mCi). **Results:** In our study a total of 181 patients were re-treated and 14 patients were re-re-treated. Median follow-up was 91 months. Patients were re-treated with a median cumulative dose of 14.9 GBq (range 3.7-16.2 GBq)/400mCi (range 100-400mCi) and re-re-treated with a median cumulative dose of 15.0 GBq (range 3.8-15.3GBq)/400mCi (range 100-400mCi). After initial therapy the median PFS and OS were 33 (**95% CI [30.4, 35.6])** and 77 (**95% CI [63.1, 91.0])** months, respectively. Median PFS after re-treatment was 14 (**95% CI [11.7, 16.3])** months and OS was 26 (**95% CI [18.9, 33.1]**) months. Median PSF and OS after re-re-treatment was 14 (**95% CI [9.8, 18.2])** months and 29 (**95% CI [4.6, 53.4])** months. Severe long-term haematological toxicity includes 2 cases of acute myeloid leukemia and 1 myelodysplastic syndrome, a total of 1.7%. No Grade III or Grade IV nephrotoxicity with regard to PRRT was seen. **Conclusion:** Salvage therapy with 177-Lu[Dota⁰,Tyr³]octreotate is a feasible treatment option in patients with a good response after initial therapy. The occurrence of severe haematological toxicity is not higher then previously reported.

OP-102

Investigation of Receptor Radionuclide Therapy with 177Lu dotatate in GEP-NEN patients with High Grade Ki67

S. Nicolini¹, S. Severi¹, M. Sansovini¹, A. Ianniello¹, P. Caroli¹, A. Bongiovanni², A. Rossi³, F. Di Mauro⁴, E. Mezzenga⁵, E. Scarpi⁶, G. Paganelli¹; ¹Nuclear Medicine and Radiometabolic Unit, Istituto Scientifico Romagnolo per lo Studio e la Cura dei Tumori (IRST) IRCCS, Meldola (FC), ITALY, ²Osteoncology and Rare Tumors Center, Istituto Scientifico Romagnolo per lo Studio e la Cura dei Tumori (IRST) IRCCS, Meldola (FC), ITALY, ³Radiology Unit, Istituto Scientifico Romagnolo per lo Studio e la Cura dei Tumori (IRST) IRCCS, Meldola (FC), ITALY, ⁴Nuclear Medicine Unit, University of Messina, Messina, Italy, Messina, ITALY, ⁵Medical Physics Unit, Istituto Scientifico Romagnolo per lo Studio e la Cura dei Tumori (IRST) IRCCS, Meldola (FC), ITALY, ⁶Unit of Biostatistics and Clinical Trials, Istituto Scientifico Romagnolo per lo Studio e la Cura dei Tumori (IRST) IRCCS, Meldola (FC), ITALY.

Background and Purpose: The WHO 2010 classification divides gastroenteropancreatic neuroendocrine neoplasia (GEP-NEN) in 3 categories based on ki67 proliferation index: NET G1: ki67<3%; NET G2: ki67 3-20%; NEC G3: ki67>20%. Accordingly, a cut-off of ki67>20% distinguishes high-grade GEP-NEC from intermediate grade; however, in clinical practice a ki67>15% is considered as a high-grade and often treated with standard schemes of chemotherapy. There is evidence that some high-grade NENs have a moderate aggressive behavior and can express somatostatin receptors (in 40-70% of cases) allowing the possibility of a targeted therapy. PRRT is one of the most important targeted therapy in the management of NET and several studies have demonstrated its efficacy in G1-G2 GEP-NETs. The aim of this study was to investigate the role of PRRT with 177Lu-DOTATATE (Lu-PRRT) in GEP-NENs with a ki67 index ranging from 15% to 70%. **Methods:** 33 patients affected by GEP-NEN with ki67 from 15% to 70% were treated with Lu-PRRT. All patients, with positive somatostatin receptor imaging (SRI+), had advanced disease and had been already treated with standard therapies. A cumulative activity of 18.5GBq or 27.8 GBq in 4 to 5 cycles was administered according to kidney and bone marrow reserve. Receiver operating characteristic (ROC) curve was used to determine the best threshold of ki67 expression to predict PD (progression disease). **Results:** The median follow-up was 43 months (range 3-69). Overall response was PR in 2 patient (6 %) and SD in 21 (64%), with a DCR of 70%. Median PFS was 23 months (95 % CI 14.9-31.0 months) and median OS 52.9 months (95 % CI 17.1-68.9 months). ROC curve analysis at 23 months revealed that the best cutoff value of ki67 expression was 35%. 24 patients had ki67≤35% and 10 patients had ki67 ranging 36-70%. Analyzing outcome according to proliferation index, in the group with ki67 ranging 15%-35% the DCR was 87% whereas in the group with ki67 >35%, DCR was 30%. The mPFS was 26.3 months (95 % CI 18.4-37.7 months) in the first group while was 6.8 months (95 % CI 2.1-27 months) in the second group (p=0.005). **Conclusion:** Lu-PRRT showed antitumor activity in advanced SRI+ high-grade GEP-NENs. DCR and PFS were significantly better in GEP-NEN patients with ki67 ≤35% compared to patients with ki67>35%. Accordingly to our experience, PRRT should be considered as a therapeutic option in patients affected by intermediate-high grade, SRI+, GEP-NEN, in particular with ki67≤35%.

OP-103

177Lu-Dotatate Peptide Receptor Radionuclide Therapy Dose Response in Small Intestinal Neuroendocrine Tumors

U. M. M. Jahn¹, E. Ilan¹, M. Sandström¹, M. Bamerny², U. Garske-Román³, M. Lubberink², A. Sundin¹; ¹Radiology, Uppsala, SWEDEN, ²Nuclear Medicine, Uppsala, SWEDEN, ³Nuclear Medicine, Gothenburg, SWEDEN.

Aim: To estimate the relationship between the absorbed tumour dose during ¹⁷⁷Lu-DOTATATE-therapy and subsequent

tumour shrinkage in small-intestinal neuroendocrine tumour (SI-NET) metastases. **Methods:** Between November 2005 and October 2014, 108 consecutive patients with inoperable and progressive SI-NETs were treated with dosimetry guided ^{177}Lu-DOTA-octreotate peptide receptor radionuclide therapy (PRRT), undergoing SPECT/CT during each therapy cycle. Thirty-one patients with at least one well-circumscribed tumour lesion on SPECT/CT were selected and analysed by extended dosimetry during the treatment administered as 3-7 cycles of 7,4 GBq ^{177}Lu-DOTA-octreotate at 6-8-weeks interval. The absorbed tumour dose was calculated from activity measurements on sequential SPECT/CT at 24, 96 and 168 h post infusion applying the unit density sphere model from OLINDA. The partial volume effects in the SPECT measurements were corrected, based on phantom measurements. The morphological response on tumour diameter, tumour volume, liver tumour volume and liver volume as well as RECIST 1.1 was evaluated by CT/MRI. Results: The absorbed tumour dose from baseline to best response (BRTR)(% tumour diameter reduction) ranged 38 to 408 Gy. The total administered activity during PRRT correlated to tumour diameter shrinkage (R^2=20% P=0,02). The mean specific activity of the 177Lu-octreotate preparations correlated to the absorbed tumour dose (R= 32%, P=0,001). No correlation was found between the absorbed tumour dose and tumour shrinkage. No correlations were found between the liver tumour volume and the liver volume or the absorbed dose and the total administered activity. The median follow up time from the start of PRRT was 17 months (range 7 to 50 months). When applying RECIST 1.1 criteria, the median time from start of PRRT to best response was 15 months. 5/26 patients developed progressive disease at 28, 29, 29, 34 and 41 months, respectively. 3/26 patients demonstrated partial response and 18/26 patients had stable disease at the latest follow up. **Conclusion:** SI-NET shrinkage correlated to the total administered ^{177}Lu-activity. The method used for calculating the absorbed dose in SI-NET tumours failed to demonstrate an absorbed tumour dose-response relationship in the chosen SI-NETs. The mean specific activity of the preparations correlated to the absorbed tumour dose. The specific activity may be an important factor and its impact needs to be considered in future research on PRRT.

OP-104

Gender-related differences in absorbed dose to risk organs in patients receiving ^{177}Lu-Octreotate therapy

M. Sandstrom, Sr.[1,2], *E. Ilan*[1,2], *K. Fröss-Baron*[1], *U. Garske-Roman*[1], *D. Granberg*[3], *B. Eriksson*[3], *A. Sundin*[1], *M. Lubberink*[1,2]; [1]*Nuclear medicine and PET, Uppsala University, Uppsala, SWEDEN,* [2]*Medical physics, Uppsala University Hospital, Uppsala, SWEDEN,* [3]*Endocrine Oncology, Uppsala University, Uppsala, SWEDEN.*

Aim: Fractionated therapy with ^{177}Lu-octreotate is an effective treatment option for patients with generalized neuroendocrine tumors. The aim of the present work was to study gender-related differences in absorbed dose to risk organs and if weight, length or lean body mass could explain gender differences for the absorbed doses to risk organs in patients receiving therapy with ^{177}Lu-octreotate. **Methods:** Five hundred patients (250 female and 250 male) with neuroendocrine tumors with high somatostatin receptor expression were included. SPECT/CT images were acquired at 24, 96 and 168 h after infusion of 7.4 GBq of ^{177}Lu-octreotate and absorbed doses to kidneys and liver were calculated using previously described methods. Absorbed doses in men and women were compared using Mann-Whitney tests. The relation between absorbed dose and gender and either body weight, length, lean body mass, or both body weight and length was assessed using multiple regression. P-values less than 0.05 were treated as significant and P-values less than 0.001 were treated as highly significant. **Results and discussion:** Absorbed doses to left and right kidneys were 4.9 and 4.6 Gy for women and 3.9 and 3.8 Gy for men, respectively ($p < 0.0001$). Absorbed doses to liver were 2.1 Gy in both men and women (n.s.). For both kidneys, absorbed dose was highly correlated to gender ($p < 0.0001$) regardless of other independent variables, but partial correlation to body weight was significant as well: p 0.013 using only gender and weight as independent variables and $p < 0.01$ when using gender, weight and length as independent variables. Partial correlations with length and lean body mass were not significant. For liver, absorbed dose was correlated primarily to body weight ($p < 0.05$), whereas partial correlations to gender, length and lean body mass were non-significant. **Conclusions:** There is a significant difference between absorbed doses to the kidneys in men and women receiving ^{177}Lu-octreotate therapy, with a much higher partial correlation to gender than to body weight. No significant differences in absorbed doses to liver between men and women were found, with liver absorbed doses correlating only to body weight. Since kidney is the dose-limiting organ in ^{177}Lu-octreotate therapy, this gender difference in absorbed doses should be taken into account in treatment planning.

OP-105

177Lu-DOTATATE therapy in radio iodine refractory differentiated thyroid cancer: a single center experience

W. Roll, B. Riemann, M. Schäfers, L. Stegger, A. Vrachimis; *University Hospital Münster, Münster, GERMANY.*

Aim: In general, differentiated thyroid cancer (DTC) patients treated by surgery and radioiodine therapy show excellent overall survival, however, radioiodine refractory DTC (RrDTC) patients suffer from a rather poor prognosis. In these situations new therapeutic options are warranted in addition to conventional external radiation therapy and surgery. To this end, novel systemic therapies such as tyrosine kinase inhibitors (TKIs) are promising, however, these are expensive and associated with serious adverse effects in more than one-fourth of patients. RrDTCs can also express somatostatin receptors, which could be employed for diagnostics and therapy using peptide radio-receptor therapy (PRRT). Hereby we present a single center experience of ^{177}Lu-DOTATATE therapy in advanced RrDTC. **Materials and Methods:** Five patients received 2 to 5 cycles

of PRRT with ^{177}Lu-DOTATATE (mean injected dose 7.0 GBq) between 5/2014 and 10/2016 in three month intervals. Inclusion criteria were RrDTC, no other therapy options as assessed by an interdisciplinary tumor board and positive ^{68}Ga-DOTATATE-PET-CT. Response to therapy was evaluated by interim and follow up ^{68}Ga-DOTATATE-PET-CT according to morphological (RECIST) and metabolic criteria (analogue to PERCIST). Additionally, thyroglobulin (Tg) levels were measured before each therapy cycle and after completion of therapy. Analysis was performed on a per-patient and per-tissue basis. **Results:** In post-therapy staging only one out of five patients (20%) showed partial response (decrease of > 30% in Tg, RECIST, and modified PERCIST), whereas three patients (60%) presented with progressive disease according to RECIST, PERCIST-like criteria and Tg levels. One patient (20%) had discordant findings regarding imaging (stable RECIST and modified PERCIST) and Tg levels (progression). On a per-tissue basis lymph node metastases and local recurrence showed more favorable results than bone metastases. **Conclusion:** In this cohort of 5 RrDTC patients, ^{177}Lu-DOTATATE therapy showed only limited efficacy, especially if bone metastases were present.

OP-106

Best Therapy Response vs Variability of Tumor Size, Absorbed Dose And Ki-67 Index After n.c.a. Lu-177 Dotatate Intra-arterial Infusions

M. Paphiti[1], I. Karfis[1], E. Z. Dimitriadi[2], S. Chondroyiannis[3], G. Nikou[1], V. Michalaki[1], G. Fragulidis[4], D. Voros[4], V. R. McCready[5], D. Rubello[3], G. S. Limouris[1]; [1]Medical Faculty, National and Kapodistrian University of Athens, Athens, GREECE, [2]Institute Claudus Regaud, University of Paul Sabatier, Toulouse, FRANCE, [3]Nuclear Medicine Department, Santa Maria della Misericordia Hospital, Rovigo, ITALY, [4]II Surgical Dept, of 'Aretaieion' Hospital, Medical Faculty, National and Kapodistrian University of Athens, Athens, GREECE, [5]Institute Cancer Research, Sutton Surrey & Royal Sussex County Hospital, Brighton, UNITED KINGDOM.

Introduction: GEP-NETs can be classified according to their Ki-67 proliferation index into grade 1 (G1), with a Ki-67 index <2%, G2 with a Ki-67 index between 3 and 20% and G3 > 20%. Focusing to liver metastasized disease, additional to the Ki-67 proliferation index the variability of tumor sizes in liver parenchyma crucially determine and contribute to their prognosis. Aiming to evaluate the tumor-volume impact on GEP-NETs response and prognosis, we compared and analyzed the correlation between their volume pattern and patients' survival. **Subjects and Methods:** We retrospectively studied a consecutive cohort of 13 patients with non-functioning, unresectable liver-metastatic GEP-NETs, undergoing intra-arterial infusions with non-carrier-added ^{177}Lu-DOTATATE (6 sessions each with 7.2 GBq per cycle, at standard intervals of about 2 mo). Patients (9, originated from pancreas and 4, from lungs) were graded as (G1/G2) and (G3) and were under long-acting somatostatin analog treatment. We classified the included patients in three groups as following: group A, with a liver metastasized tumor-size (LMTS) from 20 up to 30 mm (main diameter), group B, with a LMTS from 30 up to 40 mm and group C, with a LMTS larger than 40 mm. Response was evaluated according to RECIST criteria. Survival was analyzed according to Kaplan-Meier curve method. Cr-A was radioimmunologically measured and correlated with Ki-67 results. **Results:** The response rate regarding group A (6pts, mean tumor size 2-3cm, mean absorbed dose 450 Gy) was 50.0% as partial response, group B (3pts, mean tumor size 3-4cm, mean absorbed dose 150 Gy) was 70.0% as partial response and group C (4pts, mean tumor size 6cm, mean absorbed dose 450 Gy) was 20.0% as as stable disease. The median time of progression-free survival in group A was 53 mo, in group B, 58 mo and in group C 48 mo. Cr-A values showed a parallel to Ki-67 values, level. **Conclusion:** The final achievement to stabilize (SD) GEP-neuroendocrine liver metastasized tumours of large volume (about 6cm) after a radiobiological burden of 450 Gy (absorbed dose) compared to the partial response (PR) in pts with liver metastasized tumors of smaller volume with the same or even lower (150 Gy) absorbed dose, undeniably indicates the negative impact that the parameter volume plays, in PRRT response. The exeresis of these large volume tumors before PRRT should be a must.

| 405 | Sunday, October 22, 2017, 14:30 - 16:00, Hall E2 |

M2M: New Targets

OP-107

Radiochemistry and Preclinical Evaluation of Two Novel Peptide Analogues Targeting Glucagon Receptor for Anti-Diabetic Drug Development

I. Velikyan[1,2], M. Bossart[3], T. Haack[3], I. Laitinen[3], P. Larsen[3], O. Plettenburg[4], L. Johansson[5], S. Pierrou[5], M. Wagner[3], O. Eriksson[5,6]; [1]PET Centre, Centre for Medical Imaging, Uppsala University Hospital, Uppsala, SWEDEN, [2]Section of Nuclear Medicine and PET, Department of Surgical Sciences, Uppsala University, Uppsala, SWEDEN, [3]Sanofi-Aventis, Frankfurt, GERMANY, [4]Helmholtz Zentrum, München, GERMANY, [5]Antaros Medical AB, Molndal, SWEDEN, [6]Uppsala University, Uppsala, SWEDEN.

Introduction: Type 2 diabetes affects hundreds of millions of individuals worldwide. The development of novel anti-diabetic therapies targeting glucagon receptors (GCGR) requires employment of imaging techniques that enable in vivo investigation of GCGR engagement by the therapeutic agent to facilitate stratification of candidate drugs. Two novel peptide analogues targeting GCGR were labelled with positron emitting Gallium-68 radionuclide for imaging using positron emission tomography (PET). **Methods:** Two glucagon peptide agonists, S01-GCG and S02-GCG were conjugated to a DOTA chelate moiety and labelled with Gallium-68 available from a [68]Ge/^{68}Ga generator system. The binding affinity and specificity of the resulting imaging agents, [^{68}Ga]Ga-DO3A-S01-GCG and [^{68}Ga]Ga-DO3A-S02-GCG, were investigated in vitro using GCG receptor transfected HEK293 cells and autoradiography on cryosections of liver tissue from rat, cynomolgus monkey

and human. The organ distribution, binding specificity, and dosimetry were studied in vivo in Sprague Dawley rats. **Results:** None-decay-corrected radiochemical yield was 56.9±1.3% and 61±2%, respectively for [⁶⁸Ga]Ga-DO3A-S01-GCG and [⁶⁸Ga] Ga-DO3A-S02-GCG providing specific radioactivity of 50.2±5.4 MBq/nmol and 64.9±2.1 MBq/nmol at the time of the respective experiments. Both agents demonstrated binding and internalization in GCGR transfected cells and liver sections, which was competed by excess of each respective peptide ligand or endogenous glucagon, but not endogenous GLP-1. Affinities for the human GCG receptor were 17±8 nM and >100 nM, respectively, and thus higher for [⁶⁸Ga]Ga-DO3A-S01-GCG. The in vivo uptake and retention in rat was highest in liver, spleen and kidney. The uptake in liver and spleen was competed by co-injection of 1 mg/kg of each respective peptide, indicating GCG receptor-mediated binding in these tissues. The liver uptake of [⁶⁸Ga]Ga-DO3A-S01-GCG was over 4-fold higher than that for [⁶⁸Ga]Ga-DO3A-S02-GCG. The displacement of [⁶⁸Ga] Ga-DO3A-S01-GCG and [⁶⁸Ga]Ga-DO3A-S02-GCG in liver were 84% and 56%, respectively. The extrapolation of rat dosimetry results to human showed comparable renal doses (0.54 mSv/ MBq and 0.48 mSv/MBq) and effective doses (20.2 μSv/MBq and 16.6 μSv/MBq), that would allow for multiple annual PET examinations in healthy individuals and individuals with type 2 diabetes without exceeding the limiting radiation absorbed doses. **Conclusions:** [⁶⁸Ga]Ga-DO3A-S01-GCG and [⁶⁸Ga]Ga-DO3A-S02-GCG analogues are promising candidate peptides for in vivo monitoring of GCG receptor occupancy in humans. However, further development towards clinical use will be focused on [⁶⁸Ga]Ga-DO3A-S01-GCG due to its higher affinity and superior displaceable binding in liver in vivo.

OP-108

Development of a new 68Ga radiolabelled PET imaging agent to evaluate in vivo expression of angiomotin in malignant brain tumors

A. Moyon[1,2,3], P. Garrigue[1,2,3], P. Brige[2], M. Nollet[1], L. Balasse[2], S. Fernandez[2], M. Blot-Chabaud[1], F. Dignat-George[1,3], B. Guillet[1,2,3]; [1]UMR_S1076 VRCM, Marseille, FRANCE, [2]CERIMED, Marseille, FRANCE, [3]APHM, Marseille, FRANCE.

This study aimed at evaluating angiomotin (AMOT) as a potential molecular target for diagnosis and targeting of glioblastoma, the most common and lethal brain malignancy. We recently developed a ⁶⁸Ga-radiolabelled PET imaging agent (AM007) for assessing tissular AMOT expression as a potential predictive marker of tissue regeneration in post-ischemic condition. Data from the literature argue for AMOT involvement in glioblastoma proliferation. On this basis, we performed the first **in vivo** evaluation of AMOT-targeting ⁶⁸Ga-radiolabeled radiotracer, compared to ⁶⁸Ga-NODAGA-RGD, in mice orthotopic glioblastoma xenografts models. Human glioblastoma xenografts were achieved by injecting 3.10⁵ U87 cells into the right caudate-putamen of 7-week-old male BALB/c athymic nude mice under 2% isoflurane anesthesia. NODAGA-conjugates of AM007 were synthetized and radiolabeled with ⁶⁸Ga (25°C for

15 minutes). Gallium was obtained in ⁶⁸Ga³⁺ form using a commercial TiO₂-based ⁶⁸Ge/⁶⁸Ga generator. μPET/CT imaging was performed 1h after the injection of 7±2MBq of ⁶⁸Ga-NODAGA-AM007 or ⁶⁸Ga-NODAGA-RGD, 21 days after xenograft. **In vivo** blocking experiment was performed by injecting a 100-fold excess of cold peptide 30min before ⁶⁸Ga-NODAGA-AM007 injection. ⁶⁸Ga-NODAGA-AM007 was produced with a radiochemical purity of 93.1%±2.0 (*n*=10) and stability in serum evaluated up to 2h at 90±1.5%. In healthy mice, ⁶⁸Ga-NODAGA-AM007 showed a rapid plasmatic clearance (6.0±2.0min) and a pharmacokinetic profile compatible with PET imaging. μPET/CT imaging of mice orthotopic glioblastoma xenografts showed a high ⁶⁸Ga-NODAGA-AM007 tumor uptake (1.58±0.70% ID/g; n=5) 1h after injection of the radiotracer. ⁶⁸Ga-NODAGA-AM007 tumor uptake was significantly higher (p=0,0035; n=5) than ⁶⁸Ga-NODAGA-RGD uptake (0.48±0.14%ID/g; n=5). A 100-fold excess of cold peptide significantly reduced the ⁶⁸Ga-NODAGA-AM007 uptake (69.9%±16.0%, p=0.0032, n=3) Post-mortem histological immunohistochemistry and western-blotting analysis confirmed significant expression of AMOT in U87 cells. Based on AMOT overexpression in U87 cells, the AMOT-targeting imaging agent, ⁶⁸Ga-NODAGA-AM007, showed a specific uptake in brain tumors using μPET imaging 21 days after implementation. This uptake was 3 times higher than ⁶⁸Ga-NODAGA-RGD, allowing us to speculate that ⁶⁸Ga-NODAGA-AM007 may be considered as a potential candidate for theranostic applications in glioblastoma.

OP-109

[¹¹C]Erlotinib as a PET radiotracer to measure OATP2B1 transport activity in the human liver

M. Bauer[1], A. Matsuda[1], B. Wulkersdorfer[1], C. Philippe[1], A. Traxl[2], C. Özvegy-Laczka[3], J. Stanek[1,2], L. Nics[1], S. Poschner[4], W. Jäger[4], G. Szakács[1,3], W. Wadsak[1,5], M. Hacker[1], M. Zeitlinger[1], O. Langer[1,2]; [1]Medical University of Vienna, Vienna, AUSTRIA, [2]AIT, Seibersdorf, AUSTRIA, [3]Hungarian Academy of Sciences, Budapest, HUNGARY, [4]University of Vienna, Vienna, AUSTRIA, [5]CBMed, Graz, AUSTRIA.

The liver is a major clearance organ for many drugs. The organic anion-transporting polypeptides (OATP) 1B1, 1B3 and 2B1, which are expressed in the basolateral membrane of hepatocytes, mediate the uptake of many drugs from blood into liver and play a crucial role in drug disposition. All currently available PET radiotracers to measure OATP transport activity in the liver are not OATP-subtype specific. In this study we identified the radiolabelled tyrosine kinase inhibitor [¹¹C]erlotinib as a hepatic OATP2B1-specific radiotracer. Hepatic disposition of [¹¹C] erlotinib was studied with PET in 6 healthy volunteers without and with oral pretreatment with a therapeutic erlotinib dose (300 mg). In parallel to PET imaging, arterial blood sampling was performed and data were analysed using pharmacokinetic modelling. **In vitro** transport experiments were performed with [¹¹C]erlotinib (< 0.1 μM) in cell lines overexpressing human OATP1B1, 1B3 or 2B1. In baseline PET scans there was a high uptake of [¹¹C]erlotinib into the liver (approximately 30% of the injected dose). Following erlotinib pretreatment the rate

constant for [^{11}C]erlotinib distribution to the liver was significantly decreased (-86%) with a concomitant increase in blood exposure, pointing to the involvement of a carrier-mediated hepatic uptake mechanism. *In vitro* transport experiments revealed that [^{11}C]erlotinib is at tracer concentrations exclusively transported by OATP2B1 and that transport is inhibited at therapeutic erlotinib concentrations. Our data suggest that at PET microdoses uptake of [^{11}C]erlotinib into the human liver is mediated by OATP2B1, whereas at therapeutic doses erlotinib inhibits its own transport by OATP2B1. [^{11}C]Erlotinib may be used as a hepatic OATP2B1-specific radiotracer and erlotinib as an OATP2B1 inhibitor in clinical drug-drug interaction studies, allowing the contribution of OATP2B1 to the hepatic uptake of drugs to be revealed.

OP-110

First in vivo imaging and in vitro studies of ^{18}F-DABTA in rat model with E46K alpha synuclein mutation

B. Hooshyar Yousefi[1], K. Shi[1], S. Reder[1], S. Reder[1], M. Herz[1], M. Braeuer[1], H. Wester[2], I. Yakushev[1], T. Arzberger[3], M. Schwaiger[1]; [1]Klinikum rechts der Isar, Technical university Munich, Munich, GERMANY, [2]LS Pharm. Radiochem., Technical university Munich, Munich, GERMANY, [3]Ludwig Maximilians Universität München, Munich, GERMANY.

Increased pathological aggregation of alpha-synuclein (a-syn) is considered as an early causal factor in the pathogenesis of Parkinson's disease and other alpha-synucleinopathies. A PET tracer quantifying a-syn would be invaluable for early diagnosis of alpha-synucleinopathies and clinical trials testing of therapeutic strategies aimed at lowering a-syn levels in the brain. Recently, we developed a promising ^{18}F-DABTA based on 4,4'-diaryl-2,2'-bithiazole as specific marker for noninvasive delineating a-syn as opposed to other proteopathies (e.g. Aβ and tau). In the present work, we focused on in vivo imaging and in vitro evaluation of ^{18}FDABTA by µPET using a-syn E46K mutant rat model at age of 12-16 moths. **Methods:** A library of 4,4'-diaryl-2,2'-bithiazole derivatives was synthesized and screened towards a specific marker for a-syn. The best candidate with Ki < 10 nM and high selectivity (110 fold) was selected and converted to its ^{18}F-labeled version for in vivo and in vitro evaluation. Then, its brain specific binding kinetics have been investigated using reference Logan model on dynamic PET and confirm by in vitro evaluations using rats with a-syn E46K mutation vs WT. **Results:** We stablished an automated twostep radiosynthesis of 18F-DABTA using Neptis module with RCY ≥15% and purity >98%. The tracer was directly used in our experiments with specific activity greater than 18 GBq/µmol. The binding potential of PET data showed significant PET signal increased in a-syn abundant regions substantia nigra, thalamus, cerebellum and brainstem, confirmed by histochemistry in rats with asyn E46K mutation vs WT. **Conclusion:** The favorable properties of this tracer e.g brain entry/clearance kinetics, target affinity, excellent accumulation in the a-syn rich regions and practicability of PET imaging in E46K rats suggests that it is the first promising selective a-syn tracer that may allow early diagnosis of αsynucleinop-

athies such as Parkinson's disease and dementia with Lewy bodies. The favorable features of this tracer encourage us to further evaluative it by NHP and translation into human studies.

OP-111

Targeting αvβ6-integrin with radiometallated peptides for therapy of pancreatic carcinoma

S. Färber[1], K. Steiger[2], F. Reichart[1], M. Schwaiger[2], H. Kessler[1], H. Wester[1], J. Notni[1]; [1]Technische Universität München, Garching, GERMANY, [2]Technische Universität München, München, GERMANY.

Introduction: In most adult tissues, expression levels of αvβ6-integrin are very low. It is upregulated in many carcinomas, such as ovarian, gastric, and squamous cell carcinoma, for which it is furthermore associated with invasive growth and a poor prognosis. **Methods:** The αvβ6-integrin selective RGD-nonapeptide c(FRGDLAFp(NMe)K*) was conjugated to different chelators (DOTA, DOTAGA, DOTPI) by means of amide bonding or Click Chemistry, the latter resulting in triazole-containing linkers. The conjugates were labeled with Ga-68 or Lu-177 and their octanol-PBS distribution coefficients determined by shake-flask method. Furthermore, they were evaluated in SCID mice bearing H2009 (human lung adenocarcinoma) xenografts by means of PET or biodistribution studies, respectively. αvβ6-integrin affinities were determined by means of ELISA on immobilised integrin. Immunohistochemical (IHC) analysis of β6-integrin expression was performed for the excised tumor xenografts, and furthermore for tissue microarrays containing human pancreatic ductal adenocarcinoma (PDAC, 383 primary tumors, 7 lymph node and 8 distant metastases) and 34 pancreatic intraepithelial neoplasia (PanIN) specimens. **Results:** While the Lu(III) complexes of all 5 conjugates exhibited comparable αvβ6-integrin affinities (IC50 ranging from 0.47±0.03 to 0.82±0.17 nM), the different formal charges of the featured chelate moieties (Lu-DOTA-monoamide: 0; Lu-DOTAGA: 1; Lu-DOTPI:4) resulted in strongly varying degrees of hydrophilicity of the Lu-177 labelled compounds (logD ranging from -3.0 to -4.1). Whereas PET studies showed substantial differences of the Ga-68 labeled compounds regarding tumor uptake and background level, biodistribution of the Lu-177 labeled species were quite similar and comparable to our previously reported αvβ6-integrin PET tracer Ga-68-Avebehexin. IHC analysis of a large number of patient tissue specimens confirmed a high prevalence of αvβ6-integrin expression in PDAC primaries (88%) and in almost all metastases, as well as in PanIN (57%), underscoring a high potential of αvβ6-integrin targeted radiopharmaceuticals for diagnosis and treatment of pancreatic cancer. **Conclusion:** Lu-177 labeled αvβ6-integrin targeting radiopeptides possess high potential for endoradiotherapy of carcinomas. We confirmed that almost all pancreatic cancers are characterized by αvβ6-integrin expression. Hence, our novel radiotherapeutics appear particularly suitable for treatment of PDAC. In view of a high mortality (5-year survival rate of only 8%) and limited therapy options for this cancer type, we anticipate substantial clinical impact of αvβ6-integrin-directed PRRT.

OP-112

Imaging beta cells in patients after Roux-en-Y gastric bypass (RYGB) surgery by ⁶⁸Ga-NODAGA-exendin-4 PET/CT

M. Boss, Sr.[1], L. N. Deden[2], E. O. Aarts[3], H. de Boer[3], I. M. C. Janssen[3], M. Brom[1], F. J. Berends[3], M. Gotthardt[1]; [1]Radboud University Medical Center, Nijmegen, NETHERLANDS, [2]Rijnstate hospital, Arnhem, NETHERLANDS, [3]Rijnstate Hospital, Arnhem, NETHERLANDS.

Background: After undergoing RYGB, remission of type 2 diabetes (T2D) occurs in >60% of patients. The mechanism behind this remission is incompletely understood. Beta cell activity (BCA) and beta cell mass (BCM) could play a role. While RYGB is beneficial for the health and quality of life of most patients, a rare complication is hyperinsulinemic hypoglycaemia. Also here the mechanism is unclear, but a role for BCA and BCM is hypothesized. Measuring BCA and BCM could provide useful information on the role of beta cells in patient responses to RYGB and possibly offer predictive value. Exendin-4, a stable analogue of glucagon-like peptide-1, specifically accumulates in the beta cells. ⁶⁸Ga-exendin-4 PET/CT can be used to quantify BCM *in vivo* and could help to study the role of BCM in changes in glycemic control after RYGB. **Methods:** BCA and BCM were compared between patients with different responses after RYGB. Patients with complete remission of T2D (responders) and without complete remission of T2D (non-responders) after RYGB were included as well as patients with hypoglycaemia after RYGB. BCA was measured by an arginine stimulation test and either an oral glucose tolerance test (in responders and non-responders) or a standard meal tolerance test (in the hypoglycaemia patients). BCM was measured in all patients as pancreatic uptake of ⁶⁸Ga-exendin-4 by quantitative analysis of PET/CT scans. **Results:** In total, 12 responders and 12 non-responders will be included. So far, five responders and five non-responders were included. Preoperative patient characteristics and postoperative weight loss were comparable between the groups. BCM was 37% lower in non-responders (131±78 kBq) compared to responders (206 ± 90 kBq), although not statistically significant (p = 0.25). BCA was significantly lower in the non-responders compared to the responders, with an arginine stimulated acute C-peptide response of 0.4±0.2 and 0.9±0.3 nmol/l, respectively (p = 0.02). In total, 8 hypoglycaemia patients and 8 matched controls will be included. At this moment, three hypoglycaemia patients have completed the study and in these patients the mean BCM was 226±69 kBq. **Conclusion:** These preliminary data show that measuring BCM in vivo is possible using ⁶⁸Ga-exendin-4 PET/CT. The data suggest that BCM is lower in patients with incomplete remission of T2D compared to those with complete remission. Furthermore, BCM in patients with hypoglycaemia seems to be higher than in patients with remission of T2D after RYGB. These data may suggest a role for BCM in patient response to RYGB.

OP-113

68Ga-Pentixafor PET/CT Imaging Targeting CXCR4 chemokine receptors : The First Clinical Experience in Lung carcinoma subtypes

A. Watts[1], B. Singh[1], S. Chutani[1], N. Dhanota[1], H. Singh[1], R. Basher[1], A. Bal[1], R. Kapoor[1], S. K. Arora[1], H. J. Wester[2], B. R. Mittal[1], D. Behera[1]; [1]PGIMER, Chandigarh, INDIA, [2]Technical University of Munich, Munich, GERMANY.

Objective: To evaluate the diagnostic utility of 68Ga Pentixafor PET/CT in lung carcinoma and to correlate tumor uptake of the radiotracer with CXCR4 tumor expression/density as a function of the tumor sub-type. **Materials and Methods:** Twenty-five patients (23M: 2F; mean age= 60± 10 yrs) with histopathologically proven lung carcinoma [Non-small cell lung carcinoma - NSCLC=19 (with squamous cell in 15, adenocarcinoma in 3; NOS in 1), Small cell lung carcinoma - SCLC in 3 and primary lung Neuroendocrine tumor- NET in 3] underwent 68Ga-Pentixafor PET imaging. Biopsied lung tissue samples were subjected to fluorescence-activated cell sorting (FACS) analysis using CD184 antibody. Mean Fluorescence Index (MFI) was documented as measure of CXCR4 receptor density. 68Ga PET/CT data was reconstructed and the estimated SUVmax values were correlated with FACS results for CXCR4 expression/density. About 110-150 MBq radioactivity of freshly prepared 68Ga-Pentixafor (synthesized by using Scintomics automated chemistry module procured under DST-FIST Project Funding) was administered intravenously. Whole body contrast enhanced CT (120Kv, 200-300mAs, Pitch 0.98:1, Slice thickness 3.75mm) followed by PET from skull to proximal thighs (3min/bed position; 7-8 positions) was acquired at 1-hour post injection. Data was reconstructed using iterative method (3 iterations, 28 sub-sets) and interpreted both visually and quantitatively. **Results:** The mean 68Ga-Pentixafor SUVmax value in squamous cell and adenocarcinoma patients was 6.3±1.5 (n=15) & 8.5±1.5 (n=3), respectively. The corresponding MFI value assessed in these patients was 118± 69 and 146±53, respectively. On the other hand, in SCLC patients (n=3), the mean SUVmax value was 10.4 ± 2.5 with MFI score of 151±59. In patients with primary lung NET disease (n=3), the mean SUVmax value was 5.1±0.03 with MFI score of 80 ± 26. Our results demonstrated that among NSCLC patients, a significantly higher SUVmax was seen in adenocarcinoma variant than in squamous cell and the higher uptake correlated with higher CXCR4 expression. In SCLC, SUVmax value was significantly higher than in NSCLC and NET patients and was associated with the higher CXCR4expression/density in SCLC patients. **Conclusion:** 68Ga-Pentixafor uptake directly correlates with CXCR4 expression in lung carcinoma. SCLC demonstrates higher CXCR4 expression as compared to NSCLC. This novel PET Tracer is anticipated to pave the way for the development of CXCR4 targeting radionuclide theranostics in advanced stage malignancies.

OP-114

Evaluation of Lu-177 Labelled 6A10 Fab as Carbonic Anhydrase 12 Targeting Agent

L. Fiedler[1], M. Kellner[2], A. Gosewisch[1], G. Böning[1], S. Lindner[1], P. Bartenstein[1], R. Zeidler[2,3], F. Gildehaus[1]; [1]Department of Nuclear

Medicine, LMU, Munich, GERMANY, [2]Research Group Prevention and Immunomodulation; Helmholtz-Zentrum, Munich, GERMANY, [3]Department of Otorhinolaryngology, LMU, Munich, GERMANY.

Introduction: Typical therapy of malignant gliomas consists of surgery, followed by radiation and chemotherapy. Because of their infiltrating behaviour, the glioma cells are spread in the tumor surrounding brain tissue, which leads to local recurrence. Treatment of these infiltrated cells is the aim of the locoregional radioimmunotherapy (RIT), which is maintained by direct application of the radioimmunoconjugate into the resection cavity. The membrane enzyme carbonic anhydrase 12 (CA12) is only expressed on glioma cells and not on healthy brain tissue, and therefore a promising target for RIT. In this study the CA12 specific binding agent 6A10 Fab radiolabelled with Lu-177 is evaluated for its application in RIT. **Methods:** CHO cells were transfected with Fab coding plasmids and 6A10 Fab was purified from the culture supernatant, modified with p-SCN-Bn-CHX-A´´-DTPA and radiolabelled with Lu-177. The conjugate was characterized by MALDI-TOF, FACS and radio-TLC. In-vitro stability studies in different media were performed. Biodistribution studies (1 h, 3 h, 6 h, 24 h, 48 h, n=4 each), autoradiography examinations and ex-vivo blocking experiments on tumor slices were carried out on xenotransplanted (glioma U87-cells) SCID-mice. The tumor was visualized in first imaging experiments using planar scintigraphy and SPECT-CT techniques. **Results:** MALDI-TOF analysis revealed a molar ratio of Fab to DTPA of 1:1. FACS analysis confirmed that the biological functionality of the 6A10Fab was not inhibited by modification and radiolabelling. High radiochemical purity of > 99% (1 mg Fab; 1.5 GBq Lu-177) was verified by radio-TLC. After an incubation time of 72 h, the radiochemical purity of the product in labelling buffer (RT), human plasma (37 °C) and cerebrospinal fluid (37 °C) was still > 90%. Biodistribution study shows a moderate tumor uptake of ≤3,1% ID/g at 3 h, with a maximum tumor/muscle ratio of 14,6 at 48 h p.i. Scintigraphy and SPECT-CT imaging showed good tumor uptake at 4 h p.i. Tumor autoradiography experiments revealed an expected inhomogeneous activity distribution. Tumor uptake was decreased by 49 % (n=8) after ex-vivo blocking experiments on tumor slices with 100-fold molar excess of unmodified 6A10. **Conclusion:** Because of its high radiochemical stability under physiological conditions and the specific CA12 binding ability in-vivo and in-vitro, Lu-177-6A10-Fab is a promising agent for the RIT of gliomas.

---

406   **Sunday, October 22, 2017, 14:30 - 16:00, Hall F1**

Teaching Session 1 (Interactive): Applied Cross Sectional Anatomy and Correlative Imaging - Head and Neck

OP-115

Applied Cross Sectional Anatomy and Correlative Imaging – Head and Neck

C. Fowler; Brighton and Sussex University Hospital, Brighton, UNITED KINGDOM.

---

407   **Sunday, October 22, 2017, 14:30 - 16:00, Hall F2**

Clinical Oncology - Rapid Fire Session: Prostate

OP-116

PSMA-targeting alpha-Radiation therapy with [225]Actinium-PSMA-617: Dosimetry, toxicity and duration of tumor-control

C. Kratochwil[1], F. Bruchertseifer[2], F. L. Giesel[1], C. Apostolidis[2], U. Haberkorn[1], A. Morgenstern[2]; [1]University Hospital Heidelberg, Heidelberg, GERMANY, [2]EC-JRC, Directorate for Nuclear Safety and Security, Karlsruhe, GERMANY.

Purpose: To evaluate the potential of [225]Ac-PSMA617 for PSMA-targeting alpha-therapy of poor-prognosis advanced-stage mCRPC patients. **Methods:** An appropriate starting activity for clinical application of [225]Ac-PSMA617 was defined by a preliminary dosimetry modeling. The treatment protocol was then refined by an empirical dose escalation with n=14 patients to define a "standard operation procedure". Consecutively an additional group of n=28 was treated following this protocol. PSA and radiological response were assessed. Duration of response was compared to the duration of tumor control of preceding treatment lines. Lab tests and clinical exam was done to assess toxicity. **Results:** Assuming a RBE of 5, a mean dose of 2.3 Sv for salivary glands, 0.7 Sv for kidneys and 0.05 Sv for red marrow were estimated for 1 MBq of [225]Ac-PSMA617; comparable to an activity of 1 GB of ^{177}Lu-PSMA617. In dose-escalation phase, severe xerostomia became dose-limiting and defined the MTD even before relevant hematological toxicity was observed. 100kBq/kg BW [225]Ac-PSMA617 administered every 2 months was chosen as a first SOP. From 28 patients "intention-to-treat", n=20 were finally treated "per-protocol" and n=15 of them (75%) demonstrated a PSA and radiological response after a follow-up period of 6 months. Complete remission was observed in n=4 patients (20%). Due to early progression n=3 patients discontinued therapy at an earlier time-point, n=5 patients discontinued due to xerostomia. No grade-3/4 hematological toxicity was observed for patients with grade-0/1 values at baseline, regardless of the extent of bone involvement. PFS under PSMA-TAT was longer than the mean duration of tumor control under preceding treatment lines. **Conclusions:** First clinical results imply that PSMA-targeting alpha-radiation therapy with 225Ac-PSMA617 benefits from favorable low hematological toxicity even in "superscan"-pattern patients and also present remarkable anti-tumor activity in regard to objective response and PFS.

OP-117

68Ga-PSMA PET/CT to restage prostate cancer after radical therapy. Results of a prospective single-center trial

F. Ceci[1], P. Castellucci[2], T. Graziani[2], A. Farolfi[2], R. Renzi[2], R. Schiavina[3], M. Borghesi[3], F. Lodi[2], S. Boschi[2], S. Fanti[2]; [1]Department of Surgical Sciences, University of Bologna, Bologna, ITALY, [2]Nuclear Medicine, S.Orsola-Malpighi Hospital, University of Bologna, Bologna, ITALY, [3]Department of Urology, S.Orsola-Malpighi Hospital, University of Bologna, Bologna, ITALY.

Aim: The primary objective is to evaluate the performance of 68Ga-PSMA-PET/TC for detecting the site(s) of disease relapse in prostate cancer (PCa) with biochemical recurrence (BCR) after primary treatment. **Material and Methods**: This prospective single-center trial was approved by the Local Ethical Committee (PSMA-PROSTATA; Eudract: 2015-004589-27 OsSC). Inclusion criteria were: 1) proven PCa; 2) radical therapy (surgery or radiotherapy) for localized PCa; 3) proven BCR 4) PSA values comprised between 0.2-2ng/mL; 5) Gleason Score ≥7. From March 2016 to March 2017 were enrolled 257 patients (mean age= 68,7 years-old) matching all the inclusion criteria. This calculated sample size was adequate to evaluate the diagnostic accuracy of 68Ga-PSMA-PET/CT in a homogenous cohort of recurrent patients. The 96,5% were treated with radical prostatectomy, while the 3,5% with radical radiotherapy. The 10,1% of patients were treated with androgen-deprivation therapy at the time of PET/CT, while the 23,7% received salvage treatments during BCR. The mean PSA value at the time of the scan was 0,81 ng/mL (median-PSA=0,60 ng/mL; range=0,2-2 ng/mL). Correlative imaging with choline-PET/CT or MRI was available in the 72,3% of patients. **Results**: 68Ga-PSMA-PET/TC resulted positive, detecting at least one site of suspected PCa metastasis, in 117/257 patients, consisting in an overall detection-rate of 45,5%. On a patient-based analysis, local lesions limited to the pelvis (prostate/prostate bed and/or pelvic lymph-nodes) were detected in 57/257 patients (22,2%). The presence of at least one distant lesion (retroperitoneal or distant lymph-nodes and/or bone lesions and/or visceral lesions) was detected in 60/257 patients (23,3%). The mean PSA was significantly higher (p<0,05) in PET-positive patients (mean=0,97;median=0,86 ng/mL) vs. PET-negative patients (mean=0,68;median=0,50 ng/mL). PSA doubling-time resulted in the multivariate-analysis as statistical significant predictor for a positive 68Ga-PSMA-PET/CT scan (p<0,01). Correlative imaging with choline-PET/CT or MRI was available in 91/117 PET-positive patients resulted negative/inconclusive in the 69,2% (63/91) of cases. **Conclusion**: the results of this prospective trial confirmed the importance of 68Ga-PSMA-PET/TC for restaging PCa patients during BCR. In a homogeneous cohort of highly selected recurrent PCa patients, with a mean PSA value of 0,81 ng/mL, 68Ga-PSMA-PET/TC proved a dection-rate of 45,5%, with an incidence of systemic lesion detected in the 23,3% of cases. The validation of this new procedure in the clinical setting and its comparison with histology and/or other techniques would facilitate the routine implementation of this modality.

OP-118

Integrated 68Ga-PSMA-11 PET/MRI enhances discriminatory power of multi-parametric prostate MRI

M. Al-Bayati[1], J. Grueneisen[1], S. Lütje[1], L. Sawicki[2], S. Suntharalingam[1], S. Tschirdewahn[1], M. Forsting[1], K. Herrmann[1], L. Umutlu[1], A. Wetter[1]; [1]University Hospital Essen, Essen, GERMANY, [2]University Hospital Duesseldorf, Duesseldorf, GERMANY.

Purpose: To evaluate diagnostic accuracy of integrated 68Ga-PSMA-11 PET/MRI in patients with primary prostate cancer as compared to multi-parametric MRI. **Material and Methods:** A total of 22 patients with recently diagnosed primary prostate cancer underwent clinically indicated 68Ga-PSMA-11 PET/CT for initial staging followed by integrated 68Ga-PSMA-11 PET/MRI. Images of mpMRI, PET and PET/MRI were evaluated separately by applying PIRADSv2 for mpMRI and a 5-point Likert scale for PET and PET/MRI. Results were compared with pathology reports of biopsy or resection. Statistical analyses including ROC analysis were performed to compare the diagnostic performance of mpMRI, PET and PET/MRI. **Results:** PET and integrated PET/MRI demonstrated a higher diagnostic accuracy than mpMRI (AUC: mpMRI: 0.679, PET and PET/MRI: 0.951). The proportion of equivocal results (PIRADS 3 and Likert 3) was considerably higher in mpMRI than in PET and PET/MRI. In a notable proportion of equivocal PIRADS results, PET led to a correct shift towards higher suspicion of malignancy and enabled correct lesion classification. **Conclusion:** Integrated 68Ga-PSMA-11 PET/MRI demonstrates higher diagnostic accuracy than mpMRI and is particularly valuable in tumours with equivocal results from PI-RADS classification.

OP-119

Tc-99-MIP-1404 Imaging for the Detection of PSMA-Positive Lesions. A Pilot Study in 380 Patients with Histologically Confirmed Prostate Cancer

C. Schmidkonz, P. Ritt, C. Hollweg, M. Beck, T. I. Goetz, J. Sanders, J. Reinfelder, D. Schmidt, T. Kuwert; Universitätsklinikum Erlangen, Erlangen, GERMANY.

Introduction: Tc-99m-MIP-1404 (Progenics Pharmaceuticals, Inc., New York, NY) is a novel, SPECT- compatible Tc-99m-labeled PSMA inhibitor- for the detection of prostate cancer. We present first results of its clinical use at our institution for a cohort of 380 men with histologically confirmed prostate cancer. **Methods:** Tc-99m-MIP1404 scintigraphy was performed in 380 patients. Of these, 200, 95, and 85 were referred due to PSA relapse, for primary staging, and for restaging under therapy, respectively. Whole-body planar scintigraphy and SPECT/CT of the lower abdomen and thorax were carried out at 3 to 4 hours p.i. of 710 ± 64 Tc-99m-MIP-1404. Images were visually analyzed for presence, location and extent of abnormal uptake. In addition, quantitative analysis of the SPECT/CT data was carried out in a subset of 105 patients. Follow-up reports of subsequent therapeutic interventions were available for 58% (223) of all patients. **Results:** In total, tracer positive lesions were detected in 75% (286/380) of all patients. In 27% (104) of patients, uptake in the primary tumor was found. Local recurrence was diagnosed in 10% (37). Metastases in lymph nodes, bone, lung and other locations were detected in 37% (141), 30% (113), 4% (16), 5% (20), respectively. Detection rates were 89% at PSA levels greater than or equal to 2 ng/ml and 40% below that threshold. Quantitative analysis of PSMA-positive lesions disclosed SUV max values of on average 18.7±27.6 (0.8-262.9) and tumor-to-normal ratios of 100.7±173.9 (4.9-1325.4). The PSA level correlated significantly with total uptake of MIP-1404 in tumors (Spearman-Rho 0.64, p<0.001) and with tumor volume

(Spearman-Rho 0.47, p<0.001). The PSA level was significantly higher in patients with PSMA-positive lesions (Wilcoxon rank-sum, p<0.001). Following MIP-1404 imaging, in 76% (169/223) of those patients for whom follow-up was available therapeutic strategy was changed. These changes included initiation or adjustment of anti-androgenic therapy in 50, radiation therapy in 61, surgery in 33, initiation of chemotherapy in 10, Lu-177-PS-MA therapy in 6, and Ra-223-dichloride therapy in 9 patients. Of all patients undergoing surgery, histopathological results were available to us in 28 cases and confirmed the diagnoses of MIP-1404 imaging. **Conclusion:** SPECT/CT with MIP-1404 has a high accuracy in detecting PSMA-positive lesions in patients with elevated PSA values and has considerable therapeutic impact. Quantitative analysis showed significant correlation between PSA level, total uptake and tumor volume. Tumor-to-normal ratios are higher than those published for bone metastases of prostate cancer and Tc-99m-DPD, which could result in higher detection rates.

OP-120

Correlation Between Uptake of ^{18}F-1-amino-3-fluorocyclobutane-1-carboxylic acid (^{18}F-fluciclovine) and Expression of Amino Acid Transporters ASCT2 and LAT1 in prostate cancer

M. Kim[1,2,3], I. Saarinen[4], A. Kuisma[5], I. Jambor[6,7], J. Kemppainen[8], E. Kähkönen[9], A. Koskenniemi[10], P. Taimen[4], H. Minn[5]; [1]Gunma University, Maebashi, JAPAN, [2]Turku PET Centre, University of Turku, Turku, FINLAND, [3]Japan Society the promotion of science, Tokyo, JAPAN, [4]Department of Pathology, University of Turku and Turku University Hospital, Turku, FINLAND, [5]Turku University Hospital, Turku, FINLAND, [6]Turku University Hospital, Departments of Oncology and Radiotherapy, Turku, FINLAND, [7]Department of Radiology, Baystate Medical Center, University of Massachusetts, Springfield, MA, UNITED STATES OF AMERICA, [8]Turku University Hospital, Departments of Nuclear Medicine, Turku, FINLAND, [9]Turku University Hospital, Departments of Urology, Turku, FINLAND, [10]Turku University Hospital, Departments of Pathology, Turku, FINLAND.

Aim: ^{18}F-1-amino-3-fluorocyclobutane-1-carboxylic acid (^{18}F-fluciclovine) was recently approved by FDA for detection of recurrent prostate cancer (PCa). We aimed to evaluate expression of neutral amino acid transporter 2 (ASCT2) and L type amino acid transporter1 (LAT1) in prostatic tissue for their impact on uptake of ^{18}F-fluciclovine in localized PCa. **Materials and Methods:** Twenty-five patients with histologically confirmed PCa underwent PET/CT before robotic-assisted laparoscopic prostatectomy. Imaging was performed immediately after injection of 369 ±10 MBq of ^{18}F-fluciclovine and the uptake in PCa was expressed as SUV$_{max}$ 12-22 min from injection. Based on whole mount prostatectomy samples, the index tumours representing Gleason Scores (GS) 3+4=7 (n=10), 4+3=7 (n=8), 4+4=8 (n=1), 4+5=9 (n=4) and 5+4=9 (n=2)were selected for analysis. The expression of ASCT2 and LAT1 was studied with immunohistochemistry (IHC) in a tissue microarray (TMA) including three 1 mm cores from each patient's index tumor and one core of benign tissue from the same patient as a control. The TMA slides were scored independently by two persons based on visual intensity of carcinoma cells as follows: score 0 (negative staining), 1 (low intensity), 2 (moderate intensity) or 3 (high intensity). **Results:** The ^{18}F-fluciclovine uptake (SUV$_{max}$) in index tumour and ASCT2 score had a significant correlation (r=.468; P=.021), while that between SUV$_{max}$ and LAT1 was not (r=.250; P=.119). SUV$_{max}$ correlated with GS (r=0.435; P=0.030), while expression of amino acid transporters ASCT2/LAT1 did not show a relationship with GS. **Conclusions:** Our findings indicate that ^{18}F-fluciclovine PET/CT predicts GS and may thus assist in planning of local therapies. ASCT2 may be more important than LAT1 in mediating uptake of ^{18}F-fluciclovine in PCa.

OP-121

Impact of Ga-68 PSMA PET/CT on radiation treatment planning of prostate cancer

S. M. Schwarzenboeck[1], L. Schubert[1], H. Rennau[2], J. Kurth[1], B. J. Krause[1], G. Hildebrandt[2]; [1]Department of Nuclear Medicine, Rostock University Medical Centre, Rostock, GERMANY, [2]Department of Radiotherapy, Rostock University Medical Centre, Rostock, GERMANY.

Purpose: Radiation treatment (RT) is clinically established in PSA persistence/biochemical recurrence (BCR) as well as in primary prostate cancer (PC) as curative treatment. The aim of the study was to assess the impact of 68-Ga-PSMA PET/CT on RT planning in patients with BCR and high risk (HR) PC. **Patients and Methods:** 38 patients with BCR after radical prostatectomy (n = 27) and HR PC (n= 11) with a median PSA of 1.15 ng/ml (range 0.17-12.1) and 5.2 ng/ml (range 0.84-15.7), respectively, underwent 68-Ga-PSMA PET/CT before RT. Influence of 68-Ga-PSMA PET/CT on the extent of planning target volume (PTV) (compared to conventional PTV) and addition of PET-based boosts were assessed. 10/27 (BCR) and 5/11 patients (HR PC) were under androgen deprivation therapy during RT. Median clinical follow up of 12 months (range 3-24) was available in all patients. **Results:** 68-Ga-PSMA PET/CT was positive in 23/38 (60.5%) of patients (8/23: local recurrence (LR), 11/23: nodal recurrence/metastasis (not detected by CT, lymph node diameter≤10 mm), 1/23: LR and nodal recurrence, 2/23: solitary bone metastasis, 1/23: combined oligometastatic nodal/bone metastases). In BCR primary PTV was changed in 16/27 patients extending PTV to the lymphatic drainage (10/16), to PSMA-positive LR (3/16), bone metastases (2/16) and to both nodal/bone metastases (1/16). PET-based increase of primary PTV was 116% (median administered dose of 45 Gy (range 45-66.6)). Additional PET-based boosts were administered in 19/27 patients (local in 8/19, nodal in 10/19, both in 1/19), median boost volume was 31.3 cm3 (range 17.2-80.2) (local) and 19.7 cm3 (range 3.0-109.3) (nodal) with a median boost dose of 5.6 Gy (range 5.4-19.8) (local) and 23.1 Gy (range 5.4-34.8) (nodal). In HR PC treatment was changed in 1/11 (9%). Primary PTV was extended to the lymphatic drainage (additional RT volume of 644.5 cm3, 45 Gy), additional boost was administered to one PSMA-positive lymph node (volume of 2.7 cm3, 23.1 Gy). All patients showed biochemical response (mean

PSA decrease 88.8 +/- 14.0%). Nadir PSA was reached 10 months (range 1-17) after end of RT (median 0.07 ng/ml, range 0.002-3.96). Within a median follow-up of 12 months (range 3-22 and 8-24 in BCR and HR PC, respectively), median PSA was 0.05 ng/ml (range 0.002-8.5) (BCR) and 0.26 ng/ml (range 0.02-2.68) (HR PC). **Conclusion:** 68-Ga-PSMA PET/CT influenced RT planning in almost 63% of BCR and 9% of HR PC patients by change of PTV and addition of boosts.

OP-122

[⁶⁸Ga]Ga-PSMA-PET/CT imaging of localized prostate cancer patients for intensity modulated radiation therapy treatment planning with integrated boost

*L. Thomas[1], S. Kantz[2], A. Hung[3], D. Monaco[3], F. C. Gaertner[4], H. Strunk[5], M. Essler[4], C. R. Thomas[3], W. Laub[3], **R. A. Bundschuh[4]**; [1]Department of Nuclear Medicine, Universitaetsklinikum Bonn; Department of Radiation Medicine, Oregon Health and Science University, Portland, OR, UNITED STATES OF AMERICA, [2]LMU Munich, Department of Radiation Oncology, Munich, GERMANY, [3]Department of Radiation Medicine, Oregon Health and Science University, Portland, OR, UNITED STATES OF AMERICA, [4]Department of Nuclear Medicine, Universitaetsklinikum Bonn, Bonn, GERMANY, [5]Department of Radiology, Universitaetsklinikum Bonn, Bonn, GERMANY.*

Introduction: High-precision radiation treatment is a curative option for patients with prostate carcinoma. To improve tumour control and reduce local side effects different boost approaches are available. In this study we investigated the use of ⁶⁸Ga-PSMA-PET/CT for such treatment options and the potential gain for local tumour control and dose to organs at risk (OAR). **Methods and Materials:** 21 patients with histologicaly proven prostate cancer without previous therapy underwent ⁶⁸Ga-PSMA-PET/CT. Body contour and OAR were manually defined. PTV70 was defined as planning target volume (PTV). A PET positive volume PTV_PET was defined using an autocontouring method based on a threshold of 40% of the maximum activity in the lesion. Five treatment plan variations ranging from 70Gy on PTV70 over integrated boost plans to 95Gy just on PTV_PET were calculated for each patient (Monaco, Elekta, USA - s. table attached). Analysis of derived treatment plans was done according to QUANTEC with an in-house developed software. TCP (Tumor Control Probability) and NTCP (Normal Tissue Complication Probability) for rectum and bladder were calculated. Student's t-test method was applied for statistical analysis (paired, two-sided, p<0.05 was considered as statistically significant). **Results:** Comparing the conventional plans to the plans with integrated boost and plans just treating the PET-positive volume, we find that the TCP increased to (95.2±0.5)% for an integrated boost with 75.6Gy, (98.1±0.3)% for an integrated boost with 80Gy, (94.7±0.8)% for treatment of the PET-positive volume with 75Gy, and to (99.4±0.1)% for treating the PET-positive volume with 95Gy (all p<0.0001). For the integrated boost with 80Gy a significant increase of the median NTCP of the rectum was found, for all other plans no statistical significant increase in the NTCP neither of the rectum nor the bladder was found. Compared to their *Pros-*

tate plan results, patients with a tumour directly adjacent to the rectum wall were found to have a significantly higher NTCP_rectum if the PTV_PET was boosted. At the same time of course, these patient's median TCP of the PET-positive volume was found to be significantly improved as well. **Discussion and Conclusion:** Our study demonstrates that the use of ⁶⁸Ga-PSMA-PET/CT would allow for more individualized prostate treatment planning and better targeting of active tumour volumes. TCP values of active tumour volumes can be increased, while rectum and bladder NTCP values either remain the same or are even lower. Clinical studies should be performed to confirm the theoretical benefits of PET target optimized treatment planning.

OP-123

Intra-individual comparison of 18F-labelled PSMA-1007-PET/CT, mpMRI and radical prostatectomy specimen in patients with primary prostate cancer

*C. Kesch[1], M. Vinsensia[2], J. P. Radtke[1,3], H. P. Schlemmer[3], M. Heller[4], E. Ellert[5], T. Holland-Letz[6], S. Duensing[4,1], N. Grabe[7,8], A. Afshar-Oromieh[2], K. Wieczorek[5], M. Schäfer[9], O. C. Neels[9], J. Cardinale[9], B. A. Hadaschik[10], M. Hohenfellner[1], K. Kopka[9], U. Haberkorn[2], C. Kratochwil[2], **F. Giesel[2]**; [1]Department of Urology, University Hospital Heidelberg, Heidelberg, GERMANY, [2]Department of Nuclear Medicine, University Hospital Heidelberg, Heidelberg, GERMANY, [3]Division of Radiology, German Cancer Research Center (DKFZ), Heidelberg, GERMANY, [4]Section of Molecular Urooncology, Department of Urology, University of Heidelberg, Heidelberg, GERMANY, [5]Institute of Pathology, University Hospital Heidelberg, Heidelberg, GERMANY, [6]Division of Biostatistics, German Cancer Research Center (DKFZ), Heidelberg, GERMANY, [7]Department of Medical Oncology, National Center for Tumor Diseases (NCT), University Hospital Heidelberg, Heidelberg, GERMANY, [8]Hamamatsu Tissue Imaging and Analysis Center, University of Heidelberg,, Heidelberg, GERMANY, [9]Division of Radiopharmaceutical Chemistry, German Cancer Research Center (DKFZ), Heidelberg, GERMANY, [10]Department of Urology, University Hospital Essen, Essen, GERMANY.*

Introduction: ⁶⁸Ga-prostate-specific membrane antigen (PSMA)-11-positron-emitting-tomography (PET)/computer-tomography (CT) represents and advanced method for diagnosis of recurrent or metastatic prostate cancer but has limitations due to short half life of ⁶⁸Ga, narrow availability and urinary clearance. Objective: To examine the value of the new PET tracer ¹⁸F-PSMA-1007 for staging of local disease by comparing it to multi parametric magnetic resonance imaging (mpMRI) and radical prostatectomy (RP) histopathology. **Materials and Methods:** In 2016, ¹⁸F-PSMA-1007-PET/CT was performed in 10 men with biopsy confirmed high-risk prostate cancer (PCa). 9 patients underwent mpMRI in the process of primary diagnosis. Consecutively, RP was performed in all 10 men. Agreement analysis was performed retrospectively. PSMA-staining was added for representative sections in RP specimen slices. Localization and agreement analysis of ¹⁸F-PSMA-1007-PET/CT, mpMRI and RP specimen was done dividing the prostate into 38 sections as described in PI-RADS v2. Sensitivity (SE), specificity (SP), positive predictive value (PPV), negative predictive value (NPV) and

accuracy were calculated for total and near total agreement. **Results:** ^{18}F-PSMA-1007-PET/CT had a 68.2% NPV and 75.3% accuracy and mpMRI had 88.2% NPV ans 72.5% accuracy for total agreement. Near total agreement analysis resulted in an NPV of 91.1% and an accuracy of 92.6% for ^{18}F-PSMA-1007-PET/CT and 90.0% and 87.4% for mpMRI, respectively**. Conclusion:** The comparison with RP histopathology demonstrated that ^{18}F-PS-MA-1007-PET/CT is a very promising method to determine local staging of PCa.

OP-124

^{68}Ga-PSMA PET/CT for restaging prostate cancer patients with early biochemical recurrence and PSA values lower than 0,5 ng/mL

A. Farolfi[1], F. Ceci[1], T. Graziani[1], P. Castellucci[1], L. Esposito[1], A. Lambertini[1], E. Lodi Rizzini[1], R. Schiavina[2], F. Lodi[1], S. Fanti[1]; [1]Nuclear Medicine Unit, S.Orsola-Malpighi Hospital, University of Bologna, Bologna, ITALY, [2]Department of Urology, S.Orsola-Malpighi Hospital, University of Bologna, Bologna, ITALY.

Aim: To evaluate the diagnostic value of ^{68}Ga-PSMA-PET/CT in prostate cancer (PCa) patients with biochemical relapse (BCR) after radical prostatectomy (RP) showing prostate-specific antigen (PSA) lower than 0.5 ng/mL. **Materials and Methods:** ^{68}Ga-PSMA-PET/CT is performed in our institution as investigational procedure in PCa patients, within a prospective trial (Eudract: 2015-004589-27 OsSC). Within this cohort we retrospectively selected patients treated with RP as primary treatment, with at least 7 as Gleason Score (GS) and presenting BCR with PSA values comprised between 0.2 and 0.5 ng/mL. According to these criteria a total of 100 PCa patients were enrolled in the present analysis (mean age 66; range 53-79). Mean PSA value before ^{68}Ga-PSMA PET/CT was 0.32 ng/mL (median 0,31; SD ±0.09). 7% (7/100) were treated with androgen-deprivation therapy at the time of the scan, while 19% (19/100) already received salvage therapy during BCR. Data about clinical history, correlative imaging and PSA kinetics were all recorded and collected. **Results:** ^{68}Ga-PSMA PET/CT resulted positive in 29/100, thus resulting in an overall detection rate of 29%. ^{68}Ga-PSMA uptake was observed in the prostatic bed (2/100; 2%), in pelvic lymph nodes (14/100; 14%), in distant (retroperitoneal and above iliac-bifurcation) lymph nodes (4/100; 4%) and in bone (17/100; 17%). Multiple bone lesions (≥2 bone lesions) were observed in 6/100 patients (6%). 23/100 patients had a negative re-staging Choline-PET/CT and the 30.4% of them had a positive ^{68}Ga-PSMA scan (7/23). 19/100 patients had a negative re-staging MRI scans and the 21.1% of them had positive ^{68}Ga-PSMA (4/19). Among the 29/100 patients with positive ^{68}Ga-PSMA-PET/CT, 8/29 performed also re-staging Choline-PET/CT (1 positive and 7 negative), whereas 8/29 performed re-staging MRI (4 positive and 4 negative). No positive scans with other diagnostic procedure were recorded in PSMA negative patients. **Conclusions:** In our patient-series with PSA<0.5 ng/ml (mean PSA=0,32 ng/mL), it was observed a detection rate of 29% for ^{68}Ga-PSMA-PET/CT. According to these data, ^{68}Ga-PSMA-PET/CT is a feasible procedure and may play a role in disease re-staging, also with very low PSA levels, since one third of patients of this patient-series may benefit during the early phase of BCR detecting local or distant PCa relapse. As a consequence, these patients could be referred to metastases-directed therapy according to PET/CT results. Finally, it is notable that in this patient-series the 17% of patients presented PSMA uptake in the bone suspected for skeletal metastases.

OP-125

Oligometastatic Prostate Cancer radiotherapy treatment based on ^{68}Ga-PSMA PET/CT: preliminary results

C. Artigas[1], C. Florian[1], D. Van Gestel[1], D. Van Gestel[2], P. Flamen[1], F. Otte[1]; [1]Jules Bordet Institut, Brussels, BELGIUM, [2]Jules Bordet Institut Brussels, Brussels, BELGIUM.

Introduction and Aim: Oligometastatic disease in patients with prostate cancer (PCa) biochemical relapse (BCR) after primary treatment with curative intent is defined as the presence of up to 3 metastatic sites. Treating those lesions with stereotactic body radiotherapy (SBRT) has been demonstrated to increase disease free survival in a safe way, delaying androgen deprivation therapy for more than 2 years. However, those studies have been performed staging patients with Choline-PET. Our hypothesis is that these results can be improved using ^{68}Ga-PSMA PET/CT, which has demonstrated better accuracy in patients with BCR at low PSA levels, where the probability of oligometastatic disease is higher . The aim of this communication was to assess the efficacy of SBRT based on ^{68}Ga-PSMA PET/CT in patients with BCR. **Material and Methods:** This is a retrospective analysis of a monocentric cohort of PCa patients diagnosed with oligometastatic disease based on ^{68}Ga-PSMA PET/CT findings and treated with RT. Inclusion criteria were: histologically proven PCa, BCR after local treatment with curative intent (surgery, radiotherapy or both) and 3 or less metastatic lesions. Number and localization of metastatic sites where registered. MRI and CT coregistration were used for SBRT planning. In order to evaluate its efficacy , biochemical response was defined as a decrease of >50% of PSA (PSA$_{50}$) measured at 1 and 4 months after SBRT. Patients were followed-up until progression. **Results:** From a total cohort of 45 patients treated with RT based on ^{68}Ga-PSMA PET/CT results, 15 met the inclusion criteria. Median PSA value at the time of the scan was 2.06ng/ml. A total of 22 PSMA positive lesions were treated: 13/22 (59%) lymph nodes, 6/22 (27%) bone lesions and 3/22 (14%) lung lesions. Only 1/15 (7%) patients had a biochemical response (PSA$_{50}$) at 1 month while 8/11 (73%) patients presented a biochemical response at 4 months of follow-up . At the moment of this communication 4 patients are still responding at 1 year follow-up with no androgen deprivation therapy needed. **Conclusion:** Retrospective study preliminary results suggest SBRT based on ^{68}Ga-PSMA PET/CT to be an effective treatment in patients with PCa oligometastatic disease. Biochemical response seems to be uncomplete at 1 month and should therefore be evaluated at earliest 4 months after SBRT. Future studies measuring outcome of SBRT based on ^{68}Ga-PS-MA PET/CT should be confronted to those using other imaging techniques.

OP-126

Impact of ^{68}Ga-PSMA-11 PET/CT on salvage radiotherapy planning in post-prostatectomy patients with early biochemical recurrence

J. Calais[1], J. Czernin[1], W. P. Fendler[1,2], K. Herrmann[1,3], I. Rauscher[4], N. Hegemann[2], T. Poeppel[3], M. Cao[1], M. Eiber[1,4], N. Nickols[1]; [1]UCLA, LOS ANGELES, CA, UNITED STATES OF AMERICA, [2]Ludwig-Maximilians-University, Munich, GERMANY, [3]Universitätsklinikum Essen, Essen, GERMANY, [4]Klinikum rechts der Isar, Technical University of Munich, Munich, GERMANY.

Objectives: One main curative option for post-prostatectomy patients with biochemical recurrence is salvage radiation therapy (SRT). However up to 50% of patients treated with SRT will experience disease progression. Most prior clinical trials evaluating SRT targeted the prostate bed only. The benefit of pelvic lymph node irradiation is controversial and under investigation. ^{68}Ga-PSMA-11 PET/CT has proven to detect sites of recurrence with a higher accuracy than any other imaging modality especially at serum PSA levels of < 1 ng/ml. The aim of our study was to determine whether ^{68}Ga-PSMA-11 PET/CT localizes biochemical recurrence sites after primary surgery in patients eligible for early SRT (PSA<1 ng/ml) and how this imaging approach affects SRT planning. **Methods:** A multicenter retrospective analysis was performed on 252 men who underwent ^{68}Ga-PSMA-11 PET/CT between August 2013 and February 2017 for biochemical recurrence after initial radical prostatectomy. Four institutions participated in the study: Technical University of Munich (n=147), Ludwig-Maximilians-University, Munich (n=40), Essen University Hospital (n=36) and University of California Los Angeles UCLA (n=29). Inclusion criteria were biochemical recurrence with PSA<1 ng/ml and no prior radiotherapy. Clinical data and DICOM files of all patients were anonymized and imported on a dedicated radiotherapy workstation (MIM software). First, radiotherapy target volumes were delineated on the CT in accordance with RTOG contouring guidelines. Secondly, the ^{68}Ga-PSMA-11 PET was co-registered and target volumes were displayed in the fused ^{68}Ga-PSMA-11 PET/CT to visually assess potential differences between standard CT and ^{68}Ga-PSMA-11 PET/CT derived target volumes as a measure of impact on SRT planning. **Results:** The median PSA level was 0.45 ± 0.25 (range 0.03-1). ^{68}Ga-PSMA-11 PET/CT revealed local recurrence as the only site of recurrence in 38 (15%) patients. Pelvic nodal recurrence, extra-pelvic nodal recurrence, bone metastases and visceral metastases were present in 82 (33%), 3 (1%), 22 (9%) and 3 (1%) patients, respectively. A major impact on initial SRT planning by ^{68}Ga-PSMA-11 PET/CT occurred in 138 patients (55%): pelvic nodal radiotherapy for N1 disease in 71 (28%) patients, extension of standard RTOG target volumes in 40 (16%) patients and contraindication of SRT because of distant metastases in 27 (11%) patients. Moreover, metastasis-directed stereotactic body radiotherapy for oligometastatic disease was possible in 13 (5%) patients. **Conclusion:** ^{68}Ga-PSMA-11 PET/CT has significant impact (55%) on SRT planning in patients with early biochemical recurrence (PSA < 1ng/ml) after radical prostatectomy.

OP-127

First Clinical Experience with Ultra-High Resolution Multi-Focal Collimators for Tc-99m-PSMA Imaging

C. Schmidkonz[1], C. Hollweg[1], J. Sanders[1], M. Beck[1], D. Schmidt[1], H. Vija[2], T. Kuwert[1], P. Ritt[1]; [1]Universitätsklinikum Erlangen, Erlangen, GERMANY, [2]Siemens Medical Solutions, Hoffman Estates, IL, UNITED STATES OF AMERICA.

Introduction: Radiopharmaceuticals based on the prostate specific membrane antigen (PSMA), such as Tc-99m-MIP-1404 (Progenics Pharmaceuticals Inc., New York, NY), are used for for diagnosing and staging prostate cancer, and their broader application will most likely lead to a substantial increase in patients undergoing respective SPECT/CT exams. In order to keep the associated radiation burden for patients and medical personal as low as reasonably achievable and provide the required increased throughput, reductions in radiopharmaceutical dose and SPECT acquisition time are desirable. The prototype Siemens Ultra-High Resolution SMARTZOOM (UHRSZ) Collimator uses an astigmatic array of boreholes to offer an increase in photon sensitivity compared to the low-energy high-resolution (LEHR) collimator. The sensitivity depends on the source-detector distance and at 28cm, is at least 210 cps/MBq, compared to roughly 91 cps/MBq for LEHR. The UHRSZ features increased spatial resolution (<6 mm geometric resolution @10 cm distance) over the known SMARTZOOM collimator, which is designed for cardiac imaging. We present our first experience with the UHRSZ collimator in 15 patients with prostate cancer. **Methods:** In 15 patients, SPECT/CT of the thorax and lower abdomen was performed 2-4 h p.i. of 654.9±68.4 MBq Tc-99m-MIP-1404 using both LEHR and UHRSZ collimators. The SPECT acquisition time was 15 min for all scans. The average time difference between acquisitions was 39±14 min. Two experienced readers independently evaluated the reconstructed SPECT datasets for MIP-1404 positive lesions and the occurrence of imaging artifacts (e.g. streaks, excessive noise, and geometric distortions). Additionally, the number of photon counts for each lesion was determined from the SPECT projection data. **Results:** In 12 out of 15 patients, a total of 18 tracer positive lesions were detected (see Figure 1 for a representative example). These were located in lymph nodes (n=5), prostate (n=9), and skeleton (n=4). Agreement between images of both collimators was excellent, with 18/18 lesions detected in LEHR and UHRSZ respectively. No divergent lesions were found. Inter-reader agreement was high, with both readers identifying the same number and location or absence of lesions. No imaging artifacts were observed. The lesions' photon count levels were, on average, 67% (range 11-133%) higher for the UHRSZ acquisition, compared to the LEHR-SPECT. **Conclusion:** For diagnosing PSMA-positive lesions, UHRSZ collimators showed excellent agreement with the standard LEHR-SPECT while providing increased photon count levels, which could be used for e.g. decreasing the SPECT acquisition time or injected activity.

409 — Sunday, October 22, 2017, 14:30 - 16:00, Hall G1

Neurosciences: Imaging Amyloid and Amyloidogenesis

OP-128

Incremental value of 18F-florbetaben amyloid PET in the diagnostic work-up of most complex patients with dementia in France: a naturalistic study

E. Guedj[1], T. Jonveaux[2], A. Verger[3], P. Krolak-Salmon[4], C. Houzard[5], O. Godefroy[6], T. Shields[7], A. Perrotin[8], R. Gismondi[8], S. Bullich[9], A. Jovalekic[9], N. Raffa[10], F. Pasquier[11], F. Semah[12], S. Epelbaum[13], M. O. Habert[14], D. Wallon[15], M. Chastan[16], P. Payoux[17], NEUUS in AD study group, A. Stephens[9], M. Ceccaldi[18]; [1]AP-HM - Hôpital de la Timone, Nuclear Medicine Department, and Aix-Marseille University, CERIMED, CNRS, INT, Institut de Neurosciences de la Timone, Marseille, FRANCE, [2]CHRU de Nancy - Hôpital Brabois, Geriatric Department, Vandoeuvre-les-Nancy, FRANCE, [3]INSERM U947, IADI,, Nancy, FRANCE, [4]Clinical and Research Memory Center of Lyon, Hospices civils de Lyon, UCBL1, Inserm 1028, Lyon, FRANCE, [5]CHU Lyon, Nuclear Medicine Department, Lyon, FRANCE, [6]CHU Amiens Picardie - Hôpital Sud, Neurology Department, Amiens, FRANCE, [7]CHU Amiens Picardie - Hôpital Sud, Nuclear Medicine Department, Amiens, FRANCE, [8]Piramal Imaging, Medical Affairs, Berlin, GERMANY, [9]Piramal Imaging, Clinical Research and Development, Berlin, GERMANY, [10]Piramal Imaging, Market Access and HEOR, Berlin, GERMANY, [11]Inserm 1171, Université de Lille, CHU, DistAlz, Lille, FRANCE, [12]Univ. Lille, U1171, CHU Lille, Nuclear Medicine Department, Lille, FRANCE, [13]AP-HP - Hôpital Pitié Salpétrière, Memory and Alzheimer Disease Institute IM2A, Paris, FRANCE, [14]Laboratoire d'Imagerie Biomédicale, Sorbonne Universités, UPMC Univ Paris 06, Inserm U 1146, CNRS UMR 7371, Paris, FRANCE, [15]CHU de Rouen - Hôpital Charles Nicolle, Neurology Department, Rouen, FRANCE, [16]Centre Henri Becquerel, Nuclear Medicine Department, Rouen, FRANCE, [17]ToNIC, Toulouse NeuroImaging Center, Université de Toulouse, Inserm, UPS, Toulouse, FRANCE, [18]AP-HM - Hôpital de la Timone, Neurology and Neuropsychology Department, and Aix Marseille University, Inserm, INS, Institut de Neurosciences des Systèmes, Marseille, FRANCE.

Aim: This study investigates the naturalistic impact of florbetaben positron-emission tomography (PET) on diagnosis and management of mildly demented patients for whom the etiological diagnosis remains uncertain despite an exhaustive expert work-up. **Material and Methods:** This multicentre open label study was performed at French tertiary memory clinics in patients presenting with most complex clinical situations (ie, early-onset, atypical clinical profiles, suspected mixed etiological conditions, unexpected rate of progression), for whom cerebrospinal fluid (CSF) analysis was indicated but either not feasible, or considered as non-contributory (ie, uninterpretable due to technical problems, values close to threshold, only one or two abnormal biomarkers out of three, or result not consistent with clinical information). Therefore, this clinical trial was designed to demonstrate the potential impact of amyloid PET without interfering with the current standard practices of expert centres (ClinicalTrials.gov: NCT02681172). Following an ini-tial diagnosis, florbetaben PET was performed, and a confirmed or revised diagnosis was provided after result disclosure. PET images were visually assessed in each center by readers who had undergone appropriate training. Changes in diagnosis, diagnostic confidence and patient management after PET result disclosure were analyzed. **Results:** 205 patients (70.9±9.7 years) were enrolled with evaluable PET scans; of these, 87 had a prior lumbar puncture (42.4%). 64.4% of scans (132/205) were amyloid-positive. Scan results led to changed diagnosis in 66.8% of cases (137/205), particularly for negative scans (83.6% vs 57.6% of positive scans; p<0.0001). Improved diagnostic confidence was reported in 81.5% of cases (167/205; p<0.0001), with an overall improvement of 30.2%, leading to a confidence of 82.6% after PET disclosure. Changes in management were reported for 80.0% of patients (164/205), and considered as substantial in 50.7% (104/205) of patients (any change in initiation or withdrawal of medication, additional diagnostic tests, or referral to a new specialist). Initiation of new medication was mainly reported following amyloid-positive PET scans, whereas withdrawal of medication was exclusively reported for amyloid-negative PET scans. Results were similar regardless of patients' eligibility criteria. **Conclusions:** The results demonstrate that florbetaben PET improves diagnostic and patient management parameters when a biomarker of amyloid pathology is necessary for differential diagnosis but CSF is not helping because its results are inconclusive, or lumbar puncture is contraindicated or refused. In the context of the existing healthcare framework, high level improvement and immediate clinical utility are thus provided by selective implementation of florbetaben PET into current standard practices for the most complex dementia cases.

OP-129

Impact of 18F-Florbetaben PET on Differential Diagnosis of Unclear Clinical Routine Cases

M. Brendel[1], J. Schnabel[1], S. Schönecker[1], E. Brendel[1], J. Meyer-Wilmes[1], C. Catak[1], O. Pogarell[1], J. Levin[1], A. Schildan[2], M. Patt[2], P. Bartenstein[1], O. Sabri[2], H. Barthel[2], A. Danek[1], K. Bürger[1], A. Rominger[1]; [1]University of Munich, Munich, GERMANY, [2]University of Leipzig, Leipzig, GERMANY.

Aim: In recent years several 18-F-labelled amyloid PET tracers have been developed and obtained clinical approval. Despite widespread use in scientific investigations, studies in clinical routine settings are still limited. Therefore, we investigated the impact of 18-F-florbetaben (FBB)-PET in patients with clinical suspicion of dementia and unclear presentation after 18-F-fluordesoxyglucose (FDG)-PET. **Material and Methods:** All subjects were referred with clinical suspicion of dementia due to neurodegenerative disease from the departments of neurology and psychiatry. After undergoing an FDG-PET, patients were discussed in the interdisciplinary dementia board where an additional FBB-PET was recommended due to uncertainty on the final diagnosis. The most likely diagnosis as well as potential differential diagnoses before the FBB-PET were documented. 90-110 min p.i. recordings of FBB were interpreted visually and classified as amyloid-positive or -negative. Clinical diagnoses were

compared before and after FBB-PET. **Results:** A total of 107 patients (age 69.4 ± 9.7y) were included in the study, 65 were visually rated amyloid-positive, 42 amyloid-negative. In 83% of all former unclear cases a final clinical diagnosis could be reached after FBB-PET. FBB-PET changed the most likely prior diagnosis in 28% of all cases. The highest impact on the change of the most likely diagnosis was observed for distinguishing Alzheimer's dementia (AD) from fronto-temporal dementia (FTLD), where FBB-PET resulted in a change of the most likely prior diagnosis in 41%. **Conclusion:** FBB-PET has a high additive value in establishing the final clinical diagnosis in cases with suspected dementia when FDG-PET remains inconclusive. The differentiation between AD and FTLD resulted in the most frequent change in diagnosis and should therefore primarily be solved by amyloid-PET. A considerable impact on patient management can be supposed, especially in light of upcoming disease specific therapies.

OP-130

Reshaping the amyloid buildup curve in Alzheimer's disease? - Partial volume effect correction of longitudinal amyloid PET data

M. Rullmann, O. Sabri, H. Barthel; University of Leipzig, Department of Nuclear Medicine, Leipzig, GERMANY.

Aim: In Alzheimer's disease (AD), it is believed by many researchers that brain β-amyloid load buildup over time reaches a plateau at an early symptomatic disease stage. In the "hot-spot" imaging technique of amyloid PET, brain atrophy-related partial volume effects (PVEs) negatively impact the image signal. This cross-sectional ADNI data analysis project aimed at testing the shape of the amyloid buildup curve in AD after correcting the PET data for PVEs. **Methods:** We obtained ADNI data of 216 subjects (17 with AD dementia: 76±6 years, 8 females, 22.4±2 MMSE; 122 with early MCI: 71±8 years, 48 females, 28.3±2 MMSE; 77 with late MCI: 71±8 years, 36 females, 27.5±2 MMSE) in whom 18F-florbetapir PET, MRI (both acquisitions within ±50 days) and MMSE scoring data were available in follow-up with at least two PET visits. PVE correction of the PET data was performed in PVELab using the modified Müller-Gärtner method. Using the PVELab atlas, regional SUVRs were obtained with and without PVE correction using cerebellar cortex as reference region. Additionally, composite SUVRs were computed using the volume-weighted mean of frontal cortex, parietal cortex, occipital cortex, temporal cortex, anterior and posterior cingulate cortex. A composite SUVR threshold of 1.1 was applied to include amyloid-positive subjects only. **Results:** The PVE-corrected PET data revealed significantly higher regional and composite SUVR changes over time as compared to the non-corrected PET data (composite SUVRs: P = 0.0002). With decreasing MMSE scores, the slopes of the composite SUVR increases were significantly higher with vs. without PVEC (F = 7.1, P = 0.008). Composite SUVR changes over time were correlated to the baseline MMSE scores when the PET data were PVE-corrected (r = -0.11, P = 0.049), but not without PVEC (r = -0.07, P = 0.16). **Conclusion:** These cross-sectional PVE correction results of longitudinal amyloid PET data point to the amyloid buildup curve in AD potentially not reaching a plateau. A further prospective

evaluation of the impact of PVE correction on the in vivo characterization of time-dependent AD pathology is, thus, warranted.

OP-131

Improved Risk Stratification for Conversion from Mild Cognitive Impairment to Alzheimer's Disease with a multi-analytical Evaluation of [¹⁸F]-AV45 Amyloid PET

L. Wagner[1], M. Brendel[1], F. Scheiwein[1], A. Delker[1], J. Sauerbeck[1], P. Bartenstein[1], K. Ishii[2], C. Hosakawa[2], A. Rominger[1]; [1]Department of Nuclear Medicine, Ludwig-Maximilians-University of Munich, Muenchen, GERMANY, [2]Department of Radiology, Kinki University Osaka, Osaka, JAPAN.

Introduction: Amyloid positron-emission-tomography (PET) is used to evaluate the cerebral amyloid burden in patients with mild cognitive impairment (MCI). The most accurate interpretation in regards to conversion to Alzheimer's dementia (AD) is currently under investigation. **Subjects & Methods:** We analyzed [¹⁸F]-AV45-PET data of 396 subjects with MCI from the ADNI database. Patients had a clinical follow-up for at least two years after the initial PET-scan. Single volume-of-interest (VOI) values as well as a cortical composite VOI were generated and standard-uptake-value ratios (SUVR) were calculated using different reference regions such as cerebellar grey matter (CBL), brainstem (BST) or subcortical white matter (WM). Thresholds were obtained for each reference region by the best tradeoff between sensitivity and specificity. In addition, a visual read was performed. Receiver operating characteristics were calculated and expressed as area under the curve for the discriminatory power for conversion prediction within the observation period. Cox regression was performed for risk stratification of conversion from MCI to AD. **Results:** During the mean follow-up time of 45.6 months n = 110 converters to AD could be identified. Compared to subjects with negative results for the evaluated method, the composite VOI with WM reference showed best discriminatory power and conversion-risk stratification with a hazard ratio (HR) of 5.3. Other reference regions (HR$_{CBL}$ = 3.2; HR$_{BST}$ = 4.0) as well as the visual read (HR$_{visual}$ = 3.4) performed worse. The combination of all four methods further improved the risk stratification for conversion of MCI to AD, i.e. positivity of all four methods resulted in a HR of 12.5 compared to the absence of any positive item. Consequently, the conversion rate increased as a function of the amount of positive results, ranging between 5 to 67% within the observation period. Single region SUVR instead of the composite SUVR showed no further predictive value. **Conclusion:** Quantification using three different reference regions (CBL, BST and WM) plus the visual read showed the best conversion-risk stratification in subject with MCI according to [¹⁸F]-AV45-PET estimates. These encouraging results should be implemented in prospective clinical trials.

OP-132

Higher amyloid deposition in the striatum in familial Alzheimer's disease: a preliminary PET/CT and PET/MRI study

L. Fu, J. Zhang, B. Xu, J. Tian; Department of Nuclear Medicine, the Chinese PLA General Hospital,, Beijing, CHINA.

Purpose: It is assumed that the abnormal amyloid-β deposition is an initiating event in Alzheimer's disease (AD) and both typical and AD variants showed similar diffuse patterns of amyloid deposit as the positron emission tomography (PET) agent Pittsburgh compound-B (PIB) reflected. In the current study, we reviewed the PIB-PET images of familial AD (FAD), sporadic AD (SAD) and cognitively normal elder controls (NC) to find whether there is a different amyloid deposit pattern among groups. **Methods and Materials:** Retrospective analysis of the ^{11}C-PIB PET/CT or PET/MRI images of 5 FAD patients (Male/Femal:1/4, age range: 36-43 Yr, 39.0 ± 3.4), 10 SAD patients (Male/Femal:4/6, age range:55-68 Yr, 59.9 ± 4.0) and 10 NC subjects (Male/Female:6/4, age range:56-65 Yr, 60.4 ± 3.2) with definite clinical diagnosis and complete neuropsychological tests (such as Mini-Mental State Examination, MMSE). **PIB-PT acquisition:** All subjects received ^{11}C-PIB injection intravenously (4.44-5.55MBq/kg) 40-min prior to data acquisition, including 3 of FAD at a PET/CT (Biograph 64, SIEMENS, Germany) and 22 subjects at a PET/MRI scanner (Biograph mMR, SIEMENS, Germany). **Data analysis:** Regions of interest were drawn over cortex, the striatum and cerebellar gray matter (CGM) in CT or MRI images and their corresponding CT/MRI based attenuation corrected PIB-PET images manually. The CGM was chosen as reference region for standardized uptake value ratio (SUVR) measurement. One-way ANOVA analysis was used to assess the differences of ages, MMSE scores and SUVRs of cortical and striatum among 3 groups. **Results:** FAD patients were younger than SAD and NC subjects (F=70.02, P<0.05). Both the two AD groups' MMSE scores were significantly worse than NC (F=43.77, P<0.05). No obvious bran atrophy was detected on MRI images in 3 FAD patients. No significant difference in cortical 11C-PIB retention were observed between FAD and SAD patients, but were great higher than that of NC (F=50.61, P<0.01). Significant higher SUVR of striatum was observed in FAD than SAD and NC. In addition, the SUVR of striatum in SAD was also higher than NC (F=28.93, P < 0.01). **Conclusion:** FAD patients showed a special PIB distribution pattern including extensive striatal amyloid deposition, along with the typical cortical deposition, which might associated with their early-onset cognitive decline.

OP-133

[18F]Florbetapir PET/CT to assess the cerebral ß-amyloid binding in Parkinson's Disease Dementia - does the striatum still a key player?

M. Gennaro[1], G. Aghakhanyan[1], S. Mazzarri[1], G. Puccini[1], G. Palermo[2], D. Frosini[2], G. Manca[1], L. Antonacci[1], S. Muccioli[1], L. Fantechi[1], I. Paglianiti[1], R. Ceravolo[2], U. Bonuccelli[2], D. Volterrani[1]; [1]Regional Center of Nuclear Medicine, University Hospital of Pisa, Pisa, ITALY, [2]Unit of Neurology, Department of Clinical and Experimental Medicine, University of Pisa, Pisa, ITALY.

Aim: Cognitive impairment is a common non motor complication of Parkinson's Disease (PD), which increases in severity and frequency over time. The patients with PD are 4-6 times more likely to develop dementia (PDD) than age-matched controls. The growing evidence indicates a possible synergistic role of

Alzheimer type brain lesions containing ß-amyloid (Aß) and tau proteins with progressive cognitive decline in PD. Moreover, the recent neuropathological studies have shown that striatal Aß deposition is significantly greater in PDD patients, thus, suggesting that both cortical and also striatal Aß has pathophysiological impact in PDD. The aim of our study was to compare regional-selective cortical and subcortical amyloid burden in PDD patients in comparison to cognitively normal elder individuals. **Materials and Methods:** Fourteen consecutive PDD patients (mean age 72.1 ± 3.9; Mini-Mental State Examination, MMSE 21.1 ± 1.3) referred to our centre and six cognitively and clinically normal control subjects (mean age 72 ± 1.6; MMSE 28.8 ± 1.2) were recruited. The demographic and PD/PDD-related clinical variables (age of onset, disease duration, dementia onset, dementia duration) were collected. All subjects underwent a 20-min [18F]Florbetapir PET/CT study, acquired 50 min after intravenous injection of 370 MBq [18F]Florbetapir. The images were spatially normalized using the AV45 PET template in MNI brain atlas space (Avid Radiopharmaceuticals) and voxel-wise standardized uptake value ratio (SUVR) images were calculated using the whole cerebellum as a reference region. Subsequently, a mean SUVR was extracted from the 6 regions (cerebral cortex, cerebral white matter, precuneus, thalamus, caudate and putamen) by creating anatomical volume of interests (VOIs) in FMRIB Software Library v.5 (FSL) using Harvard-Oxford cortical/subcortical atlas. **Results** Three out of fourteen patients (21.4%) demonstrated a positive amyloid-scan after visual inspection and qualitative reading. We revealed no significant correlation between MMSE scores, clinical variables and mean SUVRs in the PDD patients. Between group analysis showed significantly higher [18F]Florbetapir retention in the putamen in PDD group compared to controls (p < 0.01). The group difference remains statistically significant after adjusting for age and further excluding the [18F]Florbetapir amyloid-positive scans. **Conclusion:** Our preliminary data confirm previous postmortem evidence showing an elevated putaminal Aß deposition in PDD patients, thus, suggesting that increased amyloid burden in the putamen may be involved in the pathophysiology of PDD. Additional large cohort studies will be required to elucidate whether increased amyloid load in the putamen contribute to cognitive decline in PDD patients.

OP-134

A Pilot Study on Hybrid 18F-Florbetaben PET/MRI in Patients with White Matter Diseases

M. Rullmann[1], S. Haars[2], P. Werner[1], R. Schmidt[2], J. Orthgieß[2], S. Tiepolt[1], M. Patt[1], D. Lobsien[3], K. Hoffmann[3], O. Sabri[1], H. Barthel[1], F. Then Bergh[2]; [1]University of Leipzig, Department of Nuclear Medicine, Leipzig, GERMANY, [2]University of Leipzig, Department of Neurology, Leipzig, GERMANY, [3]University of Leipzig, Department of Neuroradiology, Leipzig, GERMANY.

Background: PET amyloid imaging with tracers like [18F]Florbetaben allows the in vivo visualization of cortical β amyloid (Aβ) depositions as occurring in Alzheimer's disease. [18F]Florbetaben also - independent from Aβ - binds to myelin in the

brain white matter (WM). This led to the idea of employing this tracer to image multiple sclerosis, with promising preliminary results. Further studies in other WM diseases are currently missing. **Aim:** We aimed at quantifying the [^{18}F]Florbetaben in vivo uptake in patients with different WM diseases in comparison to non-WM diseased controls. By that, we hypothesized a decreased WM tracer accumulation in the patient group as a correlate of demyelinisation. **Methods:** We examined 13 patients with different WM diseases (multiple sclerosis [n=4]; progressive multifocal leukoencephalopathy [PML, n=3]; adult-onset leukodystrophy [ADLD n=3]; cerebral autosomal dominant arteriopathy with subcortical infarcts and leukoencephalopathy [CADASIL, n=3]) and concurrent mild cognitive impairment using [^{18}F]Florbetaben PET/MRI. 13 age- and gender-matched patients with cognitive impairment but without WM disease served as controls. The PET data were acquired 90-110min p.i. using a simultaneous PET/MR system (Biograph mMR, Siemens) after administering ~300MBq [^{18}F]Florbetaben. Simultaneous MR acquisition included T1 MPRAGE 3D with and without i.v. gadolinium and T2 FLAIR 3D. Segmentation of WM and generation of standard volumes of interests (AAL) was done in PMOD 3.5. WM lesions were segmented by the lesion prediction algorithm as implemented in the LST toolbox for SPM. We determined the WM SUV ratio (SUVR$_{WM}$) using the cerebellar cortex as reference region. For the WM disease patients, we additionally calculated the WM lesion SUVR (SUVR$_{WML}$) using the same reference. **Results:** In the patients, the SUVRs$_{WM}$ were significant lower as compared to the controls (1.78±0.32 vs.1.90±0.14, p=0.04). Within the patient group, WM lesions showed an even lower tracer retention compared to the WM uptake (SUVR$_{WML}$ vs. SUVR$_{WM}$: 0.98±0.22 vs. 1.78±0.32, p<0.001). These WM data were independent of the cortical tracer uptake. An additional subgroup analysis regarding WM uptake degree and distribution vs. WM disease is planned after recruitment of a larger cohort. **Conclusion:** Patients with different WM diseases show decreased [^{18}F]Florbetaben WM binding, especially in WM lesions, compared to non-WM-diseased controls. Further research using larger cohorts and including other MR parameters is justified to investigate the potential of [^{18}F]Florbetaben PET/MRI in diagnosing demyelinating diseases.

OP-135

Human Whole-body Biodistribution and Radiation Dosimetry of [^{18}F]PF-06684511, a Novel Radioligand for Brain Imaging of Beta-secretase

A. Varrone[1], R. Arakawa[1], A. Takano[1], S. Nag[1], V. Stepanov[1], P. Stenkrona[1], P. Grybäck[2], M. Bolin[2], L. Chen[3], L. Zhang[3], P. He[3], A. Villalobos[4], T. McCarthy[3], C. Halldin[1]; [1]Department of Clinical Neuroscience, Centre for Psychiatry Research, Karolinska Institutet and Stockholm County Council, Stockholm, SWEDEN, [2]Karolinska University Hospital, Medical Radiation Physics and Nuclear Medicine, Stockholm, SWEDEN, [3]Worldwide Research & Development, Pfizer Inc., Cambridge, MA, UNITED STATES OF AMERICA, [4]Worldwide Research & Development, Pfizer Inc., Groton, CT, UNITED STATES OF AMERICA.

Beta secretase (BACE) is a brain enzyme implicated in the pathophysiology of amyloid-beta (Aβ) accumulation in Alzheimer´s disease (AD). BACE inhibitors are currently under development as drugs for the prevention or treatment of AD. An imaging approach to quantify the brain BACE level would add great value to the development of inhibitors of Aβ production with regard to the selection of high-risk population and to the improvement of therapeutic outcome. The radioligand [^{18}F]PF-06684511 has been developed for in vivo imaging and quantification of BACE using positron emission tomography (PET). The aim of this study was to calculate the radiation dose from the administration of [^{18}F]PF-06684511, based on human whole-body PET/CT scans. **Methods:** Four PET/CT sessions (0-54 min; 90-144 min; 210-264 min; 330-366 min) were performed using a GE Discovery PET/CT 710 Clarity Edition for 6 hr after the injection of 111±13 MBq of [^{18}F]PF-06684511 (specific radioactivity: 42±10 GBq/μmol; injected mass: 1.2±0.3 μg) in 5 healthy subjects (2M/3F 48±5 y). Regions of interest were delineated on coronal images to calculate the percent injected dose (%ID). Urine was collected during the breaks between PET/CT sessions and the radioactivity in the urine was measured with the PET/CT system. Estimates of the absorbed radiation dose were calculated with the OLINDA/EXM software using the male adult model. **Results:** Peak uptake values were highest for the liver (25.2±2.3 %ID at 0.5 hr) and lungs (12±3 %ID at 0.2 hr), followed by the small bowel (11.8±2.9 %ID at 5.8 hr), brain (3.5±0.6 %ID at 0.4 hr), stomach (2.6±1.0 %ID at 2.2 hr), heart (2.5±0.5 %ID at 0.2 hr), pancreas and kidneys (2.3±0.7 %ID and 2.2±1.0 %ID at 0.2 hr). Up to 10±4 %ID was eliminated with the urine at 6 h. The organ receiving the largest dose was the pancreas (0.093±0.052 mSv/MBq), followed by the liver (0.071±0.006 mSv/MBq), the gall bladder and urinary bladder wall (0.058±0.041 and 0.058±0.021 mSv/MBq), and the ULI wall (0.051±0.011 mSv/MBq). The calculated effective dose was 0.025±0.001 mSv/MBq. **Conclusion:** The estimated radiation burden of [^{18}F]PF-06684511 was similar to [^{18}F]FDG (0.019 mSv/MBq) and ^{18}F-labelled radioligands used for Aβ imaging in AD ([^{18}F]AV-45: 0.019±0.004 mSv/MBq; [^{18}F]BAY94-9172: 0.015±0.001 mSv/MBq; [^{18}F]GE067: 0.034±0.003 mSv/MBq). Based on the calculated effective dose of [^{18}F]PF-06684511, the administration of 400 MBq corresponds to a radiation dose of 10 mSv, suggesting that [^{18}F]PF-06684511 can be used in clinical trials to measure the brain BACE level and/or the occupancy by BACE inhibitors in AD.

| 410 | Sunday, October 22, 2017, 14:30 - 16:00, Hall G2 |

Conventional & Specialised Nuclear Medicine: Pulmonology & Nephrourology

OP-136

The impact of Lung Perfusion Scintigraphy in the emergency management of patients with suspected Pulmonary Embolism

C. Ferrari, A. Niccoli Asabella, A. Cimino, G. Bianco, M. Fanelli, E. P. Mossa, A. Di Palo, G. Rubini; Nuclear Medicine Unit, AOU Policlinic of Bari, University of Bari, bari, ITALY.

Aim: The aim of our study was to highlight the role of Lung Perfusion Scintigraphy (LPS) in the management of patients with suspected pulmonary embolism (PE) admitted as urgent and in the "on-call" 24hrs service. **Materials and Methods**: We retrospectively revised 2166 LPS performed for PE suspicion (years 2012-2016). The relation between LPS and symptoms, risk factors (i.e. arythmia, drugs, surgery, thrauma, deep venous thrombosis), D-dimers dosage and other diagnostic imaging examination (Chest X-ray and/or Computed Tomography (CT)) were evaluated by contingency tables and Odds Ratio (OR). **Results**: 1730/2166 (79.8%) were urgent and admitted as emergency; 1026/1730 (59.3%) were performed during the on-call 24hrs service. The request of LPS came from emergency-room in 981/1730 (56.7%) patients, pneumology in 187/1730 (10.8%), neurology in 83/1730 (4.8%), internal medicine in 112/1730 (6.5%), surgery in 90/1730 (5.2%), cardiology in 57/1730 (3.3%), and other departments in 220/1730 (12.7%). LSP resulted positive for PE and treated in 294/1730 (17%) patients, while negative in 1436/1730 (83%). The presenting symptoms, single or differently associated, were chest pain in 536/1730 (31%), dyspnea in 900/1730 (52%), cough in 225/1730 (13%) and none in 69/1730 (4%); only the presence of dyspnea was significantly related to the presence of PE (OR=1.596 p=0.003); chest pain and cough were not related to PE (p> 0.005). Risk factors were present in 960/1730 (55.5%) patients and none of them were related to PE detected by LPS (p> 0.005). D-dimer dosage was increased in 1678/1730 (97%) patients and were not related to PE detected by LPS (p> 0.005). A previous diagnostic exam was performed in 1306/1730 (75.5%) patients. The Chest X-ray and/or CT resulted negative in 332/1306 (25.4%), suspected for PE in 319/1306 (24.4%), non-specific with pleural effusion in 245/1306 (18.8%) and non-specific with inflammatory interstitial diseases in 410/1306 (31.4%). LPS resulted positive for PE in 46/332 (13.8%) with negative Chest X-ray and/or CT, in 75/319 (23.4%) with suspected PE, in 37/245 (15.2%) with pleural effusion and in 60/410 (14.7%) with inflammatory interstitial diseases. The relation between LPS and other imaging resulted statistically significant ($\chi 2$=17.5 p=0.001). **Conclusions**: LPS has a key role in the assessment of PE, optimizing the management of patients who do not require admission to intensive care unit avoiding high costs and overcrowded hospitalization. Our data support the need of LPS performed as emergency in on-call 24hrs service in each metropolitan area.

OP-137

The Prognostic Significance Of Abnormal Lung Perfusion In Patients With Idiopathic Pulmonary Arterial Hypertension

L. Wang, R. Ma, D. Wu, W. Fang; Chinese Academy of Medical Science & Fu Wai Hospital, Beijing, CHINA.

Purpose: A ventilation-perfusion lung scan is recommended to be performed for patients with pulmonary hypertension, which is mainly used to exclude the diagnosis of chronic thromboembolic pulmonary hypertension according to the absence of mismatched perfusion defects. Although without this typical sign of pulmonary embolism, patients with idiopathic pulmonary arterial hypertension (IPAH) may present abnormal lung perfusion. However, evidences on the prognostic value of the presence of abnormal pattchy pattern of lung perfusion for IPAH patients are lacking. In this study, we aimed to study the abnormalities of lung perfusion to identify its prognostic value in patients with IPAH. **Methods:** Clinical database of consecutive patients with pulmonary hypertension who underwent lung ventilation-perfusion scans were reviewed. Patients diagnosed with IPAH according to current guidelines for the diagnosis and treatment of pulmonary hypertension were included in this study. Images of lung perfusion scans were analysed and categorised as patchy or normal pattern by independent experienced nuclear physicians. The relation of lung perfusion defects with patients' survival was analysed. **Results:** A total of 328 IPAH patients were enrolled. During a median follow-up period of 870 days, 14 patients were lost to follow-up. 52 patients reached the primary end-point of all-cause mortality. Of the 328 patients, 141 (43%) patients exhibited normal lung perfusion, while the other 187 (57%) patients had patchy abnormal lung perfusion. On univariate Cox analysis, the presence of patchy pattern were significantly associated with the overall survival (hazard ratio [HR]) 2.63, 95% confidence interval [CI] 1.38-5.02, p=0.003). Patients with patchy pattern had a worse outcome (patchy pattern vs normal perfusion, log-rank 9.343,p=0.009). On multivariate Cox proportional hazard analysis, the presence of patchy pattern remained a significant independent predictor of the endpoint (HR 2.42, 95%CI 1.26-4.64, p=0.008). The other significant independent covariates were mean pulmonary artery pressure, NT-pro BNP and NYHA (class III and IV). **Conclusions:** In patients with IPAH, abnormal lung perfusion largely existed and was significantly correlated with worse outcome. In the diagnostic algorithm of pulmonary hypertension, beyond exclusion of chronic thromboembolic, perfusion lung scan may be of importance to identify IPAH patients at risk of all-cause mortality.

OP-138

Assessment Of Lung Glucose Uptake In Patients With Systemic Erythematous Pulmonary Arterial Hypertension: A Quantitative FDG PET Imaging Study

L. Wang[1], Q. Wang[2], L. Zhao[3], X. Zeng[2], W. Fang[1]; [1]Chinese Academy of Medical Science & Fu Wai Hospital, Beijing, CHINA, [2]Peking Union Medical College Hospital, Beijing, CHINA, [3]Imperial College London, London, UNITED KINGDOM.

Purpose: Pulmonary arterial hypertension associated with systemic lupus erythematosus (SLE-PAH) has not been well studied. Measures for tracking pulmonary vascular disease directly in SLE-PAH patients are lacking. Enhanced glycolysis in the lung of idiopathic PAH (IPAH) patients measured by positron emission tomography imaging with fluorine-18-labeled 2-fluoro-2-deoxyglucose (FDG-PET) has been shown to correlate to pulmonary vascular remodeling. Herein we explored the potential role of FDG-PET imaging in SLE-PAH patients and aimed to investigate the relationship between the lung glucose uptake and SLE-PAH disease activity. **Methods:** Sixty-minute dynamic FDG-PET was

for the first time applied to 14 SLE-PAH patients, 20 IPAH patients and 10 healthy volunteers. Patlak analysis was used to quantify lung FDG uptake (influx rate Ki). **Results:** Lung FDG uptake in SLE-PAH patients (Ki: 0.00714 ± 0.000602 ml/g/min) was significantly increased compared to that in healthy volunteers (Ki: 0.000262 ± 0.000168 ml/g/min) (P<0.05). SLE-PAH patients with active disease (SLE disease activity score SLEDAI≥5) (Ki: 0.001075 ± 0.00055 ml/g/min) demonstrated significantly higher lung FDG uptake than those with quiescent disease (SLE-DAI<5) (Ki:0.000233 ± 0.00017 ml/g/min) (P=0.0038) and IPAH (Ki: 0.000524 ± 0.000314 ml/g/min) (P=0.0025). Lung FDG uptake in SLE-PAH significantly correlated with SLEDAI score and plasma level of complement C3 and C4 (Ki vs SLEDAI, r=0.607, p=0.021; Ki vs C3, r=-0.568, p=0.034; Ki vs C4, r=-0.661, p=0.010), suggesting patients with higher lung FDG uptake tended to have more active disease and more activated complement system consuming more C3 and C4. **Conclusions:** Lung FDG uptake significantly increased in SLE-PAH and correlated with SLE disease activity. Our data support the hypothesis that FDG lung uptake is associated with the lung inflammatory pathology in PAH. FDG-PET imaging may be developed as a potential intrapulmonary activity marker for patients with SLE-PAH.

OP-139

Comparative analysis of regional lung perfusion measurements using radiolabeled microspheres and PET/CT and fluorescence-labeled microspheres in an experimental, anesthesiological study of acute lung injury in pigs

A. Braune, A. Gueldner, J. Kotzerke, M. Gama de Abreu; University Hospital Carl Gustav Carus at the Technische Universität Dresden, Dresden, GERMANY.

Aim: Both in healthy lungs and in lungs exposed to experimental acute respiratory distress syndrome (ARDS) it has been shown that measurements of the distribution of pulmonary blood flow (PBF) determined using radiolabeled microspheres and non-radioactive, fluorescence-labeled microspheres correlate well [Glenny et al., JApplPhysiol.1993 May;74(5):2585-97; Hübler et al.: JApplPhysiol.1999 Dec;87(6):2381-5]. However, such comparisons have so far only been done for ex-vivo measurements of PBF. In this study we compared in-vivo measurements of the distribution of PBF using radiolabeled microspheres and PET/CT with ex-vivo measurements using fluorescence-labeled microspheres. **Methods:** Details of the experimental protocol are given in [Güldner et al.: Anesthesiology.120(3):673-82]. Briefly, in 7 pigs ARDS was induced by saline lavage. PBF was marked by intravenous injection of fluorescence-labeled and radiolabeled microspheres (68Ga) after 1h of mechanical ventilation superposed with >60% of spontaneous breathing. The distribution of radiolabeled microspheres was assessed by PET, and lung weight was determined by CT. The distribution of fluorescence-labeled microspheres was assessed by ex-vivo sampling of lung pieces and measurements of emitted fluorescence intensities and tissue weights. For both measurements, PBF of the left and right lungs were analyzed separately by normal-

ization of the relative intensity of each voxel/lung piece to the whole lung intensity and to its weight and volume. PBF gradient was determined by linear least-squares regression of PBF and location along the ventro-dorsal axis and slopes of regression lines were compared between measurements. Also, outer lung dimensions assessed in-vivo and ex-vivo were compared. **Results:** The resolution of PBF measurements using radiolabeled microspheres (4.06 x 4.06 x 5 mm3) was about 21 times higher than those using fluorescence-labeled microspheres (12 x 12 x 12 mm3). Excitation and drying of the lungs caused an increase of their cranio-caudal expansions by 10.8%, whereas the ventro-dorsal and left-right expansions decreased by 14.4% and 13.1%, respectively. Both measurements revealed a significant difference of ventro-dorsal PBF gradients from zero and slopes were of comparable magnitude. **Conclusion:** In this model of ARDS in pigs, ex-vivo measurements of the distribution of fluorescence-labeled microspheres and in-vivo measurements of the distribution of radiolabeled microspheres revealed comparable results in respect to the presence and magnitudes of ventro-dorsal PBF gradients. Consequently, fluorescence-labeled microspheres and radiolabeled microspheres can be used interchangeably for the determinations of PBF gradients, despite a much lower resolution of the ex-vivo measurement and the occurrence of lung deformation induced by lung extraction and drying.

OP-140

A novel, simple equation improving the accuracy of glomerular filtration rate (GFR) measurement from two blood samples

G. Arsos[1], E. Moralidis[1], D. Katsampoukas[1], E. Manou[2], C. Sachpekidis[3]; [1]3rd Department of Nuclear Medicine, Medical School, Aristotle University of Thessaloniki, Papageorgiou General Hospital, Thessaloniki, GREECE, [2]Nephrology Department, Papageorgiou General Hospital, Thessaloniki, GREECE, [3]Institute of Nuclear Medicine, Bern University Hospital, Bern, SWITZERLAND.

Aim: Glomerular filtration rate (GFR) measured by exogenous tracer plasma clearance using multiple blood samples (GFRMS) is currently the gold standard for renal function assessment. Measurement by the slope-intercept technique, limiting the number of samples at two (GFR2), is a very convenient alternative for routine clinical use. However, as it systematically overestimates GFR, proper GFR2 correction becomes mandatory. All corrective formulas proposed are only moderately satisfactory and the most widely applied Brochner-Mortensen (BM) quadratic correction underestimates considerably higher GFR values. The aim of the present study is to derive a novel equation for optimum approximation of GFRMS by GFR2. **Materials and methods:** GFR was measured for clinical purposes in 1104 adult Caucasian patients by bolus i.v. injection of ^{51}Cr-EDTA, and plasma elimination analysis by two-compartment modelling of 10 blood samples obtained between 5 and 240 min p.i., (GFR10, in ml/min). Only 721 of them with almost perfect data fit ($r^2\geq0.995$) to the biexponential model were selected for further analysis. GFR2 was calculated from blood samples at 120 and 240 min

p.i and corrected by the BM formula (GFR2BM), both in ml/min. Patients were randomized into a derivation (DG, n=376) and a validation (VG, n=345) group. A new, power function equation (NE) correlating GFR2 with GFR10 values was developed by non-linear regression analysis of DG data and its performance was evaluated in the VG. The resulting GFR2NE values in the VG were compared with GFR10 as were the GFR2BM values. Significance was accepted for p<0.05. **Results:** GFR10 in all the 721 patients was 77±36 (range 10 - 216) ml/min. DG and VG did not differ in any demographic or renal function parameter. NE was formulated as $GFR10 = 1.587 \times GFR2^{0.887}$ ($r^2 = 0.981$) and was then tested in the VG. GFR2NE showed an excellent correlation with GFR10 values ($r^2 = 0.981$). The mean difference (bias) GFR10-GFR2NE and GFR10-GFR2BM was 0.2 (ns) and 7.2 (p<0.05) with 95% confidence intervals of agreement -8.9 to 9.4 and -4.4 to 18.8 ml/min respectively. **Conclusions:** The newly developed power function equation provides corrected GFR values derived from the two samples measurement very close to the results of the multisampling full kinetic analysis and performs better than the widely applied BM correction equation in a wide range of renal function in adult patients.

OP-141

Contribution Of Isotopic Renogram And SPECT-CT In The Diagnosis Of The Complications Of The Renal Transplantation

J. Gómez Hidalgo, A. Cobo Rodríguez, A. Sainz-Esteban, C. Gamazo Laherran, M. Alonso Rodríguez, M. Ruiz Gómez, M. González Selma, R. Ruano Pérez; Hospital Clínico Universitario de Valladolid, Valladolid, SPAIN.

Objective: to evaluate the contribution of the isotopic renogram in patients with kidney transplant, and the contribution of SPECT-CT. **Material and Method:** we included 283 patients who were operated on renal cadaver transplantation from January 2011 to December 2016. At 24 hours after transplantation, after administration of 370 MBq of 99mTc-DTPA, we performed a 30 minute renogram study focusing on the abdomen in anterior projection, followed by planar images at 30 and 180 minutes. Ten patients were performed an abdominal SPECT-CT after 180 minutes image. The findings were correlated with radiological studies and clinical-analytical. **Results:** Of the 283 patients (age: 58.0 +/- 12.8, 184 men and 99 women), 69 (24.4%) presented a normal study. In 33 (11.6%) were detected surgical complications: 14 renal artery / vein thrombosis; 5 infarcts; 6 ectasias or ureteral obstructions; 1 urinoma (confirmed with SPECT-CT); and 7 urinary leaks (4 confirmed with SPECT-TC). 13 patients were operated by transplantectomy, 4 presented renal function deterioration and 1 acute rejection. In 180 patients (63.6%), there was an evidence of ischemic alteration or an acute tubular necrosis (NTA): mild in 103 (57.2%); moderate in 52 (28.9%); and severe in 25 (13.9%). Evolutionarily, 2 (1.9%) cases with mild NTA evolved to renal failure (without rejection); in moderate NTA 16 (30.7%) evolved to renal failure (2 acute rejection); and in severe NTA 11 cases (44.0%) evolved to renal failure (1 acute rejection and 4 thrombosis involving transplantectomy). A second con-trol was performed on 48 patients, normalizing the function in 15. **Conclusions:** the renogram in transplanted patients allows the detection of surgical and / or ischemic complications, facilitating the implantation of corrective measures at an early stage. SPECT-CT is especially useful in the diagnosis of urinary tract and urinary leakage, improving the assessment of its extent and location.

OP-142

The usefulness of advanced numerical parameters of kidney output in the analysis of Tc-DTPA diuresis renography

S. Beatovic[1], M. Radulovic[2], M. Jankovic[3], D. Sobic Saranovic[1], B. Ajdinovic[2], V. Artiko[1]; [1]University of Belgrade Faculty of Medicine, Center for Nuclear Medicine, Clinical Center of Serbia, Belgrade, SERBIA, [2]Institute for Nuclear Medicine Military Medical Academy, Belgrade, SERBIA, [3]University of Belgrade Faculty of Electrical Engineering, Belgrade, SERBIA.

Purpose: The aims of this study were to calculate, by means of the International Atomic Energy Agency (IAEA) software, the values of Tc-99m DTPA diuretic renogram parameters in normal kidneys, hypotonic kidneys with good drainage after furosemide and kidneys with poor response to diuretic, b) to validate the accuracy of obtained parameters by comparing with the values published by other authors and c) to assess their diagnostic utility in distinguishing poor response to diuretic from good one. **Subjects and Methods:** 146 patients (mean age: 51.1 years) with evidence of poor washout through kidney outlet were investigated. 40-minutes acquisition with 240 10-sec images was applied. Furosemide was administered after 20min (F+20). Post-void static image was acquired at 50min. Two observers analyzed each study and classified kidneys into four categories. Group A consisted of 65 normal kidneys, contralateral to affected one, without any structural or functional anomaly on previous diagnostics; group B: 124 hypotonic kidneys with complete washout after furosemide; group C: 55 kidneys with poor response to diuretic; group D: 48 kidneys with indeterminate response after diuretic. Parameters analyzed were: T_{max}, $T_{1/2}$, output efficiency at 20min (OE_{20}), output efficiency at 40min (20min after furosemide injection, OE_{F+20}), normalized residual activity at 20min ($NORA_{20}$) and normalized residual activity on post-micturition acquisition ($NORA_{PM}$). **Results** were presented as mean±SD. For group 1 they were: T_{max}: 4.2±1.0 min; $T_{1/2}$: 14.5±2.4 min; OE20: 88±5%; OE_{F+20}: 95±4%, $NORA_{20}$: 0.70±0.23; $NORA_{PM}$: 0.07±0.03. Results for group 2 were: OE_{20}: 76±10%; OE_{F+20}: 93±2%; $NORA_{20}$: 1.28±0.56; $NORA_{PM}$: 0.08±0.02. For group 3: OE_{20}: 62±12%; OE_{F+20}: 79±7%; $NORA_{20}$: 2.05±0.56; $NORA_{PM}$: 0.22±0.09. Linear regression analysis showed significant inverse linear correlation between $NORA_{20}$ and OE_{20} (r = -0.972; y = 100.4 -18.8x). ROC analysis revealed cutoff values of predicting obstruction at 82% and 0.145 for OE_{F+20} and $NORA_{PM}$, respectively. Among kidneys with equivocal findings, 32 showed OE_{F+20} and $NORA_{PM}$ values in "non-obstructive" range, in 13 kidneys both parameters were "obstructive", and in 3 kidneys, OE_{F+20} indicated

obstruction, but NORA$_{PM}$ converted the pattern into non-obstructive. **Conclusion**: The results provided evidence of excellent agreement of obtained results with previously reported values of the quantitative parameters of kidney washout. The parameters of software contribute to accurate diagnosis of obstruction and help to clarify indeterminate findings of diuretic renogram. Nuclear medicine section of IAEA should be encouraged to produce final version of the software and to release it through IAEA Web site.

OP-143

Background Subtraction in Dynamic Renal Scintigraphy Revisited

M. Samal[1], V. Ptacnik[2], H. Jiskrova[2], D. Skibova[2]; [1]Charles University, First Faculty of Medicine, Prague, CZECH REPUBLIC, [2]General University Hospital, Prague, CZECH REPUBLIC.

One of the sources of error in performing quantitative planar nuclear medicine studies is correction for the presence of background activity surrounding the area of interest. Subtracting "background" in dynamic renal scintigraphy still remains a challenge (Blaufox MD, EJNMMI 2016; 43:548-549). The aim of this study was to analyze differences in split renal function measured by integral (INT) and Patlak-Rutland plot (PRP) methods after subtracting "tissue" (perirenal), "vascular", and "both" backgrounds (TB, VB, TVB). Methods: The study was performed with data collected in public database www.dynamicrenalstudy.org including 107 adult patients with a wide range of renal function. Time-activity curves were extracted from manually defined ROIs of the heart, left and right kidneys, and automatically defined ROI of perirenal background. Missing kidneys were substituted by background area contralateral to the existing kidney. Both INT and PRP methods were applied in a fixed time interval between 1 - 2 minutes (6th to 12th 10s frames) and their results compared using Passing-Bablok regression and the mean absolute differences. Total renal function was estimated from the heart ROI curve extrapolated using gamma fit. Results: After subtracting the same type of background, INT and PRP provided identical or almost identical results with 95 % confidence intervals of individual differences well below 5 % considered as accuracy limit acceptable in clinical practice. Mean absolute difference between INT (after VB subtraction) and PRP (with implicit VB subtraction) was lower than 1 %. In comparison with no background subtraction, subtracting TB, VB and TVB resulted in mean absolute differences (with 95 % confidence interval of the mean) of 2.5 (2.1-3.0), 3.7 (3.0-4.4), and 4.6 (3.7-5.5) % in INT, and 1.1 (0.9-1.4), 0.0 (0.0-0.0), and 1.1 (0.9-1.4) % in PRP. Subtraction of VB affected split renal function more than subtraction of TB. In most comparisons, background subtraction produced individual differences inversely proportional to total renal function (weak kidneys were affected more than normal kidneys). Conclusions: Background subtraction is mandatory in INT method. Preferably both TB and VB should be subtracted to approximate PRP performance. In PRP with implicit VB subtraction, additional TB subtraction results in only a small change lower than 5 % not affecting clinical performance of the method. With PRP, no preliminary perirenal or other "tissue" background subtraction is thus necessary that also avoids uncertainty which part of background and which subtraction weight should be chosen. The study was supported by the Czech Science Foundation grant 303/07/0950.

CME 4 - Oncology: PET in Multiple Myeloma

OP-144

What is Expected from Imaging in Multiple Myeloma (MM)
C. Touzeau; CHU Nantes, Haematology, Nantes, FRANCE.

OP-145

Standard MRI in MM and Perspectives
C. Messiou; The Royal Marsden Hospital, Department of Radiology, London, UNITED KINGDOM.

OP-146

Role of PET for Initial Evaluation and Response Assessment in Multiple Myeloma: Towards New Imaging Criteria
C. Nanni; Policlinico S.Orsola-Malpighi, Department of Nuclear Medicine, Bologna, ITALY.

Joint Symposium 4 - EANM/ICRP/ICRU: Radiological Protection for Patients Receiving Radiopharmaceutical Therapy Solutions

OP-147

Tumour Response - What is Needed and What is Possible?
R. Howell; New Jersey Medical School, Division of Radiation Research, Newark, UNITED STATES OF AMERICA.

OP-148

Stochastic Effects in Patients Treated with Radiopharmaceuticals; Estimations, Observations and Possible Ways to Reduce Their Occurrence
S. Mattsson; Lund University, Medical Radiation Physics, Malmö, SWEDEN.

OP-149

Deterministic Tissue Reactions in Radionuclide Therapy, Observations and Ways to Reduce Their Occurrence
M. Konijnenberg; Erasmus MC, Radiology & Nuclear Medicine, Rotterdam, NETHERLANDS.

OP-150

Low-Dose Radiation Effects on Salivary Gland Stem Cells - Mechanisms and Clinical Relevance
R. Coppes; University Medical Center Groningen, Department of Cell Biology & Radiation Oncology, Groningen, NETHERLANDS.

504   **Sunday, October 22, 2017, 16:30 - 18:00, Hall E1**

Do.MoRe: SPECT Quantification

OP-151

Internal bremsstrahlung: a forgotten but significant effect in ⁹⁰Y SPECT and ⁹⁰Y PET imaging

S. Walrand[1], M. Hesse[2], R. Lhommel[2], J. Francois[2]; [1]Cliniques Saint-Luc, Brussels, BELGIUM, [2]Université Catholique de Louvain, Brussels, BELGIUM.

Aim: During beta decay a photon may also be emitted due to the interaction of the beta particle with the decayed nucleus. For ⁹⁰Y, this so-called internal bremsstrahlung (IB) has at 150 keV half the intensity of external bremsstrahlung (EB) in water, but supersedes it above 540 keV to become five times as higher than EB at 1500 keV (Cengiz & Almaz, Rad Phys Chem 2004). Although being above routine energy acquisition windows, these high energy x rays easily cross the collimator septa or detector shielding, and may be down scattered into the energy window. Currently, IB is not modelled in the ion source implemented in Geant4 (4.9 and 4.10), and seems unknown by most of the nuclear medicine physicists. This study investigated the impact of IB in ⁹⁰Y imaging. **Methods:** SPECT and PET imaging were simulated using Gate with photon sources modelling the EB of ⁹⁰Y and of ³²P in water, including or not their IB emission. A 1/2 inch-thick NaI SPECT camera equipped with a MEGP collimator and state of the art LSO and GSO PET systems were modelled. All models included the light guide, the PMTs, the electronic, the aluminium frame and lead shielding of the corresponding detectors. Acquisition of a ³²P source was also performed on the modelled GSO PET to validate the MC simulation. This setup is an ideal case to study bremsstrahlung emission as no positron emission and no crystal radioactivity are present. **Results:** The singles rate, the true coincidences rate and the radial profile of the ³²P PET acquisition were accurately reproduced when including EB and IB in the simulation, but with a fourfold underestimation when using EB alone. For ⁹⁰Y SPECT and PET, MC simulations showed that about 35% and 65% of the scattered events contaminating the energy acquisition window originated from the EB and from the IB X rays, respectively. MC simulations also showed that IB is the major actor of the spurious extrahepatic activity seen in most post liver ⁹⁰Y radioembolization PET imaging. **Conclusion:** MC simulations show the major impact of the IB in ⁹⁰Y imaging supporting its implementation in the ion source of Geant4. Resulting accuracy improvement in simulations will allow developing better scatter correction.

OP-152

Quantitative SPECT Neuroimaging using a Data Driven Estimation of Attenuation from the Projection Data Alone

X. Ding, A. Vija; Siemens Medical Solutions USA, Inc., Molecular Imaging, Hoffman Estates, IL, UNITED STATES OF AMERICA.

Aims: We present a method to generate a dose-less mu map derived from the SPECT emission data alone. We compare the image quality and regional quantitative uptake of reconstructions using the dose-less mu-map to that using a CT generated mu-map. **Methods:** We perform a non-attenuation compensated SPECT reconstruction using scatter data or primary emission data to generate a binary segmented anatomical volume. A sequence of morphological operations is then applied to the binary images to create a set of final images suitable for skull segmentation. A boundary tracing algorithm is used to identify the skull of the brain. Once the skull is segmented, we calculate the mu value for the skull bone and the mu value for the interior of the skull. The resulting mu-map is then used for SPECT attenuation compensated reconstruction. We compare the reconstructions using the dose-less mu-maps and the mu-maps generated from CTs on 20 clinical brain studies with Tc99m ECD (10) and I123 DATscan (10). For each reconstructed image pair, we create 5 spherical VOIs with random spatial locations within the brain tissue and with random volumes ranging from 1 mL to 10 mL. For each VOI, we calculate the mean, variance and the range of the voxel values inside the VOI. This creates three sets of 100 data pairs to measure the differences between the means, the variances, and the ranges, respectively. We perform the following statistical tests: T-test (T), Wilcoxon (W), and Kolmogorov-Smirnov (KS). **Results:** Visually, the two images reconstructed from the dose-less mu-maps and the CT mu-maps are similar. Quantitatively, the statistical tests (T, W, KS) shows no significant difference between the two reconstructions with $p > 0.5$ for means, variances, and ranges. For the differences between these two reconstructions, the mean of the VOI mean differences is $-2.2\% \pm 3.7\%$; the mean of the VOI standard deviation differences is $-1.6\% \pm 4.9\%$; the mean of the VOI range differences is $-1.6\% \pm 4.9\%$. **Conclusion:** For SPECT brain perfusion studies, quantitative measurements using spheres ranging from 1 mL to 10 mL, have no statistically significant differences between the reconstructions based on the dose-less mu-maps and the mu-maps generated from the CTs. The study indicates feasibility to provide a path to perform quantitative SPECT neuroimaging without additional CT dose. Future work will include a larger population and human observer studies to assess visual and quantitative clinical performance.

OP-153

A 3D-Printed 2-Compartment Kidney Phantom for Evaluating the Accuracy of Quantitative SPECT/CT Imaging

J. Tran-Gia, M. Lassmann; Department of Nuclear Medicine, University of Würzburg, Würzburg, GERMANY.

Aim: Partial-volume correction is among the most crucial, yet challenging corrections in quantitative SPECT/CT imaging. Therefore, the aim of this study was to mimic the renal activity distribution in radionuclide therapies by 3D printing a 2-compartment kidney phantom, and to perform accurate quantitative imaging by including a model-based partial-volume correction. **Materials and Methods:** Acquisition: Siemens Intevo Bold SPECT/CT, 0.95cm crystal, medium-energy collimator, 60 views, 30s-per-view, non-circular orbit. Reconstruction: Flash3D (6-iterations, 6-subsets, no-filtering), xSPECT (48-iterations, 1-subset, no-fil-

tering), CT-based attenuation correction, Triple-energy-window scatter correction. <u>2-Compartment Kidney:</u> Design based on ICRP 89 (Volume: 143.6mL, 70% cortex, 30% medulla). Fabrication (modelling, design, printing) as described in [1]. SPECT/CT acquisitions of the kidney (cortex: ^{177}Lu solution of 1.38MBq/mL, medulla: water) inside a water-filled NEMA body phantom. Repetition after 12 days (~2 half-lifes). <u>SPECT Quantification:</u> Predetermined Flash3D calibration factor (cylindrical 6.7L phantom): 20.22cps/MBq. xSPECT Quant directly computes activity concentration [Bq/mL]. <u>Determination of Spatial Resolution (FWHM):</u> A ^{177}Lu-filled line source (diameter: 1mm) inside a water-filled cylinder (diameter: 20cm) was placed in 5 transverse and 2 coronal positions. The FWHM (≙ resolution) in each line source was determined (average over ~60 slices), and centric-out linear fitting was performed in all 3 spatial dimensions to obtain resolution maps $FWHM_{sagittal}(x,y,z)$, $FWHM_{coronal}(x,y,z)$, and $FWHM_{transverse}(x,y,z)$. Based on these maps, position-dependent average resolutions $<FWHM_{sagittal/coronal/transverse}>$ can be calculated for any imaged object. <u>Partial-Volume Correction:</u> The extracted cortical filling volume (resolution: 0.2mm) was convolved with a non-isotropic Gaussian point-spread-function ($<FWHM_{sagittal}>$, $<FWHM_{coronal}>$, $FWHM_{transverse}>$), and the resulting matrix was resampled to SPECT voxel size (xSPECT: 2.0mm/Flash3D: 4.8mm). The partial-volume correction factor (C_{PV}) was calculated as pseudo-counts in the actual contours divided by pseudo-counts in the entire volume. Additionally, C_{PV} was calculated for spheres of equal volume (99.6mL) using the same average resolution. Finally, activities were calculated by dividing the uncorrected activity (CT-based volume) by C_{PV}. **Results:** While the activity was accurately recovered for Flash3D (deviation<1.3%), the recovery was less accurate for xSPECT (deviation<10.1%). C_{PV} differences of ~30% were found between kidney (xSPECT: 0.628, Flash3D: 0.677) and sphere geometry (xSPECT: 0.837, Flash3D: 0.871). The quantitative accuracy was equivalent (<2% difference) after 12 days. **Conclusion:** Our results suggest that recovery coefficients for partial-volume correction, which are typically assessed in spherical geometries, should instead be assessed based on more realistic geometries. Therefore, the presented combination of numerical partial-volume correction and 3D-printing based validation holds the potential of greatly improving the accuracy in quantitative SPECT/CT. **References:** [1] Tran-Gia, JNM57(12), 2016.

OP-154

Quantitative Lu-177 SPECT/CT validation to assist theragnostic procedures

S. Gnesin[1], T. Lima[2], J. Malterre[3], F. R. Verdun[1], N. Schaefer[3], J. O. Prior[3]; [1]Institute of Radiation Physics, Lausanne university hospital, Lausanne, SWITZERLAND, [2]Kantonal hospital Aarau, Aarau, SWITZERLAND, [3]Department of Nuclear Medicine and Molecular Imaging, Lausanne University Hospital, Lausanne, SWITZERLAND.

Introduction: Similar to PET, absolute quantification has recently become available on commercial SPECT/CT devices with potential benefit for predictive and post-treatment dosimetry. We present a quantitative phantom validation of a commercial SPECT/CT and quantitative protocol optimization in a patient

receiving a therapeutic administration of Lu-177-DOTATATE. **Subjects and Methods:** Quantitative Lu-177 acquisitions were performed on a Symbia Intevo xSPECT/CT (Siemens, Erlangen, Germany). System calibration relies on NIST Se-75 source. We used a NEMA/IEC and an anthropomorphic (Kyoto liver/kidney phantom) phantom including kidneys and liver insert with 20, 30 and 40mm diameter spheres to mimic lesions. Phantom activity concentrations were 20 and 200 kBq/mL in the background and spherical inserts of the NEMA/IEC phantom respectively; 100, 500 and 600 kBq/mL in the liver, lesion inserts and kidneys of the anthropomorphic phantom respectively. xSPECT/CT acquisitions (120 projections, 30s/projection, medium energy low penetration collimator) used attenuation, scatter and resolution recovery corrections. Reconstructions were performed with the proprietary iterative conjugate gradient algorithm. Activity recovery in the organs background, average and maximum recovery coefficients (RC) in lesions and image noise (coefficient of variation) were assessed as a function of iteration number (ITn range: 1-48, ITn step=4, 3D Gaussian smoothing FWHM=10mm). Signal convergence was reached when <5% signal gain was observed when increasing ITn. Average activity recovery in organs and lesions as a function of iteration number was measured in a SPECT/CT acquisition of a patient 3h after therapeutic administration of 6 GBq of Lu-177-DOTATATE. **Results:** For both phantoms, the activity recovery in the background (NEMA/IEC) and organs (anthropomorphic) was within ±6% of the actual value for ITn>16. Activity recovery in lesions ≥28mm converged for ITn≥24, while ITn≥32 was required for smaller insert sizes. In the tested conditions, the 10-mm insert (NEMA/IEC) was not recovered despite the 10:1 lesion-to-background activity concentration. Background noise was always ≤30% in all tested setups. Patient data showed that the average activity concentration converged for 4, 8, 16 and 32 iterations in liver, heart, kidneys and in a 12-mL tumour lesion located in the liver, respectively. **Conclusion:** Quantitative phantom validation showed that standardized procedures applied to Lu-177 xSPECT/CT acquisition/reconstruction protocols enables accurate activity recovery within 6% of actual values in organs. Protocol optimization and RC evaluation were performed to assess quantitative activity recovery in lesions. The validated, vendor-based xSPECT workflow potentially reduces quantitative variability in dosimetry assessment of theragnostic procedures aiming at improving patient care.

OP-155

Quantitative gamma camera imaging of ^{227}Th and ^{223}Ra with application in ^{227}Th targeted alpha therapy

E. Larsson[1], G. Brolin[1], A. Cleton[2], T. Ohlsson[1], C. Hindorf[1]; [1]Radiation Physics, Lund, SWEDEN, [2]Bayer AG, Berlin, GERMANY.

Aim: Thorium-227 (T½=18.7d) is an alpha particle emitting radionuclide and a promising candidate for targeted alpha therapy. Post-therapy gamma camera imaging of ^{227}Th poses a unique challenge due to the low activity administered in current clinical studies (1.4-7 MBq), low photon emission yield and thereby poor signal-to-background ratio. Furthermore, the

daughter-nuclide ^{223}Ra (T½=11.4d) emits photons in the same energy range as ^{227}Th, making it difficult to separate the two nuclides with conventional energy window-based techniques. Here we present a new method for simultaneous quantitative imaging of ^{227}Th and ^{223}Ra, utilizing list-mode data, energy spectrum modelling, and the conjugate-view technique. **Materials and Methods:** The SPECT/CT system (GE, NM670) allows for extraction of measurement data in list-mode format, which was used to generate count-rate energy spectrum on a pixel-by-pixel basis. The natural background spectrum in each pixel was measured and subtracted from the acquired data. For each pixel, a theoretical spectral model was fitted to the background-corrected spectra using a least-square-fit in the energy range 130-380 keV. This model includes components representing primary and scattered photons for ^{227}Th and ^{223}Ra, respectively. The primary spectrum was modelled as a sum of Gaussian functions with parameters reflecting the energy resolution, emission yield, photon attenuation and detector efficiency for every photon emission energy. Photon attenuation was considered by using X-ray scout data for estimation of water-equivalent thickness in each pixel, and model fitting to geometrical mean data. The primary component holds two fitting parameters representing the activity of ^{227}Th and ^{223}Ra, respectively. The amount of scatter is described by two additional fitting parameters. The proposed methodology was validated by measurements using a Jaszczak-phantom filled with ^{227}Th (2.6 MBq) and ^{223}Ra (0.49 MBq). Eleven acquisitions (20 min) were performed between day 0 and 52 post-preparation during which the activity ratio ^{227}Th /^{223}Ra changed from 5.4 to 0.5. **Results:** The quantified activities of ^{227}Th and ^{223}Ra were within 6% and 10%, respectively, of the theoretical values for all time-points. Furthermore, the image quality and radionuclide separation in the resulting activity images were superior to the conventional images based on energy windows acquisition, due to scatter reduction without noise amplification. **Conclusion:** We have developed a new method for quantitative planar gamma camera imaging based on pixel-by-pixel spectral modelling. This method is capable of accurate activity quantification for ^{227}Th and ^{223}Ra at clinically relevant activities and acquisition time. The image quality is superior to conventional energy window-based methods.

OP-156

Comparison of lesion SUVs between ^{99m}Tc-HDP SPECT/CT and ^{18}F-NaF PET/CT

S. Arvola[1], I. Jambor[2], A. Kuisma[3], M. Seppänen[1,4], T. Noponen[1]; [1]Department of Clinical Physiology and Nuclear Medicine, Turku University Hospital, Turku, FINLAND, [2]Department of Diagnostic Radiology, University of Turku, Turku, FINLAND, [3]Department of Oncology and Radiotherapy, University of Turku, Turku, FINLAND, [4]Turku PET Centre, Turku, FINLAND.

Aim: The aim of this study was to evaluate the feasibility of quantitative SPECT for measuring metastatic bone uptake in breast and prostate cancer by comparing the standardized uptake values (SUVs) measured with quantitative ^{99m}Tc-HDP SPECT/CT and ^{18}F-NaF PET/CT. **Materials and Methods:** 26 breast and 27 prostate cancer patients at high risk of bone metastases underwent both ^{99m}Tc-HDP SPECT/CT and ^{18}F-NaF PET/CT within 1-14 days of each other. The SPECT and PET data were corrected for decay, photon attenuation and scatter and reconstructed using the ordered subsets expectation maximization algorithms. Additionally, dead time correction was applied to PET data and collimator correction to SPECT data. SPECT SUVs were calculated using a novel commercially available software: HybridRecon-Oncology v1.3 SUV SPECT (Hermes Medical Solutions, Stockholm, Sweden). From the reconstructed images, lesions visible in both data sets were classified into benign and malignant by an experienced nuclear medicine physician and then segmented from PET images using a threshold of SUV > 15. The threshold was lowered if the resulting volume of interest (VOI) was less than 1 cm^3 and tissue with increased uptake was left outside of the VOI. Finally, the same lesions were segmented from SPECT images using SUV thresholds that resulted in VOIs with sizes similar to those in PET images. Mean and maximum SUVs of the lesions were compared between SPECT and PET, and Spearman's rank correlation coefficients (r_s) were calculated to evaluate the correlations of SUVs between SPECT and PET. **Results:** A total of 200 lesions, 110 metastatic and 90 benign, were segmented. The average thresholds were SUV = 13.0 for PET and SUV = 10.8 for SPECT. The SPECT and PET SUVs correlated strongly with each other; r_s = 0.92 between mean SUVs in metastatic lesions, r_s = 0.84 between maximum SUVs in metastatic lesions, r_s = 0.67 between mean SUVs in benign lesions, and r_s = 0.69 between maximum SUVs in benign lesions. All correlations were statistically highly significant (P < 0.001). In addition, PET mean SUVs were on average 34% higher in benign lesions and 30% higher in malignant lesions, and PET maximum SUVs were 50% higher in benign lesions and 47% higher in malignant lesions than SPECT SUVs. **Conclusion:** The very strong correlation of metastatic SUVs between ^{99m}Tc-HDP SPECT/CT and ^{18}F-NaF PET/CT suggests that quantitative SPECT is feasible for uptake measurements in bone metastases of breast and prostate cancer.

OP-157

Noise and Resolution Analysis of the xSPECT Quant Reconstruction Algorithm for ^{177}Lu

J. Tran-Gia, M. Lassmann; Department of Nuclear Medicine, University of Würzburg, Würzburg, GERMANY.

Aim: Quantitative assessment of radioactivity distributions is critical for molecular radiotherapies. Therefore, the aim of this work was to evaluate the noise and resolution characteristics of the recently presented xSPECT Quant reconstruction method for ^{177}Lu-based quantitative SPECT/CT imaging. **Materials and Methods:** Acquisition: Siemens Intevo Bold SPECT/CT, 0.95-cm crystal, medium-energy collimator, 60 views continuous, equivalent non-circular camera orbits. Reconstruction: 6 to 96 iterations, 1 subset, no filtering, CT-based attenuation correction, triple-energy-window scatter correction. Line-Source-Based Resolution: Two line-sources (diameter: 1mm) filled with a ^{177}Lu solution were placed in the central

and the outermost position (9cm off-center) of a water-filled cylindrical phantom (diameter: 20cm). By axially rotating the phantom before each acquisition, the spatial resolution at 5 different transverse positions was investigated (7.9M counts, rotation angles: 0°/90°/180°/270°). Edge-Based Resolution: Six spheres of a water-filled body phantom (PTW-Freiburg: NE-MA-NU2-2012) were filled with a ^{177}Lu solution. Additionally to a standard SPECT/CT acquisition (4.2M counts), a high-resolution CT (1-mm isotropic) was acquired to derive a numerical phantom mask. SPECT image formation was simulated by convoluting this mask with a Gaussian-shaped point-spread-function and resampling the resulting matrix to a 2-mm grid. After applying Gaussians of different FWHMs, the minimum root-mean-squared error between the reconstructed and the simulated volumes is associated to the most probable point-spread-function ($\triangleq$ resolution). Noise Analysis: SPECT/CT acquisitions were performed with a ^{177}Lu-filled cylindrical Jaszczak phantom (6.7L, 30s/60s per view, 8.0M/16.1M counts). The noise coefficient of variation was calculated as the ratio between standard deviation and mean value of counts within a large VOI (2.0L) inside the cylinder. **Results:** The resolution is considerably improved (3-fold) by an increasing number of iterations (center/off-center: 19.4/13.1mm for 6 iterations → 7.6/4.4mm for 96 iterations). The FWHM of the point-spread-function depends on the off-center distance and increases with the proximity to the detectors (about 35% difference between center and 9cm off-center). The edge-based resolution is in accordance with the centrally placed line-source (18.4mm for 6 iterations, 9.1mm for 96 iterations). While the noise level decreases with the scan duration, it increases with the number of updates (30/60s-per-view: 0.06/0.04 for 6 iterations → 0.28/0.19 for 96 iterations). **Conclusion:** In xSPECT, considerable resolution improvement by an increasing number of iterations comes at the cost of a strong noise increase. As recommended by the vendor, 48 iterations represent a reasonable trade-off between resolution enhancement and noise minimization. Despite resolution-recovery, the FWHM is not spatially invariant.

OP-158

Quantitative SPECT Imaging of Thorium-227: A phantom experiment

M. Ghaly, Y. Du, G. Sgouros, D. Thorek, E. C. Frey; Johns Hopkins University, Baltimore, MD, UNITED STATES OF AMERICA.

The radionuclide Thorium-227 and its daughter nuclide Radium-223 are important nuclides for alpha immunotherapy. However, quantitative SPECT imaging of Thorium-227 is challenging because of the low yield of photons, complicated emission spectrum and its decay to Radium-223. We have previously developed a model of the image formation process and validated it using Monte Carlo simulations. Here we incorporate that model into an OS-EM reconstruction algorithm and evaluate its ability to quantitatively reconstruct Thorium-227 activity distributions using a phantom study. Thorium-227 was purified immediately before the experiment from a laboratory scale chromatography

column, pre-treated with 80:20 mixture of methanol:nitric acid, utilizing immobilized parent Actinium-227. A 3-cm diameter sphere was filled with a solution containing 2 micro-curies of Thorium-227. We imaged the sphere placed inside an empty and a water-filled cylinder phantom using a Siemens Symbia Intevo dual-head SPECT/CT system with a 9.5 mm thick NaI(Tl) crystal and a medium energy-low penetration (ME-LP) collimator. Images were acquired at 64 views over 360, a 20% window centered at 84keV, a 15% window centered at 236keV and total acquisition time of 60 and 240 minutes for the empty and water-filled cylinders, respectively. We reconstructed the projection data using an OS-EM-based iterative reconstruction algorithm that models attenuation, scatter and the collimator-detector response (CDR) for all the relevant photopeaks. Scatter was modeled using the effective-source scatter estimation (ESSE) method; pre-computed CDR tables were used to model the interactions in the collimator-detector system including septal penetration and scatter. We evaluated the quantitative accuracy of the estimated activities in the sphere and the different imaging scenarios. A volume-of-interest over the sphere was defined based on the CT map. The percent errors in the reconstructed activities in the sphere were -11.5 +/- 4.1% and -12.4 +/- 4.9% in the empty and water-filled cylindrical phantoms, respectively. We also observed very good agreement between the Monte Carlo simulated Thorium-227 projections and those acquired on the system. Quantitative Thorium-227 imaging in the absence of its Radium-223 daughter is feasible when using good models of the image formation process. Further improvements are expected by refining the projection model and using more iterations and partial-volume compensation to reduce partial volume effects. Clinical quantitative Thorium-227 imaging is feasible by combining previously-developed Radium-223 imaging and dual isotope reconstruction methods.

---

505   **Sunday, October 22, 2017, 16:30 - 18:00, Hall E2**

M2M - Featured: Combination Therapies

OP-159

Combination Therapy: Reinforcing Current Therapy
S. U. Dalm; Erasmus MC, Rotterdam, NETHERLANDS.

OP-160

Combination of Proton Irradiation and Targeted Radionuclide Therapy with 177Lu-PSMA-617 in a Tumor Mouse Model of Prostate Cancer

C. Mueller, R. Perrin, C. Umbricht, N. van der Meulen, S. Safai, D. Weber, A. Lomax, R. Schibli; Paul Scherrer Institut, Villigen-PSI, SWITZERLAND.

Aim: Proton therapy allows the precise local deposition of therapeutic radiation doses to the tumor, whereas radionuclide therapy can target disseminated cancer cells. The combination of proton therapy and radionuclide therapy may, thus, be of unparalleled value for the treatment of patients with a non-resectable primary tumor with or without metastases. The goal of

this study was to perform the first proton therapy/radionuclide therapy combination using mice with subcutaneous prostate tumor xenografts. Furthermore, the precision of proton therapy was investigated via PET, imaging activation products in proton-irradiated tumors. **Material and Methods:** Proton irradiation was performed at the OPTIS2 facility at Paul Scherer Institut. The proton field was collimated to the tumor size with a 2.5 mm margin. Irradiation was achieved with a Spread-Out-Bragg Peak, produced from scattering and modulation of a 75 MeV beam, to achieve a uniform dose to subcutaneous PC-3 PIP prostate tumor xenografts. Radionuclide therapy was applied using ^{177}Lu-PSMA-617. Mice (Balb/c nude) were divided into four groups (n=5). Group A: untreated; Group B: 10 Gy proton therapy; Group C: treated with ^{177}Lu-PSMA-617 (5 MBq, ~20 Gy mean absorbed tumor dose); Group D: combination therapy (5 Gy proton therapy and 5 MBq radionuclide therapy). The mice of each group were monitored with weight and tumor size over a period of 9 weeks. Endpoint criteria were defined as weight loss >15% or tumor volume >1cm³. Proton-irradiated mice were scanned for 10 min using a preclinical PET/CT scanner. **Results:** High-quality static PET/CT scans revealed activation products precisely in the irradiated tumor tissue and the absence of activity in the surrounding tissue. The tumor growth inhibition at Day 16 was 83.5% (Group B), 90.8% (Group C) and 95.2% (Group D). The time to reach a relative tumor volume of 2.5 (tumor growth delay index 2.5), was 2.8-fold (Group B), 4.3-fold (Group C) and 5.5-fold (Group D), longer, respectively, as compared to untreated controls (Group A). The mean survival time was 23 days for control mice, 30 days for mice irradiated with protons and 36 days for mice treated with ^{177}Lu-PSMA-617. Combination of proton therapy (5 Gy) and radionuclide therapy (20 Gy) resulted in a mean survival time of 56 days. **Conclusions:** The encouraging results of these studies warrant detailed investigations with regard to the benefit of combining proton therapy and radionuclide therapy in tumor models of prostate cancer and other tumor types.

OP-161

In Vivo Assessment of p53 Therapy as a Way of Enhancing Therapeutic Effects of Radiation

A. C. Mortensen[1], D. Spiegelberg[1], S. Lundsten[1], C. Brown[2], D. P. Lane[2,3], M. Nestor[1]; [1]Department of Immunology, Genetics and Pathology, Uppsala University, Uppsala, SWEDEN, [2]p53 Lab, A*STAR, 8A, Biomedical Grove, #06-04/05 Neuros/Immunos, Singapore 138648, Singapore, SINGAPORE, [3]Department of Microbiology, Tumor and Cell Biology, Karolinska Institutet, Stockholm, Stockholm, SWEDEN.

Introduction: Several small HDM2-p53 antagonists are currently undergoing clinical trials as new, targeted cancer therapies either as monotherapies or in combination with cytostatic drugs. However, the role of wt p53 during radiation response mechanisms suggests a potential for utilizing such peptides in combination with ionizing radiation in order to enhance therapeutic effects. In this study, we explored the efficacy of the novel HDM2/HDMX-p53 antagonist PM2, and examined its effects in combination with external beam radiotherapy (EBRT) in both cultured human tumor cells and in tumor bearing mice. **Subjects and Methods:** The therapeutic effects of PM2-therapy *in vitro*, both as a single modality and in combination with ionizing radiation, were first evaluated in a panel of cancer cell lines using cell viability, clonogenic survival, and 3D tumor spheroid assays. Flow cytometry and Western Blot experiments assessed p53-mediated cellular responses. Potential synergistic effects of fractionated PM2-therapy and ionizing radiation were evaluated in a mouse xenograft model with wt p53 and p53 knockout (-/-) tumors, where tumor growth was followed over time. Furthermore, ^{125}I-labeled PM2 was used to study the biodistribution of the peptide *in vivo*. **Results:** PM2-therapy induced cytotoxic activity both alone and in combination with EBRT in wt p53 cell lines in both monolayer and 3D tumor spheroids, where PM2-therapy in combination with EBRT resulted in synergistic therapeutic effects. Flow cytometry and Western Blot confirmed increased apoptotic activity in the combination samples. *In vivo*, the combination of PM2-therapy and EBRT significantly prolonged survival compared to the control and single treatment groups in wt p53 xenografts. Biodistribution of ^{125}I-PM2 revealed high tumor uptake retained in the tumor for at least 24 h p.i., and digital autoradiography revealed peptide distribution throughout the tumor. Effects on p53 -/- tumors were negligible. **Conclusion:** PM2-therapy enhances the effects of EBRT in cells that retain a wt p53 expression. In the future, a clinical application of PM2-therapy in combination with radiotherapy may be a promising strategy of enhancing the effects of radiotherapy and restore quality of life in cancer patients.

OP-162

Improvement of peptide receptor radionuclide therapy effects via modulation of the DNA damage response

J. Nonnekens, M. de Jong, D. C. van Gent; Erasmus MC, Rotterdam, NETHERLANDS.

Aim: Peptide receptor radionuclide therapy (PRRT) of metastasized neuroendocrine tumors (NETs) that overexpress somatostatin receptors (SSTR) strongly increases progression-free survival and life quality. Recently phase III clinical trials using Lutetium-177 coupled to the somatostatin analogue DOTA-[Tyr³] octreotate (Lutathera® or ^{177}Lu-DOTA-TATE) were finalized. This therapy eradicates tumor cells by targeting DNA damaging radionuclides to the tumor cells with limited harm to healthy tissue. The clinical results are favorable, but most patients will eventually succumb to the disease. Therefore, adaptations of the therapy are urgently needed. We aimed to increase the damaging potential of PRRT via combination therapy with DNA damage response (DDR) inhibitors without extra harm to the healthy tissues. **Materials and methods:** To better understand the radiobiological effects of PRRT, we characterized DNA damage and the DDR induced by NET PRRT. As models, we used SSTR positive cell lines and *ex vivo* cultured human tumor slices. Cells or tissue slices were treated with different doses of ^{177}Lu-DOTA-TATE, followed by non-radioactive incubation for different periods until 7 days post treatment. During these chases the cells/ tissues were treated with inhibitors of PARP, DNA-PK or ATM.

Cells/tissues were fixed and fluorescently stained with different antibodies (53BP1, gamma-H2AX) to visualize the accumulation of DNA repair proteins to the produced DNA double strand breaks (DSBs). Cell proliferation was measured using EdU incorporation and Click-iT labeling technology. Furthermore, cellular survival was measured using colony assay and sulforhodamine B colorimetric assay. **Results:** PRRT produced different types of DNA damage and triggered the DDR in SSTR-positive cells and tumor slices. Combination treatment of PRRT with all of the DDR inhibitors showed radiosensitization and at least 2 fold increase of cell death compared to PRRT alone. PARP-inhibition increased the number of DSBs, leading to increased cytotoxicity, while ATM- and DNA-PK-inhibition caused prolonged existence of the DSBS leading to genome instability and cell death. **Conclusion:** DDR inhibitors can be used to sensitize PRRT in preclinical studies. We expect that our results will eventually improve current NET PRRT that will lead to increased patient survival rates.

OP-163

In Vitro and In Vivo Growth Inhibitory and Radiosensitizing Effects of the Anti-HSP90 agent Onalespib

D. Spiegelberg, S. Lundsten, A. C. Mortensen, A. Abramenkovs, B. Stenerlöw, M. Nestor; Department of Immunology, Genetics and Pathology, Uppsala University, Uppsala, SWEDEN.

Background and Aims: The chaperone Heat shock protein 90 (HSP90) activates and stabilizes numerous oncogenic client proteins. HSP90 overexpression is associated with increased tumor cell survival and growth. The novel HSP90 inhibitor Onalespib is currently in clinical trials, promoting degradation of oncogenic proteins, and may also act as a radio-sensitizer. The aim of this study was to evaluate the response to Onalespib treatment in combination with external beam gamma radiotherapy in 2D and 3D cell assays as well as in mouse xenograft models. **Materials and Methods:** Flow cytometry, immunoblotting, confocal microscopy and radio-immunoassays were used to evaluate the effect of Onalespib on client protein expression and cytotoxicity *in vitro*. Inhibitor effects on protein expression and tumor size were assessed *in vivo* in combination with external beam radiation. **Results:** Onalespib treatment downregulates HSP90 client proteins both *in vitro* and *in vivo*. Treatment alone and in combination with radiation reduced cancer cell proliferation, cell migration rates and increased apoptosis. Furthermore, cells accumulated in the more radio-sensitive G2/M phase of the cell cycle. *In vivo*, a minimal treatment regimen during 3 consecutive days of Onalespib (3×50mg/kg) in combination with external beam gamma radiation (3×2Gy) caused a substantial tumor growth delay and prolonged the survival by a factor of 3 compared to the control groups. **Conclusion:** Our results demonstrate that Onalespib is a potent radiosensitizer with a potentially broad therapeutic window. We speculate that the depletion and downregulation of HSP90 client proteins involved in cancer cell signaling and DNA damage repair mechanisms is the cause. Thus, individually, or in combination Onalespib has the potential to reduce tumor cell growth and may improve radiotherapy outcomes in cancer patients.

OP-164

Boramino Acid: A New Theranostic Platform Serves Imaging Guided Boron Neutron Capture Therapy

J. Li, Y. Han, Z. Liu; Peking University, Beijing, CHINA.

Objective: A new class of amino acid mimics—boramino acids (BAAs)—are described here that can serve as theranostic boron delivery agents for imaging guided BNCT cancer treatment. The structure of a BAA is identical to that of the corresponding natural amino acid, except for an exotic replacement of the carboxylate with trifluoroborate. Cellular studies demonstrate the cell uptake of BAA is strongly mediated to amino acid transporter, of which the abnormal expression is often associated with cancer. In addition, animal studies of ^{18}F labeled BAA (^{18}F-BAA) show high tumor-specific accumulation with PET (positron emission tomography), suggesting that BAA holds great promise for the development of new PET imaging probes and AAT-targeting boron agents for BNCT cancer therapy. **Method:** A boron-derived Tyrosine (B-Tyr) derivative was synthesized to mimic Tyr, of which the transportation depends on L-type amino acid transporter (LAT). [18]F-^{19}F isotope exchange reaction was conducted for radiolabeling and quality control was performed by both HPLC and radioTLC. The metabolic stability of B-Tyr was assessed both *in vitro* and *in vivo*. PET imaging were performed in mice bearing UM22B xenografts, and ^{18}F-B-Tyr is co-injected with 10 mg of unlabeled boron-derived Tyr. The animals are sacrificed right after PET scan, and organs are collected for ICP analysis. **Result:** At 60 min post injection, ^{18}F-B-Tyr shows high accumulation in UM22B tumor (11.9 ± 2.7 %ID/g) but demonstrates low uptake in the rest of the body (liver, 2.41 ± 0.36 %ID/g; muscle, 1.98 ± 0.54 %ID/g; brain, 0.35 ± 0.13 %ID/g and blood, 1.19 ± 0.47%ID/g). The tracer had predominant renal clearance but with low kidney retention. The following ICP analysis is correlated with PET imaging and shows high boron accumulation in tumor (66.7 ± 11.5 ppm) with good selectivity on healthy tissues (liver, 13.5 ± 2.1 ppm; muscle, 12.1 ± 1.9 ppm; brain, 5.9 ± 1.3 ppm and blood, 7.8 ± 2.0 ppm). **Conclusion:** A boron-derived Tyr derivative was developed and evaluated for PET-guided BNCT treatment. Administration of ^{18}F-B-Tyr allowed for clear visualization of tumor xenografts, and also delivers high concentration of boron atoms into tumor that can be promising for BNCT treatment.

OP-165

Second Generation Trifunctional PSMA Binding Ligands with Application to the Imaging of Prostate Cancer by Positron Emission Tomography and to its Treatment by Targeted Endoradiotherapy

J. M. Kelly[1], A. Amor-Coarasa[1], S. Ponnala[1], A. Nikolopoulou[1,2], C. Williams, Jr[1], D. Kim[2], J. W. Babich[1,2,3]; [1]Division of Radiopharmaceutical Sciences and MI3, Department of Radiology, Weill Cornell Medicine, New York, NY, UNITED STATES OF AMERICA, [2]Citigroup Biomedical Imaging Center, Weill Cornell Medicine, New York, NY, UNITED STATES OF AMERICA, [3]Sandra and Edward Meyer Cancer Center, Weill Cornell Medicine, New York, NY, UNITED STATES OF AMERICA.

Aim: Treatment of late-stage prostate cancer (PCa) by targeted radiotherapeutics such as ^{131}I-MIP-1095 and ^{177}Lu-PSMA-617 has shown encouraging early results. However, many patients never respond to β-particle therapy, and relapse rate remains high. Recently, treatment of PCa by targeted alpha therapy (TAT) with [213]Bi-PSMA-617 and [225]Ac-PSMA-617 has been shown to overcome resistance to beta particles, but severe, irreversible xerostomia and dry eye are dose-limiting toxicities. We recently proposed albumin binding as a strategy for improving the pharmacokinetics of PSMA-targeting small molecules and introduced a radioiodinated dual-binding ligand, RPS-027, that shows good tumor uptake and significantly reduced kidney uptake in a preclinical model. Further development is limited by the inability to independently modify either PSMA or albumin binding. We therefore devised a new class of trifunctional ligands with (1) a high affinity PSMA binding domain; (2) a chelator for radiometals such as Ga^{3+}, $^{177}Lu^{3+}$ and $^{225}Ac^{3+}$; and (3) an HSA binding group all linked by a flexible chemical moiety, and to compare these ligands in LNCaP cells and in LNCaP tumor xenografts with a view towards a next generation ligand for treatment of PCa by TAT. **Materials and Methods:** Six compounds were synthesized, incorporating a triazolylphenylurea-containing PSMA-targeting group, an N^ε-(2-(4-iodophenyl)acetyl)lysine albumin-binding group (ABG) and the bifunctional chelator DOTA. These moieties were linked by a PEG-containing polymer containing 0,3,4,6,8 or 12 repeats. The affinity of the compounds for PSMA was determined in LNCaP cells and their uptake and tissue distribution was studied in mice bearing LNCaP tumor xenografts. Imaging studies were performed using $^{68}Ga^{3+}$ and $^{66}Ga^{3+}$ and biodistribution studies with $^{177}Lu^{3+}$. RESULTS: Affinity for PSMA was in the range 1-20 nM, and it was inversely proportional to the linker length. In agreement with their binding affinities, uptake of the ligands in tumors was in the order RPS-068(PEG$_0$)>RPS-061(PEG$_4$)>RPS-066(PEG$_8$)>RPS-067(PEG$_{12}$). Important differences were observed in kidney uptake, with RPS-068≈RPS-061>>RPS-066≈RPS-067. A trend of increasing hepatobiliary excretion was observed with increasing linker length. Blood clearance was similar for all of the ligands. **Conclusion**: Although tumor uptake of RPS-068 and RPS-061 was higher than RPS-066 and RPS-067, kidney uptake of the latter compounds decreased ten-fold, leading to greater tumor-to-kidney ratios. The similar blood clearance curves indicate that this pharmacokinetic parameter is mainly driven by the ABG. Ultimately the combination of good tumor uptake and excellent tumor-to-kidney ratios makes the constructs with a linker of length PEG$_4$-PEG$_8$ the more promising candidates for TAT.

---

506   **Sunday, October 22, 2017, 16:30 - 18:00, Hall F1**

Teaching Session 2 (Interactive): Applied Cross Sectional Anatomy and Correlative Imaging - Foot and Ankle

OP-166

Applied Cross Sectional Anatomy and Correlative Imaging – Foot and Ankle

C. Fowler; Brighton and Sussex University Hospital, Brighton, UNITED KINGDOM.

---

507   **Sunday, October 22, 2017, 16:30 - 18:00, Hall F2**

Clinical Oncology: NET, a Classic!

OP-167

Peptide receptor radionuclide therapy in combination with lanreotide Autogel/Depot: a retrospective study in progressive digestive and bronchopulmonary neuroendocrine tumours (PRELUDE)

V. Prasad[1], R. Srirajaskanthan[2], C. Toumpanakis[3], C. M. Grana[4], T. Shah[5], J. Valle[6], F. Courbon[7], X. Truong Thanh[8], A. Houchard[8], L. Bodei[9]; [1]Charité Universitätsmedizin Berlin, Berlin, GERMANY, [2]King's College Hospital NHS Foundation Trust, London, UNITED KINGDOM, [3]Royal Free Hospital, London, UNITED KINGDOM, [4]Instituto Europeo di Oncologia, Milan, ITALY, [5]Queen Elizabeth Hospital, Birmingham, UNITED KINGDOM, [6]The Christie NHS Foundation Trust, Manchester, UNITED KINGDOM, [7]IUCT Oncopole, Toulouse, FRANCE, [8]Ipsen, Boulogne-Billancourt, FRANCE, [9]Memorial Sloan Kettering Cancer Center, New York, NY, UNITED STATES OF AMERICA.

Introduction Therapeutic options for progressive neuroendocrine tumours (NETs) are limited. Peptide receptor radionuclide therapy (PRRT), however, has the potential to control such tumours and has been used with somatostatin analogues such as lanreotide Autogel/Depot (LAN). The aim of the PRELUDE study is to investigate the effectiveness and safety of PRRT in combination with LAN (LAN-PRRT) in progressive gastroenteropancreatic (GEP)- and lung NETs. **Subjects & Methods** This international, retrospective, non-comparative study will analyse existing records for approximately 150 patients from France, Germany, Italy and the UK who received LAN-PRRT (NCT02788578). Key inclusion criteria for eligible adults are: a metastatic/locally advanced, well-differentiated (grade 1/2), functioning or non-functioning GEP- or lung NET; progressive disease confirmed from imaging conducted within the previous 12 months and in the 6 months before the first LAN-PRRT cycle; positive somatostatin-receptor status; ECOG performance status score ≤2; at least one LAN injection in 8 weeks prior to first LAN-PRRT cycle; no prior PRRT; continuous LAN between all cycles; total cumulative activity of ≥500 mCi of ^{177}Lu-DOTATOC or ^{177}Lu-DOTATATE. Data will be collected retrospectively for three timepoints: before treatment on day 1 of the first LAN-PRRT cycle (baseline), at the end of the last cycle, and at the last available follow-up (≤12 months after treatment). **Results** The primary endpoint is the progression-free survival (PFS) rate at the end of last LAN-PRRT cycle (response evaluation in solid tumours [RECIST] v1.1, assessed centrally). Secondary effectiveness endpoints include: PFS rate at the last available follow-up visit; best overall response; objective response rate after last cycle and at last follow-up (percentage of patients with a complete or partial response); changes from baseline to last cycle and last follow-up in the presence and severity of diarrhoea and flushing; changes from baseline to last cycle in chromogranin-A level. Safety endpoints include: changes from baseline to last cycle and last follow-up in body weight; incidences of nephro-, haemato- and hepatotoxicities; incidence of vomiting during infusion. Exploratory endpoints include: median PFS (RECIST v1.1);

median overall survival (OS); baseline factors associated with OS; association between immunoreactive and Krenning scores for somatostatin receptor 2. **Conclusion** PRELUDE will assess LAN-PRRT effectiveness and tolerability in a sizeable cohort of patients with progressive GEP- and lung NETs, and thus further our understanding of the benefits of combined somatostatin analogue and PRRT therapy. As of 20 April 2017, 38 patients have been included. *Sponsored by Ipsen*

OP-168

Clinical, tumour, and treatment parameters to predict overall survival after PRRT - a multivariate analysis in 783 patients

E. A. Aalbersberg[1], D. M. V. Huizing[1], H. R. Kulkarni[2], I. Walraven[3], B. J. de Wit - van der Veen[1], A. Singh[2], M. P. M. Stokkel[1], R. P. Baum[2]; [1]Department of Nuclear Medicine, ENETS Center of Excellence, Netherlands Cancer Institute – Antoni van Leeuwenhoek, Amsterdam, NETHERLANDS, [2]THERANOSTICS Center for Molecular Radiotherapy, ENETS Center of Excellence, Zentralklinik Bad Berka, Bad Berka, GERMANY, [3]Department of Radiation Oncology, ENETS Center of Excellence, Netherlands Cancer Institute – Antoni van Leeuwenhoek, Amsterdam, NETHERLANDS.

Introduction: Peptide receptor radionuclide therapy (PRRT) is an effective treatment option in patients with metastatic neuroendocrine tumours (NET). With increasing referral for PRRT, patient selection to benefit from treatment and prediction of the expected outcome, is becoming increasingly important. Factors such as tumour grade and Ki-67 have been shown to influence the outcome of PRRT in smaller studies. However, no large multivariate analyses on overall survival after PRRT have been performed. The aim of this study was to investigate the association between clinical factors, tumour characteristics, prior treatments, and PRRT parameters on the outcome of PRRT measured as overall survival (OS). **Materials and Methods:** All patients treated between October 2002 and August 2016 with at least three consecutive cycles of PRRT within six months of the previous cycle were included. General patient characteristics (performance status, presence of hypertension and diabetes), tumour characteristics (primary tumour location, grade, functional status, and Ki-67), prior treatment to PRRT (interferon, chemotherapy, radiotherapy, surgery of the primary tumour, ablation, or SSA), and treatment characteristics (peptide, isotope, and administered activity) were taken into account. OS was calculated as time from the last PRRT cycle to date of death or last follow-up. First, univariate cox proportional hazards analyses were performed to identify variables potentially associated with OS. Consequently, a multivariate cox proportional hazards model was constructed with variables associated ($P < 0.1$) with OS using a backward selection procedure, leaving only variables significantly ($P < 0.05$) associated with OS. **Results:** 783 patients were included in the multivariate analyses. The median OS was 44.0 months (interquartile range 21-89 months). Grade 3 tumours [HR 2.03 (95% CI 1.31 to 3.15)], performance status of either WHO 1 [HR 1.61 (95% CI 1.22 to 2.13)] or WHO 2 [HR 2.47 (95%CI 1.60 to 3.81)] compared to WHO 0, previous chemotherapy [HR 1.80 (95% CI

1.36 to 2.39)], or a previous tumour ablation [HR 1.48 (95% CI 1.05 to 2.09)] were significantly associated with a worse OS. Resection of the primary tumour was significantly associated with an improved OS after PRRT [HR 0.73 (95% CI 0.57 to 0.94)]. **Conclusion:** In 783 patients, the median overall survival after PRRT was 44 months. A higher tumour grade, poorer performance status, and previous chemotherapy or tumour ablation predict a worse overall prognosis. Resection of the primary tumour was significantly associated with improved overall survival.

OP-169

A Prospective study of Peptide Receptor Radionuclide Therapy with 177Lu-DOTATATE and Concurrent Capecitabine in Metastatic Paragangliomas

S. Ballal, M. P. Yadav, D. Yadav, C. Bal; All India Institute of Medical Sciences, New Delhi, INDIA.

Aim: Paragangliomas are rare tumors, 30% of which are malignant. They are highly aggressive and have a poor prognosis when metastatic. Peptide Receptor Radionuclide Therapy (PRRT) is currently utilized in their management due to somatostatin receptor expression in these tumors. Capecitabine has been used as a radiosensitizer during PRRT treatments for other neuroendocrine tumors. This study was done to evaluate the efficacy and toxicity of PRRT with concurrent capecitabine in patients with metastatic paragangliomas. **Methods:** 20 patients of metastatic paragangliomas who had positive somatostatin receptor expression, were enrolled in the study. All patients underwent baseline ^{68}Ga-DOTA-NOC PET/CT scans and were treated with 7.8GBq ^{177}Lu-DOTATATE therapy quarterly and concurrent oral capecitabine 1,250mg/m^2 for 15 days starting from the day of PRRT infusion. Toxicity profile and Chromogranin A (CgA) levels were recorded before, and after therapy at 2 weeks, 4 weeks and 3 months. Toxicity was assessed using CTCAE v4.0 and post therapy morphological response using RECIST1.1 criteria. **Results:** Median age of patients was 36.5yr (range 22-47). Post two to six cycles of PRRT, 18.75% patients had partial response (PR), 56.25% patients had stable disease (SD), and 25% had progressive disease (PD). Only 12.5% patients had biochemical progression whereas rest showed significant decline in CgA levels (median CgA decline 5%). The median follow up was 15 months (range 9-60). The 2-yr progression free survival was 69.2% and 2-yr overall survival was 57.8%. One patient had renal toxicity; two patients had grade II haematological toxicity while Grade III/IV toxicity was not seen in any of the patients. **Conclusion:** Concomitant Capecitabine and ^{177}Lu-DOTATATE therapy offers a good progression-free survival and overall survival with negligible toxicity noticed during the period of study. Patients with aggressive disease have limited management options and may benefit from this synergetic therapeutic approach. Longer follow-up of these patients is needed to elucidate survival advantage.

OP-170

First-in-human PET/CT Imaging of somatostatin receptor expressing tumors with the novel somatostatin receptor antagonist ^{68}Ga-NODAGA-LM3 - a comparison with ^{68}Ga-DOTATOC PET/CT

A. Singh[1], H. R. Kulkarni[1], T. Langbein[1], D. Müller[1], S. Senftleben[1], M. Fani[2], H. Maecke[3], R. P. Baum[1]; [1]Theranostics Center for Molecular Radiotherapy and Molecular Imaging, Bad Berka, GERMANY, [2]Division of Radiopharmaceutical Chemistry, University Hospital of Basel, Basel, SWITZERLAND, [3]Department of Nuclear Medicine, University Hospital Freiburg, Freiburg, GERMANY.

Aim: Since over two decades somatostatin receptor (SSTR) agonists are being used for molecular imaging of SSTR-expressing tumors. A recent clinical study with SSTR-antagonist based PET/CT reported a higher tumor detection rate in SSTR-expressing tumors than SSTR-agonist based PET/CT. This study aims to assess the suitability of ^{68}Ga-based PET/CT imaging of the SSTR-antagonist LM3 [p-Cl-Phe-cyclo(D-Cys-Tyr-D-4-amino-Phe(carbamoyl)-Lys-Thr-Cys)D-Tyr-NH$_2$] conjugated to the chelator NODAGA (1,4,7-triazacyclononane,1-glutaric acid-4,7-acetic acid) in humans with SSTR-expressing tumors, and compare it with the SSTR-agonist ^{68}Ga-DOTATOC PET/CT. **Methods**: NODAGA-LM3 was labeled with ^{68}Ga (radiochemical yield >95%, radiochemical purity >95%, specific activity 20-50 MBq/nmol). Two patients, one with pancreas NEN (P1) and other with paraganglioma (P2), who had previous ^{68}Ga-DOTATOC PET/CT within 3 months for direct comparison, were included in this study. Five other patients had ^{68}Ga-NODAGA-LM3 PET/CT (LM3), but with ^{68}Ga-DOTATOC PET/CT (TOC) performed at >3 months' time-interval, were excluded. ^{68}Ga-NODAGA-LM3 was administered to P1 (289 MBq) and P2 (286 MBq), followed by PET/CT imaging at 50 min p.i. The acquired LM3 and the corresponding TOC images were compared visually and semi-quantitatively. Tumor-to-background ratios (TBR) were calculated using volume-of-interest based SUVmax for 5 target lesions (TL) and SUVmean for reference tissue (RT) including the liver, kidney, gluteus muscle, and spleen (P2 only). **Results**: Molecular imaging with ^{68}Ga-NODAGA-LM3 PET/CT demonstrated excellent image quality with high specific uptake in the liver, lymph node, skeletal, and soft tissue metastases, as well as in multifocal paraganglioma. Visually, ^{68}Ga-NODAGA-LM3 PET/CT distinctively detected additional SSTR-expressing lesions (P1 n=10, namely, liver n=3, lymph node n=1, bone n=6; P2, n>140 skeletal metastases). The physiological uptake of ^{68}Ga-NODAGA-LM3 compared to ^{68}Ga-DOTATOC (SUVmean LM3:TOC) in RT was higher for kidney (P1, 11.7:4.6; P2, 10:6.3) and gluteus (P1, 0.73:0.35; P2, 0.44:0.38), but lower for liver (P1, 3.5:4.2, P2, 3.7:5.4) and spleen (P2, 13.9:26.5). Applying the same TL, ^{68}Ga-NODAGA-LM3 associated TBR (LM3:TOC) for P1 were higher for all RT (liver 5:0.3; kidney 1.5:0.4; gluteus 25:5); whereas, for P2, they were higher for liver (48:4) and spleen (13:7), but lower for the kidney (18:3) and gluteus (405:507). **Conclusion**: In this study, PET/CT imaging with the SSTR-antagonist ^{68}Ga-NODAGA-LM3 in comparison to the SSTR-agonist ^{68}Ga-DOTATOC demonstrated a higher rate for the detection of SSTR-expressing tumor and metastases, both visually and semi-quantitatively. Despite the limited number of patients, our findings confirm recently reported results comparing radiolabeled SSTR-antagonists with agonists. Additionally, our results emphasize the potential of the SSTR-antagonist ^{68}Ga-NODAGA-LM3 for PET/CT imaging of SSTR-expressing tumors in humans.

OP-171

Biodistribution and radiation dosimetry of ^{68}Ga-DOTA-JR11 in patients with metastatic neuroendocrine tumors

S. Krebs, J. O'Donoghue, D. Reidy, N. Pandit-Taskar, B. Beattie, L. Bodei, W. A. Weber; Memorial Sloan Kettering Cancer Center, New York, NY, UNITED STATES OF AMERICA.

Purpose: Somatostatin receptor (SSTR) imaging is widely used for the management of patients with neuroendocrine tumors (NETs). In this study we assess the utility of the novel somatostatin antagonist ^{68}Ga-DOTA-JR11 for PET imaging of NETs. Patients with advanced NETs and positive ^{111}In-pentetreotide (OctreoScan®) scans, who were candidates for peptide receptor radionuclide therapy (PRRT) with ^{177}Lu-DOTA-JR11, were imaged with ^{68}Ga-DOTA-JR11 to assess biodistribution and radiation dosimetry. **Methods:** 19 patients underwent whole-body PET/CT imaging (GE PET/CT 710 scanner; PET acquisition 60-70 minutes postinjection; 173 MBq (median) ^{68}Ga-DOTA-JR11). Volumes of interest were placed over up to 4 ^{68}Ga-DOTA-JR11 avid lesions (with uptake greater than liver). Maximum standardized uptake value (SUVmax), SUVmean and SUVpeak were measured on ^{68}Ga-DOTA-JR11 PET. Additionally, target-to-normal blood (TNR blood) and target-to-normal spleen (TNR spleen) ratios were calculated as quantitative indices. A subset (3 females, 3 males) had additional imaging for absorbed dose estimation purposes (25 min dynamic PET/CT scan of the upper abdomen including, at least partly, cardiac left ventricle, liver, spleen and kidney and a whole-body PET/CT scan at 30 min post-injection). Absorbed doses were calculated using OLINDA/EXM. **Results:** In contrast to the known biodistribution of SSTR2 agonists, no/minimal uptake above background was seen in pituitary gland, spleen, adrenals and liver; e.g. spleen SUVmean 1.49 (0.66-1.81), liver SUVmean 1.15 (0.66-1.88). A total of 40 lesions were analyzed on whole-body ^{68}Ga-DOTA-JR11 PET/CT with median SUVmax 11.7 (range: 2.87-94.47), SUVpeak 9.37 (2.46-84.07), TNR blood 9.32 (1.85-86.7) and TNR spleen 4.87 (1.87-47.63). In the 6 patients, who had dynamic imaging, tumor lesion uptake reached plateau levels by 20-30 min post-injection with SUVmax of up to 50. Maximal lesion uptake was seen in liver disease. For normal parenchymal tissues, the highest SUV at 30 min and 60 min post-injection were observed in kidneys, followed by liver and spleen. The highest absorbed dose estimates (mGy/MBq) to normal tissues were: urinary bladder wall (0.30± 0.06), kidneys (0.050± 0.013), liver (0.023± 0.014), lungs (0.021± 0.05), heart wall (0.020± 0.04) and spleen (0.016± 0.05). The effective dose was 0.025± 0.004 mSv/MBq. **Conclusion:** 68Ga-DOTA-JR11 demonstrated rapid tumor uptake, high tumor/background ratios and rapid clearance from blood. The low background uptake in the liver is advantageous and may facilitate detection of liver metastases. The dosimetric data compare favorably with previously published data of ^{68}Ga-DOTATATE and ^{68}Ga-DOTATOC (M. Sandstrom et al. JNM 2013), e.g. kidney 0.093± 0.016 mSv/MBq (TATE), 0.082± 0.02 mSv/MBq (TOC) versus 0.050± 0.013 mSv/MBq (JR11).

OP-172

First experience using LMI1195 in patients with the suspicion of pheochromocytoma or paraganglioma

C. Rischpler[1], A. M. Schlitter[1], M. Herz[1], B. Yousefi[1], A. von Werder[1], R. Tauber[1], T. Maurer[1], K. Scheidhauer[1], S. Robinson[2], C. Orlandi[2], S. G. Nekolla[1], M. Schwaiger[1]; [1]Technical University Munich, Munich, GERMANY, [2]Lantheus Medical Imaging, N. Billerica, MA, UNITED STATES OF AMERICA.

Introduction: N-[3-bromo-4-(3-(18)F-fluoro-propoxy)-benzyl]-guanidine [LMI1195], a novel, F-18-labeled radiotracer for non-invasive PET imaging of the norepinephrine transporter expression has only been evaluated in healthy volunteers so far. The aim of this study was to investigate this radiotracer in patients with the suspicion of pheochromocytoma (PHEO) or paraganglioma (PARA). **Methods:** 8 patients with suspicion of primary PHEO or PARA, 1 patient with suspicion of recurrent PHEO and 1 patient with suspicion of recurrent PARA were imaged using LMI1195 PET. On average 256±33 MBq were injected and PET/CT imaging (Siemens Biograph mCT) was started 55±11 minutes p.i. (effective dose: 6.7±0.9 mSv, imaging time: 22±2 min). Any medication potentially interfering with LMI1195 accumulation was discontinued prior to the scan according to the EANM guidelines for MIBG imaging. **Results:** After LMI1195 application no adverse events were observed. The most intense tracer accumulations were (SUVmean, organs in descending order of intensity: thyroid (SUV 25±8), salivary glands (SUV 14±4), bladder (SUV 13±15), kidneys (SUV 13±5), pancreas (SUV 13±4), stomach (SUV 10±4), left ventricle (SUV 9±2), liver (SUV 5±2), small bowel (SUV 4±2), spleen (SUV 3±1) and lungs (SUV 2±1)). In 7 patients a PHEO and in 1 patient PARAs were suspected by PET/CT (SUVmax 25±19 and 13, SUVmean 12±9 and 10; healthy adrenals: SUVmax 13±4, SUVmean 8±2). Clinical diagnosis was histologically confirmed in the resected tissue in 4 patients (PHEO) and excluded in 1 patient (endocrine-inactive adenoma). In 2 patients operation is scheduled and in 1 patient (high suspicion of multiple PARAs) a follow-up scan is scheduled. In the remaining 2 patients, there was no abnormality in PET/CT. PET image quality clearly outperformed the known limited properties of MIBG SPECT despite a 50% shorter imaging time and a comparable radiation exposure. **Conclusions:** LMI1195, a novel F-18-labeled PET-tracer, is highly promising for the confirmation, exclusion and staging of tumors of the adrenal medulla or the sympathetic trunk and further potential applications (e.g. assessment of the sympathetic innervation of the heart) should be evaluated.

OP-173

68Ga-NODAGA-exendin-4 PET/CT for the localization of insulinomas: preliminary data from a prospective multicenter imaging study

M. Boss, Sr.[1], M. Buitinga[1], M. Brom[1], D. Wild[2], V. Prasad[3], P. Nuutila[4], A. Brouwers[5], F. Pattou[6], M. Gotthardt[1]; [1]Radboud University Medical Center, Nijmegen, NETHERLANDS, [2]University of Basel Hospital, Basel, SWITZERLAND, [3]Charite University Hospital of Berlin, Berlin, GERMANY, [4]University of Turku, Turku PET Centre, Turku, FINLAND,

[5]University Medical Center Groningen, Groningen, NETHERLANDS, [6]University Hospital, Lille, Lille, FRANCE.

Background: Insulinomas are usually small, single benign tumors. Surgery is the therapy of choice and precise preoperative anatomical localization of the tumor is essential. Imaging techniques like CT, MRI as well as somatostatin receptor (SSTR) imaging have limited sensitivity. The stable glucagon like peptide-1 (GLP-1) analog exendin specifically binds to the GLP-1 receptor (GLP-1R), which is markedly upregulated/overexpressed in insulinomas. 68Ga-DOTA-exendin-4 PET/CT has been shown to be feasible in detecting insulinomas. Replacing the chelator DOTA by NODAGA in the labeling process ensures higher specific activities, allowing imaging with sub-pharmacological peptide doses. We propose 68Ga-NODAGA-exendin-4 PET/CT as a promising new method for improved localization of insulinomas. We here present the first cases of a multi center prospective imaging study to evaluate the effectiveness of 68Ga-NODAGA-exendin-4 PET/CT. **Methods:** 7 adults aged 24-65 with biochemically proven hyperinsulinemic hypoglycemia were included. PET/CT images were obtained one and two hours after injection of (5-7 µg) 95-105 MBq 68Ga-NODAGA-exendin-4. Current standard imaging was performed in all patients, consisting of CT or MRI and SSTR PET imaging. **Results:** In 2 patients standard imaging as well as GLP-1R PET/CT were all negative. Single lesions in the pancreatic body of 3 patients, and 2 lesions in the tail of 1 patient were identified by CT/MRI imaging as well as by SSTR PET/CT. At corresponding locations, GLP-1R positive lesions were clearly visualized using GLP-1R PET/CT, with low background uptake. In 1 patient an insulinoma was identified using GLP-1R PET/CT and SSTR PET/CT, which was located below the uncinate process, protruding in or against the duodenal wall. This insulinoma was not detected by MRI. None of the patients experienced any adverse effects (no hypoglycemia, nausea etc.) The 5 patients in whom lesions were identified underwent surgery and imaging findings were confirmed histologically. **Conclusion:** These preliminary results indicate the proof of principle that a low peptide amount of 68Ga-NODAGA-exendin-4 can detect insulinomas without relevant adverse effects and suggest a possible valuable role for this new imaging method.

OP-174

AZEDRA® (iobenguane I 131) in Patients with Malignant and/or Recurrent Pheochromocytoma/ Paraganglioma (PPGL): Overall Tumor Response Assessment

D. A. Pryma[1], B. B. Chin[2], R. B. Noto[3], J. S. Dillon[4], L. Solnes[5], J. Jensen[6], T. White[6], N. Stambler[6], S. Apfel[6], V. Wong[6], C. Jimenez[7]; [1]Perelman School of Medicine at the University of Pennsylvania, Philadelphia, PA, UNITED STATES OF AMERICA, [2]Duke University, Durham, NC, UNITED STATES OF AMERICA, [3]Warren Alpert Medical School of Brown University, Providence, RI, UNITED STATES OF AMERICA, [4]University of Iowa Carver College of Medicine, Iowa City, IA, UNITED STATES OF AMERICA, [5]Johns Hopkins Medicine, Providence, RI, UNITED STATES OF AMERICA, [6]Progenics Pharmaceuticals, Inc., New York, NY, UNITED STATES OF AMERICA, [7]University of Texas M. D. Anderson Cancer Center, Houston, TX, UNITED STATES OF AMERICA.

Introduction: Pheochromocytoma/paraganglioma (PPGL) are rare neuroendocrine tumors that overexpress the norepinephrine transporter (NET) that can be molecularly targeted for tumor selective therapeutic drug delivery. AZEDRA, a high specific activity, proprietary Ultratrace® form of I-131 MIBG, has been developed for the treatment of MIBG-avid metastatic and/or recurrent and/or unresectable PPGL. **Methods:** MIBG avid patients with PPGL ineligible for curative surgery, failed prior therapy or not candidates for chemotherapy, and on a stable antihypertensive regimen for tumor-related hypertension, were enrolled. 71% of patients received at least two prior lines of therapy and 31% of patients had prior conventional, low specificity MIBG therapy. Patients received a dosimetric dose (111-222 MBq) followed by up to two therapeutic doses, each at 296 MBq/kg to a maximum of 18.5 GBq, approximately three months apart. The effects on objective tumor response (RECIST) were determined and correlations to the primary endpoint (proportion of patients with at least 50% reduction of all antihypertensive medications lasting ≥6 months), number of administered doses, and prior MIBG were investigated. **Results:** 68 patients received at least one therapeutic dose (full analysis; FA). 50 patients received two therapeutic doses (per protocol; PP). The primary endpoint was met by 25% (95% CI 16%-37%) of FA patients, and 32% (95% CI 21%-46%) of PP patients, achieving the pre-specified success criteria. 23% and 30% of evaluable FA and PP populations, respectively, achieved best confirmed tumor response of partial response (PR). 69% of FA patients and 68% of PP patients achieved best overall response of stable disease (SD). Of the primary endpoint responders 41.2% experienced a PR and 0% progressive disease (PD), whereas in the non-responders 17% and 6.4% of PR and PD were observed, respectively. Similar response rates were observed, whether the patients had prior conventional low specific activity I-131 MIBG treatment or not, in their overall tumor response of PR (21.1%, 24.4%) and SD (73.7%, 66.7%), respectively. The most common (≥50%) treatment-emergent adverse events (TEAEs) were nausea, myelosuppression and fatigue. No acute drug-related hypertensive crises were observed. **Conclusions:** Objective tumor response of AZEDRA has been demonstrated in a pivotal phase 2b study. The current results suggest that tumor response correlates to the primary endpoint, patients able to tolerate additional doses of AZEDRA may experience better response, and efficacy persists regardless of previous conventional, low specificity MIBG use. Taken together, AZEDRA exhibits anti-tumor effects as well as potentially improving the debilitating cardiovascular sequelae of malignant PPGL.

---

508   **Sunday, October 22, 2017, 16:30 - 18:00, Hall K**

Cardiovascular System: Myocardial Function, Metabolism & Perfusion - From Preclinical to Clinical Practice

OP-175
The study of ^{18}F-FDG PET/CT imaging for myocardial "ischemic memory" in different degrees

Z. Na, X. Meng, Z. Bai, K. Zhang, G. Zhang, **X. Wang**; *The Affiliated Hospital of Inner Mongolia Medical University, Hohhot, CHINA.*

Objective: According to compare the change of glucose metabolism and ischemic range on ischemic myocardial under two conditions of fasting and feeding by using Micro-PET/CT ^{18}F-FDG imaging with the SD model of acute myocardial ischemia in different degrees, explore whether the"ischemic memory "correlats with the extent of myocardial ischemia and certify the time window of myocardial "ischemic memory". **Methods:** 100 male SD rats weighing 400 ± 50g. The model of acute myocardial ischemia was made by ligating the inferior one-third of left anterior descending coronary artery. According to different blood flow occlusion time, the SD model was randomly divided into mild ischemic group (ligation 10s, 30 rats), moderate ischemic group (ligation 10s, 30 rats) and the severe ischemic group (ligation 60s, 35 rats). All models were performed ^{18}F-FDG Micro-PET / CT imaging after 24 h,48 h and 72 h . we calculated the volume of the ischemic (VOI) and the Standardized uptake value (SUV$_{mean}$) to compare weather the scope of ischemic myocardium under two kinds of conditions were the same. **Results**: 1. Fast-Feed comparison group: model rats showed a "focal" myocardial ^{18}F-FDG uptake increased, the volume of myocardial imaging agent was 17.52 ± 1.14mm^3, the similar difference was observed in the same part of the model rats with the "focal" myocardium ^{18}F-FDG, and the defect volume of the myocardial imaging agent was 20.00 ± 2.85mm^3. 2. Ischemic 10s group, 30s group, 60s group after24h and 48h modeling successfully, the defect volume of the imaging agent in the left ventricular wall was 8.31 ± 0.67mm^3, 15.16 ± 0.65mm^3 and 20.15 ± 2.48mm^3, 5.38±0.51 mm^3, 5.05±1.34mm^3, 6.03±1.14 mm^3,respectively. Ischemic 10s group, 30s group, 60s group after modeling 72h successfully: For 10s group and 30s group, there has no abnormal imaging uptake of sparse area. By contrast, the defect volume of 60s group is 1.38±0.34 mm^3. The corresponding standard uptake value of the three groups was 4.64±0.85,4.85±0.74,4.66±0.90 respectively. The difference was statistically significant. **Conclusion:** The time window of myocardial "ischemic memory" was different in various degree of myocardial ischemia. As to myocardial ischemia in mild-moderate degree , the time window of myocardial "ischemic memory" can be prolonged to 48 hours. For severe degree , the time window of myocardial "ischemic memory" can be prolonged to 72 hours.

OP-176
Myocardial FDG imaging of oxidative damage underlying anthracycline cardiotoxicity

M. Bauckneht[1], F. Pastorino[2], A. Buschiazzo[1], A. Bellini[1], V. Cossu[1], A. Orengo[1], P. Piccioli[1], G. Caneva[1], L. Pellegrino[1], L. Emionite[1], S. Ravera[1], S. Morbelli[1], A. Rubartelli[1], M. Ponzoni[2], G. Sambuceti[1], C. Marini[3]; *[1]IRCCS AUO San Martino IST, Genova, ITALY, [2]G. Gaslini Institute, Genova, ITALY, [3]CNR Institute of Bioimages and Molecular Physiology, Milano, ITALY.*

Aim: Cardiotoxic effect of Doxorubicin (DXR) is at least partially related to the drug capability to impair cardiomyocyte mito-

chondrial activity through oxidative stress, that can be eventually followed by a late development of contractile dysfunction. We previously reported that the early acceleration of glycolytic flux, which can be documented as an increased left ventricular (LV) ^{18}F-FDG uptake might be considered as an epiphenomenon of DXR-related cardiotoxicity. On the other hand, we reported that in cancer cells, FDG selectively tracks the activity of a specific glucose metabolism located within the endoplasmic reticulum activated in response to the oxidative damage. In the present study, we aimed to verify whether the increased LV FDG uptake following DXR exposure might be related to oxidative stress and whether this potential biomarker of cardiotoxicity is reduced by drug delivery systems such as Liposomal-DXR administration (Lipo-DXR). **Materials and Methods:** Animal experiments were approved by the Italian Ministry of Health. Five week old female, athymic mice were injected with Neuroblastoma cells in the left adrenal gland as previously described. Subsequently, they were treated once with saline (n=5), Free DXR (Free-DXR 5 mg/kg, n=5) or commercially available Lipo-DXR (Caelyx, 5 mg/kg, n=5). All mice were fed under standard dietary conditions. FDG imaging was performed with a dedicated micro-PET system at baseline and one week after treatment. An operator unaware of mice treatment manually identified a volume of interest on the LV and implanted neuroblastoma (N). Average standardized uptake value (SUV) of both LV and N were measured. Mice were subsequently sacrificed to evaluate myocardial content of oxidized and reduced glutathione as well as NADPH/NADP ratio. **Results:** N-SUV significantly increased only in controls (from 0.93±0.1 to 1.2±0.1, p<0.05), while it remained relatively stable in both Free-DXR (from 0.98±0.2 to 1±0.1, p=ns) and Lipo-DXR treated groups (from 0.96±0.2 to 0.8±0.1, p=ns). On the other hand, LV-SUV remained relatively stable in saline (from 0.7±0.1 to 0.8±0.1, p=ns) and Lipo-DXR treated animals (from 0.7±0.1 to 0.9±0.1, p=ns). Conversely, Free-DXR significantly increased LV-SUV from 0.7±0.2 at baseline to 1.1±0.1 at PET2 (p<0.01) and caused an evident oxidative damage as documented by decreased myocardial content of reduced glutathione combined with an altered ratio of NADPH/NADP. **Conclusions:** The present data document the capability of FDG imaging to identify an oxidative damage of the LV myocardium exposed to Free-DXR. This response is at least partially prevented by drug delivery systems that, however, preserve anthracycline therapeutic potential.

OP-177

The added value on clinical impact of SPECT/CT MPI: a one year experience

M. L. De Rimini[1], G. Borrelli[1], G. Mazzarella[1], A. Russo[2], M. Bifulco[1], P. Muto[1]; [1]Nuclear Medicine Unit; AO Ospedali dei Colli - Monaldi, Naples, ITALY, [2]Cardiovascular Unit; Vanvitelli University of Campania, Naples, ITALY.

Introduction: Multimodality Imaging can improve accuracy in coronary artery disease (CAD) diagnosis and in the disease management algorithms. Purpose: to evaluate the added value and clinical impact of SPECT/CT Myocardial Perfusion Imaging (MPI).

Methods: Over a period of 1 year 3312 patients (pts), affected or suspected for CAD, underwent Stress/Rest MPI (GE-Discovery NM/CT 670, 16 slice). History of multivessel disease (MVD) in 875/3312 pts, treated with stenting. All pts underwent 6 months clinical follow-up (FU). Processing, on a Xeleris Workstation using Myovation cardiac software with ordered subset expectation maximization (OSEM), obtained images with iterative reconstruction with and without attenuation correction (IRAC/IRNC) and with NC filtered back projection (FBP). Head to head images comparison (Cedars-QPS) was performed. *P* <0.05 was considered significant. **Results:** MPI classified the following results: -Normal (pts: 1230/FBP; 1301/IRAC; 1200/IRNC); -Chronic Ischemia (pts: 728/FBP; 690/IRAC; 745/IRNC); -Mild to Moderate transient ischemia (pts: 754/FBP; 730/IRAC; 767/IRNC); -Severe transient ischemia (pts: 600/FBP; 591/IRAC; 600/IRNC). IRAC better discriminated normoperfusion and transient ischemia (<0.05). In mild-moderate ischemia, IRAC resized the stress perfusion defect extension: IRAC = <5% vs >5% in 75 pts at FBP and vs >5% in 128 pts at IRNC. Furthermore CT added, at IRAC images, the evidence of calcium scores/calcific atheromasia on the coronary vessels, respectively in the 35.3% of pts with normoperfusion and in the 42.1% of pts with mild/moderate ischemia. In the 875 pts with stenting MVD: 652/875 showed perfusion defects at MPI: -moderate ischemia in 257 and severe ischemia in 395 pts. In these pts the intrinsic metallic contrast at CT helped to match perfusion defects in specific pertaining to the stenting vessel. Moreover, in the limited field of view of the chest explored by the study, non-CAD disease findings were also obtained at CT consisting of: -Pulmonary nodules in 39 pts, later confirmed as carcinoma in 12 out of them; -Breast carcinoma: 5 patients, showing nodule/micro-calcifications at CT; - Pleural effusion: 57 pts; -Lung fibrosis : 28pts. **Conclusions:** SPECT/CT MPI can add essential information in known and suspected CAD. Thanks to perfusion and morphological correlation, it can better influence pts management or lead to prevent disease, with findings that should be taken into account by clinicians. Moreover, it can radically change the clinical approach extending the pathological scenario by defining pts with unsuspected non-CAD disease. In SPECT/CT approach, the separate CT analisys and fusion imaging (MPI/CT) are mandatory to implement the clinical outcomes of patients.

OP-178

Clinical value of myocardial perfusion imaging in patients with homozygous familial hypercholesterolemia

*J. Jiao, Q. Wang, T. Mou, L. Wang, H. Mi, **X. Zhang**; Capital Medical University affiliated Beijing Anzhen Hospital, Beijing, CHINA.*

Objective: To evaluate the features of myocardial perfusion imaging (MPI) in patients with homozygous familial hypercholesterolemia (HoFH) and the correlation between blood lipid profile and myocardial ischemia. **Methods:** Forty-two consecutive HoFH (21 female, mean age 14.8±8.4 y) patients, diagnosed by clinical and chromosome test, were performed stress and rest ^{99m}Tc-sestamibi (11.1MBq/Kg) SPECT MPI with a two-day protocol. MPI was visually analyzed by 17-segment and 5-score sys-

tem, summed stress score (SSS), summed rest score (SRS) was acquired, and summed difference score (SDS) which represents the degree and extent of myocardial ischemia, was calculated by SSS-SRS. Association between SSS, SRS, SDS and the lipid profile, which including total cholesterol (TC), low density lipoprotein cholesterol (LDLC), triglyceride (TG) and high DLC (HDLC) was analyzed. **Results:** Patients were divided into 3 groups according to age, group 1(n= 14, age <10 y, female 6), group 2 (n =14, age 10-18 y, female 6) and group 3 (n=14, age ≥19 y, 9 female). TC was 14.8±3.8 mmol/L and LDLC was 12.5±3.4 mmol/L. There were 24 (57.1%) patients with positive MPI (SSS>1) and positive MPI was found in more female (76.2%, 16/21) than in male (38.1%, 8/21) (χ2=6.22, p<0.05). More patients with positive MPI were found with increasing age (42.9% in group1, 57.1% in group 2 and 71.4% in group 3, respectively, P>0.05). Positive ATP stress test was observed in 12 patients (28.6%), and it was observed in more female (42.9%, 9/21) than in male (14.3%,3/21) (χ2=4.2, p<0.05). 63 (8.82%) myocardial ischemia (SDS≥1) segments were found, which was respectively distributed in myocardial regions supplied by left anterior descending branch (LAD) (n=38, 60.3%), left circumflex branch (n=5, 7.9%) and right coronary artery (n=20, 31.7%). SSS was positively correlated with age (OR 0.33, 95%CI 0.016-0.21, p=0.023) and HDLC (OR 0.37, 95%CI 0.50-3.57, p=0.110). SRS was positively correlated with HDLC (OR 0.60, 95%CI 1.6-3.97, p=0.0001). SDS was positively correlated with age (OR 0.34, 95%CI 0.010-0.17, p=0.029). Multivariate logistic regression analysis indicated that female was the only independent risk factor to predict positive MPI (OR 5.2, 95%CI 1.37-19.77, p=0.016). **Conclusion:** In HoFH patients, myocardial ischemia was associated with age and female was more likely to have positive MPI. Myocardial ischemia segments were more likely located in myocardial regions supplied by LAD. Preliminary study indicated that MPI was an effective and non-invasive method for detecting myocardial ischemia in HoFH patients.

OP-179

Segmental comparison of myocardial inflammation, area at risk, edema and irreversible tissue damage after acute myocardial infarction

C. Rischpler, U. Handwerker, R. Dirschinger, K. Kunze, H. Kossmann, S. van Marwick, T. Ibrahim, K. Laugwitz, M. Schwaiger, S. G. Nekolla; *Technical University Munich, Munich, GERMANY.*

Introduction: After acute myocardial infarction (AMI) diverse, partly interacting processes such as inflammation, edema and scarring take place in the heart. T2-weighted MRI allows the assessment of myocardial edema and is often used as a marker to determine the area at risk (AAR). The accumulation of FDG under fasting conditions after AMI is often interpreted as myocardial inflammation and first studies suggest that the extent of FDG uptake also corresponds to the AAR. Another important factor assessed by MRI is the late gadolinium enhancement (LGE) as a marker of irreversible tissue damage. The aim of this study was to directly compare different processes such as inflammation, edema, irreversible tissue damage and AAR after myocardial in-

farction by multimodal imaging using hybrid FDG PET/MRI and Tc-99m sestamibi SPECT. **Methods:** In 13 patients the AAR was determined by Tc-99m sestamibi SPECT with tracer injection prior to revascularization - the method of reference for the assessment of AAR. In addition, all patients received a FDG PET/MRI (Siemens Biograph mMR) under fasting conditions within the first week after AMI. The parameters AAR (MIBI SPECT), edema (T2-weighted MRI), inflammation (FDG PET) and irreversible tissue damage (LGE MRI) were directly compared in 72 segments in one central slice through the center of the infarction. **Results:** There was no significant difference in extent between the AAR (47±13%) and the edema (44±20%, p=0.68), while both AAR and edema were significantly larger than the LGE extent (31±14%, p<0.009 and p<0.02) and the FDG extent (30±11%, p<0.003 and p<0.009). No difference was observed between FDG and LGE extent (p=0.76). No correlation between edema and AAR was found (R=0.16, p=0.59), while the LGE extent was significantly associated with the FDG extent (R=0.55, p<0.05). Interestingly, the extent of edema correlated with the FDG extent (R=0.61, p<0.03) and the LGE extent (R=0.62, p<0.03). **Conclusion:** The average extent of edema estimated using T2-weighted MRI is in the same range as the AAR. However, the lack of correlation between edema and AAR and the association of edema with irreversible tissue damage and inflammation indicates that T2-weighted MRI should not be used for AAR assessment.

OP-180

Prediction of Functional Recovery After Primary PCI Estimating Myocardial Salvage in Early Gated SPECT

*R. Sciagrà, **R. Calabretta**, F. Linguanti, F. Tutino, A. Ciaccio; Nuclear Medicine, DECBS, University of Florence, FLORENCE, ITALY.*

The purpose of primary percutaneous coronary intervention (PCI) in acute myocardial infarction (MI) is to achieve myocardial salvage (MS). This parameter would be the ideal surrogate endpoint for assessing treatment effectiveness and as well be useful to predict the patient final functional outcome. Because the reference method for measuring MS requires myocardial perfusion imaging (MPI) after tracer injection before PCI, alternative approaches based on imaging performed later after PCI have been proposed, but none has gained wide acceptance in clinical routine. Since gated SPECT MPI is sometimes performed to assess infarct size (IS) after MI, we tested the hypothesis that by comparing functional and perfusion abnormalities early after MI it is possible to estimate MS and to effectively predict the left ventricular ejection fraction (LVEF) recovery at follow up. We studied 120 patients with acute MI, enrolled in protocols for primary PCI. Early (before hospital discharge) and follow-up (approximately 6 months) gated SPECT MPIs were performed to measure infarct size, MS and functional outcome. In particular MS was defined as the difference between segments with abnormal thickening (= stunned area = risk area) minus segments with abnormal perfusion (= final IS), both data expressed as percent of the total number of segments in the AHA model. LVEF was calculated using the QGS software. The risk area was 40 ± 25%, the IS 17.3 ± 16% and the MS 22 ± 19%. The early LVEF was

46.6 ± 11.6% and the late LVEF was 51.4 ± 11.6%, with 54 patients showing at least an increase > 5 LVEF units. According to ROC analysis, MS was able to predict LVEF recovery with an area under the curve (AUC) = 0.79 (p < 0.0001), and using a cutoff > 23% detected LVEF recovery with 74% sensitivity and 71% specificity. Conversely, the IS obtained an AUC = 0.53 (NS). This study demonstrates that MS assessed by a single early gated SPECT MPI can accurately predict LVEF evolution after primary PCI for acute MI. Our results support the use of this simple approach for estimating MS in clinical practice to predict patient outcome, and as a surrogate endpoint for evaluating the effectiveness of primary PCI for research purposes.

OP-181

Association of brain and cardiac glucose metabolism in patients with coronary artery disease and prior myocardial infarction

X. Lu[1], T. Mou[1], Z. Yang[1], H. Mi[1], Q. Wang[1], X. Xie[1], X. Li[2], M. Hacker[2], Y. Wei[1], **X. Zhang**[1]; [1]Beijing Anzhen Hospital, Capital Medical University, Beijing, CHINA, [2]Department of Biomedical Imaging and Image-guided Therapy, Medical University of Vienna, Vienna, AUSTRIA.

To evaluate the brain glucose metabolism (BGM) in patients with coronary artery disease (CAD) and the impact of myocardial viability and left ventricular (LV) functional parameters: (ejection fraction, LVEF, %), end diastolic volume (EDV, mL) and end systolic volume (ESV, mL) on BGM. **Methods:** Ninety-five consecutive patients (age 57±10.4 y, male 89) with CAD and prior myocardial infarction (OMI) (mean LVEF: 34±15%) who underwent ^{99m}Tc-sestamibi SPECT, ^{18}F-FDG PET/CT, and brain imaging were recruited in our study. Patients with Parkinson, Alzheimer disease and brain vascular disease were excluded. LV functional parameters by gated PET/CT were analyzed by QGS software and BGM determined by mean of standardized uptake value (SUV$_{mean}$) was analyzed by Scenium software. Furthermore, relationship between cerebellum BGM and age, insulin dose (intravenously), ^{18}F-FDG dose, blood glucose level at baseline and at injection of FDG, LV functional parameters, myocardial viability was analyzed by Pearson correlation analysis test. **Results:** BGM in cerebellum (SUV$_{mean}$) was significantly correlated with LVEF (r = 0.205, p<0.05), ESV (r = -0.217, p<0.05), and the extent of myocardial scar (%LV) (r = -0.296, p=<0.01). No significant correlation was found between BGM and age, insulin dose, blood glucose level at baseline and at injection, EDV, and the extent of myocardial viability. Multivariate analysis revealed that the extent of myocardial scar (%LV) (r = - 0.296, 95%CI -0.043-0.009, p<0.01) was the only independent predictor for cerebellum BGM. Thus, patients were divided into three groups according to the extent of myocardial scar (%LV): Group 1 (n = 35, scar < 10%), Group 2 (n = 25, scar 10-20%) and group 3 (n = 35, scar >20%). BGM was significantly different within three groups in all brain regions, including cerebellum, frontal lobe, temporal lobe, parietal lobe, occipital lobe and basal-ganglia region (all p value <0.01). Moreover, severe reduction of BGM (SUV$_{mean}$ < 4.0) was found in 57.9% (22/35) of patients in Group 3 and 13.2% (5/35)

of patients in Group 1 (p<0.0001). Age, insulin dose, and glucose level at baseline and at injection FDG did not differ among three groups (all p value >0.05). In addition, no significant difference of BGM was found in patients with severe (LVEF≤25%,n=33), moderate (25%<LVEF≤45%,n=38) and mild LV dysfunction (LVEF>45%,n=25). **Conclusion:** BGM was significantly correlated with ESV, LVEF, and extent of myocardial scar, and it was significantly decreased in patients with >20% of myocardial scar. These findings warrant further prospective investigations.

OP-182

Predictive and prognostic value of left ventricular mechanical dyssynchrony assessed by myocardial perfusion SPECT in asymptomatic patients under hemodialysis

F. Caobelli[1], C. Popescu[2], R. Laudicella[3], A. Comis[3], S. A. Pignata[3], R. Sara[2], C. Rossetti[4], Young AIMN Working Group; [1]University Hospital Basel, Basel, SWITZERLAND, [2]Niguarda Hospital, Milan, ITALY, [3]University of Messina, Messina, ITALY, [4]Niguarda Hospital, Milano, ITALY.

Introduction: Patients with end-stage kidney disease under hemodialysis have an increased risk of adverse cardio-cerebrovascular events. In these patients, myocardial perfusion scintigraphy (MPS) provides useful prognostic information at short-term follow-up. Left ventricular mechanical dyssynchrony (LVMD) has been proven to predict the onset of major adverse cardiac events (MACEs) at short-time follow-up in patients with chronic kidney disease. It remains unclear, whether the same prognostic value pertains also to patients under hemodialysis at longer follow-up. **Subjects & Methods:** Seventy patients under hemodialysis (duration range 1-8 years) with neither history nor symptoms of coronary artery disease (CAD) at the time of MPS were retrospectively evaluated. All underwent clinical evaluation and MPS with pharmacologic stress test with dipyridamole. MPS were reprocessed to derive LV ejection fraction (EF), perfusion scores (SSS and SDS), and LVMD [phase histogram bandwidth (PHB) and phase standard deviation (PSD)]. MACEs were assessed at ≥2-year follow-up (median 29 months) and defined as nonfatal myocardial infarction, hospitalisation due to cardiac symptoms, new developed ischaemia or coronary revascularisation. Statistical analysis was performed using univariate and multivariate analysis on clinical and scintigraphic data. The rate of MACEs was evaluated with Kaplan-Meyer curves and Log-Rank test. **Results:** MACEs were reported in 8 patients (11.4%). Two of 8 had a myocardial infarction and 6 of 8 underwent coronary revascularisation. At univariate analysis, a correlation was demonstrated between MACEs and PSD (p=0.02), PHB (p=0.01) and the presence of peripheral artery disease (p=0.04). At multivariate analysis, only PSD and PHB were proven independent predictors of MACEs (p=0.03 and 0.001, respectively). At survival analysis, patients with abnormal values of PSD (and PHB had a significantly shorter event-free survival (for PSD - Odd Ratio [OR] 16.8, 95% confidence interval (CI) 3.3 - 84.5, p<0.001; for PHB - OR 5.4, 95% CI 1.2 - 24.6, p=0.03, fig. 1). Perfusion scores were not proven to be predictors of the onset of MACEs (p=0.18 for SSS and p=0.20 for SDS, respec-

tively). **Conclusions:** In asymptomatic patients without known CAD under hemodialysis, LVMD is highly predictive of the onset of MACEs at ≥2-year follow-up. As perfusion scores failed to show a predictive value, a phase analysis on gated MPS should be routinely performed in these patients, in order to yield useful prognostic information.

| 509 | Sunday, October 22, 2017, 16:30 - 18:00, Hall G1 |

Neurosciences: Imaging Neurotransmission Systems in Parkinson

OP-183

Comparisons of glucose metabolism and striatal DAT binding in PD patients with different subtypes

L. Li[1], *C. Jiang*[1], *P. Wu*[1], *J. Zhao*[2], *C. Zuo*[1]; [1]PET Center, Huashan Hospital ,Fudan University, Shanghai, CHINA, [2]Department of Neurology, Huashan Hospital ,Fudan University, Shanghai, CHINA.

Aim: Parkinson's disease (PD) is characterized by loss of dopamine transporter (DAT) and a unique metabolic brain network (PDRP). The tremor-dominant subtype (TD) differs from the akinetic-rigid (AR) subtype of PD in clinical course and prognosis. The pathophysiology mechanism underlying these differences remains largely unknown. This study investigated the differences in glucose metabolic activity and striatal dopamine transporter (DAT) distribution between the two subtypes. **Materials and Methods**: Resting-state 18F-FDG PET imaging was performed in 136 patients with PD (including age and non-tremor scores-matched 75 AR-PD and 61 TD-PD) and 32 age-matched healthy controls. Among them, 100 PD patients (including age and non-tremor scores-matched 41 TD-PD and 59 AR-PD) and 17 age-matched healthy controls performed 11C-CFT PET imaging at the same time. For each 11C-CFT PET scan, sub-regional DAT binding was calculated for each hemisphere by the striatal-to-occipital ratio, defined as (striatum-occipital)/occipital counts, and these values were averaged across hemispheres. The expression of PD-related pattern (PDRP) was computed in each subject using a voxel-based network quantification algorithm based on the PDRP we previously identified in a cohort of 33 PD patients and 33 healthy controls. Comparison of regional metabolism was made on a voxel basis using SPM analysis, for which the scans from the PD patients with predominantly left-sided symptoms were flipped so that all subjects had the left hemispheres of the brain as their most affected side. Then a 4-mm radius spherical voxel of interest (VOI) centered at the peak voxel of clusters that was significant in the SPM analysis above was conducted to quantify regional cerebral metabolic rate of glucose (rCMRglc). Pearson correlation analysis was used to determine the relationship between rCMRglc and rest tremor scores. **Results:** The difference in 11C-CFT binding and PDRP scores between the TD-PD and AR-PD groups didn't show the significance by two-sample t test. Compared with AR-PD patients, TD-PD showed increased metabolism in bilateral cerebellum and left postcentral gyrus, and decreased metabolism in left medial frontal gyrus, left superior frontal gyrus and left cingulate gyrus. The rCMRglc in cerebellum demonstrated a positive correlation with rest tremor scores in TD-PD patients (P<0.05). **Conclusions:** The metabolism changes in cerebellum are related to rest tremor in PD, which maybe a clue to investigate the mechanism of tremor.

OP-184

Role of an artificial neural network classifier, a classification tree (CIT), to diagnose Parkinson's disease in early phase by using 123I-FP-CIT brain SPECT data

B. Palumbo[1], *A. Santonicola*[1], *S. Cascianelli*[2], *S. Nuvoli*[3], *M. L. Fravolini*[2], *M. Minestrini*[1], *M. Scialpi*[4], *N. Tambasco*[5], *A. Spanu*[3], *G. Madeddu*[3]; [1]Univ. of Perugia-Dept. of Surgical and Biomed. Sciences-Section of Nuclear Medicine, PERUGIA, ITALY, [2]Univ. of Perugia-Dept. of Engineering, PERUGIA, ITALY, [3]Univ. of Sassari-Dept. of Clinical and Experimental Medicine- Section of Nuclear Medicine, SASSARI, ITALY, [4]Univ. of Perugia-Dept. of Surgical and Biomed. Sciences- Section of Diagnostic Imaging, PERUGIA, ITALY, [5]Unit of Neurology- Perugia University Hospital, PERUGIA, ITALY.

Aim: To diagnose Parkinson's disease (PD) in early stage, we applied an artificial neural network classifier, a classification tree (CIT), that is composed of a set of logical rules organized as a decision tree to produce an optimized threshold based classification of data, to provide discriminative cut-off values. We applied a CIT to 123I-FP-CIT brain SPECT semiquantitave data, to obtain cut-off values of radiopharmaceutical uptake ratios in basal ganglia with the aim to classify PD versus other conditions. **Methods:** 123I-FP-CIT brain SPECT (Millenium VG, G.E.M.S.) was performed using semiquantitative analysis with Basal Ganglia (BasGan) V2 software according to EANM guidelines in 172 patients with mild movement disorders; 105 out of the 172 resulted as PD [56M and 49 F; range of age: 60-83 yrs, Hoehn and Yahr score (HY): 0.5-1.5; Unified Parkinson Disease Rating Scale (UPDRS) score: 6-38] and 67 resulted as non-PD (Essential Tremor and drug-induced PD, 33 M and 34 F; range of age 60-82 yrs). The final diagnosis was confirmed by a clinical follow-up of at least 6 months. A 10-fold cross validation was applied by repeating 1000 random experiments. This allowed the statistical evaluation of the "average performance" of CIT. **Results:** The probability of correct classification in patients obtained by CIT was 85.18±11.91% (mean±SD) for PD and 93.34±6.54%.% for non-PD patients. According to CIT, the first decision rule gave a value for the right putamen (RP) of 2.35±0.16, thus meaning that if RP values were lower than 2.35 patients were classified as PD, while if RP values were higher than 2.35 patients were classified as non-PD. To complete the classification performance, more complex CIT structures were tested, including also caudate nuclei and left putamen values as features, but they resulted as less significant. **Conclusion:** CIT allowed to accurately identify PD patients in early phase by using 123I-FP-CIT brain SPECT data and provided also reliable cut-off values able to classify PD and non-PD subjects. RP uptake values were the most discriminant and significant, probably due to a certain number of patients with initial prevalence of left clinical symptoms.

OP-185

Comparison of machine learning and semi-quantification approaches for DaTSCAN classification

J. Taylor; Sheffield Teaching Hospitals, Sheffield, UNITED KINGDOM.

Introduction: Semi-quantification and subsequent comparison with normal ranges is used routinely for objective [123I] FP-CIT (DaTSCAN) analysis. This approach is recommended by EANM clinical guidelines. Recent research has suggested that machine learning tools may be more accurate than conventional semi-quantification methods in binary image classification of DaTSCAN images into diseased or healthy groups. However, direct comparison between techniques is lacking. The aim of this study was to: • Compare the classification performance of 3 established machine learning approaches and 3 conventional semi-quantification methods using data from the Parkinson's Progressive Biomarkers Initiative (PPMI) database **Methods:** Images from 209 healthy controls and 448 patients with Parkinson's Disease were downloaded from the PPMI website (www.ppmi-info.org/data). **Machine learning algorithms:** A Support Vector Machine classifier was separately trained with three different sets of image features: 1) Image pixel intensities 2) Principal components of image pixel intensities 3) Striatal binding ratios (SBRs) from the putamen and caudate. Both linear and non-linear classifiers (using a radial basis function kernel) were considered. **Semi-quantification algorithms:** SBRs in the left and right putamen only were considered. Images with SBR results below normal limits, on either side of the brain, were classified as abnormal. Limits were set based on 3 different methods: 1) Linear regression of control data against patient age (95% confidence interval) 2) Mean of SBR results for age-matched controls (+/- 5 years, 95% confidence interval). 3) Minimum of SBR results for age-matched controls (+/- 5 years). Each machine learning and semi-quantification technique was evaluated using 5 fold cross-validation, repeated 5 times. **Results:** For the machine learning algorithms, the maximum mean accuracy using image pixels as features was: 0.96 (+/-0.01), using principal components as features was: 0.97 (+/-0.01) and using SBRs as features was: 0.96 (+/-0.02). For the semi-quantification methods mean accuracy using limits based on linear regression was: 0.94 (+/-0.02), using mean SBR was: 0.93 (+/-0.02) and using minimum SBR was: 0.90 (+/-0.03). **Conclusion:** This study provides evidence of the superior performance associated with machine learning algorithms, as compared to conventional semi-quantification analysis for binary classification of DaTSCANs.

OP-186

Abnormal striatal DAT distribution and PDRP expression in patients with rapid-eye-movement sleep behavior disorder

P. Wu[1], C. Jiang[1], L. Li[1], J. Ge[1], H. Yu[2], J. Wu[2], C. Zuo[1]; [1]PET Center, Huashan Hospital, Fudan University, Shanghai, CHINA, [2]Department of Neurology, Huashan Hospital, Fudan University, Shanghai, CHINA.

Objective: Rapid-eye-movement sleep behavior disorder (RBD) is an important risk factor for synucleinopathies such as Parkinson's disease (PD) which is characterized by loss of dopamine transporter (DAT) and a unique metabolic brain network (PDRP). This study investigated the striatal dopamine transporter (DAT) distribution characteristics and cerebral glucose metabolism features in patients with RBD and compared these imaging measures with those in patients with PD. **Methods:** Age-matched 30 healthy controls, 37 polysomnogram-confirmed RBD patients and 87 PD patients with different severity (Hoehn-Yahr (H-Y) stage I: 23 cases, H-Y II: 44 cases, H-Y III~V: 20 cases) were recruited to perform ^{11}C-CFT and ^{18}F-FDG PET imaging at the same time. For each ^{11}C-CFT PET scan, sub-regional DAT binding was calculated for each hemisphere by the striatal-to-occipital ratio, defined as (striatum-occipital)/occipital counts, and these values were averaged across hemispheres. The expression of PD-related pattern (PDRP) was computed in each subject using a voxel-based network quantification algorithm based on the PDRP we previously identified in a cohort of 33 PD patients and 33 healthy controls. **Results:** DAT distribution in caudate, anterior and posterior putamen in RBD and PD group were significantly lower than healthy controls (P<0.001). Similar with that in PD, the striatal DAT decrease followed an antero-posterior gradient in RBD. Using the Mean-2SD of healthy controls as cut-off value, RBD patients were divided into RBD with normal uptake (RBD-N) group (19 cases) and RBD with abnormal uptake (RBD-Ab) group (18 cases). The striatal DAT distribution gradually decreased along the groups of healthy controls, RBD-N, RBD-Ab, PD at H-Y I, H-Y II and H-Y III~V. In contrast, PDRP expression in RBD and PD group were significantly higher than healthy controls (P<0.001) and gradually increased along the groups of healthy controls, RBD-N, RBD-Ab, PD at H-Y I, H-Y II and H-Y III~V. **Conclusion** RBD patients present an intermediate state in striatal DAT distribution and cerebral glucose metabolism between PD and healthy controls, which demonstrates that RBD is the predromal stage of PD. Decreased DAT distribution is accompanied by increased PDRP expression from RBD to PD, which deserves further study for useful biomarkers of early diagnosis of PD.

OP-187

Striatal and extra-striatal F-Dopa PET binding potential index related to age, gender, smoker status and Carbidopa premedication

S. Toch[1], S. Poussier[1], E. Micard[1], P. Marie[1], E. Guedj[2], A. Verger[1]; [1]CHU Nancy, Nancy, FRANCE, [2]Assistance Publique des Hôpitaux de Marseille, Marseille, FRANCE.

Introduction: ^{18}F-FDOPA Positron Emission Tomography (PET) has been approved to assess the integrity of the striatal dopaminergic system in Parkinson's disease. The purpose of this study was to evaluate ^{18}F-FDOPA PET striatal and extra-striatal uptake changes related to age, gender and Carbidopa premedication. **Methods:** One-hundred and ninety-eight any known neurodegenerative nor neuro-oncologic disorder patients, who performed a whole body ^{18}F-FDOPA PET among which 21 with Car-

bidopa premedication, were retrospectively included. Cerebral images acquired 90 minutes after 4 MBq/Kg of radiotracer injection were extracted from these whole-body PET. SPM analysis was performed using an adaptive template derived from the 198 patients included and available in this article. Then, striatal Binding Potential Index (BPI) were calculated, using the occipital cortex as reference. **Results:** An age-related decrease uptake in diffuse cortical areas and an increase uptake in occipital cortex and cerebellum were found (p=0.05, FWE). Patients with Carbidopa premedication showed a significant lower putamen BPI compared to patients without Carbidopa premedication (p<0.03). Then, considering patients without Carbidopa premedication, women presented a lower left putamen BPI than men (p=0.02). Furthermore, an age-related ^{18}F-FDOPA BPI decrease in caudate nucleus (p<0.02), and a constant age-related ^{18}F-FDOPA BPI increase in putamen (p<0.01) was observed. **Conclusion:** Changes in dopaminergic system are associated with age including striatal and extra-striatal modifications likely due to atrophy phenomenon. Carbidopa premedication is not associated with a better striatum BPI.

OP-188

Validation of a reliable and convenient PET protocol for striatal dopaminergic dysfunction imaging using ^{18}F-LBT-999

N. Arlicot[1,2,3], J. Vercouillie[1,2,3], K. Mondon[1,3], V. Gissot[1,2], S. Maia[1,3], L. Barantin[1,2,3], Y. Peltier[2,3], J. Cottier[1,2,3], J. Houeto[4], J. Deloye[5], D. Guilloteau[1,2,3], M. Ribeiro[1,2,3]; [1]Centre Hospitalier Universitaire, Tours, FRANCE, [2]Université François Rabelais, Tours, FRANCE, [3]UMR U930 "Imaging and Brain", Tours, FRANCE, [4]Centre Hospitalier Universitaire, Poitiers, FRANCE, [5]Laboratoires Cyclopharma, Clermont-Ferrand, FRANCE.

Purpose: Parkinson's disease (PD) and Lewy body dementia (LBD) are characterized by a degeneration of the presynaptic dopaminergic neurons. Tropane derivatives are well established ^{123}I-ligands for SPECT imaging of the presynaptic neuronal dopamine transporter (DAT). Nevertheless, DAT SPECT studies present some drawbacks and many efforts have been made to develop PET analogs either labelled with C-11 or F-18. We report here the results of the first human study using a new DAT PET radioligand labelled with fluorine 18, the ^{18}F-LBT-999. **Subjects & Methods:** Six PD patients (age: 69±7 y, Hoehn and Yahr stage: I-II) and 8 controls (age: 69±9 y) were enrolled. 90-min dynamic PET acquisitions after iv injection of ^{18}F-LBT-999 (3.6 MBq/kg) were performed. Venous samples were concomitantly obtained for metabolites analysis. Caudate nucleus (Cd), putamen (Pu) and cerebellum regions of interest (ROI) were defined over each T1 3D MRI. Binding potential (BP) using SRTM method and ratios obtained for a 10-min image acquired between 30 and 40 min pi were calculated for Cd and Pu with cerebellum as reference region. **Results:** No adverse events or clinically detectable pharmacologic effects were reported. The parent fraction of ^{18}F-LBT-999 in plasma was 80%, 60% and 40% at 15, 30 and 45 min pi, respectively. For control group, the values were for BP 6.30±1.17 and 6.75±1.17 and for ratios 5.01±0.68 and 5.40±0.73,

for Cd and Pu, respectively. For PD group, the mean±SD BP values were 3.97±1.32 and 2.72±1.51, and the ratios 3.76±0.82 and 3.12±0.80, for Cd and Pu, respectively. For both striatal structures, BP and ratios were significantly decreased for PD patients compared to control group (*p*<0.001). **Conclusion:** These kinetics and tracer metabolism parameters, obtained from a small group of subjects, indicated that a 10-min PET acquisition, between 30 and 40 min pi of ^{18}F-LBT-999, associated to a subsequent analysis using simple ratios between striatal nuclei and cerebellum, is reliable for DAT PET imaging in the brain, allowing excellent discrimination between early PD patients and healthy controls. Such imaging procedure with ^{18}F-LBT-999 might be convenient considering its translation into clinical routine. **Acknowledgments:** This study was supported by the French National Agency for Research ("Investissements d'Avenir" no. ANR-11-LABX-0018-01), IRON and by Cyclopharma Laboratories. We thank the technical of CERRP, the nursing staff of the Service de Médecine Nucléaire, and the CIC-IT, CHRU of Tours, for their assistance.

OP-189

Validation of (S,S)-[11C]-Methylreboxetine Positron Emission Tomography in Parkinson's Disease

J. Brumberg, J. Tran-Gia, C. Kesenheimer, G. Brandt, C. Lapa, J. Volkmann, A. Buck, S. Samnick, I. U. Isaias; University Hospital Würzburg, Würzburg, GERMANY.

Purpose: To evaluate the feasibility of (S,S)-[11C]-Methylreboxetine (MRB) PET for evaluation of noradrenergic brain networks in patients with Parkinson's disease (PD). We (i) performed a phantom study, (ii) estimated binding potentials using a two-parameter multilinear reference tissue model (MRTM2), and (iii) assessed the influence of demographic and clinical parameters on first in patient scans. **Subjects and Methods:** We investigated eight men and two women with idiopathic PD (age: 60.5±6.3 years; disease duration: 4.4±4.2 years; H&Y: 1-3 stage; levodopa-equivalent daily dose (LEDD): 506±181mg) in medication-off condition (12h washout of antiparkinson medication). All subjects performed a MRI and a dynamic MRB-PET scan of 120min duration. In one instance, a 100-ml phantom filled with MRB-water-solution was placed inside the scanner to observe the noise characteristics of the PET imaging protocol. PET images were motion-corrected and co-registered to the individual's MRI images. After MRI-based normalization, several cortical and subcortical volumes of interest (VOI) were defined and transformed to the individual's PET space. VOI-specific time-activity curves were generated for scan durations of 40, 60, 80 and 100min (starting at t*=20min). MRTM2 served to calculate time-dependent non-displaceable binding potential (BP_{ND}) estimates of selected brain regions. Linear regression analysis was used to explore the association between BP_{ND} estimates with different scan durations and Spearman's rho to describe the correlation of BP_{ND} with demographic and clinical parameters. **Results:** The phantom study revealed a decay-induced coefficient of variance >20% for a scan-time of 120min, suggesting a trade-off between an adequate time coverage of the bioki-

netics and the minimization of the noise enhancement induced by later time points. Regional 80min BP_{ND} estimates exhibited a significant linear correlation with 60min BP_{ND} (R^2=0.90, p<0.001) and 100/40min BP_{ND} (R^2=0.74/0.72, p<0.001). Thalamic (p<0.01) and brainstem BP_{ND} (p<0.05) showed a negative correlation at 100, 80 and 60min scan duration with age only. **Conclusion:** Our results indicate that a 60min acquisition from 20 to 80min p.i. yields reliable estimates of BP_{ND} of MRB in PD patients. A reduction in scan duration greatly facilitates the use of this ligand in patients with advanced PD, which are unable to endure a two-hour acquisition. Also of relevance, we did not find any effect of the dose of dopaminergic medication (i.e. LEDD) on MRB binding.

OP-190

PET imaging of mGluR5 with [18F]FPEB in Parkinson's disease

Y. Kang[1], B. He[1], A. Verma[2], C. Henchcliffe[1], P. J. Kothari[1], D. Schlyer[1], K. Schmidt[2], P. C. Chiao[2], S. Vallabhajosula[1], P. D. Mozley[1]; [1]Weill Cornell Medicine, New York, NY, UNITED STATES OF AMERICA, [2]Biogen Idec, Inc., Cambridge, MA, UNITED STATES OF AMERICA.

Objective: The interaction between receptor systems is an area of intense interest for the development of new therapeutic drugs and the metabotropic glutamate receptor type 5 (mGluR5) is a potentially important regulator of the most common excitatory neurotransmitter system in the brain. The objective of this study was to explore the possibility of a correlation between mGluR5 and Parkinson's disease using the selective mGluR5 PET probe [18F]-FPEB. This is the first known imaging study of its role in Parkinson's disease (PD) in humans and we compared patients to matched healthy volunteers (HVs). **Methods:** The sample consisted of 9 patients with PD and 8 HVs. Dynamic images of the brain were acquired after the IV administration of ~183±13 MBq (~5 mCi) of [18F]-FPEB. Regions of interest (ROI) were placed with FreeSurfer on contemporaneously acquired MRI scans for the following regions: thalamus, caudate, putamen, hippocampus and amygdala. For comparison between PD patients and HVs, non-displaceable binding potential (BP_{ND}) values were calculated by the Logan reference tissue model using cerebellum white matter as the reference region. **Results:** With [18F]-FPEB, in overall brain regions, PD patients showed higher BP_{ND} values than HVs. In regional analysis, while PD patients did not show a significant difference with HVs in the caudate (9% enhancement, p=0.51), we found a significant enhancement of binding in the putamen (22% enhancement, p=0.05). In addition, hippocampus showed high enhancement but slightly less statistical significance was found (21% enhancement, p=0.06). Studies of dopamine transporter binding potential carried out on these same subjects using [11C]-PE2i showed a significant reduction in putamen (66% reduction, p<0.001) and caudate (49% reduction, p<0.001). **Conclusion:** The significant enhancement of binding of the radiotracer in the Parkinson patients when compared to the healthy controls indicate that the response to dopaminergic denervation in Parkinson's disease is mediated in part by the mGluR5 system.

Conventional & Specialised Nuclear Medicine: Paediatrics

OP-191

Comparison of FDG PET/MRI and FDG PET/CT in Pediatric Oncology: Gazi University Pediatric PET/MRI Experience

L. Ö. Atay Kapucu[1], L. Uslu Beşli[2], Ü. Ö. Akdemir[1], U. Aydos[1], M. Özçelik[1], F. G. Pınarlı[3], A. Okur[3], N. I. Karabacak[1], C. Karadeniz[3]; [1]Gazi University Medical Faculty, Department of Nuclear Medicine, Ankara, TURKEY, [2]Istanbul University Cerrahpaşa Medical Faculty, Department of Nuclear Medicine, Istanbul, TURKEY, [3]Gazi University Medical Faculty, Department of Pediatric Oncology, Ankara, TURKEY.

Aim: Pediatric patients are one of the most important indications for FDG PET/MRI, due to reduced ionizing radiation. The aim of our study is to compare FDG PET/MRI and FDG PET/CT in terms of anatomical correlation of FDG positive lesions. **Materials and Methods:** Among 47 pediatric oncology patients, that have been referred to our department for FDG PET imaging, total 34 patients (mean age: 10,6±4,4), who had both PET/MRI and PET/CT imaging performed sequentially on the same day, and/or who had additional diffusion weighted MRI images were included in our study. Following mean 3,0±1,6 mCi (111±59 MBq) iv FDG injection, PET/CT imaging (GE Discovery ST) was performed first to 25 patients in median 73 minutes and PET/MRI (GE Signa PET/MRI) was performed first in the remaining 5. Sequential PET/MRI and PET/CT imaging was performed to total 30 patients. In addition to routine T1 weighted (T1W) and T2 weighted (T2W) imaging, diffusion weighted imaging (DWI) and ADC mapping were obtained in 16 patients. Anatomical evaluation and correlation of all FDG positive lesions were performed by 2 nuclear medicine physicians separately (scoring scale:1-3, 1: negative, 2: indeterminate, 3: positive). **Results:** Sixteen sequential PET/MRI and PET/CT images were FDG negative concordantly. Total 47 FDG positive lesions (maximum 5 lesions/patient) were found in the remaining 18 sequential PET/MRI and PET/CT images; 37 of them (78,7%) were positive with CT and 46 (97,9%) were positive with at least one MRI sequence. Out of 11 discordant FDG positive lesions, 10 (2 central nervous system (CNS), 4 bone marrow, 2 lymph nodes, 2 soft tissue lesions) could not be differentiated using CT although it could be demarcated using MRI. When T1W, T2W and DWI images were evaluated separately for all FDG positive lesions, 88,6% (39/44) of the lesions were positive with T1W, 88,9% (40/45) were positive with T2W and 96,9% (31/32) were positive with DWI. Among 16 PET/MRI images with additional DWI sequences, no correlation was found between ADC and SUV values, although FDG positive lesions showed diffusion restriction on visual analysis. **Conclusions:** PET/MRI showed better anatomical correlation in FDG positive lesions compared to PET/CT in our pediatric patients. When lesions were separately evaluated, PET/MRI had better anatomical correlation in bone marrow lesions, CNS tumors, lymph nodes and soft tissue mass. Due to reduced ion-

izing radiation and better contrast resolution in soft tissue and bone marrow, FDG PET/MRI could be preferred to PET/CT in the pediatric population.

OP-192

Positive & negative predictive value of FDG PET/CT in pre-therapy assessment of Bone Marrow infiltration in pediatric lymphoma patients

M. A. Abdelwahab[1], S. A. Badr[1], M. H. Kotb[1], H. Mostafa[2]; [1]National Cancer Institute, Giza, EGYPT, [2]NEMROCK, Cairo University., Giza, EGYPT.

Objectives: to explore the Positive and negative predictive value of FDG PET/CT in assessment of bone marrow infiltration in pediatric lymphoma patient at presentation. **Methods:** 140 pediatric patients with pathologically proven lymphoma [113 Hodgkin's disease (HD), 27 non- Hodgkin's lymphoma (NHL)] were enrolled in this study. All patients had pre-therapy FDG PET/CT and bone marrow biopsy within duration not exceeding two weeks. Clinico-pathological and other radiological data were extracted from patients' files. **Results:** Among the 140 lymphoma patients FDG PET/CT revealed positive BM involvement in 41 patients with two of them were false positive with negative BMB & regional MRI results. PPV was 95.1 % for PET/CT compared to 100 % with BMB. On the other hand None of patient has positive BMI by BMB & negative FDG PET/CT for BM infiltration, on the contrary the BMB missed 25 (17.9 %) patients with statistically significant difference as regards the NPV that was 100 % with PET/CT compared to 80.2 % with BMB (P<0.05). FDG PET-CT upstaged 17.9 % of the enrolled patients. **Conclusion:** FDG PET/CT seemed to be a promising modality with optimum Negative predictive value in assessment of BMI at initial assessment of pediatric lymphoma. Also, its high sensitivity has appreciable role in upstaging cases missed with BMB.

OP-193

Grading and outcome prediction of pediatric diffuse astrocytic tumors with diffusion and arterial spin labeling perfusion MRI in comparison with 18F-DOPA PET Grading and outcome prediction of pediatric diffuse astrocytic tumors with diffusion and arterial spin labeling perfusion MRI in comparison with 18F-DOPA PET

G. Bottoni[1], D. Tortora[2], A. Piccardo[1], M. Puntoni[3], M. Severino[2], P. Nozza[2], S. Mascelli[2], A. Raso[2], A. Verrico[2], M. Garrè[2], A. Rossi[2], G. Morana[2]; [1]E.O. Ospedali Galliera, Genia, ITALY, [2]Istituto G. Gaslini, Genova, ITALY, [3]E.O. Ospedali Galliera, Genova, ITALY.

Introduction: The aim of this study was to investigate MRI derived diffusion weighted imaging (DWI) and arterial spin labeling (ASL) perfusion imaging in comparison with ^{18}F-dihydroxyphenylalanine (DOPA) PET with respect to diagnostic performance in tumor grading and outcome prediction in pediatric patients with diffuse astrocytic tumors (DAT). **Methods:** We retrospectively analyzed 26 pediatric patients with histologically proven treatment naïve low and high grade DAT who under-

went ASL and DWI performed within 2 weeks of ^{18}F-DOPA PET. Relative ASL cerebral blood flow max (rCBF max) and minimum apparent diffusion coefficient (rADC min) were compared with ^{18}F-DOPA uptake Tumor/Normal tissue (T/N) and Tumor/Striatum (T/S) ratios, and correlated with WHO tumor grade and progression-free survival (PFS). Statistics included Pearson's chi-square and Mann-Whitney U tests, Spearman's rank correlation, receiver operating characteristic (ROC) analysis, discriminant function analysis (DFA), Kaplan-Meier survival curve and Cox analysis. **Results:** ASL, DWI and ^{18}F-DOPA PET data were positively correlated. Significant differences in terms of rCBF max, rADC min and ^{18}F-DOPA uptake were found between low- and high-grade DAT (p≤0.001). ROC and DFA demonstrated that T/S and T/N values were the best parameters for predicting tumor progression (AUC 0.93, p<0.001). On univariate analysis all diagnostic tools correlated with PFS (p≤0.001), however on multivariate analysis, only ^{18}F-DOPA uptake persisted to be significantly associated with outcome (p≤0.03); a trend emerged for CBF max (p=0.09) and ADC min (p=0.08). The combination of MRI and PET data increased the predictive power for prognosticating tumor progression (AUC 0.97, p<0.001). **Conclusions:** DWI and ASL provide useful and complementary information to ^{18}F-DOPA PET for pediatric DAT grading. ^{18}F-DOPA PET parameters better correlate with progression free survival prediction. Combining MRI and PET data provides the highest predictive power for prognosticating tumor progression.

OP-194

FDG PET in response evaluation of bulky masses in paediatric Hodgkin Lymphoma patients enrolled in the Italian AIEOP LH2004 trial

E. Lopci[1], M. Mascarin[2], A. Piccardo[3], C. Elia[2], L. Guerra[4], E. Borsatti[2], A. Sala[4], A. Todisco[5], A. Todisco[5], P. Zucchetta[5], P. Farruggia[6], A. Cistaro[7], S. Buffardi[8], P. Bertolini[9], M. Bianchi[10], M. Moleti[11], F. Bunkheila[12], P. Indolfi[13], A. Garaventa[14], R. Burnelli[15]; [1]Humanitas Clinical and Research Hospital, Milano, ITALY, [2]Centro di Riferimento Oncologico, Aviano, Aviano, Pordenone, ITALY, [3]Galliera Hospital, Genova, ITALY, [4]Hospital San Gerardo, Monza, ITALY, [5]University Hospital, Padova, Padova, ITALY, [6]Ospedale dei Bambini, Palermo, Palermo, ITALY, [7]IRMET, Torino, Torino, ITALY, [8]Napoli – Pausillipon, Napoli, ITALY, [9]Azienda Ospedaliera, Parma, ITALY, [10]Regina Margherita, Torino, ITALY, [11]Università La Sapienza, Roma, ITALY, [12]Hospital San Salvatore, Pesaro, ITALY, [13]Napoli – 2° Università, Napoli, ITALY, [14]Gaslini Hospital, Genova, ITALY, [15]University Hospital S. Anna, Ferra, ITALY.

Aim: In the current report we illustrate the results concerning the role of FDG PET in response evaluation of bulky masses in paediatric Hodgkin's Lymphoma (HL) patients enrolled in the Italian AIEOP LH2004 trial. **Materials and Methods:** We analysed data derived from 703 patients (M:F=388:315; mean age 13 years) affected by HL and enrolled in 41 different Italian Centres from March 2004 till September 2012, all applying to the AIEOP-LH2004 protocol. The cohort comprised 309 patients with bulky masses, of which 238 were evaluated with FDG PET at baseline and after 4 cycles of chemotherapy. Response was determined

according to combined functional and morphological criteria. Patients were followed up for a mean period of 43 months and for each child we calculated time-to-progression (TTP), considering as reference standard clinical monitoring, instrumental and histological data. Statistical analyses were performed for FDG PET and morphological response with respect to TTP. **Results:** Overall, at response evaluation we defined 238 PET-negative (90.5%) and 25 PET-positive bulky masses (9.5%), which on log rank analysis showed a statistically significant difference in terms of TTP (p<0.0001): mean TTP of 32.67months for negative scans versus 23.8 months for positive cases. In the same cohort, the morphological response on CT showed a CR in 85 patients (32.3%), a PD in 6 patients (2.3%) and a PR in 165 cases (62.7%), which on log rank analysis for TTP resulted statistically significant: 31.1 months for CR, 7.9 months for PD (p<0.001). When specifically analysing the role of PET in PR patients, the modality could distinguish patients having different TTP (p<0.0001): PET negative 34.9 months versus 24.6 months for PET positive. **Conclusions:** After 4 cycles of chemotherapy, FDG-PET response assessment in paediatric HL with bulky masses is a good predictor of TTP and disease outcome. Moreover, in patients presenting with a partial response on CT, PET results capable of differentiating patients having a longer TTP.

OP-195
Usefulness Of FDG-PET/CT In Assessing Bone And Bone Marrow Involvement In Pediatric Hodgkin Lymphoma

P. Guglielmo[1], C. Dolci[2], A. Sala[3], M. Spinelli[3], F. Elisei[4], E. Turolla[5], C. Crivellaro[1], C. Landoni[1], L. Guerra[4]; [1]University of Milan Bicocca, Milano, ITALY, [2]Fondazione Tecnomed, ASST Monza - Ospedale San Gerardo, Milano, ITALY, [3]Fondazione MBBM, Monza, ITALY, [4]ASST - Monza, Ospedale San Gerardo, Monza, ITALY, [5]Fondazione Tecnomed, ASST Monza - Ospedale San Gerardo, Monza, ITALY.

Purpose/Introduction: Hodgkin Lymphoma (HL) is a highly curable pediatric cancer. 18F-FDG PET/CT has increasingly been introduced into guidelines and in clinical routine for staging coupled with bone marrow biopsy (BMB) to detect Bone Marrow Involvement (BMI) and stage IV of the disease. Nevertheless, PET/CT has been shown to be a sensitive diagnostic procedure for bone and BMI detection and can be more accurate than BMB. The aim of the study was to analyze the usefulness of 18F-FDG PET/CT in the assessment of BMI in staging of pediatric HL. **Subjects & Methods**: thirty-eight patients (17 females), mean age of 14.2 years (range 7.7-17.9) with histological diagnosis of HL and unilaterally trephine BMB performed at staging, were retrospectively included in the study. PET/CT studies were reviewed by 2 readers in consensus and PET/CT was considered positive if a focal uptake higher than physiological bone marrow activity was evident. **Results**: 6/38 (15.7%) patients presented with focal uptake indicating BMI, 3/6 (50%) without bone lesions at CT, 2/6 (33%) with lytic bone lesions and 1/6 (17%) with sclerotic bone lesions. In 5/6 (83%) follow-up imaging (MRI, CT or plan radiography) confirmed PET findings of bone/bone marrow involvement. In one patient with multifocal bone marrow disease at PET/CT no followup imaging was performed. Conversely, trephine BMB was positive only in 1/6 (17%)

patient with multiple focal tracer uptake at PET correlated to sclerotic bone lesions at CT. On the other side, FDG-PET/CT did not miss any patient with positive BMB. **Conclusion**: FDG PET/CT is a reference standard in the staging of Hodgkin Lymphoma. The high sensitivity of FDG-PET/CT for bone and bone marrow involvement has recently raised the issue regarding the need of a BMB and currently BMB is not mandatory when a FDG-PET/CT is performed. Although, the current study needs to be extended to a more consistent patients population, the preliminary data confirmed that PET/CT can be a valid approach to detect bone/bone marrow disease and BMB can be spared in pediatric HL.

OP-196
The Role of FDG PET/CT Metabolic Parameters In Predicting Metastatic Disease In Pediatric Osteosarcoma Patients and The Prognostic Importance

A. K. Fidan, G. Ucmak, I. Kerimel, B. E. Akkas, B. B. Demirel; S.B.U. Ankara Oncology Research and Training Hospital, Nuclear Medicine Department, Ankara, TURKEY.

Aim: Osteosarcoma is the most frequent seen primary bone tumor in pediatric patients. Metastasis is usually seen at the time of diagnosis or during follow up period. The 5-year survival of patients with local disease is about 70%, where as in patients with metastatic disease, survive rates significantly decreases to 20%. FDG PET/CT is a reliable diagnostic tool which gives important information regarding the extent of disease as well as patient prognosis. In this retrospective study, we aimed to investigate the potential prognostic role of metabolic parameters such as standardized uptake value (SUVmax), metabolic tumor volume (MTV) and total lesion glycolysis (TLG) of primary tumor in predicting distant metastasis in patients with osteosarcoma. **Method:** 37 patients with osteosarcoma (age range: 6-19 years) who underwent FDG PET/CT for initial staging and were treated with neo-adjuvant chemotherapy and surgical resection in our hospital were included in this study. After a mean clinical follow-up period of 35 months (range:4-89 months), all patients are retrospectively grouped as patient with local disease (LD) and patients with metastatic disease (MD). SUVmax, MTV and TLG levels of the primary tumorat the time of staging, were analyzed for the correlation of progressive disease and metastasis. The probability of predicting metastatic disease is investigated with ROC analysis. The association between metabolic parameters of primary tumor and progression rate of disease is analyzed by Mann Whitney-U-test. **Results:** SUVmax, MTV and TLG were significantly higher in MD compared to LD group (13.4 ±5.5, 494±342 ml and 2480±2392 gr vs. 7.9±2.8, 147±81 ml and 526±242 gr respectively,p=0.001). The cut-off values for SUVmax, MTV and TLG were 9.67, 236.5 ml, 940.5 gr, respectively. In ROC analysis, areas under curve were 82% for SUVmax, 96% for MTV, 99% for TLG. When metabolic parameters were analyzed for disease progression, we observed that TLG of the primary tumor was the only significant metabolic parameter in predicting disease progression in patients with localized disease. **Conclusion:** The metabolic parameters of initial staging PET/CT can predict progressive metastatic disease on follow-up in pediatric

patients with osteosarcoma with high sensitivity. We found that patients with high TLG have increased risk for progression even with localized disease at the time of diagnosis. Therefore, we considered that high metabolic parameters are associated with poor prognosis and may guide clinical management.

OP-197

Argentinean experience with the use of PET CT 18F DOPA in patient with suspected congenital hyperinsulinism

M. J. Bastianello[1,2]; [1]Instituto Universitario CEMIC, CIUDAD DE BUENOS AIRES, ARGENTINA, [2]Universidad Nacional de San Martin, Bs. As., ARGENTINA.

Purpose: To describe our initial experience in the use of PET / CT with 18F-DOPA for the diagnosis and differentiation of Hyperinsulinism (HIC) with focal versus diffuse pattern uptake. **Material and Method:** We studied 17 patients with clinical suspicion of HIC by administering 18F-DOPA (4.2 MBq / kg body weight) and acquiring late and early images of the abdomen and pelvis. The equipment used was a PET / CT Gemini 64 TOF. The SUV was calculated on coronal sections in regions of greater uptake of the head, body and tail of the pancreas. The SUV was calculated in a region of the baseline pancreas considered as baseline (SUVr). The SUV ratio of each region on the SUVr was obtained. If the ratio was greater than 1.5, the corresponding region was considered pathological, considering the case as focal HIC. Diffuse HIC was considered in cases where the uptake was homogeneous but with an SUV greater than 3. Normal studies were considered diffuse with an SUV of less than 3. A total of 17 patients with a mean age of 30 months +/- 49 (range 1-68 months) were studied. Those who were under 36 months of age were anesthetized to perform the study .The diagnosis with histopathological analysis and / or clinical follow-up was confirm in all Cases. **Results:** The quantification of the images showed evidence of pathological uptake in different areas according to the patients: 7 Diffuse (41.1%), 8 Focal (47.0%) and 2 Normal (11.7%). The focal points were distributed as follows: head (41.2%), neck (5.9%) and tail (5.9%) of the total number of studies. Patients with focal uptake had a mean age of 53.7 +/- 63 months versus 10.4 +/- 10 months in patients with diffuse uptake. Two of the patients with diffuse uptake and three with focal uptake did not respond to diazoxide. The genetic pattern was obtained showing an adequate concordance with the PET / CT study. In patients with focal ICH, a high correlation was observed between the anatomical region visualized as hypercaptive in PET / CT with 18F-DOPA and the surgical and anatomopathological findings. **Conclusion:** PET / CT with 18F-DOPA has allowed us to implement the international algorithms for the diagnosis of HIC with a high surgical and anatomopathological correlation.

OP-198

Lymphoscintigraphic anomalies in children with Gorham's disease

M. Pizzoferro, M. F. Villani, A. Jenkner, I. Rana, D. Barbuti, M. C. Garganese; IRCCS Bambino Gesù Paediatric Hospital, Rome, ITALY.

Purpose: Gorham-stout disease (GSD) is a rare disorder characterized by proliferating lymphatic tissue and massive osteolysis. The lymphatic malformations can arise in any anatomic location and complications are relative to interested district. Lymphoscintigraphic imaging allows assessment of the lymphatic component in bone and soft tissues showing failure of the lymph-conducting system in involved body site. The aim of this study was to investigate lymphoscitigraphic imaging findings of a group of patient affected by GSD and to evaluate the role of lymphoscintigraphy to highlight the injury to the lymphatic system in GDS. **Subject and Methods:** Four patients with confirmed diagnosis of GSD were evaluated by lymphoscintigraphy. Lymphoscintigraphy was included in the context of an extensive clinical and imaging work-up. Lower limb lymphoscintigraphy was performed in all patients by planar (dynamic, static, whole-body acquisition) and SPECT imaging up to 24h, according to a standard protocol. SPECT/CT-RMN evaluation was also performed. In one patient with humeral involvement an additional upper limb lymphoscintigraphy was performed. **Results:** In our series of four patients (1F, 3M), we studied two children (4 months, 6 years) with recent GDS diagnosis and two patients (15, 24 years) with stable disease followed by infants. Both patients with recent diagnosis had an involvement of the spinal cord and previous chylothorax: lymphoscintigraphy showed recurrence of pleural effusion and tracer stasis in the paravertebral site. Patients of follow-up group had multiple interested districts: lymphoscintigraphy showed tracer accumulation in the pelvis (female patient) and in soft tissue of left arm (patient with humeral involvement). In all patients with the exception of the newborn, lymphoscintigraphy at 24h showed presence of tracer accumulation in abdomen, corresponding to intestinal loops by fusion imaging evaluation. **Conclusion:** Our experience suggests that lymphoscintigraphy should be considered as a valuable imaging modality to investigate patients with GDS allowing a whole-body lymphatic mapping. It can be easily performed in newborns, infants and young adults without pulmonary embolism risk (even in patients with chylothorax). Our results highlight a potential application of lymphoscintigraphy in GDS diagnostic work-up (basal evaluation of lymphatic function, early diagnosis of pleural effusion in progress) and in follow-up (clinical evolution of disease and therapy response assessment). Hybrid imaging improves interpretation of lymphoscintigraphy in patients with thorax/abdominal tracer accumulation, even in newborns. Abdominal tracer stasis is an abnormal finding that could represent a preclinical detection of visceral involvement in GDS patients but further studies are needed to confirm this preliminary result.

601	Monday, October 23, 2017, 08:00 - 09:30, Hall A

CME 5 - Radiopharmacy/Drug Development/ Radionuclide Therapy/SNMMI: Theranostics and Companion Drugs

OP-199

Theranostic Concepts, Exemplified on PSMA and CXCR4
H.-J. Wester; Technical University of Munich, Faculty of Chemistry and Faculty of Medicine, Munich, GERMANY.

OP-200

Development of Novel Theranostics

C. Cutler; Brookhaven National Laboratory, Upton, UNITED STATES OF AMERICA.

OP-201

Pretargeting in the Context of Theranostics and Companion Diagnostics

J. Barbet; Arronax GIP, Saint-Herblain, FRANCE.

602	Monday, October 23, 2017, 08:00 - 09:30, Hall B

Joint Symposium 5 - EANM/ESMI: Imaging Cardiac Remodelling Solutions

OP-202

Imaging Cardiac Metabolism with PET

A. Saraste; Turku PET Centre, Turku University Hospital and University of Turku, Turku, FINLAND.

OP-203

Imaging Cardiac Metabolism with MRI

J. Prompers; Biomedical NMR, Department of Biomedical Engineering, Eindhoven University of Technology, Eindhoven, NETHERLANDS.

OP-204

Imaging Cardiac Remodelling Using PET-MRI

C. Rischpler; Department of Nuclear Medicine, Technical University Munich, Munich, GERMANY.

OP-205

Imaging Cell Trafficking in the Heart

J. Thackeray; Department of Nuclear Medicine, Hannover Medical School, Hanover, GERMANY.

603	Monday, October 23, 2017, 08:00 - 09:30, Hall C

Technologist Oral Presentations 1

OP-206

Using an asymmetric energy window improves image quality in planar bone scans

J. F. Machado[1], S. K. Doshi[1], R. Smith[2], M. Evans[1], R. N. J. Graham[1], S. Redman[1], D. Little[1]; [1]Royal United Hospitals Bath, Bath, UNITED KINGDOM, [2]Auckland District Health Board, Auckland City Hospital, Auckland, NEW ZEALAND.

Purpose: Previous work has investigated the effectiveness of using an asymmetric energy window for planar bone scans using simulation (Ruddlesden et al, Medical Physics and Engineering Conference 2010) and phantom data (Ruddlesden et al, EANM annual congress 2011). These phantom studies concluded that the asymmetric window improved both the resolution and contrast-to-noise ratio when imaging objects with high scatter. The purpose of this study was to confirm this increased image quality in patients. **Method:** Ethical approval was given for this study. Each of n=58 patients had two scans: a standard scan using an energy window of 140keV ±10% and an asymmetric window of 140keV +10%, -7.5%, using dual-head gamma camera (Infinia Hawkeye, GE Healthcare). For each patient, three radiologists independently compared the two image sets and scored them as follows: 1: asymmetric better (clinically important); 2: asymmetric better (not clinically important); 3: neither preferred; 4: standard better (not clinically important); 5: standard better (clinically important). Scores from all radiologists were pooled. The following hypotheses were tested using the sign test: H0: scores of 1 or 2 are equally likely, compared to 4 or 5; H1: scores of 1 or 2 are either more or less likely than scores of 4 or 5. **Results:** The pooled counts of each of the scores were as follows: 1: 5 2: 88 3: 66 4: 15 5: 0 For the sign test, the scores of 3 (neither preferred) are not used; the test is whether the total of 93 scores of 1 or 2 (asymmetric preferred) is significantly different from the 15 scores of 4 or 5 (standard preferred). This resulted in p<0.00001. In 5 cases, the asymmetric window images were preferred with the difference being clinically important; there were no cases where the standard window was similarly preferred. **Conclusions:** This study has confirmed in patients the improvement in image quality suggested by the previous simulation and phantom studies. Using an asymmetric energy window resulted in images which were on average preferred by the radiologists, in some cases providing extra information which was judged to be clinically important.

OP-207

Semi-quantitative analysis in salivary glands scintigraphy: a contribution for technical validation

J. S. Vale[1], D. Neves[1,2], L. Pires[3], M. F. João[2], A. I. Ferrer[2], L. F. Metello[1,4]; [1]ESS – IPP, ATC & Curso Med. Nuclear, Rua Dr. Antonio Bernardino de Almeida, 400, 4200 – 072, Porto., Porto, PORTUGAL, [2]Diaton S.A. – Unidade de Leiria, Rua de Olhalvas, Pousos, 2400 Leiria. Portugal, Leiria, PORTUGAL, [3]Diaton S.A. – Unidade de Coimbra, Urb. Espírito Santo, Lote 2 Calçada do Gato 3000-199 Coimbra, Coimbra, PORTUGAL, [4]IsoPor-Azores, Dept. de Med. Nuclear e Imagiologia Molecular, Angra do Heroismo, I. Terceira – Azores. Portugal, Açores, PORTUGAL.

Introduction: The gold standard in Salivary Glands Scintigraphy (SGS) evaluation is visual analysis, with all that it implicates in terms of subjectivity and intra/extra personal variability. Combination of visual with semi-quantitative analysis (SQA) introduces an objective parameter and reduces variability. However, it is observed a lack of standardization in protocols and the inexistence of standard values to facilitate comparisons. **Aim:** It's aimed to define a protocol for SQA in SGS with the evaluation of two functional parameters: Radiopharmaceutical Uptake (UP) and Ejection Fraction (EF) after stimulation. Additionally, it tends to contribute for the establishment of reference values for UP in the Portuguese population. Background correction (BC) relevance has been assessed as well. **Subjects and Methods:** 33

patients (7 men and 26 women; mean age: 55.58±16.39 ranging from 26 to 80 years) were included in the study. 3 images were acquired p/patient (pre and post syringe and injection site) and a 25 minutes dynamic study (20seg/frame with stimulation at 20 minutes). Patients were fasting for 2 hours previously from the administration of 5-10 mCi of ^{99m}Tc. For SQA purposes, activity effectively administered were calculated. A composite image were generated from the maximum uptake frames. ROI's were delineated in all salivary glands and in the skull, for background correction and EF for each gland was calculated. **Results:** For parotid glands uptake, in patients considered normal by visual analysis (n=3) the mean uptake was 4.16±1.27 and 4.86±1.53% with and without BC respectively, In pathological cases (n=30) was 2.34±0.79 and 2.81±0.9. For submandibular glands, in patients considered normal (n=6), the mean uptake was 2.68±0.66 and 3.03±0.68 with and without BC and in pathological cases (n=27) was 1.60±0.67 and 1.96±0.74. For EF, in patients considered normal by visual analysis (n=30), mean EF was 64.87±10.35, 65.93±7.37, 50.20±9.97 and 51.93±8.83 for the right parotid, left parotid, right submandibular and left submandibular respectively. There was only one pathological case and the referred values were 25, 58, 21 and 16%. The remaining 2 patients were considered impossible to access, due to low uptake. **Conclusion:** SQA seems to be an objective and useful tool for in SGS interpretation. The UP values obtained confirm this statement as we can see that parotid and submandibular uptake is lower in pathological cases than in normal ones for all salivary glands. There is a considerable difference between data obtained with and without background correction enhancing the need of standardization of the protocol.

OP-208

Advanced method to reconstruct SPECT image from few number of projection data

Y. Yamaguchi[1], Y. Okura[2], M. Yamamoto[2]; [1]Hiroshima International University Graduate School, Higashihiroshima-shi, JAPAN, [2]Hiroshima International University, Higashihiroshima-shi, JAPAN.

Aim: SPECT images reconstructed from few number of projection data are deteriorated by several artifacts such as streak artifact in FBP or image distortion in OSEM. The aim of this study is to develop novel method for SPECT image reconstruction from few number of projection data where the image quality is equivalent to SPECT image reconstructed from normal number of projection data to shorten acquisition time of SPECT study. **Methods:** Projection data of 24 view (15-degree step) of IB-10 brain phantom with ^{99m}Tc and Shepp-Logan numerical phantom were acquired by GCA-7200(Toshiba, Japan). Projection dataset of 12 view (30-degrees) were extracted from the 24 view datasets. We developed image reconstruction method using interpolation in the sinogram for detector direction, and the asymmetric projection data acquisition method, where relatively large step angle could be employed and opposite side data is inserted each projection direction. In this study, as interpolation method, we used the linear interpolation method. As evaluation methods, we used NMSE (normalized mean square error) and %RMSU (% Root Mean Square Uncertainty) as image quality index and image noise index, respectively. **Results:** NMSE of IB-10 brain phantom images reconstructed from 12 views, 24 views and 24 views interpolated from 12 views were 0.04195, 0.01262 and 0.02198. NMSE of Shepp-Logan phantom images reconstructed from 12 views, 24 views and 24 views interpolated from 12 views were 0.02157, 0.004099 and 0.005970. Image quality (NMSE) of reconstructed images interpolated from 12 view to 24 view was better than 12 view reconstructed images in both IB-10 Brain phantom image and Shepp-Logan phantom image. %RMSU were 33.71 % for 12 view reconstructed image, 38.35 % for 24 view reconstructed image, 38.02 % for reconstructed image interpolated from 12 view to 24 view. %RMSU of the reconstructed image interpolated from 12 views to 24 views was almost same value as the reconstructed image of 24 view which was not interpolated. **Conclusions:** We developed advanced technique for reconstruction of SPECT image. Our method applies interpolation method to the sinogram for detector direction and for asymmetric acquisition in the orbit. Image quality of SPECT image was improved by the method developed in this study. Our method will contribute to shorten the acquisition time not only SPECT study but also PET study.

OP-209

Wireless Online Monitoring of Radiation Dose Rate of Radioiodine (I-131) Ablation Patients: Saves Staff's Doses and Resources

M. C. Lehtinen Gil Compte, P. H. Puhakka, K. Levänen, M. Honkanen, S. Myöhänen, J. Heikkinen; South Savo Social and Health Care Authority, Mikkeli, FINLAND.

Introduction: In our organization, radioiodine I-131 thyroid ablation patients stay in isolation until the radiation dose rate, to which they expose their environment, has fallen under 40 µSv/h at 100 cm distance. Previously, a radiographer entered the isolation room to check the dose rate the day following the administration day. If the dose rate had not fallen under the discharge limit, she had to repeat the measurement later and be exposed to more radiation. Our aim was to minimize the radiation burden of the staff by conducting dose rate monitoring with a new wireless online measurement system. We expect that it would reduce the number of times a radiographer needs to enter the isolation room, and also the length and consequently, costs of the isolation. **Subjects and Methods:** A wireless dose rate monitor was positioned into the isolation room beside the bed, approximately 100 cm from the patient's pelvic skin. The system sent dose rate data to a server every minute. Remote monitoring of the dose rate was possible from any device with internet access. Time-dependent dose rates were analyzed for 19 radioiodine I-131 ablation patients (dose 1031-3896 MBq) during their stay at the isolation. The results were compared with the isolation times of the old system (11 patients, 2236-4026 MBq). **Results:** The new system reduced the number of times the radiographer entered the room during the isolation from average of 1.2 times to 1 time per patient. Reduction in average radiographer dose was estimated to be 2 µSv per pa-

tient. Average isolation time was reduced from 30h to 27h. The mean dose rates at the time of discharge with the old and new systems were 18 μSv/h and 20 μSv/h, respectively. Evaluated with the new system, the 40-μSv/h discharge limit was usually reached during the night, after 12.8 hours of isolation and the patients were discharged 1.3-25.4 hours (mean 13.9h) after reaching the discharge limit. **Conclusion:** Most importantly, the wireless system reduced the work load and the radiation exposure of the radiographer. Furthermore, the total isolation time was reduced, which saves the hospital resources. By studying the times of I-131 administration, reaching the discharge limit, and the realized and logistically optimal discharge, it is possible to optimize (in our case to postpone) the administration times. This could further reduce the isolation times, and consequently, reduce costs and the radiation exposure of the staff working close to the isolation room.

OP-210
The EU directive 2010/32, prevention from sharp injuries in the hospital and healthcare sector, in relation to ALARA: To recap or not?

A. F. Rekveld-van Moerkerken, K. Hart, F. Bomert, H. J. Verberne; Academic Medical Center (AMC), Amsterdam, NETHERLANDS.

Aim: The EU directive 2010/32 implies the use of safety needles. However these safety needles do not necessarily fit the sleeves used for the administration of radio-pharmaceuticals and require the needle to be removed before the syringe can be exposed of, possibly leading to higher radiation exposure. The aim of this study was to investigate if safety needles could be implemented without increasing the risk of contamination and without being exposed to a higher radiation dose. **Method and Materials:** Sixty syringes were filled with 100 MBq ^{99m}Tc-pertechnetate: thirty syringes had non-safety needles requiring a separate needle recapper and thirty syringes had safety needles. The syringes were injected into an empty vial with subsequent recapping of the needle. Thereafter, the needle and the syringe were separated and measured in a dose calibrator. Radiation exposure of the hand was calculated using the remaining dose in the needle and syringe, dose before injection, the distance from the source and the time needed to remove the needle from the syringe. In addition finger-dosimetry was assessed and radioactivity contamination was measured with a contamination monitor. **Results:** Contamination occurred once using the safety needles only (825 Bq/cm^2). The mean calculated hand dose with non-safety needles was lower compared to safety needles (0.16±0.01 μSv vs. 0.87±0.38 μSv, p <0.001). This difference was primarily driven by the time needed to remove the safety needles (4.9±1.1 seconds). These findings were corroborated by the results of the finger-dosimetry. In 2016 the total number of injections with ^{99m}Tc-labelled radio-pharmaceuticals at our department was 1658, resulting in a yearly hand radiation dose for the non-safety needles vs. safety needles of 267.20 μSv vs. 1438.79 μSv, respectively. Based on approximately 15 available workers this would have resulted in an averaged individual hand dose of 2.42 μSv vs. 13.02 μSv. **Conclusion:** The calculated radiation dose for ^{99m}Tc

using safety needles is more than 5 times higher compared to non-safety needles, primarily driven by the time needed to remove the safety needles from the syringe. However with safety needles the hand dose stays well below the maximum allowed dose (i.e. 500 mSv per year). Although there is a small risk of contamination using safety needles, this risk is most likely similar for non-safety needles. Our findings show that it is possible to use safety needles in combination with current protection sleeves without increasing the risk of contamination while staying well within the allowed exposure limits.

OP-211
The effect of PET scan time on the off-line PET image quality in proton therapy

H. Gunchul, J. joonyung, P. sejoon, C. eunsun, L. hyuk; Samsung medical center, seoul, KOREA, REPUBLIC OF.

Purpose: Proton therapy can deliver an optimal dose to tumor while reducing unnecessary dose to normal tissue as compared to the conventional photon therapy. As proton beams are irradiated into tissue, various positron emitters are produced via nuclear fragmentation reactions. These positron emitters could be used for the dose verification by using PET. However, the short half-life of the radioisotopes makes it hard to obtain the enough amounts of events. The aim of this study is to investigate the effect of off-line PET imaging scan time on the PET image quality. **Objectives and Method**: The various diameters of spheres (D=37, 28, 22 mm) filled with distilled water were inserted in a 2001 IEC body phantom. Then proton beams (100 MU) were irradiated into the center of the each sphere using the wobbling technique with the gantry angle of 0°. After 5 min of the proton irradiation, the PET/CT images of the IEC body phantom were obtained for 50 min. The PET images with different time courses (0~10 min, 11~20 min, 21~30 min, 31~40 min, and 41~50 min) were obtained by dividing the frame with a duration of 10 min. In order to evaluate the off-line PET image quality with the different time courses, the contrast-to-noise ratio (CNR) of the PET image calculated for each sphere. **Results**: The CNRs of the sphere (D=37 mm) were 0.43, 0.42, 0.40, 0.31, and 0.21 for the time courses of 0~10 min, 11~20 min, 21~30 min, 31~40 min, and 41~50 min respectively. The CNRs of the sphere (D=28 mm) were 0.36, 0.32, 0.27, 0.19, and 0.09 for the time courses of 0~10 min, 11~20 min, 21~30 min, 31~40 min, and 41~50 min respectively. The CNR of 37 mm sphere was decreased rapidly after 30 min of the proton irradiation. In case of the spheres of 28 mm and 22 mm, the CNR was decreased drastically after 20 min of the irradiation. **Conclusion**: The off-line PET imaging time is an important factor for the monitoring of the proton therapy. In case of the lesion diameter of 22 mm, the off-line PET image should be obtained within 25 min after the proton irradiation. When it comes to small size of tumor, the long PET imaging time will be beneficial for the proton therapy treatment monitoring.

OP-212
MOLY Project: a Mo-99 Production Program at ENEA TRIGA RC-1 Nuclear Research Reactor in Italy

F. Pisacane[1], O. Aronica[1], M. Carta[1], N. Cherubini[1], A. Dodaro[1,2], G. Giorgiantoni[1], M. Olivetti[1], E. Santoro[1]; [1]ENEA, Rome, ITALY, [2]Nucleo S.p.A., Rome, ITALY.

Due to the predicted ^{99m}Tc worldwide shortage, many countries are going to set up a method to produce this radioisotope, fundamental for many medical diagnostic practices. Aim of this work is to describe the feasibility of ^{99}Mo (which decays in ^{99m}Tc) production, starting from a ^{98}Mo(n,γ)^{99}Mo capture reaction through the irradiation of Molybdenum targets by using the TRIGA RC-1 nuclear research reactor (<u>T</u>raining <u>R</u>esearch <u>I</u>sotopes <u>G</u>eneral <u>A</u>tomic <u>R</u>eactor <u>C</u>asaccia <u>1</u>) in ENEA. The reactor's main features are: •Maximum power: 1 MW; •Maximum thermal neutron flux: 2.7×10^{13} $\mathrm{n \cdot cm^{-2} \cdot s^{-1}}$; •Core cooling by natural convection of demineralized water; •Irradiation facilities. To prove the possibility of achieving a significant specific activity after a suitable irradiation time, some preliminary evaluations have been performed on the basis of the following starting assumptions. 1.Metallic or sintered target of enriched ^{98}Mo. 2.Irradiation in the central channel of the core (3 cm diameter). 3.The cross-section of the capture reaction ^{98}Mo(n,γ)^{99}Mo for thermal neutrons is 136 mb. It is possible to increase this value by allowing for neutrons with energy in the resonance region. It is conceivable to assume an "effective" cross section $σ^*$, which takes into account the contributions related to intervals of the neutron spectra that include the epithermal and fast ranges. These contributions can be evaluated around 68% in the case of enriched ^{98}Mo and 78% for natural isotopic composition. Experiences in similar facilities show $σ^*$ values ranging from 400 - 500 mb up to 700 mb. 4.Total neutron flux composed by two components: the thermal component equal to 2.7×10^{13} $\mathrm{n \cdot cm^{-2} \cdot s^{-1}}$ and the fast one equal to 4×10^{13} $\mathrm{n \cdot cm^{-2} \cdot s^{-1}}$. 5.120 hours irradiation time, which corresponds approximately to two half-lives ($T_{1/2}$=66h) of the ^{99}Mo. The geometry of the central channel and the axial neutron flux of TRIGA RC-1 enable us to use, as far as the molybdenum samples are concerned, a section of 10 cm height in order to irradiate, from the neutron fluxes point of view, in most favorable conditions. In the central channel, several tens of grams of metallic molybdenum for each 120 hours session are supposed to be irradiated. As said before, a preliminary analysis confirms that, at the EOB (End Of Bombardment), it is possible to reach specific activity equal to about 30 GBq/g that could make possible a standard delivery of several radionuclide generators in health care units per week.

OP-213
F-18-FDG PET-CT Studies Reproducible Quantitative Assessment for Clinical Use

D. B. Faria[1,2,3], J. Teixeira[1,2], A. Martins[1,2], J. Fernandes[1,2], J. Pinto[1,2], J. Vale[1,2,3], J. Patrina[1,2], A. Roçado[1,2], D. Sousa[1,2], J. M. P. Oliveira[1,2]; [1]HPP - Medicina Molecular SA, Porto, PORTUGAL, [2]Lenitudes Medical Center & Research, Santa Maria da Feira, PORTUGAL, [3]School Of Health Sciences - University of Aveiro, Aveiro, PORTUGAL.

Recent improvements in PET hardware and software have been of extreme importance to reduce acquisition time, lower administered doses, improve image quality and offering new radiopharmaceutical uptake quantification possibilities. PET-CT Discovery LS (DLS) and PET-CT Discovery IQ (IQ) scanners, represent the range on Discovery BGO (GE Healthcare) clinical scanners, with improved sensitivity and count rate performances. Q. Clear™ (GE Healthcare) is a Bayesian penalized likelihood algorithm that includes a noise suppression term controlled by a penalization factor ß, that allows convergence for image quality and quantitation improvement over traditional iterative reconstructions algorithms. To ensure that data from longitudinal studies performed with these different scanners is interchangeable, it is necessary to define procedures to harmonize the quantification of SUV. **Aim:** to harmonize the quantification of PET/CT images performed with different scanner models at our department. **Methods:** A NEMA IEC Body Phantom, filled with a background activity of 6,61 and 3,72 kBq/mL and spheres with 34,312 and 19,19 kBq/mL, was scanned on a PET-CT scanner Discovery LS4 and a Discovery IQ 4 Rings for 12 minutes. DLS Images were reconstructed by OSEM (ordered subset expectation maximization) with 28 subsets, 2 iterations and IQ images with VUE Point HD (2 iterations, 24 subsets, and 6.4 mm filter) and Q. Clear β values between 50 and 500 with increment of 50. Circular volumes of interest were placed over spheres and background region, and voxel maximum activities were used to calculate recovery coefficients (RC) and contrast recovery coefficients (CRC) for all spheres. **Results:** DLS showed lower RC - 30,5% and 30,2% for the smaller sphere, reaching 107% and 102% for the 37mm sphere size; CRC ranged from 34% (smaller sphere) to 129% (biggest sphere). Images acquired with IQ, showed higher RC - 36% and 40% for VPHD reconstructions in smaller sphere size and higher CRC values, 17,9% and 22,4% for the smallest sphere and 113% and 115% for biggest sphere; Q. CLEAR reconstructed images showed a large variability in RC for smaller spheres, showing smaller RC values for higher β values; CRC showed the same tendency, with 78,4% and 82,9% for β50 and 18,3% and 25,4% for β500 for the 10mm sphere; increasing β value had less impact in RC and CRC for bigger sphere sizes. **Conclusion:** Clinical preliminary results show that harmonization for quantification in Nuclear Medicine Departments is possible and may reduce variability in quantitation if guaranteed the reproducibility of the methodology.

OP-214
Digital PET/CT in clinical routine: Dose reduction and image quality

J. Trinckauf, M. Hofbauer, M. Hüllner, I. Burger; University Hospital Zürich, ZURICH, SWITZERLAND.

Aim: With the installation of two digital PET/CT systems of the latest generation in our department, new dimensions of dose reduction and radiation protection are at hand. The possibilities offered by these new systems for dose reduction and whole body scanning have been implemented into the clinical routine. **Material and Methods:** Since January 2017, two identical GE DISCOVERY MI (DMI) PET/CT systems (64 slices CT) have been installed in our institute. For two months we had the analog DIS-

COVERY DSD PET/CT next to the new DMI for direct comparison. Due to the high detector sensitivity and the newest image reconstruction algorithms, we aimed for a reduction of the applied radiotracer dose. Based on an in-house developed BMI table, we determined the best possible dose reduction with maintained image quality with a substantial reduction for the DMI compared to the DSD PET/CT (4.5 MBq/kg): for BMI <20: 18F-FDG: 2.5 MBq/kg, BMI 20-24.5: 3 MBq/kg and BMI> 24.5: 3.5 MBq/kg. We also adapted the frame time according to dosage. While previously we acquired by default 2min / per bed position, we now acquire with 2.5min per bed position. The new scanner allows for one-stop whole-body acquisition in patients up to 2m body height. This is possible with a table extension, and patient repositioning for leg imaging is obviated. Using the reconstruction algorithm Q.clear, we were able to select different beta values for each radiotracer, yielding the optimal image quality. **Results:** Using the above mentioned BMI adapted ^{18}F-FDG dosing scheme an adequate image quality could be achieved in all patients on the DMI PET/CT compared to the higher doses on the DSD scanner with dose reduction of up to 45%. This also implies a considerable dose reduction for the technologist. The use of reconstruction algorithm Q. clear showed that an increase of the B-value is essential for lower doses. For the proposed BMI adapted ^{18}F-FDG dosing scheme an optimal value was determined at B = 450. A slightly increased (0.5min per bed position) examination time is well tolerated in clinical routine, and not inconvenient for the patient. The possibility of true whole-body examinations also facilitates clinical routine and simplifies patient preparation and positioning on the examination table. **Conclusion:** Digital PET / CT systems allow for significant dose reduction along with higher image quality.

| 604 | Monday, October 23, 2017, 08:00 - 09:30, Hall E1 |

Do.MoRe: PSMA Therapy

OP-215

Variation in the absorbed radiation dose and PSA response after serial Lu-177 PSMA radioligand therapy

C. Schuchardt, H. R. Kulkarni, S. Wiessalla, A. Singh, M. Shahinfar, D. Mueller, C. Lehmann, R. P. Baum; Zentralklinik Bad Berka GmbH, Bad Berka, GERMANY.

Aim: Prostate-specific membrane antigen (PSMA) is significantly over-expressed in prostate cancer cells. The aim of our study was to determine the inter-cycle dosimetry variation in patients with metastatic castration-resistant prostate cancer (mCRPC) undergoing at least 2 cycles of Lu-177 PSMA radioligand therapy (PRLT), in correlation with the change in serum PSA after PRLT. **Methods**: Dosimetry was performed during each PRLT cycle in 10 patients with mCRPC. PSMA expression was verified before therapy using Ga-68 PSMA PET/CT. Patients received at least 2 cycles of PRLT using 3.4-7.5GBq Lu-177 PSMA. The time-dependent biodistribution was determined based on whole-body scintigraphies and SPECT/CT. Dosimetric calcu-

lations (MIRD-scheme) were performed using OLINDA/EXM software. For intra-patient comparison, uptakes at 20h p.i. and mean absorbed doses were determined for kidneys and metastases. Variations between first and following therapy cycles were analyzed as mean with respect to the first therapy cycle (=100%). Serum PSA was determined before and every 4 weeks after the first PRLT cycle. **Results:** In 9 patients, all dosimetric parameters pertaining to metastases demonstrated variations between first and second therapy cycles: the mean uptake declined by 57% and the average dose by 64%. In contrast, the mean renal uptake increased by 62% and the average renal dose was therefore higher in the following cycles (34%), except for a lower renal dose at the second cycle in 1 patient (-17%). One of the patients showed inverse results, an increase in the tumor uptake (+84%) and dose (+154%) and a decrease in the renal uptake (-9%). However, the renal dose exhibited a mild increment (+19%). Patients with a fall in the absorbed tumor dose also demonstrated a biochemical response (decrease of serum PSA by 41%). The patient exhibiting an increasing PSA after the first cycle revealed a higher absorbed tumor dose during the second PRLT cycle. **Conclusions:** There is a significant inter-cycle variation of the absorbed tumor and kidney doses, which correlates with the change in PSA after PRLT. A decrease in serum PSA, indicating a therapy response, is therefore associated with a decrease in the absorbed tumor dose during subsequent PRLT cycle and vice versa. Whereas a decrease in tumor burden results in an increase in the absorbed renal dose due to an inverse sink effect. Administration of a higher amount of radioactivity in the first cycle seems to be reasonable, since the tumor doses tend to decrease in the subsequent cycles due to therapy Response.

OP-216

177Lu-PSMA-617 Treatment of Metastatic Castration-Resistant Prostate Cancer: Efficacy and Survival

E. Demirci[1], R. Akyel[2], O. Sahin[3], M. Ocak[4], A. Aygün[3], H. Pehlivanoglu[3], E. Karayel[3], L. Kabasakal[3]; [1]Department of Nuclear Medicine Sisli Etfal Training and Research Hospital, istanbul, TURKEY, [2]Department of Nuclear Medicine Umraniye Training and Research Hospital, istanbul, TURKEY, [3]Department of Nuclear Medicine, Cerrahpasa Medical Faculty, Istanbul University, istanbul, TURKEY, [4]Department of Pharmaceutical Technology, Pharmacy Faculty, Istanbul University, istanbul, TURKEY.

Aim: The aim of this study was to analyse efficacy of 177Lu-PSMA-617 Treatment in patients with Metastatic Castration-Resistant Prostate Cancer. **Materials and Methods:** 43 patients with metastatic castration-resistant prostate (mCRPC) cancer who underwent 177Lu-PSMA-617 treatment during period of 2014-2017 included in this retrospective study. Response to treatment evaluated according to follow up 68-Ga-PSMA PET/CT scans and weekly PSA levels. Progression-free survival (PFS) and overall survival (OS) rates were calculated according to first cycle of the treatment. **Result:** Patients were treated with an average dose of 21±7.2 GBq of 177Lu- PSMA-617. All patients had diagnosis of mCRPC with an average PSA level

of 264±108 ng/ml. 55,8% (n=24)of patients had lymph node metastasis,90,7% (n=39) of patients had bone metastasis and 18,6% (n=8) of patients had visceral organ metastasis. Grade 1 or 2 hematologic toxicity occurred in 26% (n=11) of patients and Grade 3 hematologic toxicity occurred in 7% (n=3) of patients. A decrease over 50% in PSA levels was observed in 23 (53%) patients. Among 28 patients who had a follow-up 68Ga-PSMA PET/CT 12 (27.9%) patients had progression, 16 (57.1%) patients had partial response. PFS, combined with serum PSA levels and available imaging modalities, calculated 6.5 months (%95CI:4-8,9). Median OS rate was calculated 15.9 months (95% CI: 13.1- 18.7) and 54.7 months (95%CI:51,7-58,1). In patients who had PSA decrease after treatment, OS was significantly higher compared to those who had increase (17.7 months %95CI:14,3-21,1 vs 13,8 months %95CI:10,1-17,6; p<0.05). **Conclusion:** 177Lu-PSMA-617 is a safe and effective treatment option in end-stage metastatic Castration-Resistant Prostate Cancer.

OP-217

Targeted Alpha Therapy of mCRPC: Dosimetry estimate of [213]Bismuth-PSMA-617

C. Kratochwil[1], K. Schmidt[2], F. Bruchertseifer[3], A. Afshar-Oromieh[1], A. Morgenstern[3], U. Haberkorn[1], F. L. Giesel[1]; [1]University Hospital Heidelberg, Heidelberg, GERMANY, [2]ABX-CRO, Dresden, GERMANY, [3]EC-JRC, Karlsruhe, GERMANY.

Purpose: PSMA-617 is a small molecule targeting prostate-specific membrane antigen. In this work we estimate the radiation dosimetry for this ligand labeled with the alpha-emitter [213]Bi. **Methods:** Three patients with metastatic prostate cancer underwent PET-scans 10min, 1h, 2h, 3h, 4h and 5h after injection of ^{68}Ga-PSMA-617. Source organs were kidneys, liver, spleen parotid and submandibular glands, urinary bladder, red-marrow and representative tumor lesions. The imaging nuclide ^{68}Ga was extrapolated to the half-life of [213]Bi. The residence times of [213]Bi were forwarded to the instable daughter nuclides. OLINDA was used for dosimetry calculation. Results are discussed in comparison to data for [225]Ac-PSMA-617. **Results:** Assuming a relative biological effectiveness of 5 for alpha-radiation, the dosimetry estimate revealed mean doses of 8.1 Sv/GBq for salivary glands, 8.1 Sv/GBq for kidneys and 0.52 Sv/GBq for red-marrow. Liver (1.2 Sv/GBq), spleen (1.4 Sv/GBq), bladder (0.28 Sv/GBq) and other organs (0.26 Sv/GBq) were not dose-limiting. Effective dose is 0.56 Sv/GBq. Tumor lesions were in the range 3.2-9.0 Sv/GBq (median 7.6 Sv/GBq). Kidneys would limit the cumulative dose to 3.7 GBq; red marrow might limit the maximum single dose to 2 GBq; thus, 3 cycles of 1.2 GBq might be a reasonable fractionation regime. **Conclusion:** Dosimetry of [213]Bi-PSMA-617 is in a range traditionally considered promising for clinical application. Nevertheless, the tumor-to-kidney ratio of [213]Bi-PSMA-617 is inferior compared to [225]Ac-PSMA-617 because the long half-life alpha-emitter [225]Ac can benefit from less perfusion-dependent off-target radiation and the shorter biological half-life of PSMA-617 in dose limiting organs.

OP-218

Overall survival and response pattern of castrated-resistant metastatic prostate cancer to multiple cycles of radioligand therapy using Lu-PSMA-617

H. Ahmadzadehfar, S. Wegen, A. Yordanova, R. Fimmers, S. Kürpig, E. Eppard, X. Wei, C. Schlenkhoff, S. Hauser, M. Essler; University Hospital Bonn, Bonn, GERMANY.

Introduction: Approximately 30% of patients with castrated-resistant prostate cancer (CRPC) do not show any response to the first cycle of radioligand therapy (RLT) with Lu-PSMA-617 (Lu-PSMA), measured as any decline in prostate-specific antigen (PSA). We evaluated patient response to the second and third cycles of RLT in patients that underwent at least three cycles. The second aim of this study was to calculate the median overall survival (OS) of responders and non-responders after the first cycle and after all three cycles of RLT. **Methods:** CRPC patients with distant metastases were treated with at least three cycles of Lu-PSMA, with a median interval of 8 weeks between each cycle. The tumour marker PSA was used as the main marker for response evaluation. **Results:** Fifty-two patients underwent a total of 190 cycles of RLT (3-6 cycles per patient). Of these, 80.8% showed a decline in PSA 2 months after the first cycle, with 44.2% showing a PSA decline of ≥ 50%. When compared to baseline PSA, 73.1% showed a PSA decline after the third cycle. Half (50%) of patients that did not show any response to the first cycle also did not respond to the second and third cycles. The median OS was 60 weeks. The median OS was significantly longer for patients that showed any PSA decline after the first cycle compared to patients without PSA decline (68 vs. 33 weeks). There was a significant difference in median OS between responders and non-responders for a change in PSA after the third cycle compared to baseline PSA. **Conclusion:** Patients with a positive response to RLT using Lu-PSMA (responders), regardless of the rate of decline, had a significantly longer median OS compared to non-responders. Of the patients that did not show any response to the first cycle, 50% did not respond to the second or third cycles.

OP-219

The impact of repeated cycles of Lu-PSMA-617 therapies on renal function in patients with hormone refractory metastatic prostate cancer

A. Yordanova, A. Becker, E. Eppard, S. Kürpig, C. Fisang, G. Feldmann, M. Essler, H. Ahmadzadehfar; University Hospital Bonn, Bonn, GERMANY.

Aim: Lu-PSMA-617 is a well-tolerated therapy for the treatment of metastatic prostate cancer. However, because of the mainly renal excretion of the tracer, the kidneys are one of the most limiting organs. The purpose of this study was to examine the post-therapeutic changes in renal function over time and to identify risk factors for developing renal toxicity. We also tested the reliability of markers for renal function monitoring. **Methods:** Fifty-five patients with castrate-resistant metastatic pros-

tate cancer treated with at least three cycles of Lu-PSMA-617 were investigated. Renal function was assessed through laboratory tests (creatinine, GFR, cystatin C) and Tc-99m-MAG3 measurements. Adverse events were classified according to the *Common Terminology Criteria for Adverse Events* (CTCAE) v4.0. To identify risk factors for renal toxicity, we used Pearson´s correlation coefficient and the corresponding p-values. **Results**: None of the 55 patients experienced severe nephrotoxicity (grade 3/4). In 14 patients (25%), we observed increased creatinine levels of CTC 1° or 2°. There were 16 cases of increased GFR (grade 1/2). At the baseline, only 14 patients had elevated cystatin C. However, post-therapeutic cystatin C was elevated in 32 patients (58%). A significant effect on renal function was found for age ($p = 0.049$), hypertension ($p = 0.001$) and pre-existing kidney disease ($p = 0.001$). The most reliable predictive markers of nephrotoxicity were TER-MAG3 and cystatin C. **Conclusion**: Renal toxicity in patients treated with Lu-PSMA-617 was low. There was no (sub)acute grade 3 or 4 nephrotoxicity.

OP-220

Lu-177 PSMA Radioligand Therapy might Prolong Survival in Metastatic Castration-Resistant Prostate Cancer: Results from a Single Center over 4 Years

H. R. Kulkarni[1], A. Singh[1], C. Schuchardt[1], T. Langbein[1], K. J. Pienta[2], R. P. Baum[1]; [1]THERANOSTICS Center for Molecular Radiotherapy, Bad Berka, GERMANY, [2]The Brady Urological Institute, Johns Hopkins University, Baltimore, MD, UNITED STATES OF AMERICA.

Purpose: Lu-177 PSMA radioligand therapy (PRLT) is currently a last line option in metastatic castration-resistant prostate cancer (mCRPC). This study aimed at evaluating the overall and progression-free survival in a large mCRPC patient cohort. **Subjects and Methods:** Between April 2013 and April 2017, intention-to-treat analysis was performed in 194 patients (mean age 71 years, mean Gleason score 8) with mCRPC, who were screened previously by Ga-68 PSMA PET/CT. They received 1 to 9 PRLT cycles (totally 545) using 3.5 - 10 GBq (mean 6.3 GBq) of Lu-177 labelled PSMA ligand. Previous treatments were surgery (169), external beam radiation (133), chemotherapy (96), androgen deprivation (194) and Ra-223 chloride (9). The most frequent sites of metastases were bone (148), lymph node (135), liver (25) and lungs (20), and 47 patients had diffuse bone marrow involvement. Ga-68 PSMA PET/CT was used for initial evaluation and therapy response assessment. Laboratory parameters including complete blood count, renal function and PSA levels were documented before and after therapy. **Results:** Any PSA decline was observed in 135/194 (69.6%) patients, best response was biochemical complete remission (PSA=0.0 ng/ml). Decrease in PSA by more than 50% was seen in 103 (53.1%) patients. Restaging with imaging (Ga-68 PSMA PET/CT) after at least 2 PRLT cycles in 136 patients demonstrated 6 complete remissions (5%), 70 partial remissions (51%), 11 with stable disease (8%) and 49 with disease progression (36%) according to molecular response criteria. Using RECIST 1.1, complete remission was observed in 4 (3%), partial remission in 41 (30%), stable disease in 52 (38%) and

progressive disease in 39 (29%) patients. Median overall survival was 34 months. Median progression-free survival was 13 months. There were no acute adverse effects. Mild xerostomia was reported by 9 (4.6%) patients. G3-4 hematological toxicity was observed in 9 (4.6%) patients, more frequently associated with disseminated bone marrow involvement, previous chemotherapy or Ra-223 treatment. **Conclusions:** Lu-177 PSMA radioligand therapy is a promising therapy option in mCRPC, with acceptable toxicity. An overall survival of 34 months and progression-free survival of 13 months despite extensive pretreatment, including chemotherapy, indicates that PRLT might potentially prolong the survival when compared with historical controls. However, prospective randomized control studies are needed to validate these results and to determine its place in mCRPC treatment.

OP-221

Targeted Alpha Radioligand Therapy (TART) using Bismuth-213 PSMA in End-stage Progressive Treatment-refractory PSMA-expressing Metastatic Prostate Cancer: Results of a Pilot Study

H. R. Kulkarni[1], A. Singh[1], T. Langbein[1], C. Lehmann[1], D. Mueller[2], S. Marx[3], K. J. Pienta[4], R. P. Baum[1]; [1]THERANOSTICS Center for Molecular Radiotherapy, Zentralklinik Bad Berka, Bad Berka, GERMANY, [2]Division of Radiopharmacy, Zentralklinik Bad Berka, Bad Berka, GERMANY, [3]ITG Isotope Technologies Garching GmbH, Munich, GERMANY, [4]The Brady Urological Institute, Johns Hopkins University, Baltimore, MD, UNITED STATES OF AMERICA.

Purpose: The feasibility, toxicity and efficacy of targeted alpha radioligand therapy (TART) using Bi-213 PSMA in end-stage metastatic treatment-resistant prostate cancer, having progressed under radioligand therapy using Lu-177 PSMA, were evaluated in a pilot study. **Subjects and Methods:** Bi-213 ($t_{1/2}$ 46 minutes) was obtained from a Ac-225/ Bi-213 generator (provided by ITG Isotope Technologies Garching GmbH), calibrated to elute 370 MBq of Bi-213 at the time of delivery. The labelling of PSMA-617 with Bi-213 was performed at the radiopharmacy of Zentralklinik Bad Berka. Between December 2016 and March 2017, we have treated 10 patients with Bi-213 PSMA (1-2 cycles, 2-4 applications per cycle). Extensive skeletal involvement was present in 7 patients, and 3 already suffered from G3-4 anemia and thrombocytopenia before TART. Of the 10 patients, 3 were retreated with a second cycle. The median administered activity of Bi-213 PSMA per cycle was 390 MBq (155 - 623 MBq). The very short half-life of Bi-213 necessitated at least 2 daily elutions of the generator, and 2-4 applications of Bi-213 PSMA to each patient per cycle over 2 days. Ga-68 PSMA-11 PET/CT (with contrast-enhanced CT) was used for patient selection and follow-up after TART. Response to therapy after 1 cycle was available at the time of analysis in 3 patients. Hematological status, renal function and serum prostate specific antigen (PSA) levels were documented before and after therapy. **Results:** All patients tolerated the therapy very well without any acute adverse effects; during follow-up there was no xerostomia and no additional hematological toxicity. Decrease in PSA was noted in 3/7 (43 %)

patients. Molecular response evaluation (Ga-68 PSMA-11 PET/CT) after 1 cycle of TART in 3 patients revealed stable disease/minor response, mixed response and progressive disease in 1 patient, respectively. Contrast-enhanced CT exhibited stable disease according to RECIST 1.1. One patient with disseminated bone metastases, already having received 9 cycles of Lu-177 PSMA therapy and progressing under additional 2 cycles of Bi-213 PSMA TART, died during the observation period. **Conclusions:** Targeted alpha radioligand therapy using Bi-213 PSMA is feasible in end-stage metastatic treatment-resistant prostate cancer, progressing after castration, newer hormonal agents, chemotherapy as well as after radioligand therapy using Lu-177 PSMA. With the administered radioactivities mentioned, no significant acute / subacute toxicity was noted and minor responses could be demonstrated. However, higher acitivities or more frequent cycles of Bi-213 PSMA might be required to achieve the desired response to therapy.

OP-222

Initial Theranostics Experience Using ^{68}Ga-PSMA-11 PET/CT and ^{177}Lu-PSMA-617 in a Chilean Oncology Center

H. Amaral[1,2], R. Fernández[1], V. Kramer[2], H. Lavados[1], E. Hernández[1], B. Morales[1], R. Pruzzo[1], A. Haeger[1], J. Ribbeck[2], J. Flores[1]; [1]FALP / PositronMed, Santiago, CHILE, [2]PositronPharma, Santiago, CHILE.

Patients with progressive metastatic castration-resistant prostate cancer (mCRPC) have limited therapeutic options and most of them are referred to palliative care. Several reports have confirmed that ^{177}Lu labeled prostate specific membrane antigen (PSMA) ligand is a safe and effective therapeutic option in progressive mCRPC. **Aim:** To present the initial experience in a Chilean oncology center using the theranostics concept with ^{68}Ga-PSMA-11 PET/CT and ^{177}Lu-PSMA-617 in patients with progressive mCRPC. **Subjects & Methods:** Thirteen consecutive patients with mCRPC, mean age 70±7.9 y.o. (range: 51-82), received a total of 43 doses of ^{177}Lu-PSMA-617 between June 2016 and April 2017 (eight patients: 4 doses, two patients: 3 doses, two patients: 2 doses and one patient: 1 dose). The mean administered activity per dose was 5.7±0.4 GBq (range: 4.7-6.3). All patients have a complete clinical and laboratory work-up including serum prostate specific antigen (PSA) levels before and after four weeks of every administered dose. A pre-therapy ^{68}Ga-PSMA-11 PET/CT (mCT 20, Siemens-Healthineers) was performed in all and a whole-body planar scan and SPECT/CT were acquired after each treatment application. **Results:** The ^{68}Ga-PSMA-11 PET/CT demonstrated bone metastatic involvement in all cases, additional lymphadenopathies in 62% and visceral metastases in 23%. Planar scan and SPECT/CT images after the initial treatment were in agreement with recent pre-treatment PET/CT findings. No acute adverse effects were observed after therapy. Until now no xerostomy cases has been detected. In one patient hematological toxicity grade 3 with pancytopenia was observed 4 weeks after the first dose. The initial mean PSA level was 672±1099 ng/dL (range: 3.4-4105). PSA level decreased in 7/10 patients with at least 3 doses and in 5/10 the decreased was more than 50% (71.5%, 95.1%, 97.6%, 99.7% and 99.8%, respectively). The two most significant

responses were: one patient with initial PSA level 18.3 ng/dL that decreased to 0.05 ng/dL and in a second patient the basal PSA level of 921.1 ng/dL diminished to 2.2 ng/dL, both after 4 doses of ^{177}Lu-PSMA-617. **Conclusion:** The theranostics approach with ^{68}Ga-PSMA-11 PET/CT and ^{177}Lu-PSMA-617 treatment in patients with progressive mCRPC is a safe and promising personalized therapy in a group of patients with currently limited therapeutic options. Our initial experience in Chile is in agreement with recent published data elsewhere and allows us to introduce this theranostics concept as a routine procedure in mCRPC patients.

---

605   **Monday, October 23, 2017, 08:00 - 09:30, Hall E2**

M2M: Optical/Multimodality Imaging

OP-223

Diagnostic Tumor Imaging Using Renally Excretable Nanoparticles: Focus on Active and Passive Targeting

K. Pant[1], K. Zarschler[1], C. Neuber[1], J. Pufe[1], J. Steinbach[1,2], R. Haag[3], J. Pietzsch[1,2], H. Stephan[1]; [1]Helmholtz-Zentrum Dresden-Rossendorf, Institute of Radiopharmaceutical Cancer Research, Dresden, GERMANY, [2]Technische Universität Dresden, Department of Chemistry and Food Chemistry, Dresden, GERMANY, [3]Freie Universität Berlin, Department of Chemistry and Biochemistry, Berlin, GERMANY.

Introduction: Depending on their size, shape and surface functionalities, nanoparticles can passively extravasate and accumulate in the tumor tissue through the enhanced permeability and retention (EPR) effect. Being an accumulative process, this effect favors nanoparticles with long blood retention time. Renally excretable, ultrasmall nanoparticles with short blood half-lives are therefore less prone to passive tumor targeting as they rapidly diffuse back to the vasculature and re-enter the systemic circulation, which results in only transient intratumoral presence without substantial retention. To prevent their rapid efflux from malignant tissues by increasing the interactions between nanoparticles and tumor cells as well as by improving cellular nanoparticle uptake, the strategy of active or ligand-mediated targeting is pursued. Here, we describe the development of renally excretable dendritic polyglycerols (dPGs) functionalized with different targeting units to differentiate between active and passive tumor targeting. **Methods:** Fluorescent dye labels for optical imaging and small camelid single-domain antibodies (sdAbs) as targeting units - both equipped with maleimide functionalities - were simultaneously attached in a one-pot reaction to thiol groups of the dPGs. As the presented work focusses on the epidermal growth factor receptor (EGFR) acting as a model receptor, an EGFR-specific sdAb was attached to the dPGs to obtain an active targeting probe. In parallel, a probe with similar surface characteristics but a nonspecific sdAb (passive targeting) was synthesized. Both conjugates were purified using affinity chromatography, which selectively separates the sdAb-conjugated dPGs. **Results:** In vitro binding studies on different human epithelial cancer cell lines using dye-labeled sdAb-conjugated

dPGs showed a high specificity, co-localization and a receptor-mediated cellular uptake of the EGFR-specific probes. Optical imaging studies using murine xenografts revealed a substantial accumulation of the EGFR-specific probes in comparison to its nonspecific counterparts and a minimum off-target accumulation of both conjugates. **Discussion and Conclusion:** The direct comparison of specific and nonspecific probes with similar surface characteristics allows the straight-forward preclinical discrimination between active and potential passive tumor targeting of renally excretable nanoparticles in small animal models. Furthermore, it provides important information on the extent to which ligand-mediated targeting contributes to total nanoparticle accumulation in malignant and normal tissues.

OP-224

Multicolor fluorescence click-chemistry as a means to select membrane targets for pre-targeting by function of their internalization

S. van der Wal, C. M. de Korne, L. G. L. Sand, P. C. W. Hogendoorn, K. Szuhai, F. W. B. van Leeuwen, **T. Buckle**; LUMC, Leiden, NETHERLANDS.

Introduction: The internalization kinetics of membrane receptors plays an important role in theranostic approaches, especially in those that make use of pre-targeting. To enable accurate assessment of the validity of a membrane receptor in pre-targeting based approaches (e.g. availability on the cell membrane), a novel "click" chemistry-based fluorescence quenching concept was developed. Herein the fluorescent emission of the extracellular tracer fraction can be "switched-off" or "de-activated". The efficacy of this approach was evaluated for the chemokine receptor 4 (CXCR4), a clinically relevant theranostic receptor-target that is over-expressed in e.g. multiple myeloma, breast cancer and Ewing sarcoma. Findings were compared to a targeted tracer that becomes activated following cellular internalization. **Methods:** Ac-TZ14011, a CXCR4 specific peptide, was converted into two types of receptor-targeted tracers: 1) a de-activatable tracer; a Cy5 dye that contained a chemo-selective azide handle suitable for pre-targeting applications (**N₃-Cy5-AcTZ14011**) that can react with a Cy7 quencher dye (**Cy7-DBCO**) to form the optically silent **Cy7-["click"]-Cy5-AcTZ14011** and 2) an activatable tracer; a FRET-dye construct (**Cy5-S-S-Cy3-AcTZ14011**) that is optically silent for Cy3 and becomes Cy3 fluorescent (**HS-Cy3-AcTZ14011**) upon cleavage of the disulfide bond. The photophysical properties and activation kinetics of both tracers were evaluated *in situ*. *In vitro* assessment of the binding affinity (flow cytometry; saturation binding experiments (K_D)) and internalization kinetics (fluorescence confocal microscopy; quantitative evaluation over time) was performed in CXCR4 overexpressing MDAMB 231 X4 cells. **Results:** Assessment of the binding affinity of both tracers revealed that the smaller **N₃-Cy5-COOH** had a higher binding affinity than **Cy5-S-S-Cy3-COOH** (K_D: 222.4 ± 25.2 nM vs. K_D > 500 nM, respectively). *In situ*, addition of **Cy7-DBCO** to **N₃-Cy5-AcTZ14011** resulted in >90% FRET-based reduction of the signal intensity of Cy5 fluorescence within the first 2-5 minutes. In cells, pre-targeting with **N₃-Cy5-AcTZ14011** led to membranous staining and subsequent internalization of the receptor-tracer complex. Following addition of **Cy7-DBCO,** an 80% decrease of membranous fluorescence was seen, while fluorescence of the internalized tracer-fraction was preserved and remained stable over time (0-30 minutes). The FRET efficiency of the disulfide-bridge-containing activatable tracer was 55% and a limited 45% increase in fluorescence was seen upon reduction in solution, while in cells no increase in Cy3-related fluorescence was seen. **Conclusions:** De-activatable fluorescence tracers were shown to provide a clear alternative for activatable tracers. Moreover, the click chemistry-based pre-targeting approach promises to provide an efficient read-out that for the screening of membrane receptors and their applicability in receptor-targeted theranostics.

OP-225

Multicolor fluorescence imaging as a means to reduce the toxicity during nodal dissections in prostate cancer

P. Meershoek[1,2], G. H. KleinJan[1,2], M. N. van Oosterom[1], E. M. Wit[2], N. Grivas[2], A. Mottrie[3], F. W. B. van Leeuwen[1], H. G. van der Poel[2]; [1]Leiden University Medical Center, Leiden, NETHERLANDS, [2]Netherlands Cancer Institute (NKI-AvL), Amsterdam, NETHERLANDS, [3]OLV Vattikuti Robotic Surgery Institute, Melle, BELGIUM.

Introduction: Lymphatic metastases are frequently encountered in prostate cancer. Therefore the EAU guidelines indicate an extended pelvic lymph node dissection (ePLND). Disturbance of the lymphatic flow is common after an ePLND and can result in side effects such as lymphocele and lymphedema. We reasoned accurate distinction between relevant prostate draining sentinel lymph nodes (SNs) and crucial leg draining lymph nodes (LNs) could reduce the degree of disturbance inflicted to the lymphatic flow. This study aims to intraoperatively differentiate the lymphatic drainage of the prostate from that of the legs using two complementary fluorescent signatures. **Materials and Methods:** Five pigs were included in this study. All animals were adminstered 5mL fluorescein solution (subcutaneous and intramuscular) in the hind leg(s). After allowing drainage to occur for two hours 2ml indocyanine green (ICG-) nanocolloid was intraoperatively injected into the prostate via percutaneous robot-guided needle placement (two - four deposits). Hereafter the different lymphatic drainage patterns were mapped with Firefly laparoscopic fluorescence cameras of the daVinci Si and Xi systems. **Results:** Fluorescein was detected in 29 LNs (average of 5.8 LNs/animal). Two of the five animals got a single sided injection in the right hind leg, which only resulted in the visualization of fluorescein-stained lymph nodes on that side of the anatomy. ICG-nanocolloid visualized 15 prostate related SNs (average of 3 SNs/animal) of which 8 were situated in the left pelvic area and 7 in the right. There was no overlap in the lymphatic drainage pattern of the two different dyes. While ICG-nanocolloid could only be detected using dedicated near-infrared imaging, fluorescein was also visible to the eye in the white light imaging mode. Fully integrated multispectral visualization of the complementary dyes fluorescein and ICG-nanocolloid was most succesfull with the daVinci Si set-up. **Discussion and Conclusion:** We demonstrated the

possibility to distinguish two different lymphatic flow patterns using fully integrated multicolor fluorescence imaging. These preclinical findings motivate further clinical follow-up as this approach can help to further refine lymphatic dissections and with that help maintain the quality of life of the patients.

OP-226

Development of a tumor microenvironment(FAP alpha) targeted near infrared dye for fluorescence guided surgery of cancers

J. Roy[1,2], P. S. Low[2]; [1]National Cancer Institute, Bethesda, MD, UNITED STATES OF AMERICA, [2]Purdue University, West Lafayette, IN, UNITED STATES OF AMERICA.

Aim: Fibroblast activation protein alpha (FAPα), a type II integral membrane proteinase, has emerged as a marker for cancer-associated fibroblasts (CAFs), which constitute one of the major cell types present in the solid tumor microenvironment. Because the FAPα expression is otherwise restricted to myofibroblasts and sites of wound healing/chronic inflammation, its expression in 90% of epithelial tumors has led to the development of drugs aimed at suppressing the growth of epithelial cancers. To date, however, no FAPα-targeted imaging agent has been developed for imaging of solid tumors using non-peptidic, small molecule ligand. Herein we report the in vitro and in vivo (mice xenografts) imaging with a small molecule FAPα-specific ligand(FL) linked to a near-infrared (NIR) dye for use in illuminating cancer nodules during fluorescence-guided surgery. **Methods:** Rhodamine (FL-L1-Rho) and NIR (FL-L1-NIR) conjugates were synthesized using FL linked to the dyes via a non-releasable small spacer. The expression of FAPα in MDA-MB231(M), FaDU(F), KB(K), and HT29(H) cells was determined by using FL-L1-Rho whereas the binding affinity(Kd) of FL-L1-NIR was determined by using FAPα-transfected HEK-293 cells(HEK-FAPα). Whole body and biodistribution studies were performed 2 h post-injection of M, F, K, or H xenografts with FL-L1-NIR (in the presence or absence of FL). The images were taken by using IVIS Lumina II imager. **Results:** In vitro, the cancer cells demonstrated no uptake of FL-L1-Rho indicating the absence of FAPα. The FL-L1-NIR exhibited a high binding affinity (K_d=3.7 nM) in HEK-FAPα cells. When tested in vivo the FL-L1-NIR showed FAPα mediated uptake in the tumor xenografts in which the cancer cells itself were negative for FAPα. The uptake of FL-L1-NIR was blocked in the presence of an excess of FL. Furthermore, the biodistribution study suggested that other than tumors there was minimal or no uptake in other tissues/organs except kidneys which was due to excretion of the conjugate via renal route. **Conclusion:** Through our, in vitro and in vivo studies we could demonstrate that the cancer cells itself did not express FAPα instead it is expressed by the cells of tumor microenvironment. Multiple xenografts were readily imaged following tail vein injection of the FAPα-targeted NIR dye conjugate. Because of tumor-specific uptake of FL-L1-NIR and little or no uptake in any healthy tissues/organs (except kidney during normal excretion of the dye), we conclude that FAPα constitutes an excellent tumor-microenvironment specific antigen and FAPα-targeted

imaging conjugates should prove useful in imaging most human solid tumors.

OP-227

SPECT-based navigation of fluorescence cameras during soft-tissue surgery - is it possible to use a single navigation setup for various open and laparoscopic radioguided surgery applications?

M. N. van Oosterom[1], P. Meershoek[1], G. H. KleinJan[1], K. Hendricksen[2], N. Navab[3], C. J. H. van de Velde[1], H. G. van der Poel[2], F. W. B. van Leeuwen[1]; [1]Leiden University Medical Center, Leiden, NETHERLANDS, [2]The Netherlands Cancer Institute - Antoni van Leeuwenhoek Hospital, Amsterdam, NETHERLANDS, [3]Technical University Munich, Munich, GERMANY.

Introduction: Providing real-time intraoperative visualization, fluorescence-guided surgery is increasingly gaining popularity. However, due to tissue-induced signal attenuation and scatter, the technology is mainly suitable for superficial applications (<1 cm deep). This also limits its use for surgical planning, where nuclear imaging remains the gold standard for non-invasive molecular (total-body) imaging. To compensate for the in-depth shortcomings of fluorescence-guidance, intraoperative positioning of the fluorescence camera can be achieved using the available 3D nuclear imaging data in a dedicated navigation setup. At the same time, underlying navigation inaccuracies, typically arising in soft-tissue anatomies, can be corrected for using the real-time fluorescence feedback. **Materials and Methods:** In this study, a fluorescence camera, with scopes available for both open and laparoscopic procedures, was integrated with a navigation platform, creating one setup for various surgical indications. After camera-system calibrations, navigation targets were shown as augmented reality (AR) overlays in the fluorescence-camera video feed. Using the hybrid tracer indocyanine green (ICG)-^{99m}Tc-nanocolloid, which harbors both a near-infrared fluorescent (ICG) and radioactive (^{99m}Tc) moiety, these navigation targets were generated based on either preoperative single-photon emission computed tomography/computed tomography (SPECT/CT) or intraoperative freehand SPECT (fhSPECT) imaging. The accuracy of this proposed setup was thoroughly evaluated in a phantom study. This was followed by a first-in-human (n=4) translation into radioguided-sentinel lymph node (SN) procedures for penile (open surgery) and prostate (laparoscopic surgery) cancer. **Results:** Overall, the phantom navigation studies revealed a mean tool-target distance accuracy of 2.1 (SPECT/CT) and 3.2 mm (fhSPECT) and a mean AR registration accuracy of 1.1 mm (SPECT/CT) and 2.2 mm (fhSPECT). Using intraoperative fhSPECT imaging, in-human navigation efforts during both open and laparoscopic surgery were directed towards either the primary tumor site or the SNs. In all patients, fhSPECT-based navigation of the fluorescence camera was accurate enough to localize the fluorescence signals of the targeted tissues *in vivo*; thus localizing the tissue to excise. **Conclusion:** Both phantom and in-human studies performed suggest the single navigation setup presented is applicable in both open and laparoscopic radioguided surgery.

By successfully combining the complementary imaging information of both nuclear and fluorescence imaging, the setup allowed for *in vivo* localization of the targeted tissue. Further evaluation, including larger patient groups and a greater variety of malignancies, is recommended to strengthen these results.

OP-228

Molecular imaging of malaria through fluorescent labelling of Plasmodium species within the mosquito host

B. M. F. Winkel, M. N. Oosterom, A. Bunschoten, M. M. Welling, M. C. C. Langenberg, B. Franke-Fayard, C. De Korne, S. C. Chevalley, M. Yazdanbakhsh, F. W. B. van Leeuwen, M. Roestenberg; *LUMC, Leiden, NETHERLANDS.*

Purpose/Introduction: The pre-erythrocytic stage of human malaria is a promising target for malaria vaccine development as parasite numbers are still relatively low and disease symptoms are absent. While attenuated malaria parasites (sporozoites) can be used to induce protective immunity in man, their mode of action is still unclear. In particular, analysis of the elusive human malaria skin phase is needed to improve attenuated sporozoite vaccines. Here sporozoite cell tracking can provide the solution. To realize such imaging studies, we developed a tracer-based method that targets mitochondria (both in vitro as well as within the mosquito host) that allows quantitative tracking of sporozoites in human skin. **Methods:** Sporozoites present in salivary glands of Anopheles stephensi mosquitoes infected with rodent malaria (Plasmodium yoelii or berghei) or human malaria (Plasmodium falciparum) were labelled with TCy5M2. The labelling efficacy was assessed using fluorescence confocal microscopy, conventional fluorescence microscopy and flow cytometry. For evaluation of the movements of sporozoites in the skin 10^6 in vitro TCy5M2 labelled Plasmodium yoelii or wild-type Plasmodium falciparum sporozoites were intradermally injected into human skin explants. Biopsy samples of the injection sites were imaged with fluorescence confocal microscopy for 30-60 minutes. Sporozoite motility in the skin was analysed using tailored MATLAB software. **Results:** In infected mosquito hosts (*in vivo*) and in isolated sporozoite specimens (*in vitro*) TCy5M2 was shown to rapidly accumulate in the mitochondria of sporozoites. Quantification of fluorescence showed a 100-fold increase of fluorescence compared to unstained controls. TCy5M2 labelling did not affect the viability and infectivity of sporozoites (*in vitro* or *in vivo*). Monitoring of migration of *in vitro* TCy5M2 labelled *Plasmodium falciparum sporozoites* in human skin allowed isolation of the dynamic behaviour of the sporozoites and evaluation of differences in directional movement (linear or circular), as well as measurement of velocity and displacement. **Conclusion:** In order to circumvent the need for genetic labels, we have developed a tracer-based molecular imaging method that allows imaging of different *Plasmodium* species at the single cell level. This initial proof-of-concept study shows that this technology can provide a first step towards unravelling the mystery of skin migration of malaria parasites in humans, making molecular imaging a crucial step on the path towards an effective vaccine against pathogens.

OP-229

[⁶⁸Ga]PSMA-I&F: a first successful step towards PSMA-targeted bimodal probes for radio- and fluorescence guided surgery of prostate cancer

M. Schottelius[1], A. Wurzer[1], K. Wissmiller[1], R. Beck[1], J. Notni[1], M. Koch[2], D. Gorpas[2], V. Ntziachristos[2], M. Schwaiger[3], T. Buckle[4], F. van Leeuwen[4], H. Wester[1]; [1]Pharmaceutical Radiochemistry, TUM, Garching, GERMANY, [2]IBMI, Helmholtz Center Munich, Munich, GERMANY, [3]Dept. of Nuclear Medicine, TUM, Munich, GERMANY, [4]Radiology, Leiden University Medical Center, Leiden, NETHERLANDS.

Objectives: [⁶⁸Ga/¹⁷⁷Lu]PSMA-I&T and [⁹⁹ᵐTc]PSMA-I&S are currently successfully employed for clinical PET imaging, radionuclide therapy and radioguided surgery, respectively, of prostate cancer (PC/mCRPC). To be able to exploit the high intrinsic sensitivity and spatial resolution of fluorescence imaging, a first PSMA-I&T-based bimodal agent, PSMA-I&F (nuclear imaging/fluorescence imaging; DOTAGA-k(Sulfo-Cy5)-(i-y)-(i-y)-k-Sub-KuE) has been developed and evaluated. **Methods:** PSMA-affinities (IC_{50}) of PSMA-I&F and its natGa-/natLu-complexes in comparison to the reference compounds natGa/natLu-PSMA-I&T were determined using human LNCaP PC cells and [¹²⁵I]IBA-KuE as radioligand. PSMA-specific internalization (LNCaP cells, 37°C, 0-60 min) of [⁶⁸Ga/¹⁷⁷Lu]PSMA-I&F (2 nM) was investigated in a dual tracer radioligand assay using [¹²⁵I]IBA-KuE (0.2 nM) as internal standard and via fluorescence microscopy (ligand concentration: 25nM). Biodistribution and small-animal PET imaging studies (1h p.i., 0.2 nmol [⁶⁸Ga]PSMA-I&F/mouse) were performed in LNCaP xenograft bearing SHO mice. For one animal, fully automated serial cryosectioning and fluorescence imaging was also carried out (1h p.i., 2 nmol natGa-PSMA-I&F). **Results:** Compared to the parent compounds natGa/natLu-PSMA-I&T (IC_{50}=9.4±2.9 and 7.9±2.4 nM, respectively), PSMA-I&F and its natGa-/natLu-complexes showed very similar PSMA-affinities (10.3±0.7, 10.5±2.1 and 9.6±1.7 nM), which were also reflected in equally efficient tracer internalization for [⁶⁸Ga/¹⁷⁷Lu]PSMA-I&F (103±9 and 106±2% of [¹²⁵I]IBA-KuE after 1h, respectively) compared to [¹⁷⁷Lu]PSMA-I&T (114±8% of [¹²⁵I]IBA-KuE). Fluorescence microscopy revealed PSMA-specific internalization of membrane-bound natGa/natLu-PSMA-I&F into endosomal vesicles within 1h. In vivo, relatively pronounced plasma protein binding (93.7%) resulted in slightly delayed blood clearance of [⁶⁸Ga]PSMA-I&F (2.1±0.4 %iD/g in blood at 1h p.i.). Based on its hydrophilicity (logP= -3.2), however, background accumulation of [⁶⁸Ga]PSMA-I&F was very low (0.9±0.1 and 0.5±0.2%iD/g in liver and intestines, respectively). Dynamic PET imaging confirmed specific (as demonstrated by coinjection of 1μmol PMPA) and consistently increasing uptake into the PSMA-expressing tumor (4.5±1.8%iD/g), kidneys and spleen (106±23 and 13±7%iD/g, respectively) within 1.5h, accompanied by progressive background clearance. Fluorescence imaging of the whole-body cryoslices revealed pronounced inhomogeneity of PSMA-expression in the LNCaP xenograft, homogenous probe uptake in the salivary glands and the renal cortex and in PSMA-expressing ganglia. **Conclusion:** With its high PSMA-specific uptake and its suitable pharmacokinetic profile, [⁶⁸Ga]PSMA-I&F serves as an excellent proof-of-concept

compound for the general feasibility of PSMA-I&T-based bimodal imaging. Based on these results, corresponding hydrophilic [99mTc]-labeled analogs with improved suitability for clinical application in radio- and fluorescence guided surgery of oligometastasized PC have been synthesized and are currently under evaluation.

OP-230

s-Tetrazine: a "clickable" platform for the site-specific dual-labeling of proteins

C. Canovas[1], M. Moreau[1], C. Bernhard[1], M. Cordonnier[2], J. Gobbo[3], A. Oudot[3], F. Denat[1], **V. Goncalves**[1]; [1]Université de Bourgogne, Dijon, FRANCE, [2]INSERM, UMR 866, Laboratoire d'Excellence LipSTIC, Dijon, FRANCE, [3]Centre Georges-François Leclerc, Dijon, FRANCE.

Introduction: Bioconjugates have become essential tools in biomedicine. Among them, doubly-modified proteins constitute an emerging class, which open new fields of application such as bimodal medical imaging and theranostics. Unfortunately, the multiple modification of a protein is still a fastidious and challenging task. In particular, it requires a careful control of the conjugation site(s), as the number and the localization of imaging/therapeutic payloads attached to an antibody can have a dramatic effect on its biodistribution. Here we propose an original approach, based on the use of dichloro-*s*-tetrazine as a platform, for the site-specific dual-labeling of proteins. Dichloro-*s*-tetrazine acts as a trifunctional scaffold to assist the assembly of two agents (imaging, cytotoxic or solubilizing) with a targeting biomolecule. Interestingly, thanks to its ability to undergo an iEDDA reaction, tetrazine makes possible the site-specific dual-labeling of proteins on a single non-canonical amino acid. To validate this strategy, a doubly-modified trastuzumab, suitable for SPECT/optical bimodal imaging, was prepared through site-specific labeling and evaluated in vivo. **Materials and Methods:** Dichloro-*s*-tetrazine was functionalized, by two successive S_NAr reactions, with a macrocyclic chelator (DOTA-GA or NODAGA) and a fluorophore (Rhodamine B, BODIPY or Cyanine 5.0). The bimodal probe substituted with both a DOTAGA and a disulfonated cyanine 5.0, was selected to achieve the study. Vectorization of the bimodal probe was performed via iEDDA reaction between the tetrazine derivative and an anti-HER2 antibody (trastuzumab) previously modified with a bicyclo-1,6-nonyne (BCN). The affinity of the bioconjugate was determined in vitro by BLI. The bioconjugate, radiolabeled with [111In] was injected in BALB/c nude mice xenografted with BT-474 cancer cells. SPECT-CT, optical images and biodistribution data were acquired 24h after the injection. **Results:** In order to demonstrate the simplicity and the versatility of our strategy, a library of "clickable" disubstituted tetrazines, suitable for bimodal imaging applications, was synthesized. Trastuzumab-BCN was successfully doubly-modified via a bioorthogonal reaction (protein recovery: 46%). In vitro studies confirmed the high affinity of trastuzumab for HER2. The radio-labeling by [111In] was achieved at 37°C in 3h. Evaluation in xenografted mice confirmed the favorable biodistribution properties of the dual-labeled trastuzumab and thus validated the viability of our technology. **Conclusion:**

This highly modular strategy enables the production of doubly modified proteins with an efficient control of the bioconjugation step by site-specific labeling. This technology should facilitate the production of such biomolecules and enable the explosion of this next generation of bioconjugates.

---

606   **Monday, October 23, 2017, 08:00 - 09:30, Hall F1**

Pitfalls & Artefacts 3 (Interactive) - Oncology/Inflammation & Infection/Bone & Joint: Pitfalls and Artefacts in Abdomen and Pelvis

OP-231
CT in Abdomen and Pelvis
T. Bäuerle ; *Institute of Radiology, University Hospital Erlangen, Erlangen, GERMANY*

OP-232
Pitfalls in Planar Imaging
L. Mansi ; *Università della Campania "Luigi Vanvitelli", Nuclear Medicine Department, Naples, ITALY.*

OP-233
Pitfalls in SPECT/CT
T. Kuwert; *Friedrich-Alexander-Universität Erlangen-Nürnberg, Erlangen, GERMANY*

OP-234
Pitfalls in PET/CT
L. Evangelista; *Istituto Oncologico Veneto I.R.C.C.S., Padova, ITALY*

---

607   **Monday, October 23, 2017, 08:00 - 09:30, Hall F2**

Clinical Oncology - Rapid Fire Session: What's New? Texture Analysis and More!

OP-236
Textural features assessed by dual time point 18 FDG PET/CT in locally advanced breast cancer: Relation with SUV-based variables and tumor biology

A. García Vicente[1], *G. Jimenez Londoño*[1], *D. Molina*[2], *J. Perez-Beteta*[2], *M. Amo-Salas*[3], *A. Martinez Gonzalez*[2], *M. Tello Galan*[1], *V. Perez-Garcia*[2], *A. Soriano Castrejon*[1]; [1]*General Hospital of Ciudad Real, Ciudad Real, SPAIN*, [2]*IMACI. Universidad de Castilla La Mancha, Ciudad Real, SPAIN*, [3]*Departamento de Matemáticas. Unicersidad de Castilla La Mancha, Ciudad Real, SPAIN.*

Purpose: To study the influence of dual time point 18F-FDG PET/CT in textural features and their relation with SUV-based variables and biological breast tumor characteristics. **Subjects & Methods:** 56 patients with locally advanced breast cancer (LABC) were prospectively included. All of them underwent a standard 18F-FDG PET/CT (PET-1) and a delayed acquisition

(PET-2). After segmentation, SUV variables (SUVmax, SUVmean and SUVpeak) and volume-based parameters as metabolic tumor volume (MTV) and total lesion glycolysis (TLG) were obtained. Eighteen three-dimensional (3D) textural measures were computed including: run-length matrices (RLM), co-occurrence matrices (CM) and energies features. Immunohistochemical characteristics of the tumors were collected to establish risk categories attending to molecular phenotypes: high risk [basal like or HER2 (+) pure], intermediate risk [luminal B-HER2 (-) or luminal B-HER2 (+)] and low risk [Luminal A]. Differences of metabolical variables obtained in dual time point PET/CT and their relations with biological risk categories were assessed. A significance level of p-value <0.05 and correlation coefficient values over 0.75 were taken as indicators of strong correlation. **Results:** Significant differences were found between the SUV based parameters and MTV obtained in the dual time point PET/CT, with higher values of SUV based variables and lower MTV in the PET-2 with respect to those in the PET-1. As to the textural parameters obtained in dual time point acquisition, significant differences were found for the SER (Short Run Emphasis), LGRE (Low Gray-level Run Emphasis), SRHGE (Short Run High Gray-level Emphasis), RPC (Run Percentage), LRE (Long Run Emphasis), GLNU (Gray-Level Non-Uniformity), HOM (Homogeneity) and DIS (Dissimilarity). Total energy (TE), LRE and LRHGE (Long Run High Gray-Level Emphasis) showed strong correlations with volume-based variables and phenotype risk categories. **Conclusion:** Significant differences of textural features were found in dual time point 18F-FDG PET/CT. The dynamic behavior of metabolic characteristics leads to higher heterogeneity in delayed PET acquisition compared with the standard PET. Textural features were also related to volume and biological tumor characteristics. Specifically, larger heterogeneity measures were obtained for bigger and more aggressive tumors.

OP-237

First Interim Results of the Radium-223 REASSURE Observational Study: Analysis of Patient Characteristics and Safety by Prior Use of Chemotherapy

S. Dizdarevic[1], P. Meidahl Petersen[2], M. Essler[3], A. Versari[4], J. Bourre[5], C. La Fougère[6], R. Valdagni[7], G. Paganelli[8], S. Ezziddin[9], J. Kalinovský[10], Y. De Sanctis[11], Y. Du[12]; [1]Royal Sussex County Hospital, Brighton and Sussex University Hospitals NHS Trust, Brighton, UNITED KINGDOM, [2]Rigshospitalet, Copenhagen, DENMARK, [3]Universitätsklinikum Bonn, Bonn, GERMANY, [4]Azienda Ospedaliera Arcispedale Santa Maria Nuova – IRCCS, Reggio Emilia, ITALY, [5]Centre Hospitalier Métropole Savoie, Chambery, FRANCE, [6]Universitätsklinikum Tübingen, Tübingen, GERMANY, [7]Università degli Studi di Milano and Fondazione IRCCS Istituto Nazionale dei Tumori, Milan, ITALY, [8]Istituto Scientifico Romagnolo per lo Studio e la Cura dei Tumori, Meldola, ITALY, [9]Universitätsklinikum des Saarlandes, Hamberg, GERMANY, [10]Bayer, Bratislava, SLOVAKIA, [11]Bayer, Whippany, NJ, UNITED STATES OF AMERICA, [12]Royal Marsden Hospital, London, UNITED KINGDOM.

Aim: Radium-223, a targeted alpha therapy, was shown to extend survival with a favourable safety profile during 3 years' follow-up in patients with metastatic castration-resistant prostate cancer (mCRPC) in the phase 3 ALSYMPCA trial. The REASSURE study was designed with 7 years' follow-up to determine the long-term safety profile of radium-223 and to assess potential treatment-induced secondary malignancies. Here we report the safety data and patients' characteristics from the first planned interim analysis. **Methods:** REASSURE is a global, prospective, single-arm, observational study that enrolled patients with mCRPC with bone metastases for whom radium-223 therapy was planned. It enrolled 1106 patients in North America and Europe from September 2014 to September 2016. The interim analysis by prior use of chemotherapy included data from 583 patients who had completed treatment (median duration of observation 7 months). **Results:** Out of 583 patients, 196 (34%; Group 1) had previously received docetaxel and/or cabazitaxel and 387 (Group 2) had not. At baseline, patients in Group 1 vs. Group 2 were less often ECOG 0-1 (70% vs. 81%), had more metastatic lesions (<6: 23% vs. 34% of patients; 6-20: 52% vs. 57%; >20 [not superscan]: 26% vs. 16%; superscan: 9% vs. 5%), and had higher median levels of prognostic markers (alkaline phosphatase: 162 vs. 115 U/L; prostate-specific antigen: 136 vs. 41 ng/mL). Groups 1 and 2 had similar baseline median levels of haemoglobin (11.8 and 12.3 g/dL, respectively) and platelets (236 and 233 GIGA/L, respectively). Regardless of prior chemotherapy, the majority of patients received 5 or 6 radium-223 doses (Group 1: 54% [median 5 doses]; Group 2: 68% [median 6]). In Groups 1 and 2, respectively, drug-related serious adverse events (AEs; most frequently haematological) occurred in 7.1% and 3.1% of patients and led to permanent discontinuation of radium-223 in 2.0% and 1.3%, while treatment-emergent drug-related AEs (most frequently gastrointestinal or haematological) occurred in 40.3% and 35.1% of patients and led to permanent discontinuation of radium-223 in 9.2% and 4.4%. Overall, bone marrow suppression-relevant treatments were reported for 71/583 (12.2%) patients and blood transfusions for 69/583 (11.8%) patients. Erythropoetins and colony-stimulating factors were each received by 1 (0.2%) patient. **Conclusions:** Radium-223 showed a good short-term safety profile in both groups when used in the routine clinical practice setting. Patients not previously treated with chemotherapy had less advanced disease at baseline than prior chemotherapy recipients and the majority of them completed 5-6 doses of radium-223.

OP-238

Repeatability of tumour hypoxia imaging using [¹⁸F]EF5 PET/CT in head and neck cancer

A. Silvoniemi[1,2], S. Suilamo[1,2], T. Laitinen[1], S. Forsback[1], E. Löyttyniemi[3], V. Saunavaara[1,2], O. Solin[1], T. J. Grönroos[1,2], H. Minn[1,2]; [1]Turku PET Centre, University of Turku, Turku, FINLAND, [2]Turku University Hospital, Turku, FINLAND, [3]University of Turku, Turku, FINLAND.

Introduction: Hypoxia contributes to radiotherapy (RT) resistance and more aggressive behavior of several types of cancer. [¹⁸F]EF5 is a PET tracer showing preferential uptake in hypoxic tissues. Repeatability of hypoxia imaging is of key importance

for biologically guided RT aiming to adapt the dose in poorly oxygenated tissues. This is the first study designed to evaluate the repeatability of intratumour uptake of [18F]EF5 in PET/CT scans. **Subjects & Methods:** Eleven patients with untreated head and neck cancer referred to chemoRT were enrolled. Each patient received three pre-treatment PET/CT scans: two with [18F]EF5 a median of 7 days (range 5-7) apart and one with [18F]FDG following the standard institutional protocol used in RT planning. One patient was excluded from the analyses due to extremely low tracer uptake in the primary tumour in all PET images post diagnostic tonsillectomy. The mean (SD) injected activity of [18F]EF5 was 303 (23) MBq and the 6-min acquisitions were performed a mean (SD) of 178 (9) minutes post injection. [18F]FDG images were rigidly registered with [18F]EF5 images using anatomical information from CT images. Metabolically active primary tumour volumes were defined in [18F]FDG images and transferred to [18F]EF5 images. These volumes were used as volumes of interest in the tumour and voxel level analyses. Tumour-to-muscle uptake ratio (TMR) of 1.5 was used as a threshold representing hypoxic tissue. **Results:** In the 10 paired [18F]EF5 image sets, the average tumour SUV_{mean} and SUV_{max} were 1.52 (0.18) and 2.11 (0.33), respectively. The normally distributed tumour level parameters (SUV_{mean}, SUV_{max} and TMR) showed a good correlation between the scans with the intraclass correlation coefficients of 0.81, 0.85 and 0.87, respectively. The corresponding coefficients of repeatability for these parameters were 15%, 17% and 10%, respectively. Hypoxic subvolumes of the tumours in the repeated scans had a high correlation using Spearman rank correlation test (r= 0.927). In the voxel-by-voxel uptake analysis between the repeated scans the mean of Pearson correlation coefficients (r) of individual patients was 0.65 (range 0.48 - 0.87). The mean (SD) difference of voxel-level uptake (SUV_{scan2}-SUV_{scan1}) in pooled data set was 0.06 (0.22). **Conclusion:** A high repeatability of tumour level parameters was observed in the paired [18F]EF5 PET/CT scans acquired before onset of chemoRT. The voxel-by-voxel analyses showed predominantly good or moderate correlation and agreement between the repeated scans. Our results thus encourage further evaluation of [18F]EF5 PET/CT as a tool for hypoxia targeted treatment interventions.

OP-239

Prostate-Specific Antigen Flare Induced by (223)Ra therapy in Patients with Metastatic Castration-Resistant Prostate Cancer

A. Castello[1,2], *H. A. Macapinlac*[2], *E. B. Santos*[2]; [1]*Nuclear Medicine Unit, Department of Experimental and Clinical Biomedical Sciences, Florence, ITALY,* [2]*Department of Nuclear Medicine, The University of Texas MD Anderson Cancer Center, Houston, TX, UNITED STATES OF AMERICA.*

Purpose: PSA flare is a well-known phenomenon in patients with prostate cancer treated with luteinizing hormone-releasing hormone (LHRH) and chemotherapy, but its impact on patients treated with radium-223 dichloride ($^{223}RaCl_2$) is still unclear. This alpha-emitter is the first calcium-mimetic radioisotope that has been shown to improve overall survival in metastatic castrate-resistant prostate cancer (mCRPC). We sought to evaluate the incidence and the significance of PSA flare on $^{223}RaCl_2$ and its relation on survival. **Materials and Methods**: We conducted a retrospective study of 169 patients with mCRPC who received $^{223}RaCl_2$ between August 2013 and February 2017. Baseline characteristics, disease history and PSA level before and during $^{223}RaCl_2$ therapy were collected. Overall survival (OS) and radiological/clinical progression free survival (PFS), estimated by the Kaplan-Meier method and compared using log-rank test, were evaluated to compare patient subgroups with a PSA flare, immediate decline, and without response. **Results**: An immediate PSA decline was observed in 50 patients (30%) and a PSA flare (defined as any rise after the first cycle followed by any decrease below the peak) in 40 patients (24%), whereas no responders were observed in 61 patients (36%). The 18 remaining patients (11%) had PSA flare followed by decrease below the baseline. This PSA flare subgroup was associated with a median PFS and OS of 26.2 and 23.4 months, respectively. These outcomes were not significantly different from those in patients with immediate PSA decrease from baseline, but were significantly better than in patients with persisted increase (7.4 months for PFS and 11.5 months for OS, both **p** < 0.001). Moreover, the PSA flare group was correlated with the number of $^{223}RaCl_2$ cycles and with improved (or at least stable bone metastases) status than no responder patients (**p** = 0.03). **Conclusion**: The duration of response in our patients with PSA flare after $^{223}RaCl_2$ suggests a change in the tumor environment compared to patients who develop disease progression. To our knowledge, this is the first study about PSA flare in $^{223}RaCl_2$ and its implications on mCRPC therapy. This report suggests that a flare does not necessarily indicate lack of response to $^{223}RaCl_2$ and may in fact be predictive of a positive overall response.

OP-240

The Role of Texture Features Derived from FDG-PET/CT to Characterize Lung Lesions and Predict Survival in Non-Small Cell Lung Cancer Patients Undergoing Surgery

M. Kirienko[1], *M. Sollini*[1], *L. Cozzi*[2], *L. Antunovic*[2], *E. Voulaz*[2], *G. Veronesi*[2], *N. Gennaro*[1], *R. Muglia*[1], *O. Santonocito*[1], *A. Chiti*[1]; [1]*Humanitas University, Milano, ITALY,* [2]*Humanitas Clinical and Research Center, Milano, ITALY.*

Purpose: to evaluate the ability of textural features obtained from FDG-PET/CT images to predict histotype classification (adenocarcinoma (Adk) vs squamous cell (Sqc) carcinoma) and overall survival (OS) in lung cancer patients undergoing surgery. **Methods:** we retrospectively included 185 patients (114 Adk and 71 Sqc) who performed staging FDG-PET/CT from January 2011 to February 2017. FDG-PET/CT images were segmented on AW workstation running PET-vCAR software settled with a 40% SUV_{max} trashold. LifeX software was used to extract textural features from FDG-PET/CT images. Separate analysis has been performed within the 2 datasets of patients that were scanned on the 2 PET/CT scanners present in the department: Scanner A (Discovery 690, General Electric) group (60 Adk + 40 Sqc) and

Scanner B (Biograph, Siemens) group (54 Adk + 31 Sqc). Median follow-up was 20.7 months (range 0.23-69.33). The correlations between textural features and histotype were tested. The correlations between textural features and OS were assessed within Scanner A and B group irrespectively from the histotype. Statistical analysis was performed by R package. **Results:** At univariate analysis, more than 20 features derived from shape and size, gray level co-occurrence (GLCM), gray-level run-length (GLRLM), neighborhood gray-level difference (NGLDM), gray-level zone-length matrixes (GLZLM) resulted to be significantly (p<0.05) correlated to histotype, within both Scanner A and B group. Parameters significant at multivariate analysis resulted in a very good area under the curve using ROC analysis. For more than 10 features derived from the histogram, GLCM, GLRLM, NGLDM and GLZLM it was possible to identify a threshold that was able to separate the population, both Scanner a and B group, in groups with significantly different OS. **Conclusions:** FDG-PET/CT texture analysis seems a promising tool to characterize lung lesions and stratify lung cancer patients suitable of surgery with different outcome. A validation analysis is ongoing to confirm these preliminary results.

OP-241

Transitioning New Technology into the Reading Room - A Secondary Reconstruction Approach for Evaluation of Next-generation Digital PET/CT

K. Binzel[1], J. Zhang[1], C. L. Wright[1], P. Maniawski[2], M. V. Knopp[1]; [1]The Ohio State University, Columbus, OH, UNITED STATES OF AMERICA, [2]Philips Healthcare, Cleveland, OH, UNITED STATES OF AMERICA.

Aim: When introducing a new imaging system or technology, the transition to clinical use requires some level of training regarding improvements and differences from previous technology. With the commercial release of next-generation digital PET/CT, we aimed to create a reconstruction protocol that could best approximate visual and quantitative results from a previous generation scanner, to aid in the transition from conventional to digital PET imaging. **Materials and Methods:** 25 patients had a standard of care scan on a current generation clinical system (Philips Gemini TF 64, TOF 550ps, cPET) 75 minutes post-injection of 480 MBq ^{18}F-FDG. Either immediately before or following the SOC acquisition, patients underwent a secondary scan on a pre-commercial release digital PET/CT system (Philips Vereos, TOF 325ps, dPET). Accounting for the time delay between scans, we then reconstructed the dPET raw data using various settings in order to best match both visual and quantitative characteristics from the cPET scan. Reconstruction settings included using a 144x144 matrix with 4 mm voxel lengths, use of a Gaussian filter, using a lower number of iterative subsets than default reconstruction, and finally reconstruction without Time of Flight information. Two experienced readers evaluated the images for visual comparison. Quantitative evaluation included measuring SUV_{max} of target tumor lesions and SUV_{mean} of background tissues. **Results:** Regarding image quality, we found that the use of the Gaussian filter with a lower number of subsets lead to images being overly smoothed, as compared

to cPET image quality. Readers ranked the non-TOF images with a higher number of subsets as closest in visual appearance to the cPET images. Quantitatively, we found that while the low subset, Gaussian filtered reconstructions produced SUVs most similar to cPET, the non-TOF image sets still reflected a general decrease in SUV, similar to the overall lower SUVs measured on cPET. **Conclusion:** Familiarization with the way improving technology impacts both visual and quantitative aspects of imaging is a critical step in introducing new technologies in a clinical environment. While adaptation of a phantom based assessment, EARL for example, can be performed, intra-individual comparisons of clinical data sets give a more realistic perspective. We found that non-time of flight reconstruction of digital PET data best approximates how a scan would have looked on our conventional PET system. For patients receiving follow-up imaging on a new system, this secondary reconstruction approach will help with consistent and robust evaluation of digital PET/CT images.

OP-242

Radiomics analysis predicts N- and M-stage of primary cervical cancer using multiple PET/MR-derived quantitative features

J. Grueneisen, F. Nensa, K. Herrmann, A. Bariye, M. Forsting, L. Umutlu; University Hospital Essen, Essen, GERMANY.

Purpose: Integrated PET/MRI enables simultaneous acquisition of certain morphological, functional and metabolic parameters, reflecting underlying tumorbiological features. Accordingly, the present study aimed to assess the prediction potential of multiparametric PET/MRI for the evaluation of cervical cancer patients using radiomics analysis. **Subjects & Methods :** A total of 30 consecutive patients with histopathologically proven primary cervical cancer were prospectively enrolled for a 18F-FDG PET/MR examination, prior to the initiation of any treatment. Besides morphological MR imaging (T1w- and T2w-images), the study protocol included the acquisition of several PET- and MR-derived metabolic (18F-FDG PET: standardized uptake values) and functional (DWI: apparent diffusion coefficients (ADCs); DCE-MRI: K^{trans}, Kep, Ve, and iAUC) parameters. For all tumors of the uterine cervix the gross tumor volume was manually segmented using the Fiji software. Subsequently, a voxel-wise binary image mask of each primary tumor was created and quantitative imaging features were extracted using the Radiomic Image Processing Toolbox. Statistical analysis and modeling was performed in the R software environment for statistical computing and graphics. A generalized boosted regression model based on stochastic gradient boosting was trained to predict N- and M-status using the caret package. **Results:** Forty-five different image features were calculated from native T1- and T2-weighted images, the ADC map, the parametric Ktrans map and PET images, respectively, totaling 225 features. The 20 highest ranking features, based on *P* values of univariate analyses were selected and trained on a subset of 18 observations and tested on the remaining 12 observations. For the classification of N-stage the model achieved strong predictive power in the testing

group. Receiver operating characteristic analysis revealed an area under the curve of 0.97. At 100% sensitivity the model provided 80% specificity and an accuracy of 91% (95% confidence interval [59% - 100%]). For the classification of M-stage the model achieved perfect predictive power in the testing group. ROC analysis revealed an AUC of 1.0. At 100% sensitivity the model provided 100% specificity, resulting in an accuracy of 100% (95% confidence interval [72% - 100%]). Finally, a total of 6 identical image features were found to be top predictors of both M- and N-stage. **Conclusion:** Using Radiomics analysis based on multiparametric PET/MR datasets, our results reveal strong correlations between PET and MRI-derived quantitative features and major prognostic factors of cervical cancers. Therefore, PET/MRI datasets provide a number of non-invasive biomarkers, potentially facilitating improved tumor evaluation and prediction of prognosis.

OP-243

Simultaneous whole-body ^{18}F-PSMA-1007-PET/MRI with integrated high-resolution multiparametrical imaging of the prostatic fossa for comprehensive oncological staging of patients with prostate cancer

M. T. Freitag[1], C. Kesch[2], J. Cardinale[1], P. Flechsig[2], R. Floca[1], M. Eiber[3], D. Bonekamp[1], J. P. Radtke[2], C. Kratochwil[2], K. Kopka[1], H. Schlemmer[1], U. Haberkorn[2,1], F. L. Giesel[2,1]; [1]German Cancer Research Center, Heidelberg, GERMANY, [2]University Hospital Heidelberg, Heidelberg, GERMANY, [3]Technical University Hospital Munich, Munich, GERMANY.

Introduction: To explore the clinical feasibility, reproducibility and presence of PET-artifacts using a whole-body ^{18}F-PSMA-1007-PET/MRI protocol combined with integrated multiparametric prostate imaging for imaging prostate cancer (PC) patients. **Methods:** After ^{18}F-PSMA-1007-PET/CT was performed (1h p.i.) as reference, eight patients with proven high-risk PC underwent a whole-body PET/MRI (3h p.i.) including a prostate MRI protocol according to PIRADS 2.0 guidelines using a prototype T1w CAIPIRINHA-accelerated attenuation correction for enhanced whole-body workflow. SUV$_{mean}$ quantification for reproducibility was performed using a thresholded (60%) 3D-isocontour volume of interest of SUV$_{max}$. PET-artifacts (Cohen's kappa) on a scale from 0 to 3, coregistration of prostate PET/MRI (>3mm shift between bladder outline in PET and MRI) and prostate MRI (PI-RADS 2.0) were assessed. **Results:** The examinations were well accepted by patients and comprised 1 hour. SUV$_{mean}$ values between PET/CT (1h p.i.) and PET/MRI (3h p.i.) were linear (PET/CT 9.0±5.0, PET/MRI 11.4±6.1, p<0.0003 pathological VOIs and PET/CT 19.6±7.5, PET/MRI 21.8±10.4, p<0.0001 physiological VOIs) demonstrating reproducibility. Mostly slight to moderate photopenic artifacts were noticed in PET/MRI in the abdomen, surrounding liver and kidneys (kappa 0.82 (CI 0.62-1.00)) with a mean of 1.13±0.99 (reader 1) and 1.38±0.74 (reader 2). Both readers agreed to 100% that the PET-component of the PET/MRI did not reveal any artifacts in head/neck and thorax. Both readers agreed to 100% that the PET-component of the PET/CT did not reveal any artifacts

in the four compartments defined. All acquisitions of PET and MRI of the prostatic fossa obtained simultaneously could be co-registered with optimal match of bladder volume between both modalities. All patients featured PI-RADS 5 findings indicative of PC. **Discussion and Conclusion:** The presented ^{18}F-PSMA-1007-PET/MRI protocol combines efficient whole-body assessment with high-resolution co-registered PET/MRI of the prostatic fossa, cinically feasible in 1 hour. Moderate photopenic artifacts were noticed surrounding the high-contrast areas liver and kidneys reflecting the biodistribution of the tracer. However, compared to the known artifacts that may occur in ^{68}Ga-PSMA-11-PET/MRI in the bladder region, no artifacts were noticed there using ^{18}F-PSMA-1007 which we considered beneficial for assessment of pathologies arising in the prostatic fossa. This promising protocol is proposed as a comprehensive staging for patients with prostate cancer exploiting the optimal tracer biodistribution of ^{18}F-PSMA-1007 (low bladder clearance) and the synergistic combination of T-(MRI) and N/M-staging (PET and MRI).

OP-244

Combined use of Ga-68 PSMA-HBED and multiparametric MRI imaging of patients with carcinoma of the prostate in the primary staging setting and in cases of biochemical recurrence after radical prostatectomy

Z. E. Ballok[1,2], M. Frydenberg[3], K. Marshmann[1], R. O'Sullivan[1], D. Reilly[1]; [1]BRI, Richmond, AUSTRALIA, [2]MMC, Melbourne, AUSTRALIA, [3]Australian Urology Association, Malvern, AUSTRALIA.

Background: Both multiparametric MRI and Ga-68 PSMA-HBED imaging is a rapidly growing investigation of choice for assessment of patients with carcinoma of the prostate. **Aims**: To assess the complimentary role of multipara metric MRI and Ga68 PSMA-HBED PET scanning of patients with carcinoma of the prostate **Results**: Of the 116 consecutive patients from a single urology clinic, who underwent both multiparametric MRI scan and a Ga68-PSMA scan, 57 patients were referred for primary staging and 59 patients were imaged with biochemical recurrence after prior radical prostatectomy. Age of the patients was between 42 and 90 years with a median of 69 years and between 53 years and 80 years with a median of 68 years in the primary staging and in the biochemical recurrence group, respectively. PSA levels were between 1.6 and 2300 ug/L with a median of 6.8 ug/L and between 0.06 and 28 ug/L with a median value of 0.35 ug/L in the primary staging group and in the biochemical recurrence group, respectively. In the primary staging setting Ga68PSMA HBED PET scan accurately located more extensive, multifocal or bilateral disease as compared to multiparametric MRI scan in 11 cases, showed disease only on the contralateral site as compared to mpMRI scan in 1 patient, accurately predicted pelvic nodal metastasis in 5 more patients than mpMRI scan and down staged 2 patients with suspected boney metastatic disease on mpMRI scan. In the biochemical recurrence group multiparametric MRI detected 11 more local recurrence within the prostate bed region while Ga-68 PSMA-HBED imaging detected 3 distant metastases,

was convincingly positive within regions of small pelvic nodes within the pelvis in 9 cases with equivocal or negative findings on mpMRI while imaging results were concordant in 36 patients. Biopsy of two of the prostate bed region lesions found on mpMRI showed BPH only. **Conclusion**: Ga-68 PSMA-HBED imaging is currently the most accurate examination to detect the site(s) of metastasis/recurrence of previously treated carcinoma of the prostate with biochemical recurrence; however mpMRI is more accurate to demonstrate small local residual/recurrent prostate bed region lesions when this is the only site of recurrence. Our study also suggests that Ga-68 PSMA-HBED and mpMRI scans may also play complimentary role in the primary staging setting.

OP-245

Texture analysis is more predictive than SUV in 18F-Choline PET of the aggressiveness of prostate cancer

F. Hives[1,2], A. Fagart[2], K. Bouharati-Moussa[1], M. Fares[3], L. Drelon[4], P. Danjou[5], O. Decavel[6], B. Makki[1], S. Adib[1]; [1]Service de médecine nucléaire, centre hospitalier de Béthune, Béthune, FRANCE, [2]Service de médecine nucléaire, Université Lille 2, Lille, FRANCE, [3]Service de radiothérapie, Centre Pierre Curie, Béthune, FRANCE, [4]Service d'urologie, clinique des deux caps, Coquelles, FRANCE, [5]Service d'urologie, centre hospitalier de Lens, Lens, FRANCE, [6]Service d'urologie, clinique Anne d'Artois, Béthune, FRANCE.

Aim: Nowadays, prostate cancer is the most prevalent cancer in men. The ^{18}F-Choline, a membrane proliferation marker, is mainly used for the detection of recurrent prostate cancer. Its use in the diagnosis and the initial staging is still controversial. A potential application may be to increase the detection rate of clinically suspected prostate cancer with negative prostate biopsies. The use of texture analysis in nuclear medicine shown promising results to predict tumor aggressiveness, response to therapy or survival prognostic in neoplastic diseases. Our aim was to assess the tumor aggressiveness of prostate cancer according to the Gleason scoring using the texture analysis of ^{18}F-Choline in positron emission tomography (PET). **Materials and Methods:** Our study is a retrospective analysis of 55 patients with prostate cancer who underwent ^{18}F-Choline PET in initial staging, strictly before treatment. Gleason scores were analyzed from the initial needle biopsy. They were allocated as: 3+3 (n=11, group 1), 3+4 (n=23, group 2) and >3+4 (n=21, group 3). We performed an adaptive threshold of the whole prostate to extract intensity (SUV_{mean}, SUV_{max}, SUV_{peak} and total lesion glycolysis (TLG)) and robust texture uptake (entropy, homogeneity, SRE, LRE, LGZE and HGZE). **Results:** SUV_{max}, SUV_{mean} and SUV_{peak} tented toward increase between 3+3, 3+4 and >4+3 without significant statistical difference. Also, the texture parameters tended to decrease (homogeneity, LRE) or increase (SRE, HGZE) with growing Gleason score with significant statistical difference between 3+3 and >4+3 for SRE (**p**=0.025) and LRE (**p**=0.0182). With the receiver operating characteristic (ROC), the areas under curve (AUC) between groups 1/2, 2/3 and 1/3 were higher with homogeneity, SRE and LRE than with all intensity parameters, included significant statisti-

cal differences in 1/3 with SUV_{max} (homogeneity: **p**=0.0229; SRE: **p**=0.0280; LRE: **p**=0.0432). Neither intensity nor texture parameters were correlated with prostate specific antigen (PSA). **Conclusion:** To our knowledge, our study is the first to evaluate the texture analysis in prostate cancer in ^{18}F-Choline PET. Whereas we did not find significant difference between intensity parameters and the tumor differentiation according to the Gleason scoring, the texture analysis revealed two parameters (SRE and LRE) with significant difference between 3+3 and >3+4. This result shows that the texture analysis could be more predictive of the aggressiveness of prostate cancer than SUV. Furthers studies, with higher number of patients and comparison to the survival prognostic, are necessary to ensure the efficiency of texture analysis in prostate cancer in ^{18}F-Choline PET.

OP-246

SPECT-CT visualization of sentinel and second echelon lymph nodes for lymph flow guided radiotherapy of tongue cancer

S. Novikov, P. Krzhivitskiy, Z. Radzhabova, O. Ponomareva, M. Girshovitch, S. Kanaev; N.N. Petrov Institute Oncology, St Petersburg, RUSSIAN FEDERATION.

Purpose: to evaluate patterns of lymph flow from primary lesions in patients with tongue cancer and to determine how useful can be this information for radiotherapy planning. **Materials and Methods.** In 24 primary patients with tongue cancer we performed SPECT-CT visualization of sentinel and second echelon lymph nodes (LNs). SPECT-CT examination was performed 60-90 min after 4 peritumoral injections of 99mTc-nannocolloids (100-150MBq in 0.3-0.4ml). We determined the type of lymph flow (mono-, bilateral) and localization of all LNs with tracer uptake. Finally, status of regional LN was verified by histology and/or MRI with US. **Results:** Bilateral lymph-flow was detected in 14 of 25 (58%) evaluated patients. In 10 of 14 cases distance from medial sulcus to medial border of primary tumor was 4mm or less. Monolateral lymph-flow was mentioned in remained 10 patients (42%). In 9 of 10 cases distance from medial sulcus to primary lesion was above 4mm. In 5 of 24 patients (20.8%) LNs with 99mTc-nannocolloids uptake were localized only on Ib-IIa levels. In another 15 cases (62.5%) sentinel and second echelon LNs were visualized on level Ib-IIa-III. Wide distribution (Level Ia-IIa-III-IV-VI) of LNs with tracer uptake was mentioned in 4 (16.6%) cases. In 16 of 24 patients we revealed histological and /or instrumental (MRI plus US) signs of metastatic LN involvement. In all cases LNs with tracer uptake were localized on the same level and/or more distal. According to proposed strategy of lymph flow guided radiotherapy we irradiate regional LN that localized on the level of visualized sentinel and second echelon LNs. It means that in evaluated 24 patients this strategy would permit irradiation of all metastatic LNs revealed by histology and/or by MRI/US. In the same time irradiation volumes would be decreased in 75% cases. **Conclusion:** SPECT-CT visualization of lymph flow from tongue cancer can significantly influence extent of radiotherapy fields used for irradiation of regional LNs

OP-247

18F-FDG PET/CT radiomics in endometrial cancer

C. Crivellaro[1,2], E. De Bernardi[1], D. Vicini[1], F. Elisei[2], M. Cuzzocrea[1], A. Buda[3], E. De Ponti[4], F. P. Sina[3], L. Guerra[2], R. Fruscio[1,3], C. Landoni[1,2]; [1]University Milan-Bicocca, Monza, ITALY, [2]Nuclear Medicine, ASST-Monza, San Gerardo Hospital, Monza, ITALY, [3]Clinic of Obstetrics and Gynecology, ASST-Monza, San Gerardo Hospital, Monza, ITALY, [4]Medical Physics, ASST-Monza, San Gerardo Hospital, Monza, ITALY.

Background: 18F-FDG PET/CT is a diagnostic tool for staging endometrial cancer, in particular for nodal status assessment. **Objectives**: To evaluate the role of textural and geometric shape features extracted from 18F-FDG uptake of the uterine primary lesions in endometrial cancer. In particular, we investigated if these features, inserted in a clinical model, can predict recurrence and nodal metastases by using a machine learning technique. **Methods:** 85 patients with early stage endometrial cancer who underwent preoperative PET/CT scan followed by surgery were considered. Histological and clinical data were collected. Endometrial lesions were contoured with PETVCAR (GE Healthcare) and the following parameters were extracted: SUVmax, SUVmean, MTV, TLG, 6 geometrical shape and 64 textural features (computed by CGITA software). For recurrence analysis, only patients with a follow-up longer than the maximum recurrence time (35 months) were considered. Univariate analysis for association between features and recurrence/LN metastases was performed by Mann Whitney test; the correlation between features was investigated by Spearman rank test. Two neural network multivariate models were developed to predict recurrence and LN metastases. A stepwise backward feature selection scheme was adopted and neural networks were assessed with a leave one out approach on 10 training sessions. **Results:** Recurrence rate was 29% (15/51) patients. Univariate analysis found 16 PET-features correlated with recurrence ($p<0.05$). At multivariate analysis, a 2 layers neural network with 3 inputs (myometrium invasion, Zone percentage-GLSZM and Maximum of the texture Spectrum) can predict recurrence with a sensitivity of 73% +/-4% and with a specificity of 83% +/- 1%. Nodal metastases were found in 14/78 (20%) patients submitted to lymphadenectomy. Sensitivity and specificity of PET/CT in detection of nodal metastases resulted 50% and 90%, respectively. MTV and 28 PET-features were associated with LN metastases ($p<0.01$). A 3 layers neural network with 2 inputs (Zone percentage-GLSZM and Entropy-GLCM) resulted able to predict LN metastases with a sensitivity of 50%+/-8% and a specificity of 90% +/-1%. Combining PET/CT findings at nodal level and the neural network, sensitivity resulted 83%+/-6% and specificity 88%+/-1%. **Conclusions:** In endometrial cancer, the combination of PET textural features of primary lesion and histological data can predict the presence of recurrence. Although the known role of PET/CT in nodal staging, textural features may have ad additional value in predicting nodal metastases. These preliminary data suggest a promising application of radiomics in endometrial cancer; further studies on larger populations are needed.

Committee Symposium 2 - Neuroimaging: PET/MR - Making it Clinical

OP-248

Attenuation correction - is it solved?
C. Ladefoged; Copenhagen University Hospital Rigshospitalet, Nuclear Medicine & PET, Copenhagen, DENMARK.

OP-249

Brain Tumours
I. Law; Copenhagen University Hospital Rigshospitalet, Nuclear Medicine & PET, Copenhagen, DENMARK.

OP-250

Epilepsy - what does simultaneous PET-MR achieve that PET+MR does not?
A. Hammers; King's College London, Imaging Sciences and Biomedical Engineering, London, UNITED KINGDOM.

OP-251

Dementia
A. Drzezga; University of Cologne, Nuclear Medicine, Cologne, GERMANY.

Conventional & Specialised Nuclear Medicine: Musculoskeletal (Benign)

OP-252

Low Dose Radiation 18F-Fluoride PET/CT in the assessment of Unilateral Condylar Hyperplasia of the mandible: preliminary results of a 16 patients single centre experience

G. M. Lima, S. Diodato, E. Costabile, D. Calabrò, F. Scalorbi, A. Svirydenka, G. Cicoria, S. Civollani, C. Pettinato, P. L. Guidalotti, C. Nanni, S. Fanti; S. Orsola-Malpighi University Hospital, Bologna, ITALY.

Aim: Unilateral condylar hyperplasia (UCH) of the mandible, or Hypercondylia, is a pathological condition that determines an abnormal growth of the affected condyle. Tc99m-diphosphonates Bone SPECT is a successful tool in the assessment of UCH. EANM guidelines also suggest the use of 18F-NaF PET/CT, though it leads to a higher radiation exposure. As UCH patients are young, we aimed to compare a low-injected activity 18F-Fluoride PET/CT scan to a standard-injected activity scan in terms of image quality in the evaluation of UCH. **Materials and Methods**: We prospectively enrolled 16 patients (6 males, 10 females, mean age 24.5) with UCH, who underwent 18F-NaF PET/CT to assess the hypercondylia. We administered a low activity of 18F-NaF (185 MBq) in 5 patients and a standard activity (370 MBq) in 11 patients. Activity range was chosen according to 2015 EANM guidelines. One hour after injection, a single-bed

10 minutes PET acquisition from the glabella to the chin and an attenuation correction CT were performed. To determine if the scans with low radiotracer activity were "diagnostic" such as those with standard activity, three expert nuclear medicine physicians, unaware of the administered activity, reviewed the scans and expressed a final qualitative judgment in terms of "diagnostic"/"non-diagnostic" scan. Furthermore, we compared the effective dose of a low-injected activity PET/CT to the standard one and to a Bone SPECT performed with standard-injected activity of Tc99m-diphosphonates. **Results:** Reviewers classified all scans of both groups as "diagnostic". The effective dose of a 18F-Fluoride PET/CT is about 5.0 mSv [(0.024 mSv/MBq x 185MBq) for PET + 0,15 mSv for low dose CT] in scans performed with 185 MBq and about 9.0 mSv [(0.024 mSv/MBq x 370MBq) for PET + 0.15 mSv for low dose CT] in ones performed with 370MBq. The effective dose of 99mTc-MDP bone SPECT is about 4.3 mSv [0.0057 mSv/MBq x 740 MBq of Tc99-MDP]. **Conclusion:** 18F-NaF PET/CT performed with a low radiotracer activity allows a good assessment of UCH similar to that performed with an ordinary activity. The effective radiation dose of a low-injected activity PET/CT is significantly lower than an ordinary-injected activity PET/CT and is not significantly higher than the most used Bone SPECT. The 18F-Fluoride PET/CT procedure could be performed with 185MBq to minimize the effective radiation dose received, maintaining the quality of the scan. Further studies including a larger number of patients and clinical follow-up are needed to confirm our preliminary findings.

OP-253

Diagnostic ability of bone scan index for differentiating dental diseases

S. Watanabe, K. Nakajima, N. Noguchi, S. Kawashiri, A. Mizokami, M. Inokuchi, S. Kinuya; Kanazawa University Hospital, Kanazawa, JAPAN.

Purpose: Osteonecrosis of the jaw (ONJ) is a significant side effect of antiresorptive and antiangiogenic drugs prescribed for advanced cancer patients. We have reported that a quantitative diagnosis of bone scintigraphy using bone scan index (BSI) was useful for the early detection and risk assessment before the development of stage 2 antiresorptive agent-related ONJ (ARONJ). However, common dental diseases also cause positive tracer uptakes in the jaws. The aim of this study was to validate a diagnostic ability of BSI for differentiating ARONJ from common dental diseases. **Methods:** We evaluated 147 patients who underwent both bone scintigraphy and dental examination at our hospital retrospectively. In the control group, all 130 patients underwent dental examination within 3 months of the bone scintigraphy between January 2014 and December 2014. We excluded patients who developed ARONJ. In the ARONJ group, all 17 patients were diagnosed as stage 2 ARONJ between June 2007 and March 2016 and underwent bone scintigraphy 3 months (the average 2.8±1.9 months) before the first diagnosis of stage 2 ARONJ. Dental conditions were evaluated in four blocks, namely, upper or lower jaw, and right or

left region. The tracer uptake in each block was analyzed by BSI. The software BONENAVI (FUJIFILM RI Pharma; EXINIbone, EXINI Diagnostics) could automatically detect abnormal intensities and calculate each regional BSI (rBSI). Among the rBSI, the largest one in each block was manually selected and defined as maximum BSI of the jaw (BSIJmax). We compared the BSIJmax with the dental examination, as a gold standard. Results: In the control group, mild periodontitis, severe periodontitis, apical periodontitis, and dental caries were observed in 47 blocks, 7 blocks, 13 blocks, and 19 blocks, respectively, and the average BSIJmax were 0.03±0.02, 0.05±0.03, 0.03±0.03, and 0.04±0.04, respectively. Dental extraction was performed in 13 blocks before the bone scintigraphy, and the average BSIJmax was 0.06±0.05. In the ARONJ group, stage 2 ARONJ was subsequently observed in 22 blocks, and the average BSIJmax was 0.11±0.09, 3 months before the diagnosis. The BSIJmax was significantly higher in blocks where ARONJ was subsequently observed than in blocks where common dental diseases were observed (p < 0.005). However, there was no significant difference in BSIJmax between blocks where ARONJ was subsequently observed and blocks where dental extraction was performed (p = 0.06). **Conclusion:** BSIJmax could differentiate ARONJ from common dental diseases and be useful for the early detection and risk assessment of ARONJ.

OP-254

Influence of 18F-FDG-PET/CT on therapeutic decision-making of patients with spondylodiscitis

A. Pöllmann, D. Moskopp, M. Plotkin; Vivantes Klinikum im Friedrichshain, Berlin, GERMANY.

Introduction: Inflammatory diseases of the spine may be difficult to diagnose using morphologically oriented imaging methods (MRI, CT). 18F-FDG-PET/CT has proposed as an additional tool for the detection of spondylodiscitis (SD). We examined the extent to which PET/CT affected treatment decisions in patients with SD. **Methods:** Electronic medical records of 58 patients from the period 07/2011 - 03/2015 who were examined at Vivantes Institut für Nukelarmedizin were evaluated retrospectively. The patients were divided into two sub-groups: the first group (n = 34) included all patients who were examined with PET/CT under the tentative diagnosis of SD. In the second group (n = 24) with pre-diagnosed inflammatory spinal disease (SD and/or epidural abscess), PET/CT was performed to search for an occult infection focus. We evaluated to what extent the PET/CT had an impact on the therapeutic decision-making (high, medium or low). **Results:** Group 1: PET/CT showed SD in 16/34 patients and a liver abscess in one patient. PET/CT was negative in 17 patients. The impact of PET/CT on the therapeutic decision was classified as follows: 17/17/0 (high/medium/low). For 17/34 patients MRI data were available; in the remaining patients an MRI scan could not be performed (implanted pacemaker, obesity, claustrophobia). 15 of this MRI scans were negative for SD, two showed unclear findings. In the patients with negative MRI, PET/CT showed SD in 6 cases. Of the patients with unclear MRI results, one PET/CT discovered SD. Group 2: PET/CT lead to sub-

stantial findings (previously unknown infection focus or findings suspicious for malignancy) in 4/24 patients. The impact of PET/CT on the therapeutic management was classified as follows: 04/04/16 (high/medium/low). **Discussion:** ^{18}F-FDG-PET/CT is a valuable additional diagnostic tool in the primary diagnosis of spondylodiscitis and should be used in particular when an MRI scan of the spine is contraindicated, shows unclear results or if SD is still probable in spite of negative MRI. PET/CT is not helpful for detection of inflammatory focuses in patients with already diagnosed inflammatory spinal diseases, and depicts previously unknown lesions in rare cases.

OP-255
SPECT/CT imaging in Bertolotti's Syndrome

K. Bayardo[1,2], V. Depons[2], J. Vilar[1,2], D. Muñpz[1], A. Battegazzore[2], A. Silveira[2], R. Ferrando[1,2]; [1]Clinics Hospital, University of the Republic, Montevideo, URUGUAY, [2]Ferrari Ferrando Páez Nuclear Medicine Clinic, Montevideo, URUGUAY.

Introduction: Lumbosacral transitional vertebrae (LSTV) are common congenital anomalies of the lumbosacral segment present in 3%-21% of humans. The transitional vertebra may have different morphology ranging from broadened elongated transverse processes, often unilateral, to complete fusion to the sacrum. Inaccurate identification of LSTV may lead to surgical and procedural errors and poor correlation with clinical symptoms. The relationship between low back pain and LSTV (Bertolotti's syndrome) has been debated but pain may arise from varying levels and L5 sacralization can contribute to the development of orthopedic diseases. The Castellvi classification system describes four types of LSTV with increasing levels fusion (I-IV) and unilateral (a) or bilateral (b) dysplastic transverse processes. LSTV are difficult to recognize in SPECT images and currently CT is the best imaging technique for characterization of this entity. The objective was to describe SPECT/CT findings in patients with LSTV and low back pain. **Subjects and Methods:** The study population included 63 consecutive patients (35 female), with a mean age of 22 years (range 8-49), who underwent SPECT-CT imaging in our institutions in which a LSTV was identified. Low back pain was present in all but two patients. Patients older than 50 years were excluded. **Results:** CT images identified 18 type Ia LSTV, 4 type Ib, 21 IIa, 8 IIb, 1 IIIa, 9 IIIb, and 2 type IV with SPECT showing associated increased uptake in 52 patients. Six of the 11 cases with negative SPECT had type IIIB LSTV, in which increased uptake is less likely because of bilateral complete fusion. The other cases were 4 type I and 1 IIb. The remaining type III LSTV had only mild uptake at the the vertebral body transition. All type II LSTV and 1 patient with type IV had more intense lateralized incresed uptake associated with incomplete fusion. Moderately increased sacroiliac joint uptake was present in 9 patients and facet joint uptake in 3. Associated anatomical anomalies included incomplete vertebral fusion in 3 patients and disc herniation in 2. **Conclusion:** Hybrid imaging with SPECT/CT provides a new scenario for the characterization of LSTV. Specific morphological features can be recognized while the presence of stress in the lumbosacral

transition or neoarticulation can be detected, as well as associated reactions in facet and sacroiliac joints. Bertolotti's syndrome should always be considered in radionuclide studies assessing low back pain, particularly in young patients. SPECT/CT provides new cues supporting the syndrome.

OP-256
Scintigraphy of rhabdomyolysis - cornerstone in patient management?

D. Jocius[1], D. Vajauskas[1], A. E. Tamosiūnas[1,2], A. Skrebunas[1], M. Gutauskas[1]; [1]Vilnius University Hospital Santaros Klinikos, Vilnius, LITHUANIA, [2]Vilnius University, Vilnius, LITHUANIA.

Introduction: 99mTc MDP (99mTc methylene diphosphonate) is used as a diagnostic agent in both benign and malignant bone conditions. 99mTc MDP and other phosphonates are nonspecific tracers are used in osteoblastic bone lesion imaging and muscle necrosis imaging. When the cellular damage occurs pathophysiological mechanisms such as direct cell membrane damage or ATP (adenosine triphosphate) depletion leads to elevated intracellular calcium (Ca^{2+}) level which subsequently leads to cell apoptosis [1]. Such intracellular alteration elevates 99mTc MDP accumulation in the damaged site mimicking calcium deposition though enabling to image irreversible cell damage or cellular death such as muscle necrosis [2]. **Aim** The aim of this retrospective review is to evaluate the role of 99mTc MDP scintigraphy in assessing the site and extent of muscle necrosis. **Materials and Methods:** We retrospectively reviewed three year (2014-2017) results of 99mTc MDP scan performed in 14 patients with suspected limb muscle necrosis by elevated blood myoglobin concentration and clinical symptoms of rhabdomyolysis caused by several mechanisms. Further diagnosis was confirmed either by muscle biopsy if only fasciotomy was performed (2 patients) or after histological examination of resected surgical specimen: amputation (7 patients) or necrectomy (5 patients). **Results** Arterial disease was the leading cause of muscle necrosis, found in 12 patients and the remaining two patients acquired muscle necrosis due to positional compression syndrome. 99mTc MDP scan correctly showed increased pathological tracer uptake in limb muscle for all patients suggesting muscle necrosis which further was confirmed by histological examination in all cases. In addition hybrid SPECT/CT 99mTc MDP scan identified precise location and extent of affected muscles directing surgical treatment approach. **Discussion** Conservative management (meaning fasciotomy only) was chosen when only mild intramuscular tracer uptake in a small area was seen and while more aggressive surgical tactics such as necrectomy or limb amputation were performed in more severe cases with wide areas of tissue damage and high intramuscular tracer uptake. Special notification should be made for "cold" tracer uptake spots which probably were seen in avascular sites with total myolysis. **Conclusion** This retrospective study results shows that 99mTc MDP scan is effective diagnostic tool in describing muscle necrosis and showing the location and extent of damaged tissue. 99mTc MDP scan could be used as prognostic tool also directing the choice of treatment.

OP-257

Clinical relevance of 99mTc-HDP SPECT/CT in the diagnosis of spondyloarthropathies

A. Bakos[1], Z. Besenyi[1], S. Urbán[1], R. Hemelein[2], L. Kovács[2], L. Pávics[1]; [1]Department of Nuclear Medicine University of Szeged, Szeged, HUNGARY, [2]Department of Rheumatology University of Szeged, Szeged, HUNGARY.

Introduction: Spondyloarthropathies (SpA) belong to the group of inflammatory arthritis which comprises the ankylosing spondylitis, reactive arthritis, psoriatic arthritis/spondylitis, and arthritis/spondylitis associated with inflammatory bowel diseases. The early diagnosis is extremely important for starting appropriate therapy in time. Our aim is to examine the clinical significance of 99mTc-HDP SPECT/CT in diagnosis of early and chronic axial SpA. **Materials and Methods:** Thirteen patients (6 females, 7 males, mean age: 38,69 years) were involved into the study from 2016 July. The patients were selected from the Department of Rheumatology according to the clinical features. Firstly, we performed examination of the sacroiliac joint with MRI in the following sequences: T1- weighted STIR for the bone marrow oedema (BME) and T2-weighted sequence for the fat metaplasia (FM). The HDP SPECT/CT was used within one week to examine the sacroiliac joint. Thereafter, the MRI images were fused with SPECT/CT images. On the MRI images the BME (active lesion) and FM (chronic lesion), on the CT scans the sclerotic lesions (SCL, chronic lesion) were drawn manually as volume of interest (VOI). Uninvolved cortical areas were drawn on the different modality slices as reference region (ref). Then, we determined the isotope (99mTc-labelled HDP) uptake of the different lesions and areas (mean counts/VOI): VOI_{BME}/VOI_{ref}, VOI_{FM}/VOI_{ref}, VOI_{SCL}/VOI_{ref}. **Results:** Four active sacroileitis and five chronic sacroileitis without active lesions were diagnosed according to the MRI results. On the other 4 patient's sacroiliac joints images (MRI, scintigraphy, CT scans) there were not any pathological lesions. Nineteen lesions of 13 patients were localised on the fused MRI-SPECT/CT images: 6 BME, 4 FM and 9 SCL lesions. The isotope uptake of BME was the highest (VOI_{BME}/VOI_{ref}: 2,43). The radiopharmacon uptake of sclerotic lesions was moderate (VOI_{SCL}/VOI_{ref}: 1,76). The isotope uptake of FM lesions was not different from the HDP uptake of reference regions (VOI_{FM}/VOI_{ref}: 0,96). **Conclusion:** MRI is established modality in diagnosis of axial SpA. According to the initial results, the different MRI lesions have different isotope uptake, which suggests, that the HDP-SPECT/CT can distinguish the early and chronic stage of axial SpA.

OP-258

Increased Uptake in Synchondrosis of the Lower Limbs: Added Value of SPECT/CT.

K. Bayardo[1,2], A. Zamora[1], J. Vilar[1,2], R. Ferrando[1,2]; [1]Clinics Hospital, University of the Republic, Montevideo, URUGUAY, [2]Consultorio de Medicina Nuclear Ferrari Ferrando Páez, Montevideo, URUGUAY.

Introduction: Synchondrosis is the development of a union between two bones by hyaline cartilage that mostly represents a temporary joint present during the growth phase. Usually the fusion is asymptomatic, but sometimes children may have pain resulting in limitation of movement that is nonspecific and create problems in the differential diagnosis of equivocal findings on plain radiographs.99mTc-MDP is absorbed on freshly built bone tissue like synchondrosis in the obliteration process. SPECT/CT can identify physiological uptake and better characterize equivocal lesions increasing specificity. The aim of the study was to evaluate the diagnostic utility of SPECT/CT in children and adolescents with asymmetric uptake in painful or asymptomatic synchondrosis of the lower limbs. **Subjects and Methods:** All bone scans performed in the last 5 years in our institutions in patients aged 5 to 20 years were reviewed and 9 patients (8-17 years-old, 8 male) with asymmetric or unexpected increased uptake in synchondrosis of the lower limb were identified. Bone scintigraphy included whole-body and SPECT/CT images in a GE Infinia Hawkeye 4 or a Mediso AnyScan 16 gamma camera. **Results:** Most frequently involved sites were ischiopubic junction and anterior inferior iliac spine, both of them in 3 cases. Local pain was present in one case of each. The patient with painful iliac spine had intense uptake corresponding to an avulsion fracture on CT images, and associated mildly increased uptake on the contralateral ischiopubic synchondrosis. The other patients had mild to moderate uptake correlated with swelling of the synchondrosis with a lucent expansive appearance that has been described radiographically during normal ossification. Three of the 5 patients with uptake in synchondrosis of the hip associated spondylolysis and one had a lumbosacral transitional vertebra, potentially leading to excessive weight bearing on one side with asymmetric closure of the ipsilateral synchondrosis. Two patients presented with foot pain. One had a type II accessory scaphoid and the other had a bilateral os trigonum syndrome with left predominance. Intensity of uptake was moderate in both patients. The last patient presented pain and swelling of the tibial tuberosity with moderate to intense uptake corresponding to Osgood-Schlatter disease. **Conclusion:** SPECT/CT can identify synchondrosis in the obliteration process with different levels of uptake in relation to clinical evolution and localization. Hybrid images help to recognize the normal and abnormal variants, excluding differential diagnosis like osteomyelitis or neoplastic lesions and avoiding high dose CT or more expensive high resolution studies.

OP-259

SPECT/CT is equivalent to diffusion-weighted MRI in characterizing equivocal osseous lesions detected by planar bone scintigraphy

M. Khalil[1], Y. G. Abdelhafez[1], H. Atta[1], A. A. Kandeel[2]; [1]South Egypt Cancer Institute, Assiut University, Assiut, EGYPT, [2]Faculty of Medicine, Cairo University, Cairo, EGYPT.

Aim: To evaluate the diagnostic performance of 99mTc-MDP bone scintigraphy using SPECT/CT in comparison to diffusion-weighted (DW) MRI in patients with solitary osseous lesions detected on planar bone scintigraphy. **Methods:** This ongoing prospective study recruited 46 cancer patients referred for bone

scintigraphy (staging/restaging/follow-up). Their planar whole body scan showed solitary equivocal osseous lesion. Each patient further underwent SPECT/CT (same day) & DW-MRI (12 ± 16 days after bone scan date). Studies were read independently by one experienced nuclear medicine physician and one experienced radiologist on a 5-point score: (score 1 = benign, score 2 = likely benign, score 3 = equivocal, score 4 = likely malignant and score 5 = malignant). The final diagnosis of disease status was made on the basis of subsequent clinical/imaging follow-up for at least 6 months. **Results:** In the 46 patients evaluated, 16 (35%) lesions proved to be osseous metastasis while 30 (65%) remained disease free. SPECT/CT vs DW-MRI showed sensitivity, specificity, positive predictive and negative predictive values of 75% vs 63%, 77% vs 77%, 63% vs 59%, 85% vs 79% and 83% vs 72%; respectively. Both modalities were true positive (TP) in 7 lesions, and false negative (FN) in 1 lesion. SPECT/CT correctly identified disease in 5/6 FN lesions on DW-MRI, compared to 3 FN on SPECT/CT that were correctly diagnosed by MRI. Both modalities were true negative (TN) in 18 and false positive (FP) in 2 lesions. SPECT/CT excluded disease in 5/7 FP lesions on DW-MRI and the same did DW-MRI in 5/7 FP lesions on SPECT/CT. No statistically significant difference noted in sensitivity or specificity. ROC analysis showed area under the curve (AUC) of 0.84 (95%CI: 0.71-0.93%) for SPECT/CT compared to 0.67 (95%CI: 0.51-0.79) for DW-MRI; respectively (P = 0.1). No significant difference in diagnostic performance indices was noted for either axial (n = 29) or appendicular skeletal lesions (n = 17). **Conclusions:** SPECT/CT may perform, at least, equal to MRI with diffusion in characterization of equivocal solitary osseous lesions detected on planar whole body skeletal scintigraphy.

SPS   **Monday, October 23, 2017, 08:00 - 09:30, Room 0.31-2**

UEMS/EBNM: Clinical Audit Session

Talks, Titles and Speakers TBA

701/703   **Monday, October 23, 2017, 10:00 - 11:15, Hall A**

Plenary 2: Hot Topics in Nuclear Cardiology!

OP-260

Systemic Inflammatory Response Post Myocardial Ischemia: Moving Towards Clinical Application?

E. Stroes; Department of Vascular Medicine, Academic Medical Center, Amsterdam, NETHERLANDS.

OP-261

The Role of Nuclear Medicine in Endocarditis

F. Bengel; Medizinische Hochschule Hannover, Klinik für Nuklearmedizin, Hanover, GERMANY.

OP-262

Quantification of Myocardial Blood Flow with PET

J. Knuuti; Turku University Hospital, Turku PET Centre, Turku, FINLAND.

---

801   **Monday, October 23, 2017, 11:30 - 13:00, Hall A**

CME 6 (Interactive) - Bone & Joint: Skeletal Scintigraphy Today - Accurate Diagnosis of Bone Disease with Therapeutic Impact

OP-263

High Resolution SPECT/CT and Beyond

P. Ritt; University Hospital Erlangen, Clinic of Nuclear Medicine, Erlangen, GERMANY.

OP-264

SPECT/CT Quantification

T. Kuwert; Friedrich-Alexander-University Erlangen-Nürnberg, Clinic of Nuclear Medicine, Erlangen, GERMANY.

OP-265

The End of Planar: Whole-Body SPECT as New Paradigm

Z. Keidar; Rambam Health Care Campus, Department of Nuclear Medicine, Haifa, ISRAEL.

OP-266

Top Ten Diagnoses Made Possible by SPECT/CT

G. Gnanasegaran; Royal Free London NHS Foundation Trust, Department of Nuclear Medicine, London, UNITED KINGDOM.

---

802   **Monday, October 23, 2017, 11:30 - 13:00, Hall B**

Joint Symposium 6 - EANM/EACVI: Fast-Track Cardiac Imaging: Is There an Ideal One-Stop Shop?

OP-267

Healthcare Economic Perspectives on One-Stop Shop Cardiac Imaging

S. S. Tan; Erasmus University Rotterdam, Institute for Medical Technology Assessment, Rotterdam, NETHERLANDS.

OP-268

Nuclear Medicine Physicians' Perspective on One-Stop Shop Cardiac Imaging

P. Jager; Department of Nuclear Medicine, Isala Hospital, Zwolle, NETHERLANDS.

OP-269

Radiologists' Perspective on One-Stop Shop Cardiac Imaging

T. Leiner; Department of Radiology and Nuclear Medicine, Utrecht University Medical Center, Utrecht, NETHERLANDS.

OP-270

Cardiologists' Perspective on One-Stop Shop Cardiac Imaging

D. Neglia; Fondazione G. Monasterio CNR-Regione Toscana and CNR Institute of Clinical Physiology, Pisa, ITALY.

Technologist Oral Presentations 2

OP-271

Ultra-low Dose CT for Attenuation Correction of 82Rb Cardiac PET

M. B. Sørensen, K. Bouchelouche, L. P. Tolbod; Dept. Nuclear Med. & PET-Centre, Aarhus University Hospital, Aarhus, DENMARK.

Aim: Myocardial perfusion imaging (MPI) using cardiac PET with tracers like 82Rb and 15O-water is substantially lower in radiation dose than classic MIBI-based SPECT. However, for cardiac PET, the dose contribution of CT for attenuation correction (CTAC) is typically 20-30% of the total dose. To reduce the total radiation dose of cardiac PET further, we set out to examine if the use of ultra-low dose CTAC (UL-CTAC) would affect the accuracy of the quantitative parameters related to MPI. Furthermore, we examined whether the low quality of the UL-CTAC would affect the technologist's ability to perform manual adjustment for misalignment between PET and CTAC. The CT reconstruction algorithm Q.AC was used to improve quality and consistency of the CTAC. **Method:** 23 consecutive clinical patients (BMI: 26.9 [range: 15.4-38.8]) referred for 82Rb PET rest and stress imaging were included in the study. All patient received both a normal dose CTAC (120 kVp, 0.5s rotation, 10-100 mA (Smart mA), Noise Index 46) and an UL- CTAC (100 kVp, 0.7s rotation, 10-40 mA (Smart mA), Noise Index 125) prior to the rest PET scan. The same CTAC was used for correction of both rest and stress scans. Manual adjustment for misalignment between PET and CT was performed independently for both CTAC and UL-CTAC. Data was analyzed using QPET (Cedar Sinai). Static uptake images were analyzed (%Summed Scores, %Extend, %Reversible and Total Perfusion Deficit (TPD)), and parameters were compared by using scatter plots and linear regression. CTAC radiation dose was estimated from Dose Length Product using a conversion factor of 0.014 mSv/(mGy cm). All patients were scanned on a GE Discovery MI Digital Ready PET/CT. PET images were reconstructed using Time-of-Flight, Resolution Recovery, attenuation and scatter corrections. **Results:** CTAC dose was reduced from 0.5 mSv [range: 0.1-1.1] to 0.11 mSv [range: 0.1-0.2]. Manual adjustment for misalignment between PET and CTAC was performed without any difficulties on all images. Excellent correlation between normal dose CTAC and UL-CTAC was found for all MPI parameters (Summed Scores: y=0.96x+0.02, R2=0.95; %Extend: y=0.99x+0.80, R2=0.97; %Reversible: y=0.86x+0.84, R2=0.94; TPD: y=0.99x+0.76, R2=0.97). **Conclusion:** The CTAC dose was reduced from 0.5 mSv [range: 0.1-1.1] to 0.11 mSv [range: 0.1-0.2]. Excellent correlation between the normal dose CTAC and UL-CTAC was found for the quantitative parameters related to MPI. Therefore, it seems possible to use a UL-CTAC without affecting the quantitative accuracy.

OP-272

Pediatric Anesthesia on Daily PET/CT workflow:Impact Quantification Based on Three Indicators

C. Barbosa[1], S. Mendes[1], I. Ferreira[1], P. Gil[1], P. Ribeiro[1], G. Costa[1,2], J. Pedroso de Lima[1,2,3]; [1]Centro Hospital e Universitário de Coimbra (CHUC), Coimbra, PORTUGAL, [2]Faculdade de Medicina da Universidade de Coimbra, Coimbra, PORTUGAL, [3]Instituto de Ciências Nucleares Aplicadas à Saúde, Coimbra, PORTUGAL.

Aim: 18F-FDG-PET/CT is an important method for assessing a wide variety of pathologies in any age group. Children bring special challenges to Nuclear Medicine Departments and, in some cases, the use of anesthesia must be considered. However, the specificities of the anesthesia protocol tend to extend the occupation of PET/CT's imaging room. In that context, we aimed to quantify the impact of the anesthetic procedure performed in children on the PET/CT workflow using three measurable indicators: 1) child 18F-FDG uptake period; 2) 18F-FDG uptake period of the next patient; 3) "interpatient time" defined, in this context, as the period elapsed between the end of the child PET/CT imaging acquisition and the beginning of PET/CT of the next patient. **Material and Methods**: We collected data on 18F-FDG uptake period for all pediatric patients submitted to anesthesia in our department, between April 2013 (the beginning of collaboration with the Anesthesiology Department) and February 2017. "Interpatient time", according to the above-stated definition, and the 18F-FDG uptake period of the patient immediately schedule after the child were also recorded. Finally, the averages of each one of those three indicators were calculated and compared with the corresponding time periods obtained in a regular workday, without anesthetic support. The age of the children, gender and the modality of PET/CT (brain or whole-body) were collected. **Results:** Of the 27 PET/CT examinations performed under anesthesia, 17 were brain studies (5 girls,12 boys; mean±sd age=7.5±4.8 years) and 10 were whole-body scans (9 girls,1 boy; mean±sd age=3.2±1.6 years). The 18F-FDG uptake time for anaesthetized children had a mean±sd of 01h17min±14min and for the following patient (without anesthesia) of 01h21min±19min. These periods are longer than those observed on a regular workday (01h06min±12min), without anesthetic support. The "interpatient time" was 22min±10min, also significantly longer when anesthesia was not performed (5min±2min). **Conclusion**: Anesthesia enables the acquisition of PET/CT imaging in uncooperative and unwilling children. However, is a time-consuming procedure that requires, in average in our Department, 28 additional minutes for each examination preformed under anesthesia (11min+17min for respectively 18F-FDG uptake and "interpatient time"). The quantification of the impact of anesthesia in the workflow, will help us to adjust the patients appointment intervals and the respective 18F-FDG administration timing on the days that include examinations under anesthesia.

OP-273

18F-FDG PET/CT in pediatric lymphoma patients: the role of technologist

M. Ciaccio[1], C. Nava[2], D. Bonacina[1], M. Maurizio[1], A. Perri[1], A. Renaioli[1], S. Morzenti[3], L. Guerra[1], C. Crivellaro[1,2]; [1]ASST-Monza, San Gerardo Hospital, Nuclear Medicine, Monza, ITALY, [2]University

Milan-Bicocca, Nuclear Medicine, Monza, ITALY, [3]ASST-Monza, San Gerardo Hospital, Medical Physics, Monza, ITALY.

Background: The increasing use of serial 18F-FDG-PET/CT scans in lymphoma pediatric patients raises the issue of radiation exposure. Recently, PET/CT scanners with high sensitivity allow to reduce both injected FDG-activity and CT amperage ("Low-dose" protocols) without compromising diagnostic accuracy. **Aim:** Aims of this study were: 1) to retrospectively compare dosimetric exposure of pediatric lymphoma patients submitted to serial PET/CT scans, comparing the Low-Dose vs Standard protocols, 2) to evaluate the approach of the technologist during PET/CT scan. **Methods:** Standard protocol was performed in 22 lymphoma patients by using Discovery600 (GE Healthcare) with 3,7 MBq/kg of injected activity, 2 minutes/FOV, 120kV and 40mA for CT. Low-dose protocol was performed in 8 patients scanned by DiscoveryIQ (GE Healthcare) with large axial FOV (26cm) and high-sensitivity, with 1.85 MBq/Kg, 3 minutes/FOV, 120kV and 25mA for CT. Radiation exposure calculated by ICRP 106 and by CT-expo 1.6 for PET and CT respectively, were there compared. Technologists' approach in the different phases of PET/CT and potential advantages in performing contrast-enhanced CT in a single session examination were observed. **Results:** Overall, a mean of 3 PET/CT per-patient were performed (range 2-13). The mean effective dose for PET study resulted 5.89mSv and 2,6mSv for standard and low-dose protocol, respectively (p <0,0001). The mean effective dose of CT study was 3,9mSv and 3,1mSv for standard and low-dose protocol respectively. The mean cumulative dose/patient was 31.3mSv and 18.79mSv for standard and low-dose protocol respectively. According to Biological Effects of Ionizing Radiation VII report, the risk of incidence of a second tumor for a 10-years-old male and female patient resulted 0.45/100 and 0.81/100 for standard protocol whereas the same figures were 0.22/100 (male), 0.49/100 (female) for low-dose protocol. The relationship between technologist and children is based on verbal and nonverbal communication from the acceptance of children and their parents till their dismissal. If both required, performing PET/CT and contrast-enhanced CT in a single session examination (if both required) can reduce distress for the patient, as it means a "single stressor" instead of 2 (single access to hospital, single ago-cannulae, single medical-team). **Conclusion:** The radiation exposure from serial PET/CT studies in pediatric lymphomas can be considerable. Low-dose protocols can be a valid tool to reduce radiation exposure in pediatric population without sacrificing diagnostic information. Technologists, using individual skills, have an important role in the optimization process and in patient management.

OP-274

Practical Guide for ^{18}F-Choline PET Imaging in hyperparathyroidism

M. Hofbauer, J. Trinckauf, M. Hüllner; UniversitätsSpital, Zurich, SWITZERLAND.

Purpose/Introduction: Primary hyperparathyroidism (PHPT) is the third most common endocrine disorder, with a prevalence of 0.1-1.0%. The main cause of PHPT is a solitary parathyroid adenoma (80% - 85%). There is evidence that PET imaging using ^{18}F-choline, especially in patients with negative or discrepant SPECT and ultrasound has an excellent diagnostic performance and yields promising results in the detection and correct localization of parathyroid adenomas. The aim of this presentation is to provide practical guidance for technologists using PET/CT and PET/MR scanners for the diagnostic work-up of hyperparathyroidism. **Materials and Methods:** Exams were performed on an integrated PET/MR scanner (GE Signa 3.0T) or on a sequential PET/CT+MR scanner (GE trimodality PET/CT D690 and MR 750w 3.0T). In total, more than 100 patients were scanned in one of the two modalities. After the injection of 150 MBq ^{18}F-choline, two PET datasets were acquired (early and late phase). In between a diagnostic MR scan of the neck was performed. The acquisition time for PET/CT+MR was approximately 75 minutes, while the PET/MR protocol was acquired within 45 minutes. **Results and Conclusion:** This practical guide helps technologists acquire knowledge on ^{18}F-choline PET imaging in patients with suspected parathyroid adenomas. PET/CT+MR procedure as well as PET/MR procedure, including acquisition parameters and dedicated MR pulse sequences along with pertinent work flow will be presented in a step-by-step manor. It is shown that the simultaneous PET/MR scan results in a time reduction of approximately 40% compared to the trimodality set-up, which is important for implementation in clinical routine.

OP-275

^{68}Ga-PSMA PET/CT Protocol Review

E. Poel; Academic Medical Center, Amsterdam, NETHERLANDS.

Aim: The aim of this study is to optimize the ^{68}Ga-PSMA PET/CT protocol, including the CT parameters. **Methods:** 4 academic medical centrums from the Netherlands, 1 from Belgium ,1 from Germany and 1 specialized oncological centrum from the Netherlands has been asked to share their ^{68}Ga-PSMA PET/CT scan protocol. Also PubMed, the online scientific articles' database, was consulted where the keywords "PSMA" and "PET" were used to find relevant articles. The protocols were compared to the literature. **Results:** A large difference in CT parameters is seen in de choice between a low dose CT scan (30-60 mAs) without intravenous contrast and a high dose CT scan (120-180 mAs) with intravenous contrast. Other differences are seen in PET parameters. The dose of PSMA is varying between 1,5 MBq/kg - 2,2 MBq/kg and a standard dose of 100 MBq ^{68}Ga-PSMA. The scan time per bed position variates from 2-4 minutes. All protocols prescribes that patients should be well-hydrated before the study and during the uptake time The use of Lasix is different between none use, 10 mg and 20 mg. Most hospitals start the PET/CT scan 1hr p.i. In the literature is found that an extra scan 3 hr p.i. is helpful to detect more prostate cancer lesions. **Conclusion:** The most ideal protocol will exist of 2 ^{68}Ga-PSMA PET/CT scans , 1hr p.i. and 3hr p.i. The 1hr p.i. scan low dose from the skull base to upper legs and the 3hr p.i.scan high dose of the pelvis and abdomen with intravenous contrast. 20mg of Lasix should be applied 30min prior to the late scan. The patients

should be well-hydrated before the study and during the up-take time. The best combination of dose 68Ga-PSMA and scan time per bed position should be researched in further investiga-tion and depends of the used PET/CT.

OP-276
Reducing artefacts in PSMA PET/MR due to hip prosthesis with MAVRIC SL

T. Oblasser, M. Hofbauer, J. Trinckauf, T. Berthold, K. Friedrich, I. Burger; Department of Nuclear Medicine, PET/ CT - MR Zentrum für Klinische Forschung, UniversitätsSpital Zür, Zurich, SWITZERLAND.

Aim: Metal Artefacts in PET/MR Examinations reduce MR image quality and impair the attenuation correction (AC) which is nec-essary to deliver adequate PET images. The gradient echo se-quence acquired for tissue segmentation based MR AC is espe-cially vulnerable to susceptibility resulting in large signal voids around prosthesis. There are promising new MR sequences to reduce those artifacts around metal implants such as Multi-Ac-quisition with Variable Resonance Image Combination SeLective (MAVRIC SL). We investigated the potential reduction of signal voids due to hip prosthesis using MAVRIC on Prostate Specific Membran Antigen (PSMA) PET/MR scans. **Material and Meth-ods:** The examinations were performed on a SIGNA PET/MR (GE Healthcare, 3T MR Scanner). 7 consecutive patients referred for 68Ga-PSMA PET/MR (age 69.86 ± 7.56 years) with one or two hip prosthesis were included. For imaging of the prostate gland four sequences covering the pelvic region were analysed: an MR-AC sequence (0:23min) as the reference, a Dixon (Lava Flex) Sequence (00:18 min), a T1 weighted ax sequence (2:06min) and MAVRIC SL (3:41min). The largest signal void was selected on each sequence and measured in two dimensions. The rela-tive difference between MR AC and the three other sequences was calculated. **Results:** Comparing the Lava, T1 and MAVRIC SL with the MR AC Sequence all of them showed substantial-ly reduced artefacts. For the LAVA Sequence the mean reduc-tion was 11.12% ± 17.48%, the mean reduction for the T1 was 22.98% ± 13.91% and the MAVRIC SL Sequence showed a mean reduction of 65.05% ± 10.08%. **Conclusion:** MAVRIC offers a fea-sible and relatively fast possibility to substantially reduce signal voids due to hip prosthesis for prostate PET/MR, improving MR image quality for the pelvis and potentially AC for PET.

OP-277
Improving alignment between 18F-FDG PET and CT scans by controling breathing movements during the CT-scan.

T. K. Lehnskov[1], C. P. Jønsson[2], L. B. Katz[2], D. A. Riisberg[2]; [1]Bispebjerg/Frederiksberg Hospital, København NV, DENMARK, [2]Metropolitan University College, København N, DENMARK.

Due to the short duration a lone standing CT-scan can be ob-tained during breath hold. However, when combined with a PET-scan it is not possible to perform the longer lasting PET acquisition during breath hold. The misalignment between PET and CT images is most pronounced in the lower thorax and

upper abdomen. **Aim:** The goal in the project was to train the patient during the CT scan to perform breath hold just at the end of expiration phase, in order better to align the CT-scan and PET-scans at a common level **Materials and Methods:** In our department we use a Varian system (Varian Medical Systems) to track the patient breath period under PET scanning. In conjunc-tion with a Q.Static software(GE Healthcare). With this system it is possible to perform post-hoc motion correction, where de-fined parts of the inspiration and expiration phases are deleted from the PET acquisition data. We considered several versions of breathing instructions before a CT-scan and ended by us-ing: *Breathe out gently and stop breathing*. The patients were trained to use this technique before the CT-scan. In addition they also used this breathing technique during Scout. All scan were performed on a GE Dsicorvery 710 PET/CT with the use of the Varian Breath tracking system and GE´s Q.static software. The patients we randomly CT-scanned either with or without voice instructions. The latter group consisted the control mate-rial. The Varian Breath tracking system, record all of their breath-ing movements during the CT- and PET-scan. **Results:** Fiftyone patients were included in the project. Twenty one patients were CT-scanned after voice instructions. The results showed an av-erage misalignment between PET and CT by 2.8 millimeters (Range 0.5 mm to 7.4 mm). The control group of 30 subjects showed an average misalignment by 7.19 mm (range 0.8mm to 9.8 mm). One patient was excluded because he could not collaborate according to the breathing instruction. **Conclusion:** By training the breathing technique with the patient just be-fore the CT-scan, it is possible to reduce misalignment between PET and CT-scans by approximately 60% (mean). In addition the CT-scan will be obtained during breath hold. We suggest that using this simple breathing training technique will improve the diagnostic quality of the PET/CT reading.

OP-278
Myocardium metabolic suppression protocol for 18F-FDG PET Sarcoid Scan

E. M. Bagi, A. Garcia-Campos, K. Wechalekar; Royal Brompton &Harefield NHS Foundation Trust, 77 WimpoleStreet, London, W1G 9RU, London, UNITED KINGDOM.

Introduction: 18F-fluorodeoxyglucose (FDG) PET has significant advantages in assessing disease activity and monitoring treat-ment response in patients with cardiac sarcoidosis. Normal myocytes utilize glucose as one of the major energy source, various techniques have been developed to suppress physio-logical 18F-FDG uptake in the heart to minimize false-positive results. 3 approaches have been tried: prolonged fasting, dietary modification and IV unfractionated heparin. The different proto-cols have reported varying success rates in achieving adequate metabolic suppression in the myocardium. We wanted to find out our own success rate with our protocol against this pub-lished data at our new establishment. **Method:** 100 consecutive patients underwent cardiac sarcoidosis protocol requiring 18h carbohydrate free diet followed by 18h fast (including diabet-ic patients); Dietary modification with a high-fat, high-protein

and no-carbohydrate diet was advised with menu suggestions. Diabetic patients were advised oral hypoglycaemic agents or insulin as routine until commencement of fast. Patients were informed about their preparation through a letter/email followed by a phone call during booking andat 24hprior to the scan. On arrival, patient's compliance was checked. If not, the examination was cancelled. Blood sugar level (BSL)was checked before the FDG injection with uptake time of 75mins.Half body scan (skull base-mid-thigh) with additional 10 min static acquisition of the heart on a Siemens Biograph mCT Flow scanner was acquired. Images were processed and reported on Syngo Via and Hermes software by experienced nuclear physicians. If the images showed homogeneously increase FDG uptake in the LV and RV myocardium, compliance failure was suspected and as such reported. **Results:** 100 consecutive patients were analysed: 36 (36%) women, age 54±14 years,21 (21%) diabetics (6 on insulin) mean weight 85±22kg, mean height 173±14cm. Overall mean BSL value was 5.1±1.0mmol/L; max BSL on diabetics was 8.3mmol/L and minimum was 3mmol/L.No patients needed to be cancelled due to symptomatic or reported hypoglycaemia. Good metabolic suppression of glucose in the myocardium was achieved in 99 (99%) patients and inadequate suppression was suspected in 1 (1%) diabetic patient. We did not have any symptomatic hypoglycaemia episode among diabetic or non-diabetic patients during their attendance. **Conclusions:** We report excellent patient compliance to cardiac sarcoidosis preparation protocol (99%) in our setting compared to other reported patient preparation protocols. This is achieved through patient education communication and compliance check to achieve good metabolic suppression of glucose from the normal myocardium. Diabetic patients compliedwell with this protocol.

OP-279

PET imaging with [45]Ti and the technical challenges involved

P. Costa[1], N. Arantes[2]; [1]Nuclear Medicine Department, ESS|P.Porto, Porto, PORTUGAL, [2]Independent Nuclear Medicine Technologist, Braga, PORTUGAL.

Introduction: Research has been made to test the use of unconventional PET radionuclides. Titanium-45 ([45]Ti) comes as a suitable option due to its favorable physical properties (half-life of 3.09h and positron maximum energy of 1040 keV) combined with chemical properties that allow radiolabeling of different compounds using chelation, opening new opportunities to develop new radiolabeled nanoparticles. However, the introduction of a new player into clinical routine presents some technical challenges that should be addressed. This work aims to discuss the potential role of PET imaging with [45]Ti, present and describe the best practices in this context, while addressing the opinion of Nuclear Medicine Technologists (NMT) on new imaging protocols regarding the best operating standards. **Materials and Methods:** Physical properties of [45]Ti with impact on image quality were explored using Monte Carlo simulation tools, while radionuclide production feasibility was studied in a low energy cyclotron (IBA® Cyclone 18/9). NMT's opinion was established

with the results of a survey conducted on a sample of 20 NMT's with different levels of education/training and professional experience. The survey included multiple choice questions and open answer questions. **Results and Discussion:** Experimental results demonstrate that producing [45]Ti in low energy cyclotrons is feasible. Preliminary insights regarding image quality suggest the suitability of this radionuclide to provide good PET image quality, at the same level of the one obtained using ^{11}C or even [18]F. Respondents of the survey present different insights on the necessary adjustment of technical procedures to obtain high-quality PET images. Correlation is established between professional experience on PET field, education level and their insights. Complete results of the survey will be presented and discussed, allowing to bring some topics to be addressed in future advanced education programs. Our proposal of guideline of good practices will be presented, highlighting suggestions of technical parameters regarding radionuclide production, radiopharmaceutical preparation, suggestions for administered activity and image acquisition protocols, finishing with radioprotection issues. **Conclusion:** NMT have indeed a crucial role in the implementation of new agents in the clinical routine of PET imaging. Apart from other examples that could be cited, [45]Ti could be considered an interesting option, being used in this work as a case study for the evaluation of the actual NMT's knowledge/opinion on the need of adequacy of procedures for the use of novel agents.

804	Monday, October 23, 2017, 11:30 - 13:00, Hall E1

Do.MoRe - Featured: Harmonization of Hybrid Molecular Imaging

OP-280

Molecular Imaging Systems in Harmony – Necessity and Feasibility

I. Rausch; Medical University of Vienna, Vienna, AUSTRIA.

OP-281

Feasibility of state-of-the-art PET/CT system performance harmonisation

A. Kaalep[1], T. Sera[2,3], S. Rijnsdorp[4], M. Yaqub[5], A. Talsma[6], M. A. Lodge[7], R. Boellaard[8,5,3]; [1]North Estonia Medical Centre, Tallinn, ESTONIA, [2]University of Szeged, Szeged, HUNGARY, [3]EANM Research Limited, Vienna, AUSTRIA, [4]Catharina Hospital, Eindhoven, NETHERLANDS, [5]VU University Medical Center, Amsterdam, NETHERLANDS, [6]Martini Hospital, Groningen, NETHERLANDS, [7]Johns Hopkins University, Baltimore, MD, UNITED STATES OF AMERICA, [8]University Medical Center Groningen, Groningen, NETHERLANDS.

Purpose: The aim of this study is to explore the feasibility of harmonising performance for different PET/CT systems equipped with the latest PET time-of-flight (ToF) and resolution modelling/point spread function (PSF) technologies. The second aim was producing a working prototype of new harmonising criteria with higher contrast recoveries than current EARL standards us-

ing various SUV metrics. **Methods:** Four latest generation PET/CT systems equipped with both time-of-flight and point spread function capabilities from 3 major vendors were used to acquire and reconstruct images of the NEMA NU2-2007 body phantom filled according to EANM EARL guidelines. A total of 15 reconstruction parameter sets of varying pixel size, post filtering and reconstruction type, with 3 different acquisition durations of 5, 2 and 1 minutes per bed position were used to assess and compare the quantitative performance of the systems. A target range for recovery curves was established such that it would accommodate the highest matching recoveries from all investigated systems. These updated criteria were validated on 18 additional scanners from 16 sites in order to demonstrate the scanners' ability to meet the new target range. **Results:** Each of the four investigated systems were found to be capable of producing harmonising reconstructions with similar recovery curves. The 5 reconstruction parameter sets producing harmonising results significantly increased SUV mean (24%) and SUV max (24%) contrast recoveries compared with EARL specifications currently in effect. Additional prospective validation performed on 18 scanners from 16 EARL accredited sites demonstrated the feasibility of updated harmonising specifications. Peak SUV parameter was found to significantly reduce the variability in quantitative results while producing lower recoveries in smaller (<22 mm) sphere sizes. **Conclusions:** Harmonising PET/CT systems with ToF and PSF technologies from different vendors was found to be feasible. The harmonisation of such systems would require an update to the current multi-centre accreditation program EARL in order to accommodate higher recoveries. SUV peak should be further investigated as a noise resistant alternative quantitative metric to SUV max.

OP-282

Feasibility of a brain PET harmonization program for state of the art PET/CT systems

R. Boellaard[1], S. Golla[2], A. Kaleep[3], M. Yaqub[2], T. Sera[4], S. Rijnsdorp[5], R. Kogan[1], N. Leenders[1], A. Lammertsma[2]; [1]University Medical Center Groningen, GRONINGEN, NETHERLANDS, [2]VU University Medical Center, Amsterdam, NETHERLANDS, [3]North Estonia Medical Centre Foundation, Tallinn, ESTONIA, [4]University of Szeged, Szeged, HUNGARY, [5]Catharina Hospital, Eindhoven, NETHERLANDS.

Purpose/Introduction: Use of brain PET studies in multicentre trials or as a quantitative imaging biomarker for (automated) differential diagnosis of neurogenerative diseases require harmonized quantitative image characteristics. In this study we explored the feasibility of developing a harmonizing performance standard for brain PET studies on state of the art PET/CT systems. **Subjects & Methods:** In this exploratory study 6 state of the art PET/CT systems were included: Philips Gemini TF, Ingenuity TF and digital Vereos systems, 2 Siemens Biograph mCTs and a GE 710. Only systems with EARL compliant (calibration and image quality) performances were included. A 30 min dynamic PET scan of the 3D Hoffmann brain phantom was acquired. The phantom was filled with an exact known FDG stock solution (aimed at 40 kBq/mL). Each scan was reconstructed

using various clinically relevant reconstruction settings. Depending on PET/CT system reconstruction settings were varied as follows: time of flight (TOF) on/off; resolution modelling (RM) on/off, voxel size, number of iterations/subsets and Gaussian smoothing FWHM (mm). The reconstructed images were analysed using a coregistered eroded binary map of both grey (GM) and white matter (WM). GM and WM recovery coefficients were calculated as the ratio of observed and expected activity concentrations. **Results:** For all systems distinct differences in both GM and WM recoveries and GM/WM ratios were observed between reconstructions that did or did not apply RM. Across the various systems/reconstructions a harmonized GM recovery between 0.77 and 0.85 (RM OFF) or between 0.81 and 0.94 (RM ON) seems feasible. WM recoveries (0.25 expected) were less affected by reconstruction settings, but showed a larger difference between Philips (0.28 to 0.33) versus Siemens (0.20 to 0.20) and GE (0.22 to 0.23) systems. GM/WM ratios were 4.2 to 4.4 for the Siemens and 3.7 to 4.0 for the GE systems, while the Philips systems showed somewhat lower values of 3.1 to 3.5 mainly because of difference in WM recovery. **Discussion/Conclusion:** Harmonization of PET/CT system performance for brain studies appears to be feasible, in particular for GM uptake assessment. Use of RM increases GM recovery at the cost of a wider (worse) harmonized performance range. There seems to be a vendor specific difference in WM recovery. The cause of this finding (possibly scatter correction) as well as its implication for PET/CT performance harmonization needs to be further explored. Currently, more data are being collected prospectively as part of JPND granted European networks.

OP-283

EANM/EARL FDG-PET/CT accreditation - summary results from the first 150 accredited imaging sites

*A. Kaalep[1], **T. Sera**[2,3], W. Oyen[4], B. J. Krause[5], A. Chiti[6,7], Y. Liu[8], R. Boellaard[9,10,3]; [1]North Estonia Medical Centre, Tallinn, ESTONIA, [2]University of Szeged, Szeged, HUNGARY, [3]EANM Research Limited, Vienna, AUSTRIA, [4]The Royal Marsden Hospital, London, UNITED KINGDOM, [5]Rostock University Medical Center, Rostock, GERMANY, [6]Humanitas University, Rozzano, ITALY, [7]Humanitas Research Hospital, Rozzano, ITALY, [8]The European Organisation for Research and Treatment of Cancer, Brussels, BELGIUM, [9]University Medical Center Groningen, Groningen, NETHERLANDS, [10]VU University Medical Center, Amsterdam, NETHERLANDS.*

Purpose: The European Association of Nuclear Medicine (EANM) has been running an FDG-PET/CT accreditation program under the EANM Research Ltd (EARL) initiative in order to harmonise quantitative performance of PET/CT systems, facilitate multi-centre trials and research. From 2010 until July 2016 EARL collected over 2500 phantom datasets from approximately 200 cameras and more than 150 imaging sites worldwide. The objective of this study is to report the findings and the impact of participating in the accreditation program on the standardisation and the quantitative variability of the investigated PET/CT systems. **Methods:** In order to obtain and maintain the EARL accredited status, sites were required to complete two distinct phantom scan proce-

dures - calibration quality control (CalQC) using a uniform cylindrical phantom and image quality control (IQQC) using a NEMA NU2-2007 body phantom, comprising 6 hot spheres with variable sizes. The CalQC and IQQC scans sent to EARL were analysed in a standard way, and average volumetric SUV bias and SUV recovery coefficients (RC) were calculated. In this study the EARL data were evaluated on the basis of quality control (QC) type, approval status, PET/CT camera manufacturer, and first and subsequent QC data submissions. **Results:** 5% (n=96) of all CalQC scan submissions (n=1816) demonstrated a measured SUV bias of more than 10%. Upon EARL feedback and after corrective actions, sites achieved 100% compliance within EARL specifications. Longitudinally, majority of the systems showed reproducibility within ±5% of the expected SUV. From IQQC scan submissions 30% (n=1381) of SUVmean and 23% (n=1095) SUVmax sphere recoveries failed to meet EARL accreditation criteria. After EARL accreditation, failure rate decreased to 12% (n=360) and 9% (n=254) respectively. A tendency towards positive bias was observed prior and also after EARL accreditation. Following the initial adjustment of the reconstruction parameters, the longitudinal reproducibility of the recovery values remained stable and generally within ±10% for largest 4 spheres and ±20% for smallest two spheres. **Conclusions:** Regardless of system manufacturer or model, all systems were able to comply with the CalQC and IQQC EARL specifications. Within the EARL accreditation program gross PET/CT calibration errors are successfully identified and longitudinal variability in PET/CT performances reduced by maintaining the QC experiments. The program is running successfully for more than 6 years and shows that a harmonising accreditation procedure is feasible and achievable.

OP-284

Development of the IAEA-NMQC toolkit for automated analysis of quality control tests on SPECT systems

G. L. Poli[1], *A. Vergara Gil*[2], *L. Torres Aroche*[2], *E. De Ponti*[3], *A. Kesner*[4]; [1]*International Atomic Energy Agency, Vienna, AUSTRIA,* [2]*Division of Clinical Research, Centre of Isotopes, Havana, CUBA,* [3]*Department of Medical Physics, ASST Monza, Monza, ITALY,* [4]*Memorial Sloan Kettering Cancer Center, New York, NY, UNITED STATES OF AMERICA.*

Purpose: Proper quality control (QC) procedures in SPECT play an essential role in ensuring optimized performance of imaging equipment, and are requisite for providing high quality clinical care. Because QC procedures are implemented routinely, streamlining them with automated software may offer several benefits: improved speed, reduced errors, and the standardization of calculation methods across centres. The purpose of this work was to develop a toolkit for supporting common SPECT QC data analysis procedures, and validate it using test images from multiple vendor systems and/or simulated images. **Materials and Methods**: We developed the IAEA-NMQC toolkit for performing the required image analysis of the SPECT QC procedures described in IAEA guidance documents and NEMA standards. The software is a collection of plugins which readily integrate with the freely available image analysis software

ImageJ. For validation, the plugins were tested using typical SPECT QC images acquired on machines which spanned different vendors: GE, Mediso, Philips and Siemens. The plugins were validated using test appropriate validation criteria. In some cases, software phantoms were generated and used to evaluate concordance of results with known truth. In other cases, results were compared with those from vendor software or other existing methodologies. For the plugins which are not fully automated and require some intervention by the user, the validation included inter- and intra-observer variability comparisons. **Results**: Automated and semiautomated functions were successfully developed to analyze multiple SPECT QC tests, including planar uniformity, sensitivity, spatial resolution and linearity, pixel size, centre of rotation, and tomographic uniformity, contrast and resolution. Where appropriate, measurement accuracy was assessed using "known truth" software phantoms, and in all cases results conformed to performance expectations. Validation using comparison of our plugins with standard methodologies revealed no statistically significant differences in the results. For the semi-automated tests, inter- and intra-observer variability was studied and no statistically significant differences were found. **Conclusion**: There is wide agreement that routine QC is an important aspect of any SPECT imaging program. While the field has well developed guidance for performing these tests, procedures for data analysis remain relatively established. In this work we present the IAEA-NMQC toolkit as a free resource for the community to aid with standardized, rapid analysis of QC test images using a cross vendor platform. The toolkit is freely available on the IAEA Human Health Campus (http://bitly.com/IAEA-NMQC), along with further documentation and instructions for its use.

OP-285

Implications of a FDG-PET EARL Protocol for Ga-68 PET Imaging

D. Koopman[1,2], *W. A. Noortman*[1,2], *P. L. Jager*[1], *C. H. Slump*[2], *J. A. van Dalen*[3]; [1]*Isala, Department of Nuclear Medicine, Zwolle, NETHERLANDS,* [2]*MIRA Institute for Biomedical Technology and Technical Medicine, University of Twente, Enschede, NETHERLANDS,* [3]*Isala, Department of Medical Physics, Zwolle, NETHERLANDS.*

Introduction: With the increasing use of Ga-68 PET imaging for neuro-endocrine tumours and prostate cancer, there is or will arise a need for standardization of such Ga-68 based PET scans. We have used settings as prescribed by EARL in standardisation of FDG-PET and tested these for Ga-68 PET imaging. **Methods:** We performed a phantom study using a NEMA Image Quality phantom with sphere diameters 10-37 mm. Spheres were filled with 37 kBq/mL Ga-68 and the background with 3.6 kBq/mL Ga-68. We acquired a 10 min PET scan on a state-of-the-art system (Ingenuity TF, Philips Healthcare). Data were reconstructed using a protocol that fulfils EARL specifications for contrast recovery coefficients (CRCs) using FDG-PET. Mean and maximum CRCs (CRC_{mean} and CRC_{max}) were measured for all phantom spheres. These values were compared to those obtained with Fluor-18 and to EARL specifications for FDG-PET tumour

imaging. **Results:** With Ga-68, we found relatively low CRC_{mean} and CRC_{max} values for all spheres. Values were 2% to 21% lower compared to those obtained with Fluor-18, the highest percentages corresponding to the smallest spheres. CRC_{mean} values for Ga-68 were up to 9% below the lower limit of the EARL specifications. For the small phantom spheres, CRC_{max} values were close to the lower limit, with the CRC_{max} value of the 13 mm sphere 3% below the lower CRC_{max} limit. **Conclusion:** Reconstruction settings for Ga-68 PET should be adapted towards a higher image resolution, to achieve the EARL specifications for FDG-PET. Alternatively, specific EARL accreditation specifications for Ga-68 may be defined for standardization of Ga-68 PET cancer imaging.

OP-286

Robustness of EQ•PET SUV harmonization to tumor-to-background variations

B. S. Spottiswoode[1], M. V. Mattoli[2], M. Milite[3], M. L. Calcagni[2], A. Giordano[2], L. Indovina[4]; [1]Siemens Medical Solutions USA, Inc., Knoxville, TN, UNITED STATES OF AMERICA, [2]Università Cattolica del Sacro Cuore, Rome, ITALY, [3]Siemens Healthcare Srl, Milan, ITALY, [4]Fondazione Policlinico Universitario A. Gemelli, Rome, ITALY.

Introduction: EQ•PET is a reference-based quantification technology that provides clinicians with harmonized SUVs across patient scans, even if acquired on different scanners or reconstructed with different protocols. This is achieved by aligning NEMA phantom recovery curves, either across scanners / protocols or to a standard such as EARL. Alignment involves spatial filter optimization to minimize the difference between recovery curves. Previous work has demonstrated that such an approach is relatively independent of lesion size, clinical classification, location, emission scan duration, and patient BMI (Lasnon et al. EJNMMI 2013). The aim of this work is to assess the dependence of EQ•PET on tumor-to-background variations. **Methods:** A NEMA NU2 phantom with 6 hot spheres was prepared and scanned following the PET EANM guidelines on a Biograph mCT system (Siemens Medical Solutions). Images were reconstructed using point-spread function (PSF) and ordered subset expectation maximization (OSEM3D) methods, both with time of flight. Reconstruction parameters were based on a standard clinical protocol and included a 256×256 matrix, $3.2 \times 3.2 \times 5$ mm^3 voxel dimension, 2 iterations, 21 subsets and a 2 mm Gaussian post filter. An ^{18}F-FDG solution (20.7 kBq/ml) was used to fill spheres. Three different activities were injected into the background to achieve sphere-to-background ratios (SBR) of 10, 5 and 3, respectively. An additional scan was performed without any background (SBR_{inf}). EQ•PET harmonization was performed as described previously based on SUV_{max} measured within each sphere (Kelly, Siemens White Paper, 2014), and using the EARL 2011 reference curves. The optimal EQ•PET filter from the EARL-recommended SBR_{10} was then applied to SBR_3, SBR_5, and SBR_{inf}, and harmonization effectiveness was assessed based on the mean absolute percent difference for all spheres compared to the reference recovery curve. **Results:** The optimal EQ•PET filter in the SBR_{10} scenario reduces the mean ab-

solute percent difference with the EARL reference from 39.4% to 7.1% for PSF, and from 22.0% to 9.6% for OSEM protocols. The same filters applied to the SBR_3, SBR_5 and SBR_{inf} scenarios reduces the mean absolute percent difference from 35.7% to 8.5% for PSF, and from 16.5% to 8.6% for OSEM. **Conclusion:** EQ•PET harmonization produces similar recovery curve alignment for both PSF and OSEM at a range of clinically relevant sphere-to-background ratios. These results suggest that SUV harmonization using EQ•PET is maintained in the presence of varying tumor-to-background ratios.

| 805 | Monday, October 23, 2017, 11:30 - 13:00, Hall E2 |

M2M: Peptides

OP-287

A New ^{64}Cu-Labeled, Metabolic-Resistant Peptide with Nanomolar Affinity for NPY-Y1R for Breast Cancer Targeting

M. Paquette, V. Dumulon-Perreault, S. Ait-Mohand, B. Guérin; Université de Sherbrooke, Sherbrooke, QC, CANADA.

Introduction: Neuropeptide Y1 receptor (NPY-Y1R) is overexpressed in 85% of breast carcinomas, and its presence is modulated in an estrogen-dependent manner, making NPY-Y1R a potential diagnostic target for breast cancer. Recently, ^{68}Ga-labeled [Lys(Pip-Ga-DOTA)^4, Bip^5]BVD15 allowed PET imaging of breast tumors in xenografted mice, despite low *in vitro* plasma stability (Zhang *et al.*, Mol Pharm, 2016). In our group, a series of BVD15 derivatives were tested, but compounds either had excellent stability or low-nanomolar affinity, but not both. In this work, we will present the stability along with the cell binding and uptake of a promising novel ^{64}Cu-labeled peptide with sequence D-Ile-Asn-Hyp-Lys(C6-NOTA)-Tyr-Arg-Cha-Arg-Tyr. **Methods:** Peptide was synthesized on solid phase, conjugated to NOTA chelator and radiolabeled with ^{64}Cu-acetate at pH 7.0 for 30 minutes at room temperature. In vitro stability was assessed by addition of labeled peptide to mouse plasma at 37°C sampled and analysed in a time-dependent manner. Saturation binding curves, time-dependent uptake and inhibition constant (K_i) against the ^{125}I-labeled natural ligand NPY were evaluated in MCF7 cells. Efflux was evaluated by washing and incubating cells with fresh media in a time course after a 1-hour uptake of the tracer. **Results:** Affinity of the compound for NPY-Y1R-expressing MCF7 cells was in the low-nanomolar range, with dissociation constant (K_D) reaching 9.3±3.1 nM and K_i compared to ^{125}I-NPY at 6.6±0.54 nM. Stability studies showed that 41% of the compound is still intact in mouse plasma 3 h after addition, showing a vastly improved performance over previous high-affinity analogs. Optimal uptake was reached at 1h on MCF7 cells, while a significant uptake decrease was observed upon co-application of excess unlabeled peptide between 30 to 240 minutes after tracer addition. Rapid washout from the cells was observed, with only 25% of the 1h uptake remaining 15 minutes after tracer withdrawal. **Conclusion**: The compound D-Ile-Asn-Hyp-Lys(C6-^{64}Cu/NOTA)-

Tyr-Arg-Cha-Arg-Tyr displayed both high *in vivo* stability and receptor-targeting capabilities, but with fast efflux. Further evaluation of the ^{64}Cu-peptide is currently ongoing, and PET imaging of MCF7-bearing mice will soon be carried out.

OP-288

New Radiolabeled Exendin Analogue Shows Increased Renal Clearance

L. Joosten, C. Frielink, M. Gotthardt, M. Brom; Radboud University Medical Center, Nijmegen, NETHERLANDS.

Aim: A promising imaging method for detection of small insulinomas is targeting the glucagon-like peptide-1 (GLP-1) receptor by PET/CT after injection of radiolabeled/^{68}Ga-labeled exendin-4. High accumulation of radiolabeled exendin in the kidneys via tubular reabsorption, can hamper the ability to detect small insulinomas in close proximity of the kidneys. In this study, we developed a novel exendin-analogue with a methionine-isoleucine linker between the chelator (NOTA) and the peptide, aiming at increasing the renal clearance. We examined the renal clearance and insulinoma targeting properties of this new exendin analogue in biodistribution and PET/CT studies in a nude mouse model bearing subcutaneous insulinomas. **Materials and Methods:** NOTA was conjugated via a Met-Ile-linker to the C-terminus of exendin-4 (MI-NOTA-exendin-4). Exendin with NOTA conjugated to a C-terminal lysine was used as a reference. The affinity of the peptides was determined in a competitive binding assay using GLP-1 receptor transfected CHL cells. Biodistribution of ^{68}Ga-NOTA-exendin-4 and ^{68}Ga-MI-NOTA-exendin-4 was performed in INS-1 tumor-bearing BALB/c nude mice to investigate the renal clearance and tumor targeting properties of both peptides and to assess visualization of INS-1 tumors with PET/CT. **Results and Conclusion:** Labeling of NOTA-exendin-4 and MI-NOTA-exendin-4 resulted in a maximum specific activity up to 275 GBq/μmol and 242 GBq/μmol, respectively. The affinity for the GLP-1 receptor was 9.5 nM (95% confidence interval, 7.0 to 12.8 nM) for NOTA-MI-exendin-4 and 4.0 nM (95% confidence interval, 2.5 to 6.2 nM) for NOTA-exendin-4 (p<0.001). *In vivo* biodistribution revealed a significant lower kidney uptake of ^{68}Ga-NOTA-MI-exendin-4 one hour post injection (102.6 ± 14.8 %ID/g), compared to ^{68}Ga-NOTA-exendin-4 (127.2 ± 17.3 %ID/g) (p<0.0001), which was even more pronounced four hours p.i. (34.2 ± 4.2 %ID/g vs 127.7 ± 9.5 %ID/g respectively, p<0.0001). Accumulation of ^{68}Ga-NOTA-MI-exendin-4 in the tumor was 25.0 ± 8.0 four hours p.i. and similar to that of ^{68}Ga-NOTA-exendin-4 (24.9 ± 9.3) (p>0.05). Furthermore, INS-1 tumors were visualized using PET/CT and moreover, the reduced kidney uptake of ^{68}Ga-MI-NOTA-exendin-4 compared to ^{68}Ga-NOTA-exendin-4 was clearly visible. In conclusion, ^{68}Ga-MI-NOTA-exendin-4 showed increased renal clearance of more than 60% four hours p.i. when compared to ^{68}Ga-NOTA-exendin-4, whereas tumor retention did not change significantly. Therefore, ^{68}Ga-labeled MI-NOTA-exendin-4 is a promising improved tracer resulting in better tumor-to-kidney ratios and might allow improved detection of small insulinomas, in close proximity to the kidneys.

OP-289

Metabolic fate of [^{111}In]Sarabesin 3 in mice: Identifying radiometabolites in peripheral blood as well as neutral endopeptidase as the key degrading protease

B. A. Nock[1], E. Lymperis[1], W. Sallegger[2], A. Kaloudi[1], E. P. Krenning[3], M. de Jong[4], T. Maina[5]; [1]Molecular Radiopharmacy, INRASTES, NCSR, Athens, GREECE, [2]PiChem, Graz, AUSTRIA, [3]Department of Nuclear Medicine, Erasmus MC, Rotterdam, NETHERLANDS, [4]Department of Radiology, Erasmus MC, Rotterdam, NETHERLANDS, [5]Molecular Radiopharmacy, INRASTES, NCSR "Demokritos", Athens, GREECE.

Aim: We have previously reported on the GRPR-antagonist Sarabesin 3 (SB3), [DOTA-*p*-aminomethylanilinediglycolate (AMA-DIG)-DPhe[6],Leu-NHEt[13]]BBN(6-13), suitable for labeling with medically relevant radiometals. The PET-radioligand [^{68}Ga]SB3 showed excellent targeting of GRPR-expressing prostate and/or breast cancer lesions in animals and in human. Unexpectedly, the uptake of the respective [^{111}In]SB3 in PC-3 tumors in mice was compromised (8.8±3.0%ID/g *vs*. 34.0±6.9%ID/g for [[67/68]Ga]SB3 at 4 h pi) due to inferior metabolic stability. Tumor values of [^{111}In]SB3 reached comparable to [^{68}Ga]SB3 levels (38.3±7.9%ID/g at 4 h pi) only after coinjection of the neutral endopeptidase (NEP)-inhibitor phosphoramidon (PA). In this study, we were interested to investigate the metabolic patterns of [^{111}In]SB3 in mice and the role of NEP in their formation. For this purpose, we synthesized potential SB3-metabolites and labeled those with [111]In. We subsequently compared their chromatographic behavior *vs*. actual radiometabolite patterns found in peripheral blood after administration of [^{111}In]SB3 in mice applying radio-HPLC. **Materials and Methods**: The potential SB3 metabolites M1: [DOTA-AMA-DIG]DPhe[6],Leu-OH[13]]BBN(6-13), M2: DOTA-AMA-DIG-DPhe-Gln-Trp-Ala-Val-Gly-His-OH, M3: [DOTA-AMA-DIG-DPhe-Gln-Trp-Ala-OH, M4: DOTA-AMA-DIG-DPhe-Gln-Trp-OH and M5: DOTA-AMA-DIG-DPhe-Gln-OH were synthesized on the solid support. SB3 and M1-M5 were labeled with ^{111}In in aqueous acidic (pH 4.6) medium. Each of [^{111}In]SB3 or of the predominant metabolites [^{111}In]M2 and [^{111}In]M4 was injected in the tail vein of mice without or with PA-coinjection. Mouse blood collected at 5 min postinjection (pi) was analyzed by radio-HPLC. Separate HPLC co-injections of authentic [^{111}In] M1-[^{111}In]M5 samples with 5 min blood samples of [^{111}In]SB3, [^{111}In]M2 or [^{111}In]M4 were conducted. **Results**: The major degradation products of [^{111}In]SB3 detected in peripheral mouse blood at 5 min pi were: [^{111}In]M2 (11.3%), [^{111}In]M3 (6.0%), [^{111}In]M4 (5.4%) and [^{111}In]M5 (17.7%) with no evidence of [^{111}In]M1 formation. Treatment of animals with PA resulted in full stabilization of [^{111}In]SB3. Interestingly, [^{111}In]M2 yielded [^{111}In]M3 (9%), [^{111}In]M4 (12%) and [^{111}In]M5 (43.2%) at 5 min pi in mice, but remained intact after PA-coinjection. Radiometabolite [^{111}In]M4 was in vivo stable. **Conclusions**: In agreement to previous findings, this study has confirmed the crucial role of NEP in the bioavailability of the GRPR-antagonist [^{111}In]SB3 which is of great significance for tumor uptake. Notably, the *des*-Leu[13] radiometabolite [^{111}In]M2 was also susceptible to NEP, leading to the same degradation products.

OP-290

New radiolabelled minigastrin analogues with improved CCK2R targeting for diagnostic and therapeutic use

M. Klingler[1], C. Rangger[1], D. Summer[1], J. Foster[2], J. K. Sosabowski[2], E. von Guggenberg[1]; [1]Medical University of Innsbruck, Innsbruck, AUSTRIA, [2]Barts and the London School of Medicine, London, UNITED KINGDOM.

Introduction: Medullary thyroid carcinoma and other cholecystokinin-2 receptor (CCK2R) expressing tumours can be targeted by radiolabelled minigastrin (MG) analogues showing high affinity to this receptor. We have designed four new DOTA-conjugated MG analogues aiming to increase biological stability and tumour-to-organ ratios when compared to native MG and other previously developed MG analogues. **Methods:** Based on MG11 (LAYGW-MDF-NH$_2$) four new DOTA-conjugated MG analogues with specific amino acid substitutions on position 6 and 8 were synthesized (DOTA-MGS1-4). Receptor affinity and cell uptake were tested using CCK2R-positive AR42J rat pancreatic acinar tumour cells and A431 human epidermoid carcinoma cells transfected with human CCK2R and mock-transfected cells. *In vitro* stability analyses where carried out in human serum (up to 24 h p.i.), rat liver and kidney homogenates (up to 2 h p.i.). With the two analogues showing the highest receptor affinity and cell uptake *in vivo* stability tests (10 min p.i.), dual modality single photon emission computer tomography (SPECT-CT) images and subsequent biodistribution analysis where carried out in normal or tumour bearing mice. **Results**: ^{111}In-DOTA-MGS1 and ^{111}In-DOTA-MGS4 showed high receptor affinity (IC50 <6 nM) and high receptor-specific cell uptake (~10 % in AR42J and ~20 % in A431-CCK2R) whereas ^{111}In-DOTA-MGS2 and ^{111}In-DOTA-MGS3 showed much lower affinity (IC50 >40 nM) and uptake values (<5 % in AR42J and <4 % in A431-CCK2R). ^{111}In-DOTA-MGS3 and ^{111}In-DOTA-MGS4 showed higher resistance against enzymatic degradation *in vitro* with >93 % intact radioliand in serum, and >11 % in rat tissue homogenates than ^{111}In-DOTA-MGS1 and ^{111}In-DOTA-MGS2 (serum <60 %, rat tissue homogenates <1 %). Concerning the i*n vivo* stability no intact radiopeptide was detectable for ^{111}In-DOTA-MGS1, whereas ^{111}In-DOTA-MGS4 showed a very high *in vivo* stability (>75 % in blood and liver, >24 % in kidney and urine). With both radiopeptides tumour xenografts could be clearly visualised on SPECT/CT images. ^{111}In-DOTA-MGS4 showed a high tumour uptake (10.2±2.0 % ID/g) and a favourable tumour-to-kidney ratio (2.6±0.9 % ID/g), whereas ^{111}In-DOTA-MGS1 displayed only a tumour uptake of 1.3±0.1 % ID/g and a tumour-to-kidney ratio of 1.2±0.1 % ID/g. **Conclusions:** The *in vitro* and *in vivo* characterization of the new four MG analogues developed confirmed the possibility of introducing stabilizing amino acid substitutions in the carboxy-terminal part of the peptide sequence without impairing CCK2R affinity. Alternative substitutions are currently under investigation to further optimize this approach.

OP-291

Application of SSTR radioligands in Breast Cancer

S. U. Dalm, G. N. Doeswijk, J. C. Haeck, A. M. Sieuwerts, J. W. M. Martens, C. H. M. van Deurzen, M. de Jong; Erasmus MC, Rotterdam, NETHERLANDS.

Background: Somatostatin receptor (SSTR) radioligands are successfully applied for imaging and treatment of neuroendocrine tumors. For breast cancer (BC), earlier the use of SSTR radioligands was not as successful as anticipated. These studies, performed over a decade ago, had varying results and indicated low and heterogeneous SSTR expression in BC as main limiting factors. Apart from SSTR expression, the majority of these studies did not discriminate between different BC subtypes. Furthermore, compared to the current state-of-the-art, imaging devices and radioligands used were suboptimal. The aim of our studies was to investigate once again the potential of SSTR radioligands for BC targeting, taking into account important BC characteristics and recent improvements with respect to radioligands. **Materials and Methods:** *SSTR2* mRNA expression of 915 BCs was determined and associated with BC characteristics. Also, tissues from primary BCs and corresponding metastases (n=60 pairs) were analyzed and *SSTR2* mRNA expression was compared. Furthermore, autoradiography studies using ^{111}In-octreotate were performed on 51 BC specimens to analyze SSTR protein expression. Finally, in response to the reported low and heterogeneous SSTR expression, we compared the use of a radiolabeled SSTR antagonist vs an agonist for BC targeting. SSTR antagonists have shown to be superior to SSTR agonists for targeting of neuroendocrine tumors. In vitro autoradiography studies (n=40 BCs) and in vivo SPECT/MRI studies in an estrogen receptor (ER)-positive BC mouse model (T126, n=6 per group) comparing radiolabeled DOTA-JR11, an SSTR antagonist, and radiolabeled DOTA-Tyr[3]-octreotate, an SSTR agonist, were performed. **Results:** *SSTR2* mRNA expression showed a significant correlation with ER-positivity of BCs (p<0.001). Furthermore, in the majority of cases *SSTR2* mRNA expression of primary BC and corresponding metastases (both regional and distant metastases) was equivalent. In the autoradiography studies, we found 44/51 tumors to be SSTR-positive of which 25% showed homogenous expression. In vitro binding and in vivo tumor uptake of radiolabeled DOTA-JR11 was significantly higher than that of radiolabeled DOTA-Tyr[3]-octreotate. The median (min-max) ratio antagonist/agonist binding in vitro was 3.39 (2-5). SPECT/MRI studies resulted in a tumor uptake of 1.12±0.4 and 0.8±0.1 %ID/mL (p<0.05) for the antagonist and agonist, respectively. **Conclusion:** Our findings suggest the use of SSTR radioligands for BC imaging, and perhaps also therapy, should be reconsidered. ER-positive BC patients can potentially benefit most from the application of SSTR radioligands in both primary and metastatic disease. Our results also indicate that radiolabeled SSTR antagonists are superior to radiolabeled SSTR agonists for BC targeting.

OP-292

Radionuclide tumor targeting using ADAPT scaffold proteins: aspects of label positioning and residualizing properties of the label

J. Garousi[1], S. Lindbo[2], B. Mitran[3], M. Altai[1], J. Buijs[4], A. Orlova[3], S. Hober[2], V. Tolmachev[1]; [1]Institute for Immunology, Genetics and Pathology, Uppsala University, Uppsala, SWEDEN, [2]School of Biotechnology, Division of Protein Technology, KTH Royal Institute of Technology, Stockholm, SWEDEN, [3]Division of Molecular Imaging,

Department of Medicinal Chemistry, Uppsala University, Uppsala, SWEDEN, [4]Uppsala University, Uppsala, SWEDEN.

Aim: ADAPTs are small-size (5 kDa) affinity proteins, derived from the albumin-binding domain (ABD) of streptococcal protein G. Previous studies have demonstrated the feasibility of high-contrast imaging of HER2-expressing xenografts in mice using anti-HER2 ADAPT6 site-specifically labeled at N-terminus with ^{111}In and ^{68}Ga within 1-4 h pi. Further studies identified the variant (HE)$_3$DANS-ADAPT6 as providing the best tumor-to-organ rations when labelled at N-terminus with ^{111}In using DOTA. The aim of this study is to determine if positioning of radiometal (^{111}In) and radiohalogen (^{125}I) labels at different ends of the molecule (C- vs N-termini) could affect the biodistribution. **Materials and Methods:** Two variants of (HE)$_3$DANS-ADAPT6 protein having cysteine at C-terminus (Cys[59]-ADAPT6) and N-terminus (Cys[2]-ADAPT6) were produced and labeled with ^{111}In using maleimido-DOTA or ^{125}I using ((4-hydroxyphenyl)ethyl)maleimide (HPEM). The tracers were evaluated *in vitro* and *in vivo*. BALB/C nu/nu mice bearing SKOV3 xenografts were used as a model to study biodistribution. **Results**: *In vitro* and *in vivo* data confirmed HER2-mediated binding of all four tracers to HER2-expressing cells. Internalization of conjugates by both SKOV-3 and BT-474 cells was slow. Surprisingly, the uptake in SKOV3 xenografts of radioiodinated conjugates was significantly higher than uptake of radiometal-labeled counterparts. At 4 h pi, the tumor uptake was 15±2, 22±3, 10.6±0.5, and 11.8±0.5 % ID/g for ^{111}In-DOTA-Cys[59]-ADAPT6, ^{125}I-HPEM-Cys[59]-ADAPT6, ^{111}In-DOTA-Cys[2]-ADAPT6, and ^{125}I-HPEM-Cys[2]-ADAPT6 respectively. Tumor-to-blood ratios were 277±35, 53±10, 254±37 and 61±14, respectively, at this time point. We have found that renal retention of the radioiodinated variants (renal uptake of 1.7±0.3 ID/g at 4 h p.i., regardless of position) was ca.150-lower compared to ^{111}In-labeled variants. However, the uptake in other organs was higher for radioiodine, most likely due to release of radiometabolites from kidneys into blood. Therefore, tumor-to-organ ratios (excluding kidneys) were higher for ^{111}In-DOTA labeled tracers. Overall, ^{111}In-DOTA-Cys[59]-ADAPT6 provided significantly higher tumor-to-lung, tumor-to-liver, tumor-to-spleen and tumor-to-muscle ratios compared to ^{111}In-DOTA-Cys[2]-ADAPT6. Tumor-to-organ ratios were similar for ^{125}I-HPEM-Cys[59]-ADAPT6 and ^{125}I-HPEM-Cys[2]-ADAPT6, but ^{125}I-HPEM-Cys[59]-ADAPT6 has twice higher tumor uptake and provided twice higher tumor-to-kidney ratio. **Conclusion:** Both character and position of labels had substantial influence on imaging properties of ADAPT6. Non-residualizing radiohalogen labels decreased renal uptake dramatically. An optimal position for both ^{125}I-HPEM and ^{111}In-DOTA labels is at C-terminus.

OP-293

Effectivity of a combined treatment with the m-TOR inhibitor RAD001 and Peptide Receptor Radionuclide therapy with Lu-177 DOTA TATE evaluated with Ga-68 DOTA TATE PET in a tumor model of the mouse

J. Zellmer[1], L. Vomacka[1], G. Böning[1], F. J. Gildehaus[1], J. Carlsen[1], E. Mille[1], M. Hacker[2], P. Bartenstein[1], A. R. Haug[2], **H. Ilhan[1]**;

[1]*Department of Nuclear Medicine, University Hospital of Munich, Munich, GERMANY,* [2]*Division of Nuclear Medicine, Department of Biomedical Imaging and Image Guided Therapy, Medical University of Vienna, Vienna, AUSTRIA.*

Purpose: To evaluate the efficacy of a combined treatment with the m-TOR inhibitor RAD001 (Everolimus) and Peptide Receptor Radionuclide Therapy (PRRT) with Lu-177 DOTA TATE in a somatostatin-receptor (SSTR) positive tumor model of the mouse. **Methods:** Athymic CD1-mice (10 weeks) were divided into 4 groups (Gr.) and injected with the SSTR-positive AR42J tumor cell line at day 0. A baseline Ga-68 DOTA TATE PET scan was performed 5 days after tumor injection. Therapy was started following PET at day 5. Gr. 1 (n=7) was treated with Placebo, Gr. 2 (n=8) with 5 mg/kg RAD001 weekly, Gr. 3 (n=7) with a single PRRT cycle (80 MBq Lu-177 DOTA TATE) and Gr. 4 (n=8) with a combination of RAD-001 and PRRT. Follow-up PET was performed 1, 2 and 4 weeks after start of therapy. The tumor volume was assessed manually (MTV) and threshold based in PET (biological tumor volume, BTV). PET was used to quantify the tumor to reference ratio (TRR; maximum uptake in the tumor divided by mean uptake in muscle as reference). Numbers are given as mean ±SEM. **Results:** Animals treated with Placebo and RAD001 monotherapy were euthanized according to the requirements of the local animal ethics committee at week 2 due to excessive tumor growth. One mouse of Gr. 4 died due to aspiration during application of RAD001 at day 26. All other animals of Gr. 3 and 4 were euthanized after the last PET scan 4 weeks after treatment. Tumor volume at week 2 was significantly higher in Gr. 1 compared to all other groups. Gr. 2 presented higher MTV compared to the PRRT groups (Gr. 1: 1594,4 mm^3 ±779,0; Gr. 2: 394 mm^3 ±80,0; Gr. 3: 26,0 mm^3 ±14,8; Gr. 4: 36,2 ±14,0). There was a high correlation of MTV and BTV (r^2=0,9). Mean TRR in Ga-68 DOTA TATE PET at week 2 was significantly lower in Gr. 1 and 2 compared to Gr. 3 and 4 (Gr. 1: 5,9 ±1,5; Gr. 2: 6,9 ±1,2; Gr. 3: 1,4 ±0,18; Gr. 4: 1,18 ±0,5). Mean TRR in Gr. 3 and 4 increased until week 4 and was not significantly different (Gr. 3: 4,96 ±2,18; Gr. 4: 11,17 ±3,93). **Conclusion:** Treatment with Lu-177 DOTA TATE is highly effective in AR42J tumor bearing mice. The combination of PRRT and RAD001 is equally effective and results in significantly smaller tumor-growth compared to monotherapy with RAD001 alone or Placebo.

OP-294

The Receptor UT of Urotensin-II is a New Target for Imaging Solid Tumor with Radiolabeled DOTA-Peptide Ligands

B. Poret[1,2], *L. Desrue[2], N. Perzo[2], P. M. Coly[2], J. E. Joubert[2], M. A. Bonin[3], R. Leduc[3], R. Modzelewski[1], F. Morin[2], H. Castel[2], P. Vera[1], P. Bohn[1], P. Gandolfo[2];* [1]*EA 4108, Laboratory of Computer Science, Information Processing and Systems (LITIS), team "QuantIF", Centre Henri Becquerel, Rouen, FRANCE,* [2]*Normandie Univ, UNIROUEN, INSERM 1239, DC2N, Laboratory of Neuronal and Neuroendocrine Differentiation and Communication, Mont-Saint-Aignan, FRANCE,* [3]*Department of Physiology & Pharmacology, Institute of Sherbrooke, Faculty of Medicine and Health Sciences, Sherbrooke University – Health Campus, Sherbrooke, QC, CANADA.*

Overexpression of G protein-coupled receptors (GPCRs) in tumor has been exploited to develop GPCR-targeting radioligands used *in vivo* for imaging solid tumors in cancer. In particular, somatostatin analogs labeled with [111]Indium (^{111}In-OctreoScan) are used for the diagnostic of neuroendocrine tumors. The vasoactive neuropeptide urotensin-II (UII), which shares structural analogies with somatostatin, interacts with a single high affinity GPCR named UT. We previously established that UII exhibits potent chemotactic properties to promote cell migration and angiogenesis in glioblastomas. High expression of UT in human solid tumors including lung, colorectal, prostate or breast carcinomas, suggests that UT constitutes an interesting target to design radiolabeled UII analogs for diagnostic or therapeutic approaches. In a first step, two urotensinergic ligands (UII and a biased analog of UT, urantide) containing the chelating group DOTA, able to bind radioactive isotopes, have been successfully synthetized. A radiolabeling protocol of DOTA-UII and DOTA-urantide with [111]Indium was first validated. When incubated for 3h period in human plasma, only 30% of the radioligand showed degradation. Graded concentrations of both DOTA-UII and DOTA-urantide induced a dose-dependent increase in cytosolic calcium concentration in HEK293 cells expressing UT, with similar potency and efficacy to that obtained with UII (EC_{50}: 1.26 10^{-8} M and 2.09 10^{-8} M, UII and DOTA-UII, respectively) and urantide (EC_{50}: 1.82 10^{-8} M and 1.52 10^{-8} M, urantide and DOTA-urantide, respectively). DOTA-UII was also able to promote UT internalization (ELISA and immunocytochemistry) in HEK293 cells expressing UT, whereas DOTA-urantide was ineffective, together suggesting that DOTA analogs kept ability to bind and activate human UT. To characterize the best cell line for imaging with DOTA-UII radionuclide, we have first characterized a series of human tumoral cell lines. Among 12 cell lines tested from brain, breast, lung, colorectal and prostate, 9 of them exhibited a strong expression of UT. Moreover, a treatment with UII stimulated cell proliferation (7/12) and/or cell migration (5/12). The more responsive cell lines are currently tested *in vivo* in xenografted mice. To control first the biodistribution of ^{111}In-DOTA-UII, we performed injection in C57Bl/6J mice (mUTS2R^{+/+}, mUTS2R^{-/-}, or hUTS2R^{+/+}). We observed a slight signal of ^{111}In-DOTA-UII restricted in kidney in all animals and a very fast clearance in the three groups, indicating a weak binding of UT in physiological conditions. The weak expression of UT in physiology and the strong expression of UT in solid tumors suggest that radionuclide DOTA-UII exhibits very interesting properties for the diagnosis and/or therapy.

---

806 **Monday, October 23, 2017, 11:30 - 13:00, Hall F1**

Pitfalls & Artefacts 4 (Interactive) - Paediatrics: Pitfalls and Artefacts - FDG-PET Imaging in Children

OP-295

Patient Preparation and Technical Artefacts

C. Franzius ; MR-, Nuklearmedizin und PET/CT-Zentrum Bremen Mitte, Bremen, GERMANY

OP-296

Clinical Pitfalls

R. Kluge ; Universität Leipzig, Leipzih, GERMANY

OP-297

Pitfalls in PET/MR Imaging

P. Zucchetta; Department of Nuclear Medicine, University of Padova, Padove, ITALY.

---

807 **Monday, October 23, 2017, 11:30 - 13:00, Hall F2**

Clinical Oncology: Women's Only

OP-298

Combined imaging in cervical cancer with hybrid FDG-PET/MRI for primary staging followed by Tc-99m-SPECT/CT for pre-surgical sentinel lymph node mapping

S. Sahbai[1], F. Fiz[1], F. Taran[2], S. Brucker[2], D. Wallwiener[2], A. Staebler[3], H. Dittmann[1], C. la Fougère[1]; [1]Nuclear Medicine, Tübingen, GERMANY, [2]Gynecology and Obstetrics, Tübingen, GERMANY, [3]Pathology, Tübingen, GERMANY.

Introduction: F-18-FDG-PET/MRI for primary staging in patients with cervical cancer is considered to have a high potential for initial staging and may provide prognostic information, since the presence of metastatic lymph nodes (LN) is an important prognostic factor. Currently, the use of pre-surgical sentinel lymph node (SLN) mapping in early-stage tumor is preferred and could reduce post-surgical morbidity. The aim of our study was to investigate the pre-surgical use of PET/MRI and SLN mapping combined with SPECT/CT for the detection of LN-metastases. **Methods:** Histologically proven cervical cancer patients were prospectively included and underwent initially a whole-body F-18-FDG-PET/MRI (Siemens Biograph mMR®). SLN mapping succeeded one day before surgery after peri-cervical injection of Tc-99m-nanocolloid with SPECT/CT (GE Healthcare Discovery NM 670 Pro®). Surgical SLN biopsy was performed with gamma hand probe. Pre-operative imaging results were compared to histological findings (primary tumor, location, SLNs and non SLNs). **Results:** So far, eight patients were included in this prospective study. PET/MRI was capable to detect all 8 primary tumor lesions of the uterine cervix and all 4 involved LN regions in the 2 patients with LN metastases. One patient with apparent clinical early-stage but advanced metastatic disease in PET/MRI did not receive SLN mapping and surgery. In the 7 remaining patients, SLN detection rate in pre-operative SPECT/CT was 100% and 79% based on patient and on hemi-pelvis analysis respectively. The false negative rate of metastatic LN detection was 7% (1/14) based on hemi-pelvis analysis according to SPECT/CT; this was reduced to 0% by adding PET/MRI results. **Conclusion:** The use of pre-operative PET/MRI and SLN mapping with SPECT/CT in cervical cancer could provide prognostic information prior to surgery. This combined dual-time-point imaging may avoid unnecessary systematic bilateral lymphadenectomy and additional morbidity by increasing the accuracy of LN metastases detection.

OP-299

Utility of multiparametric PET/MRI for response assessment of radiochemotherapy or neoadjuvant chemotherapy in cervical cancer patients

T. Sarabhai, Y. Erfanian, M. Forsting, K. Herrmann, L. Umutlu, J. Grueneisen; University Hospital Essen, Essen, GERMANY.

Purpose: The aim of the study was to investigate the diagnostic potential of simultaneous multiparametric PET/MRI for therapy response assessment of radiochemotherapy or neoadjuvant chemotherapy in patients with primary cervical cancer. **Subjects & Methods:** The patient cohort comprised 9 patients with a histopathologically confirmed primary cancer of the uterine cervix. All patients were prospectively enrolled for a two examination approach of simultaneous 18F-FDG PET/MR imaging: 1. prior to the start and 2. after completion of definitive radiochemotherapy.(n = 3) or neoadjuvant chemotherapy (n = 6). Therapy response was assessed based on RECIST 1.1 and PERCIST 1.0 criteria. In addition, several 18F-FDG PET- and MRI-derived metabolic (18F-FDG PET: SUVs), functional (DWI: ADC values, DCE-MRI: Ktrans, Kep, Ve, iAUC) and morphological (tumor size) parameters were determined. Histopathological verification due to biopsy or subsequent tumor resection served as the reference standard. **Results:** Simultaneous multiparametric PET/MRI has been successfully completed in all 9 patients. In accordance with the RECIST- and PERCIST-criteria, partial response (PR) or complete response (CR) could be determined in 7 patients (RECIST: CR = 1, PR = 6; PERCIST: CR = 2; PR = 5). The two remaining patients showed progressive or stable disease. Multiparametric PET/MR analysis of therapy responders revealed reduction of the mean tumor size (55mm to 20mm), perfusion parameters (Ktrans: 0.42 to 0.28, iAUC: 10.45 to 4.69), metabolic activity (SUVmax: 16.5 to 5.9; SUVmean: 7.8 to 3.5) and an increase of ADC values (ADCmean: 763 to 1032; ADCmin: 381 to 667). On the other hand, in patients with PR and CR tumor size and ADC-values remained stable, while an increase of perfusion parameters (Ktrans: 0.33 to 0.69:, Ve: 0.32 to 0.61, iAUC: 9.09 to 22.72) and metabolic activity (SUVmax 14.6 to 17.3; SUVmean: 6.7 to 7.8) was evident after treatment. **Conclusion:** In addition to commonly applied response criteria (RECIST, PERCIST), integrated PET/MRI provides certain quantitative parameters, reflecting underlying tumorbiological features, which might enable a more comprehensive treatment response assessment of radiochemotherapy and neoadjuvant chemotherapy in cervical cancer patients.

OP-300

Preoperative staging of endometrial cancer: prognostic role of PET-derived parameters

P. Mapelli[1], E. Incerti[1], A. Bergamini[2], F. Fallanca[1], P. M. V. Rancoita[3], R. Cioffi[2], M. Petrone[2], E. Rabaiotti[2], G. Mangili[2], L. Gianolli[1], M. Picchio[1]; [1]Nuclear Medicine Department, IRCCS San Raffaele Scientific Institute, Milano, ITALY, [2]Obstetrics and Gynecology, IRCCS San Raffaele Scientific Institute, Milano, ITALY, [3]University Centre of Statistics in the Biomedical Sciences, Vita-Salute San Raffaele University, Milano, ITALY.

Purpose: To investigate the preoperative prognostic role of FDG PET/CT in patients with endometrial carcinoma (EC). **Subjects & Methods:** 18F-FDG PET/CT was performed in 57 patients for EC preoperative staging (August 2009 - July 2016). Maximum and mean standardized uptake values (SUVmax, mean), metabolic tumour volume (MTV) and total lesion glycolysis (TLG) of primary tumours, at different thresholds of 40%, 50%, 60% (40-50-60), were evaluated and compared with anatomopathological features. The diagnostic performance of PET-parameters in discriminating low and high-risk disease (pT1 vs pT2-pT3-pT4 , or International Federation of Gynecology and Obstetrics - FIGO Stage I vs II-III-IV, or endometrioid vs other histotype) was evaluated with the Receiver Operating Characteristics (ROC) curve and logistic regression. Cox regression analysis and logrank test were used to assess the association with overall survival (OS) and recurrence-free survival (RFS). **Results:** Mean age at time of PET/CT was 64 years, range: 24-83 years. Categorized TLG40-50-60 with their optimal cut-off were the only parameters related to FIGO stage I versus II-III-IV (P=0.0035 for all). The cut-offs for risk stratification were 83.69, 61.81 and 41.32, respectively, with corresponding sensitivity and specificity of 60.00% and 71.43% for all parameters. TNM stage (pT2, pT3, pT4 vs pT1) was significantly predicted only by the TLG40-50 categorized with their optimal cut-off (P=0.0344 and 0.0211, respectively). The optimal thresholds were 99.55 and 77.58, respectively, with sensitivity of 50.00% for both parameters and specificity of 81.4% and 83.72%, respectively. Categorized SUVmax and SUVmean40-50-60 with the optimal cut-off (14.35, 8.55, 9.8 and 10.9, respectively) were the only parameters that significantly discriminated between endometrioid vs non endometrioid subtype (P=0.0145 for SUVmax and SUVmean50-60, P=0.0237 for SUVmean40). Corresponding sensitivity was 64.86% and 62.16% for SUVmax and SUVmean50-60 and 62.16% for SUVmean40; specificity was 70.00% for all parameters. The mean OS (mean ±SD) was 79.77% ±3.34 and the mean RFS rate was 77.89±3.73. Tumour type was the only variable significantly associated with OS (P=0.0486). The categorized TLG50 was the only variable significantly associated with RFS (P=0.0472): specifically, TLG50>77.58 cc is associated with a higher risk of relapse. **Conclusion:** TLG40-50-60 of primary EC can predict FIGO staging; TLG40-50 can predict pathological staging. These parameters, being able to discriminating between low and high risk disease, may help the preoperative prediction of EC aggressiveness.

OP-301

Prognostic value of 18F-FDG PET/CT in restaging of locally advanced cervical cancer after concomitant chemoradiation therapy

G. M. Lima, A. Matti, E. De Crescenzo, G. Polverari, A. M. Perrone, P. De Iaco, C. Nanni, S. Fanti; S.Orsola-Malpighi University Hospital, Bologna, ITALY.

Aim: The aim was to investigate the prognostic value of 18F-FDG PET/CT, in terms of overall survival (OS), in restaging of locally advanced cervical cancer (LACC) treated with concomitant chemo-radiation therapy (CCRT). We evaluated the prognostic value

of both intensity- and volume-based PET parameters (SUVmax, SUVmean, MTV and TLG). **Methods:** 78 patients (age 35-94, median 66.3) affected by locally-advanced cervical cancer (LACC, stage IB - IVA) and treated with concomitant chemo-radiation therapy (CCRT) were retrospectively enrolled. For each patient, a full clinical history, including histology, treatment (CCRT +/- boost + brachytherapy), and follow up (median 42.2 months) were available. Each patient underwent a 18F-FDG PET/CT scan both in staging (PET1) and restaging at least three months after the end of treatment (PET2). All PET/CT scans were revised by two expert nuclear medicine physicians. Post-treatment scans were classified into 4 groups according to EORTC criteria: complete metabolic response (CMR), partial metabolic response (PMR), stable metabolic disease (SMD), progressive metabolic disease (PMD). We also classified post-treatment scans on the base of percentage variation of SUVmean, MTV and TLG (CMR: no significant uptake, PMR: SUVmean/MTV/TLG reduction >25%, SUVmean/MTV/TLG increase <25% and decrease<25%, PMD: SUVmean/MTV/TLG increase >25%). The intergroups cut-offs were derived from EORTC criteria. A survival Kaplan-Meier analysis was performed to verify the prognostic significance of the PET2 response. **Results:** Among 78 patients there were 61 squamous cell carcinoma, 14 adenocarcinoma, 3 others types). In this cohort of patients, the statistical analysis with the Kaplan-Meier method showed a highly statistically significant difference in OS between patients with a CMR compared to patient with a PMR, SDM and PMD. The same statistically significant results were obtained employing SUVmax (p=0,0001), SUVmean (p<0,0001), MTV (p<0,0001) and TLG (p<0,0001) as PET evaluation parameter. The optimal OS difference was observed in CMR group vs non-complete metabolic response group (PMR, SMD, PMD). **Discussion and Conclusion:** A complete metabolic response in post-treatment 18F-FDG PET/CT scan, evaluated through SUVmax, SUVmean, MTV and TLG, predicted a lower risk of death in patients with LACC treated with CCRT. Patients with a non-complete PET/CT response after chemo-radiation therapy showed a lower OS and they may benefit from more aggressive treatment. Both intensity- and volume-based PET parameters showed a high prognostic value, in terms of OS, in our cohort of patients. Further studies including a larger number of patients prospectively enrolled are needed to confirm our preliminary findings.

OP-302

Combined FDG and 4FMFES PET Imaging in ER+ Breast Cancer Patients for Improved Diagnostic and Prognostic Value

M. Paquette, É. Lavallée, S. Phoenix, H. Senta, B. Guérin, J. E. van Lier, R. Lecomte, É. E. Turcotte; Université de Sherbrooke, Sherbrooke, QC, CANADA.

Introduction: FDG-PET is widely used for detection and treatment follow-up of breast cancer. However, FDG performs relatively poorly for luminal subtypes, which constitutes the vast majority of breast cancers. On the other hand, most luminal tumors express high levels of estrogen receptors (ER). An ongoing phase II clinical trial evaluating the novel ER PET tracer 4FMFES in ER+ breast cancer patients showed substantial gain in tumor contrast and detection rate over the widely-studied FES, with no identified drawbacks. The study focusses now on the complementary information that FDG-PET and 4FMFES-PET could provide to clinicians in order to enhance diagnostic confidence and prognostic value. **Subjects & Methods:** The preliminary, ongoing analysis includes so far 13 ER+ breast cancer patients. Each patient underwent whole-body PET/CT scans 1 hour following administration of either 186±25 MBq 4FMFES or 182±24 MBq FDG at least 48 h apart and within a maximum 2-week interval. Tumor uptake for each tracer was reported as SUV_{Max} values, and background proximal to each lesion reported as SUV_{Mean}. Except for one patient, hormone therapy was withdrawn at least 6 weeks prior to 4FMFES imaging. **Results:** A total of 78 lesions were detected using 4FMFES, whereas FDG only distinguished 66 foci**.** Twelve tumors were FDG+ and 4FMFES-, and 22 were only detected using 4FMFES. One patient was under tamoxifen therapy during the imaging protocol, and was the only patient negative to 4FMFES, likely as a result of pharmacological competition. Of note was one patient negative on FDG-PET, but positive with an extensive metastatic disease using 4FMFES. In two other patients, 4FMFES allowed restaging by detection of distant bone metastases unseen using FDG. Inversely, two liver metastases and an intestinal neoplasia were only seen using FDG in 3 other cases. Overall FDG tumor uptake was significantly higher (p < 0.001) than 4FMFES, with SUV_{Max} of 5.4 ± 3.8 and 2.7 ± 1.9, respectively. Background signal was in average significantly lower with 4FMFES (SUV_{Mean} 0.36 ± 0.09) than with FDG (SUV_{Mean} = 0.90 ± 0.43; p < 0.001). As a result, a clear trend toward better tumor-to-background ratio using 4FMFES compared to FDG was observed. **Conclusion:** While FDG PET is a well-established procedure for breast cancer detection and therapy follow-up, complementation with 4FMFES PET could further improve diagnosis and refine staging. High tumor contrast using 4FMFES could confer an advantage over FDG for small, hypometabolic ER+ lesions.

OP-303

Qualitative and quantitative analyses of ¹⁸F-FES and ¹⁸F-FDHT uptake in patients with metastatic breast cancer: an interobserver variability study

*L. H. Mammatas[1], C. M. Venema[2], C. P. Schröder[2], M. van Kruchten[2], G. Apollonio[2], A. W. J. M. Glaudemans[3], A. H. H. Bongaerts[3], O. S. Hoekstra[4], H. M. W. Verheul[1], E. Boven[1], B. van der Vegt[5], E. F. J. de Vries[3], E. G. E. de Vries[2], R. Boellaard[3,4], G. A. P. Hospers[2], C. W. Menke-van der Houven van Oordt[1]; [1]Department of Medical Oncology, VUmc Cancer Center Amsterdam, VU University Medical Center, Amsterdam, NETHERLANDS, [2]Department of Medical Oncology, University of Groningen, University Medical Center Groningen, Groningen, NETHERLANDS, [3]Department of Nuclear Medicine and Molecular Imaging, University of Groningen, University Medical Center Groningen, Groningen, NETHERLANDS, [4]Department of Radiology and Nuclear Medicine VU University Medical Center, Amsterdam, NETHERLANDS, [5]Department of Pathology & Medical Biology, University of Groningen, University Medical Center Groningen, Groningen, NETHERLANDS.

Aim: While estrogen deprivation is a cornerstone of treatment in patients with estrogen receptor (ER) positive breast cancer, androgen receptor (AR) blockade is currently under investigation. In a recent pilot study, we showed that ^{18}F-fluoroestradiol (^{18}F-FES) and ^{18}F-fluorodihydrotestosterone (^{18}F-FDHT) uptake in breast cancer lesions correlates well with, respectively, ER (sensitivity and specificity 100%) and AR (sensitivity 91%, specificity 100%) expression in biopsies. A SUV_{max} >1.9 was identified as the optimal threshold for AR-positive tumors (>10% staining), and a SUV_{max} >1.5 for ER-positive tumors (>1% staining). These techniques have the ability to visualize receptor status in all lesions of a patient, which may guide treatment decisions. Here, we examined interobserver differences, since high agreement is required for use as clinical imaging biomarkers. **Materials and Methods:** In this prospective two-center study, 2 independent observers qualitatively and quantitatively scored all lesions visible on bone scan and high-resolution CT (>1cm) on both ^{18}F-FES and ^{18}F-FDHT PET/CT in patients with ER-positive metastatic breast cancer. ^{18}F-FES and ^{18}F-FDHT PET/CT were performed ≤14 days of each other and bone scan and high-resolution CT were performed <6 weeks of the PET scans. A visually PET-positive lesion was defined as uptake above background in surrounding tissue of the same origin. Observers 1 and 2 used manual and semi-automated delineation methods, respectively. Interobserver agreement was determined by an intraclass correlation coefficient (ICC) with a 95% confidence interval (95% CI). **Results:** Ten patients were evaluated and observers 1 and 2, respectively, identified 64 and 69 positive lesions on ^{18}F-FES PET and 36 and 37 positive lesions on ^{18}F-FDHT PET. On CT and bone scan, respectively, 6 and 11 additional lesions were seen, while 55 and 33 PET-positive lesions were not identified. Comparison of qualitative and quantitative results showed a SUV_{max} >1.5 in 44% and 39% of the lesions scored visually negative on ^{18}F-FES PET by observers 1 and 2, respectively. For ^{18}F-FDHT PET, 31% and 52% of the visually negative lesions had a SUV_{max} >1.9 suggesting the importance of quantification. Interobserver agreement was excellent for ^{18}F-FES SUV_{max} (ICC 0.98, 95% CI 0.96-0.98) and good for ^{18}F-FDHT SUV_{max} (ICC 0.78, 95% CI 0.66-0.85). SUV_{max} showed a higher, although not significantly different, level of concordance compared to SUV_{peak} and SUV_{mean} with isocontour 70% of maximum. **Conclusion:** Quantification of ^{18}F-FES and ^{18}F-FDHT uptake in breast cancer lesions using SUV_{max} shows high consistency between observers, supporting use in clinical practice.

OP-304

^{68}Ga-NOTA-BBN-RGD PET/CT for GRPR and Integrin αvβ3 Imaging in Patients with Breast Cancer

J. Zhang[1,2], *F. Mao*[3], *G. Niu*[2], *L. Peng*[3], *L. Lang*[2], *F. Li*[1], *H. Ying*[4], *H. Wu*[5], *B. Pan*[5], *Z. Zhu*[1], *X. Chen*[2]; *[1]Department of Nuclear Medicine, Peking Union Medical College Hospital, Chinese Academy of Medical Sciences and Peking Union Medical College, Beijing, CHINA, [2]Laboratory of Molecular Imaging and Nanomedicine (LOMIN), National Institute of Biomedical Imaging and Bioengineering (NIBIB), National Institutes of Health (NIH), Bethesda, MD, UNITED STATES OF AMERICA, [3]Department of Breast Surgery, Peking Union Medical College Hospital, Chinese Academy of Medical Sciences and Peking Union Medical College, Beijing, CHINA, [4]Department of Medical Oncology, Peking Union Medical College Hospital, Chinese Academy of Medical Sciences and Peking Union Medical College, Beijing, CHINA, [5]Department of Pathology, Peking Union Medical College Hospital, Chinese Academy of Medical Sciences and Peking Union Medical College, Beijing, CHINA.*

Purpose: This study was designed to assess a novel GRPR and integrin αvβ3 dual targeting positron emission tomography/computed tomography (PET/CT) using ^{68}Ga-NOTA-BBN-RGD in patients with breast cancer and metastasis. **Methods:** Twenty-two patients (29-62 y, mean age 52.5±9.3 y) were recruited either with suspected breast cancer on screening mammography (n=16) or underwent breast cancer radical mastectomy (n=6). All the 22 patients underwent PET/CT at 30-45 min after intravenous injection of 1.85 MBq per kilogram of body weight of ^{68}Ga-NOTA-BBN-RGD. 11 of 22 patients also accepted ^{68}Ga-NOTA-BBN PET/CT within 2 weeks for comparison. A final diagnosis was made based on the histopathologic examination of surgical excision or biopsy. Immunohistochemical staining of tumor samples against GRPR and integrin αvβ3 was performed and correlated with ^{68}Ga-NOTA-BBN-RGD and ^{68}Ga-NOTA-BBN PET imaging. **Results:** Both the primary cancer and metastases showed positive ^{68}Ga-NOTA-BBN-RGD accumulation with high tumor/normal tissue (T/N) ratios. A total of 107 masses were pathologically confirmed, including 24 malignant breast masses, 5 benign breast masses, 16 lymph node metastases, 59 benign lymph nodes, 1 lung metastasis and 2 bone metastases. The sensitivity, specificity, positive, negative predictive values for primary breast cancer were 95.8% (23/24), 60.0% (3/5), 92.0% (23/25), 75.0% (3/4), and 75.0% (12/16), 91.5% (54/59), 70.5% (12/17), 93.1% (54/58) for lymph nodes, respectively. ^{68}Ga-NOTA-BBN-RGD PET/CT detected 23 suspected primary tumor lesions, 12 metastatic lymph nodes, 11 bone metastases, 4 lung metastases and 2 liver metastases with maximum standardized uptake values (SUVmax) of 3.84 ± 2.18, 3.78 ± 1.90, 5.50 ± 2.43, 1.40 ± 1.41 and 4.35, respectively. In comparison, ^{68}Ga-NOTA-BBN PET/CT showed relatively lower SUVmax of 2.31 ± 0.72 for primary tumor, 2.03 ± 0.76 for lymph node metastasis, 2.17 ± 0.57 for bone metastasis, and 1.55 for lung metastasis, P < 0.05). Among them, a total of 52 masses were subjected to immunohistochemical staining against GRPR and integrin αvβ3 confirming moderate correlation between SUVmax in ^{68}Ga-NOTA-BBN-RGD PET and GRPR expression (r = 0.5237, P =0.0012) and weak correlation between SUVmax and integrin αvβ3 expression (r = 0.3733, P = 0.0793). **Conclusion:** This study demonstrated significant uptake of a new type of dual integrin αvβ3 and GRPR targeting in both the primary lesions and metastases of breast cancer. ^{68}Ga-NOTA-BBN-RGD PET/CT may be of great value in discerning both primary breast cancers and metastases, suggesting the potential of ^{68}Ga-NOTA-BBN-RGD PET/CT in breast cancer diagnosis, staging and guiding surgical decision making for the patients.

OP-305

PET Imaging of Chemokine Receptor CXCR4 in Patients with Primary and Recurrent Breast Cancer

T. Vag[1], A. Rossmann[1], S. Metz[1], H. Wester[2], M. Schwaiger[1]; [1]Klinikum Rechts der Isar, Munich, GERMANY, [2]Institute of Pharmaceutical Radiochemistry, Technical University Munich, Munich/ Garching, GERMANY.

Purpose: CXCR4 is a chemokine receptor overexpressed in invasive breast cancer and plays a major role in signaling pathways of metastases. The aim of this study was to assess the feasibility of CXCR4 directed imaging in patients with breast cancer using the novel CXCR4 targeted PET probe ^{68}Ga-Pentixafor. **Material and Methods:** 13 patients with primary breast cancer and five patients with recurrent disease after primary breast cancer underwent CXCR4 targeted PET imaging using ^{68}Ga-Pentixafor. ^{18}F-FDG PET was available in 8 of 18 patients. Maximum standardized uptake values (SUVmax) and tumor-to-background ratios (T/B ratio) of primary tumors or recurrent lesions were measured for both PET probes and compared with each other. SUVmax of CXCR4 targeted PET was also compared with prognostic factors and molecular subtypes of breast cancer. **Results:** 9 of 13 primary breast cancers were visually detectable on ^{68}Ga-Pentixafor PET images (mean SUVmax of 3). The visually undetectable lesions included the two cases of invasive loubular carcinoma (ILC), and two cases of triple negative breast cancer (TNBC). Metastases of recurrent breast cancer were visually detectable in all 5 cases, exhibiting a mean SUVmax of 3.5. ^{18}F-FDG-PET demonstrated higher SUVmax in all patients compared to ^{68}Ga-Pentixafor PET. A significant correlation between SUVmax obtained from ^{68}Ga-Pentixafor PET and prognostic factors including estrogene receptor (ER), progesterone receptor (PR), HER2/neu status, Ki-67 proliferation index, tumor grade and molecular subtypes (luminal A, luminal B, basal like) was not observed. **Conclusion:** CXCR4 directed PET imaging in patients with primary and recurrent breast cancer is feasible, however tumor-detectability is lower compared to ^{18}F-FDG PET. Moreover, we did not find any significant correlation between aforementioned prognostic factors of breast cancer and CXCR4 targeted tracer accumulation. In conclusion, based on these preliminary results in a small patient cohort, CXCR4 targeted PET does not seem to demonstrate any diagnostic or prognostic benefit in Imaging of breast cancer.

Committee Symposium 3 - Inflammation & Infection/ Neuroimaging: Neurological Autoimmune Disorders

OP-306

Classification and Clinical Approach to Neurological Autoimmune Disorders

G. Gobbi; Institute of Neurological Sciences of Bologna, Child Neurology Unit, Bologna, ITALY.

OP-307

Role of Brain 18F-FDG-PET in the Syndrome-Based Diagnostic Approach to Autoimmune Encephalitis

S. Morbelli; IRCCS San Martino - IST, Department of Nuclear Medicine, Genoa, ITALY.

OP-308

PET Imaging of Brain Involvement in Systemic Autoimmune Disorders

R. Dierckx; University Medical Center Groningen, Medical Imaging Center, Dep. of Nuclear Medicine and Molecular Imaging, Groningen, NETHERLANDS.

Tomorrow's Experts Session - Best-Ranked Papers from the Under-30s

OP-309

Quantitative characterization of xSPECT algorithm: influence of reconstruction parameters (number of iterations and subsets) on image quality

L. Lorenzon[1], A. Fracchetti[1], M. Bonelli[1], M. Tredici[2], V. Zilioli[2], M. Farsad[2], M. Haller[1]; [1]Department of Medical Physics, Hospital of Bolzano, Bolzano, ITALY, [2]Department of Nuclear Medicine, Hospital of Bolzano, Bolzano, ITALY.

Introduction: Recently, Siemens introduced a new reconstruction technique, the xSPECT, which is based on a new algorithm, the Ordered Subset Conjugate Gradient Minimization (OSCGM). The aim of this study was to quantitatively characterize the xSPECT algorithm, by evaluating the influence of reconstruction parameters (number of iteration and subset) on image quality (noise, contrast and contrast-to-noise ratio). **Subject & Methods:** Measurements were performed on the NEMA IEC Body Phantom, filled with a ^{99m}Tc water solution, with a 4:1 sphere-to-background activity concentration ratio. SPECT phantom images were acquired on a Siemens Symbia Intevo 2 and reconstructed using a OSCGM method (xSpect, Siemens Medical Solutions USA, Inc., Malvern, PA), without post-reconstruction filters and varying the number of iterations and subsets. CT image was acquired at 110 kV and 100 mAs/rot, and reconstructed with B31 filter. The SPECT images, reconstructed with different number of iterations and subset, were compared calculating the noise in the homogeneous phantom region, the percentage contrast and the contrast-to-noise ratio, CNR, for the six hot spheres. **Results:** Different behavior has been observed compared to what has been reported in the literature for OSEM reconstruction technique: 1) The number of updates (the product between the subset and the iteration numbers) is not significant for noise level: the noise grows with the number of updates, but the same number of updates can generate different noise levels (t-test, $p < 0.05$). 2) For the same number of updates, the subsets which can be expressed as a power of two (2, 4, 8) generate less noise level than the subsets which are not a power of two (1,3,6,···). 3) Contrast grows with the number of updates, but over 400 updates the noise affects heavily the structures with a diameter larger than 20mm, and their contrast becomes even lower than

that of smaller spheres. 4) CNR decreases rapidly as the number of updates grows. **Conclusion:** The OSCGM reconstruction algorithm, implemented in xSPECT reconstruction technique, behaves differently from OSEM. For the same number of updates, different noise levels may result and the noise is smaller when using a number of subsets that can be expressed as a power of two. A subset number of 2 or 4 is recommended and a low number of updates (<100) in combination with a smoothing filter is suggested in order to preserve contrast and CNR.

OP-310
Dual-labeled PSMA-11 for PET/CT imaging and precise fluorescence guided intraoperative identification of prostate cancer

A. Baranski[1], M. Schäfer[1], U. Bauder-Wüst[1], M. Roscher[1], J. Schmidt[1], E. Stenau[1], T. Simpfendörfer[2], L. Maier-Hein[1], B. Hadaschik[3], U. Haberkorn[2], K. Kopka[1], M. Eder[4,1,5]; [1]German Cancer Research Center, Heidelberg, GERMANY, [2]University Hospital, Heidelberg, GERMANY, [3]University Hospital, Essen, GERMANY, [4]University Hospital, Freiburg, GERMANY, [5]German Cancer Consortium, Heidelberg, GERMANY.

Introduction: Resection of lymph node metastases using image-guided surgery is of high clinical relevance and might have considerable impact on the outcome of metastatic prostate cancer patients. In order to further improve the intraoperative accuracy of detecting PSMA-positive tumor lesions dual-labeled PSMA-inhibitors based on PSMA-11 have been designed. These novel bimodal radiopharmaceuticals allow the combination of preoperative staging by means of PET/CT and fluorescence-guided surgery for a more precise detection of metastasis or neoplastic lymph nodes. **Subjects & Methods:** A series of novel PSMA-11 based optical dye conjugates were synthesized by conjugating the parent molecule PSMA-HBED-CC with FITC, AlexaFluor488, STARRED, DyLight800 and IRDye800CW, respectively. The PSMA-binding and internalization properties were subsequently analyzed in cell based assays using human PSMA expressing LNCaP cells. For the optical investigation of affinity, internalization and intracellular distribution fluorescence was detected by microscopy and flow cytometry. To obtain a preclinical proof-of-concept, specific tumor uptake, pharmacokinetic properties and fluorescence-guided studies were performed in LNCaP (PSMA+) or PC3 (PSMA-) tumor-bearing mice and healthy pigs. **Results:** The radiolabeled fluorescent-dye conjugates showed high affinity in the nanomolar range, PSMA-specific cell uptake and effective internalization into LNCaP cells which has also been confirmed by fluorescence based assays and microscopy. Depending on the fluorescent dye, slightly varying pharmacokinetic properties have been obtained. The ^{68}Ga-labeled FITC-, AlexaFluor488-, DyLight800- and IRDye800CW- conjugates revealed a higher tumor uptake [10.9 ± 0.9 % ID/g (^{68}Ga-PSMA-HBED-CC-FITC), 9.1 ± 6.7 % ID/g (^{68}Ga-PSMA-HBED-CC-AlexaFluor488), 15.7 ± 6.7 % ID/g (^{68}Ga-PSMA-HBED-CC-DyLight800), 13.7 ± 3.7 % ID/g (^{68}Ga-PSMA-HBED-CC-IRDye800CW)] compared to ^{68}Ga-PSMA-11 (4.8 ± 1.3 % ID/g), while a similar uptake was determined for the ^{68}Ga-labeled STARRED- conjugate (5.6 ± 2.3 %lD/g). µPET studies reinforce the PSMA-specific tumor uptake and fast renal clearance of all con-

jugates. The first proof-of-concept studies in mice and healthy pigs revealed a typical organ distribution profile and specific fluorescent signals in PSMA-expressing tissue *in vivo* and *ex vivo* for the clinical relevant candidate PSMA-HBED-CC-IRDye800CW. **Conclusion:** As demonstrated in these preclinical and first *in vivo* proof-of-concept studies, dual-labeled PSMA-11 provides PSMA-specific fluorescence signals and promising pharmacokinetic properties in surgical settings indicating the high potential for future clinical translation. The dual-labeled PSMA-inhibitors investigated in this work might help to establish a novel treatment regimen for a more precise and sensitive pre-, intra- and post-therapeutic detection of prostate cancer. Research Support: We thank PD Dr. med. Arianeb Mehrabi (University Hospital Heidelberg) and his team for supporting the animal studies.

OP-311
SVM based detection of a disease specific metabolic brain pattern in a rat model for Parkinson's disease using longitudinal 18F-FDG PET imaging

M. Devrome[1], M. Crabbé[2], V. Baekelandt[3], K. Van Laere[1], C. Casteels[2], M. Koole[1]; [1]Division of Nuclear Medicine, KU Leuven, Leuven, BELGIUM, [2]Molecular Small Animal Imaging Centre, KU Leuven, Leuven, BELGIUM, [3]Division of Neurobiology and Gene therapy, KU Leuven, Leuven, BELGIUM.

Introduction: Diagnosing the early onset of Parkinson's disease (PD) is of vital importance for treatment and disease follow-up. To study the pathophysiology of PD, animal models that closely resemble the neuropathology and motor symptoms of human PD might play an important role. In this study, a rat model based on the injection of A53T alpha-synuclein rAAV vector was used and a support vector machine (SVM) classifier was applied to identify a PD-specific glucose metabolic brain pattern at a late disease stage. Subsequently, this disease-specific brain pattern was validated by evaluating the pattern expression during various disease stages. **Methods:** Rats were stereotactically injected with recombinant adeno-associated viral vector (rAAV 2/7) in the right substantia nigra, overexpressing either A53T alpha-synuclein (10 rats, PD group) or eGFP (8 rats, control group). Static ^{18}F-FDG PET scans were performed at week 3, 4, 6 and 9 after injection. At week 9, when the dopaminergic degeneration is considered to be complete and stable for the alpha-synuclein injected animals, a SVM classifier was trained to differentiate between the PET scans of the PD and control group. Accordingly, a multivariate PD-characteristic glucose metabolic brain pattern was generated. Consequently, PET scans of both groups performed at earlier time points were projected onto this PD-specific brain pattern to quantify disease progression. Projection-scores of the two groups (alpha-synuclein versus eGFP) were evaluated for statistically significant differences (Wilcoxon rank sum test, at 5% significance level). **Results:** The multivariate PD pattern allowed to identify hypermetabolism in the striatum, frontal cortex, hippocampus and sensorimotor cortex, and hypometabolism in the cerebellum. The Wilcoxon rank sum test demonstrated statistically significant differences between the disease progression scores of the alpha-synuclein

and eGFP group at week 4 (p = 0.006) and at week 6 (p = 0.002). At week 3, differences between the disease progression scores of the two groups were not significant (p = 0.96). These findings demonstrated complete and stable dopaminergic degenerating in this animal model at week 4. **Conclusion:** This study presents a proof-of-concept of a multivariate analysis to identify a disease-specific brain pattern based on preclinical ^{18}F-FDG brain PET imaging. Correlations with motor dysfunction parameters over time and comparison with univariate data analysis will further validate this PD-specific metabolic brain pattern as an imaging biomarker for monitoring disease progression and therapeutic interventions in rodent disease models using longitudinal ^{18}F-FDG brain PET imaging.

OP-312

Quantitative myocardial stress perfusion in patients with chest pain and normal coronary arteries to assess subsequent improvement of symptoms with transcutaneous electrical nerve stimulation

A. G. Monroy-Gonzalez[1], M. J. L. De Jongste[1], E. Alexanderson-Rosas[2], R. A. Tio[1], R. H. J. A. Slart[1]; [1]University Medical Center Groningen, Groingen, NETHERLANDS, [2]Department of Physiology, National Autonomous University of Mexico, MEXICO.

Introduction: Cardiac Syndrome X (CSX) is defined as the combination of chest pain and positive exercise stress test in the presence of normal coronary arteries. Improvement of symptoms in patients with CSX through Transcutaneous Electrical Nerve Stimulation (TENS) has been reported. However, the relationship of myocardial stress perfusion with PET and clinical response to TENS in patients with chest pain and normal or near normal coronary arteries is still unknown**. Aim:** We evaluated the role of absolute myocardial stress perfusion quantification with Nitrogen-13 ammonia PET in predicting good response to treatment with TENS in patients with normal or near normal coronary arteries. **Methods:** We retrospectively included 41 patients who underwent Nitrogen-13 ammonia PET for quantification of myocardial blood flow (MBF), during stress with adenosine. Patients with significant coronary artery disease (>50% stenosis) demonstrated by invasive coronary angiography were excluded. **Results:** In our population mean age was 51±10 years old, 66% of patients were female, 7% were diabetic, 34% had hypertension, and 10% were current smokers. In our population 51% of patients reported improvement of symptoms. We did not find clinical significant differences in baseline characteristics of patients with and without improvement of symptoms. However, we found an increased proportion of patients with abnormal MBF during stress in patients without improvement of symptoms when compared to patients with improvement of symptoms (50% [n=10] vs. 19% [n=4] respectively, p value = 0.04). Furthermore, we found an increased proportion of patients with the use of beta-blockers in patients with improvement of symptoms when compared to patients without improvement of symptoms (42% [n=9] vs. 10% [n=2] respectively, p value = 0.02). **Conclusion:** Absolute myocardial stress perfusion quantification and the use of beta-blockers might predict

improvement of symptoms in patients with normal or near normal coronary arteries treated with TENS. Further studies are needed in order to fully understand the role of myocardial stress perfusion in this group patients.

OP-313

TSPO-PET for high-grade glioma imaging using the novel ligand [^{18}F]GE-180 - first in human results in the course of radiotherapy

M. Unterrainer[1], D. Fleischmann[1], S. Lindner[1], A. Brunegraf[1], F. Vettermann[1], L. Vomacka[1], M. Brendel[1], R. Rupprecht[2], C. Belka[1], P. Bartenstein[1], M. Niyazi[1], N. Albert[1]; [1]Ludwig-Maximilian-University Munich, München, GERMANY, [2]University of Regensburg, München, GERMANY.

Objective: The 18-kDa mitochondrial translocator-protein (TSPO) was reported to be upregulated in high-grade gliomas (HGG). [^{18}F]GE-180, a novel 3rd generation TSPO receptor ligand, has shown an improved target-to-background contrast. Therefore, we evaluated the feasibility of [^{18}F]GE-180 PET in HGG patients, its potential for clinical use before radiotherapy and the impact of radiotherapy on the tumoral TSPO expression. **Methods:** 12 patients with histologically confirmed HGG (11 glioblastoma, 1 anaplastic astrocytoma; IDH-wildtype) underwent [^{18}F]GE-180 PET at initial diagnosis or recurrence before radiotherapy (6 medium- and 6 high-affinity binders (MAB, HAB)). The PET parameters mean background uptake (SUV_{BG}), maximal tumor uptake (SUV_{max}), maximal tumor-to-background ratios (TBR_{max}) and biological tumor volumes (BTV) using different thresholds (SUV_{BG} x 1.6, 1.8 and 2.0) were evaluated in the 60-80 minutes p.i. summation images. The different BTVs were compared to the MRI-based gross tumor volume (GTV). Follow-up PETs were performed in 8/12 patients 4-6 weeks after radiotherapy and compared to the baseline PET. **Results:** All HGG showed [^{18}F]GE-180 uptake with extraordinary high tumor-to-background contrast (median SUV_{max} 3.1 (2.5 - 5.8) and TBR_{max} 6.9 (3.9 - 9.1). No difference between HAB and MAB regarding the uptake-characteristics could be observed (p>0.05). Volumetric comparisons with GTV revealed significantly larger BTVs (p=0.002/0.003/0.008) with high [^{18}F]GE-180 uptake beyond contrast-enhancement. The spatial volumetric correlation (Sørensen-Dice coefficient) of BTVs and GTV before radiotherapy was 0.48 (BTV1.6), 0.54 (BTV1.8) and 0.58 (BTV2.0). After radiotherapy, a significant reduction of SUV_{max} (median percental reduction of 43.4% (1.1% - 61.1%), p=0.012) and of TBR_{max} (median percental reduction of 27.9% (14.1% - 54.8%), p=0.012) could be observed. All but one patients provided significant reductions of the BTVs (e.g. median percental reduction of BTV1.6: 63.2%, p=0.017). In sum, 1 patient showed an increase of 34.8% despite undergoing radiotherapy, 5 patients showed a reduction ranging between 26.1% and 63.2%, whereas 2/8 patients showed a nearly complete remission of the extent of TSPO expression (92.0% and 94.7%). **Conclusion:** This first study using [^{18}F]GE-180 in HGG patients shows a remarkably high tumor-to-background contrast. As high TSPO expression was shown in areas beyond contrast enhancement on MRI, [^{18}F]GE-

180 PET represents a promising tool for HGG delineation (with a potential influence on therapy planning). The tumoral TSPO expression was differently affected by radiotherapy, hence [18F] GE-180 PET might serve as a complementary imaging-biomarker for response assessment in HGG. [18F]GE-180 PET is of utmost interest regarding future clinical applications in terms of treatment planning and response assessment.

OP-314

Relationship between Intraprostatic Hybrid Tracer Deposition and Lymphatic Drainage Pattern in Prostate Cancer Patients

C. M. de Korne[1], T. Buckle[1], N. S. van den Berg[1], J. de Jong[2], R. A. Valdés Olmos[1], F. W. B. van Leeuwen[1], H. G. van der Poel[2]; [1]LUMC, Leiden, NETHERLANDS, [2]NKI-AVL, Amsterdam, NETHERLANDS.

Introduction: Defining the sentinel node (SN) in prostate cancer is complex as drainage may differ between segments within the prostate. While the SN procedure is based on visualization of the first tumor draining lymph node, the location of the primary tumor is currently not taken into account during tracer administration. Hence, discrepancies between the migration route of metastasizing cancer cells and the drainage pattern of the injected tracer might occur, resulting in false negative results. This study was designed to expand on an initial 19 patients proof-of-concept study[1] and aimed to evaluate the ability of the SN procedure to predict the location of lymphatic metastases based on the primary tumor site. **Methods:** 70 patients with prostate carcinoma, scheduled for robot assisted laparoscopic prostatectomy (RALP) and extended lymph node dissection with SN biopsy, were included in this study. After injection of Indocyanine green (ICG)-99mTc-nanocolloid in the peripheral zone of the prostate, SLN mapping was performed based on lymphoscintigraphy and SPECT/CT. SNs were resected using a combination of radio- and fluorescence guidance. Pathology was used to determine the primary tumor and metastatic spread. Fluorescence imaging of paraffin-embedded prostate tissue allowed visualization of the tracer deposits in the prostate. This deposition was related to the intraprostatic and lymphatic tumor spread. **Results:** In total 252 SNs and 552 non-SNs were identified. The distribution of the SNs within the pelvis was shown to correlate to the intraprostatic location of tracer administration. In 80% of the ten lymph node positive patients, positive SNs were found, with a total of 19 SNs. Two of these patients also had tumor positive non-SNs. In two patients positive non-SNs were found, without finding tumor positive SNs. In all patients, the primary tumor location could be related to the locations of lymphatic spread. **Conclusion:** The correlation between the tracer deposits within the prostate, the location of the primary tumor and the number and anatomical position of the SNs indicates that placement of tracer deposits is of influence on the visualized lymphatic drainage pattern. Moreover, the correlation between the location of the primary tumor and the location of the positive SNs suggested that placement of tracer deposits near the primary tumor site is beneficial for the identification of metastatic spread. [1] Buckle et al, JNM, 2012

OP-315

Efficacy and Safety of 177Lu-PSMA-617 Treatment in Castration Resistant Prostate Cancer with Organ Metastasis

O. E. Sahin[1], E. Akgün[1], E. Demirci[2], M. Ocak[3], A. Akgün[1], B. Akovalı[1], E. Karayel[1], H. Pehlivanoglu[1], L. Kabasakal; [1]Department of Nuclear Medicine, Cerrahpasa Medical Faculty, Istanbul University, İstanbul, TURKEY, [2]Department of Nuclear Medicine Sisli Etfal Training and Research Hospital, İstanbul, TURKEY, [3]Department of Pharmaceutical Technology, Pharmacy Faculty, Istanbul University, İstanbul, TURKEY.

Purpose: PET imaging with radiolabeled inhibitors of prostate-specific membrane antigen (PSMA) have been successfully used for imaging prostate cancer and become widespread during the recent years. Therefore PSMA targeted radionuclide therapy is increasingly being popular and using for people with advanced prostate cancer. The median survival of castration resistant prostate cancer patients with liver metastasis is reported to be 6 months which is one of the shortest median survival in prostate cancer subgroups. The aim of our study was to determine the effect of Lu177 PSMA treatment on survival and evaluate the side effects in hormone refractory prostate cancer patient with organ metastases. **Materials and Methods:** Records of patients who treated with 177Lu-PSMA-617 at our hospital from 2014 to 2016 were retrospectively examined. CRPC patients who treated with 177Lu-PSMA-617 and there wasn't clinical respond after the standard chemotherapies including docetaxel and abiraterone were included in the study. Survival rates were calculated from the first day of administered therapy. In addition, treatment nephrotoxicity was assessed by creatinine levels and hematotoxicity was assessed by using SWOG criteria. **Results:** 19 patients (median age 67.7 ± 8.1 years, range 55-82) meeting the inclusion criteria within the study timeline were included the study. 4 patients (18.2%) underwent radical prostatectomy,16 patients (84.2%) underwent curative or palliative radiotherapy. A total of 18,8 ±9,4 GBq (*average* cycle : 3 ,range :1-5) were performed in 19 patients. 16 patients (84.2%) had liver metastasis and 6 patients (31.6%) had lung metastasis before the therapy. Furthermore 18 patients (94.7%) had bone metastasis. The mean tPSA values before the therapy was calculated 557 (6 - 4499) ng/ml. Among patients whose PSA levels were regularly monitored (n:16) decreased PSA levels were seen in 6 patients (38%) and increased PSA levels were seen in 10 patients (62%). A 3,5% increase in serum creatinine was observed compared to initial levels. In 17 patients whom hematologic data could be evaluated according to SWOG criteria, grade 1 hematotoxicity were observed in 5 patients (29%) and grade 2 hematotoxicity were observed in 1 patient (6%).The median overall survival for all patients was calculated 8 months (95% Cl:5,2-10,8). **Conclusion:** 177Lu-PSMA-617 treatment is known that effective for advanced staged castration resistant prostate cancer with lymph nodes and bone metastasis. Our study show that 177Lu-PSMA-617 treatment can be safely used for patients who have castration resistant prostate cancer with organ metastasis.

EANM Young Daily Forum 2: Networking - How to Build Professional Relationships

R. Sheppard; Somerset, UNITED KINGDOM.

CME 7 - Radionuclide Therapy/Thyroid: Safety Aspects in Radionuclide Therapy

OP-321
Radiobiological Aspects in Radionuclide Therapy
J.-P. Pouget; IRCM/INSERMU896, Montpellier, FRANCE.

OP-322
Early and Late Side Effects of Radionuclide Therapy
L. Bodei; Memorial Sloan Kettering Cancer Center, New York, UNITED STATES OF AMERICA.

OP-323
Prevention of Side Effects in Radionuclide Therapy
Y. Du; Royal Marsden Hospital, London, UNITED KINGDOM.

Symposium 7 - Bone & Joint: Painful Hip Arthroplasty

OP-324
Biomechanics of Normal Hip and Hip Arthroplasty
D. Pioletti; Ecole Polytechnique Fédérale de Lausanne (EPFL), Lab. of Biomechanical Orthopedics, Lausanne, SWITZERLAND.

OP-325
What the Surgeon Wants to Know From Imaging
R. Nizard; Hospital Lariboisière - Assistance Publique – Hôpitaux de Paris, Service de Chirurgie Orthopédique et Traumatologique, Paris, FRANCE.

OP-326
Radiologic Imaging
A. Feydy; Hospital Cochin - Assistance Publique – Hôpitaux de Paris, Service de Radiologie, Paris, FRANCE.

OP-327
Hybrid Imaging: Role and Limits
F. Paycha; Hospital Lariboisière - Assistance Publique – Hôpitaux de Paris, Nuclear Medicine Department, Paris, FRANCE.

CTE 3: Prostate Imaging and Therapy

OP-328
PET-CT Imaging in Prostate Cancer
P. Castellucci; S. Orsola-Malpighi, Nuclear Medicine, Bologna, ITALY.

OP-329
Radionuclide Therapy in Prostate Cancer
T. D. Poeppel; University Hospital Essen, Essen, GERMANY.

OP-330
Radiation Therapy and PET-CT Aided Radiotherapy Planning in Prostate Cancer
A. Skanjeti; Nuclear Medicine Department, Hospices Civils de Lyon, Lyon, FRANCE.

Do.MoRe - Committee Symposium 4 - Dosimetry: Validation of Quantitative Imaging, Dosimetry & Estimates of Uncertainty

OP-331
The Need for Dosimetry Validation - A Clinician's View Point
F. Courbon; Cancer Research Centre of Toulouse, Toulouse, FRANCE.

OP-332
The Use of Monte Carlo for Validation and Uncertainty Analysis
J. R. Gustafsson; Department of Medical Radiation Physics, Lund University, Lund, SWEDEN.

OP-333
Propagation of Uncertainty Analysis for Absorbed Dose Calculations
J. Gear; Royal Marsden NHSFT & Institute of Cancer Research, London, UNITED KINGDOM.

OP-334
Validation of Calibration Protocols and the MRTDosimetry Project
A. Robinson; National Physical Laboratory, Teddington, UNITED KINGDOM.

M2M: SPECT/CT & SPECT/MRI

OP-336
Characterization of ^{111}In-labeled site-specifically conjugated anti-PSMA antibody-drug conjugates for treatment of PSMA-expressing tumors

S. Lütje[1,2], D. Gerrits[1], J. D. Molkenboer-Kuenen[1], K. Herrmann[2], G. Fracasso[3], M. Colombatti[3], O. C. Boerman[1], S. Heskamp[1]; [1]Dept. Radiology and Nuclear Medicine, Radboud university medical center, Nijmegen, NETHERLANDS, [2]Clinic for Nuclear Medicine, University Hospital Essen, Essen, GERMANY, [3]Dept. of Medicine, University of Verona, Verona, ITALY.

Aim: Prostate cancer (PCa) is the most common cancer in men worldwide. In advanced stages of the disease, PCa responds

poorly to chemotherapy. Therefore, antibody-drug-conjugates (ADCs) have been developed to allow specific and improved delivery of highly cytotoxic drug to the tumor. As the prostate-specific membrane antigen (PSMA) is overexpressed in PCa, it represents a promising target for ADC-based therapies. The aim of this study was to evaluate the therapeutic efficacy of site-specifically conjugated duocarmycin- and monomethyl auristatin E (MMAE)-based anti-PSMA ADCs with drug-antibody-ratios (DARs) of 2 and 4. **Materials and Methods:** The anti-PSMA antibody D2B was chemoenzymatically conjugated with duocarmycin or monomethyl auristatin E (MMAE) via the glycosylated site of the antibody. Preservation of the immunoreactivity of the antibody upon site-specific conjugation was investigated in vitro. Biodistribution studies and microSPECT/CT imaging (18.5 ± 2.6 MBq) with 25 μg of ^{111}In-labeled ADCs were performed in BALB/c nude mice with s.c. PSMA^{+} LS174T-PSMA xenografts. Finally, the therapeutic efficacy of the four different ADCs was assessed in mice with s.c. LS174T-PSMA tumors. **Results:** The immunoreactivity of the anti-PSMA antibody was preserved upon site-specific conjugation with the drugs. Biodistribution revealed high tumor uptake of all ADCs. ^{111}In-DTPA-D2B-DAR2-MMAE showed the highest tumor uptake, reaching 119.7 ± 37.4 %ID/g at 3 days p.i.. Tumors of mice treated with ^{111}In-DTPA-D2B, ^{111}In-DTPA-D2B-DAR2-duocarmycin, ^{111}In-DTPA-D2B-DAR4-duocarmycin, ^{111}In-DTPA-D2B-DAR2-MMAE, and ^{111}In-DTPA-D2B-DAR4-MMAE could clearly be visualized with microSPECT/CT. In contrast to 'naked' D2B or vehicle, D2B-DAR2-duocarmycin and D2B-DAR4-duocarmycin, treatment with D2B-DAR2-MMAE and D2B-DAR4-MMAE significantly impaired the tumor growth and prolonged median survival from 13 days (PBS) to 20 and 29 days, respectively. Tumor doubling time increased from 3.5 ± 0.5 days to 5.2 ± 1.8 and 9.2 ± 2.1, after treatment with D2B-DAR2-MMAE and D2B-DAR4-MMAE, respectively. **Conclusion:** The site-specifically conjugated anti-PSMA ADCs D2B-DAR2-MMAE and D2B-DAR4-MMAE efficiently targeted PSMA-expressing xenografts, effectively inhibited tumor growth of PSMA-expressing tumors, and significantly prolonged survival of mice.

OP-337

Novel high affinity affibody for radionuclide imaging of VEGFR2 in glioma vasculature: proof-of-principle in murine model

B. Mitran[1], R. Güler[2], F. P. Roche[1], E. Lindström[1], R. Selvaraju[1], F. Fleetwood[2], S. S. Rinne[1], L. Claesson-Welsh[1], V. Tolmachev[1], S. Ståhl[2], A. Orlova[1], J. Löfblom[2]; [1]Uppsala University, Uppsala, SWEDEN, [2]KTH-Royal Institute of Technology, Stockholm, SWEDEN.

Aim: Glioblastomas are rapidly growing, highly malignant brain tumors with limited therapeutics options. Due to the high vascularization of these tumors, the inhibition of angiogenesis has become an attractive therapeutic strategy in recent years. Vascular endothelial growth factor receptor-2 (VEGFR2) is a promising target for anti-angiogenic drugs. However, the successful implementation of anti-VEGFR2 therapies

requires patient stratification. The new VEGFR2 antagonistic biparatopic affibody molecule HEHEHE-ZVEGFR2-Bp2-NODA-GA (denoted as Z_{VEGFR2}-Bp$_2$, 14.4 kDa) with picomolar affinity to VEGFR2 was recently presented and demonstrated successful targeting in vivo. The aim of this study was to evaluate the biparatopic affibody construct Z_{VEGFR2}-Bp$_2$ for imaging of VEGFR2 expression in glioblastoma orthotopic tumors. **Methods:** Female C57BL/6 mice with intracranial gl261 glioma tumors were used to study the imaging properties of ^{111}In-Z_{VEGFR2}-Bp$_2$ in glioblastoma orthotopic model. The mice with MRI confirmed tumors were imaged at 2 h pi of ^{111}In-Z_{VEGFR2}-Bp$_2$ (23 MBq, 4 μg). To confirm targeting specificity, additional groups of mice were injected with 40 μg of ^{111}In- Z_{VEGFR2}-Bp$_2$ (to saturate VEGFR2 in tumor vasculature) or 4 μg of ^{111}In-Z_{taq}-Z_{taq} (size matching non-targeting affibody construct). Radioactivity distribution in brain sections was studied using autoradiography and VEGFR2 expression was assessed by immunofluorescent staining. **Results:** Intracranial orthotopic gl261 tumors were visualized using SPECT/CT. Very low radioactivity uptake was found in healthy CNS tissue. The radioactivity uptake in the tumor areas delineated by MRI was significantly higher than in the normal brain. Radioactivity uptake was also detected in lateral ventricles and pineal gland but it was significantly lower than in tumors. The tumor-to-cerebellum ratios after the injection of 4 μg ^{111}In-Z_{VEGFR2}-Bp$_2$ (3.8±0.9) were significantly (p <0.05) higher than the ratios observed for the 40 μg injected dose (2.1±0.7) and for the non-targeting conjugate (2.2±0.5). Microautoradiography of cryosectioned CNS tissue was in good agreement with SPECT/CT images. H&E staining of the slides after autoradiography confirmed the presence of tumor tissue in areas with elevated radioactivity uptake. Tumor-to-brain ratios based on autoradiography results were in agreement with SPECT/CT images (20±6 for 4 μg ^{111}In-Z_{VEGFR2}-Bp$_2$, 7±3 for 40 μg ^{111}In-Z_{VEGFR2}-Bp$_2$ and 3.5±0.9 for 4 μg ^{111}In-Z_{taq}-Z_{taq}). VEGFR2 staining with immunofluorescence showed a high vascularization specific to glioblastomas. **Conclusion:** ^{111}In-Z_{VEGFR2}-Bp$_2$ appears to be a promising probe for in vivo noninvasive visualization of tumor angiogenesis in glioblastoma.

OP-338

Development and evaluation of gonadotropin releasing hormone SPECT radioligands

R. Fjellaksel[1,2,3], J. Hansen[3], A. Oteiza[1,4], M. Martin-Armas[1,4], A. Moldes-Anaya[5,6], P. Riss[7,8,9], R. Sundset[1,5]; [1]Medical Imaging Group, Department of Clinical Medicine, UiT The Arctic University of Norway, TROMSØ, NORWAY, [2]Drug Transport and Delivery Group, Department of Pharmacy, UiT The Arctic University of Norway, Tromsø, NORWAY, [3]Organic Chemistry Group, Department of Chemistry, UiT The Arctic University of Norway, Tromsø, NORWAY, [4]Preclinical PET/SPECT/CT, Department of Clinical Medicine, UiT The Arctic University of Norway, Tromsø, NORWAY, [5]PET imaging center, division of diagnostics, UNN – University Hospital of North-Norway,, Tromsø, NORWAY, [6]Neurobiology Research Group, Department of Clinical Medicine, UiT The Arctic University of Norway, Tromsø, NORWAY, [7]Department of neuropsychiatry

and psychosomatic medicine, Oslo University Hospital, Oslo, NORWAY, [8]Realomics SFI, Department of Chemistry, University of Oslo, Oslo, NORWAY, [9]Norsk Medisinsk Syklotronsenter AS, Oslo, NORWAY.

Introduction: The Gonadotrophin-releasing hormone (GnRH) receptor density may mirror early pathologic changes leading to Alzheimer Disease (AD).[1-2] A GnRH SPECT radiotracer will contribute to the understanding of molecular disease mechanisms. **Materials and Method:** Twenty analogues were synthesized using an approach of late-stage diversification via cupper-catalysed azide-alkyne cycloreaction (Cu-AAC) and were evaluated in vitro by competitive binding assays using recombinant cells overexpressing the GnRH receptor complex.[3] We sought a route to introduce a long-lived radionuclide into the structures to allow straightforward biological characterisation. A modification of the Cu-AAC by Yan and co-workers was used, which proceeds via Cu^{II} reduction to the active cyclisation catalyst Cu^{I} by radioiodide, followed by trapping of an anionic transition state by $^{123}I^{+}$ during the cyclisation reaction. In addition as a continuation of the initial screening for GnRH-antagonists, another promising radiotracer-candidate emerged. This candidate was assessed for radioiodination based on different chain lengths by an anchimerically-assisted Finkelstein reaction. This highly promising radiotracer candidate was evaluated *in vitro* by binding assays to inhibit human GnRHR, *ex vivo* by rat gonadal and brain tissue section autoradiography, as well as *in vivo* by brain SPECT/CT imaging and biodistribution studies. **Result and Discussion:** Several promising GnRH receptor-antagonists with nM affinity have been developed.[3] Two GnRH receptor-antagonists were radiolabelled with ^{123}I by optimisation of the Cu-AAC radioiodination reaction. In addition, we found that the anchimerically-assisted Finkelstein reaction, which is an obvious candidate for application in late stage radiolabeling, has a great potential as a radiolabeling method. We have evaluated the reaction rate and how the contribution of anchimeric-assistance affects the halide exchange in the Finkelstein reaction. One compound has been successfully radiolabeled with ^{123}I by the anchimerically-assisted Finkelstein reaction and evaluated *in vitro* showing nM affinity to human GnRHR. Autoradiography in tissue sections determined the *ex vivo* receptor binding properties. Brain SPECT/CT imaging and biodistribution studies revealed the in vivo radiotracer biodistribution pattern post-injection. **Conclusion:** We have successfully synthesized and evaluated biologically a radioiodinated GnRHR antagonist with ^{123}I for further evaluation in imaging studies. *Ongoing study - Patent application number 1704681.4 IPO/UK* 1.Meethal,S.;Smith,M.; Bowen,R.;Atwood,C.,The gonadotropin connection in Alzheimer's disease. *Endocrine* 2005, *26* (3), 317-325. 2.Webber,K.M.;Perry,G.;Smith,M. A.;Casadesus,G.,The Contribution of Luteinizing Hormone to Alzheimer Disease Pathogenesis. *Clinical medicine and reserch* 2007, *5* (3), 177-183. 3.Fjellaksel,R.;Boomgaren, M.;Sundset,R.;Haraldsen,I.H.;Hansen,J.H.;Riss,P.J.,Small molecule piperazinyl-benzimidazole antagonists of the gonadotropin-releasing hormone (GnRH) receptor *Submitted to Med. Chem. Commun.* 2017.

Somatostatin receptor type 2 as a marker for pro-inflammatory macrophages

S. T. van Tiel, L. Utomo, E. J. Meester, J. de Swart, N. Kops, R. H. de Blois, M. de Jong, Y. Bastiaansen-Jenniskens, M. Bernsen; ErasmusMC, Rotterdam, NETHERLANDS.

Aim: To explore if the Somatostatin receptor type 2 (SSTR2) can be a marker for pro-inflammatory macrophages. **Materials and Methods:** Expression of SSTR2 by pro-inflammatory macrophages (IFNγ+TNFα stimulated) and human arthritic synovium, stimulated towards acute inflammation, was determined by quantitative PCR analysis. Experimental osteoarthritis (OA) was induced in mice by destabilization of the medial meniscus (DMM). The mice were euthanized between 1 and 56 days after OA induction and harvested knees were stained for F4/80 and iNOS expression to visualize (pro-inflammatory) macrophages. Specific binding of the ^{111}In-JR11 SSTR2-tracer was tested by an autoradiography assay on tissue sections from frozen human synovium. Binding of the SSTR2-tracer to pro-inflammatory macrophages is determined by an uptake assay. **Results:** SSTR2 expression was significantly higher in pro-inflammatory macrophages compared to unstimulated macrophages. SSTR2 levels were also measured in OA synovial tissue and in OA synovial tissue stimulated with IFNγ+TNFα to simulate acute inflammation. Similarly to stimulated cultured macrophages, SSTR2 was expression was significantly higher in IFNγ+TNFα stimulated arthritic synovium compared to unstimulated arthritic synovium. Immunohistochemical analysis of knees from DMM mice indicated that F4/80+ macrophages were distinctly present from day 3 onwards in developing OA in a mouse knee. The number of F4/80+ macrophages was significantly higher at day 3 than at day 1 and remained elevated until day 28, before returning to baseline at day 56. In the DMM knees, iNOS+ cell peaked between day 3 and 7 before and returned to baseline after day 14. Tracer binding studies indicated specific tracer uptake at elevated levels in cultured pro-inflammatory macrophages and synovium stimulated with IFNγ+TNFα compared to unstimulated macrophages or synovium. **Conclusion:** The Somatostatin receptor type 2 is present on pro-inflammatory macrophages and may be a marker to study macrophage activation in in vitro experiments.

Quantitative Analysis of 99mTc-DMSA Renal Scintigraphy of Animal AKI Models; Comparison with Histopathological and Biochemical Assays

K. Tanha[1], H. Fatemikia[2], M. Seyedabadi[1], K. Tanha[3], Z. Karimi[4], M. Assadi[1]; [1]The Persian Gulf Nuclear Medicine Research Center, Bushehr University of Medical Sciences, Bushehr, IRAN, ISLAMIC REPUBLIC OF, [2]Department of Physiology, Medical School, Bushehr University of Medical Sciences, Bushehr, IRAN, ISLAMIC REPUBLIC OF, [3]Department of Biostatistics, School of Public Health, Iran University of Medical Sciences, Tehran, IRAN, ISLAMIC REPUBLIC OF, [4]Shiraz Nephron Urology Research Center, Shiraz University of Medical Sciences, Shiraz, IRAN, ISLAMIC REPUBLIC OF.

Purpose: Acute kidney injury (AKI) in pre-clinical studies is commonly evaluated by biochemical markers such as blood urea nitrogen (BUN) and serum creatinine (Cr) along with histological examinations. In this study, we compared 99mTc-DMSA renal scintigraphy with biochemical and histopathological methods in two animal models of acute kidney injury. **Methods:** Nephrotoxicity was induced either by gentamicin (100mg/Kg/day for one week) or unilateral ureteral ligation (UUO). Renal scintigraphy was performed after intravenous injection of 99mTc- DMSA. Furthermore, plasma levels of blood urea nitrogen (BUN), creatinine, sodium, and potassium were determined. At the end of experiments, kidneys were excised for the measurement of activity uptake (mCi/gr) using a dose calibrator as well as histopathological examinations with hematoxylin and eosin (H&E) staining. **Results:** There was a significant decrease in 99mTc-DMSA uptake in both gentamicin and UUO groups, and it was more significant in the former. The levels of BUN and creatinine increased in both gentamicin and UUO groups, while the levels of sodium and potassium remained unchanged. Furthermore, a strong correlation was found between DMSA uptake and histopathological findings. **Conclusion:** Scintigraphy with 99mTc-DMSA is capable of detection of kidney injury in both gentamicin and UUO groups. Moreover, a significant correlation was found between scintigraphy parameters and histopathological findings. This suggests 99mTc-DMSA as a non-invasive method for the evaluation of kidney injury induced by drugs or anatomical disorders in pre-clinical studies. **Table 1.** Biochemical analysis of plasma levels of BUN, creatinine, sodium and potassium and results of tissue Tc-99m DMSA uptake in the GM, GMS, UUO and UUOS groups.

OP-341

PET/CT And SPECT/CT Based Identification of Novel Rodent BAT and Beige Depots-An Image Guided Exploration Of Human-like Thermogenic Tissues in Mice

O. K. Oz[1], F. Zhang[1], G. Hao[1], G. Hassan[1], M. Shao[1], Y. An[1], Q. Wang[1], C. Kusminski[1], K. Nham[1], Q. Zhai[2], P. Scherer[1]; [1]UT Southwestern Medical Center, Dallas, TX, UNITED STATES OF AMERICA, [2]Key Laboratory of Nutrition and Metabolism, Institute for Nutritional Sciences, Shanghai Institutes for Biological Sciences, Chinese Academy of Sciences, Shanghai, CHINA.

Aims: 18F-FDG (FDG) PET/CT imaging in humans has been invaluable to visualize active thermogenic adipose tissue. These depots are of interest due to their potential for anti-diabetic and anti-obesity effects. It is well known that mice display a prominent brown fat pad in the interscapular region (iBAT). We embarked on a systematic effort to map so far uncharacterized fat pads in mice, investigating the potential of 18F-FDG glucose and 123/125I-BMIPP fatty acid uptake as imaging guidance tools to isolate these "human-like thermogenic" depots in mice. **Materials and Methods:** Following an overnight fast, wild-type mice (n=3/group/tracer) were subjected to whole body FDG-PET/CT (~37MBq FDG/mouse, 1h uptake period, Siemens Inveon PET/CT) or 123/125I-BMIPP SPECT/CT (~175MBq/mouse, 1h uptake period, BioScan NanoSPECT/CT). In some instances mice were pre-treated for 7 days with the β3 adrenergic receptor agonist,

CL 316,243. To demonstrate that FDG or BMIPP avid sites were adipose tissue, imaging studies were carried out in the FAT-AT-TAC mouse, an inducible adipose tissue ablation model. Images guided the dissection of fat depots for histology and RNA extraction with subsequent cDNA preparation. Respective molecular markers were: brown adipose tissue: *Zic1, UCP1, Lhx8;* beige adipose tissue: *Cited1, Cd137, Epsti1, Tbx1, Tmem26*; white adipose tissue: *Tcf21.* **Results:** Both FDG-PET/CT and *I-BMIPP SPECT/CT images revealed a strong uptake in the classical iBAT. We also found regions with high metabolic activity in clavicular (supra- and infra-), cervical, axillary, scapular (supra- and infra-), spinal (pre-vertebral), inter-centrodorsal musculature posterior to spine areas and within the thigh. The β3 adrenergic receptor agonist treatment enhanced FDG and *I-BMIPP uptake. Fat depots (e.g. the inguinal, axillary anterior subcutaneous chest as well as the supraspinal fat pads) prone to absorb fatty acids as a fuel and prone to beiging were better demonstrated on the fatty acid images. FAT-ATTAC mice lost these areas of activity upon fat ablation proving their identity as adipose. Histological analysis and marker gene identification further validated and characterized these novel fat pads as brown-, beige or white-adipose tissue. **Conclusions:** The combination of FDG and *I-BMIPP image guided dissection with histological characterization and marker gene expression patterns indicate that rodents show a surprising topological similarity to regions of brown and beige adipogenesis in humans. These studies also demonstrate the utility of fatty acid SPECT/CT imaging in identifying metabolically active fat depots. Our imaging paradigm maybe useful to screen drugs as regulators of fat metabolism for obesity and diabetes treatments.

OP-342

SPECT-MRI and histological analysis to map PRRT radiobiology for a better understanding of local treatment effects

J. Nonnekens, G. N. Doeswijk, J. C. Haeck, M. W. Konijnenberg, D. C. van Gent, M. de Jong; Erasmus MC, Rotterdam, NETHERLANDS.

Aim: Radiobiological principles of external beam radiotherapy have been studied for decades, while the radiobiology of peptide receptor radionuclide therapy (PRRT) is still in its infancy. During PRRT of metastasized neuroendocrine tumors (NETs) with overexpression of somatostatin receptors, Lutetium-177 is targeted to the tumor via coupling to the somatostatin analogue DOTA-[Tyr3]octreotate (177Lu-DOTA-TATE). Lutetium-177 will induce DNA damage leading to tumor cell death with limited harm to healthy tissues. Patient treatment strongly increases progression-free survival and life quality. There is nevertheless still room for improvement, as very few patients are cured at this stage of disease. For possible future therapy optimizations, it is essential to have a better understanding of local treatment (side) effects, both in tumor and healthy tissues. To gain insight in the underlying radiobiological principles, we studied PRRT effects in mice using SPECT/MRI imaging, biodistribution, histological analysis and dosimetric calculations. **Materials and Methods:** 40 Balb/c nu/nu mice with SSTR-positive H69 xeno-

grafts were injected with a therapeutic dose of ^{177}Lu-DOTA-TATE (30MBq/0.5µg), 4 uninjected mice served as controls. Animals were grouped per 4 and sacrificed at 1 hour or 1, 2, 3, 4, 5, 7, 9, 11 or 14 days after injection. 1 animal per group was scanned with SPECT/MRI (Nanoscan, Mediso) and from all 4 animals/group organs/tumors were collected for *ex vivo* biodistribution, dosimetry and histological analysis. Organs were conserved in formalin or frozen. Furthermore, the bone marrow was extracted and prepared on cytospins. Paraffin sections were prepared for histological analysis: hematoxylin and eosin staining for morphology and immunofluorescence staining for DNA damage and cell death parameters. **Results:** SPECT/MRI imaging showed the distribution in the different organs over time which correlated well to the *ex vivo* biodistribution data. Kidney uptake was high 1h after injection (tumor-to-kidney ratio 1.0±0.2), but quickly declined over time, while tumor uptake remained high (tumor-to-kidney ratio 10.1±2.5 at day 9). DNA damage was observed in tumors until the latest time point studied (as measured with DNA double strand break markers gamma-H2AX and 53BP1). Apoptosis increased over time in the tumors (measured with TUNEL staining). Bone marrow DNA damage (due to circulating radionuclides) was observed at 1h and 1 day after injection **Conclusion:** With this study, we studied in detail the radiobiology of PRRT in a preclinical setting. Our results will contribute to a better understanding of PRRT effects, which might help to improve future patient treatment.

OP-343

Comparison study of TCO-functionalized vector systems for *in vivo* click chemistry using [^{111}In]In-DOTA-Tetrazine

P. E. Edem[1,2], J. T. Jørgensen[1,2], K. Nørregaard[1,2], E. J. L. Stéen[2], R. Rossin[3], A. Birke[4], C. Denk[5], A. Yazdani[6], J. F. Valliant[6], H. Mikula[5], M. Barz[7], M. Robillard[3], M. M. Herth[1,2], A. Kjær[1,2]; [1]Rigshospitalet, Copenhagen, DENMARK, [2]University of Copenhagen, Copenhagen, DENMARK, [3]Tagworks Pharmaceuticals, Eindhoven, NETHERLANDS, [4]Johannes Gutenberg-University Mainz, Mainz, GERMANY, [5]TUWien, Vienna, AUSTRIA, [6]McMaster University, Hamilton, ON, CANADA, [7]Johannes Gutenberg-University Mainz, Maiz, GERMANY.

Purpose/Introduction: *In vivo* click using the inverse electron demand Diels-Alder (iEDDA) reaction between a radiolabelled tetrazine (Tz) and *trans*-cyclooctene (TCO) has gained interest for pretargeted imaging. This technique was first implemented using an ^{111}In-labelled Tz and a TCO functionalized antibody to image colorectal cancer xenografts in murine models. Different radiolabelled tetrazines have since been reported, however evaluation of the accompanying *in vivo* click reaction is often lacking. This can be attributed to high costs and/or the time consuming nature in producing validated TCO-functionalized vectors in suitable animal models. Herein we compare 3 previously reported TCO-functionalized vectors and 2 new TCO functionalized polymer vectors using the ^{111}In-labelled tetrazine for pretargeted imaging with microSPECT/CT. **Subjects and Methods:** TCO functionalized mesopourous silica nanoparticles (MSN-TCO) targeting the lungs, bisphosphonates (BP-TCO) targeting bone, and antibodies (CC49-TCO) targeting tumours, were prepared as previously described.

Two TCO modified polymers: polyglutamic acid (PGA) and PGA graft copolymers functionalized with polysarcosine (PSar) were prepared, giving PGA-TCO and PGA-PSar-TCO respectively. The 1,4,7,10-tetraazacyclododecane-1,4,7,10-tetraacetic acid (DOTA) functionalized tetrazine was radiolabelled with indium-111 giving [^{111}In]In-DOTA-Tz (RCC 93-99%). Healthy BALB/c mice were administered with MSN-TCO (i.v.) or BP-TCO (i.v.), while mice bearing subcutaneous human colorectal (LS174T) xenografts or murine colorectal (CT26) tumours were administered CC49-TCO (i.v.) or the polymers (i.t.), respectively. After various time points the [^{111}In]In-DOTA-Tz was administered intravenously and SPECT/CT images were obtained at 2-3 and 22-24 h p.i. RESULTS: SPECT/CT revealed radioactivity accumulation in the lungs in mice pretreated with MSN-TCO and bone accumulation in mice pretreated with BP-TCO at 2 h and 22 h p.i. The amount of lung uptake varied for each animal, while the amount of bone uptake was more consistent. Tumour uptake was observed in mice pretreated with CC49-TCO at 2 h p.i. with improved contrast at 22 h p.i. In the case of PGA-PSar-TCO, tumour uptake was observed at 22 h p.i. while very little tumour uptake was observed in mice pretreated with PGA-TCO at either time-point. **Discussion/Conclusion:** We have shown pretargeted SPECT/CT imaging can be performed using different TCO functionalized vectors in both healthy and tumour bearing murine models using [^{111}In]In-DOTA-Tz. For healthy mice, BP-TCO was preferred over MSN-TCO due to its easier preparation and formulation. This led to improved reproducibility and good image contrast at early time-points. For the tumour models, PGA-PSar-TCO offered a cheaper and easier to synthesize alternative to CC49-TCO while maintaining good image contrast at similar time-points.

906	Monday, October 23, 2017, 14:30 - 16:00, Hall F1

Teaching Session 3 (Interactive): Applied Cross Sectional Anatomy and Correlative Imaging - Spine

OP-344

Applied Cross Sectional Anatomy and Correlative Imaging – Spine
A. van der Vliet; University Medical Centre, Groningen, NETHERLANDS.

907	Monday, October 23, 2017, 14:30 - 16:00, Hall F2

Clinical Oncology: It's in the Blood

OP-345

Functional Carbon11-Methionine and Fluorine18-Fluorodeoxyglucose PET/CT parameters in patients with multiple myeloma in a first disease staging setting: could they reflect the underlying pathophysiology?

C. Caldarella[1], D. Ripani[2], D. Pizzuto[2], T. Za[3], V. De Stefano[3], A. Giordano[2]; [1]Nuclear Medicine Unit and PET-CT Center, Policlinico "A.Gemelli", Rome, ITALY, [2]Institute of Nuclear Medicine, Università Cattolica del Sacro Cuore "A.Gemelli", Rome, ITALY, [3]Hematology Service, Università Cattolica del Sacro Cuore "A.Gemelli", Rome, ITALY.

Introduction: Carbon11-Methionine PET/CT (MET-PET) has proved to be a more sensitive tool than Fluorine18-Fluorode-oxyglucose PET/CT (FDG-PET) in evaluating multiple myeloma (MM) patients at first disease staging. Functional PET-derived parameters may be useful to depict the uptake degree of lesions in addition to visual evaluation. Aim of our study was to determine whether MET-PET and FDG-PET functional parameters in the same patients reflect the underlying pathophysiology in terms of bone marrow (BM) involvement and monoclonal Ig (mIg) production. **Subjects & Methods:** Patients with MM undergoing MET-PET and FDG-PET for first disease staging were included. Data regarding % plasma cell BM involvement and their immunological surface phenotype (%CD138), presence of serum/urine mIg, serum free-light-chains (FLCs) and their ratios were collected. Functional parameters were obtained at both MET-PET and FDG-PET: SUVmax and SUVmean of the most active lesion, background bone uptake (mean SUVmax of three vertebral bodies not focally involved) and tumour-to-background ratio (TBR) calculated as the ratio between SUVmax of the most active lesion and brain uptake (for MET-PET) or liver uptake at the right lobe (for FDG-PET). Mann-Whitney U-test was used to determine whether such PET-derived parameters significantly ($P<0.05$) reflected the presence of serum/urine mIg or BM involvement > 20%; bivariate non-parametric correlation (Spearman's ρ) was calculated between each PET-derived parameter and % plasma cell BM involvement, mIg, FLCs or %CD138 surface expression. **Results:** Seventeen patients (mean age 62y) were studied according to the aforementioned criteria. MET-PET recognized more focal lesions than FDG-PET (115 vs 24) with significantly ($P=0.012$) higher SUVmax, TBR and background bone uptake. MET-PET TBR was significantly higher in patients with presence of serum (median 4.51 interquartile range [IQR] 3.89-6.73 vs 2.58 IQR 2.16-4.43, $P=0.027$) or urine mIg (median 5.47 IQR 4.43-11.77 vs 3.83 IQR 2.49-4.74, $P=0.019$). MET-PET SUVmax, SUVmean and TBR were higher in patients with BM involvement > 10% (median 9.89 IQR 8.27-17.02 vs 5.31 IQR 4.76-7.43, $P=0.008$; median 5.46 IQR 3.77-10.83 vs 3.98 IQR 3.19-4.51, $P=0.027$; median 5.64 IQR 4.63-10.10 vs 3.24 IQR 2.31-3.93, $P=0.001$, respectively). FDG-PET derived parameters were not associated to serum/urine mIg or BM involvement > 20%. A significant correlation was found between MET-PET TBR and % plasma cell BM involvement ($ρ=0.75$), but not for FDG-PET TBR ($ρ=0.27$). **Conclusion:** Our study demonstrated that in MM patients at first disease staging MET-PET functional parameters (but not FDG-PET ones) reflect the underlying pathophysiology in terms of BM involvement and mIg production.

OP-346

Diagnostic performances of normalized FDG-PET parameters in predicting treatment response < progression-free survival after bone marrow transplantation in patients with multiple myeloma

D. Ripani[1], C. Caldarella[2], T. Za[3], D. Pizzuto[1], E. Rossi[3], V. De Stefano[3], A. Giordano[1]; [1]Institute of Nuclear Medicine, Università Cattolica del Sacro Cuore "A. Gemelli", Rome, ITALY, [2]Nuclear Medicine Unit and PET-CT Center, Policlinico "A. Gemelli", Rome, ITALY, [3]Hematology Service, Università Cattolica del Sacro Cuore "A. Gemelli", Rome, ITALY.

Background and Aim: Patients with multiple myeloma (MM) may benefit from induction chemotherapy (iChT) &lt bone marrow transplantation (BMT). FDG-PET is useful in early assessment of response to treatment &lt disease progression; several factors affect the reliability of semi-quantitative parameters in evaluating FDG uptake in lesions. Aims of our study were: to determine whether normalized semi-quantitative parameters may predict the response to treatment &lt disease progression; to determine whether such parameters could predict patients' progression-free survival. **Materials and Methods:** Patients undergoing iChT &lt BMT with baseline &lt after treatment FDG-PET were considered. Several parameters were obtained: SUVmax, SUVmean, SUVpeak, rPET &lt qPET of the most active lesion. rPET was calculated as lesion SUVmax/liver SUVmax (right lobe); qPET was calculated as lesion SUVpeak/liver SUVmean (right lobe). Baseline-to-post-treatment scan changes (Δ) were calculated for each parameter. Metabolic progression or metabolic response at follow-up FDG-PET scans were noted; time-to-metabolic-progression (TMP) was considered the interval from post-treatment scan to subsequent progression at follow-up FDG-PET. Mann-Whitney U-test was used to evaluate whether each functional parameter (baseline, post-treatment &lt Δ) was significantly ($P<0.05$) associated to metabolic progression or response. Kaplan-Meier survival curves assessed the TMP trend according to FDG-PET parameters; discriminant analysis was used to calculate a reliable cut-off for each parameter to find significant ($P<0.05$) differences between curves. **Results:** Thirty-eight patients were considered, 19 with metabolic progression during follow-up, 16 with metabolic response during follow-up (3 patients had stable disease). Significantly lower ΔrPET (median 0.06 [interquartile range (IQR) -0.22 - 0.34] vs 0.41 [IQR 0.16 - 1.13]; $P=0.023$) &lt ΔqPET (median 0.06 [IQR -0.24 - 0.45] vs 0.54 [IQR 0.15 - 1.09]; $P=0.030$) were found in patients with metabolic progression during follow-up. Significantly higher ΔrPET (median 0.41 [interquartile range (IQR) 0.17 - 1.07] vs 0.06 [IQR -0.22 - 0.48]; $P=0.023$) was found in patients with metabolic response during follow-up. According to Kaplan-Meier curves, higher post-treatment rPET &lt lower ΔrPET predicted a significantly lower TMP ($P=0.015$ and $P=0.001$, for post-treatment rPET &lt for ΔrPET respectively). Median TMP was 25 months in patients with post-treatment rPET > 1.02 &lt 21 months in patients with ΔrPET < 0.36; most patients with lower post-treatment rPET or higher ΔrPET than the cut-offs showed no metabolic progression at the end of follow-up. **Conclusions:** Our results show that normalized semi-quantitative parameters, particularly ΔrPET, may predict metabolic response or progression during follow-up &lt progression-free survival in patients with MM undergoing iChT &lt BMT.

OP-347

Diagnostic Value of ¹⁸F-FDG PET/CT in Chronic Graft Versus Host Disease (cGVHD)

C. Lasnon[1,2], N. Aide[3,4], J. Parienti[5], S. Chantepie[6]; [1]Nuclear Medicine Department, François Baclesse Centre, CAEN, FRANCE, [2]INSERM

U1086, Caen, FRANCE, ³Nuclear Medicine Department, University Hospital, CAEN, FRANCE, ⁴INSERM U1086 "ANTICIPE", Caen, FRANCE, ⁵Biostatistical Department, University Hospital, CAEN, FRANCE, ⁶Hematology Institute, University Hospital, CAEN, FRANCE.

Aim: Allogeneic stem cell transplantation (SCT) is a curative option in hematological malignancies. It results in a cGVHD in 30-70% of cases which is diagnosed by biopsies of affected organs and/or observation of clinical symptoms. This diagnosis is sometimes difficult and may be underestimated in patients with no obvious clinical signs. The improvement of cGVHD diagnosis could allow guiding the treatment after transplant and thus optimizing the outcome of allograft patients. We aimed to evaluate the diagnostic value of ¹⁸F-FDG PET/CT for cGVHD detection. **Materials and Methods:** Twenty patients treated by allogeneic SCT were prospectively included (*ClinicalTrials. gov Identifier: NCT02352064*). Whole-body ¹⁸F-FDG PET/CT were performed 4 to 6 weeks after discontinuation of immunosuppressive therapy. Images were reconstructed with PSF reconstruction optimized for diagnostic and for EARL-compliant quantification. PET/CT examinations were interpreted by two blinded nuclear physicians with a consensus reading in case of discrepancy. Location and SUV_{max} of abnormal uptakes were recorded and stratified according to a 5-point scale and finally each examination was classified as positive or negative. The gold standard was the clinical examinations based on NIH recommendations up to 3 months after ¹⁸F-FDG PET/CT (± biopsies). Sensitivity, specificity and positive and negative predictive values (PPV, NPV) were estimated. Mann-Whitney test was used to compare median SUV_{max} values. **Results:** Mean (SD) patient age was 49.9 (10.1) years and sex ratio (M:F) was 13:7. Patients had undergone allogeneic SCT for acute myeloid leukemia (55%), acute lymphoid leukemia (15%), myelodysplasia (10%) and other diseases (20%). The prevalence of cGVHD was 9/20 (45%). Before PET consensus readings, discrepancies between observers occurred in 4 patients (20%). Sensitivity and specificity of ¹⁸F-FDG PET/CT were 0.67 (95%IC: 0.31-0.91) and 0.82 (95%IC: 0.48-0.97), respectively. PPV, NPV were 0.75 (95%IC: 0.36-0.95), 0.75 (95%IC: 0.43-0.93), respectively. For both observers, there was no significant difference between median SUV_{max} value of pathological foci in cGVHD patients and median SUV_{max} value of benign lesions in disease free patients (P>0.05). Hypermetabolic lesions in cGVHD patients were localized in digestive tract (50%), ENT sphere (35%) and skin (15%) according to observer 1 and in digestive tract (40%), ENT sphere (33%), lymph nodes (13%), skin (7%) and other sites (7%) according to observer 2. **Conclusion:** ¹⁸F-FDG PET/CT based on visual assessment could be a promising tool together with clinical examinations and biopsies to help to diagnose cGVHD. Neither quantitative analysis nor whole-body scan appeared to be necessary.

OP-348
Ultrafast 8-min scan PET/MR protocol for diagnosis and follow-up of Lymphomas. Preliminary results

C. Albertti, G. Peña, E. A. Marino, P. Jaime; FUESMEN, Mendoza, ARGENTINA.

Purpose: The aim of this study is to evaluate a PET/MR protocol that reduces acquisition time to 8 minutes, minimizing image co-registration errors, as well as reducing both patient discomfort and accumulated effective dose. It is shown to keep and even to increase sensitivity and specificity levels, as compared to the PET/CT gold standard protocol in use at our facility. **Subjects & Methods:** Five patients with confirmed diagnosis of lymphoma were injected intravenously with 4.07 MBq/kg of FDG. After a 50 minute uptake period, a PET/MR scan was performed with an ultra-fast protocol of 1 min/bed (GE Signa PET/MR, Milwaukee, WI, USA). Simultaneously, MRAC sequence for attenuation correction, T1LAVA (Water, Fat, In Phase and Out Phase) in axial and coronal sequences were performed. Subsequently, 65 minutes after radiotracer administration, a PET/CT scan (GE Discovery STE) was performed with 3min/bed acquisition. Data were reconstructed with 2 iterations, 20 subsets, and scatter correction was applied in both methods. All studies were independently analyzed by 2 Nuclear Physicians, one of them also specialist in Radiological Diagnostic Imaging. Results: A total of 60 SUVmax quantifications in lesions with probable lymphoproliferative involvement and in hepatic, splenic and bone marrow parenchyma in both methods (PET/MR and PET/CT) were analyzed. 51 measurements on both sets were characterized as coincidental and 9 measures were discordant, which were only detected in PET/MR. In addition, a brain lesion and a better characterization of bone marrow lesions were found in three patients from the anatomical information of MR images, being unnoticed by the CT scan. Discussion: The first studies performed with ultrafast PET/MR protocol for diagnosis and/or follow-up of lymphomas, show similar sensitivity and specificity with less effective doses when compared to PET/CT protocols. Moreover, PET/MR provides additional findings which were undetected by PET/CT alone. The ultra-fast protocol of 8 minutes scan greatly contributes to patient comfort and cooperation. These promising results should be confirmed with a larger number of studies.

OP-349
Staging Patients with Hodgkin Lymphoma - Is Bone Marrow Biopsy Still Necessary in the Era of ¹⁸F-FDG PET?

C. Voltin¹, S. Stockter¹, C. Baues², M. Fuchs³, M. Dietlein¹, J. Mettler¹, A. Engert³,⁴, P. Borchmann³,⁴, A. Drzezga¹, C. Kobe¹; ¹Department of Nuclear Medicine, University Hospital of Cologne, Cologne, GERMANY, ²Department of Radiation Oncology, University Hospital of Cologne, Cologne, GERMANY, ³German Hodgkin Study Group (GHSG), University Hospital of Cologne, Cologne, GERMANY, ⁴Department of Internal Medicine I, University Hospital of Cologne, Cologne, GERMANY.

Introduction: Staging with 2-(¹⁸F)fluoro-2-deoxy-D-glucose (¹⁸F-FDG) positron emission tomography (PET) might be reliable to detect bone marrow (BM) involvement and advanced-stage disease in patients with Hodgkin lymphoma (HL). As ¹⁸F-FDG PET became a common procedure, BM biopsy may be omitted without impairment of the detection of advanced-stage disease. Therefore, the aim of this study was to assess the concordance

of ^{18}F-FDG PET and BM biopsy results in HL patients. **Methods**: The initial staging of all patients enrolled to the German Hodgkin Study Group (GHSG) trials HD16, HD17 and HD18 included a mandatory BM biopsy, while ^{18}F-FDG PET was a facultative procedure. We centrally reviewed all available baseline ^{18}F-FDG PET scans and categorized BM as showing focal involvement or not. All cases with diffusely increased BM uptake were documented but not interpreted as BM involvement. Additionally, we noted both the number of lesions and their localization. **Results**: A total of 832 patients who have been recruited into the above-mentioned GHSG studies until 31st December 2015 underwent a ^{18}F-FDG PET scan for staging which was assessed by the central review panel. 19 out of 20 cases with positive BM biopsy were identified by ^{18}F-FDG PET and 1 was documented to have diffusely increased BM uptake. Additional focal ^{18}F-FDG-avid BM lesions were detected in 110 patients who would have otherwise been considered negative by BM biopsy. A unifocal pattern was recorded in 43, a bifocal in 17, a trifocal in 11 and a multifocal (more than 3 lesions) in 58 cases. In addition, a diffusely increased BM uptake was noted in 152 patients. As compared to biopsy results, sensitivity, specificity, positive predictive value and negative predictive value of ^{18}F-FDG PET were found to be 95.0 % [95 % confidence interval (CI) 0.75, 1.00], 86.5 % (95 % CI 0.84, 0.89), 14.7 % (95 % CI 0.12, 0.17) and 99.9 % (95 % CI 0.99, 1.00), respectively. **Conclusion:** In our cohort, ^{18}F-FDG PET was able to detect the vast majority of cases with BM involvement according to biopsy results. Furthermore, it could identify a large number of additional cases suspicious for BM involvement who would have been considered negative by BM biopsy. This indicates that the actual incidence of BM involvement may be substantially underestimated by conventional BM biopsy. Given the high negative predictive value, baseline ^{18}F-FDG PET imaging can be safely used to exclude BM involvement in patients with HL.

OP-350

FDG-PET/CT at the end of immuno-chemotherapy in Follicular Lymphoma: the prognostic role of the ratio between target lesion and liver SUVmax (rPET)

S. Annunziata[1], A. Cuccaro[2], M. C. Tisi[2], S. Hohaus[2], A. Giordano[1], V. Rufini[1]; [1]Institute of Nuclear Medicine, Università Cattolica del Sacro Cuore, Rome, ITALY, [2]Institute of Hematology, Università Cattolica del Sacro Cuore, Rome, ITALY.

Purpose: FDG-PET/CT at the end of immuno-chemotherapy (PI-PET) in patients with Follicular Lymphoma (FL) has been recently proposed as a prognostic tool, visually evaluated by International Harmonization Project criteria (IHP) or Deauville Score (DS). Nevertheless, some limitations of the published data on this topic recently emerged, such as the absence of clear advantages of PI-PET over clinical FL International Prognostic Index at diagnosis (FLIPI). The ratio between target lesion and liver SUVmax (rPET) was recently confirmed as a strong prognostic factor in Hodgkin Lymphoma, with diagnostic and methodological advantages over visual analysis. Aim of this study was to retrospectively investigate the prognostic role of rPET in patients with FL undergoing PI-PET. **Methods:** Eighty-nine patients with FL who underwent PI-PET were retrospectively evaluated. The receiver operating characteristic (ROC) approach was applied to identify the optimal cut-point of rPET with respect to events, to calculate accuracy values and to define the area under the curve (AUC). IHP was considered positive with FDG uptake higher than the local background or higher than mediastinal blood pool (for lesions smaller or greater than 2 cm, respectively); DS 4 and 5 were considered positive. Progression-free survivals at 5-years (PFS) according to different PI-PET results (IHP, DS, rPET) and FLIPI were evaluated, considering progression, lack of complete remission and relapse after treatment as adverse events. A sub-analysis for patients who continued maintenance therapy with Rituximab was performed. **Results**: The ROC analysis for rPET as predictor of progression showed an AUC of 0.75, with an optimal rPET cut-point of 0.98. Positive IHP were 21/89 (24%) and had lower PFS compared to patients with negative IHP (50% vs 87%, p=0.0001). Positive DS were 10/89 (11%) and had lower PFS compared to patients with negative DS (30% vs 84%, p<0.0001). Positive rPET were 13/89 (15%) and had a PFS of 31%, negative rPET patients of 91% (p<0.0001). PI-PET prognostic power increased in patients who continued maintenance therapy with Rituximab (n=52/89, 58%), with a PFS of 17% in positive DS and 100% in negative IHP. FLIPI was not predictive of relapse and progression (p=0.31). **Conclusions**: rPET is a prognostic factor in patients with FL who underwent PI-PET and could be useful to identify patients with FL at risk for relapse after immuno-chemotherapy. PI-PET seems to have a stronger prognostic power in patients submitted to maintenance therapy and seems to have an incremental power over FLIPI at diagnosis.

OP-351

Interim treatment response assessment in paediatric Hodgkin's lymphoma by using Deauville and delta SUVmax in FDG PET CT

K. Shaha, S. Shah, N. Purandare, A. Agrawal, A. Puranik, V. Rangarajan; TATA Memorial Hospital, Mumbai, INDIA.

Aim: To compare Deauville 5 point score (DS) and delta SUVmax response assessment criteria used for interpretation of the interim PET in paediatric Hodgkin lymphoma (HD). **Material and Methods:** This was institutional ethics committee approved retrospective observational study. 152 consecutive paediatric (< 18 years) patients with newly diagnosed HD from January 2011 to August 2013 were enrolled in study. All patients had undergone baseline and interim 18 F FDG PET/CT (PET). Interim PET was analysed using Deauville and Delta SUVmax. Variables used in univariate analysis were sex, anaemia, hypoalbuminaemia, leucocytosis, lymphopenia, ESR, LDH, bone marrow biopsy(BMB), splenic involvement, Ann arbour stage, early versus advanced stage, anatomical residual disease, DS and delta SUVmax. DS of 1, 2 and 3 were considered negative and 4 and 5 were considered negative. Delta SUVmax cut off was considered to be 66%. Kaplan Meir survival analysis was used to calculate overall survival (OS) and event free survival (EFS). Univariate variables with significant p value (<0.05) were used for multivariate survival

analysis using COX regression analysis by forward regression method. **Results:** Median follow up was 44 months. 19 out of 152 patients had events (relapse/progression). 4 patients died in the follow up period. In univariate analysis DS, delta SUVmax, anatomical residual disease, sex, lymphompenia, spleen, early vs advanced stage and Ann arbour stage showed statistically significant EFS. In multivariate analysis only DS was significant with p value 0.000 (HR-20.21) for EFS. For overall survival DS, delta SUVmax and lymphopenia were statistically significant in univariate analysis. However only delta SUVmax was statistically significant in multivariate analysis with p value of 0.01 (HR-19.64). EFS was (38 vs 68 months) (p value <0.000) and (37 vs 67 months) (p value 0.000) in interim PET positive vs negative patients according to DS and delta SUVmax respectively. OS was (62 vs 72 months) (p value <0.001), (60 vs 72 months) (p value 0.000) in interim PET positive vs negative patients according to DS and delta SUVmax respectively. **Conclusion:** Interim PET has strong correlation with survival and hence can be used as an independent prognostic factor in HD. Deauville criteria should be used for interpretation of interim PET in HD.

OP-352

B-cell lymphoma radioimmunotherapy: effect of co-infusion of cold and radiolabelled antibody on absorbed dose to healthy tissues and tumours, a preclinical study in dogs

F. Morio[1,2], C. Ibisch[1,2], F. Nguyen[1,3], M. Berthaud[2], J. Abadie[1,3], A. Vidal[4], M. Bourgeois[4,2,5], K. Bernardeau[6], S. Becavin[1], M. Roussel[1], L. Ferrer[2,7], C. Bodet-Milin[2,5], N. Chouin[1,2], F. Davodeau[2]; [1]AMaROC, Oniris (Nantes Atlantic College of Veterinary Medicine, Food Science and Engineering), NANTES, FRANCE, [2]Team 13 "Nuclear oncology research", CRCINA, INSERM UMR1232, Université d'Angers, Université de Nantes, Nantes, FRANCE, [3]Team 8 "Stress Adaptation and Tumor Escape", CRCINA, INSERM UMR 1232, Université d'Angers, Université de Nantes, Nantes, FRANCE, [4]Radiopharmacy Department, ARRONAX Cyclotron, Saint-Herblain, FRANCE, [5]Departement of Nuclear Medicine, University Hospital, Nantes, FRANCE, [6]Recombinant Protein Core Facility of The University of Nantes, NANTES, FRANCE, [7]Institut de Cancérologie de l'Ouest, Medical Physics Department, Saint-Herblain, FRANCE.

Purpose/Introduction: Our research team, specialized in comparative oncology, developed molecular tools to address clinically relevant questions in immuno-SPECT and radioimmunotherapy of the B-cell lymphoma. This study aimed at demonstrating the feasibility and the relevance of anti-CD22 immuno-scintigraphy in dogs. Our second objective was to evaluate the interest of the systematically co-injection of labelled-unlabelled CD22 antibodies in human RIT by comparing the pharmacokinetics in dogs of an anti-CD22 antibody, radiolabelled with indium-111, with or without co-injection of the same unlabelled antibody. Subjects and methods: Six dogs (4 healthy dogs and 2 dogs bearing CD22+ B-cell lymphoma) were injected with a monoclonal murine anti-canine CD22 antibody radiolabelled with indium-111 in order to derive the antibody pharmacokinetics by SPECT imaging. Two healthy dogs and one lymphoma dog

were co-injected with a dose of unlabelled antibody (270 μg of radiolabelled antibody + 17.4mg of cold antibody), whereas the other 3 dogs received only the radiolabelled antibody (750μg). SPECT/CT images were acquired at 3 to 5 time-points following the administration (from 1h to 144h). Blood samples were also collected at 5 time-points after injection. Major organs and visible tumour lesions were delineated on CT images and the activity uptake was derived from SPECT images. Mean absorbed doses in the organs/lesions were calculated for all the dogs. **Results:** In healthy animals, the antibody residence time in blood was lower for animals injected with radiolabelled antibody only (13±1h vs 31±2h). Activity uptake in the spleen was significantly higher for dogs, which received only the radiolabelled antibody, leading to a three-fold increase in the mean absorbed dose to spleen (8.3±0.8 mGy/MBq vs 2.5±0.5 mGy/MBq). Cumulated activity within bone marrow was also 2.5 to 3 times higher in these dogs. Mean absorbed doses in other organs (kidneys, lungs, liver) were similar with or without cold antibody co-injection. In the two CD22+ B-cell lymphoma-bearing dogs, which had spleens infiltrated with disease, as assessed by ultrasound imaging, antibody uptake in the spleen was higher than in the healthy dogs indicating a specific targeting of the lymphoma cells. Infiltrated lymph nodes were also visible on SPECT imaging for both dogs. Discussion/conclusion: In the context of B-cell lymphoma RIT, with anti-CD22 antibody, co-injection with cold antibody allows for a longer residence time in blood and a limited uptake in spleen and bone marrow. Further studies should establish if these findings represent always a therapeutic advantage for patients, in regards to tumour uptake.

908	Monday, October 23, 2017, 14:30 - 16:00, Hall K

Cardiovascular System: Cardiac Sarcoidosis & Amyloidosis

OP-353

Prevalence of myocardial uptake in bone scan in the elderly population

L. Mohamed Salem, Sr., R. Reyes Marles, M. Godoy Bravo, J. Sánchez Serna, M. Castellon Sanchez, F. Nicolas Ruiz, L. Frutos Esteban, J. Navarro Ferenandez, I. Sime Loayza, M. Perez Martinez, D. Pascual Figal, M. Claver Valderas; Hospital Clínico Universitario Virgen de la Arrixaca, Murcia, SPAIN.

Introduction: Cardiac amyloidosis is a common cause of heart failure in the elderly, around 25% of patients over the age of 80 years have Amyloidosis TTR-wild Type in the heart autopsy studies, which suggests its potential contribution to the development of heart failure with preserved ejection fraction, nevertheless, the real prevalence of the disease is still unknown. According to late scientific evidence from large multicentre trial, myocardial uptake of bone tracers has a high specificity and sensitivity for the diagnosis of cardiac transthyretin amyloidosis. Purpose To determine the prevalence of myocardial uptake in bone scan in the elderly population, without previous clinical

suspicion of cardiac amyloidosis. **Subjects and Methods:** We revise retrospectively 1562 bone scans that were performed in our Department between 2010 and 2017, to elderly patients of 80 years and over, using conventional bone tracers Tc99m-HDP, Tc99m-DPD and Tc99m-HMDP, with usual bone scan clinical indications (prostate and breast cancer staging etc). Patients with clinical suspicion of cardiac amiloidosis, were excluded from the analysis. We classified the myocardial tracer uptake into 3 grades, taking as a reference the adjacent rib uptake; grade 1 is less than the rib, grade 2 equal to the rib and grade 3 more than the rib uptake **Results:** There was myocardial tracer uptake in 124 of 1562 revised bone scans (7.92%). Grade 1: 41 patients (33%), grade 2: 42 patients (34%), grade 3: 41 patients (33%). 82 patients had grade 2 and 3, which is 66% of positive patients and 5,25% of all revised bone scans, which indicates with high specificity and sensitivity, according to current evidence from literature, the presence of cardiac TTR Amyloidosis. Given that the myocardial take is highly suggestive of cardiac amyloidosis, our study indicated a prevalence of cardiac amyloidosis of almost 8%, which suggests its potential contribution to heart failure in the elderly. **Conclusion:** The prevalence of myocardial uptake in bone scan in the elderly is 7,92%. The prevalence of Transthyretin Cardiac Amyloidosis in the elderly is 5,25%. These results indicate a high prevalence of cardiac amyloidosis in the elderly as a cause of heart failure in this population.

OP-354

Prognostic impact of cardiac FDG-PET/CT using quantitative analysis in patients with cardiac sarcoidosis

T. Ando, Y. Fukushima, S. Kumita, H. Hashimoto, Y. Sugihara; Nippon Medical School, Tokyo, JAPAN.

Objective: Cardiac sarcoidosis is a potentially fatal condition in patients with sarcoidosis and ^{18}F-FDG-PET/CT can evaluate the severity of inflammation activity in cardiac sarcoidosis lesions. However, the relationships between cardiac FDG accumulation parameters and prognosis has not been sufficiently examined. The purpose of this study was to estimate the prognostic performance of cardiac FDG-PET/CT using low-carbohydrate diet and accumulation quantification software. **Materials and Methods:** A total of 20 consecutive cardiac sarcoidosis patients (6 men and 14 women, 62 ± 12 y) who underwent FDG-PET/CT using low-carbohydrate diet over 24 h (glucose intake < 10 g) were included in this study. FDG-PET images were acquired 60 min and 120 min after the administration of FDG 2.88 MBq/kg. Using accumulation quantification software GI PET, volumes of interest were automatically drawn in the myocardium setting the threshold standardized uptake value (SUV) as 1.40. Metabolic volume (MV) and total lesion glycolysis (TLG) in each lesion and entire-lesion overall values of these parameters were measured. In order to evaluate the clinical importance of overall TLG (OTLG), all patients were divided into two groups based on the value of OTLG using a receiver-operating-curve analysis. All patients were followed up over 2.1 (0.95-3.28) years from the initial FDG-PET/CT and observed for the occurrence of major adverse cardiac events, defined as cardiac death, hospitalization

due to deterioration of heart failure, development of ventricular tachycardia, and requirement of steroid therapy. **Results:** In all 20 patients, SUVmax was 3.35 (1.98-3.88), overall MV was 20 (6-132) cm^3, and OTLG was 32 (10-262). Among them, 9 were assigned to the high OTLG group while 11 were assigned to the low OTLG group. OTLG was 287 (102-479) in the high group and 11 (5-28) in the low group. Of the 20 patients, 5 (25%) experienced MACE during the follow up period. The proportion of patients that developed MACE was significantly higher in the high OTLG group than in the low OTLG group (5 of 9 versus 0 of 11 patients, p =0.008). Multivariate logistic regression analysis demonstrated that OTLG was the sole independent prognostic factor for MACE (p = 0.04). **Conclusions:** The severity of cardiac sarcoidosis activity was estimated by calculating SUVmax, overall MV, and OTLG. FDG-PET/CT using low-carbohydrate diet over 24 h as well as accumulation quantification software may have a high prognostic value for the occurrence of MACE in patients with cardiac sarcoidosis.

OP-355

Novel approach for myocardial sarcoidosis diagnosis using Ga-68-DOTATATE PET/CT: Reference values in a normal population

M. Jreige, M. Nicod Lalonde, A. van der Gucht, N. Schaefer, J. O. Prior; Centre Hospitalier Universitaire Vaudois (CHUV), LAUSANNE, SWITZERLAND.

Purpose: The emerging application of PET/CT using radiolabeled somatostatin receptor (SSTR) ligands such as Ga-68-DOTATATE for the investigation of myocardial inflammation seems to be a valuable alternative to FDG PET/CT in the emergency settings without the need for a lengthy patient preparation. This study aimed to report normal reference values of cardiac metabolic uptake of Ga-68-DOTATATE PET/CT to provide a basis for comparison for pathological cases. **Materials and Methods:** We retrospectively assessed Ga-68-DOTATATE PET/CT uptake in different cardiac regions in a population of 18 patients addressed for tumoral investigation without known myocardial inflammation or cardiac symptoms (M:F=10:8; mean age 54±14 years). Ga-68-DOTATATE PET/CT were analyzed to define SUVmax and SUVmean values in both the basal and apical myocardial regions of the left and right ventricle, as well as in the septum. We calculated the ratio of the uptake in the the basal and apical myocardial regions of the left ventricle to the intra-ventricular blood pool uptake. Results of two pathologic cases were also reported as example for comparison. **Results:** In the normal population, Ga-68-DOTATATE uptake (SUVmax/SUVmean in g/mL) was of 1.9±0.5g/mL (range 1.3-3.7)/1.1±0.3 (0.8-2.2) in basal LV, 1.9±0.5 (1.3-3.7)/1.1±0.3 (0.7-2) in apical LV, 1.7±0.7 (1-3.9) and 1± 0.5 (0.6-2.6) in basal RV, 1.6±0.5 (1-3.1)/0.9±0.3 (0.6-1.9) in apical RV, and 1.8±0.7 (1.1-3.8)/1.1±0.4 (0.6-2.1) in the septum. Mean ratios of SUVmax/SUVmean to blood pool uptake were: 1.5±0.3/1.4±0.3g/mL in basal LV, 1.4±0.2/1.3±0.3g/mL in apical LV, 1.2±0.1/1.1±0.1g/mL in basal RV, and 1.2±0.1/1.1±0.2g/mL in apical RV. As comparison, the mean ratios of SUVmax/SUVmean to blood pool uptake in 2 patients with sarcoidosis

were 2.7/2.6 in basal LV and 1.9/1.7 in apical LV with a very clear visualization on PET/CT. **Conclusions:** This study reports normal Ga-68-DOTATATE cardiac uptake in apical, basal and septal regions of the normal myocardium and provides potential normal ratios of myocardial uptake to blood pool. These reference values provide a a basis for this novel diagnosis tool for cardiac inflammation with evident differences in SUV measurements and visual assessment.

OP-356
[18F]-Florbetaben-PET/CT for Imaging of cardiac amyloidosis

M. Kircher, J. Brumberg, T. Reiter, S. Ihne, S. Knop, K. Kortüm, G. Ertl, A. Buck, W. Bauer, C. Lapa; Uniklinikum Würzburg, Würzburg, GERMANY.

Purpose: The aim of this study was to investigate the performance of [18F]florbetaben-PET/CT in comparison to CMR and scintigraphy. IntroductionCardiac amyloidosis is a rare form of restrictive cardiomyopathy which can arise from different causative conditions. Since echocardiography as the initial screening test suffers from limited specificity and myocardial biopsies are prone to sampling error, other imaging modalities including cardiac magnetic resonance (CMR) or scintigraphy with radio-labelled bisphosphonates are routinely used. Recently, positron emission tomography/computed tomography (PET/CT) emerged as a new alternative. **Subjects & Methods**: A total of 20 patients with suspicion of cardiac amyloidosis underwent [18F]florbetaben-PET/CT, CMR, scintigraphy as well as echocardiography. Qualitative and quantitative assessment of [18F]florbetaben-PET/CT was performed and compared to other imaging results. Additionally, in 2 patients a follow-up study after treatment initiation was performed after 6 and 11 weeks, respectively. **Results:** [18F]florbetaben-PET/CT was visually positive in all patients with cardiac amyloidosis independently from amyloidosis type. Of note, in two PET-negative patients, cardiac involvement could be ruled out by subsequent biopsy. PET results could be confirmed by other imaging modalities. **Conclusions/Discussion:** [18F]florbetaben-PET/CT can accurately identify cardiac amyloidosis involvement irrespective of the underlying etiology. Imaging corresponded well with CMR results. It might also prove a valuable tool in therapy monitoring.

OP-357
[18F]-Florbetaben PET/CT in cardiac amyloidosis: results from the FLORAMICAR study

D. Genovesi, G. Vergaro, A. Giorgetti, M. Emdin, E. Volpi, S. Alduini, A. Kusch, B. Favilli, S. Fucci, P. Marzullo; Fondazione CNR-Regione Toscana "Gabriele Monasterio", Pisa, ITALY.

Aim: The hypothesis is that PET/CT tracers for cerebral amyloid also bind to extracerebral amyloid deposits. The study has been proposed to evaluate and quantify the uptake of [18F]-Florbetaben in the heart of patients with cardiac amyloidosis. **Materials and Methods:** 12 patients with cardiac amyloidosis were enrolled. 6 patients had transtiretine-related amyloidosis (ATTR) while 6 patients had light chains-related amyloidosis (AL). Each patient underwent to a dynamic cardiac PET/CT scan during the injection of 300 Mbq of [18F]-Florbetaben followed by whole-body scan, brain scan and delay cardiac scan. **Results:** All patient showed a cardiac uptake of the tracer. In the AL group there was an early uptake rising to a maximum between 5 and 10 minutes after the injection and a "plateau" profile until the end of the dynamic acquisition; in the ATTR group there was the same early uptake followed by a rapid wash-out. In the first 15 minutes the median of cardiac SUV was 5,08 (range 2,88 - 8,22) in AL and 2,30 (range 2,05 - 5,42) in ATTR (P = 0,11), while in the following 50 minutes, the values were 3,73 (range 2,42 - 6,99) in AL and 1,15 (range 0,95 - 1,70) in ATTR (P = 0,02). The 15 minutes target to background ratio (TBR) was 4,14 (range 1,78 - 5,28) for AL and 2,04 (range 1,71 - 2,21) for ATTR (P = 0,20); the 50 minutes TBR was 2.58 (range 1,84 - 6,48) for AL and 1,03 (range 0,55 - 1,17) for ATTR (P = 0,02). Late cardiac scans confirmed these data showing an high cardiac uptake in the AL group and no cardiac uptake in the ATTR group. 2 ATTR patients showed a diffuse brain uptake and one of these showed also a diffuse bone marrow uptake, while 4 AL patients showed extracardiac uptake (tongue, bone marrow and lungs). **Conclusions:** [18F]-Florbetaben showed a significant uptake in the heart of patients with cardiac amyloidosis. In patient with AL the dynamic uptake shows a rapid wash-in without significant wash-out; in patients with ATTR there is a rapid wash-in followed by a rapid wash-out without significant cardiac uptake in the late cardiac scan. Brain uptake in ATTR patients suggests that brain involvement in the context of a systemic amyloidosis could not be due to the same type of amyloid deposits which involve other organs like the heart or the bone-marrow.

OP-358
Imaging amyloidosis patients with 18F Florbetapir PET - incidence and significance of non-cardiac soft tissue uptake

*J. Page[1,2], **T. Wagner**[2], M. Burniston[2], J. Ross[1,2], A. Skillen[2], D. McCool[2], T. Lane[1], R. Manwani[1], P. Hawkins[1], A. Wechalekar[1]; [1]National Amyloidosis Centre, London, UNITED KINGDOM, [2]Royal Free London NHS Foundation Trust, London, UNITED KINGDOM.*

Purpose: Amyloidosis is a rare but serious disease characterised by infiltration of abnormal protein deposits in tissues and organs throughout the body. ^{123}I-SAP (serum amyloid P) is used to image amyloid deposits in the liver, spleen and kidneys, but is only available in two centres worldwide and has low sensitivity for detecting amyloid in other organs, including the heart. As part of a study to assess the diagnostic value of ^{18}F-florbetapir in cardiac amyloidosis, we also identified other areas of soft tissue uptake and correlated these findings with ^{123}I SAP scan results. **Method:** 16 patients (14 AL, 2 ATTR) underwent dynamic cardiac PET imaging for 60 minutes following intravenous administration of 370MBq ^{18}F-florbetapir. This was then followed by a half-body PET-CT. Half-body images were assessed for areas of increased tracer accumulation and SUV_{max} for these areas was

measured. A spherical VOI was placed in the spleen and the descending aorta on the dynamic images and a spleen retention index (SRI) was calculated as the mean SUV from 10-30 minutes divided by the integral of the aorta SUV 0-20 minutes post-injection. **Results:** In the 16 patients imaged to date, uptake was seen in many different areas in which amyloid deposits are known to form (numbers of patients, range of SUV_{max}): spleen (6, 4.2-10.2), lungs (3, 6.8-37.0), fat (11, 1.6-4.3) tongue (8, 2.8-5.0), kidney (1, 4.1) and stomach wall (5, 3.6-8.6). ^{18}F-florbetapir uptake in the spleen on the half-body images was concordant with ^{123}I-SAP imaging in 13/16 patients. Taking a cut-off value of 0.03 the SRI was concordant with ^{123}I-SAP imaging in 15/16 patients. **Conclusion:** ^{18}F-florbetapir looks to be a promising, widely available PET tracer that enables the imaging of amyloid deposits in organs such as the lungs which cannot be assessed using existing imaging techniques and the spleen which can only otherwise be imaged using ^{123}I-SAP which is not widely available. Further work is needed to assess diagnostic and prognostic value as there have been very few studies yet reported.

OP-359

Cardiac amyloid imaging with [18]F Florbetapir PET - initial results from a UK study

J. Page[1,2], T. Wagner[2], M. Burniston[2], J. Ross[1], A. Skillen[2], D. McCool[2], T. Lane[1], R. Manwani[1], M. Fontanna[1], P. Hawkins[1], A. Wechalekar[1]; [1]National Amyloidosis Centre, London, UNITED KINGDOM, [2]Royal Free London NHS Foundation Trust, London, UNITED KINGDOM.

Purpose: Cardiac amyloidosis (CA) is a rare but serious disease characterised by infiltration of amyloid fibrils throughout the heart. Recently, a multi-centre study (Gilmore J. 2016, 133:2404-2412 Circulation) demonstrated the utility of ^{99m}Tc-labelled 3,3-diphosphono-1,2-propanodicarboxylic acid (DPD) in diagnosis of cardiac transthyretin amyloidosis (ATTR), but the tracer has poor sensitivity in systemic (AL) amyloidosis. Several groups have investigated brain amyloid tracers in CA patients, with promising results (Catafau A. 2015, 3:39-55 Clin Transl Imaging). **Method:** 16 patients (14 AL, 2 ATTR) underwent dynamic cardiac PET imaging for 60 minutes following intravenous administration of 370MBq ^{18}F-florbetapir. A spherical volume of interest of 1cm diameter was placed in the left ventricle (LV) chamber and the LV myocardium was manually outlined. The heart retention index (HRI) was calculated as the mean LV myocardial SUV from 10-30 minutes divided by the integral of the blood pool SUV 0-20 minutes post-injection. **Results:** Myocardial uptake of ^{18}F-florbetapir was seen in all patients. The median HRI was 0.14, (IQR=0.08-0.18). Mean HRI was lower in the ATTR patients (n=2, mean=0.06), as reported elsewhere (Dorbala S. 2014, 41:1652-1662 Eur J Nucl Med Mol Imaging). High HRI values were seen in treatment-naïve patients (n=2, mean=0.16). **Conclusion:** Our cohort confirmed 18F-florbetapir as a promising tracer for imaging cardiac amyloidosis. Median HRI in our patients is higher than others reported in the literature. This may be due to studying patients close to initial diagnosis. Further work is required to establish its role in diagnosis and monitoring of treatment.

OP-360

Cardiac FDG-PET/CT in systemic sclerosis

Z. Besenyi[1], G. Ágoston[2], R. Hemelein[3], A. Bakos[1], L. Kovács[3], A. Varga[2], L. Pávics[1]; [1]Department of Nuclear Medicine University of Szeged, Szeged, HUNGARY, [2]Department of Family Medicine University of Szeged, Szeged, HUNGARY, [3]Department of Rheumatology University of Szeged, Szeged, HUNGARY.

Aim: Systemic sclerosis (SSc) is a rare systemic connective tissue disease characterized by complex pathogenesis and multi organ involvement. Cardiac manifestation is a common complication in connective tissue diseases particularly in systemic sclerosis (SSc). In SSc the immuno-inflammatory damage leads to myocardial fibrosis and consequent myocardial dysfunction. Clinically evident heart involvement appears as a bad prognostic factor, responsible for up to 30 % of SSc-related mortality. 18F-FDG PET/CT plays an increasing role in the diagnostics of inflammatory disorders with myocardial manifestation. The aim of this study was to assess the diagnostic utility of cardiac 18F-FDG PET/CT in patients with SSc, and to evaluate simultaneously results of 2Dimensional Speckle Tracking Echocardiography (STE). **Materials and Methods:** 19 patients with systemic sclerosis (age: 57,3±10, 18 female, 1 male) where enrolled in the prospective study. After high-fat, high-protein, low carbohydrate - diet (previous 24 hours) and extended fasting (6 hours) cardiac 18F-FDG-PET/CT acquisition was performed in 2D mode and short-whole-body in 3D mode. Within 24 hours all patients underwent comprehensive echocardiography focusing on left ventricular myocardial mechanics applying STE. The recommended 17 segment model was used to assess the 18F-FDG activity and for the calculation of myocardial strain as well. On 18F-FDG PET/CT the segmental myocardial 18-FDG uptake in kBq/cc by PMOD software was calculated. The strain values were measured offline by speckle tracking EchoPAC software. **Results:** After diatery modification (mean 32,5±3,14 hours) and extended fasting (mean 18,72±5,52 hours) the mean blood glucose level of patients were 4,57±1,19 mmol/l. In 14 patients the cardiac uptake was near equal or lower than blood-pool activity. Visually there was no myocardial activity, and the muscular interventricular septum appeared "cold". In five patients (5/19) showed significantly increased 18F-FDG uptake (18,6±6,8 kBq/cc vs. 7,77±3,4 kBq/cc, p<0,01) in the myocardium. In patients with 18F-FDG increased uptake, measured global left ventricular longitudinal strain values (19,4±2,7% vs. 13,4±8%, p<0,01) were decreased. There was a negative correlation between myocardial strain and FDG uptake (p<0,05, r=-0,54). **Conclusion:** 18F-FDG PET/CT is a promising imaging tool to detect active myocardial inflammation of systemic sclerosis. In the active condition of the myocardial involvement STE provides a simple, non-invasive modality to detect metabolic activity related subtle mechanical changes in myocardium.

---

909   **Monday, October 23, 2017, 14:30 - 16:00, Hall G1**

Neurosciences: Imaging Neurodegeneration in Alzheimer's Disease by TAU and FDG Imaging

OP-361

Flortaucipir perfusion PET is a suitable replacement for FDG PET in patients with neurodegenerative diseases

J. Hammes[1], I. Leuwer[1], G. N. Bischof[1,2], A. Drzezga[1], T. van Eimeren[1,2,3];
[1]Clinic of Nuclear Medicine, University Hospital Cologne, Cologne, GERMANY, [2]INM-3, Research Center Jülich, Jülich, GERMANY, [3]Clinic of Neurology, University Hospital Cologne, Cologne, GERMANY.

Aim: Cerebral glucose metabolism measured with FDG-PET is a well established marker of regional distribution and extent of neuronal cell loss in patients with neurodegenerative diseases such as Alzheimer's disease frontotemporal lobar degeneration or atypical Parkinson syndromes. Flortaucipir PET as an in vivo marker of hyperphosphorylated and misfolded Tau-protein aggregations as they occur in these diseases is currently under evaluation and shows promising results. In this study we assess the feasibility of early Flortaucipir PET acquisitions as a marker of cerebral perfusion and as possible replacement for an additional FDG-PET examination. **Methods:** 20 patients with suspected neurodegeneration underwent Flortaucipir and FDG PET imaging. Scans were performed on a SIEMENS Biograph mCT PET/CT. Ten one-minute timeframes were acquired directly after the application of 200 MBq Flortaucipir. FDG-PET images were acquired on a different date according to standard clinical protocol. Flortaucipir timeframes were coregistered to the individual FDG-scan and normalized to MNI space using SPM 12. Voxel-wise intermodal correlations were calculated on within-subject level for every possible time-window. The optimal acquisition time was determined by identifying the window with highest pooled within-subject correlation. Z-transformed deviation maps (ZMs) and stereotactic surface projections (SSPs) were created from both FDG and early Flortaucipir images using a standard FDG-norm cohort. **Results:** Visually the regional patterns and the extent of perfusion deficits in early Flortaucipir PET were highly comparable to the metabolic deficits in FDG-PET. Best results were observed in a time window from 60-360 seconds after application of the tracer with a pooled within-subject correlation coefficients of r=0.86. Region wise analysis revealed that correlation strength ranged from r=0.96 (subcortical grey matter) to r=0.83 (frontal lobe). ZMs and SSPs of early Flortaucipir and FDG PET images were also highly similar. **Conclusion:** Early Flortaucipir PET is a good biomarker to assess extent and regional distribution of neuronal cell loss in neurodegenerative diseases. By routinely replacing FDG PET by early Flortaucipir imaging, radiation exposure and complexity of the diagnostic workup could be reduced significantly.

OP-362

The impact of education on the association between tau deposits and cognition in Mild Cognitive Impairment

*S. Trombella[1], G. B. Frisoni[2], **V. G. Garibotto**[2]; [1]Geneva University, Geneva, SWITZERLAND, [2]Geneva University and Geneva University Hospital, Geneva, SWITZERLAND.*

Aim: Years of education (YE) is a well established proxy of the reserve capacity of the brain, modulating the association between the severity of neurodegeneration and cognition in Alzheimer's disease (AD). Aim of this study was to evaluate the presence of a correlation between YE and tau deposition, as measured by 18F-AV1451 PET, in a group of amyloid positive subjects with mild cognitive impairment (MCI). **Materials and Methods:** Data were obtained from an ongoing cohort study in our Institution and from the Alzheimer's Disease Neuroimaging Initiative (ADNI) database (www.loni.ucla.edu/ADNI). 128 patients received tau-PET imaging using 18F-AV-1451, amyloid-PET imaging using 18F-Florbetapir and 3D T1 MP-RAGE MRI imaging. For this study, we included subjects with a clinical diagnosis of MCI and amyloid positivity at PET imaging (i.e. cortical SUVR higher than 1.11). 36 subjects (23/13 males/females, mean age of 76 ± 7.9, mean Mental State Examination score -MMSE- of 25.8 ± 3.8, mean YE 15.7 ± 3.2) fulfilled the inclusion criteria. Image processing was performed in SPM 12 (Function Image Laboratory, Wellcome Department of Cognitive Neurology, London, UK) with the following steps: 18-AV1451 PET images were co-registered to the subject's MP-RAGE image, normalized using the deformation matrix derived by the segmentation of each MP-RAGE image, and subsequently smoothed using an 8 mm isotropic Gaussian kernel. SUVR parametric images were calculated dividing each voxel counts by the mean cerebellar crus counts. We used two multiple linear regression analyses to evaluate the correlation between the degree of cognitive impairment (expressed by the MMSE) or YE and tau deposition, correcting for the effect of age, imaging protocol (ADNI or Geneva) and YE or MMSE. Findings meeting a height threshold of p < 0.005, uncorrected, were considered significant. **Results:** As expected, a significant negative correlation between tau binding and MMSE score was retrieved in the temporal, posterior cingulate and precuneus and frontal cortex, bilaterally, stronger on the left hemisphere. No significant positive correlation was found. For education, a significant positive correlation was found in the left posterior cingulate cortex. No significant negative correlation was found. **Conclusion:** A positive correlation between higher tau deposition and YE in amyloid positive MCI subjects was shown in the left posterior cingulate cortex, suggesting that reserve associated with education compensates for neurodegeneration in this region.

OP-363

Parametric imaging of tau load in Alzheimer's patients and controls using Flortaucipir

S. S. V. Golla**[1], E. Wolters[1,2], T. Timmers[1,2], R. Ossenkoppele[1,2], C. Groot[1], S. Verfaillie[2], P. Scheltens[2], W. M. van der Flier[2,3], L. Schwarte[4], M. A. Mintun[5], M. Devous[5], R. C. Schuit[1], A. D. Windhorst[1], A. A. Lammertsma[1], R. Boellaard[1,6], B. N. M. van Berckel[1], M. Yaqub[1]; [1]Department of Radiology & Nuclear Medicine, VU University Medical Center, Amsterdam, NETHERLANDS, [2]Alzheimer Center & Department of Neurology, VU University Medical Center, Amsterdam, NETHERLANDS, [3]Department of Epidemiology & Biostatistics, VU University Medical Center, Amsterdam, NETHERLANDS, [4]Department of Anaesthesiology, VU University Medical Center, Amsterdam, NETHERLANDS, [5]Avid Radiopharmaceuticals, Inc., Philadelphia, PA, UNITED STATES OF AMERICA, [6]Department of

Nuclear Medicine & Molecular Imaging, University of Groningen, University Medical Center Groningen, Groningen, NETHERLANDS.

Background: Flortaucipir ([[18F]AV1451) is a promising positron emission tomography (PET) tau tracer used to visualize *in vivo* tau binding in Alzheimer's disease (AD). Recently, several [18F] AV1451 studies have been published identifying the optimal tracer kinetic model to perform a full quantitative analysis of the PET data. The purpose of the present study was to evaluate the performance of several parametric methods, as well as standardised uptake values ratios (SUVr), to obtain quantitatively accurate parametric images of [18F]AV1451. **Methods:** Dynamic PET scans of 130 minutes duration, including arterial sampling, were performed in 5 AD patients and 5 controls (C). Parametric images were generated using different linearization and basis function approaches. Plasma input based Logan and Spectral Analysis (SA) were used to generate volume of distribution (V_T) images. Several reference tissue based approaches such as reference Logan (RLogan), the multilinear reference tissue models (MRTM), receptor parametric mapping (RPM), and simplified reference tissue model 2 (SRTM2) were used to obtain binding potential (BP_{ND}) images. Regional BP_{ND} and V_T values obtained from the parametric images were compared to respective values derived from reversible two tissue compartment model (2T4k_V_B). Performance of the SUV_r was assessed by comparing the values to the distribution volume ratio (DVR) and SRTM derived BP_{ND} estimates obtained using non-linear regression (NLR). **Results:** Plasma input Logan ($r^2=0.96$; slope=0.78) and SA ($r^2=0.97$; slope=0.94) estimated V_T well. RLogan ($r^2=0.93$; slope=0.77), RPM ($r^2=0.96$; slope=0.97) and SRTM2 ($r^2=0.96$; slope=0.93) correlated well with NLR estimated DVR. Regional R_1 values extracted from RPM ($r^2=0.97$; slope=0.99) and SRTM ($r^2=0.94$; slope=0.99) correlated well with the R_1 NLR estimates. Although SUVr obtained using 80-100 min scan duration correlated well with the DVR ($r^2=0.93$; slope=1.07) and SRTM BP_{ND} ($r^2=0.84$; slope=0.95), bias and precision of SUVr depended on uptake time and subject group (or underlying specific binding level). **Conclusions:** RLogan and Logan correlated well but with an underestimation when compared to respective NLR estimates. Parametric images obtained using RPM and SA seems to provide accurate parametric BP_{ND} and V_T images, respectively, and are the recommended methods for voxel level parametric kinetic analysis. Individual SUVr values appear biased when compared to DVRs and that bias varies at different uptake times and DVR values. While preliminary, this bias suggests that SUVr should be used with caution, particularly in longitudinal studies when changes in specific binding are expected.

OP-364

Association between tau deposition, amyloid-β, age and memory performance in cognitively normal subjects: influence of partial volume correction

I. Sonni[1], A. Maaß[2], S. N. Lockhart[2], S. M. Landau[2], S. L. Baker[1], W. J. Jagust[1,2]; [1]Lawrence Berkeley National Laboratory, Berkeley, CA, UNITED STATES OF AMERICA, [2]Helen Wills Neuroscience Institute, University of California, Berkeley, Berkeley, CA, UNITED STATES OF AMERICA.

Aim: We sought to investigate the association between [18F]-AV-1451 tau PET tracer uptake and age, global brain beta-amyloid, and memory performance, and the effect of partial volume correction (PVC) among cognitively normal young, middle-aged and older adults. **Materials and Methods:** We included 86 cognitively normal subjects (6 young, 6 middle-aged, and 74 older adults, aged 22.8±2.6, 53±6.4 and 77.1±5.9 y, respectively). All subjects underwent a [18F]-AV-1451 tau PET, neuropsychological testing including a measure of verbal (California Verbal Learning Test - CVLT) and visual recall, and structural 1.5T MRI (T1-weighted, MPRAGE). 76 subjects also received [11C]-PiB PET. FreeSurfer was used to segment MRIs to obtain the regions of interest (ROIs). [18F]-AV-1451 SUVR images were created based on mean uptake over 80-100 min post-injection and normalized by mean inferior cerebellar gray matter. Distribution volume ratios (DVRs) for PiB images were generated with Logan graphical analysis on PiB frames corresponding to 35-90 min post-injection using a cerebellar gray matter reference region. The PiB index (weighted-mean DVR across cortical regions) was used as a measure of global cortical PiB uptake. [18F]-AV-1451 signal was collapsed into ROIs that represented pathological Braak stages, resulting in three composite ROIs (Braak stages I/II, transentorhinal, Braak III/IV, limbic, and Braak V/VI, neocortical). Tracer binding in areas outside cortex were included in the partial volume correction using the Rousset method. Statistical analysis was conducted using Spearman rank correlations to assess associations between tau SUVR in the three Braak composite ROIs and age, global PiB and memory performance, and to determine the influence of PVC on these associations. **Results:** A moderate association was found between global cortical amyloid and tau SUVR in regions corresponding to Braak stages I/II, III/IV and V/VI. Weaker associations were found between age, memory performance and tau SUVR in Braak stages I/II and III/IV, and a very weak correlation was found in Braak V/VI. The strength of the associations between tau SUVR and age, PiB index and visual recall increased when using PVC (See Table), particularly for Braak stages V/VI. **Conclusion:** Our data collected in a heterogeneous sample of cognitively normal subjects, shows that tau SUVR is associated with global brain amyloid and this association tends to increase in all the Braak composite ROIs when using PVC, especially for Braak V/VI. A similar but weaker trend was found with age and memory ability.

OP-365

On- and Off-target binding of [18F]AV-1451 in Substantia Nigra post-mortem tissues of Alzheimer's Disease (AD) patients and Normal Control (NC) subjects

L. Gomez, Y. Lin, Q. Liang, M. Mintun, G. Attardo; Avid R.P., Philadelphia, PA, UNITED STATES OF AMERICA.

Purpose: It has been reported that the PET tracer [18F]AV-1451 binds to pathological tau inclusions in AD tissues but also at neuromelanin sites in the Substantia Nigra pars compacta (SNpc) (1). Strong uptake of [18F]AV-1451 in SNpc has been seen in

both AD patients and healthy subjects (2). The current study examines the binding profile of diverse chemical structures such as [18F]AV-1451, [18F]T808 and [18F]MK6240 in post-mortem brain tissue sections from AD and NCs. **Subjects and Methods:** Frozen sections from 6 AD, 5 NC cases were selected for this study. Autoradiography (ARG) and competition studies (10 μM cold) were performed using 20 μCi [18F]AV-1451, [18F]T808 or [18F]MK6240 on the brain sections (10 μm). The sections were then exposed to an imaging plate overnight and scanned with a FujiFilm Imaging System. The same sections were later stained with phospho-Tau AT8 antibody. Distribution of ARG signal of [18F]AV-1451, [18F]T808, and [18F]MK6240 are compared with that from the AT8 antibody. **Results:** The distribution of ARG signal of [18F]AV-1451 overlapped with clusters or occasionally with single cell/tangles that contained either neuromelanin or P-tau. In NCs with no positive AT8 regions, the ARG signal matched the distribution of neuromelanin-containing cells in the SNpc. In AD tissues containing P-tau immunostaining in the SNpc, characteristic spots of ARG signal overlapped clusters of neuromelanin cells and/or neuro fibrillary tangles (NFT). NFTs resulted in a much stronger ARG signal than isolated P-tau neurofilaments. Although there was no difference in average neuromelanin load between AD and NC tissues, the average ARG intensity in AD cases was non-significantly higher than in NCs . This resulted from a large P-tau load in the SNpc of the 2 AD tissues tested. Both [18F]T808 and [18F] MK6240 also showed uptake in SNpc. The intensity of the signal from [18F]AV-1451 and [18F]MK6240 were comparable. [18F]T808 showed lower intensity and minimal block of [18F]AV-1451 in SNpc of NCs. **Conclusion:** This study confirms previous reports showing that [18F]AV-1451 binds to a target in neuromelanin-containing cells in the SNpc. It also shows that in tissues where P-tau is abundant, the resulting ARG signal is likely to be the summation of Off- and On-target binding of the tracer. The binding to SNpc of tau radio ligands [18F]AV-1451 and [18F]MK6240 was clear and comparable in intensity, whereas the off-target binding of [18F] T808 was minimal. 1- Marquie et al., Ann Neurol. 2015 78(5): 787-800. 2- Hansen et al.,Brain 2016 137(7):2039-49.

OP-366

Clinical evaluation of ¹⁸F-PI-2620, a next generation tau PET agent in subjects with Alzheimer's disease, progressive supranuclear palsy, and non-demented controls

J. Seibyl[1], O. Barret[1], A. Stephens[2], J. Madonia[1], D. Alagille[1], A. Mueller[2], H. Schieferstein[2], M. Berndt[2], H. Kroth[3], S. Bullich[2], C. Papin[1], V. Carroll[1], C. Sandiego[1], A. Pfeifer[3], A. Muhs[3], L. Dinkelborg[2], G. Tamagnan[1], K. Marek[1]; [1]Molecular Neuroimaging, New Haven, CT, UNITED STATES OF AMERICA, [2]Piramal Imaging, Berlin, GERMANY, [3]AC Immune SA, Lausanne, SWITZERLAND.

Introduction: Intracellular tau deposition is a key pathologic feature of Alzheimer's disease (AD) and other neurodegenerative disorders. Recently, positron emission tomography tau probes have been developed for in vivo detection of brain tau load, although quantification is challenging due to high off tar-

get binding and slow kinetics. Further, different tau radiotracers have different affinities for tau species. ¹⁸F-PI-2620 is a novel tracer with a high affinity for binding to aggregated tau. ¹⁸F-PI-2620 binds specifically to tau deposits in AD brain sections from different Braak stages, Pick's, and progressive supranuclear palsy (PSP) pathologies. This first-in-human study reported here assesses the potential of ¹⁸F-PI-2620 to visualize tau deposition in subjects with AD and PSP, in comparison with non-demented controls. **Subjects & Methods:** In an ongoing clinical imaging study, participants diagnosed with mild Alzheimer's (AD, n=4), non-AD tauopathies (e.g. PSP, n=3), and non-demented controls (NDC, n=3) undergo dynamic PET imaging for over 3 h following 370 MBq bolus injection of ¹⁸F-PI-2620. Venous blood is obtained to characterize the kinetics of parent compound and metabolites. **Results:** Initial imaging data shows robust brain uptake and fast wash-out in non-target regions with peak SUV = 4-4.5. There was no increased uptake seen in choroid plexus, basal ganglia, striatum, amygdala, meninges or other regions noted in first generation tau agents. In AD, focal asymmetric uptake was evident in temporal and parietal lobes, precuneus, and cingulate. SUVr time curves demonstrate a plateau at 90-100 min post injection with resultant SUVrs of 2.5-2.8 in abnormal regions, whilst HV demonstrated shorter time to secular equilibrium (60-70 min) and lower SUVrs (1.0-1.2) in comparable brain regions. Finally, PSP subjects demonstrated focal increased uptake in the globus pallidus (SUVr = 2.0-2.1) and substantia nigra (SUVr = 2.4-2.6). Blood data confirmed fast kinetics with 20% of parent compound present at 60 min and presence of polar metabolites. Comparison of SUVr to non-invasive pharmacokinetic modeling showed a strong correlation and linear relationship with binding potential, BPnd. **Conclusion:** Initial ¹⁸F-PI-2620 PET first-in-human data in AD, PSP and NDC demonstrate excellent brain penetrance, favorable kinetics, and high target specificity with low nonspecific binding and high signal in regions of expected tau pathology.

OP-367

Metabolic patterns underlying disease heterogeneity and severity in patients with dementia with Lewy Body: a project of the European Consortium for Dementia with Lewy Body (E-DLB)

S. Morbelli[1,2], M. Brendel[3], A. Rominger[3], V. Garibotto[4], N. Nicastro[5], A. Pilotto[6,7], A. Padovani[6], B. Paghera[8,2], S. Garcia-Ptacek[9], I. Savitcheva[10], M. G. Kramberger[11], M. Trost[11], A. W. Lemstra[12], J. J. van der Zande[12], S. Pappatà[13,2], M. Calcagni[14,2], A. Cistaro[15,2], V. Berti[16,2], D. Volterrani[17,2], S. Sestini[18,2], M. Bauckneht[1,2], F. Sensi[19], A. Chincarini[19], D. Aarsland[20,21], F. Nobili[22,2]; [1]IRCCS San Martino - IST, Genoa, ITALY, [2]Neurology Study Group of the Italian Association of Nuclear Medicine, (aimn), ITALY, [3]Department of Nuclear Medicine, University of Munich, Munich, GERMANY, [4]Division of Nuclear Medicine and Molecular Imaging, Geneva University Hospitals, Geneva, SWITZERLAND, [5]Division of Neurorehabilitation, Department of Clinical Neurosciences Geneva, Geneva University Hospitals, Geneva, SWITZERLAND, [6]Neurology Unit, University of Brescia, Brescia, ITALY, [7]Parkinson's disease rehabilitation Centre, FERB ONLUS S.Isidoro Hospital, Trescore Balneario, (BG), ITALY, [8]Nuclear Medicine, Spedali Civili Brescia, University of Brescia,

Brescia, ITALY, [9]Division of Clinical Geriatrics, Center for Alzheimer Research, Karolinska Institutet, Stockholm, SWEDEN, [10]Department of Radiology, Karolinska Institutet, Stockholm, SWEDEN, [11]Department of Neurology, University Medical Centre, Ljubljana, SLOVENIA, [12]Alzheimer Center & Department of Neurology, VU University Medical Center and Neuroscience Campus, Amsterdam, NETHERLANDS, [13]Institute of Biostructure and Bioimaging, CNR, Naples, ITALY, [14]Institute of Nuclear Medicine, Fondazione Policlinico Universitario Agostino Gemelli, Università Cattolica del Sacro Cuore, Rome, ITALY, [15]Positron Emission Tomography Centre IRMET S.p.A., Turin, ITALY, [16]Nuclear Medicine Unit, University of Florence, Florence, ITALY, [17]Nuclear Medicine Unit, University Hospital of Pisa, Pisa, ITALY, [18]Nuclear Medicine Unit, U.S.L. Toscana Centro, Prato, ITALY, [19]Istituto Nazionale di Fisica Nucleare, Sezione di Genova, Genoa, ITALY, [20]Centre for Age-Related Medicine (SESAM), Stavanger University Hospital, Stavanger, NORWAY, [21]Wolfson Centre for Age-Related Diseases, King's College London, London, UNITED KINGDOM, [22]Clinical Neurology, Department of Neuroscience (DINOGMI), University of Genoa, Genoa, ITALY.

DLB is a highly heterogeneous disease both in terms of clinical presentation and related pathology. We aimed to investigate metabolic-patterns underlying core and suggestive features of DLB and the relative influence of disease severity. **Methods**: on April 2017 one-hundred and eighteen 18F-FDG PET scans of DLB patients were available on the functional-imaging database of E-DLB. Core symptoms (visual hallucinations, fluctuations, spontaneous Parkinsonism) and a main suggestive feature (REM-sleep-behavior disorder, RBD) information was available in seventy-nine patients (47 males, age:75.7±6.4, MMSE 22.1±5.1). The control group (CTR) was derived with a case-control design matching for age and gender from 156 FDG-PET scans from the Italian Normative-database (AIMN-FDG-PET). SPM8-two-sample t-test was used to compare CTR with the whole DLB group as well as with patients' subgroups according to the presence/absence of disease features. Age, gender and center were used as nuisance. To account for disease severity, analyses were repeated by including MMSE as a further nuisance. P<0.05 family-wise-error-corrected was considered significant. **Results**: Disease features at the time of FDG-PET were as follows: fluctuations (FLUC+) were present in 59%, Visual hallucinations (VH+) in 60%, Parkinsonism (PK+) in 76%, RBD (RBD+) in 39% of the patients. The whole DLB group was characterized by a large hypometabolic pattern involving occipital, posterior parietal, dorsolateral frontal cortex (DLFC), precuneus and caudate nuclei in both hemispheres. Looking at comparisons of single subgroups versus CTR, hypometabolism in bilateral posterior parietal cortex and precuneus was expressed in all clinical subtypes. A more extended occipital hypometabolism was evident in VH+ patients even after correction for MMSE score. DLFC hypometabolism was found in FLUC+ but not in FLUC- subgroup. This finding did not survived after correction for MMSE. The involvement of a larger portion of bilateral ventro-lateral and DLFC cortex was evident in PK+, not in PK- subgroup. RBD+ was the subgroup showing the wider cluster of hypometabolism in bilateral occipital, parietal, DLFC as compared to CTR even after correction for MMSE. **Conclusion**: We demonstrated in the largest available cohort of DLB patients ever studied with FDG-PET

that the hypometabolic pattern involving posterior-parietal cortex and precuneus is common to all DLB clinical subtypes. Occipital hypometabolism is a clinical correlate of VH irrespective of disease severity. The occurrence of RBD seems to reflect of more malignant phenotype in terms of extension of neurodegeneration, regardless of the severity of cognitive impairment. The highlighted patterns can represent the seeds for a functional-metabolic network-analysis in DLB.

OP-368

Diagnosis of Alzheimer's Disease Through Identification of Abnormality Patterns in Molecular Brain Imaging

N. Burgos[1,2], J. Samper-González[1,2], A. Bertrand[1,2,3], M. Habert[4], S. Ourselin[5,6], S. Durrleman[1,2], M. Cardoso[5,6], O. Colliot[1,2,3]; [1]Inria, Aramis project-team, Paris, FRANCE, [2]Sorbonne Universités, UPMC Univ Paris 06, Inserm, CNRS, ICM, Paris, FRANCE, [3]Pitié-Salpêtrière Hospital, Neuroradiology, Paris, FRANCE, [4]Pitié-Salpêtrière Hospital, Nuclear Medicine, Paris, FRANCE, [5]University College London, Translational Imaging Group, London, UNITED KINGDOM, [6]University College London, Dementia Research Centre, London, UNITED KINGDOM.

Background: In machine learning classification methods developed for dementia studies, neuroimaging features, e.g. glucose consumption extracted from PET images, are often used to draw the border that differentiates normality from abnormality. However, these features are affected by the anatomical and metabolic variabilities present in the population, which acts as a confounding factor making the task of finding the frontier between normality and abnormality very challenging. **Methods:** To reduce the confounding impact of these variabilities when trying to distinguish disease versus normal ageing, we developed a method able to extract for each individual the signal characteristic of abnormality from 18F-FDG PET data. Instead of comparing the patient's PET image to a population of healthy controls as usually done, this framework consists of creating a patient-specific model of healthy PET appearance, and comparing the patient's PET image to the model via a Z-score [1]. The resulting voxel-wise Z-score map can be interpreted as an abnormality map, as it statistically evaluates the localised deviation of the patient-specific uptake with respect to the healthy uptake distribution. We applied this method to 298 ADNI2 subjects (103 cognitively normal, 105 late MCI and 90 Alzheimer's disease subjects). The abnormality maps generated with the proposed method were then used as features to feed a classification algorithm based on linear support vector machines. We compared the classification results obtained using the abnormality maps to the classification results obtained using features from the native PET images, and using state-of-the-art Z-maps. **Results:** The balanced accuracy obtained with the proposed method when differentiating CN from late MCI and AD (80.5% and 91.6%, respectively) was found to be higher than the balanced accuracy obtained using PET SUVR values (78.3% and 88.9%) and the state-of-the-art Z-maps (78.7% and 89.6%) as features. The same trend was observed when differentiating amyloid positive from amyloid negative subjects (73.9% vs 71.5% and 71.4%). **Conclusions:** The high

classification accuracy obtained when using the abnormality maps as features demonstrates that the proposed pipeline is able to extract for each individual the signal characteristic of dementia from FDG PET data. Instead of trying to find the frontier between normality and abnormality at the population level, by transporting the problem to the individual level, the proposed method appears to offer a more effective way of differentiating dementia stages. References: [1] Burgos et al.: Subject-specific models for the analysis of pathological FDG PET data. In: MICCAI 2015, pp.651-658 (2015)

---

910 Monday, October 23, 2017, 14:30 - 16:00, Hall G2

Conventional & Specialised Nuclear Medicine: Infection & Inflammation

OP-369

Role of 18Fluorine-Fluorodeoxyglucose positron emission tomography/computed tomography in the diagnosis of endocarditis: a bicentre study on 84 patients

P. Ferro[1], D. Albano[2], C. Popescu[3], M. Bertoli[4], I. Cersosimo[5], F. Bertagna[4], R. Sara[3], G. Giubbini[4], C. Rossetti[3]; [1]Università Milano-Bicocca, Ospedale Niguarda Ca' Granda, Milano, ITALY, [2]Università Milano-Bicocca, Spedali Civili, Brescia, ITALY, [3]Ospedale Niguarda Ca' Granda, Milano, ITALY, [4]Spedali Civili, Brescia, ITALY, [5]Demographics Pro, Beijing, CHINA.

Purpose: diagnosis of infective endocarditis (IE) is challenging and involves many different tools. The latest European Society of Cardiology guidelines introduced Nuclear Medicine imaging as a diagnostic test in patients with suspected IE. The aim of this study was to assess the role of 18F-FDG-PET/CT in the diagnosis of IE, considering qualitative and semiquantitative analysis of the images, in both native (NV) and prosthetic (PV) valves. **Methods:** 84 patients (54 male, 30 female, age range 20-94, mean 62) with suspected IE who underwent 18F-FDG-PET/CT between 2010 and 2017 were retrospectively analyzed. Clinical presentation, valve type, C-reactive-protein (CRP) and white blood cells (WBC) levels, blood-cultures, ongoing antibiotic therapy, trans-thoracic (TTE) and trans-oesophageal (TEE) echocardiography results were collected for each patients. 18F-FDG-PET/CT results were correlated with the diagnosis of endocarditis by an expert team after follow up (mean 14 months) or the Duke pathological Criteria when tissue was available. Qualitative and semiquantitative (SUV max, SUV mean, valve-to-myocardium-ratio) analysis were carried out on 18F-FDG-PET/CT images with and without attenuation correction. Statistical analysis was carried out with chi-squared test and logistic regression; p-value of ≤0.05 was considered statistically significant. **Results:** on qualitative analysis 18F-FDG-PET/CT resulted positive in 26,2% (22 patients) and negative in 72,6% (61 patients). In 1 patient the examination was inconclusive. We found a statistically significant correlation between positive 18F-FDG-PET/CT on qualitative analysis and positive blood-culture or fever (even tough fever appears in 50 patients with negative 18F-FDG-PET/CT). 65% of patients with

PV resulted positive, versus 25% with NV. In 20 cases TEE was inconclusive: in 3 cases 18F-FDG-PET/CT resulted positive (true positive), in 17 negative (respectively 15 true negative and 2 false negative). In 4 cases 18F-FDG-PET/CT subverted TEE results according to modified Duke Criteria : 1 patient from rejected to definite IE, 3 from definite to rejected IE (all cases had follow up confirmation). Mean SUVmax, SUVmean, valve-to-myocardium-ratio were higher in prosthetic valve (overall mean respectively 5.94, 4.05, 2.89; PV respectively 6.38, 4.29, 3.04). No statistically significant correlation was found between any parameter of quantitative analysis and CRP/WBC level, ongoing antibiotic therapy or recurrence of endocarditis in the follow up. **Conclusion:** 18F-FDG-PET/CT is useful in the diagnosis of suspected IE, reducing the cases classified as possible by modified Duke Criteria, especially in PV. Qualitative analysis plays a central role in the diagnosis, while further investigation must be done for a better understanding of the role of quantitative analysis.

OP-370

Digestive incidentalomas in FDG-PET/CT images of patients with infectious endocarditis; relationship with the involved microorganisms

J. J. Ardila, A. Rotger, L. Reguera, M. L. Lozano, J. Ardila, J. Orcajo, C. Duran, A. Mari, R. Pascual, J. C. Alonso; Hospital General Universitario Gregorio Marañon, Madrid, SPAIN.

Purpose: To determine the frequency of digestive incidentalomas and its relationship with neoplasias and other colorectal diseases in patients who underwent FDG PET/CT for infectious endocarditis caused by a variety of microorganisms. **Methods:** This is a retrospective study of patients with FDG-PET/CT imaging perfomed under the indication of infectious endocarditis between January 2013 to January 2017 in whom colo-rectal FDG uptake was reported. We describe the nature of the colorectal disease (confirmed with endoscopy/histopathology), the image findings and the microorganism involved. **Results:** 150 endocarditis PET CT reports were revised, obtaining gastro-intestinal findings in 18 patients. Mean age was 75 years, 13 were men and 5 women. The involved microorganisms were: S.bovis (2/18), E.faecalis (5/18), S.viridans (5/18), E.coli (2/18) and others (4/18). In the PET image the uptake was diffuse in 6 of the cases and focal in the 11 remaining. Single foci were found in 9 reports and multiple in 9. Mean SUVmax was 6,2. The morphology of the lesions was: polypoid structures in 7 patients, wall thickening in 6 and uptake without radiological translation in the remaining 5. Histologically, benign lesions were found in 55,6%, premalignant in 27,7% and malignant lesions in 16,7%. Excluding S.bovis, the frequency of onset was 37,5% of premalignant lesions and 12,5% of malignant lesions. **Conclusions:** Although the relationship between S.bovis endocarditis and colorectal lesions is well known, there is also a high prevalence of premalignant pathology and colorectal carcinoma in endocarditis caused by other microorganisms, especially E.faecalis and S.viridans. Its early detection is relevant for therapeutic management and prognosis. The need to perform a PET in this type of patients seems mandatory (prevalence of 12,5%).

OP-371

Role of 18FDG PET/MR in the diagnosis and follow-up of retroperitoneal fibrosis

P. Zucchetta, F. Crimi`, C. Lacognata, R. Marcolongo, D. Cecchin, V. Bodanza, J. Doraku, D. Miotto, F. Bui; University Hospital - Padova, Padova, ITALY.

Retroperitoneal fibrosis (RPF) is an insidious disease. Vague symptoms and lack of specific biochemical markers lead often to delayed diagnosis and difficulties in treatment evaluation. Diagnosis is usually based on CT and/or MRI, but FDG PET has been proven useful particularly in assessing disease activity during treatment. We investigated the role of integrated FDG PET/MR in the diagnosis and management of RPF. We evaluated 38 patients (F 11, M 27, mean age 64 years, min 45, max 84) by integrated ^{18}F-FDG PET/MR (Biograph mMR, Siemens). The scan was repeated during the follow-up in 14 patients (total 52 examinations). Imaging was performed following the EANM guidelines for FDG imaging and included the standard Dixon sequence for attenuation correction, transverse T1-weighted, T2-weighted (HASTE) images and Diffusion Weighted Images (DWI) with calculation of apparent diffusion coefficient (ADC) maps. Images were reviewed for disease activity ad extension. Pathological FDG uptake was scored as 0- absent, 1- present but less than liver uptake, 2- present and greater than liver uptake. Suspected RPF was the clinical indication for 14 scans, the remaining (38) were performed for treatment evaluation. Mean duration of disease was 41 months (min 1 month, max 18 years). Pathological periaortic FDG uptake was detected in 24 scans (7/14 diagnostic scans, 16/38 follow-up scans) and was concordant with MR signs of active inflammation (T2 hyperintensity and diffusion restriction signs on DWI) in 22/24 scans. FDG PET and MRI were both negative in 21 scans. In 9 cases abnormal MR findings did not correspond to hypermetabolic activity.PET/MR findings prompted the start/intensification of pharmacological treatment in 8/14 patients who repeated the scan during the follow-up, leading to a reduction/disappearance of inflammation in the second exam. Basal PET/MR documented a good control of the disease in 6/14 patients, allowing a safe tapering of the treatment. The stability of the situation was confirmed in the follow-up scans, corroborating the predictive value of ^{18}F-FDG PET/MR.[18]F-FDG PET/MR appears a promising opportunity for the diagnosis and follow-up in RPF patients. The combination of metabolic and morpho-functional parameters seems to be particularly effective in evaluating treatment response, allowing a better tailoring of corticosteroid therapy.

OP-372

Comparison of F18 FDG and Ga68 citrate PET/CT in the evaluation of patient with tuberculosis

A. O. Ankrah[1,2], I. O. Lawal[1], T. M. G. Boshomane[1], M. Vorster[1], H. C. Klein[2], A. W. M. J. Glaudemans[2], M. M. Sathekge[1]; [1]University of Pretoria, Pretoria, SOUTH AFRICA, [2]University Medical Center Groningen, Groningen, NETHERLANDS.

PET/CT with F18 FDG is increasingly playing a promising role in the evaluation of patients with tuberculosis. Ga68 citrate PET/CT is a PET tracer that images infection and inflammation and preliminary studies have suggested it may be useful in the evaluation of tuberculosis. The availability of generator produced Ga68 citrate within a department makes it an attractive alternative to F18 FDG. There is currently no literature available comparing the usefulness of these two tracers in the evaluation of tuberculosis. **Aim:** To compare the usefulness of F18 FDG and Ga68 citrate PET/CT in patients with tuberculosis. **Methods:** Patients with confirmed tuberculosis were prospectively included in the study. Patients underwent an F18 FDG PET/CT scan and a Ga68 citrate scan within one week of each other. The PET/CT scans were acquired on a Siemens biograph 40 PET/CT. The patients were scanned after l hour of injection of the tracer and scan were interpreted by 2 nuclear physicians. **Findings:** Twenty-six PET/CT scans were acquired in eleven patients at different stages of tuberculosis therapy. Six (54.5%) of the patients were male and the mean age of patients was 34.4 ± 7.8 years. 83 lesions with tracer uptake by either F18 FDG or Ga68 citrate were identified in the twenty-six PET/CT scans. F18 FDG PET/CT detected eighty-two (98.8%) with Ga68 citrate detecting seventy 84.3% of these lesions. The SUV max was significantly higher for the F18 FDG PET 7.67 $\pm$ 3.54 compared to Ga68 citrate PET which was 3.14 $\pm$ 2.25 ($p < 0.0001$). On visual inspection, the F18 FDG scans yielded much better target to background ratio compared to the Ga68 citrate which was poor in areas with a high background such as around the blood vessel in the mediastinum. One lesion demonstrated tracer uptake on Ga68 citrate with no corresponding uptake on F18 FDG PET/CT suggesting there may be a complimentary role for both F18 FDG and Ga68 citrate in the evaluation of TB. Although not completely assessed in this study, in one patient who had completed therapy neither F18 FDG nor Ga 68 citrate demonstrated tracer uptake suggesting a role for Ga68 PET/CT in monitoring response to therapy. **Conclusion:** F 18 FDG PET/CT is superior to Ga 68 citrate in the evaluation of patients with pulmonary TB. Ga 68 citrate may provide complimentary information to F18 FDG study. Further evaluation of the role of Ga68 citrate in response to therapy is needed.

OP-373

The diagnostic value of ^{18}F-FDG-PET /CT, MRI and ^{18}F-FDG-PET/MRI in suspected vertebral osteomyelitis - a prospective study

l. Kouijzer[1,2], H. Scheper[3], J. de Rooy[1], J. Bloem[3], M. Janssen[1], L. van den Hoven[2], A. Hosman[1], L. Visser[3], W. Oyen[1,4], C. Bleeker-Rovers[1], L. de Geus-Oei[3,2]; [1]Radboudumc, Nijmegen, NETHERLANDS, [2]University of Twente, Enschede, NETHERLANDS, [3]LUMC, Leiden, NETHERLANDS, [4]The Institute of Cancer Research and Royal Marsden NHS Foundation Trust, London, UNITED KINGDOM.

Introduction: The purpose of this study was to compare the diagnostic value of ^{18}F-fluorodeoxyglucose positron emission tomography with combined computed tomography (^{18}F-FDG-

PET/CT), magnetic resonance imaging (MRI), and fused ¹⁸F-FDG-PET/MRI in diagnosing vertebral osteomyelitis. **Subjects and Methods:** From November 2015 until December 2016, 32 patients with suspected vertebral osteomyelitis were prospectively included. All patients underwent both ¹⁸F-FDG-PET/CT and MRI within 48 hours. ¹⁸F-FDG-PET and MRI images were fused by soft ware fusion. All images were independently reevaluated by 2 radiologists and 2 nuclear medicine physicians. **Results:** For ¹⁸F-FDG-PET/CT, sensitivity, specificity, PPV, and NPV in diagnosing vertebral osteomyelitis were 100%, 90.9%, 95.5%, and 100%, respectively. For MRI, sensitivity, specificity, PPV, and NPV were 95.2%, 90.9%, 95.2%, and 90.9%, respectively. For ¹⁸F-FDG-PET/MRI, sensitivity, specificity, PPV, and NPV for diagnosing vertebral osteomyelitis were 100%, 90.9%, 94.4%, and 100%. MRI detected more epidural/spinal abscesses compared to ¹⁸F-FDG-PET/CT. ¹⁸F-FDG-PET/CT is more valuable in detecting metastatic infectious foci. **Conclusion:** ¹⁸F-FDG-PET/CT and MRI are both valuable techniques in diagnosing vertebral osteomyelitis. An important advantage of ¹⁸F-FDG-PET/CT is the early detection of vertebral osteomyelitis and the visualization of metastatic infection, especially in patients with bacteremia. MRI is more sensitive in detection of smaller epidural abscesses. Combined ¹⁸F-FDG-PET/MRI in a 'one-stop-shop' can incorporate these qualities and should therefore become the imaging technique of choice in suspected vertebral osteomyelitis.

OP-374

¹⁸F-FDG PET/CT as a diagnostic tool for infection assessment in post-traumatic non-unions

L. Antunovic, N. Trenti, L. Di Mento, E. Malagoli, G. Cusato, L. Balzarini, A. Kirienko, A. Chiti, M. Berlusconi; *Humanitas Clinical and Research Hospital, Rozzano, ITALY.*

Introduction: Infection is a common complication in trauma patients, especially in cases with open fractures. Sometimes clinical and radiological presentations of the infection result unclear, leading to difficulties in patient management and therapy decisions. We aimed to evaluate the diagnostic performance of ¹⁸F-FDG PET/CT in detecting infection as cause of post-traumatic bone fracture non-union. **Subjects and methods:** We retrospectively reviewed 46 patients (13 females, 33 males, age 52±19), treated in our trauma center, who underwent pre-operative 18F-FDG PET/CT scan for suspected infection in the period between January 2011 and January 2017. Clinical history, diagnostic examinations, laboratory and microbiology results and patient outcome data were collected and analyzed. A visual analysis of PET/CT scans was performed by an experienced nuclear medicine physician. The results of PET/CT were confronted with microbiological examination of the specimens taken intraoperatively. Finally, diagnostic performance of ¹⁸F-FDG PET/CT was determined. **Results:** Twenty-six patients were negative for infection, while twenty patients had positive intraoperative microbiological results. PET was able to detect the infection in 14 cases, while 6 out of 20 infected patients had no significant evidence of disease on PET images and were considered as false negatives. In 6 cases PET

showed false positive results; 20/26 disease-free patients were correctly detected by PET. There was agreement between PET results and final diagnosis in 34 out of 46 cases (74%). Sensitivity, specificity, accuracy, positive predictive value and negative predictive value of ¹⁸F-FDG PET/CT were 70%, 77%, 74%, 70% and 77% respectively. Likelihood ratio for a positive test (LR+) was 3.04. Likelihood ratio for a negative test resulted 0.39. Pre-test probability of disease was 44%; post-test probability of diseas based on LR+ resulted 71%, while post-test probability based on LR- was 24%. **Conclusions:** Our data indicate FDG PET/CT as a valuable diagnostic tool in the evaluation of post-traumatic infection. Larger datasets are needed to further corroborate our preliminary evidence.

OP-375

Relationship between WBC scintigraphy with Tc99m HMPAO-labeled leucocytes and clinical outcome in patients with suspected prosthetic joint infections

T. Pellegrino[1], M. Petretta[2], V. Cantoni[3], V. Piscopo[3], G. De Matteis[3], S. Pellegrino[3], A. Cuocolo[3]; [1]Institute of Biostructure and Bioimaging, National Council of Research, Naples, ITALY, [2]Department of Translational Medical Sciences, University Federico II, Naples, ITALY, [3]Department of Advanced Biomedical Sciences, University Federico II, Naples, ITALY.

Purpose: WBC scintigraphy is considered the gold standard nuclear imaging for diagnosing infections. However, its role in the follow-up has not yet completely elucidated. We assessed the relationship between WBC scintigraphic findings and clinical outcome in patients with suspected hip or knee prosthesis infections. **Materials and Methods:** We studied 106 patients (40 men, age 63±13 years) who underwent WBC scintigraphy with Tc-99m HMPAO-labeled leucocytes for suspected hip or knee prosthesis infections. Whole-body and spot planar images were obtained 4 hours and 24 hours after reinfusion of 555 MBq of Tc-99m HMPAO-WBC. Two nuclear medicine physicians visually reviewed all WBC imaging studies. Scans were classified as "negative for infection" if no uptake was present in both early and late images or when the uptake was the same in both images, or when the uptake decreased over time and "positive for infection" when the uptake showed an increase between early and late images or when the size of the area with enhanced uptake showed an enlargement. In patients with positive result at first WBC scintigraphy, antibiotic therapy was started after imaging and a second study was performed. **Results:** At the time of the first WBC scintigraphy prosthesis infection was suspected based on clinical examination (local or general symptoms) and on blood tests including WBC counts, C-reactive protein and erithrocyte sedimentation rate. These parameters were also considered as criteria to define the outcome of patients. The first WBC scintigraphy was negative in 24 (23%) and positive in 82 (77%) of the patients. Among the 82 patients with a positive first WBC scan, an improvement of clinical symptoms and/or of blood chemistry was present in 13 (56%) of the 23 patients with a negative WBC scan at follow-up. Moreover, 43 (73%) of the 59 patients with a positive WBC scan at follow-up did not show improvement of clinical symptoms and/or of blood

chemistry (chi-square 4.3; p<0.05). Conversely, among the 24 patients with a negative first WBC scan, there were no significant differences between clinical symptoms and/or of blood chemistry and the results of second WBC scan (chi-square 0.17; p= 0.67). **Conclusions:** Our results demonstrate that in patients with suspected prosthesis infections the presence of clinical symptoms and/or of blood chemistry signs is associated with a positive WBC scintigraphy. In addition, this imaging technique seems to be a useful noninvasive tool for the follow-up of patients undergoing antibiotic therapy.

OP-376

Typical uptake distribution patterns that help the diagnosis of polymyalgia rheumatica on FDG-PET/CT

K. Nakatani, S. Yuge, K. Yoshino, T. Koyama; Kurashiki Central Hospital, Kurashiki, JAPAN.

Purpose: Polymyalgia rheumatica (PMR) is a rheumatic disease characterized by widespread aching and stiffness in elderly people. The diagnosis of PMR is often challenging, since the clinical features of PMR and the laboratory findings can also be observed in other various inflammatory conditions. PMR is considered to have specific patterns about the affected sites, and FDG-PET/CT has an advantage for assessing the disease activity of each site. The purpose of this study was to identify the patterns of FDG uptake that contribute to the diagnosis of PMR. **Subjects and Methods:** The study population included were 60 patients (mean age = 72 ± 10, male/female = 20/40) who underwent FDG-PET/CT scans for work-up examination of suspected PMR or some kinds of arthritis, enthesitis, or myopathy between July 2007 and March 2016. Final diagnoses were made by board-certified rheumatologists. The incidence of significant FDG uptake, higher than mediastinal blood pool, of the following sites were compared between PMR patients and the others — wrists, elbows, shoulders, sternoclavicular joints, acromioclavicular joints, spinous processes, ischial tuberosities, and greater trochanters. For the spinous processes, the incidence of Y-shaped uptake along the interspinous bursa was also evaluated. **Results:** 16 of 60 patients (mean age = 75 ± 10, male/female = 1/15) had definitive diagnosis of PMR by the rheumatologists. The incidence of significant FDG uptake in the definitive PMR group versus the incidence in the other group was 6% vs. 23% (p = 0.26) for wrists; 6% vs. 18% (p = 0.42) for elbows; 88% vs. 50% (p = 0.015) for shoulders; 88% vs. 25% (p < 0.01) for sternoclavicular joints; 25% vs. 18% (p = 0.72) for acromioclavicular joints; 81% vs. 52% (p = 0.072) for spinous processes; 69% vs. 27% (p = 0.006) for ischial tuberosities; and 81% vs. 48% (p = 0.037) for greater trochanters. As for the spinous processes, patients with definitive PMR showed significantly higher incidence of Y-shaped uptake than the other patients (38% vs. 9%; p = 0.016). **Conclusion:** FDG uptake distribution patterns and the shape of FDG accumulation can contribute the diagnosis of PMR. Significant FDG uptake at sternoclavicular joints is one of the characteristic findings in patients with PMR as well as the uptake at shoulders, ischial tuberosities, and greater trochanters. Y-shaped spinous process uptake may be one of the specific findings for PMR.

CME 8 - Radionuclide Therapy/Radiopharmacy/Dosimetry: Clinical Trial Design for Radionuclide Therapy

OP-377

General Aspects of Clinical Trial Design
A. Kluge; ABX - CRO advanced pharmaceutical services Forschungsgesellschaft m.b.H., Dresden, GERMANY.

OP-378

Regulatory Affairs in Radiopharmacy
C. Decristoforo; Universitätskliniken - Landeskrankenhaus Innsbruck, Medizinische Universität Innsbruck, Universitätsklinik für Nuklearmedizin, Innsbruck, AUSTRIA.

OP-379

Dosimetry for Clinical Trials
R. Gregory; The Royal Marsden NHS Foundation Trust, Institute of Cancer Research, London, UNITED KINGDOM.

Joint Symposium 8 - EANM/EANO: High Grade Glioma

OP-380

Tumour Initiation, Progression and Metabolism
R. Bjerkvig; University of Bergen, KG-Jebsen Brain Tumour Research Centre, Department of Biomedicine, Bergen, NORWAY.

OP-381

Clinical Features and Use of Amino-Acid PET
I. Law; Rigshospitalet, Dept of Clinical Physiology, Nuclear Medicine and PET, Copenhagen, DENMARK.

OP-382

State of the Art Neurosurgical Treatment
J. C. Tonn; Ludwig-Maximilians-Universität, Dept. Neurosurgery, Munich, GERMANY.

CTE 4 - Joint Session with CAMRT: Radionuclide Production

OP-383

Reactor Produced Radioisotopes Used in Nuclear Medicine
F. Rösch; Johannes Gutenberg-University Mainz, Institute of Nuclear Chemistry, Mainz, GERMANY.

OP-384

Cyclotron Produced Radioisotopes Used in Nuclear Medicine
F. Alves; Coimbra Universtiy, Institute of Nuclear Sciences Applied to Health, Coimra, SPAIN.

OP-385

Molybdenum-99 World Supply
F. Couillard; CAMRT, Ottawa, CANADA.

Do.MoRe: Dosimetry in Thyroid Disease

OP-386

First biosafety, biodistribution and dosimetry study of the gastrin analogue ¹¹¹In-CP04 in medullary thyroid cancer. Phase I clinical trial, GRANT-T-MTC

M. Konijnenberg[1], P. A. Erba[2], R. Mikolajczak[3], C. Decristoforo[4], H. Maecke[5], T. Maina-Nock[6], K. Zaletel[7], P. Kolenc-Peitl[7], I. Virgolini[4], E. Przybylik-Mazurek[8], C. Rangger[4], M. Trofimiuk-Muldner[8], K. Skorkiewicz[8], L. Ležaić[7], L. Scarpa[4], G. Di Santo[4], A. Sowa-Staszczak[8], M. de Jong[1], L. Froberg[1], P. Garnuszek[3], D. Pawlak[3], G. Göbel[4], B. Nock[6], D. Bergant[9], A. Hubalewska-Dydejczyk[8]; [1]Erasmus MC, Rotterdam, NETHERLANDS, [2]Nuclear Medicine, Azienda Ospedaliero Universitaria Pisana, Pisa, ITALY, [3]Radioisotope Center POLATOM, NCBJ, Otwock-Świerk, POLAND, [4]Nuclear Medicine, Innsbruck Medical University, Innsbruck, AUSTRIA, [5]Nuclear Medicine, University Hospital Freiburg, Freiburg, GERMANY, [6]Molecular Radiopharmacy, INRASTES, NCSR Demokritos, Athens, GREECE, [7]Nuclear Medicine, University Medical Centre Ljubljana, Ljubljana, SLOVENIA, [8]Chair and Department of Endocrinology, Jagiellonian University, Medical College, Kraków, POLAND, [9]Institute of Oncology, Ljubljana, SLOVENIA.

Introduction: The current therapeutic options in medullary thyroid cancer (MTC) patients are very limited. Although many drugs are currently under investigation an efficient treatment regimen for advanced MTC is not available yet. We herein present first promising results of the clinical part of the GRAN-T-MTC project realized under the ERA-NET TRANSCAN. First, we aimed to assess the safety of iv administration of the gastrin analogue CP04 (DOTA-(DGlu)$_6$-Ala-Tyr-Gly-Trp-Met-Asp-Phe-NH$_2$) in an amount suitable for Peptide Receptor Radionuclide Therapy, based on the high cholecystokinin subtype 2 (CCK-2)-receptor expression in MTC. Then, we were interested to acquire first biodistribution and dosimetry data of ¹¹¹In-CP04 in MTC patients, motivated by promising results from the preclinical part of the study [1,2]. **Materials and Methods**: 4 patients (aged: 30 - 59 years) with progressive/metastatic MTC were enrolled, 3 with progressive/metastatic MEN2A-related MTC with positive ¹⁸F-FDG PET-CT/CT/MRI and one (sporadic MTC) with short calcitonin doubling time. Basal calcitonin levels ranged between 279 and 824 pg/ml. During the first clinical phase of the trial each patient received ¹¹¹In-CP04 (200 MBq) using 2 different peptide kits: a) a "diagnostic" kit containing 10 μg CP04 (kit-A) and b) a "therapeutic" kit containing a higher peptide mass of 50 μg (kit-B) [1]. Biodistribution and dosimetry data were acquired based on serial planar and SPECT/CT images. **Results**: No side effects were observed during iv injection of ¹¹¹In-CP04 from either kit. In all patients ¹¹¹In-CP04 uptake was confirmed in MTC lesions. Blood and organ clearance curves for both kits were similar. The blood clearance proceeded with a terminal half-life of 38±16 min for kit-A and 22±15 min for kit-B. The effective dose ED was ED = 0.052±0.018 mSv/MBq for both kits. Kit-B led to the highest organ absorbed doses in bladder, kidneys and colon, for ¹⁷⁷Lu: 0.54±0.06, 0.32±0.13 and 0.28±0.08 Gy/GBq,

respectively. **Conclusions**: Findings from this ongoing, phase I clinical-trial have demonstrated the safety of CP04 iv-injection in both diagnostic and therapeutic kit formulations in MTC patients. Furthermore, ¹¹¹In-CP04 could visualize all active disease sites compared to established modalities. The therapeutic use of ¹⁷⁷Lu labeled CP04 will be most probably safe up to high cumulative activity (50 GBq). **Sources of Support** GRAN-T-MTC, TRANSCAN, JTC 2011: "Validation of biomarkers for personalised cancer medicine" FP7. **References**: 1. Maina T, Konijnenberg MW, KolencPeitl P, et al. Eur J Pharm Sci. 2016;91:236-42. 2. Pawlak D, Rangger C, KolencPeitl P, et al. Eur J Pharm Sci. 2016;85:1-9

OP-387

Lesion dosimetry in metstatic thyroid cancer treated with 131-I: method and preliminary results

E. Richetta, C. Cutaia, M. Pasquino, L. Sacco, A. Codegone, R. Pellerito, M. Stasi; AO Ordine Mauriziano di Torino, Turin, ITALY.

Introduction: A dosimetric approach to metastatic thyroid cancer treated with ¹³¹I should take into account not only the dose to the organ at risk (red marrow) but also to metastasis, often not evaluated because of time consuming and staff involvement. A SPECT-TC dose calculation method is proposed and verified. Dosimetry on a preliminary patients group is performed and the operating protocol standardized. **Subjects & Methods:** SPECT-TC Siemens Intevo was calibrated with a phantom (spheres 11.5,5.6,1.1 ml, cylinder 130 ml) filled with liquid ¹³¹I (13 MBq/ml). Acquisition (64views, 20s/view, circular-orbit, 256x256, Iterative*Flash3D* SC-AC corrected) on successive days allowed partial volume effects, dead-time and detector radius (25÷33cm) corrections in order to calculate activity and dose, whose accuracy was verified. Dosimetry was performed on 9 patients (6M,3F) after the therapeutic administration (for 2 patients in pre-therapy phase 74 MBq as well): 4 SPECT-TC were acquired (4÷6, 24, 48,96÷144 h p.i.). Metastases VOIs delineation with CT-based and threshold method allows dose calculation with MIRD spheres model on 37 lesions (24 bone, 7 lymph node, 6 pulmonary). **Results:** Calibration factors (cylinder:25.4, smallest sphere:1.4 kcts/MBq) confirmed partial volume effects (130ml:100%, 11ml:75%, 5.5ml:58%, 1.1ml:6%) and radius dependence (~10%). Dead-time strongly influences counts in early acquisition (up to 17 %) and it was corrected (fit (r² 0.99) between equipment's dead-time index and true counts). Mean accuracy on activity -15% [-9% ÷ -24%] and dose -13 % [-9 % ÷ -18%] for volumes larger than 2.5 cc (up to 70% for smaller volumes not suitable for dose estimation) validates the dosimetric method, according to literature (MIRD24). Dose to lesions per activity unit varies widely among patients (mean ± 1dev.st 26±38, range 0.1÷189 Gy/GBq) and within the same patient (up to +583 %) also for the same type of metastasis, confirming the need of an individualized dosimetry. Volume segmentation influences the dose: CT-based method is strongly recommended and gives in mean - 4.9 % [+0.3 ÷ -17 %] lower results compared to the isocontour threshold one. In-therapy dose values show high differences (up to -126%) compared to pre-therapy results, whose efficacy must be further investigated with more patients

also in terms of optimal activity to be administered to simulate the treatment. **Conclusions:** Lesion dosimetry of metastatic thyroid cancer treated with radioiodine can be performed accurately with SPECT-TC. The dosimetric approach provides to the physician a fundamental tool to optimize the treatment as required by the national and European laws.

OP-388

Analysis deviation of the absorbed dose of thyroid for Graves' disease with hyperthyroidism treated by iodine-131 with simplified Quimby-Marinelli-Hine formula method

Y. Chen; Quanzhou 1st Hospital, Quanzhou, CHINA.

Purpose: Deviation of the absorbed dose of thyroid (TD) was evaluated in Graves' diseases with hyperthyroidism treated by iodine-131 with the simplified Quimby-Marinelli-Hine formula method (sQMHF). **Subjects & Method:** Continuous 45 Graves' disease with hyperthyroidism (12 male, 33 female, 43.9y±12.9y) were included in this study. Thyroid masses (TM) were measured by ultrasound. Then, the average energy ($\bar{E}$) being deposited in thyroid per decay of iodine-131 was calculated. Radioiodine uptake (*RAIU*) were tested at 2h, 4-6h, 24h, 48-72h, and 96-168h, then $T_{1/2eff}$ and resident time (*RT*) was computed. According to the sQMHF, a prescribed TD set at 75Gy requires 3.7MBq/g of iodine-131 corrected by $RAIU_{24h}$. Then the real TD was computed through Standard Operational Procedures for dosimetry (SOPD) prior to radioiodine therapy of benign thyroid disease that was recommended by European Association of Nuclear Medicine (EANM), and its error was recorded as Res . The data were analyzed by *t*-test. **Results:** The TM was (35.2±22.5) g, while $\bar{E}$ was (2.83±0.05) Gy•g•d^{-1}•MBq^{-1}. The $RAIU_{24h}$, $T_{1/2eff}$ and RT was 0.543±0.132, (3.46±0.90) d, (3.15±1.15) d, respectively. The actual TD was(89.4±9.6)Gy and its Res was 5.1%±2.9%, when the prescribed TD set at 75Gy with sQMHF. They were significant difference (*t*-value 9.84, *P*<0.01) for the sQMHF ignores the absorbed dose deposited in thyroid during the first 24h which is included in the SOPD. The Res of actual TD was significantly less than the difference between actual and prescribed TD (*t*-value -32.4, *P*<0.01). **Conclusion:** When the activity of iodine-131 calculated by the sQMHF, the real TD was significantly larger than prescribed dose. The error of TD could be decreased by computing the activity of iodine-131 with SOPD. Key Words: Radioiodine uptake; effective half-life; residence time; absorbed dose

OP-389

Micro-scale Modeling for the Salivary Gland: Insights into Toxicity from ^{131}I Therapy for Thyroid Cancer

R. F. Hobbs[1], A. McGuffey[1], W. Jentzen[2], D. Plyku[1], A. Bockisch[2], G. Sgouros[1]; [1]Johns Hopkins University, Baltimore, MD, UNITED STATES OF AMERICA, [2]Universitaet Duisburg-Essen, Essen, GERMANY.

Objectives: Salivary gland toxicity is a quality of life concern in radioiodine treatment of thyroid cancer. Clinically observed toxicity is inconsistent with absorbed doses (AD) to the salivary glands calculated by absorbed fraction methods, nor by personalized Monte Carlo-based voxelized 3-dimensional radiobiological dosimetry (3D-RD) calculations, which includes accounting for dose rate effects as well as contribution to AD from outside the salivary glands. Micro-scale anatomical modeling has been proven to reconcile discrepancies between whole organ AD values and clinically or pre-clinically observed toxicities. **Methods**: We apply a micro-scale model to account for localization of radioiodine (or astatine) uptake. Uptake in the salivary glands has been shown to be primarily confined to the epithelial striated ducts which contain sodium iodine symporters. Dimensions of typical striated duct cells were obtained from the literature and S-values for the striated cells for various isotopes of iodine and astatine (^{131}I, ^{124}I, ^{123}I, ^{125}I, ^{211}At) used in clinical or pre-clinical scenarios were calculated using GEANT4 Monte Carlo. Based on the fraction of occupancy of these cells within the salivary glands, a grid of striated cells placed randomly in spheres of increasing size was used to simulate decay of activity in these cells from which ratios of striated duct AD and acinar cell AD to whole organ AD were calculated for these same isotopes. **Results**: S-values for striated duct to striated duct as well as striated duct to acinar cells as a function of distance from the striated duct were calculated, as were S-values for contents (saliva) inside the tube formed by the striated ducts to the same target cells. The grid-based Monte Carlo results showed a ductal cell AD to salivary whole organ AD ratio of 3.5 - 3.3 for ^{131}I and 14.6 for ^{211}At dependent on salivary gland size (5 - 25 ml). Ratios for ^{124}I, ^{123}I, ^{125}I were also calculated and AD distributions (DVHs) of the acinar cells were established for each isotope, normalized to whole organ AD. **Conclusions**: This is a significant step in quantifying the discrepancy between clinically observed toxicity and predicted toxicity based on whole organ AD values. This approach uses micro-scale dosimetry, which has been shown to explain similar discrepancies in different cases, particularly alpha-particle dosimetry. This study shows that while the salivary glands may be considered as parallel organs for external beam radiation, the physiology for iodine uptake means that for radiodine therapy, they have a more complex structure.

OP-390

Dose-response correlation in radioiodine therapy of hyperthyroidism from nodular thyroid disease

M. Pacilio[1], G. Ventroni[2], V. Frantellizzi[3], B. Cassano[4], E. Verdolino[4], T. Montesano[3], G. De Vincentis[3], L. Mango[2]; [1]Department of Medical Physics, Azienda Ospedaliera Universitaria Policlinico Umberto I, Rome, ITALY, [2]Department of Nuclear Medicine, Azienda Ospedaliera San Camillo Forlanini, Rome, ITALY, [3]Department of Radiological, Oncological and Anatomo Pathological Sciences, "Sapienza" University of Rome, Rome, ITALY, [4]Postgraduate School of Medical Physics, "Sapienza" University of Rome, Rome, ITALY.

Introduction: Radioiodine therapy of hyperthyroidism is a well-established modality of treatment, alternative to surgery. The EANM Dosimetry Committee recommends treatment optimization by pretherapeutic dosimetry based on the assess-

ment of the individual ^{131}I kinetics in the target tissue, after the administration of a tracer activity. Despite that, many clinicians still consider patient-specific dosimetry of doubtful value in this context, claiming that empiric methodologies or administration of fixed activities show analogous effectiveness, sparing time-consuming pretherapeutic studies. The aim of this work was to highlight the added value of patient-specific dosimetry in radioiodine therapy of hyperthyroidism from nodular thyroid disease. **Methods:** 374 patients affected by autonomous thyroid nodule and multinodular goitre underwent radioiodine therapy. All treated patients presented hyperthyroidism from blood tests (TSH, and/or FT3, FT4) before the treatment. Post-therapy follow-up lasted for at least 1 year. The healing was defined as absence of hyperthyroidism (as evidenced by blood tests) at 1 year from the therapy, after the first radioiodine treatment. 187 treatments were performed with an empiric methodology, not basing on a pre-treatment dosimetric study. 187 treatments were dosimetry-based, following the EANM Dosimetry Committee recommendations (collecting just three biokinetics points), and these include also 67 treatments based on a biologically effective dose (BED) prescription. In general, the use of the BED was also tested in the result analysis for all dosimetry-based treatments. Statistical analysis was performed by Mann-Withney and Chi-squared test, univariate receiver operating characteristics (ROC) analysis, and interpolation of dose-response data by a logistic model. **Results:** For the 120 treatments based on absorbed dose prescriptions, there were significant dosimetric differences between the unhealed and the healed group (p=0.0067), also when the absorbed dose values were converted in BED (p=0.0049), and the Area-under-curve (AUC) was 0.758 and 0.770, respectively. The absorbed dose/BED-response curves had regular trends with r-value of 0.980 and 0.984, respectively. The healing probability obtained from the BED-based treatments was not statistically different from that of treatments based on absorbed dose prescriptions (p=0.423). Considering the total 187 dosimetry-based treatments, the absorbed dose/BED-response curves confirmed regular trends with r-value of 0.979 and 0.977, respectively. The absorbed dose associated to a healing probability of 50% and 95%, was 42.6 Gy and 242.3 Gy, respectively. The probability of recurrence was 9.6%, exactly half of that associated to the empiric treatment group (19.3%, p=0.0081). **Conclusion:** Patient-specific dosimetry has proven to increase therapeutic effectiveness, reducing the recurrence frequency and the need of repeated treatments.

OP-391

First-in-human administration of the CCK-2 receptor agonist ^{177}Lu-PP-F11N in patients with metastasized medullary thyroid carcinoma - preliminary results of the "Lumed" trial

C. Rottenburger[1], G. Nicolas[1], L. McDougall[1], F. Kaul[1], E. Christ[1], R. Schibli[2], S. Geistlich[2], M. Béhé[2], D. Wild[1]; [1]University of Basel Hospital, Basel, SWITZERLAND, [2]Paul Scherrer Institut, Villigen, SWITZERLAND.

Aim: There is a clinical need to improve imaging and therapy of patients with medullary thyroid cancer (MTC). One possibility is

targeting the cholecystokinine-2 (CCK-2) receptor with radiolabeled gastrin analogues because MTC express CCK-2 receptors at a high incidence and density. Unfortunately, kidney and bone marrow toxicity precluded therapeutic applications of CCK-2 receptor specific compounds until now. The aim of this study is the feasibility testing of targeting CCK-2 receptors with the novel ^{177}Lu labelled gastrin analogue PP-F11N [DOTA-(DGlu)6-Ala-Tyr-Gly-Trp-Nleu-Asp-PheNH2] in six patients with metastasized MTC (ClinicalTrials.gov: NCT02088645). **Materials and Methods:** So far 2/6 patients received two injections of 1 GBq ^{177}Lu-PP-F11N, one injection without and the other one with Physiogel (Gelofusin) infusion for the evaluation of a possible strategy for nephroprotection. Planar scintigraphy and SPECT/CT scans were performed at several time points for up to 72 h post injection in order to calculate tumor- and organ doses using 3D voxel-based dosimetry (STRATOS software). Blood samples were taken for bone marrow dosimetry. ECG, blood count and blood chemistry were measured up to 12 weeks after the second administration of ^{177}Lu-PP-F11N in order to evaluate adverse events. **Results:** Apart from flushing, nausea and vomiting (grade 1 according to CTCAE version 4.0) at the time of injection, there were no adverse reactions observed. In both patients, multiple tumor localizations were visible on planar scintigraphic and SPECT/CT images. The median of the mean radiation dose to evaluated metastases was 9.97 Gy/GBq (range 3.29 - 19.5). The organ with the highest radiation dose was the stomach (median of the mean 2.08 Gy/GBq; range 1.75 - 2.85), followed by the kidneys. Intraindividual kidney radiation doses were lower when Physiogel was co-administered (patient 1: 1.04 versus 1.56; patient 2: 0.72 versus 1.08 Gy/GBq). The highest bone marrow dose was 0.0101 Gy/GBq. These data suggests that the administration of up to 3 cycles of 7.4 GBq ^{177}Lu-PP-F11N might be possible in individual patients before a dose limiting toxicity is reached, resulting in possible cumulative tumor doses of more than 400 Gy. **Conclusion:** The administration of ^{177}Lu-PP-F11N was safe in the first two examined patients without serious adverse reactions. Imaging and dosimetry of MTC metastases indicates tumor doses feasible for radionuclide therapy. Dosimetry studies identified the stomach and kidneys as possible dose limiting organs. However, the co-administration of Physiogel seems to be a suitable strategy for nephroprotection. These promising preliminary results warrants further clinical evaluation of ^{177}Lu-PP-F11N.

OP-392

Red marrow dosimetry in metastatic thyroid cancer treated with 131-I: a simplified method

*E. Richetta, **G. Lo Moro**, C. Cutaia, M. Pasquino, L. Sacco, G. Brusasco, R. Pellerito, M. Stasi; AO Ordine Mauriziano di Torino, Turin, ITALY.*

Introduction: A dosimetric approach to metastatic thyroid cancer treated with 131-I should calculate the dose to red marrow or blood as main organ at risk. In this study a simplified method for calculating dose is proposed. **Subjects & Methods:** According to MIRD formalism, after the 131-I administration, doses to red marrow or blood are obtained from whole body and blood residence times, derived from uptake measurements and blood

samples. Hanscheid (2009) has proposed a simplified method on a 29 patients group: under the assumption that 14 % (dt%) of the whole-body residence time can be attributed to blood, blood residence time (t_{bl}) can be calculate from whole-body time (t_{wb}) as $t_{bl}=t_{wb}\times dt\%/(100\times BLV)$, where BLV is the individual blood volume derived from weight and height. On a group of 82 patients, 102 blood residence times were calculated with standard (stdm) and simplified (sm) method, after the verification of the dt% value, both in-therapy and pre-therapy phase. Doses to red marrow and blood were compared to evaluate the overall agreement. **Results:** Blood residence time percentage (dt%) was in mean 12% (range 7%÷19%). This value was used to calculate the blood residence time for the simplified method. Both in-therapy t_{bl} (h•ml) (sm 6.39E-04 ±1.89E-04 vs stdm 6.18E-04±1.82E-04) and pre-therapy t_{bl} (h•ml) (6.35E-04±2.05E-04 vs stdm 6.15E-04±1.95E-04) were not significant statistical different (p-value > 0.05 t-test paired samples). In-therapy doses (cGy/GBq) to red marrow (sm 7.18±2.01 vs stdm 7.04±1.88) showed a mean percentage difference 2.13% (range -24%÷+34%); the Bland-Altman analysis confirmed the accuracy of the simplified method also compared to the 2 Gy dose limit. Similar results were obtained for blood doses (sm 9.35±2.61 vs stdm 9.12±2.44), with mean percentage difference equal to -1.06% (range -30%÷+41%). No statistical differences were found between in-therapy and pre-therapy doses as well. **Conclusion:** A simplified method to calculate dose to red marrow and and blood in methastatic thyroid patients treated with radioiodine was applied on a larger dataset of patients. Results confirmed the accuracy of the formalism that represents a simplified dosimetric approach, feasible for all institutions, mandatory in high dose treatments and required by national and european laws, to optimize the therapy.

OP-393

Differences in radioiodine biokinetics between papillary thyroid carcinoma low-risk patients treated with 1.11 GBq of ^{131}I-NaI and high-risk patients treated with 3.7 GBq of ^{131}I-NaI

P. Mínguez Gabiña[1], M. Domínguez Ayala[2], A. Expósito Rodríguez[2], J. Genollá Subirats[1], E. Rodeño Ortiz de Zarate[1]; [1]Gurutzeta/Cruces University Hospital, Barakaldo, SPAIN, [2]Basurto University Hospital, Barakaldo, SPAIN.

Purpose/Introduction: Administration of ^{131}I-NaI for postoperative ablation of thyroid remnants for the treatment of differentiated thyroid cancer has been performed since the 1940s. The optimal activity to administer is still a matter for discussion, as some studies have reached different conclusions after administering activities between 1.11 GBq and 3.7 GBq. In this study, we have focused on possible differences in radioiodine biokinetics between patients treated for papillary thyroid carcinoma with 1.11 GBq (low-risk patients — pT1-T2 tumours without lymph node or distant metastases.) and patients treated with 3.7 GBq (high-risk patients — pT3-T4 tumours or metastases). **Subjects & Methods:** 50 patients with papillary thyroid carcinoma were included in the study. Of them, 18 were low-risk patients and

32 were high-risk patients. Prior to radioiodine therapy, all patients underwent total thyroidectomy. Some patients had more than one remnant and in total 81 remnants were included. Low-risk patients were treated with 1.11 GBq of ^{131}I-NaI and high-risk patients with 3.7 GBq. The activity at 2 d and 7 d post-administration taken up by thyroid remnants and the mass of thyroid remnants were determined from SPECT/CT images using thresholding techniques and recovery coefficients. From these parameters, the remnant absorbed dose was calculated integrating the time-activity curve with a rectangular integration until the first time-point and thereafter assuming a monoexponentially decaying activity. The S-value was derived from interpolation of values of unit-density spheres. **Results:** For all results, mean values are given and results of low-risk patients treated with 1.11 GBq appear first. An independent samples *t*-test was performed for the analysed parameters and the *p*-value is shown. Remnant masses were 3.2 g and 3.6 g (*p*=0.43). Remnants activities at 2d post-administration were 5.2 MBq and 6.1 MBq (*p*=0.60). Remnants activities at 7d post-administration were 2.4 MBq and 0.7 MBq (*p*=0.02). Effective half-lives of the radioiodine were 99 h and 48 h (*p*=7.3x10^{-9}). Remnants absorbed doses were 38 Gy and 22 Gy (*p*=0.15). **Conclusion:** Remarkable differences were found in the biokinetics of the radioiodine in the thyroid remnants between low-risk (1.11 GBq of ^{131}I-NaI administered) and high-risk patients (3.7 GBq of ^{131}I-NaI administered) treated for papillary thyroid carcinoma. These differences may be due to the differences in the stage of the disease, or to a different response of thyroid remnants to the amount of activity delivered. This situation calls for further investigation in order to give an explanation for our results.

1005   **Monday, October 23, 2017, 16:30 - 18:00, Hall E2**

M2M: PET/CT

OP-394

Radiolabelling with carbon-11 of sulfasalazine for PET imaging of cystine transporter X_c^- involved in the radioresistance of glioblastoma

*M. Morloz, M. Ibazizene, C. Perrio, L. Barre, **F. Gourand**; Cyceron, UNICAEN, CEA, CNRS, ISTCT/LDM-TEP group, Caen, FRANCE.*

Introduction: Glioblastomas (GBMs) are aggressive brain tumors resistant to chemotherapy and radiotherapy. Tumor cells survival is related to an increased concentration of the antioxidant glutathione (GSH) which inhibits the action of Reactive Oxygen Species (ROS) produced by radiotherapy.[1] Accumulation of GSH is due to a surexpression of cystine transporter X_c^-, cystine being the precursor of GSH. The anti-inflammatory drug sulfasalazine has been reported to be an inhibitor of the system X_c^- and we sought to label this compound with carbon-11.[2] PET imaging studies using this new tracer could contribute to elucidate the role of system X_c^- in the efficacy of radiotherapies for GBMs patients. **Materials and Methods:** We examined two methods to label sulfasalazine at the

carboxylic acid position. The first strategy was the direct carboxylation with [^{11}C]CO$_2$ of sulfasalazine organomagnesium precursor. The other alternative to synthesize [^{11}C]sulfasalazine was the coupling reaction of [^{11}C]salicylic acid with a diazonium salt in basic aqueous conditions. **Results**: All attempts to obtain [^{11}C]sulfasalazine according to the direct carboxylation strategy failed. To circumvent this approach, the coupling reaction of [^{11}C]salicylic acid with the diazonium salt has been performed in presence of NaOH under different conditions (temperature, time, reagents and precursors concentrations). After optimization, [^{11}C]sulfasalazine has been obtained with a conversion rate of 40% (based on HPLC profiles). **Conclusion:** [^{11}C]Sulfasalazine was successfully obtained by a two-step radiosynthesis from [^{11}C]CO$_2$ including formation of [^{11}C]salicylic acid then coupling with a diazonium salt. Preclinical studies are in progress to better understand the role of system X$_c^-$ in GBMs. 1-Sleire *et al, Oncogene,* 2015, 34, 5951 2-Lewerenz *et al, Antioxid Redox Signal,* 2013, 18, 522

OP-395

A Successive Triple PET Tracer Approach to Characterize ER and HER2 Status In Vivo in a Breast Cancer Mouse Xenograft Model

M. Paquette, S. Beaudoin, S. Phoenix, L. Fafard-Couture, É. E. Turcotte, B. Guérin, R. Lecomte, J. V. Leyton; Université de Sherbrooke, Sherbrooke, QC, CANADA.

Introduction: Estrogen Receptor (ER) and HER2 status are two of the most important prognosis factors in breast cancer, the presence of either strongly dictating the optimal course of therapy to undertake. ER+ diseases are likely to respond well to adjuvant hormone therapies, whereas HER2-overexpressing tumors can be efficiently treated with the anti-HER2 antibody trastuzumab. This study aims at designing a preclinical PET imaging protocol for sequentially monitoring glucose consumption, ER and HER2 within a 7-day schedule using [^{18}F]-FDG, the ER radiotracer 4-fluoro-11β-methoxy-16α-[^{18}F]-fluoroestradiol ([^{18}F]-4FMFES) and the HER2-targeting ^{89}Zr-labeled trastuzumab in succession. **Subjects and Methods**: Both conjugation of *p*-isothiocyanatobenzyl-desferrioxamine (DFO) to trastuzumab and labeling with [^{89}Zr]-oxalate were carried out using known standard procedures. Purification and buffer exchange with PBS of ^{89}Zr-trastuzumab were performed by serial centrifugal filtration. ^{89}Zr-trastuzumab was radiochemically characterized using instant thin layer chromatography eluted with 0.1M DTPA. ^{18}F-4FMFES and ^{18}F-FDG were prepared as previously described. The MCF7 (ER+, HER2-) and JimT1 (ER-, HER2+) human breast cancer cell lines were engrafted subcutaneously on the shoulder of female athymic nude mice. On day 1, PET imaging was performed 45 minutes after injection of 4.5±1.9 MBq [^{18}F]-FDG. On day 2, 2.6±0.3 MBq of [^{18}F]-4FMFES was administered followed by PET imaging 1 h post-injection. The same day, mice were again injected with ~50 µg (3.9±0.4 MBq) ^{89}Zr-trastuzumab. A 20-minute PET acquisition was obtained at 2 and 6 days post-injection, followed by a low-dose CT. A semi-quantitative analysis of the tracer uptake in tumors was carried out to obtain %ID/g data. **Results**: Specific activity for [^{89}Zr]-trastuzumab reached 83 MBq/mg (25.1 TBq/mmol), with radiochemical purity ≥95%. [^{18}F]-FDG uptake averaged 2.5±0.2 %ID/g for MCF7 and 2.1±0.8 %ID/g for JimT1 tumors, respectively. Differential 4FMFES uptake was observed, reaching 2.3±1.2 %ID/g for MCF7 tumors, but only 0.8±0.3 %ID/g for ER- JimT1 tumors. [^{89}Zr]-trastuzumab uptake for the HER2+ JimT1 tumors reached 16.3±2.5 %ID/g and 19.9±3.2 %ID/g at 2 and 6 days post-injection respectively, whereas MCF7 uptake was consistently ~3-fold lower. **Conclusion**: This pilot study showed the feasibility of a triple-tracer preclinical PET imaging protocol of breast cancer within a 1-week schedule. Such a protocol enables whole-body *in vivo* discrimination between tumors having different ER and HER2 expression patterns. It could also predict therapy efficacy and help monitor ER/HER2 status switch longitudinally.

OP-396

In vivo tracking of T cells by [18F]BF4 PET/CT in a mouse model of human breast cancer

E. Kurtys[1], L. Lim[1], F. Man[1], A. Volpe[1], J. Maher[2], G. O. Fruhwirth[1,3]; [1]Department of Imaging Chemistry and Biology, Division of Imaging Sciences and Biomedical Engineering, St. Thomas' Hospital Campus, King's College London, London, UNITED KINGDOM, [2]Division of Cancer Studies, King's College London, SE1 9RT, UK, London, UNITED KINGDOM, [3]Comprehensive Cancer Imaging Centre King's College London & UCL, London, UNITED KINGDOM.

Aim: Genetically modified T cells are emerging as a promising tool for personalised anti-cancer immunotherapy. Big challenges remain for them in solid tumour therapy such as in vivo relocalization reducing on-site efficacy and on-target off-site toxicities against healthy tissues. In vivo imaging of these cellular therapeutics can not only inform their development but also inform individual therapy monitoring/dosing. The goal of the present study was to quantify anti-ErbB family Chimeric Antigen Receptor (CAR) T cells in a mouse model of human breast cancer. These therapeutic cells were rendered traceable in vivo by PET and SPECT imaging via a multi-modal multi-scale reporter gene approach. **Material and Methods:** The human sodium iodide symporter (NIS) was fused to a red fluorescent protein (RFP)[1] and co-expressed in human T-cells with the T1E28z CAR targeting the ErbB receptor family[2]. CAR::NIS-RFP Tcells were lentivirally transduced and selectively expanded via the chimeric IL-4:IL-2/15 cytokine receptor approach[3] CAR::NIS T cells were characterised in vitro for their ability to kill MDA-MB-436 cells as well as their ability to take up the NIS PET tracers [^{18}F] tetrafluoroborate ([^{18}F]BF$_4$) and [^{99m}Tc]pertechnetate (^{99m}TcO$_4^-$). MDA-MB-436 breast tumours were established in female immunodeficient NOD scid gamma (NSG) mice either orthotopically or subcutaneously. CAR::NIS T cells were injected either systemically or intratumorally into establbished tumours and followed by PET/CT imaging up to two weeks post injection. After the last scan mice were sacrificed and tissues were collected for ex-vivo biodistribution by gamm-counting and histology. **Results:** Live CAR::NIS T cells were successfully detected at various concentration levels in naïve as well as tumour-bearing animals by [^{18}F]BF$_4$

PET/CT imaging. Intratumourally administered CAR::NIS T cells could be followed in vivo over a period of 15 days. At this time point significant amounts (>66%) had left the tumour and/or died. Systemically administered (i/v) CAR::NIS T cells could be detected in primary tumours in both models within 24h of administration and were successfully tracked longitudinally at the primary tumours. Importantly, systemic administration resulted also in on-target off-site localization. Ex vivo biodistribution and histology confirmed our in vivo imaging results. **Conclusion:** NIS reporter gene imaging by [18F]BF$_4^-$ -PET is a sensitive tool for monitoring anti-cancer T cell therapy. In vivo imaging allowed quantification of T cells distribution and retention in primary tumours. Imaging informed on T cell tumour presence, which is a prerequisite for any therapeutic effect.1. J Nuc Med 2014;55(4):686-94. 2. Mol Med 2012,18,565. 3. Biol Chem 2010,285,25538.

OP-397

Differentiation of CNS lymphoma and glioblastoma with [18F]fludarabine-PET: comparison with [18F]FDG in human xenograft models

N. Hovhannisyan[1], S. Guillouet[1], M. Dhilly[1], M. Ibazizene[1], F. Fillesoye[1], S. Valable[2], B. Plancoulaine[3], L. Barré[1]; [1]Normandie Univ, UNICAEN, CEA, CNRS, CHU Caen, ISTCT/LDM-TEP group, Caen, FRANCE, [2]Normandie Univ, UNICAEN, CEA, CNRS, CHU Caen, ISTCT/CERVOxy group, Caen, FRANCE, [3]Normandie Univ, UNICAEN, INSERM, ANTICIPE, Caen, FRANCE.

Introduction: [18F]Fludarabine is a PET radiotracer [1], the specificity of which has been studied in several lymphoma models (follicular RL7, DOHH2; MM RPMI8226) and under various conditions such as cancerous tissue following therapy and inflammation [2-4]. The first-in-human study in two types of lymphoid malignancies (DLBCL, CLL) has consolidated the great potential of this innovative tool for lymphoma imaging in oncology [5,6]. The purpose of this study was to investigate whether [18F]fludarabine-PET can help differentiate between central nervous system (CNS) lymphoma and glioblastoma (GBM), considering also multimodal analyses with [18F]FDG, MRI and histology. **Methods:** Nude rats were implanted with human MC116 lymphoma- (n=10) or U87 glioma-cells (n=5). Tumor growth was monitored by MRI (7-Tesla, Bruker), with T2-weighted sequence (RARE) for anatomical features and T1-weighted (EPI) with gadolinium (Gd) enhancement for BBB permeability assessment. For PET investigation (Inveon, Siemens), ~11 MBq [18F]fludarabine or [18F]FDG were injected via tail vein and PET dynamic images were acquired up to 90 min after radiotracer injection. Paired scans of the same rat with the two [18F]-labelled radiotracers were investigated. Initial volumes of interest (tumor and healthy contralateral or cerebellum tissue) were manually delineated on T2w image and set on co-registered PET image (Pmod 3.7) and tumour-to-background ratios (TBR) were calculated to semi-quantitatively assess the tracer accumulation in the tumour. **Results:** In lymphoma model, PET time-activity curves revealed a differential response of [18F]fludarabine between tumoral and healthy tissues with average TBR varying from 2.45 to 3.16 between 5 to 90 min post-injection. In contrast, [18F]FDG demonstrated similar uptake profiles for tumoral and normal regions with TBR varying from 0.84 to 1.06 between these two time points. In GBM model, the average TBRs were from 1.67 to 1.07 for [18F]fludarabine and from 1.08 to 1.65 for [18F]FDG. Therefore, inter-model comparisons showed significantly divergent responses (p<0.001) of [18F]fludarabine between lymphoma and GBM, while [18F]FDG demonstrated considerable overlap (p=0.04) between the groups. Tumour characterisation with histology (based mainly on Hoechst, CD68 and CD79), as well as with MRI were in overall better agreement with [18F]fludarabine-PET than [18F]FDG with regard to tumour selectivity. **Conclusion:** The potential of [18F]fludarabine-PET to distinguish CNS lymphoma from GBM is quite evident and will be further investigated. Guillouet et *al.*, Mol. Imaging Biol. 2014, Dhilly et *al.*, Mol. Imaging Biol. 2014, Hovhannisyan et *al.*, EJN-MMI Res. 2015, Hovhannisyan et *al.*, Mol. Pharmaceutics 2016, Chantepie et *al.*, Blood 2015 (proceeding), Hovhannisyan et *al.*, Blood 2015 (proceeding)

OP-398

Convenient synthesis and biological evaluation of 18F-labeled MIBG analog with an improved detectability

A. Yamaguchi, H. Hanaoka, T. Higuchi, Y. Tsushima; Gunma University Graduate School of Medicine, Maebashi, JAPAN.

Aim: Radioiodine-labeled MIBG play roles in diagnosis and therapy for the neuroendocrine tumors including neuroblastoma and pheochromocytoma. To improve detectability of [123I]MIBG, efforts have been made for the development of 18F-labeled MIBG derivatives. Although 4-[18F]fluoro-3-iodobenzylguanidine (FIBG) holds a promising basic properties, its tumor imaging capability remains obscure probably because of the complexity in the radiolabeling procedure [1, 2]. In contrast, recent astonishing progress in the late-stage [18F]fluorination enabled production of 18F-labeled compounds which previously believed difficult to develop. Our aim was to establish an improved radiosynthetic method for [18F]FIBG by applying late-stage [18F]fluorination. Its usefulness as a PET imaging agent for the detection of neuroendocrine tumor was also evaluated. **Materials and Methods:** [18F]FIBG was prepared from a (mesityl)(aryl)iodonium salt precursor in the presence of a copper-catalyst, according to the procedure by Sanford and Scott [3] with a brief modification. Biodistribution studies were performed on PC-12 rat pheochromocytoma cell xenograft mice using [18F]FIBG, [125I]FIBG or [125I]MIBG. PET imaging was performed on PC-12 xenograft mice after 1 h injection of [18F]FIBG. **Results:** tetra-*N*-Boc-protected [18F]FIBG was obtained from the iodonium salt precursor in the presence of a copper-catalyst (5 equivalent) with the radiochemical yield of 18.3 ± 8.5 % (decay corrected, n = 9). Subsequent deprotection using 6 N HCl followed by HPLC purification readily produced desired [18F]FIBG. In biodistribution study in PC-12 mice, all MIBG analogs exhibited similar distribution profiles and showed highest uptake in the tumor. The tumor uptake of [18F]FIBG was slightly higher than that of [125I]MIBG though not statistically significant (41.5 ± 14.5 %ID/g and 35.4 ± 13.3 %ID/g,

respectively). In PET imaging in xenograft mice, [18F]FIBG clearly depicted the tumor, even for a small one (4 mm), as early as 1 h after injection with excellent tumor-to-background ratios, as oppose to [123I]MIBG which requires 24 h to produce high-contrast image. **Conclusion:** We successfully produced [18F]FIBG in 2 steps by using late-stage [18F]fluorination. [18F]FIBG accumulated in the tumor as high as [125I]MIBG in the PC-12 xenograft mice. Moreover, in PET imaging, [18F]FIBG clearly depicted the tumor with excellent tumor-to-background ratios. These results indicates [18F]FIBG constitute a promising PET imaging agent for the detection of neuroendocrine tumors. **References:** [1] J. Med. Chem. 1994, 37, 3655-3662 [2] J Nucl Med 1995; 36: 644-650 [3] Org. Lett. 2014; 16: 3224–3227

OP-399

Targeting glucose metabolism and EGFR signaling in oncogene-driven non-small cell lung cancer

V. De Rosa[1], *F. Iommelli*[1], *M. Monti*[2], *C. Terlizzi*[2], *S. Del Vecchio*[2,1]; [1]*Institute of Biostructures and Bioimaging, National Research Council, Naples, ITALY*, [2]*Department of Advanced Biomedical Sciences, University of Naples "Federico II", Naples, ITALY.*

Aim: In a previous study we showed that inhibition of EGFR signaling causes a metabolic switch from aerobic glycolysis to oxidative phosphorylation by reducing hexokinase II (HKII) and phosphorylated form of pyruvate kinase M2 (p-PKM2 Tyr105) and upregulation of mitochondrial complexes (OXPHOS) in NSCLC cells and animal models. Here we tested whether the simultaneous targeting of glucose metabolism and EGFR signaling may enhance tumor response to tyrosine kinases inhibitors (TKIs) in NSCLC. **Materials and Methods:** To this end, resistant H1975 and H1993 NSCLC cells were transfected with 100 nM of scrambled or PKM2, LDH-A and PDK1 targeted siRNAs using Dharmafect reagent and after 24 h they were treated with 1 μM TKIs (WZ4002, PHA-665,752) or vehicle for additional 48 h. Toxicity of combined treatment was tested by MTS assays. Furthermore, we tested the levels of HKII, PKM2, LDH-A, PDH and PDK1 along with the phosphorylation status of PKM2 and PDH in response to treatment with targeted siRNAs, selective TKIs or combination of both agents. In parallel experiments, glucose consumption and ATP production were determined in untreated and TKIs treated cells, in the presence or absence of specific siRNA. **Results:** A reduction of cell viability of both cell lines was observed in response to TKIs and was enhanced by the concomitant silencing of PKM2 or PDK1. Inhibition of EGFR signaling caused downregulation of HKII, p-PKM2, LDH-A and p-PDH. Concomitant suppression of PKM2 or PDK1 expression enhanced the effects of TKIs on downregulation of HKII, p-PKM2, LDH-A and p-PDH. In agreement with these findings, a parallel decrease of glucose consumption and a concomitant increase of intracellular ATP levels were observed in response to TKIs and both were enhanced by the concomitant suppression of PKM2 or PDK1 expression. **Conclusion:** Our findings indicate that selective targeting of glucose metabolism and EGFR signaling enhances TKIs effects on cell viability and reactivation of oxidative phosphorylation.

OP-400

A direct comparison of four different ⁶⁸Ga-labeled RGD peptides for PET/CT imaging of angiogenesis

D. Lobeek[1], *S. Y. A. Terry*[2], *G. M. Franssen*[1], *M. T. Ma*[3], *H. Wester*[4], *C. Decristoforo*[5], *W. J. G. Oyen*[1,6], *O. C. Boerman*[1], *M. Rijpkema*[1]; [1]*Radboud University Medical Center Nijmegen, Nijmegen, NETHERLANDS,* [2]*King's College London, London, UNITED KINGDOM,* [3]*King's College London, London, UNITED KINGDOM,* [4]*Technische Universität München, Garching, GERMANY,* [5]*Medical University Innsbruck, Innsbruck, GERMANY,* [6]*Institute of Cancer Research, Royal Marsden NHS Trust, London, UNITED KINGDOM.*

Objectives: $\alpha_v\beta_3$ integrins play an important role in angiogenesis and cell migration of tumours. They are highly expressed on activated endothelial cells of newly formed blood vessels and absent at almost all normal endothelial tissue. Various multimeric cyclic RGD analogues have been developed for the *in vivo* imaging of $\alpha_v\beta_3$ integrins. Here, we present a direct comparison of the *in vivo* $\alpha_v\beta_3$ integrin targeting characteristics of four commonly used RGD peptides: ⁶⁸Ga-labeled DOTA-E-[c(RGDfK)]$_2$, TRAP-(RGD)$_3$, fusarinine-C-(RGD)$_3$, and THP-(RGD)$_3$. These peptides are tested in two different human xenograft tumour models; with and without $\alpha_v\beta_3$ integrin-expressing tumour cells. **Methods:** Balb/c nude mice were subcutaneously injected with either FaDu ($\alpha_v\beta_3$ integrin negative) or SK-RC-52 ($\alpha_v\beta_3$ integrin positive) tumour cells. The dimeric DOTA-E-[c(RGDfK)]$_2$ peptide, and the trimeric TRAP-(RGD)$_3$, fusarinine-C-(RGD)$_3$, and THP-(RGD)$_3$ peptides were labeled with ⁶⁸Ga and intravenously administered to the mice (0.5 nmol per mouse, 10-15 MBq), followed by *in vivo* imaging using the Inveon microPET/CT and *ex vivo* biodistribution studies at 1 hour post injection. Uptake was expressed as percentage injected dose per gram tissue (%ID/g). For both tumour models, the non-specific uptake of the four tracers was determined by coinjecting an excess unlabeled DOTA-E-[c(RGDfK)]$_2$ (50 nmol) along with the radiolabeled radiotracers. **Results:** All four compounds showed specific tumour uptake in both tumour models. In the SK-RC-52 tumour model mean tumour uptake of ⁶⁸Ga-fusarinine-C-(RGD)$_3$ (12.5±2.5%ID/g) was significantly higher than ⁶⁸Ga-DOTA-E-[c(RGDfK)]$_2$ (5.3±1.9%ID/g, **p**<0.0005), ⁶⁸Ga-TRAP-(RGD)$_3$ (4.4±0.8%ID/g, **p**<0.0005), and ⁶⁸Ga-THP-(RGD)$_3$ (5.3±0.6%ID/g, **p**<0.0005). However, in the FaDu tumour model significantly lower uptake of ⁶⁸Ga-TRAP-(RGD)$_3$ (1.0±0.2%ID/g) compared to ⁶⁸Ga-fusarinine-C-(RGD)$_3$ (1.9±0.3%ID/g, **p**=0.026) and ⁶⁸Ga-THP-(RGD)$_3$ (2.2±0.7%ID/g, **p**=0.002) was found. Thus, different trends in mean tumour uptake were found in the two different tumour models. Different trends were also observed when assessing the tumour-to-blood ratios (TBR): 18.6 ± 6.5, 31.5 ± 15.8, 28.2 ± 11.5, 13.5 ± 1.5, and 5.9 ± 2.6, 5.0 ± 2.5, 3.1 ± 1.2, 6.8 ± 2.8, for ⁶⁸Ga-DOTA-E-[c(RGDfK)]$_2$, ⁶⁸Ga-TRAP-(RGD)$_3$, ⁶⁸Ga-fusarinine-C-(RGD)$_3$, and ⁶⁸Ga-THP-(RGD)$_3$ in the SK-RC-52 and FaDu xenograft tumour model, respectively. Both tumour models showed similar uptake pattern of ⁶⁸Ga-DOTA-E-[c(RGDfK)]$_2$, ⁶⁸Ga-TRAP-(RGD)$_3$, ⁶⁸Ga-fusarinine-C-(RGD)$_3$, and ⁶⁸Ga-THP-(RGD)$_3$ in non-tumour tissue. **Conclusions:** ⁶⁸Ga-labeled DOTA-E-[c(RGDfK)]$_2$,

TRAP-(RGD)$_3$, fusarinine-C-(RGD)$_3$, and THP-(RGD)$_3$ all allowed imaging of α$_v$β$_3$ integrin expression in both the α$_v$β$_3$ integrin negative FaDu and the α$_v$β$_3$ integrin positive SK-RC-52 xenograft models. However, individual differences in the *in vivo* targeting characteristics of multimeric cyclic RGD analogues were observed depending on the outcome measure and the human xenograft model used.

OP-401

Synthesis and biological evaluation of novel five F-18 labelled radioligands for detection of MAO-B activity

S. Nag[1], A. Jackson[2], A. Takano[1], K. Jia[1], R. Arakawa[1], M. Jahan[1], R. Ahmad[2], S. Luthra[2], R. Maior[1], C. Halldin[1]; [1]Karolinska Institutet, Stockholm, SWEDEN, [2]GE Healthcare, London, UNITED KINGDOM.

Objective: Monoamine oxidases (MAO) are important enzymes regulating the levels of monoaminergic neurotransmitters and of bioactive monoamines by catalyzing their deamination. MAO-B inhibitors are widely used in the treatment of e.g. Parkinson's disease (PD). L-deprenyl, a MAO-B inhibitor has been labelled with ^{11}C and used in PET studies to image the distribution of available MAO-B in the human brain. Carbon-11 labelled L-deprenyl is less suitable for its relatively short half life, irreversible binding kinetics and the formation of a radiometabolite methamphetamine that can enter into the brain. In this project our aim was to develop a fast and efficient synthetic method for labeling five reversible MAO-B inhibitors (GEH200439, GEH200448, GEH200449, GEH200431A and GEH200431B) with ^{18}F and their biological evaluation for the detection of MAO-B. **Method:** All five precursors and reference standards were provided by GE Healthcare. Radiolabeling was achieved by classical one-step fluorine-18 nucleophilic substitution reaction. The reaction was carried out in DMSO at 110-145 °C for 10-30 min. The stability was determined using HPLC. All five ^{18}F-labeled compounds were tested in human whole hemisphere autoradiography (ARG) experiments. Four compounds except GEH200448 were examined by PET in rhesus monkeys and radiometabolites were measured in monkey plasma using a gradient HPLC system. In addition to the baseline PET measurements, GEH200439 and GEH200431A were examined after pretreatment with L-deprenyl (1,0 mg/kg) **Results:** All the compounds were successfully radiolabeled. The incorporation yield of the fluorination reactions varied from 10% to 45% depending on the compound. The radiochemical purity was higher than 99% for all four radioligands at the end of synthesis. Specific radioactivity was 76-232 GBq/μmol at the time of administration. Radioligands were found to be stable, with a radiochemical purity of >99% at 2h after formulation in a sterile phosphate buffered solution (pH = 7,4). Although autoradiography on human brain tissue section demonstrated specific binding for GEH200449 to MAO-B, no specific uptake was observed in monkey brain PET. However, for GEH200431A, less favorable ARG result were obtained, but pronounced specific uptake in MAO-B rich regions and blocking effect by L-deprenyl was seen in monkey PET. Radiometabolite studies demonstrated that for all of the four compounds, only polar radiometabolites were formed with 25%-35% unchanged radioligand remaining 90 min post injection. **Conclusion:** Radiolabeling of five new fluorine-18 MAO-B inhibitors was successfully accomplished. Compound GEH200431A binds specifically to MAO-B in vivo monkey brain and is a potential candidate for further investigation.

1006	Monday, October 23, 2017, 16:30 - 18:00, Hall F1

Teaching Session 4 (Interactive): Applied Cross Sectional Anatomy and Correlative Imaging - Abdomen & Pelvis

OP-402

Applied Cross Sectional Anatomy and Correlative Imaging – Abdomen & Pelvis

D. Yakar; University Medical Centre, Groningen, NETHERLANDS.

1007	Monday, October 23, 2017, 16:30 - 18:00, Hall F2

Joint Symposium 18 - EANM/TBA: Treatment Landscape in Metastatic CRPC

OP-403

Current Treatment Algorithm of Metastatic CRPC
Speaker TBA

OP-404

Imaging of Metastatic CRPC in the PSMA Era
Speaker TBA

OP-405

SMA Targeted Radioligand Therapy – What Do We Know So Far?
Speaker TBA

OP-406

New Treatment Strategies and Options for Metastatic CRPC – Is There Space for PSMA RLT?
Speaker TBA

1008	Monday, October 23, 2017, 16:30 - 18:00, Hall K

Cardiovascular System: Cardiac Sympathetic Innervation - 123I-mIBG & Arrhythmias

OP-407

Standardization of MIBG Heart-to-Mediastinum Ratio Using a Phantom-based Calibration Method

K. Nakajima[1], K. Okuda[2], K. Yokoyama[3], T. Yoneyama[3], S. Tsuji[3], S. Tsuji[3], H. Oda[3], M. Yoshita[4], K. Kubota[3]; [1]Kanazawa University Hospital, Kanazawa, JAPAN, [2]Kanazawa Medical University, Uchinada, JAPAN, [3]Public Central Hospital of Matto Ishikawa, Hakusan, JAPAN, [4]Hokuriku National Hospital, Nanto, JAPAN.

Aim: In 123I-metaiodobenzylguanidine (MIBG) studies, a cross-calibration phantom method has shown to be applicable to any collimator types with Anger camera based on Japanese and European phantom studies. However, whether the approach of the simple conversion coefficient can be applicable to cadmium-zinc-telluride D-SPECT camera has not been examined. The aim of this study was to determine a phantom-based conversion coefficient for D-SPECT and validate the method by comparing heart-to-mediastinum ratios (HMR) by Anger and D-SPECT cameras. **Methods:** Calibration phantom experiments were performed with Anger and D-SPECT cameras using the same phantom validated in Japanese and European multicenter studies. A conversion coefficient to mathematically calculated reference value was determined and used as a basis for conversion among camera systems. A total of 40 patients (80 studies including early and late imaging) with suspected of having chronic heart failure and Lewy-body disease underwent 123I-MIBG studies with Anger camera (low-energy high resolution (LEHR) collimator) and D-SPECT. In Anger camera, anterior image was used while a planogram, which is nearly equivalent to an anterior planar image, was created and used for calculating HMR. The effect of correction of HMRs to both Anger camera with LEHR and medium-energy (ME) collimator conditions was examined. **Results:** Conversion coefficients for Anger camera with LEHR collimator and D-SPECT were 0.55 and 0.63, respectively. The original HMR from the Anger camera and D-SPECT were 1.76 ± 0.42 and 1.86 ± 0.55, respectively (p<0.0001). After D-SPECT HMR was converted to Anger camera conditions, corrected D-SPECT HMR became comparable values to Anger camera condition (1.74 ± 0.47, p = ns). Moreover, when both Anger camera with LEHR collimator and D-SPECT conditions were converted to standardized ME collimator conditions with conversion coefficient of 0.88, the HMRs became comparable (2.21 ± 0.65 vs. 2.20 ± 0.75, p=ns). When patients were classified into two groups with higher and lower HMR (≥ 1.6 and <1.6, respectively), the effect of correction is not significant with low-HMR patients. However, the main effect of correction was evident when HMR is more than >1.6, and was useful for differentiating both groups. **Conclusion:** The conversion coefficient of D-SPECT was determined and could be used to cross-calibrate HMR between two systems. The advantage of using phantom-based correction is possibility to calibrate HMRs between D-SPECT and Anger camera with any collimator types.

OP-408

Inter-study reproducibility of SPECT ^{123}I-mIBG left atrial innervation imaging for the identification of left atrial ganglionated plexi in patients with paroxysmal atrial fibrillation

J. Stirrup[1], U. Voss[2], S. Gregg[2], R. Baavour[3], N. Roth[3], C. Breault[3], S. Ernst[2], S. Underwood[2]; [1]Royal Berkshire NHS Foundation Trust, Reading, UNITED KINGDOM, [2]Royal Brompton and Harefield NHS Foundation Trust, London, UNITED KINGDOM, [3]Spectrum Dynamics Medical Ltd, Caesarea, ISRAEL.

Introduction: Outcomes following pulmonary vein isolation (PVI) in patients with atrial fibrillation (AF) may be improved by concomitant ablation of left atrial (LA) ganglionated plexi (GP). Single-photon emission computed tomography (SPECT) LA innervation imaging, using the noradrenaline analogue ^{123}I-metaiodobenzylguanidine (mIBG), identifies GP locations non-invasively but inter-study reproducibility is not yet known. We undertook serial SPECT ^{123}I-mIBG LA innervation imaging in patients with paroxysmal AF and assessed agreement for discrete ^{123}I-mIBG uptake areas (DUA). **Methods:** 10 patients undergoing PVI for paroxysmal AF underwent sequential LA innervation imaging 4 hours after injection of 370MBq ^{123}I-mIBG using a dedicated solid-state gamma camera. A second scan was acquired immediately after completion of the first acquisition. Where possible, images were reconstructed using ECG and respiratory gating. SPECT tomograms were co-registered with cardiac computed tomograms (CT) acquired clinically for delineation of LA and PV anatomy prior to ablation. DUAs were identified and marked on a standardized 32-segment left atrial segmentation map. Each DUA was assigned a confidence score (1: low; 2: moderate, 3: high) based on discreteness, extent of overlap with non-LA activity (e.g. LV myocardium, lung) and proximity to known GP locations. **Results:** 55 DUAs were identified (median per patient 6 [5.25 - 6]). 15, 17 and 23 DUAs were assigned confidence levels 1, 2 and 3 respectively. Overall, 33/55 (60%) DUAs were identified in the same left atrial segment on both studies. The level of agreement increased with reporter confidence (5/15 (33%), 9/17 (55%) and 19/23 (83%) for levels 1, 2 and 3 respectively). The likelihood of agreement was improved at the highest level of confidence in the 7 studies reconstructed with ECG and respiratory gating (3/11 (27%), 6/11 (55%) and 15/17 (88%) for levels 1, 2 and 3 respectively). **Conclusion:** ^{123}I-mIBG SPECT LA innervation imaging identifies GPs reproducibly and agreement is closely linked to reader confidence. When studies are acquired with ECG and respiratory gating, inter-study agreement exceeds 85% at the highest level of confidence, whilst low-likelihood areas of uptake - non-discrete, overlapping with other non-LA activity and in sites not typical for ganglionated plexi - are much less likely to be reproduced on serial imaging.

OP-409

Evaluation of the effectiveness of radiofrequency ablation of atrial fibrillation: a 123-Iodine-MIBG myocardial scintigraphy study

Y. Saushkina, V. Saushkin, K. Zavadovskiy, I. Kisteneva, I. Kostina, Z. Vesnina, Y. Lishmanov, S. Popov, R. Karpov; Cardiology Research Institute, Tomsk NRMC, Tomsk, RUSSIAN FEDERATION.

Purpose: The aim of the study was to identify scintigraphic predictors of the effectiveness of interventional treatment of atrial fibrillation (AF). **Methods and Materials:** In this study were enrolled 35 patients with essential hypertension (EH) (the duration of EH 5-20 years): 17 patients with persistent AF and 18 patients with long-standing persistent AF. All patients underwent single-photon emission computer tomography (SPECT) with 123I-metaiodbenzilguanidine (123I-MIBG) to evaluate cardiac sympathetic nervous system (SNS) activity before radiofrequency catheter ablation (RFCA). Evaluation

of the effectiveness of RFCA was carried out after 12 months by means of twenty-four hour Holter monitoring. **Results:** Patients of both groups were divided into subgroups depending on the presence of recurrence of arrhythmia in a year after interventional treatment. In the group of patients with persistent AF, the arrhythmia recurrence 12 months after RFCA were detected in 7 people. In the group of patients with long-standing persistent AF, the arrhythmia recurrence 12 months after RFCA were detected in 8 people. By ROC analysis identified the main scintigraphic predictors of the effectiveness of interventional treatment of AF. Were investigated the preoperative scintigraphic characteristics of cardiac sympathetic activity for which subgroups with and without AF recurrence had significant differences. Optimal thresholds for predicting the effectiveness of RFCA in patients with persistent AF was ≥1,7 for delayed heart-to-mediastinum ratios (HMR) (0,991 area under the ROC curve; sensitivity 100%, specificity 71%). Optimal thresholds for predicting the effectiveness of RFCA in patients with long-standing persistent AF were ≥1,69 for early HMR (0,849 area under the ROC curve; sensitivity 100%, specificity 62%); ≥1,66 for delayed HMR (0,938 area under the ROC curve; sensitivity 94%, specificity 23%). **Conclusion:** Thus, cardiac MIBG scintigraphy can be used to predict high risk of recurrence of atrial fibrillation after radiofrequency catheter ablation. The study was supported by a grant from the Russian Science Foundation No 15-15-10016.

OP-410

Value of Gated-perfusion SPECT, synchrony and I123-MIBG scintigraphy in predicting cardiac resynchronization therapy response

A. García-Burillo, P. Hinojosa, S. Aguadé, J. Pérez-Rodón, M. N. Pizzi, G. Cases, M. Andrés, N. Rivas, A. Moya; Hospital General Universitari Vall d'Hebron, Barcelona, SPAIN.

Background: Cardiac resynchronization therapy (CRT) is a well established treatment in patients with heart failure, LVEF≤35% and QRS≥120ms. However, approximately 30-40% of patients do not respond to this therapy. **Objective:** To assess the value of gated myocardial perfusion SPECT (GMPS), phase synchrony and ^{123}I-metaiodobenzyl-guanidine (^{123}I-MIBG) scintigraphy to predict response to CRT. **Methods:** In this prospective observational study, patients with a CRT indication were consecutively included. Prior to implantation, a GMPS and ^{123}I-MIBG scintigraphy were performed the same day, and latest phase mechanical activation site, LV scar percentage and heart-to-mediastinum ratio (HMR) assessed. We attempted lead concordance, defined as LV lead implantation in the area of latest mechanical activation assessed with phase analyses of GMPS, in all patients. CRT response was defined as an increase in LVEF≥5 percentage points or a reduction in LVEDV≥15% at 6 months follow-up. **Results:** Fifty-five patients were consecutively included (69±11 years, 82% male). Mean % of LVEF was 26±6. At 6 months follow-up, 58% of patients responded to CRT and lead concordance was achieved in 69% of patients. Patients that responded to CRT had lower LVEDV and LVESV and higher LVEF that patients who did

not respond (p<0.05). When lead concordance was achieved, 71% of patients responded to CRT, whereas when lead concordance was not achieved, only 29% responded (p=0.007). LV scar percentage was lower in patients that responded to CRT compared to patients that did not respond: 10±10 vs 25±14 (p<0.001). HMR was higher in patients that responded to CRT compared to patients that did not respond: 1.35±0.33 vs 1.26±0.12 (p=0.056). In multivariable analyses, only lead concordance (OR=51.184, 95% CI 3.503-747.990, p=0.004) and lower LV scar percentage (OR=0.880, 95% CI 0.788-0.983, p=0.024) were independent predictors of response to CRT. **Conclusions:** Concordance of LV lead implantation site with area of latest phase mechanical activation, assessed with phase analysis of GMPS can be achieved in nearly 70% of cases and predicts, as well as LV scar, response to CRT.

OP-411

Effect of resyncronization therapy on endothelial dysfunction and functional parameters in patients with chronic heart failure and left bundle branch block

T. Massardo[1], J. Pereira[2], C. G. Sáez[2], I. Aramburu[1], R. Morris[1], S. Brugère[1], A. Pino[1], E. Swett[1], E. Hiplan[1], R. Aguayo[3], R. Aguayo[3], G. Paillahueque[1], L. Alarcón[1], J. Torres[3], J. Spuler[1], R. Fernández[1], E. Sanhueza[1], M. Palominos[2], N. Olivares[2], G. Valenzuela[2], R. Asenjo[1]; [1]Hospital Clínico Universidad de Chile, Santiago, CHILE, [2]Pontificia Universidad Católica de Chile, Santiago, CHILE, [3]Hospital San Juan de Dios, Santiago, CHILE.

Introduction: Chronic heart failure (CHF) is a complex disease associated with systemic inflammation and endothelial dysfunction (ED) and its pathogenesis is not well understood. In the scope of a multicenter IAEA trial, we studied CHF patients submitted to resynchronization therapy (CRT). AIM: to evaluate a possible relationship between ED markers and CRT response, already observed with brachial artery flow-mediated dilation. **Methods:** We included 20 CHF patients with II-IV NYHA class with left bundle branch block (QRS≥120ms) and left ventricular ejection fraction (LVEF) ≤35% studied at baseline and 6 month post-CRT (mean age 64 years, 8 females). All with Minnesota Living with Heart Failure Questionnaire (MLHFQ); 6-min walking test (6-WT), ECHO-2D and rest gated sestamibi SPECT. Synctool® software was employed for mechanical synchronism. We determined ultrasensitive C-reactive protein (us-CRP); N-Terminal brain natriuretic peptide (pro-BNP); circulating endothelial cells number (CEC); soluble vascular cell adhesion molecule (sVCAM); soluble intercellular adhesion molecule (sICAM); interleukin-6 (IL-6); *von Willebrand* Factor (vWF) and RhoA/Rho Kinase (ROCK) pathway activation. Patients were classified as responders or non-responders to CRT, according to our trial criteria. Mean differences and correlations were analyzed. **Results:** At baseline, mean values were: pro-BNP 5290 pg/ml; us-CRP 1,7ug/mL; MLHFQ score 72; 6-WT 391 meters. CEC and vWF were over normal limits. Post-CRT, 50% of patients was responder: 11/20 patients increased at least 1 NYHA class and also ≥10% in their 6-WT; MLHFQ decreased (p<0.0001); LVEF and eccentricity improved (p=0.003 and 0.02,

respectively); end systolic volume and gated mass decreased (p=0.008 and 0.035, respectively); mean phase standard deviation (SD) and bandwidth (BW) did not change. Pro-BNP decreased (p=0.03) and us-CRP tended to decreased (p=ns). Summed rest score increased in non-responders (p=0.008); phase SD and BW were similar as well as eccentricity and gated mass (p=ns). In responders, the number of CEC decreased significantly from 67±37 to 51±17/mL (p=0.020) but still over normal limits (<10/mL) as compared with non-responders (p=ns). Pro-BNP, us-CRP, SVCAM, SICAM, IL-6, vWF and ROCK did not change between groups, however vWF remains increased. There was correlation between pro-BNP with 6-WT changes (r=0.617; p=0.004) and us-CRP with MLHFQ (r=0.617; p=0.004) and vWF(r=0.663; p=0.002). **Conclusion:** In patients with CHF and left bundle branch block there was evidence of marked ED expressed as increased CEC, a sensitive peripheral marker that significantly diminished 6 months post-CRT in responders, persisting in abnormal limits. Other cardiac function and inflammatory parameters correlated but not showed significant differences.

OP-412

MIBG scintigraphy to better identify patients who benefit from AICD in primary prevention

G. Bertuccio, G. Scrima; Ospedale S. Croce - ASLTO5, Moncalieri, ITALY.

Background: 1-2% of the adult population in developed countries has heart failure. In this population, mortality has been significantly reduced by the advent of ICD in primary prevention. About 80% of the ICD recipients will never experience an event requiring the appropriate intervention of the ICD. Currently doesn't exist a reliable screening test to select patients candidate to ICD implant. MIBG scintigraphy, such as in ADMIRE study, demonstrated very high negative predictive value for arrhythmic events in patients with Heart/Mediastinum ratio late > 1,6 and a good positive predictive value in patients with H/M late < 1,6. The aim of this study is to assess if the MIBGs should be useful to identify patients with HF who do not benefit from the ICD implantation for a low risk of arrhythmias and those who could procrastinate implant. **Methods:** This is a prospective study where patients undergoing MIBGs from February 2012 to December 2015. Inclusion criteria where: age ≥ 18 years old, LVEF ≤ 35% with idiopathic or ischemic heart disease, no previous documentation of malignant ventricular arrhythmias. Patients were divided in two groups based on of H/M late < or ≥1.60 on MIBGs. **Primary end-point:** mortality and malignant arrhythmias (MACE) RESULTS: 81 patients enrolled (median age: 69 years); 38 with ischemic and 43 with idiopathic heart disease. At the MIBG scintigraphy, 54 patients presented H/M late < 1.60 and 27 patients with H/M late ≥ 1.60. After a median follow-up of 13,7 (± 9,7) months, the primary end-point occurred in 17 patients out of 81; 16 out of 17 with MACE showed an H/M late <1,6. No arrhythmias occurred in patients with H/M late >1,6. Diabetes was associated with the occurrence of the primary end-point. **Conclusion:** This study shows that MIBGs exam with H/M late ≥ 1.60

is a positive prognostic factor with a very high negative predictive value (100% for arrhythmia and 96,3 for death) and with H/M late < 1.60 is a negative prognostic factor where the presence of diabetes predicts the occurrence of ventricular arrhythmias. In 16 patients with H/M late < 1,6 out of 54, occurred the primary end-point and the presence of diabetes was a predictor of the occurrence of ventricular arrhythmias. It confirms the idea that the deregulation of the autonomic system, as observed in diabetes, is fundamental in the occurrence of arrhythmias.

OP-413

The potential role of myocardial viability assessment using 18F-FDG PET-CT in patients with non-ischemic cardiomyopathy eligible for catheter radiofrequency ablation of ventricular tachycardias: preliminary considerations

S. Capitanio[1], R. Sara[2], C. Popescu[2], G. Colombo[2], S. Pedretti[2], P. Ferro[2], M. Milella[2], C. Rossetti[2]; [1]ASUITS Hospital, Trieste, ITALY, [2]Niguarda Hospital, Milano, ITALY.

Purpose: Catheter radiofrequency ablation (RFA) represents an important therapeutic option in non-ischemic cardiomyopathy (NICM) patients with recurrent episodes of ventricular tachyarrhythmias refractory to anti-arrhythmic drug therapy. This approach is even more relevant in NICM patients with impiantable cardiac device (ICD) and frequent painful discharges. Recently, several mapping systems have been introduced to facilitate RFA procedures. The CARTO electroanatomic mapping system is currently the most commonly used tool and it can provide three-dimensional color-coded maps of impulse propagation within the cardiac chambers. Before RFA procedure, cardiac magnetic resonance imaging (MRI) with delayed enhancement represents the gold standard for the evaluation of anomalous myocardial tissue that may harbor the arrhythmia substrate. However, evaluation of myocardial viability with FDG-PET might play a role in selecting the most appropriate mapping approach in patients with contraindications to MRI (i.e presence of ICD or severe renal dysfunction). The aim of this study was to verify whether myocardial viability assessment with FDG PET-CT might be helpful in guiding RFA. **Methods:** 6 males non-diabetic patients (mean age 61 year) with NICM underwent an FDG PET-CT study at least one day before RFA procedure. In these patients MRI was contraindicated for end-stage kidney disease in one patient and for the presence of ICD in the remaining 3 patients. An oral glucose load protocol was applied at least 30 minutes before tracer injection in order to enhance myocardial glucose uptake and suppress fatty acids utilization. A cardiac PET-CT acquisition (15 minutes) started after about 45 minutes from FDG administration. The results were displayed with QPS software (Cedars-Sinai Medical Center) to estimate global and regional cardiac uptake of FDG through 17 segment polar maps. RFA was guided by the CARTO system mapping and both left ventricular bipolar potentials and unipolar voltage maps were evaluated. **Results:** In these 6 patients we found a closely match between areas with pathological voltages at CARTO mapping and those characterized by a reduction in FDG uptake. In fact, in

these patients the clinical ventricular tachycardia was induced and successfully ablated at the exit site, which was located inside the pathological area identified at CARTO. All the patients had a significant reduction of arrhythmic events up to 8 month of follow-up. **Conclusions:** These preliminary findings suggest a potential role of myocardial viability evaluation by FDG PET-CT in the identification of myocardial substrate of arrhythmia. Therefore, this imaging technique could be helpful in guiding RFA procedure.

1010　　　　　**Monday, October 23, 2017, 16:30 - 18:00, Hall G2**

Committee Symposium 5 - Radiation Protection: CT-Optimisation of Hybrid Imaging

OP-414

Technical Optimisation

K. Bacher; Ghent University, Department of Medical Physics, Ghent, BELGIUM.

OP-415

Optimisation in Oncology

P. Veit-Haibach; University of Toronto, Joint Department of Medical Imaging, Toronto, CANADA.

OP-416

Optimisation in Paediatric Nuclear Medicine

P. Dinis de Almeida; Institute of Biophysics and Biomedical Engineering, Faculty of Sciences, University of Lisbon, Lisbon, PORTUGAL.

OP-417

The View of HERCA on Optimisation

S. Ebdon-Jackson; CRCE, Public Health England, Oxfordshire, UNITED KINGDOM.

1101　　　　　**Tuesday, October 24, 2017, 08:00 - 09:30, Hall A**

CME 9 - (Paediatrics/Inflammation & Infection: FDG PET in Paediatric infections

OP-419

FDG PET in the Evaluation of Lymphadenopathy in Children

L. Borgwardt; Clinic for Clinical Physiology, Nuclear Medicine & PET, 4011, Diagnostic Center, Copenhagen University Hospital, Rigshospitalet, Copenhagen, DENMARK.

OP-420

FDG PET in the Evaluation of the Immunocompromised Child with Fever

I. Kouijzer; Department of Internal Medicine and Infectious Diseases, Radboudumc, Nijmegen, NETHERLANDS.

OP-421

The Clinical Approach to the Immunocompromised Child with Fever

F. Karup Pedersen; Paediatric and Adolescence Clinic, Juliane Marie Centre, Copenhagen University Hospital, Rigshospitalet, Copenhagen, DENMARK.

1102　　　　　**Tuesday, October 24, 2017, 08:00 - 09:30, Hall B**

Joint Symposium 9 - EANM/EFOMP: New Developments in CT Technology

OP-422

Dual Energy CT

M. Kachelriess; University of Heidelberg, German Cancer Research Center, Medical Physics Radiology / X-Ray Imaging and CT, Heidelberg, GERMANY.

OP-423

CT Dose Optimisation Techniques

M. Kortesniemi; University of Helsinki, HUS Medical Imaging Center, Meilahti Hospital, Helsinki, FINLAND.

OP-424

CT in Hybrid Imaging Systems

M. Brambilla; Az. Ospedaliero Universitaria Maggiore della Carità, SC di Fisica Sanitaria, Novara, ITALY.

OP-425

Motion Compensation in CT

M. Kachelriess; University of Heidelberg, German Cancer Research Center, Medical Physics Radiology / X-Ray Imaging and CT, Heidelberg, GERMANY.

1104　　　　　**Tuesday, October 24, 2017, 08:00 - 09:30, Hall E1**

Do.MoRe: Preclinical & Clinical Dosimetry

OP-427

In-vivo biokinetics of ^{177}Lu-OPS201 in mice and pigs as a model for predicting human dosimetry

S. Beykan[1], M. Fani[2], G. Nicolas[2], D. Wild[2], R. Bejot[3], J. Kaufmann[3], H. Bouterfa[3], S. Jensen[4], M. Lassmann[1]; [1]Department of Nuclear Medicine, University of Würzburg, Würzburg, GERMANY, [2]Division of Nuclear Medicine, University Hospital of Basel, Basel, SWITZERLAND, [3]Octreopharm Science GmbH, Ipsen Group, Berlin, GERMANY, [4]Department of Chemistry and Biosciences, Aalborg University, Department of Nuclear Medicine, Aalborg University Hospital, Aalborg, DENMARK.

Aim: ^{177}Lu-OPS201 is a high-affinity somatostatin receptor antagonist for Peptide Receptor Radionuclide Therapy in patients with neuroendocrine tumors. Here we report a comparison between the biokinetics in animals and in patients. In addition, five inter-species extrapolation methods were examined to find the optimal method for dosimetry. **Materials and Methods:** Data on biokinetics of ^{177}Lu-OPS201 were obtained in athymic Nude-***Foxn1***^{nu} mice (28F, weight: 26±1g),

Danish-Landrace pigs (3F-1M, weight: 28±2kg), and patients (3F-1M, weight: 61±17kg) with administered activities of 0.19-0.27MBq (mice, 0.017µg of peptide), 97-113MBq (pigs, 9µg of peptide) and 850-1086MBq (patients, 55-106µg of peptide) [1,2]. In pigs and patients, kidney protection was applied. Multiple planar and SPECT/CT scans were performed until 250h (pigs) and 70h (patients) to quantify the uptake in kidneys and liver. Blood samples were taken up to 168h (patients) and 300h (pigs). Mice were euthanized at different time points (up to 168h); the organ-specific activity contents (including blood) were measured. Population-based time-dependent uptake data sets were created for each species and organ/tissue. Bi-exponential fits were applied to compare the biokinetics of kidneys liver, and blood in each species and to analyze the differences. The time-integrated activity coefficients (TIACs) were calculated by integration of the respective data. To determine the optimal extrapolation method, several scaling methods (relative organ/whole-body mass-scaling, time-scaling, combined mass- and time-scaling, allometric scaling) were compared. Blood TIAC values of mice were not included since the data for total blood volume were not available. **Results:** A fast blood clearance of the compound was observed in the first phase (<56h) for each species. In comparison to patients, pigs show higher liver retention. Based on the direct comparison of the TIACs, an underestimation in mice (liver, kidney) and an overestimation in pigs' kidneys compared to the patient data (Kidney-TIAC: Mice=1.4h, Pigs=7.7h, Patients=5.8h, Liver-TIAC: Mice=0.7h, Pigs=4.1h, Patients=5.3h) were observed. Most similar TIACs were obtained by applying time-scaling (mice) and combined scaling (pigs) methods (Kidney-TIAC: Mice=3.9h, Pigs=4.8h, Patients=5.8h, Liver-TIAC: Mice=0.9h, Pigs=4.7h, Patients=5.3h). Other methods showed higher deviations. **Conclusion:** If the organ mass ratios between the species are high, the combined mass- and time-scaling method is optimal to minimize the interspecies differences. The analysis of the fit functions and the TIACs show that, in our study, pigs better mimic human biokinetics than mice for blood and the organs considered. **References:** [1] Beykan et al, EJNMMI Research 2016, [2] Wild et al, JNM 2014

OP-428

A comparison of 2D and 3D kidney absorbed dose measures in patients receiving Lutate therapy

K. Willowson[1], H. Ru[1], A. Singh[2], P. Jackson[3], E. Eslick[2], D. Bailey[2]; [1]University of Sydney, Sydney, AUSTRALIA, [2]Department of Nuclear Medicine, Royal North Shore Hospital, Sydney, AUSTRALIA, [3]Peter MacCallum Cancer Centre, Melbourne, AUSTRALIA.

Aim: Kidneys are considered the organ-at-risk (OAR) for ^{177}Lu-DOTATATE (Lutate) treatment. Proposed OAR dose thresholds have been imported from radiotherapy, which may not be suitable for Lutate treatment given differences in radiation type, dose rate, and heterogeneity of dose distribution. Whilst the majority of literature estimating Lutate kidney dose is based on 2D planar imaging, more accurate quantitative 3D imaging is now becoming available. The aim of this study

was to compare kidney absorbed dose measures made from 2D and 3D imaging in patients receiving Lutate therapy, for the purpose of deriving accurate estimates of kidney dose to guide treatment. **Materials and Methods:** Patients underwent whole body planar imaging and kidney SPECT/CT at 0.5, 4, 24, and 96-120 hours after ~8 GBq Lutate injection. Transmission based attenuation correction was applied to planar data before conversion to units of absolute activity via two methods, using either a calibration standard or pre-voiding image counts. Regions-of-interest were used to generate time activity curves (TACs) and kidney doses were estimated in OLINDA. Quantitative SPECT (qSPECT) data were generated using CT-derived scatter, attenuation, and dead-time corrections and calibrated with a detector sensitivity factor. Volumes-of-interest were defined on the co-registered CT and TACs and dose estimates generated in OLINDA, both with and without correction for patient specific kidney volumes. 3D dose maps were also derived through dose kernel convolution (DKC) and CT-derived VOIs used to estimate kidney dose, which was treated as the gold standard. **Results:** 50 series were analysed. The average kidney absorbed dose was 2.6 ± 1.1 Gy/cycle (0.34 ± 0.14 mGy/MBq), based on the DKC method. 2D dose estimates were higher than DKC estimates by, on average, a factor of 2.3. There was no significant difference in 2D dose estimates made by the use of a calibration standard vs normalisation of counts to injected activity. Doses calculated using qSPECT and OLINDA were higher than DKC estimates by, on average, a factor of 1.3. The average difference between 3D dose estimates made with OLINDA using model kidney volumes vs patient specific kidney volumes was 3% (max 43%). **Conclusion:** Centres using 2D planar estimates for Lutate kidney absorbed dose can expect to overestimate the true exposure and should be cautious if limiting treatment cycles based on such measures and the current OAR thresholds. 3D estimates are likely to be more accurate in guiding further Lutate cycles and understanding true kidney dose-toxicity profiles for radionuclide therapy.

OP-429

Patient-specific pharmacokinetics and dosimetry over multiple therapy cycles during ^{177}Lu-based radionuclide therapy: a study for ^{177}Lu-DOTATATE and ^{177}Lu-PSMA

A. Gosewisch, L. Ermoschkin, H. Ilhan, A. Todica, L. Vomacka, P. Bartenstein, G. Böning; University Hospital Munich, Munich, GERMANY.

Aim: Both, ^{177}Lu-DOTATATE and ^{177}Lu-PSMA, evolved as promising therapy options in case of metastasized cancer disease. The aim of this work was to study ^{177}Lu-DOTATATE and ^{177}Lu-PSMA with regard to the patient-specific pharmacokinetics over multiple therapy cycles and to derive appropriate image-based dosimetry schemes. **Methods:** The kidney and tumour pharmacokinetics of 12 patients (6: 3.7-6GBq ^{177}Lu-PSMA-DKFZ-617, 6: 7.4GBq [[177]Lu-][DOTA[0]][Tyr[3]]Octreotate) was studied over the initial two therapy cycles via quantitative SPECT acquired 24, 48 and 72h p.i. (+CT). For each patient and cycle, both kidneys and three tumours were delineated and a corresponding S-value

dosimetry including a mono-exponential fit of the three data points was performed. Furthermore, for the dosimetry of the second cycle, we compared the doses derived from a modified imaging protocol, which combines a single SPECT either 24, 48 or 72h p.i. with the effective half-life of the first cycle. **Results:** For ^{177}Lu-DOTATATE the kidney mean (+/-SD) doses were 0.84+/-0.33Gy/GBq and 0.80+/-0.35Gy/GBq for cycle one and two. The dose increased in 25% of the kidneys due to an increased half-life, uptake or both. The tumour doses decreased from 4.92+/-4.01Gy/GBq to 3.91+/-1.94 Gy/GBq due to a reduction of the absorbed doses in 44% of the tumours, which is linked to a decrease in the effective half-life, uptake or both in 38% of the cases and partially due to an increase in the delineated tumour volume in 62% of the cases (40%-isocontour). For ^{177}Lu-PSMA the mean kidney doses were 0.58+/-0.23Gy/GBq and 0.61+/-0.21Gy/GBq for cycle one and two, with an increase of the dose for 50% of the kidneys mainly due to an increased uptake at 24h. The mean tumour dose decreased from 4.97+/-5.13Gy/GBq to 1.82+/-1.30Gy/GBq with a dose reduction in 83% of the tumours, mostly due to a decreased effective half-life partially accompanied by a decreased uptake. Although, a pronounced change of the effective half-lives is possible (^{177}Lu-DOTATATE: kidneys: 22+/-11%, tumours: 42+/-41%; ^{177}Lu-PSMA: kidneys: 14+/-13%, tumours: 29+/-23%), a dosimetry during the second cycle based on a single SPECT 72h p.i. reproduced all doses on average within 10%. **Conclusion:** Summarized, for both ^{177}Lu-DOTATATE and ^{177}Lu-PSMA , the first cycle constitutes the more importent contribution to the tumour dose and to the kidney dose for more than half of the cases. Using a reduced dosimetry scheme for the second cycle based on a single image acquisition 72h p.i. is thus feasible for both therapies.

OP-430

The effect of the total tumour volume on the kidneys, salivary glands and tumour BEDs for ^{177}Lu-labelled PSMA ligands

N. J. Begum[1], *A. Thieme*[2], *J. Allmann*[2], *M. Eiber*[2], *A. J. Beer*[3], *G. Glatting*[1], *P. Kletting*[1]; [1]*Medical Radiation Physics, Department of Nuclear Medicine, Ulm University, Ulm, GERMANY,* [2]*Department of Nuclear Medicine, Klinikum Rechts der Isar der Technischen Universität München, Munich, GERMANY,* [3]*Department of Nuclear Medicine, Ulm University, Ulm, GERMANY.*

Purpose: To investigate the effect of the total tumour volume on the tumour, kidneys and salivary glands biologically effective dose (BED) for prostate specific membrane antigen (PSMA) labelled with ^{177}Lu using a physiologically-based pharmacokinetic (PBPK) model. **Materials and Methods:** Eight patients with metastasized prostate cancer were included in this simulation study. An average activity of (7.2±0.3) GBq and ^{177}Lu-labeled PSMA-specific peptides of (87.7±4.1) nmol were administered. The individual parameters of the PBPK model were obtained from fits to measured biokinetic data. The biokinetics of every patient were simulated for total tumour volumes of 0.1, 0.3, 1, 3, and 10 l. Based on these simulations, the BED values were obtained

for two tumour lesions, the remaining tumour, the kidneys and the salivary glands. Furthermore, the therapeutic indices of tumours to organs at risk were calculated for every simulated total tumour volume. **Results:** The average BED values of these eight patients were (23 ± 13)Gy, (5.7 ± 2.2)Gy$_{2.5}$ and (13.9 ± 5.2) Gy$_{7.5}$ for lesions, kidneys and salivary glands, respectively. The simulated BEDs of the tumour lesions strongly depend on the total tumour volume, i.e. (28 ± 17)Gy, (26 ± 15)Gy, (22 ± 11)Gy, (15.3 ± 7.1)Gy and (7.6 ± 3.4)Gy for total tumour volumes of 0.1, 0.3, 1, 3, and 10 l, respectively. A similar dependence on tumour volume is obtained for the kidneys and salivary glands, i.e. (7.1 ± 3.2)Gy, (6.7 ± 2.9)Gy, (5.6 ± 2.1)Gy, (4.0 ± 1.2)Gy, (2.2 ± 0.7) Gy and (17.0 ± 7.3)Gy, (16.1 ± 6.6)Gy, (13.8 ± 4.9)Gy, (10.1 ± 3.2)Gy, (5.5 ± 2.1)Gy, respectively. The therapeutic indices have broad distributions for lesions to kidneys (median 3.9, range 0.2-9.5) and for lesions to salivary glands (median 1.6, range 0.1-6.3). The same applies for the relative change of the therapeutic index with increasing (simulated) tumour volumes: the mean change is 0 %, but in individual patients it could decrease or increase by up to 20 %, demonstrating the importance of the actual tumour volume for optimizing the treatment planning for an individual patient. **Conclusion:** The tumour and organ at risk BEDs are strongly affected by the total tumour volume for patients with advanced prostate carcinoma. The simulation study shows that patients with high tumour burden would benefit from higher prescribed activities as the BEDs to the critical organs and tumours are considerably lower compared to patients with lower total tumour volume. Therefore, an accurate method to identify the total tumour volume needs to be developed to be able to determine the optimal amount of peptide and activity for each patient.

OP-431

Concurrent use of ^{90}Y, ^{177}Lu and [225]Ac-labelled PSMA-binding radiopharmaceuticals can lead to improved treatment efficacy

A. M. Denis-Bacelar, A. J. Fenwick, K. M. Ferreira, J. L. Wevrett, A. P. Robinson; National Physical Laboratory, Teddington, UNITED KINGDOM.

Aim: Radiolabeled PSMA-based radiopharmaceuticals such as ^{90}Y-PSMA-J591, ^{177}Lu-PSMA-617 and [225]Ac-PSMA-617 have been shown effective for the treatment of metastatic prostate cancer. However, the different physical characteristics of the radionuclides are likely to have a significant impact upon the success of systemic treatments of microscopic metastases. The relationship between the tumour control probability (TCP) and tumour size was studied for different activity concentrations and combinations of ^{90}Y, ^{177}Lu and [225]Ac. **Materials and Methods:** Metastatic lesions were modelled as spheres with radii ranging from 100 μm to 2 cm. The radionuclides were assumed to be uniformly distributed through the volume. The EGSnrc general purpose Monte Carlo code was used to calculate the energy deposited by the beta emitters ^{90}Y and ^{177}Lu using the decay data from the RADTABS software. An equilibrium dose constant of 14.3 Gy·g/MBq/h and a relative biological effec-

tiveness (RBE) factor of 5 were used for the alpha emitter ^{225}Ac. Absorbed doses were calculated for a range of specific cumulated activities (MBq·h/g) and cocktail proportions of the three radionuclides. The TCP was calculated using the liner quadratic model and radiobiological parameters characteristic of prostate cancer cells: clonogenic cell density of 3.10^6 cm^{-3}, α/β of 3.1 Gy, α of 0.15 Gy^{-1} and repair constant μ of 0.46 h^{-1}. **Results:** Optimal tumour control for ^{90}Y, ^{177}Lu and ^{225}Ac as non-concurrent treatments was achieved for tumour radii larger than 0.1 cm, between 0.06 and 0.1 cm, and smaller than 0.07 cm, respectively. A TCP>0.95 was obtained for tumour sizes between 100 μm and 2 cm for a specific cumulated activity of 300 MBq·h/g and a 1:39 ratio of ^{225}Ac:^{90}Y. A higher specific cumulated activity of 1200 MBq·h/g and a 1:9 ratio of ^{177}Lu:^{90}Y was required to obtain a TCP of 0.75-0.95 for radii below 0.05 cm and a TCP >0.95 for larger tumours. **Conclusion:** The combination of ^{225}Ac and ^{90}Y resulted in improved curability of microscopic and macroscopic metastases as compared to ^{177}Lu and ^{90}Y. The concurrent use of cocktails of radiopharmaceuticals can lead to improved treatment efficacy for patients with metastatic prostate cancer. Future work will include non-uniform uptake distributions to study the effect of in-homogeneities and the effect of combining radiopharmaceuticals with different targeting mechanisms.

OP-432

Assessing the impact of registration methods on absorbed dose calculation in Peptide Receptor Radionuclide Therapy

S. Berenato¹, E. Grassi², F. Fioroni², D. Finocchiaro²,³, M. Iori², E. Spezi¹; ¹*School of Engineering, Cardiff University, Cardiff, UNITED KINGDOM,* ²*Arcispedale Santa Maria Nuova - IRCCS, Reggio Emilia, ITALY,* ³*Department of Physics, University of Bologna, Bologna, ITALY.*

Introduction: Peptide Receptor Radionuclide Therapy (PRRT) is currently the most effective therapy for the treatment of patients with Neuro-Endocrine Tumours. To determine the cumulated activity in volumes of interest (VOIs), serial measurements of the radiopharmaceutical activity should be performed through the analysis of multiple quantitative functional imaging. Sequential tomographic scans should be co-registered so that an accurate patient specific 3D dosimetry can be carried out. The rigid alignment between scans assumes that organs are only subjects to roto-translational movements and are unable to account for the complex internal organs motion present in the abdominal region. To accurately estimate the dose delivered to the VOIs, deformable image registration (DIR) is needed. This study focusses on developing an optimised workflow for the use of DIR algorithms in the context of a clinical trial in PRRT. **Materials and Methods:** Twenty patients treated with PRRT were imaged five times, post-injection of therapeutic administration of ^{177}Lu-labeled peptides with a SPECT/CT scanner. Sequential quantitative functional scans were registered to the reference scan and used to calculate patient specific 3D dose map using the Raydose Monte Carlo code[1]. We systematically

evaluated the impact of two different workflows involving a DIR algorithm. In the activity registration workflow (ARW), the activity maps were registered to the same reference scan before the total dose was calculated. In the dose registration workflow (DRW), the activity scans were used to calculate intermediate dose maps that were subsequently accumulated to obtain the total dose map using the deformation maps generated for the ARW. The accuracy of the DIRs was quantified using the Dice Similarity Coefficients (DSC) calculated for VOIs manually drawn on all scans. **Results:** DSC analysis confirmed excellent quality of the DIR maps, with DSC values > 0.7 in all cases. In 91% of patients, mean dose to organs at risk (OARs) calculated with DRW was higher than that calculated with ARW. The use of effective decay constants reduced this discrepancy in 16% of the cases. For lesion dosimetry, no correlation was found between total dose and registration algorithms, with percentage differences in the range [-44%, 50%]. **Conclusions:** Dose registration overestimates the absorbed dose to OARs compared to activity deformation and results in a more time-consuming workflow. The accuracy of lesions dosimetry is hampered by internal organ motion and remains a challenge that could be addressed by developing dedicated DIR strategies. **References:** [1] Marcatili Phys Med Biol. 2013 Vol 58 p 2491

OP-433

Evaluation of the Correlations Between the Absorbed Bone Marrow Dose and Bone Marrow Response During the First Cycle of 177Lu-DOTATATE Treatment

L. Hagmarker¹, J. Svensson², T. Rydén¹, B. Wängberg³, A. Sundlöv⁴, K. Sjögreen Gleisner⁵, P. Bernhardt¹; ¹*institution of clinical sciences, Göteborg, SWEDEN,* ²*Department of Oncology, Göteborg, SWEDEN,* ³*Department of Surgery, Göteborg, SWEDEN,* ⁴*Department of Oncology, Skåne University Hospital, Lund, SWEDEN,* ⁵*Department of Radiation Physics, University of Lund, Lund, SWEDEN.*

Treatment with ^{177}Lu-DOTATATE has become an established treatment option with minor side effects for patients with advanced neuroendocrine tumours. The bone marrow is one of the organs at risk and blood samples are drawn to monitor the bone marrow function during treatment. The aim of this project is to investigate if a correlation between the absorbed bone marrow dose and the bone marrow response in terms of decreased levels of haemoglobin, white blood cells and platelet counts can be established from the first treatment cycle. **Materials and Methods:** 35 patients with advanced neuroendocrine tumours treated with ^{177}Lu-DOTATATE at Sahlgrenska University Hospital between 2011 and 2016 (ILUMINET-study, EUDRACT nr 2011-etc) was included in this study. Blood samples were drawn once a week and absorbed doses to the bone marrow were calculated after the first treatment cycle. The absorbed bone marrow dose was estimated using planar gamma camera images collected at 2, 24, 48 and 168 hours post injection and a two-compartment method in the image platform PhONSAi, developed in-house. Correlations are investigated between the absorbed bone marrow doses and the nadir values and the response rates of haemoglobin, white blood cells and throm-

bocytes. The response rate is the linear slope calculated using blood values normalized to the baseline values. **Results:** The mean absorbed bone marrow in the first treatment cycle was estimated to 0.19 Gy (0.12-0.32 Gy). Already after the first treatment cycle significant correlations were found between the absorbed bone marrow dose and the decrease in platelet counts (p=0.02) and between the absorbed bone marrow dose and the response rate of platelet counts (p=0.01) and white blood cells (p=0.01). **Conclusion:** Significant correlations were found after the first treatment cycle between the absorbed bone marrow dose and the response of platelet counts and white blood cells. As a consequence of the slow response of haemoglobin, no correlations to the absorbed bone marrow dose could be found this early after treatment.

OP-434

Prospective Dosimetry and Optimization of RPT-XRT Combination Therapies

R. F. Hobbs, A. Josefsson, E. C. Frey, S. A. Terezakis, C. Meyer, D. M. Loeb, G. Sgouros; *Johns Hopkins University, Baltimore, MD, UNITED STATES OF AMERICA.*

Objectives: Metastatic osteosarcoma is a cancer of adolescents and young adults which has a very low survival rate. In general, disseminated disease requires systemic treatment, while for the localized macroscopic disease external beam radiation therapy (XRT) is a viable treatment option. At the same time, XRT is limited by adjacent normal organ toxicity, while radiopharmaceutical therapy (RPT) often has a high signal to background ratio locally. Moreover the two modalities are radiation-based, meaning that they can be combined rationally and treatment planning can be optimized based on the combined absorbed dose (AD) to the dose limiting organ(s). For metastatic osteosarcoma ^{153}Sm-EDTMP, an FDA approved bone seeking calcium mimetic, was combined with XRT for safe and effective therapy. **Methods**: Five patients have been treated thus far under this protocol. The patients underwent stem cell harvesting, then received a 37 MBq/kg pre-therapeutic dose of ^{153}Sm-EDTMP and were imaged at 4, 24 and 48 h p.i. The in-house RPT treatment planning system, 3D-RD, was used to optimized the combined plan of administered activity and XRT treatment plan by entering the RPT AD-map converted to 2-Gy equivalent AD (EQD2) into the XRT treatment planning system (Pinnacle). One week after the pre-dose, the therapeutic dose was administered, and the patients imaged at 4, 24 and 48 h p.i. AD-maps and DVHs were again generated using 3D-RD for the RPT portion of the treatment. A revised combined RPT/XRT treatment plan that incorporated the therapeutic Sm-153 dose deposition was created. **Results**: The plans gave therapeutic doses to target tumors. As an example for a pelvic tumor, the EQD2 delivered to the tumor by RPT was 19.9 Gy using an injected activity of 370 MBq/kg determined by the treatment plan as well as an XRT plan that delivered another 50.9 Gy to the tumor, resulting in a total tumor AD of 70.8 Gy. The AD to adjacent spinal cord from the combined treatments was 30.9 Gy, lower than the maximum tolerable AD of 52 Gy. the tumoricidal threshold dose of 70 Gy

would not have been possible with XRT alone. **Conclusions**: The treatment planning protocol combining RPT and XRT for metastatic osteosarcoma in pediatric patients has shown potential to treat a highly aggressive disease, while limiting the AD to normal organs to below potentially toxic thresholds. Based on the methodological success of this case other RPT-XRT combination therapies have been developed.

1105   **Tuesday, October 24, 2017, 08:00 - 09:30, Hall E2**

M2M: Automation & Production

OP-435

A 3D-Printed Automated Dual Reactor Synthesizer for Challenging Multi-Step ^{18}F-Fluorinations: Testing and Validation

A. Amor-Coarasa, J. M. Kelly, D. Kim, W. Qu, P. Kothari, J. W. Babich; *Weill Cornell Medical College, New York City, NY, UNITED STATES OF AMERICA.*

Aim: Robust, automated ^{18}F-fluorinations are vital for PET radiopharmacy production. Most automated synthesis units (ASU) are optimized for routine production of ^{18}F-FDG, the main PET tracer in clinical use. Despite the wide variety of ^{18}F imaging agents developed, production at radiopharmacies almost invariably requires adapting the new synthesis to an existing ASU. Versatile, customizable options for challenging multi-step syntheses such as the TRASIS ALLINONE™ are available, but at a very high cost. Hence, we sought to design and build a reliable, lower cost, fit-for-purpose, 3D-printed ASU capable of preparing ^{18}F imaging agents using multistep syntheses incorporating two reactors. **Methods:** All designs were drawn using Autodesk® AutoCAD® 2013 or newer. The housing was printed in poly(acrylonitrile butadiene styrene) (ABS). Moving parts were printed in nylon and heaters were printed in porcelain. High torque motors and linear actuators were used for valve turning and syringe loading/dispensing. A 24 channel USB servo controller was used for sequenced automation. The synthesis sequence was designed and uploaded onto the ASU via USB. Synthesis of the tracers consisted of (1) ^{18}F capture, elution and azeotropic drying; (2) synthesis of 2-^{18}F-fluoroethylazide at 80°C; (3) distillation of the synthon at 130°C and its trapping in a second reactor cooled to 5°C; and (4) a click reaction at 100°C following addition of Cu$^+$ and the alkyne precursor. **Results:** The total cost of design and assembly of the ^{18}F ASU was less than 5000 USD, a substantial improvement over the 100,000-200,000 USD that these units normally cost. Critical synthetic steps are controlled by a simple external push button, with several, sequential safety checkpoints. The synthesizer was validated for the synthesis of ^{18}F-RPS-040, a PSMA-targeting radiotracer. Decay-corrected radiochemical yield at the end-of-synthesis was 15.3±1.0% (n=3). There was no mechanical failure during any of the pre-testing sequences or validation runs (n>10). Synthesis time was 58 minutes after receiving ^{18}F from the cyclotron.

Conclusions: A 3D-printed, two reactor ASU was designed, manufactured and tested for a specific, multistep radiosynthesis that includes a distillation. The ASU is robust and reliable for routine clinical use, as neither leakage of liquids nor loss of radioactivity was observed even with high starting activities. Not only is the 3D-printed ASU a practical, lower-cost alternative to commercially available units, but it also represents a change of paradigm: *Do not adapt your synthesis to an existing ASU, but rather build a new ASU to accommodate your synthesis.*

OP-436

Optimization of a Novel Automated Loop Method for Production and Development of Analytical Methods for ^{11}C-Nicotine Injectable

K. Kumar, A. Ghosh, K. Woolum, M. V. Knopp; The Ohio State University, Columbus, OH, UNITED STATES OF AMERICA.

Objectives: The objective of the present study was to develop and optimize a novel automated loop method for production of ^{11}C-Nicotine Injectable and to develop analytical test methods (Identification, pH, Radionuclidic Purity, Radiochemical Purity (RCP), Chemical Purity, Specific Activity, Bacterial Endotoxin, and Sterility) and specifications for its quality control. **Methods:** In the automated production process, the ^{11}CO$_2$ was trapped at -180ºC, converted into ^{11}C-Methane and then ^{11}C-Methyl Iodide, followed by the reaction of ($\pm$) Nornicotine in the loop. The reaction mixture was purified using a semi-preparative Reversed-Phase (RP) HPLC method to remove unreacted ^{11}CH$_3$I and ($\pm$) Nornicotine. The final product was tested for the identification, RCP, chemical purity, and specific activity of ^{11}C-Nicotine by using an analytical HPLC method. The analytical HPLC method involved a Waters XTerra C$_{18}$ column (150x4.6 mm, 5 µm) at 40ºC with an isocratic mobile phase containing 80:20 mixture of 6.5 mM ammonium acetate pH 10 and acetonitrile at a flow rate of 1.0 mL/min. General methods (USP <71> and USP <85>) were used for Sterility and Bacterial Endotoxin tests, respectively. **Results:** A gas-phase produced ^{11}CH$_3$I precursor was used instead of ^{11}C-Formaldehyde or ^{11}CH$_3$I produced by the Lithium Aluminum/HI method. The reaction conditions were optimized by varying the amounts of precursor, loop temperature, and reaction times. These experiments suggested that the reaction of 2 mg precursor with ^{11}CH$_3$I for 5 minutes at 75^0, 100º, and/or 125ºC loop temperature gave ~20% (corrected) yield of the final product. An analytical HPLC method (with a 10 minutes run time) was developed with an excellent separation (retention times in min in the parenthesis) between ^{11}CH$_3$I (2.4), ($\pm$) Nornicotine (3.1), and ^{11}C-Nicotinine (5.5). Typically, ^{11}C-Nicotine (3.7mCi/mL) was produced with >99.9% RCP, no ^{11}CH$_3$I, no ($\pm$) Nornicotine, 9.8 ng/mL of Nicotine resulting 60.3Ci/µmole specific activity, 7.0 - 7.2 pH, and 20% ethanol. The product was also passed the Identification, Radionuclidic Purity, Sterility, and Bacterial Endotoxin tests. **Conclusions:** A robust and efficient process for production of high purity (>99.9%) ^{11}C-Nicotine with ~20% (corrected) yield was developed. Several analytical test methods and specifications for the quality control of ^{11}C-Nicotine were developed successfully.

OP-437

Synthesis Of 64Cu Radiopharmaceuticals For Cell Radiolabelling Using Anion Exchange Column And Labelling Of WBCs

A. Socan[1], P. Kolenc Peitl[1], M. Kroselj[1], M. Petrik[2], C. Decristoforo[3]; [1]Nuclear Medicine Department, University Medical Centre, Ljubljana, SLOVENIA, [2]Institute of Molecular and Translational Medicine, Olomouc, CZECH REPUBLIC, [3]University Clinic for Nuclear Medicine, University for Medicine, Innsbruck, AUSTRIA.

Introduction: ^{111}In labelled radiopharmaceuticals are extensively used for cell radiolabelling in routine clinical practice. Due to its half life (12.7 h) and positron emission ^{64}Cu labelled cells could possibly enable PET "in vivo" cell tracking with several attractive clinical applications (imaging of infection and inflammation, stem cell therapy). The aim of this study was to prepare (using an approach of synthesis and concentration on an anion exchange column) ^{64}Cu tracers (oxine, tropolone) and label WBCs. **Materials and Methods:** Small volumes (1-2 mL) of ^{64}Cu tracers (oxine, tropolone) in PBS of suitable radiochemical purity (n-octanol extraction) and activity (up to 102 MBq) were prepared on the anion exchange column (SepPAK QME) using a previously described method used for ^{68}Ga and ^{89}Zr labelling. WBCs were radiolabelled using modified (incubation time 20 min) EANM recommended ^{111}In-oxine WBCs labelling method. Labelling efficiency, cell viability, assessed by Trypan Blue exclusion assay and labelling stability (efflux of radioactivity) was determined at different time points after ^{64}Cu tracer radiolabelling. **Results:** Using an anion exchange column, synthesis and concentration method yield of ^{64}Cu-tropolone solution was above 92.5% with pH between 6.9-7.4 and extraction into octanol above 89.1%. Yield of ^{64}Cu-oxine solution was between 55-91.1% with pH between 6.9-7.5 and extraction into octanol above 90.6%. Labelling efficiency of WBCs s with ^{64}Cu-tropolone was above 81.1% and not dependent on the amount of cells available for radiolabelling. Labelling efficiency of WBCs s with ^{64}Cu-oxine was up to 68% and dependent on the amount of cells available. Viability of ^{64}Cu-tropolone radiolabelled WBCs before and immediately after the labelling was 92% and 85%, respectively; viability 240 min after labelling was 88 and 81%. Labelling stability of WBCs 240 min after cell radiolabelling was above 68% and remained constant up to 48h after labelling. Viability of ^{64}Cu-oxine radiolabelled WBCs immediately after the labelling was 71% (90% unlabelled WBCs) and 70% 240 min after labelling (85% unlabelled WBCs). Labelling stability of WBCs 240 min after cell labelling was above 91% but decreased to 78.1% 48h after labelling. **Conclusions:** The applied on-column synthesis and concentration method enables formation of ^{64}Cu tracers (oxine, tropolone) with good yields, quality and in small volumes suitable for cell radiolabelling. ^{64}Cu tracers radiolabel WBCs with sufficient stability and viability, this way making this approach highly promising for routine clinical use. Proof of concept in animal infection models is ongoing.

OP-438

Production and Purification of 99mTc Pertechnetate from 100Mo Targets Irradiated in a Nirta Solid Target Station on an IBA Cyclone® 18 Cyclotron

K. Buckley[1], P. Martini[2,1], M. Dodd[1], S. McDiarmid[1], V. Hanemaayer[1], B. Hook[1], J. Kumlin[1], S. Zeisler[1], P. Schaffer[1], C. Marshall[3], A. Dabkowski[3], M. Talboys[3], S. Wiltshire[3], F. Devillet[4], D. Blampain[4], B. Nactergal[4]; [1]TRIUMF, Vancouver, BC, CANADA, [2]University of Ferrara, Ferrara, ITALY, [3]Wales Research and Diagnostic PET Imaging Centre, Cardiff, UNITED KINGDOM, [4]IBA RadioPharma Solutions, Louvain-la-Neuve, BELGIUM.

Direct production of the highly utilized radioisotope 99mTc is a practical approach to self-sufficiency of supply. A TRIUMF-led consortium developed 100Mo coating technology to manufacture high current targets (Schaffer et al., J Nucl Med 2015; 56 Supp. 3: 164) and demonstrated the routine production and purification of 99mTc. The aim of this work is to implement these processes on an IBA Nirta target station and Synthera® Extension automated synthesis units. The project was implemented as discrete activities due to the geographical spread of the participants. At TRIUMF 100Mo pellets of 0.9 grams and 12.4 mm diameter were pressed and sintered. Using the method described in Zeisler et al. (http://www.qucosa.de/recherche/frontdoor/?tx_slubopus-4frontend[id]=16606) these pellets were bonded to copper alloy backings sized to fit the Nirta target station. At the Cardiff IBA Cyclone® 18 facility three targets were irradiated at 50 µA and 18 MeV for one hour and three for six hours. Target yields were estimated by measuring the whole target plate in a dose calibrator to obtain a decay curve from which the 99mTc component was extracted. At TRIUMF, separation and purification of 99mTc from 100Mo was carried out using two IBA Synthera® Extension modules. Each unit provides one syringe pump and ten pinch valves. The separation and purification scheme follows that published by Bénard et al (J Nucl Med 2014; 55:1910-1914). Initial testing used a mock solution of a dissolved target with no radioactivity. Parameters were adjusted to minimize the molybdenum content in the final product as measured by colorimetric test strips (LaMotte). When process parameters were optimized the mock dissolved target solution was spiked with 99mTc obtained from a generator. The target appearance was unaffected by irradiation. The decay curve analysis showed 13.5 ± 1.4 GBq of 99mTc for the one hour irradiation and 63 ± 6 GBq for the six hour irradiation, both corrected to EOB. These values are lower than the predicted values of 19 and 87 GBq, respectively, as they do not take into account geometric and self-shielding factors. In the purification tests, molybdenum content of the purified mock target solution was < 0.5 ppm while the mock solution spiked with 99mTc gave a purification efficiency of 98 %. In conclusion, an IBA Cyclone® 18 equipped with a Nirta solid target station and two Synthera® Extension automated synthesis units can produce and purify up to 60 GBq of 99mTc pertechnetate in a single 6 hour irradiation.

OP-439

Cyclotron production and automated new 2-column processing of [68Ga]GaCl3

M. Nair[1], S. Happel[2], T. Eriksson[1], M. K. Pandey[3], T. R. DeGrado[3], K. Gagnon[1]; [1]General Electric, Uppsala, SWEDEN, [2]Triskem, Bruz, FRANCE, [3]Mayo Clinic, Rochester, MN, UNITED STATES OF AMERICA.

Purpose/Introduction: Challenges with existing chemistry for separating 68Ga from bulk 68Zn include, high HCl concentration/volume and/or use of organic solvents/HBr, a further increase in HCl concentration if using a second column for 68Ga concentration, base-mediated pH adjustment, the use of non-commercial resins, etc.[1,2,3] With ongoing efforts towards cyclotron-based 68Ga separation and labelling using a FASTlab synthesis unit, this work describes a new two-column scheme to Ga/Zn separation that avoids many of the above noted challenges. **Methods:** Cyclotron-based 68Ga is produced by irradiating a solution of enriched (98.33%) 68Zn(NO3)2 in ~0.2 N HNO3.[1] The irradiated 2mL target volume is transferred ~50 meters to a receiving vessel and diluted to 5mL with water. The 68Ga is trapped on hydroxamate resin[2] (2mL [~700mg] ZR resin), washed with 14mL 0.1 N HNO3 and eluted as [68Ga]GaCl3 in 5mL 1.4 N HCl. The eluate is then efficiently trapped on TK200 resin (2mL [~700mg]) without the need for first increasing the HCl concentration. Finally, after purging with nitrogen, the trapped [68Ga]GaCl3 is eluted in 3mL water. **Results:** To highlight the current status, we report on three consecutive 68Ga runs performed on a PETtrace cyclotron with 1 M 68Zn-zinc nitrate at 14.0 MeV/60 min/26 µA optical post-grid irradiation current. After target transfer and automated separation chemistry, we obtained 68 ± 4 mCi (24 ± 2 mCi/mL) [68Ga]GaCl3 in "hand" at 30 minutes post-EOB and report a 77 ± 2% decay corrected separation efficiency. Select QC measurements include half-life (67.6 ± 0.2 min), pH (0.5), iron/zinc (<10 µg/GBq), RCP (99 ± 1%), and RNP @ EOB (99.8821 ± 0.0004%). **Discussion/Conclusion:** We have developed a new 2-column approach to isolate cyclotron-based [68Ga]GaCl3 on a FASTlab platform with recovered 68Ga radioactivity on par with current 68Ge/68Ga generators. The noted scheme eliminates base-mediated pH adjustment, it uses water to elute the final [68Ga]GaCl3, it uses only commercially available hydroxamate and TK200 resins, and it houses all reagent vials within a standard FASTlab cassette manifold (including those needed for column conditioning) while leaving adequate space for subsequent labelling on the same cassette. Optimization is underway to increase the separation efficiency and further reduce processing time prior to on-cassette labelling. While the efforts presented are on a liquid 68Zn target, it is anticipated that this process can be readily adapted to a solid target system. **References:** 1. Am J Nucl Med Mol Imaging 2014;4:303 2. WTTC 2016 Proceedings (http://wttc.triumf.ca):10 3. Nucl Med Biol 2015;42:842

OP-440

Fully automated GMP-compliant single-step synthesis of 18F-PSMA-1007 using SPE-cartridge purification

O. C. Neels[1], R. Martin[2], J. Cardinale[1], R. Smits[2], M. Schäfer[1], A. Hoepping[2], M. Müller[2], K. Kopka[1]; [1]German Cancer Research Center, Heidelberg, GERMANY, [2]ABX advanced biochemical compounds, Radeberg, GERMANY.

Aim: In recent years several radiofluorinated ligands targeting the prostate-specific membrane antigen (PSMA) have been reported [1,2]. Our aim was to optimize the two-step synthesis procedure of 18F-PSMA-1007 [3] towards a simplified and automated single-step synthesis, thereby fulfilling GMP compliance. **Materials and Methods:** A labelling precursor for direct nucleophilic substitution using trimethylammonium as leaving group has been developed. After azeotropic drying of [18F]fluoride using tetrabutylammonium hydrogen carbonate solution as base, the fully automated radiosynthesis of 18F-PSMA-1007 has been conducted on several commercially available automated radiosynthesizers (GE TRACERlab FX FN, MX and FASTLab, ORA Neptis Plug and RS, IBA Synthera) using 1.5 to 3.0 mg of precursor in DMSO for 10 minutes at 85 °C. The crude reaction mixture was taken up in water containing sodium ascorbate and trapped on pre-conditioned sequenced SPE cartridges (Chromafix PS-H+ and Chromafix C18ec, Macherey-Nagel). After rinsing with 5% EtOH solution, the purified product was eluted from the cartridges with 30% EtOH solution and diluted with 0.9% NaCl solution containing sodium ascorbate. After sterile filtration, quality control for 18F-PSMA-1007 was performed according to specifications set in compliance with current pharmacopoeias. **Results:** 18F-PSMA-1007 could be obtained in radiochemical yields ranging from 30-50% and radiochemical purities > 90 % in a total synthesis time of < 60 min in dependence of the type of radiosynthesizer (GE TRACERlab FX FN, MX and FASTLab, ORA Neptis Plug and RS, IBA Synthera) synthesis module used. No radiolysis of the product has been observed up to 8 hours after final batch formulation (40 GBq in 20 mL saline solution). **Conclusion:** A GMP-compliant radiosynthesis and quality control of 18F-PSMA-1007 using direct radiofluorination including a simplified purification procedure have been established on a wide range of commercially available radiosynthesizers (GE TRACERlab FX FN, MX and FASTLab, ORA Neptis Plug and RS, IBA Synthera). The product is obtained in good radiochemical yields with satisfying batch productions covering the daily clinical demand in a university hospital. Radiopharmaceutical quality will allow the initiation of prospective clinical trials. **References:** [1] Rowe SP *et al.*. Prostate Cancer Prostatic Dis. 2016 19(3):223-30. [2] Giesel FL *et al.*. Eur J Nucl Med Mol Imaging. 2017 44(4):678-688. [3] Cardinale J *et al.*. J Nucl Med. 2017 58(3):425-431.

OP-441

Automated Synthesis of Pt-195m Cisplatin for GMP Production

K. Codee-van der Schilden[1], O. Zwaagstra[1], D. van der Born[2]; [1]NRG, Petten, NETHERLANDS, [2]FutureChemistry Holding BV, Nijmegen, NETHERLANDS.

Purpose/Introduction: Imaging of the *in vivo* biodistribution of Platinum-based Cisplatin may allow to predict treatment outcome of chemo(radio)therapy in a personalized approach. We have shown the feasibility of Pt-195m SPECT imaging in mice[1], and we have adopted a known procedure[2] for the manual synthesis of Pt-195m Cisplatin for its preclinical use. To reduce synthesis time and to simplify the multistep process of the

making of Pt-195m Cisplatin, we have now developed a fully automated synthesis module, ready for GMP production. **Subjects & Methods:** First, chemical resistance of materials to *aqua regia* and concentrated hydrochloric acid was tested in a proof of concept study, and a method for the automated separation of precipitates from solution using filters was developed. Subsequently, different reaction vials, reagent vials, valves, tubing and filters were tested, and methods for dispensing, evaporation of solvents, and transfer of solutions using nitrogen gas flow were developed. A semi-automated prototype was built and tested for its performance of radioactive syntheses of Cisplatin, after which the fully automated module was designed and built. **Results:** Tests to synthesize Pt-195m Cisplatin were successfully performed with the semi-automated prototype, showing a reduction in synthesis time from 2 days to 1 day. Pt-195m Cisplatin was obtained in an overall yield of 48 %, and in high radionuclide and radiochemical purity. The automated module contains a distinguished pharmaceutical part, including a sterile section to produce sterile Pt-195m Cisplatin. All parts in contact with solvents, reagents, and the radioactive reaction mixture or the product, are fully disposable. **Discussion/Conclusion:** A fully automated synthesis module for the GMP production of Pt-195m Cisplatin has been developed. A human pilot study is under preparation. The module will also be used for the development of other Platinum-195m compounds. Since Platinum-195m is a very strong Auger electron emitter, we are currently pursuing development of Pt195m with high specific activity for therapeutic applications as well. 1: Aalbersberg, E.A., de Wit-van der Veen, B.J., Zwaagstra, O., Codée-van der Schilden, K., Vegt, E., Vogel, W.V. Preclinical imaging characteristics and quantification of Platinum-195m SPECT, Eur. J. Nucl. Med. Mol. Imaging (2017). DOI:10.1007/s00259-017-3643-2 2: Hoeschele, J.D., Butler, T.A., Roberts, J.A., Guyer, C.E. Analysis and refinement of the microscale synthesis of the 195mPt-labeled antitumor drug, *cis*-Dichlorodiammineplatinum(II), *cis*-DDP. Radiochimica Acta (1982), 31, 27-36.

OP-442

Automatic synthesis of a PSMA ligand with Al18F

J. Giglio, M. Zeni, E. Savio, H. Engler; CUDIM, Montevideo, URUGUAY.

Introduction: PSMA-targeting positron emission tomography (PET) probes have become available for prostate cancer imaging. The 68Ga-labeled PSMA ligands have been extensively studied. However, 68Ga labeled compounds are produced with generators providing limited activity per synthesis. In contrast, 18F-labelled tracers allow higher doses increasing the number of examined patients. In addition, late images can be acquired in the case of uptake in lymph nodes, to discard inflammation. It is important to transfer the manual synthesis to an automatic module, producing a batch of the radiopharmaceutical with high activity in a safe and effective way. The aim of this work was to optimize the labeling of Al18F-[GLU-UREA-LYS(AHX)-HBED-CC] in a Tracerlab-FXFN (GE) platform. **Materials and Methods:** All reagents were of analytical grade. PSMA was purchased from ABX (PSMA-11). The 18F was produced in a PET-Trace cyclotron

(16,4 MeV) and transferred directly to the Tracerlab-FX$_{FN}$ (GE). The ^{18}F was purified with a QMA cartridge (Waters) and then eluted with 500 µL acetate buffer pH=4.5 (0.5M) from vial 1 to reactor. The first step in the synthesis was the formation of the Al^{18}F. For this purpose, the reactor contained 4,5µL of 0.01M AlCl$_3$ in acetate buffer pH=4.0 (5 min at 25℃). A solution containing 60 µg of PSMA-11, 500 µL of EtOH and 700 µL of 0.5M sodium acetate was then added from vial 4. The reaction took place during 10 minutes at 50℃. The product was purified by HPLC using a C$_{18}$ column (250/10 M&N) with two mobile phases (8mL/min): buffer phosphate 10 mM, pH=6.8: EtOH [A: (98:2) for 15 min. and change to B:(92:8)]. The collected peak was transferred by sterilizing filtration to the final vial. Quality control was performed via radio HPLC and GC. **Results:** The labeling up to the reactor corroborates the formation of the complex Al^{18}F-PSMA. After purification by HPLC, the radiopharmaceutical was achieved with a radiochemical purity higher than 90%. The quality control of the final product fulfilled all the requirements in agreement with USP, such as radiochemical purity (greater than 90%) and residual solvents. Al^{18}F-PSMA was obtained with a yield of 15±2 % (n=3), not decay corrected (NCD) starting off from 500 to 1500 mCi the ^{18}F and with a radiochemical purity of 95 ± 3 %. **Conclusion:** The proposed method allowed the production of Al^{18}F-PSMA with suitable radiochemical purity in a commercial platform. High activities were achieved, with a simple and robust methodology appropriate for clinical purposes.

1106 **Tuesday, October 24, 2017, 08:00 - 09:30, Hall F1**

Pitfalls & Artefacts 5 (Interactive) - Oncology: Pitfalls and Artefacts of PET in Neuroendocrine Tumours

OP-443
18F-fluorodopa
S. Balogova; Comenius University, Faculty of Medicine & St. Elisabeth Cancer Institute, Nuclear Medicine, Bratislava, SLOVAKIA.

OP-444
Somatostatin Receptor PET/CT in Gastro-Entero-Pancreatic (GEP) NEN
V. Ambrosini; University of Bologna and S.Orsola-Malpighi Hospital, Nuclear Medicine, Bologna, ITALY.

OP-445
Somatostatin Receptor PET in Other NET
J.-N. Talbot; Hospital Tenon, AP-HP & Université P&M Curie, Paris, FRANCE.

1107 **Tuesday, October 24, 2017, 08:00 - 09:30, Hall F2**

Clinical Oncology: Cured or Not Cured?

OP-446
Accuracy of F-18-FDG-PET/CT in monitoring tumour response after neoadjuvant chemoradiotherapy (nCRT) in patients with locoregional oesophageal cancer

M. J. Valkema[1], B. J. Noordman[1], B. P. L. Wijnhoven[1], V. M. C. W. Spaander[1], J. P. Ruurda[2], G. A. P. Nieuwenhuijzen[3], M. I. Van Berge Henegouwen[4], M. N. Sosef[5], J. J. B. Van Lanschot[1], R. Valkema[1]; [1]Erasmus MC University Medical Centre, Rotterdam, NETHERLANDS, [2]University Medical Centre, Utrecht, NETHERLANDS, [3]Catharina Hospital, Eindhoven, NETHERLANDS, [4]Academic Medical Centre, Amsterdam, NETHERLANDS, [5]Atrium Medical Centre, Heerlen, NETHERLANDS.

Introduction: Neoadjuvant chemoradiotherapy (nCRT) with "CROSS" (NEJM 2012) is effective for downstaging oesophageal tumours. To safely postpone surgery, reliable clinical response evaluations (CREs) should be used to rule out residual locoregional disease without distant metastases. A multicentre feasibility study is underway (preSANO trial, NL41732.078.13) including endoscopy, (deep) biopsies, ultrasound and FDG-PET/CT with planned surgery 12 weeks after nCRT. This preliminary analysis focuses on FDG-PET/CT to predict residual tumour (substantial: >10%=TRG3-4 vs minimal: ≤10% vital cells=TRG1-2,) or metastases after nCRT. **Subjects & Methods:** FDG-PET/CT at baseline and CRE was performed according to EANM guidelines 1.0 (2.3MBq/kg F-18-FDG; scanning 60±5min.). Visual: presence of residual tumour and/or metastases; SUV and SUV/lean body mass (SUL); compared with pathology (resection specimen: golden standard). **Results:** 78 of 205 patients did not proceed to FDG-PET/CT follow-up at 12 weeks after nCRT (CRE2), including 4 with FDG-negative baseline scans and 4 with FDG-positive metastases at 6 weeks (CRE1). In 127 patients at CRE2, FDG-PET/CT was positive in 87. In 5/87, data on histology were still incomplete. 25/87 had no resection (7 postponed, 14 metastases on FDG-PET/CT, 1 died, 3 metastases peroperatively). 33/87 patients had TRG3-4 tumour; SUL-max 4.27±1.63 and SUL-max-ratio tumour/oesophagus (SULR) 2.09±0.77. 12/87 patients had (TRG2) tumour; SUL-max 3.48±0.79 and SULR 1.66±0.33. Of all 27 patients with TRG1, FDG-PET/CT was false positive in 12/27 (44%); SUL-max 3.67±1.14, SULR 1.83±0.57. In all 80 patients with TRG2-3-4-metastases, FDG-PET/CT was true positive in 66/80 (83%). In 40/127 patients at CRE2, FDG-PET/CT was negative. In 7/40 surgery was postponed. 25/40 patients had TRG1-2 tumour; SUL-max 2.28±0.65, SULR 1.22±0.21. Of all 41 patients with TRG3-4, 8/41 were missed on FDG-PET/CT (20% false negative); SUL-max 2.18±0.26, SULR 1.38±0.13. However, in 5/8 surgery was >4weeks after PET/CT. Still, in 7/8 patients radical resection was achieved. Of all patients with postponed surgery, 12 had ≥1 additional FDG-PET/CT during follow-up (25-49.7 weeks). In 6/12, FDG-signal remained low or decreased (ΔSUL-max -0.34±0.48); 6/12 had increased FDG-signal (ΔSUL-max 0.98±0.47). 4/12 had surgery; 3/4 had increased FDG-signal and TRG3-4 tumour at surgery; 1/4 patients had decreased FDG-signal and no tumour (TRG1). All four patients had radical resections. **Conclusion:** These preliminary results indicate that FDG-PET/CT is valuable in follow-up after nCRT. Positive FDG-PET/CT after nCRT predicts residual tumour in 83% of patients. However, visual and quantitative FDG-PET/CT alone is not sufficiently accurate. Therefore, final results of FDG-PET/CT combined with endoscopic ultrasound and (deep) biopsy results should be awaited.

OP-447

^{18}F-FDG-PET/CT For Evaluating Bevacizumab-Based Chemotherapy Combined With Regional Deep Capacitive Hyperthermia In Metastatic Cancer Patients

C. Ferrari[1], G. Ranieri[2], A. Niccoli Asabella[1], A. Di Palo[1], I. Marech[3], M. Porcelli[3], M. Fanelli[1], G. Rubini[1], C. Gadaleta[3]; [1]Nuclear Medicine Unit, AOU Policlinic of Bari, University of Bari, bari, ITALY, [2]Interventional Radiology Unit with Integrated section of Medicaln Oncology, National Cancer Research Centre IRCCS "Giovanni Paolo II", bari, ITALY, [3]Interventional Radiology Unit with Integrated Section of Medical Oncology, National Cancer Research Centre, IRCCS "Giovanni Paolo II", bari, ITALY.

Aim: The new treatment approach based on angiogenesis inhibitors is becoming an attractive target in cancer therapy. Bevacizumab has been investigated in combination with a range of chemotherapeutic agents, but potential synergic anti-angiogenic effects of hyperthermia, based on its ability to induce vasodilatation, improve oxygenation and then reduce hypoxic-inducible factor molecule, are never tested to date in literature. The aim of our study was to analyze the efficacy of bevacizumab-based chemotherapy associated to local deep capacitive hyperthermia (HYP) of patients affected by metastatic colorectal, ovarian and breast cancer, by using ^{18}F-FDG-PET/CT in addition to multidetector Computed Tomography (MDCT). **Methods:** a total of 23 patients with metastatic colorectal (n=16), ovarian (n=5) and breast (n=2) cancer were included in our pilot study. In addition to the standard bevacizumab-based chemotherapy regimen, all patients were treated with HYP. Treatment response assessment was performed by MDCT, taken as reference, and ^{18}F-FDG-PET/CT, at 80 days (timepoint-1) and at 160 days (timepoint-2) after therapy. Chi-squared linear test evaluated if a linear association between response groups (R/NR) and number of previous treatment (none,1,2,3), number of chemotherapy cycles (<6,6,12,>12), number of HYP sessions (<12,12,24,>24), lines of chemotherapy (I,II,III), existed. Survival curves were estimated by the Kaplan-Meier method, with differences assessed by the log-rank test. Significant difference was defined as p<0.05. **Results:** Response to therapy observed at timepoint-1 was: PR in 7/21 (33.3%) patients, SD in 11/21 (52.4%) and PD in 3/21 (14.3%), with a Disease Response Rate (DRR= CR+PR+SD) of 85.7% Eighteen/21 (85.7%) patients completed the clinical-instrumental evaluation at timepont-2: CR was achieved in 6/18 (33.3%) patients, PR in 2/18 (11.1%), SD in 5/18 (27.8%) and PD in 5/18 (27.8%), with a DRR of 72.2%. HYP was well tolerated without additional adverse effects on chemotherapy-related toxicity. A significant linear association between R/NR and lines of chemotherapy (p=0.036), number of chemotherapy cycles (p=0.015), number of HYP sessions (p<0.001), was found. Median OS was 497 days (CI: 414-580±42.3) while median TTP was 339 days (CI: 229-449±56). Both OS and TTP resulted to be influenced by number of chemotherapy cycles (p<0.001) and HYP sessions performed (p<0.001). **Conclusions:** Our pilot study suggests that the combined treatment of bevacizumab-based chemotherapy with HYP has a favorable tumor response, is feasible and well tolerated and can offer a promising option for metastatic cancer patients. Moreover, ^{18}F-FDG-PET/CT confirmed to be a useful and reliable method in evaluating and monitoring the synergic anti-angiogenetic effect of these innovative therapies.

OP-448

SUVmax from 18F-FDG PET/CT may outperform volumetric biomarkers in assessment of primary tumor response to neoadjuvant chemoradiotherapy in patients with esophageal cancer

E. R. Hassan[1], Y. G. Abdelhafez[1], M. A. Abougabal[2], C. Yeh[3], Y. Chao[4], C. Tseng[5], Y. Chang[6]; [1]South Egypt Cancer Institute, Assiut University, Assiut, EGYPT, [2]Faculty of Medicine, Cairo University, Cairo, EGYPT, [3]Chang Gung Memorial Hospital, College of Medicine, Chang Gung University, Department of Pathology, Taoyuan, TAIWAN, [4]Chang Gung Memorial Hospital, College of Medicine, Chang Gung University, Division of Thoracic Surgery, Taoyuan, TAIWAN, [5]Chang Gung Memorial Hospital, College of Medicine, Chang Gung University, Department of Radiation Oncology, Taoyuan, TAIWAN, [6]Chang Gung Memorial Hospital, College of Medicine, Chang Gung University, Chang Gung Memorial Hospital, Nuclear Medicine Department, Taoyuan, TAIWAN.

Aim: To correlate semi-quantitative measure(s) from 18F-FDG PET/CT with the pathologic tumor regression grading (TRG) in patients with locally-advanced esophageal cancer treated with neoadjuvant chemoradiotherapy (NACR) followed by surgery. **Materials & Methods:** A total of 64 patients with T3 or T4 esophageal cancer, candidates for receiving NACR prior to definitive surgical resection, underwent two 18F FDG PET/CT studies: a baseline study performed on average 31 (± 32) days prior to starting treatment; and a post-NACR study performed on average 36 (± 16) days after ending their neoadjuvant therapy. Semi-quantitative parameters measured on the primary tumor site were: SUVmax, SUVpeak, metabolic tumor volume at a threshold of 40% of the maximum pixel (MTV), mean SUV at threshold the same threshold (SUVmean) and total lesion glycolysis (TLG). Post-NACR parameters and percentage change from baseline were compared against TRG. TRG was measured on a 5-point score: 1 = no residual cancer cells, 2 = rare cancer cells, 3 = fibrosis outgrowing cancer cells, 4 = cancer cells outgrowing fibrosis and 5 = absence of regressive changes. **Results:** Area under the curve (AUC) of post-NACR SUVmax, SUVpeak, SUVmean, MTV & TLG were: 81% (95% Confidence Interval [CI]: 69-90%), 79% (67-88%), 81% (69-90%), 68% (55-79%), 71% (59-82%); respectively. AUC for post-NACR SUVmax was higher than that of MTV (Difference in AUC 12.5% & P = 0.04) and TLG (Difference in AUC 10% & P = 0.05). AUC of the percentage change from baseline study for the same parameters were: 74% (62-84%), 67% (54%-78%), 69% (57-80%), 68% (56-79%) & 69% (56-80%); respectively. AUC for the percentage change in SUVmax was higher than SUVpeak (Difference in AUC 8% & P = 0.01). Regression analysis adjusted for age, clinical T & N status identified post-NACR SUVmax as independent predictor of TRG (P < 0.0001, OR = 1.7, [95%CI: 1.3-2.3]). The best predictive cut-

off point of post-NACR SUVmax for identifying residual cancer cells was 3.9; it showed high sensitivity (93%; CI: 77-99%) albeit with low specificity was noticed (54%, CI: 37-71%). **Conclusion:** Among semi-quantitative parameters, SUVmax measured on post-NACR 18F-FDG PET/CT study may represent a better biomarker, compared to volumetric indices, in identifying residual cancer cells in patients with locally advanced esophageal carcinoma treated with neoadjuvant chemoradiation prior to surgery.

OP-449

18F-FDG PET-CT versus MRI-based External Beam Radiotherapy Volumes in Inoperable Uterine Cervical Cancer

J. A. Adam[1], H. Arkies[2], K. Hinnen[1], L. Stalpers[1], J. H. van Waesberghe[3], J. Stoker[1], B. L. F. van Eck-Smit[1]; [1]Academic Medical Center Amsterdam, Amsterdam, NETHERLANDS, [2]Isala Hospital, Zwolle, NETHERLANDS, [3]VU University Medical Center Amsterdam, Amsterdam, NETHERLANDS.

Aim: To assess the impact of 18F-FDG PET/CT (PET/CT) versus MRI on determining the external beam radiotherapy volumes in women with inoperable cervical cancer. **Materials and methods:** To determine treatment volumes for curative chemoradiation, 94 consecutive women with inoperable uterine cervical cancer (FIGO IB-IVA) had an investigation under anaesthesia (IUA), MRI and PET/CT. External beam radiotherapy (EBRT) of the pelvis is extended to para-aortal if suspicious nodes are at common iliac level or higher, and a boost is administered to suspicious nodes. Two radiation oncologists independently reassessed the RT treatment volumes for randomly presented 94 case-descriptions plus MRI-report (blinded to PET/CT), and (in random order) the 94 cases plus PET/CT-reports (blinded to MRI). The elective and boost volumes were registered by region: EBRT pelvis only or with para-aortal extension and an additional boost to suspicious nodes in 8 node regions (para-aortal, common iliac L/R, pelvic vessels L/R, inguinal L/R, presacral). Differences between the MRI or PET/CT-based EBRT volumes and additional boosts were compared by the McNemar test. The number of patients who received EBRT or boost based on the combination of MRI and PET/CT versus MRI alone were compared to assess clinical impact. **Results:** EBRT: Significantly more patients would receive para-aortic extension of the elective EBRT volume based on PET/CT compared to MRI (p = 0.003). Combining PET/CT and MRI, 26/94 patients would receive para-aortic extension of the elective EBRT volume compared to 9/94 based on MRI, leading to a changed EBRT treatment plan in 18% of patients. Boost: In all lymph node regions except right inguinal, more patients would receive additional boost based on PET/CT compared to MRI, which was significant in the para-aortal and both common iliac lymph node regions. Based on a combination of PET/CT and MRI, a change in management of suspicious lymphnodes requiring a boost was seen in 10-15% of the patients, except for inguinal (0-1%) and presacral (5%) regions. **Conclusion**: The elective EBRT treatment plan needs to be changed (i.e. extended) in 18% of patients for EBRT, and regional boost plans need to be changed in up to 15% patients when PET/CT is added to the MRI-based treatment plan. Including suspicious nodes on PET-CT in the treatment plan could result in less ex-field recurrences due to additional para-aortal EBRT and better regional node control due to additional boost to more regions, at a possible cost of more radiation toxicity.

OP-450

Low tracer availability of 68Ga-DOTATOC and 68Ga-DOTATATE in blood for patients with high SSTR density leads to non-linear correlation between SUV and K_i

E. Ilan[1,2], A. Sundin[1,3], I. Velikyan[1,3], M. Sandström[1,2], M. Lubberink[1,2]; [1]Department of Surgical Sience, Uppsala University, SWEDEN, [2]Medical Physics, Uppsala University Hospital, SWEDEN, [3]Medical Imaging Centre, Uppsala University Hospital, SWEDEN.

Introduction 68Ga-DOTATOC and 68Ga-DOTATATE are radiolabelled somatostatin analogues used for diagnosis of somatostatin receptor (SSTR)-expressing neuroendocrine tumours. In addition, their use in treatment follow-up has been proposed. However, it has been shown previously that for these tracers there exists no linear correlation with the net influx rate K_i, assumed to reflect SSTR density. This means that SUV probably does not reflect SSTR density, especially for high K_i values. The plateau in SUV for higher K_i values could be due to low availability of 68Ga-DOTATOC/68Ga-DOTATATE in the blood because of large amounts of SSTR in these patients, and hence tumor-to-blood ratio may be a better alternative than SUV. The aim of this study was to evaluate the correlation between tumor-to-blood ratio (TBR) and K_i. **Materials and methods** Ten patients with metastatic neuroendocrine tumors underwent a 45-min dynamic scan immediately after injection followed by a whole-body (WB) PET/CT scan at 1 h post injection of 68Ga-DOTATOC and 68Ga-DOTATATE on consecutive days. 50% isocontour VOIs were drawn over tumours in the whole body scan and in the last frame of the dynamic scan and transferred to all other frames, resulting in tumour time-activity curves. Net influx rate K_i was determined by nonlinear regression of an irreversible two-tissue compartment model using a descending aorta input curve. Amounts of tracer in blood was determined by drawing 70% isocontour VOIs in the descending aorta. The relation between TBR and K_i was evaluated using linear regression and compared to the relation between K_i and SUV. **Results** A linear relationship between TBR and K_i was found, with a Pearson correlation coefficient (R^2) of 0.98 and 0.99 for 68Ga-DOTATOC and 68Ga-DOTATATE respectively. For patients with high SSTR density, corresponding to high K_i values, blood radioactivity concentrations at 1 h p.i. were significantly lower ($p<0.05$) than for patients with low SSTR density both for 68Ga-DOTATOC and 68Ga-DOTATATE. **Conclusion** A linear relation with high correlation was found between TBR and Ki both for 68Ga-DOTATOC and 68Ga DOTATATE. It is likely that the non-linear relation between SUV and K_i is due to low availability of tracer in blood in patients with high SSTR density. TBR reflects SSTR density more than SUV, and is as such the preferred measure for semi-quantitative assessment of 68Ga-DOTATOC and 68Ga DOTATATE uptake.

OP-451

Evaluation of Surgically Excised Non-functioning Pancreatic Endocrine Tumors Followed Radiopeptide Treatment; To Optimize PRRT, Aiming to a Longer Term Survival

G. S. Limouris[1], G. Fragulidis[2], M. Paphiti[1], D. Voros[2], V. R. McCready[3]; [1]Medical Faculty, National and Kapodistrian University of Athens, Athens, GREECE, [2]II Surgical Dept of 'Aretaieion' Hospital, Medical Faculty, National and Kapodistrian University of Athens, Athens, GREECE, [3]Institute Cancer Research, Sutton Surrey & Royal Sussex County Hospital, Brighton, UNITED KINGDOM.

Introduction: We first report on adjuvant peptide receptor radionuclide therapy (PRRT) in 18 non-functional pancreatic neuroendocrine tumours (NF-PNETs) followed surgical lesion excision as an adopted technique in our Institution, aiming to optimize PRRT for a longer term survival. **Subjects and Methods:** Eighteen NF-PNETs received adjuvant PRRT i.a., after transhepatic infusions; 6 of them received ^{111}In-Octreotide, in a dosage of 4.0 -7.0 GBq, (12 cycles with treatment intervals of 5-8 weeks) and 12 n.c.a. ^{177}Lu-DOTATATE in a dosage of 7.4 GBq (6 cycles with treatment intervals also of 5-8 weeks), following their surgical excision as first-line treatment. Twelve patients underwent pancreato-duodenectomy and 6 distal pancreatectomy and splenectomy. Intraoperative Liver Ultrasonography was performed to enhance missed lesion detection. Liver metastases were present in 7 patients[3 bilobar, 4 unilobar]. The latter underwent hemihepatectomy or segmentectomy; in bilobar patients, concomitant major hepatectomy was planned and were subjected to pre-operative evaluation of the future liver remnant by Indocyanine Green clearance test. Prophylactic cholo-- cystectomy was planned to obviate adverse events due to the use of somatostatin analogues. Response assessment was classified according to RECIST criteria. Absorbed doses delivered to metastases, kidneys and red marrow were calculated according to OLINDA 1.0 program. CT/MRI were performed before and after the end of treatment and monthly US images for follow up. **Results:** In all 18 cases immediately resulted in a significant down slowing of the tumour aggressiveness clinically and biochemically confirmed, accelerating the therapeutic efficacy, prolonging the survival rate assessed by Kaplan-Mayer curves (50,4 mo for surgically excised pts versus 33 mo in non surgically treated pts) . **Conclusion:** In pts with metastatic liver-lesions, scheduled for surgical exeresis complementary, adjuvant radiopeptide therapy slows down the tumour aggressiveness, accelerates the therapeutic efficacy and improves the patients RECIST score assessment in favour to the partial remission scoring. The drawback of the concept is that surgical lesion debulking lurks the danger of tumour dissemination. The latter drives us to the skepsis that P R R T should precede the scheduled surgical excision by a therapeutic scheme of 2-3 cycles of n.c.a. Lu-177 DOTATATE for tumour ablation.

OP-452

^{177}Lu-PSMA Therapy Response Prediction in Metastatic Prostate Cancer Patients by Textural Heterogeneity Parameters in Baseline ^{68}Ga-PSMA PET Scans

Z. Khurshid[1], H. Ahmadzadehfar[1], F. C. Gaertner[1], L. Papp[2], N. Zsóter[3], H. Strunk[1], M. Essler[1], R. A. Bundschuh[1]; [1]Universitätsklinikum Bonn, Bonn, GERMANY, [2]Universitätsklinikum Wien, Wien, AUSTRIA, [3]Mediso Medical Imaging Systems, Budapest, HUNGARY.

Introduction: Radioactive labled PSMA analogs are of increasing importance for diagnosis and therapy of prostate cancer. In the era of personalized therapy emphasis is being placed on earlier response prediction and risk stratification of patients before the start of therapy. Analysis of textural heterogeneity parameters has been associated with determination of innately aggressive and therapy resistant cell lines thus emphasizing their importance in therapy planning. The objective of the current study was to assess the predictive ability of tumor textural heterogeneity parameters from baseline ^{68}Ga-PSMA PET prior to ^{177}Lu-PSMA therapy. **Materials and Methods:** Retrospective analysis of 70 patients with metastatic prostate cancer was performed. All patients were planned to undergo ^{177}Lu-PSMA therapy and underwent a pre-therapy ^{68}Ga-PSMA PET/CT scan. Interview Fusion (MEDISO Medical Imaging) was used for entire analysis of the PET/CT data. 3D volumes (VOIs) of 3 lesions each in bones and lymph nodes were manually delineated in static PET images (also in prostate and liver when applicable). Five PET based textural heterogeneity parameters (COV, entropy, homogeneity, contrast, size variation) were determined. Results obtained were then compared with clinical parameters including pre and post therapy PSA, alkaline phosphate, bone specific alkaline phosphate levels and ECOG criteria. Spearman correlation was used to determine statistical dependence among variables. ROC analysis was performed to estimate the optimal cutoff value and AUC. **Results:** Entropy showed a negative correlation (r_s = -0.327, p = 0.006, AUC = 0.695) and homogeneity showed a positive correlation (r_s = 0.315, p = 0.008, AUC = 0.683) with change in pre and post therapy PSA levels. Other parameters did not show statistically significant correlations. **Conclusions:** Our study showed a potential for response prediction of ^{177}Lu-PSMA therapy through one baseline ^{68}Ga-PSMA scan only. It also suggested that the more heterogeneous the tumor was in PSMA expression the more responsive it was to PSMA therapy, thus contributing efficiently towards treatment planning and improvement in overall diagnostic accuracy. This can also help in risk stratification and advanced strategy making for personalized therapy. However prospective studies need to be performed in the future to evaluate the clinical benefit.

OP-453

Dose Escalation Experience with 177Lu-PSMA-617

H. Rathke[1], F. L. Giesel[1], P. Flechsig[1], K. Kopka[2], W. Mier[1], M. Hohenfellner[3], U. Haberkorn[4], C. Kratochwil[1]; [1]University Hospital Heidelberg, Heidelberg, GERMANY, [2]Division of Radiopharmaceutical Chemistry, , German Cancer Research Center (dkfz), Heidelberg, GERMANY, [3]University Hospital Heidelberg, Department of Urology, Heidelberg, GERMANY, [4]University Hospital Heidelberg; Clinical Cooperation Unit Nuclear Medicine, German Cancer Research Center (dkfz), Heidelberg, GERMANY.

Introduction: Current treatment protocols for ^{177}Lu-PSMA-617 therapies were cautiously derived from dosimetry data, but their practical appropriateness have not yet been proven clinically. We retrospectively report our clinical observations using four different treatment activities. **Methods:** Forty patients with advanced prostate cancer and positive uptake in PSMA-imaging were treated in fractions of 4 GBq / 80 nmol, 6 GBq / 120 nmol, 7.4 GBq / 150 nmol or 9.3 GBq / 150 nmol ^{177}Lu-activity / precursor-amount (n=10, respectively) every 2 months. Blood cell count was checked every 2 weeks, PSA-response every 4 weeks; other effects were assessed per anamnesis. **Results:** PSA response presented no correlation to treatment activity. However, 2/10, 5/10, 5/10 and 8/10 patients with doses of 4, 6, 7.4 and 9.3 GBq completed all 3 cycles indicating a positive dose-response-relationship. Hematological toxicity was also irrespective of treatment activity as one grade-3 thrombocytopenia was observed in the 4 GBq and one grade-3 leukopenia in the 7.4 GBq-group, both patients had diffuse red-marrow infiltration and chemotherapeutical pretreatment. In the 9.3 GBq-group only one patient had grade-4 thrombocytopenia but in contrast to the other groups the mean platelet count for all patients chronically decreased over time. **Conclusions:** If patients with diffuse red marrow infiltration and extensive chemotherapeutical pretreatments are excluded, treatment activities up to three injections of 9.3 GBq ^{177}Lu-PSMA-617 every two months are well tolerable. We recommend no further dose escalation as the MTD seems to be reached.

1110	Tuesday, October 24, 2017, 08:00 - 09:30, Hall G2

Do.MoRe: Clinical Dosimetry for 90Y Radioembolization

OP-454

The impact of the hemoglobin level in liver radioembolization is confirmed by TOF-PET/CT based dose-response in hepatocellular carcinoma

M. Hesse, P. D'Abadie, S. Walrand, F. Jamar, R. Lhommel; Cliniques Universitaires Saint-Luc, Brussels, BELGIUM.

Background: Radionuclide therapy rarely takes into account anemia, but, as shown recently, the hemoglobin (Hb) level impacts the dose-response of non-primary hepatic metastases. Patients with hepatocellular carcinoma (HCC) treated by ^{90}Y radioembolization were retrospectively analyzed for a similar impact of the Hb level on the tumor response with respect to the mean dose (D) and to the equivalent uniform dose (EUD). **Methods:** Absorbed doses of 9 liver tumors sites in six patients post ^{90}Y radioembolization were computed by a 3D convolution of the TOF-PET based ^{90}Y distribution with a dose deposition kernel. D and EUD were evaluated from the tumors dose volume histograms and further linearly corrected for the Hb level measured on the day of the radioembolization procedure. Tumor responses at 2 and 4 months post-therapy were assessed from follow-up acetate or FDG TOF-PET scans. **Results**: Correcting for the Hb level significantly improves the linear correlation

of the dose-response both using D and EUD. The value of the parameter k modeling the Hb level impact was found in good agreement with the one previously obtained for 18 non-primary hepatic metastases sites. Furthermore a good linear correlation was also found when analyzing the dose response of the HCC tumors and of the non-primary hepatic metastases together. **Conclusions:** This study confirms a significant impact of the Hb level on the HCC tumor response similarly to the one previously observed for non-primary hepatic metastases. From our results the dose-response of HCC tumors appears similar to the one of non-primary hepatic metastases. This supports the study of methods for correcting tumor hypoxia and the introduction of liver radioembolization earlier in the treatment course, preferably before the induction of anemia by the chemotherapies or by the disease itself.

OP-455

Effect of differences in CT- and SPECT-based tumor delineation on tumor dose and dose response following 90Y Selective Internal Radiation Therapy (SIRT)

*A. Balagopal, A. Mahvash, **S. C. Kappadath**; UT MD Anderson Cancer Center, Houston, TX, UNITED STATES OF AMERICA.*

Purpose: There is no general consensus on methodology for tumor contouring for 90Y-SIRT dosimetry. The objective of this study is to investigate the effect of differences between CT- and SPECT-based tumor delineation on estimation of tumor dose and dose-response relationship. **Materials and Methods:** Quantitative 90Y-SPECT/CT for 34 HCC patients that underwent 90Y-SIRT were analyzed. 53 tumors (D>2.5cm) were segmented by an interventional radiologist on CT of SPECT/CT that was registered to the contrast-enhanced diagnostic CT or MRI of the liver. CT tumor contours were expanded (CT+5mm) and contracted (CT-5mm) by 5 mm (SPECT voxel) on all sides to represent inter-observer contouring. 4 SPECT based segmentations were performed: variable SPECT threshold to match the CT tumor volume (SPECTvol); fixed 20% and 30% SPECT threshold (SPECT20% and SPECT30%); variable SPECT threshold to match the CT contour while excluding necrotic core (SPECTnecro). 3D voxel dose maps were generated (Monte Carlo DOSXYZnrc/EGSnrc), and the mean dose was extracted for all tumor definitions. Dice Similarity Coefficient (DSC, to estimate the spatial overlap) and correlation analysis were performed between different contouring methods and the original CT (CToriginal) contours. Logistic regression was used to estimate the mean absorbed dose for 50% probability of EASL response (D50p). The Positive Predictive Values (PPV) and Negative Predictive Values (NPV) were also computed. **Results:** Absorbed doses for all tumor contour definitions were strongly correlated (r>0.94; p<0.001) with those from CToriginal. Relative to CToriginal contours, average errors observed on mean tumor doses were ±14% for CT±5mm, and 6.5%, -4.8%, 6.1%, and 4% for SPECTvol, SPECT20%, SPECT30%, and SPECTnecro contours. The median DSC value was highest for SPECTnecro (=79%) and lowest for SPECT20% (=52%) contours. D50p for CToriginal contours was 91Gy that changed to 86Gy and 115Gy for CT+5mm and CT-5mm, and to 107.3Gy, 94.8Gy,

104.5Gy, and 95.76Gy for SPECTvol, SPECT20%, SPECT30%, and SPECTnecro contours. Change in D50p relative to CToriginal was <10% only for CT+5mm, SPECT20%, and SPECTnecro contours. D50p as threshold dose provided PPV=68%, NPV=64% for CToriginal, that changed to PPV=70%, NPV=57% for SPECT20%; and PPV=61%, NPV=55% for SPECTnecro. **Conclusion:** The inter-observer variability in CT-based tumor contours translated to errors of ~15% in estimates of mean tumor dose and D50p. Although average errors in mean tumor dose and D50p with SPECT-based contours were <20%, their spatial coherence was poor. In addition, there were substantial differences in PPV and NPV for SPECT-based contours with highest values realized for CToriginal contours.

OP-456

Absorbed dose correlates with metabolic response to radioembolization of liver metastases with resin 90Y-microspheres

M. Cremonesi, M. E. Ferrari, F. Botta, F. Guerriero, C. Garibaldi, C. De Cicco, M. Colandrea, C. M. Grana, G. Varano, G. Bonomo, D. Paolo, F. Orsi, R. Orecchia; Istituto Europeo di Oncologia, Milano, ITALY.

Aim: The aim of the present study was to investigate possible correlation between absorbed dose and tumour response by means of a Tumour Control Probability (TCP) in liver metastases treated with radioembolization (RE) with resin 90Y-microspheres. To assess tumour response, the analysis of parameters from FDG-PET/CT has been preferred to RECIST criteria based on CT, as often, metabolic response has been proven to anticipate morphologic response. **Methods**: Patients with chemo-refractory liver metastases from solid tumours scheduled to receive RE underwent FDG-PET/CT scan before and 6 weeks after RE. 99mTc-MAA (75-111 MBq) were injected two weeks before RE to simulate treatment and perform previsional dosimetry based on SPECT fused to contrast CT. Response assessment was performed according to PERCIST criteria. The variations (%) of PET parameters versus basal examination were evaluated to establish Complete Response (CR), Partial Response (PR), Stable Disease (SD), and Progressive Disease (PD). **Results**: 22 patients and 29 lesions were suitable for analysis. Patients had hepatic lesions from colon-rectal (11), breast (7), ovary (1), endometrial (1), parotid (1) cancer, cholangiocarcinoma (1). All patients received a single treatment of RE, with a median activity of 1.7 GBq (range 0.6-2.9) of 90Y-microspheres. Median (range) tumour absorbed doses was 100 (30-443) Gy; average dose (standard deviation) was: 129 (100). Metabolic response rate of lesions as assessed with PERCIST was: CR=31%; PR=28%; SD=24%; PD=17%. Two different TCP curves were obtained by probit regression when considering: i) PR or CR as endpoint1; ii) CR only as endpoint2 (p<0.01 in both cases). For tumour doses > 170 Gy, only CR were observed. TCP of 20%, 50%, 75%, and 90% were obtained at: i) 51, 80, 104, and 125 Gy; ii) 81, 121, 153, and 183 Gy, respectively. **Conclusion**: Despite the variety of primary tumours, the relatively low cohort of patients, and the implicit uncertainty of the previsional dosimetry with 99mTc-MAA, our preliminary data provided evidence of correlation between response based on PET/CT parameters and absorbed dose. These encouraging results need to be confirmed with more ample dataset and possibly differentiation depending on tumour type. Other PET/CT parameters for response such as the metabolic tumour volume, and tumour lesion glycolisis are being considered for comparison with PERCIST and possible improved correlations.

OP-457

Is there any relationship between ^{90}Y-PET absorbed doses and damage to the target non tumoral liver (TNTL) after SIRT?

L. Sancho Rodriguez[1], M. Rodríguez.Fraile[1], J. Bilbao[1], M. Iñarrairaegui[1], C. Beorlegui Arteta[2], A. Benito[1], V. Moran[1], J. Martí-Climent[1], E. Guillen[1], B. Sangro[1]; [1]Clínica Universidad de Navarra, Pamplona, SPAIN, [2]Universidad de Navarra, Pamplona, SPAIN.

Aim: To identify whether a relationship exists between ^{90}Y-PET absorbed doses and damage to the TNTL after SIRT. **Material and Methods:** Retrospective analysis of patients with primary and secondary liver tumors submitted to SIRT with ^{90}Y-resin microsphere between 2012 and 2015. All patients received right lobar treatment, had pre-treatment and follow-up (8-10 weeks after SIRT) cross-sectional imaging (CT/MRI) and laboratory determinations. MIM processing software (Sureplan, MIM Software Inc, Cleveland, OH) was used for image processing and dosimetry calculation. Firstly, the volumes of interest were drawn using contrast-enhanced CT/MR to aid in anatomical delineation. Contours were automatically transferred using rigid registration and manual adjustment to fused ^{90}Y-PET/CT images. Afterwards, 3D voxel dosimetry was performed by means of the local deposition method. Absorbed dose parameters studied (D_{mean}, D_{20}, D_{50}, D_{70} y D_{90}) were obtained from the TNTL dose-volume histograms (DVHs). Finally, volumes of interest were drawn using contrast-enhanced CT/MR follow-up images to measure TNTL volume changes after SIRT. Spearman's P was performed to determine the correlation between TNTL absorbed doses and changes in TNTL volumes. Regression model was used to determine which ^{90}Y-PET absorbed dose predicts better the volume change. Changes in the TNTL volumes and laboratory determinations between baseline and 8-10 weeks post-treatment were studied using Wilcoxon test. **Results:** Fourteen patients were evaluated. The majority of them had hepatocellular carcinoma (78.6%) and suffered from cirrhosis (71.4%). The median predicted absorbed dose to the TNTL for ^{90}Y-PET was 23.3 Gy. A weak association was observed between ^{90}Y PET absorbed doses and volume changes, except for D_{20}, which is the absorbed dose that best correlates with TNTL atrophy (P=0.546, moderate association, p < 0.05). D_{90} is the next best (R=0.513, moderate association, p > 0.05). If atrophy is attempted to be predicted from ^{90}Y-PET absorbed doses, a positive relation is observed in all cases with weak determination coefficients, except for the scatter-plots between D_{20} and atrophy and for that between D_{90} and atrophy. The presence of cirrhosis does not modify the effect of the absorbed dose on atrophy. Analytical data do not significantly change between baseline data and 8-10 weeks after SIRT. **Conclusion:** The higher the absorbed dose to the TNTL,

the greater the atrophy produced. D_{20} is the parameter that best correlates with the atrophy produced in the TNTL although it has not been possible to predict the degree of atrophy from ^{90}Y-PET absorbed doses.

OP-458

Evaluation of 99TcMAA SPECT and 90Y PET similarity metrics on clinical cases with reference values from multiple realizations of phantom scans

J. Mikell, B. Majdalany, R. Srinivasa, K. Younge, Y. Dewaraja; University of Michigan Hospital and Health Systems, Ann Arbor, MI, UNITED STATES OF AMERICA.

Introduction: To implement treatment planning based on 3D dosimetry from 99TcMAA SPECT scans, it is necessary to establish that the SPECT spatial distribution is predictive of the 90Y distribution. The purpose of this work is to use clinical scanning protocols with phantom data to report baseline similarity metrics that quantify agreement between 99TcMAA SPECT and 90Y PET, and then evaluate patient scans relative to phantom metrics. **Methods:** A liver phantom with multiple lesions was filled with 99Tc and scanned five consecutive times with SPECT/CT; the procedure was repeated for 90Y PET/CT with identical uptake ratios. To account for differences in spatial resolution, Gaussian blurring was applied to PET. Rigid registration between the MAA-CT and PET-CT was performed to transform and resample the SPECT to the PET. To account for misregistration, up to +/- 3 voxel shifts were applied. 99TcMAA SPECT and Y90 PET images for radioembolization patients (n=17) were processed in an analogous manner. For both phantom and patient data, voxel-level Pearson's correlation coefficient (r) and mean squared difference (MSD) between images normalized to the maximum were evaluated. Multiple instances of metrics were generated for different blurring and registration perturbations. Additionally, threshold contours from 5 to 50% of the maximum were generated on SPECT and PET for a segmentation based similarity metric (dice). **Results:** For the 5 phantom scans, r (MSD) ranged from 0.94-0.95 (7.3e-5,9.2e-5) without misregistration and blurring. Blurring marginally improved r and worsened MSD, and misregistration widened the range to 0.69-0.95 (7.2e-05, 2.6e-04). Phantom dice values for all thresholds were > 0.7. For patients, with blurring and registration perturbations, the average r (MSD) was 0.59 +/- 0.19 (7.8e-4 +/- 8.8e-4) and ranged from 0.16 to 0.94 (3.6e-5 to 3.5e-3). Taking the maximum r from all registrations for each patient showed 2, 8, 9, and 11/17 patients had r > 0.8, 0.7, 0.6, and 0.5 respectively. The average dice was 0.64 +/- 0.22 for the 5% thresholds ranging from 0.18 to 0.89, while the 50% threshold average dice was 0.16 +/- 0.19 ranging from 0 to 0.56. Angiography-defined catheter positioning differences between the two procedures correlated (0.63) with MSD, but not with r. **Conclusion:** We quantified the contribution of imaging related effects (resolution, misregistration and noise) when evaluating similarity metrics between 99TcMAA-SPECT and Y90 PET images. In some patients similarity metrics were not in the range predicted from the phantom study due to additional clinical variability not modeled.

OP-459

Retrospective Dosimetry for Hepatocellular Carcinoma Radioembolization with Yttrium-90 Resin Microspheres Planned using Body Surface Area Method

M. Kafrouni[1,2], M. Fourcade[1], S. Vauclin[2], A. Ilonca[1], D. Mariano-Goulart[1]; [1]Montpellier University Hospital - Department of Nuclear Medicine, Montpellier, FRANCE, [2]Dosisoft SA, Cachan, FRANCE.

Aim: The body surface area (BSA) method has been the reference activity planning method in radioembolization for yttrium-90 (^{90}Y) resin microspheres for the last years. Today, interest is growing for personalized dosimetry with advanced tools similar to the ones used in external beam radiation therapy. This study aims to retrospectively analyze tumor dosimetry for hepatocellular carcinoma (HCC) patients treated with an activity of ^{90}Y-resin microspheres planned by the BSA method. **Materials and Methods:** Thirty-eight HCC patients (representing 44 different treatments) treated by radioembolization with ^{90}Y-resin microspheres (SIR-Spheres®, SIRTeX, North Sydney, Australia) were included in this study. Injected activity was planned using the BSA method. Personalized dosimetry was retrospectively performed using a dedicated software (PLANET® Dose, DOSIsoft, Cachan, France). Dose was computed using a convolution method based on voxel-S factors. This was done for both predictive and *in vivo* dosimetry respectively based on ^{99}Tc^m-MAA-SPECT and ^{90}Y-microspheres-PET images. 3D dose distribution was analyzed to the tumor delineated on the injected CT/MR beforehand. Objective response (OR) (either complete or partial response) was assessed three and six months after treatment using RECIST, mRECIST and EASL criteria. **Results:** Administered activities calculated using the BSA method ranged from 0.29 to 2.59 GBq with a median of 1.17 GBq (for target volumes from 12 to 1787 cm^3). The mean (±SD) and median predicted doses to the tumor over the 44 treatments were 70 Gy (± 47) and 55 Gy respectively. The mean (±SD) and median absorbed doses to the tumor evaluated on ^{90}Y-PET images were 63 Gy (± 41) and 54 Gy respectively. This retrospective evaluation shows a large variability of dose values and they are in most cases lower than the recommended 120 Gy threshold for treatment efficacy. This might be explained by the fact that the BSA method is not based on functional imaging which takes into account tumor uptake. Response rates were lower than 25% for any criteria used. The receiver-operating characteristic analysis was conducted in each case. Compared to the literature, the first results indicate low dose threshold values with a low significance due to the limited number of patients included and in particular of OR. **Conclusion:** These results highlight that 3D personalized dosimetry could provide more controlled and reproducible dose planning compared to the BSA approach. Dose-volume histogram analysis is ongoing and is expected to provide more robust indices to characterize the predictive value of dose distribution heterogeneity within the tumor volume.

OP-460

Assessment of dose-response correlation of selective internal radiation therapy (SIRT) for liver metastases from colorectal cancer (mCRC)

H. Levillain[1], G. Marin[1], T. Guiot[1], Z. Wimana[1], M. Vouche[2], P. Delatte[2], E. Woff[1], A. Hendlisz[3], B. Vanderlinden[1], P. Flamen[1]; [1]Nuclear Medicine Department, Jules Bordet Institute, Université Libre de Bruxelles (ULB), Brussels, BELGIUM, [2]Radiology Department, Jules Bordet Institute, Université Libre de Bruxelles (ULB), Brussels, BELGIUM, [3]Digestive Oncology Department, Jules Bordet Institute, Université Libre de Bruxelles (ULB), Brussels, BELGIUM.

Introduction: SIRT is an established and effective treatment modality for mCRC. Post-SIRT ^{90}Y-microspheres-PET/CT (^{90}Y-MS-PET/CT) enables the measurement for a patient-specific treatment dosimetry. Were this dosimetry correlated to treatment outcome, it could be a valuable tool for early treatment adaptation in case of under treatment of the lesions. This study aims at defining the dose-response correlation of SIRT for mCRC patients. **Materials and Methods:** This retrospective study was based on 17 mCRC patients treated with SIRT, who underwent pre/post-SIRT-FDG-PET/CT and post-SIRT ^{90}Y-MS-PET/CT. FDG-PET/CT image quality was assessed using predefined criteria and ^{90}Y-MS-PET/CT images were acquired and reconstructed according to the Quantitative Uptake Evaluation in SIR-spheres Therapy (QUEST) recommendations (Willowson et al., 2015). ^{90}Y-MS injected activity was computed using partition model based on ^{99m}Tc-macro-aggregates-albumin-SPECT/CT. Response assessment was performed on pre/post-SIRT-FDG-PET/CT images for lesions with a diameter >2 cm (AWserver 3.2 software, GE-Healthcare®). Lesions were delineated using a threshold corresponding to twice the normal liver mean SUV at baseline measured in a 3 cm diameter sphere. The lesion-based metabolic response was assessed by Total Lesion Glycolysis (TLG) decrease computed with SUV normalized to lean body mass. Lesions delineated on the FDG-PET/CT were projected on the anatomically registered ^{90}Y-MS-PET/CT. Voxel-based 3D dosimetry was performed on the ^{90}Y-MS-PET/CT and lesions' mean absorbed dose (D_{mean}) was measured (Planet Onco 3.0, Dosisoft®). Median[1st Quartile; 3rd Quartile] were computed for both TLG-decrease and D_{mean}. The correlation coefficient R^2 between D_{mean} and TLG-decrease was calculated using an EC50 dose-response model (GraphPad 7.01, Prism®). Finally, TLG-decrease was dichotomized into responders (≥50%) and non-responders (<50%) (Flamen et al., 2008). The D_{mean} (mean±SD) was computed for each category and a paired t-test was performed. **Results:** This study included 47 evaluable mCRC lesions. The median D_{mean} was 57[39; 82] Gy. For the TLG-decrease, the median was 97[32; 100]%. The correlation coefficient between TLG-change and D_{mean} was R^2=0.86. The D_{mean} for responders (N=32) and non-responders (N=15) was 82±46 and 36±16 Gy respectively (P<0.001). **Conclusion:** To our knowledge, this is the first study to demonstrate a correlation between the lesions' metabolic response and mean absorbed dose based on ^{90}Y-MS-PET/CT for mCRC patients treated with SIRT. This high correlation, obtained with a clinically applicable method, enables a rapid and precise prediction of the SIRT efficacy, allowing early treatment adaptation in case of under treatment of the lesions.

OP-461

On the origin of spurious extrahepatic activities observed in ^{90}Y nonTOF-PET imaging post radioembolization

S. Walrand, M. Hesse, F. Jamar, R. Lhommel; Université Catholique de Louvain, Brussels, BELGIUM.

Aim: Unlike TOF-PET, nonTOF-PET often shows spurious extra-hepatic activity in post liver ^{90}Y radioembolization imaging. We recently discovered using MC simulations how two physical effects largely unknown by the medical physicist community produce this discrepancy between nonTOF and TOF PET imaging. We think valuable for the nuclear physicians to be aware of the mechanism of these spurious extrahepatic activities generation. **Methods**: Acquisition of a ^{32}P vial was performed on a GSO PET system. This is the ideal setup to study the impact of bremsstrahlung x rays on the true coincidence rate regarding that no positron emission and no crystal radioactivity are present. Monte Carlo simulation of the acquisition was performed using Gate-Geant4. Additionally, an acquisition of a ^{111}In source was acquired on the GSO PET in order to assess its energy resolution. **Results:** Long exponentially decreasing tail in the system energy resolution was observed in the ^{111}In acquisition. This results from the poor scintillation light collection when using pixelized crystal as a consequence of the numerous photons reflections between the photoelectric location and the photo-detector. In line with recent studies (Strydhorst et al. Med Phys 2016) no explanation of the discrepancy was found using the standard Gate-Geant4 simulation tool. However, implementation in Geant4 of the internal bremsstrahlung (IB) and of the exponential tail succeeded in explaining the discrepancy between nonTOF and TOF PET imaging. IB emission during beta decay results from the beta particle interaction with the decayed nucleus. For most beta emitters, including ^{90}Y and ^{32}P, above 500 keV IB largely supersedes the external bremsstrahlung of the beta particle in water (Cengiz & Almaz, Rad Phys Chem 2004). **Conclusion:** A fraction of the high energy x rays, mainly produced by the IB, are backscattered when hitting a crystal pixel via the Compton effect and reach an opposite crystal pixel with an energy around 200 keV. Due to the long energy resolution tail, a fraction of these backscattered x rays are detected as true coincidences together with the energy deposited in the first crystal pixel hit. These faked true coincidences generate spurious extrahepatic activity in the reconstructed image. As these detections in two opposite crystal pixels are separated by a time delay being the TOF for the backscattered x ray to cross the whole field of view, they are automatically located outside the useful field of view, and thus outside the patient, by TOF based reconstruction algorithms.

1201/1203	Tuesday, October 24, 2017, 10:00 - 11:15, Hall A

Plenary 3: Radiobiology of Molecular Radiotherapy

OP-462

DNA Damage and Repair Processes at High and Low Dose Rates

D. van Gent; Erasmus MC, Department of Molecular Genetics, Rotterdam, NETHERLANDS.

OP-463

Feasibility of Non-DNA Targeted Radionuclide Therapy: Contribution of Bystander Effects

J.-P. Pouget; IRCM/INSERMU896, Montpellier, FRANCE.

OP-464

Selective Targeting of the Cell Membrane; Attacking the Tumour House of Cards

B. Bednarz; University of Wisconsin-Madison, Department of Medical Physics at Wisconsin Institutes for Medical Research, Madison, UNITED STATES OF AMERICA.

1301　　　　Tuesday, October 24, 2017, 11:30 - 13:00, Hall A

CME 10 - Neuroimaging: Brain PET and SPECT in Dementia - Beyond Alzheimer's Disease

OP-465

Brain PET and SPECT in Patients with FrontoTemporal Dementia

K. Herholz; Wolfson Molecular Imaging Centre, University of Manchester, Manchester, UNITED KINGDOM.

OP-466

Brain PET and SPECT Imaging in Lewy Body Diseases

N. Pavese; Imperial College London, London, UNITED KINGDOM.

OP-467

Brain SPECT and PET in Tau-Related Parkinsonism

J. Arbizu; Department of Nuclear Medicine, University of Navarra, Pamplona, SPAIN.

1302　　　　Tuesday, October 24, 2017, 11:30 - 13:00, Hall B

Joint Symposium 10 - EANM/ESES/IFCC: Diagnosis and Treatment of Hyperthyroidism

OP-468

Laboratory Testing in the Diagnosis of Hyperthyroidism

L. C. Giovanella; Oncology Institute of Southern Switzerland, Bellinzona, SWITZERLAND

OP-469

Nuclear Diagnostics and Therapy of Hyperthyroidism

F. A.Verburg; Philipps-University of Marburg, Marburg, GERMANY

OP-470

Surgical Treatment of Hyperthyroidism

M. Barczynski; Jagiellonian University Medical College, Department of Endocrine Surgery, Third Chair of General Surgery, JUMC, Krakow, POLAND.

1303　　　　Tuesday, October 24, 2017, 11:30 - 13:00, Hall C

Technologist Oral Presentations 3

OP-471

Feasibility of an Iodine-123 FP-CIT striatal quantitative measurement method with a partial volume effect correction

T. Kanenawa[1], S. Ota[1], A. Takaki[2], S. Ito[3]; [1]Graduate School of Health Sciences, Kumamoto University, Kumamoto, JAPAN, [2]Teikyo University, Omuta, JAPAN, [3]Facuty of Life Sciences, Kumamoto University, Kumamoto, JAPAN.

Purpose: Iodine-123 FP-CIT has been used to evaluate the distribution density of dopamine transporters in Lewy body disease (LBD), including Parkinson's disease and dementia with Lewy bodies. A new ^{123}I-FP-CIT striatal quantification method with a partial volume effect (PVE) correction was experimentally demonstrated by using a phantom study. The specific binding ratio of this method (new-SBR) has was obtained by calculating activities (MBq/ml) of both striatal and non-specific region with PVE and scatter corrections on the single photon emission tomography (SPECT) images. This method overcame the weakness in which the SBR depends on the system performance. However, the feasibility of this method in clinical studies has not been clarified. The purpose of this study was to confirm the feasibility of use of the new striatal quantification method. **Materials and Methods**: After fusion of SPECT/CT and MR images, the left- and right-side regions of interest of striatal and non-specific regions were obtained by tracing the striatal outline of the MR images. The activities of the striatal and non-specific regions were calculated by multiplying each SPECT count by the two different count-activity conversion coefficients and PVE correction factors. The PVE correction factors were experimentally determined by a striatal phantom filled with I-123 solution. Our study included 22 patients with clinically suspected LBD who had undergone ^{123}I-FP-CIT SPECT for 3 h after the tracer injection. The diagnosis was LBD in 10 patients and non-LBD in 12 patients. The new-SBR based on the activity of ^{123}I-FP-CIT SPECT was calculated, and correlation with the clinical features was analyzed. **Results**: The new-SBR values of the LBD (1.23-5.36, mean 2.12) were significantly lower than those of the non-LBD (2.78-6.88, mean 3.92, p < 0.01). The conventional SBR values of the LBD (1.28-4.45, mean 1.64) were lower than those of the non-LBD (1.53-4.13, mean 2.77, p < 0.2). The area under the curve (AUC) of the new-SBR by the receiver operating characteristic analysis was 0.821, and the AUC of the conventional SBR was 0.688. The AUC of the new-SBR was 15% higher than that of the conventional SBR. **Conclusion**: The LBD and non-LBD can be clearly distinguished by using the new SBR method with the PVE correction. This finding indicates the possibility of clinical routine study.

OP-472

Image classification of synaptic dopamine transporters ^{123}I-Ioflupane by machine learning techniques

J. Camacho-Cañamón[1], M. Guiote Moreno[2], A. Santos Bueno[2], E. Rodríguez Cáceres[2], E. Carmona Asenjo[2], J. Vallejo Casas[2], P. A.

Gutiérrez[1], C. Hervás-Martínez[1]; [1]University of Córdoba, CORDOBA, SPAIN, [2]H.U. Reina Sofia. UGC Medicina Nuclear Cordoba, CORDOBA, SPAIN.

Purpose : Apply machine learning techniques to classify functional brain imaging used in the differential diagnosis of movement disorders. **Material and methods:** In this study, SPECT images obtained after iv administration of 5 mCi of ^{123}I-ioflupane in 75 patients were analysed, in order to detect alterations in the distribution of activity (presynaptic dopamine transporter). The definitive diagnosis identified 51 % of patients with Parkinson's disease (PD) patterns, while the remaining 49 % corresponded to non-ill patients. Images were preprocessed using the PE-TRA software to orient and perform spatial normalisation, and a three-dimensional 79x95x69 matrix (i.e. 517,845 voxels) was obtained for each patient. In order to classify these images, a regularised logistic regression model using all voxels as input data was trained. The regularisation parameter was adjusted by an error estimator based on cross-validation. The model was evaluated by measuring the area under the ROC curve from a 5-fold experimental design. **Results:** The number of voxels was reduced to 259 by selecting the 0.05 % of coefficients of the logistic regression model with the highest absolute value. With these 259 voxels, the model obtained an AUC of 0.9905 with a sensitivity of 94.44 % and a false positive rate of 5.26 %. The characteristics chosen by the model were consistent with those used by skilled diagnosticians (caudate and putamen areas). However, the model highlighted other voxels outside these regions that were relevant for the task of diagnosis. **Conclusions:** The use of machine learning techniques has proved to be plausible for classification SPECT imaging of patients with PD, obtaining results similar to those of medical experts. The model obtained has shown areas of interest to the diagnostic study of PD beyond the caudate and putamen.

OP-473

Optimization Of Acquisition Time For18F-FLUTEMETAMOL PET/CT In Patients With Early-Onset Dementia

M. Isolani, A. Pieri, G. Serreli, C. Ghetti, M. Scarlattei, C. Lazzara, L. Ruffini; Azienda Ospedaliera- Universitaria Ospedale Maggiori di Parma, Parma, ITALY.

Background: Accumulation of β-amyloid in the brain plays a role in the degeneration of neurons in Alzheimer's disease and it's one of several patological characteristics implicated in Alzheimer's disease development. ^{18}F-Flutemetamol PET/CT is a diagnostic tool used to assess β-amyloid neuritic plaque density in patients with early-onset dementia, including Alzheimer's disease and other causes of cognitive decline. Patients must stay perfectly still the entire scan time and it's especially challenging to patients with dementia. Aim of the present study was to investigate the effect of decreasing acquisition time in order to improve patient compliance on ^{18}F-Flutemetamol accuracy. **Methods:** This pilot study included 10 patients evaluated for cognitive disorders. All patients were submitted to PET/CT scan (DiscoveryIQ GE Healthcare©) 90 minutes after intravenous injection of 185 MBq ^{18}F-Flutemetamol.

DiscoveryIQ PET/CT is a whole-body hybrid system operating in 3D detection mode and it provides up to 22cps/kBq. PET and CT data were co-registrated. PET acquisition was performed in LIST MODE for 20 minutes and PET images were reconstructed at different time intervals (20 minutes and 10 minutes) by VUE point and Q.Clear technologies (GE Healthcare©). Subsequently, data were processed by CortexID Suite software (GE Healthcare©). This software analyses radiotracer uptake in different brain's areas. Automated Z-scores were generated from CortexID and compared with a database of normal subjects. Z-score results of standard images and half- processed images (10 minutes) were compared by Pair T-Test (corrected by Bonferroni adjustment). **Results:** Z-score values did not show any statistically significant difference between standard images (20 minutes) and processed half-time images (10 minutes) for the evaluation of β-amyloid plaque density (P=0.01). These results mean that Z-score values were the same in brain maps at 10 and 20 minutes. **Conclusion:** The findings of this study showed that 10 minutes ^{18}F-Flutemetamol PET/CT acquisition provides accurate information regarding radiotracer uptake. Z-score values generated from CortexID Suite software suggested that acquisition time can be reduced from 20 to 10 minutes without a loss of clinical information. Reduction of acquisition time was possible using a PET/CT scan with a high sensivity detector. Using decreased time acquisition improves patients' comfort and reduces motion artifacts as well. **Keywords:** ^{18}F-Flutemetamol PET/CT ; β-amyloid plaque, processed images, acquisition time, patient comfort.

OP-474

Clinical, long term efficacy of PRRT in NEN patients with advanced, nonresectable, progressive hindgut and cancer of unknown primary (CUP)

A. D. Kolasinska-Cwikla[1], A. Lewczuk[2], L. Bodei[3], M. Kidd[4], J. R. Buscombe[5], I. M. Modlin[6], **J. B. Ćwikła**[7]*; [1]MSC Memorial Cancer Centre and Institute Maria Sklodowska-Curie, Warszawa, POLAND, [2]Medical University of Gdansk,, Gdansk, POLAND, [3]Memorial Sloan Kettering Cancer Center, New York, NY, UNITED STATES OF AMERICA, [4]Wren Laboratories, Branford, CT, UNITED STATES OF AMERICA, [5]Addenbrooke's Hospital, Cambridge, UNITED KINGDOM, [6]Yale, New Haven, CT, UNITED STATES OF AMERICA, [7]Faculty of Medical Sciences, University of Warmia and Mazury, Olsztyn, POLAND.*

Purpose: To evaluate the clinical long term effectiveness of Peptide Receptor Radionuclide Therapy - PRRT (^{90}Y or [177]Lu [DOTA0, D-Phe1, Tyr3]-octreotate), based on overall survival (OS) and progression free survival (PFS), in patients with extensive, progressive, non-resectable neuroendocrine neoplasm (NEN) hindgut or CUP (cancer of unknown primary) origin. **Materials and Methods:** Overall 22 patients with histologically proven hindgut (n=8) and CUP (n=14) NEN, were treated with PRRT (^{177}Lu-PRRT n=8; ^{90}Y-PRRT n=14). Clinical responses were assessed 6 weeks after completing therapy and then after at the 3-month intervals. The clinical efficacy was determine evaluating performance status (PS) of patients (ECOG/Karnofsky score), reduction of clinical symptoms of hormonal hyperproduction in case of secretor tumours also level of CgA. Any adverse events

(AEs) determine using CTC-NCI-AEs v. 4.01). The median OS and PFS were assessed using Kaplan Meier methods. Radiological response was classified according to RECIST 1.0.**Results**: Median OS for all subjects was 42,5 months (CI 28.7-52.5); PFS 18 months (CI 14.2-26.8). There was no significant difference in median OS between hindgut and CUP OS 48.5 (CI 25.2-71.5) vs. 28.5 (20.9-51.4) months, (P>0.05 Cox-Mantel test), but the trend favored those with hindgut NEN. Similarly, no significant difference in median PFS was noted between these groups (22.0 vs. 17.0 months). There was no difference in OS between female vs. male patients 46.0 (CI 23.8-62.0) vs. 30.0 (20.5-56.4) months and PFS 22.0 (CI 12.4 27.1) vs. 17.0 (9.6 32.9) months (P>0.05). Also, there was no significant difference in OS and PFS between those patients who were treated ^{177}Lu vs. [90]Y PRRT 45.0 vs. 28.5 months (OS), and 20.0 vs. 15.5 months (PFS), which could be related to the small number of patients in both groups [177]Lu (n=8) and [90]Y (n=14). Previous therapy with SST analogues vs. no analogues did not influence OS (42.5 vs 37 months) and PFS (17.0 vs 20.0 months). There was however a significant change in clinical stage as PS (ECOG/Karnofsky) before and 6 weeks after PRRT in all subjects.**Conclusions**: PRRT is equally effective in terms of OS and PFS in subjects with advanced non-resectable, progressive NEN, either hindgut or CUP. A more pronounced clinical effect with improved OS and PFS is seen more frequently in patients with hindgut NEN treated ^{177}Lu DOTATATE over CUP and/or [90]Y.

OP-475

A review of thyroid blockade strategies used in paediatric I[123] MIBG scintigraphy, and an evaluation of their relative effectiveness

B. Thurlow[1], T. Melhuish[2], P. Leanne[1], E. Morris[1], S. Johns[2], M. Guy[2], S. King[3], L. Biassoni[1]; [1]Great Ormond Street Hospital for Children NHS Foundation Trust, London, UNITED KINGDOM, [2]University Hospitals Southampton NHS Foundation Trust, Southampton, UNITED KINGDOM, [3]University of the West of England, Bristol, UNITED KINGDOM.

Aim: A dual centre study, to determine which medication and dosage frequency provides optimal thyroidal protection in paediatric I-123 metaiodobenzylguanidine (mIBG) scans. Purpose of the study was: 1. To compare the protective effect of potassium perchlorate versus potassium iodate; 2. To evaluate the protective effect of a single dose of potassium iodate administered 30 minutes prior to I-123-mIBG injection compared to administrations over 48 hours and over 72 hours. **Method:s** A total of 212 patients underwent I-123-mIBG scintigraphy during a 6 year period. This cohort was retrospectively categorised into two groups. In group 1, 50 patients received potassium perchlorate (KClO4) and 50 patients received potassium iodate (KIO3) according to the EANM and SPC guidelines. In group 2, 162 patients received differing dosages and frequency of potassium iodate; • Sub-group-(A) 49 patients received a single stat loading dose of KIO3 30 minutes prior to I-123-mIBG injection; • Sub-group-(B) 61 patients received a loading dose of KIO3 1 hour prior to I-123-mIBG injection with 2 further maintenance doses over 48 hours; • Sub-group-(C) 52 patients received KIO3

24 hours prior to I-123-mIBG injection, with a 2 further maintenance doses within 72 hours. Thyroid uptake was scored visually using a Likert scale (1-5) by a nuclear medicine physician blinded to the interventions received. Quantitative analysis of thyroid uptake was performed using ROIs drawn around the thyroid and a background area to calculate the counts-per-pixel and thyroid-to-background ratio. **Results:** The Mann-Whitney-U test found a statistically significant difference in the Likert responses for KClO4 and KIO3 (U=806, Z=-3.518, p=0.002). No statistical difference was noted when comparing KIO3 given over 48 and 72 hours (U=1120, p=0.455, Z=-0.748). The quantitative data indicated that 72% of patients fell within the normal distribution for thyroid activity when using KClO4 prior to I-123-mIBG injection compared to 97% when using KIO3. In subgroup-(A) Likert grading yielded 40 patients with no uptake, 7 patients with minimal and 2 patients with visible uptake. The average thyroid ROI to background ROI mean counts ratio was 1.042±0.095, showing comparable blockade effectiveness for single dose KIO3. **Discussion:** The results indicate that potassium iodate provides a greater level of protection from unbound radioiodine compared to potassium perchlorate. Furthermore, the visual and quantitative data indicate that potassium iodate given 30 minutes prior to I-123-mIBG injection provides comparable blockade effectiveness to the lengthier administrations, meaning a single stat dose is both safe and practical.

OP-476

Evaluation of the influence of adipose tissue in attenuation and scattering correction in Myocardial Perfusion SPECT/CT

B. Guerreiro[1], S. Valente[2,1], P. Pereira[1], R. Rosa[1], L. Vieira[3,4], E. Sousa[3], F. Branco[2,1], T. Freixo[2], P. Almeida[4,2], F. D. Jonge[2], T. C. Ferreira[2]; [1]Escola Superior de Tecnologia da Saúde de Lisboa, Instituto Politécnico de Lisboa, Lisboa, PORTUGAL, [2]Hospital dos Lusíadas, Departamento de Medicina Nuclear, Lisboa, PORTUGAL, [3]GIReS-Escola Superior de Tecnologia da Saúde de Lisboa, Instituto Politécnico de Lisboa, Lisboa, PORTUGAL, [4]Instituto de Biofísica e Engenharia Biomédica, Faculdade de Ciências, Universidade de Lisboa, Lisboa, PORTUGAL.

Aim: To evaluate the influence of thoracic Adipose Tissue (AT) on myocardial counts in cardiac SPECT/CT, after Attenuation Correction (AC) and Compton Scatter Correction (SC). **Materials and Methods:** We have used a tissue-equivalent anthropomorphic thorax phantom (RSD, Alderson Phantom) and a GE gamma-camera Infinia Hawkeye 4 equipped with 4 slice helical CT. Three different parts of the heart phantom, located on its superior (41.7 mL), medial (13.5 mL) and inferior (8.9 mL) regions were filled with ^{99m}Tc concentrations of approximately 0.03 MBq/mL, 0.10 MBq/mL, and, 0.16 MBq/mL, respectively. The phantom was filled with distilled water excepting for lungs and liver. The phantom was imaged and AT was simulated acquiring the phantom with different thicknesses of soft tissue (35 mm) and fat (10 mm and 30 mm). SPECT was acquired using a step and shot acquisition mode over 180º and 30 projections (64x64 pixels, zoom=1.33) for each one of the two detectors. The time from each projection varied from 25 to 44 seconds,

to correct for ^{99m}Tc decay. CT was acquired in axial mode with a slice thickness of 5 mm and 256x256 pixel matrix. The data were reconstructed using FBP, OSEM Resolution Recovery (RR), OSEM RR AC and OSEM RR AC SC methods. Semi-Quantitative analysis was made using FBP as standard. **Results:** The results show that when compared to FBP, OSEM RR, OSEM RR AC and OSEM RR AC SC a significantly higher number of counts is recovered, which is expectable. Increasing the amounts of adipose tissue leads to an increased amount of counts in all regions studied, suggesting that CT based AC may be biased. This effect is particularly visible for thicker fat layers. When the SC is added the percentage of counts are slightly decreased compared to OSEM RR AC. **Conclusion:** Quantitative data obtained for cardiac SPECT/CT using AC based CT may be biased when imaging obese patients and people using these methods should test them at their own departments before applying them to patients.

OP-477

Planar versus SPECT Acquisition in Pulmonary Embolism: comparison of some European Practices

T. C. S. Melo[1], D. Vieira[1], A. Nunes[2], C. Sibley-Allen[2], D. Dasgupta[2], H. Ahmed[2], S. M. Piekut[3], S. Mirzaei[3], C. Sonneck-Koenne[3], W. Zehetner[3], J. A. Silva[4], M. Oliveira[4], J. Nery[4], R. Castro[4], L. F. Metello[1,5]; [1]ESS-IPP, ATC & Curso Med. Nuclear, Porto, PORTUGAL, [2]Department of Nuclear Medicine Guy's and St.Thomas Hospital, London, UNITED KINGDOM, [3]Wilhelminenspital, Department of Nuclear Medicine and PET center, Vienna, AUSTRIA, [4]CHP-Hosp. Sto.António EPE, Dept. de Med.Nuclear, Porto, PORTUGAL, [5]IsoPor-Azores,Dept. de Med. Nuclear e Imagiologia Molecular, Angra do Heroismo, I.Terceira-Azores, PORTUGAL.

In recent years, the role of V/Q scintigraphy in the diagnosis of Pulmonary Embolism (PE) has diminished. Although the introduction of V/Q SPECT brought improvements in the diagnostic accuracy. The purpose of this study is to understand if SPECT brings any added value to the diagnosis of PE. In order to observe the differences between some departments in Europe, this study includes cases from 3 different Nuclear Medicine department in Europe. **Material and Methods:** 35 patients (F=18; M= 17; 60±15 years old) with clinical suspicion of PE were included in this study. All patients performed both planar and SPECT images, either for ventilation and perfusion phases. Data was acquired in three distinct European Nuclear Medicine Departments: Portugal (n=10), Austria (n=13) and the United Kingdom (n=12), using three different gamma cameras. In two of the NM Departments, ^{99m}Tc-Technegas was used for the ventilation phase, performed before the perfusion study. In the other site, [81m]Kr was used for the ventilation phase. ^{99m}Tc-MAA was used in all the patients in the perfusion phase. SPECT images were processed through Hybrid Recon-Lung v1.1.2 option in Hermes workstations using OSEM (2 iterations and 8 subsets), Butterworth 3D filter, 0.5 cycles/cm cut-off frequency and power 8.All patient data were anonymized and analyzed by seven experienced NM physicians, who were not aware about data origin or imaging protocols. Data analysis consisted in the evaluation of matched/mismatched defects in V/Q scans and if these data

was consistent between planar and SPECT acquisitions. SPSS v24.0 was used for statistical analysis and a Cohen's K test was performed to evaluate the agreement between planar and SPECT data and between physicians. Paired Wilcoxon signed-rank tests were used to compare the number of matched and mismatched defects between both techniques. **Results:** Considering 245 diagnostics (35 patients x 7 physicians, based on planar images, 29 cases (12%) were reported as positive for PE, 209 negative (85%) and 7 as indeterminate (3%). Based on SPECT, 42 cases (17%) were reported as positive for PE, 199 negative (81%) and 4 as indeterminate (2%). Considering physicians individually, 6 of them changed the report from negative to positive for PE at least in one case, but this number varied from 1 to 5. **Conclusions:** Our results suggest that SPECT, given the improved spatial resolution and thus the ability to detect smaller lesions, increases the number of cases reported as positive for PE, while slightly reducing the number of indeterminate cases.

OP-478

Preliminary results for: Optimised diagnostics of lung embolus with ventilation/perfusion SPECT/CT with use of CPAP prior to lung scintigraphy

J. P. Paludan, S. R. Andresen, J. Abrahamsen, M. S. Jensen, C. Høyer; Region Hospital Viborg, Viborg, DENMARK.

Background: When a patient is undergoing a lung scintigraphy in order to verify the presence of pulmonary embolism, the patient inhale a radioactive tracer (aerosol). If the patient suffers from chronic obstructive pulmonary disease (COPD), the gas tends to accumulate in radioactive hot spots in areas with mucus accumulations, along with reduced dispersion of the tracer in distal airways. The result is reduced quality of the scintigraphic image, and thus likely reduced diagnostic accuracy of the method. The aim of the project is to establish if it is possible to gain a higher diagnostic accuracy if Continuous Positive Airway Pressure (C-PAP) treatment is administered before inhalation of the radioactive tracer. **Method and Materials:** All patients with tracer hotspots in their initial ventilation/perfusion scintigraphy and which are deemed suitable will be invited to participate in the study. After inclusion, all patients will be randomized between an intervention group and a control group. Both groups will be asked to return between 1 and 3 days after their first ventilation/perfusion scintigraphy. The intervention group will have CPAP treatment just prior to the ventilation/perfusion scintigraphy. The control group will only have a ventilation/perfusion scintigraphy performed. After completion of both studies, all ventilation images will be evaluated. Both an objective and subjective evaluation will be performed. Objective evaluation: Regions of interest will be drawn around all tracer hotspots and also around the entire lung. A hotspot to total lung counts index will then be calculated and compared. Subjective evaluation: An experienced physician will determined which ventilation image had more tracer hotspot in comparison with the other and report the number of hotspots. **Results:** Our preliminary trial has showed a decrease in both the hotspot to total count ratio (0.20 to 0.06) and number of hotspots (5 to 3). Both results could indicate better distribution of the tracer, lead-

ing to a greater degree of certainty in the physicians report. But more trials are necessary in order to eliminate day to day variations in the ventilation image. **Conclusion:** Post CPAP treatment imaging, have shown that patients with tracer accumulation have fewer accumulation of tracer hotspots after CPAP treatment and a better hotspot to total count ratio.

1304 **Tuesday, October 24, 2017, 11:30 - 13:00, Hall E1**

Do.MoRe: Radiation Protection

OP-479

Designing a PET uptake room: ALARA does not like all concrete walls

M. Hesse, S. Walrand, F. Jamar; Cliniques Universitaires Saint-Luc, Brussels, BELGIUM.

Introduction: Today radioprotection actors demand tremendous efforts from nuclear medicine facilities to achieve always smaller absorbed dose reduction. In spite of the increasing complexity in achieving such absorbed dose reduction, basic and approximate tools based on build up factors and tabulated occupancy factors are still commonly used by radioprotection actors in most countries. These tools often overestimate the shielding requirement in PET facilities. This study reports an actual case where Monte Carlo (MC) simulations showed that an additional concrete wall, demanded by the radioprotection actors, increases the global absorbed dose to the medical staff in PET routine. **Material and Methods:** The new PET facility uptake room was intended to welcome up to 2 patients in bed. Obeying to the radioprotection actor's demand, the room was split into 2 boxes by a solid concrete wall. Absorbed dose rate to the medical staff was evaluated by MC simulations using actual occupancy factors in 4 setups: one or two patients in the room with or without the additional wall. Patients and nurse were modelled with anthropomorphic phantoms, and realistic ^{18}FDG biodistribution extracted from ICRP report 106 were used in the MC simulations. **Results:** The simulated patient self-absorbed dose was in good agreement with the OLINDA/EXM value. Averaged with the actual occupancy factors, the presence of the additional wall increases the dose rate to the nurse. Indeed in the most frequent case of only one patient in bed (80% of the time), the reduction of the working space, induced by the additional wall, decreases the distance between the nurse and the walls. As a consequence the nurse is more exposed to the gamma rays backscattered by the concrete walls. **Conclusions:** This realistic MC modeling of a real case supports that state of the art tools such as MC should be mandatory in uptake room designs. Originally developed to estimate the shielding in between the worker and the source, build-up factor based tools are not appropriate to design a shielding that surrounds the worker and the patient together. Live adaptation of the shielding to the number of patients using mobile panels might be preferable to concrete walls in PET facilities from an ALARA point of view.

OP-480

Comparison of the methods for eye lens dose measurement by a Monte Carlo method

M. Fulop[1], J. Hudzietzová[2], P. Ragan[1], J. Sabol[3], D. Solivajs[4], P. Vlk[5]; [1]Slovak Medical University, Bratislava, SLOVAKIA, [2]Faculty of Biomedical Engineering, CTU Prague, Kladno, CZECH REPUBLIC, [3]Faculty of Safety Management of PACR, Prague, CZECH REPUBLIC, [4]Slovak Legal Metrology, NGO, Bratislava, SLOVAKIA, [5]BIONT Inc., Bratislava, SLOVAKIA.

Introduction: Three systems for monitoring of eye lens exposures (SMELEs) of staff handled radiopharmaceuticals were evaluated. **Material and Methods:** The SMELEs are based on TL detectors MCP-7 and/or MCP-Ns with 3 mm built-up plate that are located in five positions on a head. The first system (SMELE-1) uses the TLD located at base of the nose root. The SMELE-2 uses two TLDs in positions above the eyebrow. The SMELE-3 is the system EYE-DTM developed in framework of ORAMED project for intervention radiology. The Monte Carlo code MCNPX and Zubal voxel head phantom with the SMELEs pinned on protective eyewear were used for calculation of angle dependence of the SMELEs responses and exposures of eye lenses irradiated by ^{137}Cs, ^{131}I, ^{99m}Tc, ^{90}Y, ^{18}F and ^{11}C point sources from angles 0°, 45°, 90° and 180° at distance of 50cm. The comparisons of the SMELEs responses and the values of eye lens exposures were performed in the same amount of averaged absorbed dose ($D_{average}$). The use of voxel head phantom allows to simulate details of the human head form face and internal structure of its tissues and cavities. The human eyes created by means of mathematical formulas contains simple constructed lenses and they were inserted into the Zubal voxel phantom to achieve a higher accuracy in the determination of the $D_{average}$ in the eye lenses. **Results:** MCNPX simulations were verified for the MCP-7 located on the polyethylene calibration cylinder phantom of diameter 20cm irradiated by ^{137}Cs source from distance of 90cm. All three SMELEs have been calibrated by the cylindrical water phantom (recommended by ORAMED project) point source ^{137}Cs at distance of 100cm in front and side of irradiation geometries. The value $D_{average}$ measured by the systems for monitoring radiation exposure of lenses were in all considered irradiation geometries higher than $D_{average}$ monitored by dosimeters located on the chest. According to results of the simulations of angle dependence of the SMELEs responses, better agreements of the $D_{average}$ values of eye lenses exposures were with the responses of SMELE-1 and SMELE-2. **Conclusions:** Monitoring of $D_{average}$ on the chest is not sufficient for the assessment of the exposure of the eye lens in the departments of nuclear medicine. SMELE-2 is recommended as a monitor of eye lens irradiation because this system is able to distinguish which eye received higher dose. Gratitude: This post arose for the project/SGS17/OHK4/1T/17.

OP-481

The Influence of Age and Gender on Bone Marrow Fat-Fraction

M. Salas-Ramirez[1], J. Tran-Gia[1], A. M. Weng[2], H. Köstler[2], M. Lassmann[1]; [1]Department of Nuclear Medicine, University of

Würzburg, Würzburg, GERMANY, [2]Department of Diagnostic and Interventional Radiology, University of Würzburg, Würzburg, GERMANY.

Aim: In adults, the active marrow is located mainly in the axial skeleton, and the active bone marrow is continuously converted into inactive bone marrow. A recently introduced magnetic resonance imaging (MRI) sequence CAIPIRINHA DIXON - Volume interpolated breathhold examination (CD-VIBE) enables a voxel-wise quantification of the fat-water fraction. The aim of this study was to investigate the effect of age and gender in the marrow conversion based on this MR technique to test if the values proposed by ICRP for a reference man are valid assumption for absorbed dose calculations in molecular radiotherapies. **Materials and Methods:** In a retrospective study, fat-water data acquired with the CD-VIBE sequence in a consecutive series of patients referred to MRI for various medical reasons were analyzed. Prior to the study, the accuracy of this technique for fat-water separation was verified in a phantom study by comparison with the MR spectroscopy (gold standard for MR-based fat-water imaging). All patients were scanned in a clinical 3T scanner (MAGNETOM Prisma, Siemens Healthcare). Only images that involved all lumbar vertebrae were included. Average values of fat-fraction were obtained by drawing VOIs in all lumbar vertebrae (L1-L5). Additionally, the fat-fraction in the os coxae and the proximal femur (head and neck) were evaluated in 11 patients. **Results:** A total of 44 patients were included in the study (21 females between 19-87 years, 23 males between 23-85 years). A linear regression analysis of the lumbar vertebrae data showed a slightly higher slope for females (0.005±0.001 fat-fraction/year) than for males (0.003±0.001 fat-fraction/year), indicating that the marrow conversion is slower in males than in females. While the absolute fat-fraction value is higher in males than in females in the life span between 20-40 years, this tendency is inverted in the interval between 40-50 years. The median/maximum/minimum fat-fraction values were 40%/70%/12% (lumbar vertebrae), 86%/92%/62% (proximal femur), and 52%/78%/40% (os coxae). In contrast, ICRP Publication 70/89 proposes 30% for lumbar vertebra, 75% for proximal femur, and 52% for os coxea in the reference man, which disagrees with our patient collective. **Conclusion:** This study demonstrates an age- and gender-dependency of marrow conversion in a collective of 44 patients. These results suggest that the constant fat-fraction values as published by the ICRP for radiation protection purposes should be replaced by a patient-specific approach to optimize the assessment of absorbed dose to the bone marrow in molecular radiotherapies.

OP-482

Doses in female carer due to a paediatric nuclear medicine patient using ICRP biokinetic data and Monte Carlo simulations

V. de Sousa[1], G. Cardoso[1], A. I. Santos[1,2]; [1]Serviço de Medicina Nuclear – Hospital Garcia de Orta, Almada, PORTUGAL, [2]Nova Medical School – Universidade Nova de Lisboa, Lisboa, PORTUGAL.

Purpose/Introduction: Nuclear medicine (NM), using low-dose radiation procedures, is increasingly contributing for the diagnostic and treatment of paediatric patients. One of the characteristics of NM is that the patients become radioactive, which results in a certain exposure to people around them. In the case of paediatric patients, they are usually accompanied by their mother, who frequently carries the children next to the chest, increasing the proximity with radiosensible organs. This scenario is of particular concern if the mother is pregnant. Dose assessment in these cases is important to ensure that it is kept acceptably low. **Subject & Methods:** Monte Carlo simulations were performed using MCNPX 2.7.0 computer program developed by the Los Alamos National Laboratory, a paediatric voxel phantom (Baby), an adult female voxel phantom (Irene) and a 24 weeks' pregnant voxel phantom (Katja). These phantoms were developed at the Helmholtz Zentrum München - German Research Center for Environmental Health. A Tc-99m source was simulated separately in the kidneys, bladder contents and total body of Baby phantom. Tally F6 (deposited energy per mass in a cell per emitted particle) was used to obtain the absorbed dose in the breast and thyroid of Irene and in Katja foetus. It was assumed that Baby started at the most extreme point in the y-axis of the female phantoms setup. Multiplying these values by the cumulated activity, the absorbed doses were estimated. The cumulated activity in the kidneys and other organs of interest, $Ã_S$, were calculated using the available ^{99m}Tc-MAG3 biokinetic data from ICRP 80. **Results:** The estimated absorbed dose in Irene's breast and thyroid was 5.49x10^{-9} and 2.20x10^{-9} mGy, respectively, and the absorbed dose in Katja foetus was 2.79x10^{-8} mGy. Using the tissue weighting factors from ICRP 103 the effective dose was also estimated as being 6.59x10^{-10} mSv for breast, 8.79x10^{-11} mSv for thyroid and 2.79x10^{-8} mSv for the foetus (since w_R=1 and $w_{totalbody}$=1). **Discussion/Conclusion:** The annual average effective dose from natural background radiation is approximately 2.4 mSv worldwide. Thus, it can be observed that the results of effective dose for breast and thyroid due to the exposure of a paediatric nuclear medicine patient are very low. When comparing these values with the results of dose in foetus, it is noticed that the effective dose is higher, although still very small, suggesting that there is no need for concern.

OP-483

Comparison between fetal dose estimates for [^{18}F]FDG PET imaging in pregnant patient using static and dynamic bladder voiding models

*C. M. Dartora[1], N. G. Cavedini[1], **A. M. Marques da Silva**[1,2]; [1]PUCRS, Porto Alegre, BRAZIL, [2]Brain Institute, Porto Alegre, BRAZIL.*

Aim: The aim of this study was to assess the effect of bladder voiding model in the pregnant patient on fetal radiation dose estimates for [^{18}F]FDG PET imaging, using Monte Carlo simulation with GATE (Geant4 Application for Tomography Emission). **Materials and Methods:** GATE version 7.1 was used to simulate a [^{18}F]FDG uptake in a 24 weeks pregnant woman voxelized phantom , named Katja [1], an altered version of the ICRP adult female reference model. All organ masses but adipose tissue,

skin, urinary bladder and uterus remained the ICRP reference masses. Two bladder emptying models were used: a dynamic model with bladder voiding after 1 hour (19.6% A_0), 2 hours (4.15% A_0) and 4 hours (0.33% A_0); and a static full bladder or no voiding model. The distribution of [^{18}F]FDG for the woman was based on Mejia et al. (1991) [2]. The uptake of fetus and placenta was 0.22% and 0.81% of the total activity distributed in the woman, respectively. The ^{18}F modeling considered both particles (positrons) and back-to-back gamma emissions. The physical processes library used in the GATE simulation was Standard and Penelope for Rayleigh scattering. Fetal absorbed doses for both bladder-emptying models were calculated and compared. **Results:** The contribution of the dynamic bladder and static bladder to the total fetal dose was 14% and 17%, respectively. The relative difference of fetal doses considering different bladder voiding models was 32% (1.56 10^{-3} mGy/MBq for dynamic voiding, and 2.06 10^{-3} mGy/MBq for no voiding). **Conclusion:** A comparison was performed between the fetal dose produced by a [^{18}F]FDG distribution in a pregnant woman voxelized phantom with two bladder emptying models using Monte Carlo GATE. The contribution of more than 10% to the total fetal dose due to maternal bladder content shows the importance of pregnant woman voiding in [^{18}F]FDG PET imaging. Bladder models for pregnant woman in literature are diverse and usually not based on real data from pregnant women. PET imaging of pregnant woman recommendations indicate the use of oral and venous hydration, diuretic drugs and bladder catheters to reduce fetus exposition. The considerable difference between the absorbed fetal doses for the voiding models points out to the importance of hydration procedures to improve the bladder emptying regimen. **References:** [1] BECKER, J et al. Pol J Med Phys Eng, 14(1), 2008. [2] MEJIA, AA et al. J Nucl Med, 32(4), 1991.

OP-484

Optimisation of administered activity for ^{18}F-FDG examination on children

J. Oddstig[1], A. Stenvall[1], H. Almquist[2], L. Jönsson[1], B. Olsson[2], C. Hindorf[1]; [1]Department of Radiation Physics, Lund, SWEDEN, [2]Department of Clinical Physiology and Nuclear Medicine, Lund, SWEDEN.

Aim: The recommendations for administered activity stated in the EANM guidelines for ^{18}F-FDG examinations of children results in an effective dose of 6.7 and 7.5 mSv for 1 and 15 years old patients, respectively. This exceeds the effective dose given to adults with up to 40 %. Since children are more sensitive to radiation the aim of this study was to investigate if the effective dose can be reduced with preserved image quality for children undergoing ^{18}F-FDG examinations. **Methods:** 46 children, aged 2-19 years and with a weight range 11-116 kg, underwent ^{18}F-FDG examination on a GE Discovery 690 PET/CT. The patients were administrated with 3 MBq/kg or more and examined 60 minutes after administration with at least 4min/bed. Acquisition in list-mode allowed studies for patients to be truncated to correspond to studies of an injected activity of 3 MBq/kg and an acquisition time of 3 and 4 min/bed, respectively. Regions-of-interest were

drawn in the liver. The SNR (signal-to-noise ratio) was calculated as the ratio of the activity concentration and the standard deviation. The SNR for the paediatric groups were compared with the SNR from 20 adult normal weighted patients (administered activity 4 MBq/kg, examined 60 minutes after administration, 2 min/bed) on the same camera and with same reconstruction parameters. **Results:** Using an administered activity of 3 MBq/kg resulted in SNR=10.9 for children < 40kg and a scan time of 4 min/bed, and in SNR=10.6 for children > 40 kg and a scan time of 3 min/bed. The normal weighted adult patients had a mean SNR of 10.9. This results in an effective dose of 2.9 mSv for a 1 year old and 4.1 mSv for a 15 years old. The corresponding effective dose using EANM guidelines would be 6.7 mSv and 7.5 mSv. The new administration schedule gives a factor of 2.3-1.8 lower effective doses than the EANM guidelines recommendation. **Conclusions:** Our result shows that it is possible to significantly reduce the administered activity and effective dose for ^{18}F-FDG examinations of children with a preserved signal-to-noise ratio.

OP-485

Validation of Siemens CARE kV for use with PET/CT: dose reduction and PET quantification

T. Jørgensen[1], M. A. Micheelsen[2], E. Dupont[3], N. A. Bebbington[4]; [1]Department of Clinical Physiology and Nuclear Medicine, Zealand University Hospital, Næstved, DENMARK, [2]Department of Clinical Physiology and Nuclear Medicine, Zealand University Hospital, Køge, DENMARK, [3]Department of Biomedical Engineering, Zealand University Hospital, Køge, DENMARK, [4]Siemens Healthineers, Aarhus, DENMARK.

Introduction: CT image quality and dose are influenced by tube voltage, mAs and patient size. On the basis of the topogram, Siemens CARE kV automatically selects the kV and reference mAs combination which gives the greatest dose saving to the patient, according to a user-defined image quality reference. However, changing tube voltage from the 120kV standard can alter CT HUs. Caution is therefore exercised in PET/CT before clinically implementing kV optimisation features, as this could affect attenuation maps and PET quantification. The aim was to assess dose savings and impact on PET quantification using CARE kV in a series of phantom conditions. **Subjects and Methods:** This investigation used four phantom conditions of varying size and density, each containing F-18 sources: 'Lungman' with no additional fat; 'Lungman' with fat layer; NEMA IEC image quality phantom with water background; Jaszczak phantom with water background. Using a CT image quality reference of 120kV/50mAs, 1 PET and 5 CT scans of each phantom were undertaken, with CARE kV on (scanner chooses optimal kV), and with tube voltages forced at 140, 120, 100 and 80kV. Dose savings were evaluated by comparing DLP to the 120kV reference scan. PET quantification was assessed by comparing F-18 activity concentrations to the 120kV reference CTAC PET reconstruction. **Results:** Dose savings up to 23% were observed with CARE kV applied (maximum dose saving with Jaszczak phantom at 100kV). None of the four phantom conditions gave low enough attenuation for the scanner to choose 80kV as the optimal

tube voltage. Forcing inappropriate kVs, lower or higher than those chosen by the scanner's CARE kV application, increased dose by up to 63% (maximum dose increase in Lungman with fat at 80kV). Despite some differences in mu-map voxel values with different kV, differences in AC PET activity concentration were considered negligible (≤0.7%) when CARE kV was applied (maximum difference found in max activity concentration in Lungman at 100kV). Although greater differences (≤2.9%) were seen across the forced kV range (maximum difference for mean activity concentration at 80kV in Lungman plus fat), differences in activity concentration were still not considered clinically significant, with most <1%. For the forced kV range it was observed that differences in PET quantification were greatest with sources in air (≤2.9%), compared with sources immersed in water (≤1.7%). **Conclusion:** Considerable dose savings can be made by applying CARE kV, and resulting kV changes have a negligible impact on PET quantification.

OP-486

Measuring, Monitoring, and Reporting Effective Dose on an Hybrid Equipment: one year results and challenges to integrate with MDCT

G. Tosi[1], A. Chiti[2], K. Marzo[1], F. Zanca[3]; [1]Humanitas Research Hospital, ROZZANO, ITALY, [2]Humanitas University, ROZZANO, ITALY, [3]GE Healthcare, BUC, FRANCE.

Purpose: The aim of this study was to measure, monitor and report effective dose in nuclear medicine and to assess current challenges in integrating these measures with CT. **Methods and Materials:** In 2014 we connected a CT-PET to a dose tracking software and started to collect dose data from CT modality; in late 2015 the software was upgraded to a version which includes a NM module for dose tracking. Data from the PET part of the scanner, in terms of administered activity and effective dose, were also collected. **Results:** Data from 11000 CT doses and 2700 PET doses were collected, mostly from: Whole Body (WB) ^{18}F-FDG (63.2%), WB ^{11}C-Choline (12.8%), WB ^{68}Ga-DOTA-TOC (5.5%), Head ^{11}C-Methionine, for a total of 18.4 % of the whole activity of the scanner. CT mean DLP (mGy*cm) data values were (range between brackets): WB ^{18}F-FDG 1481.3 (76.1-7700.9), WB ^{11}C-Choline 2451.9 (290.9-5023.1), WB ^{68}Ga-DO-TATOC 1161.8 (41.0-3728.4) and Head ^{11}C-Methionine 766.7 (52.3-2326.9). Mean effective doses (mSv) were: WB ^{18}F-FDG 15.2±4.9, WB ^{11}C-Choline 26.4±5.6, WB ^{68}Ga 13.0±3.4 and Head ^{11}C-Methionine 1.9±3.1. Mean administered activities (MBq) and effective doses (mSv) for radiopharmaceuticals used in PET were: WB ^{18}F-FDG 333.9-6.4, Head ^{11}C-Methionine 295.6-2.5, WB ^{68}Ga-DOTATOC 168.2-3.5 and WB ^{11}C-Choline 322.2-1.5. The mean total effective doses (mSv) due to both modality were: WB ^{18}F-FDG 21.5±5.2, Head ^{11}C-Methionine 4.4±3.1, WB ^{11}C-Choline 27.9±5.9 and WB ^{68}Ga-DOTATOC 16.5±3.5. **Conclusions:** The implementation of a dose tracking system to nuclear medicine is of great value for accurate and regular recording, reporting and analysis of patient's effective doses. It can help to improve the evaluation of radiation exposures in the clinical practice.

M2M: Prostate Cancer Targeting

OP-487

In vitro and in vivo characterization of a [^{18}F]AlF-labeled PSMA ligand for imaging of PSMA-expressing xenografts

S. Lütje[1,2], G. M. Franssen[1], M. Gotthardt[1], K. Herrmann[2], O. C. Boerman[1], S. Heskamp[1]; [1]Dept. Radiology and Nuclear Medicine, Radboud university medical center, Nijmegen, NETHERLANDS, [2]Clinic for Nuclear Medicine, University Hospital Essen, Essen, GERMANY.

Aim: The aim of this study was to compare the PSMA-targeting characteristics of [^{18}F]AlF-PSMA-11, radiolabeled based on chelation of [^{18}F]AlF, to those of ^{68}Ga-PSMA-11 to image PSMA-expressing xenografts with PET/CT. **Materials and Methods:** Labeling of [^{18}F]AlF-PSMA-11 via [^{18}F]AlF-complexation was performed as described by Boschi et al.. Several conditions for the quality control of the labeling of PSMA-11 via [^{18}F]AlF-complexation were evaluated to characterize the influence of ethanol, acetonitrile, and TFA on the stability of the labeled product. Internalization of [^{18}F]AlF-PSMA-11 was compared to ^{68}Ga-PSMA-11 using PSMA-expressing LNCaP tumor cells. In vivo biodistribution of [^{18}F]AlF-PS-MA-11 (0.26 nmol/mouse, 8-9 MBq/mouse) was compared to ^{68}Ga-PSMA (0.26 nmol/mouse, 7-8 MBq/mouse) in male BALB/c nude mice with PSMA-expressing s.c. LS174T-PSMA tumors by ex vivo biodistribution studies and PET/CT imaging (1 and 2 h p.i.). **Results:** In contrast to ^{68}Ga-PSMA-11, [^{18}F]AlF-PSMA-11 was not stable in PBS, TFA, ethanol and acetonitrile (radiochemical purity in PBS: 64.5% at purification - 52.7% at 120 min post purification). However, [^{18}F]AlF-PSMA-11 remained relatively stable in 25 mM NH$_4$OAc pH 6.9. Radiochemical purity was 98.5 %, 96.3%, 94.7%, 92.5% at 0, 60, 120, and 180 min post purification, respectively. Internalization of both compounds in vitro in LS174T-PSMA cells was comparable, increasing from 5.7±0.5 % at 30min incubation time to 10.8±0.4 % at 120min incubation time and 5.2±0.5 % at 30min incubation time to 13.8±0.7 % at 120min incubation time for [^{18}F]AlF-PSMA-11 and ^{68}Ga-PSMA-11, respectively. Highest tumor uptake was observed at 1h p.i. reaching 14.7±7.6 %ID/g and 10.4±2.3 %ID/g for [^{18}F]AlF-PSMA-11 and ^{68}Ga-PSMA-11, respectively. Tracer accumulation in the kidneys at 2h p.i. was significantly lower for [^{18}F]AlF-PSMA-11 (43.5±5.7 %ID/g) compared to ^{68}Ga-PSMA-11 (105.8±13.8 %ID/g). However, accumulation of [^{18}F]AlF-PSMA-11 in the bones ranged from 2.9±0.7 (1h p.i.) - 4.2±0.4 (2h p.i.) %ID/g. PSMA-expressing xenografts could be specifically visualized using both ^{68}Ga-PSMA-11- and [^{18}F]AlF-PSMA-11-PET/CT. **Conclusion:** [^{18}F]AlF-PSMA-11 shows similar internalization capacity and visualizes PSMA-expressing tumors with comparable tumor uptake as ^{68}Ga-PSMA-11. However, [^{18}F]AlF-PSMA-11 is not stable and considerable bone uptake might hamper visualization of bone lesions. Therefore, ^{68}Ga-PSMA-11 is superior to [^{18}F]AlF-PSMA-11 to image PSMA expressing tumors.

OP-488

Synthesis and Radiolabelling of a DOTA-Bisphosphonate-Conjugated PSMA Inhibitor

N. Pfannkuchen[1], F. Rösch[1], R. Bergmann[2]; [1]Institute of Nuclear Chemistry, Johannes Gutenberg University, Mainz, GERMANY, [2]Institute of Radiopharmaceutical Cancer Research, Helmholtz-Zentrum Dresden-Rossendorf, Dresden, GERMANY.

Introduction: Conjugates of bisphosphonates (BPs) with macrocyclic chelators already showed promising results for the diagnosis and radiotherapy of painful bone metastases which often occur as a consequence of prostate carcinomas. Since urea-based peptidomimetic inhibitors of the prostate-specific membrane antigen (PSMA) are widely investigated for diagnosis and therapy of metastatic prostate cancer, combination of both structures could provide a useful theranostic compound simultaneously binding to bone metastases by two mechanisms. Here we report on the synthesis and radiolabelling of a DOTA-based BP bearing the peptidomimetic glutamate-urea-lysine binding motif. **Subjects & Methods:** The BP-conjugated PSMA inhibitor was obtained in a 17 step synthesis and characterized by NMR and LC-MS. The DOTA-based BP was synthesized in 11 steps starting from cyclen. The peptidomimetic binding motif including a naphthylic linker was synthesized by solid-phase peptide chemistry in 4 steps followed by coupling of the DOTA-based BP, cleavage from the resin and deprotection. After purification by RP-HPLC the compound was labelled with n.c.a. ^{68}Ga. Radiochemical yields were determined by radio-TLC and radio-HPLC. Stability of the ^{68}Ga-complex was examined in PBS (pH 7.4) and human serum over 2 hours. **Results:** Radiolabelling of the new BP-conjugated PSMA inhibitor with ^{68}Ga in sodium acetate buffer (0.2 M, pH 4.5) provided radiochemical yields ≥95 % within 15 minutes at 95 °C. The ^{68}Ga-labelled compound showed a stability of 93-99 % in PBS as injectable solution and human serum. **Conclusion:** Successful synthesis of a BP-conjugated PSMA inhibitor and radiolabelling with ^{68}Ga as well as ongoing labelling studies with ^{177}Lu are the first steps towards a new theranostic compound for diagnosis and therapy of bone metastases as a consequence of prostate cancer. The potential of this compound will now be examined *in vivo* in biodistribution studies as well as small animal PET imaging. Ideally, we may expect an increased accumulation of the new tracer in comparison to the individual tracers, i.e. the DOTA-PSMA derivative and the DOTA-BP derivative, respectively.

OP-489

Synthesis and evaluation of ^{18}F-labeled trifluoroborate derivatives of PSMA-617 for imaging prostate cancer with positron emission tomography

H. Kuo[1], J. Pan[1], H. Merkens[1], J. Lau[1], C. Zhang[1], N. Colpo[1], D. M. Perrin[2], K. Lin[1], F. Bénard[1]; [1]BC Cancer Research Centre, Vancouver, BC, CANADA, [2]University of British Columbia, Vancouver, BC, CANADA.

Aim: Prostate-specific membrane antigen (PSMA) is a glycoprotein overexpressed on the surface of prostate cancer cells, and represents a promising imaging biomarker for diagnosis of prostate cancer. ^{18}F-DCFPyL is currently the most popular PSMA-targeting clinical PET tracer radiolabeled with ^{18}F that can be produced in a large scale and suitable for regional distribution. However, production of ^{18}F-DCFPyL is not trivial, and involves multiple synthesis steps. In this study, we designed, synthesized and evaluated two ^{18}F-labeled PSMA-617 derivatives for prostate cancer imaging, and compared them with ^{18}F-DCFPyL. Both tracers contain an ammoniomethyl-trifluoroborate (AmBF$_3$) motif that can be radiolabeled with ^{18}F via a single ^{18}F-^{19}F isotope exchange reaction directly in aqueous solution. **Methods**: The core peptidomimetic structure containing Glu-ureido-Lys, 2-naphthylalanine, and linker (4-(aminomethyl) cyclohexanecarboxylic acid for HTK01157, or 9-amino-4,7-dioxanonanoic acid for HTK01146) was constructed on solid phase. 2-Azidoacetic acid was coupled to the *N*-terminus. Azide-containing intermediates were cleaved from the resin, and reacted with *N*-propargyl-*N,N*-dimethylammoniomethyl-trifluoroborate to yield HTK01157 and HTK01146. The stability of tracers was assessed in mouse plasma and LogD$_{7.4}$ values were determined by the shake-flask method. PET imaging and biodistribution studies were conducted in mice bearing PSMA-expressing LNCaP prostate cancer xenografts. **Results**: ^{18}F-HTK01157 and ^{18}F-HTK01146 were obtained in 17±13% (n=2) and 13±7% (n=3) decay-corrected radiochemical yields with >99% radiochemical purity. Specific activities for ^{18}F-HTK01157 and ^{18}F-HTK01146 were 137±22.2 and 92.5±22.2 GBq/µmol, respectively. Both tracers were stable in mouse plasma without noticeable degradation after 2h incubation, and were highly hydrophilic (LogD$_{7.4}$: -3.52±0.21 for ^{18}F-HTK01157 and -3.24±0.03 for ^{18}F-HTK01146). All tracers enabled clear visualization of LNCaP tumours in PET images with ^{18}F-HTK01157 exhibiting higher tumour uptake (12.1±2.93 %ID/g) than ^{18}F-DCFPyL (7.95±1.64 %ID/g) and ^{18}F-HTK01146 (5.09±1.10 %ID/g) at 1 h post-injection. Tumour-to-blood and tumour-to-muscle ratios of ^{18}F-HTK01157 (17.1±5.4 and 49.7±28.5) and ^{18}F-DCFPyL (26.1±3.33 and 46.8±18.3) were comparable. Despite lower tumour uptake, the tumour-to-background ratios of ^{18}F-HTK01146 (T/B: 54.6±38.5; T/M, 117±52.1) were ~2-folds higher than ^{18}F-DCFPyL due to its faster clearance from nontarget tissues. Co-injection with DCFPyL (0.5 mg) reduced >95% uptake of ^{18}F-HTK01157 and ^{18}F-HTK01146 in tumours, demonstrating uptake was PSMA-mediated. **Conclusion**: We successfully synthesized and evaluated ^{18}F-HTK01157 and ^{18}F-HTK01146 for PSMA-targeted imaging. Both tracers clearly delineated LNCaP prostate cancer xenografts in PET images, and showed comparable (for ^{18}F-HTK01157) or even better (for ^{18}F-HTK01146) tumour-to-background contrast than ^{18}F-DCFPyL. With the advantage of facile preparation via a single ^{18}F-^{19}F isotope exchange reaction, ^{18}F-HTK01157 and ^{18}F-HTK01146 warrant further development for clinical translation for prostate cancer imaging.

OP-490

First-in-human PET/CT imaging with ^{152}Tb-DOTATOC in neuroendocrine neoplasm and of prostate cancer using ^{152}Tb-PSMA-617

A. Singh[1], R. P. Baum[1], D. Müller[1], S. Senftleben[1], M. Benesova[2,3], C. Vermeulen[2], S. Gnesin[4], U. Köster[5], K. Johnston[6], H. R. Kulkarni[1], A. Türler[7,8], R. Schibli[2,3], J. O. Prior[4], N. P. van der Meulen[2,7], C. Müller[2,3]; [1]Theranostics Center for Molecular Radiotherapy and Molecular

Imaging, Bad Berka, GERMANY, [2]Center for Radiopharmaceutical Sciences ETH-PSI-USZ, Paul Scherrer Institut, Villigen-PSI, SWITZERLAND, [3]Department of Chemistry and Applied Biosciences, ETH Zurich, SWITZERLAND, [4]Department of Nuclear Medicine and Molecular Imaging, Lausanne University Hospital (CHUV), Lausanne, SWITZERLAND, [5]Institut Laue-Langevin, Grenoble, FRANCE, [6]ISOLDE/CERN, Meyrin, SWITZERLAND, [7]Laboratory of Radiochemistry, Paul Scherrer Institut, Villigen-PSI, SWITZERLAND, [8]Department of Chemistry and Biochemistry, University of Bern, Bern, SWITZERLAND.

Objective: The lanthanide Terbium comprises several medically very interesting radionuclides for molecular imaging ([152/155]Tb) and targeted radionuclide therapy ([149/161]Tb). [152]Tb ($T_{1/2}$ = 17.5 h, $E\beta^+_{av}$ = 1140 keV, I = 20%) is suitable for PET imaging and may play a role for diagnosis and in dosimetry prior to radionuclide therapy (RNT) using radiolanthanides. The aim of this first-in-human study was to assess the suitability of [152]Tb for molecular imaging of neuroendocrine neoplasms (NEN) and prostate cancer (PCa). **Methods:** [152]Tb was produced by proton irradiation of a tantalum target, followed by on-line mass separation at ISOLDE-CERN and purification at PSI-Villigen. [152]Tb was transported >600 km to Zentralklinik Bad Berka, Germany, where radiolabeling was performed by incubating DOTATOC or PSMA-617, respectively with [152]Tb at 95°C for 15 minutes. Patient 1 (P1) with an ileum NEN was injected with [152]Tb-DOTATOC (143 MBq) and PET/CT images were acquired up to 24h p.i. Patient 2 (P2), suffering from metastatic PCa was administered [152]Tb-PSMA-617 (150 MBq) and PET/CT images were acquired up to 25h p.i. **Results:** Radiochemical yields for DOTATOC and PSMA-617 were >97% each, with specific activity = 1.37 MBq/nmol and 0.44 MBq/nmol, respectively. In P1, [152]Tb-DOTATOC PET/CT images demonstrated specific tracer uptake in lymph node, liver and skeletal metastases, with excellent retention up to 24h p.i. Physiological uptake was seen in the pituitary gland, liver, spleen, intestines, and kidneys as well as excretion of tracer in the urinary bladder. In P2, [152]Tb-PSMA-617 PET/CT allowed visualization of small lymph node and bone metastases up to 25h p.i. Physiological uptake was seen in lacrimal and salivary glands, liver, spleen, intestines, kidneys, as well as excreted activity in the urinary bladder. In comparison with previous PET/CT studies using ^{68}Ga-DOTATOC and ^{68}Ga-PSMA-617, respectively, no new metastases were identified. No adverse effects were observed after administration of [152]Tb in either case. **Conclusion:** This first-in-human studies show significant potential of [152]Tb-based PET/CT imaging in NEN and PCa. [152]Tb could be particularly useful for performing pre-therapeutic dosimetry prior to ^{177}Lu-based RNT as it allows PET imaging up to at least 25 h. Future studies could be planned with administration of larger injected activities followed by PET image acquisition performed at even more delayed timepoints. The longer half-life of [152]Tb has the advantage of its distribution over large areas as well. Currently, routine clinical application of [152]Tb is restricted due its limited availability.

OP-491

Low molecular weight target module for PET imaging and UniCAR T cell immunotherapeutic treatment of PSMA expressing tumors

R. Bergmann[1], A. Feldmann[1], M. Schäfer[2], C. Liolios[3], S. Koristka[1], N. Berndt[1], K. Kuhne[1,4], A. Höpping[5], J. Pietzsch[6,7], J. Kotzerke[8], J. Steinbach[1], K. Kopka[2,9], M. Bachmann[1,10,11]; [1]Helmholtz-Zentrum Dresden-Rossendorf, Institute of Radiopharmaceutical Cancer Research, Dresden, GERMANY, [2]Deutsches Krebsforschungszentrum, Abteilung Radiopharmazeutische Chemie, Heidelberg, GERMANY, [3]Deutsches Krebsforschungszentrum, Heidelberg, GERMANY, [4]Technische Universität Dresden, Fachrichtung Chemie und Lebensmittelchemie, Dresden, GERMANY, [5]ABX GmbH, Radeberg, GERMANY, [6]Helmholtz-Zentrum Dresden-Rossendorf, Dresden, GERMANY, [7]Technische Universität Dresden, Fachrichtung Chemie und Lebensmittelchemie, Dresden, GERMANY, [8]Technische Universität Dresden, Uniklinikum 'Carl Gustav Carus,' Klinik und Poliklinik für Nuklearmedizin, Dresden, GERMANY, [9]National Center for Tumor Diseases, Heidelberg, GERMANY, [10]Technische Universität Dresden, Uniklinikum 'Carl Gustav Carus,' UCC, Tumorimmunology, Dresden, GERMANY, [11]National Center for Tumor Diseases, 'Carl Gustav Carus' TU Dresden, Dresden, GERMANY.

Introduction: Novel PET diagnostic and immunotherapeutic treatment options, particularly for solid tumors including prostate cancer are urgently needed. The retargeting of chimeric antigen receptors transfected T cells by antibodies can cause severe adverse effects. This treatment can easily become life threatening, especially due to "on" or "off" target side effects. To overcome these problems, we recently introduced a modular CAR technology termed UniCAR: UniCAR T cells are inert but can reversibly "turn on" by application of a target module (TM). After elimination of the TM UniCAR T cells automatically "turn off". Therefore, the bioavailability of the TM determines the activation state of the UniCAR T cells. The molecular mass and consequently the blood clearance of the TM represent the main parameter of this "turn on/off" process. For proof of concept we therefore tried to convert the low molecular weight PSMA ligand PSMA-HBED-CC into a TM for in vivo imaging. **Methods:** The synthesis of HBED-CC-PSMA-E5B9 (PSMA-TM) was developed and realized at DKFZ, radiolabeling with ^{68}Ga was performed at HZDR. The radiochemical yield and purity were analyzed by radio-HPLC. Preclinically, the retargeting efficiency of ^{68}Ga-PSMA-TMwith UniCAR T cells was tested by means of cell binding assays, biodistribution experiments as well as dynamic PET imaging and metabolite analysis in LNCaP-PSCA-Luc tumor bearing mice *in vitro* and *in vivo*. Moreover, a first-in-man PET/CT study with ^{68}Ga-labelled PSMA-TM was carried out. **Results:** PSMA-TM successfully was labeled with ^{68}Ga resulting in almost quantitative radiochemical yields (&gt98%) and molar activities of 10 to 60 GBq/micromol. Tumor-to-muscle ratios of 54 plusminus 20 were reached after 2 h with SUVmean of 1.2 plusminus 0.5 in the tumor-bearing mice. Specificity of tracer-associated tumor uptake was determined by blocking with PSMA-11, 2-PMPA, and by comparison with PC3 tumors. Successful cell killing efficiency was demonstrated in vitro and in s.c. LNCaP-PSCA-Luc mouse model by optical imaging. The in vivo tumor accumulation was compared with that of ^{68}Ga-PSMA-11 which showed a similar distribution pattern. **Conclusion:** The

small molecule based PSMA-TM could be used for both retargeting of UniCAR T cells to PSMA expressing cells in vitro and in tumor-bearing mouse models, and for PSMA-11 analog PET imaging in mice, which could also be confirmed by a first-in-man study. In conclusion, the novel theranostic low molecular weight molecule HBED-CC-PSMA-E5B9 can be considered as useful PET imaging agent to non-invasively follow the progress of individualized PSMA-directed immunotherapeutic tumor treatment with the UniCAR T cell system.

OP-492
89Zr-df-IAB2M for PET/CT imaging of prostate cancer

J. S. Batra, Y. S. Jhanwar, S. Vallabhajosula, M. J. Niaz, T. Flynn, S. T. Tagawa, N. H. Bander, D. S. Scherr; Weill Cornell Medicine, New York, NY, UNITED STATES OF AMERICA.

Background: Prostate-specific membrane antigen (PSMA) is a cell surface antigen that is highly restricted to and overexpressed in prostate cancer (PC). IAB2M is an anti-PSMA minibody, derived from the humanized J591 mAb, that can be labeled with Zirconium-89 (^{89}Zr) for use as a PET radioligand. Unlike small molecule PSMA ligands that are excreted via the urinary tract which can compromise visualization of lesions within the prostate gland and pelvis, IAB2M is excreted by a hepatic route. We are conducting a Phase 2a clinical trial to image PC patients with clinically localized disease prior to their scheduled prostatectomy. **Aim:** To evaluate the ability of ^{89}Zr-df-IAB2M to detect localized, clinically significant PC, defined as: ≥ 0.5 cm^3 with Gleason pattern ≥ 4, within the gland. As a secondary endpoint, extra-prostatic uptake would also be evaluated and correlated with any available surgical tissue. **Materials and Methods:** Patients with a diagnosis of localized PC who plan treatment by radical prostatectomy are eligible for this study. Each received 10 mg of df-IAB2M conjugated with 2.5 mCi of ^{89}Zr and were scanned 2 - 4 days later at their convenience. PET/CT images were reviewed by a nuclear medicine physician. Findings were compared with conventional imaging modalities and the histopathological findings of the post-prostatectomy specimen. **Results:** To date, 9 men with median age 62 years (range 48 - 72) were enrolled between January to March 2017. Pre-surgery median PSA was 8 ng/mL (range 3.9 - 36.56), 89% had Gleason score (GS) ≥ 7 (range 6 - 9), perineural invasion (PNI) and seminal vesicle invasion (SVI) present in 25% and 12.5%, respectively. 89% had PIRADS category ≥ 4 lesions on mpMRI. Excellent targeting of PC lesions by ^{89}Zr-df-IAB2M PET/CT imaging in the prostate gland as well as in the lymph nodes has been seen. Upon radical prostatectomy, histopathology of the surgical specimen confirmed 86% had GS ≥ 7 (range 6 - 9) with visualized extra-prostatic extension in 71%, lymph node involvement, PNI and SVI each in 43% patients. No adverse events have occurred. 11 more subjects will be enrolled/imaged in this study. **Conclusion:** ^{89}Zr-df-IAB2M is safe to administer and provides favorable targeting of PC lesions within the prostate gland as well distant disease. We plan to enroll an additional 11 subjects over the next 3 months and final assessment of lesion targeting will be analyzed and presented at the meeting.

OP-493
Comparative biodistribution of the parental murine monoclonal antibody 5A10 and its humanized version for PSA-targeting in prostate cancer

T. Tran; Dept of Radiopharmacy, Stockholm, SWEDEN.

Aims: The murine IgG$_1$ antibody m5A10 targeting PSA, prostate-specific antigen, expression has earlier been evaluated by our group and was found to be a good candidate for diagnosing of prostate cancer (PCa) lesions. For future clinical studies, we developed a humanized version of 5A10 antibody and investigated the targeting properties of the newly h5A10 in PCa xenografts. The biodistribution of the parental murine 5A10 was compared with the humanized version. **Materials and Methods:** The murine and humanized 5A10 antibodies were conjugated with CHX-A''-DTPA and labeled with ^{111}In. Affinity measurements using Biacore technology were performed before and after DTPA conjugation. Micro-SPECT imaging was performed in PSA- positive LnCAP prostate-cancer xenografts at 24, 48, 72 and 168 h post-injection (hpi). Region of interest (ROI) analysis in the images were performed to determine the image contrast. Organs were collected at the last time point and measured on a gamma counter to estimate the tumor targeting properties of ^{111}In-5A10. **Results:** Conjugation of the antibodies does not appear to affect the affinity noticeably since the affinity, K$_D$, was not significantly changed. The affinities were in the range of 10-20 pM. Comparison of the biodistribution data for the humanized ^{111}In-DTPA-h5A10 with that for the parent murine antibody ^{111}In-DTPA-m5A10 revealed an unexpected and advantageous difference. The tumor accumulation was significantly higher for the humanized than for the murine, with 7.4 $\pm$ 1.4 %IA/g for h5A10 compared to 2.7 $\pm$ 0.75 %IA/g for m5A10 (p <0.001) at 7 days p.i. **Conclusions:** The humanized antibody ^{111}In-h5A10 effectively targets prostate tumours *in vivo* and exhibits an unexpectedly better tumor accumulation than its murine antibody. These findings provide compelling evidence of the better targeting properties of humanized 5A10 antibodies in the diagnosis and likely better therapeutic efficacy in the treatment of prostate cancer. **Research Support:** Swedish Cancer Foundation, Swedish Research Council, Mrs. Bertha Kamprad Foundation and Percy Falk's Foundation.

OP-494
GRPR-Targeted Radiotherapy: Influence of Chelator on Labeling and Biodistribution of Four ^{177}Lu-Labeled Analogues of the GRPR-Antagonist PEG2-RM26

A. Orlova[1], B. Mitran[1], T. Maina[2], B. A. Nock[2], S. S. Rinne[1], V. Tolmachev[1], U. Rosenström[1]; [1]Uppsala University, UPPSALA, SWEDEN, [2]INRASTES NCSR "Demokritos", Athens, GREECE.

Purpose: Gastrin releasing peptide receptors (GRPR) are overexpressed in primary prostate cancer (PCa) and soft tissue metastases. Radiolabeled GRPR-antagonists show high receptor affinity binding without physiological action, while displaying rapid renal clearance and low degree of renal reabsorption. These features

are promising for selective delivery of therapeutic radiotoxic loads to PCa lesions using suitable GRPR-antagonists as radionuclide carriers. The aim of this study was to optimize the GRPR-antagonist PEG2-RM26 for labelling with ^{177}Lu and further preclinical evaluation in a PCa model. **Methods**: The PEG2-RM26 analogue was coupled to NOTA, NODAGA, DOTA and DOTAGA and these peptide-conjugates were labelled with [177]Lu.The receptor affinity, ^{177}Lu-chelate stability, and biodistribution profile of resulting radiopeptides were studied in PC-3 xenografted mice. The in vivo metabolic stability of ^{177}Lu-NOTAGA/DOTA/DOTAGA-PEG2-RM26 was tested by HPLC analysis of peripheral mouse blood samples collected 5 min postinjection (pi) of each radiopeptide alone (control) or with coinjection of the neutral endopeptidase (NEP)-inhibitor phosphoramidon (PA). **Results**: Conjugates were labelled with ^{177}Lu in high yields (96±3% for NOTA and almost quantitative yields for the others). Affinities to GRPR of bioconjugates were found independent of chelator type in the subnanomolar range. After 1 h incubation at 37°C in mouse blood plasma 16±2% release of radioactivity was determined for the NOTA-conjugate, 4.3±0.7% for the NODAGA-conjugate and 1.5% for the DOTA/DOTAGA-conjugates. Due to the low ^{177}Lu-chelate stability, ^{177}Lu-NOTA-PEG2-RM26 was excluded from further characterisation. In vivo, 71±3% of ^{177}Lu-DOTAGA-PEG2-RM26 remained intact at 5 min pi, while 64-65% of ^{177}Lu-DOTA-PEG2-RM26 and ^{177}Lu-NODAGA-PEG2-RM26 remained intact within this period. Treatment of mice with PA resulted in full stabilization of the radiopeptides in vivo. The biodistribution of the three analogues was studied at 1 and 24 h pi in PC-3 model non-treated with PA, showing rapid renal clearance. Tumour-to-blood ratios were >15 1 h pi and tumour-to-kidney ratios were 1.3±0.2 for NODAGA, 3±1 for DOTA, and 2.8 ±0.6 for DOTAGA radioligands at 1 h pi, significantly increasing to 2.1±0.5, 5±1 and 3.0±0.3, respectively, at 24 h pi. Although the biodistribution pattern was similar for the three radiopeptides, overall results of in vivo characterisation point ^{177}Lu-DOTAGA-PEG2-RM26 as the most promising radionuclide carrier. **Conclusions**: Based on in vitro and in vivo characterisation of the four ^{177}Lu-labeled PEG2-RM26 analogues we concluded that ^{177}Lu-DOTAGA-PEG2-RM26 is the most promising member of the series for further evaluation as a candidate for GRPR-targeted radionuclide therapy of PCa. The impact of PA-treatment on therapy outcome will be also investigated.

1306　　　　**Tuesday, October 24, 2017, 11:30 - 13:00, Hall F1**

Pitfalls & Artefacts 6 (Interactive) - Dosimetry: Pitfalls and Artefacts in Pre- and Post-Therapeutic Imaging

OP-495

An Imaging Based Guide in Individualisation of Neuroendocrine Tumour Therapy

P. Manoharan; The Christie NHS Foundation Trust, Manchester, UNITED KINGDOM.

OP-496

Post-Therapy Imaging of the Treatment Effects After 177Lu-DOTA-Octreotate Therapy

U. Garske-Román; Sahlgrenska University Hospital, Gothenburg, SWEDEN.

OP-497

Prospective Dosimetry Based Treatment Planning Based on pre- (99mTc-SPECT-CT) and post- (90Y PET TOF) Radioembolisation Imaging

C. Chiesa; Foundation IRCCS Istituto Nazionale Tumori, Nuclear Medicine Division, Milan, ITALY.

1307　　　　**Tuesday, October 24, 2017, 11:30 - 12:45, Hall F2**

Clinical Oncology: Bad Brain

OP-498

[18]F-fluciclovine PET/MRI in the evaluation of brain glioma

A. Karlberg[1,2], E. M. Berntsen[1,2], H. Johansen[1], M. Myrthue[1], A. J. Skjulsvik[3,4], I. Reinertsen[5,6], M. Esmaeili[2], H. Y. Dai[3], Y. Xiao[7,8], H. Rivaz[7,8], P. Borghammer[9], O. Solheim[5,10,11], L. Eikenes[2]; [1]Department of Radiology and Nuclear Medicine, St. Olavs University Hospital, Trondheim, NORWAY, [2]Department of Circulation and Medical Imaging, Norwegian University of Science and Technology, Trondheim, NORWAY, [3]Department of Pathology and Medical Genetics, St. Olavs University Hospital, Trondheim, NORWAY, [4]Department of Laboratory Medicine, Children's and Women's Health, Faculty of Medicine, Norwegian University of Science and Technology, Trondheim, NORWAY, [5]Norwegian National Advisory Unit for Ultrasound and Image Guided Therapy, St. Olavs University Hospital, Trondheim, NORWAY, [6]Department of Medical Technology, SINTEF, Trondheim, NORWAY, [7]PERFORM Centre, Concordia University, Montreal, QC, CANADA, [8]Department of Electrical and Computer Engineering, Concordia University, Montreal, QC, CANADA, [9]Department of Nuclear Medicine & PET Centre, Aarhus University Hospital, Aarhus, DENMARK, [10]Department of Neurosurgery, St. Olavs University Hospital, Trondheim, NORWAY, [11]Department of Neuroscience, Norwegian University of Science and Technology, Trondheim, NORWAY.

Aim: The aim of this ongoing study is to improve the diagnostic accuracy and treatment planning of brain glioma using hybrid PET/MRI technology. Structural MRI and histopathological tissue sampling are routinely done as part of the diagnostic work-up of glioma patients today. Due to the heterogeneous nature of gliomas, there is however a risk of undergrading caused by histopathological sampling errors. MRI has limitations in identifying tumor grade and type, detecting diffuse invasive growth, and separating recurrences from treatment-induced changes. PET can provide quantitative information of cellular activity and metabolism, and may therefore have additional value compared to MRI alone. **Materials and Methods:** 5 pre-operative patients with suspicion of low- or high grade glioma have been included in this study. 45-minute PET list-mode acquisitions were performed simultaneously to the ordinary MRI acquisition using the amino acid PET tracer ^{18}F-fluciclovine (FACBC). Fused PET/MRI and intraoperative 3D ultrasound images were used to guide

surgical resection and histopathological tissue sampling in flu-ciclovine-avid tumors. Image-localized histopathological samples were extracted from the tumors before resection (when possible). Analyses of the samples were related to PET/MRI image data to assess the additional value of ^{18}F-fluciclovine-PET. **Results:** Histopathological examination revealed two grade II, one grade III and two grade IV tumors according to the 2016 WHO Classification of Tumors of the CNS. ^{18}F-fluciclovine uptake was present in grade III and grade IV tumors. No PET uptake was seen in grade II tumors (or grade II parts). Tumor-to-background ratio ($SUV_{max\ tumor}/SUV_{mean\ bg}$) was 3.4 for the grade III tumor and 19.2 and 25.0 for the grade IV tumors respectively. **Conclusion:** ^{18}F-fluciclovine uptake was highest where tumor grade, cell density, and cell proliferation were highest. This suggests that combined PET/MRI with this tracer has potential to improve accuracy in histopathological tissue sampling and grading. Of note, the tumor-to-background ratios in high grade tumors were considerably greater than that seen with other amino acid PET tracers, including ^{11}C-methionine and ^{18}F-FET. No PET uptake in grade II tissue might indicate that ^{18}F-fluciclovine is less suited for tumor delineation in lower grade gliomas.

OP-499

Immunohistochemically evaluated PSMA expression in 122 treatment naive glioma patients related to [^{11}C]-methionine PET and survival

T. Traub-Weidinger, N. Poetsch, T. Bachnik, A. Woehrer, J. Gesperger, W. Wadsak, M. Markus, M. Preusser, M. Hacker, O. Koperek; MEDICAL UNIVERSITY OF VIENNA, Vienna, AUSTRIA.

Background: Apart from its expression in benign and malign prostate tissue, prostate specific membrane antigen (PSMA) was shown to be also expressed in endothelium of neovascularization in solid tumors. **The aim** of this study was to evaluate immunohistochemically the PSMA expression in glioma tissue and its relation to [^{11}C]-methionine (MET) PET and survival. **Methods:** A total of 122 treatment-naive glioma patients (67 men, 55 women, mean age: 45, range 18 - 84 years) who underwent biopsy or tumor resection were included in this study. Immunohistochemical staining (IHC) for PSMA expression was performed on the paraffin embedded tissue samples and analyzed for vascular as well as non-vascular staining. Additionally, IHC for isocitrate dehydrogenase 1-R132H (IDH1-R132H) mutation was performed. IHC results were then related to the pre-therapeutic semiquantitative MET PET and patients' survival. **Results:** PSMA expression on the vessels was observed in 26 of 122 samples. Vascular PSMA expression was specific for high grade gliomas (HGG) with positive vessel staining in 81 % of glioblastomas multiforme (GBM; n=21), 10% of WHO grade III (n=4, 1 astrocytoma [AC], 3 oligodendroglial tumors [ODG]) and just 2 % of grade II gliomas (n=1, AC). No significant differences between HGG and low grade gliomas (LGG) as well as between ODG and AC were seen in quantity of PSMA staining of non-vascular cells (mean amount of PSMA staining cells: HGG: 22; LGG: 20; ODG: 26; AC: 18). Analyzed based on the IDH1-R132H mutation status, significantly higher amounts of gliomas without verifiable IDH1-

R132H mutation (NOS) showed vascular PSMA expression (p < 0.001; 35 % of NOS, 6 % of IDH1-R132H mutated). Moreover, significantly shorter median survival times were seen for patients with vascular PSMA staining in all tumors as well as HGG only (p < 0.001; OR 7.7 and 4.8). Additionally, significantly higher mean T/N ratios by MET PET were found in patients with vascular PSMA staining compared to those without (mean T/N ratio values 4.17 and 2.47, p < 0.001). **Conclusion:** Vascular PSMA expression was seen as a high grade specific feature associated with higher T/N ratio values and shorter survival times.

OP-500

Improved detection of postoperative remaining meningioma tissue with 68Ga-DOTATATE PET/CT scans compared to surgeon's estimated Simpson Grade

F. J. Vettermann[1], M. Ueberschaerr[2], M. Unterrainer[1], P. Bartenstein[1], J. Tonn[2], C. Schichor[2], N. L. Albert[1]; [1]Department of Nuclear Medicine, Ludwig-Maximilians-University, Munich, GERMANY, [2]Department of Neurosurgery, Ludwig-Maximilians-University, Munich, GERMANY.

Purpose/Introduction: The intraoperatively assessed Simpson Grade (SG) describes the extent of surgical resection of meningiomas and has been identified as prognostic marker for recurrence. However, the validity of the scoring system in contemporary neurosurgical practice has recently been doubted. Moreover, ^{68}Ga-DOTATATE PET/CT scan has been shown to be a sensitive tool for detection of meningioma tissue. Thus, we investigated the congruence between the intraoperatively estimated SG and the postoperative ^{68}Ga-DOTATATE PET/CT. **Methods:** 37 adult patients were retrospectively identified with microsurgery of either newly diagnosed or recurrent meningioma and early postoperative ^{68}Ga-DOTATATE PET/CT scans (within 30 days) between January 2011 and July 2016. The PET parameters SUV_{max}, SUV_{mean} and threshold-based biological tumor volume (BTV; SUV>2.3) were correlated with the SG (complete removal with resection (I) or coagulation (II) of dural attachment, III: complete removal without coagulation or resection of dural attachment, IV: subtotal resection, V: decompression/biopsy only). **Results:** There were 4 SG I, 4 SG II, 4 SG III and 25 SG IV resections according to surgeon's estimate. Among the cases with SG I and II, only 3/8 showed no pathological uptake, while 5/8 presented with high tracer uptake typical for meningioma tissue (3/4 SG I: median SUV_{max}=14.7; SUV_{mean}=5.06; BTV=11.5 cm^3, and 2/4 SG II: median SUV_{max}= 8.0; SUV_{mean}= 3.8; BTV=5.4 cm^3). Of the SG III cases, all 4 showed pathological ^{68}Ga-DOTATATE uptake, but 2/4 with relatively low uptake intensity and volumes (SUV_{max}= 2.6 and 2.4; BTV=0.03 and 0.02 cm^3). All 25 SG IV resected cases had high uptake of ^{68}Ga-DOTATATE (median SUV_{max}= 23.2; SUV_{mean}=6.4) with a wide range of remaining tumor volume (median BTV 21.6 cm^3; range 2.7-101.2 cm^3). **Conclusion:** ^{68}Ga-DOTATATE PET/CT seems to provide more sensitive information to delineate postoperative remaining meningioma tissue especially in cases with resection according to SG I and II. The association of postoperative ^{68}Ga-DOTATATE PET/CT with prognosis and its potential influence on patient management is currently being investigated in a prospective longitudinal study.

OP-501

Impact of chemotherapy with Temozolomide on physiological brain 18F-DOPA uptake in patients with glioma

L. Carideo[1], F. Cicone[1], C. Scaringi[2], I. Russo[2], G. Minniti[2], F. Scopinaro[1]; [1]Nuclear Medicine Unit, Sant'Andrea Hospital, Sapienza University of Rome, Italy, Rome, ITALY, [2]Radiotherapy Unit, Sant'Andrea Hospital, Sapienza University of Rome, Italy, Rome, ITALY.

Purpose: To investigate the effects of temozolomide chemotherapy on the physiological uptake of 18F-DOPA. **Subjects and Methods**: The analysis included 155 consecutive studies from 121 patients with glioma referred for F-DOPA PET/CT at our institution between July 2010 and February 2017. Patients had been previously treated with surgery, temozolomide chemotherapy, stereotactic radiotherapy, or a combination thereof. To obtain the average background uptake (SUVbckr), a large hemispherical ROI including both gray and white matter was placed above the lateral ventricles, controlateral to the tumor lesion. A semi-automatic threshold-based VOI segmentation tool (Hermes Medical Solutions) was used to delineate tumor (>1.6 x background uptake) and controlateral basal ganglia (>2.0 x background uptake). In some cases manual adjustment was needed. Average tumor and basal ganglia uptakes (SUVt and SUVbg, respectively) were calculated within each given VOI. Tumor-to-background (TBR) and tumor-to-basal-ganglia (TBG) ratios were defined as SUVt/SUVbckr and SUVt/SUVbg, respectively. All studies were divided into three groups based on chemotherapy status: ongoing treatment (Group A, n=57); treatment completed >1 months before PET (Group B, n=50); no previous treatment (Group C, n=48). Differences between groups were assessed by ANOVA with Turkey's test for multiple comparisons. **Results:** There were significant effects of chemotherapy on SUVbckr and SUVbg (p=0.02 and p=0.05, respectively, ANOVA) In particular, mean SUVbckr was significantly lower in Group A than in Group B (1.005 ± 0.2458 vs 1.144 ± 0.309, p=0.01,Turkey's test), while the difference between Group A and Group C (1.067 ± 0.2099) was not significant (p=0.43, Turkey's test). As regards SUVbg, comparisons between Groups A (2.073 ± 0.4255) and B (2.262 ± 0.5684) and between Groups B and C (2.055 ± 0.3912) showed a trend towards significance (*p* values: 0.09 and 0.07 for A vs B and B vs C, respectively, Turkey's test). Prior radiotherapy had no effect on both SUVbckr and SUVbg (data not shown). In 92 patients with PET+ tumors, temozolomide chemotherapy affected TBR (and not TBG) (*p*=0.02, ANOVA). In particular, mean TBR was significantly higher in Group A than in Group B (2.374 ± 0.537, n=41 vs 2.093 ± 0.375, n=27; p=0.03, Turkey's test) **Conclusion:** Normal brain and basal ganglia F-DOPA uptake is decreased in patients with ongoing temozolomide. As a consequence, these patients appear to have increased TBR compared to patients who never underwent or already concluded chemotherapy. This has to be taken into account when interpreting F-DOPA PET images.

OP-502

IDH1-R132H mutation and semiquantitative [¹¹C]-methionine PET: Independent prognostic factors for characterization of newly diagnosed and treatment naive gliomas

N. Poetsch, A. Woehrer, J. Gesperger, A. R. Haug, D. Wilhelm, G. Karanikas, M. Weber, I. Rausch, M. Mitterhauser, W. Wadsak, M. Hacker, T. Traub-Weidinger; Vienna General Hospital, Vienna, AUSTRIA.

Purpose: Molecular alterations are one of the main modifications in the recently updated 2016 WHO classification of gliomas. Nevertheless, only few data exist regarding the association between those molecular parameters, such the isocitrate dehydrogenase (IDH) 1/2 mutation, and L-[S-methyl-¹¹C]methionine (MET) PET in glioma patients, with respect to prognosis. **Methods:** A total of 142 glioma patients (75 men, 67 women, mean age: 44, range 18 - 84 years) were included in this study, who underwent a MET PET prior to any therapy between 2000 and 2014 at the Medical University of Vienna. The IDH1-R132H mutation status was examined by immunohistochemical staining. PET scans were evaluated semiquantitatively by the SUV tumor to background (T/N) ratio and related to IDH1-R132H mutation status and patients' survival. **Results:** Mean follow-up was 48 ± 41 months, 49 patients died. IDH1-R132H mutation was observed in 75 patients, significantly positively influencing patient survival (p < 0.001, OR = 0.26), with a mean survival of 10.1 yrs. (range: 8,6 - 11,5 yrs) for IDH1-R132H mutated tumors and 5.4 yrs (range: 4,1 - 6,6 yrs) for patients without IDH1-R132H mutation, further specified as gliomas not otherwise specified (NOS). Considering MET PET data, a significant negative correlation between the IDH1-R132H mutation status and T/N ratio value was seen (p < 0.001, correlation coefficient: -0.3), with significantly higher T/N ratio values in NOS tumors than in IDH1-R132H mutated tumors (p < 0.001, T/N ratio values: 3.19 and 2.31). Additionally, multivariate testing showed tumor crossing midline, IDH1-R132H mutation status, therapy following surgery, Karnofsky score, surgical approach, T/N ratio value, age and parietal tumor localisation as independent prognostic parameters by decreasing order of significance (p = 0.001 to p = 0.038). **Conclusion:** This analysis of a large population of newly diagnosed gliomas demonstrates the IDH1-R132H mutation status as well as the T/N ratio value as independent prognostic parameters. Moreover, a significant negative correlation between the IDH1-R132H mutation status and the T/N ratio value was seen.

OP-503

Differential Diagnosis of Recurrence and Radiation Necrosis in High Grade Gliomas Using Multiparametric Analysis of Combined Dynamic O-(2-18F-fluoroethyl)-L-tyrosine PET and MRI

D. A. Hiob[1], C. Preibisch[2], J. Gempt[3], J. Schlegel[4], C. Straube[5], C. Zimmer[2], M. Schwaiger[1], T. Pyka[1]; [1]Department of Nuclear Medicine, Klinikum rechts der Isar der TU München, Muenchen, GERMANY, [2]Department of Neuroradiology, Klinikum rechts der Isar der TU München, Muenchen, GERMANY, [3]Department of Neurosurgery, Klinikum rechts der Isar der TU München, Muenchen, GERMANY, [4]Institute of Pathology and Neuropathology, Klinikum rechts der Isar

der TU München, Muenchen, GERMANY, [5]Department of Radiation Oncology, Klinikum rechts der Isar der TU München, Muenchen, GERMANY.

Introduction: Simultaneous FET-PET/MRI promises to improve diagnostics in the often difficult but clinically relevant differentiation between tumor recurrence and treatment related changes in high grade glioma patients. In this respect, dynamic FET-PET as well as MRI, e.g. diffusion and perfusion weighted imaging (DWI and PWI), have been used to obtain valuable information. In this study, we investigate their separate and added value in a combined protocol. **Methods:** 60 contrast-enhancing lesions suggestive of recurrence in 45 high grade glioma patients were identified in follow-up MRI after combined therapy. All patients received a dynamic FET scan of 40 minutes, as well as morphologic, perfusion- and diffusion-weighted MRI on a hybrid PET/MR scanner. Lesions were manually encircled by 2-cm-spheres. Further data analysis was performed using MATLAB with parameter extraction on 90% isocontour volumes in the respective regions. **Results:** 45 lesions were classified as recurrence, 15 as radiation necrosis. Gold standard for diagnosis was histology in 16 and follow-up imaging in 44 cases. At optimal cut-off, sensitivities and specificities for static PET were 83% and 85%, increasing to 86% and 85% when including dynamic imaging, 72% and 74% for PWI as well as 70% and 63% for DWI. When analyzing receiver-operating characteristics, AUC was 0.86 for PET, 0.74 for PWI and 0.63 for DWI. Multiparametric analysis using a linear combination of PET, PWI and DWI resulted in an AUC of 0.89, improving discrimination particularly when demanding high specificity (75% sensitivity vs. 53% sensitivity at 100% specificity). **Conclusion:** Simultaneous dynamic FET-PET/ MRI was reliably feasible for imaging of recurrent high-grade glioma. While the single modalities were able to discriminate between recurrence and treatment-related changes as expected, multiparametric analysis might be of value especially when high specificity for tumor progression is desired.

OP-504

Voxel-based analysis of dynamic ^{18}F-FET-PET in gliomas : association with IDH1 mutational status and survival.

P. Blanc-Durand[1], A. Van Der Gucht[1], A. Kourilsky[2], V. Dunet[1], A. Verger[3], K. Langen[4], M. Jreige[1], M. Nicod-Lalonde[1], N. Schaefer[1], J. Prior[1]; [1]CHUV, Lausanne, SWITZERLAND, [2]Beaujon, Paris, FRANCE, [3]CH, Nancy, FRANCE, [4]Forshungszentrum, Jülich, GERMANY.

Purpose: The prognostic impact of the isocitrate dehydrogenase (*IDH*) 1 mutation has been reported by several studies. Also, PET with ^{18}F-fluoro-ethyl-tyrosine (^{18}F-FET PET) has been increasingly used to evaluate patients with gliomas, however its prognostic value remains unclear. We aimed to investigate the association between dynamic ^{18}F-FET PET, *IDH1* mutation status and survival using a voxel-based approach. **Methods:** Fifty-two patients with newly diagnosed gliomas and dynamic ^{18}F-FET PET before any histopathologic investigation or treatment were retrospectively included. Each dynamic ^{18}F-FET PET image was realigned to the first image and spatially normalized in the MNI

template. A tumor mask was semi-automatically generated from the Z-score map. Each brain tumor voxel was clustered in 3 types of curve shape (curve #1: rapidly increasing followed by slowly decreasing slope, curve #2: slowly increasing slope, curve #3: rapidly increasing and rapidly decreasing slopes) using dynamic time warping and k-means clustering. The number of voxels of each of the 3 previous curves and the tumor % of each curve in brain tumors were compared between patients with mutated and wild-type *IDH1*. The prognostic value for progression free-survival (PFS) and overall survival (OS) of each curve's proportion; *IDH1* mutation status and tumor grade was integrated into a multivariate cox regression. **Results:** Thirty-seven dynamic ^{18}F-FET PET (18 low-grade and 19 high-grade gliomas) could be segmented and retained in the final analysis. Seventeen patients were *IDH1* mutant and 20 *IDH1* wild-type. Voxel-based analysis of dynamic ^{18}F-FET PET revealed that curve #2 was positively associated with the mutated *IDH1* status (P = 0.016) whereas curve #3 was negatively associated with the mutated *IDH1* status (P = 0.009). No difference was found with the curve #1 (P = 0.13). In a multivariate model, the curve #2 remained an independent positive prognostic factor for PFS (HR 0.15, 95% CI 0.02-0.76, P = 0.02) and OS (HR 0.06, 95% CI 0.01-0.54, P = 0.01). **Conclusion:** Voxel-based analysis of dynamic ^{18}F-FET PET revealed that the proportion of slowly increasing slope (curve #2) and the proportion of rapidly increasing and rapidly decreasing slopes (curve #3) were statistically associated with the *IDH1* mutation status. Also, the curve #2 was an independent positive prognostic factor for PFS and OS in multivariate analysis.

Cardiovascular System: Myocardial Perfusion PET - 13N-Ammonia and 15O-Water

OP-505

AMMO-X: A cross-comparison study of ^{13}N-ammonia PET MPQ software tools

S. V. Nesterov[1,2], L. E. Juárez-Orozco[1], R. J. Knol[3], R. Sciagrà[4], P. Slomka[5], A. Alessio[6], F. van der Zant[3], C. Han[1], N. Kartiosuo[7], J. M. Knuuti[1]; [1]Turku PET Centre, Turku, FINLAND, [2]Institute of Evolutionary Physiology and Biochemistry, RAS, St. Petersburg, RUSSIAN FEDERATION, [3]Cardiac Imaging Division Alkmaar, Northwest Clinics, Department of Nuclear Medicine, Alkmaar, NETHERLANDS, [4]Nuclear Medicine Unit, DECBS, University of Florence, Florence, ITALY, [5]Cedars-Sinai Medical Center, Los Angeles, CA, UNITED STATES OF AMERICA, [6]University of Washington, Seattle, WA, UNITED STATES OF AMERICA, [7]Research Center of Applied and Preventive Cardiovascular Medicine, Turku, FINLAND.

Aim: ^{13}N-ammonia is widely used in myocardial perfusion quantification (MPQ) with PET. Several software packages (SWPs) enable it, and although there were cross-comparison studies for some of them, no one aimed at an exhaustive study including all packages available. Such a study was our aim. **Materials**

and Methods: At the moment of the abstract submission, five SWPs—Carimas, PMOD, QPET, Syngo.MBF, and UW-QPP—were compared using 57 clinical rest- and stress-PET myocardial perfusion scans (Siemens Biograph-16 TruePoint PET/CT). Briefly, 300 and 400 MBq of ^{13}N-ammonia were injected at rest and during adenosine (140µg/kg/min) stress. Each participating center performed MPQ (using all implemented tracer-kinetic models) blinded to the results of other SWPs. Myocardial flow reserve (MFR) was obtained as the ratio of stress to rest myocardial blood flow (MBF). Analysis was performed globally and regionally (LAD, LCx and RCA). The cross-comparison of the resulting estimates was conducted applying custom linear mixed model for repeated measures to produce two agreement metrics—intraclass correlation coefficient (ICC) and absolute difference between SWPs—calculated pairwise. Differences below 20% of median values with corresponding ICCs above 0.75 witnessed to good agreement. **Results:** Global MFR as estimated by 1TCM (DeGrado et al., 1996) in Carimas and PMOD was 2.44±0.14 and 2.99±0.14 correspondingly, with a difference of 20.6% (ICC=0.92). The most pronounced regional difference was 21.4%—in the LAD territory (ICC=0.90); the least - in RCA (14.4%, ICC=0.91). Global MFR as estimated by 2TCM (Choi et al., 1993) in PMOD and QPET was 2.95±0.14 and 2.69±0.14 correspondingly, with a difference of 9.6% (ICC=0.79). The most pronounced regional difference was 24.5%—in the RCA territory (ICC=0.51); the least - in LAD (1.1%, ICC=0.81). Finally, global MFR estimated by 2TCM (Hutchins et al., 1990) was 2.57±0.14 in Carimas, 2.33±0.14 in UW-QPP and 2.87±0.14 in Syngo.MBF; the largest difference was found between Syngo.MBF and UW-QPP (20.6%, ICC=0.84); the smallest—between Carimas and UW-QPP (9.2%, ICC=0.77). The most pronounced regional difference was 23.8% (ICC=0.46) between PMOD and UW-QPP in the RCA, while the smallest (3.0%) was found between Carimas and SYNGO in the RCA territory (ICC=0.64). **Conclusions:** There is moderate to good agreement in MPQ with ^{13}N-ammonia PET between available SWPs on global and regional levels.

OP-506

Assessment of the functional significance of coronary artery stenoses in patients with CAD using dynamic stress PET / CT with 13N-ammonium with the use of absolute values of myocardial blood flow and coronary flow reserve

I. V. Shurupova, I. P. Aslanidis, M. G. Shavman, E. P. Derevyanko, E. P. Derevyanko, I. V. Ekaeva; Bakoulev Scientific Center for Cardiovascular Surgery, Moscow, Moscow, RUSSIAN FEDERATION.

Purpose: To assess the possible contribution of the use of absolute values of myocardial blood flow (MBF) and coronary flow reserve (CFR) in the functional evaluation of coronary stenoses in patients with CAD. To compare CFR in patients with different degrees of coronary artery (CA) stenoses and ischemia severity according to semiquantitative perfusion stress PET/CT with 13N-ammonium. **Method:** 46 patients with CAD (mean age 64.7 ± 8.6 years) who underwent perfusion stress-PET/CT were examined on Biograph-64 (Siemens) in a dynamic mode. This allowed, in addition to the standard perfusion parameters (SSS

and SRS), severity of ischemia (SDS), to determine the MBF and the CFR value. Exclusion criteria were the presence of large scar in LV myocardium according to ECHO data or perfusion PET / CT, and the history of CA bypass grafting. **Results:** When comparing two groups with CA stenosis according to x-ray endovascular coronary angiography ≥75% (n = 27) and <75% (n = 19), the number of people with reduced CFR (<2.0) in the first group was 88.9%, in the second - 21.0%, the number of segments with a decreased CFR 34.8% and 5.9% respectively. There was a significant difference (p <0.001) of CFR value in the territory of CA with the most severe stenos between groups: 1.89 [1.53; 2.26] and 2.83 [2.33; 3.39], respectively. When comparing three groups: with no perfusion abnormalities (SSS ≤ 3, n = 7), insignificant (SSS = 3-8 points, n = 17) and moderate / severe disorders (SSS≥9, n = 22), CFR was significantly lower (p <0.01) in the third group (1.81 [1.39, 2.21]) compared with the first group (2.33 [2.06, 2.9]) and second group (2.83 [2.46, 3.59]). Significant differences were also found when comparing three groups with insignificant ischemia (SDS≤4, n = 15), moderate (SDS = 5-8, n = 12) and pronounced (SDS≥9, n = 19) (p <0.001) - CFR was lower in the third group (1.66 [1.27, 2.04]) compared with the first group (2.73 [2.25, 3.54]) and the second (2.67 [2.16, 2 , 97]). **Conclusion**: The value of the coronary reserve is significantly lower in patients with significant stenoses of the coronary arteries compared with the group of patients with small and borderline stenoses.Coronary reserve, calculated on the basis of absolute values of myocardial blood flow, confirms the significant differences between the group of patients with severe ischemia and patients with moderate and minor ischemia.

OP-507

Prognostic value of quantitative absolute myocardial stress perfusion in patients with chest pain and normal coronary arteries: A Nitrogen-13 Ammonia PET study

A. G. Monroy-Gonzalez[1], R. A. Tio[1], E. Alexanderson-Rosas[2], R. H. J. A. Slart[1]; [1]University Medical Center Groningen, Groingen, NETHERLANDS, [2]Department of Physiology, National Autonomous University of Mexico, MEXICO.

Introduction: Cardiac Syndrome X (CSX) has been referred as chest pain, normal coronary arteries and positive exercise stress test. Previous studies suggest that quantitative myocardial perfusion measurements can be reduced in patients with suspected CSX, independently of exercise stress test findings. Currently, the prognostic value of quantification of absolute myocardial perfusion with PET in patients with suspected CSX is unknown. **Aim:** We evaluated if abnormal absolute myocardial stress perfusion quantification with Nitrogen-13 Ammonia PET is related to higher incidence of mayor adverse cardiac events (MACE) in patients with normal or near normal coronary arteries. Methods: We retrospectively included 100 patients who underwent Nitrogen-13 Ammonia PET for quantification of global myocardial blood flow (MBF) during stress with adenosine. Normal MBF during stress was defined as ≥1.85 mL/g/min. Patients with significant coronary artery disease (>50% stenosis) demonstrated by invasive coronary angiography were excluded. MACE were

assessed as cardiac death, myocardial infarction (MI), and heart failure using the Kaplan-Meier method. **Results:** In our population 68% were female patients, mean age was 52±11 years old, 7% were diabetic, 37% had hypertension, and 20% were current smokers. Abnormal MBF during stress was found in 44% of patients. During follow up (8.9 ± 6.3 years) 6 patients presented at least one MACE. 5 patients who presented at least one MACE showed abnormal MBF during stress. Kaplan-Meier analysis showed that patients with abnormal MBF during stress had a significantly higher rate of MACE compared with those with normal MBF during stress (p= 0.02). **Conclusion:** Absolute myocardial stress perfusion quantification with Nitrogen-13 Ammonia PET predicts MI in patients with chest pain and normal or near normal coronary arteries. Further studies are needed in order to completely understand the role of MBF during stress in the prognosis of this group of patients.

OP-508

Feasibility of layer myocardial blood flow

R. Calabretta[1], *E. Milan*[2], *R. Giubbini*[3], *R. Durmo*[3], *L. Gallo*[2], *T. Kubik*[4,5], *R. Sciagra*[1]; [1]*Nuclear Medicine, DECBS, University of Florence, FLORENCE, ITALY,* [2]*Nuclear Medicine, San Giacomo Hospital, ULSS 2, Castelfranco Veneto, ITALY,* [3]*Chair of Nuclear Medicine, University of Brescia, Brescia, ITALY,* [4]*Pmod Technologies LLC, Zurich, SWITZERLAND,* [5]*Institute of Metrology and Biomedical Engineering, Warsaw University of Technology, Warsaw, POLAND.*

Previous studies suggest that myocardial blood flow (MBF) can be measured separately in the myocardial layers (subendocardium - Endo - and subepicardium - Epi) using ^{15}O-water PET. More recently, the feasibility of separate layer measurements with parametric mapping of $^{13}NH_3$ PET was demonstrated in patients with hypertrophic cardiomyopathy. Aim of the present study was to test the reliability of this method in patients with normal left ventricular (LV) wall thickness. The Dicom files of 48 patients submitted to rest and dipyridamole $^{13}NH_3$ PET for suspect or known coronary artery disease (CAD) and in whom invasive coronary angiography (ICA) was available were selected from the databases of our Institutions and anonymized. They were processed with dedicated software (PCARDP, Pmod Technologies) that calculated rest and stress MBF and coronary flow reserve (CRF) both for the entire LV wall (average) and for Endo and Epi separately. Starting from the 17 segments of the AHA model, the volume-weighted means for the three coronary artery territories and the whole LV were obtained, and then compared with ICA results. ICA identified 28 patients with significant CAD (showing > 75% stenosis in 25 territories, 100% occlusion in 10). According to ROC analysis, average CFR was the most effective for identifying CAD (area under the curve - AUC = 0.77, p < 0.003), followed by Endo CFR (AUC = 0.74, p < 0.005), stress average MBF (AUC = 0.73, p < 0.01) and stress Endo MBF (AUC = 0.73, p < 0.01). There were no differences in resting Endo and Epi MBF between normal and CAD territories, whilst they were highly significant under stress. On a territory basis, the best diagnostic performance was reached by stress Epi MBF and stress average MBF (both AUC = 0.76, p < 0.0001), followed by stress Endo MBF (AUC = 0.73, p < 0.0001). Interestingly, stress Endo MBF was the sole parameter that differentiated between segments subtended by > 75% stenosis versus 100% occlusion: (1.3 ± 0.4 vs. 1.1 ± 0.6 mL/min/g, p < 0.03). In conclusion, this study indicates that parametric $^{13}NH_3$ analysis allows the separate assessment of MBF and CFR in the myocardial layers with results that appear reasonable and compare well with the standard approach considering the entire myocardial wall. Although no specific advantage of the layer estimates could be demonstrated, the possibility that Endo MBF is more sensitive for discriminating different grades of stenosis severity deserves further attention.

OP-509

Effect of motion-induced PET-CT misalignment on cardiac function and myocardial blood flow measured using dynamic ^{15}O-water PET

M. Lubberink[1], *M. Ebrahimi*[1], *H. J. Harms*[2,3,4], *L. Poulsen Tolbod*[2], *J. Sörensen*[1,2]; [1]*Uppsala University, Uppsala, SWEDEN,* [2]*Århus University, Århus, DENMARK,* [3]*Brigham and Women's Hospital, Boston, MA, UNITED STATES OF AMERICA,* [4]*VU University Medical Centre, Amsterdam, NETHERLANDS.*

Aim: Motion-induced PET-CT misalignment artifacts are common in myocardial blood flow (MBF) measurements with ^{82}Rb and ^{13}N-ammonia. For ^{15}O-water, MBF is based on the clearance rate rather than uptake of the tracer. The clearance rate is determined by the shape of the time-activity curve, not its amplitude, and is thus not affected by attenuation correction errors. Hence, misalignment is hypothesized not to affect ^{15}O-water-based MBF to any large extent, but it may affect cardiac function measures derived from ^{15}O-water scans. The aim of the present work was to assess the effect of PET-CT misalignment on MBF, transmural MBF (MBFt), perfusable tissue fraction (PTF), cardiac output (CO), stroke volume (SV) and left-ventricular ejection fraction (LVEF) based on dynamic ^{15}O-water scans. **Methods**: 10 patients underwent 6 min PET scans after injection of 400 MBq ^{15}O-water at rest and during adenosine-induced stress on a Discovery MI PET-CT scanner. Attenuation correction was based on a respiration-averaged CT scan. Images were reconstructed using TF-OS-EM including PSF-recovery. PET-CT misalignment was induced by translation of the PET relative to the CT (1 cm caudal or cranial, 1 cm cranial + ventral, and 2.5 cm cranial + 1 cm ventral). MBF, MBFt, PTF, CO, SV and LVEF were calculated semi-automatically using aQuant software and values with and without misalignment were compared using correlation and Bland-Altman analysis. The original data, without misalignment, was analysed twice to assess intra-observer variability. **Results:** Intra-observer reproducibility was high, with $R^2 \geq 0.98$ for all parameters except LVEF during stress (R^2 0.80). CO and SV were not significantly affected by misalignment, with correlation between aligned and misaligned values >0.95 (CO) and >0.93 (SV) and no significant bias for all motions. For MBF, correlation was always >0.95 for all coronary flow territories and motions, and no significant bias was seen. For MBFt however, correlations were always lower, reducing to 0.89 in LCX for the largest misalignment at stress. LVEF

was only affected significantly for the largest misalignment. Correlation of misaligned PTF and original PTF values was lower, but no significant motion-induced bias was seen. **Conclusion**: With the exception of PTF and LVEF for >1.5 cm misaligment, misaligment-induced changes were generally similar to or slightly higher than intra-observer variability. PET-CT misalignment does not significantly affect MBF and cardiac function measures based on ^{15}O-water scans for misalignment up to 1.5 cm.

OP-510

Automatic extraction of left ventricular mass and volumes using parametric images from non-ECG-gated 15O-water PET/CT

J. Nordström[1,2], H. J. Harms[3], M. Lubberink[1,4], L. Tolbod[3], J. van den Berg[1], T. Baron[5], F. A. Flachskampf[5], T. Kero[1,6], J. Sörensen[1,6]; [1]Nuclear medicin & PET, Department of Surgical Sciences, Uppsala University, Uppsala, SWEDEN, [2]Centre for Research and Development, Uppsala University / Gävleborg County, Gävle, SWEDEN, [3]Department of Nuclear Medicine & PET Centre, Aarhus University Hospital, Aarhus, DENMARK, [4]Medical Physics, Uppsala University Hospital, Uppsala, SWEDEN, [5]Cardiology, Department of Medical Sciences, Uppsala University, Uppsala, SWEDEN, [6]Medical Imaging Centre, Uppsala University Hospital, Uppsala, SWEDEN.

Introduction: ^{15}O-water positron emission tomography (PET) is considered the gold standard for non-invasive quantification of myocardial blood flow (MBF). It has been shown to identify patients with significant coronary artery disease (CAD) with high accuracy. Hypertrophy with or without dilatation of the myocardium together with a reduction in stroke volume are common in nearly any advanced cardiac disease. Thus, in addition to MBF, assessment of left-ventricular (LV) volumes and mass provides important diagnostic and prognostic information and are vital in the clinical setting. Therefore, the aim of the present study was to investigate the feasibility of measuring LV geometry using dynamic ^{15}O-water PET/CT without ECG-gating. **Methods**: Parametric images of MBF, perfusable tissue fraction (PTF) and LV blood pool were generated automatically using kinetic modelling. Segmentation of the LV wall using PTF images generated regional MBF and PTF, and total ROI volume which was converted to LV mass (mLV). Segmentation of blood pool images generated LV end-diastolic (EDV) and end-systolic (ESV) volumes. Segmentation thresholds were studied analytically in a subset of patients. The generated values were combined to measure stroke volume (SV=EDV-ESV) and ejection fraction (EF=SV/EDV). Accuracy was determined by comparing PET to cardiac magnetic resonance (CMR) in 30 asymptomatic patients with high grade LV regurgitation (group A). Precision was determined as inter-observer variation in group A and by a test-retest PET study in 15 patients with suspected ischemic heart disease at rest (group B). Normal values were defined in nine healthy volunteers. **Results:** The accuracy of PET was good with correlations of r= 0.83, 0.88, 0.86 and 0.76 for m_{LV}, EDV, ESV and SV, respectively, compared to CMR (P<0.001 for all). EF was in the normal range (53%-75%) and had a weaker correlation of r=0.51 (P=0.004). m_{LV} was overestimated by 18%±13% com-

pared to CMR and the residuals were closely related to the eccentric remodelling (mLV/EDV) defined by CMR. EDV, ESV and SV were underestimated by 10%±10%, 19%±13%, 3%±15%, respectively, compared to CMR. EF was overestimated by 4%±5% compared to CMR. Inter-observer correlation and test-retest repeatability were excellent (r>0.97). Normal values from PET were in line with normal values from a local CMR cohort. **Conclusion**: Microvascular function and LV geometry can be measured automatically with high accuracy and precision from a single non-gated ^{15}O-water PET. The accuracy of m_{LV} from PET is affected by LV eccentricity.

1310   **Tuesday, October 24, 2017, 11:30 - 13:00, Hall G2**

Do.MoRe: Detector Technology

OP-511

A Promising PET Detector Design that Achieves 100 ps FWHM Coincidence Time Resolution

J. W. Cates, C. S. Levin; Stanford University, Stanford, CA, UNITED STATES OF AMERICA.

The past two decades have seen much improvement in coincidence timing resolution (CTR) for time-of-flight (TOF) positron emission tomography (PET). State-of-the-art clinical TOF-PET systems now achieve sub-400 ps FWHM (full-width-at-half-maximum) CTR, enabling benefits such as decreased patient radiation dose, shorter scan time, improved lesion detection and quantification, and less sensitivity to errors in data correction techniques (normalization, scatter, and attenuation). An important and long-standing milestone for clinical TOF-PET is 100 ps FWHM CTR. At that level of timing performance, more than a factor of five enhancement in reconstructed image signal-to-noise ratio is possible compared to non-TOF-PET, with the potential for a transformational impact in count starved and contrast limited imaging tasks. With advancements in silicon photomultiplier technologies, novel scintillation materials, and signal processing techniques, sub-100 ps CTR has been reported for relatively short and narrow individual scintillation crystal elements (e.g. 2x2x3 mm³). However, clinical PET requires arrays of tightly packed scintillation crystal elements with dimensions of at least 3x3x20 mm³ for high 511 keV photon detection efficiency. This increased crystal length reduces the light collection efficiency and increases the scintillation photon transit time variance, which degrade CTR. Our group has previously shown that coupling the photosensors to the long sides of the crystal elements instead of their small ends yields near-complete light collection efficiency, and reduced scintillation photon transit time jitter. In this configuration, a CTR of 102±1 ps FWHM is achievable with 3x3x20 mm³ LGSO:Ce scintillators, with the 3x20 mm² face coupled to a 6-element row of 3x3 mm² SiPMs, using simple leading edge time pickoff and a single timing channel. This is in contrast to a CTR of 137±2 ps FWHM that is achieved when the same crystals are coupled end-on to a single 3x3 mm² SiPM. Moreover, this "side

readout" configuration enables 3D position sensitivity (3DPS), which can be employed to extract more information from inter-crystal scatter events (the most likely event type), including (1) more accurate positioning of the first interaction and (2) an estimate of the incoming annihilation photon incident angle. The latter feature offers the potential to retain a high fraction of photon events that are normally rejected. These innovations can be packaged into a practical clinical detector module with mixed analog-digital multiplexing schemes that require a low number of readout channels. We present the design and proof-of-concept measurements for this advanced 100 ps FWHM CTR TOF-3DPS clinical PET scintillation detector module.

OP-512

First human images from a next generation SiPM based PET/CT system with improved time and spatial resolution

M. Casey[1], Z. Burbar[1], H. Rothfuss[1], V. Panin[1], D. Bharkhada[1], W. Howe[1], Y. Bradley[2]; [1]Siemens Medical Solutions, Knoxville, TN, UNITED STATES OF AMERICA, [2]University of Tennessee Graduate School of Medicine, Knoxville, TN, UNITED STATES OF AMERICA.

Purpose: PET/CT provides clinicians information on tumors that can be used for diagnosis, staging, and management of cancer. Silicon photomultipliers (SiPMs) offer a unique opportunity to design a PET detector with smaller crystals and better time resolution thus potentially improving the quality of the clinical findings. This paper will present both phantom measurements and patient images from a new SiPM based PET/CT prototype that incorporates these features. **Materials and Methods:** The PET/CT uses a "Block" detector based approach with a 5x5 array of 3.2x3.2 LSO crystals coupled to a 1.6 cm x 1.6 cm array of 16 SiPMs. The ratio of the SiPM array area to scintillator is 100%. 128 of these "Blocks" are incorporated into a module. 19 of the modules are used to form an 82 cm diameter detector ring. The axial dimension of the ring is 26.3 cm. The spatial resolution and sensitivity of the system was assessed according to NEMA NU 2-2012 using [18]F. Time resolution was measured with the NEMA scatter phantom as proposed by Wang (IEEE TNS 2016). To further test the system, six human subjects (3 female, 3 male) were injected with 10.4 ±0.3 mCi of FDG at the University of Tennessee Medical Center under IRB approval. The subjects were first imaged on the Siemens Biograph mCT after 66 ±3.4 minutes then reimaged on the SiPM prototype at 131 ±16 minutes. Imaging time on the mCT was 1.5 minute beds, while 3 minutes per bed was used for the prototype. **Results:** FWHM measured at 1 cm was 3.23 mm radially, 3.27 mm tangentially and 3.84 mm axially using iterative reconstruction. Time resolution was 249 picoseconds (ps) in the gantry center with 2 mCi in the phantom and 265 ps with 30 mCi. Sensitivity was measured at 15.3 cps/kBq. Detector energy resolution measured in the system is approximately 10%. Lesions in all patient images from the prototype exhibited better defined margins and improved contrast compared to the mCT images. Brain images are more clearly defined. Liver images show improved homogeneity. **Conclusions:** The large area of the SiPM array provides superior time resolution, resulting in lower image noise. The measured

spatial resolution due to the 3.2 mm crystal is much improved compared with currently available commercial whole body systems. These improvements are exhibited in both phantom and patient imaging.

OP-513

Ultra-high Definition Isotropic 1mm Voxel Reconstruction in Clinical Wholebody PET - Is Digital PET Making It a Reality?

M. V. Knopp[1], J. Zhang[1], K. Binzel[1], M. I. Knopp[1], R. Moore[1], M. Friel[1], F. Giesel[2], C. L. Wright[1]; [1]The Ohio State University, Columbus, OH, UNITED STATES OF AMERICA, [2]University Hospitals Heidelberg, Heidelberg, GERMANY.

Purpose: Current PET imaging predominantly uses voxel sizes of 3-4 mm length or matrix sizes of less than 200^2. Compared to CT and MRI, this is substantially lower. With the introduction of next-generation solid state digital detection systems and greatly improved time of flight resolution, we initially explored, demonstrated and now clinically assess the feasibility and performance characteristics of $1 \times 1 \times 1$ mm[3] image reconstruction. **Subjects & Methods:** 43 patient studies from a clinical trial that performed oncologic whole body FDG PET/CT on a next generation digital photon counting system (Vereos, Philips, dPET) were included. Ultra-high definition (UHD) isotropic 1mm reconstructions were performed from list mode data for all studies and compared to current practice isotropic 4mm (SD) reconstructions. The reconstruction methodologies have been previously optimized and validated by phantom and other clinical data Two independent, highly experienced clinical readers blinded to all clinical history were asked to identify measurable and indeterminate lesions based on the SD whole body data sets. Several days after the initial task, the readers were asked to independently review the lesions identified by the other reviewer on the SD images and classify their level of diagnostic confidence on a -5 to +5 continuous scale. Again several days later using a randomized order, the readers reviewed the lesions on the UHD images. Another nonclinical reader reviewed which lesions matched between the readers. Inter- and intra-reader assessments were performed and kappa statistics will be calculated. Additionally the readers were asked to classify overall image quality, visual noise level and artifacts. **Results:** Image quality was rated acceptable or better for diagnostic reads in all 43 SD and UHD reconstructed studies. A total of 187 lesions were evaluated. The overall confidence rating was significantly (P<.01) higher for UHD reconstruction compared to SD. The difference in confidence was most pronounced for lesions smaller than 15 mm. In no case was the confidence reduced on the UHD images compared to SD. Additionally, the image quality was consistently ranked more preferable on UHD images compared to SD, independent of the reader. **Conclusion:** Ultra-high definition reconstruction was not only feasible in all cases, it consistently enabled a higher confidence for clinical diagnostic assessment. The difference is most pronounced in small metabolically active lesions. UHD appears to fully leverage the technological advances of digital PET and it is on the verge of becoming a clinical reality which needs to be further validated in larger clinical trials.

OP-514

Evaluation of Whole-Body and Small FOV CZT Gamma Cameras

J. W. Hugg, B. W. Harris, H. Tomita; Kromek / eV Products, Saxonburg, PA, UNITED STATES OF AMERICA.

Introduction and Purpose: Pixelated semiconductor direct-conversion CdZnTe (CZT) gamma photon detector arrays have been used in several molecular imaging applications, including small-animal and whole-body human SPECT, cardiac SPECT, and molecular breast imaging (MBI). The interplay of gamma camera and collimator geometric design, gantry motion, and image reconstruction determines image quality and dose-time-FOV trade-offs. Both dose and exam time can be minimized using CZT gamma cameras without compromising diagnostic content. **Materials and Methods:** We designed a modular gamma detector (4.4 cm square with 2 mm pixel pitch) and tiled it in two array sizes to evaluate CZT capabilities: a small FOV camera (8.8 cm square, 44 x 44 pixels) and a whole-body SPECT camera (39.6 cm x 52.8 cm, 198 x 264 pixels) that we mounted on a refurbished SPECT gantry for technology demonstration. We evaluated the performance of these gamma cameras using the NEMA NU1 standard. **Results:** Compared to NaI scintillator gamma cameras: intrinsic spatial resolution improved from 3.8 mm to 2.0 mm; energy resolution improved from 9.8% to < 4 % at 140 keV; non-detection camera edges are reduced about 3-fold. We measured intrinsic flood field uniformity of ±0.8% integral and ±0.4% differential, system spatial resolution at 10 cm with an LEHR collimator of 6.8 mm and 7.5 mm without and with scatter, and intrinsic detector count rate performance of 1.4 M cps at 20% loss and 6.1 M cps maximum observed. These metrics are significantly better than scintillator SPECT systems. We have designed and are building a pixel-registered square-hole collimator to optimize the resolution-efficiency tradeoff. **Discussion and Conclusions:** Excellent energy resolution enables better scatter rejection and improved image contrast, further enhanced by excellent uniformity; the optimal FOV is increased to the entire camera area. Smaller pixels improve partial-volume dilution and quantitation. Spatial resolution is improved, even with hexagonal-hole collimators, but registered square-hole collimators provide significantly better resolution and a boost of about 30% in sensitivity which can lower dose and/or exam time. The non-paralyzable CZT cameras count at much higher count rates, enabling new first-pass and pharmacokinetic studies. Advances in detectors, collimators, and image reconstruction have significantly improved efficiency of CZT-based molecular imaging systems and the cost of CZT detectors has steadily declined.

OP-515

First Experience with Fast Imaging Using Discovery MI PET/CT

*I. Sonni, S. Park, L. Baratto, N. Hatami, G. Davidzon, S. Srinivas, S. Gambhir, **A. H. Iagaru**; Stanford University, Stanford, CA, UNITED STATES OF AMERICA.*

Introduction: We recently installed the first of a new generation PET/CT systems that bring together silicon photomultiplier (SiPM) technology first used in the SIGNA PET/MRI, with time-of-flight (TOF) and Q.Clear reconstructions. In this study, we investigated the impact of various acquisition times on image quality using this SiPM-based PET/CT. **Methods:** We reviewed data from 58 participants who were scanned using the GE Discovery MI PET/CT scanner. The administered dosages ranged 6.1-11.6 mCi (mean±SD: 9.4±1.3) and imaging started at 71-137 minutes (mean±SD: 98±17) after administration of the radiopharmaceutical. The patients' BMI ranged 17.7-46.2 (mean±SD: 26.6±5.5). We retrospectively reconstructed the raw data at 30 sec/bed, 60 sec/bed, 90/sec bed, 120 sec/bed and at the standard image acquisition time per clinical protocol (3-5 minutes/bed depending on BMI). Each reconstruction was reviewed blindly and independently by 2 nuclear medicine physicians and scored using a Likert scale (1 - poor, 5 - excellent quality). **Results:** The scores for PET images were 2.6±0.6 for the 30 sec/bed reconstructions, 3.7±0.7 for the 60 sec/bed reconstructions, 4.5±0.7 for the 90 sec/bed reconstructions, 4.8±0.3 for the 120 sec/bed reconstructions and 4.9±0.3 for the standard reconstructions. The addition of a regularized reconstruction algorithm to images reconstructed at 120 sec/bed and standard reconstruction resulted in scores of 4.7±0.7 and 4.8±0.4, respectively. Inter-reader agreement on image quality assessment was good, with a weighted kappa of 0.80 (95% CI: 0.72 - 0.81). Almost half of each reader's ratings were 5 (Excellent Quality). There was a significant positive effect of time on ratings (OR=1.05, 95%CI: 1.04-1.06, p<0.001), and significant negative effects of BMI>30 (OR=0.05, 95%CI: 0.02-0.12, p<0.001). There was no significant effect of administered dosage (OR=1.35, 95%CI: 0.95-1.91, p=0.090). **Conclusion:** Our results suggest that despite significant delays from injection to imaging compared to standard clinical operations and even in a population with average BMI>25, images can be acquired as fast as 90 sec/bed using the SiPM PET/CT and still result in very good image quality (average score >4). Additionally, one can reduce the administered dosage and still scan fast (120 sec/bed) while maintaining very good image quality.

OP-516

Phase Ia Trial Comparing Higher Definition Digital Photon Counting PET/CT with Current Photomultiplier PET/CT for Head and Neck Oncology

C. L. Wright[1], A. D. Bhatt[1], K. Binzel[1], I. R. Washington[1], P. Bhatia[1], P. Subramanian[1], J. Zhang[1], P. Maniawski[2], M. V. Knopp[1]; [1]The Ohio State University, Columbus, OH, UNITED STATES OF AMERICA, [2]Philips Healthcare, Cleveland, OH, UNITED STATES OF AMERICA.

Purpose/Introduction: Conventional photomultiplier PET/CT (cPET/CT) imaging with FDG is used clinical for the routine detection of occult malignancy, staging and assessment of treatment response. A recent technology innovation has replaced the photomultiplier tubes in the PET gantry with solid-state digital photon counting PET detectors (dPET/CT). Digital PET technology enables higher definitionPET imaging

with smaller voxel volumes and reduced partial volume effects. Our aim is to assess qualitative and quantitative imaging characteristics of dPET/CT compared to cPET/CT in patients with head/neck cancer. **Subjects & Methods:** Digital PET/CT (Vereos, Philips) was used to evaluate 30 patients in an ongoing intra-individual comparison trial and compare its image characteristics to cPET/CT (Gemini, Philips). Routine cPET/CT was performed at ~75 min p.i. using 481 MBq FDG and investigational dPET/CT either at ~55 min or ~95 min p.i. PET data was acquired in list-mode with all other acquisition aspects kept identical. Conventional PET images were reconstructed using Time-of-Flight with voxel volumes 4x4x4 mm^3 (standard definition/SD) and dPET images were reconstructed using Time-of-Flight with different voxel volumes 4x4x4 mm^3, 2x2x2 mm^3 (high definition/HD), and 1x1x1 mm^3 (ultra-high definition/UHD). Image sets were evaluated for overall quality, lesion detection, diagnostic confidence and background quality by a blinded reader panel. **Results:** For all patients, cPET and dPET images were rated as evaluable. Higher definition dPET imaging produced substantially improved image quality for qualitative and quantitative assessment of the primary malignant as well as metastatic lesions with no appreciable effect on the background FDG activity. Although UHD dPET data sets were consistently rated best, both HD and UHD dPET data sets demonstrated improved lesion detectability with sharper delineation of small lesions (≤15mm) and better characterization of larger heterogeneous lesions (>15mm) when compared with SD cPET. Quantitative SUV assessment of larger lesions using higher definition dPET yielded comparable SUVmax values whereas smaller lesions demonstrated higher SUVmax values. **Discussion/Conclusion:** FDG PET imaging in head/neck oncology is widely used and contributes tremendous clinical value to staging and therapy response assessment. Higher definition dPET/CT demonstrates improved visual and quantitative assessment of head/neck cancer patients when compared with cPET. For dPET, its faster timing resolution (~325 ps) compared with cPET (~550 ps) and its higher definition reconstructions both contribute to decreased partial volume effects and more precisely localization of FDG activity within lesions. Continued optimization and development of higher definition PET technologies will further advance precision imaging and therapy planning approaches.

OP-517

PET 20.0: a cost-efficient, 2mm spatial resolution Total Body PET with point sensitivity up to 22% and adaptive axial FOV of maximum 2.00m

S. Vandenberghe[1], E. Mikhalyova[2], B. Brans[3], M. Defrise[4], T. Lahoutte[4], K. Muylle[4], R. Van Holen[5], D. R. Schaart[6], J. S. Karp[7]; [1]MEDISIP-Ugent, Gent, BELGIUM, [2]Department of Biomedical Engineering, University of California Davis, Davis, CA, UNITED STATES OF AMERICA, [3]Department of nuclear medicine UZGent/Ugent, Gent, BELGIUM, [4]Dept of nuclear medicine, Free University of Brussels, Brussels, BELGIUM, [5]MEDISIP-Ugent-Molecubes, Gent, BELGIUM, [6]Radiation Science & Technology, Delft University of Technology, Delft, NETHERLANDS, [7]PET instrumentation Group, University of Pennsylvania, Philadelphia, PA, UNITED STATES OF AMERICA.

Aim: Total body PET (TB-PET) is a very promising concept for new applications in molecular imaging and biomedical research with the only drawback the high material costs for building the system. The aim of this study is the optimisation of the length, energy settings and configuration of a long axial TB-PET system based on 15 mm thick monolithic LYSO scintillator with SiPM readout and a transverse diameter of 63 cm. **Material and Methods:** The central point sensitivity and volume sensitivity (uniform cylinder of 20 cm transverse and 1 or 2m length) was evaluated for an axial length from 25 cm to 2m. The 1m long system was also configured for long objects (up to 2m) without increasing the cost by axially separating the 32 rings. Due to oblique data redundancy the full object can still be reconstructed (with adapted sensitivity correction) as shown already by several designs with axial gaps. Finally the effect of lowering the energy threshold on the sensitivity of the 1m long system was evaluated. **Results:** The point source sensitivity increase per additional axial ring is the largest in the range from 25-100 cm and reduces clearly for larger axial extents above 1m. For a 100 cm long water phantom the gain in total sensitivity by extending the scanner from 1m to a fully populated 2m is only 46 %. For the 2 m long phantom the gain in sensitivity is much higher: +137 %. The same 2m phantom in a 1.5 m long scanner with 33% missing rings and in a 2m long scanner with only 50 % populated rings gives respectively only 15 % and 26 % less counts than in a 1m long scanner. Lowering the energy threshold to 250 keV resulted in a point source sensitivity of 22 % for a 1 m scanner. **Conclusions:** As shown in other studies 70-100 cm seems an optimal length for maximizing the point and volume sensitivity in a realistic object (20-35 cm diameter). The cost of detectors can be reduced by 50 % by using a 1m long scanner. This system will be excellent for most of the applications. The system can be adapted by separating the rings in the axial direction for the special cases where larger axial (> 1m) FOV for eg. total body dynamic imaging is required. The loss in sensitivity can be compensated by increasing the typically short acquisition times for TB-PET.

OP-518

A New Direction to Explore to Advance Coincidence Time Resolution for Time-of-Flight Positron Emission Tomography

*L. Tao, **C. S. Levin**; Stanford University, Stanford, CA, UNITED STATES OF AMERICA.*

Introduction: We are exploring a new detection mechanism for 511keV photons that has the potential to achieve < 10ps coincidence time resolution (CTR). A limiting factor for achieving < 100ps CTR for time-of-flight positron emission tomography (ToF-PET) detectors is the intrinsic scintillation process. In order to overcome this limit, we studied the modulation of optical

properties that occurs in a crystal resulting from 511keV photon interactions, instead of scintillation, with the ultimate goal to achieve < 10ps CTR. **Materials and Methods:** The ionization charges created from 511keV photon interactions will induce fast modulations in a detector material's optical properties, which can be observed using methods of modern optics. Initial efforts used a 5×5×5mm^3 cadmium telluride (CdTe) crystal and a 5×5×5mm^3 bismuth silicon oxide (BSO) crystal. The refractive indices of both crystals are modulated as a result of a locally perturbed electric field caused by the production of ionization charges, known as *electro-optic modulation*. With a two-beam interference setup, an interference pattern is generated by one laser beam which traverses the detector crystal and another beam which does not. The refractive index modulation resulting from ionization charges was observed and quantified by monitoring the magnitude of spatial shifting of the interference pattern. We also experimented with optical cavities with the detector crystal inside. Light transmission of the cavity is very sensitive to changes in the refractive index of the detector crystal produced when ionization charges are created. For ionization sources, we employed various radionuclides as well as a laser diode. For both approaches, we also studied the influence of crystal bias voltage on the modulation signal. **Results:** With both radionuclide and laser diode as sources of ionization, sensitivity to ~10^{-6} refractive index change was observed with 1000V bias voltage and no optical cavity. The amplitude of this modulation signal is linearly dependent on the detected event rate as well as the average ionizing photon energy. We also saw that the amplitude of the modulation signal is linearly dependent on crystal bias due to charge multiplication effects, while optical amplification enabled via the optical cavity enhances the modulation signal by an additional 130-fold with 95% reflectivity cavity mirrors and a focused beam. **Conclusion:** We have shown proof of concept that the mechanism of optical property modulation can be used to detect and quantify ionizing radiation photons. Our future work focuses on achieving individual 511keV photon detection with < 10ps CTR.

YDF3   **Tuesday, October 24, 2017, 13:00 - 14:30, Hall F1**

EANM Young Daily Forum 3: Be Stronger - Mentally, Emotionally, Physically & Spiritually

R. Sheppard; Somerset, UNITED KINGDOM.

1401   **Tuesday, October 24, 2017, 14:30 - 16:00, Hall A**

CME 11 - Paediatrics/Oncology/SIOPEN: SSR Imaging and Therapy in Children

OP-519

The Importance of miBG in the International Neuroblastoma Community. Perspectives from SIOPEN Collaborations: Past, Present, Future
R. Ladenstein; St. Anna Kinderkrebsforschung, Vienna, AUSTRIA.

1404 Tuesday, October 24, 2017, 14:30 - 16:00, Hall E1

Do.MoRe - Dosimetry/Physics/AAPM: PET Auto-Segmentation: Review and Evaluation Strategies - Insights from AAPM Task Group No. 211

OP-529

State-of-the-Art of Current PET-AS Algorithms and their Advantages and Limitations for Clinical Application

M. Hatt; Centre Hospitalier Régional Universitaire Morvan INSERM, Brest, FRANCE

OP-530

Components of a Standard and a Procedure for Evaluation of PET-AS Methods

A. Kirov; Memorial Sloan-Kettering Cancer Center, New York, USA

OP-531

Design, Implementation and First Results of the Future Standard for Evaluation of PET-AS Methods

E. Spezi; Velindre Cancer Centre, Cardiff, UNITED KINGDOM

1405 Tuesday, October 24, 2017, 14:30 - 16:00, Hall E2

M2M: Nanoparticles

OP-532

An intrinsically radioactive metal-organic framework (MOF) nanomaterial for Cerenkov luminescence-triggered cancer phototherapy: focused on deep-tissue tumor

H. Hong, D. Chen, D. Yang, W. Lu; University of Michigan, Ann Arbor, MI, UNITED STATES OF AMERICA.

Purpose: As one of the cancer treatment option, the primary limitation for photodynamic therapy (PDT) is that laser used to irradiate photosensitizers can only penetrate less than 1 cm, thus PDT is more suitable for treating superficial and localized tumors. To enhance the applicability of PDT, our goal is to develop a nanoplatform with intrinsic light emission for PDT of deep-tissue tumors. Recently, we successfully incorporated ^{89}Zr into different types of metal-organic framework (MOF) nanomaterials with strong radiochemical stability. Cerenkov luminescence from ^{89}Zr can be used as an internal excitation for photosensitizer (porphyrin) inside MOF structure. In addition, the existence of ^{89}Zr enables the tracking of MOF *in vivo*. **Methods:** Porphyrin and ^{89}Zr-containing PCN-224 type MOF nanomaterial was synthesized by a hydrothermal method with tetra-kis(4-carboxyphenyl)porphyrin as the bridging ligand for Zr_6 clusters. A pyrene-derived polyethylene glycol (Py-PGA-PEG) was used to increase the dispersity of ^{89}Zr-PCN-224 and provide reaction sites for attachment of a tumor-targeting ligand (F3, against nucleolin). Fluorescence from PCN-224 can be used as a visualizer in flow cytometry and confocal fluorescence microscopy to investigate the interaction between PCN-224 and different cells. Size and physical property characterization was conducted

before *in vivo* investigation by PET imaging and biodistribution studies. The treatment efficacy of ^{89}Zr-PCN-224 was evaluated at both cellular level and *in vivo*. Toxicity evaluation of PCN-224 conjugates was also done. **Results:** PCN-224 had a size range of 40-80 nm based on TEM measurement. ^{89}Zr could be efficiently incorporated into PCN-224 structure with a specific activity up to 2.4 GBq/mg, with good radiochemical stability. PCN-224/Py-PGA-PEG-F3 had strong internalization into MDA-MB-231 cells but showed minimal interaction with L929 cells. More potent and fast accumulation of ^{89}Zr-PCN-224/Py-PGA-PEG-F3 into MDA-MB-231 tumors was observed (9.3 ± 2.4 %ID/g at 0.5 h, n = 4) compared with ^{89}Zr-PCN-224/Py-PGA-PEG (3.4 ± 2.4 %ID/g at 0.5 h, n = 4), and histological analysis substantiated the specificity of ^{89}Zr-PCN-224/Py-PGA-PEG-F3 against nucleolin-positive tumors. We confirmed that ^{89}Zr could excite the fluorescence from PCN-224 and initiate the production of ROS, which caused significant toxicity against cancer cells. PCN-224/Py-PGA-PEG did not pose acute or chronic toxicity to the test subjects at 10 mg/kg. Finally, injection of radioactive PCN-224 conjugates showed interference to the growth of deep-tissue tumors. **Conclusion:** We successfully synthesized radioactive PCN-224 MOF nanomaterial in this report. This nanoplatform can achieve triple functions: tumor detection (by PET), deep tumor treatment, and therapeutic cargo delivery (in the future).

OP-533

Formulation and in vivo biodistribution of 57Co-porphyrin-labelled hydrophobic liquid nanoparticles

P. Hervella[1], J. Dam[2], H. Thisgaard[2], C. Baun[2], B. B. Olsen[2], P. Høilund-Carlsen[2], D. Needham[1]; [1]Center for Single Particle Science and Engineering, Odense, DENMARK, [2]Odense University Hospital, Odense, DENMARK.

Introduction: In personalized nanomedicine, identification of patients most likely to respond to a nanomedicine treatment, can be identified by PET imaging. We aimed to develop a radiolabelled nanoparticle of the same size and structure as the subsequent therapeutic nanomedicines but labelled with a long-lived PET radionuclide. ^{55}Co is a PET imaging isotope for long-circulating molecules and macromolecules due to its half-life of 17.5 h and average energy of 570 keV. ^{57}Co ($t_{1/2}$ 271.6 days) is a SPECT isotope useful for preclinical studies of biodistribution and pharmacokinetics of nanoparticles. Because these ions are isoluble in a hydrophobic material, we used the hydrophobic porphyrin octaethyl porphyrin (OEP) in combination with two hydrophobic axial ligands (oleylamine, OA) to chelate cobalt to encapsulate the radionuclide inside hydrophobic liquid nanoparticles (LNP). **Methods:** LNPs were prepared by the fast ethanol injection method and were composed of a liquid core (Triolein) surrounded by a lipid monolayer (DSPC:Cholesterol:DSPEPEG). The LNPs were labelled with ^{57}Co using OEP and OA as chelators. A biodistribution study was carried out in male NOD-SCID mice inoculated subcutaneously in the right flank with 10^6 AR42J pancreatic cancer cells. **Results:** The size of LNPs loaded with a cobalt complex was 40 ± 5 nm, and the loading capacity of OEP-Co-OA in LNP was 5 mol%. In absence of the axial OA

ligands, the leakage of free [57]Co after 24 h incubation was 62%, which was significantly higher than the free [57]Co leakage from OEP-[57]Co-OA loaded LNP (only 12 %). The results demonstrate the positive effect of the additional OA ligands on the stability of the OEP-[57]Co complex. Finally, the biodistribution study showed that the concentration of LNP particles in the blood was 30% ID/g 1 h after injection with an estimated half-life of about 7.2 h. Remarkably, the accumulation of LNP in the tumor was as high as 9.5 % ID/g 24 h after injection. The most important result was that the nanoparticles could indeed accumulate in AR42J tumors up to levels that are greater than other nanoparticles like liposomes and at about half the values reported for the molecular agent [57]Co-DOTATATE. **Conclusion:** The Co^{2+} ion can be encapsulated and retained inside LNPs when the ion is chelated by the hydrophobic chelator OEP in combination with 2 OA. The method described here for labelling of LNPs with cobalt is, therefore, now ready for labelling of nanomedicines with [55]Co for preclinical *in vivo* PET-imaging.

OP-534

Pretargeted tumor imaging with a polymer: Reducing absorbed radiation dose and increasing imaging contrast

E. J. L. Stéen[1], K. Nørregaard[2], A. Birke[3], P. E. Edem[2,1], J. T. Jørgensen[2], R. Rossin[4], M. Robillard[4], A. Kjaer[2], M. Barz[3], M. M. Herth[1,2]; [1]University of Copenhagen, Copenhagen, DENMARK, [2]Rigshospitalet, University Hospital, Copenhagen, DENMARK, [3]Johannes-Gutenberg University, Mainz, GERMANY, [4]Tagworks Pharmaceuticals BV, Eindhoven, NETHERLANDS.

Introduction: Nanomedicines have demonstrated potential as targeting-vectors for diagnosis and/or therapy of cancer. Due to the leaky vasculature and reduced lymphatic drainage in some types of tumors in comparison to healthy tissue, long-circulating nano-sized agents tend to accumulate in tumors. This phenomenon is called the enhanced permeability and retention (EPR) effect.[1] The EPR effect is a relevant approach for tumor targeting in pretargeted tumor imaging, where the targeting is separated from the actual imaging step. A pretargeted approach enables the use of short-lived radioisotopes, which reduces the radiation doses for the patients and increases imaging contrast. Herein, we describe a pretargeted imaging approach, where a *trans*-cyclooctene (TCO) functionalized polyglutamic acid-*graft*-polysarcosine copolymer (PGA-*graft*-PSar-TCO) was allowed to accumulate within the tumor via the EPR effect, before a [^{111}In]In-labeled DOTA-tetrazine (Tz) derivative[2] was administered intravenously (i.v.). The latter reacts with the TCO:s on the polymer in an inverse electron demand Diels-Alder (iEDDA) reaction, which allows imaging of the polymer accumulation in the tumor. **Subjects & Methods:** The PGA-*graft*-PSar-TCO was synthesized by ring-opening polymerization of *N*-glutamic acid (Ot-Bu) carboxyanhydride, deprotection, postpolymerization modification with PSar (<40%) and functionalized with TCO (16%). The [^{111}In]In-DOTA-Tz was prepared as reported in the literature in a radiochemical conversion (RCC) of ≥99%. Analysis was performed by radio-TLC. *In vivo* stability studies and pretargeted microSPECT/CT imaging was performed using the ^{111}In-labeled PGA-*graft*-

PSar, PGA-*graft*-PSar-TCO and [^{111}In]In-Tz-DOTA in BALB/c mice bearing subcutaneous colorectal mouse tumors (CT26). **Results:** The PGA-*graft*-PSar-TCO was labeled with [^{111}In]In-DOTA-Tz via the iEDDA reaction in phosphate buffer at room temperature for 5 min in a RCC of 82-85%. I.v. injection of ^{111}In-labeled PGA-*graft*-PSar resulted in tumor accumulation after 22 h. After establishing the stability and time for clearance of the polymer, the *in vivo* iEDDA reaction was tested by injecting PGA-*graft*-PSar-TCO i.v. 72 h before i.v. injection of the [^{111}In]In-DOTA-Tz. After 24 h a clear visualization of the tumor was observed. **Conclusion:** A new easily accessible PGA-*graft*-PSar copolymer functionalized with TCO for pretargeted tumor imaging based on the EPR effect and *in vivo* click chemistry has been developed. Its utility was validated with the previously reported [^{111}In]In-DOTA-Tz. Future work is to use this polymer in pretargeted tumor imaging in companion of Tz:s labeled with short-lived radioisotopes e.g. [11]C and [18]F. **References:** 1. Matsumura Y. *et al. Cancer Research.* 1986 *46*, 6387-6392. 2. Rossin, R. *et al.*, *Angew. Chem. Int. Ed.* 2010, *49* (19), 3375-3378. 3.

OP-535

Nanoparticle-based radiopharmaceuticals: is there a future to [45]TiO2 nanoparticles?

P. Costa[1], L. F. Metello[1,2], F. Alves[3], M. D. Naia[4]; [1]Nuclear Medicine Department, ESS|P.Porto, Porto, PORTUGAL, [2]IsoPor S.A., Porto, PORTUGAL, [3]Institute for Nuclear Sciences Applied to Health, University of Coimbra, Coimbra, PORTUGAL, [4]CEMUC® - Physics Department, ECT-UTAD, Vila Real, PORTUGAL.

Introduction: Nanoparticles are being studied as drug delivery systems, and its application as vectors for radionuclide-based molecular imaging is a powerful tool of growing interest. Recent data is suggesting that functionalized titanium dioxide nanoparticles (TiO$_2$) can be surface-engineered to target cancer cells. On other hand, there is a global interest on the study of unconventional radionuclides for PET imaging. Among several examples, [45]Ti could be presented as one of the most interesting options, with physical properties (half-life of 3.09h and positron maximum energy of 1040 keV) together with results of some preclinical applications already tested providing evidences demonstrating that this radionuclide could allow good image quality. **Aim:** It is aimed to explore the potential role of [45]Ti to radiolabel biologically compatible TiO$_2$ nanoparticles for biomedical imaging applications and to describe the most favorable strategies for radionuclide and radiopharmaceutical production. **Materials and Methods:** This work departs from the presentation of our recent findings regarding the production of [45]Ti in a low energy cyclotron (IBA® Cyclone 18/9), and will be complemented with the exploration of the nanoparticle synthesis processes and radiolabeling related issues, aiming to provide a proposal for the optimization of the entire process. **Results and Discussion:** Our experimental results show that [45]Sc(p,n)[45]Ti nuclear reaction seems to be feasible for the production of [45]Ti in low energy cyclotrons, with cross-section values presenting a peak for proton beam energies of 10-14 MeV, and a thick target yield of 433.64 MBq.μA[-1]sat. Solid targetry

study is being implemented in the way to develop a prototype of target to be widely used for [45]Ti production. In what regards to nanoparticle radiolabeling, different methodologies could be used, including activation methods and synthesis based on radioactive precursors. Apart from other advantages related with the specific activity obtained, synthesis based on radioactive precursors appears to be the most simple and favorable option in this context, mainly due to the coincidence between the nanoparticle chemical nature and the radionuclide aimed to be used for radiolabeling. **Conclusion:** According to all evidences already tested and conjugated with the theoretical and prospective vision here presented, radiolabeling of TiO_2 nanoparticles with [45]Ti could constitute a tool to provide *in vitro* biodistribution studies, allowing also the *in vivo* monitoring of its biological distribution and pharmacokinetics, while could act as a theranostic tool for cancer. A proposal of a production process for [45]TiO_2 nanoparticles will be presented.

OP-536

Radiollabeling and biodistribution studies in a rat model of lipid-based nanosystems designed for the treatment of wounds.

M. Collantes[1], G. Quincoces[2], R. Ramos-Membrive[2], M. Ecay[3,4], A. Aldave[3,4], M. Pastor[5], G. Gainza[5], E. Gainza[5], I. Peñuelas[1,2,4]; [1]Nuclear Medicine, Clínica Universidad de Navarra, Pamplona, SPAIN, [2]Radiopharmacy Unit, Clínica Universidad de Navarra, Pamplona, SPAIN, [3]MicroPET Unit, Clínica Universidad de Navarra, Pamplona, SPAIN, [4]Center for Applied Medical Research, Pamplona, SPAIN, [5]Biopraxis Research AIE, Vitoria, SPAIN.

Aim: Lipid nanoparticles (NPs) for the delivery of growth factors and antibiotics lead to improve the treatment of complex wounds, allowing a controlled release of active ingredients The aim of this work was to optimize the radiolabelling of lipid-NPs under development to determine their retention time in a rat wound healing model by biodistribution studies using molecular imaging technology. **Material and methods:** Lipid-NPs were prepared by hot melt homogenisation followed by high-pressure homogenisation step. Precirol ATO 5 and Miglyol 182 were selected as core lipid and Dextran 40 as cryopreservative[1]. Lipid-NPs were radiolabelled with ^{99m}Tc by direct reaction with SnCl2-reduced ^{99m}Tc-pertechnetate. A surgical wound was created in the back of female Wistar rats under anesthesia (n=17). After 24 hours, ^{99m}Tc-lipid-NPs (5mg/3MBq, n=9) or free ^{99m}Tc-pertechnetate (negative control, 6MBq, n=8) were administered inside the wound and covered with a dressing. *In vivo* biodistribution studies were performed by SPECT/CT 1, 2, 4, 8, 12 and 24 hours post-administration and quantified by drawing VOIs over CT images transferred to SPECT and calculating the percentage of activity in organs. At the end point, animals were euthanized and organs measured *ex vivo* in a gamma-counter for the calculation of the percentage of injected dose (% ID/organ). **Results**: Radiollabeling of lipid-NPs proceeded with high yield (> 95%, radio-TLC) and used without need for further purification. SPECT/CT images showed that almost all the radioactivity (> 98%) remained in the wound until 24 hours after

administration of ^{99m}Tc-lipid-NPs. Free ^{99m}Tc-pertechnetate was absorbed in control animals, with a wound retention of 7% at 24 hours and a gradual appearance in the stomach and intestine. *Ex vivo* study allowed a separate analysis of different parts of the wound, confirming *in vivo* data. In ^{99m}Tc-lipid-NPs animals, dressing retained a 41% ID, while 57% was found in the skin, 1% in subcutaneous tissue and 0.02% in the *panniculus carnosus* muscle. In free ^{99m}Tc-pertechnetate controls these %IDs were 6%, 13%, 0.2% and 0.01% respectively, while most of the activity was found in the stomach (20.5 %) and intestines (53.1 %). **Conclusions**: The radiolabeling of lipid-NPs was achieved in a simple, efficient and stable manner. *In vivo* biodistribution studies with SPECT/CT and *ex vivo* data confirmed an excellent lipid-NPs retention in the wound at least until 24h, recommending its use as treatment-delivery systems in complex wounds. [1]G Gainza, M Pastor, JJ Aguirre et al. J Control Release 2014;185:51-61

OP-537

Chelator-free Radiolabeling of Iron Oxide Nanoparticles with [68]Ga For Dual-Modality PET/MR Imaging

*M. Karageorgou[1], J. Gallo[2], **C. Tsoukalas**[1], S. Xanthopoulos[1], M. Paravatou-Petsotas[1], D. Stamopoulos[3,4], M. Bañobre-López[2], P. Bouziotis[1]; [1]INRASTES, NCSR 'DEMOKRITOS', Athens, GREECE, [2]Advanced (magnetic) Theranostic Nanostructures Lab, INL, Braga, PORTUGAL, [3]Department of Solid State Physics, NKUA, Athens, GREECE, [4]Institute of Nanosciences and Nanotechnology, NCSR "Demokritos", Athens, GREECE.*

Aim: Dual-modality contrast agents, such as radiolabeled nanoparticles, are promising candidates for a number of diagnostic applications, since they combine the advantages of two different imaging modalities, namely SPECT or PET with MR imaging. This, in combination with hyperthermic capabilities of magnetic nanoparticles, can lead to highly-effective cancer theranostic agents. In this study, we describe the direct labeling of iron oxide nanoparticles (NPs), with the positron emitting radionuclide [68]Ga ($T_{1/2}$=67.8 min) and their subsequent *in vitro* and *in vivo* evaluation. Our goal is to evaluate the efficacy of the developed magnetic nanoparticles in passive tumor targeting. **Materials and Methods**: $Mn_xFe_{3-x}O_4@SiO_2$ nanoparticles were prepared through a two steps protocol. First, anisotropic manganese-doped magnetite nanoparticles with an average size of 13 nm were synthesized via thermal decomposition. In a second step, these particles were coated with a 20 nm silica shell. For the preparation of ^{68}Ga-labeled $Mn_xFe_{3-x}O_4@SiO_2$, the NPs were mixed with sodium acetate buffer pH 4 and 100 µL of ^{68}Ga eluate (~80 MBq, 30 min at 90°C). *In vitro* stability of ^{68}Ga-NPs was assessed in saline and serum. Radiolabeling and stability were assessed by TLC (ITLC-SG in citric acid solution, 0.1M). The *in vivo* behavior of the radiolabeled compound was evaluated in SCID mice bearing 4T1 breast cancer xenografts, at 30, 60 and 120 min post-injection of the radiotracer. **Results**: Successful labeling of the NPs was achieved with [68]Ga (purification via centrifugation, RCP ~ 98%), which was stable at RT up to 120 min post-preparation. ^{68}Ga-labeled $Mn_xFe_{3-x}O_4@SiO_2$

exhibited slow metabolic degradation in human serum (~85% at 120 min). Biodistribution studies in tumor-bearing SCID mice showed that $^{68}Ga-Mn_xFe_{3-x}O_4@SiO_2$ was mainly concentrated in the mononuclear phagocyte system (liver, spleen and lung). Moderate passive NP accumulation in tumor was observed (0.64 ± 0.19% ID/g at 120 min p.i.), with minimal uptake in other major organs. **Conclusion**: In this study we have proven the feasibility of labeling bare $Mn_xFe_{3-x}O_4@SiO_2$ magnetic nanoparticles with ^{68}Ga as a potential dual-modality imaging agent for diagnostic applications. This imaging radiotracer demonstrated high radio-labeling efficiency and high *in vivo* and *in vitro* stability, as well as moderate passive NP accumulation in 4T1 breast cancer tumors. These preliminary results prompt us to continue with the evaluation of the developed magnetic nanoparticles for passive tumor targeting, while functionalization of these nanoparticles with biomolecules (peptides, monoclonal antibodies) for active tumor targeting has been planned for the near future.

OP-538

Multifunctional Nanoprobes for Integrated PET / MR Imaging

S. Roux[1], *F. Bouraleh Hoch*[1], *V. Thakare*[2], *C. Bernhard*[2], *R. Bazzi*[1], *A. Oudot*[3], *B. Collin*[2,3], *F. Brunotte*[3], *F. Boschetti*[4], *F. Denat*[2]; *[1]Université de Bourgogne Franche-Comté, Besançon, FRANCE, [2]Université de Bourgogne Franche-Comté, Dijon, FRANCE, [3]Centre Georges-François Leclerc, Dijon, FRANCE, [4]CheMatech S.A.S., Dijon, FRANCE.*

Purpose: One important trend in molecular imaging is to combine several complementary techniques to exploit the advantages of each while overcoming their limitations. Among the numerous possibilities, the combination of magnetic resonance imaging (MRI) and positron emission tomography (PET) appears very attractive because it allies the high resolution and tissue contrast of MRI to the exceptional sensitivity of PET imaging. If the development of preclinical PET/MR scanners is in itself a significant challenge, the design of multimodal probes also constitutes an essential step for exploiting MRI/PET fused technology. **Subjects and Methods:** For achieving the development of multimodal probes for integrated MRI/PET, two strategies based on the multifunctional character of nanoparticles have been explored, keeping in mind that these nanostructured imaging agents must be removed by renal clearance. The first one consists in the synthesis of ultrasmall gold nanoparticles coated by two different types of chelator for a selective complexation of gadolinium ions (for MRI) and of positron emitters (for PET). The second strategy rests on the controlled assembly of maghemite nanoflowers detectable by MRI and of ultrasmall gold nanoparticles coated by chelators of positron emitters. Images of the biodistribution of these two kind of particles were obtained in rodents after labeling the nanoparticles with ^{64}Cu using a preclinical PET/MR scanner. **Results:** The reduction of gold salt in presence of a mixture of two different dithiolated chelators or in presence of dithiolated molecules containing two specific complexation sites provides ultrasmall gold nanoparticles (core size: 2-3 nm and hydrodynamic diameter: 6-8 nm) which are able to immobilize both gadolinium ions and 64-copper(II) ions. As a

result, the biodistribution of these nanoparticles can be monitored by T_1-weighted MRI and by PET on a same animal with the same imaging device integrating PET and MRI modalities after a single intravenous injection. The grafting of chelator coated gold nanoparticles onto superparamagnetic iron oxide nanoflowers using dopamine as linker yields also a nanoprobe (golden nanoflowers) for multimodal imaging (T_2-weighted MRI (superparamagnetic nanoflowers) and PET (radiolabeling by 64-copper). **Conclusion:** Each class of nanoparticles successfully behaves as imaging agent for integrated MRI/PET which are removed by body in large part by renal clearance. Since the ultrasmall gold nanoparticles and the golden nanoflowers are designed for remotely controlled therapy (radiosensitization with gold nanoparticles and magnetic hyperthermia with nanoflowers), the data collected by combining MRI and PET will be very precious for improving the therapeutic activity of these nanoparticles.

OP-539

Biodistribution of ^{99m}Tc-Phytate in a Sterile Inflammation Model in Mice

D. Priftakis[1], *M. Papachristou*[1], *S. Xanthopoulos*[2], *I. Datseris*[1], *P. Bouziotis*[2]; *[1]Evaggelismos Hospital, Athens, GREECE, [2]NCSR "Demokritos", Athens, GREECE.*

Purpose: When ^{99m}Tc-phytate is intravenously injected, particles in the nanometer range (150-250 nm) are formed, which are then taken up by phagocytic cells. This size can favor the radiotracer's extravasation in lesions with increased, newly formed or porous vasculature, such as inflammation and cancer, through the enhanced permeability and retention (EPR) effect. The aim of this work is the evaluation of the use of ^{99m}Tc-phytate to assess inflammation in mice. **Methods:** ^{99m}Tc-phytate was prepared by reconstitution of a commercial cold kit. The radiochemical purity was assessed by Thin-Layer Chromatography, using Whatman 1 paper and MeOH/H_2O (80/20 v/v) as the solvent system. The pH of the radiopharmaceutical was 6 and it was kept at room temperature before use. For the sterile inflammation model, 9 male Swiss albino mice were injected in the left thigh muscle with 100 μL of turpentine. The mice were then allowed to recover for 24 hours before being injected with 100 μL (3.7 MBq/100 μCi) of the radiotracer via the tail vein. A biodistribution study was performed at 1, 2 and 4 hours after the intravenous administration of ^{99m}Tc-phytate. 3 mice per time point were sacrificed by cardiectomy under slight ether anaesthesia and the main tissues and organs (blood, kidneys, liver, spleen, inflamed muscle, normal muscle etc.) were excised. Radiolabelled complex biodistribution over time was expressed as injected dose per gram (%ID/g). **Results:** The radiochemical purity of ^{99m}Tc-phytate was 98±0.5% as measured by thin layer chromatography. Biodistribution measurements reveal a higher uptake in the inflamed thigh at all time points (0.44±0.07%ID/g at 1 hour, 0.48±0.12%ID/g at 2 hours and 0.19±0.1%ID/g at 4 hours), when compared to uptake in the control tissue/non-inflamed thigh (0.14±0.08%ID/g at 1 hour, 0.2±0.14%ID/g at 2 hours and 0.13±0.07%ID/g at 4 hours), and the difference is sig-

nificant at 1 and 2 hours. The higher inflamed muscle/normal muscle ratio is 3.1 at 1 hour and showed gradual decrease over time. Moreover, there is a high uptake in the liver and spleen as expected. **Conclusions:** ^{99m}Tc-phytate has the ability to form particles of nanometer size when injected into the circulation, so it might be a non-toxic and low-cost nanoparticle-based SPECT imaging agent for the detection of inflammation. These promising preliminary results encourage us to follow the investigation with further experiments to clarify ^{99m}Tc-phytate's effectiveness in inflammation imaging and its potential use in tumor imaging.

| 1406 | Tuesday, October 24, 2017, 14:30 - 16:00, Hall F1 |

Teaching Session 5 (Interactive): Applied Cross Sectional Anatomy and Correlative Imaging - Cross Sectional CT and PETCT for the TNM Staging of Lung Cancer

OP-540

Applied Cross Sectional Anatomy and Correlative Imaging – Cross Sectional CT and PETCT for the TNM Staging of Lung Cancer

T. Lynch; Belfast, UNITED KINGDOM.

| 1407 | Tuesday, October 24, 2017, 14:30 - 16:00, Hall F2 |

Clinical Oncology - Rapid Fire Session: Mix it Up, please!

OP-541

Combination of baseline FDG-PET/CT total metabolic tumor volume and gene expression profil have a robust predictive value in patients with Diffuse Large B-Cell Lymphoma

M. N. Toledano[1], P. Desbordes[2], I. Gardin[1], P. Vera[1], F. Jardin[1], P. Ruminy[1], H. Tilly[1], S. Becker[1]; [1]Henri Becquerel Centre, Rouen, FRANCE, [2]QuantIF-LITIS, Rouen, FRANCE.

Purpose: To evaluate the predictive significance of Total Metabolic Tumor Volume (TMTV) measured on baseline FDG-PET/CT and confirm its added value to gene expression profile (GEP) with a new method of gene analysis RT-MLPA technology (Rapid Reverse Transcriptase - Multiplex Ligation - Dependent Probe Amplification Assay). **Subjects and Methods:** 114 patients with Diffuse Large B-Cell Lymphoma (DLBCL) were retrospectively included. Patients underwent FDG-PET/CT before R-CHOP or R-ACVBP regimen. TMTV was measured using 41% SUVmax thresholding method. They were classified in GCB or ABC subtypes according to the RT-MLPA method. Receiver operator characteristics (ROC) analysis was performed to determine optimal cut-off TMTV-value. Survival functions were estimated using a Kaplan-Meier method and were compared using a logrank test. Univariate and multivariate analysis were performed using a Cox proportional-hazards model. A logistic regression was also performed. P-value was corrected by Altman and Benjamini-Hoch-

berg models. **Results:** Patients had a median age of 66 years and the median follow-up was 40 months. 5 y-PFS was 54.4% and 5 y-OS was 62.3%. The optimal TMTV cut-off value was 261 cm³. Patients with a high TMTV (n=58) had a 5-year PFS and OS of 36.2% and 41.4% in comparison to 73.2% and 83.9% for patients with a low TMTV (n=56) (p=0.0038, HR=2.9 for PFS and p=0.0001, HR=4.33 for OS). ABC status was significantly associated to a worse prognosis. 5y-PFS were 55.8% *vs.* 62.9% (p=0.03, HR=1.77) and 5y-OS were 48.1% *vs.* 71% (p=0.03, HR=1.87) for ABC (n=52) and GCB (n=62) respectively. TMTV combined with molecular data identified 3 groups with very different outcome: i) patients with a low TMTV whatever the phenotype (n=56), ii) patients with a high TMTV and GCB phenotype (n=33), iii) patients with a high TMTV and ABC phenotype (n=25). These 3 groups had a 69.5%, 48.5%, 16% 5y-PFS (p<0.0001) and 83.9%, 57.6% 20% 5y-OS (p<0.0001), respectively. In multivariate analysis, TMTV, ABC/GCB phenotype and IPI score were independent prognostic factors for PFS (p=0.0454, p=0.0286 and p=0.0382, respectively) and OS (p=0.0223, p=0.0312 and p=0.0361, respectively). Logistic regression combining TMTV, ABC/GCB phenotype and IPI score was statistically meaningful between the two subgroups (p<0.0001) for PFS and OS (HR=4.47 and HR=5.53 respectively). **Discussion/Conclusion:** Combining TMTV and ABC/GCB phenotype at diagnosis individualized 3 risks categories of patients with significant different outcome. This integrative risk model could lead to a more accurate selection of patients, to increase tailor therapy.

OP-542

Improved Pulmonary Nodule Detection Using a Next Generation ^{18}F-FDG PET Imaging System

S. Park, L. Baratto, N. Hatami, G. Davidzon, S. Srinivas, V. Nair, A. Iagaru; Stanford University Medical Center, Stanford, CA, UNITED STATES OF AMERICA.

Introduction: One diagnostic indication for FDG PET is to determine whether a pulmonary nodule is benign or malignant based on the uptake of the nodule. However, FDG PET is limited by a relatively low spatial resolution (5 mm) that can lead to underestimation of tracer uptake and detectability in small lesions. The objective of this study was to evaluate the detection rate for pulmonary nodules using a next generation digital PET/CT system using Silicon Photomuliplier (SiPM) technology for increased contrast recovery and lower background variability in patients with known malignancies. **Subjects & Methods:** 76 consecutively enrolled patients who were referred for cancer staging by ^{18}F-FDG PET/CT underwent scans on the standard of care (SoC) and new digital system (Discovery Meaningful Insights) from September-December 2016. Images from the SoC PET/CT were reconstructed using time-of-flight (ToF) and ordered subset expectation maximization (OSEM) protocols. Images from digital PET/CT were reconstructed using ToF and a Bayesian penalized likelihood algorithm. Two experienced, nuclear medicine trained readers reviewed both scans for each patient in random order, blinded to clinical information and recorded the location and standardized uptake value (SUV) mea-

surement for each nodule. Differences in acquisition protocols were measured based on the distribution of the analyzed data and difference in detection rates assessed by McNemar's test. **Results:** Excluding one patient who had innumerable metastatic nodules on both scans, the number of lesions detected on the digital and standard of care PET/CT were 35 and 20, respectively. Of the 57 patients with negative standard of care scans, 7 (12%) demonstrated FDG-avid pulmonary nodules on the digital PET/CT. More lesions were detected on digital PET/CT in four patients who had nodules identified by both methods. Detection rates remained the same for 65/76 patients (86%), including 51 who were negative on both scans. Digital PET/CT nodules had a higher SUVmax compared to the standard of care (2.0; IQR 0.9-6.0 versus 1.3; 0.6-3.9, p < 0.001). **Conclusion:** Digital PET/CT system detects more FDG avid pulmonary nodules. FDG PET for diagnosing pulmonary nodules and staging metastatic disease to the lungs will require re-evaluation with this new, more sensitive platform.

OP-543

Treatment Reduction in Patients with Advanced-Stage Hodgkin Lymphoma and Negative Interim FDG-PET: Final Results of the International, Randomized, Phase 3 HD18 Trial by the German Hodgkin Study Group

C. Kobe[1], H. Goergen[2], M. Fuchs[2], H. T. Eich[3], C. Baues[4], V. Diehl[2], G. Kuhnert[1], A. Drzezga[1], M. Dietlein[1], A. Engert[2,5], P. Borchmann[2,5]; [1]Department of Nuclear Medicine, University Hospital of Cologne, Cologne, GERMANY, [2]German Hodgkin Study Group (GHSG), University Hospital of Cologne, Cologne, GERMANY, [3]Department of Radiation Oncology, University Hospital of Muenster, Muenster, GERMANY, [4]Department of Radiation Oncology, University Hospital of Cologne, Cologne, GERMANY, [5]Department of Internal Medicine I, University Hospital of Cologne, Cologne, GERMANY.

Background: In advanced-stage Hodgkin lymphoma (HL), recent clinical research indicates that metabolic response assessment early during therapy using FDG-PET (PET-2) might be suited to predict the individual outcome and eventually to adapt treatment intensity. **Aims:** We aimed to assess whether decreasing the number of eBEACOPP (dose-escalated bleomycin, etoposide, doxorubicin, cyclophosphamide, vincristine, procarbazine, and prednisone) cycles in patients with negative PET-2 is feasible without loss of efficacy as determined by progression-free survival (PFS). **Methods:** Between May 2008 and July 2014, we recruited patients with newly diagnosed advanced-stage HL aged 18-60 years. All patients received 2 cycles of eBEACOPP. PET-2 negative patients were randomly assigned to receive 6 or 2 additional cycles (i.e. 8x or 4x eBEACOPP in total, respectively). PET-positive residues after chemotherapy were irradiated. The trial was designed to exclude inferiority of 6 % or more of the group receiving only 4x eBEACOPP compared with the pooled groups receiving standard eBEACOPP at 5 years. **Results:** We enrolled 2,101 patients. 1,006 patients with negative PET-2 were randomly assigned to either standard eBEACOPP (n=504) or 4x eBEACOPP (n=502). The proportion of patients receiving radiotherapy was 3 % in total and did not dif-

fer between treatment groups. With a median follow-up of 54 months, estimated 5-year PFS in the per-protocol set was 91.2 % (88.3-94.1) with standard eBEACOPP and 92.1 % (89.3-94.9) with 4x eBEACOPP (difference +0.9 %, 95 % CI -3.1-4.9 excluding the non-inferiority margin of -6 %). In the standard eBEACOPP group, 95 % had at least one acute hematological toxicity grade 3-4 compared with 90 % in the 4x eBEACOPP group, including severe infections in 75 (15 %) and 40 (8 %) patients, respectively. Estimated 5-year overall survival (OS) in the per-protocol set was 95.7 % (93.7-97.6) with standard eBEACOPP and 97.7 % (96.2-99.3) with 4x eBEACOPP (log-rank p=0.006). **Conclusion:** Early response to the eBEACOPP regimen determined by FDG-PET allows a clinically relevant reduction of the cumulative treatment intensity from standard to only 4 cycles without loss of lymphoma control. The improved tolerability of the shortened treatment strategy results in a significant OS benefit for our patients. As both PFS and OS reach unprecedented rates, we feel safe to strongly recommend this PET-guided eBEACOPP de-escalation strategy for patients with advanced-stage HL whenever cure is the primary treatment goal.

OP-544

Experimental validation of absolute SPECT/CT quantification for response monitoring in breast cancer

A. Collarino[1], L. M. Pereira Arias-Bouda[1,2], R. A. Valdés Olmos[1,3,4], P. van der Tol[5], P. Dibbets-Schneider[1], L. de Geus-Oei[1,6,7], F. H. P. van Velden[1,5]; [1]Section of Nuclear Medicine, Department of Radiology, Leids Universitair Medisch Centrum, Leiden, NETHERLANDS, [2]Department of Nuclear Medicine, Alrijne Ziekenhuis, Leiderdorp, NETHERLANDS, [3]Interventional Molecular Imaging Laboratory, Department of Radiology, Leiden University Medical Center, Leiden, NETHERLANDS, [4]Department of Nuclear Medicine, The Netherlands Cancer Institute – Antoni van Leeuwenhoek Hospital, Amsterdam, NETHERLANDS, [5]Medical Physics, Department of Radiology, Leids Universitair Medisch Centrum, Leiden, NETHERLANDS, [6]Biomedical Photonic Imaging Group, MIRA Institute, University of Twente, Enschede, NETHERLANDS, [7]Department of Radiology and Nuclear Medicine, Radboudumc, Nijmegen, NETHERLANDS.

Purpose: ^{99m}Tc-sestamibi (MIBI) is widely used for breast cancer studies. Recent developments in iterative image reconstruction enable absolute (semi-)quantification of SPECT/CT studies by incorporating compensation for collimator-detector response attenuation and scatter, and resolution recovery into the reconstruction process (Evolution; GE Healthcare, USA). The aim of this experimental study was to assess quantitative accuracy of Evolution for clinical MIBI breast cancer SPECT/CT studies. **Materials and Methods:** Phantoms were filled with MIBI and acquired on a SPECT/CT gamma-camera (Discovery NM/CT 670 Pro; GE Healthcare) using a low-energy, high-resolution collimator, non-circular orbit, step-and-shoot mode and 120 views. A low-dose CT scan was acquired for attenuation correction purposes. All SPECT data were reconstructed using Evolution with a 128x128 matrix without zoom. Firstly, a NEMA Image Quality phantom containing six spheres was filled with a background activity concentration of 3.6 kBq/ml, reflecting clinical MIBI up-

take in the breast, with a sphere-to-background ratio of 10:1. This phantom was acquired using 20 sec per view and reconstructed using up to 8 iterations (10 subsets) to assess (1) the convergence of Evolution and (2) the recovery coefficients (RC) of standardized uptake values (SUV_{mean} obtained using a 42, 50 and 70% isocontour, and SUV_{max}). Secondly, a Jaszczak phantom (activity concentration: 38 kBq/ml) was acquired with 1 to 24 sec per view in order to assess the performance of Evolution under different count statistics. **Results:** For background compartment of the NEMA phantom, the activity concentration converged after 3 iterations, while the coefficient of variation increased from 12.3 to 44.9% with increasing number of iterations. For the remainder of the study 4 iterations were applied to ensure convergence. Depending on the count statistics, the accuracy of the reconstructed activity concentration varied between -2.61 to 5.51% (volume-of-interest covering the entire phantom) and from 9.66 to 6.49% (2 litre volume-of-interest placed in the centre of the phantom). RC of SUV_{max} was 1.56, 1.82, 1.76 and 1.47 for spheres with 37, 28, 22 and 17 mm diameter, respectively, while RC of SUV_{mean} was 0.94, 1.00, 0.95 and 0.71 (42% isocontour), 1.02, 1.12, 1.06 and 0.70 (50% isocontour), and 1.18, 1.31, 1.32 and 1.12 (70% isocontour). **Conclusion:** Absolute (semi-)quantification of SPECT/CT MIBI breast studies seems feasible (<10% deviation) when a 42% isocontour is used for delineation for tumours of at least 22 mm diameter. However, with tumour shrinkage, response evaluation should be handled with care, especially when using SUV_{max}.

OP-545

Somatostatin antagonist theranostic pair ^{68}Ga-OPS202 and ^{177}Lu-OPS201 for well-differentiated neuroendocrine tumors (NETs)

D. Reidy, N. Pandit-Taskar, S. Krebs, J. O'Donoghue, N. Raj, E. Cruz, H. Pham, A. Lashley, L. Bodei, W. A. Weber; *Memorial Sloan Kettering Cancer Center, New York, NY, UNITED STATES OF AMERICA.*

Aims: Radiolabeled somatostatin receptor 2 (SSTR2) antagonists have shown higher tumor uptake and tumor-to-organ ratios than agonists in preclinical models. We performed a phase I study to evaluate the safety and radiation dosimetry of the SSTR2 antagonists ^{68}Ga-OPS202 and ^{177}Lu-OPS201 (^{68}Ga/^{177}Lu-DOTA-JR11) in patients (pts) with metastatic well-differentiated NETs (NCT02609737). Efficacy and tolerability data after ^{177}Lu-OPS201 treatment were recorded. **Methods**: Pts with RECIST disease progression underwent a ^{68}Ga-OPS202 PET/CT to confirm in-vivo binding of the SSTR2 antagonists and, if positive, underwent treatment with 3 doses of ^{177}Lu-OPS201. The first 50 mCi dose of ^{177}Lu-OPS201 was used to calculate tumor and normal organ dosimetry. ^{177}Lu-OPS201 was then administered in divided doses ≤200 mCi for the 2nd and 3rd fractions, 8-10 weeks apart, based on dosimetry. **Results:** 19 pts enrolled (primary tumors: 1 broncho-pulmonary, 7 small-bowel, 8 pancreatic, 1 gastric, 1 rectal, and 1 renal NET). Average age was 55 y (22-73 y), 52% female; mean number of prior treatments was 3. All pts received 1 therapeutic dose of ^{177}Lu-OPS201, 7 pts received 2 doses. All tumors were visualized by ^{68}Ga-OPS202 PET/CT. With the exception of the kidneys and bladder, no organ demonstrated uptake of ^{68}Ga-OPS202 above background. Tumor radiation doses ranged from 0.15 Gy/mCi to 0.48 Gy/mCi. Subacute hematologic toxicity after cycle 1 was generally mild-moderate (G3 leukopenia in 2/19, reversed before cycle 2). 4/7 (57%) pts that received the second dose of ^{177}Lu-OPS201 exhibited G4 hematological toxicities, which occurred 4-6 weeks after administration. G3/4 toxicities in the four pts resolved to G2 or lower in 12-19 weeks; none of these pts demonstrated fever, infection, bleeding, or renal toxicity. Substantial efficacy was observed: 1 patient achieved a CR (1/19, 5%), 32% PR (6/19), 47% SD (9/19) and 16% POD (3/19). 1-year PFS was 67%. **Conclusions:** In this trial of heavily treated NETs, preliminary data are promising for the use of ^{68}Ga-OPS202/^{177}Lu-OPS201 as a theranostic combination for imaging and therapy. Additional studies are planned to optimize the therapeutic dose to minimize hematologic toxicity. The study was partly funded by the NET Research Foundation.

OP-546

Comparison of 18F-FDG PET/MRI and MRI for primary evaluation and treatment planning of cervical cancer patients

J. Grueneisen[1], T. Sarabhai[1], B. Schaarschmidt[2], M. Forsting[1], K. Herrmann[1], L. Umutlu[1]; [1]University Hospital Essen, Essen, GERMANY, [2]University Hospital Düsseldorf, Düsseldorf, GERMANY.

Purpose: To compare the diagnostic performance of integrated PET/MRI and MRI for primary tumor staging of cervical cancer patients as well as to investigate whether discrepancies of staging results between the two imaging modalities lead to different treatment recommendations. **Subjects & Methods:** 53 consecutive patients with histopathological confirmation of primary cervical cancer were prospectively enrolled for a whole-body 18F-FDG PET/MRI examination prior to the initiation of definitive treatment or lymphadenectomy. Two experienced physicians analyzed the resulting MRI data, followed by a second reading session of the PET/MR datasets. Both readers were asked to perform a dedicated TNM-staging in accordance to the 7th edition of the AJCC staging manual. Subsequently, the results of MRI and PET/MRI were discussed in a simulated interdisciplinary tumor board. The participants were blinded to the results from the pathology report of diagnostic lymphadenectomy and definitive surgical treatment as well as to findings in follow-up imaging. Finally, the most appropriate treatment strategy was determined for each patient, based on the information from clinical evaluation and imaging findings in 1. MRI and 2. PET/MRI. **Results:** PET/MRI and MRI allowed for correct determination of the T-stage in 45/53 (85%) and 46/53 (87%) cases, respectively. Furthermore, PET/MRI revealed a higher sensitivity and specificity than MRI alone for the detection of nodal positive patients (83% and 90% vs. 71% and 77%) and the identification of patients with distant metastases (87% and 92% vs. 67% and 90%). Comparing the staging results of MRI and PET/MRI revealed discrepant findings in 17 (32%) cases, which led to differences in treatment recommendations for 12 patients (23%). Among them, PET/MRI over- (n=1) and underestimated

(n=1) the actual tumor stage in two patients, which affected therapeutic decisions. In one additional patient, PET/MRI over-estimated the actual tumor stage, which was also falsely rated with MRI alone. However, incorrect ratings in MRI did not re-sulted in false treatment recommendations. Conversely, MRI revealed incorrect staging results in 9 patients (n=3, overesti-mation; n=6 underestimation). PET/MRI enabled determination of the correct tumor stage in 7 of those 9 patients. In the re-maining two cases, staging results of PET/MRI still provided cor-rect treatment recommendations. In 5 patients (11%), different imaging findings in MRI and PET/MRI did not lead to changes in therapeutic decisions. **Conclusion:** Our results demonstrate the successful application and diagnostic advantage of integrated PET/MRI imaging over MRI alone for whole-body tumor staging of cervical cancer patients, enabling more accurate treatment planning.

OP-547

[123/131I]IMAZA as a new theranostic tool in patients with advanced adrenocortical carcinoma

A. Schirbel[1], C. Blümel[1], B. Heinze[2], A. Plaß[2], C. T. Fuß[2], F. Megerle[2], T. Deutschbein[2], M. Fassnacht[2], M. Kroiss[2], H. Hänscheid[1], A. K. Buck[1], S. Hahner[2]; [1]University of Wuerzburg, Department of Nuclear Medicine, Wuerzburg, GERMANY, [2]University of Wuerzburg, Department of Medicine I, Division of Endocrinology and Diabetes, Wuerzburg, GERMANY.

Introduction: We have recently developed the metomidate analogue [123/131I]IMAZA as radiotracer for molecular imaging in adrenal tumours and radiotherapy in adrenocortical carci-noma (ACC). IMAZA selectively binds to both aldosterone syn-thase and 11ß-hydroxylase and showed in mice experiments improved binding properties to target tissue compared to io-dometomidate (IMTO). Therefore we evaluated [123I]IMAZA for imaging in a series of 36 consecutive ACC-patients with the aim to investigate the feasibility of a subsequent [131I]IMAZA-endo-radiotherapy. **Subjects & Methods:** Imaging was performed for evaluation of a potential endoradiotherapy of advanced ACC (n=36). SPECT/CT and planar images were obtained up to 24 h after i.v. administration of 180 MBq [123I]IMAZA. Additional [123I]IMTO imaging was performed in 3 patients within 1 week. Clinical and laboratory data were collected before and after im-aging. Blood samples were drawn and the metabolic stability of the tracer was analysed by radio-HPLC. After individual do-simetry first [131I]IMAZA-endoradiotherapies were performed in suitable patients. Results: [123I]IMAZA proved to be a tracer that specifically accumulated in adrenocortical tissue similar to [123I]IMTO. Uptake in the tumour lesions was heterogeneous indicat-ing variable expression of the target enzymes CYP11B1 and 2. We observed rapid clearance of unbound tracer and an up to 5-fold higher tumour uptake compared to IMTO, which signifi-cantly improved imaging quality. Analysis of blood samples by radio-HPLC demonstrated a significant higher metabolic stabil-ity of the tracer. Strong tracer uptake in all tumour lesion was seen in 42% of patients, mixed uptake in 18% and no uptake was documented in 40%. Endoradiotherapies using [131I]IMAZA

in 7 selected patients were performed with activities up to 30 GBq and were well tolerated without serious acute toxicities. High and long-lasting uptake was observed in all known lesions and resulted in tumour doses up to 265 Gy. **Conclusion:** [123I]IMAZA-SPECT shows more selective binding properties and fa-vourable metabolic stability than the reference [123I]iodometo-midate. Tracer uptake is highly specific, however the variable expression of CYP11B1/2 limits the diagnostic sensitivity. About 40% of patients are potential candidates for endoradiotherapy with [131I]IMAZA. This radiopharmaceutical has an excellent tox-icity profile and is a promising therapeutic approach in selected patients with advanced ACC.

OP-548

ImmunoPET imaging to assess target engagement: Experience from 89Zr-anti-HER3 mAb (GSK2849330) in patients with solid tumors

A. Mcgeoch[1,2], C. Menke-van der Houven van Oordt[3], M. Bergstrom[1], I. McSherry[1], D. Smith[4], M. Cleveland[1], O. Hoekstra[3], D. Vugts[3], A. Weber[5], I. Freedman[5], M. Huisman[3], C. Matheny[5], G. van Dongen[3], S. Zhang[5]; [1]GSK, Stevenage, UNITED KINGDOM, [2]University of Cambridge, Cambridge, UNITED KINGDOM, [3]VU University Medical Centre, Amsterdam, NETHERLANDS, [4]PAREXEL International, Durham, NC, UNITED STATES OF AMERICA, [5]GSK, King of Prussia, PA, UNITED STATES OF AMERICA.

Aim: Maximum tolerated dose (MTD) has historically guided dose selection in oncology. For targeted treatments and bio-logics, this approach risks exposing patients to unnecessary tox-icity and drives unsustainably high costs. A logical alternative is measuring maximal tumor target occupancy using positron emission tomography (PET) imaging with radiolabelled drugs. In this immunoPET study, we investigated biodistribution and tumor uptake of 89Zr-labelled anti-HER3 monoclonal antibody (mAb) GSK2849330, and evaluated target engagement as a function of mass dose to inform a rational dose for future effi-cacy testing. **Methods:** 89Zr-GSK2849330 distribution was mon-itored in 6 patients with HER3-positive tumors not amenable to standard treatment with PET at up to 3 occasions after adminis-tration. Uptake in normal tissues and tumor sites was quantified as standard uptake value (SUV) and through modelling related to plasma radio-pharmacokinetics. Tumor accumulation rate was established with two subsequent tracer administrations in each patient combined with different doses of unlabelled mAb. First, a low dose of 89Zr-GSK2849330 was administered to serve as baseline, and subsequently dose-dependent inhibition of 89Zr-GSK2849330 uptake in tumor tissues was evaluated after pre-dosing with increasing amounts of unlabelled GSK2849330, enabling calculation of the 50% inhibitory mass dose (ID50) of target-mediated uptake of 89Zr-mAb by unlabelled mAb. **Re-sults:** A baseline total mass dose of 8mg was found to give optimal signal in tumours. Accumulation of 89Zr-GSK2849330 was also observed in certain normal tissues such as liver and spleen. 89Zr-GSK2849330 uptakes were observed and quantita-tively measurable in tumors of 5 out of 6 patients with increas-ing accumulation seen over time on days 2 and 5 after dosing.

Pre-dosing with unlabelled mAb reduced the tumor uptake rate of ^{89}Zr-GSK2849330 in a dose-dependent manner with an ID50 of 2 mg/kg. Saturation of ^{89}Zr-mAb uptake by tumors was seen at the highest doses (30mg/kg) of competing unlabelled mAb used. **Conclusion:** In this immunoPET study with^{89}Zr-GSK2849330, we defined the mAb distribution in patients with HER3-positive tumors. The dose-dependent inhibition of tumor uptake of ^{89}Zr mAb by unlabelled mAb confirmed target engagement, i.e. the specific binding and internalization of anti-HER3 antibody by the HER3 receptors in the tumor tissues. This study further validates the use of immunoPET approach to non-invasively and quantitatively measure target engagement at the site of action (tumor) and to directly visualize tissue drug disposition in humans which offers the potential for evidence based dose selection. This study is sponsored by GSK with ClinicalTrials.gov Identifier: NCT02345174.

OP-549

FDG-PET/CT in single pulmonary nodule (SPN): a preliminary experience from a multicenter Italian Assessment of Lung Indeterminate Accidental Nodule (ITALIAN) trial

L. Evangelista[1], M. Spadafora[2], L. Mansi[3], L. Pace[4], M. Arosio[5], G. Saladini[1], S. Sanfilippo[6], M. Salvatore[7], G. Pepe[8], G. Cusato[8], M. Ferdeghini[9], A. Chiaravalloti[10], M. Giuliano[11], M. Farsad[12], S. Pellegrino[13], S. Del Vecchio[13], A. Giordano[14], A. Cuocolo[13]; [1]Nuclear Medicine and Molecular Imaging Unit, Veneto Institute of Oncology IOV - IRCCS, Padova, ITALY, [2]Nuclear Medicine Unit, Department of Imaging, S.G. Moscati Hospital, Avellino, ITALY, [3]Dipartimento Medico-Chirurgico di Internistica Clinica e Sperimentale, Second University of Naples, Napoli, ITALY, [4]Department of Medicine and Surgery, University of Salerno, Baronissi (SA), ITALY, [5]Nuclear Medicine Unit, San Gerardo Hospital, University of Milano Bicocca, Milano, ITALY, [6]Service of Nuclear Medicine, Policlinico S. Orsola Malpighi, University of Bologna, Bologna, ITALY, [7]Nuclear Medicine Unit, Department of Imaging, SDN Foundation, Napoli, ITALY, [8]Nuclear Medicine Unit, Cancer Center, Humanitas Hospital, Rozzano, Milano, ITALY, [9]Nuclear Medicine Unit, Department of Imaging, Azienda Ospedaliera Universitaria Integrata di Verona, Verona, ITALY, [10]Department of Biomedicine and Prevention, University of Rome Tor Vergata, Roma, ITALY, [11]Nuclear Medicine Unit, Department of Imaging, Medicina Futura IOS, Acerra, Napoli, ITALY, [12]Department of Nuclear Medicine, Hospital of Bolzano, Bolzano, ITALY, [13]Department of Advanced Biomedical Sciences, University of Naples Federico II, Napoli, ITALY, [14]Institute of Nuclear Medicine, Università Cattolica del S. Cuore, Roma, ITALY.

Background: The aims were to:1)determine the performance of FDG-PET/CT in SPN by considering categorical and continuous data analysis;2)assess if continuous data were correlated with intra- and extra-thoracic pathological FDG uptake and 3) evaluate if clinical, demographical or morphological variables are correlated with the presence of pathological FDG uptake (intra- and extra-thoracic) other than the lung nodule(LN). **Methods:** Between 2014 and 2016,we retrospectively selected 225consecutive patients(age:67years)investigated by FDG-PET/CT for characterization of SPN. Patients with prior cancer history and candidates to PET/CT for the staging of lung cancer were excluded. Patients were stratified, according to clinical and instrumental pre-test probability of malignancy(Brock model), in low, intermediate and high category risk. FDG uptake in SPN was visually assessed by a 4-point scoring system(from 0=absent to 3=intense)and by semiquantitative analysis of the LN(in terms of SUVmax), in the blood pool(BP)and in the liver(L)(both in terms of SUVmean). **Results:** SPN histology was available in 164 patients, while follow-up in 61. SPN was malignant in 111 patients and benign in 114. In all 225 patients, by considering categorial data(FDG uptake ≥2 vs. <2), sensitivity, specificity, positive predictive value(PPV), negative predictive value(NPV) and accuracy of FDG-PET/CT for the characterization of SPN were 79%, 75%,75%, 79% and 77%, respectively. Based on the Brock model, sensitivies and PPV were elevated in patients with intermediate and high risk patients(75% and 88%, 69% and 88%, respectively),while specificity and NPV were higher in low risk category. At Roc analysis, the cut-offs for better discriminating between benign and malignant LNs were 1.60(sens: 81% and spec. 81%)and 1.21(sens: 81% and spec. 80%)respectively for SUVmax/SUVmeanBP and SUVmax/SUVmeanL ratios. In patients at intermediate and high risk of malignancy, by including the SUVmax/SUVmeanBP ratio, the specificities shift from 71% to80% and from 64% to89%, respectively. In all patients, SUVmax/SUVmeanBP and SUVmax/SUVmeanL ratios were significantly higher in patients with intra-thoracic lesions than without(both <0.05). Furthermore, at logistic multivariate analysis, a high malignancy risk and a moderate FDG uptake in the LN were predictors of intra-thoracic pathological uptake(both p<0.05)**. Conclusions:** Visual FDG PET/CT, by 4 point scale assessment, has an acceptable performance in SPN patients, but it can significantly improve by considering semiquantitative continuous data, particularly in patients with intermediate and high risk of malignancy. Moreover, continuous data can be useful for the evaluation of disease spread in intra-thoracic site, but stratification for risk category and for FDG uptake in the LNs are predictors of intra-thoracic pathological sites.

OP-550

^{68}GaNeoBOMB1 in oligometastatic GIST: first results from a Phase-I/IIa study

L. Gruber[1], C. Uprimny[1], F. Orlandi[2], H. Margreiter[1], M. F. Mariani[2], W. Jaschke[1], C. Decristoforo[1], I. Virgolini[1]; [1]Medical University Innsbruck, Innsbruck, AUSTRIA, [2]Advanced Accelerator Applications S.r.l., Colleretto Giacosa/Ivrea, ITALY.

Introduction: Molecularly targeted therapy with Tyrosine Kinase Inhibitors (TKI) revolutionized the treatment of Gastrointestinal Stromal Tumours (GIST) but resistance to these drugs represents an important clinical challenge. Gastrin-releasing peptide receptor (GRPR) are highly overexpressed in GIST and present a promising target for molecular imaging and therapy. Within the MITIGATE project (Closed-loop Molecular Environment for Minimally Invasive Treatment of Patients with Metastatic Gastrointestinal Stromal Tumours, EU-FP7, grant agreement no 602306) a clinical trial in patients with TKI resistant GIST

was initiated in 2016. ^{68}Ga-NeoBOMB1 is a novel GRPR antagonist, which can be prepared using a kit-based preparation and was selected for this study. **Materials and Methods:** a Phase-I/IIa clinical trial (EudraCT 2016-002053-38) to evaluate safety, biodistribution, dosimetry and preliminary diagnostic performance of [68]Ga- NeoBOMB1 in patients with advanced TKI-treated GIST using PET/CT was approved by the EC and competent authority. ^{68}Ga-NeoBOMB1 is prepared using a simple kit based procedure based on a licensed [68]Ge/^{68}Ga generator. In total, 12 patients with presence of at least one surgically untreatable primary or metastatic, histologically confirmed GIST are planned to be studied with a minimum 50% of those showing documented TKI-resistance. Histopathological correlation with GRPR expression by IHC is planned in 6 patients. PET/CT includes dynamic and 1, 2 and 3-4h static PET imaging. Blood and urine sampling is performed to provide PK data. Safety parameters including vital signs, cardio-vascular, and biochemistry in blood and urine are assessed. **Results**: So far 2 TKI-resistant metastatic GIST patients were included. Kit based preparation of ^{68}Ga-NeoBOMB1 resulted in >97% radiochemical purity. ^{68}Ga-NeoBOMB1 showed favourable PK with exclusive renal excretion pattern starting within few minutes after injection and a physiologic high uptake in pancreas already 30 min p.i. Stability of ^{68}Ga-NeoBOMB1 in blood samples was high. No product-related adverse events were reported up to 2 weeks after application. Liver metastasis showed increasing SUV values with improving contrast over time. **Conclusion:** ^{68}Ga-NeoBOMB1 is a promising agent to image GIST based on the high overexpression of GRPR and so far has shown an excellent safety profile. More patients are currently enrolled and will be presented providing more information on GRPR targeting properties of this agent in patients with TKI resistant GIST.

OP-551

^{18}F-FDG PET/CT for treatment response assessment in classical Hodgkin Lymphoma (cHL), in the era of innovative immunomodulatory PD-1 blocked (nivolumab) therapy

I. Sandler[1], A. Broccoli[2], P. Castellucci[1], C. Nanni[1], C. Pellegrini[2], F. Quirini[2], P. Zinzani[2], S. Fanti[1]; [1]Nuclear Medicine Unit, University of Bologna, S.Orsola-Malpighi Hospital, Bologna, ITALY, [2]Institute of Hematology and Medical Oncology "L.&A. Seràgnoli", University of Bologna, S.Orsola-Malpighi Hospital, Bologna, ITALY.

Introduction and Aim: The intersection between immune surveillance and tumor have led to broad therapeutic advances that are now being studied in all cancer types. The IgG4 subclass PD-1 inhibiting antibodies, nivolumab and pembrolizumab, are approved for treating advanced melanoma and non-small cell lung cancer. PD-1 ligands are also overexpressed by Reed-Sternberg cells in cHL, therefore nivolumab was recently approved by the US FDA for patients with relapsed or refractory cHL. As a part of an ongoing prospective study we report our initial experience with ^{18}F-FDG PET/CT for nivolumab treatment response assessment for cHL. **Methods:** In our Center, 7 patients (5 males and 2 females, mean age 37 y.o) with relapsed or refractory cHL

are under treatment with nivolumab (3mg/kg every two weeks) since 2016. All patients underwent ^{18}F-FDG PET/CT no more than 4 weeks prior to first nivolumab administration to define disease baseline stage: 2 patients presented stage II, 2 stage III and 3 stage IV. All patients underwent 3 "interim" response assessment with ^{18}F-FDG PET/CT scan: at 2 month, 4 month and 6 month after the beginning of therapy. All ^{18}F-FDG PET/CT scans were performed according to standard procedure then were visually analyzed by two expert nuclear physicians. ^{18}F-FDG uptake was quantified by standardized uptake values (SUVmax). ^{18}F-FDG PET/CT results were classified for "immune-response" relatively to baseline as "complete" (CR; disappearance of all lesions), "partial" (PR; decrease of 50% tumor burden), "stable"(SD) and "progressive" (PD; 25% increase of tumor burden). ^{18}F-FDG PET/CT results were compared to clinical hematologic response assessment (symptoms, physical examination and laboratory). **Results:** While all patients presented complete clinical hematologic remission in 6 month of therapy (no disease symptoms, negative physical examination and laboratory results), no ^{18}F-FDG PET/CT scan showed CR after the first, second and third "interim" scans. After the third "interim" scan 3 patients showed ^{18}F-FDG PET/CT PD and 4 PR. Only 1 patient showed ^{18}F-FDG PET/CT down-staging (stage IV to stage II). No correlation between baseline stage and ^{18}F-FDG PET/CT therapy response. 4 of 7 patients showed ^{18}F-FDG uptake referred to pneumonitis and/or thyroiditis and/or rash and/or gastritis known as adverse events of the therapy. **Conclusions:** ^{18}F-FDG PET/CT findings in immunomodulatory treatment response assessment do not correlate with clinical and hematological remission. More studies should be done to understand and define this phenomenon (tumor "flare"? "Pseudo-progression"?) deciding then the right timing of ^{18}F-FDG PET/CT response assessment in cHL.

1409	Tuesday, October 24, 2017, 14:30 - 16:00, Hall G1

Neurosciences - Rapid Fire Session: Imaging Brain Physiology in Preclinical & Clinical Models

OP-552

Gender differences in the cerebral uptake of ^{18}F-FDG

*J. W. A. Sijbesma, **A. van Waarde**, D. Vállez García, H. H. Boersma, R. H. J. A. Slart, R. A. J. O. Dierckx, J. Doorduin; University of Groningen, Groningen, NETHERLANDS.*

An important issue in rodent imaging is the question whether it is possible to use both female and male animals in tracer development and evaluation, rather than animals from a single sex. For this reason, we have made repeated ^{18}F-FDG scans of the brain of adult rats (either males, or females at different phases of the estrous cycle). Our study was aimed to answer the following questions: a. Are there differences in brain metabolism between male and female rats? b. Are there differences in the cerebral ^{18}F-FDG uptake of female rats at different phases of the estrous cycle? and c. Is the test-retest variability of ^{18}F-FDG PET different in males and females? **Methods:** Long-Evans rats

(age 1 yr) were divided into three groups: 1. Males (n=8), 2. Females in metestrous (low estrogen levels, n=8), and 3. Females in proestrous (high estrogen levels, n=8). Two small animal PET scans using ^{18}F-FDG and rapid arterial blood sampling were made at an interval of 10 days in subjects anesthetized with isoflurane in oxygen (thus, 48 scans were made in total). Body temperature, heart rate, glucose levels in plasma and blood oxygenation were monitored in all rats during the scans. A preliminary analysis was performed on data from the entire brain. Data from predefined brain regions will be analyzed in the near future, using kinetic modeling. **Results:** Females showed a significantly higher brain uptake of ^{18}F-FDG than males, particularly in the initial scan (+40%, P < 0.0001). Higher estrogen levels were associated with increased brain metabolism, since the accumulation of ^{18}F-FDG was 11.5% higher in proestrous than in metestrous or other phases of the estrous cycle (P < 0.02; in the second scan, a few animals were in diestrous or estrous rather than the desired proestrous or metestrous phase). Cerebral glucose metabolism in the test and retest condition was identical in males, but females showed a significant decline (-10.5 ± 2.6%). **Conclusion:** Based on the results for this particular model, the mixing of sexes or the mixing of female rats in different phases of the estrous cycle in tracer evaluation protocols will result in an impaired test-retest stability of the PET data and a need for larger group sizes to maintain the same statistical power in group comparisons.

OP-553

Brain Metabolic Response to Prolonged Starvation: a micro-PET study

*A. Orengo[1], **A. Buschiazzo**[2], L. Emiomite[3], S. Ravera[4], V. Cossu[1], S. Bruno[5], A. Bellini[2], L. Raffaghello[6], F. Di Giulio[1], G. Bianchi[6], S. Morbelli[1], C. Marini[1,7], G. Sambuceti[1,2]; [1]Nuclear Medicine Unit, IRCCS AOU San Martino-IST, Genoa, ITALY, [2]Department of Health Sciences, University of Genoa, Genoa, ITALY, [3]Animal facility, IRCCS AOU San Martino-IST, Genoa, ITALY, [4]Department of Pharmacy, Biochemistry Laboratory, University of Genoa, Genoa, ITALY, [5]Department of Experimental Medicine, University of Genoa, Genoa, ITALY, [6]Laboratory of Oncology, G. Gaslini Institute, Genoa, ITALY, [7]CNR Institute of Bioimages and Molecular Physiology, Milan, ITALY.*

Introduction: Clinical use of brain imaging of FDG uptake relies on the assumption that this tracer accurately delineates overall glucose consumption (MRGlu) in central nervous system. We recently documented that starvation (STS) in cancer down regulates glycolysis with an increased dependency on oxidative phosphorylation. The present study was designed whether prolonged starvation causes a simultaneous decrease in glucose consumption and FDG uptake in mouse brain. **Subjects & Methods**: All animal experiments were reviewed and approved by the Italian Ministry of Health. Six-weeks-old BALB/c mice were divided into "controls" (n=7) that did not receive any treatment and "STS" (n=6) submitted to 48 hours deprivation of food before imaging. After anesthesia, both groups underwent dynamic microPET imaging (Albira, Bruker, US) according to a protocol previously validated in our lab, to estimate MRGlu by

Patlak analysis. In 2 further mice per group, not submitted to imaging, the brain was harvested soon after sacrifice by cervical dislocation. Brains were placed in the Petri dish of Ligand tracer instrument (Ridgeview, Se) whose rotation permits to cyclically move the organ from the incubation medium to the focus of a counting detector every 30 seconds. Incubation medium was enriched with 12.5 mM glucose and 6 MBq FDG. Time trend of organ radioactivity content was monitored for one hour and Patlak estimate of MRGlu was compared with directly measured glucose disappearance from incubation medium. At the end of the experiment, phospho-fructo-kinase (PFK), hexose-6-phosphate dehydrogenase (H6PD), glucose-6-phosphate-dehydrogenase (G6PD) and β-hydroxy-butyrate-dehydrogenase (β-HBD) activity were assayed in homogenates brains by standard spectrophotometric methods. **Results**: Micro-PET analysis evidenced that two-days STS significantly reduces brain MRGlu (from 14.2±3.1 nM x min^{-1} x g^{-1} to 4.6±2.3 nM x min^{-1} x g^{-1}, p<0.001 vs. controls) and similar results were obtained with ex vivo experiments. Further studies on homogenates brains showed an increase in β-HBD activity, key enzyme for ketone bodies catabolism in brain. Interestingly, PFK activity decreased to 38.9% suggesting a reduction in glycolytic flux. Moreover, the activity of cytosolic G6PD was reduced to 41.7% while the ER counterpart H6PD activity remained unchanged. **Conclusion**: The present data documented that STS caused a reduction of MRGlu probably depending on a metabolic shift of brain metabolism to oxidation of ketone bodies and to catabolism of glucose by a new ER pathway triggered by H6PD.

OP-554

Altered Insulin-Dependent Brain Glucose Metabolism During Obesity Depends On Specific Brain Areas

C. Malbert[1], S. Bahri[2]; [1]INRA, Saint-Gilles, FRANCE, [2]University of Tunis, Tunis, TUNISIA.

There is a general agreement for insulin mediated changes in brain metabolism in insulin resistance. However, the association of this phenomenon with obesity alone is unclear especially when quantitative data of glucose metabolism were obtained. Using quantitative PET, the extend of these metabolic changes involves either the entire brain (Hirvonen, 2011) or brain specific regions - some with increased and others with decreased glucose metabolism (Anthony et al, 2006). Finally, the mechanisms underlying theses modifications are unknown being potentially dependent on forward and reverse glucose transport and intracellular phosphorylation. We aimed to evaluate these modifications using quantitative PET before and after diet induced obesity either in fasting insulin or during euglycemic hyperinsulinemic clamp condition. Ten adults mini pigs were scanned using [18]FDG before and after 5 months of obesogenic diet given at 150% the recommended caloric intake (288 kcal/kg body weight wt$^{0.75}$). The extend of fat deposition was evaluated using CT scan and the resting energy expenditure was quantified using indirect calorimetry. PET images were acquired dynamically either in fasted state or during an isoglycemic-hyperinsulinemic clamp (120mU.kg^{-1}.h^{-1}). Glucose uptake rates were obtained

through model analysis of PET data and continuous arterial radioactivity measurement. Pixel-wise modelled brain volumes were also reconstructed and analysed using SPM. All animals gained weight (75.3 ± 6.01 vs 32.7 ± 2.90 kg) as a result of equal increase in visceral and subcutaneous fat-mass. The energy expenditure was about doubled (1430 ± 43.2 vs 904 ± 34.9 kcal/day) and the whole body insulin sensitivity was halved (3.9 ± 0.32 vs 6.4 ± 0.21 dL/kg.min/µU/mL.1E^{-3}). In fasting state, CMRglu was slightly but significantly less in obese than in lean condition (9.5 ± 0.47 vs 11.8 ± 1.54 µmol/min/100g) and the same reduction was found brain-wide. During insulin stimulation, CMRglu of lean animals was unchanged compared to fasting irrespective of the brain structure. On the contrary, whole brain CMRglu was significantly increase by insulin in obese compared to lean condition as a result of increased uptake in the insula, prefrontal cortex and striatum (20.6 ± 0.30 vs 12.5 ± 0.30 µmol/min/100g). This was the consequence of an increased glucose transport only. In conclusion, in the fasting state, the obese brain behaves like the remaining of the body through an overall reduction of the glucose metabolism. On the contrary, during insulin clamp, several brain structures increase their glucose metabolism in obese condition as a result of an increased glucose transport.

OP-555

Brain [11C]PK11195 and [18F]FDG PET imaging in a rat model of postoperative cognitive dysfunction

E. Kurtys[1,2], I. B. Hovens[2], C. C. Real[3], P. Kopschina Feltes[4], D. Vállez García[4], U. L. M. Eisel[2], R. G. Schoemaker[2], J. M. Verkuyl[5], L. M. Broersen[5], H. C. Klein[4], R. A. J. O. Dierckx[4], J. Doorduin[4], E. F. J. de Vries[4]; [1]King's College London, London, UNITED KINGDOM, [2]University of Groningen, Groningen, NETHERLANDS, [3]University of São Paulo, São Paulo, BRAZIL, [4]University of Groningen, University Medical Center Groningen, Groningen, NETHERLANDS, [5]Nutricia Research, Utrecht, NETHERLANDS.

Aim: Postoperative cognitive dysfunction (POCD) is a common complication after surgery that can have a long-lasting negative impact on the patient's quality of life. Although the underlying mechanism is still unknown, evidence suggests that neuroinflammation may play an important role. Here we aimed to confirm the presence of neuroinflammation in a rat model of POCD and investigated the impact of the surgical procedure on brain metabolism. Nutrition is believed to affect cognition and brain metabolism and could modulate neuroinflammation. We therefore also evaluated the impact of a multi-nutrient supplementation diet containing anti-inflammatory ingredients on surgery-induced biochemical alterations in the brain and on POCD symptoms. **Materials and Methods:** POCD after major abdominal surgery in humans was mimicked in rats by exteriorizing the gastrointestinal tract and clamping the mesenteric artery for 30 min. To assess the validity of the model, behavioral changes were evaluated in the first postoperative week. The effects of surgery on neuroinflammation and brain glucose metabolism were monitored noninvasively by positron emission tomography (PET) and postmortem by immunohistochemistry. To assess the effect of nutrition, rats were fed a control diet or

investigational diet starting either 2 weeks before or immediately after the surgical intervention. **Results:** Major surgery caused significant bodyweight loss, reduced exploratory behavior, increased anxiety and tended to decrease spatial memory. [11C]PK11195-PET imaging and immunohistochemistry confirmed the presence of neuroinflammation in several brain regions after surgery. [18F]FDG-PET imaging revealed both increased and decreased brain metabolism in distinct parts of the brain. Dietary intervention started prior to surgery had a positive impact on recovery, resulting in faster gain in bodyweight and normalization of exploratory behavior and spatial memory. This improvement was accompanied by a reversal of astrocyte activation in the periventricular zone and a normalization of brain metabolism in part of the motor cortex. Dietary intervention started after surgery reversed astrocyte activation in cerebellum and the periventricular zone and decreased brain metabolism in the piriform cortex, but had no beneficial effect on anxiety and spatial memory. **Conclusion:** This study shows that major surgery can be accompanied by neuroinflammation and changes in glucose metabolism in several brain regions. Preventive intervention with a diet containing anti-inflammatory nutrients can affect neuroinflammation and brain metabolism and has a positive effect on the recovery from abdominal surgery in rats. These results indicate that a dietary intervention can have an effect on brain physiology and warrant further investigation of this concept.

OP-556

Muscimol Reduces D2 Receptor Binding in the Mesolimbothalamic System of the Rat

S. Nikolaus[1], H. Wittsack[1], M. Beu[1], M. A. De Souza Silva[2], C. Antke[1], F. Wickrath[1], A. Müller-Lutz[1], G. Antoch[1], J. P. Huston[2], H. Müller[1], H. Hautzel[1]; [1]University Hospital Düsseldorf, Düsseldorf, GERMANY, [2]Heinrich-Heine University, Düsseldorf, GERMANY.

Purpose/Introduction: Muscimol (MUS) acts as an highly selective GABA(A) receptor (R) agonist. We have previously shown that MUS decreased D2R binding in the rat neostriatum (1). In the present study, we assessed the effect of MUS on D2R binding in neocortical and subcortical regions, employing dedicated small animal SPECT and MRT. **Subjects & Methods:** In 16 male Wistar rats, D2R binding was measured in baseline (BAS) and after application of MUS (1 mg/kg ip). After MUS challenge, motor/exploratory behavior was registered for 30 min in an open field using EthoVisionXT. Iodine-123-IBZM (26±4MBq) was injected 30 min post-challenge. Imaging data were acquired 45 min after radioligand application with the TierSPECT. Seven rats were scanned with a dedicated small animal MRT (MRS3000 Pre-clinical MRT, 3.0 T, MR Solutions, Guildford, UK) in order to gain morphological information. Based on the Paxinos rat brain atlas, regions of interest were defined on SPECT-MRT overlays. Estimations of the binding potential (BP) were obtained by computing ratios of the specifically bound compartments to the cerebellum for neostriatum (STR), ventral striatum (VSTR), thalamus (THAL), substantia nigra (SN), frontal (FC), motor (MC) and parietal cortex (PC) as well as an-

terior (aHIPP) and posterior hippocampus (pHIPP). **Results:** In BAS, BPs amounted to 2.82±.46 (STR), 2.53±.51 (VSTR), 1.92±.38 (THAL), 1.77±.39 (SN),1.65±.61 (FC), 1.56±.41 (MC), 1.18±.33 (PC), 1.49±.23 (aHIPP) and 1.47±.36 (pHIPP). After MUS, BPs were 1.92±.41 (STR), 2.40±.42 (VSTR),1.60±.41 (THAL), 1.27±.43 (SN), 1.25±.44 (FC), 1.41±.46 (MC),1.14±.30 (PC), 1.39±.30 (aHIPP) and 1.21±.40 (pHIPP). Reductions in STR, VSTR, THAL, SN and pHIPP were significant (.005≤p≤.012). In STR, VSTR, SN and pHIPP, D2R binding was negatively correlated with grooming in the first half and positively correlated with motor/exploratory behaviors in the second half of the testing time. **Discussion/Conclusion:** The MUS-induced reduction of D2R binding in STR, VST, THAL, SN and pHIPP implies an elevation of synaptic dopamine levels in these regions. Thereby, lower D2 receptor binding (and higher DA) in STR, VSTR, SN and pHIPP was associated with an increase of grooming in the first and a decrease of motor/exploratory behaviors in the second half of the testing time. Findings indicate direct GABAergic control over synaptic dopamine levels in the mesolimbothalamic system in relation to behavioral action. (1)Nikolaus et al. Pharmacol Biochem Behav 2017; 153: 76-87.

OP-557

Cross-Species Physiological Assessment of Brain Estrogen Receptor Expression Using 4FMFES PET Imaging

M. Paquette, S. Phoenix, J. A. Rousseau, O. Sarrhini, R. Lecomte; Université de Sherbrooke, Sherbrooke, QC, CANADA.

Introduction: There is evidence that the estrogen decline during and after menopause have cognitive impacts, suggesting a relationship between cognition and physiological estrogen stimulation. Previous autoradiography studies showed that many areas in the rat brain have a high estrogen receptor (ER) expression, especially in the hypothalamic region. In this work, retrospective analysis of preclinical and clinical data during evaluation of the ER PET tracer 4-fluoro-11β-methoxy-16α-[^{18}F]-fluoroestradiol (4FMFES) in mice, rats and humans with a focus on the brain uptake was performed. **Subjects & Methods:** Breast cancer tumor-bearing female athymic nude mice (n = 8), and female Sprague-Dawley rats (control, n = 3; ovariectomized, n = 3) were injected intravenously with a dose of 0.1 MBq/g 4FMFES. Twenty-minute PET acquisitions were initiated 1 hour after injection of the radiotracer. Immediately after, low-dose CT was performed in the same bed position. The rat heads were further imaged using T2-weighted proton density MRI to provide anatomical landmarks. PET/CT (and MRI) fusion images were generated and semi-quantitative analysis was conducted to extract %ID/g data. In parallel, 41 breast cancer patients were enrolled in a clinical phase II study to evaluate 4FMFES-PET for oncological assessment, but with the head included in the field-of-view; brain uptake was reported as SUV$_{Max}$. **Results:** Regardless of the species studied, 4FMFES brain uptake was near background levels, except for bilateral foci at the base of the skull, at the midsection of the brain. Anatomical localization of the PET signal using CT (and MRI for rats), indicates that the signal origins from the hypothalamus. Mice uptake in this area reached 2.8 ± 0.6 %ID/g,

a level comparable to ER+ MCF7 tumor xenografts (2.3 ± 1.2 %ID/g). Rat uptake was 0.33 ± 0.03 %ID/g for the control group and significantly higher in the ovariectomized group (0.59 ± 0.12 %ID/g; p < 0.05). Clinical assessment of human hypothalamus uptake yielded a SUV$_{Max}$ score of 0.752 ± 0.227, which is 3-fold higher than the average brain background activity. A non-significant trend toward higher uptake in post-menopausal women (SUV$_{Max}$ = 0.761 ± 0.231, n = 31) was observed compared to the pre-menopausal group (SUV$_{Max}$ = 0.707 ± 0.208, n = 10). **Conclusion:** 4FMFES allowed visualization of ER expression in the hypothalamic region in humans and two different rodent species. Contrary to what was reported previously (Khaytum *et al.*, J Nucl Med 2014;55), ER-targeting tracers accumulates mainly in the hypothalamus, not the pituitary in the brain.

OP-558

Determining the Effects of Age and Gender on Normal Pediatric Brain Metabolism Using FDG-PET

S. Turpin[1], P. J. Martineau[2], M. A. Levasseur[3], R. Lambert[1]; [1]CHU Sainte-Justine, Montreal, QC, CANADA, [2]University of Ottawa, Ottawa, ON, CANADA, [3]CHU Sherbrooke, Sherbrooke, QC, CANADA.

Introduction: Normal databases of brain metabolism can be useful when interpreting an FDG-PET brain study. While normal metabolic activity in the adult brain has been well-studied, much less is known about pediatric brain metabolism. The purpose of our study was to develop mathematical models of metabolic activity of various regions in normal pediatric brains, accounting for both gender and age, using FDG-PET data. **Methods:** 59 FDG-PET/CT brain acquisitions were performed on 59 subjects which varied between 6 months and 18 years of age. These subjects included 30 (50.8%) males. None of these patients had known collagen disease, neuropsychiatric symptoms, epilepsy or CNS neoplasm at the time of the study and none was taking medication that may influence brain uptake. These results were analyzed using commercially available software (Neuro-Q^{TM}), which provided information on the relative metabolism of 47 separate cortical and sub-cortical regions, which were normalized to whole brain activity. For each of these 47 regions, the significance of gender was examined using the Student t-test. Multiple linear and non-linear mathematical models of metabolic activity were developed for each region in order to determine the variation of local metabolism with age. Optimal models of metabolism were selected on the basis of the results of the Akaike Information Criterion (AIC). Mean predicted value and 95% prediction intervals, taking into account age and gender, were derived for all regions. Validation of models was performed analyzing a new set of 16 normal patients. **Results:** The effects of gender were found to be statistically significant only in the posterior cingulate cortex while the relative metabolism of all regions were noted to vary with subject age. For 7 regions, the optimal model was a linear function of age. For the remainder of the regions, the optimal model was non-linear with the best fit provided by a quadratic model in 13, cubic in 6, logarithmic in 11, a power law in 8, and a modified power in 4 regions. In the case of 14 paired regions, the same model could

be used in either hemisphere. Validation demonstrated that values fell within the 95% prediction interval in 95.35% of analyzed regions. **Conclusion:** Pediatric brain metabolism, as studied by FDG-PET, is a complex function of age and, in some cases, gender. This work has provided one of the largest normal pediatric databases to date.

OP-559

Impact of plasma glucose on the pattern of brain FDG uptake and on its performance for prediction of dementia in mild cognitive impairment

I. Apostolova[1], C. Lange[2], P. Suppa[3], S. Klutmann[1], L. Spies[3], M. Grothe[4], R. Buchert[1]; [1]University Medical Center Hamburg-Eppendorf, Hamburg, GERMANY, [2]University Medicine Charite Berlin, Berlin, GERMANY, [3]jung diagnostics GmbH, Hamburg, Hamburg, GERMANY, [4]German Center for Neurodegenerative Diseases, Rostock, GERMANY.

Background: Increased blood glucose level (BGL) has been reported to cause alterations of FDG uptake in the brain that mimic the characteristic pattern in Alzheimer's disease (AD). Aim of the present study was (i) to confirm this finding in well characterized normal control (NC) subjects from the Alzheimer's Disease Neuroimaging Initiative (ADNI), and (ii) to analyze its impact on the prediction of AD dementia (ADD) in mild cognitive impairment (MCI). Methods: The study included all ADNI NCs with baseline FDG PET that were cognitively stable for ≥36 months (n=87, 74.2±5.3y), and all ADNI MCIs with baseline FDG PET, baseline MRI at 3T, and ≥36 months follow-up (n=324, 71.1±7.1y). Seventy-three of the MCIs had converted to ADD within 36 months. PET images were stereotactically normalized to MNI space using SPM8. Brain parenchyma was used as reference region for intensity scaling. In the ADNI NCs, scaled FDG uptake was tested for clusters of correlation with BGL on the family-wise error corrected 5% significance level. In the ADNI MCIs, ROC analysis was used to assess the power of mean FDG uptake in a predefined AD-meta ROI for prediction of ADD after 36 months. ROC analysis was repeated after correcting mean FDG uptake in the AD-meta ROI for BGL based on linear regression in the ADNI NCs. Results: In the ADNI NCs, BGL was 98±16 (59-149) mg/dl. There was a significant cluster of negative correlation between scaled FDG uptake and BGL comprising the precuneus and bilateral parieto-occipital cortex (cluster volume 123ml, p=0.020). The cluster did not include the posterior cingulate. Linear regression of FDG uptake in the AD-meta ROI revealed: FDG uptake = 1.022-0.176*BGL(mg/dl)/1000 (one-sided p=0.059). In the ADNI MCIs, BGL was 101±17 (55-189) mg/dl. Uncorrected FDG uptake in the AD-meta ROI provided an area of 0.784±0.030 under the ROC curve for identification of MCI-to-ADD converters. Correcting FDG uptake in the AD-meta ROI for BGL did not result in significant change of the ROC curve (area=0.786±0.030). Conclusions: These findings confirm that increasing blood glucose is associated with relative reduction of FDG uptake in the cortex (compared to white matter) even in the 'acceptable' range BGL<150mg/dl. BGL-associated pattern is similar to the typical AD-pattern, but it is not identi-

cal: the pattern comprises the precuneus (more than posterior cingulate) and parieto-occipital (rather than parieto-temporal) cortex. BGL-associated variability of FDG uptake has no relevant impact on the power of FDG PET for prediction of MCI-to-ADD conversion.

OP-560

Using EQ·PET to reduce reconstruction-dependent variation in FDG PET brain imaging

M. Vanhoutte[1], R. Lopes[2], G. Petyt[3], C. Hossein-Foucher[4], A. Aziz[3], A. Jaillard[5], H. Lahousse[3], F. Semah[4], R. Fahmi[6]; [1]Siemens Healthineers / Univ. Lille, Inserm U1171, CHU Lille, F-59000 Lille, France, Lille, FRANCE, [2]Univ. Lille, Inserm U1171, CHU Lille / CHU Lille, Department of Neuroradiology, Lille, FRANCE, [3]CHU Lille, Department of Nuclear Medicine, Lille, FRANCE, [4]Univ. Lille, Inserm U1171, CHU Lille / CHU Lille, Department of Nuclear Medicine, Lille, FRANCE, [5]Univ. Lille, Inserm U1171, CHU Lille, Lille, FRANCE, [6]Siemens Healthineers, Molecular Imaging, Knoxville, TN, UNITED STATES OF AMERICA.

Aim: FDG-PET imaging is routinely used in Alzheimer's disease (AD) diagnosis, thanks to the relationship between FDG uptake and brain function. We used EQ·PET, a proprietary standardization tool based on NEMA phantom and well validated in oncology (M. Kelly, et al EJNMMI'2011, E. Quak et al., EJNMMI'2015), for reducing the quantitative variation resulting from differences in reconstruction protocols and hence allow a meaningful group analysis of longitudinal brain FDG images of AD patients. **Materials & Methods**: NEMA IQ phantom was filled with FDG according to EARL recommendations, and scanned on a Siemens mCT-Flow scanner following EANM guidelines. Images were reconstructed using two reconstruction methods: (R1) 3D-OSEM with TOF, 2 iterations and 21 subsets; and (R2) 3D-OSEM with TOF, 6 iterations and 21 subsets. EQ·PET was then used to align the recovery coefficients curves (CC) of reconstructions (R1) and (R2) with the EARL standard CC and then deduce the optimal Gaussian filter to be applied to (R2) to align it with (R1). The reduction in variability between the two reconstructions with EQ·PET was assessed on brain FDG-PET scans of nine patients with early-onset AD. We used Sum of Squared Differences (SSD) to quantify the differences between corresponding pairs of images before and after EQ·PET alignment. Three values were calculated and compared: (1) 3D spatial resolution using AFNI software (https://afni.nimh.nih.gov/), (2) regional mean SUVs, and (3) native PET voxel-wise intensities inside a brain mask. Note that for (2), calculations were performed within 116 Automated Anatomical Labeling (AAL) regions of interest in the MNI space after registering all images to a common MNI FDG template. This was achieved with Scenium software (Siemens Healthineers). To eliminate the effects of spatial registration in these cases, the same geometric transformation was applied to both reconstructions for all patients. Paired t-tests were used to compare results before and after data alignment with EQ·PET. **Results**: The optimal filter size resulting from EQ·PET experiments was FWHM=3.1mm. Averaged SSDs before (resp. after) EQ·PET alignment were: (1) 3D spatial resolution: 1.9mm³ (resp.

0.5mm³; p=1.3e-07); (2) mean regional SUVs: 0.41 (resp. 0.3; p=1.0e-06); and (3) normalized voxel-wise brain intensity: 0.74 (resp. 0.38; p=3.9e-11). **Conclusion**: EQ.PET significantly reduces reconstruction-dependent variation in brain FDG-PET measurements, enabling increased confidence in quantitative comparison of clinical images for monitoring treatment response and/or disease progression. EQ·PET could be similarly applied to reduce inter-scanner variability. Our results show the potential of using EQ·PET in Neurology applications.

OP-561

Calculation of image-derived input function for absolute quantification of clinical [18]FDG PET/MRI studies of the brain

I. Shiyam Sundar[1], O. Muzik[2], L. Rischka[1], A. Hahn[1], I. Rausch[1], R. Lanzenberger[1], M. Hienert[1], E. Maria Klebermass[1], T. Traub-Weidinger[1], T. Beyer[1]; [1]Medical University Vienna, Vienna, AUSTRIA, [2]Wayne State University School of Medicine, Detroit, MI, UNITED STATES OF AMERICA.

Aim: Absolute quantification of PET brain studies requires the knowledge of an arterial input function (IF), usually obtained invasively via arterial cannulation. Here we present a non-invasive method that allows determination of the image-derived IF (IDIF) from [18F]FDG-PET/MRI brain data. **Subjects and Methods:** As a part of an ongoing study, six subjects underwent dynamic FDG test-retest PET/MRI examinations in a fully-integrated PET/MRI system (Siemens, Biograph mMR). The protocol included a time-of-flight MR angiography (TOF-MRA) sequence used to extract an internal carotid artery mask (ICAM) as well as sparsely sampled MR-navigators for motion correction. The PET data was reconstructed using the OSEM algorithm that included both a scatter and a CT-based brain attenuation correction. Arterial blood samples (AIF) were collected as the gold standard. Calculation of the IDIF was performed in 3 steps: (1) automatic segmentation of the petrous region from the ICAM, (2) determination of activity in the PET background region surrounding the ICAM using TOF geometric information and the scanner's point spread function (PSF) and (3) performing a spill-in correction in the target region by subtracting the contribution from the background, and a spill-out correction using the recovery coefficients obtained from the ICAM and PSF. The ratio (R) of the area-under-the-curve (AUC) of the IDIF to the AUC of AIF was used as a similarity measure between the two IFs. Finally, parametric images representing cerebral metabolic rate of glucose (CMRGlc) were calculated using the standard rate constant approach. **Results:** Our results indicate a 3±7% difference for R (0.97 ± 0.07), with IDIF underestimating the true IF (AIF) due to overcorrection at later time points. Overall, regional CMRGlc values in 83 brain regions were overestimated by 3±9%. **Conclusion:** Our results indicate that using an integrated PET/MR protocol, the CMRGlc can be non-invasively determined from image data with less than 10% overestimation compared to arterial sampling. As such, this methodology appears to be well suited for assessment of CMRGlc in clinical routine.

Do.MoRe: Thyroid Cancer - Clinical

OP-562

18FDopa PET/CT is more sensitive than WB-MRI for the detection of structural disease in medullary thyroid cancer with increased calcitonin.

M. Terroir, I. Borget, C. Caramella, K. El Farsaoui, D. Deandreis, S. Grimaldi, J. Lumbroso, A. Berdelou, E. Baudin, M. Schlumberger, S. Leboulleux; Gustave Roussy, Villejuif, FRANCE.

Aim: Patients with medullary thyroid carcinoma (MTC) frequently present recurrent or persistent disease after initial surgery that is usually detected by an increased serum calcitonin (Ctn) level. The clinical challenge is to localize the disease in the neck when surgery can cure the patients, and in distant sites. The diagnostic value of 18FDopa (fluorodihydroxyphenylalanin) in MTC patients has not yet been compared to a complete imaging work-up. The aim of our study was to compare 18FDopa PET/CT and WB MRI (whole body magnetic resonance imaging) to 18FDG (fluorodeoxyglucose) PET/CT, whole body CT scan, neck US and bone scintigraphy in MTC patients with increased Ctn levels and no known distant metastases to determine the most effective imaging modality to localize the recurrent/persistent disease. **Material and Methods:** Data of 36 consecutive MTC patients with increased Ctn and no known distant metastases were prospectively recorded between September 2014 and 2016. We compared the blind interpretation of each imaging modality to the reference assessment for structural disease defined as pathology when available or agreement between two imaging modality or subsequent follow up. The detection rate of each imaging modality was determined in a per patient, per organ and per lesion analysis. **Results:** Thirty six patients (21 females, mean age 57 years) were enrolled. The median serum Ctn level was 760 pg/ml (range 21-10121) and the median Ctn doubling time was 1.5 years (range 0.4-20.7). The reference assessment demonstrated structural disease in 23 patients (64%), for a total of 65 lesions in 37 organs (9 in the thyroid bed, 15 in the neck lymph nodes, 6 in mediastinal lymph nodes, 1 in the lungs, 2 in the liver, 3 in bones and 1 in another site). At a patient level, the detection rates were 64% for 18FDopa, 40% for 18FDG, 40% for WB-MRI, 48% for CTscan. There was no correlation neither with Ctn doubling time nor with Ctn level. The per lesion detection rates were 95% for18FDopa, 52% for 18FDG, 27% for WB-MRI, 33% for CTscan. Neck US detected 58% of the neck lesions. **Conclusion:** These results suggest that 18FDopa PET/CT is more sensitive than any other imaging modality including WB MRI to detect structural disease in MTC patients with increased calcitonin and no known distant metastases.

OP-563

Role of 68Ga-DOTA RGD PET/CT in patients with TENIS (Thyroglobulin elevation with negative Iodine scintigraphy) syndrome and its comparison with 18 F FDG PET/CT

A. S. Parihar, R. Basher, J. Shukla, R. Vatsa, A. Sood, A. Bhattacharya, B. R. Mittal; Post Graduate Institute of Medical Education & Research, Chandigarh, INDIA.

Purpose: To evaluate the role of 68Ga-DOTA RGD PET/CT in patients with TENIS (Thyroglobulin elevation with negative Iodine scintigraphy) syndrome and its comparison with ^{18}F-FDG PET/CT. **Materials and Methods:** As a pilot study, 10 patients (3 Males, 7 Females) with mean age of 44.2 years (range from 16-67 years) with TENIS syndrome suggested by rising levels of Thyroglobulin (Stimulated Tg>2 ng/mL) who had undergone ^{18}F-FDG PET/CT were selected for the study. All the patients had undergone total thyroidectomy (8 papillary Ca thyroid; 2 follicular Ca thyroid) and post-surgery ^{131}I ablation therapy. On follow up, they had rising Tg levels (mean 148.8 ng/mL ; range of 85-281 ng/mL) with negative ^{131}I whole body diagnostic scintigraphy. These patients subsequently underwent ^{18}F-FDG PET/CT for disease evaluation followed by ^{68}Ga-DOTA RGD PET/CT. Quantification analysis and comparison of detected lesions in these two modalities was done using standard uptake values (SUVmax). **Result:** Of the 10 patients, two did not have any abnormal uptake of tracer on ^{18}F-FDG PET/CT. Both these patients showed uptake of ^{68}Ga-DOTA RGD in the thyroid remnant tissue or at the metastatic sites. Of the eight patients having positive FDG PET scan findings, two had additional metastatic sites (cervical lymph nodes, lung nodules) on ^{68}Ga-DOTA RGD PET/CT. Three patients had detection of the same lesions on both the diagnostic modalities, whereas in the remaining three patients ^{18}F-FDG PET/CT detected more number of lesions compared to ^{68}Ga-DOTA RGD PET/CT. The mean SUVmax of the metastatic cervical lymph nodes detected on ^{18}F-FDG PET/CT was 6.34 (range 2.5-15), that of the lung nodules was 4.5 (range 2-6) with mean blood pool SUVmax of 2.5. On ^{68}Ga-DOTA RGD PET/CT, the mean SUVmax of the cervical lymph nodes was 4.8 (range 2.5-8), that of the lung nodules was 3.2 (range 2-5) with mean blood pool SUVmax of 0.9. Remnant thyroid bed tissue was detected on ^{68}Ga-DOTA RGD PET/CT with SUVmax of 4.0 and metastatic cervical lymph nodes with SUVmax 2.5 that were negative on ^{18}F-FDG PET/CT. **Conclusion:** The use of ^{68}Ga-DOTA RGD, an angiogenesis marker targeting integrin $\alpha_v\beta_3$, in patients with TENIS syndrome can be a useful modality as an adjunct to ^{18}F-FDG PET/CT for detection of additional lesions as well as for evaluating disease activity in FDG negative cases. If ^{68}Ga-DOTA RGD PET/CT results are encouraging from multicentric studies, the FDG negative and RGD positive TENIS patients may be potential candidates for ^{177}Lu RGD therapy

OP-564

Comparison of F-18 DOPA and Ga-68 DOTA TATE in detection of recurrences or metastasis of medullary thyroid cancer

S. Asa[1], K. Sönmezoğlu[1], E. Kaymak Akgun[1], S. Razavi Khosroshah[1], S. Toksöz[2], H. Pehlivanoğlu[1], E. Karayel[1], M. Ocak[3], L. Kabasakal[1], Y. Bükey[2]; [1]Istanbul University Cerrahpasa Medical Faculty Department of Nuclear Medicine, Istanbul, TURKEY, [2]Istanbul University Cerrahpasa Medical Faculty Department of General Surgery, Istanbul, TURKEY, [3]Istanbul University Pharmacy Faculty, Istanbul, TURKEY.

Aim: The aim of this retrospective study was to compare F-18 DOPA PET/CT (FDOPA) and Ga-68 DOTA TATE PET/CT (TATE) in detection of recurrences or metastasis of medullary thyroid cancer (MTC) patients with elevated calcitonin levels during follow-up period after initial treatment. **Methods:** A total of 32 patients with high serum calcitonin levels during follow-up were enrolled in this study. All patients underwent FDOPA and TATE scans, which were performed within interval of 38 (2-120) days. PET/CT analysis was done based on per-patient basis and per-lesion basis (maximum 10 lesion/patient). Lesions with increased radiopharmaceutical uptake were examined within six categories as local, nodal (cervical, mediastinal, other), hepatic, skeletal, lung and brain. Detection rates of metastatic lesions were assessed for both FDOPA and TATE. **Results:** The study group included 19 (59,3%) females and 13 (40,6%) males with a mean age of 51,3 years. The mean calcitonin level was 1908,7 ng/L (range: 62,4-14000 ng/L). On the patient-based analysis, we observed at least one focus of abnormal uptake in 24 of 32 patients using both F-18 DOPA and Ga-68 DOTA TATE scans with a mean of calcitonin levels 2471,2 ng/L (range:125-14000 ng/L). Eight of 32 patients who had lower calcitonin levels (mean calcitonin:221,1; range: 62,4-573) did not have any pathological uptake in both imaging modalities. The difference of calcitonin level between two groups was statistically significant (T test; $p < 0.05$). There were 5 patients with FDOPA positive scan despite of negative TATE. On the other hand, in two patient, TATE was positive versus negative FDOPA scan. On the lesion-based analysis, 79 lesions were detected with FDOPA and 83 lesions with TATE scans. While 17 lesions(1 of local, 7 of servical, 3 of mediastinal, 1 of other nodal, 2 of hepatic and 1 of brain) were positive in F-18 DOPA, but negative in TATE. However, there were 21 lesions (1 of local, 7 of servical, 2 of hepatic and 11 of bone) with positive TATE scan positive, but negative on FDOPA imaging. **Conclusion:** Both F-18 DOPA PET/CT and Ga-68 DOTA-TATE PET/CT scans have clinical impact on the management of patients with MTC, according to our results. However, FDOPA imaging seems more effective modality overall on the patient-based evaluation whereas DOTA-TATE scanning is clearly better in detection of bone lesions Acknowledgements: This study was supported by Istanbul University Scientific Research Projects with project no:35236

OP-565

Characteristics of malignant thyroid lesions on [18F] Fluorodeoxyglucose (FDG) Positron Emission Tomography (PET)/Computed Tomography (CT)

H. Nasr[1,2], H. Farghaly[1,3], A. Alqarni[1], S. Al-Salem[1]; [1]Radiology Departement, Prince Sultan Military Medical City, Riyadh, SAUDI ARABIA, [2]Nuclear Medicine Unit, Kasr Al-Aini Cairo University Hospital, Cairo, EGYPT, [3]Nuclear Medicine Unit, Assuit University Hospital, Assuit, EGYPT.

Objectives: To determine the variables that can best differentiate malignant from benign thyroid lesions incidentally found on ^{18}F-FDG PET/CT. **Methods:** All ^{18}F-FDG PET/CT studies starting from 2011 to end of 2016 were reviewed for incidental thyroid lesions or metabolic abnormalities. Only patients found to have FNAB or histopathology were included. Patients with known thyroid malignancy were excluded. Patients were analyzed for age, sex, SUVmax, non-enhanced CT tissue density in

mean Hounsfield units (HU), uptake pattern (focal or diffuse) and gland morphology (MNG or diffuse). A control group of 15 patients with normal thyroid glands was used to assess tissue density (HU) for normal thyroid tissue. Pearson Chi-squar test was used to compare categorical variables, unpaired T-test and one-way ANOVA to compare means of continuous variables and ROC analysis to assess the best cut off points for SUVmax and HU. Logistic regression was used to determine the independent predictors for malignant lesions. **Results:** Thyroid abnormalities were detected in 134 patients. Histopathology could be retrieved for 48/134 patients (36%). Biopsy was unsatisfactory/indeterminate in 4/48 patients (8%). Final analysis included only 44 patients (age 55.2±14.7; 30 females (68%)) with unequivocal FNAB or histopathology. MNG was noted in 17/44 patients (38.6%). Thyroid malignancy was found in 16/44 (36.4%). Thyroid malignancies were 12 papillary, 1 follicular, 1 Hurthle cell and 2 lymphoma. Benign lesions were 21 follicular adenomas, 2 colloid nodules and 5 autoimmune thyroiditis. Focal FDG uptake was more frequently associated with malignant lesions compared to benign lesions (75% vs. 43%; *p*=0.039). The mean SUVmax and tissue density (HU) were higher in malignant than benign lesions (8.8±8.3 vs. 3.6±1.9, *p*=0.024) and (48.9±12.7 vs. 32.9±17.5, *p*=0.003) respectively. Mean HU in the control group with normal thyroid tissue was 90±7.4, significantly higher than both benign and malignant lesions (*p*<0.001). Cutoff points to best differentiate malignant from benign lesions were SUVmax >4.7 and HU >42. Sensitivity, specificity, PPV, NPV and accuracy to detect malignancy for SUVmax>4.7 were 68.8%, 78.6%, 64.8%, 81.5 & 75.0% (*p*=0.002), for HU>42 were 81.3.0%, 75.0%, 65.0%, 87.5 & 77.3% (*p*=0.0003) and for both parameters combined were 87.5%, 60.7%, 56.0%, 89.5% and 70.5% (*p*=0.002) respectively. Only HU>42 and SUVmax>4.7 were independent predictors for malignancy with odd ratios 8.98 and 4.93 respectively. **Conclusion:** Higher tissue density (HU>42) and FDG uptake (SUVmax>4.7) as well as tendency for focal uptake pattern are characteristics highly predictive of malignancy when associated with incidentally detected thyroid lesions on ^{18}F-FDG PET/CT.

OP-566

FDG+/RAI+ patients with distant metastases from differentiated thyroid cancer can benefit from RAI treatment

l. Males[1], S. Grimaldi[2], M. Terroir[3], J. Lumbroso[1], D. Deandreis[1], A. Berdelou[1], E. Baudin[1], M. Schlumberger[1], S. Leboulleux[1]; [1]Institut Gustave Roussy, Villejuif, FRANCE, [2]Serena Grimaldi, villejuif, FRANCE, [3]Marie Terroir Cassou de Mouna, Villejuif, FRANCE.

Purpose: Patients with distant metastases from differentiated thyroid cancer (DTC) with FDG uptake have the same survival rate whether they present or not radioactive iodine (RAI) uptake, suggesting that FDG could indicate resistance to RAI treatment. The purpose of this retrospective monocentric study was to evaluate tumor response rate following RAI treatment in DTC patients with distant metastases that present both FDG and RAI uptakes (FDG+/RAI+). **Method:** Thirty two FDG+/RAI+ DTC patients with distant metastases were included with following criteria i) DTC confirmed by our pathologist (ii) first RAI admin-istration between January 2007 and December 2016 (iii) distant metastases known prior to RAI administration or diagnosed on the post-therapeutic WBS iv) FDG-PET performed within 6 months of the first post-therapeutic WBS v) at least one lesion with RAI uptake and one lesion with FDG uptake vi) follow up of at least 3 months vii) availability of morphological CT examina-tion 6 months after each RAI administration. **Results:** Thirty two patients, (16 females, mean age: 60 years) treated with RAI (100 mCi following thyroid hormone withdrawal every 6 months for 2 years and annually afterwards in case of RAI efficacy). The best scintigraphic response evaluated on post-therapeutic WBS was a complete response (CR) in 1 (3%) case, a partial response (PR) in 26 (82 %). The best PERCIST response evaluated on FDG PET was a CR in 5 (15%) cases, a PR in 14 (44%) cases. The best RECIST response among 19 patients with target lesions was PR in 10 (53 %) cases and SD in 9 (47 %) cases. Thyrogobulin serum levels de-creased by more than 50% in 21 (66%) cases. The mean number of RAI administration to obtain the best response ranged from 1.7 to 2.1 depending on the method used for tumor evaluation. The mean duration of response ranged from 25 to 31 months depending on the method used for tumor evaluation. After a mean follow up of 4.4 years after the diagnostic of distant me-tastases, 7 (16%) patients died and 25 (78%) are still alive with disease (9 undergoing repeated RAI treatments, 12 (38%) under follow-up without treatment and 4 (12%) under tyrosine kinase inhibitors. **Conclusions:** FDG+/RAI patients are not cured with RAI but can benefit from RAI administration. Patients should not be excluded from RAI treatment based on FDG uptake.

OP-567

Underestimation of the risk of metastatic disease in differentiated thyroid cancer adopting the 2015 ATA guidelines

D. Albano, M. Gazzilli, M. Bonacina, R. Durmo, E. Cerudelli, M. Panarotto, F. Bertagna, R. Giubbini; Spedali Civili Brescia, Brescia, ITALY.

Aim: according to the 2015 American Thyroid Association (ATA) management guidelines, thyroid ablation by radioactive iodine therapy (RAIT), is recommended only in patients with high risk differentiated thyroid cancer (DTC) (patients with distant metas-tases or T4 stage according to AJCC 2010 classification). Meta-static disease is often not recognized at the time of diagnosis and it can be silent for a long time interval. Patients with dis-tant metastases, especially bone metastases, show poor clinical outcomes. An early diagnosis is therefore crucial, allowing an early RAIT, which can be decisive in a significant percentage of patients. Adopting the recent 2015 ATA guidelines, there is the risk of underestimating the presence of metastases in several patients. Aim of the present study was to retrospectively analyze in a consecutive cohort of patients evaluated in our institute the prevalence of metastatic disease after surgery, before or after RAIT and to evaluated the influence of the new ATA guidelines in the diagnostic work-up and/or treatment. **Materials and Methods**: between March 2010 and March 2017, 2018 patients underwent RAI ablation of residual thyroid remnant after total

or near total thyroidectomy. In 61 patients (46 female, 15 male; average age: 60 years) distant metastases were detected. In 29 patients the metastases were in the lungs, in 21 in the bones and in 11 in more than one organ, respectively. All metastases were confirmed by histology and/or other imaging modalities. **Results**: in 15/61 (25%) patients metastases were detected before RAIT, while in 46/61 (75%) were discovered after RAIT. Comparing patient with metastases detected before and after RAI, no differences were demonstrated considering age, sex, histotype, multifocality of primary cancer and metastatic localization. Metastatic DTC discovered before RAIT had higher Thyroglobulin level before ablation and received a higher RAI total activity and number of treatments. Before RAIT only 22/61 patients were categorized at high risk according to 2015 ATA guidelines, 14 at low risk and 25 at intermediate risk, respectively. Among patients with intermediate risk, only 2 presented adverse features (lymph nodes outside the central neck compartment and/or advanced age) which indicated RAI therapy; whereas in 23/25 RAI ablation of thyroid remnant would not have been recommended. **Conclusions**: following the recent ATA guidelines 61% of patients with metastatic DTC would not have been treated with RAIT, with the risk of late diagnosis and treatment.

OP-568

30 mCi Radioiodine Treatment of Thyroid Carcinoma Patients in the post ESTIMABL Era

D. Rusu[1], V. Fleury[1], C. Palpacuer[2], M. Le Thiec[1], M. Colombié[1], F. Kraeber-Bodéré[1,3,4], C. Rousseau[1,4]; [1]Nuclear Medicine, ICO Cancer Fighting Center -, SAINT HERBLAIN, FRANCE, [2]Statistics Unit, ICO Cancer Fighting Center -, SAINT HERBLAIN, FRANCE, [3]Nuclear Medicine, University Hospital, Nantes, FRANCE, [4]CRCNA, Inserm U892, CNRS UMR 6299, Nantes, FRANCE.

Aim: To investigate the effectiveness of 30 mCi ^{131}I treatment of low risk thyroid cancer patients. It has been suggested that ablation might not be as complete as with higher doses. **Methods**: 103 patients were included in this retrospective study. They were treated in our department from October 2012 until August 2016 with 30 mCi ^{131}I post total thyroidectomy and had a documented assessment of treatment response (Thyrogen stimulated Thyroglobuline and neck ultrasonography). The patients were included in the four ATA response groups. The excellent response group was subdivided in one group with detectable and one with undetectable Tg. The patient characteristics were compared according to treatment response using Chi-square test or Fisher's exact test for qualitative variables and Student's t-test or Wilcoxon's test for quantitative variables. **Results**: 82 females and 21 males with median age of 48.8 +/-14 were treated. They had mostly papillary (40.8%) or vesicular variant of papillary cancer (52.4%). 24.4% were pT1am lesions and 57.3% pT1b, 43.7% pN0, 51.5% pNx and 4.9% pN1. 38.6% of the carcinomas were fortuitously discovered. The qualitatively evaluation of scintigraphy found un absent or faint uptake in 19,6% of cases, moderate or intense in 75.5% and very intense in 4.9% pts. The median Tg during the treatment was 3, IQR : 0,3-7.7 (25.2% < 0.3; 23.3% ≥ 0.3 and < 2.5; 25.2% 2.5-7.5). The anti-Tg antibodies

were present in 11.8% pts. After at least 6 months, the stimulated Tg was < 1ng/ml in 91.3% cases, (58.3% undetectable and 33% detectable). The anti-Tg antibodies were positives in 3.1% of pts. The ultrasonography was negative in 82.5% pts and abnormal in 17,5% pts (11,65% had thyroid bed images). The ATA response was excellent in 78 pts (53 with undetectable Tg and 25 detectable), biochemically incomplete in 3, structurally incomplete in 1 and indeterminate in 21 pts. None of the analyzed variables was predictable of ATA excellent response versus other responses. By comparing the two subgroups of ATA excellent response group, the only variable predicting the detectability of Tg after treatment was the Tg during treatment. Two patients had additional surgeries (one with additional ^{131}I treatments) and three had additional radioiodine treatment. **Conclusion**: Although the excellent ATA response was the general rule post 30 mCi radioiodine treatment in our study, a quarter of patients had not that response, needing continuing observation. A third of the excellent ATA response group patients had detectable stimulated Thyroglobuline.

OP-569

Usefulness of I-123-Dx-Whole-Body Scan in planning 131I-treatment of the differentiated thyroid carcinoma in children and adolescence

M. F. Villani, A. Grossi, B. Cassano, M. Pizzoferro, G. Ubertini, S. Chiapparelli, M. C. Garganese; Bambino Gesu' Children's Hospital, Rome, ITALY.

Background: early radioiodine treatment of differentiated thyroid carcinoma (DTC) is important to avoid disease progression. Furthermore, in paediatric DTC patients, the necessity to be curative on metastatic disease is urgent, as well as the attention to minimize the risks. For these reasons, a diagnostic scan may be useful to asses therapeutic tailored activity. This is not a routine practice and many Centers are used to administer fixed doses of 131I, considering thyroglobulin levels and tumour staging. **Aim:** to evaluate the usefulness of diagnostic 123I-WBS (123I-Dx-WBS) in combination with rh-TSH, in planning radioiodine treatment in paediatric DTC. **Materials and Methods**: 101 123I-Dx-WBS of 55 patients (21 M, mean age 15 years, range 5-18 years) followed at the Bambino Gesù Pediatric Hospital for differentiated thyroid cancer from February 2004 to December 2016 were retrospectively evaluated. In 41 out of 55 patients (20 M and 21 F, mean age 14 years, range 5-18 years, 123I-Dx-WBS was performed after administration of rh-TSH (Thyrogen®) for completion of staging before radioiodine treatment with 131I. Histological examination revealed a papillary carcinoma in 37/41 (90%) patients (classic variant in 26/37-70.3%-,follicular variant 3/37-8.1%-, aggressive histological types in 7/37-18.9%-, Warthin-like in 1/37-2.7%), follicular in the other 4(10%). All patients received Thyrogen ®, 0.9 mg daily for two consecutive days (Day 1 and 2), and 123I-NaI 24 h later (Day 3); 123I-Dx-WBS was performed on Day 4. TSH levels were evaluated at baseline and on Day 3, Thyroglobulin (Tg) at baseline and on Day 5. Statistical analysis was performed. **Results**: in 41/41 (100%) cases optimal stimulation is obtained (TSH > 30 mIU / L). Mean Tg value on Day 5 was 28.49 (range

<0.2 to 300). ROC curve analysis showed that Tg is not a good predictor for staging modification (AUC=0.6855). 123I-Dx-WBS showed both remnant and lymph node in 11/41 (27%), lymph node localization alone in 1/41 (2.5%), lung alone in 1/41 (2.5%), both lymph node and lungs in 2/41 (5%), thyroid remnant alone in 26/41 (63%) patients. 123I-Dx-WBS modified patients staging in 12/41 (29%): in 3/12 (25%) for the presence of lung metastases and in 9/12 (75%) for lymph node involvement. In all these patients, administered activity of radioiodine for radionuclide therapy was then modified. **Conclusions:** Although further studies are needed, our data showed that the combined use of rh-TSH and 123I-Dx-WBS allows to obtain an accurate and complete staging of disease, in order to take the best therapeutic strategies.

1501	Tuesday, October 24, 2017, 16:30 - 18:00, Hall A

CME 12 - Translational Molecular Imaging and Therapy/Oncology/Neuroimaging: 18F-DOPA and Radiolabelled Choline PET in Recurrent Glioblastoma

OP-570

The Need of Oncologists: Can Imaging Satisfy them?
G. Lombardi; Veneto Institute of Oncology IOV – IRCCS, Oncology 1 Unit, Padova, ITALY.

OP-571

Advanced Imaging with MRI: Impact of DCE/DSC and DWI on the Diagnosis or Relapsed Gliomas
K. Salzman; University of Utah, Radiology Department, Salt Lake City, UNITED STATES OF AMERICA.

OP-572

Potential Role of F-DOPA and Choline PET in Recurrent Glioblastoma
J. Darcourt; Centre Antoine Lacassagne, Department of Nuclear Medicine, Nice, FRANCE.

1502	Tuesday, October 24, 2017, 16:30 - 18:00, Hall B

Joint Symposium 12 - EANM/EORTC: PET Criteria for Response Assessment: Quo Vadis PERCIST?

OP-573

PET Response Criteria in Solid Tumours: PERCIST and More
W. Weber; Memorial Sloan Kettering Cancer Centre, New York, UNITED STATES OF AMERICA.

OP-574

Impact of Harmonization Strategies on EORTC Criteria and PERCIST
N. Aide; University Hospital, Caen, FRANCE.

OP-575

PET Response Criteria for Patients Undergoing Target Radioligand Therapy

W. Fendler; Ahmanson Translational Imaging Division, Department of Molecular and Medical Pharmacology, UCLA, Los Angeles, UNITED STATES OF AMERICA.

OP-576

Assessing Response to Immunotherapy - Where are we?
R. Hicks; Cancer Imaging, Peter Mac Callum Cancer Institute, Melbourne, AUSTRALIA.

OP-577

Ongoing EORCT Reflexions on the Use of FDG PET and Other Imaging Biomarkers in Clinical Trials
C. Deroose; ZU Leuven, Nuclear Medicine Department, Leuven, BELGIUM.

1503	Tuesday, October 24, 2017, 16:30 - 18:00, Hall C

CTE 6 - Joint Session with Dosimetry: Imaging, Reconstruction and ROI Analysis Techniques

OP-578

Image Reconstruction and Target Delineation on PET/CT for Radiotherapy Treatment Planning
M. Josipovic; Rigshospitalet, Department of Oncology, section for Radiotherapy, Copenhagen, DENMARK.

OP-579

Technical Challenges in 99mTc-MAA SPECT and 90Y PET Based Radioembolisation Dosimetry
C. Chiesa; Foundation IRCCS Istituto Nazionale Tumori, Nuclear Medicine Division, Milan, ITALY.

OP-580

Image Based Radionuclide Dosimetry Techniques
E. Visser; Radboud University Medical Centre, Department of Nuclear Medicine, Nijmegen, NETHERLANDS.

1504	Tuesday, October 24, 2017, 16:30 - 18:00, Hall E1

Do.MoRe - Rapid Fire Session: Radionuclide Therapy, Miscellaneous

OP-581

Peptide receptor radionuclide therapy (PRRT) in ENETS Grade 3 (G3) Neuroendocrine Neoplasia (NEN) - a single-institution retrospective analysis

S. Thang[1,2], M. Lung[1], G. Kong[1], M. Hofman[1], J. Callahan[1], M. Michael[1], R. Hicks[1]; [1]Peter MacCallum Cancer Centre, Melbourne, AUSTRALIA, [2]Singapore General Hospital, Singapore, SINGAPORE.

Aims: Grade 3 NENs are aggressive tumours with poor prognosis but increasingly recognised to have well- and poorly-differentiated subgroups. Although generally responsive to chemotherapy, durability of response is poor. PRRT+/- radiosensitising

chemotherapy is a potential treatment for disease with high SSTR-expression without spatially discordant FDG-avid disease. We retrospectively evaluated the efficacy of PRRT in G3 NEN. **Methods:** Kaplan-Meier estimate was used to determine overall survival (OS) and progression-free survival (PFS), defined from start of PRRT. Subgroup-analysis was performed for patients with Ki-67≤55% and >55%. The proportions of patients treated with PRRT who achieved anatomical (N=24) and molecular imaging (SSTR imaging, N=24; FDG PET/CT, N=19) 3 months after induction PRRT were determined. Toxicity profile of PRRT was evaluated. **Results:** 29 consecutive patients (M=17; age 16-78 y.o; Ki-67≤55%=23) were reviewed. 18 patients had pancreatic , 5 small bowel, 3 large bowel, 2 bronchial and 1 unknown primary disease. Most (26/29) had significant FDG-avid disease (i.e. intensity above liver parenchyma) prior to treatment. Patients received median 4 cycles of induction PRRT (range 1-5). 21 had radiosensitising chemotherapy. Most had ^{177}Lu-DOTA-octreotate with median cumulative activity of 25.5 GBq. 90% were treated for disease progression, with 76% receiving at least one line of prior chemotherapy. 12 patients received subsequent maintenance cycles of PRRT due to recrudescent disease after response. Median follow-up was 32 months. On RECIST 1.1, the disease control rate (DCR) at 3 months was 76%; 38% (9/24) PR and 38% SD. On SSTR imaging DCR was 62%; 58% (14/24) PR and 4% (1/24) SD. On FDG PET imaging, 11% (2/19) had CMR and 37% (7/19) had PMR. Of note, 5 patients (all Ki-67≤55%) showed further imaging response up to 15 months post induction cycles of PRRT. The median PFS from start of PRRT was 9.3 months: for Ki-67≤55%, 14 months; and Ki-67>55%, 4 months. There were 17 deaths (Ki-67≤55%, 12 deaths; Ki-67>55%, 5 deaths), with median OS of 21 months: for Ki-67≤55%, 41 months; and Ki-67>55%, 7 months. Grade 3 and 4 lymphopenia and thrombocytopenia occurred in five and six patients, respectively. No renal or liver toxicity related to treatment was seen. **Conclusions:** Although proliferation rate remains an important predictor of survival in G3 NEN, PRRT achieves clinically- relevant disease control with acceptable toxicity even in patients who have already failed first-line chemotherapy.

OP-582

The HSP90-inhibitor Onalespib Potentiates ^{177}Lu-Dotatate Treatment of Neuroendocrine Tumors

S. Lundsten, A. Mortensen, A. Mäkiniemi, D. Spiegelberg, B. Stenerlöw, M. Nestor; Department of Immunology, Genetics and Pathology, Uppsala University, UPPSALA, SWEDEN.

Introduction: The HSP90-inhibitor Onalespib is in clinical trials for therapy of various tumor types. Preclinical studies have shown that Onalespib can function as a radiosensitizer in squamous cell carcinoma and adenocarcinoma in combination with external radiation. However, no studies have investigated the potential for Onalespib to enhance effects of targeted radionuclide therapy. ^{177}Lu-[DOTA^0,Tyr^3]octreotate (DOTATATE) is currently used in clinical trials for treatment of patients with neuroendocrine tumors with promising results. Thus, the aim of the study was to investigate whether Onalespib potentiates

the therapeutic effect of ^{177}Lu-DOTATATE *in vitro*. **Material & Methods:** Dose dependent effects of Onalespib were first assessed using cell viability assays in a panel of neuroendocrine cancer cell lines. Cellular uptake and binding specificity studies of ^{177}Lu-DOTATATE was then evaluated. Potential effects of Onalespib on somatostatin receptor density were assessed using Western blot. Finally, an *in vitro* 3D tumor spheroid model was used to evaluate the therapeutic effects of ^{177}Lu-DOTATATE, Onalespib, and the combination of the two. **Results:** The majority of the investigated cell lines responded to Onalespib treatment and demonstrated specific uptake of ^{177}Lu-DOTATATE. Western blot assays indicated that the expression of somatostatin receptors was not affected by treatment with Onalespib. The 3D tumor spheroid assays demonstrated clear benefits of a combination treatment. Two weeks after treatment start, fractionated therapy, using either Onalespib or ^{177}Lu-DOTATATE, reduced spheroid growth rate resulting in spheroid sizes of approximately 50% of untreated controls. However, spheroids treated with the combination had not even resumed growth at this time. **Conclusions:** By combining treatments of Onalespib and ^{177}Lu-DOTATATE in patients with neuroendocrine cancer, therapeutic effects may be improved. This could potentially lead to lower radiation doses and reduced side effects. Continued studies *in vivo* to further assess therapeutic effects and potential toxicity is warranted.

OP-583

Heterogeneity derived by somatostatin receptor PET Predicts Overall Survival in G1/2 Pancreatic NET Patients Envisaged for Endoradiotherapy

R. A. Werner[1], H. Illhan[2], M. Mooz[1], S. Lehner[2], L. Papp[3], N. Zsótér[4], I. Schatka[5], D. O. Mügge[1], T. Higuchi[1], A. K. Buck[1], P. Bartenstein[2], F. Bengel[6], M. Essler[7], C. Lapa[1], R. A. Bundschuh[7]; [1]Department of Nuclear Medicine, Universitätsklinikum Würzburg, Würzburg, GERMANY, [2]Department of Nuclear Medicine, Ludwig-Maximilians-University Munich, Munich, GERMANY, [3]Department of Nuclear Medicine, Medical University of Vienna, Vienna, AUSTRIA, [4]Mediso Medical Imaging Systems Ltd., Budapest, HUNGARY, [5]Department of Nuclear Medicine, Charité - Universitätsmedizin Berlin, Berlin, GERMANY, [6]Department of Nuclear Medicine, Hannover Medical School, Hannover, GERMANY, [7]Department of Nuclear Medicine, University Medical Center Bonn, Bonn, GERMANY.

Introduction: Neuroendocrine tumors of pancreatic origin (pNET) are a rare, but aggressive tumor entity. Early identification of rapid tumor progression could improve decision-support in patients envisaged for endoradiotherapy (ERT). We aimed to elucidate the potential of intratumoral heterogeneity determined by baseline somatostatin receptor (SSTR)-PET/CT before ERT. **Subjects and Methods**: 31 patients suffering from G1/G2 pNET were enrolled (14 females, 60 ±10 years, n=23/31 G2). Before ERT with ^{177}Lu-labeled somatostatin analogs, baseline SSTR-PET/CT was performed. After manual segmentation of 162 (median per patient, 5) metastases, intratumoral textural features were computed. The impact of conventional PET parameters (mean/maximum standardized uptake value, SUV$_{mean/}$

$_{max}$), imaging-based heterogeneity features as well as clinical parameters (e.g. Ki67, prior therapy, Chromogranin A) for prediction of both progression-free (PFS) and overall survival (OS) was evaluated. **Results**: Within follow-up of median 4.4y, tumor progression was detected after a median of 1.5y in 21 patients; 13/31 deceased after a median of 1.9y. The parameter Entropy, reflecting derangement on a voxel-by-voxel analysis, predicted OS as proven by Cox analysis (p=0.03, PFS, p>0.05). In subsequent ROC analysis, its predictive ability for OS was supported (cutoff=6.7, AUC=0.71, p=0.02). Increasing Entropy could predict a longer survival (>6.7, OS=2.5y, 17/31), whereas less voxel-based derangement portended inferior outcome (<6.7, OS=1.9y, 14/31). Besides, these findings were supported in a G2 subanalysis (>6.9, OS=2.8y, 9/23 vs. <6.9, OS=1.9y, 14/23). None of the heterogeneity features correlated significantly with Ki67. Investigating clinical and conventional PET parameters, the proliferation index holds the potential of PFS prediction (p=0.002), whereas $SUV_{mean/max}$ failed in prediction for therapy response (AUC</=0.63, n.s.). **Conclusion**: The heterogeneity parameter Entropy derived by baseline SSTR-PET demonstrated superior prognostic performance in pNET patients envisaged for ERT, in particular for "borderline" G2 tumors. Strikingly, on a quantitative voxel-by-voxel analysis, a higher ordered pattern denotes less therapeutic response to peptide-based radiotherapy whereas an increase in derangement can predict longer overall survival.

OP-584

Hyperkalemia in patients treated with radioligand or peptide receptor radionuclide therapy

C. H. Pfob[1], A. Ott[2], F. Maurer[3], P. Luppa[4], K. Scheidhauer[1], U. Heemann[5], M. Schwaiger[1], C. Schmaderer[5]; [1]Department of Nuclear Medicine, Technische Universität München, Klinikum rechts der Isar, Munich, GERMANY, [2]Biomedical Informatics, Institute of Medical Statistics and Epidemiology, Technische Universität München, Klinikum rechts der Isar, Munich, GERMANY, [3]Hospital Pharmacy Department, Technische Universität München, Klinikum rechts der Isar, Munich, GERMANY, [4]TU MunichDepartment of Pathobiochemistry, Technische Universität München, Klinikum rechts der Isar, Munich, GERMANY, [5]Department of Nephrology, Technische Universität München, Klinikum rechts der Isar, Munich, GERMANY.

Background: PSMA-targeted radioligand therapy (RLT) and peptide receptor radionuclide therapy (PRRT) lead to severe hyperkalemia when combined with a potentially nephroprotective amino-acid co-infusion. This has been reported already for PRRT. The pathophysiology behind the rapid development of hyperkalemia is incompletely understood. We hypothesized that the infusion of cationic amino acids along with the acidity of the solution itself leads to increase of hydrogen ions that causes potassium shift to the extracellular space. **Methods:** 10 patients underwent cycles of PRRT or of RLT, respectively. Prior to the first cycles excretory kidney function was assessed by mercapto-acetyltriglycine (MAG-3) renal scintigraphy and serum biochemistry. For nephroprotection all patients received

co-infusion of the cationic amino-acids L-Arginine and L-Lysine starting 30 min prior each cycle and lasting for 4hrs. Clinical symptoms, electrolytes and acid-base status were measured at baseline and after 4hrs. Results: No patient developed clinical side effects. At baseline kidney function, acid base status and electrolytes were in the normal range except two patients with minor renal insufficiency. All patients developed hyperkalemia after 4hrs and more than half exhibiting severe hyperkalemia (defined as > 6mmol/l). Base excess and HCO3- were significantly lower after 4hrs. In parallel pH dropped. Whereas chloride did rise and the anion gap dropped slightly. Conclusion: Amino-acid co-infusion during PSMA-targeted RLT or PRRT leads to hyperchloremic, normal anion gap metabolic acidosis along with hyperkalemia. The metabolic acidosis might induce hyperkalemia by favouring exchange of potassium by hydrogen ions to the extracellular space. This finding offers an easy therapeutic option by correcting acidosis with commercially available bicarbonate solutions.

OP-585

Adjuvant post-operative radiosynovectomy in patients with rare cases of ankle pigmented villonodular synovitis (PVS)

I. Iakovou[1], J. Kotrotsios[1], K. Badiavas[1], M. Potoupnis[2], V. Mpalaris[1], G. Arsos[1]; [1]Academic Nuclear Medicine dpt, Papageorgiou hsp, THESSALONIKI, GREECE, [2]Academic Orthopedic dpt, Papageorgiou hsp, THESSALONIKI, GREECE.

Background: The most common location of the local nodular form of PVS is the knee joint, followed by the finger joints. Occurrence in the ankle joint is realy rare but should be considered if clinical findings are present. Treatment consists of isolated surgical resection of the neoplastic synovium. Radiosynoviorthesis (RS) is recommended as a post-operative treatment to increase the probability of a total removal of persisting PVS cells. **Methods-Patients:** We present our experience of 5 (3 women) young (19-31yrs) athletes with PVS of the ankle joint. All patient were treated in 2 stages: surgical synovectomy (SS) with arthroplasty of the ankle joint followed by adjuvant treatment with intra-articular injection of 2 mCi Re-186 performed within 2-3 months after SS. Treatment efficacy was evaluated 2,6 and 12 months after the initial RS by a questionnaire reporting the relief of limiting the daily activities pain as a percentage of the pretherapeutic joint discomfort using a visual analog scale (VAS). Relative uptake of Tc-99m-diphosphonate in the knee joint involved on the blood pool was also taken into consideration **Results***:* In the 1 out of the 5 cases a repeated Re-186 injection was needed for better outcome. The overall response rate for all knee treatments was 80%. Results in double treated joints were significantly worse than in single treated ones. A significant improvement in blood pool bone scintigraphic signs of inflammation was noticed. On the other hand, there was no influence on late diphosphonate uptake. **Conclusion:** A combination of debulking surgery with adjuvant intra-articular injection of Re-186 for the rare cases of PVS of the ankle joints seems to be a reliable treatment method, with encouraging results

OP-586

Impact of external cooling on PSMA uptake in salivary glands

*L. W. M. van Kalmthout, M. G. E. H. Lam, B. de Keizer, A. J. A. T. Braat;
University Medical Center Utrecht, Utrecht, NETHERLANDS.*

Aim: External cooling of the salivary glands with icepacks is currently common practice in patients treated with lutetium-177-PSMA-617 for advanced prostate cancer. Cooling of both parotid and submandibular glands is believed to cause vasoconstriction, resulting in a reduced blood flow to the salivary glands. Thus lowering PSMA uptake, in the hopes of decreasing the occurrence of the reported side effect xerostomia. To date however, this rationale has not been extensively investigated. Aim of this study was to determine the impact of cooling with icepacks on PSMA uptake in salivary glands. **Materials and Methods:** Nighty one patients referred for a gallium-68-PSMA-11 PET/CT for (re)staging of prostate cancer were consecutively included in this analysis. Twenty-six patients were scanned with unilateral icepacks on the left side, allowing intra-individual analysis, and 21 patients were scanned with bilateral icepacks. A control group of 44 patients was scanned without icepacks. Icepacks were applied at least 25 minutes prior to tracer injection. All icepacks were replaced for new ones 30 minutes prior to PET/CT acquisition to ensure effective cooling of the salivary glands. PET/CT acquisition started one hour post-injection. PSMA uptake (expressed by SUVmax, SUVpeak and SUVmean) was measured on standardized EARL reconstructions in both parotid glands and submandibular glands. **Results:** Patients with bilateral icepacks showed no differences in PSMA-uptake compared to the control group (all p>0.05); right parotid gland (SUVmax 11.62 versus 13.24), left parotid gland (SUVmax 11.26 versus 13.03), right submandibular gland (SUVmax 12.09 versus 12.65) and left submandibular gland (SUVmax 11.56 versus 12.37). In the unilateral icepack-group, merely a significant decrease in SUVpeak was found in the right parotid gland compared to the left side (11.07 versus 9.87; p=0.00). Regarding SUVmax and SUVmean, no differences in PSMA uptake were found between the right and left parotid gland (SUVmax 13.90 versus 11.09; p>0.05). All parameters on PSMA uptake in the right and left submandibular gland were comparable (SUVmax 13.00 versus 12.65; p>0.05). **Conclusion:** There is no need for external cooling of salivary glands using icepacks, because it does not influence PSMA uptake in salivary glands.

OP-587

Functional imaging of the salivary glands for evaluation of radiation-induced sialadenitis before and after Lu-177 PSMA radioligand therapy

T. Langbein, H. R. Kulkarni, A. Singh, R. P. Baum; Zentralklinik Bad Berka, Bad Berka, GERMANY.

Objective: During Lu-177 PSMA radioligand therapy (PRLT) of metastatic castration-resistant prostate cancer (mCRPC), an intense uptake of the radioligand in the salivary as well as in the lacrimal glands is observed. Hence, post-therapeutic xerostomia and potentially xerophthalmia are possible adverse effects. Objective of this study was to assess the function of the parotid and submandibular salivary glands by dynamic salivary gland scintigraphy (SGS) using Tc-99m pertechnetate before and after PRLT. **Methods:** We included 35 patients (median age 67 years, range 46-81), undergoing 1-3 cycles of PRLT applying a median cumulative activity of 13.3 GBq (range 6 - 24.8 GBq). For long-term follow-up 12 patients were analyzed, who received 3-9 cycles of PRLT (mean cumulative activity 32.3 GBq, range 20.1-56.4 GBq) up to 28 month after first cycle. A total of 183 SGS studies, performed since September 2015, were investigated. Dynamic images of the parotid and submandibular salivary glands were acquired 30 minutes after injection of Tc-99m pertechnetate. The salivary gland uptake and quantitative excretion fraction after an oral secretory stimulus at 15 minutes p.i. were evaluated. A standardized questionnaire (shorted xerostomia inventory) was used to investigate the occurrence of xerostomia. **Results:** Post PRLT, 12 patients reported mild dryness of mouth (mostly at night) with no influence on their everyday life. Only 3 patients reported significant xerostomia. However, 2 of them had received external beam radiation therapy for cervical spine metastasis and had scintigraphically confirmed salivary dysfunction prior to PRLT. SGS demonstrated a worsening of the salivary gland function in only 2 of the remaining 33 patients. In the follow-up-cohort, 1 out of 12 patients reported mild xerostomia, whereas 3 of the 12 SGS revealed a slightly decreased salivary function. **Conclusion:** Salivary gland scintigraphy is a very useful and easy to perform imaging modality for the objective evaluation of xerostomia following Lu-177 PSMA radioligand therapy. No significant parenchymal dysfunction of the salivary glands was observed even after several cycles of PRLT.

OP-588

Fluorocholine PET CT parameters predictive for hematological toxicity to 223Radium Therapy

M. Sinigaglia, L. Vija Racaru, S. Kanoun, S. Zerdoud, M. Bauriaud-Mallet, D. Bastié, L. Dierickx, D. Vallot, O. Caselles, P. Pascal, F. Courbon; Institut Universitaire de Cancérologie-Oncopole, Toulouse, FRANCE.

Introduction: The main objective is to identify fluorine-18 fluorocholine (FCH) PET/CT markers predictive for hematological toxicity induced by ^{223}Ra therapy, such as metabolically active bone tumor volume (MATV) and total bone lesion activity (TLA) in castrate-resistant prostate cancer (CRPC) patients. **Methods:** Baseline FCH PET/CT was performed in 15 patients with CRPC before treatment with ^{223}Ra. Bone metastatic disease was quantified on the basis of maximum standardized uptake value (SUVmax), MATV and total lesion activity (TLA = MATV × mean SUV). Tumor burden indices derived from total skeleton PET tumor volume measurements (such as MATV/ TBV, TLA/TBV, MATV/H, TLA/H; TBV: total bone volume measured on CT, H: height in m) were also evaluated. Bone metastatic disease and FCH PET/CT bone tumor burden and activity were analyzed in order to identify which parameters could predict hematological toxicity (on Hb, platelets and lymphocytes) at the end of ^{223}Ra therapy. Pearson correlation was used to identify correlations between age,

PSA, Gleason's score and FCH PET parameters. **Results:** MATV ranged from 75.15 cm^3 to 1259.38 cm^3 (median 392.72 cm^3). TLA ranged from 342.61 to 7198.11 cm^3 (median 1853.9 cm^3). 15 patients beneficiated from 56 cycles of ^{223}Ra. At the end of the therapy 33% (5/15) of patients presented grade 2/3 toxicity on hemoglobin and lymphocytes, while 20% (3/15) presented grade 2/3 platelet toxicity. Age was negatively correlated with both MATV (r=-0.612, p=0.015) and TLA (r=-0.596, p=0.018). Age, Gleason score, previous hormonal therapy, radiotherapy and docetaxel therapy were significantly associated with TLA (p<0.001). MATV, TLA and TLA/H predicted hematological toxicity on Hb, platelets and lymphocytes at the end of ^{223}Ra cycles (p<0.001, p<0.001, p<0.01). ROC curve analysis allowed to define cut-offs for MATV (914.97 cm^3), TLA (4197.76 cm^3) and TLA/H (23.31) which predicted platelet toxicity with an accuracy of 0.92, 0.99 and 0.77 respectively. **Conclusions:** The predictive value of pre-therapeutic FCH PET/CT markers: TLA and MATV for platelet toxicity after ^{223}Ra therapy may stem from the capacity of assessing whole body visceral and bone-osteomedullary infiltration, allowing better patient selection and treatment optimization.

OP-589

Baseline 18F-Fluoride PET-derived parameters predict modification of toxicity- and response-related blood biomarkers in prostate cancer patients treated with 223Ra-Dichloride: preliminary results

V. Ceriani[1], *G. Fornarini*[1], *M. Bauckneht*[1], *S. Morbelli*[1], *E. Zanardi*[1], *E. Pomposelli*[2], *A. Buschiazzo*[1], *I. Calamia*[1], *M. Ippoliti*[1], *F. Fiz*[3], *R. Piva*[1], *P. Mataceri Bettini*[1], *F. Boccardo*[1], *G. Sambuceti*[1]; [1]IRCCS AUO San Martino IST, Genova, ITALY, [2]Nuclear Medicine Unit, A.O. SS. Antonio e Biagio e Cesare Arrigo, Alessandria, ITALY, [3]Dep. of Nuclear Medicine and Clinical Molecular Imaging University Hospital, Tübingen, GERMANY.

Aim: Beyond lesion detection and staging, 18F-NaF PET can provide semiquantitative parameters expressing skeletal tumor burden and intensity of osteoblastic reaction. 223Ra-Dichloride therapy has been shown to improve survival in prostate cancer patients, however, heterogeneous responses to 223Ra has been reported. In particular, clinical variables able to identify responders before or early in the course of therapy need to be fully elucidated. In the present study we correlated baseline 18F-NaF PET-derived parameters with modification of both toxicity- and response-related blood biomarkers in prostate cancer patients treated with 223Ra-Dichloride. **Methods**: 13 patients with hormone-refractory prostate cancer undergoing 223Ra therapy in our center were enrolled in a single-institution trial from June 2016 to March 2017. Fluoride PET/CT scan was acquired at baseline and after thee cycles of 223Ra administration. Total alkaline phosphatase (ALP) and prostate-specific antigen (PSA) as well as blood cells counts were obtained at baseline, after three cycles (interim) and at the end of therapy. Maximum standardized uptake value of the hottest lesion (hSUVmax), mean SUV of all lesions (SUVmean) and total volume of fluoride avid bone metastases (TVF) were computed on Fluoride PET/CT images. Lin-

ear regression was used to assess correlation between baseline Fluoride PET-derived parameters and blood biomarkers levels at baseline, interim and end of treatment. **Results**: To date final blood biomarkers results were available in only five of the recruited patients. Accordingly, only interim evaluation was included in the present analysis. At baseline, hSUVmax, SUVmean and TVF were 50,27 (±22.2), 27,6 (±13,9) and 1628,68 (±467,9), respectively. As expected, TVF was directly related with baseline ALP and PSA (p<0.01). However, it was also directly proportional to the interim decline in platelets count and ALP (p<0.05). On the other hand, both hSUVmax and SUVmean were directly related with the interim raise in PSA (p<0.05). **Conclusion**: According to our preliminary analysis, baseline skeletal tumor burden is able to predict early signs of both response to therapy and bone marrow toxicity in prostate cancer patients treated with 223Ra. Moreover, Fluoride PET-derived indexes of osteoblastic reaction correlate with PSA flare in the early course of treatment. Whether confirmed, these preliminary data might imply a prognostic role for Fluoride-PET in prostate cancer patients candidates to 223Ra. Recruitment is still ongoing to confirm the predictive value of fluoride PET in the end of treatment setting and to correlate these data with overall survival.

OP-590

Mechanisms of Bone Marrow Failure in Prostate Cancer Patients treated with Radium-223 Therapy

F. Fiz[1], *C. Campi*[2], *S. Sahbai*[1], *J. Schwanck*[1], *M. Weissinger*[1], *M. Bauckneht*[3], *R. Piva*[3], *C. Marini*[4], *H. Dittman*[1], *M. Piana*[3], *G. Sambuceti*[3], *C. La Fougère*[1]; [1]University of Tuebingen, Tuebingen, GERMANY, [2]National Council of Resarch - SPIN, Genoa, ITALY, [3]University of Genoa, Genoa, ITALY, [4]CNR - IBFM, Genoa, ITALY.

Introduction: Radium-223 Therapy (223-Ra) is represents a safe and effective treatment options for metastasized prostate cancer. However, our previous analysis highlighted a variable distribution of bone-seeking tracers into the trabecular bone containing hematopoietic bone marrow (BM). A higher metabolism predicted a greater hematologic toxicity. Moreover, the entity of tumor burden has been linked to a higher incidence of BM toxicity. Aim of this study is to investigate the correlation between tumor burden, 223-Ra distribution to the trabecular bone and onset of Grade III-IV hematologic toxicity events. **Methods:** Pre-223-Ra whole body bisphosphonate-SPECT/CT of 76 prostate cancer patients were analyzed with a dedicated application. The algorithm automatically analyzed the bone structure, quantifying volume, mean density (HU) and mean counts (MC) of both trabecular bone as well as of the tumor voulume (TV) i.e. the bone metastases. Tumor burden was correlated with trabecular bone MC. TV, PSA level, presence of "superscan", number of lesions and presence of tumor burden in more than 50% of appendicular skeleton were tested as predictors of Grade III-IV toxicity with MANOVA. **Results:** A tight correlation between TV and trabecular MC was found (R=0,68, p<0,001). This correlation was present in the axial skeleton as well as in the long bones (p<0,01). At MANOVA, predictors of hematologic toxicity were: trabecular MC (p<0,05), TV (p<0,05), TV in long bones (p=0,008)

and appendicular invasion (p=0,004). **Conclusions:** A greater tumor burden can increase bone metabolism within trabecular bone. This could increase the delivered activity to the BM in the course of 223-Ra therapy and expose the patient to a higher risk of hematologic toxicity.

OP-591

Prediction of hematological toxicity in Radium-223 therapy in patients with advanced metastatic castration-resistant prostate cancer

M. Ø. Fosbøl, P. M. Petersen, A. Kjaer, J. Mortensen; Rigshospitalet, Copenhagen, DENMARK.

Aim: Investigate whether automated quantitative assessment of skeletal tumor burden on bone scintigraphy (Bone Scan Index) can serve as a predictive biomarker for hematological toxicity in patients with metastatic castration-resistant prostate cancer (mCRPC) receiving Radium-223-dichloride (Ra-223). **Methods:** National study of the Danish mCRPC patients who received ≥ 1 cycle of Ra-223 therapy from March 2014 to October 2015 and for whom a baseline bone scintigraphy was available. Baseline bone scintigraphies were reviewed and graded according to extent of disease (EOD). All scintigraphies were additionally analysed with the software EXINI Bone[BSI] Version 2(EXINI Diagnostics, Lund, Sweden) to obtain Bone Scan Index (BSI). Primary outcome was occurrence of hematological toxicity grade 2-5 according to Common Terminology Criteria for Adverse Events (CTCAE) commencing within 90 days from preceding Ra-223 administration. Association between BSI and hematological toxicity was evaluated in a multivariate logistic regression analysis including the following parameters: Baseline BSI, visual grading of EOD on bone scintigraphy, B-hemoglobin, leukocyte count, thrombocyte count, serum PSA and previous use of chemotherapy. **Results:** A total of 88 mCRPC patients were included in the study. EOD by visual assessment showed 75 % of patients (n=66) had > 20 metastases or superscan. Median baseline BSI was 5.0. Median number of completed Ra-223 cycles was four and only 27 patients (31%) completed all six cycles. Hematological toxicity was the cause of early discontinuation in 21 patients (23%). Anemia grade 2-4 occurred in 51 % of patients (n=45), leukopenia grade 2-4 in 30 % (n=26) and thrombocytopenia grade 2-4 in 24 % (n=21). One patient (1 %) died due to leukopenic infection following Ra-223 therapy and one patient (1%) due to thrombocytopenia and intracranial haemorrhage. Significant predictors of haematological toxicity in multivariate regression analysis were baseline BSI (OR 1.11 per unit increase, p=0.04), B-hemoglobin (OR 1.89 per unit decrease (mmol/l), p=0.04) and leukocyte count (OR 1.37 per unit decrease (10^9/l), p=0.02). Patients with baseline BSI > 5 had odds ratio of 3.02 (95% CI: 1.2-7.8, p=0.02) for grade 2-5 toxicity compared with patients with baseline BSI ≤ 5. **Conclusion:** Hematological toxicity occurred frequently in this cohort of mCRPC patients with advanced disease. BSI at baseline was a significant predictor of haematological toxicity and can potentially aid to identify patients at high risk of toxicity, for whom alternative therapy options should be considered.

OP-592

^{90}Y PET-CT based method of dose calculation to evaluate the efficacy of internal selective radiotherapy (SIRT)

E. Kalogianni, N. Heraghty, D. Levart, B. Corcoran, N. Mulholland, M. Vadrucci, G. Vivian; King's College Hospital, LONDON, UNITED KINGDOM.

Aim: The aim of this project is to evaluate the efficacy of yttrium-90 (^{90}Y) microsphere selective internal radiotherapy (SIRT) using a patient-specific PET-CT based method of dose calculation. **Methods:** Retrospective dosimetry of the standard radioembolisation treatment with resin ^{90}Y microspheres was performed for eight patients with unresectable liver metastases (six patients with colorectal liver metastases and two with cholangiocarcinomas). Injected activity calculation was performed using the body surface area (BSA) method. A 3D radiation absorbed dose distribution was estimated for each patient, using a voxel-based semi-Monte Carlo dosimetry method on post-therapy ^{90}Y-PET-CT images, with the Hermes Hybrid Dose 3D dosimetry software. Response was examined using the tumour lesion glycolysis (TLG) on ^{18}F-FDG-PET, as measured pre and post treatment (mean 2.9 ± 0.3 months post treatment). The TLG was estimated using the metabolic tumour volume at 50% threshold. Pre-treatment ^{18}F-FDG-PET was used for the VOI delineation and calculation of TLG per metastasis and was registered with the 3D absorbed dose distribution map. All processing performed using HERMES Hybrid Viewer. A linear fixed effects model was used to assess the dose and post-treatment TLG relationship. **Results:** 36 treated metastases were identified. Mean absorbed dose was 63±37 Gy (range: 4 - 156 Gy). The biological effective dose (BED) and Equivalent Uniform BED (EUBED) were calculated ($\alpha = 0.004$ Gy^{-1}, $\alpha/\beta = 10$ Gy, $T_{1/2}^{\text{Repair}} = 1.5$). BED was 77 ± 51 Gy (range: 4-214 Gy) and EUBED was 73 ± 48 Gy (range: 4 - 208 Gy). A significant relationship was found (p < 0.001), indicating that increased absorbed dose is associated with decreased post-treatment TLG (TLG$_{post}$). A significant relationship was found (p < 0.001) between pre-treatment TLG (TLG$_{pre}$) and TLG$_{post}$, indicating that the dose response-relationship depends on the TLG$_{pre}$. A statistically significant relationship was found (p < 0.001) between the BED and EUBED and TLG$_{post}$. The experimental tumour control probability (TCP) showed that TCP(50%) was 60Gy and 90Gy for tumours with TLG>100. **Conclusion:** A statistically significant dose response relationship was found as well as a relationship between the TLG$_{pre}$ and TLG$_{post}$. Individualised treatment planning options using the Technetium-99m macroaggregated human albumin (^{99m}Tc-MAA) SPECT-CT scan could potentially improve the treatment outcome.

OP-593

Correlation of SUVmax values & liver metastasis size/number with survival of colorectal Ca patients undergoing TARE treatment

B. Sönmezer[1], A. Gülcü[2], R. Bekiş[1], B. Polack[1]; [1]Dokuz Eylül University, Faculty of Medicine, Department of Nuclear Medicine, İzmir, TURKEY, [2]Dokuz Eylül University, Faculty of Medicine, Department of Radiology, İzmir, TURKEY.

Aim: In this study we aimed to assess the correlation between survival durations and SUVmax values, largest metastatic lesion size, and SUVmax tumor/background ratio in the liver on F-18 fluorodeoxyglucose (FDG) positron emission tomography (PET)/computerized tomography (CT) images of 22 patients with colorectal Ca diagnosis treated with Y-90 glass microsphere (terasphere) transarterial radioembolization (TARE) for liver metastasis at our center. **Method:** Twenty-two patients with mean age 66.1 (± 9.8) years underwent TARE treatment a total of 32 times (twice in 10 patients, once in 12 patients). On CT imaging before treatment, the sizes of metastatic foci in the liver were measured. They were classified as larger and smaller than 5 cm. SUVmax values were measured before treatment for liver metastasis. The obtained SUVmax values and background SUVmax measured in normal liver area were used to calculate the tumor/background ratio. Additionally, treatment response was evaluated according to the PET Response Criteria in Solid Tumors (PERCIST) criteria. The correlation between calculated quantitative values and survival duration was assessed with the Kaplan Meier method. **Results:** The mean size of lesions was 4.1 (1.3) cm, with mean SUVmax value of 9.7 (4.5). On F-18 FDG PET/CT images, the survival duration of patients with tumor/background ratio in the liver above 5 was 7.0 (1.6) months, while it was calculated as 20.5 (5.0) months in patients with this ratio below 5 (p=0.05). When investigated in terms of numbers of metastatic lesions in the liver on CT images before treatment, the survival duration of patients with 1 or 2 lesions was 41.0 (± 0.2) months, while for patients with multiple lesions it was 8.7 (± 1.2) months (p=0.02). For patients with largest lesion in the liver below 5 cm on CT images before treatment, survival was 16.1 (± 4.8) months, while for patients with lesions above 5 cm survival was 11.0 (± 2.1) months (p=0.9). When SUVmax values of liver metastasis measured on PET/CT images before and after treatment are assessed according to PERCIST criteria, patients with partial metabolic response survived 17.4 (± 4.2) months, while patients without partial metabolic response survived for 6.9 (± 0.7) months (p=0.3). **Conclusion:** It is considered that number of metastatic foci in the liver and tumor/background ratio may provide predictions related to survival before TARE treatment. Using these criteria in patient and treatment choice may contribute to patient management.

1505   **Tuesday, October 24, 2017, 16:30 - 18:00, Hall E2**

Joint Symposium 15 - EANM/ESMI: Best of European Molecular Imaging Meeting - EMIM 2017

OP-594

Simultaneous Imaging of Tumor Metabolism and Vascularity During Tumor Growth with a Hybrid Positron Emission Tomography (PET) / Ultrafast Sonography (US) System

A. Garofalakis; Paris-Cardiovascular Research Center; Paris Descartes University; Georges Pompidou European Hospital, Paris, FRANCE.

OP-595

Al18F-Labelling of Heat-Sensitive Biomolecules for Positron Emission Tomography Imaging

F. Cleeren; Laboratory for radiopharmacy, University of Leuven / Department of Pharmacy and Pharmacology, Leuven, BELGIUM.

OP-596

Purinergic Receptor P2Y12: A Potential Target for PET Imaging of Neuroinflammation in Multiple Sclerosis and EAE

W. Beaino; VU University Medical Center, Department of Radiology, Amsterdam, NETHERLANDS.

1506   **Tuesday, October 24, 2017, 16:30 - 18:00, Hall F1**

Teaching Session 6 (Interactive): Correlative Imaging for Nuclear Medicine Specialists: Interactive Live Radiology and Nuclear Medicine Quiz Using the Experior Medical System

OP-597

Correlative Imaging for Nuclear Medicine Specialists: Interactive Live Radiology and Nuclear Medicine Quiz Using the Experior Medical System

T. Lynch; Belfast, UNITED KINGDOM.

1507   **Tuesday, October 24, 2017, 16:30 - 18:00, Hall F2**

Clinical Oncology: In the Air & Beyond

OP-598

Prognostic impact of pre-treatment 18FDG-PET/CT restaging in patient with HNSCC

O. Delcroix[1], J. Leclère[2], P. Robin[1], S. Querellou[1], P. Le Roux[1], P. Salaun[1], C. Guezennec[1], U. Schick[3], G. Valette[2], J. Rousset[4], R. Abgral[1]; [1]Department of Nuclear Medicine, Brest University Hospital, BREST, FRANCE, [2]Department of Head and Neck Surgery, University Hospital of Brest, BREST, FRANCE, [3]Department of Radiotherapy, Brest University Hospital, BREST, FRANCE, [4]Department of Radiology, Military Hospital of Brest, BREST, FRANCE.

Introduction: Accurate initial staging of head and neck squamous cell carcinoma (HNSCC) is essential for appropriate treatment planning and outcome prediction. Several guidelines consider fluorodeoxyglucose positron emission tomography/ computed tomography (18FDG-PET/CT) as a valuable option to assess remote extension of locally advanced stage III/IV disease. This study evaluated the yield of 18FDG-PET/CT for each AJCC subgroup and the impact of 18FDG-PET/CT results on prognosis. **Subjects & Methods:** This study retrospectively included 477 patients (414M/63W; mean age 62.3 +/-9.7) with newly diagnosed HNSCC who underwent pre-treatment 18FDG-PET/CT from 2004 to April 2014. 18FDG-PET/CT staging (Stage$_{PET}$) was compared with those of conventional workups (CWU) alone

(Stage$_{CWU}$) comprising clinical examination, cervical contrast-enhanced computed tomography (CT) and/or contrast-enhanced MRI and chest CT. 18FDG-PET/CT findings were compared to histopathology when available. The prognostic impact was assessed with overall survival (OS) and progression-free survival (PFS). Tests of statistical significance were two-sided. **Results:** 18FDG-PET/CT changed the TNM (WHO classification) Stage$_{CWU}$ in 194 of 477 patients (40.7%; 95%CI = 36.3-45.1%). 18FDG-PET/CT modified nodal Stage$_{CWU}$ in 38.2% (95%CI = 33.8-42.5%) with an upstaging rate of 26.4% (95%CI = 22.5-30.4%) and a downstaging rate of 11.7% (95%CI = 8.8-14.6). Patients with 18FDG-PET/CT nodal upstaging had significantly worse 3-year OS (44.1% versus 55.9%, *P* =0.032) and PFS (30.8% versus 43.9%, *P*= 0.019) than patients with no Stage$_{CWU}$ changes. Among the 100 cases of nodal staging comparison with histopathology, 18FDG-PET/CT showed less misclassifications than CT or MRI (34 versus 40) but without statistical significacy (*P* =0.464).18FDG-PET/CT showed unsuspected distant metastases in 20 patients (4.2%; 95%CI = 2.4-6.0%). Among the 48 synchronous proven primary tumors, 35 were uncovered by 18FDG-PET/CT but not by CWU (7.3%; 95%CI = 5.0-9.7%). 18FDG-PET/CT modified TNM classification or discovered synchronous primary tumor in 16/59 (27.1%; 95%CI = 15.7-38.6%) stage I, 27/69 (39.1%; 95%CI = 27.5-50.7%) stage II and 47/76 (61.8%; 95%CI = 50.8-72.8%) stage III.Stage$_{CWU}$ I patients with 18FDG-PET/CT upstaging had significantly worse 3-year OS (50.0% versus 86.0%; *P*= 0.002) and PFS (43.8% versus 72.1%; *P*= 0.02) than other Stage$_{CWU}$ I patients. **Conclusion:** The yield of 18FDG-PET/CT appeared substantial in patients with a clinical stage I or higher HNSCC with a powerful prognostic stratification.

OP-599

Inter-observer and inter-contouring method variability for textural analysis in head and neck cancer in pre-therapeutic 18-FDG PET/CT

C. Guezennec, J. Corre, D. Bourhis, P. Robin, O. Delcroix, Y. Gobel, U. Schick, P. Salaün, R. Abgral; CHRU Morvan, Brest, FRANCE.

Aim: Characterizing tumor heterogeneity with texture indices extracted from 18F-fluorodeoxyglucose positron emission tomography (FDG-PET) is actually highly studied. Several series have showed promising results to predict survival in patients with head and neck squamous cell carcinoma (HNSCC), analyzing various tumor segmentation methods and texture indices. This preliminary study aimed at assessing the inter-observer and inter-contouring method variability when calculating different texture indices on HNSCC pre-therapeutic 18-FDG PET/CT. **Materials and Methods:** Consecutive patients with HNSCC referred in our department for a pre-treatment 18-FDG PET/CT (Biograph mCT, Siemens) from January to March 2016 were retrospectively included. Two nuclear medicine physicians independently segmented all tumors (VOI) using 3 different contouring methods: with a relative SUV threshold (40%SUVmax), a signal-to-noise adaptative SUV threshold (Daisne) and an image gradient-based method (PET EDGE™). Six usual texture indices (homogeneity, entropy, SRE, LRE, LGZE, HGZE) were calculated

using LIFEx software (www.lifexsoft.org). An intraclass correlation test was used to assess the inter-observer reproducibility, and a Pearson correlation test was used to compare texture indices measurements within the different contouring methods. **Results:** Forty-nine patients (mean age 63.8 +/- 9.4 yo) were analyzed. A too small segmented tumor VOI could not allow texture indices calculation by the software in 11, 16 and 6 cases using respectively 40%SUVmax, PET EDGE™ and Daisne contouring method. The inter-observer reproducibility analysis revealed an excellent agreement with an intraclass correlation coefficient higher than 0.97, 0.81, and 0.96 using respectively 40%SUVmax, PET-EDGE™ and Daisne method. For each texture index, a very strong correlation between results (Pearson correlation coefficient r > 0.89) was found regardless the segmentation method used, assessing a very good inter-contouring method reproducibility. **Conclusions:** This preliminary study showed an excellent agreement between observers for textural analysis of HNSCC in FDG-PET. The different methods used were also highly reproducible among themselves to measure usual texture indices.

OP-600

PET/CT imaging of angiogenesis in head and neck squamous cell carcinoma patients

D. Lobeek[1], S. Y. A. Terry[2], M. A. W. Merkx[1], R. P. Takes[1], P. J. Slootweg[1], W. J. G. Oyen[1,3], O. C. Boerman[1], M. Rijpkema[1]; [1]Radboud University Medical Center Nijmegen, Nijmegen, NETHERLANDS, [2]King's College London, London, UNITED KINGDOM, [3]Institute of Cancer Research, Royal Marsden NHS Trust, London, UNITED KINGDOM.

Introduction: One of the features of angiogenesis is the overexpression of integrins on the cell surface of endothelial cells. To study the process of angiogenesis, we have developed an $\alpha_v\beta_3$ integrin-targeting dimeric RGD peptide for PET/CT imaging: ^{68}Ga-DOTA-E-[c(RGDfK)]$_2$ (^{68}Ga-RGD$_2$). PET/CT imaging of $\alpha_v\beta_3$ integrins may be used to characterize tumours and predict and/or assess response of (anti-angiogenic) cancer therapies. The aim of the current study is to determine the feasibility and safety of ^{68}Ga-RGD$_2$ PET/CT imaging in head and neck squamous cell carcinomas (HNSCC) and to evaluate the optimal acquisition time for ^{68}Ga-RGD$_2$ PET/CT imaging. **Subjects & Methods:** Five patients with proven squamous cell carcinomas in the oral cavity were administered intravenously with ^{68}Ga-DOTA-E-[c(RGDfK)]$_2$ (70 µg) and subsequently underwent sequential whole body PET/CT imaging at 30, 60, and 90 minutes after injection. Tracer uptake in tumour lesions was quantified as peak Standardized Uptake Values (SUV$_{peak}$); tracer uptake in muscle tissue (trapezius muscle) and blood (aortic arch) was quantified as mean SUV (SUV$_{mean}$) within a spherical volume of interest. Safety analysis included clinical examination of vital signs and analysis of blood samples taken before, during and after radiotracer injection. Additionally, immunohistochemical analysis with the anti-$\alpha_v\beta_3$ monoclonal antibody LM609 on surgically removed tumour tissue was performed to assess $\alpha_v\beta_3$ integrin expression in tumour tissue. **Results:** After intravenous injection of ^{68}Ga-RGD$_2$ (mean activity 208.66 MBq/patient, range 201-217 MBq), tracer accumulation in the tumour was visible at all imaging time

points for all patients. No drug related adverse events or changes in kidney- or liver function were observed. Tumour SUV_{peak} of ^{68}Ga-RGD_2 at the three imaging time points were 5.2 ± 0.6, 5.1 ± 1.0, and 4.4 ± 0.9, respectively. Tumour-to-muscle (TMR) and tumour-to-blood (TBR) ratios at the three imaging time points were 9.0, 10.9, 11.0, and 4.9, 6.9, 8.2, respectively. Immunohistochemical analysis confirmed $\alpha_v\beta_3$ integrin expression on the tumour neovasculature. **Conclusion:** These preliminary results show that ^{68}Ga-RGD_2 PET/CT imaging of $\alpha_v\beta_3$ integrin expression in HNSCC patients is feasible. At this dose level, no toxicities or adverse events were observed. Whereas ^{68}Ga-RGD_2 uptake in tumour lesions was highest at 30 and 60 minutes post injection, TBR further increased over time. These findings support the hypothesis for an optimal acquisition time for ^{68}Ga-RGD_2 PET/CT at 60 minutes post injection.

OP-601

Voxel based comparison and texture analysis of ^{18}F-FDG and ^{18}F-FMISO PET of 38 Patients with head-and-neck cancer

M. Kroenke[1,2], K. Hirata[2], S. Watanabe[2], S. Okamoto[2], K. Magota[2], T. Shiga[2], Y. Kuge[3], N. Tamaki[2]; [1]Department of Nuclear Medicine, Klinikum rechts der Isar, Technical University Munich, München, GERMANY, [2]Department of Nuclear Medicine, Graduate School of Medicine of Hokkaido University, Sapporo, JAPAN, [3]Central Institute of Isotope Science, of Hokkaido University, Sapporo, JAPAN.

Introduction: ^{18}F-FMISO (FMISO) is a common tracer to assess tumour hypoxia but it is far less common than ^{18}F-FDG (FDG) in the evaluation of tumours in general. Hypoxia is an important factor for treatment as it can lead to increased radiation resistance and is an independent prognostic marker for outcome. Therefore, we try to predict hypoxia from FDG PET with new techniques of voxel based analysis and texture analysis. **Methods:** Thirty-eight patients with head-and-neck cancer underwent consecutive FDG and FMISO PET scans before any treatments. ROIs enclosing the primary tumour were compared in a voxel-by-voxel manner between FDG and FMISO PET. Tumour hypoxia was defined as the volume with a tumour-to-muscle ratio > 1.25 in the FMISO PET and hyper-metabolism was defined as 50 % SUVmax in the FDG PET. The concordance rate was defined as percentage of voxels within the tumour which were both hypermetabolic and hypoxic. Texture analysis was performed by calculating 38 different parameters on all ROIs and correlated. **Results:** A moderate correlation between FDG and FMISO uptake was found by a voxel-by-voxel comparison (r=0.664, p<0.001). The mean concordance rate was 27 %, ranging from 0 to 74 %. The hypoxic tumour regions showed a twice fold increased FDG uptake compared to the non-hypoxic tumour regions (SUVmean 10.9 vs. 5.4; p<0.001). The maximum of the significant correlation coefficients between texture analysis parameters of FDG PET and tumour hypoxia was 0.524. **Conclusion:** FDG uptake was higher in hypoxic tumour regions than in non-hypoxic regions. Moderate correlations between FDG and FMISO PET were found by voxel-based analysis. However, it may be difficult to predict tumour hypoxia even with the help of texture analysis.

OP-602

Role of FDG-PET in disclosing RECIST-based pseudoprogression in non-small cell lung cancer (NSCLC) patients treated with Nivolumab

M. Bauckneht, G. Rossi, R. Piva, C. Genova, E. Rijavec, G. Barletta, F. Biello, V. Ceriani, I. Calamia, G. Dal Bello, R. Di Stefano, G. Sambuceti, F. Grossi, S. Morbelli; IRCCS AUO San Martino IST, Genova, ITALY.

Background: Anti-cancer immune reaction provided by immune check-point inhibitors (ICPIs) might initially increase total tumor burden due to inflammation and may be confused with progressive disease (PD), hampering dimensional response evaluation based on RECIST criteria. The aim of the study is to explore the potential role of FDG-PET to provide an early prognostic stratification at first response in patients classified as RECIST-PD after Nivolumab administration for NSCLC. **Methods:** 55 patients with advanced NSCLC were treated with Nivolumab (4 mg/Kg every 14 days) within a single-institutional research trial. First-response after four cycles of Nivolumab was assessed by means contrast-enhanced CT and FDG-PET. CT scans were evaluated by means of RECIST criteria. In patients classified as RECIST-PD, metabolic response was evaluated either by means of PERCIST criteria or by computing the percentage of reduction of Metabolic Tumor Volume (MTV) and Total Lesion Glycolysis (TLG). Kaplan-Meier analysis estimated the overall survival (OS) according to the different outcomes PERCIST, MTV and TLG response groups after a follow-up of 20 months. **Results:** As expected RECIST criteria were rather insensitive in the evaluation of response to Nivolumab. In fact, 28/55 patients were classified as RECIST-PD at first response (21 male, 7 female; mean age 69±2.3 years). Conversely, among PD-RECIST, at first metabolic response 14, 24 and 22 patients were classified as PD, while 2, 4 and 6 patients were classified as in partial response according to PERCIST, MTV and TLG, respectively. The stratification according to PERCIST and TGL was able to identify a subgroup of patients with longer OS. In fact, after one year, 50% of PERCIST and 60% of TLG responders were still alive. The prognostic relevance of PERCIST response was still evident after 20 months of follow-up while at one year TLG responders and non-responders curves significantly approached each other. By contrast, percentage of variation in MTV was not able to discriminate pseudoprogression in the whole group of RECIST-PD. Similarly, patients classified as PERCIST stable disease showed an OS overlapping PD PERCIST. **Conclusion**: Metabolic response according to PERCIST and TLG seems to early identify a subgroup of RECIST-PD with a better prognosis. PERCIST predicted patients' survival as long as 20 months after therapy initiation, while TLG was able to identify a larger number of RECIST pseudoprogressions losing its prognostic power one year after therapy. Metabolic response based on either PERCIST or TLG may improve the therapeutic decision-making in NSCLC patients treated with Nivolumab.

OP-603

Heterogeneity in tumours; Validating the use of textural analysis and shape analysis on 18F-FDG PET/CT scans of lung cancer patients as a prognostic tool. Preliminary analysis

M. M. K. Krarup[1], L. Nygård[1], I. Vogelius[1], M. M. Siddique[2], G. Cook[3], V. Goh[2], F. L. Andersen[1], B. M. Fischer[1]; [1]University Hospital of Copenhagen, Rigshospitalet, Copenhagen, DENMARK, [2]St. thomas', Guy's Hospital/King's College, London, UNITED KINGDOM, [3]St. Thomas', Guy's Hospital/King's College, London, UNITED KINGDOM.

Aim: The purpose of this study is to validate selected textural features (TF) and shape features in a cohort of Non Small Cell Lung Cancer (NSCLC) patients. We will evaluate TF and shape features from 18F FDG PET/CT-scans as predictors of progression free survival (PFS) in combination UICC stage, histology and Gross Tumor Volume (GTV) measured for radiotherapy. With this study we wish to determine robust data, which can support texture and shape analysis as a clinical tool. **Materials and Methods:** TF and shape features previously reported to be diagnostic, prognostic and reproducible were chosen for the textural analysis (TA). 18F FDG PET/CT scans performed for radiotherapy planning in NSCLC patients were retrospectively retrieved. An isocontour corresponding to 40% of SUVmax was drawn semi-automatically on PET images, encompassing the primary tumour. TA was performed on Feature Analysis Software Tool (FAST) to evaluate TF and shape features on PET and CT images. The features were compared with PFS by a univariate cox regression analysis. Subsequently, Spearman Rank Test was done to evaluate correlation with GTV and other TF or shape features. Significant features from the univariate analysis with minimum correlation index were chosen for inclusion in a multivariate cox regression analysis as added value to a baseline model including histology, clinical stage and GTV. The baseline model were compared with the baseline model+ TF or shape feature using cross validation (100 Bootstrap samples) with AUC as the performance metric. **Results:** TA was performed on scans from 173 patients (105 males, 68 females, mean age: 66) with clinical stage II-IV, and histology being adenocarcinoma, squamous cell, and other. Mean GTV was 115 cm^3 (SD 112 cm^3). The univariate cox regression analysis showed the following features to be significant in predicting PFS: First Order Entropy (p=0,017), Difference Entropy (p=0,006) and Grey Level Non Uniformity (GLNU) (p=0,035) from CT-images. After testing for correlation using the spearman rank test, First Order Entropy and GLNU were chosen for inclusion in the multivariate analysis. First order entropy from CT images was independently significant (p=0,018) in the subsequent multivariate cox regression analysis with the baseline model. **Conclusion:** First order entropy from CT-images shows independently significant association with PFS in the multivariate cox regression analysis including UICC stage, histology and GTV. No TF or shape features derived from PET data were independent predictors.

OP-604

Segmental FDG-PET/CT In Solitary Pulmonary Nodule: Preliminary Data Of The PET Italian Tailored Assessment of Lung Indeterminate Accidental Nodule (ITALIAN) Trial

M. Spadafora[1], L. Mansi[2], A. Cuocolo[3], L. Evangelista[4], V. Rizzo[1], L. Guerra[5], S. Fanti[6], E. Nicolai[7], A. Chiti[8], M. Zuffante[9], O. Schillaci[10], G. Peluso[11], S. Annunziata[12], A. Fracchetti[13], D. Ripani[12], C. Gridelli[14], P.

Miletto[7], L. Pace[15]; [1,2]Nuclear Medicine Unit, Department of Imaging, S.G. Moscati Hospital, Avellino, ITALY, [2]Dipartimento Medico-Chirurgico di Internistica Clinica e Sperimentale, Second University of Naples, Napoli, ITALY, [3]Department of Advanced Biomedical Sciences, University of Naples Federico II, Napoli, ITALY, [4]Nuclear Medicine and Molecular Imaging Unit., Veneto Institute of Oncology IOV - IRCCS, Padova, ITALY, [5]Nuclear Medicine Unit, San Gerardo Hospital, University of Milano Bicocca, Monza, ITALY, [6]Service of Nuclear Medicine, Policlinico S. Orsola Malpighi, University of Bologna, Bologna, ITALY, [7]Nuclear Medicine Unit, Department of Imaging, SDN Foundation, Napoli, ITALY, [8]Nuclear Medicine Unit, Cancer Center, Humanitas Hospital, Rozzano, Milano, ITALY, [9]Nuclear Medicine Unit, Department of Imaging, Azienda Ospedaliera Universitaria Integrata di Verona, Verona, ITALY, [10]Department of Biomedicine and Prevention, University of Rome Tor Vergata, Roma, ITALY, [11]Nuclear Medicine Unit, Department of Imaging, Medicina Futura IOS, Acerra, Napoli, ITALY, [12]Institute of Nuclear Medicine, Università Cattolica del S. Cuore, Roma, ITALY, [13]Department of Medical Physics, Hospital of Bolzano, Bolzano, ITALY, [14]Division of Medical Oncology, S. G. Moscati Hospital, Avellino, ITALY, [15]Department of Medicine and Surgery, University of Salerno, Baronissi (SA), ITALY.

Aim: The ITALIANtrial sought to compare the diagnostic information by segmental PET/CT(s-PET/CT)with wb-PET/CT and to estimate dosimetric and temporal impacts of segmental imaging. **Methods:** Between 2014 and 2016, we retrospectively selected 314 consecutive patients(age 67years) investigated by FDG-PET/CT for SPN characterization. Patients in staging and those with prior cancer history were excluded. Patients were stratified according to clinical and instrumental pre-test and post-test probability of malignancy. SPN FDG uptake was semi-quantitatively assessed by a 4-point scoring system(from 1=absent to 4=intense). Significant predictors of extra-thoracic metastases were assessed by logistic univariate and multivariate analyses. **Results:** A total of 331 pulmonary nodules(average diameter of 16±7 mm)were found. Based on histological and followup data, there were 36.5% malignant, 36.5% benign and 27% indeterminate pulmonary nodules. Pre and post-test malignancy prediction risks were 27±24% and 41±39%, respectively. SPN FDG uptake was from 1 to 4 point in 28%, 26%, 10% and 36%, respectively. Among all patients, 15 (5%) had an extra-thoracic FDG uptake suspected for cancer. However, only in 7/15 patients, the extra-thoracic activity was suspicious for metastatic lesions from pulmonary nodule. CT dose length product was 573±385, with an estimate of the effective dose of 8.6±5.7 mSv. FDG dose was 277±70 mBq(4.4±1.1 mSv). At multivariate analysis, SPN FDG activity, emphysema, post-test probability of malignancy and thoracic cancer sites, were independent predictors of extra-thoracic metastases(all p<0.001). The number of beds for wb-PET/CT was 6.6±1, while those to cover the chest was 2.4±0.7, with a 2.75 ratio. Compared to wb-PET/CT, s-PET/CT with a standard FDG dose saved 6 min and 3 sec for scan. Moreover, segmental scan saved about 36% of the standard FDG dose (100 vs. 277 mBq). Mean effective dose was 13 mSv for wb-PET/CT and 4.7 mSv for s-PET/CT. **Conclusions:** The preliminary results of this

multicentre trial show that it is conceivable to perform s-PET/TC in patients with SPN. This imaging approach reduces the effective dose and associated risk of cancer. Failure to identify extra-thoracic lesions seems to be negligible in patients without intense FDG uptake of SPN, emphysema and thoracic metastasis. Thus, in selected populations segmental imaging might improve cost-effectiveness.

OP-605

Quantitative 99mTc-Galacto-RGD2 SPECT/CT to Evaluate Lung Cancer Physiology and Malignancy: A Comparative Multi-center Study with 18F-FDG PET/CT

T. Wang[1], Y. Liang[2], G. Zhang[1], M. Li[3], W. Fang[4], H. Dai[5], B. He[6], X. Wang[1]; [1]The Affiliated Hospital of Inner Mongolia Medical University, Hohhot, CHINA, [2]Navy General Hospital, Beijing, CHINA, [3]First Hospital of Shanxi Medical University, Taiyuan, CHINA, [4]Fuwai Hospital, Beijing, CHINA, [5]Dianli Hospital, Beijing, CHINA, [6]University of Missouri-Columbia, Columbia, MO, UNITED STATES OF AMERICA.

Objectives: 99mTc-Galacto-RGD2 (RGD) has been reported as a feasible tracer to assess tumor angiogenesis and metastasis, but limited to quantitatively evaluate tumor physiology and malignancy by only conventional SPECT/CT imaging. We aim to quantify integrin-$\alpha v \beta 3$ expression in lung tumors with quantitative RGD SPECT and compare physiological parameters with glucose metabolism by FDG PET. **Methods:** Twenty-eight biopsy-confirmed patients with non-small cell lung cancer were enrolled to receive both RGD SPECT/CT and FDG PET/CT scans at three medical centers in China. RGD SPECT images were reconstructed with full physical corrections (attenuation, scatter, collimator blur and noise) while PET images were processed according to the clinical routine. All SPECT, SPECT/CT and PET/CT cameras were pre-qualified to enter the study and cross calibrated imaging factors to measure radionuclide concentration in (Bq/ml). Localization of tumors in lung regions was performed by SPECT-CT and PET-CT image fusion. RGD and FDG SUVmax, SUVmean and metabolic volume (MTV, threshold≥45% SUVmax) were measured and compared to assess the malignancy of lung tumors. **Results:** When measuring Tc99m and F18 radionuclide concentration in cylindrical phantom, all SPECT, SPECT/CT and PET/CT cameras were able to achieve >97% accuracy. Total number of lung tumors (41 vs 43), SUVmax (7.74±3.38 vs 8.81±2.91), SUV mean (3.67±1.23 vs 4.46±1.38) found by RGD SPECT and FDG PET were comparable. Among matched tumors (n=38), linear correlation of RGD and FDG SUVmax was strong (y=0.49x, R=0.78) while correlations for SUVmean and MTV were moderate (SUVmean: y=0.38x, R=0.67; MTV: y=0.97x, R=0.28) (All p<0.0001). Increased RGD SUVmax highly corresponded with increased FDG SUVmax to indicate elevated tumor malignancy. **Conclusions:** Quantitative 99mTc-Galacto-RGD2 SPECT/CT with full physical corrections is a feasible approach to measure tumor integrin-$\alpha v \beta 3$ expression. It can provide another insight to quantitatively assess tumor physiology and malignancy beside FDG PET/CT scan.

1508　　　　　　**Tuesday, October 24, 2017, 16:30 - 18:00, Hall K**

Cardiovascular System: Myocardial Perfusion SPECT: Quantification & Artificial Intelligence

OP-606

Evaluating stress and rest absolute quantification of uptake in myocardial perfusion SPECT using GE Q.Metrix

I. Armstrong, N. Fyfe, P. Arumugam; Central Manchester University Hospitals, Manchester, UNITED KINGDOM.

Aims: Measurement of absolute myocardial blood flow (MBF) and coronary flow reserve (CFR) using PET is now a clinical tool that potentially overcomes some of the pitfalls of relative perfusion assessment. MBF measurement with myocardial perfusion SPECT (MPS) is technically challenging. It has been suggested that differences in absolute tracer uptake for stress-rest MPS may be a surrogate for CFR. We believe this is the first report to evaluate absolute uptake differences between stress and rest in clinical MPS studies. **Method:** Static stress and rest MPS data from 65 patients (39 male; median [inter-quartile range (IQR)] weight: 77.5kg [64.3-91.3kg]; median [IQR] BMI: 27.6kg/m^2 [25.3-32.3kg/m^2]) were included. Patients were administered tetrofosmin activity according to a sliding BMI-based protocol, and scanned at a median [IQR] time of 66 [52-77] minutes post-injection. All data were acquired on a GE Optima 640 with LEHR collimators, 180-degree orbit, 6.8mm pixels and 30-seconds/projection. Reconstruction of attenuation and scatter corrected images was performed using GE Q.Metrix as per vendor-defined parameters of 4 iterations, 10 subsets and no post-filter. SUV was calculated in the entire left ventricle (LV) of the myocardium and normalised to body weight. SUV$_{max}$ and SUV$_{mean}$ were calculated with the latter using a 25% threshold of the maximum voxel. **Results:** The median [IQR] LV SUV$_{max}$ and SUV$_{mean}$ for stress images were 10.6 [9.1-13.4] and 4.3 [3.7-5.1] respectively and for the rest images they were 11.1 [8.7-12.5] and 4.2 [3.6-4.8]. The median [IQR] in absolute LV SUV$_{max}$ and SUV$_{mean}$ difference for stress, relative to rest, was +0.4 [-1.0 to +1.9] and +0.3 [-0.3 to +0.7] respectively. The median [IQR] in relative LV SUV$_{max}$ and SUV$_{mean}$ difference for stress, relative to rest, was +4.6% [-10.9% to +18.0%] and +5.9% [-8.2% to +18.4%] respectively. Differences between stress and rest across the entire group were not significant however, for the 38 cases reported as normal, the SUV$_{mean}$ was significantly greater in the stress images compared with the rest (P<0.05) with a median [IQR] relative change of +9.1% [-7.8% to +19.4%]. **Conclusion:** These initial data suggest absolute SUV quantification in MPS shows promise and may aid reporter confidence for normal cases, with follow-up required to support findings. Q.Metrix is not a cardiac package and so results from SUV polar maps may be useful. Work is on-going to develop techniques to calculate regional SUV polar maps for MPS and evaluate the impact of alternative reconstruction parameters.

OP-607

Dynamic Single Photon Emission Computer Tomography in assessment of Coronary Flow Reserve in Patients with stable coronary artery diseases

A. Mochula[1], K. Zavadovsky[1,2], S. Andreev[1], Y. Lishmanov[2,1]; [1]Cardiology Research Institute, Tomsk NRMC, Tomsk, RUSSIAN FEDERATION, [2]National Research Tomsk Polytechnic University, Tomsk, RUSSIAN FEDERATION.

Purpose: To assess the coronary flow reserve in patients with one, two and multi-vessel coronary artery diseases by dynamic SPECT using semiconductor (cadmium-zinc-telluride)-based gamma camera. **Material and Methods:** This work included forty four patients with stable coronary artery diseases. The first group included patients with multi-vessel coronary artery diseases (MVCAD) (22 males and 8 females; mean age 60,1±4,3 years) with a lesion >70% in at least 2 major epicardial vessels according to invasive coronary angiography. Second group consisted of patients with single and two-vessel coronary artery disease (STCAD) (8 males and 6 females; mean age 61,5±3,8 years) with intermediate (40-70%) and significant (>70%) coronary artery stenosis. All patients underwent rest-stress dynamic SPECT as well as conventional myocardial perfusion imaging with 99mTc-MIBI as a radiopharmaceutical. Dynamic SPECT acquisition protocol was as follows: (1) rest radiopharmaceutical injection (volume 1 mL; dose 185 MBq); 5-min list-mode acquisition; (2) stress radiopharmaceutical injection (volume 1ml; dose 740 MBq) followed by two-minute adenosine infusion (160 mcg/kg/min); then additional two-minute adenosine infusion (160 mcg/k/min). All scintigraphic images were acquired on the hybrid SPECT/CT unit (GE Discovery NM/CT 570C). Using specialized software (4DM Reserve), we estimated the following indicators: summed stress score (SSS), coronary flow reserve for the heart as a whole (gCFR) as well as for the three coronary artery territories (LAD, LCx, RCA) - regional coronary flow reserve (rCFR). Patient with STCAD underwent invasive FFR detection. **Results:** The average value of the gCFR index was lower in a MVCAD group 1.28 (1,01;1.52) than in patient with STCAD 1.67 (1.36;2.13); p<0.05. However, in these groups there was no difference in the SSS values. Regional coronary flow reserve indexes did not differ significantly in patients with MVCAD and STCAD. ROC analysis showed that the gMFR ≤ 1,42 allows to identify MVCAD with a sensitivity and specificity 68% and 86,4%, respectively. In the second group we founded a strong correlation between the rCFR and FFR (r=0.76, p<0.05). **Conclusion:** Dynamic myocardial rest-stress SPECT using semiconductor (cadmium-zinc-telluride)-based gamma camera allows to determine low coronary flow reserve and identify MVCAD with sensitivity and specificity 68% and 86,4%, respectively. There is good relationship between rCFR and invasive FFR. It will allow to assess the hemodynamic significance of coronary artery stenosis by using dynamic SPECT. The study was supported by a grant from the Russian Science Foundation (№14-15-00178).

OP-608

One-day protocol for myocardial perfusion stress-testing by combination of Rutland-Patlak analysis of 99mTc-MIBI uptake and adenosine challenge

W. Y. Ussov[1], V. M. Gulyaev[1], E. N. Karpov[2], O. Y. Borodin[1,2], E. A. Aleksandrova[1]; [1]Institute of Cardiology, Tomsk, RUSSIAN FEDERATION, [2]Tomsk Regional Institute of Oncology, Tomsk, RUSSIAN FEDERATION.

Purpose: Currently the myocardial blood flow stress-testing with 99mTc-MIBI SPECT is being carried out with two-days protocol or employs splitting of dose. We attepted to design a protocol of myocardial blood flow (MBF) rest/stress 99mTc-MIBI SPECT imaging as single study. **Subjects and Methods:** The theory of the methods was based on assumption of unidirectional transport of 99mTc-MIBI to the myocardium for early minutes after injection. As the dynamic uptake of 99mTc-MIBI to myocardium is subjected to equation $(dC_{myoc}/dt) = EF*MBF*C_{blood}$, where C-concentration in myocardium and inflowing blood, EF - extraction fraction and the MBF - myocardial blood flow, the MBF can be obtained from running slope of plot drawn in coordinates (dC_{myoc}/dt) as ordinate and C_{blood} as abscissa, corrected for EF. Then the pharmacologic stress-test can be carried out without interruption of study, and quantified as rise in plot slope value. The technique was tested in 15 patients with stenosis of two or more coronary arteries for > 60% and previous myocardial infarction. The 99mTc-MIBI was infused intravenously slowly as 65 -74 Mbq/min for up to 12 min, with acquisition of whole-chest set of 7-10 mm slices every 20 sec, using dual-head SPECT-CT scanner, with subsequent CT coronary angiography. The calculation of MBF has been carried out as described, with simultaneous acquisition of C_{blood} from left ventricle (LV) cavity and C_{myoc} from 16 segments of the LV myocardium. In everybody the adenosine test was performed at 6 min of protocol as 2 min long infusion of 140 mkg/kgBW/min. Myocardial blood flow reserve was quantified as ratio $\{MBF_{stress} / MBF_{\text{brest}}\}$. **Results:** The average myocardial blood flow at rest was obtained as high as 68 +- 7 ml/min/100 g. Perfusion reserve in stenosis - dependent regiones of myocardium was as low as 1.10 - 1.45, whereas in normal ones as big as 1.75 - 2.90. In two patients all of whom have had transmural myocardial infarction adenosin test induced extensive deterioration of myocardial blood flow concomitantly with drop of mean arterial pressure for 15 - 25 mm Hg. Plaques with micro haemorrhages were concomitant with perfusion reserve below 1,28 in everyone and thus can be reported as of high risk in every case. **Conclusion**: Quantitative dynamic 99mTc-MIBI SPECT study combined with CT coronarography provides adequate quantification of myocardial blood flow in absolute units at pharmacologic stress-tests and reveals the clinic and haemodynamic significance of the coronary stenoses.

OP-609

Modelling Factors Affecting Apparent Transmural Flow Gradient in Ungated Tomographic Myocardial Perfusion Imaging

A. Bellini[1], C. Marini[2], F. Ticconi[1], S. D. Morbelli[3], M. Bauckneht[1], F. Fiz[4], I. Calamia[1], A. Nieri[1], S. Maggio[3], G. Sambuceti[1,3]; [1]Nuclear Medicine Unit, Department of Health Sciences, University of Genoa, Genoa, ITALY, [2]CNR Institute of Bioimages and Molecular Physiology, Milan, ITALY, [3]IRCCS AOU San Martino-IST, Genoa, ITALY, [4]Nuclear Medicine Unit, Department of Radiology, Uni-Klinikum Tübingen, Tübingen, GERMANY.

Purpose: Coronary physiology implies a greater vulnerability to ischemia for inner layers of the left ventricular (LV) myocardium. Despite a number of possible approaches to describe transmural flow gradient with nuclear methods, the need for relatively long acquisition time inevitably hampers this task due to the blurring effects caused by the cyclic modification of LV shape, volume and thickness during cardiac contraction. In the present study, we used a mathematical 3D model to test the theoretical implications of heart rate and LV function on estimated transmural flow gradient. **Subjects and Methods:** The LV mathematical model was created in MATLAB with the following assumptions: parabolic shape of external and internal wall and incompressible myocardium without any transmural gradient in blood flow. LV volume curve was modeled as a function of heart rate as previously described to account for the relative increase in diastolic phase duration under bradycardia. The partial volume effect was also taken into account by considering a progressive increase in regional counting rates up to its maximum with end-systole/end-diastole recovery coefficient ratio at 1.2. Heartbeat was divided in 8 frames and a representative short-axis view of LV myocardium was considered. Thereafter, all simulated frames were overlapped into one single image to estimate the sub-endocardial/sub-epicardial flow ratio. The model was tested at different heart rates (from 45 to 120 bpm) and different ejection fractions (from 35% to 55%). **Results:** Ungated image correctly reported a homogeneous transmural flow distribution only in the presence of a normal LV function and for heart rate approaching 90 bpm. However sub-endocardial/sub-epicardial radioactivity ratio progressively increased as a direct function of heart rate from a minimum 0.74 at 45 bpm up to its maximum of 1.38 at a heart rate of 120 bpm. This direct dependence of transmural radioactivity measurements on heart rate was further enhanced by the presence of LV dysfunction whose association with bradycardia decreased sub-endocardial/sub-epicardial radioactivity ratio down to 0.38. **Conclusion:** Our mathematical model shows that cardiac contraction profoundly affects the apparent transmural distribution of radioactivity in the LV wall when ungated images are analyzed. This effect is dependent upon the effect of heart rate on the shape of LV-volume curve during cardiac cycle and is further enhanced by the presence of contractile impairment. These data suggest the need for caution in interpreting transmural flow distribution in static images and indicate a potential relevance for ECG gated acquisition to approach this issue.

OP-610

Simulation of Patient Motion with Myocardial Perfusion CZT SPECT: Data-Driven Motion Detection and Correction

D. Daou[1,2], R. Sabbah[3], Y. Alattar[1], C. Coaguila[4], H. Boulahdour[3,5]; [1]Cochin Hospital, APHP, PARIS, FRANCE, [2]EA 7334 REMES, Université Paris-Diderot, Sorbonne Paris-Cité, Paris, FRANCE, [3]CHU Jean Minjoz, Besançon, FRANCE, [4]Centre Hospitalier de Bigorre, Tarbes, FRANCE, [5]EA 4662, Université de Franche-Comté, Besançon, FRANCE.

Aim: We previously reported the feasibility and impact on myocardial perfusion imaging (MPI) of a data-driven respiratory-motion (RM) correction method (REGAT, REspiratory GATing) applicable to CZT SPECT. In this study, we aimed to evaluate the use of REGAT for the detection and correction of simulated patient motion using MPI CZT SPECT. Materials and Methods: We used an acquired patient MPI CZT SPECT study (DNM 530c) and simulated patient motion in the X, Y and Z axis by generating dynamic studies consisting each of a combination of 16 CZT SPECT studies shifted linearly using different magnitudes. These magnitudes were (pixel size at acquisition=2.46 mm): X0Y0Z6 (maximal motion=6 pixels in +Z direction); X0Y0Z-6 (6 pixels in -Z direction); X0Y6Z0 (6 pixels in +Y direction); X0Y-6Z0 (6 pixels in -Y direction); X6Y0Z0 (6 pixels in +X direction); X-6Y0Z0 (6 pixels in -X direction); X4.5Y6Z0 (4.5 pixels in +X direction and 6 pixels in +Y direction); X-4.5Y0Z3 (4.5 pixels in -X direction and 3 pixels in +Z direction); X4.5Y0Z3 (4.5 pixels in +X direction and 3 pixels in +Z direction); X4.5Y0Z-3 (4.5 pixels in +X direction and 3 pixels in -Z direction); X4.5Y0Z3 (4.5 pixels in +X direction and 3 pixels in +Z direction); X0Y6Z-3 (6 pixels in +Y direction and 3 pixels in -Z direction); and X0Y6Z3 (6 pixels in +Y direction and 3 pixels in +Z direction). All simulated dynamic SPECT acquisitions were processed with REGAT. Briefly, REGAT generates motion curves, allows the generation of patient's motion GSPECT studies based on amplitude of curves, realigns studies and provides cardiac motion magnitudes in the patient's X, Y, and Z axis. Results: Cardiac motion magnitude detected by REGAT were -1.1 / -0.5 / 4.8 pixels for X0Y0Z6; +1.0 / +0.3 / -4.6 pixels for X0Y0Z-6; +0.1 / +5.7 / -0.1 pixels for X0Y6Z0; -0.1 / -5.8 / -0.1 pixels for X0Y-6Z0; -4.5 / -0.1 / -0.7 pixels for X6Y0Z0; +5.5 / +0.2 / -0.6 pixels for X-6Y0Z0; -3.9 / +6.4 / +0.2 pixels for X4.5Y6Z0; -3.8 / -0.3 / +1.7 pixels for X-4.5Y0Z3; +2.8 / -0.1 / +2.9 pixels for X4.5Y0Z3; +3.8 / +0.3 / -2.2 pixels for X4.5Y0Z-3; -0.7 / -6.0 / -2.4 pixels for X0Y6Z-3; and -0.4 / +5.5 / +2.3 pixels for X0Y6Z3 in respectively the X, Y and Z axis. Conclusion: Data-driven motion detection with REGAT is feasible. The detected motion magnitude is well concordant with the simulated motion magnitude.

OP-611

Artificial Intelligence for Myocardial Perfusion Imaging Compared with Expert Interpretation

K. Nakajima[1], K. Kiso[2], T. Kudo[3], Y. Taniguchi[4], S. Matsuo[1], M. Nakagawa[5], T. Nakata[6], S. Hida[7], H. Tanaka[8], M. Sarai[9], K. Yokoyama[10], M. Momose[11], K. Okuda[12], L. Edenbrandt[13]; [1]Kanazawa University Hospital, Kanazawa, JAPAN, [2]National Cerebral and Cardiovascular Center, Osaka, JAPAN, [3]Nagasaki University, Nagasaki, JAPAN, [4]Hyogo Brain and Heart Center, Himeji, JAPAN, [5]Akita City Hospital, Akita, JAPAN, [6]Hakodate Goryoukaku Hospital, Hakodate, JAPAN, [7]Tokyo Medical University Hospital, Tokyo, JAPAN, [8]Tokyo Medical University Ibaraki Medical Center, Ibaraki, JAPAN, [9]Fujita Health University Hospital, Toyoake, JAPAN, [10]Public Central Hospital of Matto Ishikawa, Hakusan, JAPAN, [11]Tokyo Women's Medical University, Tokyo, JAPAN, [12]Kanazawa Medical University, Uchinada, JAPAN, [13]University of Gothenburg, Gothenburg, SWEDEN.

Aim: While application of artificial neural network (ANN) for the diagnosis of coronary artery disease (CAD) has been in-

vestigated, the diagnostic accuracy depends on how the ANN system learns expert interpretation. The purpose of this study was to create a new computer-aided diagnostic system with multicenter collaborations and to validate its diagnostic accuracy compared with nuclear cardiology expert interpretation. **Methods:** Twelve hospitals collaborated in accumulating training data for the ANN regarding presence or absence of ischemia and/or stress defects in gated stress-rest Tc-99m MIBI studies from 1,001 patients. First, an automated algorithm for detection and delineation of potential areas of ischemia or stress defects was applied. Second, an ANN was trained to classify these areas as true/false abnormality based on expert interpretations by six nuclear cardiology experts in the core center. Finally appropriate diagnostic features were adjusted for final ANN systems to provide optimal diagnostic accuracy. For the validation study, a new database consisting of 364 patients from multiple centers was used, and diagnostic accuracy of the ANN system was compared with the expert interpretation, which was used as a gold standard of abnormality. Conventional summed stress/rest/difference scores (SSS/SRS/SDS) were automatically calculated and used for comparison. Receiver-operating characteristic (ROC) was performed with area under the curve (AUC) calculation. **Results:** The training databases included ischemia and stress defect in 59% and 71% of patients, respectively. The ROC AUC for the training database was 0.91 with sensitivity/specificity of 86%/77%. The validation dataset included stress defect in 59% and ischemia in 73%, and multi-vessel disease in 40% of the patients. To identify abnormal perfusion during stress, ROC AUC of SSS was 0.82, while ANN provided better AUC (0.92, p<0.0001). Regarding stress-induced ischemia, ROC AUC of SDS was 0.75, and ANN provided significantly higher AUC (0.90, p<0.0001). ROC AUC with old myocardial infarction was 0.97 using rest-defect ANN, which was better than SRS (AUC 0.91, p=0.006). ROC AUC with and without history of revascularization using stress defect was 0.94 and 0.90, respectively, which was again better than SSS (p=0.006 and <0.0001, respectively). When the score and the probability of abnormality were compared, the SSS/SRS/SDS increased steeply when probability of abnormality was >0.80. **Conclusion:** The ANN system developed by the multicenter project showed high diagnostic accuracy in various clinical settings including history of myocardial infarction, coronary revascularization and multi-vessel diseases and could be used to assist diagnosis in patients suspected of having coronary artery disease.

OP-612

Diagnostic Performance of Artificial Neural Network for the localization of coronary artery disease

H. Shimoyama, S. Nakayama, Y. Kotake, S. Shimamoto, R. Futai; Itami City Hospital, Itami, JAPAN.

Aim: The purpose of this study was to evaluate segmental analysis of stress 99mTc-Sestamibi scintigraphy for the diagnosis and localization of coronary artery disease (CAD) using an artificial neural network (ANN) **Materials and Methods:** A total of

51 patients with CAD were studied with myocardial perfusion imaging(MPI) and coronary computed tomography angiography(CCTA). Automatic processing was carried out using ANN to obtain area of ischemia and Summed stress score (SSS) values based on the 17-segment model in the left anterior descending artery (LAD), left circumflex coronary artery (LCX) and right coronary artery (RCA) lesion. SSS more than 10% is defined ischemia. CCTA stenosis more than 50% is defined significant. We compared the coronary arterial territories diagnosis of SSS with that of ANN using CCTA as a standard of reference. **Results:** In LAD lesion, ANN showed a lower specificity than its SSS values (73vs 92%, p=0.062). In RCA lesion, ANN showed a higher specificity than its SSS values (86vs 83%, P=1.00). But difference between ANN and SSS in sensitivity and specificity for myocardial ischemia of LAD, LCX and RCA area were not significant. **Conclusion:** Although the coronary artery localization diagnosis of ANN was similar to that of SSS, ANN showed higher specificity than SSS in RCA and lower one in LAD lesion. Using ANN may contribute to lower false positive diagnosis rate in inferior ischemia patients with soft tissue attenuation artifacts, but not in LAD lesion.

| 1510 | Tuesday, October 24, 2017, 16:30 - 18:00, Hall G2 |

Do.MoRe - Featured: PET/MRI

OP-613

PET/MRI-Technology – State of the Art Systems and Future Perspectives

S. Nekolla; Clinic of Nuclear Medicine, Technical University, Munich, GERMANY.

OP-614

Methods for reducing 'halo' scatter artefact in Ga-68 PSMA PET/CT and PET/MRI

T. Sanderson, B. A. Thomas, S. Wan, J. C. Dickson; Institute of Nuclear Medicine, University College London Hospital, London, UNITED KINGDOM.

Background: Ga-68 PSMA PET images are susceptible to 'halo' scatter artefacts, where regions with high uptake such as the bladder and kidneys appear surrounded by a photopenic region. This is caused by an over-correction for scattered photons, and is prominent for Ga-68 due to the presence of a 1077 keV prompt gamma photon emission. In this study, methods for dealing with this artefact have been explored for images acquired on three scanners; Siemens mMR PET/MRI, GE D710 PET/CT, and GE DVCT PET/CT. **Methods**: Images were analysed for seven patients who received both PET/CT and PET/MRI Ga-68 PSMA imaging on the same day, and four additional patients who only received PET/MRI imaging. If an artefact was present, the image was re-reconstructed without scatter correction. Five mMR patient studies affected by the artefact were also reconstructed offline using e7 tools software. Multiple reconstructions were carried out with varying maximum scatter fractions

(MSF) (20-75%) reduced from the default 75%. Artefact severity was quantified at each MSF by drawing a 2D profile over the bladder on a transaxial slice. The bladder-to-background ratio was measured for three concentric regions surrounding the bladder (inner, central, outer). This was expressed as a percentage of the 'true' bladder-to-background ratio, defined using the default 75% MSF image and outer region. **Results**: The artefact was present on 3/3 of the DVCT images, 7/11 of the mMR images, and 0/4 of the D710 images. Reconstructions with no scatter correction removed the artefact in all cases, but resulted in noisy images which are no longer quantitatively accurate. Reducing the maximum scatter fraction reduced the severity of the artefact at the cost of increased scatter remaining in the image. For 4/5 patients, a 50% MSF gave the closest result to the 'true' bladder-to-background ratio, with an average across all regions and patients of 87% of the true ratio. For the remaining patient the best MSF was 30%. **Discussion/Conclusion**: 'Halo' artefacts were observed for studies on the GE DVCT and Siemens mMR, but not for the GE D710, indicating an improved scatter correction. The artefact can be removed by reconstructing without scatter correction, but results in noisy, non-quantitative images. For the mMR, improvements can be made by reducing the maximum scatter fraction, with best results found at 50%.

OP-615

NEMA NU 2-2007 Performance Characteristics of GE Signa Integrated PET/MR: Impact of Using Different PET Isotopes

P. Caribé[1,2], M. Koole[3], S. Vandenberghe[1], T. Deller[4], K. van Laere[3]; [1]Medical Imaging and Signal Processing – MEDISIP, UZGhent; IMEC, Ghent, BELGIUM, [2]National Council for Scientific and Technological Development – CNPq, São Paulo, BRAZIL, [3]Division of Nuclear Medicine – UZ/KU, Leuven, BELGIUM, [4]General Electric Healthcare, Waukesha, WI, UNITED STATES OF AMERICA.

The aim of this study is to assess the impact of using different PET isotopes for the NEMA NU 2-2007 performance evaluation of the GE Signa integrated PET/MR. For this purpose, NEMA NU 2-2007 performance measurements for characterizing spatial resolution (SR), image quality (IQ), noise equivalent count rate (NECR) and linearity were performed using both ^{18}F and [68]Ga. **Methods:** For the NEMA NU 2-2007 SR measurements, a ^{18}F and ^{68}Ga point source inside a glass capillary tube was positioned at 1 and 10 cm off-center in the field of view. NECR were measured using a 70-cm-long polyethylene cylinder with a diameter of 20 cm and a line source inserted axially into the cylinder 4.5 cm off-centered filed with 871.01 MBq for ^{68}Ga and 679.54 MBq for [18]F (at first frame start). PET image quality was evaluated using the NEMA IQ phantom with a 4:1 ratio for the hot sphere to background activity concentration. For ^{68}Ga, the background region was filled to 5.0 kBq/mL at scan start time, while for [18]F a background activity concentration of 3.1 kBq/mL was used. For both isotopes, the accuracy of the attenuation and scatter correction was determined from the uniform background and could lung insert regions. **Results:** The SR of ^{68}Ga increased (transaxial) by 3.1%. In the axial direction values increased by 17.8% and 27.9%

(at 1 and 10 cm off-center) respectively as compared to ^{18}F in the axial resolution measurements as compared to [18]F. The ^{68}Ga NECR was slightly lower and at a slightly higher activity concentration than measured for ^{18}F while linearity was not affected by the use of different isotopes. In terms of image quality, the average lung residual error was lower than the 3% for the both isotopes. **Conclusion:** NEMA NU 2-2007 performance measurements using ^{18}F and ^{68}Ga resulted in substantially different system characteristics, specifically in terms of SR and recovery coefficients of the IQ measurements. This is due to the anisotropic higher positron range of ^{68}Ga compared to ^{18}F, with the highest positron range aligned with the main magnetic field and thus affecting the axial more than transaxial resolution. NECR differences between the two isotopes can be explained by the lower positron branching factor of ^{68}Ga and the additional 1.077 MeV gamma emission for 3.2% [68]Ga decays, which leads to additional block business and scattering into the energy window generating additional randoms or scatter.

OP-616

Influence of ignoring bone attenuation in standard PET/MRI of carotid plaques

I. Rausch[1], J. Cal-Gonzalez[1], D. Beizke[1], A. Haug[1], X. Li[1], M. Fenchel[2], T. Beyer[1]; [1]Medical University of Vienna, Vienna, AUSTRIA, [2]Siemens Healthcare GmbH, Erlangen, GERMANY.

Aim: Evaluation of the influence of ignoring bone in standard attenuation correction (AC) in positron emission tomography/magnet resonance imaging (PET/MRI) on standardized uptake values (SUV) of carotid plaque lesions located at the carotid bifurcation. **Methods:** Up to date eleven patients, who underwent a 68-Ga PENTIXAFOR PET/MRI examination (Biograph mMR, Siemens Healthcare) were included in this ongoing study. PET data was reconstructed on a 344x344 matrix using an OSEM algorithm with point spread function correction. AC was based on either the standard Dixon-AC and a model-based AC (non-commercial prototype software, Siemens Healthcare) that inserts spatially-variant bone information (skull and cervical vertebra) into the Dixon-AC. Plaque lesions near the carotid bifurcation were delineated manually on T2-weighted TSE MR images with a pixel size of 0.6x0.6 mm by an experienced radiologist and volumes-of-interest (VOI) were copied to the respective PET images (Hybrid3D v2.0 beta, Hermes Medical, Sweden). SUVs of the maximum (SUVmax) and mean (SUVmean) pixel values were extracted from all VOIs. We report relative differences in SUV between Dixon-AC and model-based AC PET. Significant differences were tested using a paired Wilcox test considering p<0.05 as statistically significant. **Results:** In total 22 plaque lesions were delineated on MRI. On average (±SD), an underestimation of 0.5 ± 0.6% (p<0.001) and 0.4 ± 0.6% (p<0.001) was found for SUVmax and SUVmean, respectively. **Conclusion:** Ignoring bone in standard DIXON-based AC resulted in statistically significant but clinically negligible underestimation of SUV values in carotid plaques located near the carotid bifurcation in 68-Ga PENTIXAFOR examinations.

OP-617

ZTE-based attenuation correction in head and neck PET/MRI

R. de Laroche[1,2], M. Khalifé[3], D. Bequé[4], B. Sgard[1,2], F. Pérez-Garcia[3], M. Soret[1], M. Habert[1,2], F. Wiesinger[4], A. Kas[1,2]; [1]Groupe Hospitalier Pitié-Salpêtrière, Paris, FRANCE, [2]Université Paris 6 UPMC, LIB Inserm U1146, Paris, FRANCE, [3]Institut du Cerveau et de la Moelle épinière (ICM), CNRS UMR 7225 - Inserm U1127 - Université Paris 6 UPMC UMR S1127, Paris, FRANCE, [4]GE Global Research Center, Munich, GERMANY.

Aim: Attenuation correction (AC) remains a major issue in head and neck PET/MR. In this study, we applied a Zero Echo Time (ZTE)-based AC map to account for bone attenuation in this area, and explored a new AC map derived from the combination of ZTE-based and Dixon-based AC maps. **Materials and Methods**: Seven patients underwent a PET/MR scan (SIGNA PET/MR, GE Healthcare) for maxillofacial oncology 1 hour after injection of 3.7 MBq/kg of ^{18}F-FDG. PET/MR acquisition was centered at the cervical region. The available MR-based AC method consists of a two-point Dixon MRI (Dixon-AC) that generates an AC map containing 3 tissue classes: fat, soft tissue and air. In addition to routine MRI sequences, a ZTE pulse sequence was added to the protocol and used to derive an AC map containing bone (ZTE-AC). The ZTE-based AC map contained three tissue classes: bone, air and soft tissue. A hybrid ZTE and Dixon-based AC map was generated by overlaying bone voxels from the ZTE-based AC map on the Dixon-based AC map. For comparison, a CT-derived AC map was used as reference. PET images were reconstructed with the 4 AC maps using a TOF-OSEM algorithm with all corrections. SUV values (SUVmean, SUVmax) were compared on 145 volumes of interest (VOI, 3cm^3) located in bones (n=39), physiological uptakes in oral cavity (n=37), oropharynx (n=28), nasal fossa/nasopharynx (n=13), pterygoid muscle (n=14) and parotid gland (n=14), and pathological uptakes measured in malignant tumors (n=7). **Results:** The Dixon-AC method underestimated FDG uptake with respect to CT-AC method by -4.3±18.0% for SUVmean and -1.3±15.7% for SUVmax. On the contrary, the ZTE-AC method overestimated considerably SUV measurements (12.6±13.9% for SUVmean, and 13.8±14.0% for SUVmax). ZTE-AC provided AC maps with satisfying mandible segmentation. All the methods mis-segmented air in nasal fossa and upper airways. The percentage of difference of all VOIs with the combined ZTE/Dixon method was improved by approximately 45% compared with Dixon-AC, with 2.4±13.6% and 4.6±14.0% overestimation of SUVmean and SUVmax respectively, compared with CT-AC. Accuracy of FDG uptake in bones was also improved by 74% with the combined AC method compared with Dixon-AC. Tumor metabolism was overestimated by 6.0±11.2%, 15.8±8.6% and 8.5±9.9% respectively by Dixon, ZTE and combined AC methods. **Conclusion:** The hybrid ZTE/Dixon AC method improved PET quantification in head and neck PET/MR, particularly in bone regions (mandible and maxilla). ZTE-AC showed limitation due to partial volume effect in upper airways and sinuses.

OP-618

Joint Hardware and Patient Attenuation Correction for Hybrid PET/MR Imaging

T. Heußer[1], Y. Berker[1,2], M. T. Freitag[1], M. Kachelrieß[1]; [1]German Cancer Research Center (DKFZ), Heidelberg, GERMANY, [2]RWTH Aachen University, Aachen, GERMANY.

Purpose: To jointly estimate external hardware and patient attenuation distributions from the PET emission data in hybrid non-TOF PET/MR imaging. **Materials and Methods:** Attenuation correction (AC) for both hardware and patient is required for accurate PET quantification. In hybrid PET/MR imaging AC is a major challenge since the available MR data cannot directly be transformed into accurate information on the attenuation distribution. MR-based AC (MRAC), as applied in current clinical routine, does not properly account for bone attenuation and neglects attenuation of flexible hardware components such as headphones or flexible body coils. Both effects result in severe activity underestimation, limiting the clinical value of hybrid PET/MR imaging. To avoid these effects, we developed a new reconstruction approach combining ideas of our recently developed reconstruction algorithms MR-MLAA (for emission-based patient attenuation correction using MR prior information) [IEEE TNS 63(5):2443, 2016] and xMLAA (for external hardware attenuation correction) [EJNMMI Physics 4:12, 2017]. The new algorithm, xMR-MLAA, is based on maximum-likelihood reconstruction of attenuation and activity (MLAA), which estimates both attenuation and activity distributions from the PET emission data. First, the attenuation of flexible hardware components is estimated by employing the MLAA attenuation update only outside the patient and table regions. Then, considering the estimated hardware attenuation, the initial patient attenuation map is updated while incorporating MR-based anatomical prior information. The thus-estimated attenuation distribution is refined, performing additional interleaved updates on hardware and patient attenuation. The proposed method was evaluated for three clinical ^{18}F-FDG head scans acquired with a Siemens Biograph mMR. Conventional T1-weighted MR images were used to derive the patient support as well as anatomical prior information on the patient attenuation distribution. CTAC was used as a reference. **Results:** Standard MRAC results in activity underestimation in the brain, caused both by neglecting headphone attenuation and by treating bone as soft tissue during AC. Across three FDG patients included in this study, average brain activity underestimation was 14.8% compared to CTAC. Using xMR-MLAA, bone attenuation information could be accurately recovered while preserving air cavities like the nasal sinuses and the inner ears. Moreover, accurate estimates of the headphone attenuation were obtained. Average brain activity underestimation with xMR-MLAA was 2.8% compared to CTAC. **Conclusion:** We propose a method to jointly estimate hardware and patient attenuation in hybrid PET/MR imaging. The proposed method was shown to significantly reduce activity underestimation for clinical ^{18}F-FDG patient data and can, potentially, be readily included into clinical workflow.

OP-619

Comparison of quality control between PET/MRI and PET/CT systems using NEMA tests

M. Abuqbeitah[1], M. Demir[1], N. Yeyin[1], T. Toklu[2], S. Sezgin[3], H. Çetin[3], K. Sönmezoğlu[4]; [1]Istanbul university, Istanbul, TURKEY, [2]Yeditepe university, Nuclear Medicine Department, Istanbul. TURKEY, [3]epsilon laboratory, Istanbul, TURKEY.

Aim: This work targeted to compare NEMA test results among PET/CT and PET/MRI of the same providing company. **Material & Methods:** This study was carried out over General Electric (GE) Signa PET/MR and GE Discovery PET/CT systems. The rescommended NEMA tests was similarly performed using F-18 radioisotope and NEMA fantom involving Spatial Resolution, Sensitivity, Scatter Fraction/Count Rate Performance, Image Quality as well as the accuracy of correction for count losses and randoms. **Results:** Spatial Resolution results were tabulated below: The Sensitivity of PET/MRI was (22.2 cps/kBq) higher than PET/CT (5.46 cps/kBq). Peak NECR and Scatter Fraction (%) findings of PET/MRI with 17.7 kBq/cc prepared activity was 218 kcps and %43.4 respictively, while the generated values for PET/CT using activity of 27.6 kBq/cc was 137.2 Kcps for peak NECR and %39.1 for scatter fraction. Regarding to image quality, the contrast of hot lesions with 8:1 activity concentartion of PET/MRI was 56, 72, 78, and % 85 while the results were as lower as 52, 54, 70, and 78% for PET/CT. Accuracy of correction for count losses and randoms was also measured inwhich the unaccuracy of PET/MRI and PET/CT was %3.40 and %5.13 respictively. **Conclusion:** PET/MRI system seems relatively superior to PET/CT in terms of performance characteristics and image quality.

1601   **Wednesday, October 25, 2017, 08:00 - 09:30, Hall A**

CME 13 - Dosimetry/Radionuclide Therapy/Radiation Protection: Treatment Planning for Radionuclide Therapy, How Simple Can it Be?

OP-621

Legal Requirements for Nuclear Medicine Therapy Imposed by the BSS as Implemented in the Dutch Law

L. Keulemans; Dutch Ministry of health, well-being and sports, Medical radiation, The Hague, NETHERLANDS.

OP-622

Radiation Protection and Waste Management in Radionuclide Therapies

B. Godthelp; Dutch Authority Nuclear Safety and Radiation Protection ANVS, Environmental radiation, The Hague, NETHERLANDS.

OP-623

Are Traditional Fixed Activity Schedules Appropriate for Advancing in Personalised Medicine?

S. Ezzedin; Universitätsklinikum des Saarlandes, Klinik für Nuklearmedizin, Homburg, GERMANY.

OP-624

Examples of Workflow and Requirements for Patient-Specific Dosimetry-Guided Treatments

K. Sjögreen-Gleisner; Lund University, Medical radiation Physics, Lund, SWEDEN.

1602   **Wednesday, October 25, 2017, 08:00 - 09:30, Hall B**

Joint Symposium 13 - EANM/SNMMI: Standardisation of Diuresis Renography in Children

OP-626

The SNMMI-EANM Joint Guidelines for Diuresis Renogram in Children: The F+0 Protoco

D. De Palma; Circolo Hospital and Macchi Foudation, Nuclear medicine Unit, Varese , ITALY.

OP-627

The SNMMI-EANM Joint Guidelines for Diuresis Renogram in Children: The F+(20 to 30 minutes) Protocol

M. Majd; Children's National Med Center, Dept. of Diagnostic Imaging & Radiology , Washington, UNITED STATES OF AMERICA.

OP-628

The Actual Role and Clinical Impact of Diuresis Renogram in Management of Prenatally Diagnosed Hydronephrosis

A. Springer; EAPU, Medical University of Vienna, Vienna, AUSTRIA.

1604   **Wednesday, October 25, 2017, 08:00 - 09:30, Hall E1**

Do.MoRe: Image Reconstruction

OP-630

Optimisation of penalized likelihood estimation reconstruction on a digital time-of-flight PET-CT scanner for four different PET tracers

E. Lindström[1,2], A. Sundin[1,3], C. Trampal[3], L. Lindsjö[3], J. Sörensen[1,3], M. Lubberink[1,2]; [1]Department of Surgical Sciences/Nuclear Medicine & PET, Uppsala University, Uppsala, SWEDEN, [2]Medical Physics, University Hospital, Uppsala, SWEDEN, [3]PET Centre, University Hospital, Uppsala, SWEDEN.

Introduction: Resolution and quantitative accuracy of PET images are highly influenced by reconstruction method. Penalized likelihood estimation methods allow for fully convergent iterative reconstruction, leading to a higher image contrast while limiting noise compared to the current clinical standard ordered subsets expectation maximisation (OSEM). Block-sequential regularized EM (BSREM) was compared to OSEM in this study. Various strengths of noise penalization factor β were tested along with scan duration with the aim to optimise the performance and clinical use of BSREM for four tracers, both in quantitative terms and in a qualitative observer study. **Methods**: Data from clinical whole-body PET-CT scans with ^{68}Ga-DO-TATOC, ^{18}F-FDG, ^{18}F-fluoride and ^{11}C-acetate acquired on a digital time-of-flight PET-CT (Discovery MI, GE Healthcare) were included. Each scan (n_{total}=47) was reconstructed using BSREM (Q.Clear) with β 133, 267, 400 and 533, and OSEM (3 iterations, 16 subsets, 5 mm Gaussian filter) with point spread function recovery, for different acquisition time/bed. A reference VOI was placed in healthy liver tissue and lesions were delineat-

ed employing a 41% threshold of the maximum voxel value. Noise, signal to noise ratio (SNR), signal to background ratio (SBR) and maximum standardized uptake value (SUV_{max}) were analysed. A blinded image quality evaluation of ^{18}F-FDG reconstructions, rating different aspects, performed by experienced nuclear medicine physicians complemented the analysis. **Results:** The lowest levels of noise were reached with the highest β resulting in the highest SNR and in turn the lowest SBR. Noise equivalence to OSEM was found with β 400 (^{68}Ga-DOTATOC, ^{18}F-FDG, ^{18}F-fluoride) and β 267 (^{11}C-acetate), combined with a significant increase of SUV_{max} (24%, 12%, 23% and 19%), SNR (27%, 23%, 12% and 30%) and SBR (24%, 13%, 25% and 18%) compared to OSEM. Decreasing acquisition time with BSREM, by 1 or 0.5 min/bed, reduced SNR although it remained higher or equal to OSEM at full acquisition durations for all tracers at their optimal β, and gave only small differences of SUV_{max}. The observer evaluation resulted in similar scores between reconstructions, β 267 was rated highest regarding overall judgement, contrast and tumour detectability, while β 400 obtained the highest mean score and achieved a better score than OSEM concerning noise, liver background and tumour detectability. **Conclusions:** BSREM reconstruction resulted in a tracer-dependent increase in tumour SUV_{max}, SNR and SBR compared to OSEM at matched levels of noise. Observers' evaluation and semi-quantitative measures coincides and BSREM performed better than OSEM in terms of tumour detectability.

OP-631

Bayesian Penalized Likelihood Image Reconstruction (Q.Clear) in 82Rb Cardiac PET: Impact of Count Statistics

N. Christensen, L. P. Tolbod; Dept. Nuclear Med. & PET-Centre, Aarhus University Hospital, Aarhus, DENMARK.

Aim: Q.Clear reconstruction is expected to improve detection of perfusion defects in cardiac PET due to the high degree of image convergence and effective noise suppression. However, 82Rb (T½=76s) possess a special problem, since count statistics vary significantly not only between patients but also during the acquisition. Image smoothening imposed by the noise penalty (beta) of Q.Clear may vary significantly between patients leading to exaggeratedly smoothened images with poor contrast in some patients and very noise images in others. In this study, we illustrate the effect of varying count statistics using a cardiac PET phantom as well as a selection of clinical patients referred for 82Rb cardiac PET. **Methods:** The study consistent of 3 parts: 1) A thorax-cardiac phantom was scanned for 10 minutes after injection of 1110 MBq 82Rb. Frames at 3 different times after infusion were reconstructed to yield images with total number of prompts (TP) ranging from 4 to 40 MCnts. Contrast of defect-to-LV and LV-to-cavity were characterized at a range of beta factors. 2) Body Surface Area (BSA) and TP in static frames 2.5-5 min post 82Rb infusion (1110 MBq) was extracted from 75 consecutive clinical 82Rb PET scans. 3) Static and dynamic images from a set of 7 patients (BSA: 1.6-2.2 m2) referred for 82Rb cardiac PET was analyzed using a range of beta factors. Results were compared to the institution's standard clinical

practice reconstruction protocol. All scans were performed on GE DMI Digital-Ready or D690 PET/CT. **Results:** 1) Contrary to the standard images, contrast of defect-to-LV and LV-to-cavity was found to depend highly on the number of TP when using Q.Clear. 2) TP in patient scans (static) could be approximated as a linear function of BSA (TP=-5e7xBSA+2e8, R2=0.7, range TP: 20-100 MCnts, BSA: 1.5-2.5 m2). 3) Optimum performance was found at beta factors ranging of 25-100. Interestingly, MBF measurements were consistent with standard protocol results within 10% at beta factors ranging from 10-100, even though, the smoothing resulting from the noise penalty varied highly from first passage (high counts, low smoothing) to the late uptake phase (low counts, high smoothing). **Conclusion:** The Q.Clear reconstruction algorithm can be used for the 82Rb cardiac PET. For a fixed administered 82Rb dose of 1110 MBq, the optimal range of beta factors is 25-100. However, the patient specific optimal beta factor seems to depend on both administered dose and patient BSA.

OP-632

Determining the Minimum Administered Activity for Tumour FDG PET/CT Imaging that satisfies EARL Specifications, and Investigation of Bayesian Penalised Likelihood Reconstruction

T. Sanderson, J. Dickson; University College London Hospital, London, UNITED KINGDOM.

An EARL procedure has been followed to determine the minimum administered activity (MBq.min.bed^{-1}.kg^{-1}) and OSEM-TOF reconstruction parameters that satisfy EARL specifications for activity concentration recovery coefficients (RCs) and image noise in FDG PET/CT imaging. A similar procedure is also performed for a Bayesian Penalised Likelihood (BPL) reconstruction. A NEMA-IQ phantom was filled, obtaining a 10:1 sphere-to-background ratio and representing a 75 kg patient administered with 300 MBq FDG at 1 hour post-injection. The phantom was imaged for 5 min.bed^{-1} in list mode on a GE D710 system. The data was reconstructed with OSEM-TOF (2i, 24s) with a range of post-reconstruction smoothing filters (5-8.5 mm). Mean (A50%) and maximum RCs for all spheres (10-37 mm) were determined. For two chosen filters the data was re-sampled into five additional reduced min.bed^{-1} images and identically reconstructed. The mean background coefficient of variation (CoV) in each image was fitted against the min.bed^{-1} using a power law. A similar procedure was performed for a BPL reconstruction (β=400). OSEM-TOF reconstructions with an 8.5 mm filter resulted in all RCs within EARL specifications. The minimum activity to meet the maximum EARL specified CoV of 15% was 4.8 MBq.min.bed^{-1}.kg^{-1}. Reconstructions using a 6.4 mm filter resulted in increased RCs, and for two spheres were higher than the maximum specifications. Images were noisier, and the minimum required activity was 10.5 MBq.min.bed^{-1}.kg^{-1}. BPL reconstructions demonstrated significantly increased RCs (0.88-0.98 for mean A50%) with a relatively flat recovery curve. Image noise was comparable to OSEM-TOF with a 6.4 mm filter, with a minimum required activity of 11.4 MBq.min.bed^{-1}.kg^{-1}.

Edge enhancement artefacts were observed, as PSF model-ling is incorporated. For OSEM-TOF reconstructions an activity of 4.8 MBq.min.bed^{-1}.kg^{-1} can meet EARL specifications for RCs and noise. This is significantly less than the stated EANM min-imum of 14 MBq.min.bed^{-1}.kg^{-1} (PET bed overlap <30%). If 370 MBq is administered for a 75 kg patient, this corresponds to <1 min.bed^{-1}, or an 8 minute WB scan (alternatively 120 MBq ad-ministered for 3 min.bed^{-1}). The maximum EARL specifications for RCs are lower than modern PET/CT systems are capable of to ensure equivalent image quality in multi-centre trials. The higher RCs obtained with a 6.4 mm filter may be preferable, and the required minimum activity of 10.5 MBq.min.bed^{-1}.kg^{-1} is still significantly less than the EANM minimum. The BPL recon-structions result in much greater RCs, and image noise can be comparable to OSEM-TOF.

OP-633

Investigation into Optimal PET-CT Image Reconstruction for the Detection and Quantification of Inflammation and Infection Associated with Implanted Cardiac Devices

Y. Bouchareb[1,2], J. Thomas[2], G. Delanerolle[1], H. Jan[1], N. Hartman[1], A. Haroon[1]; [1]Barts Health NHS Trust, London, UNITED KINGDOM, [2]Queen Marys University, London, UNITED KINGDOM.

Purpose: To optimise and assess PET image reconstruction for the detection, localization and quantification of metabolically active foci of infection/inflammation affecting Cardiac Implant-ed Electronic Devices (CIEDs). **Materials and Methods**: An an-thropomorphic torso-phantom with balloons filled and sealed with FDG solution was used to mimic the inflammation and infection around the myocardium insert. The balloon-to-myo-cardium (40.2 KBq/mL) ratio was 10:1 (total activity was 44 MBq). A metal object was placed on top of the torso phantom where the cardiac insert is situated to replicate the CIED and its metal artefacts. A population of 10 patients (6 males and 4 females: age range of 45 -77 years) with CIEDs was also used to assess the value of TOF PET reconstruction to accurately quantity the inflammation/infection associated with CIEDs. Phantom exper-iments and patients were scanned on the Gemini TF-TOF 64 slice PET/CT Philips scanner. To optimise image reconstruction, three different reconstructions: List-mode OSEM-TOF using 3 iterations and 33 subsets (Recon1), List-mode OSEM-TOF using 3 iterations and 20 subsets (Recon2) and non-TOF 3D-RAMLA (Recon3) and were performed. To assess the effect of relaxation parameters (filter sizes), four different relaxation parameters (1, 0.7, 0.6 and 0.5) were applied with each reconstruction. A to-tal of 12 reconstructions were compared on phantom images. Activity line profiles (ALP), SUVmax, Target-to-background ratio (TBR) and Noise were used to analyse phantom and patients reconstructed images. **Results**: On phantom experiments, ALP extracted through balloons diameters in transverse slices in-dicated an improvement 7%, 13% and 21% in Recon1 recon-structed balloons diameters using a relaxation parameter of 1 over Recon2, Recon3, respectively (relaxation parameter of 1 was adopted for patient images). On this patient population, SUVmax was 4.3, 3.1 and 3.6 on wire and was 2.1, 1.9 and 1.6 on

the pacemaker for Recon1, Recon2 and Recon 3, respectively. This reflects a better indication of the inflammation/infection around the wires was detected on Recon1 images. The TBR cal-culated on the wire was 2.2, 1.1 and 1.5 and on the pacemaker was 1.4, 1.1 and 0.9 for Recon1, Recon2 and Recon3, respective-ly. The noise was in favour of Recon1 and Recon2 over Recon3. **Conclusion**: TOF FDG-PET/CT image reconstruction using 3 it-erations and 33 subsets with a relaxation parameter of 1 proved to be the most suitable reconstruction method for better detec-tion and quantification of inflammation/infection around the wire and pacemaker in patients with CIEDs.

OP-634

SMART(SiMulAtion and ReconsTruction) PET: An efficient PET simulation-reconstruction tool

E. Pfaehler, R. Boellaard, J. De Jong; UMCG Groningen, Groningen, NETHERLANDS.

Purpose: PET simulations are useful for development and per-formance evaluation of e.g. segmentation methods and quan-titative uptake metrics. Several PET simulation-reconstruction packages exist but most are either computationally demanding or lack the implementation of time-of-flight (TOF) and resolu-tion modeling (RM). The aim of this study is to develop and vali-date a new PET simulation-reconstruction tool, SMART-PET, that includes state-of-the-art features such as TOF and RM. **Meth-ods:** The simulation-reconstruction tool allows the generation of 3D PET images based on an analytical simulator (forward projection). As input it requires 3D images representing activi-ty and attenuation coefficient distributions. SMART-PET allows the user adjustable TOF, RM, noise/counts, scatter and random fractions, blurring, iterative deconvolution and use of different matrix/voxel sizes. Moreover, random spatial shifts can be in-cluded to simulate effects of repositioning patients. To validate our simulator a 3D list-mode scan of 60 min was acquired on a Siemens mCT Biograph using the NEMA NU2 image-quality phantom filled such to obtain sphere-to-background ratios of 10 and 0.5. Ten statistically equivalent replicates, representative for 30, 60, 120 and 300s scan durations, were extracted from the list-mode acquisition and reconstructed using various iterative reconstruction methods (TOF on/off, RM on/off) and matrix siz-es(256x256, 400x400). All corrections necessary for obtaining quantitative PET data, such as e.g. attenuation, scatter etc, were included. Equivalent images were generated using SMART-PET. The statistically equivalent images (measured and simulated) were further processed to obtain mean and variance images for comparison. Moreover, SUV recovery coefficient (RC) and back-ground noise (COV,%) derived from simulated and actual data were compared. **Results:** Images obtained using SMART-PET were comparable to actual phantom data. Change in counts, reconstruction settings and RM resulted in comparable chang-es in image characteristics between simulated and actual data. Moreover, variation of TOF showed variation in background noise following theoretically expected SNR changes. Sphere RCs as function of sphere size in the simulated data agreed within 12% with those found in the actual phantom scans. Regarding

mean and variance images a difference of around 2% (mean) and around 20% (variance) was found between simulated and actual image in the spheres. **Conclusion:** The SMART-PET tool simulates PET images with comparable image characteristic as those seen in actual phantom data and allows fast simulation of PET data with different settings. Small discrepancies found can be resolved by more closely matching simulation settings, e.g. scatter/randoms fractions, with those seen in actual PET data using a specific calibration process.

OP-635

Comparison of a statistical analysis method and a visual assessment of Monte Carlo based SPECT reconstruction concerning liver metastases in ^{111}In-octreotide diagnosis

E. Wikberg[1], M. van Essen[2], T. Rydén[1], J. Svensson[3], P. Gjertsson[2], P. Bernhardt[1]; [1]Department of Radiation Physics, Gothenburg, SWEDEN, [2]Department of Nuclear Medicine, Gothenburg, SWEDEN, [3]Department of Oncology, Gothenburg, SWEDEN.

Aim: This work aims to accomplish an increase in diagnostic accuracy of ^{111}In-octreotide SPECT images. This is done by improving image quality through implementation of Monte Carlo (MC) based OSEM reconstruction and by application of an analysis technique called nNUFTI. **Materials and Methods:** The nNUFTI method, developed at Sahlgrenska University Hospital, is focused on the concept of homogeneity and is a statistical approach with the assumption that uptake foci distribution differs between livers with and without tumour involvement. The distribution of the normalized number of uptake foci is plotted against a threshold index (ThI) and the quantitative measure used is ThI at 25% of maximum uptake foci. Tumour involvement will shift the curves towards higher ThI. We have previously shown that in a group of 53 randomly selected ^{111}In-octreotide tumour negative patients (iterative reconstruction with attenuation correction, IRAC OSEM) nNUFTI was able to separate the group of patients (n=40) that stayed healthy in a three-year follow-up from the group of patients (n=13) that had emergent liver tumours (p<0,01). 5 out of these 13 patients were clearly above the normal group in ThI. In the present study, the patient material has been reconstructed using Sahlgrenska Academy Reconstruction Code (SARec) to improve image quality. SARec is a MC based iterative OSEM reconstruction method where MC simulations are used in the forward projection. An observer (a trained nuclear medicine specialist) has reviewed 15 patients (of which 9 had emergent liver metastases) once again using reconstruction with IRAC OSEM and using SARec. Criteria evaluated were liver metastases yes (1) or no (0) with confidence level 1-3 (1-low/uncertain, 2-moderate/probable and 3-high/certain). The observer was aware that some patients were found to have emergent liver metastases. **Results:** The observer could not locate any liver metastases in any of the patients, neither using conventional reconstruction nor using SARec. Confidence level was higher (mean=2,7) for IRAC OSEM than for SARec (mean=1,9). **Conclusion:** Although biased (the observer knew that nNUFTI had identified patients with ThI above normal) the observer could not locate any liver metastases. Higher image quality with SARec did not change the visual outcome but lowered the observer's confidence level concerning lack of metastases. This shows the importance of and need for a quantitative measure like nNUFTI. Future plans include nNUFTI analysis using SARec and improvement of the visual quality of SARec images to increase confidence levels.

OP-636

A post-acquisition normalization to co-analyze textural features from multi-center PET images

F. Orlhac[1], S. Boughdad[1,2], C. Nioche[1], J. Alberini[2], M. Soussan[1,3], I. Buvat[1]; [1]IMIV, CEA, Inserm, CNRS, Univ. Paris-Sud, Université Paris-Saclay, CEA-SHFJ, Orsay, FRANCE, [2]Department of Nuclear Medicine, Institut Curie-René Huguenin, Saint-Cloud, FRANCE, [3]Department of Nuclear Medicine, Assistance Publique - Hôpitaux de Paris, Avicenne Hospital, Bobigny, FRANCE.

Purpose: Intratumor heterogeneity characterized by PET textural features (TF) is increasingly used in retrospective studies. Yet, several studies demonstrated that TF values are affected by the acquisition and reconstruction parameters. We proposed a method to standardize TF measured in PET. **Methods:** Patients with breast non-metastatic lesions were included. In department (dpt) A, 110 patients were scanned using a Gemini TOF PET/CT scanner (Phillips) with a list-mode iterative reconstruction algorithm (BLOB-OS-TF, 2 iterations, 33 subsets, voxel=4x4x4 mm3). In dpt B, 69 patients underwent a PET/CT using a GE Discovery LS Scanner (GMS), reconstructed with OSEM algorithm (2 iterations, 24 subsets, voxel=2.7x2.7x3.3 mm3). For each patient, VOIs of 23 ml were set in the liver, spleen, lung, muscle and healthy breast tissue. For each VOI, we built a vector of biomarkers composed of 6 TF: Homogeneity, Entropy, SRE, LRE, LGZE, HGZE. To characterize the similarity between two biomarker vectors measured in two patients, we computed the component-wise ratio between the two vectors and calculated the standard deviation over the 6 ratios, called SDM as Standard Deviation Metric. If the vectors are homothetic, SDM is 0. We used this metric to measure the similarity between biomarker vectors in different patients. We computed the averaged SDM in patients from dpt A only, in patients from dpt B only and from pairs of patients consisting of 1 from dpt A et 1 from dpt B. We compared the values for TF calculated from the original images (M1), from the images resampled to the same voxel size (2x2x2 mm3, cubic B-spline interpolation) (M2), and using M2 then dividing each TF by the median TF measured in the liver of all patients of each department separately (M3). **Results:** In spleen, we found that SDM was 0.12±0.08 for patients from dpt A, 0.12±0.08 for patients from dpt B for M1, and 0.21±0.11 between patients from dpts A and B. This suggests that the spleen TF vector is different between the two dpts (inter-center variability). Between patients from dpts A and B, spleen SDM was 0.16±0.10 for M2 and 0.14±0.09 for M3. The same trend was observed in the other four tissues. **Conclusion**: Calculating TF using the same voxel size is useful but not sufficient to remove the multi-center variation of TF. Additional normalization using a patient-indepen-

dent measurement in a reference tissue (here the median liver TF) further reduces multi-center variability. Such a standardization could facilitate multicenter studies.

OP-637

Comparison of Tumor Heterogeneity Assessed with Textural Parameters in ^{68}Ga-PSMA PET/CT and ^{177}Lu-PSMA SPECT/CT in Patients with Metastatic Prostate Cancer

L. Schwarte[1], L. Thomas[1], E. Eppard[1], M. Meisenheimer[1], C. Weiss-Wichert[2], M. Essler[1], R. A. Bundschuh[1]; [1]Department of Nuclear Medicine, Universitätsklinikum Bonn, Bonn, Germany, Bonn, GERMANY, [2]Mediso GmbH, Münster, GERMANY.

Purpose: Tumor heterogeneity in PET/CT assessed by textural parameters is gaining importance as prospective and predictive feature for multiple clinical applications. Especially in theranostics, PET and SPECT images are often performed in the same patient. Therefore, the aim of this study was to compare, if tumor heterogeneity assessed in PET/CT and SPECT/CT imaging is correlating to each other in the same lesion. This was evaluated in phantom and patient data. **Subjects and Methods:** A self-built heterogeneity phantom as well as 37 patients with metastasized prostate cancer who underwent a peptide receptor radionuclide therapy (PRRT) received a ^{68}Ga-PSMA PET/CT before and ^{177}Lu-PSMA SPECT/CT directly after each therapy cycle. Some patients only had one cycle, most had two or three, and one patient received four cycles. The variety in cycles depends on the tolerance and the survival of the patients. Both PET/CT and SPECT/CT images were processed with Interview™ Fusion software (Mediso Medical Imaging Systems). The biggest lesions were selected and manually marked in both images. Consequently 36 textural features, including deviation, entropy and different emphases were calculated. In addition, conventional parameters as tumor mean and max SUV, and tumor volume were tested as well. Results were compared using Bland-Altman Plots. **Results:** Overall, 188 metastases from 37 patients were analyzed. In Bland-Altman Plots it was shown that for the majority of the 40 parameters there is no direct comparability between PET/CT and SPECT/CT values. Using the 95% confidence interval, the best variables could be identified. Long Zone Low Grey Level Emphasis had a high accordance. 94.7% of the data were contained in 95% confidence interval. For the Short Zone Low Grey Level Emphasis it was 32.8%, 32.3% for the volume, 34.9% for TLG, 23.8% for maximum and 21.7% for the mean. Variables such as entropy which are frequently used in tumor heterogeneity have low accordance values. Only 12.2% of the entropy data are contained in the 95% confidence interval. Intensity Variation and Zone Length Non Uniformity only have results of 4.2%. Different values were found for the phantom, in which a high correlation (p<0.01) was found for the different heterogeneity parameters. **Conclusion:** This study shows, that in contrast to data obtained by phantoms, in real patients tumor heterogeneity in PET/CT and SPECT/CT is not correlating. The importance and necessity of retrospective studies looking in to the clinical value of tumor heterogeneity obtained in SPECT/CT images is still given.

M2M: Radiolabelling Methods

OP-638

First radiofluorination of LLP2A and In-vivo PET Imaging of α4β1 integrin-expressing tumors in mice

D. Perrin[1], A. Roxin[1], C. Zhang[2], K. Lin[2], F. Benard[2]; [1]University of British Columbia, Vancouver, BC, CANADA, [2]BC Cancer Research Centre, Vancouver, BC, CANADA.

Objectives: The peptidomimetic, LLP2A, is a specific, high-affinity ligand for $\alpha_4\beta_1$ integrin receptors. Our objective is to provide the first radiosynthesis of an F-18 labeled LLP2A-RBF$_3$ conjugate and investigate PET images in mice. Previously, various LLP2A conjugates were evaluated *in vivo* as imaging agents yet to date there has been no report of an ^{18}F-labeled LLP2A. Notably, F-18 is often preferred for PET imaging, yet its short half-life and general inactivity under aqueous conditions challenges peptide labeling. A simple method for labeling complex biomolecules can be achieved in a single, aqueous step by isotope exchange (IEX) on an organotrifluoroborate to readily capture ^{18}F-fluoride. **Methods**: PEGylated LLP2A was synthesized by standard solid-phase peptide synthesis to afford a C-terminal amide-linked PEG spacer terminated with an azide for eventual click conjugation to an alkyne-modified organotrifluoroborate. Following click-conjugation, the LLP2A-BF$_3$ bioconjugate was HPLC purified and aliquotted. For labeling, NCA ^{18}F-fluoride ion (~37 GBq) was trapped on a QMA cartridge and eluted into a solution of buffered aqueous DMF containing the LLP2A-BF$_3$ and heated for 15 min at 80-85 degrees. Following quench per standard protocols, radiochemically pure radiotracer was isolated in 50% ethanol following Sep-Pak desalting. Mice with xenograft tumors were imaged with standard blocking controls following injection of 3.7 MBq. Following imaging by PET in accord with standard humane use protocols, mice were sacrificed for organ dissection and biodistribution analysis. **Results**: Radiochemical yields were moderate (11%) with high specific radioactivities of 148 GBq/umol (n=5). ^{18}F-RBF$_3$-LLP2A accumulated in tumors with tumor uptake values of 10≠2%ID/g along with similar uptake values for gut and liver. Blocking controls with excess LLP2A demonstrated specific tumor uptake. Bone uptake was approximately 5%ID/g however bone uptake was blockable consistent with high $\alpha_4\beta_1$ integrin expression in bone marrow. **Conclusion**: In conclusion, we report the first labeling of LLP2A with NCA ^{18}F-fluoride ion. This is facilitated by isotope exchange in aqueous conditions by use of an organotrifluoroborate prosthetic group that affords efficient user friendly single-step labeling. Image data is promising as tumor uptake is high and T:NT ratios are high. These promising results highlight the use of RBF$_3$s for convenient labeling while indicating that other derivatives with longer PEG linkers may minimize gut/liver uptake.

OP-639

[^{18}F]fluorination of biorelevant arylboronic acid pinacol ester scaffolds synthesized by convergence techniques

G. S. Clemente[1], T. Zarganes-Tzitzikas[2], I. F. Antunes[1], A. Dömling[2], P. H. Elsinga[1]; [1]Department of Nuclear Medicine and Molecular Imaging, University Medical Center Groningen, University of Groningen, Groningen, NETHERLANDS, [2]Department of Drug Design, University of Groningen, Groningen, NETHERLANDS.

Aim: The development of small molecules through convergent multicomponent reactions (MCR) has been boosted during the last decade due to the ability to synthesize, virtually without any side-products, numerous small drug-like molecules with several degrees of structural diversity.[1] The association of positron emission tomography (PET) labeling techniques in line with the "one-pot" development of biologically active compounds has the potential to become relevant not only for the evaluation and characterization of those MCR products through molecular imaging, but also to increase the library of radiotracers available. Therefore, since the [18F]fluorination of arylboronic acid pinacol ester derivatives tolerates electron-poor and electro-rich arenes and various functional groups,[2] the main goal of this research work was to achieve the 18F-radiolabeling of several different molecules synthesized through MCR. **Materials and Methods:** [18F]Fluorination of boronic acid pinacol esters was first extensively optimized using a benzaldehyde derivative in relation to the ideal amount of Cu(II) catalyst and precursor to be used, as well as the reaction solvent. Radiochemical conversion (RCC) yields were assessed by TLC-SG. The optimized radiolabeling conditions were subsequently applied to several structurally different MCR scaffolds comprising biologically relevant pharmacophores (e.g. β-lactam, morpholine, tetrazole, oxazole) that were synthesized to specifically contain a boronic acid pinacol ester group. **Results:** Radiolabeling with fluorine-18 was achieved with volumes (800 µl) and activities (≤ 2 GBq) compatible with most radiochemistry techniques and modules. In summary, an increase in the quantities of precursor or Cu(II) catalyst lead to higher conversion yields. An optimal amount of precursor (0.06 mmol) and $Cu(OTf)_2(py)_4$ (0.04 mmol) was defined for further reactions, with DMA being a preferential solvent over DMF. RCC yields from 15% to 76%, depending on the scaffold, were reproducibly achieved. Interestingly, it was noticed that the structure of the scaffolds, beyond the arylboronic acid, exerts some influence in the final RCC, with electron-withdrawing groups in the para position apparently enhancing the radiolabeling yield. **Conclusion:** The developed method with high RCC and reproducibility has the potential to be applied in line with MCR and also has a possibility to be incorporated in a later stage of this convergent "one-pot" synthesis strategy. Further studies are currently ongoing to apply this radiolabeling concept to fluorine-containing approved drugs whose boronic acid pinacol ester precursors can be synthesized through MCR (e.g. atorvastatin). **References:** (1) Zarganes-Tzitzikas T. and Dömling A., *Org. Chem. Front.*, 2014, 1(7):834-837; (2) Tredwell M. *et al.*, *Angew. Chem. Int. Ed.*, 2014, 53:7751-7755.

OP-640

Synthesis and Evaluation of a Novel Tetrakis(3-Hydroxy-4-Pyridinone) Ligand for 89Zr-Labeling of Antibodies for ImmunoPET

C. Buchwalder[1], J. Rousseau[2], C. Rodríguez-Rodríguez[1], M. G. Jaraquemada-Peláez[1], C. Orvig[1], P. Schaffer[3,1], F. Bénard[1,2], K. Saatchi[1], U. O. Häfeli[1]; [1]University of British Columbia, Vancouver, BC, CANADA, [2]BC Cancer Agency, Vancouver, BC, CANADA, [3]TRIUMF, Vancouver, BC, CANADA.

Purpose: Zirconium-89 (89Zr) is a prominent radionuclide for antibody-targeted positron emission tomography (immunoPET) imaging. Desferrioxamine B (DFO) is currently the most widely used 89Zr-chelator, however there is concern that its hexadentate chelation may not be sufficiently stable in vivo. This has spurred recent efforts towards alternative 89Zr-ligands, which prevent the release of osteophilic 89Zr. In this study, we synthesized and evaluated a novel octadentate tetrakis(3-hydroxy-4-pyridinone) ligand (THPN) and its bifunctional derivative, as a potentially superior 89Zr-chelator for immunoPET imaging. **Methods:** The acyclic chelator THPN and its bifunctional derivative were synthesized and fully characterized. The Zr^{IV}-complex formation was studied experimentally and computationally and the concentration-dependence of 89Zr-radiolabeling was determined. The 89Zr-THPN stability was assessed in a direct transchelation challenge against DFO, in human serum, as well as in an EDTA challenge, and compared to 89Zr-DFO. The in vivo behavior of 89Zr-THPN was also studied in C57BL/6 mice. We are currently preparing and characterizing chelate-trastuzumab conjugates. Studies to assess the biodistribution and in vivo stability of these immunoconjugates in tumor-bearing mice are underway. **Results:** The chelator THPN quantitatively complexed $89Zr^{4+}$ within 10 min at ambient temperature using 10^{-6} M concentrations of the chelator and formed the monometallic 89Zr-THPN complex. Density functional theory (DFT) calculations indicate a well-ordered octadentate complex structure. A direct transchelation study demonstrated the high stability of 89Zr-THPN, which outperformed 89Zr-DFO. One equivalent of THPN ligand triggered transchelation of $89Zr^{4+}$ from 89Zr-DFO to form the THPN-complex. In contrast, 89Zr-THPN resisted a hundred-fold excess of DFO and did not transchelate. In human serum, the THPN-complex remained 93 ± 2% intact over 7 days. Challenge with a 100-fold excess EDTA did not affect 89Zr-THPN integrity at pH 6–8, and at pH 5 the THPN-complex integrity (41.6 ± 11.1%) greatly exceeded that of 89Zr-DFO, which completely disintegrated. Healthy mice rapidly cleared the 89Zr-THPN complex via urine with no substantial organ uptake. Results from the immunoconjugation of the bifunctional THPN-analogue and subsequent in vivo biodistribution results are expected shortly. **Conclusion:** The octadentate ligand THPN and its bifunctional analogue were synthesized and studied as 89Zr-chelators. THPN quantitatively formed the monometallic 89Zr-complex, which outperformed 89Zr-DFO in a direct transchelation studies. Moreover, mice rapidly excreted the radiocomplex without signs of demetallation. The investigation of the immunoconjugation and biodistribution of the chelate-trastuzumab conjugate is currently underway.

OP-641

Piscidin 1: from an antimicrobial peptide to anticancer peptide, a natural chelator for 64Cu

H. Hong, W. Lu, D. Yang, D. Chen; *University of Michigan, Ann Arbor, MI, UNITED STATES OF AMERICA.*

Purpose: Piscidins (PCD) were the first antimicrobial peptides discovered in vertebrates. Our recent investigation confirmed that one of the family members, PCD-1, possesses two unique properties: it shows decent cancer cell killing efficacy (IC_{50}: 4.8 µM for MDA-MB-231 cells), and it bears a Cu^{2+}-binding motif inside its structure. In this study, we hope to increase the cancer cell selectivity and accumulation of PCD-1, and use PCD-1 as a binding ligand for ^{64}Cu. Methods: A fused peptide containing PCD-1 sequence and another tumor-homing peptide F3 was synthesized and named PCD-1-F3. The cytotoxicity of PCD-1, natCu-PCD-1 (non-radioactive copper), PCD-1-F3, and natCu-PCD-1-F3 was measured in MDA-MB-231 cells and L929 fibroblasts by CCK-8 . Fluorescein was site-specifically introduced onto PCD-1-F3 and PCD-1 to study their interaction with cancerous and normal cells via flow cytometry and confocal fluorescence microscopy. ^{64}Cu-PCD-1-F3 and ^{64}Cu-PCD-1 was injected into MDA-MB-231 tumor bearing mice with serial PET imaging being conducted to examine their tumor accumulating behavior. Biodistribution studies and histological analysis were also carried out. A treatment study (n = 5 per group) was done in MDA-MB-231 tumor-bearing mice by using PCD-1 derivatives (5 mg/kg intravenously every other day for four weeks). Results: Both PCD-1 and PCD-1-F3 showed strong binding for copper, and natCu-PCD-1-F3 had the most potent killing efficacy for MDA-MB-231 cells. None of these PCD-1 derivatives showed significant impact for L929 growth and status. Flow cytometry and fluorescence microscopy both confirmed that the internalization of fluorescein-PCD-1-F3 into MDA-MB-231 cells was significantly stronger than that of fluorescein-PCD-1. ^{64}Cu-PCD-1-F3 was sufficiently stable to be used *in vivo* (<15% ^{64}Cu detached from it after a 4 h incubation with mouse serum). ^{64}Cu-PCD-1-F3 (~0.7 GBq/mg) had a circulation half-life of ~ 15 min in mice (from dynamic PET scans) and possessed potent and persistent uptake in MDA-MB-231 (3.6 ± 0.8 %ID/g at 24 h post-injection) than that from ^{64}Cu-PCD-1 (0.7 ± 0.2 %ID/g at 24 h p.i.), and this uptake could be successfully blocked (to 0.9 ± 0.3 %ID/g at 24 h p.i.) by co-injection of excessive amount of F3 peptide (10 mg/kg). Histological analysis of MDA-MB-231 tumors indicated that PCD-1-F3 indeed bound to nucleolin (overexpressed in tumor cell membrane) from tumors. At the treatment dose, natCu-PCD-1-F3 could significantly delay the growth of tumor burden. Conclusion: Our study confirmed the uniqueness of PCD-1 as an anti-cancer agent and a natural "chelator" for copper (radioactive or non-radioactive).

OP-642

Efficient preparation of 2-[¹⁸F]fluorophenylalanine (2-[¹⁸F]FPhe) by Cu-mediated radiofluorination

D. Modemann[1], B. Zlatopolskiy[2], J. Ermert[1], B. Neumaier[1,2]; [1]Forschungszentrum Jülich GmbH, Institute of Neuroscience and Medicine, INM-5, Jülich, GERMANY, [2]Institute of Radiochemistry and Experimental Molecular Imaging, University Clinic Cologne, Köln, GERMANY.

Objectives: 2-[¹⁸F]FPhe has been successfully applied as a PET tracer for imaging of cerebral infarction and tumors. However, the absence of convenient preparation methods of this probe precludes its broad clinical application. The aim of this work was to develop an efficient procedure suitable for the fast production of clinical doses of 2-[¹⁸F]FPhe based on the recently developed Cu-mediated ^{18}F-fluorination of (aryl)(mesityl)iodinium salts. **Methods:** Substrate for radiolabeling, Boc_2-2-[(I⁺Mes)BF_4⁻]PheOtBu, was prepared in four steps starting from HCl×HPheOt-Bu. Cu-mediated ^{18}F-fluorination was accomplished under "minimalist" conditions using only precursor, ^{18}F⁻ and Cu-catalyst. Alternatively, traces of base for ^{18}F⁻-elution were applied ("low-base" protocol)[1] The labeling conditions were optimized with respect to temperature, solvent, amount of $(MeCN)_4$CuOTf and TEABC ("low-base" approach). Boc_2-2-[¹⁸F]FPheOtBu was purified by solid phase extraction and hydrolyzed with 12 M HCl affording after HPLC-purification the desired PET probe. **Results:** The precursor was synthesized in a yield of 31%. Under optimized conditions 2-[¹⁸F]FPhe was prepared in up to 43% radiochemical yield (RCY) and with a radiochemical purity of >99% within 100 min. Unexpectedly, radiolabeling under "minimalist" conditions led to the formation of up to 20% D-enantiomer. Fortunately, adjustment of ^{18}F⁻ processing allowed to suppress racemization (*ee* >98%). Similarly, the "low-base" approach using Et_3NHCO_3 (1 mg) in MeOH enabled the preparation of enantiomerically pure 2-[¹⁸F]FPhe in 48±8% (n = 3) RCY. **Conclusions:** Clinical doses of 2-[¹⁸F]FPhe were efficiently prepared by Cu-mediated ^{18}F-fluorination of the easily accessible iodonium salt precursor under "low base" conditions. The simplicity of the translation of the proposed procedure to automated synthesis modules [2] should open up the venue for the clinical application of 2-[¹⁸F]FPhe. **Research support:** This work was supported by the DFG grant ZL 65/1-1. **Literature:** [1] B. D. Zlatopolskiy, Chem. Eur. J., 2015, 21, 5972-5979. R. Richarz, Organic & biomolecular chemistry, 2014, 12, 8094-8099. [2] J. Zischler, Appl. Radiat. Isot., 2016, 115, 133-137.

OP-643

Influence of composition of cysteine-containing peptide based chelators on biodistribution of ⁹⁹ᵐTc-labelled anti-EGFR affibody molecules

M. Oroujeni[1], K. G. Andersson[2], J. Garousi[1], M. Altai[1], A. Vorobyeva[1], X. Steinhardt[2], B. Mitran[1], S. Ståhl[2], A. Orlova[1], J. Löfblom[2], V. Tolmachev[1]; [1]Uppsala University, Uppsala, SWEDEN, [2]KTH-Royal Institute of Technology, Stockholm, SWEDEN.

Aim: Epidermal growth factors receptor (EGFR) is overexpressed in a number of malignant tumours. In vivo molecular imaging of EGFR expression may provide prognostic, predictive and pharmacodynamic information and facilitate selection of treatment and a therapy response monitoring. Earlier, we have demonstrated feasibility of imaging of EGFR expression in xenografts using ¹¹¹In-labelled anti-EGFR Z2377 affibody molecule. Feasibility of the ⁹⁹ᵐTc-labelling of anti-HER2 affibody molecules using anti-HER2 cysteine-containing peptide based chelators was shown. These chelators can be incorpo-

rated into sequence during recombinant production. In addition, the use of different amino acids permits modification of biodistribution. The aim of this study was to evaluate the use of chelators glycine-glycine-glutamate-cysteine (GGEC), glycine-glutamate-glutamate-cysteine (GEEC), and glutamate-glutamate-glutamate-cysteine (EEEC) for labelling of anti-EGFR affibody molecules with [99m]Tc. **Materials and Methods:** Variants of Z2377 containing C-terminal sequences GGEC, GEEC and EEEC were produced and characterised. The affibody molecules were labelled with ^{99m}Tc using transchelation from gluconate. In vitro characterisation was performed using EGFR-expressing A431, MDA468 and PC3 cell lines. Biodistribution of conjugates was measured in BALB/C nu/nu mice bearing A431 xenografts. To check in vivo specificity, EGFR in a part of xenografts was pre-saturated by injection of anti-EGFR antibody cetuximab. **Results:** Initial labelling experiments revealed a presence of a second binding pocket with weak binding of [99m]Tc. Incorporation of pre-purification cysteine challenge enabled obtaining of stable conjugates. The labelling yield was 83.5 ± 4.2 , 84.6 ± 4.9 and 54.9 ± 7.5 % for ^{99m}Tc-Z2377-GGEC, ^{99m}Tc-Z2377-GEEC, and ^{99m}Tc-Z2377-EEEC, respectively. After purification using size-exclusion NAP-5 cartridges, the radiochemical purity of all variants was higher than 95%. All ^{99m}Tc-labelled Z2377 variants retained specific binding to EGFR-expressing cells and high affinity. All conjugates demonstrated EGFR-specific targeting of A431xenografts. Composition of chelators had strong influence on biodistribution. Increase of number of glutamates in the chelators was associated with rapider clearance from blood and lower uptake in salivary gland, lung, liver, stomach, colon and muscle. At the same time, ^{99m}Tc-Z2377-EEEC had the highest retention in kidneys. ^{99m}Tc-Z2377-EEEC provided the highest tumour-to-blood ratio of 27±5 at 24 h after injection, which is higher than the value of ^{111}In-DOTA-Z2377 at this time point (14±4). **Conclusion**: Cysteine-containing peptide-based chelators can be used for labelling of anti-EGFR affibody molecules with preserved specificity. Amino-acid composition of such chelators has strong influence on biodistribution and can be used modification of pharmacokinetics of affibody molecules.

OP-644

H4neunpa-trastuzumab: Evaluation of a Novel Bifunctional Chelator for 111In Radiopharmaceuticals and Immuno-SPECT Imaging

S. Spreckelmeyer[1,2], C. F. Ramogida[3], J. Rousseau[4], K. Arane[1], I. Bratanovic[3], N. Colpo[4], U. Jermilova[3], G. M. Dias[4], I. Dude[4], M. Jaraquemada-Pelaez[1], F. Benard[4], P. Schaffer[3], C. Orvig[1]; [1]Medicinal Inorganic Chemistry Group, Department of Chemistry, University of British Columbia, Vancouver, BC, CANADA, [2]Dept. Pharmacokinetics, Toxicology and Targeting, Research Institute of Pharmacy, University of Groningen, Groningen, NETHERLANDS, [3]Life Sciences, TRIUMF, Vancouver, BC, CANADA, [4]BC Cancer Agency, Vancouver, BC, CANADA.

Introduction: [111]In ($t_{1/2}$ = 2.8 days) is an attractive radiometal for both therapeutic and imaging applications. Our group has developed a series of "pa" (picolinic acid) chelators with specific binding properties for a great number of radiometals.[1] Herein, we report the synthesis, potentiometric determination of stability constants and several *in vitro* as well as *in vivo* radiolabeling experiments with respect to the evaluation of H[4]neunpa-trastuzumab as a potent radiopharmaceutical in comparison to CHX-A"-DTPA-trastuzumab. **Subjects and Methods:** H[4]neunpa-*p*-Bn-NCS was synthesized starting from the backbone diethylenetriamine and the functionalization was placed on the middle nitrogen atom to keep its symmetry. Coupling of HER2/*neu* targeting antibody trastuzumab was performed via the reaction between the mAb-amine(s) with the isothiocyanate functional group of H[4]neunpa-*p*-Bn-NCS. RCYs of ^{111}In-radiolabeling and serum stability experiments were determined by radio-HPLC, size-exclusion PD-10 columns or iTLC-SG. Immuno-SPECT imaging of [^{111}In]neunpa-trastuzumab with HER2/*neu* positive tumour bearing female mice was performed compared to gold-standard [^{111}In]CHX-A"-DTPA-trastuzumab. Additionally, potentiometric stability constants were determined. **Results:** Radiolabeling with ^{111}In of the precursor H[4]neunpa-*p*-Bn-NO[2] as well as the mAb derivative, H[4]neunpa-trastuzumab, was carried out. Both chelators show labeling efficiencies >90 % within 15 minutes at room temperature and 97% or 95% human serum stability over 5 days, respectively. Immuno-SPECT imaging showed promising tumour uptake of 27.5 ± 6.2% ID/g (n = 4), with respectable blood clearance and low dosage in other organs after 5 days post-injection. **Conclusion:** The acyclic chelator H[4]neunpa-trastuzumab shows outstanding *in vitro* ^{111}In-radiolabeling kinetics with good tumour uptake *in vivo*.

OP-645

2-[^{18}F]Fluoro-5-iodopyridine ([^{18}F]FIPy): a novel thiol reactive prosthetic group for the fast site specific labeling at ambient temperature

A. Omrane[1,2], B. Zlatopolskiy[2,3], B. Neumaier[1,2,3]; [1]Forschungszentrum Juelich GmbH: Institute of Neuroscience and Medicine, INM-5, Juelich, GERMANY, [2]Institute of Radiochemistry and Experimental Molecular Imaging, University Clinic, Cologne, GERMANY, [3]Max Planck Institute for Metabolism Research, Cologne, GERMANY.

Aim: Novel ^{18}F-labeled prosthetic groups for the site specific labeling of sensitive biopolymers under mild conditions are highly sought after. The aim of this work was the study of the applicability of Pd-catalyzed *S*-arylation for indirect radiofluorination of biomolecules. To this end the simple and reliable procedure for the preparation of the suitable radiofluorinated iodo(hetero)arene should be first developed. **Methods:** Hitherto unknown [^{18}F]FIPy was chosen as a potential radiolabeled building block for Pd-catalyzed C(sp[2])-S coupling. The appropriate radiolabeling precursor, 1-(5-iodopyridin-2-yl)-1,4-diazabicyclo[2.2.2]octan-1-ium triflate (**1**), was prepared by the direct reaction of 2-bromo-5-iodopyridine with DABCO followed by anion metathesis using TMSOTf. [^{18}F]Fluoride was eluted from a QMA cartridge with **1** in MeOH. MeOH was evaporated at 45 °C (250 mbar) within 4 min, the appropriate solvent was added and the resulting solution was heated affording [^{18}F]FIPy. The latter was purified by SPE and thereafter conjugated with Boc-

Cys-OMe and glutathione (H-Glu-Cys-GlyOH) in aqueous THF using Pd-G3-Xantphos as catalyst. The both reaction steps were optimized with respect to different reaction parameters. The developed procedure was translated to an automated synthesis module. **Results:** [18F]⁻ recovery from an anion exchange resin using **1** (3 mg) amounted > 98%. Heating of the resulting [18F] fluoride onium salt in DMSO at 100 °C for 15 min afforded [18F] FIPy in radiochemical conversions (RCCs) of 98±2%. [18F]FIPy was isolated in 67±4% radiochemical yield (RCY) and excellent radiochemical purity (RCP) of > 98%. The subsequent **S**-arylation step afforded under optimized reaction conditions (0.5 μmol thiol, 0.1 μmol G3-Xantphos, 3 μmol NEt₃ 240 μL 50% THF, rt, 5 min) the corresponding conjugates in RCCs > 97%. The automated radiosynthesis furnished **S**-2-[18F]fluoropyrid-5-yl substituted glutathione in RCY of 35% (EOB) on two steps within 60 min. **Conclusion:** Pd-catalyzed **S**-arylation with [18F]FIPy is a powerful tool for the fast thiol specific radiolabeling of biomolecules under ambient conditions. [18F]FIPy is a valuable radiolabeled prosthetic group easily accessible using the "minimalist" approach.

1606 **Wednesday, October 25, 2017, 08:00 - 09:30, Hall F1**

Pitfalls & Artefacts 7 (Interactive) - Oncology: Pitfalls and Artefacts in PSMA PET Reading

OP-646
Introduction PSMA, EANM Procedure Guideline

W. Fendler; Ahmanson Translational Imaging Division, Department of Molecular and Medical Pharmacology, UCLA, Los Angeles, UNITED STATES OF AMERICA.

OP-647
Staging

M. Eiber; Technische Universität München, Nuclear Medicine, Munich, GERMANY.

OP-648
Restaging

P. Castellucci; S. Orsola-Malpighi, Nuclear Medicine, Bologna, ITALY.

OP-649
Response to Therapy

F. Giesel; Universitätsklinikum Heidelberg, Nuclear Medicine, Heidelberg, GERMANY.

1607 **Wednesday, October 25, 2017, 08:00 - 09:30, Hall F2**

Clinical Oncology: Anything Goes

OP-650
Regional hepatic glucose metabolism correlates with regional distribution of hepatic fat

A. Dunford¹, G. Keramida², M. Aplin¹, A. M. Peters³; ¹Royal Sussex County Hopsial ,Brighton, UK, Brighton, UNITED KINGDOM, ²Royal Brompton and Harefield Hospitals NHS,FT, London, UNITED KINGDOM, ³Royal Sussex County Hopsital ,Brighton, UK & Clinical Imaging Sciences Centre , Brighton Sussex Medical School, Brighton, UK, Brighton, UNITED KINGDOM.

Aim: Hepatic steatosis is associated with insulin resistance and hyperinsulinaemia. Insulin stimulates hepatic glucokinase, even in insulin-resistance, so hepatic glucose uptake (MRglu), which is the product of FDG clearance and blood glucose, is increased in hepatic steatosis. The intrahepatic distribution of fat is heterogeneous. The study aim was to test the hypothesis that, in addition to systemic stimuli, hepatic MRglu is also related to hepatic fat on a regional basis within the individual liver. **Methods:** Twenty patients undergoing routine PET/CT using 18F-fluorodeoxyglucose (FDG) also had dynamic PET for 30 min following FDG injection. They then had routine whole body PET/CT at 60 min post-injection. Hepatic FDG clearance was measured using Patlak-Rutland graphical analysis. The gradient of the Patlak-Rutland plot (Ki) was normalised to the intercept (V(0)), which represents hepatic FDG distribution volume. The 60 min CT was co-registered on to each of the 30 dynamic PET frames. Within transaxial sections, the liver was divided into multiple small regions of interest (ROI) of 5x5 pixels each in sections of 5 mm (range 118-586 ROI per liver). CT density (CTD) and Ki/V(0) were measured in each ROI. As FDG does not enter hepatic fat, normalisation of Ki to V(0) means that FDG clearance was referenced to lean liver, otherwise a correlation between Ki/V(0) and CTD would be inevitable. **Results:** The average mean grid value for Ki/V(0) for all 20 patients was 0.39 ± SD 0.23 ml/min/100 ml. There was a trend towards a negative correlation between mean grid Ki/V(0) and mean grid CTD (r = -0.39; p = 0.09). Throughout the 25-pixel ROIs in the individual liver, CTD and Ki/V(0) correlated negatively and significantly (p <0.05) in 16 of 20 patients, but significantly positively in none. A one-sample **t**-test on the entire set of correlation coefficients (μ = −0.244, σ = 0.12 and n = 20), with a null hypothesis of a correlation coefficient of zero, yielded a **p**-value of <0.0001. In some patients, parametric imaging showed a regional concordance between Ki/V(0) and hepatic fat, identified as reduced CTD. **Conclusions:** In addition to a systemically driven increase, hepatic MRglu is also regionally linked to the distribution of hepatic fat. This increased regional metabolism could be the stimulus for local fat deposition or conversely the result of increased FDG accumulation in metabolically active inflammatory cells migrating in response to regional fat deposition.

OP-651
Assessment of Effect of Fatty Infiltration on Hepatic FDG Uptake

F. Özülker¹, T. Özülker²; ¹University of Health Sciences, Okmeydanı Hospital, Department of Nuclear Medicine, Uskumruköy/Sarıyer/ İstanbul, TURKEY, ²University of Health Sciences, Okmeydanı Hospital, Department of Nuclear Medicine, Uskumruköy/Sarıyer/ İstanbul, TURKEY.

Purpose: Physiological liver FDG uptake in FDG PET/CT studies, has been used as a reference in the assessment of the FDG

uptake in pathological processes including malignancies. There is an ongoing debate on the effect of liver attenuation and the liver's FDG uptake. We aimed to assess the any possible effect of fatty infiltration on the standardized uptake value (SUV) of the liver. **Subjects and Methods:** A total of 88 patients were included in this study. Subjects were divided into 2 groups by calculating the Hounsfield unit (HU) of the liver from the unenhanced CT part of the PET/CT study and comparing it with that of the spleen. The fatty liver group included 42 patients (26 female, 16 male) with a mean age of 59,6 ±11,6, while the control group were consisted of 46 patients (22 female, 24 male) with a mean age of 60,2± 11. The patients whose mean liver attenuation value in terms of HU, equal and greater than that of spleen were enrolled in the control group, while the patients with a mean attenuation value of liver lower than spleen were assigned to fatty liver group. A subset of patients from the fatty liver group with a HU difference between liver and spleen of 10 or more (HUS-HUL >10) were evaluated separately. The age, DM and chemotherapy history, weight of the subjects, serum ALT and AST levels, simultaneous blood glucose levels during PET scan and the elapsed time between the FDG injection and beginning of PET scan were recorded. **Results:** The average SUVmean and SUVmax values were calculated as 2,7+/-0,7 and 3,6+/-0,9, in the fatty liver group, 2,8± 0,7 and 3,8 ± 1 in the HUS-HUL >10 group and 3,3+/-0,6 and 4,4+/-0,9, in the control group respectively. The average SUVmean and SUVmax values in the fatty liver group and the subset of of HUS-HUL >10 group were significantly different from the values in the control group (p < 0.05). The patients in the fatty liver group showed higher ALT (p=0,025), weight (p=0,001), glucose levels (p=0,001) and ratio of DM (p=0,002), than the patients in the control group. **Conclusion:** Hepatic steatosis causes a statistically significant decrease in SUVmean and SUVmax values in liver. Therefore we must be cautious while using the liver as an internal reference organ.

OP-652

The correlation between pathological profile and metabolic parameters of ^{18}F-FDG PET/CT in patients with gastroesophageal junction cancer

J. Song; Beijing Cancer Hospital, Beijing, CHINA.

Objective: Histopathologic features and molecular pathological indicators could affect the FDG uptake of primary gastroesophageal junction carcinoma (GEJC) and detection rate on ^{18}F-FDG PET/CT. The aim of this study was to evaluate the FDG uptake of local advanced GEJC by correlating it with the histopathologic features and molecular pathological indicators of the tumors. **Methods:** Data pertaining to patients with a histopathological diagnosis of GEJC between January 2010 and December 2015 were retrospectively analyzed. A total of 66 patients (59 years, 63.97±7.5 years) with locally advanced gastroesophageal junction adenocarcinoma who were referred for preoperative ^{18}F-FDG PET/CT scans were enrolled in this study. The maximum standardized uptake values (SUV$_{max}$), metabolic tumor volume (MTV), and total lesion glycolysis (TLG) of the primary tumor

were measured and calculated with the region of interest (ROI) technique. These relationship between metabolic parameters and Lauren's classification, histologic differentiation and the status of Ki-67, human epidermal growth factor receptor 2 (HER2), c-Met and epidermal growth factor receptor (EGFR) were investigated in all of GEJC patients. **Results:** Significant differences were observed between intestinal and no-intestinal (mixed and diffuse) adenocarcinoma in SUV$_{max}$ (8.23±2.83 vs 6.29±2.41, P = 0.008), SUV$_{mean}$ (4.85±1.47 vs 3.93±1.22,P=0.017), MTV (24.96 cm^3 vs 11.17cm^3; P = 0.004) and TLG (97.38 cm^3 vs 47.12 cm3, P = 0.005). SUV$_{max}$, MTV, and TLG of the moderately differentiated adenocarcinomas were significantly higher than those of the poorly differentiated ones. SUV$_{max}$ was significantly higher in the high Ki-67 index or c-Met-negative group (P=0.045, P=0.036). No significant correlation was found between metabolism parameters and the expression of Her2 and EGFR in GEJC. **Conclusion**: ^{18}F-FDG metabolism parameters in GEJC is associated with Lauren's classification, histologic differentiation, Ki-67 and c-Met expression. ^{18}F-FDG PET/CT may be useful for predicting the pathological characteristics and molecular pathological indicators and for determining the therapeutic strategy.**Corresponding author:**Xuejuan Wang

OP-653

Early variation of FDG-PET parameters as predictors of response after treatment in locally advanced pancreatic carcinoma patients

E. Incerti[1], P. Mapelli[1], E. G. Vanoli[1], S. Broggi[2], C. Gumina[3], N. Slim[3], P. Passoni[3], C. Fiorino[2], G. M. Cattaneo[2], L. Gianolli[1], N. Di Muzio[3], M. Picchio[1]; [1]Unit of Nuclear Medicine, IRCCS San Raffaele Scientific Institute, Milan, ITALY, [2]Unit of Medical Physics, IRCCS San Raffaele Scientific Institute, Milan, ITALY, [3]Unit of Radiotherapy, IRCCS San Raffaele Scientific Institute, Milan, ITALY.

Purpose: To assess the predictive role of FDG-PET parameters in locally advanced pancreatic cancer (LAPC) patients treated with induction and concomitant chemo-radiotherapy (CRT) on overall survival (OS), local relapse free survival (LRFS), distant relapse free survival (DRFS) and progression free survival (PFS). **Subjects & Methods:** Fifty-two LAPC patients (median age: 60 years; range: 35-85 years) were enrolled at San Raffaele Scientific Institute. Patients received 44.25 Gy in 15 fractions to the tumour: 24/52 patients received a simultaneous integrated boost (48-58 Gy) to a sub-volume infiltrating the great abdominal vessels. FDG-PET/CT was performed before CRT (PET-pre) and after CRT (PET-post) at a median time of 3 months after the end of CRT (range: 1-6 months). The predictive value of FDG-PET parameters between PET-pre and PET-post was investigated, including the percentage variation of mean/maximum standard uptake value (ΔSUV$_{mean/max}$), metabolic tumour volume (ΔMTV) and total lesion glycolysis (ΔTLG), estimated considering different uptake thresholds (40-50-60%). The percentage difference between gastrointestinal cancer-associated antigen (ΔGICA) levels measured at the same time of PET scans was also considered. For each parameters, the median percentage variation was used to categorize patients: log rank test and Cox regression were performed to assess the prog-

nostic value of the considered parameters on OS, LRFS, DRFS and PFS. **Results:** The median follow-up was 13 months (range: 4-129 months). Median OS, LRFS, DRFS and PFS after the start of the CRT treatment were 13, 12, 5, 4 months, respectively. ΔTLG50 showed borderline significance in predicting OS (*p*= 0.053; RR= 0.54) and was the most significant FDG-PET parameter correlated to LRFS (*p*= 0.001; RR= 0.22). The median value of LRFS was 33 months compared to 7 (*p* =0.0024) and 4 months (*p*= 0.0003), respectively for ΔMTV40 and ΔTLG50 lower/higher the best cut-off value. No correlation was found between the percentage variation of FDG-PET parameters and DRFS while the ΔGICA was a borderline significant predictor (*p*= 0.076; RR= 0.50). ΔTLG50 was significant in predicting PFS: a median PFS equal to 6 vs 3 months (*p*= 0.0009) was found depending on ΔTLG50 value. **Conclusion:** Early variation of FDG-PET parameters predicts LRFS in LAPC patients; in particular, a larger reduction of TLG50 was strongly associated to a better LRFS. The change of GICA values was found to be of borderline significance for DRFS. The combination of early variation of PET predictors and GICA is promising in identifying patients at higher risk of local and/or distant relapse.

OP-654

Robotic arm assisted real time ¹⁸F-FDG PET/CT guided percutaneous metabolic sampling of abdominal lesions-Initial Experience

R. Kumar, B. R. Mittal, H. Singh, T. K. Jain, A. Sood, A. Bhattacharya; PGIMER, Chandigarh, INDIA.

Objective: In this prospective study, we aimed to establish the feasibility of automated robotic arm (ARA) assisted ¹⁸F-FDG PET/CT-guided sampling of abdominal lesions and its diagnostic utility in patients with prior inconclusive conventional image-guided biopsies. **Materials and Methods:** Forty-nine patients (30 males, 19 females) with median age 51.84 years (22-78 years) with abdominal masses but prior inconclusive conventional biopsy results were subjected to ARA assisted PET/CT-guided biopsy. All patients underwent diagnostic ¹⁸F-FDG PET/CT scan prior to PET/CT-guided percutaneous biopsy. The site of biopsy was planned from the most accessible FDG avid lesion in each case. The intervention was planned 2 hours after the initial diagnostic study by obtaining a limited field of view PET/CT. The needle trajectory was planned with the help of automated robotic arm (ARA) needle navigation technique. After confirming the position of the needle tip to the target site, real time sampling was done. To check the accuracy of the interventional procedure, histopathology reports were reviewed. For confirmation of negative results, clinical or imaging follow-up was done. **Results:** Among the total 49 patients, PET-guided biopsy was performed from lesions in retroperitoneum (n=21), mesentery and anterior abdomen (n=8), iliac lymph nodes/ pelvis (n=6), liver (n= 5); kidney (n=3); pancreas (n=2), and one each from spleen, adrenal, stomach and ileocaecal junction. Diagnostic results were yielded in all biopsy procedures. Malignancy was detected in 36 patients while 7 patients with minimal residual FDG uptake on follow-up PET/CT did not show any residual tumor from the biopsy tissue. Remaining six patients had benign etiology

(tuberculosis-1 sarcoidois-1, follicular hyperplasia-1, hepatitis-1, pyelonephritis-1 and inflammation -1). Repeat biopsies were done in two patients, one with no residual tumor and other with inflammation on the previous biopsy, yielded the same results. So far, the clinical and imaging follow-up in disease negative patients was uneventful. No immediate complications or delayed life threatening event related to the procedure were noted in our patients. The diagnostic yield of real-time PET/CT-guided metabolic biopsy from abdominal lesions was 100%. **Conclusions:** ARA assisted ¹⁸F-FDG PET/CT-guided percutaneous real time metabolic sampling of abdominal lesions is technically feasible with high diagnostic yield in patients with prior inconclusive biopsies.

OP-655

The Role of ¹⁸F-Sodium Fluoride (NaF) PET-CT in the evaluation of metastatic bone disease in morbidly obese patients

S. Usmani, F. Marafi, A. Esmail, F. al kandari; Kuwait Cancer Control Center, kuwait, KUWAIT.

Purpose: Diagnostic imaging remains challenging in obese patients. The quality of conventional bone scintigraphy is generally poor in the morbidly obese due to a combination of factors including high background soft tissue activity. In comparison, ¹⁸F-sodium fluoride (NaF) PET-CT has a better target to background ratio attributed to rapid single-pass extraction and fast clearance from the soft tissues. The aim of the present study is to evaluate the emerging role of ¹⁸F-NaF PET-CT in the evaluation of bone metastases in morbidly obese patients. **Subjects and Methods:** Two hundred and twelve morbidly obese patients (BMI 45±5.1 Kg/m² and mean age, 57years; range 32-81years) with BMI >40kg/m² referred for ¹⁸F-NaF PET-CT for osseous staging of malignancy were retrospectively analyzed. All patients underwent PET-CT scan by injecting 0.06 mCi/kg of ¹⁸F-NaF. **Results:** ¹⁸F-NaF PET-CT was definitely benign in 145, possibly benign in 3; equivocal in 4; possibly malignant in 13 and definitely malignant in 47 patients. The sensitivity, specificity, PPV, NPV and accuracy of 18F-NaF PET-CT were 93.1%, 96.1%, 90%, 97.3% and 95.2% respectively (p<0.001). **Conclusions:** The results of the present study indicate that ¹⁸F-NaF PET-CT retains its high diagnostic accuracy in morbidly obese patients and may even be a preferred modality for this patient group.

OP-656

Tc-99m-DPD bone scan quantification: Metastasis of prostate cancer vs. osteoarthritis

F. Tabotta, M. Jreige, N. Schaefer, J. O. Prior, M. Nicod Lalonde; CHUV, Lausanne, SWITZERLAND.

Purpose: Bone scintigraphy with Tc-99m labeled DPD can identify metastatic prostate bone lesions with a high sensitivity but a low specificity, as benign conditions and especially osteoarthritis also trigger an osteoblastic reaction. The aim of this study is to investigated the emerging role of Tc-99m DPD

uptake quantification in order to compare the value of SUV in metastases and degenerative lesions. **Materials and Methods:** retrospectively assessed 12 patients (mean age 70±9 years) with known bone metastases of prostate cancer and 17 patients (mean age 70±12 years) with benign degenerative conditions without any known neoplastic condition. Quantitative xSPECT/CT (Siemens SYMBIA INTEVO) was acquired and SUV quantified on post-processed images with measurements of SUVmax and SUVmean (g/ml) in all bone metastasis and in the degenerative lumbar spine changes for the osteoarthritic group. We also used receiver operating characteristics (ROC) curves to determine the metastatic vs. benign origin of lesions. **Results:** A total number of 128 metastatic lesions (100 blastic, 3 lytic and 25 mixed) were analyzed showing a mean SUVmax and SUVmean (g/ml) of 46±29 (18-176) and 29±18 (11-96), respectively. In 17 osteo-arthritic lesions (mainly blastic) mean SUVmax and SUVmean were of 16.6±2.4 (12.4-20) and 11.8±1.7 (8.9-14.7) respectively. Comparison of both SUVmax and SUVmean between the metastatic and osteoarthritic groups showed a statistically significant difference with p<0.0001 for both, with SUVmax offering significantly better accuracy (AUC 0.989 vs. 0.959, p=0.009). Using a SUVmax threshold of 20 g/mL to define bone metastatic lesion, we found a sensitivity, specificity, positive and negative predictive vales of 94%, 94%, 99% and 67%, respectively. **Conclusions:** This study showed significant differences in Tc-99m-DPD uptake on bone scan between prostate metastatic lesions and osteoarthritic changes based on quantitative data analysis, with significantly higher SUVmax and SUVmean in metastases, with better accuracy for SUVmax. Thus, quantitative analysis of bone scan quantitative data can be helpful for diagnosing malignant lesions by increasing its specificity.

OP-657

Convolutional neural networks for segmentation of 49 selected bones in CT images show high reproducibility

M. Sadik[1], R. Kaboteh[1], O. Enqvist[2], J. Ulén[3], E. Trägårdh[4], M. H. Poulsen[5], J. A. Simonsen[6], P. F. Høilund-Carlsen[6], L. Edenbrandt[1]; [1]Department of Clinical Physiology, Göteborg, SWEDEN, [2]Department of Signals and Systems, Göteborg, SWEDEN, [3]Eigenvision AB, Malmö, SWEDEN, [4]Department of Translational Medicine, Malmö, SWEDEN, [5]Department of Urology, Odense, DENMARK, [6]Department of Nuclear Medicine, Odense, DENMARK.

Aim: An automated method to calculate Bone Scan Index (BSI) from bone scans has recently been established as a first imaging biomarker in patients with metastatic prostate cancer. BSI has shown to be an independent predictor of survival. PET/CT is more accurate than bone scans in detecting bone metastases. We therefore decided to develop an automated PET/CT based imaging biomarker for assessment of tumor burden in bone. The aim of this project was to develop a method for automated segmentation and volume calculation of bones in CT images, which is the first step in the process of developing a PET/CT based imaging biomarker. **Materials and Methods:** Convolu-

tional neural networks (CNN) were trained to segment 49 selected bones (12 thoracic vertebrae, 5 lumbar vertebrae, sacrum, 2 hip bones, 24 ribs, 2 scapulae, 2 clavicles and the sternum) using manual segmentations in CT images from 23 patients performed by experienced image readers. Anatomical landmarks were detected using a CNN and pruned using a shape model. These landmarks and the CT image were fed to a second CNN, segmenting the 49 selected bones. After the training process, the CNN segmented the bones in CT images in a separate validation group consisting of 46 patients with prostate cancer. All patients had undergone both 18F-Choline and 18F-NaF PET/CT within a time frame of 3 weeks as part of a previous research project. The two CT scans from each patient were segmented by the CNN and the two volumes of each bone were calculated. **Results:** The total volume of the 49 bones was on average 3,086 mL in the 46 patients. The individual bones ranged in volume from 8 mL (left 12th rib) to 440 mL (left hip bone). The reproducibility measured as ratio volume difference/mean volume was on average less than 2% for all bones except for the ribs. The mean volumes, differences and reproducibility for the bones of five anatomical regions were as follow: thoracic vertebrae 39mL, 0.6mL, 1.5%; lumbar vertebra 71mL, 0.8 mL, 1.2%; sacrum, hip bones 386mL, 0.9mL, 0.3%; ribs 26mL, 2.0mL, 8.5%; scapulae, clavicles, sternum 97mL, -0.1mL, -0.4%. **Conclusion:** Our CNN based method for automated segmentation of bones in CT images showed high reproducibility. A reproducible way to segment the skeleton and to measure the bone volume will be important in the development of a PET index relating volumes of abnormal PET tracer uptake to the bone volume.

Cardiovascular System: Myocardial Perfusion PET - 82-Rubidium

OP-658

Prognostic Value of Quantitative Coronary Artery Calcium and Myocardial Blood Flow Assessed by Hybrid Rubidium-82 PET/CT Imaging in Patients With Suspected Coronary Artery Disease

E. Zampella[1], R. Assante[1], T. Mannarino[1], G. De Simini[1], A. Genova[1], M. Panico[2], V. Gaudieri[2], C. Nappi[1], C. Mainolfi[1], W. Acampa[1], M. Petretta[3], P. Arumugam[4], A. Cuocolo[1]; [1]Department of Advanced Biomedical Sciences, University Federico II, Naples, ITALY, [2]Institute of Biostructure and Bioimaging, National Council of Research, Naples, ITALY, [3]Department of Translational Medical Sciences, University Federico II, Naples, ITALY, [4]Department of Nuclear Medicine, Central Manchester University Hospitals, Manchester, UNITED KINGDOM.

Aim: In this study we sought to evaluate the long-term prognostic value of coronary artery calcium (CAC) score and myocardial blood flow (MBF) by hybrid 82rubidium (82Rb) positron emission tomography (PET)/computed tomography (CT) imaging in a cohort of patients with low-intermediate risk of coronary ar-

tery disease (CAD). **Materials and Methods:** A total of 410 consecutive patients (mean age 56±13 years) with suspected CAD were studied. CAC score was measured according to the Agatston method and patients were categorized into 3 groups (0, 1-400 and >400). Baseline and hyperemic MBF were automatically quantified. Coronary flow reserve (CFR) was calculated as the ratio of hyperemic to baseline MBF and it was considered reduced when <2. Patients were followed up for the presence of composite endpoint of cardiac death, nonfatal myocardial infarction, or unstable angina requiring coronary revascularization whichever occurred first. **Results**: The median follow-up was 47±15 months and follow-up data were not available in 26 patients (6%). Patients who experienced events showed higher CAC score (P<0.001) and lower hyperemic MBF (P<0.05) and CFR (P<0.001) values compared to patients without events, while there were no differences in baseline MBF between the two group of patients. Event rate significantly increased with increasing of CAC score categories (P for trend <0.001) and it was higher in patients with reduced CFR (P<0.001). At multivariable analysis, CAC score >400 (P=0.006) and CFR (P=0.004) were independent predictors of events. Event-free survival decreased with worsening of CAC score category (P<0.001) and in patients with reduced CFR (P<0.005). CAC score added prognostic information to a model including in hierarchical order clinical variables, increasing the global chi-square from 23.16 to 33.70 (P=0.002). The addition of CFR to a model including clinical data and CAC score further increased the global chi-square from 33.70 to 42.45 (P=0.001). **Conclusion**: In patients with low-intermediate risk of CAD both the extent of coronary calcification and the presence of coronary vascular dysfunction are associated with increased risk of adverse cardiac events, even after adjustment for cardiovascular risk factors. CAC score and CFR are independent predictors of events, however CFR provides incremental prognostic information over established CAD risk factors and CAC score. Combined evaluation of functional and structural abnormalities by hybrid 82Rb PET/CT imaging might allow risk stratification in patients with low-intermediate risk of CAD.

OP-659

Cardiac ⁸²Rb PET/CT: The added value in diabetic Heart Transplant Patients

M. L. De Rimini[1], G. Borrelli[1], A. Russo[2], S. Carrino[3], C. Maiello[4], P. Muto[1]; [1]Nuclear Medicine Unit - AO Ospedali dei Colli - Monaldi, Naples, ITALY, [2]Cardiovascular Unit; Vanvitelli University of Campania, Naples, ITALY, [3]Pharmacy Unit - AO Ospedali dei Colli - Monaldi, Naples, ITALY, [4]Cardiac Transplant Unit - AO Ospedali dei Colli - Monaldi, Naples, ITALY.

Introduction: The integration of cardiac PET in CAD disease management algorithms, with evaluation of myocardial blood flow (MBF) and flow reserve (MFR), will advance quality of care. This capability can be even more effective in heart transplant (HTx) recipients, considering that chronic immunologic responses afflicts first small vessels rather than the main ones and that it appears to be the cause of the occlusive long term cardiac allograft vasculopa-

thy (CAV). At state, it remains unclear whether mild, diffuse intimal thickening in the epicardial arteries of HTx recipients affects the functional status of the coronary tree. Aim: To evaluate the value of cardiac PET and MFR evaluation in HTx patients (pts). Methods: 82Rb (50mCi/phase) PET/CT (Siemens, 3D PET/CT Biograph, 16 slices) was obtained in Basal conditions and after Dypiridamole (0.56 mg/kg over 4 min) in 20 HTx pts. Dynamic protocol in list-mode was obtained and these dynamic studies were reconstructed from list mode. MBF, MFR and semiquantitative perfusion analysis were obtained with Quantitative PET (Q-PET) - Cedars-Sinai (by Germano). MFR value <2.0 was considered abnormal. Pts were selected in a larger population of HTx recipients, based on the following criteria: transplantation for at least 5 years, the absence of history of acute and chronic rejection and of stenosis at coronary angiography. 9 pts out of 20 were diabetic for at least 5 years, treated with oral therapy. Results: No evidence of transient ischemia at ECG during pharmacological test. Normal perfusion scans were found in all pts (average summed scores obtained: SSS=3; SDS=1; Extension perfusion defect Dypiridamole less than 2%). MBF and MFR were shown markedly reduced in diabetic pts than in non-diabetic ones, with a range of estimated values of MFR ranging from a maximum of 1.9 to a minimum of 1.1. Discussion: Chronic rejection still remain the major drawback of long-term positive outcome after HTx. In apparently healthy HTx subjects a reduced MFR in diabetic pts, compared with the normal MFR of non diabetic ones, can be a strong and independent predictor of outcome in HTx diabetic patients without evidence of main coronary artery disease and with negative dipyridamole stress test. Conclusion: In our limited, but strictly selected population of HTx pts, diabetes can be confirmed as a factor influencing MFR. Therefore, our results suggest that PET/CT with MFR evaluation could be particularly suitable for improving detection of CAV and for clinical management of HTx pts.

OP-660

Relationship between microvascular disease assessed using myocardial flow reserve with 82Rubidium positron emission tomography and the severity of diabetic nephropathy

*L. Potier[1], R. Chequer[2], C. Amouyal[3], K. Mohammedi[4], A. Hartemann[5], M. Marre[4], R. Roussel[4], D. Le Guludec[2], **F. Hyafil**[2]; [1]Department of Diabetology, Bichat Hospital, AP-HP, PARIS, FRANCE, [2]Department of Nuclear Medicine, Bichat Hospital, APHP, PARIS, FRANCE, [3]Department of Daibetology, Pitié-Salpetrière Hospital, APHP, PARIS, FRANCE, [4]Department of Diabetology, Bichat Hospital, APHP, PARIS, FRANCE, [5]Department of Diabetology, Pitié-Salpetrière Hospital, APHP, PARIS, FRANCE.*

Introduction: Diabetes mellitus is a cardiovascular risk factor for coronary atherosclerosis but is also involved in the alteration of myocardial microcirculation. 82Rubidium PET imaging (Rb-PET) offers to assess the microcirculation through the quantification of myocardial flow reserve (MFR). Our objective in this study was to evaluate in diabetic patients the link between alterations of microcirculation in the myocardium measured with Rb-PET and the severity of diabetic nephropathy.

Methods: Myocardial flow reserve (MFR) was measured with Rb-PET in 219 patients referred for screening of CAD. Patients with CAD were excluded from the analysis. Among the 184 remaining patients, global myocardial flow were calculated on PET acquisitions at rest and under pharmacological stress (dipyridamole) using the FlowQuant software. Global MFR was calculated as the ratio between stress and RPP-corrected rest myocardial flow. Plasmatic creatinin and urinary albumin concentrations were retrospectively collected in diabetic patients for the grading of the severity of diabetic nephropathy. **Results:** Mean age of patients was 59.1 ± 10.2 years ; 55.8 % of patients were women. Among the 184 patients, 127 were diabetic patients with an average exposure to diabetes of 13.0 ± 9.2 years and a mean HbA1c of 8.5 ± 1.7 %. Micro-albuminuria was present in 35 patients (27.6%) and macro-albuminuria in 12 patients (9.4 %). Rest LVEF was similar in patients with absent, micro- or macro-albuminuria (56.0±1.0 % ; 56.2±1.8 % ; 54.1±6.0 %, respectively ; p = 0.80). Mean global MFR was lower and the prevalence of patients with MFR < 2 was higher in diabetic than in non-diabetic patients (2.7 ± 1.1 vs. 3.4 ± 1.8, p < 0.01 ; 30.7 vs. 15.8 %, p < 0.05; respectively). Patients with absent, micro- or macro-albuminuria had mean global MFR measured at 2.9 ± 1.2, 2.3 ± 1.0 and 1.8 ± 0.7, and a prevalence of abnormal MFR of 18.8 %, 42.9 % et 75.0 %, respectively (p < 0.05 for differences between groups). In logistic regression analyses using different model of adjustment, microalbuminuria and macroalbuminuria were associated with a 3 and 13-fold increased risk of impaired MFR respectively. **Conclusions:** In this study, we found a strong association between the decrease of MFR quantified with Rb-PET and the severity of diabetic nephropathy. These results suggest that microvascular dysfunction in the heart and in kidneys might share common mechanisms in diabetic patients and represent an early marker of diabetic cardiomyopathy.

OP-661

Low-dose myocardial blood flow imaging using 82Rb-PET (RUBILOW 2.0)

C. M. Hoff, L. P. Tolbod, H. J. Harms, K. Bouchelouche, J. Frøkiær, J. Sørensen; Aarhus University Hospital, Aarhus, DENMARK.

Aim: Relative and absolute measures of myocardial blood flow (MBF) can be derived from a 82Rb PET/CT scan using list mode data to extract static, gated and dynamic PET series. High doses of 82Rb are used to maximize image quality in especially static images. High doses require large eluate volumes, may degrade scanner dead time performance at first pass and decreases generator lifetime. Lower doses will expand the availability of 82Rb PET/CT and lower doses to personnel and patients. The aim of the current study was to examine MBF with a low dose (LD) 82Rb protocol compared to the institution's standard (STD) protocol. **Methods:** Twenty-one patients referred to 82Rb PET were included in the study. Patients were examined during rest and stress with repeated LD (740 MBq) and STD dose (1110 MBq) Rb-PET during the same imaging session. Regional and global rest and stress MBF values, total perfusion deficit (TPD), ejec-

tion fraction (EF) and %-perfusion using the 17-segment model were calculated using commercially available software QPET (Cedars Sinai). **Results:** Five patients had to be excluded due to motion during STD (n=2) and LD (n=3). For the remaining patients, there was excellent correlation between STD and LD global MBF (STD=0.91xLD+ 0.08, R^2=0.95, p<0.001). Mean global MBF (±SD) at rest was 1.01 ±0.31 and 1.06±0.30 mL/g/min at STD and LD (p=0.17), and at stress 2.44±0.48 and 2.57±0.55 mL/g/min at STD and LD (p=0.07), respectively. On the segmental level, correlation between STD and LD MBF was high (STD=0.91xLD+0.09, R^2=0.92, p<0.001). Mean segmental MBF (±SD) at rest was 1.01 ±0.35 and 1.06±0.35 mL/g/min at STD and LD (p<0.001), respectively. At stress mean segmental MBF was 2.44±0.70 and 2.58 ±0.75 mL/g/min at STD and LD (p<0.001), respectively. There was an excellent correlation between STD and LD TPD (STD=0.90xLD-0.42, R^2=0.95, p<0.001). Mean TPD with STD was 7.5±6.9% and 8.8±7.5% with LD (p<0.001). Mean %-perfusion with STD was 77.3±9.0% and 76.4±9.1% with LD patients (p<0.001) with a good correlation between STD and LD %-perfusion (STD=0.92xLD+7.15, R^2=0.86, p<0.001). Mean EF with STD patients was 65±9% and 65±8% in LD patients (p=0.90) with a good correlation (STD=1.06xLD-3.70, R^2=0.90, p<0.001). **Conclusions:** The 82Rb dose can be lowered to 740 MBq without loss of diagnostic accuracy for both absolute and relative measurements. The low dose protocol should be implemented into clinical routine if a modern scanner is available. This will reduce radiation burden and increase patient throughput per generator.

OP-662

Value of Rubidium-82 Flow Measurements in Patients with CABG

B. J. H. G. van Gageldonk[1], A. T. L. Fiolet[1], I. E. M. Bank[2], A. Mosterd[1], H. J. Verberne[3], J. M. H. de Klerk[1], **A. M. Scholtens**[1]; *[1]Meander Medical Center, Amersfoort, NETHERLANDS, [2]University Medical Center, Utrecht, NETHERLANDS, [3]Academic Medical Center, Amsterdam, NETHERLANDS.*

Purpose: Rubidium-82 Positron Emission Tomography (Rb-82 PET) is a reliable technique to detect ischemia. Global myocardial stress flow in native coronary arteries (cut-off 2.0mL/g/min) is strongly related to clinical outcome. However, grafted coronary arteries may have different myocardial stress flow, due to differences in blood-to-vessel wall interactions and differences in diameter between arterial and venous grafts compared to native coronary arteries. Rb-82 PET myocardial stress flow values have not been validated for grafted coronaries specifically. Therefore we investigated Rb-82 PET global myocardial stress flow in patients who had undergone coronary artery bypass grafting (CABG). **Methods:** A retrospective analysis of all Rb-82 PET scans (n=2819) performed in our institution between February 2014 and May 2016 identified 295 scans in post-CABG patients. These patients were divided based on global myocardial stress flow ((<1.8mL/g/min; low (group 1, n=106), 1.8-2.0mL/g/min; borderline-low (group 2, n=39), >2.0mL/g/min; normal (group 3, n=150)). Left ventricular ejection frac-

tion (LVEF), myocardial blood flow and summed difference scores (SDS, indicating extent of ischemia) were compared across groups. During follow-up coronary revascularizations and acute coronary syndromes (ACS) were recorded. **Results:** Group 1 was minimally older than groups 2 and 3 (74.6±7.9 vs 71.6±10 vs 71.4±9.1 years, p<0.05) and had a higher percentage of males (86.8% vs 76.9% vs 64.7%, p<0.05). Grafts in group 1 were implanted longer ago than in the other groups (Graft age 13.1±7.9 vs 9.2±6.3 vs 9.7±7.2 years, p<0.05). Rb-82 PET measurements in the 'borderline-low' and 'low' group were comparable in terms of SDS (6.1±5.4 vs 4.2±4.4, p=0.100) and both resting LVEF (50.8±15.5% vs 55.3±13.6%, p=0.203) and stress LVEF (51.2±15.5% vs 57.3±14.0%, p=0.067). The 'normal' group had lower SDS (2.4±3.5) and higher LVEF in rest and at stress (62.1±11.5% and 64.5±11.6%, respectively). There was a significant difference across groups in patients free of ACS and/or revascularization during follow-up (71.4% vs 79.5% vs 88.1%, p=0.003; mean follow-up 644 days). **Conclusion:** Established Rb-82 PET myocardial blood flow velocity cut-off values provide useful (prognostic) information in CABG patients, comparable to the evaluation of native coronary arteries.

OP-663

Higher diagnostic performances of 82Rubidium-PET in comparison to SPECT myocardial perfusion scintigraphy for the detection of three-vessel coronary artery disease

F. Hyafil[1], R. Chequer[1], E. Sorbets[2], T. Alfaiate[3], H. Regaieg[1], F. Rouzet[1], N. Mikail[1], G. Ducrocq[4], R. Ben Azzouna[1], S. Leygnac[1], M. Milliner[1], C. Estellat[3], D. Le Guludec[1]; [1]Department of Nuclear Medicine, Bichat Hospital, AP-HP, Paris, FRANCE, [2]Department of Cardiology, Avicennes Hospitall, AP-HP, Bobigny, FRANCE, [3]Unite de Recherche Clinique Paris Nord, Bichat Hospital, AP-HP, Paris, FRANCE, [4]Department of Cardiology, Bichat Hospital, AP-HP, Paris, FRANCE.

Introduction: PET-MPS provides absolute quantification of stress and rest myocardial blood flow (MBF) and might improve the detection of balanced myocardial ischemia. The aim of this study was to compare the diagnostic performance of [99m]Technetium (Tc)-MIBI-SPECT-MPS and [82]Rubidium (Rb)-PET MPS for the detection of three-vessel coronary artery disease (3V CAD) in a population with a pre-test intermediate prevalence of CAD. **Methods:** All patients underwent gated MPS with ^{99m}Tc-MIBI using CZT cameras in association to the best stress test feasible and gated MPS with [82]Rb-PET during pharmacological stress with dipyridamole. Patients with at least one MPS considered as positive were referred for coronary angiography (CA). Patients were classified as positive for myocardial ischemia in case of significant stenosis (≥ 70%, or ≥ 50 % and FFR ≤ 0.8) on CA or, in absence of CA, occurrence of cardiovascular event during the following year. **Results:** Among 292 patients after exclusion of 16 patients with missing data, 17 patients had 3V-CAD or equivalent (LM stenosis > 50 % or significant stenosis of the proximal LAD), 17 patients 1- or 2-vessel CAD and 29 no significant coronary stenosis, or normal SPECT and PET-MPS with no cardiovascular event at follow-up (n = 229). The presence of LV end-di-

astolic dilatation ≥ 20 ml between stress and rest acquisitions had sensitivity and specificity for 3V-CAD of 31 % and 96 % with SPECT-MPS and 56 % and 86 % with PET-MPS (p = 0.01 for sensitivity; p < 0.001 for specificity); the presence of LVEF difference between stress and rest ≤ - 10 % for SPECT and ≤ 0 % for PET a sensitivity and specificity of 6 % and 91 % with SPECT-MPS, and 75 % and 83 % with PET-MPS, respectively (p < 0.05 for both). Sensitivity and specificity for the detection of 3V-CAD was 94 % and 60 % for stress MBF ≤ 1.8 ml/mn/g, and 81 % and 73 % for MFR ≤ 2.0. The association of diff. LVEF ≤ 0 % and decreased global stress MBF ≤ 1.8 ml/mn/g allowed for the identification of patients with 3V-CAD with a sensitivity of 75 %, a specificity of 92 % and an accuracy of 91 %. **Conclusions:** The detection of LV dysfunction and decreased global stress MBF with Rb-PET-MPS translates into higher diagnostic performances for the detection of patients with 3V-CAD in comparison to SPECT-MPS.

OP-664

Need for Correction of Myocardium Movement during Dynamic Rubidium-82 Stress PET for Accurate Myocardial Blood Flow Quantification

S. S. Koenders[1,2], J. D. van Dijk[1], P. L. Jager[1], C. H. Slump[2], J. Ottervanger[3], J. A. van Dalen[4]; [1]Department of Nuclear Medicine, Isala, Zwolle, NETHERLANDS, [2]MIRA: Institute for Biomedical Technology and Technical Medicine, University of Twente, Enschede, NETHERLANDS, [3]Department of Cardiology, Isala, Zwolle, NETHERLANDS, [4]Department of Medical Physics, Isala, Zwolle, NETHERLANDS.

Introduction: The use of myocardial blood flow (MBF) quantification with Rubidium-82 PET is rapidly growing. However, an upward creep of the myocardium may occur during dynamic stress acquisition due to an increase in lung volume and thereby repositioning of the diaphragm and myocardium in the post-pharmacological exercise period. This effect may result in a biased MBF measurement and hence hamper diagnostic accuracy. Our aim was to determine the impact of correcting for myocardium movement on MBF quantification during Rubidium-82 stress PET. **Subjects & Methods:** We retrospectively included 46 consecutive patients who underwent dynamic rest-pharmacological induced (Regadenoson) stress PET/CT (GE Discovery 690, GE Healthcare) with Rubidium-82. Dynamic data of both the rest and stress examinations were processed using Corridor4DM (v2015.02.64) software. Myocardium contours were automatically detected in both rest and stress. Upward creep during stress was assessed by identifying differences between the contour and the activity as observed in each of 26 reconstructed time-frames. If differences were observed, manual re-alignments were performed. Rest MBF and uncorrected and motion-corrected stress MBF were calculated for the three vascular territories: left anterior descending (LAD), left circumflex artery (LCX) and right coronary artery (RCA). MBF was calculated using the one-tissue compartment model of Lortie et al. based on region of interest methodology. Furthermore, coronary flow reserve (CFR, ratio of MBF at stress to rest) was calculated. **Results:** Myocardium movement was observed in 25 (54%) of the

46 patients. The mean differences in MBF between the non-corrected and motion-corrected stress data were -0.20 (range: -1.48 to 0.74), 0.05 (-1.00 to 1.35) and 1.60 (-0.68 to 7.67) ml/min/g for the LAD (p=0.15), LCX (p=0.3) and RCA (p<0.001), respectively. Motion correction resulted in a decreasing MBF in the RCA in 23 of the 25 patients. The lower MBF of the RCA also resulted in a significant decrease in mean CFR from 4.2 to 2.7 (p<0.001). **Conclusion:** Correction of the upward creep during Rubidium-82 stress PET significantly changes myocardial blood flow and coronary flow reserve quantification of the RCA, but neither of the LAD nor LCX. Myocardium movement detection and correction during dynamic Rubidium-82 stress PET likely improves accurate MBF quantification.

OP-665

Estimation and reliability of myocardial blood flow after motion correction with dynamic PET using a Bayesian framework

A. Saillant[1,2], K. Saint[3], M. Memmott[3], I. Armstrong[3], V. Shah[2], S. Zuehlsdorff[1], J. Declerck[4], M. Jenkinson[2], M. Chappell[2]; [1]Siemens Healthineers, Knoxville, TN, UNITED STATES OF AMERICA, [2]University of Oxford, Oxford, UNITED KINGDOM, [3]Central Manchester University Hospital, Manchester, UNITED KINGDOM, [4]Siemens Healthineers, Oxford, UNITED KINGDOM.

Introduction: The measurement of myocardial blood flow (MBF) in dynamic PET can be biased by many different processes. A major source of error is motion. The objective of this study was to measure the MBF along with an estimate of confidence in MBF from dynamic PET imaging. We employed a Bayesian inference framework that represents the kinetic parameters as a probability distribution, from which a confidence was estimated. We studied the percentage change of confidence in MBF after a manual motion correction in patients. **Subjects & Methods:** A cohort of 10 patients comprising Rubidium dynamic stress datasets was examined. The datasets were screened by an independent reviewer and considered to have a significant patient motion. The blood input function (BIF) and the time activity curves (TACs) were extracted using *syngo*.via (Siemens Healthineers). The motion was corrected using a rigid frame wise manual registration, starting from the last frame as reference. Only 3D translations were applied. The TACs were fitted with a one compartment model, with spillover factor (SF). We used a Variational Bayes (VB) algorithm for nonlinear model fitting. Each parameter (K1,k2,SF) was represented by a Normal (marginal) distribution $N(\mu,\sigma^2)$, where μ is taken as the best estimated parameter value, and σ as a measure of confidence in the estimate. Here K1 is used a surrogate for MBF. The percentage difference $\sigma/\mu(K1)$ is calculated before and after correction for the global value and individual coronary territories. It is calculated as follows: 100*(Original - MotionCorrected)/ Original. **Results:** On average for all patients, there was a 39% increase in the global value after motion correction implying that the correction impacted positively the confidence. For LAD, LCX and RCA territories increase of 25%, 50% and 69% was observed respectively. A large rise was seen in the RCA on average, imply-

ing that motion correction was most important here. **Conclusion:** In this preliminary study, we have demonstrated the use of a Bayesian inference scheme for MBF estimation that permits not only kinetic parameter estimation, but also the provision of confidence estimates. This could be used to examine the effectiveness of a rigid motion correction strategy, but could be extended in future to automatically assess the effectiveness of other pre-processing tasks.

1610   **Wednesday, October 25, 2017, 08:00 - 09:30, Hall G2**

Do.MoRe: Dosimetry in Diagnostic Nuclear Medicine

OP-666

Voxel based internal dosimetry of radiopharmaceuticals in diagnostic nuclear medicine

N. Petoussi-Henss[1], J. Ocampo Ramos[2], M. Zankl[1], W. Li[1], W. Rühm[1]; [1]Helmholtz Zentrum München, Neuherberg, GERMANY, [2]Universidad National de Colombia, Medellín Branch, COLOMBIA.

Aim: The aim of this presentation is to discuss the new framework of the International Commission of Radiological Protection, ICRP, for internal dose assessment for radiopharmaceuticals and highlight the differences from the previous framework. A further aspect is to discuss the accuracy of the calculations when applied to a real patient rather than the standard individual. Effective and organ doses per administered activity for reference as well as non-reference adults and for exposures due to some frequent diagnostic nuclear medical examinations will be presented. Furthermore, the mass scaling assumption used when the organ masses of the patient are known is investigated. **Background**: Radiation dose estimates require the use of biokinetic models, radionuclide decay scheme data, and values of Specific Absorbed Fractions (SAF). Recently the ICRP has released SAF for photons, electrons, alphas and fission-spectrum neutrons derived from Monte Carlo radiation transport simulations in the ICRP reference adult male and female voxel phantoms as well as in the human alimentary and respiratory tract models (ICRP Publication 133, 2017). **Methods:** A new user-friendly computer program with graphical user interface has been developed aiming at estimating the organ and effective doses to an individual due to internal exposures in nuclear medicine once the kinetic model is defined. In contrast to other programs which utilize a single adult male and a single adult female stylized phantom of reference size, the new software is employing, besides the new ICRP SAFs, a library of pre-calculated SAFs of photons and electrons, based on several anthropomorphic voxel phantoms of non-reference size. Furthermore, the software is using the most recent nuclear decay data and has been extensively beta-tested against other methods. **Results:** 1) Organ and effective dose coefficients for the reference person will be shown for some commonly used radiopharmaceuticals, calculated using the new ICRP data set (Publication 133). These values will be compared with those of ICRP Publication 128 (2015) and potential differences will be discussed. 2). Organ

and effective dose coefficients for non-reference persons will be calculated using the respective SAFs, previously obtained with Monte Carlo methods. 3) Organ and effective dose coefficients for the non-reference persons will be calculated using the SAFs of ICRP Publication 133 based on reference phantoms and by applying the mass scaling assumption. These will be compared with those calculated as in (2). The accuracy of the calculations when applied to a real patient rather than the standard individual will be discussed.

OP-667

IDAC-Dose 2.1, an internal dosimetry program for diagnostic nuclear medicine using the official ICRP specific absorbed fractions for the adult ICRP/ICRU reference computational voxel phantoms

M. Andersson[1], L. Johansson[2], K. Eckerman[3], S. Mattsson[1]; [1]Medical Radiation Physics, Malmoe, SWEDEN, [2]Department of Radiation Sciences, Umeå, SWEDEN, [3]Center for Radiation Protection Knowledge, Oak Ridge National Laboratory, Oak Ridge, TN, UNITED STATES OF AMERICA.

Aim and Background: Committee 3 of the International Commission on Radiological Protection (ICRP) Task Group 36 estimates of absorbed dose in organs and tissue and the effective dose to patients from various radiopharmaceuticals to date have been derived using the computed program Internal Dose Assessed by Computer (IDAC). IDAC-Dose 1.0 has been used to perform the dose calculations based on photon specific absorption fractions (SAF) simulated from the mathematical phantoms created by Cristy and Eckerman in 1987. To improve the accuracy of the calculations, ICRP has now adopted a more realistic voxel phantom to incorporate in Monte Carlo (MC) simulations of new photon, electron and alpha SAF-values. The internal dosimetry computer program, IDAC-Dose, has been substantially upgraded (IDAC-Dose 2.1) and incorporates these SAF-values (ICRP 133) for calculations of the absorbed doses and the effective dose. **Material & Methods:** With IDAC-Dose 2.1 it is possible to calculate the dose from 1252 different radionuclides. The program uses the latest biokinetic models and assumptions of the ICRP TG 36, which also includes the incorporation of the Human Alimentary Tract Model (ICRP 100) and the latest tissue weighting factors (ICRP 103). The S-values are generated through mono-energetic photon, electron and alpha SAF-values given in ICRP Publication 133 generated for the adult voxel phantoms and decay data of ICRP publication 107. The IDAC-Dose 2.1 has 83 source regions where activity uptake can be placed and the program calculates the mean absorbed dose to 43 different organs and tissues. IDAC-Dose 2.1 has been harmonized with the other ICRP sanctioned computer program Dose and Risk Calculation (DCAL), which is used to estimate doses for occupational intakes of radionuclides. **Results & Conclusions:** The harmonization between IDAC-Dose and DCAL mean that there is no longer any difference in the dose calculations between decays calculated with radiopharmaceuticals or radionuclides decaying in occupational, public or environmental situations. With the update of the IDAC-Dose 2.1, more realistic absorbed dose estimations can be performed on adults and enables the implementation of the effective dose estimations defined in the ICRP Publication 103.

OP-668

Image based preclinical absorbed dose estimation through GATE Monte Carlo simulation using ^{18}F-FDG PET/CT images of mice

A. Gupta[1], M. S. Lee[1], J. H. Kim[2], S. H. Park[3], H. S. Park[3], S. E. Kim[3], D. S. Lee[1], J. S. Lee[1]; [1]Seoul National University (SNU), Seoul, KOREA, REPUBLIC OF, [2]Korea Research Institute of Standards and Sciences, Daejeon, KOREA, REPUBLIC OF, [3]Graduate School of Convergence Science and Technology, Seoul, KOREA, REPUBLIC OF.

Purpose: High level of accuracy in internal dosimetry is essential to obtain appropriate absorbed dose response-effect relationships during preclinical research. Due to the various limitations associated with organ level MIRD based dosimetry (MBD) methods, the voxel based dosimetry (VBD) which contributes to a more accurate assessment of absorbed dose has become essential. Recently, the GATE Monte Carlo (MC) simulation has gained attention in preclinical VBD application. In this study, we used real PET/CT images of mice to estimate absorbed dose using GATE MC and compared with MBD to evaluate the feasibility of GATE image-based dosimetry. **Subjects and Methods:** PET/CT imaging of C57BL/6 mice (n=4, body weight: 30.49 ± 3.62 g) in overnight fasting condition were performed using nanoScan PET/CT. Dynamic PET images were acquired in list mode for 90 min followed by a CT acquisition after IV injection of 13.50 ± 3.54 MBq of ^{18}F-FDG. GATE MC toolkit was applied to estimate absorbed dose in various organs of mice using real CT and PET images as voxelized phantom and voxelized source respectively as the input for simulation. Absorbed dose was calculated from dosemaps obtained as an output of GATE simulation using 3D VOIs drawn on organs in CT and PET images. MIRD based absorbed dose were also calculated using published S-values which were based on Moby phantom (Xie *et al* 2012 *Phys. Med. Biol.*). Organ mass correction was performed for MIRD based method. Absorbed dose estimated from GATE and the MIRD methods were compared and relative percentage differences were reported. **Results:** GATE based absorbed dose (mGy/MBq) were estimated and compared to MIRD based absorbed dose which showed comparable results. The percentage difference in brain, heart, liver, lungs, stomach, spleen, kidneys and urinary bladder were 24.32%, 9.33%, -1.72%, -73.16%, 4.78%, 17.27%, 24% and 29.52% respectively. The absorbed dose in lungs was highly overestimated by MIRD method. This was due to the difference in mass and anatomical position of lungs in Moby and real mice. The average percentage difference between GATE and MIRD method was < 5%. GATE MC simulation provided individualized absorbed dose based on specific activity distribution in each mouse when using real PET/CT images. **Conclusion:** Voxel based absorbed dose estimated by GATE simulation using real mouse imaging data would be more accurate and mouse specific. Hence, this method can be used in targeted radionuclide therapy for personalized dosimetry.

OP-669

Radiation dosimetry of the tau PET Tracer ^{18}F-PI-2620 in humans

J. Seibyl[1], O. Barret[1], A. Stephens[2], J. Madonia[1], D. Alagille[1], A. Mueller[2], H. Schieferstein[2], M. Berndt[2], H. Kroth[3], S. Bullich[2], C. Papin[1], V. Carroll[1], C. Sandiego[1], A. Pfeifer[3], A. Muhs[3], L. Dinkelborg[2], G. Tamagnan[1], K. Marek[1]; [1]Molecular Neuroimaging, New Haven, CT, UNITED STATES OF AMERICA, [2]Piramal Imaging, Berlin, GERMANY, [3]AC Immune SA, Lausanne, SWITZERLAND.

Introduction: Intracellular tau deposition is a key pathologic feature of Alzheimer's disease (AD) and other neurodegenerative disorders. Recently, positron emission tomography tau probes have been developed for in vivo detection of brain tau load, although quantification is challenging due to high off target binding and slow kinetics. Further, different tau radiotracers have different affinities for tau species. ^{18}F-PI-2620 is a novel tracer with a high affinity for binding to aggregated tau that has shown high signal in brain regions of expected tau pathology in AD and PSP subjects in an initial clinical study. The purpose of this study was to determine the biodistribution and radiation dosimetry of ^{18}F-PI-2620 in humans. **Subjects & Methods:** 6 subjects (3 male, 3 female, mean age 31 ± 9 yrs) were injected with a a single bolus of ^{18}F-PI-2620 (mean dose 354 ± 5 MBq) followed by serial whole body PET imaging scans of up to 6 hours. Urine samples collected over the imaging period were evaluated to measure the excretion of ^{18}F-PI-2620 through the urinary tract. Time-dependent source organ counts were assessed based on individualized VOIs and residence times were calculated using the area under the time-activity curve method. Radiation absorbed dose estimates based on the MIRD methodology utilizing urine data and International Commission on Radiological Protection (ICRP 30) gastrointestinal tract kinetics were determined. **Results:** ^{18}F-PI-2620 shows elimination mainly via the hepatobiliary route with some minor elimination by the urinary pathway. Target organs with highest effective dose are gallbladder wall and upper large intestine. The Effective Dose per 185 MBq (5 mCi) injection is 4.1 mSv with no bladder voiding, and 4.0 mSv with 2 hour bladder voiding interval for an adult male. **Conclusion:** The radiation dosimetry of ^{18}F-PI-2620 is suitable for human use and is similar to other ^{18}F-labelled radio-pharmaceuticals.

OP-670

Preliminay Results of Biodistribution and Dosimetric Analysis with [^{68}Ga]Ga-DOTA[ZOL]: A new bone seeking PET radionuclide

A. Khawar[1], E. Eppard[1], H. Ahmadzadehfar,[1], S. Kürpig[1], M. Meisenheimer[1], F. C. Gaertner[1], F. Roesch[2], M. Essler[1], R. A. Bundschuh[1]; [1]Department of nuclear medicine, University Hospital, Bonn, GERMANY, [2]Institute for nuclear chemistry, Johannes Gutenberg-University, Mainz, GERMANY.

Purpose/Introduction: Recently [^{68}Ga]Ga and [^{177}Lu]Lu DOTA labelled hydroxy-bisphosphonates have been proposed as new theranostic agents for metastatic skeletal disease. Animal studies have shown pharmacokinetics of [^{68}Ga]Ga-DOTA[ZOL] with high skeletal uptake and fast clearance from blood pool better than [^{18}F]NaF. This study aims at first in human biodistribution and dosimetric analysis of [^{68}Ga]Ga-DOTA[ZOL]. **Subjects & Methods**: A total of three patients (mean age: 77yr) having metastatic skeletal disease with refractory prostate carcinoma (male) and breast carcinoma (female) patients were included in this study. Patients were injected [^{68}Ga]Ga-DOTA[ZOL] intravenously (150-185MBq). All patients underwent an initial dynamic imaging of the abdomen for 30 min (list mode) followed by static PET/CT imaging (skull to mid-thigh) at 45 min and 2 h with a Siemens Biograph 2 PET/CT camera. For qualitative and quantitative analysis dynamic images were reconstructed as 6 images of 300s. Source organs were identified on qualitative analysis. Source organs VOI's were drawn on CT image and KBq/ml counts from PET image were determined using MEDISO interview fusion software. Time integrated activity coefficients were generated for source organs, marrow and urinary bladder. Organ absorbed doses and effective doses were calculated using OLINDA/EXM after applying a correction factor for patient weight. **Results:** Qualitative analysis revealed intense tracer uptake in kidneys, urinary bladder, skeletal tissue and faint uptake in liver, spleen and salivary glands. High bone to soft tissue as well as tumor to bone uptake was found. Quantitative time activity analysis showed rapid blood clearance, early uptake and fast clearance from kidneys and maximum uptake in bone achieved in less than half an hour followed by gradual decline on average. The measured effective dose was 0.016 mSv/MBq, with the urinary bladder, osteogenic cells, kidneys and red marrow receiving the highest doses of 0.22, 0.037, 0.036 and 0.026 mSv/MBq, respectively. 150 MBq of [^{68}Ga]Ga-DOTA[ZOL] results in 2.38 mSv of effective dose. **Conclusion:** These first results are showing that [^{68}Ga]Ga-DOTA[ZOL] with favourable bio kinetics and modest radiation exposure is a promising new bone seeking theranostic agent that can be labelled with [^{177}Lu]Lu for theranostic purposes. However, further large studies are required.

OP-671

PET-based human dosimetry of ^{68}Ga-NODAGA-exendin-4, a tracer for beta cell imaging

M. Boss, M. Buitinga, T. J. P. Janssen, M. Brom, E. P. Visser, M. Gotthardt; Radboud University Medical Center, Nijmegen, NETHERLANDS.

Background: The stable glucagon-like peptide-1 (GLP-1) analogue exendin-4 specifically binds the GLP-1 receptor. ^{68}Ga-NODAGA-exendin-4 is a promising tracer for beta cell imaging using PET/CT with a wide range of possible applications. In patients with insulinoma, ^{68}Ga-NODAGA-exendin-4 PET/CT shows promising results in tumour visualization. Furthermore, this technique can contribute to the knowledge of the role of beta cell mass in the pathofysiology of type 1 and type 2 diabetes (T1D, T2D, respectively). Also therapeutic approaches in diabetes, like islet transplantation in patients with T1D and remission of T2D after Roux- and Y gastric bypass can be examined using this novel tracer. Calculating the radiation dose from ^{68}Ga-NODAGA-exendin-4 is important for use in patients, to estimate the possibility of repeated PET scans to follow disease progression,

and the possibility for use in children. **Methods:** 6 patients with hyperinsulinemic hypoglycaemia (2 men, 4 women, mean age ± SD: 54.0 ± 15.5 y, mean weight ± SD: 77.1 ± 11.2 kg) were included. After intravenous injection of the tracer (105.6 ± 2.3 MBq), 4 successive PET/CT scans were obtained at 30, 60, 120 and 240 minutes post injection on a Siemens Biograph mCT-40 time-of-flight PET/CT scanner. Images were acquired of 2 bedpositions including liver, pancreas and kidneys at 10 min per bedposition and analyzed using Inveon Research Workplace software. Volumes of interest were drawn over the pancreas and kidneys and tracer activity in the remainder of body was determined. Time-integrated activity coefficients were calculated and OLINDA/EXM version 1.1 software was applied to calculate radiation doses using the reference adult male and female models. **Results:** Highest uptake was in the kidneys and pancreas. The mean effective doses were 24.6 ± 5.5, and 1.2 ± 0.4 µSv/MBq respectively. The effective dose was 32.0 ± 6.1 µSv/MBq. **Conclusion:** When using the radiopharmaceutical 68Ga-NODAGA-exendin-4 the kidneys are the dose-critical organs, which receive the highest radiation dose of 24.6 ± 5.5 µSv/MBq. The kidney dose will thus be well below 1Gy after injection of 100 MBq of 68Ga-NODAGA-exendin-4. For this injected activity , the expected effective radiation dose is 3.2 ± 0.6 mSv. This dose could be diminished in the future by optimizing protocols leading to possible reduction of injected activity. The here calculated doses show that 68Ga-NODAGA-exendin-4 can be safely used for imaging and are promising for the possibility of the use of this tracer in children in which we expect a similar biodistribution of the tracer.

OP-672

PET-based biodistribution and radiation dosimetry of [64Cu]copper dichloride, first-in-human healthy volunteer evaluation

M. A. Avila-Rodriguez[1], *C. Rios*[2], *J. Carrasco-Hernández*[1], *J. Manrique-Arias*[1], *R. Martinez-Hernández*[2], *E. Martínez-Rodríguez*[2], *F. O. García-Pérez*[3], *M. Romero-Piña*[3], *A. Jalilian*[4], *A. Díaz-Ruiz*[2]; [1]*Universidad Nacional Autónoma de México, CDMX, MEXICO,* [2]*Instituto Nacional de Neurología y Neurocirugía, CDMX, MEXICO,* [3]*Instituto Nacional de Cancerología, CDMX, MEXICO,* [4]*International Atomic Energy Agency, Vienna, AUSTRIA.*

Purpose/Introduction: In recent years Copper-64 in the chemical form of copper dichloride ([64Cu]CuCl$_2$) has been identified as a potential agent for PET imaging and radionuclide therapy targeting the human copper transporter CTR1, which is overexpressed in a variety of cancer cells. Future clinical applications of [64Cu]CuCl$_2$ will require of accurate dosimetric data, especially for therapeutic procedures; however, limited human biodistribution and radiation dosimetry data is available for this tracer. The aim of this research was to determine the biodistribution and estimate the radiation dosimerty of [64Cu]CuCl$_2$, using whole-body (WB) PET scans in healthy volunteers. **Subjects & Methods:** Six healthy volunteers were included in this study (3 women and 3 men, 54.3±8.6 y, mean weight 77.2 ± 12.4 kg). All of them signed an informed consent. After I.V. injection of the tracer (4.0 MBq7kg), 3 consecutive whole-body (WB) emission scans were acquired at 5,

30, and 60 min after injection. Additional scans were acquired at 5, 9 and 24 h post-injection. Low-dose CT scan without contrast was used for anatomic localization and attenuation correction. OLINDA/EXM software was used to calculate human radiation doses using the reference adult model. **Results:** The injection of 310±50 MBq of [64Cu]CuCl$_2$ solution in physiological saline produced no observable adverse events or clinically detectable pharmacologic effects in any of the 6 subjects. The highest uptake was in the liver, followed by lower and upper large intestine walls, and pancreas, in descending order. Elimination by urine was negligible. The critical organ was liver with a mean absorbed dose of 421±56 µGy/MBq for women and 310±67 µGy/MBq for men, while the mean effective doses were 61.8±5.2 µSv/MBq for women and 51.2±3.0 µSv/MBq for men. **Discussion/Conclusion:** To the best of our knowledge this is the first report on biodistribution and radiation dosimetry of [64Cu]CuCl$_2$ in healthy volunteers. Capasso et al. (Ann. Nucl. Med. 2015;29:482-8) obtained human biodistribution data from patients with prostate cancer and estimated dosimetric values, reporting the liver as the critical organ with a mean absorbed dose of 294 µGy/MBq, and a mean effective dose of 33.8 µSv/MBq. Note that these values are underestimated in comparison with the values obtained for healthy volunteers. However, the discrepancy could be explained by the altered biodistribution of copper in patients, as the uptake of [64Cu]CuCl$_2$ in the tumor, reduces the amount of radiotracer available for other organs and tissues. Research supported by CONACYT 233815, and International Atomic Energy Agency RC20569.

OP-673

Validation of semi Monte Carlo, voxel-based radionuclide dosimetry software using 3D printed phantom experiments with TLD measurements and patient indium-111 Exendin scans using SPECT/CT

W. D. Wormgoor[1], *A. P. W. Meeuwis*[2], *I. Sechopoulos*[2], *E. Hippeläinen*[3], *A. Sohlberg*[4], *E. P. Visser*[2]; [1]*ZGT, Hengelo, NETHERLANDS,* [2]*Radboud University Medical Center, Nijmegen, NETHERLANDS,* [3]*University of Helsinki and Helsinki University Hospital, Helsinki, FINLAND,* [4]*Joint Authority for Päijät-Häme Social and Health Care, Lahti, FINLAND.*

Purpose: The purpose of this study is to validate an experimental software package for patient-specific, voxel-based radionuclide dosimetry using both patient SPECT-CT data and another dosimetry software, and using measurements with a 3D printed phantom and thermoluminescent dosimeters (TLD). **Subjects & Methods:** A program based on semi-Monte Carlo simulations (sMC) (Hermes Medical Solutions, Stockholm, Sweden) was used to estimate the dose distributions from 18 patient 111In-Exendin SPECT-CT scans, each consisting of 3 or 5 acquisitions. The resulting mean kidney dose estimates were compared to those obtained using OLINDA/EXM 1.1 from the same SPECT-CT acquisitions. A previously developed 3D printed phantom of the pancreas and kidneys inside a shell of a NEMA IEC body phantom was filled with aqueous 111In-chloride solutions of different activity concentrations in the background and in the organs. Dose distribution estimates for both the photon and electron contribution were obtained with the sMC software of a time series of 5

SPECT-CT scans of the phantom. The absorbed dose as a result of the photon contribution was compared with local dose measurements performed using TLDs at 16 locations inside the phantom. **Results:** The mean kidney doses in the patient studies obtained using the sMC software correlated strongly with the values from OLINDA/EXM (slope = 0.86, R^2 = 0.92). The phantom study resulted in a photon contribution in the sMC software that was 1.52 times higher (SD = 0.37) than the absorbed dose as measured by the TLDs (mean factors of 1.5, 1.3, 1.8, for kidneys, pancreas and background, respectively). **Discussion / Conclusion:** Electron absorption in the walls of the phantom organs and a sub-voxel inhomogeneity could explain part of the difference between the software and the TLD measurements. Furthermore, the TLD calibration could be affected by the electrons emitted by [111]In. Therefore, further work is needed to quantify these factors and to validate the TLD measurements. Although good agreement was obtained when comparing software-based estimates, the experimental validation led to differences that could not be fully explained and need to be validated further.

1701   **Wednesday, October 25, 2017, 10:00 - 11:30, Hall A**

CME 14 - Dosimetry/Radiation Protection/Translational Molecular Imaging & Therapy: Alpha Particle Dosimetry, Does High LET Lead to High RBE?

OP-674
Preclinical Experience in Alpha Particle Dosimetry
S. Palm; University of Gothenburg, Gothenburg, SWEDEN.

OP-675
Small Scale Dosimetry and RBE of Alpha-Particles
G. Sgouros; Johns Hopkins University, Baltimore, UNITED STATES OF AMERICA.

OP-676
Ra-223: Imaging, Dosimetry and Radiation Protection
C. Hindorf; Lund university hospital, Medical physics, Lund, SWEDEN.

OP-677
Clinical Experience with 225Ac-PSMA-617 for PSMA-Targeted α-Radiation Therapy of Metastatic Prostate Cancer
C. Kratochwil; University Hospital Heidelberg, Department of Nuclear Medicine, Heidelberg, GERMANY.

1702   **Wednesday, October 25, 2017, 10:00 - 11:40, Hall B**

Joint Symposium 14 - EANM/ESSO: Head & Neck Cancer

OP-678
5-year European Survey (SENT Study) on SLNB in H&N Tumours
G. Tartaglione; Cristo Re Hospital, Department of Nuclear Medicine, Rome, ITALY.

OP-679
Hybrid Gamma- and FluorescenceImaging in SLN Detection
R. Valdés Olmos; The Netherlands Cancer Institute, Amsterdam, NETHERLANDS.

OP-680
Additional Non-SLN Metastases in Early Oral Cancer Patients with Positive SLN
R. de Bree; UMC Utrecht Cancer Center, University Medical Center Utrecht, Department of Head and Neck Surgical Oncology, Utrecht, NETHERLANDS.

OP-681a
The Added Value of PET/MR in H&N Tumours
M. Hüllner; University Hospital Zurich, Clinic of Nuclear Medicine, Zurich, SWITZERLAND.

OP-681b
Sensitivity of SLNB in H&N Melanoma Patients
A. J. M. Balm; The Netherlands Cancer Institute, Department of Head and Neck Oncology and Surgery, Amsterdam, NETHERLANDS.

1703   **Wednesday, October 25, 2017, 10:00 - 11:30, Hall C**

CTE 7 (Interactive) - Joint Session with Paediatrics: Practical and Technical Aspects of Paediatric Nuclear Medicine

OP-682
How to Set Up a Paediatric Nuclear Medicine Department
Z. Bar-Sever; Schneider Children's Medical Center of Israel, Petach-Tikva, ISRAEL.

OP-683
Paediatric Nephrology – What Do We Do With Infants?
S. Grbac-Ivanković; Clinical hospital centre Rijeka, Department of nuclear medicine, Rijeka, CROATIA.

OP-684
Paediatric Imaging Methods in Oncology - The Key is in Dosimetry, Do We Have a Solution?
A. Balenović; Dom zdravlja Zagreb-Centar /Health Care Center Zagreb, Zagreb, CROATIA.

1704   **Wednesday, October 25, 2017, 10:00 - 11:30, Hall E1**

Do.MoRe: Molecular Imaging Artefacts & Corrections

OP-685
Clinical Evaluation of Data-driven Motion Correction for PET Imaging

C. F. Uribe[1], E. Rousseau[1], F. Lacroix-Poisson[1], T. Alden[1], S. Wollenweber[2], F. Benard[1]; [1]BC Cancer Agency, Vancouver, BC, CANADA, [2]GE Healthcare, Waukesha, WI, UNITED STATES OF AMERICA.

Aim: Respiratory motion degrades the ability to detect and quantitate lung/abdomen lesions using PET. Our purpose was to evaluate data driven gating (DDG) as an approach to perform respiratory motion correction, and validate it in comparison to conventional device-based gating methods. **Methods:** Sixteen patients with liver, lung, esophageal, or gastric cancer underwent an FDG-whole-body PET/CT scan on a GE-Discovery 690 PET/CT scanner. Three methods were used to measure the respiratory waveform: 1) infrared camera with a reflective block on the abdomen, 2) a combination of data from a pressure and temperature sensors, and 3) DDG based on principal component analysis. Three 75 kBq Na-22 sources were placed fixed on the bed, and moving on the patient's chest. Data was collected over 3 bed positions for 5 minutes each with list mode enabled for retrospective reconstruction. Gated images (8-bins) were created using MATLAB-based tools using the resulting waveforms and three sub-methods: a) phase, b) displacement, and c) equal-duration displacement. Two non-gated images were also created using 100% (NGL) and 1/8 (NGS) of the data in the list file. The latter was to obtain similar statistics between gated images and NGS. Reconstructions were performed with OSEM algorithm (32 subsets, 2 iterations), and scatter/attenuation correction. ROIs were drawn around 17 lesions and sources using a 40% fixed-threshold. Volumes, displacements, SUVmax, SUVmean, and SNR were compared between gated and non-gated images using a nonparametric Kruskal-Wallis test (p=0.05). Additionally, gated images were scored (Likert scale) by two physicians based on lesion identification, noise, motion tracking, and diagnostic improvement. **Results:** Lesion displacement range was within 0.39-1.04 cm with the various methods. No significant differences in volumes (6.7±1.4 mL) were found between gating methods. Gating did not significantly increase SUVmax compared to NGS, but showed an increase of up to 40% with respect to NGL for both lesions and sources. Gating showed 16% and 28% increase in lesion SUVmean compared to NGS and NGL, respectively. For the Na-22 sources using gating, SUVmean increased up to 35% but was only significant with respect to NGL. SNR was 40% lower with respect to NGL but was comparable to NGS. The qualitative analysis demonstrated no difference between different gating methods. **Conclusion:** DDG and the other device-based gating methods were qualitatively and quantitatively similar for use in respiratory gating. Increases in SUV with gating appear to depend on image statistics and lesion displacement range, and this effect is still under investigation.

OP-686

ParaPET, A New Statistical Methodology to Derive 3D Maps of FDG-PET Kinetic Parameters

E. Colard[1], L. Padovani[2], S. Delcourt[3], S. Thureau[4], B. Farman Ara[3], P. Gouel[5], I. Gardin[6], P. Vera[6], D. Taïeb[7], D. Barbolosi[8], S. Hapdey[6]; [1]LITIS QuantIF EA4108, Rouen, FRANCE, [2]Department of Radiotherapy, La Timone University Hospital, Marseille, FRANCE, [3]Department of Nuclear Medicine, La Timone University Hospital, Marseille, FRANCE, [4]Department of Radiotherapy, Centre Henri Becquerel and LITIS QuantIF EA4108, Rouen, FRANCE, [5]Department of Nuclear Medicine, Centre Henri Becquerel, Rouen, FRANCE, [6]Department of Nuclear Medicine, Centre Henri Becquerel and LITIS QuantIF EA4108, Rouen, FRANCE, [7]Department of Nuclear Medicine, La Timone University Hospital and European Center for Research in Medical Imaging (CERIMED), Marseille, FRANCE, [8]SMARTc, INSERM, UMR 911 CR02, Marseille, FRANCE.

Purpose: We extended a statistical method recently proposed by Barbolosi et al. (Barbolosi, MBEC 2016) to generate 3D images of kinetic parameters in FDG PET: PARAPET. The major improvements rely on the integration of a new error model of PET measurement, a non-invasive blood activity measurement (NIBAM) and the measurement of 3D kinetic parameters. **Subjects & Methods**: The PARAPET method requires a late dynamic PET acquisition of 15 minutes centered over the lesion. Five images of FDG mean activity concentration, associated with five images of its variability are generated to model the errors of PET measurements necessary to our statistical approach. To avoid multiple blood samples needed for Barbolosi's method, a late NIBAM is determined from FDG PET images. Regions of interest manually drawn over blood compartment are used to extract the mean blood activity concentration and its variance. Our method is applied on each voxel to derive parametric PET images. Our approach was evaluated and compared to Patlak analysis as a reference. Hunter and Barbolosi methods (with blood samples or with NIBAM) were also investigated and compared to Patlak. Two kinetic parameters were investigated: K_i, the net influx rate and $K_{i,max}$, corresponding to the maximum value of K_i in the lesion. **Results**: The methods were evaluated on 16 non-small cell lung cancer lesions from 8 patients planned for radiochemotherapy included in the on-going ParaPET clinical trial (NCT 02821936). Patients had between 4 to 5 blood samples. Results show that our approach presents an excellent correlation with Patlak (r = 0.99) compared to Hunter (r = 0.94), Barbolosi with blood samples (r = 0.97) or with NIBAM (r = 0.95) methods. The mean errors (± SD) in $K_{i,max}$ estimate were -0.2% ± 10.2% for our approach, 40.5% ± 34.6% for Hunter, -4.9% ± 10.0% for Barbolosi and -1.3% ± 15.5% for Barbolosi with NIBAM. **Conclusion**: Our methodology allows a more accurate estimate of $K_{i,max}$ and is a non-invasive alternative to methods using multiple blood samples, using only a late PET acquisition, easily adaptable to clinical routine. It also proposed to compute a set of kinetic parameters at the voxel level, giving access to additional quantitative information. These preliminary results should be further statistically confirmed with more data. **Research Support**: The author received a grant support for education between the University of Rouen and GE Medical System. The study was also funded by the Cancéropôle PACA and the Centre Henri Becquerel.

OP-687

Assessment of whole-body scatter correction for Ga-68 PSMA PETCT

H. Bal[1], I. Hong[1], F. Buther[2], M. Aykac[1], K. Schaefers[2], M. Conti[1]; [1]Siemens Healthineers, Knoxville, TN, UNITED STATES OF AMERICA, [2]University of Muenster, Muenster, GERMANY.

Introduction*:* Multi-bed PETCT oncology studies are processed bed-by-bed in conjunction with data acquisition for efficient workflow. This process however limits the axial field of view for the scatter estimation to a single bed, leading to possible inaccuracies in the scatter shape. In this work we investigated the performance of whole-body scatter correction (WBSC) relative to single bed scatter correction (SBSC). **Methods***:* A two-bed Monte-Carlo simulation was performed for a hot bladder phantom consisting of a large cylinder containing a hot sphere (250:1 sphere to background ratio) axially centered in the bed overlapping region. Additionally, experimental data using long uniform cylinder phantoms (20 cm diameter and 37 cm diameter) and a hot bladder phantom were acquired using two-bed acquisition. Further, 8 Ga-68 PSMA clinical datasets selected based upon the indication of scatter overcorrection were also chosen for analysis. All data were reconstructed with TOF based OSEM (3it, 21 subsets) using WBSC and SBSC strategies. A background region surrounding the hot sphere was used to compute bias in the activity estimates for the simulated data. For the experimental uniform phantom data axial uniformity was computed as the maximum variation in axial planes. Clinical data were analyzed by computing SUVs in a 3D liver region of interest as well as a region suffering from scatter overcorrection. **Results:** The Monte Carlo results showed that background surrounding the hot bladder was 5% lower with whole-body scatter and 33% lower with single bed scatter relative to simulated background. The uniform phantom study had better axial uniformity with WBSC (3% (20 cm); 9% (37cm)) compared to SBSC (4% (20 cm); 12% (37 cm)). Visual assessment of hot bladder phantom indicated a more uniform background with WBSC compared to SBSC. All patient data demonstrated considerably improved visual image quality with whole-body scatter compared to single bed scatter. In general, SUVs were higher with WBSC compared to SBSC (3% for liver and 400% for scatter overcorrected regions). The pooled data of voxel-wise relative difference showed that 5% data had 50% (or greater) higher quantitative estimates with WBSC compared to SBSC. **Conclusion:** Scatter estimation with WBSC was found to be more accurate compared to SBSC due to extended axial coverage for scatter estimation. This in turn results in higher and more accurate activity estimates with WBSC compared to SBSC while also improving image quality.

OP-688

Impact of motion compensation and partial volume correction on ^{18}F-NaF PET/CT imaging of coronary plaque

J. Cal-Gonzalez[1], C. Tsoumpas[2], M. Lassen[1], S. Rasul[3], M. Hacker[3], K. Schäfers[4], T. Beyer[1]; [1]QIMP group, Center for Medical Physics and Biomedical Engineering, Medical University of Vienna, Vienna, AUSTRIA, [2]Division of Biomedical Imaging, University of Leeds, Worsley Building, LIGHT Labs, LS2 9NL, Leeds, United Kingdom., Leeds, UNITED KINGDOM, [3]Division of Nuclear Medicine, Department of Biomedical Imaging and Image-guided Therapy, Medical University of Vienna, Vienna, AUSTRIA, [4]European Institute for Molecular Imaging, University of Münster, Münster, GERMANY.

Aim: Recent studies suggest that ^{18}F-NaF PET enables visualization and quantification of plaque micro-calcification in the cor-onary tree. However, PET imaging of plaque calcification in the coronary arteries is challenging because of the respiratory and cardiac motion as well as partial volume effects. The objective of this work is to implement an image reconstruction framework, which incorporates compensation for respiratory and/or cardiac motion (MoCo) and partial volume correction (PVC), for cardiac ^{18}F-NaF PET imaging in PET/CT. **Materials and Methods**: Realistic simulations (Biograph TPTV and Biograph mCT) and phantom acquisitions (Biograph mCT) were used. Different uptake values of the plaques (spherical shape, 4 mm diameter) were evaluated in the simulated datasets, with lesion-to-background ratios (LBR) of 10, 20, 50 and 70:1. The experimental phantom included three plaque-type lesions of 18, 31 and 36 mm³ respectively, with a LBR of 70:1. After validation of the MoCo and PVC methods, they were applied to four pilot ^{18}F-NaF PET/CT patient studies. In all cases, the MoCo-based image reconstruction was performed using the STIR software. The PVC was obtained from a local projection (LP) method, previously evaluated in preclinical and clinical PET. We evaluated the noise in the image (measured in a background region) and the lesion-to-background ratio (LBR) values of the plaques, using the maximum (LBR$_{max}$) voxel value within the segmented plaque. **Results**: After applying MoCo and PVC, LBR$_{max}$ increased by 200% to 1110% in the simulated data, by 212% to 614% in the phantom experiments and by 14% to 188% in the plaques with positive uptake observed in the patients. Similar noise values were observed in all images, in contrast to the significantly higher noise observed when using respiratory or cardiac gating. **Conclusions**: A combined MoCo and PVC approach for PET/CT imaging was implemented within the STIR reconstruction framework. The simulated datasets, experimental and patient data show significant improvement in the quantification of small coronary lesions when MoCo and PVC are taken into account. **Acknowledgments:** This work was supported by the EU COST Action TD1007.

OP-689

A phantom evaluation of a commercial algorithm for photopenic artefact reduction in high contrast PET/CT and implications for ^{124}I PET/CT

P. Braad, P. F. Høilund-Carlsen; Department of Nuclear Medicine, Odense University Hospital, Odense C, DENMARK.

Purpose: Overcorrection of scatter in PET/CT images may cause photopenic artefacts in regions close to organs that have a high specific uptake of activity. On the new GE Discovery MI (DMI) PET/CT system (General Electric, USA) a scatter limit is automatically activated during image reconstruction to circumvent this problem. For non-pure positron emitters, e.g. ^{124}I, additional modelling is performed during scatter correction to account for prompt gamma coincidences (PGCs). The present phantom study aimed to validate the photopenic artefact reduction algorithm with ^{68}Ga and ^{124}I on the new DMI system. **Methods**: ^{124}I (1-50 MBq) was distributed to the spheres, background, and lung insert of the NEMA/IEC torso phantom. Scanning was performed on the DMI with and without PGC correction. Images were visually assessed. Contrast recovery, background variabil-

ity and the accuracy of activity quantification in the phantom background were measured at a sphere-to-background ratio of 5 and at lung-to-background activity ratios (LBR) of 0, 40, 120, 400, and 1200. Similar scans and subsequent analyses were performed with [68]Ga. All scans were repeated on the GE Discovery 710 (D710) PET/CT system and results compared to those obtained on the DMI. **Results:** With ^{68}Ga and [124]I, scatter appeared undercorrected on both the DMI and D710. A positive bias on activity quantification in the phantom background caused a contrast reduction between the spheres and the background at high LBRs. No spheres were visible at a LBR of 1200, the 3 ([124]I) to 4 (^{68}Ga) largest spheres could be identified at a LBR of 400 whereas all spheres were visible with both ^{68}Ga and [124]I at lower LBRs. The image quality was superior, background variability lower, and activity quantification more accurate on the DMI compared to the D710. With ^{68}Ga there were no photopenic areas or any appreciable difference between results obtained with and without PGC-correction. PGC-correction on the DMI also had no noticeable impact on [124]I-images. Photopenic areas were localized around the hot lung insert at LBRs > 40. However, these artefacts only had a minor impact on sphere detectability. Without PGC-correction enabled on the D710, scatter was significantly overcorrected in the center of images which caused large photopenic areas around the hot lung insert. PGC correction acceptably solved the problem. **Conclusion:** The new GE Discovery MI PET/CT system provides acceptable activity quantification accuracy and image quality under challenging imaging conditions where high organ-to-background activity ratios stress the accuracy of scatter correction algorithms.

OP-690

Evaluation of respiratory motion correction in PET/CT using a 3D printed phantom

J. H. Vilsbøll[1], S. W. Hasler[1], L. D. L. Duchstein[2], J. E. Wilhjelm[1], M. N. Lonsdale[2]; [1]Technical University of Denmark, Copenhagen, DENMARK, [2]Bispebjerg and Frederiksberg Hospital, Copenhagen, DENMARK.

Objective: Respiratory movement during PET/CT scan causes blurred images and misalignment between the two modalities. The aim of this study was to evaluate the performance of two motion correction algorithms, Q.Static (rejection of events during inhalation) and Q.Freeze (5 bin gated acquisition with subsequent alignment of PET and CT bins) in combination with an advanced PET reconstruction algorithm, Q.Clear. **Methods:** A 3D printed phantom was designed with six cylindrical holes of varying diameter (3mm, 6mm and 10mm) and filled with 18F-FDG. The phantom was fixed on a motor simulating breathing cycles of a patient during a PET/CT study. Data was acquired on a GE Discovery 710 PET/CT equipped with a Varian RPM respiratory gating system. PET acquisition was done in listmode with motion tracking. CT was acquired as gated CT cine and conventional helical CT. PET data was reconstructed (using Q.Clear) with Q.Static and Q.Freeze for motion correction. As recommended for clinical studies, PET Q.Freeze bin 50% and bin 70% were combined with neighboring CT cine bins (40%/60%

and 60%/80%, respectively). Q.Static PET was compared with the conventional helical CT. Using the known dimensions of the phantom, the extent and pixel values of the hot spots in the PET images and the misalignment (mean difference between center of hot spots) between PET and CT were evaluated. **Results:** The best alignment was found with PET Q.Freeze 50%/CT cine 40%, and PET Q.Freeze 70%/CT cine 60%. Compared to Q.Static/helical CT, misalignment dropped from 13.8mm to 2.7mm. A good match between bins in Q.Freeze PET and CT cine is crucial - misalignment for suboptimal matching was three times higher than for PET Q.Freeze 70%/CT cine 60%. The size of the hot spots in axial PET images was robust and more or less independent of reconstruction or slice location. Furthermore, intensity of the hot spots was reduced in Q.Freeze reconstructions, and the highest intensities were found in Q.Static reconstructions. **Conclusion:** These results show that motion correction with Q.Freeze reconstruction is effective and performs better than Q.Static, but the matching of bins and decrease in intensity is important to keep in mind.

OP-691

Evaluation of the Impact of Using TOF Technique on Metal Artifact Reduction in PET/CT Images

R. Sharifpour[1,2], P. Ghafarian[3,4], M. R. AY[1,2]; [1]Department of Medical Physics and Biomedical Engineering, Tehran University of Medical Sciences, Tehran, IRAN, ISLAMIC REPUBLIC OF, [2]Research Center for Molecular and Cellular Imaging, Tehran University of Medical Sciences, Tehran, IRAN, ISLAMIC REPUBLIC OF, [3]Chronic Respiratory Diseases Research Center, National Research Institute of Tuberculosis and Lung Diseases (NRITLD), Shahid Beheshti University of Medical Sciences, Tehran, Tehran, IRAN, ISLAMIC REPUBLIC OF, [4]PET/CT and Cyclotron Center, Masih Daneshvari Hospital, Shahid Beheshti University of Medical Sciences, Tehran, IRAN, ISLAMIC REPUBLIC OF.

Purpose: The potentials of new technique like time of flight (TOF) can positively affect metal induced artifact in PET/CT imaging. The aim of this study was to evaluate the impact of TOF reconstruction on reduction of metal artifact in PET/CT images. **Subjects and Methods:** NEMA IEC body phantom with 2:1 activity ratio was used in this study. In the first step, the phantom was adapted to hold an ICD on removable lung insert and in the second step, pacemaker generator was also fastened to the internal wall of phantom. Both ICD and battery generator were placed opposite to the sphere with 13 mm in diameter. The phantom was scanned by Discovery 690 GE PET/CT scanner, equipped with 64-slice CT. The PET images were retrospectively reconstructed using two reconstruction algorithms, including non-TOF (routine protocol in our department: OSEM+PSF with 3iterations, 18subsets, 6.4 mm post-smoothing filter) and TOF (TOF+OSEM+PSF: 2iterations, 18subsets, 6.4 mm post-smoothing filter). All images were quantitatively analyzed using the CT number, SUV_{max} and SUV_{mean}. **Results**: In analysis of hot spheres of phantom, spheres with 13 and 17 mm in diameter more than the other affected by streak artifact. The relative differences of maximum CT number in these two spheres between image with metal artifact and image without metal artifact were

327.0% and 89.8% for 13 and 17 mm sphere, respectively. TOF led to increase in SUV_{max} for all spheres except for 13 and 17 mm spheres. In these spheres that strongly affected by streak artifact, TOF decreased the SUV_{max} versus to non-TOF. In place of pacemaker generator and its surroundings a virtual activity was observed, while ICD did not produce any virtual activity. The relative differences of SUV_{max} and SUV_{mean} of the virtual activity between image with metal artifact and image without metal artifact were also considered. The image with a metal artifact that reconstructed using the non-TOF algorithm, demonstrated 71.5% and 54.1% increases in SUV_{max} and SUV_{mean}, respectively, while image with a metal artifact that reconstructed using TOF algorithm, demonstrated 38.3% and 32.7% increases in SUV_{max} and SUV_{mean}, respectively. **Conclusion:** Both the pacemaker generator and ICD produced metal artifact in CT image, but metal induced artifact was only observed for pacemaker generator in PET/CT image. That was interesting that integration of TOF technique to reconstruction, reduced metal induced artifact efficiently so that false positive activity in place of metal and near it, was obviously decreased.

OP-692

Acquisition optimization for Lutetium-177 SPECT quantification

D. M. V. Huizing[1], B. J. de Wit - van der Veen[1], E. J. Rijkhorst[2], M. P. M. Stokkel[1]; [1]Department of Nuclear Medicine, Netherlands Cancer Institute - Antoni van Leeuwenhoek, Amsterdam, NETHERLANDS, [2]Department of Medical Physics and Technology, Netherlands Cancer Institute - Antoni van Leeuwenhoek, Amsterdam, NETHERLANDS.

Introduction: Quantitative imaging in Lutetium-177 (^{177}Lu) therapy is essential for dosimetric analysis. Although in many studies single photon emission computer tomography (SPECT) is performed, there is limited consensus on imaging protocols. In this study the effects of collimators, photopeaks of ^{177}Lu, and scatter and attenuation correction (SC and AC) have been evaluated to optimize acquisition settings for ^{177}Lu-SPECT. **Materials and Methods:** A NEMA 2012/IEC phantom with sphere-to-background ratios of 1:50 and 1:10 was imaged. ^{177}Lu-SPECT acquisitions were performed on a Siemens Symbia at 13 and 20 sec/view in step-and-shoot mode (48 views) equipped with either a ^{99m}Tc/Krypton (Mullekom) or Medium Energy General Purpose (MEGP) collimator. 20% energy windows were positioned around the 113 and 208 keV photopeaks with a 10% downscatter window (reconstructed at 113, 208 and 113+208 keV). All acquisitions were reconstructed using FLASH 3D (10 iterations, 8 subsets) with AC and with or without SC. Calibration factors (CF) were calculated using three large background volumes of interest (VOI), converting counts into kBq/ml. Recovery coefficients (RC) were determined by large VOIs around the spheres and subtraction of background in all acquisitions. Line profiles of the largest sphere (37mm) were created and normalized for activity concentration. **Results:** The background standard deviation for ^{99m}Tc/Krypton ranged from 0.07-2.09 and 1.63-4.05 kBq/ml for the 1:50 or 1:10 ratios, respectively, and from 0.36-1.57 and 0.74-2.90 kBq/ml for MEGP. Moreover, better count-statistics were achieved in all MEGP reconstructions, consequently images acquired with the ^{99m}Tc/Krypton appear to have more noise. The RC-curves showed severe underestimation for spheres smaller than 17mm in all acquisitions. For 1:50 and 20 sec/view with either MEGP or ^{99m}Tc/Krypton the 13mm sphere was still accurately quantified. Due to low count-statistics 113 keV reconstructions proved less suitable for quantification. High contrast images for visual evaluation were obtained using the AC+SC 208 keV photopeak, as shown by line profiles. However, for quantification the 208 or 113+208 keV peak without SC might be more suitable given the arbitrary correction choices that some SC algorithms produce resulting in overestimation of counts by as much as 50%. **Conclusion:** For ^{177}Lu-SPECT, high contrast images suitable for quantification can be best obtained with the MEGP collimator for the Siemens Symbia at 13-20 sec/view (20% window around 208 keV photopeak) with attenuation correction. The MEGP and ^{99m}Tc/Krypton collimator perform similarly in visual assessment and quantification, yet ^{99m}Tc/Krypton has a lower signal-to-noise ratio and MEGP is more sensitive.

M2M: CNS/Neurotransmission/Brain Targets

OP-693

Injected Mass is a Limiting Factor for Small Animal PET Studies Using High-Affinity Radioligands: Evidence from a Study Using [11C]- and [18F]Fallypride

M. Toth[1], S. Nag[1], Z. Jia[1], J. Haggkvist[1], J. Mukherjee[2], A. Varrone[1], C. Halldin[1]; [1]Karolinska Institutet, Stockholm, SWEDEN, [2]University of California-Irvine, Irvine, CA, UNITED STATES OF AMERICA.

Introduction: The aim of this study was to show that extra caution should be taken with regards to the injected mass of high-affinity radioligands in small animal positron emission tomography (PET) studies. To examine the relationship between injected mass and receptor availability in mice we have used the structurally identical [^{11}C]- and [^{18}F]fallypride high affinity (0.2 nM) dopamine D_2/D_3 antagonist radioligands. Materials and Methods: [^{18}F]Fallypride was administered intravenously in a high specific radioactivity (SA) condition (45 ± 11 GBq/μmol) and low SA condition (21 ± 5 GBq/μmol) in C57BL/6J mice. To administer the same high-affinity ligand with much lower mass [^{11}C]fallypride was used with SA (153 ± 82 GBq/μmol) that was ~3 times higher than the high SA of [^{18}F]fallypride. Each animal underwent three dynamic PET measurements within two weeks with at least 1 day between the different conditions. The outcome measure was the non-displaceable binding potential (BP_{ND}) obtained with Logan graphical analysis and cerebellum as reference region. Results: BP_{ND} was 13.5 ± 1.1 for the [^{11}C]fallypride experiments. BP_{ND} obtained with [^{18}F]fallypride was 8.6 ± 2.2 with the high SA condition and 5.3 ± 1.3 with the low SA condition. The corresponding injected masses were 0.05 ± 0.04

µg with [^{11}C]fallypride, 0.11 ± 0.03 µg and 0.21 ± 0.05 µg with [^{18}F]fallypride (high SA and low SA condition respectively). BP_{ND} showed a strong negative correlation with injected mass (R2 = 0.95, P < 0.05). Conclusion: The advantage of fluorine-18 radioligands is the possibility of long distance transportation or multiple injections from one production. However, for PET studies in mice with high-affinity radioligands the amount of injected ligand is important due to the lower amount of available binding sites per gram of tissue compared with non-human primates and humans. Therefore, radioligands with high affinity such as [^{18}F]fallypride should be used in mice with precaution and specific attention to SA and mass injected.

OP-694

Quantitative PET of GABA-A receptor binding in gerbils after intra-peritoneal F-18-Flumazenil injection does not resemble accurate results obtained in rats after intravenous administration

M. Mamach[1,2], M. Kessler[1,2], J. P. Bankstahl[1], T. L. Ross[1], F. M. Bengel[1], L. Geworski[1], G. M. Klump[3,2], G. Berding[1,2]; [1]Hannover Medical School, Hannover, GERMANY, [2]Cluster of Excellence Hearing4all, Hannover/Oldenburg, GERMANY, [3]University of Oldenburg, Oldenburg, GERMANY.

Aim: Changes in the inhibitory GABAergic neurotransmitter system are of major importance in hearing disorders. This study aims to adapt and transfer established quantitative measurements of GABA-A-receptors with F-18-Flumazenil (FMZ) PET in rats to the Mongolian gerbil, which is a preferred animal model for hearing research due to its audio frequency range similar to humans. **Methods:** We compared PET results in 12 Sprague Dawley rats to those in 4 gerbils. 10-20 MBq FMZ were injected intravenously (IV) in the tail vein of rats. Gerbils were injected intraperitoneally (IP) as species specific adaptation. All animals were anesthetized using isoflurane. Scans were acquired using a Siemens Inveon PET system for 45min in rats and 60min in gerbils - to account for transfer time of tracer from the peritoneal to blood space. Frames of uptake with consecutively increasing duration were reconstructed iteratively (OSEM3D): 5x2s, 4x5s, 3x10s, 8x30s, 5x60s, 4x5min plus 1x5min, 1x10min in rats and 3x10min in gerbils. Co-57-transmission scans were employed for attenuation correction. PMOD3.6 software was used for motion correction and bio-kinetic modeling utilizing Logan plot (LP) and 2-tissue-compartment-models (2T) with an image derived input function (IDIF) of the left ventricle. Values of non-displaceable binding potentials (BPnd) for auditory cortex (AC) and inferior colliculus (IC), were calculated using pons as a reference region in rats and cerebellum in gerbils. **Results:** Besides slow tracer clearance from the peritoneal space, whole body bio-distribution was similar after both types of application. IV injection showed faster distribution in rats (left ventricle peak ≈2min, brain tissue peak ≈4min) than IP injections in gerbils (ventricle peak ≈4min, tissue peak ≈9min). The modeling approaches yielded comparable BPnds in rats in AC (LP: 1.35±0.35; 2T: 1.20±0.35) and IC (LP: 1.38±0.25; 2T: 1.31±0.30). However, BPnds in gerbils were considerably lower and showed a larger variation with both models in AC (LP: 0.09±0.14; 2T: 0.20±0.20) and in IC

(LP: 0.22±0.20; 2T: 0.45±0.20). **Conclusions:** Flumazenil allows to display GABA-A receptor binding in rats and gerbils. However, there are differences in bio-kinetic between IV and IP application, i.e. delayed kinetics after IP Injection. As a result quantitative measures of GABA-A receptor binding could not be determined with sufficient accuracy after IP application. The standard deviation of the mean BPnds approached up to 29% after IV and 156% after IP injection. The present data suggests the need to explore IV injections in gerbils as a sound basis for quantification of GABA-A receptor binding.

OP-695

In Silico, Design, Synthesis, Pre-clinical studies of [^{11}CH$_3$]-BTZ-MPP: PET neuroimaging agent for 5-HT$_{1A/1A}$/5-HT$_{1A/7}$ Dimeric Serotonin receptors

P. Jha[1,2], S. Chaturvedi[1], P. P. Hazari[1], S. Pal[1], N. Jain[2], A. K. Mishra[1]; [1]Institute of Nuclear Medicine and Allied Sciences, DRDO, Delhi, INDIA, [2]Indian Institute of Technology, Delhi, Delhi, INDIA.

Purpose: Serotonin receptors (5-HTR) sub-types, 5-HT$_{1A}$ and 5-HT$_7$ are implicated in neurological disorders. These are highly co-expressed in brain regions as heterodimers and represent an important pharmacological target for the treatment of depression, anxiety and mood regulation. 5-HT$_7$R acts as a modulator for 5-HT$_{1A}$R and the formation of 5-HT$_{1A}$R/5-HT$_7$R complex is one of the mechanisms for inactivation and desensitization of 5-HT$_{1A}$R. Imaging of 5-HT$_{1A}$R/5-HT$_7$R complex can be utilized to assess the quantitative and functional aspect of neurological disorders. We report the development of a novel ^{11}C-labelled PET radioligand for targeted imaging of 5-HT$_{1A/7}$ neuroreceptors. **Methods:** The mixed affinity ligand based on methoxyphenyl piperazine (MPP) and benzothiazolone (BTZ) was designed on the basis of physicochemical parameters predicted by ADME and the K$_i$ values reported for similar kind of structures. 3D-structures of 5HT$_{1A/7}$Rs were generated using Homology Modeling and extensively validated through Ramachandran Plot, stereochemical quality parameters, docking and MD. All intermediates and final compound were synthesised and characterized using NMR and Mass Spectrometry. Cytotoxicity studies were performed on HEK cell lines. Labelling conditions were established a prior by reaction of methyl iodide and HPLC profiling was used for characterization. **Results:** Receptor ligand interaction of [CH$_3$]-BTZ-MPP reveals the presence of conserved residues in binding sites of 5HT$_{7/1A}$Rs. The G-Score for dimeric 5-HT$_{1A}$-5-HT$_{1A}$, 5-HT$_7$-5-HT$_7$ and 5-HT$_{1A}$-5-HT$_7$Rs were -11.151, -8.816 and -9.0 respectively, which indicated good binding affinity. The values of logPo/w, logBB and logS were calculated to be 3.9, 0.35 and -3.85 respectively using QikProp. Experimental logPo/w of [^{11}CH$_3$]-BTZ-MPP was 0.26 indicating brain penetration and drug likeliness. Synthesis involved the formation of following intermediates and the respective final molecule: (a)BTZ-Cl (98%), (b) N-BOC-BEA (98%), (c) MPP-N-BOC-BEA (80%), (d) MPP-NH$_2$(99%), (e) secondary amine BTZ-MPP (90%), (e) [CH$_3$]-BTZ-MPP (98%). No significant cytotoxicity was observed at concentration range 1nM - 1mM. Radiolabeling was carried using [^{11}C]-CH$_3$I. Initial in vivo biodistribution

studies showed maximum uptake in brain corresponding to 5.19 %ID/g. Significant uptake in hippocampus (74.94%) and cortex (5.95%) indicate affinity and specificity for the dimeric 5-HT$_{1A/1A}$/5-HT$_{1A/7}$ receptors. The uptake in liver indicate hepatobiliary route of excretion. **Future Work:** The imaging studies to confirm brain uptake and selectivity studies are underway. **Conclusions:** Novel neuroimaging agent based on mixed pharmacophore MPP-BTZ to target dimeric 5-HT$_{1A/1A}$/5-HT$_{1A/7}$Rs was theoretically evaluated, synthesised and evaluated. Initial studies indicate brain penetration and preferential uptake in receptor rich regions. Further work will establish its potential application as radiopharmaceutical for neuro-receptor imaging.

OP-696

Head to head comparison of (R)-[^{11}C]verapamil and [^{18}F]MC225 in non-human primates; tracers for measuring P-gp function at the blood-brain barrier

J. Toyohara[1], *L. Garcia-Varela*[2], *T. Kakiuchi*[3], *O. HIroyuki*[3], *S. Nishiyama*[3], *T. Tago*[1], *D. Vallez-Garcia*[2], *R. Boellaard*[2], *P. H. Elsinga*[2], *H. Tsukada*[3], *G. Luurtsema*[2]; [1]*Tokyo Metropolitan Institute of Gerontology, Tokyo, JAPAN,* [2]*University of Groningen, Groningen, NETHERLANDS,* [3]*Hamamatsu Photonics, Hamamatsu, JAPAN.*

Introduction: A number of substrate for P-glycoprotein (P-gp), such as (*R*)-[^{11}C]verapamil ([^{11}C]VER), has been developed for imaging P-gp function with positron emission tomography (PET). These substrates have high affinity for P-gp and can measure decreased function which results in an increased tracer brain uptake. However, it is not possible to measure over-expression of P-gp function, because the concentration of the tracer at baseline is already extremely low. Recently developed [^{18}F]MC225 is a selective substrate for P-gp with a good metabolic stability and showed higher baseline uptake than that of other P-gp substrates. In addition, [^{18}F]MC225 is a weaker P-gp substrate than [^{11}C]VER. These properties would be suitable for measuring over-expression of P-gp in the brain, which is associated with drug resistance e.g. in case of epilepsy and depression. For clinical application in humans, direct comparison using both tracers in the non-human primate was conducted. **Subjects and Methods:** A total of 12 PET measurements with [^{11}C]VER and [^{18}F]MC225 under baseline and blocking conditions were performed in 3 conscious state male monkeys (*Macaca mulatta*) with arterial blood sampling. The blocking effect of P-gp was evaluated with tarquidar loading at a dose of 8 mg/kg. The total distribution volume (V_T) of both tracers reflects P-gp function and was calculated by Logan graphical analysis using a metabolite-corrected plasma input function. **Results:** The baseline uptake of [^{11}C]VER into the brain was low (standardized uptake value; SUV = 0.5-1) and stable till the end of PET measurements (90 min). After tarquidar infusion, the brain uptake of [^{11}C]VER was significantly increased (SUV = 2-3) and peaked at 10 min after tracer injection, and then gradually decreased to SUV=1.5-2. The baseline uptake of [^{18}F]MC225 was higher (SUV = 1-1.5) than [^{11}C]VER and also stable till the

end of PET measurements (90 min). After tarquidar infusion, the brain uptake of [^{18}F]MC225 was significantly increased (SUV = 2-3) and peaked between 20 and 30 min after tracer injection, and then stable or slight decrease till the end of PET measurements. The whole brain baseline V_T of [^{18}F]MC225 (9.5) was 2.6-times higher than that of [^{11}C]VER (3.6). Inhibition of P-gp resulted in a 3.2-times increase of whole brain V_T (11.5) for [^{11}C]VER. For [^{18}F]MC225, the increase was 1.4-times in the whole brain (13.2). **Conclusion:** Our results confirm previous research with [^{18}F]MC225 in rats and indicates that [18F]MC225 is a suitable tracer for measuring over-expression of P-gp at the human blood-brain barrier.

OP-697

Identification and development of a highly specific monoacylglycerol lipase (MAGL) PET tracer ^{11}C-PF-06809247

C. R. Butler[1], *A. Takano*[2], *S. Nag*[2], *R. Arakawa*[2], **K. P. Maresca**[1], *J. R. Piro*[1], *T. Samad*[1], *D. Smith*[1], *D. Nason*[1], *S. O'Neil*[1], *L. McAllister*[1], *S. Grimwood*[1], *P. Trapa*[1], *T. McCarthy*[1], *A. Villalobos*[1], *C. Halldin*[2], *L. Zhang*[1];* [1]*Pfizer, Inc., Cambridge, MA, UNITED STATES OF AMERICA,* [2]*Karolinska Institutet, Stockholm, SWEDEN.*

Aim: Monoacylglycerol lipase (MAGL) is a serine hydrolase highly expressed throughout the brain. It serves as a key gatekeeper regulating the tone of endocannabinoid signaling. Inhibition of MAGL is known to provide therapeutic benefits pre-clinically for a number of neurological disorders. We are interested in developing a MAGL-specific PET ligand to facilitate clinical characterization and assessment of MAGL inhibitors. Herein, we report [^{11}C]PF-06809247 as a potent and selective PET ligand that demonstrated high specific binding in vivo. **Materials and Methods:** The chemical matter was prioritized based on potency/selectivity, physicochemical, and in vitro pharmacokinetic properties. Specifically, we prioritized based on a set of CNS PET design and selection criteria, consisting of central nervous system PET multi-parameter optimization (CNS PET MPO) score; passive permeability RRCK and multi-drug resistance efflux MDR BA/AB; and brain fraction unbound Fu_b. To assess its viability as an in vivo radiotracer, [^{3}H]PF-06809247 was first prepared and evaluated in rodents for target expression (Bmax) measurement, brain bio-distribution and in vivo specific binding assessment. PF-06809247 was subsequently radiolabeled with [^{11}C] methyl iodide, followed by in vivo non-human primate (NHP) PET imaging. A cynomolgus monkey was scanned (High Resolution Research Tomograph; Siemens) for 120 minutes, at baseline and after pretreatment with a selective MAGL inhibitor. **Results:** Prioritization with aforementioned CNS PET ligand selection criteria followed by a PET-specific structure-activity relationship effort quickly identified PF-06809247 as a promising PET lead. Structurally PF-06809247 is amenable to either [^{3}H] or [^{11}C] labeling. It showed good MAGL potency (IC$_{50}$= 9 nM), high passive permeability (RRCK P$_{app}$ AB= 13.8 x 10^{-6} cm/s), low MDR efflux (BA/AB =1.6) and favorable F$_{u\_b}$ (0.04). Saturation binding of [^{3}H] PF-06809247 in rat and NHP brain homogenates revealed high MAGL expression (B$_{max}$ 75-100 nM) across species, and specific

binding across multiple brain regions (>90%), which could be dose-responsively blocked by a selective MAGL inhibitor. [¹¹C] PF-06809247 NHP PET imaging showed rapid brain uptake and sustained binding throughout the brain, consistent with MAGL distribution. The brain uptake was 2-3% injected dose at peak. A significant reduction of [¹¹C]PF-06809247 binding was observed upon pretreatment with a high dose of selective MAGL inhibitor, demonstrating the target was clearly blocked. **Conclusions:** Using PET ligand design parameters, PF-06809247 was rapidly identified with favorable in vitro attributes for PET radiolabeling. Further evaluation via in vivo NHP studies revealed high specific binding to MAGL. Altogether, these data suggested [¹¹C] PF-06809247 is a promising PET ligand for clinical imaging of MAGL.

OP-698

Development of a radiolabeled ligand targeting 5-HT$_3$ receptors in the brain

A. Takano[1], V. Stepanov[1], M. Svedberg[1], J. Häggkvist[1], L. Tari[1], M. Tóth[1], R. Krasikova[1], N. Amini[1], C. Sanchez[2], C. Bundgaard[2], M. Jessing[2], B. Bang-Andersen[2], C. Halldin[1]; [1]Karolinska Institutet and Stockholm County Council, Stockholm, SWEDEN, [2]H. Lundbeck A/S, Lundbeck Research, Copenhagen, DENMARK.

Introduction: The 5-HT$_3$ receptor is unique among 5-HT receptors since it is a ligand-gated ion channel. The 5-HT$_3$ receptor is considered to be involved in several psychiatric diseases including depression and schizophrenia. In the present study, we aimed to develop a radiolabeled ligand targeting the 5-HT$_3$ receptor and evaluate its preclinical characteristics in *in vitro* autoradiography and *in vivo* PET non-human primates (NHP) and rat brain. **Methods:** [¹¹C]2-(4-methylpiperazin-1-yl)quinazolin-4-amine was synthesized by alkylating the precursor 2-(piperazin-1-yl)quinazolin-4-amine with [¹¹C]MeOTf. *In vitro* autoradiography using [¹¹C]2-(4-methylpiperazin-1-yl)quinazolin-4-amine was performed using postmortem rat, NHP and human brain sections. Specific binding and the blocking effects by the 5-HT$_3$ receptor antagonists; ondansetron and mirtazapine, were measured. NHP PET measurements were performed in two rhesus monkeys at baseline and after pretreatment with 1.0-2.0 mg/kg of mirtazapine. Total distribution volume (V_T) was estimated by the two-tissue compartment model and Logan plot using arterial input function. Small animal PET measurements were performed in four Sprague Dawley rats at baseline and after pretreatment with mirtazapine and the cholinergic nicotinic alpha7 receptor agonist and 5-HT$_3$ receptor antagonist, encenicline. **Results:** [¹¹C]2-(4-methylpiperazin-1-yl)quinazolin-4-amine was successfully radiolabelled in good yield and high radiochemical purity (>99%). Specific [¹¹C]2-(4-methylpiperazin-1-yl)quinazolin-4-amine *in vitro* binding was detected in the hippocampus, amygdala and cortex in coronal rat and human brain sections. Total [¹¹C]2-(4-methylpiperazin-1-yl)quinazolin-4-amine binding was blocked 100% with 10 μM of ondansetron, and mirtazapine in the rat brain. However, there was no *in vitro* binding of [¹¹C]2-(4-methylpiperazin-1-yl)quinazolin-4-amine detected in the NHP brain sections. NHP

PET study showed high brain uptake (approximately 300%SUV at peak). However, no clear blocking effects were seen after pretreatment with mirtazapine. Peripherally, the uptake of the radioligand decreased in salivary gland after pretreatment with mirtazapine. Small animal PET study showed high brain uptake (approximately 200%SUV at peak). However, no clear blocking effects were seen after pretreatment with 5HT$_3$ receptor antagonists. **Conclusions:** It is shown that [¹¹C]2-(4-methylpiperazin-1-yl)quinazolin-4-amine can be used to study the *in vitro* 5-HT$_3$ receptor binding and could be used to evaluate *in vivo* peripheral 5-HT$_3$ receptor binding in salivary glands. However, it did not prove to be useful as an *in vivo* PET radioligand for the brain as no clear blocking effects were seen despite the shown good brain penetration. One possibility is that compounds with higher affinity to the 5-HT$_3$ receptor would be necessary for further development of PET radioligands for 5-HT$_3$ receptor in the brain.

OP-699

Radiosynthesis, initial evaluation and whole-body dosimetry of a beta-secretase (BACE) PET radioligand [¹¹C] PF-06684511 in non-human primates

R. Arakawa[1], L. Chen[2], A. Takano[1], M. A. Brodney[2], J. Dutra[3], V. Stepanov[1], S. Nag[1], S. Doran[3], T. McCarthy[2], C. Nolan[2], A. Villalobos[3], L. Zhang[2], C. Halldin[1]; [1]Department of Clinical Neuroscience, Center for Psychiatry Research, Karolinska Institutet and Stockholm County Council, Stockholm, SWEDEN, [2]Worldwide Research & Development, Pfizer Inc., Cambridge, MA, UNITED STATES OF AMERICA, [3]Worldwide Research & Development, Pfizer Inc., Groton, CT, UNITED STATES OF AMERICA.

Aim: Beta-secretase (BACE) is a key enzyme in the generation of beta-amyloid. BACE inhibitors are being developed to decrease beta-amyloid accumulation in the brain and to reduce the risk of Alzheimer's disease. PF-06684511 was identified by Pfizer as a candidate PET ligand for BACE. PF-06684511 bears structure moieties amenable for both F-18 and C-11 radio-labeling. We have previously reported successful radio-labeling of PF-06684511 with F-18 and desired BACE specific binding and kinetics in non-human primate (NHP) PET imaging with [¹⁸F]PF-06684511. In this study, we aimed to radio-label PF-06684511 with C-11 to develop an alternative BACE radioligand in cases that multiple PET scans in the same day and/or reduced radiation dosage to subjects are desired. [¹¹C]PF-06684511 was evaluated in NHPs with baseline/blocking measurements using a BACE inhibitor, PF-06663195. Additionally, we evaluated the radiation dosimetry of [¹¹C]PF-06684511 and [¹⁸F]PF-06684511 in NHPs with whole-body PET measurements. **Materials and Methods:** Brain PET scans of 120 min were performed in two cynomolgus monkeys twice in each NHP, one at baseline and another after intravenous administration of PF-06663195 (0.266 mg/kg bolus followed with 0.064 mg/hr/kg constant infusion). The total distribution volume (V_T) in brain regions of interest was calculated using two tissue compartment (2TC) model with radiometabolite corrected arterial plasma input function. The target occupancy was estimated using the Lassen plot.

Whole-body PET measurements with [11C]PF-06684511 and [18F]PF-06684511 were performed in two cynomolgus monkeys. The effective doses by both radioligands were estimated with the OLINDA/EXM software using the adult male model. **Results:** [11C]PF-06684511 was successfully radiolabeled with radiochemical yield from 150 to 550 MBq per run and radiochemical purity >99.8%. The brain uptake of [11C]PF-06684511 in NHPs was 2-3.5% injected dose (%ID) at the peak under the baseline condition. After pretreatment with PF-06663195, the brain uptake of [11C]PF-06684511 decreased significantly in all regions. Occupancies were 84.4% and 100.5% in two NHPs respectively. High uptake was shown in the small intestine, liver and brain for both [11C]PF-06684511 and [18F]PF-06684511. The effective dose of [11C]PF-06684511 was 0.0054 mSv/MBq while that of [18F]PF-06684511 was 0.043 mSv/MBq. **Conclusions:** [11C]PF-06684511 demonstrated high brain uptake in NHPs at the baseline and clear blocking effects after the administration of a BACE inhibitor. The radiation effective dose of [11C]PF-06684511 was smaller than that of [18F]PF-06684511. [11C]PF-06684511 was demonstrated to be a promising PET radioligand for BACE.

1707	Wednesday, October 25, 2017, 10:00 - 11:30, Hall F2

Clinical Oncology: PSMA - Saving Nuclear Medicine

OP-700

Predictor factors of 68Ga-PSMA PET/CT positivity in biochemical recurrent Prostate Cancer.

C. Artigas, R. Diamand, A. Peltier, R. Van Velthoven, F. Otte, S. Sideris, T. Gil, Z. Wimana, P. Flamen; Jules Bordet Institut Brussels, Brussels, BELGIUM.

Introduction and Aim: Prostate Specific Membrane Antigen (PSMA) is overexpressed in prostate cancer (PCa). 68Ga-PSMA PET/CT has shown better detection rates than other imaging techniques like Choline-PET/CT in patients with biochemical recurrence (BCR) at low PSA levels. The aim of our study was to analyze if parameters like PSA value, PSA kinetics and other factors are associated with a positive 68Ga-PSMA PET/CT. **Material and Methods:** We retrospectively analyzed a cohort of 248 consecutive 68Ga-PSMA PET/CT performed at our institution for PCa BCR after local treatment with curative intent (surgery, radiotherapy or both) between November 2014 and February 2017. Mean age 70y (range 51-90). Looking for predictors of positivity, multiple parameters were registered: primary treatment modality, prostate weight before treatment, initial PSA, TNM classification, OMS histological classification group, micro and macroscopic positive margins, positive lymph nodes, hormonotherapy at the time of scan, PSA value at scan and PSA kinetics. Median PSA value was 2,31 ng/mL, median PSA doubling time (PSAdt) was 8,45 and median PSA velocity (PSAv) 1,4 ng/mL/year. Statistical univariate and multivariate logistic regression analysis were performed to assess which factors were associated with positive 68Ga-PSMA PET/CT. **Results:** 68Ga-PSMA was positive in 185/248 patients (75%).

117/248 (47%) of them were considered oligometastatic (3 or less pathological foci). In the univariate logistic regression analysis, factors with significantly (p<0,05) increased probability of a positive 68Ga-PSMA PET/CT were: PSA value OR (95% CI) 2,04 (1,62-2,58) p <0,0001; PSAdt 1,47 (1,15-1,89) p 0,0025; and PSAv 2,86 (2,05-3,98) p <0,0001. However in the multivariate analysis only PSAv was a significant predictor of a positive 68Ga-PSMA PET/CT (p <0,0001). Detection rates of 68Ga-PSMA PET/CT in relation to PSAv were 42% (38/90), 82% (32/39), 80% (24/30), and 95% (62/65) in patients with PSAv values of, respectively, 1, 1-2, 2-5 and >5 ng/mL/y. **Conclusion:** This retrospective study shows that PSA value and PSA kinetics (PSAdt and PSAv) are factors significantly associated with an increased probability of a positive 68Ga-PSMA PET/CT. Of those parameters, PSAv was the only independent factor, considering it a strong predictor for a positive 68Ga-PSMA PET/CT (p<0,001).

OP-701

Ga-68 PSMA-11 PET-CT in the Evaluation of Newly Diagnosed Prostate Adenocarcinoma

N. Ergül, **T. F. Çermik**; Istanbul Training and Research Hospital, Istanbul, TURKEY.

Introduction: In newly diagnosed prostate adenocarcinoma (PC) conventional imaging modalities (CIM) like pelvic MRI and bone scintigraphy are used for staging. Ga-68 PSMA ligand PET/CT is an emerging modality to detect the metastatic disease in especially intermediate and high risk PC. In this study we analyzed the contribution of Ga-68 PSMA-11 PET/CT in staging and therapy management of newly diagnosed PC. **Materials and Methods:** A total of 78 patients with biopsy-proven PC who were referred for Ga-68 PSMA-11 PET/CT for primary staging were retrospectively analysed. The patients were divided into risk groups according to the D'amico risk stratification criteria. Some of the patients had underwent pelvic MRI and/or bone scintigraphy also. The findings of Ga-68 PSMA-11 PET/CT were compared to the CIM for staging of the disease. The SUVmax values of the primary tumors were calculated and correlated with Gleason scores and metastatic extent of the disease. **Results:** Of 78 patients 5 patients were in low risk group, 18 patients were in intermediate risk group and 55 patients were in high risk group. In 38 patients no metastasis was found. In 10 patients regional lymph node metastases and in 30 patients distant metastases were detected. In 42 out of 78 patients (53%) Ga-68 PSMA-11 PET/CT changed the staging compared to pelvic MRI and bone scan. There was significant difference between the SUVmax values of the tumors with Gleason score 6 and 7 compared to Gleason 8,9 and 10 (p=0.003). The SUVmax values were significantly different between the patients with no metastasis and patients with regional lymph node or distant metastasis (p=0.02 and p=0.002 respectively). **Conclusion:** Ga-68 PSMA-11 PET/CT is an important imaging modality for primary evaluation of newly diagnosed PC changing the disease stage substantially. Also the SUVmax of the primary tumor has a good correlation with Gleason score and metastatic extent of disease defining the prognosis.

OP-702

Initial Results with 18F-PSMA-1007 in Prostate Cancer Patients with Biochemical Recurrence

F. L. Giesel[1], L. Will[1], J. Cardinale[2], O. C. Neels[2], J. P. Radtke[3], K. Kopka[2], U. Haberkorn[1], C. Kratochwil[1]; [1]Department of Nuclear Medicine, University Hospital Heidelberg, Heidelberg, GERMANY, [2]Division of Radiopharmaceutical Chemistry, German Cancer Research Center (dkfz), Heidelberg, GERMANY, [3]Department of Urology, University Hospital Heidelberg, Heidelberg, GERMANY.

Purpose: Prostate cancer (PCa) imaging has seen a relevant improvement through the clinical introduction of ^{68}Ga-PSMA-11. Yet, Gallium-68-labeled tracers have limitations due to relatively short half-life and low production capacities. As a result, Fluorine-18-labelled ligands such as PSMA-1007 and DCFPyL were developed. PSMA-1007 has an aditional advantage as it shows low urinary clearance, resulting in better positron-emission tomography/computed tomography (PET/CT)-imaging of the pelvis. We evaluated the diagnostic potential of PSMA-1007 in PCa patients with biochemical recurrence (BCR) in this study. **Subjects and Methods:** Seven patients (median age 72) with BCR (mean PSA 1.78 ng/mL) underwent PET/CT-scans 1h and 3h after injection of ^{18}F-PSMA-1007 (mean dose 247 MBq). Biodistribution in normal organs and tumor uptake, as well as lesion morphology (size) were examined. **Results:** All 7 patients tolerated PSMA-1007 well and no adverse events occurred. PSMA-1007 PET/CT detected local recurrence in 2 patients (PSA 1.9 and 3.6 mg/mL), lymph node (LN) metastasis in 2 patients (PSA 0.16 and 2.0 ng/mL), bone metastasis in 1 patient (PSA 3.8 ng/mL) and no PET-positive findings in 2 patients (PSA 0.4 and 0.5 ng/mL). Tumor uptake increased in all lesions from 1h p.i. (mean SUV_{max} 8.4) to 3h p.i. (mean SUV_{max} 14.1). Histological validation of one patient with LN-metastasis was available and confirmed true-positive findings. Additionally, response to succeeding radiotherapy gave further clinical confirmation. Distant metastasis was not confirmed but treated with androgen-deprivation therapy. Diagnosed LN-metastases were below radiological diagnostic criteria (size). Focal therapy would not have been an option with conventional staging alone. **Conclusion:** ^{18}F-PSMA-1007 PET/CT showed a high potential for localization diagnostics in patients with recurrent PCa in this pilot study. Low background signal in bladder and urethra were seen, resulting in a good delineation of local recurrence. This might present favorable in comparison to other ligands in the setting of BCR.

OP-704

The Importance Of Ga-68 PSMA PET CT In Detection Of Recurrence Metastasis Prostate Cancer Without Biochemical Recurrence

E. Akgun[1], O. E. Sahin[1], E. Demirci[2], B. Akovali[1], M. Ocak Demirci[3], A. Aygün[1], H. Pehlivan[1], E. Karayel[1], A. R. Kural[4], L. Kabasakal[1]; [1]İstanbul University Cerrahpasa Medical Faculty, İstanbul, TURKEY, [2]Sisli Etfal Educational Research Hospital, İstanbul, TURKEY, [3]İstanbul University Faculity of Pharmacy, İstanbul, TURKEY, [4]Acıbadem University Medical Faculty, İstanbul, TURKEY.

Positron emission tomography with Gallium 68 labeled urea based prostate specific membrane antigen inhibitor (Ga-68 PSMA PET/CT) is an important modality in staging prostate cancer. It is more sensitive than morphologic imaging modalities at restaging, even low Prostate Specific Antigen (PSA) level. **Material and Methods:** In our study, we included 28 patients with prostate cancer who underwent Ga-68 PSMA PET/CT in the context of increasing follow-up PSA values (n = 17) and suspected metastatic lesions (n = 11). All patients had definitive treatment either with radical prostatectomy (RP) or radiotherapy (RT). The average age was 64,22 years and median PSA level was 0,23 ng/mL (range: 0,001-1,98 ng/mL). Among them 17 patients had RP whose PSA level lower than 0,2 ng/ml (group 1) and 11 patients had definitive RT whose PSA level lower than 2.0 ng/ml (group 2). Gleason scores were 5 (n =1, %3,57), 6 (n =5, %17,85), 7 (n =8, %28,57), 8 (n =4, %14,28), 9 (n =5, %17,85) and unknown (n =5). Lesions with higher radionuclide uptake at PSMA PET/CT were considered pathologic and their follow up based on PSA levels, control PSMA PET/CT and/or other radiologic imaging modalities. **Results:** Overall positivity rate was 50% in PSMA PET scan. In group 1; 5 of 17 (29%) patients showed pathologic uptake at PSMA PET/CT. Among these patients 4 patients had increased PSA level during follow-up and in 2 patients progression was documented by follow PSMA PET/CT. Patients who had negative PSMA PET scan 6 of 12 patients (%35,29) had increased follow up PSA level and in1 patient progression of the disease documented by PSMA PET/CT. In-group 2; 9 of 11 (64%) patients showed pathologic uptake at PSMA PET/CT. Among them 7 patients (64%) had increased PSA level during follow-up and also 3 patients's follow PSMA PET/CT revealed progressive disease. **Conclusion:** Ga-68 PSMA PET/CT shows high positivity rates in patients with prostate cancer with low PSA levels and who had suspicion of recurrence even in lower PSA levels than so called biochemical recurrence.

OP-705

Can 68Ga - PSMA PET/CT predict seminal vesicle invasion for patients undergoing radical prostatectomy?

A. Agrawal, V. Rangarajan, G. Bakshi, G. Prakash, S. Menon, N. Purandare, S. Shah, A. Puranik, N. Sable; TATA Memorial Hospital, Mumbai, INDIA.

Aim: The primary aim of the study was to assess whether Ga PSMA PET/CT could predict stage T3b which is extension of the tumor into the seminal vesicles (SV). **Materials and Methods:** 35 patients with age range of 47-73, who were diagnosed to have prostate cancer by biopsy; underwent 68Ga-PSMA PET/CT prior to undergoing a radical prostatectomy (RP). 68Ga PSMA PET/CT was visually assessed for the primary tumor and uptakes were semiquantavely assessed by SUVmax. None of these patients demonstrated metastatic sites on PSMA PET/CT. All patients underwent RP, which was either open, laparoscopic or robotically done. Histopathology post-surgery assessed the primary tumor, extra prostatic invasion (EPE), seminal vesicle invasion and nodal disease. **Re-**

sults: On per patient basis, 8 out of 35 (23%) patients were positive for seminal vesicle invasion histopathologically. On lesion wise analysis 11 out of 16 SV were positive histopathologically. On PSMA PET/CT, 7 out of 8 patients were positive for SV invasion. On lesion based analysis, PSMA was positive in 8 out of 16 SV. On per patient basis, the sensitivity (SN), specificity (SP) positive predictive value (PPV) and negative predictive value (NPV) of PSMA was 87.5%, 100%, 100%, 96.43% respectively. On lesion based analysis the SN, SP, PPV and NPV were 66.67%, 100%, 100% and 50% respectively. **Conclusion:** 68Ga PSMA PET/CT can predict SV invasion with a very high PPV. Fusion of 68Ga - PSMA PET with MR in future may still enhance the prediction of SV invasion in patients of prostate cancer undergoing radical prostatectomy.

OP-706

Dual point 18F-Choline PET/CT in the evaluation of focal hypermetabolic prostate lesions. Acquisition timing protocol

A. Díaz[1], M. Soler[2], M. Cozar[2], G. Reyes[2], E. Riera[2], Á. Jaramillo[2], J. Ferrer-Rebolleda[2], J. R. García[2]; [1]CHUC (Complejo Hospitalario Universitario de Canarias), La Laguna, SPAIN, [2]CETIR-ERESA, Barcelona, SPAIN.

Objective: The stable or increased tracer uptake over time (accumulative pattern) vs its decrease (washout pattern) has been described as a method to differentiate between benign and malign lesions. However, there is no consensus on the 18F-Choline PET/CT acquisition timing protocol. The aim of this study was to determine the optimal dual-point protocol in the evaluation of focal hypermetabolic prostate lesions. **Material and Methods:** We prospectively studied, over the first 6 months of performing 18F-Choline PET/CT scans, 43 patients with prostate cancer. We identified hypermetabolic foci in 22 patients: 10 staging and 12 biochemical recurrence scans, being the last ones: 2 post-surgery, 4 post-brachytherapy and 6 post-radiotherapy. Patients were followed up clinically, radiologically and hystologically when it was possible. The PET/CT acquisition protocol was divided in 3 steps: early static image of the pelvis, immediately after injection (1 bed); whole-body 1 hour; whole-body 2 hours. We performed visual and semiquantitative analyses, calculating the median maximum standardized uptake value (SUVmax) and its increase or decrease, in percentage terms, between the steps (early/1hour and 1hour/2 hours), to determine whether tracer uptake remained stable/increased (accumulative pattern) or decreased (washout pattern). **Results:** We identified 28 hypermetabolic foci in the prostate glands, finding 2 lesions in 6 of the patients (5 staging and 1 post-radiotherapy recurrence scans). None of the patients showed ureteral/urinary bladder activity in the early static images of the pelvis, being the evaluation of the hypermetabolic foci between the three steps non discordant. 21 lesions had an accumulative pattern. The median SUVmax was: early: 3,04 / 1 hour: 3,45 / 2 hours: 4,0. The uptake increase was: early/1hour: +18'15% ; 1hour/2 hours: +11,26%. 7 lesions had a washout pattern. The median SUVmax was: early: 3,39 / 1 hour: 2,84 / 2 hours: 2,64. The uptake decrease was: early/1hour: -17,48% ; 1hour/2 hours: -7,05%. **Conclusions:** Dual point 18F-Choline PET/CT allows differentiation between accumulative pattern (malign) and washout pattern (benign). The optimal protocol to distinguish these two patterns is to acquire early (immediately post-injection) and 1 hour images.

OP-707

Reduction of 68Ga-PSMA renal uptake with mannitol infusion: preliminary results

G. Paganelli[1], E. Mezzenga[1], P. Caroli[1], A. Moretti[2], R. Galassi[2], M. Celli[1], L. Fantini[1], V. Di Iorio[1], A. Sarnelli[1], F. Matteucci[1]; [1]IRST IRCCS, Meldola, ITALY, [2]AUSL Romagna, Forlì, ITALY.

Purpose: Urea based -PSMA ligands labelled with 68Gallium or 177Lutethium are new tracers with great potential for a theranostic approach in prostate cancer (PCa). However, clinical studies have shown that the kidney is one of the target organs along with salivary and lacrimal glands. PSMA receptor is physiologically express in the proximal tubules and mannitol is diuretic of the proximal tubules. We are investigating the use of mannitol to reduce the renal uptake after the injection of 68Ga-PSMA and 177Lu-PSMA. **Subjects and Methods:** Kidney uptake (SUVmax) in 9 patients (pts) undergoing 68Ga-PSMA PET/CT in basal conditions (b-PET/CT) and after intravenous infusion of 500 ml of 10% mannitol (m- PET/CT), was calculated. Two different infusion schemes have been used: a) slow administration (40 minutes) after the injection of 68Ga-PSMA (A-infusion); b) fast-administration (50% of the total volume of mannitol in 15 minutes before injection of 68Ga-PSMA and 50% in the next 15 minutes) (B-infusion). **Results:** In A-infusion pts, an increase in the mean value of SUV_{max} of 11.9% and 7.4% for right kidney and left kidney respectively was found. In B-infusion pts, we observed a decrease in the mean SUV_{max} value in right kidney of 24.3% and in left kidney of 22.4%. **Conclusions:** our data show that mannitol may play a role in the reduction of kidneys uptake after 68Ga-PSMA injection. The mannitol administration should be rapid and before the radioactive tracer's injection. These data warrant dosimetric studies in patients treated with 177Lu-PSMA. Mannitol administration scheme can be further optimized.

1708	Wednesday, October 25, 2017, 10:00 - 11:30, Hall K

Cardiovascular System: Atherosclerotic Plaque Imaging

OP-708

Non-invasive visualization of healing phase 2 after myocardial infarction (MI) using 68Ga-NOTA-anti-CD206-Nb: targeting mannose receptor (MR, CD206) on M2 macrophages

Z. Varasteh[1], A. Bartels[1], S. Mohanta[2], A. Steinsiek[3], Y. Li[2], M. Braeuer[1], N. López Armbruster[3], S. Nekolla[1], A. Habenicht[2], G. Raes[4], S. Hernot[4], H. Sager[3], M. Schwaiger[1]; [1]Klinikum rechts der Isar, München, GERMANY, [2]University Hospital of Ludwig-Maximilians-University, München, GERMANY, [3]Klinik für Herz und Kreislauferkrankungen, München, GERMANY, [4]Vrije Universiteit Brussel, Brussels, BELGIUM.

Introduction: Myocardial infarction (MI) is the most frequent cause of heart failure. The quality of intrinsic wound healing that occurs during the first 1-2 weeks after MI determines the fate of patients for years to come. Wound healing after cardiac ischemia is characterized by a first inflammatory phase in which the sterile wound recruits inflammatory leukocytes from the blood to the heart. Recruited monocytes differentiate into inflammatory macrophages that remove dead cells and extracellular matrix debris. The inflammatory phase is then succeeded by a reparative phase in which macrophages functionally shift from promoting inflammation to pursuing repair functions that ultimately result in a stable scar. Accordingly, an impaired resolution of inflammation consequently leads to adverse post-MI remodeling. Reparative macrophages can be distinguished from inflammatory macrophages by the surface marker mannose receptor (MR, CD206). Imaging the reparative phase of cardiac wound healing after MI is of great interest because it may early on reveal a delayed resolution of inflammation which in turn predicts adverse cardiac remodelling with development of post MI heart failure. Therefore, in this study we evaluated the feasibility of ^{68}Ga-NOTA-anti-CD206-Nb for imaging the MR expressed on alternatively activated, reparative macrophages in mice with experimental MI. **Methods**: Female C57BL/6 mice were subjected to myocardial infarction via permanent ligation of the left coronary artery. Non-operated (steady state) mice were used as controls. ^{68}Ga-NOTA-anti-CD206-Nb/PET acquisitions were taken 2, 6 and 14 days after MI. Consecutive [18]FDG/PET acquisition allowed the localization of the myocardium and the infarct zone. Upon PET/CT scans animals were euthanized and hearts were harvested. CD206-protein level on cardiac macrophages were quantified using flow cytometry. Immunofluorescent staining was executed with CD206 and CD68 targeting antibodies on cryosections. **Results**: PET/CT scans showed high ^{68}Ga-NOTA-anti-CD206-Nb myocardial uptake on day 6 after MI. Accordingly, flow cytometry experiments revealed that cardiac macrophages from day 6 after MI displayed significantly higher CD206 protein levels than macrophages from the steady state (1.236 ± 0.029 vs. 1 ± 0.018, mean fluorescent intensity (MFI)$\pm$SEM, p<0.01). Cardiac macrophages from day 2 after MI showed equal protein levels of CD206 than their counterparts from steady state (0.928 ± 0.023 vs. 1 ± 0.068 MFI/cell). Ex-vivo immunofluorescent staining on cardiac cryosections demonstrated the presence and co-localization of CD206- and CD68-positive cells (mainly macrophages), in accordance to the infected area. **Conclusion**: This exploratory study highlights the potential of ^{68}Ga-NOTA-anti-CD206-Nb to image reparative macrophages that are known to play a pivotal role in wound healing that follows acute MI.

OP-709

Non-invasive visualization of atherosclerotic plaques using ^{68}Ga-NOTA-anti-CD206-nanobody: targeting mannose receptor (MR, CD206) on M2 macrophages

Z. Varasteh[1], S. Mohanta[2], Y. Li[2], N. López Armbruster[3], M. Braeuer[1], S. Nekolla[1], A. Habenicht[2], H. Sager[3], G. Raes[4], S. Hernot[4], M. Schwaiger[1]; [1]Klinikum rechts der Isar, München, GERMANY, [2]University Hospital of Ludwig-Maximilians-University, München, GERMANY, [3]Klinik für Herz und Kreislauferkrankungen, München, GERMANY, [4]Vrije Universiteit Brussel, Brussels, BELGIUM.

Introduction: Atherosclerotic plaque phenotypes are classified based on the extent of macrophage infiltration into the lesions and certain plaque-resident macrophage subsets might be a sign for plaque vulnerability. Mannose receptor (MR, CD206) is expressed on alternatively activated (known as M2) macrophages. Recently, anti-CD206-Nanobodies (Nbs) were successfully used to specifically target tumor-associated macrophages as well as joint inflammation in rheumatoid arthritis. In the present study, we evaluated the feasibility of ^{68}Ga-NOTA-anti-CD206-Nb for imaging of CD206 expression on macrophages located in atherosclerotic plaques in apolipoprotein E-knockout (ApoE-KO) mouse model. **Methods:** NOTA-anti-CD206-Nb was labelled with [68]Ga. Binding selectivity and specificity of the radiotracer was checked in vitro. The biodistribution and in vivo specificity of the radiotracer was evaluated in control (C57BL/6) mice 1 h post injection (p.i.). For in vivo and ex vivo imaging studies, ^{68}Ga-NOTA-anti-CD206-Nb was injected into ApoE-KO and control mice and scanned 1 h p.i. For testing specificity of ^{68}Ga-NOTA-anti-CD206-Nb uptake in plaques, a group of ApoE-KO mice was co-injected with excess amount of non-labelled NOTA-anti-CD206-Nb. Upon imaging, the whole length aortas were harvested free from adipose tissue for autoradiography and Sudan-IV staining. Cryosections were prepared for immunofluorescent staining. **Results:** [68]Ga labelling provided a yield of greater than 99%. ^{68}Ga-NOTA-anti-CD206-Nb accumulated in vivo in CD206 expressing organs (i.e. liver and spleen) and showed only low residual blood signal (1.1 ± 0.1 %ID/g, 1 h p.i.). Binding specificity in receptor-positive organs was demonstrated by more than 1.5-fold reduced uptake of ^{68}Ga-NOTA-anti-CD206-Nb after co-injection of a blocking dose of non-labelled NOTA-anti-CD206-Nb. Multifocal signals could be detected in atherosclerotic plaques of ApoE-KO mice whereas no signal was detected in the aortas of control mice. ^{68}Ga-NOTA-anti-CD206-Nb uptake was detected in atherosclerotic plaques on autoradiography correlating well with Sudan-IV-positive areas. Calculated plaque-to-normal aortic tissue autoradiographic signal intensity was 7.7 ± 2.6 in aortas excised from ApoE-KO non-blocked mice. The Nb uptake in the plaques was associated with subendothelial accumulations of CD206- CD68-positive macrophages. **Conclusion:** ^{68}Ga-NOTA-anti-CD206-Nb accumulated in CD206 expressing organs and was associated with only low residual blood signal. In addition, ^{68}Ga-NOTA-anti-CD206-Nb uptake was detected in small dimension atherosclerotic plaques associated with the presence of CD206-positive macrophages suggesting that NOTA-anti-CD206-Nb represents a promising tracer for non-invasive detection of atherosclerotic plaques. Although the contribution of CD206-positive macrophages in the evolution and vulnerability of atherosclerotic plaques remains a matter of debate, it is clear that imaging of macrophage phenotypes is important in the context of plaque imaging and therapy.

OP-710

[68Ga]Pentixafor-PET/MRI for atherosclerotic plaque imaging

X. Li[1], D. Heber[2], X. Lu[3], X. Zhang[3], M. Mitterhauser[4], W. Wadsak[1], A. Haug[1], M. Hacker[1]; [1]Vienna General Hospital, Medical University of Vienna, Vienna, AUSTRIA, [2]Vienna General Hospital, Vienna, AUSTRIA, [3]Beijing Anzhen Hospital, Capital Medical University, Beijing, CHINA, [4]Ludwig Boltzmann Institute Applied Diagnostics, Vienna, AUSTRIA.

Background and Aim: Chemokines are expressed on cells of the atherosclerotic vessel wall and participate in the initial emigration of leukocytes to the sites of inflammation. The expression of chemokine receptor type 4 protein (CXCR4) was found to be co-localized with monocytes/macrophages. A novel PET tracer, Gallium-68 [68Ga]Pentixafor, a novel PET tracer with high affinity to CXCR4, has recently been introduced for the imaging of atherosclerosis. We sought to evaluate human atherosclerotic lesions using [68Ga]Pentixafor PET/MRI. **Methods:** 38 oncology patients underwent [68Ga]Pentixafor PET/MR imaging at baseline. Maximum standardized uptake values (SUV_{max}) were derived from hot lesions in seven arterial segments and target-to-blood ratios (TBR) were calculated. Spearman`s correlation coefficient and unpaired t test were performed for statistical comparison between uptake ratios and cardiovascular risk factors. The reproducibility of [68Ga]Pentixafor PET/MRI was assessed in seven patients with a PET/MRI follow-up exanimation 111±38 days after baseline. CXCR4 expression within different types of plaque lesions were estimated by Immunohistology. **Results:** 34 of 38 patients showed 611 foci with [68Ga]Pentixafor uptake that followed the contours of the large arteries. Both prevalence and mean TBR_{max} was highest in the descending aorta. There were significantly higher TBR values found in man (1.9±0.3) as compared to women (1.7±0.2; $P < 0.05$). Patients with mean $TBR_{max} > 1.7$ showed a significantly higher incidence of diabetes, hypertension hypercholesterolemia and history of cardiovascular disease than patients with mean $TBR_{max} \leq 1.7$. [68Ga]Pentixafor PET/MRI showed high reproducibility during baseline and follow-up examinations (r=0.6 for TBR_{max}, p<0.01) and there was no difference between the mean TBR_{max} values of plaque lesions ($TBR_{baseline}$ 1.8±0.3 vs $TBR_{follow-up}$ 1.8±0.3) (p=0.9). Co-locolization of CXCR4 protein expression were confirmed at fibrous plaque, atheromatous plaque and normal artery. **Conclusion:** [68Ga]Pentixafor could be detected and quantified by PET with high reproducibility. Patients with high arterial uptake showed significantly increased incidence of cardiovascular risk factors, suggesting a potential role of [68Ga]Pentixafor in the characterization of atherosclerosis. Key words: Chemokine receptor type 4, [68Ga]Pentixafor, Atherosclerosis, PET/MRI **Tables:** **Table 1.** Distribution of [68Ga]Pentixafor uptake in arterial lesions at baseline. **Table 2.** Lesional [68Ga]Pentixafor uptake at baseline compared to follow-up. P values were calculated using paired sample t-test to compare the TBR_{max} of baseline and follow-up scans.

OP-711

Imaging of LFA1 in Atherosclerotic Plaques Using a Novel SPECT Radiotracer

E. J. Meester[1], B. J. Krenning[1], M. R. Bernsen[1], G. Doeswijk[1], E. H. de Blois[1], J. P. Norenberg[2], M. de Jong[1], K. van der Heiden[1]; [1]Erasmus MC,

Rotterdam, NETHERLANDS, [2]University of New Mexico, Albuquerque, NM, UNITED STATES OF AMERICA.

Introduction: Atherosclerosis is a chronic disease of the arteries, characterised by a build-up of lipids and inflammatory cells in the vessel wall. Early detection of atherosclerosis and plaque monitoring following intervention remains a major challenge. Macrophages are attractive imaging targets for the detection of atherosclerosis, as they are involved in all phases of the disease. Lymphocyte Function associated-Antigen 1 (LFA1) is expressed on inflammatory cells including macrophages and is involved in cell migration into the vessel wall. The aim of this study was to non-invasively visualize atherosclerotic plaques through LFA1 targeted Single Photon Emission Computed Tomography/ Computed Tomography (SPECT/CT) imaging of macrophages using a novel tracer, In-111-DOTA-butylamino-Norbirt (DAN-BIRT), in a mouse model of atherosclerosis. **Methods:** Atherosclerotic mice (APOE $^{-/-}$) fed an atherogenic diet up to 20 weeks (n=10), were imaged by SPECT/CT 3 hours post injection of ^{111}In-DANBIRT (~200 pmole, ~50 MBq). *In vivo* imaging results were validated by *ex vivo* imaging and *ex vivo* autoradiography (ARG) of excised arteries. Oil Red O (ORO) staining of lipids was used to validate plaque presence in the arteries. Presence of macrophages and expression of LFA-1 in excised aortas was evaluated by immunohistochemical analysis of frozen tissue sections. Specific binding of the tracer to the target was assessed via *in vitro* ARG experiments. **Results:** *In vivo* SPECT/CT, *ex vivo* SPECT/CT, and *ex vivo* ARG showed tracer uptake inside aortic plaques. ORO staining confirmed fatty plaque build-up inside the aortic arch of all mice. *In vitro* ARG performed on mouse plaque sections confirmed specific binding, and immunohistochemistry showed macrophage and LFA1 co-localization inside plaques. **Conclusion:** Our results indicate ^{111}In-DANBIRT as a relevant tracer for non-invasive, in vivo visualization of atherosclerotic plaques and may provide a way to non-invasively monitor disease progression and therapeutic effects in patients with atherosclerosis.

OP-712

A Bradykinin Derivative Differentiates Vulnerable and Stable Atherosclerosis Plaques in Monkey

*Y. Xu[1], Z. Zhang[2], K. Lin[2], **Z. Liu[1]**; [1]Peking University, Beijing, CHINA, [2]BC Cancer Agency, Vancouver, BC, CANADA.*

Objective: Atherosclerosis is life-threatening disease that arises from the deposition of fatty plaques in the wall of arteries. Fatty plaques that can break off are called vulnerable plaques, which can be fatal as ruptured plaques would block arteries leading to acute myocardial infarction or ischemic stroke. To reduce mortality from such devastating cardiovascular events, it has been a long standing challenge to detect the presence of vulnerable plaques in high-risk but asymptomatic patients. In order to meet this challenge, recently we developed a ^{18}F-labeled bradykinin derivative (P05022) with high affinity to Bradykinin B1 receptor, which is not expressed in most tissues under normal conditions but up-regulated on vulnerable plaques. Here we report to

evaluate this PET imaging probe for identifying vulnerable atherosclerotic plaques in monkey models, and promising results have been achieved. **Method:** The receptor-binding domain of P05022 was derived from the B1R antagonist Lys-[Leu[8],desArg[9]] BK with Hyp[3] and Cha[5] substitutions to increase its in vivo stability. The binding affinity (K_i) was measured via competition binding assays using HEK293T:hB1R cell membranes. [18]F labeling was performed in NaOAc buffer (pH 4.1) at 95 °C for 10 min. Animal study was performed in rhesus monkey model, of that atherosclerosis was induced by high-fat diets over 5 years. PET image was collected at 60 min post injection. **Results:** P05022 binds B1R with high affinity (K_i = 2.3 nM), and [18F]P05022 could be prepared in high radiochemical yield (> 90 %) and purity (> 99 %). PET imaging showed the radioactivity was cleared rapidly from blood and normal tissues/organs, and was excreted mainly via the renal pathway. At 1 h p.i., atherosclerotic plaques were clearly visible in abdominal artery and femoral artery. The SUV (standard uptake value) of atherosclerotic plaque is up to 4.8, whereas the SUV of normal blood vessel, muscle and brain were 0.5, 0.4 and 0.1, respectively. **Conclusion:** P05022 selectively binds to B1R *in vivo* and generates high contrast images of vulnerable atherosclerotic plaque in monkey model. Our results suggest that P05022 is a promising PET tracer that can differentiate vulnerable atherosclerotic plaques from stable ones with significant specificity.

OP-713

Is FDG-PET/ CT a valuble diagnostic tool for verifying accelerated atherosclerosis secondary to diabetes mellitus in the aortic segments and large arteries?

G. G. Bural[1], D. A. Torigian[2], M. Houseni[3], M. K. Sozmen[1], A. Alavi[2]; [1]Izmir Katip Celebi University, Izmir, TURKEY, [2]Hospital of the University of Pennsylvania, Philadelphia, PA, UNITED STATES OF AMERICA, [3]Liver Institute, Cairo, EGYPT.

Aim: Atherosclerosis is a cardiovascular disease involving all arterial vascular beds marked by inflammation, plaque formation, and calcification. FDG-PET/CT has a well-established role for detection and quantification of atherosclerotic inflammatory disease using standardized uptake value (SUV) measurements. Detection of macroscopic arterial atherosclerotic calcification is also feasible via CT portion of PET/CT. Diabetes mellitus (DM) is a well-known risk factor which exacerbates the mechanisms underlying atherosclerosis. Thus, the inflammatory process and calcification in atherosclerosis is expected to be accelerated in subjects with DM compared to normal controls, and PET/CT could be a feasible tool evaluating both processes simultaneously. Our aim was to compare the inflammatory and macroscopic calcification processes of atherosclerosis in the aortic segments and large arteries of subjects with DM who are taking insulin compared to those of age-matched controls with no history of DM via FDG-PET/CT. **Methods:** 110 subjects who underwent FDG-PET/CT imaging were retrospectively studied. 55 were diabetics on insulin (61.5±10years old); 55 were age-matched controls (61.2±10 years old). Avarage SUVmax and SUVmean for four segments of aorta (ascending, arch, descending, abdomi-nal) and for common iliac arteries and common femoral arteries were measured and compared between subject groups. Presence or absence of macroscopic calcification on CT images for each arterial segment was also noted and compared between the two subject groups. Mann-Whitney-U test was used for continuous variables, and the chi-square test was used for categorical variables, p<0.05 was considered as statistically significant. **Results:** Avarage SUVmax and SUVmean were statistically significantly greater in subjects with DM on insulin compared to controls in all arterial segments (p<0.001). Presence of calcification on CT was more frequently encountered in six of the 8 segments in subjects with DM on insulin, and there was statistically significantly difference for the descending aorta (27/55 in DM subjects, and 14/55 in controls; p=0.01) and abdominal aorta (49/55 in DM subjects, and 35/55 in controls; p=0.0002). **Conclusion:** Our results show that inflammatory component of atherosclerosis as detected and quantified by FDG-PET/CT was more severe in all aortic segments and large arteries in subjects with insulin-dependent DM compared to those of controls. Presence of macroscopic calcification on CT was also detected to be more frequently encountered in the descending thoracic and abdominal aorta in subjects with DM. FDG-PET/CT is a valuable diagnostic tool for detecting and quantifying accelerated atherosclerotic inflammatory and calcific changes secondary to diabetes mellitus in the aortic segments and large arteries.

OP-714

Diagnosis of Deep Venous Thrombosis and Pulmonary Embolism Using ^{18}F-GP1 Positron Emission Tomography: An Exploratory Open-label Study

C. Kim[1], J. Lee[1], Y. Han[1], S. Chae[1], S. Oh[1], S. Lee[1], J. Oh[1], I. Oh[1], S. Chun[1], Y. Cho[1], T. Kwon[1], N. Koglin[2], M. Berndt[2], A. Stephens[2], D. Moon[1]; [1]Asan Medical Center, Seoul, KOREA, REPUBLIC OF, [2]Piramal Imaging, Berlin, GERMANY.

Purpose: [18F]GP1 is a new positron emission tomography (PET) tracer that binds specifically with a high affinity to activated glycoprotein IIb/IIIa receptors involved in platelet aggregation. The purpose of this study was to assess the detection rate of thromboembolic foci with [18F]GP1 PET. The safety, metabolism, biodistribution, and dosimetry of [18F]GP1 were also investigated. **Subjects & Methods:** Patients who had symptoms of acute deep vein thrombosis (DVT, n=7: 6 lower and 1 upper extremity) or pulmonary embolism (PE, n=8), and had DVT/PE focus/foci confirmed by computed tomography (CT) venography, ultrasonography or CT pulmonary angiography were enrolled. Dynamic whole-body PET images were acquired for up to 140 min after injection of 250 MBq of [18F]GP1. Analysis of DVT/PE foci included common/internal/external iliac, common/deep/superficial femoral, popliteal, tibial, peroneal, and gastrocnemius veins for DVT of the lower extremity; brachiocephalic, internal jugular, subclavian and basilic veins for DVT of the upper extremity; and main, lobar, and segmental pulmonary arteries for PE. For quantitative analysis, up to five of the largest lesions on standard images were selected. **Results:** [18F]GP1 administration and PET procedures were well tolerated in all patients. No

clinically relevant changes in safety parameters were observed. [^{18}F]GP1 PET showed initial uptake in the spleen, kidney, liver, and blood pool with rapid clearance. The determined effective radiation dose was in the range of other PET pharmaceuticals. The overall image quality was adequate for diagnosis in all patients. [^{18}F]GP1 PET identified thromboembolic foci in all 15 patients. Nine of them had both DVT and PE. Lesion based analysis revealed that [^{18}F]GP1 PET detected 43 of 49 DVT lesions (88%) in 12 patients and 112 of 185 PE lesions (61%) in 12 patients. Twelve patients had 31 distal DVT lesions on standard images, whereas [^{18}F]GP1 PET detected 46 distal DVTs in 13 patients. The number of additional distal DVT lesions identified only by [^{18}F]GP1 PET were 18 in 10 patients (1 popliteal and 17 calf veins). [^{18}F]GP1 PET also detected 3 additional PE lesions in 3 patients (1 lobar and 2 segmental arteries) which were not detected with standard imaging. The maximum standardized uptake values of reference thromboembolic foci were 5.61±2.32 for DVT and 4.39±1.92 for PE (mean ± SD). **Conclusions:** [^{18}F]GP1 may be a promising PET tracer for imaging acute DVT and PE with high sensitivity. Additionally, [^{18}F]GP1 PET may detect small previously undiagnosed thromboemboli, especially in distal veins of the lower extremity.

1801/1803   **Wednesday, October 25, 2017, 12:15 - 13:15, Hall A**

Plenary 4: Highlights Lecture

OP-715
Highlights Lecture
S. Fanti; University of Bologna, Radiological Sciences - Nuclear Medicine, Bologna, ITALY.

OP-716
Highlights Lecture
C. Decristoforo; Universitätskliniken - Landeskrankenhaus Innsbruck, Medizinische Universität Innsbruck, Universitätsklinik für Nuklearmedizin, Innsbruck, AUSTRIA.

e-Poster Walks

Cardiovascular System: Vascular Inflammation

E-PW001

The FDG-PET metabolic pattern, involving a low baseline-level and a subsequent increase, remains a landmark of less favorable outcome for the abdominal aortic aneurysms treated by endovascular prosthesis

P. Marie[1], D. Plisonnier[2], S. Bravetti[1], R. Coscas[3], M. Rouer[2], S. Haulon[4], D. Mandry[1], J. Alsac[5], S. Malikov[1], N. Settembre[1], Y. Gouëffic[6], O. Morel[7], V. Roch[1], E. Micard[1], Z. Lamiral[1], J. Michel[8], P. Rossignol[1]; [1]CHRU-Nancy, Vandoeuvre, FRANCE, [2]CHU-Rouen, Rouen, FRANCE, [3]Hôpital Ambroise Paré, Paris, FRANCE, [4]CHRU-Lille, Lille, FRANCE, [5]Hôpital HEGP, Paris, FRANCE, [6]CHU-Nantes, Nantes, FRANCE, [7]CHU-Besançon, Besançon, FRANCE, [8]INSERM Bichat, UMR 698, Paris, FRANCE.

Purpose & Introduction: The growing phases of the abdominal aortic aneurysm (AAA) treated medically are frequently associated with a ^{18}F-fluorodesoxyglucose Positron Emission Tomography (FDG-PET) imaging pattern involving: 1) a low baseline metabolism, reflecting a low parietal cellular density, and 2) a subsequent increase, presumably due to a growing inflammatory infiltrate (J Nucl Med. 2015;56:1030-1035). This prospective multicentric study was aimed at analyzing the metabolic FDG-PET patterns of the larger AAA treated by endovascular repair (EVAR). **Subjects & Methods:** Thirty-three patients referred for an EVAR of AAA (maximal diameter: 55±6 mm, total volume: 206±63 mL) underwent FDG-PET/CT before EVAR and 1- and 6-months thereafter, for monitoring the glycolytic metabolism of AAA (maximal standardized FDG uptake [SUVmax] averaged between axial-slices). Correlates of the 6-month decrease in AAA volume, defining sac shrinkage an indicator of successful repair, were analyzed. **Results:** Sac shrinkage was highly variable and could be stratified in three terciles with a first one where shrinkage was absent or very limited (0-29 mL) and a third one where it was marked (56-165 mL). Glycolytic metabolism was rather low at baseline in the 1st tercile (SUVmax: 1.73 ± 0.35) and thereafter clearly increased at 6-months (ΔSUVmax: 0.69 ± 0.65), it was much higher at baseline in the 3rd tercile (SUVmax: 2.63 ± 0.84, p=0.005 vs. 1st tercile) and stable over the 6-months (ΔSUVmax: -0.13 ± 0.52), whereas intermediate results were documented in the 2rd tercile (baseline SUVmax: 2.32 ± 0.42, ΔSUVmax: +0.53 ± 0.56). Finally, the amount of sac shrinkage was inversely related to the baseline glycolytic metabolism independently of the total AAA volume at baseline (p=0.007). **Conclusion:** The FDG-PET metabolic pattern, involving a low baseline-level and a subsequent increase, is also documented in the AAA treated by EVAR and exhibiting limited effects on sac volume and is therefore a definite landmark of less favorable outcome.

E-PW002

Prospective study comparing scintigraphy to radiolabeled leukocytes and 18F-FDG PET in patients suspected of vascular prosthesis infection

J. Pinaquy, Sr., M. Puges, X. Berard, j. Ruiz, F. Debordeaux, A. Desclaux, L. Stecken, S. Pereyre, L. Bordenave, C. Cazanave; CHU BORDEAUX, Bordeaux, FRANCE.

Introduction: Vascular prosthesis infections (VPI) are associated with high mortality rates. Diagnosis is often difficult, especially in latent infections. To improve the outcome of medical and surgical treatment, early and accurate diagnosis is essential and the actual diagnostic criteria are often insufficient. Our study aims to compare the performance of ^{18}F-fludeoxyglucose positron emission tomography (PET) and radiolabelled leukocyte scintigraphy (LS) for the diagnosis of IPV. **Material and Methods:** Prospective monocentric study including patients who received LS and PET for suspicion of VPI between April 2013 and June 2016 at the University Hospital of Bordeaux. Thoracic aortic prostheses were excluded. The diagnosis of VPI was assessed by Fitzgerald criteria at the end of follow-up. The accuracy of the two examinations was compared for each prosthesis. **Results:** Thirty-four patients were included, 14 had PVGI. Eighteen of the 93 prosthesis were infected. The sensitivity, specificity and accuracy were 88,9%, 92%, 91.4% and 89%, 85% and 86% respectively, for LS and PET. There was a significant difference (p = 0.022) between thoses two examinations. The agreement between observers was excellent for both examinations (kappa = 0.91). **Conclusion:** This study demonstrated an excellent performance of PET and scintigraphy with radiolabelled leukocytes for the diagnosis of IPV with excellent interobserver agreement. This study shows taht the scintigraphy have a better accuracy than [18]FDG-PET. Antibiotics do not seem to influence the performance of these two tests.

E-PW003

Comparison of 3 [18]FDG-PET visual interpretation scales for the diagnosis of vascular prosthesic infection

J. Pinaquy, Sr., M. Puges, C. Cazanave, J. Ruiz, F. Debordeaux, A. Desclaux, L. Stecken, S. Pereyre, L. Bordenave, X. Berard; CHU BORDEAUX, Bordeaux, FRANCE.

Introduction: Vascular prosthetic infections (VPI) are associated with high mortality rates. Diagnosis is often difficult, especially in latent infections. To improve the outcome of medical and surgical treatment, early and accurate diagnosis is essential and the actual diagnostic criteria are often insufficient. [18]FDG-PET/CT (PET), is a promising examination for the diagnosis of PVI. But criteria of interpretation remains unclear and none of the stuy use the sames parameters. We compared, from a prospective study interesting 93 prosthesis suspected to be infected, the performances of 3 visual scales. **Methods:** A monocentric prospective study including patients who underwent ^{18}F-FDG-PET/CT for suspicion of LPI between April 2013 and June 2016 at the University Hospital of Bordeaux. Thoracic aortic prostheses

were excluded. The diagnosis of VPI was assessed by Fitzgerald criteria at the end of follow-up. The performance of the 3 scales was compared for each prosthesis, 2 already published in the literature (Sah and Fukushi), the 3rd issue of our experience in PET assessment of vascular prosthesis infection. **Results:** Thirty-four patients were included, 14 had VPI. Eighteen of the 93 prostheses were infected. ROC curve analysis showes that our local scale had good performances (Sensitivity 89%, Specificity 85%, Accuracy 86%, ROC AUC = 0.87, 95% CI [0.786-0.955]), and was significantly more accurate than the scale of Fukuchi *et al.* (Sensitivity 67%, Specificity 85%, Accuracy 81%, ROC AUC = 0.76 [0.640-0.879], p = 0.04). Our local scale seems but was not significantly more accurate than the scale of Sah *et al.* (Sensitivity 83%, Specificity 72%, Accuracy 74%, ROC AUC = 0.777 [0.674-0.879], p = 0,069). For thrombosed grafts, our local scale was significantly more accurate than the scale of Sah *et al.*, but not significantly with the scale of Fukuchi *et al.* (ROC AUC = 0.963, CI 95% [0.913-1.000]; 0.778, CI 95% [0.609-0.946]) and 0.770, CI 95% [0.557-0.984], respectively, p = 0.00009 and 0.072). Inter-observer agreement was excellent for our scale, and good for the scales previously published by Sah *et al.* and Fukuchi *et al.*. **Conclusion:** This study seems to show a superiority of our visual scale visual in order to diagnose a vascular prosthesis infection especially in thrombosis prosthesis. A standardized interpretation would allow a better evaluation of the performance of [18]FDG-PET/CT.

E-PW004

18-FDG Pet-TC as tool to evaluate the efficacy of tocilizumab as a steroid-sparing agent for the treatment of Giant Cell Arteritis with Large-Vessel Involvement: a real-life single-centre case series

C. Olianti[1], G. Vitiello[2], C. Orsi Battaglini[2], N. Orsi Battaglini[3], R. Di Dato[3], S. Nicolosi[4], D. Cammelli[2]; [1]Nuclear Medicine Unit, Hospital-University Careggi, Florence, ITALY, [2]Experimental and Clinical Medicine Department, University of Florence, Florence, ITALY, [3]Nuclear Medicine Unit, University of Florence, Florence, ITALY, [4]Nuclear Medicine Unit, Hospital of Palermo, Palermo, ITALY.

Aim: To evaluate the usefulness of pre- and post-Tocilizumab (TCZ) therapy 18FDG-PET scan maximum standardized uptake value (max SUV; D TezuKa et al. JACC: cardiovascular imaging , vol 5, no. 42012 ; 422-429) for assessing disease remission in Giant cell arteritis (GCA) one of the two variants of Large-vessel vasculitis (LVV) which primarily affects medium and large sized vessels. To evaluate the efficacy and safety of TCZ as a steroid-sparing agent in patients with poor control of disease with Glucocorticoids (GC) or GC plus methotrexate (MTX). **Materials and Methods:** We retrospectively evaluated 12 GCA patients treated with TCZ (standard dose of 8 mg/kg/month) by pre- and post-therapy 18FDG-PET scan to assess activity and remission disease; post-therapy 18FDG-PET scan mean delay was 11.56 +/- 8.8 months (range 3 - 24 months) since the initiation of TCZ therapy. In addition to this, we evaluated clinical disease remission and reduction of mean GC dose. We evaluate max, mean and minimum SUV values in thoracic aorta, abdom-

inal aorta, subclavian, axillary, carotid, iliac and femoral arteries (Tool%ThresholdSUV on version V.4.5.3.40140 5.5.11 Gemini TF Philips Healthcare) and we choose maxSUV Thoracic Aorta for statistical analysis (IBM SPSS statistics 24). **Results:** maxSUV mean value has decreased from 2.05 +/- 0.64 to 1.78 +/- 0.45 (p = 0.005) after TCZ therapy; TCZ was effective in all patients, with a complete remission of the symptomatology. Mean GC dose was tapered from 26.63 +/- 13.42 mg/day to 3.3 +/- 3.1 mg/day (p < 0.0001). Overall, one half of the patients were able to discontinue GC therapy. Three patients discontinued MTX therapy without suspending GC therapy. Three patients experienced severe adverse reactions and had to stop TCZ therapy. **Conclusion:** maxSUV data could be considered a useful tool to evaluate the patients during TCZ therapy. Our maxSUV data are congruent with literature results and expressive of activity or remission of disease, as previously observed in other like-normal oncologic (1,82 +/- 0.27) and proved vasculitis (2,01 +/- 0.35) patient in our experience.

E-PW005

Tissue-to-background-ratio in major arterial vessels - comparison of 18F-FDG and 18F-fluoromethylcholine PET-CT

J. Jamsek, M. Grmek, S. Hawlina, L. Lezaic; Klinicni center Ljubljana, Ljubljana, SLOVENIA.

Background: 18F-fluoromethylcholine (18F-FCH) may be a new molecular marker of vascular inflammation. The aim of our pilot study was to directly compare metabolic activity of 18F-FDG and 18F-FCH in major arterial vessels. **Materials and Methods:** We retrospectively evaluated 18F-FDG (4 MBq/kg) and 18F-FCH (2,5 MBq/kg) PET-CT examinations of 13 male patients who had had examinations with both PET tracers within one week. TBRmean was measured in the ascending aorta (AscA), left and right common carotid arteries (LCC and RCC), thoracic aorta (TA), abdominal aorta (AA) and left and right common iliac arteries (LCI and RCI) and compared (t-test). **Results:** TBRmean for 18F-FDG and 18F-FCH in the AscA was 1.50 and 1.88 respectively (p = 0.046), in the LCC 1,57 and 1,65 (p = 0.644), in the RCC 1,45 and 1,45 (p = 0.987,), in the TA 1,46 and 2,13 (p = 0.010), in the AA 1,68 and 2,15 (p = 0.220), in the LCI 1,44 and 1,67 (p = 0.31) and in the RCI 1,64 and 1,51 (p = 0.698). **Conclusion:** 18F-FCH appears to yield comparable information on vessel wall metabolic activity in most anatomical vascular segments. For a more comprehensive analysis additional data as well as prospective studies comparing 18F-FCH and 18F-FDG are needed.

E-PW006

Correlation Between Vascular 18F-NaF Avidity and the Presence of Vascular Illness: A PET/CT Study

J. F. Alban[1], P. Lapa[1,2], M. Marques[1], A. Albuquerque[1], G. Costa[1,2], J. Pedroso de Lima[1,2,3]; [1]Centro Hospitalar e Universitário de Coimbra, Coimbra, PORTUGAL, [2]Faculdade de Medicina da Universidade de Coimbra, Coimbra, PORTUGAL, [3]Instituto das Ciências Nucleares Aplicadas à Saúde (ICNAS), Coimbra, PORTUGAL.

Purpose: Positron emission tomography/computed tomography (PET/CT) imaging using ^{18}F-sodium fluoride (^{18}F-NaF) has the potential to identify pathologically high-risk vascular microcalcification. This study aims to investigate a correlation between the presence of clinically detectable vascular disease and the vascular uptake of sodium fluoride labelled with Fluor-18 (^{18}F-NaF), and to establish a disease predictor value for maximum SUV (SUVmax). **Subjects and Methods:** We retrospectively reviewed 58 patients (22 male; 36 female), medium age 59.98 ± 40.3 years (17-82 years), submitted to PET/CT with ^{18}F-NaF between March 2011 and March 2017. The presence or absence of vascular uptake, SUVmax and localization of each uptake were recorded. The clinical charts of all patients were reviewed and two groups of patients were considered: 1) V0-no vascular uptake (n=8); 2) V1-with vascular uptake (n=50). The presence and location of clinically known vascular diseases were recorded. V1 group was then divided in 2 subgroups: 1) CV0-no clinically related vascular disease; 2) CV1-with clinically related vascular disease. According to the values of SUVmax, CV1 subgroup was subdivided into two new subgroups: 1) SM0 (SUVmax <2.15); 2) SM1 (SUVmax≥ 2.15). Statistical analysis applying Mann-Whitney test and ROC curves was performed. **Results:** For the 58 ^{18}F-NaF PET-CT studies, 129 vascular uptake locations were found (99 in CV0 and 30 in CV1 group) related to wall calcification, arterial occlusion, aneurysm, vasculitis and mitral disease. Mean SUVmax was significantly higher in the CV1 than in CV0 group (3.63 ± 5.64 vs 1.93 ± 0.64, p <0.001). For the V1 group, ROC analysis showed that SUVmax has a moderate predictive capacity for the occurrence of vascular disease (AUC=0.72, p<0.001) and the best cut-off point was 2.15 (specificity of 72% and sensitivity of 68%). For the SM1 group, when SUVmax≥2.15 and the presence of clinically known vascular disease were compared, a moderate concordance was found (k=0.316, p<0.001). **Conclusions:** There is a correlation between the presence of clinically detectable vascular disease and the vascular uptake of ^{18}F-NaF. A moderate concordance was found between having vascular uptake in ^{18}F-NaF PET/CT with SUVmax≥ 2.15 and having vascular disease at the same location.

E-PW007

Differences in semiquantitative 18F-FDG PET/CT findings of non-infectious and infectious inflammation

V. Mergen[1], I. Einspieler[1], M. Mustafa[1], H. Wendorff[2], K. Thürmel[3], M. Schwaiger[1]; [1]Department of Nuclear Medecine, Klinikum rechts der Isar TU Muenchen, Munich, GERMANY, [2]Clinic for Cardiovascular Surgery, Klinikum rechts der Isar TU Muenchen, Munich, GERMANY, [3]Department of Nephrology, Klinikum rechts der Isar TU Muenchen, Munich, GERMANY.

Objectives: The aim of the study was the evaluation and comparison of different semiquantitative parameters in patients with non-infectious large vessel vasculitis (LVV) and graft infection after aortic repair applying [^{18}F]fluorodeoxyglucose (FDG) positron emission tomography (PET)/computed tomography (CT). **Methods:** We included 17 patients with LVV and 28 patients with graft infection after aortic repair for retrospective

analysis. In the LVV group, the aorta and its major branches were analysed, whereas in patients with aortic graft infection only the graft area was evaluated. Maximum standardized uptake values (SUVmax) were obtained for all patients and different target-to-background ratios (TBRs) were calculated. 2 different background regions were defined and analysed (arterial and venous blood pool, respectively). The standard of reference for the diagnosis was defined as a combination of clinical follow-up, imaging (including PET/CT) and/or microbiological/histopathological results, if available. **Results:** SUVmax and TBRs were significantly higher in patients with graft infection compared to those with LVV (median SUVmax: 8.4 ± 3.9 vs. 4.2 ± 1.8; median TBR with arterial blood pool as background: 5.1 ± 2.2 vs. 2.1 ± 1.0; median TBR with venous blood pool as background: 5.3 ± 2.4 vs. 2.8 ± 1.1; p<0.0001). There was no substantial difference with respect to the blood pool activity in the 2 different groups. **Conclusion:** Our data show significant differences in patients with infectious and non-infectious inflammation with respect to different semiquantitative approaches. Thus, 18F-FDG-PET/CT may help to provide a better understanding of sterile and infectious inflammation.

E-PW008

18F-FDG PET/CT imaging for detection of aortic wall inflammation in patients with repaired coarctation of aorta

A. Georgakopoulos[1], N. Pianou[1], E. Oikonomou[2], A. S. Antonopoulos[2], I. Koutagiar[2], P. Kafouris[3,4], M. Metaxas[1], D. Tousoulis[2], S. Brili[2], C. Anagnostopoulos[1]; [1]Center for Experimental Surgery, Clinical and Translational Research, Biomedical Research Foundation, Academy of Athens, Athens, GREECE, [2]1st Department of Cardiology, 'Hippokration' Hospital, University of Athens Medical School, Athens, GREECE, [3]Center of Systems Biology, Biomedical Research Foundation of the Academy of Athens, Athens, GREECE, [4]Department of Informatics and Telecommunications, University of Athens, Athens, GREECE.

Purpose/Introduction: Patients with surgically repaired coarctation of aorta (RCoA) are at increased cardiovascular morbidity and mortality risk compared to general population. Endothelial dysfunction and impaired arterial elastic properties as well as relapse of arterial hypertension and pro-inflammatory stimulation could partly explain the increased cardiovascular disease risk of these patients. Positron emission tomography (PET) labeled with 18F-fluorodeoxyglucose (^{18}F-FDG) is currently considered the gold-standard imaging modality to non-invasively assess vascular inflammation in-vivo. The aim of this pilot study is to explore the role of ^{18}F-FDG PET/CT imaging in the assessment of aortic wall inflammation in RCoA subjects and the association of ^{18}F-FDG uptake with systemic inflammation and arterial elastic properties. **Subjects & Methods:** All participants underwent PET/CT imaging after intravenous administration of 140μCi/kg of ^{18}F-FDG and uptake period of around 120 minutes, preceded by at least 6 hours fasting. Target to background ratio (TBR) in the ascending, descending and abdominal aorta and their average (global aortic TBR) and coronary calcium burden

were calculated in 15 subjects with RCoA and compared with that of 15 age- and sex-matched subjects with prior history of lymphoma who needed ^{18}F-FDG-PET/CT imaging as part of their clinical follow-up and were disease free at the time of the investigation. RCoA patients also underwent assessment of central aortic mean blood pressure, arterial elastic properties and measurement of plasma levels of interleukin-6 (IL-6), transforming growth factor-beta (TGF-b) and macrophage colony-stimulating factor (MCSF) by enzyme-linked immunosorbent assay. **Results:** Global aortic ^{18}F-FDG uptake was significantly higher in RCoA compared to control subjects (1.95±0.08 vs. 1.76±0.03 respectively, p<0.05), mainly driven by differences in the descending aorta (2.04±0.07 vs. 1.76±0.05 respectively, p=0.003). The corresponding values in the ascending and abdominal aorta were 1.94±0.10 vs. 1.80±0.03 and 1.86±0.09 vs. 1.75±0.04, p=0.20 and p=0.25 respectively. There was no significant difference in coronary calcium burden between the two groups (p=0.19). In RCoA patients, aortic ^{18}F-FDG uptake was strongly correlated with plasma IL-6 levels (r=0.706, p<0.05), but not with TGF-b and MCSF levels. Moreover, patients with high aortic TBR (>median) had significantly higher central aortic mean pressure (105.2±1.9 vs. 91.6±5.3mmHg respectively, p<0.05), but not stiffness indices. **Conclusions:** Imaging of aorta by ^{18}F-FDG PET/CT detects aortic wall inflammation in adult RCoA patients. Aortic ^{18}F-FDG uptake values correlate with central hemodynamics and systemic low-grade inflammation.

E-PW009

Activity Assessment of Large Vessel Vasculitis with F18-FDG-PET(/CT)

N. Schramm[1], J. Ingenhoff[2], C. Dechant[3], F. Proft[3], H. Schulze-Koops[3], U. Hoffmann[2], A. Rominger[1], M. Czihal[2]; [1]Department of Nuclear Medicine, Ludwig-Maximilians University Hospital, Munich, GERMANY, [2]Division of Angiology, Department of Medicine IV, Ludwig-Maximilians University Hospital, Munich, GERMANY, [3]Rheumatology Unit, Department of Medicine IV, Ludwig-Maximilians University Hospital, Munich, GERMANY.

Purpose: To determine the role of 18F-Fluorodeoxyglucose (FDG)-PET/CT in activity assessment of large vessel vasculitis in patients under immunosuppressive therapy. **Materials and Methods:** 62 patients who underwent 80 PET(/CT) examinations (52 PET, 28 PET/CT) between 2004 and 2014 were included in this retrospective study. Clinical disease activity was investigated by medical history, clinical examination, laboratory tests (CRP, BSR), duplex ultrasound and/or CT/MRI and determined with established scoring systems (NIH-score, ITAS). Disease activity with PET was measured with the SUVmax of the aorta (SUVmaxAo), the SUVmax aorta/SUVmean liver ratio (ALR) and by applying a 4-point visual scale of the aortic (A) uptake vs. liver (L) uptake (3: A > L; 2: A = L; 1: A < L; 0: no uptake) and compared with the final clinical diagnosis (active vs. inactive). Correlations between clinical and PET parameters were calculated with Spearmans´s rank correlations analysis. ROC curve analysis and 4 field tables were used to determine diagnostic accuracy. Interobserver agreement of the visual PET reading was measured

with Cohen´s kappa. **Results:** Clinically, there was active disease (NIH score $\geq$ 2; ITAS-2010 6.5 $\pm$ 5.4) in 57 cases and inactive disease in 23 cases (NIH $\leq$ 1; ITAS-2010 1.1 $\pm$ 5.4). In comparison to CRP, BSR and ITAS there was a significant, but only mild to moderate correlation for SUVmaxAo (rho 0.25-0.48) and ALR (rho 0.36-0.63). With regard to the final clinical activity assessment the ROC statistics showed an area under the curve of 0.76 for SUVmaxAo and 0.9 for ALR. A cut-off of 2.6 for SUVmaxAo resulted in sensitivity of 71.4% and a specificity 73.9%; a cut-off of 1.3 for ALR resulted in a sensitivity of 84.2% and a specificity of 82.6%. Visual analysis (aortic uptake $\geq$ liver uptake: active disease) showed a sensitivity of 68.4% and a specificity of 91.3%. Interobserver reliability was excellent (kappa 0.93). **Conclusion:** Assessment of disease activity with FDG-PET(/CT) is specific and reliable if visual/semiquantitative ratios of the aortic wall to liver uptake are applied; however, sensitivity is limited.

M2M: Small Molecules

E-PW010

Clinical translation of the caspase 3/7 specific PET radiotracer [^{18}F]ICMT-11 for measuring chemotherapy induced apoptosis in breast and lung cancer

S. R. Dubash[1], s. merchant[1], F. Mauri[1], k. kozlowski[1], A. Lim[1], N. Patel[1], J. Steel[1], k. Heinzmann[1], s. Azeem[2], S. Cleator[1], R. C. Coombes[1], E. O. Aboagye[1], L. Kenny[1]; [1]ImperialL College, London, UNITED KINGDOM, [2]Imanova Ltd., London, UNITED KINGDOM.

Background: Effective anticancer therapy requires induction of tumour cell death through apoptosis. [^{18}F]ICMT-11, an isatin sulphonamide and caspase-3/7 specific PET radiotracer, has been developed for PET imaging. [^{18}F]ICMT-11 demonstrated subnanomolar affinity to caspase-3 and has shown favourable dosimetry, safety and biodistribution in healthy volunteers. Here, we report results of [^{18}F]ICMT-11-PET for detection of chemotherapy-induced apoptosis in breast and lung cancer. **Materials and Methods:** [^{18}F]ICMT-11 was synthesized as previously described. Twenty patients diagnosed with breast cancer and 2 with lung cancer were recruited. All breast patients received neo-adjuvant chemotherapy (FEC: 5-fluorouracil, epirubicin, cyclophosphamide), and the lung patients received platinum-based chemotherapy; lesions measured 2cm or more. Dynamic-PET scans were acquired over 60 min pre-and post-chemotherapy, with arterial blood sampling to measure ^{18}F radioactivity concentration and metabolites in blood and plasma. Blood samples were taken to measure cytokeratin 18 (M65 and M30) using ELISA. Lung patients underwent DWI and DCE-MRI at baseline and post-chemotherapy. Regions of interest were drawn, to derive SUV_{60mean} and SUV_{60max}. All breast patients underwent a second breast biopsy within a few hours of the second PET to correlate apoptosis with PET in breast tissue. Caspase-3 expression, Ki-67 and H&E staining were performed

on all diagnostic and research biopsies. **Results:** Seventeen patients who had early (&#8804 48h post-chemotherapy) or late (>48h) scans were evaluable. The mean (range) dose injected was 330MBq (278-353MBq) pre-chemotherapy, and 335MBq (281-259MBq) post-chemotherapy. Three breast patients (scanned >48h) displayed histograms with higher voxel-intensities post-treatment indicating "apoptosis dominant" signature. Mean percentage shift to the right in all the 3 patients was 41% and all three patients had partial responses (PRs) on histopathology at surgery after 6 cycles of chemotherapy. One patient with an "apoptosis dominant" signature showed clear staining for caspase-3, together with increased blood cytokeratin-18-derived M30, and increase of M30:M65 ratio. All lung and breast patients were responders (PR or CR) at completion of chemotherapy treatment. Overall both "apoptosis dominant" and "necrosis dominant" [18F]ICMT-11 signatures were seen, however, no correlation with IHC, PET parameters or cytokeratin analyses could be demonstrated. **Conclusion:** These are the preliminary results of the first clinical study in lung and breast cancer using [18F]ICMT-11-PET. Further clinical evaluation will reveal if [18F]ICMT-11 can be used as a potential biomarker for chemotherapy induced apoptosis.

E-PW011

18F-RPS-544: An Imaging Agent Targeting CXCR4. Imaging and Biodistribution

A. Amor-Coarasa, J. M. Kelly, S. Ponnala, C. Williams, Jr., Y. Vedvyas, D. Kim, J. W. Babich; Weill Cornell Medical College, New York City, NY, UNITED STATES OF AMERICA.

Aim*:* The emerging importance of CXCR4 to cancer progression, prognosis and patient treatment makes it a potentially valuable target for imaging by positron emission tomography (PET). Only one 18F-fluorinated CXCR4 ligand has been reported to date, and although CXCR4-positive tumors were successfully delineated, the maximum uptake was 0.5 %ID/g. We sought to develop a 18F-labeled CXCR4 ligand with improved tumor uptake. **Methods***:* A 18F-fluoropyridyl analogue of AMD-3465 (IC_{50}=4nM) was prepared by nucleophilic aromatic substitution of a NO_2 group on a 6-nitropyridine moiety by no-carrier-added [18F]fluoride in DMSO at 150°C under basic conditions. 18F incorporation was determined using radioHPLC. Deprotection of the 18F-labeled intermediate was performed using 1 mL of neat TFA at 100°C. Preparative HPLC was used to purify the final product prior to formulation for injection. PET imaging was performed in nude mice bearing bilateral (CXCR4+ and CXCR4-) PC3 xenograft tumors. A full biodistribution was carried out at 1, 2 and 4h post injection (p.i.) to quantify tissue and tumor uptake. **Results:** 18F-RPS-544 showed preferential uptake in the CXCR4+ PC3 tumor, with a CXCR4+/CXCR4- tumor ratio of 3.3±1.3 at 1h p.i. and 2.3±0.5 at 2h p.i. Maximum uptake in the CXCR4+ tumor was **3.4±1.2 %ID/g** at 1h p.i., decreasing to 1.7±0.4 %ID/g at 2h p.i. and ≈1.5 %ID/g at 4h p.i. Tumor/blood ratios were determined to be 2.5±0.4 and 3.6±0.3 at 1 and 2h p.i., increasing to more than 9 at 4h p.i. Tumor/muscle ratio was greater than 5 at all time points. Tumor/lung ratios were greater than 1.5 at all time

points. Significant uptake was observed in the liver (24.7±3.6 %ID/g at 2h p.i.), kidneys (26.3±1.8 %ID/g at 1h p.i.), the small intestine (7.1±0.8 %ID/g at 1h p.i.) and the large intestine (9 %ID/g at 4h p.i.). The circulation half-life of 18F-RPS-544 was just over 36 minutes, with a blood concentration of 1.4±0.7 %ID/g at 1h p.i., 0.5±0.3 %ID/g at 2h p.i., and less than 0.2 %ID/g at 4h p.i. All other organs showed uptake of less than 1 %ID/g at all time points. **Conclusions:** A new imaging agent (18F-RPS-544) that targets CXCR4 was designed, synthesized, radiolabeled and evaluated in vivo. Specific targeting of CXCR4-positive tumors was demonstrated, and maximum tumor uptake reached **3.4±1.2 %ID/g**, a seven-fold improvement on existing 18F-fluorinated ligands reported to date. Clearance via the hepatobiliary pathway was observed, and good tumor/blood, tumor/muscle and tumor/lung ratios led to good contrast to background.

E-PW012

In vitro characterization of [18F]THK5351 binding to melanin-containing cells

T. Tago[1], J. Toyohara[1], R. Harada[2], S. Furumoto[2], N. Okamura[3], Y. Kudo[2], J. Takahashi-Fujigasaki[1], S. Murayama[1], K. Ishii[1]; [1]Tokyo Metropolitan Institute of Gerontology, Tokyo, JAPAN, [2]Tohoku University, Sendai, JAPAN, [3]Tohoku Medical and Pharmaceutical University, Sendai, JAPAN.

Introduction: Amyloid-β plaques and neurofibrillary tangles composed of hyperphosphorylated tau protein are the neuropathological hallmarks of Alzheimer's disease. In recent years, tau positron emission tomography (PET) imaging research has undergone marked progress. However, an issue regarding off-target binding, binding to regions without tau pathology (e.g., basal ganglia and melanin-containing cells (MCCs)), remains unresolved. Melanin, a polyanionic pigment derived from the amino acid L-tyrosine, has been suggested as the binding target in MCCs for [18F]THK5351 and other tau ligands. This study characterized the binding of [18F]THK5351 to MCCs and elucidated the relationship between structure and MCCs-binding activity. **Subjects and Methods:** We conducted [18F]THK5351 autoradiography (ARG) studies using postmortem sections of the human midbrain and pons. Binding assays of [18F]THK5351 to MCCs were performed using higher- and lower-melanin-containing B16F10 and B16 murine melanomas, respectively. Binding assays with synthetic melanin were also performed. Blocking activities of about two dozen compounds (e.g., tau ligands, amyloid ligands, monoamine oxidase B (MAO-B) inhibitors, and tyrosinase inhibitors) for [18F]THK5351 binding to B16F10 cells were investigated for the structure-inhibition relationship study. **Results:** ARG confirmed [18F]THK5351 binding to MCCs of the substantia nigra and locus coeruleus in midbrain and pontine sections, respectively. Binding of [18F]THK5351 to MCCs was saturable (Kd = 230 nM, Bmax = 160 fmol/mg protein for B16F10) and dependent on levels of melanin expression. Specific binding of [18F]THK5351 to synthetic melanin was also confirmed. The tyrosinase inhibitors did not block [18F]THK5351 binding, indicating a direct interaction of [18F]THK5351 with melanin. Tau ligands including amynopyridine groups such as AV-1451, PBB3,

and a lead compound of MK-6240 showed comparable levels of [18F]THK5351 binding inhibition to the self-blocking by THK5351 (>70% at 10 μM), whereas benzothiazoles such as PiB did not (about 10% blocking at 10 μM). Inhibition rates of MAO-B inhibitors and melanin ligand were low. These results indicate the aromatic rings of melanin-binding compounds are important for the pi-stacking interaction with melanin. In addition, a certain aminopyridine group seemed to enhance the melanin-binding affinity of compounds. **Conclusions:** Binding of [18F]THK5351 to MCCs was confirmed by in vitro ARG and binding assays. These results should facilitate accurate interpretation of PET images and the development of tau probes without off-target binding.

E-PW013
Alcohol-enhanced Cu-mediated radiofluorination

J. Zischler[1,2], N. Kolks[2], D. Modemann[1], B. D. Zlatopolskiy[2], B. Neumaier[1,2]; [1]Forschungszentrum Jülich GmbH, Institute of Neuroscience and Medicine, INM-5: Nuclear Chemistry, Jülich, GERMANY, [2]University Clinic Cologne, Institute of Radiochemistry and Experimental Molecular Imaging, Cologne, GERMANY.

Introduction: The potential of many 18F-labeled (hetero)aromatics for application in positron emission tomography remains underexplored because convenient procedures for their radiosynthesis are lacking. Consequently, simple methods to prepare radiofluorinated (hetero)arenes are highly sought after. Herein, we report the beneficial effect of primary and secondary alcohols on Cu-mediated 18F-labeling of (hetero)aryl pinacolyl boronates (ArBPin), boronic acids [ArB(OH)$_2$] and stannanes (ArSnMe$_3$). **Materials and Methods**: [18F]Fluoride was eluted from a QMA cartridge with a solution of Et$_4$NHCO$_3$ in the respective alcohol into a vial containing a solution of the corresponding precursor and Cu(py)$_4$(OTf)$_2$ in DMA. The reaction mixture was stirred at 110 °C for 5-20 min under air. The reaction was quenched with water before radio-HPLC analysis was carried out. Protected 6-[18F]fluorodopamine (6-[18F]FDA) and 6-[18F]fluoro-L-3,4-dihydroxyphenylalanine (6-[18F]FDOPA) were deprotected using 12 M HCl. The desired PET tracers were isolated by HPLC. **Results and Discussion**: We observed that the presence of traces of alcohols in the reaction mixture afforded radiofluorinated arenes in unexpectedly high radiochemical conversions (RCCs). Therefore, we studied the influence of different alcohols on Cu-mediated radiofluorination of PhBPin and PhB(OH)$_2$ precursors. Noteworthy, highest RCCs (up to 99%) were obtained using *n*-BuOH/DMA mixtures as reaction solvents. To demonstrate the versatility of the procedure, we radiolabeled a series of (hetero)arylboronic and (hetero)arylstannyl substrates. Different electron-rich, -deficient, and -neutral 18F-labeled arenes including unprotected indols, phenols and anilines were prepared in RCCs mainly exceeding or averaging 80%. The clinically relevant PET probes 6-[18F]FDA and 6-[18F]FDOPA were produced in radiochemical yields (RCYs) of 34 and 40%, respectively. **Conclusion**: The efficient application of alcohols as co-solvents for Cu-mediated 18F-fluorination was demonstrated. A procedure for rapid radiolabeling of a broad range of substrates such as (hetero)arylboronic acids, pinacolyl boronates, and trialkylstannanes under the same reaction conditions was developed. This procedure allows "late-stage" access to 18F-fluorinated indoles, phenols, and anilines from unprotected precursors and obviates time-consuming azeotropic drying. The preparation of clinical doses of two PET tracers, 6-[18F]FDA and 6-[18F]FDOPA, confirmed the practicality of the method. This work was supported by the DFG grant ZL 64/1-1.

E-PW014
Novel 18F-labeled triarylphosphonium derivatives for mitochondria imaging

S. Furumoto[1], T. Tominaga[1], R. Akita[1], A. Kazama[1], Y. Ishikawa[1], R. Iwata[1], K. Ishiwata[2]; [1]Tohoku University, Sendai, JAPAN, [2]Southern TOHOKU Research Institute for Neuroscience, Koriyama, JAPAN.

Purpose: A lipophilic cation like triarylphosphonium tends to accumulate in mitochondria depending on mitochondrial membrane potential (MMP). Mitochondria imaging is expected to be applied to visualization of mitochondria-rich tissues/organs, such as heart, tumor, and brown adipose tissue. The purpose of this study is to develop a novel 18F-labeled triarylphosphonium (18F-TAP) derivative for mitochondria imaging. We devised a new one-pot synthesis method for preparing the 18F-TAPs by using a 18F-labeled triarylphosphine as an intermediate. **Methods:** 18F-TAPs were prepared from 2-([18F]fluoroethoxyphenyl)diphenylphosphine through reaction with a derivative of benzyl or alkyl halide, and then isolated by semi-preparative HPLC. 2-([18F]fluoroethoxyphenyl)diphenylphosphine was prepared from the corresponding tosylate precursor under the conditions of general radiofluorination with 18F-KF/K222. Biodistribution study in mice (n = 4) was performed for evaluation of radiopharmacokinetics of the 18F-TAPs to choose a candidate as a cardiac imaging agent. Cellular uptake assays using H9c2 cells (rat embryonic cardiomyocytes) were carried out according to the dual tracer method with 3H-tetraphenylphosphonium (TPP), a gold standard tracer for MMP measurement *in vitro*, to clarify the relationship between the cellular uptakes of 18F-TAPs and MMP. Additionally, rat-PET scans were conducted to assess the performance of cardiac imaging. **Results:** Totally 12 derivatives of 18F-TAP were prepared with moderate RCYs (ca. 30-50%) according to the new method. Most of the derivatives showed high heart uptakes (> 6%ID/g) at 60 min post-injection. Cellular uptake of 18F-TAP-018, one of the derivatives, was well correlated with that of 3H-TPP and was inhibited with carbonyl cyanide m-chlorophenyl hydrazone (CCCP, an uncoupler) dose-dependently, suggesting that the TAP accumulates in mitochondria depending on MMP. 18F-TAP-031, another one of them, showed the highest heart uptake (15 %ID/g) and heart-to-liver uptake ratio (16.4) in mice. Then, rat heart was clearly visualized through PET scanning with 18F-TAP-031. **Conclusion:** We constructed a novel convenient method for preparing a 18F-labeled TAP, which could be applicable for automated radiosynthesis. Among the TAP derivatives prepared by the method, 18F-TAP-018 and/or -031 are potentially available for cardiac imaging, although further biological characterizations and experimental validations for measuring myocardial blood flow are necessary.

E-PW015

Synthesis and initial biological evaluation of [18F] fluorotryptophans ([18F]FTrps)

B. D. Zlatopolskiy[1,2,3], J. Zischler[2,1], H. Endepols[1], M. Guliyev[1], D. Schäfer[2], E. A. Urusova[1,2], B. Neumaier[1,2,3]; [1]University Clinic of Cologne, Cologne, GERMANY, [2]Forschungszentrum Jülich GmbH, Jülich, GERMANY, [3]Max Planck Institute of Metabolism Research, Cologne, GERMANY.

Objectives: Tryptophan and its metabolites are involved in different processes linked to biosynthesis of serotonin, melatonin and niacin. Consequently, PET-tracers targeting tryptophan metabolic pathways could be applied for imaging of related pathologies like neuropsychiatric diseases (e.g. depression) and tumors. The aim of this work was the development of efficient procedures for the preparation of [18F]FTrps and their initial biological evaluation. **Methods:** Boc-4,5- and -6-BpinTrp-OtBu (**1a-c**) were synthesized from the respective bromo derivatives using Miyaura borylation. Boc-7-BpinTrp-OtBu (**1d**) was prepared from Boc-Trp-OtBu via Ir-catalyzed 2,7-diborylation followed by the selective 7-deborylation. Bpin substrates were radiolabeled according to the protocol for alcohol-enhanced Cu-mediated [18F]fluorination. Radiofluorinated intermediates were deprotected using HCl in MeOH and purified by HPLC affording [18F]FTrps as ready-to-use solutions. The metabolic stability of radiolabeled tryptophans was determined in blood serum and liver microsomes. The cellular uptake of [18F]FTrps and [18F]FET was tested in MCF7, H69, PC-3 and LNCaP C4-2 tumor cells. A brain biodistribution of [18F]FTrps, [18F]FET and [18F]FDG in healthy rats was studied using µPET. **Results:** Precursors **1a-d** were synthesized in 40-65% yields. Intermediate Boc-x-[18F]FTrp-OtBu were prepared in >90% RCC. Radiochemically and chemically pure [18F]FTrps (ee >99%) were isolated in 42-54% RCY within 50 min. All four radiolabeled amino acids were stable in blood serum and liver microsomes for at least 90 min. Uptake of [18F]FTrps in all tumor cell lines was higher or similar to that of [18F]FET. Especially, uptake of 7-[18F]FTrp in MCF7 breast tumor cells with increased Trp metabolism was significantly higher than that of [18F]FET (3.71±0.01 and 4.93±0.12% of ID vs. 2.73±0.02 and 3.26±0.05% of ID after 1 and 2 h incubation, respectively). *In vivo* brain uptake of 4- and 6-[18F]FTrp was very low, while radioactivity strongly accumulated in the skull indicating fast defluorination of tracers *in vivo*. For 5-[18F]FTrp a uniform brain distribution and a moderate accumulation of radioactivity in the skull was observed. In contrast, 7-[18F]FTrp delineated serotoninergic regions of rat brain and the melatonin-synthesizing pineal gland. At the same time [18F]FET showed a uniform brain distribution and [18F]FDG accumulated in regions with high glucose metabolism. **Conclusions:** 7-[18F]FTrp is a promising PET-probe for imaging of Trp metabolism *in vivo*, which is easily accessible via alcohol enhanced Cu-mediated radiofluorination. **Research support:** This work was supported by the DFG grant ZL 65/1-1.

E-PW016

Positron emission tomography imaging of glioblastoma with a monosaccharide-based contrast agent

H. Hong[1], D. Yang[1], D. Chen[1], W. Lu[1], X. He[2]; [1]University of Michigan, Ann Arbor, MI, UNITED STATES OF AMERICA, [2]Hanjiang University, Wuhan, CHINA.

Purpose: Compared with most other biologically active molecules, saccharide is more biocompatible, chemically versatile, and cost-effective to synthesize. However, currently there is very limited report on using monosaccharides (other than 18F-fluoro-deoxyglucose [18F-FDG]) for cancer detection, despite the frequent clinical utilization of 18F-FDG for cancer diagnosis/staging. In this study, our goal is to fill in this research blank and develop a monosaccharide-based imaging agent for cancer detection, particularly for glioblastoma. **Methods:** A glucose derivative was screened out of a monosaccharide library, which demonstrated selective binding to U87MG glioblastoma cells. The screened candidate, 5-amino-4-benzyloxy-2-benzyloxymethyl-6-(4-methoxyphenoxy)-tetrahydro-2H-pyran-3-ol, abbreviated as ABMTP, was conjugated with p-SCN-Bn-NOTA or FITC for 64Cu labeling or fluorescence visualization, respectively. The cancer cell targeting efficiency was evaluated in U87MG cells with L929 fibroblasts as a control, by both flow cytometry and confocal fluorescence microscopy. PET imaging was conducted in nude mice bearing U87MG tumors with 64Cu-labeled glucosamine as control group. Organ distribution study by gamma counting was conducted to correlate with the PET findings, while auto radiography and histological analysis were also carried out to determine the potential binding target(s) for ABMTP. **Results:** NOTA or fluorescein was successfully conjugated onto ABMTP in a decent yield, analyzed by HPLC. Fluorescein-ABMTP demonstrated strong accumulation in U87MG cells and showed minimal interaction with L929 cells, while fluorescein-modified glucosamine did not get internalized into either of the two cell lines. An interesting observation is that fluorescein-ABMTP accumulates preferably in the cell nuclei rather than cytoplasm. 64Cu could be incorporated efficiently (> 50% decay corrected yield) into NOTA-ABMTP and the resulting 64Cu-NOTA-ABMTP (specific activity: ~ 4 MBq/µg) possessed a good stability in mouse serum. 64Cu-NOTA-ABMTP had a more potent and persistent uptake in U87MG tumors (9.1 ± 0.6 %ID/g at 2 h post-injection with tumor-to-muscle [T/M] ratio of 17.6 ± 3.6, n = 4) compared with those from 64Cu-NOTA-glucosamine (2.3 ± 0.3 %ID/g at 2 h p.i. with T/M ratio of 5.4 ± 1.1, n = 4). Finally, auto radiography and proteomics analysis of U87MG tumors suggested that proteins involved in epithelial-mesenchymal transition (EMT) process could account for the tumor cell internalization of ABMTP conjugates. **Conclusion:** We successfully developed a monosaccharide derivative as a PET contrast agent. This study can further encourage the development of other saccharide candidates to be used for cancer imaging. In addition, the cell nuclei accumulation preference can enable ABMTP to be used as a useful delivering agent for Auger electron emitting isotopes.

E-PW017

The Evolving Role of Succinate in Tumor Metabolism

P. GARRIGUE[1], A. Bodin-Hullin[2], A. Moyon[2], L. Balasse[1], S. Fernandez[1], W. Essamet[2], F. Dignat-George[1], K. Pacak[3], D. Taïeb[2], B. Guillet[1]; [1]Aix-

Marseille Université, Marseille, FRANCE, ²AP-HM, Marseille, FRANCE,
³NIH, Bethesda, MD, UNITED STATES OF AMERICA.

Beyond its role in carbohydrate metabolism as a tricarboxylic acid (TCA) cycle intermediate, succinate has a hormone-like function acting in various organs and tissues. In recent years, inherited and acquired mutations in the TCA cycle enzymes have been reported. Unlike tumors with isocitrate dehydrogenase mutations, pheochromocytomas and paragangliomas (PPGL) with succinate dehydrogenase (*SDH*) deficiency are characterized by an accumulation of highly elevated levels of succinate and high 18F-fluorodeoxyglucose ([18F]-FDG) avidity. This relationship is currently only partially explained. Therefore, we hypothesised that succinate could be the major connecting hub between *SDH*-mutated tumors and [18F]-FDG uptake profile. **Design:** To test whether succinate modifies the [18F]-FDG metabolic profile of tumors, we performed *in vitro* and *in vivo* (microPET/CT imaging and autoradiography) experiments in the presence of succinate, fumarate, and phosphate-buffered saline (PBS) in different cell models. GLUT1 immunohistochemistry was performed to assess whether [18F]-FDG uptake was correlated with GLUT1 staining. **Results:** Intratumoral injection of succinate significantly increased [18F]-FDG uptake at 24 hours on microPET/CT imaging and autoradiography. No effect of succinate was observed on cancer cells *in vitro,* but interestingly, we found that succinate caused increased [18F]-FDG uptake by Human Umbilical Vein Endothelial Cells (HUVEC) in a concentration-dependent manner. No significant effect was observed after intratumoral injection of fumarate or PBS. Succinate, fumarate, and PBS have no effect on cell proliferation, regardless of cell lineage. Intramuscular injection of succinate also significantly increases [18F]-FDG uptake by muscle when compared to either PBS or fumarate, highlighting the effect of succinate on connective tissues. GLUT1 expression quantification did not significantly differ between the study groups. **Conclusions**: The present study shows that succinate stimulates [18F]-FDG uptake by endothelial cells, a finding which partially explains the [18F]-FDG metabotype observed in tumors with SDH deficiency. Although this study is an [18F]-FDG based approach, it provides an impetus to better characterize the determinants of [18F]-FDG uptake in various tumors and their surrounding microenvironment with a special emphasis on the role of tumor specific oncometabolites.

E-PW018

The Preparation of Radiolabeled Aromatic Amino Acids via Cu-Mediated Radiofluorination of Ni-Complexes

A. S. Craig; Uniklinik Köln, Cologne, GERMANY.

Objectives: Recently developed methods for Cu-mediated radiofluorinations have paved the way for the fast and efficient preparation of [18F]-labeled aromatic amino acids (AAA), including the well-established 6-[18F]FDOPA and 6-[18F]FMT tracers and the lesser-known [18F]fluorophenylalanines ([18F]Phes) and [18F]fluorotryptophans ([18F]FTrps) for improved diagnostics of tumors and neurological disorders. However, insufficient stabili-

ty and/or poor accessibility of some substrates for radiolabeling hinder the broader application of these protocols for the routine preparation of PET probes. The aim of this project was to study the feasibility of a NiBPB auxiliary as easily-removable dual-protecting group functionality for the preparation of radiofluorinated AAA *via* Cu-mediated radiolabeling. **Methods:** NiBPB-Gly was alkylated with pinacolboronyl (BPin)-substituted benzyl halides or with 4-Bpin-substituted indole methide generated *in situ* from the respective methyl *N,N,N*-trimethylammonium salt (**1**). 2-and-4-BpinBnBr are commercially available, 2-BPin-5-MOMO-BnBr and 6-BPin-3,4-di-MOMO-BnBr were prepared by radical bromination of the corresponding toluenes. **1** was prepared from 4-BPin-indole using Mannich-type reaction followed by quaternization of the intermediate gramine. Radiolabeling was carried out according to the protocol for alcohol-enhanced Cu-mediated radiofluorination affording NiBPB-2 and 4-[18F]FPhe, MOM-protected NiBPB-6-[18F]FMT, di-MOM protected NiBPB-6-[18F]FDOPA, and NiBPB-4-[18F]FTrp complexes as follows: [18F]F⁻ was loaded onto a QMA-cartridge which was subsequently washed with acetone; [18F]F⁻ was eluted with Et_4NHCO_3 in *n*-BuOH to a solution of $Cu(py)_4(OTf)_2$ and the precursor in DMF. The reaction mixture was heated (110 °C) under air for 10 min, cooled, diluted with an excess of aqueous EtOH and analyzed by HPLC. To produce 4-[18F]FTrp NiBPB-4-BPinFTrp was [18F]-fluorinated under standard conditions and the mixture was concentrated *in vacuo*. Finally, the intermediate radiolabeled nickel complex was decomposed with 6M HCl/MeOH and the desired tracer was isolated by HPLC. **Results:** Diastereomerically pure boronated NiBPB-AA complexes were prepared in 50-85% yield. The respective Ni-complexes of radiolabeled AAA were synthesized in RCCs of 41-93% in >98% diastereomeric purity. 4-[18F]FTrp was obtained in unoptimized 25% RCY (non-decay corrected) within one hour in excellent radiochemical (>98%) and enantiomeric purity (ee >96%). **Conclusions:** Easily accessible boronated NiBPB-AAA complexes have been shown to be suitable substrates for alcohol-enhanced Cu-mediated radiofluorination. NiBPB represents an ideal framework for synthesis of precursors for radiofluorinated AAA. The practicality of the novel method was highlighted by the rapid preparation of 4-[18F]FTrp. **Research support:** This work was supported by the DFG grant ZL 65/1-1.

E-PW019

Development of a tumor-associated fetal protein derived peptide as a potential tool for the targeting of estrogen receptor positive breast cancer

S. M. Okarvi, I. AlJammaz; King Faisal Specialist Hospital and Research Center, Riyadh, SAUDI ARABIA.

Objectives: Several studies have shown that estrogen action can induce and promote breast cancer; therefore decreasing estrogen production or blocking its action with antiestrogens have been the main treatments for estradiol receptor ERα- positive tumors. There is an unmet clinical need for the development of effective breast cancer prevention radiopharmaceuticals possessing high therapeutic efficacy and low systemic

toxicity. Alpha-fetoprotein (AFP) is a safe naturally occurring human serum protein produced during pregnancy, which itself has anti-estrogenic and anti-breast cancer activity. Furthermore as nearly all breast cancers initially develop as estrogen receptor-positive cells and are estrogen-driven; AFP-derived peptides may be useful for preventive as well as for therapeutic management of human breast cancers. Therefore our interest was to prepare a synthetic peptide-derived from AFP and evaluate its potential for targeting breast cancer. **Methods:** An 8-amino acids AFP-derived peptide (amino acids 472-479) was generated using standard Fmoc-based solid-phase peptide synthesis and manually coupled to DOTA chelating agent to facilitate labeling with both ^{68}Ga and ^{177}Lu to formulate theranostic pairs. The tumor cell binding ability of the radiolabeled AFP peptide analog was determined on ER positive MCF7 and T47D breast cancer cell lines and in vivo tumor targeting study was conducted on nude mice bearing MCF7 breast tumor xenografts. **Results:** The structural identity and chemical purity of the synthetic AFP-derived peptide was confirmed by mass spectrometry and HPLC. The AFP peptide revealed efficient radiolabeling (>90%) with both diagnostic (^{68}Ga) and therapeutic (^{177}Lu) radionuclides. Additionally the radiopeptide exhibited a high binding affinity to ER positive MCF7 and T47D breast cancer cell lines with the binding affinities values were below 10 nM. In nude mice bearing human MCF7 tumor xenografts, ^{68}Ga/^{177}Lu-AFP displayed rapid clearance from the blood and uptake and retention in all the major organs was found to be low to moderate levels (below 4% ID/g). The accumulation in the ER positive MCF7 tumor was 2.14±0.68% ID/g at 1 h p.i., with good tumor to blood and muscle ratios of 2.6 and 7.1. The radiolabeled AFP-derived peptide was eliminated from the body mainly through the renal system. **Conclusion:** The promising findings of this initial study suggest that further development of this AFP-derived peptide appears to be indicated because of its compelling potential to be a novel agent for the management of breast cancer. If these preclinical findings translate successfully to human trials, many at-risk women would be able to prevent breast cancer with minimal, if any, morbidity.

Clinical Oncology: Walk Mixed Tumours

E-PW020

Diagnostics of the sentinel lymphatic nodes in laryngeal and laryngopharyngeal cancer

I. Sinilkin, V.I. Chernov, E.L. Choynozonov, S.Yu. Chizhevskaya, A.Medvedeva, R.V. Zelchan, O.D.Bragina, V.S.Skur; Tomsk National Research Medical Center of the Russian Academy of Sciences, tomsk, RUSSIAN FEDERATION.

The aim of the study was to evaluate the diagnostic efficiency of ^{99m}Tc-Alotech and ^{99m}Tc-Technefyte radiopharmaceuticals (RFP) for detection of sentinel lymph nodes (SLN) in patients with laryngeal and laryngopharyngeal cancer. **Materials and Methods:** The study included 35 patients with laryngeal and laryngopharyngeal cancer. All patients were divided into 2 groups: 17 and 18 patients respectively. In the first group 99mTc-Alotech was introduced for sentinel lymph nodes visualization, the second group of patients was injected with ^{99m}Tc-Tehnefit. Injections of both RFPs were performed in 2-4 points (at a dose of 20 MBq in each injection) submucous along the perimeter of the tumor. Single-photon emission computed tomography (SPECT) of the neck area was performed on a gamma camera (E.CAM 180, Siemens) 3 and 18 hours after the administration of the radiocolloid. Evaluation of the results was carried out visually, as well as the calculation of the intensity of inclusion of RFP in SLP in comparison with the place of administration. Intraoperative detection of sentinel lymph nodes was carried out with the Gamma Finder II® gamma probe (USA) by carefully measuring of the level gamma radiation in the projection of lymphatic collectors. **Results:** In the first group of patients (n = 17), who were injected with 99mTc-Alotech, SLN were detected in all 17 patients in the number of 19 lymph nodes, while in the intraoperative radiometric study 20 SLN were identified. In the second group of patients (n = 18), who were injected with ^{99m}Tc-Tehnefit, scintigraphically succeeded in detecting 19 sentinel lymph nodes in 16 patients, and 23 SLN in 17 patients radiometrically. In the second group of patients (n = 18), who were injected with 99mTc-Tehnefyt, 19 SLN were scintigraphically detected in 16 patients and 23 SLN were revealed in 17 patients radiometrically. The intensity of ^{99m}Tc-Alotech inclusion in the SLN at the SPECT at 18 hours after the administration was 4-8% of the place of administration, with radiometry of 12-21%. When analyzing the data for ^{99m}Tc-Technefeet the values were 1.2-1.8% and 1.5-5%, respectively. **Conclusions:** Sensitivity of the sentinel lymph nodes detection using the ^{99m}Tc-Alotech radiopharmaceutical in patients with laryngeal and laryngopharyngeal cancer was 100%. While the sensitivity of detecting SLR using 99mTc-phytate was 94.4%. ^{99m}Tc-Alotech has a high level of fixation in SLN, which allows to improve the quality of visualization and to reduce the operation time.

E-PW021

PET/CT with 18F-FDG and 11C-Methionine for Assessment of Remission Status after Autologous Stem Cell Transplantation in Multiple Myeloma Patients

O. Mukhortova[1], I. Aslanidis[1], T. Katunina[1], A. Rumjantzev[1], A. Silchenkov[1], M. Solovev[2], L. Mendeleeva[2]; [1]Bakoulev Scientific Center for Cardiovascular Surgery, Moscow, RUSSIAN FEDERATION, [2]National Research Center for Hematology, Moscow, RUSSIAN FEDERATION.

Some recent data suggest that PET/CT is a promising method for diagnosis, staging, treatment assessment and estimation of prognosis for multiple myeloma (MM) patients. Effectiveness of different radiopharmaceuticals is still under discussion. **Purpose:** To compare the results of PET/CT with 18F-FDG (FDG) and 11C-Methionine (MET) in MM patients after autologous stem cell transplantation for remission status assessment. **Materials**

and Methods: All 18 patients had undergone one or two stem cell transplantation (SCT) - autologous or allogenic, at the time of PET/CT scanning had partial or complete remission status of MM: 8/18 had no M-protein secretion (NMS) and 10/18 had positive M-protein secretion (PMS). Whole-body PET/CT (including the skull) with low-dose CT scan was performed for all patients according to standard one day protocol: MET-scan in 20 min after injection (400 - 450 MBq) and 4 hours later FDG-scan in 90 min after injection (180 - 200 MBq). Visual assessment and SUVmax calculation for pathological foci were done. PET/CT results for both scans were compared with clinical and laboratory data. Analysis was performed on a patient and a lesion basis. The follow-up period was from 1 up to 9 months. **Results:** Overall 16 pathological foci were revealed on FDG scans and 28 foci on MET scans. The level of SUVmax in foci on FDG scans was lower than on MET scans: 2,7 - 3,9 vs 2,7 - 5,8. Diffuse marrow uptake of both tracers was detected in 2/18 patients. In NMS patients 3/8 had negative results in both scans (FDG and MET), 3/8 had positive results in both scans and 2/8 had positive MET but negative FDG results. In PMS patients 3/10 had negative results in both scans, 4/10 had positive results in both scans and 3/10 had positive MET but negative FDG results. In whole group the residual activity of MM was detected in 12/18 patients according to MET, whereas in 7/18 according to FDG, i.e. 5 patients were missed on FDG scans. Two patients had relapse during follow up - both with positive MET and FDG results, one from NMS and other from PMS group. **Conclusion:** According to primary results MET is a more accurate tracer than FDG for disease extension and residual activity detection in MM patients after SCT.

E-PW022

Cancer Lesions Detectability Limits in the SPECT Breast Imaging

E. Stiliaris[1], D. Maintas[2], D. Zarketan[1]; [1]National & Kapodistrian University of Athens, Athens, GREECE, [2]Institute of Isotopic Studies, Iatrikon Hospital, Athens, GREECE.

Aim: Breast imaging for early stage cancer diagnosis is still mainly relying on planar imaging techniques. Due to spatial resolution and sensitivity limitations in combination with absorption effects, whole-body PET and SPECT clinical scanners show a poor performance in tomographic level. In order to exercise in detail the detectability limits of small breast cancer lesions in a highly noisy background, a dedicated SPECT study with a breast phantom is presented here. The practical goal of the current analysis is to accurately define the tomographic limits of this method to successfully deliver accurate clinical tomographic images in a controllable signal-to-noise environment. **Materials and Methods**: A dedicated breast phantom in a cylindrical form (total volume 470 ml) has been constructed for this study. It can be filled with 99mTc water solution aiming to simulate in a proper way the noisy breast background and absorption effects normally observed in radiographic imaging detections. Four tubes and capillaries, arranged in axially asymmetric way and in various depths, can be filled with micrometric radiotracer volumes representing hot spot deposits. The breast phantom

is tomographically depicted with a small field and high sensitivity γ-Camera system consisting of a CsI pixelated scintillation crystal and a hexagonal parallel-hole collimator, all optimized for 99mTc detection. Scintillation light is read out by a Position Sensitive PhotoMultiplier Tube (PSPMT) and the position and energy information is reconstructed with an optimized Anger technique and recorded in an event-by-event mode. Entirely, 24 planar images in 15-degree steps are acquired; tomographic image reconstruction is carried out with different, well established methods, based on the Algebraic Reconstruction Technique (ART) and the Maximum Likelihood Expectation Maximization (MLEM) method. **Results**: Observed planar and tomographic images have been extensively analyzed for the various signal/background sets of the specific radioactivity. Results are presented analytically and the detection limits are given in terms of minimum detectable absolute tracer specific activity (µCi/ml). Effects of energy filtering by neglecting Compton events well below the 99mTc photo-peak are also presented. The measured efficiency of the system is finally compared to the expected ideal performance of the phantom-Camera system by means of GEANT4/GATE simulations. **Conclusion**: The current study presents in detail detectability limits for the SPECT breast imaging of clinical value with a dedicated phantom and a small field and high sensitivity γ-Camera system. Results will also serve as a feasibility study for the planned construction of a four-head γ-Camera device (Tetra-SPECT) dedicated to mammography.

E-PW023

Impact of Postoperative Diagnostic 131I Whole Body Scan with SPECT-CT on Staging, Risk Stratification and Radioiodine Therapy Planning in Low Risk Differentiated Thyroid Cancer

W. Teeyasoontranon, T. Kaewchur, S. Namwongprom, A. Klaipetch, M. Ekmahachai; Division of Nuclear Medicine, Department of Radiology, Faculty of Medicine, Chiang Mai University, Chiang mai, THAILAND.

Propose: To determine the use of postoperative diagnostic 131I whole body scan (131I DxWBS) with SPECT-CT on initial staging, risk stratification and 131I therapy planning in differentiated thyroid cancer (DTC) patients classified as low risk of recurrence based on clinical and histopathological data. **Subjects and Methods:** Seventy-one post-total thyroidectomy DTC patients (male = 7, female = 64, aged < 45 years = 34, aged ≥ 45 years = 37) classified as low risk stratification using ATA 2009 risk stratification system based on clinical and histopathology were enrolled into the study. Initial staging using AJCC/TNM staging system seventh edition was evaluated. 131I treatment planning to withhold or administer in low (1.1 GBq), medium (3.7 GBq) or high (5.5 GBq) activities of 131I was prescribed based on our institute protocol. Postoperative 131I DxWBS with SPECT-CT of neck and chest were performed at 4-6 weeks after total thyroidectomy. The additional SPECT-CT images of the specific regions based on equivocal lesions seen on planar imaging were obtained. Low activities of 131I (37 MBq) were used for 131I DxWBS. The 131I DxWBS with SPECT-CT were interpreted by two

blinded independent nuclear medicine physicians in a consensus reading. Staging, risk stratification and 131I treatment planning were re-evaluated based on additional 131I DxWBS with SPECT-CT findings. **Results:** Among 34 patients aged < 45 years, 131I DxWBS with SPECT-CT detected nodal metastases in 11 patients (32.3%, N1a = 6, N1b = 5), and distant metastasis in 1 patient (2.9%, bone and lung), which changed TNM staging in 1 patient (2.9%). Of 37 patients aged ≥ 45 years, nodal metastases were detected in 13 patients (35.1%, N1a = 7, N1b = 6) and distant metastases in 3 patients (8.1%, 2 bone, 1 lung), leading to change of TNM staging in 15 patients (40.5%). Risk stratification was changed from low risk to intermediate risk in 24 of 71 patients (33.8%) and to high risk in 4 of 71 patients (5.6%). RAI therapy planning was altered in 23 of 71 patients (32.4%). **Conclusion:** Our study results demonstrated that the postoperative 131I DxWBS with SPECT-CT altered the initial staging, risk stratification and 131I treatment planning based on the clinical and histopathology in low risk DTC patients. Nodal and distant metastases were detected leading to changing of the overall TNM staging in 22.5%, risk stratification in 39.4% and 131I treatment planning in 32.4% of our low risk DTC.

E-PW024

May 18F-Fluorocholine PET/CT Have A Role To Localize Parathyroid Adenoma In Patients With Negative 99mTc-MIBI?

F. Di Gregorio[1], M. Rensi[1], F. Vescini[2], D. Capobianco[1], F. Giacomuzzi[1], G. Ferretti[1], M. Povolato[1], O. Geatti[1]; [1]Department of Nuclear Medicine University Hospital, Udine, ITALY, [2]Department of Endocrinology University Hospital, Udine, ITALY.

Introduction: Primary hyperparathyroidism is not an uncommon disease and, being surgery the only curative treatment, a precise pre surgical localization of the adenoma is strongly recommended. Dual tracer 99mTc-sestamibi scintigraphy (MIBI), in particular when performed with SPECT/CT technique, is the most sensitive non-invasive imaging approach to localize hyperfunctioning parathyroid glands. Nevertheless its diagnostic accuracy decreases significantly in patients with very small parathyroid adenomas or multiple lesions. Aim of the study is to evaluate if 18F-Fluorocholine (FCH) PET/CT, that is commonly used in prostate cancer evaluation, can be helpful in localizing parathyroid adenoma not identified by MIBI planar and SPECT/CT. **Subjects and Methods:** 6 out of 20 consecutive patients (12 females and 8 males, age range 26-75 years) diagnosed with parathyroid adenoma on clinical and biochemical grounds, in whom MIBI scan with SPECT/CT acquisition did not detect the lesions, underwent a FCH-PET/CT acquisition (2 beds of 3 minutes) of the neck and mediastinal area after 60 minutes from i.v. injection of 350 MBq of FCH. Subsequently all the 6 patients underwent surgical neck exploration and a histo-pathological analysis was obtained. **Results:** histology confirmed parathyroid adenomas (volumes ranges 0,3 - 0,9 cm³) in all 6 patients and the localization of the lesions by FCH was correct in all the 5 patients in whom the study was positive (sensitivity: 83%). The patient with a false negative FCH had a very small lesion (0,3

cm³). **Conclusion:** our preliminary data suggest that FCH PET/CT could be an useful non invasive imaging modality to localize parathyroid adenomas in patients with a negative MIBI planar and SPECT/CT.

E-PW025

Sentinel node biopsy for bladder cancer using ICG-99mTc-nanocolloid

P. Meershoek[1,2], E. M. Wit[2], B. W. G. van Rhijn[2], G. H. KleinJan[1,2], E. Vegt[2], M. L. Donswijk[2], R. A. Valdés-Olmos[1], H. G. van der Poel[2], F. W. B. van Leeuwen[1]; [1]Leiden University Medical Center, Leiden, NETHERLANDS, [2]Netherlands Cancer Institute (NKI-AvL), Amsterdam, NETHERLANDS.

Introduction: Radical cystectomy with an extended pelvic lymph node dissection (ePLND) is considered the standard of care for non-metastatic muscle-invasive bladder cancer. The nodal status of the patient is of great importance for the prediction of disease recurrence and cancer-specific survival, hence the ePLND. The invasive nature of these procedures is, however, associated with complications like lymphocele and post-operative hematomas. We reasoned that specific targeting of the first tumor draining lymph nodes (sentinel nodes; SN) with a tracer that facilitates pre- and intraoperative guidance (indocyanine green (ICG)-99mTc-nanocolloid) could help provide a minimally invasive alternative for ePLND in bladder cancer. **Materials and Methods:** Ten patients scheduled for a radical cystectomy and ePLND with or without neo-adjuvant chemotherapy were included. Approximately eighteen hours before surgery the patients received four injections of ICG-99mTc-nanocolloid around the tumor (or random across the bladder in case of multiple tumors; under cystoscopic guidance). Preoperative SN mapping was done using planar lymphoscintigraphy (dynamic, 15 minutes, and 2h), followed by three-dimensional SPECT/CT (2h). Intraoperatively the SNs were identified using radio- and fluorescence guidance. The tumor find rate of the SN procedure an ePLND was assessed at pathology. **Results:** Cystoscopic deposition of the tracer using the endoscopic needle proved to be complex. In some patients there was leakage of the hybrid tracer into the urine, which resulted in radioactive contamination of the cystoscopy equipment. Four patients (40.0% of total) had non-visualization of SNs during preoperative SN mapping. In five of the six patients (83.3%) with SNs detected during preoperative imaging, SNs were removed successfully intraoperatively. In one patient (1/6; 16.7%) the SNs could not be removed using radio- and fluorescence guidance and could also not be found ex vivo. **Discussion/Conclusion:** Tracer administration proved to severely limit the success of performing SN biopsy in bladder cancer patients. SNs were removed successfully with radio- and fluorescence guidance in 83.3% (5/6) of the patients with SNs detected during preoperative SN mapping.

E-PW026

Correlation of hypoxia inducible transcription factor-1α, glucose transporter-1, carbonic anhydrase IX and FDG uptake in invasive ductal breast cancer

Y. Jeong, B. Choi, Y. Cho, S. Park, H. Oh, **S. Kang**; *Catholic University of Daegu School of Medicine, Daegu, KOREA, REPUBLIC OF.*

Background: Recently multiple biomarkers related to tumor hypoxic microenvironment have been discovered and offered as targets for cancer detection, treatment and monitoring, such as hypoxia-inducible transcription factors alpha (HIF-1α), glucose transporter-1 (GLUT1) and carbonic anhydrase IX (CA IX). We studied the immunohistochemical expression of HIF-1α, GLUT1 and CA IX in patients with invasive ductal breast cancer (IDC) and the correlation with SUVmax of the primary tumor (pSUVmax) as well as other biological parameters. Prognostic significance of pSUVmax, HIF-1α, GLUT1 and CA IX for the prediction of progression-free survival (PFS) was also assessed. **Materials and Methods:** One-hundred seventy four female patients with IDC who underwent pretreatment F-18 FDG PET/CT were enrolled. The pSUVmax was compared with clinicopathological parameters including ER, PR, HER2, axillary lymph node metastasis (LNM), stage, GLUT1, CA IX and HIF-1α. The prognostic value of pSUVmax, GLUT1, CA IX and HIF-1 α for PFS was assessed using the Kaplan-Meier method. **Results:** pSUVmax was significantly higher in patients with HIF-1α≥2, GLUT1≥5 and CA IX≥3 compared to patients with HIF-1α<2, GLUT1<5 and CA IX<3 (4.9±4.1 vs. 3.9±3.2, P=0.02; 6.1±4.2 vs. 3.5±3.0, P=0.003; 5.9±4.5 vs. 3.8±3.2, P=0.003). pSUVmax was also significantly higher in higher stage (P<0.001), ER-negative tumors (P<0.0001), PR-negative tumors (P=0.0009) and positive LNM (P=0.0283). pSUVmax was significantly higher in patients with progression compared to patients who were disease-free (6.4±3.5 vs. 4.1±3.6, P=0.0045). A receiver-operating characteristic curve demonstrated pSUVmax of 6.8, GLUT1 of 5 and CA IX of 3 to be the optimal cutoff for predicting PFS (sensitivity; 53.6%, specificity; 86.0%, P<0.0001; 60.9%, 72.2%, P=0.006; 56.5%, 80.8%, P=0.0054). Kaplan-Meier analysis identified pSUVmax ≥6.8 (P=0.0004), GLUT1≥5 (P=0.0005) and CA IX≥3 (P<0.0001) as predictors of recurrence. Cox proportional-hazards analysis showed that pSUVmax ≥6.8 (P=0.0338, relative risk 2.636), HIF-1α≥2 (P=0.0194, relative risk 0.331), GLUT1≥5 (P=0.0379, relative risk 3.139) and CA IX≥3 (P=0.0064, relative risk 3.829) significantly predicted recurrence. **Conclusions:** pSUVmax on pretreatment F-18 FDG PET/ CT reflect expression of HIF-1α, GLUT1 and CA IX and can be used as a good surrogate marker for the prediction of progression in patients with IDC. The amount of FDG uptake is determined by the presence of glucose metabolism and hypoxia in breast cancer cell.

E-PW027

Effect of stem cell transplantation on breast cancer-related lymphedema quantified by lymphoscintigraphy

J. A. Simonsen[1], S. Hvidsten[1], J. A. Sørensen[1,2], P. F. Høilund-Carlsen[1,2], N. M. Toyserkani[1,2]; [1]Odense University Hospital, Odense C, DENMARK, [2]University of Southern Denmark, Odense C, DENMARK.

Purpose/Introduction: Arm lymphedema is a debilitating complication of breast cancer treatment. Among different therapeutic strategies tested for, stem cell transplantation may hold promise. However, standardized methods for evaluation of the therapeutic effect have been lacking. We evaluated the effect of axillary stem cell transplantation by quantitative lymphoscintigraphy. Subjects & Methods: Ten women, aged 34-68 years, with unilateral upper limb breast cancer-related lymphedema were examined with bilateral lymphoscintigraphy before and a year after implantation of autologous fat-derived stem cells into the axilla of the lymphedema arm. From lymphoscintigraphy the mean transit time (MTT) of the tracer (Tc-99m HSA, 20 MBq in 0.1 mL) was calculated based on the uptake and retention of tracer in the upper limb; a high MTT corresponded to a slow transit and, hence, an accumulation of tracer in the soft tissue, while a fast transit was indicative of a well-functioning lymphatic drainage. The validity of this method has been reported elsewhere.1 Results: Clinically, patients experienced amelioration in terms of lower disability scores, reduced feeling of fullness and tightening, and less need for compression in five cases. Four patients suffered from recurrent skin infections before the intervention, none at one-year follow-up. Excess arm volume did not change significantly. Mean MTT±SD of the lymphedema arms was 63.4±25.4 min before the transplantation and 60.7±34.9 min after one year, p=0.65. Mean MTT of the healthy arms was 5.4±2.5 min and 7.9±2.8 min, respectively, p=0.002. Thus, these values did not suggest improved lymphatic drainage from the lymphedema arms, but a slightly delayed lymph flow in the healthy arms. Individual MTT(lymphedema arm)/MTT(healthy arm) ratios were lower after the intervention than before in all cases except one in that there was a decrease of the mean ratio from 16.2±13.7 to one of 7.9±3.4, p=0.004. One patient had a very high value before the intervention of 49.5. The mean before-ratio of the other nine patients was 12.5±8.4; hence, even a conservative judgement revealed a consistent change after one year in the balance between lymph flow in affected and healthy arm. Discussion/Conclusion: Following stem cell transplantation we observed a change in the balance of lymph flow in the two arms due to a decrease in lymph flow in the healthy arm, a finding indicating a certain systemic rather than exclusively local response to therapy. Consequently, therapeutic regimens against lymphedema should probably be monitored by methods, like our scintigraphic approach, considering the lymphatic drainage of both arms. **References:** J.A. Simonsen et al. Quantification of breast cancer-related lymphedema of the upper limbs. Abstract #2055 accepted for oral presentation at the SNMMI 2017 Annual Meeting.

E-PW028

Comparison of Magnetic Resonance Imaging (MRI) and 18F-NaF PET/CT for Detection of Spinal Bone Metastases in high-Risk Patients with Breast Carcinoma

E. Panagiotidis, A. Mistry, A. Farnworth, N. Seshadri, S. Vinjamuri; Royal Liverpool University Hospital, Liverpool, UNITED KINGDOM.

Introduction: The objective of this study was to evaluate the diagnostic accuracy of MRI and 18F-NaF PET/CT in detection of spinal metastases in patients with high-risk breast cancer. **Subjects and Methods:** Both patient and lesion-based analyses

have been performed on 66 consecutive patients (pts) (median age, 62.5 years; age range, 33-91 years) for restaging of newly diagnosed recurrent breast cancer with no previous bone metastases. All pts underwent Spinal MRI of Sagittal T1 and STIR sequences with localized axial T2 imaging along with 18F-NaF PET/CT before initiation of treatment, less than 20 days in between (median: 14 days) in our PET/CT department from September 2010 to March 2016. A nuclear medicine physician with PET/CT experience and a musculoskeletal radiologist evaluated the 18F-NaF PET/CT and MRI studies respectively. Follow-up exams with MRI, CT and 18F-NaF PET/CT as well as CT guided biopsy along with clinical follow up (22pts) (at least 12 months, median time: 19 months) were used as the standard of reference to evaluate 18F-NaF PET/CT and MRI studies. **Results:** On patient-based analysis, 26pts (39.4%) had bone metastases and 40pts (60.6%) was proven bone disease free during follow up. 18F-NaF PET/CT was positive in 40pts (60.6%) showing 97.5% sensitivity, 96.15% specificity, 97.5% positive predictive value (PPV) and 96.15% negative predictive value (NPV). Spinal MRI was positive in 39pts (59.1%) showing 95% sensitivity, 100% specificity, 100% positive predictive value (PPV) and 92.86% negative predictive value (NPV) with disease prevalence of 60.61%. There was concordance of both studies in 63pts (95.5%), MRI was superior in 2 pts (3%) and inferior in one (1.5%) pt. On lesion-based analysis, 18F-NaF PET/CT showed 175 lesions in total, 29 (16.5%) in cervical spine, 71 (40.5%) in thoracic spine, 48 (27.5%) in lumbar spine and 27 (15.5%) in sacrum. MRI revealed 190 lesions in total, 30 (15.8%) in cervical spine, 79 (41.6%) in thoracic spine, 51 (26.8%) in lumbar spine and 30 (15.8%) in sacrum. There was concordance of both studies in 52pts (78.8%), 18F-NaF PET/CT was superior in 4 pts (6%) and inferior in 10 (15.2%) pt on lesion based analysis. **Conclusion:** 18F-NaF PET/CT is a sensitive modality for detection of spine metastases caused by breast cancer. MRI shows a higher specificity but lower sensitivity than 18F-NaF PET/CT, with diagnostic advantage in detecting more spinal metastases, however of uncertain clinical benefit.

E-PW029

Evaluation of the Total Distribution Volume of 18FBPA in Normal Tissues of Healthy Volunteers by Non-Compartmental Kinetic Modeling

V. Romanov, K. Isohashi, E. Shimosegawa, T. Watabe, R. Beshr, J. Hatazawa; *Osaka University Graduate School of Medicine Department of Nuclear Medicine and Tracer Kinetics, Osaka, JAPAN.*

Background: Boron Neutron Capture Therapy (BNCT) with 4-borono-L-phenylalanine ([10]BPA) is a promising method of radiation therapy based on [10]B(n, α)[7]Li reaction inside tumor cells loaded with [10]B-labeled phenylalanine, causing cell destruction. Very short range of emerged ions (5-9 μm) reduces radiation dose to surrounding normal tissues, however the radiation dose depends on [10]B concentration in normal cells. Several studies (by Hanaoka K.; Watabe T.; Shimosegawa E.; Isohasi K.) have been performed in our laboratory to estimate [10]B concentration *in vivo* using 4-borono-2-[^{18}F]-fluoro-phenylalanine ([18]FBPA). The purpose of the current study was to evaluate total distribution

volume (Vt) of [18]FBPA in normal tissues of healthy volunteers by kinetic analysis. **Methods:** 6 healthy volunteers were injected with [18]FBPA (3-5 MBq/kg) and 7 PET-CT scans were performed subsequently. [18]FBPA radioactivity in whole blood and plasma was measured before, and 8 times after the injection within 50 minutes, using well counter. PET images have been processed by PMOD software (build 3.601). 11 volumetric regions of interest including brain, heart, right lung, spleen, liver, parotid salivary glands, esophagus, stomach, pancreas, intestines, bone marrow were drawn manually for each subject and analyzed with Logan plot (traditional and noise corrected) and Ichise multilinear (MA1 and MA2) models. Better model was defined by Akaike Information Criterion, Schwartz Criterion, Model Selection Criterion, and Coefficient of Determination. Also residual distribution was analyzed visually and using sum of squared residuals and standard deviation of the residuals. An equilibration time t* with maximal allowed error of 1% was set to 20 min for the Ichise MA2 model; to 20 and 28 min for the Ichise MA2 model; to 25 and 33 min for the Logan plot. Finally, Vt values were derived. **Results:** Ichise's MA2 model showed best fitting among all models. Vt values ranged from 0.94±0.14 ml/ccm in the pancreas to 0.15±0.01ml/ccm in the lung. **Conclusion:** Maximal Vt value of [18]FBPA did not exceed 1.09 ml/ccm, being much lower than values published for tumors as Vt itself (Grunewald C. et al., 2016) or those that could be derived from rate constants (J.C Chen et al. 2004; Imahori Y. et al., 1998), thereby reflecting lower K1/k2 ratio in normal tissues. Vt values obtained in this study could potentially be used for evaluation of [10]B concentration in normal tissues before BNCT with [10]BPA constant infusion protocol, however comparison of the estimated results with real boron concentration in normal tissues is needed.

Do.MoRe: SPECT Technology

E-PW030

Uncertainty in activity measurements using radionuclide calibrators due to source geometry effects

C. Saldarriaga Vargas[1], A. Carbutti[2], J. Dabin[1], K. Baete[3], L. Struelens[1]; [1]*Belgian Nuclear Research Centre (SCK-CEN), Mol, BELGIUM,* [2]*Politecnico di Torino, Turin, ITALY,* [3]*UZ Gasthuisberg, Leuven, BELGIUM.*

This study aimed to evaluate the uncertainty in activity measurements of clinical radioisotopes due to source geometry effects for different radionuclide calibrators (RC). Experiments were performed to assess the effect of container type and solution volume on the measurement accuracy. [18]F, ^{68}Ga, ^{99m}Tc, ^{111}In, ^{123}I, ^{131}I, [90]Y (chloride form) and [223]Ra were studied in various clinical containers, including 1-10ml plastic syringes and 2-25ml glass vials. A stock solution (SS) of each radionuclide was prepared in a standard 10ml Schott vial, and the reference activity concentrations were determined using a Fidelis Secondary Standard

RC. SS was then transferred to each container, and its reference activity was determined from the mass of the transferred solution and the SS activity concentration. The solution inside each sample was diluted with water to test for volume effects. Radioactivity was measured after preparation and following each dilution, both in the Fidelis and in RCs from Capintec and Comecer. Results showed that the activity read by all RCs is dependent on the container type. The RC response is usually higher (up to 40%) when the activity is measured in a syringe rather than in a clinical vial. This effect is stronger for radionuclides emitting low-energy photons: for ^{123}I and ^{111}In, field instruments can overestimate the activity in a syringe by 15-28%, whereas in a glass vial the activity can be underestimated by 5-15%. [18]F and ^{131}I were the radionuclides the least affected by the container type; however, measurements were not necessarily within ±5% of the reference value. In general, measurements were more accurate in the Schott vial than in clinical containers, probably because this container is more similar to the containers used by the manufacturers to calibrate the RCs (*e.g.* thin-walled glass ampoules). Regarding volume effects, the difference in activity reading between filling volumes, corresponding to about 20% and 80% of the nominal container size, was usually negligible or within 3-5% for most samples and RCs tested. Activity measurements using RCs can be strongly affected by the sample container. It is recommended to quantify these effects during acceptance/performance testing of RCs using the radiopharmaceuticals and containers most frequently used in clinical practice. If necessary, container-specific calibration (or correction) factors can be determined to improve the accuracy of radioactivity measurements in routine nuclear medicine. Finally, the accuracy of the activity reported by the suppliers of some radionuclides was also evaluated and is currently being analyzed.

E-PW031

Accuracy, Repeatability and Reproducibility of xSPECT Quant Sensitivity Calibrations using a NIST-traceable Point Source

*P. C. Holdgaard[1], H. C. Larsen[1], **N. A. Bebbington**[2]; [1]Lillebælt Hospital, Vejle, DENMARK, [2]Siemens Healthineers, Aarhus, DENMARK.*

Introduction: Before clinically interpreting quantitative values it is important to understand the error on the final measurement. A potential source of error in absolute SPECT quantification is the scanner sensitivity calibration. Sensitivity calibrations should be accurate, repeatable, reproducible, and should be representative of sensitivity across the detector. The aim was to assess accuracy, repeatability and reproducibility (over time and spatially across the detector) of sensitivity calibrations made according to the Siemens xSPECT Quant method using a NIST traceable Co-57 source. **Subjects and Methods:** Reproducibility with time: 35 sensitivity calibrations were made using a NIST-traceable Co-57 point source across two Siemens Symbia Intevo 6 systems (software version VB10), according to standard protocol, over a one-month period. Reproducibility across the detector: 11 sensitivity measurements were made across a 10cm distance in the z-direction in 1cm increments on one system.

Repeatability: 15 sensitivity calibrations were made in succession (with and without moving the source between measurements) on one system. Accuracy: a uniformity phantom filled with 51.3MBq Tc-99m-TcO$_4^-$ (as measured on a Capintec CRC15 dose calibrator) was scanned, and reconstructed with the quantitative OSCG algorithm, and the measured SUV compared to the known SUV of 1.00. **Results:** Accuracy: using a factor to correct for dose calibrator bias from prior cross-calibration between scanner and dose calibrator (as information on traceability of the dose calibrator to a primary standard was not available), the SUV of the Tc-99m uniformity phantom measured 1.00. Reproducibility with time: mean (±SD) sensitivity calibration factors (SCF) for detectors 1 and 2 were 88.5(±0.3%)cps/MBq and 88.0(±0.2%)cps/MBq for scanner 1, and 87.6(±0.2%)cps/MBq and 88.1(±0.3%)cps/MBq for scanner 2. Spatial reproducibility of SCF across the detector: Mean (±SD) SCF was 87.7(±0.4%)cps/MBq and 88.1(±0.5%)cps/MBq for detectors 1 and 2 respectively. Repeatability: without moving the source between measurements, standard deviations were 0.0% and 0.1% for detectors 1 and 2. When the source was moved between measurements, standard deviations were 0.1% and 0.2%. **Conclusions:** These findings demonstrate that xSPECT Quant sensitivity calibrations made using a NIST-traceable Co-57 point source give excellent accuracy, repeatability, and reproducibility with time and with location across the detectors. This method of sensitivity calibration thus contributes only an extremely small error to the final quantitative SPECT measurement, which is much less than is expected with manual Tc-99m calibration methods.

E-PW032

Determining the calibration factor of a SPECT/CT camera

L. Beels[1], *F. Lavent[1], I. Decostere[2], L. Tack[2], C. Van de Wiele[1], A. Maes[1]; [1]AZ Groeninge, Kortrijk, BELGIUM, [2]KU Leuven, Leuven, BELGIUM.*

Aim: Quantitative single-photon emission computed tomography (SPECT) has several important applications including monitoring tumor response after treatment and dose estimation for targeted radionuclide therapy treatment planning. The use of a calibration factor is required to obtain quantitative SPECT images. In this study, the calibration factor (CF) was determined for different acquisition and reconstruction protocols. **Materials and Methods:** A cylindrical phantom (height: 19.5 cm , diameter: 19.5 cm) was used for the SPECT/CT acquisitions (GE Discovery NM/CT 670). The phantom was filled with ^{99m}Tc, approximately 320 MBq for the first measurements and approximately 230 MBq for the second measurement that was performed to check the reproducibility of the calibration factor. The phantom was acquired four times using different acquisition parameters (change of acquisition time, matrix size, zoom factor) and the phantom was reconstructed using the GE Xeleris Volumetrix and GE Xeleris Volumetrix Evolution for Bone software. A volume of interest (VOI) (height: 15 cm, diameter: 17 cm) was drawn on the acquired images. Knowing the counts in the VOI, the volume of the VOI and the acquisition time, the count rate per unit volume was calculated. The CF was then determined by dividing the count rate per unit volume by the activity con-

centration decay corrected at the beginning of the acquisition. **Results:** The phantom reconstructed with the GE Xeleris Volumetrix resulted in a mean CF of 7.93 cpm/kBq (counts per minute per kilo Bequerel) for the 4 different acquisition protocols (CV: 0.04). Repeating this experiment resulted in a mean CF of 7.98 cpm/kBq (CV: 0.06) which only deviates 0.61% to the CF obtained during the first experiment. The phantom reconstructed with the GE Xeleris Volumetrix Evolution for Bone resulted in a mean CF of 40.51 cpm/kBq (counts per minute per kilo Bequerel) for the 4 different acquisition protocols (CV: 0.02). Repeating this experiment resulted in a mean CF of 41.29 cpm/kBq (CV: 0.02) which only deviates 1.93% to the CF obtained during the first experiment. **Conclusion:** The CF is not influenced by acquisition time, matrix size or zoom factor, but is highly influenced by the reconstruction parameters, more specifically resolution recovery (used in the GE Xeleris Volumetrix Evolution for Bone software). Therefore it is highly important when using a CF clinically to reconstruct the phantom data with the same reconstruction parameters as patient data.

E-PW033

Impact of the modelling of charge collection on the simulation of SPECT recordings from semiconductor CZT cameras

L. Imbert[1,2,3], J. Jurzcak[4], G. Karcher[1,2,5], P. MARIE[1,2,5]; [1]CHU Nancy, Vandoeuvre-lès-Nancy, FRANCE, [2]Plateforme d'Imagerie Expérimentale Nancyclotep, Nancy, FRANCE, [3]IADI, U947, Vandoeuvre-lès-Nancy, FRANCE, [4]Institut de Cancérologie de Lorraine, Vandoeuvre les Nancy, FRANCE, [5]Université de Lorraine, Faculté de Médecine, Nancy, FRANCE.

Introduction: The DSPECT CZT-camera (Spectrum Dynamics®) had already been simulated with the GATE platform, but without considering the partial collection of charges within the CZT detectors. This partial collection leads to a low energy tailing effect and is likely to deteriorate image quality. The aim of our study was to improve the Monte-Carlo simulation of the SPECT camera by the additional modeling the partial collection of charges of the CZT detectors. **Methods:** We used the Hecht equation[1], putting in relation the amount of collected charges with the depth of interaction of the γ photon within the CZT crystal, in order to model the response of the 9216 pixelated cristals of the DSPECT camera. The collimator geometry, the location and movement of each detector were modeled. A comparison was planned between the simulated and actually recorded data from punctual and spherical sources of ^{99m}Tc setting in the air or in a diffusing environment. In addition, heart images provided by the simulation with anatomic data from cardiac MRI, were compared with actually recorded SPECT images from the same patient. **Results:** The additional modeling of partial collection led to enhance the concordance between simulated and actually recorded data: 1) for the energy spectra from punctual and spherical sources, especially for experiments planed in diffusing environments, and 2) for the human SPECT images. For these latter, the myocardial contrast-to-noise ratios were 3.0 and 2.3 for simulation planed without and with the modeling of partial

collection respectively, as compared to 1.9 for the actual SPECT recording, and the corresponding sharpness indexes of myocardial walls (an index of spatial resolution) were 0.75 and 0.61 cm^{-1} respectively, as compared to 0.59 cm^{-1} for the actual SPECT recording. **Conclusion:** The additional modelling of the partial collection of charges leads to a great improvement in the simulation, through the Monte-Carlo GATE platform, of the SPECT recording from CZT-cameras, as evidenced by an enhanced agreement with actually recorded SPECT-data. *[1]Chen et al. Appl Radiat Isot 2008;66:1146-1150*

E-PW034

Simultaneous High-Sensitivity High-Resolution Molecular SPECT Imaging with Spinning Slit-Hole Collimator: A Monte Carlo Simulation Study

M. Ay[1,2], H. Mahani[3], G. Raisali[3], A. Kamali-Asl[4]; [1]Tehran University of Medical Sciences, Tehran, IRAN, ISLAMIC REPUBLIC OF, [2]Research Center for Molecular and Cellular Imaging, Tehran University of Medical Sciences, Tehran, IRAN, ISLAMIC REPUBLIC OF, [3]Radiation Application Research School, Nuclear Science and Technology Research Institute, Tehran, IRAN, ISLAMIC REPUBLIC OF, [4]Radiation Medicine Engineering Department, Shahid Beheshti University, Tehran, IRAN, ISLAMIC REPUBLIC OF.

Aim: Molecular SPECT imaging is always challenged by acquiring projection data with low statistics, leading to inferior image quality. In this study, we aim at comprehensively evaluating the performance of a novel collimation geometry, the slit-hole, using GATE Monte Carlo simulation. **Methods**: The slit-hole is a long narrow aperture embedded in tungsten body enabling high-sensitivity molecular SPECT. The collimator consists of a 0.6 mm knife-edge slit with 45 mm focal length. As the collimator measures planar projections, it spins at each regular SPECT angles, to ensure sufficient measurement of tomographic data. To assess the performance of this collimation system, a set of phantoms including a dedicated 5-point source and NEMA image quality (IQ) were simulated using the GATE Monte Carlo package. There were 16 spin angles as well as 16 SPECT angles. The planar projection data were also corrected for Compton scattering using a double-energy window method. The emission data acquired by the slit-hole were then reconstructed using an innovative 3D MLEM-based algorithm. Spatially varying system sensitivity was also molded in the reconstruction framework. **Results**: The slit-hole collimated scanner has a sensitivity of 335 cps/MBq at 30 mm distance, corrected for both scatter and background. The sensitivity of the proposed collimator shows a falling trend in field-of-view of the camera, weighted by distance from the aperture's center. A tomographic resolution of ~1.8 mm was gained at 30 mm radius-of-rotation. This spatial resolution is averaged for the 5 point sources distributed at different locations. Quantitative analyses demonstrated that 3 iterations of the developed algorithms leads to optimally reconstructed SPECT image by obtaining the highest signal-to-noise ratio. An 83% recovery of coefficient was observed for the largest rod in the NEMA IQ phantom. The slit-hole also gives rise to 4.8% image noise level for reconstruction of uniform part

the NEMA IQ phantom. **Conclusion**: The slit-hole collimation is a promising alternative to conventional pinhole and parallel-hole collimators for molecular imaging of small animals. The designed aperture shows a different resolution-sensitivity compromise by offering a high-sensitivity while keeping the spatial resolution at an acceptable level.

E-PW035

Accuracy of gamma camera efficiency determination using different experimental configurations

W. Zhao[1,2], P. L. Esquinas[1,2], X. Hou[2], C. F. Uribe[3], M. Gonzalez[4], J. Beauregard[5,6], Y. Dewaraja[7], A. Celler[2]; [1]Department of Physics and Astronomy, University of British Columbia, Vancouver, BC, CANADA, [2]Medical Imaging Research Group, Department of Radiology, University of British Columbia, Vancouver, BC, CANADA, [3]BC Cancer Agency, Vancouver, BC, CANADA, [4]Vancouver Coastal Health Authority, Vancouver, BC, CANADA, [5]Department of Radiology and Nuclear Medicine, Université Laval, Quebec City, QC, CANADA, [6]Department of Medical Imaging, CHU de Quebec – Université Laval, Quebec City, QC, CANADA, [7]Department of Radiology, University of Michigan Medical School, Ann Arbor, MI, UNITED STATES OF AMERICA.

Introduction: Accurate quantification of activity in nuclear medicine images, important for both research and clinical applications, requires determination of the camera calibration factor (CF). Although many methods have been proposed, there is still no consensus on which approach is the best. Our purpose was to compare these methods, to investigate the causes of their differences, and to propose a simple, practical and reliable camera calibration method which can be used in clinics for quantitation of radioactive isotopes for dosimetry in radionuclide therapies. **Subjects & Methods:** Experiments and Monte-Carlo simulations for three therapy isotopes (emitting beta particles and gammas: ^{177}Lu, ^{188}Re and ^{131}I) were performed. For each isotope, the data were acquired using three energy windows. The following experiments were performed: (1) planar scan of a point source in air, (2) tomographic scan of a source placed inside a cylinder filled with non-radioactive water (3) same configuration with radioactive water and (4) a cylinder filled with uniform activity. All tomographic scans were reconstructed using OSEM with CT-based attenuation and triple-energy-window (TEW) scatter corrections and CF were determined using total counts in the reconstructed image, while for planar scans, photopeak counts with (1A) and without TEW (1B) corrections were used. The experimental CFs were compared with those obtained from the corresponding simulations. **Results:** For all isotopes, the values of CF obtained from method (1A) agreed to within 5% with those from (3) and (4). However, planar scans without scatter correction (1B) produced higher CF values (20%-43%). The value of CF from method (2) CF exceeded those from other methods by 12%-15%. Analysis of simulations helped us to understand this discrepancy. It was due to inaccuracy of TEW scatter estimation which was enhanced by attenuation correction. This effect becomes less important when the source is distributed inside the phantom (configurations 3 and 4). **Conclusion:** In order to be practical,

the determination of camera CF must be simple and easy to perform. We have shown that planar acquisition of a point-like source provides the same CF as that obtained from quantitative tomographic reconstruction of an extended source, providing that self- and high-energy scatter and septal penetration are removed from planar data. But, using a tomographic scan of a source placed in non-radioactive background overestimates CF. Since activity in the patient body is usually distributed, similarly to that used in phantom (3) or (4), we conclude that method (1A) should be sufficient for CF determination.

E-PW036

Atlas-based pulmonary lobes segmentation implemented with MIM® for quantitative lung perfusion SPECT/CT analysis

C. P. L. Fulcheri[1], C. Tranfaglia[2], V. Reggioli[1], A. Chiappiniello[3], R. Tarducci[1], M. E. Dottorini[2]; [1]Medical Physics Department, Hospital Santa Maria della Misericordia, Perugia, ITALY, [2]Nuclear Medicine Department, Hospital Santa Maria della Misericordia, Perugia, ITALY, [3]Physics and Geology Department, University of Perugia, Perugia, ITALY.

Purpose: ^{99m}Tc-MAA functional lung scintigraphy is currently used in assessment of lobar function before surgical resection. Objective and accurate evaluation is possible by image quantification techniques. For years quantitation had been based on 2-d ROIs on anterior and posterior views. Nowadays, SPECT/CT provides 3-d information that can be used for a more accurate and clinically relevant definition of VOIs. To quantify radioactivity uptake in SPECT/CT, VOIs of lungs and lobes can be defined on the CT fused images. Manual or automated lung contouring is quite straightforward, whereas lobes segmentation can be time-consuming and challenging, especially when thin-slice or free-breathing/low-dose CT acquisition protocols are used. Our goal was to implement and evaluate an automated atlas-based segmentation of pulmonary lobes in order to make the contouring process fast, reliable and reproducible. **Subjects & Methods:** MIM software version 6.6.6 was used and a Single-Best Matched approach (SBM) was chosen. The reference anatomy atlas was constructed from 31 free-breathing thorax CT scans acquired with a Siemens SOMATOM Emotion 6. The contouring of right and left lungs, LM, LSD, LID, LIS, LSS was manually done by an expert clinician. The time needed for manually drawing of the ROIs was registered. Other 5 cases, with manually-created ROIs, were not included in the atlas, and were left for validation. The differences between manually and automated segmented ROIs were evaluated using the *F1-score* metric. The extra time to correct contours, if needed, was also registered. **Results:** The workflow included a rigid registration of a new patient to the template image in order to find the best atlas-matched subject and a successive deformable registration of the best matches to the patient (VoxAlign Deformation Engine). At the end of the image registration step, deformed atlas contours were transferred to the new image. Moreover, manual edit of the contours was possible. In all 5 cases the automatically generated contours needed to be slightly modified. To accurately contour all the lobes in 3 mm slice

width CT, the atlas-based segmentation and successive manual editing took 19±5 minutes per subject compared to 63±24 minutes required for completely manual segmentation. This represented a roughly 70% reduction in time. **Conclusion:** Preliminary results showed that the SBM contouring of pulmonary lobes implemented with MIM provided consistent time-saving over manual contouring. In the future the Multi-Atlas Segmentation approach will be studied as well as the effect of the contouring on the quantitative evaluation of perfusion SPECT/CT.

E-PW037
Development of a new phantom for DaTSCAN imaging

J. Taylor[1], R. Holmes[2], J. Fenner[3]; [1]Sheffield Teaching Hospitals, Sheffield, UNITED KINGDOM, [2]University Hospitals Bristol, Bristol, UNITED KINGDOM, [3]University of Sheffield, Sheffield, UNITED KINGDOM.

Introduction: Current commercially available phantoms for [123I]FP-CIT (DaTSCAN) imaging lack the flexibility to simulate realistic, patient-specific uptake patterns. Sub-resolution sandwich phantom (SSP) technology, using interleaved layers of attenuating material and printed radioactive ink patterns, has the potential to provide a practical, inexpensive solution. This proof of concept study aimed to: 1) Develop an example anatomical template, reflective of a clinical DaTSCAN patient 2) Assemble a full phantom, scan on a gamma camera and measure semi-quantification results. **Methods:** A DaTSCAN anatomical template was created through adaptation of the well-established MNI152 template. Pixel values within the caudate and putamen were set to a greyscale level that gave a printed count density ratio 8 times higher than that of the brain background (i.e. the phantom was designed with an 8 to 1 count density ratio, reflective of a healthy patient). The transaxial slices of the anatomical template were printed on to paper using a standard desktop inkjet printer (HP 8100), equipped with a black ink cartridge containing an ink and I123 Iodide mixture. Each printed paper sheet was stacked within interleaved layers of Perspex, cut to an oval shape, simulating attenuation effects within the skull. The fully assembled phantom was scanned on a Siemens Symbia T gamma camera, using LEHR collimators and standard clinical acquisition parameters. Scan time was adjusted in order to achieve > 1 million counts in the acquisition. Iterative reconstruction (8 iterations, 8 subsets) and semi-quantification was performed using MIM software, with the occipital lobe as a reference. **Results:** Phantom printing and assembly took approximately 1 hour to complete, utilising approximately 4ml of ink solution. Striatal binding ratios in the caudate and putamen were 2.91 and 2.77 respectively, on both left and right sides. Results are within the range seen for normal patients. **Conclusion:** This study demonstrated that SSP technology can be successfully adapted for DaTSCAN imaging, providing a controllable, flexible and inexpensive method for producing bespoke phantoms

E-PW038
SPECT-CT quantification of 131-Iodine - Reducing uncertainty with PSF modelling based reconstruction

L. Jenkins[1,2], A. Sohlberg[3,2]; [1]Queen Elizabeth Hospital Birmingham, Birmingham, UNITED KINGDOM, [2]Hermes Medical Solutions, Stockholm, SWEDEN, [3]Joint Authority for Päijät-Häme Social and Health Care, Lahti, FINLAND.

Introduction: Accuracy of 131-Iodine SPECT-CT quantification can be significantly improved with an iterative reconstruction algorithm incorporating full Collimator Detector Response (CDR) function modelling (septal penetration and septal scatter responses in addition to the geometric response). Furthermore, Monte-Carlo based patient scatter correction has potential to further improve quantification when compared to the Triple-Energy-Window (TEW) technique. The aim of this work was to assess whether improved SPECT-CT quantification of 131-Iodine could be achieved using full CDR function modelling and Monte-Carlo based patient scatter correction compared to current standard reconstruction using geometric response modelling and TEW scatter correction. CT based attenuation correction is used in both algorithms. **Methods:** A 34MBq 131-Iodine capsule was placed at the end of a 30cm long tube of diameter<1cm to be used within a Computed Tomography Dose Index (CTDI) body phantom. The tube was inserted into one of nine possible tubular holes (central, North/South/West/East 10mm from edge, NW, SW, SE, NW 53mm from edge) and imaged for 10s/projection and 120projections. Images were acquired at each of the nine locations for each imaging situation. The capsule was positioned at midpoint of phantom or externally (15cm away) by pushing tube through phantom and using it to suspend capsule in air. This enabled measurements to be performed in high and low attenuation/scatter conditions and allow similar contour orbits to be performed so that CDR and attenuation/scatter correction components could be assessed individually. A Siemens Symbia-T16 SPECT-CT system was used to acquire a range of images to include elliptical/26cm circular orbits with capsule in phantom and air at 0cm and 15cm z-axis offset from FOV centre. All data were reconstructed with Hybrid-Reconstruction and standard algorithms. Uptake was determined in a 5cm spherical VOI centred on the active capsule using HybridViewer (Hermes Medical Solutions). **Results:** There was substantially less variability in activity quantification using Hybrid-Reconstruction with full CDR modelling and Monte Carlo scatter correction than standard reconstruction algorithm; variability in air with capsule position was 2.9% v 42.3%. If quantification values are averaged over all imaging situations performed, then Hybrid-Reconstruction values vary from mean by -10.1% to 13.3% compared with standard reconstruction of -30.9% to 65.6%. **Conclusion:** Activity quantification was less affected by spatial location, nature of orbit and attenuation/scatter medium with Hybrid-Reconstruction than standard algorithm and images also were qualitatively superior. More accurate/reproducible SPECT-CT quantification of 131-Iodine can be achieved with commercially available reconstruction algorithms.

E-PW039
Impact of brain ventricle size on semi-quantitative index derived from 123-I-FP-CIT images using a novel 3D-striatum digital brain (3D-SDB)

H. Onishi[1], A. Furuta[1], K. Nakamoto[1], M. Takayama[1], H. Amijima[2];
[1]Program in Health and Welfare Sciences, Graduate School of Comprehensive Scientific Research, Prefectural University of Hiroshima, Mihara, Hiroshima, JAPAN, [2]Graduate School of Nursing, Hyogo University of Health Sciences, Kobe, Hyogo, JAPAN.

Aims: The quantitation of striatal dopamine transporter binding in Parkinson's disease is very important. A realistic digital brain phantom is needed to authenticate quantitative values derived from 123-I-FP-CIT SPECT images. The present study aimed to create a novel 3D-striatum digital brain (3D-SDB) phantom and assess the striatum binding ratio (SBR and SUR) to determine the effect of ventricular size 123-I-FP-CIT SPECT images. **Methods:** We constructed a 3-D striatum digital brain (3D-SDB) phantom comprising segments representing the striatum, ventricle, and brain parenchyma and skull bone using the Percentile method and other image-algorithm in T2-weighted MR images. The original image was converted to 128 × 128 matrixes to align the MR images with an added SPECT system for image resolution. A reference image was reconstructed based only on projection data sets generated from the original image. A process image was reconstructed with projection data sets generated from the original image with blurring, scatter, attenuation and static noise. Scatter, attenuation, and PSF were finally corrected in the process image. We derived the quantitative Southampton (DaTView; SBR) and anatomical normalization (DaTQUANT®; SUR) methods from reference and process images that were reconstructed to use OSEM (I = 2; S = 10). The effects of ventricle counts (0 - 200) and of a ventricle size that conformed to an Evans index between 0.2 - 0.5 (representing an enlarged ventricle) were evaluated to determine the accuracy of SBR and SUR obtained using the 3D-SDB phantom. **Results:** The practical value of a 3D-SDB phantom was assessed in a ^{123}I-FP-CIT SPECT clinical study. The true SBR values in the reference and process images were matched to calculate the SBR of the collected total striatum volume. The count and enlarged size of the ventricle caused a 5% - 10% difference in the SBR and SUR in the reference image. However, the SBR and SUR were overestimated by 18% and 8%, respectively, in the presence of ventricular counts in the process image. The effect of the enlarged ventricle (Evans index) was underestimated by 45% (SBR) and 20.5% (SUR) in the process image. **Conclusion:** This study constitutes the first step towards the accurate prediction of SBR and SUR using a 3D-SDB phantom that can conveniently reveal the basic features of ^{123}I-FP-CIT SPECT clinical images. The present findings suggested that an enlarged cerebral ventricle affects quantitative values derived from 123-I-FP-CIT SPECT images.

E. Tardelli, G. Puccini, G. Boni, M. Grosso, S. Chiacchio, I. Paglianiti, F. Guidoccio, E. Fiasconaro, S. Bola, S. Muccioli, L. Valerio, C. Giani, L. Pieruzzi, E. Molinaro, R. Elisei, D. Volterrani; University of Pisa, Pisa, ITALY.

Background: Progressive metastatic radio-iodine refractory differentiated thyroid cancer (RR-DTC) is a rare condition in which a systemic therapeutic approach is needed. Recently, AIFA has approved the use of Lenvatinib, a new Tyrosine Kinase Inhibitors (TKIs), as an optional treatment for this group of patients. **Aim:** To assess the role of [18F]FDG PET/CT in monitoring treatment efficacy and predicting prognosis. **Patients and Methods:** From December 2014 to September 2016, 33 patients with RR-DTC were enrolled at the Department of Endocrinology of the University of Pisa (M/F=17/16; mean age: 65 years+/- 8,7; histologic type: 21 papillary thyroid carcinoma, 8 follicular thyroid carcinoma, 3 poorly differentiated thyroid carcinoma, 1 oxyphilic cells) and were selected for treatment with Lenvatinib. All patients underwent a baseline FDG PET/CT scan, then repeated after about 1, 2, 6 and 12 months during therapy. All scans were performed with a PET/CT Discovery 710 scanner (GE Healthcare, Milwaukee, USA) about sixty minutes after the injection of FDG (3.7 MBq/Kg). Metabolic response to therapy was assessed in each site of disease (thyroid bed, lymph node, lung, bone, and other sites) during the follow-up by qualitative evaluation, PET Response Criteria in Solid Tumors (PERCIST 1.0), maximal standardized uptake value (SUVmax), and by metabolic tumor volume (MTV) and total lesion glycolysis (TLG) as measures of metabolic tumor burden. **Results:** All patients had metastatic high metabolic involvement disease in more than two sites. During the follow-up, 21/33 patients presented progression metabolic disease by PERCIST, 14/21 after about 1 month since the onset of therapy. Fifteen out of 33 patients died during follow-up (median of survival 19.9 months), while 18/33 patients are still alive, though with a reduced dose of Lenvatinib because of adverse effects. In multivariate analysis, SUVmax MTV and TLG of the overall malignant process in the entire body at baseline were not significantly associated with overall survival. The majority of patients had decrease in total metabolic tumor burden during treatment. Early metabolic response (after 1 month) assessed by PERCIST criteria was significantly associated with mortality. Moreover, based on logistic regression there was a significant statistical evidence (likelihood-ratio test p <0.01) that survival depended on the persistence of TLG response (total and target ΔTLG %) at lymph node level after 6 months of treatment. **Conclusion:** FDG-PET/CT can be a useful tool to evaluate tumor response during TKIs therapy. The degree of metabolic response seems to have prognostic implications.

Do.MoRe: Thyroid Cancer

E-PW040
The role of [18F]FDG PET/CT in monitoring therapy with Lenvatinib in radio-iodine refractory differentiated thyroid cancer patients

E-PW041
Comparison of ^{18}F-fluoride PET/CT, ^{18}F-FDG PET/CT and ^{131}I radioiodine diagnostic scan in patients of differentiated thyroid carcinoma with skeletal metastases: evaluation of the role of ^{18}F-FDG PET/CT in bony metastatic disease from differentiated thyroid cancer

R. V. Parghane, S. Basu; Radiation Medicine Center (BARC), Mumbai, INDIA.

Purpose: The aim of this study was to compare the diagnostic values and accuracy of ^{18}F-fluoride PET/CT, ^{18}F-FDG PET/CT and ^{131}I radioiodine diagnostic scan for the detection of bone metastases and also to determine whether the ^{18}F-FDG PET/CT scan findings changed the outcome of medical and surgical management in differentiated thyroid cancer patients. **Subjects and Methods:** Retrospective evaluation of patients of differentiated thyroid cancer who underwent diagnostic studies between January 2016- March 2017 (n=510). A total of 54 patients (40 females and 14 males; age range 26-80 years, average 55 years) were included in this study, who had been known/suspected of having bone metastases (with complaints of bony pain, lower backache, fracture history and raised stimulated serum thyroglobulin level) and had undergone ^{18}F-fluoride PET/CT, ^{18}F-FDG PET/CT and ^{131}I radioiodine diagnostic scans after total thyroidectomy. The histopathology included follicular carcinomas (n=35), follicular variant of papillary carcinoma (n=8) and papillary carcinomas (n=11). Initially stimulated serum thyroglobulin levels ranged from 12 to 475 ng/ml with an average of 247 ng/ml and these patients were followed 1-6 years with an average of 3 years after the initial diagnosis. The correlative imaging and laboratory data for evaluating skeletal metastases were available such as CT or MRI findings, histopathological examination or clinical follow-up with serum thyroglobulin level. **Result:** In patient-based analysis, the sensitivity, specificity and diagnostic accuracy of ^{18}F-fluoride PET/CT were 60.98%, 46.15% and 57.4%, respectively, those of ^{18}F-FDG PET/CT were 91.30%, 87.50% and 90.7% and those of ^{131}I radioiodine diagnostic scan were 88.37%, 90.91% and 88.8% respectively for detection bone metastases. In 11 patients (20.3%), other metastatic organ involvement was detected by ^{18}F-FDG PET/CT and also in 26 patients (48.1%) additional bony sites were demonstrated by ^{18}F-FDG PET/CT. Following ^{18}F-FDG PET/CT showing positive bony lesions, 10 patients (18.5%) underwent stabilization of fracture sites, 7 patients (12.9%) underwent EBRT and 3 patients (5.5%) underwent surgical excision of bony metastatic lesions. **Conclusion:** ^{18}F-FDG-PET/CT and ^{131}I radioiodine diagnostic scan showed high diagnostic performance in detecting bone metastases from DTC as compared to ^{18}F-fluoride PET/CT. Our results showed ^{18}F-FDG-PET/CT can detect extra metastatic bony sites, other metastatic organs, which can lead to modification of the management and improvement in the quality of life of DTC patients.

E-PW042

Incremental value of ultrasonography in incidental focal thyroid uptake at 18F-FDG PET-CT.

W. Yao; *College of Medicine, National Cheng Kung University, TAINAN, TAIWAN.*

Purpose: We aim to evaluate the incremental value of ultrasonography for further assessment of incidental focal thyroid uptake detected with 18F-FDG PET-CT in a PET center. **Subjects and Methods:** Between Jan 2015 and March 2017, a total of 2491 studies with whole-body 18F-FDG PET-CT were performed, including 558 studies for cancer screening. Focal thyroid uptake lesions were identified if they were greater than background thyroid tissue. Further evaluation of incidental focal thyroid uptake with ultrasonography was performed and assessed with TI-RADS lexicon. Patients with suspicious malignancy (category 4 or higher) went for fine needle aspiration or biopsy. **Results:** Of the 2491 PET/CT studies, 156 (5.94%) incidental focal thyroid uptake were identified in 146 patients, 117 patients for cancer work-up and 29 for cancer screening. Forty-seven nodules in 40 patients with suspicious malignancy on ultrasonography went for histological diagnosis. Seven nodules with inadequate sampling were excluded. Nigh teen were histologically diagnosed as malignant (16 papillary carcinoma, 2 anaplastic carcinoma, 1 papillary carcinoma with follicular variant) and 21 were benign lesions (19 benign follicular nodule, 2 Hashimoto's thyroiditis). In 40 histologically diagnosed nodules, malignant tumors were higher in SUVmax (11.5±8.8 vs. 4.7±2.2, p=0.0012). With cut-off value of SUVmax 6.2, the sensitivity and specificity for detecting malignancy were 73.7% and 81.0 %, respectively. **Conclusion:** Ultrasonography may increase specificity of incidental focal thyroid uptake in 18F-FDG PET-CT, avoid unnecessary invasive procedures, and provide proper recommendation for further management.

E-PW043

131I-SPECT/CT in the diagnosis and characterization of metastatic lesions in patients with differentiated thyroid carcinoma (DTC) in chronic follow-up

A. Spanu, I. Gelo, L. Mele, B. Piras, S. Nuvoli, G. Madeddu; University of Sassari, SASSARI, ITALY.

Aim: We further investigated 131-SPECT/CT usefulness in DTC current diagnosis and therapeutic post-operative protocol reassessment. **Methods:** Among a large DTC series, we retrospectively selected 79 patients (32 males and 47 females) with ascertained metastatic lesions during chronic follow-up. At surgery, 35 patients were at high risk (H), 28 at low risk (L), 16 at very low risk (VL). 131I-WBS (diagnostic in 72 and post-therapeutic in 7) was performed using a dual head gamma camera equipped with high-energy, parallel-hole collimators and with low dose x-ray tube. WBS was always followed by SPECT/CT over neck/chest and other suspect regions, for total 160 exams. **Results:** 131I-WBS detected 90 metastatic foci in 39/79 patients, 53 in and 37 outside the neck, while SPECT/CT identified 198 metastatic foci in the 79 patients, including all foci positive at WBS, 124 in and 74 outside the neck. Thus, SPECT/CT identified 108 neoplastic foci occult at WBS in 51 patients, 71 lesions being neck lymph node metastases and 37 metastases outside the neck (8 lung, 6 mediastinum, 20 bone, 3 pelvis). WBS was completely negative in 38/51 patients, 15 H, 13 L, 10 VL, two of L and10 VL being T1aN0M0 with undetermined Tg levels in 6 cases, <2.5 ng/ml in 5 and between 2.5 and 5 ng/ml in 6; moreover, 21/38 patients had single lymph node metastases and 7/21 cases (6 VL, 1L) were T1aN0M0 with undetermined Tg levels in 6 and < 2.5 ng/ml in the remaining one. Moreover, SPECT/CT also characterized as malignant 53 lesions in the neck in 19 patients and 15 outside the neck in 7 patients classified as benign or unclear at WBS; 4/19 patients (2L,2VL) with lymph node metastases

were T1N0M0 with undetermined Tg in 3 cases and between 2.5and 5 ng/ml in the remaining one. Two of these 4 cases (2VL) and further 2/19 cases (1L, 1VL) had single metastases. Five of 7 patients with 15 lesions outside the neck had Tg levels >10 ng/ml. Globally, SPECT/CT correctly changed WBS classification and patient management in 72.1% of cases. **Conclusion:** 131I. SPECT/CT proved reliable diagnostic tool in DTC follow-up localizing and characterizing iodine fixing metastatic lesions with better performance than WBS and more correct patient classification and management. SPECT/CT usefulness is more significant in patients with inconclusive WBS and Tg levels undetermined or very low, mainly in VL cases with T1aN0M0 and even more with single metastases.

E-PW044

Diagnostic Utility of Molecular and Imaging Biomarkers in Cytologically Indeterminate Thyroid Nodules: a Systematic Review and Meta-Analysis

E. J. de Koster[1], *L. F. de Geus-Oei*[2], *O. M. Dekkers*[2], *I. van Engen-van Grunsven*[1], *J. F. Hamming*[2], *E. P. M. van der Kleij-Corssmit*[2], *H. Morreau*[2], *A. Schepers*[2], *J. W. A. Smit*[1], *W. J. G. Oyen*[3], *D. Vriens*[2]; [1]Radboud university medical center, Nijmegen, NETHERLANDS, [2]Leiden university medical center, Leiden, NETHERLANDS, [3]Institute of Cancer Research, London, UNITED KINGDOM.

Introduction: Indeterminate thyroid cytology (Bethesda III and IV) corresponds to follicular-patterned benign and malignant lesions, which are particularly difficult to differentiate on cytology alone. As approximately 25% of these nodules harbor malignancy, diagnostic hemithyroidectomy is still standard-of-care. However, additional preoperative diagnostics are rapidly advancing. **Subjects & Methods:** This systematic review and meta-analysis included 164 original articles and provides an overview of the available literature on additional molecular and imaging diagnostics for indeterminate thyroid nodules, including considerations regarding cost-effectiveness, availability, and feasibility of combining techniques. The addressed diagnostic tools include gene mutation analysis, microRNA, immunocytochemistry (ICC), ultrasonography, elastosonography (USE), Tc-99m sestamibi (^{99m}Tc-MIBI) scintigraphy, fluorodeoxyglucose positron emission tomography (FDG-PET) and diffusion-weighted magnetic resonance imaging (DW-MRI). **Results:** The best rule-out tests for thyroid carcinoma were combined galectin-3/HBME-1 ICC (estimated pooled 96.6% sensitivity, 0.04 negative likelihood-ratio (LR)), semi-quantitative USE (92.1%, 0.08), qualitative USE using an alternative threshold score of 1 (98.5%, 0.08), FDG-PET imaging (94.2%, 0.12), and the Afirma® GEC (97.3%, 0.18). The best rule-in tests were BRAF mutation analysis (estimated pooled 99.9% specificity, 195 positive LR), semi-quantitative USE (93.4%, 14.04), combined galectin-3/HBME-1 ICC (94.3%, 13.47), combined BRAF/RAS mutation analysis (94.5%, 8.69) and galectin-3 ICC (90.7%, 7.07). Geographical variations in tumor genetics or cytology (e.g. incidence of Hürthle cell neoplasms) strongly influence several tests. **Discussion:** None of the diagnostics had near-perfect sensitivity, near-perfect specificity and cost-effectiveness. With the techniques currently clinically available, we propose that a multimodal stepwise approach using a sensitive rule-out and a specific rule-in test might offer the most conclusive diagnosis for indeterminate thyroid nodules. There is currently insufficient evidence in literature to reliably interpret sequentially used tests, especially combinations of (molecular) imaging and genetics. Besides choosing two accurate tests to achieve maximum diagnostic accuracy within the local patient population, the sequence of testing and costs of the selected tests and therapeutic procedures are pivotal.

E-PW045

Thyroid hormone withdrawal versus recombinant human TSH administration in radio-iodine therapy of thyroid cancer: comparison of I-131 effective half-life

K. Perisinakis, C. Donas, A. Dimitraki, S. Koukouraki; University of Crete, Medical School, Heraklion, GREECE.

Purpose/Introduction: The discharge time from the treating facility of patients subjected to radioactive iodine I-131 therapy is strongly associated with the residual I-131 activity which is governed by the effective half-life of I-131 ($Teff_{1/2}$). The aim of this study was to determine and compare the effective half-life of I-131 ($Teff_{1/2}$) in thyroidectomised patients subjected to radioiodine therapy after hormone therapy withdrawal or recombinant human TSH administration. **Subjects and Methods:** The patient cohort studied comprised 97 consecutive patients subjected to radio-iodine therapy following thyroidectomy. Administered I-131 dose was 85-200 mCi. Prior to I-131 administration, 3-week long thyroid hormone withdrawal was employed in 57 patients (group A) whereas recombinant human TSH was administered in the rest 40 patients (group B). Data regarding age, sex, weight, height, diet, administered dose were recorded prior to I-131 administration, while volume of water drunk during the first 24h after I-31 administration and size of remnant thyroid tissue were recorded at discharge from isolation room. During hospitalization, the dose rate at the level of diaphragm and 1 m distance from the standing patient was measured with an area monitor. Measurements were collected at 0, 6, 12, 24 and 30 h after I-131 administration. Plots of dose rate against time passed since I-131 administration were fitted to an exponential function and $Teff_{1/2}$ was determined. The $Teff_{1/2}$ of I-131 estimated for patients having been prepared with thyroid hormone withdrawal was compared to corresponding values obtained in patients prepared with recombinant human TSH administration, using Man-Whitney statistical test. **Results:** The mean age of patient group A and B were 46±12 and 49±16 y, respectively. The I-131 $Teff_{1/2}$ estimated for patients prepared by hormone withdrawal and patients administered with recombinant human TSH was found to be 13.4±5.2 h and 10.5±3.9 h, respectively with difference being statistically significantly ($p<0.05$). Age, sex, patient size, diet and dose administered were not found to affect $Teff_{1/2}$. Water consumption and size of remnant thyroid tissue were found to moderately affect $Teff_{1/2}$ but differences did not reach statistical significance. **Discussion/Conclusion:** Elimination rate of residual I-131 activity in thyroidectomised patients treated with radio-iodine may be significantly elevated if patient preparation involves administration

of recombinant human TSH rather than hormone thyroid with-drawal, accelerating patient's discharge from isolation room and decreasing dose received by patient healthy tissues.

E-PW046

Analyisi of long-term clinical follow-up outcome, demographic and histopathological risk factors in a large DTC series

C. Soydal, E. Ozkan, D. Nak, N. O. Kucuk, M. K. Kir; *Ankara University Medical Faculty, Nuclear Medicine Department, Ankara, TURKEY.*

Purpose: To evaluate the relationship between demographic and histopathological prognostic factors and long-term follow-up data of differentiated thyroid carcinoma (DTC) patients. **Material and Methods:** We retrospectively evaluated the long-term clinical follow-up data and baseline demographic and histopathological prognostic factors of our DTC patients. Correlation between gender, age of diagnosis, histopathological subtype, variant and diameter of tumor, multi-centricity, presence of contralateral lobe involvement, thyroiditis, capsule invasion and vascular invasion, TNM stage, ATA and ETA risk groups, preablative serum Tg level and clinical outcome were analyzed. Clinical outcome was classified as poor and good subgroups. Poor subgroup was included persistent and recurrent diseases. Good subgroup was consisted of remission and acceptable disease. **Results:** Totally 2184 (1805 F, 379 M; mean age; 44.24 ± 12.5) patients were included to the analysis. Histopathological subgroups were papillary, follicular, unclassified malign thyroid neoplasm, mixt, thyroid carcinoma with known malign potential in 1972, 131, 41, 32 and 8 patients, respectively. Mean tumor diameter was calculated as 1.66 ± 1.34 cm. While 1421 out of 2184 patients had multicenter tumor, 491 of 2184 patients had contralateral lobe involvement. Capsular and vascular invasion were detected in 1428 and 159 patients respectively. In the evaluation of relationship between histopathological risk factors tumor diameter ($P<0.001$), presence of multi-centricity ($p=0.002$), contralateral lobe involvement ($p<0.001$), capsule invasion ($p<0.001$) and vascular invasion ($p<0.001$) were found statistically correlated with poor clinical outcome. According to TNM staging system, 1850, 162, 172 was staged as 1, 2 and 3. While 1604 patients were low ATA risk group, 580 patients were in intermediate-high risk group. In ETA subgroup analysis, 1757 patients were very low-low risk group and 427patients were in high risk group. TNM stage ($p=0.025$), ATA risk group ($p<0.001$) and ETA risk group ($p<0.001$) were significantly correlated with clinical outcome. Additionally, preablative serum Tg levels ($p<0.001$) had significantly correlated with clinical outcome. **Conclusion:** The relationship between most of the demographic and histopathological risk factors and clinical outcome have been confirmed in our long-term followed up large DTC patient group.

E-PW047

FDG-PET can predict response to vandetanib treatment in patients suffering from advanced medullary thyroid carcinoma

Magdeburg, Magdeburg, GERMANY, ²Klinikum Augsburg, Augsburg, GERMANY, ³LMU München, München, GERMANY.

Introduction: Recently very promising data have been published on redifferentiating radioiodine (RAI) refractory BRAF-mutated papillary thyroid cancer using the selective BRAF-inhibitor dabrafenib in a small study population (1). Here we report on the first experiences with this novel treatment method in Germany. **Subjects & Methods:** We treated two patients with progressive and advanced radioiodine refractory BRAF-mutated papillary thyroid cancer who were not ideal candidates for systemic therapy with tyrosine kinase inhibitors. Previous RAI imaging revealed no uptake in tumor lesions. Both patients received dabrafenib (300 mg/day, compassionate use) for four weeks and had a diagnostic RAI scan after rhTSH stimulation. **Results:** In both patients redifferentiation could be achieved. One patient showed especially intense uptake in diffuse lung metastases. The other patient showed new uptake in a part of a big local relapse in the area of the upper esophageal sphincter. Both patients received therapeutic RAI (9.5 and 11.0 GB) after another 2 weeks of treatment with dabrafenib and stimulation by rhTSH. Posttherapeutic imaging confirmed the results of the diagnostic RAI scan. On follow-up thyroglobuline declined significantly in both patients. The patient with the diffuse lung metastases showed partial response on CT and a decrease in metabolism on PET imaging. In the other patient, the RAI-avid part of the tumor decreased in size, however the non-avid part slightly progressed and a tracheostoma had to be inserted (clinical progress). Dabrafenib and RAI were well tolerated with only minor toxicities. **Conclusions:** Redifferentiation using dabrafenib is a therapeutic option in radioiodine refractory BRAF-mutated papillary thyroid cancer. Patient selection and imaging are important, since, even within one patient, tumor lesions behave heterogeneously in terms of redifferentiation. Reference: (1) Rothenberg et al. Redifferentiation of iodine-refractory BRAF V600E-mutant metastatic papillary thyroid cancer with dabrafenib. Clin Cancer Res. 2015 Mar 1;21(5):1028-35

E-PW049

Lowest effective ¹³¹I activity for lymph node metastases therapy of differentiated thyroid cancer patients; Dosimetry-based model for estimation

V. Stebner, J. Phaosricharoen, K. Herrmann, W. Jentzen; Department of Nuclear Medicine, Medical Faculty, University Duisburg-Essen, Essen, GERMANY.

Aim: A theoretical dosimetry-based model was applied to estimate the lowest effective ¹³¹I activity for lymph node metastases (LM) therapy of differentiated thyroid cancer patients (DTC). **Patients, Methods:** The model is based on the distribution of the absorbed (radiation) dose per administered ¹³¹I activity and the absorbed dose threshold of 100 Gy for LM, the level believed to good response to therapy. The lower activity was considered to be equally effective to that obtained with higher activity if the (absolute) fraction difference was below 5% (Jentzen et al. Nuklearmedizin 2015:54:137). For this purpose,

¹²⁴I-PET/CT images of 36 patients, after thyroidectomy and before first radioiodine therapy, were retrospective analyzed to measure the distribution of the (average) absorbed doses to lymph node metastases per administered ¹³¹I activity between 0.7 and 12 GBq. **Results:** A total of 61 LM were included. The medians and ranges (in parenthesis) for the absorbed dose per unit ¹³¹I activity were 139 Gy/GBq (6 - 1460 Gy/GBq). The fractions of lymph node metastases receiving ≥100 Gy at different therapy activities (within parenthesis) were 80% (3.7 GBq), 93% (6.3 GBq) and 95% (9.6 GBq). The therapy activity of 3.7 GBq is considerably less effective than that of 6.3 GBq or 9.6 GBq; therapy activities were equally effective in the range between 6.3 to 9.6 GBq. **Conclusion:** On the basis of the model and the patients' data included, the lowest effective therapy activity appears to be approximately 6 GBq to therapy lymph node metastases. The results of this study may help to guide the design of prospective clinical trials.

E-PW06	**Monday, October 23, 2017, 08:30 - 09:30, e-Poster Walk Area, Level 2, Foyer A, Screen 3**

Do.MoRe: Dosimetry

E-PW050

DNA damage in blood leukocytes after internal irradiation with ⁶⁸Ga - in-vivo and in-vitro studies

S. Schumann¹, H. Scherthan², C. Lapa¹, C. Bluemel¹, J. Müller², A. K. Buck¹, M. Port², M. Lassmann¹, U. Eberlein¹; ¹University of Würzburg, Würzburg, GERMANY, ²Bundeswehr Institute of Radiobiology affiliated to the University of Ulm, Munich, GERMANY.

Introduction: The aim of this study was to investigate in-vivo the formation of radiation-induced DNA double strand breaks (DSBs) as a function of the absorbed dose to the blood (AD_{blood}) of patients undergoing PET/CT examinations with the PSMA labelled β⁺-emitter ⁶⁸Ga. Additionally, an in-vitro calibration curve for ⁶⁸Ga was established in order to compare the results. For the quantification of DSBs in blood leukocytes, the co-localizing biomarkers γ-H2AX and 53BP1 were used. **Methods:** For the in-vitro study, different ⁶⁸Ga activity concentrations were added to 37 blood samples of four volunteers to achieve absorbed doses to the blood up to 100mGy after 1h incubation on a roller mixer. For the in-vivo study, blood samples of 13 patients were obtained before and at four different time points after administration of (141 ± 34) MBq ⁶⁸Ga-PSMA. Blood sampling time points were: 15min after administration, directly before the PET/CT scan, directly after and 90-120min after the PET/CT scan. In both cases, leukocytes were isolated from the blood by density centrifugation, washed, fixed and immunofluorescently stained for γ-H2AX and 53BP1. The number of foci showing co-localizing red and green fluorescence for both DSB markers was counted manually. For the calculation of AD_{blood}, the activity in each blood sample was determined with a calibrated germanium detector. For the in-vivo study, additional external dose rate measurements of the patients were performed to determine

the γ-contribution to AD_{blood}. To estimate the CT-contribution to AD_{blood}, the $CTDI_{vol}$ was used. **Results:** For the in-vitro calibration, a linear regression was fitted to the data, which showed a good correlation (r^2=0.90) between the average number of radiation-induced foci (RIF) per cell and AD_{blood}, being in agreement with our calibration curve for β⁻-emitters [1]. In patients, AD_{blood} resulting from ^{68}Ga administration was below 4mGy. However, the number of RIF for the first two time points was higher than predicted by the in-vitro calibration curve. Directly after the CT scan, an increase of RIF was induced by the CT-contribution to AD_{blood} with $CTDI_{vol}$-values in the range of 10-20mGy. **Conclusion:** A linear in-vitro calibration curve for ^{68}Ga was established, but did not represent the RIF-values of the patients in the very low dose range (0.5 - 4mGy). To further improve the estimate of the CT-contribution to the absorbed dose to the blood and for establishing a dose-response relationship, further direct measurements of the CT doses are required. [1] Eberlein et al., PLOSONE 2015, 10:e0123174

E-PW051

Monte Carlo-Based Bremsstrahlung SPECT Reconstruction for Whole-Liver Dosimetry in Treatments with ^{90}Y-Microspheres - Comparison with ^{90}Y PET

J. Gustafsson[1], K. Knešaurek[2]; [1]Medical Radiation Physics, Clinical Sciences Lund, Lund University, Lund, SWEDEN, [2]Radiology, Icahn School of Medicine at Mount Sinai, New York, NY, UNITED STATES OF AMERICA.

Aim: In this study, the use of Monte Carlo-based bremsstrahlung SPECT reconstruction is compared with ^{90}Y PET for whole-liver absorbed-dose estimation in patients undergoing treatment with ^{90}Y-microspheres. **Materials and Methods:** Fifteen patients were imaged using both bremsstrahlung SPECT/CT (medium-energy collimator, energy window 90 keV ± 15 %) and PET/CT after administration of ^{90}Y-microspheres to the liver (activity range 0.8 GBq to 4.4 GBq). The PET images were reconstructed using OS-EM with 2 iterations, 21 subsets. Volumes of interest following the liver contour were manually defined on the PET/CT images. The outer patient contour was delineated using an automatic method and the injected activity was distributed in the patient volume relative to the PET voxel values. The mean absorbed dose to the liver (including tumours) was calculated assuming local absorption of the charged-particle energy and an assumed density of 1.04 g/cm³. The SPECT images were reconstructed (OS-EM 8 iterations, 10 subsets) using a program based on the SIMIND Monte Carlo code. The program uses SIMIND as an accurate forward projector, thereby including compensation for attenuation, scatter, and imperfect collimation, as well as a model of the overall probability of photon detection in the reconstruction. Hence, the reconstructed images are in units of MBq per voxel even without rescaling or explicit calibration. The SPECT/CT images were co-registered with the PET/CT images (CT-CT rigid registration) and the mean absorbed dose to the liver was calculated using a) the activity calculated directly in the Monte Carlo-based reconstruction and b) rescaling to the injected activity (as for the PET images). **Results**: Without rescaling of the SPECT, the difference in liver absorbed dose expressed as (SPECT - PET) was (mean ± 1 standard deviation) -3.8 Gy ± 6.9 Gy. The average relative difference was -6.5 % (range -37 % to 21 %). When rescaling the SPECT to the injected activity the corresponding results were -3.7 Gy ± 6.1 Gy and -8.4 % (range -38 % to 18 %). **Conclusions**: Monte Carlo-based reconstruction has the potential to be used for estimation of whole-organ absorbed doses from bremsstrahlung SPECT images. The absorbed doses estimated using Monte Carlo-based SPECT reconstruction are similar to the absorbed doses estimated using ^{90}Y PET with rescaling to the injected activity, both when rescaling the SPECT to the injected activity and when using the activity obtained directly from the reconstruction.

E-PW052

Safety, efficacy and outcome of Y-90-resin-microspheres radioembolization in 73 patients with unresectable intrahepatic cholangiocarcionoma: a single center experience

A. Todica, K. J. Paprottka, F. Schöppe, M. Ingrisch, P. Bartenstein, P. M. Paprottka, H. Ilhan; University of Munich, Munich, GERMANY.

Introduction: Radioembolization (RE) using yttrium-90 (Y-90) microspheres is an accepted and well established therapy option in primary or secondary liver malignancies. In patients with unresectable intrahepatic cholangiocarcinoma (ICC), systemic chemotherapy is often viewed as the only option, although efficacy is limited. Data on the value of RE in patients with ICC are limited and only few data on factors influencing prognosis are available. The purpose of our retrospective analysis was to establish factors influencing progression free survival (PFS) and overall survival (OS). **Methods:** RE was performed in accordance to current procedure guidelines in 73 Patients (103 RE procedures) with unresectable ICC. Radiologic response was evaluated by using Response Criteria in Solid Tumors (RECIST). We investigated the impact of baseline characteristics, clinical/biochemical toxicities according to CTCAE (v 4.0) criteria and response on PFS and OS. **Results:** Treatment in 73 patients (40 male) revealed no major complications. After 3 months 16 patients (22%) showed partial response (PR), 34 (47%) stable disease (SD) and 18 (25%) progressive disease (PD) according to RECIST. Mean PFS post treatment was 10.1 months (95%CI 7.9-12.2 months; median 6.4 months). Mean OS was 18.9 months (95% CI 13.9-23.9 months; median 11.8 months). PFS and OS was significantly prolonged (P < 0.001) in patients with response according to RECIST (PR or SD vs. PD; PFS: 10.5, 10.0 vs. 2.7 months; OS: 15.2, 20.9 vs. 6.6 months) or baseline CHE within regular limits (OS: 14.09 vs. 5.5 months; PFS: 6.93 vs. 3.2 months). Significant longer OS was observed in patients with a tumor burden <25% compared to those with higher tumor burden (>50%;15.2 vs. 6.6 months; P=0.036). Sex and age had no major influence. **Conclusions:** Radioembolization is an efficient and safe treatment option in patients with unresectable ICC. Patients with PR and SD show a significantly longer PFS and OS compared to patients with PD. Additional predictors for prolonged survival are baseline CHE and initial tumor burden.

E-PW053

Quantitative Y-90 PET/CT for Dosimetry in Radioembolization

H. Lim[1], N. Clinthorne[1], M. Conti[2], J. A. Fessler[1], Y. K. Dewaraja[1];
[1]University of Michigan, Ann Arbor, MI, UNITED STATES OF AMERICA,
[2]Siemens Healthcare Molecular Imaging, Knoxville, TN, UNITED STATES OF AMERICA.

Aim: The aim was to evaluate accuracy/precision of Y-90 PET/CT for dosimetry applications with a phantom study mimicking count rates, randoms fractions, scan times, activity distributions and scatter conditions that are typical for patient imaging in radioembolization. **Methods:** Y-90 PET data from 18 patients treated with microspheres (administration 0.6 - 4.2 GBq, trues 80,000 - 400,000, randoms fraction 0.85 - 0.96, scatter fraction 0.37 - 0.75) was the basis for the design of the study: a liver/lung torso phantom with 5% lung shunt, 2 MBq/mL in liver, 3 hepatic lesions (8 and 14 mL spheres, 30 mL ovoid) of 10 MBq/mL as well as low uptake (0.1 - 0.9 MBq/mL) extra hepatic objects in cold torso to assess visibility of inadvertent Y-90 deposition. The phantom was scanned for 30 min on a Siemens Biograph mCT on day0, day2, day5, day7 with total activity of 3.1, 1.8, 0.90 and 0.54 GBq, respectively, with multiple acquisitions at some time points. Data was reconstructed using OSEM with and without PSF modeling, with and without TOF and two scatter scaling options (absolute and normalized to scatter tails in sinogram). Based on contrast-to-noise ratios, 2 iterations (24 subsets) were used without TOF and 1 iteration (21 subsets) with TOF. **Results:** Randoms fractions increased from 0.88 to 0.94 while trues decreased from 363,000 to 74,000 from day0 to day7. Best results for contrast, activity recovery, noise and visibility were obtained with TOF+PSF, while alternative scatter scaling did not significantly impact these measures. With TOF+PSF, field-of-view activity estimated from the image was within 2% on day0, but overestimated by 15% at day7. In background liver, eroded by 2 pixels, activity concentration was estimated within 3% at all count-rates while noise ranged from 28 to 64%. Across all count-rates, activity recovery in CT-defined VOIs ranged from 85 - 88% for the liver (improved to 92 - 95% when outline was expanded by 2 pixels), 79 - 83 % for the largest lesion and 64 - 70% for the smallest lesion while repeatability of liver/lesion activity from multiple realizations was within 4 - 18% (all degraded values correspond to lower count-rates). **Conclusion:** Evaluations under clinically realistic conditions demonstrate that Y-90 PET/CT with state-of-the-art systems is suitable for lesion/liver dosimetry, but noise as well as activity underestimation and hence dose underestimation due to resolution effects and potential positive bias in reconstruction algorithms (e.g., due to nonnegativity constraint), should be considered.

E-PW054

Initial Experiences with Post-Interventional Imaging of Residual Yttrium-90 Activity Within Microsphere Delivery Systems using Next-Generation Digital Photon Counting PET/CT Technology

C. L. Wright[1], K. Binzel[1], J. Zhang[1], D. Konate[1], P. Maniawski[2], M. V. Knopp[1]; [1]The Ohio State University, Columbus, OH, UNITED STATES OF AMERICA, [2]Philips Healthcare, Cleveland, OH, UNITED STATES OF AMERICA.

Purpose/Introduction: Following interventional administration of Yttrium-90 (90Y) microspheres, there are typically ultra-low doses of residual 90Y activity left within the delivery system. Infrequently, residual 90Y activity within the delivery system can be higher than expected and direct examination of the radioactive delivery system may be needed to understand where the remaining 90Y activity is distributed. Yttrium-90 produces a small fraction of discrete photon pairs which can be imaged using PET technology. The aim of this study was to evaluate and assess residual 90Y activity within microsphere delivery systems using a pre-commercial release digital PET/CT (dPET/CT) system. **Subjects & Methods:** In this study, 25 microsphere delivery systems were imaged following radioembolization using a pre-commercial release dPET/CT (Vereos, Philips) to detect/localize 90Y activity. Estimated residual 90Y activities within the delivery systems were 5 - 272 MBq. Each delivery system was imaged using a single bed position in list-mode for 60 min and 7 min. List-mode clipping of the 60 min data sets were performed to reconstruct faster acquisition times (i.e., 50 to 1 min). Datasets were reconstructed with ToF using standard definition voxel lengths of 4mm. Matched comparison of dPET image characteristics for actual and subsampled data sets was performed by a reader panel. **Results:** The dPET detection of ultra-low 90Y activity within microsphere delivery system following radioembolization is practical and yields evaluable images. Residual 90Y activity was consistently detected in the source vial and sometimes in the catheter tubing when correlated with CT imaging. List-mode clipping of the 60 min dPET data sets confirmed that subsampled dPET data sets were visually similar to the 7 min true acquisition. When subsampled data sets shorter than 5 min were evaluated, there was progressive loss of the residual foci of 90Y activity within the delivery system when compared with the true 7 and 60 min acquisitions. **Discussion/Conclusion:** These results demonstrate that ultra-low levels of residual 90Y activity within microsphere delivery systems can be reliably detected and imaged using dPET/CT with image acquisition times comparable or even shorter than routine FDG PET/CT studies (i.e., 7-10 min). Further reduction in image acquisition time can significantly impact the visual detection of residual 90Y activity within the delivery system. This approach enables the rapid and precise assessment of 90Y activity within a delivery system in those instances when residual activities are greater than expected or in the case of a 90Y misadministration.

E-PW055

223Ra-Chloride Therapy: The First Multidisciplinary and Multicenter Italian Study

G. Boni[1], S. Mazzarri[1], C. Cianci[2], L. Galli[1], A. Farnesi[1], E. Borsatti[3], R. Bortulus[4], L. Fratino[5], C. Giobitti[4], E. Lamaj[5], P. Ghedini[6], E. Rodi Rizzini[6], V. Dionisi[7], S. Fanti[6], D. Volterrani[1], F. Monari[7]; [1]Nuclear Medicine Department, pisa, ITALY, [2]Medical Oncology Division, pisa,

ITALY, ³Nuclear Medicine Unit, aviano, ITALY, ⁴Radiotherapy Unit, aviano, ITALY, ⁵Medical Oncology, aviano, ITALY, ⁶Nuclear Medicine Department, bologna, ITALY, ⁷Radiotherapy Unit, bologna, ITALY.

Background. Radium-223 (^{223}Ra)-chloride, a novel alpha emitter, has been shown to improve overall survival (OS), to delay skeletal-related events and to reduce pain in patients (pts) with castration-resistant prostate cancer (CRPC) and bone metastases. Our retrospective observational study is the first multidisciplinary and multicenter Italian experience, where the efficacy and safety of ^{223}Ra therapy are evaluated in daily medical practice. **Materials and Methods.** Between August 2013/August 2016, 83 pts with metastatic CRPC (mCRPC) received ^{223}Ra therapy at three Italian Centers. ^{223}Ra-chloride (50 kBq/Kg or 55 kBq/Kg according to NIST2015) was administered every four weeks up to the programmed six cycles of therapy. Study's endpoints were OS, progression-free survival (PFS), pain according to a numeric rating scale (NRS), biomarker response, numbers of symptomatic skeletal-related events (SSEs) and toxicity. **Results.** Median age was 75 (range 53-89) years. The majority of pts had a Gleason score of 7 (n=25), 8 (n=16), or 9 (n=21). Forty-one pts completed 6 cycles of treatment; 33 discontinued treatment after 1 (n=7), 2 (5), 3 (7), 4 (5) or 5 (9) cycles. 9 were under treatment during data collection. NRS pain scores significantly improved during 6 cycles of therapy ($p < 0.000001$). Mean OS was 10.1 months; median OS had not been reached at time of reporting. Kaplan-Meier estimates for OS and PFS were 17.5 and 7.7 months, respectively. OS and PFS were significantly associated with number of ^{223}Ra cycles; most benefit occurred in pts who received all 6 cycles. By stratifying pts according to ALP's levels (≥220 and < 220), a significant difference was found between two groups in terms of expected OS and PSF according to Kaplan-Meier estimation. ^{223}Ra was well tolerated, no serious adverse events occurred during treatments. **Conclusion.** ^{223}Ra represents an important treatment option for pts with CRPC and symptomatic bone metastases and it seems to be useful in improving OS, PFS and level of pain; especially OS and PFS were better in pts with a lower tumor burden according to ALP levels.

E-PW056

Age-adjusted risk factors for patients undergoing molecular radiotherapy

J. Thurston, G. Flux; Royal Marsden Hospital, London, UNITED KINGDOM.

Purpose/Introduction: With advances in medicine, including in radionuclide therapies, the prognosis for patients suffering from a range of cancers, both for solid tumours and leukaemias, has improved significantly over the past few decades. However the implication of such improved prognoses is that the long-term risks from radionuclide therapy of inducing a second primary cancer later in life can no longer be considered to be negligible for these cohorts of patients, when carrying out Justification and when gaining informed consent from patients. **Subjects & Methods:** Whole body absorbed doses were obtained from the literature for a range of radionuclide therapies, for comparison with published ICRP data on the Effective Dose per administered activity [1] and risk coefficients for fatal cancer resulting from radiation exposure to estimate the lifetime risks associated with these procedures, including age-adjusted risk factors [2] to take into account the age of the patient when treated. The results were then further adjusted to take into account life expectancy post-therapy in relation to minimum latency periods for any radiation-induced leukaemias and solid tumours to develop. Thus risk factors were calculated as a function of the administered activity, age at treatment, and maximum life expectancy. **Results:** The wide range of absorbed doses delivered from fixed or weight based activities lead to a correspondingly wide range of potential risks, exacerbated by the range of life expectancies that are difficult to predict. Nevertheless, it is possible to generate a table of values that, although not pertaining to individual patients, may be used for reference. Example: for an administered activity of 7.4GBq I-131 labelled mIBG to treat neuroblastoma in paediatric patients and young adults, and using a published whole body absorbed dose range of 0.04 - 0.63mSv/MBq [3]. **Discussion/Conclusion:** The results indicate the range of theoretical risks suffered by patients undergoing radionuclide therapy, taking into account both the age of the patient at exposure, and their life-expectancy post-therapy. These may be used to inform Practitioners so that they can be considered as part of the Justification and Consenting processes. **References:** 1. ICRP53 + Addendums 2. ICRP103 3. Flux GD *et al*. Clinical applications of dosimetry for mIBG therapy *Q J Nucl Med Mol Imaging* 55(2), pp 116-125, 2011.

E-PW057

Renal toxicity analysis in a Peptide Receptor Radionuclide Therapy (PRRT) trial with alternated 177Lu and 90Y-DOTATOC

*E. Grassi*¹, F. Fioroni¹, M. Cremonesi², D. Finocchiaro¹,³, M. Ferrari², F. Botta², G. Castellani³, N. Lanconelli³, A. Filice⁴, A. Versari⁴, M. Iori¹; ¹Medical Physics Unit, Arcispedale Santa Maria Nuova-IRCCS, Reggio Emilia, ITALY, ²Medical Physics Unit, European Institute of Oncology, Milan, ITALY, ³Dept. of Physics, University of Bologna, Bologna, ITALY, ⁴Nuclear Medicine Unit, Arcispedale Santa Maria Nuova-IRCCS, Reggio Emilia, ITALY.

Purpose: To analyze the renal toxicity in a PRRT trial (follow-up>12 months) and to explore the dose-effect correlation in terms of normal tissue complication probability(NTCP). **Subjects & Methods:** The trial consisted in alternation of 177Lu and 90Y-DOTATOC, with activity proportion based on the patient characteristics and dosimetry. A cohort of 51 patients was recruited and divided into 2 classes: 30 patients with risk factors (hypertension, diabetes, chemotherapy), RF, and 21 without (noRF). All patients underwent organ level 3D-dosimetry study (MIRD16), after a therapeutic administration of 177Lu-DOTA-TOC (5 SPECT-CT acquisitions, Siemens-SymbiaT2). Kidney cumulative dose D, and Biological Effective Dose BED were calculated. Creatinine was assessed from blood chemistry at definite intervals up to at least 6 months after the last injection,

and creatinine clearance loss (CCL) was derived. Renal acute and chronic toxicity grade were assessed (CTCAE 4.0). NTCP curves were estimated using a probit model. **Results:** Patients were administered on average with 27% of 90Y-DOTATOC and 73% with 177Lu-DOTATOC. Kidney cumulative dose D, and BED were (mean value+/-SD) 22.7Gy+/-1.7 and 24.6Gy+/-2.2, respectively. Cumulative BED to D ratio was approximately 1.1 for both 177Lu- and 90Y. The mean+/-SD follow up period was 87+/-37 w (range 51-235w). Only G1 acute toxicity was observed in 7 patients (17% RF, 10% noRF). Low chronic toxicity was observed in noRF patients (G1=3, G2=1) and was more frequent in RF patients (G1=9, G4=1). Considering all patients, the mean CCL was 3%, 6%, 9%, 13% at 6, 12, 18, 24 months. In particular mean CCL% at 2y was 14% in RF patients and 8% in no RF patients. Higher number of cases with CCL>20%/y was observed in patients with RF (19%) compared to patients noRF (10%). Similarly with CCL>10%/y (38% RF, 29% noRF patients). The recovery of the initial creatinine value (i.e. CCL<0%) was observed in 28% of RF cases and in 24% of noRF patients. BED values (C.I.) of 35Gy(29-52), 32Gy(21-248), provided chronic NTCP of 50% for noRF and RF, respectively (significant p<0.05). **Conclusions:** Chronic toxicity was of low grade in most cases: G1 observed in 24% of pts, while higher toxicity grades were quite rare (2% G2; 2% G4). Different NTCP curves for chronic toxicity were derived for the two populations considered. For acute toxicity, poor correlation was observed between creatinine increase and dose in noRF patients. No correlation was found when all patients were considered. Work partially supported by EMPIR-MRTDosimetry project(15HLT06), co-funded by EU's Horizon-2020-programme.

E-PW058

3-Dimensional Dose Mapping after PRRT with 177Lu-DOTATATE/-TOC by One-Single Measurement after Four Days

R. A. Werner[1,2], C. Lapa[1], A. K. Buck[1], M. Lassmann[1], H. Hänscheid[1]; [1]Department of Nuclear Medicine, Universitätsklinikum Würzburg, Würzburg, GERMANY, [2]Johns Hopkins School of Medicine, The Russell H Morgan Department of Radiology and Radiological Science, Baltimore, MD, UNITED STATES OF AMERICA.

Introduction: We analyzed the accuracy of absorbed dose estimates based on one-single measurement of the activity retention in a cohort of patients treated with PRRT. **Subjects and Methods**: Activity kinetics (67 kidneys, 30 livers, 34 spleen, 52 tumors) were analyzed in patients with repeated planar whole body scans (1-4 h, 1 d, 2 d, and ≥4 d) after ^{177}Lu-DOTATATE/-TOC administration. A bi-exponential decay function was fitted to the data of each evaluable organ/tumor r_S and normalized to 100% at its maximum to deduce the relative uptake $u(r_S,t)$. This function, after integration over time to deduce the time integrated uptake $\tilde{u}(r_S)$ and normalization to a high-quality quantitative retention measurement e.g. with a SPECT/CT, can be used to determine the absorbed dose to r_S. For a function $u(r_S,t)$ decaying mono-exponentially with an effective half-live T_{eff}, $\tilde{u}(r_S)$ can be approximated by $\tilde{u}(r_S) \approx \tilde{u}_I(r_S,t_I) = u(r_S,t_I) \cdot t_I \cdot 2/\ln(2)$ from a single measurement $u(r_S,t_I)$ at a late time point t_I (1). The error is theoretically < 6% if $0.85 \cdot T_{eff} < t_I < 1.17 \cdot T_{eff}$. For each uptake function, the values $\tilde{u}_I(r_S,t_I)$ were calculated from the expected $u(r_S,t_I)$ at t_I = 24 h, 48 h, 72 h, 96 h, 120 h, and 144 h and the deviations from $\tilde{u}(r_S)$ were determined. The mean tissue specific error was calculated for each time point t_I. **Results:** For a measurement at t_I = 96 h, the deviation of $\tilde{u}_I(r_S,t_I)$ from $\tilde{u}(r_S)$ was determined to be 5% ± 6% (range, -9% to 20%) for kidneys, 7% ± 5% (range, -1% to 20%) for livers, 11% ± 8% (range, 2% to 47%) for spleens, and 2% ± 8% (range, -28% to 16%) for tumors. Accuracy is slightly reduced for measurements after 72 h (kidneys: 9% ± 6%; range, -15% to +25%) or 120 h (kidneys: -5% ± 8%; range, -25% to 8%). Inacceptable underestimates of the absorbed dose to the kidneys are observed for measurements after 24 h (-33% ± 7%; range, -61% to -18%), 48 h (0 ± 8%; range, -33% to 19%), and 144 h (-18% ± 10%; range, -41% to 7%). For calculating the absorbed dose, an activity concentration of 1 MBq/g measured in a tumor at 96 h indicates a local absorbed dose of 24 Gy. **Conclusion:** A quantitative image of the abdominal activity concentration distribution in a patient 4 days after the administration of ^{177}Lu-DOTATATE/-TOC is proportional to a map of the absorbed doses to tumors/relevant organs.

E-PW059

Bone metastases affect bone marrow response during 177-Lu-DOTATATE treatments

J. Svensson[1], L. Hagmarker[2], T. Rydén[2], R. Hermann[2], B. Wängberg[3], A. Sundlöv[4], K. Sjögreen-Gleisner[5], P. Bernhardt[2]; [1]Institution of Clinical Sciences, Dep of Oncology, Göteborg, SWEDEN, [2]Institution of Clinical Sciences, Dep of Radiation Physics, Göteborg, SWEDEN, [3]Institution of Clinical Sciences, Dep of Surgery, Göteborg, SWEDEN, [4]Clinical Sciences, Dep of Oncology and Pathology, Lund, SWEDEN, [5]Clinical Sciences, Dep of Radiation Physics, Lund, SWEDEN.

Treatment with 177-Lu-DOTATATE has proven safe according to renal function also in long time follow up, and the stated absorbed dose limits for the kidneys are being challenged. The bone marrow response to treatment is usually described as mild, but clinically relevant bone marrow toxicity does appear during treatment. Persisting bone marrow toxicity may also limit the amount of treatment cycles possible to give, and adventure future treatment options. The aim of this work was to examine if bone marrow response during the first treatment cycle could predict persisting bone marrow toxicity in the remaining treatment cycles. Patients with and without bone-metastases were also compared according to bone marrow response during treatment. **Subjects and Methods:** To date 95 patients with progressive disease of advanced SSTR-positive neuroendocrine tumours have been included in the ILUMINET study (EUDRACT nr 2011-000240-16) and treated with 177-Lu-DOTATATE in a renal dose-escalation study. 40 patients have been included in the present analyse. Post treatment planar images (2 h, 24 h, 48 h, 168 h) were used in the in-house developed image based two-compartment method for calculation of bone marrow doses. To evaluate bone marrow function and its response to treatment, biomarkers including Hb, WBC and PLT counts were

analysed baseline and weekly during all treatment cycles. **Results:** Patients with bone metastases did not receive higher absorbed bone marrow doses during treatment, but did experience more bone marrow toxicity according to platelet counts (p<0.05). Five of the six patients who had to stop treatment due to persisting leukopenia or thrombocytopenia had bone metastases. These six patients responded to the first treatment cycle more markedly showing a more pronounced decrease in platelet counts compared to the patients that could be treated as planned (p<0.0001). The decrease in white blood cells did not differ between patients with and without bone metastases, but the decrease per absorbed dose to the bone marrow was more significant for patients with bone metastases(p=0.04). This was even more pronounced for the six patients who could not receive full treatment (p=0.02). The response according to Hb counts did not differ between the groups. **Conclusions:** The more pronounced decrease in platelet counts and WBC counts per absorbed dose to the bone marrow indicates a higher individual bone marrow radiosensitivity for patients with metastases. This response pattern will be further analysed as a tool to predict bone marrow toxicity.

<0.01 to 4379 ng/mL at baseline and 0.02 to 596.3 ng/mL at follow-up. There was no correlation between NaF SUV and PSA at baseline or over time. In contrast, maximum and mean SUVs correlated to PSA at baseline (p<0.01) but changes at follow-up were not significant. At baseline, 18F NaF identified 180 (98.4%) bone lesions while 18F DCFBC detected 84 (45.7%) at 1hr and 85 (47.2%) at 2hrs. At follow-up, 18F NaF detected 120 (97.6%) and DCFBC identified 52 (44.1%) at 1hr and 55(44.4%) at 2hrs. There was no SUV correlation between the two tracers. In addition, DCFBC demonstrated focal uptake in 56 soft tissue or lymph node lesions at baseline, and at follow-up identified 40 non-osseous lesions at 1hr and 41 similar lesions at 2hrs. Conclusion: NaF had significantly higher bone lesion detection rate than DCFBC, however, this scan provides no information regarding the biological activity of each lesion. In contrast, 18F DCFBC demonstrated active metastatic lesions. 18F DCFBC was also capable of recognizing both bone and soft tissue metastases with slightly better performance at 2hrs than 1hr post injection. At baseline, PSA correlated with SUVs for DCFBC but not with NaF SUVs. 18 NaF represents both active and inactive lesions whereas 18F DCFBC provides better evidence of active metastases. PSMA agents hold great promise for characterizing all phases of prostate cancer.

Clinical Oncology: Walk the Theranostic Way of Life!

E-PW060

Detecting Prostate Cancer Bone Metastasis With 18F DCFBC (a PSMA Targeted Agent) Compared to 18F Sodium Fluoride

L. Lindenberg[1], E. Mena Gonzalez[1], I. Turkbey[1], J. Shih[1], E. Bergvall[2], A. Lindenberg[3], W. Dahut[1], M. Pomper[4], P. Choyke[1]; [1]National Cancer Institute, Bethesda, MD, UNITED STATES OF AMERICA, [2]Fort Belvoir Community Hospital, Ft Belvoir, VA, UNITED STATES OF AMERICA, [3]Fort Belvoir Community Hospital, Fort Belvoir, VA, UNITED STATES OF AMERICA, [4]Johns Hopkins University School of Medicine, Baltimore, MD, UNITED STATES OF AMERICA.

Aim: Prostate Specific Membrane Antigen (PSMA) is overexpressed in aggressive prostate cancers and is actively being pursued as an imaging and therapeutic target. 18F DCFBC is a radiolabeled PET agent that binds with high affinity to PSMA. We compared bone metastasis detection in prostate cancer patients with 18F NaF and 18F DCFBC. Materials and methods: Subjects with known or suspected prostate cancer metastases underwent 18F DCFBC PET/CT imaging performed at 1 and 2 hours post injection (p.i.) of 8 mCi 18F DCFBC. Patients also underwent a whole body 18F NaF PET/CT scan one hour p.i. of 3mCi 18F NaF within 3 weeks. Dual tracer imaging was repeated at 4-6 months. Maximum and mean Standardized Uptake Values (SUVs) were obtained for all lesions with both radiotracers. PSA levels were obtained at the time of 18F DCFBC imaging. Statistical analysis was performed with Spearman rank correlation. Results: There were 28 evaluable patients. PSA ranged from

E-PW061

177Lu-DOTA-octreotate Therapy of Advanced Pancreatic Neuroendocrine Tumors - a Single Centre Experience

K. Fröss-Baron[1], U. Garske-Roman[2,3], S. Welin[1], D. Granberg[1], B. Eriksson[1], M. Sandström[3], A. Sundin[3]; [1]Department of Medical Sciences, Uppsala University, Uppsala, SWEDEN, [2]Department of Clinical Physiology, Sahlgrenska University Hospital, Gothenburg, SWEDEN, [3]Department of Surgical Sciences, Uppsala University, Uppsala, SWEDEN.

Aim: To study progression-free survival (PFS) and overall survival (OS) and their determinants in a consecutive cohort of patients with inoperable, advanced pancreatic neuroendocrine tumours (pNET) treated with 177Lu-DOTA-octreotate in one centre. **Material and Methods:** A total of 125 consecutive patients with inoperable, metastatic pNET were treated with 177Lu-DOTA-octreotate between November 2005 and October 2014. We excluded 23 patients for final efficacy analysis: 11 patients with missing follow-up, 12 patients who could not receive more than 2 treatment cycles because of either side effects or general deterioration. The final cohort of 102 patients received 3-10 cycles at 6-8 weeks interval with mean activity 29.6 GBq (range 17-74). A total of 82 (80.4%) patients were treated according to a dosimetry-guided protocol. Out of the 102 patients, 72 (70.6%) were non-functioning, 86 (84.3%) had progressive disease before inclusion, 94 (92.1%) had received chemotherapy before PRRT (52.1% of whom more than one line of therapy) and 43 (42.1%) had their primary tumour resected. There were 9.2% G1 tumours, 83.9% G2 tumours and 6.9% G3 tumours. Mean follow up was 42 months (range 4-129). Response was evaluated according to RECIST 1.1 criteria. Toxicity analysis was assessed in the whole group of 125 patients (WHO criteria). **Results:** Median

PFS and OS were 27.5 months (95%CI 23-31) and 42 months (95%CI 31-51) respectively. Primary tumour surgery and stable disease prior to therapy start were associated with longer PFS and OS. Ki67<10% was additionally associated with longer PFS but not OS. Best morphological therapy response was as follows: Complete response (CR) in 6 patients (5.9%), partial response (PR) in 52 (51%), stable disease (SD) in 38 (37.2%), progressive disease (PD) in 6 (5.9%). Morphological response (PR+CR) correlated with longer PFS (p=0.02) and OS (p=0.0006) than stable disease (SD). In a subgroup with dosimetry-guided therapy protocol, patients reaching an absorbed dose of 23 Gy to kidneys had significantly longer PFS and OS. Any bone marrow toxicity grade 3 or 4 occurred in 17 (13.6%) pts, one patient developed fatal liver toxicity. No significant nephrotoxicity (grade 3 or 4) was observed. **Conclusions:** 177Lu-DOTA-octreotate therapy is effective in patients with advanced pNET with a median PFS of 27.5 months and a median OS of 42 months. Patients obtaining 23 Gy to kidneys and patients with morphologic response have PFS and OS benefits. In agreement with other reports, reversible bone marrow toxicity is the most frequent toxicity of this treatment.

E-PW062

The Value of Somatostatin Receptor Imaging (SRI) in Patients with NENG1/G2 Pancreatic Neuroendocrine Neoplasms (pNENs) Base on Pathological and Clinical Follow-up.

S. J. Konsek[1], A. Kolasinska-Cwikla[2], A. Lewczuk[3], L. Sawicki[2], M. Kidd[4], A. Cichocki[2], A. Nasierowska-Guttmejer[5], M. Tenderenda[2], J. B. Cwikla[1], I. M. Modlin[6]; [1]Faculty of Medical Sciences, University of Warmia and Mazury, Olsztyn, POLAND, [2]MSC Memorial Cancer Centre and Institute Maria Sklodowska-Curie, Warsaw, POLAND, [3]Medical University of Gdansk, Gdansk, POLAND, [4]Wren Laboratories, Branford, CT, UNITED STATES OF AMERICA, [5]Hospital Ministry of Internal Affairs, Warsaw, POLAND, [6]Yale University, New Haven, CT, UNITED STATES OF AMERICA.

Background: Neuroendocrine neoplasms of the pancreas (p-NEN) are common origin of GEP-NEN. The aim of this retrospective study was to review the of value of Somatostatin Receptor Scintigraphy (SRS) in initial detection and tumour extent of well and moderate differentiated (NENG1/G2) tumours in patients with confirmed p-NEN, based on histology and further clinical and/or biochemical follow-up. **Subjects and Methods:** There were 247 patients with confirmed p-NEN. The SRS was performed to evaluation of primary p-NEN, also to assess clinical stage of disease, based on current WHO classification. Overall, 696 examinations in this group of subjects were performed using 99mTc HYNICTOC (Octreotide, NCBJ; Polatom, PL). Initially whole body WB-SPECT and then WB-SPECT/CT, with standard iterative reconstruction were used in each case. **Results:** There were 143 pts with NENG1 (58%) and 104 pts with NENG2 (42%). In 58 patients (23%) with NENG1/2 seventy-two (10%) SRS were performed to assessed initial diagnosis. There were 70 (97%) true positive (TP), 2 (3%) false negative (FN), no true negative (TN) and false positive (FP) results of examinations by SRS. Sensitivity

of SRS per patient as diagnose of neoplasm is 97%. In 175 pts (71%) SRS was used in evaluation of clinical stage. Overall 548 (79%) examination were performed in this group of pts. There were TP=422 (77%), TN=115 (21%), FN=7 (1%) and FP=4 (1%) results. Sensitivity and specificity of SRS per study in evaluation of tumour extent is as follows: sensitivity 98%, specificity 97%; per patient: sensitivity 95%, specificity 94%. In 34 pts (14%) SRS was used as imaging follow-up after radical surgery, there were overall 76 (11%) studies carried out. There were 95% TN results of examinations of SRS and in 4 pts we identified the reccurance of the tumour. In total, in group of diagnose/staging and follow-up the sensitivity, specificity and accurancy of the test was 98% per study. Per patient: sensitivity 96%, specificity 97% and accurancy of the test 96%. **Conclusion:** SRS using 99mTc HYNIC-TOC acquired in WB-SPECT or WB-SPECT/CT techniques seems to be highly sensitivity and specificity and had great value as examination to evaluate in both the detection of primary p-NEN and to assess clinical stage of disease in patients with well or moderate differentiated p-NEN. The highest specificity of the test was noted in the group of patients that SRS was performed to assessed initial diagnosis and helped correctly identify those patients without the disease.

E-PW063

68Ga-PSMA-11 PET/CT in the evaluation of bone metastases in prostate cancer

C. Sachpekidis[1], P. Bäumer[2], B. A. Hadaschik[3], U. Haberkorn[1], A. Dimitrakopoulou-Strauss[1]; [1]Clinical Cooperation Unit Nuclear Medicine, German Cancer Research Center (DKFZ), heidelberg, GERMANY, [2]2Department of Radiology, German Cancer Research Center, DKFZ, heidelberg, GERMANY, [3]Department of Urology, University Hospital Heidelberg, heidelberg, GERMANY.

Aim: To compare the 68Ga-PSMA-11 PET with the ultra low-dose CT (80 kV, 30 mA) findings, as well as to provide semi-quantitative and quantitative 68Ga-PSMA-11 PET data, in bone metastases of prostate cancer (PC). **Methods:** In total 147 PET/CT scans of 137 patients were extracted from our database. 109 patients had biochemical failure after primary PC treatment with curative intent, while 28 patients suffered from primary, previously untreated PC. All patients underwent dynamic PET/CT (dPET/CT) scanning of the pelvis as well as whole-body PET/CT with 68Ga-PSMA-11. Dynamic and whole-body PET/CT assessment was based on qualitative evaluation and SUV calculation. Moreover, dPET/CT data from the pelvis underwent quantitative analysis based on a two-tissue compartment model and a non-compartmental approach leading to the extraction of fractal dimension (FD). **Results:** In total, 141 68Ga-PSMA-11 avid lesions consistent with bone metastases were detected with PET. 78 of these lesions showed a correlate on low-dose CT. On the other hand, 9 lesions were CT-positive but 68Ga-PSMA-11 PET-negative. 2 patients demonstrated disseminated skeletal 68Ga-PSMA-11 uptake, one of which with much less metastases-indicative CT findings. The mean (range) of $SUV_{average}$ and SUV_{max} for 68Ga-PSMA-11 avid bone lesions were 13.2 (1.9 - 95.0) and 20.9 (2.8 - 133.6) respectively. Dynamic PET/CT studies of

the pelvis revealed 63 lesions indicative of bone metastases with the following mean values: $K_1 = 0.21$, $k_3 = 0.28$, influx = 0.13 and FD = 1.23. In most bone lesions time-activity curves revealed an increasing ^{68}Ga-PSMA-11 accumulation during dynamic PET acquisition. The strongest correlations were found between FD and $SUV_{average}$ (r=0.95), FD and SUV_{max} (r=0.92), FD and influx (r=0.84), influx and $SUV_{average}$ (r=0.84), as well as between influx and SUV_{max} (r=0.82) (p <0.0001). A weak but significant correlation was demonstrated between PSA and $SUV_{average}$ (0.36) and SUV_{max} (0.36). Wilcoxon rank-sum revealed no statistically significant difference between bone and lymph node metastases (retrieved from our patient data pool) regarding SUVs and kinetic parameters. **Conclusion:** ^{68}Ga-PSMA-11 PET can reliably depict bone metastases of PC. Many of these bone lesions are missed on ultra low-dose CT. The amount of ^{68}Ga-PSMA-11 uptake in bone metastases correlates very strongly with tracer influx and the degree of heterogeneity of tracer distribution, and weakly with the degree of PSA plasma levels.

E-PW064

PSMA-PET MRI/TRUS robot-guided targeted prostate biopsy for detection and localisation of Primary prostate cancer

M. Mix, K. Schaal, M. Krönig, V. Drendel, U. Wetterauer, W. Schultze-Seemann, C. A. Jilg, P. T. Meyer; University of Freiburg, Medical Center, Freiburg, GERMANY.

Aim: Multiparametric MRI/TRUS-guided biopsy represents the standard tool for prostate cancer (PCa) detection in the setting of re-biopsy following negative primary biopsy. Recently, PSMA-PET/CT was introduced, targeting the prostate-specific membrane antigen (PSMA) on the surface of PCa cells, which enables powerful imaging of PCa lesions. Aim of this study was to evaluate the lesion-based detection rate for PCa from PSMA-PET MRI/TRUS fusion-robot-guided targeted prostate biopsy. **Methods:** Nine patients with tumour suspicious intraprostatic lesions on PET/CT with Ga-68-HBED-CC-PSMA underwent PET/MRI/TRUS fusion-targeted biopsies. 8/9 men received multiparametric MRI (1/9 had no MRI due to cardiac pacemaker). Areas with increased PSMA expression on PET were clinically classified by two nuclear medicine experts as PET-positive lesions (PL: highly suggestive of malignancy; showing intense focal uptake) or as PET-indeterminate lesions (IL: inhomogeneous moderate uptake). Lesions were manually contoured on fused PET/MRI images. Patients underwent a robot-guided transperineal-targeted biopsy (iSR'obot Mona-Lisa/Biobot system) of PET-PL and IL lesions and a standardized volume-adapted random saturation biopsy according to the Ginsburg study group scheme. **Results:** Mean PSA-level at biopsy was 11±4 ng/ml. The average SUV-max values were 9±8 g/ml (4 - 34) in a total of 17 intraprostatic lesions with increased PSMA expression. 9/17 lesions were defined as PL, 8/17 as IL. By histopathology, PCa was diagnosed in 7/9 men (78%). Furthermore, 8/9 (89%) prostate regions defined as PL were positive for PCa. In contrast, all 8 regions defined as IL were free of PCa. 3/8 lesions with proven PCa would have been missed by random biopsy only (lesions were not covered

by Ginsburg scheme), whereas 3 additional (PET-negative) PCa lesions had been diagnosed exclusively via random biopsy. Gleason score distribution for all PCa lesions was 2/12 (Gleason 6), 5/12 (Gleason 7a), 1/12 (Gleason 7b), 3/12 (Gleason 8), 1/12 (Gleason 9). PCa-diagnosis would have been possible in 7/7 patients by applying target biopsy only, in 6/7 men by applying random biopsies only. One patient was diagnosed with PCa (Gleason 8) with targeted biopsies only. **Conclusion:** PSMA-PET MRI/TRUS fusion-guided biopsy demonstrates strong potential for PCa detection in patients with tumour suspicious lesions on a PSMA-PET/CT after a negative primary biopsy. Targeting lesions with intense focal uptake on PSMA-PET with our biopsy system ensured high probability for PCa diagnosis, whereas lesions with only inhomogeneous moderate PSMA expression were not indicative of for PCa. The application of a limited number of PET-targeted biopsies leads to PCa diagnosis in nearly all patients.

E-PW065

Usefulness of 18F-choline PET/CT to evaluate patients eligible for Radium-223 Dichloride Therapy

E. Biggi[1], C. Fuccio[1], F. Ottalevi[1], F. D'Emidio[2], L. D'Angelo[3], A. Berbellini[1]; [1]Nuclear Medicine Unit, Ospedale "C. G. Mazzoni", Ascoli Piceno, ITALY, [2]Diagnostic Radiology Unit, Ospedale "C. G. Mazzoni", Ascoli Piceno, ITALY, [3]Medical Physics Unit, Ospedale "C. G. Mazzoni", Ascoli Piceno, ITALY.

Aim: 99mTc-diphosphonate whole-body bone scintigraphy (BS) and whole-body CT (wbCT) scan are generally used in patients with metastatic castration-resistant prostate cancer (mCRPC) potentially candidate to 223-Ra Dichloride Therapy (223-Ra) in order to evaluate the presence and the extent of metastatic spread to the bones and to exclude the presence of visceral metastases. Main aim of the study was to investigate whether 18F-choline (FCH) PET/CT may have an added value over BS or wbCT in order to correctly select patients eligible for 223-Ra therapy; secondary aim was to evaluate the extent of disease according to ALSYMPCA criteria. **Materials and Methods:** from June 2016 to February 2017, 10 consecutive mCRPC patients (median age 72,4 yr; range 61-84) potentially candidates to 223-Ra treatment were referred to our Centre. All patients showed a progression of skeletal disease at BS (performed within 12 weeks) and no visceral metastases at CT scan (performed within 6 months). All patients underwent FCH PET/CT and a complementary ultra-sound or c.e. CT of the liver. Low-dose co-registered CT images were also evaluated by a radiologist in case of equivocal findings. Patients were classified using ALSYMPCA criteria (I group <6 metastases; II group 6-20 metastases; III group >20 metastases). Validation of results was established by: a positive biopsy, a positive subsequent CT or MR or follow up. **Results:** FCH PET/CT showed unknown visceral metastases in 6/10 cases: cerebellum metastases (1), lung metastases (2), lymph-node involvement greater than 3 cm in the short-axis diameter (2), epidural spine with cord compression (1). These patients were referred to other therapies. FCH PET/CT was also able to give an accurate staging of mCRPC in 4/10 pa-

tients (that underwent 223-Ra therapy) and a better bone lesion detection rate than BS (BS positive in 232 sites vs PET positive in 389 sites), changing ALSYMPCA classification in 3/10 patients (from II to III group). **Conclusion:** FCH PET/CT can provide significant incremental data in mCRPC patients potentially eligible for 223-Ra. FCH PET/CT changed therapeutic management in 6/10 patients leading clinicians to consider other treatment options or to postpone this approach. Main limitation of this study is the small patient population enrolled.

E-PW066

64CuCl2 PET/CT and Fused-64CuCl2 PET/MRI in prostate cancer relapse. Comparison with 18F-Choline PET/CT, Fused-18F-Choline PET/MRI and multiparametric MRI

G. Ferrarazzo[1], G. Bottoni[1], F. Paparo[1], M. Puntoni[1], L. Bacigalupo[1], S. Zanardi[1], A. DeCensi[1], S. Righi[1], E. Lopci[2], M. Cabria[1], A. Piccardo[1]; [1]E.O. Ospedali Galliera, Genova, ITALY, [2]Humanitas Research Hospital, Milano, ITALY.

Aims: to evaluate the biodistribution and radiation dosimetry of 64CuCl2 in humans and to assess the ability of 64CuCl2-PET/CT and Fused-64CuCl2PET/MRI to detect prostate cancer (PCa) recurrence in patients with biochemical relapse. **Materials and Methods:** we prospectively evaluated 50 PCa patients with biochemical relapse after first-line surgery or external-beam radiation therapy. All patients underwent 64CuCl2-PET/CT, 18F-Choline-PET/CT and multiparametric magnetic resonance imaging (mpMRI) within 15 days of each other. Fused-64CuCl2PET/MRI and Fused-18F-Choline-PET/MRI images were obtained by co-registration of MRI and PET images using a dedicated software. The detection rate (DR) of each imaging modality was calculated by using histopathology, clinical or laboratory response and multidisciplinary follow-up as a reference standard. Biodistribution and Radiation dosimetry of 64CuCl2 were evaluated by means of three PET/CT acquisitions: 1, 4 and 24 hours after tracer injection. **Results:** 64CuCl2 is not excreted nor accumulated in the urinary tract, thus allowing thorough pelvic exploration. A 64CuCl2 of a 200 MBq injection translates to 5.7 mSv effective dose. In our cohort, 64CuCl2-PET/CT proved positive in 41 of 50 patients, with an overall DR of 82%. The DRs of 18F-Choline-PET/CT, mpMRI, 64CuCl2-PET/MRI and 18F-Choline-PET/MRI were 56%, 74%, 88% and 68%, respectively. The difference between the DRs of 64CuCl2-PET/CT and 18F-Choline-PET/CT was statistically significant (p=0.002). Significant differences were also found between the DRs of Fused-64CuCl2-PET/MRI and Fused-18F-Choline-PET/MRI (p=0.001) and between 64CuCl2-PET/MRI and mpMRI (p=0.023). Interestingly, on considering PSA value, 64CuCl2-PET/CT had a higher DR than 18F-Choline-PET/CT in patients with PSA <1 ng/ml . **Conclusions:** The biodistribution of 64CuCl2 is more suitable than that of 18F-Choline for exploring the pelvis and prostatic bed. The 64CuCl2 effective dose is similar to those of other established PET tracers. In patients with biochemical relapse and a low PSA level, 64CuCl2-PET/CT shows a significantly higher DR than 18F-Choline- PET/CT. In this comparative study, 64CuCl2-PET/MRI achieved the best diagnostic results.

E-PW067

Additional value of early ^{68}Ga-PSMA-11 PET Imaging in the assessment of local recurrence in prostate cancer patients with biochemical recurrence

C. Uprimny, A. S. Kroiss, J. Fritz, C. Decristoforo, E. vonGuggenberg, B. Nilica, J. Bektic, W. Horninger, I. J. Virgolini; Medical University Innsbruck, Innsbruck, AUSTRIA.

Purpose: Evaluation of local recurrence (LR) in prostate cancer patients with biochemical recurrence may be hampered by high physiologic urinary bladder activity present on 68Ga-PSMA-11 (HBEDD-CC) PET/CT exams, usually conducted 60 min after tracer injection (p.i.). This study aims to investigate whether early static PET scans could enhance diagnostic performance of 68Ga-PSMA-11 PET/CT in the detection of LR in comparison to PET imaging 60 min p.i.. **Methods:** 213 prostate cancer patients with biochemical recurrence referred to 68Ga-PSMA-11 PET/CT were analysed retrospectively (median PSA: 1.47 ng/ml). In all patients an early static scan of the pelvis was performed with a median starting time of 281 sec p.i. (range: 215-491 sec), followed by a whole-body PET/CT 60 min p.i.. Image interpretation was based on visual analysis. Furthermore calculation of maximum standardized uptake value (SUV_{max}) of pathologic lesions present in the pelvic region was performed on early PET images and on 60 min-PET scans. **Results:** On PET images 60 min p.i a LR-suggestive lesion (median SUV_{max} of 11.0; range: 4.7 - 40.9) could be detected in 28 patients (13.1 %), whereas an equivocal finding was present in 36 patients (16.9 %). In contrast, on early PET scans 52 patients revealed a pathologic lesion compatible with LR (median SUV_{max}: 5.9; range: 2.9 - 17.6) and in only 9 patients (4.2 %) an unclear finding was described. Early PET imaging led to a significant rise in the detection rate (p<0.001) and a significant reduction of equivocal findings (p<0.001). Tracer accumulation in the urinary bladder could be found in 63 patients on early PET scans (29.6 %). However, acquisition starting time of early PET scans without urinary bladder activity was significantly lower in comparison to patients with urinary bladder activity already present (median starting time of 261 vs. 321 sec p.i.; range: 215-311 sec p.i. vs. 281-491; p<0.001). Median SUV_{max} value of lesions suggestive of LR on early images was significantly higher in comparison to gluteal muscle, inguinal vessels and seminal vesicle/anastomosis (median SUV_{max}: 5.9 vs. 1.9, 4.0 and 2.4, respectively). **Conclusions:** Assessment of LR in prostate cancer patients with biochemical relapse referred to 68Ga-PSMA-11 PET/CT is improved by additional early PET imaging, enhancing the detection rate of LR and reducing equivocal findings significantly. Early PET scans should be acquired as early as 4-5 min after tracer injection in order to obviate tracer accumulation in the urinary bladder.

E-PW068

177Lutetium PSMA radioligand therapy in patients with metastatic castration resistant prostatic cancer; assessment of response, clinical evaluation, toxicity

H. R. RATHORE, 400026, G. Bhat, P. Aland, C. Kannor, C. Kale, A. Parab, P. Chaudhuri, V. Lele; Jaslok Hospital and Research center, Mumbai, INDIA.

Purpose: To evaluate the biochemical, clinical and radiological effectiveness of [177]Lutetium-PSMA-617-DKFZ radioligand therapy in patients with extensive metastatic castration resistant prostate carcinoma. **Subjects and Methods**: A total of 11 patients with biopsy proven carcinoma of prostate referred to Nuclear Medicine Department, Jaslok Hospital and Research Centre, Mumbai for 177-Lu-DKFZ-617-PSMA Radioligand Therapy. Patients underwent the scan and therapy abiding the standard protocol. Association of biochemical and clinical response to overall survival are assessed at pre therapy and post therapy at 2, 4, 6, and 10 weeks. Baseline assessment is done by correlation with WHO grade, Gleason's score, PSA level, Gallium PSMA PET Scan, EC renal scan. Clinical response by KPS and ECOG score. Bone Marrow toxicity and systemic toxicity by estimating CBC, LFT, RFT, electrolytes, ionised calcium, LDH, ALP by ECOG common toxicity criteria, CT-CAE. **Result:** All lesions detected by ^{68}Ga-HBED-CC PET-CT exhibited high 177-Lu-DKFZ-617-PSMA uptake on post therapy planar and SPECT images. 10 weeks after therapy 63.63% patients experienced PSA decline of which 18.18% experienced more than 50% PSA decline, 18.18% patients more than 30% PSA decline, 27.27% patients shows any PSA decline. 36.36% patients experienced rise in PSA out of which 27.27% experienced more than 30 % raise in PSA which shows no response to therapy, 9.09% experienced progressive disease. Relevant hematotoxicity (ECOG CTC and CTCAE) grade 3/4 anaemia in 18.18% and grade 1/2 in 27.27%, and grade 3/4 thrombocytopenia in 18.18 % and grade 1/2 leukopenia in 27.27% of patients is experienced. 27.27% with progressive disease experienced deranged LFT by grade 1/2. 9.09% has experienced grade 1 changes in RFT. There is fall in serum electrolytes as Hyponatremia - grade 3 / 4 in 18.18% and grade 2 in 9.09%. There is grade 4 raise in LDL seen in 9.09% patients, grade 3 raise in ALP in 18.18% and grade 1 in 27.27% patients, and low ionized calcium with grade 1 changes are seen in 27.27% of patients. According to fall in PSA and overall response evaluation result shows Positive response in 18.18% patients, stable disease in 45.45% patients, progressive disease in 9.09% patients and no response to therapy is seen in 27.27% patients. More than six months progression free survival is seen in 63.63% patients. **Discussion**: 177-Lu-DKFZ-617-PSMA is a novel and promising RLT for mCRPC. Our initial results indicate that radioligand therapy with 177-Lu-DKFZ-617-PSMA is safe, effective and have low side effect profile.

E-PW069

One-step kit-based radiolabeled ^{68}Ga-THP-PSMA for PET imaging of PSMA expression: Biodistribution and first clinical experience

S. Schmuck; Medizinische Hochschule Hannover, Hannover, GERMANY.

Aim: Several ^{68}Ga-labeled tracers have become available for clinical molecular imaging of PSMA expression at positron emission tomography (PET). However, the labeling process of these compounds is rather complex and time consuming, limiting the accessibility of these tracers. Recently, ^{68}Ga-trishydroxypyridinone (THP)-PSMA, a novel tracer that can be labeled in one step by reconstitution of a kit with unprocessed generator eluate, has been introduced for imaging of PSMA expression. The aim of this study was to evaluate the human biodistribution of ^{68}Ga-THP-PSMA in patients with biochemical recurrence of prostate cancer after radical prostatectomy. **Materials and Methods:** 25 men (age, 72.1±5.7 years) with elevated PSA levels (2.5±3.9 ng/ml) after radical prostatectomy underwent a whole-body PET/CT after injection of ^{68}Ga-THP-PSMA at 60 minutes post injection. The biodistribution of ^{68}Ga-THP-PSMA was analyzed by assessing physiologic uptake by assessment of standardized uptake values (SUVs) in fixed isocontour-threshold volumes-of-interest placed in various organs including the parotid glands, liver, spleen, kidneys, gluteal muscle, and the superior vena cava for blood-pool. Tracer excretion was measured in both bladder and the intestine (duodenum, jejunum, ileum, ascending colon). Pathologic uptake was quantified in metastases. **Results:** In humans, the physiologic uptake of ^{68}Ga-THP-PSMA is low in the parotid glands (SUV_{mean}, 4.0 ± 1.6 (1.6 - 8.4)), liver (SUV_{mean}, 1.3 ± 0.2 (0.8 - 1.7)), spleen (SUV_{mean}, 1.7 ± 0.4 (1.1 - 2.7)), blood-pool (SUV_{mean}, 1.4 ± 0.3 (0.8 - 2.0)), and background (gluteal muscle; SUV_{mean}, 0.3 ± 0.1 (0.2 - 0.5)). Intestinal tracer excretion was negligible, but intense urinary tracer excretion was observed (bladder; SUV_{mean}, 221.8 ± 71.8 (83.3 - 368.1)). Tracer uptake (SUV_{mean}) in lymph node metastases was 5.4 ± 4.0 (1.6 - 19.8), and 3.9 ± 3.1 (0.6 - 11.3) in bone metastases. The mean tumor to background ratio (TBR) of lymph node metastases was 27.8 ± 25.3 (5.8 - 127.4), and the mean TBR of bone metastases was 18.6 ± 14.6 (3.6 - 51.4). **Conclusion:** ^{68}Ga-THP-PSMA offers a favorable biodistribution with low physiologic uptake in organs, blood-pool and background. Tracer uptake in pathologic lesions is associated with satisfying TBRs. There is marked urinary activity. Negligible intestinal tracer excretion allows for clear visualization of retroperitoneum and abdomen.

E-PW08	Monday, October 23, 2017, 08:30 - 09:30, e-Poster Walk Area, Level 2, Foyer B, Screen 5

M2M: PET/CT

E-PW070

[18]F-Organotrifluoroborate Probes Targeting PSMA for PET Imaging of Prostate Cancer: One-step Radiosynthesis, High Tumor Uptake and High T:NT Ratios

M. L. Lepage[1], H. Kuo[2], H. Merkens[2], N. Colpo[2], F. Bénard[2], K. Lin[2], D. M. Perrin[1]; [1]University of British Columbia, Vancouver, BC, CANADA, [2]BC Cancer Research Centre, Vancouver, BC, CANADA.

Objectives: The past decade has seen the development of many PET radiotracers targeting the Prostate-Specific Membrane Antigen (PSMA) for prostate cancer (PCa) imaging, including metal chelation or ^{18}F-radiofluorination. Given the great interest in imaging PSMA for PCa diagnosis, a rapid, one-step, user-friendly, aqueous fluorination reaction that can be applied to PSMA-ligands would be of great utility. Moreover, excellent images, defined by high tumor uptake values and high T:NT ra-

tios would be equally essential to advance such a tracer to clinical applications. Organotrifluoroborates, as prosthetics afford very efficient, kit-like, one-step ^{18}F-labeling by isotope exchange (IEX). Here we have used this approach to prepare trifluroroborate derivatives of the Glu-Lys diureido scaffold to combine the advantages of one-step aqeous labeling with the production of a PSMA-specific tracer with excellent tumor images. **Methods**: To the core Glu-ureido-Lys was conjugated 2-naphthylalanine and then (4-(aminomethyl)cyclohexanecarboxylic acid) using standard SPPS. Azidoacetic acid was coupled to the N-terminus and reacted with a propargyl-pyridyl-trifluforoborate to yield a new conjugate containing a novel trifluoroborate prosthetic group. Labeling proceeded as previously reported where approximately 100 nmol of conjugate was reacted with ~1Ci of NCA ^{18}F-fluoride. PET imaging and biodistribution studies were conducted in mice bearing PSMA-expressing LNCap prostate cancer xenografts. **Results**: This new ^{18}F-RBF$_3$-Glu-ureido-Lys conjugate was labeled in yields of 10-15%, at specific activities of >104 GBq/μmol. PET imaging and correlated ex-vivo biodistribution show substantial clearance to bladder with high tumor uptake (25±8 %ID/g) along with typically high kidney uptake (81±31 %ID/g). Excellent T:Bone (35±27), T:Muscle (145±57) and T:Blood (19±8) ratios were observed. Blocking by co-injection with DCFPyL (0.5 mg) reduced >95% uptake demonstrating specific uptake by PSMA. **Conclusions**: Here we show several salient points: 1) IEX on organotrifluoroborates afford the simplicity of a one-step labeling without pre-drying of the ^{18}F-fluoride; 2) Radiosynthesis proceeds in a clinical setting within a fully shielded hot-cell within 30 min or less in reasonable yields and high specific activities; 3) Purification involves a simple Sep-Pak elution 4) Images show excellent tumor uptake values and exceptionally high T:M and T:B ratios, values that compare favorably to or exceed those seen with ^{18}F-DCFPyL. These data suggest that this compound or a closely related analog will be suitable for human clinical applications.

E-PW071

2-deoxy-glucose is a Respiratory Substrate for Endoplasmic Reticulum of Murine Breast Carcinoma Cells: New View on PET-Imaging

V. Cossu[1], S. Ravera[2], S. Bruno[3], A. Orengo[1], A. Buschiazzo[4], A. Bellini[4], F. Grillo[5], M. Bauckneht[4], M. Piana[6], C. Ghersi[1], S. Morbelli[1], C. Marini[1,7], G. Sambuceti[1,4]; [1]Nuclear Medicine Unit, IRCCS AOU San Martino-IST, Genoa, ITALY, [2]Pharmacy Department, Biochemistry Laboratory, University of Genoa, Genoa, ITALY, [3]Department of Experimental Medicine, University of Genoa, Genoa, ITALY, [4]Nuclear Medicine Unit, Department of Health Sciences, University of Genoa, Genoa, ITALY, [5]Pathology Unit, IRCCS AOU San Martino-IST, Genoa, ITALY, [6]Department of Mathematics, University of Genoa, Genoa, ITALY, [7]CNR Institute of Bioimages and Molecular Physiology, Milan, ITALY.

Introduction: The theoretical basis of ^{18}F-FDG imaging relies on the concept that, as 2-deoxy-glucose (2DG), it is trapped into the cell in its phosphorylated form. We previously documented that retention of ^{18}F-FDG and 2DG at least partially reflects the activity of an endoplasmic reticulum (ER) processing machin-

ery. This pathway is largely autonomous from the well-recognized cytosolic glycolysis and pentose phosphate pathway and is triggered by hexose-6-phosphate dehydrogenase (H6PD) whose catalytic activity recognizes both monosaccharides as substrates. Aim of this study was to verify whether ^{18}F-FDG and 2DG oxidation in the ER of cancer cells can contribute to explain the link between ^{18}F-FDG uptake and disease aggressiveness. **Subjects & Methods:** Murine breast carcinoma (4T1) cells were cultured in DMEM medium containing 11 mM glucose under standard conditions. Isolation of mitochondria and microsomes (ER) was performed by standard methods. In each cell fraction, oxygen consumption rate (OCR) was measured using an amperometric oxygen electrode while ATP synthesis was measured by the luciferin/luciferase chemiluminescence method. Response to 5 mM pyruvate + 2.5 malate (conventional substrates) or 0.7 mM NADH was tested. Similarly, response to 11 mM 2DG, glucose, glucose-6-phosphate (G6P) or galactose were tested in the presence of 0.2 mM NADP. Western blot (WB) and co-localization experiments were performed according to standard procedures. **Results:** Mitochondria conducted the oxidative phosphorylation (OXPHOS) metabolism only when stimulated with the pyruvate + malate, consuming 16.7±1.1 nmolO/min/mg and producing 24.7±2.1 nmolATP/min/mg. By contrast, microsomal fraction consumed oxygen and synthetized ATP (17.5±1.8 and 42.7±1.9 nmol/min/mg, respectively) in the presence of NADH, a substrate not suitable for mitochondria, documenting an extra-mitochondrial aerobic metabolism located in the ER. Interestingly, we observed the co-localization of subunit of the respiratory complex IV (COX1) with ER protein (calnexin). Moreover, in microsomal fraction, OXPHOS activity was present also after the addition of several hexoses and NADP, the substrates of H6PD. In particular, 2DG triggered a measurable microsomal OCR and ATP synthesis (64.1±2.2 and 182±12 nmol/min/mg, respectively), as well as glucose, G6P or galactose. This functional response well agreed with evidence of H6PD presence in microsomal fraction at WB. **Conclusion:** ER displays respiratory and ATP synthetic activities, triggered by H6PD and able to utilize 2DG as substrate. In cancer cells, the activity of this pathway is well represented and might contribute to the link between ^{18}F-FDG uptake and disease aggressiveness.

E-PW072

Assessment of pharmacokinetic properties of copper-64 and gallium-68 labelled NODAGANOC analogues for neuroendocrine tumours detection.

M. Asti[1], R. S. B. H. Schreuder[2], M. Iori[1], P. C. Capponi[1], S. Rubagotti[1], G. Cicoria[3], R. Zijlma[2], G. N. Doeswijk[4], M. De Jong[4], P. H. Elsinga[2], G. Luurtsema[2]; [1]Arcispedale Santa Maria Nuova-IRCCS, Reggio Emilia, ITALY, [2]University Medical Center Groningen, Groningen, NETHERLANDS, [3]S. Orsola-Malpighi University Hospital, Bologna, ITALY, [4]Erasmus Medical Center, Rotterdam, NETHERLANDS.

Background: Neuroendocrine tumors (NETs) are a heterogeneous group of neoplasms that can metastasize over the whole body. PET tracer ^{68}Ga-DOTATOC is frequently used in the diagnosis of NETs but the NODAGANOC analogue labelled with

gallium-68 or copper-64 might express superior features. In this study, the chemical characterization, the labelling properties and the *in vitro* behavior of ^{68}Ga and ^{64}Cu-NODAGANOC were explored and compared to those of ^{68}Ga-DOTATOC. **Methods:** Synthesis of non radioactive compounds was performed by incubating 300 µg NODAGANOC with 300 µL of 10% acetic acid and either 2 mg of copper(II) acetate or gallium(III) chloride for Cu-NODAGANOC or Ga-NODAGANOC, respectively. The crude mixture was purified by HPLC. Synthesis of radioactive compounds was performed starting from: i) ^{64}CuCl$_2$ (specific activity 420 GBq/umol) in HCl 0.1M, 74 MBq/mL solution ii) a 18 months old 1850 MBq ^{68}Ge/^{68}Ga generator (GalliaPharm, EZAG) eluted with 4 ml 0.1M HCl. 500 uL (i.e. 37 MBq copper-64 or 50 MBq gallium-68) was added to a solution containing various amounts of NODAGANOC (21, 10, 5, 3 nmol) in 1.5 M formate or acetate solution (pH: 3, 4, 5). The mixtures were heated at different temperatures (100, 50, RT °C) using various incubation times (15, 10, 7 min). Radiochemical purity (RCP) was assessed by UHPLC equipped with UV (set 220 nm) and radiochemical detector. Stability (saline and blood), lipophilicity and competitive binding were determined following published methods. **Results:** Cu-NODAGANOC and Ga-NODAGANOC were successfully synthesized and identified by LCMS-QTOF. Moreover, labeling of ^{68}Ga-NODAGANOC and ^{64}Cu-NODAGANOC was optimized and achieved a radiochemical yield (RCY) >99% and RCP >95%. Optimal radiochemical incorporation of copper-64 could be achieved at milder conditions than with gallium-68; copper-64 showed a RCY > 99% with 3 nmol of NODAGANOC for 7 minutes at RT. For gallium-68 the mildest conditions to obtain RCY >99% were 5 nmol NODAGANOC; 7 minutes at 75°C. Both radiopharmaceuticals showed high stability in plasma *in vitro* (>94 %, 2 h) and comparable lipophilicity (-1.14 and -1.63, respectively). The computed IC50 for both tracers was 0.2 nM and comparable with that of ^{68}Ga-DOTATOC. **Conclusions:** Both ^{68}Ga and ^{64}Cu-NODAGANOC appear promising radiotracers for detection of NETs tumours. Future studies are needed to assess whether ^{68}Ga and ^{64}Cu-NODAGANOC are superior to ^{68}Ga-DOTATOC in clinical practice.

E-PW073

^{18}F-FLT PET/CT imaging and inhibition of multiple signaling pathways downstream EGFR and MET receptors in resistant NSCLC

F. Iommelli[1], V. De Rosa[1], M. Monti[2], C. Terlizzi[2], M. Panico[1], S. Del Vecchio[2,1]; [1]Institute of Biostructures and Bioimaging, National Research Council, Naples, ITALY, [2]Department of Advanced Biomedical Sciences, University "Federico II", Naples, ITALY.

Aim: Simultaneous targeting of EGFR and MET receptors with a combination of selective tyrosine kinase inhibitors (TKIs) in patients with non-small cell lung cancer (NSCLC) is a strategy currently tested in clinical trials to prevent the emergence of pre-existing resistant clones in response to drug pressure, to overcome acquired MET-mediated resistance in EGFR-driven NSCLC and to exploit a synergistic effect improving clinical outcome. We previously reported that imaging with ^{18}F-FLT PET/

CT is able to detect reversal of MET-mediated resistance and to reveal synergy among different TKIs in the treatment of NSCLC. To elucidate the mechanisms responsible for the improvement of tumor response to combination therapy, we tested whether inhibition of multiple signaling pathways may converge on a common downstream effector to modulate cell proliferation. **Methods:** NSCLC cells with MET amplification and wild type EGFR (H1993) were treated with erlotinib and crizotinib, either alone or in combination and then tested for cell viability and levels of p-STAT3 (Tyr705)/STAT3, pAKT/AKT, pERK/ERK, cyclin D1 and c-Myc. Furthermore, H1993 tumor-bearing mice underwent ^{18}F-FLT PET/CT scan before and after treatment with escalating doses of EGFR and MET inhibitors, alone or in combination, and post-treatment changes of ^{18}F-FLT uptake in tumors were determined. At the end of imaging studies, tumors were removed and western blotting analysis of signaling mediators and effectors was performed on tumor lysates. Synergistic effect was evaluated for in vivo and in vitro data sets by determining the combination index (CI) using the CompuSyn software. **Results:** Imaging studies showed a significant reduction of ^{18}F-FLT uptake in response to combined treatment with escalating doses of EGFR and MET inhibitors that was higher than that obtained with treatment with single agents. In H1993 cells and excised tumors, combined treatment with EGFR and MET inhibitors caused a cumulative dose-dependent reduction of p-AKT, p-ERK and cyclin D1 levels that was stronger than that obtained by each drug alone. A synergistic effect among the two TKIs was also observed in the reduction of p-STAT3 (Tyr705) and c-Myc levels at late time points (48h-72h) in both H19993 cells and excised tumors. **Conclusion:** Our findings indicate that synergy between EGFR and MET inhibitors in determining targeted growth arrest and hence reduction of ^{18}F-FLT uptake may occur through the inhibition of multiple signaling pathways and the suppression of feedback activation of STAT3 and c-Myc which provide a compensatory cellular mechanism to escape drug injury.

E-PW074

New Sensitive Method For HEPES Quantification in [^{68}Ga]-Radiopharmaceuticals

I. F. Antunes[1], G. M. Franssen[2], R. Zijlma[1], G. L. K. van der Woude[1], C. B. Yim[3], P. Laverman[2], H. H. Boersma[1], P. H. Elsinga[1]; [1]University Medical Center of Groningen, Groningen, NETHERLANDS, [2]Radboud University Medical Center, Nijmegen, NETHERLANDS, [3]University of Turku, Turku, FINLAND.

Objective: The introduction of a GMP-certified [^{68}Ga]-generator spurred the application of [^{68}Ga]-radiopharmaceuticals. Some radiosyntheses of [^{68}Ga]-radiopharmaceuticals are more efficient and stable when performed with HEPES buffer[1,2] which is an impurity. Thus, prior to clinical use, quality control (QC) must be conducted to ensure that HEPES does not exceed the maximum dose of 200 µg/V$_{Injected}$ as described in *European Pharmacopoeia*[3]. Here we compared the TLC-method[3] with a new HPLC-method to quantify HEPES in [^{68}Ga]-radiopharmaceuticals. In addition, samples from different institutes were compared to

evaluate whether the synthesis of different [68Ga]-radiopharmaceuticals or the use of different synthesis modules could affect the amounts of HEPES. **Method:** The TLC-method was performed as described in the literature[3] with additional iodine incubation times (4, 30, 150 min and 18 h). The HPLC method (XBridge C18 column; mobile phase: ammonium formate 20mM) was validated according to ICH-M3 guidelines. Various HEPES concentrations (6-2000 μg/mL) were analysed by both methods. Samples of [68Ga]DOTATOC (n=9), [68Ga]HBED-CC-PSMA (n=8) and [68Ga]NODAGA-Exendin (n=9) from different institutes were tested with the HPLC method. **Results:** HEPES was not detected by the TLC method within 4 min incubation in an iodine saturated chamber. At 18 h, spots were only visible > 50 μg/mL. The HPLC method had a limit-of-quantification of 3 μg/mL and a limit-of-detection of 1 μg/mL. The HEPES concentrations in the final products of [68Ga]DOTATOC, [68Ga]PSMA and [68Ga]Exendin were 20±7 μg/mL, 5±6 μg/mL and 42±14 μg/mL, respectively. No significant differences were observed in the amounts of HEPES present in the same [68Ga]-radiopharmaceutical produced with similar protocols and synthesis modules, even when coming from different institutes. However, the HEPES concentration was affected when produced with a different synthesis module with different labelling reaction conditions. **Conclusion:** The TLC method described in *European Pharmacopoeia* is not sufficiently sensitive and thus unsuitable to use prior to QC release. The HPLC method was sensitive, quantitative, reproducible and suitable for QC release. With this method we were able to determine that the labelling reaction conditions may affect the amounts of HEPES in the final product. This new analytical system will be used for further studies in order to reduce the amounts of HEPES in the final product. **Acknowledgements:** This study was funded by the BetaCure project 666495. **References:** 1. R. Sasson et.*al.* , *J Radioanal Nucl Chem* **2010**, *283*, 753-756, 2. Zhernosekov KP, et *al*. *J Nucl Med* **2007**, 48:1741–1748, 3. Gallium (68Ga) edotreotide injection. *European Pharmacopoeia*. **2014**,1062.

E-PW075

Effect of Selective Endothelin B Receptor Agonist IRL-1620 on [18F]FDG Uptake in a Mouse Model of Breast Cancer

*A. Yatsyna, O. Sarrhini, M. Bentourkia, R. Lecomte, **S. V. Selivanova**; Sherbrooke Molecular Imaging Centre, CRCHUS, Université de Sherbrooke, Sherbrooke, QC, CANADA.*

Aim: Activation of endothelin type B (ET$_B$) receptors on the vasculature can produce a vasodilation or vasoconstriction of varying degrees of potency and this response depends on the cell type and tissue. ET$_B$ receptors on endothelial cells produce vasodilation, while those on vascular smooth muscle cells produce vasoconstriction. Often, tumor-associated blood vessels lack smooth muscle cells that control blood flow at normal conditions and cannot provide required auto-regulation. It was shown previously that ET$_B$ receptor agonists can produce transient effects on tumor vasculature. Consequently, ET$_B$ ligands were proposed as tools to selectively modify tumor blood flow for enhanced drug delivery. The purpose of this study was to

evaluate the effect of selective ET$_B$ agonist, IRL-1620, on [18F]FDG uptake in different organs and tissues in a mouse animal model of breast cancer. **Methods:** BALB/c mice were inoculated with MC7-L1 mouse mammary carcinoma cells and tumors were allowed to grow. Acute inflammation was induced with turpentine oil. Mice were injected with either, phosphate buffered saline or IRL-1620 (Suc-Asp-Glu-Glu-Ala-Val-Tyr-Phe-Ala-His-Leu-Asp-Ile-Ile-Trp) followed by [18F]FDG. Tissue distribution of [18F]FDG was monitored using PET and the radioactivity uptake in tumor, inflammation, muscle and other organs of interest was quantified. *Ex vivo* biodistribution (60 min after [18F]FDG injection) and histological staining were performed to validate the results. Two animals were subjected to a continuous infusion of [18F]FDG while IRL-1620 was administered to observe its effect in real time. **Results:** In PET, [18F]FDG uptake in tumor increased by ~50% on average when [18F]FDG was administered 15 minutes after the treatment with IRL-1620; tumor-to-muscle ratio rose by ~30%. Tumor-to-inflammation ratio showed negative correlation with the progression of inflammation, with or without IRL-1620. Results of *ex vivo* biodistribution revealed similar trend: while tumor uptake of [18F]FDG has substantially improved with IRL-1620 administration, the uptake in inflamed tissue depended more on the degree of acute inflammation. In infusion experiments, the rate of [18F]FDG uptake increased 1.6 and 1.8 fold potentiated by IRL-1620. **Conclusions:** IRL-1620 significantly enhanced [18F]FDG uptake in the tumors of mice bearing mammary carcinoma allografts. [18F]FDG uptake in the inflamed tissue was dependent on the degree of acute inflammation. Effect of IRL-1620 on normal tissues and organs was much less pronounced. Administration of IRL-1620 together with [18F]FDG could be a promising strategy to improve the delivery of [18F]FDG to breast cancer lesions.

E-PW076

Prediction of the synergistic efficacy of capecitabine and TAS-102 in mice with colon cnacer xenografts using [18F] fluorothymidine positron emission tomography

S. Kim[1], J. JUNG[1], H. Lee[1], H. Soh[1], S. Lee[2], S. Oh[2], S. Chae[2], J. Lee[3], S. Lee[4], Y. Hong[5], T. Kim[5], D. Moon[2]; [1]Asan Institute for Life Sciences, Asan Medical Center, Seoul, KOREA, REPUBLIC OF, [2]Department of Nuclear Medicine, Asan Medical Center, Seoul, KOREA, REPUBLIC OF, [3]Department of Nuclear Medicine, Dankook University Hospital, Cheonan, KOREA, REPUBLIC OF, [4]Department of Pharmacology, Chungnam National University College of Pharmacy, Daejeon, KOREA, REPUBLIC OF, [5]Department of Oncology, Asan Medical Center, Seoul, KOREA, REPUBLIC OF.

Purpose: We investigated whether sequential combination therapy of capecitabine and trifluridine-tipiracil (TAS-102) could synergistically enhance antitumor efficacy in colon cancer xenograft models. We also examined 3'-deoxy-3'-[18F]fluorothymidine ([18F]FLT) positron emission tomography (PET) for prediction of the therapeutic response to a sequential combination of capecitabine and TAS-102. **Subjects & Methods:** [3H]FLT uptake, [3H]-S-(p-nitrobenzyl)-6-thioinosine binding, and thymidine kinase 1 activity after 5-fluorouracil treatment *in vitro* and

[18F]FLT uptake after capecitabine (360 mg/kg/day) in athymic nude mice (Balb/c-nu) with xenografts (n = 10-12 per group) were measured using eight human colon cancer cell lines HCT8, HT29, SW620, DLD-1, RKO, COLO205, HCT116, and LOVO. The synergistic effect of sequential combinations of 5-fluorouracil and trifluridine *in vitro*, and the sequential combination of oral capecitabine (30-360 mg/kg) and TAS-102 (trifluridine 75 or 150 mg/kg with tipiracil) in six xenograft models (n = 6-10 per group) was determined. **Results:** There were significant increases in [3H]FLT uptake in all cell lines ($P < 0.05$). Likewise, equilibrative nucleoside transporter 1 increased remarkably after 5-fluorouracil treatment in most cell lines ($P < 0.05$), except for DLD-1. Thymidine kinase 1 activity was also significantly increased in five cell lines after 5-fluorouracil treatment ($P < 0.05$), but not in the HCT8, SW620 and LOVO cell lines. Serial [18F]FLT PET images after capecitabine treatment revealed a significant increase in [18F]FLT uptake ([18F]FLT flare) in five xenograft models (HT29, RKO, COLO205, HCT116 and LOVO), but not in HCT8, SW620, and DLD-1 xenografts. [18F]FLT flare after capecitabine followed by extinction of flare activity had a strong correlation with tumor growth inhibition ($\rho = -0.81$, $P = 0.02$). The effects of the combination of 5-fluorouracil and trifluridine *in vitro* were synergistic in all cell lines. Of these capecitabine-resistant HCT8, HT29, SW620, and DLD-1 xenografts, only the HT29, which had a significant [18F]FLT flare after capecitabine, showed synergistic efficacy with a percent tumor growth inhibition of 51.1%. Capecitabine-sensitive HCT116 and LOVO xenografts, which had a significant [18F]FLT flare after capecitabine, also showed synergistic antitumor efficacy of low dose capecitabine and TAS-102. **Conclusion:** The sequential combination of capecitabine and TAS-102 is synergistic in tumors with an activated salvage pathway after capecitabine in mice. [18F]FLT PET imaging may predict the response to capecitabine and the synergistic antitumor efficacy of a sequential combination of capecitabine and TAS-102.

E-PW077

[18F]-5-fluoroaminosuberic acid ([18F]FASu) superior to [18F]FDG in small animal PET/CT imaging of human xenografts

M. Colovic[1,2], H. Yang[1], H. Merkens[2], L. Southcott[1], N. Colpo[2], J. Rousseau[2], F. Benard[2,3], P. Schaffer[1,3]; [1]TRIUMF, Vancouver, BC, CANADA, [2]British Columbia Cancer Research Centre, Vancouver, BC, CANADA, [3]Department of Radiology, University of British Columbia, Vancouver, BC, CANADA.

Aim: [18F]fluorodeoxyglucose ([18F]FDG) is the most widely-used positron emission tomography (PET) tracer. The sensitivity of [18F]FDG to detect cancer varies depending on the tumour type, and is lower in organs with high background activity, such as the brain. [18F]-5-fluoroaminosuberic acid ([18F]FASu) was recently characterized as an oxidative stress imaging agent targeting a cystine transporter protein, system x_C^-. The aim of this study is to compare [18F]FASu with [18F]FDG in imaging non-small cell lung cancer and glioma xenografts in mice. **Materials and Methods:** A series of human cancer cells lines was used in this study, including a non-small cell lung cancer cell line, A549, and glio-

blastoma cell line, U-87. *In vitro* [18F]FASu uptake was measured at 20, 40 and 60 min time points, in the presence or absence of system x_C^- inhibitor sulfasalazine. For biodistribution and *in vivo* imaging studies, immunocompromised Rag2M female mice were inoculated subcutaneously with either A549 or U-87 cells in 1:1 ratio with Matrigel. Once tumours reached ~7-10 mm in diameter, mice were intravenously injected with [18F]FASu or [18F]FDG. Mice destined for biodistribution were sacrificed by CO_2 asphyxiation 60 min after radiotracer injection; their organs were harvested and measured on a PerkinElmer Wizard gamma counter. Mice destined for imaging were scanned on a Siemens Inveon Multimodality PET/CT System at 60 min post-injection, and subsequently sacrificed as described above. **Results:** [18F]FASu showed variable *in vitro* uptake in the tested cell lines, ranging from 1.84 % for MDA-MB-231 TNBC cell line, up to 11.88 % uptake/mg protein for A549 cells at 60 min. The tracer uptake increased over time, and was efficiently blocked with addition of sulfasalazine, demonstrating system x_C^-- specific uptake. We then selected the cells lines among the lowest (U-87) and highest (A549) *in vitro* uptake, for subsequent animal studies. [18F]FASu had higher tumour uptake *in vivo* than [18F]FDG, with 4.96 compared to 3.75 %ID/g for U-87 tumours, and 5.00 *versus* 2.33 %ID/g for A549 tumours, which was also evident on the PET/CT images. **Conclusion:** In murine models, [18F]FASu can be used to clearly visualize non-small cell lung cancer and glioblastoma xenografts *in vivo* better than [18F]FDG. With significantly lower background uptake, image contrast was superior to [18F]FDG. Particularly, low brain uptake of [18F]FASu highlights its potential for imaging intracranial malignancies.

E-PW078

Imaging Cancer Metastases in a Metastatic Pancreatic Ductal Adenocarcinoma (PDAC) Rodent Model Using (4S)-4-(3-18F-fluoropropyl)-L-Glutamate (FSPG) by Small-Animal PET/CT: a Preclinical Study

M. CHENG[1], Y. Huang[1], L. Hsin[2], C. Shiue[3], Y. Chang[1], R. Yen[1], Y. Tien[1]; [1]National Taiwan Universty Hospital, Taipei, TAIWAN, [2]School of Pharmacy, Molecular Imaging Center, and Center for Innovative Therapeutics Discovery, National Taiwan University, Taipei, TAIWAN, [3]National Taiwan University Hospital and Molecular Imaging Center, Taipei, TAIWAN.

Background and Aim: The System xC- transporter (xCT) mediates the sodium-independent cellular uptake of cysteine in exchange for intracellular glutamate, a pathway involved in the antioxidation process. Cancer cells show survival advantage over normal cells by higher expression of xCT. In humans, xCT is found to express in the brain, pancreas, stromal, and immune cells. FSPG is a new PET tracer reflecting cellular xCT activity. Human studies have shown intense physiologic distribution of FSPG in the pancreas. We hypothesize that xCT activity in the pancreas is upregulated during malignant transformation, which makes FSPG an ideal tracer to detect PDAC metastases. Accurate staging is of utmost importance in patients with PDAC before undergoing surgery. Here we report the result of a preclinical study comparing tumor detection rate of FSPG, com-

paring to FDG, in a metastatic PDAC rodent model. **Materials and Methods:** *In vivo* metastatic PDAC model was constructed by orthotopically injecting pancreatic cell lines (5 x 10^5 cancer cells) labeled with luciferase gene into pancreas of the SCID mice (*n*=6). FDG and FSPG small-animal PET scanning were performed in the same mouse within 1 day apart weekly for at least 2 weeks. In vivo bioluminescence imaging using the IVIS Spectrum was also done on the 2nd day after completing the dual tracer imaging. We then compared the efficiency of tumor detection between FSPG and FDG PET. **Results:** FSPG detected hepatic and peritoneal metastases from PDAC at an earlier time than FDG PET/CT. Besides, FSPG could detect more lesions at an advanced stage of cancer compared to FDG. Superior imaging characteristics of FSPG compared to FDG was also found. The tumor to nontumor ratio was 2.94±1.12 for FDG and 4.77±1.59 for FSPG. **Conclusion:** Our preliminary results suggest FSPG may be a useful PET imaging tracer in PDAC patients before undergoing surgery. Further studies in patients with PDAC are needed.

E-PW079

Potential of PET imaging to monitor upregulation of NET-1 transporter

S. M. Turnock[1], D. R. Turton[1], D. M. Ciobota[1], O. Yogev[1], L. Chesler[1], T. Wilson[2], V. Gouverneur[2], G. Smith[1], G. Kramer-Marek[1]; [1]The Institute of Cancer Research, Sutton, UNITED KINGDOM, [2]University of Oxford, Oxford, UNITED KINGDOM.

Aims: The norepinephrine analogue ^{123}I-mIBG (*meta*-iodobenzylguanadine) is widely used in diagnostic imaging of NET-1 expressing cancers such as neuroblastoma (NB). However, it is not sensitive enough to accurately assess tumour response rates to high doses of ^{131}I-mIBG in high-risk NB patients. Therefore, we have investigated the potential of ^{18}F-mFBG (*meta*-fluorobenzylguanidine) to improve imaging of NB using Positron Emission Tomography (PET) and to guide therapeutic combinations with ^{131}I-mIBG that could reduce dose and therefore toxicity, and increase efficacy by upregulating expression and/or function of the NET-1 transporter. **Materials and Methods:** ^{18}F-mFBG was radiolabelled using a recently developed copper catalysed nucleophilic fluorination from a borylated precursor. The specificity of ^{18}F-mFBG to NET-1 was analysed in a panel of NB cell lines with varying NET-1 expression levels via cell uptake assay and compared with ^{123}I-mIBG. The specificity of the radiotracer *in vivo* was evaluated in mice bearing SK-N-BE(2)C (NET-1+ve) and Kelly (NET-1-ve) subcutaneous xenografts. PET/CT images were acquired at 1 and 4 h p.i. to determine systemic radiotracer distribution. The results were compared with the distribution of ^{123}I-mIBG. At the conclusion of each imaging session, blood and major organs were collected and radioactivity accumulation measured using a γ-counter. *Ex vivo* analysis of NET-1 expression was assessed by Western blot (WB) and immunohistochemistry (IHC). To modulate ^{18}F-mFBG tumour uptake, proof of concept *in vitro* studies were done using the mTORC1/2 inhibitor, AZD2014. Upregulation of NET-1 was measured by WB, ^{18}F-mFBG and the fluorescent neurotransmission transporter cell uptake assays. **Results:** ^{18}F-mFBG uptake correlated *in vitro* with NET-1 expression in a panel of NB

cell lines and was in concordance with the results obtained for ^{123}I-mIBG. Moreover, there was also increased and dose dependent uptake of ^{18}F-mFBG in response to AZD2014. *In vivo* studies demonstrated that ^{18}F-mFBG can differentiate between NET-1 expressing (SK-N-BE(2)C) and non-expressing (Kelly) tumours at 4 h p.i. (3.58±1.40%ID/g vs. 1.25±0.14%ID/g, respectively). Tracer was eliminated quickly from the blood and normal tissues, allowing high contrast images to be acquired 4 h p.i. (T:B 6.94±1.44; T:M 2.37±0.80). A strong correlation was observed between *ex vivo* estimates of tracer concentration and the transporter expression measured in the tumour tissues (IHC, WB). **Conclusion**: ^{18}F-mFBG can quantifiably assess different levels of NET-1 transporter *in vitro* and *in vivo* therefore might provide guidance for novel therapy plans and allow for the rapid identification of responders and non-responders in future clinical trials.

Clinical Oncology: Walk FDG

E-PW080

Early response evaluation by ^{18}F-FDG-PET influences management in gastrointestinal stromal tumor patients treated with neo-adjuvant intent

S. Farag[1], N. Steeghs[1], W. T. van der Graaf[2,3], F. van Coevorden[1], D. J. Grunhagen[4], A. K. L. Reyners[5], P. A. Boonstra[5], H. J. Gelderblom[6], L. de Geus-Oei[6,7]; [1]Antoni van Leeuwenhoek Hospital, Amsterdam, NETHERLANDS, [2]The Radboud University Medical Center, Nijmegen, NETHERLANDS, [3]Institute of Cancer Research, London, UNITED KINGDOM, [4]Erasmus Medical Center - Cancer Institute, Rotterdam, NETHERLANDS, [5]University of Groningen, Medical Center Groningen, Groningen, NETHERLANDS, [6]Leiden University Medical Center, Leiden, NETHERLANDS, [7]University of Twente, MIRA Institute, Twente, NETHERLANDS.

Background: Early response evaluation by ^{18}F-fluorodeoxyglucose (FDG) positron emission tomography (PET) is effective in gastrointestinal stromal tumors (GISTs) treated with imatinib and recommended in GISTs treated with neo-adjuvant intent. Yet, it is unclear whether this effects treatment decisions. **Methods:** All patients in the Dutch GIST Registry treated with imatinib with neo-adjuvant intent were identified. Only FDG-PETs made within 8 weeks after initiation *or change* (in dose or switch) of imatinib were included. Responses were derived from radiological reports and defined in 3 categories: 1) complete response; 2) partial response; 3) no response. Change in management was defined as a difference between pre-PET and post-PET treatment plans. Four categories were defined: change in 1) surgical management; 2) systemic treatment; 3) treatment objective (from curative to palliative); 4) management regarding a second tumor. **Results:** Seventy FDG-PETs for early response evaluation in 63 patients treated with neo-adjuvant intent were identified. Forty-one patients (65.1%) had a KIT exon 11 and 22 (34.9%) had a non-KIT exon 11 mutation (15 other and 7 unknown mu-

tations). Of the 70 scans 64 (87.1%) had a baseline, 50 (71.5%) showed metabolic response (partial and complete), and 18 (25.7%) led to change in management. Change in management was strongly correlated with a lack of response (p<0.001) and a non-KIT exon 11 mutation (p<0.001). Mutational status and response were strongly correlated (p<0.001). Out of 29 FDG-PETs conducted in non-KIT exon 11 GISTs, 15 (51.7%) led to change in management: 1 (3.4%) in surgical management, 6 (20.7%) in systemic treatment, 7 (24.1%) in both and 1 (3.4%) regarding a second tumor . Out of 51 FDG-PETs conducted in KIT exon 11 GISTs, change in management was seen 3 times (5.9%): twice in systemic treatment (dose increase after partial response was seen) and once regarding a second tumor. No change in treatment objective was seen. **Conclusion:** In contrast to GIST patients harboring a KIT exon 11 mutation, in non-KIT exon 11 mutated GISTs treated with neoadjuvant intent early response evaluation by FDG-PET often leads to change in management.

E-PW081

The prognostic significance of metabolic tumor volume (MTV) and total lesion glycolysis (TLG) with F18 FDG PET / CT in non-small cell lung cancer (NSCLC)

S. Göksel, Y. Yürekli, A. Cengiz; Adnan Menderes University Medical School Department of Nuclear Medicine, Aydın, TURKEY.

Purpose: To investigate the relationship between the semi-quantitative parameters such as SUVmax, MTV and TLG and the stage of disease and histological subtype and contribution of these parameters to prediction of prognosis in NSCLC. **Subjects and Methods:** A total of 102 patients (40-89 years old) with the diagnosis of NSCLC and underwent PET/CT imaging for staging were included in the study. Histopathological diagnosis, stage of the disease, SUVmax-MTV-TLG values of mass lesions and date of diagnosis were recorded. Survival times of the patients were determined by phone calls to all patients. Mann-Whitney U test was used for statistical comparisons between the groups. The relationship between survival time and MTV, TLG, SUVmax was determined by Spearman correlation analysis. The relationship between survival time and TNM stages was determined by the Kaplan-Meier test. **Results:** 71 patients had a pathological diagnosis of squamous cell carcinoma (69.61%) and 31 patients had adenocarcinoma (30.39%). In surviving patients (27.45%) the mean MTV value was 50.21 ± 57.32, the mean TLG value was 481.02 ± 581.87, and the mean SUVmax value was 16.70 ± 8.45. In deceased patients (72.54%), the mean MTV value was 68.28 ± 75.89, the mean TLG value was 553.09 ± 662.97 and the mean SUVmax value was 14.35 ± 5.85. When the relationship between TNM stage of the disease and survival was examined, survival times were shorter in patients with advanced stage (p: 0.002). Statistically significant negative correlation was determined between MTV and survival (p: 0.020) and TLG and survival (p: 0.027). No statistically significant relationships between SUVmax and survival (p: 0.861) and SUVmax and stage of the disease (p: 0.473) have been determined. Mean MTV value was 22.32 in stage 1,2 and 68.2 in stage 3,4 (p: 0.012); The mean TLG value was calculated as 232.27 in stage 1,2 and 569.69 (p: 0.037) in stage 3,4. As the stage increased, MTV and TLG increased and survival time decreased. There was no significant relationship between the MTV and TLG and histopathological types of the lesions. SUVmax values were higher in squamous cell carcinoma (p: 0.012). **Conclusion:** MTV and TLG of FDG PET/CT contribute significantly in predicting survival and prognosis in non-small cell lung cancers independently from stage and histopathological subtype.

E-PW082

Prediction of small early lung adenocarcinoma with aggressive histopathologic subtypes using PET and CT radiomic features

C. Liu, W. Choi, S. Riyahi, W. Lu, J. Oh, J. Deasy, P. Adusumilli, W. Weber; Memorial Sloan-Kettering Cancer Center, New York City, NY, UNITED STATES OF AMERICA.

Purpose: The solid and micropapillary (MIP) histopathologic patterns have been identified as indicators for poor prognosis of patients with small early lung adenocarcinoma (ADC). Patients with these aggressive subtypes may benefit from lobectomy rather than limited resection of the tumors. This study was aimed to classify early small lung ADC with these aggressive components by using positron emission tomography (PET) and computed tomography (CT) radiomic analysis. **Materials and Methods:** The study retrospectively included 135 patients with stage I lung adenocarcinoma with tumor size smaller than 2cm. Preoperative diagnostic CT and 18F-fluorodeoxyglucose (FDG) PET were analyzed. Tumor segmentation of CT was manually contoured on axial images. A semiautomatic algorithm using two standard deviations (SD) above background FDG uptake was applied for tumor segmentation on PET images. A total 170 of radiomic features was extracted from both diagnostic CT and PET, including intensity, shape, intensity-weighted shape, and texture features. The features were used to identify the cases with aggressive subtypes, which were defined as tumors with predominant solid or MIP components according to IASLC/ATS/ERS classification. Univariate analysis was performed to evaluate each radiomic feature using area under the curve (AUC) of receiver operating characteristic (ROC) and *p*-value computed by Wilcoxon rank-sum test. For multivariate analysis, important and non-redundant features were selected by class separability feature selection (CSFS) method using between-class and within-class scatter-matrix. The prediction model was then generated by least absolute shrinkage and selection operator (LASSO) regression. A 10-fold cross-validation was repeated ten times to obtain an unbiased estimate of the model, which constructed and evaluated 100 different models. **Results:** Among 135 patients, 36 patients had aggressive subtypes (solid: 26, MIP: 10). Ninety-four features were significant (all *p*<0.05) in univariate analysis (AUC: 0.61~0.78), including 29 CT features and 65 PET features. The SD of entropy on PET and the mean of cluster shade on CT were selected in CSFS-LASSO model. The sensitivity, specificity, and accuracy of the model were 75.5±4.6%, 74.3±1.9%, and 74.6±2.3%, respectively. The AUC of the CSFS-LASSO model was 0.75±0.03 (p<0.001). **Conclusion:**

Both PET and CT radiomics features are potential biomarkers of aggressive lung ADC subtypes. The prediction model combined both imaging modalities could serve as a non-invasive classification tool for small lung ADC subtypes and provide additional information for surgery.

E-PW083

Total lesion glykolysis of the primary tumour as a biomarker derived from pre-operative FDG PET/CT outperforms established prognostic parameters in oral squamous cell carcinoma

D. Weidt[1], G. Spanier[2], T. Reichert[2], J. Meier[2], D. Hellwig[1], J. Grosse[1]; [1]*Department of Nuclear Medicine, University of Regensburg Medical School, 93059 Regensburg, GERMANY,* [2]*Department of Oral and Maxillofacial Surgery, University Hospital Regensburg, 93059 Regensburg, GERMANY.*

Objective: The purpose of this retrospective study was to investigate the impact of image derived biomarkers from FDG PET/CT prior to surgical resection in patients with initial diagnosis of oral squamous cell carcinoma (OSCC), namely maximum and mean tumoral SUV (SUVmax, SUVmean), metabolic tumour volume (MTV) and total lesion glycolysis (TLG) of the primary tumour to predict overall survival (OS). Furthermore to compare its prognostic value with established prognostic factors such as lymph node status and UICC stage. **Materials and Methods:** A total of 127 subsequent patients with biopsy-proven OSCC was included who underwent FDG PET/CT between 2006 and 2013 before surgery. The PET/CT acquisition (Biograph 16, Siemens, Germany) was started 60 min p.i. of 3 MBq FDG per kg body weight. SUVmax, SUVmean, MTV and TLG of the primary tumour were measured using ROVER (ABX, Radebeul, Germany). MTV was delineated with a relative threshold of 41% SUVmax. OS, defined as time from PET/CT until death of any cause, was estimated according to Kaplan-Meier and compared between median-splitted groups by the log-rank test. Prognostic parameters were analyzed by univariate and multivariate Cox regression. **Results:** During follow-up 52 (41%) of the patients died. All patients had a known status at 36 months after initial PET/CT. Median OS was longer for patients with lower MTV (≤5.3 mL: >95 months; >5.3 mL: 59 months; p=0.004) or lower TLG (≤38.7 g: 95 months; >38.7 g: 47 months; p<0.001). SUVmax and SUVmean failed to be significant predictors for OS (both p>0.05). Univariate Cox regression identified MTV (hazard ratio [HR]=2.260, p=0.005), TLG (HR=2.808, p=0.001), lymph node status (HR=2.234, p=0.005) and UICC stage (HR=2.095, p=0.021) as prognostic factors, but not sex, age>60 years, history of smoking or alcohol abuse and adjuvant treatment. By multivariate Cox regression MTV (HR=1.991, p=0.019) and TLG (HR=2.808, p=0.001) turned out to be independent prognostic factors for OS, even if tested against lymph node status and UICC stage, with TLG being completely independent. **Conclusion:** The pre-therapeutic FDG PET/CT parameters MTV and TLG in the primary tumour are prognostic for OS of patients with an initial diagnosis of OSCC. TLG is the strongest independent prognostic factor for OS and outperforms established prognostic parameters in OSCC.

E-PW084

Adaptive 18F-FDG-PET-guided reirradiation for recurrent and second primary head and neck cancer

J. Schatteman[1], D. Van Gestel[2], D. Berwouts[1], W. De Gersem[1], G. De Kerf[3], W. De Neve[1], B. De Ost[3], A. Olteanu[1], S. Rottey[1], T. Vercauteren[1], F. Duprez[1], I. Goethals[1]; [1]*Ghent University Hospital, Ghent, BELGIUM,* [2]*Jules Bordet Institute, Brussels, BELGIUM,* [3]*Antwerp University Hospital, Antwerp, BELGIUM.*

Purpose: To evaluate feasibility, disease control, survival and toxicity after adaptive ^{18}F-FDG-PET-guided radiotherapy (RT) in recurrent and second primary head and neck squamous cell carcinoma (HNSCC). **Subjects & Methods:** A multicenter non-randomized prospective trial investigated the feasibility of adaptive RT ± concomitant cetuximab in 10 patients with recurrent (n=5) and second primary (n=5) HNSCC. Patients were treated with static beam IMRT (n=6) or helical tomotherapy (n=4) with 3 treatment plans based on 1 pre- and 2 pertreatment PET/CT scans and consecutively delivered in 6 weeks. The range of dose painting was 66.0-85.0 Gy in the dose-painted tumoral volumes in 30 fractions with fraction doses of 2.2-3.5 Gy, 2.2-2.5 Gy and 2.2-2.5 Gy during fractions 1-10, 11-20 and 21-30, respectively. If multidisciplinary decision for concomitant cetuximab was taken, patients received a loading dose (400 mg/m^2) one week before start of RT, followed by weekly doses of 250 mg/m^2 up to 6 times concomitant to RT. The primary endpoint of the study was to achieve a 2-year grade >3 toxicity-free survival in ≥30% of patients. **Results:** Median dose of the initial RT was 67.6 Gy. Median time interval from initial RT to reirradiation was 6.3 years. Median follow-up time was only 5.2 months, reflecting the poor overall survival. One-year locoregional and distant control were 38% and 76%, respectively. Overall and disease-free survival at 1 year were 30% and 20%, respectively. No grade 4 or 5 acute toxicity was observed in any of the patients, except for arterial mucosal bleeding in one patient. Three months after RT, grade 4 dysphagia and mucosal wound healing problems were observed in 1/7 and 1/6 of the patients, respectively. Grade 5 toxicity (fatal bleeding) was seen in 2 patients, respectively at 3.8 and 4.1 months of follow-up. Late toxicity until 1 year of follow-up could only be assessed in 2 patients. Data on 2-year grade >3 toxicity-free survival is not yet available; however, since only 20% of patients are still alive, a 30% 2-year survival free of grade >3 toxicity will not be achieved. There was a significant difference in SUV$_{max}$ between the pretreatment and second pertreatment PET after fraction 18 (*p* = 0.01). No significant differences in RT treatment volumes were observed. **Conclusion:** Adaptive PET-guided reirradiation is feasible. However, the primary endpoint (to achieve a 2-year grade >3 toxicity-free survival in ≥30% of patients) could not be evaluated in this limited patient cohort with poor survival.

E-PW085

Recurrent germinal tumor carcinoma: clinical and prognostic value of FDG-PET/TC

P. Alongi[1], M. Picchio[2], F. Caobelli[3], M. Spallino[4], L. Gianolli[2], M. Midiri[1], L. Evangelista[5]; [1]*San Raffaele G.Giglio Institute, Cefalù,*

ITALY, [2]IRCSS San Raffaele Scientific Institute, Milano, ITALY, [3]Basel University Hospital, Basel, SWITZERLAND, [4]University of Milano-Bicocca, Milano, ITALY, [5]Veneto Institute of Oncology IOV - IRCCS, Padova, ITALY.

Background and Aim: The aim of this multicentre retrospective study was to evaluate the diagnostic accuracy, the impact on treatment decision and the prognostic value of [18]FDG PET/CT in patients with suspected recurrent GTC. **Materials and Methods**: 114 patients affected by GTC were evaluated. All underwent 18F-FDG PET/CT for suspected recurrent disease. Diagnostic performance of visually interpreted FDG-PET/CT was assessed using histology (17 patients), other diagnostic imaging modalities (i.e. ceCT in 89 patients and MRI in 15) and clinical follow-up (114 patients) as reference. Progression-free survival (PFS) and overall survival (OS) were computed by means of Kaplan-Meier survival analysis. The progression rate (Hazard Ratio-HR) was determined using univariate and multivariate Cox regression analysis by considering various clinical variables. **Results**: The suspicion of recurrent GTC was confirmed in 47/52 patients with pathological PET/CT findings (by histology in 18 patients and by other diagnostic imaging modalities/follow-up in 29). Sensitivity, specificity, PPV, NPV, accuracy, LR+, LR-, pre-test Odds-ratio and post-test Odds-ratio of [18]FDG PET/CT were 86,8%, 90,2%, 88,4%, 88,7%, and 88,6%, 8,85, 0,14, 0,85, 8,85 respectively. FDG-PET/CT significantly impacted the therapeutic management in 26 cases (23%). At 2 and 5-year follow-up, PFS was significantly longer in patients with a negative PET/CT scan (98% and 95% vs 48% and 38%, p<0.05). An unremarkable scan was also associated with a longer OS (98% vs 69% after 2 years and 95% vs 33% after 5 years, p<0.05). In case of a negative PET/CT, PFS and OS were significantly longer regardless of staging TNM. Conversely, a positive PET scan was associated with an increased risk of disease progression (HR=24.3, p<0.05). At univariate Cox regression analysis, progression risk further increased in case of advanced disease at diagnosis and rising HCGB or AFP values (HR=7.3 for STAGE III-PET+; HR=14.3 elevated HCGB-PET+; HR 10.7 elevated AFP-PET+); all p<0.05). Multivariate Cox regression analysis confirms the higher risk of disease progression for PET posivite scan (PET+ HR 21,5; 95%IC: 2,5-185; p=0,005) and advanced disease at TNM staging (TNM stage III HR= 4.6; 95%IC: 1.7-12; p=0,002). **Conclusion:** FDG-PET/CT has very good diagnostic performance in patients with suspected recurrent GTC and provided a change in treatment approach in 23% of patients. Furthermore, FDG PET/CT has an important prognostic value in assessing the rate of PFS and OS and to estimate risk of disease progression in this setting of patients.

E-PW086

Costeffectiveness of second line diagnostic investigation in patients included in DANTE trial

E. Lopci[1], E. Morenghi[1], D. Tanzi[1], S. Cavuto[2], F. Lutman[1], G. Chiesa[3], E. Vanni[1], A. Chiti[1], M. Alloisio[1], M. Infante[4]; [1]Istituto di Ricerca e Cura a Carattere Scientifico (IRCCS), Milano, ITALY, [2]IRCCS Arcispedale S. Maria Nuova, Reggio Emilia, ITALY, [3]Humanitas Gavazzeni, Bergamo, ITALY, [4]AIOU, Verona, ITALY.

Aim: DANTE trial is a randomized study of lung cancer screening with low-dose spiral computed tomography (LDCT). In patients with suspicious lung nodules, the implementation of PET imaging and/or CT-guided core biopsy (CTB) can help improve the diagnostic accuracy and significantly reduce unnecessary and costly surgical procedures. So far however, there is no real evidence that this approach can be cost-effective. The aim of the present study was to analyze the accuracy and economic efficiency of a work-up protocol including such second-line diagnostic investigation (PET-CTB protocol), compared to pure LDCT follow-up (standard protocol) and growth assessment prior to surgical biopsy or return to standard follow-up, in patients with undetermined lung nodules. **Materials and Methods:** Retrospective review of all surgical cases included in the DANTE trial and monitored in our Institution from 2001-2006 for lung cancer screening was performed. Overall, 246 patients and 261 lung nodules were analyzed. The study cohort was divided into patients investigated with PET imaging, CT-guided biopsy, or both (PET-CTB protocol) (N=98), compared to patients monitored with serial LDCT assessment and growth assessment (N=148). Diagnostic accuracy was computed by comparing the performances of the two protocols with tumor histology or long-term monitoring as reference standard. Invoices analyzed in the study comprised outpatient's and inpatient's costs expressed in Euro, as reimbursed by the Italian National Health System. Ineffective costs were defined as the cost of diagnostic procedures leading to potentially avoidable surgical intervention. **Results:** The diagnostic accuracy of the two protocols resulted 94% (sens. 100%, spec. 94%, PPV 36%, NPV 100%) for the standard and 90% (sens. 98%, spec. 80%, PPV 85% and NPV 98%) for the PET-CTB protocol. Average costs for outpatient's diagnostics resulted 694 and 1.462 euro, respectively, for the standard and PET-CTB protocol. Average inpatient's costs for both protocols were 12.121 euro. By applying the costs to diagnostic performance, the two protocols showed comparable effectiveness in terms of total outpatient's costs (94% and 90%, respectively; p=0.361). The inpatient's costs resulted effective for 36% of cases operated according to the standard protocol compared to 85% of cases with the new protocol. Ineffective costs corresponded to 64% and 15% respectively (p<0.0001). **Conclusion:** In front of higher average costs for outpatients diagnostics, the implementation of PET imaging with or without CT-guided core biopsy in the diagnostic protocol of patients with suspicious lung nodules results significantly cost-effective for inpatient's procedures.

E-PW087

User-guided 3D active contour segmentation of complex-shaped tumours : an efficient semi-automatic approach in FDG PET thoracic oncology

F. L. Besson[1,2], T. Henry[1], C. Meyer[1], V. Chevance[1], V. Roblot[1], E. Blanchet[3], V. Arnould[3], G. Grimon[1], M. Chekroun[1], L. Mabille[4], F. Parent[1], A. Seferian[1], S. Bulifon[1], D. Montani[1], M. Humbert[1], P. Chaumet-Riffaud[1], V. Lebon[3], E. Durand[1,2]; [1]AP-HP Universite Paris Sud, Le kremlin bicetre, FRANCE, [2]IR4M-UMR 8081 Université Paris-Sud Université Paris-Saclay CNRS, Orsay, FRANCE, [3]CEA SHFJ, Orsay, FRANCE, [4]CCML, Clamart, FRANCE.

Purpose: PET tumour segmentation is currently an active research topic in the field of radiotherapy planning and multi-parametric data quantification. Although being efficient on homogeneous spheroid-shaped tumours, classical threshold-based approaches are of limited value for heterogeneous or complex-shaped tumours, still making expert-based manual delineation the reference standard for tumour imaging, despite several limitations. In this context, the aim of this study was to assess the performances of an active contour-based approach for the PET segmentation of complex-shaped lung tumours, in comparison to an optimized expert-based manual reference standard. **Subjects and Methods**: Seventy-five thoracic tumours were segmented using the same graphical user interface (GUI) ITK snap software. For each tumour, an optimized expert-based reference standard was generated from the set of six independent expert-based manual segmentation results using the Simultaneous Truth And Performance Level Estimate (STAPLE) algorithm. In addition, four raters semi-automatically segmented the 75 PET tumours twice using the active contour based-procedure of the GUI software, with a delay time of one week between two segmentation sessions. For the 75 tumours, accuracy of the semi-automatic segmentations against the optimized expert-based reference standard was assessed using the DICE similarity coefficient (DSC). Interrater and intrarater reliability analyses were performed using the intra class correlation coefficients (ICC) estimates of the output volumes, along with their 95% confidence intervals (two-way mixed-model, individual-rating, absolute-agreement). For all tumours segmentation procedures, average time per procedure was also estimated. **Results:** Overall accuracy of the semi-automatic procedure was excellent with a DSC of 0.835 (95%CI = 0.775-0.895). Interrater reliabilities provided the following results: ICC = 0.941 (95%CI = 0.913-0.961) for the first session and ICC = 0.935 (95%CI = 0.906-0.956) for the second session. Intrarater reliabilities provided the following results: ICC = 0.993 (95%CI = 0.990-0.996) for the rater 1; ICC = 0.987 (95%CI = 0.976-0.993) for the rater 2; ICC = 0.972 (95%CI = 0.956-0.982) for the rater 3; and ICC = 0.977 (95%CI = 0.964-0.985) for the rater 4. Average time was 631 seconds for manual segmentation procedure and 130 seconds for active contour-based. **Conclusions:** Compared to the state of the art expert-based manual segmentation, the GUI-based active contour procedure provided excellent accuracy and reliability, with a mean procedure duration almost five-times faster than the manual reference procedure. ITK snap software is robust, fast, and easy enough to be routinely applied as a powerful alternative to the manual reference standard in this setting.

E-PW088

In-vivo tumour characterization of breast cancer using [¹⁸F]FDG-PET/CT and supervised machine-learning

L. Papp, T. Nakuz, H. Magometschnigg, M. Grahovac, T. Helbich, G. Karanikas, A. Haug, K. Pinker, T. Beyer, M. Hacker; Medical University of Vienna, Vienna, AUSTRIA.

Introduction: Expression of specific molecular markers such as estrogen (ER), progesterone (PR), HER2 receptors as well as pro-liferation rate (ki67) and tumor grading has direct prognostic and therapeutic implications in breast cancer patient management. To date this assessment must be performed by invasive tissue sampling and analysis. The goal of this study was to establish predictive models for these predictive and prognostic factors using [¹⁸F]FDG-PET/CT and supervised machine-learning (ML). **Subjects and Methods:** Tissue samples of 120 patients with primary breast cancer who underwent ¹⁸FDG breast PET/CT and histopathological tissue analysis including ER, PR, HER2, ki67 and grading (G1-3) before treatment were included in this IRB-approved retrospective analysis. Volume-of-Interest (VOI) of the primary lesion was delineated manually on PET/CT images using the Hybrid-3D software (Hermes Nuclear Diagnostics, Sweden). The VOI activity values were normalized to the mean of the mediastinum to calculate tumour-to-background ratio (TBR). Thirty three features, including first-order (6), histogram (6), shape (2), textural-GLCM (7), textural-GLSZM (8), textural-NGTDM (4) were extracted from the PET TBR and the CT tumour VOIs (33/PET, 33/CT, 66 total). To predict tumour grade, ER, PR, HER2 status and Ki67 values, a multi-Gaussian fuzzy classifier model was utilized for each reference value. To identify relevant features and weights, ML solutions built on evolutionary approaches were utilized in a 10-fold cross-training scheme. The optimized models were validated by comparing their predictive values to the respective reference values in a Monte Carlo cross-validation scheme. Sensitivity, specificity and accuracy were measured for binary classifiers (ER, PR, HER2, Ki67), while accuracy was measured for the multi-class grading classifier. **Results:** The cross-validation revealed the following performance values for the predictive models: Grading: 86% accuracy; ER: 90% sensitivity, 67% specificity and 82% accuracy; PR: 87% sensitivity, 73% specificity and 82% accuracy; HER2: 87% sensitivity, 55% specificity and 64% accuracy; Ki67: 75% sensitivity, 96% specificity and 82% accuracy. **Conclusions:** [¹⁸F]FDG-PET/CT and supervised machine learning allows an accurate non-invasive assessment of predictive and prognostic molecular tumor markers and thus may facilitate a personalized breast cancer treatment.

E-PW089

Evaluation of diagnostic accuracy and impact of FDG PET/CT in pre-operative managment of early breast cancers

P. Chandra, S. Nath, S. Kumar; MIOT international hospital, Chennai, INDIA.

Aim: Exact role of PET/CT in early operable breast cancers remains to be defined. Our aim of this study was to evaluate the diagnostic accuracy of staging PET/CT in early breast cancers and to assess its impact on disease management. **Patients and Methods:** We retrospectively reviewed and analyzed pre-operative PET/CT scans of 70 patients (mean age- 55yrs) done at our institute from the year 2014-2017 with clinically T1-T2 breast cancers (all tumors < 5cm, with or without palpable mobile axillary nodes). 47 patients underwent modified radical mastectomy (MRM) and 15 patients underwent breast conservation surgery (BCS) with sentinel node biopsies. Diagnostic performance of PET/CT for nodal (N) and distant metastases (M) and

its impact on disease management was analyzed using histopathology/clinical follow up as standards of reference. **Results:** PET/CT accurately identified all the primary breast tumors (T1-15 patients, T2- 52 patients, mean size- 2.8cm, mean SUVmax-9.33). 47% patients (n=33) had nodal disease confirmed on final histo-pathological evaluation (HP), noted in 44% of T1 tumors and 46% of T2 tumors. Sensitivity, Specificity, Positive predictive value (PPV), Negative predictive value (NPV), and accuracy of clinical examination for axillary N staging were 65%, 94%, 91%, 76% and 69%. Sensitivity, Specificity, PPV, NPV, and accuracy of PET/CT for axillary N staging were 84%, 89%, 87%, 86 % and 87%. PET/CT identified extra-axillary nodal disease in supraclavicular/internal mammary nodes in 15% (n=7) of patients with T2 tumors; none in T1 tumors, leading to change in radiation treatment planning in these patients. Distant metastasis was accurately identified on PET/CT in overall 11% (n=8) patients (15% of T2 patients and none in T1 patients). Site of distant metastasis included mediastinum/lung (n=5) and skeleton (n=3). 1 patient had FDG uptake in multiple liver lesions- which was identified as adenoma subsequent work up (false positive). Sensitivity, Specificity, PPV, NPV, and accuracy for M staging were 100%, 98%, 88%, 100% and 98% respectively. Surgery was deferred in all the 8 patients with distant metastasis identified on PET/CT. **Conclusion:** PET/CT has high diagnostic accuracy for N and M staging in early breast cancers. Diagnostic yield and impact of PET/CT on disease management is higher in T2 than T1 tumors and alters disease management in overall 15% of patients with T2 tumors by altering the radiation treatment plan and/or identifying distant metastasis.

Cardiovascular System: Cardial Amyloidosis & Endocarditis

E-PW090

Myocardial Technetium-99M Methylene Diphosphonate Uptake And Left Ventricular Motion In Transthyretin Related Cardiac Amyloidosis

F. Ticconi[1], A. Nieri[1], I. Calamia[1], V. Ceriani[1], F. Fiz[2], M. Canepa[3], M. Pennone[4], M. Sicignano[4], G. Villa[4], S. Morbelli[4], P. Gancitano[4], G. Sambuceti[1,4], C. Marini[5]; [1]Department of Health Sciences, University of Genoa, Genoa, ITALY, [2]Nuclear Medicine Unit, Department of Radiology, Uni-Klinikum, Tübingen, GERMANY, [3]Cardiovascular Unit, Department of Internal Medicine, University of Genoa,, Genoa, ITALY, [4]Nuclear Medicine Unit, IRCCS San Martino-IST, Genoa, ITALY, [5]CNR Institute of Bioimages and Molecular Physiology, Milan, ITALY.

Purpose: Amyloidosis is an infiltrative disease characterized by extracellular deposition of fibrillary proteins into one or multiple organs. Left ventricular (LV) involvement usually results in restrictive cardiomyopathy up to congestive heart failure. Recognizing underlying process and its severity is an import-

ant task in risk prediction. To this purpose, ^{99m}Tc-methylene diphosphonate (^{99m}Tc-MDP) scan is a low-cost, non-invasive technique with high sensitivity ($\approx$100%) and specificity ($\approx$88%) for detecting cardiac involvement in transthyretin (TTR) related cardiac amyloidosis, even at the early asymptomatic stage. Heart tracer uptake is related to the degree of cardiac amyloid deposition and to LV dysfunction and has a predictive value of major adverse cardiac events. Aim of this study was to evaluate the distribution of ^{99m}Tc-MDP uptake in LV walls of patients with TTR-related cardiac amyloidosis and its correlation with LV wall-motion. **Subjects and Methods:** Ten patients with TTR-related cardiac amyloidosis were submitted to whole body scan 180 minutes after intravenous injection of 555-740 MBq of ^{99m}Tc-MDP. Soon after planar imaging a gated SPECT acquisition was performed dividing R-R interval in eight frames and applying a 20 segments model to LV. Myocardial tracer uptake (MTU) was expressed as % of whole body counts subtracted by the bladder radioactivity content. In ungated SPECT images, uptake distribution in the different LV walls was semi-quantitatively estimated by the product % of maximum myocardial counts in each segment times MTU. Wall motion and wall thickening were estimated by the conventional QGS software. **Results:** Overall, MTU accounted for 2.6±0.7% of whole body counts. Estimated LV ejection fraction was 37±14% and was inversely correlated with MTU (R=-0.50; p<0.05). MTU was heterogeneously distributed, being higher (p<0.05) in the septum (70±6%) with respect to anterior (53±6%), lateral (52±5%) and inferior (55±7%) walls. Finally, a trend toward a negative correlation (R=-0.34, p=0.2) was observed between MTU and regional wall motion in each segment. **Conclusion** Our study supports the idea that septal wall is preferentially involved in TTR related-cardiac amyloidosis resulting in relatively higher ^{99m}Tc-MDP uptake with respect to other LV walls. The agreement between tracer uptake and amount of amyloid infiltration is further supported by the inverse relationship between MTU and functional indexes both on a global and on a regional basis.

E-PW091

Prevalence of heart failure in elderly patients with myocardial uptake on bone scan

L. Mohamed Salem, Sr., J. Sánchez Serna, J. Santos Mateo, M. Perez Martinez, R. Reyes Marles, M. Godoy Bravo, I. Sime Loayza, M. Castellon Sanchez, F. Nicolas Ruiz, L. Frutos Esteban, J. Navarro Ferenandez, M. Tomas Redondo, D. Pascual Figal, M. Claver Valderas; Hospital Clínico Universitario Virgen de la Arrixaca, Murcia, SPAIN.

Introduction: According to scientific evidence from recent literature, myocardial uptake of bone tracers has a high specificity and sensitivity for the diagnosis of cardiac transthyretin amyloidosis, which might be a common and a potential contributor to the development of heart failure with preserved ejection fraction, nevertheless, the real relationship between cardiac amyloidosis seen on bone scan and heart failure, is not fully investigated yet. **Purpose:** To investigate the relationship between myocardial uptake on bone scan and heart failure. **Subjects and Methods:** Together with Cardiology Department

of our hospital, we investigate 105 patients with myocardial uptake on bone scan, 76 men (72.4%), mean age at the moment of the scan is 81.9 (IQR 78.2 - 85.3). We study 91 of 105 patients who performed bone scan with oncological indications, mainly prostate and breast cancers, and 3 patients with rheumatological indications (3.26%). 13 patients from 25 patients, who had myocardial uptake on bone scan, without previous diagnosis of heart failure, underwent the local protocol of heart failure and cardiac amyloidosis at the Heart Failure Unit (Cardiology Department) of our hospital. We also analyzed the causes of death of 40 of 105 patients. **Results:** 25 of 91 patients are diagnosed with heart failure (27,47%), which is considerably higher the theoretical prevalence in the same population (17%). 17 of the 25 patients was hospitalized at least once because of heart failure (68%). The mean NTproBNP is 888 (IQR 233-1971). 13 of the 25 were diagnosed with heart failure after bone scan (52%). The cause of death in 28 patients of 40 (70%) with myocardial uptake on bone scan, were oncological problems, 2 (5%), terminal heart failure, 4 (10%), infection related problems, and 5 (12,5%) is unknown. **Conclusion:** The prevalence of heart failure in elderly patients with myocardial uptake on bone scan is considerably higher than the theoretical prevalence in the same population. Myocardial uptake on bone scan is an earl finding in patients who may develop heart failure later; at the moment of the scan, most patients do not have heart failure. Our results suggest that heart failure and cardiac amyloidosis should be ruled out in patients with myocardial uptake on bone scan.

E-PW092

Bone^{99m}TC-DPD Scintigraphy: More Data To Confirm Its Utility For The Diagnosis Of TTR Heart Amyloidosis In Patients With Restrictive Hypertrophic Myocardiopathy

A. Marí Hualde, E. Ardila Manjarres, R. Pérez Pascual, J. Orcajo Rincón, A. Rotger Regí, L. Reguera Berenguer, J. Alonso Farto; Gregorio Marañón Hospital, Madrid, SPAIN.

Introduction: Cardiac amyloidosis (CA) is a progressive cardiomyopathy with a poor prognosis. The diagnosis is delayed because of the limited specificity of echocardiography and the historical requirement of an histological confirmation. We aim to analyze and evaluate the diagnostic criteria of ^{99m}Tc-2,3-dicarboxypropane-1,1-diphosphonate bone scintigraphy (^{99m}Tc-DPD-BS) in a serie of patients with suspected CA. **Subjects and Methods:** Retrospective study of 54 ^{99m}Tc-DPD-BS between January-2015 and March-2017, that were remitted for suspected CA with restrictive hypertrophic cardiomyopathy by echocardiography. 35/54 were male 64.8%), mean age (79.8years). The studies were evaluated both quantitative and qualitative. Quantitatively, we performed a Left/Right Index (L/R-I) considering pathological &gt 1.5, and qualitatively according to Perugini´s criteria. In addition, the presence of other indirect signs, such as tracer deposit at deltoid and gluteus muscles, at abdominal fat and decrease activity in the femoral diaphysis, were analyzed. The findings were contrasted with those obtained in echocardiographic studies, cardiac magnetic resonance imaging (CMR), genetic tests and clinical follow-up, when pos-

sible. **Results:** Cardiac tracer uptake was evidenced in 15/54 patients (31.25%). We found a clear male predominance (80%), mean age 84.8 years. According to the visual qualitative uptake: 13patients were classified as grade3 (&gt bone) and 2patients as grade2 (= bone). Quantitatively a mean L/R-I:2.2 was found in patients with cardiac pathologic deposition and mean L/R-I:1.05 in patients without cardiac uptake. A 100% correlation was found between the two scales in which all the patients with cardiac deposition had a L/R-I &gt 1.5 and the normal ones &lt 1.5. In addition, it was possible to identify the indirect CA criteria in the 15 patients (100%). 9/15 patients presented a TTR gene sequencing, being just one positive (wild-type), with no scintigraphic differences. Two patients were diagnosed of light chain amyloidosis (LCA), which showed no cardiac deposition, as expected. **Conclusion:** ^{99m}Tc-DPD-BS is a diagnostic tool for TTR-CA (not so for LCA), avoiding the morbidity of cardiac biopsy. Scintigraphic indirect signs should be taken into account. There is a strong correlation between the qualitative scale using a pathological value above 2 and the quantitative one having a cut-off L/R-I &gt 1.5.

E-PW093

Tc99m-DPD scan in the diagnosis of Cardiac Tranthyretin Amyloidosis

L. Mohamed Salem, Sr., J. Sánchez Serna, V. Cabanas Perianes, R. Reyes Marles, M. Godoy Bravo, M. Castellon Sanchez, F. Nicolas Ruiz, L. Frutos Esteban, J. Navarro Ferenandez, I. Sime Loayza, M. Tomas Redondo, M. Perez Martinez, J. Santos Mateo, D. Pascual Figal, M. Claver Valderas; Hospital Clínico Universitario Virgen de la Arrixaca, Murcia, SPAIN.

Introduction: According to late scientific evidence from large multicenter trial, Tc99m-DPD scan has a high specificity and sensitivity for the detection of TTR cardiac amyloidosis, which might be a common cause of heart failure in the elderly. **Purpose:** Our purpose is to study the value of Tc99m-DPD scan in the diagnosis of cardiac TTR amyloidosis. Subjects and **Methods:** Together with the Haematology and Cardiology Departments of our Hospital, we revise retrospectively 50 patients with clinical suspicion of cardiac amyloidosis, who underwent a Tc99m-DPD scan, 2-3 hours after the I.V. injection of 740 MBq. The myocardial tracer uptake was classified into 3 grades, taking as a reference the adjacent rib uptake; grade 1 is less than the rib, grade 2 equal to the rib and grade 3 more than the rib uptake. We select 25 patients with positive scan to analyze their clinical cardiological and haematotological history, blood and urine tests, clinical evolution, final diagnosis, and the results of echocardiography and cardiac MRI. Results:23 patients had intense myocardial tracer uptake grade 3. 2 patients had faint myocardial tracer uptake grade 1, have been diagnosed with primary cardiac amyloidosis. 3 of 23 patients have been diagnosed with primary cardiac amyloidosis (13%). 20 of 23 patients with intense myocardial tracer uptake have been diagnosed with TTR cardiac amyloidosis (87%). **Conclusion:** Tc99m-DPD scan has a 100% specificity in the diagnosis of cardiac TTR amyloidosis. Myocardial uptake is more common in TTR amyloi-

dosis, nevertheless, primary amyloidosis can present also with myocardial uptake, so it must be ruled out in the diagnostic work-up of cardiac amyloidosis.

E-PW094

A comparison between Tc99m-DPD and Tc99m-HDP myocardial uptake in the diagnosis of cardiac amyloidosis

L. Mohamed Salem, Sr., R. Reyes Marles, M. Godoy Bravo, I. Sime Loayza, M. Tomas Redondo, M. Castellon Sanchez, L. Frutos Esteban, J. Navarro Ferenandez, F. Nicolas Ruiz, M. Claver Valderas; Hospital Clínico Universitario Virgen de la Arrixaca, Murcia, SPAIN.

Introduction: According to current scientific evidence from large multicentre trial, myocardial uptake of bone tracers, has a high specificity and sensitivity in the diagnosis of TTR cardiac amyloidosis. Purpose To compare the myocardial uptake of Tc99m-DPD and Tc99m-HDP in the detection of cardiac amyloidosis. **Materials and Methods:** We have investigated the myocardial uptake in 19 patients; 8 with the diagnosis of TTR cardiac amyloidosis, who underwent a Tc99m-DPD and a Tc99m-HPD scan for other indications, 5 with diagnosis of TTR cardiac amyloidosis with Tc99m-DPD scan, who accepted to have a Tc99m-HPD scan, and 6 patients with intense myocardial uptake who had bone scans with both traces. We perform visual inspection and quantitative analysis using heart to mediastinum (H/M) ratio, to assess the myocardial tracer uptake. **Results**: On visual inspection, myocardial tracer uptake was more intense with Tc99m-DPD than Tc99m-HDP in all patients. Individual H/M ratio was higher on Tc99m-DPD than Tc99m-HDP in all patients. Mean H/M ratio was twice higher for Tc99m-DPD (2,17), than Tc99m-HDP (1,11). **Conclusion:** Myocardial Tc99m-DPD uptake is more intense than Tc99m-HDP. Although myocardial tracer uptake would be visible with both tracers in most cases, the grading system may be underestimated, and faint uptake may be missed with Tc99m-HDP. Tc99m-DPD is the radiotracer of choice in the diagnosis of cardiac amyloidosis.

E-PW095

Myocardial uptake of bone scintigraphic agents associated with cardiac amyloidosis in daily practice

S. Fukuzawa, S. Okino, T. Uchiyama, N. Kuroiwa, Y. Iwata, M. Inagaki; Funabashi Municipal Medical Center, Chiba, JAPAN.

The bone scan is primarily used to help diagnose a number of conditions relating to bones, including: cancer of the bone or cancers that have spread (metastasized) to the bone, locating some sources of bone inflammation. Extraosseous uptake, in particular, myocardial uptake, was observed in a number of patient examined with the bone scans. Additionally, in some reports, the uptake of Tc 99m-labeled bone radiotracers in cardiac amyloidosis has been extensively documented. The aim of this study was to assess the patients with high myocardial uptake of bone scintigraphy in daily practice. We retrospectively analyzed the 3435 bone scintigraphies performed in daily practice during a 3-year period. The intensity of the myocardial uptake was graded according to a visual scale ranging from 0 to 3 points, in which the absence of uptake was assigned a score of 0 points; uptake less than that of bone (referred to as the adjacent rib), 1 point; uptake similar to that of bone, 2 points; and uptake greater than that of bone, 3 points. The distribution of the uptake in myocardium was defined as focal uptake, diffuse uptake, uptake in a ventricular wall segment, diffuse ventricular uptake, or diffuse biventricular uptake. The retrospective analysis revealed relatively intense myocardial uptake in 10 of the 3435 patients (0.3%). Eight of the 10 patients had intense Tc-99m uptake (score of 2-3) in the cardiac region, showing deposition in both right and left ventricles in every case, whereas diffuse deposition (score of 1) was observed in 2 patients. In 10 all the cases, the final diagnosis of amyloidosis was based on the results of a biopsy. Cardiac uptake of bone scintigraphic agents were revealed on 0.3% of bone scntigraphies in daily practice. This may be a sign of cardiac amyloidosis involvement which may give extraosseous bone tracer uptake its own importance and a new role.

E-PW096

Is there a relationship between clinical parameters and cardiac uptake in 99mTc-DPD scintigraphy in patients with cardiac amyloidosis?

E. Abou Jokh Casas, V. Pubul Núñez, M. Garrido Pumar, B. Sopeña, A. Varela Roman, M. Pombo Pasin, J. Cortéz, S. Argibay, Á. Ruibal; Complejo Hospitalario Universitario Santiago de Compostela, Santiago de Compostela, SPAIN.

Introduction: Cardiac scintigraphy with 99mTc-3,3-diphosphono-1,2-propanodicarboxylic acid (99mTc-DPD) has been proven useful to differenciate subtypes of cardiac amyloidosis, specially between monoclonal light chain inmunoglobulin (AL) and transthyretin (TTR). Our goal is to correlate cardiovascular risk, electrocardiograhic and ecocardiographic findings, Pro-BNP values and biopsy with different cardiac uptakes in scintigraphy. **Materials and Methods:** We reviewed 40 patients, suspected with cardiac amyloidosis. All patients underwent a 99mTc-DPD scan. Myocardial uptake was graded from 0 to 3, respect to bone uptake. We considered a high cardiovascular risk profile the presence of three or more cardiac risk factors. Electrocardiografic findings included atrial fibrillation (AF) and left bundle branch block (LBBB). Ecocardiographic findings included eyection fraction (EF) and left ventricular hypertrophy (LVH). Pro-BNP was considered positive when a result 10 times higher than normal values was obtained. Cardiac biopsy was performed in 15 patients. **Results:** From our 40 patients, 27.5% presented cardiac uptake between 0-1, 15% had uptake grade 2 and 57.5% uptake grade 3. 63% of the patients with uptake 0-1 had a high cardiovascular risk profile versus 66% in those with uptake grade 2 and 39% in the last group. AF was present in a 27% in the 0-1 group, 66% in the group with uptake 2 and 52% in the uptake 3 group. 18% had LBBB with uptake 0-1, 16% patients with uptake 2 and 34% patients with uptake 3. EF was decreased in 36% of patients with grade 0-1 versus 33% in grade 2 group and 56% in

grade 3 group. LVH was present in 90% of the patients included in the 0-1 group, versus 83% in the group with uptake 2 and 56% in the grade 3 uptake group. Pro-BNP levels were found elevated in 50% of the 0-1 group versus 56% in the grade3 group. 12 of 15 patiens with cardiac biopsy were positive for ATTR, and all of them presented grade 3 uptake. **Conclusions:** The presence of a higher 99mTc-DPD uptake was mainly related with the prevalence of atrial fibrilation and decreased EF. This was also associated with a positive biopsy for ATTR. The relationship with the cardiovascular risk profile and Pro-BNP is doubtful.

E-PW097
Clinical Utility of ^{99m}Tc-PYP and ^{201}Tl-Cl SPECT Imaging in Patients with Suspected Cardiac Amyloidosis

S. Ito, N. Kodani, K. Tanabe; Shimane University, Izumo, Shimane, JAPAN.

Introduction: The degree of myocardial 99mTc-PYP accumulations in cardiac amyloidosis (CA) is conventionally evaluated as the PYP score. This method involves qualitative visual evaluation on two-dimensional images. Recently evaluation with heart to contralateral ratio is used as quantitative analysis, but is often affected artifact. **Purpose:** We validated the ability of three-dimensional quantitative analysis. Methods: One-handed-fifty-four consecutive patients suspected CA underwent 99mTc-PYP and 201Tl-Cl SPECT. Patients received 740MBq of 99mTc-PYP and 74MBq of 201Tl-Cl. We evaluated the PYP score in five phase of the planar image. In addition, we made left ventricular myocardial mask image from 201Tl-Cl images. The mask was applied to the 99mTc-PYP images using the coordinates of the myocardium and ventricular cavity. We quantitatively analyzed on a voxel-by-voxel basis from three-dimensional coordinate axis. Thus we quantitatively calculated the PYP accumulation rates. **Results:** Mean age of population was 72±12 years, and 58% were males. Twenty-eight patients had biopsy proven systemic amyloidosis (11 ATTR, 7 AL, 10 others). When the threshold of the PYP score was defined as 3+ and that of the PYP accumulation rate as 32.6%, the sensitivity of the PYP score and PYP accumulation rate were 57.0% and 75.0% and the specificity were 80.2% and 84.1% respectively. ATTR type presented a higher accumulation rate (96.1%±11.5%) than AL type (53.6%±28.7%, p=0.012, Fig.1). **Conclusions:** Our quantitative evaluation with the PYP accumulation rates may be useful in the diagnosis of CA and type of CA compared with conventional qualitative evaluation.

E-PW098
Florbetaben Whole-Body PET/MRI for Evaluation of Systemic Amyloid Deposition

S. Park, L. Baratto, P. Gulaka, R. Herfkens, R. Witteles, A. Iagaru; Stanford University School of Medicine, Stanford, CA, UNITED STATES OF AMERICA.

Background: Florbetaben, a ^{18}F-labeled stilbene derivative (formerly known as BAY-949172, trade name Neuraceq), is a diagnostic radiopharmaceutical developed to visualize β-amyloid plaques in the brain. Here we report a pilot study evaluating patients with suspected cardiac amyloidosis for systemic extent of disease. **Methods:** We enrolled 4 men and 1 woman referred from the cardiac amyloid clinic, 61-80 year-old (mean±SD: 69.8±7.1) in a prospective study using the GE SIGNA PET/MRI. First, dynamic imaging of the heart was acquired immediately after injection of 6.0-8.1 mCi (mean±SD: 7.1±0.8) of Florbetaben. This was followed by a whole-body PET/MRI scan 60-113 minutes (mean±SD: 84.2±23.2) after injection. Cardiac MRI sequences included ECG-triggered cine SSFP, T2-weighted, and late gadolinium-enhanced imaging. Whole-body MRI sequences included MRAC and axial T1-weighted imaging. **Results:** High early uptake and delayed high uptake in the left ventricle correlated with amyloid deposition in 3 patients, while low uptake on early and delayed cardiac imaging was noted in 2 patients. Measurements of cardiac function (left ventricle ejection fraction, volumes, peak filling, peak flow, etc) were successfully measured in all participants. Areas of abnormal Florbetaben were noted on delayed whole-body imaging in the brain (2 patients), ocular muscles (2 patients), salivary glands (4 patients), thyroid (1 patient), pleura (1 patient), stomach (diffuse in 3 patients and focal in 2 patients), spleen (1 patient), kidneys (3 patients) skeletal muscles (2 patients) and bone marrow (4 patients). **Conclusions:** Florbetaben is a promising PET radiopharmaceutical for localization of systemic amyloid deposition that used in conjunction with PET/MRI may provide important structural and functional information regarding the organs involved by disease.

E-PW099
^{18}F-FDG-PET/CT as a diagnostic tool in native valve endocarditis

I. Kouijzer[1,2], M. Berrevoets[1], E. Aarntzen[1], M. Janssen[1], J. de Vries[1], A. van Dijk[1], W. Oyen[1,3], L. de Geus-Oei[4,2], C. Bleeker-Rovers[1]; [1]Radboudumc, Nijmegen, NETHERLANDS, [2]University of Twente, Enschede, NETHERLANDS, [3]The Institute of Cancer Research and Royal Marsden NHS Foundation Trust, London, UNITED KINGDOM, [4]LUMC, Leiden, NETHERLANDS.

Introduction: Diagnosing infective native valve endocarditis (NVE) is challenging. The modified Duke criteria are currently used for diagnosing infective endocarditis, but have limited sensitivity. We investigated the value of ^{18}F-fluorodeoxyglucose positron emission tomography with combined computed tomography (^{18}F-FDG-PET/CT) to diagnose NVE. **Subjects and Methods:** All patients with bacteremia and suspicion of NVE between January 2013 and June 2016 were identified from the hospitals' register and included if echocardiography and ^{18}F-FDG-PET/CT were performed within 14 days. ^{18}F-FDG-PET/CT scans were scored independently by two nuclear medicine physicians. Diagnostic accuracy of ^{18}F-FDG-PET/CT was determined using the modified Duke criteria and a multidisciplinary consensus as a reference standard. **Results:** Eighty-eight patients were included. As compared to the modified Duke criteria; sensitivity, specificity, PPV, and NPV for ^{18}F-FDG-PET/CT in diagnosing

definite NVE were 30.0%, 89.7%, 27.3%, and 90.9%. Compared to definite diagnosis by multidisciplinary consensus; sensitivity, specificity, PPV, and NPV for ^{18}F-FDG-PET/CT were 35.0%, 94.1%, 63.6%, and 83.1%. Mortality rates in patients with possible and rejected NVE according to the modified Duke criteria was higher when the heart valve region showed increased ^{18}F-FDG uptake. Metastatic infectious foci were detected by ^{18}F-FDG-PET/CT in 54.5% of patients. **Conclusions:** ^{18}F-FDG-PET/CT lacks accuracy for diagnosing NVE. In patients with possible NVE according to the modified Duke criteria, ^{18}F-FDG-PET/CT could be used in case of sustained suspicion of NVE because of its good specificity. In patients suspected of NVE, ^{18}F-FDG-PET/CT is important for detecting metastatic infection.

E-PW11 — Tuesday, October 24, 2017, 08:30 - 09:30, e-Poster Walk Area, Level 2, Foyer A, Screen 3

Neurosciences: Molecular Neuroimaging

E-PW100

Effect of blood flow on ^{18}F-Florbetaben PET quantitation: a simulation study

S. Bullich[1], N. Koglin[1], G. Becker[2], S. De Santi[3], A. Jovalekic[1], H. Barthel[3], O. Sabri[3]; [1]Piramal Imaging GmbH, Berlin, GERMANY, [2]Department of Nuclear Medicine, University Hospital Leipzig, Leipzig, Leipzig, GERMANY, [3]Department of Nuclear Medicine, University Hospital Leipzig, Leipzig, GERMANY.

Introduction: Cerebral blood flow (CBF) changes over time have been reported in Alzheimer's disease patients (van Berckel B. et al. J Nucl Med. 2013; Ottoy J. et al J Nucl Med. 2017). Standardized uptake value ratios (SUVR) are commonly used to analyze ^{18}F-Florbetaben PET scans. SUVRs, however, may be biased as surrogate marker of beta-amyloid (Aβ) load by BF effects. This is relevant in longitudinal studies and anti-Aβ therapeutic trials where a drug is administered and its effect on CBF is unknown. The objective of this study was to assess the impact of CBF changes on SUVR and non-invasive kinetic models in ^{18}F-Florbetaben PET scans. **Subjects and Methods:** Average arterial input function and rate constants (K_1, k_2, k_3 and k_4) from 10 AD subjects scanned with ^{18}F-Florbetaben PET were used to generate simulated time-activity curves by means of a two-tissue compartment model from 0 to 140 min. Two simulations were carried out: 1) regional CBF change affecting only cortical regions (i.e. average K_1 from the AD subjects (K_1=0.2) varied between 0.15 and 0.25 (±25%) while keeping K_1/k_2 constant); 2) global CBF change affecting cortical and reference regions (i.e. average K_1 varied between 0.15 to 0.25 while keeping $R_1=K_1/K_1'$ constant). The binding potential (BP_{ND}) in all the simulations was 0.59. Aβ load was quantified using the simplified reference tissue model (SRTM) (Gunn RN. et al. Neuroimage. 1997) and two multilinear reference tissue models (MRTM and MRTM2)(t^*=70 min) (Ichise M. et al. J Cereb Blood Flow Metab 2003). SUVRs were determined at 70-90, 90-110 and 120-140 min. The bias associated with CBF changes was quantified as the percent change in the Aβ load estimates from the simulated BP_{ND} ($BP_{ND,sim}$=0.59) (bias(%)=100·ΔBP_{ND}/ $BP_{ND,sim}$). **Results:** For the regional CBF change, MRTM provided accurate Aβ load estimates independent of the BF (ΔBP_{ND}=0.02 (bias=3.5%)(MRTM); ΔBP_{ND}=0.05 (8.2%)(MRTM2)). SUVR provided estimates of the Aβ load with a limited CBF effect, which got reduced at late time points (ΔSUVR-1= 0.08 (13.5%)(70-90 min); 0.06 (10.9%)(90-110 min); 0.02 (3.6%)(120-140 min)). SRTM provided CBFdependent estimates of the Aβ load (ΔBP_{ND}=0.24 (40.0%)). Global CBF change did not substantially bias the Aβ load estimates for any of the measurements (<7%). **Conclusion:** In ^{18}F-Florbetaben PET imaging, Aβ load estimates as obtained by SUVRs from late time points or by MRTM are less influenced by CBF changes. Thus, for longitudinal studies in which a maximum quantification accuracy is desired, these methods should be applied.

E-PW101

Can relative flow derived from dynamic ^{11}C-PIB scans replace FDG scans in Alzheimer disease PET studies?

T. van der Goot, F. E. Reesink, D. E. Peretti, D. Vállez García, A. T. M. Willemsen, P. P. De Deyn, R. Boellaard; UMCG, Groningen, NETHERLANDS.

Aim: Different PET biomarkers are used for the differential diagnosis of neurodegenerative diseases such as Alzheimer's disease (AD). β-amyloid plaque deposition can be assessed by ^{11}C-Pittsburgh Compound B (PIB) while ^{18}F-fluorodeoxyglucose (FDG) is used to assess cerebral glucose metabolism, which can be an indicator for synaptic dysfunction. Although FDG is a biomarker for glucose consumption, its distribution is strongly affected by cerebral perfusion. The aim of the study is to explore whether relative blood flow (rCBF) data, extracted from dynamic ^{11}C-PIB studies, can be used as a surrogate for relative FDG distributions. **Methods:** Thirty subjects (10 AD, 10 mild cognitive impairment (MCI) patients, and 10 healthy controls (HC)) underwent static ^{18}F-FDG (45-60 min p.i.) and 70 min dynamic ^{11}C-PIB PET scans. T1-MRI scans were used for anatomical labelling of brain regions. Parametric ^{11}C-PIB rCBF images (R_1: tracer delivery relative to the cerebellum) were obtained using the simplified reference tissue model 2 (SRTM2, PMOD v3.8). ^{18}F-FDG images were normalized to the cerebellar grey matter values (SUVr). The Hammers atlas was used to analyze regional correlations between R_1 and SUVr. We used SPM12 to compare SUVr and R_1 statistical parametric maps between AD and HC. **Results:** The regional analysis showed strong correlations between R_1 and SUVr for AD, MCI and HC (group average R^2 of 0.89 (AD), 0.90 (MCI) and 0.84 (HC)). Both R1 and SUVr showed similar statistical parametric maps for AD and HC which are in agreement with previous reports in literature. However, SPM based on R1 showed a smaller number of significant clusters involved than with the SPM based on FDG SUVr. In addition, the clusters found in R1 were smaller in size and T-value. For example, in the left inferiolateral parietal lobe FDG SUVr showed 2297 voxels(mean(T)=5.4) versus 999 voxels for R1(mean(T)=4.7). **Conclusion:** Relative cerebral perfusion images (R_1) obtained from ^{11}C-PIB dynamic PET acquisitions are strongly correlated with normalized ^{18}F-FDG im-

ages in all 3 groups and largely show the same SPM pattern in a group comparison. However, the observed group differences for R_1 were smaller and less significant which may be related to the lower signal-to-noise ratio of the R_1 images. These preliminary results suggest that dynamic ^{11}C-PIB PET can not only be used to asses β-amyloid plaque deposition, but that relative rCBF derived from these scans can in some cases be used to replace FDG thereby obviating the need to perform a second tracer (FDG) study.

E-PW102

Different Patterns of Dopamine and Serotonin Dysfunction in Manic, Depressive and Euthymic Phases of Bipolar Disorder

S. Nikolaus, H. Müller, H. Hautzel; University Hospital Düsseldorf, Düsseldorf, GERMANY.

Purpose/Introduction: A variety of alterations in brain neurotransmitter systems has been proposed as the underlying neurochemical cause of bipolar disorder (BD) including dopamine (DA), serotonin (5-HT) and acetylcholine (ACh). In the present study, we evaluated the contribution of the individual synaptic constituents of all assessed neurotransmitter systems by subjecting all available in vivo imaging studies in manic (BD-man), depressive (BDdep) and euthymic BD patients (BDeu) to a retrospective analysis. **Subjects & Methods:** In patients with BDman (n=39), BDdep (n=248) and BDeu (n= 265) DA synthesis, DA release or binding to DAT, VMAT2, D1 receptor [R], D2R, SERT, 5-HT1AR, 5-HT2AR, M2R and beta2-nAChR was assessed in various cortical and subcortical regions with either PET or SPECT and compared to healthy individuals. Studies were pooled and median values and interquartile ranges of percentual differences relative to controls were determined for the individual brain regions. Differences to controls were assessed with the Wilcoxon-signed-rank-test. **Results:** Findings showed elevated midbrain SERT, decreased parietal, temporal, occipital, insular and fusiform 5-HT2AR and decreased frontal D1R in BDman. BDdep was characterized by decreased hippocampal, but elevated insular SERT, elevated prefrontal, frontal, hippocampal, amygdalar and periaqueductal 5-HT1AR, decreased frontal D1R and decreased prefrontal, frontal, occipital and cingulate M2R. BDeu still showed decreased striatal, thalamic and midbrain SERT, decreased striatal DA synthesis, elevated striatal DAT, elevated thalamic and midbrain VMAT2, decreased frontal D1R and decreased striatal D2R. **Discussion/Conclusion**: From these findings, a complex pattern of dysregulations within and between neurotransmitter systems may be inferred, which is causally linked to the acute and euthymic states of BD. While increased mesencephalic and parietotemporoccipital 5-HT and increased frontal DA underlie BDman, BDdep may be characterized by decreased frontal and limbic 5-HT, increased frontal and limbic ACh and increased frontal DA. Also in euthymia, no normalization of receptor and transporter densities was observed. They act together, however, to achieve a normalization of mesencephalic, cortical and limbic 5-HT.

E-PW103

First quantification results for the new TSPO radioligand [^{18}F]GE-180 in patients with multiple sclerosis

L. Vomacka[1], N. L. Albert[1], S. Lindner[1], M. Unterrainer[1], C. Mahler[2], M. Brendel[1], L. Ermoschkin[1], A. Gosewisch[1], A. Brunegraf[1], C. Buckley[3], W. Trigg[3], T. Kümpfel[2], R. Rupprecht[4], M. Kerschensteiner[2,5], P. Bartenstein[1,5], G. Böning[1]; [1]Department of Nuclear Medicine, LMU Munich, Munich, GERMANY, [2]Institute of Clinical Neuroimmunology, LMU Munich, Munich, GERMANY, [3]GE Healthcare, Grove Centre, Amersham, UNITED KINGDOM, [4]Department of Psychiatry and Psychotherapy, University of Regensburg, Regensburg, GERMANY, [5]Munich Cluster for Systems Neurology (SyNergy), Munich, GERMANY.

Purpose: The objective of this study was to verify simplified quantification methods for the new TSPO radioligand [^{18}F]GE-180. Focal lesions and different brain regions of patients with multiple sclerosis (MS) were analysed, focusing on a high inter- and intra-patient comparability and an efficient integration into clinical routine. **Methods:** A total of 15 dynamic 90 minutes [^{18}F]GE-180 PET scans of MS patients was performed, where 7 scans were combined with manual blood-sampling for modelling based on free parent tracer in plasma. Quantification started with two-tissue-compartment (2TC) and graphical models. This was followed by an investigation regarding the least disease-affected brain tissue, which included a voxel-based comparison with data from 7 healthy controls (HC) with statistical-parametric-mapping and a comparison of brain VOI characteristics. For the definition of a final pseudo-reference region (PRR) voxels suspicious of being affected by disease were excluded by the application of an upper threshold based on mean and standard deviation from HC data in static 60 to 90 minutes images. Binding potentials (BP) estimated from static images normalized to PRR (standardized uptake value ratio SUVR, $BP_{Ref'60-90}$=SUVR-1) were correlated to BP_{ND} relative to non-displaceable uptake from 2TC model and to BP_{Ref}=V_T/V_{PRR}-1 relative to reference tissue from 2TC model, Logan-Plot and Logan-reference tissue model. SUVR was quantified for different brain VOIs and 59 focal lesions visible in PET. Lesion volumes were delineated in SUVR images with an iterative thresholding approach and a simplified threshold method. **Results:** Average SUVRmean of lesions was 1.8 (range 1.2; 3.0) and SUVRmax was 2.4 (range 1.3; 4.8). Mean SUVR in MS patients was highest in thalamus and brainstem (1.3), and lowest (1.1) in white matter (WM) and grey matter (GM). WM, thalamus and brainstem exhibited the highest mean fractions of voxels suspicious of being affected by disease (>30%) and frontal cortex (FC) the lowest (16%). Normalization to FC yielded the highest reduction in variability of healthy WM and GM. Therefore FC corrected for affected voxels was chosen as PRR. The average time-activity curves and BP_{ND} of the PRR corresponded to FC values in HC data (BP_{ND} 2.2, U-test p=0.83). BP_{ND} correlated strongly with $BP_{Ref'60-90}$ (Spearman rho=0.85), and BP_{Ref} from 2TC model and Logan methods showed very strong correlation with $BP_{Ref'60-90}$ (rho>0.9). **Conclusion:** This preliminary comparison with modelling parameters from dynamic PET scans suggest that $BP_{Ref'60-90}$ relative to not-affected frontal cor-

tex derived from static images might be suitable for [18F]GE-180 quantification in MS patients.

E-PW104

PET-Analysis: a user-friendly toolbox for epileptic seizure onset zone localization. Evaluation of the performance using simulated data

A. Niñerola-Baizán[1,2], B. Marti-Fuster[1,2], A. Martín-Pero[2], R. Tudela[1], M. Mayoral[3], X. Setoain[3,1], D. Ros[2,1], J. Pavía[3,1]; [1]Grupo de Imagen Biomédica, Centro de Investigación Biomédica en Red en Bioingeniería, Biomateriales y Nanomedicina (CIBER-BBN), Barcelona, SPAIN, [2]Unitat de Biofísica i Bioenginyeria, Facultat de Medicina, Universitat de Barcelona, Barcelona, SPAIN, [3]Servicio de Medicina Nuclear, Hospital Clínic, Barcelona, SPAIN.

Introduction: Visual inspection is commonly used in clinical practice during the assessment of [18F]FDG-PET studies for presurgical evaluation of refractory epilepsy. However, a voxel-by-voxel statistical analysis comparing the [18F]FDG-PET study of the patient to a control database can improve the localization of the hypometabolic zone related to the epileptogenic region (ER). **Aim:** To assess the clinical utility of PET-Analysis, a toolbox based on statistical parametric maps to aid clinicians in the localization of the ER in refractory epileptic patients. **Methods**: Realistic simulations based on 5 clinical studies with Magnetic Resonance Image (MRI), Computed Tomography (CT) and PET were simulated using SimSET v2.9 Monte Carlo code. The attenuation and the activity maps were obtained from structural CT and MRI and functional PET images. ERs were defined in twelve commonly observed regions in epilepsy. Activity maps (n=180) were generated together with hypometabolism levels of 15%, 30% and 45% in the ER. Simulated studies were reconstructed like the clinical data, spatially normalized into our own [18F]FDG template, smoothed with a Gaussian kernel of FWHM=8x8x8mm^3 and intensity normalized. To detect the simulated regional hypometabolism, a *t*-test between each simulated study and the control database was performed. Each resulting statistical parametric map was thresholded by a *t*-value (t_{th}) and cluster size (k_{min}) in two steps. In step one, the values of t_{th} and k_{min} were set to 3.39 (p<0.001), and 100 in line with earlier studies. In the second step, in the absence of a cluster, t_{th} was diminished and different cluster sizes were used to detect only one surviving cluster. ER was considered as detected if it intersected one of the surviving clusters in step one or the only one in step two. **Results**: As regards detectability, when the initial *t*-value and k were used (p<0.001,k=100), the number of ER detected were 4/60 for 15% hypometabolism, 41/60 for 30% hypometabolism and 59/60 for 45% hypometabolism, with more than one cluster in some images. On the other hand, when a dynamic statistical threshold was used and only one cluster was spotted, the number of ER correctly detected were 31/60 for 15% hypometabolism, 55/60 for 30% hypometabolism and 60/60 for 45% hypometabolism. **Conclusion**: PET-Analysis is a useful tool to localize the ER in refractory epilepsy. A dynamic statistical threshold is recommended to improve localization, starting with a high *t-value* (i.e. low *p*-value) and a low k_{min} and ending with a low *t-value* and a high k_{min}.

E-PW105

123I-Ioflupane scintigraphy in asymptomatic LRRK2-G2019S mutation carriers

I. Martínez-Rodríguez[1], M. Jiménez-Alonso[1], J. López-Defilló[1], J. Infante[2], M. Sierra[2], J. Jiménez-Bonilla[1], N. Martínez-Amador[1], M. De Arcocha-Torres[1], F. Gómez-de la Fuente[1], D. Meza-Escobar[1], I. Banzo[1]; [1]Nuclear Medicine Service. Marqués de Valdecilla University Hospital. Molecular Imaging Group (IDIVAL). University of Cantabria, Santander, SPAIN, [2]Neurology Service. Marqués de Valdecilla University Hospital. IDIVAL. Centro de Investigación Biomédica en Red de Enfermedades Degenerativas (CIBERNED). University of Cantabria, Santander, SPAIN.

Purpose: LRRK2-G2019S mutation is one of the known causes for Parkinson disease (PD). It has an incomplete penetrance of 30-90% at 80 years, making it difficult to know which patients are going to develop the disease. Our aim was to evaluate the contribution of 123I-Ioflupane scintigraphy as a predictor of PD development in asymptomatic mutation carrier patients. **Materials and Methods:** This prospective study included 25 subjects, asymptomatic carriers of the LRRK2-G2019S mutation (7 men; 58.2±10.3 years). An initial and 4- year follow-up 123I-Ioflupane scintigraphy were obtained in all subjects. Images were acquired 3 hours after IV injection of 150 MBq of 123I-Ioflupane. A visual and manual semiquantitative analysis was performed evaluating both the striatum globally and each nucleus separately. Occipital region was selected as background. Striatum/occipital, putamen/occipital and caudate/occipital ratios were calculated. Initial and follow-up results were compared and correlated with the clinical outcome. Three subjects developed PD at 4 years. **Results:** <u>Visual analysis</u>: Initial 123I-Ioflupane was normal in 15 out of 25 subjects (60%) and abnormal in 10 (40%), showing 6 of them a bilateral involvement. At follow-up, 123I-Ioflupane remained normal in 7 out of 25 subjects (28%) and was abnormal in 18 (72%) subjects (the 10 subjects with abnormal initial scan and 8 subjects with normal initial scan). The more intense involvement was observed at the putamen nucleus. The 3 asymptomatic subjects who developed PD had an abnormal initial and follow-up 123I-Ioflupane scan. None of the subjects with normal initial 123I-Ioflupane developed PD. <u>Semiquantitative analysis</u>: Initial striatum/occipital ratios were significantly lower (p<0.01) for the 3 PD-converters compared to the 22 non-converters (right 0.9±0.1 and left 0.9±0.1 vs. right 1.6±0.3 and left 1.6±0.4, respectively). The same behavior was observed for the follow-up examinations (right 0.6±0.1 and left 0.5±0.1 vs. right 1.3±0.3 and left 1.3±0.3, p<0.01). Visually normal subjects whom became abnormal at follow-up had initial striatum/occipital ratios lower than subjects with both normal initial and follow-up scans, but the differences were not significant (p = 0.1533 and 0.1323 for the right and left striatum, respectively). **Conclusions:** 123I-Ioflupane scintigraphy demonstrated a decline of striatal dopamine transporter binding in a high percentage of asymptomatic carriers of the LRRK2-G2019S mutation and could be a useful tool as predictor of PD development. These preliminary results should be confirmed with a longer-term follow-up.

E-PW106

Impact of Resolution Recovery Reconstruction on Quantitative Analysis of PETCT beta-Amyloid Plaque Brain Imaging

R. T. Meades[1], L. M. Perry[1], K. S. Nijran[1], Z. Win[2];
[1]Radiological Sciences Unit, Imperial College Healthcare NHS Trust, London, UNITED KINGDOM, [2]Nuclear Medicine Department, Imperial College Healthcare NHS Trust, London, UNITED KINGDOM.

Introduction: β-amyloid plaque density Positron Emission Tomography (PET) brain imaging is used for patients being evaluated for Alzheimer's Disease and computer aided quantitative analysis could be used to aid their reporting. Resolution recovery reconstruction algorithms may also be used to increase resolution, improving visual differentiation between grey and white matter in the brain which may increase diagnostic confidence. This work aimed to assess the impact of using a resolution recovery reconstruction algorithm on results from dedicated quantitative analysis software. **Method**: 12 F-18 Florbetapir (Amyvid, Ely Lilly) scans (6 negative and 6 positive) were reconstructed using Siemens TrueX resolution recovery algorithm (4 iterations, 16 subsets, 2mm Gaussian filter, 256x256 matrix, 2x zoom) as well as the recommended iterative reconstruction (4 iterations, 14 subsets, 3mm Gaussian filter, 168x168 matrix, 2x zoom). BRASS for Amyvid (HERMES Medical Solutions) was used to analyse the datasets fitting and comparing images to a reference normal template, producing SUV ratios (SUVr) for 6 regions relative to the cerebellum and an average ratio of all regions (SUVr$_{ave}$) for each scan. **Results**: When comparing the resolution recovery reconstruction with the recommended iterative reconstruction in the negative scans, statistically significant increases in SUVr were noted for 3 regions; Frontal Medial Orbital Cortex (+3.9%, p=0.02), Lateral Temporal (+4.2%, p =0.01) and Parietal (+4.4%, p=0.01). For the positive scans statistically significant increases were noted in 2 regions; Lateral Temporal (+3.3%, p=0.03) and Parietal (+4.5%, p=0.02). For all 6 negative scans, SUVr$_{ave}$ demonstrated a statistically significant increase (+2.9%, p=0.03). In 4 of the 6 positive scans SUVr$_{ave}$ increased with 2 unchanged. This change was not statistically significant (2.4%, p=0.08). **Conclusion**: The use of a resolution recovery reconstruction algorithm lead to an overall increase in region specific SUVr and SUVr$_{ave}$ compared with recommended iterative reconstruction parameters. This increase is greater in average magnitude, more statistically significant and is present in more regions for negative than for positive scans. Both negative and positive scans exhibit increases in the Lateral Temporal and Parietal regions while an increase is also observed in the Frontal Medial Orbital Cortex for negative scans. The greater effect on negative compared to positive scans highlights that care should be taken when choosing to use resolution recovery reconstruction algorithms in this setting. However, further work is required to determine the likelihood and severity of impact on clinical diagnosis.

E-PW107

Asymmetric Parkinson's disease and effects of unilateral subthalamic nucleus deep brain stimulation on neural networks: a pilot PET study

P. David[1], X. Palard-Novello[2], S. Drapier[3], M. Verin[3], F. Le Jeune;
[1]Hôpital Européen Georges Pompidou, Paris, FRANCE, [2]Centre Eugene Marquis, Rennes, FRANCE, [3]Centre Hospitalier Universitaire, Rennes, FRANCE.

Purpose: Parkinson's disease is often defined as a bilateral form of motor symptoms but some patients have a purely unilateral or very asymmetric form for many years. It is described that motor and non-motor symptoms are different between right or left form so we hypothesized that cerebral metabolism would be different depending on the side of disease. Subthalamic nucleus (STN) deep brain stimulation (DBS) is well established for many years for patients with intractable and advanced Parkinson's disease. Bilateral STN DBS has shown a significant motor improvement, but would induce metabolic changes on associative and limbic circuits and is associated with risks and costs. Unilateral surgery would be an interesting alternative for patients with extremely asymmetric symptoms. We also hypothesized that unilateral STN DBS would act differently on brain networks, depending of side of surgery. Subjects & Methods: We studied glucose cerebral metabolism in eleven patients with unilateral or asymmetric symptoms of Parkinson's disease, who underwent 18F-FDG-PET 3 months before and 3 months after unilateral STN DBS. Six patients underwent left STN DBS while five patients underwent a right surgery. Motor, psychiatric and neuropsychological assessments were also performed at each step, and Statistical Parametric Mapping software (SPM) was used for analysis data. We first analyzed pre-operative metabolism at rest of these patients compared to eleven age-matched healthy subjects and secondly we studied metabolic effects following unilateral STN DBS. **Results:** Parkinson's disease modify cerebral metabolism at resting state differently between left and right-affected hemisphere with more metabolic changes in patients candidate for right-STN DBS. The comparison between pre and post-operative metabolism showed bilateral but asymmetric effects, predominantly on the side of DBS. For patients with left symptoms, right-STN DBS induce different metabolic changes compared to left surgery, predominantly in right hemisphere and especially on limbic areas. All patients had significant motor improvement at 3 months after surgery. Discussion: The results of this pilot PET study showed that Parkinson's disease in patients with highly asymmetric symptoms modify differently the cerebral metabolism, depending on the side of hemisphere affected, possibly by acting on the Default Mode Network. Right or left surgery seems to induce different metabolic changes particularly on associative and limbic networks, probably explained by differences in functional connectivity between cortical areas and right versus left STN. These preliminary results could offer hypothesis for new therapeutic approaches such as different targets of repetitive transcranial magnetic stimulation (rTMS) depending of side of disease.

E-PW108

Cortical metabolic patterns related to CSF total tau, Aβ42 and phosphorylated tau protein in Alzheimer disease

A. Chiaravalloti[1,2], M. Ricci[3], A. Martorana[4], F. Calabria[5], P. Sannino[2], O. Schillaci[1,2]; [1]Department of Biomedicine and Prevention, University Tor Vergata, Rome, ITALY, [2]IRCCS Neuromed, Pozzilli, ITALY, [3]Nuclear Medicine Unit, University La Sapienza, Rome, ITALY, [4]Department of Neusociences, University Tor Vergata, Rome, ITALY, [5]Neuroimaging PET/MRI Research Unit, Institute of Molecular Bioimaging and Physiology, National Research Council, Catanzaro, ITALY.

Aims: physiopathological mechanisms of Alzheimer's disease (AD) are still matter of debate. Especially the role of amyloid β and tau pathology in the development of the disease are still matter of debate. Changes in tau and amyloid β peptide concentration in cerebrospinal fluid (CSF) and hypometabolic patterns at fluorine-18 fluorodeoxyglucose (18F-FDG) PET scanning are considered as biomarkers of AD.The present study was aimed to evaluate the relationships between the concentrations of CSF total Tau (t-Tau), phosphorilated Tau (p-Tau) and Aβ(1-42) amyloid peptide with 18F-FDG brain distribution in a group of patients with AD. **Materials and Methods**: We examined 131 newly diagnosed AD patients according to the NINCDS-ADRDA criteria. The mean (± SD) age of the patients was 70 (± 7) years; 57 were male and 74 were female. All patients underwent a complete clinical investigation, including medical history, neurological examination, mini-mental state examination (MMSE), a complete blood screening (including routine exams, thyroid hormones and a complete neuropsychological evaluation. Structural MRI was performed not earlier than 1 month before the 18 F-FDG PET/CT. The following patients were excluded: those with isolated deficits and/or unmodified MMSE (=25/30) on revisit (period of follow-up: 6, 12 and 18 months); patients who had had a clinically manifest acute stroke in the last 6 months with a Hachinsky score greater than 4; and patients with radiological evidence of subcortical lesions. All AD patients were taken off cholinesterase inhibitor treatment throughout the study. We performed lumbar puncture and CSF sampling for diagnostic purposes 2 weeks (± 2 days) before the PET/CT scan. The relationship between brain 18F-FDG uptake and CSF biomarkers was analysed using statistical parametric mapping (SPM8; Wellcome Department of Cognitive Neurology, London, UK) implemented in Matlab R2012b using the MMSE score, sex and age, and other CSF biomarkers as covariates. **Results:** t-Tau, p-Tau and Aβ(1-42) in CSF resulted 774±345 pg/ml, 98±64 pg/ml and 339±118 pg/ml respectively. SPM analysis showed a significant negative correlation between CSF t-Tau and 18F FDG uptake in right temporal lobe (Brodmann areas, BA, 20 and 38; P fdr and few corr < 0.001, k_e 2422), right parietal lobe (BA 40, P fdr and few corr < 0.001, k_e 548) and right frontal lobe (BA 8 and 9, P fdr and few corr < 0.001, k_e 4930). We did not find any significant relationships with other CSF biomarkers. **Conclusions:** t-Tau deposition in brain is related to temporal-parietal and frontal hypometabolism in AD.

E-PW109

18F-FDG PET brain in presurgical management of patients with periventricular nodular heterotopias related epilepsy: diagnostic features and long term outcome

C. E. Popescu[1], C. Rossetti[1], R. Mai[1], R. Sara[1], M. Milella[1], D. Redaelli[1], A. Liuni[1], F. Caobelli[2]; [1]Niguarda Hospital, Milan, ITALY, [2]University Hospital Basel, Basel, SWITZERLAND.

Introduction: Periventricular Nodular Heterotopias (PNHs) are malformations of cortical development (MCD) related to neuronal migration disorders, frequently associated with drug-resistant epilepsy (DRE). Although magnetic resonance imaging (MRI) can clearly define the morphological features of PNHs, it still remains unclear whether the metabolic activity of ectopic neurons may correlate with neurologic symptoms. The aims of our study were to compare the diagnostic performance of 18F-FDG PET/CT compared to MRI, to assess the metabolic activity of the epileptogenic foci and to evaluate the clinical and prognostic value of PET findings. **Subjects and Methods:** Fifteen patients (8 men and 7 women; age range, 23-52 years) diagnosed with PNHs-related DRE were retrospectively evaluated from a single-centre database. All underwent clinical evaluation, Stereo-Electroencephalogram (SEEG), 1.5T 3D-brain MRI and 18F-FDG brain PET/CT. PET images were superimposed on the patient-specific 3D-brain-MRI to allow for a more accurate comparison. Metabolic activity was visually assessed and classified as normal (i.e. not significantly different from that of the surrounding structures), increased, reduced or absent. All the patients underwent surgical intervention either with radiofrequency thermocoagulation only (73.3%), conventional surgery only (6.7%) or both (20%). Outcome was assessed at ≥8-month follow-up (median 28 months). A favorable outcome was defined as reduced rate of seizures (Engel outcome 1A/B/C and 2A) and/or therapy reduction. **Results:** Four patients (26.7%) had unilateral PNHs localized in the right hemisphere, 3 unilateral in the left hemisphere and 8 (53.3%) had bilateral PNHs. MRI identified a total of 23 heterotopic sites. Of these, 10(43.5%) showed on PET a normal metabolic activity, 8(34.8%) were rated hypometabolic and in 5(21.7%) FDG metabolism was absent. PET allowed to identify other metabolic alterations outside the heterotopias, correlating with neurologcal symptoms. Specifically, a hypometabolism has been observed on the anterior mesial temporal region in 8 patients (53.3%) and on posterior temporal region in 2(13.3%). At follow-up, reduced rate of seizures was reported in 13 patients (86.7%), while therapy was reduced in 5 (33.3%). At univariate and multivariate analysis, the presence of hypometabolism or absent uptake in the heterotopic sites was significantly associated with a more favorable outcome (p=0.03). **Conclusions:** 18F-FDG PET identified 13 of 23 heterotopic sites identified by MRI (56.5%). However, more metabolic alterations were detected, correlating with neurological symptoms. Furthermore, hypo- or absent metabolism on PET can predict a more favorable outcome. Brain FDG PET provides important information on metabolic activity and allows to predict the outcome of surgical therapy.

Do.MoRe: PET & PET/CT Data Analysis & Management

E-PW110

Ultra-fast or Ultra-low Count Density Wholebody PET Imaging - Pushing the Envelope with Next-generation Digital PET

M. I. Knopp, J. Zhang, K. Binzel, R. Moore, M. Friel, C. L. Wright, M. V. Knopp; The Ohio State University, Columbus, OH, UNITED STATES OF AMERICA.

Purpose/Introduction: Improving acquisition speed has been essential developments in CT and MRI to improve image quality, patient comfort and reduce artifacts. Currently most PET acquisitions are performed between 90-120 seconds per bed position. Within a clinical development program to assess next generation digital PET imaging, this study was designed to approach reduction in imaging time not via incremental improvements but instead to use a moon shot approach by attempting to accomplish 10 X improvement. While 10 X didn't appear to be feasible at the onset, it was designed to better understand boundary conditions and to accelerate the development of new pet imaging approaches. **Subjects & Methods:** A next generation, digital photon counting PET/CT system was available (Vereos, Philips), (dPET) within a clinical development program that performed whole body FDG PET scans for oncologic applications. 25 patients were included in this add on study, where we performed a 9s per bed position whole body scan immediately after performing the standard 90s scan. Patient received standard diagnostic doses of 440 MBq. Prior to performing 10 X scan time reduction on human patients, we performed the feasibility assessment using two preclinical canine subjects. An independent, blinded three reader panel was used to assess image quality, diagnostic confidence, artifacts and visual noise. Prior Phantom and preclinical assessment validated that reduction in scan time can be used as an analog for reduced count density that also directly relates to dose reduction. Different reader assessment scales were used. **Results:** 9s per bed position or < 3 min whole body acquisitions led to unexpected good image quality. While all cases were rated interpretable, 20/25 cases were rated to be diagnostically usable. As expected, all cases were rated to have more noise. 23/25 presented with exactly the same clinical findings as the 90s/20min whole body scans. Quantitative target lesion variability (SUVmax) was below 10%. Simulated 10x whole body scans were ranked equivalent to true 10x acquisitions. **Discussion/Conclusion:** The 10x reduction in scan time and count density led to most surprising good, even diagnostic, image quality using the previous optimized reconstruction approaches. SUVmax values were comparable. Listmode simulated images were found to be predictors of true reduced count acquisitions. These most encouraging findings indicate that the new generation of digital PET technology will enable ultra-fast (wholebody < 3min) or ultra-low dose imaging (FDG dose <50 MBq). These initial clinical findings will need to be further validated in larger trials

E-PW111

A Noise Smoothing Origin Ensemble Algorithm Based on Regional Filtering

K. Chuang[1], C. Chiang[1], H. Lin[2], Y. Ni[3]; [1]National Tsing-Hua University, Hsin-Chu, TAIWAN, [2]Chang Gung University/Chang Gung Memorial Hospital, Taoyuan, TAIWAN, [3]Institute of Nuclear Energy Research, Long-Tan, TAIWAN.

Aim: Origin ensemble (OE) image reconstruction algorithm is preferentially used for the reconstruction of unconventional geometrical image, e.g. in a Compton camera (CC) system. Due to the low count rate in such a system, the reconstructed image is noisy. In this study, a novel way to smooth out the noise in the OE algorithm is proposed. **Materials and Methods:** The OE algorithm is performed on the list-mode data. During the reconstruction, the algorithm stochastically modifies the current location of each detected event to a random new location (voxel) along the probable corresponding surface. The new event origin location is accepted or rejected depending on an acceptance ratio which is determined by the relative number of event origins in the voxels (event density) of the new and the old locations. Original OE technique uses single voxel to calculate the event density. In the proposed method, either the mean or median computed from the pixel values of data points within a square region centered on both the old and new locations were used to compute the event density for decision rule. A point source was used to gauge the recovery rate, point spread function, and convergence speed while a flangeless phantom cylinder with fillable thin-walled cylinders inserts (diameters: 8, 12, 16, and 25 mm; height: ~3.8 cm) were used to measure the image quality of the reconstruction. **Results:** Point source study indicates that the number of correctly assigned events increases faster with iteration number and reaches a higher plateau for the proposed OE than conventional OE algorithms. However, the profiles drawn along the point source show the edge blurring effects for both mean and median filters. The contrast recovery coefficient (CRC) and coefficients of variation (CV) measured on the flangeless phantom demonstrate significant improvement for the filtered OE algorithm. **Conclusion:** Compare to the conventional OE algorithm, the proposed methods have the advantages of: improved undersampling phenomenon, faster convergence, and smoother image. The additional computation cost of the filtering is minimum.

E-PW112

A Simultaneous Method for MRI-based Partial Volume Correction and Image Registration in Brain PET

M. Ibaraki, K. Matsubara, T. Kinoshita; Akita Research Institute of Brain and Blood Vessels, Akita, JAPAN.

Introduction: Partial volume effect due to limited spatial resolution is a critical problem especially for measuring PET signals in fine structure such as cerebral cortex (a few millimeters of cortical thickness). Although several MRI-based partial volume correction (MRI-PVC) methods have been proposed, extreme sensitivity to inaccuracy of PET-MR image registration ham-

pers clinical application. The aim of the study was to develop a simultaneous method for PVC and PET-MR image registration, that is PVC with optimized registration (PoR). **Methods:** The proposed PoR is as follows: 1) PET images are registered to individual MR images using SPM's coregister function with default setting. 2) Geometric transfer matrix method (GTM) is applied to the registered PET images, generating region-wise PV-corrected PET images (GTM-PET). 3) The GTM-PET images are smoothed with point spread function (PSF) representing effective PET resolution. The PET images (PV-uncorrected) are re-registered to the smoothed GTM-PET images. These steps (1 to 3) are repeated until the convergence. 4) Finally, region-based voxel-wise correction (RBV; Thomas BA, EJNMMI 2011) is applied to derive voxel-wise PV-corrected PET images (RBV-PET). Water PET images (^{15}O-H$_2$O) obtained from healthy volunteers for CBF study were analyzed (n = 17). Anatomical labels generated from T1-weighted MR images (MPRAGE) using FreeSurfer were merged into 16 volumes of interest (VOIs), which were subsequently used for PVC with Gaussian PSF of 7.5-mm FWHM. Regional mean and intraregional coefficient of variation (COV = SD/mean*100%) in each VOI were calculated for RBV-PET images with and without PoR. **Results:** In the visual assessment of RBV-PET images, cortical voxels with abnormally low or high values were observed due to the inaccuracy of image registration between PET and MR. Number of the abnormal voxels were greatly reduced after the application of PoR. The regional mean values were similar with and without PoR for all the cortical regions, and the differences were smaller than 10% (except for two cases). The intraregional COVs, however, were significantly smaller for RBV-PET images with PoR, 13%±1%, 12%±1%, 15%±1%, and 15%±1% respectively for frontal, parietal, temporal, and occipital cortex compared to intraregional COVs without PoR (18%±7%, 12%±2%, 20%±8%, and 17%±5%), indicating superiority in image uniformity for RBV-PET with PoR. **Conclusion:** The simultaneous method for MRI-based PVC and PET-MR image registration improves quality of voxel-wise PV-corrected PET images, and may facilitate the use of PVC in future clinical settings.

E-PW113

A lesion detection study to evaluate a weight-based dose protocol combined with Pixon Planar Processing for wholebody bone scans

N. Gunson[1], V. Militano[2], N. Ali[2], A. Spencer[2], M. J. Memmott[2], K. J. Saint[2], J. D. Thompson[3], I. S. Armstrong[2]; [1]Christie Hospital, Manchester, UNITED KINGDOM, [2]Central Manchester University Hospitals, Manchester, UNITED KINGDOM, [3]University of Salford, Manchester, UNITED KINGDOM.

Objectives: Weight-based administrations have been implemented successfully in nuclear medicine along with advanced processing methods, providing dose reduction in low-weight patients whilst maintaining the diagnostic quality of images. Guidance on weight-based administration of ^{99m}Tc-MDP for wholebody bone scanning is limited. UK guidance recommends a standard 600 MBq administration for all patients whilst

EANM state a range between 300 and 740 MBq. This study evaluates a weight-based administration of 7MBq/kg ^{99m}Tc-MDP for patients up to 85kg, combined with Siemens Enhanced Planar Processing (EPP). The work is a lesion detection study where ground truth of lesion location is known. **Method**: Anterior wholebody views from 50 bone scans for patients with body weight below 85kg, negative of metastases, were included in this work. All images were acquired on a Siemens Symbia 3 hours after injection of 600 MBq of ^{99m}Tc-MDP at a scan speed of 20 cm/minute using LEHR collimators. Lesions, mimicking those observed in breast and prostate cancer, were inserted in the images. Lesions were created by increasing pixel values in the areas of the axial skeleton according to a 2-dimensional Gaussian shape. 15 images had no lesions inserted while 1-4 lesions were inserted into the remaining 35 images. Each image was resampled to simulate 7MBq/kg activity administration. Both full-count (control) and weight-based resampled images were processed using EPP, resulting in 100 images in total. Images were presented blind to 6 observers, who were asked to locate lesions with an associated confidence score. An acceptance radius of 5 pixels for the true lesion locations was selected. The results from all observers were compared with the ground truth using a weighted Jackknife alternative free-response receiver-operating characteristic (wJAFROC) with the wJAFROC figure of merit (FOM) used to compare the two groups of images. **Results**: The wJAFROC FOMs for the weight-based resampled and control group were 0.670±0.052 and 0.699±0.056 respectively. No significant difference was observed in lesion detection between the weight-based resampled and control images. **Conclusion**: This work has demonstrated that there is no significant difference in lesion detection for patients administered a standard 600MBq or a weight-based 7MBq/kg protocol. This suggests that the weight-based administration protocol is very promising and should be considered for routine practice. In our bone scan patient population this will result in a reduction in dose to half of all patients. It will also reduce the amount of activity required by the centre.

E-PW114

Image Quantitation for LEHR-collimated Tc-99m-TRODAT-1 SPECT: An Experimental Study with Striatal Phantom

M. Wu[1], K. Lin[1], B. Hsu[2]; [1]Dept of Nuclear Medicine, MacKay Memorial Hospital, Taipei, TAIWAN, [2]Nuclear Science and Engineering Institute, University of Missouri-Columbia, Columbia, MO, UNITED STATES OF AMERICA.

Purpose: ^{99m}Tc-TRODAT-1 (TRODAT) single photon emission computed tomography (SPECT) with low-energy high-resolution (LEHR) collimation has been clinically utilized worldwide, but not yet fully investigated for its accuracy in measurement of dopamine transporter (DAT) indexes. We conducted an experimental phantom study to verify the capability of quantitative image reconstruction (QIR) associated with a method of partial volume correction (PVC) for image quantitation of LEHR-collimated TRODAT SPECT. **Methods:** A series of six line-up point sources filled with various activity concentrations of ^{99m}Tc-pertechnetate

were employed to determine image resolution (IR). Simulations of TRODAT uptakes ranging from normal to Parkinson's disease and Parkinsonism (PD/PM) in a striatal phantom were utilized to test the accuracy of DAT indexes, including specific binding ratio (SBR), SBR-symmetry (SBR-sym) and caudate-to-putamen ratio (CPR), using images reconstructed with filtered back-projection (LEHR-FBP) and QIR (LEHR-Q). DAT indexes from LEHR-Q images were further corrected with PVC coefficients derived from an exponential model of target-to-background (TB) ratio to recover absolute activity concentrations (AAC) (unit: kBq/ml) in striatal regions. **Results:** IR of LEHR-FBP was 13.48±0.37 mm and significantly improved to 6.71±0.22mm in LEHR-Q (all p<0.0001). From the analysis of linear regression, linear slopes (LS) of SBR and CPR regressed to true values were significantly higher in LEHR-Q (0.529-0.586, 0.399) than those of LEHR-FBP (0.362-0.366, 0.247), and further improved to (0.952-1.011, 0.927) with PVC (all p<0.0001, all R^2 >0.956). Post PVC, LS (0.952) and R^2 (0.988) of SBR-sym stayed close to unity (p=NS). LS and R^2 of AAC in caudate correlated with true values were (0.943-1.035, 0.970-0.984) and (0.963-0.974, 0.983-0.994) for putamen. Blend-Altman plots reveled only small bias to true values (caudate: 0.9-2.3; putamen: -2.1-10.5 kBq/ml). **Conclusions:** From the phantom study, DAT indexes measured from TRODAT SPECT with LEHR collimation can be significantly enhanced by QIR. Adding PVC additionally achieves to recover AAC close to true values in striatal regions.

E-PW115
Initial Experience with a New PET/CT System Using SiPM Detectors

S. Park, L. Baratto, N. Hatami, G. Davidzon, S. Srinivas, S. Gambhir, A. Iagaru; Stanford University Medical Center, Stanford, CA, UNITED STATES OF AMERICA.

Introduction: We installed the first worldwide of a new digital PET/CT system that brings together silicon photomultiplier (SiPM) technology with time-of-flight (TOF) and block sequential regularized expectation maximization (BSREM, Q.clear®). We report our initial clinical experience using the new Discovery Meaningful Insights (DMI) scanner and evaluate the image quality in comparison to standard PET/CT scanners with and without TOF capability. **Subjects & Methods:** Seventy-three patients were scanned first on the standard of care PET/CT followed immediately by a scan on the new Digital PET/CT system using the same scan time per field of view. Images from the Digital PET/CT were reconstructed using a conventional (non-TOF) algorithm, TOF alone and TOF in combination with Q.clear®. Images from the standard of care PET/CT were reconstructed using clinical standard of care settings. Three blinded readers randomly reviewed four datasets per patient for image quality using a 5-point Likert scale: Standard of Care, $DMI_{non-TOF}$, DMI_{TOF} and $DMI_{TOF+Q.Clear}$. Standardized uptake value (SUV) measurements for the single most avid lesion on each dataset were also recorded. **Results:** In this side-by-side comparison, datasets from the DMI showed higher image quality (*P*<0.001) and SUV measurements compared with the standard of care

systems. Scores were further improved when TOF and Q.Clear® algorithms were added for image reconstruction. Of clinical interest, nine patients demonstrated lesions that could only be visualized on images from the DMI. Noticeably less respiratory artifacts at the diaphragm were also reported in the TOF-reconstructed images. **Conclusion:** The new Digital PET/CT system outperforms the standard of care scanners in terms of image quality, with further benefits added by the use of TOF and Q.Clear® reconstruction algorithms. This may be most beneficial in detecting small tumor lesions and for more accurate disease staging.

E-PW116
Improvements of game-theoretical image segmentation algorithm using PVE correction for nuclear medicine imaging

D. Borys[1], K. Szczucka-Borys[2], I. Gorczewska[3], A. d'Amico[3]; [1]Institute of Automatic Control, Silesian University of Technology, Gliwice, POLAND, [2]Department of Nuclear Medicine and Endocrine Oncology, Maria Sklodowska-Curie Memorial Cancer Center and Institute of Oncology, Gliwice Branch, Gliwice, POLAND, [3]Department of PET Diagnostics, Maria Sklodowska-Curie Memorial Cancer Center and Institute of Oncology, Gliwice Branch, Gliwice, POLAND.

Aim: In previous studies, our group tested different nuclear medicine images segmentation algorithms [1,2]. Tests showed that game-theoretical based algorithm presents the best performance using the Jaccard Index (JI). The aim of this studies was to improve the effectiveness of the algorithm using the Partial Volume Effect (PVE) correction technique and testing different methods of distance metrics in the algorithm. **Materials and Methods:** Data has been obtained using Siemens Biograph PET/CT. The phantom used in tests was a standard cylinder with five spheres of different radius and volume (diameter from 1.3 cm up to 4 cm) filled with a constant concentration of F-18-FDG. For the PVE correction, point source measurements have been done in six different localisations in the field of view (0 to 20 cm from the center) to estimate point source response variability. The algorithm, introduced by M.Pellilo was used for segmentation purpose [3]. The main idea was to represent the image as an edge-weighted graph, where vertices correspond to pixels, and their weights reflect similarity between them. The clustering algorithm uses replicator dynamics. Allocated pixels are removed from the graph and the process is repeated until all pixels are assigned to corresponding clusters. Weights of the edges have been calculated in different ways: using intensity only, intensity and the geometrical distance metric, the neighborhood information. -The measurements of the point source response allowed to estimate Gaussian function parameters in different locations for the PVE correction. It was used in the deconvolution-based algorithm for PVE correction. Results of segmentation were compared to CT image based reference mask by using a JI, which has range [0,1] where the value one corresponds to the full similarity of sets. **Results:** Methods for weights calculation other than intensity based were much less precise producing

visually inappropriate results that gave lower JI comparing to the first method (0.2 to 0.65). The JI improved from 0.65 to 0.79 when the PVE correction was taken into account. **Conclusion:** The method based on intensity measurements was the most effective for the algorithm used in this study. PVE correction improves results of the segmentation, especially for small objects allowing to classify correctly small structures. Acknowledgment: Grant No. STRATEGMED2/267398/4/NCBR/2015. References: [1] Borys, D. et al., EJNMMI, Vol. 42, Sup. 1, p. S409-S410, 2015. [2] Borys, D. et al., EJNMMI, Vol. 43, Sup. 1, p. S496, 2016. [3] Pavan, M., Pellilo, M., IEEE CVPR, 2003

E-PW117

Large bed overlap and short acquisition time or vice versa?

T. Andersen, P. Braad, P. Hoilund-Carlsen; Odense University Hospital, Odense, DENMARK.

Purpose: The reconstruction and data acquisition in 3D PET requires an overlap between each other following bed positions to compensate for low sensitivities in the field of view (FOV) edges when data are collected in a step-and-shoot acquisition mode. A small overlap between bed positions facilitates a larger throughput, i.e. larger scan length per unit time enabling full body scans in approximately 10 min. or shorter. Such scans hence enable fast whole body scans but at the cost of an uneven sensitivity profile across bed positions due to the triangular sensitivity profile of PET scanners along the scanner axis. In the current work the noise profile and quantitative accuracy were evaluated to determine the effect of bed overlap on image quality and to determine the optimal compromise between bed overlap and acquisition time per frame. **Methods:** A NEMA IQ phantom and a custom-made 55 cm long cylindrical tube with a diameter of 5.5 cm were scanned on a digital GE Discovery MI scanner with a 20 cm field of view. The phantoms were filled with a start activity of 5 kBq/cc of ^{18}F-FDG to mimic clinical relevant activity concentrations. Five series were acquired on the scanner with overlaps ranging from 15% to 50% in list mode acquisition. The acquired data were subsequently rebinned in frames ranging from 10 s. to 10 min. per bed position and reconstructed both with a standard 17/3 OSEM reconstruction with TOF and PSF applied and a Bayesian penalized likelihood reconstruction algorithm. Noise characteristics and quantitative accuracy were evaluated in 5 ROIs distributed in each slice of the phantoms as a function of slice position along the scanner axis. **Results:** Both the standard deviation of the voxel values, i.e. the noise, and the quantitative variation along the phantom length increased with smaller bed overlaps compared to larger overlaps. This was especially evident in short acquisition frames, i.e. time per bed position < 30 s. Little effect was observed on reconstruction method where both noise variation and quantitation accuracy were similar**. Conclusion:** The results suggest that large bed overlap and shorter acquisition time pr. bed position is advantageous compared to low bed overlap and longer acquisition time pr. bed position. The effect is especially evident in low count studies as for instance dosimetry scans with ^{124}I prior to ^{131}I therapy.

E-PW118

Optimal quantitative SUV metrics over wide range of lesion sizes in advanced image reconstruction (TOF and PSF) for PET

I. Shiri[1], P. Ghafarian[2,3], S. Ashrafinia[4], A. Bitarafan-Rajabi[1,5], M. AY[6,7], A. Rahmim[8,4]; [1]Department of Medical Physics, School of Medicine, Iran University of Medical Sciences, Tehran, IRAN, ISLAMIC REPUBLIC OF, [2]Chronic Respiratory Diseases Research Center, National Research Institute of Tuberculosis and Lung Diseases (NRITLD), Shahid Beheshti University of Medical Sciences, Tehran, IRAN, ISLAMIC REPUBLIC OF, [3]PET/CT and Cyclotron Center, Masih Daneshvari Hospital, Shahid Beheshti University of Medical Sciences, Tehran, IRAN, ISLAMIC REPUBLIC OF, [4]Department of Electrical and Computer Engineering, Johns Hopkins University, Baltimore, MD, UNITED STATES OF AMERICA, [5]Cardiovascular Intervention Research Center, Rajaie Cardiovascular Medical and Research Center, Iran University of Medical Sciences, Tehran, IRAN, ISLAMIC REPUBLIC OF, [6]Research Center for Molecular and Cellular Imaging, Tehran University of Medical Sciences, Tehran, IRAN, ISLAMIC REPUBLIC OF, [7]Department of Medical Physics, School of Medicine, Tehran University of Medical Sciences, Tehran, IRAN, ISLAMIC REPUBLIC OF, [8]Department of Radiology, Johns Hopkins University, Baltimore, MD, UNITED STATES OF AMERICA.

Aim: Tumor quantification using 18F-FDG PET has significant impact on routine usage in treatment response assessment and for prognostication in cancer patient. Advanced image reconstruction techniques available in routine PET imaging lead to improved image quality and lesion detectability; yet their quantification accuracy remains a topic of debate. The aim of this study was to evaluate the accuracy of quantification metrics over these reconstruction methods, and to find the most accurate SUV quantification metric in a wide range of lesion sizes. **Material and Methods**: The NEMA-IEC body phantom was used, consisting of six standard spheres (10 to 37mm) and small lesions (2, 3,4,5,6 and 7 mm) with different contrasts (4:1,2:1) and background activities, acquired in 3D list-mode for 5 minutes-per-bed position. Images were reconstructed using 3D-OSEM algorithm with and TOF and whit PSF-modeling. Quantification of each lesion VOI was performed using SUVmean, SUV42, SUV50, SUV70, SUVNestle, SUVmax, SUVpeak1cc and SUVpeak0.5cc. Subsequently, we determined Relative Errors (RE%) with respect to true SUV values for each metric. **Result:** In spheres larger than 13mm in diameter, SUVmax, SUVpeak0.5cc and SUVpeak1cc yielded significant overestimation (RE% of 44.8, 40.1 and 37.5 respectively). SUV50 was the only quantitative metric which had no statistically significant difference with respect to the true value in sphere (RE% of 11.77 to 0.44). In the 13 and 10 mm spheres, the best quantitative performance was obtained by SUVmax and SUVpeak0.5cc. Also, in spheres smaller than 10mm, all quantification metrics had significant underestimation and high relative error (-76.32 to -34.49). **Conclusion:** Our phantom study showed that optimal quantification of the 18F-FDG tracer in PSF- and TOF-enabled reconstruction is size dependent. Even including PSF and TOF, quantification in spheres smaller than 10mm in diameter is underestimated. It is

important to also point out that incorporation of PSF and TOF in the reconstruction leads to overestimation in larger sphere for certain SUV metrics and as such, can lead to incorrect assessment of treatment response. Therefore, more caution should be exercised when using SUV metrics in the context of new PET reconstruction techniques.

E-PW119

A demonstration of the concept of numerical twins in esophageal cancer patients

F. Orlhac[1], C. Nioche[1], S. Boughdad[1,2], M. Soussan[1,3], I. Buvat[1]; [1]IMIV, CEA, Inserm, CNRS, Univ. Paris-Sud, Université Paris-Saclay, CEA-SHFJ, Orsay, FRANCE, [2]Department of Nuclear Medicine, Institut Curie – René Huguenin, Saint-Cloud, FRANCE, [3]Department of Nuclear Medicine, Assistance Publique - Hôpitaux de Paris, Avicenne Hospital, Bobigny, FRANCE.

Purpose: The characterization of tumor heterogeneity using textural features in radiomic analyses of PET images has shown promise to predict patient response or survival. In this context, the goal of this study is to identify for each patient a radiomic numerical twin who has similar radiomic feature values to learn from the numerical twin's history and guide patient management. Here, we test this concept to predict treatment response.
Subjects & Methods: 107 patients with newly diagnosed esophageal cancer underwent pre-treatment 18F-FDG PET scan (data extracted from Ypsilantis et al, PLoS ONE 10(9):e0137036). All patients received a neoadjuvant chemotherapy and were later classified as non-responders (NR=69) or responders (R=38). In each patient, the primary lesion in the baseline scan was segmented using a threshold set to 40% of SUVmax. In each resulting volume of interest, 103 radiomic features were extracted including 85 textural or fractal features and 18 histogram indices. Each lesion was associated with a vector b of biomarkers. We computed the element-wise ratio between the vector $b(p)$ of one patient p and the vector $b(i)$ of each of the other 106 patients i (i=1,P-1). A patient N was identified as the radiomic numerical twin of patient p if the distance of $b(p)/b(N)$ to 1 was the lowest among the P-1 distances. Its response to treatment was then predicted as the one observed in patient N. We evaluated the ability of this approach to predict treatment response when using 2 or 3 biomarkers in b by calculating the Youden index in a leave-one-out validation. We compared the results with logistic regression and support vector machine (SVM) models.
Results: When including two biomarkers in b, the best performance using the numerical twin concept was obtained using Kurtosis and Energy with 87% NR lesions and 63.2% R lesions accurately classified (Youden=0.50). With three biomarkers (Kurtosis, Energy and Fractal Dimension mean), Youden index increased to 0.55. With 2 or 3 biomarkers, the logistic regression and SVM models always yielded Youden index less than 0.43. **Conclusion**: This concept of radiomic numerical twins is validated in esophageal cancer to predict treatment response. We found that lesions with similar radiomic profiles consisting of only 2 to 3 biomarkers had similar response to therapy. The identification of numerical twins could assist patient manage-

ment in the future, based on the disease evolution in the patients used to identify the numerical twin.

e-Posters

Physics & Instrumentation & Data Analysis: Instrumentation

EP-0001

Conventional and microfluidic PET tracer synthesis on a novel synthesizer platform

C. Rensch[1], C. Frank[1], R. Salvamoser[1], G. Winter[1], S. Lindner[2], P. Bartenstein[2], F. Rensei[3], A. Hienzsch[4], R. Hesse[4], H. Lankau[4], M. Müller[4], A. Hoepping[4], V. Samper[1]; [1]GE Global Research, Garching near Munich, GERMANY, [2]Department of Nuclear Medicine, University Hospital Munich LMU, Munich, GERMANY, [3]GE Healthcare, Uppsala, SWEDEN, [4]ABX advanced biochemical compounds GmbH, Radeberg, GERMANY.

Introduction: Mini- and micro-scale technologies for PET tracer synthesis have been explored for more than two decades, as they hold the promise of reducing costs and improving synthesizer performance. Systems attempting downscaling of a process from an established baseline, or upscaling from exploratory studies, have encountered challenges such as spanning the different reagent volumes required, high cost of specialized components, or limited applicability to cGMP compliant routine production. The system presented overcomes these challenges. **Methods:** The core of the synthesizer is a consumable consisting of 1) a fluidic chip and 2) a reagent carrier. The chip is manufactured from a cyclic olefin co-polymer (COC) resistant to temperatures and chemicals commonly utilized in PET radiochemistry. The chip contains reactors, azeotropic dryers, pumps, and 70 individually addressable valves. All on-chip features can be routed by minor modifications of a standardized injection molded design, enabling large design flexibility at low cost. The routing channel sizes can be adapted from micro- to millimeters, enabling processing from microliter to milliliter volumes. This scalability is supported by a novel gas pressure driven fluid transport method that eliminates the need for syringe pumps whilst providing a good volume accuracy vs. range relationship, as well as a path to cGMP compliant operation by sterile filtration of the driving gases. The reagent carrier contains conventional vials, solid phase extraction (SPE) cartridges and sterile filters, providing an interface to established reagent kits and components. **Results:** For reagent volumes of microliters, the synthesizer platform was applied to research on carbon-11 radiolabeling of amino acids (Hienzsch et al., poster 441, ISRS 2017, Dresden, Germany). For conventional processing (milliliters), the GE FASTlab FDG citrate process (benchmark: 70±4% n.d.c. yield in <25min) was reproduced on the system achieving up to 65% n.d.c. yield in <25min without optimization. The fluoride-18 input activities were successfully scaled from 200 MBq to 170 GBq. **Conclusion:** The platform is capable of established stop-flow and unconventional research oriented processes, providing access to micro and conventional domains. A perspective to cGMP compliant operation is maintained by a consumable approach, interfaces to established reagent & SPE kits, as well as sterile filtration of the driving gases without use of syringes and associated tubing. Results show that this system can become a vehicle to bridge advanced synthesis design to routine production on a single platform. **Acknowledgements:** The authors gratefully acknowledge the financial support from the German Federal Ministry of Education and Research.

EP-0002

The Influence of Crystal Material and Size on the Sensitivity of Recently Developed SiPM Based Animal PET Scanner: a Monte Carlo Study

P. Ghahramani[1,2], N. Zeraatkar[2], N. Vosoughi[1], M. R. Ay[2,3]; [1]Radiation Medicine Engineering Department, Sharif University of Technology, Tehran, IRAN, ISLAMIC REPUBLIC OF, [2]Research Center for Molecular and Cellular Imaging, Tehran University of Medical Sciences, Tehran, IRAN, ISLAMIC REPUBLIC OF, [3]Department of Medical Physics and Biomedical Engineering, Tehran University of Medical Sciences, Tehran, IRAN, ISLAMIC REPUBLIC OF.

Aim: In this study, the sensitivity of an animal PET system by evaluating the influence of crystal material and size using Monte Carlo method has been optimized based on NEMA NU 4-2008 standards. **Materials and Methods:** An animal PET system with pixelated crystal has been recently designed and developed in our department. The ring diameter in the current version is 162 mm consisting of 10 modules. The sensitivity of system was evaluated for three commercial crystal materials including BGO, LYSO and GSO read out by SiPM, also for a range of crystal thicknesses (10-15 mm, 1 mm step), and for different crystal pixel sizes (1.4×1.4 - 2.2×2.2 mm^2, 0.2 mm^2 step). Each crystal block has 0.1 mm BaSO$_4$ as inner-pixel crystal reflectors. The axial field-of-view (AFOV) and energy window for all configurations respectively were 4.8 cm and 350-650 keV. The NEMA NU 4-2008 standards were used for evaluating sensitivity. According to NU-4, a ^{22}Na point source must be stepped from the beginning of the AFOV to the end of it with steps equal to slice thickness (45 steps for our system) and data should be acquired in each step. As the Monte Carlo method is slow and outputs are large, so we applied two approximations regarding to our symmetric geometry: we stepped the source in half AFOV and we increased the step length twice the NU-4. The system was well defined in the GATE Monte Carlo code in details. **Results:** For one configuration (LYSO crystal material, 10mm crystal thickness, 2×2 mm^2 crystal pixel size), the sensitivity based on NU-4 main method and after applying two approximations was respectively 1.42% and 1.45% representing 2% error due to the approximations while 75% time and volume of calculations were reduced. The sensitivity for BGO, LYSO and GSO was respectively 2.17%, 1.45%, and 0.92%. The sensitivity for 10, 11, 12, 13, 14, and 15 mm crystal thicknesses was respectively 1.45, 1.67, 1.89, 2.12, 2.35, and 2.57% and for 1.4×1.4, 1.6×1.6, 1.8×1.8, 2×2, and 2.2×2.2 mm^2 crystal pixel sizes was respectively 1.30,

1.32, 1.35, 1.45, and 1.47%. **Conclusion:** Based on the Monte Carlo results, BGO-based scanners have highest sensitivity and sensitivity of LYSO is more than GSO. By increasing the crystal thickness, sensitivity of the scanner increases due to its higher stopping power for 511 keV photons. The sensitivity also increases by increasing crystal pixel size because more photons can be detected.

EP-0003

Monte Carlo Based Performance estimation of breast PET scanners due to reduction of the ring diameter

A. Emami[1,2,3], *H. Ghadiri*[1,2], *P. Ghafarian*[4,5], *M. Ay*[1,2]; *[1]Research Center for Molecular and Cellular Imaging, Tehran University of Medical Sciences, Tehran, IRAN, ISLAMIC REPUBLIC OF, [2]Department of Medical Physics and Biomedical Engineering, Tehran University of Medical Sciences, Tehran, IRAN, ISLAMIC REPUBLIC OF, [3]International Campus, Tehran University of Medical Sciences, Tehran, IRAN, ISLAMIC REPUBLIC OF, [4]Chronic Respiratory Diseases Research Center, National Research Institute of Tuberculosis and Lung Diseases (NRITLD), Shahid Beheshti University of Medical Sciences, Tehran, IRAN, ISLAMIC REPUBLIC OF, [5]PET/CT and Cyclotron Center, Masih Daneshvari Hospital, Shahid Beheshti University of Medical Sciences, Tehran, IRAN, ISLAMIC REPUBLIC OF.*

Aim: Positron emission tomography (PET) is a useful technique to visualize biologic processes within body before or during treatment. Breast PET imaging methods continue to evolve and have been improving the limitation of the sensitivity and spatial resolution of whole body scanners. The new designs of instrumentation have vastly progressed over the past ten years. An ideal system would with high sensitivity, spatial resolution, and low cost of scanner. **Materials and methods:** We have used computer simulations to compare three designs for a breast PET scanner with different ring diameters. In three systems rings are consist of 8, 9 and 10 LYSO modules, with transaxial field of view (FOV) of 128 mm,145 mm and 162 mm. The new designs combine high spatial resolution, and sensitivity to detect small, low-contrast masses. To measure spatial resolution and sensitivity we simulated point sources in the center of the imaging FOV, where the effects of axial parallax are largest. **Results**: We developed a prototype PET scanner that can achieve a spatial resolution and sensitivity approaching the physical limits of a small-bore scanner. The simulation results showed that FOV 162 mm has better sensitivity and spatial. Based on NEMA NU 4-2008 test, the comparison between different systems indicates that the absolute sensitivity of our system is %1.42 that is appropriate that others. The sensitivity is not highlight but decreasing AFOV including some advantages such as reducing the cost of scanner. Normalized sensitivity to AFOV is 0.29 that is extremely good in comparison with other commercial systems. **Conclusions:** The PET designs of the dedicated breast PET system has improved imaging characteristics in comparison to commercial whole-body scanners, particularly when special geometry scanner design. Also the number of detectors and related electronics are much less than others which reduces the cost.

EP-0004

Measurement of 225 ps CRT on 20 mm thick monolithic LYSO and CeBr3 crystals using Temporal imaging

C. Tata Zafiarifety[1], *A. Iltis*[1], *G. Zeufack Tadonkeng*[1], *L. Rodrigues*[1], *H. Snoussi*[2]; *[1]Damavan imaging, TROYES, FRANCE, [2]Université de Technologie de Troyes, TROYES, FRANCE.*

Promising performance for TOF-PET on pixelated LYSO or LaBr3 crystal has been obtained with Phillips Digital Si-PM. However the limited thickness of the crystal in those experiment is not compatible with the use in an actual PET scanner. Thick monolithic crystals would allow much higher detection efficiency. In this work we study the timing performance of 32x32x20 mm3 monolithic LYSO and 32x32x25 mm3 monolithic Cebr3 crystals. Here the 20 mm thick LYSO crystal has an intrinsic detection efficiency of 82.45 % for 511 KeV Gamma ray. We use Depth Of Interaction (DOI) positioning in the crystal to improve the timing performance. We are correcting the delay time introduced by the scintillation photon travelling the crystal at a speed of c/n, where n is the refractive index. Whereas gamma photon travels at the speed of light c. DOI is determined using the time arrival of the first photon and least mean square root method on simulated images. Measurements were performed using Na[22] source and LYSO crystals were wrapped with ESR Vikuity. Cebr3 crystals were wrapped with Teflon. Both were coupled to DPC3200 Si-PM. For LYSO crystal energy resolution of 10.1 % was obtained and coincidence resolving time (CRT) of 503 ps FWHM was measured without correction. When applying the correction of DOI time delay, the CRT was reduced to 225 ps FWHM. For CeBr3 the measurements are still ongoing and will be available shortly. This study shows that using thick monolithic crystals and a good DOI correction through temporal imaging, it is possible to obtain in a realistic configuration a good CRT for TOF-PET system.

EP-0005

Design and Development of a Small-Animal PET Scanner Based on Pixelated Crystals and Silicon Photomultipliers

M. Ay[1,2], *N. Zeraatkar*[1], *S. Sajedi*[1], *M. Taheri*[1], *S. Kaviani*[1], *S. Sarkar*[1,2]; *[1]Research Center for Molecular and Cellular Imaging, Tehran University of Medical Sciences, Tehran, IRAN, ISLAMIC REPUBLIC OF, [2]Department of Medical Physics and Biomedical Engineering, Tehran University of Medical Sciences, Tehran, Iran, Tehran, IRAN, ISLAMIC REPUBLIC OF.*

Aim: During last two decades, the application of small animals in molecular imaging has been continuously increasing. Development of dedicated small-animal Positron Emission Tomography (PET) scanners, hence, underwent an ascending trend to provide the preclinical researchers with a molecular imaging scanner of higher spatial resolution and sensitivity to reach quantitative analysis ability. In this work, we introduce a new small-animal PET scanner called Xtrim, which we recently developed in our center. **Materials and Methods**: The Xtrim PET is a full-ring scanner composed of 10 detector blocks. Each block includes a 24x24 array of Lutetium-yttrium oxyorthosilicate (LYSO)

pixelated crystals attached to a 12x12 array of Silicon Photomultipliers (SiPMs). After pre-amplification and time-stamping, the data of all the blocks are transmitted to a main board. The main board is responsible for coincidence detection and sending the list-mode data to a computer. The axial field-of-view and bore opening of the scanner are respectively 50.3 mm and 120 mm. All calibration, correction, and data arrangement processes including positioning, energy calibration, normalization, rebinning, and image reconstruction are performed in the computer using an in-house software package. Some experiments were conducted to obtain preliminary performance parameters of the system. For this, spatial resolution and sensitivity of the system were examined using capillary and rod sources, respectively. Also, for evaluation of the animal imaging performance of the scanner, an F-18-sodium fluoride (NaF) scan using a rat was performed. **Results**: Spatial resolution of the system was measured as 1.8 mm at the center without resolution recovery. In addition, the sensitivity of the Xtrim was calculated as about 10%. The reconstructed images of the rat NaF scan revealed good imaging performance of the system resolving skeletal structure including acceptable resolutions for the vertebrae and the ribs. **Conclusion**: A dedicated small-animal PET scanner was designed and developed based on pixelated crystals and SiPM providing a potentially MR-compatible detection subsystem to be able to be merged with an MR modality and forming a PET/MR system. The preliminary performance evaluation of the system showed that Xtrim can be a reliable PET imager for numerous application in preclinical molecular imaging.

EP-0006

SiPM PET/CT vs. Standard PET/CT: A Pilot Study Comparing Semi-Quantitative Measurements in Normal Tissues and Lesions

L. Baratto[1], S. Park[1], N. Hatami[1], G. Davidzon[2], S. Srinivas[1], S. S. Gambhir[3], A. Iagaru[1]; [1]Stanford University, Division of Nuclear Medicine and Molecular Imaging, Department of Radiology, Stanford, CA, UNITED STATES OF AMERICA, [2]Stanford University, Radiological Sciences Laboratory, Stanford, CA, UNITED STATES OF AMERICA, [3]Stanford University School of Medicine, Departments of Radiology, Bioengineering, Materials Science and Engineering, Stanford, CA, UNITED STATES OF AMERICA.

Purpose: The aim of this pilot study is to determine if a new generation PET/CT scanner using silicon photomultipliers (SiPM), GE Discovery Molecular Insights - DMI PET/CT (GE Healthcare, Waukesha, WI), recently installed in our Department, provides equivalent results compared to the standard of care PET/CT scanners (GE Discovery 600 or GE Discovery 690) used in our clinic and to explore any possible differences in semi-quantitative measurements. **Materials and Methods:** We enrolled 50 patients who had a clinical indication for standard of care PET/CT. The local Institutional Review Board approved the protocol and written informed consent was obtained from each patient. All patients underwent a single injection dual imaging protocol including the standard of care PET/CT scan followed immediately by image acquisition using the DMI PET/CT scanner. We

measured SUV_{max} and SUV_{mean} of different background organs and up to 4 lesions per patient from data acquired using both scanners. **Results:** DMI PET/CT scan did not miss any of the 107 lesions detected by standard PET/CT scanners and identified additional 37 areas of focal ^{18}F-FDG uptake compatible with putative sites of disease. The results of equivalence tests on the normal tissues matched per patient showed an equivalence for all background tissues except for the cerebellum (*P* value < 0.01). The SUV_{max} measurements for all 107 lesions were 2.8 ± 2.8 higher on DMI PET/CT compared with standard of care PET/CT (*P* <0.0001) and this difference was not related to time delay between two scans (*P* <0.0001). Lesion:aortic arch ratios and lesion:liver ratios were 3.2 ± 2.6 and 1.9 ± 1.4 higher on DMI PET/CT compared with standard of care PET/CT (*P* <0.0001). **Conclusions:** The performance of SiPM PET/CT is at least comparable to that of standard PET/CT. While delayed imaging can lead to detection of additional lesions, our data suggests that in this series the lesions identified only on DMI PET/CT indicate superior performance of the scanner. Further evaluation needed to confirm our data. Differences in semi-quantitative measurements between standard PET/CT and SiPM PET/CT are important factors when adopting the new technology.

EP-0007

Optimization of the crystal thickness for a monolithic LYSO animal PET detector with anger and CSE positioning method using Monte Carlo simulation

A. Sanaat[1,2], M. Shamsaie[1], B. Teymorian[1], R. Hashemi[2,3], M. Ay[3,2]; [1]Department of Energy and Physics, AmirKabir University of Technology (Tehran Polytechnic), Tehran, IRAN, ISLAMIC REPUBLIC OF, [2]Research Center for Molecular and Cellular Imaging, Tehran University of Medical Sciences, Tehran, IRAN, ISLAMIC REPUBLIC OF, [3]Department of Medical Physics and Biomedical Engineering, Tehran University of Medical Sciences, Tehran, IRAN, ISLAMIC REPUBLIC OF.

Introduction: In nuclear medicine imaging systems' detectors, intrinsic spatial resolution and sensitivity depend on the identification and accuracy of an interacting point and the amount of interacting photons to sensitive cell. These factors is dominated by propagation of the scintillation photons in the detector crystal, positioning algorithm and physical features of the crystal. This study was intended to use Monte Carlo simulation to estimate the intrinsic spatial resolution and sensitivity of animal PET detector by using two positioning algorithm method. **Subjects & Methods:** We used Geant4 Monte Carlo simulation library to simulate the optical photon processes. Our simulation includes geometry of crystal, reflector, light guide and silicon photo multiplier SiPM and all the optical process. The validation of the simulation code was performed for a monolithic NaI(Tl) scintillator ($402 \times 246 \times 9.5$ mm³) coupled to 24 flat-panel type multi-anode photo multiplier tubes (PMT) (R6237: Hamamatsu) and results were compared with those obtained experimentally. Moreover, the code was applied to a LYSO scintillator with entrance area 50.2×50.2 mm² and various thicknesses (4 - 6 - 8 - 10 mm) coupled to a 12×12 SiPM (Sensl ArrayC-30035-144P-

PCB) for finding the best geometry and positioning algorithm. **Results:** Our simulation indicated 3.5 mm full width at half maximum (FWHM) of spatial resolution for the NaI(Tl) detector, which were in a good agreement with the experimental results. This investigation has shown that Geant4 simulation toolkit enables us to predict optical process accurately. Furthermore simulation of animal PET detector for a centric point source showed that the best resolution and sensitivity obtained in 6mm thickness (0.93 mm & 49%), also Anger and Correlated Signal Enhancement (CSE) algorithms positioning were tested and CSE algorithm showed better performance in edge and center positioning.(resolution in 25mm from center of the crystal by CSE method was calculated 31% lower than Anger). In this study the ratio of total number of scintillation photons to number of photons which are fire SiPM pixels are measured. This parameter start from 0.19% for 4mm thickness and decrease to 0.1% for 10mm thickness. **Conclusion:** The Geant4 simulation established to estimate the intrinsic spatial resolution and sensitivity of animal PET detector with Anger and CSE positioning algorithm and also different thickness. This simulation can be used to provide an optimal design of animal PET monolithic detector without physical experiment.

EP-0008

Performance Evaluation of a New High Resolution Non-human Primate (NHP) PET/CT System (LFER 150 PET/CT)

Z. Sarnyai[1], K. Nagy[2], G. Patay[2], M. Molnár[2], G. Rosenqvist[1], M. Tóth[1], A. Takano[1], B. Gulyás[1], C. Halldin[1], P. Major[2], A. Varrone[1]; [1]Karolinska Institutet, Stockholm, SWEDEN, [2]Mediso Ltd., Budapest, HUNGARY.

Aim: The LFER 150 PET/CT by Mediso is a high-resolution system for non-human primate (NHP) imaging. The objective of this study was to evaluate the performance of the system using the NEMA NU 4 standard protocol**. Materials and Methods:** The NEMA NU4 standard protocol was used for resolution, sensitivity, image quality (IQ) and noise equivalent count rate (NEC). NEC measurement was performed with the rat-like and the monkey-like phantom. A Derenzo phantom was acquired to test the resolution using 3D OSEM reconstruction. One cynomolgus monkey (4.5 kg, IV ketamine/xylazine anesthesia) was examined with the dopamine transporter radioligand [^{18}F] FE-PE2I (90 MBq) to evaluate the in vivo performance of the system. Attenuation correction was performed using a material map generated by segmentation of the CT image. List mode PET data acquired for 93 min were reconstructed into 38 frames with the Tera-Tomo™ 3D engine using OSEM algorithm. Binding potential (*BP*$_{ND}$) for caudate, putamen and substantia nigra were evaluated using the simplified reference tissue model. **Results:** Radial FWHM resolution using Fourier rebinning and 2D filtered back projection (FBP) algorithm was better than 2.2 mm and 3.2 mm in the central 60 mm and 160 mm diameter region, respectively. Maximum sensitivity in 400-600 keV and 250-750 keV energy window was 30.03 cps/kBq (3.3%) and 49.11 cps/kBq (5.4%) respectively. The uniformity in the IQ phantom was 3.3 % and the spill-over ratio for air and water was 0.1. The peak of the NEC curve was 399 kcps (149 MBq) using the rat-like phantom and

64.7 kcps (128 MBq) using the monkey-like phantom. Rods of the Derenzo phantom with 1 mm diameter could be visualised. In the NHP experiment *BP*$_{ND}$ values in the caudate, putamen and substantia nigra (4.31, 4.45 and 0.7 respectively) were similar to those previously reported in NHPs using the same radioligand and the high-resolution research tomography. **Conclusion:** The results obtained from phantom experiments and one representative PET measurement in NHP confirm that the LFER 150 is a high-resolution PET-CT system with suitable performance for brain imaging in NHPs.

EP-0009

Design optimization of partial cylindrical PET scanner based on trapezoid-shaped block detector and monolithic crystals using Monte Carlo simulation

P. Sheikhzadeh[1,2], H. Ghadiri[1,2], P. Geramifar[3], P. Ghaffarian[4,5], M. Ay[1,2]; [1]Department of Medical Physics and Biomedical Engineering, Tehran University of Medical Sciences, Tehran, IRAN, ISLAMIC REPUBLIC OF, [2]Research Center for Molecular and Cellular Imaging, Tehran University of Medical Sciences, Tehran, IRAN, ISLAMIC REPUBLIC OF, [3]Research Center for Nuclear Medicine, Shariati Hospital, Tehran University of Medical Sciences, Tehran, IRAN, ISLAMIC REPUBLIC OF, [4]Chronic Respiratory Diseases Research Center, National Research Institute of Tuberculosis and Lung Diseases (NRITLD),Shahid Beheshti university of medical science, Tehran, IRAN, ISLAMIC REPUBLIC OF, [5]PET/CT and Cyclotron Center, Masih Daneshvari Hospital, Shahid Beheshti University of Medical Sciences,, Tehran, IRAN, ISLAMIC REPUBLIC OF.

Aim: Cylindrical PET geometries with the conventional detector blocks are subject to sensitivity loss due to inter-block gap between the rectangular detector blocks. The sensitivity loss is more pronounce with pixelated crystals that suffer from lower packing fraction due to inter-pixel reflectors. One potential solution is to use trapezoid detector blocks in combination with using monolithic crystals. The objective of this work is to compare system sensitivity of PET system designs with headphone-like geometry. Our headphone-like geometry design is in fact a cylinder-like geometry with partially populated detector blocks. In this work we methodically compare the sensitivity gain across the FOV when using monolithic trapezoid detector blocks with that of pixelated rectangular blocks. **Material and Methods:** GATE Monte Carlo toolkit was used to model the PET systems. In both designs, there are 22 detector blocks per ring. The ring diameter and axial length were kept the same at 245 mm and 277 mm, respectively. We used 30 mm thick BGO crystal in the detector blocks. Block cross-section is 25.2*25.2 mm^2 at the entrance side for both designs and 31.0*31.0 mm^2 at the exit side in the trapezoid detector blocks. The BGO crystals in the rectangular block are pixelated with 2.3 mm pixels. System sensitivity of two scanner designs were measured at the center and 7 cm offset from the center of the scanner using a point-like source. **Results:** System sensitivity of 20.01% and 28.91% was calculated at the FOV center and 7 cm off-center, respectively, for the design with trapezoid monolithic crystals. The calculated values for pixelated rectangular detector block were 17.34% and

25.59%. These values show ~ 15% sensitivity gain at the FOV center and 13% gain at 7cm off-center for a point-like source. **Conclusion:** Our results show that by simply using monolithic trapezoid crystals instead of pixelated rectangular crystals we can gain ~ 15%. It is noteworthy that monolithic crystals even in trapezoid shape are cheaper to manufacture compared with pixelated arrays. The higher system sensitivity can also be used to reduce the administered patient dose or to shortening the acquisition time.

EP-0010

Feasibility of Whole Body Dynamic Acquisitions using Digital PET/CT - A Preclinical Phase I Study

K. Binzel[1], J. Zhang[1], M. I. Menendez[1], M. Friel[1], M. I. Knopp[1], R. Moore[1], C. L. Wright[1], P. Maniawski[2], M. V. Knopp[1]; [1]The Ohio State University, Columbus, OH, UNITED STATES OF AMERICA, [2]Philips Healthcare, Cleveland, OH, UNITED STATES OF AMERICA.

Aim: The future of PET/CT imaging will undoubtedly include imaging agents, acquisitions and applications beyond our current scope, as new radiopharmaceuticals are developed for specific imaging of disease states well beyond oncology and the benefit of dynamic imaging has become more evident. We explored the feasibility of performing whole body dynamic imaging enabled by the advantages provided by next-generation digital photon counting PET technology. **Materials and Methods:** We performed preclinical imaging on a pre-commercial release next-generation digital PET/CT system (Philips Vereos, dPET). dPET enables count sensitivity superior to conventional imaging systems with time of flight timing resolution of 325 ps. The potential for ultra-fast imaging protocols is being demonstrated in other preclinical as well as clinical work. We developed a feasibility study in healthy canines utilizing 10s per bed acquisitions covering a series of positions from head to pelvis, repeated up to 15 times, with imaging starting at the time of injection. From these repeated acquisitions, time activity curves or other dynamic data analysis can be generated over an area greater than the single volume dynamic field of view traditionally employed. **Results:** We found that this whole body imaging approach is readily feasible after protocol development and fine tuning performed over our first several imaging sessions. There can be different approaches such as head to feet cycling which will ensure the same temporal resolution for all locations versus head-to-feet-to-head cycling leading to varying time-lapse periods. We also found that a slower, non-bolus injection can lead to excellent imaging of the vascular phase. System performance must be fine-tuned to minimize any data transfer delays. This acquisition approach is quite strenuous from a system performance point of view. Even with cycle times of 1 - 2 min, we found that tracer uptake curves can be readily generated from any desired body region. The ultra-short acquisition time requires count sparsity optimized image reconstruction that should be regularized for relative count densities. **Conclusion:** Next-generation digital PET/CT provides a leap in technology that enables ultra-short PET acquisitions which can be expanded to whole body dynamic acquisition protocols. Performing repeated, ultra-fast acquisitions of a large volume / whole body from the time of radiotracer injection can provide insight into the biodistribution not previously possible when limited to a single bed field of view. With the development of new radiotracers for applications beyond oncology, such an imaging approach appears to be extremely valuable.

EP-02 **during congress opening hours, e-Poster Area**

Physics & Instrumentation & Data Analysis: Image Reconstruction

EP-0011

Accuracy and precision of activity concentration measurements for GE Q.Metrix absolute SPECT quantification

I. Armstrong; Central Manchester University Hospitals, Manchester, UNITED KINGDOM.

Aims: Absolute quantification packages to offer "SUV SPECT" are now available from several vendors. There are currently very few technical assessments of SUV SPECT to evaluate the accuracy and precision of metrics from images. This phantom work evaluates this using GE Q.Metrix. **Method:** SPECT/CT of NEMA image quality and anthropomorphic cardiac torso phantoms were acquired on a GE Optima 640 with LEHR collimators. Studies were ECG-gated with an external trigger to provide 8 replicate images. Total counts in each replicate were 12×10^6 and 2.3×10^6 for the NEMA and torso respectively. NEMA scans were performed with 5:1 and 10:1 sphere contrast and 3-degree and 6-degree projection steps. Images were reconstructed with corrections for attenuation, scatter and resolution using GE default parameters (4 iterations, 10 subsets, no post-filter). Maximum voxel and region mean activity concentration recovery (ACR) (ratio of measured to true) was calculated in the four largest NEMA spheres (VOIs defined on CT) and cardiac insert (40% maximum voxel threshold VOI on SPECT). Mean and standard deviation of ACR were calculated across replicates. **Results:** Maximum ACR in the NEMA spheres (37, 28, 22, 17mm respectively) was 1.33±0.03, 1.31±0.06, 0.91±0.08 and 0.53±0.07 for 5:1 contrast and 3-degree projections; 1.43±0.06, 1.39±0.10, 0.99±0.10 and 0.57±0.06 for 5:1 contrast and 6-degree projections; 1.35±0.05, 1.32±0.05, 1.21±0.07 and 0.62±0.03 for 10:1 contrast and 3-degree projections; 1.37±0.05, 1.36±0.07, 1.22±0.05 and 0.67±0.03 for 10:1 contrast and 6-degree projections. Mean ACR in the NEMA spheres was 0.89±0.01, 0.80±0.02, 0.61±0.02 and 0.44±0.05 for 5:1 contrast and 3-degree projections; 0.90±0.01, 0.82±0.03, 0.63±0.03 and 0.46±0.04 for 5:1 contrast and 6-degree projections; 0.87±0.01, 0.82±0.01, 0.68±0.03 and 0.44±0.02 for 10:1 contrast and 3-degree projections; 0.88±0.01, 0.82±0.02, 0.68±0.02 and 0.47±0.01 for 10:1 contrast and 6-degree projections. Maximum and mean ACR in the cardiac insert was 1.22±0.05 and 0.65±0.01. **Conclusions:** Positive bias is seen in maximum voxel measures in both NEMA spheres and the cardiac insert. Accuracy is good in the largest two spheres at both

contrasts with ACR>80% for mean measurements. Percentage variability for the NEMA spheres is very good (<6.0% for 10:1; <13% for 5:1) and also in the cardiac insert (2% for mean measurements). NEMA data suggests that 6-degree projections may provide marginally superior ACR, particularly as object contrast is reduced. The work also demonstrates marked ACR reductions due to partial volume effects for objects approximately 2 cm or smaller in size.

EP-0012

Impact of Point-Spread Function on the Image Quality in Small-Voxel Reconstructions of ^{18}F-FDG-PET Images

N. Assink[1,2], J. A. van Dalen[3], D. Koopman[1,2], H. Stevens[1], C. H. Slump[2], P. L. Jager[1]; [1]Department of Nuclear Medicine, Isala, Zwolle, NETHERLANDS, [2]MIRA Institute for Biomedical Technology and Technical Medicine, University of Twente, Enschede, NETHERLANDS, [3]Department of Medical Physics, Isala, Zwolle, NETHERLANDS.

Introduction: Point-spread function (PSF) modelling is an image optimization method that can partly compensate for resolution degrading effects in FDG-PET imaging. Several studies have evaluated the impact of PSF modelling as part of the image reconstruction. However, PSF modelling can also be applied as a post-reconstruction deconvolution. We have investigated the effect of this type of PSF modelling on the image quality of FDG-PET. **Subjects and Methods:** We first evaluated FDG-PET images of a NEMA image quality phantom containing 6 spheres (diameter 10-37 mm) with a sphere-to-background ratio of 4:1. Data were acquired with the Ingenuity TF PET/CT-scanner (Philips) and iteratively reconstructed using 2x2x2 mm^3 voxels and various PSF settings (1-10 iterations and 2-20 mm regularization). We determined the mean and maximum contrast recovery coefficients (CRC$_{mean}$ and CRC$_{max}$) of the spheres and the noise (standard deviation) in a homogeneous region in the background. Optimized PSF settings were derived by selecting the reconstruction with the highest CRCs without enhancing noise. This reconstruction was compared with a non-PSF reconstruction. Secondly, we included 22 oncology patients with 38 FDG-PET positive lesions varying in size and origin. Image reconstructions using previously determined PSF settings were compared to those without PSF. All lesions' mean and maximum standardized uptake values (SUV$_{mean}$ and SUV$_{max}$) were determined and the noise was measured in a homogeneous region in the liver. Furthermore, two expert readers visually assessed the image quality by a blind and randomised comparison of non-PSF and PSF images. **Results:** Optimized PSF settings were 1 iteration and 8 mm regularization, resulting in enhanced CRC$_{mean}$ and CRC$_{max}$ up to 38% and 32%, respectively. The increase in noise was kept to 3%. On patient data, PSF images resulted in enhanced SUV$_{mean}$ and SUV$_{max}$ in all lesions (mean diameter 16 mm, range 8-36 mm) with an average increase of 27% and 26%, respectively. Yet, noise increased with 11%. Visual analysis showed a preference towards the non-PSF reconstruction in 68% of the cases, although differences were considered subtle. **Conclusion:** PSF modelling as a post-recon-

struction deconvolution can be used to enhance lesions' SUV with a limited noise increase. Meanwhile, first experience by experts shows a preference towards non-PSF images, possibly because in our study all lesions could already be identified in these images.

EP-0013

A Comparison Study on Two Novel Statistical Reconstruction Algorithms Developed for Slit-Hole Collimation Data in Small Animal SPECT Imaging

H. Mahani[1,2], G. Raisali[1], A. Kamali-Asl[3], M. Ay[2,4]; [1]Nuclear Science and Technology Research Institute (NSTRI), Tehran, IRAN, ISLAMIC REPUBLIC OF, [2]Research Center for Molecular and Cellular Imaging, Tehran University of Medical Sciences, Tehran, IRAN, ISLAMIC REPUBLIC OF, [3]Radiation Medicine Engineering Department, Shahid Beheshti University, Tehran, IRAN, ISLAMIC REPUBLIC OF, [4]Department of Medical Physics and Biomedical Engineering, Tehran University of Medical Sciences, Tehran, IRAN, ISLAMIC REPUBLIC OF.

Aim: Slit-hole collimator offers simulations a high-resolution and high-sensitivity SPECT camera and measures planar projections of the object being imaged. Given the special geometry and the sophisticated imaging protocol associated with this collimator, developing novel image reconstruction techniques is mandatory. In the current research, we are aiming at comparing two innovative fully 3D in-house iterative reconstruction algorithms based on planar integral data. **Methods**: In algorithm I, the convergent plane integrals were first rebinned into parallel planar integral format. The resorted data were then reconstructed by a rotation-based MLEM algorithm. Algorithm II directly deals with the convergent planar integrals, and uses a joint plane-driven/rotation-based projector. For both, location-dependent sensitivity was also modeled. To compare the performance of the two algorithms, a 3D digital noise-free Shepp-Logan phantom, a dedicated 5-point source phantom along with NEMA image quality (IQ) were reconstructed. A fair comparison was made by assessing normalized square error (NSE), tomographic resolution, and convergence rate. There were 16 spin angles and 16 SPECT angles for data acquisition. **Results**: The NSE for the Shepp-Logan phantom reconstruction is 13% and 9% for algorithm I and algorithm II, respectively. Algorithm I results in a tomographic resolution of 1.95 mm compared with a 1.7 mm tomographic resolution obtained using algorithm II. These tomographic resolutions are averaged for the 5 point sources. The SNR of the reconstructed image using algorithm I reaches its maximum value after 2 iterations, while 3 iterations are needed for obtaining the highest SNR using algorithm II. For the same 5% noise level in reconstructed uniform part of the NEMA IQ phantom, algorithm II requires approximately a two-fold reconstruction time per iteration compared with algorithm I. **Conclusion**: Although, the performances of both algorithms are promising for reconstruction of the convergent planar projection data, algorithm II leads to superior image quality characteristics than algorithm I, but the expense of both a slower convergence rate and a larger reconstruction burden.

EP-0014

Development of Monte Carlo Simulation Based Quantitative Image Reconstruction for SPECT/CT

K. Sakaguchi[1,2,3], S. Yoshida[1], S. Watanabe[1,2], K. Matano[1], M. Okumura[1], M. Hosono[4,2], K. Ishii[4,2], T. Murakami[4,2]; [1]Department of Radiology, Kindai University Hospital, Osaka, JAPAN, [2]Division of Positron Emission Tomography, Institute of Advanced Clinical Medicine, Faculty of Medicine, Kindai University, Osaka, JAPAN, [3]Laboratory of Radiation Biology, Department of Biological Science, Graduate School of Science, Osaka Prefecture University, Osaka, JAPAN, [4]Department of Radiology, Faculty of Medicine, Kindai University, Osaka, JAPAN.

Aim: Iterative reconstruction for SPECT is composed of 5 parts, forward projection, comparison, back projection, normalization, and update. The advantage of iterative reconstruction is that, since includes various physical phenomena such as scatter, attenuation, and depth-dependent blur into a probability density matrix of forward projection, images can be reconstructed with corrections corresponding to these physical phenomena. Iterative reconstruction usually provides qualitative images but not quantitative images because the probability matrix it adopts is usually an approximate matrix, instead of a matrix that fully deals with these physical phenomena. The purpose of this study was to develop a Monte-Carlo simulation based iterative reconstruction for obtaining quantitative reconstructed SPECT images, and to evaluate its accuracy with phantom studies. **Materials and Methods:** The SIMIND Monte-Carlo program has been widely used for simulation of various scintillation camera imaging. This program is able to output list-mode data in which emission point, detection point in the crystal, photon weight, and scatter order were recorded. Since this list-mode data can be used as a probability density matrix in forward projection, we crafted a Maximum Likelihood - Expectation Maximization algorithm in which the list-mode data was incorporated into the forward projection using C-language. And we evaluated the accuracy of the proposed method with two kinds of phantom studies. In the cylindrical phantom study, two cylindrical phantoms filled with technetium-99m solution (8030.48[Bq/ml] at mid scan time) and iodine-123 solution (9392.38[Bq/ml]) were measured using SPECT/CT. In the NEMA body phantom study, two NEMA body phantoms filled with technetium-99m solution (each sphere (Diameter: 37mm, 28mm, 22mm, 17mm, 13mm, and 10mm): 37466.29[Bq/ml], background: 7622.75[Bq/ml]) and iodine-123 solution (each sphere: 39949.21[Bq/ml], background: 8108.62[Bq/ml]) were measured. [Results] In the both cylindrical phantom studies, the voxel value of reconstructed images (Technetium-99m: 8052.90[Bq/ml], Iodine-123: 9828.08[Bq/ml]) indicated a good agreement with known radioactive concentration. In the NEMA body phantom filled with technetium-99m, the voxel value of 37mm sphere, 28mm sphere and background on reconstructed images showed 37163.91[Bq/ml], 36713.40[Bq/ml], and 7605.56[Bq/ml], respectively. In the NEMA body phantom filled with iodine-123, the voxel value of 37mm sphere, 28mm sphere and background on reconstructed images showed 39481.44[Bq/ml], 37930.51[Bq/ml], and 7872.69[Bq/ml], respectively. These voxel value of reconstructed images indicated a good agreement with known radioactive concentration. [Conclusions] Our proposed method was able to estimate radioactivity concentration for more than 28mm sphere with a high accuracy. Our method opens up new possibilities for quantitative nuclear medicine procedures including dosimetry in radionuclide therapy.

EP-0015

Evaluation of optimized iterative reconstruction parameters using channelized Hotelling observer in brain receptor PET imaging

K. Matsumoto[1], H. Ogawa[1], Y. Matsumoto[1], G. Akamatsu[2], M. Senda[2], K. Murase[3], K. Endo[1]; [1]Kyoto College Of Medical Science, Kyoto, JAPAN, [2]Institute of Biomedical Research and Innovation, Kobe, JAPAN, [3]Graduate School of Medicine, Osaka University, Osaka, JAPAN.

Aim: ^{18}F-FDOPA and ^{11}C-raclopride has drawn new attention as a biomarker of regenerative therapy for Parkinson's disease with implantation of dopaminergic cells (including iPS-derived ones) or infusion of drugs with regenerating effects into the striatum. Recently, iterative reconstruction began to be used in dopamine transmitter/receptor PET images and the ordered-subset expectation maximization (OSEM) algorithm was a method used widely in some iterative algorithms. In brain receptor PET imaging using high-resolution PET scanner, optimization of reconstruction parameters is essential because the image noise influences the diagnostic performance and quantitative accuracy. The purpose of this study was to evaluate optimal reconstruction parameters of the OSEM algorithm using the channelized Hotelling observer (CHO) well correlated with human observer. **Methods:** A PET/CT scanner, GE Healthcare Discovery 690, was used to scan image of a striatal phantom (Radiology Support Devices, Inc.). To evaluate the performance of the present method, we also carried out the computer simulations with the digital brain phantom. The OSEM parameters was changing the number of subsets and iterations. The CHO was applied to 50 slices from the images of each type to compute detectability index (d_{CHO}), and the optimum image reconstruction parameter was evaluated. In this study, the channel vector elements were taken as the integrated values of the two-dimensional Fourier-transformed image within pre-defined frequency bands (or channels), and the total number of channels was taken as 16 with an equal band width, i.e., Nyquist frequency/16. **Results:** The d_{CHO} value of simulation and PET became the maximum when approximately 50 iterative updates. As for the PET study, the d_{CHO} value became the maximum when the numbers of subsets and iterations were 12 and 4, respectively. **Conclusions:** Our preliminary data suggested that the CHO was effective in reconstruction parameters setting of the OSEM algorithm. Generally the optimum reconstruction parameters of the OSEM algorithm are dependent on the statistics noise of projection data, but optimum reconstruction parameters can be quantitatively evaluated using the CHO.

EP-0016

The Impact of a Penalized Likelihood Reconstruction Algorithm on the Quantitative Evaluation of Hepatic Metastases Shown on ^{18}F-FDG-PET/CT Studies - Preliminary Results

S. Czibor, Z. Varga, A. Fekésházy, L. Jorgov, B. Kári, B. Magyar, J. Török, G. Dabasi, T. Györke; *Semmelweis University, Nuclear Medicine Centre, Budapest, HUNGARY.*

Introduction: PET/CT scans are routinely reconstructed by iterative algorithms, where a well-known limitation is the worsening of the signal-to-noise ratio when increasing the number of iterations. A novel Bayesian penalized likelihood reconstruction algorithm (BPL) has allowed more iterations without simultaneously significantly increasing noise levels that results in a better signal-background ratio. The aim of our study was to compare this algorithm with the conventional OSEM reconstruction by investigating ^{18}F-FDG-PET/CT studies. **Methods:** We investigated the ^{18}F-FDG-PET/CT studies of 9 patients (6 women, 3 men) and a total of 24 FDG-avid hepatic metastases were included in our sample. The raw data of each patient were reconstructed by both the OSEM and the BPL algorithm. A spheric VOI of 3 cm diameter was placed in the normal hepatic tissue as reference and a spheric VOI was manually adjusted to the metastases, both in an identic location in the two differently reconstructed studies of each patient. The size of the lesions were calculated by the largest axial diamater measured on the CT scans. Standardized uptake values (SUV) based on body weight were calculated, including SUVmax and SUVmean. Noise was defined as the standard deviation of the normal liver parenchyma SUV. Signal-to-noise ratio was given as SUVmean in the normal liver parenchyma divided by the noise. Signal-to-background ratio was defined by SUVmax in a lesion divided by the SUVmean in the normal liver parenchyma. Two-tailed paired sample t-tests were calculated to compare the datasets. **Results:** The average size of the lesions was 18±8,85 mm (range: 10-53 mm). The BPL algorithm resulted in significantly higher SUVmax and SUVmean values in the lesions (P<0,001): ΔSUVmax 2,12±1,75; ΔSUVmean 0,50±0,48. The signal-to-background ratio was significantly better with BPL (3,33±2,45 vs. 2,87±2,26; p<0,001) while signal-to-noise and SUVmean-to-noise ratios were not significantly different. The latter can be explained with the (nonsignificantly) higher levels of noise by using BPL. **Conclusion:** Our study showed that the BPL reconstruction algorithm resulted in better signal-to-background ratios without the decrease of the signal-to-noise ratio in FDG-avid hepatic metastases which leads to better recognition and characterization of the lesions.

EP-0017

Evaluation of FDG PET/CT lesion detectability and quantification harmonization

J. Devriese[1], L. Beels[2], E. Deboever[1], B. Decru[1], A. Maes[2], C. Van de Wiele[2], H. Pottel[1]; [1]KU Leuven campus Kortrijk, Kortrijk, BELGIUM, [2]AZ Groeninge, Kortrijk, BELGIUM.

Introduction: Standardized uptake value (SUV) is a valuable tool in quantitative ^{18}F-FDG PET/CT imaging and is used in staging and therapy follow-up. In this context as well as multicentre studies it is essential that SUV is accurate and reproducible. There are multiple biological and technical factors that can introduce variability, and several guidelines have been published with recommendations to standardize PET/CT procedures in order to reduce variability. An important factor in the scan process is the PET reconstruction protocol. Standard clinical protocols are optimized for lesion detection and this often does not match the reconstruction protocol that fulfils EARL guidelines, launched by the EANM to promote multicentre nuclear medicine and research, optimized for harmonized quantitative imaging. Different vendors aim to combine lesion detectability and quantification in one reconstruction protocol. In this study one such solution is compared to the lesion detection and EARL protocol. **Subjects & Methods:** Clinical whole-body PET/CT scans of 13 melanoma patients were reconstructed according to three scan protocols: the institution's original lesion detection protocol, EARL protocol, and Q.Clear protocol. VOIs were placed in lesions and healthy tissues according to the PERCIST criteria, SUV was normalized for lean body mass (LBM). SUVs were compared among the reconstruction protocols and variability was assessed. Anova with post-hoc Bonferroni correction was performed to detect differences between lesion SUVs among the different reconstruction protocols. **Results:** Mean (SD) liver SUV was 1.73 (0.27), 1.80 (0.32), and 1.73 (0.27) for the clinical, EARL, and Q.Clear protocol respectively, yielding coefficients of variation (CV) of 16%, 18%, and 15% respectively. 24 lesions were assessed with a maximum of 5 lesions per patient and two lesions per organ. Mean SUV_{peak} (SD) was 2.2 (1.6), 1.7 (1.4), and 2.2 (1.6) for the clinical, EARL, and Q.Clear protocol respectively. Mean SUV_{max} (SD) was respectively 4.0 (2.6), 2.5 (1.7), and 4.6 (3.3). No significant differences were detected in lesion SUV_{peak} (p = 0.382). Significant differences were detected in lesion SUV_{max} (p = 0.018). Post-hoc tests demonstrated a significant difference of lesion SUV_{max} between the EARL and clinical protocol (p < 0.001) and between the EARL and Q.Clear protocol (p < 0.001). No significant difference was found between the clinical and Q.Clear protocol (p = 0.154). **Conclusion:** These preliminary data indicate that Q.Clear is a valid alternative in replacing the original lesion detection protocol and succeeds at harmonizing lesion detection and quantification.

EP-0018

Phantom and Patient Analysis of the Impact Of Q.Clear Regularization in Texture Indices

G. Reynés-Llompart[1], J. Robles-Barba[1], E. Llinares-Tello[1], P. C. Notta[1], I. Gil-Viciano[1], A. Sabaté-Llobera[1], J. L. Vercher-Conejero[1], N. Calvo[1], C. Gámez-Cenzano[1], J. M. Martí-Climent[2]; [1]PET Unit, Nuclear Medicine Department. IDI. Hospital Universitari de Bellvitge. IDIBELL, L'Hospitalet de Llobregat, SPAIN, [2]Nuclear Medicine Department, Clínica Universidad de Navarra, Pamplona, SPAIN.

Purpose: To study the impact of Q.Clear (a fully convergent, noise constrained BSRM iterative reconstruction algorithm)

on texture indices change. **Methods:** All acquisitions were performed on a Discovery IQ PET/CT. Phantom analysis was performed using a NEMA Body IEC phantom. All six spheres were filled with a ratio of 8:1 and an activity concentration of 5.4 kBq/mL, and were acquired during 350 s on a single bed. Moreover, 10 lesions were analyzed from 8 different patients, acquired using 2.7 MBq/kg and 2 min per bed. All images were reconstructed with β values (a noise regularization parameter) of 50 to 500 using 50 intervals. For all lesions and spheres, a VOI of 40% of the SUV_{max} was performed. For each VOI, volume, SUV_{max} and SUV_{mean} were recorded. Texture indices were obtained using a resampling of 64 values between 0 and 20 units of SUV, which corresponds to units of 0.3 SUV. From the co-occurrence matrix, the second order parameters of Homogeneity and Entropy were calculated. Long-Run Emphasis (LRE) and Short-Run Emphasis (SRE) were calculated from the Gray-Level Run Length Matrix. Low-Level Zone Emphasis (LGZE) and High-Level Zone Emphasis (HGZE) were calculated from the Gray-Level Zone Matrix. **Results:** SUV_{max} and SUV_{mean} decrease as the parameter β increases, being more pronounced as the size of the sphere decreases. If we consider the set of 6 spheres at a time, the behavior of the textures against the β parameter presents two patterns: on one side Homogeneity, LRE and LGZE and on the other, Entropy, SER and HGZE. As the β increase, the first three indices increase, whereas the last three indices decrease. On the analyzed lesions, the variations of SUV and texture indices follow the same patterns as the β increases. Despite this trend, some lesions present a singular different behavior, especially on SRE and LRE parameters, making the difference in texture indices very dependent on β. Only for HGZE and LGZE a convergence of the value is achieved around a beta of 300. From these trends, a general β to maximize the texture indices difference between lesions cannot be extracted. **Conclusion:** The Q.Clear algorithm acts by modifying the contrast of the lesions with the background, being able to abruptly modify the texture indices as a function of the parameter β, so it is an important parameter to standardize in case of multicenter studies.

EP-0019

Improving Quantitative Accuracy with use of High and Ultra-high Definition PET/CT Reconstruction

K. Binzel[1], J. Zhang[1], R. Moore[1], M. Friel[1], P. Maniawski[2], M. V. Knopp[1]; *[1]The Ohio State University, Columbus, OH, UNITED STATES OF AMERICA, [2]Philips Healthcare, Cleveland, OH, UNITED STATES OF AMERICA.*

Purpose/Introduction: Next-generation digital PET/CT provides improved count statistics and sensitivity making high and ultra-high definition image reconstruction feasible. Previous clinical evaluations have shown the improvement in visual quality and lesion detectability, this study assessed the improvement in quantitative accuracy via phantom validation. **Subjects & Methods:** A NEMA phantom with hollow sphere inserts was filled with ^{18}F with 2:1, 4:1, 8:1, 16:1, 32:1 and 64:1 activity concentration ratios. Data were acquired on a pre-com-

mercial release digital photon counting system (Philips Vereos) and reconstructed. Matrix sizes used for image reconstruction included a 144x144 matrix for standard definition (SD) 4x4x4 mm³ voxel lengths, 288x288 matrix for high definition (HD) 2x2x2 mm³ voxel lengths, and 576x576 matrix for ultra-high definition (UHD) 1x1x1 mm³ voxel lengths. For each matrix size, we additionally changed the number of iterative subsets from 1-35 in increments of 5. Activity concentrations and recovery coefficients (RC) were recorded for each image set. **Results:** HD and UHD images were found to be more quantitatively accurate than SD images. For the 1 and 0.5 mL spheres, the SD RCs were 0.84 and 0.57, respectively, when using 15 subsets. For the HD reconstructions, the RCs were 0.91 and 0.64. UHD images had RCs of 0.89 and 0.65. We found that for HD and UHD reconstruction, using a larger number of subsets degraded the image quality and also biased the RCs in the larger spheres to overestimate the true activity concentrations. Thus, we found that a lower number of subsets for HD and UHD reconstructions provided was preferable, findings consistent with review of clinical data sets. **Discussion/Conclusion:** Phantom validation of the improvement in quantitative accuracy with high and ultra-high definition imaging leads to greater confidence in using such reconstruction protocols for clinical data sets. The quantification in small hot objects is improved with HD and UHD imaging, while refining the number of subsets used in reconstruction prevents overestimation of activity concentrations of larger objects, where the activity is already accurately measured on SD imaging.

EP-0020

Assessment of different reconstruction parameters for quantification of FDG-PET brain imaging

T. C. G. Moalosi[1,2,3], P. Dupont[3,4], A. Ellmann[1,3], J. Warwick[1,3], A. Doruyter[1,3], M. Du Toit[2,3], M. Mix[1,5]; [1]Tygerberg Hospital (Nuclear Medicine), Cape Town, SOUTH AFRICA, [2]Tygerberg Hospital (Medical Physics), Cape Town, SOUTH AFRICA, [3]Stellenbosch University, Cape Town, SOUTH AFRICA, [4]KU Leuven, Leuven, BELGIUM, [5]University of Freiburg, Freiburg, GERMANY.

Introduction and Aim: Reconstruction influences quantitative results in PET imaging. The aim of this study was to evaluate different image reconstruction parameters and their impact on quantification of ^{18}F-FDG PET of the brain. The reconstruction parameters studied were the number of iterations, and the use of time of flight (TOF) information. In addition, we investigated the effect of scan duration on image quality. **Materials and Methods:** A Philips® Gemini TF Big bore PET/CT was used for acquiring data of a 3D Hoffman Brain phantom. Data were acquired for 25 minutes in list mode format after injection of 40 MBq FDG, and reconstructed with a voxel size of 2x2x2 mm³ using two different iterative reconstruction algorithms: LOR-RAMLA and BLOB-OS. The number of iterations and subsets was varied successively from 3/33 (vendor default) to 30/33, acquisition scan duration from 1 to 25 minutes, and TOF switched on and off for BLOB-OS. The impact on image quality was analyzed in 15 cortical and sub-

cortical brain regions (volumes of interest, VOIs) and for gray and white matter. **Results:** Contrast increased for all regions of the brain and for grey matter (GM) /white matter (WM) ratio as the number of iterations increased. Image convergence was reached after fifteen iterations for all the algorithms. The coefficient of variation (COV) for all VOIs showed BLOB-OS with TOF to be superior to the other algorithms. The COV results for different scan durations showed only a minimal improvement after 5 minutes in high-activity regions (GM), and after 10 minutes in low-activity regions (WM). **Discussion:** These results demonstrate that optimization of the vendor's default number of iterations is possible for brain imaging and that 15 iterations is more appropriate. Furthermore, a scan duration of 10 minutes is sufficient for brain imaging. Although it is often postulated that TOF information has no impact in brain imaging, our results show a small improvement. **Conclusion:** Based on phantom data ^{18}F-FDG brain imaging for 10 minutes and reconstructed with the BLOB-OS algorithm including TOF information with 15 iterations is optimal on the Philips Gemini TF Big bore PET/CT.

EP-0021

Accelerated 3D Detector Modelling using a Lookup-table based on GATE Simulations of a single Detector Block

H. Xu, J. Scheins, M. Lenz, C. Lerche, N. Shah; Forschungzentrum Juelich, Juelich, GERMANY.

Introduction: Accurate Detector Response Functions(DRF) increase the spatial resolution and SNR for Position emission tomography (PET) in iterative image reconstruction[1]. However, full-scale 3D modelling of pixelated crystal arrays (blocks) covering all possible γ rays still remains challenging. In this abstract, we demonstrate for the Siemens BrainPET system the advantageous usage of a lookup-table(LUT) generated from GATE[2] simulations, which holds DRF for a single detector block. In this way, the DRF for each crystal combination can be derived by fetching ray-dependent LUT weights. **Methods:** Any detector block of BrainPET consists of 12×12 LSO crystals (2.5×2.5 mm^2), which is irradiated in GATE with a plane source sampling the whole field-of-view(FOV). In order to characterize all possible incident γ rays in the reference coordinate system of the block(BC), four parameters are necessary, i. e., **(x, y, θ, φ)**, where **(x,y)** denotes the intersection point with the block front surface; **θ** is the polar angle; **φ** is the azimuth angle. Each parameter is sampled as defined in table 1 and a LUT for the DRF is created. All γ rays simulated in GATE need to be sorted according to the binning of table 1 and the DRF information (crystal ID and detected counts each) is stored as sparse vector. The LUT can be used to calculate the detection probability for any Line-of-Response(LOR) by combining two specific LUT rows which are addressed by the ray coordinates in BC of the two involved blocks. **Results and Conclusion:** GATE simulations have been performed with 279.6 GBq(0.2 MBq*1398000) γ rays totally, among which 7.56x10^9 have geometrical interactions with the block and 3.91x10^9 counts are detected. The obtained LUT size is found to be 1.5 GB. For the

simulation of detector data, we have compared GATE with our LUT approach using an off-center cylindrical phantom (10 MBq activity) along axial direction. The pure calculation time for GATE and our program are 1218s and 1038s respectively (14.8% speed up). The measured counts for both are 566170 and 527498 (6.8% less due to loss of block crosstalk). However, the sinogram patterns in transaxial plane remain similar with some shadowing effects when it comes to the edge of FOV. In conclusion, the LUT method for detector simulations works properly and is feasible to provide similar results as full GATE simulations. Reference: [1] Rahmim A, et al. Medical physics, 2013, 40(6). [2] Jan S, et al. Physics in medicine and biology, 2004, 49(19):4543.

EP-0022

Sub-centimeter lesion detectability in Point-spread function (PSF) and Time of flight (TOF) reconstructed PET images

I. Shiri[1], P. Ghafarian[2,3], A. Bitarafan-Rajabi[1], M. AY[4,5]; [1]Department of Medical Physics, School of Medicine, Iran University of Medical Sciences, Tehran, IRAN, ISLAMIC REPUBLIC OF, [2]Chronic Respiratory Diseases Research Center, National Research Institute of Tuberculosis and Lung Diseases (NRITLD), Shahid Beheshti University of Medical Sciences, tehran, IRAN, ISLAMIC REPUBLIC OF, [3]PET/CT and Cyclotron Center, Masih Daneshvari Hospital, Shahid Beheshti University of Medical Sciences, Tehran, IRAN, ISLAMIC REPUBLIC OF, [4]Research Center for Molecular and Cellular Imaging, Tehran University of Medical Sciences, Tehran, IRAN, ISLAMIC REPUBLIC OF, [5]Department of Medical Physics, School of Medicine, Tehran University of Medical Sciences, Tehran, IRAN, ISLAMIC REPUBLIC OF.

Aim: Small lesion detection at early stages of disease is very important for staging and therapy performance in cancer patients. Recently, advancements in hardware and software (Time-of-Flight and Point Spread Function) have facilitated the possibility of enabling sub-centimeter lesion detectability. The main purpose of this study was to investigate small lesion detectability for PSF and TOF reconstruction. **Material and Methods:** All measurements were performed on a GE Discovery 690 PET/CT scanner using a NEMA-IEC body phantom with six spheres (having diameters of 4, 5, 6, 7, 10 and 13mm) that were filled with 2:1 as well as 4:1 contrasts and different background activities. Images were reconstructed using the 3D-OSEM algorithm with and without TOF and PSF information, and involving different post-reconstruction filters. Lesion detectability was estimated both visually by a human observer and quantitatively using the lesion over background variation (LOBV) metric which was defined according to the Rose Model of statistical detection. **Result:** In the case of 2:1 contrast, the 13 mm hot sphere could be recognized in all reconstructed PET images, and for images reconstructed with TOF the 10 mm hot sphere could also be observed. When acquisition was made with 4:1 contrast, lower limit of detectability reached 6 mm and 5 mm diameters for OSEM+PSF and OSEM+PSF+TOF respectively. Quantitative

analysis of LOBV as function of FWHM of post reconstruction filter showed stronger filter (higher smoothing) caused an improvement in LOBV of lesions 13mm in diameter. Conversely, the LOBV value trend in lesions smaller than 10mm in diameter was inverse, and deteriorated with increasing FWHM. When reconstruction was made with TOF, LOBV values was higher than without TOF information in both SBRs. **Conclusion:** TOF and PSF reconstruction improve sub-centimeter lesion detectability. Our study encourage the utilization of next generation PET technology (TOF and PSF reconstruction) in clinical PET systems which lead to substantially improvement of sub-centimeter lesion detectability

EP-0023

Impact of matrix size on metabolic tumor volume (MTV) and total lesion glycolysis (TLG) in PSF-based PET image

I. Shiri[1], A. Rahmim[2,3], S. Ashrafinia[3], P. Geramifar[4], A. Bitarafan-Rajabi[1,5]; [1]Department of Medical Physics, School of Medicine, Iran University of Medical Sciences, Tehran, IRAN, ISLAMIC REPUBLIC OF, [2]Department of Radiology, Johns Hopkins University, Baltimore, MD, UNITED STATES OF AMERICA, [3]Department of Electrical and Computer Engineering, Johns Hopkins University, Baltimore, MD, UNITED STATES OF AMERICA, [4]Research Center for Nuclear Medicine, Shariati Hospital, Tehran University of Medical Sciences, Tehran, IRAN, ISLAMIC REPUBLIC OF, [5]Cardiovascular Intervention Research Center, Rajaie Cardiovascular Medical and Research Center, Iran University of Medical Sciences, Tehran, IRAN, ISLAMIC REPUBLIC OF.

Aim: Volume-based parameters such as MTV and total lesion glycolysis (TLG=MTV×SUV_{mean}) are potentially valuable imaging biomarkers in the evaluation of response to therapy and prognostication in cancer patients. The objective of the present study was to investigate the impact of matrix size on MTV and TLG as delineated from whole-body PET images. **Material and methods:** Twenty-six patient were included in this study. PET images were reconstructed using the 3D-OSEM algorithm with and without PSF modeling, with 2 iterations, 21 subsets, 4mm FWHM of Gaussian post-reconstruction filter and different matrix sizes (128×128, 168×168, 256×256, 336×336). Twenty-nine lesions were segmented using an automatic fuzzy locally adaptive Bayesian (FLAB) method. From these segmented lesions, metabolic tumor volume and TLG were calculated. **Result:** Values of MTV and TLG were significantly higher for PSF-based reconstruction at the same matrix size. The deviations in MTV and TLG, relative to clinical standard reconstruction (3D-OSEM-168), were significantly different, depending on matrix size. At higher matrix sizes, the SUVmean was overestimated while MTV and TLG were underestimated relative to 3D-OSEM-168. **Conclusion:** These findings demonstrate the dependency of volume-based parameters (MTV, TLG) on reconstruction algorithm and matrix size. Higher matrix sizes in PET imaging may improve image quality, but do alter quantification parameters such as MTV and TLG, and their accuracy must be considered, especially in treatment response assessment.

Physics & Instrumentation & Data Analysis: Data Analysis & Management

EP-0024

Quantification of 177-Lu and 131-I: a phantom study

J. Kupferschlaeger, H. Dittmann, S. Poth, C. la Fougère; University Hospital Tuebingen/ Nuclear medicine, Tuebingen, GERMANY.

Aim: Absolute quantification is a necessary condition for the dosimetry of radionuclide treatments with 131-I and 177-Lu. Aim of this study was to investigate the accuracy of quantification, the determination of recovery coefficients (RC) for partial volume correction (PVC), the influence of CT high voltage (HV) and tube current on quantification, the influence of dead time and a comparison of planar and tomographic sensitivity. **Material and Methods:** For both isotopes we used the IEC-Phantom with hot-sphere and lung insert as well as the Anthropomorphic Torso Phantom (ATP) with lung, liver and 2 spherical inserts inside the liver. All measurements were performed on a Discovery 670 NM/CT PRO® (GE) SPECT/CT system. For each measurement we acquired CTs with different HV- and tube-current settings. Five energy windows were used in case of 177-Lu to extract the low energy (EM1:114 keV) and high energy emissions (EM2:208 keV). Dead time was determined by using vials with decaying activities over a period of 8 weeks. Quantification was done using the Q.Metrix® software (GE) with OSEM reconstruction including scatter-, CT-based attenuation correction and resolution recovery. VOI were defined for the spheres, the liver, the phantom and liver background and the cold lung inserts. For each VOI we recorded average and maximum activity concentration in Bq/ml. **Results:** CT HV and tube current has minor influence on quantification: maximum deviation is less than 2% from the activity concentrations using a reference CT for attenuation correction. The total activity in both phantoms and in the liver insert could be reproduced with a maximum error of 10% for 177-Lu(EM2) and 131-I whereas 20% for 177-Lu(EM1). RC for small lesions were always underestimated (< 0.8) in case of 131-I. RC were constant (~1) for lesion volumes larger 5 ml for 177-Lu(EM2). 177-Lu(EM1) reconstructions reveal smaller RC compared to 177-Lu(Em2). Scatter correction underestimates the scatter fraction: 20% to 50% of the background activity concentration was found in the cold lung inserts. Dead time correction is negligible in case of 177-Lu (count loss < 7% under treatment conditions) whereas dead time correction for 131-I should be considered during treatment (12% count loss for 250 MBq in the FOV). **Conclusions/Discussion:** Absolute quantification of SPECT data using the Q.Metrix® software is possible if all corrections are applied. This is valid for large structures like organs but PVC should be applied for quantification of small lesions. Further improvement of scatter correction is needed.

EP-0025

The quantitative SPECT/CT scoring of MIBG cardiac scintigraphy to identify patients with Lewy body diseases

S. Matsuo[1], H. Wakabayashi[1], K. Nakajima[1], K. Okuda[2], H. Yoneyama[1], S. Kinuya[1]; [1]Kanazawa University, Kanazawa, JAPAN, [2]Kanazawa Medical University, Kanazawa, JAPAN.

The heart-to-mediastinum ratio (HMR) of iodine-123-metaiodobenzylguanidine (MIBG) has been used to determine the uptake of the heart to evaluate sympathetic nerve activity. However quantitative SPECT scoring is still uncommon because of the inferior attenuation artifact is often found in MIBG SPECT image. Therefore we performed SPECT/CT-attenuation correction using IQ-SPECT/CT (Symbia T6, Siemens) in a short-term acquisition protocol. We investigated the relationship between quantitative SPECT/CT scoring and HMR using IQ-SPECT and conventional collimator. Furthermore we aimed to determine the SPECT scoring as well as HMR to identify Lewy body diseases (LBD). Subjects The subjects include 253 patients who underwent MIBG imaging. IQ-SPECT was used to identify LBD, including Parkinson's disease and dementia with LBD. The early- and delayed-phase cardiac images were obtained. HMR was calculated by the ratio of mean counts between heart and mediastinum areas of interest drawn on a planar image by means of automated software analysis. SPECT images were obtained by IQ-SPECT system with CT-attenuation correction. The disorders were assessed by QPS (Cedars-Sinai Medical Center, Los Angels, CA) quantitatively, using the standard 17-segment and 5-point scoring system. A neurologist expert determined the final clinical diagnosis by using international clinical diagnostic criteria. Results IQ-SPECT completed the acquisition of SPECT imaging in about 5 minutes (n=28). In part, conventional SPECT took 16 minutes (n=225). Interior decreased uptake was significantly improved by CT-attenuation correction using IQ-SPECT/CT. The quantitative QPS scoring showed significantly close relationships with HMR values (P<0.0001). The quantitative QPS scoring showed significantly close relationships with HMR values (p<0.0001). IQ-SPECT in a short time acquisition protocol was applied to the patients with dementia. SPECT scoring with IQ-SPECT identified LBD subjects (49±4 vs 4±3, p<0.0001). HMR in LBD was significantly decreased than that of non-LBD (1.4±0.2 vs 3.2±0.6, p<0.0001). Conventional collimator showed close relationship between SPECT scoring and HMR (p<0.0001). Conclusion SPECT scoring was feasible and inferior attenuation was improved. Quantitative SPECT scoring with IQ-SPECT/CT using short acquisition protocol might be feasible. Quantitative MIBG SPECT scoring might be a possible biomarker of evaluating severity of cardiac sympathetic nerve dysfunction to identify patients with Lewy body diseases.

EP-0026

Relationship between image and clinical indices in the differential diagnosis of dementia using ^{18}F-FDG-PET images and machine learning

M. Sakata[1], X. Wang[1,2], K. Ishii[1], Y. Kimura[1,3], K. Wagatsuma[1], K. Ishibashi[1], J. Toyohara[1], N. Yata[2], Y. Manabe[2]; [1]Tokyo Metropolitan Institute of Gerontology, Tokyo, JAPAN, [2]Chiba University, Chiba, JAPAN, [3]Kindai University, Kinokawa, JAPAN.

Objectives: Differential diagnosis of dementia type, such as Alzheimer's disease (AD), fronto-temporal dementia (FTD), and dementia with Lewy bodies (DLB), is necessary for treatment and care of patients with dementia. We present an automatic classification based on brain ^{18}F-FDG-PET images to support the diagnosis using the support vector machine (SVM) and propose a novel image index for assessing the severity or progression of dementia. **Methods:** We used ^{18}F-FDG-PET images from four groups: normal healthy elderly individuals (NL; n = 60; 66 ± 10 years), patients with AD (n = 64; 71 ± 10 years), with FTD (n = 23; 76 ± 8 years), and with DLB (n = 12; 61 ± 10 years). The images were anatomically normalized using parameters from the normalizations of individual T1-weighted MR images using DARTEL (Ashburner, 2007). SVM feature values were extracted from 116 VOIs using the automated anatomical labeling cortical parcellation map (Tzourio-Mazoyer, 2002) and were normalized with the cerebral global mean. The four-class classification of SVM is composed of a combination of two-class classification. We propose the signed distance from the border of the two-class classification between each group with dementia and NL (e.g. AD-NL model) as an image index for assessing the severity or progression of dementia. In the present study, precision of the four-class classification was verified using the leave-one-out cross-validation method. Furthermore, for the data (NL, n = 60, 120 scans; AD, n = 40, 79 scans; and FTD, n = 12, 23 scans) comprising the mini mental state examination (MMSE) score, the correlations between the proposed image index and MMSE score was investigated in the AD-NL and FTD-NL model. Data of each subject gathered at different times were included in these correlations. **Results:** The precision of the four-class classification was 92% , 81%, 61%, and 50% in the NL, AD, FTD and DLB groups, respectively. An imbalance in the sample size and pathological heterogeneities may have caused inadequate accuracies in the FTD and DLB groups. The correlation between the proposed image index and MMSE score was significant (p < 0.001, Spearman's rank correlation) in both the AD-NL model and FTD-NL models. The correlation coefficient in the FTD-NL model (0.27) was lower than that in the AD-NL model (0.72). **Conclusions:** The automatic classification using SMV is capable of supporting the differential diagnosis of dementia, and the proposed image index can help in assessing the severity or progression of dementia.

EP-0027

Noninvasive quantitation of rat cerebral blood flow using ^{99m}Tc-HMPAO without arterial blood sampling

C. Suzuki, M. Kosugi, Y. Magata; Hamamatsu University School of Medicine, Hamamatsu, JAPAN.

Purpose: Cerebral blood flow (CBF) assessment in small animals meaningfully enhances the understanding of pathology in model animals and facilitates evaluation of drug efficacy. We previously reported that rat CBF values is calculated dividing the brain radioactivity concentration (C_{Brain}) at 5 min post-injection of ^{99m}Tc-HMPAO by the integrated arterial blood radioactivity concentration until 19 s post-injection of ^{99m}Tc-HMPAO

(AUC_{Blood}). However, this CBF assessment procedure can not be repeated in the same animals, since arterial blood sampling is needed. In the present study, we established noninvasive quantitation of rat CBF using ^{99m}Tc-HMPAO without arterial blood sampling. **Subjects & Methods:** Acetazolamide (0, 25, or 50 mg/kg) treated rats were intravenously administered with ^{99m}Tc-HMPAO. Arterial blood sampling and chest dynamic planar imaging using single-pinhole collimator were performed for 1 min just after ^{99m}Tc-HMPAO administration. Head SPECT imaging using multi-pinhole collimator was performed from 15 to 57 min post-injection of ^{99m}Tc-HMPAO, and then brain was resected. Radioactivity in arterial blood was measured with the auto-well γ counter and integrated blood radioactivity concentration until 19 s post-injection of ^{99m}Tc-HMPAO (AUC_{Blood}**-sampling**) was calculated using the trapezoidal approximation. Radioactivity in resected brain was measured with the auto-well γ counter and radioactivity concentration in brain (C_{Brain}**-resection**) was calculated. The region of interest (ROI) was manually drawn over heart-blood pool on planar images and integrated heart-blood pool radioactivity concentration until 19 s post-injection of ^{99m}Tc-HMPAO (AUC_{Blood}**-planar**) was calculated. The ROI was manually drawn over brain on SPECT images and radioactivity concentration in brain (C_{Brain}**-SPECT**) was quantified. The rat CBF values, which were noninvasively obtained using C_{Brain}**-SPECT** and AUC_{Blood}**-planar**, were compared with the CBF estimated by the conventional method using C_{Brain}**-resection** and AUC_{Blood}**- sampling**. **Results:** AUC_{Blood}**-planar** was identical to AUC_{Blood}**-sampling**. Since our previous study showed C_{Brain} was steady from 14 s to 60 min post-injection of ^{99m}Tc-HMPAO, C_{Brain}**-SPECT** and C_{Brain}**-resection** were determined between 14 s and 60 min post-injection. C_{Brain}**-SPECT** was identical to C_{Brain}**-resection**. Noninvasively calculated CBF using C_{Brain}**-SPECT** and AUC_{Blood}**-planar** was well correlated with conventionally estimated CBF using C_{Brain}**-resection** and AUC_{Blood}**- sampling** (Spearman's rank correlation coefficient = 0.918, $p < 0.001$). **Conclusion:** Rat CBF could be noninvasively quantitated using ^{99m}Tc-HMPAO chest dynamic planar imaging and head SPECT imaging.

EP-0028

Dosimetric survey on administered activity of 11C-CHOLINE in PET/CT examinations in Sardinia from 2012 to 2016: a retrospective analysis

A. Loi[1], S. Zucca[2], M. Carta[1], D. De Vittor[1], G. Melis[3], S. Loi[2]; [1]Alliance Medical, Cagliari, ITALY, [2]C. Fisica Sanitaria Azienda Ospedaliera G. Brotzu, Cagliari, ITALY, [3]S.C. Medicina nucleare e Centro PET Azienda Ospedaliera G. Brotzu Cagliari, Cagliari, ITALY.

Due to the radionuclide short half life, exams with 11C-Choline can be provided only in PET center with cyclotron. In Sardinia, only the site at the Azienda Ospedaliera Brotzu (AOB) in Cagliari at the moment performs 11C-Choline PET/CT. In this study a retrospective analysis of administrated activities from 2012 to 2016 were reported, together with an estimate of the effective dose imparted to patient. Local Diagnostic Reference Levels (LDRL) in PET/CT for 11C-CHOLINE for the region were suggested. **Materials and Methods:** All exams performed from 2012 to 2016 were included in this survey. Data collection has been carried out through routines of automation. For each examination, administered 11C-CHOLINE activity was registered together with patient weight, height and age. From 2012 to 2015 - a standard activity was administered independently of patient size and examinations were performed on a GE DST 2D scanner. At the end of 2015 a new scanner has been installed (GE DISCOVERY IQ), and the administered activity was calculated using a reference value of 4.0MBq/Kg. Starting from the administered activity, the absorbed dose was calculated with OLINDA/EXM version 1.0 software using Male standard phantom. To take into account the variability of patient size within patient cohort, for each patient, organ masses were linearly scaled with the ratio of patient weight and the standard phantom weight (73 kg). **Results:** A total of 1206 examinations were analyzed (224@2012; 238@2013; 245@2014; 219@2015; 280@2016); The average CHOLINE injected activity was 377±22 MBq in 2012-2015 (75° percentile 391 MBq), and decreased to 316±51 MBq on 2016, 75° percentile 340 MBq) in 2016. The effective doses calculated on 2012-2015 were 1.81±0.18 mSv for patients with a weight lower than 60 kg, 1.44±0.11 mSv for patients with a weight between 60 and 80 kg, and 1.11±0.12 mSv for patients with a weight bigger than 80 kg. The effective doses calculated on 2016 were significantly lower (up to 40% for light patients) and almost constant independently on patients size : 1.13±0.01 mSv for patients with a weight lower than 60 kg, 1.13±0.01 mSv for patient with a weight between 60 and 80 kg, and 1.18±0.04 mSv for patient with a weight bigger than 80 kg. **Conclusion:** The results of the dosimetric survey highlighted the impact of new scanner technology and the optimization of the administered activity on patient dose. Moreover, LDRL for the administered activity in 11C-CHOLINE PET/CT examinations have been derived.

EP-0029

Regional-wide survey on administered activity of 18F-FDG in PET/CT examinations in Sardinia

F. Pinna[1], S. Zucca[2], D. De Vittor[3], M. Carta[3], S. Loi[2], G. Melis[4], M. Giannoni[4], A. Spanu[5], P. Marini[1], A. Loi[3]; [1]S.S.D Fisica Sanitaria Azienda Ospedaliera Universitaria, Sassari, ITALY, [2]S.C. Fisica Sanitaria Azienda Ospedaliera G. Brotzu Cagliari, Cagliari, ITALY, [3]Alliance Medical, Cagliari, ITALY, [4]S.C. Medicina nucleare e Centro PET Azienda Ospedaliera G. Brotzu, Cagliari, ITALY, [5]S.C. Medicina Nucleare e Centro PET Azienda Ospedaliera Universitaria, Sassari, ITALY.

Diagnostic Reference Levels (DRL) are a QA tool introduced by ICRP in order to monitor practice and to promote improvements in patient protection. A regional-wide survey was conducted in Sardinia to estimate the administered activity of 18-FDG in PET/CT examinations. The results were analyzed to suggest Local Diagnostic Reference Levels (LDRL) in PET/CT on a regional basis. The analysis also includes the evaluation of inter-center variability. **Material and Method:** All the FDG PET/CT examinations performed in the three PET/CT center in Sardinia in 2016 were included in the survey (A: Siemens Biograph 40 installation year 2008; B: GE DISCOVERY 710 year 2013; C: GE DISCOV-

ERY IQ installation year 2016). Data collection has been carried out through routines of automation or user-developed code (Matlab@Matworks), extracting information recorded on di-com-header data. For each examination, administered 18-FDG activity was registered together with patient weight, height and age. In order to better estimate the influence of scanner technology and optimization of diagnostic procedure on administered activity, for center C, data collected in 2016 were retrospectively compared with those registered in 2015, when a standard activity was administered with a small modulation for patient size using an older scanner (GE DST 2D). Mann-Whitney statistical test with a significance level of 0.05 was performed to compare inter-center distributions. **Results:** A total of 4406 examinations were analyzed; 1554 (35.3%) performed on A, 1039 (23.6%) on B, and 1813 (41.1%) on C. No differences were found on patient's age and weight distributions among centers. The overall average 18F-FDG injected activities were 268±62 MBq and 3.94±0.40 MBq/kg (75 percentile 307 MBq and 4.23 MBq/kg). The administered activity was statistically different among center, with a mean value of 290±65 MBq (4.28±0.39 MBq/kg) for center A, 268±56 MBq (3.88±0.12 MBq/kg) for center B and 250±56 MBq (3.53±0.31 MBq/kg) for center C. In particular, for center C, data registered in 2016 were compared with those collected in 2015 (356±45 MBq and 5.44±1.10 MBq/kg, p<0.05). For each center, the correlation between patient's weight and injected activity is affected by a non-negligible residual error, depending on automatic dispensator dose systems. **Conclusion:** LDRL for the administered activity in 18-FDG PET/CT have been derived from the analysis of all examinations performed in Sardinia in 2016. Results highlighted a variability among centers, mainly due to different installed technology, that can be minimized by standardization and optimization of diagnostic procedures.

EP-0030

Plasma to blood ratio derived parent fractions for robust plasma input based kinetic analysis of dynamic ¹⁸F-FLT PET studies in NSCLC cancer patients

A. Avendaño-Estrada[1,2,3], G. Kramer[2], V. Frings[2], D. Vallez García[1], E. Smit[4], A. Lammertsma[2], O. Hoekstra[2], R. Boellaard[1,2], QuicConcept Consortium; [1]University Medical Center Groningen, Groningen, NETHERLANDS, [2]VU University Medical Center, Amsterdam, NETHERLANDS, [3]Universidad Nacional Autónoma de México, Mexico, MEXICO, [4]The Netherlands Cancer Institute, Amsterdam, NETHERLANDS.

Purpose/Introduction: Full quantitative analysis of dynamic ¹⁸F-FLT PET studies is important to validate the use of simplified methods and metrics, such as SUVs, for early response assessment (1). However, full quantitative kinetic analysis requires the use of a metabolite corrected plasma input function. The measurement of parent fractions is often associated with poor signal to noise ratio, measurement errors and it is labor intensive. In the present work, we investigated if parent fractions could be estimated directly from plasma and blood activity concentrations thereby obviating the need to perform metabolite analysis and/

or use estimated values for quality control purposes. **Subjects & Methods:** Nine NSCLC patients underwent three 60 min dynamic ¹⁸F-FLT PET scans: at baseline within 7 days before treatment and at 7 and 28 days after start of the treatment. During each PET study 6 to 7 venous blood samples were collected to obtain blood and plasma concentrations as well as parent fractions. These data were subsequently used in combination with an image derived input function to generate a metabolite corrected input function. A plasma input reversible 2-tissue compartment model (PMOD v3.7) was applied to the tumor time activity curves, yielding tumor VTs. This analysis was repeated using parent fractions calculated from plasma to blood ratios using an equation derived from the baseline scans only. VTs derived from analysis using measured and calculated parent fractions were compared as well as longitudinal % changes in VT using both approaches. Agreement was assessed with linear regression, interclass correlation coefficients (ICC) and Bland-Altman plots. **Results:** Excellent agreement between VTs derived from measured vs calculated parent fractions was found for both early (R2=0.983[0.981-0.996 (95%CI)]; ICC=0.992[0.982-0.996]) and late response (R2=0.994[0.992-0.998]; ICC=0.996[0.991-0.998] scans. Furthermore, Bland-Altman plots showed a strong agreement for both early (percentage bias=0.284[-6.172-6.741]) and late response (percentage bias=-1.165[-7.125-4.795] studies. **Discussion/Conclusion:** The strong agreement in tumor ¹⁸F-FLT VTs as well as their longitudinal changes when obtained from input functions using measured or calculated parent fractions suggest that parent fractions can be reliably estimated using plasma to blood ratios. Plasma to blood ratio derived parent fractions could be used as an alternative when blood sample data are noisy or incomplete, to discard outliers, or when it is not possible to acquire sufficient samples for metabolite analysis. The method may be applicable to other tracers as well, but this requires further studies. **Reference:** 1. Frings et al., JNM 2014

EP-0031

Importance of algorithms in SUV calculation. Quantitative comparison of differences in SUV obtained from OSEM and Q.Clear® algorithms.Our experience

M. Agolti[1], B. Moglia[2], J. Biurrun Manresa, 3100[3], J. Bustos[2]; [1]Clinica Modelo, Parana, ARGENTINA, [2]Fundación Centro de Medicina Nuclear y Molecular Entre Ríos (CEMENER), Oro Verde, ARGENTINA, [3]Centro de Investigaciones y Transferencia de Entre Ríos (CITER) CONICET-UNER, Oro Verde, ARGENTINA.

Purpose: the standardized uptake value (SUV) is an objective measurement of FDG uptake, which is important in the evaluation of response to treatment. Using a new reconstruction algorithm (Q.Clear®), we noticed large differences in the resulting SUV values compared to the conventional OSEM algorithm. In this study we quantified these differences in order to assess their potential impact on treatment evaluation. **Subjects and Methods:** 72 FDG PET-CT scans performed with a GE Discovery PET/CT 710 were included in the study, performed in our center between December 2016 and April 2017. Scans were assessed simultaneously using the same ROI size at the same location.

Maximum SUV from both algorithms were obtained from the liver as a control (n=72), from lesions of 1 cm (n=28) and from lesions of 2 cm (n=28). Data was analyzed using Bland-Altman analysis, from which the mean difference and the 95% limits of agreement (LoA) were derived. The mean difference is a measure of systematic error, and the LoA represent the maximum differences due to random error between methods, within which 95% of the differences between measurements are expected to lie. Differences were calculated as ($SUV_{Q.Clear}$ - SUV_{OSEM}). **Results:** In average, $SUV_{Q.Clear}$ was larger than SUV_{OSEM}, but not in all individual cases. Mean differences in normal liver SUV were 0.1%, and the maximum differences ranged between -5.2% and 5.4%. Mean differences in SUV from 1 cm lesions were 7.5%, and the maximum differences ranged between -19.9% and 35.0%. Finally, mean differences in SUV from 2 cm lesions were 3.5%, and the maximum differences ranged between -6.0% and 13.0%. **Conclusion:** the differences between methods were acceptable for liver SUVs, but not for SUVs quantified from lesions. Differences were larger for smaller lesions, and the large systematic error (up to 7.5%) and random variation found (up to 35%) are clinically significant, since they could erroneously lead to a change in treatment for some patients. Therefore, SUVs obtained from different algorithms cannot be used interchangeably. These results stress the importance of visual assessment to evaluate response to treatment, since SUV is neither silly nor smart, but is rather a Simple Useful Value that has to be considered within the proper clinical context.

EP-0032

A quantitative functional and structural multiple sclerosis analysis A 99mTcECD brain SPECT study with statistical parametric mapping SPM evaluation and voxel based morphometry VBM analysis of brain MRI using CAT12 toolbox

N. Chabi[1], R. Nemati[2], M. Assadi[2]; [1]Division of Biomedical Engineering (BME), The Persian Gulf Nuclear Medicine Research Center, Bushehr University of Medical Sciences,, Bushehr, IRAN, ISLAMIC REPUBLIC OF, [2]Division of Neuroscience, The Persian Gulf Nuclear Medicine Research Center, Bushehr University of Medical Sciences,, Bushehr, IRAN, ISLAMIC REPUBLIC OF.

Introduction: This study performed a visual and quantitative analysis on secondary progressive multiple sclerosis SP-MS patients' functional and structural data. In detail, we assessed regional cerebral blood flow in SP-MS patients using statistical parametric mapping (SPM) to detect hypo perfused area on 99mTc-ECD SPECT as well as voxel based morphometry analysis of gray matter (GM) on volumetric T1-MRI scan. **Subjects and Methods:** Both MRI and SPECT were performed on 5 SP-MS patients and 20 age-matched healthy volunteers. Using statistical parametric mapping, 5 SPECT images from patients with SP-MS were compared with a control group of 20 subjects using a statistical threshold of p<0.05 (corrected for multiple comparisons). On the other hand, global GM loss has been reported in multiple sclerosis. Therefore, we want to find the regions with significantly reduced GM density. By using CAT12 software, VBM analysis

was applied to MRI data of participants. Segmented GM volumes were compared on a voxel-by-voxel basis to find regions with GM loss (P < 0.05, corrected for multiple comparisons). **Results:** All the quantitative results obtained by SPM and VBM analysis were compared with visual analyses by a nuclear physician and neurologist. Findings reveal that SPM result and nuclear physician decision, VBM result and neurologist decision were in a good agreement. Furthermore, SPM analysis of SPECT data provides information that is in complement to structural analysis of MRI. In detail, based on SPM analysis of SPECT, hyper perfusion area was seen in WM and hypo perfusion area in GM. **Conclusion:** brain perfusion SPECT can be a complementary tool to other diagnostic modalities such as MRI and clinical examinations in disease surveillance and monitoring. SPM analysis of brain SPECT and VBM analysis of MRI will provide complementary information for physicians. **Keywords**: secondary progressive multiple sclerosis SP-MS patients, 99mTc-ECD brain perfusion single photon emission computed tomography (SPECT), Magnetic Resonance Imaging (MRI), Statistical Parametric Mapping (SPM), Voxel Based Morphometry (VBM), Computational Anatomy Toolbox (CAT12), Gray matter (GM), White Matter (WM)

EP-0033

Prediction of chemotherapy response in osteosarcoma using multi-parametric PET/MRI texture feature

*Y. Park, W. Kim, B. Byun, J. Kang, C. Kong, W. Song, I. Lim, Y. Lee, B. Kim, S. Lim, **S. Woo**; Korea Institute of Radiological and Medical Sciences, Seoul, KOREA, REPUBLIC OF.*

Objectives: Intra-tumor heterogeneity assessment can improve patient management and prognosis. The aim of this study was to improve the predictability of chemotherapy response in osteosarcoma using combined information with metabolic and anatomical heterogeneity. **Methods:** Tumor heterogeneity was assessed using texture analysis and subject were a cohort of 22 patients with osteosarcoma who underwent baseline PET and MRI from May 2010 to September 2013. PET/MRI image was acquired using PET/CT (Biograph 6 PET/CT scanner, Siemens, Malvern, PA) and 3.0T MRI (MAGNETOM Trio A Tim, Siemens, Germany). Difference volume of interest (VOI) define method base on PET image can affect the prediction sensitivity, we performed the texture analysis using two difference VOI region which is PET and MRI. The F-18 FDG PET image was visualized metabolic heterogeneity through the standard uptake value (SUV) and PET VOI was defined by region growing. MRI of T2 weighted image was visualized anatomical heterogeneity through the pixel intensity and T2 VOI was defined by manually drawing. To enhance the predictability of chemotherapy response, we assessed multi-parametric texture feature. Multi-parametric texture features were extracted using T2 VOI from F-18 FDG PET and T2 weighted MRI images of global, local, and regional area. The response of chemotherapy and statistical significance of texture feature were estimated using receiver operating characteristic (ROC) and logistic regression. Results: Tumor region was identified by region growing PET VOI and manual T2 VOI. The PET VOI and MRI VOI sensitivity on F-18 FDG PET image was

61.78% and 91.86%, respectively. The chemotherapy response of PET texture features with T2 VOI has more sensitive than PET region growing VOI texture features. Logistic regression analysis of PET and MRI texture features with T2 VOI was *p* = 0.08 and *p* = 0.05, respectively. Multi-parametric texture feature logistic regression with metabolic and anatomical heterogeneity was *p* = 0.046. **Conclusions:** Prediction ability using multi-parametric texture feature which is extracted in PET/MRI was more sensitive and accurately than single parameter texture features. PET/MR multi-parametric texture features are expected to be the useful method prediction of chemotherapy response in osteosarcoma patients.

EP-0034

An efficient software tool for measuring the total metabolic tumor volume in whole body PET

C. Nioche[1], A. Cotterau[2], M. Meignan[3], I. Buvat[1]; [1]Service Hospitalier Frédéric Joliot, Imiv, Cea, Inserm, Cnrs, Univ. Paris-sud, Université Paris Saclay, CEA-SHFJ, Orsay, Orsay, FRANCE, [2]Médecine Nucléaire, Lysa Im, Hôpital Tenon et Hôpitaux Universitaires Henri Mondor, Paris, Paris, FRANCE, [3]Lysa Im, Hôpitaux Universitaires Henri Mondor, Créteil, Créteil, FRANCE.

Objectives: The total metabolic tumor volume (TMTV) estimated from FDG-PET images is a promising biomarker of the total tumor burden, especially in patients with lymphomas. However, estimating TMTV is challenging and often time consuming when multiple targets, including primary tumors, nodes and metastases, with various metabolic activities, volumes and contrasts have to be segmented. We developed a convenient and user-friendly pipeline for estimating TMTV that is now offered as part of the free LIFEx software (www.lifexsoft.org). Methods: The procedure of TMTV calculation is based on four customizable steps: The first step is a semiautomatic initialization of intermediate to high metabolic activity (typically SUV>2) volumes in which the tumor regions should be identified, yielding a possibly disconnected gross volume GV. Then, tumor volume delineation within this initial GV is refined using one or several customizable criteria in combination, including: 1) absolute SUV threshold (ie SUV>2.5), 2) region-to-liver activity threshold, 3) percent SUV-max threshold (ie, 40%), 4) adaptive threshold accounting for surrounding activity. A third step identifies groups of connected voxels, deletes clusters that are too small in volumes, and derives the resulting TMTV. Last, a final step makes it possible for the user to remove regions with physiological uptake (brain, bladder, etc) using a 1-click operation, or to add regions using a 1-click operation that runs a region growing algorithm. The TMTV value is automatically updated during these operations. All regions can be displayed using axial, sagittal and coronal slices and using a maximum-intensity-projection representation. PET volume and associated regions can also be overlapped with the CT or MR for visual analysis. The whole procedure has been implemented in the LIFEx free software (Windows, MacOS and Linux compatible) thus enabling textural indices calculation from each component of the TMTV. The results are exported in an Excel file and in the form of an image booklet displaying the regions. All regions included in the final TMTV volumes can be saved on disk for subsequent use. Results: The intuitive software interface as well as associated demo videos allow for immediate use of the tool. The calculation of TMTV is performed within 4 minutes from a whole body PET scan. Being easily accessible, the software has already been downloaded by more than 250 users over the world and is currently under evaluation to assess its ability to produce fast and robust estimates of TMTV in the context of multicenter studies of lymphoma patient cohorts.

EP-0035

Motion detection for static objects imaged with CZT cardiac camera

A. Budzynska, M. Dziuk; Military Institute of Medicine, Warsaw, POLAND.

Aim: Commercially available MDC_for_Alcyone software enables reformatting 5-minute acquisitions into 1- (Lister_1s) and 20-second (Lister_20s) bins to detect respiratory motion and patient motion, respectively. The study objective was to assess motion registered in three directions for static acquisition on CZT cardiac camera. We also aimed to determine motion cut-off safe for diagnostic outcome. **Materials and Methods**: **Stage I:** Ten acquisitions with two static 0.5ml sources (0.097mCi and 1.64mCi) without scattering medium were performed. Count rates were 1.09 and 20.13kcts/s, respectively. **Stage II:** Nine series of static heart phantom studies (three acquisitions for each series) were performed. The phantom was filled with non-radioactive water. Phantom 99mTc activity and time window between acquisitions were adjusted to obtain a count rate observed in clinical setting (2.11-4.60kcts/s). All scans were processed with the use of reformatted 1- and 20-bin data and MDC_for_Alcyone software. Detected motion was grouped according to its range in *x*, *y* and *z* direction (0, <-4mm; 4mm>, <-8mm; 8mm> and > | +/-8 | mm) and its duration reported in seconds or as a % share of acquisition time. Phantom scans results were correlated with camera-registered count rate (a surrogate for phantom radioisotope activity). **Results**: **Stage I results**: In Lister_1s bins time interval when *x*=0, *y*=0 and *z*=0 was 154s (55.91%) and 274s (99.35%) for 0.097mCi and 1.64mCi source, respectively. Over the remaining acquisition time at least one of *x*, *y* or *z* coordinates was +/-4mm (or +/-8mm for lower-activity source). In Lister_20s bins no motion was detected. **Stage II results:** In Lister_1s bins *x* and *y* direction motion of +/-4mm, +/-8mm, +/-12mm and +16mm was reported. For *z* it was +/-4mm and +/-8mm. Time interval when *x*=0, *y*=0 and *z*=0 was 23s (8.47%). Time interval when the absolute motion values were greater than 4mm was 40s (14.51%) for *x*, 38s (13.69%) for *y* and 6s (2.17%) for *z* direction. In Lister_20s bins 4mm motion was also reported. Significant motion was observed in *x* and *y* direction only (10.74% and 9.93% of acquisition time, respectively). Time interval when *x*=0, *y*=0 and *z*=0 was 233s (84.30%). No correlation between no-motion time and source activity was observed in heart phantom scans. **Conclusions**. Neither object (20-second bins) nor respiratory movements (1-second bins) are responsible for +/-4mm motion reported by MDC_for_Alcyone

software. In phantom scans *x* and *y* direction similarly showed the greatest range of motion. In the patient, however, *y* and *z* motion was the most remarkable.

EP-0036

Monte-Carlo simulated amyloid PET for testing the performance of Partial Volume Correction methods

G. Salvadó[1,2,3], A. Niñerola-Baizán[2,3], M. Garcia[2], J. Pavía[4,3], D. Ros[2,3], F. Lomeña[4,5], J. Molinuevo[1,6], J. Gispert[1,3], **R. Sala-Llonch[2]**; *[1]Barcelonaβeta Brain Research Center, Pasqual Maragall Foundation, Barcelona, SPAIN, [2]Department of Biomedicine. University of Barcelona, Barcelona, SPAIN, [3]Centro de Investigación Biomédica en Red de Bioingeniería, Biomateriales y Nanomedicina (CIBER-BBN), Zaragoza, SPAIN, [4]Servei de Medicina Nuclear, Hospital Clínic., Barcelona, SPAIN, [5]Centro de Investigación Biomédica en Red de Salud Mental (CIBERSAM)., Barcelona, SPAIN, [6]Alzheimer's Disease and Other Cognitive Disorders Unit, Hospital Clínic, Institut d'Investigacions Biomèdiques August Pi i Sunyer (IDIBAPS), Barcelona, SPAIN.*

Aim: The evaluation of Partial Volume Correction (PVC) methods with real data is limited given the unknown actual tracer distribution. We used Monte-Carlo simulated amyloid Positron Emission Tomography (PET) to evaluate the accuracy of several PVC methods. **Materials and Methods:** We performed basic and realistic simulations. We first obtained ground-truth (GT) activity and attenuation maps using Magnetic Resonance Imaging (MRI), Computed Tomography (CT) and ^{18}F-Florbetaben PET data from healthy subjects. We then obtained simulated PET images using SimSET v2.9. For the *basic simulation*, we assigned constant values to gray matter (GM) and white matter (WM) separately, so that the GM/WM ratio represented different uptake levels. We used 10 subjects and 4 different ratios. For the *realistic simulation*, GT were obtained through *BrainViset*, which sequentially compares the simulation with the real PET scan to minimize the differences by including functional information. We obtained 5 realistic simulations We tested 3 PVC methods: The Richardson-Lucy (RL) method, based on simple deconvolution, the Müller-Gärtner (MG) method, based on MRI tissue-segmentations, and the region-based voxel-wise (RBV) correction, all implemented in the *PETPVC* toolbox. We measured Standardized Uptake Value Ratios (SUVR) within the whole GM, with the cerebellum as the reference region. **Results:** *Basic simulated data* leaded to theoretical SUVR of 1, 1.56, 2.13 and 2.7, modeling different uptake levels in PET. After simulation, SUVR were overestimated in low ratios and underestimated in higher levels (from lowest to highest activity: +14%, -12%, -25% and -33%). After MG-correction, these values were more reliably estimated (+3%, -8%, -14% and -20%). RL performed worse than MG, and RBV did not improve the results. For *realistic simulations*, the average theoretical SUVR was 1.26 and the SUVR of the simulated PET scans was 12% lower. RL underestimates GM activity (-9.7%) and MG slightly overestimates it (+5.6%). RBV provided the best results (0.7% lower than the theoretical SUVR). **Conclusion:** The performance of PVC depends on the method and on the nature of the PET data. Using basic simulated data we observed

that the results of MG depend on the activity level. Realistic simulations indicate that the spatial distribution of activity has also a strong impact. Data can be slightly corrected with simple methods such as RL. The MG method, which takes into account structural information, improves the results although it overestimates GM activity. The RBV method is highly effective in realistic data, with non-uniform distribution.

EP-0037

Group-Sequential Analysis May Allow for Early Trial Termination: Illustration by an Intra-Observer Repeatability Study

O. Gerke[1,2], M. H. Vilstrup[1], U. Halekoh[2], P. Høilund-Carlsen[1,2]; *[1]Odense University Hospital, Odense, DENMARK, [2]University of Southern Denmark, Odense, DENMARK.*

Aim: Group-sequential testing is widely used in pivotal therapeutic studies, but is underused in diagnostic research. We applied group-sequential testing in an intra-observer repeatability study with normally distributed differences to demonstrate the possibility of early termination if sufficient agreement has been obtained *en route*. **Materials and Methods:** We used interim data from 45 patients in an ongoing clinical trial on the preoperative assessment of ovarian cancer by FDG-PET/CT imaging. Processing of the scans was performed twice, separated by a 2-month interval, by author MHV to investigate the intra-observer repeatability of image processing. SUVmax was measured in the primary ovarian lesion if it could be identified; otherwise, the SUVmax of peritoneal carcinosis was used. Assuming normality of differences in SUVmax between first and second reading, the sequential sample size strategy based on a one-sided hypothesis test (against the 'smaller than' alternative) was applied on the population standard deviation of these paired differences, and a type 1 error spending function was used. Two interim analyses of 1/3 (N=15) and 2/3 (N=30) of the final dataset were conducted post hoc, leading to significance levels of 0.05*1/3=0.0167 and 0.05*2/3=0.033, respectively; final analysis was done with 45 patients and a significance level of 5%. To exemplify, the level of the hypothesized population standard deviation was varied between 0.5 and 2. **Results:** At the first interim analysis (N=15), the null hypothesis could only be rejected for hypothesized population standard deviations of at least 1.5 after adjustment of multiple testing. The corresponding upper 98.33% confidence limit of the population standard deviation was 1.495. At the second interim analysis (N=30) and at the end of study (N=45), the null hypothesis could only be rejected for hypothesized population standard deviations of at least 1.75 (upper 96.67% confidence limit: 1.653) and at least 1.5 (upper 95% confidence limit: 1.288), respectively. **Conclusion:** The first interim analysis (N=15) indicated the very same hypothesised value for termination as the final analysis (N=45), illustrating both potential time and resource savings due to sequential testing. Group-sequential testing of repeatability studies offers the necessary flexibility in the planning stage when *a priori* information is scarce, but secures the experiment-wise type 1 error probability; however, fixing the hypothesized population standard deviation before

trial conduct is imperative. Further research needs to illuminate non-parametric alternatives when the assumption of normally distributed differences does not hold.

EP-0038

A [¹¹C]-(R)-PK11195 PET human brain template for spatial normalization in statistical parametric mapping of neuroinflammation

P. N. Schuck[1], A. M. Marques da Silva[1,2], C. M. Dartora[1], C. S. Matushita[2], B. Hochhegger[1,2], J. Becker[1,2]; [1]PUCRS, Porto Alegre, BRAZIL, [2]Brain Institute, Porto Alegre, BRAZIL.

Introduction: PET scans can be analyzed using voxel-based statistical methods such as Statistical Parametric Mapping (SPM) that provide statistical maps of brain abnormalities in single patients. PET templates currently are available for SPM normalization, based on [18F]FDG and [11C]PiB data. **Aim:** To create a new [¹¹C]-(R)-PK11195 PET human brain template, based on images derived from healthy controls, for spatial normalization in SPM of neuroinflammation. **Methods and Materials:** [¹¹C]-(R)-PK11195 PET data from 14 healthy subjects (age: 28 ± 8 years, weight: 75 ± 10 kg) were acquired on a PET/CT scanner (Discovery 600; General Electric). Cerebral scans were collected in list-mode immediately after injection of (359 ± 84 MBq), during 60 min. Images were reconstructed with 300 mm field of view, using VUE Point HD iterative algorithm, smoothing filter cutoff frequency 4,0 mm, 32 subsets and two iterations. A static PET SUV mean image from 10-60 min was generated for each subject, with corpus callosum trunk as origin. T1-weighted MRI from each subject was co-registered to the PET SUV image. SUV in the white matter was computed for each subject using SPM8 automatic segmentation from MRI. Normality of the group was tested using Shapiro-Wilk statistics. The PET image of the subject with SUV equal to the median value of the group was chosen as PET spatial reference image. All PET images were with spatially normalized and co-registered to this PET image reference. The SPM8 parameter settings used for estimating the spatial transformations were: template to reference PET image; source image smoothed FWHM 8mm; 25 mm cutoff; affine regularization; 16 nonlinear iterations; isotropic voxel size 2 mm. For validation purposes, [¹¹C]-(R)-PK11195 PET scans from multiple sclerosis (MS) patients with activated microglia lesions were used. Registration accuracy was evaluated using mutual information histograms. **Results:** Within a 5% significance level, the white matter SUV of the population comes from a normal distribution (W =0.9291; p=0.28776; N = 14). The median white matter SUV of the group is 0.53 g/mL (min: 0.33 max: 0.97). Z-map difference image between [¹¹C]-(R)-PK11195 PET population-based template and MS patient images, with 30% threshold, showed microglia activated lesions in the expected regions, confirmed through both T1-weighted and FLAIR MRI. **Conclusion:** The new [¹¹C]-(R)-PK11195 PET healthy population-based template allows the use of spatial normalization for SPM and voxel-based methods. [¹¹C]-(R)-PK11195 PET template-based quantification seems adequate for clinical use. Preliminary tests with MS patients show coherence with MRI findings related to neuroinflammation.

Physics & Instrumentation & Data Analysis: Radiation Exposure & Protection

EP-0039

Significantly Low Effective Dose from ¹⁸FDG PET/CT Scan Using Dose Reducing Strategies: "Lesser is Better"

M. U. Zaman[1], N. Fatima[1], A. Zaman[2], M. Sajid[3], S. Zaman[2]; [1]Aga Khan University Hospital, Karachi, PAKISTAN, [2]Dow Medical College, Dow University of Health Sciences (DUHS), Karachi, PAKISTAN, [3]Karachi Institute of Radiotherapy And Nuclear Medicine (KIRAN), Karachi, PAKISTAN.

Background: Fluorodeoxyglucose (¹⁸FDG) PET/CT imaging has become an important component of management paradigm in oncology. However, significant radiation exposure imparted by it is a matter of growing concern especially in younger population who have better odds of survival. Aim of this study was to estimate the effective dose received by patients having whole body ¹⁸F-FDG PET/CT scanning as per recent dose reducing guidelines at a tertiary care hospital. **Material and Methods:** This prospective study included 63 patients with different cancers who were referred for PET/CT study for various indications. Patients were prepared as per departmental protocol and ¹⁸FDG was injected at 3 MBq/Kg and a low dose, non-enhanced CT protocol (LD-NECT) was used. Diagnostic CT studies of specific regions were performed afterward if required. Effective dose imparted by ¹⁸FDG (internal exposure) was calculated by using multiplying injected dose in MBq with coefficient $1.9×10^{-2}$ mSv/MBq according to ICRP publication 106. Effective dose imparted by CT was calculated by multiplying DLP (mGy.cm) with ICRP conversion coefficient "k" 0.015 [mSv / (mG. cm)]. **Results:** Mean age of patients was 49 ±18 years with a male to female ratio of 35:28 (56%:44%). Median dose of ¹⁸FDG given was 194 MBq (range: 139-293). Median CTDI$_{vol}$ was 3.25 (2.4-6.2) and median DLP was 334.95 (246.70 - 576.70). Estimated median effective dose imparted by ¹⁸FDG was 3.69 mSv (range: 2.85-5.57). Similarly the estimated median effective dose by low dose (non-diagnostic) CT examination was 4.93 mSv (range: 2.14 -10.49). Median total effective dose by whole body ¹⁸FDG PET plus low dose non-diagnostic CT study was 8.85 mSv (range: 5.56-13.00). **Conclusion:** We conclude that the median effective dose from a whole body ¹⁸FDG PET/CT in our patients was significantly lower if not the lowest. We suggest adhering to recently published dose reducing strategies, use of ToF scanner with CT dose reducing option to achieve this lower if not the lowest effective dose. This would certainly reduce the risk of second primary malignancy in younger patients with higher odds of cure from first primary cancer.

EP-0040

Reducing Radiophobia in Nuclear Medicine Patients

A. Shabestani Monfared[1], M. Amiri[1], J. Cameron[2], A. Gholami[1]; [1]Babol University of Medical Sciences, Babol, IRAN, ISLAMIC REPUBLIC OF, [2]University of Wisconsin, Madison, WI 53706 USA, Madison, WI, UNITED STATES.

Introduction: This article describes a method to reduce radiation phobia of nuclear medicine patients and their families by explaining the dose in understandable words. The approach, explains the dose in terms of the time to get the same effective dose from background radiation. A medical physicist or radiation protection physicist should prepare tables for each of the nuclear medicine imaging area giving the effective dose for various standard nuclear medicine studies. A separate column should give the "Background Equivalent Radiation Time or BERT value of the patient's dose. The nuclear medicine physician or technologist should explain the dose to the patient in words, such as. "your dose from this procedure is about equal to the amount of radiation you receive from natural or background radiation in [insert the appropriate time in weeks, months or years]. In the U.S. the average background rate is about 3 mSv/year, which includes the contribution from radon progeny. It is impossible to give an exact dose for any patient, since each patient will have a different clearance time for the radionuclide. However, there here are no data to show an increased risk from modern nuclear medicine doses. If the medical staff member is asked if there is any risk or danger, an appropriate answer would be, " There is no known risk from the amount of radiation you receive in this study". The advantages of the BERT approach for explaining the dose to the patient are: 1. The BERT approach is understandable, 2. It does not mention risk, and 3. It educates the patient that we all live in a sea of natural radiation. There are many millions of natural radioactive disintegrations in our body every day. Excellent data indicate that people who live in areas with greater background radiation have less cancer than in areas with lower background levels**. Method:** The table gives the effective dose to an adult patient from a typical radionuclide dose for particular nuclear medicine procedures. A separate column gives the BERT value, the time to get the same effective dose from background in the U.S. **Conclusion:** The BERT approach is not intended as a scientific explanation. An explanation using scientific terminology would generally not be understood by a patient. The comparison with natural background does not imply nor deny any risk. It does not suggest that procedure is completely without risk, which, in any case, cannot be determined.

EP-0041

Radiation doses result from radioactive iodine therapy versus living quality

H. M. Yassin, R. M. Abdel-Halim; Cairo Univeristy, Cairo, EGYPT.

Introduction: Radioactive iodine is widely used for the therapy of various thyroid diseases. Protection issues are usually a source of worry for the patients, their families and friends. The patients are recommended to control their social and work related activities. The aim of this study was to estimate the possible external radiation dose to other individuals from patients treated with 131I and describes the results of a structured survey conducted on patients visiting selected hospital. **Materials and Methods:** A total of 510 patients were enrolled. The patients were asked about their housing, family, numbers of children, travelling modes .The hospital leaving exposure rates from the patients were measured and radiation doses to others were estimated. **Results**: According to the results the patients living in joint family system were 90%. The dose rate at one meter were 7.3., 12.1, 16.5, 19.2, 24.4 and 29.3 µSvh-1 for the administered 131I activity of 185, 370, 555, 740, 925 and 1100 MBq respectively. The corresponding doses to others from the patient were estimated as 0.93, 1.83, 2.77, 3.92, 4.95 and 5.09 mSv. The patents using public transport were 55.7% whereas 44.3 % used private transport. There were 9.4% of the patients with no children and 90.6. % of the patients had children inhabit with them. **Conclusion:** Radiation protection recommendation and regulatory requirements need to be check out keeping in view the individual patient life quality and other living conditions. Keywords: Radioactive iodine, Therapy, Radiation protection, Living quality.

EP-0042

Dosimetry and Radiation Risk in Infants after ^{99m}Tc-MAG3 Scans

J. Soares Machado, A. K. Buck, M. Lassmann; University of Wuerzburg - Universitaetsklinikum Wuerzburg, Wuerzburg, GERMANY.

Purpose/Introduction: Renal scans are among the most frequent exams performed on infants; therefore, an analysis of the stochastic radiation risk seems warranted. The aim of this study was, based on a retrospective analysis of the absorbed doses for infants undergoing ^{99m}Tc-MAG3 renal scans, to assess the associated radiation risk. **Methods:** We retrospectively analyzed data of 20 patients (14 males and 6 females; age: 1.6 to 20 months) with normal kidney function who had undergone renal scans with ^{99m}Tc-MAG3. After establishing a retrospective quantification of the kidney, bladder and whole-body time-activity curves and subsequent integration, the absorbed-dose coefficients were assessed for each patient with OLINDA/EXM. The risk estimate was performed with the Radiation Risk Assessment Tool (RadRat) for all pediatric patients individually, using the calculated absorbed organ doses as input values. The RadRat tool can be used to estimate the lifetime risk of radiation-induced cancer with uncertainty intervals following a user-specified exposure history (https://irep.nci.nih.gov/radrat). The risk models used in RadRAT are based on those developed by the BEIR VII committee for estimating lifetime risk following low-dose radiation exposure plus new risk models for seven additional cancer sites. The output of the tool is the lifetime risk of developing of radiation-induced cancer. **Results:** The mean administered activity was 17.9±2.6MBq. The mean absorbed-dose coefficients of kidneys and bladder were 0.04±0.04mGy/MBq and 0.36±0.32mGy/MBq, respectively. The mean effective dose coefficient values were 0.03±0.02mGy/MBq. For male patients, it was possible to estimate the risk for eleven organs (brain; colon; gallbladder; liver; lungs; kidneys; pancreas; red bone marrow; stomach; thyroid; urinary bladder) and for females for fourteen organs (the eleven plus three the gender-specific organs breast, uterus and ovaries). The mean excess lifetime risk estimate to develop radiation-induced cancer for the exposed organs calculated by the RadRat tool was 16.4 per 100.000 persons for newborns, about 8% high-

er than for the 1-year-old patients (15.3 per 100.000). Comparing the mean excess lifetime risk values between gender groups, the female patients showed a 26% higher excess lifetime risk than males, most likely caused by influence of the estimated risk for the gender-specific organs. **Conclusion:** This retrospective analysis provided new data on absorbed doses to infants after renal scans with ^{99m}Tc-MAG3 and an associated analysis of the corresponding age- and gender-specific excess lifetime risk. Overall, the radiation risk associated with the ^{99m}Tc-MAG3 scans is low if the injected activity follows international recommendations.

EP-0043
Effective dose of for medical workers during Y 90 microspheres radioemblization

K. Dalianis[1], F. Vlachou[2], R. Eftymiadou[3], T. Pipikos[2], J. Andreou[3], G. Kollias[1], V. Prassopoulos[2]; [1]Medical Physics Department, Hygeia SA, Marousi, GREECE, [2]Nuclear Medicine & PET/CT Department, Hygeia SA, Marousi, GREECE, [3]PET/CT Department, Hygeia SA, Marousi, GREECE.

Introduction Due to the increasing need for radioemblization of liver cancer with Yttrium 90 microspheres a new need for evaluation of the radiation exposure of the medical staff is necessary. The objective of this study is to assess occupational exposure for nuclear medicine, radiology and clinical staff involved in Y^{90} preparation and implantation. Although there are guidelines and regulation regarding the use of radioisotopes for therapy when a new teaqnic is used for first time new measurements should be perform in order to reduce the occupational radiation doses to the workers. Material & Method To estimate the effective dose from external exposure the nuclear medicine physician and the medical physicist had electronic dosimeters and TLD badges worn at the upper pocket of their overall, TLD rings on the second finger of each hand. The basics stages for radioemblization procedures involve 3 steps: measuring the Y-90 vial, segmentation of the dose, transport to radiology, implantation of the radiopharmaceutical. Results The results of our study for the average cumulative whole body dose for 22 patients (μSv±SD) at different stages were: measuring the Y-90 vial, segmentation of the dose, transport to radiology, 132±7,23 (Medical Physicist) , implantation of the radiopharmaceutical 197±6,67 (Nuclear Medicine Physician) . The mean finger exposures for the Medical Physicist were 132±76 μSv/GBq. For administration of resin microspheres, mean finger exposures for the Nuclear Medicine Physician were 197.5±90 μSv/GBq. Conclusion Medical staff performing radioembolization procedures is exposed to safe levels of radiation. The personnel dose results are significantly lower than the recommended annual dose by International Commission for Radiological Protection. However a greater effort should be made to reduce the doses further in line with the ALARA principle.

EP-0044
Radiation exposure to Allied Health personnel handling blood specimens from patients receiving radioactive iodine-131 and recombinant human TSH stimulation

K. Loke; Singapore General Hospital, Singapore, SINGAPORE.

Aim: To demonstrate that radiation exposure to allied health personnel (phlebotomist, nurse and pathologist) who handle blood specimens from and interact with post thyroidectomy patients who have recently received oral radioactive iodine therapy after Thyrogen for adjuvant treatment of thyroid carcinoma received radiation absorbed doses which are safe and within acceptable annual limits. **Materials and Method:** 30 consecutive patients who had thyroidectomy for differentiated thyroid carcinoma either recently (within 4 weeks) or in the past received thyrogen stimulation prior to radioactive I-131 therapy (30 to 200mCi). A designated nursing/medical personnel would collect the blood specimen for stimulated serum thyroglobulin and anti-thyroglobulin levels. Blood extraction was performed at 72 hours after the last injection of Thyrogen as per ATA guidelines and Thyrogen product information leaflet. The duration of the procedure and radiation exposure of the staff was recorded by way of personal dosimeter. Background radiation corrected readings were taken at varying distances from both the patient and the blood specimen to simulate the average handling distances in normal working conditions for nursing/medical personnel as well as laboratory staff in the pathology department. **Results:** In the patients whom we had collected all data, the average time for venepuncture and specimen collection was 3.6 mins. The average radiation exposure of the staff involved was 7.15microSv (range of 0 to 9microSv). Average radiation readings of the blood specimen tube at 10cm and 50cm simulating the laboratory pathologists hands and body were 0.526 and 0.319 microSv/hr respectively. **Conclusions:** Our small study showed that in patients who received Thyrogen stimulation and radioactive iodine, the average radiation exposure of nursing and medical staff who come into contact with the patient and the rate of radiation exposure to the laboratory staff who handle the radioactive blood specimen tube are very low and are safely within the annual radiation limits for non-radiation workers.

EP-0045
Occupational exposure for eye, thyroid and gonads to medical workers operating in a PET/CT facility

K. Dalianis[1], F. Vlachou[2], R. Eftymiadou[3], T. Pipikos[2], J. Andreou[3], G. Kollias[1], V. Prassopoulos[2]; [1]Medical Physics Department, Hygeia SA, Marousi, GREECE, [2]Nuclear Medicine & PET/CT Department, Hygeia SA, Marousi, GREECE, [3]PET/CT Department, Hygeia SA, Marousi, GREECE.

Purpose: Personnel monitoring results provide information on routine radiation exposure, assist in work planning and allow control of the workplace. The aim of this study was to measure the gamma dose received by dedicated medical workers operating in our PET/CT department to eye, thyroid and gonads. PET/CT studies are restricted to the use of F-18 FDG, FLT and FCH are used in our center. **Method:** To estimate the effective dose from external exposure, all 6 members of the staff (2 nurses, 2 medical physicists, 2 technologists) had TLD badges worn at plastic glasses, on the region of gonads and in front of the thyroid area. High sensitivity thermolumiscent dosimeters were

used. The measurements that were made at all stages of the PET/CT procedure: dose segmentation, injection of the radiopharmaceutical, handling the patient and positioning the patient. **Results:** Results show that the mean daily effective dose (µSv±SD) received by each member of the staff for eye were: Nurse1 13.4±5,2, Nurse2 12.19±3,2, technologist1 11.52±4, technologist2 12.10±2,3, Medical Physicist1 9,95±2,1, Medical Physicist2 8,72±3,2. The mean daily effective dose (µSv±SD) received by each member of the staff for thyroid were: Nurse1 12.46±4,4, Nurse2 12.32±3,7, technologist1 11.63±2,5, technologist2 12.44±2,4, Medical Physicist1 8,98±3,91, Medical Physicist2 8,23±2,85. Finally the mean daily effective dose (µSv±SD) received by each member of the staff for gonads were: Nurse1 11.98±3,9, Nurse2 10.26±2,3, technologist1 8.26±1,6, technologist2 11.49±3, Medical Physicist1 7,65±3,6, Medical Physicist2 7,12±2,92 **Conclusions:** From our results we can observe that the numbers are significantly lower than the recommended annual dose limit

EP-0046

Automatic CT Dose Collection Software (OpenREM) for CT Dose Audits in PET/CT and SPECT/CT

T. Sanderson, J. Dickson; University College London Hospital, London, UNITED KINGDOM.

Introduction: There is a responsibility to optimise radiation doses from CT imaging, including for the relatively low doses received in hybrid nuclear medicine. Following a recent IPEM audit of hybrid imaging CT doses in the UK, recommended Diagnostic Reference Levels (DRLs) have been proposed for PET/CT and SPECT/CT examinations [1]. In this paper we describe how a local audit of hybrid CT doses was performed using automatic CT Dose collection software to aid the optimisation of our CT exposures in PET/CT and SPECT/CT. **Methods:** CT dose data was collected using the free, open source software OpenREM (available online at *openrem.org*). OpenREM receives Radiation Dose Structured Reports directly from scanners using an inbuilt DICOM store, automatically extracts dose information into a searchable database, and produces tables and graphs. Data was collected from all CT scans performed on a PET/CT scanner and two SPECT/CT scanners over 13 months. Data was then analysed for all protocols with at least 30 adult scans during this period. This included 5 of the 6 protocols for which IPEM has recommended DRLs (WB PET/CT (n=1428), Bone SPECT/CT (n=985), Cardiac PET/CT (n=257), Parathyroid SPECT/CT (n=74), Thyroid post-ablation SPECT/CT (n=73)) and 4 additional protocols (Brain SPECT/CT (n=362), Lung VQ SPECT/CT (n=68), Brain PET/CT (n=34), and Penile SLN SPECT/CT (n=30)). **Results:** Our local CT doses were generally higher than IPEM recommended DRLs. For Bone SPECT/CT our mean and 75th percentile Dose Length Product (DLP) were 285 and 384 mGy.cm respectively, compared to a 75th percentile DRL of 180 mGy.cm. Additionally for WB PET/CT the mean and 75th percentile Dose Length Product (DLP) were 467 and 583 mGy.cm respectively, compared to a DRL of 400 mGy.cm. While for Bone SPECT/CT our local demands for high CT image quality justify the need for higher dos-

es, mA modulation factors for WB PET/CT have been adjusted to bring us within the national DRL (mean, and 75th percentile (DLP) of 328 and 386 mGy.cm respectively (n=270)) whilst maintaining acceptable image quality. **Conclusions:** OpenREM is a useful tool for automatically collecting and analysing CT dose information, and it has been used to audit CT doses in PET/CT and SPECT/CT. Using this software we have been able to optimise our hybrid imaging doses. [1] Burniston M, IPEM working party recommendations on hybrid CT DRLs, Nuclear Medicine Communications: May 2016 Volume 37 Issue 5

EP-0047

Area Monitoring in Radionuclide Treatment Ward, Surrounding Areas, and Radiation Exposure to Family Caregiver in Paediatric Patient Receiving High Dose[131]Iodine-MIBG

K. Chuamsaamarkkee[1], N. Kumwang[2], S. Monthonwattana[2], W. Changmuang[1], K. Thongklam[1], P. Charoenphun[1], A. Kositwattanarerk[1], Y. Anongpornjossakul[1], W. Chamroonrat, C. Sritara[1]; [1]Ramathibodi Hospital, Mahidol University, Bangkok, THAILAND, [2]Thailand Institute of Nuclear Technology (Public Organisation), Nakhonnayok, THAILAND.

Background: ^{131}I-metaiodobenzylguanidine (MIBG) offers an effectively targeted radionuclide therapy in paediatric patients. According to radiation protection authority in our country, the patient treated with high-dose (> 1100 MBq) radioiodine is recommended to stay in the hospital. However, unlike the adult, the paediatric patient needs exclusively supports and cares by their family caregiver, and there is difficulty to control paediatric patients to stay behind the lead shielding all the times. Therefore, this study aims to measure the radiation exposure to the family caregiver in paediatric patients receiving high dose[131]I-MIBG. Also, this study intends to measure the radiation exposure in radionuclide isolated treatment room within general paediatric ward and surrounding areas by using OSL (optically stimulated luminescence) to ensure that it is safe to other paediatric patients and their relatives. **Methods:** Environmental OSL monitoring devices (InLight®, Al_2O_3:C) were prepared and calibrated by Thailand Institute of Nuclear Technology (TINT). Twenty-five set of OSLs were placed in and surrounded the treatment room for 24 h which was included radiotracer administration process. Dose to family caregiver was recorded by digital semiconductor dosimeter (ALOKA PDM-112) also calibrated by TINT. The measurement was carried for four paediatric patients treated with ^{131}I-MIBG (activity 3700 - 5500 MBq). **Results:** The ambient doses equivalent at 10 mm depth (H*(10)) and the dose rate were analysed, the limit of 10 and 0.5 µSv/h are accepted for radiation worker and member of the public. The dose rate around the patient bed and toilet were high as expected. Dose rates at the wall of adjacent room and corridor were slightly greater than the public limit (range 1.82 to 4.48 µSv/h). Remarkably, the dose rates at caregiver chair (outside the shielding) were exceeded the limits (30.57 ± 5.69 µSv/h). Consequently, this was correlated with high personal dose equivalent in soft tissue at 10 mm depth ($H_p(10)$) to fam-

ily caregivers which listed as 175, 1632, 6760 and 7433 μSv for the patient age of 15, 5, 1 and 1 Year respectively. **Conclusion:** These radiation monitoring data provided the important information to manage radiation protection and aware of radiation exposure in an adjacent room to minimize the exposure dose for the members of public and medical staffs in the paediatric ward. The radiation exposure to caregivers were associated with the patient age; hence, caregiver exposure for younger paediatric patient tends to receive higher as the patient may require more cares and supports.

EP-0048

Efficiency evaluation of Lead Rubber aprons in Nuclear medicine applications: an approach with Monte Carlo method

F. Di Matteo[1], **F. Zagni**[2], S. Vichi[1], G. Cicoria[2], D. Pancaldi[2], D. Mostacci[1], M. Marengo[2]; [1]Montecuccolino Nuclear Engineering Laboratory, Department of Industrial Engineering, University of Bologna, Bologna, ITALY, [2]Medical Physics Department, University Hospital "S.Orsola – Malpighi", Bologna, ITALY.

Aim: Lead aprons represent the most common individual protection devices used in diagnostic radiology to protect patients and staff from radiation. In Nuclear Medicine instead, the use of protective apparels like lead rubber aprons is widely discussed as regards the real effectiveness of these devices in this field. In this work we used Monte Carlo (MC) simulations to evaluate the efficiency of these devices in Nuclear Medicine applications. **Materials and Methods:** We developed an X-ray tube model using Fluka code to study lead rubber attenuation properties and lead equivalence for a thickness of 0.25 mm and 0.50 mm, according to the CEI-EN 61331-1 regulations. The main components and materials of the X-ray tube were included in the model and it was validated by comparing the output spectrum with SpekCalc, a program designed to calculate the X-ray emission for tungsten anode x-rays tubes. The equivalent thickness of lead rubber previously evaluated at 80 and 100 kV was than used in subsequent simulations as a shielding for the digital ICRP anthropomorphic human phanton. Different radionuclides were simulated, more precisely three unshielded point sources of ^{18}F, ^{131}I and ^{99m}Tc. In this way we studied the equivalent and effective dose reduction on the phantom due to the rubber shielding. **Results:** The validation of the X-ray tube model at 80 kV and 100 kV shows a perfect agreement between the MC and SpekCalc X-ray spectra. The lead equivalence shows that 0.25 mm and 0.5 mm Lead corresponds respectively to 2.5±0.1 and 5.0±0.1 mm of Lead-Rubber. In term of effective dose, the simulations on the phantom with the two thicknesses of lead rubber, showed a percentage reduction of 4.9 % and 10.3% for ^{18}F, 8.6% and 16.3% for ^{131}I and 40.2% and 65.7% for ^{99m}Tc. **Conclusion:** This work shows that in the case of ^{18}F and ^{131}I the effective dose reduction is almost negligible. For the ^{99m}Tc the dose reduction is higher. However, considering the real practice in Nuclear Medicine, it must be noted that the same dose reduction is easily achievable by increasing the distance according to the inverse-square law. Moreover an operator will tend to work at the right distance

from the source rather than wearing a lead rubber apron that is heavy and not much practical. In conclusion, because of the weight and the low attenuation properties, lead rubber aprons are unsuitable in Nuclear Medicine applications.

EP-0049

Ionising radiation exposure of children during the course of neuroblastoma or other oncological diseases due to diagnostic procedures- a preliminary report

J. Iwanowski, H. Piwowarska-Bilska, D. Skupiński, J. Peregud-Pogorzelski, A. Walecka, B. Birkenfeld; Pomeranian Medical University in Szczecin, Szczecin, POLAND.

Introduction: Diagnosis and follow-up of neuroblastoma among others is based on imaging studies in which patients are exposed to a certain dose of ionizing radiation. In the course of neuroblastoma physicians often recommend a multiple diagnostic CT and SPECT/CT or PET/ CT procedures. Recent radiobiological findings have shown that the tissues of infants and young children are more radiosensitive than the adult organs. The younger age the child is exposed to radiation, the more serious can be later biological effects. **Material:** The study comprised the group of 36 children diagnosed and treated with neuroblastoma or other oncological diseases in 2007-2016 at the Department of Paediatric Oncology. They had multiple CT and SECT/CT studies performed at the Department of Nuclear Medicine and the Department of Diagnostic Imaging and Interventional Radiology during the course of the diagnosis, treatment and follow-up. **Results** The group consisted of 22 boys and 14 girls aged from several months to 17 years. All the children had several whole body and SPECT/CT scintigraphy using I131- MIBG and CT scanning over years. Total number of examinations varied among children but the highest number of examinations employing ionizing radiation per year was observed in a 7-year-old girl - it was three I131-MIBG scintigrams and eleven CT scans. The total effective dose received by individual children during the course of treatment and follow-up varied strongly and ranged from about 30 to 500 mSv. **Conclusions:** 1. Children with neuroblastoma can be exposed to significant doses of ionizing radiation over the entire diagnostic, treatment and follow-up period. 2. Physicians who refer children with oncological diseases for imaging studies using ionizing radiation should know the patient ionising radiation exposure history. 3. In paediatric patients who received a significant radiation effective dose the possibility of further imaging with MRI or US techniques should be considered. Table 1. Effective doses received by children from whole body and SPECT/CT scintigraphy using I131- MIBG and CT scanning (NM -Nuclear Medicine, CT - Computed Tomography).

EP-0050

Dose rates from diagnostic nuclear medicine patients

V. de Sousa[1], G. Cardoso[1], A. I. Santos[1,2]; [1]Serviço de Medicina Nuclear – Hospital Garcia de Orta, Almada, PORTUGAL, [2]Nova Medical School – Universidade Nova de Lisboa, Lisboa, PORTUGAL.

Purpose/Introduction: Nuclear Medicine (NM) patients are a source of ionising radiation to the general public. The aim of this work is to evaluate the dose rate emitted by the patient when leaving the department. **Subject & Methods:** Two diagnostic exams were considered, Myocardial Perfusion Scintigraphy (MPS) - rest/stress - (^{99m}Tc-Sestamibi) and Renograms (^{99m}Tc-MAG3). Dose rate measurements were performed with a portable dose rate monitor, during one minute, at a distance of 1 meter of the patient, throughout their stay in the department and immediately before they left it. Twenty-seven patients undergoing MPS and 11 patients undergoing Renograms were evaluated. Regarding MPS, only patients undergoing a two-day study protocol were considered. Gender, weight and administered activity were collected. The dose rate values measured immediately before the patient left the department were compared to a recommended dose limit from U.S.NRC Regulatory Guide 8.39 for the release of a patient undergoing diagnostic nuclear medicine procedures. **Results:** The sample of MPS comprised 11 women (mean weight 68.18 kg) and 10 men (mean weight 80.40 kg), with an average administered activity of 755.81 MBq (standard deviation 1.04 MBq) and 799.94 MBq (standard deviation 1.28 MBq), respectively. The Renogram sample consisted of 5 women (mean weight 67.60 kg) and 6 men (mean weight 73.50 kg), with an average administered activity of 127.21 MBq (standard deviation 0.29 MBq) and 128.58 MBq (standard deviation 0.24 MBq), respectively. Considering MPS procedures, the mean dose rate recorded immediately before the patient left the department was 3.91 µSv/h (for the female group) and 4.28 µSv/h (for the male group). While for the Renograms, the average of dose rates were 0.51 µSv/h and 0.57 µSv/h, for female and male group, respectively. It was also verified that between the first and the last dose rate measurements there was a mean reduction of 24.24% and 21.04% for the female and male patients undergoing MPS procedures, respectively. For Renograms, the mean reduction was 54.05% and 46.09% for the female and male patients, respectively. **Discussion/Conclusion:** It was verified that none of the values measured before the patient left the department exceeded the limit of 0.58 mSv/h established by U.S.NRC. On the other hand, it was also possible to note that in the case of patients submitted to Renograms, to whom bladder emptying is requested during the stay in the department, there is a more pronounced dose rate reduction over time.

EP-0051

Personnel dose saving in dispensing of beta emitters-labelled radiopharmaceuticals using automatic device

F. Fioroni[1], E. Grassi[1], M. Asti[2], C. Benini[3], G. Guidi[3], A. Versari[2], M. Iori[1]; [1]Medical Physics Unit, Arcispedale Santa Maria Nuova - IRCCS, Reggio Emilia, ITALY, [2]Nuclear Medicine Unit, Arcispedale Santa Maria Nuova - IRCCS, Reggio Emilia, ITALY, [3]Comecer SpA, Castel Bolognese (RA), ITALY.

Aim: The use of beta emitters-labelled radiopharmaceuticals has been one of the most interesting therapeutic applications adopted in nuclear medicine in recent years. When handling unsealed radiation sources, considering the physical characteristics of beta emitters, the skin of the hands is the organ most at risk and the corresponding annual dose limit of 500 mSv might be exceeded. The aim of this work was to evaluate the equivalent dose saving of the staff involved in ^{90}Y/^{177}Lu-labelled radiopharmaceuticals synthesis and fractionation, using an automatic dispensing system (Febo-Comecer). **Materials and Methods:** Febo is a dispenser for safe and accurate fractionation of radiopharmaceuticals. Before the clinical use, it was properly calibrated to guarantee correct measures of beta-pure emitters, taking into account the large dependence on geometry, volume and amount of radioactivity. Personal dose measurements were carried out with a series of thin active layer ultrasensitive dosimeters fixed at the operator's fingertips to evaluate the skin equivalent dose, replaced after each procedure. Shielded aprons and anti-X gloves were used. The staff wore also direct reading personal devices to monitor the external radiation exposure during labelling and dispensing. The analysis was carried out through the comparison of the data collected in 90 procedures. The mean handled activity was 36.01 GBq (^{177}Lu) and 11.84 GBq (^{90}Y). **Results:** The fingertip dosimetric data were normalized to the activity used in each procedure to enable a comparison between the different sessions and the different equipment used. For the chemist, the mean values (95th percentile) of Hp(0.07) before and after Febo introduction were respectively 0.021 (0.096) and 0.014 (0.045) mSv/GBq. The multivariate analysis of covariance was applied to evaluate the impact of Febo use on staff doses. Collected data showed a reduction in the skin-equivalent dose ($P<0.05$). Mean personal body equivalent doses absorbed by the chemists before and after Febo introduction were 2.1 µSv (range: 0-21 µSv) and 1.8 µSv (range: 0-28 µSv) in terms of Hp(10) respectively, and 8.9 µSv (range: 0-39 µSv) and 5.4 µSv (range: 0-35 µSv) in terms of Hp(0.07) respectively. **Conclusion:** Febo positively affects the dose saving of the chemists in handling beta emitters-labelled radiopharmaceuticals. Exposure of the hands of nuclear medicine staff to radiation needs to be addresses, particularly when handling high-energy β-emitter. The use of appropriate devices and procedures allow staff skin dose to be limited.

EP-0052

Belgian Diagnostic Reference Levels for Radiopharmaceuticals in Daily Practice

T. Vanaudenhove[1], M. Vandecapelle[1], F. Jamar[2], G. Moulin-Romsee[3], R. Hustinx[4], B. Dehaes[5], K. Bacher[6], A. Fremout[1]; [1]Federal Agency for Nuclear Control, Brussels, BELGIUM, [2]Cliniques universitaires Saint-Luc, UCL, Brussels, BELGIUM, [3]Sint-Andries ziekenhuis, Tielt, BELGIUM, [4]Centre Hospitalier Universitaire de Liège, Liège, BELGIUM, [5]Ziekenhuis Oost-Limburg, Genk, BELGIUM, [6]Ghent University, Ghent, BELGIUM.

Aim: To analyze the distribution of activity administered to patients in Belgian nuclear medicine (NM) departments and determine national diagnostic reference levels (DRLs) for typical scintigraphy procedures and radiopharmaceuticals used in daily practice. **Materials and Methods:** Since the 1st of January

2015, all NM departments in Belgium register their values of administered activity for one specific diagnostic procedure either during 3 months or for 30 patients. These data are collected by the Federal Agency for Nuclear Control (FANC) and used to determine the national DRL for that specific diagnostic procedure. This value is compared to national and international recommendations. If adequate, the DRLs are also calculated as a function of the patient's weight. First and third quartiles are computed and used to determine the relative position of an individual department. Belgian DRLs are determined as mean activity for an adult of 70 kg. So far, distributions of the administered activities and DRLs have been determined for eight diagnostic procedures concerning adult imaging : bone scintigraphy (^{99m}Tc-phosphates), myocardial perfusion scintigraphy (^{99m}Tc-radiopharmaceuticals - single injection, one-day and two-day protocols - and ^{201}Tl-chloride), thyroid scintigraphy (^{99m}Tc-pertechnetate and ^{123}I-NaI), pulmonary perfusion scintigraphy (^{99m}Tc-MAA), PET-scan (^{18}F-FDG), cerebral blood flow (^{99m}Tc-HMPAO and ECD), renography (^{99m}Tc-MAG3 and DTPA) and renal cortical scintigraphy (^{99m}Tc-DMSA), and gastric emptying (^{99m}Tc labelled compounds). One survey was dedicated to four pediatric procedures: bone imaging, renal scintigraphy, gastroesophageal reflux and PET-scan. **Results:** Most of the Belgian DRLs are within 10% deviation from national recommendations, indicating good compliance to them, with the exception of thyroid scintigraphy with ^{99m}Tc-pertechnetate, pulmonary perfusion with ^{99m}Tc-MAA, and renography with ^{99m}Tc-MAG3. The DRLs are also in concordance with international guidelines. A roughly linear increase of the mean and quartiles was observed in function of the patient's weight for the bone, myocardial perfusion and PET-procedures with no relationship to body weight for the others. For children, the administered activities are globally close to those recommended by the EANM dosage card. **Conclusion:** Thanks to the large participation (close to 100% for all procedures), the determined DRLs are representative of the Belgian situation. In order to optimize the administered activities in daily practice, every single NM department in Belgium receives elaborate feedback on the national and on their individual situation compared to the general one. This enables them, where needed, to take corrective actions and adapt their administered activities conform to the national and international guidelines.

EP-0053

Exposure of eye lens as a possible limiting factor?

J. Hudzietzova[1], M. Fülöp[2], J. Sabol[3], J. Doležal[4], P. Povinec[5], D. Baček[5], D. Solivajs[6], Z. Zelenka[7]; [1]Faculty of Biomedical Engineering CTU in Prague, Kladno, CZECH REPUBLIC, [2]Slovak Medical University, Bratislava, SLOVAKIA, [3]Faculty of Safety Management of PACR, Prague, CZECH REPUBLIC, [4]Department of Nuclear Medicine,University Hospital, Hradec Králové, CZECH REPUBLIC, [5]Nuclear Medicine Clinic, BIONT, Bratislava, SLOVAKIA, [6]Slovak Legal Metrology, Bratislava, SLOVAKIA, [7]NUVIA Dosimetry, s.r.o., Prague, CZECH REPUBLIC.

Purpose: The aim of the paper is to evaluate whether eye lens can present a limiting organ in nuclear medicine during some selected risky procedures. **Subjects and Methods:** The eye lens measurement was performed at selected PET departments. Workers wore specially modified glasses with TLDs for monitoring $H_p(3)$. The TLDs were placed at positions corresponding to three well-known eye lens exposure monitoring configurations. 5 MCP-7 dosimeters were placed 2.5 cm above the right and left eye lenses, on the outside corners of the eyes, and between the eyes at the root of the nose, where a MCP-Ns dosimeter was also placed to control the presence of positrons in the radiation field. The workers wore glasses only during the preparation and administration of radiopharmaceuticals labelled with ^{18}F and ^{11}C. Currently, the eye lens exposure is routinely controlled based on monitoring $H_p(10)$, $H_p(3)$ and $H_p(0.07)$ on the chest, so besides the glasses with TLDs, each monitored person was also equipped with an additional personal dosimeter, worn only with the above mentioned glasses. Each worker was monitored for a time during which $H_p(10)$ was in the range of 50 - 100 µSv. During the monitoring of workers video shots of individual activities were taken. It has been performed experimental as well as Monte Carlo (MC) simulations of risk procedures where the exposure of the eye lens may be higher than the exposure of the monitors placed on the chest (e.g., during the manipulation with unshielded syringe near to the eyes, administration of radiopharmaceuticals while in the bow). **Results:** Based on present measured data (workplace experiments are still going on), it can be seen that exposure of the right and left eye lenses is similar. In contrast to local hand exposure, exposure of the eye lens appears to be lower during the same manipulations involving ^{18}F application. This will be verified for radiopharmaceuticals labelled with ^{11}C emitting more energetic positrons than ^{18}F. Based on the MC simulation it was found that during the manipulation with unshielded radionuclide ^{11}C the eye lens may be exposed with positrons. **Conclusion:** Three systems of monitoring eye lens were experimentally compared. Place the dosimeter on the root of the nose appears as the most practical system. Experimental measurements continue at department with radiopharmaceutical labelled with ^{11}C, where it is necessary to verify the irradiation of eyes lens of the positrons. **Acknowledgment:** The work was supported by project SGS17/113/OHK4/1T/17.

EP-0054

Radiation Protection and Dosimetry for worker used 18F-FDG

H. M. Yassin[1], M. S. El-Nagdy[2], A. Wabdan[2]; [1]Cairo Univeristy, Cairo, EGYPT, [2]Helwan Univeristy, Cairo, EGYPT.

Introduction: Positron Emission Tomography (PET) is acquiring explosive growth due to its ability to accurately detect and stage many types of cancer and follow the progress of treatments. An increasing demand for use of 18F-FDG PET in oncology has been the main reason for its growth. The physical characteristics of positron emissions result in higher radiation risk for staff and growing use of PET/CT for diagnostic purposes increase radiation exposure. An understanding of the radiation protection and safety issues are very important

to keep clinical and occupational exposure as low as reasonably achievable (ALARA). **Method:** In the present study we investigated radiation doses to the PET staff. The whole-body doses received by physicist, technician and nurses were measured by dosimeter and the finger doses by ring dosimeter during a period of 3 months. **Result:** In 42 PET/CT studies, the mean whole-body dose per study to physicist, technician and nurses were 1.85±0.17, 2.35±0.59, 1.08 µSv, respectively. The mean finger doses per study received by physicist, technician and nurses were 290.65±56.12, 55.13±2.8 and 29.57±6.05 µSv, respectively. The average time in contact with 18F-FDG was 9.70±0.09, 47.07±2.03 and 2.19±0.44 minutes per study for physicist, technician and nurses respectively. Technician received highest mean effective whole body dose per study and physicist received the highest finger dose per study. Radiation doses measured by thermo luminescent dosimeters (TLD) for staff working in PET. **Conclusion:** it is found that the radiation exposure of PET technicians was higher than that physicist working conventional general nuclear medicine studies at the beginning. After implementing radiation protection measures and procedures, PET technicians doses significantly reduced. Since high energy photons of positron emitters, facility design for radiation protection, including shielding, containments of sources, strict radiation protection measures should be implemented to working environment design.

EP-0055

Estimation of Organ and Effective Doses for CT Scan During Whole Body PET/CT examination

L. Chipiga[1,2], *V. Golikov*[1], *C. Bernhardsson*[3]; [1]*Institute of Radiation Hygiene after Prof. P.V. Ramzaev, St. Petersburg, RUSSIAN FEDERATION,* [2]*Federal Almazov North-West Medical Research Centre, St. Petersburg, RUSSIAN FEDERATION,* [3]*Scane University Hospital, Malmo, SWEDEN.*

The aim of this study was to compare organ and effective doses during whole body CT examinations measured with physical pediatric and adult phantoms with doses calculated by software programs and to estimate the values of conversion coefficients from dose length product (DLP) to effective dose for whole body CT examinations based on the results of measurements. **Material and Methods:** In order to measure organ doses TL detectors were positioned into the 1-year-old, 5-years-old and adult ATOM series phantoms. For calculation organ and effective doses were used the following dedicated software: CT-Expo 2.3.1, VirtualDose™CT and NCICT beta version 1.00. The CT protocols applied were the same as clinically used for patients undergoing whole body PET/CT examinations. **Results and Discussion:** The results of whole body irradiation during the CT examination are shown that the relative differences of doses for the majority of organs in different phantoms were within 15%, exception is the organs with different positions in phantoms. Therefore, an accuracy of organ dose estimation for individual patient is achieved 15%, additional uncertainty of patient organ dose estimation is defended from body size. The direct measurements of doses using physical phantom is the most, time-consuming

and expensive method and unusable in routine clinical practice. Using this method increases the uncertainties connected with different size of patients and human factor. The software is more convenient to use, cheaper compared to TLDs, manufacture-protocol specific and is potentially more flexible to adjust the phantom dimensions to meet that of a specific group of patients. Based on the effective doses estimated with TLDs, conversion coefficients from DLP to E for whole body CT scans have been established according to ICRP Publication 60 and ICRP Publication 103 that were 0,036 mSv/(mGy·cm) for 1-year-old phantom; 0,030 mSv/(mGy·cm) for 5-years-old phantom; 0,017 mSv/(mGy·cm) for adult phantom. **Conclusions:** Overall good agreement was observed by the different methods investigated and the results show that all these methods are suitable for estimation of effective dose during whole body CT scans. Although, the dimension and geometry of the phantoms, the size and location of the organs as well as the position for TLD inserts in the organs have a significant impact on the resulting doses. Based on the effective doses estimated with TLDs, conversion coefficients from DLP to E for whole body CT scans have been established.

EP-0056

Effects of Nanoparticle and Radiation Doses on Red Blood Cells

J. Lee, *M. Hur, S. Yang, J. Park; korea atomic energy research institute, Jeollabuk-do Jeongeup-si, KOREA, REPUBLIC OF.*

Aim: Radioisotope-incorporated nanoparticles have been used for several applications including but not limited to drug delivery, biodistribution, biological circulation half-life and pharmacokinetics. However, red blood cells (RBCs) can be damaged by nanoparticles (NPs) and radiations. The damage is correlated with the dose and the concentration of the nanoparticles used. Studies carried out so far seem to be insufficient and further research on radiolytic stability and effect of nanoparticle concentrations on RBCs is needed. Thus, to fulfill the scientific curiosity we evaluated the hemolysis of RBCs as the function of radiation dose and concentration of nanoparticles. **Materials and Methods:** RBC Isolation Blood collection was carried out using K2 EDTA sample collection tubes to avoid the calcium depletion. 1 mL of isolated RBCs were washed thoroughly using 1 mL of ice cooled 1xPBS (pH 7.4). RBC suspensions were centrifuged at 1500 rpm for 20 min and supernatant was discarded. Nanoparticle and Radiation Stress Evaluation Nanoparticle and radiation stress on RBCs were assayed in the presence of an anticoagulant using silica nanoparticles applying various radiation doses of ^{68}Ga. Varying ratios of RBC-NPs and RBC-NP-^{68}Ga with 1 % hematocrit were agitated (24 rpm) for 2 hours at 37 ^{0}C. The hemoglobin released from the RBCs during assay time was measured by UV-Vis. The hemolysis % of RBC was calculated as: (Absorbance of sample-Absorbance of negative control)/(Absorbance of positive control-Absorbance of negative control)x100% **Results and Conclusion:** Through 2 hours of incubation, radiation and mechanical stress caused hemolysis

of 15% and 29%, respectively. These results are close to that of hemolytic level of normal RBCs and were comparable with the morphological appearance of the normal RBC. Hemolysis was observed in RBCs adsorbing more than 1 mg of nanoparticles. In this study, we were able to optimize the amount that can reduce the damage by nanoparticles to RBCs, and it was observed that when the RBCs were exposed to the optimized concentration of nanoparticles and radiations, the hemolysis was negligible. This study will help us in understanding the administration of nanoparticle quantities and radiation dose causing the optimal damage in the biological systems.

EP-0057
Patient release after Lu-177 DOTATATE and Lu-177 PSMA 617 therapies

C. Mair, B. Warwitz, S. Buxbaum, I. J. Virgolini; LKH Universitätskliniken Innsbruck, Univ.-Klinik für Nuklearmedizin, Innsbruck, AUSTRIA.

Aim of the study: As TRTs are gaining importance in palliative treatment of patients suffering from neuroendocrine tumors as well as castration resistant prostate cancer, radiation protection for patients, staff, family members and general public is of increasing interest and has to be taken into account as well. In this study we want to define guidelines for patient release according to our national radiation safety law and Austrian Standards in radiation protection. **Materials and Methods:** We have been calculating patient doses based on the MIRD principle at our institute for over a decade. Planar whole body images are recorded at different time points after injection of the radiopharmaceutical. These scans with anterior and posterior projection respectively are performed at approximately 0.5, 4, 24, 72 and 96 hours p.i. Residence times out of the respective time-activity-curves are calculated subsequently based on the conjugated view method. Residence times for critical organs are fed into the commercial OLINDA software to calculate organ doses. The doses of tumors and salivary glands are calculated via their self-irradiation by approximation with spheres of equivalent volume. Kidney volumes are gained by organ segmentation, volumes of all other organs are estimated by means of OLINDA and BMI corrected. **Results:** Patient dosimetry is performed individually alongside the first therapy cycle of every patient, since the specification of the illness, tumor load and metabolism - among other parameters - differ from one patient to another. Nevertheless it has been tried to calculate reference points for patient release out of the whole-body curves. Therefore 40 patients with NETs and 20 patients with CRPCs have been evaluated and mean values as well as standard deviations calculated. In pateints with NETs the variation is much smaller, which allows for a reasonable prediction of release dates, the latter not only being crucial for radiation protection, but also making therapy planning much easier. The situation looks a little different for PSMA therapies, where the variation is much larger due to different tumor loads as well as heavy pre-treatment with established therapies, due to which critical organs like kidneys may have already been damaged. **Conclusion:** While patient release for Lu-177 DOTATATE is quite well predictable, further studies

have to be carried out in the case of Lu-177 PSMA for a better understanding of the effects of pre-treatment.

EP-0058
Radiation dose rates of post Y90 therapy patients - Is it safe to nurse or visit them?

M. Tong, H. Cheng, J. M. Lara; National University Hospital, Singapore, SINGAPORE.

Purpose/Introduction: Y90 treatment involves the administration of radioactive Y90 resin microspheres to the liver. Y90 is a pure beta-emitter with a physical half-life of 64.2 hours, 0.94 MeV decay energy, and an average penetrative depth of 2.4mm in human tissue. The patients are administered with a mean activity of 0.92 Gbq ($\pm$ 0.42). After treatment, the patients become a radiation source/concern mainly to the nurses during the hospital stay, and to visiting family members. The study strives to explore if the concerns are warranted. **Methods:** The external radiation exposure rates of 30 patients were measured using a calibrated ionization survey meter. The measurements were taken at 1 meter, 2 meters, and 3 meters from the patients' supine body axis (liver to pelvis), immediately post therapy, and at 24 hours and 48 hours. Urinary excretions in 8 patients were also measured to estimate the potential risk from the discharge into the sewage system. **Results:** Dose rates of 16.6 ($\pm$ 1.3), 8.5 (+ 1.2), and 1.1 (+ 1.1) μSv/hr were measured at 1, 2, and 3 meters respectively immediately post therapy. All patients had exposure rates below 1 μSv/hr by 24 hours at 1 meter from the liver. The urinary bag had a maximum dose rate recorded at 1.2 μSv/hr at 6 hours post therapy. The conservative assumption of a nursing staff or family member at an interaction distance of 1 meter from a patient at these dose rates for a continuous 6 hours based on the measurements is less than 0.1 mSv of radiation dose exposure, with decay taken into consideration. Mean TEDE dose was 0.04 mSv. **Discussion and Conclusion:** The dose exposure from Y90 microsphere administered patients is very low, with the beta dose delivery mainly confined to the liver. There is minimal biologic elimination of Y90 from the patient's bodies, with only trace amounts detected.

EP-0059
Justification of New Radiofarmaceuticals and Methods in Nuclear Medicine

A. Andersen, Sr.; Norwegian Radiation Protection Authority, Østerås, NORWAY.

Aim: Medical radiation exposure is an essential tool in diagnosis and treatment of different conditions and diseases. However, ionizing radiation is associated with cancer induction and in some cases, acute tissue reactions. New methods in nuclear medicine, some with new radiopharmaceuticals, are continuously under development. To ensure safe introduction of new methods in nuclear medicine, it is important to properly address and evaluate the radiation detriment associated with medical radiation exposure. This risk/benefit evaluation is the rationale behind the

requirement for generic justification of medical radiation exposure in the international and European Basic Safety Standards (BSS) on radiation protection. The Nordic radiation protection authorities recommend integrating this risk/benefit evaluation into established methods for assessments of new health technologies as an approach to strengthen the generic justification process. **Material and Methods:** In Norway, The National System for Managed Introduction of New Health Technologies within the Specialist Health Service in Norway was launched in 2013. Systematic use of health technology assessments (HTA) to inform decision-making was the main ambition behind the establishment. The aim of this system is to: •improve patient safety •ensure that patients gain equal access quickly to new methods that have proved to be effective and fulfill safety and cost-effective requirements •provide an appropriate decision-making platform for priority setting based on HTAs •ensure rational use of resources •establish a systematic and predictable process for the introduction of new methods. **Results:** The Norwegian Radiation Protection Authorities became a part of this national system in 2014, having the following role: •Ensure that radiation assessments are taken into account in the generic evaluation of new methods involving medical radiation exposure. •Contribute to rapid and full HTA that involves medical radiation exposure. The main advantage is that the radiation detriment is part of the total assessment and decision making process and not evaluated in a separate and isolated system. So far, two relevant methods has been evaluated (one ongoing) in the system: •Ra-223 (Xofigo) for treatment of castration resistant metastatic prostate cancer (mCRPC) (with progression on docetaxel) •177Lu- DOTA0-Tyr3-Oktreotat (Lutathera; lutetium-177) for treatment of inoperable gastroenteropancreatic neuroendocrine tumors. **Conclusion:** HTA is recognized as a valuable tool in promoting generic justification of medical radiation exposure. A close cooperation between national radiation protection authorities and relevant national bodies, like competent HTA bodies, is essential to succeed with the development of this approach.

Physics & Instrumentation & Data Analysis: Quality Control, Performance and Standardisation

EP-0060

Optimizing Administered Ga-68-DOTATOC Activity for PET Imaging

D. Koopman[1,2], W. A. Noortman[1,2], P. L. Jager[1], N. Schreuder[3], C. H. Slump[2], J. A. van Dalen[4]; [1]Isala, Department of Nuclear Medicine, Zwolle, NETHERLANDS, [2]MIRA Institute for Biomedical Technology and Technical Medicine, University of Twente, Enschede, NETHERLANDS, [3]GE Healthcare Radiofarmacy, Zwolle, NETHERLANDS, [4]Isala, Department of Medical Physics, Zwolle, NETHERLANDS.

Introduction: The EANM procedure guidelines for PET/CT tumour imaging with Ga-68-octreotide analogues (DOTA-conjugated peptides) recommend an administrated Ga-68 activity of 100 to 200 MBq, depending on the characteristics of the PET device. These guidelines do not take into account the impact of patient's size on the image quality of Ga-68-DOTA PET scans. However, when using a fixed activity, a degraded image quality can be expected for obese patients due to enhanced photon attenuation. Our aim was to assess an optimized relation between Ga-68-conjugated-edotreotide (DOTATOC) activity and patient's size, to provide PET images with constant quality across patients. **Subjects & Methods:** We evaluated Ga-68-DOTATOC PET studies from 25 patients on a state-of-the-art PET/CT scanner (Ingenuity TF, Philips). For each patient, a PET scan was acquired 60 minutes after intravenous administration of 150 MBq Ga-68-DOTATOC, using a fixed scan duration of 4 minutes per bed position. Images were reconstructed using a 3D List-mode Ordered-Subset Expectation-Maximization iterative Time-Of-Flight technique with CT-based attenuation correction. Image quality was assessed by measuring the signal-to-noise ratio (SNR) in a selected homogeneous area in the liver. The SNR was defined as the ratio between mean pixel value and standard deviation. We used the body mass index (BMI) as a measure for patient size. The dependence of SNR on patient's BMI was evaluated, to calculate the optimal activity to be administered for a constant image quality between patients. **Results:** The mean BMI across all patients was 25 kg/m^2 (range 17-37 kg/m^2). The use of a fixed Ga-68 activity, resulted in a strong decrease in SNR for increasing BMI (p < 0.001). From BMI 17 to BMI 37 kg/m^2, the SNR decreased by a factor of 3. The optimal amount of activity to be administered should be scaled with BMI to the power 1.9, where c is a constant depending on scanner type and t is the acquisition time per bed position: Ga-68 activity $= c / t \cdot BMI^{1.9}$. This protocol implies that obese patients (BMI > 30 kg/m^2) should be administered with an activity at least 2.4 times the activity to be administered to underweight patients (BMI < 19 kg/m^2). **Conclusion:** A fixed Ga-68 activity is suboptimal for Ga-68-DOTATOC PET imaging. Our study suggests that using BMI in a power law based calculation of Ga-68 activity administration, results in a more constant image quality across patients.

EP-0061

Optimisation of Scintigraphic Imaging of the Novel Therapeutic Agent Ra223 in the Treatment of Metastatic Castration Resistant Prostate Cancer

S. Maguire, P. Gilligan, M. Carson; Mater Private Hospital, Dublin 7, IRELAND.

Purpose/Introduction: Imaging of radionuclide therapy agents is useful in determining biodistribution, verification of correct pharmaceutical and to rule out extravasation in clinical administrations. The aim of this study was to optimise imaging of Ra-223 dichloride (Xofigo™) for patients with metastatic castration resistant prostate cancer. **Materials and Methods:** A Jaszczak phantom and bar resolution phantom were used with 0.8MBq of Ra-223 to evaluate image quality for a range of collimators, energy windows and matrices for planar and SPECT imaging (Siemens ECam, Erlangen). Clinical imaging was carried out twenty minutes

post injection of Ra-223. Four sets of static images were obtained on two patients undergoing treatment, pre and post optimisation. **Results:** Optimum imaging parameters were found using planar imaging with a Xenon-133 energy window (80kV photopeak, 20% energy window), 128 x 128 matrix. A medium energy collimator resulted in higher resolution images with reduced image noise compared to a low energy general purpose collimator. These parameters allowed for clinically acceptable image quality with an imaging time acceptable for patient comfort (20 minutes). Clinical imaging allowed visualisation of structures post administration of Ra-223. Post optimisation images were of better quality although pre and post optimisation images were clinically useful. **Conclusion:** Useful clinical information can be obtained from scintigraphic imaging of Ra-223. The quality of imaging improved with optimisation of imaging parameters.

EP-0062

Pre-Clinical Assessment of the 99mTc-DMSA Renal Scintigraphy Using HiReSPECT; A Small-Animal SPECT System

K. Tanha, H. Fatemikia, M. Seyedabadi, M. Assadi; The Persian Gulf Nuclear Medicine Research Center, Bushehr University of Medical Sciences, Bushehr, IRAN, ISLAMIC REPUBLIC OF.

Purpose: The physical properties of the imaging system as well as the amount of injected activity, are influencing the quality of the scintigraphic images. In this study, we assessed the pre-clinical 99mTc-DMSA renal scan using a recently developed high-resolution, dual-head animal SPECT system. **Methods:** Radionuclide injection was performed with an activity range of 0.1 mCi to 10 mCi. Renal uptake determined in terms of the activity of the kidneys, count rate per pixel (CRPP) and the kidney to background ratio (KBR) using HiReSPECT. **Results:** Maximum KBR was achieved for the administration of about 2 mCi of the radionuclide. Activities bellow 1 mCi did not show a uniform renal cortex and could not be considered as acceptable. Higher amounts of activities decreased the KBR. **Conclusion:** An activity of 2 mCi is recommended for the 99mTc-DMSA renal scan using HiReSPECT small-animal imaging system. Table 1- Measured activity of the kidneys, CRPP and the KBR for different activities of 99mTc-DMSA. Kidney activities measured by a dose calibrator. The amounts of CRPP of the kidneys was calculated as kidney counts per second divided by the pixel number in selected ROI. KBR calculated as kidney counts divided by the sum of kidney and total counts of the image, multiplied by 100.

EP-0063

Matching and Optimisation of CT Protocols Using Automatic Exposure Control in PET/CT

S. Gould, J. Mackewn, S. Chicklore, G. Cook, L. Pike; King's College London & Guy's and St Thomas' PET Centre, London, UNITED KINGDOM.

Aim: The Siemens Biograph mCT Flow 64 PET/CT scanner recently installed at our centre implements CT automatic exposure control (AEC) based on a reference tube current (Quality Reference mAs) and a dose modulation strength setting, whereas our existing GE Discovery 710 scanners perform AEC based on acceptable image noise. The aims of this study were to match the CT protocol used for attenuation correction and localisation across vendors in terms of image quality and radiation dose and to evaluate the iterative reconstruction algorithm provided by Siemens. **Materials and Methods:** After matching acquisition parameters as closely as possible, the Phantom Laboratory Catphan phantom was used to establish an appropriate Siemens Quality Reference mAs by matching CTDI$_{vol}$ and image noise to our clinical GE protocol. 33 patients scanned on the Siemens scanner were matched by gender, height, weight and scanning position (arms up/down) to patients scanned on the GE scanner and the images compared in terms of image noise in the patient's liver and CTDI$_{vol}$. Based on these results, the dose modulation strength setting was reduced for obese patients. The matched patient study was repeated for a further 27 patient pairs and size specific dose estimates (SSDEs) calculated for this group according to the protocol in AAPM Report No. 204. To optimise the reconstruction algorithm, CT data from Siemens patient scans will be reconstructed with a range of settings. The resulting reconstructions will be scored for image quality and compared to matched GE patient images by clinicians experienced in PET/CT reporting. **Results:** In the first matched patient study the mean percentage difference in CTDI$_{vol}$ for Siemens compared to GE was -10.7% (range -41.7% to 50.1%) and the mean percentage difference in noise was 7.6% (range -31.0% to 76.8%). For matched obese patients (n=8, BMI>30) the mean and maximum differences in CTDI$_{vol}$ were 6.7% and 50.1%. Following the change in dose modulation strength, for obese patients (n=6) the mean and maximum differences in CTDI$_{vol}$ were -18.2% and -4.4%. The mean percentage difference in SSDE for Siemens compared to GE was -18.7% (range -38.9% to 13.4%). Scores from the reconstruction evaluation study will inform protocol setup and allow comparison with GE image quality. **Conclusion:** Matching of CT acquisition and reconstruction parameters across scanners from different vendors is important to ensure comparable patient dose and image quality. We undertook a matched patient study to verify comparability of our scanners and justify optimisation for obese patients.

EP-0064

Evaluation of Parameters of Radioisotope Studies to Reduce the Radiation Exposure to the Patient in the Diagnosis of Bone Metastases

I. Tleulessova[1,2], A. Saduakassova[1,2]; [1]Medical Center Hospital of President`s Affair Administration of the Republic of Kazakhstan, Astana, KAZAKHSTAN, [2]National Laboratory Astana, Astana, KAZAKHSTAN.

The aim of the work is to evaluate the parameters of hybrid radioisotope studies to reduce the radiation exposure to the patient in the diagnosis of bone metastases. A routine method for diagnosing bone metastases is osteoscintigraphy. However, thanks to the introduction of hybrid technologies, it has become

possible to perform SPECT/CT scan of the osteoarticular system to obtain volumetric images. Diagnosis of osteolytic bone metastases may be performed on a PET/CT scan. However the use of hybrid technologies leads to an increase in radiation dose on the patient. According to the principle of optimization of radiation protection, optimization is not just a reduction of the individual dose, but the maximization of the benefit-harm ratio. In diagnostic studies the maximum benefit-harm difference is achieved with a reduction in irradiation to a minimum level, at which qualitative diagnostic information is technically provided. Maximizing the benefit-harm difference in diagnostics also requires improving the quality of the images obtained. Materials and methods: SPECT/CT of osteoarticular system, whole body PET/CT. Results of the research. Based on this principle, the parameters for the collection of PET/CT and SPECT/CT data were assessed. PET/CT studies were performed on a 40-slice scanner. In 18F-FDG whole body PET/CT scan, a "low-dose" CT was used for attenuation correction of PET image. Using those parameters, quality of CT images was evaluated as "satisfactory", the total effective equivalent dose (EED) from the study was around 7-13mSv. To improve the quality of obtained CT images, the parameters were then optimized: 120kV, 70mAs, pitch 1.0, matrix 24×1.2mm, rot.time 0.5s. Using these parameters, quality of CT images was rated as "good", the EED was around 9-15mSv. SPECT/CT studies of osteoarticular system were performed on 6-slice SPECT/CT scanner. Using those parameters, quality of CT images was rated as "good", the EED was around 5-8mSv. To reduce the radiation dose of the patient, CT scan parameters were then optimized: 130kV, 90mAs, pitch 0.8, matrix 6x2mm, rot.time 1.0s. Using these parameters, quality of CT images was evaluated as "good", and the EED was around 3.5-6mSv. As a result, radiation dose was reduced, on average, by 27% while maintaining the quality of the images. Conclusion. Studies have shown that optimizing the data collection parameters of standard protocols for radioisotope studies is necessary to achieve two goals: obtaining good image quality, and maintaining a low radiation dose on patient. The parameters can vary depending on the goal of the study.

EP-0065

Intensity Quantisation Effects in Texture-based Tumor Heterogeneity in FDG-PET

*A. Forgacs[1,2], L. Balkay[2], I. Garai[1], M. L. Lassen[3], T. Beyer[3], **M. D. DiFranco**[3]; [1]Scanomed Nuclear Medicine Center, Debrecen, HUNGARY, [2]Division of Nuclear Medicine, Department of Medical Imaging, Faculty of Medicine, University of Debrecen, Debrecen, HUNGARY, [3]Center for Medical Physics and Biomedical Engineering, Medical University of Vienna, Vienna, AUSTRIA.*

Purpose: Reliable tumor heterogeneity quantification from FDG-PET images could lead to more accurate treatment selection and patient follow-up assessment. Texture features are being actively studied as heterogeneity measures, but the errors produced by intensity quantization, an essential step in texture calculation, can lead to unreliable results. **Subjects & Methods:** We investigated the effects of intensity quantization errors on texture-based heterogeneity parameters by measuring gray-level co-occurrence matrix (GLCM) texture indices (TIs) at varying quantization bin widths, and by applying bin location shifts. Three data sets were investigated: simulated spherical homogeneous volumes of interest, spherical volumes of interest from the livers of human lung tumor patients (n=58), and lung lesion volumes of interest (n=63) from the same patient cohort. Results: Lung lesions showed a positive linear relationship between bin width and voxel-level quantization error. For homogeneous uptake regions in the liver, the quantization error peaked at a bin width = 0.8. Mean values of GLCM TIs for lung lesions varied monotonically with bin width, with variances remaining stable. In homogeneous regions represented by both simulated and liver regions, the variations of mean GLCM TIs exhibited local peaks or troughs around specific bin widths, and in some cases the variance was sensitive to bin width. Shifting quantization bin boundaries resulted in changes to relative TI values for liver lesions, with the instability becoming more pronounced with increasing bin width. **Discussion:** SUV quantization is an essential step in GLCM-based TI calculation, but it introduces an error on the underlying values. Furthermore, the magnitudes of TIs commonly used as heterogeneity parameters vary as a function of quantization bin width. For homogeneous SUV regions such as the liver, peaks appear in the TI vs. bin width curve due to the low variance of SUV values, leading to unpredictable TI values for homogenous regions relative to more heterogeneous ones. Bin boundary shifts result in TIs taking on different values for the same data at certain bin widths. **Conclusion:** GLCM-based TIs are sensitive to the bin width used for quantizing the SUV values, with regions of homogeneous SUV being susceptible to errors introduced by quantization. The mathematical limitations of GLCM-based TIs must be better understood to achieve reliable and robust tumor heterogeneity quantification for inter-patient comparisons and radiomics systems.

EP-0066

An Assessment of Quantitative Analysis Software in Nuclear Medicine Gastric Emptying Studies

S. Maguire[1], P. Giligan[1], S. Ross[2], H. McKeown[1]; [1]Mater Private Hospital, Dublin 7, IRELAND, [2]Dublin Institute of Technology, Dublin 8, IRELAND.

Introduction: Gastric emptying studies are useful in the assessment of altered gastric emptying and motility. Standardised protocols have been published to improve the clinical utility of the study and establish normal ranges. Gastric emptying reporting requires both qualitative and quantitative image analysis. Common parameters reported are time to 50% emptying and gastric retention at 2 and 3 hours post ingestion. The purpose of this study is to validate a number of software systems used to produce quantitative results in gastric emptying studies. **Materials and Methods:** Three methods of analysis were assessed; Siemens gastric emptying software (Siemens Healthcare, Germany), GE analysis software (GE Healthcare, USA) and an in-house developed spreadsheet. A gastric emptying phantom was constructed using a saline bag, Perspex and

a programmable infusion pump to simulate gastric emptying at pre-defined rates. The phantom was imaged on a Siemens ECam (Siemens Healthcare, Germany) according to SNM guidelines for a range of clinically relevant emptying rates. Acquired images were analysed using in house analysis software and vendor proprietary software. The phantom was also scanned on a GE Discovery SPECT/CT system (GE Healthcare, USA) for a single emptying rate and analysed using vendor's software. Accuracy of the analysis software was compared with pre-defined emptying rates. **Results:** Accuracy of the phantom emptying rate was confirmed prior to the imaging study. In house quantitative analysis was found to be accurate across the range of emptying rates. One of the vendor's software was found to give erroneous results in comparison to the in-house software. **Conclusion:** In house gastric emptying quantitative analysis software was confirmed to be accurate and suitable for use in a clinical setting. Vendor software was shown to have inaccuracies across a range of clinically significant emptying times. Further evaluation of the vendor software should be carried out to determine the source of the inaccuracies. Verification of quantitative software should be included as part of any gastric emptying quality assurance program. Phantom based assessment is useful in the verification of software generated quantitative results in gastric emptying.

EP-0067

Audit of Radionuclide Injection Administered Activity for VQ imaging with Tc-99m MAA

L. M. Perry, *R. T. Meades, M. Vartzokas, Z. Win, K. S. Nijran; Imperial College Healthcare NHS Trust, London, UNITED KINGDOM.*

Introduction: The diagnostic reference level (DRL) stated in the UK ARSAC guidance notes for ^{99m}Tc-MAA for planar V/Q imaging is 100MBq. Locally we define the DRL as 100MBq for non-pregnant patients and 50MBq for pregnant patients with a tolerance of ±10%. This was taken as the audit standard. An audit cycle was completed to measure current practice against audit standard, identify and implement change and re-audit to evaluate impact of change. **Method:** An initial audit between May 2016 and November 2016 required department staff to record dispensed and residual ^{99m}Tc-MAA activities and times of measurement on a paper record sheet. Administered ^{99m}Tc-MAA activity was calculated from decay-corrected dispensed and residual activities. Compliance with the audit standard was evaluated. As a result of the the initial audit an allowance for residual activity was defined and applied when dispensing activity for these studies. Following this change the dispensed, residual and administered activities were recorded together with times of measurements for all patients electronically on the new Radiology Information System (Soliton Radiology +). A second audit was performed to assess any change in compliance with audit standard for studies performed between January and April 2017. **Results:** Data was collected for 43 patients including 7 pregnant patients for the initial audit. Compliance with the audit standard was 14% (8% for non-pregnant patients, 43% for pregnant patients). Residual activity was identified as a cause of poor compliance with standard. Dispensed activity showed

allowance for residual for pregnant but not for non-pregnant patients. Mean residual activity was 35MBq (SD ±16MBq) for non-pregnant and 20MBq (SD ±6MBq) for pregnant patients. A change in practice was implemented to allow for these mean residual activities when dispensing ^{99m}Tc-MAA for planar V/Q imaging. The re-audit included 99 patients of whom 11 were pregnant. Compliance with the audit standard was 57% (58% for non-pregnant patients, 45% for pregnant patients). Mean residual activity was 22MBq (SD ±12MBq) for non-pregnant and 20MBq (SD ±5MBq) for pregnant patients. **Conclusion:** Compliance of injected activity with audit standard was improved by making allowance for residual activities. Residual activity was different for non-pregnant patients between the two audit cycles requiring further investigation. Further adjustment to dispensed activity for this change could lead to increased improvement in compliance with the audit standard. Data collection was more efficient using electronic recording on RIS.

EP-0068

Influence of multiple lesions in the detection of Sentinel lymph nodes

R. Ringler, *K. Gmey, K. Schuller, P. Hammer, L. Bluemlein, M. Stich; Technische Hochschule Amberg-Weiden, Weiden, GERMANY.*

Introduction: The infestation of sentinel lymph nodes (SNL) determines the prognosis and the choice of a therapy. With the help of a gamma hand-held probe, the monitoring of radioactively marked lymph nodes are located and removed intraoperatively. The aim of the study was to investigate the influence of multiple lesions in the detection of SNL. First aim was to determine the minimum distance between different activities to be detected as two sources/lesions. Second to determine the minimum distance if two sources/lesions are placed in different depth to the surface/skin. **Methods:** With a newly developed SNL hybrid phantom (US & Röd & NUK), two or more vials filled with Technetium Tc-99m simulate the lesions in SNL scintigraphy. The vials can be placed in the phantom at different distances in one depth to simulate the lesions/sources. Furthermore the sources can be placed in six depth positions. With a 2D-motor positioning unit, controlled by LabVIEW, a Gamma-hand-held-probe is automatically moved along the SNL hybrid phantom to detect the lesions. The measurement (cps of the vials) is recorded by an automatic count rate acquisition. The cps values and the resolution of multiple lesions are evaluated with Matlab. The measurements were carried out at different lateral distances and six different depths of the vials with Tc-99m (max. 300kBq/vial). **Results:** The results show that the sources/lesions in the same depth can be separated from each other from a minimal distance of 10 mm at a depth position of 8.5 mm. An increase of the depth position to 18.5/28.5/38.5 mm, the two sources need a minimal distance of 18/22/28 mm to be seperated. Two sources at different depth e.g. 8.5/18.5mm or 8.5/48.5 lead to a minimal distance of 15 mm and >30 mm respectively. Lesions with different acitivity (e.g. 300 kBq and 350 kBq) can be clearly distinguishe by the count rate (cps). **Conclusions:** The closer the SLN-lesion is placed to the skin/phantom surface, two

lesions can seperated by the change in the count rate. Therefor a surgery can be more minimal invasive. By increasing the depth position, a greater distance of the sources is necessary in order to be able to clearly distinguish two lesions from each other.

EP-0069

Investigation of the axial sampling rate of helical mode multi-pinhole SPECT dedicated for human brain imaging with a Multi-Disk phantom

A. Forgacs, Á. Krizsán, I. Garai, S. Szabó; Scanomed Ltd, Debrecen, HUNGARY.

Aim: Multi-Pinhole SPECT technology using organ specific apertures holds the potential to exceed the image quality of conventional parallel-hole SPECT imaging. Helical SPECT acquisition mode intended to extend the relatively small size of field of view in axial direction, and diminish differences due to the non-uniform 3D sensitivity profile, but at the expense of sensitivity and spatial resolution. We assembled a multi-disk phantom (even called Defrise phantom), originally developed for tomographic technics that use cone-beam projected data (typically CT). Furthermore our aim was to determine the optimal pitch factor (translational movement of patient bed) for the Multi-Pinhole SPECT acquisition based on visual and numerical evaluation of phantom measurement. **Materials and Methods:** The multi-disk phantom was assembled from 6 piece of Styrofoam disks (20mm thick, 110mm diameter) placed in 4mm distance next to each other, and the entire setup was inserted into a hollow plastic cylinder tube. The scanner in the investigation was a triple headed SPECT/CT system (Mediso AnyScan TRIO) equipped with organ specific multi-pinhole apertures dedicated for human brain imaging. Series of helical SPECT/CT scans were performed about multi-disk phantom that was filled with Tc99m water solution and positioned on the head holder. Scan parameters were 72 views, 128x128 image matrix, [0-8] cm axial bed motion. Total counts were identically ~100Mcts. For the iterative reconstruction with attenuation and scatter correction a spiral CT scan followed the SPECT acquisition. The reconstructed images were evaluated visually, by calculating line profiles and coefficient of variation on each active slices of the phantom. **Results:** The quality of reconstructed image is sensitive to the table motion length during the scan. The range of 4-6 cm of bed motion provided the lowest geometric distortion (ranking visually), along with the best coefficient of variation (<5%). **Conclusion:** Reconstructed data of multi-disk phantom measurements are sensitive indicators to express the impact of axial sampling rate in helical Multi-Pinhole SPECT technology. The results of this study indicate that this method is applicable for protocol optimization of patient examinations with multi-pinhole apertures.

EP-0070

Comparison of estimated and measured pixel variance in Whole Body PET affecting SUV uncertainty

Á. K. Krizsán[1], G. Nagy[2], M. Szolik[1], I. Garai[1], M. Dahlbom[3], L. Balkay[2]; [1]ScanoMed Nuclear Medicine Centers, Debrecen, HUNGARY,

[2]Department of Nuclear Medicine, University of Debrecen, Debrecen, HUNGARY, [3]Ahmanson Translational Imaging Division, David Geffen School of Medicine, UCLA, Los Angeles, CA, UNITED STATES OF AMERICA.

Aim: During the clinical reading process of Whole Body ^{18}F-FDG PET images constant signal-to-noise ratio (SNR) properties would be preferable, therefore a method to correctly determine SNR values for each slice would be necessary. The most straightforward way for this is repeated scans of the same subject, however this is mainly limited to phantom scans and cannot be performed at the human clinical level. Estimation of image pixel variance from image sets reconstructed using parts of a single acquisition raw data may provide results close to the expected repeated scan SNR values, and therefore give important information on regional SUV variance of WB PET images. **Materials and Methods:** We proposed a method that uses a special algorithm to assign an SNR value to each voxels of the reconstructed image. These values were calculated from the list-mode files of the routine clinical patient scan durations, while performing sub-reconstructions of identical image sets by splitting the original scan duration per bed position to 7, 6, 5, 4 and 3 parts identically. Standard deviation (Std) and mean values for each image voxel were determined for all of the image sets. From the Std/Mean images of shorter acquisitions the SNR values of each image voxel for the original scan duration/bed position scan were estimated with a linear regression method. On the other hand, Std/Mean calculations on series of the original time duration/bed position patient scan routine were also performed. SNR values of the estimated and measured noise image sets were investigated in the axial direction using a central region of interest (ROI) analysis. We performed PET scans of uniform cylindrical and various activity filled phantoms along with reconstructions from real human list mode data using the method described above. **Results:** SNR values gained using the estimation and the conventional method showed a high correlation qualitatively looking at the images and quantitatively after the ROI analysis. Differences between the estimated and repeated scan SNR values remained under 10% for both the phantom and patient scans. Body mass indices (BMI) of the investigated patients varied between 28 - 42, however, no major differences were found in SNR due to the applied time-of-flight reconstructions. **Conclusion:** With our method, the noise of individual PET-studies was simply measurable, and used for the determination of SUV variance during patient scan optimizations.

EP-0071

Robustness and reproducibility PET image radiomic features: the impact of delineation and segmentation

I. Shiri[1], A. Rahmim[2,3], H. Abdollahi[1], P. Geramifar[4], A. Bitarafan-Rajabi[1,5]; [1]Department of Medical Physics, School of Medicine, Iran University of Medical Sciences, Tehran, IRAN, ISLAMIC REPUBLIC OF, [2]Department of Radiology, Johns Hopkins University, Baltimore, MD, UNITED STATES OF AMERICA, [3]Department of Electrical and Computer Engineering, Johns Hopkins University, Baltimore, MD, UNITED STATES OF AMERICA, [4]Research Center for Nuclear

Medicine, Shariati Hospital, Tehran University of Medical Sciences, Tehran, IRAN, ISLAMIC REPUBLIC OF, [5]Cardiovascular Intervention Research Center, Rajaie Cardiovascular Medical and Research Center, Iran University of Medical Sciences, Tehran, IRAN, ISLAMIC REPUBLIC OF.

Aim: Radiomics (quantification of tumors phenotype by extracting and mining large number of quantitative metrics) and radio-genomics (linking radiomics and genomics) are active areas of research in cancer diagnosis, prognosis and treatment response evaluation. As crucial steps for subsequent informatics analyses in radiomics, methods of Gross Tumor Volume (GTV) delineation (manual or automatic) have varying impacts on radiomic feature values. The main aim of this study was to evaluate impact of different delineation and segmentation methods on PET image radiomic features. **Material and Method:** Thirty-two patients who underwent 18F-FDG PET/CT scans were subjected to the study. GTVs were delineated using manual segmentation on CT, and on PET using the following segmentation methods: 42, 50 and 70 % of the maximum SUV threshold, as well as Nestles and fuzzy locally adaptive Bayesian methods. Following 3D segmentation, 55 quantitative radiomic features including SUV-based, histogram-based, shape-based, and texture-based methods including those based on gray level co-occurrence matrices (GLCM), gray level run length matrices (GLRLM), neighboring gray-level dependence matrix (NGLDM) and gray-level zone length matrix (GLZLM) were extracted. **Result:** SUVmax, SUVpeak and SULpeak from SUV-based/ Entropy and Energy from histogram-based/ sphericity and compacity from shape-based/ Homogeneity and Entropy form GLCM/ SRE, LRE, GLNU and RP from GLRLM/ Coarseness from NGLDM / SZE, ZP and GLNU from GLZLM showed very good robustness and reproducibility over segmentations method. SUVstd from SUV-based/ skewness from histogram-based/ Energy and Contrast from GLCM/ LGRE, SRLGE and RLNU from GLRLM/ Busyness from NGLDM/ LGZE and LZHGE from GLZLM exhibited poor robustness and reproducibility across delineation and segmentation methods. **Conclusion:** The robustness and reproducibility of PET radiomic features due to different segmentation methods is feature dependent. Despite increasing use of such quantitative metrics as potential imaging biomarkers, robustness and reproducibility of radiomic features in different delineation and segmentation methods must be considered. Quantitative radiomic features with high robustness and reproducibility could be considered as good potential imaging biomarkers in different applications.

Physics & Instrumentation & Data Analysis: Miscellaneous

EP-0072

Comparison of estimated and measured isotope specific spatially variant point spread functions on the HRRT PET scanner

J. M. Anton Rodriguez[1], G. Krokos[1], M. Asselin[1], F. Kotasidis[2], P. Julyan[3], A. Archer[1], O. Morris[1], J. C. Matthews[1]; [1]Wolfson Molecular Imaging Centre-University of Manchester, Manchester, UNITED KINGDOM, [2]Geneva University Hospital Faculty of Medicine, Geneva, SWITZERLAND, [3]Christie NHS Foundation, Manchester, UNITED KINGDOM.

Aim: To compare spatially variant isotope specific point spread functions (PSF) derived from published positron range data with measured data on a the high resolution research tomograph (HRRT, Siemens). **Materials and Methods:** Spatially variant PSFs have previously been measured using an array of printed sources between 5-mm Perspex sheets for Fluorine-18 and Carbon-11 on the HRRT scanner [1]. In this work, these measurements were extended to Gallium-68 after modifying the method to use 1) a concentrated isotope solution of 0.50 GBq/mL, 2) thicker 10-mm Perspex sheets, and 3) points spaced hexagonally 2.4 mm apart to account for the longer positron range. Additionally, using the Fluorine-18 measurements and previously published data on positron range simulations [2,3], we have estimated PSFs for Carbon-11 and Gallium-68. For the estimated and measured PSFs, a double 3D Gaussian function was fitted to each printed source and used to model the PSF response over the scanner field of view (FOV). Differences between the measured and estimated PSFs were quantified using full-width-at-half-maximum (FWHM) and full-width-at-tenth-maximum (FWTM) in the tangential, radial and axial directions. **Results:** For Carbon-11, (radial, tangential, axial) FWHM of (2.95, 2.92, 2.99) mm and FWTM of (5.58, 5.52, 5.67) mm were measured at 15mm radially from the FOV centre, increasing to (3.13, 2.77, 3.10) mm and (5.88, 5.26, 5.84) mm at 35mm. For Gallium-68, the FWHM and FWTM were (4.19, 4.19, 4.14) mm and (8.56. 8.52, 8.47) mm at 15mm and (4.37, 4.09, 4.34) mm and (8.73, 8.31, 8.63) at 35mm. The estimated PSFs were generally in agreement with the measured PSFs. In comparison, and when using the data from [2], the PSFs had wider tails with FWHM values 3-7% and FWTM values 5-9% higher for Carbon-11, and 0-3% (FWHM) lower and 9-15% (FWTM) higher for Gallium-68. When using the data from [3], better agreement was observed with FWHM values 1-4% and FWTM values 1-5% higher for Carbon-11 and 2-5% (FWHM) and 0-3% (FWTM) lower for Gallium-68. **Conclusion:** Spatially variant isotope specific point spread functions can be estimated with a good degree of accuracy from Fluorine-18 measurements and published positron range data. We have validated this approach for Carbon-11 and Gallium-68, but such an approach may be appropriate for other isotopes such as Oxygen-15 for which measurements are not practical. **References:** [1] F.A. Kotasidis *et al,* MP 2014 [2] L. Jodal *et al*, PMB 2012 [3] J. Cal-Gonzalez *et al*, PMB 2013

EP-0073

Computational 3D Preoperative Simulation As Useful Tool For Sentinel Lymph Node Detection In Breast Carcinoma Surgery

M. Matovic[1], D. Nikolic[2], N. Filipovic[2], M. Jeremic[1], S. Jankovic[3], S. Ninkovic[4], A. Cvetkovic[5], M. Vlajkovic[6]; [1]Dpt. of Nuclear Medicine Clinical Center Kragujevac, Kragujevac, SERBIA, [2]University of

Kragujevac Faculty of Engineering, Kragujevac, SERBIA, [3]Dpt. of Clinical Pharmacology Clinical Center Kragujevac, Kragujevac, SERBIA, [4]Dpt. of Surgery Clinical Center Kragujevac, Kragujevac, SERBIA, [5]Dpt. of surgery Clinical Center Kragujevac, Kragujevac, SERBIA, [6]Dpt. of Nuclear Medicine Clinical Center Nis, Kragujevac, SERBIA.

Background: Hybrid Single-Photon Emission Computed Tomography (SPECT) / Computerized Tomography (CT) system with 3D interactive modeling is reliable, sensitive and rapid method for location of sentinel lymph nodes in patients with breast cancer. However, availability of such systems is limited to small number of highly equipped medical centers in developed countries. **Objective:** The aim of our study was to pilot new method of 3D interactive modeling which integrates images obtained by separate SPECT and Multi Slice Computed Tomography (MSCT) modalities with help of original software. **Method:** We used ^{99m}Tc-colloid rhenium sulphate for labeling sentinel lymph nodes with radioactivity in seven patients with breast cancer. The markers made of lead pearls wrapped with cotton wool soaked in pertechnetat were placed on the skin of the patients in the form of a triangle. Using original software, two separate 3D models were made after SPECT and MSCT imaging, and then merged into hybrid 3D model which enabled precise visualization and localization of the sentinel lymph nodes. **Results:** In all cases the position of the sentinel lymph nodes established by our method was successfully verified using manual probe equipped with Geiger Muller counter. Duration of the sentinel lymph node identification and extirpation was significantly reduced below 10 minutes per patient. **Conclusion:** Precise identification and biopsy of sentinel lymph nodes are much faster and easier using this integrated SPECT/MSCT 3D modeling in comparison with the "classic" method, based on just radioactivity detection probe. In addition, our method is accurate, user-friendly, and associated with low costs. **Key Words:** breast cancer; sentinel lymph node; biopsy; integrated SPECT/CT; 3D modelling

EP-0074

Monte Carlo simulation of ^{90}Y PET imaging requires the modelling of internal bremsstrahlung and of long energy resolution tail

S. Walrand, M. Hesse; Université Catholique de Louvain, Brussels, BELGIUM.

Aim: Unlike to pure positron emitters, the true coincidences (cc) sinogram radial profile in ^{90}Y-PET acquisition exhibits tails increasing with the radial distance (Conti & Erikson EJNMMI Phys 2016). This behaviour is suspected to hamper tails-tuned scatter correction methods and to produce spurious extrahepatic activity in nonTOF-PET imaging post liver radioembolization. However, Gate simulations using the Geant4 ion source do not predict this profile shape (Strydhorst et al. Med Phys 2016). This study investigates whether two effects not modelled in Geant4 could explain this unexpected mismatch, namely internal bremsstrahlung (IB) and long tail energy resolution. IB results of the emitted beta particle interaction with the decayed nucleus. **Methods:** To study true cc rate resulting only from bremsstrahlung x rays, a ^{32}P vial was acquired using a GSO PET system afterwards accurately modelled in Gate. Gamma histogram sources modelling EB and IB were used, as IB is not modelled in Geant4 ion source. A ^{111}In source was also acquired. **Results:** Singles energy spectrum of the ^{111}In source showed an energy resolution made of a 20%-FWHM gaussian plus a long decreasing exponential tail. The measured ^{32}P true cc sinogram radial profile in the [450,650] keV window had a smooth concave shape with a central sharp valley corresponding to the vial attenuation print. This profile was accurately predicted by the simulation using the EB+IB source and the measured energy resolution. When removing the IB or the exponential tail in the simulation, only 18% or 11% of the measured true cc were predicted, respectively (only 4% when removing both). The Gate hit file sorting provided the explanation: a fraction of the high energy x rays, mainly produced by the IB (Cengiz & Almaz, Rad Phys Chem 2004), are backscattered when hitting a crystal pixel and reach an opposite crystal pixel with an energy around 200 keV. Due to the long energy resolution tail, a fraction of these backscattered x rays are detected as true cc together with the energy deposited in the first hit crystal pixel. A similar behaviour was also observed in additional ^{90}Y-PET simulations. **Conclusion:** MC simulations show the major impact of the IB in ^{90}Y PET imaging supporting its implementation in the ion source of Geant4. Resulting accuracy improvement in simulations will allow developing better correction methods for scatter ^{90}Y PET and for spurious extra-hepatic activity in nonTOF PET (TOF information automatically discards these spurious cc).

EP-0075

Modelization of trues over prompts events ratio to optimize individual posology on a high-sensitive BGO PET/CT system

D. Vallot, M. Bauriaud, S. Brillouet, L. Dierickx, S. Kanoun, S. Zerdoud, F. Courbon, O. Caselles; Institut Universitaire du Cancer de Toulouse, Toulouse, FRANCE.

Aim: The aim of this study was to find new rules to optimize injected activity of F18-FDG exams, based on trues/prompts ratio analyzed on phantoms and patient studies. **Materials and Methods:** This study was made on a non-TOF, high sensitive BGO PET/CT system (Discovery IQ, GEHC). A program using Matlab® was written to extract automatically the relevant data from raw data of phantoms and patients PET exams. The first step was to establish a relationship between the activity located in the field of view (FOV) and the trues over prompts (T/P) events ratio. For this, various geometric phantoms (CEI 61675-2, 20 cm cylinder phantom) filled with different F18-FDG activities were scanned in several conditions. Then, a retrospective analysis on 19 oncologic patient exams was performed for each bed position to determine T/P. **Results:** *Phantom study* The phantom acquisitions allowed us to find a Weibull fitting model (trues/prompts = a-b*exp(-c*activity^d)) for T/P depending on the activity in the FOV. This mathematical relationship was not dependent on the phantom's form (thoracic or cylindrical, more

or less diffuse material) and worked well within a large range of activities (up to 300 MBq). A T/P superior to 50% matched to an activity below 80.8 MBq in the FOV. Conversely, this model over-estimates the trues/prompts ratio in presence of a radioactive source outside the FOV. _Clinical study_ For all the patients, T/P was retrospectively analyzed on the whole body scans. This ratio varied between 22.5% and 86% with a mean ratio of 44.2%. The corresponding calculated injected activity given by our Weibull model is in average 4.6 times the injected activity corrected by the radioactive decay (R^2=0.96). As we noticed for the phantom studies with activity outside the FOV, our Weibull model overestimates T/P in patients' scans. Based on T/P, it seemed also that the injected activity could be reduced with our system. **Conclusion:** This study showed that the use of standard phantoms to optimize injected activity of F18-FDG has some limitations as they don't allow to reproduce faithfully what happens in a real body, especially the presence of activity outside the FOV.

EP-0076

Comparison of SUVmax obtained by Non-Time of flight PET system with Time of flight PET system: a phantom based study

A. K. Jha, S. Mithun, A. D. Puranik, N. C. Purandare, S. Shah, A. Agrawal, V. Rangarajan; Tata Memorial Hospital, Mumbai, INDIA.

Aim: Discovery IQ PET/CT (D-IQ,GE Medical Systems, USA) with a 5-ring detector configuration was installed in 2014 in our department in addition to existing time of flight (TOF) PET/CT system Gemini TF64 (Philips Medical System). D-IQ is a BGO based PET system and has two different reconstruction techniques, namely, VPHD and QClear. The objective of our study was to compare the SUVmax obtained by QClear and VPHD reconstructed images of D-IQ system with that of Gemini TF64 system based on phantom study. **Material and Method:** Average 40.69MBq 18F-FDG was filled in NEMA IQ phantom, Biodex Inc., USA. Out of six spherical inserts two larger spherical inserts were filled with normal water and four smaller inserts were filled with radioactivity water in known target to background ratio (TBR). PET/CT acquisition was performed in clinical imaging protocol for 3min per bed position in list mode. Phantom imaging were performed in four different TBR i.e. 4:1, 8:1, 16:1 and 32:1 respectively on D-IQ as well as Gemini TF64 PET/CT system. Two image sets, namely, VPHD and QClear were reconstructed from each study performed on D-IQ system generating 8 image sub-sets namely VPHD4 and QClear4 (TBR:4:1), VPHD8 and QClear8 (TBR:8:1), VPHD16 and QClear16 (TBR:16:1) and VPHD32 and QClear32 (TBR:32:1). One image set for Gemini TF64 (64TF) was reconstructed for each study performed and total 4 image sub-sets, namely, 64TF4 (TBR:4:1), 64TF8 (TBR:8:1), 64TF64 (TBR:16:1) and 64TF32 (TBR:32:1). SUV-max of four hot inserts and background were obtained by drawing 3D ROI over the lesions for all 12 image sub-sets. Two tailed Wilcoxon Signed-Rank Test was performed for statistical analysis of the data. **Result:** Lesion and background SUVmax obtained on two systems are summarized in Table:1. The difference in the SUVmax of VPHD and 64TF was 23.65% and of QClear and 64TF was 2.14% averaging across all the lesion size and TBR. SUVmax

versus size of lesion graph is shown in Figure:1. Wilcoxon Signed-Rank Test shows significant difference between the SUVmax obtained by VPHD and 64TF as well as Qclear and 64TF in all the TBR range. **Conclusion:** Our study concludes that _Non-TOF PET system with Q.Clear and VPHD reconstruction_ shows significant difference in mean values of SUVmax of all lesions in same TBR range with that of TOF system. However, SUVmax obtained by Qclear and 64TF were of higher range in comparison with SUV-max obtained by VPHD in all TBR ranges.

EP-0077

Yield estimation for ^{62,63}Zn via proton induced reactions using GEANT4

M. Rostampour[1], **M. Aboudzadeh Rovais**[2], M. Sadeghi[2], S. Hamidi[1], S. Hosseini[3]; [1]Department of Physics, Arak University, Arak, IRAN, ISLAMIC REPUBLIC OF, [2]Nuclear Science and Technology Research Institute, Tehran, IRAN, ISLAMIC REPUBLIC OF, [3]Payeme Noor University, Tehran, IRAN, ISLAMIC REPUBLIC OF.

Introduction: The optimization of radioisotopes production is an important factor in maximizing the production yield and minimizing the associated costs. The ^{63}Zn and ^{62}Zn radioisotopes are positron-emitting isotopes of zinc that have potential to be used as PET biomarkers of zinc kinetics in animal and human studies. In this study, the GEANT4 code was employed to calculate the saturation yield of ^{62,63}Zn from proton-induced reactions. Furthermore, the reported experimental saturation yield data were compared with the estimated values using GEANT4. **Method:** In this study, the physics list was constructed with several built-in modules available in the Geant4 Toolkit. The range of proton in different targets calculated using the G4EmStandardPhysics are found to be in better agreement with SRIM-2013 data than those of the other electromagnetic models. Therefore, the G4EmStandardPhysics package is considered for the electromagnetic processes. In addition, the G4 Hadron Elastic Physics, and G4HadronInelastic QGSP_BIC_HP packages were considered for proton elastic interactions, and inelastic hadron interaction. The geometry and structure of the target set were simulated by the Geant4 code. In this study, ^{63}Cu, ^{65}Cu, and ^{nat}Cu are considered as targets. A cylindrical target having a diameter of 1 cm has been implemented into the simulation code. The cylindrical targets were assembled in an aluminum target boat. The thickness of cylindrical targets was calculated by considering G4EmStandardPhysics. The beam was designed to reach the target at 90° angle and impinge on the target in the z-direction. A statistics of 1000,000 primary particles have been run for all simulations. In this study, the simulation output consists of the total number of produced isotopes inside the target. The saturation yields using GEANT4 were estimated by considering time of irradiation, produced isotopes, and decay constant of produced isotopes. **Results and discussion:** The saturation yields are in the range of 80 %- 90% of the predicted theoretical value for ^{63}Zn and ^{62}Zn. **Conclusion:** Good agreement between saturation yields using GEANT4 and reported experimental data indicate that this Monte Carlo code can be used for estimating the saturation yield of beta emitter nuclides.

EP-0078

Validation of the GAMOS Monte-Carlo Toolkit for Nuclear Medicine Dosimetry

P. Ritt[1], K. Reuss[1], J. C. Sanders[1,2], N. Lanconelli[3], M. Pacilio[4], T. Kuwert[1]; [1]University Hospital Erlangen, Erlangen, GERMANY, [2]Pattern Recognition Lab, Friedrich-Alexander-University Erlangen-Nürnberg, Erlangen, GERMANY, [3]Department of Physics and Astronomy, Alma Mater Studiorum, University of Bologna, Bologna, ITALY, [4]Department of Medical Physics, Azienda Ospedaliera S. Camillo Forlanini, Rome, ITALY.

Purpose: Monte-Carlo simulations (MCS) are frequently used in tasks of Nuclear Medicine dosimetry, e.g. for calculating dose-kernels for voxel based dosimetry of Y-90 and Lu-177 therapies. A large variety of MCS are available. The GAMOS MCS framework is based on GEANT4 routines and aims at simplified usability. Consequently, the different physics modules known from GEANT4 are also available in GAMOS. So far, the accuracy of GAMOS has only been shown for external beam radiation and brachytherapy settings. The aims of this study were 1) to evaluate the accuracy of GAMOS for application in voxel based dosimetry of Nuclear Medicine therapies using Lu-177 and Y-90 and 2) to compare the dose values obtained from standard electromagnetic (EM) and Penelope physics modules. **Methods:** Using GAMOS, the voxel-wise deposited energy dose from radiation sources was simulated. Sources were mono-energetic electrons (range 10-2100 keV) and mono-energetic photons (set of energies for most common Lu-177 and Y-90 gamma transitions). Additionally, the decays of radionuclides Lu-177 and Y-90 were directly simulated. Absorbing tissue types included soft tissue and compact bone. The obtained data were compared to reference values from literature, obtained by other MC-codes. Additionally, the dose values obtained from EM and Penelope physics modules were compared. **Results:** Differences between GAMOS and reference data were: 1a) Photons: <5% for central voxel and energies below 1 MeV. For high photon energies and non-central voxels, larger differences of up to 20% were found. 1b) Electrons: <1% for central voxel and energies up to 2.1 MeV. For non-central voxels, larger differences of up to 5% were found. 1c) Lu-177: ~3.2% for central voxel for soft and bone tissue. For non-central voxels slightly higher, with on average 4.0% and 3.7% for soft and bone tissue, respectively. 1d) Y-90: ~0.4% for central voxel for soft and bone tissues. For non-central voxels higher, with on average 3.5% and 2.2% differences for soft and bone tissue, respectively. 2) Physics modules: Only minor differences (<1%) were found for central voxels and Lu-177 and Y-90. Larger differences (up to 10%) occurred for Y-90 for distances which correspond to the bremsstrahlung region. **Conclusion:** Energy dose values obtained from GAMOS show good agreement with those available from literature. For this, GAMOS is suitable for application in Nuclear Medicine therapies with Lu-177 and Y-90. Between standard EM and Penelope physics modules, only minor differences were found.

EP-0079

Partial volume correction changes intra-tumoral heterogeneity in 18F-FDG PET

I. Shiri[1], A. Rahmim[2,3], G. Hajianfar[4], H. Abdollahi[1], P. Geramifar[4], P. Ghafarian[5,6], A. Bitarafan-Rajabi[1,7]; [1]Department of Medical Physics, School of Medicine, Iran University of Medical Sciences, Tehran, IRAN, ISLAMIC REPUBLIC OF, [2]Department of Radiology, Johns Hopkins University, Baltimore, MD, UNITED STATES OF AMERICA, [3]Department of Electrical and Computer Engineering, Johns Hopkins University, Baltimore, MD, UNITED STATES OF AMERICA, [4]Research Center for Nuclear Medicine, Shariati Hospital, Tehran University of Medical Sciences, Tehran, IRAN, ISLAMIC REPUBLIC OF, [5]Chronic Respiratory Diseases Research Center, National Research Institute of Tuberculosis and Lung Diseases (NRITLD), Shahid Beheshti University of Medical Sciences, Tehran, IRAN, ISLAMIC REPUBLIC OF, [6]PET/CT and Cyclotron Center, Masih Daneshvari Hospital, Shahid Beheshti University of Medical Sciences, Tehran, IRAN, ISLAMIC REPUBLIC OF, [7]Cardiovascular Intervention Research Center, Rajaie Cardiovascular Medical and Research Center, Iran University of Medical Sciences, Tehran, IRAN, ISLAMIC REPUBLIC OF.

Aim: PET images suffers from the partial volume effect (PVE), a consequence of the limited spatial resolution and the tissue fraction effect. Several partial volume correction (PVC) methods have been developed to enable appropriate quantification for PET images. In the present study, we investigated impact on intra-tumoral heterogeneity by PVC methods as applied to 18F-FDG PET. **Material and Methods:** Thirty-seven lesions from twenty patients were included in the current study. 3D tumor segmentation was performed on CT images, and following tumor delineation, three methods of PVC including Richardson-Lucy (RL), Reblurred Van Cittert (RVC) and Single Target Correction (STC) were used to compensate for PVE. Intra-tumoral heterogeneity was assessed by 31 textural features including gray level co-occurrence matrices (GLCM), gray level run length matrices (GLRLM), gray-level zone length matrix (GL-ZLM) and neighboring gray-level dependence matrix (NGLDM). Subsequently, we determined the Relative Change (RC %) with respect to uncorrected PET image. **Result:** 46, 75 and 39% of textural features had RC more than 10% for RL, STC and RVC respectively. Homogeneity (RC: 11-43%), Contrast (RC: 12-53%) and Correlation from GLCM (RC: 12-43%), LGRE (RC: 56-84%), LRLGE (RC: 46-86%) from GLRLM, Busyness (RC: 85-211%) from NGLDM, LGZE (RC: 52-82%), SZLGE (RC: 48-79%), LZHGE (RC: 13-173%) from GLZLM exhibited the greatest RC between textural features. **Conclusion:** Our results demonstrated that PVC methods substantially altered intra-tumoral heterogeneity. This change must be considered in quantitative analysis of PET images particularly in radiomics and radio-genomics applications.

EP-0080

Relationship between intra-tumoral heterogeneity indices and metabolic parameters in 18F-FDG PET

I. Shiri[1], H. Abdollahi[1], P. Geramifar[2], A. Bitarafan-Rajabi[1,3]; [1]Department of Medical Physics, School of Medicine, Iran University of Medical Sciences, Tehran, IRAN, ISLAMIC REPUBLIC OF, [2]Research Center for Nuclear Medicine, Shariati Hospital, Tehran University of Medical Sciences, Tehran, IRAN, ISLAMIC REPUBLIC OF, [3]Cardiovascular Intervention Research Center, Rajaie Cardiovascular

Medical and Research Center, Iran University of Medical Sciences, Tehran, IRAN, ISLAMIC REPUBLIC OF.

Aim: Quantification of intra-tumoral heterogeneity using textural features in 18F-FDG PET has significant potential for treatment response assessment and prediction of survival in cancer patient. The objective of the present study was to explore relationship between textural features and conventional parameters (SUV$_{max}$, SUV$_{mean}$, SUV$_{peak}$, MTV and TLG) for quantification of 18F-FDG PET. **Material and Methods:** 104 lesion from 96 patient were pooled into the current study. All lesions were segmented using the fuzzy locally adaptive Bayesian (FLAB) method. Conventional indices including SUV$_{max}$, SUV$_{mean}$, SUVpeak, MTV and TLG and 67 textural features including gray level co-occurrence matrix (GLCM), neighborhood gray-tone difference matrix (NGTDM), gray-level size zone matrix (GLSZM), gray-level run-length matrix (GLRLM), normalized GLCM, neighboring gray level dependence (NGLD), texture feature coding (TFC) and Texture Spectrum were extracted from 3D segmented lesion volumes. Relationship between each pair of textural features and metabolic parameters was characterized by the Pearson correlation coefficient. **Result:** Weak correlation between SUV$_{max}$, SUV$_{mean}$, SUV$_{peak}$ and some textural feature was found (RL $|r|$=0.29, RP $|r|$=0.30, LIZE $|r|$=0.29, correlation $|r|$=0.46, coarseness $|r|$=0.47 for SUV$_{max}$/ Busyness $|r|$=0.37, ZP $|r|$=0.30, HIZE $|r|$=0.38 for SUVmean/ Correlation $|r|$=0.54, Coarseness $|r|$=0.57, Mean Convergence $|r|$=0.41 for SUV$_{peak}$). The remaining textural features did not exhibit any significant correlation with SUV$_{max}$, SUV$_{mean}$, or SUV$_{peak}$. Textural features was strongly correlated with MTV and TLG with $|r|$=0.31-0.92 and $|r|$=0.28-0.59 respectively, and a little number of textural features haven't any significant correlation with MTV and TLG (LIRE, LISRE, LIZE, LISZE, Max spectrum and coarseness for MTV/SAM ,LIRE, LISRE, Busyness, LZE LIZE, HIZE, LISZE, LILZE, HILZE, Entropy, Homogeneity and LZE for TLG). **Conclusion:** The current study provides evidence for relationship between conventional quantification parameters and textural features in PET imaging. The correlation between conventional quantification parameters and textural features may lead to similar performance in treatment response assessment and prediction of survival in cancer patient. Also the poor correlation between metabolic parameters and textural feature shows this parameter can capture complementary information for intra-tumoral heterogeneity which can be used in data mining and radiomics.

EP-07   **during congress opening hours, e-Poster Area**

Molecular & Multimodality Imaging: PET/CT

EP-0081

The role of 18F-FDG PET-CT in patients with fever of unknown origin

I. Kostadinova[1], A. Demirev[1], M. Baimakova[2]; [1]Clinic of nuclear medicine, City Clinic Oncology, Sofia, BULGARIA, [2]Military Medical Academy, Sofia, BULGARIA.

Currently, 18F-FDG PET-CT is considered an imaging method of choice in patients with Fever of Unknown Origin (FUO) for visualization and localization of inflammation/ infection/ tumors due to the possibility of conducting a whole body examination. The aim of our study was to share our experience, including 30 patients with FUO, who were examined by PET/CT in the period 2014-2016. Twenty four of them had concomitant antibiotic treatment due to inability to control the fever and 7 received corticosteroid therapy prior exam. The cause of FUO was confirmed in 21 (70%) of these 30 patients, by the use of all contemporary clinical, para-clinical and conventional imaging modalities (excluding PET-CT), data comparable to the results from other authors. Applying PET-CT, additionally in 3 patients from the group with unconfirmed diagnosis it was clarified. In all investigated with a final diagnosis (24/30), a true positive results was obtained in 14 patients -12 of them had - infection/inflammation: (abscess, pneumonia, spondylodiscitis, vasculitis, arthritis, thrombophlebitis and 9 of whom received concomitant antibiotic therapy), and 2 had lymphoma. True negative findings were observed in 2 patients, false-negative in 8 (3 of them were with toxoplasmosis or Still's disease). There were no false positive results. PET-CT examination itself contributed to establishing the final diagnosis in a total of 16/30 patients- 53.3% and in the group with the confirmed diagnosis the a sensitivity was of 66.7% and specificity - 100%. In 4/6 patients with unconfirmed/ false negative result, corticosteroid therapy had been applied, which have been determined it as one of the main factor for a lower diagnostic sensitivity. **In conclusion** we consider that PET-CT is recommended imaging method which has to be applied early in the diagnostic algorithm in patients with FUO after routine clinical and laboratory tests, before therapy, in order to detect and localize a region with an increased glucose metabolism which has to be etiologically clarified and an appropriate therapy to be initiated.

EP-0082

Thoracic duct lesion: Detection by [124]I-heptadecanoic acid PET/CT

H. Petersen, S. Inglev, P. Braad, S. Hvidsten, P. Høilund-Carlsen, J. A. Simonsen; Department of Nuclear Medicine, Odense University hospital, Odense, DENMARK.

Aim: Surgical cure of lesions of the thoracic duct depends on proper localization of the leakage. ^{123}I-labeled heptadecanoic acid (HDA) is useful for scintigraphy after oral administration, since the chain length of HDA allows absorption by intestinal lymphatics. However, ^{123}I-HDA has not been commercially available in Europe for the last decade. [124]I PET/CT has superior imaging properties compared to ^{123}I SPECT/CT. Consequently, we wanted to elucidate if PET/CT was feasible by labeling HDA with [124]I. **Materials and Methods:** A 56-year old man who suffered from accumulation of chyle in the pleural and abdominal cavities following resection of a caudal oesophagus tumour was referred for PET imaging. HDA was synthesized by halogen exchange of the corresponding bromine-analogue, 17-Bromo-HDA (Aaron Chemistry GmbH, Germany) using [124]I-Iodine in NaOH (BV Cyclo-

tron VU, The Netherlands). [124]I-HDA was administered orally in salad oil and served with a milk chocolate bar. Potassium iodide was administered to block thyroid uptake. PET/CT scans of the thoraco-abdominal region were obtained 16, 48, and 196 min after ingestion with late images after 21 h using a Discovery 690 PET/CT scanner (GE Healthcare, USA). **Results:** With a labeling efficiency of 14%, 12 MBq of [124]I-HDA was produced and administered to the patient. The effective patient dose was estimated to 4.6 mSv. PET/CT scans showed high tracer activity within the lumen of the gastrointestinal tract, and very quickly extra-intestinal activity was visualized left of the oesophageal-ventricular anastomosis. From there it diffused to the contralateral pleura and downwards to the abdominal cavity. From this it was concluded that the leak occurred to the left side within the thoracic cavity. A closed thoracic compartment was constructed surgically in order to apply a counter pressure to the chyle leakage. The operation was complicated by aspiration pneumonia and sepsis, but slowly the patient recovered. **Conclusion:** In this case of therapy resistant chylothorax PET/CT images pointed out the site of chyle leakage and successfully guided surgical treatment. Hence, PET/CT imaging with [124]I-HDA may be a promising modality for visualization of thoracic duct leakage. Labeling of [124]I-HDA is feasible, but should be optimized.

EP-0083

The value of dual-time FDG PET/CT for differentiating primary lung cancer from inflammatory nodules with an initial standard uptake value greater than 2.5 in a tuberculosis-endemic area, A preliminary retrospective study

*J. wang[1], **J. J. wang**[1], C. Y. Pu[1], J. G. Yang[2]; [1]Chinese Armed force police General Hospital, Beijing, CHINA, [2]Beijing Friendship Hospital affiliated to Capital Medical University, Beijing, CHINA.*

Objective: To evaluate the value of dual time Fluorodeoxyglucose (FDG) Positron emission tomography/Computed Tomography(PET/CT) imaging in the differentiation of lung carcinoma from inflammatory with an initial maximum standard uptake value(SUVmax) greater than 2.5 in a tuberculosis-endemic area, to assess its diagnostic performance and find out the optimal cut-off value of Retention index-(RI). **Material and Methods:** Fifty-three patients underwent dual time-point FDG PET/CT imaging(DTPI). There are 36 cases(67.9%) received biopsy or surgical removal of the nodules, the rest 17 cases (32.1%) did not have histological diagnosis and were confirmed as benign disease by clinical regular CT follow-up. SUVmax in each lesion were calculated on initial imaging(SUV1) and delayed imaging (SUV2) and the relative change of SUV2 to SUV1 for each lesion on dual-time imaging was calculated (Retention index,RI). Routine histological findings were considered as the gold standard. **Results:** Thirty-two pulmonary nodules were confirmed malignancy through histopathology and clinical follow-up. The rest twenty-one nodules were demonstrated to be benign disease, including tuberculosis granulomas(n=10), Cryptococcus neoformans granulomas(n=2), non-specific granu-

lomatous inflammation(n=9). When TB granulomas were included in analysis, the SUV1 and SUV2 as well RI between the benign and malignant group have no significant difference. However, when tuberculosis granulomas were excluded from the group, a significant difference in SUV2 and RI between the two groups was observed. SUV2 for benign and malignant lesions were 3.84±0.68 vs 7.17±4.40(P=0.017). Median RI of benign and malignant groups were 10.97±11.17 and 26.29±11.92 (P=0.001). (Using a cut-off>10% as an indicative of malignancy, a sensitivity of 87.5% and a specificity of 45.4% were obtained. Receiver operating characteristic curve(ROC) analysis indicated the area under the curve (AUC) was 0.827 (p=0.001). Based on analysis of ROC curve, the optimal cut-off value of RI on DTPI for diagnosis of malignancy was 19.05%. Using RI>19.05%, a sensitivity of 71.9% with a specificity of 81.8% were acquired. **Conclusion:** Our findings suggested that dual-time point FDG PET/CT imaging is unable to distinguishing pulmonary cancer from active inflammation, such as active tuberculosis with an initial SUVmax>2.5 in a tuberculosis-endemic area. But this method is still potentially helpful to differentiate malignancy from inactive or chronic pulmonary inflammation. Using a cut-off of RI>19.05 on DTPI as indication of malignancy, the optimal diagnostic performance could be achieved.

EP-0084

Uptake patterns and pecularities of metabolic tumor pointers on initial staging FDG PET/CT in patients with untreated primary gastrointestinal extranodal lymphomas

E. Alagoz[1], K. Okuyucu[1], S. Ince[1], S. Ozaydin[2], N. Arslan[1]; [1]Gülhane Training and Research Hospital, Department of Nuclear Medicine, Ankara, Turkey, Ankara, TURKEY, [2]Gülhane Training and Research Hospital, Department of Medical Oncology, Ankara, Turkey, Ankara, TURKEY.

Objective: Non-Hodgkin's lymphomas (NHLs) arising from the tissues other than primary lymphatic organs are called primary extranodal lymphoma (PEL).PEL of gastrointestinal system (PGISL) is a NHL originating from the lymphatic tissues of gastrointestinal tract. FDG-PET/CT has a high prognostic value with respect to overall survival and disease-free survival (DFS) in lymphomas. Our aim was to research uptake patterns, pecularities of low-grade and high-grade PGISL; investigate metabolic tumor indices on primary staging FDG-PET/CT for prognosis estimation in high-grade PGISL. **Methods:** 39 patients having PGISL were enrolled in this retrospective cohort study between 2014-2015. Primary staging FDG-PET/CT were performed and quantitative parameters of SUVmax, SUVmean, metabolic tumor volume (MTV), total lesion glycolysis (TLG) were calculated for all patients before the treatment. Low-grade and high-grade PGISL were compared according to metabolic tumor parameters. Cox regression models were performed to determine related factors with DFS in high-grade PGISL. **Results:** There was statistically significant difference between high-grade and low-grade PGISL according to SUVmax, SUVmean, MTV, TLG, recurrence, ex, DFS and OS. After univariate and multivariate cox regression mod-

el were performed for all potential risk factors (sex, age, organ, SUVmax, SUVmean, MTV, TLG) impacting recurrence, female sex remained the only risk factor. Metabolic tumor parameters were not statistically significant after multivariate analysis. **Conclusion:** Metabolic tumor parameters are not useful in prognosis estimation of high-grade primary gastrointestinal lymphomas despite their high values, especially in diffuse large B cell variant and primary gastric lymphoma and not appear to play a role in patient management. **Keywords**: 18-fluorodeoxyglucose positron emission tomography/computed tomography; metabolic tumor parameters; primary gastrointestinal lymphoma.

EP-0085

Correlation of lymph node size with PSMA expression & SUVmax values on Ga-68 PSMA PET/CT imaging

B. Sönmezer[1], E. Acar[1], E. Erkoyun[2], G. Çapa Kaya[1]; [1]Dokuz Eylül University, Faculty of Medicine, Department of Nuclear Medicine, İzmir, TURKEY, [2]Dokuz Eylül University, Faculty of Medicine, Department of Public Health, İzmir, TURKEY.

Aim: To evaluate whether there is a correlation between lymph node size and SUVmax values observed with PSMA expression on Ga-68 PSMA PET/CT images. **Method:** A total of 178 patients with prostate cancer diagnosis and Ga-68 PSMA PET/CT tests performed at our center from February 2015 to February 2017 were assessed.According to imaging results, 25 patients with lymph node metastasis and no bone metastasis were included in the study.Imaging was performed for staging in 10 patients(40%), for re-staging in 11 patients(44%) and to assess response to treatment in 4 patients(16%).Lymph nodes with Ga-68 PSMA involvement differentiated from the background activity in the literature were accepted as positive.As a result, all lymph nodes with PSMA expression differentiated from background activity had short axis diameters and SUVmax values measured on axial images.Lesion-based statistical analysis was completed with SPSS v22.0(IBM,USA).The correlation between lymph node size and PSMA expression was tested with the Spearman correlation test, while differences in PSMA expression of lymph nodes 8 mm and smaller or larger than 8 mm were analyzed with the Mann Whitney U test. **Results:** The mean age of patients was 70±7.0 years.Mean PSA value was 58.1±85.1 ng/ml, with mean Gleason score calculated as 8±1.1.In 25 patients, a total of 88 lymph nodes were identified as having PSMA expression.Of these 6 were lymph nodes located in cervical/thoracic region, 35 were abdominal and 47 were located in the pelvic region. The mean size of cervical/thoracic lymph nodes was 14.3±10.2 mm and mean SUVmax value was 6.9±8.5. For abdominal lymph nodes,mean size was 8.4±5.6 mm with mean SUVmax value of 11.5±9.5.Pelvic lymph nodes had mean size of 9.2±6.8 mm with mean SUVmax value of 7.3±7.1. When all lymph nodes are assessed together, lymph nodes with size 8 mm and smaller (2.7-8.0)had mean SUVmax value of 5.5±3.6, while those larger than 8 mm(8.1-31.4)had mean SUVmax value of 15.5±10.5.PSMA expression was identified even in the 2.7 mm lymph node(SUVmax: 3.1). The correlation between lymph node size and SUVmax expression was at moderate levels and significant (r:0.68, p<0.001).The SUVmax measurements for lymph nodes of 8 mm and smaller size were significantly different to those from lymph nodes above 8 mm in size(p<0.05). **Conclusion:** To the best of our knowledge, there is no study in the literature researching the correlation between PSMA expression and lymph node size.Our findings show that the lower limit for detection of PSMA expression is below 8 mm.Additionally, as lymph node size increases,PSMA expression increases.

EP-0086

18FDG PET-CT for Characterization of Adrenal Lesions in Cancer Patients

A. Tzonevska, M. Garcheva, I. Kostadinova; Acibadem City Clinic, Sofia, BULGARIA.

The purpose of the study was to differentiate benignant from malignant adrenal lesions in PET-CT study applying standard image reconstruction and reconstruction algorithm QClear. **Material and methods:** 18FDG PET-CT is performed in 19 cancer patients with adrenal lesions (known from previous CT) using hybrid scanner Discovery IQ, GE Healthcare and standard study protocol. The PET reconstruction is made using OSEM (Ordered Subsets Expectation Maximization) and QClear algorithm for reconstruction (Regularized Reconstruction Iterative Algotitm). The quantitative analysis of 18FDG uptake is performed with SUV_{max} measurement using both reconstructed images from OSEM and QClear in adrenal lesions, liver, mediastinum. The CT images are used for density measurement in adrenal lesions in HU. We accepted the following criteria for differentiation benignant from malignant lesions: SUV_{max}. in the lesion ≤ SUV_{max}. in the liver, SUV_{max} in the lesion < 3,0 and CT density <30HU. **Results:** The assessment of SUVmax in mediastinum in OSEM and QClear images was mean 2,34 ±0,46 vs 2,49±0,67. The assessment of SUVmax in liver was mean 3,13±0,58 vs 3,41±0,54. No significant difference was fond,p<05.The adrenal lesions in 6 patients were defined as malignant. The lesions' SUVmax. in OSEM images was mean 6,45±3(3,3÷16), in QClear- mean SUVmax. 11,94±7,1(7÷22), p<0,001.CT density was mean 39(32÷48). In 17 lesions/13 patients the measurements of SUVmax. in OSEM images was mean 1,7±0,5(0,9÷2,6); in QClear images SUVmax was mean 2,1±(2÷3); HU mean 13(2÷27) significantly different from HU in malignant lesions, p=0,017. These lesions were defined as benignant. The assessment of the images, reconstructed with Q.Clear show better quality and increased quantification accuracy. **Conclusion:** The differentiation of benignant from malignant lesions of adrenal glands in cancer patients applying the accepted PET-CT criteria for adrenal lesion characterization and the new reconstruction algorithm QClear, increase the diagnostic capabilities and suggest higher study accuracy.

EP-0087

Ratio of mediastinal lymph node to primary tumor FDG uptake improves prediction of nodal metastases in lung cancer

F. Al-Lhedan, R. Klein, J. Gardner, L. S. Zuckier, W. Zeng; The Ottawa Hospital, Ottawa, ON, CANADA.

Introduction: When staging lung cancer with FDG PET, moderate or intense FDG uptake by mediastinal lymph nodes is usually considered predictive of nodal metastases; mild uptake with a low maximum standard uptake value (SUV_{LNmax}) is regarded as equivocal. Mediastinal lymph node to primary tumor SUV_{max} ratios ($SUV_{N/T}$) have been proposed as superior to absolute lymph node SUV_{LNmax}, but findings in the literature are inconsistent. In this study we compare SUV_{LNmax} and $SUV_{N/T}$ as predictors of nodal metastases in a series of over 100 consecutive patients with NSCLC, including a subgroup with SUV_{LNmax} of 1.0-3.0. **Methods:** This retrospective study examined patients with newly diagnosed NSCLC who underwent FDG PET/CT for initial staging followed by mediastinal nodal resection. 107 consecutive patients who met the inclusion criteria over 6 months were included. Intensity and size of the primary lung tumor and lymph nodes were recorded. Measured SUV_{LNmax}, derived $SUV_{N/T}$ values, and nodal size, were correlated with pathology results. ROC curves were generated for $SUV_{N/T}$, SUV_{LNmax}, and lymph node size. Area under the ROC curve (AUC) was compared amongst all 3 parameters. Optimal benign/malignant cut-off values and their corresponding sensitivities and specificities were derived from the coordinate which minimized the Euclidean distance to the ideal coordinate. **Results:** 181 lymph nodes were analyzed in 107 patients (age: 67.0 ± 9.9, F:M=55:52). The average SUV_{max} was 12.8±7.8 for primary lung tumors and 4.7±4.1 for lymph nodes. A median interval of 27 days elapsed between scan and surgical resection. AUC was greater for $SUV_{N/T}$ than SUV_{max} (0.803 vs. 0.569, n=98, p=0.001) in patients with SUV_{LNmax} of 1.0-3.0. Optimal cut-off sensitivity and specificity were 78.3% and 73.3% for $SUV_{N/T}$, and 52.2% and 65.3% for SUV_{LNmax}, respectively. No benefit of $SUV_{N/T}$ over SUV_{LNmax} was noted in patients with SUV_{LNmax} >3.0. The volume of lymph nodes did not have any predictive value when SUV_{LNmax}<3.0 (AUC:0.467) but had slight value when SUV_{max}>3.0 (AUC:0.651). **Conclusion:** In patients with SUV_{LNmax}<3.0, the ratio of SUV_{LNmax} to primary tumor SUV_{max} is more predictive than SUV_{LNmax} alone. One should consider FDG avidity of the primary tumor when evaluating uptake in mildly FDG-avid lymph nodes.

EP-0088

Artifacts and physiologic soft tissue activities on NaF PET/CT bone images

I. Sarikaya[1], A. Elgazzar[1], M. Alfeeli[2], A. Sarikaya[3]; [1]Kuwait University Faculty of Medicine, Kuwait, KUWAIT, [2]Mubarak Al Kabeer Hospital, Kuwait, KUWAIT, [3]Trakya University Faculty of Medicine, Edirne, TURKEY.

Aim: The use of NaF PET/CT bone imaging is increasing. It is important to be aware of certain artifacts as well as physiologic soft tissue distribution of 18F-Fluoride. In this study we aimed to identify specific artifacts and normal soft tissue activities on NaF PET images. **Materials and Methods:** In this study, we retrospectively reviewed forty (40) NaF PET/CT images taken at our institute. Cases with artifacts were identified and physiologic soft tissue distributions of 18F-Fluoride were noted. **Results:** In addition to common well known minor PET/CT artifacts, in 4

patients there were prominent asymmetric or symmetric cold defects in bone and soft tissues in the lower thoracic, abdominal and pelvic regions on attenuation corrected PET images acquired in arms down position. Whereas cold defects were identified in the skull in 3 patients imaged in arms up position. In addition to physiologic intense renal and bladder activity in every case, there was mild diffuse physiologic blood pool activity in the heart and large blood vessels in majority of the patients which was more prominent on early images. Activity in the choroid plexus of the lateral ventricles and varying degree of bowel activity (mild or moderate) were more common than occasional mild diffuse activity in the liver, gallbladder, spleen, muscles and stomach. **Conclusion:** In routine NaF PET/CT studies, we recommend acquiring whole body images in arms up position to eliminate cold defects in the spine, ribs and pelvic bones, particularly in obese patients. Head and neck region should be imaged in arms down position. Mild diffuse activity in the spleen is likely due to blood pool activity. Faint diffuse activity in the liver could be from both blood pool activity and hepatocellular uptake. Occasional mild activity in the gallbladder is likely secondary to hepatobiliary excretion of activity which can also explain bowel activity. Mild diffuse muscle activity could be physiologic.

EP-0089

Normal tissue 18-FDG activities are similar after either 60 or 90 minute uptake

*D. W. Ap Emyr[1], P. A. Fielding[1], C. Marshall[2], **N. C. D. Morley**[2]; [1]Cardiff and Vale University Health Board, Cardiff, UNITED KINGDOM, [2]Cardiff University, Cardiff, UNITED KINGDOM.*

Purpose: Comparison of standardised uptake value (SUV) in normal tissues, between scans after 60 or 90 minute (min) FDG uptake period. **Introduction:** There is quiet controversy about optimal uptake period for FDG in oncology PET/CT. 3 published studies of dynamic tumour FDG PET reported that increasing uptake over the first 120 min (and sometimes beyond) is a feature of malignancy. We use 90 min for most work in our centre, along with some similar centres in our country. Longer uptake decreases overall activity due to decay and excretion, and requires workflow time and space, which are always under pressure. Current EANM guidance is 60 min. To enable drug trial participations, our first-daily scan is performed after 60 min uptake. We obtain scans at both 60 and 90 min with otherwise similar parameters and hypothesised a difference in uptake values between these two scan types, in particular: greater blood pool SUV on the earlier studies. **Subjects and Methods:** Oncology FDG body scans, 4MBq/kg of 18F labelled FDG, supine uptake period. LYSO PET/CT, 3 min bed position, attenuation correction and time of flight reconstruction. Patients consented to retrospective research. We excluded lymphoma patients (often extensive avid disease or recent chemotherapy). Twenty 60 min subjects were identified, along with the best-match that day regarding height, mass and blood glucose concentration, as a 90 min control. SUVmax and SUVmean were recorded from blood pool (mediastinal vessels), liver parenchyma (central right lobe), muscle (gluteals) and cerebellar vermis (SUVmax only, sagittal

reconstruction to avoid upper slice noise). Manual 2.5cm spherical region of interest, supervised by an experienced PET/CT reporter, Xeleris workstation. Graphical and statistical analysis of data including uptake/time plots, case/control histograms and unpaired t-tests. **Results:** No clear correlations were seen in the graphical analyses. (No gradient on time activity plots, or dichotomy of population histograms). Mean blood pool SUVmean was lower after 90 min uptake, 2.22 versus 2.48, with p of 0.06. The 95% confidence interval of the difference was (-0.51 to +0.0076). The statistical power of that comparison is 76%, alpha 5%. **Discussion:** These findings do not support our hypothesis that uptake values or blood pool activity are different in normal tissues between 60 and 90 minute scans. Observed differences are not statistically significant, though the study is underpowered and inconclusive. We plan to extend this study to 40 paired observations (power estimate > 90%) and collect data on subjective assessments of scan quality.

EP-0090

Irisin, an exercise-induced hormone, targets glioblastoma tumor in vivo PET/CT imaging may serve as a novel theranostic agent

Y. Lin[1], H. Chiu[1], W. Chang[1], Y. Lin[1], Y. Chung[1], T. Yen[1], F. Huang[2], **C. Huang**[1]; [1]*Chang Gung Memorial Hospital, Taoyuan, TAIWAN, [2]National Taiwan University, Taipei, TAIWAN.*

Introduction: Exercise has beneficial effects on cancer. Specifically, exercise delays cancer development and progression. Herein, we reported that an exercise-induced myokine, irisin, not only can inhibit cancer cell proliferation and invasion and even retard tumor growth, but also has tumor-targeting capabilities that may facilitate its use as a new theranostic gent. **Methods:** U-87 MG cells (5×10^6) were subcutaneously injected into the front flanks of 6–8-week-old male nude mice. The resultant tumors were allowed to grow until they reached volumes of 200–500 mm^3 in volume. The acquired PET/CT images through 15-minute static scans 10 minutes after U-87 MG glioma xenograft mice (n = 6) were injected with radiolabeled ^{68}Ga-DOTA-irisin (6.6-7.4 MBq). All images were generated with scatter correction, random correction and attenuation correction (AC). The average radioactivity concentration within the tumor or organ of interest was obtained by determining the mean pixel values within the multiple ROIs (% ID/g). The tumor-to-normal organ radioactivity ratio, which was calculated for organs such as the muscles, heart, lung, liver, kidney and brain, was also calculated for comparisons. At the end of each scan, the tumor and major tissues/organs were dissected, and *ex vivo* autoradiography and immunohistochemistry images were acquire to confirm the tracer distribution results. **Results:** Other than the kidneys (19.55 ± 2.14% ID/g) and urinary bladder, in which the level of radiolabeled irisin uptake was influenced by excretion, intriguingly, the highest level of uptake occurred in U-87 MG tumors (5.74 ± 1.86% ID/g). The tumors were clearly delineated and displayed significant tumor-to-background contrast. The liver (4.67 ± 0.82%ID/g), lung (3.255 ± 0.28%ID/g), heart (2.2 ± 0.08%ID/g), spleen (1.45 ± 0.23%ID/g),

pancreas (1.14 ± 0.28%ID/g), bone (0.43 ± 0.19%ID/g), muscle (1.03 ± 0.27%ID/g) and brain (0.26 ± 0.07%ID/g) displayed comparatively low levels of ^{68}Ga-DOTA-irisin uptake. The levels of ^{68}Ga-DOTA-irisin uptake in white and brown adipocytes were 1.69 ± 0.06%ID/g and 1.71 ± 0.08%ID/g, respectively, values that were more than 60% higher than those in muscle, results consistent with those of previous reports showing that irisin is taken up by fat. **Conclusion:** For the first time, the *in vivo* positron emission tomography (PET) imaging was performed to investigate the biodistribution profile of radio-isotope-labeled irisin in a tumor xenograft mice model. The low median hepatobiliary excretion and background uptake values characteristic of ^{68}Ga-DOTA-irisin indicate that it is an attractive compound whose usefulness as a tumor molecular-targeting agent should be investigated further.

EP-0091

Somatostatine receptor PET/CT imaging in patients with sarcoidosis - preliminary report

J. Kunikowska[1], D. Pawlak[2], L. Królicki[1]; [1]Nuclear Medicine Department, Medical University of Warsaw, Warszawa, POLAND, [2]National Centre for Nuclear Research, Radioisotope Centre POLATOM,, Otwock, POLAND.

Sarcoidosis is a chronic inflammatory multisystem disease. Disease activity take important role in strategy treatment planning. Somatostatin receptor scintigraphy (SRS) can visualize sarcoid granulomas through binding of a radionuclide-coupled somatostatin analog to somatostatin receptors that are expressed in sarcoidosis. However, number of papers described using SRS in sarcoidosis are very limited. Currently wildly use PET technique with the better resolution allows use gallium labeled somatostatine analogues in diagnosis of sarcoidosis. The aim of the study was to analyses possibility of use ^{68}Ga-DOTATATE PET/CT in patients with suspicion or know of sarcoidosis to test organ involvement. **Material and Methods:** The study included 13 patients (6 man, 7 females, aged 51.5± 14.7) with suspicion or known sarcoidosis. All patients underwent somatostatin receptor imaging (SRI) with ^{68}Ga-DOTATATE PET/CT (60 minutes post injection of 120-160 MBq). PET/CT examinations underwent visual analysis on intensity uptake and semi quantitative analysis - measured by SUVmax. The SUVmax of involvement organ/ lymph node was compare to uptake in mediastinum. The active organ/lymph node was described if it was visualize and uptake was greater than mediastinum. PET/CT findings was compared with CT. **Results:** The median mediastinum SUVmax was 1.1±0.3. The main localization of sarcoidosis was chest lymph nodes (n=12/13) with median SUVmax 3.2. Additionally, two of them had active pulmonary lesions with SUVmax 2.2 and 2.7. Interesting, that extrapulmonary disease was found in 85% of the patients. Five patients demonstrated axillary and femoral lymph nodes involvement with median SUVmax 2.5. One patient had active disease in neck lymph node with SUVmax 3.7 and one in abdomen paraortic lymph node with SUVmax 2.3. Two patients had except lymph node, heart involvement with SUVmax 3.3 and 3.8, which changes treatment strategy. In one patient with

neurological disorders and problem with walking - muscularly sarcoridosis was suspect (SUVmax 2.0) and confirmed by muscle biopsy. One patient demonstrated eye localization (SUVmax 2.9) and in one additional focus in bone was found (SUVmax 4.5). SRI improved the yield of visualization compare to CT in 8 patients. **Conclusions:** Somatostatin receptor imaging using ^{68}Ga-DOTATATE PET/CT provides a useful imaging technique to organ involvement in patients with sarcoidosis.

EP-0092

Liver-spleen axis: hepatic and splenic metabolic activities are linked

G. Keramida[1], A. Dunford[2], C. D. Anagnostopoulos[3], A. M. Peters[4]; [1]Royal Brompton and Harefield Hospitals, NHS, FT, London, UNITED KINGDOM, [2]Brighton and Sussex Univerity Hospitals NHS Trust, Brighton, UNITED KINGDOM, [3]Biomedical Research Foundation Academy, Athens, GREECE, [4]Brighton and Sussex Univerity Hospitals NHS Trust, Clinical Imaging Sciences centre, Brighton Sussex medical School, Brighton, UNITED KINGDOM.

Aim: Splenic enlargement in non-alcoholic hepatic steatosis has created the concept of the liver-spleen axis. Our aim was to investigate the hypotheses that liver and spleen are metabolically coupled and that splenic metabolic activity is increased in hepatic steatosis. **Methods:** Splenic and hepatic FDG clearances were measured from 30 min dynamic PET using Patlak-Rutland graphical analysis and abdominal aorta for arteria input in 60 patioents undergoing routine clinical PET/CT.The gradient of the Patlak-Rutland plot (ki) was divided by the intercept (V(0)) to give FDG clearance normalised to distribution volume and multplied by glucose to give glucose uptake rate (MRGlu) in μmol/min/ml. Statistical "noise" in the plot was quantified as the normalised root mean standard deviation (NRMSD) of points from the regression line. CT density as a measure of hepatic fat content and SUV of tissues and left ventricular cavity (SUVLV) were measured from whole body PET/CT 60 min post-injection. Relations between variables where assessed using Pearson corellation analysis. We avoided corellations where a variable was present in both cp-ordinates; e.g splenic versus hepatic MRglu(glucose). SUV was based on weight so splenic SUV was correlated with ratio hepatic SUV/SUVLV, from which weight and blood glucose cancel out. **Results:** There was no significant difference in splenic MRglu between 8 patients with inactive (non-FDG avid) lympho-proliferative disease (LPD) , 26 patients with other avid malignancies and 13 patients with normal scans but was increased, on average approximately 2-fold, in 13 patients with active LPD.Hepatic MRglu was similar in all 4 groups. Active LPD patients were therefore excluded from further analysis. Splenic Ki/V(0) correlated positively with blood glucose (n=47; r=0.31;p =0.03) consistent with sensitivity of the spleen to insulin. Splenic Ki/V0 correlated with hepatic Ki/V0(r=0.60;p<0.0001). This correlation was stronger in studies with low NRMSD (r=0.69) compared with high NRMSD(r=0.57), arguing against an artefactual relation from using the same arterial input function. Moreover, splenic SUV correlated with hepatic SUV/SUVLV (r=0.30, p=0.04). Splenic (r=-0.32; p=0.03)

and hepatic (r=-0.50; p=0.003). MRglu correlated inversely with hepatic CT density, indicating increased metabolic activity in hepatic steatosis. **Conclusion:** Hepatic and splenic metabolic activities are coupled. Positive correlations of splenic Ki/V(0) with blood glucose and hepatic fat suggest that the slpeen , like the liver, is insulin-sensitive , partially explaining their metabolic linking.

EP-0093

Towards Diagnostic Reference Levels in PET-CT in Finland

J. Liukkonen, S. P. Kaijaluoto, P. M. Toroi, R. Bly; STUK - Radiation and Nuclear Safety Authority in Finland, Helsinki, FINLAND.

Introduction: The role of PET-CT has been significantly growing in the past years. The patient effective dose related to CT scanning varies based on the objective of the study. In numerous cases studies can be performed with notably lower doses compared to diagnostic CT. However, national DRLs have not been set. The aim of the current study was to assess patient doses related to PET-CT. **Methods:** The survey was conducted in 2015 by e-mailing a questionnaire to the all eleven departments equipped with PET-CT in Finland. The responses were asked for each equipment separately. Background information consisted manufacturer, model, the maximum number of slices and commission year. The questionnaire was limited to 18F-FDG studies on metabolism of brains, heart and whole body. For each target and the most common studies at least ten PET-CT examinations were asked to report. The following information was gathered: delivered activity [A]=MBq, volume CT dose index [CTDIvol]=mGy, dose-length product [DLPw]=mGy*cm, weight of patient [w]=kg, tube voltage [U]=kV and if contrast agent was used. Supplementary data included information on collimation, reconstructed slice thickness, pitch, rotation time, dose modulation, tube current, iterative reconstruction and phantom used for the dose calculation. Effective doses for 18F-FDG were calculated based on ICRP publication 128. CT-doses were evaluated based on literature (STUK-B 169, in Finnish). The questionnaire was made with Microsoft Excel 2010. R version 3.2.2 was used for data analysis. **Results:** The response rate was equal to 100%. In total 216 individual examinations were reported. Proportions between brains, heart and whole body examinations were 26%, 19% and 57%, respectively. 3D or 3D&TOF -techniques were used in 90% of cases. The medians of delivered activities were 225 MBq for brain, 260 MBq for heart and 309 MBq for whole body. The corresponding doses were 4.3, 4.9 and 5.9 mSv. Median doses due the CT imaging were 0.1, 1.6 and 3.6 mSv, respectively. The upper quartiles for CTDIvol were 3.5 mGy (brains), 3.1 mGy (heart) and 5.5 mGy (whole body). **Discussion:** Based on the current data the 18F-FDG dose is dominant. Nevertheless, all examinations involving use of ionizing radiation should be performed in accordance with the ALARA (As Low As Reasonably Achievable) principle. This requires optimization of CT-doses. As upper quartiles of CTDIvol values are significantly lower than DRLs for diagnostic CT, introducing specific DRLs for PET-CT studies may be beneficial for optimization of CT-doses.

EP-0094

Motion correction during dynamic FDG-PET/CT studies performed in the staging of breast cancer

T. Tokes[1], K. Kajáry[2], M. Dank[1], Z. Lengyel[2]; [1]Semmelweis University Center of Oncology, Budapest, HUNGARY, [2]Pozitron PET/CT Center, Budapest, HUNGARY.

Purpose: To evaluate interchangeability of different VOI delineation and motion correction methods in the assessment of dynamic FDG-PET/CT studies in breast cancer patients as well as to assess the interrater reliability of these methods. **Methods:** In our prospective study we included patients with malignant invasive breast tumors sized more than 20 mm without any distant metastases. Dynamic PET acquisition lasted for 60 minutes after tracer (FDG) injection. Every study was assessed by the same two experienced observer. To assess plasma activity we delineate sphere VOIs in the left ventricle of the heart sized 15 mm in diameter. To delineate tumor VOIs we applied 15 mm sized sphere VOIs placed over the tumors by using two different approaches to correct motion artifacts: I) subjective VOI location over the tumor with manual motion correction and II) semi-automatic VOI replacement by centering the sphere VOIs to the maximal detected activity in the tumor lesion on every time frames. Thereafter time activity curves were defined by both methods and FDG two compartment kinetic modelling was applied to assess K1, k2, k3 coefficients and to calculate Ki (the tracer flux constant, mL/min) and MRFDG (the FDG metabolic rate in the tissue, μmol/min/100g tissue). **Results:** 35 lesions detected during 34 dynamic studies were included in this current analysis. Interrater reliability of both methods proved to be excellent (ICC=0.89-0.99), except Ki measured by Method I, whereas only moderate agreement was found between the two observers (ICC=0.66). When applying Bland-Altman analysis to assess the agreement between the two methods, we find that Method II resulted in significantly lower values than Method I regarding k3 and Ki in case of both observers. In case of K1, k2 and MRFDG the two methods were considered to be in good agreement. **Conclusion**: Both applied methods proved to be reproducible and reliable, especially Method II, whereas every measured kinetic parameter showed excellent interrater reliability. Additionally, it seems like there could be significant effect of the different approaches of motion correction on the results of the kinetic modelling.

EP-0095

Mismatch Between68Ga-PSMA-HBED-CC PET/CT And mpMRI In Prostate Cancer Lesion Detection: Relation With Gleason Score, PSA Kinetics And Previous Therapy

G. Ferreira, I. Lucena Sampaio, L. Sobral Violante, J. Teixeira, H. Duarte; Instituto Português de Oncologia Francisco Gentil, Porto, PORTUGAL.

Purpose: To compare 68Ga-PSMA-HBED-CC PET/CT and multiparametric magnetic resonance imaging (mpMRI) ability to detect prostate cancer lesions and identify possible sources of diagnostic mismatch. **Subjects and Methods:** Thirty-seven male patients (mean age 71,1 ± 5,6 years) with suspected initial, recurrent or persistent prostate cancer underwent both 68Ga-PSMA-HBED-CC PET/CT and mpMR imaging. A maximum time threshold of 90 days between both exams was defined (mean 37,84 +- 25,25 days). Images were evaluated independently and only highly suggestive findings for prostate cancer lesions in the abdominal and pelvic region were considered. The diagnostic performance of each imaging modality for local and metastatic disease was accessed and the mismatch for malignancy detectability was determined using McNemar's test. Gleason Score, PSA kinetics (total PSA level, PSA doubling time and PSA velociy), previous primary therapy, including radical prostatectomy and external-beam radiotherapy, and androgen deprivation therapy (ADT) concomitant to imaging, were tested to predict false negative results using Fisher's exact test for nominal variables and Wilcoxon-Mann-Whitney test for independent samples (p<0.05). **Results:** Thirty patients had at least one pathologic finding demonstrated by either PET/CT or mpMRI, of which 25 (83.3%) had local disease and 10 (33.3%) metastatic involvement. Local disease detection performance was superior in mpMRI: 23 (92.0%) detected patients against 15 (60.0%) by PET/CT (p=0.039). PET/CT failure to detect local malignancy was associated with lower median total PSA level (U=35.0; p=0.022) and PSA speed (U=16.5; p=0.041). Patients under ADT were also associated with PET/CT false negative results (p=0,007). PET/CT detected all 10 patients with metastatic disease, while mpMRI failed to detect 4 patients with regional lymph node metastasis, 1 with bone metastasis and 1 with both lymph node and bone involvement. This mismatch was also statistically significant (p= 0.031). MRI failure to identify pathologic findings was associated with higher Gleason score (U=41.0; p=0.043). The remaining tested variables were not associated with false negative results. **Conclusion:** This study stated the importance of PET imaging in the correct staging of advanced prostate cancer, as well as the added value of mpMRI in detecting local disease, particularly in patients with low total PSA and PSA velocity or under ADT. 68Ga-PSMA uptake may be impaired due to a dynamic progression in the downregulation of PSMA expression during androgen deprivation, possibly leading to false negative results in PET/CT.

EP-0096

Measurement of urinary radiation dose of PET patient by using Compton camera

D. Kano[1], R. Enomoto[2], S. Hosokawa[3], R. Wakamatsu[4], T. Watanabe[5], Y. Nakagami[1], M. Yamaguchi[1]; [1]National Cancer Center Hospital East, Kashiwa, JAPAN, [2]ICRR, University of Tokyo, Kashiwa, JAPAN, [3]University of Hirosaki, Hirosaki, JAPAN, [4]College of Science, Ibaraki University, Ibaraki, JAPAN, [5]Tokyo Metropolitan University, Tokyo, JAPAN.

Purpose: Standardized Uptake Value (SUV) is the most common estimate of metabolic activity used in clinical PET. Variation caused by urinary excretion of FDG influences the accurate measurement of SUV; however, we do not measure radioac-

tivity concentration in the urine. In this study, we developed a measuring system that could easily estimate quantity of the radiopharmaceutical during the urination by using Compton camera equipped with crystal scintillators. **Material and Methods:** The detector which we developed used four scintillation counters(CsI(Tl)) which were readout by photomultipliers. A photon was scattered with the first crystal (Compton scattering), and these photoelectric absorption events were sorted by using the second crystal, estimating an arrival direction of the gamma ray by applying Compton kinematics. Because we could squeeze a field of view without shielding, we could measure only specific source even when there were several sources. Based on the number of the gamma ray, we estimated radioactivity concentration in the urine. We initially performed simulation to determine whether we could measure only gamma rays from spurious urine. We focused on the restroom in the nuclear medicine institution where a toilet stool was located axis of the detector placed in the adjacent room. In this measurement experiment, we located a large source (spurious patient 200 MBq) near a small source (spurious urine 44MBq) in the toilet stool. **Results:** When there was not a spurious patient, the number of the events agreed with approximately 10% of errors. We compared spurious urine using the five-seconds energy spectrum that we measured with or without the spurious patient. We determined that in both cases energy spectrum detected 511keV gamma beam derived from FDG similarly. However, when there was the spurious patient present, there was increase of events at 300 keV or less. From these results, the detector which we developed demonstrated that we could measure only urinary radiation in the toilet stool when there was patient in the restroom. **Conclusion:** In the simulation of measuring urinary radioactivity concentration by using the Compton camera with limited field of view, even in the presence of patients after FDG administration, we can estimate only the quantity of the drug included in the urine.

EP-0097

Effects of iMAR on CT and PET reconstructions in patients with metal hip implants

P. Holdgaard[1], L. Grønnemark[1], N. Bebbington[2]; [1]Sygehus Lillebælt, Vejle, DENMARK, [2]Siemens Healthineers, Århus, DENMARK.

Aims: iMAR (iterative Metal Artifact Reduction) reduces metal artefacts in CT reconstruction, and can therefore impact on quantification of attenuation-corrected PET images. Having previously assessed improvements in CT and PET quantification in a phantom with hip prosthesis, the aim was to evaluate effects of iMAR on CT and PET data in patients with metal hip prostheses. **Materials and Methods:** This study comprised 20 [18F]-FDG oncology/infection patients (10 males, 10 females) with bilateral (n=10) and unilateral (n=10) hip prostheses ('prosthesis group'), and 10 sex and age-matched controls without prostheses ('control group'), scanned on a Siemens Biograph mCT Flow-64. CT data for the prosthesis group were reconstructed both with iMAR and without ('standard' reconstruction), and AC PET data reconstructed both with iMAR CT and with standard CT

reconstructions. Standard CT and PET data were reconstructed for controls. VOIs were assigned to a reference region (prostate/vagina) in syngo.via. Differences in CT HU and PET SUV were compared between iMAR and standard CT reconstructions in the prosthesis group using paired t-tests. iMAR reconstructions in the prosthesis group were also compared with controls using unpaired t-tests. Reconstructions were also qualitatively scored (0-5) by one expert observer. **Results:** CT iMAR versus standard reconstructions in prosthesis group: Mean HUs were significantly greater on iMAR (31.5±15.0HU) compared with standard reconstructions (-34.7±87.6HU) (p=0.002), and SD in HUs were significantly lower on iMAR (22.7±4.5HU) compared with standard reconstruction (87.8±76.0HU) (p=0.001). Quality scores were significantly better on iMAR (4.3±0.6) compared with standard reconstruction (1.3±1.3) (p<0.001). CT iMAR reconstructions in prosthesis group versus controls: Mean HUs for controls (37.9±4.1HU) were not significantly different to the iMAR prosthesis group, but SD in HUs was significantly lower for controls (16.5±2.4HU) compared with iMAR prosthesis group (p=0.001). PET iMAR versus standard reconstructions in prosthesis group: There was a small but significant difference in mean SUVmax for iMAR (2.9±0.5) and standard reconstructions (2.8±0.5) (p=0.002). Differences in SUVmean, SD and quality score were not significant. PET iMAR reconstructions in the prosthesis group versus controls: SUVmax for controls (2.9±0.5) was not significantly different to iMAR reconstructions in the prosthesis group (p=0.70), but SUVmean was significantly greater in controls (2.2±0.3) compared with the iMAR prosthesis group (1.9±0.3) (p=0.05). **Conclusions:** iMAR dramatically improves CT data in patients with hip prostheses, giving results that are almost comparable to patients without prostheses, and gives a small but significant improvement in accuracy of SUVmax, although PET differences are not visually noticeable.

EP-0098

[18F] - NaF positron emission tomography assessed microcalcifications in symptomatic and asymptomatic human carotid plaques

*H. Hop[1], S. A. de Boer[1], M. Reijrink[1], D. J. Mulder[1], P. W. Kamphuisen[1], M. H. de Borst[1], R. A. Pol[1], C. J. Zeebregts[1], J. L. Hillebrands[1], J. Doorduin[1], H. H. Boersma[1], **R. H. J. A. Slart**[1,2]; [1]University Medical Center Groningen, Groningen, NETHERLANDS, [2]University of Twente, Enschede, NETHERLANDS.*

Introduction: The appearance of microcalcifications in atherosclerotic plaques is associated with their vulnerability. Recently, [18F]- Sodium Fluoride ([18F]-NaF) positron emission tomography (PET) has been shown to target microcalcifications. To gain more insight in [18F]-NaF as marker of plaque vulnerability, we compared *ex vivo* PET assessed [18F]-NaF uptake between symptomatic and asymptomatic human carotid plaques. Furthermore, we compared [18F]-NaF uptake with established calcification assessed with high resolution computed tomography (CT). **Methods:** Carotid plaques from patients undergoing carotid endarterectomy were collected. Renal artery specimens from healthy kidney donors were used as negative controls. All tissue samples

were incubated in 49.4±7.2 Mbq [^{18}F]-NaF for 60 minutes. Then, a micro PET and a micro CT scan was performed. The average PET [^{18}F]-NaF uptake in each tissue sample was calculated and expressed as percentage of the incubation dose per gram of tissue (%Inc/g). PET and CT images of carotid plaques were co-registered, after which the distribution of PET positive volumes (microcalcification) was compared with CT positive volumes (macro- and microcalcification). **Results:** 23 carotid plaques (17 symptomatic, 6 asymptomatic) from 23 patients (median age 72 years, interquartile range [IQR] 61-75, 85% male) and 15 renal artery specimens from healthy kidney donors (median age 55, IQR 41-63, 33% male) were included. The average [^{18}F]-NaF uptake in symptomatic carotid plaques was comparable with the uptake in asymptomatic carotid plaques (median 2.32, IQR 1.98-2.81 vs. median 2.35, IQR 1.77-3.00 %Inc/g, P=0.92), and the uptake in carotid plaques was significantly higher than in renal arteries (median 2.32, IQR 1.86-2.80 vs. median 0.44, IQR 0.18-0.68 %Inc/g, P<0.00). In carotid plaques, a discordant pattern between CT assessed and [^{18}F]-NaF PET assessed calcifications was seen. Only a median of 10 % (IQR 4-25) of the total CT positive volume showed increased [^{18}F]-NaF uptake, while merely a median of 35 % (IQR 6-42) of the total PET positive volume was visible on CT scan. In renal artery specimens, no CT assessed calcifications could be identified. **Conclusion:** [^{18}F]-NaF PET may represent a different calcification-related process than CT and may therefore have potential additional value. We observed no clear differences in [^{18}F]-NaF PET uptake or pattern between symptomatic and asymptomatic plaques of high risk patients, indicating that this method may be of more value in earlier stages of carotid artery stenosis development.

EP-0099

FDG-PET/CT for evaluation of inflammation in the lumbar spine following surgery for lumbar disc herniation

C. C. Støttrup[1,2], M. Zadeh[3], C. Constantinescu[4], S. O'Neill[1], M. Ø. Andersen[1,2], A. Alavi[3], P. Høilund-Carlsen[4,2]; [1]Lillebaelt Hospital, Middelfart, DENMARK, [2]University of Southern Denmark, Odense, DENMARK, [3]University of Pennsylvania, Philadelphia, PA, UNITED STATES OF AMERICA, [4]Odense University Hospital, Odense, DENMARK.

Purpose: Back pain has great socio-economic impact, typically in the shape of prolonged sick-leave and increased use of pain killers. Patients with lumbar disc herniation (LDH) are often part of the labor force, and their condition greatly limits their work capacity and social life. Using FDG-PET/CT, this study evaluated changes in the lumbar spine of patients undergoing surgical intervention for their LDH. **Subjects and Methods:** 21 patients, aged 40-65 years, with first-time LDH found eligible for surgery were included. FDG-PET/CT was performed preoperatively, 6 weeks and 6 months post-operatively. Using a standardized protocol for patient reported outcome (PRO) and quantitative sensory testing (QST) patients' pain perceptions were registered pre- and post-operatively. Using ROVER software (ABX, Radeberg, Germany), the volume of interest, including the relevant disc and vertebra immediately above or beneath, was marked. Comparison was made between the three time points and correlated to clinical data (PRO and QST). **Results:** In general, patients with LDH had some degree of inflammation at their level of herniation prior to surgery (average SUVmean 2.97), an increase shortly after surgery (6 weeks - mean 5.68) followed by a later decrease (6 months - mean 3.27). However, this pattern was only seen in 16/21 (76%) of the patients, while in 5/21 (24%) there was a more variable pattern with a primarily increasing trend over time. At baseline, these two groups showed little difference in SUVmean (2.97 vs 3.19, p=0.41). However, over time a significant difference appeared: 6 weeks 5.68 vs 3.62, p=0.06; 6 months 3.27 vs 6.63, p=0.01. Correlating PRO-data with PET/CT measurements showed that patients with increased SUVmean also had more intense radicular leg pain both prior to surgery, but also predictive of 1 year outcome (r_s 0.49, p=0.02 & r_s 0.62, p=<0.01). Looking at back specific measures of pain perception and tolerance, we found multiple correlations at a statistically significant level. **Conclusion:** FDG-PET/CT showed distinct patterns of pre- and post-operative inflammation in the lumbar spine following surgery for LDH. There was an increase in FDG uptake immediately after surgery followed later by a decrease in most patients. This pattern was prevalent in ¾ of patients, whereas in ¼ there was a continued increase over time, which apparently was associated with more intense radicular leg pain and altered pain perception and tolerance. FDG-PET/CT in musculoskeletal conditions is a novel field; the current data point to a potentially useful application in the management of LDH.

EP-0100

Diagnostic performance of ^{18}F-FDG PET/CT semiquantitative analysis in the management of sarcoidosis

C. Altini, A. Niccoli Asabella, C. Ferrari, A. Cimino, C. Magarelli, E. P. Mossa, M. Fanelli, G. Rubini; Nuclear Medicine Unit, DIM, University of Bari "Aldo Moro", bari, ITALY.

Aim: To evaluate the clinical usefulness of ^{18}F-FDG PET/CT and its semiquantitative parameters for the assessment of treatment efficacy in patients with sarcoidosis. **Materials and Method:** Thirtyone consecutive patients (12 male, 19 female; median age 58 years, range 25-77 years) who performed ^{18}F-FDG PET/CT for sarcoidosis assessment were selected. All subjects performed ^{18}F-FDG PET/CT before any treatment (PET1) and after 6-12 months (PET2). SUVmax and SUVmean on PET1 and PET2 were collected. SUVs values were employed to evaluate the ratios with the liver (R-LIVERmax, R-LIVERmean) and the blood (R-BLOODmax, R-BLOODmean). The difference between the PET1 and PET2 values were evaluated (ΔSUVmax, ΔSUVmean, ΔR-LIVERmax, ΔR-LIVERmean, ΔR-BLOODmax, ΔR-BLOODmean). Patients were classified as Responders (R), Partial-Responders (PR) and Non-Responders (NR). Cohen's K test was used as a measure of agreement between clinical staging and PET1 staging. Comparisons between PET1 and PET2 semiquantitative parameters were performed by t-student test. The chi-square test was performed to evaluate the association between the response groups and the clinical staging and the therapy performed. ANOVA tests, followed by student-newman-keuls

post-hoc test, were performed to assess the differences of the Δ semiquantitative parameters into the response groups, stage groups (Thoracic, Extrathoracic and Systemic) and therapies groups (None, Corticosteroids and Corticosteroids and Immunosuppressive drugs). Relationship between Δ semiquantitative parameters and number of involved sites was detected using Pearson's correlation coefficient. **Results:** Seventeen patients (54.8%) had a complete metabolic response (R), 4 (12.9%) were PR while 10 (32.3%) had no metabolic response (NR). A fair agreement between clinical staging at the time of PET1 and stage of disease resulted by PET1 was found by Cohen's K (K=0.398). The chi-square test showed that response groups were not related neither to stage of disease (p=0.59) nor to therapy performed (p<0.079). The comparison between each Δ semiquantitative parameter showed a statistical significant decrease from PET1 to PET2 (0.0001<p<0.002). The comparison between Δ mean values in relation to response groups showed to be statistically significant (0.001<p<0.005). Conversely, they did not show statistical significancy in relation to the clinical stage groups and to the kind of therapy performed (p>0.05). Pearson's coefficient demonstrated a reverse correlation between number of sites still involved by disease after therapy and each Δ semiquantitative parameters (p≤0.0001). **Conclusion:** ^{18}F-FDG PET/CT is a useful technique for the evaluation of sarcoidosis and semiquantitative parameters should be considered. Further studies are needed to determine the long-term impact of ^{18}F-FDG PET/CT on clinical outcomes.

EP-0101

Comparisons of cerebral glucose metabolism and striatal DAT binding in PD patients with and without RBD

Q. Xu, P. Wu, C. Jiang, H. Yu, J. Wu, C. Zuo; Huashan Hospital of Fudan University, Shanghai, CHINA.

Abstract Objective: REM sleep behavior disorder (RBD) can appear in any clinical course of Parkinson's disease (PD) which is characterized by loss of dopamine transporter (DAT) and a unique metabolic brain network (PD-related pattern, PDRP). It is regarded as a prodromal stage of synucleinopathies and also to be related with an aggressive course of PD. This study aims to identify the differences of functional neuroimaging phenotype between PD patients with RBD (PD+RBD+) and without RBD (PD+RBD-) by using a dual-tracer design. **Methods:** Two groups of PD patients were recruited in this study, including 38 with PD+RBD+ (age 63.8±5.6years) and 38 with PD+RBD- (age 64.3±6.2years), which were matched with age, sex and disease duration. 17 age-matched healthy volunteers were also included as controls. All subjects undertook PET imaging with both 11C-CFT and 18F-FDG at the same time. Sub-regional dopamine transporter (DAT) tracer uptake of bilateral caudate, anterior putamen and posterior putamen was calculated respectively using ScAnVp software to measure the striatal dopaminergic dysfunction. The expression of PDRP was computed in each subject using a voxel-based network quantification algorithm based on the PDRP we previously identified in a cohort of 33 PD patients and 33 healthy controls. Normalized regional FDG metabolism between groups was compared voxel-to-voxel using two-sample t-test by application of statistic parametric mapping (SPM). **Results:** The striatal DAT distribution significantly decreased in PD patients compared with healthy controls, and the patients with PD+RBD+ tended to lose more DAT than PD+RBD- group although it didn't reached significance. PDRP expression was significantly elevated in PD patients compared with healthy controls, and it was also found elevated in PD+RBD+ patients relative to PD+RBD- patients (P<0.05). Regional FDG uptake in right palladic-putamen area, right thalamus and bilateral rectal gyrus were increased in PD+RBD+ cohort compared with PD+RBD- cohort (P<0.001). **Conclusion:** These findings suggest that PD patients, paralleling with RBD, may have more damage of DAT distribution and have specific spatial metabolism pattern, which may provide a clue to understand the clinical features.

EP-0102

Quantification and Reduction of respiratory induced errors in attenuation correction of PET data using respiration averaged CT: a simulation study

P. Ghaffarian[1,2], F. Fatemi[3], P. Geramifar[4], M. Ay[3,5]; [1]PET/CT and Cyclotron Center, Masih Daneshvari Hospital, Shahid Beheshti University of Medical Sciences, Tehran, IRAN, ISLAMIC REPUBLIC OF, [2]Chronic Respiratory Diseases Research Center, National Research Institute of Tuberculosis and Lung Diseases (NRITLD), Shahid Beheshti University of Medical Sciences, Tehran, IRAN, ISLAMIC REPUBLIC OF, [3]Department of Medical Physics and Biomedical Engineering, Tehran University of Medical Sciences, Tehran, IRAN, ISLAMIC REPUBLIC OF, [4]Research Center for Nuclear Medicine, Tehran University of Medical Sciences, Tehran, IRAN, ISLAMIC REPUBLIC OF, [5]Research Center for Molecular and Cellular Imaging, Tehran University of Medical Sciences, Tehran, IRAN, ISLAMIC REPUBLIC OF.

Purpose: We investigated the impact of using the ACT data (respiration-averaged CT) in attenuation correction process in order to reduce the amount of respiratory artifacts produced in thorax region in Positron Emission Tomography/Computed Tomography (PET/CT) images. We evaluated the improvement in parameters such as maximum standardized uptake value (SUVmax) and size in different respiratory traces for multiple lesion sizes in different locations of the thorax and abdomen in PET images. **Subjects and Methods:** Respiratory motion patterns were simulated in 4D XCAT phantom based on common breathing cycle and pattern in real patients. Lesions with different diameters were simulated in different locations of liver and lungs. The emission data produced by XCAT was then converted into PET sinograms using the software for tomographic image reconstruction (STIR). The attenuation in PET sinograms were corrected using end inhalation CT (EICT), end exhalation CT (EECT), and average CT (ACT) respectively. It should be noted that stationary PET images (without the respiratory motion) were reconstructed, and evaluated as the stationary truth. **Results:** Using EICT for attenuation correction, the respiration pattern with 35-millimeter diaphragm motion results in %53 error in SUVmax estimation in comparison with the stationary images for a 9-milimeter lesion in the liver. For the same tumor and di-

aphragm motion, the use of EECT results in %139 overestimation of the tumor volume relative to the stationary image, and hence this results in %40 underestimation of SUVmax , which is significant. The use of ACT in attenuation correction can reduce this amount of error in SUVmax estimation up to %10 for this lesion. Other diaphragm motions (15 and 25 mm), and lesion sizes (15 and 21 mm), follow the same pattern, and the ACT based attenuation correction shows lower errors. The ACT-based attenuation correction shows significant improvement in SUVmax (p-value=0.003, 0.041 for 9-mm and 15-mm lesions respectively). **Conclusion:** The amount of respiratory induced errors in the quantified values of both SUVmax and the volume of the tumors depend on the location of the tumor, its diameter, the amplitude of the diaphragm motion, and the CT image we use for attenuation correction. Overall, ACT shows better results in comparison with the aforementioned techniques for attenuation correction of PET data in thorax region.

EP-0103

Is the incremental diagnostic value of Mammi PET higher than MRI on detection and characterization of breast lesions with equivocal conventional imaging modalities?

L. Pan, M. Sun; Fudan University Shanghai Cancer Center, shanghai, CHINA.

Purpose: The aim of our work is to evaluate the added diagnostic value of a dedicated breast PET (MAMMI) and breast MRI in detection and characterization of breast lesions with equivocal mammography and/or ultrasound. **Subjects & Methods:** 45 patients with total 60 breast lesions with mammography (n=24) and/or ultrasound (n=43) were enrolled. Final histopathological evaluation was performed within one week after all patients went MAMMI with 18F-fluorodeoxyglucose and breast MRI. **Results:** For ultrasound, 19 of 58 lesions were considered positive, 20 of 58 negative and 17 of 58 equivocal, while for mammography, 7 of 39 lesions were considered positive, 18 of 39 negative and 14 of 39 equivocal. Most lesions that can't be determined were classified as BIRADS 4 on both ultrasound (11/17, 64.7%) and mammography (11/14, 78.6%). By percutaneous or surgical biopsy or further excision, all the undetermined lesions were confirmed. In all 31 equivocal lesions from ultrasound and/or mammography, 15 and 2 were correctly classified by MAMMI as positive and negative respectively with one false negative lesion while 11 and 2 were correctly classified by MRI with 5 remained equivocal. The overall accuracy of MAMMI was 98.3%. When equivocal lesions on MRI were classified as positive, the overall accuracy of MRI was 98.3%, the same as MAMMI, while the figure was dropped to 91.7% when classified as negative. **Conclusion:** Results indicate that MAMMI seems superior to breast MRI in diagnosing breast lesion, reducing ultrasound and mammography ambiguous findings and increasing the overall accuracy, although further evaluation are required.

EP-0104

The diagnostic performance of a dedicated breast PET (MAMMI) in patients with small and dense breasts in China

L. Pan, M. Sun; Fudan University Shanghai Cancer Center, shanghai, CHINA.

Purpose: The currently standard breast cancer screening tools such as mammography and breast MRI were reported to be unpromising in tumor detection in women with dense breast tissue. However, unlike women in Europe and the United States, women in Asia usually have rather small breasts with dense tissue. The purpose of this study was to evaluate the diagnostic performance of a dedicated high-resolution breast PET (MAMMI) in those women. **Subjects & Methods:** 93 consecutive patients with suspicious breast lesions and planning for further operation were enrolled. MAMMI was performed after 5 mCi FDG administration in patients with breast lesions. The macroscopical findings at operation and/or histopathological analysis were regarded as golden standard. MAMMI findings were compared with mammography, ultrasound and breast MRI. **Results:** 78/93 patients had malignant and 15/93 benign findings. The sensitivity values were 93.6%, 76.5%, 67.6% and 55.9% and specificity values were 66.7% 81.8%, 63.6% and 50% for MAMMI, MRI, mammography and ultrasound, repectivley. The positive predictive value for MAMMI in differential diagnosis of malignant and benign breast lesions was 93.6% and NPV was 66.7%. The diagnostic accuracy was 89.2%, 77.8%, 66.7% and 57.8(P<0.05) for MAMMI, MRI, mammography and ultrasound, respectively. **Conclusions:** MAMMI which providing metabolism information yielded better sensitivity, accuracy and PPV than other conventional imaging modalities for detecting malignant lesions in woman with small, dense breast tissues. Combining MAMMI and MRI may improve the whole diagnostic performance compared to MAMMI alone.

EP-0105

FDG uptake in a dedicated breast PET (MAMMI): correlation with histopathological prognostic factors

L. Pan, M. Sun; Fudan University Shanghai Cancer Center, shanghai, CHINA.

Purpose: To assess the correlation of primary breast tumor maximum standardized uptake values (SUVmax)and tumor to non-tumor SUVmax ratio (T/N ratio) of MAMMI with histopathological prognostic factors such as oestrogen receptor(ER),progesterone receptor (PR),human epidermal growth factor receptor 2 (HER2) status and Ki-67 proliferation index. **Subject & Methods:** Between October 2016 and April 2017, 45 consecutive patients with breast cancer were enrolled. The traditional prognostic factors (age, menopausal status, tumor size, histopathological type, histologic grade, hormone receptor status and Ki-67 level) were evaluated with SUVmax of MAMMI. Spearman's rank correlation, Wilcoxon and $\chi^{(2)}$ test were utilized for statistical analysis. **Results:** The mean SUVmax of the 45 tumors was 24.21±14.20 and the mean T/N ratio was 5.17±2.86. There was a positive correlation between SUVmax and T/N ratio (r=0.85, P<0.05). T/N ratio was superior to SUVmax as they both were significantly correlated with histological type, histological grade, estrogen receptor and Ki-67. Though SUVmax and T/N

ratio were both higher in larger tumor size, PR(+) and HER2 (+) cases, there's no significant correlation was found between SU-Vmax and T/N ratio with tumor size, PR and HER2 status. There was no influence of age or menopausal status on SUVmax and T/N ratio. **Conclusion:** SUVmax and T/N ratio reflecting the expression of some biological features of primary breast tumors had a strong relationship with some known prognostic parameters and may be useful for predicting the prognosis of breast cancer. And T/N ratio is more valuable served as a potential factor than SUVmax.

EP-0106

Contribution of ^{18}F-FDG PET/CT to conventional imaging techniques in the suspicion of recurrence in patients with uterine cervical cancer: preliminary results

P. Garcia - Talavera[1], F. Gómez-Caminero[1], C. A. Achury[1], L. G. Diaz[1], M. J. Doyague[2], P. Soria[3], J. Corredera[2], B. Pérez[1], P. Tamayo[1]; [1]Nuclear Medicine Department. Hospital Universitario de Salamanca, Salamanca, SPAIN, [2]Gynecology and Obstetrics Department. Hospital Universitario de Salamanca, Salamanca, SPAIN, [3]Radiotherapy Department. Hospital Universitario de Salamanca, Salamanca, SPAIN.

Purpose: To evaluate the contribution of ^{18}F-FDG PET/CT to conventional imaging techniques in the suspicion of recurrence in patients with locally advanced uterine cervical cancer. **Subjects and Methods:** Seventeen patients with locally advanced uterine cervical cancer (3 adenocarcinoma and 14 squamous cancer) were included. Most of them had been treated with chemo and radiotherapy, and, in some cases, combined with surgery. A total of 21 ^{18}F-FDG PET/CT were performed to these patients, from October 2014 to December 2016, at the University Hospital of Salamanca (Spain), in a Biograph mCT Flow PET/CT (SIEMENS). Other imaging techniques (MRI, and/or CT and/or ultrasonography) as well as gynecological examination were previously performed to all patients. For the PET/CT acquisition all patients fasted for at least 4-6 hours (glycaemia inferior to 150 mg/dl). A total body scan (from skull base to mid thigh) was acquired 60 minutes after the intravenous administration of 5 MBq/kg of the radiotracer. PET/CT interpretation was cualitative, with the support of the semicuantitative parameter SUVmax, and it was reported by an experienced nuclear medicine physician. PET/CT results were correlated with anatomo-pathological study and/or clinical/radiological follow up. The median follow up was 12,3 +/- 6,7 months. **Results:** With the results of conventional techniques, before performing PET/CT, patients were classified into three groups: With recurrence (12), without recurrence (1) and with doubtful recurrence (8). With PET/CT results, patients were classified as: With recurrence (10), without recurrence (7) and with doubtful recurrence (4). PET/CT made a significant contribution to all cases of negative PET/CT results (7/7) and to 60% (6/10) of the cases with positive results in PET/CT. In 4/10 positive PET confirmed the result of the conventional techniques. **Conclusions:** ^{18}F-FDG PET/CT is an useful technique in the diagnosis of patients with suspicion of recurrence of uterine cervix cancer, avoiding unnecessary surgeries, helping to classified doubtful cases of other imaging techniques and confirming recurrence, previously to a curative treatment with radical intention. Because of these, we recommended the inclusion of this technique in the diagnostic assessment of these patients.

EP-0107

Combined model-based and patient-specific dosimetry for ^{18}F-DCFPyL, a PSMA-targeted PET agent

R. F. Hobbs, D. Plyku, E. Mena, S. P. Rowe, Z. Szabo, S. Y. Cho, M. G. Pomper, G. Sgouros; Johns Hopkins University, Baltimore, MD, UNITED STATES OF AMERICA.

Objectives: Prostate-specific membrane antigen (PSMA), a type II integral membrane protein highly expressed in prostate cancer, has been extensively used as a target for imaging and therapy. Among the available PET radiotracers, the low-molecular-weight agents that bind to PSMA are proving particularly effective. We present the complete dosimetry results of ^{18}F-DCF-PyL in nine patients with metastatic prostate cancer. **Methods**: Nine patients were imaged using sequential PET/CT at approximately 1, 12, 35, 70 min with a final PET/CT approximately 120 min after the intravenous administration of 320 MBq (8.7 ± 0.2 mCi) ^{18}F-DCFPyL. Time-integrated-activity coefficients were calculated and used as input in OLINDA/EXM software to obtain dose estimates for the majority of organs of interest. For the lacrimal gland and lens, S-values were calculated using Monte-Carlo models based on idealized anatomy of the lacrimal gland eye, lens and tear film covering the eye. Patient-specific volumes and activity from the PET/CT scans were then input into the S-value to obtain lacrimal gland and lend AD values. Monte-Carlo based models were also developed for the dose calculation to two major salivary glands (parotid and submandibular) using CT-based, patient-specific gland volumes for S-values and AD calculations. **Results**: The highest mean AD per unit administered activity of ^{18}F was calculated for the lacrimal glands, followed by the kidneys, urinary bladder wall, submandibular and parotid glands. The resultant mean effective dose was 17.1 ± 2.0 μSv/MBq, less than for ^{18}F-DCFBC (19.9 ± 1.3 μSv/MBq). The **S**-values for the lacrimal glands to the eye-lens (0.40 mGy/MBq-h), the tear-film to the eye-lens (1.78 mGy/MBq-h) and the lacrimal glands' self-dose (574.10 mGy/MBq-h) were calculated. Average **S**-values for the salivary glands are 3.58 mGy/MBq-h for the parotid self-dose and 6.78 mGy/MBq-h for the submandibular self-dose. The mean cross-dose **S**-value was 0.011 mGy/MBq-h from parotid gland to submandibular and 0.075 mGy/MBq-h from submandibular gland to parotid gland. **Conclusions**: Dosimetry evaluation of the complete ^{18}F-DCFPyL patient data set and previously unavailable Monte-Carlo model based dose estimates for the EL, LG and SMG for ^{18}F confirmed that the PET imaging with ^{18}F-DCF-PyL is feasible and safe. The Monte-Carlo models established in this study provided previously unavailable **S**-values for the dose calculation to the non-standard organs such as EL, LG, and SG for [18]F. These models can be used in future studies for dose estimation to these organs from other radio-isotopes that may be of interest for both diagnostic and therapeutic purposes.

EP-0108

Determinants of C-X-C motif chemokine receptor CXCR4 Expression after myocardial infarction with [68Ga] Pentixafor-PET/CT in correlation with cardiac MRI

M. Kircher, T. Reiter, A. Schirbel, S. Kropf, R. Werner, G. Ertl, A. Buck, H. Wester, W. Bauer, C. Lapa; Uniklinikum Würzburg, Würzburg, GERMANY.

Aims: Non-invasive imaging of the C-X-C motif chemokine receptor CXCR4/stromal cell-derived factor-1α axis with positron emission tomography/computed tomography using the radiolabeled chemokine ligand [68Ga]Pentixafor might offer new insights on the myocardial healing after acute ischemia. CXCR4 expression after myocardial ischemia was analyzed regarding its temporal orchestration, spatial distribution as compared to cardiac magnetic resonance tomography (CMR) as well as its prognostic value. **Methods:** 22 patients with (sub-)acute myocardial infarction (after catheterization) were included. Day 2 to Day 13 after the acute event were gaplessly covered by imaging with [68Ga]Pentixafor-PET/CT and CMR. Location and volumes of infarcted myocardium visualized by both modalities were derived. For analysis of a systemic inflammatory response, standardized uptake values (SUV) were obtained for bone marrow of thoracic vertebral bodies and the spleen and compared to a control patient cohort. Patient outcomes were assessed 1 to 14 months after initial ischemia. **Results:** In 17/22 patients (77.3%), upregulation of CXCR4 in the infarcted myocardium could be identified. CXCR4- and LGE-positive areas of infarcted myocardium substantially overlapped with larger extent in CMR. CXCR4 expression was independent from all clinical or CMR parameters and could be observed at all time points. However, intensity of [68Ga]Pentixafor uptake decreased with time after infarction (r=-0.73, p<0.01). No systemic inflammatory response could be demonstrated in comparison to controls. At follow-up, no prognostic value of intensity or extent of CXCR4-positivity could be demonstrated. **Conclusions:** In this pilot study, upregulated CXCR4 expression was present in the majority of patients up to 2 weeks after infarction. Chemokine receptor expression peaked early after ischemic injury, most likely due to inflammatory cell infiltration. Further studies are needed to fully disclose the underlying biology as well as individual prognostic implications for therapy and patient outcomes.

EP-0109

Development of low dose CT protocols with acceptable CT image quality for CTAC of PET data:Phantom Study

Z. Mojabi[1,2], P. Ghafarian[3,4], H. Ghadiri[1,2], M. Bakhshayeshkaram[3,4], M. Ay[1,2]; [1]Department of Medical Physics & Biomedical Engineering, Tehran University of Medical Sciences, Tehran, IRAN, ISLAMIC REPUBLIC OF, [2]Research Center for Molecular and Cellular Imaging, Tehran University of Medical Sciences, Tehran, IRAN, ISLAMIC REPUBLIC OF, [3]Chronic Respiratory Diseases Research Center, National Research Institute of Tuberculosis and Lung Diseases (NRITLD), Shahid Beheshti University of Medical Sciences, Tehran, IRAN, ISLAMIC REPUBLIC OF, [4]PET/CT and Cyclotron Center, Masih Daneshvari Hospital, Shahid Beheshti University of Medical Sciences, Tehran, IRAN, ISLAMIC REPUBLIC OF.

Aim: Our purpose was to minimize the radiation exposure of CT for whole-body PET/CT imaging by reducing tube current (mAs) and tube voltage (kVp) while keeping CT image quality in acceptable level. **Methods:** For optimization, baseline dose was defined from a whole-body PET/CT examination of all patients, and then QA and cylindrical phantom were scanned with Discovery 690 GE PET/CT scanner that equipped with 64-slice CT. The fixed tube current (mA) methods was performed with various tube voltage (80, 100, 120, 140 kVp), tube current (10- 100 mA), 1s rotation time, Standard (STD) and PETAC filters, and slice thickness (3.75 mm). Optimization of low dose CT protocol was designed based on both qualitative and quantitative factors (MTF, contrast to noise ratio (CNR) and image noise). To assess the influence of new CT protocol on PET images, a house-made image quality phantom, including 6 cylindrical inserts, was filled with an F-FDG solution with a 2:1 radioactivity ratio compared to the background. **Results:** At 80 kVp and 100 mA, 3.75 mm slice thickness, the CNR and SD was 111.79 HU, 8.1 with STD filter while CTDI and CNR decreased 90%, 70% at 10 mA, Noise increased by factor of three. By increasing kVp from 140 to 100, at 50 mA, CNR decline 31% and MTF demonstrated 86.3%, 77.7%, 61.2%, and 44.4% , also 88.4%, 78.4%, 57.1%, 35.7%, when spatial resolution were 0.75, 1, 1.5, 2 lp/cm and each group includes 5 slits. PET data shown SUV was 1.8 while mA reduced from 100 to 30 mA at 80 and 120 kVp therefore CTDI decline almost 70% for both kVp. SNR was 16.8 for 37 mm insert at 120 kVp, 100 kVp where tube current was 50 mA. CV was 5.1 at 120 kVp, 10 to 50 mA while it reduced to 4.2 at 80 kVp at the same mA. **Conclusion:** This study demonstrates the possibility of reduction patient dose from CT while image quality could sustain for diagnostic radiology goals. At 10mA, SNR reduced 11% by decreasing kVp from 120 to 80 for 13 mm insert while DLP was diminished. It should be noted, using ultralow fixed mA compared with high mA method may cause to miss smaller lesions, but, choosing desirable low tube current and tube voltage cause to reduce patient dose while diagnostic radiology goals will be preserved. The developed protocol is under evaluation in clinical environment with patient data.

EP-0110

The relationship between Ga-68 PSMA accumulation intensity and Gleason score, PSA levels in primary staging and evaluation of biochemical recurrence of prostate cancer: The preliminary results

G. Ege Aktas, 22030[1], V. Çaloglu[2], N. Can[3], H. Akdere[4], F. Ustun[1], G. Durmus Altun[1]; [1]Trakya University Medical Faculty Department of Nuclear Medicine, Edirne, TURKEY, [2]Trakya University Medical Faculty Department of Radiation Oncology, Edirne, TURKEY, [3]Trakya University Medical Faculty Department of Pathology, Edirne, TURKEY, [4]Trakya University Medical Faculty Department of Urology, Edirne, TURKEY.

Purpose/Introduction: Prognostic behavior of prostate carcinoma is defined histopathologically by Gleason score (GS). GS

is the sum of GS-1, GS-2; GS-1 is determined based on the appearance of most common cell morphology and GS-2 is based on the second prominent morphology or commonly the most aggressive part. Prostate specific antigen (PSA), GS, stage, histologic grade are the factors in determining the risk group, therapy selection. Prostate cancer cells exhibit varied degree of increased expression of prostate-specific membrane antigen (PSMA); its level correlates with poorly prognostic factors such as high GS. PSMA can be visualized by Ga-68 PSMA-PET/CT, increasingly used for staging, detection of local recurrence, or metastases. The aim of this study was to assess the relationship between intensity of Ga-68 PSMA uptake in the lesions and GS, PSA level at initial, at time of PET/CT. **Material-Methods:** Patients with histopathological diagnosis of prostate cancer who were referred for Ga-68PSMA-PET/CT were retrospectively reviewed. PET images were analyzed visually, semiquantitatively; SUVmax of the primary tumor, lesions suspicious for lymphatic or distant metastases, prostate bed, liver were noted. SUVmax of the lesions were compared to physiologic liver activity and Lesion/Liver index was calculated. The correlations between Lesion/Liver index and PSA level at initial, at the time of PET/CT and GS-1, -2, total GS were assessed. **Results:** Fifty patients were enrolled to the study. The mean age and mean PSA value of the patients at the time of diagnosis were determined as 67.31±8.54, 64.96±89.64, respectively. GS of the patient population was determined as mean: 7.74±1.22 (6-10). Mean Lesion/Liver index was 2.55±2.24. Ga-68-PSMA PET/CT indicated local disease in 22, distant metastasis in 28 patients. There were pelvic lymph node metastases in 26 while 8 patients exhibited metastasis in distant lymph nodes. 26 patients showed bone metastases; only five patients had visceral metastasis. GS of the patients with systemic metastasis were significantly higher (p:0.04). Lesion/Liver index was correlated with initial PSA level, GS-1, -2 and total GS (spearman's rho; r:0.516-p<0.001, r:0.519-p<0.001, r:0.536-p<0.001, r:0.638- p<0.001, respectively). We could not determine a significant correlation between PSA level at time of PET/CT and Lesion/Liver index (r:0.238, p:0.092). PSA level at the time of PET/CT was associated with number of lesions detected on PET/CT and the presence of systemic metastasis (p=0.036). **Results:** Our preliminary results suggest that GS and initial PSA level correlates with the intensity of Ga-68 PSMA accumulation in primary and metastatic lesions of prostate cancer patients.

EP-0111

Application of F-18-Sodium Fluoride (NaF) dynamic PET-CT (dPET-CT) for defect healing: comparison of biomaterials in an experimental osteoporotic rat model

C. Cheng[1], V. Alt[2], L. Pan[1], U. Thormann[2], R. Schnettler[3], A. Dimitrakopoulou-Strauss[1]; [1]DKFZ, Heidelberg, GERMANY, [2]University Hospital Giessen-Marburg GmbH, Giessen, GERMANY, [3]University Hospital Giessen-Marburg GmbH, giessen, GERMANY.

The aim of current study was to measure and compare the efficacy of the multifunctional bioabsorbable implant in an animal model of bone defect healing using ^{18}F-Fluoride dPET-CT. **Meth-ods:** Osteoporosis was induced by ovariectomy and a calcium restricted diet in each rat. Alternatively, a sham-operation was performed in the control group (n = 8). After three months, rats were operated to create a 4mm wedge-shaped defect using an oscillating saw in the distal metaphyseal femur that was internally fixed with a metal plate without using any biomaterial. In addition, we examined another 8 groups of osteoporotic rats (n = 8) that have been treated with different biomaterials (Table 1). 18 weeks after osteoporosis induction and 6 weeks following femoral surgery, dPET-CT studies scan were performed with F-18-Fluoride (representative Fig 1). Standardized uptake values (SUVs) were calculated, and a 2-tissue compartmental learning-machine model (calculation of K1-k4, VB) and the influx (INF) as well as a non-compartmental model based on the fractal dimension (FD) were used for quantitative analysis of all rats. Multivariate analysis was used to evaluate the kinetic data. **Results:** The comparison of different biomaterials in the osteoporotic rats demonstrated that FD and SUV were the most sensitive parameters and revealed the best differentiation between empty defects and the biomaterial group (Wilcoxon rank-sum test, p<0.05). Among these biomaterials, the defect with PPGC+S (3:7) takes up most fluoride as strontium carbonate acts as a catalysator for the fixation of calcium. Further evaluation between two different biomaterials revealed k3 was the most sensitive parameter. **Conclusion:** Biomaterials have the potential to stimulate bone healing and improve treatment outcome for rats with osteoporotic fractures. We found PET scanning using ^{18}F-Fluoride to be a sensitive and useful method for evaluation of the development of bone healing with bone biomaterials. **Keywords:** Dynamic PET-CT, ^{18}F-Fluoride, osteoporosis, bone healing, biomaterials **Table 1.** The information of biomaterials **Figure 1.** A representative 3D fused PET-CT image (Left: CT; Middle: SUV; Right: fused PET-CT image).

EP-0112

Correlation between FDG uptake in the lung and pulmonary function in sarcoidosis patients treated with infliximab

M. Schwillens-Dirkx, M. Vredenduin, D. Hartmans, R. Keijsers; Sint Antonius Hospital, Nieuwegein, NETHERLANDS.

Introduction: Changes in forced vital capacity (FVC) are the most used measure of response to therapy in sarcoidosis patients. FDG PET/CT is used to identify inflammation in patients with active sarcoidosis. Earlier studies demonstrated that SUVmax correlated with pulmonary function tests (PFT). Establishing the correlation between the SUVmean and PFT can be of additional clinical significance in the assessment of therapy response in patients with diffuse parenchymateus sarcoidosis. The use of a lung segmentation tool may allow for a more precise measurement of FDG uptake in the total lung. **Subjects & Methods:** In a retrospective study we included 40 patients that underwent FDG PET/CT and pulmonary function tests prior to and after infliximab therapy. Metabolic activity of pulmonary sarcoidosis was measured by using a lung segmentation program provided by Hermes Medical Solutions (Stock-

holm, Sweden). Hounsfield units of low-dose CT determined the volume of interest (VOI) in PET to measure SUVmean and total lung glycolysis (TLG). FVC, forced expiratory volume in 1 second (FEV1) and diffusion capacity of the lung for carbon monoxide (DLCOc) was evaluated pre- and post-therapy. The percentage predicted of these PFT was used. We determined the correlation coefficient (r) and the statistical significance (p) between SUVmean of the lungs and PFT and between TLG and PFT. Furthermore the interobserver agreement for the use of the segmentation tool was determined. **Results:** Inter observer agreement was performed in 80 PET scans. Intraclass Correlation Coeffient (ICC) for SUVmean was 1.00 (95% CI 0.99 to 1.00) and for TLG 0.96 (95% CI 0.93 to 0.97). In the total group of patients the correlation between ΔSUVmean and ΔFVC was -0.36 (p<0.05). The correlation between initial SUVmean and DLCOc was - 0.43 (p<0.01) and between initial TLG and DLCOc was -0.33 (p<0.05). After infliximab treatment the correlation between TLG and FVC was -0.35 (p<0.05). No other correlations between SUV or TLG and other PFT was found. **Conclusion:** The Hermes lung segmentation program demonstrates an excellent inter observer agreement in sarcoidosis patients and seems therefore a reliable tool in evaluating pulmonary disease. The change in SUVmean and FVC showed a significant correlation in sarcoidosis patients pre- and post-therapy. In patients prior to infliximab treatment, a significant correlation was found between SUVmean and DLCOc as well as TLG and DLCOc. However, no significant correlation between the change in TLG and change in PFT was found.

EP-0113

The value of SUVmax is related with major chemotherapy-related tumor markers expression and serum tumor markers in gastric adenocarcinoma patients

X. Duan; the First Affiliated Hospital of Xi'an Jiaotong University, Xi'an, CHINA.

Aim: Previous research found that ^{18}F-fludrodeoxyglucose (^{18}F-FDG) positron emission tomography/computed tomography (PET/CT) is used as an important non-invasive tool for maximal measuring standardized uptake value (SUVmax) in patients with various tumors, including gastric adenocarcinoma. In our previous studies, we found that the expression of p53 was significantly correlated with SUVmax in non-small-cell lung cancer (NSCLC) patients. Hence, the aim of this present study was to assess whether there is a correlation between SUVmax and the status of the chemotherapy-related tumor marker expression or serum tumor markers in gastric adenocarcinoma patients. **Materials and Methods:** Immunohistochemistry was performed to detect lesions changes of Her-2, p53 and Survivin. ELISA analysis were used to quantify serum CA72-4, CA19-9 and CEA in gastric adenocarcinoma patients. The relationship between these parameters was assessed by Spearman correlation analysis. **Results:** Our results showed that SUVmax was associated with Her-2 and p53 which reflected chemotherapy-resistant of cancer patients. Moreover, the relationship between SUVmax and serum tumor markers was analyzed by linear correlation

analysis. At last, Serum CA72-4 and CA19-9 was used as independent parameters to establish equations for SUVmax by the linear regression models. **Conclusions:** These results suggested that SUVmax which was calculated either by 18F-FDG PET/CT or serum tumor markers, could be used to predict and evaluate Her-2 or p53 related chemotherapy resistant of gastric adenocarcinoma patients.

EP-0114

Adrenal Glands Uptake Patterns in 18F-Fluoroethylcholine PET/CT

E. J. Bialek[1,2], P. Kwasiborski[3], M. Dziuk[1,2], A. Mazurek[1,2], E. Witkowska-Patena[2], A. Giżewska[1,2], S. Piszczek[1,2], S. Osiecki[2]; [1]Affidea Mazovian PET/CT Centre, Warsaw, POLAND, [2]Department of Nuclear Medicine, Military Institute of Medicine, Warsaw, POLAND, [3]Angiology and Hemodynamics Laboratory, Regional Specialistic Hospital in Miedzylesie, Warsaw, POLAND.

Purpose: Adrenal glands present relatively wide range of radioactive choline uptake patterns and intensities on Positron Emission Tomography/Computer Tomography (PET/CT) scans. The reasons for why that is the case remain unknown. The aim of the study was to retrospectively correlate available data to check for their possible impact on radioactive choline adrenal uptake in prostate or renal cancer patients who underwent 18F-fluoroethylcholine (18F-FCH) PET/CT. **Subject:** Fifty 18F-FCH PET/CT studies (98 adrenal glands) were analyzed with respect to the adrenal glands shape, uptake pattern and maximum standardized uptake value (SUVmax) normalized by lean body mass. Thirteen parameters were recorded, assessed or counted, ratios of chosen parameters were calculated, and all above were checked for correlation with adrenal glands 18F-FCH uptake. Most important data included: SUVmax of the liver (automatic measurement - SUVmax.aut, and from the maximum right lobe parenchyma volume - SUVmax.vol), SUVmax and SUVmean of blood pool and SUVmax of a pituitary gland. Ratios of adrenal SUVmax to the liver, blood pool and pituitary gland SUVmax were also calculated. Correlations between pure adrenal SUV and their liver/pituitary ratios and patient's age, adrenal gland thickness, hormonal therapy were also assessed. **Results:** Adrenal glands presented diffused, focal or mixed uptake patterns. SUVmax of the right (4,3±1,2 SD) adrenal gland positively correlated with the thickness of the parenchyma at the point of maximal SUV value (5,3mm±1,5) (p=0,000). SUVmax of the right and left adrenal gland, as well as mean adrenal gland SUVmax, correlated with SUVmax of the pituitary gland (p=0,000, p=0,000 and p=0,001, respectively), with SUVmax.aut (p=0,008, p=0,000 and p=0,010, respectively) and SUVmax.vol of the liver (p=0,015, p=0,000 and p=0,019, respectively). Left adrenal maximum SUVs also correlated with mean liver SUVaut (p= 0,006) and SUVvol (p=0,009). Neither hormonal treatment nor patients' age significantly correlated with SUVmax values of adrenal glands in the studied group. **Conclusions:** There is a positive correlation between SUVmax values of adrenal glands and liver in 18F-FCH PET/CT images. SUVmax of adrenal glands also positively correlate with SUVmax of the pituitary gland and SUVmax values of the right

adrenal gland correlate with the thickness of its parenchyma. However, we speculate that normal adrenal glands FCH uptake depends on many determinants. Further prospective studies need to be conducted to define the factors influencing their normal radioactive choline uptake pattern.

EP-0115

Fluorodeoxyglucose-positron emission tomography disease activity assessment in patients with biopsy-proven giant cell arteritis

M. Simó[1], I. NAVALES[2], J. MESTRES[1], F. MARTINEZ[1], R. SOLANS[1], M. SALCEDO[1], M. BARIOS[2], M. BORONAT[2], J. CASTELL[1]; [1]HOSPITAL UNIVERSITARI VALL DE HEBRON, BARCELONA, SPAIN, [2]UNITAT IDI. HOSPITAL UNIVERSITARI VALL DE HEBRON, BARCELONA, SPAIN.

Aim: Disease activity assessment and spread in large vessel vasculitis is often challenging for physicians. In this study, we analyzed the intensity and distribution of FDG uptake at different vascular territories in patients with newly diagnosed Horton's disease. **Materials and Methods:** 40 consecutive patients with biopsy-proven giant cell arteritis were studied by two observers. For each patient visual analysis according 4 grade scale liver score reference (considering positive: grade equal or >2) and maximal standardised uptake value (SUVmax) were calculated at axillary, carotid, subclavian and vertebral arteries, brachiocephalic trunk, three aortic segments and in iliac territory. Half of them were treated with corticosteroids bolus on the days prior to the scan due to ischemic symptoms included (jaw claudication and visual symptoms). The study was performed from the skull to mid-thigh. Clinical data, blood tests and PET/CT results were recorded. **Results:** A total of 40 patients [30 women (75%), median age 72 (55-90)] involving 14 arteries and 42 Rois(3 for each territory) or Vois were selected for the analysis. PET/CT was performed after (median, intercuartilic range) 6.5 days (2 - 10 days) after symptoms. According liver score reference, 35 patients (87.5%) were positive and 5 (12.5%) were negative. Taking into account individual experience, two positive patients were finally classified as indeterminate/no conclusive result. No statistical differences were found between both observers to characterize as positive or negative each scan either to characterize each single territory (T student). Mean maximal standard uptake values (SUVmax) per patient measured at all the arterial territories were of 5.4 (2.9-13.3). In PET positive patients, the mean number of territories with a score ≥ 2 were 6 and with a score > 3 (greater than liver) were 4.5. In 34 patients, the highest vascular uptake was located in supraortic branches, remarking that 18 of them the most active territory was the vertebral. It could be related with visual symptoms and/or jaw claudication present in 65.7% of all patients of our serie. A polymyalgia FDG-PET pattern was observed in 9/50 patients (18%). **Conclusions:** FDG-PET characterizes good the extent and degree of inflammatory activity in patients with biopsy-proven giant cell arteritis even in those who have received previous corticoid treatment and with very good agreement between observers. In our serie, the territory most affected were the vertebral arteries.

EP-0116

Automated evaluation of normal uptake in different skeletal parts in ¹⁸F-sodium fluoride (NaF) PET/CT using a new convolutional neural network method

S. Lindgren Belal[1], M. Sadik[2], R. Kaboteh[2], O. Enqvist[3], J. Ulén[4], H. Kjölhede[5], O. Bratt[5], L. Edenbrandt[2], E. Trägårdh[1]; [1]Department of Translational Medicine, Division of Nuclear Medicine, Lund University, Malmö, SWEDEN, [2]Department of Clinical Physiology, Sahlgrenska University Hospital, Göteborg, SWEDEN, [3]Department of Signals and Systems, Chalmers University of Technology, Göteborg, SWEDEN, [4]Eigenvision AB, Malmö, SWEDEN, [5]Department of Translational Medicine, Division of Urological Cancers, Lund University, Malmö, SWEDEN.

Introduction: Understanding normal skeletal uptake of ¹⁸F-sodium fluoride (¹⁸F-NaF) in positron emission tomography/computed tomography (PET/CT) is important for clinical interpretation. Quantification of tracer uptake in PET/CT is often performed by placing a volume of interest (VOI) to measure standard uptake values (SUVs). Manual placement of this VOI requires a subjective decision and can only measure uptake in a specific part of the bone. The aim of this study was to investigate normal ¹⁸F-NaF skeletal activity in patients with prostate cancer at a stage of the disease prior to development of bone metastases, by using a new method that quantifies uptake in entire skeletal parts. **Material and Methods:** Patients with biopsy-verified high-risk prostate cancer and a negative or inconclusive bone scintigraphy and no metastatic lesions on ¹⁸F-NaF PET/CT (performed March 2008 - June 2010) were retrospectively included (n=48). Whole-body PET scans were acquired 1-1.5 h after i.v. injection of 4 MBq/kg ¹⁸F-NaF (max 400 MBq). CT scans were obtained immediately after the PET scan. Thoracic and lumbar vertebrae, sacrum, pelvis, ribs, scapulae, clavicles and sternum were automatically segmented in the CT images, using a method based on a convolutional neural network, to obtain the volume of each skeletal region. The network was trained using a separate group of CT scans with manual segmentations. Mean and maximum SUV (SUV_{mean} and SUV_{max}) were subsequently measured for each skeletal part in the PET scans. **Results:** Average (SD) SUV_{mean} for the skeletal regions were: Thoracic vertebrae 0.98 (0.20), lumbar vertebrae 0.96 (0.19), sacrum 0.75 (0.15), pelvis 0.73 (0.16), ribs 0.41 (0.11), scapulae 0.46 (0.11), clavicles 0.50 (0.16) and sternum 0.61 (0.13). Average (SD) SUV_{max} for the skeletal regions were: Thoracic vertebrae 1.95 (0.66), lumbar vertebrae 2.10 (0.78), sacrum 2.22 (0.77), pelvis 1.99 (0.82), ribs 1.19 (0.35), scapulae 1.94 (0.98), clavicles 2.00 (1.03) and sternum 1.68 (0.44). **Conclusion:** We present a new method to segment and quantify uptake in skeletal regions in ¹⁸F-NaF PET/CT. Various parts of the bone have different SUVs in patients with regional prostate cancer. Vertebrae and pelvis have higher SUVs than ribs. The highest SUV_{max} were found in the thoracic and lumbar vertebrae. The findings are of importance for interpretation of ¹⁸F-NaF PET/CT.

EP-0117

18FDG-PET/CT clinical impact in patients with pure testicular seminoma and residual retroperitoneal mass post-chemotherapy treatment

M. Arceluz, 1986, C. Gonzalez, S. Traverso, C. Tinetti, A. Osorio, G. Bruno; Fundación Centro Diagnóstico Nuclear, CABA, ARGENTINA.

Purpose: The purpose of the present study is to evaluate the clinical impact of 18FDG-PET/CT in patients with pure testicular seminoma (PTS) and residual retroperitoneal mass after chemotherapy in the post-treatment control CT. **Materials and Methods:** We analyzed retrospectively, between January 2009 and January 2016, 40 patients with the histological diagnosis of PTS, after surgical treatment and completed chemotherapy, with residual retroperitoneal mass by CT. They were all evaluated with 18FDG-PET/CT performed 6 weeks after chemotherapy was completed. Images were acquired on a GE Discovery STE-16 scan. For the assessment of metabolic activity visual parameters were taken into account. There were considered potentially active malignant tumor (positive PET scan) any area with an 18FDG uptake greater than the physiological blood-pool uptake, and also taking into account the maximum Standardized Uptake Value (SUVmax). The PET validation results were based on the histopathologic diagnosis in surgical patients or clinical/imagine followed up with CT or/ and 18FDG-PET/CT. **Results:** Overall 40 patients, 15 (37.5%) had negative 18FDG-PET/CT and 25 (62.5%) positive. From these last group, 2/25 (8%) the surgical specimens confirmed the PET scan findings; 15/25 (60%) were managed with chemo/radiotherapy showing response in the clinical/radiological followed up; 3/25 (12%) had disease progression. All these cases were considered true positive (TP). 5/25 (20%) did not receive treatment nor show disease progression therefore were considered false positive (FP). Those patients with negative 18FDG-PET/CT followed for a period between 1 and 8 years and showing no relapse disease were considered true negative (TN). 18FDG-PET/CT sensitivity, specificity, negative predictive value (NPV), and positive predictive value were 100%, 75%, 100%, and 80%, respectively. Also a significant difference of SUVmax values were found between TP and FP PET/ CT (p-value < 0.002), with a mean SUVmax of 6.6 for TP and 2.6 for FP. **Conclusion:** 18FDG-PET/CT is a potential useful tool to study patients with PTS and residual retroperitoneal mass post-chemotherapy, because of the high NPV, precluding unnecessary treatment and reducing morbid-mortality. Also, despite that not all 18FDG-PET/CT positive lesions had histological confirmation, we found that the SUVmax may help to differentiate TP and FP PET/ CT, because we found a significant metabolic activity difference between both groups. Further validation is needed with a large number of cases.

EP-0118

Clinical implications of FDG PET/CT in left ventricular assist device (LVAD) infection

*J. M. Sohns[1,2], **H. Kröhn**[1,2], J. D. Schmitto[1], A. Schöde[1], A. Haverich[1], F. M. Bengel[1]; [1]Hanover Medical School, Hanover, GERMANY, [2]*abstract contributed equally, Hanover, GERMANY.*

Purpose: LVADs are increasingly utilized for treatment of advanced heart failure. In recipients, device infection remains a significant risk and a diagnostic challenge. FDG PET/CT may aid in detection, localization and severity assessment, but its clinical impact is not yet well established. **Materials and Methods:** A consecutive series of 85 FDG PET/CT studies in patients with clinical signs of LVAD infection was included. FDG uptake was quantified by SUV and attributed to four different LVAD segments: driveline entry, subcutaneous driveline pathway, aggregate, and outflow prothesis. Clinical follow-up was obtained over a median period of 106 d after imaging, to identify changes of therapy and hard events. **Results:** PET identified focal inflammatory FDG hot spots (verified on attenuation-corrected and non-corrected images) in all cases. The driveline was most frequently affected (65/85 for driveline entry, and 74/85 for driveline pathway, 42/85 for aggregate and 49/85 for outflow tract). SUVs decreased with distance from the driveline entry point. For the driveline entry, where microbiologic samples were consistently available, ROC analysis identified a fair diagnostic accuracy of PET for presence of bacteria, with an optimal SUVpeak cutoff at 2.45 (AUC=0.72, p<0.001). In 31% of cases, PET triggered short-term surgical interventions (vacuum therapy, driveline revision, device replacement). Of note, the number of hospital admissions in the year following PET tended to be lower in subjects with PET-based therapy adjustment vs those without (5.2 vs 5.5). During long-term follow-up, there were 14 deaths due to sepsis, 8 deaths due to organ failure, 15 transplantations and 46 LVAD replacements. Kaplan-Meier analysis revealed no significant survival difference between subject with superficial vs deep LVAD segment infection by PET criteria (p=0.56). However, there was a trend towards adverse outcome in those subjects where PET identified lymph node involvement in addition to device infection (p=0.04). **Conclusions:** FDG PET-based assessment of localization and severity of inflammation in LVAD infection frequently leads to changes in therapeutic management, which translate into a reduction of subsequent hospital admissions. Scan results of a broader spectrum of LVAD recipients, including subjects with lower infective burden, may be necessary for in-depth analysis, but the systemic pattern of FDG distribution may provide prognostic information about the individual disease status.

EP-0119

Assessment of Effective Dose estimation in hybrid imaging (PET/CT)

G. Tosi[1], K. Marzo[1], A. Chiti[2], F. Zanca[3]; [1]Humanitas Research Hospital, ROZZANO, ITALY, [2]Humanitas University, ROZZANO, ITALY, [3]GE Healthcare, BUC, FRANCE.

Purpose: The aim of this study is twofold: 1) assess typical doses associated with hybrid imaging for PET FDG /CT exams (cumulative and contribution of each modality) for a large population; 2) assess the difference in effective dose estimation associated with PET/CT exams when fixed activity is administered vs patient-adapted activity for the same protocols. Differences in doses to the critical organ (urinary bladder) after FDG admin-

istration will be also estimated for the PET exam. **Methods and Materials:** DoseWatch tracking system will be used to collect patient information and dose data for WB PET FDG/CT exams. Effective dose and organ dose (for PET part only) associated with a fixed injected activity are obtained from DoseWatch, by retrospectively analyzing existing data. Specifically, for CT exams DLP values and effective dose values will be collected; for the PET part of the exams DoseWatch provides the administered activity, the effective dose as well as organ doses, based on the ICRP 103. Effective dose and organ dose (for PET part only) associated with a PET/CT exam where the administered activity is adapted to the patient weight will instead be estimated starting from the same retrospective database as above but using theoretical calculation as described in "FDG PET/CT: EANM procedure guidelines for tumor imaging: version 2.0" in Eur J Nucl Med Mol Imaging (2015) 42:328-354 or similar. For this theoretical calculation, the patient weight as well as the protocol information will also be taken from DoseWatch. The dose to the urinary bladder for the PET part will also be based on theoretical calculations **Results:** Data from 6900 CT doses and 1700 WB 18F-FDG doses were collected. CT mean DLP (mGy*cm) data values were (range between brackets): 1481.3 (76.1-7700.9). Mean effective doses (mSv) were: WB 18F-FDG 15.2±4.9. Mean administered activities (MBq) and effective doses (mSv) for radiopharmaceuticals used in PET were: WB 18F-FDG 333.9-6.4. The mean total effective doses (mSv) due to both modality were: WB 18F-FDG 21.5±5.2. Organ dose as well administered activity adapted to the patient weight are at the moment work in progress. **Conclusions:** The implementation of a dose tracking system to nuclear medicine is of great value for accurate and regular recording, reporting and analysis of patient's effective doses. It can help to improve the evaluation of radiation exposures in the clinical practice.

EP-0120
Impact of Specific Activity of ^{68}Ga-PSMA-11 on its accumulations in PSMA-expressing Tumors

A. Ahad, H. Zhang, A. Sadique, S. Larson, N. Pillarsetty, W. Weber; Memorial Sloan Kettering Cancer Center, New York, NY, UNITED STATES OF AMERICA.

Aim: ^{68}Ga-PSMA-11 PET imaging is now commonly used clinically for staging and restaging of prostate cancer. Because of the short physical half-life of ^{68}Ga the specific activity (SA) at the time of injection may vary significantly in clinical practice. A decrease in SA may decrease quantitative measures of tumor uptake of ^{68}Ga-PSMA-11 (such as SUVs), but also detection of lesions with low or moderate PSMA expression. To our knowledge, however, the magnitude of this effect is not well studied. Thus, we investigated how much uptake of ^{68}Ga-PSMA-11 decreases with decreasing SA in PSMA expressing prostate cancer cells *in vitro* and in tumor-bearing mice. **Materials and Methods**: PSMA-11 was labeled with ^{68}Ga for PET imaging and ^{67}Ga for *in vitro* studies. The SA was adjusted by addition of unlabeled PSMA-11. LNCaP and PC3-PIP cells were utilized for *in vitro* and *in vivo* evaluation. *In vitro*, LNCap and PC3-PIP cells were incubated for 5 min to 120 min with ^{67}Ga-PSMA-11 of different SA and the cell surface

bound and internalized fraction was measured. The *in vivo* uptake of ^{68}Ga-PSMA-11 was assessed with dynamic (60 min) PET/CT imaging. **Results**: *In vitro* studies in both LNCaP and PC3-PIP cells showed rapid uptake and internalization (14% for LNCaP and 27% for PC3-PIP of total) of radioactivity reaching 26±1.7% and 40±0.6% of the added activity, respectively, for a specific activity of 22 MBq/nmol. At a specific activity of 7.4 MBq/nmol, uptake in LNCaP and PC3-PIP cells decreased to 9±0.09% and 26±0.6%, respectively (p<0.001). However, *in vivo* imaging of LNCaP xenografts showed that the tumor uptake at 50-60 min was not significantly different between the high (SA 42.7MBq/nmol, 6.4±0.29%) and intermediate (10.7 MBq/nmol, 6.2±0.35%, p<0.8) SA of ^{68}Ga-PSMA. Only when the SA at the time of injection was decreased to 2.7 MBq/nmol, tumor uptake decreased to 2.8±0.12 %ID/g (p<0.004). **Conclusion**: Tumor uptake of ^{68}Ga-PSMA-11 *in vivo* was stable over a 4-fold variation of SA (2 physical half-lives of ^{68}Ga) and reduced only by 50% by a 16-fold decrease in SA (4 physical half-lives of ^{68}Ga). This suggests that quantitative measurements of tracer uptake in patients will be relatively insensitive to variations in specific activity. The data also supports the central production and shipping of ^{68}Ga-PSMA-11 over several hours.

EP-0121
Digestive incidentalomas in FDG-PET/CT images of patients with infectious endocarditis; relationship with the involved microorganisms

J. Ardila Mantilla, A. Rotger Regí, L. Reguera Berenguer, L. Lozano Murgas, J. Ardila Manjarres, J. Orcajo Rincón, C. Duran Barquero, A. Mari Hualde, R. Pascual Pérez, R. Pascual Pérez, J. Alonso Farto; Hospital Gregorio Marañón, Madrid, SPAIN.

Purpose: To determine the frequency of digestive incidentalomas and its relationship with neoplasias and other colorectal diseases in patients who underwent FDG PET/CT for infectious endocarditis caused by a variety of microorganisms. **Methods:** This is a retrospective study of patients with FDG-PET/CT imaging perfomed under the indication of infectious endocarditis between January 2013 to January 2017 in whom colo-rectal FDG uptake was reported. We describe the nature of the colorectal disease (confirmed with endoscopy/histopathology), the image findings and the microorganism involved. **Results:** 150 endocarditis PET CT reports were revised, obtaining gastro-intestinal findings in 18 patients**.** Mean age was 75 years, 13 were men and 5 women. The involved microorganisms were: S.bovis(2/18), E.faecalis(5/18), S.viridans(5/18), E.coli(2/18) and others(4/18). In the PET image the uptake was diffuse in 6 of the cases and focal in the 11 remaining. Single foci were found in 9 reports and multiple in 9. Mean SUVmax was 6,2. The morphology of the lesions was: polypoid structures in 7 patients, wall thickening in 6 and uptake without radiological translation in the remaining 5. Histologically, benign lesions were found in 55,6%, premalignant in 27,7% and malignant lesions in 16,7%. Excluding S.bovis, the frequency of onset was 37,5% of premalignant lesions and 12,5% of malignant lesions. **Conclusions:** Although the relationship between S.bovis endocarditis and col-

orectal lesions is well known, there is also a high prevalence of premalignant pathology and colorectal carcinoma in endocarditis caused by other microorganisms, especially E.faecalis and S.viridans. Its early detection is relevant for therapeutic management and prognosis. The need to perform a PET in this type of patients seems mandatory (prevalence of 13.3%).

EP-0122

Usefulness Of PET-CT In Non-Oncology Pathology: A Review Of Cases Of Patients Diagnosed With Erdheim-Chester Disease

M. Godoy Bravo, R. Reyes Marles, I. Sime Loayza, L. Frutos Esteban, L. Mohamed Salem, J. Navarro Fernandez, M. Castellon Sanchez, F. Nicolas Ruiz, M. Claver Valderas; Hospital Clinico Universitario Virgen de la Arrixaca, Murcia, SPAIN.

Purpose: To assess the importance of PET-CT as a complementary imaging technique in Erdheim-Chester disease (EC) diagnosis and its role in monitoring therapeutic response. **Subjects & Methods:** A total of four patients were analyzed by a retrospective study from 2012 to 2016, 3 males and 1 female aged between 46 and 76 years. At diagnosis, 3 of them presented constitutional syndrome and the fourth one had pain in the renal fossa. As common imaging diagnostic findings, all of their CT scans showed retroperitoneal fibrosis and bilateral hydronephrosis grade 2, as well as all patients had whole-body bone scintigraphy which findings were compatible with clinical suspicion. PET-CT was performed at diagnosis in all patients to complete extension study and to evaluate initial metabolic activity, and two more PET-CT were performed to assess metabolic response to treatment. **Results:** Identical findings were shown both in PET-CT and CT at initial diagnosis of the studied EC cases, although PET-CT findings added bone affectation not described in CT, but showed in bone scintigraphy. **Conclusion:** We highlight the importance of PET-CT performing as a complementary technique in the diagnosis of EC as it allows delimiting its extension and the possible bone affectation in only one diagnostic imaging test, as well as to evaluate therapeutic response. Unlike CT, PET-CT can determine the possible metabolic disease progression / regression in a comparative study with the same anatomical extension.

EP-0123

18 F FDG PETCT uptake patterns in the diagnosis of vascular graft infection

J. R. Orozco Cortés[1], H. Bowles[2], J. Ambrosioni[2], G. Mestres[2], M. Hernandez-Meneses[2], M. Almela[2], J. Llopis[2], D. Fuster[2], A. Moreno[2], V. Riambau[2], F. Lomeña[2], J. Miró[2], Hospital Clinic Endocarditis Study Group; [1]Hospital Clinic Valencia, Valencia, SPAIN, [2]Hospital Clinic Barcelona, Barcelona, SPAIN.

Introduction: Prosthetic vascular graft infection (PVGI) is a severe complication associated with high morbidity and mortality. Clinical diagnosis is complex, especially in low grade deep infections, requiring image testing such as CT angiography or scintig-

raphy, which have considerable limitations. The aim of this study was to evaluate the sensitivity and specificity of PET/CT with 18F-FDG in patients with suspected PVGI. **Subjects and Method:** Retrospective study with 49 patients, median age 63±12 years. Three uptake patterns were defined following published recommendations: (i) focal, (ii) patched (PAVGI criteria) and (iii) diffuse (no PAVGI criterion). Volumetric 3D reconstruction was performed to determine if the captures observed in the PET/CT were located in the wall of the VG or in the adjacent tissues, and if they overlapped with the suture points or puncture cannulas. The definitive diagnosis was established by means of a microbiological and/or histopathological evaluation of VG and/or clinical follow-up. **Results:** Median time of VG placement prior to PET/CT was seven months (IQR=2-36) and antibiotics were administered before the surgery in 44 patients (89.8%). There were no significant differences in PET/CT results with prior administration of antibiotics or with VG placement time (p>0.05). The sensitivity and specificity of 18F-FDG PET/CT were 88% and 73%. 18F-FDG PET/CT was able to identify in 15/17 cases of PVGI showing a focal (n=10) or patched pattern (n=5) and was true negative in 24/32 cases with either a diffuse pattern (n=14) or without uptake (n=10). Five of the eight false positive cases (63%) showed a patched pattern, and all of them were coincident with the application of adhesives for VG placement. Excluding these cases, the specificity of PET/CT was 94%. Additionally, PET/CT identified extra-prosthetic infections in seven cases: catheter (n=1), aneurysm (n=3), osteomyelitis (n=1) and infected hematoma (n=2). In six of these seven cases, the planimetry with subsequent volumetric reconstruction was determinant in establishing that infection was unrelated to VG, and also in correctly identifying all the focal uptake patterns secondary to suture (n=4) and cannula inflammation (n=3). **Conclusion:** PET/CT with 18F-FDG is a useful technique for the diagnosis of PVGI with a high specificity, particularly where volumetric reconstruction is performed. The patched pattern on PET/CT in which adhesives were applied for VG is not an indicator of infection.

EP-0124

Polyostotic Fibrous Dysplasia in McCune-Albright Syndrome Resembling Malignant Bone Dissemination: Pitfalls in PET/CT Interpretation

G. Horvatic Herceg[1], I. Bracic[1], M. Hrabak Paar[2], R. Petrovic[1]; [1]Department of Nuclear Medicine and Radiation Protection, University Hospital Center Zagreb, Zagreb, CROATIA, [2]Department of Diagnostic and Interventional Radiology, University Hospital Center Zagreb, Zagreb, CROATIA.

Background: McCune-Albright syndrome (MAS) is a rare disease defined by the triad of polyostotic fibrous bone dysplasia (FD), café-au-lait skin pigmentation, and premature puberty. FD can involve one or more skeletal sites, presents with a limp and/or pain, and occasionally has an associated pathologic fracture. There are only few reports on the use of 18F-FDG PET in MAS. Case report: Diagnostic CT scan revealed a liver mass in a 52 year-old female with a history of MAS, after which she was referred for 18F-FDG PET/CT for the clarification of tumor nature and

detection of malignant dissemination. Numerous foci of moderate-to-intense metabolic activity were scattered throughout the skeleton (SUVmax: 3.47-8.43). These matched the ground-glass lesions with sclerotic margins seen on CT scan, and were attributed to polyostotic FD. The right liver lobe mass appeared as a large, hypermetabolic lesion with a hypervascularized rim and rapid contrast washout. According to morphologic criteria, liver cancer could not be ruled out and the mass was surgically removed. Histopathology of the mass identified it as a hepatic adenoma. **Conclusion:** The low incidence of MAS leaves the potential for misinterpretation of multiple hypermetabolic bone lesions connected with polyostotic FD. Such lesions should be correlated with previous imaging results and biopsied in case of ambiguity. We want to emphasize the importance of interpreting FDG PET/CT scans in the overall clinical context.

EP-0125

Persistent Pneumothoraces Observed Following Percutaneous Transthoracic Needle Biopsy of Lung Nodules Mandates Vigilance when Interpreting PET-CT Images

L. S. Zuckier, J. Sommerfeldt, T. L. Miao, A. Gupta; The Ottawa Hospital, Ottawa, ON, CANADA.

Aim: To characterize the prevalence and characteristics of pneumothorax (PTX) following transthoracic needle biopsy (TTNB) as detected on PET-CT imaging. PTX has been characterized as a critical finding which mandates prompt communication with the referring physicians. **Materials and Methods:** 2,603 patients who underwent PET-CT scanning for characterization of solitary lung nodule in years 2013-14 were retrospectively identified. 336 patients (12.9%) had undergone TTNB at our institution between 1-21 days prior to PET-CT (mean 9.2±6.0 d). 3 studies were excluded due to presence of pleural catheters at the time of PET-CT scanning. All CT biopsies were performed using a 19G introducer and biopsies under fluoroscopic or ultrasound guidance were performed using 22 or 25G needles. 2 board-certified radiologists independently assessed the presence and size of PTX in all 336 CT scans; discrepancies were resolved by consensus. Demographic and other features were reviewed. **Results:** Of the 333 patients, 123 (36.9%) had PTX identified on 30' post-biopsy plain radiographs. 31.7% of these (39/123) were visible on the subsequent CTs performed in the days following biopsy. An additional 14 patients with PTX detected on subsequent CT scan did not have PTX identified on the initial post-biopsy plain films, of which 4 were medium and 4 were large size. Representative prevalence of PTX on CT were 47% at 1 day, 26% at 3 days and 10% at 1 week following biopsy. Average size of PTXs declined over the course of 16 days; no PTXs were detected after day 17 with the exception of 1 on day 20. **Conclusion:** Prevalence of PTX at PET-CT performed one day following TTNB is over 40%; of these, many were not visible on the post-procedure chest radiography. Furthermore, post-biopsy PTXs may persist for up to several weeks, and may not be readily visible unless studies are properly windowed and reviewed. As a critical finding which should be promptly assessed and reported, a high level of vigilance is recommended to identify PTX in patients who have undergone prior TTNB, even when no pneumothorax was apparent immediately following the biopsy procedure.

EP-0126

FDG-PET/CT in multiple myeloma: dual time point imaging results can predict response to treatment in patients recieving high dose chemotherapy

B. Oestergaard[1], R. Taghvaei[2], A. L. Nielsen[1], M. Z. Zirakchian[2], W. Y. Raynor[2], J. T. Asmussen[1], P. Holdgaard[3], T. Plesner[3], N. Abildgaard[1], A. Alavi[2], P. F. Hoilund-Carlsen[1]; [1]Odense University Hospital, Odense, DENMARK, [2]University of Pennsylvania, Philadelphia, PA, UNITED STATES OF AMERICA, [3]Vejle Hospital, Vejle, DENMARK.

Aim: In other settings, dual time point (DTP) FDG-PET/CT imaging has proved useful in differentiating malignant from benign lesions because increasing uptake from 1 to 3 hours is characteristic of malignancy. Our aim was to evaluate the potential predictive role of DTP FDG-PET/CT for response assessment of chemotherapy in multiple myeloma (MM). **Material and methods:** 19 patients (aged 53-75 years) with ≥ 2 focal lesions of at least 10 mm were selected. All underwent FDG-PET/CT as part of a prospective study before and two months after high dose chemotherapy with stem cell support. Scans were performed 60 and 180 min after tracer administration. Images were analyzed using an adaptive thresholding algorithm (ROVER software; ABX, Radeberg, Germany). Focal malignant lesions were localized on pre-treatment scans; maximum standard uptake value (SUVmax), mean SUV (SUVmean), and partial volume corrected SUVmean (pvcSUVmean) were obtained for each lesion. Lesional response to chemotherapy was classified as complete or partial in the post-treatment scan. A complete response meant complete resolution of the lesion in the post-treatment scan, partial response meant a still visible lesion. All statistical analyzes were done in SPSS 24 using repeated measurements-ANOVA. **Results:** All focal lesions in each patient were evaluated. In the pre-treatment PET studies, the increase in pvcSUVmean from 1 to 3 hours was significantly higher for lesions with partial response (n=35) compared to the lesions with complete response (n=108): 36.7% vs. 27.3%; P=0.020. Based on this lesion based analysis 6/19 patients had complete response in that all lesions showed complete resolution at end of treatment, whereas in 13/19 patients there was only partial response in at least one lesion. **Conclusion:** Our preliminary results suggest that a significant increase of FDG uptake at DTP PET/CT imaging before treatment is associated with a relatively poor lesion response to chemotherapy in patients with MM. The increase in pvcSUVmean is an appropriate indicator to evaluate DTP findings for this purpose.

EP-0127

FDG PET/CT in multiple myeloma: changed FDG uptake in the brain of patients receiving high dose chemotherapy

B. Oestergaard[1], S. P. Shamchi[2], R. Taghvaei[2], M. Z. Zirakchian[2], W. Y. Raynor[2], A. L. Nielsen[1], P. Holdgaard[3], T. Plesner[3], N. Abildgaard[1], A.

Alavi², P. F. Hoilund-Carlsen¹; ¹Odense University Hospital, Odense, DENMARK, ²University of Pennsylvania, Philadelphia, PA, UNITED STATES OF AMERICA, ³Vejle Hospital, Vejle, DENMARK.

Aim: Multiple Myeloma (MM) is caused by proliferation of a single clone of plasma cells in the bone marrow. Chemotherapy is one of the most commonly used treatments in these patients usually as a combination of corticosteroids or immune modulating agents. We examined the alterations in brain FDG uptake in MM patients before and after chemotherapy. **Materials and Methods:** Data were collected prospectively as part of the FULIMA project, a prospective study of dual FDG PET/CT and diffusion weighted MRI in MM patients without a history of prior chemotherapy. Patients with other inflammatory conditions, recent biological therapies, recent radiotherapy or surgery were excluded. FDG PET/CT was performed at baseline, before induction treatment and two months after high dose chemotherapy and stem cell transplantation. Supratentorial (including individual measurements for frontal, parietal, occipital and temporal lobes) and cerebellar FDG uptakes were measured by manual placement of regions of interest (ROIs) over these regions based on predefined criteria for each of them. The SUVmean across all slices was then calculated for each lobe and region, using OsiriX software, Bemex, Switzerland). **Results:** 30 MM patients, 7 females and 23 males, mean age 64.9 years (50; 81), were included. In patients who have received high dose treatment (n=20), the supratentorial brain SUVmean was 7.19±1.27 on before treatment scans compared to 6.81±1.03 after treatment (p<0.0001). The cerebellar SUVmean was also lower after treatment (decline from 6.39±1.03 to 6.0±0.63, p<0.0001). In patients who received non-high dose treatment (n=10), the supratentorial SUVmean was 7.04±1.46 before treatment compared to 6.92±1.92 after treatment (p=0.028). However, the cerebellar SUVmean was unchanged: before 6.48±1.18 versus after 6.46±1.57 (p=0.19). The average reduction in supra- and infratentorial uptake in patients with high dose treatment was 0.38 and 0.39, respectively. Corresponding values in patients with non-high dose treatment were 0.12 and 0.02, respectively. **Conclusion:** These findings confirm lower 18F-FDG uptake in supratentorial brain and cerebellum after combined induction treatment, high dose chemotherapy and stem cell transplantation.

EP-0128

NaF-PET/CT in multiple myeloma: assessing bone remodeling at baseline in newly diagnosed myeloma patients compared to a healthy control group

B. Oestergaard¹, M. Z. Zirakchian², W. Y. Raynor², R. Taghvaei², A. L. Nielsen¹, P. Holdgaard³, J. T. Asmussen¹, T. Plesner³, N. Abildgaard¹, A. Alavi², P. F. Hoilund-Carlsen¹; ¹Odense University Hospital, Odense, DENMARK, ²University of Pennsylvania, Philadelphia, PA, UNITED STATES OF AMERICA, ³Vejle Hospital, Vejle, DENMARK.

Aim: Multiple myeloma (MM) is characterized by a malignant proliferation of plasma cells primarily in the bone marrow, with potential extra medullary and extra osseous disease. Preliminary reports suggest that ^{18}F-sodium fluoride (NaF) PET imaging has strength in portraying bone remodeling. We examined the feasibility of a novel NaF-PET based method that quantifies global bone formation in pelvis and the whole skeleton based on CT segmentation in MM patients. **Methodology:** Baseline NaF scans of 19 newly diagnosed myeloma patients who underwent high dose chemotherapy and bone marrow transplant were collected at two centers in the Region of Southern Denmark (clinical trial NCT02187731) with the aim of evaluating new imaging technologies in MM. Scans were performed prior to any given anti-myeloma treatment. The skeleton was isolated on the fused PET/CT images using CT segmentation with an iterative thresholding algorithm (OsiriX ; Pixmeo SARL; Bernex, Switzerland). First, a threshold of 150 Hounsfield units was used to delineate bony structures with high attenuation, and then a contour-smoothing algorithm was applied to obtain the whole skeleton, allowing for semiautomatic quantification of total NaF uptake reflecting bone activity. For whole skeletal measurements, the skull and extremities more than 20 cm distal to the glenohumeral joint and more than 10 cm inferior to the lowest part of the ischium were excluded. For measurements of the pelvis, everything superior to the sacrum apart from the ilium was excluded. The global mean standardized uptake value (global SUVmean) was computed as a metric representing total bone formation in the body and studied in the whole skeleton at the baseline and compared to a healthy control group. **Results:** A significantly higher SUVmean of the global skeletal of patients before treatment compared to that of the control group was observed (3.59 and 2.70 respectively, P =0.001). The same trend was observed for the Pelvis and the SUVmean was significantly higher in before treatment compared to the control group (4.16 and 3.10, P=0002). **Conclusion:** In our study the global SUVmean of patients before treatment was significantly higher than that of a control group. It is well known that F-18 NaF uptake depends on increased vascularity and reflects osteoblastic reaction, where NaF accumulates in newly mineralizing bone, including other causes for bony reconstruction such as degenerative change or trauma. So, the higher NaF uptake in these patients could be related to the high number of insufficiency fractures in the bone before treatment.

EP-0129

Role of F18-FDG-PET/CT in malignant otitis externa. Preliminary study

L. Rodriguez-Bel¹, E. Llinares-Tello¹, M. Cortés-Romera¹, J. Robles-Barba¹, X. González-Compta², M. Santín-Cerezales³, S. Castañer-Llanes⁴, A. Sabaté-Llobera¹, L. Gràcia-Sánchez¹, C. Majós-Torro⁴, C. Gámez-Cenzano¹; ¹PET Unit. Department of Nuclear Medicine. IDI., L'Hospitalet de Llobregat. Barcelona, SPAIN, ²Department of Otorhinolyngology. Hospital U. De Bellvitge-IDIBELL, L'Hospitalet de Llobregat. Barcelona, SPAIN, ³Department of Infectious disease. Hospital U. de Bellvtge-IDIBELL, L'Hospitalet de Llobregat. Barcelona, SPAIN, ⁴Neurorradiology Unit. Department of Radiology. IDI. Hospital U. de Bellvitge-IDIBELL, L'Hospitalet de Llobregat. Barcelona, SPAIN.

Aim: Malignant otitis externa (MOE) is an infrequent but severe invasive infection of the external auditory canal generally

caused by Pseudomonas aeruginosa, which mostly affects elderly diabetic patients. The aim of this study was to investigate the potential use of FDG-PET/CT in initial diagnosis/disease spread of MOE and evaluation of treatment response, comparing the results with MRI. **Material and Methods:** Retrospective study of 4 patients with MOE (3 men; 3 diabetic), mean age 67,5 years (range 42-84 years). A total of 7 FDG-PET/CT scans were obtained (4 initial diagnosis; 3 during the follow-up). All patients underwent a dedicated head and neck acquisition and a torso imaging FDG-PET/CT. FDG-PET/CT scans were analyzed on the basis of visual interpretation. Maximum standardized uptake values (SUVmáx) were also calculated. FDG-PET scans were co-registered with MRI (PET/MRI). **Results:** All FDG-PET/CT (7/7) studies showed increased uptake of F18-FDG in the otomastoid region (3 unilateral and 4 bilateral). In 5/7 scans it was also a disease spread including both bone and soft tissue involvement. The mean SUVmax of all lesions was 7,89 g/ml (range 5,1-13,3 g/ml). The concordance between PET and MRI findings was superior in initial studies (4/4) than in the follow-up ones (2/3). In one case, the infection revealed by FDG-PET/CT was more widespread than detected by MRI, and it was confirmed later by clinical and radiological evolution. **Conclusions:** FDG-PET/CT can be helpful in determining disease extent and inflammatory activity in MOE, allowing evaluation of both soft tissues and bony structures. FDG-PET/CT may also be used in monitoring treatment response. The information provided by MRI and FDG-PET/CT is complementary, but further studies would be needed to determine whether FDG-PET/CT scan findings could be used as predictor of treatment outcome and identifying resolution of disease that could help unify recommendations for when to terminate therapy for MOE.

EP-0130
Role of ^{18}F-FDG PET/CT in radiotherapy planning for patients with non-small cell lung cancer

P. Garcia - Talavera[1], Á. Matías- Pérez[2], C. Cigarral[2], F. Gómez-Caminero[1], L. A. Pérez-Romasanta[2], M. E. Martín[1], E. Martín[1], B. Pérez[1], P. Tamayo[1]; [1]Nuclear Medicine Department. Hospital Universitario de Salamanca, Salamanca, SPAIN, [2]Radiotherapy Department. Hospital Universitario de Salamanca, Salamanca, SPAIN.

Purpose: To evaluate the advantages of planning radiotherapy treatment, using 18F-FDG PET/CT with intravenous contrast for patients with non small cell lung cancer. **Subjects and Methods:** Twelve patients were included (7 squamous cancer, 4 adenocarcinoma, 1 non small cell lung cancer without confirmation of histologic type). Ten men, with a mean age of: 74,4 +/- 9,9 years old. An intravenous contrast CT, as a staging technique, was previously performed to all patients. The following stages were found: I-II (7 patients), IIIA (2 patients), and IIIB (3 patients). Two patients received neoadjuvant chemotherapy. PET/CT after intravenous administration of 5 MBq/Kg of ^{18}F-FDG (6 hours fast; glycaemia < 150 mg/dl) was acquired for all patients in positioning conditions for radiotherapy treatment. **Results:** SUVmax of the primary lung lesion was 11,28 +/- 4,4. In one of the two patients with neoadjuvant chemotherapy (IIIB staging), a liver

metastasis was detected. As for the other 10 patients: out of the 7 patients with I/II stages, in 3 of them PET helped to differentiate the mass from the component of atelectasis and in one of them, it detected bone metastasis. Out of the two patients with IIIA staging, in one of them PET helped to differentiate mass from associated atelectasis. In the patient with IIIB stage, it detected bone and brain metastasis. Consequently, three patients were excluded from radiotherapy treatment, due to the detection of metastasis in PET/CT. In the rest (9 patients), the localization of the mass (central or peripheral) was important for the assessment of PET/CT utility. PET/CT helped to delimitate the mass inside the atelectasis in 3/5 patients with central localization. For peripheral nodules (4), it was useful just in one, which associated a small area of atelectasis. **Conclusion:** Performing a ^{18}F-FDG PET/CT before radiotherapy in non small cell lung cancer is a useful practice, allowing the detection of distant metastasis, not detected by conventional imaging techniques (25% of patients). Volume delimitation is more precise when the metabolic imaging is added to that of the contrast CT, especially for central tumours with associated atelectasis.

EP-0131
TSPO Brain PET using [18F]FEPPA in a lipopolysaccharide induced animal model

W. Huang[1], Y. Huang[2], Y. Kuo[3], C. Shiue[4,5], H. Yeh[6]; [1]Department of Nuclear Medicine, Taipei Veterans General Hospital, Taipei, Taiwan, Taipei, TAIWAN, [2]PET Center, Department of Nuclear Medicine, National Taiwan University Hospital, Taipei, TAIWAN, [3]Graduate Institute of Medical Sciences, National Defense Medical Center, Taipei, Taiwan, Taipei, TAIWAN, [4]PET Center, Department of Nuclear Medicine, National Taiwan University Hospital, Taipei, Taiwan, Taipei, TAIWAN, [5]Molecular Imaging Center, National Taiwan University, Taipei, Taiwan, Taipei, Taiwan, TAIWAN, [6]Brain Research Center, National Yang-Ming University, Taipei, Taiwan, Taipei, TAIWAN.

Objectives: Inflammation plays a critical role in the development and progression of many neurodegenerative disorders. [18F]-FEPPA, has been synthesized and evaluated, *in vitro* and *ex vivo*, as a potential positron emission tomography (PET) radioligand targeting TSPO for the quantification of neuroinflammation. The study aimed to evaluate effects of [18F]-FEPPA, a specific TSPO radioligand, on a neuroinflammatory animal model induced by a systemic LPS administration. **Methods:** The model was created in male C57BL/6JNarl mice (20-25 g, n=10) by intra- peritoneal injection of a single dose of lipopolysaccharide, i.e. LPS (E. Coli O111:B4, 5 mg/kg). Under anesthesia, 250 μCi of [18F]-FEPPA was injected via tail vein 24 hrs after LPS injection. The other 5 in breed mice served as the controls. Dynamic sinograms were acquired with 12 x10 sec, 3 x60 sec, 3 x 300 sec, 4 x 600 sec, 2 x 900 sec frames using an Argus microPET/CT scanner. The static whole brain PETs were acquired 90 min after injection. Data were processed by eXplore Vista PET-CT MMWKS software and analyzed by PMOD version 3.4(Zurich, Switzerland) and were expressed in time-activity curves (TAC) of the dynamic study and SUVmax/mean of the static study in certain

brain regions of interest, i.e. Midbrain (MB),Thalamus(TH),Hypothalamus(Hypo),Cerebellum(CB),Cortex(CTX) ,Striatum,Hippocampus(Hippo),Amygdala. Analysis the [18F]-FEPPA binding (V_T) to mice brains was analyzed using repeated measures analysis of variance with SUV. **Results:** The dynamic images showed significantly increased brain [18F]-FEPPA TAC with time in ROIs of the LPS treated group compared to those of the controls. There were also higher brain static [18F]-FEPPA uptake in ROIs than the controls (MB: **0.79±0.06** vs. **1.28±0.06**; TH: **0.72±0.05** vs. **1.21±0.06**; Hypo: **0.86±0.03** vs. **1.33±0.03**; CB: **0.82±0.02** vs. **1.36±0.04**; CTX: **0.69±0.04** vs. **1.16±0.04**; Striatum: **0.67±0.04** vs. **1.13±0.04**; Hippo: **0.78±0.04** vs. **1.30±0.04**; Amygdala: **0.71±0.02** vs. **1.16±0.02** p<0.05 each). The uptake results appear consistent with those of immunohistochemistry. **Conclusion:** [18F]-FEPPA micro PET provided a good mouse imaging quality and may also allow quantitative interpretation of TSPO activity that appear potentially to be useful in various clinical or pre-clinical studies.

EP-0132

Semi-quantitative assessment with PETRA soft-platform of 18F-Florbetaben PET in patients with cognitive impairment

R. Sánchez-Vañó[1], S. Prado-Wohlwend[1], M. Gómez-Río[2], F. Segovia-Román[3], P. Sopena Novales[1], E. Uruburu-García[1], M. Martínez-Lozano[4]; [1]Nuclear Medicine Department Hospital Nisa 9 de Octubre, VALENCIA, SPAIN, [2]Nuclear Medicine Department University Hospital Virgen de las Nieves, Granada, SPAIN, [3]Dept. Signal Theory, Networking and Communications, UGR, Granada, SPAIN, [4]Memory and Dementia Unit. Hospital La Magdalena., Castellón, SPAIN.

Purpose: The semi-quantitative evaluation of 18F-Florbetaben (FBB) amyloid-PET is usually carried out using programs based on population data on MR images as CortexID-Suite. PETRA is a computer aided diagnosis system designed to assist neurological disorders, performing statistical analyses of the PET/CT exploration using the CT itself. Our aim was to compare PETRA with CortexID-Suite quantitative analysis and the visual reading by experts, in 18F-FBB scans of clinically diagnosed patients with cognitive imparment (CI). **Subjects and Methods:** Twenty-two prospectively and consecutively recruited subjects with CI, fulfilling Amyloid-PET criteria (Johnson) underwent PET-CT brain acquired in GE-STE system 90-min after 370MBq of 18F-FBB injection. FBB blinded and random images were classified as Alzheimer Disease (AD) and no-AD (negative for AD or abnormal but no AD) by three nuclear medicine experts, reaching final diagnosis by consensus. CortexID-Suite quantified FBB-PET, obtaining standardized uptake value ratio (SUVR) of multiple regions with a positive threshold SUVR value >1.17, according to literature. Discrepant cases were revised and solved with clinical diagnosis (follow up of at least two years and FDG-PET assessment). FBB-PET were processed using PETRA. TC images were segmented (VBM8-Toolbox) and normalized spatially regarding standardized template. By atlas (AAN-MNI-Montreal) activity was quantified in 116 regions of interest (ROI) as the medium uptake rate relative to mean uptake in cerebellum gray mat-

ter. We analyzed the ROI based analysis of the target areas of patients with AD and no-AD. **Results:**The visual and Cortex-ID assessment of the scans were clearly positive and concordant in 8 patients and clearly negative in 11, concordant with clinical diagnosis and supported by FDG-PET. In two cases quantitative FBB assessment classified AD whereas readers graded non-AD for FBB, but they were classified as AD after revision and one patient obtained non-AD by FBB quantification whereas visual FBB reading graded AD with clinical diagnosis of AD. The PETRA semi-quantitative analysis by ROIs between the two subgroups showed higher mean values in AD than in no-AD subjects in all the studied regions, with statistical significance in most of them (specially in olfactory, cingulum anterior, amygdala, precuneus and left temporal superior lobe regions), according to the Cortex-ID and the visual assessment. **Conclusion:** In our preliminary series FBB quantification with PETRA showed excellent agreement with FBB reading and Cortex-ID quantification. This software could be a usefull tool in cognitive impairment assessment, but more studies with longer subject series are necessary.

EP-0133

Tumour Primary and possible Pitfalls in Paediatic PET/CT

A. A. Nawwar[1], M. Abou Gabal[1], A. Tawakol[1], W. Omar[2], H. Mostafa[1]; [1]Faculty of Medicine, Cairo University, Cairo, EGYPT, [2]National Cancer Institute, Cairo University, Cairo, EGYPT.

Introduction & Purpose: Two of the most common indications for PET/CT scans in paediatric population are pretreatment and follow-up scans for Hodgkin's lymphoma and MIBG negative neuroblastoma. Physiological and benign tracer distribution sites may present major interpretation difficulties in both diseases; affecting scan interpretation and inturn, management. The aim of our study is to assess possible pitfalls and artifacts and compare those of these two malignancies. The aim of that is to understand whether the type of primary affects potential pitfalls; particularly in paediatrics, which is in itself challenging. **Subjects & Methods:** Retrospective analysis of PET/CT scans of 253 pediatric patients undergoing staging evaluation for malignancy at children's cancer hospital, Egypt. Scans were reviewed by two nuclear medicine physicians who underwent visual and quantitative analysis of scans. Debatable scans were reviewed by an additional third specialist. Relevant detailed clinical and procedure data were obtained. **Results:** The study population was found to constitute of 159 Hodgkin's Lymphoma patients (62.9%), 65 Neuroblastoma patients (25.7%) and 25 patients (11.4%) of various primary tumours. Pitfalls and artifacts were characterized into physiological uptakes, technical artifacts, benign lesions and therapy-related artifacts. Although Lymphoma showed significantly higher prevalence, a some-what similar pattern of pitfalls was found in the two common diseases as regards therapy related artifacts and technical artifacts. On the other hand, a statistically significantly higher percentage of physiological uptake related pitfalls (89.9%) was seen in lymphoma (highest in the head and neck) as compared to the 38.4% found in neuroblastoma (P=0.01). However, a higher percentage of benign lesions; 21.5%, was found in neuroblastoma

patients, as compared to 12.6% found in lymphoma patients, with a P value 0.04. **Discussion & Conclusion:** We have found that tumour primary "does" affect possible pitfalls and artifacts to some extent. For instance, due to the nature of lymphoma as well as the active and diffuse lymphatic tissue nature in the paediatric population, possible pitfalls were vast, in particular physiological uptake sites eg. thymus. Also, different sites become of concern depending on primary type; eg. cranial uptake in neuroblastoma. This helps to know what to look closer into. Paediatric scans are trickier but with a deeper understanding of their different physiology and possible pitfalls, more accurate diagnosis and inturn better treatment and prognosis can be achieved.

EP-0134

Radio-metabolomics: association between CT radiomics features and metabolic indices in 18F-FDG PET

I. Shiri[1], H. Abdollahi[1], P. Geramifar[2], A. Bitarafan-Rajabi[1,3]; [1]Department of Medical Physics, School of Medicine, Iran University of Medical Sciences, Tehran, IRAN, ISLAMIC REPUBLIC OF, [2]Research Center for Nuclear Medicine, Shariati Hospital, Tehran University of Medical Sciences, Tehran, IRAN, ISLAMIC REPUBLIC OF, [3]Cardiovascular Intervention Research Center, Rajaie Cardiovascular Medical and Research Center, Iran University of Medical Sciences, Tehran, IRAN, ISLAMIC REPUBLIC OF.

Aim: Intra-tumoral heterogeneity is frequently assessed by radiomics features in CT images. The main aim of current study was to preliminarily assess a hypothesis of possible correlation between 18F-FDG PET metabolic parameters and radiomics features as derived from CT image. **Material and Methods:** 112 patients undergoing integrated PET/CT were included to this study. Gross tumor volume (GTV) as delineated from CT images were used for subsequent radio-metabolomics analysis. Then, Laplacian of Gaussian (LoG) spatial band-pass filters with different values (Fine σ=0.5, Medium σ=1 and Coarse σ=2.5) were used to highlight different anatomical scales. 1403 radiomics features including intensity histograms (IH), gray level run-length (GLRLM), gray level co-occurrence (GLCM), gray level size-zone texture matrices (GLSZM) and neighborhood-difference matrices (NDM) were extracted following each filter value (generating 4209 radiomics features for each patient). Correlations between PET metabolic indices (SUVmax, SUVmean, SULpeak and TLG) and CT radiomics feature were assessed by Pearson's correlation analysis. **Result:** A total of 127 lesions were analyzed in this study, and 16836 correlation coefficients were calculated for patient cohorts. A weak correlation between TLG and Difference Entropy |r|=0.36, Dissimilarity |r|=0.29, Energy |r|=0.34, entropy |r|=0.23 and 50Percentile |r|=0.35 existed. Also no significant (p<0.05) association between any radiomic features from CT images and SUVmax, SUVmean and SULpeak were found. **Conclusion:** No significant correlation between metabolic parameters of PET (SUVmax, SUVmean and SULpeak) and CT radiomic features were found, except between few CT features and TLG, and this may be due to the nature of TLG (TLG=MTV×SUVmean, CT radiomics feature are dependent on tu-

mor volume). Although, using CT radiomic features along with PET metabolic parameter still has the potential to improve early response assessment in cancer patient which needs to be carefully assessed.

Molecular & Multimodality Imaging: SPECT & SPECT/CT

EP-0135

The influence of gene polymorphism, cetptaq1b, cetp1405v, abca1, in the influence of myocardium ischemia with spect imaging, in patients with familial hypercholesterolemia

A. Iakovidou, F[1,2], V. Kolovou[1,2], A. Theodorakos[1,2], D. Degiannis[1,2], M. Koutelou[1,2], G. Kolovou[2]; [1]Onassis Cardiosurgery Center, Athens, GREECE, [2]Nuclear Medicine Department Cardiology Department, Onassis Cardiac Surgery Center, Athens, GREECE.

Background: Familial hypercholesterolemia is a common autosomal dominant inherited disorder characterized by elevated levels of ldl cholesterol and premature atherosclerosis. The aim of the study is to evaluate the effect of gene polymorphism associated with lipid metabolism CETPTaq1B, CETP1405V, ABCA1 insofar extent of myocardial ischemia, assessed by scintigraphic studies of myocardial perfusion in patients with familial hypercholesterolemia. **Method:** This is a retrospective study and involves 84 patients, 43 patients with coronary artery disease and FH, 30 with coronary artery disease without FH and 11 without CHD in FH, aged 35-80 years, who have already been examined for polymorphisms and the degree of ischemic area will be studied scintigraphically between 2000 and 2016. The tests have been already carried out in the Nuclear Medicine department, at the Onassis Cardiac Surgery Center. **Results:** In 43 patients who have both coronary heart disease CHD and familial hypercholesterolemia FH their single photon emission computed tomography SPECT showed ischemia or infarct area in 32 patients. In addition patients with CHD but not FH presented pathologic SPECT in half portion 16 out of 30 patients and finally in 11 patients with FH but not CHD only one SPECT was ischemic. **Conclusion:** Familial Hypercholesterolemia FH influences myocardial imaging in patients with coronary heart disease CHD . However when no CHD exists, the FH alone may not influence the myocardial perfusion imaging MPI .

EP-0136

Gastric & Intestinal Scintigraphy in Adhesive Small Bowel Obstruction

N. Kudryashova, P. Yartsev, A. Lebedev, E. Migunova, O. Sinyakova, I. Selina, E. Trofimova; Sklifosovsky Research Institute for Emergency Medicine, Moscow, RUSSIAN FEDERATION.

The study of the intestine passage in patients with small bowel obstruction (SBO) in the absence of strangulation pattern, re-

quires emergency surgery, is especially important for the choice of treatment tactic. With this **purpose** we used a two-stage scintigraphy to evaluate the gastric empting, to determine the time of indicator output into the colon and the level of obstruction. **Material and Method:** We analyzed 100 pts with adhesive SBO (group 1 - 76 operated and group 2 - 24 conservatively treated). These patients (in around the clock operating nuclear medicine department) were examined with Infinia II (GE, USA). The gastric and intestinal scintigraphy were performed with 99mTc-technefit, the sulphur colloid analogue (per os 100 MBq + 50 ml of water; 0.94 mSv), in combination with panoramic x-ray and ultrasound of the abdomen. The protocol of the study: 1 - gastric empting study (dynamic recording for 20 min - 1 frame/1 min); 2 - static scintigraphy of the intestine (200 s/frame) every 2 hours with a marker set at the level of the umbilical ring. **Results:** Signs of SBO revealed by scintigraphy in 73 (96%) pts of group 1: delay of the indicator in the small intestine local area with the constant pattern at 2, 4 and 6 h, the absence of the cecum visualization in 2-6 hours. The slow gastric empting was registered in 65 pts (85.5%). In the resolution of SBO on the conservative treatment (group 2) the gastric empting was slow in 83.3% pts, but the passage was traceable, the small intestine loops during 10-12 h became free from colloid, the cecum and other parts of the colon visualized on delayed frames. Scintigraphic signs of passage were in line with clinical improvement and objective confirmed the SBO resolving. **Conclusion:** The study shows that gastric and intestinal scintigraphy is low-dose and informative method. It has a high accuracy for SBO and allows proving of the conservative treatment in some patients with adhesive SBO.

EP-0137
Diagnosis of Urinary Leakage with Scintigraphy

E. Migunova, A. Pinchuk, B. Khubutia, N. Kudryashova, O. Sinyakova; Sklifosovsky Research Institute for Emergency Medicine, Moscow, RUSSIAN FEDERATION.

Urinary leakage is an early postoperative complication after kidney transplantation. Being delayed diagnosed it significantly reduces both graft and recipients' survival rate and increases the treatment duration. The absence of clinical evidence in some cases and diagnostic insufficiency of ultrasound determine the difficulty of prompt diagnosis of urinary leakage in patients after kidney transplantation. **Aim:** Analysis of renal scintigraphy efficiency in diagnosis of urinary leakage after kidney transplantation. **Material and Method:** 523 patients after kidney transplantations were studied: male 275 (52.6%), female - 248 (47.4%), the age ranged from 18 to 72 years old (median was 46 [35; 56] years). In 15 pts (2.9%), the early postoperative period was complicated by the urinary leakage without the characteristic clinical signs. It was diagnosed by scintigraphy with 99mDTPA 120-150 MBq (0.6-0.8 mSv), using Infinia II and Discovery 670 NM/CT (GE, USA). **Results:** despite the absence of clinical manifestations, the urinary leakage was diagnosed by scintigraphy in all 15 pts at different study periods in the form of an extrarenal indicator accumulation in the projection of the urinary tract and scrotum. In two patients with a satisfactory function of the graft, the uri-

nary leakage was visualized during 20 min of investigation. In 13 pts with graft function impairment, the extrarenal uptake of the indicator was detected on the delayed frames in 1-6 hours after the study start. Previously, the detection of a urinary leakage allowed in the shortest time to perform a surgical correction and save the transplant. **Conclusion:** renal scintigraphy with the delayed frames is the effective method for timely reliable diagnosis of urinary leakage after kidney transplantation.

EP-0138
LM/SL with SPECT/CT in cervical cancer : A Systematic Review of the Literature Data

T. Z. Belhocine[1], M. Prefontaine[2]; [1]Biomedical Imaging Research Centre (BIRC), Western University - London, ON, CANADA, [2]London Health Sciences Centre (LHSC), Western University - London, ON, CANADA.

Purpose: A systematic review of the literature data was performed to assess the added-value of SPECT/CT to lymphatic mapping and sentinel lymphadenectomy (LM/SL) in cervical cancer. **Subjects & Methods**: A literature search was performed on PubMed and Google using the key-words: 1- "SPECT/CT" AND "cervical cancer" AND "sentinel lymph node"; 2- "SPECT-CT" AND "cervix"; 3- "SPECT/CT" AND "ICG" AND "cervical cancer"; 4- "sentinel lymph node" AND "cervical cancer" AND "gynaecological cancers". 5- "sentinel lymph node" AND "cervical cancer" AND "ICG". Data were extracted from the included articles. Case reports and abstracts were excluded from the systematic review. **Results**: From January 2006 to March 2017, 15 articles were included into the systematic review (10 prospective and 5 retrospective studies) including 580 patients (mean=36; 7-132) with the FIGO stages Ia-IIa (4 studies) Ia2-Ib1 (3 studies), Ib1-IIa1 (2 studies), Ia1-IIb (2 studies), Ia1-Ib2 (1 study), Ia1-Ib1 (1 study), Ia1-IIIa (1 study); not precised in one study. Laparotomy and/ or laparoscopy and/or robotics were performed for LM/SL in a 1-day and/or 2-day protocols. Mean DR was 96% for SPECT/CT (97.6% with GPG+BD) and was 95.5% for NIR-ICG. Mean bilateral DR was 69.5% for SPECT/CT (11 studies), 78.6% for SPECT/CT vs. 75.7% for planar lymphoscintigraphy (4 studies), and 61% for SPECT/CT vs. 95.5% for NIR-ICG (1 study). SLNs were detected in predictable and unpredictable lymphatic pathways. SLN pathology was performed with frozen section (7 studies), routine HE/HPS (11 studies), IHC (9 studies) with CKAE1/A3 antibodies (6 studies) and serial sections (50μm-300μm); not precised in 4 studies. Mean %SLN+ was 17.2%. With SPECT/CT, mean Sv was 95.9% (98.9% w/GPG+BD), mean DAc. was 98.7%, mean NPV was 98.6% (99.2% w/GPG+BD) and mean FNR was 3.6% (1.1% w/GPG+BD). In the prospective IAEA multicenter trial (n=15), SPECT/CT overall DR was 80% vs. 73.3% for planar imaging. In the retrospective European multicenter trial (n=144), overall DR and bilateral DR were 100% (NSD) and 98.5% (SD) for ICG-NIR versus 96% and 76.3% for combined 99mTc/BD tracers with SPECT/CT when required. **Conclusion**: In early-stage of cervical cancer, SPECT/CT is of incremental value for anatomic and functional imaging of SLNs in 3D with a DR, Sv and NPV approaching 100%. SPECT/CT increased the bilateral DR of SLNs compared

to planar imaging and allowed a laparoscopy and/or robotics approach for LM/SL and ultrastaging. NIR-ICG increased the bilateral DR compared to SPECT/CT. SPECT/CT with MRI software fusion may open promising perspectives for LM/SL.

EP-0139
Added value of SPECT/CT over planar bone scintigraphy in the diagnosis and management of patients with breast or prostate cancer

A. Gafita[1], M. Mereuta[1], G. Andries[1,2]; [1]'Iuliu Hatieganu' University of Medicine and Pharmacy, Cluj-Napoca, ROMANIA, [2]Department of Nuclear Medicine, County Emergency Clinical Hospital, Cluj-Napoca, ROMANIA.

Purpose: The purpose of this study was to investigate the additional benefit of single photon emission tomography/computed tomography (SPECT/CT) over whole-body planar bone scintigraphy (planar BS) in the assessment of equivocal results by planar BS in patients with confirmed breast or prostate cancer and clinical suspicion of bone metastases. **Subjects & Methods**: 361 consecutive patients (245 with breast cancer, 116 with prostate cancer) who underwent planar BS with ^{99m}Tc-hydroxymethylene diphosphonate (HDP) (mean dose 550 MBq) between 2014 and 2015 were retrospectively analyzed. In 47 patients (35 with breast cancer, 12 with prostate cancer, mean age 61 years), further evaluation by combined SPECT/CT system was needed. **Results:** In 13% of the patients who underwent planar BS, results were unclear and required SPECT/CT assessment. Images of 83% (39/47) of the patients who underwent SPECT/CT could be classified, of whom 72% (28/39) were defined as benign and 28% (11/39) as malignant. In 17% of the patients (8/47) the lesions remained unclear and required further investigation. One third of SPECT/CT scans were performed for unique lesions, of which 67% were evaluated as benign, 13% as malignant and 20% remained unclear. **Conclusion:** The hybrid SPECT/CT technique is an advanced imaging modality that can improve the diagnostic performance in the assessment of patients with equivocal lesions in planar bone scintigraphy and also can have further implications in patient management.

EP-0140
An incidentally detected breast cancer on ^{99m}Tc-MIBI SPECT/CT parathyroid imaging

T. Costa, A. Sanches, C. Cruz, A. Pepe, D. Solano; Hospital Português, Salvador-BA, BRAZIL.

Introduction: Parathyroid scintigraphy is a useful technique for localize one or more hyperfunctioning parathyroids in patients with high serum levels of PTH, which has been improved by the new hybrid methods (SPECT/CT). The main radiotracer employed is 99mTc-MIBI, that concentrates in tissues with high density of mitochondrias, representing the significant energetic demand. When a non-physiological focal 99mTc-MIBI uptake is detected in other organs, complementary investigation should be necessary, considering that neoplasic tissues not rarely con-

centrate this radiotracer. Subjects & Methods: An 88-year-old woman with high serum levels of PTH underwent a 99mTc-MIBI SPECT/CT parathyroid study for identificate a possible adenoma/hyperplasia of parathyroid. The study shows no evidence of hyperfunctioning parathyroid. However, a focal uptake was visualized in a nodular image localizated in upper outer quadrant of the right breast. A subsequent digital mammography performed was inconclusive (BI-RADS classification: 0). RESULTS: A core biopsy of the previously described breast nodule showed a ductal invasive carcinoma, estrogen receptor-positive (ER+), progesterone receptor-positive (PR+) and HER-2 negative. The patient was conducted to staging breast cancer, that showed no distant secondary lesions, so she underwent a surgery and hormonal therapy with good response in the surveillance. CONCLUSION: Nuclear Medicine frequently envolves global evaluations of the body's patient, that are not just restricted to the main purpose of the requested exam. It's very important that the Nuclear Physician be aware of this essential purpose. In this way, many patients could be benefit by the careful imaging analysis.

EP-0141
Usefulness of SPECT/CT with ^{99m}Tc-Methylene Diphosphonate Bone Scintigraphy in Patients with Chest Wall Pain

S. Park[1], J. Hwang[1], J. Park[2], J. Hwang[2]; [1]Soonchunhyang University Hospital, Seoul, KOREA, REPUBLIC OF, [2]Soonchunhyang University Bucheon Hospital, Bucheon, KOREA, REPUBLIC OF.

Purpose: SPECT/CT can improve sensitivity and specificity for identifying abnormal bone lesion than conventional planar bone scan. We investigated and compared diagnostic performance of planar bone scan and SPECT/CT detecting chest wall lesion in patient with chest wall pain. **Subjects and Methods:** We analyzed planar bone scan and SPECT/CT of 59 patients who were referred for chest wall pain. Bone scintigraphy and SPECT/CT were performed on a dedicated hybrid SPECT/CT scanner 3 hours after intravenous injection of Tc-99m methylene diphosphonate. Anterior and posterior whole-body images and bilateral anterior oblique and bilateral posterior oblique spot images of the chest region were obtained and followed by SPECT/CT. CT-based attenuation corrected (AC) and non-attenuation corrected (NonAC) SPECT images were reconstructed and fused with the CT. Planar bone scan, AC and NonAC SPECT/CT of each patient were reviewed focusing on abnormal radioactive uptake in the chest wall including bilateral 1st-12th ribs, T1-T12 spines, sternum, bilateral clavicles, and bilateral scapulae. Number and location of the chest wall lesions were investigated and the final diagnosis was determined by analysis of all data. **Results:** The 59 study subjects were 54 ± 18 y in age (range, 15 to 88 y), and 33 were males. Of the 59 patients, 46 had a trauma history and 13 had no significant trauma related to the chest wall pain. Symptom duration was 39 ± 70 days (range, 2 to 360 days). Most common diagnosis was post-traumatic change of the rib (395 lesions), spine (47 lesions) and others (27 lesions), which was followed by bone metastasis (15 lesions). Total of 52 subjects (88.1%) with

492 bone lesions were detected on SPECT/CT. SPECT/CT correctly changed location of chest wall lesions shown on bone scan in 5 subjects (8.5%). AC and NonAC SPECT/CT detected additional chest wall lesions than planar bone scan in 36 subjects (61.0%) with total of 483, 492, and 320 lesions, respectively (p-value of both < 0.001). In subgroup analysis according to bone location, AC and NonAC SPECT/CT also detected more lesions than planar bone scan both for rib (398 and 406 vs. 256 lesions, p-value of both < 0.001) and other than rib (85 and 86 vs. 64 lesions, p-value = 0.004 and 0.007, respectively). However, there was no significant difference between AC and NonAC SPECT/CT. **Conclusion:** SPECT/CT is useful in patient with chest wall pain by sensitive detection and by specific diagnosis of chest wall lesion.

EP-0142

Optimisation of acquisition duration in extremities SPECT/CT

A. C. A. Gomes Moura, A. Nunes, A. Eccles, F. Hassan, D. Dasgupta; Guy's and St Thomas NHS Foundation Trust, London, UNITED KINGDOM.

Aim: The aim of this study is to compare the diagnostic quality of a 10 seconds/ view SPECT with a 20 seconds/view SPECT in patients having SPECT-CT studies of their extremities (wrists and feet). **Materials & Methods:** 20 SPECT/CT bone scans of the extremities were considered, 10 of the feet and 10 of the wrists/ hands. These patients were injected with 750MBq (+/-10%) of ^{99m}Tc-MDP as per departmental protocol. 20 seconds/frame SPECT/CT was performed as per protocol. Philips Precedence was used for this data acquisition and EBW workstation was used for data reconstruction. The Precedence system is able to acquire multiple SPECT scans with differing times per frame at the same time. This facilitated the acquisition of just one SPECT per patient. Data was analysed by 3 experienced Nuclear Medicine Consultants that report these scans regularly. Each scan was anonymised and scored regarding image quality and reporting confidence on a scale from 1-5. **Results:** Regarding the wrists scan, the image quality scoring for the 10 seconds/frame SPECT had a mean of 3.67, while for the 20 seconds/frame the scoring was 3.53. Reporting confidence scoring was also higher for the 10 seconds/frame SPECT with 3.87 and 3.77 for the 20 seconds/frame SPECT.For the feet scan, the image quality scoring for the 10 seconds/frame was 3.23, while for the 20 seconds/ frame was slightly higher with 3.63. Regarding reporting confidence, the mean scoring was 3.67 for the 10secondss/frame SPECT and 4.2 for the 20 seconds/frame SPECT.**Conclusion**This data attests that the image quality is not significantly affected when decreasing the acquisition time for the wrists SPECT with the reporting confidence being also higher for the 10 seconds/ frame scans compared to the 20 seconds/frame SPECT. For the feet SPECT the data shows that the image quality and reporting confidence scoring is higher for the 20 seconds/frame. This study will contribute to inform the decision about the length of SPECT-CT studies to adopt in new protocols in the department. Further studies will be structured to keep the trend of reducing imaging time for other areas as knees, hips, etc. as long as the image quality is not affected as well as the reporting confidence.

EP-0143

Complex radionuclide evaluation of response to cardiac resynchronization therapy

V. Saushkin, K. Zavadovsky, I. Kostina, D. Lebedev, S. Popov; Cardiology Research Institute, Tomsk, RUSSIAN FEDERATION.

Background: On today complex radionuclide studies play important role in the diagnosis cardiac functional state special in patients with heart failure. We consider that the assessment of cardiac sympathetic activity and ventricular dyssynchrony will help to develop new predictors of the outcome of cardiac resynchronization therapy (CRT). **Methods:** The study comprised 59 patients with severe contractility dysfunction of the left ventricle (LVEF <30%; NYHA III-IV) (mean age of 49±8 years). All patients underwent a comprehensive clinical and functional examination including gated SPECT myocardial perfusion imaging (gSPECT-MPI), I-123 MIBG imaging and gated blood-pool SPECT (GBPS). Systolic and diastolic functions (EDV, ESV, and EF) as well as mechanical intraventricular dyssynchrony of both ventricles were analyzed. Moreover, we analyzed abnormalities of 123I-MIBG (summed 123I-MIBG score) and 99mTc-MIBI accumulations (normalized SSS and SRS) in the left ventricular (LV) myocardium. All examinations were performed using GE Discovery NM/CT 570C with cadmium-zinc-telluride detectors. **Results:** In all patients, decreases in contractility and dilatation of both ventricles were detected: median LV EDV was 401 mL (312-511 mL); median right ventricular (RV) EDV was 280 mL (216-388 mL); median LV EF was 26% (17-27%); and median RV EF was 23% (21-44%). Based on GBPS data, severe mechanical dyssynchrony of both ventricles was detected. The median value of LV intraventricular dyssynchrony was 129 ms (103-161 ms); RV intraventricular dyssynchrony was 123 ms (82-152 ms). The value of interventricular dyssynchrony was less than 50 ms. According to stress and rest gSPECT-MPI, all patients had heterogeneous myocardial perfusion pattern. The median values of normalized SSS and SRS were 13% (12-19%) and 5% (2-7%), respectively. The summed 123I-MIBG score was 26% (21-31%) which was significantly greater than normalized SSS and SRS (p=0.03 and p=0.04, respectively). Areas of reduced 123I-MIBG accumulation matched the myocardial perfusion defects localizations. **Conclusion:** Our findings suggest that in patients with chronic heart failure sympathetic activity/perfusion disturbances mismatch was detected. These data will be used in the follow-up study after CRT device implantation in order to develop new predictors of CRT outcomes. Acknowledgements: The study was supported by a grant from the Russian Science Foundation (N 15-15-10016).

EP-0144

Rare paranganglioma localizations caught by MRI and CT hybrid 123I-MIBG SPECT imaging.

M. Pontico, G. Follacchio, V. Frantellizzi, L. Cosma, M. Ricci, M. Liberatore, F. Monteleone, G. DeVincentis; Università di Roma Sapienza, Rome, ITALY.

Introduction: Paragangliomas are rare neuroendocrine tumours arising from extra-adrenal paraganglia, consisting of spe-

cialized catecholamine-secreting chromaffin cells. We present two rare paranganglioma localizations cases in female pelvic region. **Subjects and Methods:** A 77 years old woman came to our attention after she underwent a TURV for removing a pathologic tissue located in the posterior wall of the bladder. Histopathologic analysis revealed a neoplasm infiltrating the muscolar tissue of the bladder with morphophenotipic features compatible with paraganglioma. CT scan showed surgical scarring reffered to recent TURV and a thin hypervascular thickening of the posterior wall of the bladder. A 24 years old woman complained hypertensive crises with headache, palpitations and fainting when urinating and pelvic MRI showed a disomogenous enhancing mass between the urinary bladder and left ovary. After thyroid bloking, i.v. injection of 185 mBq of ^{123}I-MIBG (AdreView, GE Healthcare) was performed and images were obtained using a dual-head SPECT scanner (Infinia, GE Healthcare) equipped with LEHR collimators after 4 and 24 hours. Whole body, planar and SPECT images of the abdomino-pelvic region were acquired, with the following acquisition parameters: 120 projections, 64×64 matrix and 20s acquisition time per projection. For iterative reconstruction of the SPECT data, 4 iterations and 4 subsets were used with a Butterworth filter. SPECT scans were transferred to the workstation and fused semiautomatically with the above mentioned MR/CT scan previously obtained, by using dedicated software. **Results**: ^{123}I-MIBG SPECT images showed an area of increased uptake on the right side of posterior wall of the bladder, more clear in the delayed phase images. This finding was compatible with residual paranganglioma in that location. Hybrid SPECT-CT fused images confirmed that the area with increased uptake in the bladder matched with the parietal thickening advised in the CT study. In the second case planar and SPECT images shows a tissue with a pathologic ^{123}I-MIBG concentration just in correspondence of the mass pointed out by MRI exam. Despite of the complexity in the interpretation of nuclear imaging in the pelvic region, even more in bladder localizations due to the high activity present in this organ, we've obtained an optimal morpho-functional correlation by matching CT/MRI and SPECT imaging, after appropriate reconstruction and post-processing work, capable of reaching an accurate diagnostic power. **Conclusions**: The hybrid SPECT/CT and SPECT/MRI imaging, even if taken separately, showed an increasing diagnostic confidence in image interpretation and enhancing sensitivity in tricky paranganlioma localization as in these cases.

EP-0145

Sagliker Syndrome in A patient with Secondary Hyperparathyroidism and Chronic Renal Insufficiency: A Case Report

s. shakeri, S. Zareparvar Moghadam, N. Ayati; Mashhad university of medical science, Mashhad, IRAN, ISLAMIC REPUBLIC OF.

Introduction: Sagliker syndrome, the most severe form of skeletal changes in secondary hyperparathyroidism, describes with uglifying face, skeletal abnormalities, severe secondary hyperparathyroidism, and chronic renal failure. This is a rare syndrome which was accidently noted in our patient. **Subjects and Method**: This report describes a 44-year-old male patient, referred to our center for parathyroid scan. ^{99m}Tc-MIBI scintigraphy was in favor of parathyroid hyperplasia. The patient underwent parathyroidectomy for three of parathyroid glands which proved hyperparathyroidism pathologically. Short stature, changes in facial appearance such as mandibular deformity, chronic renal failure and severe secondary hyperparathyroidism with high level of alkaline phosphatase and parathyroid hormone encouraged us to search for a syndrome like disease which was clinically and paraclinically matched with Sagliker syndrome. **Conclusion**: Sagliker syndrome is a rare form of renal osteodystrophy presents with severe skeletal deformities resulted from untreated secondary hyperparathyroidism. Evidence of high levels of PTH in a patient with chronic renal failure and uglifying face appearance are in favor of this extremely rare abnormality. **Keywords:** Sagliker syndrome, hyperparathyroidism, renal osteodystrophy, skeletal deformity, uglifying face

EP-0146

Comparison of reporting outcomes for Simultaneous and Sequential perfusion SPECT in VQ SPECT/CT

C. Sibley-Allen, H. Ahmed, S. Johnson, D. Dasgupta; Guy's and St Thomas' NHS Foundation Trust, London, UNITED KINGDOM.

Background: VQ SPECT using [81m]Kr gas for ventilation offers the possibility of simultaneous ^{99m}Tc-MAA perfusion imaging. This reduces the scan time, movement artefacts and improves departmental workflow. However, crosstalk between the [81m]Kr (190keV) ventilation and [99m]Tc (140 keV) perfusion photopeak may reduce image quality and confidence of interpretation. The aim of this study was to compare the reporting outcomes of simultaneous and sequential perfusion SPECT. **Methods:** VQ-SPECT/CT reports from Jan 2015-Jun 2016 were extracted from the hospital radiology system. 8 positive reports with subsegmental unmatched perfusion defects and 10 negative reports for pulmonary embolism were selected in chronological order. All patients had [81m]Kr ventilation SPECT, simultaneous perfusion SPECT followed by sequential perfusion SPECT with 200 MBq of ^{99m}Tc-MAA. A localisation CT scan using 110 kV, and 16 effective mAs was acquired, except for one pregnant patient. Images were acquired with a Siemens Symbia T16, MELP collimators, 128x128 matrix and 15% energy windows around 190 and 140 keV photopeaks. Ventilation and simultaneous perfusion SPECT were acquired with 64 projections of 15 seconds. Sequential perfusion SPECT was acquired with 64 projections of 12 seconds. Reconstruction used a 2DOSEM iterative algorithm with 4 iterations, 16 subsets and a 10mm FWHM Gaussian filter. Images were reviewed blinded by 2 experienced nuclear medicine clinicians. The number of mismatched defects, positive or negative status for pulmonary embolism and image quality scored between 1 (non-diagnostic) and 5 (excellent) were reported. **Results:** Both clinicians had concordant reporting of positive/negative results in 17/18 of the sequential perfusion images and 16/18 of the simultaneous images. The intra-observer kappa score was 0.89 for sequential and 0.78 for simultaneous

images. In 1 study both clinicians gave a different outcome to the original sequential report, however this was noted in both simultaneous and sequential perfusion images. Image quality scores ranged from 2 to 5 for both sequential and simultaneous scanning, with a median image quality score of 4. **Discussion:** Overall, clinicians gave consistent reporting outcomes, with each other and the original report. Consistency didn't depend on the type of perfusion imaging performed. Absence of clinical history may have resulted in the 1 disagreement with the original report. Sequential and simultaneous perfusion images were rated with similar image quality. **Conclusions:** In this study, simultaneous and sequential perfusion SPECT gave similar clinical outcomes in VQ SPECT/CT. A larger prospective review with measurement of crossover fraction would be helpful to improve clinician confidence.

EP-0147

Manual fused single photon emission tomography/ computed tomography in 123I-MIBG scintigraphy: a 13 years' experience

M. F. Villani, M. Pizzoferro, A. Castellano, M. Longo, A. Serra, E. Villanucci, M. C. Garganese; Bambino Gesu' Children's Hospital, Rome, ITALY.

Background: 123I-metaiodobenzylguanidine (123I-MIBG), an analogue of norepinephrine labeled with 123I, is an ideal tumor specific agent for scintigraphic imaging in neuroblastoma (NB). Advantages of single photon emission tomography (SPECT) in comparison to planar scanning (better anatomic localization and better lesion definition) are widely known since many decades. Nevertheless, pathologic findings are sometimes difficult to localize anatomically and the role of integration with computed tomography (CT) in increasing the accuracy is well established. Purpose: to underline the feasibility of manual single photon emission tomography/computed tomography (SPECT/CT) fusion, sometimes supported by radiologist contribution. **Materials and Methods:** we retrospectively evaluated 850 123I-metaiodobenzylguanidine (123I-MIBG) scintigraphies (planar and SPECT images) of 253 children (112 males, age range at presentation 1 month - 15 years) which referred to our Institution for neuroblastoma from 2003 to 2016. Since 2009, all SPECT studies (389 SPECT, 183 patients) were processed by manual fusion with CT by a dedicated software. Fusion images were read by a nuclear medicine physician in collaboration with a radiologist. **Results:** in 66/389 (17%) studies, SPECT/CT fused images confirmed the absence of 123I-MIBG uptake showed by planar images; in 238/389 (61%) studies, SPECT/CT fused images provided additional information about number and site of uptake foci revealed by planar acquisition (osteomedullary in disease in 37, thoracic disease in 33, residual disease in the abdomen in 168); in 85/389 (22%) SPECT/CT fused images confirmed planar images findings. **Conclusion:** in our experience, SPECT/CT provided additional information as widely known. Also in absence of a hybrid tomograph, image fusion is feasible; collaboration between nuclear medicine physician and radiologist increases diagnostic accuracy.

EP-0148

The usefulness of SPECT/CT and neck pinhole SPECT (P-SPECT) as complementary tools to planar parathyroid scintigraphy in hyperparathyroidism (HPT)

A. Spanu, S. Sanna, S. Galassi, M. Stazza, B. Piras, F. Chessa, A. Falchi, S. Nuvoli, G. Madeddu; University of Sassari, SASSARI, ITALY.

Aim: To assess the usefulness of SPECT/CT and neck P-SPECT as complementary tools to planar parathyroid scintigraphy in the preoperatively detection of hyperfunctioning parathyroid glands in HPT patients scheduled to parathyroidectomy. **Methods:** We retrospectively reviewed a consecutive series of 34 patients (age: 29-76 years) affected by HPT, primary in 31 cases, including 3 patients with HPT associated with MEN syndromes, and secondary in 3 cases. All patients underwent neck surgery and had definitive histology. Before surgery, planar dual-tracer (99mTc-pertecnetate/99mTc-MIBI) parathyroid scintigraphy followed by neck pinhole-SPECT and SPECT/CT of neck/mediastinum region was performed in all cases. At surgery, 23/34 patients had a parathyroid adenoma each (in ectopic site in 4 cases), while in the remaining 11/34 patients 20 hyperplastic glands (2 of which ectopic) were resected. **Results:** Planar scintigraphy was true positive in 28/34 (82.3%) patients, while both SPECT/CT and P-SPECT in 31/34 (91.1%) of cases. Overall per-lesion sensitivity was 86% for P-SPECT, 81.4% for SPECT/CT and 72.1% for planar scan. The difference in sensitivity between P-SPECT and planar scan was statistically significant (p<0.05). SPECT/CT identified more adenomas than P-SPECT and planar scintigraphy (95.5% vs 91.3% and 82.3%, respectively), while P-SPECT detected a higher number of hyperplastic glands than planar and SPECT/CT (80% vs 65% and 55%, respectively). One ectopic adenoma deeply located in upper mediastinum was evidenced only at SPECT/CT that also gave a precise anatomic localization, as did in all the other ectopic lesions. Another adenoma was evident only at planar scan, probably due to a rapid MIBI washout, while 3 hyperplastic glands were evident only at P-SPECT. **Conclusion:** These preliminary data seem to suggest that both tomographic procedures, either SPECT/CT and P-SPECT, may improve the sensitivity of conventional planar scintigraphy. In particular, SPECT/CT, also giving anatomical details, should be included in parathyroid scintigraphy protocols as a complementary tool to conventional planar scanning to plan the surgical treatment, especially in patients with ectopic glands. However, the employment of the less available high-resolution neck P-SPECT should also be considered, in selected patients, given the highest sensitivity demonstrated in the detection of hyperplastic glands.

EP-0149

Diagnostik Value of Quantitative 99mTc-DPD-SPECT/CT for the detection of prosthetic loosening in patients with hip- and knee joint replacement

*M. Braun[1], M. Cachovan[2], G. Pagenstert[1], A. H. Vija[2], D. Wild[1], **M. Kretzschmar**[1]; [1]University Hospital Basel, Basel, SWITZERLAND, [2]Siemens Healthcare GmBH, Molecular Imaging, Forchheim, GERMANY.*

Purpose: To evaluate the diagnostic accuracy of maximum standardized uptake values (SUV max) of ^{99m}Tc-DPD in periprosthetic bone of patients with painful hip- and knee joint replacement regarding the detection of prosthetic loosening. SUVs were derived by a modern SPECT/CT scanner that enables standardized (NIST traceable) quantitative SPECT measurements. **Methods:** We evaluated 36 patients with a total of 50 joint replacements of the hip or knee joints with clinical suspicion of prosthetic loosening, and all presenting with pain in these joints. Seventeen patients had knee joint replacements and 18 patients hip joint replacements. In 14 cases joint replacements were implanted at both sides. All patients underwent a 99mTc- Dicarboxypropan-diphosphate (DPD) -SPECT/CT examination with a standardized protocol: Quantitative SPECT/CT scans were performed 3h after injection of 740 MBq of 99mTc- DPD on a hybrid quantitative SPECT/CT camera (Symbia Intevo, Siemens Healthcare, Germany). Quantitative SPECT data were reconstructed with Siemens' xSPECT Quant and with xSPECT Bone, using the CT not only for attenuation correction but also to incorporate tissue boundary delineation from a CT for bone SPECT imaging. xSPECT Bone images depict voxelized uptake in kBq/ml in soft tissues and bone tissues while maintaining the separation of the tissue types at the resolution of the CT. Maximum SUVs of xSPECT Quant and xSPECT Bone data were compared with the definite diagnosis of a prosthetic loosening according to either intraoperative findings or the long-term clinical outcome of at least 1 year. Sensitivity and specificity were calculated using receiver operator characteristics (ROC). **Results:** Using the xSPECT Quant reconstructed SPECT data mean SUV max of loose joint replacements was significantly higher compared to stable joint replacements (18,2 ± 4,7 vs. 11,9 ± 4,2, p < 0.0001). The ROC analysis revealed an area under curve of 0.86 (p < 0,0001). With a cut off value of 12 the estimated sensitivity and specificity was 94% and 71%. Compared to the xSPECT Quant reconstruction xSPECT Bone reconstructed data showed a significantly higher mean SUV max of both, loosened and stable joint replacements (16,9 ± 6,3 vs. 14,1 ± 5,3, p = 0,016). **Conclusion:** Uptake quantification of periprosthetic bone metabolism in patients with painful joint replacements using quantitative 99mTc-DPD-SPECT/CT offers a promising quantitative marker that is likely to improve the accuracy for the diagnosis of prosthetic loosening.

EP-0150
Value of hybrid imaging in the detection of bone abnormalities in brucellosis

O. Ben Hamida, F. Hamza, I. Jardak, W. Amouri, M. Maaloul, F. Kallel, S. Charfeddine, K. Chtourou, F. Guermazi; Habib Bourguiba Hospital, Sfax, TUNISIA.

Aims: To assess the usefulness of SPECT CT in combination with bone scintigraphy in the detection of bone and joint abnormalities in brucellosis. **Methods and Results**: We present 2 brucellosis patients with osteoarticular involvement and normal plain radiography. They were evaluated with Tc-methylene diphosphonate bone scanning with quantification of sacroiliac joint uptake to improve the sensitivity for the detection of sacroiliitis. Single photon emission computed tomography (SPECT) in combination with low-dose computed tomography (CT) were performed in the patients, systematically. **Results:** For the first case, planar scintigraphy (vascular inflow, soft tissue phase and delayed phase images) showed a discreet increased radio-nuclide uptake in the left sacroiliac joint. Furthermore, we notify a second localization in the dorsal spin. For the second case, planar scintigraphy showed a normal whole body uptake. With SPECT, increased uptake in the affected joint was heterogeneous and non-symmetrical without lesions on CT. In the two cases, bone uptakes correspond to the symptomatic joint. The diagnosis of skeletal brucellosis was retained. **Conclusion**: Single-photon emission computed tomography (SPECT) in combination with low-dose computed tomography (CT) can increase the sensitivity of planar bone scintigraphy for the diagnosis of sacroiliitis. It must be systematically indicated for an individualized approach to the diagnosis of axial spondyloarthritis in brucellosis, particularly in patients with clinical symptoms and negative bone scintigraphy.

EP-0151
Concordance Among SPECT-CT, Peroperative Gamma probe Sentinel Localisation and Patent Blue Dye Technique for mapping hidden Sentinel nodes in Early Stage Breast Cancer patients

M. Siddique, A. Hassan, H. Bashir, M. K. Nawaz, A. I. Khan; Shaukat Khanum Memorial Cancer Hospital and Research Centre., Lahore, PAKISTAN.

Objective: To compare the detection efficacy of SPECT-CT using Tc-99m Sulphur Colloid versus Patent Blue Dye(PBD) technique for sentinel Lymph Node(SLN) detection in breast cancer patients with undetectable nodes on Planar Scintigraphy (PS) and to determine which modality is better for SLN detection. **Material and Methods:** Retrospective study of 1024 early stage (tumors<3cm) breast cancer patients referred for SLN mapping using radioisotope and PBD between April 2014 and March 2016. Out of these, patients with non-visualization of SLN/equivocal PS findings undergoing SPECT-CT (n=134) followed by peroperative detection of counts with gamma probe and/or PBD technique were included. Visually blue stained radioactive/non-radioactive nodes were surgically removed and evaluated histopathologically. The detection rate by individual method was calculated. Cohen's Kappa statistics were applied to calculate overall agreement between radioisotope and PBD techniques for diagnostic value assessment. **Results**: 134 female patients underwent SPECT-CT and PBD injection for obscure SLN on PS. Median age: 47 years (age range:26-82 years). 49(36.6%) had T1, 85(63.4%) T2. 131(97.8%) had positive SLN detected by radioisotope and/or PBD technique. 105/134 had SLN localization by SPECT-CT lymphoscintigraphy, later peroperatively gamma probe detected hot nodes in additional 20 cases. Out of nine cases with no detectable radioactivity in the axilla, SLNs were identified only by PBD staining in six, while none of the cases was identified only by radioisotopic detection (hot-only); illustrating failure rates of 2.2%(3/134) by PBD and 6.7%(9/134) by radioiso-

tope mapping. Therefore, the contribution of PBD to sentinel nodes identification was relevant for only 4.5%(6/134) patients. None of the cases developed allergic reaction with PBD. Three remained negative on both radioisotope and PBD localization. On subsequent axillary nodal dissection, all had metastatic nodal disease. All SLNs detected on SPECT-CT showed blue dye uptake. In 112 cases, more than one SLN was surgically removed. Frozen section analysis in total 536 excised nodes showed metastatic disease in 31%. Overall moderate agreement(k-value=0.54) was calculated between radioisotope/gamma probe detection and PBD. Statistically significant difference(p=0.01) was noted in SLN mapping between radioisotope and PBD technique where lymphoscintigraphic findings were negative. **Conclusion:** The role of PBD to reduce the false-negative rate of SLN mapping is only limited to occasional cases where no radioactivity is detectable in the axilla by SPECT-CT and/or gamma probe detection(<5%). When a radioisotope mapping has localised SLN, the use of PBD should be limited. Moreover, SPECT-CT had added value added value only for preoperative surgical planning in case of unusual node localization.

EP-0152
Challenges of low count in vivo imaging

S. T. van Tiel, E. J. Meester, J. de Swart, G. N. Doeswijk, L. Utomo, M. de Jong, M. R. Bernsen; ErasmusMC, Rotterdam, NETHERLANDS.

Aim: To define challenges that may be encountered during in vivo imaging of low count targets. **Materials and Methods:** Three disease models in mice were used to non-invasively image presence of somatostatin receptor 2 (SSTR2) positive macrophages (=pro-inflammatory macrophages) using the tracer ^{111}In-Octreoscan. These models were a Collagenase Induced Osteo Arthritis (CIOA) model, a Destabilization of the Medial Meniscus (DMM) model, and a atherosclerotic plaque model. These models represent disease models with small and low count imaging targets. At various time points during disease development animals were injected with 50-60 MBq/200 pmol ^{111}In-Dotatate or ^{111}In-Octreoscan. Imaging was performed on a MILabs USPECT -II/CT system using a mouse collimator with 1.0mm pinholes. SPECT was followed by a CT scan. During the scans the mouse was warmed and under 2% isoflurane anaesthesia. SPECT data sets were reconstructed using the POSEM algorithm; 30 iterations, 4 subsets and a voxel size of 0.4mm. CT was reconstructed using FBP. SPECT and CT were registered and the SPECT data were corrected for attenuation using the CT data. The resulting data was analysed using Invicro Vivoquant software. In addition phantom samples containing ^{111}In-Chloride at a concentration of 3 MBq/ml were also prepared. Different volumes of this solution were pipetted in an Eppendorf tube (500, 50, 5 and 0.5 ul). Scan parameters were kept the same as the in vivo scans. Scans of a single Eppendorf were made every 2-4 days to obtain increasingly lower count samples in order to study its effect on image quality. **Results:** Imaging of SSTR2 positive macrophages, with ^{111}In-labelled somatostatin peptide analogs in small targets in vivo, was proven to be challenging. The amount of radioactivity present in the diseased tissue is very low, resulting in images full of noise and imaging artifacts. Phantom studies affirmed that when there is a low amount of radioactivity present in a certain volume the images become noisy. Longer scan times resulted in less noisy images, but are not desirable for in vivo imaging. High signal objects (bladder, thymus) in the neighborhood of a low signal (knee, plaque) also interfere with the detectability of the low count targets. **Conclusion:** For imaging not only the activity concentration is crucial for image quality, but also the volume and total activity determines image quality. Imaging of small, low count targets in vivo is challenging and complicated when high activity objects are in close proximity.

EP-0153
Usefulness of examining hepatic functional volumetry with Tc-99m galactosyl serum albumin (GSA) using SPECT/CT in patients with liver disease

K. Maruyama, K. Utsunomiya, N. Kan, Y. Kono, Y. Ueno, N. Tanigawa; Kansai Medical University, Hirakata, JAPAN.

Aim/Introduction: To perform functional volumetric analysis of Tc-99m galactosyl serum albumin (GSA) using SPECT/CT scanner in chronic hepatitis or cirrhosis. Indocyanine green (ICG) is used as a maker in assessment of liver function. We examined liver volumetric function by SPECT, in comparison with biochemical test results using ICG retention rate at 15 min (ICG-R). **Subjects and Methods:** This retrospective study comprised 102 consecutive patients (91 chronic hepatitis and 11 cirrhosis) who underwent GSA scintigraphy and ICG test between May 2016 and March 2017. After the intravenous injection of Tc-99m GSA, dynamic planar imaging followed by SPECT/CT imaging was performed. The value of intravenously injected activity (201 ± 17 MBq) at the time of SPECT scan calculated from injected dose with decay correction. Functional activity was evaluated from the volume of interest with the outline extraction method from SPECT data. Total lesion of function (TL) was calculated by multiplying the functional volume with mean uptake per volume of liver. Percent injected dose (%ID) was account for % liver uptake of intravenously injection. SPECT parameters (mean uptake per volume, functional volume, TL, %ID) in relationship to ICG-R were statistically evaluated, and compared in disease severity (chronic hepatitis vs cirrhosis). **Results:** Quantitative SPECT parameters (mean uptake per volume, TL, %ID) in cirrhosis were significantly lower than those in hepatitis (p = 0.02, p < 0.001, p < 0.001, respectively). The mean value of %ID was 64 ± 14% in all, 67 ± 12% with chronic hepatitis and 45 ± 19% with cirrhosis. There was no difference in intravenously injected activity between chronic hepatitis and cirrhosis (ns). Functional volume, %ID of liver had no correlation with intravenously injected activity. The mean ICG-R was 25 ± 19%. Fourteen patients (all with hepatitis) had normal ICG-R (≤ 10%), and 88 patients (77 with hepatitis, 11 with cirrhosis) had elevated ICG-R (> 10%). Both %ID and TL were inversely correlated with ICG-R (r = -0.59 and r = -0.47, both p < 0.001). **Conclusion:** Functional volumetric analysis with Tc-99m GSA SPECT/CT provides useful information on patients with chronic hepatitis and cirrhosis. Under the

ICG test as the standard for hepatic function, the close relationships between %ID of liver and ICG-R indicate that %ID is a reliable parameter for evaluation of focal liver function.

EP-0154
SPECT/CT mapping of sentinel lymph nodes in patients with breast cancer

P. Krzhivitsky, S. Kanaev, S. Novikov, P. Krivorotko, N. Popova; *Petrov research oncology institute, Saint-Petersburg, RUSSIAN FEDERATION.*

Purpose: to evaluate the ability of SPECT-CT to determine the individual anatomic localization of sentinel lymph nodes in patients with breast cancer. **Materials and Methods:** SPECT-CT mapping of sentinel lymph nodes (SLN) performed in 159 patients (pts) with primary early-stage (cT1-2N0) breast cancer. Age of patients varied from 27 to 79 years (mean 56). In all cases, the results of clinical and instrumental (ultrasound) studies indicated no evidence of axillary lymph nodes abnormality. The rutine SPECT-CT imaging of SLN was performed 45-60 minutes after intra- or peritumoral injection of 0.2-0,3 ml (70-100MBq) of 99mTc -radiocolloids with particle size of 300-1000 nm. The large particle size of radiocolloids provided preferential visualization of SLN without concomitant transport of radiopharmaceutical to the second-echelon LN. Acquisition was performed on SPECT-CT (Symbia T16, Siemens) using a low-energy high-resolution collimator and step-and-shoot protocol of 20s/3degrees for a total of 60 views per camera head, 128x128 matrix, zoom factor 1,0. CT parameters included: 80 mAs, 100 kV, rotation tube time of 0.5 seconds, scan time of 10-15 seconds, a pitch of 1 mm, slice thickness of 5 mm with reconstruction interval of 1.5 mm. Post-processing fusion of SPECT and CT images was done on the workstation Siemens. All of SLNs was divided into the following 2 main groups: axillary with central, pectoral and lateral subgroups and internal mammary nodes (IMN). The additional Ђnon-standardЇ localization of SLN were intrapectoral and subpectoral. **Results:** SPECT-CT visualization of SLN demonstrated variability of their localization. Axillary SLN detected in 155 (97%) and internal mammary nodes (IMN) in 30 (19%) of 159 patients with breast cancer. In 26 (87%) patients sentinel IMN were identify with axillary SLN together and in 4 (13%) cases separately. In the axilla SLN were detected in central 94 (61%), pectoral 77 (50%) and lateral 6 (4%) subgroups. The additional intrapectoral and subpectoral localisation of SLN revealed in 35 of all patients (22%). **Conclusion:** SPECT-CT has ability to determinate the different anatomic localization of SLN in patients with breast cancer. At least in 22% cases SPECT-CT help to identify SLN in the Ђnon-standardЇ intrapectoral or subpectoral sites. Internal mammary sentinel nodes were visualized by SPECT-CT in 19% cases.

EP-0155
Dual tracer SPECT/CT utility for the localization and exclution of discordants spots

J. L. Pou, Sr., A. Armesto, R. Balbuena; *DIAGNOSTICO MAIPU, Buenos Aires, ARGENTINA.*

Introduction: Infections are not uncommon in prosthetic knee implants. The localization of the loosening prosthesis knee area or the source of infections can be complicated particularly because of its size or the attenuation artifacts caused by the same adjacent metal implant, requiring multiplanar or tomographic scintigraphic techniques. **Subjects and methods:** 56 year old male. Dual tracer Tc99m-MDP (25 mCi) and Tc99m-Ciprofloxacin (25 mCi) SPECT/CT knee study are done. **Results:** A right gonarthrosis are presented after 16 month of the bicompartmental femorotibial prosthesis implantation. Right knee radiography showed periprosthetic radiotransparent line. The three phase bone scintigraphy showed increased radiotracer uptake of the right knee in bloodpool and bone phases at the tibial component levels at the expense of the internal component. Posteriorly a scintigraphy with Tc99m-ciprofloxacin was done visualizing normal periprosthetic uptake and a diffuse mild uptake at subcutaneous cellular tissue level interpreted as inflammatory origin with late wash-out. **Conclusion:** The conduction and correlation of the dual tracer SPECT/CT study has helped for the precise localization and interpretation of the right peri-prosthetic knee pathology related to aseptic loosening prosthetic knee, a situation that would have had an erroneous diagnostic impression (false positive) if already relied on static projections scintigraphic images because of the avidity of the Tc99m-ciprofloxacin in subcutaneous cellular localization hardly identified by other not SPECT techniques.

EP-0156
Interobserver decreased variability by optimizing the SPECT/CT imaging fusion technique

J. L. Pou, A. Armesto, R. Balbuena; *DIAGNOSTICO MAIPU, Buenos Aires, ARGENTINA.*

Purpose: To demonstrate the usefulness of SPECT / CT with correct image fusion process regarding the SPECT images to improve interobserver variability. **Subjects and Methods:** 310 images from 155 bone SPECT / CT with 99mTc-MDP from the same center (90 of spine, 20 hips, 15 knees, 20 feet and 10 hands) acquired by gamma camera SPECT / CT GE Healthcare Infinia Hawkeye 4 were analyzed in the period 2015 to 2016 (1 year). They were analized by 2 nuclear medicine physicians with more than 10 years of experience in the field. Their results were compared with second reports made by observing the SPECT images alone of those same studies. **Results:** 155 SPECT/CT and 155 SPECT images (isolated from the same studies) were obtained. 150 images of those 155 SPECT/CT images (97%) were corrected by manual registry process. The two reporting doctors managed to locate the hyperactive lesions in 140 images (Kappa = 0.9) of those SPECT/CT images and 93 images of those SPECT alone (Kappa = 0.6). SPECT/CT technique with a correct methodology in the registration process of the anatomical and functional imaging has increased by 0.3 the Kappa coefficient. **Conclusions:** It is essential to have a good image processor to perform a correct anatomic-functional images registration process. Hybrid SPECT / CT cameras increase the confidence in reporting physicians and interobserver variability decreased by 33 % compared to the exclusive functional imaging technique (SPECT).

EP-0157

No added diagnostic value of contrast-enhanced CT versus low-dose CT in dual phase MIBI parathyroid SPECT/CT

*T. B. Andersen[1], **R. Aleksyniene**[1], S. K. Boldsen[1], M. Gade[2], H. C. Bertelsen[1], L. J. Petersen[1]; [1]Aalborg University Hospital, Aalborg, DENMARK, [2]Aalborg University, Aalborg, DENMARK.*

Purpose of the Report: The purpose of this study was to investigate the contribution of contrast-enhanced CT (CE-CT) on localization of parathyroid adenomas compared to dual-phase Tc-99m MIBI SPECT with low dose CT (LD-CT). **Materials and Methods:** This retrospective study included consecutive patients with primary hyperparathyroidism referred to pre-operative dual-phase MIBI SPECT/CT imaging followed by surgical resection. Standard of care was dual phase MIBI SPECT/CT acquired with LD-CT in the early phase and CE-CT in the late phase (SPECT/CE-CT). The presence and localization of positive sites were extracted from study reports. To examine the role of CE-CT, patient cases were independently re-reviewed with the early LD-CT fused with early and late SPECT (SPECT/LD-CT). We compared the two CT methods for sensitivity and positive predictive value (PPV) with histopathology as reference. **Results:** In total 138 patients were included. The investigation was positive for suspected adenomas in 124 patients using SPECT/CE-CT and in 122 patients with SPECT/LD-CT. The per-patient sensitivity was 87.5% (95% CI: 80.7-92.6%) for SPECT/CE-CT which not statistically significantly different from SPECT/LD-CT (85.3%; 78.2-90.8%) (*p*=0.39). The PPV was 95.2 (95.4-99.9%) with SPECT/CE-CT versus 100% (96.8-100%) with SPECT/LD-CT. For small adenomas (≤ 500 mg), the sensitivity was low with SPECT/CE-CT (67%) as well as SPECT/LD-CT (64%). **Conclusions:** Late CE-CT, compared to late LD-CT, did not significantly improve diagnostic sensitivity of dual-phase Tc-99m MIBI parathyroid SPECT/CT in a population of patients with primary hyperparathyroidism. These findings were consistent despite the size of the adenomas, histology, or location of the adenomas.

EP-0158

Collagen-based scaffolds and Non-Invasive SPECT/CT Bone Defect Pre-Clinical Imaging

E. Fragogeorgi, III[1], M. Rouchota[2], J. Daich[3], M. Georgiou[2], P. Bouziotis[1], G. Loudos[1,4]; [1]National Center for Scientific Research, Aghia-Paraskevi, GREECE, [2]BioEmission Technology Solutions, Athens, GREECE, [3]Bioimag Soluciones de Contraste, S.L., Caceres, SPAIN, [4]Technological Educational Institute of Athens, Department of Biomedical Engineering, Egaleo-Athens, GREECE.

Aim: Non-invasive imaging gains interest in the evaluation of novel synthetic scaffolds in bone tissue engineering as an alternative approach to the clinical gold standard treatment (autografting). Herein, we employ collagen-based scaffold materials as bone implants labelled with magnetic nanoparticles (MNPs) and with ^{99m}Tc. The *in vitro* labelling studies including stability and enzyme activity assessment in principle permit us to *in vivo* follow the fate of new bone grafts using MRI, SPECT and CT. Therefore, in the early stage of the *in vivo* evaluation of bone regeneration, we established a SPECT and CT based evaluation procedure for the longitudinal assessment of bone healing. **Materials & Methods:** The two collagen scaffolds studied are collagen free (CF) and coated with MNPs collagen (MFC). Radiolabeling with ^{99m}Tc was performed by the direct method using SnCl$_2$. The assessment of their *in vitro* stability was performed in relation to temperature, in an isotonic solution, in culture media at 37°C and in the presence of cysteine at three different concentrations. Measurements of collagenase activity were performed following incubation of collagenase (1 mg/mL) at 37°C with the radiolabeled collagen preparations used as substrate. To generate longitudinal SPECT combined with CT datasets a craniotomy is created at a rat model and each group of animals (empty defects (control) and defects filled with collagen gel) is injected with ^{99m}Tc-MDP and then imaged at predetermined time points up to 10 weeks. **Results:** Direct radiolabeling was performed in high yields (<98%) using 40μg SnCl$_2$ with neither radiocolloid nor free pertechnetate present in the final preparations. Radiolabeled collagen scaffolds, CF and MFC, was higher when kept at 4°C even after 24h. Radiolabeled collagen samples in saline remained stable up to 5h. Degradation in medium started after 3h, while ~50% remained intact after 24h. The rate of trans-chelation of ^{99m}Tc from radiolabeled collagen samples to cysteine was increased with cysteine concentration. A linear increase in collagenolytic activity occurred over time for both radiolabelled collagen samples, while colorimetric experiments of collagen degradation after being exposed to a series of enzymes are ongoing. In vivo imaging experiments allowed for a detailed evaluation and assessment of bone regeneration with and without the collagen-based scaffold implants. **Conclusion:** Following the satisfactory results obtained so far via the tested *in vitro* assays, an *in vivo* protocol is established based on rat models with calvarial bone defect to monitor the healing process over time by using the collagen-based scaffold materials.

EP-0159

Additional Value of SPECT-CT Versus SPECT in Progressive Necrotizing External Otitis Management

L. ZAABAR, D. BEN SELLEM, B. LETAEIF, M. BEN SLIMENE; Salah Azaeiz Institute, Ezzahra, TUNISIA.

Aim: ^{99m}Technetium- methylene diphosphonate (^{99m}Tc-MDP) is an early valuable tool to confirm progressive necrotizing external otitis (PNEO) diagnosis and assess extension, particularly, the SPECT modality. The aim of this study is to evaluate additional diagnostic value of fused single photon emission computed tomographic (SPECT) and computed tomographic (CT) images (SPECT-CT). **Materials and Methods:** Over one-year period, we explored 25 diabetic patients aged from 49 to 78 years old (73 years old median), with trailing and resistant otitis. We injected intravenously a mean activity of 740 MBq (20 mCi) ^{99m}Tc-MDP, and performed 2-3 h later, static planar scintigraphy views in anterior, posterior, lateral positions focused on skull. Thirteen patients (8 women, 5 men), underwent additional SPECT-CT scan. SPECT and SPECT-CT images were retrospectively then

separately interpreted: Firstly, the reviewer interpreted bone scan results (planar and SPECT), afterward, few days later, he/she interpreted fused SPECT/CT images and focused on additional value of fused images. **Results:** On planar acquisition qualitative analysis, we noticed increased temporal uptake was objectified in 9 patients. Three patients had uptake spreading towards midline, suspecting skull base invasion. The remaining four patients, had normal and symmetric temporal bone uptake. On SPECT images, we noticed mastoid uptake in 7 cases with additional limited petrous bone extension in two cases and further extension to petrous apex in three cases. Sphenoid extension was noted in one patient, and temporomandibular joint involvement in three patients. No new abnormalities were objectified on the four patients with normal planar images. On SPECT/CT images, no changes on the final report were noted (complete maching). **Conclusion:** Despite the known higher diagnostic value of SPECT-CT in suspected metastatic bone assessment, our preliminary study did not bring more accuracy in bone infection pathology in SPECT/CT modality.

EP-0160

SPECT CT in patients with non-specific hand and wrist pain

O. Ben Hamida[1], W. Amouri[1], F. Hamza[1], Y. Hentati[2], I. Jardak[1], F. Kallel[1], S. Charfeddine[1], Z. Mnif[2], F. Guermazi[1]; [1]Habib Bourguiba Hospital, Sfax, TUNISIA, [2]Hedi Chaker Hospital, Sfax, TUNISIA.

Aim: In this work, we investigated the usefulness of SPECT/CT combined with three-phase bone scan in assessing 12 patients with non-specific hand and wrist pain. **Materials and Methods**: In a retrospective study, 12 patients (9 women and 3 men with mean age of 44 years) were referred for non-specific pain of the hand with normal plain radiographs. Three-phase planar bone scan was performed with early dynamic acquisition after injection of 700MBq 99mTc-methylene diphosphonate (99m Tc-MDP). Two hours later, a static acquisition of the hands was performed followed by Single photon emission tomography coupled to diagnostic CT (SPECT/CT). The reconstructed SPECT/CT images were interpreted by a nuclear medicine physician and a radiologist. The planar bone scan was analyzed firstly alone and then in conjunction with SPECT/CT data. Reading criteria were lesion detection and localisation, type and etiology of the underlying pathology. **Results:** The diagnosis of algodystrophy was made by planar bone scan in 4 patients (33%)having either a diffusely increased tracer uptake in carpal and metacarpal regions on early and late phase images (in 3 patients) or a decreased radiotracer uptake on all 3-phases images (in 1 patient). SPECT/CT images helped to determine the etiology in 50 % of cases when revealing an occult stress fracture of radial tuberosity and an osteonecrosis of the large carp bone. In the 8 other patients (67%), planar bone scan showed indeterminate foci of uptake in the carp (for 6 patients) and the metacarpi (for 2 patients). SPECT/CT imaging concluded to an osteonecrosis of the lunate in 4 patients, a degenerative disease in 3 patients and arthritis in 1 patient. **Conclusion:** In complex joints such as those in the hand and wrist, SPECT/CT allows accurate localization of pathological uptake and provides better lesions characterization. This hybrid imaging technique improves test specificity and diagnostic confidence when coupled to three -phase bone scan.

EP-0161

The Value of Somatostatin Receptor Imaging (SRI) in Patients with Broncho-Pulmonary Carcinoids (BPCs) including Large Cell NEC Base on Pathological and Clinical Follow-up

S. J. Konsek[1], M. Franecka[1], M. Lowczak[1], A. Kolasinska-Cwikla[2], A. Lewczuk[3], M. Kidd[4], A. Nasierowska-Guttmejer[5], M. Tenderenda[2], J. B. Cwikla[1], I. M. Modlin[6]; [1]Faculty of Medical Sciences, University of Warmia and Mazury, Warszawska 30, Olsztyn, POLAND, [2]MSC Memorial Cancer Centre and Institute Maria Sklodowska-Curie, Warsaw, POLAND, [3]Medical University of Gdansk, Gdansk, POLAND, [4]Wren Laboratories, Branford, CT, UNITED STATES OF AMERICA, [5]Hospital Ministry of Internal Affairs, Warsaw, POLAND, [6]Yale University, New Haven, CT, UNITED STATES OF AMERICA.

Purpose: The aim of this retrospective study was to review the of value of Somatostatin Receptor Scintigraphy (SRS) as initial diagnosis, evaluation of tumour extent and in case of radical surgery as imaging follow-up patients with confirmed Broncho-Pulmonary-Carcinoids (BPCs) and LCNEC. **Subjects and Methods:** Overall 177 patients with confirmed in pathology BPCs or LCNEC were included. The type of the primary was based on current pTNM classification, including evaluation of clinical stage. Overall 332 SRS were performed using 99mTc HYN-lCTOC (Octreotide, NCBJ; Polatom, PL). Initial whole body WB-SPECT and then WB-SPECT/CT were used with standard iterative reconstruction in each case. **Results:** There were 70 patients with typical carcinoids (TCs), 76 pts with atypical carcinoids (ACs) and 31 with large cell neuroendocrine carcinoma (LCNEC). SRS was performed as initial diagnosis only in 10 of them, all subjects with TCs/ACs. SRS was true positive (TP) in 8 (80%), false negative (FN) in 2 (20%), no false positive (FP) and true negative (TN). In 92 patients SRS was used to assess stage of disease, overall 187 (56%) studies were performed. There were TP=62 (33%), TN=88 (47%), FN=32 (17%) and FP=5 (3%). The overall sensitivity of the SRS per study was 66% and specificity 95%. The sensitivity and specificity per patient 65% and 96%. Imaging follow-up was performed in 44 subjects, overall 91 studies. There were TP=13 (14%), TN=68 (75%); FN=9 (10%) and single FP (1%) results. The sensitivity and specificity per study: 59% and 99%; per patient: 50% and 97%. In group of LCNES two pts were diagnosed by SRS both TP. In this group of subjects, SRS was used in 26 subjects to evaluation of tumour extent; overall 38 examinations were carried out. There were: TP=6 (16%), TN=5 (13%), FN=27 (71%), no FP results. The sensitivity per study was very low 18%, and very high specificity 100%. The sensitivity and specificity per patient: 17% and 100%. Only 3 subjects with LC-NEC had follow-up studies, single TP and TN, 2 subjects had FN results, no FP study recorded. **Conclusion:** The test specificity was very high in both groups TCs/ACs and LCNEC. The highest test sensitivity was noted in evaluation of staging in TCs/ACs and slightly less in patients who had imaging follow-up. In com-

parison, the test was less useful in evaluation of primary diagnosis, evaluation of tumour extent and functional imaging follow up in group of LCNEC.

EP-0162

Hepatobiliary Scintigraphy Combined With SPECT/CT In Predicting Liver Failure Before Major Hepatectomy: Preliminary Results Of The HIBA-Index At A Single Center

m. serenari[1], c. pettinato[1], l. zanoni[1], c. collaud[2], m. levorato[1], l. esposito[1], c. bonatti[1], s. brocchi[1], a. cappelli[1], a. cucchetti[1], r. golfieri[1], a. d. pinna[1], s. fanti[1]; [1]sant'orsola-malpighi hospital, Bologna, ITALY, [2]hospital italiano de buenos aires, Buenos Aires, ARGENTINA.

Aim: Hepatobiliary scintigraphy (HBS) combined with single photon emission computed tomography (SPECT/CT) would potentially estimate future liver remnant function (FLR-F) more accurately than planar acquisitions and may be useful to predict post-hepatectomy liver failure (PHLF) before major hepatectomy. Existing cut-off values for PHLF (FLR-F < 2.69%/min/m2) had been previously set using only planar acquisitions and the described low rates of positive predictive value may render these values not completely reliable especially if using SPECT/CT to calculate the distribution of function within the FRL. A new index, the so-called Hospital Italiano De Buenos Aires index (HIBA-*i*), has been recently used to measure sectorial liver function in two-stage hepatectomy setting. **Materials and Methods**: Between November 2016 and April 2017, 18 patients were submitted to major hepatectomy (defined as resection of 3 or more segments) according to preoperative volumetry at Sant'Orsola-Malpighi Hospital (Bologna, Italy). PHLF was defined according to the International Study Group of Liver Surgery (IS-GLS) criteria. Data regarding preoperative HBS were retrospectively reviewed. Our HBS protocol included a first dynamic acquisition using the Geometric mean datasets, followed by the SPECT/CT phase. Total liver function (TL-F) and total liver uptake (TL-U) were calculated as well as FLR-F and HIBA-*i*, as previously described (De Graaf W et al. J Nucl Med. 2010;51:229-236. Serenari et al. Ann Surg. 2017 Jan 24). **Results**: Eighteen patients were submitted to major hepatectomy (9 right hepatectomy, 4 left hepatectomy, 4 right trisectionectomy, 1 left trisectionectomy). Mean TL-F was 9.58% ± 2.67 %/min, whereas TL-U was 48.90% ± 7.81%. FLR-F and HIBA-*i* differed between patients with (n=6) and without PHLF (n=12). Mean FLR-F and HIBA-*i* in patients with PHLF were 1.27% ± 0.73 %/min/m2 of the body surface area and 11.60% ± 6.83 %, respectively. Whereas, in patients without PHLF, mean FLR-F and HIBA-*i* were 2.88% ± 2.29 %/min/m2 and 26.64% ±17.08 %, respectively. **Conclusion**: The HIBA-*i* seems a promising tool able to estimate future liver remnant function. Prospective clinical trial are warranted to define more precise cut-offs for PHLF.

EP-0163

Use of wall-less radionuclide doped gel phantoms to determine the influence of non-active phantom walls in ⁹⁹ᵐTc and ¹²³I SPECT/CT activity quantification and outlining of tissue volume

I. Ceric '[1], S. Leide-Svegborn[2], M. Sydoff[2,1]; [1]Clinical Physiology and Nuclear Medicine, Helsingborg, SWEDEN, [2]Medical radiation physics, Malmö, SWEDEN.

Introduction and Aim: Activity quantification of tomographic images, such as Single photon emission computed tomography (SPECT) images, is an important tool to convert imaging data into activity concentration values. It is of great importance to have a high level of accuracy in the quantification of activity, since it is used in studies of the biokinetics and dosimetry of radiopharmaceuticals in nuclear medicine. It is also important in volume assessment for correct delineation of tumor volumes e.g. for grading of skeletal metastases from prostate cancer. The most common types of phantoms used in activity quantification in SPECT utilize fillable, hollow spheres placed in a circular cylinder which can be filled with a chosen activity concentration to simulate tumors in a hot or cold background. However, the occurrence of a cold sphere wall surrounding the hot-spot activity in images of this kind of phantoms could pose a problem since the lesion-to-background contrast is decreased and the delineation of volumes becomes less accurate on account of the cold sphere wall. **Materials and Methods:** We are verifying the use of a new type of phantom without cold sphere walls for the quantification of activity and outlining of tissue volume in SPECT measurements. Gelatin hot-spots of three different sizes were molded in custom made aluminum molds, and placed in a Jaszczak phantom together with hollow plastic spheres of the same sizes containing the same activity concentration. ⁹⁹ᵐTc and ¹²³I SPECT measurements were made with zero background activity and with lesion-to-background activity concentrations of 10:1 and 5:1. The background corrected relative volume reproducing threshold, T was calculated for both the gelatin and the plastic spheres. **Results and Conclusion:** The results show that the threshold, T drops with increasing background for the plastic spheres. For the gelatin spheres, this background dependence is not present. A decrease of the lesion-to-background contrast is seen for the plastic spheres compared to the gelatin spheres for both radionuclides.

EP-0164

Whole body SPECT/CT significantly improved inter-reader agreement compared to planar skeletal scintigraphy in detection of osseous metastases

R. Maklad[1], Y. G. Abdelhafez[1], M. Abd ElKareem[2], M. Abougabal[2]; [1]South Egypt Cancer Institute, Assiut University, Assiut, EGYPT, [2]Faculty of Medicine, Cairo University, Cairo, EGYPT.

Aim: To compare inter-reader agreement of whole body (WB) SPECT/CT compared with planar bone scans (PBS) for detection of bone metastases. **Materials and Methods:** Retrospective analysis of 106 patients who underwent 99mTc-MDP WB PBS and 2-bed SPECT/CT covering the region from the base of the skull to the upper thigh. Studies were anonymized and presented to 2 independent readers (R1 & R2) with 12- & 3-year experience; respectively. A 3-month interval was allowed between planar and SPECT/CT reading. The skeleton was divided

into 10-subsites (sternum, ribs, clavicles & scapulae, shoulders & humeri, cervical spine, dorsal spine, lumbar spine, sacrum, pelvis and femora). A 6-point score (0 = free, 1 = benign, 2 = probably benign, 3 = equivocal, 4 = probably metastatic or 5 = metastatic findings) was used to assess different sites (site-based) and patient overall (patient-based). The final diagnosis of disease status was made on the basis of subsequent clinical/imaging follow-up for at least 6 months. **Results:** Fifty-four patients were having metastases (51%). Sensitivity of WB SPECT/CT for R1 & R2 were 98% (95% Confidence Interval [CI]: 96-100) & 96% (CI: 93-100) while their respective specificity values were 96% (CI: 92-100) & 88% (CI: 82-95). Accuracy from ROC analysis were 98.4% (CI: 94-100) & 97% (CI: 91-99); respectively. Differences in sensitivity, specificity & accuracy were 2% (P = 1.0), **8% (P = 0.13)** & 2% (P =0.5); respectively. Sensitivity of WB PBS for R1 & R2 were 78% (CI: 70-86) & 81% (CI: 74-89) while specificity were 94% (CI: 90-99) & 83% (CI: 75-90); respectively. Their respective accuracy values were 87.3% (CI: 79-93) & 84% (CI: 76 - 90). Differences in sensitivity, specificity & accuracy were 4% (P=0.7), **12% (P=0.07)** & 3% (P=0.3); respectively. On patient-basis, kappa agreement between R1 & R2 were 68.1% for PBS & 72.9% for SPECT/CT. On site-basis, agreement varied according to the site from 10 to 76% for PBS and from 68 to 86% for SPECT/CT. The difference was statistically significant in most sites. **Conclusion:** Inter-reader agreement was higher for whole body SPECT/CT compared to planar skeletal scans. It has the potential to improve inter-reader agreement for different anatomical sites between readers with different experience. Identification of subgroups who benefit the most from WB SPECT/CT is necessary and warrant further studies.

EP-0165

Does whole body SPECT/CT significantly improve accuracy over planar skeletal scintigraphy in all cancer types?

M. Abd ElKareem[1], Y. G. Abdelhafez[2], R. Maklad[2], M. Abougabal[1]; [1]Faculty of Medicine, Cairo University, Cairo, EGYPT, [2]South Egypt Cancer Institute, Assiut University, Assiut, EGYPT.

Aim: To compare diagnostic performance of whole body (WB) SPECT/CT compared with planar bone scans (PBS) in patients with different primary tumors. **Materials and Methods:** Retrospective analysis of 106 patients who underwent 99mTc-MDP WB PBS and 2-bed SPECT/CT covering the region from the base of the skull to the upper thigh. Studies were anonymized and presented to one experienced reader (12-year experience). A 3-month interval was allowed between planar and SPECT/CT reading. A 6-point score (0 = free, 1 = benign, 2 = probably benign, 3 = equivocal, 4 = probably metastatic or 5 = metastatic findings) was used to assess the scan overall (patient-based analysis). Skeleton was divided into 10 sites and the reader was requested to record whether their decision per site was based on uptake intensity/pattern, CT findings or combination. The final diagnosis of disease status was made on the basis of subsequent clinical/imaging follow-up for at least 6 months. **Results:** A total of 54/106 patients were having metastases (51%). Sensitivity and specificity for WB SPECT/CT were 98% (95% Confidence Interval [CI]: 96-100) & 96% (CI: 92-100) compared to 78% (CI: 70-86) & 94% (CI: 90-99) for WB PBS; respectively. WB SPECT/CT was significantly more sensitive (P < 0.001). ROC analysis showed higher accuracy for WB SPECT 98.4% (CI: 94-100) compared to 87% (CI: 79-93) for PBS (P = 0.003). Fifty-six patients had breast cancer (BC), 50 with other cancers (NBC); of them 25 had uro-genital cancer (UGC). Prevalence of skeletal metastases in these groups were 45%, 58%, and 48%; respectively. ***In BC patients***, WB SPECT/CT & PBS showed accuracy of 97% (CI: 88-100) & 90% (CI: 80-96); respectively ***(P = 0.2)***. These figures were, respectively, 100% (CI: 93-100) & 85% (CI: 72-93) ***for NBC group (P = 0.005)*** and 100% (CI: 86-100) & 84% (CI: 64-95); ***for UGC group (P = 0.07)*** Diagnosis was based on CT findings only in 25/131 (19%) positive sites in BC group compared to 23/95 (24%) in NBC and 11/40 (28%) in UGC; respectively (P = 0.5) No statistically-significant difference in patients' scores or site predilection for metastases among different groups. **Conclusion:** When cancer site is considered, accuracy of WB SPECT/CT shows was not higher than PBS in unselected group of breast cancer patients, while it performs significantly better in non-breast cancer patients.

Molecular & Multimodality Imaging: PET/MR

EP-0166

Impact of reduced injected activity on the quantification of [18F]FLT and [18F]FDG SUV in NF2 patients with vestibular schwannomas

J. M. Anton Rodriguez[1], I. Djoukhadar[1], P. Julyan[2], D. Russell[3], G. Evans[4], A. Jackson[1], J. C. Matthews[1]; [1]Wolfson Molecular Imaging Centre-University of Manchester, Manchester, UNITED KINGDOM, [2]Christie NHS Foundation, Manchester, UNITED KINGDOM, [3]East Cheshire NHS Trust, Manchester, UNITED KINGDOM, [4]Genomic Medicine, Central Manchester University Hospital, NHS Foundation Trust, Manchester, UNITED KINGDOM.

Aim: Retrospective study to assess the impact of reductions in injected radiotracer activity on SUV quantification of [18F]fluorothymidine (FLT) and [18F]fluorodeoxyglucose (FDG) within vestibular schwannomas (VS) lesions of neurofibromatosis type II (NF2) patients and its effect on the ability to discriminate growing lesions. **Materials and Methods:** Our previous study showed that both FDG and FLT have utility in the differentiation of growing VS lesions in NF2 patients [1]. For this work, data collected on a Siemens Biograph TrueV PET/CT was used. These data were from six patients with VS lesions (5/6 bilateral, 11 in total), with the patients injected with 200 MBq of FLT and FDG on two separate occasions. Collected 30 minute listmode data were resampled with replacement (bootstrapped) 50 times for each of five counts levels corresponding to 5, 10, 20, 50, and 100% of the original counts [2]. This resampled data were subsequently reconstructed with and without resolution modelling (RM) (4 iterations 21 subsets, 4500 reconstructions in total). Regions of interest defined on co-registered contrast enhanced

T_1-weighted MRI were then used to calculated mean, peak and maximum standardised uptake values (SUV) for each image. For each count level, the distribution of SUV values was estimated at approximately 75-105 minutes post injection, either directly or from the interpolation of earlier and later scan data. To evaluate the impact on the ability to discriminate growing lesions, further resampling was conducted to calculate a distribution of area under the curve of the receiver operator characteristic curve (ROC-AUC). **Results:** The deterioration in SUV precision with reduced counts was greatest for: SUVmax; small lesions with low uptake; and for VS lesions close to brain (for FDG) or sphenoid bone (for FLT). For FDG/FLT, SUVmean precision (standard deviation) was 4(1-14)/6(2-14)% (median(range)) at 100% counts which reduced to 18(7-47)/18(7-67)% at 5%. For the ROC-AUC for both FDG and FLT, there was only a small reduction in ROC-AUC, with the greatest reduction with SUVmax and no RM. For FDG/FLT and using SUVmean without RM, ROC-AUC values were 0.83±0.02(0.86-0.79)/0.76±0.02(0.80-0.73) (mean+/-std(range)) for 100% reducing to 0.81±0.07(0.94-0.66)/0.76±0.07(0.94-0.66) for 5% counts. **Conclusion:** Despite a modest loss in SUV precision, doses could be reduced to 5-10% without a significant loss in the ability to discriminate when the location of the lesion is known. The development of PET-MR scanners enables such co-localisation. **References** [1] Anton-Rodriguez et al, CP J Nucl Med 2016 57:628 [2] Herholz K. et al ,EJNMMI 2014 41:2144:2149

EP-0167

Accuracy of tumor segmentation from multi-sequence MRI and 18F-choline PET/CT for focal prostate cancer therapy applications

M. R. Piert, P. Shankar, J. Siddiqui, V. Rogers, L. P. Kunju, J. Montgomery, J. Hearn, M. S. Davenport; University of Michigan, ANN ARBOR, MI, UNITED STATES OF AMERICA.

Purpose: We tested the accuracy of MRI and 18F-choline PET/CT for tumor segmentation of significant prostate cancer (PCa) relative to pathological truth from prostatectomy specimen. Methods: 18F-choline PET/CT and multi-parameter MRI (mp-MRI) were performed in 10 subjects undergoing prostatectomy. All subjects had one single biopsy-confirmed Gleason ≥7 cancer. Two fellowship trained expert prostate MR radiologists (reader1, reader2) were tasked to determine tumor boundaries based on all available MRI sequences. 18F-choline data were co-registered with T2-weighted (T2W) 3D-sequences and a semi-automatic segmentation routine based on choline uptake was used to define tumor volumes. We facilitated registration of whole-mount pathology to in-vivo imaging by performing ex-vivo prostate specimen MRI, 3D-printing of custom-made molds, and gross sectioning of the specimen within the mold. All PCa foci were outlined by the pathologist on whole-mount HE slices registered to the *ex-vivo* MRI to be transferred into the *in-vivo* 3D T2W MR and registered PET volumes. The consensus between manually created contours by expert radiologists, PETEdge segmented lesions and ground truth was determined by commonly applied similarity coefficients (Hausdorff-Distance, MDA, Dice on MIM Software). **Results:** Histological tumor

volumes ranged from 0.15 - 6.31 mL; the smallest lesion (0.15 mL) was not identified by both readers (and 18F-choline) and excluded from analysis. One reader missed a 1.35 mL lesion. Visual tumor border segmentation based on MRI significantly underestimated the true tumor volumes (reader1 by 72%; reader2 by 76%, P<0.02), while PETEdge segmented volumes were not significantly different from truth. However, similarity coefficients obtained from MRI and PET contours were equally misplacing tumor disease compared to pathological truth (Hausdorff-Distance: reader 1 = 7.92, reader 2= 9.14, PETEdge = 8.58 mm). We tested whether a 5-mm contour expansion in all directions would improve tumor coverage. Indeed, the missed tumor volume decreased significantly compared to the original segmentation (reader1: from 1.16 to 0.07 mL; reader2: from 0.84 to 0.18 mL; PETEdge: from 0.73 to 0.04 mL, p<0.001). However, depending on tumor shape and the identification of the lesions' center, minimum contour expansions between by 8 (reader1), 14 (reader2) or 11 (PETEdge) mm would have been needed to cover all Gleason ≥7 disease. **Conclusion:** Visual tumor segmentation based on MRI significantly underestimates the true volume of Gleason 7 PCa, which is an important consideration for focal PCa treatments. Substantial safety margins are needed to include all Gleason ≥7 disease. **Support:** United States DOD GRANT10953301

EP-0168

Early assessment of radiation treatment response in liver cancer by dual-tracers PET/MRI in preclinical study

Y. C. Chung, C. Huang, F. Chen, C. Yu, J. Hong, T. Yen; Chang Gung Memorial Hospital, Taiwan, Tao-Yuan, TAIWAN.

Imaging probes/biomakers associated with the molecular changes or tumor microenvironment structure altered have been applied not only in cancer diagnosis but also in the assessment of cancer treatment efficacy. The purpose of this study is to assess the early response to radiation treatment in liver cancer by dual PET tracers, ^{18}F-FDG and ^{68}Ga-RGD as well as MRI diffusion-weighted images(DWI). **Methods:** Six weeks old BALB/c mice were orthotopic injected hepatocellular carcinoma cells into the right lobe of the liver. The MRI and PET with two tracers were performed on day-1, 1, 3, 6 and/or 9 after 15Gy radiation therapy with a 2 x 2 cm cone. The sizes of tumors were determined in the coronal planes of MRI T2. The apparent diffusion coefficient (ADC) values of DWI were quantified with a threshold of below (maximum-minimum)*50% of ROI, matching the tumor burden. The quantification of tumor uptake in FDG and RGD PET were carried on with a threshold of above (maximum-minimum)*50% of ROI, contouring the tumor margin. The tumors were stained with CD31, PIMO, and Hoechst33342 after last imaging scan to verify that the effect of radiation on the molecular change or tumor microenvironment altered. All the data (RT group and non-RT group) were normalized to day-1 and compared at each time-point using student's t-test. **Results:** The tumor size of RT group (n=6, 4.31±3.75) is significantly decreased in day 9, respectively compared with non-RT group (n=5, 8.16±3.15; p<0.05). The ADC values of RT

group were slightly increased than non-RT group in the whole period of observing time. FDG radioactivity of the tumors in RT group was significantly lower than that of non-RT group on day 6 (RT: 0.93±0.22; non-RT:2.03±0.7, p<0.05), indicating the cellular density and glucose metabolism of the tumor were significantly altered on day 6 after radiation. RDG radioactivity of the tumors in RT group was significantly higher than that of non-RT group on day 3 (RT: 1.11±0.18; non-RT: 0.76±0.04, P<0.05) and day 6 (RT:1.14±0.07; non-RT:0.94±0.02, p<0.05). The less vessel density of tumor in the RT group was demonstrated in CD31; on the contrary, the increased perfusion function in RT group was shown with Hoechst33342 staining on day 9 after radiation, which is corresponding to the diminished hypoxia effect (PIMO). **Conclusion:** The angiogenesis altered, better perfusion, less cellular density, and decreased glucose metabolism were characterized as the earlier radiation treatment response than the morphological change using dual-tracers PET/MRI in vivo imaging.

EP-0169

First use of Bruker Albira and ICON multimodal bed for acquisition of PET/CT/MRI images

J. D. Steinberg, N. de Wit, E. Semenova; Netherlands Cancer Institute, Amsterdam, NETHERLANDS.

Aim: PET/CT is a well-established multimodal imaging method that combines the functional information of PET with the structural information of CT. However, CT has poor soft tissue contrast, which makes it difficult to visualize certain tumors. Thus, there is an interest in combining PET and MRI to allow for better visualization of the tumor. Bruker introduced a multimodal bed that is compatible between the Albira PET/CT and ICON 1T MRI to create PET/CT/MRI with the mouse in the same orientation for easy registration. We will present our first results acquiring PET/MRI for the various mouse models at our imaging center. **Materials and Methods**: The study uses a small cell lung cancer (SCLC) model that was created by intratracheal injection of the CMV-Cre adenovirus in mice over-expressing Nfib to delete Trp53 and Rb1, leading to the development of SCLC lesions. Cisplatin was used for treatment, and tumor response was monitored on both an Albira PET/CT and ICON 1T MRI using Bruker's multimodal bed. Each mouse was injected with 10-15 MBq of 18F-FDG 1 hour prior to the 18F-FDG PET/CT examination. The mice were fasted overnight and kept warm during and after injection using a heated bed. Following the PET/CT scans, the mice were transferred to the MRI while still remaining inside the multimodal bed, where the lungs were scanned with both axial and coronal T1-FLASH. The PET/CT and MRI were registered using a semi-automated rigid registration within Pmod. **Results**: The SCLC model showed extensive tumor burden in the lung from both the MRI and CT. However, it was difficult from the CT alone to distinguish between healthy and malignant tissue, whereas delineation of the tumor was possible with the MRI. Thus, from the MRI it was determined that there was visible FDG uptake in some parts of the tumor but not in other parts of the tumor. We know from ex vivo analysis that there are different tumor populations within the tumor, so it is possible that the different tumor populations took up different amounts of FDG. Thus, FDG PET/MRI might be able to distinguish the two populations, which would help determine how each distinctive cell population responds to treatment. **Conclusion**: PET/MRI has the potential to replace PET/CT as the preferred method of imaging in tumor models. The soft tissue contrast of MRI makes it an ideal partner with PET for imaging the tumor and delineating the tumors from healthy tissue.

EP-0170

Comparison of ZTE and atlas attenuation correction for brain [15O]H2O-PET/MR imaging

T. Hjørnevik[1,2,3], A. P. Fan[2], M. Khalighi[4], H. Gandhi[2], D. Holley[2], P. K. Gulaka[2], B. Shen[2], J. H. Park[2], F. T. Chin[2], G. Zaharchuk[2]; [1]Oslo University Hospital, Oslo, NORWAY, [2]Stanford University, Stanford, CA, UNITED STATES OF AMERICA, [3]The Norwegian Medical Cyclotron Centre, Oslo, NORWAY, [4]GE Healthcare, Menlo Park, CA, UNITED STATES OF AMERICA.

Purpose: MR-based attenuation correction (AC) is still challenging in hybrid PET/MR systems. Recently, a new bone imaging technique, based on proton density-weighted, single-echo zero-echo time (ZTE) acquisition, has been developed for PET/MR AC (ZTE-AC)[1]. This study compares the effect of atlas-based AC (Atlas-AC) and ZTE-AC on image-derived input functions (IDIF), [15O]H$_2$O PET uptake values and quantitative cerebral blood flow (CBF) estimations. **Subjects and Methods:** 10 patients with Moyamoya disease were examined with [15O]H$_2$O-PET/MR (SIGNA PET/MR; GE Healthcare). Images were reconstructed (OSEM; 3 iterations, 28 subsets; 30x1 sec, 10x3 sec, 12x5 sec, 12x10 sec) and corrected for scatter and attenuation using two different AC maps: 1) Atlas-AC: derived from T1-weighted liver acquisition with volume acceleration flex images (LAVA-FLEX), 2) ZTE-AC: derived from ZTE images by applying tissue segmentation and assigning continuous attenuation values to the bone. CBF values were estimated in PMOD3.6 using a novel IDIF method[2] and 3 min of dynamic PET data. The percent differences (%Diff) in the IDIF peak, regional CBF values and summed PET uptake values were calculated between the AC methods. **Results:** ZTE-AC resulted in a significant increase in the IDIF peak (mean ± SD, 11.1 ± 4.2 %; range: 5.3-17.3 %; paired t-test, p<0.001). ZTE-AC also resulted in higher PET uptake values in all regions of the brain, in particular the temporal lobe and the cerebellum (%Diff; 7.1 ± 2.7 % and 5.9 ± 3.2 %, respectively). CBF values estimated using ZTE-AC were lower than with Atlas-AC, with the largest difference in the frontal lobe and insula (%Diff; 9.5 ± 8.8 % and 9.3 ± 5.2 %, respectively). **Conclusion:** Accurate AC is crucial for quantitative PET imaging. The choice of AC method influences both the IDIF and PET uptake values, both highly important for estimating CBF. The observed higher PET uptake in the temporal lobe and cerebellum could be caused by ZTE misclassification of air and bone in the mastoid and nasal areas as reported by others[3]. Lower CBF values due to ZTE-AC are most likely due to the increased peak of the IDIF, which is estimated from the cervical arteries near the skull base. Future work will include comparing these results to the gold standard CT-based AC. **References:** 1 Wiesinger et al.,

Magn Reson Med (2016) 2 Khalighi et al., J Cereb Blood Flow Metab (2017) 3 Sekine et al., J Nucl Med (2016)

EP-0171

Total Activity method: A fully automated approach to calculate the image-derived input function from [18]FDG PET/MRI brain studies

l. Shiyam Sundar[1], I. Rausch[1], O. Muzik[2], L. Rischka[1], A. Hahn[1], R. Lanzenberger[1], M. Hienert[1], E. Maria Klebermass[1], T. Traub-Weidinger[1], T. Beyer[1]; [1]Medical University Vienna, Vienna, AUSTRIA, [2]Wayne State University School of Medicine, Detroit, MI, UNITED STATES OF AMERICA.

Aim: To assess the performance of a method that uses the activity balance between sub-locations of a large region that contains both the internal carotid artery and tissue background for extraction of an image-derived input function (IDIF) from simultaneously acquired PET/MR image data. The method is neither dependent on the point-spread-function (PSF) of the scanner, nor it is affected by minor subject motion. **Material and Methods:** Seven subjects underwent dynamic FDG test-retest PET/MRI examinations in a fully-integrated PET/MRI system (Siemens, Biograph mMR). The protocol included a time-of-flight MR angiography (TOF-MRA) sequence used to determine an internal carotid artery mask (ICAM) as well as sparsely sampled MR-navigators for motion correction. The PET data was reconstructed using OSEM with scatter and a CT-based brain attenuation correction. Arterial blood samples (AIF) were collected as the gold standard. Initially, the petrous portion of the ICAM was obtained using an automated segmentation algorithm. Subsequently in the co-registered PET frame, a large region (volume V_T and total activity C_T) containing the petrous activity (C_A) along with the background activity (C_B) was defined by dilating the petrous ICAM mask 4 mm from its edges (volume, V_T; concentration, C_T). The FDG concentration (C_B) in the background region (V_B) was estimated from values at the outer surface of the dilated region. The activity balance in these 3 volumes can be then expressed as $C_T V_T = C_A V_A + C_B V_B$. This equation can be solved for Ca, yielding the true FDG concentration in the ICAM (i.e. IDIF) for each dynamic PET frame. The ratio (R) of the areas-under-the-curve (AUC) obtained for the IDIF and the AIF was used as a similarity measure between the two input functions. **Results:** We obtained a 4±9% difference for R (1.04 ± 0.09), with the IDIF overestimating the true IF (AIF) due to underestimation of background activity (C_B) at later time points. As a result, the accuracy of this method is dependent on selection of a large region that permits precise estimation of the average background activity. **Conclusion:** The total activity method allows non-invasive determination of the arterial input function that is insensitive to low-level subject motion and independent from scanner PSF. Thus it has potential for being relevant in clinical routine for quantitative assessment of FDG PET studies.

EP-0172

Multi-radiotracer PET/MR Truncation Correction by Segmentation of TOF-NAC-PET Images with F18-FDG, Ga-68 PSMA and O-15-H$_2$O

J. Teuho[1], V. Saunavaara[2,3], M. Lahesmaa[1], M. Teräs[2,4]; [1]Turku PET Centre, University of Turku, Turku, FINLAND, [2]Department of Medical Physics, Turku University Hospital, Turku, FINLAND, [3]Turku PET Centre, Turku University Hospital, Turku, FINLAND, [4]Institute of Biomedicine, University of Turku, Turku, FINLAND.

Introduction: Truncation of the arms due to the limited MR field-of-view (FOV) poses a challenge in PET/MR imaging and needs to be compensated in MR-based attenuation correction (MRAC). On the Philips Ingenuity TF PET/MR, truncation correction is clinically conducted by segmentation of non-attenuation corrected PET images (NAC-PET), which is feasible for F18-FDG as it exhibits a clear accumulation in the skin. This allows delineation of the patient contour from NAC-PET. However, other radiotracers without any clear accumulation in the patient outline such as Ga-68 prostate-specific membrane antigen (PSMA) and O-15 H$_2$O create a challenge for PET-based truncation correction. In addition, obese subjects are a challenge when using F18-FDG. Our intention was to investigate and to show that using time-of-flight (TOF) NAC-PET images improves the delineation of the arms in F18-FDG and allows to accurately delineate the arms with Ga-68 PSMA and O-15 H$_2$O. **Materials and Methods**: Truncation corrected attenuation maps were created by segmentation of NAC-PET images and TOF-NAC-PET images with 525 ps timing resolution. Two obese subjects with F18-FDG, two subjects with Ga-68 PSMA and one subject with O-15 H$_2$O were included to our initial evaluation. We intend to include more patients in the future. MRAC maps and the resulting PET images were inspected visually for artifacts and accuracy in delineation of the arms. SUVmax was measured in one Ga-68 PSMA subject from randomly selected four regions of interest the arms and one region of interest in the trunk. **Results:** The visual inspection of the attenuation maps revealed small artifacts with two of the obese subjects when using NAC-PET and F18-FDG. The PET accumulation in these subjects was not significantly changed. With the two subjects with Ga-68 PSMA, the attenuation maps revealed large regions which were not effectively compensated. In O-15 H$_2$O, the arm of the subject was partially missing. Using TOF-NAC-PET allowed better delineation of the arms with F18-FDG. TOF-NAC-PET allowed to effectively compensate the regions which were not visible in NAC-PET with Ga-68 PSMA and O-15 H$_2$O. SUVmax increase in the truncated regions with TOF-NAC-PET was in the range of 12.5 % to 25 % with mean increase of 17.9 %. SUVmax was not significantly changed in the trunk. **Conclusions:** TOF-PET imaging is beneficial for truncation correction in MRAC. Truncation correction by segmentation of TOF-NAC-PET images is superior to NAC-PET, allowing improved delineation of the arms using multiple radiotracers.

EP-0173

Impact of MR-based attenuation correction on the evaluation of time-activity-curves and time-to-peak analysis in F-18 FET PET/MRI

I. Rausch[1], A. Ziterl[1], A. Haug[1], R. Aghamohammadi-Sareshgi[1], M. Fenchel[2], M. E. Mayerhoefer[1], T. Beyer[1], T. Traub-Weidinger[1]; [1]Medical

University of Vienna, Vienna, AUSTRIA, ²Siemens Healthcare GmbH, Erlangen, GERMANY.

Aim: Evaluation of the influence of different magnetic resonance based attenuation correction (MR-AC) on uptake patterns of dynamic F-18 FET positron emission tomography/magnetic resonance imaging (PET/MRI) brain cancer examinations. **Methods:** 24 patients with suspected brain tumours undergoing a 40 min dynamic 18F-FET PET/MRI examination (Biograph mMR, Siemens) and a subsequent low dose computed tomography (CT) scan of the head were included in this study. PET data was reconstructed into 8 time frames (2x2 min, 4x4 min, 2x10 min) using an OSEM algorithm and with the following attenuation correction (AC) approaches: CT-AC, standard DIXON- and UTE-AC and a model-based approach incorporating spatially variant bone information into the DIXON-AC (non-commercial prototype software, Siemens Healthcare). Time activity curves (TAC) and time to peak (TTP) using different region-of-interest (ROI) and volume-of-interest (VOI) definitions were extracted for all lesions and reconstructions. TACs extracted from (A) ROIs and (B) VOIs defined by a 90% threshold of the maximum uptake within the lesion were categorized into two curve patterns: constantly rising or TTP <20min followed by a descent. TACs extracted from (C) ROIs and (D) VOIs defined by a threshold of 1.6 times the background and (E) VOIs with a fixed volume of 2mL placed in the maximum uptake region within the lesion were categorized into three curve patterns: constantly rising, TTP >20min followed by a plateau or TTP<20min followed by a descent. Changes in TTP and TAC patterns compared to CT-AC based PET were reported. **Results:** TTP changed in 8%, 8% and 8% (A), 0%, 17% and 4% (B), 13%, 13% and 17% (C), 6%, 6% and 12% (D), 4%, 8% and 8% (E) of patients following DIXON-, UTE- and model-based AC, respectively. No change in TAC pattern was observed in (B) and (E). However, TAC pattern changed for (A) in 0%, 4%, 0%, for (C) in 8%, 4% and 8% and for (D) in 6%, 0% and 6% of the patients, respectively. **Conclusion:** Using different AC approaches in PET/MRI can affect the TTP and TAC pattern in dynamic F-18 FET examinations. The difference is assumed to be caused by variations in the anatomical region included in ROI or VOI when using different AC approaches.

EP-0174

Assessing the impact of different attenuation correction methods on clinical image-derived input functions extracted from 18F-FDG PET/MRI brain data

I. Rausch[1], L. Shiyam Sundar[1], O. Muzik[2], L. Rischka[1], A. Hahn[1], R. Lanzenberger[1], M. Hienert[1], E. Klebermass[1], M. Fenchel[3], T. Traub-Weidinger[1], T. Beyer[1]; ¹Medical University of Vienna, Vienna, AUSTRIA, ²Wayne State University School of Medicine, Detroit, MI, UNITED STATES OF AMERICA, ³Siemens Healthcare GmbH, Erlangen, GERMANY.

Aim: To assess the impact of different attenuation correction (AC) methods on image-derived input function (IDIF) calculated from 18F-FDG PET/MRI studies. **Material and Methods:** To date, 7 subjects were studied. Subjects underwent dynamic 18F-FDG PET/MRI examinations in a fully-integrated PET/MRI system (Siemens, Biograph mMR). The protocol included standard Dixon- and UTE-based AC sequences and a time-of-flight MR angiography (TOF-MRA) sequence for delineation of the carotid arteries. Following the PET/MRI examination, subjects underwent a low-dose CT scan in order to obtain a CT-based AC. PET data was reconstructed using OSEM with four different AC methods: (1) Dixon-based AC, (2) UTE-based AC, (3) Atlas-based AC (non-commercial prototype software adding spatially variant bone information to Dixon-based AC, Siemens Healthcare), and (4) CT-based AC. Arterial blood samples were collected to determine the arterial input function (AIF) as the gold standard. The IDIF was calculated in 3 steps: (1) automatic segmentation of the petrous region of the internal carotid artery (ICA) in order to obtain an ICA mask (ICAM), (2) determination of activity in the background region surrounding the ICAM using TOF geometric information and the system's PSF and (3) application of a partial volume correction for activity in the center of the ICAM, following subtraction of the spillover contribution from background activity. IDIFs were extracted individually for PET images obtained using the four different AC methods, resulting in four different IDIFs (Dixon, UTE, Atlas, CT). The relative difference (RD) between the areas-under-the-curve (AUCs) of the four IDIFs and the AUC of the AIF was calculated. The RD of the AUC of the MRI-based AC methods to the AUC of the $IDIF_{CT}$ was used as a similarity measure between the input functions. **Results:** The RDs between the AUC of the individual IDIFs and the AUC AIF was calculated as -40±4% (Dixon), 4±13% (UTE), -28±6% (Atlas) and -4±5% (CT). The RDs between the AUC IDIFs of the MRI-based AC methods and the $IDIF_{CT}$ was -37±4% (Dixon), 9±16% (UTE) and -25±5% (Atlas). **Conclusion:** The $IDIF_{CT}$ and $IDIF_{UTE}$ approximate the AIF reasonably well. However, given the large variance of $IDIF_{UTE}$, the UTE AC is suboptimal for IDIF calculation. The $IDIF_{Atlas}$ and $IDIF_{Dixon}$ severely underestimated the AIF but with a similar variance as $IDIF_{CT}$.

EP-0175

An in vivo PET study of a rat fluid-percussion-induced traumatic brain injury model with [¹¹C]PBR28 and [¹⁸F] Flumazenil - A preliminary study

P. Padmanabhan, Z. Wang, C. Yang, K. K. GHOSH, C. Halldin, B. Z. Gulyás; LKC Medicine, NTU, Singapore, SINGAPORE.

Background and Objectives: Traumatic brain injury is recently receiving great attention due to the increasing number of human mortality and morbidity related to war and terrorism. To study the cellular and molecular changes of TBI observed in humans, a lateral fluid-percussion-induced (LFPI) rodent model was developed. It is an extensively utilized animal model of TBI due to its capability of reproducing the physiological, pathological and behavioural aspects under different well controlled clinical conditions in rodents. We previously demonstrated that the neuroinflammatory response and neuronal loss in rat TBI model can be quantified by PET imaging using [¹¹C]PBR28 and [¹⁸F] Flumazenil tracers. Here, we aimed to evaluate whether there are any demonstrable changes in the affected and the control

hemisphere. **Materials and Methods:** The device used to create the TBI model consists of a Plexiglas cylindrical reservoir filled with saline. Five Sprague Dawley rats were anesthetized prior to the surgical procedure. The pendulum was placed at a height that would inflict server injury by defining the force of the fluid pressure pulse transmitted through the saline reservoir. After the LFPI procedure on the right hemisphere of the brain, Day2 post operation 3D dynamic PET scans were performed. The animals, following an initial MRI scan, were first scanned in the PET scanner with [^{11}C]PBR28 for 60minutes. Then [^{18}F]Flumazenil was injected 80minutes later and the animals were scanned for 90minutes. **Results:** The quantitative image data suggests that changes in the level of TSPO, indicating neuroinflammatory activities, changes can be observed in the TBI rodent model with the help of [^{11}C]PBR28, whereas changes in the uptake of [^{18}F]Flumazenil were not marked. When comparing the affected and control hemispheres, an increase of uptake of [^{11}C]PBR28, caused by the LFPI procedure, was demonstrable in the affected hemisphere, whereas the uptake of [^{18}F]Flumazenil were similar in both hemispheres, indicating that local increases due to physical impact caused neuroinflammation can be observed in the LFPI TBI rodent model. Conversely, the lack of changes in [^{18}F]Flumazenil uptake between the two hemispheres may indicate either the lack of neuron density changes or the inappropriateness of the radioligand for indicating neuron density changes. **Conclusions:** Although our datasets are not yet comprehensive, our results demonstrated clearly that it is possible to quantify with [^{11}C]PBR28 PET scans the regional changes of neuroinflammation, caused by a local physical impact on the brain, whereas the demonstration neuron density changes with [^{18}F]Flumazenil PET imaging needs further investigations.

EP-0176

Image fusion analysis of ^{18}F-Choline-PET-CT and MRI in patients with recurrent or persistent hyperparathyroidism (HPTH)

J. Kronbichler, J. Röper-Kelmayr, J. Pilz, S. Jäger, M. Hatzl, H. Huber, M. Gabriel; Kepler University Hospital, Linz, AUSTRIA.

Aim: There is certain evidence, that coregistration of multimodal imaging is a useful method to increase the accuracy of preoperative assessment, especially in patients who had already undergone surgical treatment. The aim of our investigation was to estimate the usefulness of ^{18}F-Choline-PET-CT/MRI coregistration based on retrospective software fusion in patients with recurrent or persistent hyperparathyroidism. **Methods:** In this ongoing retrospective analysis we enrolled 6 Patients so far, 5 female, 1 male, 45-75 years (mean±SD: 65±11.3). Image fusion between ^{18}F-Choline-PET and MRI was performed using HER-MES Software (Hermes Medical Solutions) and was manually coregistered with the aid of anatomic landmarks. The fusion was anatomically plausible in all 6 patients. After blinded and independent viewing of each modality by a nuclear medicine physician (PET-CT) and a radiologist (MRI) the fusioned images were reported in consensus. **Results:** ^{18}F-Choline-PET-CT MRI showed a matching result in 3 of 6 patients. Foci in the thyroid bed were detected in all patients. In 3 patients discrepancies were observed between both modalities. In one 74 year old male patient equivocal uptake was found in PET on the left neck side which turned out to be non- specific in the soft tissue. In a 45 year old female patient foci were found on both neck sides, but there was no correlation in MRI findings. However, the coregistrated images showed positive results. In a 55 year old patient, a focus was found close to the lower pole of the left thyroid lobe, but no corresponding lesion in the MRI was detectable. Again, the coregistrated images revealed a positive result. Overall, the results of all patients were confirmed by surgery or by follow up investigation. **Conclusions:** ^{18}F-Choline-PET-CT/MRI image fusion provides significant improvement of localization and reliability of PET findings in patients with recurrent or persistent hyperparathyroidism. Our approach is a relatively inexpensive and an easy-to-use method to also provide surgeons exact anatomic localization prior to surgical Intervention.

EP-0177

Image fusion analysis of ^{68}Ga-PSMA-PET-CT and MRI for initial evaluation in suspected prostate carcinoma patients

J. Kronbichler, J. Röper-Kelmayr, J. Pilz, S. Jäger, M. Hatzl, H. Huber, M. Gabriel; Kepler University Hospital, Linz, AUSTRIA.

Aim: There is certain evidence, that coregistration of different imaging modalities is a powerful aid to increase the accuracy of preoperative assessment and to also guide the treatment planning in several malignant tumours. The aim of this still ongoing study is to estimate the usefulness of ^{68}Ga-PSMA-PET-CT/MRI image fusion in patients with suspected prostate carcinoma. **Methods:** We enrolled 8 patients so far, 58-79 years old (mean±SD: 67±6,2), in a retrospective analysis. Patients underwent both modalities, because malignancy of the prostate gland was suspected. In all of the patients, a suspicious histopathological biopsy result was obtained. Image fusion between ^{68}Ga-PSMA PET-CT and MRI was performed using HER-MES Software (Hermes Medical Solutions) and was manually coregistered with the aid of anatomic landmarks. The fusion was anatomically plausible in all 8 patients. After blinded and independent viewing of each modality by a nuclear medicine physician (PET-CT) and a radiologist (MRI) the fusioned images were reported in consensus. **Results:** ^{68}Ga-PSMA-PET-CT/MRI coregistration showed true negative results in 4 patients. The use of image coregistration provided a high degree of confidence. True positive findings were obtained in 3 patients. In a 66 year old patient an increased ^{68}Ga-PSMA uptake was found in several abdominal lymph nodes, corresponding to pathologically enlarged lymph nodes in the MRI. In a 63 year old patient, an increased uptake was found in the left side of the prostate, corresponding to a highly suspicious alteration of the prostate in the MRI. One patient showed increased uptake in the prostate and in the base of the seminal vesicles. The MRI findings revealed highly suspicious corresponding alterations of the prostate as well as the seminal vesicles. In one patient a mismatch between ^{68}Ga-PSMA-PET-CT and MRI was found in terms of suspicious findings close to the right kidney in PET. In this pa-

tient, ^{68}Ga-PSMA-PET-CT/MRI coregistration was a useful aid to avoid a false positive result. It also showed a good performance in ruling out distant metastases. Overall, the so far obtained results show good correlation of ^{68}Ga-PSMA-PET-CT and MRI concerning bone metastases as well as lymph node metastases. **Conclusions:** [68]Ga68-PSMA-PET-CT/MRI image coregistration provides significant improvement of diagnostic efficacy even for initial diagnosis of suspected prostate carcinoma. It is also a useful aid to avoid diagnostic pitfalls if there is a mismatch between PET and MRI findings. Furthermore, it is a cost effective and easy-to-use method, as it can be retrospectively performed in unclear situations.

EP-0178

Monte Carlo Simulation for Scatter Correction in Brain PET/MRI based on GPU Acceleration

B. Ma[1,2], L. Caldeira[1,3], L. Tellmann[1], P. Lohmann[1], J. Scheins[1], E. Kops[1], H. Xu[1], C. Lerche[1], N. J. Shah[1], U. Pietrzyk[1,3]; [1]Institute of Neuroscience and Medicine (INM-4), Forschungszentrum Jülich GmbH, Jülich, GERMANY, [2]Institute of High Energy Physics, Chinese Academy of Sciences, Beijing, CHINA, [3]School of Mathematics and Natural Sciences, University of Wuppertal, Wuppertal, GERMANY.

Introduction: Accurate scatter correction is essential for qualitative and quantitative PET imaging. Up to now, scatter correction based on Monte Carlo simulation (MCS) has been recognized as the most accurate method. However, the major disadvantage of MCS is the long associated computational effort. In this work, a newly developed implementation of PET MCS using GPU acceleration is employed to allow full Monte Carlo-based scatter correction in clinical 3D PET imaging. Compared to two approaches proposed by other researchers [1-2], our method includes a physically accurate modeling of the interactions in all volumes, especially the patient's head. **Methods:** The computing power of GPU is exploited in order to facilitate the use of PET MCS. Starting from voxelized images, the annihilation photons are tracked through to their detection in PET scanner, while retaining the information of their associated interactions. The scatter distribution provided by the simulation can subsequently be used to correct measured datasets. The proposed approach is presented and evaluated within the context of a hybrid brain PET/MR scanner, the 3T MR-BrainPET developed by Siemens Healthcare. The results are validated by comparison with GATE simulation and a vendor-provided single scatter simulation (SSS) approach. **Results:** The running time of our approach on a single GPU (Geforce GTX 690) was compared with the standard GATE simulation on a single CPU core (Intel Core i7, 3.4 GHz), showing an acceleration factor of 170 for a voxelized brain phantom. The differences in photoelectric and Compton interactions between standard GATE and our approach are 0.09% and 0.04 %, respectively, with ten million generated annihilation photon pairs (30 seconds on GPU). A comparison of SSS and MCS for a NEMA sphere phantom experiment showed that MCS-based corrections could achieve an improvement in the recovery coefficients from 11.8 % to 15.8 % for the hot spheres; a ^{18}F-FDG patient measurement showed that MCS could improve the contrast of the reconstructed images. **Conclusions:** The GPU-accelerated MCS represents a major step towards a clinically feasible and physically accurate scatter correction. It allows overcoming the tail-fitting step necessary for SSS and thus constitutes a much more robust scatter correction approach. [1] C. H. Holdsworth et al. IEEE Trans. Nucl. Sci.2002; 49 83-9. [2] K. S. Kim et al. IEEE J. Biomed. Heal. Informatics 2014; 18 148-56. ***Acknowledgement:*** *This work was financially supported by China-Germany OCPC scholarship program and China Postdoctoral Science Foundation(2015M570154).* **Keywords:** PET, Scatter correction, GPU, MCS

EP-0179

Gadobutrol and ^{18}F-FDG Do Not Interact When Combined in a Single Syringe for Combined Contrast PET/MRI

B. Wilk[1,2], J. Hicks[2], F. S. Prato[1,2], J. D. Thiessen[1,2]; [1]University of Western Ontario, London, ON, CANADA, [2]Lawson Health Research Institute, London, ON, CANADA.

Introduction: Hybrid PET/MRI systems can simultaneously track PET tracers and MR contrast agents. In the heart, simultaneous PET/MRI can follow the process of scar formation after a myocardial infarction from a combined anatomical, functional, metabolic and molecular perspective [1,2]. In previous research by our group, ^{18}F-fluorodeoxyglucose (FDG) and the gadolinium-based contrast agent, Gd-DTPA (Magnevist) were combined in a single syringe prior to a one-hour constant infusion to investigate infarcted tissue in a canine model with dynamic PET/MRI [3]. In humans, there is concern when using Gd-based contrast agents with linear chelators such as Gd-DTPA. Therefore, the gadolinium with a macrocyclic chelator, gadobutrol, is used. In order to demonstrate their independent pharmacokinetics and safety when injected into the human body, the potential interactions between FDG and another gadolinium-based contrast agent, gadobutrol (Gadovist, provided free on an educational grant from Bayer) must be evaluated. As such, the aim of this project was to determine whether there are chemical changes when combining FDG and gadobutrol prior to simultaneous PET/MRI. **Materials and Methods:** FDG was prepared by GE FASTLab cassette method and passed all QC specification at the time of release. Approximately 1 GBq of FDG was added to 5 mL of gadobutrol in a 10 mL PP/HDPE syringe. The syringe was inverted thrice to mix and left flat at room temperature. At 5, 10, 30, 60, 90 and 120 min, samples were analyzed for appearance, radiochemical identity and purity by TLC, and pH. **Results:** There was no change in the FDG or gadobutrol. The ^{18}F label remained on the FDG with no binding to gadobutrol after 2 hours. Appearance and pH remained within FDG release specifications. **Conclusion:** FDG and gadobutrol may be combined in a syringe and the labeling will not change during average imaging times. Additional tests are needed to confirm these initial results and extend them to other Gd-based contrast agents. Combined contrast experiments may allow tracers to penetrate areas of low flow and yield new insights when incorporated into a combined contrast kinetic model. This research provides a stepping stone to using this type of tracer delivery in humans

with hybrid PET/MRI. **References:** [1] Kim et al., Circulation, 1999 [2] Dahl et al, Journal of Nuclear Medicine, 1997 [3] Wilk et al., SNMMI, 2016

EP-0180
Feasibility of Multi-Week PET Studies with a Single Injection of 89Zr-phosphate on a Clinical PET/MRI

J. D. Thiessen[1,2], J. Sykes[1], L. Keenliside[1], H. Biernaski[1], J. Butler[1], N. Cockburn[1], D. E. Goldhawk[1,2], R. T. Thompson[1,2], F. S. Prato[1,2]; [1]Lawson Health Research Institute, London, ON, CANADA, [2]Western University, London, ON, CANADA.

Aim: ^{89}Zr-labelled *p*-isothiocyanato-desferrioxamine (^{89}Zr-DBN) is a promising new cell labeling agent that has the potential to label and track a variety of cells over multiple days (Bansal *et al. EJNMMI Res* (2015) 5:19). In order to better understand the inflammatory process after myocardial infarction, we are developing methods to track ^{89}Zr-DBN labeled monocytes over multiple weeks. The aim of this study was to assess the feasibility of multi-week ^{89}Zr studies on a clinical PET/MRI using a single injection of ^{89}Zr-phosphate, measuring the uptake and longevity of the tracer in target organs. **Subject & Methods:** A 24.5 kg bred-for-research hound was injected intravenously with 80 MBq of ^{89}Zr-phosphate (3D Imaging LLC). Whole-body PET/MRI (Siemens Biograph mMR) was acquired under anesthetic at 3 hours and 4, 8, 12, and 16 days after injection. Acquisitions consisted of 5-6 bed positions (20 cm each), with 15-30 minutes/bed position. After 20 days, a head and neck PET/MRI acquisition (45 minutes/bed position) preceded measurement with a whole body shadow shield gamma detector. Regions of interest included whole-body, lungs, liver, kidneys and bone (vertebrae, sacrum, sternum, ribs, scapula) and were defined using a threshold in the PET image with additional reference to anatomy in the MRI (3D Slicer). All experiments were approved by the local animal care committee. **Results:** At 3 hours, 97% of the injected dose (ID) was measured in the whole-body scan, with activity concentrated in the lungs, liver, and blood. Whole-body activity decreased to 73% ID by day 4 and stayed relatively stable thereafter: $(71 \pm 2)\%$ ID when averaged over days 8-16. Uptake in different regions was also stable by day 8, with SUV = 3.3 ± 0.2 (liver), 3.2 ± 0.3 (lungs), and 10.6 ± 1.5 (bone) when averaged over days 8-16. After 20 days, whole-body activity was approximately 1 MBq, yet bones in the head and neck were still clearly visible. **Conclusion:** Longitudinal studies with ^{89}Zr benefit from a long half-life (78.4 hours) but are limited by lower injected dose and less PET-visible activity. With its increased sensitivity and additional anatomical information, the mMR is well-suited to long-term ^{89}Zr studies. With a branching ratio of 0.2275, 1 MBq ^{89}Zr is equivalent to a PET scan of 0.24 MBq ^{18}F. Despite this ultra-low dose, we were still able to delineate bones in the head and neck at day 20, demonstrating the feasibility of multi-week PET studies using ^{89}Zr-labelled cells.

EP-0181
PET/MRI technique role in Alzheimer disease

D. Vieira[1], R. Vardasca[2,3], J. M. Tavares[1]; [1]INEGI, Faculty of Engineering, University of Porto, Porto, PORTUGAL, [2]LABIOMEP, UISPA-LAETA-INEGI, Faculty of Engineering, University of Porto, Porto, PORTUGAL, [3]Medical Imaging Research Unit, University of South Wales, Pontypridd, UNITED KINGDOM.

Introduction: Hybrid or multimodal imaging has provided excellent opportunities to meet the needs inherent in the management of neurodegenerative diseases, especially in Alzheimer Disease (AD) context. Recent PET/MRI equipment for simultaneous data acquisition attempts to address this challenge. The aim of this review was to compile the main advantages related with PET/MRI along with the detection of the main challenges which remain to be resolved for a full clinical validation of the technique in Neuroimaging field are identified. **Methods:** A literature review was performed, following a PICO methodology with the question: "What is the role of PET/MRI technique in the diagnosis of neurodegenerative diseases, specifically in context of Alzheimer's disease?". Based on the formulated question, keywords and key phrases were identified for scientific database research: "Alzheimer", "neurodegenerative disease" "brain" and "PET/MRI" (disambiguation terms applied). The SCOPUS platform was used as digital repository of research. Only "article review" publications since 2010 in English language were considered. Articles feasibility was verified based on exclusion criteria: access to full version publications, verification of redundant items and empirical analysis of abstracts based on their relevance to the research question. **Results:** Based on the methodology and the inclusion criteria used, a total of 60 publications were initially obtained, which after applying the exclusion criteria dropped to a final number of 41 scientific publications. The results obtained were stratified into five categories: PET/MRI Equipments - Design and Components, Attenuation Correction in PET/MRI, image data reconstruction, PET/MRI in Clinical Neuroimaging, PET/MRI exam Protocols. **Discussion and Conclusion:** AD has been extremely influenced by the results and imaging capabilities achieved by neuroimaging techniques. PET/CT has been successfully applied in clinical practice with superior results to dedicated PET or CT options. However, the ability of MRI to obtain higher spatial resolution levels especially in soft tissues (especially critical factor in the context of the brain region) as well as the non-use of radiation made evident the need to include this technique as a new component to be included in a multimodality solution. PET/MRI bridge the limitations of PET/CT at the brain level and improving the results achieved through a simultaneous real-time combination of quantitative neurophysiological information from PET and accurate MRI morphological information, with greater radiological safety. PET/MRI technique presents high potential for diagnostic and follow-up studies. Despite the advantages, several challenges arise and PET/MRI adoption in AD imaging still need technical and clinical validation of its promising imaging characteristics.

EP-0182
Effect of attenuation and its correction in brain PET/MR imaging: a phantom study

M. Soret[1], J. Maisonobe[1], M. Khalifé[2], A. Kas[1]; [1]HU Pitié Salpetrière, Paris, FRANCE, [2]Institut du Cerveau et de la Moëlle épinière, Paris, FRANCE.

Aim: In PET/MR brain imaging, attenuation correction (AC) is critical as the head coil introduces a medium attenuating around the patient's head. In clinical routine, the AC in brain PET/MR is based on a human atlas. However, this method cannot be used for phantoms. Instead, DIXON MRI is used to separate air, soft tissues and fat, and assign them attenuation coefficients at 511keV. Nevertheless, the usually used phantoms are composed of materials different from human tissues. We suggest to use a CT derived AC as an alternative for brain phantom imaging in PET/MR. **Materials and Methods:** Acquisitions were performed with a 3D Hoffman phantom filled with 55 MBq of 18F-FDG using a SIGNA PET/MR (GE Healthcare) system and a Biograph mCT Flow PET/CT (Siemens Healthcare). Five images were reconstructed from each acquisition: two with the PET/CT (with and without AC) and three with the PET/MR (without AC, using MR-based AC and using the CT obtained with the PET/CT for AC). Mean activity concentrations were measured in white (WM) and grey (GM) matter, in anterior (A), posterior (P), right (R) and left (L) regions segmented using the CT of the phantom. Errors in activity concentrations were calculated considering the PET/CT corrected from AC as a reference. To evaluate the effect of the attenuation and AC on different regions, ratio between A/P and R/L regions were also measured. **Results:** Without AC, activity concentrations as measured in PET/MR in GM and WM were underestimated by 90% and 88%, respectively; a strong A/P asymmetry with a ratio of 1.2 was measured for both WM and GM was also measured. Without AC, the underestimation was of 86% in GM, and 87% in WM in PET/CT. The A/P asymmetry was not observed in PET/CT without and with AC, and disappeared in PET/MR after AC. A R/L asymmetry has never been observed in any PET images With CT-AC, the activity concentrations measured in PET/MR in GM and WM were of -2% and -1% respectively, compared to PET/CT. With MR-AC, the activity concentrations were underestimated by -60% (WM) and -58% (GM) due to an incorrect attenuation map in PET/MR. **Conclusion:** Without AC, an important A/P asymmetry appeared in brain PET/MR due the presence of MR coil. All attenuation corrections suppressed this asymmetry in PET/MR. However, MR-based AC was quantitatively inaccurate for the Hoffman phantom. With CT-based AC, activity concentrations and ratios were similar for PET/MR and PET/CT.

EP-0183

11C-Choline, multiparametric MR and T2 mapping for the study of prostate cancer with simultaneous PET/MRI

E. A. Marino[1,2], G. Peña[1], R. Isoardi[1], V. Rada[1]; [1]FUESMEN, Mendoza, ARGENTINA, [2]CNEA(Comision Nacional de Energía Atómica), Mendoza, ARGENTINA.

Introduction: The purpose of this work is to evaluate sensitivity and specificity of PET/MRI for the analysis of diagnosis and tumor relapse in prostate cancer using C11-Choline, multiparametric (mp-MR) and T2 mapping sequence. **Subjects & Methods:** Four patients diagnosed with suspected a prostate cancer and one patient with confirmed prostate cancer (undergoing hormonal treatment) were intravenously administered optimized doses of 2.035 MBq/kg C11-Choline. After a 5-minute uptake period, a PET/MR scan was performed with a protocol of 3 min/bed (GE Signa PET/MR, Milwaukee, WI, USA). Simultaneously, MRAC (for correction attenuation), T1LAVA, T2 SSFSE and DWI sequences were acquired. Then, mp-MR prostate study was performed to obtain T2W, T1W, DWI, DCE images. In addition, T2 mapping sequence in prostate was implemented.PET data were reconstructed using 3D OSEM with 2 iterations and 20 subsets, scatter and attenuation correction was applied. All studies were analyzed by a qualified physician in both Nuclear Medicine and MR methods. **Results:** For all patients, a suspected tumor lesion was detected in prostate peripheral zones (PZ). Four patients with suspected prostate cancer lesions were detected in T2W, DWI, ADC Map, enhancement curve and pathological C-11-Choline uptake. In addition, T2 mapping images were measured in Functool GE software by tracing ROI in the suspected lesion area for all patient (T2mean=65.95 +/- 13.25 ms) and compared with T2 value in normal parenchyma of the contralateral PZ (T2mean=105.86 + /- 0.83 ms). As for the patient with confirmed diagnosis, the suspected malignancy region was only detected with PET with pathological uptake of the radiopharmaceutical, as multiparametric MR scan resulted negative. In addition, T2 values were obtained in the suspected area (T2mean=53.7 ms) and normal tissue of the contralateral PZ (T2=91.47 ms). Prostate cancer for all suspected lesions was then confirmed by anatomical pathology. **Discussion:** In this preliminary study, C11-Choline PET/MR scan and mp-MR, associated with T2 mapping coincide with anatomical pathology in areas of suspected malignancy in PZ for all cases studied. These findings are in agreement with previously published studies. The findings previously described in the T2 mapping sequence, contribute to a more accurate diagnosis and follow-up of prostate cancer patients. Therefore, the described protocol is proposed as a new powerful clinical tool while keeping short acquisition times. These promising results should be consolidated with a larger number of studies.

EP-0184

GE Signa Integrated PET/MR: NEMA NU 2-2007 Performance Characteristics for ^{68}Ga PET Imaging

P. Caribé[1,2], M. Koole[3], S. Vandenberghe[1], T. Deller[4]; [1]Medical Imaging and Signal Processing – MEDISIP, UZ Ghent; IMEC, Ghent, BELGIUM, [2]National Council for Scientific and Technological Development – CNPq, São Paulo, BRAZIL, [3]Division of Nuclear Medicine – UZ/KU, Leuven, BELGIUM, [4]General Electric Healthcare, Waukesha, WI, UNITED STATES OF AMERICA.

Highly specific ^{68}Ga-labeled PET tracers such as ^{68}Ga-PSMA targeting the prostate-specific membrane antigene or ^{68}Ga-labeled tracers targeting the somatostatin receptor expressed by neuro endocrine tumors are considered a key application for combined PET/MRI. The purpose of the study is to evaluate the

PET performance of the GE SIGNA integrated PET/MR system for ^{68}Ga according to the NEMA NU 2-2007 protocol. **Methods:** The following measurements were performed according to the NEMA NU 2-2007 protocol: spatial resolution (SR), Image Quality (IQ) sensitivity, scatter fraction, noise equivalent count rate (NECR) and linearity. SR measurements, a ^{68}Ga point source inside a glass capillary tube was used. Sensitivity measurements were based on a 70-cm-long polyethylene tube, filled with 8.67 MBq of [68]Ga. Scatter fraction and count rates were measured using a 70-cm-long polyethylene cylinder with a diameter of 20 cm and a line source (871 Mbq of 68Ga) inserted axially into the cylinder 4.5 cm off-centered. IQ was assessed using NEMA IQ phantom with a background activity concentration of 5.3 kBq/mL at start time of the experiment and a 4:1 ratio for activity concentration in hot spheres compared to the background. In addition, the accuracy of the attenuation and scatter correction was analyzed. **Results:** Transaxial SR was 4.1 and 5.1 mm full width at half maximum (FWHM) at 1 and 10 cm off-center respectively. In the axial direction, the values were 7.16 and 8.76 mm, respectively. The system sensitivity was 17.1 cps/kBq along the center and 16.7 cps/kBq at 10 cm off-center. The measured NECR peak was 205.6 kcps at 20.4 kBq/ml. The scatter fraction at peak NECR was 42.9 % and the specific count rates for 17.5 kBq/mL and 30.0 kBq/mL were 202.5 kcps and 197.2 kcps respectively. Image contrast recovery values were 36.3, 47.2, 59.7, 73.2, 86.5 and 92.1% for the six spheres (10- to 37-mm diameter). The background variability was between 7.5 % (10 mm sphere) and 2.1 % (37 mm sphere). The average lung residual error was lower than the 10%. **Conclusion:** The ^{68}Ga NEMA measurements confirm adequate system performance of GE Signa integrated PET/MR for ^{68}Ga PET imaging. However, since specific ^{68}Ga-labeled tracers can yield much higher tumor to background ratios than the 4:1 ratio used for NEMA image quality assessment, future IQ measurements will be extended with higher hot sphere to background ratios to better characterize system performance for relevant tumor to background ratios

EP-0185

Assesssment of acute response to bone loading in humans with 18F-NaF PET/MRI: a pilot study

B. Haddock[1], A. P. Fan[2], C. Suetta[1], F. Kogan[2], G. E. Gold[2,3]; [1]Dep. of Clinical Physiology, Nuclear Medicine and PET, Rigshospitalet, Glostrup, DENMARK, [2]Department of Radiology, Stanford University, Stanford, CA, UNITED STATES OF AMERICA, [3]Department of Bioengineering, Stanford University, Stanford, CA, UNITED STATES OF AMERICA.

Purpose: The acute effect of loading on bone tissue is of growing interest in the study of bone physiology. With the increased use of NaF in non-oncological studies of the skeleton, there is considerable interest in measuring in NaF uptake as an early indication of bone degradation in diseases such as osteoarthritis [1]. Previous animal studies using NaF have found acute increases in uptake using heavy loads on bone [2]. However, the acute response of bone to a more physiological stimulus is still poorly understood and has not been studied with 18F-NaF PET. The aim of this study is to measure acute changes in NaF uptake in human bone due to exercise-induced impact. **Materials and Methods:** One subject (M, 43yrs) was recruited for the pilot examination consisting of a baseline and post-exercise NaF-PET scan on a GE Signa time-of-flight PET/MRI. Each scan covered the lower leg (mid- femur to feet) with 3 min beds acquired starting 60 min after the injection of 93 +/-2 MBq ^{18}F-sodium fluoride. On the first day the subject arrived after having abstaining from exercise for 24 hours and a baseline scan was performed. The subject then performed an exercise using the right leg to step up onto a 25 cm high stool and hopping down, landing on the left leg 100 times. A single bed control scan -without injection- was then performed to control for any changes in the activity of the first injection. Lastly, at approximately 8 minutes after the exercise stop, the second injection was administered and the second scan was performed 60 minutes post-injection. Images were then coregistered and the second image was corrected for activity remaining from the first injection. A study of 10 subjects with this paradigm will be completed in June 2017. **Results:** There was a mean increase in ^{18}F-Sodium Fluoride uptake (mean or maximum standardized uptake value?) in the knee (70%), tibia (53%) and foot (100%) of the left landing leg as opposed to the right lifting leg which had a mean increase in the knee (73%) but not the foot (-3%) or tibia (4%). **Conclusion:** A distinct response to bone loading was imaged using NaF-PET/MRI. This can prove to be a necessary consideration when interpreting reproducibility of NaF images and a promising tool in research of biomechanics and bone physiology.

EP-0186

18F-FDG PET/MR imaging in optimizing monitoring and management of patients with sarcoidosis

D. Jurgilewicz[1,2], P. Szumowski[1,3], M. Mojsak[1,2], B. Kubas[1,2], B. Kuklinska[4], M. Hladunski[1,2], A. Amelian[1,2], J. Mysliwiec[1,3], R. Mroz[1,4]; [1]Medical University of Bialystok, Bialystok, POLAND, [2]Laboratory of Molecular Imaging Medical University of Bialystok, Bialystok, POLAND, [3]Nuclear Medicine Department Medical University of Bialystok, Bialystok, POLAND, [4]Pulmonology Clinic University Hospital of Bialystok, Bialystok, POLAND.

Introduction: Sarcoidosis is a multi-organ disease characterized by the appearance of inflammatory granulomas in various organs. Lungs and intrathoracic lymph nodes are mostly affected, but clinical manifestation is variable and other organs like: eyes, skin, liver, spleen, muscles, heart, bones, brain and salivary glands may be involved. Aim: The purpose of the study is to evaluate the utility of [^{18}F]fluorodeoxy-d-glucose (18F-FDG) PET/MRI in sarcoidosis staging and therapy optimization. **Subjects and Methods**: 18F-FDG PET/MR study was performed in 52 patients (F/M: 33/19), mean age: 48 years (range: 25-72) with diagnosed and histologically confirmed pulmonary sarcoidosis. Patients were recruited to the study upon the symptoms like dyspnoea, chest pain, fatigue, headache, dizziness, muscle and joint pain exacerbation. PET/MR scans were obtained 60 min after intravenous 18F-FDG injection with mean dose of 297±45 MBq. Additional subsequent CE-MRI of the thorax using 3-tesla

Biograph mMR scanner (Siemens) with proper MR sequences: T1 VIBE, T2 HASTE, T2 BLADE were performed in all patients. The obtained images were analyzed with visual and semi-quantitative SUVmax measurement methods. Disease staging based on presence and number of FDG-avid nodes was performed by two nuclear medicine and one radiology experienced specialists. **Results**: 18F-FDG PET/MR confirmed metabolically active disease in 48 (92%) patients, in 4 (8%) no morphological changes in MR and no increased activity of 18F-FDG in the lungs were found . Sarcoidosis staging upon 18F-FDG PET/MRI changes in thorax classified patients respectively as: n=29 (56%) stage I, n= 15 (29%) stage II, n= 4 (8%) stage III. There were no patients with stage 4. Increased 18F-FDG uptake in PET/MR study, with SUV-max: 2,43-8,7, as a new additional metabolically active foci were found as follows: abdominal lymph nodes in 10 (19%), musculo-skeletal system in 2 (3%), skin in 1 (2%) patients. Inhomogeneous cardiac 18F-FDG uptake in left ventricule were found in 2 (3%) patients. Additionally, in 12 patients (23%) changes in maxillary and sphenoid sinuses were found in MR images only. The mean SUVmax =6,45 in the lung parenchyma changes, mean SUVmax =4,96 in active mediastinal lymph nodes, has been estimated. Steroid treatment has been ceased in 2 and enhanced in 8 patients according to study results. **Conclusion**: 18F-FDG PET/MR is useful diagnostic tool in inflammatory activity assessment and treatment optimization in patients with sarcoidosis. The clinical utility should be especially dedicated to patients with non-specific symptoms and those for whom steroid therapy alteration is considered.

Molecular & Multimodality Imaging: Biology (Benign Disease)

EP-0187

Longitudinal PET studies on bone uptake of F-18-fluoride in healthy mice with respect to age, sex and circadian rhythm

N. Beindorff[1], V. Dorau[1], K. P. Huang[2], C. Rosner[2], O. Schulze[2], M. Lukas[2], C. Lange[2], E. J. Koziolek[1], B. Gregor-Mamoudou[1], I. G. Steffen[2], W. Brenner[2]; [1]BERIC, Charité - Universitaetsmedizin Berlin, Berlin, GERMANY, [2]Department of Nuclear Medicine, Charité - Universitaetsmedizin Berlin, Berlin, GERMANY.

Aim: The aim of this longitudinal study was to establish normal values for F-18-fluoride bone uptake with respect to age, sex, and circadian rhythm in healthy mice. **Materials and Methods**: In isoflurane anesthetized 12 female and 12 male C57BL/6 mice PET images of 30 min duration were acquired (nanoScan PET/MRI, Mediso) starting at 90 min after intravenous injection of approx. 20 MBq F-18-fluoride. Each mouse was imaged in follow-up studies up to 24 months (A: 1 month, puberty; B: 3 months, sexually mature, but not fully grown; C: 6 months, fully grown; D: 12 months; E: 24 months, senile). In order to monitor circadian rhythm, animals were imaged during light (sleep

phase (SP)) as well as during night conditions (awake phase (AP)). Image viewing and quantification were performed using PMOD 3.5. The percentage tracer uptake of the injected activity is expressed as median [interquartile range; IQR]. Differences between groups were analysed using Mann-Whitney-U test and paired Wilcoxon test. **Results**: Maximum uptake of F-18-fluoride occurred after 109 min [90-110]. While aging, uptake changed significantly (P<0.001). Pubertal mice (A) showed the highest uptake (66 [62-72]) compared to age B (47 [44-49]; P<0.001), with no further change at C (45 [40-49]; P=1.0) and D (44 [40-50]; P=1.0), and thereafter with a slight rise at E (51 [47-59]; P<0.1). At all ages no effect of sex was observed: A (female 66 [62-72], male 65 [62-71]; P=0.8), B (female 48 [45-49], male 46 [43-48]; P=0.3), C (female 47 [41-51], male 42 [38-48]; P=0.2), D (female 48 [41-51], male 42 [40-48]; P=0.2) and E (female 51 [48-59], male 47 [42-50]; P=0.1). An effect of circadian rhythm was detectable in females (SP 51 [48-63], AP 45 [41-50]; P<0.001) but not in males (SP 47 [42-54], AP 43 [39-60]; P=0.18). **Conclusion**: This study showed significant effects of age and circadian rhythm on bone uptake of F-18-fluoride in healthy mice. Pubertal mice had the highest uptake irrespective of sex and circadian rhythm. After puberty, mice showed a significantly lower but rather constant bone uptake. Interestingly, only in females bone uptake was depending on circadian rhythm. In summary, for the design of longitudinal bone studies in mice it is mandatory to consider age and circadian rhythm as significant parameters.

Molecular & Multimodality Imaging: Optical Imaging

EP-0188

In Vitro and In Vivo Bioaffinity Determination of FDG-Conjugated Magnetic Nanoparticles

V. Yasakci, P. Unak, O. Guldu, V. Tekin; Ege University, İzmir, TURKEY.

Aim: The aim of this work is to design and synthesis, iron oxide based MNPs (magnetic nanoparticles) with dual mode for lymph node imaging and hyperthermia. This approach makes use of the 'Warburg effect', utilizing the fact that cancer cells have a higher metabolic rate than normal cells. Material and **Methods:** For this purpose, magnetic nanoparticles (MNP) were synthesized and their surface were silicated and modified with TEOS, then coated with hyaluronic Acid (HA) to enhance their bioavailability. The modified MNPs were conjugated with Fluorodeoxyglucose ([19]FDG). The synthesized MNPs were optically labeled by Indocyanine green (ICG). In addition, they were radiolabeled with I-131 and then the radiolabeled MNPs were subjected to MCF-7 human breast adenocarcinoma cells and PC3 human prostate adenocarcinoma cells. *In vivo* perfusion studies were performed on Sprague-Dawley rats with optical labeled FDG-MNP molecule to see organ biodistribution. **Results and Conclusion:** The hydrodynamic diameter and zeta potential measurements at each step were measured on a Malvern Nano-ZS DLS instrument. Scanning Electron Microscopy (SEM)

and Transmission Electron Microscopy (TEM) images were also acquired. It is seen that the 19FDG-MNP has dimensions of 20-30 nm. FT-IR presented that Fe-O bond vibrations at around 570 cm^{-1} can be distinguished, and Si-O stresses around 1000-1100 cm^{-1} give us a distinctive result about the silanated MNPs. Quality control studies of radiolabeled FDG-MNPs were performed by TLRC and HPLC. Cell incorporation studies were performed and binding efficiencies were found using with the Packard Liquid Scintillation counter. The involvement in PC-3 cell lines appears to be approximately 2-fold greater than the involvement in MCF7 cells. *In vivo* perfusion studies were performed with Sprague-Dawley Rats. HPLC method was applied to see organ biodistibution of MNPs. Besides using standard histological assessment and fluorescent TUNNEL staining, we observed no detrimental impact of FDG-MNP on tissue morphology at any time point. The results demonstrate that FDG conjugated Fe$_3$O$_4$ nanoparticles enhance the involvement of cancer cells and that these particles may be theranostic agents due to their favorable properties for dual imaging (MRI and optical) with hyperthermia in cancer cells.

EP-0189

The influence of structural alterations on asymmetric cyanine 5 dyes on the photophysical properties and protein conjugation characteristics

S. J. Spa, A. Hensbergen, S. van der Wal, J. Kuil, T. Buckle, F. W. B. van Leeuwen; Leiden University Medical Center, Leiden, NETHERLANDS.

Purpose/Introduction: Far red fluorescent dyes are popular fluorophores applied in (bio)medical diagnostics, including image guided surgery trials. Their signal intensity and emission in the far red region of the light spectrum (>650 nm) allow for good tissue penetration depths. In the clinic, methylene blue and the more potent Cy5 have proven diagnostic value in image guided surgery trials. When multiple fluorescent dyes are conjugated to a protein, within 8 nm distance, they quench the fluorescence of each other. Realizing that fluorescent dyes represent relatively large conjugated systems, the degree of labelling can influence the binding specificity and affinity of a targeting vector. While on average one dye/targeting vector is generally aimed for, samples consist of a mixture of non- one- or di-conjugated tracers, which given the above could influence the value of the imaging agent. Finally there are multiple examples that underline that some dyes have high affinities for serum proteins, a feature that will influence the overall tracer pharmacokinetics. Since molecular interactions drive these phenomina, we performed a systematic study to illustrate how the chemical structure of asymmetrical Cy5 dyes influences the serum interaction, labelling behaviour and photophysical properties. **Subjects and Methods:** To gain more insight in the self-aggregation and labelling efficiency of cyanine dyes, a matrix of ten structurally different Cy5 fluorophores (Cy5-(R$_1$)R$_2$-(R$_3$)R$_4$; R represents the substituents varied) were investigated in comparison with methylene blue. Of these compounds we analysed the stacking, chemical-stability, serum protein interaction, and conjugation efficiencies. To validate the dye compatibility with clinically available imaging hardware and image guided procedures, visibility and photo-stability of the dyes was studied using a clinical grade fluorescence laparoscope. **Results:** Besides minor differences in self-aggregation (only Cy5-(Ar)SO3-(Ar)COOH and methylene blue self-aggregated), clear differences were observed in the labelling efficiencies and non-specific interaction with serum proteins. Overall, Cy5-(SO3)SO3-(SO3)COOH, Cy5-(SO3)Me-(SO3)COOH, and Cy5-(SO3)QAmine-(SO3)COOH stood out in terms of fluorescence brightness (ε = ~240.000 M$^{-1}\cdot$cm^{-1}, Q$_f$ = 23%) and < 20% non-specific interactions with serum proteins. From these three, the most homogeneously labelled Ubiquitin samples were obtained with Cy5-(SO$_3$)SO$_3$-(SO$_3$)COOH. **Discussion/Conclusion:** Our findings indicate that altering the chemical composition of Cy5 dyes prominently influences the interaction with serum proteins as well as the conjugation behaviour. The presented data provides a valuable resource for the use of fluorescent dyes in future tracer developments.

EP-0190

Optimization of cytotoxic T-cell activation by tracking of dendritic cell migration using reporter gene imaging

H. Lee[1], H. Lee[2], Y. Jeon[2], S. Jeong[2], S. Lee[2], J. Lee[2], B. Ahn[2]; [1]Dongnam institute of radiological & medical sciences (DIRAMS), Busan, KOREA, REPUBLIC OF, [2]Kyungpook National University School of Medicine and Hospital, Daegu, KOREA, REPUBLIC OF.

Purpose: The aim of this study is to optimize the dendritic cell (DC)-mediated T-cell activation using reporter gene imaging and flow cytometric analysis in living mice. **Subjects & Methods:** A murine dendritic cell line (DC2.4) co-expressing effluc, green fluorescent protein (GFP) and Thy 1.1 genes were established by transfection with retroviral vectors. Thy1.1 positive cells were sorted by magnetic bead separation system (DC2.4/effluc). Cell proliferation assay and phenotype analysis to determine the effects of gene transduction on the function of dendritic cells between parental DC2.4 and DC2.4/effluc were performed. To optimize the DC-mediated immune response by cell number or frequency, different cell number (5×10^5, 1×10^6 and 2×10^6 DC2.4/effluc) or different frequency of DC2.4/effluc (first, second and third injections) were injected in the right footpad of mice. The migration of the DC2.4/effluc into draining popliteal lymph node of mice was monitored by bioluminescence imaging. Flow cytometric analysis was performed with splenocytes to determine the cytotoxic T-cell population after injection of DC2.4/effluc. **Results:** Parental DC2.4 and DC2.4/effluc exhibit no significant differences in their proliferation and phenotype. Bioluminescent signals were observed in draining popliteal lymph node at day 1 after injection of DC2.4/effluc in 1×10^6 and 2×10^6 cells-injected groups. The highest bioluminescent signal intensity was detected in 2×10^6 cells-injected mice. On day 11, the bioluminescent signal was detected in only 2×10^6 cells-injected group but not in other groups. Optimized cell numbers (2×10^6) were injected in three animal groups with a different frequency (first, second, and third injection groups). The bioluminescent signal was detected at day 1 and main-

tained until day 7 in first injection group, but there is low signal intensity in second and third injection group. Although the expression levels of Thy1.1 gene in the first injection group were very high, there reveals no expression of Thy1.1 gene in second and third injection groups. CD3+ and CD8+ double positive T-cells were higher in the first injection group when compared with second and third injection groups. **Conclusion:** Successful optimization of DC-mediated cytotoxic T-cell activation in living mice using reporter gene imaging and flow cytometric analysis was achieved. The optimization of DC-mediated cytotoxic T-cell activation could be applied for the future DC-based immunotherapy.

EP-0191

Evaluation of non-peptidic small molecule targeted imaging and therapeutic agents LHRH receptor expressing tumors

J. Roy[1,2], P. S. LOW[2]; [1]National Cancer Institute, Bethesda, MD, UNITED STATES OF AMERICA, [2]Purdue University, West Lafayette, IN, UNITED STATES OF AMERICA.

Aim: Luteinizing hormone-releasing hormone receptor (LHRH-R) is overexpressed in various cancers whereas its expression in healthy tissues/organs is limited to pituitary glands and reproductive organs. To date, only the natural peptide ligand, LHRH or its analogs have been used to develop LHRH-R targeted conjugates. To avoid unwanted side-effects of peptide ligands such as rapid metabolism and, non-specific uptake by peptide scavenger receptors we have developed a non-peptidic, small molecule LHRH-R targeting ligand (BOEPL) conjugate for imaging (NIR or 99mTc) and therapeutic (tubulysin,TubBH) applications. These conjugates were then evaluated in vitro and in vivo (tumor mouse xenografts) to demonstrate their ability to image and kill LHRH-R positive cells. **Materials and Methods:** BOEPL was conjugated to an NIR dye (BOEPL-L3-NIR), 99mTc (BOEPL-L3-Tc) or tubulysin B hydrazide (BOEPL-L3-TubBH) via a releasable or non-releasable linker. In vitro and in vivo binding studies were performed by using LHRH-R positive and negative cancer cells (LHRH-R(+/-)). In vitro binding and in vivo uptake of the optical imaging conjugate was determined by fluorimetry and IVIS Lumina II correspondingly. In vitro binding (K_d) and in vivo uptake (%ID/g) of BOEPL-L3-Tc was determined by gamma scintigraphy. The in vitro cytotoxicity of BOEPL-L3-TubBH was determined by 3H-thymidine incorporation assay. **Results:** The BOEPL-L3-NIR(K_d,4.43 nM) and BOEPL-L3-Tc(K_d,14.39 nM) conjugates have shown high binding affinity in vitro and accumulated rapidly in vivo in LHRH-R(+) tumors at 2 h post injection ((Tumor/muscle):17.5/1). In vivo, the excess of both the conjugates was excreted either via the renal or hepatic route. The cytotoxic conjugate BOEPL-L3-TubBH demonstrated receptor-mediated killing of cancer cells both in vitro (IC$_{50}$,26 nM) and in vivo. After three weeks of treatment, a complete response was observed in LHRH-R(+)xenografts whereas no reduction in tumor-volume was noticed in LHRH-R(-)xenografts. Mice did not show any side-effects associated with free TubBH. The receptor-me-

diated uptake of LHRH-R targeted conjugates were shown by blocking studies with an excess of BOEPL. **Conclusion:** Because the uptake of BOEPL-L3-NIR and BOEPL-L3-Tc by healthy tissues was negligible and retention in kidney/liver was due to excretion of the conjugate, we suggest that BOEPL-L3-NIR has a potential to be used for fluorescence guided surgery and BOEPL-L3-Tc may be valuable for detection and monitoring the progression of LHRH-R(+) tumors. As expected the BOEPL-L3-TubBH demonstrated the anti-tumor effect in LHRH-R(+) cancer cells while sparing healthy tissues. In conclusion, we successfully demonstrated the use of the non-peptidic, small molecule BOEPL to deliver various payloads to LRHR-R(+)cells with minimal side-effects.

EP-0192

Lysine as a versatile platform for the design of multimodal (optical/SPECT or PET) imaging probes

C. Goze[1], C. Bernhard[1], N. Maindron[1], M. Ipuy[1], D. Lhenry[1], M. Moreau[1], V. Thakare[1], A. Dubois[1], F. Boschetti[2], F. Denat[1]; [1]ICMUB, Dijon, FRANCE, [2]Chematech, Dijon, FRANCE.

Aim: Dual-labeling of biological vectors with both a fluorescent dye and a radiometal chelate for PET or SPECT imaging has gained increasing interest both for preclinical and clinical purposes. Thanks to this double modification, one can inject into the patient a unique imaging agent that allows for i) the diagnosis and staging of the patient by whole body nuclear imaging and, ii) provide guidance of the surgeon, by fluorescence imaging of the intraoperative field during the surgery. Labeling the biovector with a single molecule containing both probes, called MOMIP (MonomOlecular Multimodal Imaging Probe), presents numerous advantages compared to the conventional dual-labeling approach. However, as the properties of the MOMIP may strongly affect the behavior of the resulting imaging agent, being able to finely modulate the different components of the bimodal probe is of major importance. The aim of this work is to provide a versatile tool for an easy access to a wide variety of MOMIP. **Material and Methods:** The design of a MOMIP requires the use of a trifunctional platform. We have chosen a lysine carefully protected with orthogonal protecting groups as a building block, to introduce sequentially the three components of the MOMIP: a fluorescent dye (Cy5, BODIPY, fluorescein), a chelator (DOTA or DOTAGA for ^{111}In labeling, NODAGA for ^{68}Ga or ^{64}Cu labeling), and a bioconjugatable handle (isothiocyanate, azide or tetrazine group, dithiolane ring). Several examples of MOMIP have been synthesized, characterized (including photophysical studies), and conjugated to different biomolecules (full antibodies, antibody fragments, peptides) or nanoparticles. The radiolabeling (^{111}In, ^{68}Ga) of some resulting bimodal bioconjugates has been investigated. Whole-body fluorescence images were recorded after injection in tumor bearing mice. Ex-vivo imaging was performed to provide semi- quantitative information about the tracer biodistribution. **Results:** A broad family of new bimodal probes has been prepared and some of them have been investigated after conjugation to biomolecules. The properties of the resulting bioconjugates (radiolabeling efficiency,

fluorescence properties, hydrophilic/lipophilic balance, biodistribution profile), may be easily modulated by changing independently one of the components of the MOMIP. **Conclusion:** This work shows the versatility of a new method for the construction of MOMIP, differing by the nature of the chelator and/or the fluorescent dye and/or the function for bioconjugation, thus providing access to optimized bimodal imaging agents for a given application.

EP-0193

Pretargeted imaging of peritoneal carcinomatosis using bioorthogonal chemistry

A. Rondon[1,2], N. Ty[1], J. Bequignat[1], M. Quintana[1], A. Briat[1], T. Witkowski[1], B. Bouchon[1], C. Boucheix[3], E. Miot-Noirault[1], J. Pouget[2], J. Chezal[1], I. Navarro-Teulon[2], E. Moreau[1], F. Degoul[1]; [1]INSERM U1240, Clermont-Ferrand, FRANCE, [2]INSERM U1194 IRCM, Montpellier, FRANCE, [3]INSERM U935, Villejuif, FRANCE.

Aim: Bioorthogonal chemistry represents a challenging approach in pretargeted radioimmunotherapy (PRIT) based on fast, strong and biocompatible covalent interaction between *trans*-cyclooctene (TCO) conjugated antibodies (mAbs) and radiolabelled probes linked to tetrazine (TZ) (Rossin et al., 2010; Houghton et al., 2017). However, both the number of TCO engrafted per mAb and the linker length between mAbs and TCO can influence the efficiency of PRIT. We studied the influence of the number of TCO conjugated per mAb and the effect of several PEGylated linkers (Rahim et al., 2015) in order to determine the optimal mAb-$(PEG)_n$-TCO structure. **Methods**: Two models of colorectal cancer were used, a subcutaneous model of colon (HT29) using Ts29.2 mAb specific for tetraspanin 8 (Maisonial et al., 2017) and an orthotopic peritoneal carcinomatosis (PC) model (A431-CEA-Luc) using mAb 35A7 targeting CEA (Boudousq et al., 2013). Different amount of TCO (0, 5, 10, 15, 20 and 30 equivalents) were incubated with mAbs, and the corresponding number of linked TCO quantified using MALDI-TOF MS. mAbs-$(PEG)_n$-TCO were evaluated in immunofluorescence assays. Three PEG lengths were compared (i.e. PEG_0, PEG_4 and PEG_{12}) through *in vitro* and *in vivo* experiments using a fluorescent TZ probe. **Results**: MALDI-TOF MS showed that the number of TCO grafted per mAb was higher for PEG_4 or PEG_{12} compared to PEG_0. Immunofluorescence quantifications of Ts29.2-PEG_0 and Ts29.2-PEG_{12} showed an increase of the fluorescent signal respectively to the number of TCO grafted while for Ts29.2-PEG_4 a peak was reached at 10 equivalents. 35A7 PEG_4 showed the same pattern as Ts29.2-PEG_4 and a plateau was observed for PEG_0 and PEG_{12} at 10 equivalents. We then selected the TCO-mAb conjugates obtained with 10 equivalents of TCO to compare PEGylation. On both models the antigen recognition was not significantly altered by mAbs modifications. When reported to the number of TCO grafted per mAb, the mean fluorescence intensity significantly decreased for PEG_4 compared to PEG_0 and even more for PEG_{12} compared to both PEG_4 and PEG_0. *In vivo*, on both models, mAbs-PEG_{4-12}-TCO roughly induced two times less fluorescent signal in tumors than corresponding non-PEGylated mAbs. **Conclusion**: Results

suggest that addition of PEG linkers did not alter significantly the antigen recognition of TCO-mAb conjugates but caused an alteration of the TCO/TZ interaction which could be explained by a decrease of available reactive TCO per mAb. We here demonstrated that mAb-TCO without PEG linker will represent the best candidate to perform PRIT studies on PC.

EP-0194

3D tumor margin demarcation combined with sentinel node resection using the hybrid tracer ICG-^{99m}Tc-nanocolloid

P. Meershoek[1,2], N. S. van den Berg[1], G. H. KleinJan[1,2], C. A. H. Lange[2], B. van der Hiel[2], R. A. Valdés-Olmos[1], W. M. C. Klop[2], A. J. M. Balm[2], F. W. B. van Leeuwen[1]; [1]Leiden University Medical Center, Leiden, NETHERLANDS, [2]Netherlands Cancer Institute (NKI-AvL), Amsterdam, NETHERLANDS.

Introduction: For radical resection of squamous cell carcinoma of the oral cavity, a tumor free margin of 5 mm is required. While achieving this margin is relatively easy on the surface of the tissue, the difficulty lies in establishing a margin in depth. It has previously been shown that the hybrid sentinel node (SN) tracer indocyanine green (ICG)-Technetium-99m (^{99m}Tc)-nanocolloid can be used to generate temporary markings at the site of administration. Here, we studied the feasibility using this feature of ICG-^{99m}Tc-nanocolloid for Ultrasound-based 3D tumor demarcation of primary tongue tumors and combining this with SN resection. **Materials and Methods:** 33 patients with clinical T1-2 tongue tumors that were scheduled to undergo SN biopsy and resection of the primary tumor were included. ICG-^{99m}Tc-nanocolloid was injected peritumorally, under ultrasound guidance, in six deposits in thirteen patients (superficial and in-depth; tumor margin demarcation) and in four superficial deposits in twenty patients. After tracer deposition, SN mapping was performed using lymphoscintigraphy and SPECT/CT. In the patients who received tumor margin demarcation, prior to and after tumor excision, fluorescence imaging was used to evaluate if the tracer deposits could be visualized. *Ex vivo*, the (paraffin-embedded) tumor samples of these patients were studied to relate the location of the tracer deposits to the tumor and its margins. **Results:** Intraoperatively and *ex vivo,* the tracer deposits of the tumor margin demarcation could be detected surrounding the primary tumor using fluorescence imaging in all thirteen patients who received the tumor margin demarcation. However, it proved difficult to place deposits of equal size. The different administration routes did not result in significant differences in the number of SNs identified; 39 (mean 3.0 per patient) and 55 (mean 2.8) in patients with six or four injections, respectively (p=0.540). **Discussion/Conclusion:** Preoperative SN mapping can also be done while using the hybrid tracer for tumor margin demarcation and does not negatively influence the SN procedure. In addition, the fluorescent nature of ICG-^{99m}Tc-nanocolloid allowed visualization of the tracer deposits in the resection margins and could be of value when preoperative data indicates that intraoperative margin assessment will be complex.

Molecular & Multimodality Imaging: Miscellaneous

EP-0195

Utility of combined CT coronary angiography and SPECT myocardial perfusion imaging for the detection of functionally relevant coronary stenoses

P. Mohan, A. Vaidya, U. Kaul, H. Mahajan; Mahajan Imaging, NEW DELHI, INDIA.

Aim: Noninvasive imaging techniques to exclude coronary artery disease (CAD)with a high certainty and to detect its functional consequences at an early stage to guide patient management have been developed. Currently both gated SPECT and multislice CT are available for functional imaging i.e. assessing the haemodynamic consequences of CAD and anatomical imaging i.e. visualizing the coronary artery tree respectively. The aim of the current study was toevaluate the diagnostic performances and incremental clinical values of combined computed tomography coronary angiography (CTCA) and single photon myocardial perfusion imaging (MPI) for the detection of functionally relevant coronary stenoses (FRCS). **Materials and Methods**: In total, 150 patients underwent Gated SPECT for MPI, 64-slice CT for CTCA & coronary angiography within 30 days. Coronary arteries on multislice CT angiography were classified as having no CAD, insignificant stenosis (<50% luminal narrowing), significant stenosis, or total or subtotal occlusion (>90% luminal narrowing).Gated SPECT findings were classified as normal or abnormal (reversible or fixed defects) and were allocated to the territory of one of the various coronary arteries. **Results**: The diagnostic performances of CTCA and combined CTCA plus MPI for the detection of significant coronary stenoses (≥50%) were calculated on the patient or vesselbased levels and included the indices of sensitivity (SN), specificity (SP), positive predictive value (PPV), negative predictive value (NPV) and accuracy (AC). Mean patient age was 64±5 years (72% male). On the patientbased level, the SN for CTA alone was 90.6%, SP 59 %, PPV 57% , NPV 92% and AC was 68% . After combining CTA and MPI, SN was 96.9%, SP 72.9%, PPV 69%, NPV 95.4% and AC respectively. On the vesselbased level, the SN, SP, PPV, NPV and AC of CTCA alone or combined with MPI in the detection of FRCS were 90.3 and 90.3, 87.6 and 98.9, 54.9 and 93.3, 98.2 and 98.4 and 88.0 and 97.7%, respectively. The PPV, SP and AC of combined CTCA and MPI in the detection of FRCS were significantly improved compared with CTCA alone (all values, P<0.05). **Conclusion:** The diagnostic performance of combined CTCA and MPI in the detection of FRCS not only retains a high SN and NPV, but also markedly improves SP, PPV and AC, which should play an incremental and significant role in the decisionmaking process for the revascularization therapy of coronary artery disease (CAD).

EP-0197

Engineered DOTA antibody reporter with infinite affinity for in vivo tracking of lymphocytes

S. Krebs[1], A. Ahad[1], H. Zhang[1], J. Dozier[1], S. M. Larson[1], S. Gottschalk[2], P. Adusumilli[1], V. Ponomarev[1], W. A. Weber[1]; [1]Memorial Sloan Kettering Cancer Center, New York, NY, UNITED STATES OF AMERICA, [2]Center for Cell and Gene Therapy/TXCH, Baylor College of Medicine, Houston, TX, UNITED STATES OF AMERICA.

Objectives: There remains an urgent need for the non-invasive tracking of the transfused chimeric antigen receptor (CAR) T cells to determine their biodistribution, viability, expansion and anti-tumor functionality. Preliminary studies in cancer cell lines expressing DOTA antibody reporter 1 (DAbR1) demonstrated irreversible binding to the probe yttrium-/lutetium-(S)-2-(4 acrylamidobenzyl)-DOTA (*Y/*Lu-AABD) *in vitro* and *in vivo*. The aim of this study was to investigate whether DAbR1 can be expressed on lymphocytes and used for tracking their distribution *in vivo*. **Methods:** DAbR1, which consists of the single-chain Fv (scFv) fragment of the anti-Y-DOTA antibody 2D12.5/G54C fused to the human T cell CD4 transmembrane domain, was subcloned together with the gene for GFP into an SFG retroviral vector. In addition, we used an SFG retroviral vector encoding for a second generation mesothelin (MSLN) CAR. RD114 pseudo-typed retroviral particles were used to transduce CD3/CD28-activated human T cells. Transduction of T cells was judged based on GFP (for DAbR1) and/or staining for the MSLN CAR. *In vitro and in vivo* accumulation of the reporter probe ^{177}Lu -AABD were determined. For *in vivo* imaging 3×10^6 and 5×10^6 DAbR1-T cells were implanted s.c. in immuno-compromised (SCID) mice followed by i.v. injection of ^{177}Lu-AABD. **Results:** We generated a panel of DAbR1-expressing T cells derived from human primary T cells and genetically engineered MSLN CAR T cells. Successful cell surface expression of DAbR1 on human PBMCs and MSLN CAR T cells was confirmed using FACS analysis (range of transduction: 72%-86%) and based on binding assays with radio-labelled AABD. *In vitro* DAbR1-T cells exhibited a rapid accumulation of the added radioactivity, rising from 4.6% at 30 min to 7.2% at 120 min, whereas % uptake of NT cells remained at 0.6% at 30 min and 120 min. *In vivo* experiments demonstrated binding of ^{177}Lu-AABD on implanted DAbR1 T cells using SPECT/CT. Repeated imaging of intratumoral implanted DAbR1 T cells after a 2nd dose was feasible. In contrast, uptake of AABD in non-transduced cells and normal murine organs was minimal. **Conclusion:** Our results demonstrate that DAbR1-transduced T cells express membrane-bound DAbR1 enabling specific binding of the radiolabeled reporter probe AABD *in vitro* and *in vivo*. This approach is now being further developed to track adoptively transferred CAR T cells in tumor bearing mouse models. **Research Support:** NIH (K12-CA184746)

EP-0198

Development of PET in Europe

A. Stevens; Medical Options, London, UNITED KINGDOM.

Purpose: To track the development and use of PET in Europe. The provision and level of scanning of PET (PET, PET/CT and PET/MR) in Europe varies widely both between and within countries where workload volume differs between providers. The large differences

between facilities in terms of scan volumes and the range of tracers in use precluded a simple sampling approach and required identification of all European PET providers. **Subjects and Methods:** Facilities with PET and or cyclotron(s) were identified from a number of sources primarily equipment manufacturers and sites providing PET. Sites were invited to describe their operation including their equipment profile, the number and types of patient studies performed and their use of radiotracers. We were able to identify over 95% of the PET cameras and cyclotrons operating in Europe. Over 60% of these sites provided workload numbers for 2016. To project total workload we employed a segmentation scheme for each country or region which identified ten types of facility allowing us to estimate more accurately patient numbers at sites who did not contribute workload data. **Results:** In 2016 there were 719 providers of PET and/or CT or MR in Europe of which 18 were mobile. PET/CT accounted for over 90% of the installed systems. PET cameras which comprised 3.8% of the total were almost entirely operating in research settings while PET/MR represented 4.8% of systems. FDG studies accounted for 93% of the total patient workload with oncology examinations accounting for 91% of FDG scans. Tracers other than FDG accounted for 9% of studies and of these Fluorine 55%, Gallium 33%, buoyed by the introduction of PMSA, and Carbon 7% were the significant nuclei in use. Studies to identify prostate disease accounted for 53% of studies with F-choline and 68Ga PSMA accounting for 85% of these investigations. Scan numbers rose by 9.5% from the 1.36m scans estimated for 2014 versus 9.3% between 2012 and 2014. There are wide variations across Europe both in terms of scans performed and patient throughput. In some cases this is due to reimbursement and in others working practices and patient catchment. **Conclusions:** Across Europe there is an opportunity to double the use of FDG if the proportion of patients in countries with low adoption meets that of high adopters. The increasing use of compounds other than FDG bodes well for a further expansion of PET over the coming years.

EP-0199

Tumor alignment in proton therapy using the onboard functional imaging

H. Lin[1,2], H. Chang[3], T. Chao[4,1,2], Y. Ni[5,6], C. Shih[7], K. Chuang[6]; [1]Medical Physics Research Center, Institute for Radiological Research, Chang Gung University/Chang Gung Memorial Hospital, Taoyuan, TAIWAN, [2]Department of Radiation Oncology, Chang Gung Memorial Hospital, Taoyuan, TAIWAN, [3]Environmental Protection and Chemistry Section, Kuosheng Nuclear Power Station, Taiwan Power Company, New Taipei, TAIWAN, [4]Department of Medical Imaging and Radiological Sciences, College of Medicine, Chang Gung University, Taoyuan, TAIWAN, [5]Health Physics Division, Institute of Nuclear Energy Research, Atomic Energy Council, Taoyuan, TAIWAN, [6]Department of Biomedical Engineering and Environmental Sciences, National Tsing Hua University, Hsinchu, TAIWAN, [7]3D Printing Medical Research Center, China Medical University Hospital, China Medical University, Taichung, TAIWAN.

Aims: Traditional geometrical alignment performed primarily by x-ray transmission modalities cannot provide tumor information for target alignment. The alignment error may introduce significant underdose or overdose to tumor target in proton therapy. For reducing the alignment error, we proposed an additional functional imaging for multidimensional geometric verification in proton therapy. **Materials and Methods:** Since both the functional imaging for tumor location and prompt gamma (PG) imaging for proton range verification require a gamma camera but with different collimators, we develop a dual mode gamma camera that can switch between the "PG-based" and "SPECT-based" collimator. Before the proton treatment, the location of target volume was verified by an emission scan with a pre-injected radionuclide 99mTc using the SPECT-based gamma camera. During the proton irradiation, the proton range was detected by the camera equipped with knife-edge slit collimator that images PG emitted along the proton tracks in the patient. Monte Carlo studies with GATE/GEANT4 were performed to assess the feasibility of such a system for tumor localization in proton therapy. The effects of tumor size, tumor-to-background (TB) ratio, and phantom shift on target location will be studied in a rectangular PMMA phantom. Finally, the performance of this system was evaluated using a Zubal phantom with an embedded brain tumor. **Results:** The results indicated that the detection ability of the SPECT-based camera was dependent on the tumor size and TB ratio. The TB ratio must be greater than 4 for tumor to be detected. For those detected tumors, the location errors are within 0.5 mm for the weighted center of tumors and within 1 mm for the boundary of tumors. Both the PG-based collimator and SPECT-based collimator can achieve reasonable accuracy and good response to the phantom shift. For Zubal phantom, a linear relationship between the detected shifts of the weighted center of tumors and simulated tumor shifts was presented. The mean localization error for the weighted center of tumors detected by the SPECT-based camera is about -1.89 mm. **Conclusion:** We conclude that the functional imaging using the designed dual-mode gamma camera have potentials for accurately tumor alignment in proton therapy.

EP-0200

Development Of Multimodal Mannosylated Dextran For Sentinel Lymph Node Detection With SPECT/ PET And Optical Imaging

A. Shegani[1], A. Papasavva[1], I. Roupa[1], C. Karachaliou[1], L. Palamaris[1], C. Kiritsis[1], C. Tsoukalas[1], C. Triantis[1], G. Loudos[1], P. Kyprianidou[1], P. Bouziotis[1], M. Pelecanou[2], M. Papadopoulos[1], I. Pirmettis[1]; [1]INRASTES, NCSR DEMOKRITOS, ATHENS, GREECE, [2]IB-A, NCSR DEMOKRITOS, ATHENS, GREECE.

Introduction: Sentinel lymph node biopsy (SLNB) is a common practice in the management of patients with tumors. The introduction of mannose molecules to 99mTc or 68Ga labeled macromolecules such as dextrans, showed that these agents can be trapped selectively by the mannose receptors of lymph node macrophages. In addition to the presence of a radioactive element, the introduction of a fluorophore on the dextran may combine preoperative planning and intraoperative localization of deeply located sentinel lymph nodes with direct optical guid-

ance in a single lymphatic tracer. **Purpose:** Aiming at the development of multimodal mannosylated dextrans for SLND, we report herein the synthesis and biodistribution of a new mannosylated dextran DCM20-NODAGA-FITC carrying cysteine and NODAGA as a chelator for labelling with ^{99m}Tc and ^{68}Ga respectively and fluorescein isothiocyanate (FITC) as a short-term fluorophore. **Subjects and Methods:** DCM20, **1** was synthesized according to the literature. Subsequently, reaction of the NODAGA NHS with free amine groups of **1** resulted in the formation of the DCM20-NODAGA, **2**. DCM20-NODAGA-FITC, **3** was synthesized by reacting of **2** with FITC in bicarbonate buffer/DMSO solution, for 18 hrs at rt. The final product **3** was purified by fast ultrafiltration and characterized by NMR. ^{99m}Tc (or ^{68}Ga) labelling was achieved by addition of ***fac***-[^{99m}Tc(CO)$_3$(H$_2$O)$_3$] 0.5 mL (or ^{68}GaCl$_3$ 0.5 mL) to a 0.1 mL solution of **3** (100 µg) and incubation at 100 °C for 40 min (or at 40 °C for 20 min). Quality control and stability studies were performed by RP-HPLC. The biological evaluation was performed by biodistribution studies in Swiss albino mice after subcutaneous injection (20 µL) in the footpad. **Results:** The preliminary biological testing of ^{99m}Tc and ^{68}Ga complexes showed high accumulation in the popliteal lymph node 4.09 and 4.39 % ID and fast injection site clearance 59.37 and 40.61 % ID at 120 min p.i. respectively. These data are comparable with previous data of ^{99m}Tc-DCM20, indicating that the attachment of NODAGA chelator and FITC fluorophore did not alter its biodistribution. Furthermore, dynamic imaging study confirmed the rapid elimination rate from the injection site. **Conclusion:** In this study a new hybrid fluorescence and radioactive tracer for sentinel lymph node was developed. The new DCM20-NODAGA-FITC labeled compound did reveal attractive biological features as a novel multimodal imaging agent combining sentinel lymph node radioimaging with ^{99m}Tc (SPECT) or ^{68}Ga(PET) and direct optical guidance by FITC, justifying further investigations in animals and humans.

EP-13   **during congress opening hours, e-Poster Area**

Radiopharmaceuticals & Radiochemistry: Radiopharmaceuticals - PET

EP-0201

A Total Synthesis of High Optically Pure ^{18}F-FP-(+)-DTBZ and Its Validation as a PET Imaging Agent for VMAT2

P. Zou, C. Liu, X. Li, J. Tang, C. Zhao, Z. Chen; Key Laboratory of Nuclear Medicine, Ministry of Health, Jiangsu Key Laboratory of Molecular Nuclear Medicine, Jiangsu Institute of Nuclear Medicine, Wuxi, CHINA.

Introduction: Imaging vesicular monoamine transporter type 2 (VMAT2) with PET has provided a valuable measurement for neurodegenerative disorders such as Parkinson's disease. Fluoride[^{18}F]-9-fluoropropyl-9-desmethyl-(+)-α-dihydrotetrabenazine (^{18}F-FP-(+)-DTBZ) was becoming a potential VMAT2 PET imaging agent due to its excellent affinity and specificity. During its on-going wide clinical route application, a total synthesis of high optically pure ^{18}F-FP-(+)-DTBZ including its precursor was required. **Methods:** We herein developed a synthetic scheme for preparing high optically pure ^{18}F-FP-(+)-DTBZ. Firstly, racemic 9-benzyl-9-desmethyl-(±)-dihydrotetrabenazine (BnO-(±)-DTBZ) was ynthesized from 3-(benzyloxy)-4-methoxybenzaldehyde by reduction, annulation, and followed by addition reaction. Then, this racemate was resolved to give BnO-(+)-DTBZ with an optical purity of >98%, the key intermediate for synthesizing the precursor. This enantiomer was consequently deprotected under H$_2$ to yield 9-desmethyl-(+)-α-dihydrotetrabenazine. Lastly, the tosylated precursor TsOP-(+)-DTBZ was synthesized from the 9-demethyl compound. Chiral HPLC was used to analyze its optical purity. With the optically pure TsOP-(+)-DTBZ, ^{18}F- FP-(+)-DTBZ was synthesized in a one-step reaction under K$_{222}$ and K$_2$CO$_3$ in DMSO followed by purifying with HPLC. Biodistribution, blocking test, and microPET imaging in normal and 6-hydroxydopamine semi-lesioned PD rats were performed to validate its in vivo bioactivity. **Results:** The precursor TsOP-(+)-DTBZ showed an optical purity of >97% and was characterized with MS and ^{1}HNMR. ^{18}F- FP-(+)-DTBZ was synthesized from TsOP-(+)-DTBZ at over 98% radiochemical purity. Biodistribution studies show that ^{18}F- FP-(+)-DTBZ displayed a high brain uptake (1.3%ID) at 2min after an intravenous injection and a high target-to-nontarget ratio (striatum/cerebellum) of 6.1 at 60 min. The uptake of ^{18}F-FP-(+)-DTBZ in the striatum could be blocked by DTBZ, a VMAT2 inhibitor, but not by dopamine transporter inhibitor. MicroPET imaging in normal rat brain gave excellent images with high symmetrical radioactivity in striatum, resulting in a maximum ST/CB ratio of 8.2 at 80-120 min. By contrast, the 6-OHDA semi-lesioned rats gave asymmetrical striatum images with dramatically lower radioactivity on the lesioned side than unlesioned. **Conclusions:** A Synthetic method of high optically pure ^{18}F-FP-(+)-DTBZ including its precursor was developed and validated for ***in vivo*** VMAT2 PET imaging. Combined with other reports, our studies further confirmed that ^{18}F-FP-(+)-DTBZ has high affinity and specificity to VMAT2. **Acknowledgements:**

EP-0202

[^{18}F]Fluoride retention and elution in a SAX microcartridge included in a lab-on-chip for radiopharmaceuticals

L. Fernandez-Maza[1], B. Salvador[2], A. Corral[1], D. Orta-Castello[1], I. Fernandez-Gomez[1], A. Luque[2], J. Quero-Reboul[2]; [1]Centro Nacional de Aceleradores. Universidad de Sevilla. CSIC. Junta de Andalucia, Seville, SPAIN, [2]Departamento de Ingenieria Electronica. Escuela Tecnica Superior de Ingenieria. Universidad de Sevilla, Seville, SPAIN.

Introduction: Microfluidic devices for PET radiopharmaceuticals have increasing interest for dose on demand synthesis, mainly at centres with no cyclotron facilities. In order to reduce shielding needs, more compact microfluidic devices are being

developed. Our group has integrated a strong anion exchange (SAX) microcartridge in a polydimethylsiloxane (PDMS) chip. The aim of the study was the characterisation of the cartridge. **Materials and Methods**: The chip mould was made of 8-epoxy-based negative photoresist resin on a printed circuit board to define the channels for the liquids. This mould was covered with a 3D-printed enclosing box, including a 2 mm rod to form the hole in which the SAX resin would be hosted. Then, PDMS was poured into the mould, degassed for an hour in a vacuum chamber, and cured at 65° for 45 minutes. Inlet and outlet orifices were drilled, and the chip was closed with a PDMS membrane. The microchip was cured again at 80° for an hour. 10 mg of quaternary methyl ammonium resin (QMA, Waters) with 60 µm of particle size were inserted and two polyethylene frits enclosed the cartridge. 60 microcartridges were tested to establish the best conditions of activation and elution to recover the maximum amount of [^{18}F]F$^-$ at the reactor. Activation with K_2CO_3 0.5M was tested from 0-3 mL. Doubled volumes of deionized water to clean the excess of K_2CO_3 were used and different flow rates were also tested at activation, [^{18}F]F$^-$ loading, and elution steps. The activated cartridges were dried before [^{18}F]F$^-$ loading. Dosis of 500 µCi of [^{18}F]NaF were loaded into the cartridges, and eluted with 30 µL of a mixture of K_2CO_3 0.5M + K2.2.2 1M in acetonitrile. Radioactivity of irradiated water eluted, and fluoride eluted solution were measured in a Capintec CRC ll activimeter. The tubing and PDMS cartridge residual activities were also measured in the activimeter. **Results:** [^{18}F]F$^-$ retention rate was 91-100%, elution rate of 94-97%. K_2CO_3 clogging appeared in PDMS channels when the same microcartridge was re-used. In order to avoid clogging phenomena, K_2CO_3 activation was discarded. [^{18}F]F$^-$ recovered at reactor was above 95%. **Conclusion**: Retention of [^{18}F]F$^-$ was 91-100%, elution of 94-97%. K_2CO_3 activation could be avoided if the chip is used for single use purpose, to avoid cross contamination. In any case, the microcartridge can be regenerated with K_2CO_3 for more than ten runs.

EP-0203

High yield ^{18}F-FET production on AllinOne (Trasis) at commercial scale

T. Vergote, M. Otabashi, C. Vriamont, C. Desfours, C. Warnier, J. Morelle, G. Philippart; Trasis SA, Ans, BELGIUM.

Introduction: O-(2-[^{18}F] fluoroethyl)-L-tyrosine ([^{18}F]FET), one of the first ^{18}F-labeled amino acids for imaging amino acid metabolism in tumors, is showing high uptake in the so called primary brain tumors. [^{18}F]FET is overcoming disadvantages of [^{18}F]FDG and [^{11}C] methionine tracers: [^{18}F]FET is a more specific tracer than FDG and benefit of a really longer half-life than [^{11}C] methionine. Accordingly, [^{18}F]FET PET is a highly relevant tool for patient management [1-3]. Therefore, a robust synthesis combined with a high yield is requested and has been achieved under cGMP conditions by Trasis on the AllinOne synthesizer. **Methods:** [^{18}F]FET is prepared from the protected compound O-(2-tosyloxyethyl)-N-trityl-tyrosine tert-butylester (TET), see Figure 1. TET is labelled with fluorine-18 at 120°C via direct nucleophilic radiofluorination to give the O-(2-fluoroethyl)-N-trityl-tyrosine

intermediate. This compound is subsequently hydrolyzed at 100°C with hydrochloric acid 0.5 M to afford the [^{18}F]FET compound. Finally, this crude solution is purified by HPLC to isolate the [^{18}F]FET and formulated for injection. **Results:** The average Non-Decay Corrected yield is about 50%, with highest values around 55%. This synthesis is performed in 45 minutes. The radiochemical purity is higher than 98% and the enantiomeric purity always above 97%. The formulated product is stable over at least 10 hours. **Conclusions:** The fully automated production of [^{18}F]FET developed and optimized by Trasis on an AllinOne synthesizer module is appropriate for routine commercial scale purposes. **References:** [1] M .Zuhayra et al., *Bioorg. Med. Chem.*, **2009**, *17,* 7441-7448, [2] V. Dunet et al., *J. Nucl. Med.*, **2012**, *53,* 207-214, [3] K.-F. Langen et al., *Nucl. Med. Biol.*, **2006**, *33,* 287-294

EP-0204

PET imaging of Pheochromocytoma with a novel ^{18}FAl labeled exendin-4 analog

D. Pan[1,2], Y. Xu[1], Y. Wang[1], Y. Yue[1], L. Wang[1], J. Yan[1], X. Wang[1], R. Yang[1], M. Yang[1]; [1]Jiangsu Institute of Nuclear Medicine, Wuxi, CHINA, [2]Jiangnan University, Wuxi, CHINA.

Purpose: Glucagon-like peptide 1 receptor (GLP-1R) is overexpressed in pheochromocytoma and becomes interest targets for diagnosis and therapy of the tumor. ^{18}F-Al-NOTA-MAL-Cys[39]-exendin-4 holds great promise for GLP-1R imaging. Therefore, the feasibility of the ^{18}F-labeled peptide for pheochromocytoma imaging was investigated. **Methods:** MicroPET imaging was performed in PC-12 tumor-bearing mice after injection of ^{18}F-Al-NOTA-MAL-Cys[39]-exendin-4 with or without unlabeled peptides. Pathological studies were also performed. **Results:** PC-12 pheochromocytoma xenografts were clearly imaged under baseline conditions, whereas no tumor was visualized under blocking conditions. At 30, 60 and 120 min postinjection, the tumor uptakes were 2.48±0.10 %ID/g, 2.15±0.22%ID/g and 1.46±0.37%ID/g respectively. The presence of cys[39]-exendin-4 significantly reduced the tumor uptake (0.71±0.15 %ID/g at 60 min p.i.). The tumors to muscles were improved significantly with the increase of time due to rapid clearance of the tracer from normal organs (7.79±0.51 at 30min p.i and 29.27±3.56 at 2h p.i respectively). Immunohistochemistry results confirmed GLP-1R expression in PC-12 tumors. **Conclusion:** Primary studies revealed that PET imaging pheochromocytoma with the specific GLP-1R probe was feasible. **Acknowledgement:** This work was partially supported by National Natural Science Foundation (81401450,51473071,81472749,21504034,21401084,31671035), Jiangsu Province Science and Technology Foundation (BE2014609 and BE2016632), Jiangsu Provincial Medical Innovation Team (H201529 and Q201406).

EP-0205

Influence of Enzyme Inhibitors on FSHR PET Imaging

M. Yang[1,2], Y. Xu[1,2], D. Pan[1], Y. Wang[1], Y. Yue[1], L. Wang[1], J. Yan[1], X. Wang[1], R. Yang[1]; [1]Jiangsu Institute of Nuclear Medicine, Wuxi, CHINA, [2]Nanjing Medical University, Nanjing, CHINA.

Aim: FSHR is an important biomarker of cancer. Previous studies showed that radiolabeled FSH1 and its analogs successfully visualized FSHR positive tumors. However, poor metabolic stability may decrease the contrast of images and hamper the clinical use. Co-administration of specific enzyme inhibitors would improve the pharmacokinetics of the peptides. To validate the hypothesis, the effect of an endopeptidase inhibitor (phosphoramidon, PA) and a protease inhibitor (Aprotinin) co-injection with FSH1 derives (FSH4) were investigated in tumor model. **Methods:** FSH4 (YTRDLVYKDPARPKIQKTCTFNDRGGG) was conjugated to NOTA-MAL, then radiolabeled with Al[18]F complex. The tumor-targeting potential and pharmacokinetic profile of the ^{18}F-labeled tracer alone or after coinjection of inhibitors were evaluated using PC3 human prostate tumor models. **Results:** ^{18}F-Al-NOTA-MAL-FSH4 can be efficiently produced within 30 min with a non-decay corrected yield of nearly 20% and radiochemical purity of more than 95 %. The PC3 human prostate tumor xenografts were visible after injection of ^{18}F-Al-NOTA-MAL-FSH4 via microPET. At 30, 60 and 120 min postinjection, the tumor uptakes were 3.32±0.13 % ID/g, 1.36±0.27 %ID/g and 0.42±0.06 %ID/g, respectively. FSHR-binding specificity was also demonstrated by reduced tumor uptake of ^{18}F-Al-NOTA-MAL-FSH4 after coinjection with an excess of unlabeled FSH4 peptide. The tracer was excreted mainly through the renal system. It was noted that the coadministration of inhibitors significantly increase uptakes in tumors. The tumor uptakes ranged from 4.37± 0.53 %ID/g to 1.81± 0.40 %ID/g at 30 min and 2h after coinjection of the tracer with PA respectively. Meanwhile, the radioactivites in tumors kept ~8% ID/g from 30min to 2h after injection of ^{18}F-Al-NOTA-MAL-FSH4 with Aprotinin. **Conclusions:** ^{18}F-Al-NOTA-MAL-FSH4 appears to be a promising candidate for FSHR-positive tumor imaging. Coadministration of enzyme inhibitors can effectively prolong the accumulation of radiolabeled peptides in the tumors. Detailed mechanism will be studied in the future.

EP-0206

Synthesis Of Novel Copper-64 Labeled Rhodamine: A Potential Pet Myocardial Perfusion Imaging Agent

I. Aljammaz; kfshrc, riyadh, SAUDI ARABIA.

Myocardial infarction is the leading cause of death in most of the countries, and myocardial perfusion imaging (MPI) is an important tool in the evaluation of myocardial ischemia and infarction. Currently, MPI are usually performed using single-photon radiopharmaceuticals such as ^{99m}Tc-MIBI, ^{99m}Tc-tetrofosmin and ^{201}Tl-chloride. Unlike single-photon emission computed tomography (SPECT), Positron emission tomography (PET) imaging offers several advantages imaging in MPI application including better sensitivity, higher spatial resolution and an improved attenuation correction. The currently used PET tracers for MPI

studies ([13]NH₃, [82]Rb and ^{15}O-water) have limitations such as high cost or the need of on-site cyclotron for production. Due to the ideal physical properties of fluorine-18, various ^{18}F-tracers for MPI were developed. Rhodamine dyes are known to accumulate in the heart; therefore, several [68]Ga- and ^{18}F-labeled esters of rhodamine B were reported recently as potential MPI agents. Due to the various advantages offer by ^{64}Cu, many ^{64}Cu-based imaging agents have already been developed and tested in humans. Thus, as part of our on-going research effort to develop novel radiotracers for MPI studies, we here report the synthesis and preclinical evaluation of new ^{64}Cu-NOTA-rhodamine conjugate. The synthetic approach for the preparation of ^{64}Cu-NOTA-rhodamine conjugate was straightforward. Solution of [64]CuCl₂ (37-300 MBq) were reacted with NOTA-rhodamine conjugate (20 μg) in acetate buffer (pH ~5) at room temperature and different time range. Work up of these conjugates gave ^{64}Cu-NOTA-rhodamine conjugate in quantitative radiochemical yield and purity as assessed by TLC and HPLC in less than 30 min. The synthetic approaches hold considerable promise as rapid and simple method for radiolabeling of rhodamine with ^{64}Cu in high radiochemical yield and in short time. The stability of ^{64}Cu-rhodamine conjugate was determined in human plasma and revealed that this radioconjugate remained stable during incubation at 37°C for at least 4 h. **In vivo** characterization in normal Fischer rats at 60 min p.i., showed high myocardial uptake (~ 5 % ID/g). Initial cardiac imaging study using animal PET/CT imaging modality; demonstrate that this radioconjugate may be useful for MPI studies using PET. However, further evaluation is in progress.

EP-0207

A Modified Procedure for the Synthesis of a Potential Tau Imaging Agent [¹⁸F]T807 Employing a Neutral Mobile Phase Containing Acetonitrile and a Buffer for Semi-preparative HPLC Purification

M. CHEUNG, N. NG, K. LIU, C. HO; HONG KONG SANATORIUM & HOSPITAL, HONG KONG, HONG KONG.

Aim: [¹⁸F]T807 is a PET tracer for neurological imaging of paired helical filaments of tau pathologies with promising results for dementia. However, repeated attempts to synthesize [¹⁸F]T807 following the literature procedure gave two inseparable products at low yield and long retention times during HPLC elution and purification procedures. We, therefore, proposed a set of modified reaction conditions and an efficient HPLC purification procedure to achieve the desired product. **Materials & Methods:** With the Sumitomo F121R synthesizer, the protected precursor, tert-butyl 7-(6-nitropyridin-3-yl)-5H-pyrido[4,3b]indole-5-carboxylate was fluorinated and de-protected concurrently at different temperature settings (130-150°C) to compare the yields. For comparison of desorption efficiency, aqueous acetonitrile (ACN) of different compositions was used instead of ethanol to desorb the crude product from solid phase extraction (SPE) cartridge before proceeding to semi-preparative HPLC purification. To avoid forming two compounds and to keep the solvent homogeneity, the mobile phase used in HPLC was changed from acidic to a neutral

mixture of ammonium formate solution and ACN. Their ratios were varied to optimize the retention time and appearance of the product peak by using a reverse phase C18 column. **Results:** By testing different combinations of the above variables in reaction temperature, SPE desorption solvent, HPLC column and mobile phase used, the optimal setting was found when the concurrent fluorination and de-protection reaction was carried out at 150°C. 70% ACN was found to desorb the crude product from SPE with high efficiency (85%). This desorption solvent was homogeneous with the mobile phase, ammonium formate and ACN in the ratio of 7:3, eluting the single pure product [^{18}F]T807 at about 13 minutes. The radiochemical identity was verified by means of spiked standard analysis. The radiochemical purity of the product was found >99% by analytical HPLC and the reaction yield was 20.10±0.82%. The HPLC purified fraction was formulated into an injectable solution, which passed all quality control requirements and was suitable for patient administration. **Conclusions:** Synthesis of the tau imaging agent [^{18}F]T807 was achieved in our radiopharmacy laboratory using a Sumitomo F121R synthesizer with an average yield of 20.10±0.82% (n=4) and >99% radiochemical purity. This was comparable to the literature reported results, but only after significant modifications in reaction temperature and other purification procedures including SPE desorption solvent, HPLC column, mobile phase compositions and pH.

EP-0208

A Modified Procedure for the Synthesis of a Potential Tau Imaging Agent [^{11}C]PBB3

M. CHEUNG, N. NG, K. LIU, C. HO; HONG KONG SANATORIUM & HOSPITAL, HONG KONG, HONG KONG.

Aim: Phenyl/pyridinyl-butadienyl-benzothiazoles/benzothiazoliums (PBBs) represent a class of tau imaging ligands, of which [^{11}C]PBB3 has been shown to have effective binding to tau pathologies in patients with Alzheimer's disease (AD). Notably, the high-level retention of [^{11}C]PBB3 in the AD hippocampus, wherein tauopathy is enriched, is sharply in contrast with that of β-amyloid PET probe, [^{11}C]PIB. However, repeated attempts to synthesize [^{11}C]PBB3 following the literature conditions were unsuccessful. Therefore, we proposed a modified procedure for the synthesis of [^{11}C]PBB3. **Materials & Methods:** With the Sumitomo F121R synthesizer, N-desmethylated O-(tert-butyldimethylsilyloxy) protected precursor was used to react with freshly prepared [^{11}C]methyl iodide at different temperature settings (45 to 125°C) in the presence of different forms of potassium hydroxide (dry pellet or dry powder) in DMSO. The subsequent hydrolysis reaction was performed at 50°C to compare its efficiency with that performed at room temperature. Finally, variation in volume (0.1 to 0.13 mL) of 10% phosphoric acid added to the reaction mixture before proceeding to HPLC purification was tested to compare the yield of final product. **Results:** By testing different combinations of the above variables in temperature, reagent and reagent volumes, the optimal setting was found when the N-methylation reaction was carried out at 80°C for 5 minutes followed by hydrolysing the

intermediate N-methylated compound at 50°C for 2 minutes. The yield of the desired product was improved when 0.1 mL of 10% phosphoric acid was added to the reaction mixture before entering the HPLC purification column. At this setting, [^{11}C]PBB3 could be synthesized and isolated at a RCP of >99% by analytical HPLC and with a yield of 12.67±1.62%. The radiochemical identity was verified by means of spiked standard analysis. This compound was then formulated into an injectable solution for patient administration after passing all quality control requirements. **Conclusions:** The synthesis of the potential tau imaging agent [^{11}C]PBB3 was successful in our radiopharmacy laboratory using a Sumitomo F121R synthesizer with an average yield of 12.67 ± 1.62% (n=7) and >99% radiochemical purity. This was comparable to the results reported in the literature, but only after significant tuning and adjustment of different reaction temperature and reagent settings.

EP-0209

Fully automated 18F-FAZA production on AllInOne (Trasis) at commercial scale

T. Vergote, M. Otabashi, C. Vriamont, C. Desfours, J. Morelle, G. Philippart; Trasis SA, Ans, BELGIUM.

Introduction: Tumor hypoxia is a common feature of many solid malignant tumors. Hypoxic cells are known to be more than three times more resistant to radiation therapy than those with normal oxygenation levels. It's believed that during the process of hypoxia-driven malignant progression, tumors develop an increased potential for local invasive growth [1]. The identification and quantification of such type of tumors will improve their monitoring and treatment. Many radiotracers have been used to diagnose this kind of tumors including [^{18}F]FRP-170, [^{18}F]FETNIM, [^{18}F]FETA, [^{18}F]FMISO and [^{18}F]FAZA [2]. Among them, [^{18}F]FMISO and [^{18}F]FAZA [3] are the most widely PET tracers used in the diagnostic of hypoxia. The comparison between both radiotracers showed that much better images are obtained with [^{18}F]FAZA with a very high contrast due to its quick clearance from blood and non-target tissues [4]. **Methods:** The radiosynthesis of [^{18}F]FAZA is achieved under standard nucleophilic substitution conditions. 1-(2,3-di-O-acetyl-5-O-tosyl-a-D-arabinofuranosyl)-2-nitroimidazole precursor is labelled with ^{18}F-fluoride, in presence of the phase transfer agent TBA-HCO$_3$. Sodium hydroxide is then used to remove acetyl protecting groups. The solution is neutralized by addition of acetic acid, then purified by preparative HPLC using a methanol-water mixture as eluent. The collected fraction is reformulated on a cartridge. After elution with ethanol followed by saline [^{18}F]FAZA is ready for Quality Control (QC) and dispensing. **Results:** Labeling yield is about 80% under the following conditions: 100°C within 3 minutes using 5 mg of precursor. Hydrolysis is performed with 1 mL of 0.05 N NaOH at 40°C for 1 min. The automated process gives a reproducible radiochemical yield of 30 ± 4 % non-decay corrected after approximately 45 minutes of synthesis. The radiochemical purity is higher than 98%, in line with radiopharmaceuticals QC specifications. **Conclusions:** The fully automated production of [^{18}F]FAZA with ready to use reagent kits and cassettes has been

developed and optimized by Trasis on an AllInOne synthesizer module. This automated synthetic pathway is appropriate for routine commercial scale purposes. **References:** [1] M. Hokel, P. Vaupel, Journal of the National Cancer Institute **2001** *93(4)* 266-276 [2] S.J. Oh et al., Nucl. Med. Biol. **2005** *32(8)* 899-905 [3] P. Kumar et al., Appl. Radiat. Isot. **2002** *57(5)* 697-703 [4] D. Sorger et al., Nucl. Med. Biol. **2003** *30(3)* 317-326

EP-0210

Synthesis of Two Neurological PET Tracers, ^{18}F-FEPPA and ^{18}F-NAV4694 on a FlexLab Synthesizer

L. Morandeau[1], A. Asad[1], J. Ioppolo[1], S. Poniger[2,3], A. Wilson[4], R. Price[1,5]; [1]Medical Technology and Physics Dpt, Sir Charles Gairdner Hospital, Nedlands, AUSTRALIA, [2]iPHASE technologies Pty Ltd, Melbourne, AUSTRALIA, [3]The Austin Hospital, Melbourne, AUSTRALIA, [4]Centre for Addiction and Mental Health, Toronto, ON, CANADA, [5]School of Physics, University of Western Australia, Nedlands, AUSTRALIA.

Introduction: Neuroinflammation is a common feature in neurodegenerative disorders. Several ^{18}F-PET tracers have recently been developed to circumvent the limitations of the short-lived reference neuroinflammation imaging tracer, ^{11}C-PK11195. Among these, ^{18}F-FEPPA has shown promise in patients. ^{18}F-NAV4694 is a PET tracer for imaging of β-amyloid plaques in Alzheimer's disease (AD). It showed almost identical imaging characteristics to those of the benchmark radiotracer ^{11}C-PIB. The aim of this work was to develop the synthesis of ^{18}F-FEPPA and ^{18}F-NAV4694 on a FlexLab Synthesizer (iPHASE technologies Pty Ltd) for clinical applications. **Materials and Methods:** ^{18}F-FEPPA and ^{18}F-NAV-4694 were produced on a fully automated dual reactor FlexLab synthesizer. For both tracers, ^{18}F-Fluoride (56-107 GBq) was trapped on a pre-conditioned QMA and eluted into reactor 1 with 1 mL of K_{222}/K_2CO_3 eluent solution and dried azeotropically. For ^{18}F-FEPPA, 5 mg of precursor (N-[[2-[2-[[(4-methylphenyl)sulfonyl]oxy]ethoxy]phenyl]methyl]-N-(4-phenoxy-3-pyridinyl)-acetamide) in 1 mL anhydrous acetonitrile was reacted at 80 °C for 10 min. After cooling, the reaction was quenched with 4.25 mL of a formic acid/methanol solution and purified via semi-preparative HPLC. For ^{18}F-NAV4694, 3 mg of precursor ([5-(5-ethoxymethoxy-benzofuran-2-yl)-6-nitro-pyridin-2-yl)]-methylcarbamic acid tert-butyl ester) in 1 mL anhydrous dimethylsulfoxide were reacted at 80 °C for 6.6 min. After cooling, the reaction mixture was hydrolysed with 0.5 mL HCl 6 N for 5 min at 70 °C, diluted with 3.5 mL of 50% methanol in water and purified via semi-preparative HPLC. The ^{18}F-FEPPA or ^{18}F-NAV-4694 HPLC fractions were collected and diluted in 0.08 N sodium bicarbonate or water respectively, before transfer through a preconditioned t-C18 SepPak cartridge (Waters). After rinsing the SepPak with water, the final product was eluted off with 1 mL ethanol, further diluted with saline or sodium ascorbate solution, and transferred through a sterile filter into a vented sterile vial. **Results:** The synthesis of ^{18}F-FEPPA was successfully validated with an average yield (n=5) of 11.9% ± 3.3% EOS. The radiochemical purity was greater than 99% and the EOS specific activity ranged between 182 and 320 GBq.µmol^{-1}. The quality control passed all requirements. ^{18}F-NAV-4694 was also successfully synthesized with an average yield (n=2) of 27.8% ± 0.8% EOS. The radiochemical purity was greater than 97% and the product was chemically pure as assessed by analytical HPLC. **Conclusion:** ^{18}F-FEPPA and ^{18}F-NAV-4694 were successfully synthesized on a FlexLab synthesizer. ^{18}F-FEPPA was fully validated and is ready for clinical applications. ^{18}F-NAV-4694 is still under development with encouraging initial test runs.

EP-0211

Triphenylphosphonium Modified ^{18}F-Silica Nanoparticles as Tumor Targeting Agent for PET Imaging

Y. Kim[1], J. Lee[2], G. Kim[2,3], J. Park[2], S. Kim[1]; [1]Dongguk university, gyeongju, KOREA, REPUBLIC OF, [2]Korea Atomic Energy Research Institute, Jeongeup, KOREA, REPUBLIC OF, [3]Dongguk University-Gyeoungju, Gyeoungju, KOREA, REPUBLIC OF.

Aim This study was aimed to develop effectual tumor targeting silica nanoparticles. To achieve this goal, surface modified silica nanoparticles (SNPs) using cationic triphenylphosphonium (TPP) were synthesized. The positive charge of TPP enables them to infiltrate lipid bilayers easily and high accumulation into intracellular fluid may be achieved because of the plasma membrane potential (-30 to -60 mV). In cancerous cells, the plasma membrane potential is reported to be higher than that in normal cells which facilitates the accumulation of positively charged nanoparticles in the cancerous cells than normal cells. In this study, TPP modified ^{18}F-SNPs have been synthesized and evaluated for tumor uptake. Materials and Methods Different amounts of TPP in DMF were mixed with EDC and NHS as coupling agent and triethylamine in the molar ratio of 1:1.2:1.2:2 respectively. Amine-modified SNPs were added in each mixture and were stirred at room temperature for 24 h. TPP modified SNPs (TPP-SNPs) were dried at room temperature for 24 h. After this, labeling procedure was carried out in constant stirring condition at 100 °C for 1 h in which TPP-SNPs were suspended in acetonitrile and ^{18}F was added to the suspension. To introduce ^{18}F directly, TFA was added in mixture and stirred at 100 °C for 1 h. ^{18}F-labeled TPP-SNPs were collected by centrifugation and washed with water and saline. *In vivo* study was carried out in colon cancer cell (CT-26) xenografted balb/c mice weighing about 20 g. To measure PET image, ^{18}F-labeled TPP-SNPs were intravenously (i.v) injected in mice tail. Results and Conclusion The radiochemical yield and purity of ^{18}F-labeled TPP-SNPs were 9% and >99% respectively. By measuring the zeta potential, it was confirmed that the surface charge of TPP layer of silica nanoparticles was highly positive ~ +31.5 mV in the most surface modified SNPs. Acquired PET images after 5 min i.v injection of ^{18}F-labeled TPP-SNPs, clearly indicated its high uptake in the tumor. In particularly, the uptake value of positive charged silica nanoparticles (+31.5 mV) was higher in tumor site than that of others. Also, the uptake value of the tumor was strongly dependent on the surface charge of the nanoparticles and the same was confirmed by the *in vivo* experiments. From this studies we can conclude that the positively charged nanoparticles modified using TPP can be used as a tumor targeting agent for PET imaging.

EP-0212

[68Ga]Nivolumab: a novel PET tracer to detect PD-1 expressing tumors

S. Migliari, A. Sammartano, B. Pellegrino, V. Regina, D. Cavazzini, S. Ottonello, G. Missale, A. Musolino, L. Ruffini; AOU Pr, Parma, ITALY.

In recent years, the blockade of immune checkpoint molecules with monoclonal antibodies, like those targeting the PD-1/PD-L1 pathway, has enabled the development of breakthrough therapies in oncology, leading to delayed tumor growth and increased survival. Non-invasive methods permitting whole-body detection of PD-1 and PD-L1 at high sensitivity and resolution could thus be highly useful in patient selection and monitoring of PD-1/PD-L1 expression during disease progression and treatment. Aim of this study was to develop an immunoPET tracer for imaging PD-1 using a checkpoint-blocking antibody with proven antitumoral activity. We conjugated a 1,4,7,10-tetraazacyclododecane-1,4,7,10-tetraacetic acid (DOTA) chelator to Nivolumab (BMS-936558, ONO-4538, or MDX1106, trade name Opdivo; Bristol-Myers Squibb, Princeton, NJ, USA) the first-in-human immunoglobulin G4 (IgG4) PD-1 immune checkpoint inhibitor antibody for radiolabelling with Gallium-68. The buffer of Nivolumab (10 mg/ml) protein solution was readily exchanged by loading the protein onto a Biorad micro Bio-Spin 6 columns, pre-equlibrated in Sodium Phosphate 0.1M, pH 8.5; p-SCN-Bn-DOTA powder was dissolved in the same buffer at a concentration of 10mg/ml. The mixture of p-SCNBn-DOTA and Nivolumab was incubated overnight at 4°C. Binding affinity of DOTA-Nivolumab to T-cell blasts expressing PD-1 receptor was assessed by its capacity to inhibit fluorescently-labeled PD-1 binding, measured by flow cytometry. Unconjugated DOTA showed no binding, while a titration curve of Nivolumab and DOTA-Nivolumab showed comparable binding affinity for PD-1 receptor. Then the complex was radiolabelled with 30-50 MBq of Ga-68 in 500 µl of sodium acetate buffer (pH 5.1) at room temperature. The radiolabelling efficiency of [68Ga]DOTA-Nivolumab was determined using instant thin layer chromatography (TLC): the radiolabelling efficiency was approximately 75% and the free Ga-68 remained at the origin of the TLC plate. Collectively, these initial biological and radiochemical results suggest that our [68Ga]DOTA-Nivolumab is a promising candidate for PET imaging of PD-1 expressing tumors.

EP-0213

Preparation and preclinical evaluation of 64Cu-NOTA-anti MUC1 as a radioimmunoconjugate for diagnosis of MUC1 breast cancer by PET

B. Alirezapour[1,2], M. Davarpanah[3], J. Mohammadnejad[4], A. Jalilian[1], S. Rajabifar[1], E. Maadi[3], M. Hashemizadeh[3], N. Soltani[3], F. Bolourinovin[1], P. Ashtari[1], G. Aslani[1]; [1]Nuclear Science and Technology Research Institute, Tehran, IRAN, ISLAMIC REPUBLIC OF, [2]Pars Isotope Company, Teharn, IRAN, ISLAMIC REPUBLIC OF, [3]Pars Isotope Company, Tehran, IRAN, ISLAMIC REPUBLIC OF, [4]Department of Life Science Engineering, Faculty of New Sciences & Technologies, University of Tehran, Tehran, IRAN, ISLAMIC REPUBLIC OF.

Purpose: Radioimmunoscintigraphy (RIS) has attracted considerable clinical application in tumor detection. Underglycosylated MUC1 antigen is one of the early hallmarks of tumor genesis and is overexpressed in more than 80% of breast cancers. PR81 is a new murine anti-MUC1 monoclonal antibody (mAb). In this study, as the first step, we have developed an efficient indirect labeling method of PR81 with ^{64}Cu ($T_{1/2}$ = 12.8 h, β+ = 17%, β− = 39%, EC = 43%) through using NOTA (p-SCN-Bn-NOTA) bi-functional chelator and performed preliminary biodistribution studies in mouse bearing breast adenocarcinoma. **Methods:** Anti-MUC1 (PR81) was conjugated with NOTA (Macrocyclics B-605), the average number of the chelator conjugated per mAb was calculated and total concentration was determined by spectrophotometrically. NOTA-Anti-MUC1 was labeled with ^{64}Cu then Radiochemical purity and immunoreactivity, internalization study by MCF7 cell line and serum stability of ^{64}Cu-NOTA-Anti-MUC1 were determined. The biodistribution studies and radioimmunoscintigraphy were performed in female BALB/c mouse bearing breast carcinoma tumor (^{64}Cu-NOTA-Anti-MUC1i.v., 100 µl, 20±5 µg mAb , 6, 12, 24 and 48 h). **Results:** ^{64}Cu-NOTA-Anti-MUC1was prepared (RCP >98% ± 0.4, Specific activity 5.2 ± 1.2 µCi/µg). Conjugation reaction of chelator (50 molar excess ratio) to antibody resulted in a product with the average number of chelators attached to a mAb (c/a) of 4.1 ± 0.5. Labeling yield with ^{64}Cu in 400µg concentration of bioconjugate was 96.5% ± 2.1. Immunoreaction of ^{64}Cu-NOTA-Anti-MUC1complex towards MUC1 antigen was determined by RIA and the complex showed high immunoreactivity towards MUC1. *In vitro* and *in vivo* stability of radioimmunoconjugate was investigated respectively in PBS and blood serum by RTLC method. *In vitro* stability showed more than 94% ± 1.26 in the PBS and 81% ± 2.62 in the serum over 24 h. The Immunoreactivity of the radiolabeled Anti-MUC1 towards MCF7 cell line was done by using Lindmo assay protocol. Under these conditions, the immunoreactivity of the radioimmunoconjugate was found to be 0.82. The biodistribution of ^{64}Cu-NOTA-Anti-MUC1complex in the mice with normal and breast tumor at 6, 12, 24 and 48 h after intravenous administration, expressed as percentage of injected dose per gram of tissue (%ID/g). Biodistribution and imaging studies at 24 and 48 h post-injection revealed the specific localization of complex at the site of tumors. **Conclusion:** ^{64}Cu-NOTA-Anti-MUC1 is a potential compound for molecular imaging of PET for diagnosis and follow up of MUC1 expression in oncology.

EP-0214

Combination of [18F]F ion into Aromatic Ring Using Pinacol Boran Derivative for the Synthesis of LAT 1 tracer [18F]FBPA

S. Naka[1], Y. Kanai[1], Y. Ota[2], Y. Hattori[2], H. Takenaka[2], K. Uehara[3], T. Sakai[4], E. Shimosegawa[1], M. Kirihata[2], J. Hatazawa[1]; [1]Osaka University Graduate School of Medicine, Suita, Osaka, JAPAN, [2]Osaka Prefecture University, Sakai, Osaka, JAPAN, [3]Stella Pharma, Sakai, Osaka, JAPAN, [4]Hanwa Intelligent Medical Center, Sakai, Osaka, JAPAN.

Object: 4-Borono-2-[18F]fluoro-L-phenylalanine ([18F]FBPA) combined 18F into the 2-position of the aromatic ring of 4-bo-

rono-L-phenylalanine (BPA), is used as a radiotracer for Positron Emission Tomography (PET) to predict accumulate to tumor before Boron Neutron Capture Therapy (BNCT). Currently, [18F] FBPA has been generally prepared according to the [18F]F$_2$ gas method described by Ishiwata et al (*Appl Radiat Isot 1991*). However, this method has disadvantage that the radioactivity of the final product is very low because mass-production of ^{18}F with a cyclotron is difficult. In this study, we tried to develop new synthesis method using [18F]hydrogen fluoride ([18F]HF). **Method:** In this study, the [18F]HF method was used for the directly [18F]F reaction into the aromatic ring. As a precursor, a phenylalanine derivative combined with pinacol borane was used. The catalyst for fluorination was investigated about radiochemical yield with six copper reagents containing tetrakis (pyridine) copper (II) triflate (Cu(OTf)$_2$Py$_4$). In the copper reagent obtained highest radiochemical yield, was investigated additional amount relative to the substance amount of the precursor (no addition, 0.5, 2 times, 5 times, 10 times and 20 times). Then, the reaction solvents (N,N-dimethylformamide, dimethyl sulfoxide and acetonitrile) were examined using optimized copper reagents. **Result:** The radiochemical yield was highest at 65% by using Cu(OTf)$_2$Py$_4$ as a copper reagent. However, in other copper reagents, reaction hardly progressed. Further, Radiochemical yield was approximately 0, 17, 43 and 65 % with no addition, 0.5, 2 and 5 times of precursor amount respectively. By increasing additional amount of Cu(OTf)$_2$Py$_4$ more than 10 times, radiochemical yield was decrease. In the organic solvent used for the reaction, radiochemical yield was over 50% with N,N-dimethylformamide and 12% and less than 1% with dimethyl sulfoxide and acetonitrile. **Conclusion:** In this study, we developed a method to combine ^{18}F into aromatic rings with high radiochemical yield using [18F]HF.

EP-0215

Feasibility of radioiodine labeled gold nanoparticle using AS1411 DNA aptamer for targeting of nucleolin-expressing glioma

M. Kim, K. Kim, S. Woo, T. Lee, K. Lee, J. Kang, Y. Lee; Korea Institute of Radiological and Medical Sciences, Seoul, KOREA, REPUBLIC OF.

Purpose: Nucleolin is highly expressed in various cancer cells. DNA aptamer (AS1411) binds nucleolin in the plasma membrane and has anti-proliferative activity. The purpose of this study was to target nucleolin-expressing glioma tumor using radioiodine labelled nucleolin-targeted AS1411 aptamer conjugated with gold nanoparticle (AnNP) probes. **Subjects & Methods:** Nucleolin-targeted AS1411 aptamer was conjugated with gold nanoparticle (AuNP) probes, and then labeled with radioiodine ($^{124\ or\ 125}$I-AuNP-AS1411). For evaluation of nucleolin-expressing tumor targeting efficiency, human U87MG cells were used for tumor xenografted model. Small-animal positron emission tomography (PET)/computed tomography (CT) imaging was performed at 1, 4 and 19 h after injection. Biodistribution studies performed at 1 and 4 h after injection. Transmission electron microscopy (TEM) analysis was performed at 1 h after injection to observe accumulation of AS1411 aptamer conjugated

with AuNP in tumor tissue. **Results:** ^{125}I was efficiently labeled to AuNP-AS1411 (99.07±0.24%) at 60 min after reaction. Small-animal PET/CT imaging showed that the ^{124}I-AuNP-AS1411 targeted U87MG glioma tumor *in vivo* at 1 h after injection. Biodistribution results showed that 2.96±2.91% of ^{125}I-AuNP-AS1411 uptake in tumor tissue at 1 h after injection. Also, TEM images confirmed that ^{125}I-AuNP-AS1411 accumulated in tumor tissue at 1 h after injection. **Conclusion:** These results show that AS1411 DNA aptamer conjugated, radioiodine-labeled gold nanoparticle probe has potential for specific targeting to nucleolin-expressing tumor.

EP-0216

[18F] FBPA synthesis from pinacol boran precursor and [18F] fluoride ion with copper reagent

Y. Kanai[1], Y. Ohta[2,3], Y. Hattori[2], H. Takenaka[3], K. Uehara[3], S. Naka[1], T. Sakai[4], E. Shimosegawa[1], M. Kirihata[2], J. Hatazawa[1]; [1]Osaka University Graduate School of Medicine, Suita, JAPAN, [2]Research Center of Boron Neutron Capture Therapy, Osaka Prefecture University, Sakai, JAPAN, [3]STELLA PHARMA CORPORATION, Sakai, JAPAN, [4]Hanwa Intelligent Medical Center, Sakai, JAPAN.

Objectives: 2-[18F] Fluoro-4-borono-phenylalanine (FBPA) is a PET tracer for determination of Boron Neutron Capture Therapy (BNCT) application. Nowadays [18F] FBPA is mostly produced from [18F] F$_2$ gas. Final product of [18F] FBPA radioactivity is small in amount, because of nuclear reaction yield is smaller in ^{20}Ne (d, α) ^{18}F nuclear reaction compared to ^{18}O (p, n) ^{18}F. Recently [18F] fluorination of aromatic ring with pinacol boran derivatives and copper reagent was reported. We tried to adopt this method for [18F] FBPA synthesis from [18F] F$^-$ which is produced by ^{18}O (p, n) ^{18}F nuclear reaction. **Methods:** We used pinacol boran precursor and copper reagent was used for [18F] fluorination step. About 100 MBq of [18F] KF in DMF was added to reaction vial containing 5 mg of precursor and copper reagent (0.3~20 molar equivalents for precursor). Reaction solution was heated to 80~160 ^{0}C for 5~20 minutes. After cooling to room temperature, reaction mixture was purified by cartridge column for remove copper reagent. Then 86 mg of bis(pinacolato)diboron, 5.5 mg of bis(dibenzylideneacetone)palladium(0), 6.8 mg of tricyclohexylphosphine and 48 mg of potassium acetate were added to reaction mixture for boration. Reaction temperature and time were 100 ^{0}C and 30 minutes in boration step. After boration, 0.25 ml of hydriodic acid (57 %) was added to reaction mixture and heated to 100 ^{0}C for 10 minutes for hydrolysis of protection group in precursor. Finally, we analyzed reaction mixture by TLC and HPLC and calculate the reaction efficiency from [18F] F$^-$. **Result:** Radiochemical yield in [18F] fluorination step was 70 % with 5 mg of precursor and 5 molar equivalents of copper reagent at 120 ^{0}C and 20 minutes reaction. [18F] FBPA was synthesized via boration step and hydrolysis step. Total radiochemical yield was 10 % from [18F] F$^-$ via three steps. Our method is not needed the purification step in the middle of reaction. **Conclusion:** We succeeded to synthesis [18F] FBPA from [18F] F$^-$ with pinacol boran precursor and copper reagent. Our method is simple and reliable.

EP-0217

Synthesis and *in vitro* evaluation of ^{68}Ga-labeled peptides for metalloproteinase (MT1-MMP/MMP-14) targeting on HT1080 cells

C. Liolios, U. Bauder-Wüst, M. Schäfer, K. Kopka; Department of Radiopharmaceutical Chemistry, German Cancer Research Center (DKFZ), Heidelberg, GERMANY.

Introduction: Controlled cell migration is fundamental in many physiological processes and once it's lost it facilitates disease progression e.g. during tumorigenesis and tumor dissemination. One of the critical proteinases involved in cell migration is membrane-type 1 matrix metalloproteinase (MT1-MMP/MMP-14)[1]. We synthesized two ligands based on a peptide sequence (**MP**) previously identified as a specific binder for MT1-MMP[2]. Two chelator groups were linked with MP via an aminohexanoic acid spacer: the acyclic N,N'-bis[2-hydroxy-5-(carboxyethyl)benzyl] ethylenediamine-N,N'-diacetic acid chelator (HBED-CC), **MP-1H**, and the well-known chelator DOTA, **MP-1D**. The two ligands were labeled with ^{68}Ga and tested in vitro on the HT1080 (human sarcoma cell line). **Methods: MP-1H** and **MP-1D** were accessible via solid-phase peptide chemistry on a Wang (Leu) resin[3]. The peptides were purified with preparative RP-HPLC and their masses were determined with MALDI-MS. Radiolabeling with [Ga-68] Ga^{3+} eluate was accomplished within 10 min and resulted in a single peak. [68]**Ga-MP-1H** and [68]**Ga-MP-1D** (30 nM) were tested *in vitro* (at 37 °C) without further purification for specific binding, and internalization rates on HT1080 cells (10^5 cells/well)[4]. Specific binding was determined by blocking experiments with excess addition of the non-labeled ligand, **MP**, (30 uM). **Results:** In vitro assays for [68]**Ga-MP-1H** and [68]**Ga-MP-1D** on HT1080 cells (after 45 min of incubation time) showed specific binding for both compounds. Results expressed as percentages (± SD) of the total non-blocked cell-related counts showed that after blocking the amount of bound ligand was reduced to nearly half of the initial value i.e. surface bound (at 37 °C), [68]**Ga-MP-1H**: 66.7 ± 0.1, blocked 26.9 ± 0.2 % and [68]**Ga-MP-1D**: 50.65 ± 0.1, blocked 33.4 ± 0.1 % and internalized, 33.2 ± 0.1, blocked 17.9 ± 0.6 %; 49.5 ± 0.1, blocked 35.5 ± 0.1 % respectively. The main fractions of the ligands were surface bound in both cases, while [68]**Ga-MP-1H** showed slightly higher binding. **Conclusion:** Two new tracers, [68]**Ga-MP-1H** and [68]**Ga-MP-1D**, were synthesized, labelled with ^{68}Ga and tested in vitro for MT1-MMP/MMP-14 targeting on HT1080 cells. Preliminary results showed specific binding for both, with the main fractions of the ligands being cell surface bound. [68]**Ga-MP-1H** showed slightly improved binding. Further studies are under way based on the here described lead structures. **References:** [1] Itoh Y, *IUBMB Life,* 2006;58(10): 589-596. [2] Min K, et al. *PLoS One,* 2015;10(10): 1-12. [3] Liolios CC, et al. *Eur.J.Inorg.Chem.* 2012;2012(17): 2877-2888. [4] Eder M, et al. *Eur.J.Nucl.Med.Mol.Imaging* 2008;35(10): 1878-86.

EP-0218

Radiosynthesis of 6-[^{18}F]Fluoro-α-methyl-L-tryptophan - a prospective tracer for in vivo studies of tryptophan metabolism

A. Vazquez-Romero[1], E. Revunov[1], R. Krasikova[1,2], M. M. Moein[1], S. Cervenka[1], S. Erhardt[3], C. Halldin[1], M. Schou[1,4]; [1]Department of Clinical Neuroscience, Center for Psychiatry Research, Karolinska Institutet and Stockholm County Council, Stockholm, SWEDEN, [2]Institute of Human Brain of the Russian Academy of Science, St. Petersburg, RUSSIAN FEDERATION, [3]Department of Physiology and Pharmacology, Karolinska Institutet, Stockholm, SWEDEN, [4]AstraZeneca PET Science Centre, Department of Clinical Neuroscience, Karolinska Institutet, Stockholm, SWEDEN.

Aim: [^{11}C]Alpha-methyl tryptophan (AMT) is an established tool for the study of tryptophan metabolism in human subjects using positron emission tomography (PET) [1, 2]. Despite its documented utility, the cumbersome preparation and the short half-life of ^{11}C has restricted the use of [^{11}C]AMT to only a few PET centers in the world. In an effort to address these shortcomings, we herein report the synthesis and radiolabeling of an analog of AMT that is fluorinated in the 6-position of the aromatic ring. **Materials and Methods:** Copper mediated radiofluorination was performed with minor modifications to previously published procedures [3, 4]. Briefly, a protected (*N*-Boc and *O*-Me) 6-pinacolyl boronic ester precursor was radiofluorinated in a mixture of *N,N*-dimethyl formamide and acetonitrile. Subsequent deprotection was effected by sequential addition of aqueous hydrochloric acid and sodium hydroxide. Crude 6-[^{18}F]Fluoro-α-methyl-L-tryptophan was purified using semi-preparative high performance liquid chromatography and isolated using mixed mode solid phase extraction (Oasis MCX, Waters). Following elution of the product using a solution ammonium hydroxide in methanol, solvents were evaporated and the residue was redissolved in phosphate buffered saline (pH 7.4). **Results:** Under non-optimized conditions, the radiochemical conversion of [^{18}F]fluoride into *N*-Boc-6-[^{18}F]Fluoro-α-methyl-L-tryptophan methyl ester was 41% and the overall radiochemical yield was 2% (not corrected for decay). The final product was obtained in a radiochemical purity exceeding 99%. **Conclusions:** 6-[^{18}F]Fluoro-α-methyl-L-tryptophan was successfully prepared at high radiochemical purity. The in vivo evaluation of this tracer is underway. **References:** [1] P.K. Chakruborty, T.J. Mangner, D.C. Chugani, O. Musik, H.T. Chuguni, NUCLEAR MEDICINE AND BIOLOGY, 1996, 23, 1005-1008. [2] H.T. Chugani, A.F. Luat, A. Kumar, R. Govindan, K. Pawlik, E. Asano, NEUROLOGY, 2013, 81, 674-680. [3] M. Tredwell, S.M. Preshlock, N.J. Taylor, S. Gruber, M. Huiban, J. Passchier, J. Mercier, C. Genicot, V. Gouverneur, ANGEWANDTE CHEMIE-INTERNATIONAL EDITION, 2014, 53, 7751-7755. [4] D. Schafer, P. Weiss, J. Ermert, J.C. Melean, F. Zarrad, B. Neumaier, EUROPEAN JOURNAL OF ORGANIC CHEMISTRY, 2016, 4621-4628.

EP-0219

Radio-synthesis of [^{18}F]NKO028 as a L-type amino acid transporter 1 (LAT 1) PET tracer for cancer diagnosis

S. Naka[1], Y. Kanai[1], T. Watabe[1], S. Nagamori[1], T. Sakai[2], H. Kato[1], K. Isohashi[1], M. Tatsumi[1], E. Shimosegawa[1], Y. Kanai[1], J. Hatazawa[1]; [1]Osaka University Graduate School of Medicine, Suita, Osaka, JAPAN, [2]Hanwa Inteligent Medical Center, Sakai, Osaka, JAPAN.

Object: L-type amino acid transporter 1 (LAT1) is expressed specifically in some tumor cells. Therefore LAT1 is a good target of anti-tumor drug development. NKO 028, LAT1 inhibitor, was developed as an anti-cancer agent in Osaka University. NKO 028 is derivative of aromatic amino acid. NKO 028 has high affinity for LAT1. NKO 028 is good candidate for cancer diagnosis. We tried to establish radiolabeling method of NKO 028 with fluorine-18. **Method:** In radiolabeling of [^{18}F]NKO 028, we investigate concentration of precursor (1, 4, and 10 mg/mL) reaction temperature (60 and 80 °C), reaction time in fluorination step (5 and 7 min) and appropriate base (potassium carbonate, tetrabutyl ammonium hydroxide, cesium carbonate and cesium hydrogen carbonate). Then, hydrolysis condition was investigated concentration of hydrochloric acid (1.0 and 5.0 mol/L) and reaction time of hydrolysis step (5 and 10 min). We confirm the fluorination efficiency and radiochemical purity (and optical purity) with TLC and HPLC method respectively. **Result:** More than 5 mg/ml of precursor concentration, 80 °C of reaction temperature and 5 minutes of reaction time gave high radiochemical yield in [^{18}F] NKO 028 radiolabeling. Acetonitrile was best for reaction solvent, because solubility for NKO 028 precursor is very high. Under the optimized condition, F-18 fluorination efficiency was more than 70 %. Potassium carbonate gave 50 % of [^{18}F] NKO 028 racemate. Tetrabutyl ammonium hydroxide gave high optical purity (> 90 %), but resulted in low radiochemical yield because of low solubility for acetonitrile. In hydrolysis step, 1.0 mol/L hydrochloric acid resulted in 30 % of radiochemical yield. **Conclusion** Under the optimized condition, we succeeded to synthesize [^{18}F]NKO 028 with 30 % of radiochemical yield within 80 minutes from end of bombardment.

EP-0220

Minimising residual activities in daily 18F-FDG administrations. Preliminary results

P. Z. Stavrou, D. Priftakis, K. Kouvelis, M. Papachristou, I. E. Datseris; General Hospital of Athens "Evaggelismos", Athens, GREECE.

Purpose/Introduction: 18F-FDG is a radiotracer, which is frequently used in oncologic field. Due to its short-lived nature, activity management is a daily issue to consider. Procedural guidelines suggest taking note of activities before (administered activity) and after injection (residual activity). Dilution of the administered volume can also be considered to minimize residue, but with caution, to avoid the risk of extravasation. The aim of this study is to calculate the percentage of residual activity during daily administrations of 18F-FDG and to identify an ideal volume of dilution of the injected dose, where that percentage is minimal. **Subjects and Methods:** The administered dose for each patient was prepared by the department's radiopharmacist in M 5cc syringe and diluted to either 1, 2, 3, 4 or 5 ml using 0.9% NaCl solution. The needle of the syringe was replaced prior to the administered activity measurement, to ensure that it is free of FDG. For each patient, a venous access with a three-way valve was obtained. All administrations were performed manually by three nuclear medicine physicians/residents and consecutively post-injection residual activity was measured in the syringe. In some cases, residual activity was also measured in vein cannulas. **Results:** 116 administrations were included in the study. Percentages of residual activity in the syringes ranged from 0.41% to 7.85% (mean: 1.86%). In 34 cases the percentage of residual activity in the vein cannula was also measured and ranged from 0.01% to 3.33% (mean: 0.41%). Mean residual activities for each of the dilution volumes were as follows: for 1ml injections the mean percentage was 2.81%, for 2ml injections it was 1.96%, for 3ml injections it was 1.54%, for 4ml injections it was 1.59% and for 5ml injections it was 1.04%. It is also notable that for dilution volumes 3-5ml, the mean percentage of residual activity in vein cannulas was lower than 0.1%. **Conclusion:** Preliminary results suggest that a 3ml volume of dilution should be ideal to guarantee an acceptable percentage of residual activity with minimal risk for extravasation during the injection. Also, if the venous access needs to be maintained until the completion of the examination, measurements should be accurate without the need to measure the residual activity in the vein cannula for doses with a dilution volume equal or over 3ml.

EP-0221

Ga-68 Labeled Neurotensin Peptide for PET Receptor-targeting Imaging and its first human study

L. Huo[1], G. Hu[1], L. Wang[1], S. Yao[1], Z. Li[2], Z. Wu[2], F. Li[1]; [1]Peking Union Medical College Hospital, Beijing, CHINA, [2]University of North Carolina at Chapel Hill, North Carolina at Chapel Hill, NC, UNITED STATES OF AMERICA.

Purpose: Neurotensin (NT) receptor is over expressed in various tumor entities like pancreatic or colon carcinoma. Therefore, it represents an interesting target for the diagnosis of pancreatic cancer by positron emission tomography (PET). This study aimed to synthesize 68Ga-DOTA-NT, and to assess the feasibility of this receptor-targeting PET imaging tracer for specific diagnosis of pancreatic tumor in human. **Methods:** DOTA-NT was synthesized according to procedure published previously. 68Ga was eluted from a 68Ge/68Ga generator (ITG). The mixture was incubated at 100°C for 10 min, then passed Sep-Pak light C-18 column for purification. 68Ga-DOTA-NT safety evaluation and biodistribution study were performed in 20 mice. Tumor avidities were observed in 4 type (HEPG-2, BXCP-4, Melanoma and PAN-1) xenografts. 5 patients with pancreatic lesions were recruited in this study. Each patient underwent both FDG and 68Ga-DOTA-NT PET/CT within one week. 68Ga-DOTA-NT PET/CT imaging were acquired in 5 and 60min separately after injection. **Results:** 68Ga-DOTA-NT was synthesized in about 70% yield within 20min .The radiochemical purity of final product was over 97%. In animal studies, the kidneys had the highest concentration at 5 min (49.82±14.62 %ID/g) after injection, and declined to a low level at 120 min (19.93±4.04%ID/g).The rest tissues (such as lung, heart, intestine and pancreas) experienced a relatively high uptake at 5 min and reduced gradually over the 120 min experimental assays. The lowest radioactivity uptake was found in brain (0.02±0.01%ID/g). Imaging studies both in mice and in human further confirmed this biodistribution results. Tumors in 4 type xenografts showed moderate to high uptake of 68Ga-

DOTA-NT, and the target/muscle (T/M) ratio elevated with time passing on. T/M fluctuated from 2.3(Melanoma) to 4.2 (PANC-1) on the basis of various NT receptor expression. In the patients study, no adverse effects were observed for 24 h post tracer injection. The lesions of 3 patients with pathological pancreatic adenocarcinoma and 1 patient with IPMN(moderate atypical hyperplasia proved by surgical pathology) were positive in FDG PET/CT (SUVmax 3.3-5.4), but all were negative in 68Ga-DOTA-NT PET/CT imaging. The lesion of 1 patient with chronic pancreatitis (follow-up more than 6 month) was negative in both PET/CT studies. **Conclusion:** Although animal studies prove that 68Ga-DOTA-NT is a promising tracer to pancreatic tumor detection, the evidence achieved from our pilot first-in-human study shows its limited value in the diagnosis of pancreatic adenocarcinoma and moderate atypical hyperplasia IPMN. Further clinical studies in other malignant tumors are warrented.

EP-0222
Four Runs of [18F]FDG on a Single Cassette

C. Warnier, *C. Vriamont, T. Vergote, J. Masset, M. Otabashi, C. Desfours, J. Morelle, G. Philippart; Trasis, Ans, BELGIUM.*

Introduction: [18F]FDG (2-Deoxy-2-[18F]Fluoro-D-glucose remains by far the most widely used Positron Emission Tomography (PET) tracer worldwide, due to its versatility as a radiotracer for the diagnosis and staging of various cancers or inflammation zones. With thousands of doses produced every day around the globe, cost management, production rationalization and synthesis efficiency are of central concern for all producers.[1,2] We herein describe a method for the production of four batches of [18F]FDG on one single cassette and one reagent kit, in compliance with cGMPs and Pharmacopoeias (Europe and US). **Methods:** The FDG 4-run production method was implemented on the AllinOne synthesizer unit from Trasis. The cassette uses 21 three-way valves built in 4 manifolds and several commercial components such as SEP cartridges, tubes and filters. The method was fully automated to perform 4 identical FDG runs, using the well-known solid phase supported alkaline hydrolysis method.[3,4] **Results:** The fully-automated 4-run production delivered 74±3% of [18F]FDG in 21 minutes (n=36, consecutive, non-decay-corrected, tested on multiple machines and sites and up to 310 GBq of incoming activity). In order to remain compliant with the cGMP's and efficient in terms of synthesis yields, a comprehensive rinsing of the reactor, manifolds, syringes, and cartridges between the runs was included in the process. The optimized automated sequence and cassette rinsing processes were such that no yield drop could be observed between the 1st and 4th run while all Quality Controls on the FDG from all the runs showed similar and compliant results. Ongoing microbiological validations will define the extent of usage time between the placement of the consumables on the machine and the start of the 4th run, currently estimated to be 7 days. **Conclusion:** This new automated multi-run production method of [18F]FDG allows optimal production yields (74±3% n.d.c.), while minimizing production costs, manual operations and radiation exposure of the operator. **References:** [1] Burns, M. *Market for*

PET Radiopharmaceuticals and PET imaging (Abstract); Marina Del Rey, CA, 2014; [2] Knuuti, J. et al., *Heart* **2008**, 94(3), 360-367; [3] Füchtner, F. et al., *Appl. Radiat. Isot.* **1996**, *47* (1), 61-66 ; [4] Lemaire, C. et al., *J. Label. Compd. Radiopharm.* **2002**, *45* (5), 435-447.

EP-0223
Development of novel lipophilic [18F]thiosemicarbazone gallium fluoride complexes

D. H. R. Stimson[1], T. K. Venkatachalam[1], G. K. Pierens[1], P. V. Bernhardt[2], K. Mardon[1], D. C. Reutens[1], R. Bhalla[1]; [1]University of Queensland, Centre for Advanced Imaging, St Lucia, QLD, AUSTRALIA, [2]University of Queensland, School of Chemistry and Molecular Biosciences, St Lucia, QLD, AUSTRALIA.

Purpose/Introduction: Fluorine-18 labelling strategies involving the formation of stable metal-fluorine bonds have been reported previously.[1,2] However, these metal-[18F]fluorine complexes are hydrophilic and there is a need to develop more lipophilic metal-fluoride moieties which can be incorporated into new radiopharmaceuticals for potential applications in brain imaging. **Materials and Methods:** A series of substituted thiosemicarbazone gallium chloride complexes have been synthesised. We have investigated the exchange of the chloride with a variety of ligands and have been able to synthesise the methoxide and nitrate analogues. Complexes of diphenylthiosemicarbazone gallium fluoride were prepared by reacting the nitrate derivative with fluoride.[3] Imaging studies of [18F]diphenylthiosemicarbazone gallium fluoride in mice have been performed. **Results and Conclusion:** Attempts to form diphenylthiosemicarbazone gallium fluoride from the corresponding chloride by direct exchange were unsuccessful. However, the desired diphenylthiosemicarbazone gallium fluoride complex was successfully obtained first by reaction of the chloride precursor with silver nitrate followed by fluoride (both 19F and 18F). The resultant fluoride complex is neutral and has a measured logP of 1. Preliminary PET studies of mice show rapid uptake of the complex in the brain with an injected dose per gram of around 2 to 3%. These initial studies highlight the potential of the [18F]thiosemicarbazone gallium fluoride into new radiopharmaceuticals for applications in neuroimaging using PET. **References** 1. McBride WF et al. EJNMMI Research 2013; 3:36. 2. Bhalla R et al. Chem Sci, 2014; 5: 381. 3. Venkatachalam TK et al. Aust J Chem. 2016; 69:9.

EP-0224
Optimization of C-11 labeled methyl iodide production

E. V. Nemeth[1], D. Szikra[1], I. Jószai[1], V. Forgács[1], P. Mikecz[1], P. Larsen[2]; [1]University of Debrecen, Faculty of Medicine, Debrecen, HUNGARY, [2]Scansys Laboratorieteknik ApS, Copenhagen, DENMARK.

INTRODUCTION: 11C labelled tracer synthesis in most cases the labeling procedure is methylation with [11C]methyl-iodide reagent. We applied the Tracer Maker synthesis panel developed by Peter Larsen to produce [11C]MeI and [11C]Me-Triflate in

order to synthesize [11C] isotope labeled radiotracers. METH-ODS: We produced [11C]MeI by the gas phase method using the Tracer Maker synthetizer. [11C]CO2 generated in the target was reacted with H2 at 360 °C in the presence of Ni catalyst. The resulting [11C]CH4 was separated from the waste gases by freezing at 190 °C on Hayesep adsorbent. Upon heating the Hayesep the [11C]CH4 was released at 10 °C and directed to the recirculating circuit containing an iodine column where methane reacted with the sublimated iodine vapours at 720 °C. The formed [11C]MeI was adsorbed on Hayesep again, and released by heating to 200 °C. The operational parameters of the module were systematically varied in order to find those, which are influencing the yield. The pressure drop in the system was minimized using a multi stage leak check program. We determined the decay corrected radioactivity produced in the cyclotron with 44 µA beam current and 2 minute irradiation time. The activity of the produced [11C]MeI with the same parameters was compared to this value. We varied the time of the regeneration of the adsorbents, the flow rate of the target gas, the temperature of the iodine and the high temperature furnace and the flow rate of the recirculation circuit. in order to study the dependence of the yield on these parameters. RESULTS: The activity of the [11C]CO2 produced by the cyclotron was 12 GBq in our measurements. The initial yields of the system with default settings were 36 ± 3%. With the increase of temperature of the iodine oven only 2 % increase was achieved. We observed no change in yield by increasing the flow rate of the recirculation circuit and the temperature of the high temp. oven. Optimization of the target gas flow, increase of the regeneration time, achieving appropriate starting temperature and minimizing pressure drops of each stages of the process resulted in a 52 ± 2% [11C]MeI yield. The radiochemical purity was more than 98%. CONCLUSION: Based on our measurements, the critical part of the synthesis process was found to be the adsorption of the [11C]CO2 on the molecular sieve. The other parameters showed only minor effect on the yield.

EP-0225

In-vitro and in-vivo evaluation of 2 enantiomers of Nanocyclix(R) EGFR targeted PET radiotracer

C. BERTHET[1,2], *O. RAGUIN*[1,2], *C. MOTHES*[3,2], *P. PROVENT*[1,2], *G. SERIN*[1,2], *X. TIZON*[1], *A. OUDOT*[4,2], *P. WALKER*[5], *J. HOFLACK*[1,2], *G. VIOT*[3,2]; [1]ONCODESIGN, DIJON CEDEX, FRANCE, [2]Pharmimage, Dijon, FRANCE, [3]Cyclopharma, SAINT-BEAUZIRE, FRANCE, [4]Centre Georges François Leclerc, DIJON, FRANCE, [5]CHU François Mitterand, DIJON, FRANCE.

Aim: IMA*kinib*® program is an innovative approach to develop new PET radiotracers, based on Nanocyclix® chemistry technology. We developed ODS2004436, a novel radiotracer to target the epidermal growth factor receptor (EGFR) and its mutated forms. One of the mutation, T790M, is involved in resistance to first-line treatment in advanced non-small cell lung cancer (NSCLC). ODS2004436 could be a valuable tool to stratify patients for EGFR activity and responsiveness to EGFR-targeted therapies. Clinical evaluation of this radiotracer is ongoing (first in-man phase 0/I clinical trial NCT02847377). **Material and Methods:** Two enantiomers of ODS2004436 were characterized regarding their binding capabilities for EGFR (wild-type *versus* mutated). Biochemical EGFR activity, kinome selectivity, cellular activity in NSCLC cell lines, efficiency in radiochemistry, in-vivo biodistribution were performed to select the best enantiomer able to selectively bind to double mutant L858R/T790M EGFR. Our study was conducted on the *Pharmimage* radiochemistry and imaging platforms using a new PET/MRI prototype. **Results:** Both enantiomers displayed a similar biochemical profile on EGFR wild-type and eight mutated/deleted isoforms (*i.e.* L858R). Interestingly the (R)-enantiomer showed an improved activity on EGFR L858R/T790M (IC_{50}: 55 nM (R) *vs* 1011 nM (S)). Selectivity score S(50%) on a panel of 320 wild-type kinases was better for (S) *versus* (R) enantiomer (respectively 0.6% and 2.5%, 100 nM). In NSCLC cell lines, (R) enantiomer was the most active as it appeared slightly more potent than the (S) enantiomer. Both enantiomers showed a marked cytotoxic activity in NCI-H3255 cells (L858R; $IC_{50} \approx 10\text{-}50$ nM), a weak activity in NCI-H1975 cells (L858R/T790M; IC50≈10-20µM), and no cytotoxicity in NCI-H441 cells (wild-type; IC50>25µM). F-18 radiolabeling of both enantiomers achieved a similar specific activity. Their biodistribution in healthy Sprague-Dawley rats was evaluated using PET imaging and *ex vivo* γ-counting showing a similar distribution pattern for both compounds without any preferential organ accumulation. They were rapidly cleared from blood and mainly eliminated through kidneys and liver. Based on these results, the (R)-enantiomer was selected to study the differential tumor uptake in rats and compare *in vivo* binding to various forms of EGFR. **Conclusion:** *In vitro* and *in vivo* characterization of ODS2004436 as a radiotracer targeting EGFR led to the selection of the (R)-enantiomer, with improved binding to EGFR double mutant L858R/T790M. This radiotracer is a promising tool to assess sensitivity or resistance of patients with tumors acquiring EGFR mutation upon first-line EGFR-targeted therapies.

EP-0226

Radiosynthesis of 3/5-[¹⁸F]-fluoropyridines by TEMPO-mediated radiofluorination of pyridinyl iodonium salts

M. Pauton[1], *C. Aubert*[2], *G. Bluet*[2], *F. Gruss-Leleu*[2], *S. Roy*[2], *C. Perrio*[1]; [1]Normandie Univ, UNICAEN, CEA, CNRS, ISTCT-FRE2001, LDM-TEP, Cyceron, CAEN, FRANCE, [2]SANOFI R&D, Vitry sur Seine, FRANCE.

Aim: The pyridine moiety is encountered in numerous drugs, and some PET radiotracers contain a [¹⁸F]-fluoropyridine framework.[1] Although advantageous for stability, introduction of [¹⁸F]-fluorine atom at positions 3 or 5 remains challenging. Radiofluorination of pyridinyl iodonium salts using microfluidics was found to be efficient but no scope was reported so far.[2] The radical scavenger TEMPO is known to be a very efficient agent for the enhancement of diaryliodonium [¹⁸F]-radiolabellings.[3,4] Herein, we report the TEMPO-mediated radiofluoration of pyridinyl iodonium salts as a general method for the preparation of functionalized 3/5-[¹⁸F]-fluoropyridines. **Methods:** We prepared a series of pyridinyl iodonium salts (tetrafluoroborates, tosylates or triflates) from the corresponding iodopyridines and

either anisole, mesitylene or thiophene. Radiofluorination reactions were conducted manually or using automated systems with [18F]FK-K2.2.2 complex in different solvents (ACN, DMF or DMSO) for 10 to 60 min, at temperature between 85 and 150°C, in the presence of TEMPO (0- 5 equiv) and K_2CO_3 (0- 4 equiv). [18F]-Fluoropyridines were identified by coelution with reference compounds on analytical HPLC. RCYs were determined after purification on semi-preparative HPLC. **Results:** The efficacy of the radiofluorination reaction was strongly dependent on the starting iodonium salts and the amounts of TEMPO and K_2CO_3. The optimal RCYs (24-83%) were obtained by treatment of pyridinyl iodonium triflates containing an anisole group in the presence of TEMPO (1 equivalent) and K_2CO_3 (2 equivalents) in DMF at 130°C for 30 min or in DMSO at 100-130°C for 15-30 min. Radiofluorination reactions were compatible with various substituents on the pyridine ring (chloride, alkyl, alkoxy, cyano or amide groups). **Conclusion:** The TEMPO-mediated radiofluorination of pyridinyl iodoniums has been proved to be useful for the synthesis of 3/5-[18F]-fluoropyridines. Application to the development of new radiotracers is underway. **Acknowledgements:** We thank the ANRT (Association Nationale de la Recherche et des Technologies), CIFRE grant 2015/0665. **References:** [1] Preshlock S, Tredwell M, Gouverneur V, *Chem. Rev.* **2016**, *116*, 719-766. [2] Chun JH, Pike VW, *Chem. Commun.* **2012**, *48*, 9921-9923. [3] Carroll MA, Woodcraft J, WO2007141529 A1 [4] Warnier C, Lemaire C, Becker G, *et al.*, *J. Med. Chem.* **2016**, *59*, 8955-8966.

EP-0227

Uptake of the MCHR1 PET-tracers [18F]FE@SNAP and [11C]SNAP-7941 in BAT: an adrenergic beta-3 receptor mediated effect?

T. Balber[1,2], K. Benĉurová[1], M. Mitterhauser[1,3], W. Wadsak[1,4], H. Viernstein[2], M. Hacker[1], C. Philippe[1,2]; [1]Biomedical Imaging and Image-Guided Therapy, Division of Nuclear Medicine, Medical University of Vienna, Vienna, AUSTRIA, [2]Department of Pharmaceutical Technology and Biopharmaceutics, Faculty of Life Sciences, University of Vienna, Vienna, AUSTRIA, [3]Ludwig Boltzmann Institute Applied Diagnostics, Vienna, AUSTRIA, [4]CBmed GmbH, Center for Biomarker Research in Medicine, Graz, AUSTRIA.

Background: Recent µPET studies showed uptake of the melanin-concentrating hormone receptor 1 (MCHR1) ligands [18F]FE@SNAP and [11C]SNAP-7941 in brown adipose tissue (BAT) of naïve rats. Moreover, administration of SNAP-7941 (15mg/kg BW) led to increased [18F]FDG accumulation in rat BAT suggesting a BAT activation by SNAP-7941. Interestingly, expression of MCHR1 in BAT has not been described so far. Since the adrenergic beta-3 receptor (ADRB3) is mainly expressed in the BAT and involved in the regulation of lipolysis and thermogenesis [1], the aim of the present study was to identify if the two MCHR1 ligands (FE@SNAP and SNAP-7941) show binding affinity to the ADRB3. **Materials & Methods:** To explore binding affinity of FE@SNAP and SNAP-7941 to ADRB3, conventional competition experiments (filtration method, Brandel® Cell Harvester) using [3H](−)-CGP12177 and ADRB3 expressing membranes were performed. Additionally, a real-time kinetic assay (LigandTrac-

er®, Ridgeview Instruments AB) using ADRB3 transfected CHO-K1 cells and [125I]Cyanopindolol as radioligand was established. **Results:** K_i values for known ADRB3 ligands were reproduced using the conventional competition assay: Carazolol K_i=2.33±0.7nM (n=3) compared to the published K_i of 2.0nM [2], Pindolol 44.5±24nM (n=3) compared to the K_i of 44.1nM, which was obtained from the literature [3]. FE@SNAP and SNAP-7941 applied in nM-concentrations, were not able to displace [3H](−)-CGP12177 binding. Estimated K_i values are > 10µM (n=2). In competition assays, performed in real-time, concentrations above 50µM (n=2) led to displacement of [125I]Cyanopindolol. **Conclusion:** The obtained affinity values in µM-range do not explain the observed effects of the PET-tracers [18F]FE@SNAP and [11C]SNAP-7941 as they are applied in pM-concentration. Nevertheless, pharmacological concentrations of the respective cold compounds, as they were used in µPET blocking experiments, may exert effects in BAT via ADRB3. The upcoming real-time experiments of [18F]FE@SNAP and [11C]SNAP-7941 on CHO-K1-ADRB3 and BAT-cells will elucidate the observed BAT uptake of the two MCHR1 PET-tracers. **References:** 1. D'Allaire F et al. Characterization of β1-and β3-adrenoceptors in intact brown adipocytes of the rat. British journal of pharmacology. 1995;114(2):275-82. 2. Méjean A et al. Carazolol: a potent, selective β3-adrenoceptor agonist. European Journal of Pharmacology: Molecular Pharmacology. 1995;291(3):359-66. 3. Hoffmann C et al. Comparative pharmacology of human β-adrenergic receptor subtypes—characterization of stably transfected receptors in CHO cells. Naunyn-Schmiedeberg's archives of pharmacology. 2004;369(2):151-9.

EP-0228

Alcohol-supported Cu mediated 18F-flluorination of iodonium salts under "minimalist" conditions

V. V. Orlovskaya[1], O. F. Kuznetsova[1], D. Modemann[2], O. S. Fedorova[1], B. D. Zlatopolskiy[2,3,4], E. A. Urusova[2,3], B. Neumaier[2,3,4], R. N. Krasikova[1]; [1]N.P.Bechtereva Institute of the Human Brain RAS, Saint-Petersburg, RUSSIAN FEDERATION, [2]Institute of Neuroscience and Medicine, INM-5: Nuclear Chemistry, Forschungszentrum, Julich, GERMANY, [3]Institute of Radiochemistry and Experimental Molecular Imaging University Clinic, Cologne, GERMANY, [4]Max Planck Institute for Metabolism Research, Cologne, GERMANY.

Aim: Recently published Cu-mediated radiofluorination of (aryl)(mesityl) iodonium salts (AMI) enables the preparation of radiolabeled (hetero)arenes including electron rich ones from nucleophilic 18F-. Especially, the application of the "minimalist" approach to this protocol enables high-yielding preparation of 18F-fluorinated (hetero)aromatics on a preparative scale using only Cu-catalyst, iodonium salt and 18F- regardless the substrates electronic properties. The "minimalist" approach circumvents azeotropic drying and the application of base and any other additives. However, the solvent evaporation step remains necessary. The aim of this work was further refinement of Cu-mediated radiofluorination under "minimalist" conditions, which allows omit any evaporation steps. **Materials and Methods:** [18F]fluoride was eluted from QMA cartridge with a solution of

the appropriate iodonium salt precursor (22 μmole) in ROH/DMF mixture. The eluate was directly collected in a vial preloaded with a solution DMF (0.6 mL) of Cu(CH$_3$CN)$_4$OTf (22 μmole). The mixture was heated at 85°C for 20 min, diluted with water, and radiochemical conversions (RCCs) were determined using radioTLC and/or HPLC. Deprotection of the respective intermediate (10 M HCl, 110 °C, 10 min) afforded 2- and 4-[18F]FPhe which were isolated by HPLC. **Results:** Over 90% recovery of 18F- from the anion exchange resin was achieved using solutions of AMI precursors in 20% MeOH/DMF. 4-[18F]Fluoroanisole, [18F]fluorobenzene and 3-[18F]fluorobenzaldehyde were prepared in RCCs of 81-95%. Protected 2- and 4-[18F]FPhe were furnished in 27 and 81% RCC, respectively. The desired radiolabeled amino acids were isolated in 22 and 69% RCY (EOB) in excellent radiochemical (over 98%) and enantiomeric purities (ee over 96%) within 60 min. **Conclusions:** We demonstrated for the first time that alcohols are suitable co-solvents for Cu-mediated 18F-fluorination of iodonium salts. The radiofluorination protocol based on this finding enables the simple, fast and efficient preparation of labeled (hetero)arenes and should be well-suited for the translation to an automated synthesis module. Its practicality was confirmed by the production of clinical doses of two PET tracers, 2- and 4-[18F]Phe, in reasonable yields. This work was supported by Russian Foundation of Basic Researches, grant 16-54-12062/16 and DFG grant ZL 65/1-1.

EP-0229

Microdose Study for Amino Acid Imaging Using D-[18F]FMT PET in Human Brains

K. Lee[1], B. Byun[2], B. Kim[2], I. Lim[2], C. Choi[2], S. Youn[3], C. Rhee[3], S. Chu[4], C. Park[4], H. Kil[4], B. Lee[4], D. Chi[4,5], S. Lim[2]; [1]KIRAMS, Division of RI-Convergence Research, Seoul, KOREA, REPUBLIC OF, [2]KIRAMS, Department of Nuclear Medicine, Seoul, KOREA, REPUBLIC OF, [3]KIRAMS, Department of Neurosurgery, Seoul, KOREA, REPUBLIC OF, [4]FutureChem Co. Ltd., Seoul, KOREA, REPUBLIC OF, [5]Sogang University, Department of Chemistry, Seoul, KOREA, REPUBLIC OF.

Objectives: The aim of the present phase 0 study was to obtain information about distribution, toxicity, pharmacokinetics, and optimal scan time of *O*-([18F]fluoromethyl)-D-tyrosine (D-[18F]FMT) [1][2]. **Methods:** Six control subjects (median age = 23.0 y) and 3 patients (median age = 55.0 y) with primary or metastatic brain tumor were enrolled (M: F = 4: 5). We acquired 5 times of whole-body PET images during 4 hours (4 control subjects) after injection of 370 MBq of D-[18F]FMT or a 60 min dynamic brain PET image (2 control subjects and 3 patients). The distribution of D-[18F]FMT in each organ was assessed on whole-body PET dataset and the standardized uptake value (SUV) of brain tumor was measured on each dynamic brain PET dataset and. All adverse effects during the clinical trial periods were collected. **Results:** D-[18F]FMT was synthesized by the nucleophilic [18F]fluorination of triazolium salt leaving group-tethered precursor [3] and the subsequent deprotection under acid condition in 40% radiochemical yield (non-decay corrected). After injection, the highest uptake of D-[18F]FMT was observed in the kidney and urinary bladder. The brain showed little uptake and the liv-

er showed mild uptake, which decreased over time. In patients with a meningioma (n = 1) metastatic brain tumor from rectal cancer (n = 1), the maximum SUV of brain tumor was 3.5 and 2.0, respectively. In these patients, the SUV of brain tumor reached a peak before 15 min after injection of D-[18F]FMT then continuously decreased over 60 min. In a patient with glioblastoma multiforme (highly malignant primary brain tumor), however, the SUV of brain tumor continuously increased during the first 25 min after injection of D-[18F]FMT and showed little change over 60 min. The maximum SUV of brain tumor was 2.5 in this patient. No adverse event was observed. **Conclusion:** D-[18F]FMT is safe and its kinetic behavior is suitable for amino acid imaging in the brain. Further clinical investigations are needed to determine the optimal scan time according to the type of brain tumor. **Aknowledgements:** This work was supported by the National Research Foundation of Korea (NRF) grand funded by the Korean government (MSIP: Ministry of Science, ICT and Future Planning) (2014M2A2A7066472, 2014M2A2A7066474) **References** [1] Tsukada, H. et al., *J. Nucl. Med.* **2006**, *47*, 679-688. [2] Burger, I. A. et al., *J Nucl. Med.* **2014**, *56*, 1778-1785. [3] Park, C. et al., *Org. Lett.* **2013**, *15*, 4346-4349.

EP-0230

Implementing [18F]FB-IL2 synthesis in GMP

J. G. Hessels-Scheper, P. Maarsingh, E. L. van der Veen, I. F. Antunes, R. Zijlma, H. H. Boersma, G. Luurtsema, P. H. Elsinga, E. F. J. de Vries; UMC Groningen, Groningen, NETHERLANDS.

Aim: [18F]FB-IL2 is a radiopharmaceutical that was successfully used for detecting activated T-cells in rodents. For application of this PET tracer in clinical trials, a GMP-compliant production method was set up. Here, we describe the challenges encountered in the implementation and validation of the GMP-compliant production of [18F]FB-IL2. **Methods:** [18F]SFB was used as a reagent for the labeling (50°C, 10 min) of human recombinant IL2 (Proleukin®) in the presence of borate buffer pH 8.3. For GMP-compliant production of [18F]FB-IL2 for human use, several modifications had to be made to the previously described procedure [1]. **Results:** Conversion of the partly manual labelling procedure for preclinical studies [1] into an automated GMP-compliant method proved challenging. First, Proleukin was found to degrade in the warm hotcell during the long synthesis procedure. Second, an impurity in [18F]SFB interfered with the conjugation of IL2 and consequently the SepPak purification method had to be replaced by HPLC purification followed by a formulation step. Third, after modification of the [18F]SFB purification, our GMP-compliant synthesis modules had insufficient functionalities to accommodate the whole 4-step labelling procedure. Therefore, [18F]SFB was produced in a non-classified hotcell and transferred to the GMP cleanroom facility as a reagent and conjugated to Proleukin using a synthesis module with disposable cassettes. Forth, recovery of [18F]FB-IL2 from the HPLC column and sterilization filter was poor, due to its high lipophilicity and tendency to aggregate. Purification of the product by solid-phase extraction over a tC2 cartridge could overcome this problem. Retention of [18F]FB-IL2 on the GV ster-

ilization filter could not be prevented by saturation with HSA, but was reduced to approximately 25% by using 13-mm diameter filters, irrespective whether the filter was saturated with HSA. Fifth, an excipient in the final formulation of the product occasionally precipitated (9% ethanol, 4.5% glucose, 0,5% HSA, 0.09% SDS and 0.02% phosphoric acid). Precipitation of the excipient proved pH-dependent and could be avoided at pH 5-6. After these modifications, [18F]FB-IL2 could reliably be produced in an average radiochemical yield of 4.0±1.6%, radiochemical purity of 98±1% and specific activity of 157±35 GBq/µmol. **Conclusion:** The transformation of a manual non-GMP production of [18F]-IL2 into an automated GMP production proved challenging. However, we have now established a stable and reproducible GMP-compliant production of [18F]-IL2 for human use, although radiochemical yield remains low. **References:** [1] Di Gialleonardo et al., *J. Nuc. Med.*, **2012**, 53(5):679-86

EP-0231

Preparation of [18F]fluoroalkenyliodonium salts and their application for radiolabeling by Sonogashira coupling reactions

S. Humpert[1], B. Zlatopolskiy[2,3], M. Holschbach[1], B. Neumaier[1,2,3]; [1]Forschungszentrum Jülich GmbH, Institute of Neuroscience and Medicine, INM-5: Nuclear Chemistry, Jülich, GERMANY, [2]Institute of Radiochemistry and Experimental Molecular Imaging, University Clinic Cologne, Köln, GERMANY, [3]Max Planck Institute for Metabolism Research, Cologne, Köln, GERMANY.

Aim: Fluoroalkenyliodonium salts can be obtained by nucleophilic addition of fluoride to the triple bond of alkynyliodonium salts. They are valuable building blocks in palladium catalysed cross coupling reactions like Stille-, Heck- or Sonogashira couplings [1]. The aim of this work was the preparation of 18F-labeled fluoroalkenyliodonium salts. The feasibility of this prosthetic group for indirect radiolabeling by Sonogashira cross coupling reactions should also be evaluated. **Methods:** Alkynyl(aryl)iodonium salts were radiolabeled with [18F]fluoride in aqueous organic media in the presence of different bases and K[2.2.2]. The reaction parameters were optimized with respect to temperature, time, solvent and the amount of different bases and precursor. The effect of different substituents at the triple bond (R_1), counter ions (X^-) and aryl moieties (Ar) on the radiochemical conversions (RCCs*) was studied. One pot Sonogashira cross coupling of (*Z*)-2-[18F]fluorohexen-1-yl(phenyl)iodonium tosylate to several model compounds (hex-1-yne, N_ε-propargyloxycarbonyl- and N_ε-propioloyllysine derivatives) was evaluated. **Results:** The nucleophilic addition of [18F]fluoride to the triple bond furnished [18F]fluorohexenyl(phenyl)iodonium salts in RCCs of up to 60 % using K[2.2.2]/$KHCO_3$ in DMSO/water (2:1) at 75 °C within 10 min. Remarkably, the reaction afforded highest RCCs in aqueous media without time consuming azeotropic drying. Radiolabeling of phenylethynyl-derived iodonium salts generally resulted in lower RCCs of 20-30%. Different counter ions (OTs^-, OMs^-, BF_4^-) did not have a significant influence on RCCs. In the case of BF_4^- the molar activity of the resulting labeled iodonium salts decreased significantly (OTs^-: 30 GBq/mmol vs. BF_4^-:1.5 GBq/µmol, 100MBq isolated yield). The one pot Sonogashira reaction

at room temperature furnished the respective radiofluorinated compounds in RCCs of up to 88% within 10 min. The total synthesis time including HPLC purification amounted to 34 min. **Conclusion:** [18F]Fluorohexen-1-yl(phenyl)iodonium tosylate is a valuable and easily accessible prosthetic group for indirect radiolabeling of biomolecules using Sonogashira cross coupling. The application of this method for the labeling of the prostate specific membrane antigen (PSMA) targeting Glu-Urea-Lys motiv is in progress. *RCCs based on HPLC results Literature: [1] M. Yoshida, Tetrahedron, 2006, 62, 8636-8645

EP-0232

Highly Improved and GMP compliant synthesis of [11C]UCB-J: in situ generation of boronic acid precursor

M. Onega[1], H. Chong[1], A. Roble[1], C. Plisson[1], M. Huiban[1], J. Mercier[2], M. Vandergeten[2], J. Passchier[1]; [1]Imanova Limited, London, UNITED KINGDOM, [2]UCB Biopharma, Braine l'Alleud, BELGIUM.

Introduction: The synaptic vesicle glycoprotein 2A (SV2A) is a transmembrane protein expressed in secretory vesicles nearly ubiquitous in the CNS, as well as in endocrine cells. It is critical for synaptic function and it serves as a specific binding site for certain antiepileptics.[1] Recently, [11C]UCB-J was presented as an excellent PET ligand for the delineation of SV2A and as a marker for synaptic density in the central nervous system *in vivo*.[2,3] While the ligand is very promising, the current chemistry leaves room for improvement. Initially, it was believed that the trifluoroborate precursor was the reactive species in the Suzuki-Miyaura cross coupling. Since then, it was confirmed that the corresponding boronic acid actually engages in the reaction. However, this compound is not stable and degrades quickly over time. To address this, a mixture of the trifluoroborate and the boronic acid (3-10%) is used. This approach is not compatible with GMP preparation of precursor material and leads to variable yields due to inevitable degradation of the boronic acid over time. Here we present an approach to generate the boronic acid in situ and highlight the improvement in process yield and stability. **Materials and Methods:** UCB-J reference material and chiral trifluorophenylpyrrolidinone precursor were provided by UCB Biopharma, Belgium. GMP grade 3-pyridyl trifluoroborate was supplied by ABX, Germany. An automated procedure was developed in-house using an Eckert and Ziegler Modular-Lab system coupled with a semi-preparative HPLC system. Quality control methods for clinical batches of [11C]UCB-J were developed in accordance with Eudralex, EP and ICH requirements.[4] **Results and Conclusion:** Initial tests confirmed the feasibility of hydrolysing the trifluoroborate precursor to successfully carry out the cross coupling reaction with [11C]CH_3I. This approach was fully automated and resulted in reproducible high yields (2.4±0.3 GBq, n=6). This approach provides an excellent method to support clinical and preclinical evaluation of [11C]UCBJ. This tracer has now been validated at Imanova in compliance with GMP requirements and is undergoing clinical evaluation as part of the highly innovative MIND-MAPS programme. Generation of the reactive boronic acid species immediately prior to or as part of the automated process for the synthesis of [11C]UCB-J pro-

vides greatly improved reaction yields and process stability. **References** 1] Löscher W *et al.* CNS Drugs. 2016 Nov;30(11):1055-1077. 2] Nabulsi NB *et al.* J Nucl Med. 2016 May;57(5):777-84 3] Finnema SJ *et al.* Sci Transl Med. 2016 Jul 20;8(348):348ra96. 4] https://ec.europa.eu/health/documents/eudralex/vol-4_en

EP-0234

Optimization of a Novel Automated Loop Method for Production and Development of an Analytical HPLC Method for 11C-PK11195

K. Kumar, A. Ghosh, K. Woolum, M. V. Knopp; The Ohio State University, Columbus, OH, UNITED STATES OF AMERICA.

Objectives: The objective of the present study was to develop and optimize a novel automated loop method for production of ^{11}C-PK11195 and development of an analytical HPLC method for its quality control. **Methods:** In the automated production process the [11]CO_2 was trapped at -180°C, converted into ^{11}C-Methane and then ^{11}C-Methyl Iodide. The [11]CH_3I was reacted with Desmethyl PK11195 in the loop (~1 mg Desmethyl PK11195, dissolved in 100 μl anhydrous DMSO saturated with 30 mg KOH) at a desired temperature and time. The reaction mixture was purified by using a semi-preparative Reversed-Phase (RP) HPLC method (involving a 150x10 mm, 5 μm XTerra column, a 40:60 mixture of 0.1 M ammonium formate and acetonitrile as a mobile phase, flow rate 5.5 mL/min) to remove unreacted [11]CH_3I and Desmethyl PK11195 and by a SepK cartridge to remove salts and acetonitrile. The final product, ^{11}C-PK11195, was analyzed using a model 1100 Agilent HPLC system involving a quaternary pump, degasser, a temperature controlled column compartment, an auto-injector and multi-wavelength diode-array UV (254 nm) and radioisotope detectors. A 150x4.6 mm, 5 μm XTerra column at 30°C was used with 40:60 mixture of 0.1 M ammonium formate and acetonitrile as a mobile phase at a flow rate of 1.0 mL/min. **Results:** A gas-phase produced [11]CH_3I precursor was used instead of ^{11}C-Formaldehyde or [11]CH_3I produced by the Lithium Aluminum/HI method. The reaction conditions were optimized by varying the loop temperature and reaction times. These experiments suggested that the reaction of 1 mg precursor with [11]CH_3I for 5 minutes at 80°C loop temperature gave ~25-30% (corrected) and ~10% (uncorrected) yield of the final product. An efficient reversed-phase semi preparative HPLC method, with 8 minutes purification time, was developed for selectively removing [11]CH_3I and the starting material, Desmethyl PK11195, and collecting the pure product, ^{11}C-PK11195, in PBS buffer(pH 7) with ~20% ethanol. In the analytical HPLC method, the retention times were 2.4, 2.9, 3.7 minutes, for [11]CH_3I, ^{11}C-PK11195, and desmethyl ^{11}C-PK11195, respectively. **Conclusions:** A robust and efficient process for production of high purity (>99.9%) ^{11}C-PK11195 with ~25-30% (corrected) yield was developed. An analytical HPLC method for the quality control of the final product was developed.

EP-0235

O-TRENSOX, a new chelating agent for ^{68}Ga radiopharmaceutical

J. Leenhardt[1,2], M. Desruet[1,2], L. Djaileb[3,2], A. Jullien[1], C. Ghezzi[2], P. Bedouch[1], A. Du Moulinet D'Hardemare[4]; [1]Radiopharmacy/ pharmacy department, Grenoble Alpes University Hospital (CHUGA), Grenoble 38000, FRANCE, [2]INSERM Unit U1039, Radiopharmaceutiques Biocliniques, University of Grenoble Alpes-Faculté de Médecine, Grenoble 38000, FRANCE, [3]Department of nuclear medicine, Grenoble Alpes University Hospital (CHUGA), Grenoble 38000, FRANCE, [4]DCM-Department of Molecular Chemistry, UMR5250, University of Grenoble-Alpes, 301 Rue de la Chimie, BP 53 GRENOBLE cedex 9, FRANCE.

Positron Emission Tomography (PET) is a high resolution molecular imaging technic used for diagnostic test. [18]Fluor-Fluorodeoxyglucose (^{18}F-FDG) is still the most important radiopharmaceutical applied in PET imaging; nevertheless production and short half-life constraints limit the development of fluorinated tracers to cyclotron centers. The positron-emitting isotope [68]Gallium, present the great advantage to be produced by a long-lived isotopic generator ([68]Ge/^{68}Ga), making possible the preparation of clinical or preclinical PET radiotracers as needed and on-site, independently from cyclotron supply constraints. Since several years, study of ^{68}Ga complexation from [68]Ge/^{68}Ga generator significantly increased. The ^{68}Ga complex must be stable under physiological conditions and preferably be prepared in high yield>95% at room temperature and in a short time. The choice of the chelating subunit is fundamental to obtain such a properties and today, NOTA, HBED, DOTA and there derivatives, are promising ligands, however none are without shortcomings. But, siderophores like Desferrioxamine B (DFO), which are naturally occurring ligand having high affinities for Fe^{3+}, are also molecules of interest in this context because Ga^{3+} is very close to Fe^{3+} in terms of charge density, ionic radius and coordination preferences. In one of our laboratory (Department of Molecular Chemistry), we have synthesized the abiotic siderophore O-TRENSOX with exceptional capability to bind very strongly Fe^{+3}. As Ga^{3+} is a mimic of Fe^{3+}, we decided to establish the potential of O-TRENSOX for the complexation of $^{68}Ga^{3+}$ for PET imaging. In this study we investigated the radiolabeling of 68Ga with O-TRENSOX in comparison with two of the currents standards chelators HBED and DOTA.

EP-0236

Biodistribution And Micro-TEP Imaging Of68GA-NODAGA-RGD, A New Radiotracer For Tumor Angiogenesis: Human Glioblastoma Xenograft Model In Mice

S. ISAL[1], A. Clément[2], J. Pierson[2], C. Collet[2], N. Veran[2], S. Frezier[2], S. Poussier[2], G. Karcher[1], P. Marie[1], F. Maskali[2]; [1]Nuclear Medicine and Nancyclotep imaging platform CHRU Nancy, Nancy, FRANCE, [2]Nancyclotep imaging platform, CHRU Nancy, Nancy, FRANCE.

Introduction: ^{68}Ga-NODAGA-RGD is a radiotracer consisting of cyclic and multimeric arginine-glycine-aspartic (c(RGDyK)) peptide, and NODAGA complexing agent, which allows gallium-68 labeling. This radiotracer could show good characteristics for PET imaging of αvβ3 integrins expression. The involvement of αvβ3 integrins in tumor-induced angiogenesis is well de-

scribed. Objectives. We propose to investigate the biodistribution of ^{68}Ga-NODAGA-RGD in micro-PET imaging, compared to ^{18}F-FDG, a reference in preclinical Oncology imaging, with human glioblastoma xenograft model in mice. We also study the specificity of fixation to integrins with in vivo (blocking test with micro-PET) and ex vivo (immunohistochemistry) studies. **Methods:** 48 nude mice bearing human U87MG glioblastoma tumor xenograft were studied. When a target tumor volume of 500 ± 300mm³ was reached, two successive micro-TEPs imaging ^{68}Ga-NODAGA-RGD and ^{18}F-FDG were performed. In vivo biodistribution properties, and blocking tests with co-injection of an excess of unlabeled NODAGA-RGD were analysed in micro-PET. Ex vivo autohistoradiography (μ-Imager™), and immunohistochemistry (αvβ3 integrins and Ki67 expression in tumor) studies, were also compared. **Results:** The biodistribution curves of ^{68}Ga-NODAGA-RGD: 1) showed rapid hepatic and especially renal excretion 2) defined the optimal acquisition delay of 60 minutes after injection, for imaging of a sufficient tumor activity, clearly superior to the blood activity. The saturation tests showed that specific binding of ^{68}Ga-NODAGA-RGD to αvβ3 integrin, was 50% at 60 minutes and increased to 70% at 120 minutes after injection. Compared to ^{18}F-FDG, the ^{68}Ga-NODAGA-RGD tumor binding is lower, but more specific, with a lower extra-tumor activity (except hepatic and urinary elimination). Finally, the tumor uptake of ^{68}Ga-NODAGA-RGD, observed by autohistoradiography (μ-ImagerTM), was heterogeneous with a maximum in the highly proliferation areas of tumor and correlated with αvβ3 integrin expression in immunohistochemistry. **Conclusion:** PET imaging of αvβ3 integrins is possible with ^{68}Ga-NODAGA-RGD with an optimal acquisition delay of 60 minutes after injection. This radiotracer could be evaluated for tumor diagnosis and for monitoring response to anti-angiogenic treatment.

EP-0237

Evaluation Of Nucleophilic Synthesis Of [18F]-FDOPA HPLC Free On Fastlab Platform

E. Cazzola[1], A. D'Angelo[1], L. Mora[2], A. Purgato[1], C. Malizia[2], D. Peruzzi[1], S. Costa[2], J. Amico[1], F. Lodi[2], G. Gorgoni[1]; [1]Sacro Cuore Hospital, Negrar, ITALY, [2]Sant'Orsola Hospital, Bologna, ITALY.

Introduction: The [^{18}F]F-L-6-Fluoro-3,2-dihydroxyphenylananine [^{18}F]-FDOPA is an established radiotracer for diagnosis of integrity and function of the nigrostriatal dopaminergic system by PET and recent studies have emphasize the usefulness of [^{18}F]-FDOPA for diagnosis of neuroendocrine tumors. Historically the [^{18}F]-FDOPA are made by electrophilic pathway with several important limitation like, deuteron cyclotron beam option available, low [^{18}F]-F$_2$ activity made form target prospective, low process yield. All of this points allow to have long working time for few patients doses available. The introduction of nucleophilic pathway on [^{18}F]-FDOPA synthesis makes an important step over in the tracer availability, due to the possibility to have a wide range on inlet activity . Many different approaches are presents on literature with different yield and purification steps like HPLC or HPLC free. The aim of this study is to evaluate the quality of the [^{18}F]-FDOPA product with Ge FASTLab synthesiz-

er by using nucleophilic pathway, the reliability of the method used in terms of yield stability at different conditions of inlet activity and with the same activity in different runs. **Methods:** The method used on Ge FASTLab synthesizer is made by ABX by using the new non carrier added precursor ABX (1336). All the reagents are included on a single use commercial cassette. The [^{18}F]Fluorine was trapped on QMA and eluted with a mixture of TBAHCO$_3$/ACN after drying at 125°C on synthesis reactor, the ABX precursor dissolved on DMSO was added to proceed with the nucleophilic [^{18}F]-Fluorination. The reaction mixture was heated up at 110°C for 20 min after the reaction step the mixture was cooled at 55°C to starting the pre-purification step followed to oxidation and acid hydrolysis after this step the final purification and formulation take place. The total process takes place on 110 minutes. **Results:** We performed test a different inlet activity with two different cyclotron and targets shapes. S.Orsola Hospital (Bologna) with a Ge PETtrace and Sacro Cuore Hospital (Negrar) with ACSI TR-19, both of them are equipped with Nb Target. All the [^{18}F]FDOPA batches was fully evaluated on quality control in terms of general indications of European Pharmacopoeia Monography. **Conclusion:** All the syntheses performed at Sacro Cuore Hospital and the preliminary data at S.Orsola Hospital showed that the Radiochemical yield are stable at different range of inlet activity and all the quality control parameters evaluated are aligned to the general requirements of European Pharmacopoeia.

EP-0238

Synthesis and Biological evaluation of 68Ga labeled NOTA-Capsaicin for Targeting Colon Cancer CT-26

G. Kim[1,2], S. Kim[2], M. Hur[1], S. Yang[1], J. Park[1]; [1]korea atomic energy research institute, jeongeup, KOREA, REPUBLIC OF, [2]Dongguk University, Gyeongju, KOREA, REPUBLIC OF.

Aim: Capsaicin (trans-8-methyl-N-vanillyl-6-nonenamide) is a compound of vanilloid family and binds specifically to the vanilloid receptor. A vanilloid receptor is expressed in colon cancer cells. NOTA is conjugated with capsaicin to label positron-emitting nuclear species ^{68}Ga. We believe using this feature to develop diagnostic agents selectively accumulating in colon cancer for PET. **Materials and Methods:** ^{68}Ga^{3+} was eluted from a ^{68}Ge/^{68}Ga generator with 0.05 N HCl and used directly for the reaction after adjusting the pH 4. The labeling method of ^{68}Ga^{3+} (37 MBq) was performed in 1 M sodium acetate buffer with NOTA-capsaicin (1 mg) and the mixture was stirred for 10 min at room temperature. The mixture was purified by RP-HPLC. The stability in human serum was evaluated for 120 min at 5 time points (5, 15, 30, 60 and 120 min). ^{68}Ga labeled NOTA-capsaicin was dissolved in PBS/1-octanol for lipophilic test and solvents respectively measured by γ-counter. The cellular uptake of ^{68}Ga labeled NOTA-capsaicin was evaluated using CT-26 and A549 cells (control). **Results and Conclusion:** The products were obtained in >98% radiochemical yields and a radiochemical purity of >99% checked by chromatography method. The stability of ^{68}Ga labeled NOTA-capsaicin in human serum was over 95% for 120mins. The partition coefficient (Log P value) was mea-

sured -2.16, which is an indication of the hydrophilic agent. Cellular uptake evaluation of ^{68}Ga labeled NOTA-capsaicin was CT-26 and A549 cells over incubation periods of 15, 30, 60 and 120mins. (CT-26: 0.23ID% at 15mins, 0.40 ID % at 30mins, 0.49 ID % at 60mins and 0.77 ID % at 120mins and A549: 0.11 ID % at 15mins, 0.20 ID % at 30mins, 0.27 ID % at 60mins and 0.49 ID % at 120mins). In conclusion, we successfully synthesized a ^{68}Ga labeled NOTA-capsaicin. This compound showed high stability in human serum and close to hydrophilic. In cellular uptake, ^{68}Ga labeled NOTA-capsaicin showed higher uptake on CT-26 cells than controls. These results can suggest that ^{68}Ga labeled NOTA-capsaicin could be a potential CT-26 targeted agent for PET.

EP-0239

One-pot Synthesis of Surface Modified Gallium Incorporated Zeolitic Imidazolete Framework (ZIF-8) as a PET probe

P. Choi[1,2], J. Lee[1], G. Kim[1], S. Kim[2], J. Park[1]; [1]Korea Atomic Energy Reaserch Institute, jeongeup, KOREA, REPUBLIC OF, [2]Dongguk University Gyeongju, Gyeongju, KOREA, REPUBLIC OF.

Aim: The nano-sized metal-organic framework (MOF) of zeolitic imidazolete Framework (ZIF-8) have been used as drug delivery probe. ZIF-8 consists of Zn^{2+} metal ion and 2-methylimidazole (2-MID) as an organic linker synthesized through self-assembly nucleation. ^{nat}Ga was partially incorporated in lattice of ZIF-8 instead of Zn ions for measuring the PET images. Surface modification of folic acid provides ZIF-8 with the properties that could actively target the folate-receptor on the surface of cancer cells with EPR effect of nano-materials and improve biocompatibility of ZIF-8. The obtained nano-sized ^{68}Ga incorporated ZIF-8 with the modified surface using folic acid (^{68}Ga-ZIF8-FA) may be used as an effective PET probe for cancer diagnosis **Materials and Methods:** ^{nat}Ga-ZIF8-FA was synthesized in one step utilizing CTAB and 1-hexanol by reverse micro-emulsion method at room temperature. Concentration ratio (w) between CTAB and water was ~ 20. 0.01 M $GaCl_3$ was allowed to react with 0.05 M $Zn(NO_3)_2$ and 0.1 M 2-MID for 1h. ^{nat}Ga-ZIF8-FA structure and morphology was characterized using UV, IR, TEM, XPS, XRD, EDX, DLS, Zeta potential. **Results and Conclusion:** We were successful in synthesizing ^{nat}Ga-ZIF8-FA in 1 h by reverse micro-emulsion method. Characterization of the synthesized ^{nat}Ga-ZIF8-FA shown that it was 25 nm uniform nanospheres. ^{nat}Ga was successfully incorporated in ZIF-8 with imidazolic nitrogen of ZIF-8 partially instead of Zn and not the inner capsule of the molecule which was confirmed using EDX and XPS spectra, while surface modification of folic acid was confirmed with UV, IR, XPS. Surface charge was changed from +8 to -20.7 due to surface modification ZIF-8 by of folic acid. This studies form the basis for one-pot synthesis of ^{nat}Ga-ZIF8-FA which is suitable as a PET probe if ^{68}Ga radioisotope is introduced in ZIF-8. ^{68}Ga-ZIF8-FA stability is highly effective due to direct ^{68}Ga incorporation in ZIF-8. By the folic acid surface modification, ^{68}Ga-ZIF8-FA could be selectively targeted in cancer cells which is expressed by the folate-receptors having improved biocompatibility for the normal cells. Stability and biological studies are due using ^{68}Ga-ZIF8-FA.

EP-0240

Fully automated one step [18F]F-PSMA-1007 production on AllinOne (Trasis)

A. Fasel[1], M. Otabashi[2]; [1]ABX advanced biochemical compounds, Radeberg, GERMANY, [2]Trasis SA, Liege, BELGIUM.

Introduction: The prostate-specific membrane antigen (PSMA) targeted positron-emitting-tomography (PET) tracer 68Ga-PSMA-11 and HBED has proved very good performances in the diagnosis of prostate cancer. However 68Ga has a rather short half-life and its high β energy blurs somewhat the images. This has encouraged the development 18F-labelled alternatives. In particular the [^{18}F]-PSMA-1007 has been synthesized and studied by Cardinale et al 1. Giesel et al 2 have demonstrated that PSMA-1007 is good alternative for 68Ga- PSMA-11. **Methods:** The radiosynthesis of [^{18}F]-PSMA-1007 is achieved in a single step by aromatic nucleophilic substitution of 18F on a Trimethyl ammonium leaving group of the PSMA-1007 precursor (named below) in presence of $TBAHCO_3$ at 90°C, followed by SEP cartridges purification. The final [^{18}F]-PSMA-1007 is formulated in a dilute solution of ethanol in saline, stabilized with sodium ascorbate. Precursor:5-((S)-4-carboxy-1-((S)-4-carboxy-1-(4-((S)-1-((S)-5-carboxy-5-(3-((S)-1,3-dicarboxypropyl)ureido)pentylamino)-3-(naphthalen-2-yl)-1-oxopropan-2-ylcarbamoyl)benzylamino)-1-oxobutan-2-ylamino)-1-oxobutan-2-ylcarbamoyl)-N,N,N-trimethylpyridin-2-aminium 2,2,2-trifluoroacetate **Results:** The NDC yield was in a range of 35 to 45% using around 1.5 mg of precursor. The process is carried out in about 45 minutes. The chemical and radiochemical purities are both >98% and the product is stable for at least 6 hours. **Conclusions:** A fully automated production of [^{18}F]-PSMA-1007 with ready to use kits developed and optimized by ABX is available on the AllinOne synthesizer module and appropriate for routine commercial scale purposes. **References:** 1. J Cardinale et al. J Nucl Med 58 (3), 425-431 2. Giesel, F.L., Hadaschik, B., Cardinale, J. et al. Eur J Nucl Med Mol Imaging (2017) 44: 6789.

EP-0241

High activity automated production of Lu-177 radiopharmaceuticals using the Modular Lab-Eazy system

M. J. Latter[1], S. Tapper[1], J. Seemann[2]; [1]Royal Brisbane and Women's Hospital, Herston, AUSTRALIA, [2]Eckert and Ziegler, Berlin, GERMANY.

Purpose/Introduction: The use of theranostic pairs has seen considerable growth in the clinical demand for Ga-68 and Lu-177 radiopharmaceuticals, particularly those with applications in neuroendocrine and prostate cancer. Increasing demand can be met with the use of automated modules to manufacture higher activities, without compromising on product quality or increasing staff dose. In addition to the computer controlled module, method templates and hardware/reagent kits specific for each radiopharmaceutical are available from commercial suppliers. The combination of these components provides an extra level of consistency as variability between choice of reagents, preparation methods and operator techniques is minimised. **Subject**

& Methods:This presentation will describe radiolabelling of DOTA-TATE and -PSMA with Lu-177. Synthesis was done on the ML Eazy module, with an emphasis on testing the limits of the system by manufacturing radiopharmaceuticals using extremely high activity inputs of up to 60 GBq per synthesis run. **Results**: Radiolabelling of both DOTA-TATE and -PSMA analogues have been conducted to optimise precursor quantities for high activity batches using the commercially available method template provided with the ML Eazy module. Comprehensive quality control data will be presented to demonstrate the product is suitable for clinical use in PET centres. **Discussion/Conclusion**: The true practical benefit from this project is the improvement in manufacturing efficiency from the perspective of the radiochemistry laboratory. The success of high activity radiolabelling processes translates to fewer batches of the same radiopharmaceuticals to be produced for equivalent or increasing demand, which in a clinical PET Department is a considerable cost saving in staff time. Ensuring the quality of the product over an extended period (relative to half-life of the incorporated radioisotope) also increases flexibility in patient scheduling per manufactured batch. **Acknowledgements**: ABX Advanced Chemicals and AN-STO Health are acknowledged for providing precursors (PSMA HBED-CC and PSMA-617) and 177LuCl3 respectively to undertake this project. Technical support from Chris Quinn (Imaxeon Pty Ltd) is also appreciated. MJL also acknowledges the support of a Churchill Fellowship.

EP-0242

Fully automated production of [^{18}F]LBT999, a dopamine transporter (DAT) radiopharmaceutical, for preclinical and clinical PET studies

C. Vala[1,2], C. Mothes[1,3], P. Magadur[2], G. Viot[1,2], J. Deloye[1,2], R. Bidault[2,4], G. Chicheri[2,4], Y. Peltier[2,4], N. Arlicot[2,4,5], D. Guilloteau[2,4,5], J. Vercouillie[2,4,5]; [1]Cyclopharma Laboratories, Saint Beauzire, FRANCE, [2]CERRP, Tours, FRANCE, [3]Pharm'image, Dijon, FRANCE, [4]INSERM U930, Tours, FRANCE, [5]CHRU Bretonneau, Tours, FRANCE.

Aim: Fluorine labeled 8-((E)-4-fluoro-but-2-enyl)-3β-p-tolyl-8-aza-bicyclo[3.2.1]octane-2β-carboxylic acid methyl ester ([^{18}F]LBT999), is a highly selective Positon Emission Tomography (PET) radioligand for the dopamine transporter (DAT) and thus may be an useful tool for in vivo quantification of DAT[1,2]. DAT is involved in many neurodegenerative and psychiatric diseases, like Parkinson's disease (PD), and accurate quantification of DAT can help in early and differential diagnosis of brain disorders. In order to satisfy preclinical and clinical demands for PET studies, the objective of this work was to develop a fully automated radiolabeling procedure of the [^{18}F]LBT999 on two available commercial modules, the GE Tracerlab FXFN and the Trasis AllinOne (AIO). **Material and Methods:** The automated radiosynthesis of [^{18}F]LBT999 was first developed on the Tracerlab FXFN module, based on a direct one-step nucleophilic fluorination from the corresponding chlorinated precursor [3,4] in DMSO at 165°C for 10 min. Then, the same labelling process was applied on the AIO module, using disposable-cassettes to comply with GMP production. This industrial production transfer on AIO required

few optimizations on the fluorination reaction (time, temperature···) and the purification. For each module, an automated in-house program was developed to perform the radiofluorination, followed by a semi-preparative HPLC purification and the final formulation of the product. A quality control procedures of [^{18}F]LBT999 were established for preclinical and clinical human uses according to the US and Ph. Eur. requirements. **Results:** By using the Tracerlab FXFN, [^{18}F]LBT999 was obtained with a good radiochemical yield of approximately 35 % (decay-corrected, n=16), with a total synthesis time of 65 min. After optimization of the labelling process on the AIO module, the synthesis of [^{18}F]LBT999 was performed in less than 50 min with radiochemical yields > 40 % (decay-correted, n=12). The quality control was tested and validated for human use (first in man phase 0/1, EUDRACT 2014-004229-42). **Conclusion:** We reported here the first automated production of [^{18}F]LBT999 on two commercial platforms. The whole process is performed with good reproducibility, high radiochemical yield, purity and specific activity (up to 500 GBq/µmole). Both modules can be used for routine clinical production, with an advantage for AIO and its disposable-cassettes. **References:** [1] Varrone et al., *J. Nucl. Med.* 2011, 52, 1313-1321; [2] Sérrière et al., *Nucl. Med. Biol.* 2014, 41, 106-113; [3] Dollé et al, 2008, EP1925615A1; [4] Dollé et al., *J. Label. Compd. Radiopharm.* 2007, 50, 716-723.

EP-0243

Improvement of [^{11}C](+)-PHNO synthesis by evaluation of reaction temperatures

S. Pfaff[1,2], C. Philippe[1], V. Pichler[1], A. Weidenauer[3], M. Willeit[3], M. Hacker[1], M. Mitterhauser[1,4], W. Wadsak[1,2,5], L. Nics[1,6]; [1]Department of Biomedical Imaging and Image-guided Therapy, Division of Nuclear Medicine, Medical University of Vienna, Vienna, AUSTRIA, [2]Department of Inorganic Chemistry, University of Vienna, Vienna, AUSTRIA, [3]Department of Psychiatry and Psychotherapy, Medical University of Vienna, Vienna, AUSTRIA, [4]Ludwig Boltzmann Institute Applied Diagnostics, Vienna, AUSTRIA, [5]Centre for Biomarker Research in Medicine, CBmed GmbH, Graz, AUSTRIA, [6]Department of Nutritional Sciences, University of Vienna, Vienna, AUSTRIA.

Purpose/Introduction: [^{11}C](+)-PHNO ([^{11}C]-(+)-4-Propyl-3,4,4a,5,6,10b-hexahydro-2*H*-naphtho[1,2-*b*][1,4]oxazin-9-ol) is used for imaging of the dopaminergic system as it is an agonist for the dopamine D2/3 receptor. The synthetic procedure is quite demanding as in-loop Grignard reactions and a reduction with LiAlH$_4$ are involved. As a result, the yields for [^{11}C](+)-PHNO are generally quite low and long reaction times are additionally leading to a low specific activity. Nevertheless, especially agonistic radiotracers require a high specific activity. Therefore, any improvement of the synthesis is of major interest. Aim of this study was to enhance the radiochemical yield by increasing the conversion as well as reducing the synthesis time. **Subjects and Methods:** Lithium aluminium hydride (LiAlH$_4$) and the precursor HNO (GMP grade) were obtained from ABX (Advanced Biochemical Compounds, Radeberg, Germany). The synthesis was performed on a TRACERlab™ FX C Pro synthesis platform (GE Healthcare, Uppsala, Sweden). (1) LiAlH$_4$ was added at -40°C,

-15℃ and room temperature. Additionally, for the reduction at room temperature all reaction steps (except for the release of [^{11}C]CO$_2$ from the molecular sieve) were performed without heating or cooling. **Results:** The reduction of the carbonyl function using LiAlH$_4$ could be successfully performed at all tested temperatures. No decline of by-products was observable at lower temperatures as described previously. (2) Quite on the contrary, the best results were obtained for syntheses at ambient temperature due to a drastic decrease of synthesis time. Preliminary results showed an overall time reduction of 7 min, which resulted in a remarkable gain in radioactity yield of 27%. **Discussion/Conclusion:** As lower temperatures could not reduce the formation of side products, it is not necessary to spend time on cooling down (and re-heating) the reaction mixture. It was seen that it is more important to counteract the decay of a short-lived radionuclide by gaining time. In this study, the yield could be distinctly improved as no time was needed for heating and cooling resulting in reduced synthesis time. (1) Christina Rami-Mark, Johanna Ungersboeck, Daniela Haeusler, Lukas Nics, Cecile Philippe, Markus Mitterhauser, Georgios Karanikas, Wolfgang Wadsak, Appl. Radiat. Isot., 2013, 82, 75-80 (2) Alan A. Wilson, Patrick McCormick, Shitij Kapur, Matthaeus Willeit, Armando Garcia, Doug Hussey, Sylvain Houle, Philip Seeman, and Nathalie Ginovart, J. Med. Chem., 2005, 48, 4153-4160

EP-0244

Evaluation of benzoxazolone based TSPO selective PET radiotracer to access microglial activation in ishemic rat brain

N. Kumari[1,2], S. BHAGAT[3], A. K. Tiwari[1]; [1]INSTITUTE OF NUCLEAR MEDICINE AND ALLIED SCIENCES, DRDO, DELHI, INDIA, [2]DELHI UNIVERSITY, Delhi, INDIA, [3]DELHI UNIVERSITY, DELHI, INDIA.

Aim: In neuropsychiatric disorders or brain injury the Translocator protein (TSPO) is considered as an efficient biomarker to trace the area of neuroinflammation. The quantification of translocator protein density in a specific region can be used as a tool for monitoring the progression of disease or recovery after treatment. In this work our main objective was to design the TSPO targeted ligands which can overcome the limitation of first generation and second generation TSPO ligands. So herein we are reporting the synthesis and biological evaluation of ^{11}C- MNBP for PET imaging in ishemic rat brain. **Material and Methods:** By utilizing Benzoxazolone as a basic scaffold, series of TSPO ligands have been designed followed by their screening through in silico studies. Synthesis has been planned by employing convergent methodology in six high yielding steps. For the synthesized ligands the in vitro assay was performed to determine the binding affinity in term of K_i. On ischemic rat brain, autoradiography studies were also carried to check the specificity and affinity of the designed radiolabelled ligand for TSPO. **Results:** Better G_{Score} for MNBP in comparison to the reference ligand promoted it for wet lab synthesis. Synthesis of MNBP was successfully carried out and characterized by spectroscopic techniques (FTIR, NMR and HRMS). In vitro binding assay showed high binding affinity $K_i = 8.1 + 0.8$ for TSPO over central benzodiazepine receptor (CBR) $K_i > 100$. ARG studies indicated higher uptake of ^{11}C- MNBP on the lesion side compared with that on the non-lesion side of ischemic rat brains. Displacement experiments with unlabelled ligand had minimized the difference in uptake between the two sides which indicates the specificity of the ligand towards TSPO receptor. **Conclusion:** Biological evaluation in ischemic rats have proved [^{11}C]MNBP as a potential PET imaging agent for TSPO targeting.

EP-0245

Measurement of the Stability of [^{18}F]FDOPA with High Activity Concentration

T. Bali, A. Richárd, G. Tihanyi, T. Cservenyák, Z. Áncsán, T. Csipak, B. Bojtor, I. Repa, G. Bajtek, P. Mikecz; University of Kaposvár, Kaposvár, HUNGARY.

Introduction: 6-[^{18}F] fluoro-3,4-dihydroxy-L-phenylalanine (FDOPA) is one of the oldest PET radiopharmaceuticals. Its synthesis was first described in 1983. Earlier mainly used for neuropsychiatric diseases, movement disorders and malignant brain lesions. Nowadays its uses are in a wider range, for example, it has been successfully used to diagnose neuroendocrine tumors. The widespread use of this tracer was inhibited, because of the only available complex electrophilic substitution reaction. An increasing number of methods were developed to implement high-yield nucleophilic synthesis in the early 2000s. Our goal was to synthetize this tracer in high radioactivity concentration and study its stability during prolonged storage. **Methods:** The synthesis was performed with cassette-based AllinOne synthesizer installed with the appropriate software developed by Trasis SA. The synthesis was performed without any modification of the firms' software. When it was necessary, into the buffer for formulation vial ethanol was added. The product was purified by semi-preparative HPLC column, and it was formulated with citrate buffer. The product was sterilized by filtration. The quality control tests were carried out by gas, thin layer and liquid chromatography and gamma spectrometry. The stability of the product was followed for minimum 14 hours. **Results:** We manufactured pharmacopeia compliant quality batches. The average decay corrected yield was 70%, resulting about 70 GBq [^{18}F]FDOPA. The activity concentration of these batches was between 4.1 and 2.8 GBq/ml. The radiochemical purity measured by HPLC was typically < 99.5%, and the enantiomeric purity was found about 97%. The product was free of organic solvents that used for the production except for the ethanol content which was 3-4,7 mg/ml. Each batch was sterile and non-pyrogenic. The free [^{18}F]fluoride content measured by TLC has shown a continuous increase from 1 to 5-6 % in 14 hours. In the case of added ethanol, the fluoride content was limited below 4 %. At elevated temperature (40 ℃) even the ethanol did not help to prevent the radiolysis of [^{18}F]FDOPA over 5 %. **Conclusion:** Since the manufacturer had decreased the concentration of the citrate buffer in the production kit, it became necessary to measure the influence of this change. We had found that the less concentrated citrate did not have enough stabilizing power. Adding ethanol to the final product helped to cap the free fluoride content. On the basis of the results obtained we had applied for a marketing authorization at OGYEI (National Institute of Pharmacy and Nutrition).

EP-0246

[11C]Me@NEBIQUINIDE: A Real Third Generation TSPO PET Tracer?

N. Berroterán-Infante[1,2], S. Schmitl[3], T. Kalina[4], H. Spreitzer[3], M. Hacker[1], M. Mitterhauser[1,5], K. Pallitsch[4], W. Wadsak[1,6]; [1]Division of Nuclear Medicine, Department of Biomedical Imaging and Image-guided Therapy, Medical University of Vienna, Vienna, AUSTRIA, [2]Institute of Inorganic Chemistry, Faculty of Chemistry, University of Vienna, Vienna, AUSTRIA, [3]Department of Pharmaceutical Chemistry, Faculty of Life Sciences, University of Vienna, Vienna, AUSTRIA, [4]Institute of Organic Chemistry, Faculty of Chemistry, University of Vienna, Vienna, AUSTRIA, [5]LBI Applied Diagnostics, Vienna, AUSTRIA, [6]Center for Biomarker Research, Graz, AUSTRIA.

Introduction & Aim: The Translocator Protein (TSPO) has become an important biomarker for several pathophysiological conditions. Its overexpression has been described in cancer, heart failure and especially neurologic disorders. Unfortunately, high non-specific binding and mainly a single nucleotide polymorphism in the *TSPO* gene (rs6971) have hampered the development of successful TSPO PET tracers, due to different binding affinity profiles described for subjects with distinctive genotype; classifying them in high-affinity-binders (HAB), mixed-affinity-binders (MAB) and low-affinity-binders (LAB). Hence, the aim of this work was the (radio)synthesis and affinity evaluation of the new PET ligand [11C]Me@NEBIQUINIDE. **Methods:** Me@NEBIQUINIDE (N-(*sec*-butyl)-1-(2-chloropyridin-3-yl)-N-methylisoquinoline-3-carboxamide) as reference standard and its precursor NEBIQUINIDE (N-(*sec*-butyl)-1-(2-chloropyridin-3-yl)isoquinoline-3-carboxamide) were synthesized in 8 and 7 steps procedures, respectively. The affinity of Me@NEBIQUINIDE towards the TSPO of subjects previously genotyped as HAB and MAB was determined in a competitive experiment using platelets membrane, as described previously [1]. Moreover, 11C-labeling was automated in a GE TRACERlab FX C Pro Synthesizer using [11C]methyl triflate as methylation reagent. Binding to α1AGP and *log* P were also determined using spin desalting columns and a HPLC method, respectively. **Results:** The affinity of Me@NEBIQUINIDE towards the TSPO was found to be in the nanomolar range for both groups (HAB and MAB) with no difference in the binding affinity profile. Binding affinity towards LAB is still in progress, since no LAB subject has been found in our cohorts. [11C]Me@NEBIQUINIDE was successfully synthesized using a suspension of sodium hydride in DMSO for 2min at 75°C using 4mg/mL of precursor NEBIQUINIDE with a RCY of 2,2±0,1% (non-corrected for decay, non-optimized conditions) and a molar radioactivity of 98±9 GBq/μmol (n=3). Binding to α1AGP and *log* P were reduced in comparison to the established TSPO PET tracer [11C]PK11195. **Conclusions:** The presented results point towards the suitability of the new TSPO PET tracer, [11C]Me@NEBIQUINIDE, for future *in vivo* evaluations. Moreover, low sensitivity towards the rs6971 polymorphism is expected, since no difference between HAB and MAB was found. References: [1] Owen, D et al; *J Cereb Blood Flow Metab*; 2012; 32:1-5

EP-0247

68Ga(III) complex with morin for kidney cancer cells labeling

K. Kilian, A. Sentkowska, &. Cheda, K. Pyrzyńska; University of Warsaw, Warszawa, POLAND.

Aim: Morin (3,5,7,2`,4`-pentahydroxyflavone) is well known natural antioxidant and medically important flavonoid. Morin possesses antioxidant, anti-inflammatory, anticancer and cardioprotective properties thus acts as chelating agent and its complexes play significant role in human health. The main purpose of this work was to examine the methodology for the synthesis of 68Ga(III)-morin complex. UV-Vis, IR and mass spectrometry were used to characterize the complex. The knowledge gained from this study was used for efficient labeling of ranal cancer cells. **Materials & Methods:** 68Ga was obtained from 68Ge/68Ga generator by elution with 0.1 mol/L hydrochloric acid. Cells: Caki-1 HTB-46™ (Human, kidney, clear cell carcinoma), Caki-2 HTB-47™ (Human, kidney, clear cell carcinoma), ACHN CRL-1611™ (Human, kidney, renal cell adenocarcinoma) and 786-O CRL-1932™ (Human, kidney, renal cell adenocarcinoma). 68Ga-morin complex was synthesised using "kit-concept" as for technetium diagnostics radiopharmaceuticals. 100μg of morin was dissolved with 200 μl of DMSO and added to the 68Ga eluate equilibrated to pH5 with sodium hydroxide and acetate buffer to total volume 5 mL. Sample was vortexed and gently heated in 60ºC for 5 minutes. After cooling to room temperature solution was distributed to Eppendorf vials with cells cultures. **Results:** 68Ga-morin complex was used for labelling of human kidney cancer cells. For Caki-2, ACHN and 786-O (n=3) the efficiency was about 30% (24.9±1.2, 31.2±2.3 and 29.8±1.6% respectively), while for Caki-1 (n=3) more than twice (61.6%±2.8) of activity was immobilized on cancer cells. Cellular viability was satisfactory and reached 51-65% for Caki-2, ACHN and 786-O with increase to 71-76% for Caki-1. **Conclusion:** This study examined the interaction of gallium(III) ions with morin in aqueous-ethanol solution. The spectroscopic data shows the importance of 3-OH group and the carbonyl group of the ligand for forming the coordination site. As the flavoniods are recently widely studied for their pharmacological properties, the presented strategy of Ga-morin synthesis can be potentially used in development of new PET radiopharmaceuticals labelled with 68Ga and for further studies on flavonoids behaviour *in vivo*.

EP-0248

Evaluation of arylpiperazinyl analogues as PET radioligand for 5HT7

A. K. Tiwari; Institute of Nuclear Medicine & Allied Sciences, Delhi, INDIA.

Objective: 5-HT_7 is one of the subset of serotonin receptor. Till date, no 5-HT_7 PET ligand is available for human studies. Here, we present the radiosynthesis and biological evaluation of arylpiperazinyl -alkyl bezoxzolone/benzothiazolone as a possi-

ble PET radiotracers for 5HT$_7$. The functions of this receptor is very important in sleep and memory related cognitive functions. **Methods:** Radioligands were synthesized by reacting desmethyl precursor with [^{11}C]CH$_3$OTf in the presence of NaOH. The distributions of these ligands were assessed by autoradiography in rat brains. Autoradiograms obtained after 30 min. of incubation with a constant in vitro radiotracer concentration in those binding areas described as rich in 5-HT$_7$ receptors, Cerebral cortex (Cb), Hippocampus (Hi), Thalamus (Th), Hypothalamus (Hy), Striatum (St) ,Cerebellum (Ce) and Pons-Medulla (PM) regions. **Results:** Preliminary PET study in rat brain showed fast accumulation of radioactivity in the brain ranging 1.75-3.00 SUV. Radioactivity measured in displacement experiments was reduced markedly after the addition of cold reference and SB269970, a 5-HT$_7$ receptor antagonist. Diminution in binding of cerebral cortex was −84% and in the hippocampus, thalamus and pons-Medulla were −83.9%, −81.2%, and −82.5%, respectively. **Conclusion:** Further investigation in multiple animal models having increased 5-HT$_7$ expression may optimize these ligands for clinical use.

EP-14　　　　　during congress opening hours, e-Poster Area

Radiopharmaceuticals & Radiochemistry: Radiopharmaceuticals - SPECT

EP-0249

Development of [^{123}I] 6-iodo-deoxy glucose ([^{123}I] 6-IDG) with composite polymer precursor for imaging of brain glucose metabolism with SPECT.

Y. Kanai[1], H. Tanaka[2], A. Nagasaki[3], S. Naka[1], T. Sakai[4], T. Kamiya[1], G. Horitsugi[1], E. Shimosegawa[1], T. Takahashi[5], J. Hatazawa[1]; [1]Osaka University Graduate School of Medicine, Suita, JAPAN, [2]Tokyo Institute of Technology, Tokyo, JAPAN, [3]Iwaki Seiyaku Co.,Ltd, Tokyo, JAPAN, [4]Hanwa Inteligent Medical Center, Sakai, JAPAN, [5]Yokohama University of Pharmacy, Yokohama, JAPAN.

Object: In synthesis of radiopharmaceuticals, HPLC purification and formulation step including evaporation are time consuming and cumbersome process. Nowadays many novel radio-synthesis methods without HPLC purification and formulation step were reported. We focused a composite polymer. Composite polymer is generally large molecule. When we use composite polymer as precursor in radio-synthesis, it is easy to separate composite polymer precursor and objective substance. In this study we paid an attention to 6-iodo deoxy glucose (6-IDG) as a brain sugar metabolite imaging agent. We tried to synthesize [^{123}I] 6-IDG using composite polymer precursor without HPLC purification and formulation methods and take an image of [^{123}I] 6-IDG in small animals for evaluation of [^{123}I] 6-IDG basic property as a brain glucose metabolism imaging agent. We employed a composite polymer method which enabled high radiochemical yield and purity of [^{123}I] 6-IDG. **Method:** Composite polymer precursor (30 mg) and [^{123}I] NaI (80 MBq) in acetonitrile was reflux at 100 degree C for 1 hour.

After purified reaction mixture by silica gel cartridge column and evaporate the reaction solvent, 0.5 % H$_2$SO$_4$ was added for hydrolysis. Finally [^{123}I] 6-IDG solution was obtained after purification with ion-exchange column. Radiochemical purity was determined by HPLC analysis. In animal imaging, about 3 MBq of [^{123}I] 6-IDG was administered to each rat via tail vein. Dynamic images are acquired with gamma camera (e.cam, Siemens) for 0~45 minutes after injection. After dynamic imaging, SPECT images are taken for 15 minutes. **Result:** Radio-chemical yield of [^{123}I] 6-IDG was about 30 % from [^{123}I] NaI and Radio-chemical purity is more than 95 %. Synthesis time of [^{123}I] 6-IDG was about 1.5 hours. [^{123}I] 6-IDG dynamic and SPECT imaging were obtained successfully. We confirmed that [^{123}I] 6-IDG uptake in rat brain was reached maximum at 10-15 minutes after injection and wash out from brain rapidly. **Conclusion:** We succeeded to synthesize [^{123}I] 6-IDG by means of composite polymer method without HPLC purification and formulation step. We successfully took images and observed pharmacokinetics of [^{123}I] 6-IDG in rat.

EP-0250

In vitro assessment of the accumulation of highly specific radiochemical compounds based on ^{99m}Tc-labeled recombinant molecules

O. Bragina[1,2], M. Larkina, E. Stasyuk, V. Chernov, R. Zelchan, A. Medvedeva, Sinilkin I., M. Yusubov, V. Skuridin,; [1]Tomsk National Research Medical Center of the Russian Academy of Sciences, Tomsk, RUSSIAN FEDERATION, [2]National Research Tomsk Polytechnic University, Tomsk, RUSSIAN FEDERATION.

Purpose: to produce a chemically stable radiochemical compound for targeted imaging of cells overexpressing Her-2/neu. **Materials and Method:** The study was performed using 2 cell lines. The human breast adenocarcinoma HER2-overexpressing cell line BT-474 was chosen to detect specific binding. As a control, HER2-negative human breast adenocarcinoma MCF-7 was used. The human breast adenocarcinoma BT-474 and MCF-7 cell lines were seeded in chamber-slides at the density of 35000 cells/ml in trypsin-EDTA (PanEco) medium and grown overnight at 37 °C. After that both cell lines were washed with Phosphate buffered saline (PBS) and distributed into test tubes to 1 ml (5 millions cells in each). After adding 100 μl (70 MBq) studied complex of ^{99m}Tc-DPAH-DARPin9_29 was incubated for 40 min at + 4 °C. Washing was performed three times with buffer PBS and 5% Bovine Serum Albumin (BSA). Characteristics of the binding specificity of the test set with the HER-2/neu receptor were determined by direct radiometric and planar scintigraphy. To evaluate the differences between quantitative traits between the groups non-parametric Mann-Whitney test. **Results:** Output of the labeled complex was more than 91%, with a radiochemical purity of more than 94%. When carrying out a visual scintigraphic assessment much greater intensity accumulation of radiotracer was observed in the studied cell culture surface receptor overexpressing Her-2/neu The results of direct radiometric also showed higher accumulation of the radiopharma-

ceutical in the adenocarcinoma cell line BT-474 human breast cancer overexpressing Her-2/neu compared to the control group. **Conclusion:** Preclinical studies demonstrated high in vitro stability study compound, as well as its accumulation in the cell group overexpressing Her-2/neu.

EP-0251

The First Experience of Using a Radiopharmaceutical Based on Derivative of Glucose Labeled with Technetium-99m in Breast Cancer Imaging

R. Zelchan[1,2]*, A. Medvedeva, I. Sinilkin, O. Bragina, V. Chernov, E. Stasyuk, A. Rogov, E. Il'ina, V. Skuridin;* [1]*Tomsk National Research Medical Center, Russian Academy of Science, Tomsk, RUSSIAN FEDERATION,* [2]*National Research Tomsk Polytechnic University, Tomsk, RUSSIAN FEDERATION.*

Purpose: to study possibility of using 1-thio-D-glucose labeled with 99mTc for breast cancer imaging. **Materials and Method:** the study included 11 patients with stage $T_{1-4}N_{0-1}M_0$ breast cancer who underwent SPECT with «99mTc-1-thio-D-glucose» for visualization of primary tumor and regional metastases. SPECT was performed 20 minutes after intravenous injection of 500 MBq of «99mTc-1-thio-D-glucose» into a qubital vein opposite from the tumor side. In addition, the tumor / background index was calculated. **Results:** the primary breast tumor was visualized in all patients. Sensitivity of SPECT with «99mTc-1-thio-D-glucose» in the diagnosis of breast cancer was 100%. Metastases in regional lymph nodes were detected in 8 patients out of 10. Thus, the sensitivity of SPECT with «99mTc-1-thio-D-glucose» in detecting regional metastases in breast cancer was 80%. The mean values of the index tumor / background were 3.91±0.2. **Conclusion:** the present study demonstrated that «99mTc-1-thio-D-glucose» is a prospective radiopharmaceutical for the breast cancer visualization. This study has shown that SPECT with «99mTc-1-thio-D-glucose» can be one of the supplementing methods in detection of primary breast tumors and regional metastases.

EP-0252

Preparation of ^{131}I-iodohexadecanoic acid: a tracer to localize lymphatic leakage lesions

H. Kvaternik, S. Stanzel, R. M. Aigner; Medical University of Graz, Graz, AUSTRIA.

Intoduction: Radio-iodinated long-chain fatty acids were originally used to detect areas of inadequate myocardial perfusion, but were soon replaced by others. Only a small application segment in the scintigraphic localization of lymphatic leakage sites remained. Our aim was to establish the preparation of n.c.a. 16-^{131}I-iodohexadecanoic acid (^{131}I-IHDA) for localization of central conducting lymphatic anomalies (1). **Methods:** The procedure based on a nucleophilic radio-iodine for brome exchange (2,3) of 16-bromohexadecanoic acid (16-BrHDA) was carried out on a cassette-based Scintomics GRP Module, manually operated with the software. Due to the poor availability of

iodine-123, iodine-131 was used for labelling. 10 µl of a 1.0 M aq. ammonium acetate, 10 µl of aq. sodium bisulfite (2 mg/mL) and 70 MBq ^{131}I-NaI was added to a reaction vial containing a solution of 1 mg 16-BrHDA in 1.0 ml ethanol. The evaporated reaction mixture was heated for 10min at 130°C and processed by HPLC (Nucleosil 100-5C18, 4×190 mm). ^{131}I-IHDA was eluted with a mobile phase of ethanol/0.07 M aq. acetic acid 74/26 (v/v) at a flow rate of 0.7ml/min (UV 205 nm). Then 1 ml of isolated ^{131}I-IHDA was slowly suspended in 9 ml of 4% human serum albumin and passed over a 0.22 µm Millex-GV filter ready for oral administration. **Results:** At the nucleophilic exchange reaction in dry state, the addition of sodium bisulfite (20 µg) to the mixture prevented the formation of volatile ^{131}I during evaporation. The following solid phase reaction of 16-BrHDA with n.c.a. ^{131}I-NaI under catalysis ammonium acetate improved the labeling yield to 85%. ^{131}I-IHDA (tr=18 min) was separated quantitatively from the precursor 16-BrHDA (tr=15 min) by HPLC. Without further optimization 32 MBq n.c.a. ^{131}I-IHDA (46%) was obtained with a specific activity >3 MBq/µg. The RCP of ^{131}I-IHDA was assessed with radio-TLC and radio-HPLC by comparison with an authentic nonreactive reference sample and was >98%, remaining stable up to 24 hours. Sterility and apyrogenicity were tested according to the European Pharmacopeia. **Conclusion:** Radio-labelled long-chain aliphatic fatty acids are not commercially available in Europe anymore. We apply a synthesis pathway for fatty acid to the preparation of 131I-IHDA and demonstrated that a hospital radiopharmacy is able to prepare these tracers on demand for scintigraphic detection of lymphatic leakage lesions. (1)Kettner BI, et al. J Nucl Med 1998; 39: 2141-2144; (2)Angelberger P, et al.: in Radioaktive Isotope in Klinik und Forschung 1982, 249-264; (3)El-Wetery AS, et al. J. Radioanal Nucl Chem 1997; 222: 133-140

EP-0253

A new method for the preparation of astatine-211([211]At) and iodine-123(^{123}I) labelled amino acid analogues of phenylalanine, [211]At-Phe and ^{123}I-Phe, for radionuclide therapy and SPECT imaging applications

Y. Shirakami[1]*, H. Ikeda*[2,3]*, J. Hatazawa*[1]*;* [1]*Osaka University Graduate School of Medicine, Suita, JAPAN,* [2]*Cyclotron and Radioisotope center, Tohoku University, Sendai, JAPAN,* [3]*Research Center for Electron Photon Science, Tohoku University, Sendai, JAPAN.*

Purpose: This study aims to develop a new method for preparation of astatine-211([211]At) labelled phenylalanine ([211]At-Phe) using 4-borono-L-phenylalanine as a precursor molecule. [211]At (α particle emitter, $T_{1/2}$=7.2hr) is known as one of the promising nuclides for radiotherapy and behaves as a halogen, however, the analogy between astatine and iodine is not well elucidated yet since astatine has no stable isotopes. We investigated the chemical properties of [211]At comparing to those of radioactive (^{123}I) and stable isotopes of iodine. **Materials and Methods:** Astatine-211([211]At) was produced by a nuclear reaction of [209]Bi (α, 2n) [211]At at Research Centre of Nuclear Physics Osaka University and supplied as an aqueous solution. Iodine-123 (Na[123]I) was purchased from Japan Isotope Association (Tokyo).

4-Borono-L-phenylalanine (BPA) and other reagents were purchased from Nacalai tesque (Kyoto). An aliquot of BPA (10mg/ml) dissolved in 7% sodium hydrogen carbonate solution and the ^{211}At solution (5MBq/ml) was poured into a reaction vial. Then N-chlorosuccinimide (NCS, 4mg/ml) solution was dropped in the vial and the mixture was stirred for 30 minutes at room temperature. The reaction mixture was analyzed by a thin layer chromatography (plate: Silicagel 60, Merck; solvent: acetonitrile/methanol/trifluoroacetate=66/33.5/0.5) and an electrophoresis (strip: cellulose acetate membrane; electrolyte: 0.06M Baribital buffer solution, pH8.6) for the assessment of radiochemical yields. **Results:** ^{211}At-labelled phenylalanine was obtained from the reaction of ^{211}At and BPA by using NCS as an oxidizing agent. The borono-group in the precursor molecule, BPA, was replaced by ^{211}At resulting in the production of ^{211}At-4-astato-L-phenylalanine (^{211}At-Phe) with more than 90% of RCY. The high RCY was achieved under the mild reaction conditions at room temperature in 30 minutes. There is no need of protection groups on the precursor molecule which require a time consuming process of deprotection during a course of manufacturing. We also conducted the reactions by using ^{123}I and stable iodine as well instead of ^{211}At under the similar conditions and obtained the corresponding products, i.e., ^{123}I-Phe and I-Phe. The extraction mass of I-Phe, 291.983Da, was measured and the chemical form of 4-iodo-L-phenylalanine was confirmed by LC-MS. No other side products were observed in the reaction mixtures except for Phe which is the degraded product from BPA. **Conclusion:** ^{211}At-Phe was synthesized by using BPA and NCS as the oxidizing agent with high radiochemical yield. The borono-substituted molecule is convenient for a site specific labelling of ^{211}At under the mild reaction conditions. This work was supported by JSPS KAKENHI Grant number T16K102770.

EP-0254

Current status of stress myocardial perfusion imaging pharmaceuticals and radiation exposure in Japan: Comparison with European nuclear cardiology practice

R. Otsuka, Y. Miyazaki, N. Kubo, M. Kawahara, J. takaesu, K. Fukuchi; Osaka University Graduate School of Medicine, Suita, JAPAN.

Introduction: Because reducing the medical imaging radiation exposure, the use of ^{201}TlCl in stress myocardial perfusion imaging (MPI) have been decreased in many countries. In addition, American Society of Nuclear Cardiology published an information statement that a total radiation exposure of ≤9 mSv could be achieved in 50% of the studies in 2010. However, in Japan, many facilities still use ^{201}TlCl in MPI. In this study, we investigated the current status of radiopharmaceutical use in stress MPI and its radiation exposure in Japan. We also compare these data with IAEA Nuclear Cardiology Protocol Study of European countries (INCAPS-EU). **Subjects and Methods:** A nationwide survey was conducted from June through July 2016. The questionnaires on the radiopharmaceuticals used and their administered doses during stress MPI were sent to 641 nuclear medicine facilities which described that they performed stress MPI

on their website. The responses were collected and effective dose (ED) for an adult with standard body weight (60kg) was calculated. **Results:** The responses were collected from 431 facilities. Forty three facilities used only ^{201}TlCl, 35% used only ^{99m}Tc radiopharmaceuticals, and the remaining 22% used both. The two main reasons for using ^{201}TlCl than ^{99m}Tc radiopharmaceuticals were familiarity with the usage of ^{201}TlCl than ^{99m}Tc radiopharmaceuticals" and "apprehension about increasing the burden of physicians performing tracer injection twice". The mean ED of stress MPI was 14.0 ± 5.5 mSv and the percentage of the tests of EDs ≤ 9 mSv was 43.3 %. **Discussion:** Compared to mean ED of INCAPS-EU (8.7 ± 3.1 mSv), the Japanese ED estimated from our survey seemed to be higher. Despite only 2.8 % of MPI tests were performed using ^{201}TlCl in INCAPS-EU, more than 50% of the facilities still use ^{201}TlCl in Japan, the percentage of the tests of EDs ≤9 mSv was also smaller than INCAPS-EU (58.8 %).

EP-0255

Synthesis And Radiolabeling Of Temozolomide Loaded Solid Lipid Nanoparticles

K. Arı, S. Teksöz, C. Ichedef, E. Uçar, A. Yurt Kılçar, E. &. Medine; Ege University, Izmir, TURKEY.

Solid lipid nanoparticles are colloidal systems that have received considerable interest in recent cancer treatment research because of their biocompatibility, targeting of anticancer drugs and their ability to provide controlled release. In this study, it is aimed to synthesize radiolabeled solid lipid nanoparticles (SLN) as a carrier and imaging system for temozolomide (TMZ), an anticancer agent. Temozolomide loaded nanoaprticles (TMZ-SLN) were prepared by emulsification and low temperature solidification methods. Characterization and morphological properties of nanoparticles were determined by Dynamic Light Scattering (DLS), Zeta Potential Measurement (ZP) and Scanning Electron Microscopy (SEM) methods. The DLS analysis showed that the particle size was found as 120 ± 20 nm, the zeta potential value was measured as -30.4 mV. In addition SEM images show that the particles have a particle size ranging from 70-200 nm with spherical morphology. Drug loading capacity of of these solid nanoparticles was calculated as 49.25%. Radiolabeling yield of [^{99m}Tc(CO)$_3$]-TMZ and [^{99m}Tc(CO)$_3$]-TMZ-SLN were calculated as 99,3±0,35%, 90,04±0,3 % by Thin Layer Radiocromatography (TLRC) and High Performance Liquid Chromatography (HPLC). In this study, radiolabeled solid lipid nanoparticles were evaluated on U87 MG Glioblastoma-astrocytoma) and Daoy (human medulloblastoma) cell lines by in vitro. The results show that [^{99m}Tc(CO)$_3$]-TMZ-SLN did not show cytotoxic effect on both cell line. On the other hand TMZ showed IC50 values of 1241 μM and 501 μ M on U87 MG and Daoy cell lines respectively at 48 hours. When the binding activity on the cells was analyzed over time, it was observed that the highest binding efficiency for the [^{99m}Tc(CO)$_3$]-TMZ-SLN on the U87 MG cell line was found to be 33.36 ± 3.77 % at 240 minutes. This study was carried out by funding support of TÜBİTAK 1001 project. (Project no: 113S369)

EP-0256

Partition Coefficient,Plasma Protein Binding Percentage and Pharmacokinetic Studies of $^{99}Tc^m$-ZL and $^{99}Tc^m$-ZLM for New Bone-imaging Agents

H. Wang, P. Zou, M. Xie, Y. Liu, J. Wu, H. Wu; Jiangsu Institute of Nuclear Medicine, Wuxi, CHINA.

Aim: The purpose of this study was to evaluate partition coefficient,plasma protein binding percentage and pharmacokinetic of $^{99}Tc^m$-ZL (Zoledronate) and $^{99}Tc^m$-ZLM (2-(2-methyl-imidazol-1-yl)-1-hydroxyethane-1,1-diphosphonic acid). **Materials and Methods:** In this study, the preparation of $^{99}Tc^m$-ZL and $^{99}Tc^m$-ZLM were carried out by the reduction of $^{99}Tc^mO_4^-$ in the presence of stannous chloride. Partition coefficient of $^{99}Tc^m$-ZL and $^{99}Tc^m$-ZLM were obtained in n-octanol/water system. Plasma protein binding percentage of $^{99}Tc^m$-ZL and $^{99}Tc^m$-ZLM were tested. After intravenous injection $^{99}Tc^m$-ZL or $^{99}Tc^m$-ZLM in rats, blood was collected at 5min, 15min, 30min, 60min, 120min or 240min and the radioactivy of the samples was measured by γ-counter. **Results:** Radiochemical purity of $^{99}Tc^m$-ZL and $^{99}Tc^m$-ZLM determined by TCL were over 95%. Partition coefficient of $^{99}Tc^m$-ZL and $^{99}Tc^m$-ZLM were 16.54 and 7.44 at pH 7.40, respectively. Plasma protein binding percentage of $^{99}Tc^m$-ZL and $^{99}Tc^m$-ZLM were 17.40% and 18.88%, respectively. The elimination of $^{99}Tc^m$-ZL and $^{99}Tc^m$-ZLM from blood has a biexponential pattern. The important kinetic parameters of $^{99}Tc^m$-ZL and $^{99}Tc^m$-ZLM were as follows: $T_{1/2\alpha}$=1.506min and 2.731min, $T_{1/2\beta}$=53.140min and 35.888min, $V_{(d)}$=44.223ml and 19.992ml, K_{21}=0.265min^{-1} and 0.130min^{-1}, K_{12}=0.0345 min^{-1} and 0.056 min^{-1}, respectively. **Conclusion:** These results indicated $^{99}Tc^m$-ZL and $^{99}Tc^m$-ZLM had very rapidly and widely from blood to tissues. Their partition coefficient and plasma protein binding percentage were suitable for the drug requirement. So, $^{99}Tc^m$-ZL and $^{99}Tc^m$-ZLM may be very potential candidate for bone-imaging agents. **Keywords:** partition coefficient, plasma protein binding percentage, pharmacokinetic, $^{99}Tc^m$-ZL, $^{99}Tc^m$-ZLM

EP-0257

Design Of A Radiolabeled Polymeric Drug Carrier System $^{99m}Tc(CO)_3$-Oxaliplatin-PEG-PLA

K. Senocak, S. Teksoz, A. Yurt Kılçar, E. Uçar, B. Aydın; Ege University Institute of Nuclear Sciences, Izmir, TURKEY.

In recent years, polymer based colloidal systems are under investigation as drug carriers in order to develop biodistribution and accumulation of drugs in the target region. In this study, oxaliplatin, a chemotherapeutic drug, loaded polymer based nanodrug carrier system was designed. It is aimed to examine the radiopharmaceutical potential of the prepared system in vitro by radiolabeling with $^{99m}Tc(CO)_3^+$. In our study, technetium-99m was used as the imaging radionuclide with ideal half-life and gamma energy ($T_{1/2}$ = 6 hours, E_γ= 140 keV). As an anti-cancer agent model, oxaliplatin used for rectal and colon cancer treatment was chosen. Oxaliplatin loaded PEG-PLA polymeric nanoparticles were prepared and characterized by Dynamic Light Scattering (DLS) and Zeta Potential Measurement (ZP). The PEG-PLA polymeric nanoparticles dispersed in water had an average hydrodynamic diameter of 640 nm and a polydispersity index of 0.592. The zeta potential of the synthesized nanoparticles was measured as -14.8 mV. Oxaliplatin loaded nanoparticles were radiolabeled with $^{99m}Tc(CO)_3^+$ core. Then the quality control studies of the complex were carried out by TLRC (Thin Layer Radiocromatography) method. The radiolabelling yield of nanoparticles was found to be 92.31 ± 1.86. Finally, incorporation studies on cancer cells have been carried out. The data obtained in this study suggest that PEG-PLA nanoparticles radiolabeled with $^{99m}Tc(CO)_3^+$ may contribute to the use of these polymer based nanoparticles as a carrier system and an imaging agent for oxaliplatin. This study was carried out by funding support of Ege University Scientific Research Project. (Project no: 2012-NBE-014)

EP-0258

Evaluation of the SPECT Image Using Probe 123I-EISB for SPECT of the Systemic Amyloidosis

K. Kashiwa[1], K. Fukuda[2], Y. Ando[3], K. Tomiyoshi[4]; [1]Graduate School of Health Science, Department of Radiological Science Kumamoto University, Kumamoto, JAPAN, [2]Radiation Oncology, Yokohama City University Hospital, Kanagawa, JAPAN, [3]Graduate School of Medical Science, Department of Neurology,Kumamoto University, Kumamoto, JAPAN, [4]Department of Medical Physics, Faculty of Life Science, Kumamoto University, Kumamoto, JAPAN.

Aim: We synthesized 1-(2-123I-ethoxy)-2,5bis (phenylstyryl) benzene ([123I]EISB) and injected 123I-EISB to both of normal mice (NM) and amyloid mice (AM). Our aim is to examine visual and quantitative evaluation to compare SPECT/CT imaging for NM and AM with their bio-distribution. **Material and Methods:** 123I-EISB is a new imaging probe for detecting systematic amyloidosis with SPECT/CT examination. An FX3300 pre-clinical imaging system (Gamma Medica USA) was used to acquire SPECT and CT imaging. In 30 minutes after injected 123I-EISB in NM and AM, SPECT/CT imaging of NM and AM were obtained. The count/voxel (C/V) of liver and spleen both NM and AM were measured from SPECT/CT imaging. The mice were killed immediately after SPECT/CT imaging acquisition and tissues of interest were counted for its radioactivity. **Result:** From SPECT imaging, Counts/voxel(C/V) of Liver and Spleen in NM were 1696.2 and 76.9, and these C/V of Liver and Spleen in AM were 1511.9 and 608.0 respectively. Similarly, from radioactive counts of bio-distribution, Liver and Spleen in NM were 1383.7 +/- 719.9kBq and 12.4 +/- 1.9kBq/g and these in AM were 603.3 +/- 249.5 and 186.7 +/- 17.2kBq/g respectively. There were also a small different C/V between NM and AM in heart, large intestine, and kidney. **Conclusion:** There were a good correlation between C/V in SPECT/CT imaging and counts (kBq/g) in bio distribution. Based on a quantitative evaluation of SPECT/CT imaging, we were able to confirm the differences between NM an AM, but not able to confirm visual differences on the imaging between them.As a result, 123I-EISB is useful for detecting systematic amyloidosis with SPECT/CT quantitative evaluation

EP-0259

99mTc-Al2O3 - new radiopharmaceutical for sentinel lymph nodes visualization: first experience in oncogynecologic cancer patients

V. Chernov[1,2], R. Zelchan[1,2], Lyapunov A., Sinilkin I., Chernyshova A, Ochirov M., Kolomiets L., Medvedeva A.; [1]Tomsk National Research Medical Center of the Russian Academy of Sciences Cancer Research Institute, Tomsk, RUSSIAN FEDERATION, [2]National Research Tomsk Polytechnic University, Tomsk, RUSSIAN FEDERATION.

The purpose of the study was to evaluate the feasibility of using the new radiopharmaceutical, based on technetium-99m-labeled gamma-alumina (^{99m}Tc-Al_2O_3) in comparative to and 99mTc-fitat, for the detection of sentinel lymph nodes (SLN) in oncogynecologic cancer patients. **Materials and Methods:** Nanocolloid 99mTc-Al2O3 with size of nanoparticles 80-100 nm coated with organic covering was studied. During passage through the lymphatic way nanoparticles lose organic coating and strongly accumulate in the sentinel lymph nodes without redistribution. Nanocolloid 99mTc-fitat has size of nanoparticles 50-100 nm. The study included 60 patients with cervical cancer of stage $T_1a_2N_xM_0$ - $T_{1b1}N_xM_0$ and 17 patients with cancer corpus uteri of stage $T_1aN_xM_0$ - $T_{3a}N_xM_0$. To identify sentinel lymph nodes with cervical cancer patients a ^{99m}Tc-Al_2O_3 was administered to 30 patients (first group) and ^{99m}Tc-fitat was injected to 30 patients (second group). Patients with cancer corpus uteri were also divided into two groups. The first group of patients with cancer corpus uteri (5 patients) to determine SLN was injected a 99mTc-Al2O3 and 99mTc-fitat was injected to 12 patients (second group). Nanocolloid was injected paracervical in four points to 20 MBq one day prior to the planned operation. SPECT study was performed at 18 hours after injection, intraoperative detection was executed by gamma probe at 20 hours after injection. **Results:** In the first group in all cervical cancer patients 38 SLN were identified by SPECT and 43 SLN by gamma probe. In the first group in all patients of cancer corpus uteri 6 SLN were identified by SPECT and 8 SLN by gamma probe. Accumulation of 99mTc-Al2O3 in SLN was 7-11% by SPECT and 18-24% by gamma probe (in compare to spot of injection). In the second group by SPECT in cervical cancer 26 patients 32 SLN were identified and by gamma probe in 29 patients 39 SLN were visualized. In the second group by SPECT in 9 patients with cancer corpus uteri 14 SLN were identified and by gamma probe in 11 patients 18 SLN were visualized. Accumulation of 99mTc-fitat in SLN was 1.5-2% by SPECT and 3-7% by gamma probe (in compare to spot of injection). **Conclusions:** the clinical study of ^{99m}Tc-Al_2O_3, a new radiopharmaceutical agent, have shown that the studied nanocolloid has high uptake level in SLN and can be successfully used for visualization of SLN in patients with cervical cancer and cancer of corpus uteri.

EP-0260

Evaluation of the labeling parameters of 99mTc-Nanocoll-ICG® for multimodal imaging of the sentinel lymph node

J. Dinet[1], P. Bonijol[1], Q. Becheras[2], C. Faure[3], D. Daugeron[4], F. Giammarile[5], D. Kryza[5]; [1]GCS Lumen, Lyon, FRANCE, [2]Université Claude Bernard Lyon 1, Lyon, FRANCE, [3]Centre Léon Bérard, Lyon, FRANCE, [4]Université d'Auvergne, Montluçon, FRANCE, [5]Hospices Civils de Lyon - Université Claude Bernard Lyon 1, Lyon, FRANCE.

Introduction: Sentinel node (SN) mapping by colorimetric and isotopic methods increases the sensitivity and specificity of the detection. However, the use of patent blue can lead to severe anaphylaxis reaction with an estimated incidence rate of 0.5 to 1%. The aim of this study was to evaluate the indocyanine green (ICG) labeling conditions on ^{99m}Tc-colloidal albumin (^{99m}Tc-Nanocoll®) in order to propose a routine method for a bimodal tracer allowing the intraoperative guidance by gamma camera and the use of an optical camera in the surgical unit to facilitate the detection of the lymph nodes and their possible excision. **Materials & Methods:** ICG (Infracyanine® 25mg) was reconstituted in 10mL (5% glucose) and then diluted to obtain a 1mg.mL^{-1} concentration solution. Nanocoll® (GE healthcare) was prepared by adding 400 to 800 MBq of sodium pertechnetate in a volume of 2 mL (concentration at 0.25mg.mL^{-1}). After labeling with technetium 99m, 500-800 µL of ^{99m}Tc-Nanocoll® were added to 100-210 µL of the diluted ICG. Different labeling parameters such as time reaction and temperature on the binding kinetics of ICG have been evaluated. The binding efficiency of ICG was carried out using Amicon filters (Millipore®) and a UV-visible spectrophotometer. The radiochemical purity was determined according to the Nanocoll® manufacturer's instructions. A purification method using a sephadex G25 column (exclusion chromatography) was also evaluated. Finally, the binding stability of the ICG on the ^{99m}Tc-colloidal albumin as well as the emission spectra of ICG were determined over 72h. **Results & Discussion:** The binding efficiency of ICG on ^{99m}Tc-Nanocoll varied from 51 to 59% by mixing 500 µL of 99mTc-Nanocoll® with 150 µL of ICG for 30 minutes at room temperature. Heating at 37 ° C for 30 minutes allowed us to increase the yield to 64% without influence of an increase incubation time. The exclusion chromatography column purification method allowed us to obtain the bimodal tracer with a radiochemical purity> 99% and less than 1% of free ICG. Stability was greater than 24 hours, compatible with a 2 days SN protocol. **Conclusion:** The ^{99m}Tc-Nanocoll®-ICG bimodal tracer is an alternative to the use of patent blue. The labeling and purification conditions are compatible with a routine use. Studies on murine models are currently investigated to evaluate the *in vivo* influence of the purification method on the bimodal tracer uptake by the lymph nodes.

EP-0261

Optimization of affibody molecule for imaging of HER3 expression: negatively charged metal-chelator complex increases imaging contrast

S. S. Rinne[1], B. Mitran[1], C. Dahlsson Leitao[2], S. Ståhl[2], J. Löfblom[2], V. Tolmachev[1], A. Orlova[1]; [1]Uppsala University, Uppsala, SWEDEN, [2]KTH Royal Institute of Technology, Stockholm, SWEDEN.

Aims: In recent years HER3 has emerged as an attractive molecular target for anti-cancer therapy. The development of HER3-targeting therapeutics simultaneously demands development of

suitable methods for patient stratification. Radiolabeled affibody molecules have previously demonstrated to be suitable agents for imaging of HER3 expression *in vivo*. However, low target expression in tumors and high endogenous expression of HER3 especially in liver, remains to be a challenge in HER3-targeting. The combination of chelator and radionuclide can influence the biodistribution of affibody molecules and provides a tool for optimization of imaging sensitivity and specificity. The aim of this study was to investigate the influence of chelators NOTA, NODAGA, DOTA and DOTAGA on the biodistribution of anti-HER3 affibody molecule Z_{08698} labelled with indium-111. **Methods**: Chelators NOTA, NODAGA, DOTA and DOTAGA were conjugated to affibody molecule Z_{08698} via C-terminal cysteine. The constructs were radiolabeled with indium-111. Stability, binding specificity, and cellular processing were evaluated *in vitro* in HER3-expressing cell lines, BxPC-3 (pancreas carcinoma) and DU145 (prostate carcinoma). Binding affinity was measured using LigandTracer. Biodistribution was investigated in Balb/c nu/nu mice bearing BxPC3 xenografts at 4h and 24h pi. **Results**: All indium-111-labelled conjugates were stable *in vitro*. Specific binding to HER3 *in vitro* was preserved after labeling. Binding affinities were in low picomolar range for all conjugates. *In vitro*, overall internalization rate of radiolabeled conjugates was low and the majority of cell associated activity was membrane bound during observation time. Only minor differences were seen between tested conjugates and cells lines. *In vivo*, no significant differences in tumor uptake between conjugates were observed 4h and 24h pi. All conjugates showed elevated initial uptake in organs with endogenous expression of HER3, especially liver. Hepatic uptake at both time points was the highest for ^{111}In-Z_{08698}-NOTA, containing a positively charged chelator-radionuclide complex. ^{111}In-Z_{08698}-DOTAGA carrying a negatively charged complex at C-terminus had 2-fold lower uptake in liver than positively charged NOTA complex at 4h pi. Tumor-to-organ ratios did not differ significantly between NODAGA, DOTA and DOTAGA containing constructs. However, 24h pi ^{111}In-Z_{08698}-NOTA had about 2-fold lower tumor-to-blood-ratio (10.0±0.4) than the other conjugates (a range from 17 to19), due to slower blood clearance. **Conclusions**: The choice of chelator influences the biodistribution of indium-111 labeled anti-HER3 affibody molecules. Increase of negative charge of the chelator/metal complex at C-terminus facilitated blood clearance and reduced uptake in organs with endogenous expression of HER3 without significant influence on tumor uptake.

EP-0262

Preparation of 99mTc-labelled hydroxyapatite nanoparticles and their in vitro/in vivo characterisation

Z. Novy[1], M. Petrik[1], S. Gurska[1], J. Kozempel[2], M. Vlk[2], V. Lobaz[3], J. Kucka[3], M. Hruby[3], J. Drymlova[4], M. Hajduch[1]; [1]Palacky University Olomouc, Olomouc, CZECH REPUBLIC, [2]Czech Technical University in Prague, Praha, CZECH REPUBLIC, [3]Czech Academy of Science, Praha, CZECH REPUBLIC, [4]University Hospital Olomouc, Olomouc, CZECH REPUBLIC.

Purpose: Preclinical screening of selected hydroxyapatite (HAP) nanoparticles modified with various biocompatible polymers (HAP-PEG5000, HAP-POX5000, HAP-POX10000 a HAP-PHP-MA12000). The goal of this work was indirect radiolabeling of newly prepared nanoparticles with radioisotope 99mTc via clinically used radiopharmaceutical 99mTc-HDP and subsequently to verify the stability of such labelled nanoparticles *in vitro* and then to reveal their *in vivo* biodistribution in normal mice using microSPECT/CT system. The future intention of the project is to use these nanoparticles and 99mTc-HDP as two-staged imaging agent in visualisation of tumors based on enhanced retention and permeability (EPR) effect. **Subjects & Methods:** Studied nanoparticles were radiolabeled with 99mTc-HDP for 60 minutes in room temperature. Subsequently radiochemical purity control was employed using ITLC with two different mobile phases (ammonium acetate and acetone). Stability studies of labelled nanoparticles were performed in two environments - saline and human plasma (2h, 4h and 24h). *In vivo* microSPECT/CT biodistribution study was performed with labeled nanoparticles as well as with 99mTc-HDP itself and was registered 1h, 3h, 6h a 24h after application of studied compound. Cytotoxicity tests of chosen nanoparticles (in unlabeled form) were done using MTS method in six cell lines (B2, BJ, MRC5, HCT116, HCT116p53-/-, CCRF-CEM) employing high-throughput instrumentation with incubation time of 72 hours. The IC50s were calculated from obtained in vitro results. **Results:** Cytotoxicity of nanoparticles - studied nanoparticles were considered nontoxic according to their IC50s obtained using above mention cell lines (IC50 >1000 µg/mL resp. > 2000 µg/mL). Radiolabeling of all studied nanoparticles with 99mTc-HDP resulted in radiochemical purity over 90%. Stability studies of such prepared radiopharmaceutical revealed decrease in radiochemical purity of maximum 10.7% in saline and 11.0% in human plasma respectively after 24 hours. SPECT/CT imaging showed very specific biodistribution of nanoparticles concentrated in liver and spleen even 24 p.i. for all tested compounds. The accumulation of activity was observed in heart and bladder in earlier time points (1h and 3h p.i.). **Conclusion:** Tested nanoparticles show relatively facile radiolabeling with clinically used radiopharmaceutical 99mTc-HDP. Their stability in saline and human plasma is in highly satisfactory level. Biodistribution studies revealed significant accumulation in liver and spleen, whereas part of injected dose is excreted via kidneys. *In vitro* toxicity of the nanoparticles is relatively very low. All these parameters suggest the potential of these compounds for future studies aimed into tumor imaging based on EPR effect *in vivo*.

EP-0263

Cytotoxicity, In vitro binding and imaging evaluation of radiolabeled-DOTA-SP90 in 4T1 breast cancer model

M. Chen, Y. Huang, S. Lee, S. Lo, L. Chen, C. Chang; Institute of Nuclear Energy Research, Taoyuan City, TAIWAN.

Introduction: Targeted delivery of drugs to tumors represents a significant advance in cancer diagnosis and therapy. A new targeting peptide (SP90), which is capable of binding specifically to the cell surface of breast cancer cells, is identified by phage display system. This study investigated the cytotoxicity

of ^{177}Lu-DOTA-SP90 and in vitro binding and SPECT/CT imaging of ^{111}In-DOTA-SP90 in 4T1 mammary cancer cell line. **Methods:** SP90 was labelled with ^{111}In or ^{177}Lu in Institute of Nuclear Energy Research. Cytotoxicity assay was performed in 96-well plates. Each well was seeded with 1.5 x 10^3 cells. At 4 h after cell seeding, ^{177}Lu or ^{177}Lu-DOTA-SP90 (1 mCi,0.5 mCi,0.25 mCi,0.125 mCi and 0.0625 mCi) were added to each well of 96-well plates, respectively. After 48 h incubation of ^{177}Lu or ^{177}Lu-DOTA-SP90, the medium was replaced with fresh medium. Then, the cells were incubated at 37°C for 24 h. Cell viability was evaluated with alamarBlue assay. The binding assay of ^{111}In-DOTA-SP90 in 4T1 and CL1-5 cells was determined using a γ-counter. The 4T1 and CL1-5 cells were seeded in 24-well plates. After 24 hours incubation, 0.1 μCi of ^{111}InCl$_3$ or ^{111}In-DOTA-SP90 was added to the control well or to SP90 wells at intervals of 0.5, 2, 4, and 24 hours. In animal study, tumor xenografts were performed in 6-wk-old female BALB/c mice by subcutaneous injection of 2 x 10^6 4T1 cells. At 14 days after tumor inoculation, nanoSPECT/CT imaging was performed at 0.5, 2, 4, and 24 hours after injection of ^{111}In-DOTA-SP90. **Results:** The labeling efficiency of ^{177}Lu-DOTA-SP90 was more than 90%. The significant changes were found in the viability of 4T1 cells incubated with ^{177}Lu-DOTA-SP90 in 0.125, 0.25, 0.5 and 1 mCi group. No significant change of viability in 4T1 cells were observed in each ^{177}Lu group. In vitro binding assay showed that compared with control groups, significant high-binding affinity of ^{111}In-DOTA-SP90 in 4T1 cells. The high tumor-to-organ ratios for the ^{111}In-DOTA-SP90 (at 2 h after injection: tumor-to-muscle ratio, 7.6; and tumor-to-liver ratio, 2.3) were confirmed by nanoSPECT/CT images in the subcutaneous 4T1 tumor model. **Conclusions:** This study revealed that ^{177}Lu-DOTA-SP90 could improve the cytotoxic effect, and ^{111}In-DOTA-SP90 also showed the high-binding affinity in 4T1 mammary tumor cell line. The nanoSPECT/CT imaging demonstrated that ^{111}In -DOTA-SP90 could accumulate in tumor sites. These results suggested that potential benefit and advantage of ^{111}In-DOTA-SP90 was suitable as a diagnostic tracer for the imaging of breast cancer.

EP-0264

Radiolabeled AMO conjugated nanoparticle for in vivo tumor imaging in cervical cancer

L. Kang, *Y. Huo*, *R. Wang*, *C. Zhang*, *P. Yan*; *Peking University First Hospital, Beijing, CHINA.*

Anti-microRNA oligonucleotide (AMO) has been used for genetic regulation and as a potential therapeutic agent. However, the low ability to pass through the cell membrane and lack of proof in target delivery in vivo limits AMO success in vivo application. Meanwhile, nanotechnology provides potential and effective vectors for target delivery in vivo. Therefore, in this study, AMO-phospholipids conjugates were developed to overcome the AMO backbone structures and to enhance the AMO delivery efficiency, and was further radiolabeled with ^{99m}Tc for tumor imaging in tumor xenografts. ^{99m}Tc radiolabeled miR-155 targeted AMO with partial 2'-OMe and PS chemical modification was prepared via the conjugation to NHS-MAG3. This radiolabeled AMO was then linked with phospholipids as a component of nanoparticles to embed the hydrophobic part. AMO-phospholipids with cationic lipids and DSPE-PEG2000 were fused to form AMO-phospholipid enveloped nanoparticle (AMO-DSPE). Radiolabeled AMO-DSPE was confirmed by gel electrophoresis and evaluated for its serum stability, inhibitory ability and cellular uptake in HeLa cells. Moreover, the biodistribution and in vivo imaging were performed HeLa tumor bearing mice. The labeled AMO-DSPE showed good conjugation between AMO and DSPE at the ratio more than 1:3 by gel electrophoresis. It showed highly stable in human serum. Western blotting results showed that the unconjugated and conjugated AMOs could up-regulate its target C/EBPβ protein, one of target proteins of miR-155 in HeLa cells, proving the ability in the specific binding and inhibition. The cellular uptake of ^{99m}Tc labeled AMO-DSPE was significantly higher than that of unconjugated AMO. After the system administration, the distribution and in vivo imaging results revealed the significant difference between ^{99m}Tc labeled AMO-DSPE and negative control probe in HeLa tumor xenograft models, which suggested the specific binding and effective delivery ability of ^{99m}Tc labeled AMO-DSPE in vivo. Therefore, This study supports the effectiveness and efficiency of cellular and in vivo delivery of ^{99m}Tc radiolabeled AMO-DSPE in cervical tumor and suggests a prospective candidate for future tumor imaging.

EP-0265

Proof of Concept for Nucleolipids as potential SPECT tracer: Synthesis and Evaluation of Uridine derived Nucleolipid as Targeted Imaging Agent

S. Mishra[1], S. Chaturvedi[1], A. Kaul[1], S. Paul[1], P. Barthélémy[2], B. Singh[3], A. K. Mishra[1]; [1]Division of Cyclotron and Radiopharmaceutical Sciences, Institute of Nuclear Medicine and Allied Sciences, Delhi, INDIA, [2]INSERM U869 and Université de Bordeaux, Bordeaux,F-33076, FRANCE, [3]Department of Chemistry, Banaras Hindu University, Varanasi, INDIA.

Objective: Nucleosides are structural modules and play fundamental role in all biosystems. Their enhanced uptake in the rapidly proliferating cells like tumor leads to a differential concentration vis a vis normal cells. This differential concentration build up is the key to their application in imaging of cellular proliferation and results in the required contrast for imaging. The work was undertaken primarily with the aim to explore the potential of nucleolipid as imaging agent capable of penetrating a non-compromised blood brain barrier (BBB). Presently, brain tumor imaging is dominated by positron emitting radionuclide labelled tracers which include fluorine labelled FDG, FLT and FIAU. The tracers even though selective for tumors cannot cross the intact BBB and cannot detect early stages when the BBB has not been compromised. Nucleolipids can provide a solution for both selectivity by virtue of being nucleoside based and penetrating BBB because of the high lipophilicity. **Materials and Methods**: Uridine has been conjugated with 16- hentriacontanone at 2', 3' using ketal linkage. The resulting nucleolipid was conjugated with DTPA that serves as the chelator for radionuclide (NL-DTPA). For comparison, non-lipidic analog of uridine with DTPA

has also been synthesized (NS-DTPA).The compounds and intermediates have been characterized through NMR and Mass spectrometry. After radiolabeling, the NL-DTPA and NS-DTPA have been evaluated for brain entry. Cytotoxicity studies were performed using HEK cell lines through SRB and MTT toxicity assay. ^{99m}Tc radiolabeling was performed using stannous tartarate. Biodistribution and SPECT imaging studies have been carried. **Results:** Multi-step synthesis leads to the final compound (NL-DTPA) with a yield of 85% and m/z was observed at 1050. Parallel NS-DTPA was also synthesized and characterized. The cytotoxicity studies (SRB and MTT) using HEK cell lines indicate no appreciable toxicity upto 72h. Radiolabeling with stannous tartarate lead to high radiolabeling efficiency of 98% for NL-DTPA and 99.83% for NS-DTPA. The complexes (^{99m}Tc-NL-DTPA and ^{99m}Tc-NS-DTPA) were found to be stable over a period of 24 h. The bio-distribution studies show 1.6% I.D/g uptake in brain at 5 min for NL-DTPA as against 0.6% I.D/g for NS-DTPA. Excretion follows hepatic and renal route. **Conclusion**: In the work, we have attempted to modify the nucleolipid as a SPECT tracer by appending with the acyclic chelator DTPA, known to be an excellent chelator for ^{99m}Tc. Initial studies indicate better penetration ability of NL-DTPA as compared to NS-DTPA. Further work will concentrate on targeting of NL-DTPA in brain tumor model.

EP-0266

Exendin-4 labeled with ^{99m}Tc, ^{111}In and ^{68}Ga - a comparative pharmacokinetics evaluation

B. Janota, U. Karczmarczyk, E. Laszuk, P. Garnuszek, R. Mikołajczak; National Centre for Nuclear Research Radioisotope Centre POLATOM, Otwock, POLAND.

Introduction: The ^{99m}Tc-HYNIC-Ahx-^{14}Met-Exendin-4 imaging of GLP-1 receptors has been documented in patients with insulinoma and MTC in our earlier studies [1]. However, the oxidation of ^{14}Met may compromise the receptor affinity of this tracer to GLP-1 receptors *in vivo*. Explored methods used for preventing the oxidation of methionine are the addition of L-methionine to the radiolabeling mixture or replacing the ^{14}Met with norleucine (Nle). Aim: To investigate an influence of the method for enhancing ^{14}Met oxidation on the Exendin-4 derivatives pharmacokinetics in normal Swiss mice. **Materials and Methods:** ^{99m}Tc-HYNIC-Ahx-^{14}Met-Exendin-4, ^{99m}Tc-HYNIC-Ahx-^{14}Nle-Exendin-4, ^{99m}Tc-HYNIC-Ahx-^{14}Met-Exendin-4 (with L-Methionine to prevent oxidation of ^{14}Met), ^{68}Ga-NODAGA-Ahx-^{14}Nle-Exendin-4 and ^{111}In-DTPA-Ahx-^{14}Met-Exendin-4 were administered intravenously to mouse. For each investigated tracer the mass of the injected peptide was 0.28 μg. The biodistribution of the radiolabelled peptides was assessed at different time points (10 min, 0.5 h, 1 h, 2 h, 4 h, 24 h) except for ^{68}Ga-NODAGA-^{14}Nle-Exendin-4, which was investigated at: 10 min, 0.5 h, 1 h, 2 h, 3h p.i.v. GraphPad Prism software was applied for non-linear regression analysis of pharmacokinetics data. **Results and Conclusion:** All tested Exendin-4 derivatives were successfully labelled with ^{99m}Tc, ^{111}In and ^{68}Ga with radiochemical yields over 90% controlled by HPLC and TLC. The obtained specific activities, SA, were 105 GBq/μmol for: ^{99m}Tc-HYNIC-^{14}Met-Exendin-4, ^{99m}Tc-HYN-IC-^{14}Nle-Exendin-4, ^{99m}Tc-HYNIC-^{14}Met-Exendin-4 (with L-Methionine) and ^{111}In-DTPA-^{14}Met-Exendin-4, and 31 GBq/μmol for ^{68}Ga-NODAGA-^{14}Nle-Exendin-4. The pharmacokinetics data showed tracers accumulation in organs naturally expressing GLP-1R (stomach, lungs, pancreas) and rapid clearance from the blood ($T_{1/2}$ ca. 0.2h). Out of the five compared complexes, ^{111}In-DTPA-^{14}Met-Exendin-4 and ^{99m}Tc-HYNIC-^{14}Met-Exendin-4 (with L-Methionine) showed the highest uptake in GLP-1R positive organs (lungs: 17.2 %ID/g and 12.7 %ID/g, pancreas: 16.3 %ID/g and 9.2 %ID/g, stomach: 1.9 %ID/g and 2.5 %ID/g, respectively, at 30min p.i.v.). Kidneys were the critical organ with significant uptake of the radioactivity. For ^{99m}Tc labelled Exendine-4 derivatives the radioactivity concentration in kidneys decreased (from 100-150 %ID/g at 10min p.i.v. to 15-30 %ID/g at 24h p.i.v.), whereas for the ^{68}Ga-NODAGA-Exendin-4 and ^{111}In-DTPA-Exendin a time dependent association of radioactivity in kidneys was observed (from 130-140 %ID/g at 10 min p.i.v. to > 200 %ID/g at 3-24h p.i.v.). These pharmacokinetics results suggest ^{99m}Tc-HYNIC-^{14}Met-Exendin-4 (with L-Methionine) may have higher diagnostic potential than the derivatives in which ^{14}Met was replaced with Nle, however this still needs to be confirmed clinically. **References:** [1] A. Sowa-Staszczak et.al., Eur J Nucl Med Mol Imaging 2013, 40:524-531 [2] D. Pach et.al., J. of Endocrinology 2013, ID 384508, http://dx.org/10.1155/2013/384508

EP-0267

Radiolabeling and preclinical assessment of ^{188}Re-HYNIC-trastuzumab for Radioimmunotherapy

B. Alirezapour[1,2], M. Davarpanah[2], S. Rajabifar[1], H. Abbasi[2], B. Aziz Kalantari[2], F. Johari Daha[1], M. Hashemizadeh[2], E. Maadi[2], N. Soltani[2], H. Masoumi[2], S. Moradkhani[2]; [1]Nuclear Science and Technology Research Institute, Tehran, IRAN, ISLAMIC REPUBLIC OF, [2]Pars Isotope Company, Tehran, IRAN, ISLAMIC REPUBLIC OF.

Purpose: Radiolabeled monoclonal antibodies have shown great promise for cancer diagnosis and therapy. Trastuzumab is a humanized IgG1 monoclonal antibody directed against the extracellular domain of the Human Epidermal Growth Factor Receptor2 (HER2). HER 2 receptor is overexpressed in 20-30% of the early-stage breast cancers and these patients may be candidates for Herceptin treatment. Has been attempted to label trastuzumab with ^{188}Re ($T_{1/2}$ = 16.9 h, E_β- max= 2.12 Mev, Eγ= 155 KeV (15%)) through using (HYNIC) BFC in order to shows that trastuzumab and radiation treatment combined will increase therapeutic efficacy. In this regard, cell based assays as well as biodistribution studies in HER2$^+$ cell lines and normal mice have been performed, respectively. **Methods:** The high radionuclide and radiochemical purity of the ^{188}Re-perrhenate solution was eluted from ^{188}W/^{188}Re generator which was manufactured by Pars Isotope Company**.** Trastuzumab was conjugated with HYNIC. HYNIC-trastuzumab was labeled with ^{188}Re then Radiochemical purity as well as immunoreactivity, Cell Cytotoxicity and internalization studies by SkBr3 cell line (HER2$^+$ cell line) and serum stability of ^{188}Re-HYNIC-trastuzumab were determined. The biodistribution studies and radioimmunoscintigraphy were performed in normal mice (^{188}Re-HYNIC-trastuzumab i.v., 100 μl,

25±5 μg mAb, 12, 24 and 48 h). **Results:** [188]Re-HYNIC-trastuzumab was prepared (RCP >97% ± 0.8, Specific activity 4.8 ± 1.2 μCi/μg).. Labeling yield with [188]Re in 400μg concentration of bio-conjugate was 93.1% ± 2.4. Immunoreaction of [188]Re-HYNIC-trastuzumab complex towards HER2 antigen was determined by RIA and the complex showed high immunoreactivity towards HER2. *In vitro* and *in vivo* stability of radioimmunoconjugate was investigated respectively in PBS and blood serum by RTLC method. *In vitro* stability was more than 88% ± 2.1 in PBS and 70% ± 3.1 in serum over 24 h. The Immunoreactivity of the radiolabeled trastuzumab towards SkBr3 cell line was done by using Lindmo assay protocol. Under these conditions, the immunoreactivity of the radioimmunoconjugate was found to be 0.76. Cell Cytotoxicity study by MTT assay showed increased effects of [188]Re-HYNIC-trastuzumab on cell death of HER2-overexpressing breast cancer cell in camparison to unlabeled trastuzumab. The biodistribution of [188]Re-HYNIC-trastuzumab complex in the normal mice at 12, 24 and 48 h after intravenous administration, expressed as percentage of injected dose per gram of tissue (%ID/g). The accumulation of the radiolabeled antibody in lungs, liver, spleen and other tissues demonstrates a similar pattern to the other radiolabeled anti-HER2 immunoconjugates. **Conclusion:** [188]Re-HYNIC-trastuzumab is a potential compound for Radioimmunotherapy of HER2 expression in oncology.

EP-0268

Validation of alternative methods for quality control of [^{99m}Tc-EDDA-HYNIC-D-Phe[1], Tyr[3]]-Octreotide

M. A. Hernandez Fructuoso[1], S. Ruiz Llama[2], B. Santos Montero[1], C. Beltran Gracia[2], E. miñana Olmo[1], J. Castell Conesa[1]; [1]Hospital Universitari Vall d'Hebron - Institut de Diagnòstic per la Imatge, Barcelona, SPAIN, [2]Hospital Universitari Vall d'Hebron, Barcelona, SPAIN.

Purpose: During the labeling of [^{99m}Tc-EDDA-HYNIC-D-Phe[1], Tyr[3]]-Octreotide, 3 impurities can be produced: [99m]TcO$_4^-$, ^{99m}Tc-colloidal and ^{99m}Tc-coligand (^{99m}Tc-EDDA). The method of radiochemical purity testing (RCP) according to the summary of product characteristics (SPC-method), only evaluates [99m]TcO$_4^-$ and ^{99m}Tc-colloidal. The aim of this study is to validate an alternative method of RCP testing that quantifies the ^{99m}Tc-EDDA to obtain more accurate RCP values. **Material and Method**: We compared three different methods. SPC-method: 1 ITLC-SG strip with acetonitrile / water (1: 1) to determine ^{99m}Tc-RH and 1 ITLC-SG strip with MEK for [99m]TcO$_4^-$. Method-1: 1 ITLC-SG strip with 0.1M sodium citrate to determine [99m]TcO$_4^-$ and ^{99m}Tc-EDDA. Method-2: Sep-Pak®C-18 with 95% Ethanol and NaCl0.9%. The ^{99m}Tc-EDDA was prepared adding 5 μg SnCl2 * 2H2O + 0.25 mg EDDA + 5 mCi [99m]TcO4^{-} and heating for 20 minutes. The RCP of ^{99m}Tc-EDDA was determined by both methods. Unpaired t-test analysis was used (GraphPad Prism). **Results**: The RCP of the ^{99m}Tc-Octreotide (n = 10) according to the SPC-method was superior to the other methods (97.70 ± 0.38%), with statistical significant differences: SPC versus Method-2 (p <0.0001) and method- SPC versus Method-1 (p <0.0001). Using method-1 we obtained higher values (93.30 ± 0.66%) than method-2 (91.51 ±

0.62%), statistically non-significant (p = 0.0604). ^{99m}Tc-EDDA (n = 12) RCP using method-1 was 97.96 ± 0.30% and with method-2 was 92.75 ± 1.05%, which showed statistical significant differences (p <0.0001). We verified that the corresponding activity of the ^{99m}Tc-EDDA is eluted in Sep-Pak® fraction A (NaCl0.9%) (method-1) and Rf value is 1 in ITLC sodium citrate (method-2). The ^{99m}Tc-EDDA Rf value is 0 for ITLC-SG MEK) and Rf = 1 for ITLC-SG Acetonitrile / water, as well as for ^{99m}Tc-Octreotide. **Conclusions**: Using the method of RCP testing recommended by SPC we do not separate the ^{99m}Tc-EDDA impurity because it has the same Rf value as ^{99m}Tc-Octreotide. We recommend the use of these alternative methods that allow the determination of all the impurities and so we will obtain more accurate RCP values.

EP-15 during congress opening hours, e-Poster Area

Radiopharmaceuticals & Radiochemistry: Radiopharmacy

EP-0269

Theranostic probe Lu-177-DOTA-NIR790 for multimodal diagnosis and therapy of cancer

C. Peng, Y. Shih, P. Chiang, Y. Kuo, T. Luo; Isotope Application Division, Institute of Nuclear Energy Research, Taoyuan, TAIWAN.

Cancer-targeted theranostic probe labeled with radionuclides has been developed to provide multi-modalities for NIR fluorescence (NIRF) and nuclear imaging and for photothermal therapy (PTT) and radiotherapy of cancer. In this study, we prepared NIR dye-based probe DOTA-NIR790, which could be chelated with Lu-177 for nuclear imaging and radiotherapy of cancer. In addition, the dye allowed the probe to have multi-functions in NIR imaging and photothermal therapy. Animal experiments confirmed that ^{177}Lu-DOTA-NIR790 could target to tumor for SPECT imaging and near-infrared fluorescence imaging as cancer detection. The SPECT/CT images showed a high detection capability for deep tumor, and NIRF images showed a better tumor-targeted image in the superficial tumor. The ^{177}Lu-DOTA-NIR790 also delayed the tumor growth by beta-emission. After laser irradiation, the tumor temperature could be effectively increased to about 48.6 °C, resulting in tumor ablation. The cancer-targeted theranostic probe(^{177}Lu-DOTA-NIR790) had been developed to provide multi-modalities for NIR fluorescence and SPECT imaging and for PTT and radiotherapy of cancer.

EP-0270

Stability assessment after reconstitution and investigation of the biodistribution in a pre-clinical mouse model of 99mTechnetium-Sestamibi (Cardiovis™)

C. Mak[1], S. A. Barker[1], J. K. Sosabowski[2], J. M. Foster[2], N. G. Hartman[3]; [1]UCL School of Pharmacy, London, UNITED KINGDOM, [2]John Vane Science Centre, Queen Mary University, London, UNITED KINGDOM, [3]Barts Health NHS Trust, London, UNITED KINGDOM.

Background: ^{99m}Tc-Sestamibi is used clinically as a cardiac imaging agent for the diagnosis of coronary heart disease. This study aims to investigate its stability in a range of storage conditions and to evaluate its biodistribution in a pre-clinical mouse model. **Methods:** ^{99m}Tc-Sestamibi (Cardiovis™, ROTOP Pharmaka GmbH, Germany) was reconstituted as per the Summary of Product Characteristics (SPC). Aliquots were stored at 4-7°C, 20-22°C and 35°C, with radiochemical purity (RCP) testing being conducted initially and every 2 hours for 14 hours, using instant Thin Layer Chromatography as described by the UK Radiopharmacy Group. Separate aliquots were adjusted to pH 4, 6, 7.4, 8 and 10 with phosphate buffer and stored at 20-22°C, with RCP analysis at time 0 and 4, 8 and 12 hours. ^{99m}Tc-Sestamibi was administered via the tail vein to a BALB/c mouse (1 year, male, 34 g, anaesthetised with isoflurane), to assess its overall biodistribution. Dynamic planar images and SPECT/CT images were obtained using a NanoSPECT/CT® system (Mediso). Dynamic planar images were taken at the rate of 200 frames per second immediately post injection. A CT scan of the mouse was conducted 20 minutes post injection and was followed by a 30 minute SPECT acquisition. **Results:** ^{99m}Tc-Sestamibi (Cardiovis™) reconstituted as per the SPC showed RCP stability at all three conditions studied (4-7°C, 20-22°C, 35°C) for 14 hours. Reconstituted samples stored at pH 4 and 6 showed RCP stability at 20-22°C for 12 hours, with progressively higher pHs leading to lower RCP stability. Planar images showed that ^{99m}Tc-Sestamibi was taken up into the heart rapidly after injection, reaching a peak of 56 % uptake at 3 seconds, reducing to a steady state of 8 % uptake at 50 seconds post injection. ^{99m}Tc-Sestamibi was rapidly cleared renally, with measureable amounts being detected 4 seconds post injection, rising very rapidly to a steady state of 62 % uptake thereafter. SPECT/CT imaging allowed a clear 3-dimensional view of the myocardium of the mouse, with radioactivity also being detected in other organs. **Conclusion:** This study suggests that ^{99m}Tc-Sestamibi is stable for longer and over a wider temperature range than stated in the SPC, supporting short-term excursions from these recommended storage conditions (maximum 25°C for 12 hours). The in vivo imaging in the mouse is broadly similar to that observed in humans, but shows greater cardiac uptake (8 % cf 1.5 %), due to differences in mouse and human physiology.

EP-0271

Evaluation of the physicochemical properties of ^{99m}Technetium-Exametazime (Medi-Exametazime™) and its biodistribution in a pre-clinical mouse model

W. Ahmed[1], S. A. Barker[1], J. Sosabowski[2], J. M. Foster[2], R. Soanes[3], N. Hartman[3]; [1]UCL School of Pharmacy, London, UNITED KINGDOM, [2]John Vane Science Centre, Queen Mary University, London, UNITED KINGDOM, [3]Barts Health NHS Trust, London, UNITED KINGDOM.

Background: ^{99m}Tc-Exametazime is utilized clinically in the diagnosis of neurodegenerative diseases. The aims of this study were to explore its stability, physico-chemical properties and biodistribution in a pre-clinical mouse model. **Methods:** ^{99m}Tc-Exametazime (Medi-Exametazime™, Radiopharmacy Laboratory Ltd,

Hungary) was reconstituted as per the Summary of Product Characteristics (SPC). Aliquots were stored at 20-22°C and tested for radiochemical purity (RCP) over 5 hours, using instant Thin Layer Chromatography as described in the SPC. Lipophilicity (logP) of the radiolabelled product was assessed using the octanol-water shake-flask partition method. Protein binding of the unlabelled product (Medi-Exametazime™ reconstituted with 0.9 %w/v NaCl) was assessed by comparing the UV absorbance of a 4 %w/v bovine serum albumin solution in the presence and absence of the ligand. ^{99m}Tc-Exametazime was administered via the tail vein to a C57 mouse (male, 45.92 g, anaesthetised with isoflurane), to assess its overall biodistribution. Dynamic planar images and SPECT/CT images were obtained using a NanoSPECT/CT® system (Mediso). Dynamic planar images were taken for 300 seconds immediately post injection. A SPECT scan of the mouse was conducted 20 minutes post injection and was followed by a CT scan. The CT and SPECT scans were repeated 3 hours post injection. **Results:** ^{99m}Tc-Exametazime (Medi-Exametazime™) reconstituted as per the SPC showed RCP stability at 20-22°C for 90 minutes post reconstitution, 30 minutes longer than is stated in the SPC. The stability of the product decreased thereafter. Planar images showed that ^{99m}Tc-Exametazime was taken up into the brain fairly rapidly after injection, reaching a peak of 13 % uptake at 25 seconds. Radioactivity was retained in the brain over the duration of the study, with circa 3 % of the original dose being retained at both 1 and 3 hours post-injection. ^{99m}Tc-Exametazime was also taken up by the heart and kidneys. SPECT/CT imaging allowed a clear 3-dimensional view of the biodistribution of the tracer. Log P was measured as 1.1 suggesting that ^{99m}Tc-Exametazime is somewhat lipophilic. ^{99m}Tc-Exametazime demonstrated limited protein binding at 11 %. Both of these data help explain the uptake of the tracer into the brain and other tissues. **Conclusions:** This study suggests that ^{99m}Tc-Exametazime is stable for slightly longer than stated in the SPC. The in vivo imaging in the mouse is broadly similar to that observed in humans, but shows greater brain uptake and retention, presumably due to differences in mouse and human physiology.

EP-0272

Validation of a Cost Effective Alternative Radiochemical Purity Analysis Method

F. P. Ekoume[1,2], S. M. Rubow[2], H. H. Boersma[3]; [1]Yaounde General Hospital, Yaounde, CAMEROON, [2]Stellenbosch University, Cape Town, SOUTH AFRICA, [3]University Medical Center, Groningen, NETHERLANDS.

Introduction: In low-income settings, it may not be possible to use compendial analytical methods or expensive equipment for radiochemical purity (RCP) testing of Tc-99m labelled radiopharmaceuticals (RP). All radiochemical analysis methods should be validated against compendial or otherwise proven methods. To ensure the efficacy of RP prepared at Yaoundé General Hospital (YGH), this study compared a cost effective routine chromatographic method using counting equipment available at YGH, against the method used at the GMP

compliant radiopharmacy at the University Medical Center Groningen (UMCG). **Aim:** To validate a cost effective routine chromatography method using counting equipment available at YGH, by comparison against the method used at the GMP compliant radiopharmacy at the UMCG. **Experimental Methods:** MIBI, HMDP and DMSA kits currently used at YGH were reconstituted with freshly eluted sodium pertechnetate as described by the manufacturer and spiked with eluate of the same generator to reach different sample concentrations. Five µl of Tc-99m-RP was spotted on a 1x10 cm strip of iTLC-SG medium as stationary phase (2 cm from the lower end of the strip). The strips were developed in appropriate mobile phases. Each strip was first scanned on the chromatogram scanner used routinely at UMCG (standard method), and thereafter the strip was cut in 2 pieces and radioactivity from each portion of the chromatogram was counted with the RadEye B 20 survey meter, equivalent to that available at YGH (proposed method). The percentage of radiochemical purity of each strip was calculated for each counting method. The validation parameters, as well as acceptance criteria used were those recommended by pharmacopeia, ICH-guidelines and regulatory bodies. For statistical analysis, Student's paired t-test was used. A value of p less than 0.05 was considered significant. Chromatography results using the survey meter at YGH will be reported. **Results:** The proposed method using the RadEye counter proved to be linear (r^2 more than 0.99 for all 3 radiopharmaceuticals), precise (RSD less than 2%), and specific, with a clear separation of impurity from the labeled compound on the chromatogram. The method was also robust, with no influence of environmental factors such as the humidity or operative variable of the chromatography performance. **Conclusion:** The proposed method compared well with the standard method and is reliable to determine radiochemical purity. The validated method can easily be used in any low-income unit.

EP-0273

Analysis of the new rules of clinical trials with drugs in Spain

*L. Sanz-Ceballos, Á. Ramírez-Navarro, **J. García-Redondo**, J. M. Llamas-Elvira; Hospital Universitario Virgen de las Nieves, Granada, SPAIN.*

Introduction: Clinical Trials (CT) within the world of Nuclear Medicine have greater relevance given the significant development of new radiopharmaceuticals in recent years. The new Regulation of the European Parliament and the Council on CT of medicines for human use (536/2014) repeals Directive 2001/20/EC. The Spanish State promulgated the Royal Decree (RD) 1090/2015 that incorporates and repeals the previous (RD 223/2004), developing local aspects of national legislation. **Objective**: To analyze the main changes introduced by the RD 1090/2015 to regulate medicine CT, the Committees for Research Ethics medicines (CREM) and the Spanish Registry CT from the previous regulations. **Material and Methods**: We compared RD 1090/2015 front RD 223/2004 and differences between the two standards were analyzed. **Results:** The RD 1090/2015 provides

as novelties: - Creation of concept "low level of intervention CT", subject to less stringent rules on monitoring, content master file or traceability, while maintaining security. - It develops the concepts of "auxiliary medicinal product" and "temporary halt". - Authorization CT: just an evaluation with a positive opinion of one accredited Ethics Committee and the approval of the Competent Authority. It expires in 2 years if not recruit any subject and it is required to publish results a year after the date of completion. - Only record CT with two parts: Part I (documentation for the European Union, EMA) and part II (national documentation, AEMPS). All data will be sent to a database and a web portal of the European Union public. It develops the Spanish Registry of clinical studies regulations. - It incorporates the figure of the representative legally designated for incapable and minor subjects and stipulates new conditions in emergency situations, pregnant and breastfeeding periods, as well as the informed consent. - Creation of "promoter of non-commercial clinical trials", to promote research within the National Health System and the Universities. - It defines key dates: Start, completion and early termination of a CT. - It distinguishes the Ethics Committee of Clinical Research (ECCR) from CREM and additional requirements to be met by ECCR who want to be accredited as CREM. There is active participation of patients in decisions that concern them, and their inclusion in these committees. **Conclusions:** RD 1090/2015 deepens transparency and simplified administrative procedures. It expedites and promotes the realization of simultaneous multi-center studies in Europe. It increases efficiency in communication and evaluation processes and it improves the delineation of responsibilities of all stakeholders.

EP-0274

Overview of 2.5 years experience of manual synthesis of in-house 68Ga labelled radiopharmaceuticals using non metallic 68Ge/68Ga column generator: An institutional experience

***B. S. Shetye, Sr.**, P. Monteiro, M. Pathan, V. Rangarajan; Tata Memorial Hospital, Mumbai, INDIA.*

Introduction: Doorstep availability of self-shielded, GMP complied generator provided in-house facility of labelling of 68Ga labelled radiopharmaceuticals. It has given us ease of synthesis as per patient requirement. Hence, we evaluated labelling performance of ITG 68Ge/68Ga generators (n=5, 30 mci) for synthesis of 68Ga-DOTANOC and 68Ga-HBED-PSMA-11 by optimising its use. **Subjects and Methods:** Conjugate of peptide DOTANOC and HBED-PSMA-11 were procured from ABX, Germany. Labelling was done manually in internally shielded fluidic module. $68Ga^{3+}$ was obtained using 0.05N HCl as eluent. 25µg of DOTANOC peptide and 5µg of DKFZ- PSMA 11 peptide in 0.25M sodium acetate buffer, C-8 (DOTANOC), C-18 (PSMA) cartridge were used in labelling procedure. 1 to 2 labelling procedures were done per day to optimise use of generator keeping minimum interval of 4 hrs between two elutions to obtain optimum elution yield. Radiochemical and radionuclidic purity, stability of the product were determined. RCP was performed by ITLC method using 0.1M sodium citrate as a sol-

vent. **Results:** Total 618 labelling procedures (68Ga-DOTANOC =236, 68Ga-PSMA = 382) were performed using 5 generators. Low yield of final product 23-50% for DOTANOC (n=49) and PSMA (n=16) was reported. Labelling efficiency of 68Ga-DOTANOC as 68% (n=31, STDEV= 0.062 pH= 5.5) and 68Ga-PSMA as 78% (n=8, STDEV= 0.046, pH= 5.5) was reported using 1st generator. To improve labelling efficiency operational errors were minimised by conditioning cartridge at a time to start elution, maintaining desired temperature, preventing contamination of reagents. Using 2nd generator labelling efficiency for 68Ga-DOTANOC as 76% (n=38, STDEV= 0.003) and 68Ga-PSMA as 76%(n= 40, STDEV= 0.005) was obtained. It improved further in the range 77 to 79 % for DOTANOC and 76 to 80 % for PSMA for remaining generators. Radiochemical purity was >96 % for 68Ga-DOTANOC and >98% for 68Ga-PSMA. In-vitro stability of the product was evaluated up to 2 hrs. It was more than 94%. 68Ge breakthrough in the final product was zero which confirmed purification effectiveness of C-8 and C-18 cartridge. **Conclusion:** Our data exhibited good labelling efficiency and consistent RCP results for labelled 68Ga radiopharmaceuticals by implementing proper protocols. It will facilitate use of 68Ge/68Ga generator for in-house 68Ga labelling pharmaceuticals widely and cost effectively.

EP-0275

Computer platform for radiopharmaceuticals prescription

J. García-Redondo, E. Morillo-Martínez, Á. Ramírez-Navarro, J. M. Llamas-Elvira; Hospital Universitario Virgen de las Nieves, Granada, SPAIN.

Introduction: The development of computer systems in health care is modifying certain aspects of clinical practice. With the appearance of the digital medical history, an electronic system for the prescription of radiopharmaceuticals used in different Nuclear Medicine services is necessary. **Aim:** To implement a computer tool for radiopharmaceuticals prescription. **Material and Methods:** Computer tool developed in Java language whose database is located in the Oracle management system. It has double communication with digital medical history and Medical appointment computer application. On the other hand this platform allows access to different options according to professional category, allowing prescription of the radiopharmaceutical by the physician, the preparation of a clinical history with the most important aspects for exploration to be carried out by the nursing staff and the access of the radiopharmacy staff to the prescription data of the radiopharmaceutical for later dispensation. In addition, it offers a compilation of the most relevant data of the patient and the radiopharmaceutical for further elaboration of the clinical report by the physician. **Results:** This computer tool has made possible to unify in a single system the prescription, nursing history, dispensation and registry. It has also facilitated the preparation of the medical report, compiling the most relevant data about patient and radiopharmaceutical, as well as recording all the prescriptions made in the Nuclear Medicine Service. **Conclusions:** This computer system improves the previous prescription method incorporating

new functions that streamline the entire procedure and adapts to the framework of computer development that is being imposed on our daily practice of care.

EP-0276

Leukocyte scintigraphy : biologic criteria for the decision of realization of the scintigraphy using the benchmark method of in vitro 99mTc-HMPAO (Ceretec®) granulocytes labeling

K. Casagrande[1], J. Woillard[2], I. Quelven[1]; [1]CHU Dupuytren, Nuclear Medicine Department, Limoges, FRANCE, [2]CHU Dupuytren, Pharmacology and Toxicology Department, Limoges, FRANCE.

Purpose: 99mTc-HMPAO labeled granulocytes imaging is the benchmark technique for leukocyte scintigraphy. It requires an *in vitro* labeling involving blood handling and a complex cells separation. In accordance with gamma-cameras performances, we established that 99mTc-labeled leukocytes activity must be higher than 185MBq to be administrated to patients. Otherwise labeled cells are not injected and a less specific and less sensitive alternative method is performed: 99mTc-Leukoscan®, a single-injection technique with *in vivo* radiolabeling. The aim of this study is to set out a biologic criterion which is predictable of the possibility to complete the scintigraphy with the *in vitro* labeling method, avoiding that this heavy, time-consuming and expensive preparation procedure was realized uselessly. **Material and Methods:** From December 2014, for 101 patients which underwent leukocyte scintigraphy, we collected: neutrophils count (PNN), sedimentation rate (VS) and activity obtained after labeling. Receivers operating characteristic (ROC) curves were constructed using Medcalc© to determine a threshold value of PNN or VS above which the examination can be completed using the *in vitro* benchmark labeling method with satisfactory sensitivity and specificity. As references values differ, two groups were considered for the VS depending of the VS measurement method used: sedimentation (visual or automated) (n=91) or red blood cells aggregation (TEST 1 - Alifax®) (n=10). **Results:** The ROC curve area under the curve (AUC) was not significant for PNN. For the VS measured with sedimentation method the AUC was 0,920 (95% CI: 0,843 - 0,966) and the threshold value, determined by Yuden index, was 5mm with sensitivity (Se) and specificity (Sp) of 97,7% and 75% respectively. For the VS determined by aggregation the AUC was 0,625 (95% CI: 0,283 - 0,893); Se and Sp were 50% and 100% respectively for a 18mm threshold value. **Conclusion:** The VS seems a predictive factor to estimate the success of *in vitro* 99mTc-HMPAO labeling method. According to the VS determination method, the predictive threshold value differs. For aggregation method, we need to increase number of patients to obtain significant value. Regarding sedimentation method, VS was higher than 5 mm in 97,7% of leukocyte scintigraphy performed using the *in vitro* method and in 75% of cases that we had to switch to *in vivo* method, the VS was 5 mm or lower. We propose to use the VS with a cut-off of 5 mm (when measured by sedimentation) as the biological criterion to determine the preferential labeling method to realize leukocyte scintigraphy.

EP-0277

Optimization of Gallium-68 radiolabelling methods : feedback in Centre Jean Perrin cancer institute

H. Nicolas[1], M. Tempier[1], P. Auzeloux[2], M. Galmier[2], S. Tarrit[2], F. Cachin[1,2], R. Chevrier[1], S. Levesque[1]; [1]CRLCC Jean Perrin, Clermont ferrand, FRANCE, [2]Université Clermont d'Auvergne, INSERM U1240, Imagerie Moléculaire et Stratégies Théranostiques, Clermont ferrand, FRANCE.

Introduction: In France, ^{68}Ga-labeled compounds are not widely used, as they are mainly injected in the framework of clinical trials or compassionate use. However, since 2016 a pharmaceutical grade [68]Ge/^{68}Ga generator (Galliapharm®, Eckert&Ziegler) is now available. We managed to optimize both manufacturing and analytical control processes of [^{68}Ga]Ga-DOTA-NOC in order to allow the use of this radiotracer for clinical applications. **Subjects and Methods:** The manufacture of [^{68}Ga]Ga-DOTA-NOC was performed in an automated synthesis module Mini-AIO (TRASIS), using the process without pre-purification of the generator eluate (Acetate buffer, 110°C/7 min, HLB purification cartridge). Three criteria affecting synthesis yield were evaluated: quality of eluate, reconstitution and transfer of peptidic precursor available in France and final filtration step. Simple and fast analytical procedure to evaluate radiochemical purity was developed and validated using radio-HPLC. **Results:** Thirteen [^{68}Ga]Ga-DOTA-NOC synthesis, allowing the optimization of our methods, were realized. The total production duration is about 26 min. Regarding the quality of gallium chloride eluate, in order to obtain a sufficient synthesis yield (>50%, decay-corrected) a correlation study shows the generator must be pre-eluted twice at most 48 hours before the production (p=0.00003). The Iason peptidic precursor vial cannot be used and we must dissolved DOTA-NOC in 1 mL of acetate buffer 0.7N before it transfer into a suitable vial compatible with the automated radiosynthesis. Concerning the sterilizing filters, there is a significant difference of percentage of the final product retained between the two references used (19.5% Millex®-GS **vs** 10.6% Sterifix®). Regarding the radio-HPLC method used for both determinate chemical and radiochemical purity, the use of an isocratic method (Poroshell C18 column, TFA in acetonitrile 70:30) allows a short time of analysis (r_t=5.35 min) compatible with a clinical use. This method was validated: linearity r^2>0.99, limit of detection 0.145 µg.mL^{-1} with p=0.01 and limit of quantification 0.236 µg.mL^{-1} with p=0.01). **Conclusion:** Trasis method of production of [^{68}Ga]Ga-DOTA-NOC was adapted with success in our Radiopharmacy unit. Radiochemical yield is 59% (74% decay-corrected, n=6) and all quality controls required for the pharmaceutical delivery, including radio-HPLC, can be done in less than one hour after starting generator elution.

EP-0278

Routine GMP production of ^{68}Ga-radiopharmaceuticals using two [68]Ge/^{68}Ga generators in sequence

G. M. Franssen[1], M. van Riel[1], D. Gerrits[1], R. Bongaerts[1], C. M. van Rij[1], S. Kropf[2], H. J. Wester[2], P. Laverman[1]; [1]Radboud university medical center, Nijmegen, NETHERLANDS, [2]Scintomics GmbH, Furstenfeldbruck, GERMANY.

Objective: The introduction of GMP-certified or even approved [68]Ge/^{68}Ga generators and the development of several automated synthesis modules dramatically increased the acceptance of ^{68}Ga radiopharmaceuticals in nuclear medicine. Due to the decrease of output due to parent decay and the short half-life of the daughter [68]Ga(III) (68 minutes), it would be favorable to elute several generators in sequence for radiopharmaceutical production. Our aim was to develop a safe, fast and efficient method for the elution of two [68]Ge/^{68}Ga generators in sequence for the routine clinical production of ^{68}Ga radiopharmaceuticals using a Scintomics GRP 4V module. **Method:** The elution of two generators in sequence was performed on a Scintomics GRP 4V module (Scintomics GmbH, Fürstenfeldbruck, Germany) connected to two [68]Ge/^{68}Ga generators, (1850 MBq, GalliaPharm®, Eckert and Ziegler, Berlin, Germany). Generators were two and seven months old, respectively. Elution of the generators was performed fully automatic, using a custom-made cassette for the valves 16-20. Elution was done via valves 19 and 20, connected to a standard ABX labeling cassette (SC-01) via valve 7 for the production of ^{68}Ga-HBED-cc-PSMA, ^{68}Ga-DOTA-TOC, ^{68}Ga-DOTA-[RGD]$_2$ and ^{68}Ga-NODAGA-exendin. To minimize decay during the elution of the second generator, first the oldest, then the second generator was eluted, each with 8 mL 0.1 N HCl. The lines were flushed with 2 mL of WFI. Eluates of both generators directed to and concentrated on a single PS-H$^+$ cartridge and eluted for production of one of the four ^{68}Ga-radiopharmaceuticals. Yield was measured using a dose calibrator, quality control included RP-HPLC, ITLC (colloid), pH, endotoxin and sterility testing and [68]Ge breakthrough measurement. **Results:** With the same amount of precursor, high activity amounts ^{68}Ga-radiopharmaceuticals with high specific activity were produced. Yield was up to 1.6 times higher as compared to a single generator production. Radiochemical purity (> 98%), pH and ^{68}Ga colloid (<2%) were comparable. No [68]Ge was detected by gamma spectroscopy after decay (< 0.001%). Endotoxin levels were < 10 EU/mL, all products proved sterile. Total synthesis time was only 8 min longer as compared to a single generator production. **Conclusion:** We developed a fully automated, GMP-compliant method to produce ^{68}Ga-radiopharmaceuticals in high activity amounts using two generators in sequence allowing for a much more efficient and economical use of the [68]Ge/^{68}Ga generators.

EP-0279

Establishment of Glomerular Filtration Rate reference values measured by 51Cr-EDTA clearance in patients over 75 years

I. Gil-Viciano[1], I. Romero-Zayas[1], P. Saldaña-Gutiérrez[2], M. Roca-Engronyat[1], E. Pineda-Fernández[1], M. Bueno-Raspall[1], A. Rodriguez-Gasén[1], J. L. Vercher-Conejero[1], L. Gracia-Sánchez[1], J. Rodríguez-Rubio[1], L. Rubio-Alvarez[1], C. Munuera-Sañudo[1], N. Calvo-Malvar[1], C. Gamez-Cenzano[1]; [1]Radiopharmacy Unit and Nuclear Medicine-

PET Department. IDI. Hospital Universitari de Bellvitge-IDIBELL., L'Hospitalet de Llobregat. Barcelona. Spain., SPAIN, 2Medical Physics Department. ICO., L'Hospitalet de Llobregat. Barcelona. Spain., SPAIN.

Aim: In the literature there are no normal values for patients over 75 years, because data come from kidney donors. So, for elderly patients values for 75 years are used as the reference. The aim of the study was to assess how the Glomerular Filtration Rate (GFR) depends on age in patients over 75 years and to establish our own population reference values. A second aim was to compare our reference values with those calculated from the equation for patients up to 75 years recommended by the *"Guidelines for the measurement of glomerular filtration rate using plasma sampling. Nucl Med Commun 2004;25:759-769"* and find out if this is useful for elderly patients. **Material and Methods**: GFR was performed to 93 cancer patients aged 75-87 years with no other associated pathology and normal renal function. The GFR was determined with ^{51}Cr-EDTA, according to the method recommended by the guidelines. Blood samples were taken at 2, 3 and 4h post-injection. The correlation between the values of GFR and age of each patient was performed to obtain an equation to calculate our own population reference interval values. These data were compared with the values calculated with the equation recommended in the guidelines, notwithstanding it is only for patients aged between 50 and 75 years. **Results**: Our 93 GFR values followed a normal distribution with a ±2SD of ±29 mL/min/1.73m^2, instead of 24 mL/min/1.73m^2 that was found in the literature to patients up to 75 years. The dependence of GFR on age was, *GFR=185,66-1,4152*age* and the root mean squared error (RMSE) of the predicted values with our equation respect sample values was 13.9. Using guidelines equation, *GFR=148-age*, the RMSE was 14.9. The observed differences in the RMSE were statistically significant (p=0.03). The reference interval values (mean ± 2SD) of our population were: 46-103 ml/min/1.73m^2 whereas the values according literature equation were: 46-94 ml/min/1.73m^2. **Conclusions**: It has established our own GFR references values for patients over 75 years from our population. Our equation is more accurate to obtain the GFR and the reference values for elderly patients because its RMSE was lower than the used in the guidelines adopted by the British Nuclear Medicine Society, as it is based on experimental results.

EP-0280

Peptides labelling with ^{64}Cu and ^{68}Ga on heterogeneous phase using a microfludic system

*D. Seifert, M. Kleinova, A. Cepa, J. Ralis, P. Hanc, **O. Lebeda**; Nuclear Physics Institute of the CAS, Rez, CZECH REPUBLIC.*

We present a new approach in peptides labeling on a solid phase in a microfluidic system. It is composed from a chip out of PMMA matrix containing 20 mg of the c18t reverse phase filled in a volume of 100 μl. The chip allows for labeling on solid phase at elevated temperatures up to 100 °C. The labeling was performed in the three steps: adsorption of a selected peptide from liquid to solid phase, applying activity on the chip from the same mobile phase, elution of the labeled compound with an organic mobile phase. The product needn't be further purified. As a model peptide we chose DOTA-TOC and labelled it with ^{64}Cu. The system was chosen intentionally, because DOTA chelator isn't suitable for copper isotopes. DOTA-TOC (60 mg) dissolved in water (0.5 ml) was applied on the microfluidic čhip activated with 2 ml of water and 2 ml of EtOH and finally washed with 0.1M MES mobile phase at pH = 5.5. The chip was heated up to 95 °C. The flow-rate was set to 0.1 ml/min. After reaching the set temperature, the Cu-64 activity was injected in the chip in the amount of 300 MBq in the volume of 0.3 ml in 0.1 M MES at pH = 5.5 achieving retention of 90%. The activity was then eluted with 0.1 ml of EtOH (180 MBq, not decay corrected). The labeling yield reached 60 % after 25 min. Radiochemical purity determined with HPLC was 98 %. Labeling technique on the PMMA microfluidic chip with a suitable sorbent seems to be very promising and simple method. Even without any optimizing, we obtained product of very high radiochemical purity and in reasonable yield.

EP-16   **during congress opening hours, e-Poster Area**

Radiopharmaceuticals & Radiochemistry: Radiometals

EP-0281

Holmium-166 Phytate: From Suspension To Microspheres

*E. Szemenyei, S. Keresztes, N. Halász, Z. Kiss-Gombos, P. Buszlai, D. Zsolnai, **J. Környei**; Institute of Isotopes Co. Ltd., Budapest, HUNGARY.*

Aim: Holmium-166 phytate suspension injection is registered in Hungary for radiosynoviorthesis. Low leakage (less than 0.9% totally, after 24 hrs) indicates stable bonds between holmium and phytate within the particles of 0.5-1.2 μm size. The aim of the present pilot study is to utilize these strong interactions also for much larger particles. The concept is to bind phytate to carrier particles with anion exchanger properties, followed by labelling with holmium-166. **Materials and Methods:** Phytic acid dodecasodium salt came from Sichem (Germany). Phytate carriers like Dowex-1x2 (Sigma-Aldrich, 200-400 mesh, 40-80 μm, 'DO1') and YMC-BioPro-Q30 (YMC Europe, Germany, 30 μm, 'MS30') were chosen. Natural holmium was irradiated in research reactor (Budapest and Swierk-Otwock). Carriers were loaded with phytate solution of 25 mg/mL at pH=7. Washed and dried samples of the phytate-covered carriers were labelled with various volumes of holmium-166 precursor containing 5 mg/mL Ho and 75-225 MBq activities, by simple mixing and incubation at room temperature. Molar ratios between holmium and phytate were adjusted to 2:1 (like in the original suspension), furthermore to 3:2 and 2:3. Labelled samples were washed in several steps. The released holmium-activities were measured and the bound-holmium/phytate molar ratios were calculated. **Results:** 10 mL 'DO1' with capacity of 0.6 meq/mL bound 660 mg phytate. During washing, phytate release was

below the detection limit (0.1 mg/mL). In case of „MS30" microspheres, a volume of 10 mL bound 97.2 mg phytate (only 12% of the capacity). After labelling, holmium-release from phytate-covered 'DO1' was found at the adjusted molar ratios of Ho/Phy = 2:1 and 3:2 but stable holmium-binding was at Ho/Phy = 2:3. In case of 'MS30' holmium-release was observed at each adjusted molar ratios with asymptotically decreasing Ho content to Ho/Phy = 1:3. **Conclusions:** 'DO1' and 'MS30', covered by phytate, can bind holmium at Ho/Phy = 2:3 and 1:3, respectively. The higher Ho-binding of 'DO1' can be explained by the higher density of functional groups ensuring that phytate molecules are nearer to each other. On the other hand, the stable Ho/Phy ratio (2:3) is really less than that of the suspension (3:2), indicating that a part of the phosphate groups of the phytate cannot interact with holmium since they are bound to the carrier. Since Ho/Phy molar ratio of 1:3 could be sufficient to attain a specific activity of 2.5 GBq holmium-166/g carrier, microspheres with higher ion exchange capacity should be chosen for further developments.

EP-0282

Optimal molecular design of radiocopper-labelled affibody molecules

V. Tolmachev[1], C. Yim[2], J. Garousi[1], Y. Yue[3], S. Grimm[3], J. Rajander[2], A. Perols[3], M. Haaparanta-Solin[2], T. J. Grönroos[2], O. Solin[2], A. Orlova[1], C. Anderson[4], A. Eriksson Karlström[3]; [1]Uppsala University, Uppsala, SWEDEN, [2]Turku PET Centre, Turku, FINLAND, [3]KTH Royal Institute of Technology, Stockholm, SWEDEN, [4]University of Pittsburgh, Pittsburgh, PA, UNITED STATES OF AMERICA.

Aim: Clinical affibody-based imaging at several hours after injection improves discrimination between metastases with high and low HER2 expression. The use of long-lived copper positron-emitting isotopes might be preferable for this purpose. Earlier, ^{64}Cu-NODAGA-ZHER2:S1 and ^{64}Cu-NOTA-ZHER2:S1 affibody molecules demonstrated suboptimal imaging at 6 and 24 h p.i., presumably because of release of radiometabolites from kidneys. The aim of this study was to evaluate if the use of a cross-bridged chelator 4,11-bis(carboxymethyl)-1,4,8,11-tetraazabicyclo[6.6.2]hexadecane (CB-TE2A) for radiocopper-labelling of affibody molecules would improve imaging contrast. **Materials and Methods:** CB-TE2A was conjugated to N-terminus of synthetic ZHER2:342 affibody molecules using either glycine (conjugate designation CB-TE2A-G-ZHER2:342) or glycine-triglutamate (CB-TE2A-GEEE-ZHER2:342) as a spacer. The triglutamyl spacer was used since earlier studies demonstrated that increase of negative charge at N-terminus of affibody molecules reduces hepatic uptake. Biodistribution of ^{64}Cu-CB-TE2A-G-ZHER2:342 and ^{64}Cu-CB-TE2A-GEEE-ZHER2:342 in BALB/C nu/nu mice bearing HER2-expressing SKOV-3 xenografts was measured at 2, 6 and 24 h p.i. and compared with biodistribution of ^{64}Cu-NODAGA-ZHER2:S1, which had the best targeting properties in the previous study. Ramos lymphoma xenografts were used as a HER2-negative control. **Results:** CB-TE2A-G-ZHER2:342 and CB-TE2A-GEEE-ZHER2:342 were labelled with ^{64}Cu with an isolated yield of 80-90%. The radiochemical purity of conjugates was over 98%. The specific activity was ~29 GBq/μmol. Both conjugates demonstrated specific binding to HER2-expressing cells in vitro. Uptake of both ^{64}Cu-CB-TE2A-GEEE-ZHER2:342 and ^{64}Cu-CB-TE2A-G-ZHER2:342 in HER2-postive SKOV-3 xenografts at 2 h (14.5±4.8 and 16.8±1.9 %ID/g, respectively) was significantly (p< 0.001) higher than the uptake in HER2-negative Ramos xenografts (0.16±0.02 and 0.40±0.06%lD/g, respectively). This demonstrated that targeting of HER2 in vivo was highly specific. There was no significant difference between tumour uptakes of different conjugates at any time point. The renal uptake of all variants decreased between 2 and 24 h p.i. The pattern of uptake of conjugates in other normal organs was quite different. The uptake of NODAGA-conjugated variant increased with time in blood, liver, lung, spleen, stomach, muscle and bone, while uptake of CB-TE2A-conjugated variants decreased with time. Uptake of ^{64}Cu-CB-TE2A-GEEE-ZHER2:342 in normal tissues was typically lower than the uptake of ^{64}Cu-CB-TE2A-G-ZHER2:342. The most pronounced was a sevenfold difference in the hepatic uptake. ^{64}Cu-CB-TE2A-GEEE-ZHER2:342 provided the best tumour-to-organ ratios. At optimal time point, 6 h p.i., tumour-to-blood and tumour-to-liver ratios were 185±66 and 13±4, respectively. **Conclusion**: The use of the cross-bridged chelator CB-TE2A in combination with the trigutamyl spacer is the most preferable approach to labelling of affibody molecules with radiocopper.

EP-0283

Radiometals Production by only one Solid Target System

M. Malinconico[1,2], F. Boschi[1], G. Guidi[1], C. Lang[2], J. Asp[2], P. Takhar[2]; [1]COMECER SPA, Castelbolognese, ITALY, [2]SAHMRI, Adelaide, AUSTRALIA.

Aim: Ga-68, Cu-64 and Zr-89 are radionuclides widely used in studies of selective tumor targeting. The aim of this work is to demonstrate the feasibility of production of all these metal isotopes by only one automated Solid Target system. The system uses dedicated disposable cassette and specific automatic recipes for each production avoiding any cross-contamination. **Materials and Method:** By irradiation of a solid target via (*p,n*) nuclear reaction Ga-68, Cu-64 and Zr-89 can be produced. Nickel and Zinc powders were electroplated into a shuttle, commercial yttrium foil was inserted in. ^{64}Ni plating, ^{68}Zn plating and ^{89}Y foil were bombarded with an energy range 12-15MeV by a medical cyclotron (with a typical current from 35uA to 10uA). After irradiation, the shuttles were transferred fully automatically to the dissolution module. Every irradiated targets were dissolved in HCl: Cu-64 by hot 6M acid, Zr-89 by drop-by-drop acid and Ga-68 by hot 10M HCl. The dissolved solution was purified to recovery the enriched starting material and collect the final product: a dedicated disposable kit was used to process the radio-metal to completely avoid cross-contamination between the different productions. Dissolution and purification steps were managed by automatic recipes. Cu-64 and Ga-68 were eluted from an ion

exchange resin in ^{64}Cu- and ^{68}Ga-chloride form, with respectively 6M HCl and 1M HCl. ^{89}Zr-oxalate was obtained eluting an hydroxamate resin with 1M oxalic acid. All phases (electroplating, delivery to cyclotron, dissolution and purification) were executed automatically by the Comecer ALCEO Solid Target. This system is composed by one irradiation unit, one dissolution/transfer unit and one purification module. Using dedicated dissolution circuits and disposable purification kits is possible to avoid cross-contamination. **Results:** In succession within few days, productions of Ga-68, Cu-64 and Zr-89 were performed using only one Solid Target automatic system (updated Comecer ALCEO) . The electroplating yields were up to 90%. The found EOB yield were up to 2mCi/uAh for 64Cu, up to 0,45mCi/uAh for 89Zr and the saturation yield for 68Ga was 25mCi/μA. The isotopes were produced with very high radio-purity and high chemical-purity. **Conclusion:** This work describes one possible way to produce different PET-isotopes (Ga-68, Cu-64, Zr-89) with a medical cyclotron and only one commercial Solid Target System, using the updated Comecer ALCEO.

EP-0284
Radiolabeling with ^{68}Ga and ^{44}Sc in a capillary reactor

D. Szikra[1], G. Nagy[2], G. Trencsényi[1], N. Dénes[1], V. Forgács[1], E. Berényi[1], I. Garai[2]; [1]University of Debrecen, Debrecen, HUNGARY, [2]Scanomed Ltd., Debrecen, HUNGARY.

Aim: A capillary system, designed for the optimization of labeling conditions chelators with ^{68}Ga and ^{44}Sc, was applied to choose the best chelator from the examined derivatives. The system was modified in order to handle larger activities. **Materials and Methods:** The operation of the capillary system is based on the coinjection of the reagent solutions into a heated loop. The labeling reaction takes place among stopped flow conditions in order to minimize activity loss. The reaction mixture is injected onto a HPLC column for the determination of radiochemical yield or purification of the product. **Results:** Maleimide derivatives of DOTA, DOTAGA, NOTA and NODA-GA chelators were used as model compounds, and their radiolabeling yield was compared in the case of ^{68}Ga and ^{44}Sc using 10-10 ul chelator and radiometal solutions. DOTAGA and NODAGA redivatives were found to be applicable for both radiometals. NODAGA RGD was used to test the scale up capabilities of the system. 100 ul gallium and 100 ul peptide solution was injected into a 200 ul loop, and heated for 10 minutes. After chromatographic separation on a Kinetex column, the product could be collected in 250 ul volume. The eluate was evaporated to dryness and the labelled product was redissolved in PBS (80% overall yield) and used in preclinical experiments. **Conclusion:** Besides the fast optimization of labeling conditions, the constructed capillary system can be used for labeling with higher activities. The online coupled HPLC system enables the precise determination of radiochemical yield. After the determination of optimal reaction conditions, the system can be converted to preparative scale by simply changing the reactor loop.

EP-0285
High yield separation of ^{67}Cu from irradiated zinc targets

P. Martini[1,2], A. Boschi[3], M. Pasquali[1,2], G. Cicoria[4], L. Mou[2], C. Rossi Alvarez[2], S. Carturan[2], S. Canella[2], J. Esposito[2], L. Uccelli[5,3], A. Duatti[6], F. Haddad[7], T. Sounalet[7], G. Pupillo[2]; [1]University of Ferrara, Physics Department, Ferrara, ITALY, [2]Legnaro National Laboratories, National Institute for Nuclear Physics (LNL-INFN), Legnaro (Pd), ITALY, [3]University of Ferrara, Laboratory of Nuclear Medicine, Department of Morphology, Surgery and Experimental Medicine, Ferrara, ITALY, [4]Department of Nuclear Medicine, St. Orsola Hospital, Bologna, ITALY, [5]Department of Nuclear Medicine, St. Anna Hospital, Ferrara, ITALY, [6]University of Ferrara, Deparment of Chemical and Pharmaceutical Sciences, Ferrara, ITALY, [7]GIP ARRONAX, Saint-Herblain, FRANCE.

The radionuclide ^{67}Cu is still attracting considerable interest owing to its favorable nuclear properties for theranostics. It decays through the emission of a medium-energy β-particle (E_β =141keV) and γ-radiation (E_γ =185keV), which makes it suitable for both therapy and diagnosis. Production of ^{67}Cu is very challenging due to the very low cross-sections of all potential reactions. Generally, ^{67}Cu can be produced using zinc targets eg. by ^{68}Zn(p,2p) reaction, which requires high energy and high intensity proton beams and long irradiation times. Under these irradiation conditions, a variety of radionuclides are generated including ^{67}Ga ($T_{1/2}$=3.2617d), which presents the same γ-lines of ^{67}Cu and heavily interferes with the measurement of ^{67}Cu yield. This work was aimed at investigating a highly efficient separation process of Cu radioisotopes from the Zn target and, in particular, from the Ga impurities. Therefore, this procedure could be employed for the precise measurement of the nuclear cross-sections of the various possible routes to ^{67}Cu production and for yield optimization studies. Ion-exchange solid phase extraction was employed as separation method. In preliminary simulation experiments, a mock solution containing the cold metal ^{nat}Zn was spiked with radionuclides impurities tracers ^{65}Zn, ^{64}Cu and ^{68}Ga. The separation procedure comprised the following steps: removal of Ga isotopes by passing the radioactive solution through a cation exchange resin; evaporation of the resulting solution to adjust the HCl concentration and purification of Cu isotopes from bulk zinc by anion exchange resin. Once optimized, the procedure was applied for ^{67}Cu extraction in five irradiation runs performed by proton bombardment of a Zn metallic target. The yield of the chemical process was checked for each irradiated target foil by considering the activity of tracer radionuclides (^{61}Cu, ^{66}Ga, ^{65}Ga) before and after application of the chemical procedure. The complete procedure lasted approximately four hours and the preliminary recovery yields of all tracer radionuclides in each final solution was determined by HPGe γ-spectrometry (^{64}Cu:99.43%, ^{68}Ga:99.15% and ^{65}Zn:99.91%). Data of chemical yields from irradiated targets are under elaboration. The new separation procedure allowed a quantitative separation of the elements Cu, Zn and Ga based on the optimized efficiency of the ion exchange resins. It is worthy to note that this procedure can be easily automated and remotely controlled to ensure an effective operator's radiopro-

tection and to maximize the reproducibility of the separation process. Furthermore, it can be readily translated to obtain sterile and high purity ^{67}Cu solutions for human use.

EP-0286

Production of Sc radionuclides by separation of scandium from calcium target using UTEVA resin

D. Pawlak, W. Wojdowska, J. L. Parus, M. Żółtowska, P. Garnuszek, R. Mikołajczak; National Centre for Nuclear Research Radioisotope Centre POLATOM, Otwock, POLAND.

Introduction: Significant interest in medical applications of scandium radioisotopes (Sc-43, Sc-44, Sc-47) has been recently observed. Due to its favorable nuclear properties ^{44}Sc ($t_{1/2}$=3.927 h, 94.3% β$^+$, E_{max}=1474 keV) and ^{43}Sc ($t_{1/2}$=3.97 h, 88.1% β$^+$, E_{max}=1198 keV) are radiometals holding great potential for PET application. Their therapeutic 'twin' is ^{47}Sc ($t_{1/2}$=3.35 d, $E_γ$ = 159.4 keV (68.3%), Eβ$^-_{max}$=600 keV). This low-energy β$^-$ emitter can be utilized for targeted radiotherapy thus Sc offers an ideal theranostic set of radionuclides. All these radionuclides can by produced by either proton or neutron irradiation of appropriate enriched calcium targets, followed by chemical separation of Sc. From the number of various methods of scandium separation from calcium we investigated the extraction chromatography with UTEVA resin (Triskem International) [1]. **Materials and Methods:** To simulate a target dissolution mixture, 10 mL of solutions containing 40 mg of Ca and 0.3 μg of Sc in 9 M HCl spiked with either ^{46}Sc (50 kBq) or ^{45}Ca (100 kBq) was loaded on the column containing 130 mg of UTEVA resin (Dipentyl Pentylphosphonate, DPPP, as extractant). Then, the column was rinsed with 5 ml of 10 M HCl to remove calcium. Finally scandium was eluted with 5 mL of 0.01 M HCl with the flow rate 0.5 mL/min. The content of ^{46}Sc or ^{45}Ca was measured in each collected fraction using a well-type scintillation counter and LSC counter. The effluent from the UTEVA column obtained during sample loading on the column was pooled together with the fraction collected during washing the column with 10 M HCl. The 11 g of dry $(NH_4)_2CO_3$ was added to this solution and the mixture was heated at 80ºC for 2 h. The obtained $CaCO_3$ precipitate was separated by centrifugation for calcium recovery. **Results and Conclusion:** The recovery of scandium using UTEVA extraction chromatography was higher than 90%. More than 99% of calcium was found in the fractions collected from the column for calcium recovery. The concentration of calcium in the scandium fraction was below the detection limit less than 4μg/mL. This study confirms the usefulness of UTEVA resin for efficient separation of Sc radionuclides from irradiated calcium targets. **Acknowledgements:** This project was supported with the funds awarded by the National Centre for Research and Development in Poland within the Applied Science Program, grant no PBS3/A9/28/2015. References: [1] H. Valdovinos, R. Hernandez et.al., *Appl. Radiat.Isot.* **2015**, *95*, 23-29

EP-0287

Development of solid target and automated synthesis module for the production of scandium-44 and scandium-44 labeled peptides

I. Hajdu, V. Forgács, A. Fekete, E. Várhalminé Németh, D. Szikra; University of Debrecen, Debrecen, HUNGARY.

Introduction: Scandium-44 (^{44}Sc) is a promising radionuclide that has favorable half-life ($t_{1/2}$ = 3,97 h) and decay characteristics (Eβ$^+_{av}$ = 632 keV) for PET imaging. Currently, natural calcium or enriched calcium carbonate-graphite powder mixture is used as target material, moreover automated synthesis module is not available to produce ^{44}Sc labeled peptides. Our goal was to develop a solid target and elaborate a fully automated synthesis procedure from the solid target dissolution to the ^{44}Sc labeled peptide synthesis and purification. **Methods:** After irradiation of calcium target the dissolution, purification and the peptide labeling was prepared manually and with automated synthesis module and the results were compared. Solid target dissolution: The irradiated calcium target was dissolved in 3 molar ultra-pure hydrochloric acid. Purification: the crude ^{44}Sc solution was loaded onto the DGA column. To remove the impurities, 3 molar HCl and 1 molar HNO_3 was passed through the column. ^{44}Sc was eluted with 0.1 molar HCl. Before the labeling the pH was adjusted to 4.2 with ammonium-acetate buffer. The labeling efficiency of ^{44}Sc was tested with different concentration of DOTA solution and DOTA-PSMA, NODAGA-AMBA and NODAGA-RGD peptides. **Results:** In case of manual synthesis 115 MBq activity was loaded onto the filter. The trapped activity was 114 MBq and 109 MBq remained after the washing. Eluted activity was 89.3 MBq in 0.1 M HCl. The labeling efficiency was > 98% by 0.2 micro molar DOTA solution and the synthesis yield was over 80% using DOTA-PSMA, NODAGA-AMBA and NODAGA-RGD peptides. Using automated synthesis module the starting activity was much higher (500 ± 40 MBq). The eluted activity was 400 ± 20 MBq in 0.1 M HCl. The labeling efficiency was > 98% by 1 micro molar DOTA solution and the synthesis yield was over 60% using DOTA-PSMA, NODAGA-AMBA and NODAGA-RGD peptides. The automated synthesis procedure takes 56 minutes. **Conclusion:** ^{44}Sc labeled peptide synthesis was successfully prepared using fully automated synthesis module which is essential in clinical routine of nuclear imaging because it allows to increase the starting activity and reduces received dose by the clinical workers. In our next step, we are planning to increase the starting activity and use enriched calcium carbonate that is necessary to produce isotopically pure ^{44}Sc and allowing its use for clinical PET imaging.

EP-0288

Preliminary experimental tests of ^{64}Cu production in combination with ^{18}F

L. Auditore[1], E. Amato[2], G. Cicoria[3], M. Marengo[3], S. Baldari[1]; [1]Nuclear Medicine Unit, University Hospital "G. Martino", Messina, ITALY, [2]Radiological Sciences Section, BIOMORF Dept., Messina, ITALY, [3]Medical Physics Department, University Hospital "S. Orsola-Malpighi", Bologna, ITALY.

Aim: ^{18}F for Positron Emission Tomography is routinely produced with low energy cyclotrons by the reaction ^{18}O(p,n)^{18}F induced on H$_2$(18)O target. The emitted neutrons can be used to produce ^{64}Cu in a Zn target properly coupled to the H$_2$(18)O

target. The aim of this work is to evaluate the ^{64}Cu activity obtainable during a routine ^{18}F production. **Materials and Methods:** Preliminary experimental tests of ^{64}Cu production were carried out during a routine production of ^{18}F at S. Orsola-Malpighi University Hospital in Bologna. During the first test, a natZnCl$_2$ pellet, 847 mg, 13 mm-diameter and 2.35 mm-thickness, was positioned close to the H$_2$(18)O target and irradiated for 2 h with 15.3 MeV protons, 58 μA current. The second test was carried out irradiating 8 metal zinc discs (99.99% purity), 10 mm diameter, 1 mm thickness. Six discs were positioned in three different positions around the H$_2$(18)O target and, for practical reasons, two discs were positioned on the cooling flange next to the H$_2$(18)O target. Each position counted for two Zn discs. Targets were simultaneously irradiated for 108 min with 15.3 MeV protons, 54 μA curren NatZnCl$_2$ pellet and pure Zn discs was analysed in gamma-ray spectrometry using a HPGe N-Type detector with a 30% relative efficiency and a resolution of 1.8 keV at 1,332 keV. The spectrometry system was calibrated in the 59-1,836 keV range by means of a multi-radionuclide certified reference solution, obtained from an accredited Standardization Laboratory. **Results:** The spectrometry analysis of the irradiated natZnCl$_2$ pellet indicated the presence of ^{64}Cu and an activity of about 60 kBq was estimated 3 h later the End Of Bombardment (EOB). ^{38}Cl, ^{65}Ni, ^{65}Zn, ^{69m}Zn and ^{71m}Zn radionuclides were also detected in the irradiated pellet. Same analysis was carried out on Zn metal discs. For the six discs positioned around the H$_2$(18)O target a ^{64}Cu activity of about 75 kBq for each disc was estimated 3 h later the EOB. For the discs positioned on the cooling flange, the measured activity was about 35 kBq. Activities were measured with an uncertainty of about 6 % for a measuring time of 1 h. ^{65}Ni, ^{65}Zn, ^{69m}Zn and ^{71m}Zn radionuclides were also detected in the irradiated discs. Results were compared with Monte Carlo simulations. **Conclusions:** Preliminary experimental tests of ^{64}Cu production with neutrons emitted during a routine ^{18}F production suggest that optimizing the zinc target cumulative activities useful for pre-clinical studies can be obtained.

EP-17   during congress opening hours, e-Poster Area

Radiopharmaceuticals & Radiochemistry: Radiopharmacokinetics & Drug Development

EP-0289
11C-choline pharmacokinetics in recurrent prostate cancer

M. Grkovski, K. Gharzeddine, P. Sawan, H. Schöder, W. A. Weber, J. L. Humm; Memorial Sloan Kettering Cancer Center, New York, NY, UNITED STATES OF AMERICA.

Purpose: To investigate pharmacokinetic analysis for quantifying ^{11}C-choline uptake in patients with metastatic prostate cancer. **Subjects and Methods**: 128 patients with clinical suspicion of recurrent prostate cancer based on rising PSA and with inconclusive standard-of-care imaging underwent ^{11}C-choline PET imaging. Dynamic PET acquisitions (0-8-min) were performed over the pelvic region, followed by a whole-body scan and an additional 6 min static acquisition at ~25 min post-injection. Regions of interest (ROIs) were drawn over sites of disease identified in 53 patients by an experienced nuclear medicine physician. ^{11}C-choline uptake and pharmacokinetics were evaluated (by standardized uptake value (SUV) on the last frame, graphical analysis (Patlak plot; slope K_i^P) and 1- and 2-compartment pharmacokinetic models to estimate the kinetic rate constants K_1, K_1/k_2, k_3, k_4 and macro-parameter K_i^C. The input function was defined on the femoral artery and was corrected for metabolites. 17 local recurrences, 54 lymph nodes and 12 osseous metastases were included in the analysis (n=83), which was subsequently repeated for ROIs placed over non-diseased gluteus maximus muscle and adipose tissue.. **Results**: Median PSA and Gleason score were 2.4 ng/ml (range, 0.3-82.9 ng/ml) and 7 (range, 6-9), respectively. According to Akaike Information Criterion, 2-compartment irreversible model ($k_4=0$; $2C_{IR}$) was most appropriate in 85% of lesions, supporting the applicability of Patlak analysis. ^{11}C-choline equilibration time was 9±8 min. Mean SUV and K_i^P were 3.7±2.0 and 0.27±0.17 min^{-1} in lesions compared to 1.03±0.42 and 0.07±0.03 min^{-1} in muscle and 0.26±0.07 and 0.01±0.00 min^{-1} in adipose tissue (p<0.01, 2-tailed t-test). Pharmacokinetic modeling with $2C_{IR}$ resulted in: $K_1=0.80±1.05$ min^{-1} (range, 0.10-7.17 min^{-1}), $K_1/k_2=2.17±2.26$ (range, 0.17-13.10), $k_3=0.59±0.83$ min^{-1} (range, 0.05-4.98 min^{-1}) and $K_i^C=0.18±0.11$ min^{-1} (range, 0.04-0.53 min^{-1}). Spearman's ρ between SUV-K_i^P was 0.92, whereas between SUV-K_i^C it was lower, ρ=0.67, primarily due to lesions with $K_1/k_2>>1$. ρ between SUV and K_1, K_1/k_2, k_3 and PSA was 0.74, 0.36, 0.26 and 0.25, respectively. Cases were identified where intra-patient lesions had similar SUV but different pharmacokinetics (very high K_1 with low k_3, or average K_1 with very high k_3), as visualized by substantial dissimilarity in time-activity curve shapes. Despite having similar SUV (4.29±1.26 and 4.09±2.22), osseous metastases had significantly higher K_1 compared to local recurrences (1.27±1.02 min^{-1} and 0.46±0.30 min^{-1} respectively; p=0.01). **Conclusion**: High correlation between SUV and K_i^P supports the use of SUV in the clinic. However, pharmacokinetic modeling has a potential to uncouple the contributions of perfusion/vascular permeability and specific binding of ^{11}C-choline.

EP-0290
Development of ^{18}F-labeled α-methyl L-phenylalanine for tumor specific imaging

H. Hanaoka[1], A. Yamaguchi[1], Y. Ohshima[2], T. Higuchi[1], N. S. Ishioka[2], Y. Tsushima[1]; [1]Gunma University, Maebashi, JAPAN, [2]National Institutes for Quantum and Radiological Science and Technology, Takasaki, JAPAN.

Purpose: Fluorine-18-labeled amino acids are promising radiopharmaceuticals with excellent tumor specificity due to their low background accumulation. Among them, α-methyl-substituted non-natural amino acids hold great potential because α-methyl group provides selectivity for L-type amino acid transporter type 1 (LAT1) that is overexpressed in many types of tumor. In this study, three ^{18}F-labeled α-methyl L-phenylalanine derivatives, 2-^{18}F-α-methyl L-phenylalanine (2-^{18}F-FAMP),

3-^{18}F-α-methyl L-phenylalanine (3-^{18}F-FAMP) and 4-^{18}F-α-methyl L-phenylalanine (4-^{18}F-FAMP) were designed, and their potential as a tumor imaging agent was evaluated. **Materials and Methods:** ^{18}F-labeled α-methyl L-phenylalanine was prepared from α-methyl L-phenylalanine by electrophilic fluorination using ^{18}F-acetyl hypofluorite, then purified by reverse-phase HPLC. Cellular uptake studies were performed using a human colorectal cancer cell line, LS180. Biodistribution studies were performed on normal mice or LS180 xenograft mice using ^{18}F-FAMPs and 3-^{18}F-α-methyl-L-tyrosine (^{18}F-FAMT) which is already in clinical use. PET imaging were performed on LS180 tumor-bearing mice after 1 h injection of 2-^{18}F-FAMP or ^{18}F-FAMT. **Results:** Each ^{18}F-FAMP was successfully prepared. In biodistribution studies, 2-^{18}F-FAMP showed blood clearance faster than 3-^{18}F-FAMP, 4-^{18}F-FAMP and ^{18}F-FAMT (1.04 ± 0.57, 2.32 ± 0.36, 2.27 ± 0.39 and 0.89 ± 0.28 % ID/g at 1 h after injection, respectively), and showed renal accumulation lower than 3-^{18}F-FAMP, 4-^{18}F-FAMP and ^{18}F-FAMT (4.55 ± 0.97, 6.05 ± 0.46, 5.58 ± 1.05 and 16.7 ± 3.10 % ID/g at 1 h after injection, respectively). 2-^{18}F-FAMP was taken up by LS180 cell and its uptake was inhibited by a LAT1 specific inhibitor. In biodistribution study in tumor-bearing mice, 2-^{18}F-FAMP exhibited higher tumor accumulation than ^{18}F-FAMT (10.0 ± 1.46 %ID/g and 4.55 ± 0.48 %ID/g at 1 h after injection, respectively). In PET imaging in xenograft mice, 2-^{18}F-FAMP clearly visualized the tumor as early as 1 h after injection with excellent tumor-to-background ratios which is much better than that of ^{18}F-FAMT. **Conclusion:** 2-^{18}F-FAMP exhibited preferred pharmacokinetics and high tumor accumulation in LS180 tumor, and showed LAT1 specific cellular uptake in vitro. Moreover, in PET imaging, 2-^{18}F-FAMP clearly visualized the tumor with excellent tumor-to-background ratios. These findings suggest that 2-^{18}F-FAMP constitute a potential new PET tracer for tumor specific imaging.

EP-0291

Synthesis and evaluation of ^{125}I-labeled tetrazine prosthetic group for an efficient bioorthogonal radiolabeling of trans-cyclooctene containing biomolecules

S. Mushtaq[1,2], M. Choi[1], H. Shim[1], S. Yun[1], C. Lee[1], S. Park[1,2], D. Choi[1], B. Jang[1], J. Jeon[1,2]; [1]Korea Atomic Energy Research Institute, Jeongeup, Jeonbuk, KOREA, REPUBLIC OF, [2]Korea University of Science and Technology, Deajeon 34113, KOREA, REPUBLIC OF.

Inverse-electron demand Diels-Alder reaction (IEDDA) between tetrazine and trans-cyclooctene (TCO) is known to have extremely fast reaction kinetics and excellent bioorthogonality. Several radioisotopes labeled tetrazine or trans-cyclooctene have been reported for in vitro radiolabeling of biomolecules and (or) in vivo pre-targeting strategy. Radiolabeled products provided by this method were successfully applied to various molecular imaging studies. In this report, we present a new radioactive iodine labeled tetrazine and its applications to efficient radiolabeling of cyclic RGD peptide and human serum albumin (HSA). A stannylated precursor was synthesized and used for the radioiodination of tetrazine structure to give [^{125}I]**1**

. Tran-cyclooctene derived cRGD peptide and human serum albumin were synthesized to evaluate the labeling efficiency of [^{125}I]**1**. Radioiodination of these substrate by using [^{125}I]**1** was carried out under mild conditions to give radioiodinated cRGD peptide[^{125}I]**2** and radioiodinated human serum albumin [^{125}I]**3** . We also compared the in vivo stability of [^{125}I]**3** and human serum albumin radioiodinated by chloramine-T method. tetrazine prosthetic group [^{125}I]**1** was easily synthesized with 65.8% radiochemical yield and >99% radiochemical purity. Rapid and bioorthogonal radiolabeling reaction using [^{125}I]**1** provided ^{125}I-labeled cRGD peptide [^{125}I]**2** and ^{125}I-labeled HSA[^{125}I]**3** with excellent RCY (>99%). In the biodistribution study, ^{125}I-labeled HSA ([^{125}I]**3**) was proved to be highly stable and showed significantly lower uptake in the thyroid. Therefore the radiolabeling method in the present study provided both excellent radiochemical results and highly stable ^{125}I-labeled product against in vivo deiodination. We anticipate that the present radiolabeling method will be extensively applied to radioactive iodine labeling of biomolecules containing a TCO group.

EP-0292

Generation and evaluation of single chain fragments for molecular imaging of CD44v6-expressing cancers

A. Haylock[1], J. Nilvebrant[2], A. C. Mortensen[3], I. Velikyan[4], R. Falk[5], M. Nestor[3]; [1]Department of Surgical Sciences, Department of Immunology, Genetics and Pathology, Uppsala University, UPPSALA, SWEDEN, [2]Division of Protein Technology, School of Biotechnology, Royal Institute of Technology, STOCKHOLM, SWEDEN, [3]Department of Immunology, Genetics and Pathology, Uppsala University, UPPSALA, SWEDEN, [4]Department of Medicinal Chemistry, Uppsala University, UPPSALA, SWEDEN, [5]Department of Neuroscience, Karolinska Institutet, STOCKHOLM, SWEDEN.

Aim: The aim of this study was to generate and characterize scFv antibodies directed to human CD44v6, and to radiolabel and evaluate top candidates *in vitro* and *in vivo* for their potential use in CD44v6-targeted molecular imaging in cancer patients. **Materials and Methods:** Phage display selections were used to isolate CD44v6-specific scFvs. A chain shuffling strategy was employed for affinity maturation based on a set of CD44v6-specific first-generation clones. Two second-generation scFv clones were then chosen for labeling with ^{111}In or ^{125}I/[124]I and assessed for CD44v6-specific binding on cultured tumor cells. *In vivo* uptake and distribution was evaluated in tumor-bearing mice using a dual tumor model. **Results:** Two affinity-matured clones, CD44v6-scFv-A11 and CD44v6-scFv-H12, displayed promising binding kinetics. Seven out of eight radiolabeled conjugates demonstrated CD44v6-specific binding. *In vivo* studies on selected candidates demonstrated very advantageous tumor-to-organ ratios, in particular for iodinated conjugates, where ^{125}I-labeled scFvs exhibited favorable kinetics and tumor-to-blood ratios above five already at 24 hours p.i.. A proof-of-concept small animal PET-CT study was in line with the biodistribution data, clearly visualizing the high CD44v6-expressing A431 tumor. **Conclusion:** The single chain fragments, CD44v6-scFv-A11 and CD44v6-scFv-H12 specifically bind to CD44v6, and the labeled

counterparts provide high tumor-to-blood ratios and fast clearance from organs and blood. We conclude that radioiodinated CD44v6-scFv-A11 and CD44v6-scFv-H12 possesses highly suitable features for stringent molecular imaging.

EP-0294

Does nanocarrier tumour uptake increase with increasing size?

*V. Schmitt, C. Rodriguez-Rodriguez, J. L. Hamilton, R. A. Shenoi, J. N. Kizhakkedathu, **K. Saatchi**, U. O. Hafeli; University of British columbia, Vancouver, BC, CANADA.*

Purpose: Given the lack of a spatially homogenous tumor microenvironment and the enormous variability of tumor types and locations, non-invasive platforms to study the distribution and circulation time of novel drug carrying nanomedicines to treat cancer must be explored. In this study long circulating radiolabeled macromolecules of different molecular weights were injected into tumor bearing mice and their pharmacokinetics, biodistribution, tumor uptake and EPR effect determined. The goal was to expose differences in the circulation and accumulation characteristics caused by nanocarrier sizes. **Methods:** Hyperbranched polyglycerols of 25, 50, 100, 200, 300 and 500 kDa were synthesized, functionalized and radiolabeled with ^{67}Ga. The tracers were injected intravenously via the tail vein into rag2m mice with subcutaneous tumors and dynamically assessed over a period of 192 h using SPECT/CT (MILabs VECTor/CT) outfitted with an ultra-high resolution mouse multi-pinhole collimator. Following the final scan, a sacrifice-based biodistribution of all organ systems was conducted. The average activities of specific organs were calculated placing two spherical volumes of interest (VOI) inside the organs and tumor. The mean activity in each VOI (counts/pixel) was multiplied by the calibration factor to result in an organ activity concentration (MBq/mL). Data was expressed as standardized uptake value (SUVs) to account for variations in injected dose and animals' body weight. **Results and Conclusion:** Our study explores the advantages of quantitative SPECT/CT imaging of radiolabeled nanocarriers to determine their organ and tumor distribution. Furthermore, the use of SPECT/CT was compared to the classic biodistribution methodology. The VOI analysis allowed us to determine pharmacokinetic parameters such as the plasma half-life in mice without blood sampling, but rather monitoring the activity concentration in the organs with simple spherical VOIs. Interestingly, the tumor concentration of the nanocarrier on day 8 was size independent at 12.5% ± 2.8% of the remaining activity in the body for the tested range of MWs which had a hydrodynamic radius between 3.3 and 7.8 nm. These results will allow the prediction of drug concentrations in the tumor that could lead to more rational cancer treatment.

EP-0295

Radiolabeling and biodistribution study of engineered antibody-like protein with ^{99m}Tc for tumor therapy

D. Lee[1], S. Mushtaq[1,2], S. Yoon[1], J. Rho[3], J. Lee[3], J. Kang[1], D. Choi[1], H. Kim[3]; [1]Korea Atomic Energy Research Institute, Jeongeup, KOREA,

REPUBLIC OF, [2]Korea University of Science and Technology, Deajeon 34113, KOREA, REPUBLIC OF, [3]Korea Advanced Institute of Science and Technology (KAIST), Daejeon 34141, KOREA, REPUBLIC OF.

Recently, antibody-mimetic proteins have received a great deal of interest in diagnosis and therapeutic applications. Since, antibody-mimetic proteins possess intrinsic features that are often required for tumor imaging and therapy, they have potential to be used as platforms for integrating imaging and therapeutic functions. Intrinsic issues that are associated with therapeutic application of antibody-mimetic proteins, particularly in cancer treatment, include an efficient and straightforward radiolabeling for understanding in vivo biodistribution and excretion route, and monitoring therapeutic responses. Repebody is an antibody-mimetic proteins that consist of highly diverse leucine-rich repeat (LRR) modules, it has been constructed to bind to interleukin-6 for cancer therapy. Herein, to investigate the biodistribution and blood clearance, repebody was successfully radiolabeled with the $[^{99m}Tc(OH_2)_3(CO)_3]^+$ by using a site-specific direct labeling method via hexahistidine-tag. The repebody was radiolabeled with ^{99m}Tc-tricarbonyl at 37°C within 1 h. The radiochemical purity of radiolabeled repebody (^{99m}Tc-repebody) was estimated to be greater than 99% and the specific activity was 925 MBq/mg.^{99m}Tc-repebody was highly stable up to 24 h for both *in vivo* SPECT/CT and in vitro histidine challenge study. Biodistribution results showed that most of intravenous or intraperitoneal doses of ^{99m}Tc-repebody were found in kidneys, and other organs were found with subsequent remaining. When we examined the whole-body distribution of ^{99m}Tc-repebody via SPECT/CT images, especially after intravenous administration, ^{99m}Tc-repebody was preferentially found in the kidney at early time point. Even after 6 h, the radioactivity in the kidney remained high compared to the surrounding tissue. This result indicates the main excretion route of ^{99m}Tc-repebody was through renal clearance. These biodistribution studies of repebody will be useful for development of therapy strategy along with their systemic information.

EP-0296

Evaluation of 89Zr Complexes With Dicarboxylic Acids for PET-Diagnosis of Inflammatory Processes and Metabolic Skeletal Disorders

A. Larenkov, A. Maruk, M. Zhukova, A. Krasnopyorova; Burnasyan FMBC, Moscow, RUSSIAN FEDERATION.

The positron-emitting ^{89}Zr ($T_{1/2}$=78.42h), is being increasingly studied for PET. Ionic forms of zirconium have a high affinity for bone tissue. This fact is considered by scientific groups, mainly as a negative one, requiring special control of the stability of ^{89}Zr complexes. However, should we disregard the diagnostic potential of simple ^{89}Zr compounds?! In our work, we decided to study the possibility of effective visualization of foci of inflammatory processes and skeletal lesions using ^{89}Zr complexes with carboxylic acids both for a long time and at the earliest possible time after administration. Complexes of ^{89}Zr with oxalic, malonic, succinic and lactic acids were investigated. 60 minutes

after intravenous administration of [89]Zr-oxalate/-malate/-suc-cinate/-lactate, its concentration in the bloodstream is about 30-35% of the initial (mouse, rabbit). In the inflammation sites and bone calluses, an average radioactivity accumulation was 6-8%/g and 10%/g of the administered dose (respectively). In intact bone tissue, the amount of [89]Zr accumulated is at least 2 times lower than in lesions of the bone callus. As expected, there was no significant difference in the pharmacokinetics of [89]Zr-oxalate/-malate/-succinate/-lactate complexes. Only for [89]Zr-malate a statistically higher accumulation in pathological foci was found (on average 2%/g for fracture and 1.5%/g for in-flammation foci). Effective visualization of pathologies is possi-ble for a long time (10-12 days), but only after a certain interval (5-24 hours) between the introduction and PET-scanning. So, it was decided to use transferring-blocking solution injection [A.Larenkov et al // J.Nucl.Med., 2015. 56, 5(2), 14]. Preliminary or joint with [89]Zr preparation intravenous administration of small amount of Fe(III)-citrate allows to reduce the content of [89]Zr in the blood stream significantly and to accelerate its ac-cumulation in pathological foci: an hour after administration, the blood content is 2.5%/g from the administered dose. And in the fracture and focus of inflammation it is 14%/g and 10%/g, respectively. This fact points to the important role of transferrin and, probably, other transport proteins in the mechanisms of biodistribution of zirconium. It is noteworthy that in the case of the introduction of [89]Zr-oxalate without additional procedures within 6-8 days, approximately 30% (decay corrected) of the in-jected radioactivity is excreted from the body. The remaining part is firmly retained in bone tissue and pathological foci. When the transferrin is blocked the same amount is excreted in the urine during the first hour (30-40%), and no significant removal of zirconium was observed subsequently.

EP-0297

Bioaffinity testing of 68Ga/177Lu-DOTA-Neurotensin and neurotensin fragments as teranostic agent in colon cancer

D. Niculae[1], D. Draganescu[1,2], E. A. Min[1,2], A. Raicu[1], L. Chilug[1,3], G. Manda[4], R. A. Leonte[1,3], I. Manea[5], M. Costache[5]; [1]Horia Hulubei National Institute for Physics and Nuclear Engineering, Magurele Ilfov, ROMANIA, [2]University of Medicine and Pharmacy "Carol Davila", Bucharest, ROMANIA, [3]University Politehnica, Bucharest, ROMANIA, [4]Victor Babes National Institute for Pathology and Biomedical Sciences, Bucharest, ROMANIA, [5]Colentina Clinic Hospital, Bucharest, ROMANIA.

Introduction: Neurotensin is a natural peptide, pGlu-Leu-Tyr-Glu-Asn-Lys-Pro-Arg-Arg-Pro-Tyr-Ile-Leu, produced mainly in the central nervous system and in N endocrine cells of the gas-trointestinal tract. As it is involved in the proliferation of many types of cancers, an overexpression of neurotensin receptors being an early event that occurs in many tumors compared to normal tissues. Targeting neurotensin receptors for both detection and treatment is envisaged for tumors showing an increased level of NTSR1 subtype of neurotensin receptor NTR: colon, breast, lung cancers and ductal pancreatic adenocarci-nomas. **Methods:** DOTA-neurotensin (DOTA(pGlu-Leu-Tyr-Glu-Asn-Lys-Pro-Arg-Arg-Pro-Tyr-Ile-Leu)) and several analogs based on neurotensin peptide fragments (6-13) and (8-13) were developed for diagnostic and therapeutic targeting neuroten-sin receptors of colonic tumors, thus radiolabelled with Ga-68 and Lu-177. We performed comparative testing of cellular uptake and retention on colonic cell lines HT29 and CaCo2, as indicators of protein-cell receptor interaction that can provide useful information regarding the dosage, latency and duration of effect of the radiolabelled compound. **Results:** Elution, label-ing and purification procedures were performed in 25 min with a radiochemical yield over 85%. The radiochemical purity of the final product performed by HPLC was over 99%. The bioaffinity profile of ^{68}Ga/^{177}Lu-DOTA-NT and NT fragments analogs show rapid and high uptake of the radiolabelled peptide in both cell lines, faster on HT29, while the retention was found to be 30% on CaCo2 cells and 80% on HT29 cells, over 30 min. The profile of the retention curves shows a fast fall down at 30% followed by stabilization in the case of CaCo2 cell ine and a slowly de-crease of only 20% of retained activity in the case of HT29 cell line. *In vivo* binding to colon tumor bearing mice was confirmed by PET scans.The binding profile and retention-efflux curves will be presented comparatively for each compound. **Discussion/ Conclusion:** The optimisation of parameters for the radiosyn-thesis, purification processes and automation leads to a short time for preparation with good radiochemical yield and high radiochemical purity of final products, ^{68}Ga/^{177}Lu-DOTA-NT and NT fragments analogs. The radiolabeled compounds exhibiting good uptake in the both cell lines and very good retention in the HT29 colon cancer cells, over a sufficient period for a PET scan. ^{177}Lu-radiolabelled neurotensin requires further in vivo in-vestigations, as a promising candidate for the targeted systemic radiotherapy of the colon cancer. This work was supported by the program Partnerships in Priority Areas - PN II, implemented with the support of MEN-UEFISCDI, project 228/2014.

EP-0298

n.c.a. Lu-177-Dotatate Kinetics Comparison With In-111-DTPA-Oc in Intra-arterially Infused Liver Metastasized GEP-NET Patients; From Bench to Bedside

G. S. Limouris[1], M. Paphiti[1], S. Chondroyiannis[2], D. Rubello[2], V. R. McCready[3]; [1]Medical Faculty, National and Kapodistrian University of Athens, Athens, GREECE, [2]Nuclear Medicine Department, Santa Maria della Misericordia Hospital, Rovigo, ITALY, [3]Institute Cancer Research, Sutton Surrey & Royal Sussex County Hospital, Brighton, UNITED KINGDOM.

Introduction: Compared with [DTPA[0]]octreotide the soma-tostatin analogue [DOTA[0],Tyr[3]]octreotate has a 9-fold higher affinity for the somatostatin receptor subtype II (sst2). Labelled with ^{177}Lu, clinical results have classified it, so far, as perhaps the most effective radiopharmceutical for the confrontation of GEP-NETs. We aimed to compared the pharmacokinetic of ^{177}Lu-DO-TATATE (13 pts) and ^{111}In-DTPA-OC (18 pts), intra-arterially in-fused, for GEP-NETs treated patients, evaluating their absorbed dose, pharmacokinetic differences and efficacy, based on their survival rate in long-term. **Subjects and Methods:** Blood sam-

ples were drawn and quantified at 1 minute before and 30 min, 2, 4, 8 and 24 hours post-infusion. Urine was collected and quantified once before and up to 24hours post-injection. Planar scintigraphic images were obtained at 24, 48, 96 and 120 hrs post injection, and ROIs were drawn manually on the anterior and posterior spot views for tumor, liver, spleen, and kidneys in order to determine their residence time and absorbed dose [from effective half-lives and radionuclide uptake]. The background region was placed close to the ROIs for background correction. The geometric mean value, derived from the anterior and posterior scans, was taken and corrected for attenuation and physical decay. Dosimetric calculations were performed using the patient specific scintigraphic data by applying the OLINDA/EXM (1.0) code, assuming a sphere for tumour having 20 gr mass density. Tumor diameters were measured by US, CT or MRI. The bone marrow residence time was calculated from the plasma activity concentration curve. Statistical correlation analysis was performed using the unpaired Student's t-test. **Results:** n.c.a.^{177}Lu-[DOTA0,Tyr3]octreotate blood radioactivity, expressed as a percentage of the injected dose, was significantly lower than ^{111}In-[DTPA^0] octreotide (p <0.05); the background-corrected tumour uptake was significantly higher than ^{111}In-[DTPA^0] octreotide but without any significant difference in other organs (spleen, kidneys, liver). The organ average radiation dose (mGy/MBq) expressed as ^{111}In /^{177}Lu ratios were: (a) liver tumour 11.2/35.0 mGy/MBq, (b) liver 0.14/0.03-0.1 mGy/MBq, (c) kidneys 0.41/0.02-0.5 mGy/MBq, (d) spleen 1.4/0.02-1.2 mGy/MBq and (f) bone marrow 0.0035/0.008-0.04 mGy/MBq. **Conclusion:** Using ^{177}Lu-[DOTA^0,Tyr^3]octreotate, a 3-fold higher absorbed dose to tumour tissue was achieved compared to ^{111}In-[DTPA^0] octreotide. However, the resident time of n.c.a. ^{177}Lu-[DOTA^0,Tyr^3]octreotate results in a significantly higher absorbed dose to bone marrow compared with ^{111}In-[DTPA^0]octreotide. However, a drawback of ^{111}In-[DTPA^0]octreotide therapy is that the number of administrations would need to be almost doubled in order to achieve an equal therapeutic outcome to ^{177}Lu-[DOTA^0,Tyr^3]octreotate.

EP-18   during congress opening hours, e-Poster Area

Radiopharmaceuticals & Radiochemistry: Antibodies & Peptides

EP-0299
New 99mTc labeled peptide for EGFR tumor targeting

N. Rahmanian[1], S. Hosseinimehr[2], A. Khalaj[1], Z. Noaparast[2], S. Abedi[2]; [1]Tehran University of Medical Sciences, Tehran, IRAN, ISLAMIC REPUBLIC OF, [2]Mazandaran University of Medical Sciences, sari, IRAN, ISLAMIC REPUBLIC OF.

Introduction: The epidermal growth factor receptors (EGFRs) are a family of cell surface receptors that play multiple roles in normal cellular functions mainly including cell growth, proliferation and cell survival. Several reports indicated that enhances in EGFRs expression (e.g. HER1 and HER2) disrupt the mechanism of normal cells and consequently lead to cellular proliferation, angiogenesis, migration and invasion. The aim of this study was to evaluate a new ^{99m}Tc targeted GE 11 peptide that has high tendency to accumulate in tumors with high level of epidermal growth factor receptor (EGFR) expression. **Material and Methods:** The 12-mer GE11 peptide (YHWYGYTPQNVI) was modified on N-terminus using the serylserylserin amino acids and HYNIC as spacer and bifunctional chelating agent, respectively. The HYNIC-(Ser)$_3$-GE11 peptide was purchased from ProteoGenix (Schiltigheim, France) and labeled with ^{99m}Tc using tricine and mixture of EDDA/tricine as the coligands. The efficacy of radiolabeling of peptides were analyzed on ITLC-SG and also by reversed-phase high-performance liquid chromatography (RP-HPLC). **Results and Conclusion:** HYNIC-SSS-GE11 were labeled with ^{99m}Tc using both labeling approaches with more than 95% efficiency and showed high stability in buffer and serum. The affinity of new radioconjugated peptides for binding to EGFR were investigated on various cell lines with different levels of EGFR expression in which human ovarian carcinoma cells showed higher affinity and was used for further in vitro and in vivo investigations. The *in vitro* experiments showed good affinity to human ovarian carcinoma cells using both radioconjugated peptides. Biodistribution studies in normal female mice and mice xenograft tumor model revealed that the both radioconjugated peptides had high in vivo stability and high renal excretion. However tricine-coliganded radiolabeled peptide showed higher liver and intestine uptake compared than EDDA/tricine coliganded radiolabeled peptide. The gamma scintigraphy showed good tumor visualization. From the results of this investigation it appears that, the new radioconjugated peptide might be a promising radiotracer for SPECT imaging of ovarian tumor.

EP-0300
Biodistirbution study of ^{111}In-anti-CDH17 minibody using CDH17-positive gastric cancer xenograft mice

K. Fujiwara[1,2], K. Koyama[2], H. Akiba[3], H. Iwanari[4], T. Higashi[1], K. Tsumoto[5], T. Hamakubo[4], T. Momose[6]; [1]Department of Molecular Imaging and Theranostics, National Institute of Radiological Sciences, National Institutes of Quantum and Radiological Science and Technology, Chiba, JAPAN, [2]Department of Radiology, Graduate School of Medicine, The University of Tokyo, Tokyo, JAPAN, [3]Laboratory of Pharmacokinetic Optimization, Center for Drug Design Research National Institutes of Biomedical Innovation, Health and Nutrition, Osaka, JAPAN, [4]Department of Quantitative Biology and Medicine, Research Center for Advanced Science and Technology, The University of Tokyo, Tokyo, JAPAN, [5]Department of Bioengineering, School of Engineering, The University of Tokyo, Tokyo, JAPAN, [6]Department of Radiology, Faculty of Medicine, International University of Health and Welfare, Chiba, JAPAN.

Purpose: CDH17 is a membrane protein that contributes cell-cell adhesion. CDH17 might have potential as a target protein for PET imaging of gastric cancer with high sensitivity and high specificity, because CDH17 is expressed at high level in not only primary site of gastric cancer, but also metastatic lymph nodes. We previously reported a PET imaging study using ^{64}Cu-labeled

anti-CDH17 monoclonal antibody (IgG) against CDH17-positive gastric cancer xenografts. Although ^{64}Cu-anti-CDH17 IgG showed high tumor uptake, relatively long retention of agent in blood was observed. In order to improve the blood clearance of agent, we developed an anti-CDH17 minibody which is small molecule of anti-CDH17 IgG. In this study, we performed the biodistribution study of anti-CDH17 minibody labeled with ^{111}In and compared with that of anti-CDH17 IgG. **Materials and Methods:** The specificity of anti-CDH17 minibody was evaluated by cell ELISA. We conjugated anti-CDH17 minibody and anti-CDH17 IgG with 1, 4, 7-triazacylononane, 1-glutaric acid-4, 7-acetic acid (NODAGA). Then, those were labeled with ^{111}In. CDH17-positive AGS xenograft mice were injected 370 kBq of ^{111}In-anti-CDH17 minibody or 370 kBq of ^{111}In-anti-CDH17 IgG via tail vein. Mice were euthanized at at 3, 6 and 24 hours post injection (p.i.). Tumor and normal tissues were collected. The percentage of injected dose per gram of tissue (%ID/g) was calculated for each organ. **Results:** Cell ELISA using AGS cell line demonstrated the specificity of anti-CDH17 minibody for CDH17 antigen. In addition, we confirmed that NODAGA conjugation and radiolabeling did not impair the affinity of anti-CDH17 minibody. In the biodistribution study, tumor uptake of ^{111}In-anti-CDH17 minibody and ^{111}In-anti-CDH17 IgG was 10.2% and 19.2%ID/g at 24 h p.i., respectively. Rapid blood clearance of ^{111}In-anti-CDH17 minibody was confirmed (0.78%ID/g at 24 h p.i.) compared with ^{111}In-anti-CDH17 IgG (11.6%ID/g at 24 h p.i.). Tumor-to-blood ratio of ^{111}In-anti-CDH17 minibody and ^{111}In-anti-CDH17 IgG was 13.0 and 1.7 at 24 h p.i., respectively. ^{111}In-anti-CDH17 minibody showed relatively high uptake in the liver, spleen and kidney compared with ^{111}In-anti-CDH17 IgG. **Conclusion:** Anti-CDH17 minibody has a potential for a promising PET agent for CDH17-positive gastric cancer and might contribute to determine the management of gastric cancer such as indication for neoadjuvant chemotherapy.

EP-0301

^{68}Ga-labelled Neuropeptide Y short analogue: A potential PET/CT tracer for breast cancer imaging

M. E. Cardoso[1], K. Zirbesegger[2], E. Savio[2], H. Engler[2], M. Terán[1], A. M. Rey[1]; [1]Área Radioquímica, Facultad de Química, UdelaR, Montevideo, URUGUAY, [2]Uruguayan Centre of Molecular Imaging (CUDIM), Montevideo, URUGUAY.

Breast cancer is the most common cancer in women worldwide and consequently the development of new radiopharmaceuticals to improve diagnosis is of considerable importance. Radiolabelled peptides are interesting tracers since many peptidic receptors are overexpressed in proliferative processes. Researchers found that non-neoplastic breast tissue expresses neuropeptide Y (NPY) receptors subtype 2. However, NPY subtype Y1 is the dominant receptor in breast carcinomas. The aim of the present study is to develop and characterise a ^{68}Ga-labelled NPY analogue with potential application in breast cancer imaging. The peptide sequence (H-Lys(NOTA)-Tyr-Arg-Leu-Arg-BPA-Nle-Pro-Asn-Ile-OH) was selected because of its reported high affinity to the NPY receptor subtype Y1 and

includes the well known chelator NOTA. The ligand (100 µg, 5.85x10^{-5}mmol) was incubated with [^{68}Ga] GaCl$_3$ (60-100 MBq, 0.2 mL) and sodium acetate solution to adjust the pH to 4,5 at 95ºC for 10 minutes. Radiochemical purity (RP) was assessed by reverse phase HPLC using CH$_3$CN/0.1% TFA and H$_2$O/0.1% TFA as mobile phases. Stability of the labelled compound in reaction milieu and in the presence of human plasma was studied for up to 4 hours and 2 hours respectively. Binding to plasma proteins was determined by size exclusion chromatography. Lipophilicity was studied through the apparent partition coefficient between n-octanol and sodium phosphate buffer (pH=7.4). The complex was incubated with 100 fold molar excess of diethylenetriaminepentacetic acid (DTPA) at 37°C and the mixture studied by HPLC. ^{68}Ga-(NOTA)-NPY was obtained with RP> 95% and was stable for at least 4 hours in labelling milieu and 2 hours in human plasma (RP>90%) The complex is hydrophilic (Log P= -3.2 ±0.1) and presented a protein binding of 28.3±0.4% and 35.2±0.6% (30 and 60 minutes respectively). Challenge with DTPA revealed no gallium *trans*-chelation. In conclusion, the radiolabelled peptide was obtained with high RP and shows, remarkable stability in labelling milieu, human plasma and in the presence of an excess of a competitive ligand. It exhibited low lipophilicity and intermediate binding to plasma proteins. These results are promising and in vitro affinity studies are being performed in order to conclude about the potentiality of this radiotracer as radiopharmaceutical for breast cancer imaging. **Acknowledgements:** Pedeciba-Química.

EP-0302

A novel peptide targeting GPC3 for HCC PET/CT imaging

Y. Qin[1], Y. Li[2], S. Zou[1], D. Zhu[1], H. Wu[2], L. Zhu[3], X. Zhu[1]; [1]Tongji Hospital, Tongji Medical College, Huazhong University of Science and Technology, Wuhan, CHINA, [2]The First Affiliated Hospital of Xiamen University, Xiamen, CHINA, [3]Emory University School of Medicine, Atlanta, GA, UNITED STATES OF AMERICA.

Objective: Glypican-3 (GPC3) has proven to be a specific marker for hepatocellular carcinoma (HCC) detection. In this study, we aim to identify a peptide that can bind with GPC3 with high affinity and specificity. The HCC diagnostic potency of this peptide is evaluated by non-invasive fluorescence imaging and PET imaging. **Methods:** Phage display screening was conducted in vivo and in vitro with GPC3 positive tumor xenograft and recombinant GPC3 protein. The obtained peptide, denoted as TJ12P2, was synthesized and labeled for subsequent evaluations such as ELISA, cell binding, non-invasive *in vivo* imaging and ex vivo study. **Results:** The apparent Kd between TJ12P2 and GPC3 was calculated as 158.2 ± 26.25 nM. After fluorescent dye labeling, Cy5.5-TJ12P2 was found capable of binding with human hepatocellular carcinoma HepG2 and SMCC-7721 cells that overexpressed GPC3, as well as human tissue of hepatocellular carcinoma (GPC3 positive). No fluorescence signal can be observed when using Cy5.5-TJ12P2 to label human prostate carcinoma cell line PC3 (low GPC3 expression), human tissue of cholangiocarcinoma and normal liver (GPC3 negative), indicating that Cy5.5-TJ12P2 is able to differentiate cells and tissues with differ-

ent GPC3 expression. The dynamic PET imaging showed that HepG2 and SMMC-7721 tumors were clearly visualized from 10 min after intravenous administration of ^{18}F-AlF-NOTA-TJ12P2 with extremely low liver and intestines accumulation. From static PET/CT imaging, ^{18}F-AlF-NOTA-TJ12P2 accumulation in HepG2 and SMMC-7721 tumors reached 1.825 ± 0.296%ID/g and 1.575 ± 0.520%ID/g at 30 min p.i, respectively. The accumulation of ^{18}F-AlF-NOTA-TJ12P2 in tumors can be effectively blocked with excess TJ12P2 and only 0.446±0.074%ID/g (HepG2) and 0.379±0.051%ID/g (SMMC-7721) were observed. In addition, little accumulation (0.533±0.078%ID/g) of ^{18}F-AlF-NOTA-TJ12P2 was found in PC3 tumors. **Conclusion:** A novel peptide targeting GPC3, TJ12P2, was obtained using phage display screening technique with high affinity and specificity as confirmed in vitro and in vivo. Our results demonstrated that TJ12P2 could be a novel imaging probe for PET imaging of HCC with great translational potency.

EP-0303

99mTc-HYNIC-ramucirumab: in vitro studies on binding to VEGFR2 and internalization in VEGFR2-positive cells

J. Janousek, Jr., P. Barta, F. Trejtnar; *Faculty of Pharmacy in Hradec Kralove, Hradec Kralove, CZECH REPUBLIC.*

Aim: The tumor angiogenesis is a fundamental complex process that enables solid tumor development. One of the most important angiogenesis regulator is the vascular endothelial growth factor (VEGF) family. VEGF proteins bind to the three types of receptor with tyrosine-kinase activity of which VEGF receptor 2 (VEGFR2) is a key receptor in angiogenesis. Ramucirumab (RAM) is a fully humanized monoclonal antibody targeted the extracellular domain of human VEGFR2 that binds receptor with greater affinity than its natural ligand and thus inhibits its function. As several types of cancer are known to overexpress VEGFR2, RAM labeled with appropriate radionuclides could be potentially used for scintigraphic imaging in oncology. However, the radiolabeling process may negatively affect RAM binding ability. The aim of the present work was to determine the binding characteristics of prepared ^{99m}Tc-HYNIC-ramucirumab. **Materials and Methods:** Two VEGFR2 expressing cell lines were used in the binding studies. Ramucirumab was indirectly labeled with ^{99m}Tc using HYNIC as a chelator. Radiochemical purity and stability were evaluated using instant TLC and SE-HPLC. For evaluating of binding characteristics we used saturation and internalization studies. The saturation method was based on real-time radioimmunoassay performed on LigandTracer Yellow instrument. The tested cells were incubated with two consecutive concentrations followed by washout. The internalization studies were performed with the manual method at a selected concentration of RAM. **Results:** The labeling method enabled effective labeling of RAM with [99m]Tc. Radiochemical purity was higher than 95% and the radiopreparation was stable in the course of the experiments. The data from *in vitro* saturation and internalization studies provided information on binding characteristics of the radiolabeled RAM. The RAM's receptor affinity was slightly lowered but preserved. With employment of the manual method

we were able to detect a considerable VEGFR2 internalization. **Conclusion:** The introduced labeling method is convenient for radiolabeling of RAM with [99m]Tc. The binding assays provided basic information on important biological characteristics of radiolabeled RAM in the VEGFR2 positive cells**.** The obtained experience may be utilized in the further preclinical studies of radiolabeled RAM *in vitro* and *in vivo. This project was supported by Charles University: GAUK(998216/C/2016), SVV(260414) and PRVOUK P40.*

EP-0304

Development of ^{90}Y-DOTA-nimotuzumab: a specific tool for testing a new probe potentially suitable for β⁻ radio-guided surgery

T. Scotognella[1], D. Maccora[2], G. Bancivenga[3], N. Misceo[3], C. Martelli[4], V. Marzano[4], F. Marini[4], I. Fratoddi[5], I. Venditti[5], A. Cartoni[5], E. Solfaroli-Camillocci[6], S. Morganti[6], C. Mancini-Terraciano[6], F. Collamati[6], D. Rotili[7], M. Chinol[8], M. Castagnola[4], R. Faccini[6], A. Giordano[2]; [1]Nuclear Medicine Unit, Policlinico "A. Gemelli", Rome, ITALY, [2]Institute of Nuclear Medicine, Università Cattolica del S. Cuore "A. Gemelli", Rome, ITALY, [3]PET-CT Center, Radiopharmacy Unit, Policlinico "A. Gemelli", Rome, ITALY, [4]Institute of Biochemistry and Clinical Biochemistry, Università Cattolica del S. Cuore "A. Gemelli", Rome, ITALY, [5]Department of Chemistry, Sapienza University, Rome, ITALY, [6]Department of Physics, Sapienza University, Rome, ITALY, [7]Department of Drug Chemistry and Technologies, Sapienza University, Rome, ITALY, [8]Division of Nuclear Medicine, European Institute of Oncology, Milan, ITALY.

Aim: Nimotuzumab is a humanized anti-EGFR monoclonal antibody, currently employed to treat head and neck cancer and tested for other tumours. Some researchers of our group have developed a radio-guided probe able to detect β⁻ emissions for an innovative radio-guided surgical approach (Solfaroli-Camilloci et al. 2016). Aim of our study was to verify labelling procedures of nimotuzumab with ^{90}Y, based on preliminary experiences of Beckford-Vera et al. (2011) using ^{177}Lu and Martinez et al. (2014) using [90]Y. **Methods:** Synthesis of ^{90}Y-DOTA-nimotuzumab was performed according to Beckford-Vera: at day one, the starting solution of nimotuzumab (5 mg/ml, CIMAher®, Oncoscience) was concentrated using Vivaspin 20 and mixed with p-SCN-Bn-DOTA (50 fold molar excess, Macrocyclics). The immunoconjugate was incubated overnight at 4°C. The following day, DOTA-nimotuzumab was purified using a PD-10 desalting column and concentrated with Vivaspin 0.5. Bradford assay was used to evaluate the protein concentration. A mixture containing 20 µl of nimotuzumab, 300 µl of ammonium acetate (50 mM, pH 7.0) and 80 µl of [90]YCl₃ (Perkin Elmer), was incubated for two hours at 37°C. The excess of unchelated [90]Y³⁺ was trapped through the addition of 20 µl of DTPA (50 mM, pH 6.0). The radiochemical purity (%R.P.) was evaluated using an ITLC-SA strip and 10% ammonium acetate:methanol (1:1). ^{90}Y-DOTA-nimotuzumab was incubated both at room temperature and at 37°C, either in NaCl (0.9%) and human plasma (rather than in serum as performed by Beckford-Vera). Stability of the samples

was evaluated immediately and 4, 24, 48 and 72 hours after the labelling procedure; each control was repeated for three times. **Results:** The immunoconjugate concentration ranged from 6.0 to 9.0 mg/ml, in 5 separated tests. Although in all incubation conditions the %R.P. was greater than 95%, our results clearly showed that the radioimmunoconjugate was more stable in plasma (from medium value - M - of 95.3% at T0 to M=85.7% at T72) than in 0.9% NaCl (from M=95.2% at T0 to M=45.9% at T72) at room temperature. Similar results were obtained when the radioiommunoconjugate was incubated at 37°C; ^{90}Y-DO-TA-nimotuzumab was more stable in plasma (from M=95.2% at T0 to M=82.0% at T72) than in 0.9% NaCl (from M=95.6% at T0 to M=71.0% at T72). **Conclusions:** The procedure to conjugate DOTA to nimotuzumab and the labelling with ^{90}Y resulted simple and effective. We are now ready to assess the biodistribution of ^{90}Y-DOTA-nimotuzumab in animal models and the sensitivity and specificity of β[-] radio-guided probe.

EP-0305

Site-specific Bimodal Labeling of Proteins on Cysteine Residues with Chlorotetrazines

C. Canovas, M. Moreau, C. Bernhard, F. Denat, V. Goncalves; ICMUB, UMR 6302, CNRS, Université de Bourgogne Franche-Comté, Dijon, FRANCE.

Introduction: Proteins labeled with radiometals serve daily as diagnostic and therapeutic agents in nuclear medicine departments. Yet, a new generation of bioconjugates begins to emerge. It consists in doubly-modified proteins, which have optimized properties and open new fields of application such as bimodal medical imaging and theranostics. For instance, these last years have seen the emergence of bimodal imaging agents based on a biovector labeled with both a fluorescent dye and a chelator for a radiometal, and some of them have been already used in clinic for surgery assistance. Similarly, antibodies have been labeled with both a cytotoxic drug and an imaging probe, to give ADCs with theranostic potential. The development or these new families of bioconjugates is currently hampered by the technical difficulties associated with their construction. Here, we will show how a small heterocycle, i.e. dichloro-s-tetrazine, can be used as a robust and modular, ternary platform to enable the site-specific, double-labeling of proteins on cysteine residues in fully biocompatible conditions. **Materials and Methods:** s-dichlorotetrazine was substituted with DOTAGA and NODAGA metal chelating agents. The selectivity and kinetics of reaction of the resulting molecules with proteins' nucleophiles were determined by HPLC/MS on model peptides. The strategy was then validated on a model protein, bovine serum albumin, which bear a unique accessible cysteine residue (BSA). Incubation of BSA with 10 equivalents NODAGA-chlorotetrazine (1 h, pH 5.15, RT) followed by a purification by ultracentrifugation, afforded site-selectively labeled BSA- tetrazine-NODAGA. The conjugate was then clicked with Cyanine 5.0-BCN in aqueous buffer at 37°C, pH 7.13, overnight, and purified by size exclusion chromatography to give a site-selectively, doubly-modified, BSA, as determined

by nanoLC-MS and gel electrophoresis. **Results:** Commercially available *s*-dichlorotetrazine, once monosubstituted with metal chelating agents, reacted within minutes and under biocompatible conditions, with peptides and proteins through a nucleophilic aromatic substitution reaction. This reaction exhibited an excellent selectivity for thiols over amines, at near neutral pH, enabling the site-specific labeling of proteins on cysteines. The resulting disubstituted tetrazines could further react with strained alkynes and alkenes to form site-specifically dual-labeled proteins. The strategy was successfully exemplified with the bimodal PET/optical dual-labeling of BSA. **Conclusion:** s-dichlorotetrazine is a modular platform that allows the site-specific double-labeling of proteins on cysteine residues, with a variety of therapeutic/imaging agents. This robust technology, that does not require any advanced skills in organic chemistry or synthetic biology, should facilitate the production of clinically relevant doubly-modified proteins.

EP-0306

Feasibility of Z Domain-Mediated Conjugation of PNA to Antibodies for Radionuclide Pretargeting

A. Vorobyeva[1], M. Altai[1], K. Westerlund[2], A. Al-Ramadan[1], V. Tolmachev[1], A. Eriksson Karlström[2]; [1]Uppsala University, Uppsala, SWEDEN, [2]KTH Royal Institute of Technology, Stockholm, SWEDEN.

Aim: Pretargeting may improve imaging contrast and shorten time between injection of a radiolabeled probe and image acquisition compared with directly labeled monoclonal antibodies (mAbs). Peptide Nucleic Acids (PNAs) are stable nucleic acid analogues. Fast hybridization rates, bioorthogonal properties and biocompatibility make them attractive tags for pretargeting. Site-specific conjugation of PNA to antibodies is important to provide a homogeneous product with a defined degree of modification and predictable pharmacokinetics. The Z domain of protein A binds to the Fc domain of IgG. The aim of the current study was to test if Z-PNA chimera is suitable for site-specific decoration of mAbs with a PNA-based hybridization probe. **Methods**: The HP1 hybridization probe was coupled using sortase to Z domain containing photoactivable linker. The Z-HP1 was site-specifically and covalently conjugated to the Fc-region of anti-HER2 antibody trastuzumab using photoactivation, providing the primary agent trastuzumab-Z-HP1. The secondary agent, the complementary PNA probe HP2, was conjugated to DOTA and labeled with ^{111}In and [68]Ga. Trastuzumab-Z-HP1 and parental trastuzumab were directly radioiodinated. *In vitro* binding specificity of ^{125}I-trastuzumab-Z-HP1 to HER2-expressing cells was tested by saturation of HER2. The specificity of ^{111}In-HP2 and ^{68}Ga-HP2 binding to trastuzumab-Z-HP1-pretreated cells was tested using a binding saturation assay with large excess of trastuzumab and non-labeled HP2 or using ^{111}In/^{68}Ga-HP2 only. Binding affinities of ^{125}I-trastuzumab-Z-HP1 to HER2-expressing cells and affinities of ^{111}In-HP2 to trastuzumab-Z-HP1-pretreated cells were measured using LigandTracer. *In vitro* cellular processing and retention of trastuzumab-Z-HP1:[111]In-HP2 adduct by HER2-expressing cells was measured. **Results**: Photoconjugation resulted in 40% efficiency yielding 0.8 Z-HP1 per antibody mole-

cule. Binding of ^{125}I-trastuzumab-Z-HP1 to cells with high (SKOV3, BT474) and low (DU145) HER2-expression was HER2-specific. The binding affinities of ^{125}I-trastuzumab-Z-HP1 to HER2-cells were comparable to ^{125}I-trastuzumab (0.5-2 nM). Hybridization of trastuzumab-Z-HP1 and HP2 *in vitro* was fast. Pretargeting of ^{111}In-HP2 and ^{68}Ga-HP2 to trastuzumab-Z-HP1-pretreated cells was PNA-specific with high affinities (pM range). Both SKOV3 and BT474 cells demonstrated very good (over 60% at 24 h) retention of the trastuzumab-Z-HP1:[111]In-HP2 adduct. **Conclusions**: Site-specific attachment of HP1 to trastuzumab provides production of a uniform conjugate with a controllable degree of modification. This methodology could potentially be used for modification of any antibody of interest. The *in vitro* affinity data shows that the conjugation of HP1 to trastuzumab does not impair its binding to HER2-expressing cells. The feasibility of PNA-mediated antibody-based pretargeting for SPECT and PET imaging was demonstrated *in vitro* and should be further evaluated *in vivo*.

EP-0307

First application of radionuclide labeling and imaging studies to assess the pharmaceutical stability of reconstituted trastuzumab (Herceptin) stored under correct or incorrect conditions

C. Chan[1], J. Seki[2], R. Kwong[2], R. M. Reilly[1,3]; [1]Departments of Pharmaceutical Sciences and Medical Imaging, University of Toronto, Toronto, ON, CANADA, [2]Department of Pharmacy, Princess Margaret Cancer Centre, Toronto, ON, CANADA, [3]Toronto General Research Institute, University Health Network, Toronto, ON, CANADA.

Aim: Occasionally, monoclonal antibody pharmaceuticals may be stored by accident under incorrect conditions but there is little information on the effects of storage conditions on product stability to understand the implications. Our aim was to assess the stability of reconstituted trastuzumab (Herceptin) stored incorrectly at room temperature (RT) by using radionuclide labeling and imaging studies to assess HER2-binding affinity and targeting to HER2-positive tumours in vivo in mice. **Methods:** Four lots of trastuzumab (D1 to D4) stored incorrectly at RT for 12 h were compared to one lot stored correctly at 4 °C (P1). The purity and homogeneity of all lots were evaluated by SDS-PAGE and size exclusion HPLC (SE-HPLC). The UV-visible spectrum (200-900 nm) was obtained. Trastuzumab lots were buffer-exchanged into 0.1 M $NaHCO_3$ pH 8.2 and 2.2 mg was reacted with a 10-fold excess of 2-(4-isothiocyanatobenzyl)-diethylenetriaminepentaacetic acid (BzDTPA). BzDTPA-trastuzumab was labeled with [111]In (0.2-0.8 MBq/µg). The radiochemical purity was measured by instant thin-layer silica gel chromatography (ITLC-SG). HER2 binding affinity of ^{111}In-BzDTPA-trastuzumab was determined in a direct (saturation) binding assay using SK-Br-3 breast cancer cells (1.3×10^6 HER2/cell). MicroSPECT/CT imaging and biodistribution studies were performed in CD1/nude mice with s.c. HER2-positive SK-Ov-3 ovarian cancer xenografts (1.0×10^6 HER2/cell) at 72 h p.i. of 4.8-44.4 MBq (60 µg) of ^{111}In-BzDTPA-trastuzumab. **Results:** SDS-PAGE showed one major band for all lots of trastuzumab under non-reducing conditions with the expected M_r=170 kDa. SE-HPLC showed a single peak with identical reten-

tion time (t_R=11.8 mins) for all lots. The UV-visible spectrum of all lots showed λ_{max} at 230 nm and 260-280 nm. Trastuzumab was conjugated to 2-3 BzDTPA chelators. The radiochemical purity of ^{111}In-BzDTPA-trastuzumab was >90%. All lots exhibited high affinity specific binding to HER2 with K_d-values of 3.7±0.4, 3.6±0.4, 2.2±0.2, and 4.4±1.0 nM, respectively for lots stored incorrectly, which were not significantly different than those stored correctly (K_d = 3.1±0.4 nM; p=0.2-0.5). The B_{max} values ranged from 0.75-0.98×10^6 HER2/cell. Imaging and biodistribution studies are in progress and will be presented, but differences are not expected between correctly and incorrectly stored lots based on analytical results. **Conclusion:** Radionuclide labeling and imaging/biodistribution studies provide a useful tool to assess the stability of antibody pharmaceutical products stored under different conditions. There was no effect of storage of reconstituted trastuzumab under RT for 12 h compared to 4 °C on purity and homogeneity and HER2 binding affinity. We do not expect differences in localization in HER2-positive tumours in mice.

EP-0308

Biological evaluation of hybrid peptide radiolabeled with ^{68}Ga emitter as melanoma targeting probe

M. H. AL Qahtani, Y. H. Al-Malki; King Faisal Specialist Hospital & Research Center, Riyadh, SAUDI ARABIA.

Melanoma is a tumor of constantly accumulative occurrence for which novel methods of imaging and targeted therapy are generally pursued. Developing a newly hybrid short peptide that been labeled with position emitter Ga-68 will be discussed. Gallium-68 is a metallic positron emitter with a half-life of 68 min that is ideal for labelling small peptides as radiopharmaceuticals **Aim:** In order to evaluate the potential relevance of positron emitter labeled hybrid short peptide with enhanced melanoma targeting capacity, the uptake of ^{68}Ga-hybird short peptide was investigated in SK-MEL 28 melanoma cell. **Materials and Methods:** The radiolabeling approach for the hybrid ^{68}Ga-hybrid short peptide entailed a one-step reaction. High performance liquid chromatography (HPLC) system and Thin Layer Chromatography (TLC) were used for quality control purposes. The radiochemical purity were > 99.00% (n=5). The stability was persistent over 6 h and amounted to > 98.55% ±0.35% (n=5). The uptake of ^{68}Ga-hybrid short peptide was high by pheomelanotic SK-MEL-28 human melanoma cells. In vitro receptor binding was performed on SK-MEL28 cell line and biological evaluation was done in normal and mice bearing SK-MEL28 cell xenograft. Animal PET/CT using ^{68}Ga-hybrid short peptide was performed in murine models of melanoma. **Results and Conclusion:** As determined by HPLC, the ^{68}Ga-hybrid short peptide efficiency was >70% and radiochemical purities always > 99% in short reaction time. These synthetic approaches hold substantial promise as a rapid and efficient method amenable for automation for the labelled of peptides with high radiochemical yield and short synthesis time. In vitro tests have shown that significant amount of the ^{68}Ga-hybrid short peptide associated with melanoma cell fractions. ^{68}Ga-hybrid short peptide animal PET/CT yielded a

high tumor-to-background ratio at 1 h and at 2h. In vivo characterization in normal mice revealed rapid blood clearance of ^{68}Ga-hybrid short peptide with excretion by both urinary and hepatobiliary pathways. In vivo imaging using animal PET/CT is confirming the later findings. These results demonstrate that ^{68}Ga-hybrid short peptide may be useful as molecular probes for detecting and staging of melanoma and their metastasis. Due to its easy handling and quite high uptake by melanoma cells, we expect that this hybrid peptide could be successfully used in routine application for melanoma imaging or eventual radiotherapy suggesting great potential for noninvasive clinical evaluation of suspected metastatic melanoma

EP-0309
Evaluation of Monochloramine as a Novel Reagent for Radiolabeling of Peptides and Proteins

K. Kumar, K. Woolum; The Ohio State University, Columbus, OH, UNITED STATES OF AMERICA.

Objectives: Radiolabeling of peptides and proteins is routinely performed by using various oxidizing agents such as Chloramine T, Iodobeads, and Iodogen reagent and radioactive iodide (I-). Hypochlorite was recently reported as a reagent for radiolabeling of peptides. The objective of the present study was to develop a novel and inexpensive reagent for radiolabeling of peptides and proteins. **Methods:** An inorganic mono chloramine (NH_2Cl), prepared from the reaction of ammonia and hypochlorite, was investigated as a novel reagent for radiolabeling of a tyrosine residue in peptides and proteins. A known amount of carrier-free [125]I Na activity was added to a 100 µL of 0.1 M Sodium Phosphate (pH 7.4) buffer solution containing a known amount of tyrosine amino acid or a cyclic peptide (cRGDyK, cyclo Arg-Gly-Asp-d-Tyr-Lys) or a protein (BSA, Bovine Serum Albumin) in a 1.5 mL Eppendorf centrifuge tube. Excess NH_2Cl in PBS buffer was added next and the reaction mixture was incubated at room temperature for 20 minutes. Excess NH_2Cl was reduced by the addition of sodium metabisulfite. The crude reaction mixture was purified by using either a Sep-PaK C_{18} Light cartridge or a PD-10 column. The final product was analyzed by a Reversed-Phase High Performance Liquid Chromatography (RP-HPLC) analytical method. **Results:** The RP-HPLC and Matrix-Assisted Laser Desorption Ionization (MALDI) mass spectral analysis of cold iodinated Tyrosine and cRGDyK suggested the formation of mono and di iodinated Tyrosine and cRGDyK. Radiolabeling efficiency (i.e., incorporation of ^{125}I label) was >80% for radiolabeling of Tyrosine, cRGDyK, and for BSA. Reversed-Phase (for radiolabeled Tyrosine and cRGDyK) and Size-Exclusion (for radiolabeled BSA) HPLC analysis showed >99% Radiochemical Purity (RCP) of the radiolabeled materials. **Conclusions:** A novel reagent, inorganic mono chloramine, for radiolabeling of peptides and proteins was developed successfully.

EP-0310
Development of ^{64}Cu-labelled Monomeric and Trimeric RGD-recognising Integrin Ligands via 2-Cyanobenzothiazole/1,2-Aminothiol Click Addition

F. Gao, K. Nguyen, K. Chen, Y. Seimbille; TRIUMF, Vancouver, BC, CANADA.

Purpose: A versatile bioorthogonal reaction between 2-cyanobenzothiazole (CBT) and 1,2-aminothiol was recently reported. This condensation reaction enabled fast, efficient and site-specific labelling of macromolecules in solution and on living cells' surface without the need of a catalyst; and we successfully applied this attractive ligation approach to the radiolabelling of peptides and antibodies on biogenic *N*-terminal cysteine residues for PET imaging. Herein, we developed two bifunctional chelates - pyCBT-NOTA and (pyCBT)$_3$-TACN - for the preparation of monomeric and trimeric peptides via CBT/Cys-mediated click addition to image angiogenesis. **Methods:** Synthesis of pyCBT-NOTA and (pyCBT)$_3$-TACN was straightforward from 2-cyano-6-hydroxybenzozthiazole and the corresponding macrocyclic intermediates. c(RGDyK) was modified for the click reaction by incorporation of a polyethylene glycol linker containing a *N*-terminal cysteine residue. pyCBT-NOTA and (pyCBT)$_3$-TACN were labelled with ^{64}Cu in MES buffer (0.2 M, pH 6.2) at RT for 20 min, while the condensation reactions between CBT-chelators and cysteine residues were carried out at 37 °C in PBS buffer (0.2 M, pH 7.4). **Results:** [64Cu]Cu-NOTA-pyCBT and [64Cu]Cu-TACN-(pyCBT)$_3$ were obtained with radiochemical yield over 95%. Kinetic studies showed fast coupling of [64Cu]Cu-NOTA-pyCBT and [64Cu]Cu-TACN-(pyCBT)$_3$ with L-cysteine to form [64Cu]Cu-NOTA-Luc and [64Cu]Cu-TACN-(Luc)$_3$. The coupling yields were over 50% in 20 min and quickly reached 94% in 30 min. [64Cu]Cu-NOTA-Luc and [64Cu]Cu-TACN-(Luc)$_3$ were stable in PBS and human serum for 12 h. Using this convenient labelling method, [64Cu]Cu-NOTA-luc-PEG$_2$-c(RGDyK) and [64Cu]Cu-TACN-(luc-PEG$_2$-c(RGDyK))$_3$ have been successfully prepared by click ligation between radiolabelled CBT-chelators and Cys-PEG$_2$-c(RGDyK) in 60 min with radiochemical yields above 90%. **Conclusion:** We clearly demonstrated that this bioorthogonal method affords an efficient and site-specific approach to label biomolecules containing a *N*-terminal cysteine. A monomeric and a trimeric ^{64}Cu-labelled RGD-recognising integrin ligand were successfully prepared by CBT/Cys ligation. *In vitro* receptor binding affinity assays, integrin specificity assays, and µPET evaluation of the new radiotracers are underway.

EP-0311
Development of HER2-targeted Molecular Imaging Probes via a Facile 2-Cyanobenzothiazole (CBT)/1,2-Aminothiol Ligation Approach

K. Chen, F. Gao, C. Ieritano, Y. Seimbille; TRIUMF, Vancouver, BC, CANADA.

Purpose: Low molecular weight peptide-based targeting vectors have been extensively used in nuclear medicine. However, site-specific incorporation of an imaging reporter into tumour-targeting peptides remains a major challenge. Herein, we described a rapid and chemoselective strategy for the preparation of human epidermal growth factor receptor 2 (HER2)

imaging probes through the bioorthogonal CBT/1,2-amino-thiol cycloaddition. **Methods:** In our study, we employed an artificial heptapeptide (KSPNPRF) that was recently identified to bind specifically to the extracellular domain (ECD) of HER2. The peptide was functionalized with a short linker - GGGSK(C) - bearing a 1,2-aminothiol click functional group allowing the selective attachment of imaging reporters containing the complementary CBT click functionality. Fluorescent and radioactive reporters were synthesized and clicked to the HER2-targeting peptide (HER2pep) to demonstrate the efficiency and versatility of our ligation approach. **Results:** The imaging reporters - fluorescein-CBT, NODAGA-CBT and DOTA-CBT - were prepared according to three steps chemical syntheses from 2-cyano-6-hydroxybenzozthiazole with satisfactory yields of 58%, 57% and 46%, respectively. Synthesis of HER2pep with an addressable 1,2-aminothiol group was accomplished by solid phase peptide synthesis. Chemoselective ligation of KSPNPRFGGGSK(C)-NH$_2$ and fluorescein-CBT provided fluorescein-luc-HER2pep in 61% yield after reversed phase HPLC purification. Labelling of HER-2pep with [^{64}Cu]Cu-NODAGA-CBT and [^{64}Cu]Cu-DOTA-CBT was successfully achieved under mild aqueous conditions (PBS buffer, 0.2 M, pH 7.4, 37 °C). ^{64}Cu-HER2pep probes were obtained in 60 min with a radiochemical yield above 90%. **Conclusion:** We demonstrated that this rapid and facile bioorthogonal approach is very attractive to label sensitive peptidic vectors. A peptide, targeting HER2-ECD, has been successfully labelled by this approach with fluorescein and ^{64}Cu. *In vitro* binding affinity and *in vivo* distribution of the radiolabelled HER2pep probes are currently being tested. Our study not only confirms the potential of this efficient methodology to label biomolecules at a specific site, but also paves the way to pre-targeting imaging and theranostic applications.

Radiopharmaceuticals & Radiochemistry: New Targets

EP-0312

The Novel, Stapled HDM2/HDMX-p53 Antagonist PM2 Has Potent Antitumorigenic Activities and Enhances the Effects of External Radiotherapy

A. C. Mortensen[1], D. Spiegelberg[1], C. Brown[2], D. P. Lane[2], M. Nestor[1]; [1]Department of Immunology, Genetics and Pathology, Uppsala University, Uppsala, SWEDEN, [2]p53 Lab, A*STAR, 8A, Biomedical Grove, #06-04/05 Neuros/Immunos, Singapore 138648, Singapore, SINGAPORE.

Introduction: Exposure to ionizing radiation activates the p53 tumor suppressor, a key mediator of cellular stress and DNA damage response cascades. Thus, amplifying wild-type p53 (wt p53) expression by targeting negative regulators such as HDM2 and HDMX in combination with radiotherapy may result in increased therapeutic effect. Thus, we investigated the antitumorigenic effects of PM2, a novel, stapled HDM2/X-p53 antagonist, and the possibility of utilizing the peptide in combination with

ionizing radiation. **Materials and Methods:** Effects of PM2 and potential PM2-induced radiosensitivity were first assessed in a panel of cancer cell lines, using 2D cell viability assays. Western Blot and flow cytometry helped clarify the mechanism behind the observed effects in samples treated with either PM2, external beam radiotherapy (EBRT), or the combination of the two. Furthermore, the potency of combining PM2-treatment and EBRT was evaluated using an *in vitro* 3D tumor spheroid model. **Results:** In 2D cell culture, PM2 induced cytotoxic activity alone and in combination with EBRT in wt p53 cells, whereas no significant PM2-mediated effect was observed in p53 mutated or Human Papillomavirus positive cells. Decreased viability following PM2-treatment was observed in all wt p53 cell lines both with and without EBRT. Western Blot confirmed a sixfold increase in p53 expression 24 hours post treatment as well as an increase in apoptosis at later time points in all PM2-treated samples. Flow cytometry confirmed p53-mediated apoptosis through increased levels of cleaved caspase-3 and Noxa in all PM2-treated samples. The combination of PM2-treatment and EBRT proved more potent than either treatment alone in an *in vitro* 3D tumor spheroid model, causing growth inhibition and complete spheroid disintegration as a result of fractionated treatments. **Conclusion:** We conclude that PM2 has potent HDM2/X-p53 antagonistic properties. Additionally, PM2 potentiates the effects of EBRT and shows great promise as a new, targeted therapy of wt p53 cancers.

EP-0313

Preliminary Results Of The Production Of Gallium-68 With Cyclotron

G. Cicoria, F. Zagni, S. Vichi, L. Mora, M. Marengo; Policlinico S.Orsola-Malpighi, Bologna, ITALY.

In the last few years there has been a significant increase in the use of ^{68}Ga for the labeling of different PET radiopharmaceuticals. The current production system of ^{68}Ga through the ^{68}Ge/^{68}Ga generator is readily available and easy to use but it's unable to meet the current clinical requirement, as well as having high costs. In this work we present a feasibility study for the production of ^{68}Ga by liquid target with a biomedical cyclotron. The cross section data were downloaded from the IAEA EXFOR database. Through the SRIM software, the proton stopping power for different materials was calculated: havar, niobium and target material. Subsequently the ^{68}Ga saturation activity and its impurities were estimated. Experimental irradiation tests were performed through the liquid niobium target dedicated to the production of ^{18}F of the GE PETtrace cyclotron. The irradiated solution was prepared by dissolving metallic ^{nat}Zn with HNO$_3$ 6M, the final concentration of Zn(NO$_3$)$_2$ was 1.7 M in HNO$_3$ 0.2N. Cold tests were carried out to evaluate the transfer time and the mass of the solution. In addition, 5 minute up to 5μA to 50μA irradiation tests were performed to evaluate the target resistance to the stress produced by the solution's acidity and to the pressure within the niobium chamber. Irradiated solutions were characterized by gamma spectrometry with an HpGe detector. The main contaminant radionuclide produced results to

be 67Ga through the nuclear reaction 68Zn(p, 2n)67Ga. This reaction has a threshold of 12.2 MeV. Since this radionuclide can't be chemically removed at the end of the irradiation, it is necessary to minimize its production during irradiation. Experimental tests, with entering energy into the target material of 15.7 MeV, showed an optimum target seal, constant delivery times and a recovery of 97% of the solution. The gamma spectrometry analyzes samples of irradiated $^{nat}Zn(NO_3)_2$ showed the presence of different isotopes of Cu,Ga and Co as predicted by the theoretical estimates. The average saturation yield of ^{68}Ga on natural zinc was 146.5 MBq/μA. This result leads to an estimated saturated yield on enriched target of about 780 MBq/μA. In a typical production run at 40μA for 30 minutes, the estimated activity of ^{68}Ga is greater than 8 GBq. Estimated saturation yield for ^{68}Ga using an enriched $^{68}Zn(NO_3)_2$ solution is very promising. However, further experimental tests have to be carried out to evaluate different aspects: evaluation of radionuclidic purity, purification of ^{68}Ga and ^{68}Zn recovery.

EP-20   **during congress opening hours, e-Poster Area**

Radiopharmaceuticals & Radiochemistry: Miscellaneous

EP-0314

Structural Requirement of the 11b-Poisition Chirality of Tetrabenazine Analogs as VMAT2 Imaging Ligands: Synthesis and in vivo Evaluation

Z. Chen[1], D. Xue[2,1], C. Liu[1], X. Li[1], J. Tang[1], L. Cao[2,1], Y. Liu[2]; [1]Key Laboratory of Nuclear Medicine, Ministry of Health, Jiangsu Key Laboratory of Molecular Nuclear Medicine, Jiangsu Institute of Nuclear Medicine, Wuxi, CHINA, [2]Jiangsu Key Laboratory of New Drug Research and Clinical Pharmacy, School of Pharmacy, Xuzhou Medical University, Xuzhou, CHINA.

Introduction: Tetrabenazine (TBZ, chemically named 3-isobutyl-9,10-dimethoxy-1,3,4,6,7,11***b***-hexahydro-2H-pyrido[2,1-a] isoquinolin-2-one) and its analogs have shown potential for vesicular monoamine transporter type 2 (VMAT2) imaging agents in mammalian brain. While some structure-activity relationship between TBZ analogs and VMAT2 binding properties have been investigated, there is no information about the independent role of 11***b-position*** chirality of TBZ ring for *in vivo* bioactivity. **Methods:** We herein designed, synthesized and *in vivo* evaluated two ^{18}F labeled TBZ analogs with eliminated chirality in the 11***b***-position by inserting a 1,11***b***-double bond into the parent TBZ ring, ^{18}F-FP-9-(3-fluoropropoxy)-3-isobutyl-10-methoxy-3,4,6,7-tetrahydro-2H-pyrido[2,1-a]isoquinolin-2-one (^{18}F-FP-DeHTBZ) and ^{18}F-9-(2-fluoroethoxy)-3-isobutyl-10-methoxy-3,4,6,7-tetrahydro-2H-pyrido[2,1-a]isoquinolin-2-one (^{18}F-FE-DeHTBZ), for in vivo VMAT2 binding anaylsis. ^{18}F-FP-DeHTBZ and ^{18}F-FE-DeHTBZ were synthesized from the corresponding tosylate precursors in a one-step reaction. MicroPET imaging studies of these two ^{18}F labeled compounds in rat brain were performed and compared with the known VMAT2 ligand ^{18}F-FP-(+)-DTBZ. Furthermore, nonradioactive FP-DeHTBZ, FE-DeHTBZ and another TBZ analog with eliminated chirality in 11***b***-position, 3-isobutyl-9,10-dimethoxy-3,4,6,7-tetrahydro-2H-pyrido[2,1-a]isoquinolin-2-one (DeHTBZ), were synthesized. Then in vivo bioactivity of these three compounds were assayed and compared with TBZ via competition studies using ^{18}F-FP-(+)-DTBZ as VMAT2 tracer. **Results:** Fluoride[^{18}F] labeled ^{18}F-FP-DeHTBZ and ^{18}F-FE-DeHTBZ were synthesized at radiochemical purity of >93% and radiochemical yield of >30% (decay corrected). MicroPET imaging studies of these two ^{18}F labeled compounds in rats brain showed negligible radioactivity uptake in VMAT2 enriched region (striatum) in 0-2 hour after injection as compared with ^{18}F-FP-(+)-DTBZ. Moreover, nonradioactive compounds FP-DeHTBZ, FE-DeHTBZ and DeHTBZ displayed dramatically lower in vivo VMAT2 binding ability than TBZ as evaluated by competition studies. **Conclusions:** These results demonstrated that the loss of the chiral center in the 11***b***-position of TBZ dramatically decreased *in vivo* VMAT2 bioactivity, indicating that the chiral C in the 11***b***-position is essential for *in vivo* VMAT2 binding. Our studies provided a theoretical basis or a lab experience for developing new VMAT2 ligands.

EP-0315

Central Conducting Lymphatic Anomaly in Neonatal Chylothorax Visualized after Oral Administration of [^{131}I] IHDA

S. Stanzel[1], H. Kvaternik[1], K. Pfurtscheller[2], R. Ulreich[2], R. M. Aigner[1]; [1]Medical University of Graz, Department of Radiology, Division of Nuclear Medicine, Graz, AUSTRIA, [2]Medical University of Graz, University Children's Hospital, Pediatric Intensive Care Unit, Graz, AUSTRIA.

Purpose: Congenital malformations of the thoracic duct (central conducting lymphatic anomalies, CCLA) are extremely rare. CCLA are leading to chylothorax, which is the accumulation of chyle in the pleural space from the thoracic duct. The difficulty is that these anomalies are difficult to delineate with conventional radiological methods. Lymphatic leakage lesions can be localized by scintigraphy after oral admission of radio-iodinated long chain fatty acids. The aim was to localize the thoracic duct after preparation and oral administration of n.c.a. 16-[^{131}I]iodohexadecanoic acid ([^{131}I]IHDA) in a 3-month-old female with chylothorax and central conducting lymphatic anomaly (CCLA) by [^{131}I] IHDA lymphoscintigraphy. **Subjects and Methods:** A 3-month-old female with a known cystic intrathoracic mass in the posterior inferior mediastinum which became apparent already in fetal sonography was referred to the Division of Nuclear Medicine for localization of the thoracic duct. Overall, 3.6 MBq [^{131}I]

IHDA was suspended in pasteurized breast milk and applied via the gastric tube. Anteroposterior and lateral planar scintigraphic images were acquired 0 - 4 h and 24 h after ingestion. Images were acquired with a Symbia T2 (Siemens) and a Discovery NM/CT 670 Pro (GE), dual head gamma camera, fitted with a high energy collimator for ^{131}I. **Results:** After oral administration, two hours and 50 min. post applicationem a malformed, blind ending thoracic duct was localized by scintigraphy. The chylothorax could not be visualized by scintigraphy but revealed indirectly through radioactivity measurement of the aspirated chylus out of the thorax drain. Totally, 26% of the applied radioactivity was found in the collected aspirated chylus, the highest radioactivity concentration was observed in the fraction of about 8 h after administration. **Conclusion:** The described application of the labeled fatty acid [^{131}I]IHDA presented a suitable approach for a scintigraphic detection of CCLA.

EP-0316

Influence of the use of cryoprotectant on the ladiolabelling of poly(lactic-co-glycolic acid) (PLGA) nanoparticles with ^{99m}Tc

R. Iglesias-Jerez[1], M. D. Cayero-Otero[2], L. Martín-Banderas[2], I. Borrego-Dorado[1]; [1]HU VIRGEN DEL ROCÍO. Avda Manuel Siurot s/n. 41013, Sevillla, SPAIN, [2]Dpt. Farmacia y Tecnología Farmacéutica. Facultad de Farmacia. Universidad de Sevilla. c/Prof. Gracía González nº2, 41012., Sevilla, SPAIN.

Introduction: Radiolabelled nanoparticles have gained a widespread application in the diagnosis and therapy of several diseases (inflammation/infection, cancer, and others). PLGA Nanoparticles (NPs) prepared by solvent emulsion evaporation method have shown more suitable characteristics with regard to those produced by nanoprecipitation: better size, a higher homogeneity and higher encapsulation efficiency. The radiolabelling of PLGA nanoparticles (platforms with excellent biodegradability and biocompatibility) with ^{99m}Tc; could allow obtaining a suitable nanosystem for theranosis. On the other hand, the cryoprotector has demonstrated its effectiveness improving the dispersion of the PLGA nanoparticles, so that, the radiolabel could be altered in some way. The purpose of our work is to study the influence of the use of cryoprotectant on this labelling process. **Materials and Methods:** PLGA nanoparticles were prepared using the nanoprecipitation method. Then, 5 mg of lyophilized NPs were dispersed in 1 mL 0.9% NaCl and stored in a vacuum vials. Different amounts of stannous fluoride in aqueous solution (30, 20, 4, 2, 1 and 0,1 μg) were added. Then, was added ≈74 MBq (2 mCi) of ^{99m}Tc in 1 mL of 0.9% NaCl. Finally, the suspension was incubated for 10 min. ^{99m}Tc -NPs suspensions were analyzed by thin layer chromatography (TLC) with silica gel strips (10 x 2,5 cm). With 0.9% NaCl as the mobile phase, free pertechnetate ran with the front, meanwhile particles stayed in the start. Using a solution of pyridine: acetic acid: water (3: 5: 15), radiocolloids remained at start, NPs migrated with Rf = 0.3 and free pertechnetate moved with Rf = 0.7-0.8. **Results:** Preliminary results obtained so far, indicate that the labeling yields are much higher, under any circumstances, with the use of the cryopro-

tectant. In addition, using 1 μg of SnF$_2$ as a reducing agent, PLGA nanoparticles (with and without cryoprotectant) were labeled with ^{99m}Tc with a yield ≥ 90 %. **Conclusions:** Results obtained, indicate that procedures of nanoparticle synthesis with cryoprotectant, radiolabelling and quality control were reproducible and appropriate for designing a biodegradable nanosystem suitable for *in vivo* theranosis.

EP-0317

Gamma Ray Spectroscopy for Determination of Absolute Activities of Cyclotron-Produced Technetium Product Impurities and Waste

L. A. Stothers[1,2], X. Hou[2], M. Vuckovic[3], K. Buckley[4], P. Schaffer[4], F. Bénard[3], T. J. Ruth[3,4], A. Celler[2]; [1]The University of British Columbia, Vancouver, BC, CANADA, [2]Medical Imaging Research Group, Vancouver, BC, CANADA, [3]BC Cancer Agency, Vancouver, BC, CANADA, [4]TRIUMF, Vancouver, BC, CANADA.

Purpose: Proton irradiation of ^{100}Mo (cyclotron-produced ^{99m}Tc) is a reliable alternative to reactor-based production of ^{99m}Tc, the most commonly used isotope in diagnostic imaging. We have already shown that selecting irradiation conditions can minimize impurities in the ^{99m}Tc product. However, small quantities of Tc isotopes other than ^{99m}Tc, and other long-lived isotopes including Re and Mo, will remain in the product after purification. The potential increase of patient dose due to these isotopes must be determined. Additionally, since waste isolated during ^{99m}Tc purification will contain long-lived isotopes, which may impact its handling, storage and disposal, the waste activity needs to be evaluated. Therefore, the aim of this study was to determine the activities of isotopes present in the ^{99m}Tc sample and waste produced during irradiations at BCCA and TRIUMF. **Methods:** Gamma ray spectroscopy was performed to identify isotopes produced during the 18MeV proton irradiation of 99.815%-enriched ^{100}Mo. Eighteen diluted product/waste samples were measured using a high-purity germanium detector at end of beam (EOB) and at days 1, 3-4, 6-8 and 28-35 after EOB. Hyperlab 2009 software was used to identify and quantify isotopes present in all samples. The results were compared with those from a 24MeV proton irradiation to determine which isotopes can be present in the waste after higher energy irradiations. **Results:** Due to chemical properties similar to Tc, ^{181}Re, ^{182}Re, ^{183}Re, ^{184}Re and ^{99}Mo still remained in the purified ^{99m}Tc product. The cyclotron produced ^{99m}Tc already increases patient dose by 0.56% as compared to pure ^{99m}Tc. For injections at expiration time, these impurities would further increase dose by 0.12%. For each 1GBq of cyclotron-produced ^{99m}Tc, the total activity at EOB of the 41 isotopes identified in the waste samples was $2.76 \times 10^{-2} \pm 0.01 \times 10^{-2}$GBq. Reactions on ^{100}Mo led to the production of ^{99}Mo($2.26 \times 10^{-2} \pm 0.08 \times 10^{-2}$GBq), ^{96}Nb($1.678 \times 10^{-3} \pm 0.006 \times 10^{-3}$GBq) and ^{181}Re($1.4 \times 10^{-3} \pm 0.3 \times 10^{-3}$GBq) per 1GBq ^{99m}Tc. Additionally, target impurities/support material resulted in the production of ^{198}Au($1.1 \times 10^{-4} \pm 0.4 \times 10^{-4}$GBq), ^{120}Sb($6 \times 10^{-8} \pm 2 \times 10^{-8}$GBq), and ^{43}K($3.0 \times 10^{-4} \pm 0.9 \times 10^{-4}$GBq) per 1GBq ^{99m}Tc. The isotopes with the longest half-lives were ^{57}Co(272 days), ^{195}Au(186 days) and ^{184}Re(169 days). Waste samples from high

energy (24MeV) irradiations contained five additional isotopes: [72]As, [76]As, [77]As, [97]Nb and [124]Sb. **Conclusion:** Non-Tc impurities in the ^{99m}Tc product result in only a 0.12% dose increase at expiration. Waste produced by 18MeV protons amounts to 0.0276GBq per 1GBq ^{99m}Tc, and decays to $3.61\times10^{-6}\pm0.04\times10^{-6}$GBq after 1 year. Although the majority of activity comes from reactions on [100]Mo, target impurities make a non-negligible contribution to the total waste activity.

EP-0318

Radiolabeling optimization of radioaptamers as new heterotrimeric theranostic systems for antimetastatic therapy

R. Ramos-Membrive[1], G. Gan[2], *M. Collantes*[3], F. Pastor[4], M. Martínez-Soldevilla[4], I. de Miguel[5], M. Villalba[6], J. Oyarzabal[5], A. Calvo[6], I. Peñuelas[3,1]; [1]Radiopharmacy Unit, Clínica Universidad de Navarra, Pamplona, SPAIN, [2]University College, London, UNITED KINGDOM, [3]Nuclear Medicine, Clínica Universidad de Navarra, Pamplona, SPAIN, [4]Aptamers and Small Molecules Unit, Center for Applied Medical Research (CIMA), Pamplona, SPAIN, [5]Molecular Therapies, Center for Applied Medical Research (CIMA), Pamplona, SPAIN, [6]Program in Solid Tumors and Biomarkers, Center for Applied Medical Research (CIMA), Pamplona, SPAIN.

Purpose/Introduction: Radioaptamers are heterotrimeric conjugates composed of an aptamer, a deoxyribonucleotide linker and a diagnostic or therapeutic radiometal attached by a chelator. This type of molecule would serve as a new *in vivo* monitoring system for tumor detection and as combined antimetastatic and/or radiometabolic therapy. The aim of the present work was to develop the radiolabeling of the newly designed radiopatamer E07-pNT-NODAGA with gallium-67 and to analyze the stability of the radiolabeled complex. **Subjects & Methods:** An anti-EGFR aptamer (E07) was produced by in vitro transcription and was coupled by hybridization to a complex (pNT-NODAGA) formed by an extension of deoxyribonucleotides bound to the NODAGA chelator and synthesized from pNCS-benzyl-NODAGA. [^{67}Ga]GaCl3 was obtained by acidification of gallium-67 citrate with HCl and fractional purification (12x30 µl) with C18 cartridges. Fractions with the highest activity were pulled together and brought to pH=3.4 or 5 with HEPES and incubated (40 °C, 30') with 32.5 pmoles of E07-nt-NODAGA. The kinetics of labeling (1,3,5,10,20 and 30min) and its stability at 1 and 5 days were analyzed by radio-TLC. As controls, pNTNODAGA (2 nmoles) and E07 aptamer (2 nmoles) were also labeled. **Results**: The conversion yield from gallium-67 citrate HCl to [^{67}Ga]GaCl3 was> 80%. E07-pNT-NODAGA showed a more favorable reaction kinetics and higher radiochemical purity (≥95%) than pNT-NODAGA (≈ 50%) or E07 (70%); the last two were purified by tangential filtration to remove [67]Ga^{3+}. Yield was higher at pH=5 in all cases. All complexes were stable for 5 days with a gallium-67 release <3%. **Discussion/Conclusion:** The labeling of the radioaptamer E07-pNT-NODAGA with gallium-67 is feasible and occurs in high yield. However, the results of the controls seem to indicate that the 3D structure of the aptamer may be responsible for the binding of the major part of the gallium.

EP-0319

Forecasting the production of medical radioisotopes at Extreme Light Infrastructure - Nuclear Physics gamma-beam system

D. Niculae[1], F. D. Puicea[2,3], S. Ilie[1,3], W. Luo[4], P. V. Cuong[2,5], G. Cata Danil[3], C. A. Ur[2], D. Balabanski[2]; [1]Horia Hulubei National Institute for Physics and Nuclear Engineering, Magurele Ilfov, ROMANIA, [2]Extreme Light Infrastructure - Nuclear Physics, "Horia Hulubei" National Institute for Physics and Nuclear Engineering, Magurele Ilfov, ROMANIA, [3]Politehnica University, Bucharest, ROMANIA, [4]School of Nuclear Science and Technology, University of South China, Hengyang, CHINA, [5]Centre of Nuclear Physics, Institute of Physics, Vietnam Academy of Science and Technology,, Hanoi, VIET NAM.

Purpose: The applications of radioisotopes in molecular nuclear medicine require high specific activities, which can be usually obtained using nuclear reactions induced by high intensity accelerated beams or neutrons coming from nuclear reactors. In the latter case, the radioactive element is transmuted from the target isotope and can be easily separated by chemical procedures (carrier free). This method involves also high reaction cross-sections, spanning from few barns to thousands of barns. **Methods:** One of the alternative route for production of emerging radioisotopes for nuclear medicine employ (γ,n) nuclear reaction to produce such radioisotopes, with relevant quantity and quality. Gamma beams can efficiently excite a nucleon into an unbound state leading to photo-dissociation and creation of a new isotope. Using the new beam facilities compact targets could be exposed to the gamma radiation and undergo photonuclear reactions such as (γ, γ'), (γ, n), (γ, p) to form radioisotopes. The existing gamma beam facilities have flux densities below 10^{14} γ/cm^{2}s, leading to specific activities below 10^{-5} Ci/g. Prospective radioisotopes to be produced by (γ,n) reactions simulations of the target geometry and estimation of activity of some radioisotopes of interest for nuclear medicine will be presented. We propose to utilize the intense laser beam backscattered on high energy electron bunches to produce monoenergetic directed brilliant pulsed gamma-rays by the Compton backscattering process. **Results:** Even the reaction cross-sections are as low as 0.1 barn for (γ,n) reaction, the flux densities and the narrow band at the new gamma facility at Extreme Light Infrastructure - Nuclear Physics (ELI-NP) will allow in the first stage the possibility of production of radioisotopes with higher specific activities. At ELI-NP, the spectral density is designed to be higher than $0.5\cdot10^4$ photons/s·eV, number of photons/s within FWHM bandwidth are 10^8-10^9 and linear polarization over 95%, while the energy of the photons will reach 19.5 MeV in the second phase of the project development. **Discussion/Conclusion:** Alternative routes for reliable production of emerging radioisotopes will open the way for completely new clinical applications of radioisotopes. [195m]Pt could be used to monitor the patient's response to chemotherapy with platinum compounds before a complete treatment is performed, using low-energy γ transition for SPECT imaging. In targeted radionuclide therapy the short-range Auger and conversion electrons resulted from [195m]Pt could enable a very local treatment. [62]Cu, ^{64}Cu, [186]Re and [225]Ra/[225]Ac are also evaluated for production on this route.

Cardiovascular System: Basic Science

EP-0320

Quantification of Myocardial Perfusion Defect in Rats with Ultra-high Resolution SPECT System using QPS Software: Comparison with High-resolution Autoradiography

H. Wakabayashi[1], J. Taki[1], A. Inaki[1], T. Hiromasa[1], K. Shiba[2], S. Kinuya[1]; [1]Dept. of Nuclear Medicine, Kanazawa University Hospital, Kanazawa, JAPAN, [2]Advanced Science Research Center, Kanazawa University, Kanazawa, JAPAN.

Commercially available software packages have become available to quantify myocardial perfusion defects in small animal study. Novel ultra-high resolution SPECT/CT system using multiple pinhole collimators has been applied to image small rodents. To determine the accuracy of perfusion defects quantified by QPS (Cedars-Sinai Medical Center, US), we compared the area of myocardial infarction (MI) determined by *in-vivo* SPECT/CT with that of high-resolution autoradiography in rats with coronary artery occlusion and reperfusion. **Methods:** After thoracotomy, the left coronary artery was occluded for 20-30 min and reperfused (n=9). Then ^{99m}Tc-MIBI (185MBq) was injected to perform *in-vivo* SPECT/CT and high-resolution autoradiography. Additionally, healthy rats (n=20) were scanned to create normal database. The image size was magnified by 10 times (scaling factor 10) in order to approach the human reference heart volume. The MI area (defect area) on SPECT/CT images (U-SPECT system, MIlabs, the Netherlands) was automatically analyzed by QPS software using a normal database. For autoradiography images, the MI area was analyzed by Image J software (NIH, US). The MI was defined as the area with less than 50% of the maximum myocardial count. The MI area was set in each short axial image in every 1mm slices. **Results:** MI was confirmed in every rat on both SPECT and autoradiography. MI size in SPECT/CT correlated well with that of autoradiography (defect area on QPS software vs autoradiography; r^2=0.86, y=745x+33788, p=0.0002 and summed rest score vs autoradiography; r^2=0.81, y=5653x+31006, p=0.0008, respectively). However, small MI was not recognized as perfusion defect on QPS analysis. **Conclusions:** The SPECT/CT with QPS software can evaluate the severity of MI on myocardial perfusion images in rats semiquantitatively, which was well correlated with the results of autoradiography. The widely available software in clinical use will be useful for the evaluation of small animal cardiac imaging.

Cardiovascular System: Clinical Science: Perfusion, Metabolism and Receptors

EP-0321

Evaluation of diagnostic ability of an artificial neural network for detecting ischemia in myocardial perfusion imaging

T. Yoneyama[1], K. Nakajima[2], S. Tsuji[1], K. Yokoyama[1], T. Michigishi[1]; [1]Public Central Hospital of Mattou Ishikawa, Hakusan, JAPAN, [2]Department of Nuclear Medicine, Kanazawa University Hospital, Kanazawa, JAPAN.

Aim: We investigated usefulness of an artificial neural network (ANN) for patients with coronary artery disease (CAD) in myocardial perfusion imaging (MPI) with D-SPECT and conventional Anger SPECT systems. **Methods:** A total of 30 patients (male 23, age: mean 67.4 ± 9.2 years, range 45-85) suspected of having CAD who underwent stress and rest MPI by both D-SPECT and conventional Anger SPECT systems were included. Coronary stenosis was confirmed by coronary angiography which used ≥75% stenosis as the gold standard. In ANN analysis, an ANN value was calculated from subtraction of stress and rest images to indicate the probability of ischemia. The probability of ischemia using the ANN value was used to evaluate the presence of ischemia. In visual analysis, a scoring method based on 4-grade points (0, normal; 1, possibly abnormal; 2, probably abnormal; 3, definitely abnormal) was used to classify the probability of ischemia. Ischemia was defined as scores of 2 and 3 grade points. Receiver-operating characteristics curve (ROC) analysis was performed, and the area under the curve (AUC) was calculated to evaluate diagnostic ability. **Results:** Coronary stenosis was detected in 18 of 30 cases. Concordance of evaluating the presence or absence of ischemia in left ventricular myocardium between ANN and visual analyses using D-SPECT was 80%, and that using conventional SPECT was 77%. ROC analysis showed no significant difference between ANN and visual analyses for evaluating ischemia in left ventricular myocardium using D-SPECT and conventional SPECT. With conventional SPECT, sensitivity and specificity for identifying significant coronary stenosis were 78% and 50%, respectively for both ANN and visual analyses. With D-SPECT, sensitivity and specificity were 83% and 50%, respectively for both methods. In visual analysis, ROC AUC of conventional SPECT and D-SPECT were 0.73 and 0.76 (p=n.s.), respectively, whereas in ANN analysis, they were 0.65 and 0.72 (p=n.s.), respectively. **Conclusion:** Diagnostic ability of an artificial neural network for detecting ischemia was comparable to visual analysis in both D-SPECT and conventional Anger SPECT systems, when difference between stress and rest images was used.

EP-0322

Lower Annual Cardiac Events in Diabetics with A Normal Exercise GMPI And A Functional Capacity ≥7 METS on Treadmill

N. Fatima[1,2], M. u. Zaman[1,2], D. J. M. baloch[3], A. U. Hussiaini[3], S. Z. Rasheed[3]; [1]Aga Khan University Hospital, Karachi, PAKISTAN, [2]Dept of Nuclear Cardiology, Karachi Institute of Heart Diseases (KIHD), Karachi, PAKISTAN, [3]Karachi Institute of Heart Diseases (KIHD), Karachi, PAKISTAN.

Introduction: Good exercise capacity has a high negative predictive value (NPV) in patients with known or suspected coronary artery disease (CAD) similar to a normal gated myocardial perfu-

sion imaging (GMPI). However, previous studies have suggested that diabetic patients undergoing single photon emission computed tomography (SPECT) myocardial perfusion imaging (MPI) are at greater risk for cardiac events than non-diabetic patients with both normal and abnormal MPIs. Aim of this study was to evaluate NPV of functional capacity during treadmill exercise in diabetics with normal GMPI in Pakistani population. **Methods:** This was a prospective study which included 338 diabetics with normal exercise GMPI. On the basis of metabolic equivalents (METS) achieved during exercise, these patient were divided into Group A: ≥7 METS (140 patients) and Group B: <7METS (198 patients). These patients were followed up on telephone (for 18 ±3 months) for fatal or non-fatal myocardial infarction (FMI and NFMI respectively). Regarding risk factors in Group A and B, like obesity (50 vs. 54%), hypertension (61 vs. 60%), smoking (14 vs. 15%), dyslipidemia (32 vs. 42%) and family history (32 vs. 30%), no significant difference was found. **Results:** The mean age predicted HR (MAPHR) achieved in group was significantly higher than Group B (86% vs. 83%). No significant difference was found between LV functional parameters (like ejection fraction, end diastolic and systolic volumes) of two groups. During follow up period, the overall all cardiac events reported in Group A was 03 (all NFMI and no FMI) while in Group B 16 events (15 NFMI and 01 FMI) were reported. Annualized event rate for overall events, NFMI and FMI in two groups were 1.43 vs. 5.39%, 1.43 vs. 5.05 and 0% vs. 0.3% respectively. **Conclusion:** We conclude that NPV of a normal GMPI is higher in diabetic patients with a functional capacity ≥7 METS than their counterparts who could achieve <7 METS on treadmill.

EP-0323

The application of ATP stress SPECT cerebral blood flow perfusion imaging in ischemic cerebrovascular disease

R. Wang[1], L. Yin[2], J. Yan[2], J. Liu[2], R. Xu[2], C. Jin[2]; [1]Peking University First Hospital, Beijing, CHINA, [2]China-Japan Friendship Hospital, Beijing, CHINA.

Aim: To investigate the value of adenosine triphosphate (ATP) stress cerebral blood flow perfusion imaging in diagnosis of ischemic cerebrovascular disease (ICVD). **Methods:** 32 patients with ischemic cerebral ischemia and cerebral infarction in Chinese-Japan Friendship hospital (male 26, female 7, average 63 years) were underwent rest and ATP stress cerebral blood flow perfusion imaging method, respectively. Region of interests (ROIs) were drew and the regional cerebral blood flow (rCBF) was automatic calculated. The images of post and pre-ATP stress were compared and the data of rCBF were analyzed. The reactions to ATP stress cerebral blood perfusion were divided into 5 types. A type, both perfusions before and after ATP stress CBF were normal. B type, the resting perfusion was normal, while the load perfusion decreased. C, the resting perfusion decreased and load perfusion decreased more seriously. D type, resting perfusion decreased while load perfusion improved or became normal. E type, no change of hypoperfusion between resting and load images. **Results:** The positive rate of rest and ATP stress CBF perfusion imaging are 53% (17/32) and 65.5% (21/32),

respectively. While the positive rate of rest+ ATP stress CBF perfusion imaging is 100%. The average rCBFs of vascular stenosis side in resting and load images are (65.8 13.2) and (62.7±13.3) ml (100g⁻¹·min⁻¹) respectively. The average rCBF in resting is higher than that of load imaging; The average rCBFs of the contralateral side in resting and load imaging are (67.4±13.3) and (65.9±13.0) ml (100g⁻¹·min⁻¹) respectively. There was no significant differences between them. 16 patients had bilateral multivessel disease (including anterior circulation and posterior circulation). The average rCBF in resting is (62.5±13.9) ml (100g⁻¹·min⁻¹), while that in load imaging is (57.5±11.6) ml (100g⁻¹·min⁻¹). The average rCBF in resting is higher than that of load imaging. There was significant differences between them (t=3.5, P<0.05). 32 cases of ATP stress reaction were divided into 15 cases of type B, 6 cases of type C and 11 cases of type D. The result showed that cerebral blood flow reserve decreased in 21 cases. **Conclusions:** ATP stress combined with rest cerebral blood flow perfusion imaging will raise positive rate remarkably and help to evaluate the cerebral blood flow reserve. Thus they may be more helpful for ICVD patients. **Keyword**: Adenosine triphosphate, Cerebral blood flow perfusion, Ischemic cerebrovascular disease (ICVD), Cerebral blood flow reserve, Three-dimensional arterial spin labeling (3D ASL)

EP-0324

Investigation of the Impact of Early Imaging on Systolic and Diastolic Dysfunction Parameters on Gated Myocardial Perfusion Scintigraphy

*A. O. Karacalioglu, **T. Haciosmanoglu**, O. Emer, S. Ince, E. Alagoz, K. Okuyucu, N. Arslan; Gulhane Training and Research Hospital, Department of Nuclear Medicine, Ankara, TURKEY.*

Introduction: While performing gated myocardial perfusion scintigraphy, generally it has been waited for at least 30 minutes to reduce the extracardiac activities such as liver activity after the exercise. This results in reduction of the effects of increased exercise-induced sympathetic nervous system activity over the heart. The aim of this study is to evaluate the impact of elapsed time after exercise on systolic and diastolic functions of the heart. **Material and Methods:** This study included 30 patients consecutively (17 female, 13 male, mean age: 55 years) referred to our clinic for gated myocardial perfusion scintigraphy (gMPS)..All the patients were injected 7±1 mCi (259±37 MBq) of Tc99m-MIBI when they reached at least 85% of the targeted heart rate according to Bruce protocol on treadmill. The effort continued at least one more minute after the injection. Dual-time gMPS imaging was performed post-exercise (early: 7±2 minutes and late: 30±5 minutes, respectively) on solid state cardiac gamma camera. The images were analyzed by a commercially available software programme (QGS-QPS). **Results:** Left ventricular systolic and diastolic volumes were significantly increased; ejection fraction, peak filling and emptying rates of left ventricle decreased on late images in statistical comparison of early and late images. **Conclusion:** According to first impressions of this study, as post-exercise imaging period is prolonged, the systolic and diastolic functions of heart seems to be dimin-

ishing with exercise-induced sympathetic nervous system activation. This situation is similar to wall motion disorders occuring after exercise-induced ischemia (stunning) which are detected in a decreased rate proportionally with time lapse.

EP-0325

Measurement of Cardiac Function Before and After TAVI (Transcatheter Aortic Valve Implantation) Using Myocardial Scintigram

K. Yamaguchi; St. Marianna University School of Medicine, Kawasaki, JAPAN.

Objective: In patients with severe aortic stenosis (AS), left ventricular hypertrophy is associated with increased myocardial stiffness and dysfunction linked to cardiac morbidity and mortality. We aimed at systematically investigating the degree of left ventricular mass regression and changes in left ventricular function before and after transcatheter aortic valve implantation (TAVI) using cardiac SPECT image analysis. **Materials and Methods:** Myocardial scans were performed in eighty AS cases before and after TAVI. Seventy-three cases (male 21, female 52, mean age: 83 years old) of non-small heart cases (ESV>20ml) were analyzed. The gated SPECT image was obtained using the E.com (Toshiba), and 740Mbq ^{99m}Tc-labeled tetrofosmin. The study group was divided into two groups based on SRS, mild ischemia group (SRS 0-3) and severe ischemia group (SRS 4 or more). Cardiac function was analyzed by Cardio Repo (FRP). Ejection fraction (EF), peak filling rate (PFR) and bandwidth (BW) for phase analysis were compared before and after TAVI in each group. **Results:** EF did not significantly differ between pre- and post-TAVI in both mild and severe ischemia groups (57.4 % vs. 58.0 % in mild ischemia (NC) 50.0% vs. 52.6 % in severe ischemia (NC) . PFR significantly increased post-TAVI in the mild ischemic group (pre 1.8 vs. post 2.2 (ml/sec) P<0.001, paired t-test). No significant differences were observed in the severe ischemia group between pre- and post-TAVI (1.8 vs. 2.2 (ml/sec)). BW significantly decreased in the mild ischemia group (43 vs. 38.6 (p<0.04, paired t-test) in mild ischemia, 57 vs. 63 (NC) in advanced ischemia). **Conclusion:** TAVI effectively improved AS patients' left ventricular dilatation in the mild myocardial ischemia group in early post-operative period. This result suggests that the first step of the recovery from the pressure overload status by TAVI is dilatation recovery prior to the systolic function recovery, which has previously been known for the systolic function recovery to occur first. The reason for improvement of BW in the mild ischemia group is not clear. The one possibility for improvement of BW might stem from improvement of myocardial ischemia.

EP-0326

Myocardial perfusion and neurotropic SPECT features in patients with primary pulmonary hypertension

A. A. Ansheles[1], E. G. Valeeva[1], T. V. Martynyuk[1], R. S. Karpov[2], V. B. Sergienko[1]; [1]Russian Cardiology Research Center, Moscow, RUSSIAN FEDERATION, [2]Cardiology Research Institute, Tomsk, RUSSIAN FEDERATION.

Introduction/Purpose: Primary pulmonary hypertension (PPH) is associated with sympathetic nervous system activation. Besides regulating of pulmonary endothelial function, it affects myocardium, in some cases in advance of right ventricular (RV) failure. PPH can also manifest with cardialgias, suspecting myocardial ischemia. The aim or current research was to compare cardiac ^{123}I-MIBG and ^{99m}Tc-MIBI SPECT data in patients with PPH. **Subjects & Methods:** The study included 40 patients with confirmed diagnosis of PPH, with clinical status assessment, Holter ECG monitoring and rest cardiac ultrasound (US) data. All patients, as well as a group of healthy volunteers (n=20) underwent myocardial perfusion SPECT with ^{99m}Tc-MIBI at rest and after treadmill exercise test, and myocardial neurotropic SPECT with ^{123}I-MIBG, performed in 15 min (early phase) and 4 hours (delayed phase) after MIBG administration. LV perfusion abnormalities were evaluated using standard SSS and SDS parameters, RV was assessed visually, and RV/LV uptake ratio was calculated. Global sympathetic activity (SA) was assessed with delayed heart/mediastinum ratio (H/M$_d$) and MIBG Washout Rate in 4 hours (WR). Regional SA abnormalities were assessed using early Summed MIBG Score (SMS$_e$). MIBG RV/LV and LV IVS/lateral wall (LW) uptake ratios were calculated. **Results:** All myocardial SPECT parameters, both perfusion (SSS, SDS, RV/LV) and neurotropic (H/M$_d$, WR, SMS$_e$, RV/LV, IVS/LW), were significantly worse in PPH patients compared to the control group (all p<0.01). Perfusion SPECT showed no significant (SDS>4) transient LV ischemia in all patients, but in 95% of cases IVS perfusion was stably impaired (SSS=9±3), presumably due to IVS compression by dilated RV, suggesting that it may be responsible for angina-like symptoms. MIBI RV/LV ratio was 0.60±0.11, indicating that RV was clearly visible, with inhomogeneous MIBI uptake in all cases, but without reliable perfusion defects. Values of H/M$_d$ were 1.84±0.18, WR: 27±8%, with no reliable correlations with perfusion parameters. Regional SA defects also were located in IVS predominately, causing SMS$_e$ mean value of 10±4 and IVS/LW of 0.79±0.09, both parameters correlated with SSS (r=0.44, p=0.04, r=-0.48, p=0.02, respectively). All parameters, except MIBG RV/LV ratio, had reliable correlations with systolic pulmonary artery pressure (SPAP) assessed by cardiac US, especially MIBI RV/LV (r=0.64, p<0.01), MIBG WR (r=0.55, p=0.01) and MIBG IVS/LW (r=-0.49, p=0.02). **Conclusion:** Combination of myocardial neurotropic and perfusion SPECT has a certain diagnostic value in patients with PPH, since MIBG SPECT reflects SA downregulating, and MIBI SPECT reveals specific microcirculatory abnormalities in these patients, both possibly caused by myocardial pressure overload.

EP-0327

Rest/Stress vs. Stress only Myocardial Perfusion Imaging. How many exams could be avoided? Our experience

*S. Sollaku, **V. Frantellizzi**, G. A. Follacchio, J. Lazri, M. Ricci, M. Liberatore, F. Monteleone, G. De Vincentis; Sapienza University of Rome, Rome, ITALY.*

Aim: Myocardial Perfusion Imaging (MPI) is used as non invasive method for evaluating severity of coronary artery disease. When

Stress imaging is normal, Rest images couldn't be required. But often, Rest images are acquired prior to Stress acquisition. The aim of this study is evaluate how many rest perfusion imagings are not necessary. **Materials and Methods:** Two cardiac imaging experienced physicians collected data from a period of one calendar year (2016). Image processing and recostruction was done on a Xeleris 3 Workstation (GE, Milwaukee), using QPS/QGS software in order to generate three plane slices, polar plots and quantitative perfusion images. Only One Day protocol data were collected. 275 patients, 170 males, mean age 69 years (51-83) and 105 females, mean age 71 years (57-81) underwent MPI using both Rest and Stress protocol. Rest images were obtained using 8-10 mCi of 99mTc-SestaMIBI and Stress images using 20-30 mCi of 99mTc-SestaMIBI, after exercise or dipyridamole (0,56 mg/kg). Summed Stress Score (SSS), Summed Rest Score (SRS) and Summed Difference Score (SDS) were calculated for each study. Correlation between two observers was done using spearman correlation coefficient. **Results:** Correlation was determined as 0.96 (p<0.001) for SRS and 0.94 (p<0.001) for SSS. Considering an exam as positive when SRS or SSS was >2, 203/275 (75%) exams were negative at Rest imaging and 132/275 (48%) exams were negative at Stress imaging. **Conclusions:** Stress only protocol, when normal, can lead to lower radiation exposure to patients and shorter exam time. Also, lower occupation exposure for nuclear medicine department staff could be achived.

EP-0328

The relationship between myocardium sympathetic innervation dysfunction with the occurrence of ventricular tachycardia in patients with coronary artery diseases and implantable cardioverter defibrillator

S. I. Sazonova[1,2], T. A. Atabekov[1], R. E. Batalov[1], J. N. Ilushenkova[1], N. V. Varlamova[2], E. A. Nesterov[2], A. S. Semenov[2], S. V. Popov[1], Y. B. Lishmanov[1]; [1]*Cardiology Research Institute, Tomsk NRMC, Tomsk, RUSSIAN FEDERATION,* [2]*Tomsk Polytechnic University, Tomsk, RUSSIAN FEDERATION.*

Despite advances in the treatment of coronary artery disease and the use of implantable cardioverter defibrillators (ICD), sudden cardiac death (SCD) is a leading cause of mortality. So, the early detection of persons with high risk of life-threatening ventricular arrhythmia is an important problem. The heart/mediastinum (H/M) ratio, assessed by myocardial scintigraphy with ^{123}I-MIBG, was previously proposed as a predictor of SCD in patients with heart failure (HF). We made an attempt to compare correlations between characteristics of the ventricular tachycardia episodes (VTE) during 6 month follow-up and different scintigraphic indexes of myocardial ^{123}I-MIBG scintigraphy in patients with myocardium infarction (MI) and ICD. **Purpose:** To assess the correlation between VTE characteristics and different indexes of ^{123}I-MIBG myocardium scintigraphy in patients with IM and ICD during 6 month follow-up. **Methods:** 35 patients (5 female and 16 male), mean age 66,7±8,98 years, with MI (I-III HF by NYHA) referred for ICD implantation were included into the research. Ejection fraction of the left ventricle (LVEF) was in

a whole group 46,2 ± 15,6%. All patients before ICD implantation underwent cardiac scintigraphy with ^{123}I-MIBG. Planar and SPECT images were acquired at 15 minutes (early) and 4 hours (dealed) after i.v. administration of ^{123}I-MIBG (185 MBq). Early H/M ratio, delayed H/M ratio, and ^{123}I-MIBG washout rate (WR) were calculated. A semi-quantitative myocardial ^{123}I-MIBG distribution was analyzed by a 17-segment model with a 4-point scoring with summed ^{123}I-MIBG score (SS %) calculation. Results of scintigraphy were compared by the frequency and duration of VTE during 6 month follow-up. **Results** During 6-month follow-up no ICD shocks were registered. The number of VTE was 1,26±0,85 with duration 17,59±21,37 sec. In a whole group H/M early was 1,84±0,39, H/M delay 1,7±0,58, the SS early 21,8±16,55 %, SS delayed 27,24±22,26 %. WR was 36.7±30,64 (min 2.98, max 128.57). Both early and delayed ^{123}I-MIBG SS correlated with LVEF (r= -0,46; p=0,021 early; r= -0,47, p=0,018 delayed), with the number (r=-0,62; p=0,001 early; r=-0,41, p=0,042 delayed) and duration of VTE (r=-0,63; p=0,001 early; r=-0,6, p=0,001 delayed). We failed to find any correlation between H/M, WR and functional class of HF or VTE characteristics. **Conclusion:** These preliminary results showed that index of regional innervation (SS %), assessed by cardiac ^{123}I-MIBG imaging is more perspective predictors for arrhythmic events then H/M and WR in patients with previous myocardial infarction and implantable cardioverter defibrillator. Supported by the Russian Science Foundation (project N 15-15-10016).

EP-0329

Myocardial Glucose Metabolism Evaluated by Fasting 18Fluorodeoxyglucose-Positron Emission Tomography in Pulmonary Hypertension

T. Nakamura, N. Tahara, M. Bekki, Y. Sugiyama, A. Tahara, A. Honda, E. Kumagai, S. Igata, Y. Fukumoto; *Department of Internal Medicine, Division of Cardiovascular Medicine, Kurume University School of Medicine, Kurume, JAPAN.*

Background: The myocardium changes its energy substrate from fatty acid oxidation to glycolysis under increased afterload. 18F-fluorodeoxyglucose (FDG)-positron emission tomography (PET) can provide clinical information about myocardial glucose metabolism.**Purpose:** We aimed to investigate the myocardial glucose metabolism in patients with pulmonary hypertension (PH).**Methods:** We studied 50 patients with pre-capillary PH (41 females; mean age 55 ± 16 years; pulmonary arterial hypertension n=35, chronic thromboembolic PH n=5 and PH associated with chronic lung disease n=10), who underwent magnetic resonance imaging and FDG-PET. FDG uptake in the right ventricle (RV) and left ventricle (LV) was measured by maximum standardized uptake values (SUV) corrected for partial volume effect. The SUV ratio of RV to LV was calculated ($SUV_{R/L}$) to evaluate RV glucose metabolism. Further, we examined whether disease targeting therapy for PH could shift the myocardial glucose metabolism in 33 patients. **Results:** The $SUV_{R/L}$, mean pulmonary arterial pressure (mPAP) and RV ejection fraction (RVEF) were 1.34±0.66, 38.4±11.6mmHg and 36.0±10.0%, respectively. Univariate analysis revealed that $SUV_{R/L}$ was significantly cor-

related with heart rate, mPAP, cardiac index (inversely), RVEF (inversely), uric acid and N-terminal pro-B-type natriuretic peptide (NT-proBNP). In multiple stepwise regression analysis, RVEF (*p<0.001*), mPAP (*p<0.01*) and NT-proBNP (*p<0.05*) were independently associated with $SUV_{R/L}$ (R^2=0.506). Disease targeting therapy for PH including pulmonary vasodilators or balloon pulmonary angioplasty significantly decreased $SUV_{R/L}$ and NT-proBNP, and improved hemodynamics and RVEF. The change in RVEF was a sole and independent determinant with that in $SUV_{R/L}$ after treatment (R^2=0.457). **Conclusions:** The present study reveals that $SUV_{R/L}$ is associated with disease severity of PH, suggesting that myocardial glucose metabolism may contribute to its clinical importance of patient care.

EP-0330

Left ventricular diastolic dysfunction in patients with typical angina pectoris and angiographically normal or near normal coronary arteries

E. Khachirova, L. Samoylenko, O. Shevchenko; Moscow, Moscow, RUSSIAN FEDERATION.

Findings on left ventricular diastolic function (LVDF) in patients with ischemic symptoms and angiographically normal or near normal arteries are somewhat controversial. Aims: to assess LVDF in patients with ischemic chest pain and without obvious angiographically obstructive coronary artery disease (CAD) using gated single photon emission computed tomography (gSPECT). **Methods:** 35 patients (m/f - 15/20; mean age 62.8 yrs) with chest pain, positive stress test and angiographically normal or near normal epicardial coronary arteries were underwent rest/stress 99mTc-MIBI gSPECT (group 1) by two-day protocol. 10 patients (m/f - 6/4; mean age 63.2 yrs) without cardiovascular diseases were studied as a control (group 2). Patients with previous myocardial infarction, LV hypertrophy, cardiomyopathies, heart failure or systolic dysfunction (EF<45%), valvular heart diseases, and other conditions could compromised coronary perfusion, were not included in the study. Peak filling rate (PFR), mean filling fraction (MFR/3), time-to-peak filling from end-systole (TTPF), and secondary peak filling rate (PFR2) were analyzed. **Results**: There was not found significant difference in rest PFR between two groups (2.18±0.5 vs 2.3±0.28, respectively; p>0.05). Significant difference was observed in rest MFR/3 (1.09±0.3 vs 1.57±0.2, respectively; p<0.05) and rest TTPF (173.1±28.0 vs 140.0±9.0; p<0.05). Rest PFR2 was detected in 7 patients (14.3%) of group 1 only. During the stress-test significant difference was found in PFR (1.67±0.35 vs 2.7±0.27, respectively; p<0.05), MFR/3 (0.88±0.28 vs 1.7±0.16, respectively; p<0.05), and TTPF (201.4±44.0 vs 151.0±9.0, respectively; p<0.05). Stress PFR2 was detected only in 11 patients (31.4%) of group 1. Evaluation of diastolic function in the same patients by means of two-dimensional transthoracic echocardiography showed diastolic dysfunction only in 4 cases. **Conclusion:** Patients with chest pain, positive stress test and angiographically normal or near normal epicardial coronary arteries showed presence of rest LV diastolic dysfunction. There was found further deterioration of LVDF during stress. These patients might constitute a risk group for

development of heart failure with preserved ejection fraction. gSPECT might be useful tool in assessment and risk stratification of the patients with chest pain, positive stress test and angiographically normal or near normal epicardial coronary arteries, so it could detect diastolic dysfunction earlier than conventional echocardiography.

EP-0331

Higher event rate in patients with high risk Duke Treadmill Score despite of normal exercise gated MPI

*N. Fatima[1], **M. U. Zaman**[1], A. Zaman[2], R. Tahseen[3], S. Zaman[2], U. Zaman[3]; [1]Aga Khan University Hospital, Karachi, PAKISTAN, [2]Dow Medical College, Dow University of Health Sciences (DUHS), Karachi, PAKISTAN, [3]Civil Hospital, Karachi, PAKISTAN.*

Background: An exercise normal gated SPECT myocardial perfusion imaging (GSPECT MPI) has a high negative predictive value (NPV) with an annual event rate <1%. Similarly low risk Duke Treadmill Score (DTS ≥5) has 99% survival at 4 years while high risk (DTS ≤ -11) has a 79% survival at 4 years. Aim of this study was to find negative predictive value of various DTSs in patients with normal MPI. **Methods**: This was a prospective study conducted from August 2012 till July 2013 and 603 patients who had normal exercise GSPECT MPIs were included. These patients were followed for 02 years for fatal and non-fatal myocardial infarction (FMI and NFMI). Follow-up was not available in 23 patients, leaving a cohort of 583 participants. **Results:** DTS was low risk (≥5) in 286, intermediate risk (between 4 and -10) in 211 and high risk (≤ -11) in 86 patients. Patients with high and intermediate risk DTS were significantly elder than low DTS cohort. Patients with high DTS had significantly higher body mass index (BMI) with male preponderance compared to other groups. No significant difference was found among 03 groups regarding incidence of diabetes, hypertension, dyslipidemia, smoking, family history and left ventricular ejection fraction. On follow-up, single fatal MI was observed in high DTS group (Logrank test value = 5.779, p = 0.056). Five non-fatal events were observed in high DTS (94.2% survival; Logrank Test Value = 19.398, P =0.0001; significant) as compared to 02 events each in low and intermediate risk DTS (non-significant). **Conclusions:** Patients with normal exercise MPI with low and intermediate DTS have significantly low non-fatal MI. High risk DTS despite of normal exercise MPI was found to be associated with high non-fatal MI.

EP-0332

Arterial Age Estimation in Patients with Suspected Coronary Artery Disease: a Suitable Tool to Predict Myocardial Ischemia

C. Nappi[1], V. Gaudieri[2], A. Genova[1], G. De Simini[1], P. Buongiorno[1], V. Cantoni[1], R. Green[1], E. Zampella[1], R. Assante[1], S. Daniele[2], W. Acampa[1], M. Petretta[3], A. Cuocolo[1]; [1]Department of Advanced Biomedical Sciences, University Federico II, Naples, Italy, Naples, ITALY, [2]Institute of Biostructure and Bioimaging, National Council of Research, Naples, Italy, Naples, ITALY, [3]Department of Translational Medical Sciences, University Federico II, Naples, Italy, Naples, ITALY.

Aim: Chronological age is considered as surrogate of atherosclerotic burden. Nevertheless, individuals with the same age may have different atherosclerotic burden due to other risk factors. Arterial age, based on conversion of chronological age to age derived from vascular imaging findings, may lead to a more accurate assessment of cardiovascular risk. The role of arterial age to predict myocardial ischemia in patients with suspected coronary artery disease (CAD) has not been assessed. We sought to assess the role of arterial age, by a convenient transformation of coronary artery calcium (CAC) into a year's scale, in predicting myocardial ischemia in patients with suspected CAD. **Materials and Methods:** A total of 717 subjects referred to CAC scoring and ^{82}Rb PET/CT stress-rest myocardial perfusion imaging for suspected CAD were studied. CAC score was measured according to the Agatston method and arterial age (Â) was estimated by equating estimated CAD risk for chronological age and CAC using the formula: $\hat{A} = 39.1 + 7.25 \times \ln(CAC +1)$. Regional myocardial perfusion was assessed using 17-segment standardized model. The summed stress score, summed rest score, and summed difference score were automatically calculated. Ischemia was defined by a summed difference score ≥2. **Results:** Stress-induced myocardial ischemia was present in 105 (15%) patients. Chronological age and arterial age were higher in patients with ischemia compared to those without (P<0.001). In patients with ischemia, arterial age was higher compared to chronological age (75.1±18.6 years vs. 66.1±8.9 years, P<0.001). Differently, in patients without ischemia, arterial age was lower compared to chronological age (56.1±19.1 years vs. 60.9±9.7 years, P<0.001). At multivariable logistic regression analysis male gender, age, and arterial age resulted independently associated with stress-induced myocardial ischemia. At incremental analysis for predicting myocardial ischemia, arterial age significantly improved the model including clinical variables, increasing the global chi-square from 68.8 to 106.4 (P<0.001). The continuous net reclassification improvement of adding arterial age to clinical data was 0.610 (95% bootstrap confidence interval 0.407-0.803). **Conclusion:** In patients with suspected CAD, stress-induced myocardial ischemia is associated with higher arterial age and chronological age. Patients with myocardial ischemia have higher arterial age than chronological age. Arterial age provides incremental value over clinical variables in predicting stress-induced myocardial ischemia.

EP-0333

Pathological Asynchrony and Progressive Local Reduction of Myocardial Perfusion at the Apex as Important Sign of the Coming Loss of Heart Transplant

E. N. Ostroumov[1], E. D. Kotina[2], E. V. Migunova[1], N. E. Kudryashova[1], V. A. Ploskikh[2], A. V. Babin[2], S. Y. Shemakin[1], V. V. Golubitsky[1], M. V. Vovchenko[1]; [1]N.V. Sklifosovsky Research Institute for Emergency Medicine, Moscow, RUSSIAN FEDERATION, [2]Saint Petersburg State University, Saint-Petersburg, RUSSIAN FEDERATION.

Introduction: Acute cardiac allograft rejection (ACAR) and cardiac allograft vasculopathy (CAV) remain the main causes of death in the early period and after the first year after the heart transplantation (HTx). Endomiocardial biopsy and coronary angiography play important role in the management of recipients because of their high level of indication of rejections and complications. Nevertheless, they can be significantly less sensitive towards detecting of early functional disorders in comparison with non-invasive methods. **Aim:** The aim of the research is to use gated-SPECT with phase images to determine the most characteristic disorders of perfusion and the function of the heart transplant in patients who had lost it in the follow-up period. **Materials and Methods:** For assessment of perfusion and function of myocardium of left and right ventricles 207 recipients had been observed at various times after HTx (from 1 month to 12 years). The patient population comprised of 179 men and 28 women. All of them underwent gated-SPECT with phase images from 1 month after HTx and for the second time when needed. **Results:** For the follow-up period 6 recipients lost the transplant (4 of them - in the period of from 3 to 5 years after the HTx, one after 2 months and another - after 14 months past the HTx). All the 6 explanted transplants had been histologically examined. In 3 patients, ACAR was verified, 2 patients had ACAR and CAV, and one patient had CAV. 2 cases of difference between results of histological examination and clinical diagnosis had been observed (in one case the cause of the transplant dysfunction was not clinical revealed). Results of retrospective assessment of gated-SPECT reveal that in all 6 patients the first predictor of future complications was pathological asynchrony, which eventually localized at the apex. Disorders of perfusion were indicated for all the patients, but for only 4 of them with HTx periods from 3 to 5 years these disorders were progressing from study to study and became maximally profound at the apex by the time of transplant's loss. **Conclusion:** Pathological asynchrony at the apex can be important predictor of the coming loss of the heart transplant even in the absence of such signs of this via endomyocardial biopsy and coronary angiography.

EP-0334

Possibility of software program provided Artificial Neural Network (ANN) analysis supporting interpretation of medical staffs in myocardial perfusion SPECT

K. Koyama[1], H. Yamada[1], T. Ogura[1], M. Kanou[1], K. Maehara[1], T. Ino[1], H. Hoshizaki[1], S. Oshima[1], T. Toyama[2]; [1]Gunma Cardiovascular Center, Maebashi, JAPAN, [2]Toyama internal medicine and cardiovascular clinic, Maebashi, JAPAN.

Purpose: It is important to understand myocardial perfusion SPECT imaging (SPECT) better for better treatment of patients with coronary artery disease. To assist medical staffs, using the software program provided Artificial Neural Network (ANN) is expected. It is the method that based on many characteristics from Japanese data base. And it interprets abnormality in SPECT comprehensively. We investigated the possibility of software program supporting interpretation of medical staffs in SPECT **Methods:** Thirty patients suspected coronary artery disease were enrolled in this study. Stress and rest SPECT studies were performed. Five medical staffs and two expert physicians

in nuclear medicine detected myocardial abnormality. SPECT data were also analyzed by software program. Inter-observer variability for abnormality in SPECT reported by different medical staffs were calculated. Concordance rate with the results of expert physicians was obtained in patient based, coronary artery based and area based. **Results:** In patient based, concordance rate of five medical staffs (concordance M) and software program (concordance S) with expert physicians were 80% +/- 7 %(mean+/- SD), 100% in stress study and 82% +/- 8%, 90% in rest study, respectively. In coronary artery based, concordance M and concordance S were88%+/-11%, 100% in stress study and 92%+/-8%, 90% in rest study in LAD, respectively. In RCA, concordance M and concordance S were 66%+/-15%, 80% in stress study and 82%+/-16%, 80% in rest study, respectively. In area based, concordance M and concordance S, in apex, anterior, septal, inferior and lateral were 82%+/-8%, 100%, 86%+/-9%, 90%, 92%+/-8%, 90%, 72%+/-13%, 70%, 100%, 90%, respectively in stress study. Concordance M and concordance S, in apex, anterior, septal, inferior and lateral were 88%+/-16%, 100%, 94%+/-9%, 90%, 90%+/-7%, 90%, 82%+/-16%, 80%, 100%, 100%, respectively in rest study. **Conclusion:** There were low concordance rate and large SD in RCA area or inferior wall in interpretation of myocardial perfusion SPECT obtained both from medical staffs and from software program. It needs to pay attention to variation of coronary artery distribution and sensitivity of software program.

EP-0335

Myocardial Perfusion Imaging With CZT SPECT: Impact of Prone Versus Supine Imaging Positions on Cardiac Respiratory-Motion Magnitude

D. Daou[1,2], R. Sabbah[3], Y. Alattar[1], C. Coaguila[4], H. Boulahdour[3,5]; [1]Cochin Hospital, APHP, PARIS, FRANCE, [2]EA 7334 REMES, Université Paris-Diderot, Sorbonne Paris-Cité, Paris, FRANCE, [3]CHU Jean Minjoz, Besançon, FRANCE, [4]Centre Hospitalier de Bigorre, Tarbes, FRANCE, [5]EA 4662, Université de Franche-Comté, Besançon, FRANCE.

Aim: We previously reported the feasibility and impact on CZT SPECT myocardial perfusion imaging (MPI) of a data-driven respiratory-motion (RM) correction method (REGAT, REspiratory GATing). Imaging in both the prone and supine positions has been suggested to increase the performance of CZT SPECT. In this study, we aimed to evaluate the impact of patient's positioning (prone versus supine) on cardiac RM magnitude evaluated with REGAT applied to MPI CZT SPECT. **Materials and Methods:** We included 10 nonconsecutive randomly retrieved MPI studies in 9 patients (9 stress and 1 rest study) imaged in the prone and supine positions. All patients had stress MPI (2 MBq/Kg 99mTc-Tetrofosmin, 5-min acquisition) than rest MPI 3-hours later (6 MBq/Kg, 5-min acquisition). In our department, patients are preferably imaged in the prone position only (supine if prone positioning is uncomfortable for the patient). This is followed by supine imaging if the physician in charge decides to image the patient in a second position (prone if supine has been the first imaging position). All acquisitions were made on CZT SPECT (DNM 530c) and processed with REGAT. REGAT generates RM

gated reconstructed SPECT volumes (pixel size=4mm) which were summed either without realignment or after rigid realignment. It provides cardiac RM magnitudes in the patient's cranio-caudal (CC), ventral-dorsal, and right-left axis. Modifications in RM magnitudes due to positioning were considered non-significant when the difference was < 2 mm (0.5 pixels), limited when it was between 2 and 4 mm (0.5 to 1-pixel), moderate when it was between 4 and 8 mm (1 to 2-pixels), and severe when it was > 8 mm (2-pixels). **Results:** Time between prone and supine imaging was 10±14 min. In 2/10 studies, supine imaging was done before prone imaging. Supine total cumulated counts were higher than prone total cumulated counts: 1,304,737±360,321 vs 1,009,257±399,976 (P<0.005). CC cardiac RM magnitude was the dominant movement in both supine and prone imaging: 10.4±3.8 mm (Max=19mm) vs 8.8±6.8 mm (Max=21mm) (NS) respectively. Interestingly, when comparing supine to prone positioning, modification of cardiac RM in the CC axis was not significant in 3/10 studies, limited in 2/10 studies (decreased in 1/10 and increased in 1/10), moderate in 3/10 studies (decreased in 2/10 and increased in 1/10), and severe in 2/10 studies (decreased in 1/10 and increased in 1/10). **Conclusion:** Patients' positioning in supine or prone posture presented variable impact on CC RM magnitude with sometimes severe modifications.

EP-0336

One week extension of a ketogenic diet provides a further decrease in myocardial FDG uptake and a high detectability of myocarditis by FDG PET in rats

A. Clement[1], S. Poussier[1], H. Boutley[1], J. Pierson[1], M. Lhuillier[1], A. Kolodziej[2], J. Olivier[2], G. Karcher[1,3], P. Marie[1,3], F. Maskali[1]; [1]Nancyclotep, Experimental Imaging Platform, Vandoeuvre-Les-Nancy, FRANCE, [2]Department of Biochemistry and Molecular Biology, CHRU-Nancy, Nancy, FRANCE, [3]Department of Nuclear Medicine, CHRU, Vandoeuvre Les Nancy, FRANCE.

Introduction: Up to 24-hours periods of fasting and/or low carbohydrate diet have been proved beneficial for decreasing the myocardial uptake of ^{18}F-fluorodesoxyglucose (FDG) and enhancing the detectability of inflammatory heart diseases by FDG positron emission tomography (PET). This study aimed at determining whether this benefit is further higher when a low-carbohydrate ketogenic diet is prolonged up to 7-day in normal- and myocarditis-rats. **Methods:** Twelve males Wistar rats were referred to serial FDG-PET images planed after a 24-hours fasting and thereafter, after 2-, 4- and 7-days of a ketogenic diet (3% carbohydrate) and they were compared to a control group of 7 rats submitted to the same protocol but with normal diet (44% carbohydrate). The PET/ketogenic protocol was also applied in two rats with immune myocarditis. **Results:** Ketogenic diet was associated with: 1) a sustained increase in circulating ketone bodies all along the 7-days of diet and at an equivalent level than that reached after 24-hours fasting, 2) a progressive decrease of FDG uptake within normal myocardium reaching a lower level compared to 24-hours fasting at the 7th day (mean myocardial standardized uptake

values: 0.81±0.41 vs. 1.95±1.01, p<0.05), and 3) a high FDG-PET detectability of the inflammatory and fibrotic myocarditis areas. **Conclusion:** A one-week extension of ketogenic diet provides a further decrease in myocardial FDG uptake and a high detectability of myocarditis by FDG-PET, in line with the ongoing gradual metabolic changes already documented for such diets.

EP-0337

Comparison of the tolerability of Regadenoson and Adenosine in patients undergoing myocardial perfusion scintigraphy

A. Tsaroucha[1], O. Bourogianni[1], M. Stathaki[1], E. Papadaki[1], M. Alefantinou[1], K. Galanopoulos[1], H. Mavrakis[2], M. Marketou[2], S. Koukouraki[1]; [1]Department of Nuclear Medicine, University Hospital of Crete, Heraklion, GREECE, [2]Department of Cardiology,University Hospital of Crete, Heraklion, GREECE.

Purpose: To evaluate and compare the tolerability of regadenoson and adenosine as pharmacologic stress agents for myocardial perfusion imaging (MPI), assessing the frequency and duration of reported symptoms. **Subjects and Methods:** 87 patients were referred to the Nuclear Medicine Department for pharmacologic stress test preceding MPI (January 2017-March 2017). Patients were randomized to undergo regadenoson or adenosine stress procedure, except 7 patients with COPD in whom regadenoson was specifically selected as optimal stress agent. 48/87 patients (mean age: 72,05 years) underwent regadenoson stress test - regadenoson group (RG): 24 men (12: known CAD, 12: suspected CAD), 24 women (5: known CAD,9: suspected CAD). 39/87 patients (mean age:72,05 years) underwent adenosine stress test - adenosine group (AG): 14 men (4: known CAD, 10: suspected CAD), 25 women (4: known CAD, 21: suspected CAD). **Results:** 55% of patients (58% of men and 52% of women) in the RG experienced at least one adverse effect-symptom, versus 74% (71% and 76% respectively) in the AG. The main reported symptom in both groups was dizziness (32% of the patients in RG vs 25,6% in AG), followed by weakness/fatigue (12,5% in RG vs 20,5% in AG). The frequency of other symptoms reported in RG and AG respectively was: chest pain (8,3 vs 18%), flushing (9,3% vs 5,1%), discomfort (7,3% vs 18%), nausea-vomiting (3.1% vs 2,5%), paresthesia (3,1% vs 5,1%), headache (1% vs 5,1%). No dyspnea was reported in the RG vs 12,8% in the AG. This is to be highly considered, taking into account the fact that all patients with COPD were included in RG. Palpitations, somnolence and anxiety were reported only in the RG (2% of the patients, 1%,1% respectively). The average duration of symptoms was 4,2 min (0,35-35min) in RG vs 3,2min (1-18 min) in AG. The median duration of symptoms was 2 min for RG vs 3 min for AG. All symptoms reversed in time with no need of remedy rescue. The image quality of MPI was generally reported good for both stress agents. **Conclusion**: In our initial experience, regadenoson was overall better tolerated than adenosine. This fact, combined with its simple administration protocol, makes it an easily usable stress agent in daily clinical practice.

EP-0338

SPECT myocardial perfusion assessment in asymptomatic patients with hypercholesterolemia using new quantitative parameters

A. A. Ansheles, L. A. Martirosyan, I. V. Sergienko, V. B. Sergienko; Russian Cardiology Research Center, Moscow, RUSSIAN FEDERATION.

Introduction/Purpose: Visual inhomogeneity of myocardial perfusion SPECT images nowadays can not be explained only with probable technical reasons. Initial diffuse myocardial perfusion impairments are visually observed in patients with diabetes, rheumatoid arthritis, asymptomatic atherosclerosis, etc, and may have prognostic significance. Standard parameters (defect extents, summed scores) in such cases usually are in normal limits. We presented more sensitive parameters, calculated as standard deviations of relative perfusion values (in %) in 17 polar map segments, in reference to maximal 100% (severity sigma, σ_{sev}) and to arithmetical mean value (heterogeneity sigma, σ_{het}). The aim of current research was to validate those parameters with visual analysis and to examine them on a clinical group of asymptomatic patients with hypercholesterolemia (HCh). **Subjects & Methods:** 60 patients with HCh (total cholesterol >7.5 mmol/L and/or LDL cholesterol >4.9 mmol/L), with no symptoms and comorbidities, as well as 20 healthy volunteers, underwent myocardial ^{99m}Tc-MIBI rest/stress SPECT with CT-attenuation correction. Two experts independently observed obtained images and concluded them as homogeneous (visual group 1, VG1), focal inhomogeneous (VG2) and diffuse inhomogeneous (VG3). New sigma parameters, as well as standard perfusion parameters, were assessed. **Results:** Inter-observer agreement in assessing visual perfusion inhomogeneity was good (Cohen's kappa - 0.92). Rest σ_{sev} differed significantly between VG1, VG2 and VG3 (18.1±2.6, 20.9±1.9, 21.7±2.7, respectively, p_{1-2}=0.045, p_{1-3}<0.01). Patients with HCh were assigned to VG3 in 45% of cases, while only 20% of control group cases (p=0.07), all of latter were physically trained males. Patients with HCh demonstrated more severe inhomogeneity of LV MIBI uptake, compared with control group, Rest σ_{het} = 6.5±1.2 and 5.9±0.9, respectively, p<0.05, while differences in standard parameters (rest/stress extent, SRS, SSS, TPD) in visual and clinical groups were not significant. Positive correlation between Rest $\sigma_{sev}/\sigma_{het}$ with TCh/LDL-C levels was observed (r=0.33, p<0.01; r=0.37; p<0.01; r=0.29; p=0.02; r=0.32; p=0.01, respectively). **Conclusion:** Quantitative assessment of initial impairments and inhomogeneity of left ventricular myocardial perfusion with SPECT using proposed σ_{sev} and σ_{het} parameters reflects expert visual interpretation better than standard parameters. $\sigma_{sev}/\sigma_{het}$ may be suitable for therapy effects assessment in patients with subtle perfusion abnormalities, for instance, in patients with HCh on statin treatment.

EP-0339

Cardiac contraction motion compensation in gated Myocardial Perfusion SPECT

N. Salehi[1,2], M. Farahani[2], E. Fatemizadeh[3], S. Farzanefar[4], M. Ay[1,2]; [1]Tehran university of medical sciences, Tehran, IRAN, ISLAMIC REPUBLIC

OF, [2]Research Center for Molecular and Cellular Imaging, Tehran, IRAN, ISLAMIC REPUBLIC OF, [3]Electrical Engineering Department, Sharif University of Technology, Tehran, IRAN, ISLAMIC REPUBLIC OF, [4]Department of Nuclear Medicine, Vali-Asr Hospital, Tehran University of Medical Sciences, Tehran, IRAN, ISLAMIC REPUBLIC OF.

Introduction: Cardiac contraction and respiratory motion are main factors which degrade gated myocardial perfusion SPECT images quality by inducing image blurring and quantification inaccuracies. As images are acquired in different time frames, photon counts are limited. Hence, reconstructed "low-count" images, have poor statistical image quality. Therefore, motion compensated temporal processing can have a major impact on gated images quality. **Materials and Method:** 50 patients without known heart condition has undergone gated Myocardial perfusion SPECT. A 3D diffeomorphic log domain-demon algorithm was applied to warp all image phases to fit the end-diastolic (ED) phase. Warped images provide ED representation of LV but contain counts from all the time intervals. Myocardial wall thickening form ED(End-Diastolic) to ES(End-Systolic) frames, myocardial to blood pool contrast and image CNR were measured in summed images before and after compensation (BC and MC respectively). Quantitative study of Image sequences were conducted after importing image sequences to cardiac SPECT system's work station. BC and MC summed image parameters were automatically derived and calculated on the basis of sex specific normal limits obtained from the same healthy population using standard Cedars-Sinai software. **Result:** Myocardial wall thickening from ED to ES before compensation was 0.86±0.66 mm and after compensation 0.38±0.48 mm (P<0.0001). Myocardial to blood pool contrast in MC images are greater than the corresponding summed images before compensation (BC) 14% (P<0.05) CNR has increased 33% (P<0.05) in MC images compared to corresponding BC images. TPD (Total Perfusion Defect) measure after compensation are in good agreement with corresponding images TPD derived after motion freezing with Cedars-Sinai software and there was no statistically significant difference between them (P=0.13). **Conclusion:** This technique is topology preserving; therefore, transformation fields between frames are physically plausible. In small hearts which lost their resolution in ES frame due to partial volume effect, this technique can find the displacement vectors between ES and ED frames. Myocardial wall thickening significant decrease after compensation indicates, that motion blurring has been compensated in lateral wall to some extent, while preserving image SNR. However, apparent myocardium/blood pool contrast and CNR have increased which means signal cross contamination between myocardium and blood pool has been effectively reduced. Since, derived clinical quantification factor (TPD) is in good agreement with a gold standard software, it can be concluded that this technique can be developed to be used in routine patient studies, which needs to be investigated in clinical researches.

EP-0340

Prognostic Value of Left Ventricular Shape Index Assessed by Gated SPECT Myocardial Perfusion Imaging

V. Gaudieri[1], C. Nappi[2], W. Acampa[2], E. Zampella[2], R. Assante[2], T. Mannarino[2], A. Genova[2], S. Daniele[1], G. Melluso[2], G. De Simini[2], M. Petretta[3], A. Cuocolo[2]; [1]Institute of Biostructure and Bioimaging, National Council of Research, Naples, ITALY, [2]Department of Advanced Biomedical Sciences, University Federico II, Naples, ITALY, [3]Department of Translational Medical Sciences, University Federico II, Naples, ITALY.

Aim: Left ventricular (LV) remodeling is a subset of compensatory changes of myocardium and vascular system consisting of progressive structural modifications in ventricular mass, composition and volume. It has been demonstrated that LV remodeling is associated with adverse cardiovascular events. Endocardial and epicardial contours of LV can be obtained automatically by gated single-photon emission computed tomography (SPECT) program, providing quantitative indexes of 3-dimensional LV geometry, such as the LV shape index (SI). This study sought to assess the prognostic value of LVSI assessed by gated SPECT in a cohort of patients without overt coronary artery disease (CAD) and normal LV ejection fraction (EF). **Materials and Methods:** We prospectively evaluated 646 patients with suspected CAD with normal myocardial perfusion (summed stress score ≤3) and normal LVEF (>45%) at stress gated-SPECT imaging. An automated software program was used to calculate indices of LV volumes, LVEF, parameters of diastolic function and LVSI. A LVSI at end-systole ≤0.54 was considered normal. **Results**: Follow-up was 96% complete and the median follow-up was 37 months. In 646 subjects, 25 cardiac events occurred (13 cardiac deaths, 8 nonfatal myocardial infarctions, and 4 revascularizations for unstable angina) with cumulative event rate of 3.8% and an incidence rate of 1.25 per 100 persons/year (95% confidence interval 0.85-1.85). Patients with events were older, had higher prevalence of diabetes and higher end-systolic and end-diastolic LVSI values as compared to patients without events (all P<0.001). At multivariable Cox-regression analysis, age (P<0.01) and end-systolic LVSI (P<0.001) resulted independent predictors of cardiac events. At incremental analysis, end-systolic LVSI added prognostic information in a model including clinical variables, increasing the global chi-square from 1.23 to 15.33 (P <0.001). At the event-free survival analysis, patients with abnormal end-systolic LVSI had the worst outcome (P<0.001). **Conclusion:** End-systolic LVSI may identify patients with normal myocardial perfusion and normal LVEF at higher risk of cardiac events. Thus, shape indexes by gated-SPECT imaging seem to be useful for identifying early LV remodeling in patients with suspected CAD.

EP-0341

Clinical Value of Late post stress Imaging of Gated SPECT Myocardial Perfusion Scintigraphy after Stress-only injection

M. Garcheva-Tsacheva, A. Tzonevska, S. Shalamanov, S. Avramova; AcibademCityclinic-Sofia, Sofia, BULGARIA.

Background and Objectives: The Myocardial Perfusion Stress/ Rest Gated SPECT scintigraphy has been accused to produce

high exposure to patients, but it gives important prognostic information, related to the extent of ischemia and to the change in post stress functional parameters of left ventricle (LV). The stress images are the most important part of examination, determining the Summed Stress Score (SSS) and the post stress LV ejection fraction (PSLVEF) and kinetic. The comparison with rest LV parameters is important to prove an post ischemic dysfunction, but the comparison not always can be properly done by using different modalities. The aim of the study is to obtain additional information for the rest left ventricular (LV) function from decay corrected late registered images without reinjection. The considerable reduction of radiation exposure by 60% would be obtained. **Methods:** Twenty patients with proved or observed coronary artery disease and no prevous data of myocardial infarction were examined on GE Discovery SPECT/CT by 2 registrations after 1 stress injection (exercise). The exclusion criteria: left bundle branch block (LBBB). The early registration was done at the 15-th min. post stress application, the late registration - 1.5 hours later. The second registration was prolonged from 25 sec/pr. to 30 sec/pr. in order to obtain the equal count statistics for determination of the functional parameters. **Results:** The rest functional parameters differed in 12 of examined patients: concerning only regional transit abnorm kinetic (n=7) (proving the severety of the stenosis), or global function improvement (n=5), defining a high risk group. Discussion. According to De Winter the free of Major Cardiac Events survival depends on the extent of ischemia and on the post stress LV ejection fraction (PSLVEF). We had 3 groups of patients that needed rest examination: patients with moderate SSS, but not preserved PSLV fraction; patients without perfusion abnormalities, but low PSLV fraction and patients with significant SSS, but preserved PSLV fraction. By revealing transit post stress LV dysfunction a strong suggestion for coronary anatomy evaluation, and for decision to revascularize is obtained. As to the transit kinetic abnormalities, the severety of the stenosis even in territories with attenuation was obtained. **Conclusion:** The results show opportunity to increase the information, obtained by stress-only application of 99m Tc tetrofosmin concerning the functional part of examination and to add important prognostic information, supporting also the management process.

EP-0342

Quantitative myocardial-perfusion SPECT. Comparison of three cardiac software programs

S. Alexiou[1,2], *P. Georgoulias*[1], *G. Angelidis*[1], *V. Valotassiou*[1], *I. Tsougos*[3], *D. Psimadas*[1], *D. Tsivaka*[3], *V. Lakiotis*[2], *A. Kaspiri*[2], *D. Alexopoulos*[4], *D. Apostolopoulos*[2], *P. Vassilakos*[2]; [1]Department of Nuclear Medicine, University Hospital of Larissa, LARISSA, GREECE, [2]Department of Nuclear Medicine, University Hospital of Patras, Patras, GREECE, [3]Department of Medical Physics, Medical School, University of Thessaly, LARISSA, GREECE, [4]Department of Cardiology, University Hospital of Patras, Patras, GREECE.

Purpose/Introduction: Quantitative assessment of myocardial perfusion indices is complementary to the visual, qualitative interpretation of myocardial scintigrams and enhances their diagnostic accuracy in patients with known or suspected coronary artery disease. Summed stress score (SSS) and perfusion defect size (PDS), are the most commonly applied semi-quantitative parameters, which can be measured using Emory Cardiac Toolbox (ECTb), Myovation and Quantitative Perfusion/Gated SPECT (QPS-QGS) cardiac software programs. The aim of the present study, was to compare the three aforementioned software packages in estimating SSS and PDS variables. **Subjects and Methods:** The study cohort consisted of 634 consecutive patients (419 men, mean age 64.0years ±10.6 years) who underwent one-day stress/rest Tc[99m]-Tetrofosmin gated -SPECT studies. Data processing and quantification analysis were performed on a central workstation, Xeleris 3 (General Electric Medical Systems), using ECTb, Myovation and QPS/QGS algorithms. Polar maps were formed for all examinations. Left ventricle was automatically divided into 17 segments. Tracer uptake in each segment was scored based on a five-point scale (0: normal, 1: mildly, 2: moderately, 3: severely reduced uptake, 4: absent). The extent of perfusion defect size (PDS) was expressed as a percentage of left ventricle myocardium. Variations in SSS and PDS between the algorithms were investigated for the overall population and for several subgroups, formed according to: SSS values (normal: SSS≤3), several patient/protocol related factors (gender, exercise according to Bruce protocol or vasodilator stress and presence of diabetes mellitus). **Results:** The concordance between the software was good to excellent in the overall population and SSS>3 subgroup (Interclass Correlation Coefficients, ICCs: 0.76-0.99). Regarding SSS≤3 sub-population, the correlation of the three algorithms was suboptimal, (ICCs: 0.30-0.83). In pair comparisons, Myovation algorithm displayed significantly higher SSS and PDS values in comparison to ECTb and QPS/QGS. An additional analysis showed that mean differences between the three software were significant according to sex (p<0.001), Bruce protocol (SSS p=0.041, PDS p<0.001) and vasodilator stress test (p<0.001). Finally, no similar discrepancies were noticed between the computer programs, in patients with or without diabetes mellitus. **Discussion/Conclusion:** Despite the relatively, favorable concordance among the algorithms in the evaluation of SSS and PDS indices, differences in the mean values between them, should always be taken into consideration, particularly when a new algorithm is introduced, or if more than one software packages are used in the same nuclear medicine department.

EP-0343

Higher non-fatal cardiac events in diabetics with HBA1C >7.3 and normal stress myocardial perfusion scan

N. Fatima[1,2], *M. U. Zaman*[1,2], *D. J. M. Baloch*[2], *A. U. Hussiaini*[2], *S. Z. Rasheed*[2]; [1]Aga Khan University Hospital, Karachi, PAKISTAN, [2]Dept of Nuclear Cardiology, Karachi Institute of Heart Diseases (KIHD), Karachi, PAKISTAN.

Aim: To find out clinical outcomes in diabetics with normal stress myocardial perfusion scans (MPS) having glycosylated hemoglobin (HBA1C) > 7.3 or ≤ 7.3. **Material and Method:** This prospective study was conducted at nuclear cardiology

department of Karachi Institute of Heart Diseases (KIHD), Karachi, Pakistan. Total 251 diabetics who had a normal stress MPS were included. On the basis of their HBA1C, these patients were categorized into Group A (HBA1C >7.3) and Group B (HBA1C ≤ 7.3). This cut-off was taken from our previously published study performed upon early cohort. These patients were followed for 05 years for fatal and non-fatal myocardial infarction (FMI and NFMI). Follow-up was not available in 29 patients, who were excluded and leaving a cohort of 222. **Results**: Group A included 57 while Group B had 165 diabetics with a mean age of 59 vs. 57 years and male to female ratio of 42:58% vs. 40:60% respectively (non-significant). Mean body mass index (BMI) in Group A and B was 28.318 vs. 27.532 kg/m^2 (non-significant). Mean HBA1C and fasting blood glucose in Group A were significantly higher than Group B (8.363 vs. 6.630 and 135 mg% vs. 120 mg% respectively). No significant difference was seen in prevalence of hypertension, dyslipidemia, family history of coronary artery disease (CAD) and smoking between two cohorts. Persantin (Dipyridamole) stress was used in 58% vs. 56% in Group A and B respectively (non-significant) while no significant difference was seen in effort tolerance (Metabolic Equivalent Task; METS) of participants of both groups during dynamic exercise. In both groups stress MPS was normal with normal left ventricular function parameters (non-significant). During 05 years follow-up, significantly higher NFMI was seen in Group A as compared to Group B [11 (19.301%) vs. 04 (2.420%), significant p value] only in last 03 years. FMI was non-significant in both groups [02 (3.510%) vs. 01 (0.606%), non-significant p value]. **Conclusion:** Higher non-fatal MIs were observed in diabetics with impaired glucose control (HBA1C >7.3) and normal MPS. Event rate was significantly higher after 2nd years of follow-up in these patients.

EP-0344

Hemodynamic and left ventricular mechanical dyssynchrony parameters in patients with ischemic dilated cardiomyopathy: a study with Tc-99m sestamibi stress-rest MPI using adenosine

G. Kumar, A. Sood, A. Ashwathanarayana, M. Parmar, B. Mittal; Post Graduate Institute of Medical Education and Research, Chandigarh, INDIA.

Introduction: Hemodynamics and left ventricular (LV) dyssynchrony evaluation play an important role in assessment of ischemic burden in ischemic dilated cardiomyopathy (IDCM) patients. This study evaluates the role of these parameters in patients undergoing adenosine stress-rest myocardial perfusion imaging (MPI). **Material and Methods:** Twenty-two patients (13 males) who underwent adenosine stress-rest ^{99m}Tc-sestamibi MPI between January 2014 and February 2017 with a final diagnosis of IDCM were chosen for retrospective analysis. Hemodynamic parameters such as LV ejection fraction (EF) reserve (stress EF-rest EF) and heart rate (HR) response (stress HR-rest HR) were obtained following stress and rest studies. Following imaging, LV dyssynchrony parameters namely phase bandwidth and standard deviation (SD), expressed in degrees, were also obtained. Studies were interpreted by two experienced

nuclear physicians. Correlation between different variables was assessed with Pearson's coefficient (R). Cox proportion hazards model was employed for regression analysis. Results were tabulated with p<0.05 being considered as statistically significant. **Results:** Mean age of the patients was 60.2±12.2 years. Among the hemodynamic and dyssynchrony parameters used, significant negative correlations were drawn between following parameters: EF reserve and SD response (R= -0.496, p=0.019), EF reserve and bandwidth response (R= -0.467, p=0.028) and HR response and bandwidth response (R= -0.430, p=0.046). Following the identification of perfusion defects on MPI scans, the study sample was trifurcated based on the extent and reversibility of these defects. Accordingly, 9 patients had predominantly fixed defects (group 1, mean total defect size 13.2±11.3%), 6 had predominantly reversible defects (group 2, 22±20.8%) and 7 had co-existent fixed and reversible perfusion defects (group 3, 22.6±12.5%). The patients in group 3 in comparison to group 1 and 2 showed significantly lower values of LV phase bandwidth in post-stress (135.1±21.7° vs 164±21.6° vs 158.6±34.4°, p=0.036) and rest studies (136.7±12.4° vs 167.7±21.2° vs 154±13.7°, p=0.003) with independent samples t-test. The phase standard deviation did not show statistically significant difference among three groups (p>0.05). Linear regression analysis revealed that increasing age, presence of HR response > 10, and positive EF reserve were associated with larger fixed/reversible perfusion defects (Nagelkerke's R^2=0.555, p=0.034). **Conclusion:** Assessment of hemodynamic parameters in patients with IDCM using adenosine stress-rest MPI yielded valuable information regarding behaviour of LV dyssynchrony. LV phase bandwidth particularly showed significant differences among the patients' subgroups depending on status of the perfusion defects. Hemodynamic variables also helped in predicting the extent of myocardial involvement in these patients.

EP-0345

Gated Myocardial Perfusion Scintigraphy and Coronary Arteriography Correlation- A Retrospective Evaluation of Our Clinical Experience

B. T. Okudan[1], Ö. Uçar Elalmış[2], B. Özyazgan[2], N. Coşkun[1], P. Arıcan[1]; [1]Health Science University Ankara Numune Research and Training Hospital, Nuclear Medicine Clinic, Ankara, TURKEY, [2]Health Science University Ankara Numune Research and Training Hospital, Cardiology Clinic, Ankara, TURKEY.

Background: Early diagnosis of coronary artery disease (CAD) is crucial in preventing morbidity and mortality. Gated myocardial perfusion scintigraphy (GMPS) provides important diagnostic and prognostic information for CAD. The aim of this retrospective study is to investigate the correlation of GMPS and coronary arteriography (CAG) and to share our clinical experience. **Methods:** In this study, 9800 patients who were referred to our clinic between the years of 2012-2015 were screened retrospectively. 193 patients (63 males and 130 females with a mean age of 57.4 ± 10.7 years) who underwent both GMPS and CAG, with a maximum period of 6 months between them, were included in the study. GMPS was performed using Tc-99m MIBI (350-700

MBq, 45-60 minutes before imaging) with double day stress/rest protocol (165 patients with exercise stress and 28 with pharmacological stress). **Results:** The results of GMPS evaluation were grouped according to coronary artery anatomy and personal anatomic variations were ignored. Areas of hypoperfusion were as follows: anterior wall (left anterior descending artery, LAD) in 40 patients, inferior wall (right coronary artery, RCA) in 29 (15%) patients, lateral wall (circumflex artery, Cx) in 11 patients (5.7%), lateral and inferior walls in 10 patients (5.2%), anterior, lateral and inferior walls in 23 (11.9%) patients. GMPS was reported as normal in 53 (27.5%) patients. These findings were then compared with CAG results. GMPS and CAG results were discordant in 48 (25%) patients, compared to 145 (75%) patients in whom GMPS and CAG were compatible (p <0.001). Coronary stenosis was mild or moderate in 33 patients (17%) with a normal GMPS and abnormal CAG. CAG was reported as defective in 23 (11%) of patients with a normal GMPS, which was thought to be related to development of collateral vessels. **Conclusion**: GMPS, being performed intensively in our clinic, is an important method in evaluation of myocardial perfusion defects and follow-up of patients with a preliminary diagnosis of CAD. In our hospital, GMPS is used as an important selection criterion to evaluate patients before CAG, an invasive procedure, especially those with a low pre-test probability.

EP-0346

Left Ventricular Dyssynchrony: Influence of Attenuation Correction in Myocardial Perfusion Scintigraphy in an Overweight/Obese Population

A. Sá Pinto[1], T. Vieira[2], V. Alves[1], S. Chaves[1], A. Oliveira[1], T. Faria[1], J. Pereira[1]; [1]Centro Hospitalar de São João, Porto, PORTUGAL, [2]HPP - Medicina Molecular, SA; Lenitudes Medical Center & Research, Santa Maria da Feira, PORTUGAL.

Introduction: Left ventricular (LV) mechanical dyssynchrony evaluation by myocardial perfusion scintigraphy (MPS) has prognostic value in patients with heart failure and is a predictor of Cardiac Resynchronization Therapy response. It can be impaired in overweight/obese patients, even when ejection fraction is normal. These patients present a higher prevalence of attenuation artefacts due to increased body fat, so it is the current practice in our Nuclear Medicine Department to perform MPS with computed tomography for attenuation correction (AC). To our knowledge, there are not previous studies on the influence of AC on phase analysis parameters. **Aim:** To evaluate the influence of AC in LV dyssynchrony evaluation in an overweight/obese population. **Methods:** We reviewed data from 45 overweight/obese consecutive patients who underwent gated-MPS in our Department. The patients performed a stress adenosine protocol, being injected with an activity of 370 MBq or 925 MBq. Functional and perfusion parameters of the LV were assessed with Quantitative Gated SPECT (QGS) software, and dyssynchrony was evaluated with Emory Cardiac Toolbox - with and without AC. The influence of AC in phase analysis standard deviation (sd) parameter was assessed by multiple linear regression between sd with AC (sdAC) and sd without AC (sdNAC). In a multi-

variate analysis, the following variables were tested: Body Mass Index (BMI), hypertension (HTA), diabetes, dyslipidemia, ECG alterations, Chronical Kidney Disease (CKD), previous myocardial infarction (MI) and the presence of a perfusion defect. Multiple linear regression was performed with IBM SPSS 23. **Results:** 45 patients (25 women) presented a mean age of 64.11±9.875 years old and median BMI of 36.57 kg/m^2 (range = 27.39 - 54.82 kg/m^2). 12 patients had documented HTA, 8 had diabetes, 5 had dyslipidemia, 36 had ECG alterations, 4 had CKD and 8 had a previous MI. Regarding the LV function and perfusion, MPS with AC analysis registered a median ejection fraction of 57% (range 19 - 78%) and "mild" to "severe" perfusion deffects in 33 patients. A strong, positive correlation between sdAC and sdNCA was found: sdAC = 11.359 + 0.833 sdNAC, R = 0.833, *p* < 0.0001. The remaining variables analysed did not influence significantly the sd parameter. **Conclusion**: With this study, we demonstrate a strong correlation between phase analysis sd parameter determined with and without AC. We thus propose a model to a more accurate evaluation of LV dyssynchrony in this population, to be validated on further studies.

EP-0347

Influence of Stress Test Activity in Left Ventricular Dyssynchrony Evaluation in an Overweight/Obese Population

A. Sá Pinto[1], T. Vieira[2], V. Alves[1], S. Chaves[1], A. Oliveira[1], T. Faria[1], J. Pereira[1]; [1]Centro Hospitalar de São João, Porto, PORTUGAL, [2]HPP - Medicina Molecular, SA; Lenitudes Medical Center & Research, Santa Maria da Feira, PORTUGAL.

Introduction: Obesity is a multifactorial condition and an independent risk factor for cardiovascular diseases, associated with high morbidity and mortality. Left ventricular (LV) mechanical dyssynchrony is a valuable prognostic tool in predicting Cardiac Resynchronization Therapy response and can be assessed by myocardial perfusion scintigraphy (MPS). Even in the presence of normal ejection fraction, it can be impaired in overweight and obese patients. MPS may be challenging in these patients, presenting a higher prevalence of attenuation artefacts due to increased body fat. The current practice in our Nuclear Medicine Department is to perform MPS with computed tomography for attenuation correction (AC) in these patients. **Aim:** To study the influence of injected stress test activity in LV dyssynchrony evaluation in an adenosine MPS protocol acquired with and without AC, in an overweight/obese population. **Methods:** We reviewed data from 45 overweight/obese consecutive patients who underwent gated-MPS in our Department. The patients performed a stress adenosine protocol, with an activity of 370 MBq (Group 1) or 925 MBq (Group 2). Functional and perfusion parameters of the LV were assessed with Quantitative Gated SPECT (QGS) software and dyssynchrony was evaluated with Emory Cardiac Toolbox - with and without AC. Wilcoxon test was performed with IBM SPSS 23. **Results:** 45 patients (25 women), mean age of 64.11±9.875 years old and a median Body Mass Index (BMI) of 36.57 kg/m^2 (range = 27.39 - 54.82 kg/m^2). 12 patients had documented hypertension, 8 diabetes, 5 dyslipidemia, 36 had ECG

alterations, 4 had Chronical Kidney Disease and 8 had a previous myocardial infarction. Regarding the LV function and perfusion, MPS with AC analysis registered a median ejection fraction of 57% (range 19 - 78%) and "mild" to "severe" perfusion deffects in 33 patients. 15 patients were included in the Group 1 and 30 in the Group 2. Comparing the phase analysis parameters with and without AC, within the two groups, we obtained a significant difference in standard deviation (sd) parameter for Group 1 and Group 2 (p = 0.036 and p < 0.0001, respectively). Regarding histograma bandwith (hb) parameter, we obtained a significant difference withing the Group 2 (p < 0.0001), but no differences were observed within the Group 1 (p = 0.108). **Conclusion:** Phase analysis sd parameter is influenced by AC, independently of the administered activity. Concerning hb parameter, for higher stress activities, there is a significant influence of AC.

EP-0348

Cardiac sympathetic neuronal damage precedes myocardial fibrosis in patients with Anderson-Fabry Disease

T. Pellegrino[1], M. Imbriaco[2], V. Piscopo[2], M. Petretta[3], A. Ponsiglione[2], C. Nappi[2], M. Puglia[2], S. Dell'Aversana[2], E. Riccio[4], L. Spinelli[2], A. Pisani[4], A. Cuocolo[2]; [1]Institute of Biostructure and Bioimaging, National Council of Research, Naples, ITALY, [2]Department of Advanced Biomedical Sciences, University Federico II, Naples, ITALY, [3]Department of Translational Medical Sciences, University Federico II, Naples, ITALY, [4]Department of Public Health, University Federico II, Naples, ITALY.

Purpose: Cardiac sympathetic denervation may be detectable in patients with Anderson-Fabry disease (AFD), suggesting its usefulness for early detection of the disease. However, the relationship between sympathetic neuronal damage measured by ^{123}I-metaiodobenzylguanidine (MIBG) imaging and the presence of myocardial fibrosis on cardiac magnetic resonance (CMR) is still unclear. **Materials and Methods:** Cardiac sympathetic innervation was assessed by ^{123}I-MIBG single-photon emission computed tomography (SPECT) imaging in 25 patients with genetically proved AFD. Within one month from ^{123}I-MIBG imaging, all patients underwent contrast enhanced CMR. ^{123}I-MIBG defect size and fibrosis size on CMR were measured for the left ventricle (LV) and expressed as %LV. **Results:** Patients were divided in 3 groups according to ^{123}I-MIBG and CMR findings: (1) matched normal (n=10), without ^{123}I-MIBG defects and without fibrosis on CMR images; (2) unmatched (n=5), with ^{123}I-MIBG defect but without fibrosis on CMR images; (3) matched abnormal (n=10), with ^{123}I-MIBG defect and fibrosis on CMR images. The 3 groups were comparable as regards to age, gender, α-galactosidase, proteinuria, glomerular filtration rate, and troponin I, while New York Heart Association (NYHA) class (p=0.008), LV hypertrophy (p=0.05), and enzyme replacement therapy (p=0.02) were significantly different among groups. In patients of group 3 there was a significant correlation between the ^{123}I-MIBG defect size and the area of fibrosis at CMR (r=0.87, p=0.001). **Conclusions:** Sympathetic neuronal damage measured by ^{123}I-MIBG SPECT is frequent in AFD patients and may precede signs of myocardial damage, such as fibrosis. Thus, ^{123}I-MIBG imaging can be considered a challenging technique for the early detection of cardiac involvement in AFD.

EP-0349

Relationship between focal reduction in cardiac I-123 metaiodobenzylguanidine uptake and left ventricular longitudinal function in patients with Anderson-Fabry Disease

T. Pellegrino[1], L. Spinelli[2], V. Piscopo[2], C. Giudice[2], S. Pellegrino[2], G. De Matteis[2], M. Imbriaco[2], B. Trimarco[2], A. Cuocolo[2]; [1]Institute of Biostructure and Bioimaging, National Council of Research, Naples, ITALY, [2]Department of Advanced Biomedical Sciences, University Federico II, Naples, ITALY.

Purpose: We investigated the relationship between abnormalities of cardiac sympathetic innervation and left ventricular (LV) function in patients with Anderson-Fabry disease (AFD). **Materials and Methods:** We performed I-123 metaiodobenzylguanidine (MIBG) cardiac imaging and speckle tracking echocardiography in 23 patients (11 men, mean age 43±13 years) with genetically proved AFD and preserved LV ejection fraction and in 10 age and gender-matched control subjects. From planar and single-photon emission computed tomography (SPECT) MIBG images heart to mediastinum (H/M) ratio and regional defect score were calculated. The total defect score (TDS) was calculated as the sum of the segmental tracer uptake using the standardized 17-segment model. Global and segmental longitudinal systolic strain was obtained by speckle tacking echocardiography. **Results:** At SPECT MIBG imaging, TDS was 0 in 10 AFD patients (group 1) and ranged from 1 to 54 in the remaining 13 patients (group 2). Late H/M ratio was below two-fold standard deviation of control subjects (≤1.75) in 8 AFD patients of group 2 and in none of group 1. Patients of group 2 had significantly higher LV mass index (177±47 g/m2 vs. 103±21 g/m2, p=0.001), relative wall thickness (0.51±0.07 vs. 0.41±0.07, p=0.003), left atrial volume (58±10 ml/m2 vs. 37±12 ml/m2, p=0.001) and systolic pulmonary artery pressure (37±6 mmHg vs. 27±4 mmHg, p=0.001) compared to patients of group 1. On the contrary, global longitudinal strain was significantly lower in patients of group 2 compared to those of group 1 (-14±3.7% vs. -19±3.5%, p=0.001). In the whole patient population, a significant correlation between MIBG TDS and global longitudinal strain (r=0.599, p=0.003) and left atrial volume (r=0.498, p=0.016) was found. At multivariable linear regression analysis, global longitudinal strain was the only independent predictor of TDS ≥1 (**β=2.14, p=0.018**). **Conclusions:** The results of this study indicate that reduced regional cardiac MIBG uptake parallels impairment in LV longitudinal function in AFD patients. Noteworthy, focal derangement of cardiac sympathetic activity may be present even in patients with preserved H/M ratio.

EP-0350

A novel clinical risk prediction model for myocardial infarction, coronary revascularization and cardiac death according to clinical, exercise and gated SPECT variables (VHRs)

A. García-Burillo, G. Romero-Farina, S. Aguadé-Bruix, J. Candell-Riera, J. Castell-Conesa, D. García-Dorado; Hospital General Universitari Vall d'Hebron, BARCELONA, SPAIN.

Objective: To create a risk score for hard event (HE) according to clinical, exercise and gated SPECT variables. **Methods:** We analyzed consecutive 5707 patients; 3181 patients (age 64.5 ± 11, male 59.6%) had no previous myocardial infarction (MI) or coronary revascularization (CR), and 2526 patients (age 63.3 ± 11, male 81.7%) had previous MI or CR. During a follow-up of 4.1 ± 2.7 years the HE (nonfatal MI, CR and cardiac death) was evaluated. **Results:** In patients without previous MI or CR; age (p< 0.001), gender (p= 0.001); hyperlipidemia (p < 0.001); nitrates (p= 0.04); ejection fraction (EF) (p= 0.001); summed stress score (p< 0.001); METs (p< 0.001); exercise angina (p= 0.006); and mm of ST segment depression (p= 0.004); were the independent predictors of HE (C-statistic: 0.8; p< 0.001). In patients with previous MI or CR, EF (p< 0.001), summed difference score (p= 0.001); age (p< 0.001); smoker (p= 0.002); nitrates (p= 0.003); exercise angina (p= 0.001); METs (p< 0.001); and mm of ST segment depression (p= 0.011); were the independent predictors of HE (C-statistic: 0.7; p< 0.001). The risk score obtained from these variables allows stratify patients in five risk levels: very low risk (≤ 0.4%/year), low risk (0.5 to < 1%/year), moderate risk (≥ 1 to < 3%/year), high risk (≥ 3 to 5%/year) and very high risk (> 5%/year). **Conclusion:** The cardiac risk stratification by mean of clinical, exercise and gated SPECT variables is an objective aid to assessing an individual's cardiac risk.

EP-0351

Assessment of normal values of quantitative parameters of tissue muscle perfusion scintigraphy in population without peripheral artery disease - first experience

N. Manevska[1], S. Stojanoski[1], D. Pop Gjorceva[1], L. Todorovska[2], D. Miladinova[1], V. Majstorov[1]; [1]Institute of Pathophysiology and Nuclear medicine, Skopje, MACEDONIA, THE FORMER YUGOSLAV REPUBLIC OF, [2]Institute of Medical Physiology and Antropology, Skopje, MACEDONIA, THE FORMER YUGOSLAV REPUBLIC OF.

Introduction: The muscle perfusion is a physiologic process that can undergo quantitative assessment and thus define the range of normal values of perfusion indexes and perfusion reserve. The investigation of the changes in microcirculation has a crucial role in muscle perfusion. **Aim:** To design protocol for diagnostic method of tissue-muscle perfusion scintigraphy of lower limbs with 99mTc-MIBI and establish the normal values of lower limb perfusion indexes, as well as perfusion reserve, for both rest and stress phase (after workload). Materials and method Prospective study with 30 patients, 24 - 74years of age, was performed. They were without known history of peripheral artery disease (PAB), normal findings on Doppler ultrasonography of lower limbs as well as pedo-brachial index. 21/30 had one or more risk factors for PAB. This method is a non-invasive, functional method that evaluates tissue perfusion in resting condition "rest study" and after workload "stress study", through quantitative parameters. Rest study was started with a dynamic

phase or tissue-muscle vascularization of both calves after i.v application of 300MBq of 99mTc-MIBI, followed by whole body scan (WBS). Stress study started with 30 flexion / extension of the feet, i.v application of 600MBq of 99mTc-MIBI and another 30 flexion / extension of the feet performed (dynamic phase of both calves), followed by WBS. Inter-extremity index and perfusion reserve were calculated for both studies. **Results:** The examinees with risk factors in comparison with those without risk factors, had insignificant lower values of LT/RT and LC/RC in rest phase. Both groups of examinees had insignificant different values of LT/RT and LC/RC in stress phase as well (0.98±0.06vs0.98±0.05; 1.01±0.09vs0.99±0.05 consequent). In the group with risk factors present, compared with the group without risk factors, insignificant lower perfusion reserve was registered of LC, LT, and RC and insignificant higher for RT. The age had no significant impact on the perfusion reserve of LC, LT, RC and RT. The examinees older than 50 years had insignificantly lower perfusion reserve of these parameters compared with those younger than 50, LC (p=0.25), LT (p=0.74), RC (p=0.2) and RT (p=0.81). **Conclusion:** Tissue muscle perfusion scintigraphy with 99mTc-MIBI is a non-invasive scintigraphic method that allows in healthy individuals to determinate the range of normal values of muscle perfusion at rest and stress condition. Thus it allows to implement this values in clinical evaluation of patients with peripheral artery disease.

EP-0352

Clinical Follow-Up Post Coronary Artery Bypass Grafting in Patients with Viable Myocardium on 18F-FDG PET

A. S. Kokkadan, M. Shankar, S. H. Venkat Rao, G. K. Chaithanya; Narayanan Hrudayalaya, Bangalore, Karnataka, INDIA.

Purpose: To evaluate improvement in clinical symptoms and left ventricular ejection fraction (LVEF) post coronary artery bypass grafting (CABG) in patients who have viable myocardium on 18F-FDG PET (Fluorine-18 fluorodeoxyglucose positron emission tomography) and to correlate improvement in LVEF with extent of viable myocardium on 18F-FDG PET prior to CABG. **Subjects and Methods:** 55 patients were enrolled in the study. Rest myocardial perfusion scan with technetium 99m sestamibi followed by 18F-FDG PET was done. The patients who had undergone CABG after detected to have viable myocardium on 18F-FDG PET were followed up. Mean time of follow-up was 150 days. During follow-up their New York Heart Association (NYHA) functional class and echocardiographic LVEF were assessed. **Results:** This study showed that there is statistically significant difference in the extent of viable myocardium between patients with improvement in LVEF (percentage change in LVEF ≥ 5%) and patients without improvement in LVEF (percentage change in LVEF < 5%). P = 0.023. The mean of percentage viable myocardium in those with improvement in LVEF was 34.43 +/- 11.12% and in those without improvement was 26.96 +/- 10.17%. Receiver operating characteristic (ROC) curve analysis showed a cut off level of >25% viable myocardium yielded the optimum sensitivity and specificity (86% and 54%, respectively) for predicting improvement in LVEF after CABG. There was only

a weak positive correlation between percentage viable myocardium prior to CABG and percentage change in LVEF after CABG (r=0.138). 76% of patients with > 25% viable myocardium showed improvement in NYHA class after CABG and the mean change in NYHA class was at least one grade. Among patients with >25% viable myocardium, mean end diastolic volume (EDV) was higher in patients who did not show improvement in LVEF (EDV = 170.18 +/- 63.69 ml) than those who had improvement in LVEF (EDV = 126.72 +/- 36.06 ml). **Conclusion:** Patients who had a higher percentage viable myocardium showed improvement in LVEF after CABG compared to patients who had lesser percentage viable myocardium. A cut-off level of > 25% of viable myocardium yielded the optimum sensitivity and specificity for predicting improvement in LVEF after CABG. There was only a weak positive correlation between percentage viable myocardium and improvement in LVEF. Improvement in NYHA functional class was higher in patients with higher amount of viable myocardium. Patients with higher baseline EDV are unlikely to improve LVEF after CABG even if they have viable myocardium.

EP-0353

Evaluation of multipoint pacing-cardiac resynchronization therapy (CRT) by Gated SPECT myocardial perfusion phase analysis and cardiac 123I-MIBG.

I. Casáns-Tormo[1], R. Ruiz-Granell[2], L. Bondanza-Saavedra[2], R. Díaz-Expósito[1], V. López-Prior[1]; [1]Nuclear Medicine. University Clinic Hospital, Valencia, SPAIN, [2]Cardiology. University Clinic Hospital, Valencia, SPAIN.

Introduction: The purpose of the present study was to assess the contribution of the evaluation of left ventricular dyssynchrony assessed by Gated SPECT myocardial perfusion phase analysis and cardiac sympathetic nerve activity by 123I-MIBG, to determine significant functional recovery after CRT by multipoint pacing in heart failure patients. **Material and Methods:** We have studied 22 patients (6 women, mean age: 66±5, 57-77 y/o) with dilated cardiomyopathy (6 ischemic, 16 non-ischemic) and CRT indication. We performed basal cardiac 123I-MIBG obtaining early and late heart to mediastinum ratio (EHM and LHM), washout rate (WR) and myocardial GSPECT at rest with 99mTc-MIBI with assessment of left ventricular ejection fraction (LVEF), end-diastolic (EDV) and end-systolic (ESV) ventricular volumes and parameters of LV dyssinchrony by phase analysis (standard deviation (SD), histogram bandwidth (HB) by Synctool ECToolbox. The patients underwent clinical follow-up with new assessment of cardiac 123I-MIBG and myocardial GSPECT 12 months after CRT implantation, available in 13/22 patients with a total of 72 performed explorations. **Results:** Mean basal LVEF was 20.7±6.3% (10-33), with EDV: 235.1±71.7ml, ESV: 189.1±71.4ml, EHM: 2.25±0.54, LHM: 2.05±0.47, WR: 30.6±15.2, SD: 50.6±14.7, HB: 160.1±59.6. After 12 months follow-up, mean follow-up LVEF was 26.7±12.6% (10-47), with improved LVEF and/or lower volumes in 8 patients and LVEF lower than basal or without changes in the other 5. Comparing patients with and without functional recovery, we found significant differences in follow-up EHM: 2.53±0.33 vs 1.83±0.45 (p:0.01), LHM: 2.48±0.46 vs 1.69±0.38(p:0.01), SD: 38.7±7.1 vs 58.7±7.8 (p:0.002), HB:122.3±37.6 vs 202.2±15.1 (p:0.002). The basal values tended to be higher in patients with functional recovery, but without statistical significance: EHM: 2.42±0.73 vs 2.16±0.33, LHM: 2.14±0.56 vs 2.01±0.37, and lower SD: 46.5±4.8 vs 56.3±23.1 and HB: 141.6±29.0 vs 200.5±96.9. **Conclusion:** In our group of patients the evaluation of cardiac sympathetic nerve activity by 123I-MIBG and LV dyssynchrony by Gated SPECT myocardial perfusion phase analysis showed significant changes after CRT by multipoint pacing in relation with functional recovery (higher LVEF and/or lower volumes), with improved innervation and lower dyssynchrony and could help to select patients to cardiac resynchronization therapy.

EP-0354

Hemodynamic Effects of Regadenoson Administration With Respect to MPI Findings: 6 Month Institutional Experience in Greece

J. Koutsikos, G. Angelidis, E. Ilia, M. Vogiatzis, J. Mamarelis, V. Stefanidis, A. Zafirakis, K. Lazaridis, N. Dimakopoulos; Army Share Fund Hospital (417 NIMTS), ATHENS, GREECE.

Aim: Regadenoson is a selective A2A adenosine receptor agonist recently approved for clinical use in Greece. Similarly to other adenosine receptor agonists, regadenoson can cause an increase in heart rate and may induce hypotension. According to previous clinical trials, an increase in heart rate and a small decrease in blood pressure were observed in the majority of patients receiving regadenoson as the stress component of myocardial perfusion imaging (MPI) studies. We investigated the hemodynamic effects of regadenoson administration with respect to MPI findings, based on our 6 month institutional experience. **Materials and Methods:** We enrolled 108 consecutive patients (80 males, 28 females, mean age 68.7 y.o) referred to the Department of Nuclear Medicine, for a clinically indicated pharmacological stress MPI. All participants were ≥20 years of age without meeting any of the contraindications to regadenoson administration. Sixty-eight patients reported no history of CAD. Patients underwent regadenoson stress test, combined with both stress and rest MPI. Data on the hemodynamic effects of regadenoson administration were recorded. Based on the visual interpretation of stress and rest images, patients were categorized into two groups; group A (normal studies) and group B (abnormal studies). Subsequently, the influence of hemodynamic changes on MPI findings was assessed according to t-test values. **Results:** Forty-two patients had normal MPI studies (group A). Sixty-six studies were abnormal (group B patients). The mean change in heart rate was 41.14±15.69 bpm in group A and 39.79±17.53 bpm in group B (P=0.39). The mean change in systolic blood pressure was 4.28±5.29 mmHg in group A and 5.11±6.34 mmHg in group B (P=0.31), while the corresponding values for the mean change in diastolic blood pressure were 8.89±10.00 mmHg and 8.02±9.30 mmHg, respectively (t-test=0.37). **Conclusions:** No statistically significant associations were found between hemodynamic effects of re-

gadenoson administration and MPI results (normal vs. abnormal studies). Notably, the magnitude of heart rate increase has been correlated to patient prognosis, independently of the presence of absence of a perfusion defect. However, due to the recent application of regadenoson MPI at our institution, additional data (including coronary angiography findings and follow-up evidence) are not currently available for the study cohort.

Cardiovascular System: Clinical Science: Plaque and Vascular Imaging

EP-0355

A novel concept of F-18 NaF PET/CT: Molecular Calcium Scorring measured by F-18 NaF PET/CT in detection and global quantification of cardiovascular molecular calcification

H. Onner, i. Ak Sivrikoz, E. Entok; Eskisehir Osmangazi Unuversity School of Medicine, Department of Nuclear Medicine, Eskişehir, TURKEY.

Aim: Coronary artery calcifications are a complex biological process that is considered as a pathognomonic finding of atherosclerosis and is an independent risk factor for cardiovascular events. Because calcification process in atherosclerosis is thought to use similar cell types, signals and metabolic pathways for new bone formation, F-18 NaF PET / CT imaging is thought to show areas of calcium remodelling and new calcification areas in diseased coronary arteries. In this study, we assessed the relations of Global Cardiac Molecular Calcium Score (GCMCS) /Aortic Molecular Calcium Score (AMCS) obtained from the F-18 NaF PET / CT images and coronary artery risk factors of patients. **Material and Methods:** A total of 87 patients (43 man, 44 women; mean age of 61.8 ± 8.48 years) undergoing F-18 NaF PET / CT to investigate bone metastasis were evaluated retrospectively. Cardiac/aortic SUVmax values, GCMCS and AMCS were generated using a software program on Siemens Biograph 6 PET/CT camera The correlations between GCMCS/AMCS and age, gender, HT, DM, LDL values, smoking history, CAD history, and Framingham risk score of the patients were assessed. The study was approved by local ethics committee. **Results:** In patients with HT, cardiac region SUVmax values indicating F-18 NaF uptake were significantly higher than those without (p = 0.032). Both GCMCS and AMCS were significantly higher in smokers than non-smokers (p = 0.009 and p = 0.025, respectively). Cardiac and aortic SUVmax values were found to be significantly higher (p = 0.05, p = 0.019 and p = 0.006, respectively) in patients with CAD history. Significant correlation was found between LDL ratios and cardiac SUVmax values (r = 0.640, p <0.0001). Significant correlation was also observed between LDL and both GCMCS and AMCS (r = 0.367 p = 0.002; r = 0.309 p = 0.009, respectively). Between the Framingham score and cardiac SUVmax (r = 0.576, p = 0.000), GKMCS (r = 0.440, p = 0.000), Aort SUVmax (r = 0.573, p = 0.000) and GAMKS (r = 0.352,

p = 0.003) significant correlation were detected. **In conclusion;** the increased cardiac F-18 NaF uptake corresponds to a high cardiovascular risk profile. F-18 NaF PET / CT imaging can be a molecular imaging modality to demonstrate global calcification of the heart and aorta.

EP-0356

Comparison of different semiquantitative approaches for the diagnosis of graft infection after thoracic and abdominal aortic repair using F18-FDG-PET/CT

V. Mergen[1], I. Einspieler[1], M. Mustafa[1], H. Wendorff[2], K. Thürmel[3], M. Schwaiger[1]; [1]Department of Nuclear Medecine, Klinikum rechts der Isar TU Muenchen, Munich, GERMANY, [2]Clinic for Cardiovascular Surgery, Klinikum rechts der Isar TU Muenchen, Munich, GERMANY, [3]Department of Nephrology, Klinikum rechts der Isar TU Muenchen, Munich, GERMANY.

Objectives: The aim of this study was the evaluation and comparison of different semiquantitative parameters for the diagnosis of graft infection after thoracic or abdominal aortic repair applying [^{18}F]fluorodeoxyglucose (FDG) positron emission tomography (PET)/computed tomography (CT). **Methods:** 50 patients who underwent [^{18}F]-FDG PET/CT for suspected aortic graft infection were retrospectively analysed. Besides, 13 oncological patients with aortic repair but without graft infection were included in the analysis. Maximum standardized uptake values (SUV$_{max}$) were obtained for all patients and different graft to background ratios were calculated. The diagnostic accuracy of SUV$_{max}$ and different target-to-background ratios (TBRs) was assessed by receiver-operating-characteristic (ROC) analysis. Overall, 8 different background regions were defined and analysed (blood pool activity within the left cardiac ventricle, 4 different aortic segments, the vena cava and the pulmonary trunk as well as FDG wall uptake in non inflammatory aortic segments). A combination of clinical follow-up, imaging (including PET/CT) and/or microbiological/histopathological results, if available, served as the standard of reference for the final diagnosis. **Results:** 28 infected and 35 uninfected grafts were identified. SUV$_{max}$ was the most powerful predictor for the diagnosis of graft infection according to the ROC analysis (area under the curve: 0.978, CI: 0.904-0.999). ROC analysis suggested an SUV$_{max}$ cut off value of >4.48 to differentiate between infected and non-infected grafts (p<0.0001). Notably, there was no substantial difference between SUV$_{max}$ and other semiquantitative approaches according to the area under the curve. **Conclusion:** Semiquantitative approaches and in particular SUV$_{max}$ provide a good reference to assess graft infection after thoracic or abdominal aortic repair and may increase the diagnostic accuracy of [^{18}F]-FDG-PET/CT in the setting of suspected graft infection.

EP-0357

Metabolic Findings Of 18F-FDG PET/CTIn Patients With Suspected Inflammatory Vascular Disease

I. Plaza de las Heras, B. Rodriguez Alfonso, R. de Teresa Herrera, C. Field Galán, L. Canales Rodriguez, S. Seijas Marcos, J. Mucientes

Rasilla, M. Mitjavila Casanovas; University Hospital Puerta de Hierro, Majadahonda, SPAIN.

Introduction: 18F-fluorodeoxyglucose (FDG) accumulates in inflammatory cells due to an increased metabolic rate. Therefore, 18F-FDG positron emission tomography (PET) represents a promising imaging technique in patients with inflammatory vascular disease. The aim of this study was to assess the metabolic findings with 18F-FDG PET/CT in patients with suspected inflammatory vascular disease. **Subjects and Methods:** We performed a retrospective analysis of the metabolic findings in PET/CT studies adcquired from January 2011 to April 2017 in patients with suspected inflammatory vascular disease (either because clinical or analytical criteria or because of the existence of a predisponent condition or illness) or for follow-up of vasculitis. A visual analysis was carried out considering positive studies those which showed an intensity of uptake in the wall of vessels equal or superior to liver uptake. **Results:** A total of 92 studies were performed on 78 patients. 18F-FDG PET/CT was ordered because of suspected inflammatory vascular disease in 34 patients, based on clinical and / or analytical criteria. A total of fifty eight studies were ordered because vasculitis or illnesses commonly associated with inflammatory vascular disease, of which fourteen were referred for follow up of vasculitis (Takayasu n=17, polymyalgia rheumatica resistant to corticoid based therapy n=11, giant cell arteritis n=8, polyarteritis nodosa n=2, Wegener's granulomatosis n=2, Bechet syndrome n=1, idiopathic aortitis n=7, aneurysms n=5, carotidynia n=2, immune-mediated inner ear disease n=2 and Cogan's syndrome n=1). Fiveteen of the 92 studies (16.3%) were considered positive (12 patients). Three of these studies were referred for follow-up to assess response to treatment. The greatest intensity of uptake was observed in large vessels, (thoracic aorta, supra-aortic trunks, abdominal aorta and iliac arteries), except in a patient with Bechet syndrome that affected the superior mesenteric artery. Pathological uptake in the femorotibioperoneal arteries was not observed in any patient. **Conclusions:** In our institution there is a low positivity of PET/CT studies in patients with suspicion of inflammatory vascular disease, vasculitis and follow-up of vasculitis, which indicates the need to redefine or get a better grasp of the reasons for the request. The best results are obtained in the suspicion of vasculitis of large vessels. The positive findings modified the clinical management of the patient and intensified the therapy.

EP-0358
Role Of Positron Emission Tomography In The Early Diagnosis Of Infective Endocarditis

E. Abou Jokh Casas, V. Pubul Núñez, M. Garrido Pumar, A. Martinez, M. Pombo Pasin, A. Anxo Martínez, C. Abou Jokh Casas, P. Fierro, I. Dominguez, S. Argibay, Á. Ruibal; Complejo Hospitalario Universitario Santiago de Compostela, Santiago de Compostela, SPAIN.

Introduction: The early diagnosis of infective endocarditis (IE) is a medical challenge, thus the importance of a muldisciplinary approach to improve its fatal prognosis. Our aim is to evaluate the usefulness of 18FDG-PET in the diagnosis of this desease. **Materials and Methds:** We retrospectively evaluated 33 patients, 3 females and 30 men, clinically suspected with infective endocarditis, between 2015-2017. All patients underwent transesophagic ecocardiography (ETE) and a 18-FDG-PET; these results were later compared with respect to diagnosis accuracy. In order to avoid heart radiotracer uptake, all patients performed a low-carbohydrate, rich- fatty acids diet, and an injection of a sodium heparin bolus. We defined positive PET criteria as an increase of FDG uptake in cadiac valves or in intracardiac devices. Ecocardiographic criteria included the visualization of valve thickenings or vegetation chords. **Results:** From thirty three patients suspected of IE, the diagnosis was confirmed in 24/33 (72,7%) cases, 19 showed FDG uptake on cardiac valves (6 natives and 13 prosthetic), and 5 patients on cardiac devices (pacemaker). From the total cases with a final diagnosis of IE, 18FDG-PET was positive in 21 of them, being concordant in 7 cases with ecocardiography findings. 18FDG-PET sensitivity (S) was 87%, specificity (P) 100%, positive predictive value (PPV) 100% and negative predictive value (NPV) 75%. Ecocardiography presented a S, P, PPV and NPV of 26%, 100%, 100% and 33% respectively. **Conclusions:** Although ecocardiography has a high specificity in the diagnosis of IE, it presents serious limitations in its sensibility. Due to the importance of making an early diagnosis, its is vital the use of a more sensitive and specific tecnique, specially in those patients where the clinical suspicion is high and the diagnosis can not be delayed. In this number of patients 18-FDG-PET has demonstrated its usefulness, stablishing a final diagnosis in 87% of the cases.

Cardiovascular System: Imaging Systems

EP-0359
Myocardial ischemia in female patients with rheumatoid arthritis

*C. Sioka, K. Papadimitropoulos, A. Papadopoulos, **J. Al-Boucharali**, L. Lakkas, T. Kotrotsios, K. Pappas, A. Fotopoulos; University Hospital of Ioannina, Ioannina, GREECE.*

Introduction: The goal of this study was to evaluate the rate of cardiovascular disease in female patients with rheumatoid arthritis (RA) with non-specific cardiac symptoms. **Materials and Methods:** Myocardial perfusion imaging (MPI) with 99mTc tetrofosmin stress - rest single photon emission computer tomography (SPECT) of 13RA female patients with atypical cardiac symptoms was compared to 44 weight and age-matched females with similar cardiac complaints (control group). Smoking, hypertension, diabetes mellitus, dyslipidemia, obesity and cardiac heredity were recorded and compared between the study and control group. MPI was assessed using17 segment polar map and with a scale of 0 to 5 scoring. **Results:** Patients with RA subjected to MPI for atypical cardiac symptoms had higher

cardiovascular risk (46%) compared to control individuals (17%). **Conclusions:** RA patients with atypical cardiac complaints are at higher risk for cardiovascular disease; early detection and monitoring of this patient group could potentially reverse or successfully manage the consequences of the upcoming cardiovascular disease.

EP-0360

Improving nuclear cardiology efficiency: Novel CZT technology in combination with ⁹⁹ᵐTc-tetrofosmin and regadenoson

S. Kranz, Sr.; Nuklearmedizin Wandsbek Markt, Hamburg, GERMANY.

Aims: Myocardial perfusion scintigraphy (MPS) is one of the best evaluated methods to assess patients with coronary artery disease (CAD), with high diagnostic (sens/spec at least 85%) and prognostic accuracy. Over time, several radiation-free methods e.g. stress echocardiography have been established, meaning cardiologists now have a choice of imaging techniques which can be used, driving considerations around radiation exposure. Additionally, a fast, cost effective diagnostic is required demanding an increase in efficiency in the nuclear medicine departments. To meet these criteria of maintaining or improving image quality whilst optimising dose exposure, cost effectiveness and speed, we assessed the impact in our department of using cadmium zinc telluride camera technology (CZT) with ⁹⁹ᵐTc-tetrofosmin and regadenoson. **Materials & Methods:** For pharmacological stress testing, regadenoson with 50 watts treadmill exercising was used. Ten minutes after 150MBq ⁹⁹ᵐTc-tetrofosmin injection, image acquisition was initiated (using the GE Discovery 530c system), with a total acquisition time of typically seven minutes, achieving 700-1000 kCounts with a 70 kg standard patient. Target radiation exposure was 1 mSv per study. **Results:** Use of regadenoson saved time since it was delivered as a single bolus injection. Additionally, use of ⁹⁹ᵐTc-tetrofosmin with a more rapid liver and background tissue clearance compared to ⁹⁹ᵐTc-sestamibi enabled the image acquisition to be started earlier after injection. Use of CZT-⁹⁹ᵐTc-tetrofosmin-regadenoson enabled 4 stress-examinations per hour, with a total of up to 30 stress scans plus 30 rest scans to be done per day. The duration of the patient's stay in the department was less than one hour for the whole stress testing and 30 minutes for the rest-scans, using both one and two-day protocols. **Conclusions:** MPS is established in the diagnostic pathway for the assessment of CAD. Due to the development of other myocardial perfusion imaging procedures MPS is under increasing pressure. We have shown that use of novel CZT technology as well as suitable radiopharmaceuticals such as ⁹⁹ᵐTc-tetrofosmin with rapid liver clearance and time-saving pharmacological stress procedure such as regadenoson, it is possible to improve the high diagnostic level of MPS (sens/spec at least 85%) while increasing the efficiency with higher patient throughput. In addition, the significantly higher sensitivity of the CZT technique comparing to Na(I) gamma cameras reduced radiation exposure to a very acceptable level (1 mSv can be achieved for a stress test only).

EP-0361

Advantages of simultaneous dual-isotope SPECT imaging using a cardiac semiconductor camera

T. Niimi[1], M. Nanasato[1], M. Sugimoto[1], H. Maeda[2]; [1]Nagoya Daini Red Cross Hospital, Nagoya, JAPAN, [2]Nagoya University School of Health Sciences, Nagoya, JAPAN.

Purpose: High-speed and high-resolution single-photon emission computed tomography (SPECT), based on semiconductor detectors, presents a unique possibility for nuclear cardiac imaging. Above all, high-energy resolution provides a new possibility for the combination of simultaneous dual-isotope (SDI) SPECT imaging such as Tc-99m and I-123 (Tc-99m/I-123), which was impossible in the conventional Anger SPECT. In a previous report, we evaluated the energy resolution, detector sensitivity, and spatial resolution of the Tc-99m/I-123 D-SPECT system (Spectrum Dynamics, Israel) by phantom experiment, and confirmed this system to be largely superior to Anger SPECT by quantitative analysis. In this study, we assessed whether simultaneous Tc-99m/I-123 dual-isotope SPECT imaging with D-SPECT had benefits for clinical study, such as inspection under the same physiological conditions, reduction of injection dose, and improvements in patient throughput. **Methods and Materials:** We estimated the injection dose, timing of the injection, and acquisition times for SDI SPECT based on the data from the D-SPECT phantom study. In this experiment, we used a combination of Tc-99m-sestamibi (MIBI) and I-123-beta-methyl iodophenyl pentadecanoic acid (BMIPP) to diagnose vasospastic angina (VSA) among patients with acute myocardial infarction. Thirteen clinical studies were conducted under these conditions, and the accuracy of the D-SPECT examination and effectiveness of the diagnosis were evaluated. In addition, we assessed the clinical usefulness of the semiconductor SPECT by comparing it with conventional TlCl/I-123-BMIPP. **Results:** The injection dose, calculated from the myocardium uptake of Tc-99m-MIBI/I-123-BMIPP in SDI of D-SPECT, was 370 MBq/111 MBq. The collection time at these doses was 15 minutes (if both left ventricular counts were to be over 1 M). The appropriate scan start time after injection was considered to be 30 minutes. On clinical study, mismatch between Tc-99m-MIBI and I-123-BMIPP appeared in 3 of 13 cases, and the diagnosis of VSA was established. By changing from conventional TlCl (111 MBq)/I-123-BMIPP (148 MBq) to a combination of Tc-99m-MIBI and I-123-BMIPP for patients suspected of having VSA, the injection dose could be reduced by 45% and examination time shortened to 20%. **Conclusion:** Simultaneous Tc-99m/I-123 dual-isotope SPECT imaging of D-SPECT offers many advantages, such as inspection under the same physiological conditions, reduction of injection dose, and improvements in patient throughput.

EP-0362

Assessment of the impact of small cardiac motions according to motion direction for SPECT images provided by different Anger- and CZT-cameras

L. Imbert[1,2,3], J. Salvadori[4], Y. Petegnief[5], S. Rémi[5], H. Boulahdour[5], G. Karcher[1,6,7], P. Y. Marie[1,6,7]; [1]CHU Nancy, Vandoeuvre-lès-Nancy,

FRANCE, ²Plateforme d'Imagerie Expérimentale Nancyclotep, Vandoeuvre-lès-Nancy, FRANCE, ³IADI, U947, Vandoeuvre-lès-Nancy, FRANCE, ⁴Institut de Cancérologie de Lorraine, Vandoeuvre-lès-Nancy, FRANCE, ⁵CHRU de Besançon, Hôpital Jean Minjoz, Besançon, FRANCE, ⁶Plateforme d'Imagerie Expérimentale Nancyclotep, Nancy, FRANCE, ⁷Université de Lorraine, Faculté de Médecine, Nancy, FRANCE.

Introduction: Small cardiac motions remain a frequent cause of artefactual SPECT defects for myocardial perfusion imaging planed with Anger- or CZT-cameras. However, the mechanisms of these artefacts are poorly known, especially their relation to motion direction for different cameras, detectors and collimation systems. This phantom-based study was aimed to analyze the magnitude and location of SPECT artefacts, according to the direction of small cardiac translations, and in a comparative way between Anger-cameras, equipped with parallel-hole (Conv.SPECT) or astigmatic (IQ.SPECT) collimators, and the Discovery NM-530c (GE) and DSPECT (Spectrum Dynamics) CZT-cameras. **Methods:** A left ventricular insert, which walls were filled-in with 10 MBq of a ^{99m}Tc solution, was recorded at the center of the field of view for each camera, and after a 5- or 10-mm translation applied in 6 different orthogonal directions (-X/+X, -Y/+Y et -Z/+Z). Motions occurring at half of SPECT recordings were simulated by mixing projections from the first half of the untranslated acquisition with projections from the second half of each translated acquisition. In addition, the reconstructed images from translated and non-translated acquisitions were merged to provide a clear visualization of the exact places of the phantom walls before and after translation in a single set of 3D fusion images. **Results:** Motion-artefacts were particularly uncommon with the D.SPECT camera, whatever the motion direction, a property that was however conditioned by the use of its model-based reconstruction system. For the other cameras and systems, artefacts were mainly documented for 10-mm axial (X or Y) translations and for segments setting: 1) orthogonal to the translation direction and thus, with the larger distance between the locations of translated and non-translated walls, and/or 2) in areas showing a rather low activity at baseline, an observation that only concerned the 2 Anger cameras for which the homogeneity was the lowest at baseline. **Conclusion:** This phantom-based study shows that the SPECT artefacts induced by cardiac translations are mainly documented for segments setting both orthogonal to axial translations and in areas of rather low activity at baseline**.** The CZT-cameras appear less vulnerable to these translations than Anger-cameras, a property that is mainly attributable to a better homogeneity preexisting at baseline and to difference in reconstruction methods.

EP-0363

Radionuclide renoscintigraphy and biochemical markers in the detection of renal dysfunction in patients undergoing myocardial revascularization

Z. Vesnina, Y. Arsenjeva; Cardiology Research Institute, Tomsk, RUSSIAN FEDERATION.

Introduction: Nonpulsatile blood flow plays an important role in the pathogenesis of renal dysfunction in patients with extracorporeal circulation. Therefore, search for highly efficacious methods for early diagnostic of renal dysfunction in patients undergoing cardiac surgery is an important task of present-day cardiology. **Aim:** To evaluate diagnostic value of radionuclide renoscintigraphy and biochemical markers in detecting of renal dysfunction in patients with coronary artery disease (CAD) in the early postoperative period after coronary artery bypass grafting (CABG). **Materials and Methods:** The study included 108 CAD patients (all men, mean age 59.94 ± 0.72 years), who underwent direct myocardial revascularization by CABG. All patients underwent dynamic renal scintigraphy with ^{99m}Tc-DTPA before and 6-7 days after operative treatment. As a result of scintigraphy glomerular filtration rate (GFR) was calculated (total and separately for each of the kidneys). Forty pts were subjected to measuring the concentration in blood serum of lipocalin before and 5 hours after CABG and cystatin C before and 24 hours after surgery. **Results:** After CABG a significant decrease in the average value of total GFR and GFR for each of the kidneys was noted. Wherein severe renal dysfunction under the influence of non-pulsating blood flow (reduction of total GFR by 15% or more from baseline) developed in 35% of cases. As well a statistically significant increase in the concentration of s-NGAL and cystatin C in blood serum was observed. In the postoperative period also creatinine clearance decreased significantly. Statistical regression analysis showed a high degree of correlation between the duration of extracorporeal circulation and dynamics of GFR (R = 0.42; p = 0.017) and the level of s-NGAL (R = 0.39, p = 0.02) in patients undergoing cardiac surgery. **Conclusion:** Radionuclide method is not inferior to its diagnostic value and informativeness than biochemical markers in the evaluation of early postoperative renal dysfunction.

EP-25	during congress opening hours, e-Poster Area

Cardiovascular System: Miscellaneous

EP-0364

The use of fatty acids labeled with technetium-99m for visualization of the cardiac muscle

A. Rogov¹, E. Stasyuk¹, N. Varlamova¹, V. Sкuridin¹, E. Nesterov¹, S. Sazonova²,¹, V. Sadkin¹, E. Ilina¹, V. Chernov³,¹, Z. Konstantin³,¹; ¹National Research Tomsk Polytechnic University, Tomsk, RUSSIAN FEDERATION, ²Cardiology Research Institute, Tomsk, RUSSIAN FEDERATION, ³TOMSK CANCER RESEARCH INSTITUTE, Tomsk, RUSSIAN FEDERATION.

Introduction: The results of studies on the development of methods for the synthesis of new X-ray diagnostic tools based on a modified fatty acid are presented. Labelled technetium-99m fatty acid is necessary for a detailed scintigraphic evaluation of myocardial metabolism. In the process of synthesis of the radiopharmaceutical, the interaction of the substance with technetium-99m in an alcohol medium was studied using etha-

nol as a solvent. **Aim:** Developing methods for the synthesis of a new radiopharmaceutical based on modified fatty acid labelled with technetium-99m. **Methods:** This agent is intended for studying the metabolism of cardiac muscle and this will allow differentiating viable heart and scar tissue. An important task of cardiology is the diagnosis of viable myocardium, since its presence in an ischemic area is a direct indication for invasive correction of coronary insufficiency. As a substance for radiolabelling fatty acid was synthesized derivative (PDA-DTPA). PDA-DTPA molecule includes two structural fragments ensuring successful functioning of the radiopharmaceutical. The first is that provided bioavailability acid fragment of the radiopharmaceutical to myocardium. The second fragment which serves for chelate binding of ^{99m}Tc. Ethanol was used as solvent for PDA-DTPA but it acts as a reducing agent for $SnCl_2 \cdot 2H_2O$. To perform labelling 1mg PDA-DTPA dissolved by heating in 1.0 ml 96% ethanol. Then 1.0ml ^{99m}Tc, 50 mcl Sn(ll) solution and 50mcl ascorbic acid as a stabilizing additive were successively placed in a test tube. Determine radiochemical purity was carried out by thin layer chromatography. Determine radiochemical purity was carried out by thin layer chromatography. As mobile phases have been identified Chloroform and Acetone. Acetone was selected for comparing mobility ^{99m}Tc(VII). Determine radiochemical purity was carried out by thin layer chromatography. As mobile phases have been identified Chloroform and Acetone. Acetone was selected for comparing mobility ^{99m}Tc(VII). Radiometer «RIS-A1» was used to measure the total activity of the vial. After incubating the mixture for 15min and it is heated on a steam bath for 30min at temperature to 98°C. Then was carried out repeated sampling for chromatography in the same media. **Conclusions:** The experiments carried out show that receiving PDA-DTPA-^{99m}Tc, having a pH of~6, the desired product yield is insufficient. The next stage of our research will be the study of PDA-DTPA behavior in aqueous media and effect on solubility of the pH medium.

EP-0365

Quantitative evaluation of DNA damage in peripheral blood lymphocyte in patients after cardiac ^{201}Tl/^{123}I-BMIPP study

K. Okuda, N. Watanabe, M. Hashimoto, M. Doai, Y. Kawai, T. Takahashi, T. Arikawa, K. Ooiso, K. Iwabuchi, K. Kajinami, H. Tonami; Kanazawa Medical University, Uchinada, JAPAN.

Objectives: The aim of this study was to quantitatively evaluate DNA double strand breaks (DSBs) of peripheral blood lymphocyte in patients who underwent cardiac dual-isotope SPECT imaging in clinical practice. A phosphorylated histone variant H2AX (γ-H2AX) has been used as a biomarker for detection of radiation-induced DSBs. **Methods:** We prospectively evaluated radiation-induced DSBs in five patients who underwent dual-isotope SPECT imaging with 74 MBq of ^{201}Tl and 111 MBq of ^{123}I-labeled beta-methyl-p-iodophenyl-pentadecanoic acid (BMIPP). Peripheral blood lymphocytes isolated from the blood samples were immunostained with anti-γ-H2AX antibody. Additionally, the nuclei of peripheral blood lymphocytes were also immunostained with 4',6-diamidino-2-phenylindole (DAPI). The number of γ-H2AX foci in the nucleus was determined before the SPECT scan, and at 6 h and 24 h following the SPECT scan. The average number of γ-H2AX foci per nucleus was calculated from 50 lymphocytes. The percentage of lymphocytes in G1, S, and G2/M phases of the cell cycle, which was determined by flow cytometric analysis, was also used to assess DNA damage and repair. **Results:** Median values of γ-H2AX foci per nucleus were 0.18 before the SPECT scan, and 0.64 and 0.40 at 6 h and 24 h respectively, after the SPECT scan, in five patients. In one patient, the number of γ-H2AX foci significantly increased at 6 h and 24 h in comparison with that before the SPECT scan (0.92 ± 1.17 vs. 0.07 ± 0.29, *p* = 0.0016 and 1.45 ± 1.48 vs. 0.07 ± 0.29, *p* < 0.0001, respectively). However, the value of mean γ-H2AX foci per nucleus was significantly lower at 24 h than that at 6 h (0.32 ± 0.74 vs. 1.12 ± 1.35, p=0.0020) in another patient. The other three patients did not show any significant increase or decrease in value of mean γ-H2AX foci after the SPECT scan. There was no significant change in the percentage of cells in G1 phase before the SPECT scan and at 6 h and 24 h after the scan (Median: 87.7,85.8,and 88.3); neither was there a significant change in percentage of cells in S phase (Median: 1.91, 1.63, and 1.52) nor in G2/M phase (Median: 3.93, 5.51, and 3.57), respectively. **Conclusions:** By using γ-H2AX foci as a biomarker for DNA damage in peripheral blood lymphocyte, radiation effect of cardiac ^{201}Tl/^{123}I-BMIPP SPECT scans was evaluated quantitatively. Radiation-induced DNA damage in the ^{201}Tl/^{123}I-BMIPP study was observed to be limited.

EP-0366

Cardiac twist quantified by gated myocardial perfusion SPECT: a new insight into nuclear cardiology

*H. Javadi[1], A. Keshavarz[2], N. Shayestehnia[2], M. Mansouri[2], **M. Assadi**[3]; [1]Golestan Research Center of Gastroenterology and Hepatology (GRCGH), Golestan University of Medical Sciences (GUOMS), Gorgan, IRAN, ISLAMIC REPUBLIC OF, [2]Department of Electrical Engineering, Persian Gulf University, BUSHEHR, IRAN, ISLAMIC REPUBLIC OF, [3]The Persian Gulf Nuclear Medicine Research Center, Bushehr University of Medical Sciences (BUMS), BUSHEHR, IRAN, ISLAMIC REPUBLIC OF.*

Purpose/Introduction: Nowadays, there has been fast growing interest in LV torsion and its association with symptomatic and pre-symptomatic disease processes. Torsion gives useful additional information about myocardial tissue performance which gets ready pivotal information on myocardial mechanics that complements standard pump function indices in both systolic and diastolic function. Now, this index is quantified with cardiovascular magnetic resonance and also echocardiographic speckle tracking . In this research twist of left ventricle has been estimated with myocardial perfusion Gated SPECT Images. **Subjects & Methods**: Myocardial perfusion gated tomograms at rest were selected retrospectively for 38 patients who had normal myocardial perfusion imaging .Two assumptions have been considered in the proposed algorithm: each region of the myocardium has a unique count pattern and variation of voxel count

from one frame to the next is low. In total, at least 8 steps were done for the torsion calculation. **Results**: In total, peak apical rotation was 15.4°±2.5° and peak basal rotation was -5.4°±1.1°. The twist was 20.7°± 1.8°. **Discussion/Conclusion**: The study may demonstrate that myocardial perfusion Gated SPECT seems to be a feasible noninvasive imaging modality to measure cardiac twist ; although , it is readily carried out in majority of MPI gated SPECT examinations, standardized procedures of calculation are highly recommended.

EP-0367

Cardiac SPECT as a predictor of cardiotoxicity in patients with prostate cancer treated with abiraterone acetate after docetaxel therapy

S. S. Medina-Ornelas, F. O. García-Pérez; Instiuto Nacional de Cancerologia, Mexico City, MEXICO.

Background: Abiraterone is a selective, potent, and irreversible inhibitor of CYP17, a key enzyme in testosterone synthesis, and improves overall survival in postdocetaxel metastatic castration resistant prostate cancer (mCRPC). According to the international literature the overall incidence of adverse cardiac effects is lower, the frequency of cardiac failure is less of 5%. Heart failure is the most common manifestation of chemotherapy induced cardiotoxicity. The purpose of this study is to evaluate the incidence of heart failure by using gated cardiac SPECT with ^{99m}Tc-MIBI, in asymptomatic patients post-treatment with abiraterone acetate plus prednisone after docetaxel therapy. **Methodology:** Twenty patients with mCRPC after docetaxel therapy (overall 4 to 6 cycles) and at least one comorbidity (hypertension, diabetes mellitus or elevated serum creatinine level), and previous to received abiraterone acetate, were examined using gated ^{99m}Tc-MIBI SPECT (8 gates/cardiac cycle) 60 minutes after tracer injection at rest, between February 2014 to September 2016. End-diastolic/End-systolic volumes (EDV, ESV), and ejection fraction (LVEF) were calculated from gated ^{99m}Tc-MIBI SPECT using QGS software. **Results:** Twenty patients aged 68.6 years (45% had hypertension, 35% had diabetes mellitus and 20% both), and the average serum creatinine level were 1.15mg/dl. The overall LVEF was 53.8±1.4%, EDV 102ml, ESV 51ml; and the basal perfusion pattern was abnormal in 8 patients (2 patients with hypertension, 2 patients with diabetes mellitus and 4 patients with both). During follow-up period of 20 months±2 months; 5 patients (4 patients with hypertension and diabetes mellitus; and 1 patient with hypertension, the average of serum creatinine level of this 5 patients was 1.29mg/dl) developed heart failure, characterized by decline in LVEF of at least 5% to less than 55% with accompanying signs and symptoms of congestive heart failure, such as third heart sound (S3) gallop, tachycardia, dyspnea, peripheral edema and asthenia, after two-four doses of abiraterone acetate. The value of gated SPECT was higher obtaining sensitivity, specificity and PPV of 100%, 80% and 75% respectively. **Conclusion:** We conclude that perfusion gated SPECT is a useful noninvasive screening test and may be proposed to help identify cardiac failure after the treatment with abiraterone acetate in patients mCRPC with

hypertension, diabetes mellitus and chronic renal damage underlying with a high risk of poor clinical outcome. Abiraterone acetate plus prednisone treatment was generally well tolerated, and safety results were consistent with previous studies; however, this is the first study that includes postdocetaxel asymptomatic patients with more than two comorbidities.

EP-0368

Left and Right Ventricular Performance and Cardiovascular Risk in Patients on Maintenance Hemodialysis - an Assessment with Radionuclide Ventriculography at Rest and During Exercise

N. Topuzović[1], S. Topuzović[2], I. Mihaljević[1,2]; [1]Osijek University Hospital, Osijek, CROATIA, [2]Faculty of Medicine, University of Osijek, Osijek, CROATIA.

Aim: To investigate left (LV) and right ventricular (RV) function at rest and exercise in chronic hemodialysis patients after correction of anemia with erythropoietin (EPO), and to identify independent predictors of hemodialysis treatment outcome. **Patients and Methods:** Forty patients undergoing regular hemodialysis with severe renal anemia (hematocrit < 0.25) were treated with EPO in adjustable doses and were followed up. Radionuclide ventriculography were performed at rest and exercise on three occasions: 1) before EPO therapy, 2) after reaching target hemoglobin (Hb) of 100g/L, and 3) after 12 months of maintained EPO therapy. The outcome measures were cardiovascular complications and overall mortality at the end of follow-up. The independent variables were identified with the multiple linear regressions. **Results:** Mean age of patients was 38 ± 11 years, mean duration of dialysis 5.3 ± 3 years). Median follow-up was 11.2 years. Hb was increased from 72 ± 8 g/L to 111 ± 12 g/L during 3.8 ± 1.6 months and was maintained thereafter. During exercise, no significant difference was observed in increase of heart rate, mean blood pressure, LV and RV ejection fraction, peak ejection rate (PER) and time to PER before and after treatment with EPO. At peak stress patients after correction of anemia achieved a higher workload (72.5 ± 18.1 vs. 90.4 ± 14.3 W, p<0.05)) and longer exercise duration (8.4 ± 2.2 vs. 11.3 ± 1.4 min, p<0.05). At rest, LV peak filling rate (PFR) was significantly reduced from 2.94 ± 1.3 to 2.33 ± 1.0 end-diastolic volume (EDV) per second, while during exercise was no significant difference. LV time to PFR was prolonged during EPO therapy from 158 ± 34 to 183 ± 29 msec at rest, and from 102 ± 22 to 130 ± 29 msec during exercise, p<0.05. While RV PFR remained unchanged at rest during therapy (2.78 ± 0.98 vs. 2.57 ± 0.63 EDV/s), RV time to PFR was prolonged from 163 ± 51 to 208 ± 57 msec, p<0.05, but no significant difference was obtained during exercise. Multivariable regression analysis showed direct relationship between reducing in LV-PFR at rest and increasing death risk, as well as cardiovascular complications. **Conclusion:** LV and RV systolic function at rest and exercise was unchanged during correction of anemia with EPO in chronic hemodialysis patients, LV and RV diastolic function was worsened. But, multiple regression analysis identified only LV-PFR at rest as one of the significant determinants for survival.

EP-0369

Exercise MPI coupled with impedance cardiography for better cardiac workload assessment - preliminary results

S. Osiecki, S. Piszczek, E. Witkowska-Patena, M. Dziuk; Military Institute of Medicine, Warszawa, POLAND.

Purpose: The aim of the study was to combine standard myocardial perfusion imaging (MPI) protocol with impedance cardiography (IC) for better assessment of heart workload during exercise. IC is a non-invasive method of heart monitoring that allows to continuously measure several parameters such as cardiac output, stroke volume, and cardiac work index. **Subjects and Methods**: Forty-three patients undergone exercise MPI coupled with IC and were divided in two groups: control group (n=16) - primary diagnostics, exercise level over 7 METs, negative cardiac SPECT and study group (n=27) - with low exercise tolerance - patients who met diagnostic stress test criteria before achieving exercise level of 7 METs. Exercise tests were performed on the treadmill using Bruce or modified Bruce protocol. Following IC parameters have been compared and correlations between them assessed: cardiac index (CI) - which is cardiac output (CO) divided by body surface area (BSA), left cardiac work index (LCWI) - which takes into account CO, BSA and arterial blood pressure as afterload, and percentage of target heart rate (HR%) estimated for age (220/min - age). **Results:** Mean age was 51 years (range: 35-67), mean exercise level was 10,6METs (8-13,5) in control group and 67 years (52-81) and 6,5 METs (5,2-6,8) in exercise intolerance group, respectively. In two groups there have been no significant differences between HR% (p=0,6) with mean HR% of 94% and 95% in control and study group, respectively. Significant differences have been found between peak CI (p=0,006) and peak LCWI (p=0,03). Mean peak CI was 10,1 l/min/m^2 (7,2-14,6) vs 8,2 l/min/m^2 (4,7-13,2) and peak LCWI was 15,1 kg*m/m^2 (10,1-12,9) vs 12,6 kg*m/m^2 (7-20,9) in control group vs study group, respectively. Twenty one percent of study group patients did not achieve minimal LCWI level observed in control group. **Conclusion:** Impedance cardiography may allow for a better definition of cardiac workload than standard HR. In some cases achieving 85% of target HR may not be precise enough to indicate sufficient workload, thus influencing sensitivity of MPI procedure. In uncertain cases conversion to pharmacological stress test should be considered.

Neurosciences: Basic Science

EP-0370

Amantadine Influences Motor/Eyploratory Behavior, but not D2 Receptor Binding in the Rat

S. Nikolaus[1], M. Beu[1], M. A. De Souza Silva[2], F. Wickrath[1], A. Müller-Lutz[1], C. Antke[1], H. Hautzel[1], J. P. Huston[2], H. Müller[1], G. Antoch[1], H. Wittsack[1]; [1]University Hospital Düsseldorf, Düsseldorf, GERMANY, [2]Heinrich-Heine University, Düsseldorf, GERMANY.

Purpose/Introduction: Amantadine (AMA) acts as a D2 receptor (R) agonist and a NMDAR antagonist. It is known to increase dopamine (DA) synthesis and release in the rat striatum. In the present study, we assessed the effect of AMA on motor and exploratory behavior and on cerebral D2R binding in the same rats with the method of small animal SPECT. **Subjects & Methods:** In 22 male Wistar rats, D2R binding was measured in baseline (BAS) and after application of AMA (40 mg/kg ip). After AMA challenge, motor/exploratory behavior was registered for 30 min in an open field using EthoVisionXT. In 16 further rats, D2 receptor binding and behavior were assessed after pre-treatment with vehicle (VEH; 0,9% NaCl). Iodine-123-IBZM (25±4MBq) was injected 30 min post-challenge into the lateral tail vene. Imaging data were acquired 45 min after radioligand application with the TierSPECT. Furthermore, all rats were scanned with a dedicated small animal MRT (MRS3000 Pre-clinical MRT, 3.0 T, MR Solutions, Guildford, UK) in order to gain morphological information. Based on the Paxinos rat brain atlas, regions of interest were defined on SPECT-MRT overlays. The equilibrium ratios of the distribution volumes of the specifically and the non-specifically bound compartment (V3''=V(ROI)/V(REF)-1) were computed as estimates for the binding potentials in neostriatum, ventral striatum, thalamus, substantia nigra and prefrontal, motor and parietal cortex as well as anterior and posterior hippocampus. **Results:** V3'' did not differ in any region between BAS and challenge (.396≤p≤.913). After AMA locomotion was decreased in min 1-5, 6-10 and 11-15 relative to vehicle (.001≤p≤.042), whereas in min 25-30 an elevation was observed (p=.031). Conversely, sitting was elevated in in min 1-5, 6-10 and 11-15 relative to VEH (.0001≤p≤ .029), but reduced in min 25-30 (p=.006). Rearing behavior was decreased in min 1-5, 6-10 and 11-15 relative to VEH (p≤.0001), whereas head-shoulder motitlity was elevated in min 1-5, 6-10 and 11-15 (.0001≤p≤.045). **Discussion/Conclusion:** The increase of motor/exploratory activities in min 1-15 post-challenge and their decrease in min 15-30 can be interpreted to reflect an elevation of DA in the first 15 min and its subsequent decrease. Consistently, no regional alterations of D2R binding were observed in the in vivo imaging studies, which were conducted 75 min post-challenge.

EP-0371

Bicuculline Elevates D2 Receptor Binding in the Rat Thalamus

S. Nikolaus[1], H. Wittsack[1], M. Beu[1], M. A. De Souza Silva[2], C. Antke[1], F. Wickrath[1], A. Müller-Lutz[1], G. Antoch[1], J. P. Huston[2], H. Müller[1], H. Hautzel[1]; [1]University Hospital Düsseldorf, Düsseldorf, GERMANY, [2]Heinrich-Heine University, Düsseldorf, GERMANY.

Purpose/Introduction: Bicuculline (BIC) acts as an highly selective GABA(A) receptor (R) antagonist. We have previously shown that BIC increased motor/exploratory behaviors, but had no effect on neostriatal D2R binding (1). In the present study, we assessed the effect of BIC on D2R binding in ventral striatum (VSTR), neostriatum (STR), thalamus (THAL), substantia nigra (SN) as well as neocortical and limbic regions, employing dedicated small animal SPECT and MRT. **Subjects & Methods:** In 16 male Wistar

rats, D2R binding was measured in baseline (BAS) and after application of BIC (1 mg/kg ip). After BIC challenge, motor/exploratory behavior was registered for 30 min in an open field using EthoVisionXT. Iodine-123-IBZM (26±4MBq) was injected 30 min post-challenge. Imaging data were acquired 45 min after radioligand application with the TierSPECT. Seven rats were scanned with a dedicated small animal MRT (MRS3000 Pre-clinical MRT, 3.0 T, MR Solutions, Guildford, UK) in order to gain morphological information. Based on the Paxinos rat brain atlas, regions of interest were defined on SPECT-MRT overlays. Estimations of the binding potential (BP) were obtained by computing ratios of the specifically bound compartments to the cerebellum for VSTR, STR, THAL, SN, frontal (FC), motor (MC) and parietal cortex (PC) as well as anterior (aHIPP) and posterior hippocampus (pHIPP). **Results:** In BAS, BPs amounted to 2.32±.70 (VSTR), 2.53±.75 (STR), 1.59±.33 (THAL), 1.29±.43 (SN),1.45±.49 (FC), 1.37±.22 (MC), 1.10±.28 (PC), 1.29±.24 (aHIPP) and 1.37±.31 (pHIPP). After BIC, BPs were 2.32±.46 (VSTR), 2.65±.40 (STR),1.80±.27 (THAL), 1.40±.23 (SN), 1.54±.47 (FC), 1.46±.33 (MC), 1.05±.24 (PC), 1.35±.28 (aHIPP) and 1.38±.27 (pHIPP). The elevation of D2R in the THAL relative to BAS was significant (p=.047). In the THAL, D2R binding correlated negatively with sitting duration and sitting frequency and positively with travelled distance and rearing frequency in min 1-5. **Discussion/Conclusion:** The increase of D2R binding in the THAL is likely to reflect a decrease of DA levels in this region. The early behavioral effects of BIC indicate an almost immediate decline of synaptic DA. At the time of in vivo imaging studies, no alterations of D2R binding were detected in any other of the investigated areas, which may be interpreted in terms of a vast compensation of diminished DA levels. (1)Nikolaus et al. Pharmacol Biochem Behav 2017; 153: 76-87.

EP-0372

Bilateral stimulation of the abdominal vagus modifies dopamine connectivity in acquired obesity

C. Malbert[1], C. Picq[2], J. Divoux[2], C. Henry[3]; [1]INRA, Saint-Gilles, FRANCE, [2]Axonic, Valloris, FRANCE, [3]Livanova, Clamart, FRANCE.

Introduction: We recently demonstrate that bilateral abdominal VNS restores insulin sensitivity of the cingulate and prefrontal cortices in obese animals (Diabetes, 2017). These areas were also inhibited in obese patients. Furthermore, animals data show that extracellular dopamine was increased in the prefrontal cortex of VNS treated subjects (Manta et al, 2012). This suggest that abdominal VNS may act on dopamine transmission. We aimed to characterize the effect of abdominal VNS on metabolic connectivity and dopamine transmission in an animal model of acquired obesity. **Subjects & Methods:** Bilateral abdominal VNS was applied on 10 adults mini-pigs during 2 months while sham procedure was achieved on 10 additional animals. All animals were made obese after 5 months of obesogenic diet prior the onset of stimulation. Stimulation electrodes were placed on the vagus using laparoscopy and connected to a stimulator placed under the skin. PET [18]FDG and SPECT DATscan were acquired on all subjects. CMRglu and DAT receptor binding maps were constructed with pixel wise modeling (Patlak-FDG and Ichise-

DAT). Glucose uptake and DAT receptor binding were analyzed separately using SPM and a join analysis using parallel ICA was also achieved together with the identification of metabolic connectivity with group ICA. **Results:** The weight of VNS animals was 25% less than sham. This was associated with an increased glucose metabolism of the anterior cingulate cortex, the anterior prefrontal cortex, the putamen and of the anterior thalamus. The same areas have also an increased DAT receptor binding with the exception of the anterior thalamus. No areas other than those identified by SPM FDG were found with different DAT binding. Connectivity analysis using the correlators from FDG and DATscan demonstrated a more than doubled connectivity in VNS compared to sham group. **Conclusions:** Bilateral abdominal VNS modified brain metabolism and connectivity of anterior structures that were altered by obesity through a restored dopamine transmission.

EP-0373

Metformin Effect on Brain Metabolism: the Role of Endoplasmic Reticulum

A. Buschiazzo[1], A. M. Orengo[2], S. Ravera[3], L. Emionite[4], V. Cossu[2], A. Bellini[1], S. Morbelli[2], M. Bauckneht[1], L. Raffaghello[5], D. Gandolfo[2], G. Bianchi[5], S. Bruno[6], G. Sambuceti[1,2], C. Marini[7,2]; [1]Nuclear Medicine Unit, Department of Health Sciences, University of Genoa, Genoa, ITALY, [2]IRCCS AOU San Martino-IST, Genoa, ITALY, [3]Department of Pharmacy, University of Genoa, Genoa, ITALY, [4]Animal Facility, IRCCS AOU San Martino-IST, Genoa, ITALY, [5]Laboratory of Oncology, G. Gaslini Institute, Genoa, ITALY, [6]Department of Experimental Medicine, University of Genoa and IRCCS-AOU San Martino-IST, Genoa, ITALY, [7]CNR Institute of Bioimages and Molecular Physiology, Milan, ITALY.

Aim: Clinical use of brain imaging of FDG uptake relies on the assumption that this tracer accurately delineates overall glucose consumption (MRGlu) in central nervous system. We recently documented that, in cancer, the link between FDG retention and glucose disposal is relatively loose and profoundly dependent upon the activity of a specific glucose processing machinery located in the endoplasmic reticulum (ER) and triggered by hexose-6-phosphate-dehydrogenase (H6PD). This study was designed to verify whether metformin (MTF) capability to inhibit H6PD function affects FDG uptake also in nervous tissue. **Materials and Methods:** All animal experiments were reviewed and approved by the Italian Ministry of Health. Six-weeks-old BALB/c mice were divided into 2 groups: "controls" (n=7) did not receive any treatment; MTF (n=6) were studied after one-week treatment with 750 mg/Kg/die MTF. Both groups underwent dynamic microPET imaging (Albira, Bruker, US) according to a protocol previously validated in our lab, to estimate MRGlu by Patlak analysis. In 2 further mice per groups, not submitted to imaging, the brain was harvested soon after sacrifice by cervical dislocation. Brains were placed in the Petri dish of Ligand tracer instrument (Ridgeview, Se) whose rotation permits to cyclically move the organ from the incubation medium to the focus of a counting detector every 30 seconds. Incubation medium was enriched with 12.5 mM glucose and 6 MBq FDG. Time trend of

organ radioactivity content was monitored for one hour and Patlak estimate of MRGlu was compared with directly measured glucose disappearance from incubation medium. At the end of the experiment, H6PD expression was estimated by Western blot while enzyme activity was assayed following the reduction of NADP at 340 nm. **Results**: In vivo, one week MTF virtually halved brain MRGlu from 14.2±3.1 nM x min^{-1} x g^{-1} to 6.0±2.1 nM x min^{-1} x g^{-1}. In ex vivo studies, MRGlu predicted by FDG uptake well agreed with direct measurement of glucose disposal under control conditions. By contrast, MTF significantly decreased the lumped constant (i.e. the ratio between FDG uptake and glucose consumption) from 1 to 0.6. Autoradiography confirmed the gray matter location of FDG uptake in ex vivo experiments. This finding well agreed with the molecular response to MTF treatment characterized by a reduction of 24.1% in brain H6PD expression and of 66.7% in enzyme activity. **Conclusion**: The present data document that H6PD triggered metabolism within ER significantly contributes to FDG uptake in the central nervous system.

EP-0374

Activations in the gerbil auditory system can be demonstrated in ^{18}F-FDG PET scans during anesthesia with fentanyl but not if ketamine/xylazine is used

M. Kessler[1,2], *M. Mamach*[3,2], *R. Beutelmann*[4], *J. Bankstahl*[1], *T. Ross*[1], *F. Bengel*[1], *G. Klump*[4,2], *G. Berding*[1,2]; *[1]Department of Nuclear Medicine, Hannover Medical School, Hannover, GERMANY, [2]Cluster of Excellence Hearing4all, Hannover and Oldenburg, GERMANY, [3]Department of Medical Physics and Radiation Protection, Hannover Medical School, Hannover, GERMANY, [4]Animal Physiology and Behaviour Group, Department for Neuroscience, School of Medicine and Health Sciences, University of Oldenburg, Oldenburg, GERMANY.*

Introduction: Having an auditory frequency range overlapping with that of humans, gerbils are a well-suited model to study effects of age-related hearing loss. In this context PET measurements of activity in the gerbil auditory system during processing of binaural stimuli, which deteriorates with age-related hearing loss, are of interest. However, such measurements require stimulation via headphones, which only is possible in gerbils under anesthesia. Therefore, we investigated the detectability of activation in the auditory pathway in gerbils with PET using different anesthetics. **Methods:** For measuring brain activity, gerbils (n=8) were injected with 15MBq ^{18}F-fluorodeoxyglucose (FDG) intraperitoneally, and acoustic stimulation (30-40min, in sound-shielding box) was performed: (i) in awake gerbils, (ii) under anesthesia with ketamine/xylazine(KX) or (iii) fentanyl/midazolam/medetomidin(FMM) - always with two different acoustic free-field conditions (30dB laboratory background noise (BG); 90dB frequency modulated sounds (FM)). Thereafter, 30min acquisitions were performed using a Siemens Inveon PET/CT. Blood glucose was measured before and after scanning. For data analysis, PMODv3.7 software and statistical parametric mapping (SPM8) were used. FDG-uptake was normalized to pons. Anatomical locations were assigned after implementing a

VOI-template based on high-resolution images of a stereotaxic brain-atlas of the Mongolian gerbil (Radtke-Schuller et al. 2016). **Results:** Compared to BG-condition FM-stimulation revealed a significant increase of mean activity (16%) in the inferior colliculus (IC) of awake gerbils (1.02±0.04 vs. 1.18±0.06; p=0.0002). Under FMM anesthesia a significant increase of 12% from BG to FM (1.21±0.03 vs. 1.33±0.07; p=0.016) was seen. No difference was observed between both conditions under KX (1.16±0.05 vs. 1.13±0.06). Blood glucose levels were consistently low for both time-points in awake gerbils (5.76mmol/l±0.47 vs. 6.14mmol/l±0.84), and values were significantly higher during FMM- and KX-anesthesia for both time-points. However, for the first time-point values during KX were significantly higher compared to FMM (17.29mmol/l±0.42 vs. 13.83mmol/l±2.06 p=0.011). **Conclusions:** Processing of (binaural) auditory stimuli has been successfully investigated in gerbils during KX-anesthesia using electrophysiological methods. However, in the present study no functional correlate of auditory processing could be revealed using FDG-PET during KX, which is likely to be due to a significant increase in blood glucose hampering FDG-uptake. In contrast, during FMM-anesthesia as significant activation of the IC similar to that in FDG-studies with awake gerbils could be demonstrated. These results support the use of opioid-based anesthesia in hearing research in gerbils consistent with registered auditory evoked potentials and implicit memories post anesthesia with this type of anesthesia in humans.

EP-0375

^{18}F-FET, ^{18}F-FCH and ^{18}F-DOPA uptake on human glioblastoma T98G cells: in vitro study

M. Hodolic[1], *M. Persico*[2], *L. Lodola*[3], *C. Aprile*[4], *R. Nano*[5], *F. Pasi*[6]; *[1]Nuclear Meidicine Research Department, Iason, Graz, AUSTRIA, [2]Department of Oncohaematology, Nuclear Medicine Unit, Fondazione IRCCS Policlinico San Matteo; Scuola Universitaria Superiore IUSS, Pavia, ITALY, [3]Department of Oncohaematology, Nuclear Medicine Unit, Fondazione IRCCS Policlinico San Matteo, Pavia, ITALY, [4]4Department of Oncohaematology, Nuclear Medicine Unit, Fondazione IRCCS Policlinico San Matteo; CNAO - National Center of Oncological Hadrontherapy, Pavia, ITALY, [5]Department of Biology and Biotechnology "Lazzaro Spallanzani", University of Pavia,, Pavia, ITALY, [6]Department of Oncohaematology, Radiotherapy Unit, Fondazione IRCCS Policlinico San Matteo, Pavia, ITALY.*

Introduction and Aim: O-(2-[18F]fluoroethyl)-l-tyrosine (^{18}F-FET) is a radiolabelled modified natural amino acid which accumulates in glioblastoma cells. Choline is a substrate for the synthesis of phosphatidylcholine, major component in the cell membranes of prostate cancer but also glioma, for that reason ^{18}F-methyl-choline (^{18}F-FCH) is commonly used in molecular imaging. ^{18}F-dihydroxyphenylalanine (^{18}F-DOPA) is an analogue of L-DOPA, used to image the dopaminergic pathway and to evaluate striatal dopaminergic presynaptic function but also gliomas. Aim of this study was to evaluate ^{18}F-FCH, ^{18}F-FET and ^{18}F-DOPA uptake by human glioblastoma T98G cells. **Materials and Methods:** Human glioblastoma T98G or human dermal fi-

broblasts cells, seeded at a density to obtain 2 x 10⁵ cells per flask, grew adherent to the plastic surface at 37°C in 5% CO_2 in complete medium. Equimolar amounts of radiopharmaceuticals were added to cells for different incubation times (20 to 120 minutes) for ¹⁸F-FCH, ¹⁸F-FET and ¹⁸F-DOPA respectively. All experiments were carried out in duplicate and repeated three times. Data (expressed as mean values of % uptake of radiopharmaceuticals) were compared using parametric or non-parametric tests as appropriate. **Results:** A significant uptake of ¹⁸F-FCH was seen in T98G cells at 60, 90 and 120 minutes. The percentage uptake of ¹⁸F-FET in comparison to ¹⁸F-FCH was lower by a factor of more than 3, with different kinetic curves. ¹⁸F-FET showed a more rapid initial uptake up to 40 minutes and ¹⁸F-FCH showed a progressive rise reaching a maximum after 90 minutes. ¹⁸F-DOPA shows the lowest uptake in T98G cells, less than a half in comparison to ¹⁸F-FET. Uptake kinetic was characterized by an early maximal activity at 40 minutes, thereafter tending to a plateau pattern. **Conclusions:** ¹⁸F-FCH, ¹⁸F-FET and ¹⁸F-DOPA are candidates for neuro-oncological PET imaging: ¹⁸F-FET could be the most appropriate oncological PET marker in the presence of reparative changes after therapy, where the higher affinity of ¹⁸F-FCH to inflammatory cells makes it more difficult to discriminate between tumour persistence and non-neoplastic changes. The lowest uptake of ¹⁸F-DOPA in tumour cell line together with a physiological accumulation in basal ganglia might indicate a less suitable candidate for in vivo imaging.

EP-0376

Preclinical evaluation of non-invasive imaging molecules of growth differentiation factor-11 for aging-related diseases' uses

M. C. Weng, M. H. Wang, C. H. Yang, W. M. Li, W. J. Lin; Institution of Nuclear Energy, Taoyuan, TAIWAN.

Purposes: The increasing levels on health-care budget of governments that is owing to neurodegenerative diseases accompanied with aging have been defined in Europe and Taiwan. According to recent studies, scientists have evaluated genes and proteins associated with aging, including growth differentiation factor 11 (GDF-11) which has been defined its capability of improvements on muscular function when treated in aged mice. However, the distribution of GDF-11 in whole body and central nervous systems still needs more evaluation. Here we have tried to develop radiolabeled non-invasive imaging molecules of GDF-11 that can be used to clarify the biological mechanisms of GDF-11 in mice. **Materials and Methods:** GDF-11 was first conjugated with DTPA under room temperature for 24 h and purified by centrifuge; the original and final molecular weights of molecules were both checked by a MALDI TOF/TOF. After radiolabeled with In-111, the radiochemical purity (R.C.P.) and stability tests in PBS and serum were investigated. ¹¹¹In-GDF-11 was then intravenously (i.v.) or intraventricularly (i.b.) injected into both normal and neurodegenerative mice for SPECT/CT imaging at 1, 4, 24 and 48 h. **Results:** The R.C.P. of ¹¹¹In-GDF-11 was checked as >95%; results of stability tests in PBS and serum were found as >90% within 120 h. Results of SPECT/CT imaging

showed significant liver uptake in whole body in 48 h. After i.b. injection of ¹¹¹In-GDF-11, the collection was found mainly in hippocampus, thalamus, cerebellum and olfactory bulb region at 48 h, which is similar to the distribution of intrinsic GDF-11 RNA that is defined by *in situ* hybridization in previous studies (ALLEN BRAIN ATLAS). **Conclusions:** In this study, radiolabeled imaging molecules of growth differentiation factor-11 (¹¹¹In-GDF-11) were successfully developed for non-invasively monitoring the biological mechanisms in our preclinical evaluation. For several potential uses of GDF-11, more studies in aging-related diseases can be evaluated through the uses of these novel molecules in further preclinical and clinical research in the future.

EP-0377

Imaging of basal metabolic activity in primary visual cortex in mice. A FDG-microPET study

A. Buschiazzo[1], J. F. Maya-Vetencourt[2], F. Ticconi[1], L. Emionite[3], C. Eleftheriou[2], C. Marini[4,5], S. Icardi[5], A. Bellini[1], C. Ghersi[5], A. M. Orengo[5], F. Benfenati[2,6], G. Sambuceti[1,5]; [1]Department of Health Sciences, University of Genoa, Genoa, ITALY, [2]Center for Synaptic Neuroscience and Technology, Istituto Italiano di Tecnologia, Genoa, ITALY, [3]Animal Facility, IRCCS San Martino-IST, Genoa, ITALY, [4]CNR, Institute of Bioimages and Molecular Physiology, Milan, ITALY, [5]Nuclear Medicine Unit, IRCCS AOU San Martino-IST, Genoa, ITALY, [6]Department of Experimental Medicine, University of Genova, Genoa, ITALY.

Background: Previous experiments performed in our lab focused on evaluation of primary visual cortex (V1) metabolism in a recognized rodent model of Retinitis Pigmentosa. In order to perform future studies of neuronal plasticity during early development, we evaluated V1 metabolic response to alterations of vision in mice by means of FDG-PET. **Materials and Methods**: Sixteen C57BL/6 mice (25±2 days old) were subjected to FDG-PET three days after surgical closure of the right eye. All mice were kept under fasting conditions with free access to water for 6 hours under the same artificial light. Mice were weighted and anaesthesia was induced by intra-peritoneal administration of ketamine/xylazine (100 and 10 mg/kg, respectively). Serum glucose level was tested soon before the injection of 3-4 MBq ¹⁸F-FDG through a tail vein. Animals were maintained under the same light (5 lux) for 40 minutes and then positioned on the bed of a dedicated micro-PET system to undergo a scan acquisition of 600 seconds. We identified a volume of interest (VOI) in the left and right V1 and also used the whole cortex of the left and right hemisphere to measure average standardized uptake value (SUV). We utilized paired *t*-test to compare the experimental data (*p* value <0.05). **Results**: Comparing whole cortical areas in the two hemispheres, we found the same average SUV (1.21±0.20 right and 1.22±0.17 left). The mean SUV in right cortex, corresponding to physiologic metabolism of V1, was 1.31±0.15. Interestingly, left V1, contralateral to the deprived eye, showed a mean SUV of 1.24±0.17. These data revealed a significant decrease (*p*=0.02) of basal metabolic activity specific to the left V1 after right eye closure. **Conclusions**: Our findings reveal a specific decrease of basal metabolic activity in V1 of

mice after short-term monocular deprivation during early development. This study suggests the possibility to follow-up V1 plasticity after alterations of sensory input using *in vivo* imaging by means of micro FDG-PET in mice brain.

Neurosciences: Dementia

EP-0378

Brain network alterations in Alzheimer's disease identified by early-phase PIB-PET

L. Fu[1], J. Zhang[1], B. Xu[1], Y. Fan[2], J. Tian[1]; [1]Department of Nuclear Medicine, the Chinese PLA General Hospital,, Beijing, CHINA, [2]Department of Radiology, Perelman School of Medicine, University of Pennsylvania, Philadelphia, PA, UNITED STATES.

Purpose: Early uptake of the amyloid-β tracer ^{11}C-PIB on PET images is mainly determined by cerebral blood flow (CBF) and shows a high correlation with ^{18}F-FDG uptake. In the current study, we identify brain networks from early-phase of ^{11}C-PIB (perfusion PIB, pPIB) data and evaluate the brain networks for differentiating Alzheimer's disease (AD) vs. cognitively normal (CN) and mild cognitively impaired (MCI) vs. CN. **Methods:** Forty participants (14 CN, 12 MCI and 14 AD) underwent ^{11}C-PIB- and ^{18}F-FDG-PET studies. Pearson correlation between the ^{18}F-FDG image and sum of early ^{11}C-PIB frames was maximized to identify the optimal time-window for ^{11}C-pPIB. Parallel independent component analysis (pICA) was used to jointly identify independent components of pPIB and FDG and their association. Two-sample *t*-test was used to evaluate differences of pPIB and FDG measures between AD and CN and between MCI and CN in the highest correlated pair of pPIB and FDG components. **Results:** A pair of correlated components of pPIB and FDG was identified across all subjects, depicting correlated brain networks of FDG and pPIB. Within the correlated networks, decreased FDG uptake was correlated with decreased rCBF in the frontal, parietal and temporal regions, including the medial frontal gyrus, anterior cingulate cortex, posterior cingulate cortex/Precuneus, and superior temporal gyrus. Group comparisons between AD and CN and between MCI and CN revealed similar spatial patterns on FDG and pPIB data, and hypometabolic regions highly co-localized with the hypoperfusion areas. **Conclusion:** Our results revealed brain networks of brain perfusion (early-phase ^{11}C-PIB) in the resting state with AD-specific neurodegenerative changes, which was similar with the networks of glucose metabolism (^{18}F-FDG) and highly co-localized with default mode network, indicating that pPIB derived from the early-phase ^{11}C-PIB could provide complementary information for ^{18}F-FDG examination in AD.

EP-0379

Accuracy of brain FDG PET for detection of Alzheimer's disease in geriatric inpatients with newly manifested cognitive impairment

C. Lange[1], I. Apostolova[2,3], A. Mäurer[4], P. Suppa[1,5], H. Amthauer[1], W. Brenner[1], R. Buchert[1,3]; [1]Department of Nuclear Medicine, Charité - Universitaetsmedizin Berlin, Berlin, GERMANY, [2]Department of Radiology and Nuclear Medicine, University Hospital Magdeburg, Magdeburg, GERMANY, [3]Department of Nuclear Medicine, University Medical Center Hamburg-Eppendorf, Hamburg, GERMANY, [4]Evangelisches Geriatriezentrum Berlin, Berlin, GERMANY, [5]jung diagnostics GmbH, Hamburg, GERMANY.

Purpose: Determination of the etiology of cognitive impairment in acutely hospitalized geriatric patients can be challenging, but is important in order to effectively treat potentially life threatening causes or identify underlying neurodegenerative disease. This prospective study evaluated the accuracy of brain FDG PET for detecting Alzheimer's disease (AD) in cognitively impaired geriatric inpatients (WHO Trials Registry DRKS00005041). **Methods:** The study enrolled 103 patients hospitalized due to (sub)acute admission indications in 11 different geriatric units. The main inclusion criterion was newly manifested cognitive impairment with clinically uncertain suspicion of AD or cerebrovascular disease (CVD) or mixed pathology (MD=AD+CVD) as underlying disease. Brain FDG PET was performed according to common guidelines. Two readers in consensus categorized PET findings as positive or negative for AD-typical alterations by visual inspection of reconstructed FDG uptake images and hypometabolism t-maps obtained by voxel-based single subject testing against 32 age-matched normal control subjects. Reduction of FDG uptake in the posterior cingulate/precuneus area was required for PET to be AD-positive. Reduction of FDG uptake in parietotemporal association cortices was assumed to confirm AD-positivity, but was not required. Clinical follow-up including detailed neuropsychological testing after ≥12 months was performed at the patients' home. Etiological diagnosis at follow-up was used as gold standard to assess the accuracy of FDG PET to detect AD in these patients. **Results:** Follow-up after 16±3 months was completed in 67 patients (46 females) aged 81.0±5.4 years at baseline (range 69-96 years). Etiological diagnosis at follow-up comprised AD (n=18), CVD (n=21), MD (n=14), neurodegenerative disease other than AD (n=7) and other non-neurodegenerative etiology (e.g. delirium or depression, n=7). Thus, 32 of 67 patients (48%) were diagnosed to have AD, either rather purely or with concomitant CVD. Sensitivity, specificity and accuracy of baseline FDG PET to identify these patients was 84.4%, 88.6%, and 86.6%, respectively. FDG PET was interpreted as normal for age in 3 of the 5 false negative cases, and as abnormal but not typical for AD in the remaining 2 cases (posterior cortical atrophy, frontotemporal lobar degeneration). All false positive cases showed the 'full' AD pattern including parietotemporal association cortices. Neither false negative cases nor false positive cases differed from true positive cases with respect to duration of follow-up (Mann-Whitney test, p=0.521 and p=0.505). **Conclusion:** FDG PET provides similar accuracy for detection of AD in de novo cognitive impairment in acutely hospitalized geriatric patients as in less 'difficult' settings such as outpatient memory clinics.

EP-0380

Clinical value of ¹⁸F Florbetaben Amyloid-β PET in a memory clinic.

B. de Kwaasteniet, Jr., *D. Raaymakers, senior, J. de Klerk, senior; Meander Medical Center, Amersfoort, NETHERLANDS.*

Introduction: Accumulation of both amyloid-β and tau proteins in the brain are considered key processes in the pathophysiology of Alzheimers disease (AD), which is the main cause of dementia. Abnormal accumulation of both proteins are thought to begin 10 to 20 years before the onset of symptoms. Therefore, the development of biomarkers to detect amyloid-β in the brain is of huge clinical importance in the diagnosis of AD. Until now the diagnostic impact of amyloid-β PET has only been investigated in clinical trials. This study was the first to investigate the clinical value of [¹⁸F] Florbetaben Amyloid-β PET in a memory clinic. **Subjects and Methods:** In this study 24 patients underwent a [¹⁸F] Florbetaben amyloid-β PET scan in which there was no diagnosis after a standard work-up. Only patients younger than 70 year were referred for an amyloid scan. The amyloid-β PET scans were interpreted as amyloid negative or positive based on visual rating by especially trained nuclear medicine physicians. Furthermore, patients were only included when the differential diagnosis included both AD and a psychiatric disorder, a personality disorder, frontotemporal dementia (FTD), vascular dementia, cognitive decline after traumatic brain injury or normal aging. After the amyloid-β PET scan the differential diagnosis was reevaluated. **Results:** Results showed that the amyloid-β PET scan was positive in 11 patients which all were finally diagnosed with AD. The amyloid PET was negative in 13 patients in which 12 patients were finally diagnosed with an alternative diagnosis, including depressive disorder, FTD, burn out, normal aging and cognitive decline after brain injury. One patient was diagnosed with early onset AD despite the negative scan. **Conclusion:** These findings show that [¹⁸F] Florbetaben amyloid-β PET has a good clinical value in a memory clinic when there is no certain diagnosis after standard work-up in patients with suspected AD. Since amyloid-β PET has a high negative predictive value an alternative diagnosis can reliably be made in case of a negative amyloid-β PET scan. In patients <65 years with mild cognitive impairment (MCI) and a positive amyloid-β PET AD can reliable be diagnosed. However, with increasing age scans are more likely to be false-positive since amyloid-β aggregation increases with age in healthy controls. Furthermore, an amyloid-β PET scan is a good alternative when there are contra-indications for CSF or neuropsychological investigation.

EP-0381

Diagnostic accuracy of FDG-PET/MR for dementia—Estimation of the impact of commercial atlas-based MR attenuation correction

T. Sekine[1], A. Buck[2], G. Delso[3], E. ter Voert[2], M. W. Huellner[2], P. Veit-Haibach[4], G. Warnock[2]; [1]Nippon Medical School, Tokyo, JAPAN, [2]University Hospital Zurich, Zurich, SWITZERLAND, [3]GE Healthcare,

Waukesha, WI, UNITED STATES OF AMERICA, [4]University of Toronto, Toronto, ON, CANADA.

Aim: The PET/MR system has been clinically available. One of the best targets of PET/MR is the evaluation of dementia. However, incomplete MR-attenuation correction (MRAC) on commercial PET/MR cause the error of PET images, which may lead to decrease the accuracy of the evaluation. The purpose of this study was to estimate the impact of commercial MRAC on FDG-PET evaluation of Alzheimer's disease (AD). **Materials and Methods:** We obtained FDG-PET data of AD, MCI (mild cognitive impairment) and normal control subjects (n=203) from the Alzheimer's Disease Neuroinitiative database (ADNI). To clarify the statement of prediction of AD, PET probability score was calculated by using PALZ (Pmod) which software is widely used for FDG-PET/CT dementia study. Separately, we recruited 14 patients (6 males, median age 66, range 56 to 80) who underwent both PET/CT and PET/MR (GE SIGNA) examination. Two FDG-PET data was generated based on MRAC (Atlas-based method) and CTAC from the identical PET raw data on PET/MR. After the spatial normalization and smoothing for these PET images which procedure is the same as PALZ protocol, we calculated the error-map of PET where PET based on MRAC was divided by that on CTAC in each patient. We multiplied each 14 error map and each 203 ADNI data to which the same normalization and smoothing was performed as above. Totally, we could get 203*14=2842 dataset. We performed PALZ evaluation to these simulated PET dataset. The diagnostic accuracy of the discrimination of AD and of predicting progression to AD was estimated in each 14 error map. **Results:** The accuracy, sensitivity and specificity for the discrimination of AD-patients from the normal control was not impaired by MRAC (Original vs. Error; 83.2%, 83.3% and 83.1% vs. 81.3% [range 77.6-83.2%], 82.6% [range 79.2-85.4%,] and 80.3% [range71.2-86.4%]). The accuracy, sensitivity and specificity for predicting progression from MCI to AD during 2-year follow-up was not impaired either by MRAC, either (Original vs. Error; 57.0%, 60.6% and 65.1% vs. 56.9% [range 54.2-59.8%], 61.5% [range 54.5-72.7%] and 64.5% [range 54.0-73.0%]). **Conclusion:** It is estimated that clinical PET/MR system using atlas-based MRAC could discriminate AD-patients from the normal control and predict the progression from MCI to AD based on the same manner with the same database for FDG-PET/CT. FDG-PET on clinical PET/MR system has enough accuracy to diagnose AD.

EP-0382

18F-FDG PET/CT Usefulness In Primary Progressive Aphasia (PPA) Variants And In Fronto-Temporal Dementia (FTD) Or Alzheimer's Disease (AD) Development

S. Nuvoli[1], M. R. Piras[2], S. Contu[1], B. L. J. Pung[1], L. Calderoni[1], B. Piras[1], A. Nieddu[3], A. Spanu[1], G. Madeddu[1]; [1]Unit of Nuclear Medicine, Clinical and Experimental Medicine DPT, University of Sassari, Sassari, ITALY, [2]Unit of Neurology, Clinical and Experimental Medicine DPT, University of Sassari, Sassari, ITALY, [3]Geriatrics DPT, Policlinico Sassarese, Sassari, ITALY.

Introduction: We evaluated ¹⁸F-FDG PET/CT usefulness in PPA variant early initial diagnosis, since Logopenic Aphasia (LPA)

variant is closely related to AD, while Progressive Non-Fluent Aphasia (PNFA) variant and Semantic Variant (SV) might develop FTD. **Methods:** We investigated 26 consecutive patients, 13 with uncertain symptoms attributable to PPA (Group 1) and 13 with ascertained PPA but with symptoms suspected also for early AD or FTD (Group 2). All patients underwent brain ^{18}F-FDG PET/CT using GE Discovery tomograph. Images were evaluated both qualitatively and quantitatively with automated analysis program (Cortex ID, GE Healthcare); brain metabolic map and normal age matched control group comparative analysis was produced. **Results:** ^{18}F-FDG PET/CT showed different hypometabolic patterns with reduced cortical uptake in the two patient groups. Group 1: widespread in 1/13 cases, diffuse and bilateral in fronto-parietal and fronto-temporal regions in 1/13, bilateral in temporo-parietal regions in 2/13, in left frontal/parietal inferior regions in 5/13 cases, in bilateral inferior-frontal and temporal regions in 3/13 and in left inferior-frontal regions in 1/13. Group 2: diffuse in 2/13 cases, in bilateral frontotemporal and fronto-parietal regions in 6/13 and in bilateral temporo-parietal regions in 5/13. The 9 Group 1 patients with hypometabolic areas only in inferior-frontal regions as well as in inferior-parietal and temporal regions were clinically classified as PNFA at risk to develop FTD, while the two patients with bilateral hypometabolism temporo-parietal regions was classified as LPA, eventually anticipating AD. However, in the two patients with diffuse hypometabolism, diagnosis remained uncertain. The six Group 2 patients with hypometabolism in frontotemporal and fronto-parietal areas were considered PNFA and SV, respectively, both associated to FTD, while the five patients with temporo-parietal hypometabolism were classified as LPA associated to AD. However, diagnosis remained uncertain in the remaining two cases with diffuse hypometabolism. **Conclusions:** The present study confirms the difficulty in clinical differential diagnosis of PPA different variants that could develop AD/FTD. ^{18}F-FDG PET/CT proved valuable tool in supporting both primary PPA clinical diagnosis and uncertain AD/FTD differential diagnosis with PPA symptoms, being diagnosis more confidential in 84.6% of PPA our cases and also hypothesizing the PPA associated symptoms with AD/FTD disorders in 84.6%. However, ^{18}F-FDG PET/CT could not clarify the four cases with diffuse cortical hypometabolism, diagnosis remaining uncertain; a more accurate clinical and instrumental investigation and a close follow up might guide to correct diagnosis. Only a larger number of cases monitored over time could confirm these data.

EP-0383

Midbrain Serotonin transporter (SERT) evaluation by 123I-FP-CIT: a one-year retrospective study

M. Ricci, S. Sollaku, V. Frantellizzi, J. Lazri, F. Monteleone, M. Liberatore, G. De vincentis; Università di Roma "Sapienza", roma, ITALY.

Introduction: SPECT 123I-FP-CIT imaging is widely used for the differential diagnosis of degenerative parkinsonisms by exploiting the high affinity of the radiotracer for the dopamine transporter. Dopaminergic availability is known to linearly decline in Parkinson's disease (PD). In contrast, temporal charac-

teristics of serotonergic markers like the serotonin transporter (SERT) in relation to clinical staging of PD and non-motor symptoms are less clear. Extent of neurodegenerative process may extend beyond nigrostriatal system defining PD as a multi-systemic disease. The serotonergic (5-HT) system is one of these and has been extensively studied in PD, also although affinity of 123I-FP-CIT to serotonin transporter (SERT). It is known that SERT blockade might effectively alleviate PD symptoms, retarding use of L-DOPA and limiting as well typical side effects. We have exploited the affinity of the same radiotracer 123I-FP-CIT for the serotonin transporter to investigate SERT levels in the midbrain in order to focus on correlation between SERT expression and clinical presentation of disease (using Hoehn&Yahr scale). **Subjects and Methods:** 80 patients submitted to 123I-FP-CIT SPECT in one year (2016) were selected. SPECT were obtained in 128x128 matrix using a dual headed gamma camera equipped with LEHR collimators (Infinia®, GE Healthcare). Regions of interest (ROIs) were placed on the midbrain, where the binding of 123I-FP-CIT is associated mainly with 5-HT, and the cerebellum, which was assumed to represent non-displaceable activity. From each set 3 consecutive transaxial slices with highest midbrain activities were summed and a standard ROI (10.68 x10.68 mm rectangle) was positioned on the midbrain. The regions were manually positioned using a brain atlas and the SPECT image itself as a guide. Three consecutive slices representing the cerebellum were also added, and a standard ROI (14.24 x24.92 mm rectangle) was placed on the cerebellum. Right and left cerebellar values were averaged for subsequent analysis. An uptake activity ratio was evaluated in each patient [(midbrain - cerebellum)/cerebellum activity] and compared to clinical presentation. **Results**: Uptake ratio resulted not related to Hoehn&Yahr scale (linear regression test: p value 0,5; R square < 0,01). Furthermore in our population 26 patients presented previous or concurrent psychiatric symptoms and Uptake ratio resulted significantly higher (Mann-whitney test *p* 0,0004) than in patients that presented mainly motor symptoms. **Conclusion:** These data suggest that SERT evaluation should be considered in order to personalize clinical management of PD, especially for non-motor symptoms, and that serotonin metabolism influence on PD should be studied.

EP-0384

Topographical overlap of β-amyloid deposition in patients with Alzheimer's disease and mild cognitive impairment - a voxel-wise [^{18}F]Florbetapir PET/CT study

G. Aghakhanyan[1], M. Gennaro[1], S. Mazzarri[1], A. Vergallo[2], V. Nicoletti[2], S. Cintoli[2], G. Manca[1], L. Garau[1], G. De Laurentis[1], E. Spinelli[1], S. Bola[1], M. Grosso[1], C. Radicchi[2], G. Tognoni[2], U. Bonuccelli[2], D. Volterrani[1]; [1]Regional Center of Nuclear Medicine, University Hospital of Pisa, Pisa, ITALY, [2]Unit of Neurology, Department of Clinical and Experimental Medicine, University of Pisa, Pisa, ITALY.

Purpose: We aim to determine a common whole-brain pattern of the β-amyloid (Aβ) tracer uptake in patients with Alzheimer's disease dementia (AD) and mild cognitive impairment (MCI) by using whole brain voxel-wise analysis of 18F-Florbetapir PET

scans. **Materials and Methods:** We enrolled mild to moderate AD patients and single or multiple-domain amnestic MCI patients (both according to the clinical core of the NIA-AA, 2011 diagnostic criteria), and healthy older individuals with subjective cognitive impairment (SCI) as a control group. All subjects underwent to standardized neurologic and neuropsychological examinations and a 20-min [18F]Florbetapir PET/CT study, acquired 50 min after intravenous injection of 370 MBq [18F]florbetapir. The inclusion criteria were a positive amyloid-scan for AD and MCI group, and negative amyloid-scan for SCI subjects by visual inspection. All images were spatially normalized using the AV45 PET template in MNI brain atlas space (Avid Radiopharmaceuticals). Subsequently, the voxel-wise standardized uptake value ratio (SUVR) images were calculated using the whole cerebellum as a reference region. Differences in Aβ load among the groups were estimated on a voxel-by-voxel basis using analysis of covariance (ANCOVA) in SPM12 accounting age as a nuisance covariate. Multiple comparisons across space were controlled using family-wise error (FWE) rate. **Results:** Overall, sixteen AD patients (mean age 70 ± 7.9; Mini-mental State Examination, MMSE 22.4 ± 3.6), ten amnestic MCI patients (mean age 72 ± 6.2; MMSE 25.3 ± 2.4) and six SCI subjects (mean age 72 ± 1.6; MMSE 28.8 ±1.2) were recruited. The global cortical SUVRs in AD and MCI groups were significantly higher compare to SCI group (p < 0.05). No correlation was found between the global cortical SUVR and MMSE scores. Whole-brain voxel-wise analyses of SUVR images in AD patients compared to SCI group revealed a large cluster of increased relative [18F]florbetapir uptake in the precuneus (p < 0.05, corrected). The MCI group compared to SCI, displays three clusters of elevated SUVRs in the precuneus, left paracentral lobule and right medial prefrontal cortex with extension to the left anterior cingulate (p < 0.05, corrected). **Conclusion:** Our results highlight the common concurrence of the regional-specific Aβ deposition pattern in both AD and MCI patients. The topographical overlap in significant amyloid burden in AD and MCI patients, strictly related to precuneus, suggests that these two clinical entities may represent one continuum. In addition precuneus early dysfunction, in AD pathology, might represent a marker of conversion from MCI to dementia.

EP-0385

The impact of FDG and amyloid PET-CT in a clinical setting consisting of patients with suspected dementia: the Ferrara experience

A. Farolfi[1,2], I. Rambaldi[2], D. Gragnaniello[3], P. Milani[3], S. Panareo[2], I. Santi[2], S. Taralli[2], M. Bartolomei[2], V. Tugnoli[3], C. Cittanti[2]; [1]Nuclear Medicine Unit - S. Orsola-Malpighi Hospital - University of Bologna, Bologna, ITALY, [2]Nuclear Medicine Unit - Azienda Ospedaliero Universitaria, Ferrara, ITALY, [3]Neurology Unit - Azienda Ospedaliero Universitaria, Ferrara, ITALY.

Purpose: To evaluate the impact of sequential use of PET-CT with 18F-FDG and 18F-Florbetapir (Eli Lilly™) in a clinical setting consisting of patients with cognitive impairment and suspected dementia referring to Ferrara University Hospital and to assess the accuracy of FDG and amyloid PET-CT to correctly lead clinicians during diagnostic work-up in this patient population. **Subjects and Methods:** From our clinical cases of patients studied with PET for brain metabolism evaluation, we retrospectively extrapolated 42 subject (20M; 22F) who underwent both FDG and amyloid PET-CT from October 2015 to January 2017. The FDG-PET has always preceded the execution of PET with florbetapir. Before any scan the reference clinician filled out a form with the clinical suspicious and the diagnostic question. Data about clinical history, neuropsychological tests, neuro-imaging and patient treatment were all recorded for further evaluation. Studies were acquired on a Biograph mCT Flow PET-CT scanner (Siemens Healthcare) after 30 minutes post-injection of 18F-FDG (187±20MBq) and 45 minutes after administration of 18F-Florbetapir (338±47MBq). Images were interpreted by two trained nuclear physicians. **Results:** In our population mean MMSE before FDG PET-CT was 23.1 (11-30). Mean age of subjects at the time of FDG scan was 67 years (55-72) and mean follow-up was 342±272 days. FDG PET-CT was concordant with clinical suspicious in 19 patients (45.2%) and therapy was changed in 13 patients (31%) after FDG study. Furthermore, after the subsequent amyloid PET-CT, clinical orientation was compatible with Florbetapir results in 23/42 scans (54.8%) and therapy was modified in further 9 patients (21,4%). On the basis of clinical follow-up, final diagnosis was fully concordant with FDG PET-CT in 19/42 patients (45,2%) whereas was consistent with amyloid PET-CT results in 38/42 patients (90.5%). The accuracy of FDG PET-CT in diagnosis of Alzheimer disease (AD) was 71.4% (sensitivity 58.8% and specificity 71.4%); whereas amyloid accuracy was 90.5% (sensitivity 88.2%, specificity 92%). Moreover FDG accuracy for fronto-temporal dementia (FTD) was 88.1% (sensitivity 57.1%, specificity 94.3%); meanwhile amyloid scans in FTD patients show absence of deposition in 7/7 cases. **Conclusion:** In this study we found that both FDG and amyloid PET-CT are feasible and have a significant impact in "everyday" clinical practice. Together they have high accuracy in the diagnosis of AD and FTD and FDG PET-CT leads clinicians to change therapy in one third of patients whereas amyloid PET-CT, used as a next step after the FDG, shows very high correlation with the final diagnosis.

EP-0386

Change of glucose metabolism in white matter of AD patients using F-18 FDG PET

Y. Jeong, H. Yoon, J. Jeong, D. Kang; Dong-A University Hospital, Busan, KOREA, REPUBLIC OF.

Purpose: In Alzheimer 's disease (AD), neuroinflammation is an important process related to the deposition of amyloid-beta plaques and the activation of microglia. Deposition of amyloid-beta plaques and activated microglia occur not only in the gray matter of the brain but also in the white matter (WM). We hypothesized that the glucose metabolism of WM would increase due to the activation of glial cells in AD patients. We measured the glucose metabolism of WM in patients with AD and evaluated the difference of the value between AD patients and healthy controls. **Subjects & Methods:** Eighteen AD patients (66.9 ± 8.2 years) who were positive in amyloid PET and

18 age-matched normal subjects (69.3 ± 8.5 years) who were negative in the same study underwent F-18 FDG PET. F-18 FDG PET images were coregistered each subject's MRI image and the WM was segmented using by PMOD 3.7. Mean SUV of the global and regional WM of the brain were checked and the values were converted based on the cerebellar WM uptake as a reference site. First, we evaluated the difference of the global and regional WM values between AD patients and normal controls. Second, in AD patients, we assessed the correlation between the global WM values and MMSE score, CDR-sum of boxes (SOB) score and global deterioration scale (GDS), respectively. **Results:** (1) In F-18 FDG PET images, the global WM uptake value of AD patients was significantly higher than that of normal controls (14.9 vs 12.9, p=0.036). In the regional analysis, the value of WM of the frontal area (16.6 vs 14.3, p=0.033) and the temporal area(11.1 vs 97, p=0.041) was higher in AD patients group. Although there was no statistical significance, the value of WM of the parietal area (21.5 vs 18.8, p=0.053) and occipital area (11.5 vs 10.5, p=0.157) was higher than that of the normal controls. (2) In the correlation analysis, the global WM uptake value of AD patients was significantly correlated with GDS (r=-0.577, p<0.001), MMSE score (r=0.522, p=0.001) and CDR-SOB score (r=0.507, p=0.002). **Conclusion:** We could measure the glucose metabolism of the WM using F-18 FDG PET. In AD patients, glucose metabolism of the WM was significantly higher and well correlated with scores of the clinical test. Although we think that F-18 FDG PET could be used as an indicator of neuroinflammation like TSPO PET, further research is needed on a direct comparison between the two tests.

EP-0387

How Useful is Amyloid PET in Clinical Diagnosis? A Systematic Review and Meta-analysis

E. R. Fantoni[1], *A. Chalkidou*[2,3], *G. Farrar*[1], *A. Hammers*[4]; [1]*GE Healthcare, Amersham, UNITED KINGDOM,* [2]*King's College London, St Thomas' Hospital, London, UNITED KINGDOM,* [3]*King's Imaging Technology Evaluation Centre, St Thomas' Hospital, London, UNITED KINGDOM,* [4]*King's College London, London, UNITED KINGDOM.*

Background: With the availability of ^{11}C-PiB and four ^{18}F tracers for imaging amyloid with PET, this diagnostic modality has gained increasing traction in both research and clinical evaluation of patients with cognitive impairment (CI). While several studies have endeavoured to quantify amyloid PET (aPET) utility, this work is the first comprehensive meta-analysis of the existing literature for use of aPET as an adjunct to AD diagnosis. **Methods:** This systematic review and meta-analysis covers all clinical and research studies published in English language between 2000 and 2017, which conformed to pre-determined inclusion criteria. The impact of visual aPET imaging on the differential diagnosis of CI subjects in the absence of prior FDG-PET or CSF sampling was assessed with respect to change in diagnosis before and after aPET imaging. Results: Of 1142 patients from 7 studies meeting the inclusion criteria [1-7], 65.7% cases had an initial clinical diagnosis of AD, 29.6% non-AD and 4.7% indeterminate. In patients with an initial diagnosis of AD, a positive scan

confirmed the diagnosis in 98.8% of cases. In patients with initial diagnosis of Non-AD neurocognitive decline, physicians ruled out AD diagnosis in 100% of the cases where the aPET scan turned out negative. Amyloid PET results discrepant with the pre-aPET diagnosis were found in 31.5% of AD cases and 39.9% of non-AD cases, leading to an average change in diagnosis, respectively, 86.4% and 74.1% in these cases. For all confirmed diagnoses a trend of accompanying diagnostic confidence increase was observed. Overall, the analysis suggests that 93.6% of final diagnoses reflect the aPET outcome and 31.3% of diagnoses are changed following aPET due to discrepant pre-aPET diagnosis. **Conclusion:** This meta-analysis shows that use of aPET significantly impacted diagnostic decision-making by helping physicians to either ascertain AD diagnosis or to rule out the disease in 93.6% of the patients. The utility of aPET integrated with other imaging modalities and/or in selected populations and with respect to patient management is currently being explored as an extension of this analysis. **References:** [1] Zwan MD *et al.*, Alzheimers Res Ther 2017:1-8. [2] Boccardi M *et al.*, JAMA Neurol 2016;73:1417-24. [3] Mitsis EM *et al.,* Mol Neurodegener 2014;9:10. [4] Pontecorvo MJ *et al*., Br Nucl Med Soc Spring Meet 2016;1:P42. [5] Sanchez-Juan P *et al.,* Neurology 2014;82:230-8. [6] Ishii K *et al*., Alzheimer's Assoc Int Conf 2016:P4-14. [7] Grundman M *et al*., Alzheimer Dis Assoc Disord 2013;27:4-15.

EP-0388

Coupled imaging with 18F FBB and 18F FDG in AD subjects show a selective association between amyloid burden and cortical dysfunction in brain

A. Chiaravalloti[1,2], *A. Castellano*[2], *P. Sannino*[2], *M. Zinzi*[2], *E. Di Giorgio*[2], *F. Scalone*[1], *R. Giancipoli*[1], *O. Schillaci*[1,2]; [1]*Department of Biomedicine and Prevention, University Tor Vergata, Rome, ITALY,* [2]*IRCCS Neuromed, Pozzilli, ITALY.*

Aims: novel radiotracers for amyloid imaging in Alzheimer's disease (AD) proved to be useful in the non-invasive detection of amyloid burden in brain and in the differential diagnosis between AD and other types of dementia, but the role of amyloid pathology in AD is still matter of debate. Changes in fluorine-18 fluorodeoxyglucose (18F-FDG) cortical consumption has been evaluated for at least 15 years in AD subjects but the relationships between cortical glucose consumption and amyloid pathology are still unclear. The present study was aimed to evaluate the relationships between the concentrations of cortical amyloid burden as detectable by means of 18F Florbetaben (18F FBB) and brain glucose metabolism of 18F-FDG in a group of patients with AD. **Materials and Methods**: We examined 38 newly diagnosed AD patients according to the NINCDS-ADRDA criteria. The mean (± SD) age of the patients was 68 (± 7) years; 19 were male and 19 were female. All patients underwent a complete clinical investigation, including medical history, neurological examination, mini-mental state examination (MMSE), a complete blood screening (including routine exams, thyroid hormones and a complete neuropsychological evaluation. The average interval between 18 F-FDG and 18F FBB PET/CT was 1 month. We excluded with isolated deficits and/or unmodified

MMSE (=25/30) on revisit (period of follow-up: 6, 12 and 18 months); patients who had had a clinically manifest acute stroke in the last 6 months with a Hachinsky score greater than 4; and patients with radiological evidence of subcortical lesions. The relationship between brain ^{18}F-FDG and 18F FBB uptake was analysed using statistical parametric mapping (SPM8) implemented in Matlab R2012b. A region of interest (ROI) mask including the whole cortex was generated on 18F FBB scans using WFU Pickatlas and a multiple regression analysis was performed on 18F FDG scans using the data obtained from the ROI after a normalization process. **Results:** SPM analysis showed a significant negative correlation between 18F FDG and 18F FBB uptake in left temporal lobe (Brodmann areas, BA, 21, 22 and 39; P fdr and fwe corr < 0.001, k_e 636-1000), left parietal lobe (BA 31 and 40 P fdr and fwe corr < 0.001, k_e 775). **Conclusions:** combined imaging with 18F FBB and 18F FDG show that amyloid deposition in brain is related to a cortical dysfunction of left temporal and parietal lobe in AD.

EP-0389

Evaluation of Magnetic Resonance and PET/CT methods with FDG-18F in the diagnosis of Alzheimer' s disease

B. L. Ferrari, G. C. Campos Neto, A. C. Felício, E. Amaro, S. L. Silva, L. F. Gamarra; Hospital Israelita Albert Einstein, São Paulo, BRAZIL.

Aim: It is well established that both Fluorine 18 fluorodeoxyglucose (FGD) positron emission tomography (PET) and structural magnetic resonance (MR) imaging can demonstrate evidences of the neurodegenerative process associated with Alzheimer's disease (AD), even in preclinical stages. A well-known hypothetical model for biomarkers dynamics posits that synaptic dysfunction evidenced by FDG PET or functional MR precedes the structural changes detected by volumetric MR. However, although synaptic dysfunction, neurodegeneration and atrophy are certainly interconnected entities, some studies point significant discrepancy between metabolic and structural findings (regarding spatial distribution and amplitude) and there are published data suggesting that these events may, actually, be concomitant. Considering that multiple studies confirm the hippocampus as one of the earliest sites of AD pathology, we decided to specifically investigate the correlation between hippocampal volumetry and glucose metabolism in patients being evaluated for possible AD. **Materials and Methods:** We retrospectively studied 38 patients undergoing evaluation for possible AD and who underwent FDG PET and MR within 90 days. Patients of both genders were included (22 women), aged 46 to 89 years (68.3 ± 11.2 years). All patients underwent neuropsychological testing and had clinical follow-up for 8 to 43 months (23 ± 11 months). The final diagnosis, used as the standard for sensitivity, specificity and accuracy calculation, was defined using the pooled information from the clinical evaluation (based on NIA/AA guidelines and DSM-V), neuropsychological tests, both imaging studies and laboratory test results. FDG PET quantitative parametric and qualitative analyses were compared with MRI volumetry of the hippocampal formation. **Results:** Qualitative FDG PET analysis showed greater accuracy,

sensitivity and negative predictive value compared to the other tests and specificity and positive predictive value similar no MR considering percentile 5 as the cut-off point for hippocampal volumetry. Comparing the two FDG PET analysis methodologies, the qualitative one presented higher accuracy, sensitivity, specificity, negative and positive predictive values than the quantitative. **Conclusion:** The performance of FDG PET qualitative analysis was significantly better when compared to MR volumetry. At least in part, this observation could corroborate the sequential hypothesis of AD pathophysiology, which posits that functional changes (synaptic dysfunction) precedes the structural ones (atrophy). The results of qualitative PET analysis were also significantly better compared to quantitative measurements, showing higher values of sensitivity and specificity suggesting that quantification analysis could be used as an adjunct tool, but should not replace visual interpretation.

EP-0390

Semiquantitative analysis of amyloid PET/CT and the performance of its own CT images for ROI's delimitation

*F. Segovia Roman[1], **N. Testart Dardel**[2,1], R. Sanchez Vaño[1,3], P. Sopena-Navales[3], A. Gonzalez-Jimenez[2], R. Sanchez Sanchez[2], E. Triviño-Ibañez[2], J. Ramírez Pérez de Inestrosa[1], M. Gomez-Rio[2]; [1]Universidad de Granada, Granada, SPAIN, [2]Hospital Virgen de las Nieves, IBS, Granada, SPAIN, [3]Hospital 9 de octubre, Valencia, SPAIN.*

Objectives: Semiquantitative analysis of amyloid PET/CT is usually performed by different software based on the extraction of population data from MRI images, which could eventually be unreliable, especially in patients with cortical atrophy. Nowadays, most of the PET centers are equipped with PET/CT devices. Therefore, our objective is to analyze and determine the performance of the CT images from the PET/CT study to be considered as a basis for the semiquantitative analysis of the amyloid PET/CT. **Patients and Methods:** Florbetaben PET/CT studies were performed in 29 patients following international recommendations for acquisition. Florbetaben PET/CT interpretation was visual and binary, according to manufacturer's instructions. The semiquantitative analysis was performed in a multimodal station (PETRA), starting from the PET registered in MNI through SPM8 (minimizing the quadratic difference between the template and the images). Similarly, the CT images segmentation and normalization was performed according to a standardized template. As a starting point, the normalized CT imaging was the basis to obtain an exclusive grey matter cortex mask, specific for each patient in each ROI. By the use of automated anatomical labeling the activity will be quantified in 116 different ROIs according to the CT mask. The quantified index of the medium uptake respect to the medium cerebellum grey matter uptake was determined for each ROI. **Results:** The visual analysis of the studies resulted positive in sixteen patients (13 diffuse patterns and 3 focal patterns) and negative in thirteen. The semiquantitative analysis for each ROI between those two subgroups showed statistically significative differences in the majority of the ROIs. Those with a better capacity for discrimination or more distant to the mean value, were the basofrontal

cortex (bilateral), prefrontal cortex and right precentral gyrus (t-test; p<0.05). **Conclusions:** In our pilot study, our preliminary results suggest that it is possible to use the CT from the PET/CT for the semiquantitative analysis of the amyloid PET; however, larger series are needed to validate these results.

EP-0391

FDG PET as a golden standard in the evaluation of diagnostic significance of metabolic ratios measured with multivoxel H-MRS

J. Khomenko, G. Kataeva, E. Gromova, E. Chernysheva, D. Susin, A. Bogdan; N.P. Bechtereva Institute of the Human Brain, RAS, St.Peterburg, RUSSIAN FEDERATION.

Search for neuroimaging markers for Alzheimer disease (AD) detection on the earliest stage is of great importance. **Purpose:** study cerebral metabolism in patients with AD-type mild cognitive impairment (MCI-AD) and MCI accompanying cerebrovascular diseases (MCI-CVD) using positron emission tomography with 18F-fluorodesoxyglucose (FDG PET) and multivoxel magnetic resonance spectroscopy (H-MRS). **Methods:** 14 patients with MCI-CVD (4 male, 10 female, age 59.7±10.5) and 11 with MCI-AD (2m, 10f, age 67.8±8.7) underwent standard neuropsychological examination. PET was performed on Scanditronix-2048 and GE-Discovery-710, normalized with SPM8. Cerebral glucose metabolism rate (CMRglu) in Brodmann areas (BA) calculated using WFU-Pickatlas. H-MRS in supraventricular region performed on Achieva-3T, Philips (2D-PRESS, TE/TR=53/2000 ms); area 8*9 voxels 10*10*15 mm, whole volume 80*90*15 mm was divided into 9 regions of interest (ROI): 6 in semioval centers white matter (WM) (3 for each hemisphere) and 3 ROIs in medial cortex gray matter (GM). NAA/Cr, NAA/Cho, Cho/Cr, MI/NAA ratios were analyzed (NAA - N-acetyl-aspartate (neural integrity marker), Cr - creatine, Cho - choline (membrane turnover marker), MI - myo-inositol (glial activity marker)). As multivoxel MRS allows to evaluate ratio of metabolite content in WM and GM, NAA-WM/NAA-GM, Cho-WM/Cho-GM and Cr-WM/Cr-GM ratios were calculated. **Results:** In MCI-AD group in comparison with MCI-CVD decrease of CMRglu in left frontal (BA 6,8,9,47), parietal (BA 7,39,40), temporal (BA 21,22,37) regions, insular cortex and nucleus caudatus were found (p<0.05). CMRglu in hippocampus and anterior cingulate were decreased bilaterally (p<0.05). H-MRS revealed the following differences: Cho/Cr in WM, MI/Cr and MI/NAA in GM were higher in MCI-CVD group; NAA/Cho, Cr-WM/Cr-GM and NAA-WM/NAA-GM - in MCI-AD (p<0.05). MI/Cr in GM correlated negatively with CMRglu in left BA9, 22 and 37 (r=-0.5, p<0.05), Cho/Cr in WM - with CMRglu in BA 20,21,37 and insular cortex in right hemisphere (r=-0.5, p<0.05). ratios were higher in MCI-AD (p<0.05). Cr-WM/Cr-GM correlated positively with CMRglu in left anterior cingulate (r=0.5, p<0.05) and left and right posterior cingulate (r=0.7, p<0.01 and r=0.5, p<0.05). **Conclusions:** CMRglu in left frontal, parietal and temporal regions, insular cortex, bilateral cingulate and hippocampus shown significant differences, that was expected, since the diagnostic value of FDG PET for

different types of dementia is known. H-MRS allowed to reveal several ratios that possibly have diagnostic value, and these ratios correlated with CMRglu. Among them not only traditional metabolites indexes, but also ratios of concentrations in white and gray matter, but to clarify their diagnostic value follow-up studies are required.

EP-0392

Diagnostic implications of total hemispheric glucose metabolism ratio in Mild cognitive impairment and Alzheimer´s disease

E. A. Segtnan[1], A. Majdi[2], C. Constantinescu[1], P. Grupe[1], H. Dali[1], O. Strøm[1], J. Holm[1], M. S. Vafaee[1], A. Alavi[3], S. Sadigh-Eteghad3[2], L. Wermuth[1], A. Gjedde[1], P. Høilund-Carlsen[1]; [1]Odense University Hospital, odense, DENMARK, [2]Neurosciences Research Center (NSRC),, Tabriz, IRAN, ISLAMIC REPUBLIC OF, [3]Division of Nuclear Medicine, Department of Radiology, Perelman School of Medicine, Hospital of the University of Pennsylvania, Philadelphia, PA, UNITED STATES OF AMERICA.

Introduction: Recent reports have pointed to brain connectivity as a potential biomarker of Alzheimer's disease (AD), mainly on the basis of fMRI and EEG studies. We hypothesized that examination for brain diaschisis (brain damage remote from focal or regional lesions) by means of FDG-PET/CT may be of potential diagnostic value. **Method and Materials:** FDG-PET/CT images of 15 AD patients (mean age 62 years, range 53-78), 8 patients with mild cognitive impairment (MCI) (mean age 66 years, range 54-74), and 10 neurologically healthy individuals (HI) (mean age 62.5 years, range 43 -75) were analyzed and compared. Total hemispheric glycolytic rate (THG) in the suspected diaschitic hemisphere was divided by that of the contralateral hemisphere to yield the total hemispheric glycolysis ratio (THGr) in cerebrum (Ce) and cerebellum (Cb), respectively, with the purpose of detecting lateralized hemispheric glucose metabolism, i.e., diaschisis. Qualitative assessment of diaschisis was performed by a PET neuroimaging specialist. Receiver operating characteristics (ROC) provided optimal cut-offs for combinations of cerebral (Ce) and cerebellar (Cb) THGr in the diagnostic test. **Results:** Median THGr (Ce) estimates were 0.95 (range 0.65-1.00), 0.86 (range 0.64-0.98) and 0.64 (range 0.43-0.99) for HI, MCI and AD groups, respectively (*p*<0.01). Similarly, median THGr (Cb) estimates were 0.84 (range 0.75-0.96), 0.70 (range 0.48-0.81), and 0.70 (range 0.18-0.98), respectively (p<0.02). Qualitative analyses revealed cerebral diaschisis in 10/15 (67%) of AD and 0/8 (0%) of MCI patients, and cerebellar diaschisis in 7/15 (47%) and 1/8 (12,5%), respectively. Cerebrocerebellar diaschisis, i.e diaschisis in cerebrum and cerebellum, was qualitatively assessed in 6/15 (40%) and 0/8 (0%) of AD and MCI patients, respectively. When both THGr (Ce) and THGr (Cb) failed to reach ROC area under the curve (AUC), this "positive" result had 100% positive predictive value for detection of AD/MCI brains, while the "negative" test result had 80% negative predictive value for differentiating healthy brains from AD/MCI brains. ROC-AUC thresholds for sub-differentiating AD and MCI had a "positive" result with 100% positive predictive value for AD, at the expense of a negative predictive value of

50% for MCI. **Conclusion:** THGr calculations provided high sensitivity and fair-to-low specificity for differentiating healthy brains from AD/MCI brains. The cerebral glucose metabolic imbalance was more pronounced in AD than in MCI patients, and the combined diaschisis test had high sensitivity but poor specificity for differentiating among these subtypes of dementia.

EP-0393

Clinical Utility of the Brain SPECT with Ioflupane 123I-FP-Scan in the Imagiological Diagnosis of Possible Dementia with Lewy Bodies

J. F. Alban[1], M. J. Cunha[1], M. Marques[1], A. Albuquerque[1], G. Costa[1,2], J. Pedroso de Lima[1,2,3]; [1]Centro Hospitalar e Universitário de Coimbra, Coimbra, PORTUGAL, [2]Faculdade de Medicina da Universidade de Coimbra, Coimbra, PORTUGAL, [3]Instituto das Ciências Nucleares Aplicadas à Saúde (ICNAS), Coimbra, PORTUGAL.

Purpose: To establish the predictive value of brain *SPECT* with 123I-Ioflupane (123I-FP-SCAN) in the final diagnosis of dementia with Lewy Bodies (DLB). **Subjects and Methods:** Patients with dementia submitted to 123I-FP-SCAN, between April 2007 and January 2017, for differential diagnosis between Alzheimer and DLB were selected. We found 49 patients with a mean±sd age=70.5±7.2 years (range: 54-84 years). After reviewing, the 123I-FP-SCAN were classified in 4 groups: DAT0 - normal uptake in all regions (n=13); DAT1 - asymmetric activity with a putamen showing reduced uptake (n=18); DAT2 - bilateral absence of uptake in the putamen (n=11); DAT3 - bilateral absence of uptake in the putamen and severe reduction in one, or both, caudate nuclei (n=7). The 123I-FP-SCAN results were correlated with the final clinical diagnosis of DLB (FCDDLB). **Results:** The proportion of DCL is significantly different for the 4 123I-FP-SCAN groups (p <0.001). FCDDLB was present in 1/13 of the patients (7.7%) in DAT0, in 15/18 (83.3%) in DAT1, in 10/11 (90.9%) in DAT2 and in all 7 patients (100%) in DAT3 group. For DAT1 group we found a significant agreement with the FCDDLB (K: 0.741; P <0.001). For DAT2 we found a significant agreement with FCDDLB (K: 0.832; P <0.001); For DAT3 we also found a significant agreement with FCDDLB (K: 0.894; P <0.001). **Conclusion:** 123I-FP-SCAN is an important tool in the imaging diagnosis of clinical suspicion of DLB, presenting a statistically significant difference for the 4 results of the exam, with a progressive increase in agreement with FCDDLB and specificity when its degree of abnormality increases. A prospective multidisciplinary study (nuclear medicine, neurology and psychiatry) with postmortem pathological confirmation is necessary to establish the definitive predictive value of 123I-FP-SCAN in this entity.

EP-28   during congress opening hours, e-Poster Area

Neurosciences: Psychiatry

EP-0394

The Metabolic Basis of Cognitive Insight in Psychosis: a Positron Emission Tomography Study

G. Marotta, E. Caletti, G. Delvecchio, R. A. Paoli, M. Cigliobianco, C. Prunas, P. Brambilla, C. A. Altamura; Fondazione IRCCS Ca' Granda Ospedale Maggiore Policlinico, Milano, ITALY.

Purpose: Cognitive insight is the degree of awareness in psychosis and the patient's ability to assess the nature and severity of his disease. The purpose of this study was to investigate the relationship between cognitive insight and cerebral metabolism in psychosis. **Methods:** Sixty-three inpatients (17 woman and 46 men), age between 18 and 65 years, with acute psychosis according to the DSM-IV-TR criteria were enrolled in the current study. Thirty-six were diagnosed with affective psychosis (all with bipolar disorder type I) and twenty-seven with non-affective psychosis (10 with schizophrenia, 17 with psychosis NOS). FDG-PET scanning was performed within 7 days of insight and symptom assessment. The statistical analyses were performed using SPM8. Subjects were divided into four groups considering the BCIS score (low insight with R-C=<5 and high insight with R-C>5) and the diagnosis (affective vs non affective psychosis). **Results:** The comparison between the four groups, non affective psychosis with low and high insight and affective psychosis with low and high insight, showed significant metabolic differences in fusiform gyrus, superior temporal gyrus and insula, in the right hemisphere, and in precuneus and superior temporal gyrus extended to insula, in the left hemisphere (ANOVA, p<0.005). The post-hoc two-samples t-test analyses, between the entire group with low insight compared to the one with high insight, revealed in the group with low insight decreased metabolism in fusiform gyrus, superior temporal gyrus and insula, in the right hemisphere, and in precuneus and superior temporal gyrus extended to insula, in the left hemisphere, and showed increased metabolism in left orbito-frontal gyrus. The post-hoc two-samples t-test analyses, between the non-affective group with low insight compared to the one with high insight, revealed that the group with low insight showed decreased metabolism in right superior temporal gyrus and insula, in left precuneus, in left superior temporal gyrus extended to insula as well as increased metabolism in left orbito-frontal gyrus. The post-hoc two-samples t-test analyses, between the affective group with low insight, compared to the one with high insight, revealed in the group with low insight had decreased metabolism in right inferior temporal gyrus and increased metabolism in right orbito-frontal gyrus. Finally, the analysis of covariance showed a positive significant correlation between the metabolism in right precuneus and the insight score (p<0.005). **Conclusion:** Our findings suggest reduced posterior (occipito-temporal and parietal cortices) and increased anterior (orbitofrontal) cerebral metabolism supporting low cognitive insight in psychosis.

EP-0395

Cerebral metabolism changes and neurocognition in patients with somatic symptoms and related disorder, and dissociative disorders: a qualitative PET study

G. Capriotti[1], M. Conte[1], A. Del Casale[1], G. Lauretti[1], L. Carideo[1], P. pizzichini[2], D. Prosperi[2], F. Scopinaro[1]; [1]Sapienza University, Rome, ITALY, [2]Sant'Andrea Hospital, Rome, ITALY.

Introduction and Aim: Much of what classical psychopathology used to classify as "hysteria" ended-up in the "Somatic Symptoms and Related Disorders" (SSRDs) and "Dissociative Disorders" (DDs) diagnostic categories of the DSM-5. These disorders are psychopathologically, neuropsychologically, and neurobiologically heterogeneous. We aimed to analyse such heterogeneity. **Subject & Methods:** We recruited 10 patients, including five with DSM-5 SSRDs (all women, mean age 44.6) and five with DDs (three men and two women, mean age 35.4). Within six weeks from their index episode, patients underwent psychopathological and neurocognitive testing, and ^{18}F-fluoro-deoxy-glucose (^{18}F-FDG) positron emission tomography (PET). **Results:** Compared to patients with DDs, those with SSRDs performed significantly worse on the Wisconsin Card Sorting Test (WCST), with more total and perseverative errors and responses. They were also less accurate in recognising disgust on the Facial Emotion Recognition Test. Moreover, they showed reduced temporal cortical metabolic rate of glucose utilisation (CMRglu), mainly left-sided, which was associated with a worse performance on the WCST, and reduced CMRglu in the left striatum. **Conclusions**: SSRDs appear to be associated with a greater impairment of both neurocognitive functions and regional glucose metabolic rate alterations than DDs. Our data support the DSM-5 nosography, which distinguishes between DDs and SSRDs.

EP-0396

Protective and restorative effects of the traditional Chinese medicine Jitai tablets against methaphetamine-induced dopaminergic neurotoxicity

S. Xu[1], S. Tu[1], J. Gao[1], J. Liu[1], Z. Guo[1], J. Zhang[2], X. Liu[3], J. Liang[4], Y. Huang[5], **M. Han**[1]; [1]Beijing Normal University, Beijing, CHINA, [2]Chinese PLA General Hospital, Beijing, CHINA, [3]Huashan Hospital, Fudan University, Shanghai, CHINA, [4]Peking University School of Pharmaceutical Sciences, Beijing, CHINA, [5]Yale University School of Medicine, New Haven, CT, UNITED STATES OF AMERICA.

Rationale: Methamphetamine (METH) is a psychostimulant with high abuse liability that affects the monoamine neurotransmitter systems, particularly the dopamine system. Currently there are no effective medications for the treatment of METH abuse to restore METH-induced dopaminergic dysfunction. The Jitai tablet (JTT), a commercial traditional Chinese medicinal preparation, has been shown to modulate the dopaminergic function both in heroin addicts and in morphine-dependent rats. Objectives: The purpose of this study was to investigate, in a rodent model, whether JTT can protect against METH-induced neurotoxicity, and/or restore METH-damaged dopaminergic function. **Methods:** Immunohistochemical staining and/or autoradiography staining were used to detect tyrosine hydroxylase (TH)-positive neurons in the substantia nigra, and to examine the levels of dopamine transporter (DAT), dopamine D2 receptor (D2R) and TH expression in the striatum. Using a stereotyped behavior rating scale, we evaluated the inhibitory effect of JTT on METH-induced behavioral sensitization. **Results:** Repeated METH administration induced obvious stereotyped behavior and neurotoxicity on the dopaminergic system. Pre-treatment with JTT significantly attenuated METH-induced stereotyped responses, and interdicted METH-induced changes in the levels of DAT, D2R and TH expression. Treatment with JTT after METH administration restored DAT, D2R and TH expression to normal levels. **Conclusions:** Our results indicated that JTT protects against METH-induced neurotoxicity and restores the dopaminergic function, and thus might be a potential treatment for the dopaminergic deficits associated with METH abuse.

EP-0397

Brain hypothyrodism induces the elevation of serotonin 1A receptor bindings in the limbic system

J. Lee[1], Y. Ryu[1], J. Park[2], K. Lee[2], K. Kim[2], **J. Choi**[2]; [1]Gangnam Severance Hospital, Yonsei University College of Medicine, Seoul, KOREA, REPUBLIC OF, [2]Korea Institute of Radiological & Medical Sciences, Seoul, KOREA, REPUBLIC OF.

Purpose: The aim of the present study is to elucidate the effects of hypothyroidism on serotonin 1A receptors in rodents. **Methods:** Five thyroidectomized male Sprague-Dawley (SD) rats and five hypophysectomized SD rats were used as animal models of hypothyroidism; the same number of sham-operated SD rats served as age-matched controls. After hypothyroidism was confirmed by thyroid function tests, dynamic PET was performed for 120 min. All PET data were spatially normalized to T2-weighted magnetic resonance imaging templates, and then time-activity curves of the hippocampus, septum, and cerebellum were extracted using predefined volume-of-interest templates. Non-displaceable binding values in the hippocampus and septum were calculated using a multilinear reference tissue model and parametric maps were constructed. **Results:** Both volume-of-interest and voxel-based analyses showed higher brain uptake in the thyroidectomized and hypophysectomized rats compared to the respective sham-operated rats. Time-activity curves showed that the brain uptake values for the thyroidectomized and hypophysectomized groups were 21-52% higher than were those in the respective control groups. In the thyroidectomized group, the binding potential values for the hippocampus and septum were 20-26% higher than were those in the sham-thyroidectomized group. In the hypophysectomized group, the binding value for the hippocampus was 23% higher than was that in the sham-hypophysectomized group, whereas the septal binding value was not significantly different from that in the sham-hypophysectomized group. Parametric maps for hypothyroidism also showed significantly higher binding values than did those for controls. **Conclusion:** Our results demonstrate that hypothyroidism elevates serotonin 1A receptor binding in the limbic system.

EP-0398

Striatal Dopaminergic Dysfunction in Patients with Gambling Disorder

D. Di Giuda[1], F. Cocciolillo[2], M. Pettorruso[3], I. Bruno[4], V. Valenza[1], G. Camardese[3], G. Conte[3], L. Janiri[3], A. Giordano[1]; [1]Institute of Nuclear Medicine, Università Cattolica del Sacro Cuore, Rome, ITALY, [2]Nuclear Medicine Unit, Ente Ecclesiastico Ospedale Generale

"F. Miulli", Acquaviva delle Fonti, Bari, ITALY, ³Institute of Psychiatry, Università Cattolica del Sacro Cuore, Rome, ITALY, ⁴Nuclear Medicine Unit, Policlinico "A. Gemelli", Rome, ITALY.

Introduction: Gambling disorder (GD) is characterised by persistent and recurrent maladaptive gambling behaviour leading to impaired functioning. Increasing evidence shows similarities between this behavioural addiction and substance use disorders. Although GD pathophysiology is poorly understood, existing research suggests a mesocorticolimbic dopaminergic dysfunction. Dopamine role is further supported by the association of behavioural addictions with dopaminergic medications in Parkinson's disease (PD). Reduced Dopamine Transporter (DAT) availability in the right striatum is reported in PD patients with GD compared to those without GD; it might predate and predict susceptibility to the addictive behaviour development. We assessed DAT availability in GD using ¹²³I-FP-CIT SPECT. **Subjects and Methods:** Fourteen treatment-seeking patients (13 males, age:46±13 years) diagnosed with GD (DSM-5) were enrolled. Exclusion criteria included comorbid psychiatric disorders, neurological or medical illnesses, previous or current drug abuse other than nicotine and use of psychotropic medications. GD severity and craving were assessed using the Gambling Symptom Assessment Scale and Pathological Gambling-Yale Brown Obsessive-Compulsive Scale. The Gambling Timeline Followback (G-TLFB) was employed to estimate gambling behaviour in the month prior to enrolment. Anxiety, depression and anhedonia symptoms were evaluated through the Hamilton Anxiety Rating Scale, Hamilton Depression Rating Scale and Snaith Hamilton Pleasure Scale. The Barratt Impulsiveness Scale was used to assess impulsivity traits. ¹²³I-FP-CIT SPECT was performed 3.5 hours after 185 MBq intravenous injection. Specific to non-specific binding ratios (SBRs) were calculated using the BasGan(V2) software. Twenty-two healthy subjects (HS; 18 males, age:46±15 years) served as control group. **Results:** Patients and controls did not differ in age, gender distribution, education and smoking status. In comparison with HS, GD patients showed lower SBRs in the right caudate (p<0.05). Inverse correlations were found between the number of gambling days assessed by G-TLFB and SBRs in caudate nuclei and right putamen (p<0.05). The number of abstinence days positively correlated with SBRs in caudate nuclei and right putamen (p<0.05). Similarly, positive correlations were observed between the number of days elapsing from last gambling activity to SPECT and SBRs in caudate nuclei and right putamen (p<0.05). There were no associations between SBRs and GD severity or other psychiatric scores. **Conclusion:** Our findings suggest a dysfunction of dopamine transmission in GD pathophysiology. Although results are in line with previous reports in other addictions, the small sample size prevents from drawing a definite conclusion. A functional DAT down-regulation may be hypothesised. However, it is not possible to rule out a genetically-determined lower DAT expression.

EP-0399

Anatomo-Functional Correlations of Personality Traits to Aggression and Aggressive Behavior in Cocaine Addicts

R. Ferrando, C. Pascovich, M. Langhain, A. Negrin, A. Silveira; Clinics Hospital, University of the Republic, Montevideo, URUGUAY.

Introduction: Limbic dyscontrol and prefrontal dysfunction have been proposed as mechanisms underlying aggressive behaviour in drug abusers. Both features are also intertwined in the pathophysiology of addiction. An association of cocaine abuse with this kind of behaviours is supported in the forensic and clinical literature. Smoked forms of cocaine have been particularly linked to criminal and violent acts, representing a challenge for health and public security. The objective of the study was to assess the neural basis of aggressiveness in cocaine abusers using SPECT. **Subjects and Methods:** Thirty-nine chronic cocaine users (>1 year of use, <10 days of abstinence; 21 inhaled cocaine hydrochloride, 18 smoked cocaine) and 23 normal controls underwent resting 99mTc-ECD SPECT. Age (18-35 ys) and gender did not differ between groups. Verbal or physical (object or persons) hetero or auto-aggressiveness was evaluated using the Overt Aggression Scale (OAS, Yudofsky et al, 1986). Aggressive traits were assessed with the Inventory of Personality Organization (IPO, Clarkin, Foelsch & Kernberg, 2001). SPM8 was used to compare cocaine users with controls and to look for correlations between images and scales. Uncorrected voxel p values lower than 0.001 and clusters containing more than 100 voxels were reported. Trends to significance were also reported at p<0.01 uncorr. **Results:** Cocaine users showed bilateral dorsolateral prefrontal, orbitofrontal, mesial frontal, anterior cingulate, thalamic and midbrain hypoactivity, as well as left mesial temporal, right lateral temporal and ipsilateral posterior parietal hypoperfusion. OAS was available in 32 subjects (mean score 20.3±4.1%, range 0-75%). Al least one type of aggressive behaviour was present in 19 of them (59.4%). IPO was available in 30 patients (mean score 38.8±1.6%, range 24-63%). OAS and IPO showed significant correlation (Pearson coefficient 0.64, p<0.001). Image correlations with OAS were found in bilateral subgenual anterior cingulate, left rostral frontal mesial cortex and posterior temporoparietal cortex. Correlations with IPO were found in left orbitofrontal and anterior ventromedial frontal cortex, bilateral subgenual anterior cingulate, bilateral posterior ventromedial frontal cortex and midbrain. **Conclusion:** Aggressive traits and behaviour correlated with mesial and ventral prefrontal dysfunction in cocaine abusers. These paralimbic regions play a major role in emotional control and adapted behaviour. Significant overlapping with dysfunction of the reward system responsible for conditioning, dependency and craving in addicts is seen. Results provide new insights into the neural substrates of predisposition to aggressive behaviour in cocaine addiction.

Neurosciences: Neurodegeneration

EP-0400

11C-Pittsburgh Compound B PET in Primary Intracerebral Hemorrhage

R. Yen, H. Tsai, L. Tsai, Y. Chen, J. Jeng; National Taiwan University Hospital, Taipei, TAIWAN.

Background: ^{11}C-Pittsburgh Compound B (PiB) positron emission tomography (PET) can be used to detect brain amyloid deposition in patients with cerebral amyloid angiopathy (CAA). The diagnostic utility of PiB PET in patients with primary intracerebral hemorrhage (ICH) has not been investigated before. **Methods:** Seventy-seven primary, spontaneous ICH patients were recruited in this study. CAA was diagnosed by the Boston criteria. All patients (11 CAA, 66 non-CAA) underwent PiB PET to evaluate the brain amyloid retention. The amyloid burden was visually assessed and dichotomized as PiB (+) and PiB (-). The global standardized uptake value ratio (SUVR) was also calculated using cerebellum as the reference. **Results:** Using visual ratings, 10/11 CAA patients were PiB (+), as compared with 10/66 non-CAA patients (sensitivity=91%, specificity=85%). Quantitative assessment using global SUVR > 1.23 as cutoff value had similar findings (sensitivety=91%, specificity=89%). There was no difference in the diagnostic performance between visual ratings and quantitative assessment (p=0.51). Combining binary visual ratings and SUVR could further increase the specificity to 94%. **Conclusions:** PiB PET can be used as diagnostic tool for CAA in patients with primary ICH with high sensitivity and specificity. Visual ratings had similar diagnostic efficacy as quantitative method, and could be readily applied to the clinical practice.

EP-0401

Divergent Metabolism in Brain and Spinal Cord in Patients with Amyotrophic Lateral Sclerosis: A FDG-PET/CT Study

A. Buschiazzo[1], C. Marini[2], M. Piana[3], C. Campi[3], A. Bellini[1], A. Cistaro[4], A. Chiò[5], C. De Vecchi[3], I. Calamia[1], A. M. Massone[3], F. M. Nobili[6], C. Caponnetto[7], S. D. Morbelli[8], F. Fiz[9], M. Bauckneht[1], G. Sambuceti[1,8]; [1]Nuclear Medicine Unit, Department of Health Sciences, University of Genoa, Genoa, ITALY, [2]CNR Institute of Bioimages and Molecular Physiology, Milan, ITALY, [3]Department of Mathematics, University of Genoa, Genoa, ITALY, [4]Positron Emission Tomography Centre IRMET S.p.A., Euromedic inc., Turin, ITALY, [5]Department of Neuroscience "Rita Levi Montalcini", University of Turin, Turin, ITALY, [6]Clinical Neurology, IRCCS AOU San Martino-IST, Genoa, ITALY, [7]Department of Neuroscience, IRCCS AOU San Martino-IST, Genoa, ITALY, [8]IRCCS AOU San Martino-IST, Genoa, ITALY, [9]Nuclear Medicine Unit, Department of Radiology, Uni-Klinikum Tübingen, Tübingen, GERMANY.

Introduction: Amyotrophic lateral sclerosis (ALS) is a fatal late-onset neurodegenerative disorder of adult life, characterized by a progressive impairment of motor function. We have recently reported the potential of Hough transform in delineating the spinal cord (SC) structure and metabolism by clinical ^{18}F-FDG PET/CT scanning in ALS patients. The aim of our study was to extend this analysis to the primary motor cortex Brodmann area 4 (BA4) and primary somatosensory cortex Brodmann area 3-1-2 (BA3-1-2) to verify the relationship between the ALS metabolic effect on cortex and SC. **Subjects and Methods**: We studied 40 ALS patients at different clinical stage, submitted to ^{18}F-FDG brain and whole-body PET/CT imaging. Patient population was compared to 40 matched healthy controls, randomly selected from a published normalcy database. All images were preprocessed using SPM12. Original DICOM images were converted to NifTI-1 format using SPM DICOM Import. Images were normalized using to Montreal Neurological Institute (MNI) space with an FDG-PET template, and subsequently smoothed with a 8-mm full width at half maximum Gaussian kernel. Volumes Of Interest (VOI) masks were created using WFU PickAtlas. We are interested in BA4, BA3-1-2 and in whole-brain. We used NiftyReg to register the Atlas's reference image on each patient's PET; using these transformations we were able to register each mask on the corresponding PET image, in order to extract the average SUV from each VOI. The analysis of SC of each patient and control subject was performed as previously described. **Results**: Significant relative reduction in glucose metabolism was found in ALS patients as compared with controls in BA4 (mean SUV 5.84±1.29 vs 6.87±1.98, p<0.01) and in BA3-1-2 (mean SUV 5.37±1.19 vs 6.31±1.80, p<0.01). Similarly, whole brain mean SUV was lower in ALS patients than in controls (5.21±1.13 vs 6.01±1.67, p<0.01). By contrast, the present data confirmed a slight yet significant increase in FDG-SC uptake of ALS patients, most evident in the cervical spine segments. **Conclusion**: The major finding of the present study is the evidence of different ALS effects on glucose metabolism in brain and in SC, suggesting a differential neuro-pathological state or different temporal sequence in disease progression.

EP-0402

Hypothalamic dysfunction is related to sleep impairment and CSF biomarkers in Alzheimer Disease

A. Chiaravalloti[1,2], C. Liguori[3], M. Nuccetelli[4], F. Izzi[3], G. Sancesario[5], A. Cimini[1], S. Bernardini[4], O. Schillaci[1], N. Mercuri[3], F. Placidi[3]; [1]Department of Biomedicine and Prevention, University Tor Vergata, Rome, ITALY, [2]IRCCS Neuromed, Pozzilli, ITALY, [3]Sleep Medicine Centre, Neurophysiopathology Unit, Department of Systems Medicine, University Tor Vergata, Rome, ITALY, [4]Clinical Biochemistry and Molecular Biology, University Tor Vergata, Rome, ITALY, [5]Neurology Unit, Department of Systems Medicine, University Tor Vergata, Rome, ITALY.

Background: hypothalamus is a key brain region regulating several essential homeostatic functions, including the sleep-wake cycle. In fact, nuclei controlling the alternation of sleep and wake states are sited from the anterior to the posterior regions of this brain area and are named suprachiasmatic nucleus (SCN), orexinergic nucleus, melanin-concentrating hormone nucleus, tuberomammillary (TBM) nucleus. It has been described in post-mortem studies that hypothalamus is affected by the Alzheimer's Disease (AD) pathology, and in particular SCN, orexinergic and TBM regions showed the reduction of these populations of neurons in AD patients. Since dysfunctions in these areas detected in *post-mortem* AD brains have been related to the sleep-wake cycle impairment, we investigated the possible *in vivo* alteration of the hypothalamus and its correla-

tions with sleep impairment and cerebrospinal-fluid (CSF) AD biomarkers changes in a population of AD patients compared to non-demented elderly controls. **Materials and Methods:** we measured the polysomnographic sleep, the CSF AD biomarkers and orexin levels, and the hypothalamic [18F]FDG uptake by means of Positron Emission Tomography (PET) in a population of AD patients compared to two control groups matched for age and sex with the AD population. The first group of controls underwent PSG and CSF biomarkers and orexin analysis (Control 1), and the second group underwent [18F]FDG PET assessment (Control 2). **Results:** we documented the significant reduction of hypothalamic [18F]FDG PET uptake in the AD group (n=18) compared to the Control 2 group (n=18) (p<0.01). Moreover, we found the increase of CSF orexin levels coupled with the marked alteration of the nocturnal sleep in the AD group as compared to the Control 1 group (n=15) (p<0.05). Finally, we observed the significant association linking the reduction of both sleep efficiency and REM sleep to the reduction of hypothalamic [18F]FDG PET uptake in the AD group. Moreover, [18F]FDG PET hypothalamic uptake correlated with the higher ratio of total-tau/beta-amyloid$_{42}$ CSF levels (index of more marked neurodegeneration). Finally, we documented a connection between the hypothalamus and the limbic system in the control group, which was not evident in the AD group. **Conclusions:** we documented the *in vivo* dysfunction of the hypothalamus in AD patients, which was correlated with both the impairment of nocturnal sleep and the CSF index of more marked AD neurodegeneration.

EP-0403

Cognitive Reserve (CR) interacts with brain metabolism in regions independent of the PD-related network: an 18F-FDG PET study in Parkinson disease (PD) de novo patients

H. Efetürk[1], M. Bauckneht[1], D. Arnaldi[2], A. Buschiazzo[1], R. Piva[1], F. Ticconi[1], M. Pardini[2], F. Massa[2], A. Bugnolo[2], N. Girtler[2], J. Accardo[2], G. Sambuceti[1], F. Nobili[2], S. Morbelli[1]; [1]IRCCS San Martino - IST, University of Genoa, Genoa, ITALY, [2]Clinical Neurology, University of Genoa, Genoa, ITALY.

CR is the hypothesized capacity of an adult brain to cope with brain damage in order to minimize symptomatology. While 18F-FDG PET has been extensively used to assess the effect of CR in Alzheimer's Disease (AD) patients, no data have been to-date provided on interactions between CR and brain metabolism in PD. We aimed to investigate the interactions between education as reserve proxy and brain metabolism as marker of neurodegeneration in de novo PD patients. **Methods:** 56 de novo PD patients underwent 18F-FDG PET/CT (18 females, age 71 ±7.3 years, mean education 10±4.4 years, range 4-19 years, MMSE score 27 ±2.2, UPDRS-III score 23±11.9). Based on the median value of years of formal education, patients were divided into highly (n=28, 10 female, age 70 ±7.2 years, education 14±2.5, MMSE score 27±1.6; UPDRS-III score 22±14.6; High-PD) and poorly (n=28, 8 female, age 73 ±7.3 years, education 7±1.8, MMSE score 27±2.6; UPDRS-III score 23±10.7; Low-PD) edu-

cated PD subgroups. Images were preprocessed in SPM8 and High-PD and Low-PD were compared amongst each other and independently with a healthy-elderly control group (n=48) as well as with education-matched subgroups. Finally, to further investigate interaction between CR and neurodegeneration in PD, the correlation between education and brain metabolism was assessed by means of SPM multiple regression analysis. Age and MMSE score were included as nuisance variables in all the analyses. Uncorrected p<0.005 at voxel level was accepted as significant. **Results:** Both High- and Low-PD subgroups showed hypometabolism in large clusters involving the posterior parietal cortex in both hemispheres (FWE-corrected p<0.05). No differences in brain metabolism were highlighted when PD subgroups were compared within each other. Education showed a significant inverse correlation with brain metabolism in the bilateral posterior cingulate (uncorrected p<0.005). All results were confirmed after correcting for MMSE and age. **Conclusion**: In de novo PD patients, CR seems to interact with brain metabolism in a region not included in the typical PD-related network. This finding is further supported by the fact that, differently from what previously reported for AD patients, the severity and extent of hypometabolism in PD patients is not affected by their level of education. The inverse correlation between education and posterior cingulate, a well-known marker of AD-related pathology, suggests that, even in PD patients, CR might reflect the interaction between amyloid load and neurodegeneration. Analyses on DATSPECT in this de novo PD group are ongoing to further investigate CR pathophysiology in PD.

EP-0404

Evaluation of age-related metabolic changes in healthy subjects: an italian brain 18F-FDG PET study

V. Berti[1], M. Allocca[1], F. Linguanti[1], M. L. Calcagni[2], A. Cristaro[3], U. P. Guerra[4], F. Nobili[5], S. Pappatà[6], S. Sestini[7], D. Volterrani[8], F. Tutino[1], A. Ciaccio[1], R. Sciagrà[1]; [1]Nuclear Medicine Unit, Department of Experimental and Clinical Biomedical Sciences "Mario Serio", University of Florence, Florence, ITALY, [2]Institute of Nuclear Medicine, Fondazione Policlinico Universitario Agostino Gemelli, Università Cattolica del Sacro Cuore, Rome, ITALY, [3]Positron Emission Tomography Centre IRMET S.p.A., Turin, ITALY, [4]Department of Nuclear Medicine, Poliambulanza Foundation, Brescia, ITALY, [5]Clinical Neurology, Department of Neuroscience (DINOGMI), University of Genoa, Genoa, ITALY, [6]Institute of Biostructure and Bioimaging, CNR, Naples, ITALY, [7]Nuclear Medicine Unit, U.S.L. Toscana Centro, Prato, ITALY, [8]Nuclear Medicine Unit, University Hospital of Pisa, Pisa, ITALY.

Introduction: 18F-fluorodeoxyglucose (FDG) positron emission tomography (PET) has been extensively used to detect metabolic alterations in several neurological diseases vs. normal aging. Our aims was to evaluate age-related changes in cerebral glucose metabolism in a cohort of healthy subjects, and to assess the effect of gender. **Subjects and Methods:** Brain FDG-PET scans of 152 subjects (67/85 M/F, 20-84 y.o) were selected from the Italian Normative Database of the Italian Association of Nuclear Medicine. Regions of interest (ROI) were drawn over

all grey matter anatomical regions and Brodmann areas using Pickatlas toolbox and intensity normalization was performed using white matter as reference. SPM12 multiple regression and full factorial designs were used to find age and gender effects on cerebral metabolism. P<0.05 family-wise-error-corrected was considered significant. Besides, linear regression analyses were performed using SPSS software and ROIs values to investigate age-related effects and gender differences. **Results:** SPM analysis demonstrated a significant negative correlation between age and cerebral metabolism involving frontal lobes bilaterally, especially medial frontal cortices, insular regions bilaterally, several areas of temporal lobes, including hippocampi, and few regions of parietal lobes. No significant correlation was found between age and glucose metabolism in occipital lobes and in primary sensory-motor cortex. A significant relative positive correlation was found between age and glucose metabolism in cerebellum and brainstem. This pattern of age-related changes was similar in both males and females, although with wider clusters of negative correlation with age in females as compared to males. SPSS analysis confirmed previous SPM analysis, both using anatomical and Brodmann areas, demonstrating the same pattern of metabolic correlation with age, and wider and stronger correlations in females than in males. **Conclusion:** Our study demonstrated age-related metabolic reductions in frontal, especially medial, insular, hippocampal cortices, more evident in female than in male subjects. Thorough knowledge of age- and gender-related cerebral metabolic changes is critical for accurate detection of abnormal findings and for investigating metabolic alterations in neurological disorders.

EP-0405

Voxel and surface-based structural and functional imaging study in patients with idiopathic REM sleep behavior disorder

X. Han[1], X. Li[1], W. Tang[2], H. Yu[3], P. Wu[1], C. Zuo[1]; [1]PET Center, Huashan Hospital, Fudan University, Shanghai, CHINA, [2]Department of Radiology, Huashan Hospital, Fudan University, Shanghai, CHINA, [3]Department of Neurology, Huashan Hospital, Fudan University, Shanghai, CHINA.

Aim: Idiopathic rapid eye movement sleep behavior disorder (iRBD) is a complex parasomnia harboring diverse neurodegenerative diseases, such as Lewy body diseases (LBD) and multiple system atrophy (MSA). Brain anatomical and functional abnormalities have been identified in iRBD, respectively; whereas researches combining the two neuroimaging approaches have never been reported. We aimed to explore the relationships between glucose metabolism and gray matter volume (GMV) as well as cortical thickness (CT) alterations in iRBD. **Materials and Methods:** ^{18}F-FDG PET and magnetic resonance imaging (MRI) were performed in 20 patients with iRBD and 20 age-matched healthy controls. Computational anatomy toolbox (CAT12) based on statistical parametric mapping (SPM12) was employed to detect GMV and CT changes in patients. SPM12 was applied to determine the voxel and surface-based metabolic activity changes and identify the overlapping regions between metabolism and GMV as well as CT alterations in patients. **Results:** The results of voxel-based analysis showed that significantly increased GMV was found in the anterior lobes of bilateral cerebellum and right middle temporal gyrus, with reduced GMV in left superior frontal gyrus and right postcentral gyrus in patients. Patients showed increased metabolism in the anterior lobes of right cerebellum and right middle temporal gyrus, but decreased metabolism in left superior frontal gyrus. Consistent alterations were found in the anterior lobes of right cerebellum, right middle temporal gyrus and left superior frontal gyrus. The results of surface-based analysis revealed that patients exhibited pronounced cortical thinning in bilateral inferior frontal gyrus, cingulate gyrus, and right fusiform gyrus, and left superior frontal gyrus, middle temporal gyrus. Reduced metabolism in patients was found in bilateral inferior frontal gyrus cingulate gyrus, and right fusiform gyrus, superior temporal gyrus. Overlapping regions were located in bilateral inferior frontal gyrus, cingulate gyrus, and right fusiform gyrus in patients. **Conclusion:** We presented the first dual-modality study using voxel and surface-based analysis in iRBD and revealed that glucose metabolism changes in specific brain regions corresponded well with structural changes; nevertheless, the two analysis methods emphasized different overlapping regions, suggesting that combining the above-mentioned methods might provide complementary and related information to understand the underlying neuropathological process of neurodegeneration. Besides, we captured iRBD-related structural anomalies, which were similar to those visualized in LBD and MSA, indicating that iRBD might possess a common morphological abnormality with neurodegenerative synucleinopathies.

EP-0406

[18F]FDG PET imaging study in early phase of unilateral 6-OHDA Parkinson disease rats model submitted to treadmill exercise protocol

C. C. Real, K. H. Binda, P. C. Garcia, C. G. Carneiro, C. A. Buchpiguel, D. P. Faria, L. R. G. Britto; University of São Paulo, São Paulo, BRAZIL.

Introduction: Parkinson's disease (PD) is the second most common neurodegenerative disease in the elderly people. An intervention that has demonstrated beneficial effects in PD is exercise. Thus, it is important to study non-invasive methods for early diagnosis and therapeutic interventions evaluation. We aimed to evaluate treadmill exercise effects on motor behavioral and brain metabolism in an early phase of PD rat model by [18F] Fludeoxyglucose (^{18}F-FDG) PET imaging. **Methods:** PD rat model was induced in three months Wistar rats (n=6) by unilateral striatal 6-hydroxy-dopamine (6-OHDA-6µg) injection whereas control animals received saline injection. Two days after injection the animals were subjected to a treadmill exercise protocol (10 meters/min, 40 minutes, 3 times/week during 4 weeks). Animals were divided in four groups, SED (control sedentary animals); SED+6-OHDA (PD sedentary animals); EX (control exercised animals); EX+6-OHDA (PD exercised animals). On day -1 (baseline), 10 and 30, motor behavioral was analyzed by a 5-min cylinder test, and brain metabolism was measured

by a 30-min PET scan, performed 45 min after tracer injection. ^{18}F-FDG images were analyzed with PMOD™ software and the uptake ratio between brain hemispheres was made to perform ANOVA statistical analysis. **Results:** An increase in the asymmetric use of forelimb (p<0.01) was observed in SED+6-OHDA group on day 10, while exercise reversed this effect. No difference was observed in other groups. On day 30, no differences were observed. When compared to baseline, ^{18}F-FDG uptake on day 10 demonstrated that SED+6-OHDA group showed a decreased ^{18}F-FDG uptake in the caudate putamen (p<0.0001), motor cortex (p<0.01), hippocampus anterodorsal (p<0.0001), posterior hippocampus (p<0.05) and midbrain (p<0.05), while EX+6-OHDA rats did not change ^{18}F-FDG uptake. On day 30, there was a decrease in the SED+6-OHDA, EX and EX+6-OHDA in the caudate putamen (p<0.05). Motor cortex revealed a decrease in the SED+6-OHDA (p<0.0001) and EX (p<0.01). In the somatossensorial cortex there was an increase in the SED group (p<0.05), and a decrease in the SED+6-OHDA (p<0.01). In the posterior hippocampus SED+6-OHDA group revealed an increase in the ^{18}F-FDG uptake. **Conclusion:** A worse forelimb use and changes in brain metabolism of sedentary rats subjected to the PD model were observed. These results could explain cognitive (decrease in ^{18}F-FDG hippocampus uptake) and motor (decrease in ^{18}F-FDG caudate putamen and midbrain uptake) symptoms of PD. Beneficial exercise effects could be measured through ^{18}F-FDG PET imaging and were correlated to an improvement in the asymmetric forelimb use. **Financial support:** FAPESP, CNPq

EP-0407

Therapeutic effects of dietary intervention on neuroinflammation and brain metabolism in a rat model of photothrombotic stroke

E. Kurtys[1,2], C. Casteels[3], C. C. Real[4], U. L. M. Eisel[5], J. M. Verkuyl[6], L. M. Broersen[6], H. C. Klein[2], R. A. J. O. Dierckx[2], J. Doorduin[2], E. F. J. de Vries[2]; [1]King's College London, London, UNITED KINGDOM, [2]University of Groningen, University Medical Center Groningen, Groningen, NETHERLANDS, [3]Catholic University Leuven, Leuven, BELGIUM, [4]University of São Paulo, São Paulo, BRAZIL, [5]University of Groningen, Groningen, NETHERLANDS, [6]Nutricia Research, Utrecht, NETHERLANDS.

Aim: One of the possible targets for stroke management is modulation of neuroinflammation. Evidence suggests that food components may exert anti-inflammatory properties. Therefore, we investigated the effects of a diet containing anti-inflammatory ingredients, on focal ischemic brain damage induced in the somatosensory cortex of rats by photothrombotic stroke. **Material and Methods:** Rats were fed a control diet or an investigational diet, starting either 2 weeks before or immediately after the induction of ischemia by photothrombotic stroke. The effects of ischemia and the investigational diet on lesion size, neuroinflammation, brain glucose metabolism and motor function were assessed with immunohistochemistry, positron emission tomography (PET) and behavioral tests. **Results:** Ischemia caused focal brain damage and transient lateral movement

impairment. The brain lesions were surrounded by strong astrogliosis and accompanied by a trend towards global decrease in glucose metabolism. On day 21, activated astrocytes were still present, but brain glucose metabolism was not significantly different from control rats anymore. The investigational diet applied two weeks before the ischemia did not affect astrocyte activation on day 7, but improved the normalization of brain glucose metabolism. If the investigational diet was started immediately after the ischemia, increased astrocyte activation and decreased global glucose metabolism were still observed on day 7. Twenty-one days after the induction of ischemia the investigational diet completely reduced astrocyte activation when started after stroke induction, whereas only a partial reduction was observed when started before stroke. Only the investigational diet started after stroke tended to inhibit the growth in lesion size between day 7 and 21. **Conclusion:** This study reveals potentially beneficial effects of diet containing elevated amounts of anti-inflammatory nutrients on the recovery from ischemic brain damage.

EP-0408

Comparison of [18F]FE-PE2I and [18F]fluorodopa/ PET images in the LPS-induced Parkinsonian rat model

K. Ma[1], H. Ko[1], S. Weng[1], T. Chou[2], C. Tsai[3], Y. Huang[3], R. Yen[3], C. Shiue[2,3], C. Halldin[4]; [1]Department of Biology and Anatomy, National Defense Medical Center, Taipei, TAIWAN, [2]Department of Nuclear Medicine, Tri-Service General Hospital, National Defense Medical Center, Taipei, TAIWAN, [3]Department of Nuclear Medicine, National Taiwan University Hospital, Taipei, TAIWAN, [4]Department of Clinical Neuroscience, Centre for Psychiatry Research, Karolinska University Hospital, Karolinska Institutet, Stockholm, SWEDEN.

Aims: Parkinson's disease (PD) is a neurodegenerative disorder characterized by the degeneration of dopaminergic neurons in nigroatrial pathway. Several lines of evidences have indicated that neuroinflammation may be involved in the pathogenesis of PD. The [18F]FE-PE2I is a novel PET imaging agent which target to dopamine transporters *in vivo*. In this study, we compared the imaging quality of [18F]fluorodopa and [18F]FE-PE2I/ PET in a rat model of PD induced by an endotoxin, lipopolysaccharide (LPS). **Materials and Methods:** The PD rat model were created by injecting different dose of LPS (45 μg or 60 μg) in the striatum of rat brain. The rotarod performance test, [18F]fluorodopa/animal PET/animal PET, [18F]FE-PE2I/animal PET, and immunochemistry were performed to evaluation the PD severity in the LPS-induced rats, respectively. **Results:** The rotarod test showed that the injections of LPS induced motor deficits in the rats. Both the imaging studies of the [18F]fluorodopa and [18F]FE-PE2I coupled with small animal-PET showed that there were lower uptakes in the lesion side of striatum than those of contralateral side in PD model rats. The immunostaining results of tyrosine hydroxylase (TH) and dopamine transporter (DAT) in the rat brains also showed paralleled trend with those of behavioral and PET imaging data. **Conclusions:** Our results suggest that the [18F]FE-PE2I/PET is a feasible method for the measurement of PD severity in the LPS-induced rat

model. Moreover, this imaging technique coupled with the LPS-induced rat model may provide a platform to screen the therapeutic drugs for Parkinson's disease.

EP-0409

Evaluating the status of serotonin transporters in the LPS-induced rat model using 4-[^{18}F]-ADAM/PET

C. Cheng[1], K. Ma[2], T. Ho[2], S. Weng[2], T. Chou[1], C. Shiue[1]; [1]Department of Nuclear Medicine, Tri-Service General Hospital, National Defense Medical Center, Taipei, TAIWAN, [2]Department of Biology and Anatomy, National Defense Medical Center, Taipei, TAIWAN.

Aims: The neuroinflammation may lead to the pathogenesis of several neurological disorders such as Parkinson's disease and depression. During the neuroinflammatory response, the microglia were activated with changing in morphology and released various pro-inflammatory cytokines. In this study, we aim to evaluate the status of serotonin transporters (SERT) in the depression-like rat model using 4-[18F]-ADAM/PET. **Materials and Methods:** The depression-like rat model was induced by systemic lipopolysaccharide (LPS) administration (0.5 mg/kg or 5 mg/kg, i.p.). The open field test, [^{18}F]FDG and 4-[^{18}F]-ADAM coupled with small animal-PET imaging, and immunohistochemistry(IHC) studies were performed to access the depression-like behavior and the alteration of serotonergic systems, respectively. **Results:** The results of open field test in LPS-treated group showed obviously decrement than that of the sham group. The uptakes of [^{18}F]FDG showed markedly changes at 1 week after LPS injection, but they demonstrated comparable to the controls at 2 weeks after LPS injection. The uptakes of 4-[^{18}F]-ADAM displayed a trend of increment at 3 days and 3 weeks after LPS injection. The IHC studies of SERT presented a paralleled result to the 4-[^{18}F]-ADAM images. **Conclusions:** These results suggest that the systemic administration of LPS may result in the depression-like behavior in rat. Moreover, 4-[18F]-ADAM coupled with small animal-PET is a useful technique for imaging SERT in the depression-like rat model.

EP-0410

Disease-related Metabolic Brain Patterns Associated with Parkinsonian and Cerebellar Subtypes of Multiple System Atrophy

P. Wu[1], J. Wang[2], J. Wu[2], C. Jiang[1], J. Ge[1], Y. Ma[3], Y. Ma[3], C. Zuo[1]; [1]PET Center, Huashan Hospital, Fudan University, Shanghai, CHINA, [2]Department of Neurology, Huashan Hospital ,Fudan University, Shanghai, CHINA, [3]Center for Neurosciences, Feinstein Institute for Medical Research, Manhasset, NY, UNITED STATES OF AMERICA.

Objective: Multiple system atrophy (MSA) is associated with a disease-related metabolic brain network (MSARP) based on 18F-FDG PET. MSARP expression was elevated in MSA patients relative to healthy controls as well as patients with Parkinson's disease (PD) and correlate with clinical indices, suggesting that this network marker can assist in differential diagnosis and assessing disease severity. However, the previous studies included patients mostly with a parkinsonian (MSA-P) and also with a cerebellar (MSA-C) subtype. It remains In this study, we investigated unknown if unique brain network can characterize each of the two clinical subtypes of MSA. **Methods:** Age-matched 16 Chinese patients with MSA-P, 16 MSA-C and 16 healthy controls underwent FDG PET imaging. MSAPRP and MSACRP were identified in the combined patients and control subjects by an automated network computation using SSM/PCA toolbox. The MSA-related patterns were determined from a linear combination of select principal components (PCs) whose expression in individual cases gave the maximum separation between the patients and control groups. The network expression in each PET scan was represented by a Z-transformed score using subject scores of the normal controls. The reliability of each pattern was assessed by a voxel-based bootstrap estimation procedure (5). **Results:** For the MSA-P cohort, the first 4 PCs accounted for 55% of the subject × voxel variance. A logistic regression model including all these PCs demonstrated their linear combination produced a MSAP-related pattern (MSAPRP), characterized by metabolic decreases in the bilateral caudate, putamen and cerebellum and in the left thalamus. Voxel weights in these regions were reliable (N=1000, P=0.01). For the MSA-C cohort, the first 3 PCs accounted for 54% of the subject × voxel variance. The linear combination of PC1 and PC3 (42% VAF) produced a MSAC-related pattern (MSACRP), characterized by bilateral metabolic decreases in the cerebellum. Voxel weights in these regions were highly reliable (N=1000, P=0.001). Both MSAPRP and MSACRP scores were elevated (P<0.001) in the patients relative to the controls. **Conclusions:** This is the first study to investigate the specific metabolic brain networks corresponding to MSA-P and MSA-C using FDG PET imaging. The differing topographies of these two network patterns are consistent with manifestation of motor symptoms in each of two clinical subtypes of MSA but may represent different expression of cerebral metabolic substrates in response to the same neuropathophysiologic process. The specific MSAPRP and MSACRP may be helpful in differential diagnosis, therapy monitoring and patients recruitment for clinical trials.

EP-0411

Chronic Exposure to Resveratrol Improves Cerebral Blood Flow and Cognitive Function in Aged Rats

P. Garrigue, Y. Mouhajir, E. Seree, M. Alessi, F. Dignat-George, B. Guillet; Aix-Marseille Université, Marseille, FRANCE.

Resveratrol is a natural stilbene found in grape skin and seeds, known for its antioxidant activity in the vascular and nervous systems. The present study investigated the influence of resveratrol on aging in vivo, focusing on cerebral blood flow (CBF) and cognitive function. 3 months Sprague-Dawley rats (n=8 per condition) were fed with water supplemented with resveratrol (50 mg/L, ad libitum) for 5 months (resveratrol group) or with plain water ad libitum (control group). At the age of 8 months, rats underwent a 99mTc-HMPAO μSPECT/CT coupled with a novel object test (NOT), to assess CBF during a cognitive stimulation, and to evaluate the cognitive function respectively.

Experiments were performed according to an Ethics Committee agreement by trained and competent researchers. Resveratrol-treated rats got significantly higher CBF than the control rats (6.404±0.6644 vs 3.914±0.5442 %ID/mm3 99mTc-HMPAO, respectively, P<0.001) but also significant better results with the NOT (discrimination index 0.5691±0.2821 vs 0.1486±0.1373 respectively, P<0.05). Molecular biology micro-arrays performed on brain tissues of the same animals showed a pronounced activation of anti-inflammatory and anti-oxydative genes in the resveratrol-treated group. We therefore speculate resveratrol chronic administration could be an interesting option to prevent pathophysiological cerebral cognitive impairments due to aging.

EP-0412

Effects of Pioglitazone on Amyloidogenesis, Neuroinflammation and Cognition in a Transgenic Amyloid Mouse Model

M. Brendel[1], M. Deussing[1], B. Zott[2], T. Blume[1], Y. Shi[3], G. Kleinberger[3], C. Focke[1], S. Lindner[1], F. Gildehaus[1], P. Bartenstein[1], K. Baumann[4], C. Haass[3], H. Adelsberger[2], A. Rominger[1]; [1]*University of Munich, Munich, GERMANY,* [2]*Technical University of Munich, Munich, GERMANY,* [3]*DZNE, Munich, GERMANY,* [4]*F. Hoffmann-La Roche, Basel, SWITZERLAND.*

Aim: Pioglitazone treatment improves cognition in amyloid mouse models by modulation of neuroinflammation. We objected to perform a pioglitazone therapy in an amyloid mouse model and investigated the effects on glial activation and amyloid accumulation by means of dual *in vivo* PET monitoring. 18kDa translocator protein (TSPO) PET imaging of neuroinflammation may therefore facilitate a responder identification. **Methods:** PS2APP (TG) mice and C57Bl/6 (WT) mice were randomly stratified in pioglitazone (N=13 TG, N=8 WT) and placebo treatment (N=10 TG, N=7 WT) at the age of 8 months. Therapy was conducted for 5 months. All mice were scanned with the TSPO ligand (F-18-GE180) at baseline, after 0.5 mo, 2.5 mo and 5 mo. Amyloid-PET (F-18-Florbetaben) was performed at baseline and after 5 mo. Forebrain tracer uptake was assessed for each timepoint. Cognitive testing (Morris Water Maze) after the terminal PET scan was followed by biochemical and histological analyses. **Results:** Pioglitazone treatment resulted in a reduction of -13% (p < 0.001) in the TSPO-PET signal of TG mice compared to the TG placebo group at study termination. The amyloid-PET signal increase in TG mice during treatment was significantly larger during pioglitazone treatment (+16%) when compared to placebo (+13%; p < 0.05). Increase of amyloid signal and decrease of TSPO signal in treated TG mice correlated inversely for the whole treatment period (R= -0.62; p < 0.05). Early TSPO decrease correlated with cognitive improvement at study termination (R= 0.66; p < 0.05) and allowed responder identification. Biochemistry indicated lower soluble Aβ in the TG treatment group when compared to placebo. **Conclusions:** TSPO-PET signal reduction was associated with consecutive amyloid-PET signal increase, probably related to more condensed amyloid plaques but increased clearance of soluble Aβ. Early serial TSPO-PET facilitates responder prediction showing better cognitive outcome despite increasing plaque load after long term pioglitazone treatment.

Neurosciences: Neurotransmission

EP-0413

Dopaminergic, Serotoninergic And Glucose Metabolism Disorders At Early Stage Of Disease In Accelerated Mouse Model Of Synucleionopathy

E. Levigoureux[1,2], C. Bouillot[3], T. Baron[4], L. Zimmer[1,2,3], S. Lancelot[1,2]; [1]*Université Claude Bernard Lyon 1, INSERM, CNRS, Lyon Neuroscience Research Center, Lyon, France, Lyon, FRANCE,* [2]*Hospices Civils de Lyon, Lyon, FRANCE,* [3]*CERMEP, Imagerie du vivant, Lyon, FRANCE,* [4]*ANSES, Lyon, FRANCE.*

Aim: Alpha-synuclein (α-syn) aggregation is a neuropathological hallmark of neurodegenerative diseases called synucleinopathies, including Parkinson's disease, dementia with Lewy bodies and multiple system atrophy. The aim of this study was to evaluate *in vivo* early dopaminergic and serotoninergic disorders and glucose metabolism in an accelerated mouse model (M83) of synucleinopathy. **Material and Methods:** This study used a model of mouse (M83) expressing in an accelerated manner the human A53T mutated α-syn. Control animals were C57Bl/6S mice presenting a deletion of the α-syn locus (KO α-syn) and C57Bl/6S mice (wild type). MicroPET acquisitions were performed using five radiotracers: [11C]raclopride, a D_2 receptor antagonist radiotracer, [11C]PE2I, a dopamine transporter radiotracer, [18F]MPPF, a $5HT_{1A}$ receptor antagonist radiotracer, [11C]DASB, a serotonin transporter radiotracer and [18F]FDG. 7T-MRI images were acquired for extraction of regional time-activity curves in PET studies. For all radiotracers (except for [18F]FDG), PET data were analyzed in two ways: MRI-based VOI method and voxel-by-voxel analysis (SPM). **Results:** In terms of dopaminergic neurotransmission, results obtained with the MRI-based VOI method showed a significant increase of [11C]raclopride uptake in the caudate area of M83 mice. Voxel-based SPM analysis revealed a significant regional increase in [11C]raclopride uptake in these mice compared to KO α-syn mice and two significant clusters were identified in the caudate and the thalamus. An increasing trend of [11C]PE2I uptake in KO α-syn mice versus M83 and WT was found in caudate. Voxel-based SPM analysis revealed no significant differences for [11C]PE2I uptake between the 3 groups of mice. In terms of serotoninergic neurotransmission, a significant increase of [18F]MPPF uptake was found in the frontal and the cingular cortex of M83 mice. Voxel-based SPM analysis revealed a significant regional increase in [18F]MPPF uptake in M83 mice compared to KO α-syn mice with a cluster in hippocampus and the thalamus. No significant differences for [11C]DASB uptake were observed between the 3 groups. Finally, a decrease of [18F]FDG uptake was measured in M83 mouse in

the whole brain. **Conclusion:** These results suggest that M83 mice have overexpressed D_2 and $5HT_{1A}$ receptors at the early stage of the disease, without dopamine and serotonin transporter modifications, suggesting a preserved neuronal density, and associated with a carbohydrate hypometabolism. This neurotransmitter modifications suggest pathophysiological mechanisms that could be explored in a translational manner in Parkinson's disease patients.

Neurosciences: Movement Disorders

EP-0414
123I-MIBG Cardiac Scintigraphy And123I-IOFLUPANE SPECT Combined Use In Uncertain Parkinsonian Syndromes

S. Nuvoli[1], M. R. Piras[2], A. Mulas[1], B. L. J. Pung[1], B. Piras[1], A. Santonicola[3], B. Palumbo[3], A. Spanu[1], G. Madeddu[1]; [1]Unit of Nuclear Medicine, Clinical and Experimental Medicine DPT, University of Sassari, Sassari, ITALY, [2]Unit of Neurology, Clinical and Experimental Medicine DPT, University of Sassari, Sassari, ITALY, [3]Section of Nuclear Medicine, Surgical and Biomedical Sciences DPT, University of Perugia, Perugia, ITALY.

Introduction: Vascular lesions (VL) in basal ganglia (BG) represent a clinical problem in uncertain parkinsonian syndromes (UPS) differential diagnosis. A low[123]I-Ioflupane SPECT accuracy has been observed in these conditions also showing diagnostic overlap in pathological SPECT cases. In the present study, we used ^{123}I-MIBG cardiac scintigraphy, which evaluates presynaptic postganglionic sympathetic system, to support ^{123}I-Ioflupane SPECT in UPS patients with VL in BG. **Methods:** We enrolled 46 patients with VL in BG at MR; 24 patients had differential diagnosis between Parkinson's disease and Vascular Parkinsonism (PD/PV), 12 between PD and other Neurodegenerative Parkinsonism (PD/NP) and 10 between Lewy Body Dementia and Alzheimer Disease (LBD/AD). All patients underwent brain SPECT, 3-4 hrs after 148 MBq ^{123}I-Ioflupane i.v. injection, using dual head gamma camera, also defining striatal dopaminergic activity as binding potential (BP) with 3.3 cut-off in both caudate and putamen. After 15-21 days, cardiac planar scintigraphy in anterior and left anterior oblique views in both early (15 min.) and delayed (240 min.) phases, was performed after 111 MBq ^{123}I-MIBG i.v. injection also calculating heart/mediastinum (H/M) ratio with 1.56 cut-off. **Results:** ^{123}I-Ioflupane uptake was normal in 9/46 patients while it showed striatal defects in 37/46 cases, with BP values under cut-off at least in one of the striatal nuclei.[123]I-MIBG uptake was normal in 21/46 patients, 5 of whom with normal and 16 with striatal ^{123}I-Ioflupane defects, all of them with H/M ratio>1.56, and reduced in 25/46 cases, 4 of whom normal and 21 with striatal ^{123}I-Ioflupane defects with H/M ratio <1.56 in all cases, in both early and delayed phases, with no statistical difference comparing the two phase data. Combining both procedures, a more reliable diagnosis was ob-tained in 42/46 cases properly classifying 16 PD, 10 PV, 7NP, 5 LBD and 4 AD. Only in four patients with normal ^{123}I-Ioflupane and reduced ^{123}I-MIBG uptakes, the diagnosis remained uncertain and they are still monitoring in a close follow-up. **Conclusions:** ^{123}I-Ioflupane SPECT alone was not able to differentiate between UPS with VL in BG. Only with the combined use of ^{123}I-MIBG cardiac scintigraphy, also calculating H/M ratio, even with the early acquisition alone, a more appropriate diagnosis was obtained in 91.3% of cases better defining disease progression and prognosis, thus allowing the most appropriate treatment. However, in those cases with normal ^{123}I-Ioflupane and reduced ^{123}I-MIBG uptakes, a close follow-up is suggested since sympathetic damage could precede striatal disorders in PD and LBD early stage.

EP-0415
Effects of different reconstruction methods on ^{123}I-FP-CIT (DaTSCAN) SPECT quantification

A. Smith[1], J. Niedbala[2], Y. Dewaraja[2], J. C. Dickson[1]; [1]University College London Hospital, London, UNITED KINGDOM, [2]University of Michigan, Ann Arbor, MI, UNITED STATES OF AMERICA.

Quantification of ^{123}I-FP-CIT (DaTSCAN) specific binding ratios (SBRs) has an increasing role in single and mutli-centre trials both as a cross-sectional measurement for entrance criteria and for longitudinal imaging pre and post a therapeutic drug. However, there is no understanding of the bias and precision of quantification with different reconstructions and/or gamma cameras. The aim of this Quantitative Imaging Biomarkers Alliance (QIBA) supported investigation is to look at two contemporary SPECT/CT systems to understand the effects of different reconstruction strategies on SBR, and the effects this may have when planning multi-centre trials. **Method:** Using a striatal phantom, clinically relevant count concentrations were used to represent normal (right side) and abnormal (left side) uptake distributions. This was achieved with equal caudate and putamen concentrations on the right side, while the left side had a 50% reduction in left putamen concentration. Using GE Discovery D670 and Siemens Intevo scanners with LEHR collimators, five 3 million count SPECT/CT acquisitions were performed. Data were reconstructed using Filtered Back Projection (FBP), FBP with Chang attenuation correction (FBP Chang); and OSEM with no corrections (NC), with measured CT attenuation correction (AC), with AC and scatter correction (ACSC), with AC and resolution recovery (ACRR), and with AC, SC and RR (ACSCRR). SBRs were calculated using manual VOIs defined on the phantom CT. Bias was calculated by comparing SBRs to filling concentrations. Precision was defined as standard error of the mean (SEM) from the 5 acquisitions. **Results:** Bias across reconstructions ranged from 45-64% (D670), 56-67% (Intevo) for the right putamen. Left putamen was 48-62% (D670), 55-65% (Intevo); right caudate 62-74% (D670), 63-73% (Intevo); left caudate 63-75% (D670), 61-72% (Intevo). Lowest bias was typically found using ACSCRR, with highest bias with NC. SEM showed a variability in precision across reconstructions with a range of 0.01 - 0.08 (D670) and 0.01 - 0.04 (Intevo). D670 showed the best

precision with FBP and worst for ACSC. There was no clear difference in the precision of reconstructed Intevo data. **Conclusion:** There was variability across different reconstructions and systems. Full correction provided the smallest bias, while subtractive TEW scatter correction methods affected precision on the D670. Differences in collimator design between manufacturers also brings variability to bias and precision. This demonstrates the importance of using consistent reconstruction methods in multi-centre trials and the significance of using the same gamma camera for longitudinal studies.

EP-0416

Right versus left onset Parkinson's disease metabolic patterns: a FDG PET study.

X. Palard-Novello[1], P. David[2], J. Houvenaghel[3], A. Riou[3], G. Robert[4], S. Drapier[3], M. Vérin[3], F. Le Jeune[1]; [1]Centre Eugène Marquis, Rennes, FRANCE, [2]Hôpital Européen Georges Pompidou, Paris, FRANCE, [3]CHU Rennes, Rennes, FRANCE, [4]CH Guillaume Régnier, Rennes, FRANCE.

Aim: At disease onset, patients with Parkinson's disease (PD) typically report one side of the body to be more affected than the other associated with asymmetric dopaminergic degeneration in the brain. Research on the cognitive repercussions of this asymmetric degeneration showed cognitive difficulties associated with the side of disease onset, like visuospatial or vocal emotion deficits for left-sided symptoms onset (LSO) PD patients and verbal expression for right-sided symptoms onset (RSO) PD patients. Our objective was to analyze differences in brain metabolism measured with FDG-PET between LSO and RSO PD patients. **Materials and Methods:** A total of 102 non-demented and non-depressive PD patients were categorized into RSO (n = 53) and LSO (n = 52) PD patients groups. Patients underwent in the same week a motor assessment, a neuropsychological assessment and a resting state FDG-PET assessment 3 months before deep brain stimulation (DBS). Cerebral glucose metabolism for RSO patients and LSO PD patients were compared to 11 healthy controls patients, using a two sample t-tests at every voxel, with age as covariates. Clusters with a threshold of p < 0.001 (corrected for multiple comparison) were considered to be significantly different. **Results:** No statistical differences were observed between RSO and LSO PD patients concerning age, sex ratio, stimulation site (pallidal or sub-thalamic), disease duration, right-handed/left handed ratio, Mattis dementia rate scale, Montgomery-Asberg Depression Scale and motor scores (UPDRS I, II, III and IV tests ; Schwab and England test and Hoehn and Yahr test). For both RSO and LSO PD patients, compared to healthy controls, results showed significant hypermetabolism cluster from the postcentral gyrus in the ipsilateral side of the predominant brain side disease and significant hypermetabolism cluster from the precentral gyrus in the contralateral side of the predominant brain side disease. Furthermore, for LSO PD patients, results showed significant hypometabolism cluster from the medial frontal gyrus in the ipsilateral side of the predominant brain

side disease. **Conclusion:** Whatever side of disease onset, hypermetabolism was observed in the postcentral gyrus in the ipsilateral side of the predominant brain side disease, which could be related to an ipsilateral somesthesic compensation and significant hypermetabolism cluster from the precentral gyrus in the contralateral side of the predominant brain side disease which could be related to a controlateral motor compensation. Furthermore, LSO PD patients showed significant hypometabolism cluster from the medial frontal gyrus in the right side, which could be related to right-sided cognitive difficulties.

EP-0417

Evaluation of an automated classification method for DaTscanTM SPECT using a volumetric approach to the Southampton Method

*D. Mirando, A. Kruzer, **A. S. Nelson**; MIM Software, Cleveland, OH, UNITED STATES OF AMERICA.*

Purpose: To evaluate a method for differentiating Parkinson's Disease (PD) from healthy controls (HC) using the specific binding ratio (SBR) statistic. **Methods:** 391 subjects were selected from the Parkinson's Progression Markers Initiative (PPMI) database (www.ppmi-info.org/data). This group was separated into a "training dataset" (71 HC, 125 PD) and a "testing dataset" (70 HC, 125 PD). SBRs were calculated using the semi-automatic Southampton Method described by Bolt et al (2006), modified so that all regions were defined in three dimensions. DaTscan SPECT images from each subject were automatically registered to a template using a two step affine registration, with the 1st step focused on the whole brain and the 2nd focused on independent hemispheres. Left and right striatal volumes of interest were drawn according to the dimensions specified by the Southampton Method, with thickness increased from 44mm to 54mm to better account for the partial volume effect. A reference region was then generated following the procedure outlined by the Southampton Method. SBRs were recorded for each hemisphere, and subjects were split into 4 age ranges selected to contain similar numbers of database subjects. Kappa values from the "training dataset" were used to optimize SBR cutoffs for differentiating PD from HC in each age range. These cutoffs were then compared to the SBR results from the "testing dataset", and a PD classification was applied if either hemisphere's SBR value was below the SBR cutoff. PD classification was also applied if either hemisphere's SBR value exceeded that of the other hemisphere by at least 20%. **Results:** The four age groups were defined as <50, 50-59, 60-69, and 70+ years old, and their corresponding optimized SBR cutoffs were 4.70, 4.59, 4.79, and 3.56, respectively. This classification scheme achieved 89.2% accuracy in the testing dataset, with 92.8% sensitivity and 82.9% specificity. **Conclusion:** We have described a method for automatically classifying DaTscan SPECT using SBR calculated through a volumetric version of the Southampton Method and age-specific cutoff values, demonstrating >89% accuracy. We plan to perform future investigations into combining SBR with results from other classification methods.

EP-0418

Hypometabolism of the putamen and the pallidum in 18F FDG PET is predictive of clinical disability in multiple system atrophy

F. Hives[1], A. Pavy-Le Traon[2], J. Dupouy[3,4], F. Ory-Magne[5,6], C. Brefel-Courbon[5,6,7], O. Rascol[8,9], A. Hitzel[1], P. Payoux[10,1]; [1]Department of Nuclear Medicine, University Hospital of Toulouse, Toulouse, FRANCE, [2]Institute of Cardiovascular and Metabolic Diseases, National Institute of Health and Medical Research (INSERM), UMR-1048,, Toulouse, FRANCE, [3]Pharmacoepidemiology Research Unit, INSERM 1027, University of Toulouse, Toulouse, FRANCE, [4]Academic Department of Family Medicine, Faculty of Medicine Toulouse, University of Toulouse, Toulouse, FRANCE, [5]INSERM UMR1214, Imagerie cérébrale et handicaps neurologiques, Toulouse, FRANCE, [6]Department of Neurology, University Hospital of Toulouse, Toulouse, FRANCE, [7]Department of Clinical Pharmacology, University Hospital of Toulouse, Toulouse, FRANCE, [8]Department of Clinical Pharmacology and Neurosciences, University Hospital and University of Toulouse 3, Toulouse, FRANCE, [9]INSERM CIC1436 and UMR825, Toulouse, FRANCE, [10]INSERM UMR825, Imagerie cérébrale et handicaps neurologiques, Toulouse, FRANCE.

Aim: Multiple system atrophy (MSA) is a progressive, sporadic, adult-onset neurodegenerative disorder characterized by varying severity of parkinsonism, cerebellar ataxia, autonomic failure and corticospinal impairment with two phenotypes according to predominant symptoms (P with predominant parkinsonism or C with predominant cerebellar ataxia). ^{18}F-fluorodeoxyglucose (FDG) in positron emission tomography (PET) is used in MSA to help to the diagnosis. Hypometabolisms are located mainly in striatum and cerebellum. As FDG PET, diffusion-weighted imaging (DWI) in magnetic resonance imaging (MRI) can contribute to differentiate MSA-P from the others parkinsonian syndromes. It has been reported that higher apparent coefficient diffusion (ADC) in the putamen and the pallidum was related with the clinical progression of the disease. Our aim was to study the correlation between clinical disability and brain metabolism on FDG PET in MSA. **Materials and Methods:** Retrospective analysis of 32 patients with MSA (22 MSA-P and 10 MSA-C) who underwent brain FDG PET/computed tomography (CT) and who were clinically evaluated with the Unified Multiple System Atrophy Rating Scales (UMSARS) and cardio-vascular-autonomic testing (CVAT). We performed a voxel-based morphometry (VBM) and confirmed the results with regions of interest (ROI) analysis using Scenium software (Siemens Molecular Imaging). Scenium software provides quantification assessment of ROI with comparison *versus* database of normal subjects. We considered threshold of $p<0.01$ uncorrected and cluster > 10 voxels for VBM, and $p<0.05$ for ROI analysis, as significant. **Results:** The metabolism of bilateral putamen and pallidum was negatively correlated with UMSARS I (daily living), UMSARS II (motor function), UMSARS IV (global disability) and the sum of UMSARS I+II+IV. The strongest associations were with UMSARS I and UMSARS I+II+IV (family wise error corrected with $p<0.05$). All these correlations were confirmed with the ROI analysis. In the subgroup of MSA-P, bilateral putamen and right pallidum were negatively correlated with all UMSARS sub-scales (except right pallidum with UMSARS IV). We did not find correlation in the subgroup of MSA-C. VBM and ROI analyses with CVAT were nonsignificant. **Conclusion:** To our knowledge, our study is the first to highlight negative correlation between metabolism of putamen and pallidum and clinical disability according to the UMSARS. We did not find abnormal cerebral metabolism according to the autonomic dysfunction; this result is congruent with a medullar predominant mechanism of dysautonomia in MSA. The metabolism of putamen and pallidum is more than a diagnosis tool in MSA, it could be an additional quantitative tool to monitor the disease progression.

EP-0419

What is the diagnostic accuracy of FDG-PET in the Atypical Parkinsonian Syndromes

A. Buschiazzo[1], A. Chincarini[2], D. Volterrani[3], G. Puccini[3], B. Paghera[4], U. P. Guerra[5], M. Gregianin[6], V. Fiore[6], S. Sestini[7], C. Mazzeo[7], A. Cistaro[8], F. Ticconi[1], D. Arnaldi[9], G. Sambuceti[1,10], S. Morbelli[10], F. Nobili[9]; [1]Department of Health Sciences, University of Genoa, Genoa, ITALY, [2]National Institute of Nuclear Physics (INFN), Genoa section, Genoa, ITALY, [3]Department of Translational Research and Novel Technologies, University of Pisa, Pisa, ITALY, [4]Nuclear Medicine Spedali Civili and University of Brescia, Brescia, ITALY, [5]Nuclear Medicine Fondazione Poliambulanza-Istituto ospedaliero, Brescia, ITALY, [6]Nuclear Medicine Unit, San Giacomo Hospital, Castelfranco Veneto, ITALY, [7]Department of Diagnostic Imaging, Nuclear Medicine Unit N.O.P.-S. Stefano, U.S.L. Toscana Centro, Prato, ITALY, [8]Positron Emission Tomography Centre IRMET S.p.A. Euromedic inc., Turin, ITALY, [9]Clinical Neurology, Department of Neuroscience (DINOGMI), University of Genoa and IRCCS AOU, San Martino-IST, Genoa, ITALY, [10]Nuclear Medicine Unit, IRCCS AOU San Martino-IST, Genoa, ITALY.

Background: Atypical Parkinsonian Syndromes(APS) are a cluster of different pathologies including Progressive Supranuclear Palsy(PSP), Multiple System Atrophy(MSA), Cortical Basal Syndrome(CBS) and Dementia with Levy Bodies(DLB), with their variants especially numerous and intriguing in PSP and CBS. Classically, they can be difficult to be distinguished from Parkinson Disease(PD) only on a clinical ground, especially in the mild stages. The aim of this study was to characterize the different FDG-PET brain metabolic pattern in these pathologies with PD taken as a control. **Subjects and Methods:** We retrospectively enrolled 113 patients (mean-age 70±8; mean-MMSE score=23±5) with APD from six Italian center (Genoa, Brescia, Pisa, Turin, Prato and Castelfranco Veneto) in the frame of a spontaneous, multicenter study promoted by the Neurology study group of the Italian Association of Nuclear Medicine(AIMN). Patients were submitted to FDG-PET at the time of diagnosis, which was then clinically established after at least a 1-y follow-up (unblinded to the results of FDG-PET). We divided patients based on diagnosis into 25PSP, 13MSA, 22CBS, 28DLB and 25PD. FDG-PET scans were preprocessed with SPM on an AAL atlas, to get 120 intensity-averaged ROIs. Overall intensity normalization was taken on the whole brain. Pattern

analysis was carried out with bi-clustering and correlation-networks techniques. For each clinical diagnosis class, subjects were clustered using hierarchical methods to give one or more subclass sharing similar ROI values. For each subclass we computed the correlation networks, finding a number of patterns which are expected to be characteristic of diagnosis class/subclass. Finally, all dataset was projected on the patterns, giving out a single score per subject and per pattern. A leave-k-out procedure was then applied to estimate the classification performance. **Results:** The main results show that it is possible to discriminate among diagnosis class with relatively high accuracy for all pathology classes, if we make use of different patterns. For instance: the Area Under the Curve (AUC) was 0.93 on CBD vs. PSP, and 0.98 on DLB vs. PSP (projection on the PSP pattern); 0.94 on DLB vs. MSA and 0.85 on MSA vs. PD when projected onto the DLB pattern. **Conclusion:** FDG-PET can be of help in the differential diagnosis between APS and PD on the one hand, and among the various forms of APS. These results highlight the diagnostic accuracy of metabolic brain network pattern computations and further stress the relevance of specific-Parkinsonism related metabolic patterns reported in independent patient groups.

EP-0420

Negative correlation between dopamine transporter activity at caudate nucleus and the symptom duration at FP-CIT PET/CT in Parkinson disease

J. Park[1], J. Park[1], A. Lee[1], J. Hwang[1], S. Park[2]; [1]Soonchunhyang University Bucheon Hospital, Bucheon, KOREA, REPUBLIC OF, [2]Soonchunhyang University Seoul Hospital, Seoul, KOREA, REPUBLIC OF.

Purpose: To evaluate any significant relationship between subregional striatal dopamine transporter activity (DTA) in FP-CIT PET and the clinical data in Parkinson disease (PD). **Subjects & Methods:** Fourty PD without cognitive impairment or vasculopathy and 6 age matched non-PD(3 DIP, 1 ET and 2 Jaw tremor) FP-CIT PET/CT (128m PET/CT scanner) at 3 hours after injection from 2015 to March. 2016 were investigated. FP-CIT PET maximum intensity projection (MIP) images were visually classified into three groups (group I [n=17], decreased DTA in putamen; group II (n=13), wide angle between caudate and putamen with preserved long shape of caudate nucleus; group III (n=10), wide angle between caudate and putamen with short caudate body-tail). Four subregional striatal analysis were performed in (caudate nucleus head [CAU_H]/body-tail [CAU_B], putamen anterior [PUT_A]/posterior [PUT_P]) and background analysis in cerebellum using simple volume of interest. **Result:** The symptom duration showed significant difference among the visual groups (group I, II and III, 1.4 ± 1.8 yrs, 1.9 ± 1.4 yrs and 4.0 ± 2.4 yrs, p<0.01). There was no significant difference of sex, age (68.2 ±9.0 yrs, 70.9 ± 8.2 yrs, 68.3 ± 12.1 yrs) and Hoen-Yahr stage (1.7 ± 0.7, 1.9 ± 0.7, 2.3 ± 0.9) among the groups. Striatal subregional DTA ratios to those of non-PD were significantly different (group I, II, III, 74.1% [SD 11.5], 63.5% [18.9], 47.9% [16.8] for CAU_H, 73.1% [11.7], 65.3% [20.0], 47.1% [24.5] for CAU_B; 64.6% [11.6], 50.6% [15.6], 40.2% [14.6] for PUT_A, 40.9% [9.8],

35.8% [11.5], 27.9% [8.9] for PUT_P, respectively. We observed negative correlation of DTA % of caudate nucleus (Spearman rho = -0.48, p <0.005 for % CAU_H, rho = -0.47, p <0.005 for % CAU_B, rho = -0.36, p <0.05 for % PUT_A) with the symptom duration. However putamen posterior did not show significant correlation with the symptom duration (rho = -0.24, p=ns for % PUT_P). We observed significant negative association between symptom durations and both DUR of CAU_H (-2.7, p<0.01), CAU_B (-2.8, p<0.01) using linear regression model analysis. **Conclusion:** DTA at caudate nucleus showed strong negative correlation between the symptom duration of PD. In use of high resolution of FP-CIT PET imaging, DTA at caudate nucleus shows a significant correlation the symptom duration. And FP-CIT PET MIP imaging can provide useful information about visual subregional grading of both caudate nucleus and putamen for PD progression.

Neurosciences: Data Analysis & Quantification

EP-0421

Cerebral ¹⁸F-FDG PET in macrophagic myofasciitis : an individual SVM based approach for computer aided diagnosis

P. Blanc-Durand[1], A. van Der Gucht[1], E. Guedj[2], M. Abulisi[1], M. Sebaiti[1], A. Verger[3], L. Lerman[1], F. Authier[1], E. Itti[1]; [1]Henri-Mondor, Créteil, FRANCE, [2]La Timone, Marseille, FRANCE, [3]CH Strasbourg, Strasbourg, FRANCE.

Introduction: Macrophagic myofasciitis (MMF) is an emerging condition with highly specific myopathological alterations. As a peculiar spatial pattern of a cerebral glucose hypometabolism involving occipito-temporal cortex and cerebellum have been reported in those patients we built a support vector machine (SVM) to classify patients between healthy or macrophagic myofasciitis (MMF) status using ¹⁸F-FDG brain scans. **Methods:** ¹⁸F-FDG PET brain images of 119 patients with MMF and 64 healthy subjects were retrospectively analyzed. The whole-population was divided into two groups; a training set (100 MMF, 44 healthy subjects) and a testing set (19 MMF, 20 healthy subjects). Dimensionality reduction was performed using t-map from statistical parametric mapping (SPM) and a SVM with a linear kernel was trained on the training set. **Results:** The SPM12 analysis on the training set exhibited the already reported hypometabolism pattern involving occipito-temporal and fronto-parietal cortices, limbic system and cerebellum. The SVM procedure, based on the t-test mask generated from the training set, correctly classified MMF patients of the testing set with following sensitivity, specificity, positive predictive value, negative predictive value and accuracy: 89%, 85%, 85%, 89%, and 87%. **Conclusion:** We developed an original approach including a SVM to classify patients between healthy or MMF metabolic brain profile using ¹⁸F-FDG-PET. Machine learning algorithms are promising for computer-aided diagnosis but will need further validation in prospective cohorts.

EP-0422

An investigation for intra-observer reproducibility of FP-CIT SPECT in patients with DLB

A. Okizaki, M. Nakayama, K. Takahashi; Asahikawa Medical University, Asahikawa, JAPAN.

I-123 labelled 2β-carbomethoxy-3β-(4-iodophenyl)-N-(3-fluoro-propyl) nortropane (FP-CIT) single photon emission CT (SPECT) imaging is useful for evaluation of parkinson's disease, parkinson syndrome, and dementia with lewy bodies (DLB). A quantitative or semi-quantitative analysis is useful for the evaluation of FP-CIT accumulation. Tossici-Bolt et al. reported a method to calculate the FP-CIT specific binding ratio in striatum (SBR). The method is frequently used in our country, however, SBR is sometimes unstable, and the reproducibility may be limited. The purpose of this study is to investigate the intra-observer reproducibility in patients with DLB using Bolt's method. Moreover, we devised modified method to improve the reproducibility. The second purpose of this study is to evaluate the intra-observer reproducibility of our method. Eighty-six striatum from 43 patients with DLB were studied. The diagnoses of DLB were made clinically by a psychiatrist. FP-CIT SPECT scans were performed, and the SBR were evaluated twice independently by a nuclear medicine physician using Bolt's (SBR-Bolt's) and our method (SBR-ours). In our method, striatal VOI were semi-automatically placed based on accumulation of FP-CIT and volume of striatum. Reference VOI was also automatically positioned based on weighted histogram and 3-dimensional relationships to the striatum. The weight parameters for the histogram were related to the distance from center of brain on the image, consequently the histogram had bifid peak. Where, first peak may represent the voxels outside the body, and second peak may represent tracer uptake inside the brain. Therefore, we assumed between the first and second peak was comparable to the surface of brain. Wilcoxon matched-pairs signed rank test was used to test the intra-observer reproducibility. The average of SBR-Bolt's with first measurement was 2.63 ± 1.31, and it with second measurement was 2.52 ± 1.27. There was statistically significant difference between SBR-Bolt's with first and second measurement (p < 0.01). On the other hand, SBR-ours with the measurements were completely matched in all striatum. The average of SBR-ours were 2.90 ± 0.58. The intra-observer reproducibility by Bolt's method was limited in this study. On the other hand, our method was reproducible and therefore might be useful to calculate SBR in patients with DLB.

EP-0423

Impact of Computer Aided Diagnosis (CAD) on DaTSCAN reporting: a pilot study

J. Taylor[1], M. Kinsella[1], Y. Yong[1], I. Azam[1], R. Balachandar[1], V. Balian[1], M. King[1], C. Lo[1], O. Bandmann[2], J. Fenner[2]; [1]Sheffield Teaching Hospitals, Sheffield, UNITED KINGDOM, [2]University of Sheffield, Sheffield, UNITED KINGDOM.

Introduction: Numerous machine learning algorithms have been applied to [123I]FP-CIT (DaTSCAN) images, many of which have demonstrated accurate binary classification of patients into diseased or healthy groups. However, little research has been conducted into the impact of such algorithms when used as an aid to diagnosis in the clinic. The aims of this pilot study were to: 1) Assess the impact of a CAD algorithm on reporting performance 2) Obtain feedback based on radiologists' experience of using CAD for DaTSCAN. **Methods:** In the context of automated classification of DaTSCAN images, an established classification method was selected, incorporating a Support Vector Machine with input features based on Principal Component Analysis of image voxel intensities. Output from the algorithm was a probability, indicating the likelihood of a Parkinsonian Syndrome being present. Two sets of historical data from Sheffield Teaching Hospitals were used: 305 images for algorithm training and 30 images for evaluating radiologist performance (the test set). Assessed independently, the algorithm achieved an accuracy of 0.97 on the test set. Seven junior radiologists were trained to interpret DaTSCAN images and were then challenged to classify each patient in the test set according to a 5 point scale (where 1 = definitely abnormal and 5 = definitely normal), without the aid of CAD. In phase two of the pilot study the reporting procedure was repeated twice, once with and once without the aid of CAD. Each radiologist was given a questionnaire to assess their opinions of reporting with CAD assistance. **Results:** The mean area under the Receiver Operator Curve (AUROC) was 0.97 and 0.95 for the repeated reporting exercise, without exposure to CAD. AUROC was 0.97 after CAD had been introduced. The CAD system caused a change in classification score in 15% of cases. Analysis of questionnaire results showed that all radiologists felt the CAD system had either a small or moderate impact on their reporting decisions and a majority reported that the CAD tool would be of benefit if used as a training tool. A majority of the participants felt that the addition of a localiser, showing the position of likely abnormalities, would be of assistance during reporting. **Conclusion:** This investigation demonstrates that CAD can have a moderate impact on radiologists' reporting decisions. However, for this small pilot study metrics of overall performance were relatively unchanged as a result. Performance gains may be more apparent for image sets containing more borderline cases.

EP-0424

Low-dose PET/MRI of patients with non-lesional epilepsy

J. Cal-Gonzalez[1], G. Schramm[2], K. Vunckx[2], I. Rausch[1], L. Shiyam Sundar[1], J. Nuyts[2], T. Traub-Weidinger[3], T. Beyer[1]; [1]QIMP group, Center for Medical Physics and Biomedical Engineering, Medical University of Vienna, Vienna, AUSTRIA, [2]KU/UZ Leuven, Department of Imaging and Pathology, Division of Nuclear Medicine, Leuven, BELGIUM, [3]Division of Nuclear Medicine, Department of Biomedical Imaging and Image-guided Therapy, Medical University of Vienna, Vienna, AUSTRIA.

Aim: To evaluate the effect of reducing the ^{18}F-FDG injected activity on the quantitative accuracy of brain PET images of patients with non-lesional epilepsy. **Materials and Methods**: Five healthy volunteers and four pilot patients with non-lesional

epilepsy have been scanned on a Siemens Biograph mMR PET/MR system. Acquisitions were performed in listmode (LM) for 60 min immediately after the injection of (226±18) MBq of ^{18}F-FDG. A virtual reduction of the injected dose levels was performed by randomly removing counts from the LM data prior to image reconstruction. We used LM-data from the last 10 min of the scan; images were reconstructed with and without post-filtering. The following virtual activities were simulated: 50%, 35%, 20% and 10% of the total activity. In addition to the standard (OSEM) and resolution recovery (PSF) reconstructions available with the vendor tools, we evaluated two maximum-a-posteriori (MAP) algorithms: the AMAP and asymmetrical Bowsher methods. Four cylindrical volumes of interest (VOI) located in the white matter (WM) and one covering the entire gray matter (GM) were defined. In addition, we evaluated a VOI in the epilepsy focus (lesion), identified from the PET image. The GM-to-WM ratio (5 volunteers + 4 patients), uniformity within the WM (5+4) and lesion-to-GM ratio (4) were evaluated. **Results**: In general, the GM-to-WM ratios were reduced when reducing the injected activity, while the lesion-to-GM ratios were slightly increased (worse identification of the epileptic focus). The uniformity within the WM was degraded when reducing the activity. These dependences on the injected activity were reduced when applying a post-filter to the images or when increasing the prior weights in the MAP reconstructions. Visual inspection of the images reveals no substantial changes in the quality of the images up to 35% of the total activity level. For this case we observed: a decrease of the GM-to-WM ratio between -1.0% (PSF, 3 mm Gaussian post-filter) and -2.6% (AMAP, low weights); an increase of noise between 23.7% (PSF, 3 mm Gaussian post-filter) and 57.2% (AMAP, low weights); and a increase of the hypometabolic-to-GM ratio between 0.2% (AMAP, high weights) and 2.7% (AMAP, low weights). Higher image contrast at similar noise level was observed in the MAP reconstructions (higher GM-to-WM and lower lesion-to-GM ratio values). **Conclusions**: The evaluations performed in this work suggest that injected activity can be potentially reduced up to 35% without substantial changes in the quantification accuracy if adequate reconstruction settings are used.

EP-0425

The effect of image reconstruction algorithms on topography of characteristic metabolic brain network for Parkinson disease

L. Jensterle[1], P. Tomše[1], M. Grmek[1], Z. Pirtošek[2], V. Dhawan[3], D. Eidelberg[3], Y. Ma[3], M. Trošt[2]; [1]University Medical Centre Ljubljana, Department of Nuclear Medicine, Ljubljana, SLOVENIA, [2]University Medical Centre Ljubljana, Neurology Department, Ljubljana, SLOVENIA, [3]The Feinstein Institute for Medical Research, Center for Neurosciences, New York, NY, UNITED STATES OF AMERICA.

Introduction: We have recently identified and cross-validated a characteristic metabolic brain network associated with Parkinson Disease (PD) in Slovenian population - PD Related Pattern (PDRP-Slovenia). It is currently not known how this pattern and its clinical performance change with respect to the use of various image reconstruction methods available. Our objective was to investigate the effect of different image reconstruction algorithms on network topographies and their diagnostic accuracy in discriminating PD patients from Normal Controls (NC). **Materials and Methods:** We used 18F-FDG-PET scans of 20 PD patients and 20 NC acquired with Siemens Biograph mCT. Scaled Subprofile Model/Principle Component Analysis (SSM/PCA) was performed to identify PDRP-Slovenia from images reconstructed using six reconstruction algorithms: FBP, FBP+TOF, OSEM (iterations 6, subsets 21), OSEM+TOF (6, 24), OSEM+PSF with incorporated point spread function (6, 21) and OSEM+PSF+TOF (6, 24). Differences between the six patterns were assessed by comparing the region weights in a set of 30 standardized volumes of interest (VOIs) and on a voxel-by-voxel basis over the whole brain, ability to discriminate PD patients and NC, ROC analysis, and correlation with clinical motor ratings for PD. **Results:** Region weights of the patterns from the images reconstructed by the six algorithms highly correlated with each other (r≥0.995; p<0.0001). Expressions of PDRP-Slovenia were significantly elevated in PD subjects relative to NC, for each version of PDRP-Slovenia (p<0.0001). All six patterns manifested good diagnostic accuracy and at the optimal cut-off of pattern expression showed specificity >90%, and sensitivity of 85% for OSEM+PSF and OSEM+PSF+TOF and specificity/sensitivity of >75% for others. PDRP-Slovenia subject scores significantly correlated with MDS-UPDRS-III ratings (r≥0.47; p<0.05). **Conclusion:** Our study confirms that PDRP-Slovenia is highly consistent across different image reconstruction algorithms, with small deviations between analytical and iterative algorithms. These findings further prove that PDRP provides a robust and reproducible imaging biomarker for Parkinson's disease irrespective of image reconstruction techniques.

EP-0426

Application of Attenuation Correction for Quantitative Brain Perfusion SPECT in Patients with Dementia

A. K. Kondakov[1], D. Y. Mosin[2], D. S. Kharina[2], A. V. Grechko[3], I. A. Znamenskiy[1]; [1]Pirogov RNRMU, Moscow, RUSSIAN FEDERATION, [2]Central Clinical Hospital of the RAS, Moscow, RUSSIAN FEDERATION, [3]Federal Research and Clinical Center of Intensive Care Medicine and Rehabilitology, Moscow, RUSSIAN FEDERATION.

Purpose of this study is to evaluate different methods of attenuation correction (AC) in SPECT/CT for quantification of regional cerebral blood flow (rCBF) in patients with different types of dementia and influence of each method on the study diagnosis. Twenty brain perfusion SPECT studies with 99m-Tc-HMPAO were retrospectively selected for this study: 7 cases represented Alzheimer disease, 5 cases - vascular dementia, 3 cases - fronto-temporal degeneration and 5 cases were included as control subjects. Brain perfusion tomograms were reconstructed by iterative algorithm with application of Chang's AC, CT-based AC and without attenuation correction for each study. For each AC method, rCBF was quantified using Lassen's equation (alpha value 1,5, reference rCBF in cerebellum 60 ml/100 g/min) in regions of interest (ROIs) corresponding to basal ganglia and

frontal, temporal (anterior and posterior parts), parietal and occipital lobes on the same levels. Number of counts and calculated rCBF were compared between methods of AC and non-AC rCBF calculations with Wilcoxon test for paired samples. All SPECT images were blindly reviewed by experienced physician and final diagnosis in report were compared between methods of AC. As a result of the study it was found that number of counts in selected ROIs and calculated rCBF hadn't stitistically significant difference in comparison of Chang's and CT-based AC methods (p>0.05). On the other hand, each of AC methods was significantly different compared with non-AC studies: in non-AC methods number of counts was lower (Chang's AC p=0,006, CT-based AC p=0.0048) and rCBF was higher (Chang's AC p=0,017, CT-based AC p=0.017). Average rCBF in grey matter of unaffected lobes was 55.3 ml/100 g/min for non-AC reconstructions, 48.2 ml/100 g/min for Chang's AC and 47.9 ml/100 g/min for CT-based AC. In the final reports there were no significant difference between diagnoses, and both methods of AC and non-AC images correlate with high correlation coefficient. Study showed that different methods of AC provide comparable results for rCBF calculation, but significantly differ from rCBF's calculated in non-AC images. This finding confirms results of previous studies and points out the need for proper identification of the study parameters by interpreting physician. The choose of AC method or rejection of AC don't influence on image interpretation by physician in patients with dementia and don't lead to a shift in the diagnosis. Chang's AC method is preffered due to absence of additional radiation exposure of the patient.

EP-0427

Comparison of an image-based to an atlas-based set of volumes of interest for DaTScan quantification

R. Fahmi, S. Zuehlsdorff; Siemens Healthineers, Knoxville, TN, UNITED STATES OF AMERICA.

Aim: The aim of this study was to compare the performance of two sets of striatal volumes of interest (VOIs) for semi-quantitative evaluation of Parkinson's disease (PD) using ^{123}I-Ioflupane SPECT (DaTScan) images. **Materials and Methods:** The atlas-based VOIs were created by editing the standard Automated Anatomical Labeling (AAL) striatal regions. The image-based VOIs were generated by segmenting the striatum from a DaTScan template that was created in the MNI space from a set of 42 spatially and intensity normalized DaTScan images (R. Buchert et al, Nuc. Med. Comm.'2015). The image-based VOIs were enlarged to ensure complete enclosure of the anatomical structures even in cases of inaccurate stereotactic normalization. Both sets of VOIs were composed of caudate, anterior/posterior putamen, and were mirrored around the brain midline. Distribution volume ratios (DVRs) were computed on DaTScan images registered to the MNI DaTScan template, using 100% (resp. 75%) of voxels with the highest uptake within the atlas-based (reps. image-based) VOIs. VOIs were automatically placed and their position adjusted on the registered images and no further manual repositioning of VOIs was performed. Correlations of mean ratios between the two methods were calculated for 40 Healthy controls (HC) and 50 baseline-PD subjects from the PPMI (www.ppmi-info.org) database. In addition, DaTScan images of 153 HC subjects from the PPMI database were used to generate reference values, for each set of VOIs, as a function of age. The corresponding regression lines together with the upper/lower bounds (±95% CI) were used to classify the 90 test subjects as either HC or PD based on their regional DVR values after correction for age effect. **Results:** Correlation of mean ratios between the two sets of VOIs were: caudate (0.915), putamen (0.957), anterior putamen (0.957), posterior putamen (0.945), and striatum (0.983). Overall, using mean of left and right DVR values, 99.16% (resp. 72.8%) classification accuracy was achieved with the image-based VOIs for HC (resp. PD), and 95.4% (resp. 69.6%) accuracy with the AAL-based VOIs for HC (resp. PD). The best PD classification was obtained with posterior putamen for both methods (43/50 or 86%), whereas for HC data all regional DVRs led to ~100% accuracy for both methods. **Conclusion:** The two tested sets of VOIs were shown to perform equally well in classifying HC subjects, however the enlarged image-based VOIs led to an overall better classification accuracy for PD subjects. This is mainly due to robustness of the image-based VOIs to registration inaccuracies.

EP-0428

Comparison of tissue time activity curve based image derived input function estimation methods in simulation for non-invasive CBF imaging

N. Kudomi[1], H. Watabe[2]; [1]Faclty Of Medicine, Kagawa University, KAGAWA, JAPAN, [2]Cyclotron and Radioisotope Center, Tohoku University, Sendai, JAPAN.

Aim: Quantification of cerebral blood flow (CBF) is important for the understanding of normal and pathologic brain physiology. When CBF is assessed using PET and $H_2^{15}O$, calculation requires input function, which requires invasive arterial blood sampling, and some methods have been proposed to derive an image derived input function (IDIF)[1-3] using tissue time activity curves (TACs). The aim of the present study was to compare those methods by testing accuracy and precision in simulation. **Methods:** We tested three procedures: input expression, tissue TAC (tTAC) division, and optimization. For the input expression, we tested two types, differential-based expression using tTAC and its derivative with rate parameters (Diff-based) [3], and integration based (Integ-based) [1,2] using the tTAC and its integration with the rates. For tTAC division, area under the curve (AUC-based) [3], moment-based clustering [2], and K-means-based methods were tested. For optimization, all rates were estimated in a single optimization procedure applying all tTACs (Single-opt), and in multiple optimization procedures for all possible pairs of two tTACs (Pair-opt). One hundred of images were generated with noise based on water kinetics. CBF distribution and noise level was obtained from our clinical data as in our previous study [3]. Using the generated images, inputs were estimated. For the estimated inputs, CBF was calculated using a tTAC generated assuming CBF=0.5 ml/min/g, and bias and deviation were ob-

tained. **Results:** The obtained biases and deviations were: for AUC-based dividing, 1.9±2.2% and 5.0±0.9% for Single-opt and Pair-opt with Diff-based method, and -3.3±0.6 and -0.2±0.4% for Single-opt and Pair-opt with Integ-based method. For Cluster mode, those were 15.2±0.34% and 0.8±0.9% for Single-opt and Pair-opt with Diff-based method, and -14.4±0.6 and 1.1±0.7% for Single-opt and Pair-opt with Integ-based method. For K-means mode, those were -0.5±0.48% and -5.7±1.5% for Single-opt and Pair-opt with Diff-based method, and 1.2±0.3 and -2.9±2.6% for Single-opt and Pair-opt with Integ-based method. **Conclusion:** The presented results made reveal that the bias and deviation in CBF was the smallest by the Integ-based with Pair-optimization in AUC-based dividing method among the applied combinations, suggesting that combination of estimation procedure would be the best for IDIF. Reference: [1] Watabe et al J Cereb Blood Flow Metab, 1996;16:311-9. [2] Naganawa et al Neuroimage 2008;40:26-34. [3] Kudomi et al Phys Med Biol 2016;61:5755-67.

EP-0429

Validation of non-invasive tracer kinetic analysis of ^{18}F-Florbetaben PET using a patient-friendly dual time-window acquisition protocol

S. Bullich[1], A. Jovalekic[1], N. Koglin[1], G. Becker[2], S. De Santi[3], O. Sabri[2], H. Barthel[2]; [1]Piramal Imaging GmbH, Berlin, GERMANY, [2]Department of Nuclear Medicine, University Hospital Leipzig, Leipzig, GERMANY, [3]Piramal Pharma Inc, Boston, MA, UNITED STATES OF AMERICA.

Introduction: Amyloid PET quantification is necessary in longitudinal observation studies and in anti-Aβ therapeutic trials. Currently, most of the studies are analyzed using semi-quantitative methods such as standardized uptake value ratios (SUVRs) because of their simplicity. However, a SUVR-based approach may be biased by blood flow or tracer clearance changes. This bias is especially important in therapeutic trials. We have already shown for ^{18}F-Florbetaben (FBB) that non-invasive (cerebellar cortex reference) kinetic measures and SUVRs correlated well with the invasive (arterial blood sampling) kinetic modeling data, and that SUVRs overestimated DVRs by 21% (Becker et al., J Nucl Med. 2013). The objective of this study was to validate a non-invasive kinetic modeling approach using a patient-friendly acquisition protocol. **Subjects and Methods:** Twenty subjects (10 ADs / 10 HVs) were scanned dynamically up to 140 min. Arterial samples were collected during scan acquisition and corrected for blood radioactive metabolites. Full tracer kinetic analysis using time-activity curves (TACs) and arterial input function was performed using a 2-tissue compartment model (2TC). Binding potential (BP_{ND}) obtained from the full kinetic analysis was compared to non-invasive tracer kinetic methods (simplified reference tissue model (SRTM), and multilinear reference tissue model (MRTM2)). Cerebellar gray matter was used as reference region. Different approaches to shorten and/or interrupt acquisition times were compared to the results of the invasive full acquisition (0-140 min) modeling approach (standard of truth, SoT). When an interrupted acquisition was used, the missing points of the time-activity curve were interpolated

using the average TAC scaled using the function that provided best fitting to the acquired points ($TAC_{interpolated}=(a+b \cdot time) \cdot TAC_{average}$ or $TAC_{interpolated}=(a \cdot e^{-b \cdot time}+c) \cdot TAC_{average}$ where the parameters were determined using least-squares. The average TAC was based on data of all subjects leaving out the subject being interpolated. **Results:** A 0-30 and 120-140 min dual time-window dynamic non-invasive acquisition protocol provided the best compromise between patient comfort and quantification accuracy. Here, an excellent agreement was found for the BP_{ND} as compared to the SoT (2TC) ($BP_{ND}= 0.00+ 0.80 \cdot BP_{ND,2TC}$, $R^2=0.82$ (MRTM2); $BP_{ND, SRTM}= 0.02+ 0.72 \cdot BP_{ND,2TC}$, $R^2= 0.74$ (SRTM)). Excellent agreement was found also between BP_{ND} obtained using full and interrupted acquisition protocols ($BP_{ND,INT}= 0.01+ 1.00 \cdot BP_{ND,FULL}$, $R^2=0.97$ (MRTM2); $BP_{ND,INT}= 0.05+ 0.92 \cdot BP_{ND,FULL}$, $R^2=0.93$ (SRTM)). **Conclusions**: This study demonstrates the feasibility to perform accurate kinetic modeling of FBB PET scans using a non-invasive protocol with two imaging time-windows, thus promising increased patient comfort.

EP-0430

Validation of a dose reduction simulation for neurodegenerative brain indications in 18F-FDG PET/MR

M. Soret[1], J. Maisonobe[1], M. Khalifé[2], A. Kas[1]; [1]APHP, Hôpital Pitié-Salpêtrière, Paris, FRANCE, [2]Institut du Cerveau et de la Moëlle epinière, Paris, FRANCE.

Aim: Given the high sensitivity of PET/MR and considering that a longer acquisition time is needed in brain neurodenerative ^{18}F-FDG indications due to MRI sequences, a reduction of injected activity might be feasible without degradation of image quality. However, the intra-individual study of the influence of different injected doses is not ethical. We validated a method to retrospectively simulate dose reduction using a partial reconstruction of the acquired list mode data on a phantom acquisition. **Materials and Methods**: Acquisitions were performed with a 3D Hoffman phantom filled with 15 MBq of ^{18}F-FDG using the SIGNA PET/MR (GE Healthcare) system. List-mode data were recorded during 20-minutes, simulating a brain patient acquisition (PET_{STD}). This acquisition was also used to generate a 10-minutes image (PET_{simuLD}) to simulate a low-dose injection, reducing the amount of data collected. A second acquisition of 20 minutes was performed 110 minutes later to obtain an acquisition with half the activity (PET_{LD}). For all acquisitions, the attenuation map was derived from a CT scan of the phantom. Data was reconstructed using OSEM3D (all corrections applied) but with different parameters to obtain an equivalent signal-to-noise ratio in all PET reconstructions. SUV was measured in white and grey matter, segmented using a CT scan of the phantom. **Results:** The number of prompt coincidences detected for the Hoffman phantom between low dose count rate during 20 minutes and simulation of low dose with standard count rate during 10 minutes was 125.7 millions and 121.6 millions, respectively. A good visual agreement was found between PET_{LD} and PET_{simuLD}. The difference introduced by simulating low dose with shorter acquisition time (PET_{simuLD}) compared to actual low dose acquisition (PET_{LD}) on mean SUV was -0.2%

and +0.3% in white and grey matter, respectively. The impact on grey to white matter ratio was of 0.5%. **Conclusions:** These Hoffman phantom acquisitions demonstrated that activity dose reduction by a factor 2 is visually and quantitatively similar to a reduction of PET duration by the same factor in our medical context. The assumption that tracer dose reduction is equivalent to a reduction of PET duration by the same factor is a simplification of the complex process of PET data acquisition; however, it is valid for optimizing dose in brain neurodegenerative FDG imaging in patients for the range of activity used in clinical settings.

EP-0431

PET Kinetic Modeling with Arterial Sampling of ^{18}F-Choline Uptake in Patients with a Suspected Initial Diagnosis of High Grade Glioma

S. Rubí[1,2], *P. Bibiloni*[3], *M. Galmés*[4], *M. Toscano*[1], *M. Oporto*[1], *M. Villar*[1], *M. Ortiz*[1], *J. Valera*[1], *G. Matheu*[1], *J. Molina*[1], *M. Brell*[1,2], *M. González*[3], *A. Mir*[3], *C. Peña*[1,2]; [1]*Hospital Universitari Son Espases, Palma de Mallorca, SPAIN,* [2]*Institut d'Investigació Sanitària Illes Balears (IdISBa), Palma de Mallorca, SPAIN,* [3]*Grup Scopia, Universitat de les Illes Balears (UIB), Palma de Mallorca, SPAIN,* [4]*Hospital QuirónSalud Palmaplanas, Palma de Mallorca, SPAIN.*

Purpose/Introduction: There is an increasing interest in using ^{18}F-fluoromethylcholine (FCho) as a PET radiotracer for brain tumor assessment. Following its transport across blood-brain-barrier (BBB), FCho is intracellularly phosphorylated. This preliminary study aims at quantifying FCho tumor uptake using kinetic modeling in patients with newly diagnosed high-grade-glioma. **Subjects & Methods:** Seven patients with suspected initial diagnosis of high-grade-glioma underwent a 45 min dynamic brain PET scan immediately after a FCho bolus injection (5 MBq/Kg). Plasma input functions were obtained using manual arterial blood sampling from a radial catheter, and parent fractions for metabolite correction were determined by thin-layer-chromatography. Tumoral time-activity curves were derived from a 70%-threshold VOI drawn in averaged PET frames. These experimental data were fitted to several 1- and 2-tissue-compartment models, and the selection was based on the Akaike-Information-Criteria (AIC). Additionally, the effect of scan time (30 vs 45 min) on the estimation of the rate constants was evaluated. The kinetic parameters were also compared to the SUV_{max} of the tumor. **Results:** The 2-tissue-4-parameter model accounting for blood volume fraction (2T4k+vB), which yielded the lowest AIC score in 6/7 patients, was selected as the best model. Estimated values of the reversible step parameter k_4 were small compared to the other exchange rate constants: K_1 [range: 0.061-0.220 ml·cm^{-3}·min^{-1}], k_2 [0.049-0.930 min^{-1}], k_3 [0.109-0.712 min^{-1}], k_4 [0.002-0.029 min^{-1}], vB [0.041-0.142]. In 6/7 patients, these parameters were relatively unchanged after reducing the scan time from 45 to 30 min, being the k_3 the most affected one, with a mean change of 14.4% with respect to those at 45 min. The K_1 and the influx macroparameter $K_i=K_1*k_3/(k_2+k_3)$ were very robust with respect to scan time (mean change of 1.9% and 3.4%, respectively). One patient's model presented more unstable parameters (e.g. k_3 increased by 222%). Tumor SUV_{max} values were highly correlated to K_i (r^2=0.97), and to a lesser degree to K_1 (r^2=0.77). Following surgery, a glioblastoma was confirmed in five patients, while the other two had a final diagnosis of metastasis. **Discussion/Conclusion:** FCho uptake kinetics in the aggressive brain tumors studied is best explained by a 2T4k+vB compartmental model. Reliable estimates of rate constants seem achievable with a scan time as short as 30 min. Correlations in this small sample suggest that SUV_{max} adequately reflects the FCho influx rate (K_i), and that transport through the BBB (represented by K_1) might have a strong influence in FCho tumor uptake.

EP-0432

Assessment of the Impact of Repeat Scanning on Centiloid Scaling Values using PMOD Image Quantification Software

M. Battle, C. Buckley; *GE Healthcare, Amersham, UNITED KINGDOM.*

Introduction: The Centiloid scale, a standardised quantitative imaging analysis method for measuring the uptake of βamyloid imaging PET tracers in Alzheimer's disease (AD), has been promoted by the Global Alzheimer's Association Information Network (GAAIN), with established process pipelines reported by various groups [1,2]. We previously reported data showing the value of Centiloid scaling for [^{18}F]flutemetamol subjects. For those studies, images were acquired from 90 to 110 minutes post injection of [^{18}F]flutemetamol, and Standard Uptake Value ratio (SUVr) values were scaled to a [^{11}C]PiB-equivalent before conversion to Centiloid. Here we investigate the robustness of Centiloid scaling in subjects with test-retest scans, comparing the Centiloid values. The methodology of creating Centiloid values has an in-built subtraction of average healthy control SUVr's to zero, therefore providing a more robust measure than direct SUVr percentage differences. Also, the percentage differences in Centiloids are more closely associated with measures of binding potential (BP) percentage differences (BP can be approximated by SUVr-1)[3,4]. **Methods:** Using the Centiloid Volume of Interest (VOI) regions, previously established as an atlas in PMOD, [^{18}F] flutemetamol images for subjects imaged in Phase II with Alzheimer's disease (with retest scans acquired within one week of test scan) were processed using PMOD, following the methods described by Klunk *et.al.*[2]. SUVr for the VOI regions were generated, and Centiloid values calculated. These are presented, together with the SUVr differences, for the same images. These subjects were also processed using SPM8 (as described by Klunk *et al.*) in order to compare the PMOD- versus SPM8-supported Centiloid pipelines. **Results:** For the AD subjects test-retest scans, we found that the difference between test and retest scan was approximately 2% for SUVr, generated using PMOD with whole cerebellum reference region, and was 5% for SUVr-1. When converted to Centiloid values, there was approximately 5% difference in the values between test and retest scans. These results were comparable with the SPM8 pipeline, where the differences for both the SUVr-1 and the Centiloid values were again approximately 5% for test-retest subjects who had [^{18}F] flutemetamol SUVr's in the range 1.6 to 2.0. **Conclusions:** For

[¹⁸]flutemetamol, the test-retest difference, as obtained with the Centiloid cortex VOI with whole cerebellum as reference, when calculated on the Centiloid scale were approximately 5% average between test and retest. **References** 1. www.gaain.com 2. Klunk WE, *et al*. Alzheimer's & Dementia 11 (2015) 1-15 3. Klunk *et al*. Pages 10-11 4. Klumpers UM, *et al*. Nucl Med Commun. 2012;33:422-430.

EP-0433

xSPECT derived absolute SUV: An emerging accurate tool for I-123-ioflupane analysis

M. Jreige[1], F. Tabotta[1], M. Nicod Lalonde[1], R. Fahmi[2], N. Schaefer[1], G. Allenbach[1], J. O. Prior[1]; [1]Centre Hospitalier Universitaire Vaudois (CHUV), LAUSANNE, SWITZERLAND, [2]Siemens Medical Solutions USA, Inc., Knoxville, TN, UNITED STATES OF AMERICA.

Aim: Quantification of I-123-ioflupane uptake within basal ganglia using the latest SPECT scanners may add valuable precision in the diagnosis of neurodegenerative diseases of the nigro-striatal pathway. We investigated the role of absolute and relative SUV quantification of I-123-ioflupane in comparison to relative semi-quantitative metric methods (SSSA based on Flash-3D or xSPECT) in differentiating between normal and pathologic DATscan. **Methods:** In total, 7 individuals were scanned (Symbia Intevo, Siemens Healthineers) and images were reconstructed using iterative reconstruction (Flash 3D) and the xSPECT providing PET-like SUV values. Three scans were scored as normal and four as abnormal. Data were analyzed using Scenium. It co-registers individual tomographic data to a reference template and subsequently applies a standard set of volumes of interest (VOI), extracting in a fully-automated way mean regional counts and SUV values for the left and right caudate nucleus, putamen and striatum, as well as for the occipital region, taken as reference region for the calculation of the distribution volume ratio (DVR) and rSUV. We compared SUVmean and relative metrics techniques in normal and abnormal subgroups for each region of interest as well as the uptake asymmetry. **Results:** Absolute SUVmean, but not relative methods (SSSA based on Flash-3D or xSPECT), allowed to differentiate between normal and pathological DATscan in the caudate nucleus (p<0.002 vs. p>0.1). All methods detected the difference between normal and pathological, but with more pronounced significance using absolute SUVmean for putamen (p<0.0009 vs. p<0.006) and striatum (p<0.0005 vs. p<0.05). Quantitative xSPECT was able to detect significant asymmetry in caudate, putamen and striatum in pathological DATscan (p<0.03), while Flash-3D was not (p>0.1). There was significant asymmetry in pathological DATscan vs. normal DATscan in putamen and striatum (p<0.03) but not caudate nucleus (p>0.13) with meanSUV, while it was only detected in putamen with Flash-3d (p<0.03). The variation among "normal" DATscan is less pronounced with SUV (xSPECT) than with Flash-3D. When using the Putamen/Caudate ratio, all processing methods significantly made the difference between normal and pathological DATscan in our population. **Conclusions:** xSPECT-derived absolute SUV detected smaller differences in I-123-ioflupane uptake than the regular semi-quantitative approach. This has the potential for detecting earlier pathological changes or, with more accuracy, the difference between normal and pathologic areas.

EP-0434

Decline with Age in Normal Cerebral and Cerebellar Glucose Metabolism in Women and Men Determined by FDG PET/CT

F. Seifar[1], N. Parnianfard[1], C. Constantinescu[2], K. Shakouri[1], P. F. Høilund-Carlsen[2]; [1]Tabriz University of Medical Sciences, Tabriz, IRAN, ISLAMIC REPUBLIC OF, [2]Department of Nuclear Medicine, Odense University Hospital, Odense, DENMARK.

Aim: Age-related changes in cerebral and cerebellar glucose metabolism in women and men constitute the background for differentiation between pathological and physiological conditions. The aim of this study was to investigate by FDG PET/CT the change in glucose uptake in the cerebral and cerebellar hemispheres with normal aging in a population of healthy control subjects. **Method and Materials:** 42 healthy subjects, 15 women (57.8±10.9 years) and 27 men (50.1±16.2 years) underwent FDG PET/CT as part of a prospective study. Scans were acquired 180 minutes post tracer injection (4 MBq/kg) and analyzed using ROVER™ software (ABX, Radeberg, Germany). The brain was divided into 4 volumes of interest, two for left and right cerebral (Ce_L and Ce_R) and two for left and right cerebellar (Cb_L and Cb_R) hemispheres. FDG uptake was assessed using standard uptake values (SUV) per body weight. The liver SUVmean was used (according to EANM 2.0 guidelines) as the lower threshold for each patient, and the volume of all for hemispheres, their SUVmean, and the product of volume and SUVmean (SUVmean-total) were recorded. **Results:** The average values for the 15 females and 27 males were: (A) Females: Ce_L VOL 794.768cc, SUVmean 6.756±1.254, SUVmean-total 5406.01; Ce_R VOL 705.863cc; SUVmean 6.974±1.287; SUVmean-total 4971.111; Cb_L VOL 60.768cc, SUVmean 6.851±1.267, SUVmean-total 418.541; Cb_R, VOL 57.5cc, SUVmean 6.532±1.194, SUVmean-total 379.987. (B) Males: Ce_L VOL 877.635cc, SUVmean 6.685±1.279, SUVmean-total 5853.024; Ce_R VOL 843.362cc, SUVmean 6.625±1.06; SUVmean-total 5637.753; Cb_L VOL 67.547cc, SUVmean 6.686±1.268, SUVmean-total 449.118; Cb_R VOL 67.122cc, SUVmean 6.637±1.338, SUVmean-total 442.576. Average declines per age decade were: (C) Females: Ce_L VOL -4.09%, SUVmean -4.92%, SUVmean-total -7.28%; Ce_R VOL -4.94%, SUVmean -4.50%, SUVmean-total -7.44%; Cb_L VOL -0.39%, SUVmean -3.67%, SUVmean-total -4.23%; Cb_R, VOL -2.17%, SUVmean -1.93%, SUVmean -total -4.02%. (D) Males: Ce_L VOL -1.04%, SUVmean -3.49%, SUVmean-total -4.16%; Ce_R VOL -1.89%, SUVmean -3.66%, SUVmean-total -4.97%; Cb_L VOL -0.68%, SUVmean -2.90%, SUVmean-total -3.34%; Cb_R, VOL -0.20%, SUVmean -3.47%, SUVmean-total -3.43%. **Conclusion:** Using ROVER software, we found a significant age-related decline in mean and mean-total SUVs in both cerebral and cerebellar hemispheres. All male hemispheres were larger than corresponding female hemispheres, but the relative decline in FDG uptake with age was similar in men and women.

EP-0435

Assessment of False-Positive Results in SPM SPECT Group Comparisons

R. Ferrando, C. Pascovich, S. Parra, M. Langhain; Clinics Hospital, University of the Republic, Montevideo, URUGUAY.

Introduction: Recent concern has arisen about fMRI false-positive results in group comparisons using voxel-based parametric statistics. Although PET or SPECT analysis is simpler, false-positive rates remain almost unexplored. The objective is to assess the presence of false-positive results in a group comparison of SPECT images. **Subjects and Methods:** 54 normal controls evaluated by 99mTc-ECD SPECT in a Mediso Nucline Spirit DH-V gamma camera were divided in two similar groups of 27 individuals matched for age and gender. Group 1: 20-87 years, mean 47.5±21.1, 12 male; Group 2: 23-89 years, mean 47.0±18.6, 11 male. Scans were spatially normalized to the SPM SPECT template using default options and smoothed with a 16 mm FWHM. T-test were conducted in SPM8 with proportional scaling to cerebral global mean. Voxels were interrogated at p<0.01 FWE corr, p<0.001 uncorr and p<0.01 uncorr. Cluster level was extended to 100 voxels, p<0.05 uncorr and p<0.05 corr. Subsequently, two groups of 14 subjects with opposite ages were extracted from the same population. Group A: 22-34 years, mean 29.7±6.4, 6 male; Group B: 63-89 years, mean 72.1±9.0; 3 male. SPM analysis was repeated. **Results:** No significant voxels were detected when comparing Group 1 and Group 2 with a p threshold of 0.001 uncorr. At p<0.01 uncorr, Group 1 presented a cluster of lower perfusion (kE=298, p=0.212 uncorr) in left occipital cortex and Group 2 showed a cluster of lower activity in left posterior frontal white matter (kE=243, p=0.258 uncorr). Group B showed hypoperfusion compared to Group A in frontal, anterior cingulate and anterior temporal cortex, insula, basal ganglia and thalami (p<0.001 uncorr voxel level, p<0.05 corr cluster level). Widespread hyperperfusion was detected in Group B mainly affecting white matter. No clusters >100 voxels survived FWE correction. **Conclusion:** In a regular SPM SPECT group comparison no false-positive results were detected at a p<0.001 uncorr voxel value and no significant clusters (p<0.05 uncorr) were detected at a lower level of 0.01. Expected age differences were detected at p<0.001 uncorr but did nor survive FWE correction. Hyperactivity detected in elderly subjects can be interpreted as false-positive resulting from decreased whole brain blood flow. A p threshold of 0.001 uncorr at the voxel level and 0.05 uncorr for the cluster level seems to offer adequate results, and valid significant clusters may even be reported at a lower voxel p value. Correcting for multiple comparisons can significantly compromise sensitivity in SPECT studies.

Neurosciences: Miscellaneous

EP-0436

The Effect of Obesity on the Availability of Dopamine and Serotonin Transporter

K. Pak[1], Y. Lim[2], S. Kim[2]; [1]Pusan National University Hospital, Busan, KOREA, REPUBLIC OF, [2]Pusan National University Yangsan Hospital, Yangsan, KOREA, REPUBLIC OF.

Background: Dopamine and serotonin are neurotransmitters that involved in the regulation of food intake and body weight. We investigated the relation of obesity, age, and sex with the availabilities of striatal dopamine transporter (DAT) and extrastriatal serotonin transporter (SERT) in ^{123}I-FP-CIT single-photon emission computed tomography (SPECT). **Methods:** Data used in the preparation of this article were obtained from PPMI database (www.ppmi-info.org/data). The study population consisted of healthy controls with screening ^{123}I-FP-CIT SPECT. Specific binding of ^{123}I-FP-CIT regarding DAT and SERT was calculated using a region of interest analysis. A standard set of volume of interest (VOI) defining putamen, caudate nucleus, striatum (putamen + caudate nucleus), and thalamus based on the Automated Anatomical Labeling (AAL) atlas as well as a spherical VOI for pons and midbrain was defined. The cerebellum was chosen as a reference region. VOI template was applied to measure specific binding ratios (SBRs) of putamen, caudate nucleus, striatum, thalamus, pons, and midbrain as follows; SBR= (target- cerebellum)/cerebellum. **Results:** None of SBR of DAT and SERT except for pons (r=0.2217, p=0.0026) correlated with BMI of 182 subjects. SBR of midbrain correlated negatively with BMI of obese subjects (r=-0.3126, p=0.0496), and positively with that of non-obese (r=0.2327, p=0.0053). SBR of caudate nucleus (r=-0.3175, p<0.0001), striatum (r=-0.226, p=0.0022), and thalamus (r=-0.1978, p=0.0074) showed a reduction with aging. **Conclusion:** Obesity has an opposite effect on midbrain SERT availability. In addition, BMI was not correlated with striatal DAT availability, but with pontine SERT.

EP-0437

Interpretation and analysis of PET hypermetabolism in children with epilepsy

R. Wang, Z. Tong, Y. Fan, L. Cai, X. Liu, J. Zhang; Peking University First Hospital, Beijing, CHINA.

Aim: We observed 24 children with epilepsy to investigate the the possible etiological factors of positron emission tomography (PET) hypermetabolism and the diagnostic value of PET/CT. **Methods:** We retrospectively reviewed PET brain studies in patients with childhood epilepsy for evidence of hypermetabolism. We retrospectively reviewed the metabolic abnormality, magnetic resonance imaging (MRI) findings and electroencephalography (EEG) and we reviewed the histopathology and surgical outcome of patients who underwent surgery. **Results:** PET hypermetabolism was identified in 24/396 (6%) of studies. Fourteen patients had seizures before or during their PET studies. Consistency of hypermetabolism localization between PET/CT and MRI was 63%. Consistency of hypermetabolism localization between PET/CT and EEG was 81%. Eleven patients underwent surgery; in 6 patients, the site of resection was convergent with the region of PET hypermetabolism. **Conclusion:** Regions of glucose hypermetabolism were observed most frequently

in the frontal and parietal lobes, with or without hypometabolism. The hypermetablism can occur during the ictal and interictal state. In the patients who underwent surgery, MCD is the most common histological type. **Key Words**: Epilepsy; PET/CT; ^{18}F-FDG; Increased metabolism; Video electroencephalography monitoring **Fund program**: 1.National Special Fund for the Development of Major Research Equipment and Instrument (2011YQ03011409); 2. National Science and Technology Pillar Program of the Twelfth Five-year Plan (2014BAA03B00)

EP-0438
Brain death scintigraphy

P. Sirucek[1,2], D. Novakova[1], M. Havel[1,2], O. Kraft[1,2]; [1]University hospital, Ostrava, CZECH REPUBLIC, [2]University of Ostrava, Department of Imaging Methods, Ostrava, CZECH REPUBLIC.

Introduction: Retrospective analysis of statistical data of brain death scintigraphy from a period of 2003 - 2016 performed on the Department of Nuclear Medicine University Hospital Ostrava. **Method:** Since 2003 till the end of 2016 (13 years), we examined 220 ventilated patients in a deep coma with areflexia above C1. We performed 229 scintigraphy acquisitions to confirm brain death. Immediately after the intravenous administration of ^{99m}Tc-HMPAO there was performed dynamic scintigraphy, followed by static scintigraphy in the front, back and both side projections. Prior to administration of the radiopharmaceutical the radiochemical purity was always checked. All adult patients had during the application of the radiopharmaceutical mean arterial pressure more than 80 mmHg. Most frequent indication for this examination was to include the patient into the transplantation program; exceptionally brain death was diagnosed to stop the intensive care. **Results:** Majority of the patients were men (151, 69 %), less than a third were women (69, 31%). Patients had a mean age 43 years, the youngest patient was a 10-day newborn, the oldest was 68 years old. This examination was indicated in 25 children. The cause of coma and subsequent cerebral oedema was in 39 % trauma (traffic accidents, falls, suicide - jumping, gunshot wounds of the head), 61% were other causes - AV brain malformation, stroke, complications of epilepsy, complications of anticoagulation therapy, drowning, CO intoxication, brain tumours, abscesses, encephalitis, etc.). Investigations are evaluated qualitatively. Brain death was confirmed, if there was no accumulation of radiopharmaceuticals supra- and infratentorial. Brain death was detected in 207 patients (94 %), 13 patients at first examination had partially preserved brain perfusion. In the transplant program were enrolled 183 patients (83%), multiorgan harvesting was done in 80 patients (44 %), otherwise kidneys and heart were removed. **Conclusion:** Brain death scintigraphy is an important diagnostic tool in the process of brain death diagnosis, not only before the removal of organs for transplantation, but also before the termination of anesthesiology and intensive care. It is most often used in patients after cranial trauma and after neurosurgical decompression.

EP-0439
Ictal SPECT injector commercially available: EpiJET

X. Setoain, F. Campos, J. Pavia, O. Vernet, P. Paredes, M. Mayoral, M. Carreño, F. Lomeña; Hospital Clínic de Barcelona, Barcelona, SPAIN.

Purpose: To present the main features of the first remotely controlled automated injector system for ictal SPECT (epiJET, LemerPax, Nantes, France) used in patients with refractory epilepsy. We report the results of injection time (Ti) and seizure focus (SF) localization with ictal SPECT using epiJET. **Method:** Ti and SF localization using epiJET in 23 patients were compared with Ti (t-test) and SF localization (X^2) of the retrospective database of the historic pool of 126 patients injected manually during 2011-2015. Injection dose error and radiation dosimetry were analyzed. **Results:** EpiJET injects the full volume of the perfusion radiotracer (3-8 ml) in 3,5 s on average (2-6 s) and all injections were performed without any problem. Ti with epiJET, using the remote control system and doing the injection from the control-EEG room was 12±7,2 s. Manual Ti was 17±11,7 s on average (p<0,001). Otherwise, when the manual injection took place with the operator waiting the seizure from the control room (same conditions used in epiJET), the Ti in these group of 54 patients was 24±12 s (P<0,001). When the manual injection took place with the operator waiting the seizure inside the patient room (bedside and worse conditions compared with epiJET), the average Ti in these 72 patients were 13±9,7 s (P=0,6). Ictal SPECT with epiJET localized SF in 18/21 (85%) patients and with manual injection in 89/117 (76%) of patients (p>0.05). EpiJET calculate the volume to inject in real-time accounting of the ^{99m}Tc decaying. The system error in prescribed dose administration using epiJET was less than 5%. With manual injection, to compensate for radioactive decay of ^{99m}Tc, the volume is readjusted once during the 4-h period and the theoretic error between programed and injected dose may be 12%. EpiJET reduce the risk of radiation contamination and decreases radiation dosimetry of nurses. The syringe with the radioactive tracer is assembled in the shielded cartridge in the radiopharmaceutic unit. The closed cartridge avoid any manipulation of radioactive tracer in the epilepsy unit. Radiation exposure is also very low, so with the syringe filled with 3700 MBq of ^{99m}Tc, the radiation exposure at 50 cm was 0.07 μSv/h. **Conclusion:** EpiJET, the first commercially available dedicated automated injector for ictal SPECT simplify the methodology for injecting radioactive doses during seizure, making ictal SPECT more accessible. First results using epiJET are promising in reducing injection time and improving SPECT accuracy.

EP-0440
Neuromodulatory effects of galvanic white noise vestibular stimulation after bilateral labyrinthectomy in the rat

M. Lindner[1], E. Eilles[1], L. Günther[1], A. Gosewisch[1], L. Vomacka[1], G. Xiong[1], R. Oos[2], P. Bartenstein[2], R. Beck[1], A. Zwergal[3]; [1]Deutsches Schwindel - und Gleichgewichtszentrum (DSGZ), Klinikum der Universität München, Klinik und Poliklinik für Nuklearmedizin, Klinikum der Universität München, München, GERMANY, [2]Klinik und Poliklinik für Nuklearmedizin, Klinikum der Universität München, München, GERMANY, [3]3Deutsches Schwindel - und

Gleichgewichtszentrum (DSGZ), Klinikum der Universität München, Institut für klinische NeurowissenschaftenNeurologische Klinik, Klinikum der Universität München, München, GERMANY.

Purpose: Investigation of modulatory effects of galvanic whitenoise vestibular stimulation (GWS) on the locomotor behavior and cerebral glucose metabolism after bilateral labyrinthectomy (BL) of the **Subjects and Methods:** 17 SD rats were subjected to a BL by the transtympanic injection of bubivacaine / arsenilate. 8 animals were stimulated with galvanic white-noise on the mastoid (200μA, 30min) , 9 animals underwent a Shamstimulation on days 1,3,7,15,30,60 post BL. On the respective days the cerebral glucose metabolism was measured by means of [^{18}F] FDG-μPET. The locomotion behavior was recorded in the Cat-Walk system before the stimulation to represent the therapeutic long-term effects on days 1,3,15,30,60 post BL. Furthermore, the therapeutic acute effect on gait stability was examined on day 6 post BL in a direct comparison before and after GWS / Sham stimulation. **Results:** While no therapeutic effect of the GWS could be demonstrated in the longitudinal course by means of gait analysis, a significant improvement of the postural instability was found in the direct comparison of pre / post GWS on day 6 post BL. In the [^{18}F] FDG-μPET, an activation of cerebral locomotor centers (day 1: medial septal nucleus and globus pallidus, day 30: globus pallidus, day 60: medial septal nucleus p <0.005 uncorrected) was found in the GWS group in comparison to the Shamstimulated group. **Conclusion:** GWS improves postural instability transiently when applied in the acute phase after BL but does not change gait parameters on the long-term. However, by means of [^{18}F] FDG-μPET persistent neuromodulatory effects of GWS on cerebral locomotor centers can be demonstrated

EP-0441

Cardiac selectivity of autonomic sympathetic alteration in Parkinson Disease

A. Nieri[1], R. Piva[1], G. Borgonovo[1], V. Ceriani[1], M. Pennone[2], G. Siclari[2], F. Ticconi[1], M. Sicignano[2], G. Villa[2], G. Sambuceti[1,2], C. Marini[3]; [1]Nuclear Medicine, Department of Health Sciences, University of Genoa and IRCCS AOU San Martino-IST, Genova, ITALY, [2]Nuclear Medicine Unit, IRCCS San Martino-IST, Genova, ITALY, [3]CNR Institute of Bioimages and Molecular Physiology, Milan, ITALY.

Purpose: Parkinson disease (PD) often results in a damage to both central and peripheral autonomic nervous system. This association is exploited for diagnostic purposes by imaging of myocardial innervation using ^{123}I labeled meta-iodo-benzyl-guanidine (MIBG). As a norepinephrine analogue, MIBG is concentrated in post-ganglionic sympathetic neurons and in cells of neuroectodermal origin, where it is stored in vesicles by VMAT2 protein. However, whether the systemic autonomic alteration also results in abnormal uptake in further organ beyond the heart, it has been scarcely investigated. Purpose of this study was to verify whether PD also affects MIBG uptake in thyroid and liver. **Subjects & Methods:** We recruited a total of 37 patients (20 males and 17 females) with suspicion of PD or atypical parkinsonism; 12 patients were administered with

potassium perchlorate to prevent thyroid uptake of unlabeled [123]I. All patients were imaged 30 minutes after injection of 111-185 MBq of ^{123}I-MIBG with a total body scan. 19 had a preserved myocardial MIBG uptake (12 males and 7 females; Group 1); 18 patients had an absent cardiac tracer retention and were thus diagnosed as PD (9 males, 9 females: Group 2). Total whole body counts were assessed and used to normalize radioactivity measured in regions of interest drawn on the heart (H), thyroid (T) and liver (L). **Results:** Pretreatment with potassium perchlorate did not affect at all MIBG uptake in all studied organs and mostly in T in both disease groups. By contrast, PD was indeed associated with lower values of H uptake (1,69±0,52% vs 2,13±0,64%, respectively, p<0,01) and with a lower H/mediastinum ratio (1,17±0,09 vs 1,55±0,17, respectively, p<0,01) with respect to atypical parkinsonism. Tracer uptake in T was remarkably similar in the two groups (0,63±0,23% vs 0,63±0,26%, respectively, p=ns). By contrast, L tracer retention was higher in PD than in remaining patients (13,8±3,5% vs 11,2±2,2%, respectively, p<0,05). **Conclusion:** Response of thyroid handling of MIBG is independent from the mechanisms affecting tracer uptake in the heart. Conversely, the statistically significant difference observed in the liver might indicate either an increased MIBG availability in the blood in PD eventually resulting in hepatic processing of injected tracer or derived metabolites.

EP-0442

Brain ^{18}F FDG abnormalities in Neurobechet Disease

A. Chiaravalloti[1,2], F. Ursini[3], S. D'Angelo[4], A. Padula[4], M. Gilio[4], P. Leccese[4], P. Sannino[2], E. Di Giorgio[2], F. Calabria[5], O. Schillaci[1,2], I. Olivieri[4]; [1]Department of Biomedicine and Prevention, University Tor Vergata, Rome, ITALY, [2]IRCCS Neuromed, Pozzilli, ITALY, [3]Department of Healt Sciences, University Magna Graecia, Catanzaro, ITALY, [4]Azienda Ospedaliera Regionale San Carlo, Potenza, ITALY, [5]Neuroimaging PET/MRI Research Unit, Institute of Molecular Bioimaging and Physiology, National Research Council, Catanzaro, ITALY.

Introduction: Neurological involvement of Neuro-Behçet's disease (NBD) is a relatively uncommon but potentially life-threatening manifestation. The gold-standard imaging modality for NBD is Magnetic Resonance Imaging (MRI) that is able to demonstrate both parenchymal and non-parenchymal disease. However a number of patients presents with neurological complaints (headache, cognitive impairment orneuropsychiatric manifestations) despite a normal MRI suggest that other imaging techniques could be useful in the evaluation of such patients. Aim of this preliminary study was to investigate the differences in brain glucose consumption as detectable by means of 2-deoxy2-(^{18}F) fluoro-D-glucose (^{18}F FDG) Positron Emission Tomography/Computed Tomography (PET/CT) in a selected population with NBD. **Methods:** Six subjects (1 males and 5 females, mean age 42 (±12) years old, Table 1) with BD classified according to the International Criteria for Behçet's Disease (ICBD) and neurological involvement (NBD) were enrolled in this study. NBD was diagnosed by clinical evaluation (including neurophysiological studies when appropriate) and

MRI findings. Seventeen healthy subjects (CG group), 3 males and 14 females, mean age 40 (±12) years old) and 7 BD without neurological involvement (BD group) were enrolled as control groups. All the subject underwent a 18F-FDG PET/CT at rest in the same experimental conditions after the i.v. injection of 185-210 Megabequerels of 18F FDG. Differences in brain glucose consumption were evaluated by means of statistical parametric mapping (SPM8) using age, sex and scholarship as covariates. The voxel-based analyses were performed using a two sample t-test. **Results:** As compared to CG, NBD showed a significant reduction of brain glucose consumption (Pfwe corr. < 0.001) in left and right cingulate gyrus [Brodmann Area (BA) 24, BA 23 and BA36], left precuneus (BA7) and in left temporal lobe (BA 38). At a sub-cortical level, we found a significant reduction of brain glucose consumption (Pfwe corr. < 0.01) in right brainstem that involved mainly the midbrain. We did not find any area of increased glucose consumption in NB as compared to CG. No significant differences were found in glucose consumption when CG and BD were compared. However, when NDB and BD were compared, we found a significant reduction of brain glucose consumption in right and left parahippocampal gyrus (BA 30 and 19) and in right posterior cingulate cortex (BA23) in NBD patients**. Conclusions***: Our preliminary results demonstrate a cortical and brainstem dysfunction in NBD patients, but not in patients with BD without neurological involvement.

EP-0443

Post traumatic olfactory dysfunction assessment by 99mTcHMPAO brain imaging

I. Konstantinidis[1], I. Iakovou[2], E. Tsakiropoulou[1], V. Mpalaris[2], V. Athanasiou[2], D. Katsampoukas[2], D. Lo Presti[2], S. Georga[2], G. Arsos[2]; [1]Academic ORL dpt, Papageorgiou hsp., THESSALONIKI, GREECE, [2]Academic Nuclear Medicine dpt, Papageorgiou hsp., THESSALONIKI, GREECE.

Aim: Psychophysical olfactory tests are useful in clinical practise however they have limitations as they are depended upon the patients' response. The aim of this study was to use 99mTc HMPAO Brain SPECT in order to detect possible areas of brain activation in response to supra-threshold odour stimulation in patients with post-traumatic impaired olfaction in comparison to a group of normal subjects. Material- **Methods:** Thirty-two patients with post-traumatic olfactory disorders and ten normosmic controls were enrolled in this prospective study. The clinical diagnosis of smell impairment was based on olfactory testing using the Sniffin Sticks battery. A total of 84 Brain SPECT studies were performed; all subjects underwent brain imaging in two consecutive days: one with suprathreshold olfactory stimulation with phenyl-ethyl-alcohol (test) and the second without (baseline examination). **Results:** The mean Sniffin Sticks score was 35.2 for the normosmic and 16.4 for the group of post-traumatic olfactory dysfunction. SPECT analysis showed significantly increased cortical perfusion in post-stimulation values of normal volunteers compared with the anosmic patients. Maximal activation was observed in orbitofrontal regions followed by the

temporal region. It is worthy to note that in almost all anosmia post-traumatic cases there was agreement of the clinical test values and SPECT imaging findings (16/15). However this was not the case with the hyposmic patients as they could not be distinguished by the normosmics. SPECT detected additional hypofunctional areas in 4 anosmic patients (25%). In 2 patients (one normosmic and one hyposmic) baseline hypofunctional areas were functional with phenyl-ethyl-alcohol stimulation. **Conclusion:** Brain SPECT is a valuable imaging technique in the assessment of olfactory disorders especially the post-traumatic anosmia cases. It could be an additional objective method of olfactory function assessment in medicolegal cases

EP-0444

99mTc HM-PAO Brain Spect Qualitative And Quantitative Analyses (QLA/QNA) In Fibromyalgia Syndrome (FMS) Treated With Hyperbaric Oxigen Therapy (HOT)

S. Nuvoli[1], A. Bolognini[2], G. Motroni[3], L. Calderoni[1], B. Piras[1], A. Spanu[1], G. Madeddu[1]; [1]Unit of Nuclear Medicine, Clinical and Experimental Medicine DPT, University of Sassari, Sassari, ITALY, [2]Hyperbaric Center, Sassari, ITALY, [3]Unit of Functional Recovery and Rehabilitation AOU Sassari, Sassari, ITALY.

Introduction: FMS is painful chronic disease with subjective pain perception related to brain final processing of peripheral signal. HOT, inducing neuroplasticity and increasing brain function, seems to reduce clinical symptoms and improve life quality. We studied 99mTc HM-PAO brain SPECT usefulness in evaluating perfusion changes induced by HOT. **Methods:** We investigated five consecutive FMS female patients, who underwent 40 daily HOT treatment, 5 days/week. In all cases, brain SPECT was performed, at baseline and 3 weeks after the end of HOT course, by dual head gamma camera after 740 MBq 99mTc HM-PAO intravenous injection. SPECT images were evaluated by both QLA and QNA, using a software based on voxel by voxel comparative analysis with normal healthy age matched controls (C). QNA for each Brodmann Area (BA) was expressed as Standard Deviation (SD) than C (cut-off: -1.5 SD). **Results:** At baseline, in all five patients QLA and QNA showed bilateral reduced perfusion in secondary sensorimotor cortex (BA5 and BA7) and in medial temporal, parahippocampal and temporal pole cortex (BA 20, BA 22, BA 28, BA 36, BA 38), but also in other different adjacent cortical areas. During follow-up, at clinical evaluation performed both immediately and 3 months later after HOT course end, different degrees of clinical symptom improvement were evidenced in all cases. QLA comparative evaluation before and after treatment identified perfusion improvement only in 2/5 cases with no variation in the other 3/5. QNA confirmed significant perfusion improvement in the 2/5 patients and no variation in a third patient as also evidenced by QLA. However, QNA permitted to ascertain significant improvement in a forth patient but worsening in the remaining fifth case. **Conclusions:** These data confirm that HOT can be useful in FMS therapy since in all five treated cases clinical symptoms and life quality improved. Moreover, the improvement in 3/5 patients after treatment was also confirmed at 99mTc HM-PAO SPECT, mainly

with QNA evaluation, which already in basal conditions had evidenced brain cortical damage in specific BA areas confirming cortical involvement in FMG pain processing. Thus, perfusion BA improvement at QNA could support hypothesis that HOT may contribute to functional neuroplasticity resumption. Regarding the 2 cases unchanged or even worsened at QNA, unlike clinical data, it will be necessary closely clinical and SPECT QNA follow-up to better interpret these data also for therapeutic purpose. Wider casuistries monitored over time occurs to confirm these preliminary data.

EP-0445
18F-FDG PET/MRI allows improved detection of epileptogenic focus in patients with normal MRI

C. E. Popescu[1], F. Caobelli[2], R. Mai[1], R. Sara[1], M. Milella[1], A. Liuni[1], C. Rossetti[1]; [1]Niguarda Hospital, Milano, ITALY, [2]University Hospital Basel, Basel, SWITZERLAND.

Introduction: In approximately 25% of patients with drug resistant focal epilepsy undergoing pre-surgical evaluation, magnetic resonance imaging (MRI) is normal or discordant with clinical and EEG data. A major challenge in pre-surgical evaluation is the correct delineation of the seizure onset zone (SOZ), which often requires invasive EEG recordings. We aimed at assessing the clinical value of 18F-FDG PET coregistered with MRI (18F-FDG PET/MRI) in localizing epilepsy prior to intracranial EEG recordings. Furthermore, we tested the predictive value of 18F-FDG PET/MRI on the postoperative outcome. **Subjects and Methods:** Sixty patients with neocortical epilepsy (mean age at epilepsy onset 13.3±8.12 years) with normal 1.5T 3D brain MRI were retrospectively evaluated. For each patient, we collected clinical characteristics, localizing features on preoperative diagnostic tests (ictal video-electroencephalogram (VEEG), intracranial EEG (iEEG), FDG PET/MRI images), histopathological findings and surgical outcome. PET images were reprocessed, fused with MRI using FSL software (Oxford Centre for Functional MRI brain) and compared to invasive EEG recordings. Surgery was performed 1 to 43 months after PET (median 9 months). Outcomes were assessed according to Engel's classification at follow-up until 66 months (median 32 months). A favorable outcome was defined as reduced rate of seizures (Engel IA-IB-IC-2A) and/or reduced antiepileptic therapy. **Results:** In 47 patients (73.3%), PET/MRI could detect foci of decreased uptake. Compared to invasive EEG recordings, PET/MRI correctly identified SOZ in 42 patients (70%), detected foci discordant to EEG in 5 (8.3%) and resulted falsely negative in 13 (21.7%). Pooled sensitivity was 76.4%, positive predictive value 89.4%, positive likelihood ratio 76.4%, posttest probability 89.4%. A positive PET/MRI examination did not show a significant correlation with a poorer outcome (p=0.16) or with the need of increasing antiepileptic therapy (p=0.47). **Conclusions:** PET/MRI allowed for a correct, noninvasive identification of SOZ in 70% of patients with an unremarkable MRI examination. The presence of a hypometabolic focus on PET/MRI is not predictive of a worse outcome after surgery. Brain PET/MR should be routinely performed before surgery and may limit the need of a preoperative invasive assessment.

EP-0446
Radionuclide cisternography in the detection of cerebrospinal fluid leakage

D. Ben Sellem, L. Zaabar, B. Dhaoadi, I. El Bez, B. Letaief, M. F. Ben Slimene; University of Tunis El Manar, Tunis, TUNISIA.

Introduction: Cerebrospinal fluid leak occurs when there is an osseous and dural defect at the skull base, with direct communication of the subarachnoid space to the extracranial space. Recognition of the leak site and source and appropriate treatment are necessary to avoid complications. Radionuclide cisternography, functional imaging, is a sensitive tool to detect these leaks. The aim of this study was to evaluate the contribution of this examination to the diagnosis, localization and quantification of osteo-meningeal breachs. **Subjects and Methods:** Nine patients (5 children aged from 3 months to 10 years and 4 adults aged from 23 to 57 years), with suspected osteo-meningeal breach, were sent to our department for radionuclide cisternography. The main indication was recurrent meningitis observed in 5 patients. Two patients had intermittent rhinorrhea and one patient a left otorrhea. The last patient suffered head injury which occasioned the fracture of the anterior skull base. Examination was performed after lumbar intrathecal administration of ^{99m}Tc-DTPA and consisted of early and late static images up to 24 hours. A count of activity of nasal and ear pledgets was carried out 24 hours post radionuclide injection. **Results:** Radionuclide cisternography confirmed the diagnosis of osteo-meningeal breach in 6 patients. In one case, it well localized the defect in the left sphenoid sinus. In 3 others cases, it objectified the accumulation of the radiotracer within the nasal cavity heralding a positive finding that suggests a cerebrospinal fluid leak without adequate localization. In 2 cases, planar images showed no direct or indirect signs of leak: diagnosis was made by measuring a high activity of the radiotracer within the pledgets removed when the patient returned 24 hours later. In the three remaining cases, it has not been able to establish this diagnosis. In one of these cases, there were no measures of the activity within the pledgets which have fallen. **Conclusion:** The diagnosis of cerebrospinal fluid leak is essential to avoid serious complications such us meningitis. Radionuclide cisternography seems to be a valuable tool to facilitate the diagnosis of osteo-meningeal breach. The placement of pledgets in the nasal cavities and the measurement of their activity 24 hours later increase the sensitivity of the examination and help to quantify the importance of the leak. The SPECT/CT fusion imaging will better localize cerebrospinal fluid leakage sites.

EP-0447
Brain death scintigraphy - a 12 year experience

A. Fernandes[1], T. Faria[1], A. Oliveira[1], J. Pereira[1], P. Coelho[2]; [1]Hospital de São João, Porto, PORTUGAL, [2]Universidade Fernando Pessoa, Porto, PORTUGAL.

Introduction: Brain death is defined slightly differently by various organizations, but the overlying concept is of complete and irreversible loss of function of the brain. An accurate and timely

determination of brain death is necessary to best address the grief and anxiety of family members and to allow timely assessment for possible organ donation. The study aims to describe and characterize the requests received for brain death assessment with brain perfusion scintigraphy (740 MBq of HMPAO-Tc-99m) at our Department. **Subjects/Methods**: An existing database of performed clinical exams was analysed. The transplantation service database was consulted in order to investigate which patients were organ donors and which organs were donated. Descriptive statistical analysis was performed using SPSS v.24.0 software for Mac. **Results**: A total of 54 exams were requested from January 2005 to April 2017. Of those 54 patients, 19 were women (35.1%) and 35 were men (64.9%). The average age of the examined patients was 59.67± 12.66 years. The most common cause of death was Traumatic Brain Injury (n=24, 44.4%), followed by brain haemorrhage (n=8, 14.8%), ischemic stroke (n=4, 7.4%) and aneurism (n=4, 7.4%). Only four of the exams requested were negative for brain death. Of all the positive exams (n=50), 31 became organ donors. The most donated organ was the kidney (n=29), followed by the liver (n=19) and the heart (n=12). Other donated organs included the pancreas, the stomach, colon and lung. The direct costs related with the brain death scintigraphy are approximately 250 Euros. **Discussion/Conclusion**: Brain death scintigraphy is highly specific and even though it is well described in the brain death assessment guidelines it is not very requested at our hospital. When Intensive care doctors request this evaluation by the Nuclear Medicine department the result is majorly confirmatory of brain death. We postulate that one of the causes this exam is not more frequently requested is because it is assumed to be expensive. However, the direct costs for one day at the intensive care unit are 1,383± 398 Euros (vs 250 Euros, the direct cost of the exam). In this way, asking for this exam can, not only prove to be cost effective, but also allow avoiding unnecessary procedures and probably increase the number and the viability of donated organs. We suggest that this information and this exam should be widely divulged to the Intensive Care Units.

EP-0448

First results of combined brain perfusion SPECT and EEG measurements during speech processing in cochlear-implant users

M. Kessler[1,2], I. Schierholz[2,3], M. Mamach[2,4], F. Wilke[4], A. Hahne[5], L. Geworski[4], A. Büchner[3,2], F. Bengel[1], P. Sandmann[6], G. Berding[1,2]; [1]Department of Nuclear Medicine, Hannover Medical SchoolHannover Medical School, Hannover, GERMANY, [2]Cluster of Excellence Hearing4all, Hannover and Oldenburg, GERMANY, [3]Department of Otolaryngology, Hannover Medical School, Hannover, GERMANY, [4]Department of Medical Physics and Radiation Protection, Hannover Medical School, Hannover, GERMANY, [5]Saxon Cochlear Implant Center, University Hospital, Dresden, GERMANY, [6]Department of Otorhinolaryngology, University of Cologne, Cologne, GERMANY.

Introduction: Variable quality of speech comprehension in cochlear-implant (CI) users has been attributed to cognitive fac-

tors. Therefore, we aim to implement the simultaneous, synergistic use of two methods reflecting cognitive processes (brain perfusion-SPECT and EEG) to further clarify this issue. By combination of these methods we, in a first step, simultaneously evaluated speech perception scores, event-related potentials and activation of speech-related brain areas in response to speech stimuli. **Methods**: Four CI-users have been characterized using audiometric and neuropsychological tests. On different days perfusion-SPECT scans were performed with or without auditory stimulation during injection of 740MBq Tc-99m-HMPAO. In the stimulation condition, HMPAO was injected 2min after the onset of a semantic recognition task and EEG was recorded simultaneous for in total 7min. During the task subjects had to classify semantically correct and incorrect sentences. Hit-rates of accurate classification of sentences were calculated. SPECT-scans were acquired 1.5h p.i. aiming for 9 million total counts. After iterative reconstruction including attenuation correction, z-difference images were calculated using a Matlab based tool supplemented in SPM2. This tool includes stepwise proportional scaling. Thereafter, VOI-based analysis was applied using PMODv3.7. The mean scaled counts of the 30% hottest voxels in Brodmann areas(BA) 21, 22, 41 and 42 were calculated for both conditions. To assess percent activation in BAs, mean counts of the respective 30% hottest voxels at stimulation were related to the mean counts of the entire BA at baseline. **Results:** Z-maps indicated a distinct activation in auditory BAs contralateral to the stimulation side in 3 cases. Mean percent activations of the contralateral side were 14%±3.7% in BA22, 12%±3% in BA41, 13%±3.1% in BA21 and 6%±0.8% in BA42. Statistical analysis revealed a significant increase of mean counts in the 30% hottest voxel due to the semantic recognition task for BA21(p=0.014) and BA22(p=0.024). EEG showed typical N1 and P2 event-related potentials for sentence onset (e.g. subject1: N1 at 204ms, -1.056μV; P2 at 264ms, 1.165μV). The mean hit-rate of correct sentence classification was 82%±2%. **Conclusions:** A speech task designed to register the quality of speech comprehension and auditory evoked potentials enables additional measurement of activations in brain areas involved in speech processing using perfusion-SPECT. Due to the different strength of both methods with respect to higher temporal (EEG) and spatial resolution (SPECT) it can be expected that both methods synergistically help to disentangle and avoid reasons for limited speech comprehension after cochlear Implantation.

EP-0449

Value of MIBG myocardial scintigraphy in the differential diagnosis of neurodegenerative disorders

L. Mohamed Salem, Sr., M. Godoy Bravo, R. Reyes Marles, I. Sime Loayza, M. Castellon Sanchez, L. Frutos Esteban, F. Nicolas Ruiz, J. Navarro Ferenandez, J. Marín Muñoz, S. Manzanares Sánchez, F. Noguera Perea, C. Antúnez Almagro, M. Claver Valderas; Hospital Clínico Universitario Virgen de la Arrixaca, Murcia, SPAIN.

Introduction: The differential diagnosis of neurodegenerative disorders, Dementia with Lewy bodies (DLB), Alzheimer Disease (AD), Frontotemporal Dementia (FTD), , Parkinson's Disease (PD),

Progressive Supranuclear Palsy (PSP), Multiple System Atrophy (MSA) and Corticobasal Degeneration (CBD), may be a very challenging task, specially at early stages, according to scientific evidence from recent literature, 123-I-MIBG myocardial scintigraphy, is a very helpful tool to differentiate these conditions. **Purpose:** To assess the value of 123-I-MIBG myocardial scintigraphy in the differential diagnosis of neurodegenerative disorders. **Subjects and Methods:** Together with Dementia Unit of our hospital, we investigate retrospectively 18 patients, mean age 63,3 (IQR 56-71.5), who were referred to our department for the differential diagnosis (DD) of neurodegenerative disorders. Chest planner images were acquired, 15-30 minutes and 4 hours after the intravenous injection 370 MBq of 123-I-MIBG. Heart to mediastinum (H/M) ratio was calculated using the 4 hours image, according to the following formula: Heart ROI mean count density / Mediastinum ROI mean count density. We compare the finding with the results of other nuclear medicine diagnostic techniques, such as Dopamine Transporter SPECT (DAT-SPECT), Brain Perfusion SPECT-CT, Amyloid PET, neuropsychological tests, and clinical history. **Results:** - 8 patients with abnormal DAT-SPECT were referred for DD of PD versus Parkinson-plus, 6 had abnormal MIBG scan with severe denervation, suggestive of PD, 2 with normal MIBG scan, suggestive of Parkinson-plus. - 4 patients with clinically uncertain DLB with normal DAT-SPECT, had also normal MIBG scan, and the diagnosis of DLB was ruled out. - 1 patient who was referred for DD of AD at early stages versus DLB, had abnormal MIBG scan and normal Amyloid PET scan, was diagnosed with DLB. - 1 patient who was referred for DD of FTD at early stages versus DLB, had abnormal MIBG scan and normal Brain Blood Perfusion SPECT CT, suggestive of DLB, was diagnosed with DLB. - 6 patients who were referred with clinical suspicion of various neurodegenerative disorders, had no other nuclear medicine tests, but according to the clinicians the MIBG scan report seems to be compatible, with neuropsychological tests and clinical history in most of the patients. **Conclusion:** 123-I-MIBG myocardial scintigraphy is a very useful tool in the differential diagnosis and management of patients with neurodegenerative disorders.

EP-0450

Advanced FDG PET Imaging of the Orbits using an Ultra-High Definition Digital PET/CT Approach

C. L. Wright[1], *K. Binzel*[1], *M. Mohamed*[1], *J. Zhang*[1], *P. Maniawski*[2], *M. V. Knopp*[1]; [1]*The Ohio State University, Columbus, OH, UNITED STATES OF AMERICA,* [2]*Philips Healthcare, Cleveland, OH, UNITED STATES OF AMERICA.*

Purpose/Introduction: Digital photon counting PET detector (dPET) technology represents a technical innovation which enables higher definition whole-body PET imaging with smaller voxel volumes. The aim of this study is to assess the clinical capabilities of higher definition dPET/CT imaging of the orbits and compare its imaging characteristics to conventional photomultiplier tube-based PET/CT (cPET/CT) imaging. **Subjects & Methods:** Fifteen oncologic patients without known orbital malignant/metastatic disease agreed to participate in an ongoing clinical trial using pre-commercial release dPET/CT (Vereos,

Philips) and cPET/CT (Gemini TF 64, Philips) systems. Standard whole-body cPET/CT was performed with 481 MBq FDG with imaging at ~75 min p.i. whereas investigational whole-body dPET/CT was performed at ~55 or ~95 min p.i. Conventional PET/CT images were reconstructed using Time-of-Flight with $4\times4\times4$ mm^3 voxel volumes (standard definition/SD). Digital PET/CT images were reconstructed using Time-of-Flight with $4\times4\times4$ mm^3 (SD), $2\times2\times2$ mm^3 (high definition/HD) and $1\times1\times1$ mm^3 (ultra-high definition/UHD) voxel volumes. Image characteristics for cPET/CT and dPET/CT images of the orbits were assessed by intra-individual comparison by a blinded reader panel using an Intellispace Portal workstation. **Results:** All 15 whole-body cPET and 45 whole-body dPET data sets were rated as evaluable with no FDG-avid pathologic lesions identified within the orbits. In general, there was better anatomic delineation, more confident identification and more precise FDG characterization of the orbital structures with higher definition dPET/CT. Although UHD dPET/CT images were rated best, HD dPET/CT also improved overall image quality when compared with SD cPET for both qualitative and quantitative assessment of the orbits. With higher definition dPET enabling more precise localization of FDG activity into smaller voxel volumes, physiologic FDG uptake within orbital soft tissues led to slightly higher SUV_{max} values and this is likely due to a reduction in partial volume effects. **Discussion/Conclusion:** Routine detection and quantification of small FDG avid-orbital malignant/metastatic lesions is currently challenging with standard definition whole-body PET/CT approaches. There remains an unmet clinical need for improved visualization and characterization of both normal and pathologic orbital soft tissues on FDG PET/CT. Using higher definition approaches enabled with digital PET detector technology, improved FDG PET/CT imaging of the orbits is practical and even achievable with routine whole-body PET acquisitions. In the future, higher definition FDG dPET/CT studies in patients with known orbital neoplasms will be essential in further developing and validating this new precision imaging approach.

EP-0451

Brain SPECT Findings In Patients With Malformations Of The Corpus Callosum: Clues For Neuroimaging Reports

L. Wichert-Ana[1,2], *A. C. Trevisan*[1], *C. E. P. Baltazar*[1], *L. Alexandre-Santos*[1], *F. A. Pitella*[1], *E. N. Itikawa*[1,2], *M. Kato*[1], *M. V. Simões*[1], *M. V. Santos*[1], *H. R. Machado*[1], *A. C. Sakamoto*[1], *A. C. Santos*[1]; [1]*Ribeirão Preto Medical School, University of São Paulo - USP, Ribeirão Preto - SP, BRAZIL,* [2]*Bioengineering Interunits Postgraduation Program, São Carlos Engineering School, University of São Paulo - USP, São Carlos - SP, BRAZIL.*

Introduction: Malformations of the corpus callosum, MCC, is one of the most common brain malformations observed in humans, and in particular, in patients with pharmacoresistant epilepsy. It is a complex condition, which can result from a disruption in any one of the steps of the brain development, such as cellular proliferation and migration, axonal growth or glial patterning at the midline. Importantly, MCC may be a challenge during brain SPECT and PET reports, since the anatomy of the

medial cortex is ruptured. This study aimed to describe the brain SPECT findings associated to MCC. **Subjects and Methods:** Patients with significant changes in corpus callosum morphology, retrieved from the results of 3T magnetic resonance imaging, MRI, exams performed at our institution, were included in this retrospective study. They also underwent to interictal SPECT scans with 99mTc-ECD during the presurgical workup for epilepsy. Patients MRI and SPECT exams were fused enabling the detailed analysis of the brain anatomy. Additionally, the subtraction between ictal and interictal SPECT, SISCOM, was performed to exhibit the cerebral regions involved in seizures. **Results:** Interictal SPECT scans showed similar findings in all patients with MCC. Comparatively to the normal brain anatomy on SPECT, perfusion images of MCC revealed elongation of the anterior mesial frontal cortex, elongation of the posterior mesial cortex and loss of normal curvature of brain mesial cortex, being the last more evident in cases with total agenesis. This altered perfusion anatomy should be known by nuclear medicine physicians. In fact, the corpus callosum cannot be visualized in cerebral perfusion SPECT because it contains only bundles of axons and no neurons. A presumption of its anatomy is made by the cortex that is anchored therein. The SISCOM areas did not present any specific critical perfusion patterns associated with MCC. Otherwise, SISCOM was more associated with the presence of epileptogenic lesions such as Polymicrogyria. **Conclusions:** The perfusional anatomy of the medial cerebral cortex may show changes on brain 99mTc-ECD SPECT and possibly on 18F-FDG PET/CT in patients with MCC. These changes should be kept in mind by nuclear medicine physicians on reporting these neuroimaging techniques.

EP-0452
Importance Of Using Portable Mini-Gamma Camera In Scintigraphic Brain Death Diagnosis

M. Godoy Bravo, R. Reyes Marles, A. Abella Tarazona, I. Sime Loayza, M. Castellon Sanchez, L. Mohamed Salem, L. Frutos Esteban, J. Navarro Fernandez, F. Nicolas Ruiz, M. Claver Valderas; Hospital Clinico Universitario Virgen de la Arrixaca, Murcia, SPAIN.

Purpose: To emphasize the importance of the possibility of diagnosing brain death by cerebral perfusion scintigraphy in the Intensive Care Unit (ICU) thanks to the portable mini-gamma camera (PMC). **Subjects & Methods:** Cerebral perfusion scintigraphy study is performed after an intravenous bolus injection of stabilized (925MBq) ^{99m}Tc-HMPAO immediately followed by 10cc saline, acquiring static planar cerebral images in both lateral projections 15 minutes after injection, each lasting for 300 seconds, using PMC provided with a 2.5mm diameter pinhole collimator. Scintigraphic criteria include the total absence of tracer uptake in both cerebral cortex and posterior fossa, which houses cerebellum and brain stem. Images showing tracer uptake in these regions or of doubtful interpretation definitively rule out the scintigraphic diagnosis of brain death. **Results:** There is increasing request for this imaging test in our hospital due to the recent introduction of PMC in scintigraphic brain death diagnosis. Previously, this test was performed at the Nu-

clear Medicine department, involving both the transfer of patients and specialized medical required team to ensure their hemodynamic stability. The success of the current test lies in the use of the PMC allowing its performance in the ICU, thus avoiding such difficulties. A total of 22 studies were carried out from May 2016 to April 2017, 19 of them met criteria for brain death diagnosis and 3 of them failed to brain death diagnosis due to scintigraphic cerebral perfusion persistence. **Conclusion:** We highlight the importance of using PMC in scintigraphic brain death test which offers a precise, fast and more practical diagnosis, as it allows performing the test in ICU, thus avoiding patient transferring to Nuclear Medicine department.

EP-0453
Location Of Cerebrospinal Fluid (CSF) Leaks And Treatment With Epidural Blood Patch (EBP) In Spontaneous Intracraneal Hypotension Syndrome (SHI) And Assesment Of Neuroimaging, MRI And Radionuclide Cisternography

P. Plaza[1], N. Mayolas[2], N. Morollon[2], E. Rivera[2], B. Domenech[1], P. Pifarre[1], J. Oglio[2], A. Banguero[2], R. Belvis[2]; [1]Hospital Quironsalud Barcelona, Barcelona, SPAIN, [2]Hospital Universitario Dexeus, Barcelona, SPAIN.

Objective: To evaluate the usefulness of the neuroimaging, MRI and cisternography, in the diagnosis and localization of CSF leaks in patients with spontaneous intracranial hypotension. **Material and Methods:** Retrospective longitudinal observational study of seven patients with definitive diagnosis of SHI who were treated with an EBP. Clinical presentation: orthostatic headache was the main symptom. Other associated symptoms included nuchal rigidity, neck pain, vertigo, nausea, vomiting, tinnitus and diplopia. There was no history of trauma or iatrogenia. All patients underwent cranial MRI with paramagnetic endovenous contrast; five of the patients had additional studies of spinal MRI with intravenous contrast (cervical, thoracic and lumbar). The cisternography with 0.5mCi In111 DTPA had been performed in patients with disabling postural headache without clinical improvement after conservative treatment. **Results:** There was a significant delay in the definitive diagnosis in all 7 cases. Radionuclide cisternography: macroscopic leakage was found in all cases (1 cervical, 5 high thoracic, 2 lumbar). No CSF flow progression to cerebral convexity. No nasal or optic fistulas were seen. Cerebral MRI identified enhancement of pachymeninges, subdural fluid collections, sagging brainstem, inferior displacement of the cerebellar tonsils, and engorgement of venous structures. In all cases, the spinal MRI revealed either subdural or epidural fluid collections, engorgement of epidural veins, pachymeningeal enhancement, and the "C1-C2 sign" was shown. Treatment was performed using EBP-guided imaging with one or two patches, showing progressive and complete resolution of the symptons and without side effects. No patient required further surgical treatment. **Conclusions:** SHI is a rare entity with a difficult diagnosis. It requires high quality neuroimaging tests for its detection and early treatment. The evaluation of both techniques, MRI and Radionuclide Cisternography, allow to specifically determinate the level of CSF leakage. EBP-guided

imaging, according to clinical practice, provides a better chance of therapeutic success compared to a blind performance.

EP-0454

Prognostic Contribution Of SISCOM In The Presurgical Evaluation Of Patients With Refractory Epilepsy And Negative 3T MRI

L. Wichert-Ana[1,2], *E. N. Itikawa*[1,2], *L. Alexandre-Santos*[1], *F. A. Pitella*[1], *J. H. Silvah*[1], *A. C. Trevisan*[1], *M. Kato*[1], *V. Alexandre-Junior*[1], *A. P. Martins*[1], *F. N. Nakano*[1], *T. R. Velasco*[1], *A. P. Martins*[1], *M. V. Simões*[1], *A. C. Sakamoto*[1], *A. C. Santos*[1]; [1]Ribeirão Preto Medical School, University of São Paulo - USP., Ribeirão Preto - SP, BRAZIL, [2]Bioengineering Interunits Postgraduation Program, São Carlos Engineering School, University of São Paulo - USP, São Carlos - SP, BRAZIL.*

Purpose: To assess the practical localizing value of subtraction of ictal SPECT corregistered with MRI regarding the findings of presurgical evaluation in patients with refractory epilepsy and negative 3T MRI. **Subjects and Methods**: We studied forty patients with refractory epilepsy and negative 3T MRI who underwent presurgical evaluation including ictal and interictal video EEG monitoring, neuropsychological, neuropsychiatric evaluations, and ictal interictal SPECT studies. SISCOM was performed and we visually determined whether the SISCOM focus agreed to show the cerebral cortex exhibiting prominent abnormalities on scalp EEG of the presumed epileptogenic zone, PEZ, obtained by consensus of presurgical evaluation. **Results**: Eleven female and 29 male were selected for this study. The mean age was 34.25 ± 12.09 years, range 18 - 62 years, the mean seizure onset was 11.26 ± 6.51, range birth to 25 years, and the mean epilepsy duration was 22.99 ± 11.53 years, range 7 - 43 years. The MRI was normal 23 patients, 57.5%, and unspecific for epilepsy etiology in 17 patients, 42.5%. Video EEG was abnormal in 36 patients, 90%, and inconclusive findings in four patients, 10%. Ictal SPECT showed hyperperfusion focus in 35 patients, 87.5%, and was multifocal in five, 12.5%, interictal SPECT showed hypoperfusion focus in 25 patients, 62.5%, no abnormality in ten, 25%, and sparse hypoperfusion in five, 12.5%. SISCOM focus was determined in 37 patients, 92.5%, and was multifocal in three, 7.5%, patients. So far, 17 patients had a consensus about the PEZ in the presurgical evaluation, and SISCOM showed the same focus in ten patients, 58.8%. Within this group, five patients underwent epilepsy surgery and four of them showed Engel IA and one showed Engel III seizure outcome. In seven patients, 41.2%, SISCOM showed different areas of activation from the consensus. Four patients of this group underwent epilepsy surgery and three of them showed Engel III and one patient showed Engel IA. **Conclusions**: Resection of the area localized by SISCOM together with the consensus of presurgical evaluation is a reliable predictor of favorable postoperative seizure outcome in patients with refractory epilepsy and negative 3T MRI.

EP-0455

Contribution of 18F-FDG PET/CT to the clinical diagnosis of Autoimmune Encephalitis: VISUAL vs VOXEL-BASED ANALYSIS

B. Garcia-Garcia, *D. Moreno-Ajona, E. Prieto, E. Guillen, A. Minguez, M. Morales, M. Riverol, J. Gallego-Perez Larraya, J. Arbizu; Clinica Universidad de Navarra, Pamplona, SPAIN.*

Aim: The recently proposed diagnostic criteria for Autoimmune Encephalitis (AE) provides a clinical quick approach, which did not include ^{18}F-FDG-PET/CT-imaging (Graus et al. Lancet Neurol. 2016). Our aim was to evaluate the contribution of ^{18}F-FDG-PET/CT in AE patients by comparing its diagnostic yield to the aforementioned criteria, and ascertaining the differences between visual and voxel-based methods of brain-imaging assessment. **Materials and Methods:** We studied 7 patients evaluated by the Neurology Department (4 men and 3 women, ranged 17-77 years) with definitive AE diagnosis. Clinical features included cognitive impairment (5/6 patients), behavioural disorders (4/7), and seizures (6/7). All patients underwent initial CSF study, MRI, EEG, and autoantibodies test. ^{18}F-FDG-PET/CT (Brain±Whole-Body) was performed using a Siemens-Biograph-mCT. Brain[18]F-FDG-PET images were evaluated by visual assessment (2 independent observers) and voxel-based analysis by means of SPM8 (20 healthy control subjects included for group comparisons; height threshold p<0.005, extent threshold 100 voxels) and Siemens-database comparison stereotactic surface projection software (DBC-SSP). **Results:** CSF analysis only revealed lymphocytic pleocytosis in 3/7 patients. Definitive autoantibodies-based AE diagnosis resulted in 1 NMDAR patient; and 6 Limbic Encephalitis (LE): 1 Seronegative, 3 LGI-1, 1 Paraneoplastic, 1 CASPR2. LE cases that underwent brain[18]F-FDG-PET/CT exhibited metabolic abnormalities, while MRI was positive in 3/6 patients, and EEG was positive in 6/6 patients. All LE cases showed hypermetabolism on the medial temporal cortex (m-T) and also extra-limbic abnormalities: hypermetabolism in cerebellum and basal ganglia with frontal hypometabolism in 2/2 LGI-1; anterior-cingulate and insular hypermetabolism with hypometabolism in Broca's area, primary-motor cortex (PMCx), precuneus, and temporal-parietal-occipital junction (TPO) in the Paraneoplastic case; posterior-cingulate hypermetabolism with hypometabolism affecting anterior-cingulate gyrus, frontal, temporal-lateral region (l-T), and TPO in the Seronegative patient. NMADR depicted hypermetabolism compromising l-T, cerebellum, parietal and insular cortex, with hypometabolism in the contralateral l-T, frontal and PMCx. Visual-assessment showed m-T hypermetabolism in 2/5 LE, and global hypometabolism in 2/2 LGI-1. Most of the m-T and extra-limbic hypermetabolism were only observed using voxel-based analysis. SPM8 was less sensitive than DBC-SSP for noticing both hypermetabolism (similar findings in 1/6 cases) and hypometabolism (SPM8 was superior only in 1 patient). Brain[18]F-FDG-PET/CT follow-up was performed in 2/7 patients, showing concordance between clinical outcome and brain[18]F-FDG changes on the previously affected areas. **Conclusions:** Regarding AE diagnosis/follow-up, brain[18]F-FDG-PET/CT reveals pathological findings even when MRI is normal, matching concrete metabolic patterns to the specific antibodies involved. Visual-assessment lacks sensitivity when detecting hypermetabolism and benefits from voxel-based analysis, specifically DBC-SSP.

EP-0456

Varying Standards for Brain Death Scintigraphy Across National and Professional Societies

L. S. Zuckier[1], T. L. McFarland[2]; [1]The Ottawa Hospital, Ottawa, ON, CANADA, [2]University of British Columbia, Kelowna, BC, CANADA.

Aim: To compare and contrast standards for evaluation of brain blood flow in the determination of brain death across professional societies and national guidelines. **Materials and Methods:** Web-based nuclear medicine and neurologic professional web sites were reviewed to identify procedure guidelines for brain death determination. In addition, online search engines were employed to identify published national or society-based guidelines for brain death confirmatory/ancillary studies. Areas of agreement and disparity were identified and tabulated. **Results:** Guidelines were obtained for 4 imaging societies (Society of Nuclear Medicine, American College of Radiology, Society of Pediatric Radiology and the European Association of Nuclear Medicine) and 2 professional societies (American Association of Neurology and the American Association of Pediatrics). An additional 2 statements of national societies/consensus groups were identified and reviewed (Belgian Society for Nuclear Medicine and the Canadian Forum). Most significant area of variability was regarding suitability of non-lipophilic radiopharmaceuticals for determination of brain death. Less critical areas included questions of relative desirability of specific agents in each radiopharmaceuticals category, and technical details such as the need for scalp tourniquet, need for uptake delay, and specific dosages to be employed. **Conclusion:** In spite of the great import of brain death studies, variability exists in promulgated performance guidelines. This is most manifest regarding preference of lipophilic over non-lipophilic radiopharmaceuticals, and the specific agents preferred in each category. Other difference relate to technical matters and are less critical in nature.

EP-0457

Brain Perfusion Scintigraphy As Confirmation Test Of Absent Cerebral Blood Flow

T. Samardzic, R. Petrovic, A. Golubic, J. Ljevak, V. Stambolija; University Hospital Centre Zagreb, Zagreb, CROATIA.

Aim: The aim of this study is to evaluate the effectiveness of single photon emission tomography (SPECT) with Tc-99m HMPAO in the diagnosis of brain death (BD). It is widely accepted that BD is a clinical diagnosis, but sometimes confirmatory tests are recommended when clinical testing cannot be evaluated reliably. In our study we compared the outcome of planar brain scintigraphy with Tc-99m pertechnetate, with Tc-99m HMPAO brain SPECT for the assessment of brain blood flow in patients suspected of BD. **Methods and Materials:** In a period of five years (2012-2107) 36 patients with a clinical diagnose of BD (22 men and 14 women, age 6-86 y) were referred to our department for the confirmation of a clinical diagnosis of BD. We performed planar brain scintigraphy with Tc-99m pertechnetate 21 times, and Tc-99m HMPAO brain SPECT 20 times in patients. In 4 of 36 patients brain scintigraphy were performed few times because of doubtful findings. Flow images are acquired at the time of the injection of 1110 MBq of selected radiopharmaceutical with one-second dynamic images for a period of 60 seconds. Anterior, posterior and both lateral static images were obtained within 5 minutes after dynamic images, and than late static images when we use pertechnetate as a radiopharmaceutical. When we use Tc-99m HMPAO, brain SPECT images were obtained in addition to flow and early static images. **Results:** In 21 planar brain scintigraphy with Tc-99m pertechnetate we confirmed a clinical diagnose of BD in 10 patients (47,6%) while in 11 of them (52,4%) we found different signs of cerebral blood flow. In 2 of them we performed a brain SPECT with Tc-99m HMPAO in few days and found the absence of brain perfusion. In 20 brain SPECT with Tc-99m HMPAO we confirm a clinical diagnose of BD in 15 patients (75%), while 5 cases (25%) were not consistent with BD. **Conclusions:** Our results suggest that Tc-99m HMPAO brain SPECT is a non-invasive procedure, more sensitive in confirmation of clinical diagnosis of brain death than planar scintigraphy. SPECT also could facilitate the interpretation of doubtful planar images. So, we propose cerebral perfusion SPECT with Tc-99m HMPAO as a reference standard in the diagnosis of brain death wherever is possible, considering patient conditions and organization possibilities to perform it.

EP-0458

Betahistine improves vestibular compensation after unilateral labyrinthectomy: a [18F]FDG-µPET study in the rat

M. Lindner[1], E. Eilles[1], L. Günther[1], A. Gosewisch[1], L. Vomacka[1], G. Xiong[1], R. Oos[2], P. Bartenstein[2], R. Beck[1], A. Zwergal[3]; [1]Deutsches Schwindel - und Gleichgewichtszentrum (DSGZ), Klinik und Poliklinik für Nuklearmedizin, Klinikum der Universität München, München, GERMANY, [2]Klinik und Poliklinik für Nuklearmedizin, Klinikum der Universität München, München, GERMANY, [3]Deutsches Schwindel - und Gleichgewichtszentrum (DSGZ), Neurologische Klinik, Klinikum der Universität München, München, GERMANY.

Purpose: To investigate the effect of i.v. versus s.c. betahistine treatment on compensation of acute vestibular imbalance using behavioural testing and serial [18F]Fluorodesoxyglucose ([18F]FDG)-µPET in a rat model of unilateral chemical labyrinthectomy. **Material and Methods:** Unilateral chemical labyrinthectomy (UL) was performed by transtympanic injection of bupivacaine and arsenilate. In the first group 10 rats underwent i.v. betahistine treatment twice a day from day 1-3 after UL. For control saline was applied i.v. in 10 other rats. The second treatment group received s.c. application of betahistine (9 rats), respectively saline (8 rats) via subcutaneously implanted osmotic pumps Nystagmus, postural imbalance and head roll tilt were rated by clinical assessment on days 1, 2, 3, 7, 9, 15,30 post surgery. Clinical scoring was followed by sequential whole-brain [18F]FDG-µPET-scans on the respective days. **Results:**Postural asymmetry and head roll tilt significantly improved in the i.v. treatment group at days 1-3 after surgery compared to the control group (p<0.05). The [18F]FDG-µPET-scans revealed a significant relative increase of cerebral glucose metabolism in

the contralateral vestibular nucleus on days 1 and 3 post after UL in the i.v. betahistine group (p<0.005, uncorrected).In the s.c. treatment groupsigns of vestibular imbalance improved more significantly and persistently as compared to the i.v. treatment group (i.e. postural imbalance: day 1-30, p<0.05; head roll tilt: day 1-3, p<0.05). The [18F]FDG-μPET-scans showed a relative increase of cerebral glucose metabolism in the contralateral vestibular nucleus at day 1 and cerebellum at day 3 after UL in the s.c. treatment group (as compared to the control group). **Conclusion:** Betahistine treatment improves compensation of postural symptoms in acute unilateral vestibulopathy. A continuous s.c. application as a higher effect and longer persistency as compared to i.v. treatment. [18F]FDG-μPET data suggest a mode of betahistine action via vestibulo-cerebellar circuits.

EP-0459
Role of 18 F FDG PET/CT in documenting the disease burden in Pott's spine

S. Gambhir; Sanjay Gandhi Post Graduate Institute of Medical Sciences, lucknow, INDIA.

Aim: The authors demonstrate the potential of F-18 Fluro-deoxyglucose Positron emission tomography (PET)/Computerized tomography (CT) and magnetic resonance imaging (MRI) at disease onset and its complementary role along with MRI in elucidating the pott's spine involvement. This may have a possible role in planning duration of treatment in scenario of TB resurgence and reported increase in multi-drug resistance (MDR) and extensively drug resistant (XDR TB) in patients with past history of TB. **Materials and Methods**: 19 patients with definite Potts spine, based on clinical, CT/MRI scan and CSF criteria were prospectively studied and subjected to whole body 18F FDG PET CT imaging and MRI. ^{18}F-FDGPET/CT results were independently reviewed and results were compared with MRI spine and other conventional imaging modalities (CT and X-Ray). **Results**: There were 19 patients with Potts spine whose median age was 47 (range, 18-75) years and the median duration of illness was 4 (range, 0.5- 8.0) months. ^{18}F-FDG PET/CT confirmed the MRI findings in all the patients, revealed additional details in the body, such as extensive lymph-nodal involvement in 10 cases, joint involvement in 2 cases, lung lesions in 4 cases, bilateral psoas abscess in 2 cases, pectoralis major muscle abscess in 1 case, retro-pharyngeal abscess in 1 case. **Conclusion**: [18] F-FDG PET/CT helps in documenting upfront disease burden in diagnosed cases of tuberculosis, thus prognosticating the cases and deciding upon the length of the therapy and preventing disabling complications. Also whole body imaging by PET-CT might shorten the time period in the diagnosis and staging of disease burden especially in developing countries. **Keywords**: 18 F -FDG-PET; Potts spine; MRI; disease burden **Acknowledgement**: IAEA, Coordinated research Project E 15021

EP-0460
Reproducibility Of DAT SPECT Quantification

L. Wichert-Ana[1,2], L. W. Alexandre-Santos[1], A. C. Trevisan[1], E. N. Itikawa[1], F. A. Pitella[1], M. Kato[1], M. V. Simões[1], V. Tumas[1]; [1]Ribeirão Preto Medical School, University of São Paulo - USP., Ribeirão Preto - SP, BRAZIL, [2]Bioengineering Interunits Postgraduation Program, São Carlos Engineering School, University of São Paulo - USP, São Carlos - SP, BRAZIL.

Introduction: Molecular imaging of DAT gives differential information in research of neurodegenerative diseases, such as Parkinson's Disease, PD, when properly approached quantitatively. Yet, each method used in clinical routine may give, or not, different results when the quantifications are applied in images of several activity levels. Hence, this study assessed the reproducibility intra and inter observer of DAT SPECT quantification methods, based in ROIs. **Materials and Methods**: Twenty three DAT SPECT images were acquisitions of anthropomorphic striatal phantom filled with different activity concentrations of [99m]Tc. For each acquisition performed, the specific chambers, caudate and putamen chambers, to large chamber, simulating nonspecific background activity, was filled with solutions activity of different specific to nonspecific ratios, 10, 8, 6, 4 and 2 to 1. The images were reconstructed by an iterative algorithm, corrected to attenuation effects. The extracted values were analyzed by the specific binding ratio, SBR. Two observer independent applied five quantification DAT SPECT methods using ROIs were assessed: Manual technique: (A) draw freehand ROIs on SPECT images. Standard size ROIs: (B) TwoBox and (C) ThreeBox Methods. VOIs using structural images: (D) MRI and (E) CT. Reproducibility of methods was assessed by variability of 2 set of values of each observer through of the reliability test by intraclass correlation coefficient (ICC) and Bland Altman plot. **Results**: The SBR index founded to manual technique showed increase variability of results in the intra-observer assessment (1.55% - 12.66%), while methods B and C (2.52% - 3.07%), D and E methods (0.02% - 0.8%) showed values of less dispersion between set values by same observer. All methods presented excellent reliability (ICC > 0.8) to p < 0.05. In the assessment inter-observer, the SBR values of method A showed even higher variability values that results intra-observer (8.37% - 22.9%) to low and middle reliability (0.38 < ICC < 0.52). Standard size ROI and VOI structural methods presented a low variability and high reliability (ICC > 0.99) in the investigation DAT-SPECT images with Tc-99m. **Conclusion**: The manual method showed lower reproducibility in assessment SBR index to different activity levels, while the methods standard size ROI and VOI structural demonstrated be excellent tools in research of SBR values in DAT-SPECT imagens.

Basic Oncology: Preclinical Imaging

EP-0461
Pilot Study of [64]Cu(I) for PET Imaging of Melanoma

L. Jiang[1], Z. Cheng[2]; [1]Zhongshan Hospital, Shanghai, CHINA, [2]Molecular Imaging Program at Stanford, Stanford University, Stanford, CA, UNITED STATES OF AMERICA.

Purpose: Copper, an essential dietary metal, plays an important role in many crucial physiological and biochemical processes in vivo, and also is required for cell proliferation and tumor angiogenesis. At present, ^{64}Cu(II) labeled tracers including ^{64}CuCl$_2$ have been widely applied in the research of molecular imaging and therapy. Human copper transporter 1 (hCTR1) is the major high affinity copper influx transporter in mammalian cells, which is specially responsible for the transportation of Cu(I) but not Cu(II). Thus, in this study, we investigated the feasible application of ^{64}Cu(I) for PET imaging of malignant melanoma. **Methods:** ^{64}Cu(II) was reduced to ^{64}Cu(I) with the existence of sodium L-ascorbate, DL-Dithiothreitol or cysteine. Cell uptake and efflux assay of ^{64}Cu(I) was investigated using B16F10 and A375 cell lines, respectively. Small animal PET imaging and biodistribution studies of ^{64}Cu(I) were performed in both B16F10 and A375 tumor-bearing mice. In addition, radiation absorbed doses for the major tissues of a human adult male were calculated based on the mouse biodistribution. **Results:** Compared with ^{64}Cu(II), ^{64}Cu(I) exhibited higher uptake by both B16F10 and A375 cell lines, which could be effectively inhibited in the blocking groups. However, there was no obvious difference in cell efflux of ^{64}Cu radioactivity between ^{64}Cu(I) and ^{64}Cu(II) groups. Both B16F10 and A375M could be clearly visualized by ^{64}Cu(I) and ^{64}Cu(II) PET imaging at 1 h post-injection. Small animal PET quantitative analysis and biodistribution data revealed that the biodistribution of ^{64}Cu radioactivity in B16F10 (or A375M) tumor and other normal tissues of ^{64}Cu(I) were similar to those determined after the injection of ^{64}Cu(II). Calculations of radiodosimetry for $^{64/67}$Cu(I) and $^{64/67}$Cu(II) were also similar, which suggested that although melanoma were with high radiation absorbed doses, high radioactivity accumulation by liver and kidney should be noticed for the further application of radionuclide copper. **Conclusion:** Compared with ^{64}Cu(II), ^{64}Cu(I) exhibited higher cellular uptake by melanoma, which further testified CTR1 specially influx of Cu(I). However, due to oxidation reaction in vivo, no significant difference between ^{64}Cu(I) and ^{64}Cu(II) was observed through PET images and biodistribution. The in vivo stability of ^{64}Cu(I) should be further studied to evaluate it as a PET imaging radiotracer.

EP-0462

Prognostic value and monitoring after2-3years of patients subject to a SSNB on melanoma inside our service

F. S. Zelaya Reinquet, Jr., A. Renda Alcalde, M. Castrillon, C. Castillo, B. Nuñez, F. Loira, J. Nogueiras, D. Ruiz, L. Campos; Complejo hospitalario de vigo hospital meioxeiro, vigo, SPAIN.

Introduction: The Selective Sentinel Node Biopsy(SSNB),is currently considered as the most specific and sensitive method for the detection of melanoma micro-metrastasis at regional nodules,with lower morbidity and less secondly effects than the lymphadenectomy.Our purpose is to prove the Negative Predictive Value(NPV)from the Sentinel Node(SN)in order to avoid the lymphadenectomy,in the case the SN(+)determine if there is correlation with the Mitotic Index(MI). **Subjects and Methods:** Retrospective study of melanoma diagnosed

patients from General Surgery and Dermatologic from Vigo's and Pontevedra's Hospitals, who were assessed with a SSNB, through a period of 3years. (2012to2015). Inclusion Criteria: Patients diagnosed with melanoma with anatomicopathological study of the SN and monitoring during at least two years after diagnosis. **Result:** The representative sample was about 35patients. The averaged aged captured at the SSNB realization was 58,6years old (from a sample between18to85years old). With male dominance around60% (21patients) and40%-Women(14patients). The lesions localization was25.71%at trunk,22.86%on head or neck,20%at left upper limb,11.43%on lower left limb,11.43%on lower right limb and8.57%left,on upper right limb.The biopsy result showed SN(+)of37%from the sample(13patients)and SN(-)in the remaining62%(22patients).From the patients with SN(+),lymphadenectomy was performed to76.92%of the sample(10patients).Whit negative result in all of them.Being an average of fourteen nodules removed(a range of9to23).to the23.07%(3patients) no lymphadenectomy was performed because of distant metastases. From the sample a22,86%passed away (8 patients) before the two monitoring years. From this62,5%of the sample(5patients) caused to cerebral metastases,25% (2patients) due to a distance metastases and12,5%(1patient) owing to other reasons. **Discussion:** Recent studies have shown that80%of patients SSNB undergoing have a negative result. In our study,37%of SN have showed metastases,which is consistent with the literature.This suggests that the indication and method used in our survey was correct.AJCC Melanoma Staging Database shows a negative correlation between increased MI and the survival.AJCC has included MI≥1/mm2of primary melanoma as T1b in the TNM classification due to its association with lower survival rate, but there is insufficient data to determine the risk of lymph node micrometastases in patients with a MI≥1/mm2.In our study, a greater percentage of patients with positive SN(61.5%)had a MI≥1 mm2,but the differences were not statistically significant,this can be explained because the size of ours survey is small.A relevant fact in our sample is that the deceased patients presented MI≥3/mm². **Conclusion:** The SSNB is an established and useful procedure to minimize the unnecessary lymphadenectomies. As all the patients with SN(-)results have not presented distance metastasis or local relapsed.In this study there was no correlation found between SN(+)and the IM.More over, from the patients with SN(+)who underwent thought lymphadenectomy,this gave negative results in all cases.

EP-0463

Preparation of ^{99m}Tc-labeled HER2:V2-Pemetrexed for HER2-Positive lung tumor imaging

X. Zhao, J. Liu, T. Ma, Y. Zhang, F. Jing, T. Yu; The Fourth Hospital of Hebei Medica; University, Shijiazhuang, CHINA.

Purpose: Human epidermal growth factor receptor type 2 (HER2) overexpression has been reported in various malignant tumors. This study aimed to develop a novel integration of diagnosis and treatment probe, technetium-99m (^{99m}Tc) labeled

HER2:V2-Pemetrexed using -G(Gly)GGC(Cys) as a chelator, and to evaluate its imaging characteristic in HER2-positive lung xenografts. **Methods:** The HER2-binding $Z_{HER2:2395-}$Pemetrexed molecule probe with a C-terminal chelating sequence -G(Gly)GGC(Cys), called HER2:V2-Pemetrexed, was synthesized by Fmoc/tBu solid phase synthesis and chemical method. The molecular HER2:V2-Pemetrexed was labeled with ^{99m}Tc. The labeling efficiency and radiochemical purity were analyzed by reversed-phase high performance liquid chromatography (RP-HPLC). Molecular imaging studies were performed in BAL-B/c nude mice bearing lung A549 (high HER2 expression) or lung H23 cells (low HER2 expression) carcinoma xenografts. In addition, to investigate the specificity of the probe toward HER2 and the potential applications in monitoring therapies non-labelled HER2:v2-Pemetrexed was test as blocking agent in SPECT imaging. **Results:** The molecular probe was successfully synthesized and stably labeled with ^{99m}Tc with the labeling efficiency of 99.52±0.21% (n=5). The SPECT imaging showed clear localization of ^{99m}Tc-HER2:V2-Pemetrexed in the lung A549 xenografts shortly after injection but not in liver and other organs except for the kidneys or bladder. In vivo imaging, A549 tumor-bearing mice were visualized as early as 1 h and were shown most clearly at 8 h after the administration of ^{99m}Tc-HER2:V2-Pemetrexed. Whereas, the lung H23 xenografts with low HER2 expression were weakly imaged at any time after the injection of ^{99m}Tc-HER2:V2-Pemetrexed. Meanwhile, the A549 xenografts could be blocked by pre-saturation of receptors with unlabelled HER2:V2-Pemetrexed and were weakly imaged. The tumors in A549 tumor-bearing mice accumulated obviously more radioactivity than did the H23 xenografts or the blocked A549 xenografts, with significantly difference T/NT (tumor/non tumor) ratios (p<0.05, n=5). **Conclusion:** This study showed that ^{99m}Tc-HER2:V2-Pemetrexed is a promising imaging agent for HER2 over-expression lung tumors. It may be a potentially radiopharmaceutical agent for lung cancer integration of diagnosis and treatment. Fund: This work was supported by the National Natural Science Foundation of China (NSFC) project (81571702) and Hebei Provice Government Founding for Clinical Excellent Talent Project (2016).

EP-0464

Investigation of MSH receptor expression using ^{68}Ga- and ^{44}Sc-labeled molecules

G. Nagy[1], A. Kis[2], N. Dénes[2], I. Hajdu[2], I. Kertész[2], J. Hunyadi[2], E. Berényi[2], I. Garai[2,1], D. Szikra[2,1], G. Trencsényi[2,1]; [1]Scanomed Ltd., Debrecen, HUNGARY, [2]University of Debrecen, Debrecen, HUNGARY.

Aim: Alpha melanocyte stimulating hormone (alpha-MSH) enhances melanogenesis in malignant melanoma by binding to melanocortin 1 receptors (MC1R). Previous studies showed that MSH analogues (e.g. NAPamide) specifically binds to MC1R receptor, and radiolabeled NAPamide is a promising radiotracer for the detection of melanoma tumors by Positron Emission Tomography (PET). In this present study the MCR1 specificity of our newly developed ^{44}Sc-labeled DOTA-NAPamide was investigated using melanoma tumors. **Materials and Methods:** For *in vitro* experiments and tumor induction MC1R positive (B16-F10) and negative (A375) melanoma cell lines were used. Cells (1×10^6/ml tube) were incubated in the presence of 0.74 MBq of ^{44}Sc- or ^{68}Ga-labeled DOTA-NAPamide. After the incubation time (30 and 60 min) samples were washed and the radioactivity was measured with calibrated gamma counter. For the induction of tumor models 1×10^5 A375 or B16-F10 tumor cells were injected subcutaneously into the left shoulder area of CB17 SCID or C57BL/6J mice, respectively. For PET/MRI imaging studies mice were injected intravenously with 13±1.2 MBq of ^{44}Sc/^{68}Ga-labeled DOTA-NAPamide 15±1 days after tumor cell inoculation. 20-min static whole body PET scans were acquired 60 min after radiotracer injection using preclinical PET/MRI instrument. Radiotracer uptake was expressed in terms of standardized uptake values (SUVs). **Results:** *In vitro* and *in vivo* experiments showed that ^{68}Ga- and ^{44}Sc-labeled DOTA-NAPamide specifically bind to MC1 receptors of B16-F10 cell and tumors. B16-F10 cells showed significantly (p≤0.01) higher *in vitro* radiotracer accumulation than that of A375 cells. In imaging experiments, significantly (p≤0.01) higher ^{68}Ga-DOTA-NAPamide (SUVmean: 0.38±0.02), and ^{44}Sc-DOTA-NAPamide (SUVmean: 0.52±0.13) uptake was observed in the subcutaneously growing receptor positive B16-F10 tumors, than in A375 tumors, where the SUVmean values of ^{68}Ga-DOTA-NAPamide and ^{44}Sc-DOTA-NAPamide were 0.04±0.01 and 0.07±0.01, respectively. We found that the tumor-to-muscle (T/M SUVmean) ratios were approximately 14-fold higher than the T/M ratios of A375 tumors, and this difference was also significant (p≤0.01) using both radiotracers. No significant difference was found between ^{68}Ga- and ^{44}Sc-labeled DOTA-NAPamide uptakes. **Conclusion:** The investigated ^{44}Sc-DOTA-NAPamide, as a newly developed PET radiopharmaceutical specifically binds to MC1 receptors of melanoma cells. Due to the physicochemical properties of ^{44}Sc and its high selectivity, ^{44}Sc-DOTA-NAPamide is a promising PET radiotracer for the detection of melanocortin 1 receptor positive malignant melanoma for the clinical use.

EP-0465

Positron loss in small objects in preclinical PET

J. de Swart, M. W. Konijnenberg, M. de Jong, M. R. Bernsen, S. F. Petit; Erasmus MC, Rotterdam, NETHERLANDS.

Aim: MicroPET is used to image small objects adjacent to air, like tumour samples or xenografts in the chicken chorioallantoic membrane (CAM) model. In small tissue samples positrons may escape however; the positron range may lead to annihilation outside the tissue sample and thereby to loss of signal. In a phantom experiment we characterized the signal loss in relation to object size for the radionuclides ^{18}F and ^{68}Ga. **Method:** To model small tissue samples, circular pieces of coated, absorbing paper with a diameter of 5.5mm and a thickness of 0.22mm were used. These paper tissue phantoms were subsequently wetted with 0.22 MBq ^{18}F or 1.65 MBq ^{68}Ga in 5 µL. Sheets of 0.5mm thick polystyrene, density 1 g/cm^3, were used to provide

surrounding material to slow down the positrons to annihilation, and to study their influence on the signal detected by the PET system. Polystyrene sheets were stacked in increasing numbers under and on top of the paper tissue phantoms; for ^{18}F to a maximum of 3.5mm and for ^{68}Ga to 9.5mm, corresponding to their respective maximum positron range in water. Resulting samples were placed on the nylon mesh of a cell strainer. The cell strainers were placed in a six well plate. To mimic the situation in scanning tissue samples, a sheet of paper was also scanned with 3mL PBS added to the well cavity. Imaging of the phantom samples was performed on a Siemens Inveon microPET. A 30 minutes emission scan was followed by a transmission scan using two ^{57}Co sources. The PET scans were reconstructed using the OSEM3D/MAP algorithm. Recovery of the radioactivity in the sheets of paper was determined by VOI drawing. A recovery of 1 was a full recovery, a deviation of 0.1 was considered acceptable. **Results:** Recovery of the radioactivity in the paper tissue phantoms without surrounding material was only 0.27 for ^{18}F and 0.09 ^{68}Ga. Recovery increased with increasing thickness of surrounding material and reached 1±0.1 for ^{18}F when the polystyrene had a thickness of 1.0mm. For ^{68}Ga this recovery was reached at a thickness of 2.0mm. When 3mL PBS was added to the well the recovery improved to 0.68 and 0.34 for ^{18}F and ^{68}Ga, respectively. **Conclusion:** Measurement of the radioactivity in small objects using a PET system may result in severely underestimated values when the thickness of tissue-like material is less than 1mm for ^{18}F and less than 2mm for ^{68}Ga.

EP-0466

Molecular imaging of APN/CD13 receptors using 68Ga-labelled NGR peptides

A. Kis[1], N. Denes[1], J. Peline Szabo[1], T. Nagy[1,2], I. Kertesz[1], I. Hajdu[1], G. Mező[3], G. Farkasinszky[1], G. Nagy[2], I. Garai[2], E. Berenyi[1], G. Trencsenyi[1,2]; [1]University of Debrecen, Faculty of Medicine, Division of Nuclear Medicine, Debrecen, HUNGARY, [2]Scanomed Ltd., Debrecen, HUNGARY, [3]MTA-ELTE, Research Group of Peptide Chemistry, Budapest, HUNGARY.

Purpose: Aminopeptidase N (APN/CD13) is a zinc dependent, transmembrane exopeptidase. It plays an important role in neo-angiogenic process and metastatic tumor cell invasion. Our previous studies have already shown that ^{68}Ga-labelled NGR peptides specifically bind to APN/CD13 expressing chemically induced tumor cells. The ^{68}Ga labelled NGR peptides were enabled to investigate the neo-angiogenic process with Positron Emission Tomography (PET). The aim of this study was to investigate and compare the ^{68}Ga-NOTA-c(NGR), ^{68}Ga-NODAGA-NGR (tioether) and ^{68}Ga-NODAGA-NGR (sarcosine) specificity of APN/CD13 in hepatocellular carcinoma (He/De) and mesoblastic nephroma (Ne/De) tumor models using PET/MRI. **Subjects and Methods:** He/De (hepatocellular carcinoma) and Ne/De (mesoblastic nephroma) cells were used for the induction of heterotopic transplanted (subcutaneously (n=4) and under the left kidney capsule (n=4)) tumor models in Fischer-344 rats. Whole body PET/MRI (nanoScan PET/MRI, Mediso Ltd, Hungary) scans and ex vivo biodistribution studies were performed using tu-

mor-bearing and control (n=3) animals 90 min after intravenous injection of 6.9±0.2 MBq ^{68}Ga-NOTA-c(NGR) or ^{68}Ga-NODAGA-NGR (tioether) or ^{68}Ga-NODAGA-NGR (sarcosine) and two weeks after tumor cell implantation. The imaging of neoangiogenetic process with ^{68}Ga-NOTA-c(NGR) was compared with ^{68}Ga-NODAGA-NGR (tio) and ^{68}Ga-NODAGA-NGR (sar) tracer. Aminopeptidase N receptor expression of He/De and Ne/De tumors was verified by western blot analysis. **Results:** In control animals using ^{68}Ga-NOTA-NGR high SUVmean values were observed in abdominal organs, however, in the case of ^{68}Ga-NODAGA-NGR (tioether) and ^{68}Ga-NODAGA-NGR (sarcosine) it was much higher. SUVmean and Tumor/Muscle(SUVmean) ratios were found higher after injection of ^{68}Ga-NOTA-NGR, than the administration of ^{68}Ga-NODAGA-NGR (tioether) or ^{68}Ga-NODAGA-NGR (sarcosine) in Ne/De tumor bearing animals. In the case of He/De tumor bearing animals comperable SUVmean and Tumor/Muscle(SUVmean) values were detected. Higher SUVmean and Tumor/Muscle(SUVmean) ratios were measured after the injection of ^{68}Ga-NOTA-NGR, than after that of the ^{68}Ga-NODAGA-NGR (tioether) or ^{68}Ga-NODAGA-NGR (sarcosine). The *in vivo* PET/MRI results correlates with *ex vivo* biodistribution results. The APN/CD13 receptors attendance was demonstrated with western blot analysis. **Conclusion:** Among the investigated radiopharmacons the ^{68}Ga-NOTA-c(NGR) showed the highest binding affinity to APN/CD13 positive tumors by PET/MRI imaging. Therefore, ^{68}Ga-NODAGA-NGR (tioether) showed sufficient and ^{68}Ga-NODAGA-NGR (sarcosine) showed the worst properties for the detection of APN/CD13 expression. Therefore, ^{68}Ga-NOTA-c(NGR) is the most suitable tracer for the detection of APN/CD13 positive He/De and Ne/De tumors *in vivo.* This project was supported by the János Bolyai Research Scholarship of the Hungarian Academy of Sciences.

EP-0467

Application of 68Ga-NODAGA and 68Ga-HBED-CC conjugated procainamide derivates for preclinical melanoma modeling

N. Dénes[1], G. Trencsényi[1,2], G. Nagy[2], A. Kis[1], A. Vida[3,4], J. P. Szabó[1], F. Farkas[1], T. Kovács[3,4], P. Bay[3,4,5], E. Berényi[1], I. Garai[2], J. Hunyadi[6], I. Kertész[1]; [1]University of Debrecen, Faculty of Medicine, Division of Nuclear Medicine, Debrecen, HUNGARY, [2]Scanomed LTD, Debrecen, HUNGARY, [3]University of Debrecen, Department of Medical Chemistry, Debrecen, HUNGARY, [4]MTA-DE Lendület Laboratory of Cellular Metabolism, Debrecen, HUNGARY, [5]Research Center for Molecular Medicine, Debrecen, HUNGARY, [6]University of Debrecen, Department of Dermatology, Debrecen, HUNGARY.

Introdcution: Malignant melanoma is a metastatic skin cancer which initiates from the pigment-producing skin cells (melanocytes), most commonly from the existing naevus. Although, only 3-5 percent of the skin cancer is melanoma, it possesses the worst prognosis. However, in case of early detection, melanoma is a completely curable disease. Nowadays one of the most efficient methods in tumor diagnostics is PET imaging; therefore, several recent studies focus on the development of melanoma specific tracer. Previous researches have shown that

benzamide derivatives (e.g. PCA) were proven to be specific markers for detection of melanoma. The aim of this study was to radiolabel the NODAGA and HBED-CC chelator conjugated PCA derivative with Ga-68, and in order to PET imaging, to apply the labeled compounds on animal models of melanoma. Moreover, we aimed an extensive testing of the compounds under in vitro and in vivo conditions. **Subjects and Methods:** The free amino group of procainamide (PCA) was conjugated with macrocyclic NODAGA and acyclic HBED-CC chelators. The complete ligands were purified with RP-HPLC and then were lyophilized. The product was characterized by ESI-MS and ^{1}H-NMR. The [68]Ge/^{68}Ga generator (Eckert-Ziegler, Obninsk) was eluted by using 0.1 M with 5 mL HCl. The labelling was accomplished on pH=4.5-4.6 in NaOAc buffer at room temperature and at 95ºC for five minutes. The melanin specificity of ^{68}Ga-HBED-CC-PCA and ^{68}Ga-NODAGA-PCA was investigated *in vitro* and *in vivo* using amelanotic (MELUR and A375) and melanin containing (B16-F10) melanoma cell lines. Tumour-bearing animals were prepared by subcutaneous injection of B16-F10, MELUR and A375 melanoma cells into C57BL/6 (n=10) and SCID (n=9) mice. **Results:** Procainamide derivatives conjugated with two different chelators were prepared successfully. The compounds possessed excellent radiochemical purity (≥ 98%). Concentration range for quantitative labelling was determined after optimization experiments. The octanol-PBS partition coefficients (LogP) of the two radiolabelled compounds were determined. Based on the results of the in vitro measurements the ^{68}Ga-NODAGA-PCA showed significantly (p≤0.01) higher accumulation than the ^{68}Ga-HBED-CC-PCA on the B16-F10 cell line. **Conclusion:** Two ^{68}Ga labelled PCA derivatives were developed, which could selectively accumulate in melanin producing melanoma cells. The uptake values of the compounds are diverse and the in vivo preclinical measurements have confirmed, that the ^{68}Ga-NODAGA-PCA possessed higher uptake on tumour models. Therefore, it was proven that the heterobifunctional chelators also served as pharmacokinetic modifiers, and by their selection the distribution profile of the radioligands within the organism can be considerably modifiable.

EP-0468

In Vivo Imaging Of Ischemia-Reperfusion Using (68)Ga-Labeled Peptides

G. Farkasinszky[1], N. Denes[1], J. S. Peline[1], T. Nagy[1], G. Trencsenyi[1,2], I. Kertesz[1], A. Kis[1], G. Mező[3], J. Hunyadi[4]; [1]*Division of Nuclear Medicine, Faculty of Medicine, University of Debrecen, DEBRECEN, HUNGARY,* [2]*Scanomed LTD, Debrecen, HUNGARY,* [3]*Research Group of Peptide Chemistry, MTA-ELTE, BUDAPEST, HUNGARY,* [4]*Department of Dermatology, University of Debrecen, DEBRECEN, HUNGARY.*

Introduction: Angiogenesis is the process of new blood vessel formation. One can be observed physiologically in wound healing and embryogenesis but it has discovered in several human pathological disorders such as tumors, coronary artery disease or retinopathia diabetica. The asparagine-glycine-arginine (NGR) peptide sequence known as a possible biomarker of angiogenesis. Previous studies have shown that the NGR peptides are specifically bind to APN/CD13 molecules expressed by tumors. Ga-68 labeled NGR peptides allowed the preclinical PET conducted non-invasive imaging of neo-angiogenic processes. **Methods:** The cyclic NGR peptide was prepared successfully by solid phase peptide synthesis. The NGR derivate was conjugated with NOTA macrocyclic chelator. The complete ligand was purified by RP-HPLC and then was lyophilized. The product was characterized by ESI-MS and 1H-NMR. The labeling optimization experiments were accomplished with Ga-68 at room temperature and at 95ºC. The partition coefficient of 68Ga-NOTA-c(NGR) was expressed as log P by measuring the distribution of radioactivity in 1-octanol and PBS-solution. Left eye of rats (Fischer-344) (n = 5) were ligated surgically using a cannula guided loop. Ischemia can be induced by tightening the noose (90 min.) furthermore it can be terminated by loosening it. The upper mentioned surgical procedure suitable to develop lesions that occur during reperfusion. One day after ischemia-reperfusion (I/R) induction labeled radioligand (15 MBq in 150 µl saline) was injected intravenously (lateral tail vein) to surgical and non-surgical control (n = 2) groups. After the appropriate incubation time (90 min.) the radiopharmaceutical distribution was determined in vivo using PET (MiniPET-II small animal PET scanner) and CT (Micro-CT). **Results:** NGR peptides conjugation with NOTA chelator was prepared successfully. 68Ga-NOTA-c(NGR) was produced with high specific activity (5.13-5.92 GBq/µmol) and with excellent radiochemical purity (95%<), at all cases. The quantitate labeling range was determined. It was over 10 µmol/dm³. The octanol-PBS partition coefficient (LogP) of the radiolabeled compound was successfully defined.In the left bulbus of the surgical group significantly (p≤0.05) higher tracer uptake was observed (SUV mean) compared to the control (internal control) and non-surgical control group. Western blot analysis confirmed the presence of neo-angiogenic markers (APN / CD13). **Conclusion:** The above outlined application suitable for study in vivo I/R mediated receptor expression in rat eye model. Thus, creates an opportunity to develop modern diagnostic methods in various pathological processes.

EP-0469

Impact of Hypoxia on the Expression of Amino Acid Transporters and the Uptake of [^{11}C]methionine

M. Kim[1,2,3], T. Ishizu[1,2,4], S. Forsback[1], O. Eskola[1], E. Arponen[1], J. Tuomela[4], H. Minn[1,5], T. J. Grönroos[1,2,6]; [1]*Turku PET Centre, University of Turku,, Turku, FINLAND,* [2]*MediCity Research Laboratory, University of Turku, Turku, FINLAND,* [3]*Graduate School of Medicine, Gunma University and apan Society the promotion of science, Gunma and Tokyo, JAPAN,* [4]*Department of Cell Biology and Anatomy, University of Turku, Turku, FINLAND,* [5]*Department of Oncology and Radiotherapy, Turku University Hospital,, Turku, FINLAND,* [6]*Department of Oncology and Radiotherapy, Turku University Hospital, Turku, FINLAND.*

Aim: Two amino acid transporters are known to be overexpressed in cancer and upregulated by hypoxia, the L-type amino acid transporter 1 (LAT1) by HIF-2 and xCT through HIF-1. The aim of this study was to determine whether the expression level of LAT1 and xCT transporters is upregulated by hypoxia in

head and neck (UT-SCC-74A), prostate (PC-3) and breast (MDA-MB-231) cancer cell lines and furthermore evaluate whether the uptake of [^{11}C]-L-methyl-methionine ([^{11}C]MET) is affected by the expression level of these proteins. In addition, the uptake of [^{18}F]FDG and the hypoxia tracer [^{18}F]EF5 will be determined in order to evaluate the glycolytic activity and hypoxic properties of the selected cell lines. **Materials and Methods:** Selected cell lines were grown in 6-well plates until ~70-80% confluency under normoxia or different time periods (3, 6, 12, 24, 48 and 72 h) of hypoxia (1% O$_2$) in a hypoxia workstation (Invivo2, Ruskinn Technology Ltd). Cells (n = 4-6 for each cell line and circumstance) were collected, lysed in RIPA buffer and proteins (LAT1, xCT) were separated with SDS-PAGE. The expression levels of the proteins were detected by immunoblotting. Separate sets of cells were incubated with [^{11}C]MET for 1 hour. After the incubation period, cells were counted and measured for radioactivity using a Wizard gamma counter (Perkin-Elmer). The uptake of [^{11}C]MET into the cells was related to the amount of viable cells. **Results:** The uptake of [^{11}C]MET was 5-10 times higher in breast and prostate cancer cell lines compared to that seen in head and neck cells. Hypoxia increased [^{11}C]MET uptake in prostate cancer cells, whereas no such effect could be detected in breast or head and neck cells. The expression rate of LAT1 and xCT transporters were not increased in prostate cancer cells, whereas an increased expression level was detected in breast (xCT) and head and neck cancer cells (LAT1 and xCT). The expression level of mTOR, HIF-1α and HIF-2α will be determined. **Conclusions:** Our preliminary results indicate that the expression rate of the amino acid transporters LAT1 and xCT do not affect the uptake of [^{11}C]MET in the selected cell lines used in this study.

EP-0470

Multimodal imaging of tumor invasion by targeting integrin α$_v$β$_3$ in a preclinical model of lung metastasis

F. Iommelli[1], V. De Rosa[1], M. Monti[2], C. Terlizzi[2], M. Gramanzini[1], S. Gargiulo[1], S. Del Vecchio[2,1]; [1]Institute of Biostructures and Bioimaging, National Research Council, Naples, ITALY, [2]Department of Advanced Biomedical Sciences, University "Federico II", Naples, ITALY.

Aim: Metastatic dissemination is the primary cause of death in cancer patients. Among the key proteins involved in this multistep process, a prominent role is played by members of the integrin family. Here we developed a preclinical model of lung metastasis as a tool to test the effects of antimetastatic drugs including α$_v$β$_3$ targeted agents using Fluorescence Molecular Tomography and micro-CT. **Methods:** human fibrosarcoma HT1080 cells were tested for the expression of α$_v$β$_3$ integrin by flow cytometry and then intravenously injected in Balb/c female nude mice. Development of lung metastases in mice was monitored by serial imaging studies with microCT (eXplore Vista, GE Healthcare). CT data sets were then transferred in DICOM format to an OsiriX workstation for image processing. Mice bearing lung metastases were subjected to optical imaging studies and i.v. injected with 2 nmol of fluorescent small molecule α$_v$β$_3$ antagonist (PerkinElmer). After 2h from injection to allow probe

biodistribution, the animals were subjected to Fluorescence Molecular Tomography (FMT 4000 fluorescence tomography imaging system, PerkinElmer). At the end of imaging studies, lungs were surgically removed, subjected to ex vivo optical imaging and fixed in buffered 4% formaldehyde. Finally, the number of lung metastases was determined by staining lung sections with hematoxylin and eosin. **Results:** Flow cytometry analysis found high levels of α$_v$β$_3$ integrin in HT1080 cells. Axial CT images of mice showed development of lung nodules approximately 3-4 weeks after cell injection. Volumetric segmentation of CT images using thresholds for normal lung parenchyma showed a strong reduction of aerated lung volume in mice with lung metastases as compared to that observed in healthy animals. Optical imaging of mice revealed a signal from lungs and metastatic lung nodules were clearly detected in excised lungs and confirmed by histopathological examination. **Conclusions:** Our findings indicate that multimodal imaging with Fluorescence Molecular Tomography and micro-CT may be used in a preclinical model to test the effects of antimetastatic drugs including α$_v$β$_3$ targeted agents

EP-0471

Optimization of High Throughput ^{18}FDG Murine Imaging Using a Clinical Digital PET/CT System

K. Briley[1], K. Binzel[1], M. Friel[1], R. Moore[1], J. Ellis[1], J. Zhang[1], P. Maniawski[2], M. V. Knopp[1]; [1]The Ohio State University, Columbus, OH, UNITED STATES OF AMERICA, [2]Philips Healthcare, Cleveland, OH, UNITED STATES OF AMERICA.

Purpose/Introduction: High throughput PET/CT imaging of rodents would allow for cost effective screening and dose-response optimization of emerging novel therapeutics agents. The aim of the current study was to optimize the PET and CT acquisition and reconstruction to simultaneously image multiple mice (n=6) using a next generation clinical digital PET/CT (Philips Vereos)(dPET). **Subjects & Methods:** A sample holder allowing for the administration of isoflurane to multiple mice (n=6) in the clinical dPET/CT system was constructed. Wild type mice were administered 18FDG in dose range of 1.8-18 MBq via tail vein injection. Imaging was performed 20-90 minutes post injection in order to determine the optimal 18FDG dose and time post injection for the dPET imaging of multiple mice. CT acquisition (Philips Ingenuity) was optimized to allow for best soft tissue contrast and co-registration with the dPET fine tuning KV, mAs, FoV, and reconstruction parameters to allow for simultaneous multiple CT mice imaging. The dPET bed acquisition time (600, 180, and 18 seconds) was then evaluated using n=5 tumor bearing (RIF1) nude mice with one control mouse also scanned. The mice were sacrificed and the tumors removed immediately after dPET/CT. The excised tumors were gamma counted to determine 18FDG uptake and scanned ex vivo in order to validate system sensitivity. **Results:** The results of the study concluded that a dose of 3.7 MBq 18FDG with dPET image acquisition 30-60 minutes post tail vein injection allowed for optimal dPET imaging of n=6 mice. Additionally, optimal CT soft tissue contrast was obtained using 80kV, 150 mA, FoV=166,

matrix 1024x1024, iDose 6, and SharpC reconstruction for the CT acquisition of n=6 mice. 18FDG imaging of the RIF1 mice using the optimal imaging methodology allowed for clear visualization of the tumors. No significant variation in the SUV of the tumors was observed for the 600, 180 and 18 second dPET bed acquisition times. Gamma counting of the ex vivo tumor showed 3.8±1.4 % uptake of the total 18FDG dose injected in the tumor at the time of imaging. Additionally, ex vivo imaging of the tumors demonstrated the feasibility of tissue sample imaging. **Discussion/Conclusion:** After optimization, the next generation dPET/CT allowed for high throughput / simultaneous (n=6) 18FDG imaging of tumor bearing mice. This method enables cost and throughput effective, dynamic screening for biodistribution, diagnostic and therapeutic pre-clinical studies.

Basic Oncology: Metrics & Intervention

EP-0472

Endoscopic non-ablative fractional laser irradiation suppresses early tumor growth in orthotopic colon tumor model

S. Yoo[1,2], G. Oh[3], A. Safi[2], S. Hwang[2], Y. Seo[4], K. Lee[5], H. Song[6], H. Bom[1], J. Min[1], Y. Kim[7], E. Chung[2,3]; [1]Department of Nuclear Medicine, Chonnam National University Hwasun Hospital, Jeollanam-do, KOREA, REPUBLIC OF, [2]Department of Biomedical Science and Engineering, Institute of Integrated Technology (IIT), Gwangju Institute of Science and Technology (GIST), Gwangju, KOREA, REPUBLIC OF, [3]School of Mechanical Engineering, Gwangju Institute of Science and Technology (GIST), Gwangju, KOREA, REPUBLIC OF, [4]R & D center, WONTECH Co., Ltd., Daejeon, KOREA, REPUBLIC OF, [5]Department of Pathology, Chonnam National University Hwasun Hospital and Medical School, Jeollanam-do, KOREA, REPUBLIC OF, [6]Department of Nuclear Medicine, Chonnam National University Hospital, Gwangju, KOREA, REPUBLIC OF, [7]Weldon School of Biomedical Engineering, Purdue University, West Lafayette, IN, UNITED STATES OF AMERICA.

Purpose: Colorectal cancer is the second frequent cause of cancer-related death in the US and colonoscopy is firmly established as the mainstay of cancer prevention. Several options for treating early colorectal cancer therapy via endoscopic procedure are available, such as snare polypectomy, endoscopic mucosal resection, and endoscopic submucosal dissection. However, these treatment strategies bring complications such as bleeding or even bowel perforations. Therefore, there exists a compelling need for less invasive, therapeutic modality for early colorectal cancer treatment. In this study, we developed an endoscopic non-ablative fractional laser (eNAFL) irradiation system to test its therapeutic effect on early stage tumor. Utilizing an orthotopic colon cancer model to match the tumor's microenvironment, we examined the clinical usefulness of fractional laser as cancer therapeutic modality. **Materials and Methods:** We combined thulium fiber-based fractional laser system with multi-channel endoscopy system. The thulium laser was coupled with multimode fiber and inserted through the instrumental channel of endoscopy. Orthotopic tumor model with SL4-DsRed mouse colon cancer cell was generated with various kinds of cancer cell implantation methods. After selecting most appropriate orthotopic tumor model, six orthotopic tumor mice were randomly separated into two groups, irradiation group or control group. After one day from cancer cell implantation, irradiation group received four eNAFL irradiation spots. Total 70 mJ of energy (35 mJ/sec × 2 sec) was delivered to each spot via multimode fiber tip with contact mode. control group mice didn't receive any irradiation. Follow-up endoscopic image was done with fluorescence and white light imaging. In vivo thermal imaging and numerical simulation was performed to evaluate thermal distribution after eNAFL irradiation. **Results:** Smaller tumor growth was observed in the eNAFL irradiated group than control group by both white light and fluorescence images. Visual scoring of the tumor growth revealed smaller tumor grade in the eNAFL irradiated group. Statistical significance between two groups was observed in the day 6 and 7 after cancer cell implantation. Thermal imaging and numerical simulation showed minimal thermal damage that is only confined to the irradiated spot sparing adjacent tissue. **Conclusion:** eNAFL irradiation has a great potential as a minimally invasive therapeutic intervention at an early stage of tumorigenesis.

Basic Oncology: Tumour Biology

EP-0473

Fluciclovine is a potential imaging biomarker of glutamine utilisation in breast cancer

E. J. Teoh, E. M. Bridges, M. Morotti, C. E. Zois, S. R. Lord, F. V. Gleeson, A. L. Harris; University of Oxford, Oxford, UNITED KINGDOM.

Purpose/Introduction: To determine the uptake mechanisms of the amino acid PET tracer fluciclovine (anti-1-amino-3-fluorocyclobutane-1-carboxylic acid / FACBC) in breast cancer cell lines, and explore its potential utility as an imaging biomarker of early response to therapies modulating the glutamine pool. **Subjects & Methods:** Fluciclovine (^{14}C) uptake was assessed in a panel of 6 breast cancer cell lines. This was correlated with the expression of amino acid antiporters ASCT2 and LAT1, reported as main contributors to fluciclovine transport in prostate cancer. In a smaller panel of 3 cell lines (MCF7, HCC1806, BT474), the effect of competitive inhibition with the ASCT2 inhibitor L-γ-Glutamyl-p-nitroanilide (GPNA) and system A inhibitor methylaminoisobutyric acid (MeAIB), ASCT2 and LAT1 siRNA, on fluciclovine uptake was assessed. Competitive inhibition with a panel of 14 natural amino acids was performed. For drug response assessment, assays were performed 48-hours after drug exposure, with sensitivities based on 5-day treatments. **Results:** There was a statistically significant correlation between uptake and ASCT2 expression (p<0.05), but not with LAT1 expression.

Fluciclovine (^{14}C) uptake was markedly decreased to 22-28% in the presence of GPNA, and 16-28% with ASCT2 knockdown. There was no significant difference in uptake in the presence of MeAIB, control siRNA and LAT1 knockdown. There was a minimally additive effect of LAT1 knockdown in the presence of GPNA on inhibition of uptake. High-affinity substrates of ASCT2 (glutamine, alanine, serine, cysteine and threonine) inhibited fluciclovine (^{14}C) uptake to 14-21%, while the reduction of uptake was less with high-affinity substrates of LAT1 (41-82%). Change in fluciclovine uptake following treatment with glutaminase inhibitor CB-839, and metformin were evaluated. In a sensitive cell line HCC1806, fluciclovine uptake increased by 1.7-fold following CB-839 treatment (p<0.01), consistent with accumulation of intracellular glutamine allowing greater exchange for influx of fluciclovine. Metformin treatment of sensitive cell lines MDA-MB-468 and MCF7 resulted in reduction of fluciclovine uptake (64% and 78% of control respectively, p<0.05), with no significant change in resistant cell line MDA-MB-231. This is consistent with our previous findings of increased glutamine dependence in sensitive cell lines following metformin exposure, leading to decreased intracellular glutamine availability to exchange for influx of fluciclovine. **Discussion/Conclusion:** Fluciclovine is predominantly transported by high-affinity glutamine transporter ASCT2 in breast cancer and may inform on the dynamics of intracellular glutamine levels. This raises the potential for future clinical use in early imaging response to inhibitors of glutamine metabolism and pathways which augment glutamine consumption.

EP-0474

Diagnostic Importance of 18F-FDG PET/CT Parameters And Total Lesion Glycolysis (TLG) in Differentiating Between Benign And Malignant Adrenal Lesions

E. Ciftci, B. Turgut, A. Cakmakcilar, S. Erturk; Cumhuriyet University, School of Medicine, Department of Nuclear Medicine, Sivas, TURKEY.

Purpose: Benign adrenal lesions are frequently come acrossed in oncologic imaging and make difficulties in the diagnosis of metastatic disease. The purpose of this study is evaluation the diagnostic importance of metabolic, volumetric and metabolovolumetric parameters measured by 18F-FDG PET/CT in differentiating between benign and malignant adrenal lesions in cancer patients. **Subjects & Methods:** In this retrospective study we evaluated 18F-FDG PET/CT parameters of adrenal lesions of follow-up cancer patients referred to our clinic between January 2012 and November 2016. Diagnosis of adrenal malignant lesions was based on interval growth or reduction after chemotherapy. Patient demographics, analysis of metabolic parameters as SUVmax (maximum standard uptake value), T/LR (tumor SUVmax/liver SUVmean ratio), morphologic parameters as size, Hounsfield Units (HU) and CT volume and metabolovolumetric parameters as metabolic tumor volume (MTV) and total lesion glycolysis (TLG) of adrenal lesions were calculated. PET/CT parameters were assessed by using Mann Whitney U-test and receiving operating characteristic analysis. **Results:** 186 adrenal lesions in 162 cancer patients (108M/54F); mean±SD

age, 64±10.9 years were underwent FDG PET/CT for evaluation of spreadtumor. SUVmax values (mean±SD) were 2.8±0.8 and 10.6±6; TLG were 10.8±9.2 and 124.4±347.9; T/LR were 1±0.3 and 4.1±2.6 in benign and malignant adrenal lesions, respectively. Based on AUC, adrenal lesion SUVmax and T/LR had the similar highest diagnostic performance for predicting malignant lesion (AUC:0.993 and 0.991, p<0.001), respectively. Multivariate logistic regression analysis revealed that T/LR, adrenal lesion SUVmax and HU was an independent predictive factor for malignancy rather than TLG. **Conclusion:** Whether TLG, which proposed as a new parameter in the literature, is statistically highly significant for differentiating benign from malignant lesions, it did not reach the expected performance with low NPV. It's thought that, it may be due to the malignant but small and benign but large lesions on metabolovolumetric calculation.

EP-0475

Does F18FDGPET/CT is Able to Differentiate Between Histological Subtypes of Lung Adenocarcinoma (LADC) and Their Mutation Status (ALK, EGFR) - Tertiary Referral Centre Experience

L. Calovi Motschenbacher, A. Parsai, M. Sheaff, S. Ellis, T. O'Shaughnessy, H. Jan, E. Nowosinska; Barts Health, London, UNITED KINGDOM.

Introduction: Lung adenocarcinoma (LADC) is a major histological subtype of lung cancer known for its heterogenicity including histological subtypes, molecular alterations and responses to chemotherapy and targeted therapy. Whilst LADC patients benefit less from conventional chemotherapy, targeted treatment has been associated with great achievements towards improving the clinical outcomes. Hence, currently Epidermal Growth Factor Receptor (EGFR) and Anaplastic Lymphoma Kinase (ALK) mutations are routinely assessed in clinical practice before decision regarding the treatment options and for the prediction of therapy response. Increasing numbers of studies have focused on the histological subtypes of LADC following the novel classification proposed by the International Association for the Study of Lung Cancer/American Thoracic Society/European Respiratory Society (IASLC/ATS/ERS). Finding the association between the histological subtype and mutation status of LADC patients is crucial. Numerous studies have previously evaluated the association between EGFR mutation, ALK status and histological subtype. However, the results of these studies have been controversial. **Aim:** To demonstrate correlation between histological subtype, tumour size, ALK and EGFR mutations and ^{18}F-FDGPET/CT SUV max in patients with lung LADC. **Materials and Methods:** All the patients who underwent pre-operative evaluation with ^{18}F-FDGPET/CT between July 2013 and March 2017 were retrospectively analised. The patients were stratified according to IASLC/ATS/ERS classification. Tumour size, histology subtype, EGFR, and ALK status were correlated with F18 FDGPET/CT. **Results:** 81 patients (45 females) were included in the analysis. The mean age was 68 (range 32-88). EGFR mutations were identified in 79% and ALK mutations were detected in 91% of cases. Four major histologic patterns were identified:

Lepidic (30%), Acinar (30%), Papillary (7%) and solid (33%). There was a significant correlation between SUV max and tumour size *(p<0.001)*. However, there was no significant association between EGFR *(p=0.79)*, ALK *(p=0.81)* status, histologic pattern *(p=0.13)* and SUV max. **Conclusion:** 1. F18FDGPET/CT is a valuable tool in LADC patients' stratification prior to surgery, and cannot differentiate between histological subtypes of ADC and their mutation status . 2. Evaluation of those variables has been now in progress on a larger cohort of patients.

EP-0476

Neutrophil Extracellular Traps as a New Target for Imaging of Integrin-Dependent Dissemination of Cancer Cells

M. Monti[1], F. Iommelli[2], V. De Rosa[2], M. V. Carriero[3], G. Di Minno[1], S. Del Vecchio[2,4]; [1]Department of Clinical Medicine and Surgery, University "Federico II", Naples, ITALY, [2]Institute of Biostructures and Bioimages, National Research Council, Naples, ITALY, [3]Department of Experimental Oncology, National Cancer Institute, Naples, ITALY, [4]Department of Advanced Biomedical Sciences, University "Federico II", Naples, ITALY.

Aim: Neutrophil extracellular traps are web-like structures composed of nucleic acids, histones and selected cytoplasmic proteins that are released by activated neutrophils to entrap and kill different pathogens. In addition to their function as a host defense mechanism, neutrophil extracellular traps are reported to promote metastatic dissemination of cancer cells by entrapment of circulating tumor cells. Here we tested the role of integrins α5β1 and αvβ3 in the adhesion of cancer cells to neutrophil extracellular traps and explore the possibility that these web-like structures may serve as targets for imaging of dissemination of cancer cells. **Methods**: HL60 cells were differentiated with DMSO in neutrophil-like cells and then stimulated with calcium ionophore A23187 for 4 hours at 25 µM to produce large amounts of neutrophil extracellular traps. K562 cells endogenously expressing α5β1 integrin (K562) and its derived clone overexpressing αvβ3 integrin (K562αvβ3) were subjected to adhesion assays using neutrophil extracellular traps as an adhesion substrate. Negative controls included the addition of DNAse 1, blocking antibodies against α5β1 or αvβ3, RGD cyclic peptides and Proteinase K. Neutrophil extracellular traps were also analyzed for their protein content by western blotting and confocal microscopy for co-immunolocalization studies. **Results:** Neutrophil extracellular traps obtained from neutrophil-like cells were positively stained for chromatin structures with Sytox Green cell-impermeable nucleic acid dye, for citrullinated histone H3 and myeloperoxidase, all recognized markers of neutrophil extracellular traps. Adhesion assays using neutrophil extracellular traps as substrate showed that 59% ± 8% and 80% ± 3% of K562 and K562αvβ3 cells, respectively, were adherent to coated plates. As expected DNAse 1 treatment strongly inhibited adhesion of both cell lines to neutrophil extracellular traps. An equivalent significant reduction of cell adhesion was obtained after treatment of cells with blocking antibodies against α5β1 or αvβ3 indicating that both integrins were able to mediate cell adhesion to neutrophil extracellular traps. Western blot analysis and immunoprecipitation experiments showed a dose-dependent increase of fibronectin levels in samples from stimulated neutrophil-like cells and a direct or indirect interaction of fibronectin with histone H3. Finally, co-immunolocalization studies with confocal microscopy showed that fibronectin and citrullinated histone H3 co-localize inside the web-structure of neutrophil extracellular traps. **Conclusions**: Our study showed that α5β1 and αvβ3 integrins mediate cell adhesion to neutrophil extracellular traps by binding to their common substrate fibronectin. Structural components of neutrophil extracellular traps may serve as potential targets for imaging of integrin-dependent dissemination of cancer cells.

EP-0477

Volumetric metabolic parameters on FDG-PET independently predicts PD-L1 expression in patients with non-small cell lung cancer (NSCLC)

M. Jreige, I. Letovanec, J. O. Prior, N. Schaefer; Centre Hospitalier Universitaire Vaudois (CHUV), LAUSANNE, SWITZERLAND.

Purpose: Humanized anti-PD-L1 or anti-PD-1 IgG1 monoclonal antibody can restore tumor-specific T-cell immunity by inhibiting the binding of PD-L1 to PD-1. It is considered as an emerging novel therapy in non-small cell lung cancer (NSCLC). Herein, we investigate the correlation of tumoral metabolic activity on FDG-PET with tumoral tissue expression of PD-L1 in resection or biopsy sample from NSCLC patients. **Materials and Methods:** All patients with a confirmed NSCLC who were investigated by immunohistochemistry (IHC) for PD-L1 (Roche-Ventana Clone SP263) on biopsy sample or on resection specimen and who had a FDG-PET prior to surgery or biopsy, were retrospectively included. From January 2016 to Mars 2017, 50 patients (M:F=29:21; mean age 67±12 years) were investigated. Sampled surgical and biopsy tumor specimens were analyzed by immunohistochemistry (IHC) for PD-L1 tumor expression. FDG-PET images were analyzed to define in biopsied or resected lesions the values of SUVmax, SUVmean, metabolic tumor volume (MTV) and total lesion glycolysis (TLG) with a threshold of 42% of SUV_{max}. Metabolic information on FDG-PET was correlated with the positivity of expression of PD-L1 in corresponding tissue using Spearman correlation and linear regression analysis. **Results:** Thirty-two adenocarcinomas (ADC), 13 squamous cell carcinomas (SCC) and 5 NSCLC were analyzed. All tumors showed metabolic FDG-PET uptake with mean SUVmax 12.3±6.3 g/ml (range: 3.2-27), SUVmean 6.8±3.4 g/ml (range: 1.9-14.9), MTV 38±49 cm^3 (range: 1.2-257) and TLG 307±576 g*cm^3/ml (rang: 1.2-3730). There was no dependency of FDG-PET uptake on histologic type (p=0.18). We found a statistically significant correlation between MTV and TLG (rho=0.34, p=0.02 and rho=0.32, p=0.02), but not SUVmax and SUVmean with PD-L1 tumor expression (p≥0.2). Wilcoxon rank-sum test showed significant differences in MTV and TLG according to PD-L1 tumor expression ≥10% (25±32 vs. 67±66, p=0.039 and 190±296 vs. 498±834, p=0.027 respectively). On multivariate analysis using SUVmax, MTV, TLG and histology, only MTV significantly predicted the PD-L1 expression (beta=0.65, p<0.0001). **Conclusions:** This

study shows a direct association between metabolic FDG-PET parameters, in particular MTV and TLG, and the expression of PD-L1, suggesting a higher metabolic FDG activity load in PD-L1 positive NSCLC patients, thus potentially predicting tumor microenvironment based on metabolic features.

Basic Oncology: Animal Models

EP-0478

Brachytherapy of Biodegradable Microspheres for Hepatocellular Carcinoma in Rats by Intra-arterial Chemoembolization

P. Chiang, C. Peng, Y. Shih, T. Luo; Institute of Nuclear Energy Research, Taoyuan, TAIWAN.

The global incidence of liver cancer is increasing and has a poor prognosis, particularly when the tumor is unresectable. Transcatheter arterial chemoembolization (TACE) is a way of delivering cancer treatment directly to a tumor through minimally-invasive means that affords significant reductions in systemic toxicity. The aim of this study was to investigate the effects of biodegradable microspheres (Re/DOX@MS) on hepatocellular carcinoma in F-344 rats by intra-arterial Chemoembolization. In the experiment, we used biodegradable and biocompatible polymer Poly(D,L-lactide-co-glycolide)(PLGA) to prepare micron particles. Through double emulsion, the microspheres contain water-soluble polymers, Poly(vinylsulfonic acid, sodium salt) solution (PVSA). Doxorubicin is absorbed in microspheres by ionic exchange process, resulting in slow release and [188]Re-tin-colloid is embedded to fill the pores of microspheres, leading to brachytherapy. The effects of Re/DOX@MS were evaluated through ex vivo and in vivo using bio-distribution, NanoSPECT/CT imaging and ultrasonography. Experimental results show that 50mg PVSA/PLGA microspheres absorbed 2.5mg doxorubicin within an hour. Microspheres were embedded with [188]Re-tin-colloid and performed in a rat hepatocellular carcinoma model. NanoSPECT/CT imaging and bio-distribution showed the microspheres were still in the liver after 72 hours. The tumor growth was more profoundly inhibited by treatment with Re/DOX@MS than others by ultrasonography during 4 weeks observation period. To conclude, the present study is to develop a novel biodegradable drug delivery system that investigates the feasibility of Re/DOX@MS combined with chemotherapy and radiotherapy for transcatheter delivery to liver tumors. Transcatheter arterial embolization of Re/DOX@MS is a potential agent for treatment of liver cancer. In the future, the drug delivery system for cancer therapy could maximize the effects on hepatocellular carcinoma.

EP-0479

18F-FDG-PET imaging of genetically engineered mouse models elucidates oncogenic function of Nlp and FAM135B

W. Xiao[1], D. Dong[1], D. Li[1], S. Han[2], H. Yan[3], L. Wan[3], Q. Xie[2], Q. Zhan[1]; [1]National Cancer Center/Cancer Hospital, Chinese Academy of Medical Sciences, Beijing, CHINA, [2]Department of Biomedical Engineering, Huazhong University of Science and Technology, Wuhan, CHINA, [3]Hubei Raydata Technology Co., Ltd, Ezhou, CHINA.

Purpose: Nlp is a significant centrosome associated protein that is essential for centrosome maturation, microtubule development and spindle assembling chromosome separation during mitosis. FAM135B is a potential oncogene in various cancer including esophageal squamous cancer, hepatoma, ovarian cancer, lung cancer and breast cancer. To evaluate the oncogenic function of Nlp and FAM135B in vivo, we constructed Nlp-deficient mouse model and FAM135B overexpression mouse model, and examined tumorigenesis with ^{18}F-FDG-PET scanning. **Materials and Methods:** Mouse models: Nlp-deficient DMBA-induced tumorigenesis mouse model: C57BL/6J Nlp-deficient mice constructed by genomic UPA trap were backcrossed to N8 generation to achieve genomic background purified. Then filial generation of Nlp$^{+/-}$ deficient mice were intraperitoneal-injected with DMBA 14 days after birth. FAM135B overexpression mouse model: C57BL/6J mouse oosperms were pronucleus injected to generate transgenic mice contain randomly inserted CAG-fam135b-HA-3flag gene. Both of the two mouse models were fed by regular deit and observed constantly. Reagents: 2-Deoxy-2-(^{18}F)fluoro-D-glucose(^{18}F-FDG) Equipments: Trans-PET ® BioCaliburn ® 700 (Raycan Technology Co., Ltd, Suzhou, China) Methods: Mice were administered FDG intraperitoneally 60 minutes before they were placed on the PET bed for 10 min PET acquisition (inhaled anesthesia with 2% isoflurane). PET-deduced measures of tumor FDG retention, including standardized uptake value (SUV)-based quantification, was evaluated. After PET scanning, complete necropsy was performed to the mice after euthanization. Selected tissues were H&E stained following fixing, paraffin embedding and section. **Results:** ^{18}F-FDG-PET scanning results of 28 Nlp-deficient mice and 13 wild-type mice showed that Nlp-deficient mice exhibited higher FDG uptake in liver area compared to wild-type mice at 8 to 10 months after DMBA injection. Signals of Nlp-deficient mice were elevated, showing tumor profile and high metabolic intensity, while wild-type mice were low in signal. H&E staining showed that Nlp gene-deficient mice had a higher proportion of hepatoma, and the tumor nodules were larger; while the proportion of wild-type mice was lower in liver cancer, and the nodules were smaller and these mice were mostly liver injury. PET scanning results of 7 FAM135B overexpression mice and 3 wild-type mice showed that after 1 year of normal feeding, the abdomen of two FAM135B overexpression mice showed abnormally elevated metabolism, and were found to be hepatoma and ovarian cancer, while wild-type mice showed no abnormal abdominal metabolism, no obvious tumor after anatomy. **Conclusion:** The elevated ^{18}F-FDG uptake indicated that Nlp-deficient mice were more susceptible to DMBA carcinogenesis, and FAM135B overexpression mice were more prone to spontaneously developed tumor.

Basic Oncology: Miscellaneous

EP-0480
FDG-PET/CT in the incidental diagnosis of tumour thrombosis

C. Castillo Berrio, **J. M. Nogueiras Alonso**, M. A. Castrillon Sanchez, F. Zelaya Reinquet, A. Renda Alcalde, F. Loira Bamio, D. Ruiz Hernandez, L. Campos Villarino, B. Núñez de De Oliveira, R. Guitian Iglesias; Hospital do Meixoeiro, Vigo, SPAIN.

Objective: Our aim is to explore the prevalence, clinical data and metabolic features of patients with tumour thrombosis (TT) incidentally detected in 18F-FDG-PET/CT studies. **Material and Methods:** Of 10027consecutive 18F-FDG-PET/CT scans (January 2013-December 2016) performed for malignant disease, the images of 7 patients with vascular tumour thrombosis as an incidental finding were retrospectively assessment through a visual and semiquantitative analysis. The FDG uptake pattern of affected vessel was divided by visual analysis as linear or focal. For the semiquantitative analysis the SUVmax was measured, drawing regions of interest at the site of thrombosis and in the tumours confirmed in CT/MRI. **Results:** The prevalence of tumour thrombosis was 0.059% (1 not confirmed). Seven patients with tumour thrombosis were identified, 6 with CT and/or MR confirmation and 1 diagnosed as vascular fibrosis by MR. Six had pulmonary carcinomas (2-adenocarcinomas, 3-microcytic, 1-undifferentiated non-small cell), 4 with involvement of pulmonary veins, one on superior cava vein and one of the left renal vein associated with ipsilateral adrenal mass; and 1 with renal cell carcinoma with involvement of right renal vein and inferior cava vein. Uptake pattern was linear in 5 patients and focal in 2 (one not confirmed by anatomical study). The SUVmax at the tumour thrombosis site: 10.3g/ml (4.2g/ml-27.2 g/ml) and in the primary tumours: 12.7g/ml (6.5 g/ml - 25 g/ml). Survive 3 patients, including unconfirmed of tumour thrombosis with SUVmax.4.9g/ml and two patients with thrombus SUVmax of 5.7g/ml and 5.9g/ml, the lowest in the sample. **Conclusions:** With an incidental prevalence of TT 0.059%, 18F-FDG-PET/CT can help to diagnosed occult tumour thrombosis, based on the linear uptake pattern and significant activity respect to normal vascular uptake, change the staging and modified with the correct treatment, the sample is small but we can suspect that intensity uptake has additional prognosis information.

EP-0481
Ex-vivo experience with beta- Radiation and Radioguided Surgery Technique in meningioma and neuroendocrine patients

C. M. Grana[1], R. Faccini[2], M. Schiariti[3], M. Colandrea[1], E. Solfaroli Camillocci[2], S. L. V. Fracassi[1], L. Gilardi[1], S. M. Baio[1], P. A. Rocca[1], L. L. Travaini[1], S. Papi[1], S. Morganti[4], M. Cremonesi[1], M. E. Ferrari[1], V. Bocci[4], C. Mancini Terracciano[2], A. Russomando[5], F. Collamati[6], E. Bertani[1], E. Pisa[1], L. Funicelli[1], N. Fazio[1], L. Bodei[7], R. Ghisini[1], M. Chinol[1]; [1]Istituto Europeo di Oncologia, Milano, ITALY, [2]Dipartimento di Fisica, Sapienza Università di Roma; INFN Sezione di Roma, Roma, ITALY, [3]Istituto Neurologico Besta, Milano, ITALY, [4]INFN Sezione di Roma, Roma, ITALY, [5]Center for Life Nano Science@Sapienza, Istituto Italiano di Tecnologia, Roma; Centro Científico Tecnológico de Valparaíso-CCTVal, Universidad Tecnica Federico Santa Maria, Chile, Roma, ITALY, [6]INFN Sezione di Roma; Dip. Scienze di Base e Applicate per l'Ingegneria, Sapienza Univ. di Roma, Roma, ITALY, [7]Memorial Sloan Kettering Cancer Center, New York, NY, UNITED STATES OF AMERICA.

Introduction: Radioguided surgery (RGS) is a technique aimed at assisting the surgeon to reach a complete resection of the tumoral lesion, while minimizing the amount of healthy tissue removed. RGS with beta- radioisotopes, as 90Y, is a novelty under investigation: one of the main advantages is its capability to detect small lesions after the injection of low activities. This novel approach allows to develop a new probe which, detecting electrons and operating with low background, provides a clearer delineation of the margins of lesions with low radiation exposition for surgeons. **Aim:** To explore the applicability of this new technique and to overcome the limits of gamma-RGS, extending the applicability of RGS in different tumors. **Materials and Methods:** We started evaluating tumors highly expressing somatostatin receptors (SSR), where we can study the uptake of 90Y-DOTATOC, first in meningioma and then in neuroendocrine tumors. These studies started from PET images with 68Ga-DOTATOC and, assuming that the biodistribution of the tracer did not change when labeled with 90Y, with a simulation program (FLUKA) estimated the signal rate on the probe. So far, 4 pts with meningioma and 1 pt with bowel neuroendocrine tumor (NET), received 68Ga-DOTATOC/PET, two weeks prior to surgery in order to know the uptake in the lesions. Twenty-four hours before surgery, the patients were injected with a median activity of 4.5 mCi (we started with 8 mCi in the first patient and we decreased to 2.5 mCi in the last meningioma patient); the NET pt received 5 mCi of 90Y-DOTATOC. Before surgery the probe was placed in proximity to the skin of the patient to estimate the background. **Results:** Surgery was performed as clinical indicated in meningioma and NET pt. Tumors and the around tissues were sectioned in different samples and the probe was put in contact with each sample to measure its activity: all the samples identified by the probe as malignant were actually of tumor tissue, as histologically routine detected in meningioma. Data about NET pts are still in evaluation and results will be provided during the congress. **Conclusions:** These first ex-vivo RGS tests showed that through this probe we could discriminate very strongly between tumor and nearby healthy tissues by the administration of low activities of 90Y-DOTATOC. We are planning to enroll new NET patients, as it is well known that a complete surgery could better the prognosis of this disease, and to further better the probe.

EP-0482
Influence of androgens (AND) and androgen metabolites on the Expression of the prostate specific Antigen (PSMA) and the cell cycle in in Vitro models of castration resistant prostate carcinoma

B. Meller, P. Thelen, V. Unterkircher, C. Breunig, C. Sahlmann, C. Bouter, L. Trojan, J. Meller, F. Bremmer; Georg-August-University Göttingen, Göttingen, GERMANY.

Purpose: In some patients with CRPC a tumor regression was observed after withdrawal of androgen deprivation and the resulting increase in androgen supply. The aim was to investigate the influence of different androgens and its metabolites on proliferation, cell cycle and PSMA expression of cell lines with wild-type and mutated androgen receptors. **Methods:** For our investigation the CRPC human cell lines LNCaP und VCaP (ATCC) were used. In LNCaP the castration resistance based on androgen receptor (AR) mutations (AR-T878A) while in VCaP a wild-type (WT) AR overexpression has been observed. VCaP were grown permanently with testosterone (T, revCRPC) or without T (CRPC). RevCRPC cultures represent therefore the androgen sensitive cell type, CRPC the castration resistant VCaP (CRPC). All three cell lines were incubated for 48 h with one androgen or androgen metabolite like 1 nmol/L T, dihydrotestosterone (DHT) and R1881 or 5nmol/L 3β-androstanediol (A) and 3α-A. Thereafter, cell cultures were incubated with 300 kBq ^{68}Ga-PSMA-11 for 3 h and the uptake as well as proliferation and the percentage of the cells in the different phases of the cell cycle were determined. **Results:** In the AR-mutated LNCaP the incubation with AND did not influence the radiopharmaceutical uptake significantly. In androgen-sensitive revCRPC the uptake of ^{68}Ga-PSMA-11 increased >30 % (p <0.05) after AND withdrawal. After incubation with testosterone the uptake doubled in CRPC (p<0.05). The incubation with 3αA, R1881 und DHT resulted in an increase of the radiopharmaceutical uptake of >400 % (p <0.01). This increase was associated with an increase of cell fraction in the G0/G1 cell cycle arrest (p <0.05) and a significant decrease (p <0.005) of the cell fraction in the other phases of cell cycle. **Conclusions:** In cell lines with wild-type androgen receptors different experimental designs leaded to a cell cycle arrest associated with increased expression of PSMA.

EP-0484

Evidence of therapeutic effect of Atorvastatin enhances initial penetration of trastuzumab to solid tumors in a HER2-positive gastric cancer model

J. Kim, Y. Lim, S. Lim; Korea Institute of Radiological & Medical Sciences, Seoul, KOREA, REPUBLIC OF.

Introduction: The limited penetration of monoclonal antibodies (mAb) into solid tumors restricts their antitumor efficacy. We investigated the effect of atorvastatin for enhancement of trastuzumab into tumor. **Subjects & Methods:** Nude mice were inoculated with HER2-positive NCI-N87 cancer cells. Alexa-488-trastuzumab was intravenously injected and atorvastatin was administered via oral gavage for 3 days. Tumors were harvested, flash frozen and sliced at 3 days after injection of Alexa-488-trastuzumab. The penetration of Alexa-488-trastuzumab, density of functional vessels, and circularity of cell nucleus were calculated. **Results:** Atorvastatin markedly enhanced the penetration of Alexa-488-trastuzumab compared with Alexa-488-trastuzumab alone, and similar to with Alexa-488-trastuzumab co-administration with cyclophosphamide. In addition, atorvastatin also increased antitumor efficacy of Alexa-488-trastuzumab. Furthermore, we examined whether atorvastatin-induced abnormal hair regrowth in mice, hair was depilated on the dorsal surface of the back in C57BL/6 mice, as a results atorvastatin do not induced abnormal hair regrowth of mice as compared with those of cyclophosphamide-treated mice. **Discussion/Conclusion:** Our study suggests that atorvastatin is new promising therapeutic strategy for enhancement of drug delivery by co-administration with atorvastatin to solid tumor, without side effects in hair growth.

EP-0485

Inhibition Of Autophagy During Epithelial To Mesenchymal Transition In Renal Cell Carcinoma Cells: Potential Therapeutic Role With mTOR Inhibitor

S. Bhattacharyya, M. Singla; Postgraduate Institute of Medical Education and Research, Chandigarh, INDIA.

Introduction: Most of the anti-cancer agents induce autophagy which can limit their antitumor efficacy. Primary neoplasias are still treatable but metastasis poses a major threat to cancer patients. It is very important to understand the mechanism of metastasis, especially to cure advanced cancers. Growing evidence suggests that the process that helps in the progression of cancer toward invasive and metastatic disease is associated with the reactivation of an embryonic development program, epithelial-to-mesenchymal-transition (EMT). Epithelial to mesenchymal transition-like phenotype is observed during the malignant transformation of renal epithelial cells in renal cell carcinoma. There exists a complex relation between autophagy, epithelial-to-mesenchymal-transition and metastasis. Cells undergoing epithelial-to-mesenchymal-transition require autophagy activation for survival during metastatic spread; on the other hand, autophagy acts as an oncosuppressive signal to inhibit early metastasis. In this study, we evaluated the role of autophagy inhibition alongwith mTOR inhibitor in epithelial-to-mesenchymal-transition induced cells. **Methods:** Epithelial-to-mesenchymal-transition was pharmacologically induced in A498 cells by transforming growth factor-beta (TGF-β). The changes in the morphological parameters of the cells were noted by light microscopy and atomic force microscopy. Autophagy was assessed by acridine orange staining. Cell viability in presence of temsirolimus alone and in combination with the autophagy inhibitor chloroquine was determined by cell viability assay using MTT-(4,5-dimethylthiazol-2-Yl)-2,5-diphenyltetrazolium bromide. The effect of combination treatment of temsirolimus and chloroquine was confirmed by various apoptosis assays. **Results:** The cells acquired a fibroblastic appearance on treatment with TGF-β. The migratory ability and invasiveness of these cells also increased signifying the onset of epithelial to mesenchymal transition. A higher autophagic flux was observed in A498 cells treated with TGF-β. It was observed that addition of chloroquine alongwith with temsirolimus to epithelial-to-mesenchymal-transition induced cells decreased their vi-

ability. Annexin-propidium iodide assay and sub-G1 population analysis showed a significant apoptosis in epithelial-to-mesenchymal-transition-induced cells treated with combination of chloroquine and temsirolimus. In addition, we observed higher DNA fragmentation, bax expression and caspase 3/7 activation in cells treated with combination of chloroquine and temsirolimus. **Conclusion:** Epithelial-to-mesenchymal-transition induced cells survived the therapy stress due to temsirolimus by enhanced autophagic flux. The epithelial-to-mesenchymal-transition induced cells were more susceptible to cell death when autophagy was inhibited. Our results suggest that addition of an autophagy inhibitor like chloroquine with temsirolimus may be a more effective approach to target the metastatic cells in renal cell carcinoma.

Clinical Oncology: Brain

EP-0486

Survival prediction of Glioma based on the combined analysis of in-vivo [¹¹C]Methionine -PET, ex-vivo and patient-characteristic features utilizing machine learning approaches

L. Papp, N. Pötsch, M. Grahovac, V. Schmidbauer, M. Mitterhauser, W. Wadsak, T. Beyer, M. Hacker, T. Traub-Weidinger; Medical University of Vienna, Vienna, AUSTRIA.

Introduction: [¹¹C]Methionine (MET) is well established in PET imaging of glioma. Nevertheless, diagnosis is still based on histopathological analysis. Our goal was to establish a machine learning-driven survival predictor model based on the combined analysis of in-vivo MET-PET, ex-vivo and patient-characteristic features and to identify key features playing important role in survival prediction. **Subjects and Methods:** To date, 105 glioma patients who underwent MET-PET between 2000-2013 prior to therapy were included. Days of survival information was dichotomized with a 36-mo threshold to build up two predictor models. Those patients whose survival information was not available for at least 3 years after the MET-PET acquisition were excluded from the analysis. Delineation of the primary tumour and a contra-lateral background region serving as reference for tumour-to-background calculations of each case were performed manually in PET using the Hybrid3D software (Hermes Nuclear Diagnostics, Stockholm, Sweden). The delineated VOI voxels were resampled to 1x1x1 mm size in order to increase the number of samples for stable statistical evaluation. Overall, 41 features were collected for each tumour: 33 in-vivo features including first-order (6), histogram (6), shape (2), textural-GLCM (7), textural-GLSZM (8), textural-NGTDM (4) were extracted from tumour VOIs; furthermore, 5 patient (age, weight, height, BMI, Karnofsky-score) and 3 ex-vivo features (Histology, WHO-2007 grading, IDH1+/-) were collected. A multi-layer machine learning algorithm was utilized to automatically select and weight relevant features in order to build a 36-mo survival predictor model. The machine learning-derived predictor outcomes were subject of the Monte Carlo cross-validation scheme where dichotomized survival values served as reference. **Results:** Applying the exclusion criteria resulted in 70 cases for the analysis. The 36-mo predictor model resulted in 81% sensitivity, 80% specificity, 81% accuracy, 90% positive-predictive-value and 68% negative-predictive-value in the cross-validation. The most prominent features (> 50% of maximum weight) of the 36-mo predictor were all in-vivo MET-PET features. **Conclusions:** The combined analysis of in-vivo MET-PET based features yields stable predictor models for survival in patients with glioma.

EP-0487

Diagnostic Value of PET with [¹¹C] Methionine in Recognizing Early Progression of Cerebral Glioma from Pseudoprogression

T. Skvortsova, D. Zakhs, Z. Savintseva, A. Gurchin, S. Medvedev; N. P. Bechtereva Institute of the Human Brain of Russian Academy of Sciences, Saint-Petersburg, RUSSIAN FEDERATION.

The purpose of the study was to assess the diagnostic value of PET with [¹¹C]methionine (PET-Met) for distinction between true tumor progression (TP) and pseudoprogression (PsP) after combined therapy of gliomas. **Material and Methods**: 54 patients with suspected glioma progression on contrast-enhanced MRI within first 3 months after radiation therapy were investigated by PET with [¹¹C]methionine. The primary tumor type was low-grade glioma (n=7), anaplastic glioma (n=13), glioblastoma (n=34). Patients had received radiation therapy with concomitant temozolomide (n=39) or other radiochemotherapy scheme (n=8), radiotherapy/radiosurgery only (n=7). Final diagnosis was verified on the basis of the pathological study (surgery-15, autopsy-2) or clinical course with MRI and PET follow-up on an average 18 months (range 1,5 - 74). Imaging results were also related to progressive free survival (PFS) in 44 patients. 8 patients also had pretreatment or immediately postoperative PET study. PET examinations were assessed by visual inspection and calculating [¹¹C]methionine uptake index (UI) as the ratio of the mean lesion uptake (hot spot 10 mm in diameter) to normal cortex. **Results:** 24 patients were considered to exhibit PsP. The UI was 1,5±0,3 (mean±SD), range 1,0-2,14. In recurrence group (30 pts) PET-Met showed significant higher focal [¹¹C]methionine uptake in the lesion (p<0,0001). The UI was 2,34±0,8 **(**range 1,5-4,8). In comparison with pretreatment PET in time of radiological impairment patients with PsP showed decrease [¹¹C]methionine uptake in the tumor on an average by 26%. Using cutoff value of UI >1,86 ROC analysis showed a sensitivity of 76% and a specificity of 96% for differentiating early glioma progression from pseudoprogression. The area under ROC curve was 0,894. For all grades of gliomas UI higher than 1,86 was statistically associated with a shorter progressive free survival (median PFS 9 vs 24 months, p=0,04, log-rank test). **Conclusion:** PET-Met has been shown to be a promising tool for early detection of glioma progression after primary or second-line therapy. Metabolic imaging using Met might help to avoid a loss of time due to repeated MRI scan.

EP-0488

18F-Fluorocholine PET/CT in patients with newly diagnosed glioma: association with tumor biology. Preliminary analysis (FuMeGA study)

G. A. Jimenez Londoño, Sr., F. J. Pena Pardo, A. M. García Vicente, M. Villena Martin, J. Gonzalez García, M. P. Talavera Rubio, M. J. Tello Galán, Á. M. Soriano Castrejón; Hospital General Universitario de Ciudad Real, Ciudad Real, SPAIN.

Objective: To evaluate the association between 18F-Fluorocholine uptake, metabolic tumor volume (MTV), tumor grade and proliferative activity in patients with newly diagnosed gliomas. **Methods:** Prospective study (FuMeGA B-176/2016). A pre-operative 18F- Fluorocholine PET/CT was performed in patients with diagnosis of glioma. The PET/CT was considered as positive (uptake higher than background) or negative (similar uptake to background). The SUVmax and MTV were derived from PET images. The %SUVmax threshold to calculate MTV in each lesion (MTV %SUVmax threshold) was selected (10%, 20%,30% or 40% of SUVmax) by agreement between two nuclear physicians (in case of disagreement, there was a third evaluator). Tumor grade and proliferative activity (Ki-67 index) were estimated in tissue specimens. Correlation between PET/CT (positive/negative) and tumor grade (low/high-grade) was assessed using the Chi-square test. Receiver operating characteristic (ROC) analyses were used to assess the SUVmax for predicting tumor grade (low/high-grade) and the ability of SUVmax and MTV for predicting a Ki-67 level>10%. To determine MTV% SUVmax threshold, an inter-observer agreement was estimated using Cohe´s kappa coefficient. **Results:** Fifteen patients were include, 12 with high-grade and 3 with low-grade tumors. The mean of Ki-67 was 28.6%±22.1 (range 1 to 70%). PET/CT was positive in 14 patients. The mean of SUVmax and MTV was 3.0±2.1 (range 0,4 to 7,4) and 46.4ml±35.05 (range 10,99 to 144ml) respectively. PET/CT was positive in all high-grade gliomas and negative in one low-grade tumor (χ^2 =4.2, **p**<0.03). The ROC curve analysis of SUVmax for predicting tumor grade showed an AUC of 1 (**p**=0.009) with Sensitivity (Se) and specificity (Sp) of 100% using an SUVmax cut-off of 1. The best SUVmax cut-off value for predicting a Ki-67>10% was 1 with an AUC of 0.944 (**p**=0.01), Se of 100% and Sp of 75%. The optimal MTV cut-off value for predicting Ki-67>10% was of 11.82 ml (AUC=1, **p**=0,11). Agreement between the two nuclear physicians for determining MTV %SUVmax threshold was fair (Kappa coefficient= 0.42, **p**= 0.03) and variable among lesions. **Conclusion:** According to our preliminary results, 18F-Fluorocholine PET/CT is a useful technique for imaging of brain gliomas. The SUVmax seems to be a useful tool to determine the tumor grade and proliferative activity in gliomas. Regarding to MTV, further studies are needed to establish the optimal %SUVmax threshold and its usefulness in gliomas.

EP-0489

18F-FDOPA PET And IDH Mutation As Prognostic Factors Of Velocity Of Diameter Expansion In Newly Diagnosed Diffuse Grade II-III Gliomas

S. Isal[1], G. Gauchotte[2], F. Rech[3], M. Blonski[4], S. Planel[5], M. Chawki[1], G. Karcher[1], P. Marie[1], L. Taillandier[4], A. Verger[1]; [1]Nuclear Medecin, CHU Nancy, Nancy, FRANCE, [2]Anatomopathology, CHU Nancy, Nancy, FRANCE, [3]Neuro-surgery, CHU Nancy, Nancy, FRANCE, [4]Neuro-oncology, CHU Nancy, Nancy, FRANCE, [5]Neuro-radiology, CHU Nancy, Nancy, FRANCE.

Introduction: 18F-FDOPA Positron Emission Tomography (PET) imaging has been reported in many studies for detection and grading gliomas, but its prognostic value remains debated. IDH mutation, a molecular parameter, is a factor of good prognosis. In daily clinical practice, iterative Magnetic Resonance Imaging (MRI) is useful to predict tumor growth with the velocity of diameter expansion (VDE), >4mm/year being considered as poor prognosis. The aim of this study was to assess, in newly diagnosed diffuse grade II-III gliomas, relationships between 18F-FDOPA PET uptake and common prognosis factors (MRI VDE and molecular parameters). **Methods:** Twenty patients (42±10 years, 10 female) with newly diagnosed diffuse grade II and III gliomas, histologically confirmed, for whom a 18F-FDOPA PET was planned less than two months after the first MRI, were included. Two MRI (MRI1 and 2) were performed for each patient with an average time of 82 (+/- 29) days to determine VDE. 18F-FDOPA PET uptake was quantified by ratios of tumor uptake to the contralateral normal brain tissue (SUVmax T/N) and striatum (SUVmax T/S). **Results:** in univariate analysis, all gliomas which presented a SUVmax T/N >2 presented a VDE ≤4mm/year and were IDH mutants. In multivariate analysis SUVmax T/N>2 and IDH mutant were predictive of MRI VDE in a logistic regression model to define groups of good, poor and unknown prognosis. **Conclusion:** Combining 18F-FDOPA PET and IDH mutation could predict tumor growth in newly diagnosed diffuse grade II-III gliomas. **Keywords:** Glioma; 18F-FDOPA PET; MRI; IDH mutation; prognosis

EP-0490

Relationship between MRI contrast enhancement and 18F-Fluorocholine PET/CT to improve radiotherapy planning in resected high grade glioma patients

N. Testart Dardel[1,2,3], M. Revelles Paniza[4], E. Triviño Ibañez[1], M. Zurita Herrera[4], A. Jorques Infante[4], R. Luque Caro[4], A. Gonzalez Jimenez[1], M. Gomez-Rio[1], J. Llamas-Elvira[1]; [1]Hospital Virgen de las Nieves, IBS, Granada, SPAIN, [2]CHU - Lyon, Lyon, FRANCE, [3]Universidad de Granada, Granada, SPAIN, [4]Hospital Virgen de las Nieves, Granada, SPAIN.

Objectives: Even though major improvements in high grade gliomas (HGG) treatment have occurred in the past few years, the prognosis remains poor. The aim of our study is to evaluate the relationship between MRI-contrast-enhancement and 18F-Fluorocholine-PET/CT to define therapeutic targets prior to radiotherapy and improve the delimitation of treatment volumes. **Patients and Methods:** Prospective study of adults with resected HGG prior to radiotherapy. The standard protocol for determination of radiation therapy volumes is based on MRI: pre-surgical, early post-surgical (<72h) and delayed post-surgical (4weeks). The proposed protocol includes the

additional information provided by 18F-Fluorocholine PET/CT performed during the week before radiotherapy, estimating the probability of tumour presence. Treatment targets are determined according to fluorocholine uptake and its relation with T1-Gd-enhanced area. The definitive radiotherapy target volumes are established after the analysis of both imaging procedures: MRI and 18F-Fluorocholine-PET/CT, separated and fused, providing a final consensual report to the radiotherapist. **Results:** Seventeen eligible patients (10 males and 7 females; mean age: 58.4 years [range: 22-75]) were included (14 glioblastoma, 2 anaplastic astrocytoma, 1 gliosarcoma). In five glioblastoma patients, no MRI-T1-Gd-contrast-enhancement neither fluorocholine uptake were observed, compatible with total resection (they all remain alive and recurrence free). In two partial resection glioblastoma patients, there was an exact coincidence between MRI-T1-Gd-contrast-enhancement and increased fluorcholine uptake. In seven glioblastoma patients, there were discrepancies between the intensity of the T1-MR-Gd-enhancement and fluorocholine uptake: one patient showed a highly intense heterogeneous uptake and in the remaining six, the area of fluorocholine uptake was smaller and comprised into the T1-MRI-Gd-enhancement area. In the three non-glioblastoma patients, also discordances were observed; with two presenting fluorocholine uptake small subcentimetric areas outside the margins of T1-MRI-Gd-enhancement and one gliosarcoma with both: fluorocholine outside the T1-MRI-Gd-enhancement but also enhanced areas without fluorocholine uptake. The planned volumes of treatment did not change in any patient. **Comments:** Our preliminary results showed discrepancies in the intensity of MRI-T1-Gd-enhanced areas and the intensity of fluorocholine uptake that differed according to the histology. In all the glioblastoma patients, the area of fluorocholine uptake was similar or smaller to the MRI-T1-Gd-contrast-enhancement area, while in the rest, fluorocholine uptake was observed outside the margins of MRI-T1-Gd-contrast-enhancement area, probably revealing infiltration. In our small series, the addition of 18F-Fluorocholine-PET/CT in the pre-RT evaluation of these patients has no impact in the expected treatment approach and does not modify the planned volumes for treatment, although, larger studies are needed.

EP-0491

FBPA PET/CT of brain tumors after radiotherapy: a differential diagnosis between tumor recurrence and radiation necrosis

R. Beshr, K. Isohashi, T. Watabe, V. Romanov, E. Shimosegawa, J. Hatazawa; Osaka University, Graduate School of Medicine, Yamada Oka 2-2, Suita City, Osaka, JAPAN.

Objectives: Radiation therapy is essential in the management of patients with primary and metastatic brain tumors, however, post radiation cerebral necrosis is a common side effect. Magnetic resonance imaging (MRI) is regularly performed for those patients after treatment as the standard imaging modality to detect tumor recurrence, yet, it is still challenging to distinguish tumor recurrence from post radiation cerebral necrosis by MRI alone, or with other anatomical and functional diagnostic modalities like positron emission tomography (PET). 4-borono-2-18F-fluoro-phenylalanine (18F-FBPA) is an amino acid tracer with a selectivity of L-type amino acid transporter 1 (LAT1) which is specifically expressed in cancer cells. In this study, we aimed to assess 18F-FBPA PET/CT as a method to differentiate between these two entities. **Methods:** 12 patients of glioblastoma (9), malignant meningioma (1), hemangiopericytoma (1), and metastatic brain tumors (1) who had been previously treated with radiotherapy were investigated by FBPA PET/CT scan. A diagnosis of recurrent tumor or radiation necrosis was made on the basis of clinical course and MRI. 18F-FBPA (3.7MBq/kg) was administered intravenously for each patient after fasting for four hours. Whole-body PET/CT scan, using Eminence SOPHIA SET-3000 BCT/X (Shimadzu, Kyoto, Japan), was acquired 60 minutes after 18F-FBPA administration. Scan data were analyzed using PMOD image analysis software (PMOD Technologies). Spherical volumes of interests (VOI) were set by encompassing the lesion with reference to an MRI. Volume-based parameters were measured, which included metabolic tumor volume (MTV) using blood SUVmean as a threshold, and total lesion (TL) FBPA uptake (MTV * SUVmean). **Results:** MTVs and TL FBPA uptake values of FBPA PET/CT scan were significantly higher for tumor recurrence than for radiation necrosis. The mean MTV in tumor recurrence was 44.9 ±28.9 (mean±1SD), while in radiation necrosis it was 10.7 ±8.5 (P< 0.01). The mean TL FBPA uptake in tumor recurrence was 121±50.5, while in radiation necrosis it was 12.4±9.7 (P<0.001). **Conclusion:** 18F-FBPA PET/CT is a promising method to differentiate tumor recurrence from radiation necrosis in patients with primary or metastatic brain tumors who have received radiation therapy. 18F-FBPA as an LAT1 specific PET biomarker can be used to selectively detect cancer cells and aid in the accurate diagnosis and proper management of these patients.

EP-0492

Utility of delayed-phase C-11 methionine PET in the evaluation of focal brain lesions with high methionine uptake: A preliminary study

K. Takanami, Y. Toyama, M. Saito, K. Takase; Tohoku University Hospital, Sendai, JAPAN.

Purpose/Introduction: Low-grade-/non-malignant brain lesions sometimes demonstrate high C-11 methionine (MET) uptake. The purpose of this study was to determine whether additional delayed-phase C-11 MET PET can help to evaluate the focal brain lesions that demonstrate high MET uptake. **Subjects & Methods:** We retrospectively investigated the early- and delayed-images of C-11 MET PET studies for the focal brain lesions detected on MRI, and this study included the brain lesions that demonstrated a high C-11 MET uptake with SUVmax of 2.5 or higher on the early images. The early- and delayed-images were scanned at 20-30 and 30-40 minutes after the administration of C-11 MET (10 mCi), respectively. C-11 MET uptake (SUVmax) in the focal brain lesions and background on the early and delayed images were obtained, and the lesion-to-background SUVmax

ratio (SUVratio) on the early- and delayed-images and the retention index of C-11 MET uptake (delayed-SUVratio / early-SUVratio) were calculated. Low-grade-/non-malignant lesions were diagnosed based on the pathological findings (grade 1 or 2 on WHO classification) or no progression within 1 year on follow-up MRI, and the others were diagnosed as malignant lesions. Mann-Whitney test was used for comparing the results between the low-grade tumors/non-malignant lesions and the malignant lesions. P value < 0.05 was set as a statistically significance. The receiver-operating characteristic (ROC) analysis was performed and the areas under the curve (AUC), sensitivity, and specificity for the detection of the low-grade-/non-malignant lesions were calculated. **Results:** Twenty three brain lesions demonstrated SUVmax of 2.5 or higher on the early images. The 23 lesions consisted of 5 low-grade-/non-malignant lesions, and 18 malignant lesions. The median of the early-SUVmax, delayed-SUVmax, early-SUVratio, delayed-SUVratio, and retention index were 4.05, 3.70, 2.73, 2.64, and 0.99 for the low-grade-/non-malignant lesions, and 4.04, 4.05, 3.03, 2.68, and 0.89 for the malignant lesions, respectively. There was a significant difference only in the retention index between the low-grade-/non-malignant lesions and malignant ones (p < 0.05). The AUC by ROC analysis were 0.52 for early-SUVmax, 0.60 for delayed-SUVmax, 0.67 for early-SUVratio, 0.67 for delayed-SUVratio, 0.88 for retention index. The sensitivity and specificity for detecting low-grade-/non-malignant lesions using a cutoff retention index of 0.95 or higher was 85% and 100%, respectively. **Discussion/Conclusion:** In the presence of high C-11 MET uptake in the focal brain lesions on routine C-11 MET PET imaging, immediately delayed phase imaging and calculating the retention index may help to distinguish low-grade-/non-malignant lesions.

EP-0493

Dynamic 18F-FET-PET predicts a highly malignant epigenetic signature of IDH wildtype and IDH mutant glioma.

M. Röhrich[1], *K. Huang*[2], *A. Dimitrakopoulou-Strauss*[3], *A. von Deimling*[2], *U. Haberkorn*[1]; [1]*Klinik für Nuklearmedizin, Heidelberg, GERMANY,* [2]*Institut für Neuropathologie, Heidelberg, GERMANY,* [3]*Klinische Kooperationseinheit Nuklearmedizin, Heidelberg, GERMANY.*

Introduction: 18F-FET-PET is a powerful diagnostic tool for glioma, especially for biopsy planning and diagnosis of recurrence. 18F-FET-PET time activity curves (TAC) allow differentiation between histologically low grade and high grade glioma. Next to IDH 1/2 mutation and 1p19q co-deletion, new molecular methods like epigenetic profiling are of dramatically rising importance for glioma grading and allow subclassification. Here, we analyzed dynamic 18F-FET-PET data and corresponding histological and epigenetic features of 57 grade II,III and IV glioma. **Subjects and Methods:** Dynamic 18F-FET-PET was performed in 57 Patients with newly diagnosed, untreated glioma (19 grade II, 17 grade III and 21 GBM) including 4 grade II and 2 grade III oligodendroglioma. All patients underwent stereotaxic biopsy or tumor resection after FET-PET imaging. Next to histology and

analysis of IDH1/2 and 1p19q status, DNA of all tumors was subjected to epigenetic analysis using Illumina 850 K methylation array. Dynamic 18F-FET-PET Parameters (SUVmax, TAC, kinetic modeling using 2 compartment and fractal Dimension models) were correlated with histology and with molecular and epigenetic signatures. **Results:** 18-FET-PET TAC were divided into steadily increasing TAC typical for histological low grade glioma (LGG-like TAC) and peaking TAC suspicious for high grade glioma (HGG-like TAC). We observed increased 18F-FET uptake in 10/19 histologically grade II glioma (8 LGG-like TAC, 1 HGG-like TAC), in 12/17 histologically grade III glioma (7 LGG-like TAC, 5 HGG-like TAC) and in 19/21 histologically glioblastoma (7 LGG-like, 12 HGG-like). Epigenetic profiles of 1 grade II glioma and 2 grade III glioma lead to upgrading to GBM. 3 grade III glioma were subclassified as high risk subtype after epigenetic profiling. These Tumors included all grade II/III glioma with HGG-like TAC except 1 grade III oligodendroglioma. Methylation-based GBM subgroups and GBM-typical chromosomal alterations like 7p loss / 10q gain and genetic alterations like EGFR-amplification were almost equally distributed between GBM with LGG-like and HGG-like TAC. **Discussion/Conclusion:** Integrated diagnosis including methylation data is currently changing the practice of glioma grading and allows glioma subgrouping. Our data revealed a close correlation between HGG-TAC in F18-FET-PET and a highly malignant epigenetic signature in glioma. The prediction of high malignancy through F18-FET-PET TAC seems to become significantly more precise when epigenetic data is included into the diagnosis compared to histological diagnosis alone. The diagnosis of grade II/III glioma should be complemented with epigenetic profiling in cases with HGG-TAC.

EP-0494

Value of early and delayed Imaging for 18F-FDOPA PET high grade gliomas evaluation

M. Paquet[1], *J. Doyen*[1], *L. Mondot*[2], *E. Saada Bouzid*[1], *P. Bondiau*[1], *F. Almairac*[2], *D. Fontaine*[2], *S. Chanalet*[2], *M. Ouvrier*[1], *C. Zwarthoed*[1], *A. Schiazza*[1], *D. Benisvy*[1], *O. Humbert*[1], *V. Bourg*[2], *J. Darcourt*[1]; [1]*CAL, nice, FRANCE,* [2]*CHU, nice, FRANCE.*

Introduction: MR is often of limited value during the follow-up of patients treated for high grade gliomas both for differential diagnosis between recurrence (REC) and radiation necrosis (RN) and for prognostic evaluation. We studied the value of early and delayed 18F-FDOPA in this context. **Method:** 35 patients mean age 60 yo were prospectively evaluated (34 glioblastomas; 1 anaplastic oligoastrocytoma). They were studied after initial same treatment associating surgery, radiation therapy and chemotherapy (Stupp protocol) by 18F-FDOPA PET. Two 10 min static PET-CT images were obtained 20 min and 90 min post injection of 2 MBq/kg of 18F-FDOPA. MRI T1 weighted images were coregistered to PET data. Early images were graded visually using Lizarraga et al. criteria (JNM 2014). PET was considered positive for a score > 1. Quantitative analysis was performed using 3D VOIs: over striatum (S), brain tumor (T) (75% of striatal SUVpeak) and background (Bgd) on 20 and 90 min images. For diagnostic evaluation, results were compared to surgical results

for 15 patients (43%) and to MR follow-up for the rest. For prognostic evaluation, progression-free survival (PFS) and overall survival rates (OS) were calculated. **Results:** A total of 60 18F-FDO-PA PET evaluations were analyzed. The median follow-up was 41.6 months. 18F-FDOPA PET was considered positive for REC at visual analysis of early images in 50/60 evaluations and negative in 10. Sensitivity and specificity were 95.8% and 72.7%. Only the quantitative analysis of the early images had a diagnostic contribution. The SUVmeanL/SUVmeanS and SUVmeanL/SUVmean-Bgd ratios were the most discriminating parameters for the differential diagnosis between REC and RN (AUC 0.863 and 0.858). The 2-year PFS was 25.1%. Only the tumor metabolic volume (MTV) measured at 20 min was predictive of PFS (p = 0.005, RR = 0.32 [0.12-0.86]). The 2-year OS was 38.7%. Only the SUVmeanL/SUVmeanS at 90 min was correlated with OS (p = 0.02 and RR = 0.12 95% CI [0.02-0.73]). No parameter measured at 20 min was correlated to OS. **Conclusion:** 18F-FDOPA PET is a sensitive and specific examination for the detection of REC. This is the first study evaluating the diagnostic and prognostic value of early and late acquisitions of 18F-FDOPA PET. For diagnosis, only the interpretation of early images is relevant. For prognosis, the MTV measured at 20 min is a predictive factor for PFS and the SUVmeanS/SUVmeanS ratio at 90 min is a predictive factor of OS.

EP-0495

FET PET in Brain Tumors: Higher Background Activity under Dexamethasone Therapy and in Female Patients

C. Stegmayr, G. Stoffels, E. Rota-Kops, C. Filß, L. Phillip, B. Neumaier, K. Langen; Forschungszentrum Juelich, Juelich, GERMANY.

Objectives: With the O-(2-[F-18] fluoroethyl)-L-tyrosine (FET) PET of brain tumors, the tumor activity is determined by the tumor/brain quotient (TBR). An experimental study with rats showed significantly lower TBR after treatment with dexamethasone due to a higher background activity in the brain (1). In this study, we investigated this phenomenon in patients with brain tumors. **Methods:** In a prospective study, the FET-PET of 160 brain tumor patients (80 men, 80 women) was evaluated, 40 each were treated with dexamethasone (Dex) (0.5-24 mg/day). The SUV in the brain tissue was determined by a volume-of-interest of 15.5 ml (SUV-B) contralateral to the tumor. In addition, the FET accumulation with and without Dex was compared intra-individually in nine patients. The influence of Dex on the TBR was investigated. **Results:** The SUV-B was significantly increased in both men (1.31 ± 0.28 vs. 1.06 ± 0.16; P <0.001) and women (1.45 ± 0.25 vs 1.33 ± 0.19; P = 0.018). Furthermore, there was a highly significant difference between men and women (1.06 ± 0.16 vs 1.33 ± 0.19, P <0.001). The maximum difference of the SUV-B between men without Dex and women with Dex was 37%. In individual cases, a significant increase in SUV-B under Dex therapy was observed in 8/9 cases and a corresponding drop in TBR was observed. Furthermore, the tumor volume was underestimated in patients under Dex therapy. **Conclusion:** The results confirm a selectively higher FET accumulation in the normal brain after Dex therapy. In addition, there is a significant difference between men and women. The higher SUV-B leads to

smaller tumor volumes and decreased TBR in a threshold-based evaluation. In addition, the follow-up after the initialization/discontinuation of a Dex therapy is impaired. The causes of the phenomenon are still unclear. Research Support (1) Stegmayr et al. EJNMMI 2016; 43:1115-23

EP-0496

F18-FET tumour to background ratio is a predictor of rate of disease progression in post surgery patients with Glioblastoma

J. R. Cain[1,2], *M. Bynevelt*[2], *A. Nowak*[3], *N. Loh*[3], *L. Morandeau*[3], *R. Francis*[3]; [1]Lancashire Teaching Hospitals, Preston, UNITED KINGDOM, [2]Neurological Intervention & Imaging Service of WA, Perth, AUSTRALIA, [3]Sir Charles Gairdner Hospital, Perth, AUSTRALIA.

Aims: To determine if a novel PET imaging tracer has value in the assessment of the prognosis and treatment response in patients with Glioblastoma. O-(2-[18F]-fluoroethyl)-L-tyrosine Positron Emission Tomography (FET-PET) is an amino acid agent. In contrast to MRI gadolinium enhanced studies amino acid agents uptake in glioma appears independent of a disrupted blood brain barrier and may be present in non-enhancing sites of tumour, potentially allowing more sensitive detection of active tumour. **Materials and Methods:** A longitudinal prospective imaging cohort study was performed with matched tumour biospecimens to assess FET-PET in patents with Glioblastoma . FET PET scan (200 MBq of F18 FET) was performed post surgery and 4 weeks before the start of radiotherapy (t1), an additional FET-PET scan was performed 7-14 days after completion of radiotherapy (t2). F18 FET PET-CT studies were independently assessed by 2 PET physicians. Semi-quantitative analysis was performed with representative volumes of interest drawn at the site of maximum intensity of tumour activity, using the PET manufacturer's standard software (Siemens Syngo Via). F18 FET tumour to background ratio (TBR) was calculated using SUVmax of the tumour compared to SUVaverage in contralateral normal brain. Patients continued to have regular routine follow up MRI scans as per clinical protocol. Date of clinical progression was assigned retrospectively on consensus of Radiologists and Oncologists. **Results:** 19 patients were recruited to the study. 13 of the 19 patients have progressed clinically and/or on conventional MRI imaging at time of reporting. There was a significant difference in TBR between t1, pre radiotherapy, (4.2 mean) and t2, post radiotherapy, (3.1) p =0.005. Mean time to progression was 202 days. On initial analysis there was a dichotomisation of survival of the subjects with high TBR and low TBR. A TBR threshold value of 3 was set; Kaplan-Meier survival analysis was performed. Mean survival of subjects with TBR <3: 297 days (SD 65 days), TBR >3: 144 days (SD 23 days). Log rank regression (6.07) p-value 0.01) this relationship was present at both t1 and t2. **Conclusions:** This initial data suggests that F18-FET tumour to background ratio both prior to radiotherapy and after radiotherapy is a predictor of the rate of disease progression in patients with Glioblastoma. MRI assessment of these patients is hampered by both post surgical and post radiation effects, FET-PET may prove to be a valuable additional tool in the assessment of Glioblastoma.

EP-0497

Stereotactic histologic correlation of dynamic FET-PET/MRI in untreated high-grade glioma patients

T. Pyka[1], J. Gempt[1], M. Lukas[1,2], J. Schlegel[1], F. Ringel[1,3], S. Förster[1,4], C. Zimmer[1], C. Preibisch[1], M. Schwaiger[1]; [1]TU Munich, Munich, GERMANY, [2]Charité Universitätsmedizin Berlin, Berlin, GERMANY, [3]Universitätsmedizin Mainz, Mainz, GERMANY, [4]Klinikum Bamberg, Bamberg, GERMANY.

Introduction: Multiparametric 18F-Fluoroethyl-L-Tyrosine-(FET)-PET/MRI promises to improve the diagnostic work-up of glioma patients. However, not much is known about the pathologic correlates of the determined imaging parameters, particularly FET uptake dynamics; an early peak and consecutive negative slope of FET uptake is said to correlate with higher malignancy, possibly through increased expression of amino acid transporters (AT), with LAT-1 proposed as a major contributor to FET uptake recently. In this study, we look into correlations between imaging and histologic parameters through stereotactic biopsies. **Methods:** In a prospective protocol approved by the local ethics committee, patients with suspected high-grade glioma received a dynamic FET scan over 40 minutes, as well as morphologic and perfusion-weighted MRI on a hybrid PET/MR scanner before treatment. Stereotactic biopsies were obtained during surgery. Histologic evaluation included cellularity, SLC7 (AT), CD31 (vascular proliferation), Ki67/MIB1 (tumour proliferation) and CAIX (tissue hypoxia). **Results:** 44 samples from 13 patients (12 glioblastomas, 1 anaplastic astrocytoma) were obtained (study ongoing). Static FET uptake was positively correlated with cellularity and amino acid uptake. Rather unexpectedly, regions with negative dynamic FET-PET slope did not show increased tumour proliferation (Ki67) or expression of AT, but were associated with increased vascular proliferation, which also showed some correlation with perfusion-weighted MRI. Furthermore, increased AT expression could be demonstrated in regions with positive slope in FET-PET. No stable correlations could be established between tissue hypoxia and the different imaging markers. **Conclusion:** While static FET uptake appears to correlate well with cellularity and AT expression in high grade gliomas, spots with negative FET slope did not show particularly high AT levels or cellular proliferation, but exhibiting instead increased vascular proliferation. On the other hand, elevated AT expression was predominantly seen in regions with positive FET slope. As a possible explanation, steady FET uptake over time might be facilitated by AT, while wash-out of FET could be enhanced by increased vascularity - possibly associated with malignant behavior as reported in previous studies.

Clinical Oncology: Head & Neck

EP-0498

Prognostic significance of restaging 18-FDG PET/CT parameters for post-index irradiation recurrence of head and neck squamous cell carcinoma

K. Musaieva[1], B. Musaiev[1], Y. Kmetyuk[1], O. Solodianykova[2]; [1]All-Ukrainian Center of Radiosurgery, Kyiv, UKRAINE, [2]National Cancer Institute, Kyiv, UKRAINE.

Purpose: The aim of this study was to establish the value of metabolic and/or volumetric 18-FDG PET/CT measurements in prognostication of overall survival of patients with local or regional recurrence of head and neck squamous cell carcinoma (HNSCC). **Subjects & Methods:** Sixty-nine restaging/surveillance 18-FGD PET/CT studies of patients with locoregional recurrent HNSCC were selected for the retrospective analysis. The maximum standardised uptake value (SUVmax), metabolic tumour volume (MTV) and total lesional glycolysis (TLG) of recurrent tumour (Tr) and lymph node (LN) were analysed, and results were correlated with overall survival (OS), using Kaplan-Meier analysis. **Results:** Whole body metabolic tumor volume (WB MTV) was the best predictor of outcome. Optimal WB MTV cutoff (OC) was derived from receiver operating characteristic curve WB MTV = 21,5 cm^3. Median surveillance of the first group (WB MTV < 21,5 cm^3) was 28 months; while median surveillance of the second group (WB MTV ≥ 21,5 cm^3) was 10 months. Kaplan-Meier plot of survival in recurrent HNSCC patients by WB metabolic volume cut-off (≥21,5 vs < 21,5 cm^3) showed significant split of the survival curve. Further analysis showed survival curve split by the location of the recurrence (local, isolated nodal, locoregional) that is consistent with the prevalence of subjects with high WB MTV in the latest group. We also performed a subgroup analysis among 24 patients who underwent re-irradiation. The absence of re-irradiation within patient's salvage treatment plan was a distinguishable parameter that demonstrated hazard ratio HR 2,92 (95% CI: 1,16; 7,31; p = 0,02) in Cox regression analysis and a significant split of survival curves. **Conclusion:** As is discovered in previous studies, post-index 18-FDG PET/CT imaging is a reliable tool in diagnostics of early and late HNSCC recurrence. However, decisive quantitative metabolic cut-offs, enabling patients' stratification, have been lacking to date. Our analysis indicates that whole body metabolic tumour volume WB MTV has potency in estimating the overall survival. High WB MTV (over 21,5 cm^3) corresponds with poor prognosis and low one- and two-years survival rates (56,0% of patients will not survive over 12 months); on the other hand, one-year survival at WB MTV < 21,5 cm^3 is estimated as 93,2%. This observation remained robust even after accounting for other known prognostic factors including salvage re-irradiation and recurrence location. A more extensive study is warranted to decide if this cut-off point is acceptable for subgroup of patients who will undergo a salvage re-irradiation.

EP-0499

Predictive value of 11C-Metionine PET/CT (MET-PET) in the restaging of adenoid cystic carcinoma (ACC) of head and neck

F. Scalorbi[1], E. Lodi Rizzini[1], D. Calabrò[1], G. Lauretti[2], P. Castellucci[1], F. Dionisi[3], A. Tarsitano[4], S. Battaglia[4], D. Borsetto[5], G. M. Lima[1], S. Fanti[1]; [1]Department of Nuclear Medicine, S Orsola-Malpighi University Hospital, Bologna, ITALY, [2]Department of Nuclear Medicine, S Andrea University Hospital, Rome, ITALY, [3]Operative Unit of

Protontherapy, S Chiara Hospital, APSSTN, Trento, ITALY, [4]Operative Unit of Maxillofacial Surgery, S. Orsola- Malpighi University Hospital, Bologna, ITALY, [5]Operative Unit of Otolaryngology and Otosurgery, Department of Neuroscience, University Hospital of Padova, Padova, ITALY.

The ACC is a rare tumour characterized by poor survival because of the onset of distant metastasis even many years after the treatment. Moreover, the surgery cannot be radical because of the typical perineural infiltration and the localization of the disease. The purpose of this study was to assess the predictive value of MET-PET in the restaging of the disease. This retrospective study includes seventeen patients (11 female, 6 male, mean age 56, range 37-80 years) that were admitted to our centre between March 2011 and December 2016 for the restaging of ACC. Before MET-PET four out of seventeen have been treated with surgery, six with heavy-ion radiotherapy and seven with both treatments. MET-PET imaging were visually evaluated by three experienced nuclear medicine physicians. Each examination was classified as negative or positive. In addition, each patient was evaluated as positive or negative for the presence of primary localization, lymphadenopathy or distant metastasis. The PET findings were validated by clinical and radiological follow-up (mean time of FU 8.2 months, range 2-19). The FU was performed by MRI, except in case of distant metastases that have been validated by CT-scans or bone scintigraphy. Among the four patients that underwent surgery, two had a negative MET-PET while two were positive (one for local relapse, the other for distant skeletal metastasis). The two negative cases were lately confirmed to be true negative (TN) in one case and was false negative (FN) in the other one. The two positive cases were both confirmed as true positive (TP). The patients with negative MET-PET underwent surgery a few months before the PET examination. Among the six patients that underwent heavy-ion-radiotherapy, four had negative MET-PET and two had positive examination. These last were confirmed to be TP. Three MET-PET were TN and one was FN. In that case MET-PET showed faint uptake misinterpreted as post-actinic reaction. Among the seven patients treated with surgery and heavy-ion radiotherapy before MET-PET, three were TP, three TN and the last was doubt for lymph-nodal involvement but TN for local disease. This case was considered TN; further investigations are underway to clarify lymph-nodal metastasis. MET-PET showed a very good positive predictive value (7/7, 100%) for the restage of the disease. Negative predictive value of MET-PET was not excellent (6/10, 60%), as already reported by other studies. Further investigations are needed in order to assess the role of MET-PET in the restaging of ACC

EP-0500

Parotid incidentalomas on positron emission tomography: what is their clinical significance?

R. Barbara, D. Pawaroo, C. Beadsmoore, N. Hujairi, D. Newman; Norwich Radiology Academy, Norwich, UNITED KINGDOM.

The increased use of PET/CT for cancer staging has resulted in incidental foci of uptake in unexpected locations, making this a challenge for the interpreting radiologist. The aim of this retrospective study was to determine the frequency of parotid incidentalomas and to assess the ability of PET/CT to characterize these masses. During a five-year period, 4,044 patients had a whole-body PET/CT scan at the Norfolk and Norwich University Trust and in 70 of these patients, abnormal 18F-FDG uptake in the parotid glands was identified. The prevalence of parotid incidentalomas in our institution was 1.73%, which was higher than reported in the literature of up to 0.45%[1]. This could be due to our patient demographics but the mean age of our patients was significantly higher than the study cohort of Wang et al (2010) and Makis, Ciarallo & Gotra (2015) (71 compared to 61 and 62.3 years respectively). 49% of our patients had an ultrasound of their parotids. Of these, 10% had no identifiable focal lesion identified. One-third of our patients had a biopsy, which demonstrated that the most frequent pathology was of benign tumours (87%). However, in 13% of cases the histopathology demonstrated metastatic deposits from the patients' known primary tumours, with the primary carcinoma being neuroendocrine colon carcinoma, high grade B-cell Non-Hodgkin's Lymphoma and melanoma respectively. None of our patients being investigated for lung cancer were found to have parotid metastases. The predominant benign tumour discovered in our study was Warthin's tumour and the majority of these patients had a primary lung carcinoma. Considering that the main predisposing factor for both pathologies is smoking, we suggest that there is a significant association between the incidence of primary lung carcinoma and Warthin's tumour. In ten patients (14%) in our study, the parotid lesion had a standardized uptake value (SUV) of or below 3.2 and these patients had either no identifiable lesion on ultrasound or no malignant features on histology, therefore, we propose that an SUV cut-off of 3.2 on PET/CT can be used to differentiate between physiological or benign parotid uptake from malignant FDG uptake in the parotid gland. References: 1. Makis W, Ciarallo A & Gotra A. Clinical significance of parotid gland incidentalomas on 18F-FDG PET/CT. *Clin Imaging* 2015; 39(4):667-671. 2. Wang H-C, Zuo CT, Hua FC, et al. Efficacy of conventional whole body 18F-FDG PET/CT in the incidental findings of parotid masses. *Ann Nucl Med* 2010; 24:571-577.

EP-0501

Diagnostic efficacy of FDG-PET/CT in head/neck carcinoma of unknown primary with cervical lymph node metastases

F. E. Noltenius, A. Pfestroff, D. Librizzi, M. Luster; Philipps-Universität Marburg, Marburg, GERMANY.

Aim: The detection of the primary tumor in a head/neck Cancer of Unknown Primary (CUP) situation is of great clinical importance for the therapeutic strategy and consequently the patients' prognosis. The aim of this study is to analyze the diagnostic efficacy of FDG-PET/CT in head and neck CUP with cervical lymph node metastases. **Material and Methods:** A retrospective analysis of 31 patients with a head/neck CUP based on histologically proven cervical lymph node metastases who received a PET/CT between June 2009 and March 2015 was

performed. Follow-up was collected until May 2015 in order to evaluate the result of PET/CT against other diagnostic and cytological/histological results. **Results:** In 15/31 (48%) of patients the PET/CT scan was positive, with an increased FDG uptake suggesting a potential localization of the primary tumour. Compared to results obtained during post-PET/CT follow-up, PET/CT findings were classified as true positive in 12, true negative in 10, false positive in 1 and false negative in 6 patients. 2 patients had to be excluded from the final evaluation due to missing follow-up. A suspicious tracer accumulation in the sense of further metastases was found in 32% (10/31) of the patients. Overall the PET/CT examination provided clinically relevant information in 77% (24/31) of the cases. These findings result in a sensitivity of 67%, a specificity of 91%, a positive predictive value of 92% and a negative predictive value of 63% for the detection of a primary tumour in head/neck CUP. **Conclusion** FDG-PET/CT has a high added clinical value in terms of detection of the primary tumour as well as revealing further information relevant to treatment in patients with head/neck CUP. This high value is all the more evident if one considers that most patients undergoing PET/CT in head/neck CUP have already undergone extensive prior clinical and imaging examinations.

EP-0502

⁹⁹ᵐTc sestamibi spect in evaluation of neoadjuvantchemotherapy effectiveness in larynx/ laryngopharynx cancer patients

A. Medvedeva[1,2], V. Chernov, R. Zelchan, Yu. Belevich, S. Chizhevskaya, E. Choynzonov, I. Sinilkin; [1]Tomsk National Research Medical Center of the Russian Academy of Sciences Cancer Research Institute, Tomsk, RUSSIAN FEDERATION, [2]National Research Tomsk Polytechnic University, Tomsk, RUSSIAN FEDERATION.

Purpose: assessment of the role of SPECT with ⁹⁹ᵐTc-MIBI of neoadjuvant chemotherapy response prediction in patients for larynx/laryngopharynx cancer. **Materials and Methods:** The study included 32 patients with cancer of the larynx/laryngopharynx. SPECT studies were carried out 15-20 minutes after the injection of 740 MBq of ⁹⁹ᵐTc-MIBI using ECAM-180 gamma-camera (Siemens). Studies was conducted before treatment and after two courses of neoadjuvant chemotherapy. The imagines were quantitatively assessed using the tumor/submandibular salivary gland (T/SSG index), tumor/parotid gland (T/PG index) and tumor/background (T/B index). Indices were compared with clinical effect which was assessed by RECIST scale. **Results:** When analyzing obtained results indexes were used (T/SSG index, T/PG index, T/B index) that in the group of patients with tumor regression of more than 30%, a decrease of the calculated parameters was also more than 30%. At the same time calculated indices showed a decrease of less than 30% in patients with tumor regression of less than 30% on a scale RESIST. **Conclusion:** Thus, the present study demonstrated that SPECT with ⁹⁹ᵐTc-MIBI may be regarded as a method of assessing the state of malignant neoplasm of larynx/laryngopharynx during neoadjuvant chemotherapy. The values of these indicators before treatment and after two courses of che-

motherapy, most fully reflect the dynamics of changes in the tumor tissue.

EP-0503

Textural and shape features of pretreatment lymph nodes images of FDG PET/CT: correlation to extranodal extension and impacts on survivals of N-positive oral cavity squamous cell carcinoma

N. Cheng[1], Y. D. Fang[2], T. Yen[3]; [1]Chang Gung Memorial Hospital, Keelung, Keelung City, TAIWAN, [2]Department of Biomedical Engineering, National Cheng Kung University, Tainan City, TAIWAN, [3]Chang Gung Memorial Hospital, Linkou, Taoyuan City, TAIWAN.

Introduction: Extranodal extension (ENE) of lymph nodes has been associated with poor prognosis in oral cavity squamous cell cancer (OCSCC). In this study, we intended to use texture and shape analyses for quantifying lymph nodes heterogeneity and irregularity and investigated the correlation of those parameters with the ENE and survivals. **Subjects & Methods:** Enrolled patients received staging FDG-PET scans followed by radical surgery of primary tumor and cancerous lymph nodes. We used 40% of SUV maximum (T40) for delineation of lymph node lesions for exploratory study. SUV 2.5 was applied as threshold for segmentation for validation purpose. Optimal cut-offs of the FDG-PET parameters were obtained by receiver operating characteristic (ROC) curve analyses. The prognostic significance of PET textural features was examined using Kaplan-Meier method and Cox regression analysis. Disease-specific survival (DSS) and overall survival (OS) served as the main outcome measurements. **Results:** 67 patients with pathologically positive lymph node were enrolled. 103 lymph nodes were analyzed. ENE-positive lymph nodes (n = 58, 56.3%) have higher SUV maximum (P = 0.069), larger volume (P = 0.024), more heterogeneous uptakes (higher ZSNU, P = 0.026) and irregular shape (higher asphericity, P = 0.001). Nevertheless, only lymph nodes SUV maximum significantly correlated with DSS and OS (both P = 0.001) in multivariate Cox analyses in both exploratory and validation studies. Those with higher lymph node SUV maximum (>10.03) had significant higher risk for distant metastases (odds ratio: 12.29, P = 0.003). **Conclusion:** Our study indicated that ENE lymph nodes were more heterogeneous in FDG uptakes and irregular in shape. Higher SUV maximum of lymph nodes is an independent predictor of outcomes in patients with N-positive OCSCC and may improve prognostic stratification before radical operation.

EP-0504

Sentinel lymph node in early oral cavity squamous cell carcinoma

*R. C. Capuzzo, **E. Rocha**, L. F. Bicalho, W. E. Furlan, A. L. Carvalho; Hospital de Câncer de Barretos, Barretos, BRAZIL.*

Introduction: Squamous cell carcinoma (SCC) of the head and neck typically spreads to regional neck lymph nodes (LN) and

distant metastasis is a late event. Lymph node involvement is the most important prognostic factor and patients with regional lymph node metastases present a 50% reduction in survival. Controversies exist as to the best method of evaluating the presence of lymph node metastases. However, all forms of evaluation are not fully effective in the detection of lymph node involvement and approximately 30% of patients with neck N0 present metastases in the pathological evaluation of lymph node cervical emptying (EC). The objective was to evaluate the 5 - year survival rate and the regional control rate. **Material and Methods:** We included 44 patients aged 29-94 (mean 58), 33 M and 11 F evaluated between 2008 and 2013 with a mean follow - up of 57 months. Including criteria: neck N0, M0 and tumor T1 - T2 (48 and 52%); Excluding criteria: synchronic / metachronous tumor disease, previous cervical incision and radiotherapy (RT). Evaluation of lymphatic drainage was performed with peritumoral injection in three or four points, 72MBq of phytate-Tc99m with dynamic acquisition in 20 minutes. Results: Lesions were 64% in the tongue and 27% in the floor of the mouth, 39% were on the right side and 43% on the left, invasive SCC in 98% and in situ in 2%; Smoking was related in 75% and alcoholism in 25%. With regard to laterality, in 34 (77.5%) were on the same side of the lesion, in 7 bilateral, 1 contralateral and 2 in the midline. In 34 patients, up to two lymph nodes with depth varying from 2 - 42mm were collected. Cervical recurrence was found in three cases. Overall survival in T1 was 88.4% → LN (-) in 80% with lymph nodes <7mm in 82%; T2 65.2% → LN (+) in 57.1% with lymph nodes> 7mm in 50%. Overall survival considering all patients was 76.2%. Regional control rate with LN + was 100% and LN- was 92%. Currently there are 30 patients alive, without disease; And 1 live patient with disease. FN (false negative) 8%, S (sensitivity) 70%, E (specificity) 100%, NPV 92% and PPV 100%, accuracy of 93%. Conclusion: Sentinel lymph node screening is a reliable and safe tool to support neck surgeries. It showed excellent correlation with survival and local control, which recommends observation in T1-T2 negative patients.

EP-0505

Morphologic and Metabolic differences between HPV-positive and HPV-negative Oropharyngeal cancer patients as detected with FDG F18 PET/CT

A. M. El-Sabbagh, Z. Asiri, A. Rayan, S. Frye, F. Ahmed, R. Walker, R. Muzaffar, M. M. Osman; Saint Louis University, Saint Louis, MO, UNITED STATES OF AMERICA.

Objective: Human Papilloma Virus (HPV)-positive oropharyngeal cancer (OPC) has been on the rise and is becoming one of the major causes for head and neck cancers. The purpose of this study was to retrospectively evaluate the differences in the morphologic (CT) and metabolic (PET) characteristics of the primary tumor, locoregional nodal disease and distant metastasis in HPV positive vs negative (+/-) OPC. **Material and Methods:** A total of 161 OPC patients were included in the study. Baseline pretreatment ^{18}F-FDG PET/CT scans were reviewed to select matched HPV +/- OPC patients based on age, gender, tobacco

and alcohol use. A log was kept to record the size and metabolic activity of the primary tumor, nodal metastasis and presence of distant metastasis. For statistical analysis, paired T-Tests were used to compare results. **Results:** Among the 161 patients, 44 were tested for HPV and the characteristics are in the table below. Of the 20 HPV+ OPC patients, only 1 (5%) had distant metastasis compared to 4 (17%) of the HPV- OPC patients. There was no statistical difference in the mean baseline SUVmax of HPV+ primary tumor 8.11±4.1 or cervical lymph nodes 4.7±5.6, compared to HPV- primary tumor 10.33± 5.1 or cervical lymph nodes 4.5±3.9 with p-value of 0.126 and 0.87, respectively. However, there was statistical significance between the HPV+ mean baseline primary tumor size 2.0±1.6 cm and the largest cervical lymph node short-axis measurement 1.9± 0.4, compared to HPV- primary tumor size 4.5±3.4cm and the largest lymph node measurement 1.0± 0.1cm with p-value of <0.05 in both. **Conclusion:** We continue to accrue data, but our initial results suggest HPV+ OPC have no difference in the metabolic activity of the primary tumor or nodal metastasis compared to HPV- OPC. However, HPV+ OPC had a smaller primary tumor, larger nodal metastasis, less frequent distant metastasis, less frequent recurrence and an overall better prognosis. In contrast, HPV- OPC had more distant metastasis and recurrence, a greater association with a history of tobacco and alcohol use, and overall a worse prognosis. The differences in patterns of second malignancies are still being evaluated.

EP-0506

18F-FDG-PET/CT In Locoregional Staging in Oropharynx, Oral Cavity and Lip Tumors and Correlation with Sentinel Lymph Node Biopsy

F. Gomez-Caminero Lopez, P. Garcia-Talavera San Miguel, B. Perez Lopez, P. Blanco Perez, J. Serradilla Lopez, C. Achury Murcia, L. Diaz Gonzalez, P. Tamayo Alonso; Complejo Asistencial Universitario de Salamanca, Salamanca, SPAIN.

Aim: Analyze the correlation between lymph node status in malignant tumors of oral cavity, oropharynx and lip by means of 18F-FDG-PET-CT and anatomopathological findings in sentinel lymph node biopsy (SLNB). **Material and Methods:** Prospective study where patients with malignant tumors of oral cavity and lip (clinical stage T1-T2 N0) were included. All of them underwent staging 18F-FDG-PET-CT. Lymphatic mapping was performed by peri-tumoral intradermal injection of Technetium-labeled (Tc-99m) nanocolloid. Sentinel node (SN) localization was performed by dynamic study, static and lateral images (depending on the location of the tumor) and SPETC/CT to properly define the localization of the sentinel node. SN detection was done with a hand-held gamma probe and correlated with the 18F-FDG-PET-CT and histological findings. **Results**: We enrolled 15 patients (10 males and 5 females) with mean age 65.49 years (SD ± 8.27). Lesions were located in tongue (50%), retromolar trigone (28.5%), lower lip (14.3%) and sublingual tonsil (7.2%). Staging PET/CT was negative for lymphatic disease in 10 patients (66,7%) and positive in 5 (33,3%). In 11 cases, 2 or more SN were identified in the lymphadenec-

tomy specimen (73,3%). In 7 patients (46,7%) PET/CT and histological results agreed in N0 staging, in 3 patients (20%) PET/CT was positive for lymphatic disease and were confirmed by histology. Although, 2 cases (13,4%) were N1 by PET/CT and N0 by histology. The opposite occurred in 2 cases (13,4%) where PET/CT was negative (N0) but pathological anatomy found lymphatic metastases. **Conclusion**: 18F-FDG-PET-CT staged most of the patients studied correctly regarding lymphatic disease. We believe that, despite the sample, PET-CT has proved to be an useful tool for the optimal staging of oropharynx, oral cavity and lip tumors.

EP-0507

Head-and-neck dedicated acquisition after whole-body 18F-FDG PET/CT in head-and-neck tumours: can it provide a real added value?

M. C. Marzola, S. Chondrogiannis, G. Grassetto, E. Milan, M. L. Manerchia, A. M. Maffione, L. Tamiso, L. Rampin, D. Rubello; *Nuclear Medicine - PET/CT centre, Santa Maria della Misericordia Hospital of Rovigo, Rovigo, ITALY.*

Introduction: 18F-FDG PET/CT whole-body acquisition (from the base of the skull to the mid- tight) is an useful and reliable diagnostic tool in staging and restaging head-and-neck tumors. Moreover, PET resolution couldn't be enough, in some cases, to completely identify small cervical, metastatic lymph-nodes showing only slight FDG uptake. The aim of our work was to evaluate the usefulness and reliability of a "dual-phase" protocol (including whole-body and subsequent head and neck dedicated acquisition) in patients with head-and-neck tumors. **Materials and Methods:** From February to September 2016, 89 patients with tumors involving head-and-neck (in 27 cases with the primary in site) underwent both whole-body acquisition (128x128 matrix, 6-7 beds, 3 minutes/bed) and dedicated head andneck acquisition (256x256 matrix, 2 beds, 7 minutes/bed) in our department. From the analysis of the data, several parameters have been obtained and compared between the two acquisitions: number of lymph-nodes identified, number of primary lesions identified, SUVmax normalized for the background (SUVmax /SUVmean of the sternocleidomastoid) for the primary tumor and for the lymph-nodes (considering the lymph-node with the higher and, when it's possible, with the lower uptake). **Results:** 51/89 patients showed at least one pathologic uptake site ("positive" patients), while the other 38 were considered "negative". Primary tumor was identified in all 27 patients by both acquisitions, but normalized SUVmax was higher using head-and-neck acquisition (18.6, vs. 14.3 for whole-body, respectively). In 22 of the 51 patients in which cervical lymph-nodes were identified, head-and-neck and whole body acquisition revealed the same number of cervical lymphnodes, while in the others 29 head-and-neckacquisition identified more lymph-nodes than whole-body. The medium value of normalized SUVmax was higher in dedicated acquisition than in whole-body for both high-uptake lymph-nodes (11.2 vs. 8.9) and low-uptake ones (4.1 vs. 2.8). In 3 patients, head-and-neck was the only acquisition able to detect

a pathologic accumulation in the unique metastatic lymph-node. **Conclusion:** Thanks to some specific technical parameters (matrix, time/bed), head-and-neck PET/CT dedicated acquisition can provide better quality images than whole-body only. It's especially useful in patients with suspicious relapse, for detecting small lymph-nodes with relatively slight uptake, not clearly seen at whole-body acquisition. For these reasons, the proposed "two-phases" protocol can provide a real "added value" in evaluating patients with tumors involving head-and-neck site.

EP-0508

FDG PET/CT And MRI For The Assessment Of Therapeutic Response In Nasopharyngeal Cancer

F. Aydin, T. Bukulmez, K. Karaali, S. Bozkurt, M. Genc; *Akdeniz University Medical School, Antalya, TURKEY.*

Objective: This study aimed to investigate the effects of fluorodeoxyglucose positron emission tomography/computerized tomography (FDG PET/CT) and diffusion-weighed magnetic resonance imaging (DW-MRI) on assessing therapeutic response and survival in patients with nasopharyngeal cancer (NC). **Materials and Methods:** The study was performed in a retrospective fashion with 43 patients (11 female and 32 male patients between 12-76 years old) who had received chemo-radiotherapy (CRT), (Table). Study endpoints were apparent diffusion coefficient (ADCmean) values as measured by DWM-RI and maximum standardized uptake value (SUVmax), metabolic tumor volume (MTV), and total lesion glycolysis (TLG) as measured by PET/CT. **Results:** After CRT, primary tumor (PT) and pathological lymph nodes showed increased ADCmean and decreased SUVmax, MTV, and TLG. While SUVmax of PT of 8 patients were below 11 before CRT, those of 24 patients were above 11. When these two groups were compared in terms of disease-free survival (DFS), these were 100% to 58%, respectively at the end of 80-month follow-up. SUVmax<11 before CRT was significantly associated with prolonged duration of DFS (p<0.05). When DFS was compared in terms of MTV of PT before CRT, it was 91% vs 55% at the end of 73-month follow-up in patients with MTV<10 mL (n=11) and MTV>10 mL (n=9), (p=0.05). DFS was also compared based on SUVmax response rate of lymph nodes (<80% vs >80%) after simultaneous CRT. At the end of 58-month follow up, this was 36% (n=11) vs 100% (n=7). Response rates of SUVmax above 80% were found statistically significant (p=0.026). Fourteen patients having DW-MRI examination was evaluated. When DFS was compared in patients with ADCmean value <0.85 (n=6) and ADCmean value >0.85 (n=8), it was 16% vs 87%, respectively at the end of 42-month follow-up. ADCmean values above 0.85 was detected to be statistically significant in affecting DFS (p=0.029). **Conclusion:** DW-MRI and PET/CT reflects different biological characteristics of tumor. ADCmean and SUV are important in predicting therapeutic response and survival in NC. We believe that tandem evaluation of ADCmean and SUV parameters will provide better information about the prognosis in this cancer.

EP-0509

The impact of PET/CT in therapeutic management of patients with lymph node metastasis and cancer of unknown primary

P. Nikolova, V. Hadzhiyska, T. Petrov; University Hospital Alexandrovska, Sofia, Bulgaria, Sofia, BULGARIA.

Recent data suggest that cancer of unknown primary (CUP) accounts for approximately 3-5 % of all malignant neoplasm's. Despite of general poor prognosis of these patients, the favorable sub-sets are proven to respond to treatment and have better life expectancy. **The aim** of the study is to evaluate the role of positron emission tomography/computed tomography (PET/CT) in detecting primary site in patients with lymph node metastasis and guide treatment management. **Material and Methods:** Fifty three patients (aged from 35 to 72 years) were evaluated and followed up since 2012 to 2016 period by FDG-PET/CT on GE Discovery 16T, using the weight adjusted activity, 60 minutes delay between injection and registration, hydration of patients with diuretic stimulation by furosemide and oral/ i.v. contrast intake.. The inclusion criteria were patients with proved malignant histology by lymph node biopsy or by highly suspicious data from other imaging modalities, which were divided into several groups according to the primary location - (gr.LN neck, n= 39),(gr.LN axilar, n=6), (gr.LN inguinal, n=3),(gr.LN mediastinal, n=2) and (gr.LN retroperitoneal and pelvic, n=3). **Results:** By performing PET/CT the primary tumor was successfully found in 19 (35,8 %) of the patients with highest positive rate in head and neck region (9p, 16,9%) , followed by lung cancer (5p, 9,4%), breast cancer (2p, 3,7 %), sarcoma (1 p), lymphoma (1 p), prostate cancer (1 p). Six patients (11,3%) were found to be TN (true negative) with no further treatment after the PET/CT examination. There were two false negative (FN) results, which are proved in the time to be carcinoma of breast and nasopharynx and one false positive result, which was not confirmed by the guided biopsy. In twenty-five (47,1 %) patients the primary site was not found and they were guided for different types of treatment according to the extent of the disease. The calculated average survival rate, based on the date of pet/ct examination and the date of initial diagnosis were 238,9 days and 324,8 days, respectively. **Conclusion:** Our results demonstrates positive PET/CT findings in almost one third of the patients with highest positive rate in the diagnosis of head and neck tumors. PET/CT is a valuable tool in planning treatment strategy, following up therapy response and could be used successfully for more precise determination of the so called"favorable subgroups", which are proved to have better prognosis and benefits of the treatment.

EP-41   **during congress opening hours, e-Poster Area**

Clinical Oncology: Thyroid

EP-0510

Effect of postoperative thyrotropin suppression on bone mineral density in postmenopausal women with differentiated thyroid carcinoma

D. Wang, Y. Huo, C. Ma; Affiliated Xinhua Hospital of Shanghai Jiaotong University School of Medicine, Shanghai, CHINA.

Objective: To investigate the effect of postoperative TSH suppression on bone mineral density (BMD) in postmenopausal women with differentiated thyroid carcinoma (DTC). **Methods:** Postmenopausal women with postoperative DTC, and undergoing thyroid residual ablation or for metastases treatment at Xinhua Hospital between September 2009 and December 2014 were collected and followed for two years. They were divided into a suppressed TSH group (median TSH<0.3 mU/L; Group 1) and a nonsuppressed group (median TSH≥0.3 mIU/L; Group 2). Lumber 1-4 BMD levels (T scores) were measured by a dual energy x-ray absorptiometry bone densitometer at baseline, 12 and 24 months. All patients had calcium and vitamin D supplementation after TSH suppression. The T scores were compared with independent t-test. **Results:** Out of 792 patients treated in our hospital, 126 met the inclusion criteria, including 65 in Group 1 and 61 in Group 2. The baseline characteristics of the patients in the two groups were comparable. The T scores in Group 1 and Group 2 at baseline, 1 year and 2 years follow-up were -0.82±1.22 and -0.51±1.56 (t=-1.050, P=0.220), -1.39±1.13 and -0.68±1.33(t=-2.530, P=0.013), -1.34±1.33 and -0.37±2.21(t=-2.140, P=0.036). **Conclusion:** TSH suppression significantly increases the risk of postoperative osteoporosis. The BMD should be followed up annually in postmenopausal DTC patients. **Disclosure:** This work was supported by the National Natural Science Fund (grant 81271612).

EP-0511

Stratification of recurrent differentiated thyroid cancer with elevated thyroglobulin and negative I-131 whole body scan by restaging 18F FDG PET/CT

K. Okuyucu, S. Ince, E. Alagoz, O. Emer, H. San, E. Balkan, A. Ayan, B. Gunalp, A. O. Karacalioglu, N. Arslan; Gulhane Training and Research Hospital, Department of Nuclear Medicine, Ankara, TURKEY.

Introduction: In nearly 20-30% of patients with differentiated thyroid carcinoma (DTC) relapse and 7% of them die during the next 10 years after initial diagnosis. In 10-30% of patients with DTC after ablation therapy during the follow-up show a negative iodine-131 (131I) whole-body screening test (131I WBS) and increased serum thyroglobulin (Tg) level. Loss of ability of DTC metastatic lesions to trap 131I is associated with pure survival and often aggressive disease. Several studies have shown that in DTC cases non trapping 131I, fluorine-18-fluorodeoxyglucose positron emission tomography (18F-FDG PET) can detect recurrence or metastasis with high sensitivity (80-90%). The purpose of this study was to investigate the clinicopathologic features and other related risk factors of patients with DTC having elevated Tg levels and negative 131I WBS in which recurrence was detected by 18F-FDG PET/CT. We tried to study and stratify patients in this grey zone who could benefit from 18F-FDG PET/CT for the detection of metastasis/recurrence according to predefined risk factors not investigated before. **Materials and Methods:** We studied retrospectively 100 DTC patients with el-

evated Tg levels and a negative 131I WBS during their follow-up between 2004-2013. Recurrence was found in 47% of the patients on restaging with 18F-FDG PET/CT and were compared with nonmetastatic group according to predefined risk factors. These factors were also evaluated in true positive and false negative cases. **Results:** The sensitivity and specificity of 18F-FDG PET/CT for detecting recurrent/metastatic disease were 88% and 95%, respectively. No apparent predefined risk factor impacting a false negative 18F-FDG PET/CT was found. Findings in follicular carcinoma, Hürtle cell carcinoma and papillary carcinoma were not different according to a positive PET. The variants of papillary carcinoma also had no statistically difference with regard to 18F-FDG results. **Conclusion:** The most important factors affecting a true positive 18F-FDG PET/CT study were: Extrathyroidal extension in initial histopathology, high total 131I dose and the SUVmax values over 4,5.

EP-0512

SPECT/CT somatostatin-receptor scintigraphy in Medullary Thyroid Cancer

S. Sergieva[1], M. Atanasova[2], A. Fakirova[3], B. Robev[4], A. Saint-Georges[1]; [1]Sofia Cancer Center, Sofia, BULGARIA, [2]Central Hospital, Plovdiv, BULGARIA, [3]Military Medical Academy, Sofia, BULGARIA, [4]UH"St.Ivan Rilsky, Sofia, BULGARIA.

The medullar thyroid cancer /MDC/ is a rare neuroendocrine tumour - made up of 5% to 8% of thyroid neoplasms. During the last decades, the somatostatin receptor scintigraphy with 99mTc-EDDA/HYNIC-TOC has been introduced for imaging of neuroendocrine tumors. The purpose of this study was to determine the role of SPECT/CT with 99mTc-Tektrotyd in patients with MTC. Twenty one patients, (14F/7M) with MTC underwent somatostatin-receptor scintigraphy. Three of them were studied for initial pre-operative N/M-staging, 18/21 were follow-up after surgery. Plasma calcitonin level was measured as a tumor marker. SPECT/CT studies of the neck and chest and/or abdomen and pelvis were carried out 2-4 hrs. post i.v. administration of average 740 MBq activity dose of 99mTc-Tektrotyd /Polatom/ in all pts. Initial pre-operative staging showed high tracer uptake in the primary tumor and metastatic regional lymph nodes in all 3 cases and false negative imaging of small military 1-4 mm lung metastases in 2 cases, visualized only on the CT part of the fusion images. These results correlated with the high level of serum calcitonin. In the group of patients studied after surgery, true negative results were obtained in 5 cases after thyroidectomy, corresponding to the very low calcitonin value. True positive results were obtained in 1 case with tumor persistence, in 11 patients with paratracheal and/or retrotracheal local recurrence in the thyroid bed and enlarged cervical, mediastinal and/or supraclavicular lymph nodes. Osteolytic bone metastases were obtained in 2 patients, lung nodules with size more than 10 mm were positive in one patient. SPECT-CT study in the region of abdomen identified hepatic metastases in a patient with high background activity in the liver. False positive result was in 1 case with benign ovary cyst. Plasma level of calcitonin vary from 94 to 5496 pg/ml in all 13 patients with local recurrence and/or

metastatic lesions. Sensitivity of SPECT/CT with 99mTc- Tektrotyd in the studied group was 88,8% (16/18); specificity 83,3% (5/6) and accuracy 87.5% (21/24). In conclusion our results showed that SPECT-CT somatostatin-receptor scintigraphy should be used in the MTC imaging as follows: 1. For pre-treatment correct N/M staging of MTC 2.For monitoring of surgical treatment 3.For early determination of recurrence/metastases in cases with clinical and biochemical indices for presence and extent of MTC. 5.For precise topography of metastatic foci in patients with disease extension. 6.To assess SSTR tumor status.

EP-0513

Diagnostic Accuracy of [99mTc]Tc-Sestamibi in the Assessment of Thyroid Nodules

A. Yordanova[1], S. Mahjoob[2], P. Lingohr[3], A. Türler[4], H. Palmedo[5], H. Biersack[1], G. Kristiansen[6], M. Essler[1], H. Ahmadzadehfar[1]; [1]Nuclear Medical Department of the University Hospital of Bonn, Bonn, GERMANY, [2]Institute of Radiology and Nuclear Medicine, BG Kliniken Bergmannsheil, Bochum, GERMANY, [3]Department of Surgery of University Hospital Bonn, Bonn, GERMANY, [4]Department of General and Abdominal Surgery, Johanniter-Krankenhaus, Bonn, GERMANY, [5]Institute of Radiology and Nuclear Medicine and PET-CT Center, Bonn, GERMANY, [6]Institute of Pathology of University Hospital Bonn, Bonn, GERMANY.

Purpose: [99mTc]Tc-Sestamibi (MIBI) is an increasingly used non-invasive tool for the evaluation of thyroid nodules. However, there is still sparse evidence about the accuracy of this diagnostic method in the European population. The aim of this study was to assess the utility of MIBI for the differentiation of thyroid nodules in a larger patient cohort. Furthermore, we constructed a reliable image interpretation method, adapted to the studied population. **Subjects and Methods:** 161 patients underwent MIBI, followed by a thyroid operation. We used a double dual phase MIBI-imaging-protocol. The interpretation of the images included a scoring system from score 0 (absent) to score 3 (increased) accumulation of the tracer to scale the uptake of the thyroid nodule in comparison to the paranodular thyroid tissue. Additionally, we evaluated the tracer-uptake trend in late images compared to early images. We used the final histopathology as a reference (gold standard). **Results:** Scores 0-1 in early images, scores 0-2 in late images and absent uptake-increase in the thyroid nodule in late images showed the best predictive value to exclude malignancy, respectively (NPV 89%). A positive predictive value of 32% could be reached in nodules with an increasing uptake in late images. Highest sensitivity (91%) for malignant nodules showed early images with score 1-3. Highest specifity (91%) was obtained when the negatives were defined as an absent uptake-increase in the nodules. **Conclusion:** The current study confirms that the most valuable feature of MIBI is the good NPV. Thus, with the appropriate image interpretation method a high sensitivity, specifity and moderate PPV can be obtained.

EP-0514

68Ga-DOTA-NOC and 18F-FDG PET/CT for the Diagnosis of Iodine-refractory Differentiated Thyroid Cancer : pilot studies

S. Li, F. Wang, X. Yao, R. Liu, L. Zhang; *Nanjing First Hospital, Nanjing, CHINA.*

Purpose: The aim of this study was to evaluate the role of ^{68}Ga-DOTA-NOC PET/CT in the diagnosis of iodine-refractory thyroid cancer (RAIR) and compare with ^{18}F-FDG PET/CT. **Methods:** Fourteen patients confmed with iodine-refractory thyroid cancer, in our single center (5 male and 9 female, age range 42 to 68, mean 57 ±9) were enrolled in this study, all of them previously received 2-4 cycles of radioiodine therapy, mean of total cumulative activity of 131 I of > 400 mCi. RAIR-DTC was confirmed according to Criteria? by evaluate of serum Tg level and TgAb level, quantitative 131I uptake in metastases on post-therapy WBS, and also by anatomical imaging with CT scan and MRI follow up at least 1 year. The rate of metastases of these 14 patients were: lung> neck lymph nodes > mediastina lymph nodes> bone. ^{68}Ga-DOTA-NOC PET/CT and ^{18}F-FDG PET/CT were performed for all the patients. PET images were analyzed by an experienced radiologist and two experienced nuclear medicine physicians, respectively. **Result:** On patient based analysis, ^{68}Ga-DOTA-NOC PET/CT was positive in 12 patients (12/14,85.7%) with RAIR-DTC,[18]F-FDG PET/CT was positive in 13 patients (13/14,92.8%), there is no significant correlation (P=0.204). On lesion based analysis,46/57 lesions (80.7%) were detected by ^{18}F-FDG PET-CT, and 36/57 lesions were detected by 68Ga-DOTA-NOC PET-CT (P<0.005). 18F-FDG PET-CT was more sensitive in pulmonary metastatic (P <0.001), while 68Ga-DOTA-NOC PET-CT was superior in detecting bone metastasis. For lymph nodes adenopathy, no significant difference between two modality (P> 0.05). Additionally, ^{68}Ga-DOTA-NOC PET-CT confirmed a patient with multiple-endocrine -neoplasia, pancreatic neuroendocrine tumors and medullary thyroid cancer was detected . **Conclusion:** Both ^{68}Ga-DOTA-NOC PET/CT and ^{18}F-FDG PET/CT serve as valuable tools for the confirmation of with RAIR-DTC, and high sensitivety for the detection of lymphadenopathy and remote metastasis, further study is needed.

EP-0515

The role of air pollution in the incidence and mortality of thyroid cancer (TC) in 27 countries of the European Union for the years 1992, 2002,2012

E. Giannoula[1], I. Katsikavelas[2], G. Giannoula[3], I. Iakovou[1]; [1]Academic Nuclear Medicine dpt, Papageorgiou hsp., Thessaloniki, GREECE, [2]Aristotle University, Thessaloniki, GREECE, [3]Faculty of General Medicine, Comenius University, Bratislava, SLOVAKIA.

Introduction: During the past decades, an increasing incidence of TC has been reported, while its mortality is almost constant and comparatively low. It is currently unclear whether the observed increases are real or due to increased diagnosis, as there exist many analyses stating a real increase in the incidence and mortality of TC of all sizes and stages, with different distribution depending on gender, race, age and environmental conditions. Recent studies are examining risk factors such as diet and exercise, benign thyroid diseases as well as genetic factors. There are only few epidemiological studies examining the effects of exposure to chemical agents on TC's "behavior". Therefore the study of environmental factors, potentially influencing the onset and prognosis of TC, such as air pollution is a research field of great interest, given its documented literature carcinogenicity. **Objective***:* The aim of this study is to investigate the role of air pollution in the incidence as well as in mortality from TC in 27 countries of the European Union (EU) for the years 1992, 2002, 2012. **Methods:** The present study is an analytical, ecological, observational study. There were conducted a thorough literature review, data collection from online databases, statistical processing and analysis of information. This ecological study used age-adjusted incidence and mortality rates of thyroid cancer for the year 2012 with respect to 23 air pollutants as well as 179 socioeconomic confounding factors in the EU for the years 1992, 2002, 2012. **Results:** Data analysis of air pollutants revealed a positive correlation between male incidence of 2012 and male mortality of 1992 of TC and levels of benzo(k)[benzo(k)fluoranthene] (P=0,04, r2=0,21) and Hg (P=0,04,r2=0,17) respectively. Socioeconomic factors examined as confounders, presenting a positive correlation between male incidence of 2012 and Gross-National-Income-per-capita, purchasing-power-parity as well as between male mortality of 1992 and adjusted-net-national-income-per-capita, adjusted-net-national-income-per-capita, hospital-beds-per-1,000-people, Gross-Domestic-Product, Gross-National-Income-per-capita and purchasing-power-parity. Multiple linear regression did not reveal any statistically significant correlation between the above epidemiological and confou nding factors. **Conclusions:** A positive correlation between the incidence and mortality of TC and benzo(k)[benzo(k)fluoranthene] & Hg levels was revealed. Although higher socioeconomic status was associated with increased incidence and mortality, no apparent confounding effect was detected in TC's correlation to air pollution. In order to avoid ecological fallacy, it is made clear that the conclusions of the study are limited and concern the countries examined for the years 1992, 2002, 2012

EP-0516

Role of radioguided occult lesion localization (ROLL) in the management of cervical recurrences from differentiated thyroid cancer

V. Garbaccio[1], M. Menga[2], G. Mensa[3], D. Deandreis[1], R. E. Pellerito[4]; [1]Nuclear Medicine AOU S. Giovanni Battista, Città della Salute e della Scienza, Torino, ITALY, [2]Nuclear Medicine Arcispedale Santa Maria Nuova - IRCCS, Reggio Emilia, ITALY, [3]General and Oncologic Surgery, Thyroid Unit AO Ordine Mauriziano Umberto I, Torino, ITALY, [4]Nuclear Medicine AO Ordine Mauriziano Umberto I, Torino, ITALY.

Purpose: Surgery is the treatment of choice for cervical lymph-node and soft tissue recurrences of differentiated thyroid cancer (DTC). Reintervention after previous surgery is technically demanding because of scar tissue and distorted anatomy, with increased risk of failure and morbidity (injury to the recurrent laryngeal nerves and parathyroid glands). We explored the feasibility and the efficacy of radioguided localization of occult lesion (ROLL) to improve the surgical resection of locoregional DTC recurrences. **Subjects and Methods:** Fifteen patients (2

patients being operated twice) that underwent ROLL between December 2013 to October 2016 for DTC recurrence were considered. DTC recurrence was confirmed with FNA in all patients. A few hours prior to surgery, ^{99m}Tc-albumin macroaggregates (MAA) were injected intralesionally (45 MBq in 0,2 ml) under US guidance. During surgery a handheld gamma probe helped to localize the lesion and to confirm complete removal. Patients were then followed up by thyroglobulin and neck ultrasound according to guidelines. **Results:** In 15 patients DTC recurrence was diagnosed after a median follow-up of 34 months from last treatment. It was localized in locoregional lymphnodes (n=8), neck soft tissue (n=6) and in both (n=1). A total of 27 lesions were radiolabeled (mean size 16,8 mm) before surgery. No side effects were observed after radiotracer injection. The radiolabelled lesions were identified and excised without nerve injury or hypoparathyroidism related to reintervention. In presence of lymphnode metastases modified radical neck dissection was performed, while for soft tissue recurrence mini-invasive excision guided by ROLL was preferred. Histopathology confirmed metastatic involvement of 100% of the radiolabelled lesions (27/27) and it showed 11 additional metastases in other nodes. 11/15 patients received subsequent radioactive iodine treatment after radiosurgery for persistently elevated Tg or AbTg levels. After a median follow up of 16 months 5/15 patients were classified in excellent response without evidence of disease, 3/15 patients had persistently elevated Tg or AbTg levels without structural evidence of disease (biochemical incomplete response) and 7/15 patients showed structural incomplete response with persistent cervical disease (n=4), lung metastases (n=2), and both (n=1). **Conclusions:** despite the small population of the study, we confirm that ROLL is a simple, reliable and safe procedure in the management of DTC locoregional recurrences to guide surgery. This technique seems to be particularly useful in patients already submitted to previous surgery and neck lymphnodes dissection and/or with small size recurrence hidden in scar tissue.

EP-0517

The relevance of the BRAFV600E mutation in the treatment of the Papillary Thyroid Carcinoma

O. Ajuria, T. Navarro Martinez, B. Lorente Castro, J. Castro Beiras; Hospital Ramon y Cajal, Madrid, SPAIN.

Purpose/Introduction: There are multiple studies analyzing the prevalence of BRAFV600E mutation and its relationship with other clinical-pathological risk factors reported with controversial conclusions. The aim of this study is to determine the prevalence of BRAFV600E mutation in our hospital and to correlate the association of the positivity of BRAFV600E mutation with poor prognosis of papillary thyroid carcinoma (PTC) and its consequent need to change the management of these patients. Subjects and **Methods:** 73 patients with PTC that were treated with radioiodine (1110-5550MBq) after total thyroidectomy, neck dissection or recurrence surgery between January 2014 and April 2016 were included in this retrospective study. Patients with microcarcinoma diagnosis were excluded. BRAFV600E mutation was tested by PCR-single-strand confor-

mation polymorphism analysis before surgery. The follow up period was 3 years, with an anual control. Total remission was considered when clinical examination, cervical ultrasound, I131 SPECT-CT and whole body scan were negative and stimulated Tg < 1ng/l and Tg antibodies <20UI/ml. Patients were divided according their age (<45 or >45), BRAFV600E mutation (positive/negative) and clinical stage (I, II-III and IV). Then, in each group we assessed the number of iodine administrations and the number of patients in remission or with disease. **Results:** In the <45 years group: 28 patients, 16/28(57,1%) BRAFV600E negative and 12/28(42,9%) BRAFV600E positive, all of them I stage. Only 2/16(12,5%) BRAFV600E negative and 1/12(8,3%) BRAFV600E positive did not reach remission. In the >45 years group: 45 patients, 20/45(44,5%) BRAFV600E negative (8/20(40%) I stage, 9/20(45%) II-III stage and 3/20(15%) IV stage) and 25/45(55,5%) BRAFV600E positive (6/25(24%) I stage, 14/25(56%) II-III stage and 5/25(20%) IV stage).Out of the 20/45(44,4%) BRAFV600E negative patients: 6/20(30%): 0/8(0%) I stage, 3/9(30%) II-III stage and 3/3(100%) IV stage had disease in spite of several iodine treatments.Out of the 25/45(55,5%) BRAFV600E positive patients 0/6(0%) I stage, 7/14(50%) II-III stage and 4/5(80%) IV stage did not reach remission. It must be highlighted that in the >45 years II-III stage group with BRAFV600E negative remission is reached in 6/9(66%) while when BRAFV600E was positive remission was reached on the 7/14(50%), but without statistical significance p=0,67. **Conclusion:** The prognosis value of BRAFV600E varies depending on the age and the clinical stage of the PTC. In older than 45 years the prognosis was worse, especially when associated with II-III stage. There is no evidence that BRAFV600E should modify the therapeutical management of the PTC patients even though further studies with more patients and longer follow up are required.

EP-0518

An audit of Differentiated Thyroid Cancer (DTC) patients, post-surgery and Radioiodine therapy in a tertiary care centre and the effect of the ATA 2015 on them in terms of risk stratification and use of RAI

V. Rangarajan, A. Agrawal, S. Choudhury, G. Pantavaidya, P. Pai, S. Shah, A. D. Puranik, N. Purandare, A. K. D'Cruz; Tata Memorial centre, Mumbai, INDIA.

Aim: The study aim was to conduct an audit of patients with DTC in post total thyroidectomy setting and risk stratify them using ATA 2009 and ATA 2015 and to see how many of them would change their risk stratification category according to the new ATA 2015 guideline and if the changed risk stratification would affect the use of radio-active iodine. **Methods:** This was retrospective observational study approved by institutional ethics committee. 128 patients of DTC who had undergone total thyroidectomy followed by radioiodine treatment in year 2014-and 2015 were recruited in study. These patients were risk stratified according to ATA 2009 and 2015 guidelines. **Results:** Out of 128 patients 81(63.2%) had loco-regional lymph node metastases and 8 had distant metastases Histologically 31were follicular variant of differentiated papillary carcinoma, 8 were high

risk type of papillary carcinoma (tall cell-1, columnar cell-2, solid variant-2 and insular variant-3), 3 were differentiated follicular carcinoma, 4 were hurthle cell carcinoma and rest were classical variant of papillary carcinoma. According to the 2009 risk stratification criteria 21 out of 128 were found to be of low risk, 74 intermediate risk and 33 high risk. However according to the 2015 modification 23 were low risk, 64 intermediate risk and 41 high risk. Overall 7.8 % patients changed their risk stratification category. The patients that changed risk stratification categories, were all intermediate category patients according to 2009 guidelines. Amongst them 8 (6.25 %) got upstaged to high risk. As for the intention of RAI use goes only 3 (2.3 %) patients got down staged to only remnant ablation from adjuvant therapy, 2 of them on the virtue of being changed to low risk patients and 1 on account of having a low volume central neck nodal disease without any high-risk features. **Conclusion:** Patients with lymph-node metastases are primarily affected by the modified 2015 ATA risk stratification system. Modified 2015 risk stratification system changed RAI use in only 2.3% of patients, however all these patients could now be considered for remnant ablation with 30 mCi of RAI on OPD basis. Long term follow up is needed to understand the prognostic significance of the modified risk stratification of ATA 2015

EP-0519

Serum Calcitonin Increase-guided evaluation of MTC in Patients with Multinodal Goiter and correlation with Tc99m-DMSA (V) scintigraphy

V. Sukhov[1], P. Kirichenko[1], A. Marin[1], W. Wiedemann[2], K. Zaplatnikov[2];
[1]Military Medical Academy, ST. PETERSBURG, RUSSIAN FEDERATION,
[2]MAZ Nuclear Medicine, Nürnberg, GERMANY.

Aim: Medullary thyroid carcinoma (MTC) is associated with a high concentration of serum calcitonin. Routine measurement of serum calcitonin concentration has been advocated for detection of MTC among patients with nodular thyroid diseases. We evaluated the usefulness of routine Calcitonin test in these patients with presence of hypoechogenic nodes (0,3-3,7 cm) and use of DMSA (V) as nonspecific agent for detection of above-mentioned pathology. **Methods:** Routine radio immunological measurements of serum calcitonin concentrations were performed in 1,548 patients (415male; 1,133 female) with ultrasonography (US) revealed nodular thyroid diseases and Pentagastrine or Calcium stimulation in some of them. The average age was 44 years (range 8-86 years). Additional examination included thyroid Tc-99m scan, measurements of thyroid hormones, TSH and antithyroid autoantibodies, DMSA (V) Tc-99m scan. **Results:** We found that 44 (2,8%) of all patients with nodular thyroid diseases by US had serum calcitonin level by RIA above 10 pg/mL. Among them 10 patients (22,7%) presented histologically confirmed MTC. 6 of 10 patients with MTC had basal serum calcitonin level above 100 pg/mL. The remaining 4 patients had moderate elevation of basal serum calcitonin (range, 12-66 pg/mL). Serum calcitonin concentration increased to more than 100 pg/mL after administration of Calcium i.v. in all patients with MTC (2.4x to 47.7x increase). 4 of 34 pts with

Calcitonin levels from 10-33 pg/ml and negative Test with stimulation had C-cell hyperplasia; the rest had renal failure or other diseases. All of Calcitonin positive patients were underwent to DMSA (V) Tc-99m scan and had focal uptake of tracer in all 10 histologically verified patients. **Conclusion:** These results suggested that routine RIA measurement of serum Calcitonin is useful for early detection of MTC among patients with nodular thyroid diseases, especially in presence of hypoechogenic nodes of different size. Calcium or Pentagastrine stimulation test may also be a reliable way for evaluating thyroid nodular patients with mild or moderate elevation of serum Calcitonin concentrations. Scan with non-specific, nevertheless very sensitive agent, as Tc-99m-DMSA (V) will bring a lot of additional information and help to localize tumor node.

EP-0520

Correlation between stimulated thyroglobulin levels and positive 18F-FDG PET/CT findings in DTC patients with radioiodine refractory disease

D. Srbovan, S. Lučić, A. Peter, E. Matovina, V. Cimbaljević; Institut of oncology Vojvodina, Sremska Kamenica, SERBIA.

Purpose: To analyze the correlation of stimulated thyroglobulin (Tg) levels and Tg elevation rate in DTC patients (pts) with radioiodine refractory disease (RRD) and positive findings of ^{18}F-(FDG) PET/CT scan. **Subjects & Methods:** In 46 pts with DTC (41 papillary and 5 follicular) and diagnosed RRD, with stimulated Tg>1.5ng/ml and negative ^{131}I-NaI whole-body scans, ^{18}F-FDG-PET/CT examination has been performed, and the findings were compared in regard to Tg value. Dependently on the Tg level range, pts were divided in four groups, (group 1: Tg 0-20ng/ml (21 pts); group 2: Tg 20-40ng/ml (13pts); group 3: Tg 40-80ng/ml (9pts); and group 4: Tg 80-100ng/ml (3pts)). Data were analyzed by Pearson's correlation test and Spearman's rank correlation coefficient; significance level $p<0.05$. **Results:** ^{18}F-FDG-PET/CT findings were positive in 21 (45.65%), and negative in 25pts (54.35%).The most common location of pathological foci in positive ^{18}F-FDG-PET/CT scans were in 16/21 pts loco regional (jugular, paratracheal, retroclavicular and in thyroid bad), mediastinal lymph nodes in 2/21 pts, and distant metastasis were found in 3/21 pts. Tg value range in the whole group (46 pts) was 1.59-95.92ng/ml (mean 29,57±2.607ng/ml); in pts with positive scans Tg range was 3.66-95.92ng/ml (mean Tg 37.8271±2.746ng ng/ml), and with negative scans range 1.59-93.29ng/ml (mean Tg 22.634±2.317ng/ml). In group 1 average Tg value was 8.69ng/ml, in 6/21 pts with positive scans average Tg=10.34ng/ml, and in 15/21 pts with negative scans average Tg=8.03ng/ml. In group 2 average Tg=27.98ng/ml, in 6/13 pts with positive scans average Tg=30.57ng/ml, and in 7/13 pts with negative scans average Tg=28.89ng/ml. In group 3 average Tg=60.32ng/ml, in 6/9 pts with positive scans average Tg=61.46ng/ml, and in 3/9 pts with negative scans average Tg=57.70ng/ml. In group 4 average Tg=90.30ng/ml, in 2/3 pts with positive scans average Tg= 88.81ng/ml, and in 1/3 pts with negative scan average Tg=93.29ng/ml. Statisticaly significant correlation between Tg level and PET/CT findings was established in the whole group of pts (r=0.293;*p*=0.048 & rho=0.34;*p*=0.021),

but separate groups analysis did not indicate any significant correlation (group 1: r=0.216;*p*=0.515 & rho=0.279;*p*=0.221); group 2: r=-0.199;*p*=0.346 & rho=-0.247;*p*=0.415; group 3 r=0.173;*p*=0.657 & rho=0.274;*p*=0.476; and group 4: r=-0.342;*p*=0.778; Spearman N/A (due to small pts number). **Conclusion:** Since the weak correlation between Tg and PET/CT findings was determined, seemingly dependently related to the value of Tg, we are of opinion that there may be the place to determine the cut-off Tg value as a possible predictor for positive PET/CT finding by further investigation.

EP-0521

Retropharyngeal lymph nodes metastases in differentiated thyroid carcinoma might be under estimated

D. Benisvy, I. Birtwisle Peyrottes, J. Santini, C. Zwarthoed, A. Schiazza, O. Humbert, J. Darcourt; Centre Antoine Lacassagne, Nice, FRANCE.

Aim: Retropharyngeal lymph node metastases (RPNM) are rare during the course of thyroid carcinoma. This diagnosis is difficult because this region is hard to explore with usual tools, and due the preconceived opinion that this site is hardly ever involved. The aim of this observational study is to highlight tools allowing the diagnosis of such lesions and to correlate RPNM finding to clinical and pathological features. **Materials and Methods:** We retrospectively studied 11 cases of patients treated with radioiodine in our institution, from 2009 to 2017, for thyroid carcinoma in whom RPNM were discovered either with ^{131}I SPECT-CT and/or with 18F-FDG-PET at the time of diagnosis or during follow-up. For each patient we studied clinical features, pathological subtypes, scintigraphic results, localization of the primary tumor, TNM classification (7th), therapeutic approach and follow up. **Results:** We included 11 patients with known RPNM. Patients were 9 to 72 years old at time of diagnosis of thyroid carcinoma (mean 43), sex ratio was 5/6. Seven of these patients were diagnosed for RPNM at the time of initial treatment. Two patients were diagnosed retrospectively on persistent biological abnormalities. We were not able to prove that RPNM were present at the time of initial treatment for the last 2 patients due to lack of imaging. For most patients, the RPNM radioiodine uptake was hardly visible on the whole body scan, due to physiological mouth activity. In those cases only SPECT-CT, and or PET-CT allowed the diagnosis confirmed by MRI. RPNM were always related to papillary carcinoma, 9/11 were associated with multifocal tumor, 8/11 with aggressive pathological subtypes, such as diffuse sclerosing carcinoma, large lymphatic spread traits (carcinomatous lymphangitis, numerous psammomes) and loco regionally advanced forms (8/11 T3-T4).5/11 patients had surgery in addition to radioiodine therapy. On follow up, all patients are still alive with 4/11 in complete remission and only one patient has progressive disease. **Conclusion:** We found that RPNM, when diagnosed, are mostly present since the beginning of the disease. They are associated with pejorative pathological papillary features, loco regional extend, multifocality. This probably reflects the very lymphophilic caracter of such tumor. Although, RPNM does not seem to be related to a poorer prog-

nosis, it should be systematically looked for, using ^{131}I SPECT-CT or ^{18}F-FDG PET in patients with aggressive papillary subtypes and in cases of biological disease without evidence of structural disease by conventional imaging.

EP-0522

Evaluation of calcium stimulation test for the diagnosis and follow-up of medullary thyroid cancer: comparison with pentagastrin test

E. Rainer, A. Gessl, M. Krebs, B. Niederle, C. Scheuba, A. Haug, M. Hacker, S. Li; Medical University of Vienna, VIENNA, AUSTRIA.

Purpose: Calcitonin (CT) is an important tumour marker for the diagnosis and follow-up of medullary thyroid cancer (MTC). The aim of this study was to evaluate the reliability of calcium stimulation test (CST) for MTC diagnosis and follow-up as compared with pentagastrin test. **Subjects and Methods:** A total of 256 patients (123 females and 133 males, mean age of 56 ± 27 years, range 21 to 83 years) had both pentagastrin (0.5 µg/kg body weight) and calcium (2.5mg/kg body weight calcium gluconate) stimulation tests. Among them 28 patients with thyroid goiter had thyroidectomy after both CST and pentagastrin test. **Results:** Stimulated CT levels after administration of pentagastrin or calcium were significantly correlated in all groups. The Cut-off values with best sensitivity and specificity to differentiate between MTC and C-cell hyperplasia (CCH) plus healthy individuals were above 727 pg/ml for men and above 395 pg/ml for women. The Cut-off values for differentiation between MTC plus CCH and healthy individuals were above 590 pg/ml in men and above 160 pg/ml in women. **Conclusion:** CST seems to be a reliable, safe and effective test and may replace the pentagastrin test for the diagnosis and follow-up of MTC.

EP-0523

Usefulness Of SPECT/CT Imaging In Patients With Differentiated Thyroid Carcinoma

S. Ucak Semirgin[1], T. Basoglu[1], Z. Sahin[2], M. Sahin[1], O. Yapici[1]; [1]Ondokuz Mayis University Nuclear Medicine Department, Samsun, TURKEY, [2]Yıldız Medstar Hospital, Antalya, TURKEY.

Aim: SPECT/CT fusion imaging offers anatomical and functional information together and improves the sensitivity and specificity of I-131 wholebody imaging (WBI) in patients with differentiated thyroid carcinoma (DTC). In our study, diagnostic value of the SPECT/CT method in evaluating patients with DTC was investigated. **Materials & Methods:** A total of 72 patients (8M, 64F) previously undergone total thyroidectomy were included (20-79 yr, mean age 48,7 ± 13,1). 57 patients underwent diagnostic WBI and 15 posttherapeutic WBI using a dual head gama camera. Excluding obvious physiological uptake sites, any focal or diffuse uptake of higher than surrounding background activity on planar images was considered as pathologic. Regional SPECT/CT imaging was performed immediately after WBI in all patients with inconclusive findings. **Results:** On WB images, 61 pathological foci were detected in 72 patients. From 38 foci

compatible with thyroid remnant on planar imaging, 7 were not observed on SPECT/CT; 3 were evaluated as lymph node and 2 were located at dental and nasal structures. SPECT/CT images detected 3 additional residual foci that were not seen on WB images. From 4 foci compatible with lymph nodes on WB images, 2 were confirmed whereas other 2 were not seen on SPECT/CT. In 13 focal uptake sites located in the thoracic region on WB images, bone/soft tissue differentiation could not be done. On SPECT/CT images, these were determined as: 2 mediastinal lymph nodes, 2 bone lesions, 7 lung lesions and 2 breast lesions. SPECT/CT detected 3 additional iodine accumulating lesions, located in bone(2) and lung(1). On WB images, 5 foci were determined in the abdominopelvic region. On SPECT/CT images, 2 were compatible with reactive/inflammatory findings associated with IM injections, other 3 foci were not seen. One upper appendicular lesion was confirmed with SPECT/CT imaging. SPECT/CT determined exact localization in 22 of 61 lesions (36%). In 19,7 % of WPI detected foci (12/61), SPECT/CT could not confirm the presence of a lesion. **Conclusion:** SPECT / CT improves interpretation of WBI, especially in lesion localization and distinguishing malignant foci from physiologic accumulations. It has also a role in determining additional pathological foci when compared to planar WB imaging.

EP-42   **during congress opening hours, e-Poster Area**

Clinical Oncology: Breast

EP-0524
The Role of 18F-FDG PET/CT In the Evaluation of Tumor Marker Increase In Breast Cancer

I. Goktaş, H. Cayvarli; Ordu State Hospital, Clinic of Nuclear Medicine, Ordu, TURKEY.

Introduction: Breast cancer is the most frequently diagnosed cancer and the leading cause of cancer related death among females worldwide. Locoregional recurrence and/or distant rmetastasis in breast cancer can occur after 15 years or even more following primary theraphy. Early detection of recurrence can improve long term survival rates and life quality, so routine follow-up of these patients should never be given up. Serum tumor markers are routinely used in the follow-up of breast cancer. In this study we aimed to assess the diagnostic performance of PET/CT in the follow-up of breast cancer patients, who underwent a PET/CT scan because of having a suspicion of recurrence due to serum tumor marker (CA 15-3 and CEA) increase. **Methods:** 77 consecutive patients were included in this study. PET/CT scan results were compared with the final diagnosis which were obtained from the histopathological sampling or a minimum 6 months of radiological follow-up. The sensitivity, specificity, positive predictive value, negative predictive value and the diagnostic accuracy of PET/CT for detecting recurrence were calculated. **Results:** Of all 77 patients, all of them had increased (>25 U/ml) serum CA 15-3 levels and 37 of them had increased (>3.8 ng/ml) serum CEA levels. According

to PET/CT scan results, 59 of 77 patients (PET/CT positive) had local recurrence and/or distant metastasis while there was no pathological finding in 18 patients (PET/CT negative). In a minimum 6 months of follow-up, in 58 of "PET/CT positive" patients tumor recurrence is confirmed while in 16 of "PET/CT negative" patients no tumor recurrrence is detected. According to these results the sensitivity, specificity, positive predictive value, negative predictive value and the diagnostic accuracy of PET/CT for detecting recurrence on a per-person basis were calculated as 98%, 88%, 96%, 94% and 96% respectively. **Conclusion:** 18F-FDG PET/CT is a noninvasive imaging modality that enables to scan the whole body at once. In the case of serum tumor marker increase, 18F-FDG PET/CT has a high diagnostic accuracy in detecting tumor recurrence in patients with breast cancer and it is an effective modality that can be used in addition to conventional imaging modalities.

EP-0525
Diagnostic accuracy of mammography and scintimammography with 99м Tc-MIBI in detection of early breast cancer

S. Novikov, S. Kanaev, A. Chernaya, P. Krzhivitskiy, P. Krivorotko, L. Jukova, A. Artemyeva; N.N. Petrov Institute Oncology, St Petersburg, RUSSIAN FEDERATION.

Purpose: to compare the diagnostic performance of mammography (MG) and scintimammography (SMG) with 99mTc-MIBI, alone and in combination, for the diagnosis of breast cancer (BC). To evaluate usefulness of both methods for detection of minimal (<10mm) BC in women with normal and mammographically dense breasts. **Material and Methods:** 437 women with "suspicious for malignancy" breast lesions were included in this prospective single center study. Digital MG was done according to standard clinical protocol. Routine planar SMG was performed in prone position 5-10 min after i/v injection of 740 MBq of 99mTc-MIBI with acquisition time of 10min for every lateral and anterior projection. Final diagnosis was established after biopsy or surgery. **Results:** According to histopathological examinations BC was diagnosed in 367 patients and benign disease in remaining 70 cases. MG correctly detected 346 cancer and 51 benign lesions. It was false positive in 19 and false negative in another 21 cases. SMG was true positive in 341, true negative in 44, false positive in 26 and false negative in another 26 women. Diagnostic performance of MG and SMG were as follows: Sen -94% vs 93%; Sp-73% vs 63%; AC - 91% vs 88%. As expected, we mentioned significant differences in diagnostic performance of MG in 266 women with mammographically low (grade 1-2) and 171 patients with high (grade 3-4) breast density. Sen and Sp in this diagnostic groups were 95% vs 89%; 82% vs 71%. On the contrary we didn't mention any correlation between breast density and diagnostic performance of SMG. In low and high density breasts Sen and Sp of scintimammography were comparable: 91% vs 94%; 64% vs 63%. 108 women had normal breasts or suspicious lesions less than 10mm in diameter. BC was diagnosed in 61 patients of this group: Sen, Sp and Ac of mammography were 72%, 74%, 73%; for SMG- 62%, 51%, 57%. **Combination of**

MG and SMG provide significant gain in Sen (up to 93%). In 53 of 108 women with "no or minimal lesions" and dense breasts Sen, Sp and Ac of mammography were 40%, 71,4%, 64%. **Sen of scintimammography was two times higher (82%)** with 55% Sp and 60% Ac. **Conclusion:** Combination of MG and SMG can significantly increase delectability of early (10mm or less) breast cancer, especially in women with dense breasts.

EP-0526

Comparison of the efficiency for Tc-99m Tin-colloid and Tc-99m Phytate in sentinel node detection in breast cancer patients

J. Seok; Chung-Ang University Hospital, Seoul, KOREA, REPUBLIC OF.

Objectives: Lymphoscintigraphy and sentinel node biopsy has become a standard method for detection of axillary lymph node metastasis in breast cancer patients, but the standard radiopharmaceutical was not prepared. About detection of axillary lymph node metastasis by lymphoscintigraphy and sentinel node biopsy in breast cancer patient, we compared the results of Tc-99m Tin-colloid and Tc-99m Phytate by subareolar injection. **Methods:** This study included 956 breast cancer patients who were performed operation during 2001-2017. Four hundred twelve patients were injected 0.8 ml of Tc-99m Tin-colloid (37-185 MBq) by subareolar injection. Five hundred forty four patients were injected 0.8 ml of Tc-99m Phytate (37-185 MBq). Lymphoscintigraphy was performed in supine position and sentinel node localization was performed by hand-held gamma probe in operation. **Results:** Among 412 patients by Tc-99m Tin-colloid, 374 cases (90.8%) were localized the sentinel node by lymphoscintigraphy and 367 cases (89.1%) were localized by gamma probe. Among 544 patients by Tc-99m Phytate, 527 cases (96.9%) were localized by lymphoscintigraphy and 529 cases (97.2%) were localized by gamma probe. The detection rate by lymphoscintigraphy and gamma probe was superior for Tc-99m Phytate compared to that for Tc-99m Tin-colloid, with a statistically significant difference. (p<0.05, p<0.05). **Conclusions:** Tc-99m Phytate is a better choice for localization of sentinel node than Tc-99m Tin-colloid in breast cancer patients.

EP-0527

Comparison of subareolar Injection lymphoscintigraphy with the 1 day and the 2 day protocol for the detection of sentinel lymph nodes in patients with breast cancer

J. Seok; Chung-Ang University Hospital, Seoul, KOREA, REPUBLIC OF.

Objectives: Lymphoscintigraphy and sentinel node biopsy were used for the detection of axillary lymph node metastasis in breast cancer patients. We compared the results of subareolar injections on the day of surgery (1 day protocol) with injections the day before surgery (2 day protocol). **Methods:** This study included 956 breast cancer patients who underwent surgery between 2001 and 2017. For the 1 day protocol 0.8 ml of Tc-99m Tin-Colloid (37MBq) was injected in 614 patients in the subareolar region on the morning of the surgery. For the 2

day protocol 0.8 ml of Tc-99m Tin-Colloid (185MBq) was injected in 342 patients on the afternoon before surgery. Lymphoscintigraphy was performed in the supine position and sentinel node identification was performed by hand-held gamma probe during surgery. **Results:** Among 614 patients with the 1 day protocol, 582 cases (94.8%) were identified by sentinel node lymphoscintigraphy, and 587 cases (95.6%) were identified by gamma probe. Among the 342 patients, in the 2 day protocol, 319 cases (93.3%) had the sentinel node identified by lymphoscintigraphy, and 309 cases (90.4 %) had the sentinel node identified by the gamma probe. There was no significant difference in the identification rate of the sentinel node between the 1 day and 2 day protocol by lymphoscintigraphy and the gamma probe. **Conclusions:** The results of the identification of the sentinel node according to 1 day or 2 day protocols showed no significant differences. Because the 2 day protocol allows for an adequate amount of time to perform the lymphoscintigraphy, it is a more useful protocol for the identification of sentinel nodes in patients with breast cancer.

EP-0528

Volumetric Retention Indexes by Early Delayed Dual-time-point FDG PET/CT Do Not Correlate with Prognostic Factors in Invasive Breast Cancer

H. Song; Jeju National University School of Medicine, Jeju-si, KOREA, REPUBLIC OF.

Purpose: This retrospective study investigated the correlation between volumetric parameters on tumor assessed by early delayed dual-time-point FDG PET/CT (edPET) with prognostic factors of invasive breast cancer. **Subjects & Methods:** Forty-five women were enrolled. All patients underwent mastectomies and edPET before surgery. They underwent conventional FDG PET/CT (1) followed by the early delayed scan (2) without additional CT and repositioning. The patients with the primary tumors of below maximal standardized uptake value (SUV) 2.5 were excluded. Total lesion glycolysis (TLG) and tumor metabolic volume (TMV) in the primary tumors were evaluated with cut-off value of SUV 2.5 and the percentage changes between TLG and TMV of PET/CT1 and PET/CT2 calculated (retention indexes; TLGRI = (TLG2-TLG1)/TLG1, TMVRI = (TMV2-TMV1)/TMV1). Statistical analysis was performed to find the correlation of prognostic factors with TLGRI and TMVRI. **Results:** PET/CT2 was conducted 19.3 ± 1.2 min after PET/CT1 without additional CT and repositioning. Significant statistical differences between mitotic count (1 to 3, p = 0.016, 0.023), lymph node stage (p = 0.019, 0.012) and pathologic stage (p = 0.013, 0.026) in TLGRI and TMVRI. Otherwise TLGRI and TMVRI did not showed any relationship with Ki-67, tumor size, number of lymph node metastasis, T stage, histologic grade, tubular differentiation, nuclear pleomorphism, ER, PR, Her2/neu, p53, EGFR, CK5/6 and E-cadherin. **Conclusion:** Volumetric retention indexes assessed by edPET do not correlate with most of well-known prognostic factors in invasive breast cancer. Considering about conventional retention index such as maximal SUV, these parameters are not useful for predicting the prognosis in invasive breast cancer.

EP-0529

Evaluation of Metabolic Character of Breast Cancer with F-18 FDG PET/CT

H. Önner, E. Entok, M. Dinçer, S. M. Erkasap; Eskişehir Osmangazi Üniversitesi, Eskişehir, TURKEY.

The aim of our study was to investigate the relationship between histopathological and immunohistochemical prognostic factors and metabolic parameters in patients undergoing F-18 FDG PET/CT imaging for preoperative and neoadjuvant pre-treatment breast cancer diagnosis and appropriate for clinical use. Our series consisted of 94 female patients. There was a significant relationship between T-stage, M-stage and grade of tumor with SUVmax, SUVmean, MTV, TLG and SUVmax/kc SUVmean values in the tumor, but no significant correlation was found between histopatholagic types and menopausal status. There was a significant difference between lymph node metastasis status and tumor's MTV, TLG and SUVmax/kc SUVmean values, but the relation with other metabolic parameters was insignificant. Significant correlations were found between tumor ER, HER-2 receptor status, Ki-67 levels, and molecular subtypes and metabolic parameters other than MTV. Significant correlations were found between PR status and metabolic parameters other than MTV and TLG values. The Ki-67 value, which is the indicator of tumor proliferation, was the SUVmax value of the most correlated metabolic parameter's of tumor. In conclusion, our study showed that SUVmax value in relation to prognostic factors of tumor was better than other metabolic parameters. However, the association of TLG, which reflects both volumetric and glycolytic activity of the tumor, is significant in relation to axillary lymph node involvement, meaning that it is meaningless with other metabolic parameters and that the significance value in the case of distant metastasis is better than other metabolic parameters suggests that it may reflect tumor biology and behavior.

EP-0530

CEA, CA15.3 and 18-FDG PET in the follow-up of early breast cancer patients: a prospective, multicentric, randomized trial—KRONOS patient-oriented new surveillance study Italy

E. Barbieri[1], C. Zamagni[1], M. Gion[2], L. Mariani[3], P. Stieber[4], D. Rubino[1], R. Wirtz[5], A. Bernardi[1], N. Cacciari[1], S. Quercia[1], M. Lenzi[1], M. Cubelli[1], C. Pizzirani[1], M. Carapelle[1], M. Pagliaro[1], S. Tomasini[1], S. Toracchio[1], R. Baum[6], S. Fanti[1]; [1]Policlinico S. Orsola - Malpighi, Bologna, ITALY, [2]Centro Regionale Indicatori Biochimici di Tumore, Mestre, ITALY, [3]Istituto Nazionale Tumori, Milano, ITALY, [4]Institute of Clinical Chemistry, Munich, GERMANY, [5]STRATIFYER Molecular Pathology GmbH, Cologne, GERMANY, [6]Zentralklinik Bad Berka, Bad Berka, GERMANY.

In the last twenty years new findings about biology, treatment and the introduction of cutting-edge diagnostic technologies such as 18-FDG PET have deeply modified our knowledge about breast cancer. As a consequence current recommendations for breast cancer surveillance in asymptomatic patients which include only mammography and physical examination and arise from two trials conducted in the 80's may not be updated to the present times. On this basis we designed this prospective randomized trial to verify if the serial measurement of CEA and CA15-3 followed by 18-FDG PET can anticipate the diagnosis of breast cancer recurrence compared to control arm by estimation of the difference of restricted mean survival time between the two arms. If the end-point will be met a subsequent extension trial will investigate the impact of the earlier diagnosis of distant metastases on survival. Patients diagnosed with stage I-III breast cancer, who underwent adequate surgery are eligible. Special histologies and low-risk cases according to St. Gallen criteria are excluded. The study includes patients at the beginning of the follow-up after the conclusion of primary treatment (cohort 1), and patients that have concluded without relapse the first 5 years of follow-up (cohort 2). Eligible patients will be randomized in a 1:1 ratio to follow-up according to local practice (control arm) or to three-monthly serial dosing of CEA and CA15-3 and subsequent 18 FDG-PET only in case of an increase of CEA and/or CA 15.3 greater than a critical difference compared to baseline (experimental arm). The following stratification factors will be used: node negative *vs* positive, HER2 negative *vs* positive, ER positive *vs* negative. Eight-hundred pts will be enrolled over 3 years. For such a calculation, we made the assumption of a 20% baseline 5year incidence of relapse. The target reduction of three months in restricted means survival times implies a median time of diagnostic anticipation, conditional on having breast cancer recurrence, of 10 months. The follow-up will continue until 10 years from surgery. Since 23rd October 2014 616 pts have been enrolled. The present trial was approved by the Ethical Committee of each participating centre and is registered on clinicaltrials.gov (NCT02261389).

EP-0531

Evaluation of metastatic breast cancer patients on FDG PET scan with PERCIST 1.0: Experience from University Hospital Oman

A. Jain, A. K. Mittal, S. Raniga, K. Al Baimani, S. Kumar, H. Al Dhuhli; Sultan Qaboos University Hopsital, Muscat, OMAN.

Introduction: RECIST 1.1 is widely used for response assessment of solid tumors, however it designates numerous lesions as non-measurable, which cannot be quantified and remains a substantial metastatic disease burden. **Purpose:** 1. To evaluate the non measurable disease burden in breast cancer 2. Quantitative response evaluation of non-measurable disease using PERCIST 1.0 criteria and to study its impact in patient management. **Subjects and Methods:** Retrospective analysis of locally advanced/ metastatic breast cancer patients with FDG PET/ low dose non contrast CT scans were performed between April 2016 and March 2017 after ethics committee approval. All baseline and follow up scans were acquired with similar doses of FDG and acquisition protocols (Biograph mCT, Siemens heathcare, Erlangen Germany). Metabolic quantitative values of target lesions (hottest maximum five) were

calculated in form of peak standardized uptake value corrected for lean body mass(SULpeak). The percentage of change in SULpeak of target lesions was calculated in follow-up scan using following formula: {follow-up target lesion SULpeak-baseline target lesion SUL peak/ baseline target lesion SUL peak}X100 Metabolic response was categorised according to PERCIST 1.0 a) Complete metabolic response (CMR), b) Partial metabolic response (PMR), c) Stable metabolic response (SMR), d) Progressive metabolic disease (PMD). Change in patient management was also recorded. **Results:** Total 45(93%) patients had non-measurable disease by RECIST 1.1 (26 with only non measurable and 19 with both measurable and non measurable disease). Out of 19 patients 14 patients had upstaging of disease when non-measurable components were considered in evaluation. 22 patients had bone metastases; others had inflammatory breast disease, small lymph nodes, lung nodules, pleural disease, musculoskeletal disease, liver lesions and adrenal gland disease as non measurable lesions. CMR was seen in 7 (15.5%) patients, PMR in 11 (24.4%) patients, SMD in 4 (8.8%) patients and PMD in 15 (33.3%) patients. 8 (17.7%) patients could not be grouped in above categories. We are still exploring and quantifying the clinical impact of follow-up PET scan in patient management. **Conclusion:** Overall PET quantification could pick disease in smaller lesions, early stage disease causing upstaging of disease with better quantification of response assessment, causing significant change in management. Challenges in terms of false positive and difficulty in grouping all patients still remains to be answered. Key words: Breast cancer, FDG PET scan, PERCIST 1.0, RECIST 1.1

EP-0532

Axillary staging for breast cancer during pregnancy. Feasibility and safety of sentinel lymph node biopsy

S. N. Han[1], F. Amant[1], E. H. Cardonick[2], S. Loibl[3], F. A. Peccatori[4], O. Gheysens[1], C. A. Sangalli[3], V. Nekljudova[3], K. Dahl Steffensen[5], M. Mhallem Gziri[6], C. P. Schröder[7], C. A. R. Lok[8], A. Verest[1], A. Smeets[1], G. Pruneri[4], **M. Cremonesi**[4], O. Gentilini[9]; [1]University Hospitals Leuven, Leuven, BELGIUM, [2]Cooper Medical School at Rowan University, Camden, NJ, UNITED STATES OF AMERICA, [3]German Breast Group, Neu-Isenburg, GERMANY, [4]Istituto Europeo di Oncologia, Milano, ITALY, [5]Vejle Hospital, Vejle, DENMARK, [6]University Hospital Gasthuisberg, Leuven, BELGIUM, [7]Universitair Medisch Centrum Groningen, Groningen, NETHERLANDS, [8]Antoni van Leeuwenhoek-Netherlands Cancer Institute, Amsterdam, NETHERLANDS, [9]Ospedale San Raffaele, Milano, ITALY.

Purpose: Safety of sentinel lymph node (SLN) biopsy for breast cancer during pregnancy is insufficiently explored. We investigated efficacy and local recurrence rate in a large series of pregnant patients. **Methods:** Women diagnosed with breast cancer who underwent SLN biopsy during pregnancy were identified from the INCIP (International Network on Cancer, Infertility and Pregnancy), the GBG (German Breast Group) and the Cancer and Pregnancy Registry. Chart review was performed to record technique and outcome of SLN biopsy, loco-regional and distant recurrence and survival. **Results:** We identified 145 women

with clinically N0 disease who underwent SLN during pregnancy. The SLN detection techniques were as follows: ^{99m}Tc-labeled albumin nanocolloid-only (n=96; 66.2%), blue dye-only (n=14; 9.7%), combined technique (n=15; 10.3%), or unknown (n=20; 13.8%). Mapping was unsuccessful in one patient (%) and she underwent an axillary lymph node dissection (ALND). Mean number of SLN's was 3.2 (range, 0-22; missing n=15). Positive SLN's were found in 43 (29.7%) patients and 34 subsequently underwent ALND. After a median follow-up of 48 months (range, 1 to 177), 123 (84.8%) patients were alive and free of disease. 11 patients experienced a loco-regional relapse, including 1 axillary recurrence (0.7%). 11 (7.6%) patients developed distant metastases, of whom 9 (6.2%) died of breast cancer. No neonatal adverse events related to SLN procedure during pregnancy were reported. **Conclusions:** SLN biopsy during pregnancy has a low axillary recurrence rate comparable to SLN in non-pregnant women. Therefore, this method can be considered during pregnancy instead of standard ALND for early stage, clinically node negative breast cancer.

EP-0533

68Ga-PSMA PET-CT in the evaluation of Metastatic Breast Cancer

S. S. Medina Ornelas, F. O. García-Pérez; Instituto Nacional de Cancerologia, Mexico City, MEXICO.

Background: Selective inhibition of angiogenesis is a key strategy in breast cancer. This process requires early identification when first-line therapy fails. Current research indicates that PSMA is related to angiogenesis of many solid tumors. However, studies are limited in the use of this agent in metastatic breast cancer. The purpose of this study is demonstrate PSMA expression in tumor neovasculature of primary and metastatic breast cancer sites, to assess the potential use as theragnostic agent, regardless of the hormonal status and histology. **Methodology:** Eleven patients of our institution with breast cancer were studied. 3 patients estrogen receptors and progesterone (+), 2 patients estrogen and progesterone (-), 3 patients were Her-2neu (+), and 3 patients Her-2neu (-). Metastatic to bone confirmed by bone scintigraphy were evaluated by PET-CT with 68Ga-PSMA one month prior to receiving QT cycle; the purpose of assess the degree of avidity of metastatic lesions, under the hypothesis of the neovasculature of the tumor microenvironment of metastasis in breast cancer. **Results:** Of the eleven patients evaluated similar uptake patterns were obtained in 3 of them: Four patients with Infiltrating ductal carcinoma; ki-67 70%, Her-2 (+); multiple bone metastases were observed and primary lesion; Three patients with infiltrating ductal carcinoma; ki-67 30%, Her-2 (-) multiple bone metastases were observed; Two patients with Invasive lobular carcinoma; ki-67 5% Her-2 (-); not greedy bone metastases were observed PSMA, but two liver metastases unsuspected; One patient with Invasive lobular carcinoma; ki-67 5% Her-2 (+); not greedy bone metastases, but brain only metastases seen were observed by PSMA; One patient with Infiltrating ductal carcinoma; ki-67 70%, Her-2 (+); only two metastases were observed and primary lesion. **Conclusion:**

Expression levels in tumor neovasculature PSMA differ between the primary site and metastasis. Our study showed expression of PSMA in metastatic sites were observed in 100%. A PET / CT with 68Ga-PSMA demonstrating metastatic disease can help in the selection of tumors with high expression of PSMA to provide targeted therapy with 177 Lu-PSMA, particularly in patients with invasive ductal carcinoma regardless of the status of the Her-2neu, with failure to second-line treatment

EP-0534

Clinical Experience of a dedicated Breast PET and Whole Body PET / CT for Breast imaging with F-18 FDG

K. Uno[1], H. Sasamori[1], J. Wu[1], M. Irie[1], T. Nakajima[1], Y. Akiba[1], Y. Tsuchiya[1], N. Baba[2]; [1]gaienhigashi clinic, Tokyo, JAPAN, [2]Tokyo kyousai Hospital, Tokyo, JAPAN.

Purpose: The aim of this study is to compare the performance of a dedicated breastPET (dbPET) with its of whole body PET/CT (WB-PET/CT) in patients with newly diagnosed breast cancer. **Subjects and Methods:** We introduced a dbPET with ring-shaped scanner (MAMMI, Oncovision co. Spain) to using for detection and diagnosis of breast cancer. We compared the images obtained by prone position between dbPET and WB-PET/CT (Biograph 16 truePoint, Siemens.co. Germany). A total of 76 Japanese women(mean age at 52 years) with histologically proven breast lesions were retrospectively enrolled. Patients were administered 3.5~4.0MBq/kg of F-18 fluorodeoxyglucose (FDG) intravenously, and 60min and90min after injection WB-PET/CT and dbPETimages were acquired, respectively. Primary tumor detection was assessed and FDG uptake was calculated as maximum standardized uptake value (SUVmax). **Results:** In our data, dbPET was able to visualize the tumor in more detailed than WB-PET / CT. There was positive correlation of SUV values between them and it was confirmed that the SUV value of dbPET was about twice higher than that of WB-PET / CT. Whereas, dbPET (54/76, 71%) is less detected tumors compared to WB-PET/CT (67/76, 88.2%). Base on breast imaging, our findings were classified into the following patterns: 1) similarly evaluated by dbPET and WB-PET/CT: 51 (67.1%): 2) Positive findings, could not be detected on WB- PET/CT, was visualized with dbPET 3 (3.9%): 3) dbPET image able to visualize tumor shape in more detail and examined up to daughter nodule 6 (7.9%): 4) Positive findings, shown on WB-PET/CT but abnormality could not be detected in dbPET 16 (21.1%). **Conclusion:** Our results suggest dbPET is useful for detailed analysis of breast cancer lesions. However, there was a limitation to demonstrate the primary tumors in the vicinity of the thoracic wall. It is necessary to consider for usefulenss both dbPET and WB-PET/CT for detection of breast cancer.

EP-0535

Clinical value of prone position ^{18}F-FDG PET/CT and MRI for predicting nipple-areolar complex involvement in breast cancer

J. Yoo, B. Kim, J. Chung, H. Yoon; Ewha Womans University School of Medicine, Seoul, South Korea, Seoul, KOREA, REPUBLIC OF.

Purpose: We aimed to evaluate the predictive value of prone positioned dual time point (DTP) ^{18}F-FDG PET/CT for identifying malignancies involved in the nipple-areolar complex (NAC) in breast cancer patients. **Methods:** We enrolled 66 patients who underwent preoperative DTP PET/CT and magnetic resonance imaging (MRI) between October 2015 and February 2017. We calculated the NAC-Standard Uptake Value (SUV) ratio using the following formula: maximum SUV (SUV_{max}) of the NAC in the malignant breast /SUV_{max} of the NAC in the contralateral normal breast on early (NAC-SUV_{early}) and delayed (NAC-SUV_{delay}) phase images. MRI was used to measure the distance between the tumor and the NAC and to analyze NAC enhancement patterns. Univariate and multivariate analyses were performed to determine the significant predictive factors for NAC involvement. **Results:** Twelve patients were confirmed to have pathologic NAC involvement. NAC symptoms, NAC-SUV_{delay}, MRI-based tumor-to-NAC distance, and linear enhancement to NAC were independent predictable factors for NAC involvement (all p < 0.05). Combined criteria for each MRI feature and NAC-SUV_{delay} increased the predictive accuracy for NAC involvement from 69.7% to 90.9% and from 72.7% to 87.9%, respectively. **Conclusions:** Delayed prone ^{18}F-FDG PET/CT is complimentary to MRI for evaluation of pathologic NAC involvement in breast cancer patients. Acknowledgements: This research was supported by grants from the National Research Foundation (2015R1C1A1A02037051, 2012M3A9B6055379, 2015R1C1A2A01054113) of South Korea.

EP-0536

Comparison of 18 F FDG PET CT and tumor marker findings in advanced breast cancer patients with progression

E. E. Bayar[1], E. Ö. Gür[2], G. G. Bural[1]; [1]Katip Çelebi University Atatürk Training and Research Hospital, Department of Nuclear Medicine, Izmir, TURKEY, [2]Katip Çelebi University Atatürk Training and Research Hospital, Department of General Surgery, Izmir, TURKEY.

Purpose: F-18 FDG PET/CT is an effective and accurate imaging modality in the evaluation of response to treatment in breast cancer. Also serum markers are the only validated approach for monitoring treatment in patients with advanced disease. Our aim was to compare F-18 FDG PET/CT and tumor markers in patients with advanced breast cancer. **Method:** 49 subjects (47 female; 2 male) ages 30-78 years, with metastatic breast cancer who had a PET/CT scan before and after chemotherapy and had progression on PET CT findings after chemotherapy were involved in this retrospective study. F-18 FDG PET/CT images before and after treatment were evaluated and compared with Ca15.3 tumor marker levels. **Results:** Initially all patients had distant metastases and after comparison between pre and post chemotherapy PET/CT images all showed progression after treatment. In 30 subject with 49 progression patient new metastatic lesions were detected (% 61). In 49 subject with progression 25 had increase in Ca 15.3 level (% 51) but 24 had normal tumor marker levels pre and post- treatment. In 30 subjects with new metastatic disease 18 had increase in Ca 15.3 levels (%60)

and in 12 tumor markers were with in normal limits (%40) pre and post- treatment. **Conclusion:** F-18 FDG PET/CT is an effective imaging modality in evaluating response to chemotherapy in the detection of progression or regression of metastases. It can also evaluated the whole body in single session and can detect new metastases. However tumor markers were unable to detect progression of disease in % 49 of patient who showed progression on F-18 FDG PET/CT. It is not possible to decide on treatment based solely on the increase in tumor marker level.

EP-0537

Prediction of breast tumor response to neoadjuvant chemotherapy through quantitative 99mTc sestamibi Molecular Breast Imaging (MBI)

S. C. Kappadath, B. Lopez, B. Adrada, K. Hess, G. Rauch; UT MD Anderson Cancer Center, Houston, TX, UNITED STATES OF AMERICA.

Purpose: To characterize 99mTc-sestamibi uptake by invasive breast cancers using novel quantitative metrics in Molecular Breast Imaging (MBI) and to assess their potential to predict tumor response in a pilot study of patients undergoing neoadjuvant chemotherapy (NAC). **Materials and Methods**: In a prospective IRB-approved clinical trial, patients with invasive breast cancer (T1-T4, N0-N3, M0) were imaged with MBI (99mTc-sestamibi 296 MBq injected activity, CC and MLO views) at baseline (T0), after 2 cycles (T1), and at the completion of NAC (T2). Following NAC, patients underwent surgery to determine pathologic response. Three quantitative metrics of 99mTc-sestamibi uptake were calculated in physician-drawn regions of interest (ROI) following novel scatter and attenuation correction. [1] Tumor-to-Background Ratio (TBR) = (Tumor Counts/Area) / (Background Counts/Area). [2] Fractional Activity Uptake (FAU) = (Tumor Uptake) / (Administered Activity), where Tumor Uptake = (Tumor Counts / System Sensitivity). [3] MBI-specific Standardized Uptake Value (SUV) = (Tumor Uptake / Volume) / (Administered Activity) / (Patient Weight). The clinical range, correlations, and changes observed in these novel MBI metrics were quantified. ROC analysis was performed to assess each metric's ability to predict complete pathologic response (pCR). **Results**: Analysis was performed on 25 enrolled patients (median age 49 years, range 31-77). Clinical ranges of the metrics (reported as the median and 2.5%-97.5% quantile values) across all time points and views were: TBR = 3.19 (0.63-14.47), FAU = 2.80e-4 (1.06e-5 - 4.81e-3), and SUV = 1.57 (0.31-6.69). The median values of all 3 metrics in all patients decreased significantly (p<0.01) with NAC, i.e., between T0 and T2. TBR change was negatively correlated with tumor area (r =-0.35, p<0.001) but not with breast thickness. 11 of 25 (or 44%) patients had pCR. Absolute TBR values at T1 and T2 and relative SUV difference between T2 and T0 were most predictive of pCR. TBR at T1 had an AUC=0.81 (p=0.01, 95%CI 0.63-0.99) and TBR at T2 had an AUC=0.78 (p=0.015, 95%CI 0.59-0.97). Change in SUV between T2 and T0 had an AUC=0.80 (p=0.02, 95%CI 0.60-1.00). **Conclusion**: Quantitative tumor uptake metrics in clinical MBI show initial promise as early, non-invasive predictors of complete pathological response in breast cancer patients undergoing neoadjuvant chemotherapy. Further investigations on the differenti-

ation of MBI metrics between responders and non-responders is underway as patients continue to enroll and complete participation in the on-going clinical trial.

EP-0538

Contribution of Morphologic Assessment of Axillary Lymph Nodes to the Staging of Invasive Lobular Breast Cancer in FDG PET-CT Imaging

S. Yıldız[1], A. Yıldız[2], M. Özdoğan[3], B. Özcan[4], A. Özlük[4], S. Yılmaz[5]; [1]Department of Radiology, SBU Antalya Education and Research Hospital, Antalya, TURKEY, [2]Department of Nuclear Medicine, Medstar Hospital, Antalya, TURKEY, [3]Department of Medical Oncology, Medstar Hospital, Antalya, TURKEY, [4]Department of Surgery, Medstar Hospital, Antalya, TURKEY, [5]Department of Radiology, Medstar Hospital, Antalya, TURKEY.

Purpose: Invasive lobular breast cancer (ILBC) is a relatively rare breast cancer type with a rate of 10-15%. Metabolic activity is usually low in FDG PET-CT examination. This study investigated the contribution of axillary evaluation that is performed with metabolic and morphological data at preoperative stage to the diagnosis in patients with ILBC diagnosis. **Subjects and Methods:** Thirty cases, which were examined for the purpose of preoperative staging and diagnosed with early stage ILBC between January 2012 and December 2016, were assessed retrospectively. Bilateral ILBC was diagnosed in 1 of the cases and a total of 31 axilla were evaluated. Axillary evaluation was performed with sentinel lymph node in 14 cases, core needle biopsy in 2 cases, axillary dissection in 17 cases and with histopathological study. In addition to metabolic activity, the contribution of CT images to assessment was investigated. Morphologically, the presence of at least one of the findings of diffuse or asymmetric cortical thickening, size, contour irregularity and the loss of fatty hilum was interpreted to be pathological. Late images were obtained in prone position at the 2nd hour after standard PET-CT metabolic activity measurements were repeated. **Results:** Axillary lymph nodes were reactive in 10 patients and metastatic in 21 patients in the histopathological assessment. Sensitivity and specificity were found as 95%, 81.8% only with morphological assessment; when the threshold value was taken as SUVmax: 2, they were found as 60%, 81.8%, respectively. When the lymph node showing a late metabolic increase was taken as metastatic, sensitivity was 25% and specificity was 63.6%. The best values in ROC analysis were found as 1.55 for the early SUVmax (area under the curve: 0.82), sensitivity: 85%. When morphology and metabolism were interpreted with general assessment findings together, a patient with a sarcoid reaction was correctly identified and the sensitivity was found as 85% and the specificity was found as 90.9%. Statistically significant difference (p = 0.004) was found when the SUVmax values of the reactive and metastatic cases were compared, however there was no significant difference in size and cortical thickness of the lymph nodes (p = 0.16). **Conclusion:** Morphological evaluation in PET-CT provides important contribution to the detection of axillary metastasis in ILBC. Late imaging is not useful for this purpose. However, further studies are necessary with higher number of cases.

EP-0539

Value Of 18F-FDG PET/CTIN Locally Advanced Breast Cancer Patiens Treated With Neoadjuvant Chemotherapy

I. Acevedo Báñez, R. Fernandez Lopez, A. Bonilla Damia, L. Caballero Gullón, F. Frutos Arenas, L. Alfaro Galan, A. Montaño Periañez, B. Vieites Perez-Quintela, I. Borrego Dorado; *Hospital Universitario Virgen Del Rocio, Sevilla, SPAIN.*

Aim: To assess the use of 18F-FDG PET / CT in initial locoregional staging and in the evaluation of the response to treatment of locally advanced breast cancer patients treated with neoadjuvant chemotherapy. **Material and Methods:** We analyzed prospectively 35 women with an average age of 52 years (range:28-73) diagnosed of breast carcinoma who underwent neoadjuvant chemotherapy. Stages at diagnosis were: IIA (7 patients), IIB (13), IIIA (6), IIIB (7) and IIIC (2). All patients were performed conventional morphological study (ultrasonography, mammography and MRI) as well as 18F-FDG PET/CT for initial staging (PET1), early evaluation after 2 cycles of chemotherapy (PET2) and final evaluation to chemotherapy treatment before surgical intervention (PET3). The concordance of the different diagnostic techniques in the locorregional staging of primary tumor was correlated. SUVmax of primary tumor was calculated in different PET studies and correlated with histopathological characteristics of the tumor. Anatomopathological response was classified according to RCB index (residual cancer burden) and regrouped considering as responders to groups 0, I and II, and as non-responders to III. A ROC analysis was performed to obtain a cut-off value of Δ%SUVmax that was useful in the prediction of type of responses. **Results:** Concordance between conventional morphological techniques and PET1 in local tumor staging was moderate with a weighted kappa index of 0.56 and 0.5 in case of PET3. There was no statistically significant relationship between SUVmax, hormone status, HER-2 and molecular subtypes, but a significant relationship with Ki-67 (p = 0.03) was detected. In the analysis of ROC curves, a Δ%SUVmax ≥ 69.89 between PET1 and PET3 allowed the differentiation between non-responder and responders with sensitivity, specificity, PPV, NPV and accuracy of 71.4%, 61.5%, 33,3%, 88.9% and 63.6%, respectively. Whereas a Δ%SUVmax ≥ 52.97% between PET1 and PET2 showed results of 66.7%, 52.2%, 26.7% 85.7% and 55.2%. **Conclusion:** 18F-FDG PET/CT is a useful tool to evaluate response to treatment in breast cancer patients allowing the early distinction between responder and non-responder patients. A statistically significant relationship between tumor uptake and Ki-67 proliferation index was observed, not being related to other histopathological features. There was also a moderate concordance between 18F-FDG PET/CT and conventional morphological techniques in locorregional staging, so both techniques are not exclusive.

EP-0540

Diagnosing recurrent breast cancer: Accuracy and interrater agreement of FDG-PET/CT and bone scintigraphy

Z. A. Farahani[1], J. Holm[1], C. Baun[1], K. Falch[1], O. Gerke[1], P. Hoilund-Carlsen[1], A. Alavi[2], **M. G. Hildebrandt**[1]*; [1]Odense University Hospital, Odense, DENMARK, [2]Department of Radiology, Perelman School of Medicine, Pennsylvania, PA, UNITED STATES OF AMERICA.*

Aim: To investigate the interrater agreement of FDG-PET/CT and bone scintigraphy for diagnosing distant and bone recurrence in breast cancer patients. **Material and Methods:** Prospectively, 100 women with suspected recurrence of breast cancer underwent planar whole-body bone scintigraphy (BS) with ^{99m}Tc-DPD and FDG-PET/CT, within a median time period of 3 days (Range: 0-24). Scans were evaluated independently by two experienced nuclear medicine physicians, Reader 1 (R1) and Reader 2 (R2); readers were also blinded to other test results. Images were visually interpreted using a 4-point assessment scale, and data were dichotomized (0/1 versus 2/3) for accuracy results. The reference standard was biopsy along with treatment decisions and clinical follow-up (median 17 months). Sensitivity, specificity, proportions of agreement, and Cohen's kappa values were calculated. **Results:** Of 100 patients, 22 (22%) were verified with distant recurrence and 18 of these had bone involvement. For distant recurrence the sensitivity and specificity of FDG-PET/CT was 100% (95% confidence interval: 85.1-100) and 91.0% (82.6-95.6) for R1, and 100% (85.1-100) and 93.6% (85.9-97.2) for R2, respectively. For bone recurrence the sensitivity and specificity of FDG-PET/CT was 100% (82.4-100) and 97.6% (91.5-99.3) for R1, and 100% (82.4-100) and 96.3% (89.8-98.7) for R2, while the sensitivity and specificity of BS was 77.8% (54.8-91.0) and 86.6% (77.6-92.3) for R1, and 77.8% (54.8-91.0) and 90.2% (81.9-95.0) for R2, respectively. The proportions of agreement between readers were 80% for distant recurrence and 93% for bone recurrence with FDG-PET/CT, while it was 47% with BS. The strengths of agreement between readers with FDG-PET/CT was 'substantial' for diagnosing distant recurrence and 'almost perfect' for diagnosing bone recurrence according to Cohen's kappa values of 0.65 (0.52-0.78) and 0.82 (0.70-0.95), respectively. The agreement between readers with BS was 'fair' with a Cohen's kappa value of 0.28 (0.18-0.39). **Conclusion:** The agreement between readers was significantly higher for FDG-PET/CT than for BS when diagnosing bone recurrence. With high values of sensitivity and specificity for FDG-PET/CT, higher than those for BS, our results indicate that FDG-PET/CT should be preferred when examining distant and/or bone recurrence in breast cancer patients.

EP-0541

Prognostic Value Of Initial 18F-FDG PET/CT IN ER+/HER2- Locally Advanced Breast Cancer Patients

M. Martinez de Bourio, A. Jiménez-Ballvé, O. Salsidua-Arroyo, A. Serrano-Palacio, M. García García-Esquinas, C. Rodríguez Rey, A. Ortega Candil, J. A. García-Sáenz, M. E. Fuentes Ferrer, J. L. Carreras Delgado; HOSPITAL CLINICO SAN CARLOS, MADRID, SPAIN.

Objective: To evaluate the prognostic value of PET/CT volumetric parameters, such as metabolic tumour volume (MTV) and total lesion glycolysis (TLG), compared to Standardized Uptake Value (SUVmax), in the initial staging PET/CT of patients with ER+/HER2- locally advanced breast cancer (LABC). **Ma-**

terials and methods: Retrospective study including 72 ER+/HER2- LABC women from January/2010 to July/2013 (follow-up until December/2016).[18]F-FDG PET/CT scan for initial staging was performed prior neoadyuvant treatment. We analyzed the following metabolic parameters: SUVmax, MTV and TLG in the primary tumour and in all lesions (sum of the primary tumour and lymph node metastases). **Results:** The median follow-up was 62.9 months. Only 11.1% (8/72) of them presented recurrence: local disease (n=1), distant metastases (n=6) and both (n=1), and 2.8% (2/72) died, all of them presenting recurrence. SUVmax and TLG in both primary tumour (T) and in all lesions (WB) were higher in those patients with recurrence, compared to those without recurrence (p=0.005 and p=0.026 in T; p=0.007 and p=0.034 in WB, respectively). We also observed that MTV and TLG values in both T and WB were higher in patients who died, despite the small size of patients who did not survive. In the ROC curve analysis, we obtained an area under the curve (AUC) for T SUVmax 0.805 (CI: 0.695-0.915) and for WB SUVmax 0.795 (CI: 0.662-0.928). The best cut-off values for SUVmax in the primary tumour and SUVmax in all lesions to predict recurrence were ≥ 10.1 (sensitivity 75% and specificity 80%) and ≥ 15.7 (sensitivity 63% and specificity 78 %), respectively. **Conclusions:** SUVmax in primary tumour and in all lesions could be a useful parameter in order to predict recurrence risk in ER+/HER2-locally advanced breast cancer patients. TLG could also be a good predictor, however a larger sample size is needed in order to define a cut-off value and to assess its effect on the recurrence rate.

EP-0542

Successful Diagnosis of a CT-Negative, Bone Scintigraphy-Negative and FDG-PET-Negative Metastatic Recurrence Case Using ER-Targeting 4FMFES-PET

M. Paquette, É. Lavallée, S. Phoenix, H. Senta, J. E. van Lier, R. Lecomte, B. Guérin, É. E. Turcotte; Université de Sherbrooke, Sherbrooke, QC, CANADA.

Introduction: A 58 years old woman was diagnosed 11 years earlier with a T1N0M0 breast adenocarcinoma. A mastectomy was conducted, followed by a multi-chemotherapy treatment with a 5-year adjuvant tamoxifen therapy. The breast area was also irradiated with 25 fractions of 2 Gy each. The patient was followed yearly with bone scintigraphy, and has since been considered in complete remission. Eighteen months ago, the patient showed vague clinical signs of recurrence, including lower body lymphedema, inguinal pain and slight ocular problems. Considering the history of the patient, a series of extensive examinations was carried out to detect a possible recurrence. **Subjects & Methods:** The patient was enrolled in a clinical phase II study aiming at evaluating the novel estrogen receptor (ER) targeting agent 4-fluoro-11β-methoxy- 16α-[18F]-fluoroestradiol (4FMFES). Meanwhile, a CT scan was first obtained, followed by a bone scintigraphy exam. Further investigation was conducted and FDG-PET was performed one week prior the experimental 4FMFES-PET scan. **Results:** CT exam was overall within normal range, with no clear sign of oversized lymph

nodes or osteoblastic process. Bone scintigraphy was negative, with the exception of an inflammatory process in the cervical area. FDG-PET revealed a few ubiquitous foci in breast nodes and the mediastinal area, with the rest of the exam within normal range. So far, in the light of those standard evaluations the patient was still considered in complete remission, in contradiction with recent clinical signs. Further assessment using 4FMFES-PET revealed, in stark contrast with previous examinations, an extensive metastatic burden which included a retroorbital lesion, and multiple neck, mediastinal and inguinal foci. The latter were biopsied, and pathology report confirmed the presence of ER+/PR+/HER2- lobular carcinomas. Following this finding, a taxol treatment along with palliative inguinal radiotherapy was conducted. Six months later, FDG and 4FMFES PET scans were obtained to follow-up the therapy response. Unsurprisingly, FDG-PET returned negative, whereas 4FMFES-PET showed a significant reduction of the inguinal burden following radiotherapy, along with an apparent partial response in the mediastinal and neck region resulting from the chemotherapy protocol, in concordance with the overall improvement reported by the patient. **Conclusion:** The case presented here has been completely misdiagnosed using standard procedures. Opportune 4FMFES PET imaging allowed adequate patient management and therapy follow-up. The ongoing phase II study shows excellent complementarity between 4FMFES-PET and FDG-PET in breast cancer management.

EP-0543

Contribution Of 18FDG PET-CT For Staging And Prognosis Of Primary Breast Neuroendocrine Carcinoma

E. Arslan[1], T. Cermik[1], F. Can Trabulus[2], E. Kelten Talu[3]; [1]İstanbul Health Science University Education and Research Hospital Clinic of Nuclear Medicine, İstanbul, TURKEY, [2]İstanbul Health Science University Education and Research Hospital Clinic of General Surgery, İstanbul, TURKEY, [3]İstanbul Health Science University Education and Research Hospital Department of Pathology, İstanbul, TURKEY.

Aim: Primary neuroendocrine carcinomas (NEC) of the breast are rare tumors (1% of all breast carcinomas). Their clinical course, except for small cell subtypes, has better prognoses compared to the frequently observed breast malignant tumors. In this retrospective study, fluorodeoxyglucose positron emission tomography-computed tomography (FDG PET-CT) findings in patients diagnosed with primary breast NEC were evaluated comparatively with findings from invasive ductal carcinoma (IDC). **Materials and Methods:** Data from 481 malignant lesions were obtained from a total of 481 cases (age, mean ± SD: 54.77 ± 13.06) diagnosed with breast cancer between March 2009 and February 2017. Primary neuroendocrine breast cancer was detected in 12 cases, while primary NEC was detected in a total of 14 lesions in the breast. Two of them were bilateral. IDC was detected in 377 out of the 472 cases. IDC was compared with the SUV$_{max}$ values, which were semiquantitative data obtained from the primary tumors in the PET-CT imaging of primary breast NEC for staging purposes. In addition, the

presence of lymph node metastasis and distant organ metastasis was retrospectively reviewed. **Results:** A total of 481 lesions were detected in 472 breast cancers patients. In twelve of patients, primary NEC of the breast had a total of 14 lesions (mean ± SD SUV_{max} values: 9.95 ± 4.6), IDC was detected in 377 lesions (mean ± SD SUV_{max} values: 11.78 ± 8.33). Axillary lymph node metastases were detected in 6(50%) of the 12 NEC-diagnosed patients. While distant metastases were detected in 3(25%) cases. Axillary lymph node metastasis was detected in 247 (65%) of the 377 cases diagnosed with IDC. Distant metastases were detected in 84 (22%) cases diagnosed with IDC. **Conclusion:** FDG PET-CT findings of the rare primary breast neuroendocrine tumor and the most common invasive ductal carcinoma were presented in this study. It has been previously reported in the literature that the SUV_{max} value of rare subtypes is significantly lower than that of invasive ductal carcinoma. In this study, we determined that the rate of lymph node metastasis was also lower in patients with NEC compared to IDC, which is consistent with previous reports. There was no significant difference on the rate of the presence of distant metastasis between the two tumor types.

EP-0544

18F FDG PET-CT To Stage And Determine Rarely Seen Apocrine Type And Basal Like-Triple Negative Breast Adenocarcinoma

E. Arslan[1], T. Cermik[2], F. Can Trabulus[3], E. Kelten Talu[4]; [1]İstanbul Health Science University Education and Research Hospital, İstanbul, TURKEY, [2]İstanbul Health Science University Education and Research Hospital Clinic of Nuclear Medicine, İstanbul, TURKEY, [3]İstanbul Health Science University Education and Research Hospital Clinic of General Surgery, İstanbul, TURKEY, [4]İstanbul Health Science University Education and Research Hospital Department of Pathology, İstanbul, TURKEY.

Aim: Apocrine type breast carcinoma is a rare, high-grade form of breast tumors and is defined as a subtype of invasive ductal carcinoma. The androgen receptor (AR) is expressed in apocrine type breast carcinoma, while the estrogen (ER) and progesterone receptors (PR) are negative similar to the basal like-triple negative (ER (-), PR (-), CerbB2 (-)) carcinomas. The frequency ranges from 0.3 to 1% and the triple negative subtype has been observed in 10-15% of the cases studied. Receptor status in breast cancer has been used as an important criterion for treatment selection and prognosis. In this study, FDG (fluorodeoxyglucose) PET-CT (Positron emission tomography-computed tomography) findings of apocrine type and basal like-triple negative breast carcinoma subtypes were retrospectively compared. **Materials and Methods**: Four hundred eighty one malignant lesions were detected from 481 breast cancers (age, mean ± SD: 54.77 ± 13.06) patients who were admitted to our clinic between March 2009 and February 2017. Twenty of the cases were diagnosed as apocrine subtype invasive ductal carcinoma and 42 were diagnosed as the triple negative subtype. Maximum standard uptake values (SUV_{max}), which are semi-quantitative data obtained from primary tumors, were compared in PET-CT

imaging for staging of apocrine type and basal like-negative type carcinomas. In addition, lymph node metastasis and distant metastasis were retrospectively screened. **Results:** Twelve of 20 patients diagnosed with apocrine type breast carcinoma were Cerb B2 (+) (mean±SD SUV_{max} values: 11.81 ± 6.54) and 8 patients were CerbB2 (-) (mean±SD SUV_{max} values: 13.89 ± 6.59). Axillary LN metastasis was found in 10 (83%) of 12 CerbB2 (+) cases and distant organ metastasis was observed in 1 (8%) case. Axillary lymph node metastasis was detected in 6 (75%) cases of a total 8 of Cerb B2 negative cases and distant metastasis was detected in 1 (12%) case. In addition, axillary lymph node metastasis was found in 33 (78%) of 42 basal like / triple negative cases. distant metastasis was detected in 6 cases (14%). **Conclusion:** In this study, F^{18}-FDG PET-CT findings of apocrine type and triple negative/basal type carcinomas were presented. There are few studies in the literature on this subject. Considering the significance of SUV_{max} between the subgroups according to the presence of the hormone receptor and the Cerb B2 oncogene, we put forth the notion that this determine value may aid in the management of the disease as well as prognosis.

EP-0545

Clinical Significance of Partial-volume Corrected SUVmax of Axillary Lymph Nodes suggesting Intraoperative Examination of Sentinel Lymph Nodes in Early Breast Cancer

S. Kang[1,2], S. Ha[1,2], H. An[1], J. Lee[1], G. Cheon[1,3], J. Park[4], W. Han[4], D. Lee[1], J. Chung[1], K. Kang[1]; [1]Department of Nuclear Medicine, Seoul National University Hospital, Seoul, KOREA, REPUBLIC OF, [2]Department of Molecular Medicine and Biopharmaceutical Sciences, Graduate School of Convergence Science and Technology, Seoul National University, Seoul, KOREA, REPUBLIC OF, [3]Seoul National University College of Medicine, Seoul, KOREA, REPUBLIC OF, [4]Department of Surgery, Seoul National University Hospital, Seoul, KOREA, REPUBLIC OF.

Introduction: Sentinel lymph node biopsy is a safety device to determine patients who have to undergo axillary lymph node dissection (ALND). However, according to recently reported study, complete ALND does not improve survival in patients with clinical T1-2 tumors with less than three metastatic lymph nodes followed by systemic therapy. Clinical significance of partial-volume corrected SUVmax of axillary lymph nodes on ^{18}F-FDG PET/CT that is able to predict three or more pathologic metastatic lymph nodes was investigated in patients with early breast cancer. **Methods:** The study group comprised 132 women patients with T1-2 invasive breast cancer who underwent pretreatment ^{18}F-FDG PET/CT and had surgical treatment. Maximum standardized uptake values (SUVmax), metabolic tumor volume (MTV), and total lesion glycolysis (TLG) were measured on ^{18}F-FDG PET/CT. Partial volume-corrected SUVmax (PVC-SUVmax) using the recovery coefficient method was also calculated. Parameters from other preoperative imaging, ultrasonography and contrast CT, were also extracted for analysis. Independent t-test and multivariate logistic regression were used to identify significant independent predictors of three or more metastatic

lymph nodes. **Results:** Of the 132 patients, 11 (8.3 %) had ≥ 3 lymph nodes, 21 (16 %) had 1-2 lymph nodes and 100 (76 %) were negative. PVC-SUVmax was significantly higher in patients with ≥ 3 lymph nodes than in those with < 3 lymph nodes (3.95 vs. 2.06; *P* = 0.003). High PVC-SUVmax of axillary lymph node was significantly associated with ≥ 3 lymph nodes (odds ratio, OR, 1.341; *P* = 0.012) in univariate analysis. In multivariate analysis with clinicopathologic factors and other imaging modalities, PVC-SUVmax (OR, 1.341; *P* = 0.012) was a significant independent predictor of three or more metastatic lymph nodes. **Conclusions:** High PVC-SUVmax on ^{18}F-FDG PET/CT was significantly associated with pathologic metastasis more than three lymph nodes. ^{18}F-FDG PET/CT may be a useful imaging modality to select patients who require intraoperative examination of sentinel lymph nodes in T1-2 early breast cancer.

EP-0546

Assessment of biological, clinical aggressiveness of invasive ductal breast cancer using baseline fluorine-18 fluorodeoxyglucose positron-emission tomography/computed tomography-derived volumetric parameters

G. Ege Aktas[1], E. Tastekin[2], A. Sarıkaya[1]; [1]Trakya University Medical Faculty Department of Nuclear Medicine, Edirne, TURKEY, [2]Trakya University Medical Faculty Department of Pathology, Edirne, TURKEY.

Objective: To evaluate the relationship of baseline fluorine-18 fluorodeoxyglucose positron-emission tomography/computed tomography (F-18 FDG PET/CT)-derived volumetric parameters for the primary tumor with clinicopathological risk factors and molecular subtypes in patients with invasive ductal breast carcinoma (IDBC). **Methods:** We evaluated 65 patients who underwent F-18 FDG PET/CT for initial BC staging. The association of maximum and mean standardized uptakes (SUVmax and SUVmean, respectively), metabolic tumor volume (MTV), and total lesion glycolysis (TLG) with clinicopathological risk factors and molecular subtypes was investigated and the discriminative power of significant features was assessed. **Results:** All volumetric parameters were significantly higher for tumors measuring >2 cm and exhibiting a Ki-67 index of ≥20. Estrogen receptor (ER) and progesterone receptor (PR)-negative (ER–/PR–), human epidermal growth factor receptor 2-positive (HER2+), and triple-negative (TN) tumors exhibited increased SUVmax. SUVmax and SUVmean were higher for TN and HER2+ IDBC than for ER+/HER2− IDBC (median SUVmax: 12.1, 11.2, and 6.9, respectively; median SUVmean: 7.5, 6.2, and 4.4, respectively). MTV and TLG showed no differences among subtypes. All volumetric parameters correlated with tumor size (SUVmax: r = 0.516, SUVmean: r = 0.496, MTV: r = 0.718, TLG: r = 0.828; p < 0.001 for all) and Ki-67 index; these correlations differed among the different subtypes. Patients with systemic metastases exhibited significantly higher TLG (median: 76.5 vs. 36.7, p = 0.04). Receiver operating characteristic analysis revealed that SUVmax had the highest discriminative power for the different subtypes (area under the curve (AUC), 0.782; p < 0.001), whereas TLG had a

statistically significant discriminative power for systemic metastasis (AUC: 0.644; p = 0.03). **Conclusions:** SUVmax may appropriately reflect the immunohistochemical characteristics of IDBC, while TLG is associated with clinical risk factors and systemic metastasis. Our preliminary findings suggesting different relationships between volumetric parameters and the clinical tumor size and Ki-67 index for different subtypes need further evaluation. **Key words:** positron-emission tomography, computed tomography, breast cancer, metastasis, TNM staging, standardized uptake value

EP-0547

[99mTc]-Sestamibi Molecular Breast Imaging (MBI) compared with digital mammography plus ultrasound in preoperative breast cancer detection: preliminary experience

S. Chiacchio[1], G. Angelini[2], D. Mazzotta[3], S. Muccioli[1], S. Caputo[1], D. Fontanelli[1], M. Gennaro[1], M. Roncella[3], C. Marini[3], D. Volterrani[1]; [1]Regional Center of Nuclear Medicine-Ospedale Santa Chiara, Pisa, ITALY, [2]Università di Pisa-Ospedale Santa Chiara, Pisa, ITALY, [3]Senology Unit-Ospedale Santa Chiara, Pisa, ITALY.

Aim: To compare the diagnostic performance of 99mTc-Sestamibi Molecular Breast Imaging (MBI) to digital mammography (DM) plus ultrasound (US) in a restrospective preliminary study. Material and **Methods:** We retrospectively enrolled 35 women (mean age: 62,3 ±11,6 SD), between January 2015 and February 2017, with 47 suspicious breast lesion after clinical examination, DM/US and core needle biopsy (CNB). They underwent MBI followed by pathologic analysis from surgical specimens or from CNB (in case of 2 benign lesions and 1 carcinoma, not operated for metastases). DM/US findings were categorized according to BI-RADS® and considered as positive with a BI-RADS® score greater than R4b/U4b. MBI was performed 10 minutes after i.v. injection of 296 MBq of 99mTc-Sestamibi by using cameras in semiconductor cadmium zinc telluride (CZT) for single photon planar imaging of the immobilized breast. MBI was interpreted in conjunction with DM/US and qualitatively evaluated as positive (focal moderate or marked increased uptake) or negative (completed negative or mild uptake). Chi square test, sensibility, specificity and Cohen's k coefficient were performed by using SPSS® 23. **Results:** We analyzed 35 patients, with a total of 47 breast lesions. Pathological correlation demonstrated 41 malignant foci of tumor (32 non special type carcinomas, 5 in-situ ductal carcinomas, 2 invasive lobular carcinomas, 1 invasive tubulo-lobular carcinoma and 1 mucinous carcinoma) and 6 benign lesions. Sensitivity and specificity of DM/US are 83.5% and 62.5%. Sensitivity and specificity of MBI are 87.8% and 50%. 0.4 is the value of Cohen's k coefficient for DM/US, showing a moderate agreement with histological results, while for MBI the value is 0.36. **Conclusions:** Our initial experience with MBI supports the use of this modality in addition to DM/US, especially when magnetic resonance may not be performed. Our data have shown a greater sensitivity of MBI than DM/US, in particular in case of small lesions (less than 1 cm). According to our results, MBI represents a useful technique to increase the detection rate

in preoperative assessment of multi-focal/centric breast cancer and sometimes it may contribute to change surgical management. t;1 cm).

EP-0548

Lymph node staging in primary breast cancer patients: supine FDG PET/CT compared to prone PET/CT, MRI and prone PET fused with MRI

M. J. Ribelles, M. Rodriguez, A. Fernadez-Montero, L. J. Pina, L. Sancho, E. Prieto, M. Santiesteban, N. Rodriguez-Spiteri, M. A. Idoate, F. Martinez-Regueira, A. Elizalde, M. J. Garcia-Velloso; Clinica Universidad De Navarra, Pamplona, SPAIN.

Purpose: To evaluate the diagnostic accuracy of prone FDG-PET/CT, against supine PET/CT, magnetic resonance imaging (MRI), and prone PET fused with MRI for the detection of lymph node metastasis in patients with newly diagnosed primary breast cáncer. **Subjects and Methods:** This retrospective study included 68 consecutive women, with 73 biopsy-proven invasive breast cancers. The mean age was 51.8 ± 10.2 years. FDG PET/CT scans with time-of-flight (TOF) and point-spread-function (PSF) reconstruction, prone PET/CT, and MRI were performed in all patients. A radiologist and a nuclear medicine physician independently examined the studies, and prone PET fused with MRI images were analyzed by consensus. Qualitative interpretation using a 4-point scale (0 = negative, 1 = questionable, 2 = moderately intense, and 3 = very intense) and semi-quantitative assessment of lymph nodes was performed using SUVmax when point-scale in PET/CT was equal or higher than "questionable". The data were analysed blindly, and histopathology and/or at least 1 year of follow-up served as the standard of reference. **Results:** There was histologically confirmed lymph node metastasis in 42(62 %) patients and 44 tumors. Sensitivity and specificity of prone PET/CT in the detection of axillary lymph node metastasis were 70.5% and 90%, respectively; whereas the values of supine PET/CT, MRI, and prone PET fused with MRI were 73% and 86%, 45% and 90%, and 70% and 79%, respectively. Prone and supine PET/CT had significantly higher accuracy than MRI (p&lt 0.05). The areas under the curve (AUC) for prone PET/CT, supine PET/CT, MRI and prone PET fused with MRI were 0.828, 0.826, 0.700, 0.761, respectively (p&lt 0.05), with statistically significant difference between both PET/CT modalities and MRI. PET/CT detected 10 additional extra-axillary locoregional lymph node metastasis in 7 patients (4 internal mammary), all of them were negative on MRI. Metastatic lymph nodes, axillary and extra-axillary, mostly presented with visual grade 2 (14 %) or 3 (73 %) and median (IQR) SUVmax were 0.6 (0.5-0.6) and 2.1 (1.2-8.2) respectively. FDG uptake in primary tumors with lymph nodes metastases (median SUVmax: 3.9; IQR: 2.4-6.5) was significantly higher than in tumors without lymph node involvement (median SUVmax: 2.3; IQR: 1.5-5.1, p&lt 0.05). **Conclusion:** PET/CT is more accurate than PET fused with MRI and MRI for initial lymph node staging in primary breast cancer patients. Prone PET/CT performed better than supine PET/CT. However, its low sensitivity is insufficient to replace histopathology for lymph node staging.

EP-0549

The Localization of Nonpalpable Suspicious Breast Lesions and Sentinel Lymph Node with Single Injection: Our SNOLL Experience

P. Arıcan[1], B. T. Okudan[1], G. Dağlar[2]; [1]Ankara Numune Hospital, Nuclear Medicine Clinic, Ankara, TURKEY, [2]Ankara Numune Hospital, General Surgery Clinic, Ankara, TURKEY.

Aim: Nowadays the development of breast imaging methods has increased the number of non-palpable suspicious breast lesions. These susceptible lesions have excisional biopsy indication. Operation technique is planned according to localization of lesion and sentinel lymph nodes (SLN) hence it is important to localize suspicious lesions precisely before operation. Nowadays, wire localization is the gold standard for intraoperative tumor localization. Radio guided occult lesion localization (ROLL) as a new method for the localization of nonpalpable breast lesions has been developed in recent years. SLN biopsy is used to evaluate axillary lymphatics in early stage breast cancer. The combination of both ROLL and SLN biopsy within the same surgical session is described as Sentinel Node Occult Lesion Localization (SNOLL). The aim of this retrospective study was to evaluate the contribution of SNOLL technique in the localization of both nonpalpable suspicious breast lesions and SLN before operation. Materials and **Methods:** Thirty nine patients (19-77 yrs) with suspicious ultrasonography and mammography who were not detected by physical examination were included in this study. Four to six hours before operation, 0.3 μCi / 0.2 mL Tc-99m nanocolloid was injected intratumorally in all patients under ultrasonography guidance. Preoperative lymphoscintigraphy was performed as planar and thoracic SPECT/CT imaging following injection after 15 and 120 minutes. According to images Lesion and if present SLN were removed guided by intraoperative gamma probe (IGP) during the surgery. Histopathologic examination of resected tumor and lymph node were performed. It was considered to be a negative disease if the nearest distance between the surgical margin and tumor tissue was at least 1 mm. **Results:** The lesion was totally excised in all 39 patients with IGP. Eleven invasive ductal carcinoma, one ductal carcinoma in situ and 28 benign pathologies were detected histopathologically. The mean size of the lesions was 21.5 mm ± 16 (5-38 mm). The closest surgical border in 38 patients was negative and infiltrated with tumor in one patient. SLN was detected in 31 of 39 patients (79.4%) with planar images and SPECT/CT. In 12 patients with malign pathologies, SLN was excised with IGP. Two (1.6%) patients with metastases had axillary dissection. **Conclusion:** SNOLL is a simple, noninvasive and effective technique that enables an intraoperative localization of nonpalpable suspected breast lesions in combination with a SLN biopsy. In this study, we have experienced that both non-palpable breast lesion and SLN localization can be successfully performed with a single radiopharmaceutical injection.

EP-0550

Role of (18)F-3'-deoxy-3'-fluorothymidine (18F-FLT) PET/CT in early prediction of response in patients with breast

cancer (BC) treated with neoadjuvant chemotherapy (NCT): preliminary results

L. Fantini[1], A. Fedeli[1], P. Caroli[1], M. Celli[1], A. Rocca[1], A. Moretti[2], R. Galassi[2], M. Dall'Agata[1], P. Serra[1], G. Paganelli[1], F. Matteucci[1]; [1]IRST IRCCS, Meldola (FC), ITALY, [2]Morgagni-Pierantoni Hospital, Forli' (FC), ITALY.

Background and Aim: 18F-FLT is a thymidine analogue used as a cell proliferation tracer: its cellular uptake reflects thymi-dine-kinase-1 activity (TK1). Clinical studies showed a significant FLT uptake reduction in human BC cells after only 3 days from the first NCT administration. Our purpose is to evaluate 18F-FLT-PET/CT role in early NCT response. **Materials and Methods:** We studied 15 patients (pts) with operable (T>2cm, cT2-3, N0-N2, M0) or locally advanced potentially operable BC (T4, N0-N2, M0), with HER2 over-expression or amplification undergoing chemo-therapy (6 cycles of doxorubicin encapsulated with liposomes plus docetaxel plus trastuzumab plus Metformin). 18F-FLT-PET/CT was performed 50 minutes after 100-200 MBq 18F-FLT in-travenous injection, before the NCT beginning (FLT1) and in the days immediately prior to the second NCT cycle (FLT2). All patients underwent surgery within 2-4 weeks of NCT end and histopathological findings were correlated with 18F-FLT-PET/CT results. **Results:** 14 pts performed both FLT1 and FLT2 and 1 was excluded from the study for metastatic lesions comparison. In 7 pts FLT1 was positive only at breast (M+), while in 7 there were lesions both at breast and in axillary lymph-nodes (M+N+). FLT2 was negative in 4 patients (2M+ and 2M+N+ at FLT1), while in 10 pts FLT2 was positive at breast in 7 (4M+ at FLT-1 and 3M+N+ at FLT1); specifically, the 4 pts M+ to FLT1 showed a SUV reduction of 29% (range 9-49), while in 3 M+N+ at FLT1, FLT2 show a complete disappearance of lymph-node uptake and reduced in breast (SUV decrease of 49%). In 3 pts, FLT2 re-sulted positive both at breast and lymph-node level: in partic-ular in 2M+N+ at FLT1, a stable uptake was observed at both level, while 1 pt showed a progression disease at lymph-node. Histopathological findings resulted completely concordant with FLT2 results in 9 pts (64%): 4 with FLT2 negative, 4 with only residual disease in breast and in 1 with positive FLT2 both in breast and lymph-node. In 2 pts, histopathological findings resulted partially concordant with FLT2: 1 had FLT2 and breast positive histology, but false-positive lymph-nodes at FLT2. In 1 with FLT2 negative, histopathological analysis showed lymph-nodes disease. In 3, histopathology findings are completely dis-cordant with FLT2 both at primary lesion and lymph-nodes: 1 pt resulted false positive in FLT2 and in 2 pts FLT2 resulted falsely negative. **Conclusion:** Our preliminary study suggests FLT-PET/CT potential utility to predict early NCT response; however fur-ther studies are needing.

EP-0551

Myocardial perfusion defects after radiation therapy for left-sided breast cancer:is stress study necessary?

M. Amoui[1], D. Askari[2], M. Bakhshandeh[2], H. R. Mirzaee[3], S. Saifollahi[4], M. Malekzadeh[3], E. Pirayesh[1], M. Pishgahi[5], A. Rakhsha[3], S. Azghandi[3], P. Hajian[3], A. Yousefi Kashi[3], M. Hoshiari[3], M. Mosavizadeh[3]; [1]Department of Nuclear Medicine, Faculty of Medicine, Shahid Beheshti University of Medical Sciences, Tehran, IRAN, ISLAMIC REPUBLIC OF, [2]Department of Radiology Technology, Faculty of Allied Medical Sciences, Shahid Beheshti University of Medical Sciences, Tehran, IRAN, ISLAMIC REPUBLIC OF, [3]Department of Radiation therapy, Faculty of Medicine, Shahid Beheshti University of Medical Sciences, Tehran, IRAN, ISLAMIC REPUBLIC OF, [4]Department of Nuclear Medicine; Arad Hospital, Tehran, IRAN, ISLAMIC REPUBLIC OF, [5]Department of Cardiology; Faculty of Medical Sciences, Shahid Beheshti University of Medical Sciences, Tehran, IRAN, ISLAMIC REPUBLIC OF.

Purpose: Radiation-induced cardiovascular damage (RICD) has been reported in some studies for left-sided Breast cancer, prominently by rest Myocardial Perfusion Imaging (rest-MPI). This prospective study was planned to evaluate various scinti-graphic patterns in stress-rest MPI after completion of radiation therapy (RT) by modern breast RT techniques. **Materials and Methods:** Stress/rest MPI with Tc-99m MIBI was carried out in 23 patients with left-sided BC before and six months after com-pletion of RT. **Results:** Perfusion defects appeared in 13 (56.5 %) patients in rest study. Stress study revealed additional perfusion defects in 6 (26%) patients. Totally, Stress-rest MPI was abnor-mal in 19 (82.6%) patients after RT which in compared to base-line study was statistically different (P value= 0.000). Myocardial perfusion defects were reversible, partial reversible or fixed in 26.09%, 34.78% and 21.74% of cases. Semi-quantitative factors such as SSS, SDS and SRS were 0.91, 0.65 and 0.26 in baseline study which were respectively changed to 8.21, 3.82 and 4.39 after RT with significant statistically difference (P-value=0.000, 0.000 and 0.002). **Conclusion**: The current quasiexperimental study demonstrated that either stress and rest MPI are neces-sary to identiy various patterns of radiation-induced myocardial perfusion changes in left-sided breast cancer and it is import-ant not to miss one-forth of perfusion changes detected only in stress-induced MPI SPECT. A combination of ischemic, infarcted or hibernating myocardium are hypothetically supposed in la-tent phase of irradiation when notably myocardial mirovasula-ture is concerned. Moreover, it may be clinically useful in symp-tomatic patients or with known coronary artery disease who are proposed for RT in order to diagnose and treat high risk patients as well as for preventive strategies for RICD. **Keywords:** Breast Cancer, Radiation Therapy, Cardiac Toxicity, Myocardial Perfu-sion Imaging, Radiobiology

EP-0552

Restaging Infiltrating Lobular Breast Cancer Patients With Nuclear Medicine

D. Grigolato, F. Pellini, A. Invento, E. Filippi, M. Cucca, L. Locantore, M. Zuffante, G. P. Pollini, M. Ferdeghini; Azienda Ospedaliera Universitaria Integrata, Verona, ITALY.

Aim: To evaluate if FDG PET/CT and Bone Scintigraphy (BS) are able to detect metastases from infiltrating lobular breast carci-noma (ILC), which shows very peculiar metabolic characteristics

and represents a challenge nowadays. Breast cancer can metastasize anywhere, the most common sites are bones, liver, lungs and brain. **Methods:** we reviewed and analyzed the cancer database at our University Hospital of Verona. We found 1050 patients with ILC followed up from 2000 to December 2016. All of them had surgery and chemotherapy according to the TNM status and expression of phenotypes. Fifty-one patients experienced metastases (range: 34-79 years). As being symptomatic or for the rising of CA 15-3 level, these patients received diagnostic imaging with contrast-enhanced CT, PET/CT, BS and MR in case of further uncertain findings. **Results:** Pathological foci were observed in the skeleton (75% of the patients), in the liver (40%), peritoneum (12.5%), brain (10%), thoracic wall (7.5%), gastrointestinal tract (5%), adrenal and kidney (2.5%). PET/CT and CT completely agreed in 6 patients, PET/CT had 4 false negative results (FN): three patients with bone metastases (all osteoblastic lesions) and one patients with duodenal focus. Contrast-enhanced CT had 3 FN results (all lymph nodes) and one FP result (vertebral collapse due to osteoporosis). Bone scintigraphy was completely inaccurate in six patients, where the lesions were diffusively osteoblastic, although this imaging can only examine the skeleton. Overall CT saw more lesions in the liver, brain, lung and GI tract, conversely PET/CT better revealed pathologic nodes and bone lesions. We noticed a wide spectrum of FDG uptake, from faint to very high SUV, sometimes in the same patient, stressing on the fact that the FDG uptake depends on several factors, mainly the histologic and biologic characteristics of the breast tumor, the higher the grade and the tumor proliferation index, the more intense the FDG concentration. **Conclusions:** metabolic imaging must be assessed with the knowledge that metastases from ILC are more difficult to detect compared to other types of breast cancer because of possible low FDG uptake in pathological foci. So far, in these patients, all the unusual finding on hybrid CT with normal FDG uptake should be considered and reported (i.e: osteoblastic lesions, visceral enlargement, peritoneal nodules). On the whole, FDG PET-CT, if negative, cannot be considered a reliable method to exclude a metastatic spread.

Clinical Oncology: Lung

EP-0553

Clinical use of F-18 FDG PET/CT in pulmonary pleomorphic carcinoma

K. Hayasaka, T. Saitoh, H. Inoue, M. Fukasawa, Y. Shiraishi, K. Yoshimori, F. Kikuchi, H. Gotoh; Fukujyuuji Hospital, Anti-tuberculosis Association, Tokyo, JAPAN.

Objective: Pulmonary pleomorphic carcinoma (PPC) is a rare and unresearched subtype of non-small cell lung cancer (NSCLC). The present study aimed to determine whether F-18 fluorodeoxyglucose (FDG) positron emission tomography (PET)/computed tomography (CT) could play a role in the diagnosis of PPC and the prognosis of patients. **Materials and Methods:** We assessed 20 of 23 patients (male, n = 19; age, 51 to 88 years) when the initial stage with PPC was diagnosed and 21 at follow up using FDG-PET/CT. The maximum standardized uptake (SUVmax) of F-18 FDG during one hour was measured and we reviewed the FDG PET/CT findings of primary lung tumors, recurrent tumors, lymph nodes and distant metastasis. All data were statistically analyzed using SPSS Version 11.0 software (SPSS Inc., Chicago, IL, USA). Statistical significance was set at $p < 0.05$ (Kaplan-Meier method with log rank test). **Results:** Pulmonary pleomorphic carcinoma was confirmed in 20 surgical and three surgical biopsy specimens. The mean (SD) of tumor dimension (mm) and SUVmax was 39.5 (16.7) and 10.9 (7.4), respectively. The SUVmax of FDG did not differ according to age, sex, tumor dimension, location, histology (sarcomatoid or epithelioid), nodal metastasis, pleural invasion or pathological stage. Pearson correlation analysis revealed a statistically significant association between dimension of whole tumor, location, epithelioid (adenocarcinoma) and sarcomatoid (spindle cell) components vs those of SUVmax. One patient had distant metastasis in muscle and abdominal lymph nodes at the time of initial staging. Sites of initial recurrence in patients during follow-up were locoregional (mediastinal nodes, pleural and intrapulmonary; n = 2 each) and distant (bone, n = 3; small intestine, brain, pancreas, kidney and adrenal gland, n = 1 each). Kaplan-Meier analysis revealed significant differences between lower and higher SUVmax values (p=0.0187), stages 1 - 2 and 3 - 4 (p = 0.0014) and pleural invasion (pl) 0-1 and 2-3 (p = 0.0082), but not between tumor size (p = 0.1240) or age (p = 0.857). **Conclusion:** The SUVmax of the primary site did not significantly differ with respect to age, sex, tumor dimension, tumor location, histology (epithelioid or sarcomatoid component), node metastasis, pleural invasion and pathological staging. However, FDG-PET seems helpful to assess prognosis, pre-surgical diagnosis and post-surgical management.

EP-0554

Whole-body bone scintigraphy in comparison with bone metabolism in lung cancer patients

J. Weissensteiner[1], E. Babusikova[2]; [1]Hospital Poprad, Poprad, SLOVAKIA, [2]Comenius University in Bratislava, Jessenius Faculty of Medicine in Martin, Department of Medical Biochemistry, Martin, SLOVAKIA.

Introduction: Primary lung cancer is the most commonly diagnosed cancer. Osteocalcin (OC - marker of bone formation) is the main non-collagenous, hydroxyapatite-binding protein, which has a regulatory role in mineralization. Beta-carboxyterminal cross-linking telopeptide of type I collagen (ß-CTx - maker of bone resorption) is a specific marker for the degradation of mature type I collagen in bone. The aim of this study was to correlate serum concentration of OC and ß-CTx with the presence of bone metastases detected by whole-body bone scintigraphy in lung cancer patients. **Material and Methods:** We measured serum concentration of biochemical marker of bone metabolism (OC, ß-CTx) in 60 patients (46 men, 14 women) with lung

cancer. The mean age was 66.65 years (range: 50-84 years). In healthy control were 10 persons without malignant disease (2 male, 8 female, mean age 52.3, range 34-67 years). All participants of study were examined by whole-body bone scintigraphy using a hybrid SPECT/CT scanner with ^{99m}Tc-MDP. The study populations included 50 non-small-cell lung cancers (NSCLC), 9 small-cell lung cancers (SCLC), 1 patient with typical carcinoid of lung. NSCLC included 21 squamous cell carcinomas, 20 adenocarcinomas, 3 large cell carcinomas, 3 non-small-cell lung cancers with neuroendocrine component, 3 undetermined non-small-cell lung carcinomas. **Results:** The bone metastases by whole-body bone scintigraphy were in 15 cases (25 %), probably bone metastases in 11 cases (18.33 %) and 34 patients (56.67 %) were without bone metastases. In healthy control of 10 persons were serum concentrations of OC and ß-CTx in reference range; only in one case was serum concentration of OC and ß-CTx below reference range. We did not find significant difference of OC concentration in patients with bone metastases in comparison with healthy control (p=0.60). The significant difference in β-CTx concentration between patients and healthy control we did not notice (p=0.09). We observed significant difference in β-CTx concentration between patients with bone metastases and healthy control (p=0.02). Patients with bone metastases had higher concentration of β-CTx than healthy control and slightly increased than patients without bone metastases (p=0.06). **Conclusion:** The bone metastases findings by whole-body bone scintigraphy were not correlated with the serum concentrations of OC, but were correlated with the serum concentrations of ß-CTx in lung cancer patients. The determination of osteocalcin probably does not have diagnostic importance, determination of beta-carboxyterminal cross-linking telopeptide of type I collagen could be a diagnostic marker in lung cancer patients with suspected bone metastases.

EP-0555

The utility of dynamic F-18 FDG PET/CT in differentiating histology of primary lung carcinoma

Y. Otomi[1], T. Shinya[2], K. Takechi[3], M. Yamanaka[1], K. Terazawa[1], M. Kubo[1], N. Uyama[1], H. Otsuka[4], M. Harada[1]; [1]Tokushima University Hospital, Tokushima, JAPAN, [2]Okayama University Hospital, Okayama, JAPAN, [3]Tokushima Red Cross Hospital, Tokushima, JAPAN, [4]Tokushima University Graduate School, Tokushima, JAPAN.

Purpose: This prospective study aimed to compare the diagnostic ability of dynamic fluorodeoxyglucose-positron emission tomography/computed tomography (F-18 FDG PET/CT) to differentiate malignancy from benign lesions in patients with lung carcinoma with that of dual-time-point (DTP) F-18 FDG PET/CT. In addition, we investigated the utility of dynamic F-18 FDG PET/CT in differentiating histology of lung carcinoma. **Subjects & Methods:** We performed dynamic and DTP PET/CT studies on 81 consecutive patients (60 males, 21 females; mean age 70.5 years old) with suspected lung carcinoma. Sixty-seven were pathologically proven to have primary lung carcinoma (50 males, 17 females; mean age 70.7 years-old; 36 cases of adenocarcinoma, 20 cases of squamous cell carcinoma, 4

cases of small cell carcinoma, 3 cases of adenosquamous cell carcinoma, and 4 cases of other carcinomas), and 14 had benign lesions (10 males, 4 females; mean age 69.3 years old). The dynamic PET/CT studies were divided into 3 phases (phase 1: 5-15 minutes, phase 2: 15-25 minutes, phase 3: 25-35 minutes). We evaluated the SUVmax of the primary lesions of 5 phases [dynamic phase 1, dynamic phase 2, dynamic phase 3, the early phase (60 minutes), the delayed phase (120 minutes)]. We also calculated the retention index (RI) of the dynamic PET/CT study (dynamic phases 1-3) and the DTP scan (early to delayed phase). The diagnostic performance for distinguishing malignancy from a benign lesion was assessed by analyzing the receiver operating characteristic (ROC) curve. Bonferroni's correction of p-values for multiple comparisons was applied. **Results:** In the ROC analysis, the areas under the curve for differentiating lung carcinoma from benign lesions of SUVmax (dynamic phase 1), SUVmax (dynamic phase 2), SUVmax (dynamic phase 3), SUVmax (early phase), SUVmax (delayed phase), RI (dynamic phases 1-3), and RI (early to delayed phase) were 0.76, 0.77, 0.77, 0.77, 0.78, 0.76, and 0.76, respectively. Significant differences were found between the RI (dynamic phases 1-3) of adenocarcinoma and squamous cell carcinoma (p=0.003) and between RI (early to delayed phase) of adenocarcinoma and squamous cell carcinoma (p=0.003). **Conclusion:** Both the RI obtained from the dynamic PET/CT study and the RI obtained from the DTP PET/CT study made it possible to improve the diagnostic ability in distinguishing adenocarcinoma from squamous cell carcinoma, which are the two major subtypes of non-small cell lung carcinoma. When differentiating between two subtypes, a dynamic PET study can omit delayed scans and shorten the PET/CT examination time in clinical practice.

EP-0556

Prognostic assessment of 18F-FDG uptake using dual point imaging and partial volume correction in resected non-small cell lung cancer patients

H. Kaida[1], K. Azuma[2], A. Kawahara[3], S. Takamori[4], J. Akiba[3], K. Fujimoto[5], R. Axel[6], K. Ishii[7], T. Murakami[1], M. Ishibashi[8]; [1]Department of Radiology, Kindai University Faculty of Medicine, Osakasayama, JAPAN, [2]Division of Respirology, Neurology, and Rheumatology, and Department of Internal Medicine, Kurume University School of Medicine, Kurume, JAPAN, [3]Department of Diagnostic Pathology, Kurume University Hospital, Kurume, JAPAN, [4]Department of Surgery, Kurume University School of Medicine, Kurume, JAPAN, [5]Department of Radiology, Kurume University School of Medicine, Kurume, JAPAN, [6]Department of Nuclear Medicine, Ludwig Maximilians University Hospital Munich, Munich, GERMANY, [7]Department of Radiology, Kindai University Faculty of Medicine, Osakasayama City, JAPAN, [8]Division of Nuclear Medicine, PET Center, and Department of Radiology, Fukuoka Tokushukai Hospital, Kasuga, JAPAN.

Aim: To investigate the relationship between the prognosis and glucose transporter-1 (Glut-1) expression and fluorine-18 fluorodeoxyglucose (^{18}F-FDG) uptake using partial volume correction (PVC) and dual point imaging in surgically resected non-small cell lung cancer (NSCLC) patients. **Materials and Meth-**

ods: Our patient population consisted of 108 NSCLC patients (64 men and 44 women), and the median age was 71 (range, 45-90) years. The maximum standardized uptake value at 1hr (SUV1), SUV max at 2hr (SUV2), PVCSUVmax, and retention index (RI) [RI= (SUV2-SUV1)/SUV1×100] of primary lesions were calculated. Recovery Coefficient (RC) method was performed to obtain the PVCSUVmax. Excised tumor tissues were analyzed by immunohistochemistry using monoclonal antibodies for Glut-1, as follow: the intensity multiplied by immunostained area. Patients were classified into two groups using the cutoff value, namely, those with low and high values of SUV1, SUV2, RI and PVCSUVmax and Glut-1 expression. Overall survival (OS) and Disease free survival (DFS) were estimated by Kaplan-Meier methods, and the difference in survival between subgroups was analyzed by log-rank test. The Cox proportional hazard model was applied to evaluate the effects of PET parameters and Glut-1 expression while adjusting for potential confounding factors. **Results:** The optimal cutoff value of SUV1, SUV2, PVCSUVmax, RI and Glut-1 was 3.18, 4.32, 3.51, 65%, and 70.0, respectively. On the Kaplan-Meier survival curves, the patients with high SUV1, SUV2, and PVCSUVmax showed significantly worse prognosis than those with low values, and the patients with high Glut-1 expression group showed significantly worse prognosis than those with low Glut-1 expression [SUV1: DFS, P=0.001, OS, P=0.003; SUV2: DFS, P=0.002, OS, P=0.004; PVCSUVmax : DFS, P<0.001, OS, P=0.013; Glut-1: DFS, P=0.012, OS, P=0.002]. There was statistical significant difference between RI and DFS but not OS [DFS, P=0.02, OS, P=0.293]. With adjustment for several clinicopathological variables, Cox regression analysis revealed that SUV1, SUV2 and PVCSUVmax, and Glut-1 were significantly associated with both DFS (SUV1: hazard ratio (HR)=2.301; 95% confidential interval (CI), 1.146-4.618; P=0.019; SUV2: HR=2.483; 95%CI, 1.257-4.905; P=0.009; PVCSUVmax: HR=2.205; 95%CI, 1.038-4.686; P=0.04; Glut-1: HR=2.095; 95%CI, 1.086-4.041; P=0.001) and OS (SUV1: HR=3.197; 95%CI, 1.339-7.633; P=0.009; SUV2: HR=3.599; 95%CI, 1.521-8.516; P=0.004; PVCSUVmax: HR=8.655; 95%CI, 2.048-36.658; P=0.003; Glut-1: HR=2.427; 95%CI, 1.146-5.140; P=0.021). RI had no significant association with DFS and OS [DFS; HR=1.642; 95%CI, 0.610-2.212; P=0.648, OS; HR=1.60; 95%CI, 0.735-3.481; P=0.236]. **Conclusion** PVCSUVmax, SUVmax and Glut-1 expression might be more significant prognostic factors for OS and DFS than RI in surgically resected NSCLC patients.

EP-0557
PET in radiotherapy planning for lung cancer

O. Solodyannikova; Institute of cancer, Kiev, UKRAINE.

Introduction: In recent years, the role of positron emission tomography (PET) in the delineation of macroscopic tumor volume (MTV) based on metabolic imaging to determine the optimal format for radiotherapy (RT) planning has been considered in the literature. **Aim:** determination of macroscopic tumor volume (MTV) with 18F-FDG-PET/CT in the RT planning of lung cancer (LC) patients. **Materials and methods:** The examinations were carried out in the PET-center using Siemens RDS

Eclipse RD cyclotron (energy - 11 MeV) on the combined PET/CT scanner Biograph-64 TruePoint (Siemens) in the accordance with the EANM recommendations for Siemens devices with the 3D data collection mode. **Results:** The RT planning using PET/CT was performed in 25 patients. In 19 patients the non-small cell LC was diagnosed, in 6 cases - small cell LC. The structure of the group by stages was as following: IIA - 2 cases, IIB - 3, IIIA - 8, IIIB - 7, and IV - 5. We compared the data of irradiated MTV obtained by CT and 18F-FDG-PET/CT (Table 1, 2). Table 1. Indices of MTV from CT and 18F-FDG-PET/CT in non-small cell LC. As it can be seen from the table 1, the volume determined with 18F-FDG-PET/CT was less than the CT score. The decrease was 15.6%. The index of intramodal variability was 21.5% for CT values and 7.4% for 18F-FDG-PET/CT, respectively. This coincides with the data of other authors and is probably due to the inaccuracy of the determination of atelectasis areas in the lungs by CT. Table 2. Indices of MTV from CT and 18F-FDG-PET/CT in small cell LC. In this group of patients the volume determined with 18F-FDG-PET/CT was less different from the CT score. The decrease was 7.2%. The index of intramodal variability was 7.4% for CT values and 9.3% for 18F-FDG-PET/CT, respectively. **Conclusion:** LC is heterogeneous in terms of biological characteristics and radioresistance, so it is important to take this factor into account when determining the irradiation volumes.

EP-0558
Role of metabolic parameters evaluated from baseline F18-FDG PET/CT as prognostic markers in non-small cell lung cancer (NSCLC) patients undergoing platinum-based chemotherapy

A. Sharma, A. Mohan, A. S. Bhalla, S. Vishnubhatla, M. C. Sharma, C. J. Das, A. K. Pandey, C. D. Patel, C. S. Bal, R. Kumar; All India Institute of Medical Sciences, Delhi, INDIA.

Purpose: To prospectively evaluate the role of various quantitative and semiquantitative metabolic parameters evaluated from baseline F18-FDG PET/CT in prediction of overall survival in biopsy proven NSCLC patients planned to undergo platinum-based chemotherapy. **Subjects & Methods:** Sixty patients with biopsy proven NSCLC and mean age 59.55 ± 10.06 years who were planned to undergo platinum-based chemotherapy were enrolled in the study. Each patient underwent a baseline dynamic and whole body F18-FDG PET/CT scan after injecting 5.18-7.77 Mbq/Kg of F18-FDG intravenously. Two dynamic PET/CT parameters i.e. Net influx constant (Ki) and glucose metabolic rate (MR-glu) at 30 minutes and 60 minutes were evaluated. Along with this the whole body PET/CT parameters i.e. maximum standardized uptake value(SUVmax), average SUV(SUVavg), tumor to background ratio(TBR), metabolic tumor volume of primary tumor(MTV), total lesion glycolysis of primary tumor (TLG), whole body MTV (MTVwb) and whole body TLG (TLGwb) were evaluated. Cut-offs for all significant parameters (p&lt0.05) were calculated using ROC analysis. Survival analysis was performed using log rank test, Kaplan-Meier curves and Cox proportion hazard model to determine the prognostic markers for overall survival. **Results:** The median follow-up period was 4.4 months (range:

8 days - 15.9 months). All the four dynamic PET/CT parameters were statistically non-significant in prediction of overall survival. Out of seven whole body PET/CT parameters, the four metabolic tumor burden parameters i.e. MTV, TLG, MTVwb and TLGwb were significantly associated with overall survival with cut-off values 120, 800, 160 and 1350 and hazard ratios 3.64 (p=0.001), 3.359(p=0.002), 2.512(p=0.019)and 2.694(p=0.008) respectively. In multivariate survival analysis, MTV was found to be the independent prognostic marker for overall survival in NSCLC patients. **Conclusion:** The baseline metabolic tumor burden parameters evaluated from primary tumor(MTV, TLG) as well as the whole body tumor lesions (MTVwb and TLGwb) are the reliable prognostic markers of overall survival in NSCLC patients undergoing platinum-based chemotherapy. However, other baseline whole body PET/CT parameters (SUVmax, SUVavg, and TBR) and Dynamic PET/CT parameters (Ki, MRglu) have no significant role as predictors of overall survival in these patients.

EP-0559

Effect of Respiratory Gating System on PET Image of Lung Cancer: Relationship with Location and Size

T. Kamibayashi, N. Shuke, C. Miyazaki, T. Onishi, S. Aoyagi, K. Saito; Kushiro Kojinkai Memorial Hospital, Kushiro, JAPAN.

Purpose: The aim of our study was to evaluate the effect of respiratory gating on detection of lung cancers with PET/CT, focusing on the relationship to their locations and sizes. **Methods:** FDG uptakes of fifty lung cancers in 46 patients (23 men and 23 women mean age 68.2±10.2 years) were retrospectively analyzed in both standard and respiratory gating PET/CT images. The lung cancers had a maximum diameter of 8—56 mm (mean±SD, 22.48±11.69 mm). The size was determined on CT scan (lung window). PET/CT was performed on Discovery 710 (GE Healthcare) with phase based respiratory gating method (GE: Q static). A camera-based respiratory gating system (RPM, Varian Medical Systems) was adopted for monitoring patients' respiratory motion. The locations of lung cancers were visually classified into 3 groups (16 cancers in the upper, 18 cancers in the middle, and 16 cancers in the lower lung field) on the MIP images. Maximum standardized uptake values (SUVmax) were assessed on both standard and respiratory gating PET/CT images. Standard SUVmax and percentage difference of SUVmax (SUV%difference: 100(standard SUVmax - respiratory gating SUVmax)/ standard SUVmax) were compared between 3 locations. Correlation between SUVmax%difference and lesion size was also analyzed. Paired Student's t-test was used to compare the mean values of SUVmax between groups. Correlation of SUVmax%diference and lesion size was analyzed with Spearman test. **Results:** In standard PET/CT, SUVmax values (mean ± SD) were 7.2 ± 5.0 in upper, 6.7 ± 5.3 in middle, 8.0 ± 5.5 in lower lung field. In respiratory gating, SUVmax values (mean ± SD) were 9.1 ± 6.3 in upper, 8.1 ± 6.6 in middle, 8.9 ± 6.1 in lower lung field. In all locations, SUVmax showed significant increase in respiratory gating (P<0.05). SUVmax%difference values (mean ± SD) were 4.56 ± 10.65 in upper, 12.96 ± 14.26 in middle, 21.97 ± 15.94 in lower lung field, showing significant difference in all

locations (P<0.05), and the difference became greater in order of upper to lower location, indicating location-dependent effect of respiratory gating. In middle field, we observed a statistically significant inverse correlation between SUVmax%diference and lesion size (p<0.05), indicating size-dependent effect of respiratory gating. In other locations, however, no statistically significant correlations were observed. **Conclusion:** Characterization of lung lesions with PET/CT was better with respiratory gating. The respiratory gating PET/CT technique was a valuable clinical tool in diagnosing lung cancer.

EP-0560

Diagnostic abilities of Dynamic and dual-time-point F-18 FDG PET/CT for lymph node metastasis in patients with lung carcinomas

M. Yamanaka[1], T. Shinya[2], Y. Otomi[1], K. Terazawa[1], K. Takechi[3], M. Kubo[1], H. Otsuka[4], M. Harada[1]; [1]Tokushima Univ. Hospital, Tokushima, JAPAN, [2]Okayama Univ. Hospital, Okayama, JAPAN, [3]Tokushima red cross hospital, Tokushima, JAPAN, [4]Tokushima Univ. Graduate School, Tokushima, JAPAN.

Aim: This prospective study clinically assessed the diagnostic abilities of dynamic F-18 FDG PET/computed tomography (CT) scans compared with dual-time-point F-18 FDG PET/CT for lymph node metastasis in patients with lung carcinomas. **Materials and Methods:** Dynamic PET studies were performed with F-18 FDG on 63 consecutive patients with pathologically proven lung carcinoma. These participants had not received any therapy before the PET/CT examination. The dynamic PET scans were performed in list mode, beginning at 5 min after injecting the tracer and continuing for 30 min (dynamic phases 1, 2, and 3, 5-15, 15-25, and 25-35 min, respectively). The dual-time-point PET/CT was performed at 60 and 120 min after the intravenous injection. The maximum standardized uptake value (SUVmax) in each dynamic phase and the retention index (RI) [RI-SUV (dyn) = {SUV (3) - SUV (1)}/SUV (1) × 100%, where SUV (1) and SUV (3) are the SUVmax in dynamic phases 1 and 3, respectively; RI-SUV (D) = {SUV (120 min) - SUV (60 min)/SUV {60 min} × 100%] were compared. Receiver operating characteristic (ROC) curve analysis was performed to evaluate the predictive performance of calculating the SUVmax of primary tumors for differentiating the groups with and without metastatic lymph nodes. Discrimination was assessed by the area under the curve (AUC). **Results:** There were significant differences in SUVmax and RI-SUV at all time points between the tumor groups with and without lymph node metastasis (p < 0.05). The ROC curve for diagnosing the lung carcinomas with metastatic lymph node revealed that the appropriate cut-off SUVmax value could be set in all dynamic phases with a sensitivity of 82.8%-86.2% and a specificity of 61.8%-70.6%. The AUC values were 0.728-0.749. The appropriate cut-off SUVmax values were set at 60-min early and 120-min delayed phases with sensitivities of 72.4% and 72.4% and specificities of 67.6% and 64.7%, respectively. The AUC values were 0.728-0.749. For RI-SUVmax, the ROC curve analysis revealed that the appropriate cut-off RI-SUV (dyn) and RI-SUV (D) values were 67.41% and 65.34% with sensitivities of 62.1% and 72.4%

and specificities of 67.6% and 61.8%. The AUC values were 0.713 for RI-SUV in the dynamic and dual-time-point scans. **Conclusion:** Dynamic and dual-time-point F-18 FDG PET/CT studies had moderate diagnostic performances for discriminating the lung carcinomas with lymph node metastasis from without lymph node metastasis using the analyses of SUVmax and RI-SUV in primary lung tumors.

EP-0561

Quantitative Analysis of Respiratory-Gated PET/CT Images for the Evaluation of Hilar Lymph Nodes in Non-Small Cell Lung Cancer

L. Hehenwarter[1], L. Rettenbacher[1], F. Zehentmayr[2], C. Pirich[1];
[1]Department of Nuclear Medicine and Endocrinology, University Hospital Salzburg, Salzburg, AUSTRIA, [2]Department of Radiotherapy and Radiation-Oncology, University Hospital Salzburg, Salzburg, AUSTRIA.

Acquisition and reconstruction parameters might have impact on radiotherapy planning of NSCLC with respect to inclusion of hilär lymph nodes. **Aim:** To evaluate the impact of respiratory gated [^{18}F]FDG PET/CT image acquisition and thin reconstruction using 2mm slice thickness compared to standard 4mm reconstruction slice thickness. **Material and Methods:** Seven male and six female patients (mean age 68±10 years) underwent PET/CT imaging using a Philips Ingenuity TF PET/CT scanner. Images were acquired one hour p.i. Subsequently gated PET/CT images were continuously acquired using a belt (Medspira Bellows IBC) as gating device. Static images were reconstructed with 4mm slice thickness and 2mm slice thickness. Gated image reconstruction was performed dividing the gated raw data into four phases, each 25% of one breathing cycle. Different Standard-Uptake-Value (SUV)-based volumes of interest (VOI) were drawn at 90% 85% 80% and 75% of a lymph node's SUVmax and by defining the cut-off value for best anatomical correlation. The highest SUVmax among different breathing phases was determined for every lymph node (Gmax). Several background areas were defined as large regions of interest (ROI) in the mediastinum, liver and muscle tissue for the calculation of the Tumor-to-Background Ratio (TBR) for both SUVmax (TBRmax) and SUVmean (TBRmean). Applying different cut-off values SUVmean, TBRmean and volumes were calculated for each lymph node. **Results:** Results are shown for 2mm and 4mm reconstruction slice thickness. SUVmax: 6.89 (±2.83) vs. 5.13 (±2.40); p=0.031, TBRmax mediastinum: 3.82 (±1.52) vs. 2.78 (±1.20); p=0.016, TBRmax liver: 2.85 (±1.05) vs. 2.11 (±0.88); p=0.015, TBRmax muscle: 10.22 (±4.53) vs. 7.53 (±3.62); p=0.035, TBRmax all: 4.92 (±1.93) vs. 3.62 (±1.57); p=0.018, TBRmean90 mediastinum: 3.50 (±1.33) vs. 2.62 (±1.15); p=0.029, TBRmean85 mediastinum: 3.37 (±1.27) vs. 2.56 (±1.19); p=0.039, TBRmean80 mediastinum: 3.35 (±1.32) vs. 2.51 (±1.18); p=0.038, TBRmean90 liver: 2.61 (±0.92) vs. 2.00 (±0.85); p=0.031, TBRmean85 liver: 2.52 (±0.87) vs. 1.96 (±0.87); p=0.045, TBRmean80 liver: 2.50 (±0.91) vs. 1.91 (±0.88); p=0.042, TBRmean90 all: 4.50 (±1.68) vs. 3.42 (±1.52); p=0.035, TBRmean85 all: 4.34 (±1.59) vs. 3.34 (±1.56); p=0.048, TBRmean80 all: 4.32 (±1.68) vs. 3.27 (±1.56); p=0.045.

The comparison of all parameters obtained with Gmax and 2mm reconstruction demonstrated no significant differences. **Conclusion:** 2mm reconstruction revealed significantly higher SUV and TBR values in hilar lymph nodes as compared to standard 4mm reconstruction. This might have a clinical impact on radiotherapy planning when including hilar lymph nodes based on SUV or TBR cut-off values to be addressed in future trials.

EP-0562

18F-FAZA PET/CT to assess hypoxia in non-small cell lung cancer: comparison with glucose metabolism and immunohistochemistry

P. Mapelli[1], E. Incerti[1], V. Bettinardi[1], F. Fallanca[1], G. Negri[2], F. Rossetti[2], A. Coliva[1], C. Doglioni[3], L. Gianolli[1], M. Picchio[1];
[1]Nuclear Medicine Department, IRCCS San Raffaele Scientific Institute, Milano, ITALY, [2]Department of Thoracic Surgery, IRCCS San Raffaele Scientific Institute, Milano, ITALY, [3]Pathology Unit, IRCCS San Raffaele Scientific Institute; Vita-Salute San Raffaele University, Milano, ITALY.

Purpose: To assess the capability of 18F-FAZA PET/CT in identifying intratumoral hypoxic areas in early and locally advanced non-small cell lung cancer (NSCLC) patients and to compare 18F-FAZA PET/CT with 18F-FDG PET/CT and histopathological biomarkers. **Subjects & Methods**: Seven patients with NSCLC were prospectively enrolled (3 men, 4 women; median age: 71 years; range 63-80) between March 2015 and September 2016. All patients underwent to 18F-FDG PET/CT and 18F-FAZA PET/CT before surgery. Maximum standardized uptake value (SUVmax) was used to evaluate 18F-FDG PET/CT images, while 18F-FAZA PET/CT images have been interpreted by using tumour-to-blood (T/B) and tumour-to-muscle (T/M) ratio. Surgery was performed in all patients well as immunohistochemical analysis for hypoxia biomarkers CA-IX and HIF-1. **Results:** All lung lesions showed intense uptake of 18F-FDG (mean SUVmax: 7.35; range: 2.35/25.20). A faint uptake of 18F-FAZA was observed in 6/7 patients (T/B < 1.2) while significant uptake was present in the remaining 1/7 (T/B and T/M=2.24). On both 2 and 4 h imaging after injection, no difference was observed between T/M and T/B (p=0.5), suggesting that both blood and muscle are equivalent in estimating the background activity for image analysis. One patient had a lesion >9cm, while the remaining patients had lesions <3cm. Immunohisotchemical analysis showed low or absent staining for hypoxia biomarkers in 3 patients (HIF-1: mean 3.3%, range 0-10; CA-IX:0%). Two patients showed staining for HIF-1 of 5%, with CA-IX being 60% and 30% respectively; in 1/7 HIF-1 was 10% and CA-IX was 50%. In P1 high staining of both HIF-1 and CA-IX (20% and 70%, respectively) was present. **Conclusion:** All lung lesions showed 18F-FDG uptake, confirming the usefulness of this imaging modality in the preoperative staging of lung cancer. The faint 18F-FAZA uptake was concordant with absent/low immunostaining for hypoxia biomarker and the presence of 18F-FAZA uptake in one patient was concordant with staining for hypoxia biomarkers. T/M and T/B ratio seems to be equivalent and

could be mutually used to evaluate hypoxia in NSLCC patients undergoing 18F-FAZA PET/CT. **Acknowledgments**: This work was supported by the Italian Ministry of Health, Ricerca Finalizzata GR-2009-1575612

EP-0563

FDG PET-derived parameters as prognostic tool in post-treatment progressive malignant pleural mesothelioma patients

E. Incerti[1], P. Mapelli[1], S. Broggi[2], A. Fodor[3], M. Cuzzocrea[4], A. M. Samanes Gajate[1], C. Fiorino[2], I. Dell'Oca[3], L. Gianolli[1], N. Di Muzio[3], M. Picchio[1]; [1]Unit of Nuclear Medicine, IRCCS San Raffaele Scientific Institute, Milan, ITALY, [2]Unit of Medical Physics, IRCCS San Raffaele Scientific Institute, Milan, ITALY, [3]Unit of Radiotherapy, IRCCS San Raffaele Scientific Institute, Milan, ITALY, [4]University of Milano-Bicocca, Milan, ITALY.

Purpose: To evaluate the predictive role of FDG PET-derived parameters in treated malignant pleural mesothelioma (MPM) patients on overall survival (OS), local relapse free survival (LRFS) and distant relapse free survival (DRFS). **Subjects & Methods:** Fifty-five MPM patients (44 male and 11 female; median age: 67 years; range: 39-82 years), treated with FDG PET/CT guided salvage helical tomotherapy (HTT) after previous surgery plus chemotherapy, were retrospectively evaluated between March 2006 and February 2015 at San Raffaele Scientific Institute. Univariate Cox regression analysis was performed to assess FDG PET-derived parameters: biological target volume (BTV), mean and maximum standard uptake value (SUVmean-max), metabolic tumour volume (MTV) and total lesion glycolysis (TLG), measured at different uptake threshold 40-50-60%. By considering patients with OS, LRFS and DRFS inferior and superior to the corresponding median time, a logistic regression was performed to FDG PET-derived parameters able to better select patients with the worst prognosis. **Results:** Median OS was 9.2 months (range: 0 - 69.6 months) after the end of HTT; 54/55 patients were dead at the last follow-up. BTV (p= 0.0007; RR= 1.001) and TLG40-50-60 (p< 0.0001, RR= 1.001) were the most significant predictors of OS. The median values of MTV60 (p= 0.015; RR= 2.1) and TLG40 (p= 0.0047; RR= 2.4) significantly predict OS; a median OS equal to 4.8 months was found for patients with MTV60> 5 cc and for TLG40> 334.4 cc compared to 13.8 and 16.1 months, respectively for patients with smaller MTV60 and TLG40. Median LRFS and DRFS were 6.2 months (range: 1.2 - 39.4 months) and 6.5 months (0 - 66.4 months), respectively. TLG40-50-60 were found significantly (p< 0.015) correlated to LRFS, but a median value not discriminate patients. Almost all FDG PET-derived parameters were found significantly correlated with DRFS. In particular, a median DRFS equal to 6.4 and 6.2 months was found for patients with a MTV40> 39.6 cc and TLG40> 334.4 cc compared to 17 and 18.8 months for patients with MTV40 and TLG40 smaller than these values. **Conclusion:** FDG PET-derived parameters well discriminated patients with poor OS, LRFS and DRFS. The predictive role of FDG PET-derived parameters may be helpful in identifying patients with the worst prognosis, potentially allowing a better selection of MPM patients for salvage HTT.

EP-0564

Tumor heterogeneity, hypoxia and immune markers in patients with non-small cell lung cancer candidate to surgery

E. Lopci[1], L. Toschi[1], F. Marchesi[1], D. Rahal[1], G. Castino[1], N. Cortese[1], S. Marchetti[1], G. Finocchiaro[1], S. Rossi[1], P. Allavena[2], F. Grizzi[1]; [1]Humanitas Clinical and Research Hospital, Milano, ITALY, [2]Fondazione Humanitas per la Ricerca, Milano, ITALY.

Aim: The current study aimed at investigating the prognostic role of tumor heterogeneity on FDG-PET and assess differences in terms of hypoxia and other markers of tumor-related immunity in resected non-small cell lung cancer (NSCLC). **Materials and Methods:** Overall, 44 patients (M:F=33:11; median age 69.5 years) referred to our Institution for NSCLC resection and investigated with FDG-PET prior to surgery were analyzed. Surgical tumor specimens were assessed by immunohistochemistry for HIF1a (hypoxia-inducible factor-1a), CD68-TAMs (tumor-associated macrophages), CD8-TILs (tumor-infiltrating lymphocytes), PD1-TILs and PD-L1 expression. FDG-PET images were analyzed semi-quantitatively using SUVmax, SUVpeak, SUVmean, and metabolic tumor volume (MTV), and for texture heterogeneity by considering tumor sphericity, skewness (asymmetry of the gray-level distribution in the histogram), kurtosis (gray-level distribution relative to normal), entropy (randomness of distribution), and energy (uniformity of distribution). Parameters were correlated with disease-free survival (DFS) considering a median follow-up of 22.7 months. **Results:** All tumors resulted positive at FDG-PET. Pooled together with texture heterogeneity, SUVmax (cut-off 7.9; p=0.015), SUVpeak (cut-off 6.7; p=0.013), SUVmean (cut-off 5.5; p=0.028), MTV (cut-off 3.6cm^3; p=0.027) and entropy (cut-off 1.89; p=0.045) showed a statistically significant association with DFS. Also the presence of high expression of HIF1a in the cytoplasm (score 3) resulted associated to shorter DFS (HR 0.09; p=0.003). All FDG-PET parameters resulted significantly different in terms of mean and median values (p<0.05) in between tumors with higher (>1.89) or lower entropy (≤1.89). Among immune-markers, a significantly higher level of mean CD8-TILs was also seen in tumors with higher entropy (p=0.041). **Conclusions:** Metabolic parameters on FDG-PET, tumor heterogeneity and the expression of hypoxia result prognostic factors in NSCLC patients candidate to surgery. Higher levels of entropy seem associated to increased presence of CD8-TILs.

EP-0565

FDG-PET/CT features of cavity-related primary lung cancers

N. Kawano, H. Otsuka, Y. Otomi, M. Otomo; Tokushima University Hospital, Tokushima, JAPAN.

Purpose: In FDG-PET/CT of primary lung cancers, we often encounter lesions that are considered to have arisen from the bulla wall and those with cysts and cavities. The objective of this study was to investigate FDG-PET/CT features of cavity-related primary lung cancers. **Methods:** We classified FDG uptake of

106 pathologically proven primary lung cancers (Ad: 60 lesions, Sq: 46 lesions) into 6 patterns: 1. single nodular, 2. thin ring-like, 3. irregular thick ring-like, 4. ring-like+nodule, 5. multifocal/segmental, and 6. massive. We further evaluated the SUVmax on PET and the tumor size, size and number of cysts/cavities, and presence or absence of emphysema/interstitial change on CT. **Results:** The single nodule pattern was the most frequent, followed by the irregular thick ring-like patterns. The SUVmax was high in the massive patterns. More than 60% of the lesions had emphysema/interstitial changes in the background. Single nodule pattern lesions tended to be smaller and show lower FDG uptake compared with irregular thick ring-like pattern lesions. 1. single nodular : n=56, SUVmax 5.69±4.22, tumor size 25.29±8.51mm, 2. thin ring-like : n=1, SUVmax 1.7, tumor size 32mm, 3. irregular thick ring-like : n=21, SUVmax 13.1±5.93, tumor size 49.86±14.60mm, 4. ring-like+nodule : n=5, SUVmax 6.86±3.07, tumor size 37.2±9.58mm, 5. multifocal/segmental : n=16, SUVmax 6.07±3.48, tumor size 46.88±15.49mm, 6. massive : n=7, SUVmax 15.2±14.1, tumor size 66.86±28.36mm. **Conclusion:** Small cavities and thin walls could be identified on CT, but difficult to identify by PET, because FDG defects were masked by the tumor uptake, and thin walls occasionally failed to be delineated as FDG-positive tissue due to the spatial resolution of the PET system. Even lesions with small cavities show a ring-like uptake pattern since FDG does not accumulate in degenerated/necrosed contents. If degenerated/necrosed contents are drained by the airway, the cavity enlarges morphologically and begins to show ring-like accumulation. In primary lung cancers, glucose metabolism is considered to be enhanced, and the solid part to enlarge, with progression of the disease, and degeneration/necrosis of the interior to advance with enlargement of the tumor. The progression and activity of the lesion can be evaluated according to the SUVmax and FDG uptake pattern of PET, and background pulmonary emphysema, interstitial change, and morphological information on the lesion can be evaluated by CT.

EP-0566

FDG-PET in the assessment of metabolic response in patients with NSCLC treated with nivolumab: Preliminary results

L. Goldfarb, B. Duchemann, A. Chouahnia, G. Pop, L. Gomez, L. Zelek, M. Soussan; Hôpital Avicenne, APHP, Bobigny, FRANCE.

Introduction: Immunotherapy becomes a standard treatment in non-small-cell lung carcinoma (NSCLC), locally advanced or metastatic, after prior chemotherapy. Because of systemic involvement and heterogeneity of the tumoral disease, methods of assessment are complex and the role of PET-FDG is not well established. The objective of the present study is to describe the results of FDG-PET in the evaluation of patients with NSCLC treated with checkpoint inhibitor (OPDIVO®, Nivolumab) in our academic center. **Subjects & Methods:** A retrospective analysis of FDG-PET's data was performed in 25 patients (performance status: 1), with NSCLC (21 adenocarcinoma, 3 squamous cell carcinoma and 1 large cell neuroendocrine carcinoma) and

progression after at least one line of treatment, and treated with Nivolumab. All patients had an FDG-PET before and at 2 months (M2) of treatment. Patients showing progression at M2 had a third PET at M3 to confirm disease progression. Disease responses were assessed according to PERCIST criteria. Patients were considered as responders to Nivolumab treatment, if the treatment was pursued at least 6 months, or as non-responders if the treatment was pursued less than 6 months. Pseudo-progression was defined as a disease progression at M2, which was not confirmed on FDG-PET control at M3. **Results:** Assessment by FDG-PET after 2 months of treatment showed 11/25 partial metabolic responses (PMR), 12/25 progressive metabolic diseases (PMD), 1/16 stable metabolic disease (SMD) and 1/25 complete metabolic response (CMR). Among the patients with PMR, SMD or CMR at M2 (n = 10), 92% (12/13) were considered as responders and 8% (1/13) as non-responders. Nivolumab was discontinued in patients with PMD. One patient showed a pseudo progression at M2 (PMR at M3). **Conclusions:** These results show an association between the metabolic response at M2 and the continuation of the treatment with Nivolumab in NSCLC patients. More than 90% of patients with early metabolic response showed a sustained response with Nivolumab. FDG-PET could be helpful in the therapeutic strategy of these patients and deserves to be assessed in prospective trials including a cost/benefit evaluation.

EP-0567

FDG-PET findings provide insights into thyroid-related side-effects in patients with Advanced Non-Small Cell Lung Cancer (NSCLC) treated with the immune checkpoint inhibitor Nivolumab

I. Calamia, M. Albertelli, E. Nazzari, M. Bauckneht, G. Rossi, E. Rijavec, C. Genova, G. Barletta, F. Biello, G. Dal Bello, R. Piva, M. Giusti, G. Sambuceti, M. Bagnasco, D. Ferone, F. Grossi, S. Morbelli; IRCCS AUO San Martino IST, Genova, ITALY.

Background: Immune checkpoint blockade is associated with several endocrine-related adverse events including thyroid dysfunction that, however, still needs to be fully characterized. As several studies documented increased FDG uptake in thyroid gland in patients with thyroid autoimmunity, FDG-PET/CT images might further disclose the nature of thyroid disease onset after immunotherapy. In the present study, we aimed to evaluate the metabolic correlates of thyroid-related side-effects in NSCLC patients during therapy with Nivolumab (PD-1 receptor monoclonal antibody). **Methods**: 74 patients with advanced NSCLC underwent Nivolumab administration (4 mg/Kg every 14 days) within a single-institutional translational trial encompassing FDG-PET/CT every 4 cycles. 55/74 patients were evaluable for metabolic response assessment. Blood samples were collected at baseline and every cycle in order to monitor thyroid function and autoimmunity. Thyroid FDG uptake was semiquantitatively estimated by means of average SUV value (SUVmean). Presence/absence of focal uptake was also recorded. Finally, intensity of thyroid uptake was score-based assessed according to Deauville scale (DS). **Results**: At baseline, 6 patients showed

impaired thyroid function (5 showed low and 1 increased TSH). During treatment, 4 patients developed transient thyrotoxicosis evolving to hypothyroidism in 3 cases. These patients showed increased autoantibodies, mainly anti-tireoglobulin (AbTg) and TSH after 6 months from therapy initiation. On the other hand, 8 patients developed hypothyroidism, with negative thyroid autoimmunity. No significant raise in SUVmean was highlighted (1.6±0.2 at baseline vs 1.9±0.3 after 6-8 months of therapy). Focal FDG thyroid uptake was recorded in one patient at baseline, while it appeared in two patients during therapy, corresponding to thyroid nodules in the absence suspected ultrasound features, thyroid dysfunctions or autoantibodies abnormalities. In the subgroup of 12 patients with thyroid-related side effects, changes in DS during treatment reflected better than SUVmean the alterations of thyroid function and autoimmunity. However, in 10/12 patients DS unexpectedly decreased during treatment. Moreover, in patients with hypothyroidism as well as and in a substantial percentage of the whole group of patients, DS score 1 more frequently occurred after treatment with respect to baseline, further testifying a reduction in thyroid FDG-avidity related to Nivolumab administration. **Conclusion:** Thyroid function abnormalities confirm to be the main endocrine adverse event related to Nivolumab. Hypothyroidism seems to be the most frequent of these effects. Autoantibodies type (mainly AbTg), the decrease in DS and their time-trend, support the hypothesis of a non-autoimmune pathophysiology underlying a substantial part of immunotherapy-related thyroid toxicity.

EP-0568

Comparison between PERCIST and EORTC criteria in the evaluation of response to immune check-point inhibitors in Non-Small Cell Lung Cancer (NSCLC) patients

R. Piva, G. Rossi, M. Bauckneht, C. Genova, V. Ceriani, E. Rijavec, G. Barletta, F. Biello, I. Calamia, G. Dal Bello, R. Di Stefano, G. Sambuceti, F. Grossi, S. Morbelli; IRCCS AUO San Martino IST, Genova, ITALY.

Aim: Immune check-point inhibitors block inhibitory signaling, enhancing T-cell activity against tumor cells. CT-based RECIST assessment showed a sub-optimal capability to describe antitumor response, supporting the need of immune-related response criteria that, however, has not yet been validated. To date none of the available FDG PET-based criteria have been systematically tested in NSCLC patients to assess response to Nivolumab a human IgG4 program-death-1 (PD-1) antibody. In the present study we compared PERCIST and EORTC criteria in the assessment of FDG-PET-based response to Nivolumab in NSCLC patients. Moreover, we assessed the relationship between PERCIST and EORTC classification on one side and patients' overall survival on the other. **Methods:** 55 patients with advanced NSCLC were treated with Nivolumab (4 mg/Kg every 14 days) within a single-institutional trial. Each patient underwent FDG-PET/CT every four cycles of Nivolumab. We evaluated metabolic response to treatment by means of both PERCIST and EORTC criteria and their concordance was computed with kappa value. Kaplan-Meier analysis was performed to estimate the overall survival after a follow-up time of 20 months in the

different PERCIST and EORTC response groups. **Results:** A low overall concordance between PERCIST and EORTC criteria was observed (k=0.500). This finding was mainly due to the different classification of patients in Stable Disease (SD). In fact, 54% of patients defined as SD by PERCIST were classified in other response groups by EORTC (20% in Progressive Disease -PD- and 34% in Partial Response -PR-). Moreover, PERCIST outperformed EORTC in prognostic stratification. Accordingly, overall survival of PERCIST-PR was significantly longer with respect to PD and SD subgroups (p=0.034). Furthermore, 55% of PR-PERCIST versus 35% of PR-EORTC patients were still alive at 20 months. Of note, both criteria showed to be not informative in case of PD and SD classes. In fact, according to PERCIST criteria, SD and PD Kaplan-Meier curves substantially overlapped while according to EORTC criteria, SD group demonstrated a shorter OS with respect to PD patients. **Conclusion**: PERCIST has greater prognostic value than EORTC criteria in capturing the heterogeneous response to Nivolumab in NSCLC patients. Concordance between PERCIST and EORTC criteria seems to be lower with respect of what highlighted for conventional therapies. The peculiar mechanism of action of Nivolumab makes FDG-PET-response assessment according to both criteria not informative in case of PD or SD.

EP-0569

Prognostic features in non-small cell lung cancer: difference in metastatic behavior between adenocarcinoma and squamous cell carcinoma

E. A. Usmanij[1], A. Posthuma[1], N. Hugen[1], R. P. J. van den Ende[1], I. D. Nagtegaal[1], J. Bussink[1], L. F. de Geus-Oei[2]; [1]Radboudumc, Nijmegen, NETHERLANDS, [2]Leiden University Medical Center, Leiden, NETHERLANDS.

Background: Clinical studies in non-small lung cancer (NSCLC) have suggested a difference in metastatic patterns between different adenocarcinoma (AC) and squamous cell carcinoma (SCC). In this study the different sites of metastases are evaluated systematically. **Methods:** A nationwide retrospective review of pathology records in the Netherlands of 2798 patients with NSCLC was performed, who underwent an autopsy between January 2001 and December 2010. These autopsies were selected from the Dutch pathology registry (PALGA). To correlate pathology findings, metastatic patterns were compared with a single center cohort on all patients with NSCLC who underwent ^{18}F-fluoro-deoxy-glucose positron emission tomography /computed tomography (FDG PET/CT) between January 2012 and May 2013 for initial staging workup. **Results:** From the PALGA database a total of 2798 NSCLC patients were selected, 1128 AC and 875 SCC. AC more frequently had metastases compared with SCC (49.7% in AC versus 24.8% in SCC, **P** < 0.001). Differences in metastatic patterns between stage IV AC and stage IV SCC were found. Adrenal gland metastases (40.0% in AC versus 22.9% in SCC) and bone metastases (30.2% in AC versus 18.2% in SCC) were found more often in AC, compared to SCC (P = 0.002). Kidney metastases were found more often in SCC vs AC (21.6% versus 12.0%, P < 0.001). Furthermore, female AC patients devel-

oped significantly more liver metastases (18.8% versus 27.2%, P < 0.001), lung metastases (16.4% versus 26.0%, P < 0.001) and kidney metastases (5.1% versus 8.6%, P < 0.05), compared with male AC patients. Correlation with initial staging FDG-PET/CT cohort was performed in a total of 143 NSCLC patients, of which 70 AC and 73 SCC. In this cohort metastatic disease was present in 26 patients, 7 SCC and 19 AC. On initial staging AC revealed more distant metastases and metastasized significantly more to the bones ($P = 0.007$) and the adrenal glands ($P = 0.003$) **Conclusion:** Differences in metastatic potential and patterns have been found between AC and SCC. The findings of this study should be taken into account for future staging and follow-up of NSCLC.

EP-0570

Volume-dependent comparative analysis of positron emission tomography and diffusion-weighted magnetic resonance imaging parameters in lung adenocarcinoma tumourous tissue

S. Lucic[1], I. Djan[2], M. Bjelan[1], S. Pena-Karan[3], A. Peter[2], N. Andjelic[4], O. Sveljo[5], K. Koprivsek[1], D. Kozic[1], M. A. Lucic[1]; [1]Oncology Institute of Vojvodina/Medical Faculty University of Novi Sad, Sremska Kamenica/Novi Sad, SERBIA, [2]Oncology Institute of Vojvodina, Sremska Kamenica/Novi Sad, SERBIA, [3]Institute of Pulmonary Diseases of Vojvodina, Sremska Kamenica/Novi Sad, SERBIA, [4]Medical Faculty University of Novi Sad, Novi Sad, SERBIA, [5]Oncology Institute of Vojvodina/Faculty of Technical Sciences University of Novi Sad, Sremska Kamenica/Novi Sad, SERBIA.

Purpose: The aim of the study was to explore possible correlation and interconnection between the values of apparent diffusion coefficient (ADC_{mean}), obtained by diffusion weighted magnetic resonance imaging (DWI), and standardized uptake value (SUV_{max}), obtained by ^{18}F-FDG PET/CT in the lung adenocarcinoma tumourous tissue, in regard to the tumour volume. **Subjects & Methods:** Thirty-five newly diagnosed patients with verified lung adenocarcinoma underwent chest MRI examination on 3T MRI unit, that included respiratory triggered DWI (3 diffusion-encoding gradient directions, with 2 b values (0 and 1000 s/mm^2), TR 5000ms/TE 80ms, slice thickness 4mm, inter-slice gap 0.8mm) measurements, followed by ^{18}F-FDG PET/CT examination within the maximally 24-48h interval. A region-of-interest (ROI), covering the exactly same area of the tumour in each single patient was determined, and maximal standard uptake values (SUV_{max}) and mean ADC values (ADC_{mean}) were analyzed and measured by one independent radiologists and one nuclear medicine specialists, and one both nuclear medicine specialist and radiologist, and numerical data sets from both diagnostic modalities were obtained. Maximal adenocarcinoma volume (V_{max}) was calculated and determined, and patients were grouped into group 1 (V_{max}<10000mm^3; n=16), group 2 (10000mm^3<V_{max}<20000mm^3; n=9), and group 3 (V_{max}>20000mm^3; n=9). The data sets were statistically analyzed by use of two-tailed Pearson's correlation coefficient (r), and Spearman's rank correlation coefficient (ρ), with the level of confidence determined at p<0.05. **Results:** Though on the border level, in the whole group of pa-

tients, regardless of V_{max} we haven't found significant correlation between SUV_{max} and ADC_{mean} values (r=0.327;*p*=0.055 and ρ=0.201;*p*=0.248). In the group 1 (V_{max}<10000mm^3), significant correlation between both SUV_{max} and ADC_{mean} values was encountered (r=0.539;*p*=0.031 and ρ=0.535;*p*=0.033). In the group 2 and 3 correlation between two observed biomarkers was not significant (group 2: r=-0.202;***p*=0.601** and ***ρ*=-0.200;*p*=0.606**; group 3: r=0.339;*p*=0.373 and ρ=0.100;*p*=0.798), yet SUV_{max} values solely demonstrated significant correlation with V_{max} in the group 2 (r=0.749;*p*=0.020). **Conclusion:** Our results suggests that mutual interconnection between SUV_{max} and ADC_{mean} varies depending on the tumour volume, indicating that ^{18}F-FDG PET/CT and DWI are complementary diagnostic modalities, providing not the uniform and/or exactly the same, but rather differently acquired and based information in both assessment of lung adenocarcinoma metabolism and cancer tissue cellularity, successively. We are of opinion that these two tumourous hallmarks are the most probable causes of the correlation absence in more voluminous adenocarcinomas with pronouncedly heterogeneous internal structure, affirming SUV_{max} and ADC_{mean} as possible separate, however complementary biomarkers for tumourous tissue internal bioarchitectonics scrutinizing.

EP-0571

Diagnostic value of SUVmax cut-off in assessment of lymph node metastases among patients with NSCLC imaged by 18F-FDG PET/CT

J. Teodorczyk[1], B. Brockhuis[1], G. Romanowicz[1], W. Cytawa[1], I. Wenzel-Duszynska[1], J. Kozlowska-Gladki[1], P. Lass[1,2]; [1]Medical University of Gdansk, Nuclear Medicine Department, Gdansk, POLAND, [2]Division of Molecular Spectroscopy, Institute of Experimental Physics, University of Gdansk, Gdansk, POLAND.

Objective: Previous studies did not provide a definitive answer as to the status of the SUVmax parameter used as the sole criterion for lymph node evaluation in NSCLC. Many authors do not see the clinical utility of using a fixed SUV cut-off value. Study aims to assess diagnostic value of purely quantitative evaluation of lymphonodal metastases utilizing selected SUVmax cutoff thresholds in patients diagnosed by 18F-FDG-PET/CT. **Materials and Methods**: Study included 89 patients and 436 nodal stations. In order to assess the potential benefits of using the fixed thresholds of SUVs to differentiate metastatic lymph nodes from benign, the ROC curve was used as the evaluation criterion. Pathological status of operatively resected lymph nodes served as the "gold standard". **Results:** The minimal sum of false results was obtained with a relatively high SUVmax cut-off value - 5.2. Very high specificity (98.6%) obtained at this level was unfortunately associated with a low sensitivity of 55%. The NPV and PPV values were 95.9% and 78.6%. At lower cutoff level - SUVmax 3.3 - the highest sum of sensitivity and specificity was obtained (minimal sum of FNR and FPR) - sensitivity and specificity at this level was 75% and 87.4% respectively. Quantitatively obtained sensitivity was better than the value obtained by qualitative (visual) assessment, where a level of 56.8% was obtained. The quantitative specificity with the cut-off point

of 3.3 is, however, lower than the value obtained qualitatively (87.4% quantitatively vs. 91.0% qualitatively). Data present in the literature suggested the optimal SUVmax cut-off 2.5 what cannot be recommended in the present study. Using proposed cutoff value (2.5), sensitivity of the test was slightly improved, but at a price of a deep reduction in specificity in comparison to the results obtained at the 3.3 SUVmax threshold (sensitivity for SUVmax cut-off 2.5 was 80%, specificity was 67.8%). **Conclusions:** The SUVmax cut-off value that minimizes the sum of false results is 5.2 and is higher than recommended in the majority of literature reports. Sensitivity at this level was 55 %, specificity was 98,6 %. Clinically optimal SUVmax cut-off value was set to be 3.3, what gives satisfactory sensitivity (75 %) with relatively small decrease of specificity (87,4 %). Relatively low SUVmax cut-off value frequently present in the literature - 2.5 - is not recommended.

EP-0572

Detection and monitoring of thoracic sarcoidosis using F-18 FLT PET/CT: Comparison with F-18 FDG PET/CT

Y. Yamamoto, T. Norikane, H. Dobashi, Y. Nishiyama; Kagawa University, Kagawa, JAPAN.

Purpose: We investigated the feasibility of 3'-deoxy-3'-^{18}F-fluorothymidine (FLT) positron emission tomography/computed tomography (PET/CT) for the detection and monitoring of thoracic sarcoidosis, in comparison with 2-deoxy-2-^{18}F-fluoro-D-glucose (FDG) PET/CT. **Materials and Methods:** A total of 18 patients with newly diagnosed thoracic sarcoidosis were examined with FLT and FDG PET/CT studies. A follow-up PET/CT scan was also performed after immunosuppressive therapy in 5 patients. PET/CT imaging was performed at 60 min after each radiotracer injection. For the analysis of sarcoidosis involvement, evaluation was done using 2 sites: mediastinal/hilar lymph nodes and pulmonary parenchyma. For visual analysis, focal radioactivity that was greater than the mediastinal blood pool activity and the background uptake in the lungs was interpreted as involvement of mediastinal/hilar lymph nodes and pulmonary parenchyma, respectively. Multiple lesions in each site were defined as one lesion. For visualized lesions, the maximal standardized uptake value (SUVmax) in each site was calculated. **Results:** Before therapy, 12 patients had mediastinal/hilar lymph nodes involvement and 6 had both mediastinal/hilar lymph nodes and pulmonary parenchymal involvements. All 18 mediastinal/hilar lymph nodes involvements and 6 pulmonary parenchymal involvements were visually identified with both FDG and FLT PET/CT studies. The mean FDG SUVmax of mediastinal/hilar lymph nodes and pulmonary parenchymal involvements were significantly higher than those of FLT SUVmax (p<0.001 and p<0.008, respectively). The mean FDG SUVmax and FLT SUVmax of mediastinal/hilar lymph nodes involvements after therapy were lower than those of before therapy (p<0.05 and p<0.01, respectively). **Conclusion:** These findings suggest that FLT PET/CT could detect and monitor thoracic sarcoidosis as well as FDG PET/CT, although uptake of FLT in involvement of sarcoidosis was significantly lower than that of FDG.

EP-0573

Role Of PET CT In Management Of Resectable Non Small Cell Carcinoma Lung

P. Gupta, R. Mishra, M. Gupta, P. Choudhury; Rajiv Gandhi Cancer Institute, West DELHI, INDIA.

Aim: Accurate pre-operative staging and restaging of mediastinal lymph nodes with potentially resectable non small cell lung carcinoma (NSCLC) cases is a major determinant of treatment options offered. In case of PET-CT positive mediastinal lymph nodes, targeted tissue confirmation is indicated. When there is no uptake in lymph nodes on PET-CT, blind nodal staging is indicated. Our study was aimed at determining accuracy, sensitivity and specificity of PET-CT in identifying and classifying the presence of metastatic intra-thoracic lymph nodes. **Methods:** 35 operable NSCLC cases underwent PET-CT. Visually significant lymph nodes on PET-CT were compared with histopathological findings. The receiver operating characteristic (ROC) curve was generated to determine the diagnostic efficiency of PET-CT. **Results:** In these 35 cases total 393 lymph nodes, 32 were significantly visualized on PET-CT. Of these 32 lesions, 20 were proven positive pathologically. 12 remaining lesions were labeled false positives. Out of 361 PET-CT negative lymph nodes, 353 were proven negative histopathologycally. 8 of these visually insignificant lesions came out to be pathologically positive (false negatives). The lesion based sensitivity, specificity and accuracy were 71.4%, 96.7% and 94.9%. The PPV and NPV were 62.5% and 97.8%. Factors associated with false negatives were: Centrally located tumor and subcentimeteric lymphnodes. The ROC curve had an area under curve (AUC) of 0.835 (95% CI 0.735-0.905). In order to maximize accuracy, optimal cut-off SUVmax value was identified. The value found was 6.1. With SUVmax of 6.1 or greater, sensitivity was 70.3% with an increased PPV of 82.6%. False positives were reduced from 12 to just 4. The accuracy also remarkably rose to 96.7% from 94.9%. False positives were mainly attributable to the chronic granulomatous inflammation. **Conclusions:** Our study demonstrated that PET-CT is a valuable imaging tool for staging the cases of NSCLC in deciding the treatment modality. Generally EBUS or mediastinoscopy is sufficient for further treatment decisions, but not all mediastinal lymph nodes are routinely reachable by these means. PET-CT can hereby assist and reduce mediastinoscopy owing to a high negative predictive value, although granulomatous conditions are a deterrent in a developing country. **Keywords:** PET-CT, SUV max, ROC and Area under Curve.

EP-0574

Prognostic value of metabolic tumor volume measured by 18F-FDG PET/CT in patients with non-small cell lung cancer ≤ 3 cm in size

S. Pellegrino[1], R. Fonti[2], E. Matano[3], M. Ottaviano[3], V. Damiano[3], L. Pace[4], S. De Placido[3], S. Del Vecchio[1,2]; [1]Department of Advanced Biomedical Sciences, University "Federico II", Naples, ITALY, [2]Institute of Biostructures and Bioimages, National Research Council, Naples, ITALY, [3]Department of Clinical Medicine and Surgery, University

"Federico II", Naples, ITALY, [4]Department of Medicine and Surgery, University of Salerno, Salerno, ITALY.

Purpose: The aim of this study was to evaluate the prognostic value of imaging parameters derived from 18F-FDG PET/CT in non-small cell lung cancer (NSCLC) patients with malignant nodules ≤ 3 cm in diameter. **Subjects and Methods**: Twenty-six patients (20 men, 6 women; mean age ± SD, 65 ± 12y; range 38-82y), with histologically proven malignant nodules ≤ 3 cm in diameter who had undergone whole-body 18F-FDG PET/CT before any therapy, were included in the study. Ten patients in stage I and 1 patient in stage II were grouped for statistical purposes. Among the remaining patients, 4 were in stage III and 11 in stage IV. 18F-FDG PET/CT scans were performed after fasting for 8 h and 60 min after i.v. injection of 370 MBq of 18F-FDG using an integrated PET/CT system. Imaging parameters including SUVmax, SUVmean, metabolic tumor volume (MTV) and total lesion glycolysis (TLG) were determined. For MTV, a 3-dimensional region of interest including the malignant nodule was drawn using a SUVmax-based automated contouring program setting the threshold at 50% of SUVmax. For TLG, each value of MTV was multiplied for the correspondent value of SUVmean. The median follow-up period after 18F-FDG PET/CT scan was 10 months. Univariate and multivariate analysis of clinical and imaging variables were performed using Cox proportional hazards regression. Survival analysis was performed using Kaplan-Meier method and log-rank tests. **Results**: Malignant nodules included in the analysis had a mean diameter of 2.2 cm ± 0.53 cm (SD) with a range between 1.4 cm and 3 cm. Mean values of SUVmax, SUVmean, MTV and TLG were 9.27 ± 4.34, 6.23 ± 3.03, 2.89 ± 2 and 17.41 ± 13.95, respectively. Univariate analysis showed that, among the variables tested, lesion size (p=0.0027), stage (p=0.0043), MTV (p=0.0008) and TLG (p= 0.0063) predicted overall survival in NSCLC patients. At multivariate analysis only MTV was retained in the model for prediction of overall survival (p=0.0008). By Kaplan-Meier analysis and log-rank testing, overall survival was significantly better in patients showing a MTV ≤ 3.3 cm^3 as compared to those having MTV > 3.3 cm^3 (p=0.0001). **Conclusion**: Our findings indicate that metabolic tumor volume is a strong and independent prognostic parameter that predicts overall survival in patients with malignant lung nodules ≤ 3 cm in size.

EP-0575

Metabolic features measured on 18F-FDG PET and aerogenous spread are prognostic factors for disease-free survival in early stage non-small cell lung cancer patients treated by curative surgical resection without adjuvant therapy

Y. Kang, Y. Song, W. Lee, S. Kim; Seoul National University Bundang Hospital, Seoul National University College of Medicine, Seongnam, KOREA, REPUBLIC OF.

Purpose: For early stage non-small cell lung cancer (NSCLC) patients, surgical resection is the curative treatment of choice. According to the National Comprehensive Cancer Network (NCCN) guideline, low-risk patients with tumours of T1-2, negative lymph node and negative surgical margin, adjuvant therapy is generally not performed after the surgical resection. We attempted to predict disease-free survival (DFS) in the low-risk NSCLC patients undergoing curative resection without adjuvant therapy using postoperative pathologic and 18F-FDG PET/CT findings. **Subjects and Methods:** 150 NSCLC patients who underwent preoperative 18F-FDG PET/CT and curative surgical resection were enrolled retrospectively. Inclusion criteria were as follows; (1) pathologic T stage 1-2, (2) pathologic N stage 0, (3) microscopically negative surgical margin, and (4) no adjuvant therapy. Clinical and postoperative pathologic profiles were investigated by medical record review. Maximum SUV corrected by lean body mass (SUL$_{max}$), tumour-to-liver ratio (TLR; SUL$_{max}$ corrected by the mean SUL of the liver), mean SUL (SUL$_{mean}$) and metabolic tumour volume (MTV; 50% of SUL$_{max}$ as isocontour threshold) were measured for primary tumours on 18F-FDG PET/CT. Significant prognostic factors for DFS were selected by univariate survival analyses and stepwise multivariate survival analyses. **Results:** Tumours recurred in 25 patients (16.7%) during the follow-up period (61.1±21.4 months). In univariate survival analyses, SUL$_{max}$ (1.91 as threshold), TLR (1.35 as threshold) and SUL$_{mean}$ (1.23 as threshold) were significant predictors for DFS, among which SUL$_{max}$ was the most significant factors (hazard ratio 22.71; *P*<0.001). Pathologic factors such as tumour size (1.9 cm as threshold), visceral pleural invasion, lymphatic invasion and aerogenous spread were also significant predictors. In the multivariate survival analysis using SUL$_{max}$ and all pathologic factors selected by the univariate analysis, SUL$_{max}$ and aerogenous spread were proven to be independent prognostic factors (*P*<0.001 for both). **Conclusion:** We suggest high 18F-FDG uptake and aerogenous spread as independent poor prognostic markers in low-risk NSCLC patients treated by curative surgical resection without adjuvant therapy. Further studies are warranted to investigate the need for adjuvant therapy in patients with tumours of low risk but with high FDG uptake and aerogenous spread.

EP-0576

Association of 18Fluorodeoxyglucose (FDG), complete pathological response and overall survival in patients with Pancoast tumours treated with trimodality therapy

S. McArthur[1], K. Perera[1], B. Thapa[1], M. Newman[1], T. Fancourt[1], S. Lee[1], S. Berlangieri[1], A. Scott[1,2], S. Knight[1], S. Barnett[1]; [1]Austin Health, Melbourne, AUSTRALIA, [2]Olivia Newton-John Cancer Wellness and Research Centre, Melbourne, AUSTRALIA.

Induction chemoradiotherapy (CRT) and surgical resection is considered standard care for treatment of node negative Pancoast tumours. This study was conducted to investigate whether baseline 18F-FDG positron emission tomography (FDG-PET) scan parameters or changes post induction treatment may predict pathological complete response (pCR) to CRT and hence obviate the need for subsequent resection in patients with pCR. We conducted a retrospective review of our prospectively maintained single institution database with supplemental chart

review to evaluate FDG-PET, histopathological, and clinical outcome parameters in consecutive patients undergoing curative intent trimodality treatment of Pancoast tumours from 2001 to 2015. Parameters based on the standardised uptake values (SUV) were calculated including SUVmax (maximum SUV value), SUVPTL (peak tumour-to-liver ratio), and TGV (total glycolytic volume, mean SUV x tumour volume). Two pathologists independently reviewed specimens to assess percentage viable tumour in resected tumours. Nineteen patients (9 males:10 females), median age 61 (range 42-75) years completed trimodality treatment with cisplatin and etoposide chemotherapy, 45Gy radiotherapy and subsequent resection. Histopathological data was available for all patients. Of the 19 patients, baseline PET was available in 15 and post induction FDG-PET in 13. Baseline TGV > 441 was associated with reduced overall survival (OS) (mean 2.05 vs 8.80 years, p=0.04) disease and reduced disease free survival (DFS) (0.90 vs 8.82 years, p =0.002). In our series of patients, high baseline TGV was associated with lower DFS and OS. Although this is not sufficient to obviate surgical resection, it does suggests that despite good local control there is a cohort of patients who do poorly despite optimal therapy. If confirmed in a larger cohort, including multivariate analysis of other prognostic and predictive factors, these patients may benefit from more aggressive induction or even post operative adjuvent therapies.

EP-0577

Prognostic value of ¹⁸F-FDG PET/CT parameters in patients with operable non-small cell lung cancer: comparison with known high-risk clinicopathologic factors

S. Boo, H. Park, H. Kim, I. Yoo; Seoul St Mary's Hospital, College of Medicine, The Catholic University of Korea, Seoul, KOREA, REPUBLIC OF.

Purpose: To evaluate the prognostic value of metabolic and volumetric parameters obtained from ¹⁸F-FDG PET/CT compared to high risk factors where adjuvant chemotherapy is recommended in patients with operable non-small cell lung cancer (NSCLC). **Subjects & Methods:** FDG PET/CT images from 2009 to 2014, performed for initial staging of NSCLC undergoing curative surgery were retrospectively reviewed. We excluded cases with comorbidity other cancer, history of neoadjuvant therapy, double primary tumors, or imperceptible FDG uptake in primary tumor. PET parameters were acquired from the primary tumor; maximum standardized uptake value (SUVmax), peak standardized uptake value (SUVpeak), metabolic tumor volume (MTV), and total lesion glycolysis (TLG). To define the margin of the primary tumor, various SUV cutoffs, including fixed value of 2.5, were used. In addition to the PET parameters, basic patient characteristics (age, sex, smoking history, histologic subtype, T stage, N stage, TNM stage), high-risk factors for considering adjuvant chemotherapy (differentiation grade, visceral pleura involvement, vascular invasion and tumors >4cm), and molecular mutation status (EGFR, KRAS and ALK) were studied. Median values of each parameter were used to dichotomize the patients. Statistical analysis was

done using Cox regression analysis and Kaplan-Meier method. **Results:** A total of 340 patients were included and the median follow-up was 42.5±20.8 months. 54 patients (15.9%) had died and median overall survival (OS) was 40.1 months (range 0.7-97.8 months). 80 patients (23.5%) had recurrence and median disease free survival (DFS) was 35.5 months (range 0.7-92.8 months). On multivariate analysis, lower SUVpeak and N0 were associated with longer OS. Also, lower SUVmax, lower stage, and no vascular invasion were associated with longer DFS. The hazard ratio (HR) for OS was 6.68 (95% CI 2.28~19.57) for high SUVpeak, and 2.32 (95% CI 1.18~4.57) for presence of metastatic lymph node. The HR for recurrence was 2.16 (95% CI 1.24~3.73) for high SUVmax, and 3.06 (95% CI 1.88~4.99) for presence of vascular invasion, and 2.45 (95% CI 1.29~4.64) for stage III vs. stage I. **Conclusion:** Higher SUVmax, higher SUVpeak from FDG PET/CT, presence of metastatic lymph node, presence of vascular invasion, TNM stage in patients with operable NSCLC were each independent prognostic factors for recurrence or survival. SUVpeak in particular showed the highest HR for OS. Thus SUVmax and SUVpeak could be factors for considering adjuvant chemotherapy.

EP-44   during congress opening hours, e-Poster Area

Clinical Oncology: Liver, Upper GI & Pancreatic Cancer

EP-0578

Clinical significance of FDG uptake of bone marrow on PET/CT in patients with gastric cancer

J. Lee[1], M. Lee[2], S. Lee[3]; [1]Catholic Kwandong University College of Medicine, Incheon, KOREA, REPUBLIC OF, [2]Soonchunhyang University Hospital, Cheonan, KOREA, REPUBLIC OF, [3]Soonchunhyang University Hospital, Cheonen, KOREA, REPUBLIC OF.

Purpose: The purpose of this study was to evaluate the relationship between F-18 fluorodeoxyglucose (FDG) uptake of bone marrow (BM) on positron emission tomography/computed tomography (PET/CT) and clinical factors and to assess the prognostic value of FDG uptake of BM in patients with gastric cancer. **Subjects & Methods:** We retrospectively enrolled 309 patients with gastric cancer who underwent staging FDG PET/CT and subsequent curative surgical resection. FDG uptake of primary tumor was visually classified as positive or negative FDG uptake. Mean FDG uptake of BM (BM SUV) and BM-to-liver uptake ratio (BLR) were measured. The relationships of BM SUV or BLR with clinical factors were evaluated. The prognostic values of BM SUV, BLR, and other clinical factors for predicting recurrence-free survival (RFS) and overall survival (OS) were assessed. **Results:** Of 309 patients, 38 patients (12.3%) experienced cancer recurrence and 18 patients (5.8%) died. Patients with advanced gastric cancer, positive FDG uptake, and recurrence had higher values of BM SUV and BLR than those with early gastric cancer, negative FDG uptake, and no recurrence (*P* < 0.05). BM SUV and BLR were significantly correlated with hemoglobin level, neutrophil-to-lymphocyte ratio, and platelet-to-lymphocyte ratio (*P*

< 0.05). On multivariate analysis, multiple tumors, T stage, lymph node metastasis, tumor involvement of resection margin, and BLR were significantly associated with RFS (P <0.05). T stage, lymph node metastasis, hemoglobin level, and BLR were significantly associated with OS (P < 0.05). **Conclusion:** Patients with advanced gastric cancer and recurrence had higher FDG uptake of BM and FDG uptake of BM was significantly correlated with serum inflammatory markers. BLR on PET/CT was an independent prognostic factor for RFS and OS in gastric cancer patients with curative surgical resection.

EP-0579

Diagnostic value of TOF-^{18}F-FDG PET/CT in patients with suspected pancreatic cancer

S. Stanzel[1], F. Quehenberger[2], B. Pernthaler[1], R. Weinke[3], R. M. Aigner[1]; [1]*Medical University of Graz, Department of Radiology, Division of Nuclear Medicine, Graz, AUSTRIA,* [2]*Medical University of Graz, Institute for Medical Informatics, Statistics and Documentation, Graz, AUSTRIA,* [3]*University Hospital of Graz, Department of Radiology, Division of General Radiological Diagnostics, Graz, AUSTRIA.*

Purpose: Evaluation of the advantages of time-of-flight (TOF) in ^{18}F-FDG-PET/CT in the detection and characterization of pancreatic lesions in patients with suspected pancreatic cancer. Furthermore, the maximum standard uptake value (SUVmax) was assessed. TOF should improve image noise, local resolution and thus the demarcation of small lesions. **Subjects and Methods:** TOF-^{18}F-FDG PET/CT was prospectively performed in 54 patients with suspected pancreatic cancer. In all patients, a histopathologic confirmation was made. PET/CT images were performed 30 and 90 min. p.i. including a diagnostic CT of the upper abdomen with contrast medium and pancreas protocol in 41 patients and a diagnostic CT of the upper abdomen without contrast medium in 13 patients. SUVmax of the lesions was measured and compared with and without TOF in the 30 and 90 min. p.i. images. Lesions with an increase of SUVmax on the delayed images of at least 20% compared to the early images were assessed as malignant, whereas lesions with a decrease of SUVmax were assessed as benign. **Results:** Of 54 patients 38 patients had malignant and 16 patients a benign pancreatic lesion. The mean lesion size was 2.9 cm ± 1.57. In four patients IPMN (2), serous microcystic adenoma (1) and NET (1) was diagnosed correctly only with TOF. 51 pancreatic lesions diagnosed with diagnostic CT showed increased tracer-uptake with TOF-PET/CT. 42 lesions diagnosed with diagnostic CT were detectable without TOF. Thus, significantly more pancreatic lesions were identified with the aid of TOF than without TOF (p=0,002). Based on the histopathologic findings sensitivity, specificity and diagnostic accuracy for TOF were 97%, 77% and 91% versus 81%, 85% and 82% without TOF. Receiver operating characteristics curve analysis of SUVmax with TOF 30 and 90 min p.i. yielded a cut-off value of 5.0 and 6.6, respectively with a sensitivity and specificity of 80% and 87% and 81% and 88%, respectively. **Conclusion:** Among patients with suspected pancreatic cancer, the use of TOF-PET/CT correlated due to a better anatomical localization and identification of pancreatic lesions with higher sensitivity and diagnostic accuracy. Signifi-

cantly more pancreatic lesions could be identified with the aid of TOF than with conventional PET/CT. However, pancreatic lesion assessment still remains a diagnostic issue resulting in a lower specificity of TOF-PET/CT compared to conventional PET/CT.

EP-0580

Effectiveness of dual-time-point F-18 FDG PET/CT imaging between fatty liver patients and FDG accumulation in the liver

M. Nakayama, A. Okizaki, K. Takahashi; Asahikawa Medical University, Asahikawa, Hokkaido, JAPAN.

Purpose: Among the fatty liver patients, hepatic accumulation possibly increase as a back ground. We evaluated the influence of fatty liver on Fluorine-18-fluorodeoxyglucose (FDG) accumulation and the effectiveness of the delayed imaging. **Subjects and Methods:** During the period from January 2015 to December 2016, 84 patients (35 males and 49 females) who had dual-time-point FDG positron emission tomography/computed tomography (PET/CT) imaging including the liver among the cancer patients other than hepatocellular carcinoma were covered. F-18 FDG PET/CT scan was performed at 60 min (early scan) and at 120 min (delayed scan) after the injection. The maximum standardized uptake value (SUVmax) of the liver were obtained in both the early and delayed images of FDG PET/CT images. The retention index (RI-SUVmax) to evaluate the change of tracers in the liver was also investigated. The relationship between SUVmax of fatty liver patients and non-fatty liver patients was determined using the Wilcoxon rank-sum test. **Results:** Whereas early SUVmax of hepatic accumulation in patients with fatty liver was significantly higher than those with non-fatty liver (P < 0.0001), delayed SUVmax of hepatic accumulation in patients with fatty liver showed no significant difference with in those with non-fatty liver. RI-SUVmax significantly decreased in fatty liver patients than non-fatty liver (P < 0.0001). **Conclusion:** The lesion may be overlooked by only early images due to the increase of the hepatic background accumulation, but scanning the delayed images can provide the equivalent images to the ones of non-fatty liver. For fatty liver patients, it may be better to positively scan the delayed images.

EP-0581

Significance of ^{11}C-acetate PET/CT in the evaluation of post-treatment recurrence for Gastrointestinal Stromal Tumor

S. Chen, S. Cheung, K. Cheng, Y. Leung, K. Wong, Y. Wong, C. Ho; Hong Kong Sanatorium & Hospital, Hong Kong, HONG KONG.

Purpose: Patients with Gastrointestinal Stromal Tumor (GIST) have higher chance of recurrence in the presence of high mitotic rate, large size and exo-luminal location. ^{18}F-FDG PET/CT has a proven role in identifying these parameters for primary GIST; but for recurrence, false negative (FN) results are often encountered. This study aims to explore the role of ^{11}C-acetate PET/CT in the detection of GIST recurrence. **Subjects & Methods:** We consecutively recruited 10 patients (M: 9, F: 1; mean age = 62.8 ± 13.1

y) who had undergone resection with (8/10) or without (2/10) adjuvant Imatinib therapy for primary high/intermediate or low risk GIST, respectively based on NCCN guidelines, but clinically suspected to have tumor recurrence. They were referred for a same-day ^{11}C-acetate and ^{18}F-FDG PET/CT. Biopsy or resection histopathology after PET/CT was the gold standard for diagnosis of recurrent GIST for all patients. **Results:** Preoperative ^{18}F-FDG PET/CT was positive in 8/8 (100%) high/intermediate and 1/2 (50%) low risk primary GISTs. Interval between primary GIST operation and follow-up PET/CT ranged from 15 to 84 months. All patients were found to have recurrent GIST with a total of 26 lesions (size = 3.7 ± 2.8 cm, liver: 14, peritoneum: 10, adrenal: 1, retroperitoneal lymph node: 1). Follow-up ^{18}F-FDG PET/CT detected 4/26 (15.4%) lesions in 2/10 (20%) patients, which gave a false impression that no active treatment was necessary in 8/10 (80% FN) patients. Instead, ^{11}C-acetate PET/CT detected 25/26 (96.2%) lesions in 10/10 (100%) patients, with SUV_{max} ranging from 3.4 to 11.6 (mean = 6.4 ± 2.5), which prompted resection in 5 patients, resuming Imatinib in 2 patients, and changing to Sunitinib in 3 patients. **Conclusion:** Although ^{18}F-FDG PET/CT is useful in the detection, risk stratification and monitoring of adjuvant drug treatment of primary GIST, it is suboptimal for surveillance of recurrent GIST. It is not clear if the ^{18}F-FDG FN cases were related to kinase inhibition by Imatinib coupled with altered KIT mutation; but since ^{11}C-acetate is a molecular probe of fatty acid metabolism independent of kinase mechanism, it is likely a more suitable PET tracer for follow-up of recurrent GIST, particularly in post-Imatinib cases.

EP-0582

Incremental role of C11-acetate PET/CT in Hepatocellular carcinoma

S. Z. Ali[1,2], *A. Sinha*[2], *H. Loi*[2], *L. Khor*[2]; [1]*Khoo Teck Puat Hospital, Singapore, SINGAPORE,* [2]*National University Hospital, Singapore, SINGAPORE.*

Objectives: To evaluate the role of C11-acetate PET/CT in the evaluation of Hepatocellular carcinoma (HCC). **Methods:** Retrospective analysis was performed in fifteen patients who had undergone C11-acetate PET/CT scan in addition to one or more of the standard imaging techniques for HCC, namely F18-FDG PET/CT, dedicated CT or MRI scan. Scans were performed either for pre-liver transplant screening or unexplained rising alpha-fetoprotein (AFP) levels in patients with prior history of HCC. C11-acetate PET/CT was obtained with initial limited acquisition through liver at 10 minutes after injection followed by whole body imaging at 20 minutes, using PET/CT scanner (Biograph 16, Siemens Medical Solutions, USA). Calculation of the maximum standardized uptake value (SUVmax) was performed for all sites with visibly increased metabolism. **Results:** Overall sensitivity of C11-acetate PET/CT for lesion detection is 53.9% (CT sensitivity 42.9%, MRI sensitivity 66.7%, F18-FDG PET/CT sensitivity 57%). Negative predictive value (NPV) of C11-acetate PET/CT is 25% (95% Confidence Interval (CI): 0.15-0.37). The addition of C11-acetate PET/CT changed management in 4 patients (26%) with detection of either occult bone metastasis or

confirmation of primary disease recurrence, indeterminate on CT/MRI scans. The metastatic bone lesions positive on C11-acetate PET/CT were not detected on Tc-99m MDP bone scans. C11-acetate PET/CT did not show any significant difference in sensitivity of lesion detection between rising AFP group and pre-transplant group (P value 0.447). In addition, although there is no significant difference in sensitivity between C11-acetate PET/CT and F18-FDG PET/CT in the detection of liver recurrence (P value 0.57), bone metastases were conclusively detected only on C11-acetate PET/CT. Also, the mean SUVmax of lesions detected by C11-acetate PET/CT were higher as compared to F18-FDG PET/CT (P value 0.03). False negative cases on C11-acetate PET/CT were noted in poorly differentiated HCC's, while moderately differentiated HCC showed increased C11-acetate uptake. **Conclusion:** C11-acetate PET/CT is especially useful in identifying occult distant bone metastasis in cases of HCC with unexplained rising AFP levels. It also has a role in the assessment of primary disease recurrence for lesions which are indeterminate on standard imaging techniques.

EP-0583

Prognostic value of F-18 FDG PET/CT in the Pre-transplant Evaluation of Patients with for Hepatocellular Carcinoma Patients without Treatment

B. Choi, **S. Kang**; *Catholic University of Daegu School of Medicine, Daegu, KOREA, REPUBLIC OF.*

Background: Although several prognostic factors are used to predict recurrence and to select adequate candidates for liver transplantation for hepatocellular carcinoma (HCC), these prognostic factors have some clinical limitations. The purpose of this study was to evaluate prognostic value of F-18 FDG PET/CT (PET/CT) in the pre-transplant evaluation of patients with HCC. **Materials and Methods:** The study included a total of 41 HCC patients (35 men and 6 women; age: 56±8) who underwent PET/CT and subsequent liver transplantation. All patients did not undergo any treatment before PET/CT and were followed up for more than 1 y (mean, 26 ±22 months), and recurrence of tumor was monitored. Three PET parameters—maximal standardized uptake value of primary tumor (pSUVmax), ratio of p SUVmax to normal-liver SUVmax (pSUVmax/nSUVmax), and ratio of pSUVmax to normal-liver mean SUV (pSUVmax/nSUVmean)—were tested as prognostic factors and compared with conventional prognostic factors. **Results:** pSUVmax, pSUVmax/nSUVmax, pSUVmax/nSUVmean, tumor size and T stage were significantly higher in patients with recurrence (P=0.0066, 0.0106, 0.0185, 0.031 and 0.0362). A receiver-operating characteristic curve demonstrated pSUVmax/nSUVmax of 1.14 to be the optimal cutoff for predicting PFS (sensitivity; 64.7%, specificity; 79.2%, P=0.0115). Kaplan-Meier analysis identified pSUVmax/nSUVmax ≥1.14 (P=0.0208) as predictors of recurrence. **Conclusions:** In this study, PET/CT was an independent and significant predictor of recurrence of HCC. In liver transplantation for HCC, PET/CT can provide effective information on the prognosis for tumor recurrence and the selection of candidates for liver transplantation.

EP-0584

Does TLG (total lesion glycolysis) superior value over SUVmax for pancreatic cancer assessment in operable cases and inoperable cases?

R. Ideguchi[1], A. Myssayev[2], T. Kudo[1]; [1]Department of Radioisotope Medicine, Atomic Bomb Disease Institute, Nagasaki University, Nagasaki, JAPAN, [2]Depatrment of Radioisotope Medicine, Graduate School of Biomedical Sciences, Nagasaki University, Nagasaki, JAPAN.

Aim: Pancreatic cancer is a poor prognostic cancer which requires proper diagnosis of tumor invasion to determine therapeutic decision. If we can predict tumor invasiveness with FDG PET, it would be hugely beneficial. However, there are many FDG parameters such as standardized uptake value(SUV), target to background ratio (TBR) and TLG (Total lesion glycolysis). We hypothesized that FDG parameter with volume information such as TLG has better accuracy than parameter that without such as SUVmax and TBR. Histopathogical findings of surgically resected pancreatic cancer and preoperative FDG PET parameters are correlated. Also, difference between operative and inoperative cases were analyzed. **Materials and Methods:** 51 consecutive pancreatic cancer patients who underwent preoperative FDG PET were analyzed. FDG images were obtained 60min after injection. SUVmax, SUVpeak, TLG of main tumor and TBR at each time point. For TBR calculation, average SUV of normal liver was used for "background" activity. Histopathological parameters such as lymphatic(ly), vascular(v) and perineural(ne) invasion were determined on resected surgical specimen. Each parameter of invasion was classified into 4 grading system (0=no invasion, 3=severe invasion). Those histopathological parameters were correlated with FDG PET parameters. Comparison of FDG parameters between patients who were able to go surgery and who were diagnosed inoperative were also analyzed. **Results:** 27 cases underwent surgery. One case of solid-pseudopapillary tumor and one case of IPMN were excluded. One case of preoperative chemotherapy performed between FDG PET and operation was also excluded. In three cases, tumor FDG uptake was too low to measure SUV or TLG. Remaining 21 cases were separated into two groups which has 0~1 invasive grade and 2~3 invasive grade for each of "ly", "v" and "ne" parameters because of too small case number of invasive parameter classified into "0" and "3". SUVmax, SUVpeak and TBR showed difference between "v" grade0~1 and grade2~3. For "ly" and "ne" invasions, no significant difference was observed. Interestingly, TLG parameters did not showed any difference in all parameters. When we compare between those 21 operative case and 24 inoperative cases, only TLG showed significant difference. SUVmax, SUVpeak and TBR did not show any significant difference. **Conclusion:** For predicting tumor invasiveness, FDG PET may useful for evaluating vascular invasion but not for lymphatic and perineural invasion. Adding volume information to FDG uptake does not showed incremental value on those invasiveness prediction. On the other hand, for operability determination, tumor volume parameter has significant impact.

EP-0585

^{18}F-FMISO PET/CT as a preoperative prognostic factor in patients with pancreas cancer

T. Yamane[1], M. Aikawa[2], M. Yasuda[3], A. Seto[1], I. Kuji[1]; [1]Department of Nuclear Medicine, Saitama Medical University International Medical Center, Hidaka, JAPAN, [2]Department of Gastroenterological Surgery, Saitama Medical University International Medical Center, Hidaka, JAPAN, [3]Department of Diagnostic Pathology, Saitama Medical University International Medical Center, Hidaka, JAPAN.

Purpose: Tumor hypoxia in pancreas cancer is known as one of the important prognostic factors. The aim of this study is to test the feasibility of ^{18}F-fluoromisonidazole (^{18}F-FMISO) PET/CT as a preoperative prognostic factor in patients with pancreas cancer. **Subjects & Methods:** The institutional review board approved this study, and a written informed consent was obtained from all the participants. We enrolled 16 patients with pancreas tumor who had been initially planned for surgery. PET/CT was performed at 2.5 h after intravenous injection of 7.4 MBq/kg ^{18}F-FMISO. Regions of interest were drawn on the pancreas tumor and the descending aorta, and tumor blood ratio (TBR) was calculated by dividing SUVpeak of the tumor by SUVmean of the aorta. For the patients who underwent surgery, the expression of HIF-1α in the tumor was measured by immunohistochemistry. The patients were dichotomized by TBR, and recurrence-free survival was analyzed using Kaplan-Meier method. A *p* value of less than 0.05 was considered to be significant. Data expressed with plus/minus indicates mean and standard deviation. **Results:** As a result of thorough clinical examinations other than ^{18}F-FMISO PET/CT, 3 patients were considered inoperable. Their TBR was significantly higher than that in the operative patients (1.93 ± 0.52 vs 1.17 ± 0.24, *p* < 0.05, Mann-Whitney U test). Among the 13 patients who underwent surgery, HIF-1α was overexpressed in 4 patients. Their TBR was significantly higher than the others (1.39 ± 0.33 vs 1.07 ± 0.11, *p* < 0.01, Mann-Whitney U test). The patients were dichotomized at TBR of 1.18, and the higher group showed shorter recurrence-free survival than the other (median 145 vs 318 days, *p* < 0.05, Wilcoxon test). **Conclusion:** ^{18}F-FMISO PET/CT has the possibility to be a preoperative prognostic factor in patients with pancreas cancer.

EP-0586

New exponential functions based on CT density to estimate the precentage of liver that is fat

G. Keramida[1], A. M. Peters[2]; [1]Royal Brompton and Harefield Hospitals NHS,FT, London, UNITED KINGDOM, [2]Royal Sussex County Hopsital & Clinical Imaging Sciences Centre,, Brighton, UNITED KINGDOM.

Aims: In FDG PET/CT, hepatic standardised uptake value (SUV) is reduced through 'signal dilution' by hepatic fat because FDG does not enter hepatocyte fat droplets. As it will tend to be located in a low fat region of liver, maximum SUV (SUV_{max}) will be less affected by signal dilution than mean SUV (SUV_{mean}). Accordingly, hepatic SUV_{max}/SUV_{mean} correlates with hepatic fat.

SUV_{mean} can be corrected for signal dilution using an equation that relates hepatic CT density (CTD) to %fat. However, the 2 previously published equations (one linear and one sigmoid) disagree widely at low and high fat contents. Our aim was to exploit the relationships between hepatic SUV indices and CTD to compare these 2 equations against each other and against two new exponential equations for estimating %fat from CTD. **Methods:** The study population comprised 465 patients having routine FDG PET/CT. SUV_{max}, SUV_{mean} and CTD were measured from a 3 cm-diameter ROI over the liver. The new exponential equations assume that CTD of 31 HU corresponds to 14.5% fat, which is where the linear and sigmoid equations cross, and that 100% fat corresponds to CTD of -50 or -100 HU. The proportion of liver occupied by fat (P_F) was estimated from all 4 equations, as follows. $P_F = (55.8 - CTD)/170$ (1) (Ricci, J Hepatol 1997;27:108-13) $P_F = \exp[-\exp([0.051*CTD] - 0.915)]$ (2) (Kodama, AJR 2007;188:1307-12) $P_F = \exp[-0.0238*(CTD+50)]$ (3) $P_F = \exp[-0.0147*(CTD+100)]$ (4) Fat-corrected SUV_{mean} is given as $SUV_{mean}/(1-P_F)$. The ideal equation should give SUV_{mean} approaching but not exceeding SUV_{max} and give fat-corrected SUV_{mean}/SUV_{max} that shows no correlation with CTD. **Results:** Equation 1 fails at CTD values exceeding 56 HU because it gives negative P_F values. Moreover, it gave fat-corrected SUV_{mean}/SUV_{max} values that still correlated (negatively) with CTD. Equation 2 grossly over-corrected SUV_{mean} at low CTD. Thus at CTD <20 HU), it gave ratios of fat-corrected SUV_{mean}/SUV_{max} approaching 3. It grossly under-corrected SUV_{mean} at high CTD as a result of giving values of %fat of zero when CTD >45 HU. Equations 3 and 4, in contrast, gave very few ratios exceeding unity at any CTD value and moreover produced no correlation between fat-corrected SUV_{mean}/SUV_{max} and CTD. **Conclusion:** Equation 2 (sigmoid) is unsuitable for estimating %fat from CTD. Equation 1 (linear) generally performed well but gave nonsensical negative values of %fat at CTD levels not uncommonly encountered. Equation 3 (exponential) that assumes that 100% fat corresponds to -50 HU performed best.

EP-0587

Study on diagnosis of primary liver cancer by PET/CT multimodal imaging

*X. Wu, X. Meng, K. Zhang, Z. Bai, **X. Wang**; The Affiliated Hospital of Inner Mongolia Medical, Hohhot, CHINA.*

Objective: To explore the diagnosis value of PET/CT multimodal imaging in primary liver cancer by the ^{18}F-FDG PET/CT dual-phase imaging and combination of ^{18}F-FDG and ^{11}C-CHO PET/CT imaging in the positive detection rate of primary liver cancer. **Methods**: Twenty-three patients with primary liver lesions have not been confirmed on the examinations of ultrasound, CT or MRI from March 2014 to October 2015. All cases were examined on ^{18}F-FDG PET/CT imaging examination and liver regional delayed and ^{11}C-CHO imaging. The region of interest (ROI) was outlined on the neoplastic focus and the maximum standard uptake (SUVmax) was generated automatically as a semi-quantitative indicators .Tumor tissue uptake was higher than the surrounding normal liver tissue on ^{18}F-FDG (^{11}C-CHO)imaging:

T/L (tumor/liver) ≥1 was positive imaging. On delayed regional liver ^{18}F-FDG imaging, ΔSUVmax≥10% was positive imaging of malignant ; ΔSUVmax<10% was a negative imaging of benign lesion. 17 cases of benign lesions were excluded by confirmation of pathology or clinical follow-up results and 36 cases of primary liver cancer were included in the study with pathology or biopsy confirmation. **Results:** (1) The lesion SUVmax of dual phase imaging were 5.38±2.87 and 6.44±4.11(t=2.965, p <0.05) on ^{18}F-FDG PET/CT dual phase imagin of 23patients ;Tumor/liver (T/ L) values were 3.63±2.16 and 5.26±3.15(t=5.019, p<0.05); T/L value on whole body imaging was lower than delayed imaging. The positive detection rate of primary liver cancer was 65.2% (15/23) on whole body PET/CT imaging, while the diagnosis detection rate was 78.26% (18/23) on dual-phase imaging. (2) 23 abnormal radioactivity uptake lesions of liver were found on ^{18}F-FDG and ^{11}C-CHO PET/CT imaging and primary liver cancer was confirmed by pathology or clinical follow-up result. SUVmax of liver background on ^{18}F-FDG and [11]C- CHO imaging were 1.58±0.29 and 5.41±1.85; t=3.783, p<0.05;The lesion SUVmax on ^{18}F-FDG and ^{11}C-CHO imaging were 4.54±2.26, 7.43±3.45(t=3.016, p<0.05); T/L value on ^{18}F-FDG and ^{11}C-CHO imaging were 2.85±1.23 and 1.47±0.92(t=10.200, p<0.05);The positive detection rate of primary liver cancer was 57.14% (12/21) on ^{18}F-FDG PET/CT imaging, while the positive detection rate on combination of ^{18}F-FDG and ^{11}C-CHO PET/CT imaging was 90.48% (19/21), the combination of two kinds imaging agent could improve the positive detection rate of primary liver cancer (p<0.05). **Conclusion:** Dual-phase ^{18}F-FDG PET/CT imaging and combination of ^{18}F-FDG and ^{11}C-CHO PET/CT multimodal imaging could improve the positive detection rate of primary liver cancer and had important clinical value in the making of early diagnosis, treatment measures and prognosis.

EP-0588

Improvement Of Survival In Patients With Hepatocellular Carcinoma After 90Y RESIN Microsphere Radioembolization: Our Experience

F. Di Gregorio[1], M. Rensi[1], A. Vit[2], G. Ferretti[1], F. Giacomuzzi[1], D. Capobianco[1], M. Povolato[1], L. Peressini[3], M. Sponza[2], F. Bonutti[4]; [1]Department of Nuclear Medicine University Hospital, Udine, ITALY, [2]Department of Radiology University Hospital, Udine, ITALY, [3]University Hospital, Udine, ITALY, [4]Department of Medical Physics University Hospital, Udine, ITALY.

Introduction: Hepatocellular carcinoma (HCC) is a common cause of cancer related mortality. Among the therapeutic procedures selective internal radiation therapy with 90Yttrium resin microspheres (SIRTEX) has demonstrated high efficacy across the whole spectrum of HCC from early to advanced stages. The aim of this study was to assess the improvement of overall survival in patients with HCC after radioembolization using SIRTEX. **Subjects and Methods:** 87 patients (79 Males; 8 Females; median age: 66 ± 9 years) with locally advanced HCC were enrolled in the study. As defined by Barcelona Clinic Liver Cancer 26 patients were in stage A, 21 patients in stage B, 26 patients in stage C and 14 in stage D. Median size of lesion was 6,0 ± 2,8

cm. 65 patients had a single lesion 53 of them localized in right lobe and 12 of them in left lobe, while 22 patients had multifocal disease. All patients underwent radioembolization with SIRTEX and received a median activity of 2,7 ± 0,6 Gbq. Patient survival was summarized using Kaplan-Meier method. Log-rank test (Wilcoxon test) was applied to calculate the significance of the difference between the survival curves. **Results:** The overall survival for all patients was 21,9 months, which varied by disease stage (stage A: 55,0 months; stage B: 27,3 months; stage C: 11,3 months; stage D: 4,1 months). The improvement of survival was significant in stage A patients in comparison with patients in stage B and C (p< 0,001) and was not significant in stage D, confirming the poor indication for SIRTEX in advanced stage of HCC. No significant influences on survival by number and size of the HCC lesions was observed. **Conclusion:** Our results suggest that radioembolization with SIRTEX can provide a clinically relevant benefit in survival of patients with HCC across different tumor stages and particularly in early stage.

EP-0589

Prognostic value of a computer based, machine learning-driven survival model for pancreatic cancer in treatment naïve patients

T. S. Nakuz[1], Y. Bican[1], L. Papp[1], W. Wadsak[1], A. Al-Mukhtar[2], A. Haug[1], M. Hacker[1], G. Karanikas[1]; [1]Medical University of Vienna, Department of Biomedical Imaging and Image-guided Therapy, Division of Nuclear Medicine, Vienna, AUSTRIA, [2]Medical University of Vienna, Department of Biomedical Imaging and Image-guided Therapy, Division of Radiology, Vienna, AUSTRIA.

Aim: To integrate image and laboratory parameters into a machine learning based model for two-year survival prediction in treatment naïve patients with pancreatic cancer. **Materials and Methods:** To date 25 patients aged 43 to 88 (mean age of 62.7 years) were included in this retrospective study. All patients underwent pre-therapy ^{18}F-FDG-PET/CT scan as well as laboratory analysis and were followed at least for 24 months from the date of the PET/CT acquisition. Delineation of the primary tumours and the mediastinum serving as reference for tumour-to-background calculations were performed manually in PET/CTs using the Hybrid3D software (Hermes Nuclear Diagnostics, Stockholm, Sweden). Both the PET and CT tumour VOIs were the subject of image-derived feature extraction including first-order (6), histogram (6), shape (2), as well as textural (19) features (33/image, 66 overall). In addition, 12 laboratory features (CA19-9, CEA, Keratinin, Gamma-GT, Alkaline phosphatase, GOT, GPT, Bilirubin, a-Amylase, Lipase, CRP, Leukozytes) were collected for each case as well. This way each tumour was characterized with a total number of 78 features. A multi-layer machine learning algorithm was utilized to automatically select and weight relevant features in order to build a 24-month survival predictor model. The machine learning-derived predictor outcomes were the subject of the Monte Carlo cross-validation scheme where dichotomized survival values served as reference. **Results:** The average life expectancy in the cohort was 18.4 months (range of 4 months to two year survival). The machine learning driv-

en 24-month prognostic model resulted in 84% sensitivity, 85% specificity, 84% accuracy, 79% positive-predictive-value and 89% negative-predictive-value in the cross-validation. **Conclusions:** The preliminary results demonstrate that there is a high potential in machine learning-driven 24-month pancreatic survival predictor models.

EP-0590

18F FDG PET CT, Circulating Tumor Cells and Alpha Fetoprotein in Patients With Hepatocellular Carcinoma on the Waiting List for Liver Transplantation

J. Navarro Fernandez, L. Frutos Esteban, M. Laroussi, P. Ramirez Romero, M. Godoy Bravo, R. Reyes Marles, L. Sáenz Mateos, P. Cascales-Campos, E. Llàcer Millán, M. González Sánchez, M. Sánchez Lorencio, S. Veganzones de Castro, E. Díaz Rubio, P. Parrilla Paricio, M. Claver Valderas; H U Virgen de la Arrixaca, Murcia, SPAIN.

The aims of this study were determination the relationship between the number of circulating tumor cells (CTCs) in patients with hepatocellular carcinoma (HCC) in compliance with the Milan criteria and on the waiting list for hepatic transplantation with the of α-fetoprotein levels (AFP) and 18F FDG PET CT findings. **Patients and Methods**: An oncologycal evaluation with 18 F FDG PET CT, CTCs, and AFP was conducted in 24 consecutive patients with HCC eligible for orthotopic liver transplantation according to the Milan criteria. The diagnosis of HCC was made according to clinical, biological, and radiological findings. **Results:** We detected CTCs in peripheral blood in 21 of 24 patients (87.5%) before liver transplantation, with a mean number CTCs of 156 ± 370 (range, 2 to 1768) with statistically significant association between number of CTCs detected in peripheral blood and the time within the waiting list (P < .05), but not betwen AFP levels and standard uptake value (SUV) and time to orthotopic liver transplantation (P > .05). **Conclusions:** 18 F FDG PET-TC, CTCs, and AFP levels could be an essential key for the correct management of the patients with HCC on the waiting list for liver transplantation

EP-0591

Role of PET-CT with ^{18}F-FDG in the Detection of Pancreatic Neoplasm Recurrence: Preliminary Study

A. Sabaté Llobera[1], J. J. Robles Barba[1], P. Notta[1], E. Llinares Tello[1], L. Rodríguez Bel[1], J. Mestres Martí[1], G. Reynes Llompart[1], J. Fabregat Pous[2], N. Calvo Malvar[1], C. Gámez Cenzano[1]; [1]Unitat PET-Servicio de Medicina Nuclear. IDI. Hospital U. de Bellvitge-IDIBELL., L'Hospitalet de Llobregat, SPAIN, [2]Servicio de Cirugía General. Hospital U. de Bellvitge-IDIBELL, L'Hospitalet de Llobregat, SPAIN.

Aim: To evaluate the utility of FDG-PET/CT (PET) in the detection of recurrence of pancreatic neoplasms. **Material and Method:** Retrospective analysis of PET studies in 36 patients (21 males, median age 69 years) with clinical/radiological/serological suspicion of recurrence of pancreatic neoplasia. The location and metabolic activity of the lesions (PET+ / PET-), the impact on the therapeutic management (CT/MRI) and the subsequent evolu-

tion of the patients (follow-up 7-24 months) were studied. **Results:** Twenty-six patients (72%) were PET+, of whom 1 was a primary pulmonary tumor and another one was a false positive due to infection. In 5 patients (19%) relapse was exclusively local, in 6 (23%) regional and in 14 (54%) distant metastasis. The most hipermetabolic lesions were located at the surgical bed (6), lymph nodes (7), liver (8), lung (3), bone (1) and peritoneum (1). The median of SUVmax in surgical bed lesions was 4.0, while for the set of lesions was 5.4. In 11 patients (42%), PET detected more lesions than CT/MRI, and in 7 (27%) changed stage and management. At follow-up, 12 patients (33%) remain free of disease (6 PET+, 6 PET-; the positive ones with local disease (1), lymph nodes (3), hepatic (1) and synchronous pulmonary neoplasm (1)); 5 showed progression (14%, all of them PET+), and 19 (53%) deceased (15 PET+, 4 PET-). In the 4 PET- exitus, CT/MRI were negative too and patients died between 4-16 months after PET/CT (false negatives). Overall survival was 10.5 months (2-23); 8.5 months for PET+ and 12 months for PET-. **Conclusions:** In our preliminary study, FDG-PET/CT for detection of recurrence of pancreatic neoplasms visualized more lesions than conventional imaging techniques, changing the therapeutic management in up to 25% of the patients. Survival was lower in patients with PET+ than in those with PET-.

EP-0592
The benefits of 18FDG-PET/CT in the evaluation of pancreatic IPMN

E. Tabacchi[1], C. Nanni[1], E. Lodi Rizzini[1], P. Ghedini[1], D. Santini[2], A. De Leo[2], F. Minni[3], N. Pagano[4], C. Ricci[3], L. Calculli[5], R. Casadei[3], S. Fanti[1]; [1]Department of Nuclear Medicine, S. Orsola-Malpighi Hospital, University of Bologna, Italy, Bologna, ITALY, [2]Anatomy, Pathological Histology Unit, S.Orsola-Malpighi University Hospital, Bologna, Italy, Bologna, ITALY, [3]General Surgery Unit, S.Orsola-Malpighi University Hospital, Bologna, Italy, Bologna, ITALY, [4]Gastroenterology Unit, S.Orsola-Malpighi University Hospital, Bologna, Italy, Bologna, ITALY, [5]Radiology Unit, S.Orsola-Malpighi University Hospital, Bologna,Italy, Bologna, ITALY.

Aim: Intraductal papillary mucinous neoplasms (IPMN) (20-50% of all cystic neoplasms) can be divided into benign, borderline and malignant lesions (carcinoma). An effective stratification of patients at very high risk of cancer is of utmost importance to avoid unnecessary surgery. The association between IPMN and adenocarcinoma of the pancreas as distinct entity is reported as a relatively common event: thus IPMN could be considered as a target for the identification of sporadic pancreatic adenocarcinoma. The aims of this study are: 1)to evaluate accuracy, sensitivity and specificity of 18FDG-PET/CT in the detection of malignant IPMN in comparison to histological/cytological exam or follow-up (CT, MRI, EUS) and with the data reported in the literature; 2)to identify the percentage of patients with IPMN and adenocarcinoma of the pancreas as different entity and compare it with literature. **Materials and methods:** We retrospectively evaluated 135 18FDG-PET/CT from January 2009 to July 2016 (99 patients) with an imaging-based (CT, MRI, EUS, ERCP) diagnosis of IPMN. All 18FDG-PET/CT scans had to be performed within 3 months after diagnostic conventional imaging for IPMN, following standard procedure. Results were validated by histological/cytological confirmation or by follow-up through CT/MRI/EUS (mean follow-up was 10 [5-14] months). Clinical history, follow up and imaging have been used to assess the presence of association between IPMN and adenocarcinoma. **Results:** 18/135 18FDG-PET/CT (13.3%) showed increased uptake at the site of IPMN (mean SUVmax:10). 17/135 (12.6%) were true positive for cancer, 1/135 (0.7%) false positive. One hundred seventeen on 135 (86.7%) 18FDG-PET/CT showed no increased uptake at the site of IPMN, with 115/135 (85.2%) true negative and 2/135 (1.5%) false negative. 18FDG-PET/CT showed accuracy:98%, sensitivity:89%, specificity:99%, positive predictive value:94% and negative predictive value:98% in the evaluation of malignant IPMN. These results were consistent with literature (reported accuracy:97%, sensitivity:88%, specificity:98%). Thirteen of 135 (9.6%) 18FDG-PET/CT scans were performed in patients with adenocarcinoma of the pancreas in a distinct site from IPMN: 7/13 (54%) presented concomitant adenocarcinoma and 6/13 (46%) prior adenocarcinoma. 7/99 (7%) patients with IPMN therefore presented concomitant/no concomitant adenocarcinoma according to literature (2.5% - 9.2%). **Conclusions:** 18FDG-PET/CT seems advisable for routine use in IPMN monitoring and could be a valid tool for detecting early malignant degeneration, implementing conventional imaging methods. This small preliminary study suggests a correlation between IPMN and distinct adenocarcinoma of the pancreas recommending a close surveillance not only to assess IPMN malignant degeneration but also to check all pancreatic parenchyma.

EP-0593
Simultaneous FDG-PET/CT and contrast-enhanced CT in cholangiocarcinoma: just pretty images?

A. Farolfi[1], A. Lambertini[1], L. Zanoni[1], C. Mosconi[2], S. Brocchi[2], I. Pettinari[2], V. Rossetti[3], F. Mangiacotti[1], D. Mascherini[1], R. Golfieri[2], S. Fanti[1], C. Nanni[1]; [1]Service of Nuclear Medicine, S. Orsola-Malpighi Hospital, University of Bologna, Bologna, ITALY, [2]Radiology Unit, Department of Diagnostic and Preventive Medicine, S. Orsola-Malpighi University Hospital, Bologna, ITALY, [3]Nuclear Medicine Department, ASUITS, Trieste, ITALY.

Purpose: To assess the performance of [18]FDG PET/ceCT simultaneously acquired, contemporary read and finally discussed by a nuclear medicine physician and a radiologist in a group of cholangiocarcinoma patients. **Methods:** We analyzed a cohort of patients, diagnosed with cholangiocarcinoma (CC), who underwent a combined ^{18}F-FDG-PET/CT and contrast-enhanced CT (PET/ceCT) scan, for both staging and re-staging of disease. The resulting images, simultaneously acquired on the same tomograph, were read and reported on by experienced nuclear medicine and radiology physicians. **Results:** We retrospectively analyzed, between December 2012 and March 2017, a total of 52 patients (23F, 29M; mean age 59, range 39-84) with histologically confirmed CC (34 intrahepatic, 15 peri-hilar, 3 distal). 6 scans were performed during staging, 46 during re-staging

of disease. None of the patients experienced immediate severe adverse reactions relating to the procedure. 45/52 (86.5%) PET/ceCT scans turned out positive, while 7 were negative. Among positive patients, the average maximal standard uptake value (SUVmax) was 8.5 (range: 2.1 to 53.6; median SUVmax: 6.9). In 34/52 patients (65.4%), PET/CT and ceCT were completely concordant in detecting liver disease. CeCT alone determined a significant impact on the interpretation of liver disease in 15/52 patients (28.8%), PET/CT alone in 3/52 (5.8%). Regarding the detection of metastatic lymph nodes, complete concordance was achieved in 38/52 cases (73.1 %), while PET/CT alone detected hyper-metabolic lymph nodes in 4/52 cases (7.7%). CeCT alone showed positives in 7/52 (13.5%); additional positive lymph nodes, though related to different findings and therefore not concordant, were observed by both techniques in 3/52 patients (5.8%). Metastatic disease was detected by both PET/CT and ceCT in 42/52 cases (80.8%). CeCT alone was positive in 5/52 cases (9.6%), PET/CT in 2/52 (3.8%). Discordant positive findings of metastatic disease were again observed in 3/52 patients (5.8%). Overall, ^{18}F-FDG-PET/CT alone played a significant role in the final evaluation of extra-hepatic spread of disease in 12/52 cases (23.1%). **Conclusions:** In our cholangiocarcinoma patients we found that combined ^{18}F-FDG-PET/ceCT may be feasible and time-saving, providing useful information for both staging and re-staging of disease. CeCT is more accurate in the assessment of liver involvement and showed significant advantages in the detection of smaller lesions, particularly sub-centimetric pulmonary nodules. ^{18}F-FDG-PET/CT may add value to ceCT in characterizing abdominal lymph nodes as in detecting distant metastasis. Nevertheless, the prognostic value of ^{18}F-FDG-PET/CT during follow-up and therapy response evaluation should be further investigated.

EP-0594

The Contribution of Metabolical and Morphological Evaluation in FDG PET/CT in the Staging of Signet Ring Cell Carcinoma of the Stomach

A. Yıldız[1], B. Özcan[2], M. Özdoğan[3], H. Dikici[4], C. Ertuğrul[4], A. Gürkan[2], Z. Şahin[1]; [1]Nuclear Medicine, Medstar Hospital, Antalya, TURKEY, [2]General Surgery, Medstar Hospital, Antalya, TURKEY, [3]Medical Oncology, Medstar Hospital, Antalya, TURKEY, [4]Gastroenterology, Medstar Hospital, Antalya, TURKEY.

Purpose: Hypometabolism is usually observed in signet ring cell subtype of stomach cancer due to low GLUT-1 expression. Therefore, the success of FDG PET-CT in detecting local spread and metastasis is much lower than other gastric cancer subtypes. The diagnostic contribution of assessment in the combination of multiplanar diagnostic CT using contrast enhanced and MDCT features of PET-CT was investigated in the study. **Subjects and Method:** A total of 37 signet ring cell gastric carcinomas patients composed of 18 patients who were examined for the purpose of preoperative staging and then underwent palliative surgery due to obstruction and 19 patients who underwent curative total gastrectomy and lymph node dissection were included in the retrospective study. All imaging data were compared with postoperative pathological data in all cases. The CT component of FDG PET was performed with IV contrast agent, standard dose and technique. In addition to metabolic activity, the contribution of the CT images to the evaluation was investigated. **Results:** No metastasis was detected in 19 of the cases and metastasis was detected in 18 of the cases. The metastases were peritoneal in 15/18 cases, nodal in 8/18 cases, ovarian in 4/18 cases, osseous in 3/18 cases and were hepatic in 3/18 cases. Peritoneal metastasis was observed in 83.3% of cases in form of diffuse infiltration. In 5/18 (38.8%) of the cases, metastases were only peritoneal and could be morphologically detected in contrast-enhanced MDCT slices of PET-CT. Peritoneal lesions were in form of focal involvement in 11 cases (61.1%) and was in form of diffuse infiltrative spread in other cases. SUVmax values of primary mass were statistically indifferent between metastatic and non-metastatic cases (p = 0.085), however, there was significant difference between metastatic cases (10.86+6.9) and non-metastatic cases (5,7+2.6) when a case (30.1), in which a high non-metastatic activity was observed, was excluded from the analysis. The involvement of the stomach appeared diffusely infiltrative in 23/38 of cases. A weak (r = 0.45) but statistically significant correlation was detected between SUVmax and the presence of metastasis (P = 0.006). Conclusion: Signet ring cell carcinoma of the stomach can often cause peritoneal metastasis and peritoneal spread can be successfully detected by the combined assessment of PET and CT slices. SUVmax shows positive correlation with metastasis and may be correlated with the prognosis.

Clinical Oncology: Neuroendocrine Tumours

EP-0595

The effect of long acting somatostatin analogue administration on ^{68}Ga-DOTATATE uptake in primary and metastatic NET lesions

N. Ayati[1], S. Lee[2], R. Zakavi[1], K. Pathmaraj[2], L. Qatawneh[3], A. Poon[2], A. Scott[2,4,5]; [1]Mashhad Univesity of Medical Sciences, Mashhad, IRAN, ISLAMIC REPUBLIC OF, [2]Department of Molecular Imaging & Therapy, Austin Health, Heidelberg, AUSTRALIA, [3]Nuclear Medicine and Cyclotron Unit, King Hussein Medical Center, Jordanian Royal Medical Services, JORDAN, [4]Olivia Newton-John Cancer Research Institute; and School of Cancer Medicine, La Trobe University, Heidelberg, AUSTRALIA, [5]Department of Medicine, University of Melbourne, Austin Health, Heidelberg, AUSTRALIA.

Introduction: Synthetic somatostatin analogs have been posed as a potential source of error in somatostatin receptor imaging by interfering with tumor detection; however, experimental models and clinical studies have shown a complex mechanism of octreotide effect on tumors. This study aimed to assess whether ^{68}Ga-DOTATATE uptake differs before and after treatment with long-acting somatostatin analogs. **Subjects & methods:** Thirty patients with intermediate to well differenti-

ated neuroendocrine tumors who underwent 68Ga-DOTATATE PET/CT scanning before and after receiving Sandostatin LAR were included in the study. The maximum and the mean standardized uptake values (SUV$_{max}$ and SUV$_{mean}$) of healthy target organs, residual primary tumor and up to five lesions with the highest SUV$_{max}$ in each organ were compared before and after octreotide treatment. **Results:** Thirty patients (15 males) with a mean age of 64.6±13.4 years were studied. The mean time interval between the two 68Ga-DOTATATE studies was 9.6±7.2 months, and the mean time gap between the last Sandostatin LAR injection and the second 68Ga-DOTATATE study was 25.1±14.8 days. The pre-treatment mean SUV$_{max}$ and SUV$_{mean}$ were both significantly higher in the thyroid, liver, spleen and residual primary tumor (P<0.05) than the values measured after administration of Sandostatin LAR. No significant differences were found among the uptake indices for any metastatic lesions of the liver, bone, lung or lymph nodes before and after Sandostatin LAR administration (P>0.05). **Conclusion:** Long-acting octreotide treatment diminished 68Ga-DOTATATE uptake in the liver, spleen, and thyroid gland as well as in residual primary tumor but did not compromise tracer uptake in metastatic lesions. These findings have direct impact on the interpretation of 68Ga-DOTATATE PET/CT scans.

EP-0596

68Ga-DOTA-TOC PET/CT predicts exact tumor staging in head and neck paragangliomas, compared to 18F-DOPA PET/CT and 123I-MIBG SPECT/CT

A. S. Kroiss[1], C. Uprimny[1], L. Gruber[1], B. L. Shulkin[2], I. J. Virgolini[1]; [1]Medical University Innsbruck, Innsbruck, AUSTRIA, [2]St Jude Research Hospital, Memphis, TN, UNITED STATES OF AMERICA.

Purpose: MIBG labeled with 123I, and somatostatin receptor (SST) imaging, labeled with 111Inpentetreotide, respectively, are functional imaging modalities, which achieve moderate sensitivity in localizing extraadrenal paragangliomas (PGL). However both functional imaging modalities are limited in detecting (malignant) head and neck PGL due to limited resolution of planar scintigraphy and of single photon emission computed tomography (SPECT) compared to positron emission tomography (PET), respectively. We compared functional imaging modalities in the diagnosis and staging of head and neck PGL, using 68GaDOTATOC PET/CT (diagnostic CT), 18F-DOPA PET("low-dose" CT) and 123IMIBG scintigraphy, including SPECT/CT ("low-dose" CT). Functional and anatomical imaging (combined crosssectional imaging) referred as reference standard. **Methods:** Three male and eight female patients (age range 26 to 73 years) with anatomical and/or histologically proven disease were included in this study. Comparative evaluation included morphological imaging with CT, functional imaging with 68GaDOTATOC PET, 18F-DOPA PET and 123IMIBG imaging. Imaging results were analyzed on a perlesion basis. Results: the overall detection rate of 68GaDOTATOC PET on a perlesion basis was 100% (McNemar p<0.5), of 18F-DOPA PET 67.9% (McNemar p<0.01) and that of 123IMIBG imaging was only 8.0% (McNemar p<0.0001) and of SPECT/CT was 12.0 % (McNemar p<0.0001), respectively. Both,

68GaDOTATOC PET and anatomical imaging identified 28 lesions. 18F-DOPA detected 19 manifestations, 123I-MIBG imaging identified only 2 lesions and SPECT/CT 3 lesions. Two additional lesions were detected by 68GaDOTATOC PET, but negative in both, 123IMIBG and CT imaging. **Conclusion:** 68GaDOTATOC PET/CT predicts exact tumor staging in head and neck paragangliomas, compared to 18F-DOPA PET and to 123IMIBG imaging, including SPECT/CT, respectively.

EP-0597

Indication of MDP bone scan after MIBG scintigraphy in patients with neuroblastoma

K. Chaurasiya, E. Kireeva, I. Krupina, Y. Likar; Dmitry Rogachev National Research and Practical Center of Pediatric Hematology, Oncology and Immunology, Moscow, RUSSIAN FEDERATION.

Introduction: Scintigraphy with 123I-MIBG and 99mTc-MDP are widely used in diagnosis and staging of neuroblastoma. 123I-MIBG is the specific marker for neuroblastoma whereas 99mTc-MDP scintigraphy can distinguish bone metastasis and bone marrow involvement in 123I-MIBG positive neuroblastoma patients. **Purpose:** Determine the indications of 99mTc-MDP scintigraphy after 123I-MIBG scintigraphy in patients with neuroblastoma and evaluate the sensitivity of both methods in patients with neuroblastoma IV-stage. **Materials and Methods:** The study includes 107 patients, aged 0-14 years (median age 1.5 years), who had not previously performed MIBG and MDP scintigraphy, underwent both diagnostic procedures at interval of less than 30 days (mean 13 days) using standard protocols. **Results:** 94 (88%) patients were MIBG positive and 13 (12%) MIBG negative. Out of the total patients (n=107), 82 were with neuroblastoma IV-stage. 123I-MIBG-scintigraphy had revealed skeletal metastasis in 78 out of the 82 patients with neuroblastoma IV-stage, whereas 99mTc-MDP-scintigraphy was able to detect bone metastasis only in 55 patients. Out of all MIBG-positive patients (n=94): 78 (73%) were MIBG positive for skeletal metastasis ± primary tumors; out of them only 51 (47.6%) were MDP positive. 16 (14.9%) patients were MIBG positive only for primary tumors; all of them were MDP negative. Only in MIBG negative patients (n=13), MDP had played an important role to detect bone lesions in 4 (3.7%) patients. A significant difference has been noted in the number of identified metastatic lesions: 123I-MIBG-scintigraphy has identified 951 lesions and 99mTc-MDP-scintigraphy only 268. **Conclusions:** According to our study the scintigraphy with 99mTc-MDP is indicated only in patients with 123I-MIBG-negative neuroblastoma. Sensitivity of 123I-MIBG scintigraphy significantly exceeds the sensitivity of bone scan in detection of metastasis in patients with neuroblastoma IV-stage. To analyze the outcome of treatment and prognostic value in patients with bone metastasis detected by 99mTc-MDP-scintigraphy and in other patients with neuroblastoma IV-stage, a longer observation period is needed.

EP-0598

The role of 18F Fluorocholine PET/CT in the imaging of recurrence of parathyroid cancer after surgery

A. Florczak, I. Gorczewska, A. d'Amico; Maria Sklodowska-Curie Memorial Cancer Center and Institute of Oncology, Gliwice Branch, Poland, Gliwice, POLAND.

Introduction: Parathyroid carcinoma is an extremely rare endocrine malignancy. It accounts for between 0.5% and 5% of all cases of primary hyperparathyroidism. The only known curative treatment is complete primary excision of a parathyroid tumour and surrounding structures. The recurrence rate in patients who have undergone en-block resection is 33% and who have undergone suboptimal resection is 50%. Parathyroid cancer and his recurrences commonly present severe hypercalcemia due to osteoporosis with fractures, pain, chondrocalcinosis, nephrolithiasis with impaired renal function, disorders of digestive tract like peptic ulcers and pancreatitis, hypertension disease. May also cause neuropsychiatric symptoms, decreased quality of life. Hypercalcemia disease is a life-threatening emergency. Finding metastases can be difficult, especially in the neck. With persistent or recurrent disease it is important to exclude metastases to the lung or bone before reexploration of the neck. The aim of the study was to show that the 18F Fluorocholine PET/CT examination is a valuable tool for finding and imaging the recurrence of parathyroid cancer. Subjects and Methods: Three women after a few surgeries of parathyroid glands because of parathyroid cancer with a high level of PTH in the serum underwent 18F Fluorocholine PET/CT examination. Obtained results showed metastases in each case. Results: 1. 49-year-old woman after ten surgeries because of recurrences of parathyroid cancer, last operation two months before PET/CT examination, with persistent hypercalcemia and high PTH serum level: there was one lymph node found in the right supraclavicular area in the PET/CT examination. The histopathology proved the obtained result. 2. 69-year-old women after operation of parathyroid cancer ten years before the examination, after radiotherapy of the neck because of recurrence eight years before PET/CT and stereotactic radiotherapy lung metastases two years before PET/CT with high serum level of PHT: there were four small new metastases found in the right lung. 3. 46-year-old women after two operations of parathyroid cancer in the neck localisation, last operation four months before examination and after operation of metastases to mediastinum and skin ten months before PET/CT: there were three recurrences found on the neck, located paratracheal and one lesion in the mediastinum. The histopathology proved the result. Conclusion: the 18F Fluorocholine PET/CT examination is a valuable and very sensitive tool for finding and imaging the recurrence of parathyroid cancer.

EP-0599

Orbital Metastasis Detected by Ga-68 Somatostatin Receptor PET/CT in Patients with Neuroendocrine Tumors

Z. Awange[1], R. Baum[2]; [1]ministry of Health Malaysia, Melaka, MALAYSIA, [2]Zentralklinik Bad Berka, Zentralklinik, GERMANY.

Aim: Ocular metastasis considered rare. The aim of this study is to report the frequency of the disease and the outcome of neuroendocrine tumors metastasis to the orbital region. **Meth-**

od: The clinical data of 30 patients with neuroendocrine tumors from 1999 to 2017 who underwent PRRT in Bad Berka Zentralklinik, Germany were analyzed. **Results:** Thirty patients (n=30), mean age 72 year; range: 56-91 years. The male: female ratio was 12:18. Primary neuroendocrine tumor sites were ileum (n=12), pancreas (n=5), CUP (n=4), rectum (n=3), lung (n=3), jejunum (n=1), pheochromocytoma (n=1) and small bowel (n=1). Grade of the neuroendocrine tumors were G1 (n=7), G2 (n=15), G3 (n=1) and NA (n=7). Number of PRRT cycles received in patients with orbital metastases were one cycle (n=1), two cycles (n=3), three cycles (n=2), four cycles (n=8), five cycles (n=4), six cycles (n=3), seven cycles (n=6), eight cycles (n=1) and two patients did not received PRRT. Disease status last reported after PRRT with orbital metastasis were disease progression (n=23), stable disease (n=6) and partial remission (n=1). Distant metastases spreading to liver, lymph nodes, ovaries, skin, breast, cardiac, bone and orbital region. The locations of the orbital metastases were right orbit (n=12), left orbit (n=12) and bilateral orbital region (n=6). Patients with orbital metastases have been treated with radiotherapy (n=3), tumor resection (n=1) and partial resection (n=2). The overall mean survival after first diagnosis of neuroendocrine tumors with orbital metastases was 84 months and overall mean survival after first therapy with Lu-177 DOTA-TOC and Y-90 DOTATOC was 42 months. **Conclusion:** We have reported 30 cases of patients with Gallium-68 DOTATOC PET/CT from 1999 to 2017, which has the highest number of orbital metastasis reported in neuroendocrine tumors in single center. With the limited role of physical and ophthalmologic finding in orbital metastases, imaging with Ga-68 DOTATOC PET/CT could be the primary means in detecting this entity. The overall median survival after the first diagnosis with neuroendocrine tumors with orbital metastases was 84 months and overall mean survival after first therapy with PRRT was 42 months, which are higher than previously reported in the literature. Further study is needed to better define the role of PRRT with chemotherapy, surgery and radiotherapy in this subset of patients.

EP-0600

Performance of somatostatin receptor scintigraphy (SRS) and fluorodeoxyglucose (FDG) PET/CT in initial staging of gastro-entero-pancreatic neuroendocrine tumors (GEP-NET)

S. P. Dhake, A. Agrawal, M. Ramadwar, N. Purandare, S. Shah, A. Puranik, V. Rangarajan; Tata Memorial Hospital, Mumbai, INDIA.

Background: NETs are uncommon neoplasms that arise from neural crest cells. SRS is considered a sensitive test for diagnosis, particularly in low grade NETs. FDG PET/CT has been shown to be sensitive in high grade NETs. However, there is variability in uptake of SRS and FDG in intermediate grade of NET. **Aim:** Correlation of SRS and FDG PET scan findings with that of histological grade of NET and to determine quantitative parameters **Materials and Methods:** This was a retrospective single center study. 81 patients with biopsy proven GEP-NET who had undergone paired baseline ^{68}Ga-DOTANOC PET/CT and ^{18}F-FDG PET/CT were included in study. Patients were classified according

to WHO criteria into three grades based on Ki67 index: G1: ≤2 %, G2:3-20 % and G3:>20 %. The G2 grade was subclassified as G2-1 with Ki67 index 3-10% and G2-2 with Ki67 index 11-20%.All lesions were assigned Krenning score (for SRS) and 3-point score (for FDG). Uptake on Krenning score: 0:none, 1:very low, 2:less than or equal to liver, 3:more than liver, 4:more than spleen. Uptake on 3-point score: 0:none, 1:less than liver, 2:equal to liver, 3:more than liver. The grades of NETs were correlated with SUVmax of SRS and FDG by one way ANOVA. Correlation of grade with Krenning score (for SRS) and 3-point score (for FDG) was performed with Pearson's chi square test. **Results:** Total of 299 lesions were identified, 96 in G1, 136 in G2-1, 45 in G2-2 and 22 in G3. Lesions positive for SRS and FDG were 91/96 (95%) vs 53/96 (55%) in G1, 127/136 (93%) vs 84/136 (62%) in G2-1, 39/45 (87%) vs 32/45 (71%) in G2-2 and 8/22 (36%) vs 20/22 (91%) in G3 tumors respectively. Significant correlation was found between grade and SUVmax of lesions on SRS (P<0.001) and FDG (P<0.001). Significant correlation was found between grade with Krenning score on SRS (P<0.001) and 3-point score on FDG (P<0.001).The DOTANOC SUVmax and FDG SUVmax values were 50.72 vs 5.63 in G1, 25.22 vs 6.74 in G2, and 13.74 vs 13.07 in G3 tumors respectively. **Conclusion:** The SRS and FDG expression shows good correlation with the grade of the tumor; SRS expression being higher in low grade NETs than in high grade NETs and vice-versa for FDG.A greater number of lesions were detected on SRS for Ki67 index of 3-10% as compared to that of 11-20% amongst patients with G2 tumors.

EP-0601

Cell dediferrentiation & somatostatin receptors expression can coexist in neuroendocrine carcinomas?

*V. Ippolito, G. Annunziata, c. Mocerino, D. Scala, F. Scavuzzo, I. Valenti, **M. Catalano**; aorn cardarelli, Naples, ITALY.*

Aim: To correlate neuroendocrine neoplasms (NEN) pathological data WHO 2010 classification based to ^{111}In-pentetreotide uptake at receptorial scintigraphy (OctreoScan). Well differentiated NEN overexpress somatostatin receptors and show high degree radiopharmaceutical uptake at OctreoScan, while poorly differentiated neuroendocrine carcinomas (NEC) are usually negative at receptorial imaging. Because of dedifferentiated tumors OctreoScan positivity, sometimes observed in clinical practice, the authors have looked for a link between cell dediferentiation and somatostatin receptors expression of different type of NEN. **Materials and Methods:** 116 patiens (pts) with pathological diagnosis of neuroendocrine neoplasms (NEN) were studied for receptorial imaging. 94 pts were affected with gastro-entero-pancreatic tumors (GEP) and 22 with thoracic tumors (T). In GEP-NET group, 43 tumors rose from pancreas, 9 from stomach, 5 from duodenum, 9 from ileum, 9 from colon, 5 from rectum and 1 appendix. T-NEN group included 10 tipic carcinoid, 4 atipic carcinoid, 1 tipic/atipic carcinoid, 2 non small cell lung cancer (NSCLC), 3 small cell lung cancer (SCLC). According to WHO 2010 classification, based on ki-67 proliferative index and necrosis evidence limited to thoracic tumors, all pts were categorized in G1-NET (33 GEP, 10 T), G2-NET (13 GEP, 8 T)

and G3-NEC (12 GEP, 4 T). All pts underwent ^{111}In-pentetreotide scintigraphy. In pts affected with G3-NEC, OctreoScan was performed because of discordance between morphological characteristics, synaptophysin and/or CD56 expression, and grading or because of negative ^{18}F-FDG PET-TC. **Results:** According to pathological data, all G1 and G2 GEP-NET were positive at OctreoScan before surgery and negative for metastasis if the scintigraphy was performed post-surgery. According to current literature data, 5/12 pts with G3 GEP-NEC were negative at OctreoScan but 7/12 pts showed high ^{111}In-pentetreotide uptake (score 3-4). Likewise, all G1 and G2 T-NET had ^{111}In-pentetreotide uptake; in G3 T-NEC 2/4 pts were OctreoScan negative, while 2/4 pts showed an abnormal behavior because one pt with ki67 &gl 80%, synaptophysin and CD56 positivity, revealed an unexpected labeled somatostatin analogue uptake (score 2); furthermore another pt affected with SCLC showed a higher radiopharmaceutical uptake (score 3). **Conclusion:** Our data are too small to draw conclusions, but show that tumor cell dedifferentiation, expressed by high proliferative index, don't rule out somatostatin receptor expression on tumor cell surface so that receptorial imaging may be indicated in G3 NEC too. These findings could help to better understand NET behavior and could suggest to associate somatostatin analogues therapy/ PRRT to the standard of care in G3 NEC.

EP-0602

Advanced Digestive Neuroendocrine Neoplasms: prognostic role of 18-F-FDG-PET

D. Prosperi[1], M. Cucinotta[1], M. Rinzivillo[1], F. Panzuto[1], G. Capurso[1], G. Capriotti[1], E. Iannicelli[1], M. Pacilio[1], L. Carideo[1], E. Pilozzi[1], E. Merola[1], O. Schillaci[2], G. Delle Fave[1], F. Scopinaro[1]; [1]Sant'Andrea University Hospital of Rome, Rome, ITALY, [2]University of Rome Tor Vergata, Rome, ITALY.

Aim: The role of ^{18}F-FDG-PET to predict clinical outcome in advanced digestive neuroendocrine neoplasms (dNENs) is still unclear. The aim of this study was to determine the ability of ^{18}F-FDG-PET to predict disease progression (DP) in patients with advanced dNENs. **Materials and Methods**: We performed a retrospective analysis of prospectively enrolled consecutive patients with histologically confirmed, metastatic or locally advanced, unresectable dNEN. All patients underwent a ^{18}F-FDG-PET/CT scan. ^{18}F-FDG-PET uptake was quantified using maximum standardized uptake value (SUVmax). The analysis of variables for prediction of DP was performed by univariate and multivariate analysis using Cox proportional odds method. Progression Free Survival (PFS) and Overall Survival (OS) analysis was performed using Kaplan-Meier method. **Results**: A total of 60 patients (46.6% males, median age 60 years) with a median follow-up of 32 months were evaluated. At the time of study enrollment 38 (63.3%) patients had radiological documentation of DP whereas the remaining 22 (36.6%) patients had stable disease (SD). In the group of patients with DP, 36/38 (94.7%) had positive ^{18}F-FDG-PET, while the remaining 2/38 (5.2%) had negative ^{18}F-FDG-PET. In the group of patients with SD, 2/22 (9%) had positive ^{18}F-FDG-PET. On the contrary, ^{18}F-FDG-PET was negative

in the other 20/22 (90.9%) patients with SD. Significantly longer PFS (not reached) was observed in ^{18}F-FDG-PET negative patients in comparison with ^{18}F-FDG-PET positive ones (12.5 months) (p<0.001). According with the tumor grading, median PFS was 16 months in NET G1, 12.5 months in NET G2, and 9 months in NEC G3 group, respectively (p=0.04). Significantly longer OS was observed in ^{18}F-FDG-PET negative patients (35 months) in comparison with ^{18}F-FDG-PET positive ones (24 months) (p=0.002). Median OS was 41 months in NET G1, 28 months in NET G2 and 15 months in NEC G3 patients, respectively (p=0.02). At univariate analysis, ^{18}F-FDG-PET positivity, grading system and proliferative index Ki-67 as a continuous variable were associated with DP. When multivariate analysis was performed, ^{18}F-FDG-PET and Ki-67 were confirmed to be independent variables associated with increased risk of tumor progression. **Conclusion**: although this is an ongoing study, first data suggest that ^{18}F-FDG-PET should be considered in the imaging approach of patients with advanced dNEN in order to better predict the risk of DP.

EP-0603

Differences in uptake between ^{68}Ga-Dotatate and ^{68}Ga-HA-DOTATATE in normal organs and tumour lesions: a retrospective study in 342 patients

E. A. Aalbersberg, B. J. de Wit - van der Veen, M. M. Geluk - Jonker, L. Bonsen, M. P. M. Stokkel; Department of Nuclear Medicine, Netherlands Cancer Institute - Antoni van Leeuwenhoek, Amsterdam, NETHERLANDS.

Introduction: Gallium-68-somatostatin receptor PET/CT has significantly improved the functional imaging of neuroendocrine tumours (NETs). Different ^{68}Ga-conjugated peptides have been developed, including DOTATATE and High-Affinity-DOTATATE (HA-DOTATATE). Several articles have been published by the same centre describing the similarities in receptor affinity, distribution, and dosimetry between DOTATATE and High-Affinity-DOTATATE. The aim of this study was to retrospectively evaluate the distribution of ^{68}Ga-DOTATATE and ^{68}Ga-HA-DOTATATE in normal organ tissue and tumour lesions in a larger independent patient population. **Materials and Methods:** All whole-body ^{68}Ga-DOTATATE and ^{68}Ga-HA-DOTATATE PET/CT scans acquired between 11-2011 and 04-2016 and acquired 45±10 minutes post-injection were retrospectively evaluated. The SUVmax and SUVpeak was determined for the liver, spleen, aortic arch, renal cortex, and pituitary-, adrenal-, parotid-, and thyroid glands in each patient. For tumour measurements, SUV was determined only in the lesion with the highest uptake in 7 categories: primary tumour, or metastasis in liver, bone, lung, abdomen (including lymph nodes), lymph nodes (not in the abdomen), and other. Tumour-to-background ratios were calculated using the liver as background organ. An independent-samples T-test was used to determine the difference in uptake between the cohorts imaged with ^{68}Ga-HA-DOTATATE and ^{68}Ga-DOTATATE. **Results:** 342 PET/CT scans were available for normal organ tissue analysis, 110 scans after injection of ^{68}Ga-DOTATATE and 232 scans after injection of ^{68}Ga-HA-DOTATATE. For tumour lesion analysis 158 PET/CT scans were available, 64 with

^{68}Ga-DOTATATE and 94 with ^{68}Ga-HA-DOTATATE. SUVmax was significantly increased with ^{68}Ga-HA-DOTATATE compared to ^{68}Ga-DOTATATE in the liver, spleen, kidney, adrenal gland, pituitary gland, and thyroid gland. There was no difference in the SUVmax of the parotid gland. In the blood pool measured in the aorta, the SUVmax was lower with ^{68}Ga-HA-DOTATATE. SUVpeak showed the same pattern. SUVmax was significantly increased with ^{68}Ga-HA-DOTATATE compared to ^{68}Ga-DOTATATE in the primary tumour, but no difference was seen in tumour metastases in the liver, bone, abdomen, lymph nodes, or other organs. For SUVpeak, the only difference was seen in abdominal metastases where the uptake of ^{68}Ga-HA-DOTATATE was higher . There is no significant difference in SUVmax or SUVpeak of ^{68}Ga-HA-DOTATATE or ^{68}Ga-DOTATATE in the tumour-to-background ratio in any of the measured tumour lesions. **Conclusion:** ^{68}Ga-HA-DOTATATE and ^{68}Ga-DOTATATE have a different distribution in vivo as demonstrated in these 342 patients. Uptake of ^{68}Ga-HA-DOTATATE is significantly increased in most organs, but only at some tumour sites. This difference should be taken into account when choosing a peptide for somatostatin imaging or treatment.

EP-0604

Fifty months of somatostatin receptor SPECT/CT with 99mTc-EDDA Hynic Toc: What have we learned?

N. Girotto, E. Kukić, M. Maršić, S. Rac, S. Grbac; Clinical Hospital Centre Rijeka, Rijeka, CROATIA.

The aim of this work was to evaluate performance of SRSPECT/CT imaging in diagnosis and follow up of patients with neuroendocrine tumors (NETs) in a four year period. **Patients and Methods:** Between 1/2013 and 2/2017, 204 patients were referred to SRSPECT/CT, with overall 280 studies performed. In this work, only 120 patients (62 male, 58 female, age median 62.5 years) with histologically proven NETs were included. Forty two underwent 2 to 5 control studies, with altogether 196 imaging procedures. Regarding tumour site, there were 32 pancreatic, 25 lung, 13 gastric, 12 colon, 9 small bowel NETs, 21 in other locations and 8 patients with unknown primary tumor. Immediately after 555-740 MBq 99mTc-EDDAHynicToc application, whole body (WB) planar imaging was performed, followed with WB SRSPECT/CT on dual head SymbiaT SPECT/CT system at 2 and 4 hours. **Results:** Primary lesion was visible on SRSPECT/CT in 56 patients, but 47 pts were referred for staging when primary lesion was already removed. In the remaining 17 pts, lesions showed no accumulation, including 8 pts with unknown primary lesion. In 45/56 patients primary lesion was visible early, on bloodpool images. Metastases were revealed in 57/120 pts; in 46 patients they were also visible on bloodpool images. In 11 patients they were spotted only on "low dose"CT, without 99mTc-EDDAHynicToc accumulation. 18F-FDGPET/CT was performed in 45 patients, in 21 postoperatively. Out of the remaining 24 patients, primary lesions was visualized in 18. Metastases with FDG accumulation were found in 26 pts. Overall, including primary lesions and metastases, findings were consistent with SRSPECT/CT in 27/45 pts. Only FDG positive findings were pres-

ent in 11, and only SR positive in 7 pts. Chromogranine A (CgA) values were available for 70 patients. Levels above normal (cut-off 100 pmol/l) were found in 42 pts (mean value 249 pmol/l). **Conclusions:** Calculated sensitivity of SRSPECT/CT in patients with proven NETs was 77% for primary lesion, 83% for metastases and better than of 18F-FDGPET/CT with sensitivities of 75% and 76%, respectively. Early visualization of majority of lesions points to the fact that their perfusion can be reliably detected and commented on. Normal CgA values should be taken with caution because of its low negative predictive value. Data on this population of patients show high value of SRSPECT/CT in evaluation of NET, especially when metastatic spread is suspected. Also, in patients with negative SRSPECT/CT findings, 18F-FDGPET/CT should be considered.

EP-0605

Biodistribution of [68Ga]Ga-DATATOC in comparison with [68Ga]Ga-DOTATOC in normal tissues and neuroendocrine tumour lesions

B. Schmidt-Kreppel[1], T. Plum[1], F. C. Gaertner[1], E. Eppard[1], J. Sinnes[2], H. Strunk[1], R. A. Bundschuh[1], F. Rösch[1], M. Essler[1]; [1]University Medical Center Bonn, Bonn, GERMANY, [2]Johannes Gutenberg-University Mainz, Mainz, GERMANY.

Aim: [68Ga]Ga-DATATOC is a somatostatin-analogue for PET imaging of neuroendocrine tumours. Its advantage over DOTA-conjugated somatostatin-analogues is especially the possibility for labelling with gallium-68 quickly at room temperature with high labelling efficiency without the need for purification of the product, which facilitates radiochemical production and paves the way for the development of a kit-type labelling method. **Materials and Methods:** 19 patients imaged with DATATOC were retrospectively analysed. SUV_{max} and SUV_{mean} were measured in normal organs (pituitary gland, adrenal glands, brain, lungs, mediastinal blood pool, liver, spleen, kidneys, and muscle) and in tumour lesions (primary tumour, hepatic and lymph node metastases). Lesion-to-background ratios were calculated for tumour lesions. Results were compared with a cohort of 19 patients imaged with [68Ga]Ga-DOTATOC. **Results:** PET imaging with DATATOC delivered high image quality suitable for detection of neuroendocrine tumour lesions. Quantitative analysis revealed a significantly lower lesion-to-background ratio of DATATOC in lymph nodemetastases (4.9 vs. 9.7) and hepatic metastases (2.6 vs. 4.8) in comparison to DOTATOC. Furthermore, uptake in primary tumours was lower for DATATOC, however this was not significant. Regarding normal organs with physiologic expression of the somatostatin receptor, uptake in the pituitary gland, adrenal glands and spleen were significantly lower for DATATOC (SUV_{mean} 1.7 vs. 2.1; 4.1 vs. 6.4; 12.7 vs. 19.2). Regarding unspecific background uptake, DATATOC showed a higher retention in the mediastinal blood pool and the lungs (SUV_{mean} 1.4 vs. 0.9; 0.4 vs. 0.3). In contrast normal liver tissue uptake was significantly lower for DATATOC (3.3 vs. 4.8). No significant differences were observed for brain, kidney, bone and muscle uptake. **Conclusion:** This is the first study showing the feasibility of PET imaging with DATATOC

in patients with neuroendocrine tumours. Visual image quality was high which allowed for specific detection of tumour lesions. Therefore, DATATOC seems promising as a PET tracer with the potential for kit-type labelling, which allows a wide applicability. Quantitative analysis in comparison to a different cohort of patients imaged with DOTATOC showed a lower uptake of DATATOC in organs with physiologic expression of the somatostatin receptor. Though the lower uptake of DATATOC in normal liver tissue seems advantageous for detection of liver metastases, the tumour-to-background ratios of DATATOC were lower for hepatic and lymph node metastases. Further studies are warranted to evaluate if these results have a clinical impact on lesion detectability of DATATOC in comparison to established DOTA-conjugated somatostatin analogues, preferably in prospective Settings.

EP-0606

Comparison of ^{68}Ga-DATATOC & ^{68}Ga-DOTANOC PET/CT Imaging in Patients with Neuroendocrine Tumours

D. Yadav, M. Tripathi, N. A. Damle, C. Bal; All India Institute of Medical Sciences, New Delhi, INDIA.

Purpose: Recently the DATA (6-Amino-1,4-diazepine-triacetate) chelator has been introduced, which has the advantage of high yield and radiolabeling of DATA based octreotide derivative TOC at room temperature in contrast to DOTA that needs 95°C for effective labeling. The aim of this study was to compare the diagnostic efficacy of ^{68}Ga-DATATOC with ^{68}Ga-DOTANOC in patients of gastroenteropancreatic neuroendocrine tumors (GEP-NETs). **Methods**: Twenty-one patients with biopsy-proven GEP-NETs were included in the study. Patients age ranged from 30 to 75 years (mean 49.3 years). There were eight patients with well-differentiated neuroendocrine tumour (WDNET) grade1, ten patients with WDNET grade 2 and three patients with poorly differentiated neuroendocrine carcinoma (PDNEC) grade 3. All patients underwent two consecutive PET studies with a similar dose of ^{68}Ga-DATATOC and ^{68}Ga-DOTANOC within a period of 7 to 10 days. All images were evaluated visually and maximum standardized uptake values (SUVmax) were calculated for semi-quantitative evaluation. The SUVmax of the liver and muscle, and the tumor-to-liver (T/L) and tumor-to-muscle (T/M) SUV ratios were computed. For the purpose of comparison patient-wise as well as lesion-wise analysis was carried out. A maximum five lesions per organ were chosen on ^{68}Ga-DATATOC and each lesion was compared with corresponding lesion on ^{68}Ga-DOTANOC. The student's t-test (paired) was applied to calculate p-value. **Results**: On visual evaluation the bio-distribution and image quality of ^{68}Ga-DATATOC was similar to ^{68}Ga-DOTANOC. Liver and spleen uptake values did not show any significant difference (p=o.797). On a patient-wise analysis, both ^{68}Ga-DATATOC and ^{68}Ga-DOTANOC was lesion positive in 17 (80 %) patients and lesion-negative in 4 (20 %) patients. On a lesion-based analysis, 75 lesions were compared and ^{68}Ga-DATATOC had 98.6% concordance with ^{68}Ga-DOTANOC (74 out of 75 lesions detected). The mean tumor SUVmax on ^{68}Ga-DATATOC and ^{68}Ga-DOTANOC was 40.02 and 42.24 re-

spectively (p=0.392). The T/L SUVmax ratios were also not significantly different (4.875 Vs 4.762, p=0.80). The T/M SUmax ratio was higher with ^{68}Ga-DATATOC than ^{68}Ga-DOTANOC (34.524 Vs 30.762, p=0.402), though the difference was not statistically significant. **Conclusion:** ^{68}Ga-DATATOC PET/CT imaging produced results that were comparable to ^{68}Ga-DOTANOC imaging, which is the current standard for imaging NET. Keeping in mind the ease of preparation and better yield in case of ^{68}Ga-DATATOC, it can be effectively used in place of ^{68}Ga-DOTANOC with similar results.

EP-0607

Association Between Somatostatin Receptor Scintigraphy And Chromogranine Levels In Patients With Neuroendocrine Tumors

R. H. Reyes Marlés, Sr., M. Castellón Sanchez, F. Nicolas Ruiz, L. Mohamed Salem, J. Navarro, L. Frutos Esteban, M. Godoy Bravo, I. Sime loayza, M. Tomás Redondo, E. Fernandez Muñoz, M. Claver Valderas; Hospital Clinico Universitario Virgen de la Arrixaca, El Palmar, SPAIN.

Objective: To analyze the association between somatostatin receptor scintigraphy (SRS) and Chromogranin A (CgA) levels in patients with clinical diagnosis or suspicion of neuroendocrine tumors (NEDT). **Methods:** GRS performed in our service in 2015 (162 studies) were retrospectively evaluated, selecting those diagnosed or suspected of NEDT and determining CgA levels 3 months prior, or 3 months after SRS (78 studies), which were classified in two groups: A (Diagnostic SRS) and B (follow-up SRS). In both groups, the CgA values were reviewed and the Chi-square test was performed between categorical variables 1. SRS (positive, negative and doubtful), and 2. CgA (positive or increasing and negative). **Results:** There was no statistically significant association between SRS outcome and CgA levels in group A (p = 0.259), nor in group B (p = 0.507); However, when analyzing the percentage values of the data association tables, it can be observed that in the group of diagnostic SRS, 83.33% of SRS with findings compatible with the presence of NEDT had elevated or elevated levels of CgA. **Conclusion:** Although there was no statistically significant association in our series, between the SRS results and the CgA levels, a high percentage of diagnostic SRS compatible with TNED, had a positive or rising CgA, suggesting a possible relationship between both tests, useful in the diagnosis of patients with TNED.

EP-0608

Quality Of Life in Patients with Neuroendocrine Gastroenteropancreatic Tumors Treated with Peptide Receptor Radionuclide Therapy

A. Georgakopoulos[1], T. Liotsou[2], S. N. Chatziioannou[1,2]; [1]Biomedical Research Foundation of the Academy of Athens, Clinical and Translational Research, Nuclear Medicine Division, PET/CT section, Athens, GREECE, [2]2nd Radiology Department, "Attikon" University Hospital, Athens Medical School, National and Kapodistrian University of Athens, Nuclear Medicine Division, Athens, GREECE.

Purpose/Introduction: Peptide receptor radionuclide therapy (PRRT) is a treatment modality with very good results in patients with metastatic gastroenteropancreatic neuroendocrine tumors (GEP-NETs). Self-reported health-related quality of life (HRQoL) is an important outcome for the effect of a therapy in patients with malignant diseases. The aim of this study is to evaluate the HRQoL in patients with somatostatin receptor positive, metastatic GEP-NETs treated with PRRT. **Subjects & Methods:** Twenty seven patients (mean age 58, SD ± 37.3) received 2-4 therapies with labeled peptide either with Lutetium 177 (Lu-177) or with Yttrium 90 (Y-90). Before receiving the first therapy and 6 months after the last, patients completed the quality of life questionnaire (QLQ) core module (C30) which is an instrument for measuring general cancer HRQoL and has been developed by the European Organization for Research and Treatment of Cancer (EORTC). It consists of 30 items divided into five functional scales, nine symptom scales and a scale representing global quality of life. Responses were transformed to produce 0-100 scores with higher functional scale scores indicating better HRQoL, and higher symptom scale/item scores indicating higher level of symptoms. In accordance to previous validated studies a mean change in score between 0 and 5 was regarded as not clinically important, a change between 5 and 10 as a "little" subjective change, whereas a change between 10 and 20 as a "moderate" change, and more than 20 as a "significant" change. **Results:** A moderate improvement in the global health status (GHS) /QoL scale score was observed at 6 months after the last therapy [mean GHS (SD): 64.11 ± 24.15 six months after the end of therapy versus 53.59 ± 28.49 at the beginning]. There were no clinically important changes in the functional scales (physical, role, cognitive and social functioning). A small exception only occurred in the emotional functioning (EF) with minor clinical relevance [mean EF (SD): 80.74 ± 21.98 six months after the end of therapy versus 75.11 ± 22.14 at the beginning]. Also, no clinically important changes were observed in all the symptom scales (fatigue, nausea and vomiting, pain, dyspnea, insomnia, appetite loss, constipation, diarrhea and financial difficulties). **Conclusion:** Our results indicate that PRRT in GEP-NETs improves the GHS/QoL. Compared to the initial state, no clinically important deterioration in symptom scales was observed several months after the end of treatment.

EP-0609

Quantification of 6-[^{18}F]fluoro-L-3,4-dihydroxyphenyl alanine Uptake in Neuroendocrine Tumour Lesions: The Effect of Specific Activity

R. S. B. H. Schreuder[1], A. H. Brouwers[1], P. H. Elsinga[1], R. H. J. A. Slart[1], A. M. E. Walenkamp[2], A. W. J. M. Glaudemans[1], G. Luurtsema[1]; [1]Department of Nuclear Medicine and Molecular Imaging, University Medical Center Groningen, Groningen, NETHERLANDS, [2]Department of Medical Oncology, University Medical Center Groningen, Groningen, NETHERLANDS.

Aim: ^{18}F-FDOPA can be used for the detection and follow-up of neuroendocrine tumours (NETs). ^{18}F-FDOPA synthesized via electrophilic substitution leads to ^{18}F-FDOPA with a low specific

activity (SA): ^{18}F-FDOPA-L. A new method for the production of radionuclides involves irradiation with protons via the double shoot method, resulting in ^{18}F-FDOPA with higher SA (^{18}F-FDO-PA-H). This new production method results in a ten-fold higher SA. Therefor the aim of this study was to investigate if SA affects the ^{18}F-FDOPA uptake in background organs and lesions in NET patients by calculating standardized uptake values (SUV). **Methods:** We conducted a retrospective analysis in 50 NET patients who received both ^{18}F-FDOPA-L PET and ^{18}F-FDOPA-H PET. 100 scans (performed according to EARL guidelines) were evaluated and stratified in three different groups according to NET tumor load. Group I: no metabolic active NET on both scans (22 patients). Group II: ≤ 2 minor lesions visible on both scans (10 patients). Group III: low tumor load and slight disease progression between the two scans (18 patients). All scans were analyzed using syngo.via software (Siemens) and quantification was performed using SUV max in tumor lesions and SUV mean in background organs. Statistical analyses were performed between the old and new production method for each group using the Wilcoxon rank test and statistical significance was considered if $p<0.05$. **Results:** The SUV of ^{18}F-FDOPA-L vs ^{18}F-FDOPA-H differed significantly in background organs and in tumor lesions. In group I, statistical significant differences were observed in background organs: striatum, heart, kidneys, and the right adrenal gland. In group II no statistical significant differences were obtained for the background organs. In group III, statistical significant differences were obtained for the striatum, aorta, right kidney and the left adrenal gland. Group III also showed a statistical significant difference between both tracers in tumor lesions. **Discussion:** Statistical significant differences in uptake in background organs and lesions in patients with NETs is observed between ^{18}F-FDOPA-H PET and ^{18}F-FDOPA-L PET. Therefore, it is important to consider that differences in SA could affect the uptake and the SUV calculations. This is of clinical relevance when quantitatively comparing scans of the same patient in longitudinal studies in which the two production methods are applied.

EP-0610

The role of Ga 68-DOTANOC PET-CT in treatment management of recurrent medullary thyroid cancer

A. Aliyev[1], A. Aliyeva[1], I. Aliyeva[2], E. Mehdi[3], **F. Novruzov**[3]; [1]Azerbaijan National Centre Of Oncology, Department Of Head and Neck Surgery, Baku, AZERBAIJAN, [2]Azerbaijan Medical University, Department of Internal Medicine, Baku, AZERBAIJAN, [3]Azerbaijan National Centre Of Oncology, Department Of Nuclear Medicine, Baku, AZERBAIJAN.

Medullary thyroid cancers are the third most common of all thyroid cancers. They make up about 3% of all thyroid cancer cases. We investigated the benefit of 68Ga-labelled [1,4,7,10-tetraazacy-clododecane-1,4,7,10-tetraacetic acid]-1-Nal3-Octreotide (68Ga-DOTANOC) positron emission tomography computed tomography (PET-CT) in 4 patients with recurrent medullary thyroid carcinoma which has been widely used for imaging of neuroendocrine tumours. We reviewed 68Ga-DOTANOC PET-CT images of 4 patients with suspicion of recurrent medullary thyroid cancer, who has elevated calcitonin levels and enlarged cervical lymph nodes in conventional imaging. All of these patients have a history of radical thyroidectomy with proven pathology of medullary thyroid cancer. **Results:** There were distant metastases (lung, liver and bone) in two of them which were suitable for radiolabelled peptide treatment with Lutetium-177. The cervical lymph nodes dissection was performed on other two patients who had high uptake of radiotracer in only cervical lymph nodes. The calcitonin levels decreased to normal values in one year follow-up. **Conclusion:** 68Ga-DOTANOC PET-CT was able to localize the disease recurrence and influence the treatment management in patients with medullary thyroid cancer. In addition, in cases with biochemically recurrent medullary thyroid cancer 68Ga-DOTANOC PET-CT is useful for detection of sources of calcitonin production, especially where conventional anatomic imaging methods is negative.

EP-0611

F-18-DOPA PET/CT in medullary thyroid carcinoma patients

A. T. Golubić[1], E. Pasini[1], M. Zuvic[1], S. Kusacic Kuna[1,2], T. Samardzic[1], M. Despot[1], D. Huic[1,2]; [1]Department of Nuclear Medicine and Radiation Protection, University Hospital Centre Zagreb, Zagreb, CROATIA, [2]School of Medicine, University of Zagreb, Zagreb, CROATIA.

Introduction: Thyroid carcinoma is currently the topic of many discussions and there are ongoing debates on the best moment for F-18 dihydroxyphenylalanine PET/CT scan. The aim of this study was to examine the value of F-18-DOPA PET/CT scan in patients with medullary thyroid carcinoma and increased calcitonin levels. **Subjects and Methods:** Twenty-eight patients with medullary thyroid carcinoma after initial total thyroidectomy and rising calcitonin levels were scanned with F-18-di-hydroxyphenylalanine (DOPA) PET/CT from November 2012 to April 2016. Conventional imaging findings (ultrasound or MSCT) suggestive for active disease were equivocal or negative. Mean patient age was 57 years (range 13-78 years). Mean calcitonin level was 108.5 pmol/l (range 6.7-290 pmol/l) and mean CEA level was 15.7 ug/l (range 1.1-221.9 ug/l). The mean follow-up period was 19.7 months (range 6-47 months). **Results:** Sixteen patients had a positive F-18-DOPA PET/CT scan (57%). Increased tracer uptake was found in the neck and mediastinal lymph nodes, with a mean SUVmax value 5.6 (range 2.7-10.9). Bone metastases were found in six patients, with the mean SUVmax value 4.7 (range 2.9-6.2). A positive scan was reported in four patients (25% of positive scans) with a calcitonin value lower than 49.9 pmol/l. Change of management or therapy approach was reported 16 patients in the follow-up period. Surgical procedure was performed in eight patients, radiotherapy or palliative bone radiotherapy was started in five patients and chemotherapy in two patients. **Conclusions:** Functional imaging with F-18-DO-PA PET/CT provides clinicians with valuable information in patients with medullary thyroid carcinoma. It presents additional data necessary for individual patient management, especially in patients with low and moderately elevated calcitonin levels as tumor volume in these patients is small and treatment can be personalized and made more efficient.

EP-0612

Frequency of physiological 111In-DTPA-octreotide SPECT/CT uptake in pancreatic uncinate process: retrospective study on a large 198 patients review and comparison with 68Ga-DOTATOC PET/CT

P. Schwartz, CHU de Bordeaux, Pessac, FRANCE.

Aim: The aim of this study is to evaluate the frequency of physiological 111In-DTPA-octreotid uptake in the pancreatic uncinate process, on SPECT/CT acquisitions. **Methods:** We analysed retrospectively 247 patients 111In-DTPA-octreotid SPECT/CT images realized in the nuclear medicine department of CHU de Bordeaux, France, between June 2012 and March 2015. Intensity uptake of pancreas uncinate process was classified in comparison with physiological liver and spleen uptake. When positive, an uptake was considered as physiologic when radiological investigations (CT, MRI or echoendoscopy) didn't show anatomical lesion in the pancreatic head, or if no lesion appeared during clinical and radiological follow-ups. For patients who underwent both 111In-DTPA-octreotid SPECT/CT and 68Ga-DOTATOC PET/CT, we compared the uncinate process uptake patterns. **Results:** One hundred ninety eight patients without uncus and cephalic pancreatic lesion were analysed. Forty two percent had a physiological 111In-DTPA-octreotide uptake in the pancreatic uncinate process. Uptake intensity was significant (greater than or equal to liver uptake) in 17%. Sixteen patients underwent both 111In-DTPA-octreotid SPECT/CT and 68Ga-DOTATOC PET/CT. SUVmax, SUVmean and SUVpeak values had good linear correlation coefficients with intensity uptake on 111In-DTPA-octreotid SPECT. **Conclusion:** Intense physiological 111In-DTPA-octreotid uptake of the pancreatic uncinate process can occur in 17% of cases on SPECT/CT acquisitions. This tracer accumulation can mimic malignancy in pancreatic head. Uptake in the pancreatic uncinate process should be correlated with morphologic examinations, such as CT, MRI or somatostatin PET/CT if available.

EP-0613

Complementary role of 18F-FDG and 68Ga-DOTATOC PET-TC in patients with cystic pancreatic lesions

M. Cucca, L. Locantore, D. Grigolato, M. Zuffante, M. Ferdeghini; Nuclear Medicine Unit, University Hospital of Verona, Verona, ITALY.

Purpose/Introduction : Cystic pancreatic lesions (CPN) encompass a varied group of abnormalities, including serous cystic neoplasm (SCN), mucinous cystic neoplasm (MCN), intraductal papillary mucinous neoplasm (IPMN), solid pseudopapillary neoplasm (SPN), cystic neuroendocrine neoplasm (NET). An accurate lesion characterization is fundamental for risk stratification and decision treatment making. 18F-FDG PET-CT (FDG PET) could be useful for metabolic characterization of pancreatic cystic lesions, but large population studies are not currently available. 68Ga-DOTATOC PET-CT (DOTATOC PET) is an established diagnostic tool in patient with suspected neuroendocrine pancreatic lesions. We assessed if a combined approach with both FDG and DO-TATOC PET could be useful in patients with CPN. **Subject & Methods**: Twentyseven patients (15 F-12 M, mean age 58.3, range 34-80) with CPN, respectively suspected IPMN (=8), SCN/MCN (=5), SPN (=4) and cystic NET (=10). Patients underwent FDG and DOTATOC PET (a total of 54 studies) after performing unconclusive exams (MR=20; CT=18; abdominal US=24). PET images were analyzed both qualitatively and semiquantitatively (SUVmax). FDG results were compared to DOTATOC results in a lesion-by-lesion analysis. Lastly, both findings were compared to cytologic/bioptic (=18) or histological data (=9). **Results:** According to FDG, pancreatic lesions were negative in 17 and positive in 10/27 of the cases (SUVmax range 3-33). According to DOTATOC 14 lesions showed increased uptake (SUVmax range 5.6-82) and 13 lesions had no significant uptake. Three lesions were positive both at FDG and DOTATOC scan; 6 lesions were totally negative according to both. In 7/27 of the patients, FDG scan was positive with negative DOTATOC findings. In 11/27 of the patients DOTATOC scan was positive with FDG negative results. Histological data showed in 5/7 of the patients positive at FDG but negative at DOTATOC PET: 3 adenocarcinoma, 1SPN, 1 IPMN. Ten pNET were found in 10/11 of the patients positive at DOTATOC with negative FDG. In 2 patients with FDG positivity/DOTATOC negativity, 1 with DOTATOC positivity/FDG negativity, cytology was negative for neoplastic cells. Patients classified as negative according to both exams (5), were all "true negative". In all patients (=3) with FDG and DOTATOC positivity histological data showed NET. **Discussion/Conclusion**: FDG and DOTATOC may have a complementary role in patients with cystic pancreatic lesions. The metabolic activity assessment using FDG PET could be sufficient in case of FDG unambiguous positive findings, being pivotal in guiding biopsy. In patients with FDG negative/doubtful findings, an additional DOTATOC scan should be recommended to avoid false negative results.

EP-0614

Role of 68Ga DOTANOC PET/CT in patients of paraganglioma and comparison with 131I-MIBG SPECT/CT scintigraphy

S. Arora, M. Tripathi, R. kumar, C. Bal, R. kumar; All India Institute of Medical Sciences, AIIMS, New Delhi, New Delhi, INDIA.

Objective: To find out diagnostic accuracy of 68Ga DOTANOC PET/CT in patients of paraganglioma and compare with 131I-MIBG SPECT/ CT in different subgroups (Head & Neck, Abdomen/ Pelvis and uncommon sites). **Methods**: A total of 76 (Mean age: 35.8±15.35 years; Male-31, Female-45) paraganglioma patients {59 for staging, 9 for both staging and restaging and 8 for restaging only} were enrolled. All patients underwent 68Ga-DOTANOC PET/CT and 131I-MIBG scan within 2 weeks of each other. Histopathology and/or clinical/imaging follow up (minimum-6 months) were used as reference standard. **Results**: Seventy six patients underwent a total of 85 68Ga - DOTANOC PET/CT scans. On patient wise analysis, 68Ga-DOTANOC PET/CT

was positive in 66 and negative in 19 scans, with overall sensitivity of 97%, specificity of 94%, positive predictive value of 98% and negative predictive value of 94%. All patients also underwent ^{131}I MIBG SPECT/CT, which showed a sensitivity of 43% and specificity of 100%. On lesion wise analysis, a total of 131 lesions were analyzed. PET/ CT was positive in 111 lesions and negative in 20 lesions. Among these, 110 were true positive and one lesion was false positive with sensitivity of 97% and specificity of 94%, whereas ^{131}I MIBG SPECT/CT had sensitivity of 35% and specificity of 100%. There was significant difference in accuracy between ^{68}Ga DOTANOC PET/CT vs ^{131}I MIBG scintigraphy (P< 0.0001). On region wise analyses, in head and neck paragangliomas (52 lesions), ^{68}Ga DOTANOC PET/CT showed 100% sensitivity and specificity, while ^{131}I MIBG scan showed sensitivity of only 19% and specificity of 100%. In abdominal paraganglioma (44 lesions), sensitivity of MIBG scan improved significantly to 81% with specificity of 100%. In detection of metastasis (13 patients) ^{68}Ga DOTANOC PET/CT showed sensitivity of 96% compared to ^{131}I MIBG scan which showed sensitivity of only 25%. **Conclusion**: ^{68}Ga-DOTANOC PET/CT showed high diagnostic accuracy in patients with paraganglioma. In addition, it demonstrated other synchronous paraganglioma. ^{68}Ga-DOTANOC PET/CT was superior to ^{131}I MIBG SPECT/CT for these cases especially in head & neck, uncommon sites of involvement and metastatic lesions.

EP-0615

Advantages of Simultaneous PET/MRI in the Evaluation of Neuroendocrine Tumors with Ga-68 DOTATATE

D. Franceschi, R. Matthews, R. Chimpiri, N. Relan; *SUNY at Stony Brook, Stony Brook, NY, UNITED STATES OF AMERICA.*

Introduction: A new hybrid technology combining positron emission tomography (PET) with magnetic resonance imaging (MRI) has been increasingly used in cancer imaging. We evaluated its utility in patients with neuroendocrine tumors using Ga-68 DOTATATE as a radiotracer. **Material and Methods:** We performed total of 33 PET scans with Ga-68 DOTATATE in period of five months following its FDA approval. In 31 of these patients imaging was done for staging and restaging of known gastroenteropancreatic neuroendocrine tumors. In 18 patients PET/MRI was used, and in 13 patients PET/CT was performed. Images were compared visually for quality using 4-point (1-4) scoring scale, for morphological correlation and for coregistration. **Results:** The visual scoring for the PET/MRI quality was significantly higher in comparison to PET/CT image quality (3.85 for PET/MRI vs 3.04 for PET/CT; P < 0.05). Anatomical alignment was better with PET/MRI due to misalignment of the abdominal organs in more than 50% cases on PET/CT. This was mostly related to respiratory motion and bowel movement. In 2 patients with intestinal lesions PET foci were not aligned with bowel loops but localized in the adjacent mesentery on PET/CT. Morphological correlates for abnormal PET foci were seen much more frequently on MRI images than on CT. In cases of abnormal PET foci in the liver, 87% of underlying lesions were identified on MRI images and just 32 % on non-contrast CT. Tiny abnormal PET foci, smaller than 1 cm and in particular in the bones, were not

readily identified on both, underlying MRI and CT images. **Conclusions:** PET-MRI with Ga-68 DOTATATE proved to be a feasible and effective modality in staging and restaging of patients with neuroendocrine tumors providing superior image quality, better anatomical alignment, and identifying significantly more morphological correlates than PET/CT.

EP-0616

Indium 111 pentetreotide in Neuroendocrine Tumors: SPECT CT is truly needed

M. L. De Rimini[1], A. Di Sarno[2], N. De Rosa[3], A. Settembre[4], F. Lassandro[5], C. Bergaminelli[6], P. Muto[1]; [1]Nuclear Medicine Unit - AO Ospedali dei Colli - Monaldi, Naples, ITALY, [2]Oncology Unit - AO Ospedali dei Colli - Monaldi, Naples, ITALY, [3]Pathology Unit - AO Ospedali dei Colli - Monaldi, Naples, ITALY, [4]Surgery Unit - AO Ospedali dei Colli - Monaldi, Naples, ITALY, [5]Radiology Unit - AO Ospedali dei Colli - Monaldi, Naples, ITALY, [6]Thoracic Surgery Unit - AO Ospedali dei Colli - Monaldi, Naples, ITALY.

Introduction: ^{111}In-pentetreotide-DTPA, Octreoscan (Oct), specifically binds to somatostatin receptors (SR), allowing SR Scintigraphy (SRS). Many NET centers switched to PET-based imaging, using mainly ^{68}Ga-DOTA peptides as the SRS gold standard, nevertheless in a lot of centers, as well as in our Institution, SPECT-based tracer remains the SRS approach for NET imaging. **Aim:** To evaluate the added value of SPECT/CT vs only SPECT diagnostic performance in the NET imaging. Methods: From January to April 2017, 18 patient (pts) with suspected/known NET (-lung, n.7 pts; -mediastinum, n.1; -ileum, n.5; -hepathic metastases with unknown origin, n.1; -pancreas, n.4) underwent Oct-SRS. Pts were selected on the basis of: clinical history (e.g. surgery for NET in 6/18 pts), high serum levels of NSE and chromogranin, positive FNAB. Early (4hrs) and Delayed (24hrs) scans (GE-Discovery NM/CT 670, 16 slice) after Oct administration (200 MBq/pt) were obtained in: WB planar spots and SPECT with co-registered Low Dose CT, used for attenuation correction (AC) and anatomical cross. SPECT uncorrected (NAC), AC and CT images were visually analyzed and the AC/CT fused images were used for cross evaluation. NAC and AC images were compared on a head-to-head basis. Semiquantitative analysis for SUV evaluation was also obtained for SPECT/CT images (QMetrix-GE Software). Clinical implications of scan results were discussed by the Multidisciplinary Group for NET of Naples, ENETS Center of Excellence. **Results:** Planar images were inconclusive vs the NAC and AC ones. A total of 28 lesions were detected on both AC/NAC images, but the AC correctly defined the anatomical cross in all lesions, where the main limits of SPECT alone was the absence of anatomical cross and the false-positives, due to aspeciphic uptake (fecal, gallbladder, ureter activities), causing over-estimation of lymph node extension and hepatic metastases. At a patient-basis analisys, additional 12 lesions were defined at only AC images vs NAC, pertaining lymph nodes and metastases, which were found to be true-positive on follow-up. Among these, particular clinical impact was achieved thanks AC images and SUV evaluation, in better discriminating lesions, particularly for liver metastases, for the project of ptswork-up. **Conclusion:** In the clinical setting of pts affected with NET, OCT-SPECT/CT

takes significant advantages vs SPECT only respectively in: lesion detection, improving specificity and in the prediction of pts responder to therapy. On this basis, and considering the prevalent role of PET-based imaging, multimodality technique with SPECT/CT could be mandatory to use in the case of SPECT-based scans. (On behalf of the Multidisciplinary Group for NET of Naples, ENETS Center of Excellence)

EP-46   **during congress opening hours, e-Poster Area**

Clinical Oncology: Colorectal Cancer

EP-0617

Preliminary results in the evaluation of PET/CT colonography in preoperative obstructive colorectal cancer diagnosed by incomplete optical colonoscopy

D. Fuster, M. Pagès, A. Ginés, E. Buxó, D. Momblan, F. Campos, F. Pons, N. Sánchez, A. Tapias, F. Lomeña; Hospital Clinic, BARCELONA, SPAIN.

Introduction: Optical colonoscopy is the method of choice for diagnosis of colorectal cancer (CRC) in standard clinical routine. However, obstructive masses can impede its completion so the presence of synchronous malignancies or potentially malignant polyps cannot be excluded which is critical when deciding the extension of surgical management. The aim of this prospective study was to evaluate if integrating whole-body PET/CT with CT colonography (PET/CTC) can improve preoperative diagnosis of obstructive CRC. **Subjects & Methods:** We performed PET/CTC in 20 consecutive patients (11 men and 9 women with a mean age of 69±15 years old) suspected of having CRC by optical colonoscopy which was not completed due to obstructive masses. To perform PET/CTC a Foley catheter of small caliber was inserted to distend the colon with a CO_2 insufflation. Before the patient was scanned, a preview image was obtained to estimate the distention and PET/CT scans were acquired with patient in the supine and prone positions. A radiologist and a nuclear medicine physician analyzed PET/CTC images. Polyps measuring ≥10mm were considered as high risk of malignancy. The sensitivity and specificity of PET/CTC and CTC alone were calculated for local lymph node involvement and metastatic disease. Surgical resection and/or biopsy of the lesions served as the gold standard and, when indicated, an optical colonoscopy was performed as follow-up. **Results:** CRC was localized in the sigmoid (n=6), rectosigmoid junction (n=5), rectum (n=3), descending (n=3), ascending (n=2) and transverse (n=1) colon. All tumors showed FDG uptake (mean±sd SUVmax=16.7±10.6). One synchronic tumor also showed pathological FDG uptake (SUVmax=17). A total of 6 polyps were found by CTC: <10mm (n=4) and ≥10mm (n=2). Both polyps ≥10mm showed FDG uptake (SUVmax= 7.8 and 4.7) but none of the <10mm polyps could be identified by PET. Pathological lymph nodes were diagnosed in 13/20 cases after surgical removal with a sensitivity and specificity for CTC and PET/CTC of 61% and 87% and 69% and 100%, respectively. Liver metastases were confirmed in 4 patients (one case along with lung metastases) showing a sensitivity and specificity for CTC and PET/CTC of 75% and 89% and 75% and 100%, respectively. **Conclusion:** PET/CTC is a reliable technique useful to stage CRC and to diagnose synchronous tumors. PET/CTC showed a potential use to rule out polyps at high risk of malignancy in this series.

EP-0618

Clinical role of 18F FDG PET CT in recurrence of colorectal cancer with suspected conventional image findings irrespective of tumour markers

E. Kaya[1], H. Temiz[1], A. L. Güner[1], T. Aksoy[1], E. Vardareli[1], M. Emi[2], A. Karaman[3]; [1]Acıbadem University Medical Faculty, Department of Nuclear Medicine, Istanbul, TURKEY, [2]Acıbadem Kayseri Hospital, Department of Radiodiagnostic, Kayseri, TURKEY, [3]Acıbadem University Medical Faculty, Department of Gastroenterology, Istanbul, TURKEY.

Background: Fluorine 18 fluorodeoxyglucose positron emission tomography/computed tomography (18F-FDG PET/CT) is used for diagnosis, staging, restaging and evaluation of response to therapy of malignant disease and generally shows higher diagnostic accuracy compared to conventional imaging. **Aim:** The purpose of this study is to evaluate clinical role of 18F-FDG PET/CT in detection of recurrence colorectal cancers in patients with suspected conventional image findings irrespective of tumour markers. **Material and Method:** This was a prospective study consisting of 43 patients (27 male, 16 female) to detect recurrence in primary site and evaluate metastatic areas of patients referred to our clinic in whom suspected of having recurrence by conventional imaging modalities (ultrasonography, computed tomography, magnetic resonance image, colonoscopy). Tumour markers were not concidered. All pathological 18F-FDG uptake sites were declerated for further clinical investigation and to the final diagnose. The number and sites of suspected lesions on conventional imaging were correlated by 18F-FDG-PET/CT. Recurrence site and metastatic focus on 18F-FDG PET/CT and convantional images, were evaluated at least two experience nuclear medicine specialist and radiological specialist, the final decision was made by concensus. Sensitivity, specificity, positive predictive value (PPV) and negative predictive value (NPV) were calculated on patient base and lesion base. **Results:** 18F-FDG PET/CT scan located recurrent site and metastatic focus in 28 patients (28/43, 65%), and 77 lesion (77/110, 70%). On patient base, the sensitivity, specificity, PPV and NPV were, 87%, 19%, 73%, 20%, respectively. The sensitivity, specificity, positive PPV and NPV on lesion base were 75%, 40%, 76%, 37%, respectively. **Conclusion:** 18F-FDG PET/CT is provide considerable diagnostic contribution in detection of recurrence colorectal cancers in patients with suspected conventional image findings. **Keywords:** Colorectal cancer, recurrence, 18F FDG PET/CT

EP-0619

Correlation between metabolic tumor volume and prognostic hematological parameters in patients with colorectal cancer

A. Cengiz, Y. Yürekli; Adnan Menderes University Medical School Department of Nuclear Medicine, Aydın, TURKEY.

Introduction: Colorectal cancer (CRC) is the 3rd most commonly diagnosed cancer in the world. Among the various inflammatory markers, elevated neutrophil-to-lymphocyte ratio (NLR) and platelet-to-lymphocyte ratio (PLR) have been shown to be with poorer clinical outcomes in various cancers. Serum carcinoembryonic antigen (CEA) level is the most widely used tumor marker for CRC and is associated with poor clinical outcome. Metabolic parameters in positron emission tomography/computed tomography (PET/CT) such as metabolic tumor volume (MTV) have been reported to be a prognostic marker in various cancers including CRC. The aim of this study is to evaluate the correlation between serum NLR, PLR, CEA and MTV in patients with CRC. **Subjects & Methods:** Ninety patients (30 female, 60 male) (32-85 years, mean 63.5±11.8) with CRC who underwent 18-F FDG PET/CT for initial staging were evaluated retrospectively. Patients with hematological disease, chronic infections, prior chemotherapy, radiotheraphy or surgery for CRC were excluded. MTV was delineated with the SUV2.5 isocontour and was calculated automatically with a software program. Hematological parameters were taken within seven days of the PET/CT imaging. Pearson's correlation test was used for statistical analyses. **Results:** MTV ranged from 2.14-230.36 cm^3 and NLR ranged from 0.91-25.1. There was statistically significant positive correlation between NLR and MTV (r=0,444, p=0.000). PLR ranged from 23.77-432.65 and CEA values ranged from 0.53-1117.8 (ng/mL). PLR and CEA values were not correlated with MTV. SUVmax of primary tumor was not correlated with hematological parameters. **Conclusion:** NLR is significantly correlated with MTV in patients with CRC. MTV can contribute to prognostic evaluation of these patients.

EP-0620

Relationship between metabolic parameters and ras mutation status

*E. Karci[1], **C. Soydal**[2], G. Utkan[1], Y. Urun[1], H. Akbulut[1]; [1]Ankara University Medical Faculty, Medical Oncology, Ankara, TURKEY, [2]Ankara University Medical Faculty, Nuclear Medicine, Ankara, TURKEY.*

Purpose: The aim of this study was to investigate the relationship between metabolic parameters on 18F-FGD PET/CT and neutrophil lymphocyte ratio (NLR),platelet lymphocyte ratio (PLR), serum carcinoembrionic antigen (CEA) and ca-19.9 levels and RAS mutational status in colorectal cancer patients. **Methods:** We retrospectively evaluated 45 (30M, 15F, mean age: 62) patients with pathologically confirmed metastatic colorectal adenocarcinoma. While 20 patients metastatic at the time of diagnosis, 25 patients developed metastases during follow-up after initial treatment. All the patients underwent 18F-FDG PET/CT at the time of metastatic disease. For statistical analysis data of serum sampling within 1 month period before PET/CT was used. NLR was defined as neutrophil/lymphocyte ratio, PLR as platelet/lymhocyte ratio. NLR and TLR was calculated using

laboratory data when PET/CT performed. Ras mutational status was evaluated from histopathological examination of primary surgical speciment. Difference between mean standardized uptake value (SUV) and total lesion glycolysis (TLG) of metastatic lesions of Ras mutant and nonmutant groups were analyzed by Student T test. Relationship between NLR, TLR, serum CEA and Ca19-9 levels and PET parameters were analyzed by Lineer Regression Model. **Results:** Totally 18 (40%) of patients were RAS mutant. Median NLR, TLR, serum CEA and Ca19-9 levels were calculated as 2.36 (min-max: 1-8), 133.5 (min-max: 41-404), 16 NG/mL (min-max:115-227) and 19 U/ml (min-max: 200-495). In the evaluation of metabolic parameters in 18F-FDG PET/CT, median SUV and TLG of metastatic lesions were calculated as 10.5 (min-max: 3-44) and 150.63 (min-max:13-2723). Although mean SUV of RAS mutant and nonmutant groups were not significantly different (13.6 vs 11.9, p=0.34), mean TLG of those groups were significantly different (455.96 vs 320.98, p=0.02). In the Lineer Regression Model, relationship between serum CEA levels and TLG was found statistically significant (p=0.19). NLR, TLR and serum Ca19-9 levels and PET parameters had not significant relationship. **Conclusion:** Despite the limited number of included patients, results of this study revealed that TLG and RAS mutation status have a significant correlation in metastatic colorectal cancer patients. Although its is not routinely recommended in that patient group, 18F-FDG PET/CT seems to have a prognotic role.

EP-0621

The FOXFIRE/SIRFLOX/FOXFIRE-Global randomised studies of first-line selective internal radiation therapy for metastatic colorectal cancer

N. K. Sharma[1], P. Gibbs[2], G. Van Hazel[3], V. Heinemann[4], J. Ricke[5], M. P. Findlay[6], V. Gebski[7], J. Moschandreas[8], P. Virdee[8], P. Dutton[8], J. Taieb[9], M. Peeters[10], P. Tait[11], P. Boardman[12], V. Lewington[11], A. Al-Nahhas[11], H. Wasan[13], R. A. Sharma[14]; [1]Penn State Hershey Cancer Institute, Hershey, PA, UNITED STATES OF AMERICA, [2]The Royal Melbourne and Western Hospitals, Melbourne, AUSTRALIA, [3]University of Western Australia, West Perth, AUSTRALIA, [4]University of Munich, Munich, GERMANY, [5]University of Magdeburg, Magdeburg, GERMANY, [6]University of Auckland, Auckland, NEW ZEALAND, [7]University of Sydney, Sydney, AUSTRALIA, [8]University of Oxford, Oxford, UNITED KINGDOM, [9]Georges Pompidou European Hospital, Paris, FRANCE, [10]Antwerp University Hopital, Antwerp, BELGIUM, [11]Imperial College Healthcare NHS Trust, London, UNITED KINGDOM, [12]Oxford University Hospitals NHS Trust, Oxford, UNITED KINGDOM, [13]Hammersmith Hospital, London, UNITED KINGDOM, [14]University College London, London, UNITED KINGDOM.

Aim: The FOXFIRE, SIRFLOX and FOXFIRE-Global (FF-SF-FFG) randomised studies assessed the efficacy and safety of adding selective internal radiation therapy (SIRT) using yttrium-90 (Y90) resin microspheres to first-line mFOLFOX chemotherapy in patients with liver metastases from colorectal cancer (mCRC). This is the first analysis of activity planned and delivered in this combined dataset. **Materials & Methods:** FF-SF-FFG included

chemotherapy-naïve mCRC patients (performance status 0 or 1) with liver-only or liver-dominant metastases not suitable for curative resection/ablation. Patients were randomized (1:1) to mFOLFOX6 or OxMdG chemotherapy (± a biologically targeted agent) alone (Arm A) or with SIRT (Arm B). A single session of SIRT was planned on day 3 or 4 of cycle 1 of chemotherapy in SF-FFG and on day 3 or 4 of cycle 2 in FF. The primary endpoint was overall survival (HR 0.8, 80% power, two-sided 5% significance). Y90 resin microspheres were prescribed as a single treatment to the whole liver or one lobe using previously published activity tables based on a body surface area formula. Variations in SIRT administration, dosing variations and association with outcomes were assessed in the intent to treat population. **Results:** Patient characteristics and primary outcomes have been previously presented. Median follow-up was 43.3 months. Of the 1103 patients randomized, 554 were included in Arm B and 507 received SIRT at a median activity of 1.4 (range 0.2-2.8, 25th percentile:1.06, 75th percentile: 1.80) GBq. SIRT was delivered to the right lobe, the left lobe and both lobes in 48, 8 and 449 patients (2 unavailable), respectively. Of the FF patients who did not receive the intended SIRT, the most common cause was inappropriate arterial distribution. Objective response rate (*p*=0.001) and liver-specific progression-free survival (HR 0.51, CI 0.43-0.62, p<0.001) were improved with the addition of SIRT. Association between absorbed (Gy) dose and clinical outcomes will be presented at the EANM meeting. **Conclusions:** This is one of the largest prospective, randomised studies performed in the history of Nuclear Medicine. The addition of SIRT to first-line chemotherapy for patients with liver-only and liver-dominant mCRC improved objective response rate and liver-specific progression-free survival. Variations in implantation techniques/dosimetry and the association with clinical outcomes will be presented at the meeting to yield insights into the findings of this seminal prospective trial.

EP-0622

Diagnostic value of 18F-FDG PET/CT in follow up of patients with locally advanced rectal cancer treated with neoadjuvant chemoradiation before surgery

C. Altini, A. Niccoli Asabella, A. Di Palo, V. Lavelli, A. Cassano, E. P. Mossa, G. Rubini; *Nuclear Medicine Unit, AOU Policlinic of Bari, University of Bari, bari, ITALY.*

Aim: The aim of this study was to prospectively investigate the value of the follow up ^{18}F-FDG PET/CT in patients with locally advanced low-rectal cancer (LARC) treated by neoadiuvant chemoradiation (nCRT) before surgery. **Matherials and Methods:** 58 patients (39 male, 19 female; mean age 66 years old) performed 18F-FDG PET/CT 3 months later the eradicative surgery for LARC. All patients previously performed nCRT ended 8 weeks before surgery. Patients were considered Responders to the nCRT if ypStaging were 0 or I and Non-Responders if were II or III. Sensitivity (Sen), Specificity (Spe), Accuracy (Acc), Positive Predictive Value (PPV) and Negative Predictive Value (NPV) of 18F-FDG PET/CT were evaluated in

all patients and in the two groups about local relapses, liver, lungs and lymphnodes involvement. **Results:** Sen, Spe, Acc, PPV and NPV in all patients were respectively 87.5% (95%CI: 47.3%-99.7%), 86% (95%CI: 73.3%-94.2%), 86%, 50% (95%CI: 32.4%-67.6%) and 97.7% (95%CI: 87.3%-99.6%) for local relapse; 75% (95%CI: 19.41%-99.37%), 94% (95%CI: 84.61%-98.84%), 93%, 50% (95%CI: 22.5%-77.5%) and 98% (95%CI: 90.3%-99.64%) for liver metastases; 100% (95%CI: 54.07%-100%), 94% (95%CI: 84.05%-98.79%), 95%, 67% (95%CI: 40%- 85.71%) and 100% for lung metastases; 100%, 82.46% (95%CI: 70.09%-91.25%), 83%, 9% (95%CI: 5.39%-14.93%) and 100% for lymphnode metastases. According ypStaging 28 patients (48.3%) were Responders and 30 (51.7%) Non-responders. Sen, Spe, Acc, PPV and NPV in Responders patients were respectively "not-valuable", 89.29% (95%CI: 77.77%-97.73%), 89%, 0% and 100% for local relapse; 50% (95%CI:1.26%-98.74%), 100% (95%CI: 86.77%-100%), 96%, 100%, 96.3% (95%CI: 86.67%-99.05%) for liver metastases; 66.67% (95%CI: 9.43%-99.16%), 92% (95%CI: 73.97%-99.02%), 89%, 50% (95%CI: 17.49%-82.51%) and 95.83% (95%CI: 82.22%-92.13%) for lung metastases; 50% (95%CI: 1.26%-98.74%), 85.71% (95%CI: 67.3%-95.97%), 86%, 20% (95%CI: 4.55%-56.71%) and 96% (95%CI: 85.62%-98.98%) for lymphnode metastases. Sen, Spe, Acc, PPV and NPV in Non-responders patients were respectively 87.5% (95%CI: 47.35%-99.68%), 81.82% (95%CI: 59.72%-94.81%), 83%, 63.64% (95%CI: 40.98%-81.52%) and 94.74% (95%CI: 74.01%-99.13%) for local relapse; 100%, 89.29% (95%CI: 71.77%-97.73%), 90%, 40% (95%CI: 18.62%-66.01%), 100% for liver metastases; 100%, 96.15% (95%CI: 80.36%-99.9%), 97%, 80% (95%CI: 36.92%-96.47%) and 100% for lung metastases; 100%, 85.14% (95%CI: 62.27%-95.81%), 83%, 20% (95%CI: 9.19%-38.18%) and 100% for lymphnode metastases. McNemar revaled differences statistically significant between sensitivity about the liver (χ^2=19.43, p<0.0001), lung (χ^2=11.69, p=0.0006) and lymphnodes (χ^2=10.43, p<0.0001) localizations. **Conclusion:** 18F-FDG PET/CT in wholebody evaluation of patients with LARC in follow up have a good performance independently by their response to nCRT.

EP-0623

Prognostic value of 18F-FDG PET/CT visual assessment and semiquantitative analysis in locally advanced rectal cancer trated with neoadjuvant chemoradiation

C. Altini, A. Niccoli Asabella, C. Ferrari, V. Lavelli, S. Sisto, M. Fanelli, G. Rubini; *Nuclear Medicine Unit, AOU Policlinic of Bari, University of Bari, bari, ITALY.*

Aim: the aim of our study was to prospectly assess the prognostic value of 18F-FDG PET/CT in patients with locally advanced rectal cancer (LARC) previously treated with neoadjuvant chemo-radiation therapy (nCRT). **Materials and Methods**: 58 patients with LARC (39 male, 19 female; mean age 66 years old) performed 18F-FDG PET/CT scans twice (baseline and 5-6 weeks post-nCRT). All patients performed 8 weeks later the same surgery procedure. Semiquantitative parameters were collected both baseline and post-nCRT and were SUVmax, SU-

Vmean, MTV, TLG, and Response indexes (RImax% and RImean% =[(SUVbaseline−SUVpost-nCRT)/SUVbaseline]x100). Visual response assesment (VRA) on 18F-FDG PET/CT post-nCRT categorized patients in Complete-Response (CR), Partial-Response (PR), Stable-Disease (SD) and Progressive-Disease (PD). CR and PR was considered together "Responders" while SD and PD "Non-responders". Overall survival (OS) was defined as the time from surgery until death or to last follow-up. Disease-free survival (DFS) was defined as the time from surgery to the documented local or distant recurrence or last follow-up. OS ad DFS rates were estimated by Kaplan-Meier method and compared with the log-rank test. Quantitative data were expressed as medians and compared with Fisher's exact test. Univariate analysis assessed the correlation of semiquantitative paramenters with OS and DFS. Hazard ratios (HR) were derived from Cox regression analysis. **Results**: at the end of the observation 46 patients (79.3%) were alive and 12 (20.7%) death; 33 (56.9%) had relapses while the remnant 25 (43.1%) don't. OS was 83.51 months (SD 3.30) and DFS was 45.72 months (SD 5.79). 12 patients were CR, 36 were PR, 6 were SD and 4 were PD. The OS was longer in PR patients while DFS in SD patients but the differences among VRA groups were not statistically significant (χ^2=2.872 p> 0.005; χ^2=3.802 p> 0.005). OS in "Responders" and "Non-responders" were respectively 83.44 (SD 3.64) and 79.35 months (SD 7.38). DSF in "Responders" and "Non-responders" were respectively 83.44 months (SD 3.64) and 79.35 months (SD 7.38); differences were not statistically significant (p> 0.005) Differences in semiquantitative parameters mean values among VRA groups were not significant (p>0.005). Cox regression analysis showed that none of the semiquantitative parameters was related to OS and DSF; only the age was significantly related to the OS (OR=1.123 p=0.007). **Conclusion**: our results, although requiring confirmation in larger cohorts, showed 18F-FDG PET/CT potential in assisting physicians on individualized management decisions in patients with LARC, suggesting if patients can benefit of "wait and see" strategy after nCRT.

EP-0624

18F FDG PET CT vs CT Scan in patients with pulmonary metastases previously operated on for colorectal liver metastases

J. Navarro Fernandez, L. Frutos Esteban, V. Lopez-Lopez, M. Laroussi, M. Godoy Bravo, R. Reyes Marles, R. Robles Campos, R. Brusadin, A. Lopez Conesa, P. Parrilla Paricio, M. Claver Valderas; H U Virgen de la Arrixaca, Murcia, SPAIN.

Aim: The aim of this study was to analyze the benefits of preoperative 18F FDG PET CT for detecting pulmonary or extrapulmonary disease in patients operated on for colorectal liver metastases (CRLM) when the CT scan detected pulmonary metastases from colorectal cáncer (PMCRC) during the follow-up. We compared the findings obtained by the CT scan and the 18F FDG PET CT in patients operated on for these PMCRC with the histological findings of the surgical specimen. Additionally we analyzed the cost of the 18F FDG PET CT vs CT can. **Materials and Methods:** We designed the study pro-

spectively performing 18F FDG PET CT on all patients operated on for CRLM where the CT scan detected PMCRC during the follow up. We only included patients who were operated on for PMCRC because the histological findings were taken as a control. **Results:** Of the 101 pulmonary nodules removed in 57 patients, the CT scan identified a greater number (89 nodules) than the 18F FDG PET CT (75 nodules) (p 0.001). Sensitivity was greater with the CT scan (90% vs 76%, respectively) with a lower specificity (50% vs 75%, respectively) than with the 18F FDG-PET CT. There were no differences between in terms of PPV and NPV. 18F FDG PET CT detected more pulmonary nodules in 4 patients (one PMCRC in each of these patients) and more extrapulmonary disease in 6 patients (four mediastinal lymph nodes, one retroperitoneal lymph node and one liver metastases) that CT scan had not detected. The cost of the 18F FDGPET CT was 2.5 times higher than the CT scan. Since we detected more disease in 10 patients (17.5%) in whom the CT scan had not detected it, leading us to reflect on whether the use of 18F FDG PET CT could be economically justified. **Conclusions:** Although the CT scan has a greater capacity to detect PMCRC, the 18F FDG PET CT could be useful in the detection of more pulmonary and extrapulmonary disease not identified by the CT scan.

EP-0625

Diagnostic value of 18F-FDG-PET/CT in the assessment of colorrectal liver metastasis with neoadjuvant therapy pre-metastasectomy

A. M. Santos Bueno[1], M. V. Guiote Moreno[1], L. M. Mena Bares[1], E. Carmona Asenjo[1], F. R. Maza Muret[1], E. Ortega Moreno[1], E. Rodríguez Cáceres[2], J. A. Vallejo Casas[1]; [1]HU Reina Sofía, Córdoba, SPAIN, [2]IMIBIC, Córdoba, SPAIN.

Purpose/ Introduction: Assesment the utility of 18F-FDG/PET-CT in the evaluation of colorrectal liver metastasis (CRLM) that were treated with neadjuvancy previous to metastasectomy. **Subjects & Methods:** Observational retrospective study performed in 2016. Patients with CRLM who were treated with neoadjuvant therapy and who were candidates to curative surgery (according to the pre-operative studies) were included. All patients had a pre-treatment 18F-FDG/PET-CT study and another one at the end of it. The respond to neoadjuvant therapy was measured by the intensity of 18F-FDG/PET-CT's uptake. The total amount of liver metastasis pre-treatment was defined by the findings in PET-CT (and other image studies) and the number of metastasis post-treatment was defined with the pathological study. **Results:** 25 patients (89,3%) were positive for metastasis before receiving neoadjuvant therapy. 17 of them (60,71%) were clasified only with 18F-FDG/PET-CT. The total amount of lesions described by 18F-FDG/PET-CT and other imagen studies before the neoadyuvancy were 50 CRLM, with a mean of 1,96 (typical deviation of 1,67) lesions per patient. It was observed (with the 18F-FDG/PET-CT after neoadjuvantcy) an absence of uptake in 10 patients and 18 of the studies presented changes in the uptake (increase, decrease and/or new hipermetabolic lesions). 41 pathologic lesions were described after treatment,

corresponding with 18 patients. All patients suffered surgery. 27 of the excised lesions obtained pathologic confirmation for metastasis, 8 of them were false negatives and 1 was false positive. Sensitivity obtained was 68% and specificity 66%. The positive predictive value was 94% and negative predictive value was 20%. **Discussion/Conclusion:** The main utility of 18F-FDG/PET-CT in the reevaluation of CRLM patients is the confirmation of the presence of CRLM before metastasectomy (predictive positive value). The negative study not exclude the viability in the liver metastases, but is very important for evaluated absence of extrahepatic disease.

EP-0626

The Role of 18F-FDG PET/CT in Restaging and Management of Patients with Colorectal Carcinoma

G. Mateva, I. Kostadinova; Acibadem City Clinic Cancer Center, Sofia, BULGARIA.

Colorectal carcinoma is the third most common cancer worldwide. It consists mainly (95%) of adenocarcinomas which are FDG-avid. Thus the evaluation of patients with known or suspected recurrent colorectal carcinoma is an widely accepted indication for FDG-PET/CT imaging. We analyzed a total number of 50 consecutive patients. Almost half of them were diagnosed with histopathologically verified colon cancer and the rest were diagnosed with rectal cancer. All of them has undergone surgical resection of the primary tumor and chemotherapy. Additional procedures such as radiation therapy of the primary tumor or metastases, local ablation or resection of lung and liver metastases were performed in some of the cases. The patients included in the study met the following criteria-either there was clinical or biochemical suspicion of recurrence of the disease, equivocal results from another imaging study or a need of reassessment of the extent of the disease after treatment or after confirmed recurrence. Based on the existing response evaluation crieteria (such as EORTC , RECIST, PERCIST) we have established modified criteria regarding size, number and the metabolic activity (measured by SUVmax) of the lesions for evaluation of the treatment response. According to their results we have divided the patients in four groups as follows: A\ Complete response B\ Partial response C\ Stable disease D\ Progressive disease As a result of the performed studies we have managed to confirm malignancy in more than 2/3 of the patients with elevated tumor markers or equivocal results from another imaging study. The PET/CT accessment has added certainty and specificity to the restaging process and in some cases has helped to avoid overtreatment or undertreatment of the patients. However there is a great need for unified PET/CT criteria for evaluation of treatment response for solid leasons since it will minimise the individual mistakes of judgement and will contribute to more accurate management of the patients. In conclusion we could say that PET/CT is a technique of choice for restaging patients with colorectal cancer and adjustment of the treatment strategy. As a result of the performed PET/CT studies in all of the patients with progressive disease the treatment plan was changed.

Clinical Oncology: Urogenital

EP-0627

Role of 11C-Choline PET/CT in prostate cancer patients with biochemical recurrence after brachytherapy

J. Garcia, M. Cozar, M. Soler, G. Reyes, A. Diaz, J. Ferrer, E. Riera; CETIR ERESA, Esplugues. Barcelona, SPAIN.

Objective: Prostate brachytherapy is a radical treatment for low-risk prostate cancer patients that meet the D´Amico criteria. After the procedure, prostate inflammation may lead to a transitory increase in PSA values, thus difficulting the definition of biochemical recurrence. However, the early detection of cancer recurrence allows rescue therapies to be implemented. This study aimed to assess the value of 11C-Choline PET/CT in those patients with prostate cancer already treated by brachytherapy and subsequent increase in PSA levels, as well as their therapy outcome after early detection of disease recurrence by 11C-Choline PET/CT. **Materials and Methods:** Sixty one patients were retrospectively studied (PSA ≤ 10 ng/ml, Gleason score <7 and <T2c stage) with no severe urinary symptomatology (flow test ≥15 ml/s), and progressive increase in PSA values. Patients were referred to our clinic for recurrence detection by means of an 11C-Choline PET/CT study. Mean time from brachytherapy to biochemical recurrence time was 55.93 months (12-144 months). **Results:** Recurrence rate assessed by 11C-Choline PET/CT was 67.2%. PSA values in negative cases were lower than in positive cases (7.6 ng/ml vs.11.2 ng/ml). Sites of disease recurrence were: prostate 39.3%; infradiaphragmatic invasion 11.5%; bone involvement 4.9%; and other involvement sites 11.5%. Mean increase in PSA values was proportional to recurrence site: prostate: 8.1 ng/ml; infradiaphragmatic invasion: 9.7 ng/ml; bone involvement: 14.5 ng/ml; and multiple sites: 20.3 ng/ml. The detection of confined recurrence allowed implementing rescue therapy in up to 50.8% of patients in whom 11C-choline PET/CT was positive. **Conclusion:** 11C-Choline PET/CT proved its usefulness for assessment of recurrence in prostate cancer patients treated with brachytherapy, with a rate detection of 67.2%, and showed a major impact on their treatment outcome.

EP-0628

Assessing the value of mediastinal lymph node uptake on ¹⁸F-choline PET/CT scans

V. Sousa, C. Loewenthal, M. Vieira; Hospital da Luz, Lisbon, PORTUGAL.

Aim: Prostate cancer is the most common cancer among men. The use of ¹⁸F-choline positron emission tomography (PET)/ computed tomography (CT) to study these tumors has become mainstream. The aim of this review was to study the significance of mediastinal lymph node uptake in a population evaluated with ¹⁸F-choline PET/CT through histological evaluation and/or

follow-up. **Materials and Methods:** Of 344 oncologic patients (pts), average age of 67±7, examined by ^{18}F-choline PET/CT (total of 413 studies) from September 2009 to August 2016, 36 pts (10%) had mediastinal lymph node uptake. Prostate specific antigen (PSA), clinicopathological and imaging findings were retrospectively reviewed. Patients without at least 5 months follow-up were excluded (n=4). The remaining patients (n=32) had a median follow-up of 26 months (min 5, max 63). **Results:** Four pts (4/32) were evaluated for initial staging and 28 (28/32) for biochemical recurrence. Of 32 pts with abnormal mediastinal lymph node ^{18}F-choline uptake, 72% (23/32) had biochemical/imaging progression or initiated systemic therapy with stabilization of disease (Group 1) and 28% (9/32) did not have biochemical/imaging progression (Group 2). Histological confirmation was obtained in only 2 pts. In one pt prostate cancer metastases was confirmed and the other had a lung cancer, and there was no biochemical recurrence in this latter patient. The mean SUV_{max} of mediastinal lymph nodes of Group 1 pts was 6.59±3.1 (median 6.2) and of those of Group 2 was 5.07±2.9 (median 4.69). The PSA levels, as well as Gleason score, were not significantly different between the two groups. Of those patients from Group 1, 52% (12/23) had additional distant metastatic disease and 9% (2/23) died 29 months (average) after ^{18}F-choline PET/CT. Among the pts with only mediastinal lymph node uptake (9/32), with a median SUV_{max} 4.85, 66% (6/9) showed progression or stabilization of disease under systemic therapy whereas 33% (3/9) have not shown progression of prostate disease. **Conclusions:** The significance of mediastinal lymph node uptake of ^{18}F-choline should not be overlooked as it may have some bearing on prognosis, which should be confirmed in larger pt populations. The possibility of finding a second tumor, namely lung, should be considered.

EP-0629

F-18 Fluorocholine PET/CT In Restaging Prostate Cancer Patients With Biochemical Recurrence After Radical Prostatectomy

*S. K. Vadi, **B. Singh**, S. K. Singh, A. Watts, R. K. Basher, A. Sood, N. Kakkar, A. Lal; Post graduate institute of medical education and research, chandigarh, INDIA.*

Purpose: To evaluate the diagnostic performance of F-18 Fluorocholine positron emission tomography / computed tomography (FCH PET/CT) in restaging prostate cancer (PC) patients with biochemical recurrence (BCR) following radical prostatectomy (RP). **Materials and Methods**: Twenty patients (mean age = 67.25 ± 7.94 ; range = 51-79 years) who had previously undergone RP, had undetectable (<0.2 ng/mL) serum prostate specific antigen (PSA) postoperatively and with BCR (PSA ≥0.2 ng/mL) twice during post-operative period were recruited. The mean time from RP to the BCR in the group was 48.45±52.50 months (range=6-192). A written and informed consent was taken from all the study subjects. All the study subjects underwent FCH PET/CT (Discovery PET/CT 710 scanner GE, Healthcare, Milwaukee, USA) after documentation of BCR. The doubtful PET/CT findings were validated either by TRUS or CT guided

biopsy and histopathological analysis. **Results**: The initial mean Gleason's score was 6.3 ± 1.53 (range 4-9). The mean PSA levels at the first time point of relapse were 1.98 ± 2.87 (median value=0.98; range 0.24-13.2 ng/mL). The corresponding PSA values repeated after a minimum time interval of 4 weeks were 3.23 ± 3.30 ng/mL (range 0.6-14.7). FCH PET/CT results were positive in the primary tumor recurrence in the prostate bed, pelvic lymph node, pelvic skeletal sites in 7 (7/20=35.0%), 9 (9/20=45.0%) and 2 (2/20=10.0%) patients respectively. The gold standard histopathological findings were positive in 8 patients True positive PET/CT findings were observed in 7 (7/9=78.0%) patients. A positive correlation (Spearman's correlation coefficient= 0.872) was observed between SUVmax values and PSA levels for pelvic lymph nodes recurrence. However, no correlation was observed between the PSA levels and SUV max values of the metastatic lesions (skeletal and prostatic fossa) on FCH PET/CT. The sensitivity for detecting the recurrence in FCH PET/CT was found to be 87.5% (95% CI of 47.35% to 99.68%), while specificity was found to be 75.0% (95% CI of 42.81%-94.51%). Additionally, the whole body FCH PET/CT detected extra pelvic distant metastases in 4 (4/20=20%) patients with skeletal in 2, lung in 1 and adrenal metastases in one patient respectively. **Conclusion:** FCH PET/CT proved a useful tool in recurrence evaluation and management in BCR post RP in this small patient group with low recurrent PSA level.

EP-0630

11C-Choline PET/CT in the Diagnostics of Bone Metastases in Prostate Cancer Patients with Biochemical Relapse

D. M. Pursanova[1], I. P. Aslanidi[1], O. V. Mukhortova[1], T. A. Katunina[1], V. I. Shirokorad[2], D. A. Roshchin[3]; [1]A.N.Bakoulev Scientific Center for Cardiovascular Surgery of the Ministry of Health of the Russian Federation, Moscow, RUSSIAN FEDERATION, [2]Moscow City Oncology Hospital №62, Moscow, RUSSIAN FEDERATION, [3]N.Lopatkin Scientific Research Institute of urology and Interventional Radiology - Branch of the National Medical Research Radiological Centre of the Ministry of Health of the Russian Federation, Moscow, RUSSIAN FEDERATION.

The detection of skeletal involvement in prostate cancer (PCa) patients with biochemical relapse is crucial for further treatment approach. **Purpose:** To evaluate the usefulness of 11C-Choline PET/CT in the detection of bone metastases in PCa patients with biochemical relapse after radical treatment. **Materials and Methods:** PET/CT was performed in 157 patients on PET/CT scanner (Biograph-64, Siemens) 10 min after injection of 11C-Choline (400-550 Mbq). The mean PSA value in the group was 2.8±2.9 (0.2-14.5) ng/ml, median - 1.8 ng/ml. **Results:** Overall, 11C-Choline PET/CT detected PCa relapse in 50% (79/157) of cases, of which 34% (27/79) had bone metastases: 19 patients after radical prostatectomy and 8 - after radiation therapy. The mean PSA value in patients with revealed bone metastases was 5.0±3.7 (0.4-13.6) ng/ml, median - 3.8 ng/ml. In 59% (16/27) patients the PSA doubling time was less than 6 months. Isolated skeletal involvement was identified in 44% (12/27) patients. The rest of patients with bone metastases had extraosseous lesions: loco-regional recurrence - in 33% (9/27), iliac and distant lymph

nodes - in 19% (5/27) and lung metastases - in one patient (4%). Importantly, that 37%(10/27) of PET-positive patients with bone metastases had no structural abnormalities on CT images (CT-negative cases), corresponding to isolated involvement of bone marrow. Bone metastases in 67% (18/27) patients were presented by single lesion, 8 of which (44%) were CT-negative. Several (two-four) and multiple lesions were detected in 26% (7/27) and 7% (2/27) patients, respectively. 48% (13/27) of results were confirmed by repeated PET/CT, of which 7 were presented with single bone metastases, including 2 patients with isolated single bone marrow lesions. **Conclusion:** 11C-Choline PET/CT was able to detect and correctly identify bone metastases in 34% of patients with PET-positive PCa relapse. This modality is useful in the diagnosis of skeletal involvement in patients with low PSA levels (median 3.8 ng/ml), as well as in cases with no structural abnormalities on CT, corresponding to isolated involvement of bone marrow.

EP-0632

^{68}Ga PSMA PET/CT in prostate cancer - A single centre experience from India

A. Sasikumar[1], A. Joy[1], M. Pillai[1], R. Nanabala[1], S. Bindu[1], J. Madhavan[2], B. Thomas[2], S. S R[2], R. Thomas[2]; [1]KIMS-DDNMRC, Trivandrum, INDIA, [2]KIMS Hospital, Trivandrum, INDIA.

Purpose: Describe the potential applications of ^{68}Ga PSMA PET/CT in prostate cancer (PCa) from diagnosis to treatment response evaluation. **Subjects & Methods:** Retrospective analysis of ^{68}Ga-PSMA PET/CT for PCa during the period from 01.05.2015 to 14.01.2017 was done. 417 scans were done in 405 patients during this period. The indications for the scan and its usefulness in the clinical scenario was analysed. **Results:** Lesion characterisation (153 cases) in suspected PCa patients revealed presence of foci suspicious of PCa in 90 (59%) patients and they were advised biopsy correlation. Scan negative patients 63 (41%); an immediate biopsy was avoided and put on follow up. ^{68}Ga-PSMA PET/CT as staging work up prior to initiating treatment was done in 65 patients. Primary site in prostate showed abnormal tracer uptake in 64 patients (98.5%) and excluded distant metastasis in 40 patients. 24 patients showed at least one site of metastasis. 160 patients underwent ^{68}Ga-PSMA PET/CT for suspected recurrence evaluation and the culprit lesion/lesions could be identified in 140 (87.5%) patients. 10 cases ^{68}Ga-PSMA PET/CT was used for RT planning and it provided accurate identification of involved sites. 12 cases follow up ^{68}Ga-PSMA PET/CT was done after 4-6 cycles of chemotherapy and six cases showed scan concurrence with clinical/biochemical response. Five cases ^{68}Ga-PSMA PET/CT was done prior to ^{177}Lu-PSMA scan to assess feasibility of therapy. **Conclusion:** The main indications for ^{68}Ga-PSMA PET/CT in PCa include lesion characterisation in suspected prostate cancer, initial staging work up in newly diagnosed cases and recurrence evaluation in suspected biochemical/clinical disease recurrence. ^{68}Ga-PSMA PET/CT also has potential application in radiotherapy planning, assessment of response to chemotherapy and in theranostics which requires to be validated further.

EP-0633

Therapeutical changes in the management of patients with biochemical relapse of prostate cancer and positive ^{11}C-Choline PET/CT

F. J. Gómez-de la Fuente, I. Martínez-Rodríguez, R. Quirce, M. De Arcocha-Torres, J. L. López-Defilló, M. Jiménez-Alonso, B. Lucas-Velázquez, D. F. Tovar-Echeverri, G. Molina-Mendoza, I. Banzo; Nuclear Medicine Service. Marqués de Valdecilla University Hospital. Molecular Imaging Group (IDIVAL). University of Cantabria, Santander, SPAIN.

Purpose: To evaluate the role of ^{11}C-Choline PET/CT in the management of patients with prostate cancer (PC) and a diagnosis of biochemical relapse submitted from the Radiotherapy department. **Methods:** We have retrospectively included 100 consecutive patients (mean age: 70±6.6 y.) with biochemical relapse of PC. Mean serum PSA level at the time of study was 6.6±10.5 ng/ml. Initial PC treatment was radical prostatectomy (RP) with/without external beam radiotherapy (EBRT) or hormonotherapy (HT) in 33 patients, EBRT with/without prostatic brachytherapy (PB) in 21 patients, and EBRT with/without PB or HT in 46 patients. All patients had a positive ^{11}C-Choline PET/CT. PET/CT scans were acquired 20 minutes after i.v. injection of 370-740 MBq of ^{11}C-Choline. Medical records were reviewed to evaluate the changes in the therapeutic approach resulting from PET/CT reports. The minimum active surveillance period was 12 months. **Results:** One hundred and forty-eight pathological ^{11}C-Choline sites were reported in the 100 PET/CT scans performed: 62 in prostate or prostatic bed, 30 in pelvic or inguinal lymph nodes, 38 in mediastinal lymph nodes, 8 in bone, 4 in seminal vesicles, 3 in adrenal glands and 3 in lungs. Final diagnosis was malignant process in 86 out of 148 sites, a benign process in 21, PET/CT findings were no longer studied in 28 sites, and record data were not available in 13. ^{11}C-Choline results led up to a change in the initial therapeutic approach in 52 out of 100 patients (52%): 20 received HT, 16 PB, 7 EBRT, 3 chemotherapy, 2 HT + PB, 2 HT + EBRT, and 2 HT + chemotherapy. Initial therapeutic plan was not changed in 46 out of 100 patients, but in 16 of them disease progression was reported afterwards, with subsequent management change in 11 patients. No clinical data after PET/CT was available in 2 out of 100 patients. Additionally, a second malignancy was detected in 4 patients (lung cancer in all of them). **Conclusions:** ^{11}C-Choline PET/CT had a key role in patients with PC and biochemical relapse, leading to a change in the initial therapeutic approach in more than half of positive ^{11}C-Choline patients.

EP-0634

Oligometastatic disease (OMD) in prostate cancer (PCa) detects by 18F-Choline (FCH) PET/CT in patients with PSA levels < 5 ng/mL

L. Cuppari[1], A. Guttilla[2], M. Gardi[3], A. Agostini[3], A. Cervino[1], P. Reccia[1], M. Burei[1], G. Saladini[1], M. Hodolic[4], L. Evangelista[1]; [1]Veneto Institute of Oncology IOV - IRCCS, Padova, ITALY, [2]Camposampiero Hospital, Camposampiero (PD), ITALY, [3]Hospital of Sant'Antonio, Padova, ITALY, [4]Nuclear Medicine Research Department, Iason, Graz, AUSTRIA.

Introduction: OMD is defined as solitary or <5 metastases usually confined to a single organ. In PCa, OMD can be divided into patients with a rising PSA following primary therapy or those with castrate resistant PCa(CRPC). The aim of the study was to assess the ability of FCH-PET/CT to detect OMD in patients with early recurrence of disease (PSA≤5ng/mL), both in those after primary therapy (not undergoing androgen deprivation therapy-ADT) and in subjects with a CRPC (undergoing ADT). **Materials and Methods:** Between 2010 and 2016, from a single institutional database composed by 1293 patients who underwent FCH PET/CT, 324 patients with PCa and PSA levels≤5ng/mL were selected. The mean(SD)age was 71(10)years. Gleason score was ranged between 5 and 10. All patients were treated with a radical prostatectomy±lymphadenectomy, following by radiation treatment in 69 subjects(21.3%). 122 patients were under ADT at the time of PET/CT, while 205 did not. Mean(SD) PSA at the time of PET/CT was 1.33(1.19)ng/mL, mean(SD) PSAdt was 10(12)months and mean(SD) PSAvel was 1.94(3.31) ng/mL/year. **Results:** 193(59.6%)patients had a negative FCH PET/CT, while 131(40.4%) had a positive scan for OMD. Of these latter patients, 35 had a significant FCH uptake in the prostatic fossae, 59 in lymph nodes and 37 in bone. The presence of OMD was similar in patients without ADT and those undergoing ADT(chi-square test;41.3% vs. 39%; p=0.653). PSA levels were significantly different between patients with a positive than those with a negative scan(chi-square test;p<0.001), independently from ADT intake. FCH-PET/CT was negative in the majority of patients with a PSA≤ 1ng/mL(122; 63.2%). More than 60% of patients with a PSAdt≤6 months had a positive FCH-PET/CT for OMD, being the distribution similar for patients with and without ADT(chi-square test;p=0.107). PSAvel resulted higher in patients with a positive scan than those with a negative one. However, in patients with a positive scan, PSAvel was <1ng/mL/year in 52% vs. 24% in those without and undergoing ADT, respectively(chi-square test;p<0.01). At logistic univariate analysis, PSA level, PSAdt and PSAvel were predictors of a positive FCH-PET/CT for OMD, while at multivariate analysis only PSA level and PSAdt resulted as independent predictors(both p<0.01). **Conclusions:** In patients with early recurrence of PCa, FCH-PET/CT is able to detect OMD in 40.4% of cases, moreover PSA levels and PSAdt are predictors. This finding has an important impact on the detection of PCa recurrent lesions that could be treated by local therapy to achieve long-term survival or cure.

EP-0635

The effects of 18F-FDG-PET/CT on the management and prognosis of patients with bladder (Bca) and upper urinary tract urothelial carcinoma (UTUC)

L. Evangelista[1], F. Zattoni[2], E. Incerti[3], V. Lowe[4], i. Rambaldi[5], S. Panareo[6], R. Schiavina[7], J. R. Karnes[8], M. Moschini[9], V. Ficarra[2], M. Colicchia[8], S. Fanti[10], A. Briganti[11], M. Picchio[3]; [1]Nuclear Medicine and Molecular Imaging Unit., Veneto Institute of Oncology IOV - IRCCS, Padova, ITALY, [2]Department of Urology, Hospital of Udine, Udine, ITALY, [3]Nuclear Medicine Department, IRCCS Ospedale San Raffaele, Milano, ITALY, [4]Division of Nuclear Medicine, Mayo Clinic, Rochester, MN, UNITED STATES OF AMERICA, [5]Nuclear Medicine Unit, Diagnostic Imaging e Laboratory Medicine Department, University Hospital of Ferrara, Ferrara, ITALY, [6]Nuclear Medicine Unit, Diagnostic Imaging e Laboratory Medicine Department, University Hospital of Ferrara, Padova, ITALY, [7]Department of Urology, Sant'Orsola-Malpighi Hospital, Bologna, ITALY, [8]Department of Urology, Mayo Clinic, Rochester, MN, UNITED STATES OF AMERICA, [9]Division of Oncology/Unit of Urology, URI, IRCCS Ospedale San Raffaele, Milano, ITALY, [10]Service of Nuclear Medicine, Policlinico S. Orsola Malpighi, University of Bologna, Bologna, ITALY, [11]Division of Oncology/Unit of Urology, URI, IRCCS Ospedale San Raffaele; Vita-Salute San Raffaele University,, Milano, ITALY.

Objectives: To evaluate the role of FDGPET/CT in the management and in the prognosis for patients with bladder cancer(Bca)and upper urinary tract urothelial carcinoma(UTUC)**. Methods:** Between 2007 and 2015, data of patients undergoingFDG PET/CT for the suspicious of recurrenturothelial carcinoma(UC), after primary treatment,were retrospectively collected in amulticenter (San Raffaele Hospital; IOV-Padua; Hospital of Ferrara, Mayo Clinic, Sant'Orsola Malpighi Hospital- Bologna) study. Inclusion criteria were: 1) patients with a known history of Bcaand/or UTUC; 2) FDG PET/CT images after cystectomy and/or nephrouretectomy; 3) morphological imaging modalities (ceCT and MRI) performed within 3 months from PET/CT 4) available gold standard (final pathology or if not available clinical evaluation/conventional imaging) for the assessment of PET/CT findings. Exclusion criteria were other abdominal tumors and chemotherapy administration concomitant to imaging and non-urothelial cancer variants. The change of management after the introduction of FDG PET/CT in the diagnostic algorithm was assess in all patients. Kaplan-Meier and log-rank analysis were computed for survival assessment. A Cox regression analysis was used to identify predictors of recurrence and death,separately for bladder cancer, UUTand concomitant bladder and UUT cancer. **Results:** Overall, 287 patients were collected. Two-hundred thirteen patients (74,2%) had an history of BCa, 38 (13,2%) of UTUC and 36 (12,5%) of concomitant Bcaand UTUC. Patient's management was changed in 114 (39.7%) cases by the inclusion of FDG PET/CT. After a mean period follow-up of 21 months (1-117 mo.), 136 patients(47.4%) had a recurrence/progression of disease. Moreover 131 subjects (45.6%)died. At Kaplan-Meier analyses, patients with bladder cancer and positive PET/CT had a worse overall survival than those with a negative scan(log-rank<0.001). Furthermore, a negative PET/CT scan was associated with a lowerrecurrence rate than a positive examination, independently from the primary tumor site. At multivariate analysis, in patients with Bca, the presence of pT3-pT4, lymph node involvement and a positive FDG PET/CT were independent predictors of disease-free and overall survival (p<0,01). In patients with UTUC and concomitant Bcaand UTUC, a positive FDG PET/CTwas a significant predictor of recurrence/progression,atunivariate analysis (HR:5.55;95%CI: 1,25-24,73, p<0.05 and HR: 3,13;95%CI: 0,98-9,97, p<0.05). **Conclusion:** FDGPET/CT is able to change patients' management in 39% patients with UC. Further, it can be considered a valid prognostic tool after primary treatment, in patients with recurrent UC.

EP-0637

Predictive value of 11C-Acetate PET-CT in metastatic renal cell carcinoma

B. Małkowski[1,2], V. Pankowska[1], B. Malkowski[1], K. Roszkowski[1]; [1]Oncology Centre Bydgoszcz, Bydgoszcz, POLAND, [2]Collegium Medicum BydgoszczUMK Torun, Bydgoszcz, POLAND.

Background: Renal clear cell carcinoma poses considerable diagnostic difficulties in the identification of distant metastases. We used an ^{11}C-Acetate PET/CT examination to determine metastases in patients diagnosed with renal cell carcinoma. The aim of this study was to establish whether the degree of metabolic activity (based on SUV) of metastases in advanced metastatic renal cell carcinoma may be a prognostic factor. **Methods:** The study was conducted in 113 patients with renal cell carcinoma in whom numerous distant metastases were detected using an ^{11}C-Acetate PET/CT examination. The patients were divided into two subgroups depending on the standardized uptake value (SUV): those with the highest SUV ≤ 8 in all lesions (n=75; subgroup I); those with the highest SUV > 8 in all lesions (n=38; subgroup II). All patients were subjected to sunitinib chemotherapy at appropriate doses. **Results:** In subgroup I, median SUV was 5.3, while in subgroup II, median SUV was 10.8. Overall survival periods were longer in the subgroup of patients with higher SUV values: 33 months and 60 months, respectively (p=0.02; log-rank test). **Conclusions:** The longer overall survival of patients with advanced renal cell carcinoma characterized by higher SUV values can be associated with a fast metabolism of tumor cells. These cells are probably more sensitive to the treatment with a protein kinase inhibitor. These preliminary results demonstrate that patients with advanced renal cell carcinoma and SUV values above 8-9 may be a good target for effective treatment. For ultimate confirmation of the results under the presented project, it will be necessary to recruit a much larger group of patients and conduct a long follow-up to allow correlation of the results of the analyses with clinical effects.

EP-0638

Prostate Specific Antigen (PSA) and Gleason Score (GS) as gatekeepers for bone scintigraphy in a resource restricted setting

K. M. G. Mokoala[1,2], M. H. W. Vangu[1,2]; [1]Charlotte Maxeke Johannesburg Academic Hospital, Parktown, Johannesburg, SOUTH AFRICA, [2]University of the Witwatersrand, Johannesburg, SOUTH AFRICA.

Aim: Prostate cancer is one of the leading cancers in males worldwide. Osseous metastases are very common and important for the prognosis. Early detection of bone metastases is critical in the management of patients. Bone scintigraphy (Bone scan) plays a great role for their detection. In this study we evaluate the correlation between PSA, Gleason score and findings on bone scan. **Materials and Methods:** We reviewed data of 940 patients referred for bone scans from 2010 -2014. The PSA and Gleason score were recorded. Fisher's probability exact test and Pearson Chi square test were used in the analysis of data. Odds ratios and confidence intervals were also used to assess correlation as an outcome. The strength or magnitudes of associations / relationships were evaluated using the Phi and Cramer's V tests. Univariate and multivariate logistic regression analyses were used to assess the predictors in patients with positive bone scans. **Results:** We found osseous metastases in 243 (26%) patients. We were able to determine whether a scan was requested for staging or not in 633 cases. Four hundred and fourty three (70%) were staging bone scans and 25 % of them had evidence of metastases. There was a significant relationship between PSA and bone scan findings (p = 0.0001). For patients with a PSA ≥ 20ng/mL there was a risk of developing metastases [OR=1.253 (95 % CI: 0.843 - 1.862)]. Using a cut-off of 20ng/mL for PSA levels, the measured sensitivity, specificity, NPV and PPV for predicting metastases were 73.3%, 74%, 87.1% and 54.1%, respectively. In 237 patients with a Gleason score > 7, eighty-seven (36.7%) had positive bone scans. When the Gleason score was > 7, patients were at risk of developing metastases with an OR of 1.322 (95% CI: 0.838 - 2.086). Using a Gleason score of at least 7, the sensitivity, specificity, NPV and PPV for predicting metastases were 78.8%, 26.8%, 77.8% and 28.1% respectively. **Conclusions:** In this study, we found that two-thirds (70%) of scans that are referred to our institution are for staging and a quarter (25%) of them are found to have bone metastases as compared to other studies. Patients with a PSA ≥ 20 and Gleason score > 7 should be considered to undergo a bone scan. For patients with PSA < 20 or a Gleason score < 7, the decision for a bone scan should be considered after evaluation of other clinical parameters.

EP-0639

Value of ^{18}F-fluorocholine PET/CT for Targeted Prostate Re-Biopsies in Patients with Rising PSA Levels

P. Koranda[1], Š. Kudláčková[2], M. Hodolič[1], A. Fellerová[1], L. Quinn[1], R. Formánek[1], E. Buriánková[1], M. Kamínek[1]; [1]Dept. of Nuclear Medicine, Univ. Hospital and Palacký University, OLOMOUC, CZECH REPUBLIC, [2]Dept. of Urology, Univ. Hospital and Palacký University, OLOMOUC, CZECH REPUBLIC.

Purpose: Rising prostate-specific antigen (PSA) levels even after a previously negative biopsy indicate the need for a prostate re-biopsy. The aims of the study were two-fold: to determine the ^{18}F-fluorocholine uptake patterns indicating increased risk of prostate cancer in this group of patients; and to estimate whether targeting re-biopsies by the ^{18}F-fluorocholine PET/CT findings improves prostate cancer detection. **Subjects & Methods:** Within the prospective clinical trial (time period: October 2012 - July 2015), an ^{18}F-fluorocholine PET/CT was performed in 41 patients with rising PSA following a previously negative prostate biopsy. Of this group, 39 patients subsequently underwent a ^{18}F-fluorocholine PET/CT targeted re-biopsy, and 2 patients were followed up clinically (without any signs of prostate malignancy). All patients were pre-treated with doxycycline. The ^{18}F-fluorocholine PET/CT acquisition started 40 minutes

after injecting the radiopharmaceutical. The assessed PET/CT parameters were: localization of the ^{18}F-fluorocholine uptake to target the re-biopsies, the ^{18}F-fluorocholine uptake patterns (16 diffuse, 12 focal, 9 diffuse+focal, 4 negative) and SUVmax (SUVmax 5.6 ± 1.7). **Results:** Untreated prostate cancers were detected in 16 out of 39 biopsied patients (41%). This ratio is distinctly higher than in the re-biopsies performed using the transrectal ultrasound-guided approach only (10-20%)*. The ^{18}F-fluorocholine uptake patterns in 16 patients with malignant biopsies were 9 focal (56%), 3 diffuse (18%), 2 focal+diffuse (13%), and 2 negative (13%). The ^{18}F-fluorocholine uptake patterns in 25 patients without signs of malignancy (23 patients - benign biopsies and subsequent follow-up, 2 patients - clinical follow up only) were 12 diffuse (52%), 6 diffuse+focal (26%), 3 focal (13%), and 2 negative (9%). Malignant biopsies were significantly accompanied by focally increased ^{18}F-fluorocholine accumulation (p = 0.020). The risk of prostate cancer was 3.75 times higher in patients with focal PET/CT findings, than in patients with a diffuse increase of ^{18}F-fluorocholine accumulation. SUVmax values, measured in the group of prostate cancer patients (6.5 ± 2.1) were significantly higher than in patients with benign biopsies 5.2 ± 1.2 (p = 0.037). **Conclusions:** A focal ^{18}F-fluorocholine uptake pattern and a high SUVmax indicate increased risk of prostate cancer. Targeting prostate re-biopsies through the use of a ^{18}F-fluorocholine PET/CT improves the identification of prostate cancer in patients with rising PSA levels. * (Djavan B, et al. Prospective evaluation of prostate cancer detected on biopsies 1, 2, 3 and 4: when should we stop? J Urol 2001;166:1679-1783).

EP-0640

223Radium: analysis of effect of treatment in bone oligo-metastatic CRPC patients

V. Frantellizzi, G. A. Follacchio, M. Pontico, L. Cosma, A. Farcomeni, F. Monteleone, M. Liberatore, G. De Vincentis; Sapienza University of Rome, Rome, ITALY.

Aim: It is well established that in men with CRPC and symptomatic bone metastases, 223Radium-Dichloride (223Ra) has shown to improve overall survival. The purpose of our study was to assess the efficacy of 223Ra treatment in bone oligo-metastatic subjects. **Materials and Methods:** 55 KBq/Kg IVq4w of 223Ra were administered to 98 consecutive patients affected by bone metastatic CRPC from July 2015 to December 2016. Number of metastases at bone scan, serum level of Prostate-Specific Antigen (PSA) and total Alkaline Phosphatase (tALP) values at baseline and at the end of therapy were taken into account. **Results:** 43/98 patients [mean age 73 (50-81)] completed all six cycles. Of whom 5 patients showed only 2 metastatic foci at baseline bone scan. In this subgroup of subjects at baseline mean PSA value was 12.3 ± 3, whereas tALP mean value was 121 ± 8. At the end of 223Ra therapy PSA mean value resulted 4.6 ± 2.3 and tALP mean value was 95.2 ± 11. Interestingly, at bone scan performed 3 months after the last cycle, bone metastasis completely disappeared in 3 patients, while a partial response was observed in the remaining 2 with as a decreased uptake of di-

phosphonates. After a median 12 months follow up all patients are alive. **Conclusions:** 223 Ra treatment at the onset of metastatic disease, seems to allow, in some cases, a complete control of bone metastatic pathology, as evidenced by the complete regression at the bone scan examination. Another impressive datum is decrease of both tALP and PSA values in responsive patients subgroup. The role of baseline tALP as predictive factor in 223Ra treatment is well known, while the role of PSA remain controversial. In the oligo-metastatic patients, also PSA decrease at the end of therapy, appear as a reliable marker. We emphasize that in bone oligo-metastatic patients 223Ra treatment gives excellent results.

EP-0641

Analytical validation of an automated method for segmentation of the prostate gland in CT images

E. Polymeri[1], M. Sadik[2], R. Kaboteh[2], O. Enqvist[3], J. Ulén[4], E. Trägårdh[5], M. H. Poulsen[6], J. A. Simonsen[7], P. F. Høilund-Carlsen[7], L. Edenbrandt[2], Å. Johnsson[1]; [1]Department of Radiologi, Göteborg, SWEDEN, [2]Department of Clinical Physiology, Göteborg, SWEDEN, [3]Department of Signals and Systems, Göteborg, SWEDEN, [4]Eigenvision AB, Malmö, SWEDEN, [5]Department of Translational Medicine, Malmö, SWEDEN, [6]Department of Urology, Odense, DENMARK, [7]Department of Nuclear Medicine, Odense, DENMARK.

Aim: Uptake of PET tracers in the prostate gland may serve as guidance for management of patients with prostate cancer. PET studies alone do, however, not allow for accurate segmentation of the gland, instead the corresponding CT images contain the required anatomical information. Our long-term aim is to develop an objectively measured PET/CT imaging biomarker reflecting PET tracer uptake. In this study we take the first step and develop and validate a completely automated method for 3D-segmentation of the prostate gland in CT images. **Methods:** A convolutional neural network (CNN) was trained to segment the prostate gland in CT images using manual segmentations performed by a radiologist in a group of 100 patients, who had undergone 18F-FDG PET/CT. After the training process, the CNN automatically segmented the prostate gland in CT images in a separate validation group consisting of 45 patients with prostate cancer. All patients had undergone a 18F-choline PET/CT as part of a previous research project. The CNN segmentations were compared to manual segmentations performed independently by two radiologists. The volume of the prostate gland was calculated based on segmentations by the CNN and radiologists. The Sørensen-Dice index was used to analyse the overlap between the segmentations by the CNN and the two radiologists. **Results:** The prostate volumes were on average 79mL (range 9-212mL) in the 45 patients, measured as mean volumes for the two radiologists. The mean difference in prostate volumes between the two radiologists was 14mL (SD 29mL). The mean volume difference between the CNN segmentation and the mean values from the two radiologists was 22mL (SD 43mL). For the subgroup of patients with prostate volumes <100 mL (n=36), the difference between the radiologists was

9mL (SD 11mL) compared to difference CNN vs radiologists of 7mL (SD 15mL). The Sørensen-Dice index was 0.69 and 0.70 for the comparison between CNN segmentation and the two radiologists, respectively and 0.83 for the comparison between the two radiologists. The corresponding Sørensen-Dice index in the 36 patients with volumes <100 mL were 0.74, 0.75 and 0.83, respectively. **Conclusion:** Our CNN based method for automated segmentation of the prostate gland in CT images show good agreement with the corresponding manual segmentations by two radiologists, especially for prostate glands with a volume less than 100 mL.

EP-0642

Convolutional neural network based quantification of choline uptake in PET/CT studies is associated with overall survival in patients with prostate cancer

R. Kaboteh[1], E. Polymeri[2], **M. Sadik**[1], O. Enqvist[3], J. Ulén[4], M. Ohlsson[5], E. Trägårdh[6], M. H. Poulsen[7], J. A. Simonsen[8], P. F. Høilund-Carlsen[8], Å. Johnsson[2], L. Edenbrandt[1]; [1]Department of Clinical Physiology, Göteborg, SWEDEN, [2]Department of Radiologi, Göteborg, SWEDEN, [3]Department of Signals and Systems, Göteborg, SWEDEN, [4]Eigenvision AB, Malmö, SWEDEN, [5]Department of Theoretical Physics, Lund, SWEDEN, [6]Department of Translational Medicine, Malmö, SWEDEN, [7]Department of Urology, Odense, DENMARK, [8]Department of Nuclear Medicine, Odense, DENMARK.

Aim: To develop a convolutional neural network (CNN) based automated method for quantification of 18F-choline uptake in the prostate gland in PET/CT studies and to study the association between this measure, clinical data and overall survival in patients with prostate cancer. **Methods:** A CNN was trained to segment the prostate gland in CT images using manual segmentations performed by a radiologist in a group of 100 patients, who had undergone 18F-FDG PET/CT. After the training process, the CNN automatically segmented the prostate gland in the CT images and SUV values in the corresponding PET images were automatically analyzed in a separate validation group consisting of 45 patients with biopsy-proven hormone-naïve prostate cancer. All patients had undergone an 18F-choline PET/CT as part of a previous research project. Voxels localized in the prostate gland and having a SUV >2.65 were defined as abnormal, as proposed by Reske S et al. (2006). Automated calculation of the following five PET measurements was performed: maximal SUV within the prostate gland - SUVmax; average SUV for voxels with SUV >2.65 - SUVmean; volume of voxels with SUV >2.65 - VOL; fraction of VOL related to the whole volume of the prostate gland - FRAC; product SUVmean x FRAC defined as Total Lesion Uptake - TLU. The association between the automated PET measurements, age, PSA, Gleason score and overall survival (OS) was evaluated using a univariate Cox proportional hazards regression model. Kaplan-Meier analysis was used to estimate the survival difference (log-rank test). **Results:** TLU and FRAC were significantly associated with OS in the Cox analysis while the other three PET measurements; age, PSA and Gleason score were not. Kaplan-Meier analysis showed that patients with SUVmax <5.3, SUVmean <3.5 and TLU <1 showed significantly longer surviv-

al times than patients with values higher than these thresholds. No significant differences were found when patients were stratified based on the other two PET measurements, PSA or Gleason score. **Conclusion:** Measurements reflecting 18F-choline PET uptake in the prostate gland obtained using a completely automated method were significantly associated with OS in patients with hormone-naïve prostate cancer. This type of objective quantification of PET/CT studies could be of value also for other PET tracers and other cancers in the future.

EP-0643

Correlation between molecular active tumor volume evaluate with 68Ga-PSMA PET-CT and levels of antigen prostatic specific

F. O. García-Pérez, **S. S. Medina-Ornelas**, B. L. Abundiz-Lopez, A. Arellano-Zarate; Instituto Nacional De Cancerologia, Mexico City, MEXICO.

Background: Patients with Prostate cancer (PC) a that has recurred after local therapy or that has disseminated distantly usually respond to androgen deprivation therapy (ADT); however, despite this management, most patients eventually experience disease progression within a median of 18-24 months. **Objective:** Investigate the association between molecular active tumor volume (MATV) evaluate with 68Ga-PSMA-PET/CT and levels of Trigger-PSA for patients with PC. **Materials and Methods:** One hundred sixty-three consecutive patients who underwent 68Ga-PSMA-PET/CT imaging for recurrent PC were studied. Only patients with PSA levels on the same week of the 68Ga-PSMA-PET/CT (Trigger-PSA), were included. Eighty-four patients were included. Sixty patients had received ADT at last 6 months before the examination. The median of the Trigger-PSA was 8.9 ng/mL (range 0.2-127 ng/ml) **Results:** The median MATV among all neoplastic activity was 58.9 (range: 3.3-3748.1). The median MATV of bone metastatic disease was significantly higher than that in metastatic lymph nodes (LN) and prostate bed (139.5 versus 17.7; p<0.05). When analyzing positive results by location, in 8 patients (9.5%) the disease was limited to the prostate bed; loco-regional and/or distant lymph node disease was detected in 21 patients (25%); metastatic bone disease was found in 32 patients (38.1%); and more than 3 sites was found in 23 patients (27.39%). Respect to Trigger-PSA values, the median Trigger-PSA levels of patients with tumors that were limited to the prostate bed (median Tigger-PSA 2.8ng/ml); loco-regional and/or distant lymph node disease (median Tigger-PSA 6.8ng/ml) and metastatic bone disease (median 46.8ng/ml (p<0.05). The MATV 68Ga-PSMA-PET/CT in the primary tumor was higher in patients with Trigger-PSA levels ≥4ng/ml than those with Trigger-PSA values <1 ng/ml, exhibiting a median MATV of 7.9 vs 77.3, respectively (p < 0.001). Positive patients had a mean Trigger-PSA of 4.3ng/mL vs 1.5ng/mL in negative patients (P <0.05). We established several threshold points for Trigger-PSA level and studied the detection rate for each one: Trigger-PSA ≤1ng/mL, detection rate 47.3%; Trigger-PSA 1-4ng/mL, 68.4%; Trigger-PSA ≥4ng/mL, 96.7%. When analyz-

ing the best association between Trigger-PSA and MATV, we found that when Trigger-PSA was >4ng/mL, was greater for patients with a higher MATV (p<0.001). **Conclusion:** The correlation of a low MATV has greater influence than the level of Trigger-PSA, which may have an impact on the timely change of the therapeutics used. A complete detection of the site of metastatic disease could lead to an appropriate therapeutic strategy, particularly avoiding the same scheme of ADT.

EP-0644

18F-choline PET/CT as a prediction diagnostic tool of the disease progression in patients with castration resistant prostate cancer

M. Grmek, S. Hawlina, L. Lezaic; University medical centre Ljubljana, LJUBLJANA, SLOVENIA.

The aim of the study is to find out the value of 18F-choline PET/CT to predict disease progression in patients with castration resistant prostate cancer (CRPC). **Patients and Methods:** 21 men with CRPC (without prostatectomy, chemotherapy naive) were included in the study. Patients were on average 75±6 years old. In all patients two 18F-choline PET/CT studies were preformed, initial study and a follow up study after 115±12 days. Patient's therapy wasn't altered between studies. Injected activity per study was 2,5 MBq/kg. Acquisition on PET/CT (Siemens, Biograph mCT) started 45 minutes after 18F-choline administration. A low dose CT scan followed by PET acquisition was used. Scan evaluation: SUV max 4 for prostate and SUV max 2 for bone lesions and lymph nodes were considered as malignant. (Only lymph nodes around big abdominal vessels and in pelvic cavity were evaluated.) The results of both studies were compared and classified as: Stable disease- no new lesions were detected and SUV max in know lesions was not increased more than 25%; Local progress- increase in SUV max in prostate for more than 25%; Slow progress- combined number of new lesions and already known lesions with SUV max increase of 25% or more was three or less; Rapid progress- combined number of new lesions and already known lesions with SUV max increase of 25% or more was four or more. **Results:** Initial study: 2 patients had no lesions, 6 patients had recurrence of prostatic cancer (RPC) only, 6 patients had RPC and bone metastases (BM), 2 patients had RPC and lymph nodes metastases (LNM), 5 patients had RPC+BM+LNM. Follow up: in 1 of 2 patients without pathologic lesions local progress was detected; 4 of 6 patients with RPC had stable disease and 2 patients local progress; 3 of 6 patients with RPC+BM had stable disease, 1 patient had local and 2 patients slow progress; 1 patient with RPC+LNM had slow and 1 patient rapid progress; 1 of 5 patients with RPC+LNM+BM had slow and 4 patient rapid progress. **Conclusion**: 18F-choline PET/CT can be used as a prognostic diagnostic tool to predict CRPC progression. We can predict relatively stable disease in patients where malignant process is located only in the prostate. In patients where malignant process is located in prostate and bone we can predict that the disease will progress slowly. Patients with the disease located in prostate, lymph nodes and bone have the worst prognosis.

EP-0645

Bone Scintigraphy Versus PSMA PET-CT in Primary Staging of Prostate Cancer

P. Kaldeway, H. van Melick, J. Lavalaye; St Antonius Hospital Nieuwegein, Nieuwegein, NETHERLANDS.

Purpose: The aim of this retrospective study was to compare the results of planar ^{99m}Tc bone scintigraphy with the results of ^{68}Ga-PSMA-11 PET-CT in patients with newly diagnosed prostate cancer. **Methods:** Records of patients who received PSMA PET-CT in our clinic between April 2015 and March 2017 were reviewed. All patients with histologically proven prostate cancer, who received a bone scintigraphy 3 months prior to PSMA PET-CT, were included in the study. Indication for PSMA PET-CT was primary staging in patients with high risk for metastases. Bone scintigraphy was scored as positive (M1b), negative (M0) or equivocal (Mx). PSMA PET-CT was scored as disease limited to the prostate (N0M0), loco regional lymph node metastases (N1M0), distant lymph node metastases (M1a), distant skeletal metastases (M1b) or distant visceral metastases (M1c). Results of the bone scintigraphy and PSMA PET-CT were tabulated. **Results:** Eighty-five patients were included in the analysis. Bone scintigraphy was scored negative in 73 patients, positive in 6 patients and equivocal in 6 patients. Out of 73 patients with a negative bone scan, PSMA PET-CT scored N0M0 in 30 patients, N1M0 in 16 patients, M1a in 11 patients, M1b in 13 patients and M1c in 3 patients; in this last group 2 patients also showed skeletal metastases. Out of six patients with a positive bone scan, one patient showed no bone metastases and only local disease on PSMA PET-CT. In five patients bone metastases was confirmed on PSMA PET-CT. In 20% of the patients a disagreement between bone scintigraphy and PSMA PET-CT regarding the skeletal status was observed. **Conclusion:** PSMA PET-CT is more sensitive than bone scintigraphy in detecting bone metastases in prostate cancer in the primary setting. Furthermore, PSMA PET-CT will detect distant lymph node or visceral metastases in a significant number of patients, which were not visualized by other modalities. Prospective studies are required to evaluate the role of PSMA PET-CT in primary staging of prostate cancer in terms of cost effectiveness, disease outcome and quality of life, but PSMA PET-CT looks promising for primary staging in patients with high risk prostate cancer.

EP-0646

Comparison between 18F-Choline (FCH) PET/CT and Conventional Imaging (CI) in Intermediate-high risk prostate cancer (PCa) patients: design and preliminary data of a phase III Italian Multicenter Randomized Trial

L. Evangelista[1], B. Eugenio[2], M. Farsad[3], G. Trifirò[4], S. Agostini[5], E. Bombardieri[6], T. Baresic[2], A. Golemi[3], E. Brugola[4], F. Chierichetti[5], M. Hodolic[7], G. Saladini[1]; [1]Nuclear Medicine and Molecular Imaging Unit, Veneto Institute of Oncology IOV - IRCCS, Padova, ITALY, [2]Department of Nuclear Medicine, Centro Regionale Oncologico (CRO), Aviano (PD), ITALY, [3]Department of Nuclear Medicine, Hospital of Bolzano, Bolzano, ITALY, [4]Department of Nuclear Medicine, Fondazione Salvatore Maugeri IRCCS, Pavia, ITALY,

[5]Department of Nuclear Medicine, Hospital of Trento, Trento, ITALY, [6]Department of Nuclear Medicine, Istituto Humanitas Gavazzeni IRCCS, Bergamo, ITALY, [7]Nuclear Medicine Research Department, Iason, Austria Palacky University, Olomouc, CZECH REPUBLIC.

Introduction: A prospective, randomized multicenter trial has been designed to evaluate the role of FCH-PET/CT for the initial staging of patients with intermediate-high risk PCa in comparison to CI(bone scintigraphy-BS, ceCT and MRI). The aim of the present study was to report details of the study design and some preliminary enrollment data. **Methods:** We have planned to enroll 390 patients, 195 for each arm (ratio 1:1 in two arms; a significant level(α) of 5%, and a power of test of 80%). The patients will be randomized in two groups: Group 1(control arm) will undergo CI, and Group 2(experimental arm) will undergo CI and FCH-PET/CT. The examinations will be performed not more than 1 month one from each other. Inclusion criteria were: 1) intermediate-high PCa patients (according to NCCN classification; version 2.2013); 2) age >18 years; 3) candidates to prostatectomy or radiotherapy or systemic therapy; 4) patients accessible to the follow-up information. Histopathological results from radical prostatectomy and lymphadenectomy will be used as gold standard. CeCT, MRI, BS and FCH-PET/CT were performed in accordance with the established protocols and visually assessed by two radiologists and two nuclear medicine physicians. **Results:** From 15th February 2016 to 21st April 2016, six Italian centers received the approval for this trial from the Ethical Committee (IOV - IRCCS of Padova, Hospital of Bolzano, Fondazione Maugeri of Pavia, Humanitas-Gavazzeni of Bergamo, Hospital of Trento and CRO of Aviano). Eighty-eight patients were enrolled. The patient randomization was: 45(51.1%) in the control arm and 43(48.9%) in experimental one. Thirty-two patients (36.4%) were at intermediate risk and 56(63.6%) at high risk. Sixteen out of 32 patients (50%) and 27/56(48%), respectively at intermediate and high risk were randomized in experimental arm. The median value of PSA was 19 ng/mL (range: 4-56)and Gleason Score(GS)ranged from 6 to 10. Furthermore, the most of patients (n=45, 51.1%)were at Grade 4 and 5(primary and secondary GS: 4+4 and 4+5 or 5+4 or 5+5). Finally, median (range) PSA levels were 26.5 ng/mL(4-56) and 20 ng/mL(6-55), respectively for control and experimental arm. **Conclusions:** The trial is ongoing and no definitive conclusions are available. The next step is to involve other Italian centers, like the Hospital of Ferrara, Mestre, Legnano, Arezzo and IEO of Milan. The enrollment of patients should be stopped within December 1, 2017. We expect that this multicentre randomized trial will show that FCH-PET/CT and MRI are "the first line" imaging modalities, in patients with intermediate-high risk PCa.

EP-0647

^{68}Ga-PSMA PET/CT; current impact on management in prostate cancer

F. Intema, A. Kooistra, A. P. Lont, L. P. J. Hendriks, J. P. Esser, R. Lange, J. M. H. de Klerk; Meander Medical Center, Amersfoort, NETHERLANDS.

Introduction: Just shortly after its introduction, promising results of ^{68}Ga-PSMA PET/CT (PSMA-PET) have led to a striking expansion in availability and usage. Meanwhile the use of this novel diagnostic tool is suggested in recent guidelines even though its role in diagnosis and management of prostate cancer (PC) has not been fully clarified yet. The aim of this study is to describe current use of ^{68}Ga-PSMA PET/CT and postulated impact on management of PC patients. **Subjects & Methods:** Retrospective cohort study of all consecutive patients from the Meander Medical Center who underwent PSMA-PET between October 2016 and February 2017. Outcome parameters included indication for PSMA-PET, disease stage, and impact on individualized treatment strategy as interpreted by two observers. **Results:** Eighty patients were included. Indications for PSMA-PET included primary staging in 32%, biochemical recurrence in 48%, castrate resistant prostate cancer (CRPC) with PSA rise in 15% and suspected prostate cancer in biopsy negative cases in 5%. In primary staging, 42% showed solely local disease, 23% additional regional lymph node metastasis and 35% osseous metastasis. In patients with biochemical recurrence, there was no PSA substrate in 16%, local recurrence in 5%, regional lymph node metastasis in 32% and distant metastasis in 47%. In patients with CRPC, 8% showed lymph node metastasis and 92% osseous metastasis. In biopsy negative cases despite high PSA, PSMA-PET was negative in 75%. In primary staging the PSMA-PET had impact on the management in 38% (10/26) if compared to conventional diagnostic work-up. In half of these patients surgery was abandoned because of distant metastasis. PSMA-PET lead to change in management in 29% (11/38) of patients with biochemical recurrence; five patients were shown to be candidates for stereotactic radiotherapy (RT) or salvage lymph node dissection whereas intended salvage therapy with curative intent was abandoned in six because of distant metastasis. Repeated biopsy was omitted because of negative PSMA-PET in 75% (3/4) in patients with suspected PC based on PSA level and negative earlier biopsy. No conclusions could be drawn regarding impact on management in CRPC patients with PSA rise. Overall, PSMA-PET had clear impact on management in 30% of patients (24/80). **Conclusion:** Currently applied indications for ^{68}Ga-PSMA PET/CT are divers because of lack of thorough validation. However, PSMA-PET had impact on management in 30% of patients in comparison to conventional imaging. In 46% of these patients, therapy with curative intent had to be abandoned because of unfavourable findings.

EP-0648

Relationship between metabolic parameters of 18F-FDG PET of prostate cancer bone metastases

r. g. yang[1], z. j. ren[2], w. z. huo[1], h. x. wang[1], y. liu[1], q. kong[1]; [1]Shandong Cancer Hospital affiliated to Shandong University, Shandong province, CHINA, [2]Shandong Jining No.1 People's Hospital, Shandong province, CHINA.

Introduction: To investigate the relationship between metabolic parameters of ^{18}F-fluorodeoxyglucose (^{18}F-FDG) PET/CT of bone metastases and serum markers in the patients with prostate cancer. **Methods:** Retrospective analysis was carried out in 48 patients with prostate cancer hospitalized in Shandong

Cancer Hospital Affiliated to Shandong University from January 2012 to December 2014. The patients underwent ^{18}F-FDG PET/CT examination within a week after admission. The relationship between metabolic parameters of ^{18}F-FDG PET/CT such as number of metastatic bone lesion, maximum standardized uptake value (SUVmax), mean SUV (SUVmean), metabolic tumor volume (MTV) and total lesion glycolysis (TLG) and the serum tumor markers in the corresponding period was analyzed. **Results:** The number of metastatic bone lesion of 8 was set as the best cutoff point to predict the overall survival (OS) of the patients with prostate cancer, who were divided into no bone metastasis group, limited bone metastasis group (1-8 lesions) and diffuse bone metastasis group (more than 8 lesions). Except that there was significant difference in the level of ALP between limited bone metastasis group and no bone metastasis group, the levels of tPSA, fPSA and ALP were statistically significant. The positively correlated relationship was shown between the number of metastatic bone lesion and the corresponding levels of tPSA, fPSA and ALP (r=0.604, P=0.02; r=0.531, P=0.03; r=0.478, P=0.018). Except that there was no correlation between SUVmax value of metastatic bone lesion and the level of ALP, between SUVmean value of metastatic bone lesion and the levels of ALP and fPSA, the rest parameters and biomarkers were correlated. **Conclusion:** The number of metastatic bone lesion of 8 is the optimal cutoff point to predict the OS of patients with prostate cancer. tPSA, fPSA and ALP can be used as clinical blood biochemical indicators for diffuse bone metastasis in the patients with prostate cancer. Σ_{MTV} and Σ_{TLG} combined with tPSA, fPSA and ALP are better than SUVmax and SUVmean in evaluation of bone metastases. Σ_{TLG} could be used to evaluate the prognosis of prostate cancer.

EP-0649

^{68}Ga-PSMA-PET/MRI, ^{11}C-acetate-PET/CT and stand-alone multi-parametric MRI with histopathology as reference in intermediate- and high-risk prostate cancer - preliminary data

S. Strandberg[1], K. Sandgren[1], J. Jonsson[1], J. Axelsson[1], M. Ögren[1], T. Nyholm[1], C. Thellenberg Karlsson[1], L. Blomqvist[1], M. Skorpil[1], K. Riklund[1], B. Friedrich[2], A. Bergh[3]; [1]Radiation Sciences, Umea, SWEDEN, [2]Surgical and Perioperative Sciences, Umea, SWEDEN, [3]Medical Biosciences, Umea, SWEDEN.

Introduction: Although most prostate cancers (PCs) are low-risk, mortality numbers rise in untreated intermediate- and high-risk PC, where curative treatment options are available in terms of surgery and radiotherapy. However, treatment decision-making requires improved pre-therapeutic staging. Diagnostic imaging offers CT, multi-parametric (mp) MRI, bone scintigraphy, SPECT/CT and PET/CT for staging of PC. PET radiotracers ^{18}F-choline, ^{11}C-choline and ^{11}C-acetate are used for this indication but have limited sensitivity and specificity. ^{68}Ga-PSMA is a promising new radiotracer that may outperform choline/acetate tracers. The aim of this prospective study is to evaluate ^{68}Ga-PSMA-PET/MRI, [11]C -acetate-PET/CT and stand-alone mpMRI with histopathology as reference in intermediate- and high-risk PC. **Methods**

and Materials: 55 consecutive intermediate- and high-risk PC patients referred for radical prostatectomy at the Department of Urology, Umeå University Hospital, will be included in the study, starting from November 2016. Patients will pre-operatively be examined with [11]C -acetate-PET/CT and ^{68}Ga-PSMA-PET/MRI. After resection, the prostate specimen will be examined with stand-alone T2W MRI. Histopathological findings will be compared with imaging characteristics. The mpMRI included in the PET/MRI will be evaluated in accordance with PI-RADS v2. In the scientific evaluation, readers will be blinded to all information from other imaging modalities and clinical records except inclusion criteria. **Results:** Preliminary non-blinded data for clinical use from the first four patients showed a dominant intra-prostatic lesion (DIL) in the right transition zone in the first patient ([11]C -acetate -, ^{68}Ga-PSMA +, mpMRI - PI-RADS 2), confirmed with histopathology as a Gleason 4+4. The second patient had a DIL in the right peripheral zone (PZ) ([11]C -acetate -, ^{68}Ga-PSMA -, mpMRI + PI-RADS 4), Gleason 3+4. The third patient had a DIL in the left PZ ([11]C -acetate +, ^{68}Ga-PSMA+, mpMRI + PI-RADS 5), Gleason 4+3. The fourth patient had a DIL in the left PZ ([11]C -acetate +, ^{68}Ga-PSMA -, mpMRI + PI-RADS 5), Gleason 4+3. **Discussion:** The first preliminary results show some discrepancies, where different PCs appear to be either [11]C -acetate- or ^{68}Ga-PSMA-avid or both, while some show no uptake at all. Likewise, some are visible in mpMRI while some are not. These data were used for clinical decision-making and cannot be used at present for scientific evaluation of the separate imaging methods, but will be evaluated later in a blinded manner. In conclusion, preliminary data indicate that diagnostic imaging for staging of PC might require a combination of methods to cover PCs with different characteristics.

EP-0650

Hormonal therapy impact on 18F-Fluorcholine PET-CT detection rates in recurrent prostate cancer

E. Triviño-Ibáñez, I. Puche-Sanz, A. Rodríguez-Fernández, A. González-Jiménez, E. Moratalla-Aranda, B. El Fahimi, F. Vázquez-Alonso, M. Gómez-Río, J. Llamas-Elvira; Virgen de las Nieves University Hospital, Granada, SPAIN.

Aim: To analyze the influence of hormonal therapy on 18F-Fluorocholine PET/CT (FCH-PET/CT) detection rates to locate the disease in biochemical recurrence (BR) of prostate cancer (PC). **Materials and Methods**: Observational and retrospective study included patients with biochemical relapse of PC or castration resistance (RC) according to the European Association of Urology criteria, who underwent a FCH-PET/CT between January 2010 and September 2016. The results of the FCH-PET/CT study were categorized in positive and negative. We confirmed the results with other imaging techniques, pathology reports or clinical follow-up. The relationship between FCH-PET/CT and the initial treatment (radical therapy or hormone therapy) and PSA kinetics (PSA doubling time and PSA velocity elevation) were studied. **Results:** 203 patients (mean age: 64.3±7.2years) were included. The overall detection rate of FCH-PET/CT was 43.3% (88/203 patients). Of these, 35/88 (39.8%) presented local

recurrence, 21/88 (23.9%) had pelvic lymph node involvement and 32/88 (36.4%) distant metastases. In the bivariate analysis between the negative and positive FCH-PET/CT groups, PSA diagnosis (13.5±18.5 vs 41.0±69.8 ng/mL), PSA trigger (2.7±3.9 vs 12.2±15.3 ng/mL), PSAdt (14.5±7.6 vs 7.5±7.5ng/mL), PSAve (1.8±3.7 vs 8.37±14.8 ng/mL), radical retropubic prostatectomy (RP) (64.3% vs. 18.2%), external beam radiotherapy (EBRT) (31.3% vs. 58%) and hormone therapy (73.9% vs. 26.1%), showed statistically significant differences (p<0.001). FCH-PET/CT detection rate in the subgroup with CR was 89.1% (41/46), significantly higher in comparison with radical treatment group (PR or EBRT) of 29.9% (47/157), p<0.001, and higher in the subgroup with radical treatment that received adjuvant hormonal treatment (54.2% vs 19.3%, p<0.01). In the multivariate analysis, RP, EBRT, hormonal therapy and PSA kinetics were independent predictors. **Conclusions:** FCH-PET/CT is useful in the detection of the disease in BR of CP, especially in patients with RC. Hormone therapy and PSA kinetics (PASdt and PSAve) were the main factors to consider when selecting patients.

EP-0651

Alkaline phosphatase (ALP) is a good predictor of skeletal metastasis in prostate cancer patients

K. M. G. Mokoala[1,2], M. W. H. Vangu[1,2]; [1]Charlotte Maxeke Johannesburg Academic Hospital, Parktown, Johannesburg, SOUTH AFRICA, [2]University of the Witwatersrand, Johannesburg, SOUTH AFRICA.

Aim: In white South African males, prostate cancer has been found to be the second most prevalent cancer. However, it is evident that black males are increasingly at risk of prostate carcinoma and often develop an aggressive type of prostate cancer. No local data exists regarding the value of alkaline phosphatase (ALP) levels for predicting bone metastasis on bone scintigraphy. We retrospectively assessed the value of ALP in predicting bone metastasis in our environment. **Material and Methods:** A total of 940 patients with histological diagnosis of prostate carcinoma were included. All had bone scans as part of the clinical management. Both Fisher exact test and Pearson Chi square test were used together with a logistic regression to determine if ALP could be an independent predictive factor for osseous metastases on bone scan. **Results:** Metastases were found on bone scan (BS) in 64% of patients with high ALP levels. A significant relationship was found between ALP levels and bone scan findings (p= 0.0001). A Mann Whitney *U*-test was done as a post-hoc test and revealed a significant difference in the ALP levels of patients with positive (Mean Rank = 276.24, N= 253) versus negative bone scans (Mean Rank = 146.24, N = 253), U = 4868, z = -10.883, p = 0.000, r = 0.56. Direct logistic regression analysis revealed that PSA (OR = 1.001; 95% CI = 1 - 1.003; p 0.017) and ALP (odds ratio = 1.013; 95% CI = 1.007 - 1.018; p < 0.001) were the predictive factors for detecting bone metastases. **Conclusion:** Our study revealed a high portion (63%) of patients with positive BS had high ALP. We also found that ALP was an independent predictive factor for the presence of bony metastases from logistic regression and that ALP was superior

to PSA in predicting for the presence of skeletal metastases on bone scintigraphy. The ALP is of great value and may be used in conjunction with the PSA and Gleason score in assessing for the presence of skeletal metastases in the management of patients with prostate cancer. Our results may serve as a guide to clinicians when deciding on the use of bone scintigraphy for patients with prostate cancer. This may impact on the number of requests that we receive and hence alter the waiting time for a bone scan.

EP-0652

Dual-phase 18F-FDG PET/CT Combined Diuretic for Restaging of Bladder Cancer

Q. Zhao, Y. Jia, J. Li, L. He, F. Zhao, X. Zhuang, F. Zhang; General Hospital of Ningxia Medical University, Yinchuan, CHINA.

The aim of this study was to investigate the role of dual-phase 18F-FDG PET/CT imaging combined diuretic and oral hydration in restaging of invasive bladder cancer. **Materials and Methods:** 20 patients (female 4, male 16, age 65.35±11.31 years old) with invasive bladder cancer (16 without cystectomy, 4 with total cystectomy and urinary diversion) were included in this study between March 2013 and September 2016. All the patients underwent 18F-FDG PET/CT from head to the mid-thighs 60 min after the intravenous injection of 370MBq of 18F-FDG. Delayed pelvic imaging was acquired 2 h after the intravenous injection of 20 mg furosemide and oral hydration. PET/CT findings were confirmed by cystoscopy or biopsy. **Results:** Delayed imaging combined diuretic PET/CT detected bladder lesions in 10 of 16 patients without cystectomy, with 9 recurrences and 1 residual lesion. SUVmax of the lesions in delayed PET/CT was 5.85±2.78. Pelvic lymph nodes metastases were detected in 7 of 20 patients only in delayed imaging, whereas 3 in standard imaging. Distant metastases in prostate, lung, skeleton and kidneys were visualized in 10 patients. These results changed the restaging and therapeutic strategies of 12 of 20 patients (60%). The sensitivity and specificity of delayed PET/CT combined diuretic was 80% and 75%. **Conclusion:** Dual-phase18F-FDG PET/CT combined application of diuretic, which overcomes the disadvantage caused by the excess FDG in the urinary tract, is better in the restaging of invasive bladder cancer. Local recurrent, residual bladder tumors and pelvic lymph nodes metastases can be dramatically detected.

EP-0653

68Ga-PSMA-11 PET/MRI in Primary Intermediate/High-Risk Prostate Cancer

S. Park, C. Zacharias, C. Harrison, L. Baratto, N. Hatami, A. Iagaru; Stanford University Medical Center, Stanford, CA, UNITED STATES OF AMERICA.

Introduction: Extensive investigation of 68Ga-PSMA-11 PET has shown high detection rates in men with recurrent prostate cancer after treatment. However, data is limited for evaluation (alone or as a hybrid system) at initial diagnosis. We report the

diagnostic performance of ^{68}Ga-PSMA-11 PET/MRI prior to prostatectomy in patients with intermediate or high-risk cancer. **Subjects & Methods:** We recruited twenty men without metastatic disease on conventional imaging (CT or MRI and bone scintigraphy) who were scheduled for radical prostatectomy with pelvic lymph node dissection. A mean dose of 4.2 ± 0.6 mCi (155.4 ± 22.2 MBq) of ^{68}Ga-PSMA-11 was administered. Whole-body images were acquired starting 43-61 minutes post-injection using a GE SIGNA PET/MR, followed by an additional pelvic PET/MRI acquisition (including conventional multiparametric MRI sequences) 42-67 minutes later. PET/MRI findings were compared to preoperative diagnostic MRI and correlated with final pathology. **Results** Preoperative: ^{68}Ga-PSMA 11 PET identified intraprostatic cancer foci in all 20 patients, whereas mpMRI alone identified PIRADS 4 or 5 lesions in 16 patients and PIRADS 3 in two patients. PET/MRI demonstrated focal uptake in pelvic lymph nodes in three patients. Final pathology confirmed cancer in the prostate of all patients, as well as nodal metastasis in two. No patient with normal pelvic nodes on PET/MRI had cancer in the nodes on final pathology. Tracer accumulation increased overall at later acquisition times, with higher SUVs (mean: 16.6 vs 13.4, P=0.006). However, no additional lesions were identified on delayed imaging. **Conclusion:** ^{68}Ga-PSMA-11 PET/MRI correctly identifies foci of cancer within the prostate while MRI provides detailed anatomical guidance for the location of abnormal uptake. ^{68}Ga-PSMA-11 PET/MRI provides valuable information even in the setting of negative conventional imaging, and may inform the need for and extent of pelvic node dissection.

EP-0654

^{68}Ga-PSMA for radioimaging of prostate cancer: an in-vitro study using LNCaP cells and PC3 cells

P. Cuber[1], M. Heuschkel[1], J. Rabenstein[2], A. Hohn[1], W. Rutz[1], O. W. Hackenberg[2], D. Fischer[3], B. J. Krause[1]; [1]Department of Nuclear Medicin Rostock, Rostock, GERMANY, [2]Department of Urology Rostock, Rostock, GERMANY, [3]Department of Paediatrics, Rostock, GERMANY.

Background: Prostate specific membrane antigen (PSMA), also known as glutamate carboxypeptidase II is an enzyme preferentially expressed in the prostate and in minor amounts in kidney and endocrine glands. In prostate cancer, PSMA is frequently upregulated and the utilization of ^{68}Ga labelled peptides (^{68}Ga-PSMA) with high specificity for binding to the catalytic extracellular domain has been proposed as a measure for the detection of metastatic disease and for early evaluation of treatment response. Inhibition of the interaction between PSMA at the cell surface and ^{68}Ga-PSMA with low doses of 2-(Phospho-nomethyl)-pentandioic acid **(**2-PMPA) might be helpful to reduce damage in other PSMA expressing tissues [1]. **Material and Methods:** PC3 and LNCaP cells were purchased from LGC Standards (ATCC, Wesel, Germany). Medium (Hams F12 and RPMI-1640 for PC3 and LNCaP cells, respectively) was supplemented with FCS (10%) and penicillin (100 u/l) /streptomycin (100 mg/l). Cells were cultured in a humidified atmosphere (5%CO_2, 37°C)

and PSMA expression was verified by immunofluorescence and western blotting of protein lysates, respectively. To this end, the PSMA-specific antibodies GCP04 (Exbio, Prag, CZ) and YPSMA1 (Abcam, Cambridge) in combination with appropriate secondary antibodies were used and 2-PMPA (Tocris, Bristol, UK) served as specific inhibitor of ^{68}Ga-PSMA uptake. ^{68}Ga-PSMA was prepared by utilization of PSMA-11 (ABX Radeberg, Germany) and a GRP modul (Scintomics, Fürstenfeldbruck). Cells were grown to subconfluency and uptake of ^{68}Ga-PSMA was investigated prior and after pre-treatment of cells with docetaxel. All experiments were performed in a total volume of 200 μl at 37°C with constant shaking and utilization of 0.5 MBq ^{68}Ga-PSMA. **Results:** PSMA was readily detectable by immunofluorescence of intact LNCaP cells as well as by western blotting of cell lysates. By contrast, either method failed to detect PSMA in PC3 cells. Consequently, binding of ^{68}Ga-PSMA ligand occurred in LNCaP cells only and can be inhibited by 2-PMPA with an IC_{50} of 1.72 μM. Pre-treatment of cells with docetaxel did not affect ^{68}Ga-PSMA uptake, i.e. cytotoxic treatment comes along with a reduced number of viable cells but did neither effect ^{68}Ga-PSMA uptake per cell nor up- or downregulation of PSMA in surviving cells. **Conclusion:** Uptake of ^{68}Ga-PSMA is restricted to PSMA-positive prostate cancer cells and can be inhibited by 2-PMPA. The utilization of ^{68}Ga-PSMA for monitoring cytotoxic therapy in PSMA-positive prostate cancer is worth to be evaluated further in appropriate animal models.

EP-0655

Comparison of Ga-68 PSMA-11 PET, Tc-99m DPD bone SPECT and computed tomography for the detection of bone metastases in patients with metastatic prostate cancer

H. Ilhan[1], S. Reinhardt[1], W. P. Fendler[1], A. Todica[1], F. J. Gildehaus[1], C. Cyran[2], C. Gratzke[3], A. Herlemann[3], V. Wenter[1], P. Bartenstein[1], A. Rominger[1]; [1]Department of Nuclear Medicine, University Hospital of Munich, Munich, GERMANY, [2]Institute for Clinical Radiology, University Hospital of Munich, Munich, GERMANY, [3]Department of Urology, University Hospital of Munich, Munich, GERMANY.

Purpose: To compare the diagnostic performance of Ga-68 PSMA-11 PET (PSMA PET), Tc-99m DPD bone scintigraphy including SPECT (BS) and computed tomography (CT) for the detection of bone metastases in patients with metastatic prostate cancer. **Methods:** 35 patients with prostate cancer bone metastases who received PSMA PET/CT and BS including a SPECT/CT within three months without change in medical treatment were included in this retrospective analysis. The reference standard for the evidence of bone metastases was the consensus of two experienced readers evaluating PSMA PET, CT (diagnostic CT with contrast agent from Ga-68 PSMA-11 PET/CT), BS, clinical information and follow-up data in each patient. Follow-up imaging included at least one PSMA PET/CT or bone scan. A lesion-by-lesion analysis was performed in a total of 240 bone metastases. Additionally a region-based analysis including the identification of bone metastases in 6 bone regions (skull and skull base, spine and sacrum, clavicle and scapula, ribs and sternum, pelvic bone,

upper and lower extremities) was performed. **Results:** 214/240 (89 %) bone metastases were detected in PSMA PET. 180/240 metastases (75 %) showed a correlate in CT and 162/240 (67,5%) in Tc-99m DPD scintigraphy and SPECT (CT data from SPECT/CT was not evaluated). Diagnostic performance of PSMA PET was also superior to CT and BS in the region based analysis (4 skull and skull base lesions: 100% vs. 50% vs. 100%; 67 lesions in the spine and sacrum: 85% vs. 67%, vs. 58%; 20 lesions in the clavicle and scapula: 75% vs. 55% vs. 65%; 75 rib and sternum lesions: 93% vs. 77% vs. 71%; 55 pelvic lesions: 89% vs. 89% vs. 73%; 19 lesions in the extremities: 100% vs. 79% vs. 73%). The highest diagnostic performance for PSMA PET was observed in bone metastases in the extremities, the skull / skull base and the pelvic bone. **Conclusion:** Ga-68 PSMA-11 PET showed a very high sensitvity and detected more lesions in patients with prostate cancer bone metastases compared to CT and Tc-99m DPD bone scintigraphy including SPECT. The accurate assessment of involved bone regions is improved by PSMA PET. These results confirm earlier findings and indicate that PSMA PET outperforms conventional imaging and bone scan in the staging of prostate cancer bone metastases.

EP-0656

18F-Choline (FCH) PET/CT for initial staging of patients with intermediate and high risk prostate cancer (PCa) in routine use: results and perspective

C. Rousseau[1,2], M. Barbaud[1], L. Ferrer[3,2], V. Fleury[1], M. Le Thiec[1], D. Rusu[1], L. Campion[4,2], F. Kraeber-Bodéré[1,2]; [1]ICO Cancer Center, Nuclear Medicine Unit, Saint Herblain, FRANCE, [2]CRCINA, Inserm U1232, CNRS UMR 6299, Nantes, FRANCE, [3]ICO Cancer Center, Medical Physics Unit, Saint Herblain, FRANCE, [4]ICO Cancer Center, Biometrics Unit, Saint Herblain, FRANCE.

Purpose: Routine imaging modalities, performed at initial staging in intermediate and high risk (IHR) PCa, have limited accuracy in nodal/bone involvement. Recently, focal treatments have been developed and could be legitimately proposed if a more accurate exhaustive disease evaluation than conventional one (CT, whole-body bone scan) could be achieve. Currently, there is a strong demand for FCH PET/CT examination for these patients at initial stage to allow a personalized therapy. This study evaluated FCH PET/CT efficiency to detect lymph-node/bone involvement in IHR PCa patients, and treatment impact of this imaging procedure based on patients outcome. **Subjects & Methods**: we retrospectively studied 71 consecutive patients (median age 66.2, IQR [61.3-74.3]) who underwent FCH PET/CT for the initial staging of IHR PCa. All of them had bone scan and abdominal-pelvic CT doubtful or normal. FCH PET/CT diagnostic performance was reported as a per patient basis of the population. All hotspots, except physiological uptakes, were classified as positive. Histological specimens or follow up data were used as the standard of reference. Kaplan-Meier and log-rank analysis were computed for survival assessment. **Results**: The population comprised 53.5% patients with high risk PCa. While the conventional imaging was either normal or doubtful, FCH PET/CT overall sensitivity, specificity and positive/negative pre-

dictive values for lymph-node involvement were respectively 77.0%, 83.1%, 84.8% and 79.0%. For bone assessment, the sensitivity and specificity of FCH PET/CT were respectively 100% and 85.3%. FCH PET/CT revealed 17% of metastatic patients with a predominance of bone foci. FCH PET/CT has changed treatment plan in 26 patients (36.6%): from curative strategy to another one (5 patients, 19.2%), from palliative to curative treatment (8 patients, 30.8%) and from curative to palliative treatment (13 patients, 50%). When FCH PET/CT was positive only in prostate bed (group 1), treatment was modified in 22.2% (8/36) versus 51.4% (18/35) if FCH PET/CT was positive beyond prostatic bed (p = 0.011) (group 2). As treatments were tailored on FCH PET/CT results, no difference on relapse free survival between these 2 groups was observed (p = 0.598), whereas group 2 had a more advanced disease. **Conclusion**: In intermediate and high risk PCa, FCH PET/CT efficiency in detecting both bone and lymph-node involvement at initial staging was found to be better than conventional imaging and notably, patients benefit from treatment tailoring decided according to FCH PET/CT results. Obviously, clinical trials are warranted to confirm these findings.

EP-0657

What factors should be considered before proposing 18-F-Choline (FCH) PET/CT in rising PSA prostate cancer patients who are being considered for targeted therapy ?

M. Barbaud[1], L. Ferrer[2,3], V. Fleury[1], M. Le Thiec[1], D. Rusu[1], T. Rousseau[4], G. Bochereau[5], H. Monsaint[6], F. Kraeber-Bodéré[1,3], L. Campion[7,3], C. Rousseau[1,3]; [1]Nuclear Medicine Unit, ICO Cancer Center, Saint Herblain, FRANCE, [2]Medical Physics Unit, ICO Cancer Center, Saint Herblain, FRANCE, [3]CRCINA, Inserm U1232, CNRS UMR 6299, Nantes, FRANCE, [4]Urologic Clinic Nantes-Atlantis, Saint Herblain, FRANCE, [5]Urologic Unit, Saint Augustin Clinic, Nantes, FRANCE, [6]Urologic Unit, Urologic Medipole Group, Vannes, FRANCE, [7]Biometrics Unit, ICO Cancer Center, Saint Herblain, FRANCE.

Aim: In prostate cancer (PCa) with biochemical failure after therapy, FCH PET/CT has emerged in recent years as an accurate tool for early PCa recurrence detection. However, location is important to provide a personalized treatment depending on disease extension. Fast PSA doubling time (PSAdt) and high PSA velocity (PSAvel) are recognized factors influencing FCH PET/CT positivity in biochemical recurrence PCa patients. The study aims at investigating whether one can refine these factors and if other clinical and/or biological data would be able to predict positive FCH PET/CT results. **Materials and Methods**: We retrospectively analysed 134 FCH PET/CT, performed between 2013 and 2016, in 132 patients with rising PSA and PSAdt ≤ 6 months after radical prostatectomy (RP), radiation therapy (RT) or androgen deprivation therapy (ADT). All hotspots, excepted physiological uptake, were classified as positive. Histological biopsies or follow up data were used as the standard of reference. Positive studies were classified in 3 groups, according to disease locations: prostatic bed, loco-regional disease (ie: pelvic lymph nodes+/- prostate area), or distant metastases. **Results:** Overall, 109/134 FCH PET/CT were positive (detection rate 81.3%). Among positive FCH PET/CT, 12, 54 and 40 examinations were

respectively local recurrence (11.3%), lymph node recurrence (51%) or distant metastases (37.7%). ADT was not significantly associated with a better detection rate (p=0.155). Positive FCH PETscans have significant higher PSA trigger (median 4.3 [2.5-8.7] vs 2.1 [1.5-3.7], p<10^{-3}), higher PSA level (median 6.1 [3.2-16.4] vs 2.9 [1.8-5.3], p=0.025) and shorter PSAdt (median 3 [2.0-4.6] vs 4.3 [2.9-5.5], p<10^{-3}) than negative FCH PET/CT. Alternatively, high Gleason (≥7 p<10^{-2}) and D'Amico (>2-3 p<10^{-3}) scores were found as FCH PET/CT positive factors. In a univariate analysis, only PSAvel was significantly different according to recurrence sites (local, lymph node or metastatic) (p=0.04). A PSAvel cut-off value of 6.5 ng/ml/yr was associated with a higher risk of distant metastases (p<10^{-2}). **Conclusion:** In a patient population with rising PSA and PSAdt ≤ 6 months, FCH PET/CT identified a site of recurrence in a large majority of patients and local pelvic recurrence representing the most common site. PSAvel should be taken into account for patient eligibility to FCH PET/CT examination. Furthermore, a PSAvel value higher than 6.5 ng/ml/yr should suggest an extrapelvic recurrence, which should be controlled by FCH PET/CT to determine precisely metastases localization. Thus, this could legitimate a tailored treatment as hypofractionated stereotactic radiotherapy to oligometastases for this advanced disease patients.

EP-0658
Ga68 PSMA-11 PET/MRI: Influence of Scan Time on Image Quality

*S. Park, L. Baratto, H. Gandhi, P. Gulaka, **A. Iagaru**; Stanford University School of Medicine, STANFORD, CA, UNITED STATES OF AMERICA.*

Objectives: Ga68-PSMA 11 is now used worldwide to evaluate patients with prostate cancer (PC). In this study, we investigated the impact of various acquisition times which simulate low-dose images on image quality for Ga68-PSMA 11 PET/MRI conducted at initial staging of patients with intermediate and high risk prostate cancer. **Methods:** The data was acquired using a GE SIGNA PET/MR (GE Healthcare, Waukesha, WI). Images were acquired mid-thigh to head in 6 bed positions for all but 3 subjects, which were acquired in 5 bed positions. PET images were reconstructed using a fully 3D time of flight iterative ordered subsets expectation maximization (OSEM) algorithm with 2 iterations/28 subsets and a 5 mm Gaussian filter. Attenuation correction used the two-point Dixon technique. Further the list mode PET data was retrospectively under-sampled and reconstructed to simulate acquisition times of 30 seconds/bed, 1 minute/bed, 2 minutes/bed and 4 minutes/bed. The latter is the standard image acquisition time per bed position in the existing protocol to accommodate simultaneous MR imaging sequences. Each PET reconstruction was reviewed blindly and independently by 2 nuclear medicine physicians and scored for image quality using a Likert scale (1 - poor, 5 - excellent quality). **Results:** We enrolled 23 male participants (55-74 year-old, mean±SD: 66.5±4.1 yr.) in this study. The administered dosages of Ga68-PSMA 11 ranged 2.9 - 5.0 mCi (mean±SD: 4.2±0.6) and imaging started at 41-61 minutes (mean±SD: 51.1±5.3) after administration of the radiopharmaceutical. The scores for PET

images were 1.9±0.5 for the 30 sec/bed reconstructions, 3.2±0.5 for the 1 min/bed reconstruction, 4.7±0.5 for the 2 min/bed reconstructions and 4.7±0.4 for the 4 min/bed reconstructions. All differences were statistically significant (*P* < 0.05), except for the 2 min/bed reconstruction vs. the 4 min/bed reconstruction (*P*: 0.0823). **Conclusion:** Data acquisition of 2 min/bed results in high quality Ga68-PSMA 11 PET images similar to 4 min/bed acquisition. Therefore, fast exams can be acquired if the duration of MR sequences can be limited to 2 minutes at each PET position.

EP-0659
68Ga PSMA PETCT improves initial management plan of patients with intermediate and high risk prostate cancer

A. Al-Ibraheem, A. Alsharif, A. Al-Daghamen, S. Salah, J. Khader, M. Alkhaldi, M. Abu Nasser, J. Khzouz; King Hussein Cancer Center, Amman, JORDAN.

Background & Objective: Conventional staging of patients with intermediate-risk to high-risk prostate cancer includes either CT or MRI accompanied by bone scintigraphy. Evaluation of lymph nodes using CT or MRI solely depends on morphological information, and metastatic lymph nodes are mainly detected on the basis of increased size which is insufficient criterion in many situations. Bone scan has high sensitivity but with limited specificity. Despite superiority of 68-Ga-PSMA-PET/CT in recurrent prostate cancer, its potential role in initial management of intermediate /high risk prostate cancer patients has not been adequately explored. Our goal in this study is to evaluate the added value of 68-Ga-PSMA-PET/CT in patients with intermediate/high risk prostate cancer and equivocal radiologic or scintigraphic findings prior to any therapeutic intervention. **Materials and Methods:** We retrospectively reviewed electronic files and images of patients with biopsy proven intermediate/high risk prostate cancer patients who underwent conventional staging procedures (CT or MRI) and bone scan in addition to 68-Ga-PSMA-PET/CT at KHCC prior to initiation of any treatment. We examined the added value of 68-Ga-PSMA-PET/CT in staging these patients. Twenty patients from August 2015 until January 2017 matched our inclusion criteria and enrolled for this study. PET/CT was acquired by TOF Biograph mCT flow (64) EARL accredited PET/CT scanner 90 minutes after injection of 150 mBq 68 Ga- PSMA (HBED-CC). We performed patient-based analysis. Organ-based sub-analysis concerning LNs, bone, LNs & bone, soft tissue lesions is planned. Uni- and multivariate analysis were performed; age, PSA and Gleason score. **Results:** A total of 20 patients in the period from August 2015 until end of March 2017 were included in this study. Median age was 72 years (range 56-79). Average Gleason score was 8. Median initial PSA was 25. There were 9 patients with equivocal lymph nodes on CT or MRI, 7 with equivocal bone scan findings, 4 with questionable soft tissue metastases or synchronous tumours. Overall PET provides more accurate staging in 11 patients (55%) and changed patient management in 7 patients (35%).On uni- and multivariate analysis, Gleason score was the only significant predictor.

The odds of PET changing decision-making for Gleason 8-10 disease was 4 times that of Gleason 7 disease (p = 0.02). **Conclusion:** 68-Ga-PSMA-PET/CT has the potential to significantly changing patient management by confirming or excluding suspicious lesions on conventional imaging or by detecting new previously non detected lesions.

EP-0660
Seminal vesicles infiltration

L. Holody, M. Tarnawska-Pierscinska, M. Obarzanowski, J. Jaskulski, J. Kopczynski, P. Kedzierawski; Swietokrzyskie Centrum Onkologii, Kielce, POLAND.

Aim: The aim of our research was to evaluate infiltration of seminal vesicles in PET/CT with 18F-FCH examination in patients with prostate cancer from middle and high risk groups before surgical treatment. **Materials and Methods:** In Nuclear Medicine Department of Swietokrzyskie Centrum Onkologii, we examined 92 patients, average age 62, with prostate cancer. These patients had the disease confirmed by sextant prostate gland biopsy. PET/CT with 18F-FCH was performed in two independent acquisitions with a dose of 3,5 MBq/kg. The first one was dynamic, limited to the area of pelvis, conducted between 1' and 8' after intravenous administration of the radioisotope. The other one was static, from skull to femur, 60' from injection. In both acquisitions SUV value was measured in seminal vesicles. All the patients were operated up to two months after the examination. **Result:** In our research two methods were analysed statistically. In the first one, we recognised infiltration of seminal vesicles when SUV value was 2,5 in static examination. In the other one, infiltration was recognised when SUV value in static examination was higher than in dynamic one, independently on the SUV value itself. In the static acquisition there was a strong correlation between SUV value and histopathological examination, where SUV was 2,5 (p-value 0,0002). Sensitivity, specificity, accuracy were 72%, 93%, 89%, respectively. We achieved a high value of NPV, which was 93%. There was no statistical significance when using the second method (p-value 0,44). **Conclusion:** PET/CT with 17F-FCH examination seems to be a useful tool in evaluating seminal vesicles infiltration in prostate cancer with SUV value of 2,5. In our examination we showed lack of correlation between the increase of SUV value and presence of cancerous infiltration.

EP-0661
Impact of Whole Body 99m-Tc-HDP SPECT-CT On Tretament Decisions In Patients With High Risk Prostate Cancer

K. E. Esa Kauppila; Seinäjoki Central Hospital, Seinäjoki, FINLAND.

Purpose: For accelerating development of prostate cancer (PCa) treatment precise diagnostic tools are warranted. This report retrospectively explores our clinical practice of use of 99-mTc-HDP-Whole-Body-SPECT-CT imaging in high risk prostate cancer, its impact on treatment decisions and initial outcomes. Subjects and **Methods:** Patients (n = 104, mean age 73 years ± SD 8.8 years) with new PCa or with biological failure of previously radically treated PCa without evidence of metastases, scanned with 99-mTc-HDP-WB-SPECT-CT, were included in the analysis. **Results:** 0, 1, 1-5 and widespread osteoblastic metastases were found in 63 (77 %), 9 (11%), 3 (4 %) and 4 (5 %), respectively. There were 2 equivocal osteoblastic findings (2 %). On CT there were suspicious N positive disease in 6 patients (7%). Repetition or monitoring of the nuclear imging (NM) finding, staging MRI, evaluation of CT finding, follow up of incidental finding was performed in 3.9 %, 8.7 %, 5.8 %, 3.8 %, respectively. The most significant CT co-morbidity was aortic aneurysm (AA); (n =5), leading to one death, one urgent surgery, and otherwise to follow up. Treatment options were surgery (S), radiotherapy (R), hormonal therapy (H), chemotherapy (C), or watchful waiting (W). If bone metastases were noted, n=18, 45 % received H, 44 % C, 5.6 % W, if not, n= 78, 45 % received HR, 28 % H, 10 % S, 10 % W, 1 % C, respectively. Follow up PSA is available in 82 patients (3/2017). Initial decrease of PSA > 50 % occurred in 74 %, with response to < 0.1 µg/l in 15 %, and to < 1 µg/l in 52%, and without response or progression in 18 %. **Conclusions:** Bone WB-SPECT-CT directed treatment decisions in high risk prostate cancer with relatively few equivocal findings on NM component. Low dose CT did not only guarantee the accurate NM finding interpretation, but revealed other significant non-malign and malign findings for the patients benefit. Confirmatory imaging was used rarely. Outcome evaluation is ongoing.

EP-0662
Correlation of Prostate specific antigen and Gleason score with Standardized uptake values of 68Ga PSMA PET/CT in initial staging of prostate cancer

A. Agrawal, K. Shaha, G. Prakash, G. Bakshi, S. Menon, N. Purandare, S. Shah, A. Puranik, V. Rangarajan; Tata Memorial Hospital, Mumbai, INDIA.

Aim: The aim of the study was to assess the uptake of PSMA semiquantitatively, using maximum Standardized uptake values(SUVmax) in the primary tumor and in metastases of prostate cancer (PC) and to determine if this correlates with Prostate specific antigen (PSA) and Gleason score (GS); in initial staging of prostate cancer. **Materials and Methods:** 73 biopsy proven cases of PC, who underwent [68]GA PSMA PET/CT for initial staging, prior to start of any form of treatment were included in this analysis. The uptake in the primary and in metastases were analyzed both visually and by SUVmax. The GS ranged between 7 and 10 and range of PSA was 0.5 to 11,631ng/ml, median 49ng/ml. SUVmax in the primary and metastases was assessed in relation to PSA and GS. **Results:** 97% (71/73) of patients demonstrated increased tracer accumulation in the primary tumor greater than the background (range - 0 to 143, median 24). 35% of patients were non metastatic (M0), and 65% were metastatic (M1a,b,c). In patients with PSA < 20ng/ml (28%), the mean SUVmax was 15.44 and in patients with PSA>20ng/ml (72%) the mean SUVmax was 37.70 in the primary tumor; the mean SUVmax in metastases was 17.28 and 43.58 respectively. Both were

statistically significant (0.001). In patients with GS of 7, 8, (47% of patients) the mean SUVmax was 25.32 and in those with GS of 9, 10 (53%), the mean SUV was 37.08 in the primary lesion. In the metastatic lesions the mean SUVmax was 30.17 in the GS 7,8 group and 41.77 in the GS 9,10 group. Though this was not statistically significant in both groups (0.066 and 0.067 respectively), there was a trend towards higher SUVmax in patients with a higher GS. **Conclusion:** In our study the PSMA uptake was significantly higher in patients with high PSA (>20ng/ml) as compared to patients with lower PSA (<20ng/ml) with good statistical significance. Whereas there was trend of higher uptake was seen in patients with GS >9, as compared to those with GS <8; though this was not statistically significant; which could be due to lesser number of patients with GS of <7. 68Ga PSMA is an ideal modality to stage patients of intermediate and high risk prostate cancer.

EP-0663

Somatostatin receptor expression in renal cell carcinoma: a new perspective on an old knowledge

L. Locantore, M. Cucca, D. Grigolato, M. Zuffante, M. Ferdeghini; Nuclear Medicine Unit, University Hospital of Verona, Verona, ITALY.

Background/Aim: 18F-FDG PET/CT (FDG PET) is considered as an effective diagnostic tool in patients treated for renal cell carcinoma (RCC). Unfortunately, many lesions from RCC are not 18F-FDG avid. RCC may be a target for somatostatin receptor (SSTR) based imaging, due to the reported SSTRs expression. PET/CT using 68Ga-labelled DOTA0-Tyr3octreotide (DOTATOC) is one of the imaging tools for SSTRs assessment. At this time, experience with DOTATOC PET/CT (DOTA PET) in RCC is very limited. We aimed to investigate if DOTA PET could be helpful in patients with recurrent/metastatic RCC. **Patients/Methods:** Eight patients (7 males, 1 woman, mean age 61) who had surgery for RCC underwent DOTA PET for suspected tumor recurrence. Patients previously performed other exams (ceCT=7/8), brain MRI (=1/8); FDG PET (7/8). DOTA PET scan was performed after 1 hour from 68Ga-DOTATOC administration. Images were analyzed both qualitatively and semiquantitatively (SUVmax). Results were compared to ceCT, MRI and FDG PET findings, adding clinical and radiological follow-up data (at least 6 months). **Results:** DOTA PET was positive in 6 patients; SUV max of the lesions ranged from 2,1 to 26. With respect to CT uncertain findings, PET images showed disease in pancreas (=3) and lung (=3). In patient undergone MRI, DOTA PET confirmed cerebral lesions. Totally, in half of the patients with positive DOTA PET, additional sites of suspected lesions were detected. Two patients had DOTA PET scan negative (lung was the site of CT suspected recurrence). No uncertain results were found. Compared to FDG PET, 3/7 of the patients were positive at DOTA PET with a negative FDG scan; one patient with indeterminate FDG results was classified as positive according to DOTATOC/PET images. Two patients had both FDG- and DOTA PET scans negative (lung). One patient was positive to both FDG and DOTA PET, even though DOTA PET detected an additional secondary lesion. DOTA PET findings changed management in 100% cases. In 100% of the patients with positive DOTA PET candidated to surgery, histologic data confirmed RCC origin. One patient with negative DOTA PET had negative cytologic findings (radiologic follow-up also showed lesion stability). **Conclusions:** In patients with RCC DOTA PET is a powerful tool for evaluation somatostatin receptor expression of the lesions, especially when radiologic/FDG PET findings are negative/doubtful. This approach permits a better tumor characterization and a more accurate staging, adding the potential advantage to detect further additional lesions, suitable for biopsy (usually required for appropriate diagnosis).

EP-0664

PSA cutoff for ordering NaF PET/CT bone scan in patients with newly diagnosed prostate cancer

I. Sarikaya[1], A. Elgazzar[2], A. Baqer[3], P. Sharma[2], M. Alfeeli[3]; [1]Kuwait University Faculty of Medicine, Kuwait, KUWAIT, [2]Kuwait University Faculty of Medicine, Kuwait, KUWAIT, [3]Mubarak Al Kabeer Hospital, Kuwait, KUWAIT.

Aim: The use of NaF PET/CT bone imaging is increasing because of its higher image resolution, lesion detection efficiency, sensitivity and specificity over standard bone scintigraphy. Various studies previously reported that bone scintigraphy should be ordered when PSA level is greater than 10 or 20 ng/ml in asymptomatic newly diagnosed prostate cancer patients. In this retrospective study, our goal was to determine a PSA cutoff level for ordering NaF PET/CT imaging. **Methods:** Newly diagnosed prostate cancer patients who had NaF PET/CT scan and PSA measurements available within 2 mos of PET scan were selected for this study. When available other parameters (gleason score, clinical stage, alkaline phosphatase levels, skeletal symptoms, and correlative imaging findings) were recorded. Receiver operating characteristics (ROC) analysis was performed to determine a PSA cutoff value for NaF PET/CT imaging. **Results:** Twenty six (26) patients met the inclusion criteria. PET was positive in 7 patients. In 5 asymptomatic PET positive patients, PSA was above 20 ng/ml in 4 patients and below 10 ng/ml in 1 patient (gleason score:8). In 2 symptomatic PET positive patients PSA levels were above 100 ng/ml. ROC analysis indicated that PSA cutoff for PET positivity was > 20 ng/ml. PET was negative in 8 and suspicious/indeterminate in 11 patients. **Conclusion:** This preliminary study indicates that PSA cutoff value for NaF PET/CT positivity is >20 ng/ml. However, in symptomatic or high risk patients NaF PET/CT can be ordered at lower levels of PSA (≤ 20 ng/ml). A study with larger number of patients with follow-up NaF PET/CT scan, correlative radiological imaging, or histopathological confirmation to determine a PSA cutoff level for ordering NaF PET/CT bone imaging is underway.

EP-0665

The value of Ga-68 PSMA-11 PET/CT in the primary staging of biopsy proven prostate cancer

H. Ilhan[1], D. Schmidt[1], V. Wenter[1], A. Todica[1], C. Cyran[2], A. Herlemann[3], C. Gratzke[3], F. J. Gildehaus[1], P. Bartenstein[1], A. Rominger[1], W. P.

Fendler[1]; [1]Department of Nuclear Medicine, University Hospital of Munich, Munich, GERMANY, [2]Insititute for Clinical Radiology, University Hospital of Munich, Munich, GERMANY, [3]Department of Urology, University Hospital of Munich, Munich, GERMANY.

Introduction/Purpose: Current guidelines recommend bone scintigraphy, CT or MRI in asymptomatic patients with biopsy proven PC in case of PSA >10 ng/ml. The diagnostic performance of Ga-68 PSMA-11 PET/CT is superior to conventional imaging. The aim of the current study was to assess the value of PSMA PET/CT in patients with biopsy proven PC stratified on the basis of PSA values and Gleason Score (GS). **Methods:** 46 patients (median 71 years, range: 53 - 80) with biopsy proven PC prior to therapy were included in this retrospective analysis. Risk stratification by PSA and GS was performed in analogy to D'Amico classification. PET/CT was analyzed visually and semi-quantitatively and included the visual detection rate of the primary tumor (VDR; positive, negative and equivocal), the measurement of SUV_{max} in the primary tumor (SUV_{max}), the detection of a local infiltration (seminal vesicles, bladder, rectum), lymph node metastases and distant metastases (including non-regional lymph node metastases). **Results:** Median GS was 8 (range 6 - 10; 8 patients GS 6, 7 patients GS 7, 8 patients GS 8 or higher). The mean PSA was 25,5 ±81 ng/ml (range: 3,2 - 167 ng/ml). VDR was positive in 38 of 46 patients (83%), negative in 5 (11%) and equivocal in 3 patients (6%). Median PSA in patients with negative and equivocal VDR was 8,9 ng/ml. Mean SUV_{max} of the primary tumor was significantly higher in patients with PSA ≥20 ng/ml (21,5 ±12,7) compared to PSA ≤10 ng/ml (12,5 ±12,4) and 10-20 ng/ml (13,9 ±7,6; p<0,05). According to D'Amico classification 2 patients were classified as low, 9 as intermediate and 35 as high risk patients. 4 of 9 patients with intermediate risk (44%) showed local infiltration, 7 (78%) regional lymph node metastases and 4 (44%) distant metastases. In high risk patients local infiltration was seen in 20 (57%), regional lymph node metastases in 23 (66%) and distant metastases in 19 patients (54%). Out of 13 patients with a PSA ≤10 ng/ml, 6 (46%) showed local infiltration, 7 (54%) regional lymph node metastases and 6 (46%) distant metastases. **Conclusion:** Ga-68 PSMA-11 PET/CT demonstrates local and distant metastases in a significant number of patients particularly at a PSA ≤10 ng/ml. The clinical significance of the improved sensitivity with Ga-68 PSMA-11 PET/CT remains to be established.

EP-0666

Semiquantitative analysis of ^{18}F-choline uptake in prostate gland of patients with untreated cancer: relationships with Risk Assessment Score and patient's outcome

M. Castellani[1], **L. Florimonte**[1], M. Vadrucci[2], V. Longari[1], E. Orunesu[1], R. Benti[1]; [1]Department of Nuclear Medicine, Fondazione IRCCS Ca' Granda - Ospedale Maggiore Policlinico, MILAN, ITALY, [2]Department of Nuclear Medicine, King's College Hospital NHS Foundation Trust, London, UNITED KINGDOM.

Introduction: ^{18}F-choline PET/CT is used to restage prostate cancer patients (with a biochemical relapse or when metastases are suspected after primary treatment) and, in selected cases, to stage patients with risk of local or distant metastases on the basis of PSA levels, Gleason score and T grade (Risk Assessment Score: RAS). In both cases, proper evaluation of the extent of disease is crucial to define the best therapy and for risk stratification. ^{18}F-choline prostate gland uptake, RAS and the extent of cancer in prostate bioptic cores were analyzed, and the role of PET/CT in assessing clinical outcome was explored. **Subjects & Methods:** PET/CT of 42 males (mean age: 67.6; range: 49-84 yrs) with increased PSA levels (median value 9.3; range: 2.4-329) and recent histological diagnosis of prostate cancer, were retrospectively evaluated. Images of the pelvis and whole-body were obtained 5 and 60 minutes after injection. The SUVmax values of prostate gland and the percent of positive specimens were related to RAS. The relationship between SUVmax and the outcome expressed as stable disease or biochemical progression at follow-up (median: 19.8 months; range 3-47) was also assessed. **Results:** Mean levels of early and late SUVmax were different (p<0.05) in patients with low, intermediate and high risk (early: 3.9±1.1, 4.1±1.1, 6.2±2.5, late: 6.1±1.2, 6.2±2.3, 8.1±2.8). Differences (p<0.05) in the percentage of cancer positive specimens (0.22±0.16, 0.34±0.25, 0.66±0.33) were also found. Significantly greatest values of early (4.5±1.09 vs 6.4±2.0; p<0.05) and late (6.3±2.3 vs 8.7±2.1; p<0.05) SUVmax were observed in patients with metastases whose frequency increased from low (1/12) to intermediate (1/9) and high risk (11/21) subjects. Similar differences were found when the mean number of cores involved (0.36±0.26 vs 0.70±0.37; p<0.05) were considered. Greater mean values of early (SUVmax 6.2±2.6) and late (SUVmax 9.4±3.0) choline uptake were found in 9 patients with biochemical progression at follow up (median PSA value: 76.5; range 0.25-1202), whereas 33 patients with a good outcome (median PSA level: 0.09; range 0-27) had an early and late SUVmax values of 4.8±1.09 and 6.5±1.9 (p<0.01), respectively. ROC analysis of late SUVmax values provided a NPV value of 90% for a cut-off greater than 8.3. **Conclusion**: These data suggest that a measure of prostate ^{18}F-choline uptake could be useful in monitoring the local activity of disease and in prognostic evaluation of patients with prostate cancer.

EP-0667
PSMA Avid Liver Hemangioma

K. Oksuzoglu, T. Ones, H. T. Turoglu, S. Inanir, T. Y. Erdil; Marmara University School of Medicine, Nuclear Medicine Department, Istanbul, TURKEY.

Introduction: The prostate specific membrane antigen (PSMA) is a transmembrane glycoprotein with significantly elevated expression in prostate cancer cells compared to benign prostatic tissue. Although 68-Ga PSMA PET/CT is a promising, highly sensitive and specific new modality for the detection of primary and metastatic prostate cancer, there are a growing number of reports on the presence of significant PSMA uptake in extra-prostatic benign and malign lesions. We report a case of a benign liver hemangioma with PSMA uptake on 68-Ga PSMA PET/CT. **Case Report:** A 70-year-old man with prostate ade-

nocarcinoma (Gleason Score: 3+4, PSA: 10 ng/ml) underwent 68-Ga PSMA PET/CT. He had undergone radiation therapy, and received hormonoteraphy 3 years ago. Follow-up Tc-99m MDP bone scintigraphy demonstrated mildy increased heterogen activity in the pelvic bones. 68-Ga PSMA PET/CT was performed for restaging because of abnormal bone scintigraphy. Heterogen mild activity uptake (SUVmax:4.8) in the prostate gland was seen on 68-Ga PSMA PET/CT but there was no foci of receptor positive metastatic disease in pelvic bones. 68-Ga PSMA PET/CT showed a PSMA-positive lesion in the liver (SUVmax: 16.3; 3 cm), which was not detectable in the corresponding low-dose CT. In order to evaluate PSMA-positive lesion in the liver, MRI was performed. Contrast-enhanced T1-weighted images showed homogenous enhancement in both arterial and portal phases. The portal phase showed no washout of the contrast medium. The findings were characteristic for benign liver hemangioma. **Discussion:** PSMA is highly expressed not only in prostate cancer, but also in the neovasculature of other neoplasms. In recent reports, high uptake of 68Ga-PSMA has been shown in various malignant lesions such as lymphoma, thyroid carcinoma, rectal carcinoma, renal cell carcinoma, gastrointestinal stromal tumour and also in some benign lesions such as adrenal adenoma, schwannoma, sarcoidosis, vertebral hemangioma, fracture, and subacut stroke. In the literature, there has been a single case report of PSMA-avid liver hemangioma on PET/CT. The bones and lymph nodes are the most common sites of extraprostatic tumor spread. Although liver metastasis from prostate cancer are not very rare, it is a late manifestation of systemic disease and most often occurs in patients after extensive therapy with hormone and/or chemotherapy. Isolated liver metastasis from prostate cancer is rare. **Conclusion:** Liver hemangioma should be kept in mind when interpreting 68-Ga PSMA PET/CT images in patients with PSMA-positive lesions in the liver and additional further diagnostic imaging is also necessary to separate liver metastasis from liver hemangioma.

EP-0668

The Value of ⁶⁸Ga-PSMA PET/CT in Biochemical Recurrence of Prostatic Carcinoma (Pca)

E. Abamor[1], T. Çakır[1], A. Çakır[2], A. Bilici[3], S. Güven[4], T. Atasever[1]; [1]Medipol Mega University Hospital, Department of Nuclear Medicine, ISTANBUL, TURKEY, [2]Medipol Mega University Hospital, Department of Pathology, ISTANBUL, TURKEY, [3]Medipol Mega University Hospital, Department of Oncology, ISTANBUL, TURKEY, [4]Medipol Mega University Hospital, Department of Urology, ISTANBUL, TURKEY.

Aim: To analyze lesion detectability of ⁶⁸Ga-PSMA PET/CT according to PSA values. **Materials and Method:** 76 patients (pt) with biochemical recurrence of Pca were evaluated with PSMA PET/CT, retrospectively. Gleason scores were between 6 to 10 (3pt GS-6, 30pt GS-7, 18pt GS-8, 20pt GS-9, 5pt GS-10). We analyzed patients in four groups according to PSA values (ng/ml): G-I (0-2; mean 1.03), G-II (2-10; mean 5.6), G-III (10-20; mean 14.6) and G-IV (mean >20). **Results:** Local recurrence was positive in 44 of 76 (57.8 %) and overall metastases were positive in 57 of 76 (75 %). Nineteen pt in G-I had overall metastases of 57.9% and local recurrence of 31.6%. Regional nodal metastases were positive in 36.8% and 5.8% in distant nodal stations. Bone metastases were detected in 26.3% and soft tissue metastases in 21%. Twenty one pt in G-II had overall metastases of 71.4% and local recurrence of 57.1%. Regional nodal metastases were positive in 42.8% and 19% in distant nodal stations. Bone metastases were detected in 57.1% and soft tissue metastases in 14.2%. Eleven patents in G-III had overall metastases of 91% and local recurrence of 63.6%. Regional nodal metastases were positive in 81.2 % and 18.2% in distant nodal stations. Bone metastases were detected in 72.7 % and soft tissue metastases in 27.3%. Twenty five patients in G-IV had overall metastases of 92% and local recurrence of 76%. Regional nodal metastases were positive in 76% and 25% in other nodal stations. Bone metastases were detected in 72% and soft tissue metastases in 28%. There was good correlation (r: 0.69 - 0.81) between rising PSA levels and overall metastatic disease detection, as well as primary recurrence, pelvic nodal metastases and bone metastases rates. No significant rate difference was observed in detecting distant nodal and soft tissue metastases between all groups. The detectable lesion rates of local recurrence, regional nodes and bone metastases, increased between G-I&G-II. Lesion detection rate was higher in G-III&G-IV, however there was no significant difference between them. **Conclusion:** PSMA PET/CT can be helpful in patients who has PSA recurrence under 2ng/ml with high risk factors. Lesion detection rates start to increase with PSA levels over 2ng/ml. Remarkable rates of local recurrence, regional nodes and bone metastases with PSA levels 2-10 ng/ml was observed. Highest lesion detection found over 10ng/ml but no significant difference was observed in detectability rates within patients having PSA recurrences over 10ng/ml.

EP-0669

Does delayed FDG PET/CT imaging improve diagnostic sensitivity in lymph node staging of muscle invasive bladder cancer?

A. Girard, Jr., S. Taconet, A. Girma, D. Vilain, M. Rouanne, C. Radulescu, E. Le Stanc, J. Grellier; Hôpital Foch, Suresnes, FRANCE.

Purpose/Introduction: Accurate lymph node (LN) staging is of major importance in the management of patients with muscle invasive bladder cancer (MIBC), in order to select those who could benefit from induction chemotherapy. The aim of this study is to evaluate the interest of delayed ¹⁸F-2-fluoro-2-deoxy-D-glucose (FDG)-PET/CT imaging to improve the sensitivity in pelvic LN staging of non-metastatic MIBC. **Subjects & Methods:** Here we present the preliminary results of a prospective study ongoing from May 2015 to May 2017 in which 120 patients are to be included. Patients were referred to our nuclear medicine department for initial staging of biopsy proven MIBC. For all patients, PET/CT images were acquired 60 minutes after FDG injection from vertex to thigh. Additional delayed images of the pelvis were acquired 120 minutes after FDG administration. Four experimented investigators blindly interpreted these images, two of them for each series. Comparison of diagnostic

performances for pelvic LN staging was based on three strategies: FDG-PET/CT images acquired 60 minutes after injection only (S1), FDG-PET/CT images acquired 120 minutes after injection only (S2), and delayed images only when there was no positive LN on the 60 minutes series (S3). Analyses were made by LN pelvic regions (left and right) and by patients. The gold-standard was the pathologic data after LN dissection. Sensitivities and specificities were compared using pairwise Mc Nemar test with Bonferroni alpha adjustment. **Results:** This preliminary analysis included 71 patients. Distant metastases were diagnosed in 15 (21.1%). LN dissections were performed in 98 pelvic regions from 49 patients. At least one metastatic LN was found in 21 (21.4%) regions from 15 (30.6%) patients. By regions, sensitivities and specificities were respectively 38.1 and 94.8% with S1, 66.7% and 89.6% with S2, and 71.4% and 89.6% with S3. By patients, sensitivities and specificities were respectively 53.3% and 94.1% with S1, 73.3% and 82.4% with S2, and 80.0% and 82.4% with S3. Sensitivity by regions with S3 was 33.3% higher than with S1 (p=0.016). The other differences between sensitivities or specificities were not statistically significant. **Discussion/Conclusion:** Despite the lack statistically significant difference in the by patients analysis with these preliminary results, we showed a statistically significant improvement of sensitivity in the by pelvic regions analysis with the dual-time strategy, with no significant loss of specificity. In common practice, delayed images could be performed to improve sensitivity when no positive LN is found on images obtained 60 minutes after FDG injection.

EP-0670

The influence of postdiuretic late phase imaging in visual and quantitative evaluation of uroepithelial tumors by F-18 FDG PET/CT

Z. Koç, P. Özcan Kara, E. Sezer; Mersin University Hospital, Mersin, TURKEY.

Aim: Although F-18 FDG PET/CT is a valuable imaging method in most of the malign tumors it has limited diagnostic ability in uroepithelial tumors due to high physiologic urine activity. The aim of this study is to evaluate the effect of postdiuretic late phase imaging to visual and quantitative evaluation of uroepithelial tumors. **Materials and Methods**: Two patients with ureter and 24 patients with bladder tumors who were referred for staging or restaging or treatment response evaluation were included in the study (3 F, 23E; mean:68±7.73 years old). Late phase (at second hour) images including renal pelvis and bladder region after administration of approximately 20 mg furosemide injection were obtained after standard oncologic F-18 FDG PET/CT imaging to the patients. Paired samples T test were used to decide the significance of difference between early and late phase images and p<0.05 considered significant. **Results:** The activity accumulation in primary or recurrent lesions in bladder or ureter were observed in 12 patients (early SUVmax=15.4±11.2 and late SUVmax=19±14.1; p=0.004), lymph node metastases in 13 patients (early SUVmax=7.8±4.9 and late SUVmax=10.7±6.6; p=0.004) and distant metastases included in late phase image field in 5 patients (early SUVmax=11±6.1

and late SUVmax=15.4±7.1; p=0.008). The difference between early and late phase images was statistically significant. Additionally in 7/26 patients (18%) the primary tumor in bladder was only determined in late phase images due to high background urine activity and additional lymph node metastases adjacent to bladder/ureter were observed in diuretic late phase images. **Conclusion:** Late phase imaging after diuretic administration must be implicated in case of non-visualization of primary tumor in bladder. Late phase diuretic imaging revealed significant influence in visual and quantitative evaluation of uroepithelial tumors. **Key Words:** uroepithelial, bladder, ureter, diuretic, PET.

EP-0671

Sarcoid-like reaction in prostate cancer patients assessed by 18-F-choline PET-CT

N. Eftychiou[1], M. Wong[1], J. Hunter[2], S. Dizdarevic[1,2]; [1]Brighton and Sussex University Hospitals, Brighton, UNITED KINGDOM, [2]Clinical Imaging Science Centre BSMS, Brighton, UNITED KINGDOM.

Purpose: 'Sarcoid-like' reaction in malignancy has been described in patients who had 18F-FDG-PET-CT scans. It is characterised by bilateral non-malignant uptake in hilar and mediastinal lymph nodes. The aim of this study is to assess the prevalence of 'sarcoid-like' reaction in prostate cancer patients undergoing 18F-choline PET-CT. **Method:** A total of 271 patients with prostate cancer underwent 289 PET-CT scans between 01/01/2014-20/04/2017. Forty-six patients demonstrated hilar and/or mediastinal uptake, 5 of which had a repeat PET-CT. Visual analysis was performed by two experienced reporters and 3 groups were specified according to the pattern of uptake: Group 1 (bilateral hilar and mediastinal nodal uptake reported as 'sarcoid-like' reaction), Group 2 (inflammatory/reactive hilar and/or mediastinal nodal uptake due to co-existing lung changes/infection) and Group 3 (different patterns of uptake reported as suspicious for malignancy). Maximum standardized uptake value (SUVmax) of the most avid intrathoracic node was obtained in all patients. **Results:** 'Sarcoid-like' reaction (Group 1) was reported in 34/271(12.5%) patients, (SUVmax range: 1.84 - 7.64; mean 4.16) and was confirmed either histologically/EBUS, by repeat imaging (PET-CT or CT) and biochemical (PSA) follow up or combination of above in 17/34(50%) patients. Thirteen of 34 are recent cases and clinically stable under clinical observation. No follow-up data in 4/34 patients. In Group 2 there were 6/271(2.2%) patients (SUVmax: range: 3.13 - 4.95; mean 4.3). In Group 3 there were 6/271(2.2%) patients (SUVmax range 2.88 -14.26; mean 6.44). This group included 2 patients with widespread intense nodal uptake (SUVmax: 5.88 and 8.52) and avid bone lesions; 1 patient with unilateral mediastinal (SUVmax: 14.26) and retroperitoneal uptake and 1 patient with one avid mediastinal (SUVmax: 3.94) and one groin node. There were 2 patients with widespread nodal uptake (SUVmax: 2.88 and 3.16) reported as suspicious for synchronous pathology e.g. lymphoproliferative disease. Thirty-four out of 46 (74%) patients with avid nodes were due to sarcoid-like reaction, while only 6/46 (13%) were due to malignancy. **Conclusion:** 'Sarcoid-like' reaction was identified in 12.5% of prostate cancer patients who

underwent 18F-choline-PET-CT and hence should be taken into consideration when reporting to avoid false-positive results. Majority of choline positive bilateral mediastinal/hilar lymph nodes were due to 'sarcoid-like reaction rather than malignancy. Pattern of uptake and coexisting disease elsewhere may help to differentiate benign from malignant mediastinal and hilar lymph nodal uptake. Highest SUV values were reported in malignant nodes, but SUVmax malignant threshold should be determined in larger prospective studies.

EP-0672

Early 68Ga-PSMA PET/CT imaging in assessment of prostate cancer and its impact on patient's management comparing to standard protocol

M. Beheshti[1], Z. Paymani[1,2], H. Geinitz[3], G. Broinger[4], D. Gehring[1], T. Leopoldseder[1], B. Gruy[1], W. Loidl[5], W. Langsteger[1]; [1]PET-CT Center Linz, St. Vincent's Hospital, Linz, AUSTRIA, [2]Research Center for Nuclear Medicine, Shariati Hospital, Tehran, IRAN, ISLAMIC REPUBLIC OF, [3]Radiation Oncology, St. Vincent's Hospital, Linz, AUSTRIA, [4]Clinical Pathology, St. Vincent's Hospital, Linz, AUSTRIA, [5]Urology, St. Vincent's Hospital, Linz, AUSTRIA.

Aim: This prospective study evaluated tumor characteristic on early (20 min. p.i.) 68Ga-PSMA-11 PET/CT acquisition vs. standard protocol and its impact on patient's management in staging or biochemical recurrent prostate cancer. Furthermore, we assessed its consequence on institutional workflow and cost of examination. **Methods:** Fifty prostate cancer patients (25 Staging, 25 biochemical recurrence) were enrolled in this study. All patients received an intravenous dose of 2.0 MBq/kg/bw 68Ga-PSMA-11 using HBED-CC-PSMA Cold Kit - ANMI, followed by an early (20 min. p.i.) semi-whole body and delayed (100 min. p.i.) abdominopelvic PET/CT imaging. A reference VOI was defined on bone, soft tissue, blood pool and prostate background to assess pattern of physiologic uptake in various tissues in both acquisition times. A 20% change in SUVmax was considered as the cut-off to present the pattern of tracer uptake between the two phases. Histopathology or clinical- or imaging follow-up were considered as the standard of truth. **Results:** Physiologic soft tissue and bone uptake in the reference regions showed significantly (p<0.001) increase in SUVmax (mean: 0.97±0.29 to 1.38±0.44 and 1.04±0.43 to 1.53±0.84, respectively) on delayed images while it was no significant (p=0.48) change in blood pool activity (1.92±0.52 to 1.83±0.94). In patient-based analysis, the clinical stage of the disease was not changed between early and standard delayed studies. In lesion-based analysis overall 157 lesions (49 prostate, 45 bone and 63 lymph nodes) were analyzed. There was significant (P<0.001) increasing pattern of SUVmax in suspicious prostate (11.21±8.2 to 14.51±10.85) and lymph nodes (9.72±5.9 to 12.34±8.8), while bone lesions show no significant increase (p=0.188) on delayed images (8.46±5.6 to 9.20±7). However, SUVmax value of suspicious lesions on early images was adequate to support the criteria for correct interpretation (mean SUV max 9.83±6.7). In 26/157 Lesions (13 bone, 4 prostate, 17 LN) a decreasing pattern of SUV was seen, mostly in subcentimetric lesions in patients with multiple metastases. However, decreasing pattern didn't affect the stage of the disease or

patient's management. **Conclusion** Early 68Ga-PSMA-11 PET/CT images seem to provide comparable findings to standard protocol without any appreciable effect on disease staging or patient's management. Additionally, it offers more flexibility in acquisition protocol allowing more examinations per single generator elution and cold kit consumption leading to better institutional time management and less cost.

EP-0673

18F-Choline PET/CT & functional parameters in treatment evaluation of patients with castration resistant prostate cancer submitted to Abiraterone: preliminary data

D. Pizzuto[1], S. Annunziata[1], D. Ripani[1], C. Altini[1], C. Caldarella[2], V. Rufini[1]; [1]Institute of Nuclear Medicine, Università Cattolica del S. Cuore "A. Gemelli", Rome, Roma, ITALY, [2]PET-CT Center, Policlinico "A. Gemelli", Rome, Roma, ITALY.

Introduction: Abiraterone is an irreversible inhibitor of androgen biosynthesis and showed to be useful in treating patients with castration resistant prostate cancer (CRPC). Radiolabeled choline PET/CT (Cho-PET) is currently used for staging, restaging and monitoring therapy in patients with prostate cancer. Aim of this study was to determine the role of 18F-Cho-PET (visual and semi-quantitative parameters) in assessing response to Abiraterone in CRPC patients. **Subjects & Methods:** CRPC patients undergoing Cho-PET at baseline (bPET) and six month after the beginning of treatment with Abiraterone (ePET) were retrospectively evaluated. PSA levels at baseline (bPSA) and during treatment (ePSA) were collected. Both qualitative and semi-quantitive analysis were performed, the latter by means of such parameters: SUVmax, SUVmean, functional-tumor-volume (FTV) and total-lesion-activity (TLA) of target-lesion, SUVmax of target lesion/SUVmean of spleen (splPET). Variations between bPET and ePET were assessed to classify treatment response according to EORTC: complete (eCR), partial response (ePR), stable (eSD) and progressive disease (ePD). Clinical, biochemical (PSA) and imaging (including Cho-PET) evaluations one year after the beginning of treatment were used as reference to assess the response to Abiraterone: patients were classified as with progressive (PD) or non-progressive disease (NPD). **Results:** Thirteen patients with CRPC submitted to bPET and ePET were considered. According to follow-up, seven patients had PD and six patients NPD. Total lesion number was 45 at bPET and 49 at ePET. Total lesion number increased in 4/7 PD patients and decreased or was unchanged in 6/6 NPD patients. Among PD patients, 5/7 showed new uptake sites at ePET, (bone involvement in three and distant lymph-node metastases in two patients). Functional parameter variations were not associated with PD nor NPD. Among PD patients, 6/7 showed ePD with > 50% increase in ePSA levels in 5 patients; among 6 NPD patients, two showed eCR, three ePR, one eSD, with > 50% decrease in ePSA levels in 5. **Conclusion:** From this preliminary study in a small series of patients, Cho-PET seems to be useful in monitoring patients during treatment with Abiraterone to predict eventual progressive disease. Moreover, Cho-PET response during therapy seems to be associated with eventual non-progressive disease. Variations of functional parameters seem to predict neither pro-

gressive disease, nor non-progressive disease, maybe due to new uptake sites in most PD patients. Further prospective studies are needed to assess the role of Cho-PET and functional parameters in monitoring therapy with Abiraterone.

EP-0674

Appropriateness of prescription of 18F-Choline PET/CT in 218 patients with prostate cancer

S. Chondrogiannis, M. C. Marzola, G. Grassetto, G. Borotto, E. Tommasi, L. Tamiso, A. M. Maffione, L. Pavan, L. Rampin, D. Rubello; Nuclear Medicine - PET/CT centre, Santa Maria della Misericordia Hospital of Rovigo, Rovigo, ITALY.

Aim: To evaluate the appropriateness of prescription of 18F-Choline PET/CT (18FCH) in 218 prostate cancer (PC) patients, in a single PET/CT centre. **Materials and Methods:** We have evaluated data of 218 consecutive patients with prostate cancer (mean age: 74 years; range: 56-91), who were referred to our centre to perform 18F-Choline PET/CT (mean PSA: 19.77 ng/ml; range: 0.01-525 ng/ml). As reference criteria to establish the appropriateness of the examination we used the indications for 18F-Choline PET/CT as proposed 1) by the guidelines on prostate cancer of the European Association of Urology (EAU) published on 2016, 2) by the guidelines on prostate cancer of the European Society of Medical Oncology (ESMO) published in 2015, 3) a recently published meta-analysis including 19 original papers on 18FCH PET/CT performed in a total of 1555 patients and the regional guidelines on prostate cancer (PDTA of Veneto region, Italy). In agreement with the previous mentioned documents 18F-Choline PET/CT was considered appropriate 1) in the staging of patients with intermediate or high risk PC; 2) in the restaging of patients with biochemical PC relapse with PSA>1 ng/ml or PSA<1 ng/ml associated to fast PSA kinetics (PSAvel >1 ng/mL/year e PSAdt <3 months) and 3) in monitoring systemic therapy with PSA elevation. **Results:** The overall Detection Rate (DR) of 18F-Choline PET/CT was 64% (139/218). In both univariate and multivariate logistic regression analysis, trigger PSA was significantly correlated to DR of 18FCH PET (p<0.05). Moreover, 61% of the patients (134/218) performed 18F-Choline PET/CT for restaging the disease (mean PSA 6.85 ng/ml, DR: 53%), 16% (35/218) for initial staging (mean PSA 36 ng/ml; DR: 97%) and 21% (46/218) for monitoring the systemic treatment (mean PSA 45.25 ng/ml, DR: 67%). The overall appropriateness of prescription of 18FCH PET/CT was 82% (180/218); in particular: 85% (115/134) in the restaging group, 82% (29/35) in the staging group and 82% (38/46) in the monitoring the systemic treatment group. **Conclusion:** In our centre the prescription of 18F-Choline PET/CT resulted appropriated in the 82% of the cases which can be considered a good reference. Guidelines of the nuclear medicine communities on Choline PET/CT have not yet been published and are mandatory in order to have precise indications and perform appropriate Choline PET/CT examinations that can help the management of prostate cancer patients.

EP-0675

68Ga-Psma Hbed Pet/Ct in the assessment of biochemical recurrence in radically treated prostate cancer patients

P. Caroli[1], M. Celli[1], R. Gunelli[2], V. Lanzetta[3], V. Di Iorio[3], A. Romeo[4], L. Fantini[1], M. Pancisi[1], A. Moretti[1], R. Galassi[1], T. Zenico[2], G. Paganelli[1], F. Matteucci[1]; [1]Nuclear Medicine Unit IRCCS IRST, Meldola, ITALY, [2]Urology Unit AVR, Forlì, ITALY, [3]Radiopharmacy Unit IRCCS IRST, Meldola, ITALY, [4]Radiotherapy Unit IRCCS IRST, Meldola, ITALY.

Introduction: The aim of our prospective study is to compare the diagnostic accuracy of 68Ga-PSMA PET/CT with the clinical standard 18F-FCH PET/CT to image the source of biochemical relapsing patients radically treated for prostate cancer (PCa) with negative/equivocal conventional imaging. **Subjects and Methods:** Starting from December 2015, we have enrolled 148 patients with biochemically recurrent Pca. Our cohort included patients with PCa with initial Gleason ranging from 6 to 10, initially treated with either radical prostatectomy (RP - 97 patients), or external beam radiotherapy (RT - 47 patients), or brachytherapy (BT - 4 patient). At enrollment, all patients had a serum PSA value > 0.2 ng/ml (PSA range: 0,2 - 12,8 ng/ml). All patients had a negative / equivocal restaging 18F-FCH PET/CT and had been off hormonal and radiation therapy for at least 6 months. 68Ga-HBED-CC-PSMA was prepared according to national regulations, good radiopharmaceutical practice (GRP) as outlined in EANM guidelines, using an Eazy® synthesis module (Eckert and Zieckert, Germany). PET/CT scan was performed from skull vertex to mid-thigh, 70 minutes after intravenous administration of body-weighted activity of 68Ga-PSMA (range 100-200 MBq 68Ga-PSMA). 68Ga-PSMA PET/CT scans were performed on a Biograph mCT Flow® (Siemens Healthineers, Erlangen Germany). Acquisition was made on Flow mode (0,7 mm/sec) in 3D mode. Results: 68Ga-PSMA PET/CT was positive in 106 patients (72%), equivocal in 6 patients (4%) and negative in 36 patients (24%). In particular, local uptake (prostate bed or prostate gland) was observed in 49/148 patients (33% of pts); 12 of these patients also showed nodal disease and in 7 more patients bone disease was revealed. Nodal uptake was described in the pelvis for 31/148 patients (21% of pts), while 9/148 patients (6% of pts) had retro-peritoneal uptake. In 5/148 patients (3% of pts) retro-peritoneal nodal and bone uptake co-existed; 10/148 patients (8% of pts) only showed bone uptake and in 2/148 (1%) pts lung focal uptake was found. For PSA ranges of 0.2 - 1 ng/mL, 68Ga-PSMA PET/TC resulted positive in 36/64 patients (positivity rate=56%). For PSA levels >1 ng/ml 68Ga-PSMA PET/CT resulted positive in 72/148 patients (positivity rate=48%). **Conclusion:** Our ongoing experience confirms 68Ga-PSMA PET/CT as a highly sensitive and accurate restaging tool in biochemically-relapsing prostate cancer with negative or equivocal conventional imaging also for PSA < 1.0 ng/ml. Confirmation of these results will prompt clinical validation of 68Ga-PSMA PET/CT, potentially granting earlier detection of clinical recurrence, improving patient care and prognosis.

EP-0676

The Role of 68Ga-PSMA PET/CT in Newly Diagnosed Primary Prostatic Carcinoma (Pca)

E. Abamor[1], T. Çakır[1], A. Çakır[2], A. Bilici[3], S. Güven[4], T. Atasever[1]; [1]Medipol Mega University Hospital, Department of Nuclear

Medicine, ISTANBUL, TURKEY, ²Medipol Mega University Hospital, Department of Pathology, ISTANBUL, TURKEY, ³Medipol Mega University Hospital, Department of Oncology, ISTANBUL, TURKEY, ⁴Medipol Mega University Hospital, Department of Urology, ISTANBUL, TURKEY.

Aim: 68Ga-PSMA PET/CT is a suggestive tool in recurrent Pca. We aimed to evaluate the role of 68Ga-PSMA PET/CT in primary Pca for detecting primary tumour and metastatic spread. **Materials and Method:** 62 patients (pt) (mean age: 67,5) of newly diagnosed Pca were evaluated by PSMA PET/CT, retrospectively. Gleason scores (GS) were between 6 to 10 (3pt GS-6, 23pt GS-7, 13pt GS-8, 20pt GS-9, 3pt GS-10). PSA values were between 1,5 - 600 (mean 93,3). All patients also had radiological and clinical risk factors. PSMA uptake over vascular bed was accepted as positive. **Results:** Primary tumour PSMA uptake was positive in 58 of 62 pt (93.5 %) and overall metastases were positive in 31 of 62 pt (50%). Primary tumour was PSMA negative in 2 and suspicious in 2 pt. Overall lymph nodes metastases were detected in 44%. Only pelvic nodal metastases were positive in 10% of pt and both pelvic-distant nodal metastases were positive in 34%. Bone metastases were detected in 40,3% and distant organ (pulmonary or liver) metastases in only 6.4%. Bone and lymph nodes metastases were found together in 33,8 of pt. Local tumour invasion was also detected in 12 pt (19,4%) which were in seminal vesicle region (11,3%), through urinary bladder (6,4%) and in penil root (1,6%). There was moderate correlation between overall metastases - PSA values (r:0,38) and relatively low correlation (r:0,29) between overall metastases - GS. Moderate correlation between nodal metastases - PSA values (r:0,39) and GS (r:0,40) was observed. Correlation between bone metastases - PSA values (r:0,48) was higher than correlation between bone metastases - GS (r:0,35). **Conclusion:** Although there was moderate correlation rates between metastatic findings and PSA values-GS; PSMA PET/CT detected metastatic disease in considerable extent. PSMA PET/CT detected overall metastases in about one-half of pt with primary Pca while only 10% of pt had intrapelvic disease. Distant organ metastases rate was low at diagnosis but distant nodal metastases and bone metastases rates were higher, respectively (between 30-45%). Primary tumour was detected with or without local invasion nearly all pt. Local invasion was also observed in nearly 20% percent of pt. Our findings show that PSMA PET/CT has a suggestive value for staging and theraphy planning in primary Pca pt.

EP-0677

Extracting more information from ⁶⁸Ga-PSMA-11 PET/CT performed for primary staging of prostate cancer

*O. Sahin¹, E. Kaymak Akgun¹, **E. Demirci²**, M. Ocak³, A. Aygün¹, H. Pehlivanoglu¹, E. Karayel¹, A. Kural⁴, L. Kabasakal¹; ¹Department of Nuclear Medicine, Cerrahpasa Medical Faculty, Istanbul University, istanbul, TURKEY, ²Department of Nuclear Medicine Sisli Etfal Training and Research Hospital, Istanbul, istanbul, TURKEY, ³Department of Pharmaceutical Technology, Pharmacy Faculty, Istanbul University, Istanbul, istanbul, TURKEY, ⁴Department of Urology, Acibadem University, istanbul, TURKEY.*

Aim: Current morphological imaging techniques have limited sensitivity to detect lymph node metastasis in prostate cancer. 68Ga-PSMA-11 PET/CT can be added to staging protocol of intermediate to high risk prostate cancer (PCa) to assess mainly lymph node metastasis. However, 68Ga-PSMA-11 uptake of the primary tumour may provide additional information that can help clinical decisions. In our study, we investigate correlation between 68Ga-PSMA-11 uptake in the primary tumour and other clinical factors. **Materials and Methods:** 32 patients with PCa who underwent 68Ga-PSMA-11 PET/CT before radical prostatectomy (PR) during period of 2015-2016 included in this retrospective study. PET images evaluated semi-quantitatively and correlation between the uptake of primary tumor and histopatological parameters were investigated. **Results:** Average dose of 68Ga-PSMA-11 was 229.6±66.3 MBq. According to RP results, PCa with gleason score (GS) of 6,7,8 and 9 were detected in %9.4 (n=3), %62.5 (n=20), %15.6 (n=5) and %12.5 n=4, respectively. SUVmax values of primary tumours, with an overall average of 9.5±9.6, are correlated with GS and calculated 4±0.6, 7.6±5.22, 7.7±2.3 and 25.1±19.96 for GS scores of 6,7,8 and 9, respectively (p<0.005). Pearson correlation coefficient between SUVmax of primary tumor (PT) and PSA levels, primary, secondary, combined gleason scores were 0.64, 0.29, 0.46 and 0.54 (p:<0.0005, 0.105, 0.009 and 0.001 respectively). Upstaging from prostate biopsy to radical prostatectomy was observed in 18.8% (n=6) of patients and due to low sample size no further statistics were performed. According to binary logistic regression analysis SUVmax values of PT is a predictor of lymph node metastasis (p<0,05). **Conclusion:** PSA levels and GS, secondary and combined, are correlated with uptake of 68Ga-PSMA-11 in primary tumors of PCa. Additionally, SUVmax values of PT may predict presence of lymph node metastasis.

EP-0678

Role of [¹⁸F]Choline PET/CT guided stereotactic body radiotherapy in patients with oligometastatic prostate cancer

R. Boni¹, A. Marciano², R. Zanca², M. Sollini³, E. Notini⁴, D. Baldaccini⁴, F. Matteucci⁴, P. Cocuzza⁴, P. Ferrazza⁴, G. Coraggio⁴, F. Paiar⁴, G. Pasqualetti⁵, L. Galli⁶, L. Mannelli⁷, F. Pasqualetti⁴, P. Erba²; ¹ASST Papa Giovanni XXIII-Nuclear Medicine, Bergamo, ITALY, ²Nuclear Medicine, Department of Translational Research and New Technologies in Medicine, Pisa, ITALY, ³Humanitas University, Milan, ITALY, ⁴Radiation Oncology, AOUP, Pisa, ITALY, ⁵Geriatric Unit, University of Pisa, Pisa, ITALY, ⁶Medical Oncology, AOUP, Pisa, ITALY, ⁷Radiology, Memorial Sloan-Kettering Cancer Center, New York, NY, UNITED STATES OF AMERICA.

Purpose/Introduction: in an attempt to achieve a PSA control, patients with oligometastatic disease could eventually be managed by treating all the active lesions revealed by [18F]Choline ([18F]FMCH) PET/CT with local therapy, either surgery or ablative stereotactic body radiotherapy (SBRT). This study aims to assess in a prospective manner the impact of [18F]Choline ([18F]FMCH) PET/CT guided SBRT in patients with oligometastatic PCa. **Subjects & Methods:** Between May 2011 and December

2016, 53 patients with oligometastatic PCa (defined as ≤3 synchronous active lesions detected with [18F]FMCHPET/CT) out of 98 patients with biochemical relapse of PCa were enrolled in the present prospective clinical trial. All patients were treated with salvage SBRT until the occurrence of a multimetastatic disease (>3 active synchronous metastases). Primary endpoint analyzed was the length between the baseline PET/CT and the beginning of systemic therapy. **Results:** A total of 85 lesions were treated with SBRT. After a median follow-up of 20.3 months, 32 pts started systemic therapy after 39.7 months from the first PET/CT whereas 23 did not. Toxicity related to SBRT greater than G2 where not recorded. Results of semiquantitative parameters and texture features analysis are under evaluation. **Discussion/ Conclusion**. Salvage [18F]FMCHPET/CT-guided SBRT is feasible, well tolerated and succeeded in deferring the initiation of systemic therapy in selected patients with oligometastatic PCa.

EP-0679

Castration-Resistant Prostate Cancer Patterns of Metastasis Evaluated by 68Ga-PSMA PET/CT

M. Silva[1], R. Silva[1,2], P. Lapa[1,3], G. Costa[1,3], J. Pedroso de Lima[1,2,3]; [1]Centro Hospitalar da Universidade de Coimbra, Coimbra, PORTUGAL, [2]Instituto das Ciências Nucleares Aplicadas à Saúde (ICNAS), Coimbra, PORTUGAL, [3]Faculdade de Medicina da Universidade de Coimbra, Coimbra, PORTUGAL.

Aim: Prostate cancer (PCa) is the most frequently diagnosed cancer and the second leading cause of cancer related death in men. Although most patients with localized disease may be cured with interventional therapies, approximately 10-20% develop castration-resistant prostate cancer (CRPC) within 5 years of follow-up. CRPC is defined as biochemical or radiological progression with castrate serum testosterone levels and it's associated with frequent metastases, poor quality of life and low survival rates. It's usually thought that the skeleton is the most common metastatic site, followed by soft tissue metastases, mainly the lymph nodes. 68Ga-PSMA PET/CT is a promising new imaging technique in PCa, with high diagnostic accuracy. With this study, we aimed to evaluate the CRPC patterns of metastasis, as assessed by 68Ga-PSMA PET/CT. **Methods:** All CRPC patients who performed 68Ga-PSMA PET/CT where retrospectively selected. All relevant and available data was recorded. Patterns of metastasis were defined according to the 68Ga-PSMA PET/CT clinical reports. Due to the clinical context, histopathologic findings were not available. Lymph node metastasis were considered either regional or distant, according to AJCC 7th edition manual. The small axis diameter of the largest lymph node metastasis was recorded. Also, the SUVmax of the highest intensity lymph node and bone metastasis was recorded. **Results:** A total of 26 CRPC patients (72.2±7.0years; average PSA:11.0±7.6ng/mL; median Gleason:7, 1Q:6,3Q:8.25) were selected. Baseline PSA level, PSA velocity and PSA doubling time were not available. Regional and distant lymph node metastasis were detected in 10/26 (38.5%) and 12/26(46.2%) patients, respectively. Overall, lymph node metastasis were diagnosed in 16/26(61.5%) patients (average SUVmax:20.2±17.8, 1.8-63.5g/mL). Also, a significant percentage of patients presented with infra/pericentimetric small axis lymph node metastasis (15.1±9.8mm, 7-45mm, 43.8%≤10mm), which could go undetected in conventional imaging techniques. Bone metastasis were detected in 11/26(42.3%) patients (average SUVmax:34.8±29.5, 5.8-87.0). Nine patients presented with lymph nodes metastasis without bone metastasis (2 regional, 4 distant and 3 both regional and distant lymph nodes), and 4 patients only had bone lesions. **Conclusion:** In our sample lymph, node metastasis not only were more frequent than expected, they were more common than bone metastasis. Also, in a significant percentage of patients, lymph node involvement could go undetected in conventional imaging techniques, due to their small size. These results underline the need for more accurate and reliable imaging techniques, particularly for the detection of lymph node involvement, so appropriate patient management decisions can be made early in this disease stage.

EP-48   **during congress opening hours, e-Poster Area**

Clinical Oncology: Gynaecological

EP-0680

Can We Predict the Sites of the Recurrence of Tuba-Ovarian Cancer by F18-FDG PET/CT Depending on CA-125 Level?

E. Ciftci[1], B. Turgut[1], S. Erturk[1], Z. Hasbek[1], B. Cetin[2], H. Aker[3]; [1]Cumhuriyet University, School Of Medicine, Department Of Nuclear Medicine, Sivas, TURKEY, [2]Recep Tayyip Erdogan University, School Of Medicine, Department Of Internal Medicine, Division Of Oncology, Rize, TURKEY, [3]cumhuriyet University, School Of Medicine, Department Of Pathology, Sivas, TURKEY.

Purpose: The purpose of the present study is to predict the sites of the recurrence with PET/CT by CA-125 level and to detect the cut off value of CA-125 for metastatic tuba-ovarian cancer (TOC) in comparison with F-18 fluorodeoxyglucose (FDG) positron emission tomography (PET)/computed tomography (CT) examination in patients with suspicion of recurrent TOC. **Subjects and Methods:** 39 patients with histologically proven stage III-IV TOC and 59 18F-FDG PET/CT studies referred for suspicion of relapsing of TOC at the time of rising in CA-125 level and that of normal CA-125 with suspicious imaging findings were studied. Each positive PET/CT image was assessed as positive or negative in 4 categories based on similar location as (I) local recurrence, (II) peritoneal metastasis, (III) lymph node metastases and (IV) distant metastases. Patients were divided into five groups according to the levels of CA-125. The results of PET/CT imaging were compared with the level of CA-125. Clinical and imaging follow-up were taken as gold standard. **Results:** Recurrence was confirmed in all FDG-PET/CT studies. In 7 of them (%11.9) CA-125 levels were normal (mean:18.9 ±5.9) whereas in 52 of them (88%) CA-125 levels were high (mean: 433.9 ± 798.3). Moderate but highly significant positive correlation between CA-125 level and the number of metastatic foci detected by PET/CT.

There is no statistically significant difference in between CA-125 level subgroups and metastatic sites. However, the difference between CA-125 levels and location of metastasis is statistically significant only for distant metastasis and peritoneal metastasis with moderate accuracy (71% and %66, respectively). **Conclusion:** CA-125 has an important clinical impact on the management of TOC patients with moderate but highly significant positive correlation with the number of metastatic foci, however it may not predict the localization of the recurrence. When suspicious findings were reported at morphologic imaging techniques in TOC patients, FDG-PET is a useful technique for detecting recurrent ovarian carcer regardless of CA-125 level.

EP-0681
Differential between ovarian tumor with solid portions and Stage I malignant ovarian cancer by FDG PET/CT

R. Nakamoto, Y. Nakamoto, T. Ishimori, A. Kido, K. Togashi; Kyoto University Hospital, Kyoto, JAPAN.

Objectives: Preoperative diagnosis of borderline ovarian tumors (BOTs) is important, because limited resection and fertility-sparing surgery could be selected. The SUVmax of FDG-PET/CT is thought to be useful to differentiate malignant ovarian tumors (MOTs) from BOTs. However, BOTs with high FDG uptake are sometimes experienced in everyday clinical practice. The purpose of this study was to evaluate the diagnostic performance of FDG PET/CT to differentiate Stage I BOTs with solid portions from Stage I MOTs. **Materials and Methods:** We retrospectively reviewed preoperative FDG-PET/CT images of 30 patients who had pathologically proven ovarian tumors of either early stage MOTs (FIGO stage I) or BOTs. The enrolled patients were divided into two groups; the BOT group (n=16) or the MOT group (n=14). We assessed five quantitative parameters (SUVmax, SUVpeak, SUVmean, MTV and TLG) in order to differentiate between BOTs and MOTs. **Results:** Based on histopathological results, there were seromucinous borderline tumors (n=7), endometrioid borderline tumors (EBT) (n=4), granulosa cell tumor (n=2), serous borderline tumors (n=2), and mucinous borderline tumor (n=1) in BOT, and clear cell carcinomas (n=8), endometrioid cancers (n=5), and a malignant mixed Müllerian tumor (n=1) in MOT. The SUVmax, SUVpeak, and SUVmean in the BOT group were significantly lower than those in the MOT group (SUVmax: 7.2±9.1 vs 8.7±3.1, SUVpeak: 5.6±7.1 vs 6.6±2.8, and SUVmean: 4.5±5.8 vs 4.8±2.0). On the other hand, there was no significant difference between the two groups in both MTV and TLG. When comparing 8 BOTs that had been suspected to be malignant by MR and 14 MOTs, no significant difference of SUVmax was observed between the two groups. All EBTs had been suspected malignancy by MR, and there was no difference of SUVmax(peak, mean) between EBTs and endometrioid cancers. **Conclusion:** Our preliminary data indicate that FDG-PET/CT had a limited clinical value for differentiating MOTs from BOTs.

EP-0683
Incidence and clinical Significance of Neck Node metastasis in Patients With cervix malignant lesion

S. Yoon; Women's Cancer Center, Cheil General Hospital, Dankook University College of Medicine, Seoul, KOREA, REPUBLIC OF.

Objective: Cervix cancer is usually localized disease compared with other ovarian/endometrial malignant lesion with systemic disease. Usually distant node metastasis is rare in the gynecologic malignancy, We performed F-18 FDG PET/CT for staging and evaluation of metastasis in 3440 patients with cervix malignant lesion. Therefore we evaluated the incidence and imaging characteristics in case of neck node metastasis using F-18 fluorodeoxyglucose positron emission tomography (FDG-PET) in the patients with the cervix cancer patients. **Material and Method**: Material and method: Between 2009 and 2016, we retrospectively analyzed PET/CT scans with pathological-proven gynecologic malignancies including cervix cancer (3440 patients). Neck node metastases were proved by sono guided biopsy of the neck nodes or clinical follow up. We compared the tumor marker according to the multiplicity of FDG uptakes outside of the neck and only single uptake in the neck. **Results**: Incidence of metastatic cervical neck node metastasis in 3440 patients with cervix malignancy was 24 patients (0.7%). Fourteen patents (28%) among 24 patients were confirmed clinically due to extensive lesions in chest, abdomen and pelvis. 22 patients were further studied due to only single neck node uptake outside abdomen/pelvis. Among 22 patients performed pathologic aspiration of node for evaluation of metastasis, 10 patients (45%) were pathologically confirmed as metastatic nodes including one metastatic papillary carcinoma from thyroid carcinoma and remaining 12 patients (55%) were no malignant cell or benign reactive node. Tumor marker of 4 patients (44%) among 9 patients with only single node uptake and metastasis from cervix cancer in the neck node were within normal range. **Conclusions**: We found that the incidence of neck node metastases in the cervix cancer was very low (0.7%). Four patients with single neck node metastasis showed normal tumor marker in spite of node metastasis. Neck node uptake on PET/CT could be due to metastatic node and benign reactive nodes. Therefore, we should rule out the neck node metastasis in case of neck node uptake above diaphragm on the PET/CT even though very lower incidence of neck node metastasis and normal tumor marker in cervix cancer.

EP-0684
Comparison of Diagnostic Value of PET/CT and Ca-125 Assay in Detection of Residual and Recurrent Tumor in Follow-up Ovarian Cancer

G. Çekin[1], I. Bezircioğlu[2], S. Yiğit[3]; [1]İzmir Katip Çelebi University, Atatürk Training and Reseach Hospital, Nuclear Medicine Department, Izmir, TURKEY, [2]Izmir University of Economics, Medical Faculty, Obstetric and Gynecology Department, Izmir, TURKEY, [3]İzmir Katip Çelebi University, Atatürk Training and Research Hospital, Pathology Department, Izmir, TURKEY.

Purpose: The purpose of our retrospective study was to compare the efficacy of ^{18}F-FDG PET/CT and serum Ca-125 levels in the early detection of residual/recurrent disease during the

follow-up period of patients with ovarian cancer. **Material and Methods:** 42 patients with histologically proven ovarian cancer were included in the study. All patients completed their treatment which included surgery and adjuvant chemotherapy. During the follow-up period, the patients with the clinical or radiological suspicions or elevated Ca-125 levels were evaluated by ^{18}F-FDG PET/CT. Total 49 ^{18}F-FDG PET/CT imaging were performed in 42 patients. The mean age of our patients was 58.2 ± 9.8 years. The tumor histopathology was derived from epithelial origin in 39 (92.8%) patients and non-epithelial origin in 3 (7.2%) patients. Detailed Ca-125 levels of patients are shown in Table 1. Increased ^{18}F-FDG uptake according to physiological distribution was considered as positive for tumor tissue after being correlated with abnormal findings on CT. ^{18}F-FDG PET/CT imaging results and Ca-125 levels at the time of imaging were compared to histopathological diagnosis after biopsy or surgical procedures that followed imaging. **Results:** Residual/recurrent disease was diagnosed histopathologically in 43 of 49 (87.7%) PET/CT scans. PET/CT scan was positive in all residual/recurrent disease except one. Lymph nodes were the most frequent site of metastasis place. The involvement areas were abdominal-pelvic lymph nodes in 33 (67.3%), peritoneal involvement in 23 (46.9%), thoracic lymph nodes in 6 (12.2%), cervical lymph nodes in 2 (8.1%), lung in 1 (2%), liver in 2 (4.1%) and primary tumor areas in 12 (24.4%) PET/CT scans. When evaluated according to histopathological diagnosis, 3 true negative, 1 false negative and 3 false positive results in PET/CT, 5 true negative, 26 true positive, 1 false positive and 17 false negative results in Ca-125 were obtained. Overall sensitivity, specificity and accuracy of PET/CT were 97.6%, 50%, 91.8%, respectively, whereas those of Ca-125 were 60.4%, 83.3%, 63.2%, for the detection of residual/recurrent disease in the patients with ovarian cancer. **Conclusion:** Compared to Ca-125, ^{18}F-FDG PET/CT has been found more efficient in detecting recurrence after the treatment of ovarian cancer. PET/CT imaging, which demonstrates the patient's tumor burden and anatomical/metabolic characteristics of the lesions with high accuracy and sensitivity, has been found as a valuable modality for detecting residual/recurrent disease in ovarian cancer patients. Key words: Ovarian cancer, residue, recurrence, PET/CT, Ca-125.

EP-0685

Effect of XbaI G > T Polymorphism of the Glucose Transporter 1 Gene on F 18 FDG Uptake in Gynecological Cancers

O. Yaylali[1], A. Koseler[2], D. K. Sakarya[3], D. Yuksel[1], T. Sengoz[1], V. Fenkci[3]; [1]Pamukkale University Dept of Nuclear Medicine, Denizli, TURKEY, [2]Pamukkale University Dept of Biophysics, Denizli, TURKEY, [3]Pamukkale University Dept of Gynecology, Denizli, TURKEY.

Introduction: PET/CT usingtheglucose analog F-18 FDG provides an opportunity to gain both anatomic and metabolic information about a tumor. Because of the capability of rapidly growing cancer cells to increase glucose metabolism, F-18 FDG accumulates within tumor cells. The standardized uptake value (SUV) was determined in tumor tissue as a measure of F-18 FDG uptake using a region-of-interest technique and correcting for body weight. After the transportation of F-18 FDG via glucose transport proteins (GLUT) have been accumulated in related tissue. Most malignancies overexpress GLUT family members, especially, the GLUT1 are most frequently overexpressed in cancer cells. Single-nucleotide polymorphisms (SNPs) are variations of the DNA sequence occurring when a single nucleotide of the genome differs between members of a species.This SPNs may influence dominantly gene expressions and the protein functions. The possible functional influence of GLUT1—XbaI G&gtT (rs2754218) on F-18 FDG uptake has not been investigated in gynecological cancers. We aimed to investigate the effect of GLUT1—XbaI G&gt T (rs2754218) polimorfism in the GLUT1 gene to the uptake of 18F-FDG in gynecological cancers. **Material and Methods:** In 13 individuals with gynecological cancer, a diagnostic PET/CT scan was obtained, and the SUVmax was determined as a measure of F-18 FDG uptake. And also, probable accompanying metastatic foci and their SUVmax values were investigated. The blood samples were taken just before PET/CT examination. Genomic DNA was isolated from peripheral blood samples. The GLUT1—XbaI G&gtT (rs2754218)polymorphism were determined,and than its effect to the uptake of F-18 FDG investigated in gynecological cancer patients. **Results:** The mean SUVmax value was 11.54±7.73 for our 13 patients (mean age; 54.61±15.39). There were no metastases in 9/13 patients. Metastases were present in 4/13 patients.GLUT1—XbaI G&gtT was absent in 3 patients and the SUVmax values were 24.30, 25.22 ve 19.37, respectively. GLUT1—XbaI G&gtT was positive in 10 patients and the minimum SUVmax value was < 2.50, the maximum SUVmax value was 13.70. **Conclusion:** Our investigation as a preliminary study continues and it's early to express how is the effect DNA GLUT1—XbaI G&gtT (rs2754218) polymorphism in the GLUT1 gene to the uptake of F-18 FDG in gynecological cancers. When our work is completed we will evaluated the relationship between the DNA GLUT1—XbaI G&gtT (rs2754218) polymorphism and the uptake of F-18 FDG in gynecological cancers and we will report to the literature whether its contribution as a prognostic factor.

EP-0686

[18]FDG PET with Low Dose CT versus Contrast Enhanced CT in the Detection of Recurrent or Residual Tumor in Ovarian Cancer

A. Repetto[1], N. Orta[1], C. Sampol[2], S. Rubí[2], M. Oporto[1], H. Navalón[1], M. Toscano[1], C. Peña[2]; [1]Hospital Universitari Son Espases, Palma, SPAIN, [2]Hospital Universitari Son Espases/IdISPa, Palma, SPAIN.

Aim: The aim of the study was to compare [18]FDG PET with low dose CT ([18]FDG PET-CT) versus Contrast Enhanced CT (CE-CT) in the detection of recurrent or residual tumor in ovarian cancer. **Materials and Methods:** Retrospective study from February 2012 to November 2016 of patients previously diagnosed of ovarian cancer and remitted for the detection of recurrent or residual tumor with [18]FDG PET-CT (Discovery™ PET/CT 600, GE). Each patient had a previous CE-CT study. We analyzed demographic/clinical data and image findings. The findings were

divided into 4 categories following TNM-FIGO classification of 2013 (pelvic, peritoneum, retroperitoneal lymph-nodes, distant metastasis). The final diagnosis was based on histopathology results or follow-up data (image and/or clinical data). **Results:** 66 [18]FDG PET-CT and CE-CT studies were performed in 48 patients, mean age of 58 years old with ovarian cancer disease. At the diagnosis the most frequent histological subtype was serous carcinoma (80.3%), stage IIIC (69.2%), high grade (83.3%).71.2% of patients were referred for suspicion of recurrent disease by clinical data (2.1%), by image (40.4%), tumor marker (27.7%) or a mixture of them (29.8%). 28.8% of patients were referred for monitoring the response to treatment.[18]FDG PET-CT and CE-CT had coincident findings in 42.4% (29.6% in pelvis and peritoneum respectively, 22.2% in distant metastasis and 18.5% in retroperitoneal lymph-nodes). [18]FDG PET-CT detected more findings in 43.9% studies (31.9% in retroperitoneal lymph-nodes, 27.8% in peritoneum, 26.4% in distant metastasis, 13.9% in pelvis), which were all true positive findings.CE-CT detected more findings in 13.6%, most of them were distant metastasis, of which only one third were true positive.[18]FDG PET-CT had a sensitivity of 94.6%, specificity of 70.0%, PPV of 94.6% and a NPV of 70.0%.CE-CT had a sensitivity of 85.7%, specificity of 10.0%, PPV of 84.2% and a NPV of 11.1%. **Conclusions:** [18]FDG PET with low-dose CT has a higher sensitivity and PPV compared to CE-CT. The increased sensitivity of [18]FDG PET-CT is overall due to detection of disease in retroperitoneal lymph-nodes. The values of specificity and NPV may be not reliable due to the sample number.

EP-0687

The role of PET/CT in the detection of residual/recurrent tumor in patients with ovarian cancer whose Ca-125 value is within normal limits

G. Cekin[1], I. Bezircioglu[2], S. Yiğit[3]; [1]İzmir Katip Celebi University, Atatürk Training and Research Hospital, Nuclear Medicine Department, Izmir, TURKEY, [2]Izmir University of Economics, Medical Faculty, Obstetric and Gynecology Department, Izmir, TURKEY, [3]İzmir Katip Celebi University, Atatürk Training and Research Hospital, Pathology Department, Izmir, TURKEY.

Purpose: The purpose of our retrospective study was to investigate the efficacy of 18F-FDG PET/CT in the detection of residual/recurrent tissue in the follow-up of patients with ovarian cancer whose serum Ca-125 level is within normal limits. **Materials and Methods**: 18 patients with histologically proven ovarian cancer were included in the study. All patients completed their treatment which included surgery and/or adjuvant chemotherapy. The study group consisted of follow-up patients who underwent PET/CT imaging either after clinical suspicion or abnormal radiological imaging findings. Total 22 18F-FDG PET/CT imaging were performed in 18 patients. The mean age of the patients was 57.7 ± 9.4. The tumor histopathology was derived from epithelial origin in 15 (83.3%) and non-epithelial origin in 3 (16.7%) patients. Increased 18F-FDG uptake according to physiological involvement was assessed as positive for tumor tissue after being correlated with abnormal finding in CT. 18F-FDG PET/CT imaging results were compared with histopathological diagnosis after biopsy or surgical procedures following imaging. **Results:** Residual/recurrent disease was diagnosed histopathologically in 17 of 22 PET/CT scans. PET/CT showed positive finding in all residual/recurrence disease except one. The most common metastasis places in PET/CT imaging were the lymph nodes. The involvement areas were abdominal-pelvic lymph nodes in 12 (54.5%), thoracic lymph nodes in 2 (9%), cervical lymph node in 2 (9%), peritoneal involvement in 7 (31.8%), liver in 3 (13.6%) and primary tumor areas in 4 (18.1%) PET/CT imaging. The values of mean SUV max±standard deviation were calculated 9.2 ± 4.8 in abdominal-pelvic lymph nodes, 5.8 ± 4.1 in thoracic lymph nodes, 4.9 ± 2.9 in cervical lymph nodes, 12.7 ± 5.9 in peritoneal involvement areas and 6.0 ± 1.7 in primary tumor areas. When evaluated according to histopathological diagnosis, 16 true positive, 2 true negative, 1 false negative and 3 false positive results were obtained in PET/CT. Sensitivity, specificity, positive predictive value, negative predictive value and accuracy rate for PET/CT were 96.3%, 40%, 84.2%, 66.6%, and 81.8% respectively for the detection of residual/recurrent tissue in the patients with ovarian cancer. **Conclusion:** FDG-PET/CT imaging, which demonstrates the patient's tumor burden and anatomical/metabolic characteristics of the lesions with high accuracy and sensitivity, which helps the clinicians in diagnosis and treatment planning is a valuable tool in detection of residual/recurrent disease in follow-up ovarian cancer patients with normal Ca-125 level. Key words: Ovarian cancer; residual/recurrent tumor; PET/CT; normal tumor markers.

Clinical Oncology: Lymphoma

EP-0688

Prognostic value of metabolic criteria with 18F-FDG PET / CT in patients with follicular lymphoma

M. Cozar Santiago[1], J. Garcia Garzon[2], M. Soler Peter[2], C. Igua Saenz[1], R. Sanz LLorens[1], R. Sanchez Jurado[1], J. Aguilar Barrios[1], V. Faus Rodrigo[1], E. Riera Gil[1], J. Ferrer Rebolleda[1]; [1]ERESA-General Universitary Hospital, Valencia, SPAIN, [2]CETIR-PET Unit, Esplugues, SPAIN.

Aim: To evaluate the prognostic value of the different metabolic criteria in the 18F-FDG PET/CT baseline and interim study in patients with follicular lymphoma **Material and Methods:** 36 patients (20 women / 16 men, age 59.97 ± 13.3) who underwent three 18F-FDG PET/CT studies: at baseline, after 2-4 cycles of chemotherapy (interim) and at the end of treatment. The variables Total Glycolysis Tumor (TGT) and Tumor Metabolic Volume (TMV) of the lesion with higher uptake in the baseline 18F-FDG PET/CT (TGT1, TMV1), in the interim study (TGT2, TMV2) and the reduction between both (%ΔTGT and %ΔTMV) using the MIMvista® software (PET-edge tool). The ROC curves are obtained to determine the optimal cut-off of parameters to predict response. A 40-month follow-up is performed with 18F-FDG PET/CT at the end of treatment, clinical follow-up, analytical and by

imaging techniques, according to medical criteria. **Results:** In the initial ^{18}F-FDG PET/CT study we obtained significantly different values in patients with relapse during follow-up of those who remained disease free: TGT1 (418.13 vs 342.23) and TMV1 (51.56 vs 71.35). Taking the 305 cut-off point for TGT1 and 54 for TMV1, survival rates with statistical significance (Log Rank, p = 0.029, p = 0.01) were obtained. In the interim study we obtained 26 ^{18}F-FDG PET/CT negative and 10 positive. The values obtained in patients with relapse and those who remain disease free were TGT2 (29.29 vs 10.8) and TMV2 (14.25 vs 6.48). The percentages of TGT and TMV reduction were calculated: %ΔTGT (88.61 vs 85.57) and %ΔTMV (88.37 vs 68.55). Taking as a cut-off point 81.92 for the %ΔTGT and 53.72 for the %ΔTMV the survival rates were higher although there were no significant statistical differences. **Conclusion** Metabolic criteria in the initial ^{18}F-FDG PET/CT in patients with follicular lymphoma shows a prognostic value with a cut-off value of 305 for TGT1 and 54 for TMV1. However, in the interim study, these metabolic criteria do not present significant prognostic significance

EP-0689

Outcome and survival of patients with primary testicular lymphomas delineated by control or restaging FDG PET/CT

E. Alagoz, K. Okuyucu, s. ince, N. Arslan; Gülhane Training and Research Hospital, Department of Nuclear Medicine, Ankara, Turkey, Ankara, TURKEY.

Introduction: Primary testicular lymphoma (PTL) is an extranodal non-Hodgkin's lymphoma (NHL) with primary origin of testis and accounts for 1-2% of all NHLs.Metastasis is mostly seen as local recurrence and in central nervous system (CNS). FDG-PET/CT has a high prognostic value with respect to overall survival (OS) and disease-free survival (DFS) in many cancers and lymphomas.We aimed to evaluate clinical outcome and survival of patients with PTL from control (evaluation of treatment response or restaging) FDG-PET/CT. **Material and Methods:** 12 patients with PTL of DLBC variant only were enrolled in the study. The cases were histopathologically proven by excisional biopsy. Control (evaluation of treatment response) or restaging or FDG-PET/CT were performed for all patients after the treatment.We retrospectively examined response to treatment and outcome of the patients.We compared common prognosticators impacting metastasis. **Results:** Mean OS and DFS was 44 and 33.5 months.50% patients died,57.5% developed recurrence and/or metastasis during the follow-up. OS at 1st year was 92%,57.5% at 2nd year,50% at 3rd year.DFS at first year was 92%,50% at second year. Local recurrence was seen in 4 patients.Four patients developed CNS metastasis. After the comparison all potential risk factors (bulky disease, age, serum LDH, ESR, SUVmax, SUVmean,MTV,TLG) impacting recurrence by univariate analysis, we found SUVmax, SUVmean, MTV, TLG and LDH as significant parameters. Multivariate analysis of these factors couldn't be evaluated due to undersampling.ROC curve drawing with cut-off values and their related sensitivity, specificity; Kaplan-Meier test for survival analyses were not performed because of the same reason. **Conclusion:** PTL is a fatal variant with recurrences

and metastases especially in CNS.FDG-PET/CT is the absolute tracker in the follow-up showing metastatic disease. **Keywords:** Primary testicular lymphoma, 18F-fluorodeoxyglucose positron emission tomography/computed tomography.

EP-0690

SUVmax of 10 is a Highly Specific and Moderately Sensitive Cutoff Between Aggressive and Indolent Non-Hodgkin Lymphoma: Analysis of 331 Patients with FDG -PET/CT

G. Alobthani, K. Isoahshi, T. Watabe, K. Matsunaga, H. Kato, M. Tatsumi, E. Shimosegawa, J. Hatazawa; Osaka University, Osaka, JAPAN.

Purpose: The main aim of this study is to find a reasonable SUVmax cutoff of FDG that can discriminate between indolent and aggressive non-Hodgkin's lymphomas (NHLs) to support biopsy findings in the challenging equivocal cases which frequently referred for FDG - PET/CT. **Methods:** Three hundred thirty-one patients were retrospectively selected among patients with NHL who were scanned by FDG-PET/CT between 2008 - 2016. Selected cases have biopsy-proven NHL subtype, time interval between biopsy and FDG -PET/CT scanning was less than 90 days in new cases, recurrent cases should be more than 6 months since last therapy, no history of transformation. **Results:** Aggressive NHLs (55.8%, n=185), indolent NHLs (44.1%, n=146). New aggressive NHLs (n =152) have an extremely significant higher SUVmax than new indolent NHLs (n=108); 15.2 ± 8.7 v 5.3 ± 3.5, (P< 0.0001). Recurrent aggressive NHLs (n=33) have a very significant higher SUVmax than recurrent indolent NHLs (n=38); 13.6 ± 11.64 v 7.6 ± 3.3, (P=0.0048). New aggressive NHLs tend to have a higher SUVmax than recurrent aggressive NHLs; 15.2 ± 8.7 v 13.6 ± 11.64, but the difference was not significant (P = 0.36). Unlike aggressive NHLs, new indolent NHLs have a significantly lower SUVmax than recurrent indolent NHLs; 5.3 ± 3.5 v 7.6 ± 3.3 (P=0.0009). SUVmax of 10.3 was the most reasonable cutoff point between new aggressive and new indolent NHL (both were 78.5% of the study population, 260/331) with 0.86 as the area under the curve (AUC) of receiver operating characteristic (ROC), the specificity was 91.6%, and the sensitivity was 73%. **Conclusion:** SUVmax of 10 is a balanced cutoff between new aggressive and new indolent NHL. However, this cutoff should be used only in cases where biopsy is not conclusive, inaccessible or contraindicated.

EP-0691

^{18}F-FDG PET/CT in Primary Extranodal Lymphoma: Evaluation of Treatment Response and Prognosis

B. Salvatore[1], R. Fonti[1], A. De Renzo[2], S. Pellegrino[2], I. L. Ferrara[2], C. G. Mainolfi[2], L. Marano[2], C. Selleri[2], F. Pane[2], S. Del Vecchio[2], L. Pace[3]; [1]IBB-CNR, NAPLES, ITALY, [2]University "Federico II", NAPLES, ITALY, [3]University of Salerno, Salerno, ITALY.

Introduction: Nowadays, ^{18}F-FDG PET/CT is routinely used in staging, response assessment and follow-up of lymphoma.

Primary Extranodal Lymphoma (PEL) is a clinic-pathological rare type of lymphoma whose optimal management has remained largely undefined. Therefore, the aim of our study was to evaluate the role of ^{18}F-FDG PET/CT in tumor response assessment and prognosis of PEL patients. **Materials and Methods**: We evaluated retrospectively, 56 (32 men, 24 women; mean age±SD, 54.4±14.6 y) PEL patients: 31 with aggressive diffuse large B cell lymphoma (DLBCL) and 25 with indolent lymphoma (20 mucosa-associated lymphoid tissue lymphoma-MALT and 5 follicular lymphoma). All patients had undergone ^{18}F-FDG PET/CT at diagnosis (PET-I). Fifty of these patients underwent also a second ^{18}F-FDG PET/CT after therapy (PET-II). Moreover, 52 patients were subjected to a mean follow-up period of 76 months (range 3-141 months; median 78 months). **Results**: PET-I was positive in 50 (89%) patients with a mean SUVmax value of 10.3±6.7 (range 3.3-27.6). According to histological type, 30/31 (97%) DLBCL, 16/20 (80%) MALT PEL and 4/5 (80%) follicular PEL were positive at PET-I. Analysis of variance showed a significant difference of SUVmax values among the 3 histological groups, with the mean value of SUVmax significantly higher in DLBCL (12.4±7.4) than in MALT (6.9±3.3) and in follicular PEL (6.9±1.3) (p<0.05). In the assessment of tumor response, qualitative analysis of PET-II showed: 80% sensitivity, 85% specificity, 84% accuracy, 57% Positive Predictive Value and 94% Negative Predictive Value. At follow-up, patients in complete or partial remission were compared to those with progressive disease or dead, additionally, survivors were compared with those who had died. Univariate analysis showed that age, performance status, prognostic index and Deauville score predicted Progression Free Survival (PFS) (*p*<0.05), while, performance status, prognostic index and Deauville score predicted Overall Survival (OS) (*p*<0.05). At multivariate analysis only Deauville score was retained in the model for prediction of both PFS (*p*<0.05) and OS (*p*<0.05). By Kaplan-Meier analysis and log-rank testing both PFS and OS were significantly better in patients showing a Deauville score <4 than those with ≥4 score (p<0.01). **Conclusion:** ^{18}F-FDG PET/CT represents a useful tool in the detection of disease response and in the evaluation of outcome in PEL patients.

EP-0692

Diagnostic value of dynamic F-18 FDG PET/CT in patients with malignant lymphoma

K. Terazawa[1], T. Shinya[2], Y. Otomi[1], M. Kubo[1], K. Takechi[3], H. Otsuka[1], M. Harada[1]; [1]Tokushima University Hospital, Tokushima, JAPAN, [2]Okayama University Hospital, Okayama, JAPAN, [3]Tokushima Red Cross Hospital, Komatsushima, JAPAN.

Purpose: The purpose of this study was to assess the diagnostic capacity of dynamic fluorodeoxyglucose-positron emission tomography (F-18 FDG PET)/computed tomography (CT) for differentiating indolent lymphoma from aggressive lymphoma compared with dual-time-point (DTP) F-18 FDG PET/CT. **Subjects and Methods:** We performed dynamic PET studies on 13 consecutive patients with 21 lymphoma lesions. All participants had undergone a dynamic F-18 FDG PET/CT at our institution and received no therapy before the PET/CT examination. Dy-

namic PET acquisition was performed in list mode, beginning at 5 min after the tracer injection and continuing for 30 min (Dynamic 1, 5-15 min; Dynamic 2, 15-25 min; Dynamic 3, 25-35 min). We compared the maximum standardized uptake value (SUVmax) and the retention index (RI-SUVmax) for each dynamic phase and for early and delayed phases between 4 indolent and 17 aggressive lymphoma cases. A receiver operating characteristic (ROC) curve analysis was performed to evaluate the predictive performance for discriminating aggressive lymphoma from indolent lymphoma. Discrimination was assessed by the area under the curve (AUC). **Results:** There were significant differences in the SUVmax on all phases between the indolent and aggressive lymphoma specimens (all p values < 0.05). For RI-SUVmax, a significant difference was noted for the dynamic phase (p=0.04). No significant difference was detected for RI-SUVmax in the DTP study (p=0.574). The ROC curve for diagnosing aggressive lymphoma revealed that the appropriate cut-off SUVmax values could be set at the dynamic 2 and 3 phase, early phase, and delayed phases with a sensitivity of 94.1% and a specificity of 100% for each phase. All AUC values were 0.985 (95% confidence interval [CI]: 0.941-1.000, p=0.003). For RI-SUVmax for the dynamic phase, the ROC curve analysis revealed the appropriate cut-off RI-SUVmax value to be 34.98 with a sensitivity of 100.0% and a specificity of 75.0%. The AUC value was 0.941 (95% CI: 0.821-1.000, p=0.007). **Conclusion:** Dynamic and DTP F-18 FDG PET/CT studies showed high diagnostic performance for discriminating indolent lymphoma from aggressive lymphoma with analyses of the SUVmax for each phase and the RI-SUVmax for the dynamic phase. Dynamic PET scans may be useful for discriminating indolent lymphoma from aggressive lymphoma, and a delayed scan is not necessarily required.

EP-0693

Limited Benefit of Additional Contrast-Enhanced CT to End-of-Treatment PET/CT Evaluation in Patients with Follicular Lymphoma

G. Paone, M. Raditchkova-Sarnelli, L. Giovanella, E. Zucca, L. Ceriani; Oncology Institute of Southern Switzerland, Bellinzona, SWITZERLAND.

Introduction: Follicular lymphoma (FL) is generally characterized by a moderate metabolic activity (FDG-avidity) in nodal and extra-nodal sites and by the frequent detection of residual disease in post-treatment PET scans. Since median age at diagnosis is over 60 years, in many FL patients several conditions that affect the elderly often occur in combination with the tumor, thus complicating and limiting the use of conventional imaging for lymphoma staging and response assessment. For this reason, the choice of the imaging technique should take into account clinical needs (preservation of renal function, reduction of diagnostic radiation exposure) as well as the necessity to constrain health care costs. **Purpose:** The aim of the study was to investigate if there is any advantage in the use of contrast-enhanced CT (ceCT) vs. unenhanced low-dose CT (ldCT) in routine protocols for end-of-therapy PET/CT evaluation of patients with FL. **Subjects and Methods:** Forty-four FL patients who underwent

end-of-therapy PET/CT protocol with ldCT and ceCT were analyzed retrospectively. Two different observers evaluated PET/ldCT and PET/ceCT in a blinded manner. Number and sites of nodal or extra-nodal disease were compared, using PET/ceCT as gold standard in order to evaluate if the type of CT could result in changes of the DS and therapeutic strategy. **Results:** In 34 of 44 patients (77%) PET/ldCT showed the same number and sites of lesions highlighted by PET/ceCT. The inter-observer concordance and overall concordance between imaging procedures were excellent with a very high Cohen's kappa (respectively 0.87 and 0.95). 90% of lesions (138/153) were found by PET/ldCT and in 10 of 44 patients (23%) PET/ceCT provided additional nodal lesions in the mesenteric and iliac regions (10 mesenteric nodes and 5 iliac node). In these 10 patients, DS and consequently the therapeutic strategy were not changed after additional ceCT findings. PET/ldCT accuracy, sensibility, specificity, positive predictive value and negative predictive value and NPV were respectively 95%, 94% (95% CI, 0.80% to 0.98%), 100% (95% CI, 0.72% to 1%), 100% and 83%. **Conclusion:** Our results indicate that the clinical impact of PET/ceCT in assessing end-therapy evaluation in FL is limited. The PET/ldCT could be suggested as primary imaging modality of choice, thus limiting the acquisition of PET/ceCT images only for doubtful cases of residual disease in mesenteric area. This diagnostic approach would be less expensive, minimize diagnostic radiation exposure, and preserve renal function.

EP-0694

Application of Quantitative Indexes on FDG PET to Treatment Response Evaluation of Indolent Lymphoma

H. Kim, J. Paeng, T. Kim, M. Kim, G. Cheon, D. Lee, J. Chung, K. Kang; Seoul National University Hospital, Seoul, KOREA, REPUBLIC OF.

Purpose: FDG PET is a standard imaging modality for response evaluation in FDG-avid lymphoma, for which the current recommendation is based on visual grading instead of quantitative PET indexes. Additionally, there is no recommendation regarding low FDG-avid lymphoma. The purpose of this study was to investigate how to adopt quantitative indexes in response evaluation of indolent lymphomas. **Methods:** A total of 57 patients with indolent lymphoma (39 follicular and 18 marginal zone B-cell lymphoma) who completed R-CVP regimen of chemotherapy were retrospectively enrolled. FDG PET/CT scans were performed at baseline, interim (after 2-3 cycles) and end-of-treatment (EOT). Response at the EOT was determined by Lugano classification, and progression-free survival (PFS) was determined by follow-up data. Maximum standardized uptake value (SUV$_{max}$), metabolic tumor volume (MTV) and total lesion glycolysis (TLG) with margin threshold of SUV 3.0 were measured in the single hottest lesion (Target A) or 5 hottest lesions (Target B), and their efficacies regarding response evaluation and PFS prediction were evaluated. **Results:** On EOT PET, SUV$_{max}$ of Target B was the most significant index to determine treatment response (P = 0.0154). MTV of Target B was also significant (P = 0.0160). However, the differences (%Δ) from the initial PET were not significant for any of the tested indexes. In predicting PFS,

SUV$_{max}$ of Target B was the most significant index (P = 0.0002), and MTV and TLG were also significant (P = 0.0005 and 0.0004, respectively). These indexes showed comparable predictive power to Lugano classification. On interim PET, SUV$_{max}$ and its %Δ of Target B were significant for predicting final response and PFS (P < 0.05 for all). Regarding MTV, %Δ of MTV was significant for predicting final response while MTV per se was not (P = 0.0069 vs. 0.1699). **Conclusion:** PET is an effective tool for response evaluation even in indolent lymphoma. SUV$_{max}$ and MTV measured from multiple lesions are effective quantitative indexes for evaluating treatment response and predicting PFS. Regarding interim PET, it appears that %Δ of indexes need to be considered as appropriate quantitative indexes for response evaluation.

EP-0695

Does PET reconstruction method affect Deauville scoring in lymphoma patients?

B. Enilorac[1], C. Nganoa[1], C. Fruchart[1], A. Gac[1], S. Chantepie[1], G. Damaj[1], C. Lasnon[2,3], N. Aide[1,3]; [1]CHU de Caen, Caen, FRANCE, [2]Centre François Baclesse, Caen, FRANCE, [3]INSERM U1086 "ANTICIPE", Caen, FRANCE.

Background: When scoring FDG PET with the Deauville scale (DS), quantitative evaluation of tumour and reference organs limits the problem of optical misinterpretation. However, compared to conventional OSEM reconstruction, advanced algorithms such as point spread function (PSF) modeling significantly increase SUV metrics in tumour lesions but not in the liver. Consequently, they could affect DS. This retrospective study aimed to investigate this issue and to seek whether the EANM/EARL accreditation program is efficient in overcoming it. **Materials and Methods:** Included were 34 diffuse large B cell Lymphoma (DLBCL) patients (13 females, 21 males, mean+/-SD age: 63+/-12 years) treated with RCHOP (n=29) or RACVB (n=5) regimen. PET data were reconstructed with an OSEM EARL-compliant algorithm (4 iterations/8 sub-iterations/5mm Gaussian filtering) and with PSF reconstruction (3 iterations/21 sub-iterations/no post filtering). Additionally, a 6mm filter was applied to PSF images to meet the EANM/EARL requirements (PSF$_{EARL}$). Fifty scans were analyzed: 13 early interim PET (post 2 cycles, i-PET2), 13 interim PET (post 4 cycles, i-PET4) and 24 end-of-treatment PET (EoT-PET). SUV$_{max}$ in the liver and aorta were determined using automatic VOIs and compared to SUV$_{max}$ of the residual mass harboring the highest FDG uptake. DS5 was defined as 2 times the normal liver uptake. **Results:** Overall, using conventional OSEM reconstruction, patients were classified as DS1, DS2, DS3, DS4 and DS5 in 18, 6, 11, 11 and 4 cases, respectively. Using PSF, patients were classified as DS1, DS2, DS3, DS4 and DS5 in 18, 3, 10, 15 and 4 cases, respectively. Concordance (Cohen's unweighted Kappa) between OSEM and PSF Deauville scoring was 0.81 (95%CI:0.68-0.94). Amongst the 7 discordances (14% of scans) that occurred between OSEM and PSF, 3 patients moved from DS2 to DS3 (1 i-PET2, 1 i-PET4 and 1 EoT-PET), and 4 patients moved from DS3 to DS4 (1 i-PET2, 1 i-PET4 and 2 EoT-PET). When applying a 6mm Gaussian filter to PSF images, patients

were classified as DS1, DS2, DS3, DS4 and DS5 in 18, 5, 11, 12 and 4 cases, respectively. Concordance between OSEM and PSF$_{EARL}$ Deauville scoring was 0.84 (95%CI:0.72-0.96). Kaplan-Meier analysis in the EoT-PET group showed a better discriminative power of OSEM for Progression-free survival, compared to PSF. **Conclusion:** PSF reconstruction affects DS by providing higher scores. This may be an issue in trials with a PET response-adapted design. The EARL harmonization program partially overcomes this issue. Another option could be to disable PSF reconstruction in lymphoma trials.

EP-0696

Do PET textural features have an additional value over visual assessment for the diagnosis of bone involvement on baseline FDG PET scans in diffuse large B cell lymphomas patients?

N. Aide[1,2], **M. Talbot**[3], C. Nganoa[1], C. Fruchart[4], G. Damaj[4], C. Lasnon[5,2]; [1]Nuclear Medicine Department, University Hospital, CAEN, FRANCE, [2]INSERM U1086 "ANTICIPE", Caen, FRANCE, [3]Normandy University, CAEN, FRANCE, [4]Hematology Institute, University Hospital, CAEN, FRANCE, [5]Nuclear Medicine Department, François Baclesse Centre, CAEN, FRANCE.

Background: ^{18}F-FDG-PET is a well-validated tool for bone marrow (BM) assessment in newly-diagnosed diffuse large B cell lymphomas. Its diagnosis is based on visual assessment leading to a pooled sensitivity (Se) and specificity (Sp) equal to 88.7% and 99.8%, respectively, according to a recent meta-analysis. However, negative ^{18}F-FDG-PET findings in patients with positive bone marrow biopsy (BMB) occurred in approximately 3% of patients, suggesting that BMB can't be omit in PET negative patients. We aimed to investigate if quantitative assessment of BM involvement based on PET textural features could overcome visual assessment's drawbacks. **Materials and Methods:** From December 2008 to December 2015, 82 baseline ^{18}F-FDG-PET examinations of patients with newly-diagnosed DLBCL (38 females, 44 males, mean±SD age: 62±13 years) who had BMB were retrospectively included. All examinations were reconstructed with PSF reconstruction (3 iterations/21 sub-iterations/no post-filtering). For each examination, (i) a visual assessment of BM was made by 2 experienced readers in consensus, (ii) axial skeleton was segmented using CT images with MIM software and (ii) PET textural features (TF) (2nd order: entropy, dissimilarity, correlation, 3rd order: HGZE, ZP) were extracted and computed from these VOIs using LifeX software. For ROC analysis, Se and Sp calculations, BMB-/PET- patients were considered to be disease-free (D-) whereas BMB-/PET+, BMB+/PET- and BMB+/PET+ patients were considered to have BM involvement (D+). **Results:** Fifty-eight (70.7%) and 24 (29.3%) patients were D- and D+, respectively (58 BMB-/PET-, 13 BMB-/PET+, 2 BMB+/PET-, 9 BMB+/PET+). Clinical characteristics (age, sex, BMI, B symptoms) were not statistically different between D- and D+ patients. Apart correlation, all textural features were significantly different between normal-weight (BMI≤25) and overweight (BMI>25) patients. Focusing on BMI≤25 patients (n=49, 37 D-, 12 D+), all TF were statistically different between

D- versus D+ patients. Areas under the ROC curves for the most discriminative TFs, HGZE and ZP, were 0.89 and 0.85. Optimal cut off-value was 109.7 for HGZE (Se = 83.3%, Sp = 97.3%) and 0.035 for ZP (Se =66.7%, Sp = 94.6%). Over 38 PET- patients, 1 had a positive BMB. Applying the cut-off values in PET- patients both HGZE and ZP allowed to identify the BMB+ patient at the cost of 1 and 2 false positive cases, respectively. **Conclusion:** Evaluation of heterogeneity of BM uptake with TFs is hampered by its sensitivity to noise level in overweight patients but may bring additional diagnostic value over visual assessment in normal-weight and PET- patients.

EP-0697

MTV and TLG of staging PET/CT as predictors of outcome in Hodgkin Lymphoma patients: preliminary results of a single center study

M. Spallino[1], M. Cuzzocrea[1], C. Spadavecchia[2,3], S. Morzenti[3], E. De Ponti[3], S. Bolis[4], C. Landoni[1,5], L. Guerra[5]; [1]University of Milan-Bicocca, Milan, ITALY, [2]Post graduate school of Medical Physics, Milan, ITALY, [3]Medical Physics Department, San Gerardo Hospital, Monza, ITALY, [4]Department of Hematology, San Gerardo Hospital, Monza, ITALY, [5]Department of Nuclear Medicine, San Gerardo Hospital, Monza, ITALY.

Recently, total metabolic tumor volume (tMTV) on positron emission tomography / computed tomography (PET/CT) has been shown to be prognostic factor in some subtypes of non-Hodgkin's lymphoma. However, currently it is not well defined whether the tMTV can be a predictive factor for clinical outcome in HL. The objective of the present study is to evaluate if tMTV is correlated to clinical outcome in terms of progression free survival (PFS) and overall survival (OS) in HL patients. Forty patients (23 men; mean age: 36 years, range 20 - 69) with newly diagnosed HL, disease stage I-IV (6 stage I, 23 stage II, 10 stage III, 1 stage IV) referred to our Hospital between October 2006 and May 2012 were retrospectively evaluated. All patients were studied with 18F-FDG PET/CT prior to treatment (baseline PET), after two cycles of chemotherapy (interim-PET) and at the end of treatment (nd-of-Treatment-PET). tMTV was calculated at baseline PET/CT by two nuclear medicine physicians in a consensus with a commercial software (PET-VCAR, GE Healthcare, Milwaukee, WI) with a fixed threshold of 41% of maximum. For any lesion, MTV, TLG (total lesion glycolysis), SUVmax and SUVpeak were defined. Then MTV ad TLG of any lesion were summed to obtain tMTV and t(total)TLG.At the time of writing the median follow up duration was 78 months, 6/40 (15%) patients relapsed and no patient died. tMTV, tTLG, SUVmax and SUVpeak of not relapsed patients resulted respectively as follows: 124.8 ± 135.1 cm^3 (median value 72.3, range 6.8 - 627.3), 699.6 ± 950.9 g/ml cm^3 (median value 447.9, range 37.4 - 5112.6), 11.8 ± 4.0 g/ml (median value 12.4, range 4.9 - 20.6), 9.8 ± 3.7 g/ml (median value 9.8, range 3.9 - 17.8). The same parameters for relapsed patients were: 113.8 ± 166.4 cm^3 (median value 50.0, range 23.8 - 449.7), 890.7 ± 1445.9 g/ml cm^3 (median value 264.7, range 151.1 - 3824.7), 14.8 ± 6.0 g/ml (median value 13.9, range 6.5 - 24.6), and 12.3 ± 5.2 g/ml, (median value 12.0, range 4.7 - 20.0). No sta-

tistically significant difference was found comparing metabolic parameters relative to relapsed and non-relapsed patients using the rank sum test. The preliminary results of the present study do not indicate any correlation among clinical outcome and metabolic quantitative data in HL patients. Nevertheless, these results need to be confirmed in a larger population.

EP-0698

Prognostic role of final FDG-PET in relationship to absolute monocyte count at diagnosis for Diffuse Large B Cell Lymphoma (DLBCL)

A. Franceschetto[1], R. Marcheselll[2], R. D'Apollo[1], L. Massi[1], A. Casolo[1], S. Sacchi[2], N. Prandini[1]; [1]Nuclear Medicine, Modena, ITALY, [2]Clinical Oncology, Modena, ITALY.

Purpose/Introduction: FDG-PET-CT (PET) has high predictive value for PFS. However, about 20% of PET negative patients will relapse, while only 30-40% of PET positive patients can be rescued with salvage treatments. In order to increase the already high predictive value of PET, this study combined end of treatment PET (EOT-PET) results with absolute monocyte count (AMC) at staging, a prognostic factor related to lymphoma microenvironment. **Subjects & Methods:** We studied 63 patients with DLBCL and treated at Modena Cancer Center from 2007-2014 with R-CHOP or CHOP-like regimens: 61% were in stages III-IV and 26% had an International Prognostic Index (IPI) score 3-5. Eligibility criteria were: availability of clinical characteristics, blood differential, basal and end of treatment PET scan (BAS-PET and EOT-PET), and survival outcome. Response evaluation was based on 2007 Cheson criteria. The PET results were revised using Deauville Score (DS); AMC at diagnosis > 630/mmc were considered predictive of poor prognosis. PFS was assessed by Kaplan-Meier estimates and compared to risk groups using the log-rank (LR) test. **Results:** At EOT 48 patients reached a CR and 15 achieved PR or progressed during treatment. After a median follow-up of 50 months (range: 1-104 months) 3-year PFS was 83%. At EOT-PET analysis 13 patients were positive (DS ≥ 4): the predicted 3-year PFS was 90% for negative and 58% for positive patients. The predicted 3-year PFS by AMC was 87% for AMC ≤ 630/mmc and 70% for AMC > 630/mmc. Given the predictive value of both BAS-PET and AMC, we stratified patients into 3 groups: the low risk level (negative EOT-PET and AMC ≤ 630/mmc/L) had a 3-year PFS of 91% (95% CI: 80-96%), the intermediate level (EOT-PET positive or AMC > 630/mmc/L) had a 3-year PFS of 82% (95% CI: 55-85%), and the high risk level (EOT-PET positive and AMC > 630/mmc/L) had a 3-year PFS of 50% (95% CI: 1-49%). **Discussion/Conclusion:** Our retrospective study shows that both EOT-PET evaluated with DS and AMC are strong prognostic factors, able to discriminate patients with different PFS. We hypothesize that similar trend of the two curves (PET and AMC) expresses two aspects of DLBCL, with positive PET reflecting the persistence of the lymphoma, and elevated AMC at diagnosis in peripheral blood as a biomarker of the tumor microenvironment/cytokines. Our hypothesis based on the prognostic value of the combination of both parameters must, however, be validated in a larger and independent patient case.

EP-0699

Quantitative and qualitative analyses of metabolic response at end of treatment 18F-FDG PET-CT scan can predict outcome in diffuse large B-cell lymphoma

L. Baratto[1], F. Wu[1], J. Sabile[2], T. Liang[3], J. Rosemberg[3], R. Adavni[2], E. Mittra[1]; [1]Stanford University, Division of Nuclear Medicine and Molecular Imaging, Department of Radiology, Stanford, CA, UNITED STATES OF AMERICA, [2]Stanford University, Department of Medicine, Division of Medical Oncology, Stanford, CA, UNITED STATES OF AMERICA, [3]Stanford University School of Medicine, Department of Radiology, Stanford, CA, UNITED STATES OF AMERICA.

Aim: The goal of this study was to evaluate different response criteria (Lugano, EORTC-European Organization for Research and Treatment of Cancer, PERCIST - PET Response Criteria in Solid Tumors, and IHP - International Harmonization Project) as well as various other metabolic parameters from 18F-FDG PET/CT in patients with Diffuse Large B-cell Lymphoma (DLBCL). **Materials and Methods:** This retrospective study was approved by the Institutional Review Board. We enrolled patients older than 18 years with biopsy proven DLBCL, who had both baseline and end of treatment (EOT) 18F-FDG PET/CT scans at our institution. Images were independently analyzed by two experienced nuclear medicine physicians according to Lugano, EORTC, PERCIST and IHP response criteria; any disagreements were resolved by consensus. EOT PET was classified into two categories: complete metabolic response (CR) and residual metabolic disease (RD), which included partial response, stable disease and progressive disease. Metabolic Tumor Volume (MTV), Total Lesion Glycolysis (TLG), SUVmax, SUVmean and the SUM of all these metabolic parameters (obtained by adding together all lesions' values) were also measured at baseline and EOT PET/CT. All datasets were correlated to Overall Survival (OS) and Progression Free Survival (PFS). **Results:** 79 patients (45 males, 34 females) who met the inclusion criteria were identified from the lymphoma database; median age was 58 years (SD=16). Median follow up was 50 months for OS and 44 for PFS. All patients were treated with R-CHOP chemotherapy. 15/79 had also external beam radiation therapy. IPI score was 0-1 for 27/79 patients; 2 for 18/79; 3 for 18/79 and 4-5 for 16/79. Sensitivity/specificity for each criterion were: Lugano (99%/44%), EORTC (94%/56%), PERCIST (94%/67%), IHP (96%/67%) (see table). Log-rank tests showed that EOT 18F-FDG PET/CT was predictive of OS when Lugano, EORTC, or PERCIST criteria were used (p<0.001, p=0.02, and p=0.04, respectively), but not IHP (p=0.25). None of the individual criteria were predictive of PFS (all p>0.43). No radiological measurements at baseline were predictive of OS, but percentage change of MTV SUM and TLG SUM from baseline to EOT were significant predictors of PFS (p=0.003 and p=0.022, respectively). **Conclusions:** In our data-set the Lugano criteria was the best predictor of OS at the EOT FDG PET/CT. EORTC and PERCIST criteria were also useful, but to a lesser extent. The percentage change in MTV and TLG SUM were the only metabolic parameters significant for PFS. Further evaluation in a larger cohort of patients are needed to confirm these findings.

Clinical Oncology: Leukaemia & Myeloma

EP-0700

Investigation of correlation between PET/CT findings and clinical parameters in patients with multiple myeloma

R. Wang, L. Di, J. Zhang, G. Zhao, Y. Fan, Z. Fu, X. Zhang, Q. Jiang; Peking University First Hospital, Beijing, CHINA.

Aim: The purpose of this study was to investigate the correlation between PET/CT findings and clinical parameters in patients with multiple myeloma. **Methods:** Fifty-five patients diagnosed with multiple myeloma were enrolled in this study. The SUVmax of each patient reflecting glucose metabolic activity was recorded. The relationships of SUVmax between different pathological types and clinical stage including D-S and ISS were analyzed. The relationship between lesions and serum lactate dehydrogenase level was also analyzed. **Results:** In 35 patients with newly diagnosed MM, the SUVmax of patients with pathological type of immunoglobulin and light chain was 5.55±3.15, 5.07±2.69 (t=0.42, P=0.68) respectively. According to the D-S staging system, the SUVmax of lesions for phase III and other phases was 5.63±2.76, 3.59±1.68 (t=2.41, P=0.02) respectively. While according to the ISS staging system, the SUVmax of lesions for phase III and other phases was 4.18±2.76, 6.18±2.53 (t=-1.73, P=0.10) respectively. The serum lactate dehydrogenase level for patients with more than and less than twenty lesions according to PET/CT findings was 235.79±188.15 (IU/L), 157.40±29.93 (IU/L) (t=2.19, P=0.04) respectively. While there was no significant statistical difference between SUVmax and serum lactate dehydrogenase levels (r=-0.02, P=0.91). **Conclusion:** There is partly positive correlation between PET/CT findings and clinical parameters in MM patients. The higher the SUVmax is, the later the D-S staging is. The serum lactate dehydrogenase level is higher in those patients with more lesions. **Key words:** Multiple myeloma; Positron-emission tomography; Staging; Standard uptake value; Lactate dehydrogenase **Fund program**: 1.National Special Fund for the Development of Major Research Equipment and Instrument (2011YQ03011409); 2. National Science and Technology Pillar Program of the Twelfth Five-year Plan (2014BAA03B00)

EP-0701

Application of F-18-FDG PET/CT in staging and metabolic activity assessment of multiple myeloma

R. Wang, L. Di, J. Zhang, Z. Fu, Y. Fan, X. Zhang, G. Zhao, Y. Cui, M. Liu, L. Kang, X. Liao, Y. Wang; Peking University First Hospital, Beijing, CHINA.

Aim:The paper of this study was to investigate the clinical value of F-18-FDG PET/CT in staging and assessing the glucose metabolic activity of multiple myeloma (MM). **Methods**: A total of 25 MM patients (13 males, 12 females, age: 39-67 years) newly diagnosed by Peking University First Hospital from May 2010 to April 2015 were enrolled in this retropective study. The SUVmax of

each patient reflecting the metabolic activity was recorded. D-S plus staging according to F-18-FDG PET/CT was compared with the traditional D-S staging. The SUVmax and the percentage of plasmacytes of bone marrow of phase III and non-phase III (phaseI and II) according to D-S plus staging were compared. One-way analysis of variance was used to analyze the data. **Results:** In 25 MM patients, the range of SUVmax of lesions was 1.8-12.0 and the mean value was 5.15±2.74. According to D-S staging, the numbers of phase I, II and III were 7, 4 and 14, respectively. While the numbers were 3, 1 and 21, respectively on the results of F-18-FDG PET/CT according to D-S plus staging. Based on the D-S plus staging system, staging of 7 patients (28%, 7/25) was changed. According to the D-S plus staging system, the SUVmax between phase III and non-phase III patients was significantly different (5.75±2.54 vs 3.00±0.70, F=4.49, P<0.05), while the percentage of plasmacytes of bone marrow between the two groups had no significant difference (27.66±28.76 vs 19.33±17.13, F=0.30, P>0.05). **Conclusion**: F-18-FDG PET/CT is of great clinical importance for MM staging and metabolic activity assessment of MM. **Key words**: Multiple myeloma; Staging; Durie-Salmon plus; Positron-emission tomography and computed tomography; Fluorodeoxyglucose F18 **Fund program**: 1.National Special Fund for the Development of Major Research Equipment and Instrument (2011YQ03011409); 2. National Science and Technology Pillar Program of the Twelfth Five-year Plan (2014BAA03B00)

EP-0702

18F-FDG-PET/CT In Solitary Plasmacytoma: Metabolic Behavior And Possible Role In Prediction Of Progression To Multiple Myeloma

D. Albano, F. Bertagna, M. Bertoli, G. Bosio, M. Bonacina, E. Cerudelli, R. Durmo, M. Gazzilli, R. Giubbini; Spedali Civili Brescia, Brescia, ITALY.

Aim: Solitary plasmacytoma (SP) is a rare plasma cell neoplasm which can develop both in skeletal or soft tissue and frequently progresses to multiple myeloma (MM). The prognosis is influenced by the risk of transformation to MM, which occurs in most cases, especially in solitary bone plasmacytoma. Many possible factors for progression to MM are investigated with controversial results. The role of 18F-FDG-PET/CT in this field is not well understood. Our aim was to study the metabolic behavior of SP and the impact of 18F-FDG-PET/CT in the evaluation of the risk of progression to MM. **Materials and Methods**: between 2006 and 2016 sixty two patients (20 female, 42 male; average age: 64 years) with histologically-confirmed diagnosis of SP who underwent 18F-FDG-PET/CT for staging before any treatment were included. The primary site was osseous in 53 cases and extramedullary in the remaining 10. PET images were qualitatively and semi-quantitatively analyzed by measuring the maximum standardized uptake value body weight (SUVbw), lean body mass (SUVlbm), body surface area (SUVbsa), metabolic tumor volume (MTV), total lesion glycolysis (TLG) and compared with epidemiological (age at diagnosis, sex), site of primary disease and morphological (diameter max lesion) characteristics. A multivariate analysis was made for evaluating prognostic factors predictive of transformation in MM. Time to transformation to

myeloma (TTMM) were calculated using the Kaplan-Meier method. **Results**: 48/62 (41 osseous, 7 extramedullary) patients had positive 18F-FDG-PET/CT showing FDG uptake at the plasmacytoma lesion (average SUVbw was 8.7±4.5; SUVlbm 6.2±3.2; SUVbsa 2.1±1; MTV 43.8± 44.7; TLG 220±278); the remaining 14 (12 osseous, 2 extramedullary) were not 18F-FDG-avid. 18F-FDG avidity was significantly correlated with tumor size (p=0.04) and was not influenced by primary site of disease, sex or age. SUVbw, SUVlbm, SUVbsa, MTV and TLG were not correlated with any features (age, sex, site, tumor size). Progression to MM occurred in 29 patients within an average time interval of 18 months (range 6-40). MM was more likely to develop in patients with bone SP compared extramedullary (p= 0.02), in patients with 18F-FDG-avid plasmacytoma (p=0.01), with high SUVlbm (p=0.02) and high SUVbsa (p=0.03). Progression to MM was not correlated with sex, age, tumor size, SUVbw, MTV and TLG. TTMM was significantly shorter in patients with SUVbsa>3 and SUVlbm>5.2. **Conclusions**: 18F-FDG avidity was noted in 77% of SP and is correlated with tumor size only. SUVlbm and SUVbsa are predictive factors to evaluate the risk of transformation in MM and TTMM.

EP-0703

Association between 18F-fluorodeoxyglucose uptake and CD38, CD138 expression in myeloma cells and clinical parameters in patients with multiple myeloma

A. Cengiz[1], H. Ü. Arda[2], F. Doger[3], I. Yavaşoğlu[4], Y. Yürekli[1], A. Z. Bolaman[4]; [1]Adnan Menderes University Medical School Department of Nuclear Medicine, Aydın, TURKEY, [2]Adnan Menderes University Medical School Department of Internal Medicine, Aydın, TURKEY, [3]Adnan Menderes University Medical School Department of Pathology, Aydın, TURKEY, [4]Adnan Menderes University Medical School Department of Hematology, Aydın, TURKEY.

Introduction: Bone marrow plasma cells can exhibit strong CD38 and 138 expression in patients with multiple myeloma (MM). Some laboratory parameters such as anemia, hypoalbuminemia, hypercalcemia, elevated beta-2 microglobulin, C-reactive protein (CRP), creatinine and lactate dehydrogenase (LDH) are parameters relevant to prognosis in patients with MM. The aim of this study was to evaluate the association between the degree of F-18 FDG uptake and CD38, CD138 expression in myeloma cells in bone marrow and other clinical parameters in patients with MM. **Subjects & Methods:** Patients with the diagnosis MM who underwent 18F-FDG PET/CT for initial staging were evaluated retrospectively. Patients who were treated with chemotherapy, radiation therapy or hematopoietic growth factor previously and had history of another cancer were excluded. We analyzed a total of 36 patients (43-83 years-old, mean: 64.7 ±9.7). Hematological and biochemical tests including hemoglobin, CRP, β2-microglobulin, creatinine, albumin, LDH, erythrocyte sedimentation rate was recorded for all patients. In the bone marrow samples, plasma cell ratio and CD38, CD138 immunohistochemical staining were evaluated. For semi-quantitative evaluation, mean standardized uptake value (mSUV) of right anterior and posterior iliac crest and right proximal femora were recorded by semi-automatic image registration software package. The correlation between average mSUV of bone marrow and CD38, CD138 expressing myeloma cells and other clinical parameters were analyzed by Spearman's correlation test. p values <0.05 were considered as statistically significant. **Results:** There was statistically significant correlation between bone marrow FDG uptake and percentage of plasma cells in bone marrow and CD38 and CD138 expression in plasma cells. (r=0.390, r=0.398 and r=0,469). There was also correlation between bone marrow FDG uptake and serum beta-2 microglobulin levels (r=0.690). There was negative correlation between bone marrow FDG mSUV and hemoglobin and hematocrit values (r=-0. 377 and r=-0,368). Other hematological parameters were not correlated with FDG uptake in bone marrow. **Conclusion:** Increased FDG uptake is correlated with the percentage of and CD38 and CD138 expression in plasma cells in bone marrow. In addition to initial staging, 18F-FDG PET/CT is useful in treatment planning and prognostic evaluation in MM patients.

EP-0704

18F-FDG PET/CT In Premalignant Stages Of Multiple Myeloma: Preliminary Analysis

F. J. Pena Pardo, G. A. Jiménez Londoño, A. M. García Vicente, A. Palomar Muñoz, N. D. Disotuar Ruiz, Á. Soriano Castrejón; Nuclear Medicine Service. Hospital General Universitario de Ciudad Real, Ciudad Real, SPAIN.

Aim: To assess the role of 18F-FDG PET/CT in the prediction of progression of monoclonal gammopathy of unknown significance (MGUS) and smoldering multiple myeloma (SMM) to symptomatic multiple myeloma (MM). **Materials and Methods:** Analysis of data from a prospective multicenter trial. Patients undergoing PET/CT in this setting, with at least 3 months of follow-up after last examination, were included. If available, stages of International Staging System (ISS), serum monoclonal protein, free light chain (FLC) ratio, immunoglobulin subtype and the percentage of clonal marrow plasma cells were collected. We grouped Mayo Clinic risk stratification scores for MGUS and SMM into three categories: low (0-1), intermediate (2) or high risk (3 factors). PET/CT interpretation. We considered a scan as positive if any of these patterns was present: focal bone or extramedullary uptake, not explainable by other causes, bone marrow diffuse uptake higher than liver one, or both. **Results:** Forty-two patients (26 female, median age of 69 years) were included: 18 with MGUS and 24 SMM. They underwent a total of 71 PET/CT scans, ranging for 1 to 5 per patient (mean of 1.65), with a median time interval of 7 months. The evolution time between the diagnosis and the first PET/CT was 1-204 months (mean 42), and the mean follow-up since that examination to last clinical control was 14.70 months (3-49). The majority of patients were ISS stage 1 and have intermediate risk. In 36 patients previous imaging tests (mainly whole body skeletal X-Ray) were available: 30 negative and 6 doubtful. A progression, leading to initiation of treatment, was documented in 8 patients (1 MGUS and 7 SMM). Four had at least a positive PET/CT scan, but in other 4 was negative. PET/CT was positive en 6 patients (14%), 2 MGUS and 4 SMM. Four of them started treatment, but only 2

due to that result; in the other two the main reason to treat was a progression in bone marrow (BM) aspirate, plus anemia in one of them. One PET+ patient was 83 year old and follow-up was decided, and the other PET+ patient underwent thyroid FNAB because of an incidental finding in the scan and is awaiting for rib and BM biopsies. **Conclusion:** PET/CT seems to have a limited role in the prediction of progression to symptomatic MM. A larger series is needed to find which factors could serve to identify the patients who would beneficiate for a PET/CT scan.

EP-0705

¹⁸F-fluorocholine versus ¹⁸F-fluorodeoxyglucose for PET/CT in staging, follow-up or suspected relapse of multiple myeloma

J. Zhang-Yin[1], O. Benesty[1], A. Cottereau[1], M. Gauthé[1], M. Calzada[1], K. Kerrou[1], J. Ohnona[1], V. Gaura-Schimidt[1], V. Nataf[1], F. Montravers[1], L. Garderet[2], J. Talbot[1]; [1]hôpital Tenon, Paris, FRANCE, [2]hôpital Saint-Antoine, Paris, FRANCE.

Aim: The usefulness of ¹⁸F-fluorodeoxyglucose (FDG) PET/CT in multiple myeloma (MM) has been proven for several years but its sensitivity is imperfect. In a pilot study, we showed that ¹⁸F-fluorocholine (FCH) is able to pinpoint lesions with a less intense metabolism and/or located in the skull, in recurrent MM. The aim of the present study was to compare the diagnostic performance of PET/CT using FCH and FDG, in various settings of MM: staging, follow-up or suspected relapse. **Materials and Methods:** FDG and FCH PET/CTs were both performed within few days, in 68 consecutive patients with MM referred between November 2015 and April 2017. For each patient and each tracer, we determined the number of foci (intraosseous and extraosseous) and their intensity of uptake measured by their SUVmax and the corresponding target/non-target ratio (T/NT). Bone spread was divided into three patterns: innumerable foci (more than 10), countable bone foci (less or equal to 10) or diffuse bone marrow infiltration. **Results:** The 68 patients with MM underwent 80 FDG and FCH PET/CTs: 17 for staging, 33 for follow-up (some patients had iterative PET/CTs) and 30 for suspected relapse. No foci were found in 34 exams (6 for staging, 17 for follow-up and 11 for suspected relapse). Uncountable foci were observed in 9 cases with both tracers, with mismatched FDG/FCH foci in 1 case. Concerning countable foci, in 7 staging exams FDG showed 25 foci vs. 30 FCH foci, in 12 follow-up exams 29 FDG foci vs. 26 FCH foci, in 15 cases of suspected relapse 40 FDG foci vs. 60 FCH foci (+50%). During follow-up, only FDG foci were visible in 1 patient and only FCH foci in 2 patients. Median SUVmax and T/NT was overall greater for FCH than for FDG, significantly in case of suspected relapse. Of the 3 cases of diffuse bone marrow infiltration, 1 was better detected with FDG and 2 with FCH. Extramedullary spread was detected in 2 patients, foci of similar intensity being visible with both tracers. In 3 patients, the management decided on basis of FDG PET/CT was changed in view of FCH PET/CT. **Conclusion:** These findings suggest that FCH PET/CT could have a role in all settings of MM, in particular suspected relapse. In which patients it is worthwhile and significance of mismatched lesions require further investigation.

EP-0706

Monoclonal gammopathy of undetermined significance (MGUS): Computational analysis of PET/CT images

R. Piva[1], A. Nieri[1], C. Campi[2], F. Fiz[3], A. Bellini[1], M. Bauckneht[1], A. Borra[1], S. Morbelli[1], A. Buschiazzo[1], A. Orengo[1], A. Massone[4], M. Piana[2], G. Sambuceti[1], C. Marini[5]; [1]IRCCS AUO San Martino IST, Genova, ITALY, [2]Department of Mathematics, University of Genoa, Genova, ITALY, [3]Nuclear Medicine Unit, Department of Radiology, Uni-Klinikum, Tübingen, GERMANY, [4]CNR SPIN (Superconductors, oxides and other innovative materials and devices),, Genova, ITALY, [5]CNR Institute of Bioimages and Molecular Physiology, Milan, ITALY.

Aim: Monoclonal gammopathy of undetermined significance (MGUS) is an asymptomatic condition, characterized by a proliferation of monoclonal plasma-cells in the hematopoietic bone marrow (BM) that can evolve in smoldering or overt multiple myeloma (MM). The possible role of FDG-PET/CT in MGUS is still uncertain, despite the documented relationship between skeletal structure and BM metabolism already reported in MM. In the present study, we applied a computational analysis to the whole-body images to verify skeletal and BM response to MGUS. **Materials and Methods:** 18F-FDG-PET/CT images of 18 MGUS patients (13 males, mean age 71±7,5 years) were analyzed. The algorithm identified and quantified the volumes of trabecular (intra-bone volume, IBV), compact bone (CBV) and total skeletal volume (SV, i.e. the sum of IBV and CBV) in the CT images. Within these volumes, it calculated the mean attenuation coefficient value (HU) and extracted the mean SUV from the corresponding PET images. Moreover, the program quantified the volume of active "red" BM, using a published PET threshold criterion. The analysis considered the vertebrae (axial skeleton) and the long bones (appendicular skeleton) separately. All data were compared with corresponding findings in 18 sex/age-matched controls from a published normalcy database. **Results:** Total SV was larger in MGUS than in controls. This difference was particularly evident in appendicular bones (906±250 vs. 547±170 ml, p<0.01). In this area, bone alterations particularly involved IBV, whose increase was markedly larger with respect to the corresponding change in CBV. As a result, IBV/SV ratio was markedly increased in MGUS patients with respect to controls (38±5% vs 28±3%, p<0.01). These findings were associated with a marked effect on bone mineral content: MGUS patients had a relevant decrease in shaft HU with respect to controls, both in IBV (158±53 vs. 233±65, p<0.05) and in CBV (912±297 vs 1114±65, p<0.01). Metabolic activity of RBM was not significantly different between patients and controls. However, RBM volume in long bone shafts was increased in MGUS subjects (11,2±2,4 vs. 5,2±2 ml/Kg of ideal body weight, p<0.01). **Conclusions:** MGUS is associated with a significant increase of the IBV/SV ratio paralleled by an increase of CBV volume with respect to controls. These features are more evident in the appendicular bones and are co-localized with an increase in the RBM volume. This study suggests the presence of a signaling between neoplastic clone and stroma cells, eventually resulting in bone remodeling.

EP-0707

11C-Methionine versus 18F-Fluorodeoxyglucose PET/CT imaging in patients with multiple myeloma and other plasma cell malignancies: initial staging and re-staging

M. I. Morales-Lozano, B. Garcia-Garcia, S. Villar, E. Guillen, P. Rodriguez Otero, F. Grissanti, L. Sancho, R. Ramos, V. Moran, J. San Miguel, J. Richter, M. J. Garcia-Velloso; Clinica Universidad de Navarra, Pamplona, SPAIN.

Purpose: To compare 11C-Methionine (11C-MET) and 18F-Fluorodeoxyglucose (18F-FDG) PET/CT imaging outcomes for staging and re-staging patients with MM or other plasma cell malignancies. Furthermore, the potential added value of 11C-MET for the detection of active lesions was assessed. **Methods:** A total of 41 patients (23 males; mean age, 58±11 years, range 31-76 years) were retrospectively evaluated by means of 11C-MET and 18F-FDG PET/CT. Thirty-four patients had MM, 3 smouldering multiple myeloma (SMM), and 4 plasmacytoma. Fifty-two PET/CT studies were included in the analysis, 11 patients were referred for staging, 32 for response evaluation and 9 for relapsed disease. Qualitative and semi-quantitative image analyses were performed. Bone marrow (BM) and maximal lesion SUVmax were compared for both, 11C-MET and 18F-FDG. Histopathology and/or data extracted from electronic medical records served as the standard of reference. Differences among groups and their correlations were analysed using Mann-Whitney U test. **Results:** 11C-MET detected active lesions in 32/37 (86%) studies performed, whereas 4 of them were missed with 18F-FDG. In addition, in 18 (56%) studies 11C-MET identified more focal lesions. The SUVmax of the most avid lesion was significantly higher for 11C-MET (median 6.3; IQR 3.1-9.1) than for 18F-FDG (median 3.3, IQR 1.7-4.5; p<0.01) in 32 studies. On the other hand, 18F-FDG revealed focal active lesions in two patients without 11C-MET uptake. One of that focal uptakes demonstrated no tumor infiltration in the histopathological analysis (false positive) and the other one became negative at follow-up. Normal BM SUVmax was significantly (p<0.01) higher for 11C-MET (2.3±0.5) than for 18F-FDG (1.5±0.4). At staging 11C-MET demonstrated diffuse bone marrow infiltration in two patients, one with SMM (SUVmax=9) and another patient with MM (SUVmax=3.4), whereas 18F-FDG did not depict active disease. In the remaining patients, both tracers yielded comparable results. Extramedullary MM was identified in 4 patients with 11C-MET (median SUVmax=6.2; IQR 4.5-7.6) and in 3 with 18F-FDG (median SUVmax=4.3; IQR 3.4-7.6). **Conclusion:** 11C-MET PET/CT presented better outcomes than 18F-FDG in the assessment of active disease, being able to detect more medullary and extramedullary active lesions. 11C-MET PET/CT appears to be an accurate biomarker for active disease detection with a significant added value in the diagnostic imaging work-up of MM patients.

EP-0708

Diagnostic Value Of 18F-FDG PET/CT Imaging In Patients With Multipl Myeloma

*U. Telci, **S. Ucak Semirgin**, M. Sahin, T. Basoglu; Ondokuz Mayis University Nuclear Medicine Department, Samsun, TURKEY.*

Aim: Multiple myeloma is a hematological malignancy which is proceeding with the uncontrolled proliferation of plasma cells in bone marrow. We aimed to evaluate the value of FDG PET/CT, one of the methods most frequently used in oncology, in the diagnostic approach of multiple myeloma in our study. **Material and Methods**: Patients who have multipl myeloma or related monoclonal gammopathy and FDG PET/CT scan were investigated retrospectively. Finally, 40 female and 48 male patients who had bone marrow biopsy, biochemical tests and bone survey and/or MRI were included in the study. Patients were evaluated according to revised IMWG diagnostic criteria. Italian Myeloma Criteria for PET used for visual and quantitative F-18 FDG PET/CT assesment without clinical information. **Results**: Patients were diagnosed with MGUS (n=14), SMM (n=9) and MM (n=65). In bone survey, 9/25 of patients with no abnormal findings showed pathological focus in MRI and/or F-18 FDG PET/CT. All patients with pathological bone survey findings (15/15) were also abnormal in all FDG PET/CT images and in 14/15 patients in MRI. In 3/20 (15%) patients with normal MRI findings, FDG PET/CT study showed pathological focus. In the other hand, in 4/23 patients with pathological MRI findings, the results of FDG PET/CT were normal. Lytic lesions were detected in 44/65 patients in FDG PET/CT examinations. There was at least one paramedullary lesion in 21/44 patients with lytic lesions. There was also at least one fracture in 11/65 patients on the group of MM and 2/9 patients on the group of SMM. SUVmax value of focal lesions were found as 4,9 (1,23-15,75) and the value of Deauville score (DS) was 4 (2-5) in metabolic imaging. There was a correlation between lesion SUVmax value and lesion DS (r=0,86; p<0,001). There was a correlation between lesion SUVmax and number of lytic lesion (r=0,50; p=0,001) and DS and number of lytic lesion (r=0,55; p<0,001). **Conclusion**: Demonstrations of lesions glycometabolic activity and pathological foci without bone findings with FDG PET/CT are possible as well as detection of lytic lesions. FDG PET/CT is superior to conventional methods and has the advantage over MRI, because outside the MRI area can be detected. DS which provides standardization of the lesion metabolic activity is considered useful.

EP-51   **during congress opening hours, e-Poster Area**

Clinical Oncology: Bone

EP-0709

Osteoarthritis of the knee evaluated using images of bone uptake of myocardial perfusion agent

R. Tanaka, M. Ebine; Chiba Institute of Science, Choshi, JAPAN.

Purpose: Cellular uptake of the myocardial perfusion agent 99mTc-sestamibi (MIBI) is related to mitochondrial membrane potential activity. In the present study, we administered MIBI to patients with osteoarthritis of the knee and examined the relationship with osteomyelitis using bone uptake and magnetic resonance imaging (MRI). **Methods:** This study included 39 patients with osteoarthritis of the knee, who were hospitalized for tests for knee replacement surgery, and 10 healthy individ-

uals as controls. Planer images of the knee were acquired 30 min after the administration of MIBI injection. Regions of interest were set for the bone substance of the knee and for the quadriceps femoris muscles from the planar images. The mean radioisotope (RI) count was then calculated. Short-tau inversion recovery (STIR) MRI of the same site was taken, and the presence or absence of osteomyelitis was determined based on the contrast value. **Results:** The mean RI count for the bone substance was significantly higher at 20.8 ± 6.3 in the osteoarthritis group compared to 6.4 ± 1.6 in the control group (p < 0.001). The mean RI count for the quadriceps femoris muscles was 20.9 ± 8.0 in the osteoarthritis group and 23.1 ± 4.0 in the control group, with no significant difference observed between the two groups. The mean contrast value on STIR MRI was 921.4 ± 138.9 for the healthy area and 1993.7 ± 666.0 for the affected area, with a significant difference observed (p < 0.001). Furthermore, the RI count on planer images of the bone substance in the osteoarthritis group and the contrast value on STIR imaging had a significant correlation of r = 0.74 (p < 0.001). **Conclusion:** Osteoclasts and osteoblasts seem to have increased with bone remodeling activity in patients with osteoarthritis of the knee accompanied with osteomyelitis, due to which the data showed an increase in MIBI uptake on planer imaging. Moreover, the degree of MIBI uptake showed a correlation with MRI images, suggesting that it could serve as an indicator in the evaluation of osteomyelitis severity.

EP-0710

Extraosseous Accumulation of Tc-99m-MDP on Bone Scan in a Four-years-old Boy With Acute Lymphoblastic Leukemia: A Case Report

F. Banezhad Jannati, S. Zakavi, N. Ayati; Mashhad University of Medical Sciences, Mashhad, IRAN, ISLAMIC REPUBLIC OF.

Introduction: Extraosseous accumulation of technetium-99m-methyl diphosphonate(TC-MDP) on bone scan is not common. This phenomenon is often attributed to abnormality of calcium metabolism and has been reported in a variety of conditions including metabolic diseases and malignancies. **Methods**: We are presenting a four-years, nine months-old boy that was admitted to the pediatric emergency with poor health and severe respiratory distress. The patient had been suffering from fatigue, respiratory symptoms, weight loss, intermittent fevers, anorexia, nausea and vomiting, edema of legs and abdominal distension from one month earlier. The initial laboratory analysis also revealed hypercalcemia. The patient was referred for whole body bone scan with suspicion of malignancy and bone metastasis. After IV injection of 2mci of Tc-99m-MDP bone scan was performed in multiple spot and SPECT views. The bone scan revealed highly increased radiotracer uptake in both lungs in the perfusion and blood pool phases. Delayed images also showed increased activity in lungs and gastric wall. The skeleton was not seen clearly. Bone marrow aspiration was done and established the diagnosis of ALL. The patient received packed cells, platelets and broad-spectrum antibiotics. He deceased due to respiratory failure 20 days later. **Results**:

According to the literature two patients with ALL have been reported with exraosseous accumulation of ^{99m}Tc-MDP. We have not find any report from pediatric patients with ALL and high ^{99m}Tc-MDP lung uptake in Medline. Highly increased diffuse lung uptake in this patient was consistent with respiratory failure and poor prognosis. It is reported that bone scan may be of clinical utility in assessing the extent of metastatic calcification and instituting appropriate management to prevent organ failure. **Conclusion:** In conclusion, diffuse lung uptake of ^{99m}Tc-MDP in pediatric patients with ALL may have important prognostic value.

EP-0711

Clinical value of ^{99m}Tc-MIBI scintigraphy for bone lesions with indefinite diagnosis by ^{99m}Tc-MDP bone imaging

Z. J. Ren[1], r. g. yang[2], w. z. huo[2], h. x. wang[2], y. liu[2], q. kong[2]; [1]Shandong Jining No.1 People's Hospital, Shandong province, CHINA, [2]Shandong Cancer Hospital affiliated to Shandong University, Shandong province, CHINA.

Introduction: To investigate the clinical value of ^{99m}Tc-MIBI scintigraphy in differential diagnosis of bone lesions in tumor patients. **Methods:** Fifty-two patients with bone isolated lesions (≤3) found by ^{99m}Tc-MDP bone scintigraphy was enrolled from June 2014 to November 2015. However, whether the bone lesions were malignant was not clear on ^{99m}Tc-MDP imaging. ^{99m}Tc-MIBI double-phase (10 min and 30 min after injection of ^{99m}Tc-MIBI) SPECT/CT imaging was performed in a week after ^{99m}Tc-MDP bone scintigraphy. The final diagnosis was made according to results of more than two imaging modalities (CT or MRI or PET/CT) and/or follow-up (≥6 months). The diagnostic efficiency of ^{99m}Tc-MIBI SPECT/CT imaging was calculated. The clinical data of chemotherapy were also collected. Patients with bone metastasis were grouped as the treatment response (CR+PR, SD+PD). Retention index (RI) of metastatic lesions was calculated and compared between the 2 groups(two-sample t test). The relationship between RI and chemotherapy efficacy was investigated by Spearman correlation analysis. **Results:** A total of 12 benign lesions and 84 malignant lesions were eventually diagnosed. The sensitivity, specificity, positive predictive value (PPV), negative predictive value (NPV) and Youden index of ^{99m}Tc-MIBI scintigraphy were 96.43%(81/84), 83.33%(10/12), 97.59%(81/83), 76.92%(10/13), and 0.80, respectively. The RI was statistically different between CR+PR, group and SD+PD group: -0.142±0.036 vs -0.384±0.067(t=2.367, P<0.05). The RI of ^{99m}Tc-MIBI in bone metastases was positively correlated with the chemotherapy efficacy (rs=0.78, P<0.01). **Conclusions:** The ^{99m}Tc-MIBI scintigraphy is helpful in differential diagnosis of bone lesions with indefinite diagnosis by ^{99m}Tc-MDP bone scintigraphy in tumor patients. The ^{99m}Tc-MIBI RI of bone metastasis may predict the efficacy of chemotherapy efficacy.

EP-0712

Interobserver agreement in the evaluation of Sodium Fluoride-PET/CT for the evaluation of bone metastases in prostate cancer

H. D. Zacho[1], R. F. Fonager[1], J. B. Nielsen[1], C. H. Nielsen[2], H. W. Hendel[2], L. J. Petersen[1]; [1]Dept of Nuclear Medicine, Aalbrg University Hospital, Aalborg, DENMARK, [2]Dept of Nuclear Medicine, Herlev Hospital, Herlev, DENMARK.

Purpose: The objective of this study was to assess the observer agreement among trained observers in the interpretation of sodium fluoride PET/CT (NaF PET/CT) in a population of patients with prostate cancer at different stages. **Materials and Methods:** The study group consisted of 84 patients with prostate cancer at various stages (newly diagnosed, with biochemical recurrence, undergoing ADT or chemotherapy). The patients had been participating in four prospective studies conducted at Aalborg University Hospital. The NaF PET/ with low dose CT was conducted as a part of a study related procedure. The NaF-PET/CT images were blindly evaluated by two nuclear medicine physicians experienced with evaluation of NAF PET/CT (five and ten years of experience, respectively). The two observers were blinded to all clinical data except for the diagnosis of prostate cancer. Each NaF PET/CT was classified on a patient level using a three category scale (M0: no bone metastases, Me: equivocal for bone metastases and M1: bone metastases present) and subsequently on a dichotomous scale (bone metastasis absent or present). Positive and negative controls were included in the group. Finally, if there was disagreement between the observers, they were asked to re-evaluate the NaF-PET/CT and provide a consensus diagnosis. **Results:** According to the consensus diagnosis 39 of 84 patients were M1, 8 patients had equivocal status of bone metastases (Me), and 37 were deemed M0. Crude agreement on the three category scale was seen in 80/84 patients (95 %). The kappa value was 0.95 (95% confidence interval: 0.78-1.0) corresponding to almost perfect agreement. The use of a dichotomous scale increased the crude agreement slightly (82/84, 98 %) with a resultant increase in the kappa value (kappa 0.98, 95% confidence interval: 0.76-1.0). However, no statistical significant difference between using a three category scale or a dichotomous scale was observed. **Conclusion:** There is a high level of agreement among trained observers for evaluation of NaF PET/CT in patients with prostate cancer on a three-category scale. The agreement was numerically slightly higher - though not significantly - when a dichotomous scale was used. A three category scale is suggested as it previously have been shown to be easier adaptable to the clinical setting and can be used without decreasing the agreement between readers.

EP-0713

Feasibility Of Nuclear Medicine In Prognosis And Evaluation Of Effectiveness Of Therapy By Bisphosphonates

V. Sukhov[1], A. Marin[1], P. Kirichenko[1], K. Zaplatnikov[2]; [1]Military Medical Academy, ST. PETERSBURG, RUSSIAN FEDERATION, [2]MAZ Nuclear Medicine, Nuernberg, GERMANY.

SZoledronic acid (ZA) is a unique synthetic analogs of bone matrix - bisphosphonate (BF), third generation that containing 2N atoms, making it more active among other BFs for bone resorption caused by MTS or bone-degenerative processes and directly acting against tumor cells. ZA most strongly inhibits activity of osteoclasts, as it has ability to block synthesis of mevalonate (osteoclast stimulator). ZA also differ from other BPs by it's selective effect on bone tissue, w/o affecting normal bone remodeling, direct antitumor effect, ability to suppress proliferation and cause apoptosis of tumor cells, potentiate antitumor and analgetic effect of other drugs. Study was conducted to determine possibility for use of "Resoscan,99mTc" for prognosis and efficacy assessment of ZA treatment and included 210 patients with Cr of prostate, breast, thyroid, kidney, lymphomas, multiple myeloma, mean age 51 years, 126 m/84 w, who had Rx, CT or MRI mts bone deposits, including osteolytic. Based on whole body scan (WBS) with Rezoscan treatment with 90 mg of pamidronate and 4 mg of ZA was indicated to 63 and 147 patients, respectively, by IV infusions every 3-4 weeks. All patients underwent repeated WBS procedures during and after the BP treatment course. High uptake of "Rezoscan" in metastatic foci (also lytic) was detected in all patients. After the first WBS and detection of high uptake, patients received more than 2 Tx procedures (from 1 to 6). In most patients WBS noted positive response to BP-therapy. In 86% (126 of 147 patients) of treated with ZA, partial response (PR) was achieved, which resulted in a decrease in foci number and decrease of tracer uptake and levels of biochemical markers of bone metabolism. In 21 patients, despite the treatment of ZA and in all patients treated with pamidronate, no PR was observed (stabilization or progression of the disease), that requires change of therapeutic scheme. Positive response to treatment with BP can be predicted and evaluated using WBS with Rezoscan as labeled analog of the therapeutic agent as it correlated with focal tracer uptake. PPV was very high that led to use of BP to prevent the further development of the disease and to obtain a therapeutic effect. Pathophysiology of bone metastatic lesions at different stages and in various diseases can undergo changes. This requires use of different schemes of using BPs. WBS with Rezoscan can help to choose therapeutic regimen and specific BP.

EP-0714

When there is no other option: Utility of Bone Scintigraphy in Oncology in a resource constrained environment

E. N. B. Hammond; Ghana Atomic Energy Commission/ National Centre for Radiotherapy and Nuclear Medicine, Accra, GHANA.

Purpose: To evaluate bone scans done in the past year for purposes of oncology in our department and the usefulness of the information obtained to referring physicians and clinicians. **Methodology:** We retrospectively reviewed bone scan data of 483 patients with histologically confirmed malignancies. These were then analysed looking at the age and sex of the patients, the diagnosis, indication or reason for referral and the presence of metastases. We also compared scans of patients who had 2 or more scan to assess for disease progression. **Results:** A total of 483 patients were included comprising 397 males (82.2%) and 86 (17.8%) females. The age range of patients was from 12 years to 88 years with both median and modal age being 66 years. Ca prostate patients made up 80.1% (387) of the total number

of patients whilst breast Ca was 14.9% (72). Other oncological diagnosis such as Ca cervix, Nasopharyngeal Ca, Ca lung, Thyroid Ca and Ca of unknown primary make up the remaining 5% (24 patients). Patients who were referred for exclusion of bone metastases totaled 439, which made up 90.9% of the total number of patients. 41 patients (8.5%) had follow-up scans to assess for disease progression whilst 3 patients (0.6%) were referred for other reasons Of the 483 patients included in the study, 162 (33.5%) were positive for bone metastases, 286 (59.2%) were negative for bone metastasis whilst only 35 (7.2%) had equivocal studies. Table 1.1 shows groups the scan findings according to patient diagnosis. Table1.1: scan findings grouped according to diagnosis When those with scans showing bone metastases were grouped according to age, 78.9% of patients below 40 years had bone metastases whilst 38.4 % of patients between 40 - 60 years had metastases. Those between 61- 80 years and above 80 years had 28.6% and 33.7% respectively showing metastases (p value 0.00) Of the 41 patients with previous scans, 39 were analyzed. 51.3% of these patients showed diseases progression whilst 41% remained unchanged with only 7.7% showing improvement. **Conclusion:** Bone scans are still a very valuable resource in the management of oncology patients, especially in low resourced countries and play a significant role in management planning. There should be a low threshold for performing bone scans in younger patients as they have higher risk of developing bone metastases. Regular and frequent follow-up of patients with bone scan is also be very helpful in assessment of disease progression.

EP-0715

Comparison of ^{99m}Tc-MDP Bone Scintigraphy and ^{18}F-FDG PET/CT to predict histologic response to neoadjuvant chemotherapy in patients with osteosarcoma

B. Byun, S. Lim, K. Lee, C. Kong, J. Choi; Korea Institute of Radiological and Medical Sciences, Seoul, KOREA, REPUBLIC OF.

Purpose: We compared the usefulness of ^{99m}Tc-MDP bone scintigraphy and ^{18}F-FDG PET/CT in predicting histologic response in patients with osteosarcoma receiving neoadjuvant chemotherapy. **Subjects & Methods:** We retrospectively enrolled 62 patients with high-grade osteosarcoma treated with two cycles of neoadjuvant chemotherapy (NAC) and surgery. All patients underwent ^{99m}Tc-MDP bone scintigraphy and ^{18}F-FDG PET/CT before and after NAC. ^{99m}Tc-MDP uptake of primary tumor was measured quantitatively as the maximum tumor-to-nontumor ratio (T/NT) and ^{18}F-FDG uptake was measured as the maximum SUV (SUV) before and after NAC. The percent changes of T/NT (%T/NT) and SUV (%SUV) after NAC were calculated respectively, and the correlations between these parameters were evaluated. After surgery, the effects of NAC were graded histopathologically (good vs. poor) and the optimum cut-off values of %T/NT and %SUV for predicting histologic response were assessed by ROC curve analysis respectively. **Results** %T/NT and %SUV positively correlated with each other (r = 0.549, p < 0.001). Based on ROC curve analysis, both %T/NT (AUC = 0.768, p < 0.001) and %SUV (AUC = 0.829, p < 0.001) predicted good histologic response.

However, there was no significant difference between the AUCs of %T/NT and %SUV (p = 0.373). The sensitivity and specificity for predicting good histologic response were 83.3% and 75.0%, for the criterion of %T/NT < -10% and 80.0% and 81.2%, for the criterion of %SUV < -45%. **Conclusions** Both ^{99m}Tc-MDP bone scintigraphy and ^{18}F-FDG PET/CT are useful for predicting histologic response after NAC in osteosarcoma.

EP-0716

The usefulness of maximum standardized uptake value of quantitative bone SPECT/CT

M. Ishibashi, Y. Tanabe, T. Ogawa; Faculty of Medicine, Tottori University, Yonago, JAPAN.

Aim: A new SPECT/CT has enabled to quantify bone uptake as standardized uptake value (SUV) in bone scintigraphy. The aim of this retrospective study was to evaluate the usefulness of quantification on bone SPECT/CT for the differentiation among bone metastases, degenerative changes, and fracture. **Materials and Methods:** We analyzed 69 male patients (mean age 72.1±8.7 years, age range, 49 - 95 years) with newly diagnosed prostate cancer who underwent bone SPECT/CT between February 2016 and April 2017. SPECT/CT was performed after approximately 3 hours after injection of Tc-99m HMDP. Maximum SUV (SUVmax) was measured for normal vertebrae, normal rib, degenerative change, benign fracture and osteoblastic bone metastasis on SPECT/CT images reconstructed by the ordered subset conjugate gradient minimization (OSGCM) methods. We compared the SUV max of normal vertebrae, normal rib, degenerative change, benign fracture and bone metastases. **Results:** Twelve patients of them had bone metastases. The mean ± standard deviation of SUVmax were 6.2±2.4 for normal vertebra (n=57), 4.6±1.0 for normal rib (n=44), 13.7±5.2 for benign rib fracture (n=8), 22.1±5.6 for benign compression fracture (n=3), 14.9±4.7 for degenerative change of vertebra (n=42), 23.6±9.2 for rib metastases (n=8), and 38.6±15.1 for vertebral metastases (n=9). The SUVmax of vertebral metastases was significantly higher than those in normal vertebra and degenerative change (P<0.01). The SUVmax of rib metastases was significantly higher than that of normal rib (P<0.01). On the other hand, there was no significant difference in SUVmax between benign rib fracture and rib metastases. **Conclusions:** The evaluation of SUVmax on bone SPECT/CT would be useful to distinguish bone metastasis from degenerative changes.

EP-0717

Tc^{99m} MDP SPECT-CT based modified Mirel's classification - a new approach to evaluate for impending pathologic fractures

S. Riaz[1], H. Bashir[1], I. K. Niazi[2], S. Butt[3], F. Qamar[4]; [1]Nuclear Medicine department, Shaukat Khanum Memorial Cancer Hospital & Research Centre (SKMCH&RC), Lahore, PAKISTAN, [2]Radiology department, SKMCH&RC, Lahore, PAKISTAN, [3]Radiation Oncology department, SKMCH&RC, Lahore, PAKISTAN, [4]Surgical Oncology department, SKMCH&RC, Lahore, PAKISTAN.

Purpose/Introduction: Osseous metastases predispose the bones to impending risk of fracture. Conventional Mirel's scoring system quantifies the risk of sustaining a pathologic fracture in weight bearing long bones based on radiographs. Our study proposes SPECT-CT based modified Mirels' scoring system and its comparison with conventional Xray based Mirel's scoring. **Material & Methods:** A prospective review of Tc99m MDP SPECT-CT scans performed in patients referred to Shaukat Khanum Memorial Cancer Hospital and Research Centre, Lahore, Pakistan, between July 2016 and April 2017. A total of 32 metastatic lesions in weight bearing long bones were evaluated in 16 patients; aged 35 to 75 years, 11 males and 5 females. As per Mirel's criteria each lesion was assessed for the site (upper limb, lower limb, Peritrochanteric), type (blastic/mixed/lytic), MDP avidity (avid, mixed, non-avid), size on X-ray (<1/3rd, 1/3-2/3, >2/3rd) and pain (mild, moderate, functional). For modified Mirel's scoring system same variables were observed using the Tc99m MDP SPECT-CT scans. Additional parameters recorded include: cortical lysis, circumferential involvement and extra-osseous soft tissue. Clinical recommendations were derived for both the scores as: <7 (radiotherapy and observation), 8 (clinical judgment), >9 (prophylactic fixation). Statistical difference between the two scoring systems was evaluated by applying Chi-square test (p<0.05). **Results:** Out of 32 lesions, 21 (66%) were peritrochanteric and 11 (34%) involved shaft of the femurs. X-ray based Mirel's scores were; <7 [n=5,21.8%], 8[n=15,46.9%] and >9 [n=12,37.5%]. SPECT-CT based Mirel's score were; <7 [n=8,25%], 8[n=15,46.9%] and >9 [n=9,28%]. On bivariate analysis, there was statistically significant difference in the results of two scoring systems with an overall change in scores in 6 lesions (p<0.01). Cortical lysis was noted in 8(24%) lesions on SPECT-CT versus only 2 (6.3%) on X-rays. SPECT-CT showed that 65% of lesions involved more that 50% of the circumferential diameter on axial images. One patient had extra-osseous soft tissue extension. **Conclusions:** Our pilot study shows that a modified Mirel's scoring system based on bone SPECT-CT can yield useful information about predicting risk of fracture in skeletal metastases.

EP-0718

Diagnostic impact of quantitative bone SPECT/CT for patients with bone metastasis caused by castration resistant prostate cancer

Y. Fukushima, S. Kumita, G. Kimura, J. Akatsuka, T. Hamana, Y. Sugihara, T. Ando; Nippon Medical School, TOKYO, JAPAN.

Introduction: Ra-223 is an alpha-ray emitting radiopharmaceutical designed for the treatment of bone metastasis in patients with castration resistant prostate cancer (CRPC). Its therapeutic efficacy has been evaluated by calculating bone scan index (BSI) using BONE NAVI. However, the analysis using this software is based on conventional planar images which are often unclear and have low contrast. Recently, new quantification software (GI BONE) based on SPECT/CT images has been introduced. In comparison to planar imaging, bone SPECT/CT produces clearer, high-contrast images. The purpose of this study was to assess the diagnostic performance of quantitative SPECT/CT when using Ra-223 therapy for patients with CRPC and bone metastasis. **Materials and methods:** A total of 24 consecutive patients (74 ± 7 y) between Jun 2016 and April 2017, who were diagnosed to have CRPC with bone metastasis and indicated for Ra-223 therapy, were included in this study. All patients underwent pre-treatment bone scintigraphy via both planar and SPECT/CT imaging and were scheduled to receive Ra-223 therapy. Planar images were acquired 2 hours after the administration of ^{99m}Tc-HMDP 740MBq. Immediately after the planar acquisitions, SPECT and low-dose CT images were acquired using a SPECT/CT combined system: Symbia T2. SPECT data were reconstructed using CT attenuation correction, and SPECT/CT images were created by hardware fusion. BSI was calculated from planar images using BONE NAVI. SUVmax and overall total bone uptake (OTBU) were derived from SPECT/CT images using GI BONE. All patients were observed for a median of 5.2 (3.9-5.8) months until the end of treatment or death. The correlations between clinicopathological characteristics, including prostate specific antigen (PSA) and bone alkaline phosphatase (BAP), severity of bone metastasis, including BSI and OTBU, and patient outcomes were analyzed. **Results:** BSI, SUVmax, and OTBU were 2.25 (0.58-5.24), 33.78 (21.18-46.12), and 912648.56 (200837.71-1651571.82), respectively. BSI, SUVmax, and OTBU were not correlated with PSA. BSI and OTBU were correlated significantly with BAP (r = 0.86, p < 0.001; r = 0.61, p = 0.005; respectively) and SUVmax was not (r = 0.20, p = 0.410). Patients with high OTBU had poorer prognoses than those with high BSI [8 of 10 (80%) vs. 10 of 14 (71%)]. OTBU was a better prognostic factor for predicting patient outcomes than BSI. **Conclusions:** Quantitative parameters, such as OTBU, derived from bone SPECT/CT, may have a higher diagnostic performance compared to parameters from planar imaging, such as BSI, for patients with bone metastasis caused by CRPC.

EP-0719

Hybrid bone scintigraphy in gastrointestinal malignancies

*N. Rashid, **H. Bashir**, S. Riaz, A. Hassan; Nuclear Medicine department, Shaukat Khanum Memorial Cancer Hospital & Research Centre (SKMCH&RC), Lahore, PAKISTAN.*

Purpose: Bone metastases in GI malignancies are uncommon and known to be predominantly lytic thus rendering a limited role for conventional bone scintigraphy. The aim of the study is to review Tc^{99m}MDP bone scans performed in patients with known gastrointestinal malignancy and the utility of SPECT/CT in characterisation of bone lesions. **Material & Methods:** Retrospective review of bone scans done between June 2014 to December 2016 in patients with known gastrointestinal malignancy, using electronic Hospital Information System (HIS). **Results:** A total of 110 patients (60 males, 50 females; age range: 22 - 84 years) had bone scan over the 30 months period. The commonest indications for referral was suspected bone metastasis on other imaging [CT (n 56), MRI (n 10), PET/CT (n 6)], musculoskeletal pain (n 37), pathological fracture (n 1), neurological symptoms (n 1), hypercalcemia (n 1) or others (n 14). Metastatic lesions were identified in 32 (29%) patients while 78 (71%) patients had benign non-aggressive lesions or normal bone scans. Amongst 32 patients with osseous metastasis unifocal lesion

(25%) were identified in 8: axial skeleton (n 2) appendicular skeleton (n 6). 24 (75%) patient had multifocal lesions; axial skeleton (n 6), appendicular skeleton (n 6) and both axial + appendicular (n 12). Only 4 (12%) patients had concurrent visceral metastasis along with osseous metastasis. In our cohort, based on the location of primary tumor the frequencies of osseous metastasis were; esophagus 35% (15 out of 43), gastric 39 %(7 out of 18), gastroesophageal junction 1.5% (1 out of 8) and colorectal 22.5% (9 out of 40). SPECT/CT was acquired in 29 out of 110 patients, which characterised metastatic lesions (n 12) and benign looking non-aggressive entities (n 17). Overall, bone scan upstaged disease in 31% and down staged 15% patients. **Conclusion:** Bone metastases in GI malignancies, though uncommon, show an aggressive pattern, with axial and appendicular involvement, and can be readily identified with hybrid bone scintigraphy in symptomatic patients. **Key words:** hybrid imaging, Tc^{99m} MDP, bone metastases, gastrointestinal malignancies

EP-52	during congress opening hours, e-Poster Area

Clinical Oncology: Soft Tissues & Sarcoma

EP-0720

Diagnostic Performance Of F18 FDG PET/CT In Recurrence Evalaution Of Chondrosarcoma -A Tertiary Care Centre Experience

S. K. Vadi, A. K. R. Gorla, A. Sood, A. Sood, R. K. Basher, N. Kakkar, A. Bhattacharya, B. Singh, B. R. Mittal; Post graduate institute of medical education and research, chandigarh, INDIA.

Purpose: To evaluate the diagnostic performance of contrast enhanced F-18 FDG PET/CT in patients with recurrent chondrosarcoma. **Materials and Methods:** Thirty-one histologically proven chondrosarcoma (29 conventional and 2 mesenchymal) patients (mean age 41.4 years, range 17-69 years; male 20) underwent F-18 FDG PET/CT (46 studies; 15 repeat studies) for recurrence evaluation (February 2010-December 2016) were retrospectively analyzed. All the patients were treated previously (n=46 studies; surgery alone 24, surgery and chemotherapy in 6, surgery and radiotherapy in 7 and all three modalities in 9 studies) prior to FDG PET/CT with interval of 2-72 months between last treatment and PET/CT, (mean duration 17) for residual or recurrent disease evaluation. Any abnormal FDG uptake with corresponding CECT lesion were taken as positive. Histopathological / clinical or imaging follow up were taken as gold standard. **Results:** FDG PET/CT detected abnormal FDG uptake in 20/31 patients (study-wise: 30/46 = 65.2%). Out of total 46 FDG PET/CT studies, uptake was noted at recurrent primary site (mean SUV max 8.23; range: 2.3-26.0) in 23 (50%), regional lymph node metastasis (mean SUV max 6.9; range: 2.3-23.0) in 8 (17.3%) and distant metastatic lesions in 17 (36.9%) studies. The metastatic disease alone without recurrent primary was seen in 6 studies. Recurrence at primary site alone was noted in 7 out of 23 studies and the remaining 16 studies had associated regional/systemic metastases (regional lymph nodes in 7, distant lymph nodes

in 3, associated lung lesions in 7, liver lesion in 1, muscular lesions in 3 and skeletal in 2 studies). The lesion based analyses of 17 studies with distant metastases showed involvement of lymph nodes, lung, muscular, skeleton and liver metastases in 4, 13, 4, 2 and 1 studies respectively. One patient with mesenchymal chondrosarcoma from the kidney showed FDG avid (SUV max 17.0) filling defect in the inferior vena cava. Out of the 22 patients (30 studies) in which PET/CT showed recurrence, true positivity was found in 17 patients (24 studies). On a per study basis, the sensitivity, specificity, PPV and NPV were 88.9% [95% CI: 70.8% to 97.6%], 68.4% [95% CI: 43.4% to 87.4%], 80.0% [95% CI: 67.0% to 88.7%] and 81.2% [95% CI: 58.8% to 92.9%] respectively for residual/recurrence detection. **Conclusion:** FDG PET/CT showed high diagnostic utility in recurrence evaluation of chondrosarcoma patients in the present study and should be validated with large scale prospective studies as an important imaging armamentarium in this rare disease.

EP-0721

The diagnostic ability of dynamic positron emission tomography with F-18 fluorodeoxyglucose and C-11 methionine in patients with musculoskeletal lesions

T. Shinya[1], Y. Otomi[2], K. Terazawa[2], M. Kubo[2], M. Harada[2], S. Kanazawa[1]; [1]Okayama University Hospital, Okayama-city, JAPAN, [2]Tokushima University Hospital, Tokushima-city, JAPAN.

Aims: The aim of this prospective study was to assess the discrimination abilities of dynamic positron emission tomography/computed tomography (PET/CT) with F-18 fluorodeoxyglucose (FDG) and C-11 methionine (Met) in musculoskeletal lesions in clinical practice. **Materials and Methods:** We performed dynamic PET studies with F-18 FDG and C-11 Met on 17 consecutive patients with 5 benign musculoskeletal lesions (2 schwannomas, 1 osteochondromatosis, 1 synovial osteochondromatosis, 1 hematoma) and 12 malignant musculoskeletal neoplasms (5 primary sarcomas, 4 metastatic soft tissue neoplasms, 3 diffuse large B-cell lymphoma). All participants had undergone dynamic PET/CT with F-18 FDG and C-11 Met on a different day. All of them had received no therapy before the PET/CT examination. The dynamic PET scans were performed in list-mode, beginning at 5 min after the tracer injection and continuing for 30 min (Dynamic 1 phase, 5-15 min; Dynamic 2 phase, 15-25 min; Dynamic 3 phase, 25-35 min). We had compared the maximum standardized uptake value (SUVmax) on each dynamic phase and the retention index [RI-SUVmax = {SUV(3)-SUV(1)}/SUV(1)×100%, where SUV(1) and SUV(3) are the SUVmax on dynamic 1 and 3 phases, respectively]. Receiver operating characteristic (ROC) curve analysis was performed to evaluate the predictive performance of differentiating benign lesions and malignancy. Discrimination was assessed by the area under the curve (AUC). **Results:** There were significant differences in the SUVmax on all dynamic phases and in the RI-SUVmax between benign and malignant lesions on F-18 FDG and C-11 Met PET/CT (all p values < 0.05). The ROC curve for diagnosing malignant musculoskeletal neoplasms revealed that the appropriate cut-off SUVmax values could be set on all dynamic phases in F-18 FDG PET

study and on dynamic 3 phase in C-11 Met PET study with a sensitivity of 100.0% and a specificity of 100.0%. All AUC values were 1.000 (95% CI; 1.000-1.000, p=0.004). For RI-SUVmax, the ROC curve analysis revealed the appropriate cut-off RI-SUVmax values were 1.20% with a sensitivity of 91.7% and a specificity of 75.0% on F-18 FDG PET study and -10.44% with a sensitivity of 83.3% and a specificity of 75.0% on C-11 Met PET study. The AUC values were 0.896 (95% CI; 0.722-1.000, p=0.021) on F-18 FDG PET study and 0.875 (95% CI; 0.690-1.000, p=0.029) on C-11 Met PET study. **Conclusion:** Dynamic F-18 FDG and C-11 Met PET/CT studies had the high diagnostic performance for discriminating the benign musculoskeletal lesions from the malignant musculoskeletal neoplasms with the semiquantitative analyses.

EP-0722
Interval from first symptoms to diagnosis in high-grade primary osteosarcoma and Ewing sarcoma of bone in relation to metabolic activity on FDG-PET/CT

A. C. M. Luijtgaarden[1], E. A. Usmanij[1], L. F. de Geus-Oei[2], J. J. W. de Rooy[1], U. E. Flucke[1], S. E. J. Kaal[1], V. L. M. N. Soomers[1], C. A. H. P. van Riel[1], H. W. B. Schreuder[1], W. J. G. Oyen[3], W. T. A. van der Graaf[3]; [1]Radboudumc, Nijmegen, NETHERLANDS, [2]Leiden University Medical Center, Leiden, NETHERLANDS, [3]The Institute of Cancer Research & Royal Marsden Hospital, London, UNITED KINGDOM.

Introduction: Diagnostic delay in osteosarcoma (OST) and Ewing's sarcoma (ES) may facilitate tumour growth and metastatic spread. Nevertheless, no negative impact of a long diagnostic interval on survival has been published, which suggests an important role of intrinsic tumour biology on prognosis. We analyzed the relationship between diagnostic interval and tumour metabolism depicted by maximum standardized uptake value (SUV_{max}) on FDG-PET/CT to better understand the relationship between tumor biology, diagnostic interval and outcome **Subjects and Methods:** In 41 patients diagnosed between January 2007 and April 2016 with OST (48.8%) or ES (51.2%) without synchronous metastases Spearman's ρ correlations were calculated between diagnostic interval and SUV_{max}. SUV_{max} was compared between short (< 75th percentile) and long diagnostic interval groups and impact of delay on overall survival (OS) in months was calculated. **Results:** Median SUV_{max} in all patients with short diagnostic interval was 8.2 versus 7.0 in the long interval group (ρ =-0,197 p=0.224); in OST, SUV_{max} was 8.9 versus 6.6 (ρ =-0.504 p=0.023) and in ES 7.6 versus 5.1 (ρ =-0.058 p=0.809) respectively. Median OS was longer in OST patients with long delay (70 versus 18 months, p=0.016) but not in the total (87 versus 62, p=0.055) or ES group (78 vs 76, p=0.854) **Conclusion:** We demonstrated that tumour metabolism at diagnosis was inversely correlated with diagnostic interval and patients with a long diagnostic interval showed a better survival in OST but not ES, suggesting that delay is at least partially caused by a more latent tumour biology. Results should be confirmed in a larger prospective series.

EP-0723
Diagnostic performance of 18F-FDG PET/CT in patients with Kaposi sarcoma: a preliminary retrospective study

S. Annunziata[1], A. Borghetti[2], S. Di Giambenedetto[2], A. Rizzo[1], M. L. Calcagni[1], A. Giordano[1], V. Rufini[1]; [1]Institute of Nuclear Medicine, Università Cattolica del Sacro Cuore, Rome, ITALY, [2]Institute of Infectious Diseases, Università Cattolica del Sacro Cuore, Rome, ITALY.

Purpose: Kaposi sarcoma (KS) is a rare soft-tissue cancer, originating by endothelial cells and generally shows muco-cutaneous lesions, but may also have nodal and visceral localizations. Diagnosis of KS is commonly based on clinical evaluation or biopsy. KS is more common in immuno-compromised patients (e.g. HIV), who often show synchronous primary tumours and inflammatory diseases. The role of imaging techniques in the different clinical settings is not defined yet. To our knowledge, only few reports about 18F-FDG PET/CT in patients with KS have been published until now. Aim of this study was to retrospectively evaluate the diagnostic performance of 18F-FDG PET/CT in patients with KS. **Methods:** All patients with KS submitted to 18F-FDG PET/CT in different clinical settings from January 2007 to December 2016 were retrospectively analyzed. The diagnostic performance of PET/CT in terms of positive predictive value (PPV), negative predictive value (NPV), sensitivity and specificity were calculated on a patient-based analysis, using histological or radiological examinations at follow-up as reference for the diagnosis of KS. Moreover, PPV and specificity of PET/CT for the diagnosis of both KS and possible synchronous primary tumours were evaluated. **Results:** Eighteen consecutive patients with KS were submitted to 18F-FDG PET/CT in the following clinical settings: staging (5/18, 28%), restaging (9/18, 50%), treatment evaluation (2/18, 11%), follow-up (2/18, 11%). Fourteen patients had a positive scan (14/18, 78%). On a patient-based analysis, true positive and false positive cases for the diagnosis of KS were 7 and 7 respectively (PPV of 50%). False positive cases resulted to be synchronous primary tumours (5/7) or inflammatory diseases (2/7), respectively. Four patients had a negative scan (4/18, 22%) and all were confirmed to be true negative (no false negative, NPV of 100%). Consequently, sensitivity and specificity were 100% and 36% respectively. Considering a diagnosis of both KS and synchronous primary tumours as true positive, PPV and specificity improved (85% and 67% respectively). **Conclusion:** In this preliminary retrospective study, 18F-FDG PET/CT seems to be an accurate diagnostic tool to exclude lesions from KS. Nevertheless, false positive findings such as synchronous primary tumours and inflammatory diseases could affect the accuracy of FDG-PET/CT in the diagnosis of KS, even though the detection of a synchronous tumour has an impact on clinical management. Larger prospective studies about the role of FDG-PET/CT in KS are needed, especially in order to compare PET/CT with other diagnostic tools and to evaluate the possible impact on clinical management.

EP-0724
The F-18 FDG PET/CT and CT evaluation of plevral plaques

Z. Koç, P. Özcan Kara, Y. Balcı; Mersin University Hospital, Mersin, TURKEY.

Aim: Pleural plaques have the possibility of bearing malignancy thus investigation of this entity is important and the most important indicator of malignancy in general is FDG accumulation in radiological appearance. However there is discrepancy between results of previous studies in the literature about this subject. The aim of this study is to analyze the standadized uptake value of pleural plaques and the cut off levels for malignancy in comparison with CT. **Materials and Method:** Seventy one patients were included in the study (27F, 44M; mean: 59,9±13,1 years). Oncologic F-18 FDG PET/CT was performed to all the subjects for a different primary tumor. Pleural plaques (18 bilateral, 35 right, 21 left) were identified in all patients in CT component of PET/CT examination. The mean SUVmax levels of the lesions with FDG uptake were mean 6,5±4,4 (n=46) and 7,1±3,8 (n=25) respectively in right and left hemithorax. Twenty patients were out of follow up. The PET/CT and CT images were evaluated by an experienced Nuclear Medicine and Radiology physician independently according to the gold standard pathology. **Results:** The diagnostic sensitivity, specificity and accuracy of CT was; 41%, 75% and 56% respectively and if the cut off SUVmax level was accepted '4' the diagnostic sensitivity, specificity and accuracy of PET was 71%, 47%, 62% respectively. **Conclusion:** The most appropriate cut off level for evaluation of pleural plaques in PET examination was '4' according to the study results. The sensitivity and accuracy of PET was higher compared to CT with this cut off value. **Key words:** pleural plaques, FDG, PET, CT.

EP-0725

Ga68 DOTATATE PETCT Imaging In Oncogenic Osteomalacia - Experience From A Tertiary Hospital In Southern India

J. Hephzibah, T. V. Paul, D. Mathew, N. Shanthly, R. Oommen; Christian Medical College, Vellore, VELLORE, INDIA.

Purpose: Utility of Ga68 DOTATATE PETCT imaging to localise cause for oncogenic osteomalacia. **Subjects and Methods**: Retrospective analysis between 2015 -17 of patients who presented with nonspecific generalized / localized unexplained bone pains, proximal myopathy with hypophosphatemia and who underwent Ga68 DOTATATE PETCT imaging. Following biochemical parameters were estimated at baseline: Serum phosphate mg/dL (S.P), Serum Calcium mg/dL (S.Ca), Parathyroid hormone pg/ml (PTH), Serum Alkaline phosphatase U/L (SAP), Fibroblast growth factor 23 [C-terminal] RU/ml (FGF23), 24 hour urine phosphorous in mg/L, Vitamin D levels ng/ml. Bone scan when applicable. Tubular maximum phosphorus reabsorption/glomerular filtration rate (Tmp/GFR in mmol/L) was calculated as a product of fractional tubular reabsorption of phosphate (TRP) and S.P. **Results:** Total of 21 patients were analysed; age range 18-65 years, 8 females, 13 males. Fourteen out of 21 (66.6%) were found to be positive for a possible mesenchymal tumour and 7/21 (33.33%) were negative. Of the positives, 8 were in lower limbs, 3 in head and neck (2 in ethmoid, 1 in left choana), 1 presacral, 1 multiple neurofibroma, 1 in right 7th rib. Of these, 5 patients underwent surgery, 1 had curettage - biopsy was reported as mesenchymal tumour. Biochemical

parameter ranges were as follows: FGF23 47-1500, SAP 104-433, S.Ca was within normal, S. P 0.9 -2.2, PTH 3.1 to 222, 24 hour urine phosphorous 269-1200. Tmp/GFR was calculated in 9/14 patients, it was found to be between 0.1 - 0.51mmol/L (Normal range 0.8-1.35mmol/L). S.P levels was normalised in all 5 who underwent surgery with a range of 2.8 to 5.2. Serum FGF was done in 3 /5, was 5 - 95.2. Of remaining positives 8/21 received medical management with neutral phosphate. At follow up within 6 months, phosphorous level was normalised in 4, remained low in 2 and not done in 2. Seven patients with negative DOTATATE scan with S.P between 1.4 -2.0, 6/7 received medical management. On follow up S.P was done in 5 patients, was normalised only in one patient. **Conclusion:** In patients presenting with severe weakness of extremities, musculoskeletal pain, oncogenic osteomalacia should be considered as a possible cause. Although localisation of these small mesenchymal tumours are challenging, it should be extensively investigated and excised as clinical and biochemical changes are possibly reversible. In our observation, we found Ga68-DOTATATE PET/CT is a useful investigatory modality for localizing cause for oncogenic osteomalacia.

EP-0726

Quantification of tumor blood flow in sarcomas from dynamic ^{99m}Tc-MIBI SPECT : Validation and clinical employment

W. Y. Ussov[1], V. M. Gulyaev[1,2], E. V. Barysheva[3], O. Y. Borodin[2], I. I. Anisenia[4], Y. I. Tyukalov[4]; [1]Institute of Cardiology, Tomsk, RUSSIAN FEDERATION, [2]Tomsk Regional Institute of Oncology, Tomsk, RUSSIAN FEDERATION, [3]Clinical and Diagnostic Center, Tomsk, RUSSIAN FEDERATION, [4]Institute of Oncology, Tomsk, RUSSIAN FEDERATION.

Purpose: Although ^{99m}Tc-MIBI has been shown and widely used for imaging of bone sarcomas, quantitative analysis of ^{99m}Tc - MIBI uptake remains unemployed in routine diagnosis and follow-up of musculoskeletal tumors. We analysed uptake kinetics of ^{99m}Tc-MIBI to bone sarcomas as a technique for quantification of blood flow in vital tumor tissue as part of SPECT-MRI multimodal imaging. **Subjects and Methods:** Assuming ^{99m}Tc-MIBI uptake to sarcoma unidirectional for early few minutes after injection, the Gjedde-Rutland-Patlak (GRP) approach was applied, delivering classic equation: $C_{tum}(t)/C_h(t) = K*\{\int C_h(\tau)d\tau / C_h(t)\} + V_0$, where $\boldsymbol{C_{tum}(t)}$ is radioactivity in sarcoma, $\boldsymbol{C_h}$ -blood concentration of ^{99m}Tc-MIBI, $\boldsymbol{K}$ - transport constant. Plotting$\{\int C_h(\tau)d\tau / C_h(t)\}$as X, and $C_{tum}(t)/C_h(t)$ as Y, the $\boldsymbol{K}$ can be obtained as slope . $\boldsymbol{K}$ is clearance equal to product **(retention fraction) * (tumor blood flow): K = E * TBF**. TBF can be then calculated as ratio **K/E**. **E** was obtained from **A(t)** and $\boldsymbol{C_h(t)}$ time series as asymptote of ^{99m}Tc-MIBI retention function $\boldsymbol{h(t)=F^{-1}\{F[A(t)]/F[C_h(t)]\}}$, where **F** is Fourier transforms. In 32 patients with various musculoskeletal tumors the dynamic SPECT (in twelve) or scintigraphy (in twenty) were performed with bolus injection of 540 MBq of ^{99m}Tc -MIBI and acquisition of tumor uptake of radioactivity with simultaneous blood sampling. From the blood input and tumor curves the TBF were calculated as descibed above. Vali-

dation study with intraaortal catheter injection of ^{99m}Tc-labelled macroaggregates of albumin (MAA) was carried out in 12 patients. **Results**: Validation with ^{99m}Tc-MAA revealed significant correlation (r=0,89; p<0,002) between TBF values calculated from dynamic ^{99m}Tc-MIBI uptake data and from ^{99m}Tc-MAA reference method. TBF values observed in patients varied from 49,5 (sd 2,6) ml/min/100 g in malignant osteoblastoclastomas and 31.7 (sd 10,1) ml/min/100 g in osteogenic sarcomas down to 23,1 (sd 1,6) ml/min/100 g in reticulosarcomas, 17,4 (sd 7,2) ml/min/100 g in Ewing sarcomas, 14,3 (sd 2,1) ml/min/100 g in fibrosarcomas, 12,6 (sd 0,6) ml/min/100 g in chondrosarcomas. In 3 patients (Ewing's sarcoma, reticulosarcoma and haemangiopericytoma), in whom the chemotherapy was proven effective later on from analysis of bioptate we observed early (within three days) postchemotherapy drop of TBF for > 1/3 of initial value. In patients with no effect of chemotherapy there was no early decrease in TBF. **Conclusion**: Dynamic analysis of ^{99m}Tc-MIBI kinetics in sarcomas provides quantification of blood flow in absolute units. Early postchemotherapy decrease in tumour blood flow predicts the efficiency of chemotherapy in bone sarcomas.

EP-0727

Applying radiomics and machine learning on PET images to predict lung metastases in soft tissue sarcoma patients

I. Shiri[1], A. Rahmim[2,3], H. Abdollahi[1], P. Geramifar[4], A. Bitarafan-Rajabi[1,5]; [1]Department of Medical Physics, School of Medicine, Iran University of Medical Sciences, Tehran, IRAN, ISLAMIC REPUBLIC OF, [2]Department of Radiology, Johns Hopkins University, Baltimore, MD, UNITED STATES OF AMERICA, [3]Department of Electrical and Computer Engineering, Johns Hopkins University, Baltimore, MD, UNITED STATES OF AMERICA, [4]Research Center for Nuclear Medicine, Shariati Hospital, Tehran University of Medical Sciences, Tehran, IRAN, ISLAMIC REPUBLIC OF, [5]Cardiovascular Intervention Research Center, Rajaie Cardiovascular Medical and Research Center, Iran University of Medical Sciences, Tehran, IRAN, ISLAMIC REPUBLIC OF.

Aim: Soft tissue sarcoma (STS) presents highly heterogeneous tumors, with metastases to lungs as main sites. The prognosis of lung metastases in STS patients is poor. The aim of this study was to investigate use of PET image radiomics and machine learning to predict lung metastases in STS patients. **Material and methods:** Fifty-one STS patients (33 without and 19 with developed lung metastases) from the Cancer Imaging Archive (TCIA) were subjected to this study. Gross tumor volume (GTV) delineation was done on T1-weighted MRI images registered to PET images. Subsequently, 100 3D quantitative radiomic features from different feature categories including shape, SUV and intensity histogram, gray level co-occurrence matrix (GLCM), neighborhood gray-tone difference matrix (NGTDM), gray-level size zone matrix (GLSZM), gray-level run-length matrix (GLRLM), normalized GLCM, neighboring gray level dependence (NGLD), texture feature coding (TFC), TFC GLCM and texture spectrum were extracted. Supervised machine learning methods (multinomial logistic regression, decision tree C4, multilayer perceptron (MLP), bagging, AdaBoost and Naive Bayes) were used to predict lung metastases from PET radiomic features. **Result:** The results of the constructed prediction models showed high overall classification performance. By using area under ROC curve (AUC) as an assessment index, multinomial logistic regression, Decision tree C4, multilayer perceptron (MLP), bagging, AdaBoost and Naive Bayes with 0.711, 0.777, 0.950, 0.811, 0.789 and 0.772, respectively, showed high prediction power, with MLP performing particularly favorably (0.950). **Conclusion:** Use of PET image radiomics features towards imaging biomarker discovery hold great promise for prediction of metastases to lung in STS patients. In our study, the best predictive model using PET radiomics was achieved by the MLP method. The proposed method can effectively predict lung metastases in STS by application of advanced machine learning to radiomic features.

| EP-53 | during congress opening hours, e-Poster Area |

Clinical Oncology: Melanoma

EP-0728

Voxel-based analysis of I-123 IMP in patients with uveal malignant melanoma: comparison with ROI analysis

M. Yoshimura[1], T. Aida[2], D. Hakamata[2], K. Uchida[2], K. Suzuki[1], H. Goto[1]; [1]Tokyo Medical University, Tokyo, JAPAN, [2]Tokyo Medical University Hospital, Tokyo, JAPAN.

Purpose/Introduction Sometimes I-123 IMP is the only or the best tool to evaluate malignant melanoma. So it is thought very important to establish the objective quantification. Conventional ROI analysis sometimes miss the small or flat lesion, and sometimes impossible to draw reproducible ROIs. This time we assess the utility of voxel-based analysis for I-123 IMP SPECT/CT in uveal malignant melanoma, and compared with conventional ROI analysis. **Subjects & Methods** Fifty-two patients were examined. Thirty-one patients had malignant melanoma (group A), and 21 patients had either benign pigmented lesions or tumor except for malignant melanoma (group B). Early image was obtained 20 minutes after the intravenous injection of I-123 IMP, and delayed image was obtained after 24 hours. Early and delayed I-123 IMP SPECT/CT images were applied a two-dimensional ROI at the level of lesion (ROI analysis) and the three-dimensional region of interest (VOI) around the eye ball (VOI analysis). Both ROI and VOI were drown largestly inside the orbit. Retention index (RI=(delayed ratio- early ratio) / early ratio x 100) and tumor-to-nontumor ratio of the delayed phase (T/N) were calculated in each case by using ROI and VOI analysis. **Results** ROI analysis: RI and T/N were significantly higher in group A, relative to group B. In the ROI analysis, RI and T/N had cutoff value of 31.41 and 1.07, with AUC values of 0.916 and 0.932. VOI analysis: RI and T/N were significantly higher in group A, relative to group B. In the ROI analysis, RI and T/N had cutoff value of 6.13 and 1.14, with AUC values of 0.932 and 0.966. **Discussion/Conclusion** RI and T/N by VOI analysis was superior to ROI analysis in the differentiation of malignant melanoma from other lesions. Moreover VOI analysis had two advantages to the ROI

analysis. Firstly by VOI analysis the accumulation of the lesions could be picked up reproducibly and objectively because the orbit was obvious on the SPECT/CT, but in the ROI analysis selection of the slice depends on the operator. Secondly, by VOI analysis the accumulation of the lesions could be picked up totally and correctly especially when the tumor shape was flat and/or the tumor accumulation is blurred. In VOI analysis, T/N was more accurate and convenient than RI.

EP-0729

Lymphoscintigraphy and sentinel node biopsy optimal visualization in thick and high risk melanoma- five years experience

A. Koljevic Markovic[1], S. Tasic[1], L. Mijatovic Teodorović[1,2], I. Markovic[1,3], M. Buta[1,3], R. Džodić[1,3], M. Janković[4]; [1]National Cancer Research Center Serbia, Belgrade, SERBIA, [2]Faculty of Medicine, University of Kragujevac, Kragujevac, SERBIA, [3]Faculty of Medicine, Univeristy of Belgrade, Belgrade, SERBIA, [4]School of Engineering, University of Belgrade, Belgrade, SERBIA.

Aim: Evaluation of lymphoscintigraphy (2012.-2017.) and sentinel node detection in melanoma patients. **Patients and Method:** 105 melanoma patients median age 53(18-81) were gathered for evaluation. Among them low risk melanoma was present in 72 (68%) patients (Breslow I and II, in this group thickness median was 1,5mm). Anatomical locations of melanoma were: in trunci 81(77%), in arm/leg 20(19%) and in head/neck 4(4%). Early dynamic phase, planar late scans and SPECT images were performed on Siemens ecam gamma camera, following EANM guidelines (2009); IBA CIS nanoparticles (32-178nm). Supporting intraoperative gama probe enabled the biopsy harvest of hottest sentinel nodes(SLN). **Results:** In 105pts total off 153 lymph nodes were visualized in 95(90%)pts. Following standard acquisition protocol respectively, in early phase up to 30min lymph nodes and aberrant lymph routs were visualized in 18(17%)pts and the region of interest time/activity curves clearly depicted the slow transit nodes and aberrant vessels. In delayed planar and SPECT acquisitions sentinel nodes were visualized in 77(73%)pts. In 27(26%)pts lymph nodes were detected in more than one basin (truncal and leg melanoma). Histopathology revealed in 10(9,5%)pts melanoma metastases (only one had micrometastases); Breslow II (3pts), III (5pts) and IV (2pts); anatomical location: in trunk (6pts), leg(2pts), arm(1pts) and ear(1pts). Sentinel nodes in this group were visualized in late scans after 30min(!). The number of SLN per pts varied from 2 to 22, and in only three pts multiple basins were involved. The sensitivity of our multiphase scintigraphy was 90% (one false negative), and negative predictive value was 95%. Follow up in the group of 33(32%) patients with high risk (Breslow III/IV): in total of 9(8,6%) pts (SLN biopsy was positive in five) progression developed: local recurrence (in two pts), one had liver metastases, and in five pts multiple metastases were developed as lenticular and central nervous system lesions. **Conclusion:** Our results confirm the usefulness of preoperative dual phase lymphoscintigraphy protocol: a.) in identification of basins at high risk, b.) facilitated identification of true sentinel nodes in aberrant lymph routes

after excision of thick melanoma, c.) the following SLN biopsy had high efficacy for high risk melanoma patients.

EP-0730

Absolute number of new lesions in ¹⁸F-FDG PET/CT is more predictive of clinical outcome than SUV changes in metastatic melanoma patients receiving ipilimumab

H. Anwar[1], C. Sachpekidis[1], J. Winkler[2], A. Kopp-Schneider[3], U. Haberkorn[4], J. Hassel[2], A. Dimitrakopoulou-Strauss[1]; [1]Clinical Cooperation Unit Nuclear Medicine, German Cancer Research Center, Heidelberg, GERMANY, [2]National Center for Tumor Diseases, Heidelberg, GERMANY, [3]Department of Biostatistics, German Cancer Research Center, Heidelberg, GERMANY, [4]Division of Nuclear Medicine, University of Heidelberg, Heidelberg, GERMANY.

Aim: Immune checkpoint inhibitors such as the cytotoxic T-lymphocyte-associated protein 4 (CTLA-4) antibody ipilimumab have revolutionized oncological treatment options. Treatment response evaluation of immunotherapy is, however, still a matter of debate. Aim of the present study was to perform metastatic melanoma treatment response evaluation to ipilimumab by means of ¹⁸F-FDG PET/CT, using the patients' clinical response as reference. **Methods:** 41 metastatic melanoma patients scheduled for ipilimumab therapy underwent ¹⁸F-FDG PET/CT before and after administration of the four cycles of ipilimumab treatment. After determination of the best clinical response, the PET/CT scans were retrospectively reviewed and a separate independent analysis of the post-therapy PET/CT scans was performed. The analysis was focused on the number of newly emerging ¹⁸F-FDG avid lesions, on their functional size, on their location as well as on the SUV changes during therapy. **Results:** Based on their clinical response, patients were dichotomized in responders and non-responders. The responders' group included patients with stable disease (SD), partial response (PR), and complete response (CR) (n= 31 patients), while the non-responders' group involved patients with progressive disease (PD) (n=10 patients). The application of a threshold of 4.5 newly emerging ¹⁸F-FDG avid lesions in the post-therapy PET/CT led to a sensitivity (correctly predicting responders) of 87% and a specificity (correctly predicting non-responders) of 90%. Respectively, a threshold of 3.5 lesions, led to a sensitivity of 84% and a specificity of 100%, yielding a higher Youden index. Moreover, when the functional size of newly emerging lesions exceeded 1.0 cm, the application of a cut-off of 2.5 new lesions yielded a sensitivity of 90% and a specificity of 90%. Respectively, when the functional size of the newly emerging lesions exceeded 1.5 cm, the use of a cut-off of 1.5 lesions led to a 94% sensitivity and a 90% specificity. The location of newly emerging lesions as well as SUV changes during therapy did not correlate with clinical response. **Conclusion:** Our results show that using the cut-off of 4 newly emerging ¹⁸F-FDG avid lesions in post-therapy PET/CT gives a reliable indication for treatment failure in metastatic melanoma patients receiving ipilimumab. Moreover, the size of the new lesions is predictive of the clinical outcome of these patients.

EP-0731

FDG-PET/CT in the Evaluation of Non-Melanoma Skin Cancers

A. Sabaté-Llobera[1], **P. C. Notta**[1], E. Llinares-Tello[1], J. R. Ferreres[2], R. Tarragona-Fernández[3], T. Soler-Monsó[4], L. Rodríguez-Bel[1], A. Lucas-Calduch[5], J. L. Vercher-Conejero[1], M. Cortés-Romera[1], C. Gámez-Cenzano[1];

[1]PET Unit, Department of Nuclear Medicine-IDI. Hospital Universitari de Bellvitge-IDIBELL, L'Hospitalet de Llobregat (Barcelona), SPAIN, [2]Department of Dermatology. Hospital Universitari de Bellvitge-IDIBELL, L'Hospitalet de Llobregat (Barcelona), SPAIN, [3]Department of Plastic Surgery. Hospital Universitari de Bellvitge-IDIBELL, L'Hospitalet de Llobregat (Barcelona), SPAIN, [4]Department of Pathology. Hospital Universitari de Bellvitge-IDIBELL, L'Hospitalet de Llobregat (Barcelona), SPAIN, [5]Department of Radiation Oncology-Institut Català d'Oncologia. Hospital Duran i Reynals-IDIBELL, L'Hospitalet de Llobregat (Barcelona), SPAIN.

Aim: squamous and basal cell carcinomas (SCC and BCC respectively) account for approximately 99% of non-melanoma skin cancers (NMSC). Such malignancies rarely metastasize, though certain risk factors (RF) determine a more aggressive behavior. The aim of this work is to evaluate the role of FDG-PET/CT in assessing disease extension in patients with high-risk NMSC. **Material and Methods:** between 2013-2016, 25 patients (22 men, median age 79 years) with NMSC were studied with FDG-PET/CT. In 2 patients (8%) the primary lesion was a BCC, while in 23 (92%) was a SCC. Eleven patients (44%) were referred for initial staging (IS) and 14 (56%) for restaging of recurring disease (RS). Included RF were: location and size of the primary tumor, degree of differentiation in SCC (G) or subtype in BCC, perineural invasion, and immune status. We evaluated the ability of FDG-PET/CT to detect the primary lesion (if present), lymph node involvement (N) and distant metastasis (M). Patients' evolution was also assessed. **Results:** in 9/25 patients (36%) the primary lesion was in a high-risk area (H). Among patients referred for IS, 7 had the lesion in a H area. Of those referred for RS, 9 had a cutaneous relapse (4 in a H area) and 5 a lymphatic one. The size of the cutaneous lesions was 0.9-19 cm. Among SCC 2 were G1, 15 G2, 5 G3 and 1 G4; the two BCC had an aggressive growth pattern. Fourteen lesions had perineural invasion (including one BCC). Immunologically, 3 patients had a concurrent chronic lymphocytic leukemia and one hepatitis-C virus. FDG-PET/CT detected all present cutaneous lesions (12). Overall, 15/25 patients (60%) had N (6 at IS), and 2/25 (8%) M (1 at IS). Five patients did not have lesions at FDG-PET/CT. During evolution, 4/11 IS patients (36%) relapsed (3-12 months), all with the primary in a H area. At follow-up (median 17 months), 8 patients are free-of-disease, 2 have stable disease, 2 are progressing and 13 died (9 of them due to disease complications). In a per-patient basis, median SUVmax of the most hypermetabolic lesions in deceased patients was 14.2, while in the rest of patients it was 11.7. **Conclusion:** FDG-PET/CT could be useful in studying NMSC, both at IS and at RS, as it can detect unsuspected dissemination. No differences in SUVmax of the most hypermetabolic lesions were observed between patients who died due to disease complications and the rest of patients.

EP-0732

Is whole body 18F-FDG PET/CT including the extremities routinely warranted in melanoma patients?

K. Pinker-Domenig[1,2], H. Schoeder[1], G. Ulaner[1], T. Saidon[1], K. Juluru[1], S. Huang[1], W. A. Weber[1], C. C. Riedl[1]; [1]Memorial Sloan Kettering Cancer Center, New York, NY, UNITED STATES OF AMERICA, [2]Medical University of Vienna, Vienna, AUSTRIA.

Purpose: In patients with melanomas [18]FDG-PET/CT is commonly used for staging and is often performed as a as whole body scan including the upper and lower extremities. Imaging of the extremities significantly increase the time of examination, is a associated with a non-trivial increase in radiation dose and its clinical value is not well established. The aim of this study was to investigate how frequently new information is obtained from [18]FDG-PET/CT imaging of the upper and lower extremities in melanoma patients. **Subjects & Methods:**The hospital database was searched for melanoma patients who underwent whole body (WB) [18]FDG-PET/CT scanning in our institution between 2012-2016. The imaging reports searched for findings in the extremities and subsequently analyzed for malignant findings that would have not included in a scan ranging from the skull base to mid thighs, the range routinely used for 18FDG-PET/CT in most other malignancies. All [18]FDG-PET/CT findings were classified using a certainty lexicon grading the likelihood of malignancy on a scale from 1-5. Findings in the extremities which were less likely to be malignant (<25%) were considered not to be relevant as they generally are not subjected to further assessment in our center. Findings in an extremity that were related to the primary tumor and/or its treatment as well as findings in cases of disseminated disease were also considered not relevant. **Results:** [18]FDG-PET/CT scans in 1975 melanoma patients were identified. There were findings in the extremities in 27.5% (543/1975) scans and 14% (276/1975) were classified as a malignant (primary/recurrence, local or distant metastases). 50.4% (139/276) patients with malignant findings in the extremities presented with disseminated disease. In 1.6% (32/1975) we identified metastases in an extremity that would not have been covered by an "eyes-to-thighs" scan or a scan of the extremity afflicted by the primary tumor. In 93.8% (30/32) of these patients there was disseminated disease and thus WB [18]FDG-PET/CT detected relevant metastases in the extremities in only 0.1% (2/1975) of melanoma patients. **Conclusions:** Metastases in an extremity that was not the origin of the primary tumor were identified in only 1.6% of the scans in melanoma patients. In melanoma patients where the origin of primary was not in the extremities, WB [18]FDG-PET/CT did not provide an additional value in the vast majority (99.9%) of patients.

EP-0733

Clinical Relevance of Imaging the Lower Limbs When Staging or Restaging Malignant Cutaneous Melanoma Using 18F-FDG PET/CT

N. Plouznikoff, F. Arsenault; Centre Hospitalier de l'Université de Montréal (CHUM), Montréal, QC, CANADA.

Aim: Malignant cutaneous melanoma can theoretically metastasize nearly anywhere in the body through lymphatic and vascular spread. At first glance, this suggests the use of true whole-body imaging when staging or restaging cutaneous melanoma. The purpose of this study was to assess the clinical relevance of imaging the lower limbs when using ^{18}F-FDG PET/CT for patients without previous known or suspected cutaneous melanoma lesions in the lower limbs. **Materials & Methods**: We retrospectively reviewed 880 consecutive whole-body ^{18}F-FDG PET/CT scans performed at the University of Montreal Health Centre in a context of possible melanoma covering a 5 year period (January 2011 to December 2015), as well as the associated clinical, pathological and radiological records until at least 6 months after the end of the study. 461 PET/CT scans for adults with histopathologically proven cutaneous melanoma but with a priori no known or suspected melanoma lesions in the lower limbs were included in the study and tabulated. Descriptive statistics and Wilson 95% confidence intervals for proportions were calculated. **Results**: Scans were performed for patients 60.1 years old on average, mostly men (62.5%), known for superficial spreading or nodular melanomas (respectively 44.3% and 38.1% of scans), mainly originating from the back, head or upper limbs (respectively 33.4%, 21.9% and 18.9%), with an average Breslow index of 4.3 mm, and mostly stage II or III (respectively 39.6% and 48.0%). 109 scans (23.6%) showed lower limb abnormalities, but at most 21 scans showed melanoma lesions in the lower limbs (4.6%, CI: 3.00%-6.86%). No scan showed malignant lesions solely in the lower limbs (0%, CI: 0%-0.83%), with lower limb lesions overwhelmingly (85.7% of cases) being part of extensive disease or associated with multiple lymph node or bone metastases. In only 1 in 461 scans (0.22%, CI: 0.04%-1.22%) did imaging the lower limbs change the clinical management of the melanoma, with the discovery of an asymptomatic left distal femur bone metastasis and subsequent preventive radiotherapy in an otherwise multi-metastatic patient headed for palliative care. Moreover, stopping the scan at the proximal thighs saves 17.2 minutes of PET/CT camera time per patient on average. **Conclusion**: For patients with malignant cutaneous melanoma without known or suspected melanoma lesions in the lower limbs, true whole-body ^{18}F-FDG PET/CT imaging provides little additional clinically relevant information and our study, the largest of its kind, confirms that stopping at the proximal thighs has essentially no clinical impact while saving valuable resources.

EP-0734

A portable hybrid camera for fused optical and scintigraphic imaging: clinical experience in 90 patients with melanoma

C. A. Tapias, Sr., N. Sanchez, R. Pigem, R. Rull, p. paredes, p. perlaza, S. Vidal-Sicart; hospital clinic de Barcelona, barcelona, SPAIN.

Aim: Portable gamma cameras (PGCs) have been helpful to produce real time visual localisation of sentinel lymph nodes (SNs); however, sometimes nuclear physicians or surgeons have difficulties to interpret PGC images due to the lack of anatomical information. The aim of the present study was to clinically test the prototype of a new portable hybrid camera (PHC), which adds optical to γ-imaging, in a preoperative and intraoperative setting. **Materials & Methods:** PGC (Sentinella S102; Oncovision) equipped with a 4-mm pinhole collimator was upgraded with an optical module to build a PHC. This system offers real-time superimposition of an optical image onto the scintigraphic image. During preoperative and intraoperative imaging, the PHC is positioned at 15 cm distance (overview) and at <5 cm (close-up). Errors in the optical image co-registration were evaluated by means of the laser pointer integrated in the PHC system with a 5 mm accuracy for each patient. **Results:** Ninety patients with melanoma were introduced for this evaluation. In the PHC overview images, the optical module offered fused optical and γ-imaging indicating the image field of view and anatomical SN locations. The spatial information provided on the screen is quite similar to the real-life situation that is observed. Average optical image co-registration errors were 1.0 cm (range 0-2.0 cm). At least 1 SN was located in all patients, 294 SNs were resected (3.2 nodes/patient), 33 SNs were metastatic (in 19 patients), portable gamma camera found 10 nodes not clearly detected. by hand-held gamma probe after SN removal (2 with micromets). Most of errors came from objects with more irregularities in the imaging plane surface (the curved shaped patient's body contour, intense light of the operation room lamps). **Conclusions:** Fused optical and γ-imaging with a prototype PHC increased nodal visualization in several clinical scenarios. The optical image is helpful to orientate the γ-image field of view of the PHC, enabling SN localization in an anatomical context. A more stable software is being developed to correct small image co-registration errors of the PHC prototype.

EP-0735

18-F-FDG-PET/CT In Head And Neck Mucosal Melanoma

R. Durmo, F. Bertagna, D. Albano, M. Bertoli, M. Bonacina, M. Gazzilli, E. Cerudelli, R. Giubbini; spedali civili brescia, brescia, ITALY.

Aim: Mucosal melanoma (MM) represents about 1.3% of all melanomas and it is a rare disease with a very poor prognosis. The nasal cavity, paranasal sinuses, and oral cavity are the most common locations. MMs are now recognized to have distinct molecular alterations and different clinical behaviour compared to cutaneous or uveal melanomas showing a greater tendency to metastasize and poorer prognosis. The aim of our retrospective study was to evaluate glucidic metabolic behaviour and imaging findings of head and neck MMs studied with 18F-fluorodeoxyglucose positron-emission tomography/computed tomography (18F-FDG PET/CT). **Materials and Methods:** Between 2005 and 2016 twenty seven patients (19 female, 8 male, average age 65,8 years, range 20-87 years) with histologically-confirmed diagnosis of head and neck MM underwent 18F-FDG PET/CT (13 staging; 14 re-staging; patients of restaging group underwent more than one PET/CT). A total of 58 PET/CT images were qualitatively and semi-quantitatively analyzed by measuring the maximum standardized uptake value (SUVmax). No patient was affected

by primary melanoma in any other site at the time of diagnosis. **Results:** Twenty-four MMs were located in the nasal cavity and/or ethmoidal/maxillary sinus while 4 in the oral cavity. All MMs of patient who underwent PET/CT for staging were 18F-FDG avid at the site of primary tumor (average SUVmax 14,4; range: 5.25-30.5); three patient showed also cervical lymph nodes involvement (average SUVmax 5.9; range: 4.77-6.6) and one patient showed axillary lymph node positivity (SUVmax= 4.77); no distant metastasis were found. In the group of patients who underwent 18F-FDG-PET/CT for re-staging and/or follow up, primary site recurrence was demonstrated in 7 patients (average SUVmax 16.5; range: 12.5-22), lymph node metastasis in 6 patients (average SUVmax 11.4; range: 4.2-18.8) and distant metastasis in 4 patients (2 in liver: SUVmax 13.7 and 8.6 respectively; 1 in lung: SUVmax 12.4; 1 multiple bone metastasis). **Conclusion:** Head and neck MMs are 18F-FDG avid tumors; 18F-FDG PET/CT could be a valuable imaging for staging, re-staging and follow up of patients.

EP-0736

Does SPECT/CT Improve Sentinel Node Detection in Melanoma Patients

K. Nikoletic[1], S. Tonjer[1], S. Hegg[1], M. Møll Dalen[1], E. Spangen Hoset[1], M. Knezevic[2]; [1]Drammen hospital, Nuclear Medicine Department, Drammen, NORWAY, [2]Bærum hospital, Department of Surgery, Bærum, NORWAY.

Introduction: Use of SPECT/CT is highly recommended as an additional diagnostic tool in sentinel lymph node detection (SLND). The aim of the study is to investigate utility of SPECT/CT compared to planar images in SLND in melanoma patients. **Subjects & Methods:** We investigated retrospectively total of 64 patients (January `16 - Mars `17), 43 male/21 female, mean age 61.8 (19-86). In all patients SPECT/CT was performed in addition to planar images. Most common localization of melanoma was trunk (26), upper arm (15), foot/lower leg (8), thigh (6), shoulder (5), gluteus (2), forearm (1) and penis (1) retrospectively (head/neck localization is performed in another hospital). Initially 62 patients underwent excisional biopsy before SLND (in 2 pts SLND was performed before primary excisional biopsy). SLN biopsy and margins enlargement surgery were performed 1 day after SLN scintigraphy in 40 pts, however 22 pts had already been operated with margins enlargement surgery before SLND. Dynamic images were acquired immediately after application of 99mTc-Nanocoll, planar images after 15-60 min and SPECT/CT after 45min-2 h. **Results:** We detected SLN in 63/64 patients, detection rate 98.4%. If no lymph nodes were detected after dynamic images, massage of injection site was performed. In some patients certain lymph nodes were visualized on SPECT/CT not prior detected on planar images. A mean of 2.43 sentinel nodes were reported with planar images only (range 1-8) and mean of 2.61 nodes with SPECT/CT images (range 1-2). Malignant melanoma metastases were detected in 7 pts/11 nodes (11%) with a mean Breslow thickness of 1.97 mm. In 57 pts (89%) nodes were benign, mean Breslow was 1.7 mm. **Conclusion:** SPECT/CT helps surgeons in correct anatomical localization providing three-dimensional images with better contrast and spatial reso-

lution, thus leading to higher overall SLN detection rate (mean of 2.61 nodes vs 2.43 with planar images only). SPECT/CT was particularly significant in evaluating sentinel nodes located next to injection site. We highly recommend use of SPECT/CT in all SLND patients, especially for groin and axillary area.

EP-0737

Comparison of 123I-IMP SPECT, 18F-FDG PET/CT, and 18F-FDOPA PET/CT in Detection of Choroidal Malignant Melanoma

K. Kato[1], T. Odagawa[1], T. Tsutsumi[1], M. Honda[1], K. Kunimoto[1], R. Mukumoto[1], S. Matsuzawa[1], S. Abe[2], S. Naganawa[1]; [1]Nagoya University Graduate School of Medicine, Nagoya, JAPAN, [2]Nagoya University Hospital, Nagoya, JAPAN.

Aim: Previously we showed that 123I-IMP SPECT is a sensitive and accurate method for detection of choroidal malignant melanoma. The feasibility and usefulness of 18F-FDOPA PET for detection of choroidal malignant melanoma have not yet been established. The purpose of this study is to compare the usefulness of 123I-IMP SPECT, 18F-FDG PET/CT, and 18F-FDOPA PET/CT for detection of choroidal malignant melanoma. **Materials and Methods:** Fifty-eight patients with suspected choroidal malignant melanoma were examined by 123I-IMP SPECT, 18F-FDG-PET/CT, and 18F-FDOPA PET/CT. **Results:** In 40 of 58 study patients, 123I-IMP SPECT showed markedly increased uptake in the site corresponding to the ocular tumor. In 36 of the 40 patients showing increased uptake of 123I-IMP, the ocular tumors were confirmed histopathologically or clinically to be choroidal malignant melanoma. The ocular tumors in 3 of the other 4 patients showing increased uptake of 123I-IMP were diagnosed as small choroidal melanocytic lesions, and that in 1 patient was a metastatic lesion. The 18 123I-IMP SPECT-negative cases comprised 7 small melanocytic lesions, 1 choroidal hemangioma, 1 adenoma, and 2 melanocytoma, 2 metastases, 3 hemorrhages, and 2 unknown benign lesion. Twenty eight cases were positive in 18F-FDG PET/CT and 18F-FDOPA PET/CT. The uptakes of both 18F-FDG and 18F-FDOPA were much weaker than that of 123I-IMP. The range and mean ± SD of SUVmax for 18F-FDG and 18F-FDOPA in choroidal malignant melanoma were 1.70-10.35, 3.56 ± 1.81 and 0.74-4.63, 1.13 ± 1.53, respectively. The difference between the uptakes of both tracers was statistically significant. Thus the uptake of 18F-FDOPA was weaker than that of 18F-FDG. **Conclusion:** 123I-IMP SPECT is superior to 18F-FDG and 18F-FDOPA PET/CT for detection of choroidal malignant melanoma. Efficacy of 18F-FDOPA PET/CT is for detection of choroidal malignant melanoma is low compared with 18F-FDG PET because of its weak uptake into choroidal malignant melanoma.

EP-0738

Functional Radiographic Profiling of Immunotherapy Related Toxicities with 18F-FDG-PET/CT in Patients with Metastasized Malignant Melanoma

Y. Zhuwu, S. Nekolla, J. Kohlmeyer, A. Krackhardt, M. Schwaiger, M. Mustafa; Klinikum rechts der Isar, Munich, GERMANY.

Purpose: FDG PET/CT is the most accurate imaging procedure in metastasized malignant melanoma for initial staging of distant metastases and in therapy monitoring. During the last years the introduction of targeted therapy with BRAF/MEK inhibitors and immunotherapy with checkpoint inhibitors has impressively prolonged PFS and OS. On the downside of this a considerable amount of patients (pts) receiving checkpoint inhibitors develop grade III and IV toxicities, up to 54% of pts when using combination therapies. Many of the toxicities can be visualized on hybrid 18F-FDG-PET/CT, rendering serial PET/CT scanning also useful in detecting serious side effects. Therefore the aim of this retrospective study is to investigate the sensitivity of FDG-PET/CT in diagnosing immune related toxicities. **Methods:** We retrospectively evaluated 85 pts, with metastasized malignant melanoma AJCC stage IV who presented themselves to and were treated with targeted therapies and/or immunotherapy at the interdisciplinary melanoma group of our institution in 2012 - 2016. 68 pts received at least one total body FDG-PET/CT-scan, 44 patients were monitored before and after treatment with BRAF/MEK inhibitors or/and checkpoint inhibitors. The average number of PET/CT-scans was 3 (range 1-11 scans). In 23 pts a treatment with BRAF/MEK inhibitors was monitored with PET/CT, in 38 pts immunotherapy treatment was monitored with PET/CT (change of therapy regime at progress under BRAF/MEK inhibitors). Clinical toxicities and their time point of occurrence during therapy monitoring were correlated to FDG-PET findings. **Results:** Of all 49 pts who were treated with checkpoint inhibitors 14 pts developed immune related toxicities during followup (29%). In total 25 different toxicities were documented in 14 pts (3 pts developed different toxicites under different medication). The documented autoimmune reactions were hypophysitis, thyreoditis, pleuritis, pneumonitis, hepatitis, enteritis/colitis, dermatitis/vitiligo, Sjögren Syndrom and sarcoidlike lesions. FDGPET depicted 8 immune related toxicities in 7 pts. Time until FDG PET of FDG-avid lesions was significantly shorter than for those reactions not depicted on FDG-PET (8,3 vs. 21,7 weeks). **Conclusion:** FDG-PET is a sensitive tool for diagnosing immune related toxicities. The main confounder in our study was the long time interval between occurrence of laboratory parameters or clinical symptoms and conduction of PET/CTscan. In conclusion, a PET/CTscan within the duration of immunotherapy in the sense of an early response evaluation and detection of immune related toxicities is recommendable, especially in the advent of multiple combinational immunotherapy.

EP-0739

18FFluorodeoxyglucose Positron Emission Tomography/ Computed Tomography Findings In Ocular Melanoma

J. Benouhoud, S. Choukry, Y. Shimi, A. Guensi; CHU Ibn Rochd, Casablanca, MOROCCO.

Introduction: The 18 fluorodeoxyglucose positron emission tomography/computed tomography (PET/CT) is a very useful tool used in staging in staging of melanoma. The ocular localization of the melanoma is not frequent and initial staging define the prognosis of patients. We report the experience of nuclear medicine unit of the nuclear medicine department of the University Hospital Ibn Rochd of Casablanca in using of FDG PET/CT in initial staging of ocular melanoma. **Materials and Methods:** We collected all PET-CT examinations performed in the initial staging of ocular melanoma between January 2015 and December 2016 at the nuclear medicine department of the University Hospital Ibn Rochd of Casablanca. We conducted our tests using a SIEMENS BIOGRAPH engine starting in 2011. We achieved the acquisitions 60 minutes after injection of 3.5 MBq / kg of 18-FDG. **Results:** We collected 8 patients, 5 of them were female. The mean age was 30.4 years. The locations of the melanomas were: the conjunctiva (3 patients), choroid (3 patients), iris and eyelid. The mean SUVmax lesions were 10,48 with extremes of 2.71 and 24.46. Cervical and mediastinal lymph nodes were found in 2 cases and we found metastatic lung and liver lesions in the same 2 cases. The other 6 patients had localized disease. The surgical treatment was an evisceration in 4 cases. Conclusion: The contribution of PET/CT to diagnosis and treatment ocular melanoma is actually proved. The PET/CT imaging can also be used to assess ocular melanomas for their response to treatment.

EP-0740

Necrosis determines FDG-avidity in cerebral metastases of malignant melanoma - correlating 18F-FDG-uptake with histological parameters

M. Mustafa, H. Einhellig, M. Boxberg, T. Pyka, J. Kohlmeyer, A. Krackhardt, M. Schwaiger; Klinikum rechts der Isar, Munich, GERMANY.

Purpose: FDG PET/CT is the most accurate imaging procedure in metastasized malignant melanoma for therapy monitoring of distant metastases. Our group recently reported the importance of including the skull in regular staging / restaging 18F-FDG-PET/CT scans with a sensitivity of 65 % and a specificity of 98% for cerebral metastases. One of the most significant factors of FDG-PET-visibility of cerebral metastazation seems to be the size of the metastases. This analysis looked into histological parameters of resected metastases - correlating them to FDG-avidity. **Methods:** We retrospectively evaluated 168 pts, with metastasized malignant melanoma AJCC stage IV who presented themselves to and were treated at the interdisciplinary melanoma group of our institution in 2011 - 2016. 37 pts that developed cerebral metastases were included in this analysis, of these 14 patients had complete resection of the largest symptomatic cerebral metastasis. Histological findings -melanin content, hemosiderin, necrosis, proliferation and lymphocytic cell influx were correlated to FDG avidity. **Results:** Of the investigated parameters only necrosis reached significant correlation, low count of necrotic tumor areas seemed to correlate to hypermetabolic cerebral metastases. **Conclusion:** FDG-PET is able to depict cerebral metastases of a certain size with high specificity. Lesions with low necrotic areas were more prone to being depicted as hypermetabolic lesions. An ongoing analysis is investigating the change of histological parameters under targeted therapies and immune therapies and the influence on FDG-avidity.

Clinical Oncology: Paediatric Cancer

EP-0741

Post-therapy outcome in initially positive FDG PET/CT for Bone marrow infiltration in pediatric lymphoma patients

M. A. Abdelwahab[1], S. A. Badr[1], M. H. Kotb[1], H. Mostafa[2]; [1]National Cancer Institute, Giza, EGYPT, [2]NEMROCK, Cairo University., Giza, EGYPT.

Purpose: To assess the prognostic outcome in terms of response and survival of pediatric lymphoma patients initially diagnosed with bone marrow involvement on basis of 18F-fluoro-deoxy- glucose (FDG)**. Methods:** 39 pathologically proved pediatric lymphoma patients with pre-therapy FDG PET/CT that showed criteria for positive BMI were enrolled in this study. BMB, clinical, radiological and follow up data were also collected. **Results:** Within the 39 positive PET/CT cases for BMI, those with maximum of standard uptake value (SUV max) of bone marrow more than 6.8 were significantly associated with worse therapy outcome (*P*<0.05).Also the overall survival and 2 years relapse free survival were compared between the 39 PET/CT BMI patients and other PET/CT negative groups (101 patients) no significant statistical difference in 2 years overall survival between the patients with negative PET/CT for BMI and those with positive PET/CT for BMI (92.9 % ± 0.036% vs. 94.3 % ± 0.04%; *P*=0.44), while a significant difference was demonstrated in 2 years relapse free survival between the two groups (95.4 % ± 0.029% vs. 81.8 % ± 0.097 %; P<0.05) in negative and positive PET/CT groups for BMI respectively. **Conclusion:** Positive PET/CT criteria for BMI seem to correlate well and predict the post-therapy outcome in pediatric lymphoma patients

EP-0742

Can FDG PET/CT predict the outcome of pediatric rhabdomyosarcoma?

E. Elkholy[1,2], I. Al-Antabily[3], E. ElNadi[4,5], S. Ahmed[6], M. Saad Zahhlol[6], H. Hafez[7], O. Shawky[7], T. Rafaat[8], N. El-Kilini[9], A. Younis[10], G. Taha[11], E. Khalid[12]; [1]Nuclear Medicine National cancer Institute (NCI) Egypt, Cairo, EGYPT, [2]Childern Cancer Hospital Egypt, Cairo, EGYPT, [3]Nuclear medicine National cancer Institute (NCI) Egypt, Cairo, EGYPT, [4]Pediatric Oncology Beniswif Univeristy, Cairo, EGYPT, [5]CCHE, Cairo, EGYPT, [6]Radiotherapy CCHE, Cairo, EGYPT, [7]Pediatric Oncology CCHE, Cairo, EGYPT, [8]Radiology CCHE, Cairo, EGYPT, [9]Pathology CCHE, Cairo, EGYPT, [10]Surgery CCHE, Cairo, EGYPT, [11]Surgey CCHE, Cairo, EGYPT, [12]Statistic department CCHE, Cairo, EGYPT.

Purpose: to establish whether initial 18F-FDG SUV can add prognostic information to clinical staging in pediatric rhabdomyosarcoma patients. **Subjects and Methods:** 98 patients (48 female, 50 male, Age ranged 4 mo-17.5 years, mean age: 5.8±4.5) with pathologically proven RMS underwent PET/CT for initial cancer staging were included in the study. We retrospectively assessed whether or not FDG PET/CT using primary SU-

Vmax and primary/liver ratio, could predict event-free survival (EFS) or overall survival (OS) in patients with pediatric RMS who received specific therapy according to the standard Children Cancer Hospital-Egypt (CCHE) protocol. Correlation with other prognostic factors was also obtained. **Results:** High SUVmax was significantly related to the presence of nodal or distant metastasis. With marked cutoff values of (3.6) and (2.1) by ROC curve for SUV primary and SUV primary/liver ratio respectively, OS (for 36 months) and EFS proved to be higher in patients with SUVmax below these values. Patients with SUVmax primary/liver less than the cutoff of 2.1 had OS 60.8% and EFS 48.1% compared to 44.5% and 14.8% to those above the cutoff, yet, this semiquantitative evaluation failed to attain statistical significance. (P value 0.92 & 0.16 respectively). Similar results were obtained in assessment of primary SUVmax with (P value 0.76 and 0.62 respectively). There was prevalence of high SUV primary and SUV primary/liver ratio among those patients with less favorable clinico-pathological features (unfavorable primary site, high and intermediate risk & alveolar pathological type), yet was not statistically significant. **Conclusion:** In this preliminary study, FDG PET/CT may be an additional predictor of outcome in pediatric rhabdomyosarcoma, further studies are needed to correlate between assessment of therapy response by PET/CT and final outcome and survival. **Key words:** FDG PET/CT, rhabdomyosarcoma, prognosis.

EP-0743

How can FDG PET CT add benefits in staging pediatric rhabdomyosarcoma?

E. Elkholy[1,2], S. Abd El-Giad[1], H. Fathy[1]; [1]Nuclear Medicine National Cancer Institute (NCI) Egypt, Cairo, EGYPT, [2]Childern Cancer Hospital Egypt, Cairo, EGYPT.

Purpose: This study aimed to evaluate the added value of FDG PET/CT in initial staging of pediatric RMS patients, as compared to conventional imaging. **Subjects and Methods:** This is a retrospective study including total 112 patients with pathologically proven RMS (60 males, 52 female; mean age, 5.8 years, with predominant embryonal type), PET/CT results were compared with CT and/or MRI. SUVmax of the primary lesion, LNs and distant metastases were calculated in an individual analysis. Clinical follow-up (mean, 27 months), and histo-pathological data were served as the standard of reference. **Results:** Among 112 patient, 40 (29%) patients proved metastatic by PET/CT, and 5 was Indeterminate with nodal lesions. Both diagnostic CT and PET/CT shows comparable results for primary tumor site. Extremities was the most common primary site in metastatic patients (17 patient, 42.5%), while Alveolar type was more prevalent pathological type (51%) and had the highest SUVmax as well. PET/CT upstage 13 patients (32.5%) (6 with nodal metastases, 5 with bone marrow, 1 peritoneal and 1 patient with solitary acetebular bone lesion). Additional 60 lesions were detected by PET/CT (21 nodal, 16 osseous, 3 peritoneal, 5 ST nodules, 5 bone marrow involvement). Unusual suprarenal, spermatic cord and IVC thrombotic metastases were detected in individual patients by both modalities. The sensitivity and PPV for PET/CT were (100%,

92.4%), (92.5%, 96%), (100%, 98%), (100%, 100%), (100%, 100%), for nodal, pulmonary, osseous, peritoneal and ST metastases respectively as compared to (66%, 93.6%), (100%, 93%), (73%, 97%), (50%, 67%), (70%, 100%) for diagnostic CT. **Conclusion:** This study shows that FDG PET-CT can be useful in initial staging of patients with RMS as compared to CT regarding nodal, bone, bone marrow, peritoneum, and soft tissue metastatic lesions, except for pulmonary deposits. **Key words:** FDG PET/CT, rhabdomyosarcoma, metastases, staging.

EP-0744

The value of volumetric 18F-FDG PET parameters in pediatric patients with bone sarcoma

E. Ozkan, M. Khalizadeh, C. Soydal, N. Tacyildiz, N. O. Kucuk, M. K. Kir; Tip Fakultesi, Ankara, TURKEY.

Aim: To determine the value of pre- and post-neoadjuvant chemotherapy metabolic and volumetric 18F-FDG PET/CT parameters in evaluation of therapy response and prediction of clinical outcome in pediatric patients with bone sarcomas. **Material and Method:** A total thirty-two patients with bone sarcoma [22 osteosarcoma (OS), 10 ewing sarcoma (ES); mean age: 12.31± 3.43] were included to the study. All patients underwent to 18F-FDG PET/CT scan before (PET-0) and after (PET-1) neoadjuvant chemotherapy. In all of the patients, metabolic (SUV and TLG) and volumetric (MTV) parameters of the primary tumor lesions, were measured from PET-0 and PET-1 scans. Also additional pathologic uptake in different parts of body and new lesions were recorded. The metabolic and volumetric PET parameters were compared with the histopathological examination reports obtained from surgical specimen and clinical follow-up results. ΔSUVmax, ΔMTV and ΔTLG were calculated form the % change between PET-0 and PET-1 parameters. **Results:** According to clinical follow-up results, patients were evaluated in two groups (progression group (PG): 15 pts and remission group (RG): 17 pts). Although, mean SUVmax (p=0.43; p=0.71), MTV (p=0.44; p=0.60) and TLG (p=0.27; p=0.56) obtained from PET-0 and PET-1 is higher in PG than RG, this difference could not reach the significance level. Moreover, in the comparison based on necrosis rate (<90% vs ≥90%) despite ΔSUVmax (p=0.28), ΔMTV (p=0.36) and ΔTLG (p=0.96) difference values have calculated higher in RG patient groups, there was no statistically significance in both groups. In the analysis of parameters including demographic, histopathological and PET parameters, presence of the metastasis at diagnosis was found significant to predict to disease progression (p=0.009) **Conclusion:** Although, our study results could not reach statistically significance, we think that pre- and post-neoadjuvant chemotherapy metabolic and volumetric 18F-FDG PET parameters could be a guide for prediction of clinical outcome and response to therapies in pediatric patients with bone sarcoma.

EP-0745

123I-MIBG scintigraphy and diffusion-weighted whole-body RMI with background body signal suppression (DWIBS) : comparison in HR-Neuroblastoma

C. Olianti[1], A. Tondo[2], A. L. Perrone[3], C. Favre[2], C. De Filippi[3]; [1]Nuclear Medicine Unit, Careggi University-Hospital, Florence, ITALY, [2]Oncohematology Unit, Meyer Pediatric University-Hospital, Florence, ITALY, [3]Radiology Unit, Meyer Pediatric University-Hospital, Florence, ITALY.

Aim: To assess agreement between 123I-metaiodobenzylguanidine (MIBG) and diffusion-weighted whole-body imaging with background body signal suppression (DWIBS) in high and intermediate risk neuroblastoma (HR-NB), a retrospective review was performed on MIBG and DWIBS paired scans acquired at diagnosis and response-to-therapy steps. **Materials and Methods:** 66 paired MIBG and DWIBS scans were acquired for 23 patients (8 female and 15 male) between 06/2009 and 02/2017 within 30 days, without intercurrent therapy. For 123I-MIBG scan 5.18 MBq/kg was administered, with a maximum dose of 370 MBq and 24h whole-body and SPECT images were performed according EANM GL (Eur J Nucl Med Mol Imaging 2010 37:2436-2446) on a Picker Philips Medical System. DWIBS sequences were acquired using a short TI inversion recovery echo-planar imaging (STIR-EPI) sequence with free breathing and performed on a 1.5 T unit (Intera; Philips Medical Systems). SIOPEN Semi-quantitative scoring systems for NB with 12 body sections was applied at whole body MIBG and DWIBS images acquired to evaluate the disease extent at diagnosis and the response-to-therapy (Decarolis B, J Clin Oncol 2013; 31:944-954). We evaluated specificity, sensibility, overall accuracy, VPP and VPN of DWIBS respect MIBG considered as gold standard, (SE Sharp et Al in Nucl Med 2009;50: 1237-1243). **Results:** DWIBS and MIBG were congruent in 728 out of the 792 body areas analyzed: 637 negative concordant sites (80,4 %), 91 positive concordant (11,4) ; 48 DWIBS positive but MIBG negative sites (6,1 %), 16 DWIBS negative but MIBG positive sites (2%), with high agreement between the two techniques (κ=0.64, P < 0.0001 and Chi2 1312.1 P < 0.0001). If we consider MIBG as gold standard, MR overall accuracy was 92%; sensibility 85%; specificity 93%; VPP 65%; VPN 97%. Otherwise if we consider DWIBS as gold standard, MIBG overall accuracy was 92%; sensibility 65%; specificity 97%; VPP 85%; VPN 93%. Thus, MIBG and DWIBS SIOPEN scoring resulted superimposable (Rho of Spearman = 0,88, p < 0,0001). **Conclusions:** DWIBS and MIBG showed very high concordance, so MR may represent an alternative especially in weak-avid MIBG tumors.

EP-0746

Contribution of FDG PET/CT In Staging and Management of Pediatric Patients with Osteosarcoma

A. K. Fidan, G. Ucmak, I. Kerimel, B. B. Demirel, B. E. Akkas; S.B.U. Ankara Oncology Research and Training Hospital, Nuclear Medicine Department, Ankara, TURKEY.

Aim: Osteosarcoma is the most frequent seen primary bone tumor in pediatric patients. Metastasis is usually seen at the time of diagnosis or during follow up period. 5 year survival of patients with local disease is about 70% where as overall survive significantly decreases in metastatic disease. The importance of FDG PET/CT in staging/restaging of osteosarcoma has increased

on last decade. In recent studies, it is seen that PET/CT is more sensitive and specific than the conventional radiologic imaging techniques, in the diagnosis of metastases other than lungs. In our study, we aim to investigate the contribution of PET/CT in the staging and management of patients with osteosarcoma. **Method:** 37 patients who are diagnosed with osteosarcoma and underwent FDG PET/CT imaging on staging were included in our study. After treated with neoadjuvant chemotherapy and surgery, all patients were followed up for mean 35 months (range: 4-89). Findings which are suspicious for metastasis on PET/CT were verified either histopathologically or based on the findings of clinical and/or imaging results on follow-up.Results: In all patients, primary tumors were detected successfully on PET/CT. The FDG uptake was increased on all primary lesions as well as on metastatic sites. Pulmonary nodules in 14 patients, lymph node metastasis in 12 patients, lytic bone metastasis which were negative on bone scan in 2 patients and intra-medullary skip metastasis in 6 patients were detected on PET/CT at the time of diagnosis. All pulmonary nodules which are seen in contrast enhanced thorax CT imaging are all detected on PET/CT. Lymphatic metastases were only detected by PET/CT and 5 of these patients (41 %) were upstaged (stage 4) by PET/CT for lymph nodes were the only site of distant disease. **Conclusion:** FDG PET/CT can detect distant metastases with high accuracy and provided accurate information on the extent of disease. We considered that PET/CT plays an important role on initial staging and must be a part of clinical management algorithm of patients with osteosarcoma.

EP-0747

Correlation of Tumor Necrosis Ratio and Metabolic Parameters of Initial Staging FDG PET/CT In Pediatric Patients with Osteosarcoma

G. Ucmak, A. K. Fidan, I. Kerimel, B. E. Akkas, B. B. Demirel; S.B.U. Ankara Oncology Research and Training Hospital, Nuclear Medicine Department, Ankara, TURKEY.

Aim: Tumor necrosis ratio (TNR) after neo-adjuvant chemotherapy is an important factor affecting treatment protocol and prognosis in patients with osteosarcoma. Standardized uptake values (SUVmax), metabolic tumor volume (MTV) and total lesion glycolysis (TLG) are metabolic parameters that are shown to correlate with patient prognosis in several malignancies. The aim of this study is to analyze if metabolic parameters obtained by initial staging FDG PET/CT may predict TNR in pediatric patients with osteosarcoma. **Method:** 33 patients with osteosarcoma (age range:6-19) are included in our study. SUVmax, MTV and TLG of the primary tumor were measured. After 2 cycles of chemotherapy with adriamicine, cisplatin and methotrexate, all patients underwent surgical resection. Based on pathology results of the surgical specimen, patients were classified as low TNR group (0-89%) and high TNR (90-100%) groups. The correlation of metabolic parameters and TNR was analyzed. **Results:** The median SUVmax, MTV and TLG were 10, 399 ml and 1648 gr respectively in patients with low TNR (n:18). Whereas, the median SUVmax, MTV and TLG were calculated as 9.1, 130 ml and 605 gr, respectively in patients with high TNR (n:15). MTV

and TLG were significantly higher in low TNR group compared to high TNR group (p=0.02). In addition, we observed significant negative correlation between TNR and both of these two metabolic parameters (p=0.03). **Conclusion:** We observed that metabolic parameters such as MTV and TLG have strong negative correlations with TNR after neo-adjuvant chemotherapy in patients with osteosarcoma. The findings of this study indicate that higher MTV and TLG predict an insufficient response to chemotherapy and primary tumors with high MTV and TLG may need to be treated with more intensive chemotherapy regimens. We considered that further prospective clinical trials are warranted to prove the findings of this study in order to provide longer progression free and overall survival.

EP-55   during congress opening hours, e-Poster Area

Clinical Oncology: Imaging Guided Surgery (including Sentinel Lymph Node)

EP-0748

Sentinel lymph node biopsy (SLNB) before and after neo-adyuvant chemotherapy (NAC) in locally advanced breast cancer, our results

J. M. Espejo Niño, A. Esteban Figueruelo, E. Rodeño Ortiz De Zárate, P. Cobos Baena, L. Andres Alvarez; Hospital Universitario Cruces, Barakaldo, SPAIN.

Purpose: We assessed the contribution of SLNB performed before to NAC (B-NAC) or after NAC (A-NAC) in locally advanced breast cancer patients regarding tumour and lymph node response and metastatic disease. **Subjects and Methods:** Retrospective study (January/2012-February/2017). Eligibility criteria: consecutive patients selected for NAC with: radiologic studies assesing tumour size and localization (TNM-AJCC-7th-Edition), axillary clinical involvement (cN+/cN0), histological types, predominantly infiltrating ductal carcinoma (IDC) and high grade ductal in-situ carcinoma (DISC-HG), tumour markers, chemotherapy protocols: docetaxel+cyclophosphamid+-doxorubicin scheme (DCD 6 cycles), and DCD (4 cycles) plus docetaxel+trastuzumab (4 cycles) in HER2 gene overexpression patients, who underwent to SLNB-B-NAC or SLNB-A-NAC, including the assessment of tumoral response to the treatment following radiological and pathological criteria (RECIST1.1 and Miller&Payne). **Results:** We reviewed 58 patients selected to NAC, we exclude 24 patients that didn´t met eligibility criteria. A total of 34 patients were included, 2 with bilateral breast disease (mean age:49.5 years). We performed 20 SLNB-B-NAC and 16 SLNB-A-NAC. In the B-NAC group, 9 patients were cN(+). 7 SLNB positive (SLNB+), 12 SLNB negative (SLNB-) and 1 SLNB with micrometastatic disease (SLNBmic). After chemotherapy, 8 patients showed complete response (CR); 2 didn´t respond (NR); 4 showed partial major response (PMR) and 6 showed partial minor response (PmR). We completed axillary lymphadenectomy (ALND) to the positive SLNB: Two of these were positive ALND (ALND+) and non-responder patients too, and 5 were negative

ALDN (ALND-): 3-CR, 1-PMR and 1-PmR. Only 1 patient had metastatic disease, with SLNB(+), PmR and ALND(-). The SLNB(mic) presented CR. There were no relapses or metastatic disease in SLNB(-). In the A-NAC group, 14 patients were cN(+) and 2 cN(0) before the chemotherapy. 7 were SLNB(+), that in the clinical follow-up presented: 6-PmR and 1-PMR. In 3 patients there were unsuccessfull detection of the SLN: 2 patients with PmR and 1 with PMR with hepatic and bone metastatic disease. The 4 SLNB(-) presented: 2-CR, 1-PMR and 1-PmR. 2 patients were SLNB(mic): 1-PMR and 1-PmR. 13 of 16 patients underwent to ALND. We obtained 10 ALND(+). In these patients there were 6 SLNB(+), 3 unsuccessfull detection and 1 SLNB(-). In 3 cases we didn´t perform ALND: 2 were cN(0) with SLNB(-): and 1 SLNB(+) with DISC-HG diagnosis, with contralateral DIC and ALND(+). **Conclusions:** In our series the detection rate of SLNB-B-NAC was 100% and in the SLNB-A-NAC of 81%, with 6% of false negatives. There were no relapses in the SLNB(-) B-NAC.

EP-0749

Comparison of the diagnostic value of preoperative sentinel lymph node (SLN) imaging using conventional scintigraphy and SPECT/CT in penile cancer patients with non-palpable inguinal lymph nodes

U. Lützen, B. Egeler, M. Jüptner, Y. Zhao, M. Marx, C. M. Naumann, K. Jünemann, M. Zuhayra; UKSH, Campus Kiel, Kiel, GERMANY.

Purpose/Introduction: The aim of the current study is to evaluate the diagnostic worth of preoperative SLN-imaging via SPECT/CT and conventional planar scintigraphy in patients with penile cancer and impalpable inguinal lymph nodes. **Subjects and Methods:** We performed preoperative radioactive marking of the SLNs after intradermal perilesional injection of 150 MBq Tc-99m -labelled nanocolloids according to the two-day protocol. Acquisition of conventional lymph scintigraphies was done by means of a twin head gamma camera (Siemens, ECAM, Symbia S) as well as indirect body contouring. Immediately after this, we performed SPECT/CT-images of the abdomen incl. groins using a twin head hybrid system (Siemens Symbia T, Symbia Intevo6). Prospective evaluation of 52 groins in 26 examined patients of this tumour entity was done for all image files obtained by both techniques by two experienced experts in consensual assessment. **Results:** Preoperatively, 71 SLN in 37 groins were identified by means of conventional scintigraphy. In the planar images, no radioactive lymph nodes were visualized in 15 out of 52 groins (28.8%). The hybrid-images showed a total of 82 SLN in 42 groins. In 19.2% (10 of the 52 groins), there was no visualization of lymph nodes in this technique. 8 SLN in 7 groins that were visualized in the conventional technique were found to be false positive by SPECT/CT. 19 SLN in 16 groins that were overlooked by planar imaging could only be detected by SPECT/CT. In contrast to planar scintigraphy, SPECT/CT-imaging enabled clear identification and accurate anatomical localization of SLN in all 42 groins where radioactive SLNs were detectable. The statistical evaluation (sign-test) of our data showed a significantly higher number of detected SLN with the hybrid- in comparison to the planar technique (p=0.002). **Discussion/**

Conclusion: In patients with penile cancer and impalpable inguinal lymph nodes SPECT/CT-imaging is capable of visualizing SLNs that cannot be detected in planar imaging. In addition, the hybrid-technique reduces the number of false-positive findings from planar SLN-imaging and is able to show anatomic SLN localization more accurate. If possible, preoperative SLN-imaging should be performed by using SPECT/CT-technique in patients with penile cancer.

EP-0750

Diagnostic Accuracy Of Sentinel Lymph Node Biopsy In Patients With Endometrial Cancer

S. Sanz-Viedma, T. Gomez, A. Fernandez-Molina, M. De La Torre-Baca, P. Espejo, I. Egea, A. Eslava, J. Jimenez Hoyuela, L. Gonzalez, J. Oliva; University Hospital Virgen de la Victoria, Malaga, SPAIN.

The surgical approach to endometrial carcinoma is a controversial issue. In cases considered high-risk, lymphadenectomy has shown therapeutic benefits and there is consensus about its need. However, in cases of low and medium risk, its usefulness has not been demonstrated. **Aim:** To evaluate the applicability and results of SLN technique in endometrial cancer. **Methods:** From 2014 to 2016, 35 patients with preoperative diagnosis of low- and medium-risk endometrial carcinoma underwent sentinel lymph node procedure (SLN). The day before surgery, an injection of 111 MBq 99mTc- nanocolloid in the cervix and a subsequent SPECT/CT lymphoscintigraphy were carried out. Blue dye was injected at the same location intraoperatively. A laparoscopic gamma probe was used to identify SNs. An intraoperative biopsy of the sentinel nodes was performed. Regardless of the outcome, a complete pelvic lymphadenectomy was performed in all cases. In the definitive histopathological analysis lymph nodes were analyzed by conventional techniques while sentinel lymph nodes were analyzed by immunohistochemistry techniques. **Results:** The sentinel node detection rate was 74.3%, with a bilaterality of 50%. False negative rate was 0% .Negative predictive value and sensitivity were 100%. There were no surgical complications resulting from sentinel node sampling. 88.9% of the lymphadenectomies performed in low- and medium-risk cases were negative. After the final histopathological analysis, 22.9% of the patients in the study had a greater tumor risk than the preoperativel one according to MRI and biopsy data. A discordance of 20% was recorded for biopsy and 58% for MRI.The overall incidence of metastasis, regardless of tumor risk, was 17.1%. By groups, the lymph node involvement was 13.3% at low risk, 8.3% at medium risk and 37.5% at high risk. The application of immunohistochemical techniques in the sentinel node increased a 5.7% the detection of lymph node metastases. **Conclusion:** SLN procedure is a safe and feasible method in endometrial cancer. It has a good detection rate and provides representative information of the lymphatic drainage of endometrial cancer.

EP-0751

Tc-99m-PSMA-guided intraoperative lymph node localization in recurrent prostate cancer

M. C. Schmidt[1], D. Pfister[2], C. Kobe[1], M. Dietlein[1], M. Dietlein[1], A. Heidenreich[2], A. Drzezga[1]; [1]University Hospital of Cologne, Dpt. of Nuclear Medicine, Cologne, GERMANY, [2]University Hospital of Cologne, Dpt. of Urology, Cologne, GERMANY.

Introduction: PSMA-PET/CT is the most sensitive diagnostic tool in biochemical recurrent prostate cancer to detect minimal metastatic disease. However, it may be difficult to localize small PSMA-positive lymph nodes intraoperatively. Therefore, it was the aim to compare PSMA-PET/CT with Tc-99m-PSMA imaging and to investigate whether preoperative Tc-99m-PSMA targeting may improve intraoperative tumor localization with the aid of a gamma probe. **Patients and Methods:** In 13 Patients Ga-68-PSMA-PET/CT identified iliac lymph nodes in patients suitable for salvage lymph node dissection. On the day before operation a mean activity of 470 MBq Tc-99m-PSMA was injected and gamma camera scintigraphy + SPECT was performed 4-5 hours after tracer application. About 24 hours after tracer application a salvage lymph node dissection was performed on the side of initial suspicious lymph node metastases. PET/CT results were correlated with SPECT results and diagnostic values were calulated for gamma probe use. **Results:** In 9 / 13 patients PSMA-positive metastatic lymph nodes were identified in Ga-68 PSMA-PET/CT. Tc-99m-PSMA was positive in 8/13 patients, most lymph nodes detected had a short axis diameter above 1 cm or a SUV max above 10. Intraoperatively, a total of 156 lymph nodes were removed with 14 lymph nodes in 9 patients being positive in histopathologic examination. Sensitivity, specifity, pos and neg. predictive values for PSMA PET/CT and gamma probe were 85% and 79%, 99% and 100%, 85% and 100% and 99% and 98% respectively. In one patient only gamma probe use identified a pathologic lymph node. **Conclusion:** Gamma probe guided salvage lymph node dissection in PSA recurrent prostate cancer is feasible and had a high concordance with PSMA-PET/CT. However, the additional diagnostic benefit is limited compared to PSMA-PET/CT because in only one patient (7%) a positive lymph node could be identified with the use of the gamma probe outside the standard operative area in salvage lymph node dissection.

EP-0752

Wire-guided localization vs ¹²⁵I radioactive seed localization in nonpalpable breast lesions

R. Sánchez Sánchez, A. González Jimenez, A. Rebollo Aguirre, E. Triviño Ibañez, E. Moratalla Aranda, S. Menjon Beltran, J. Llamas Elvira; Hospital Virgen de las Nieves, Granada, SPAIN.

Purpose: To show our preliminary result in using of ¹²⁵I radioactive seed (RSL) for guidance during surgical resection of nonpalpable breast lesions and to assess the therapeutic outcomes against wire-guided localization, the current gold standard. **Methods:** Patients undergoing breast procedures after radiologic localization during 2015-2016 were included. Wire guided localization (WGL) as RSL (B) were preferentially conducted under ultrasound guidance and were performed under mammographic guidance if the lesion was no sonographically visi-

ble. RSL was performed with a 4.5 mm by 0.8 mm titanium seed containing 3.7-11.1 MBq of ¹²⁵I. The radioactive seed is loaded into and 18G spinal needle after occluding the tip with sterile bone wax. The day selected was determined by radiology and operative suite scheduling (up to five days). At the time of operation a gamma probe is set to detect 27 KeV (¹²⁵I) source. The incision was made at the point of greatest activity. Seed removal within the specimen is assured by detecting the ¹²⁵I source of radioactivity within the excised specimen and no ¹²⁵I source remaining within the wound. Sentinel lymph node were performed in patients with no contraindication. Margins of excision were considered negative when no invasive cells or carcinoma in situ cells were present on the inked edge of the excised specimen. The volume of the resection was estimated using the formula for the volume of an ortoedro. Dimensions of the resection margin were measured in the pathology department. **Results:** WGL group (n: 53): CDI 84.9%, malignant tumor size (cm) mean-1.8. RSL group (n: 45), CDI 82.2%, malignant tumor size (cm) mean-1.5. No major complications occurred during surgery. All seed were removed. The mean rates of positive involved resection margins were 22.6% in WGL group vs 15.6% in RSL group. The mean rates of re-interventions were 13.2% in WGL group vs 7.5% in RSL group. The median resection volume was statistically significant lo wer in RSL group (189.37 cm³ vs 128.68 cm³). **Conclusion**: In our institution RSL is a feasible procedure that shows promising results. Use of RSL has enabled precise breast conserving surgery and show low positive resection margin rates and significantly lower resection volumes. It is necessary increased the number of patient and good preliminary results encourage us to continue working on it.

EP-0753

Time to relapse is associated with altered lymphatic drainage and sentinel node location in recurrent breast cancer

P. Borrelli[1], S. Teixeira[2], S. Vidal-Sicart[3], M. van Essen[1], H. van Tinteren[2], R. A. Valdés Olmos[2,4]; [1]Sahlgrenska University Hospital, Göteborg, SWEDEN, [2]Netherlands Cancer Institute, Amsterdam, NETHERLANDS, [3]University Hospital Clinic, Barcelona, SPAIN, [4]Leiden University Medical Center, Leiden, NETHERLANDS.

Introduction: During recent years sentinel node procedures in relapsed breast cancer patients have increased. Various aspects like migration percentages, metastasis rates and drainage to non-typical sentinel node areas have been evaluated in the literature. However, the issue considering whether and how time until relapse affects migration patterns remains still undocumented. **Subjects and Methods:** Data from various participating centres were analysed retrospectively and 93 female patients who underwent sentinel node procedures for staging during breast cancer relapse were evaluated. Median age was 59 years (range: 24-87). Patients were divided in two groups: an early relapse group (group 1), from 1 to 120 months to relapse, and a late relapse group (group 2), beyond 121 months. **Results:** Out of 93 patients with SN visualization ipsilateral lo-

co-regional migration was visible in 34 patients (36.5%), non-ipsilateral migration in 39 (41.9%) and to both areas in 20 (21.5%). Ipsilateral migration rate was 68,6 % in group 1 (early relapse) versus 52,9 % in group 2. Migration rate to non-ipsilateral areas increased from 52,4 % in group 1,to 73,8 % in group 2. Ipsilateral loco-regional migration included drainage to axilla in 37 patients, intramammary or interpectoral in 10 patients, while 7 patients had SN visualization both in ipsilateral axilla and intramammary/interpectoral areas. **Conclusion:** In patients with breast cancer recurrences scheduled for sentinel node biopsy, time to relapse seems associated with altered lymphatic drainage patterns. Early relapse cases tend to have a higher migration rate to ipsilateral loco-regional areas (axilla/ intrammamary/ interpectoral) whereas relapses after 10 years show a trend to drainage to non-ipsilateral areas.

EP-0754

Sentinel Lymph Node Biopsy in Cutaneous Melanoma: Analysis of 362 Patients from a Single Institution

L. Jaukovic, M. Radulovic, M. Rajovic, L. Kandolf-Sekulovic; Military Medical Academy, Belgrade, SERBIA.

Background: Sentinel lymph node (SLN) biopsy is widely accepted staging procedure for cutaneous melanoma patients who are at risk of clinically occult nodal metastases. Numerous predictive factors for regional lymph node metastases have been identified, however, few have been found to be reproducibly significant. **Aim:** We present a single institution study looking at characteristics predictive of a positive SLN biopsy result in our population. **Methods:** We performed a retrospective review of 362 cutaneous melanoma patients who underwent lymphoscintigraphy and SLN biopsy at our Institution in period 2010-2016.y. To delineate the relation of each variable (demographical, clinical and pathological variables as well as the presence of in- transit nodes, number of draining basins and SLN localization on scintigraphy) with positive SLN status, we used univariate logistic regression with odds ratios representing effect size. We performed multivariate regression analysis using only the factors that were significant in the univariate analysis. **Results:** In all, 18.4 % of patients had one or more positive SLNs. Breslow thickness (p&lt0.001), primary ulceration lesion (p=0.001), and lymphovascular invasion (0.007) were strongly correlated with SLN positivity. Site of primary tumor (p=0.023), inflammatory infiltrate (p=0.024) and sex (p=0.025), were also significantly associated with SLN status. Multivariable analysis with 362 cases included in model revealed Breslow thickness and inflammatory infiltrate to be significant independent predictors of SLN status (p&lt0.05). The remaining variable regressed, were no more significantly associated with SLN status. **Conclusion:** Beside the well established primary tumor thickness as the predictor of SLN positivity, we also observed a significant association for body site of primary. Increase in Breslow depth of 1 mm enhanced the chances for SLN positivity by 2.6 folds. Using the acral site as a referent, melanoma of the trunk showed 74% less chances for metastatic involvement of SLN. Our findings on possible relation between the acral localization and SLN metastasis needs further clarification.

EP-0755

Incidence and implications of atypical lymphatic drainage in patients with Primary Cutaneous Malignant Melanoma

M. Oporto[1], C. Sampol[1,2], A. Repetto[1], N. Orta[1], H. Navalon[1], S. Rubi[1,2], M. Villar[1], C. Peña[1,2]; [1]hospital Universitari Son Espases, Palma, SPAIN, [2]IdISPa, Palma, SPAIN.

Purpose: To determine the frequency and importance of Atypical Sentinel Lymph Node Drainage(ASLND) in patients with Primary Cutaneous Malignant Melanoma(PCMM). **Materials and Methods:** We retrospectively evaluated 165p with PCMM who underwent SLNB (Sentinel lymph node biopsy) between 2012-2015. We classified in 5 categories according melanoma´s localization: 1)Head and Neck,2)Anterior truncal,3)Posterior truncal,4) Upper extremity and 5)Lower extremity. Preoperative lymphoscintigraphy was performed in all patients the day before surgery with 4 intradermal injections peritumoral or around the scar of 99mTc-nanocolloid. Early planar, dynamic post-injection, delayed images, SPECT-CT were taken on region of interest. Unusual lymph node location were defined as epitrochlear and popliteal for extremities and ectopic/interval (in-transit or any other nonstandard lymph node-bearing area)for truncal and head and neck. Intraoperatively SLN identification was determined by gamma probe detection. Finally, patients were followed for recurrence and complications until 2017. **Results:** Out of 165p included, median age 57.8 years (23-94years), 91 female and 74 male, all diagnosed of PCMM (63 nodular,73 superficial spreading,16 lentigo-maligna and 14 acral-lentiginous)with medium thickness on Breslow scale of 1,81 mm(0,42-9,1mm). The number of patients for group was 1)23p,2)19p,3)32p,4)38p,5)53p. A total of 479 sentinel lymph node were identified and excised(median per patient:2,46).26p had ASLND with a total of unusual sentinel lymph node of 44. The number of patients with unusual sentinel lymph node and number of SLN and location for category was:1)=7p (retroauricular=4, occipital=3, temporal=2;2)=3p (in-transit-shoulder blade=1, breast=1, internal mammary chain=1);3)=11p (upper-clavicle=14,in-transit-shoulder blade=6,-cervical=2, breast=1); 4)=3p (epitrochlear=6);5)=3p(popliteal=3). Among this 26p, 3p (11,53%) had lymph node metastasis in ASLND. In 2p the only positive SLN was from the unusual site (7,69%),1 occipital and 1 in-transit-shoulder blade. With a median follow-up of 38 months, the ASLND group had 15,38% of nodal relapse, being similar to the non-ASLND group (15,10%), having all of them an initial positive SLNB. All patients from both groups died, being the global mortality in our serie, including nodal and extranodal relapse, of 22,42%. **Conclusion:** In our study, the most frequent incidence of ASLND, in nearly one-third of cases, was in posterior truncal melanoma, followed by head and neck. Preoperative lymphoscintigraphy and SPECT-CT is highly recommended to achieve the correct identification and location of ASLN. The excision of these nodes is crucial because may represent the only site of lymph node metastases, being in these cases decisive for the prognosis and therapeutic decision-making. In our study the nodal relapse and mortality were similar in both groups, being more related to the positivity of the SLN rather to the presence or absence of ASLND.

EP-0756

Our Experience with ROLL and SNOLL techniques in clinically occult breast carcinoma

S. M. Nieves Maldonado[1], Z. Bravo Ferrer[1], C. Lancha Hernandez[1], I. Nuñez Cambre[1], J. Rodriguez[2], J. Corredoira[3], A. Rodriguez Pan[3]; [1]Nuclear Medicine Department. Hospital HM- Modelo de la Coruña, La Coruña, SPAIN, [2]Surgery Department. Hospital HM- Modelo de la Coruña, La Coruña, SPAIN, [3]Radiology Department. Hospital HM-Modelo de la Coruña, La Coruña, SPAIN.

Purpose: To evaluate our experience after implementation of lymphoscintigraphic method for radioguided occult lesion localisation (ROLL) and sentinel node and occult lesion localisation (SNOLL) techniques in clinically occult breast carcinoma at our institution. **Methods:** 81 consecutive patients (39-85 years old, mean age 59,3 years) suspected to have clinically occult breast carcinoma, and without palpable axillary lymph nodes were enrolled in the study over the last three years. Breast carcinoma patients after NeoAdjuvant Chemotherapy (NAC) treatment were also included to facilitate breast-conserving therapy. On the day before surgery, 0,2-0,5 ml solution of nanocolloids with 74 MBq of technetium-99m was injected under sonographic (73 patients) or stereotaxic (8 patients) guidance into the lesion in order to perform ROLL (29 patients) and SNOLL (52 patients). Scintigraphic images were acquired to verify the correct tumor localisation and lymph node detection. In cases of no lymphatic migration, retroareolar injection was performed. All patients underwent open surgical biopsy guided by gamma probe. An intraoperative macroscopic examination of the specimen with margins evaluation was performed. SLN was considered to be positive if macrometastases or micrometastases were found, and in such cases axillary dissection was consequently implemented. **Results:** The procedure was always successful helping to accurately locate the occult breast lesions on lymphoscintigraphy. Images showed axillary drainage in 51 SNOLL patients, internal mammary chain drainage in 3 patients, and intramamary drainage in 1 patient.Pathological findings revealed breast carcinoma in 70/81 patients (86%) and benign lesions in 11 (14%).There were 53/70 cases of infiltrating carcinoma (76%) and 17/70 of intraductal carcinoma (24%). Intraoperative detection was successful and allowed a precise tumoral bed excision in most patients (28/29, 97%). Tumor margin was involved in one patient (3%), therefore a mastectomy was performed along with lymphadenectomy due to macrometastasis. ROLL was performed in 3/29 patients (10%) for tumor placement after NAC without complications, and these patients underwent lymphadenectomy. Axillary SLN were resected in 51 patients, and intraoperative examination of them were histologically negative for metastases in 44 patients (86%) and revealed metastatic involvement in 7 patients (14%). 4 additional SLNB were differed to a second surgical act after ROLL. **Conclusion:** We have implemented of performance of ROLL and SNOLL techniques as useful choices for accurate localisation of non-palpable lesions and sentinel nodes in our institution with promising results, thus replacing the use of a hook-wire mark. These techniques have been precise and reproductible, facilitating accurate surgical approach and avoiding reinterventions.

EP-0757

Prognostic Significance Of The Effect Of Delay Time Between Primary Melanoma Biopsy And Sentinel Lymph Node Biopsy

M. L. Dominguez[1], J. P. Suarez[2], P. Fernandez[3], J. I. Rayo[4], O. D. Rodriguez[1], F. M. Gonzalez[1]; [1]Nuclear Medicine Department. Central University Hospital of Asturias, Oviedo, SPAIN, [2]Nuclear Medicine Department. San Pedro de Alcantara Hospital, Caceres, SPAIN, [3]Clinical investigation and trials unit. Virgen del Rocío University Hospital, Sevilla, SPAIN, [4]Nuclear Medicine Department. University Hospital Infanta Cristina, Badajoz, SPAIN.

Purpose: To investigate the effect of delay time between primary melanoma biopsy and sentinel lymph node biopsy (SLNB) on recurrence and survival. **Subjects & Methods:** We retrospectively reviewed 184 consecutive cutaneous melanoma patients who underwent a SLNB from December 2005 to December 2015. Clinical characteristics of patients, histologic features of primary melanoma, SLNB technique, lymph node dissection and follow-up were analised. The main variable defined as delay time, was categorised using the minimum p-value approach which consisted of performing multiple log-rank tests to compare survival curves and determine the optimal cutoff point for separating the patients into two groups. The optimal cutoff was established at 50 days for "overall survival" and at 30 days for "melanoma-specific survival". Associations between delay time and other variables were investigated using chi-square tests. Survival curves were generated using the Kaplan-Meier (KM) nonparametric method and compared using the log-rank test. **Results:** Median of delay time was 53 days (8.25-70.75) and follow-up 43.5 months (23.25-63.75). 16 patients (8.69%) died, and 23 (12.5%) developed any recurrence (local, satellitosis, regional lymph node and systemic). 38 patients (20.70%) had a positive sentinel lymph node, so lymph node dissection was subsequently performed. A delay time ≤ 50 days had *statistical significance with* overall survival (p=0.003), melanoma-specific survival (p=0.035) and disease-free survival (DFS) by satellite lesions (p=0.045). A delay time ≤ 30 days had *statistical significance with* melanoma-specific survival (p=0.014), DFS by any type (p=0.018), DFS by local recurrence (p=0.005) and DFS by satellitosis (p=0.003). *KM curves showed* an *association* between a delay time > 50 days with better survival (p=0.026, p=0.019 in negative sentinel lymph node). **Conclusion:** In our population, a relatively prolonged delay in sentinel node dissection from the initial melanoma biopsy does not adversely affect sentinel node status, recurrence, nor survival. The scarce number of patients of our study could complicate the generalization of these results.

EP-0758

Evaluation Of The Influence Of Preoperative Wire-Guided Localization And Radiopharmaceutical Injection With Or Without Radiological Guidance In Global Detection Of Sentinel Lymph Node Biopsy In Patients With Breast Cancer

*V. López-Prior, **A. Amr-Rey**, R. Díaz-Expósito, Sr., I. Casáns-Tormo, J. Orozco-Cortés, J. Sabater-Sancho; Servicio de Medicina Nuclear. Hospital Clínico Universitario de Valencia, Valencia, SPAIN.*

Purpose: We analyzed the detection of the sentinel node (SN) in breast cancer after radiotracer injection, with radiological guidance (RG) (ultrasound or stereotaxy) or without it (NRG). We evaluated whether the placement of a preoperative wire influenced the detection. **Methods:** Retrospective study in 603 patients, aged 57.24 y/o (range 28-86), with infiltrating carcinoma 483 (80.1%), histological grade I 203 (33.7%) and II-III 398 (66.0%), luminal immunohistochemical profile 440 (72.97%), HER2 (+) 70 (11.6%), triple negative 46 (7.63%). Mean tumor size 12.74 ± 8.8 mm. Neoadjuvant chemotherapy 192 (31.84%). External quadrants 361 (59.87%), internal 178 (29.51%) and retroareolar 64 (10.61%). There were 270 (44.78%) patients with wire and intratumoral injection of 99m-Tc nanocolloid, with ultrasound guidance (217/270, 80.37%) or stereotaxy (53/270, 19.62%). In 333 (55.22%), NRG injection: 107 (32.13%) intratumoral and 226 (67.87%) periareolar (63 preoperative wire). The total number of patients with preoperative wire was 333. If necessary, periareolar reinjection (84/603, 13.93%). We performed planar lymphoscintigraphy, surgical detection with gamma probe and intraoperative anatomopathological analysis (OSNA). **Results:** The global SN detection after RG injection was 249/270 (92.2%) and NRG 317/333 (95.2%) (NS). In RG injected patients, the detection when we analyzed exclusive intratumoral injection was similar (ultrasound guide: 156/217, 71% and stereotaxy: 37/53, 69.8%). After periareolar reinjection, the detection was substantially increased: (ultrasound 199 / 217, 91%, stereotaxy 50 / 53, 94.3%). In 306/333 (91.8%) of the patients with preoperative wire, the detection was significantly lower (p = 0.02) than in patients without it (260/270, 96.2%). In those intratumorally injected, detection was significantly lower (p = 0.00) in tumors with preoperative wire (193/270; 71.5%) vs without it 93/107 (86.9%). Extraaxillary drainage, evaluating exclusive intratumoral injection, tended to be higher RG (39/51; 76.4%) than NRG (12/51; 23.6%) (NSS). When we analyzed patient characteristics, tumor size was significantly greater (p = 0.00) in NRG patients injected intratumorally (18.5 ± 8.5 vs 10.2 ± 5.6 mm). There were no significant differences in clinical-tumor characteristics of the patients with preoperative wire (with or without radiological guidance). **Conclusion:** The SN detection after intratumoral injection of the radiopharmaceutical and wire placement was lower (71.5%) than optimal values (95%), with no differences according to the guidance by ultrasound or stereotaxy. There were no differences in the detection of patients injected RG or NRG.

EP-0759

Internal Mammary Lymph Node in Breast Cancer as a Predictive Value in a High Risk Asymptomatic Population

A. Mestre-Fusco[1], J. Jimeno[2], M. Suárez-Piñera[1], I. Espallargas[1], M. Vernet[3], J. Corominas[4], S. Vidal-Sicart[5]; [1]Radiology & Nuclear Medicine Department, IMI. Hospital del Mar, PSMar., Barcelona, SPAIN, [2]Surgery Department. Hospital del Mar, PSMar., Barcelona, SPAIN, [3]Gynecology Department. Hospital del Mar, PSMar., Barcelona, SPAIN, [4]Pathology Department. Hospital del Mar, PSMar., Barcelona, SPAIN, [5]Nuclear Medicine Department. Hospital Clínic., Barcelona, SPAIN.

Introduction: The internal mammary lymph node (IMLN) drainage has been considered a prognostic factor in breast cancer. However randomized trials have failed to demonstrate a survival benefit from surgical IMLN dissection. The aim of this study was to evaluate the clinical impact of IMLN metastases in breast cancer in a high risk asymptomatic population. **Subjects & Methods:** A retrospective study was performed in two university hospitals between December 2001 and June 2015 involved 206 breast cancer patients underwent preoperative lymphoscintigraphy (99mTc-colloid) who demonstrated radioisotope uptake to the internal mammary node chain. Analysis was performed including demographic data, size and localization of tumor, histopathology findings and sentinel lymph node (SLN) drainage. Local and systemic recurrence and overall survival (log-rank test, SPSS) were calculated. **Results:** Lymphoscintigraphy demonstrated uptake to the internal mammary chain drainage in 206 patients. Thirty nine patients (18.9%) were excluded due to the retrosternal drainage, non-surgically accessible. A total of 167 patients with IMLN removed in surgery were finally included in the analysis. Nodal metastases in IMLN were diagnosed in 19 out of 167 patients (11.4%). Median age: 56 year-old (range 27-90). A 51% of the patients were diagnosed through the screening program. Tumor diameter: 15.3±9 mm. Median follow-up after surgery was 80.5±43 months. The most frequent localization was superior outer quadrant (27%) followed by superior inner quadrant (22.3%). The probability of IMLN metastases has been observed to increase with tumor size (18.1±8.7 versus 14.3±8,5 mm; p=0.068). The probability was not associated with other tumor variables. However, a higher recurrence (log-rank test; p<0.001) and low survival (log-rank test; p=0.001) were observed in case of axillary sentinel lymph node (ASLN) metastases. Patients with negative ASLN showed a lower percentage of IMLN metastases (9.3% versus 90.7%; p=0.028). **Conclusion:** Our results showed that IMLN metastases in patients with IMLN drainage has neither been significantly associated with worse prognosis nor with other risk factors. Positivity of ASLN is the main predictive factor in recurrence and survival in breast cancer patients.

EP-0760

Within-patient comparison of two sentinel lymph node tracers: 99mTc-Senti-Scint and (ICG-)99mTc-nanocolloid

P. Meershoek[1,2], M. L. Donswijk[2], G. H. KleinJan[1,2], N. S. van den Berg[1], B. van der Hiel[2], R. A. Valdés-Olmos[1], J. A. van der Hage[2], W. M. C. Klop[2], F. W. B. van Leeuwen[1]; [1]Leiden University Medical Center, Leiden, NETHERLANDS, [2]Netherlands Cancer Institute (NKI-AvL), Amsterdam, NETHERLANDS.

Introduction: The standard radiocolloid used in Europe for the sentinel node (SN) procedure is the albumin-based 99mTc-nanocolloid (diameter 20-100 nm). This tracer can be combined with

indocyanine green (ICG) to yield ICG-^{99m}Tc-nanocolloid. Since radiocolloids have to be administered in a standardized fashion, interpatient variations may severely influence the degree of drainage. In some cases this results in over saturation of the SNs, yielding overflow to clinically irrelevant higher echelon nodes (LNs[he]). An unwanted effect that dictates the longitudinal scanning procedure used today to e.g. differentiate SNs from LNs[he] in the head and neck area. Reduction of the number of LNs[he] has been a target for new efforts in tracer development including the development of ^{99m}Tc-Senti-Scint, a "larger" (100-600 nm) albumin-based radiocolloid. Via an interpatient comparison of ^{99m}Tc-Senti-Scint with (ICG-)^{99m}Tc-nanocolloid, we studied if the increased particle size could reduce the amount of LN[he], while preserving the SN identification. **Materials and Methods:** 25 patients with (re-)excision of melanoma were included, all of which received a two-day SN procedure. On the first day 90 MBq (±10%) ^{99m}Tc-Senti-Scint was administered intracutaneously in four deposits of 0.1 mL around the melanoma (scar); injection sites were marked with indelible ink. Lymphatic drainage was mapped using: dynamic lymphoscintigraphy, static lymphoscintigraphy (15 minutes and 2 h) and SPECT/CT (2h). On the second day a static lymphoscintigraphy of the residual activity of ^{99m}Tc-Senti-Scint, was made prior to administering 90 MBq (±10%) ICG-^{99m}Tc-nanocolloid (four 0.1 mL deposits at the marked sites), followed by the above mentioned imaging protocol. **Results:** In total 108 lymph nodes (LNs) were found with ^{99m}Tc-Senti-Scint of which 58 (53.7%) were considered SNs and 50 (46.3%) LNs[he]. For ICG-^{99m}Tc-nanocolloid these numbers were 123 LNs (difference +15; p=0.036, 95% CI -1.159; -0.041), of which 58 SNs (47.2%; difference 0; p=1.000; 95% CI -0.169:0.169) and 65 LNs[he] (52.8%; difference +15; p=0.033; 95% CI -1.146:-0.054), respectively. Of the LNs that were identified 106 LNs were classified identically with both tracers. On a patient basis this resulted in 16 (64%) patients that were identically classified. **Discussion/Conclusion:** In line with the expectations, ^{99m}Tc-Senti-Scint yielded a lower amount of LNs[he]. This was realized, while preserving the SN detection rate under standard conditions. Nevertheless, the longitudinal scanning procedure proved to remain a critical component in the SN identification process as it helped prevent a ±50% over estimation for the amount of SNs with both tracers.

EP-0761

Importance of in-transit sentinel node in patients with cutaneous melanoma

E. Noriega-Álvarez[1], J. Rodríguez-Rubio Corona[1], M. Bajén Lázaro[1], R. Jaller Vanegas[1], A. Benítez Segura[1], J. Marcoval Caus[2], R. Penin Mosquera[3], J. Bermejo Segu[4], C. Gámez Cenzano[1]; [1]Nuclear Medicine-PET Department. IDI. Hospital Universitari de Bellvitge-IDIBELL, L'Hospitalet de Llobregat. Barcelona, SPAIN, [2]Dermatology Department. Hospital Universitari de Bellvitge-IDIBELL, L'Hospitalet de Llobregat. Barcelona, SPAIN, [3]Pathology Department. Hospital Universitari de Bellvitge-IDIBELL, L'Hospitalet de Llobregat. Barcelona, SPAIN, [4]Plastic Surgery Department. Hospital Universitari de Bellvitge-IDIBELL, L'Hospitalet de Llobregat. Barcelona, SPAIN.

Objective: Analyze the relationship between pathological state (PS) of in-transit sentinel lymph node (TSN) and the draining node basin (NB) in patients with cutaneous melanoma. **Material and Method:** -Retrospective study from January/2014 to December/2016 of 100 patients (p), diagnosed of cutaneous melanoma with selective sentinel node biopsy - Lymphoscintigraphy was performed following administration of 5 mCi of 99m-Tc-Nanocoloid the day before surgery. - Parameters studied: • Number of TSNs detected in scintigraphy • Number of TSNs surgically excised • PS of TSN • PS of NB • Number of patients in which staging changes with TSN • Follow-up of patients with metastatic TSN. **Results:** • Number of TSNs detected in scintigraphy: 17 • Number of TSNs surgically excised: 12 • PS of TSN: 7 tumor-negative and 5 metastatic • PS of NB: 10 tumor-negative and 2 metastatic • Number of patients in which staging changes with TSN: 5p (42% of TSN surgically excised) with metastatic TSN. § 3p with negative NB pass from N0 to N2c § 2p with metastatic NB pass, respectively, from N2a and N2b to N3 • Follow-up of patients with metastatic TSN: § 3p with negative NB: after 18 months of media (between 12 and 24 months) are free of disease § 2p with metastatic NB: 1p presents cutaneous recurrence and bone metastases and 1p has been recently operated. **Conclusion:** Although the number of patients studied is small, the results obtained reflect the importance of TSN dissection whenever feasible; due to lymph node staging (according to TNM) changes.

EP-0762

Implementation of sentinel lymph node for cervical and endometrial cancer: early experience

S. Seijas Marcos, A. Prieto Soriano, J. Cardona Arboniés, I. Plaza de las Heras, R. De Teresa Herrera, L. Canales Rodriguez, A. Sanfiel Delgado, J. Mucientes Rasilla, M. Mitjavila Casanovas; Hospital Universitario Puerta de Hierro, Majadahonda, Madrid, Spain, Madrid, SPAIN.

Purpose: The aim of this study was to analyse our experience in the implementation of sentinel lymph node biopsy in cervical and endometrial cancer. **Subjects and Methods:** Patients with cervical cancer (stages IA1, IA2, IB1, IIA1) and endometrial cancer (stage I) were selected for sentinel lymph node scintigraphy. Patients received a standardised cervical injection of radiotrazer and images were acquired at 30 minutes and 2 hours after the injection. A laparoscopic gamma probe was used for the detection, and detection rate was analysed. **Results:** In our center we have realized a total of 20 procedures, 7 patients had cervical cancer and 13 endometrial cancer. In cervical cancer 6 of them had successful sentinel lymph node mapping: bilateral external iliac 3, unilateral left external iliac 2, unilateral right common iliac 2, unilateral left common iliac 1 and unilateral obturator 1. Pelvic lymphadenectomy was done in these patients. 5 of them had negative sentinel lymph nodes and had no metastasic disease. 1 of them had a positive lymph node, without no more metastasic disease. The detection rate was 85%. 10 out of 13 endometrial patients had successful sentinel lymph node mapping: bilateral external iliac 2, unilateral left external iliac 1, unilateral right external iliac 4, uni-

lateral common iliac 3, unilateral right obturator 1, unilateral left mesorectum 1. Surgery was cancelled in two of them because of adverse events. Of these 8 patients, 1 was positive and 7 were negative. The detection rate was 77%. **Conclusion:v**Our sentinel lymph node detection rate in cervical cancer is similar to others published studies. According with good anatomopathological correlation, this technich could be validated, saving patients from lymphadenectomy morbility. In endometrial cancer even though detection rate is still low, more experience is needed.

EP-0763

Comparison between planar and tomographic SPET/CT acquisition on sentinel node identification on patients affected by breast cancer and melanoma

S. Chondrogiannis, M. C. Marzola, G. Grassetto, A. M. Maffione, A. Zompa, L. Tamiso, E. Milan, A. Bassan, L. Rampin, D. Rubello; Nuclear Medicine - PET/CT centre, Santa Maria della Misericordia Hospital of Rovigo, Rovigo, ITALY.

Purpose: To compare planar (static and dynamic) acquisition with tomographic SPET/CT acquisition and evaluate the clinical utility of SPET/CT images on lymphoscintigraphy for sentinel node identification on breast cancer and melanoma patients. **Materials and Methods:** From 01/2014 to 07/2016, we evaluated data of 28 patients affected by breast cancer and of 31 patients affected by coutaneous melanoma who performed planar and tomographic lymphoscintigraphy for sentinel node (SLN) detection. We evaluated data concerning the pathology, the method (site and number of injections, site(s) of lymphatic drainage), the number of SLN removed during operation, the histology and the number of SLN detected by planar acquisition and SPET/CT acquisition. Moreover we evaluated the added value/clinical utility of SPET/CT as reported by two nuclear medicine physicians and by the two most experienced surgeons on radioguided surgery on our hospital (breast surgeon and dermatologist). **Results:** Regarding the 28 patients affected by breast cancer (26 female, 2 male, median age 58 years; range 36-78) the detection rate was 100% on both static and SPET/CT images. 11/28 patients (39%) presented at least one metastatic node and underwent lymphadenectomy. In 9 patients SPET/CT identified more nodes than planar imaging (33 vs 19), in 7 patients planar images erroneously showed more nodes (18 vs 12), while in 12 patients SPET/CT and planar imaging showed the same number of nodes (33 linfonodi). Regarding the 31 patients affected by melanoma (10 female, 21 male, median age 64 years, range 27-87) the detection rate was 97% on both static and SPET/CT images. 7/31 patients (22%) presented at least one metastatic node and underwent lymphadenectomy. In 9 patients SPET/CT identified more nodes than planar imaging (27 vs 13), in 2 patients planar images erroneously showed more nodes (8 vs 5), while in 19 patients SPET/CT and planar imaging showed the same number of nodes (n.42). SPET/CT was very useful also for localizing the SN on 15 cases of breast cancer patients and on 28 cases of melanoma patients. **Conclusion:** On both breast cancer and melanoma patients SPET/CT identified more radioactive nodes than planar static or dynamic

imaging. Moreover it has been proven very useful not only for the identification of the exact number of the radioactive nodes that should be removed by the surgeon but also for their localization. SPET/CT is an accurate preoperative imaging procedure that helps optimizing radioguided surgery procedures, particurarly on complex anatomic regions like head and neck region.

EP-0764

Sentinel Lymph Node Biopsy In Patients With Breast Cancer And Axillary Involvement Treated With Neoadyuvant Chemotherapy

S. Sanz-Viedma, V. Scholz -Gutierrez, F. Fernandez-Garcia, C. Lacalle, R. Gomez, M. Martinez Del Valle, L. Vicioso, J. Jimenez Hoyuela; Hospital Clinico Virgen de la Victoria, Malaga, SPAIN.

Aim: Neoadjuvant chemotherapy (NAC) in patients with breast cancer does not increase survival, compared to post-surgical adjuvant chemotherapy. In the neoadyuvant setting, the utility of the sentinel lymph node biopsy (SLNB) is controversial. The aim of this study was to evaluate the feasibility and accuracy of SLNB in patients with breast cancer (N1) treated with neoadjuvant chemotherapy. **Material and Method:** We prospectively included 42 patients with breast cancer and positive lymph nodes (N1) who underwent NAC and were clinically node negative (cN0) by physical examination after NAC. Surgery and SLNB was performed. Regardless of the outcome, a complete axillary lymphadenectomy was performed in all cases. Dual tracer (radioisotope and blue dye) was used for the detection of the sentinel node. Tumorectomy was performed in 29 cases (76.3%) and mastectomy in 9 cases (23.7%). The sentinel node was detected only in 35 patients. Mean age: 51 years (range: 26-71), histological type: invasive ductal (hormone receptor positive 52.6% and HER-2 positive 47.4%), mean tumor size: 30 mm (range: 10-80 mm). The number of lymph nodes removed was ≥ 2 in 71.1% of the cases. The sentinel nodes were positive in 42.1% of the cases. The detection rate was 83.3%. The false negative rate: 17.1%. The sensitivity and specificity was 73.9% and 100%, respectively. Related to anatomopathological parameters, false negatives tended to be associated with hormone receptor positive, HER-2 positive and Ki-67> 15% tumors. **Conclusion:** SLNB does not report enough accuracy because the false- negative rate is not <10%, That is recommended in this clinical context. New improvements must be carried out such as: remove at least 3 sentinel lymph nodes, immunohistochemical study to detect micrometastases and the use of a metal clip for the correct identification and removal of the biopsy-proven positive lymph node (N1) at the initial diagnosis .

EP-0765

Relationship Between Sentinel Lymph Node Metastasis Size In Cutaneous Melanoma Patients And The Number Of Lymphadenectomies With Presence Of Additional Lymph Nodes Metastasis

J. Rodriguez-Rubio Corona[1], M. Bajén-Lázaro[1], E. Noriega-Álvarez[1], A. Rodríguez-Gasén[1], J. Suils-Ramón[1], E. Llinares-Tello[1],

A. Benítez-Segura[1], J. Mora-Salvadó[1], J. Ferreres-Riera[2], M. Soler-Monsó[3], D. Pérez Sidelnikova[4], C. Gámez-Cenzano[1]; [1]Nuclear Medicine-PET Department. IDI. Hospital Universitari de Bellvitge-Idibell, L'Hospitalet de Llobregat (Barcelona), SPAIN, [2]Dermatology Department. Hospital Universitari de Bellvitge-Idibell, L'Hospitalet de Llobregat (Barcelona), SPAIN, [3]Pathology Department. Hospital Universitari de Bellvitge-Idibell, L'Hospitalet de Llobregat (Barcelona), SPAIN, [4]Plastic Surgery Department. IDI. Hospital Universitari de Bellvitge-Idibell, L'Hospitalet de Llobregat (Barcelona), SPAIN.

Purpose: To analyze the relationship between the size of the lymph node metastases detected by sentinel node (SN) biopsy in patients with cutaneous melanoma and the number of lymphadenectomies with additional lymph node metastases. **Material and Methods:** We retrospectively studied 100 patients diagnosed with cutaneous melanoma who underwent SN biopsy between January/2014 and December/2016. In all cases a lymphoscintigraphy was performed after the intratumoral injection of 185 MBq of 99mTc-nanocolloid the day before surgery. In those patients with metastatic SN, a lymph node dissection of the lymphatic station of the SN was performed. The analyzed parameters were: SN surgical detection, number of lymphatic stations detected on the lymphoscintigraphy, number of metastatic SN, size of the SN metastasis, number of lymphadenectomies, number of lymphadenectomies with presence of additional lymph nodes metastasis, and size of those metastasis in the lymphadenectomies. **Results:** Up to 98 patients achieved surgical SN detection and in these patients lymphoscintigraphy showed 102 lymphatic stations. Lymphadenectomies were performed in 31 patients, 8 of them (26%) showed additional metastatic lymphadenopathies, all with a metastatic SN (> 2mm in 5 patients and >0.2-2mm in 3 patients). SN metastases were founded in 33 lymphatic stations and were classified in 3 groups according: 1) >2 mm: 20 SN (5 of them with additional lymph node metastases), 2) >0.2-2mm: 11 SN (3 of them with additional lymph node metastases), and 3) ≤0.2mm: 2 SN (without other evidenced lymph node metastases). **Conclusions:** According to our results more than a quarter of patients with cutaneous melanoma can show additional metastatic lymphadenopathies in the lymphadenectomies. So this intervention and further imaging studies as PET should be considered when metastasis of any size are found in the sentinel node.

EP-56   during congress opening hours, e-Poster Area

Clinical Oncology: External Beam Radiation Therapy Planning

EP-0766

Gated Reconstruction in 18F-FDG PET-CT Quantitative Imaging: Impact on SUV Estimation of Tumor Motion Inside the Lung and Respiration Gated Radiotherapy Treatment with Dynamic Thorax Phantom

M. Zuffante, E. Zivelonghi, F. Sciumè, D. Grigolato, M. Cucca, L. Pavanello, L. Locantore, P. Polloniato, F. Dusi, C. Cavedon, M. Ferdeghini; AOUI Verona, Verona, ITALY.

Introduction and Purpose: Breathing-induced motion of lung tumors represents a considerable problem both in PET/CT imaging and during the delivery of the radiotherapy treatment. In this study we intend to provide guidelines for the selection of the Varian's Real-time position Management™ (RPM) respiratory gating technology to compensate for lung tumor motion during PET/CT imaging and radiotherapy treatment. **Materials and Methods:** We employed a dynamic anthropomorphic thorax phantom to simulating the PET/CT acquisition with and without therespiratory gating system for different spherical targets filled with ^{18}F-FDG.To simulate respiratory motion, the phantoms were driven in the superior-inferior direction with a sinusoidal motion pattern with a period of 4 s and a real patient breathing trace with different amplitudes. Maximum standardized uptake value (SUV_{max}) and target volume analysis were performed in gated and nongated PET. In the second part of the work the dynamic thorax phantom was used to simulate the radiation therapy with and without the respiratory gating system for different cranial-caudal target excursions with a sinusoidal and a real breathing trace. The discrepancies between the distribution of static dose and dose distribution with moving target, obtained with and without respiratory gating technique, were measured with Gafchromic™ EBT3 films in the phantom. **Results:** In PET/CT, the lesion SUV_{max} underestimation depends on both the amplitude of respiratory motion and the lesion volume. The 4D acquisition was able to recover most of the apparent loss in SUV. SUV_{max} value increases with the number of bins. The decrease of the therapeutic dose to the target depends not only on the amplitude of tumor motion but also on the patient specific breathing pattern. The convolution of the static dose distribution with the probability density function (PDF) is a good approximation of the dose distribution with target motion. Respiratory-gated radiation therapy using the RPM gating system, with a duty cycle of 40% reduced the blurring effects on the dose distribution **Conclusion:** The 4D-PET/CT successfully recovers most of the loss induced by the respiratory motion with 5-bin gating acquisition. We found that targets which are smaller than 4 cm with PDF standard deviations larger than 0.4 cm are most susceptible to loss of coverage; in these case the use of the respiratory-gated technique is advisable.

EP-0767

Investigation of automatic thresholding on PET images for volume delineation of lung lesions in radiation therapy treatment

T. Osman[1], B. McBride[2], T. Hennessy[2], S. Downes[2], A. Rosenfeld[1], A. Malaroda[1]; [1]University of Wollongong, Australia, Wollongong, AUSTRALIA, [2]Prince of Wales Hospital, Randwick, AUSTRALIA.

In radiation therapy treatment planning, 4D-PET/CT scans can significantly improve the accuracy of lung tumour localisation and delineation. Typically, volumes on PET images are delineated by applying an automatic fixed threshold of ~40%. However, depending on lesion specific metabolism, as well as different

noise properties, a single threshold value might not be an appropriate choice. This study aimed to investigate optimal PET thresholds, accounting for source-to-background ratio (SBR), lesion size and motion. Static and gated PET/CT images of the NEMA IEC body phantom were acquired, for 2.5 and 10 minutes respectively for PET, on a Philips Ingenuity 128 TF PET/CT scanner with the use of the Philips Bellows respiratory motion tracking system for the 4D acquisitions. The six hollow spheres of the phantom (diameters between 10-37mm) were filled initially with 93.47 kBq/ml of 18F-FDG, and Optiray-350 for CT contrast enhancement, and imaged sequentially (SBR of 9:1, 6:1 then 3:1). Gated scans, with 10 phases per respiratory cycle (1min/phase), were acquired by placing the phantom on a moving platform, to simulate respiratory motion of 2.6cm in amplitude and frequency 16 breaths/minute. PET images were reconstructed using Philips Astonish TF algorithm and both the static and gated PET/CT images were analysed using an in-house MATLAB-R2015a code which generated the gated MIPs, determined the optimal threshold and automatically contoured the volumes. The Dice Coefficient (DC) was used to assess concordance of internal target volumes (ITV) between the PET and CT volumes as identified with the optimal threshold. Optimal thresholds, ranging between 32-90%, were found to increase with decreasing sphere diameters and SBRs, and were ~10% lower for the gated data. Good agreement between PET and CT volumes delineated using the optimal threshold was also found, with concordance highest for the largest sphere (DC = 0.97). The 4D data showed more consistent agreement over all the sphere sizes and SBRs (DC range = 0.86-0.96 for SBR=9:1). A maximum discrepancy of 5.4% was found between the PET volumes at the optimal thresholds compared to the expected volumes. These preliminary results show that under the noise properties, sizes and motion considered in this study, optimal threshold varied significantly from the standard choice of ~40%: for the moving 37mm diameter sphere, it varied between 32% (SBR=9:1) to 41% (SBR=3:1). As determined by the Dice coefficient, volumes delineated on PET images based on the optimal threshold were in good agreement with the expected volumes and the CT volumes.

EP-0768

Volume-based assessment of different image reconstruction algorithms and thresholds for FDG-PET/CT based on dose-painting concept

P. Ghafarian[1,2], A. Ketabi[3,4], M. A. Mosleh-Shirazi[5], M. R. Ay[6,4]; [1]Chronic Respiratory Diseases Research Center, National Research Institute of Tuberculosis and Lung Diseases (NRITLD), Shahid Beheshti University of Medical Sciences, Tehran, Iran., Tehran, IRAN, ISLAMIC REPUBLIC OF, [2]PET/CT and Cyclotron Center, Masih Daneshvari Hospital, Shahid Beheshti University of Medical Sciences, Tehran, Iran, Tehran, IRAN, ISLAMIC REPUBLIC OF, [3]Department of Medical Physics and Biomedical Engineering, Tehran University of Medical Sciences, Tehran, Iran., Tehran, IRAN, ISLAMIC REPUBLIC OF, [4]Research Center for Molecular and Cellular Imaging, Tehran University of Medical Sciences, Tehran, Iran., Tehran, IRAN, ISLAMIC REPUBLIC OF, [5]Medical Imaging Research Center, and Physics Unit, Department of Radiotherapy and Oncology, Namazi Hospital, , Shiraz University of Medical Sciences, Shiraz, Iran., Tehran, IRAN, ISLAMIC REPUBLIC OF, [6]Department of Medical Physics and Biomedical Engineering, Tehran University of Medical Sciences, Tehran, Iran, Tehran, IRAN, ISLAMIC REPUBLIC OF.

Purpose: PET/CT-imaging based on dose-painting is very prone to variations by technical factors. In this work, the impact of technical imaging aspects, variability of volume-based indices such as Metabolic Tumor Volume (MTV) and Total Lesion Glycolysis (TLG) was investigated **Materials and Methods:** All PET acquisitions were performed on a GE D-690 PET/CT scanner. An in-house produced NEMA phantom with six cylindrical insert (diameters 10 to 37 mm), the background activity level of 5.3 kBq/mL, and Signal-to-Background-Ratio (SBR) of 4:1 and 2:1 was applied. All images were reconstructed with four different reconstruction algorithms: OSEM, OSEM+PSF, OSEM+TOF, OSEM+TOF+PSF with Gaussian filter 3, 5 and 6.4 mm. To investigate inter-thresholds variation, The MTV was defined as the voxels within the VOI with SUV ≥ X% * SUV_{max} that X was the threshold value at 10% intervals ranged from 40% to 90%. Later, inter-methods comparisons were performed at threshold 50%. The percentage of the relative differences in MTV (called *Mismatch*) was determined as *Real Volume* subtracted from *MTV_{recon}* divided by *Real volume* multiplied by 100. TLG were also calculated. **Results:** Maximum inter-method variation was obtained in threshold value from 50% to 60% at SBR2 and from 40% to 50% at SBR4 for all reconstruction methods. Mean Mismatch (%) in all target volumes among reconstruction-methods ranged from -6.1 to 20.7 at SBR4 and from -24.6 to 11.3 at SBR2. It is interesting that in the smallest target volumes up to 74% variation was seen in Mismatch by changing the filter size from 3 mm to 6.4 mm. The differences between SBR4 and SBR2 increased by decreasing targets volume in all reconstruction-methods; the mean differences form largest to smallest target volume changed from 2.4% to 120.8%. The mean inter-method differences for TLG were 0.9 g at both SBRs. **Conclusion:** Quantification of MTV is highly dependent on reconstruction method, thresholds and SBRs; although the impact of reconstruction-method is smaller for TLG value.

EP-0769

The role of 18F-Choline (FCH) PET/CT for the prediction of long-term response to radical radiotherapy (RT) in patients with localized prostate cancer (PCa)

L. Cuppari[1], M. Sepulcri[2], M. Fusella[3], A. Zorz[3], M. Paiusco[3], L. Corti[2], G. Saladini[1], L. Evangelista[1]; [1]Nuclear Medicine and Molecular Imaging Unit., Veneto Institute of Oncology IOV - IRCCS, Padova, ITALY, [2]Radiation Oncology Unit., Veneto Institute of Oncology IOV - IRCCS, Padova, ITALY, [3]Medical Physics Unit., Veneto Institute of Oncology IOV - IRCCS, Padova, ITALY.

Purpose: This study aims to determine if metabolic parameters provided by FCH PET/CT are able to predict the long-term response to radical radiotherapy (rRT) in patients with

localized PCa. **Methods:** Between 2011 and 2016, from a mo-no-centric database, we retrospectively reviewed pre-treatment FCH PET/CT scans of 37 patients who underwent RT for the definitive treatment of localized PCa. For each PET/CT scan, different metabolic parameters were assessed, such as maximum standardized uptake value (SUVmax), average SUV (SUVavg), metabolic tumor volume (MTV), total lesion choline kinase activity (TLCKA) and FCH multifocality. In all patients, the value of PSA before RT (PSAp) was recovered. All patients underwent rRT for a total equivalent dose of 78-80 Gy, with a standard or hypofractionated schedule (2 Gy or 2.5Gy /fraction). Patients were classified as disease free (DF) if the increase of PSA value after RT was less than 2 ng/mL respect to PSA nadir value, conversely with an increase of PSA higher than 2 ng/ml they were classified as recurrent (not disease free, NDF). Only patients with at least 1-year follow up, after rRT, were enrolled in this study. **Results:** In all 37 patients, median (range) values of SUVmax, SUVavg, MTV, TLCKA, and PSAp were 6.6 (0.2-29.6), 3.62 (0.1-9.4), 7.79 (0.03-167.9), 20.1 (0.1-462.2) and 12.7 ng/mL (2.2-88.7 ng/mL), respectively. Moreover, 16 (43%) patients had a multifocality FCH uptake in prostate gland. After 1-year of follow-up, 30 patients were considered as DF and 6 patients were considered as NDF. All metabolic parameters were lower in DF than NDF patients (Table 1), in particular TLCKA and SUVavg. Furthermore, FCH multifocality was more frequent in NDF than DF patients (36.7% vs. 83.3%; p=0.036). At multivariate logistic regression analysis, only multifocality resulted a predictors of rRT failure (OR: 9.98; 0.88-11.26; p=0.063). **Conclusion:** High values of TLCKAresult predictive of poor outcome after 1-year follow-up forpatients with a multifocal intraprostatic lesionand who are candidates to rRT. The present findings, taking into account the radiobiology of PCa (which benefits of hypofractionation and higher prescription dose), suggest to increase the dose inside the primary tumor. Further work has to be done to assess a risk-adapted prescription protocol for patients with multifocal lesions and high values of TLCKA, who could benefit of an increased dose to the IntraprostaticDominant Lesion.

Clinical Oncology: Therapy Response Assessment

EP-0770

Automated quantification of reference levels in liver and mediastinum (blood pool) for the Deauville therapy response classification using FDG-PET/CT in lymphoma patients

M. Sadik[1], E. Lind[2], O. Enqvist[3], J. Ulén[4], E. Polymeri[5], E. Trägårdh[6], L. Edenbrandt[1]; [1]Department of Clinical Physiology, Göteborg, SWEDEN, [2]Department of Medicine, Göteborg, SWEDEN, [3]Department of Signals and Systems, Göteborg, SWEDEN, [4]Eigenvision AB, Malmö, SWEDEN, [5]Department of Radiologi, Göteborg, SWEDEN, [6]Department of Translational Medicine, Malmö, SWEDEN.

Aim: To develop and validate a convolutional neural network (CNN) based method for automated quantification of reference levels in liver and mediastinum (blood pool) for the Deauville therapy response classification using FDG-PET/CT in lymphoma patients. **Methods:** CNNs were trained to segment the liver and the mediastinum, defined as the thoracic part of the aorta, in CT images from 81 consecutive lymphoma patients, who had undergone FDG-PET/CT examinations. Trained image readers segmented the liver and aorta manually in each of the CT images and these segmentations together with the CT images were used to train the CNN. After the training process, the CNN method was applied to a separate validation group consisting of six consecutive lymphoma patients (17-82 years, 3 female). First, the liver and mediastinum were automatically segmented in the CT images. Second, voxels in the corresponding FDG-PET images, which were localized in the liver and mediastinum, were selected and the median standard uptake value (SUV) was calculated. The CNN based analysis was compared to corresponding manual segmentations by two experienced radiologists. The Dice index was used to analyse the overlap between the segmentations by the CNN and the two radiologists. A Dice index of 1.00 indicates perfect matching. **Results:** The mean Dice indices for the comparison between CNN based liver segmentations and those of the two radiologists in the validation group were 0.95 and 0.95. A corresponding comparison between the two radiologists also resulted in a Dice index of 0.95. The mean liver volumes were 1,752ml, 1,757ml and 1,768ml for the CNN and two radiologists, respectively. The median SUV for the liver was on average 1.8 and the differences between median SUV based on CNN and manual segmentations were less or equal to 0.1. The mean Dice indices for the mediastinum were 0.80, 0.83 (CNN vs radiologists) and 0.86 (comparing the two radiologists). The mean mediastinum (aorta) volumes were 147ml, 140ml and 125ml for the CNN and two radiologists, respectively. The median SUV for the mediastinum was on average 1.4 and the differences between median SUV based on CNN and manual segmentations were less or equal to 0.14. **Conclusion:** A CNN based method for automated quantification of reference levels in liver and mediastinum show good agreement with results obtained by experienced radiologists, who manually segmented the CT images. This is a first and promising step towards a completely objective treatment response evaluation in patients with lymphoma based on FDG-PET/CT.

EP-0771

Variability in reference levels for Deauville classifications applied to lymphoma patients examined with 18F-FDG-PET/CT

M. Sadik[1], E. Lind[2], O. Enqvist[3], J. Ulén[4], E. Polymeri[5], E. Trägårdh[6], L. Edenbrandt[1]; [1]Department of Clinical Physiology, Göteborg, SWEDEN, [2]Department of Medicine, Göteborg, SWEDEN, [3]Department of Signals and Systems, Göteborg, SWEDEN, [4]Eigenvision AB, Malmö, SWEDEN, [5]Department of Radiologi, Göteborg, SWEDEN, [6]Department of Translational Medicine, Malmö, SWEDEN.

Aim: 18F-FDG-PET/CT is increasingly being used in the follow up assessment of treatment response in lymphoma patients. To standardize the interpretations, the Deauville five-point scale has been proposed and is now internationally accepted. The Deauville scale ranges from 1 to 5, where 3 is defined as lymph uptake above uptake in the mediastinum (aorta), but below or equal to uptake in the liver. Each of the FDG-avid or previously FDG-avid lymph nodes is compared to the mediastinum and the liver. The aim of this study was to analyse the standard uptake values (SUV) for these reference regions in a group of lymphoma patients. **Methods:** A group of 87 consecutive patients with lymphoma who had undergone 18F-FDG-PET/CT were studied. Eight of the patients comprised two PET/CT scans. The complete liver and the aorta from above the aortic root to the diaphragm was segmented in the CT images. SUV for PET voxels localized in these two volumes were used to calculate the median SUV for liver and aorta for each patient. The median was used in order to reduce the influence of voxels with high SUV representing abnormal areas. **Results:** The median SUV was on average 1.9 (SD 0.3) for the liver and 1.5 (SD 0.2) for the aorta. The ratio "median SUV liver/median SUV aorta" was on average 1.3 (SD 0.1) with a 95% confidence interval 1.1 to 1.6. The ratio "median SUV liver/median SUV aorta" was on average 1.3 also for the eight patients with two scans each. The absolute difference in ratio between the two scans ranged from 0.0 to 0.5. **Conclusion:** The results of this study show a considerable variation in FDG uptake in liver and aorta for lymphoma patients. The ratio between the SUV in the two reference regions show variability also between different studies from the same patient. This may influence the performance of the Deauville criteria and further validation is warranted.

EP-0772

The value of PET-CT in the evaluation of response to treatment in patients with prostate cancer treated with Radium223

S. S. Medina Ornelas, F. O. García-Pérez; *Instituto Nacional De Cancerologia, Mexico City, MEXICO.*

Introduction: It has been postulated that the molecular response evaluated by PET-CT with Fluxesoxyglucose (FDG) may be a useful tool in the evaluation of bone metastases response; however, compared with the radiotracer sodium fluoride (NaF), it has been shown to be superior for the detection of blastic metastatic disease; becasuse the mechanism of incorporation into the blastic lesions is very similar to Radium-223 (^{223}Ra); The recent introduction of ^{68}Ga-PSMA (prostate-specific membrane antigen) has been particularly useful in patients with suspected visceral disease.The purpose of this study is to determine if PET-CT with 18F-NaF and 68Ga-PSMA can predict response to ^{223}Ra treatment. **Methodology:** From November 2014 to December 2016, fifteen patients with metastatic castration-resistant prostate cancer (mCRPC), and seven patients with high-grade prostate cancer (hgPC), were evaluated by ^{18}F-NaF and ^{68}Ga-PSMA PET-CT prior to receipt ^{223}Ra therapy a standard dose (55kBq/kg), and 4-6 weeks after the last dose, with simultaneous measurements Prostate specific antigen (PSA) and alkaline phosphatase

(AP). A semiquantitative analysis of each patient allowed to establish 3 study groups based on the molecularly active volume: low-overall burden (<1000 cm^3), medium-overall burden (1001-3000 cm^3); and high-overall burden (> 3001 cm^3). Thus, 7 patients were classified as high burden, 9 patients as medium burden and 6 patients as low burden. **Results:** Fourteen patients completed 6 cycles (7-hgPC, 8-mCRPC), of which 6 were of low burden and 8 of medium burden, which showed a decrease in PSA and AP levels (p <0.05); Of the other patients we obtained variable results according to the number of doses; the value of ^{18}F-NaF and ^{68}Ga-PSMA as a predictive tool in response therapy according to the degree of overall tumor burden. Patients with overall tumor burden <1000 cm^3 treated with ^{223}Ra showed to be a predictor of good prognosis in response to treatment; while patients with overall-tumor burden >3001 cm^3 have a high probability of do not complete the 6 cycles. **Conclusion:** The PET-CT in the evaluation of response to ^{223}Ra is an extremely useful tool in the selection of those patients who are likely to improve according to their degree of overall tumor burden, in addition to timely evaluation of therapeutic efficacy.

EP-0773

Unicentric experience in the treatment of metastatic castration-resistant prostate cancer with Ra223

E. Rodeño Ortiz de Zarate, P. Mínguez Gabiña, I. Fernández Tercero, A. Gómez de Iturriaga Plña, R. Llarena Ibarguren, A. Urresola Olabarrieta, A. Esteban Figueruelo, J. Espejo Niño, A. Sánchez Salmón; Gurutzeta/Cruces University Hospital, Barakaldo, SPAIN.

Purpose/Introduction: The purpose of this study was to evaluate the clinical outcome, the response patterns (biological and metabolic), and the toxicity after Ra223 treatment of patients with skeletal metastases of castration-resistant prostate cancer (CRPC). **Subjects & Methods:** Between April and November 2016, eleven consecutive patients with CRPC treated with Ra223–6 cycles of 55 kBq/kg–were prospectively studied. Two patients died during the therapy and another could not finish the 6 cycles due to renal failure. In the other 8 patients, the clinical outcome, the biological (alkaline phosphatase (ALP) and prostate-specific antigen (PSA)) and metabolic (Tc99m-HDP whole body scan (WBS) and PET/CT F18 Choline) response, and the toxicity were evaluated. Ra223 uptake in some of the cycles was evaluated as well. To date, four patients have ended the 6 cycles, one patient four cycles, two patients three cycles and one patient one cycle. **Results:** All patients reported lower levels of pain. Decrease in ALP levels was observed in seven patients, and decrease in PSA levels in 5. From Tc99m-HDP WBS, patients were categorised according to metastatic extension before therapy: one patient had 1 focus; another patient had less than 6 foci; 2 patients had between 6 and 20 foci; 3 patients had more than 20 foci and 1 patient had a superscan. In Tc99m-HDP WBS, uptake was homogeneous and decreased during therapy, except for those patients with less than 6 foci. In F18 Choline PET images, the areas with a greater Ra223 uptake were hypometabolic and in CT images an extensive sclerosis was seen in lesions and around them. One patient

showed grade-3 thrombocytopenia and one patient grade-1 anemia. Ra223 uptake was observed in the bigger lesions with the greater uptake in Tc99m-HDP WBS. A variable Ra223 uptake was observed between the cycles in which images were acquired. **Conclusion:** During CRPC therapy with Ra223 there is clinical improvement, and also biological and metabolic response in those lesions with the higher metabolism. This can be observed in the Tc99m-HDP WBS, and in the F18 Choline PET/CT images, with hypometabolism and extensive bone sclerosis in those lesions which showed Ra223 uptake.

EP-0774

Outcomes Of Treatment With Ra223 In Patients With Castration-Resistant Prostate Cancer with symptomatic bone metastases and no known visceral metastatic disease

R. H. Reyes Marlés, Sr., M. Castellón Sanchez, L. Mohamed Salem, F. Nicolas Ruiz, J. Navarro, L. Frutos Esteban, M. Godoy Bravo, I. Sime Ioayza, M. Tomás Redondo, E. Fernandez Muñoz, M. Claver Valderas; *Hospital Clinico Universitario Virgen de la Arrixaca, El Palmar, SPAIN.*

Objectives: The aim of this study was to evaluate the use of Ra223 in the treatment of patients with prostatic Ca, performing clinical and analytical follow-up considering alkaline phosphatase (FA), prostate specific antigen (PSA), hemoglobin (HgB), platelet (PLT) and neutrophils (N), to determine their clinical relevance, and side effects. **Methods:** We evaluated 18 patients who received Ra223 as a treatment for castration-resistant prostate cancer, with symptomatic bone metastases and without visceral metastases, previously assessed by oncology unit. Haematologic control was made before each treatment, as well as the subjective pain rating scales and analgesics required for pain control. **Results:** Of the 18 patients who started treatment with Ra223, 3 died, one after the end of treatment (sepsis), and two during treatment, all due to causes beyond the administration of the treatment. 5 patients have completed the treatment, 1 was suspended due to disease progression and was referred to chemotherapy, and 10 are still in the process of being administered. No patient presented immediate adverse effects to the administration of the drug, 7 reported gastrointestinal symptoms (nausea, vomiting, diarrhea, dysgeusia, dyspepsia, loss of appetite or weight loss), and 2 more required transfusion because of low HgB. No significant decrease in PSA or AF was found, and in patients who were not transfused there was no clinically relevant variation in haematological parameters. Of the 5 patients who have completed the treatment, in 4 the pain decreases, based on the numerical rating scales, requiring less doses of analgesic medication. **Conclusion:** Ra223 as a treatment for patients with prostate Ca and bone metastases, has few clinically relevant adverse reactions, which makes it a safe therapeutic alternative, with the additional advantage of a decrease in pain and the dose of analgesic medication.

EP-0775

Is the averaged SUV from several hottest voxels an alternative to SUV$_{peak}$ for quantification of large heterogeneous or small lesions in oncological PET imaging?

A. Ketabi[1,2], P. Ghafarian[3], S. Masjoodi[1], M. A. Mosleh-Shirazi[4], M. R. Ay[1,2]; [1]*Department of Medical Physics and Biomedical Engineering, Tehran University of Medical Sciences, Tehran, IRAN, ISLAMIC REPUBLIC OF,* [2]*Research Center for Molecular and Cellular Imaging, Tehran University of Medical Sciences, Tehran, IRAN, ISLAMIC REPUBLIC OF,* [3]*PET/CT and Cyclotron Center, Masih Daneshvari Hospital, Shahid Beheshti University of Medical Sciences, Tehran, IRAN, ISLAMIC REPUBLIC OF,* [4]*Medical Imaging Research Center, and Physics Unit, Department of Radiotherapy and Oncology, Namazi Hospital, Shiraz University of Medical Sciences, Shiraz, IRAN, ISLAMIC REPUBLIC OF.*

Purpose: SUV_{max} and SUV_{peak} are common indices for clinical quantification which are adversely affected by noise and heterogeneous uptake or lesions size. The aim of this work was to analyze the averaged SUV from several hottest voxels in small- to large-sized lesions to determine its impact on quantification of MTV and TLG. **Materials and Methods:** a body phantom with six cylindrical insert (diameters 10 to 37 mm) were scanned with Discovery 690 GE PET/CT scanner. The background activity level of 2.6 kBq/mL and sources-to-background-ratio 4:1 was applied. All PET images were reconstructed with four reconstruction algorithms (OSEM, OSEM+PSF, OSEM+TOF, OSEM+TOF+PSF) and 3 mm Gaussian filter. SUV_{peak} was calculated using a 3D 1.0 mL spherical volume (SUV_{S_peak}) equal 41 voxel and a cubic $3\times3\times3$ matrix (SUV_{C_peak}) equal 9 voxel. Later, SUV_{41} (average 41 hottest voxels) and SUV_9 (average 9 hottest voxels) was calculated. SUV_{max}, SUV_{S_peak}, SUV_{41}, SUV_{C_peak} and SUV_9 were applied for MTV and TLG measurements. **Results:** In the small- to large-sized lesions (diameter > 2 times the image resolution) showed $SUV_{max} > SUV_{S\_peak} > SUV_{C\_peak} > SUV_{41} > SUV_9$, so that SUV_9 showed the least relative difference with ideal SUV. In the smallest volume, as a border that in less than it peak SUV was not applicable, relative difference were -2.60, 3.90, -7.41 and -4.18 at HD, PSF, TOF and TOFPSF, respectively. The mean relative difference between SUV_{S_peak} and SUV_4 was 15.3% and between SUV_{C_peak} and SUV_9 was 21.3%. The MTV calculation showed the least relative difference (<10%) with real insert volume obtained using averaged SUV from several hottest voxels in small volumes. **Conclusion:** averaged SUV from several hottest voxels is most robust method for quantification of large heterogeneous or small lesions, especially where quantification is highly sensitive to volume of interest definitions. **Key Words:** FDG-PET, SUV, hottest voxels

Clinical Oncology: Miscellaneous

EP-0776

Back pain in oncology patients does not equal spinal metastases

L. Louw, M. Vangu; *University of the Witwatersrand, Johannesburg, SOUTH AFRICA.*

Aim: A retrospective study undertaken in patients with solid tu-

mour malignancies to evaluate the association of back pain with abnormal ^{99m}Tc-MDP uptake on SPECT/CT images of the spine. **Materials and Methods:** A total of 116 adult patients (72 males, 44 females), aged 19-83 years, referred for bone scan from January 2013 - May 2015 and complaining of back pain were included. SPECT/CT reconstructed images of the spine (thoracic and lumbar) were acquired for localization of abnormal foci. All the images were visually analyzed. Focal uptake in the pedicle or posterior aspect of the vertebral body, or diffuse uptake in the vertebral body was considered as likely malignant. **Results:** The presence of back pain was correlated with the total number of lesions detected in the spine, but there was no significant association (p=0.45). A trend was seen only between back pain and lesions in the lumbar spine (p=0.07). Back pain was then correlated with the number of likely malignant lesions in the spine, but again no significant association was found (p=0.27). The anatomic location of vertebral uptake was correlated with back pain. No significant association was found with any of the locations considered as likely malignant (p=0.58). A significant association was found between back pain and uptake in either anterior vertebral osteophytes (p=0.027), or in the lateral articular aspect of the vertebral bodies (p=0.014). **Conclusion:** According to our results, there is no significant association between back pain and spinal metastases in oncology patients. As in the general population, back pain remains multi-factorial. It may simply be a more common complaint in patients with benign changes in the spine, such as degenerative processes, regardless of the extent of malignant involvement.

EP-0777

A Systematic Review And Meta-Analysis Of FDG-PET/CT As A Screening Tool For Occult Malignancy In Unprovoked Venous Thromboembolism

S. Hess[1,2,3], E. C. Frary[1,4], P. F. Høilund-Carlsen[1,3], O. Gerke[1,5]; [1]Dept. of Nuclear Medicine, Odense University Hospital, Odense, DENMARK, [2]Dept. of Radiology and Nuclear Medicine, Hospital Southwest Jutland, Esbjerg, DENMARK, [3]Dept. of Clinical Research, Faculty of Health Sciences, University, Odense, DENMARK, [4]Department of Cardiology, Nephrology, and Endocrinology, Nordsjællands Hospital Hillerød, Hillerød, DENMARK, [5]Centre of Health Economics Research, University of Southern Denmark, Odense, DENMARK.

Purpose/Introduction: Venous thromboembolism (VTE) and occult malignancy are associated. Within one year of unprovoked VTE (i.e. no major risk factors), incidence of occult malignancy is around 10%. Some propose screening VTE patients for underlying malignancy with limited (e.g. history and basic findings) or extended (imaging-based) approaches, but no established management strategies exist. FDG-PET/CT is employed in other settings of suspected occult cancer and has been suggested. We present a systematic review of FDG-PET/CT as a screening tool for occult malignancy in unprovoked VTE. **Subjects and Methods:** PubMed and EMBASE were searched systematically with a research librarian using comprehensive variations of "positron emission tomography" and "venous thromboembolism". Papers were screened and evaluated for eligibility independently

by two authors. Inclusion criteria were original human studies, comprising > 10 patients, in English/Scandinavian languages and about occult malignancy screening with FDG-PET/CT in patients with VTE. Eligible papers were assessed by QUADAS-2 criteria, and FDG-PET/CT detected cancer prevalence was meta-analyzed with a fixed effects model. **Results:** A total of 2120 articles were screened by title and abstracts, 1913 were excluded. Thus, 207 full-texts were assessed, 203 were excluded [irrelevant (n=185), not original/full papers (n=13), duplicates (n=3), animal studies (n=2)]. Studies included two prospective, one retrospective, and one randomized controlled trial comparing FDG-PET/CT to limited screening. Median number of patients (range) was 50 (40-173), pooled FDG-PET/CT-detected cancer prevalence (95% CI) was 6.77% (4.12%-9.42%). Large heterogeneity was observed across studies (I^2=71.2%): Observed cancer prevalence ranged from 2.5 to 26%; one study included only patients 50+ years, while the others included all adults; in one study a quarter of included patients were thrombophilic, one study did not exclude patients with obvious VTE risk factors (e.g. recent travels, and previous VTE). All studies had high negative predictive values (NPVs), whereas two reported false positive (FP) rates of 24%. One study found no significant difference between CT and FDG-PET/CT, another reported three times higher cancer detection rate, a higher proportion of early cancers, less cancer-related deaths, and less false negatives in the PET/CT-group compared to the limited screening group, albeit without statistical significance. **Discussion/Concusion:** FDG-PET/CT seems feasible as screening tool for occult malignancy in unprovoked VTE, but reported prevalences were highly variable. Sensitivity may be better than with limited screening strategies, NPV was higher with PET/CT, but with considerable FP findings. The literature is sparse and heterogeneous. Further studies are needed to define the role of PET/CT in unprovoked VTE.

EP-0778

Use of ^{18}F-FDG PET/CT in early diagnosis of primary neoplasm site in patients with neurologic paraneoplastic syndromes

A. Sowa-Staszczak, M. Opalińska, M. Trofimiuk-Müldner, W. Lenda-Tracz, M. Buziak-Bereza, A. Brzozowska-Czarnek, A. Hubalewska-Dydejczyk; Chair and Department of Endocrinology, Jagiellonian University, Medical College, Kraków, POLAND.

Introduction: Paraneoplastic neurological syndromes (PNS) are rare disorders associated with neoplastic process which are not caused by local tumor invasion (infiltration or local suppression) nor metastases to the central nervous system. PNS is diagnosed in less than 1% of all patients with cancer. The causes of PNS remain unknown, but their autoimmune origin is strongly suggested. Properly in case of neoplasm organism produces antibodies against cancer cells, but in rare cases that antibodies additionally attack the structures of the nervous system (onco-neural antibodies). These antibodies are rather specific for the malignancy than for PNS, it means there are different antibodies associated with the same syndrome so immunological diagnosis is often difficult. In 80% of patients PNS preceded other symp-

toms of neoplasm and in average the primary tumor is detected 4-6 months after the onset of PNS. The risk of PNS is the highest in patients with small cell lung cancer, neuroblastoma or thymus cancer. **Aim of study:** The aim of our study was to evaluate the diagnostic efficacy of ^{18}F-FDG PET/CT examination in detection of primary neoplasm site in patients with PNS. **Materials and Methods:** The analysis included 10 patients (3 women and 7 men) with PNS manifestation as progressive limb paresis (3 patients), cerebral palsy (3 patients, in 1 case the pNMA2 (Ma2/Ta) antibodies connected to thymus and testicular neoplasms were detected), amyotrophic lateral sclerosis (1 patient), motor neuron disease (1 patient) and subacute sensory neuropathy (2 patients). PET/CT examination of 18F-FDG was performed according to standard procedure. **Results:** The neoplastic process has been identified in 5 cases. The primary sites include: large intestine (transverse colon) - 1 person, lung with presence of metabolically active mediastinal and thoracic lymph nodes - 1 person, prostate - 1 person, endometrium with presence of metabolically active metastases to lungs - 1 person. In 1 person involvement of mediastinal and thoracic lymph nodes suggesting lymphoma was detected. The remaining 5 patients (50%) did not demonstrated the pathological metabolism of ^{18}F-FDG. **Conclusions:** A PET/CT examination with ^{18}F-FDG may be useful in diagnosis of a cause of PNS. Its value result, among other, from the possibility of the whole body examination, which in the case of varied (chest, abdomen, pelvis) localization of the neoplastic disease may substantially accelerate detection of the neoplasm site leading to faster onset of treatment.

EP-0779

Metabolic characterization of anterior mediastinal mass in adult patients by F-18 FDG PET/CT

Z. Koç, P. Özcan Kara, E. Ayan; Mersin University Hospital, Mersin, TURKEY.

Aim: The thymus tumors, lymphoma, and benign tumors might cause anterior mediastinal mass. The aim of this study is to investigate the results of metabolic characterization of anterior mediastinal mass by F-18 FDG PET/CT. **Materials and Methods:** 16 patients with diagnosis of anterior mediastinal mass (6F, 10M; 17-83; mean:56.5±19.51 years old) who were referred to our department for metabolic characterization of mediastinal mass were included in the study. **Results:** Anterior mediastinal mass (mean: 54.4±38.6 mm) were defined by CT in all the patients previously. FDG accumulation was observed in all the patients' masses (mean SUVmax=9.5±6.3) except two (who were not operated exceptionally) and additional lymph node metastases in 8 patients, distant primary tumor in 4 patients and pleural plaques in 3 three patients were observed in PET/CT. The final diagnoses in patients were thymic carcinoma in 4, lung carcinoma in 5, lymphoma in 3, carcinoid metastases in 2 and schwannoma in one patients. **Conclusion:** Anterior mediastinal masses may originate from different primary tumors in adult patient group and F-18 FDG PET/CT imaging might provide an easier cite to evaluate or another diagnostic method for an unexpected primary tumor. **Key words:** anterior mediaten, mass, FDG ,PET.

EP-0780

Clinical Usefulness Of 18F-FDG PET/CT For The Evaluation Of The Atypical Adrenal Tumors

A. Rubio Rodriguez; Institut Diagnòstic per la Imatge, Girona, SPAIN.

Aim: To evaluate 18F-FDG PET/CT results in patients with an atypical adrenal incidentaloma. **Methods:** Fifteen patients with a radiological diagnostic of adrenal incidentaloma (adrenal lesion with more than 10 UH in a CT and/or lesions with lack of T1 signal lost in phase and out of phase by MRI) were studied with 18F-FDG PET/CT. We retrospectively evaluated the SUVmax lesion and the tumor/hepatic SUVmax ratio (SUVmax T/H). We considered as a malignant, lesions with SUVmax>5.2 and SUVmax T/H>1.5. The final diagnosis were obtained by surgery in ten patients, biopsy in two, and with a 2 years clinical follow-up in three patients which surgery were dismissed. **Results:** 11 incidentalomas were classified as benign: 2 non-functioning adenomas (SUVmax: 2,3±0,4; SUVmaxT/H:0,8±0,2), 3 functioning adenomas (SUVmáx: 2,2±0,1; SUVmáxT/H:0,94±0,03), 4 pheochromocytomas (SUVmax: 4,2±1; SUVmaxT/H: 1,16±0,2), 1 hemangioma (SUVmax: 2.9; SUVmaxT/H: 0.71) and 1 granulomatous tumor (SUVmáx: 9,1; SUVmáxT/H: 1.83). 4 incidentalomas were classified as malignant: 2 functioning adrenal carcinomas (SUVmax: 11,6±0,6; SUVmaxT/H: 2,7±0,1), 1 non-functioning oncocytic tumor (SUVmax: 18,9; SUVmaxT/H: 7,8) and 1 renal carcinoma metastasis (SUVmax: 3,6; SUVmaxT/H: 1,36). A SUVmax value >5.2 and a SUVmaxT/H value >1.5 identify all the malignant lesions, with the only exception of the renal carcinoma metastasis. All the benign lesions, except the inflamatory lesion, presented a SUVmax value <5.2 and a SUVmax T/H value <1.5. **Conclusion:** 18F-FDG PET/CT is useful in patients with an atypical adrenal incidentaloma, identifying the malignant ones. The inflamatory adrenal lesions can produce false positive results.

EP-0781

Retrospective Study of Bone Marrow Disease Detection with 18F FDG PET/CT and Correlation with Positive Bone Marrow Biopsies for Haematological Malignancies

M. Hamidian[1], J. Crook[2], H. Rizvi[2], N. Swalding[2], Y. Bouchareb[2], S. Hallam[2], K. Shahabuddin[2], H. Jan[2], **A. Haroon[2];** *[1]Kowsar Hospital Nuclear Medicine Department, Shiraz, IRAN, ISLAMIC REPUBLIC OF, [2]Barts Health NHS Trust, London, UNITED KINGDOM.*

Purpose: To evaluate the detection of bone marrow infiltration due to haematological malignancies on 18F FDG PET-CT and correlate the findings with bone marrow biopsies. **Subjects and Methods:** We performed retrospective electronic search for bone marrow biopsies performed over 2 years (1/1/2014 - 18/10/2016). Bone marrow trephines with histological evidence of infiltration by haematological malignancies (based on a standardised local panel comprising routine Haematoxylin and Eosin stain, Reticulin stain, Immunostains for CD20, CD3 and CD79a and where relevant CD30, CD15 and MUM1) were

retrieved. This yielded a total of 270 bone marrow trephines showing involvement by lymphoma. Those cases where 18F FDG PET were available were included. The PET/CT images were acquired on a Philips Gemini TF TOF 64 slice PET/CT scanner (Philips Healthcare, Cleveland, Ohio) at a single site. Those patients who had received recent treatment were excluded. Based on the above we had 42 cases included in the study. **Results:** There were 12 females and 30 males; age range 27-87 years (average 59.4 years). The case mix was as follows

-18F FDG PET-CT was negative in 5 cases and positive in 37 cases.
- Negative 18F FDG PET-CT cases included
- Positive 18F FDG PET-CT included

SUVmax range for positive PET CT scans was 1.56-14.46 and SUVmax range for negative PET CT scans was 1.85-3.3. **Conclusion:** This retrospective study showed that ^{18}F-FDG PET has good concordance with the results of bone marrow biopsy for the detection of bone marrow infiltration in the staging of patients with haematological malignances. ^{18}F-FDG PET may complement the results of bone marrow biopsy and its performance may vary according to the type of lymphoma.

EP-0782
Incidental lesions in FDG-PET/CT scans

G. Sipka[1], Z. Besenyi[1], Z. Lengyel[2], L. Pavics[1]; [1]University of Szeged, Szeged, HUNGARY, [2]Pozitron-Diagnosztika Központ, Budapest, HUNGARY.

Introduction: In modern oncological diagnostics are FDG-PET/CT unevitable. During the metabolic information gaining process we often discover different, incidental lesions, which aren't connected to the primary tumours. Our goal in the study was to retrospectively specify the origins of these freshly discovered, independent FDG-avid lesions on „routine" FDG PET/CT. **Subjects & Methods:** We revised 326 FDG-PET/CT exams' results, performed indifferent oncologic indications, from 2006 February to 2012 January (229 men, 97 women; average age: 57,4 year). According to the written results we classified the PET findings and separate those FDG-avid lesions, which aren't connected to the primary malignancies. Under the 2 years follow up the incidentalomas exact locations, states and malignancies were evaluated. Histological identifications and the long term follow up were taken into account for the identification of true positive findings. **Results:** 119 abnormal, unexpected, focal lesions were confirmed in 112 patients out of 326. Overall 18 (5,5 %) newly detected, separate, primary malignancies were proved, while 19 (5,8%) metastases and 82 (25,1%) benign diseases have been were found. The majority of the incidental lesions were in the gastrointestinal tract and in the head and neck region (35-35), while the respiratory- and urogenital system, the skin and other locations contained the rest of cases (30%). In the digestive tract several FDG-avid lesions in the colon (24/42) were described, but all of them was false positive. In the stomach and pancreas were decisively more aggressive abnormalities. The head and neck lesions were often related to the primary diseases (10/13).

Surprisingly no histological confirmed malignant lesion was detected in the thyroid gland. The other findings in the suprarenal gland and in the lung were equally metastases and newly discovered, primary malignant tumours. **Conclusion:** In summary, unexpected incidental lesions are common on FDG-PET/CT scans. Most of them are benign, although one third of FDG-avid lesions are progressive, malignant, pathological diseases, which raise the patients' mortality. The most common false positive findings were in the gastrointestinal system.

EP-0783
Synchronic and Metachronic Tumors Detected by PET / CT in the Staging of Primary Tumors

B. Perez Lopez, F. Gomez-Caminero Lopez, P. Garcia-Talavera San Miguel, C. Achury Murcia, L. Diaz Gonzalez, E. Martin Gomez, E. Martin Gomez, P. Tamayo Alonso; Complejo Asistencial Universitario de Salamanca, Salamanca, SPAIN.

Aim: To evaluate the usefulness of 18F-FDG-PET-CT staging in primary tumors and the detection of synchronous and metachronous tumors. **Material and Methods:** We reviewed retrospectively staging 18F-FDG-PET-CT performed between January 2015 and January 2017. Of the total of 2200 cases we selected 160 patients with suspicion of synchronic tumor. Finally, analysis only was made in 88 patients due to lack of clinical information. 18F-FDG-PET-CT findings were correlated with histological analysis. **Results:** 88 patients, 66 males and 22 females with average age of 66.7 (SD ±9.9) years old, and known primary tumor, mainly located in: oto-rhino-laryngology area (48.4%), lung (17.6%), gastrointestinal tract (13.6%), gynecological (10.2%), genitourinary tract (2.3%) and others (7.9%). Histological types encountered of known tumor were epidermoid carcinoma in 57.1%, adenocarcinoma in 25.3%, sarcoma in 3.3% (osteosarcoma, chondrosarcoma), invasive ductal carcinoma in 3%, small-cell carcinoma in 1.1%, urotelial carcinoma in 1.1%, and others types in 9.1%. In all patients, PECT/CT detected another hypermetabolic lesion which might be a synchronic tumor due to its metabolic characteristics (SUVmax mean: 13.1 ± 8.4). Lesions were located in: gastrointestinal tract (57.9%, where large bowel represented the 84.3%), lungs (9.1%), genitourinary tract (3.4%), breast (2.3%), thyroid (2.3%), adrenal gland (1.1%) and hypophisis (1.1%). After PET/CT findings, histological analysis was performed in all patients. Diagnosis of malignancy was confirmed in 64.8% and discarded in 35.2% of the patients. Regarding histological type, adenocarcinoma was the most common type found (25.4%) for malignancy, and adenoma (19.8%) for non-malignancy. **Conclusion**: Detection of a second tumor in staging 18F-FDG-PET-CT is not an uncommon finding. Patients with known tumors can have other tumors in unexpected places and 18F-FDG-PET-CT can identify, localize and metabolic characterize these tumors for an early diagnosis, which will prevent the development of these second neoplasms.

EP-0784
Diagnostic Performance of Gallium-68 SSR PET-CT in patients with TIO: A Meta-analysis

K. Agrawal, B. M. Padhy; All India Institute of Medical Sciences, Bhubaneswar, INDIA.

Aim: Tumor-induced osteomalacia (TIO) is a rare paraneoplastic syndrome, which is usually caused by small benign mesenchymal tumors. Localization of these small tumors by anatomical imaging is often challenging. Aim of our study is to meta-analyse the published data about the diagnostic performance of Gallium-68 (Ga-68) somatostatin receptor (SSR) positron emission tomography-computed tomography (PET-CT) in patients with TIO. **Materials and Methods:** A comprehensive computer literature search of studies published in Pubmed and Google Scholar databases was performed. No beginning date limit was used; the search was updated until 3rd April 2017 and no language-based restriction was used. References of the retrieved articles were also searched for additional studies. The exclusion criteria were: (a) articles not within the field of interest of this review, (b) review articles, editorials or letters, comments, conference proceedings (c) Sample size <3 patients (d) duplicate data. **Results:** Seven studies comprising of seventy eight patients were included in this meta-analysis. The pooled sensitivity and specificity of Ga-68 SSR PET-CT in detecting tumors causing osteomalacia were 91% (95% confidence interval [95% CI]: 82-96%) and 94% (95% CI: 82-99%) respectively, on a per patient-based analysis. The area under the ROC curve was 0.95. **Conclusion:** Ga-68 SSR PET-CT showed high sensitivity and specificity in localizing tumors in patients with TIO. Therefore, it should be considered as first line imaging modality in patient with TIO.

EP-0785

Association Between Gastric FDG Uptake in PET-CT and 14-C UBT Results in Patients Referred for Non-Gastric Cancer PET-CT Studies

A. Hassanzadeh-Rad, F. Farsiabi, M. Eftekhari, A. Fard-Esfahani, B. Fallahi, A. Emami-Ardekani, D. Beiki; Research Center for Nuclear Medicine, Tehran, IRAN, ISLAMIC REPUBLIC OF.

Introduction: Patients referred for evaluation of non-gastric cancers with FDG-PET-CT study may have variable degrees of FDG uptake in the gastric region. This diffuse FDG uptake may-be caused by H. Pylori infection with positive 14-C Urea Breath Test (UBT) results. In this research, we want to evaluate the association between degree of FDG uptake in FDG-PET-CT study and C14-UBT results. **Subjects and Methods:** Study groups are selected from non-gastric cancer patients who are referred for FDG-PET-CT study. All selected patients undergo C14-UBT by ingesting a capsule containing 1 microCurie C-14 Urea and exhale in to a HELIPROBE™ breath card, until reaching the chemical equilibrium of acid-base reaction. After that, breath card is inserted in to HELIPROBE Analyzer for beta counting and Disintegrations Per Minute (DPMs) of the sample solutions are calculated. Results are interpreted as negative (DPM <25) and positive (DPM >50). Patients from both UBT positive and UBT negative groups undergo FDG-PET-CT study, using Siemens BIOGRAPH T6 Series™. Gastric FDG uptake are divided as: grade 0: absent uptake, grade 1: uptake below mediastinal background, grade 2: uptake between mediastinal and liver background, grade 3: uptake moderately increased than liver, grade 4: uptake markedly increased than liver. Regions Of Interest (ROIs) are drawn over stomach and SUVmax values of gastric uptake are calculated for the patients with grade 3 or 4 FDG uptake. Data was analyzed by SPSS ver 22 (SPSS, Inc). **Results:** 80 Patients in two groups (40 UBT positive and 40 UBT negative results) were selected. The prevalence of increased gastric FDG uptake (grades 3 and 4) was significantly higher in UBT positive group as compared to UBT negative group (83 % versus 35 %, P-value < 0.001). Besides, in the subgroup with increased gastric FDG uptake, there was significant positive correlation between DPMs of 14-C UBTs and SUVmax values (r= +0.67, P-value < 0.05). **Discussion/Conclusion:** Results of our study shows a significantly higher prevalence of increased gastric uptake in UBT positive patients and a significantly positive correlation between DPM and SUV max of gastric region. Therefore we suggest that in those patients with non-gastric cancers who are evaluated by FDG-PET-CT, if there is moderately or markedly increased gastric FDG uptake, 14C-UBT may be helpful. With a high probability of a positive UBT result in these patients, appropriate and on-time treatment of H-pylori can lead to eradication of this microorganism.

EP-0786

Clinical Contribution of the Second Primary Cancers Detected by FDG PET/CT

A. Yıldız[1], M. Özdoğan[2], S. Yılmaz[3], B. Özcan[4], N. Öz[5], A. Gürkan[4], Z. Şahin[1], H. Dikici[6], A. Kargı[6]; [1]Nuclear Medicine, Medstar Hospital, Antalya, TURKEY, [2]Medical Oncology, Medstar Hospital, Antalya, TURKEY, [3]Radiology, Medstar Hospital, Antalya, TURKEY, [4]General Surgery, Medstar Hospital, Antalya, TURKEY, [5]Thoracic Surgery, Medstar Hospital, Antalya, TURKEY, [6]Gastroenterology, Medstar Hospital, Antalya, TURKEY.

Purpose: Accurate diagnosis of the second primary cancers by FDG PET-CT has the potential to influence the staging, treatment approach and prognosis. The aim of the study is to present the role and clinical significance of PET-CT in detecting incidentally the second primary cancers and to determine the contribution to patient management. **Subjects and Method:** A total of 7684 FDG PET-CT examinations performed between February 2012 and December 2016 were reviewed retrospectively and 511/7684 (6.6%) patients, who were specified to have probably a second primary malignancy in the report, were evaluated. A total of 235/511 (45.9%) patients (125 males, 110 females), who were assessed histopathologically from the point of a second primary, were included in the study. In the assessment of tomographic component of PET/CT, morphologic images incompatible with metastasis, metabolic activity difference, atypical localization, lesions showing no change or progression despite treatment response were assessed to be compatible with a second primary cancer. The tomographic component of PET/CT was performed using IV contrast agent at diagnostic dose. **Results:** Second primary cancers were detected in 145 (61.7%) of 235 cases with histopathological evidence. Thirt-five (38.8%) of the 90 false negative patients were detect-

ed to have metastasis and 19 (21.1%) of them were detected to have benign lesion. Secondary cancers were synchronous in 51.9% of the cases and were metachronous in 48% of the cases. The distribution of first cancer diagnoses were lung (15.2%), colorectal (13.5%), head and neck (12.2%), lymphoma-myeloma (10.5%), breast (22.8%), gynecological (6.3%), genitourinary (4.2%), esophagus, stomach and duodenum (2.5%), malignant melanoma (1.2%), pancreas (1.6%), bone and soft tissue (2.1%), prostate (3.8%), liver and bile ducts (1.6%) and other organs (1.6%). The distribution of 145 patients was detected as breast (22.9%), lung (15.3%), colorectal (13.6%), head and neck (12.3%), hematologic (10.6%) and other cancers (25.1%). 3 synchronous primary malignancies were detected in 5 patients. **Conclusion:** Radiologic features and oncological data are important as well as metabolic activity in the detection of the second primary cancers by PET/CT. The likelihood of detecting second cancers may lead to misleading results both for the diagnosis of primary cancer and therefore for the treatment approach; so it is important from the point of treatment to be planned and may change the clinical approach.

Radionuclide Therapy & Dosimetry: Preclinical Studies (Animal & In Vitro)

EP-0787

Neurotensin receptor-1 expression in human prostate cancer and lymph nodes metastases

C. Morgat[1,2,3], V. Molinié[4], H. de Clermont Gallerande[1], G. Macgrogan[5,6], V. Vélasco[5,6], G. Robert[7,8], B. Malavaud[9], P. Fernandez[1,2,3], E. Hindié[1,2,3]; [1]Department of Nuclear Medicine, University Hospital of Bordeaux, Bordeaux, FRANCE, [2]CNRS, INCIA UMR-5287, Bordeaux, FRANCE, [3]University of Bordeaux, INCIA UMR 5287, Bordeaux, FRANCE, [4]Department of Pathology, University Hospital of Fort de France, Fort de France, MARTINIQUE, [5]Surgical Pathology unit, Department of BioPathology, Institut Bergonié, Bordeaux, FRANCE, [6]INSERM, ACTION U1218, Bordeaux, FRANCE, [7]Department of Urology, University Hospital of Bordeaux, Bordeaux, FRANCE, [8]Department of Medical Sciences, University of Bordeaux, Bordeaux, FRANCE, [9]Department of Urology, University Hospital of Toulouse, Toulouse, FRANCE.

Purpose: Neurotensin and its receptor NTR_1 are involved in the growth of various tumors. No data are available regarding NTR_1 expression in normal and tumoral human prostate tissues. **Methods**: NTR_1 expression was assessed using immunohistochemistry in samples of 12 normal prostate tissue, 11 benign prostatic hyperplasia (BPH), 34 prostate cancers and five related metastatic lymph nodes. **Results**: NTR_1-staining was negative in normal prostate and BPH samples. NTR_1-overexpression was seen in 11.8% (4/34) of primary tumors. Primary tumors from node-positive patients expressed more frequently NTR_1 (3/7; 42.9%) than those from pN_{0-x} patients (1/27; 3.7%; *P* = 0.021). NTR_1-overexpression was more frequent in metastatic lymph

nodes (4/5; 80%) than in primary tumors (*P* = 0.004). **Conclusions**: NTR_1 overexpression in primary prostate cancer is associated with the risk of lymph node invasion. The presence of this target in metastatic lymph nodes may open new perspectives for imaging and radionuclide therapy of prostate cancer.

EP-0788

Determination of the Rat Kidney Uptake of 99mTc-DMSA Using the Quantitative Radionuclide Imaging and a Computational Method: A Comparison Study

K. Tanha[1], H. Fatemikia[2], M. Assadi[1]; [1]The Persian Gulf Nuclear Medicine Research Center, Bushehr University of Medical Sciences, Bushehr, IRAN, ISLAMIC REPUBLIC OF, [2]Department of Physiology, Medical School, Bushehr University of Medical Sciences, Bushehr, IRAN, ISLAMIC REPUBLIC OF.

Purpose: The aim of this study was to evaluation of the absorbed radionuclide calculation using radionuclide imaging of 99mTc-DMSA renal scan in the rat. Also, we introduced a computational method for estimation of the radionuclide uptake in the kidneys based on the injected activity and effective half-life of the radionuclide. **Materials and Methods:** after injection of a range of activities between 0.1 mCi to 5 mCi of 99mTc-DMSA, planar images were acquired using HiReSPECT; a small-animal SPECT. At the end of the experiments, kidneys were excised for the measurement of activity uptake using a dose calibrator. **Results:** The relative error in estimation of radionuclide uptake in the kidney were 19.6 % for imaging method and 18.03 % for the computational method. The results were more accurate for injection activities higher than 2 mCi Both of the methods underestimate the amount of the radionuclide uptake. **Conclusion:** the results of this study indicate that the HiReSPECT imaging system has acceptable accuracy in determination of kidneys radionuclide uptake in the 99mTc-DMSA renal scan. Application of attenuation corrections in the future studies may increase the accuracy of both of the imaging method and the computational method.

EP-0789

The difference of tumor accumulation between conventional and site-specific Ga-67 radiolabeled anti-HER2 antibody

Y. Kono[1], K. Utsunomiya[2], Y. Ohira[3], H. Sato[3], N. Kan[1], Y. Matsumoto[4], Y. Ueno[1], K. Maruyama[1], N. Tanigawa[1]; [1]Kansai Medical University, Osaka, JAPAN, [2]Kansai Medical University Medical Center, Osaka, JAPAN, [3]Perseus Proteomics Inc., Tokyo, JAPAN, [4]Kansai Medical University, Radioisotope Research Center, Osaka, JAPAN.

Purpose: To compare the accumulation of Ga-67 labeled anti-HER2 antibodies with novel homogeneous site-specific conjugation versus conventional chemical, heterogeneous site, conjugation in HER2-positive tumors. **Subjects & Methods:** First, anti-HER2 antibody was chemically conjugated with deferoxamine. The resulting chemical conjugate was radiolabeled with Ga-67 (Chem-Ab). Second, site-specific anti-HER2 antibody

conjugation was performed with 67-Ga radiolabeled transglutaminase (SSC-Ab). In vitro, binding activity of HER2 to both antibodies, Chem-Ab and SSC-Ab, was evaluated using ELISA with fluorescent antigen labeling. In vivo, a xenograft mouse model consisting of subcutaneously transplanted CHO cells with HER2 overexpression was established. We divided the subjects into the Chem-Ab group (n=7) and the SSC-Ab group (n=7). Planar images were acquired over three days, for both groups, after antibody injection and the tumor / whole body count ratios (T/WB ratio) was measured. On the fourth day, pharmokinetic analysis was used to compare the Chem-Ab group to the SSC-Ab group, in both whole organs and tumor, for Ga-67 accumulation of. **Results:** SSC-Ab was found to have a higher binding capacity than Chem-Ab. The T/WB ratio increased in both groups. On the third day, the SSC-Ab group had a significantly higher T/WB ratio than the Chem-Ab group (p=0.03). In the SSC-Ab group, the antibody accumulation was significantly higher than the Chem-Ab group in not only the tumors (20.37, 15.08 %ID/g, p=0.016), but also in the liver and spleen. **Conclusion:** The site-specific conjugation method enhanced the accumulation of the anti-HER2 antibody labeled with Ga-67 in tumors and also in in the liver and spleen as well.

EP-0790

Improvement of therapeutic efficacy by combing 90Y-ITGA6B4-mediated radioimmunotherapy (RIT) with dual PI3K and mTOR inhibitor NVP-BEZ235

W. Aung[1], A. B. Tsuji[1], H. Sudo[1], A. Sugyo[1], Y. Ukai[2], K. Kouda[2], Y. Kurosawa[3], T. Furukawa[4], T. Saga[5], T. Higashi[1]; [1]Department of Molecular Imaging and Theranostics, National Institute of Radiological Sciences, National Institutes for Quantum and Radiological Science and Technology, Chiba, JAPAN, [2]Perseus Proteomics Inc., Tokyo, JAPAN, [3]Innovation Center for Advanced Medicine, Fujita Health University, Toyoake, JAPAN, [4]Department of Radiological and Medical Laboratory Sciences, Nagoya University Graduate School of Medicine, Nagoya, JAPAN, [5]Department of Diagnostic Radiology, Kyoto University Hospital, Kyoto, JAPAN.

Aim: We have previously studied the Radioimmunotherapeutic effect and toxicity of Yttrium-90 labeled anti-integrin $\alpha_6\beta_4$ antibody (^{90}Y-ITGA6B4) in a pre-clinical mouse pancreatic cancer model. The severe myelotoxicity caused by an overdose is a major problem in radioimmunotherapy (RIT). The phosphatidylinositol 3-kinase (PI3K)/Akt/mammalian target of rapamycin (mTOR) pathway is frequently mutated in human cancers and its activation alters a number of cellular processes that are stimulating proliferation, cell growth, and survival. NVP-BEZ235 (BEZ235) can potently inhibit the PI3K and mTOR kinase activity and has been used in preclinical studies in many cancers with excellent results of anticancer effects. Here, we explored whether the therapeutic effect of RIT could be improved by BEZ235 in pancreatic cancer model. **Materials and Methods:** The phosphorylation of Akt (p-Akt), mTOR (p-mTOR) and downstream effector eukaryotic initiation factor 4E (eIF4E) binding protein 1, 4EBP1 (p-4EBP1) were evaluated in BxPC-3 human pancreatic cancer cells treated with ^{90}Y-ITGA6B and BEZ235 by using

western blotting method. Radiosensitization effect of BEZ235 was investigated with colony formation assay. Enhancement of therapeutic efficacy by BEZ235 oral administration was evaluated by using mice bearing BxPC-3 xenograft tumors. Tumor volume measurements and immunohistochemical analyses (cell proliferation marker Ki-67, DNA damage marker p-H2AX and, p-4EBP1 staining) of tumors were performed for evaluation of effects of combined treatment ^{90}Y-ITGA6B4 plus BEZ235, or each arm alone. **Results:** We found that expressions of p-Akt and p-4EBP1 were inhibited and cell colony forming was also synergistically suppressed by RIT and BEZ235. Treatment groups showed reduction in tumor volumes (P < 0.05), decreased Ki-67-positive cells and increased p-H2AX-positive cells and decreased p-4EBP1 expression. **Conclusion:** These results demonstrate that it is possible to improve the therapeutic efficacy by combing ^{90}Y-ITGA6B4 with PI3K and mTOR inhibitor BEZ235.

EP-0791

Preferential Tumor Accumulation in Mice bearing Human Head and Neck Cancer using Radionuclide-carrying Liposomes aiming for Radiotheranostics

I. O. Umeda, S. Hamamichi, H. Fujii; National Cancer Center, Kashiwa, JAPAN.

Purpose/Introduction: Radionuclide-carrying liposomes are promising for tumor imaging and radionuclide therapy because they can accumulate in the tumor. However, they also accumulate in the normal tissues, especially in the liver, hindering their clinical application. Previously we found that the liposomal degradation was rapid in the liver, and successfully removed radionuclide from the liver after liposomal degradation, keeping high level in the tumor, by combination of liposomes and new radionuclide-ligand complex, ^{111}In-ethylenedicysteine (EC). However, it was also revealed that liposomal degradation rate in the liver was different among mouse strain. In this study, we expanded our strategy to mouse xenograft models bearing human cancer. **Methods:** BALB/c-nu/nu mice bearing human head and neck cancer FaDu were used. To confirm degradation of the liposomes, tumor and liver homogenates were ultracentrifuged at 105,000 x *g*, and resulting supernatants were analyzed by HPLC equipped with a GPC column to separate intact liposomes from small molecules. *In vivo* images were acquired by using a small animal dedicated SPECT/CT scanner. **Results:** Our results indicated that liposomal lipid dose was very important factor to achieve our strategy. At 2 μmole as phospholipid/mouse, there was no difference between ^{111}In-EC liposomes and control liposomes (^{111}In-DTPA liposomes); i.e., 40 % of administered dose /g (%AD/g) was still left in the liver at 24 h after administration. On the other hand, at 0.5 μmole/mouse or less, significant liver reduction (less than 5% AD/g) was observed only with ^{111}In-EC liposomes. Subsequent HPLC analysis demonstrated that liposomes remained intact in the liver under high dose whereas they were well degraded under the reduced dose. Another problem occurred when reduced liposomal dose caused the decrease of tumor accumulation; however, PEGylation of liposomes solved the contradiction. Injection of 0.2 μmole/mouse

of ^{111}In-EC PEGylated liposomes successfully achieved both sufficient tumor accumulation and rapid liver clearance. *In vivo* SPECT/CT imaging also depicted it well. **Conclusions:** In human cancer xenograft model, we attained high tumor accumulation, as well as rapid background clearance by using ^{111}In-EC-PEGylated liposomes, consequently, radionuclide accumulated almost only in the tumor. Our concept is applicable to diagnostic and therapeutic radionuclides, such as ^{111}In, ^{90}Y, and [177]Lu. These findings should become driving force targeting radionuclide therapy and theranostics for solid tumors. **Research support:** This study was supported by Grants-in-Aid from the Japan Society for the Promotion of Science (JSPS), Health Labour Sciences Research Grant by MHLW and the National Cancer Center Research and Development Fund.

EP-0792

Combination Therapy of Medullary Thyroid Cancer Using Radiation and Vandetanib

V. Sandblom[1], J. Spetz[1], E. Shubbar[1], J. Swanpalmer[2], E. Forssell-Aronsson[1]; [1]Department of Radiation Physics, Institute of Clinical Sciences, Sahlgrenska Cancer Center, Sahlgrenska Academy, University of Gothenburg, Gothenburg, SWEDEN, [2]Department of Medical Physics and Biomedical Engineering, Sahlgrenska University Hospital, Gothenburg, SWEDEN.

Introduction: Most patients diagnosed with medullary thyroid cancer (MTC) present with metastatic disease. MTC are rare neuroendocrine tumours that occur either sporadically or in a hereditary form. Surgical resection of the thyroid gland followed by external beam radiotherapy (EBRT) or the use of tyrosine kinase inhibitors are current clinical methods for management of MTC. Unfortunately, the 10-year survival for patients with metastatic disease is only about 40%. However, many MTC tumours overexpress somatostatin receptors as molecular targets. Therefore, one option for patients with MTC is systemic treatment with radiolabelled somatostatin analogues (*e.g.* ^{177}Lu-octreotate) that bind with high affinity and specificity to somatostatin receptors on the tumour cells. In addition, the tyrosine kinase inhibitor vandetanib has recently been approved for single-agent treatment of MTC by the U.S. Food and Drug Administration (FDA). The aim of this study was to investigate the potential synergistic effect of combining irradiation and vandetanib for treatment of MTC. **Subjects & Methods:** BALB/c nude mice were transplanted with patient-derived MTC cells (GOT2). When developed tumours reached a volume of about 500 mm³, the mice were treated with EBRT, vandetanib or a combination of both. The radiation dose and the amount of vandetanib were chosen to give moderate effect as single treatment to enable detection of any increased effect from the combination. Tumour volume was followed and compared with that in untreated mice. **Results:** We found that the largest treatment effect over time was seen for the animals receiving a combination of both EBRT and vandetanib. Given as single-agent treatment, EBRT and vandetanib resulted in a reduction in tumour size or in tumour growth arrest. For example, at two weeks after start of treatment, the tumour volume was reduced by 64%, 52%, and 73% compared with the untreated control group, for the animals treated with single EBRT, single vandetanib, and the combination, respectively. **Conclusion:** The results indicate that an additive or even synergistic effect could be achieved when combining irradiation with vandetanib for treatment of patients with MTC. Further studies are needed to investigate the possibility of using ^{177}Lu-octreotate for treatment of MTC, both as single-agent treatment or in combination with vandetanib.

EP-0793

Receptor Binding Kinetics of PSMA-Specific Peptides Determined by Surface Plasmon Resonance Measurements

G. Winter[1], A. Vogt[1], G. Glatting[2], P. Kletting[2], A. J. Beer[1]; [1]Department of Nuclear Medicine, Ulm University, Ulm, GERMANY, [2]Medical Radiation Physics, Department of Nuclear Medicine, Ulm University, Ulm, GERMANY.

Introduction and Aim: Diagnostic and therapeutic approaches of prostate cancer treatment are often based on targeting the prostate-specific membrane antigen (PSMA). The PSMA-specific peptides PSMA-11 and PSMA-617 are increasingly used for diagnosis and therapy. Current standard methods to determine the binding characteristics are based on cell assays and are frequently performed at non-physiological temperature. Furthermore, the results do not explicitly include binding kinetics parameters, i.e. association rate (k_{on}) and dissociation rate (k_{off}). Therefore, we used surface plasmon resonance (SPR) spectroscopy for cell-free determination of these rates and the resulting equilibrium dissociation constant (K_D). **Material and Methods:** The PSMA protein (R&D Systems) was covalently bound to the dextran chain on the surface of various CM5 chips (GE Healthcare). Using a Biacore X100 (GE Healthcare, Freiburg, Germany), variable concentrations in ascending order in the range of 0.1 fold to 10 fold of the expected K_D of the peptides of interests, PSMA-11, (Ga)PSMA-11, PSMA-617 and (Ga)PSMA-617 (ABX, Radeberg, Germany) were applied to various PSMA-CM5-chips performing the device specific single-cycle kinetics program. Each chip was regenerated and reused multiple times to replicate measurements at least three times. Assuming a standard 1:1 interaction model the results were analysed with the Biacore software and statistically evaluated using the Kruskal-Wallis H test and Mann-Whitney U test (p<0.05 was assumed significant). **Results:** The kinetic parameter obtained were in the range of k_{on}: (2.0 x 10⁶ to 5.5 x 10⁶) (Ms)⁻¹ and k_{off}: (5.4 x 10⁻⁵ to 4.2 x 10⁻⁴) s⁻¹. The resulting K_Ds determined for PSMA-11 and GaPSMA-11 were (0.07±0.02) nM and (0.04±0.02) nM at 25℃, and (0.07±0.04) nM and (0.10±0.08) nM at 37℃. For PSMA-617 (0.01±0.01) nM at 25℃ and (0.1±0.06) nM at 37℃ were obtained. PSMA-11 and GaPSMA were not significantly different at 37℃ and 25℃, while for PSMA-617 K_D differed significantly at these temperatures. **Conclusion:** SPR measurements allow highly reproducible determination of interaction data at physiological temperature. The results are of great value for peptide development and optimization and can be implemented in a physiologically-based pharmacokinetic (PBPK) model. This will improve individualized

treatment planning of molecular radiotherapy using PBPK modelling.

EP-0794
Radioiodination Of Small Stapled Peptides For p53 Therapy

S. Lundsten[1], D. Spiegelberg[1], V. Agmo Hernández[2], C. Brown[3], K. Edwards[2], D. Lane[3,4], M. Nestor[1]; [1]Department of Immunology, Genetics and Pathology, Uppsala University, UPPSALA, SWEDEN, [2]Department of Chemistry - BMC, Uppsala University, UPPSALA, SWEDEN, [3]p53Lab, A*STAR, SINGAPORE, SINGAPORE, [4]Department of Microbiology, Tumor and Cell Biology, Karolinska Institutet, Stockholm, SWEDEN.

Background: We have investigated two small stapled peptides, PM2 and VIP-116, HDM2/HDMX-p53 antagonists that protect p53 from degradation. Thus, they can reduce viability of various p53 wildtype tumour cells, but could also result in radiosensitisation. It is interesting to assess the possibility of radiohalogenation of the peptides in order to follow binding kinetics and biodistribution, as well to create potential radiotherapeutic agents. Furthermore, by utilising tumour targeting PEG-stabilised nanodiscs (lipodisks) as peptide delivery vectors, a more tumour specific effect may be obtained. **Methods:** A ^{125}I-labelling protocol using chloramine-T was first optimised for most advantageous labelling yield with minimal oxidative exposure on the peptides. The function of the radioiodinated peptides was investigated through interaction assays and tumour cell dose response studies. The biodistribution of iodinated PM2 was assessed in tumour bearing mice. The interaction between peptides and lipodisks was also characterised using quartz crystal microbalance with dissipation monitoring (QCM-D) and LigandTracer. **Results:** The optimised labelling protocol resulted in a yield of approximately 55% and size exclusion chromatography eliminated free [125]I. The iodination was shown to be stable after 48 hours. Biodistribution data showed promising results with retained radioactivity in and around the tumour. The interaction assays demonstrated a strong association between peptides and lipodisks. **Conclusion:** We have successfully optimised radiohalogenation of PM2 and VIP-116, and demonstrated retained cytotoxic effect of the compounds. The novel combination of a radiohalogen and an HDM2/HDMX-targeting peptide could potentially result in synergistic therapeutic effects. The investigated lipodisks can potentially serve as a delivery system for small stapled peptides.

EP-0795
Radium-223 and metastatic prostate cancer: new insights from cellular studies

I. A. Marques[1], A. M. Abrantes[1,2,3], A. R. Neves[1], A. S. Pires[1,2,3], G. Costa[4], F. Caramelo[1,5], T. Rodrigues[6], P. Matafome[6,7], E. Tavares-Silva[1,8], R. Seiça[6], A. Figueiredo[8], M. F. Botelho[1,2,3]; [1]Biophysics Institute, IBILI-Faculty of Medicine, University of Coimbra, Coimbra, PORTUGAL, [2]CIMAGO, Faculty of Medicine, University of Coimbra, Coimbra, PORTUGAL, [3]CNC.IBILI, University of Coimbra, Coimbra, PORTUGAL, [4]Department of Nuclear Medicine, CHUC, Coimbra, PORTUGAL, [5]Laboratory of Biostatistics and Medical Informatics, IBILI-Faculty of Medicine, University of Coimb, Coimbra, PORTUGAL, [6]Laboratory of Physiology, IBILI-Faculty of Medicine, University of Coimbra, Coimbra, PORTUGAL, [7]Department of Complementary Sciences, Coimbra Health School (ESTeSC), Polytechnic Institute of Coimbra, Coimbra, PORTUGAL, [8]Department of Urology and Renal Transplantation, CHUC, Coimbra, PORTUGAL.

Purpose: Prognosis for patients with metastatic castrate-resistant prostate cancer(mCRPC) is poor. Radium-223([223]Ra) has given hope to these patients, however, little is known about its mechanisms of action. Given this, our aim is to study radiobiological effects induced, directly or indirectly, by [223]Ra in metastatic Prostate Cancer(mPCa) cell lines differing on hormonal receptors and metastatic potential to optimize the application of this radiopharmaceutical. **Materials and Methods:** Previous studies presented last year showed that [223]Ra is uptake, internalized by cells, enters the nucleus and kept inside the cells. Also, it was observed a decrease in survival factor in the same cell lines. To complement this information and to trying understand the mechanisms that leads to presented radiossensitivity, studies to evaluated cell proliferation, oxidative stress, signaling pathways and angiogenesis have been performed. For this, two cell lines of PCa will be irradiated, PC3 (without hormonal receptors, representative of mCRPC) and LNCaP (with hormonal receptors, representative of early stage of mPCa). Cell proliferation were accessed by sulphorhodamine-B assay. Formation of hydrogen peroxide were evaluated by a fluorescence assay. Response to DNA damage were accessed by western blot through a DNA Damage Antibody Sampler Kit. Angiogenesis were evaluated by aortic ring assay. **Results:** Per SRB assay,[223]Ra leads to proliferation decrease in more than half percent, in a dose-dependent manner, at low doses (until 10 mGy) for mPCa cell lines. These results were associated with distinct activation of CHK2, a nuclear protein involved in cell cycle arrest. Preliminary results showed an increase of peroxides production, when cells are irradiated with 10 mGy of [223]Ra. In aortic ring assay, [223]Ra also leads to a dose-dependent decrease of endothelial cell migration and organization, with statistical significance. **Discussion/Conclusion:** Results showed that [223]Ra leads to survival and proliferation decrease in mPCa cell lines, what can enhance the great potential in using this radiopharmaceutical in mCRPC patients. This also suggest that [223]Ra have a direct effect in mPCa cell that are presenting in bone metastatic niche, and with potential to reduce the aggressiveness of those cells. Studying radiobiological effects show that both direct and indirect damage contribute to induce the activation of important pathways and systems that leads to cell death. Related to angiogenesis, [223]Ra as a determinant role in decrease of progression and metastization and consequently the aggressiveness of this stage of disease. The authors would like to thank Foundation for Science and Technology (FCT) (Strategic Project CNC.IBILI: UID/NEU/04539/2013), COMPETE-FEDER for financial support.

EP-0796
Cell Survival in Colorectal Cancer under Yttrium-90 and Megavoltage X-ray

N. Forwood[1,2], Y. Gholami[3], R. Harvie[4], K. Willowson[3], R. Bromley[5], V. Howell[4], H. Ryu[6], Z. Kuncic[7], D. L. Bailey[1,6]; [1]Department of Nuclear Medicine, Royal North Shore Hospital, St Leonards, AUSTRALIA, [2]Faculty of Health Sciences, Sydney University, Sydney University, AUSTRALIA, [3]Institute of Medical Physics, Sydney University, Sydney, AUSTRALIA, [4]Kolling Institute, St Leonards, AUSTRALIA, [5]Department of Radiation Oncology, Royal North Shore Hospital, St Leonards, AUSTRALIA, [6]Faculty of Health Sciences, Sydney University, Sydney, AUSTRALIA, [7]School of Physics, University of Sydney, Sydney, AUSTRALIA.

Introduction: Personalized dosimetry in radioembolisation is being increasingly pursued in clinical practice. The maximum tolerable dose to the normal liver has been adopted from external beam radiotherapy (EBRT) and this has been used in dose planning. Radionuclide therapy (RNT) uses particulate radiation delivered at a lower dose rate over a longer period. The tolerable and toxic doses used in EBRT have not been validated in an RNT setting. This study investigates the relative difference between cell survival in EBRT and RNT specifically using colorectal cancer cell lines and Yttrium-90. Aims: To compare the cell survival for colorectal cancer using Yttrium-90 radiation and compare with cell survival for megavoltage x-ray beam radiation. To compute the α/β ratio that is derived from the linear quadratic model of cell survival for the two irradiation modalities. **Methods:** Colorectal cancer cell lines HT29, HCT116 and SW48 were irradiated with either 6 MV photons in the range 1-8 Gy or mixed with Y-90 chloride solution of amounts up to 230 kBq corresponding to 1 to 60 Gray of absorbed dose. Cell lines were cultured for 8 days and the cell survival was measured using the MTS viability assay and compared with control cell lines. **Results:** The resulting cell survival curves were fitted with the LQ model and the α/β ratio derived. The values for the different cell lines are shown in the table. **Conclusions:** The computed α/β ratios demonstrate a significantly different radiobiological response between the two types of radiation. This experimental method can be used for further exploration of these radiobiological differences. The accepted radiation dose limits for Y-90 may need to be revised.

EP-0797

Potential use of PRRT with 177Lu-octreotate beyond NETs : preliminary in vitro data in melanoma and multiple myeloma

W. Delbart, Z. Wimana, M. Vercruyssen, N. Meuleman, G. Ghanem, P. Flamen; Jules Bordet Institute, Brussels, BELGIUM.

Introduction: Octreotate (DOTATATE), a somatostatin analog, has been radiolabeled with Gallium-68 and Lutetium-177 and used for the Peptide Receptor Radionuclide Therapy (PRRT) theranostic approach of neuroendocrine tumors (NETs). This successful approach takes advantage of the overexpression and turnover of somatostatin receptors (sstr) (mainly sstr subtype 2) of NETs. $Sstr_2$ expression has been demonstrated in other malignancies than NET, such as melanoma and multiple myeloma. Positive OctreoScans using ^{111}In-pentetreotide have been reported in the latter. The present study explores the potential use of PRRT in melanoma and multiple myeloma. **Material & Methods:** Octreotate binding/uptake was assessed in melanoma (MM074, MM161), multiple myeloma (COLO-677, EJM) and a positive control neuroendocrine pancreas carcinoma (MIA-PACA-2) cell lines. Radiobinding was performed with ^{68}Ga-DOTATATE and cell viability with ^{177}Lu-DOTATATE using MTT assay. **Results:** Increased specific uptake of ^{68}Ga-DOTATATE was observed with increasing activities and incubation time in all tested cell lines, equivalent to half of the uptake in the neuroendocrine cancer cell line. A significant effect on cell survival was already observed 24h after 1h under 5kBq ^{177}Lu-DOTATATE, with a higher clear sensitivity of myeloma cell lines. **Conclusion:** Taken together our preliminary results show specific uptake of ^{68}Ga-DOTATATE in melanoma and multiple myeloma cell lines. Furthermore, ^{177}Lu-DOTATATE treatment shows potency already at low doses, with increasing therapeutic effect observed over time. This warrants further mechanistic and pre-clinical investigations aiming at proposing a translational theranostic approach in these malignancies.

EP-0798

Improving Image Quality in Preclinical ^{18}F-FDG TOF PET through Higher Definition Image Reconstruction

M. I. Menendez, J. Zhang, R. Moore, M. Friel, K. Binzel, M. V. Knopp; The Ohio State University, Columbus, OH, UNITED STATES OF AMERICA.

Aim: In preclinical PET/CT imaging precise measurement of SUV is critical, due to the smaller subject size. Recently, the utilization of larger matrices and smaller voxel volumes in reconstruction has been proposed with the potential for substantial quantitative benefits. The aim of this study was to assess the impact of reconstruction parameters on visualization and quantification, using 2x2x2 mm³ voxels sizes (8 mm³ voxel volume), high definition (HD) compared to the standard t 4x4x4 mm³ (64 mm³ voxel volume) standard definition (SD) reconstruction. **Materials and Methods:** Five mature healthy dogs underwent ^{18}F-FDG PET/CT under general anesthesia. List mode time of flight (TOF) raw data was acquired on a Gemini 64 TF PET/CT with Astonish (Philips). Four millimeter (mm) slice thickness CT data (512x512 matrix size using a 450 FOV) were used for attenuation correction. Subjects were injected with a dose of 110 MBq and imaged 30 minutes post-injection. Images were reconstructed using the system default reconstruction parameters with the SD reconstruction: 33 subsets (s) and 3 iterations (i). Additionally, the 2 mm HD reconstructions were performed varying the number of subsets: 5, 7, 9, 11, 15, 21, 29, 33 subsets with 3 iterations. The Philips IntelliSpace Portal was utilized for image analysis by 3D ROI, placed on measurable lesions as well as healthy liver and para-spinal musculature. Image quality of each data set was assessed by two independent, blinded readers. **Results:** Substantial differences in visual quality were noted in the HD reconstructions among the 8 parameter sets, with the 11 subset reconstruction being consistently rated as most preferable. HD image sets with greater than 11 subsets were deemed too noisy. We found that HD reconstructions generally exhibited SUVs in background tissue comparable to those

of SD image sets, while small hot regions of interest demonstrated increases in SUV previously validated in phantom models. Unlike SD reconstruction which requires a larger number of subsets, we found that HD images reached convergence after about 7-9 subsets. Thus the 11 subset images had a high level of quantitative robustness, while balancing good image quality. **Conclusion:** Smaller voxel volume (2mm) and thus higher definition reconstruction is feasible even on current generation TOF PET/CT. HD reconstruction leads to advanced image quality and lesion details. Furthermore, when reducing the voxel volume, reconstruction parameters, especially the number of subsets, need to be adjusted and optimized to account for the reduced count density and different iterative convergence.

EP-0799

Radiotherapeutic Nanoparticles Containing a Ruthenium-Based Radiosensitizer for EGFR-Positive Oesophageal Cancer

M. R. Gill[1], J. U. Menon[1], R. C. Carlisle[1], J. A. Thomas[2], P. J. Jarman[2], **K. A. Vallis**[1]; [1]*University of Oxford, Oxford, UNITED KINGDOM,* [2]*University of Sheffield, Sheffield, UNITED KINGDOM.*

Aim: Oesophageal cancer is a frequently lethal and aggressive form of cancer. Current non-surgical treatments are based on radiotherapy and DNA-damaging chemotherapy such as cisplatin. However, survival rates remain poor. Targeted radionuclide therapy (TRT) offers cell-specificity and cytotoxic ionising radiation. An emerging concept is how best to combine TRT with other therapies. The goal of this study was to develop a delivery system for simultaneous delivery of the Auger electron-emitting radionuclide, indium-111, and a ruthenium-based DNA intercalator/radiosensitizer to EGFR-positive oesophageal cancer cells for a combined therapeutic effect. **Materials and Methods:** PLGA (polylactic-co-glycolic acid) nanoparticles containing a ruthenium-based radiosensitizer were prepared, surface functionalized with human epidermal growth factor (hEGF) peptide and radiolabelled with [111]In. Nanoparticles were characterised by standard techniques. Cellular uptake was determined by intracellular radioactivity and inductively coupled plasma mass spectroscopy (ICP-MS) for ruthenium content. The impact of nanoparticle formulations on cell proliferation was determined by clonogenic survival. DNA damage response pathway (DDR) activation and γH2AX generation were assessed by immunoblotting and immunofluorescence. **Results:** [111]In radiolabelled hEGF-PLGA nanoparticles (130 nm diameter) are radiotoxic towards EGFR over-expressing oesophageal squamous cell carcinoma at a specific activity of 1 MBq/mL and greater, with minimal impact towards oesophagheal cancer cells with normal EGFR expression. Nanoparticle internalization was two-fold higher in EGFR-overexpressing versus normal cells and blocking with unlabelled hEGF confirms uptake to be EGFR-mediated. Increased levels of γH2AX foci correlate with radiotoxicity and DDR signalling indicates pChk1 and pChk2 generation, consistent with nanoparticle-conjugated ^{111}In activating both double-strand break and single-strand break repair pathways. The inclusion in the nanoparticles of a ruthenium-based intercalator

with comparable radiosensitizing effects as cisplatin, increases overall radiotherapeutic potency two- to five-fold. Quantification of γH2AX foci indicates enhanced DNA damage induced by dual-agent nanoparticles, equating to the sum of single-agent nanoparticle treatment groups. **Conclusions:** PLGA nanoparticles can be employed to co-deliver radiotoxic ^{111}In and a ruthenium-based radiosensitizer to achieve enhanced DNA damage and corresponding cytotoxicity in EGFR overexpressing oesophageal squamous carcinoma cells. These findings are rationalised by increased EGFR-mediated nanoparticle internalization and an additive relationship between the two DNA-damaging agents.

EP-60   **during congress opening hours, e-Poster Area**

Radionuclide Therapy & Dosimetry: MIBG & Peptides Therapy

EP-0800

Improving quality of life in patients with pancreatic neuroendocrine tumor following peptide receptor radionuclide therapy assessed by EORTC QLQ-C30

M. Marinova, M. Mücke, L. Mahlberg, M. Essler, H. Cuhls, L. Radbruch, R. Conrad, **H. Ahmadzadehfar**; *University Hospital Bonn, Bonn, GERMANY.*

Introduction: Neuroendocrine tumors (NETs) have proven to be appropriate neoplasms for peptide receptor radionuclide therapy (PRRT), as the majority of these slow-growing malignancies overexpress somatostatin receptors. As PRRT of pancreatic NET (P-NET) is still considered as an investigational treatment, the aim of this study was to evaluate changes in quality of life (QoL) of patients with P-NET following PRRT. **Methods:** Sixty-eight patients with P-NET (31 female, mean age 61.4 y) underwent PRRT: 12 with NET of grade 1, 40 of grade 2, 8 of grade 3 (grade non-available n=8). Prior to treatment 39 patients showed ECOG 0, 26 patients ECOG 1, and 3 patients ECOG 2. Clinical assessment included evaluation of QoL and symptom changes using standardized questionnaire (EORTC QLQ-C30) and was performed at baseline and every three months following each therapy cycle up to 12 months. **Results:** Up to four treatment cycles PRRT were performed in each patient with P-NET. The median cumulative administered activity was 28.2 GBq. Compared to baseline status, QoL was improved revealing increased global health status (3 months after 1st, 2nd, 3rd and 4th treatment cycle p=0.048, p=0.002, p<0.001, and p=0.008, respectively), emotional functioning (3 months after 1st-3rd cycle p=0.003, p=0.049, and p=0.001, respectively) and social functioning (3 months after 1st and 2nd p<0.001, after 3rd and 4th cycle p=0.015 and p=0.049, respectively). Furthermore, some symptoms were significantly alleviated compared with baseline: fatigue (after 1st-4rd cycle p=0.026, p=0.050, p=0.008 and p=0.029, respectively), nausea and vomiting (after 1st and 2nd cycle p=0.006 and p=0.001, respectively), dyspnea (after 3rd cycle p=0.025), appetite loss (after 1st-4th cycle p=0.010, p=0.001, p=0.009, and p=0.015, respectively), constipation (after 1st-3rd

cycle p=0.050, p=0.003, and p=0.060, respectively). **Conclusion:** PRRT is an effective treatment of P-NET improving QoL of patients in terms of increasing global health, emotional well-being and the mitigation of physical complaints.

EP-0801

I-131-mIBG therapy in high-risk neuroblastoma patients at end of induction chemotherapy

M. C. Schmidt[1], B. Hero[2], B. Decarolis[2], A. Eggert[3], F. Berthold[2], A. Drzezga[1], T. Simon[2]; [1]University Hospital of Cologne, Dpt. of Nuclear Medicine, Cologne, GERMANY, [2]University Hospital of Cologne, Dpt. of Pediatric Hemato-Oncology, Cologne, GERMANY, [3]Charité Berlin, Dpt. of Pediatric Hemato-Oncology, Berlin, GERMANY.

Introduction: Randomized trials on mIBG therapy in the first-line treatment of high-risk neuroblastoma are not available. Therefore, we analyzed the national neuroblastoma data base on the impact of I-131-meta-iodobenzylguanidine (mIBG) therapy, local radiotherapy, and single agent ch14.18 immunotherapy in the first-line therapy of high-risk neuroblastoma. **Patients and Methods** Patients of two consecutive national neuroblastoma trials were included if they met all key criteria: (1) stage 4 neuroblastoma, (2) age at diagnosis >18 months, (3) N5/N6 induction chemotherapy, (4) diagnosis between 1997 and 2014. mIBG therapy prior to the myeloablative chemotherapy was scheduled for non-progressing mIBG positive lesions. Local radiotherapy 36-40 Gy was delivered to unresectable mIBG positive residual at the primary site. Single agent ch14.18 immunotherapy was stratified according to open trials. **Results:** A total of 264 patients were included. The median observation time was 8.9 years. The presence of mIBG positive metastases at the end of induction chemotherapy was associated with inferior EFS (5yEFS 29.0+/-4.5% vs 41.3+/-4.1%, p=0.049). It had no impact on OS (5yOS 49.7+/-5.1% vs 51.2+/-4.2%, p=0.655). Among 108 patients with residual MIBG positive metastatic disease the EFS was similar between patients who underwent mIBG therapy (5yEFS 31.8+/-6.3%) and patients who did not (5yEFS 25.2+/-6.4%, p=0.238). The OS was better after mIBG therapy (61.2+/-6.6%) compared to no mIBG therapy (5yEFS 37.7+/-7.2%, p=0.038). Multivariable analysis of all 264 patients including the variables MYCN, mIBG therapy, local radiotherapy, and immunotherapy with ch14.18 revealed an independent impact of MYCN amplification (p=0.034, hr 1.445) and ch14.18 treatment (p<0.001, hr 0.455) on EFS, and MYCN amplification (p=0.001, hr 1.894) and ch14.18 treatment (p=0.001, hr 0.475) on OS. **Conclusion:** mIBG therapy can improve the outcome of high-risk neuroblastoma patients with incomplete metastatic response to induction chemotherapy. These results warrant a prospective multicenter trial on mIBG therapy. In addition, this analysis confirmed the long term effect of immunotherapy with ch14.18.

EP-0802

Phase 1/2 open-label trial to assess the safety and preliminary efficacy of ^{177}Lu-OPS201 as peptide receptor radionuclide therapy in patients with somatostatin receptor-positive, progressive neuroendocrine tumours

G. Nicolas[1,2], R. P. Baum[3], K. Herrmann[4,5], M. Lassmann[4], R. J. Hicks[6], A. R. Haug[7], S. Navalkissoor[2], H. Oberwittler[8], T. Wang[9], D. Wild[1]; [1]University of Basel Hospital, Basel, SWITZERLAND, [2]Royal Free Hospital, London, UNITED KINGDOM, [3]Zentralklinik Bad Berka, Bad Berka, GERMANY, [4]University Hospital Würzburg, Würzburg, GERMANY, [5]UCLA, Los Angeles, CA, UNITED STATES OF AMERICA, [6]Peter MacCallum Cancer Centre, East Melbourne, AUSTRALIA, [7]Medical University of Vienna, Vienna, AUSTRIA, [8]Ipsen, Les Ulis, FRANCE, [9]Ipsen, Cambridge, MA, UNITED STATES OF AMERICA.

Introductions: Peptide receptor radionuclide therapy (PRRT) with radiolabelled somatostatin receptor (SSTR) agonists is highly effective and has become an integral part of neuroendocrine tumour (NET) treatment. However, tumour uptake and tumour-to-tissue dose ratios may be higher with radiolabelled SSTR antagonists than agonists. OPS201 (DOTA-JR11) is a very promising next-generation SSTR antagonist selective for SSTR2 (expressed by NETs). This phase 1/2, international, single-arm, open-label study will evaluate ^{177}Lu-OPS201 as PRRT in 45 adults with unresectable, SSTR-positive, progressive gastroenteropancreatic (GEP)-NETs, lung NETs, phaeochromocytomas and paragangliomas. **Subject & Methods:** Patients are recruited at 15 study centres in Australia, Europe, and the US with experience in the use of PRRT (or other radionuclide therapy). The core trial comprises phases A and B. Phase A: six patients receive three cycles of [177]LuOPS201 at 4.5 GBq over 24 weeks; a further nine patients receive three cycles of [177]LuOPS201 at 4.5 GBq, or an activity not evoking dose-limiting toxicity, dependent on initial safety/dosimetry data. Phase B: 30 patients receive three cycles of [177]LuOPS201 at up to 7.4 GBq, dependent on phase-A safety/dosimetry data. In a subsequent long-term follow-up, tumour response (centrally reviewed [response evaluation criteria in solid tumours v1.1]) will be assessed using computed tomography/magnetic resonance imaging every 3 months from the end-of-core-trial visit for 2 years, or until progressive disease/death. This core study and long-term follow-up are together expected to last 42-45 months. **Results:** The primary endpoint is safety and tolerability (based on physical examination, vital signs, electrocardiogram, clinical laboratory measurements, adverse events, dose-limiting toxicities, concomitant medication, pituitary markers and bone marrow aspirate in case of persisting toxicities of grade 3 or more). Secondary endpoints include: biodistribution and pharmacokinetics (maximal uptake, area-under-curve, terminal half-life); radiation dosimetry; preliminary efficacy (tumour response, progression-free survival), and quality of life. Additional endpoints include: exploratory efficacy (tumour growth rate, tumour markers, and tumour micro-environment and markers in biopsies) and exploratory safety (DNA damage in lymphocytes and renal toxicity markers). As of April 2017, the first patient has been recruited. **Conclusions:** This study will provide important information regarding the safety and efficacy of the radiolabelled SSTR antagonist ^{177}Lu-OPS201 as PRRT in patients with SSTR-positive, progressive GEP-NETs, lung NETs, phaeochromocytomas and paragangliomas (EudraCT 2015-002867-41; NCT02592707). *Sponsored by Ipsen*

EP-0803

Association between uptake on ^{68}Ga-DOTATOC and ^{18}F-FDG PET/CT with uptake and mean absorbed dose on ^{177}Lutetium-SSA gamma imaging during PRRT

D. M. V. Huizing[1], E. A. Aalbersberg[1], C. Schuchardt[2], B. J. de Wit - van der Veen[1], I. Walraven[3], A. Singh[2], H. R. Kulkarni[2], M. P. M. Stokkel[1], R. P. Baum[2]; [1]Department of Nuclear Medicine, ENETS Center of Excellence, Netherlands Cancer Institute - Antoni van Leeuwenhoek, Amsterdam, NETHERLANDS, [2]THERANOSTICS Center for Molecular Radiotherapy, ENETS Center of Excellence, Zentralklinik Bad Berka, Bad Berka, GERMANY, [3]Department of Radiation Oncology, ENETS Center of Excellence, Netherlands Cancer Institute - Antoni van Leeuwenhoek, Amsterdam, NETHERLANDS.

Introduction: ^{177}Lutetium-labelled somatostatin analogues (^{177}Lu-SSA) are used in peptide receptor radionuclide therapy (PRRT) of neuro-endocrine tumours, enabling quantitative gamma imaging for dosimetry. Therapy is expected to be more effective in cases of high ^{68}Gallium-SSA (^{68}Ga-SSA) and low ^{18}F-fluoro-2-deoxyglucose (^{18}F-FDG) uptake on PET/CT, demonstrating high somatostatin receptor expression in well-differentiated tumours. In this study the association between diagnostic imaging, mean absorbed dose, and uptake was evaluated. **Materials and Methods:** 107 patients treated with ^{177}Lu-SSA between August 2004 and June 2016 at Zentralklinik Bad Berka with dosimetry in the first cycle of therapy were included. Whole-body planar imaging was performed 0.5, 3, 20, 45 and 68 h.p.i. with Mediso SPIRIT DH-V (MEGP collimator, 208 keV photopeak, 15% energy window, 15 cm/min). A maximum of five tumour lesions per patient were selected for dosimetry. The time-activity curve, uptake (mSv/MBq) and mean absorbed dose (Gy) were fitted using ORIGIN PRO 8.1G and calculated by OLINDA/EXM. SUVmax, SUVpeak, and Bq/ml were measured in the same lesions on both ^{68}Ga-DOTATOC and ^{18}F-FDG PET/CT scans, prior to- and within 6 months after PRRT. Univariate linear mixed modelling was applied to determine the association between diagnostic imaging parameters, uptake in percentage of injected activity at 20hours post-injection, and mean absorbed dose. For ^{68}Ga-DOTATOC analysis (n = 73) only patients treated with ^{177}Lu-DOTATOC were included, and for ^{18}F-FDG analysis (n = 72) patients treated with any ^{177}Lu-SSA were included. Different models were constructed to account for potential influencing effects of intra-patient correlation and organ location. Random intercepts and slopes were examined to assess model improvement. The fit of the models was compared using the Likelihood ratio test. For one point increased uptake in diagnostic imaging, the estimate B represents the increase in ^{177}Lu-SSA uptake or dose. **Results:** 192 ^{68}Ga-DOTATOC lesions and 125 ^{18}F-FDG lesions were analysed. Both SUVmax [B 0.011 (95% CI 0.003 to 0.019)] and the highest quartiles of SUVpeak 24.9 to 78.94 [(B 0.000 (95% CI 0.483 to 1.622)], Bq/ml max 2.16×10^4 to 7.82×10^4 [(B 0.020 (95% CI 0.094 to 1.071)], and Bq/ml peak 1.74×10^4 to 9.19×10^4 [(B 0.004 (95% CI 0.227 to 1.160)] of ^{68}Ga-DOTATOC were significantly associated with an increased uptake of ^{177}Lu-DOTATOC. All ^{18}F-FDG parameters were not associated with ^{177}Lu-SSA accumulation. **Conclusion:** SUVmax, SUVpeak, and Bq/ml of ^{68}Ga-DOTATOC PET/CT, but not of ^{18}F-FDG PET/CT imaging, were significantly associated with an increased uptake of ^{177}Lu-DOTATOC, thus suggesting pre-therapy uptake prediction on a lesion basis.

EP-0804

Quality of Life Improvements in Patients with progressive Midgut Neuroendocrine Tumors: the NETTER-1 Phase III Trial

J. Strosberg[1], E. Wolin[2], B. Chasen[3], M. Kulke[4], D. Bushnell[5], M. Caplin[6], R. P. Baum[7], P. Kunz[8], T. Hobday[9], A. Hendifar[10], K. Öberg[11], M. Lopera Sierra[12], P. Ruszniewski[13], E. Krenning[14]; [1]Moffitt Cancer Center, Tampa, FL, UNITED STATES OF AMERICA, [2]Montefiore Einstein Center for Cancer Care, Bronx, NY, UNITED STATES OF AMERICA, [3]The University of Texas MD Anderson Cancer Center, Houston, TX, UNITED STATES OF AMERICA, [4]Dana-Farber Cancer Institute, Boston, MA, UNITED STATES OF AMERICA, [5]University of Iowa, Iowa City, IA, UNITED STATES OF AMERICA, [6]Royal Free Hospital, London, UNITED KINGDOM, [7]Zentralklinik, Bad Berska, GERMANY, [8]Stanford University Medical Center, Stanford, CA, UNITED STATES OF AMERICA, [9]Mayo Clinic College of Medicine, Rochester, MN, UNITED STATES OF AMERICA, [10]Cedars Sinai Medical Center, Los Angeles, CA, UNITED STATES OF AMERICA, [11]University Hospital, Uppsala University, Uppsala, SWEDEN, [12]Advanced Accelerator Applications, New York, NY, UNITED STATES OF AMERICA, [13]Hopital Beaujon, Clichy, FRANCE, [14]Erasmus Medical Center, Rotterdam, NETHERLANDS.

Aims: Neuroendocrine tumor progression is associated with deterioration in quality of life, both due to tumor and hormone-related symptoms. We aim to determine the impact of treatment on time to clinically relevant change (deterioration) in health-related quality of life (HRQoL). **Materials:** The NETTER-1 trial is an international phase III study which enrolled patients with progressive, somatostatin receptor positive midgut neuroendocrine tumors. Patients were randomized to receive treatment with ^{177}Lu-DOTATATE (^{177}Lu; Lutathera) versus high-dose (60 mg) Octreotide LAR (Oct). EORTC questionnaires QLQC-30 and G.I.NET-21 were assessed during the trial to determine the impact of treatment on HRQoL. Methods: Patients completed EORTC QLQC-30 G.I.SNET-21 questionnaires at baseline and every 12 weeks thereafter until progression was centrally confirmed. QoL scores were converted to a 100-point scale according EORTC instructions and individual changes from baseline scores were assessed. The time to deterioration was defined as the time (in months) between randomization and the first QoL deterioration ≥10 points for each patient in the corresponding domain scale. This magnitude of variation was considered clinically relevant. **Results:** Time to QoL deterioration was significantly longer in the ^{177}Lu-DOTATATE arm vs the control arm for the following domains: global health status (hazard ratio (HR) 0.406; p=0.0006), physical functioning (HR 0.518; p=0.0147), role functioning (HR 0.580; p=0.0298), fatigue (HR 0.621; p=0.0297), pain (HR 0.566; p=0.0247), diarrhea (HR 0.473; p=0.0107), disease related worries (HR 0.572; p=0.0176) and body image (HR 0.425; p=0.0058). In the other domains time to deterioration did not reach statistical significance be-

tween the arms. **Conclusions:** This analysis demonstrates that ^{177}Lu-DOTATATE provides a significant quality of life benefit for patients with progressive midgut NETs compared to high-dose octreotide, in addition to the meaningful increase in progression-free survival already reported. **Keywords:** ^{177}Lu-DO-TATATE, PRRT, NET, Quality of Life

EP-0805

Monte Carlo Based SPECT Activity Quantification and Tumor Dosimetry for 177Lu-DOTATATE Treatments

l. Marin[1], J. Svensson[2], T. Rydén[1], E. Wikberg[1], A. Elf[3], V. Johansson[3], P. Bernhardt[1]; [1]Department of Radiation Physics, Gothenburg, SWEDEN, [2]Department of Oncology, Gothenburg, SWEDEN, [3]Department of Surgery, Gothenburg, SWEDEN.

Aim: Peptide receptor radionuclide therapy (PRRT) with ^{177}Lu-DOTATATE has shown to be an effective palliative treatment for neuroendocrine tumors. [177]Lu emits primarily electrons, but also photons, which enable gamma camera imaging. Dosimetric calculations are generally performed only for risk organs using planar gamma camera images. Estimations of the absorbed dose to tumors are normally not made. This work aims to estimate absorbed dose to neuroendocrine tumors and to investigate the tumor dose response relationship. Establishing such a relationship could aid in the selection of patients suited for treatment with ^{177}Lu-DOTATATE. **Method:** Neuroendocrine tumors were identified and measured in 51 patients by a radiologist according to the response evaluation criteria in solid tumors (RECIST). Out of these, 24 patients were possible to include in the study. Planar imaging was performed at day 0, 1, 2 and 7 after ^{177}Lu-DOTATATE infusion and single photon emission computed tomography (SPECT) at day 1. SPECT images were reconstructed using Sahlgrenska Academy Reconstruction code (SARec), which is an iterative method using Monte Carlo simulated forward projection. Tumors were segmented manually in single photon emission computed tomography/computed tomography (SPECT/CT) and planar gamma camera images. In 7 patients, manual segmentation was compared with an automated 42% thresholding method by determining a ratio between the doses acquired using each method. SPECT was used for absolute activity quantification and planar images for determining the biokinetics of the radionuclide in each patient. Absorbed dose was calculated by presuming local energy deposition by electrons. **Results:** The mean tumor absorbed dose and specific mean tumor absorbed dose (mean tumor absorbed dose per injected activity) were 65 Gy and 2.5 mGy/MBq, respectively. The mean and median ratios between doses acquired using a 42% threshold segmentation and manual and were 4.7 and 2.0 respectively. No significant correlation between absorbed tumor dose and tumor response could be established. **Conclusions:** Automated tumor segmentation resulted in larger doses than manual segmentation. The method for segmentation thus greatly affects dose estimation and needs to be further investigated. No correlation between absorbed dose to tumors and tumor response could be established in this study.

EP-0806

Haematological toxicity in patients with somatostatin receptor positive tumours showing high bone and bone marrow involvement treated with 177Lu-Dotatate

M. Cremonesi[1], M. E. Ferrari[1], L. Bodei[2], F. Botta[1], M. Colandrea[1], S. M. Baio[1], P. A. Rocca[1], G. Prisco[1], G. Buonsanti[1], D. Militano[1], C. Garibaldi[1], R. Orecchia[1], C. M. Grana[1]; [1]Istituto Europeo di Oncologia, Milano, ITALY, [2]Memorial Sloan Kettering Cancer Center, New York, NY, UNITED STATES OF AMERICA.

Aim: Therapy with 177Lu-DOTATATE shows generally low incidence of bone marrow (BM) toxicity. BM uptake is typically negligible from NM images, leading to cumulative absorbed doses <2Gy. However, patients with high Bone and BM (B-BM) involvement show anomalous biodistribution with very high B-BM uptake, raising doubts about tolerability. The aim of this study was to assess toxicity in such patients and to estimate B-BM uptake. **Methods:** Whole body(WB) images of patients treated with 177Lu-DOTATATE were acquired at 24h p.i. Images were visually selected and included in the study for B-BM uptake >5% of the total image. ROIs were drawn around source organs and muscle (representative of the remainder-of-the-body, RB). B-BM uptake was determined by subtraction of source organs and RB counts from WB. One patient underwent a complete dosimetry study (imaging at: 2,24,50,170h). Haematological toxicity (WBC,Hb,PLT) was evaluated (CTCAE-4.0), every 2 weeks up to 2 months after last cycle, and every 3 months later on. **Results:** Images from 19 NET (9 GEP; 8 lung, 1 thymoma, 1 unknown origin) out of 557 patients corresponded to selection criteria. Patients received multiple cycles with mean(SD) activity of 17(12) GBq, range 2-42 GBq. Mean(SD) follow-up lasted 18(13) months, range 2-37. The mean(SD) uptake% normalised to image at 24h were: B-BM: 23(13), range:6-47%; kidneys: 7(4)%; RB: 45(14)%. The dosimetry analysis gave an effective half-life for B-BM lesions of 95h, and WB image at 24h was 30% of the injected activity, comparable with 34% obtained from another dosimetry study. Applying these hypotheses, the mean(SD) uptake% at 24h normalised to injected activity were: B-BM: 8(5)%, range:2-16%; kidneys: 3(1)%; RB: 15(5)%. The extrapolated time-integrated activity coefficient for B-BM was: mean(SD)= 10.5(6.2)h, possibly distributed in BM(50%) and bone(trabecular 25%; cortical 25%). Nonetheless, the step of estimating the BM absorbed dose based on uniform activity distribution was not applicable. Toxicity was almost always of grades G1 (WBC=42%, Hb=53%, PLT=37%) and G2 (WBC=21%; Hb=26%, PLT=5%). Only 3 patients manifested transient G3-G4 toxicity, and had 11% (WBC,G3), 41% (PLT,G3), and 45% (PLT,G4) of B-BM uptake at 24h. No myeloproliferative diseases (myelodysplastic syndrome, acute leukaemia) were observed. **Conclusion:** Haematological toxicity in patients with high B-BM involvement is acceptable (G1,G2) in the majority of cases, indicating 177Lu-DOTATATE treatments as feasible. This is most probably due to the low range of 177Lu beta-particles in B-BM and to the uptake inhomogeneity, which does not allow to derive BM mean dose estimates compatible with G1-G2 toxicities.

EP-0807

A long term efficacy of PRRT in patients with advanced, non-resectable paraganglioma/pheochromocytoma tumours, related to SDHx gene mutation

A. D. Kolasińska-Ćwikla[1], M. Pęczkowska[2], I. Michałowska[2], A. Lewczuk[3], L. Bodei[4], M. Kidd[5], I. M. Modlin[6], **J. B. Ćwikła[7]**; *[1]MSC Memorial Cancer Centre and Institute Maria Sklodowska-Curie, Warsaw, POLAND, [2]Institute of Cardiology, Warsaw, POLAND, [3]Medical University of Gdansk, Gdańsk, POLAND, [4]Memorial Sloan Kettering Cancer Centre, New York, NY, UNITED STATES OF AMERICA, [5]Wren Laboratories, Branford, CT, UNITED STATES OF AMERICA, [6]Yale University, New Haven, CT, UNITED STATES OF AMERICA, [7]Faculty of Medical Sciences, University of Warmia and Mazury, Olsztyn, POLAND.*

Purpose: To evaluate the clinical effectiveness of PRRT (^{90}Y DOTA0, D-Phe1, Tyr3]-octreotate), based on overall survival (OS) and progression-free survival (PFS), in patients with extensive paraganglioma-pheochromocytoma (PGL), related to SDHx gene mutation. **Materials and Methods:** 12 patients with histologically proven PGL with SDHx genetic mutations, 6 with SDHD (PGL1) and others with SDHB (PGL4). All patients had advanced, non-resectable, hormonally active, progressive tumours base on radiology/clinically/biochemically criteria, 8 of them had distant metastases. All subjects were treated i.v. [90]Y DOTATATE, mean activity 8.1GBq (range 3,7-14.8). Clinical responses were assessed 6 weeks after completing therapy and then after each of the 6-month intervals. The efficacy of PRRT was evaluated base on OS and PFS (KaplanMeier estimator), radiological response was based on RECIST 1.0. Hormonal active tumours were evaluated using serum fractionated free catecholamines: normetanephrine, metanephrine and metoxy-tyramine **Results**: Initially, there were 8 secretor tumours, with elevated free plasma catecholamines, after therapy 6 (75%) had normalization. Six Months after PRRT, 8 subjects had a clinical response, the rest (n=2) were stable (SD) or exhibited disease progression n=2 (DP). There was significant difference between clinical stage performance status - PS (ECOG/Karnofsky) before, 6 weeks and 6 months after PRRT. Median OS for all subjects was 74.5 months (CI 40.5-98.8), PFS 47.5 months (CI 26.7-90.6). Median OS and PFS were not significantly different between male and female 80 vs. 68 and 60 vs. 35 months (Cox-Mantel P>0.05). Significantly longer median OS were noted between patients with PGL1 compared to subjects with PGL4 median OS 119.5 vs. 24 months, (P=0.01); PFS was also significant 119 vs. 12 months, (P=0.0036). There was significant difference in OS in those patients who respond clinically on PRRT (evaluated after 6 M), compare to those who has SD or DP, median OS 102.0 vs. 22.5 months (P=0.0018). Also there was significant difference in patients with distant metastases compare to those without. Median OS 27.5 vs. 124.5 months (P=0.029) and median PFS 15.5 vs. 124.5 months (P=0.003). **Conclusions**: PRRT is a very effective therapy in selected population of patients with germline mutation of SDHx, in those with locally advanced, non-resectable tumours, especially in patients with PGL1. Furthermore, it is effective in patients with secretory and non-secretory tumours.

Patients who respond clinically on PRRT had better prognosis. In those patients with PGL4 and those with distant metastases, PRRT could be used as an option, but the clinical efficiency is uncertain.

EP-0808

Red Bone Marrow Dosimetry and Haematotoxicity in 177Lu-DOTATATE PRRT

S. Tshori[1], *S. Glasberg[2], D. Luder[2], Y. Krausz[2], D. Gross[2], A. Schwartz[2], N. Freedman[2,3]; [1]Kaplan Medical Center, Rehovot, ISRAEL, [2]Hadassah Hebrew University Medical Center, Jerusalem, ISRAEL, [3]Tel Aviv Sourasky Medical Centre, Tel Aviv, ISRAEL.*

Introduction: Lu177-DOTATATE PRRT is an important treatment modality for patients with neuroendocrine tumours (NET's), becoming more widely available. Lu177-DOTATATE is administered as an intravenous infusion of a standard dose of 7.4 GBq, repeated at intervals of 5-8 weeks. Unlike external beam radiotherapy, radiation dose in PRRT is not planned in advance, but can be calculated after each treatment. Dosimetry may be useful for planning ongoing serial treatments to deliver sufficient tumour dose, while avoiding radiation damage to kidneys and/or red bone marrow (RBM). More data is needed to standardize dosimetry and to understand its impact on patient treatment. **Subjects and Methods:** 151 NET patients received 446 PRRT treatments (range 1-7 treatments) in Hadassah Medical Centre between 2011 and 2016. Serial post-therapy SPECT/CT and planar whole body images were acquired on GE Discovery 670. Dosimetry data were extracted using GE Dosimetry Toolkit, and processed using an in-house IDL application using OLINDA to calculate absorbed doses. RBM self-dose was calculated from activity in serial blood samples. **Results:** Tumour and organ absorbed doses were highly variable between patients, and the distribution was not normal. Liver and kidney doses significantly decreased (p<0.0001 and 0.0004, respectively) from first to second treatment. The reason for this is unknown. However, slight increase in spleen dose and only slight decrease in RBM dose with borderline significance were observed (p=0.0418 and 0.0367, respectively). Mild neutropenia was observed in one patient, while incidence of moderate thrombocytopenia increased from 1.6% before treatment to 15.8% after 3rd treatment. Cumulative dose after 4 treatments (n=60) was 0.315 Gy (IQR 0.229-0.423, maximum 1.294), lower than the current 2 Gy limit, partly because treatments were stopped earlier in patients with high RBM dose. No correlation was found between RBM dose and either neutropenia or thrombocytopenia. Surprisingly, highly significant correlation was found between age and RBM dose for first treatment (Spearman's r(131)=0.344, p=0.0001). RBM dose for patients younger than 50 (n=29) was 0.084 Gy (IQR 0.061-0.107), and for patients over 70 (n=26) was 0.173 Gy (IQR 0.118-0.214), respectively. **Conclusion:** Dosimetry requires considerable resources in terms of camera and technologist time, Nuclear Medicine physicians and physicists, as well as patient cooperation. However, our results indicate that dosimetry provides an important contribution to optimizing personalized PRRT. Our results also raise questions regarding the biology of

organs under internal radiation. Most patients can safely undergo more than 4 treatments, but special attention might be required for older patients.

EP-0809

Safety, Biodistribution, and Efficacy of ⁶⁷Cu-SARTATE targeted therapy in somatostatin receptor expressing tumours in mice

E. M. van Dam[1], C. M. Jeffery[1], J. L. Stoner[2], A. V. Hedt[1], M. J. Harris[1]; [1]Clarity Pharmaceuticals, Sydney, AUSTRALIA, [2]Idaho State University, Pocatello, ID, UNITED STATES OF AMERICA.

Introduction: Over the past decade, radiolabelled somatostatin analogues such as octreotate have been developed and show promise for diagnosis, staging, prognosis, therapy, and monitoring response to treatment in neuroendocrine tumours (NETs) and in other cancers expressing the somatostatin receptor (SSTR). The diagnostic imaging radionuclide can be replaced with a therapeutic radionuclide in what is referred to as a "theranostic". For many years copper isotopes have been discussed as the "perfect pairing" for a theranostic tracer due to the ideal characteristics of two isotopes, Cu-64 and Cu-67. Cu-64 enables precise biopharmaceutical imaging due to its half-life of 12.7 hours, thus producing images at suitable time points for biologics, for studying changes in biodistribution over time and for prospective dosimetry estimations using PET imaging. Cu-67 has similar energy characteristics to other therapy isotopes in current use, however, the shorter half-life of 61.8 hours provides greater flexibility for optimally dosing tumours and reducing potential side-effects. ⁶⁴Cu-SARTATE, consisting of a bifunctional chelator, MeCOSar, conjugated to (Tyr³)-octreotate, has been successfully trialled as an imaging agent and dosimetry tool in ten patients diagnosed with NETs. **Methods**: To progress ⁶⁷Cu-SARTATE as a therapeutic in clinical trials, preclinical safety, efficacy, and biodistribution studies were performed. To determine the intravenous repeat dose toxicity, mice were administered 4 weekly doses of Cu-SARTATE at either 0, 0.2, 1 or 2mg/kg. Furthermore, the effect of a single administration of ~21 MBq of ⁶⁷Cu-SARTATE on the health and behaviour of mice was determined. For biodistribution and efficacy studies, a small cell lung cancer (SCLC) xenograft mouse model with high expression of SSTR2 was used. To determine efficacy, a single dose of ⁶⁷Cu-SARTATE, varying from 5 to 30 MBq, was administered to mice bearing NCI-H69 SCLC xenografts. Furthermore, to allow for prospective dosimetry calculations, the biodistribution of ⁶⁴Cu-SARTATE and ⁶⁷Cu-SARTATE in NCI-H69 tumour bearing mice was compared directly. **Results**: Repeat administration of Cu-SARTATE showed no significant toxicities except for transient clinical signs in females at the 2 mg/kg dose levels. Furthermore, ~21 MBq of ⁶⁷Cu-SARTATE was well tolerated and caused no adverse effects in healthy mice. The uptake of SARTATE in the tumour was good, with low background in the liver and clearance through the kidney. The results of the ⁶⁷Cu-SARTATE efficacy and biodistribution studies in tumour bearing mice show promise as a therapeutic agent. **Conclusions**: ⁶⁷Cu-SARTATE has a good safety profile and shows promise as a therapeutic agent to treat SSTR2 expressing cancers.

EP-0810

Treatment of 28 Paragangliomas with 177Lu-octreotate based PRRT

*D. Smit Duijzentkunst, **T. Brabander**, J. Hendriks, A. van Linge, R. Feelders, R. Oldenburg, E. Krenning, D. Kwekkeboom, W. de Herder; Erasmus MC, Rotterdam, NETHERLANDS.*

Introduction: Paragangliomas (PGL) are a heterogeneous group of rare tumours that can express high numbers of somatostatin receptors on their cell surface and can be targeted with peptide receptor radionuclide therapy (PRRT) using the radiolabelled somatostatin analogue [lutetium-177-DOTA-Tyr3-] octreotate (177Lu-octreotate). **Materials and Methods:** From a larger cohort treated with PRRT, all Dutch patients with histologically proven inoperable or metastatic PGL were selected. The intended dose of 177Lu-octreotate was 4x 7.4 GBq, administered with intervals of 6-12 weeks. Data were prospectively registered, Kaplan-Meier analysis was used to express survival. **Results:** Eleven patients with extra-adrenal (EA) and 17 with head and neck (HN) PGL received a total of 104 administrations. No severe (sub-)acute bone marrow or kidney toxicity was observed. A subacute, mild adverse event due to catecholamine release occurred in one patient. Best tumour response (RECIST 1.1) was partial response in 6 (21%), stable disease in 18 (64%) and progressive disease in 4 (14%) patients. Disease control was observed in 15 out of 19 (79%) patients with progressive disease at baseline. Median progression free survival was 30 months for all patients; 14 in EA-PGLs versus not reached in HN-PGL (median follow-up 49 months). **Conclusion:** This study shows that PRRT is a safe and effective treatment for inoperable or metastatic PGL, and supports the implementation of PRRT into the treatment algorithm.

EP-0811

Siopen Scoring System to quantifying response to 131-MIBG metabolic treatment in HR-NB relapse: review of local experience

C. Olianti[1], P. Saletti[2], G. Simontacchi[3], A. Tondo[4]; [1]Nuclear Medicine Unit - Careggi University Hospital, Florence, ITALY, [2]Health Physic Unit, Careggi University Hospital, Florence, ITALY, [3]Radiotherapy Unit, Careggi University Hospital, Florence, ITALY, [4]OncoHematology Unit, Meyer University Hospital, Florence, ITALY.

Aim: Semi-quantitative Curie-scoring system used for quantifying the extension of disease and treatment-response in patients with high-risk neuroblastoma treated with high-activity of 131I-mIBG : review of our local experience. **Material and Methods:** Between November 2009 and February 2017, seven children (mean+/-SD age : 4+/-1,2 years) 6 with mIBG-avid high-risk neuroblastoma relapse and 1 child with mIBG-avid un-resectable NB were treated with high-activity 131I-mIBG radiometabolic therapy for a total number of treatment performed 12, range 1-4, median 1. All children underwent two diagnostic 123I-mIBG scans before and 1-2 month after completing the treatment, and 131I-mIBG post-therapy scans with-

in 7-10 days. All scans were reviewed by two independent expertise nuclear medicine physicians using semi-quantitative Curie-scoring system that includes evaluation of 10 anatomic regions with the scoring of each site (0-3) based on the extent of disease. **Results:** The administered activity range was 0,44-0,66 GBq/kg, mean activity was $0,5 \pm 0,1$ GBq/kg, cumulative administered activity was $7,8 \pm 1,7$ GBq. One patient with HR-NB relapse was treated on the basis of proposed Veritas Protocol using a first 131I-mIBG activity of 0,44 GBq/kg administered, cumulative administered activity was 10,6 GBq, obtaining a whole-body absorbed-radiation dose of 2,24 Gy. A contemporary dosimetric study was performed in order to calculate a whole-body absorbed-radiation dose and to estimate the required activity for the second 131I-mIBG treatment with the target to deliver a combined whole body radiation dose of 4 Gy. The second treatment performed after 60 days employed 131 I-mIBG activity of 0,4 GBq/kg, cumulative administered activity of and 9,6 GBq, so to obtain one 1,99 Gy adsorbed dose. Totale absorbed dose was 4,2 Gy. Qualitative assessment of mIBG scans demonstrate a scintigraphic response rate (complete + partial response, CR+PR) in all patients with CR in 1 and PR in 6 out of 7 patients. Semi-quantitative assessment demonstrates overall 63 % reduction of Curie-scores (non-parametric Wilcoxon rank test showed a significative difference p <0,03) between Curie-score pre-and post therapy 123I-mIBG scans. The last patient with important pulmonary relapse, as multiple nodules, had a very good partial response, a dimensional reduction about of 70% of estension of disease respect pre-treatment 123I-MIBG. The procedure was well tolerated by all the patients without necessity of recovery in Pediatric-Hospital nor hemo-transfusions. Nevertheless today 5 of them died for progression of disease, 2 are still alive, the one treated for unsesectable-NB without evidence of disease.

EP-0812

Outcome of Lutetium DOTANOC therapy in metastatic neuroendocrine tumor: Preliminary experience

P. K. Pradhan, D. Datta, S. Gambhir, A. Mishra, A. Agarwal; SGPGIMS, Lucknow, INDIA.

Introduction: Peptide receptor radionuclide therapy (PRRT) is a systemic treatment for well differentiated metastatic NET, exploiting the abundance of SSTRs, especially sst2. **Objective:** To evaluate the outcome of Lu177 DOTANOC therapy **Subjects and Methods:** 13 patients of proven NET of different tissue origins [GEP carcinoid-1 (7%), NET unknown origin 04 (32.5%), gastrinoma 01 (7%), pancreatic NET 01(7%), VHL-01(7%), Poorly differentiated carcinoma thyroid 01(7%), Medullary carcinoma thyroid 04(7%)] were treated with 1-4 cycles of Lutetium -177 DOTANOC therapy. **Results:** The outcome was evaluated using change in the tumor-specific biomarkers, QoL scores (EORTC), KPS and blood parameters. Each of the QoL scores and KPS at the baseline were compared with the scores after each cycle. Hence, change in the scores (negative or positive) after each cycle was evaluated and categorized as < -20 ; (-20)- (-10) ; (-10)- (-5) ; (-5 to 5) , 5-10, 10-20 and > 20

and were assumed for the subjective change in the quality of life. All patients had received 150 to 200 mCi of 177Lu-DOTA-NOC in each cycle and followed up within 3 (range: 02-04) months. Medians scores at baseline and after each cycle of PRRT were compared with each using Wilcoxon-signed rank test. 07 out of 13 patients died during the course of treatment of which 2 were MCT with extensive sclerotic skeletal metastasis, 3 patients had anterior mediastinal NET of unknown origin with skeletal metastasis, 1 patient had VHL syndrome (post cerebellar tumor excision) and 1 patient had gastric fundal NET with extensive nodal and cerebral metastasis. There was no significant difference noted in any of the sub-scores (comprising QoL) after any cycle, except for the improvement in the global- health score after the 2nd cycle (p-0.03). **Conclusion:** Its noted that global health score improved following minimum two cycles of Lu 177 DOTANOC therapy that those patients with skeletal involvement were having increase incidence and persistence of thrombocytopenia and mortality in comparison to those without skeletal involvement. Thus, it seems, Lutetium -177 DOTANOC therapy can be used with caution in NETs with skeletal involvement as none showed clinical or biochemical improvement.

Radionuclide Therapy & Dosimetry: Radioimmunotherapy (RIT)

EP-0813

SUVmax predicts survival in patients with diffuse large B-cell lymphoma who received radioimmunotherapy using ^{131}I-rituximab as consolidation therapy

J. Choi[1], I. LIM[1], B. Byun[1], B. Kim[1], C. Choi[1], S. LIM[1], D. Shin[2], H. Kang[1]; [1]Korea Cancer Center Hospital, Korea Institute of Radiological and Medical Sciences, Seoul, KOREA, REPUBLIC OF, [2]Seoul National University Hospital, Seoul, KOREA, REPUBLIC OF.

Purpose: We evaluated the prognostic value of ^{18}F-FDG-PET/CT for patients with diffuse large B-cell lymphoma (DLBCL) after ^{131}I-rituximab consolidation therapy. **Methods:** The patients who achieved complete response after six to eight cycles of R-CHOP (rituximab, cyclophosphamide, vincristine, doxorubicin, and prednisolone) with advanced stage (Ann Arbor III or IV) or bulky stage II DLBCL were recruited in this study. They received radioimmunotherapy (RIT) as consolidation treatment. ^{18}F-FDG-PET/CT scans were performed before the R-CHOP as initial staging. The Mann-Whitney test was used for comparing the difference of SUVmax in each group. Receiver-operating characteristic curves (ROCs) of SUVmax were calculated and the areas under the curves (AUCs) were applied for assessing the optimal cut-off values of SUVmax. Kaplan-Meier curve survival analysis was performed after dividing the patients using the cutoff values of SUVmax. **Result:** A total of 15 patients (M: F = 12: 3, Age: 55 ± 12) were enrolled. All the fifteen patients underwent consolidation RIT after complete response. Among them, 4 patients were relapsed and 4 patients died during follow up. The median value

of relapse free survival was 59 months (range 1-108), and overall survival was 64 months (range 11-108). The patients without relapse showed higher SUVmax than the patients with relapse (23.1 vs. 12.7, p = 0.021). ROC curve analysis revealed that SUVmax of 13.2 at initial stage was a cut off value for determining whether the patients relapsed or not (AUC 0.944; sensitivity / specificity; 100% / 92%; p < 0.0001). Patients with lower SUVmax showed worse overall survival (65 M vs. 40M, p = 0.0001) and worse relapse free survival (43 M vs 27 M, p = 0.002) than patients with higher SUVmax. **Conclusion:** Higher SUVmax at the initial staging ^{18}F-FDG PET/CT demonstrated better survival in the patients with DLBCL after RIT consolidation following R-CHOP. Initial ^{18}F-FDG PET/CT can stratify the patients with DLBCL after RIT consolidation following R-CHOP in terms of prognosis.

EP-0814

FDG uptake at baseline may predict absorbed dose in tumor lesions in indolent Non-Hodgkin lymphoma patients treated With the novel antibody-radionuclide-conjugate 177Lu-lilotomab satetraxetan

A. Londalen[1,2], J. Blakkisrud[2], J. Dahle[3], M. Revheim[1,4], H. Holte[5], A. Kolstad[5], C. Stokke[2,6]; [1]Division of Radiology and Nuclear Medicine, Oslo University Hospital, Oslo, NORWAY, [2]Department of Diagnostic Physics, Oslo University Hospital, Oslo, NORWAY, [3]Nordic Nanovector ASA, Oslo, NORWAY, [4]Faculty of Medicine, University of Oslo, Oslo, NORWAY, [5]Department of Oncology, Radiumhospital, Oslo University Hospital, Oslo, NORWAY, [6]Oslo and Akershus University College of Applied Science, Oslo, NORWAY.

Aim: ^{177}Lu-lilotomab satetraxetan is a novel anti-CD37 antibody-radionuclide-conjugate (ARC) under development for treatment of indolent non-Hodgkin lymphoma. Four different treatment regimens have been investigated in a dose escalating phase 1 study. Patients in arm 1 and 4 received cold lilotomab as pre-dosing; 40 mg fixed and 100 mg/m^{2}, respectively, on the same day as ^{177}Lu-lilotomab satetraxetan, while patients in arm 2 and 3 did not. Administered activity of ^{177}Lu-lilotomab satetraxetan was 10, 15 or 20 MBq/kg. FDG PET/CT imaging was performed at baseline, and at 3 and 6 months after treatment. The aim of this work was to investigate correlations between baseline FDG uptake and tumour absorbed dose at the lesion level. **Material and Methods:** In eleven patients, a total of 33 lesions were eligible for tumour dosimetry (1-5 lesions/patient). Lesions were included based on visual identification on low dose CT and activity on SPECT. Tumour absorbed doses were determined from SPECT/CT images obtained at different time points. Peak standardized uptake value (SUV_{peak}) according to EANM procedure guidelines for tumour imaging:version 2.0 at baseline PET/CT were registered for each lesion. Based on pre-dosing, patients were separated into two groups: lilotomab(+) and lilotomab(-), with and without pre-dosing respectively. Tumours were further grouped into two as, "high" and "low" FDG-avid tumours based on the SUV_{peak} 50% percentile cut-off and the absorbed dose was corrected for ARC dosage. **Results:** Mean SUV_{peak} for all lesions at baseline was 7.34 (range 3.5 - 12.3). Mean dosage-corrected tumour absorbed doses for the lilotomab(+) group were 19.2 and 25.7 cGy/(MBq/kg) for tumours with

high and low-SUV_{peak}, respectively (P = 0.34). For the lilotomab(-) patients the mean absorbed tumour doses were 12.3 and 20.2 cGy/(MBq/kg) for high and low-SUV_{peak} tumours respectively (P = 0.18). **Conclusion:** A tendency towards higher absorbed doses in tumours with low FDG uptake at baseline PET/CT was observed. The difference seemed to decrease when pre-dosing with cold lilotomab before ^{177}Lu-lilotomab satetraxetan treatment was given. This may indicate that pre-dosing increases the availably of ^{177}Lu-lilotomab satetraxetan for tumours and evens out the difference in relative absorbed doses between high and low FDG avid lesions.

EP-62 during congress opening hours, e-Poster Area

Radionuclide Therapy & Dosimetry: Thyroid

EP-0815

Effect of selenium supplement for protection of salivary glands from I-131 radiation damage in patients with differentiated thyroid cancer

J. Lee[1], H. Son[1], S. Lee[2]; [1]Catholic Kwandong University College of Medicine, Incheon, KOREA, REPUBLIC OF, [2]Soonchunhyang University Hospital, Cheonan, KOREA, REPUBLIC OF.

Purpose: The aim of this study was to examine whether selenium supplementation during I-131 treatment had a radio-protective effect for salivary glands in patients with differentiated thyroid cancer. **Subjects & Methods:** Sixteen patients with differentiated thyroid cancer were prospectively enrolled in the study. All patients underwent total thyroidectomy and were scheduled to undergo high-dose I-131 treatment. Enrolled patients were divided into two groups before I-131 treatment; 8 patients in the selenium group and 8 patients in the control group. Patients in the selenium group received 300 μg of selenium orally for 10 days, from 3 days before to 6 days after I-131 treatment. The control group received a placebo over the same period. To assess salivary gland function, salivary gland scintigraphy was performed before and 6 months after I-131 treatment. Serum amylase and whole blood selenium levels were measured before and 2 days and 6 months after I-131 treatment. Using salivary gland scintigraphy, maximum uptake ratio (MUR), maximum secretion percentage (MSP), and ejection fraction (EF) of each salivary gland were calculated. **Results:** Baseline clinical characteristics, baseline amylase and selenium levels, and parameters of baseline salivary gland scintigraphy were not significantly different between selenium and control groups (p>0.05). On a blood test performed 2 days after I-131 treatment, the selenium group showed a significantly higher whole blood selenium level (p=0.008) and significantly lower serum amylase level (p=0.009) than the control group. On follow-up salivary gland scintigraphy, the control group showed significantly decreased MUR of the bilateral parotid and left submandibular glands, MSP of the bilateral parotid and submandibular glands, and EF of the left submandibular glands (p<0.05), while the selenium group only had a significant decrease in MSP of the right submandibular gland and EF of the left submandibular gland (p<0.05). **Con-**

clusions: Selenium supplements during I-131 treatment were effective to reduce salivary gland damage by I-131 radiation in patients with differentiated thyroid cancer.

EP-0816

Higher Body Weight and Distant Metastasis are Associated with Higher Radiation Exposure to the Household Environment from Patients with Thyroid Cancer after Radioactive Iodine Therapy

S. Kuo[1], J. Lin[2], M. Liou[2], B. Huang[1], K. Chiang[1], R. Cheng[1]; [1]Chang Gung Memorial Hospital, Keelung, TAIWAN, [2]Chang Gung Memorial Hospital, Taoyuan, TAIWAN.

Purpose: To evaluate the radiation exposure to the household environment from patients with thyroid cancer after radioactive iodine (RAI) therapy. **Subjects and Methods:** Patients with papillary or follicular thyroid cancer who received 3.7 GBq (100 mCi) RAI were enrolled in this prospective hospital-based study. The enrolled patients were asked to place a thermoluminescent dosimeter (TLD) in the living room, bedroom and bathroom of their houses for 4 weeks to measure radiation exposure to the household environment. **Results:** A total of 43 patients (18 men and 25 women; mean age, 51 ± 13 years) who received 100 mCi (3.7 GBq) RAI completed the study. The mean value of total radiation exposure over 4 weeks from the patients to the bedroom, bathroom, and living room (eliminating the background radiation factor) was 0.446 ± 0.304 (0.088-1.382) mSv. We divided the patients into two groups, those with more than and less than the mean value of total radiation exposure to the bedroom, bathroom, and living room. Factors associated with the higher amount of radiation exposure from the patients to the household environment were patient body weight [p = 0.025, univariate analysis; p = 0.037, multivariate analysis, odds ratio (OR) (95% confidence interval [CI]) = 1.067 (1.004-1.134)] and distant metastases based on ^{131}I post-therapy scanning (p = 0.041, univariate analysis; p = 0.058, multivariate analysis, OR (95% CI) = 6.453 (0.938-44.369)]; age, sex, body mass index (BMI), renal function, serum stimulated thyroglobulin level, and recombinant human thyroid stimulating hormone (rhTSH) use were not associated with the amount of radiation exposure from the patients to the household environment. **Conclusions:** Higher body weight and distant metastases may be the best predictors for higher radiation exposure to the household environment from patients with thyroid cancer after RAI therapy.

EP-0817

Abnormal Uptake Of 131 Iodine On Surgical Clips, A Case Report

A. Buitrago[1], M. Gallet[1], H. Lasolle[1], C. Bournaud[1], F. Giammarile[1,2], E. Levigoureux[1,2]; [1]Hospices civils de Lyon, Groupement Hospitalier Est, Bron, FRANCE, [2]Université Lyon 1 Claude Bernard, Lyon, FRANCE.

Introduction: We report the case of a 78-year-old female with skull uptake on the whole-body scan (WBS) after radioiodine (RAI) therapy for a pT3N0 papillary thyroid carcinoma. **Materials and Methods:** After total thyroidectomy and recombinant TSH stimulation (257 mUI/L), the patient received an activity of 3700 MBq of 131-I. Thyroglobulin was 1.4 µg/L without thyroglobulin antibody. Planar and head and neck SPECT-CT were acquired 5 days after treatment. **Results:** The WBS disclosed physiological distribution of 131-I, the expected uptake of thyroid remnant, and abnormal uptake on the left skull. The SPECT-CT localized this focus of uptake on left parietal bone, around metallic surgical clips. No lesion suggestive of cerebral or bone metastases was observed. The patient had undergone previous surgery for a cranial trauma with hematoma 50 years before. **Discussion, Conclusion:** Interpretation of post-radioiodine WBS implies knowledge of the physiological distribution of 131-I outside thyroid tissue (for example salivary glands, stomach, bowel, and urinary tract) but also of the variants of uptake, as far as they can be misinterpreted as thyroid cancer foci. Several examples of false-positive uptakes of radioiodine have been described in the literature, but only 2 similar cases of uptake on surgical clips have been so far reported [1-2]. The physiopathological mechanisms of uptake could rely on increased perfusion and vasodilatation which enhance locally the capillary net. These hematological modifications may be the consequences of the old hematoma [3], the persistence of a low chronic inflammation due to the presence of the foreign materiel [3-4], and passive diffusion of iodine between skull and meninges [5].In vivo oxidation of iodine induced by chemical species of the clips could also explain the uptake. A last hypothesis would be a chelation of iodine by the calcifications around the clips. Other clinical and chemical studies are needed to test these latter hypotheses. Bibliography : 1. Modoni S, et al. Clin Nucl Med 2000. 2. Campenni A,et al. Nuklearmedizin 2002. 3. Jong-Ryool O, et al. Am J Nucl Med Mol Imaging 2012. 4. Rudoni S, et al. Ann Endocrinol (Paris) 1997. 5. Salvatori M, et al. Clinical nuclear medicine 1997.

EP-0818

Clinical Significance of Iodine-131 ablation therapy post total thyroidectomy in differentiated thyroid cancer

K. Utsunomiya[1], H. Iwai[2], K. Suzuki[2], N. Kan[1], Y. Kono[2], K. Maruyama[2], Y. Ueno[2], N. Tanigawa[2]; [1]Kansai Medical University Medical Center, Moriguchi, JAPAN, [2]Kansai Medical University Hospital, Hirakata, JAPAN.

Purpose: To evaluate the efficacy of postoperative low dose (30mCi) Iodine-131 ablation therapy in high-risk group patients with differentiated thyroid cancer. **Subjects and Methods:** Forty one postoperative (total thyroidectomy) patients in the high-risk group were included in this study. Twenty nine patients underwent total thyroidectomy for thyroid cancer, the primary operation (PO) group, and 12 patients underwent total thyroidectomy for recurrent thyroid cancer post subtotal thyroidectomy, the reoperation (RO) group. To ensure I-131 accumulation into thyroid tissue (thyroid bed), To increase blood TSH level, patient L-thyroxine administration to patients was suspended for one month. Alternatively, rhTSH (Thyrogen®) was injected into muscle. Eight patients were enrolled in the the L-thyroxine suspension group and 33 patients were enrolled in the rhTSH injec-

tion group. After pre-treatment, all patients were were injected with 30 mCi of I-131 -for thyroid ablation. Iodine-131 SPECT/CT scans were acquired 72 hours post-injection to visually assess thyroid bed accumulation. Follow-up SPECT/CT I-131 scans were also performed at 4 to 6 months post- ablation to evaluate therapy efficacy in a 19 patient sub-group (12 in PO group, 7 in RO group). An ablation was considered successful if I-131 accumulation in the thyroid bed was not visually observed, failure as visual evidence of I-131 remaining in the thyroid bed. Ablation success and thyroid cancerrecurrence post I-131 ablation were evaluated in both groups (PO and RO). The observation period after I-131 ablation was 3-48 months (mean 23.9±9.25) in the PO group, and 3-45 months (mean 23.1±10.3) in the RO group. **Results:** Ablation success rate was 58.3% in the PO group (7/12), 42.8% in the RO group (3/7), 50.0% in the Suspension group (2/4), and 53.3% in the rhTSH group (8/15). Thyroid cancer recurrence was observed in five of the total 41 patients; 3.4% in the PO group (1/29), 33.3% in the RO group (4/12). No thyroid cancer recurrence was observed in any PO group patient who underwent a successful ablation. In the RO group, thyroid cancer recurrence was observed in 3 of 4 patients with ablation failure; only one case underwent successful ablation. **Conclusion:** I-131 ablation therapy was not found to be effective in patients with recurring cancer post initial subtotal thyroidectomy.

EP-0819

Acceptable radiation exposure to contacts of patients treated with low dose radioactive iodine (I-131) post family counseling can pave the way for high dose I-131 therapy on outpatient basis

K. Salman[1], S. Yassin[1], T. Munshy[1], M. Almalki[2], S. Zatari[1], Z. Khan[1], S. Elmorsy[1], D. Abdelmoety[1], M. Al-Ezzi[1], M. Al-Otaiby[1], H. Fedah[1], M. Alhazmi[1], N. Ali[1]; [1]King Abdulla Medical City (KAMC), Makka, SAUDI ARABIA, [2]Ministry of health, KSA, Riyad, SAUDI ARABIA.

Purpose: To numerically ensure acceptable radiation exposure to family members of Saudi patients treated with low dose I-131 therapy on outpatient basis after family counseling with proper explanation of radiation protection instructions. Also to demonstrate that cumulative radiation exposure (CRE) is well below radiation exposure constraints of 1mSv and to verify any factor that can significantly affect CRE. This would serve as a preparatory step prior to possible giving high dose of I-131 therapy on outpatient basis **Subjects and Methods:** Patients with cancer thyroid or hyperthyroidism referred for low dose I-131 therapy were included. Detailed radiation protection instructions were given to the patient and to family members going to be in contact with the patient post-therapy, after which thermoluminescent dosimeters (TLD's) were dispensed to all contacts explaining how to be employed. TLD's were collected 5 days post-therapy and individual CRE was measured, with studying different factors that can affect CRE. **Results:** Forty-seven patients (39 females & 8 males) were included; 29 had thyroid cancer and 18 had toxic goitre. All received 30 mCi or less of I-131 on outpatient basis, the mean dose was relatively higher in the former group. Included household family members were 212 with a mean age of

28.9±17.3 years and 50% were females. The mean period of contact with the patient was 9.1±6.5 hours. CRE of family members ranged from 109 to 991 uSv, with a median of 212 and 25th and 75th percentiles of 165 and 321 uSv, respectively. In this dataset, there was no statistically significant association of CRE with patient or family contact age or gender, patient educational level, given dose of I-131, time spent with the patient, or household area. **Conclusion:** Post family counseling for Saudi patients treated with low dose I-131 there is CRE evidently below the radiation exposure constraints of 1 mSv, with a median value less than its one fourth and no single factor of statistically significant impact on CRE. Our numerical data ensures that post family counseling there is good compliance to radiation protection instructions with acceptable radiation exposure levels, paving the way for possible giving high dose of I-131 therapy on outpatient basis.

EP-0820
Thyroid Cancer and Galectin-3

Z. Hasbek[1], G. DUMAN[1], T. CANDAR[2], S. A. ERTURK[1], A. CAKMAKCILAR[1]; [1]Cumhuriyet University School of Medicine, SIVAS, TURKEY, [2]Ufuk University School of Medicine, ANKARA, TURKEY.

Aim: It was reported that immunohistochemically measured Galectin-3 (ihGal-3) was detected positive in differentiated thyroid cancer patients in several study. Although the role of Galectin-3 in cancer development is not well known, it was notified that overexpression of Galectin-3 changes adhesion and motility of tumor cells and increases metastasis rate. Sensitivity of ihGal-3 is high but specifity of this marker is low in thyroid cancer patients. Aim of this study is the investigation of whether or not serum galectin 3 (sGal-3) levels are related with prognosis of differentiated thyroid cancer patients who were undergone with bilateral total thyroidectomy and referred for high dose radioiodine ablation theraphy to Nuclear Medicine Department. **Material and Methods:** Chemiluminescent microparticle immunoassay was used for the quantitative determination of sGal-3 in human serum. Patients who have normal physical examination, normal low dose diagnostic whole body scan (WBS), have no distant and local lymphatic metastases and have very low thyroglobulin levels in TSH stimulation period (stimulated Tg <1ng/ml or non-stimulated Tg <0.2 ng/ml) was accepted as ablation success and have good prognosis. **Results:** Forty eight thyroid carcinoma patients were included in this study. There were 42 female and 6 male patients with a mean age of 47.35±11 years (range; 25-73 years). sGal-3 levels were found at upper limits in only 2 patients. Metastatic activity accumulation in WBS was seen only in one patient. ihGal-3 was found positive in 25 patients and negative in 23 patients by immunohistochemically. When assessing the relationship between ihGal3 and sGal-3; sGal-3 was negative in all patients whether ihGal3 positive or negative.There were six patients with lymph node metastasis at the time of diagnosis and sGal-3 was found negative in these patients. ihGal-3 was investigated in two of them and was found positive. There was not a statistically significant relationship between ablation success and sGal-3 levels (p=0.812). **Conclusion:** In our preliminary study, sGal-3 levels were found nega-

tive even if patient with positive ihGal-3. And we did not found statistically significant relationship between ablation success and sGal-3 levels. We think that the reason for this was absence of significant tumor burden because of radioablation therapy. sGal-3 levels were elevated in patients with exicence of tumor burden in body. We think that normal sGal-3 levels at the time of ablation is related with good prognosis.

EP-0821

BRAF^{V600E} and ^{99m}Tc-MIBI scintigraphy are usefull diagnostic tools in identifying metastatic differentiated thyroid cancer patients refractory to radioiodine therapy

A. Campenni'[1], M. Siracusa[1], M. Stipo[1], S. Pignata[1], F. Di Mauro[1], R. Ruggeri[2], S. Baldari[1]; [1]Unit of Nuclear Medicine of Messina, Messina, ITALY, [2]Unit of Endocrinology of Messina, Messina, ITALY.

Aim: Papillary Thyroid Cancer (PTC) is generally associated with favorable outcome. However, in a small number of metastatic PTC patients, tumor cells lose the capacity to uptake radioiodine. Many Authors have already reported how radioiodine uptake in metastatic cells is reduced or lost in BRAF^{V600E} positive patients. ^{99m}Tc-MIBI scintigraphy is an easy diagnostic method, useful in detecting metastases in PTC patients. The aim of our retrospective study was to verify if ^{99m}Tc-MIBI scintigraphy and BRAF^{V600E} analysis can be useful tools in identifying metastatic PTC patients refractory to radioiodine therapy (RAIT). **Material and Methods:** We retrospectively reviewed the records of 15 PTC metastatic patients (F= 10, M= 5; F/M ratio= 2:1; mean age 44.3±13.3, range 20-68) with persistent or recurrent bio-chemical disease (serum Tg levels > 2 ng/ml after rhTSH-stimulation) during follow-up. In all cases BRAF^{V600E} analysis was obtained on primary tumor samples. At follow-up, neck-ultrasonography and ^{99m}Tc-MIBI scintigraphy of the neck-thorax regions were obtained in all cases. Thyroglobulin-antibodies were negative. Then, all patients underwent RAIT with high radioiodine activities (mean activity= 5614±903.8 MBq, range 3700-6882 MBq). At RAIT, TSH was ≥ 30 µUI/ml in all patients. A post-therapy whole body scan (pT-WBS) was acquired 5-7 days after RAIT. **Results:** In 10 out of 15 patients (67%), pT-WBS showed abnormal radioiodine uptake (+ve 131I). In 9 out of 10 patients (90%), abnormal radioiodine uptake was located in the neck (i.e.lymph-node metastases). A female patient showed both lymph-node and lung metastases. ^{99m}Tc-MIBI scintigraphy had shown abnormal tracer uptake in the neck in 6 out of 10 patients (+ve MIBI) while in the remaining patients no abnormal tracer uptake was observed (-ve MIBI). BRAF^{V600E} gene mutation was not found in 9 out of 10 patients (90%) (-ve BRAF^{V600E}). One female patient only had BRAF^{V600E} mutation (+ve BRAF^{V600E}). In 5 out of 15 patients (33%), pT-WBS did not show abnormal radioiodine uptake (-ve 131I). Interestingly, in all these patients ^{99m}Tc-MIBI scintigraphy did not show abnormal tracer uptake (-ve MIBI) and the BRAF^{V600E} mutation was found (+ve BRAF^{V600E}). Considering the association between -ve MIBI scintigraphy and +ve BRAF mutation as suspicious for radioiodine resistant, the overall sensitivity, specificity, accuracy, PPV and NPV in identifying radioiodine refractory patients reached 100%. **Conclusion:** Our results, albeit obtained in

a small retrospective series, show how the association between BRAF^{V600E} +ve mutation and MIBI -ve scintigraphy is a negative prognostic factor in DTC metastatic patients, predicting refractoriness to radioiodine therapy.

EP-0822

Investigation Of The Effect Of Vitamin C On Oxidative Stress Parameters Due To Radioiodine Treatment In Hyperthyroidism Patients

S. Ozdemir[1], K. Ukinc[2], D. Ulker Cakir[3], Y. Ziya Tan[1], M. Aşik[4], F. Celik[1]; [1]Canakkale Onsekiz Mart University, Faculty of Medicine, Department of Nuclear Medicine, Canakkale, TURKEY, [2]Canakkale Onsekiz Mart University, Faculty Of Medicine, Department of Endocrinology and Metabolic Disease, Canakkale, TURKEY, [3]Canakkale Onsekiz Mart University, Faculty of Medicine, Department of Biochemistry, Canakkale, TURKEY, [4]Canakkale Onsekiz Mart University, Faculty of Medicine, Department of Endocrinology and Metabolic Disease,, Canakkale, TURKEY.

Objective and Aim: The radioactive I-131 (RAI) treatment is a adjuvant treatment option that increasingly applied in hyperthyroidism, toxic nodular goiter and Graves' disease. Current project was aimed to investigate the possible radioprotective role of Vitamin C in I-131(RAI) treatment in hyperthyroid patients. **Material and Methods:** Two groups of RAI treated patients were investigated. In control group I (24 patients) no Vitamin C was received but the second group of RAI treated (28 patients) patients were received Vitamin C by starting 1 day prior of the treatment in 1000mg/day dose orally for a one week. The peripheral bloods samples were optained for two times (before begining of the treatment and seventh day of treatment) from all individuals for both groups. The oxidative stress parameters such as; malonyl dialdehyde (MDA), total antioxidant status (TAS), total oxidant status (TOS), ischemia modified albumin (IMA) and 8 hydroxydeoxyguanosine (8-OHdG) were analysed biochemically by ELISA kit protocols in plasma serum samples. The oxidative stress parameters that obtained from both groups were statistically compared to reveal the possible Vitamin C radioprotective effect in I-131 RAI treatment. **Results:** The preliminary results from the current project showed that Vitamin C is to reduce the effects of oxidative stress and therapeutic radiation during the I-131 RAI treatment in hyperthyroid patients. In conclusion, results revealed the crucial protective role of the vitamin C in radioactive administered patients.

EP-0823

Influence of coexisting Hashimoto thyroiditis on the postoperative residual thyroid tissue ablation success after the first dose of 3.7 GBq of iodine-131 in patients with differentiated thyroid carcinoma

M. P. Rajic, M. Vlajkovic, S. Ilic, M. Stevic, I. Misic, M. Kojic; University of Niš Medical School, Nis, SERBIA.

Introduction: Radioiodine ablation of residual thyroid tissue (RRA) is a standard procedure in the majority of patients with

differentiated thyroid carcinoma (DTC) after thyroidectomy. It reduces the chances of recurrence by targeting the microscopic tumor foci, increases the sensitivity of follow-up whole body scan (DxWBS) and specificity of serum thyroglobulin (Tg) levels to detect recurrence. The aim of the study was to assess the influence of coexisting Hashimoto thyroiditis and other factors on the RRA success after the first dose of 3.7 GBq of iodine-131 in patients with DTC. **Subjects and Methods:** After six to 12 months the results of RRA were analyzed in 59 patients with DTC, aged 14 - 69 years. The successful ablation was defined as visually undetectable thyroid bed activity or elsewhere on the DxWBS, stimulated thyroglobulin (st-Tg) serum levels < 2 ng/ml and anti-Tg antibodies negative at the same time of DxWBS. **Results:** There were 84.7% women and 15.3% men. 91.5% of patients had papillary and 8.5% had follicular carcinoma. pT1 category of tumor was found in 49.2%, pT2 in 33.9%, pT3 in 8.5%, pT4 in 1.7% and pTx in 6.8% of patients. DTC was associated with pathologically confirmed Hashimoto thyroiditis in 25.4% of patients. A successful ablation was achieved in 71.2% of patients. A successful response to therapy was registered in a larger number of women than men ($\chi 2$ =7.42, p<0.01). Pre-ablative st-Tg was significantly lower in patients with successful than with unsuccessful ablation (3.51±3.53 ng/ml vs. 6.69±5.99 ng/ml, p<0.05). Logistic regression analysis showed that tumor histology and T category of the tumor were not recognized as predictors of unsuccessful therapy response. On the contrary, gender and Hashimoto thyroiditis [OR=0.229; (95%) CI=0.053-0.996; p=0.049] had influence on ablation success. **Conclusion:** Results showed that a considerable number of patients with DTC had successful residual thyroid tissue ablation after first administration of 3.7 GBq of radioiodine. Patients with successful ablation had significantly lower st-Tg than those with unsuccessful ablation. In relation to gender, the better success of ablation was demonstrated in women. Hashimoto thyroiditis had a protective effect for the unsuccessful outcome of ablation. Key words: Differentiated Thyroid Carcinoma, Hashimoto thyroiditis, Residual thyroid tissue ablation, Iodine-131

EP-0824

Risk factors for predicting osteoporosis in patients who receive tsh-supressive levothyroxine treatment for differantiated thyroid carcinoma

C. Soydal[1], E. Ozkan[1], D. Nak[1], A. H. Elhan[2], N. Kucuk[1], M. K. Kir[1]; [1]Ankara University Medicel Faculty, Nuclear Medicine, Ankara, TURKEY, [2]Ankara University Medicel Faculty, Biostatistics, Ankara, TURKEY.

Purpose: To define the additional risk factors to develop of osteoporosis inrpatients who receive TSH-suppressive Levothyroxine treatment for differentiated thyroid carcinoma (DTC). **Material and Method:** This study included prospective and retrospective parts and approved by Ethical committee of Ankara University Medical Faculty. All the patients who received TSH-suppressive Levothyroxine treatment following radioiodine treatment for DTC were included to the study. After filling a patient inclusion form that consist of information on possible

risk factors for osteoporosis (gender, age, menopausal state, smoking, family history of osteoporosis, preoperative thyroid hormone status, postoperative hypoparathyroidism history, mean serum TSH levels, duration of TSH suppression), bone mineral densitometry of femur and lumbar vertebrae, serum D vitamin and parathyroid hormone measurements were performed. Relationship between duration of TSH suppression and development of osteoporosis was analyzed by Kaplan Meirer method. Effect of other risk factors to presence of osteoporosis was analyzed by Cox-regression analysis. **Results:** Totally 929 (813F, 116M, mean age: 52.33±7.2) patients were included to the analysis. Median duration of TSH suppression was calculated as 7 (min-max: 1-26) years. During this period osteoporosis was detected in 89 (%9.6) patients. Menopausal stage (p<0.001) and family history of osteoporosis (p=0.001) was found statistically significant parameters to detection of osteoporosis. Osteoporosis detection rates were calculated as 0.6%, 15% and 12% in premenopausal, postmenopausal women and men respectively. Postmenopausal women have 18-fold risk in comparison to premenopausal women. Interestingly men have found 20-fold risk in comparison to premenopausal women. Although patients with family history of osteoporosis have a 13% osteoporosis rate, patients without have 8%. Patients with a family history of osteoporosis have 2-fold risk for osteoporosis development in comparison to without. Although preoperative thyroid hormone status was found significant in the Chi Square analysis (p=0.003), this significance lost in the multivariate Cox Regression analysis. Despite mean serum TSH level was not a significant factor for the presence of osteoporosis, osteoporosis detection rate seems to decrease in patients with higher than 0.4 mIU/ml mean TSH levels. **Conclusion:** Postmenopausal women, men and patients with family history of osteoporosis have a higher rate of osteoporosis under TSH-suppressive Levothyroxine treatment. Although they were not reach the significant level preoperative hyperthyroidism and mean serum TSH levels seems to be another possible predictors. For these reasons, shortening of the duration of TSH-suppressive Levothyroxine treatment might be beneficial in low/intermediate risk group men/postmenopausal women DTC patients with family history of osteoporosis.

EP-0825

National survey and harmonization of practices of I-131 therapy for thyroid cancer in Finland

T. E. J. Noponen[1], M. Tenhunen[2], J. Heikkinen[3], V. Tunninen[4], H. Mäenpää[2]; [1]Department of Clinical Physiology Nuclear Medicine, Turku University Hospital, Turku, FINLAND, [2]Department of Radionuclide Treatments, Cancer Centre, Helsinki University Hospital, Helsinki, FINLAND, [3]Department of Medical Physics, Etelä-Savo Hospital District, Mikkeli, FINLAND, [4]Department of Nuclear Medicine, Satakunta Central Hospital, Pori, FINLAND.

Introduction: I-131 therapy is globally the most common radionuclide treatment. It is used to treat patients with hyperthyroidism or residual thyroid cancer and its metastases after partial or complete thyroidectomy. The I-131 cancer therapies

involve carefully implemented radiation protection and after therapy imaging procedures. **Material and Methods:** We conducted a survey to find out the status of radiation protection and imaging practices related to I-131 therapy in Finnish nuclear medicine departments. The questions dealt with dose measurement and delivery, patient in-hospital isolation and discharge and after-treatment imaging practices. Our final aim is to harmonize the I-131 cancer therapy practices by developing a national recommendation for the length of in-hospital radiation isolation, national radiation-protection instructions for patients after the discharge of isolation and the guidelines for imaging procedures. **Results:** We received answers to the survey from all Finnish 22 nuclear medicine departments operating in public hospitals. The results of the survey showed the need for standardization. Dose calibrator measurement before administration, the dose rate level to terminate the radiation isolation and imaging time points should be standardized between centers. According to the answers, the length of in-hospital radiation isolation periods varies from 1 to 4 days. The dose rate level to terminate the radiation isolation measured with a gamma-beta radiation survey detector at 1 meter from a patient range from 15 to 70 µSv/h in different hospitals. Some hospitals carried out a second dose-rate measurement during the after-therapy follow-up scanning visit to shorten or completely terminate the radiation protection requirements. One hospital utilized a remotely readable dose meter in an isolation room. The imaging time-points and gamma camera techniques differ clearly between hospitals when after-therapy imaging procedures were compared. The common desire was to achieve the national radiation protection instructions for patients after the discharge of radiation isolation. **Discussion and Conclusions**: During the ongoing year the national guideline has been prepared for thyroid cancer treatment in Finland. The results of this survey were utilized in those recommendations. The nationally harmonized practices will improve patient care and decrease the costs of treatment especially when the in-hospital isolation periods will shorten. Also common national radiation-protection instructions decrease the uncertainty among patient, if they compare the publicly available radiation protection instructions between the hospitals or use the services in different hospitals.

EP-0826

Predictive factors of a disease-free status in post-operative differentiated thyroid cancer patients treated with [131]I

P. Gouveia, T. Alves, A. Amado, R. Teixeira, R. Brito, R. Castro, I. Amorim, A. Silva, M. Oliveira, A. M. Costa, A. Carvalho, C. Freitas, F. Borges; Centro Hospitalar do Porto, Porto, PORTUGAL.

Aim: Although predictors of differentiated thyroid cancer (DTC) prognosis have been investigated by several studies, the results are inconsistent among them. The purpose of our study was to investigate potential predictive factors influencing the achievement of a disease-free status after the first ^{131}I ablative therapy (IAT) in post-operative DTC patients. **Materials and Methods:** Four hundred and sixty three patients with differenti-ated thyroid cancer were evaluated retrospectively. All patients underwent total thyroidectomy and IAT. A disease-free status was established as: undetectable TSH suppressed Tg levels, whole body imaging scan without local-regional uptake or distant metastases and negative cervical ultrasounds or thoracic CT scan. Clinical and tumoral factors such as sex, age, size of tumor, pathologic type, capsular invasion, tumor distribution pattern, tumor invasion pattern, lymph node (LN) metastasis, distant metastasis, Tg after thyroidectomy and Tg before IAT were analyzed. Multiple regression analysis was performed on selected influential parameters in univariate analysis (Tg before thyroidectomy, Tg before IAT, capsular invasion, LN metastasis) and in other clinical relevant parameters (sex and age). **Results:** Among 463 patients (360 women, 103 men; mean age 47 years), 287 (62%) achieved disease-free status. Multiple logistic regression analysis showed that age, Tg before IAT and LN metastasis were significant predictors for the disease-free status: age < 45 years (OR = 4.94; 95 % CI = 1.11 - 5.28; p<0.05), Tg level < 0.1 ng/ml before IAT (OR = 3.59; 95 % CI = 0.98 - 13.088; p<0.05) and presence of LN metastasis (OR = 0.44; 95 % CI = 0.23 - 0.84; p<0.05). **Conclusion:** This study revealed that age, Tg before IAT and LN metastasis are significant predictors for achieving a disease-free status by the first IAT. Patients younger than 45 years old, with low pre-ablation Tg levels and without LN metastasis would be likely to achieve a disease-free status.

EP-0827

Radioiodine uptake by thyroglossal duct remnant after radioiodine therapy for differentiated thyroid carcinoma

M. Jinguji, M. Nakajo, A. Tani, T. Yoshiura; Kagoshima University Graduate School of Medical and Dental Sciences, Kagoshima, JAPAN.

Aim: To evaluate the frequency of radioiodine (I-131) uptake by thyroglossal duct remnant (TGDR) after I-131 therapy and its response to ablation. **Materials and Methods:** The subjects were 79 patients (24 males and 55 females; mean age, 56.44 years; age range, 19-85 years) with differentiated thyroid cancer who underwent I-131 therapy after total thyroidectomy and neck SPECT/CT 48 to 72 hours after the initial I-131 therapy. We divided the abnormal neck uptakes into three groups; uptakes along the thyroglossal duct (TGDR uptake), peritracheal thyroid bed uptakes (peritracheal uptake) and other uptakes including those in the metastases (other uptake). We examined the association between presence or absence of TGDR uptake and the serum thyroglobulin level, age, sex, and I-131 dose (1110 or 3700 MBq), using Mann-Whitney U test or Fisher's exact test. For 61 patients who underwent follow-up I-131 scintigraphy six to nine months after initial therapy, we evaluated residual neck visualized lesions in the three regions (TGDR, peritracheal and other) and examined whether there was statistically significant difference in the incidence of residual uptake between TGDR and non-TGDR (peritracheal or other) using Fisher's exact test. We also examined the association between presence or absence of residual TGDR uptake and serum thyroglobulin level, and I-131 dose (1110 or 3700 MBq) for initial therapy using Mann-Whitney

U test and Fisher's exact test, respectively. **Results:** On the initial therapy, TGDR, peritracheal and other uptakes were found in 53.2% (42/79), 62.5% (49/79) and 27.5% (20/79), respectively. No significant association was found between presence or absence of TGDR uptakes and any of the examined factors. The follow-up I-131 imaging revealed residual TGDR, peritracheal and other uptakes in 48.4% (16/33), 10.3% (4/39) and 15.8% (3/19), respectively. Residual visualization was significantly higher in TGDR than in non-TGDR (P=0.0027). There were no significant differences in the incidence of residual TGDR visualization on follow-up I-131 images by initial treatment dose or post-treatment serum thyrogroblin level. **Conclusion:** TGDR uptake after I-131 therapy is seen relatively frequently, and is resistant to I-131 therapy.

EP-0828

Comparison of the Prescribed Dose of Radioiodine Ablation (Low Dose versus High Dose) in patients with Intermediate to High Risk Thyroid Cancer: An Inverse Probability of Treatment Weighting Analysis

Y. Iizuka, T. Katagiri, K. Ogura, T. Mizowaki; Kyoto University, Kyoto, JAPAN.

Background and Aim: Radioiodine remnant ablation (RRA) is performed to destroy residual normal thyroid tissue after surgical resection for differentiated thyroid carcinoma (DTC). Few studies have compared the prescribed dose in patients with intermediate to high risk according to the American Thyroid Association (ATA). We used 1,110 MBq of [131]iodine (I) (low dose) as outpatient therapy and 1,850-3,700 MBq (high dose) as inpatient therapy. This study aimed to compare the clinical results between these doses. **Materials and Methods:** Patients who underwent RRA for DTC without macroscopic residual lesions or metastatic lesions after surgical resection were retrospectively evaluated. Between December 2011 and August 2016, 147 patients underwent RRA. Patients whose distant metastases were confirmed during RRA and whose initial pathological stage or RRA result was unknown were excluded; thus, 119 patients were evaluated. Inpatients underwent a 3-week I intake restriction with thyroxin withdrawal, whereas outpatients underwent a 2-week I intake restriction with recombinant human TSH administration. Then, 3 to 12 months after RRA, the thyroglobulin (Tg) concentration was measured, and ^{131}I scintigraphy (370 MBq) was performed. The initial success of RRA was defined as disappearance of the uptake of ^{131}I at the thyroid bed and a Tg concentration <2.0 ng/mL. Patients who did not undergo ^{131}I scintigraphy were evaluated based on the Tg value, and those who had an anti-Tg antibody were evaluated based on ^{131}I scintigraphy. Results of ablation were compared between the high-dose and low-dose groups using the Fisher´s exact test, and inverse probability of treatment weighting (IPTW) analysis was performed on age, sex, performance status, the ATA risk classification, and period between the operation and RRA. **Results:** Seventy-nine patients had an ATA intermediate risk, and 40 had a high risk. The initial RRA goal was achieved in 50/68 patients (73.5%) in the low-dose group, and in 36/51 patients (70.6%) in the high-

dose group. Among intermediate-risk patients, 42 (73.6%) in the low-dose group and 11 (50.0%) in the high-dose group were successfully treated. Among high-risk patients, 8 (72.7%) treated in the low-dose group and 25 (86.2%) in the high-dose group were successfully treated. There was no significant difference in the RRA success rate between groups (p=0.84). Moreover, IPTW analysis showed no significant difference between the low and high doses (p=0.63). **Conclusion:** About 70% of intermediate or high-risk patients with DTC achieved initial RRA goals. There was no significant difference between the low and high doses.

EP-0829

False positive thymus uptake on 131-I post therapeutic scan of DTC patients

I. Iakovou, E. Giannoula, K. Michailo, V. Mpalaris, K. Badiavas, V. Athanasiou, D. Katsampoukas, D. Lo Presti, S. Georga, E. Moralidis, G. Arsos; Nuclear Medicine Academic dpt, Papageorgiou hsp, THESSALONIKI, GREECE.

Aim: to identify clinical conditions closely associated with thymic uptake on 131-I post therapeutic scan in DTC patients. **Methods:** Post therapeutic 131-I SPECT/CT scans of 303 consecutive patients were retrospectively reviewed. Radioiodine Thymus gland Uptake (RTU%), was observed in just 13 (4,2%) patients (2 male). Although, without histological confirmation, all patients had a CT scan suggestive of residual thymus. A possible relation with age, sex, type and TNM stage of DTC, total administered 131I dose, number of therapies, type of TSH stimulation (withdrawal or rhTSH), and TSH, Tg, AbTg levels was assessed. **Results:** Mean age of patients with thymic uptake was significantly lower (p<0.001). LT4 withdrawal and repeated 131I therapies also proved to be significant indicators for RTU% (p:0.03). Logistic regression analysis revealed that only the fact of repeated radioiodine therapies and young age were correlated with RTU% (p<0.001). **Conclusion:** Especially in young patients, with repeated 131I therapies, physiological radioiodine concentration by the thymus gland is a potential cause of false-positive therapy 131I scans.

EP-0830

The long term effect after 10 years of radioiodine therapy in patient with subclinical hyperthyroidism

S. S. Abdelrazek, P. Szumowski, M. Sykala, A. Polak, J. Mysliwiec; Department of Nuclear Medicine, Medical University of Bialystok, Bialystok, POLAND.

Introduction: The clinical diagnosis of subclinical hyperthyroidism (SHT) is very difficult in the absence of the typical symptoms of hyperthyroidism Radioisotope scan is important to confirm the provisional diagnosis. There is no established strategy for the management of SHT. The aim of our study was to evaluate the long-term (10 years) effect of radioiodine therapy (RAIT) on the achievement of euthyroidism, and prevention evolvement to overt hyperthyroidism. **Material and Methods**: We treated 920 patients, aged 18-76 years, 88% of them were females

and 12% males. 330 patients with multinodular goitre (MNG), and 590 patients with autonomous nodule (ATN). Qualification of these patients were based on: clinical features, normal levels of serum fT3 and fT4 ,low levels of serum TSH (<0.1mU/L), characteristic appearance on thyroid scans, Malignant changes were excluded in all nodules by fine needle aspiration biopsy. All the patients had serum TSH levels <0.1 mU/l and effective half life measured by the use of T24 and T48 was more than 3 days at the time of treatment. The activity dose was calculated by the use of Marinelli's formula and ranged between 200 and 800 MBq. The absorbed dose (Gy) for MNG ranged between 150 and 260, and for ATN: 200-300. Follow up control was done every 6 weeks in the first year. Then every 6 months for the next 7 years. **Results**: In general the success of treatment after 1 year was: 99% of patient with ATN and 92% of patient with MNG achieved euthyroidism. 1% of patient with ATN and 7% of patient with MNG develop hypothyroidism. 1% of the patients had persistent hyperthyroidism and received second dose of radioiodine therapy. After 5 years of RAIT 2% of patient with ATN and 9% of patient with MNG develop hypothyroidism. After 10 years of RAIT 3% of patient with ATN and 10% of patient with MNG develop hypothyroidism. In all the patients the symptoms and signs of subclinical hyperthyroidism disappeared (palpitation, tachycardia, atrial fibrillation, exercise tolerance improved, the blood pressure normalised and the quality of life improved). **Conclusions**: The achievement of euthyroidism and the remission of the symptoms and signs of subclinical hyperthyroidism, were due to good diagnosis, well preparation of the patients; accurate measurement of administered activity, effective half-life, and well-organised follow up.

EP-0831

Usefulness of radioiodine therapy in low risk patients with papillary thyroid cancer

E. Takacsova, M. Bartovic, R. Kralik; St. Elisabeth Cancer Institute, BRATISLAVA, SLOVAKIA.

Aim: The aim of our retrospective study was to evaluate a persistent/recurrent disease in eight-year follow-up in two different groups of low risk patients with papillary thyroid cancer (PTC). In the first group, there were patients who underwent total thyroidectomy with central neck dissection and in the second group the patients underwent total thyroidectomy without neck dissection. **Materials and Methods:** Our study included 126 of low-risk (T1-2N0(x)M0) patients with PTC - 56 patients, who underwent total thyroidectomy with prophylactic central neck dissection (with known lymph node status) and 70 of all patients underwent total thyroidectomy without neck dissection (without known lymph node status, although without clinically suspected lymphadenopathy). All patients were operated between years 2009 - 2011, and after initial surgery they received radioiodine (^{131}I) treatment. The persistent/recurrent disease was detected by imaging methods (neck ultrasonography, and/or ^{131}I-SPECT/CT, and/or ^{18}F-fluorodeoxyglucose-PET/CT), in most of the cases, it was done on a combination with the elevated level of stimulated serum thyroglobulin (>2 ng/ml), and in some cases

histologically after reoperation. **Results:** In eight-year follow-up (median seven years), we discovered the persistent/recurrent disease in 3 of 56 patients (5,4%) from the first group of patients who underwent total thyroidectomy with central neck dissection (all metastases were detected in lymph nodes of the lateral neck compartment), and in 17 of 70 patients (24,3%) from the second group of patients who underwent total thyroidectomy without neck dissection. In 85,0% of all 20 patients with the persistent/recurrent disease, the metastases were detected in lymph nodes of the neck. **Conclusion:** Radioiodine ablation has an important therapeutic/diagnostic role, not only in case of high-risk patients, but it is also found useful in case of low-risk PTC patients (T1-2N0(x)), especially in the patients without neck dissection at the time of initial surgery. It means that in case of patients without known lymph node status, although without clinically suspected lymphadenopathy - we discovered the persistent/recurrent disease in 24,3% of them in eight-year follow-up.

EP-0832

Radioiodine Treatment of Thyroid Papillary Carcinoma in Patient on Hemodialysis: Treatment Protocol and Dosimteric Results

J. Bang, H. Lee; Department of Nuclear Medicine, Seoul National University College of Medicine, Seoul National Univer, Seongnam, KOREA, REPUBLIC OF.

Purpose: For proper I-131 therapy, effective radiation dose to remnant thyroid tissue, while minimizing the risk of total body radiation is required. Because, the principle route of I -131 excretion is via kidneys, more consideration should be placed on I-131 therapy for patients on hemodialysis. Several studies reported the radiation dosimetry and treatment recommendations for such patients; however, consensus has not been achieved. Thus, objectives of this study were to assess the radiation dose for remnant thyroid tissue and organs in a patient receiving hemodialysis using hybrid SPECT/CT images, and determine the I-131 treatment protocol for patient requiring hemodialysis. **Methods**: A 63-year-old female patient suffering from end-stage renal disease and undergoing hemodialysis was treated with 80mCi of I-131 for pT3N1b papillary thyroid cancer after total thyroidectomy. After withdrawal of levothyroxine and low-iodine diet for two weeks, she admitted to the hospital right after the hemodialysis, and received 80mCi of I-131 (Day 0). Planar whole-body imaging and regional SPECT/CT were acquired right after I-131 administration, Day1, and 2 (before and after dialysis). She underwent hemodialysis on Day 2. For defining the organ's residence time (RT), 4 consecutive SPECT/CT images were automatically co-registered using the latest CT image as a reference. Organ segmentation was done for lungs, heart, cervical spines, and liver from CT images and remnant thyroid activity from SPECT images. Total body count was assessed via serial planar whole body images. Using the pre-dialysis RT, radioactivity was estimated for in case of not undergoing hemodialysis on Day 2, and compared with actual radioactivity on discharge day. Radiation dose was measured at 1m distance from patient using survey meter. **Results**: From

serial SPECT/CT images, half-life of remnant thyroid activity was 6.9 days. After hemodialysis on Day 2, 36.5% of the dose administrated was removed. If hemodialysis was not performed on Day 2, estimated residual radioactivity at the time of discharge was assumed as 2.8 time for lungs, 2.3 times for heart, 1.3 times for cervical spines, 1.7 times for liver and 2.2 times for total body higher than actual radioactivity on discharge day. Radiation dose was 13.3 mR/hr before hemodialysis on Day 2 and 3.4 mR/hr after hemodialysis. **Conclusion**: For patient with poor renal function and needed hemodialysis, I-131 therapy for remnant thyroid ablation could be successfully performed with hemodialysis on Day 2. Dosimetry with SPECT/CT would be helpful for specific condition of I-131 therapy.

EP-0833

Comparison Between Preablative Tc-99m Pertechnetate Scintigraphy and Postablative I-131 Whole Body Scan for Evaluation of Remnant Thyroid Tissue in Differentiated Thyroid Cancer

G. Mutevelizade, Y. Parlak, 45030, E. Sayit, **G. Gumuser**; *Celal Bayar University, Manisa, TURKEY.*

Aim: Total thyroidectomy and radioiodine (I-131) ablation have been used for patients with differentiated thyroid cancer (DTC). Before radioiodine ablation theraphy, thyroid scintigraphy with Tc-99m pertechnetate is performed to evaluate the remnant thyroid tissue existence and to investigate possible metastatic regions in the neck. **Methods:** Twenty eight patients who received radioiodine ablation for DTC were examined retrospectively. Every patient had Tc-99m pertechnetate scintigraphy 3-6 weeks after the surgery and postablative (RxWBS) I-131 whole body scan 7-10 days after the radioiodine ablation theraphy. Remnant tissue localizations and number of foci were compared. **Results:** Thirteen (46.4%) of 28 patients have exactly the same number of foci at the same localizations at both images. Tc-99m pertechnetate scintigraphy showed no uptake of remnant thyroid tissue at 2 (7.1%) out of 28 patients, while RxWBS exposed radioiodine avid remnant tissues. 7 (25%) patients had more number of remnant foci at Tc-99m pertechnetate scintigraphy; 6 (21.4%) patients had more at RxWBS. **Conclusion:** Eight patients had more number of foci at RxWBS than Tc-99m pertechnetate scintigraphy due to different uptake mechanisms of these two agents. 7 (25%) patients had more number of foci at Tc-99m pertechnetate scintigraphy due to star artifact. As a result while evaluating the remnant thyroid tissue existence there was no prominent difference between these two scanning procedures. Tc-99m pertechnetate scintigraphy is easy to perform and cost-effective; it is appropriate to evaluate the remnant thyroid tissue before radioiodine ablation of differentiated thyroid cancer. **Key Words:** Thyroid cancer, remnant, I-131, Tc-99m pertechnetate

EP-0834

The difference of clinical characteristics and outcome according to FDG avidity in pulmonary metastases of differentiated thyroid cancer

S. Wu, H. Wang; Xinhua Hospital Affiliated to Shanghai Jiaotong University School of Medicine, Shanghai, CHINA.

Purpose: To evaluate differences in clinical characteristics and outcome between pulmonary metastasis with and without FDG avidity in thyroidectomized differentiated thyroid cancer(DTC) patients with pulmonary metastasis who underwent high dose 131I treatment(RAI). **Methods:** A total of 92 DTC patients with pulmonary metastasis (age, 44.4±17.3 years; women/men,65/26) were included. The cumulative dose of treatment ranged from 5.41-89.19 GBq (200-3300mCi), mean 828.4mCi. The mean follow-up period was 118.7±98.4 months. Clinical characteristics, chest CT, FDG PET/CT and thyroid stimulating hormone (TSH)-stimulated serum thyroglobulin(s-Tg) level were compared between patients with and without FDG uptake in metastatic lung lesions. The response to RAI was evaluated by the changes of s-Tg level and the size changes on CT images. **Results:** 23 patients (25.3%,F+) showed high FDG uptake and 68 patients (74.7%, F-) did not. Among the F- group, 53 patients (77.9%) showed radioiodine uptake on post RAI WBS(I+). Only 15 patients(22.1%) were non-131I avid(I-). Univariate analysis shows changes on s-Tg were influenced by age, operation method, the intial s-Tg level and the accumulation of 131I (p values 0.012,0.049,0.001 and 0.001 respectively). Multivariate analyses reveals that the initial s-Tg level and 131I-avidity had a significant impacts on it (OR=4.691;95% CI=1.453-15.143,p=0.01 and OR=8.014;95% CI=2.353-27.290,p=0.001,respratively).A so-called "flip-flop" phenomenon was also seen in this study, which explains a reverse relationship between iodine and FDG accumulation in thyroid cancer lesions. In our study, F+/I- was only in 14/91(15.4%), but F-/I+ was seen more, about 53/91(58.2%). As evaluating from the CT changes,11 patients achieved CR(12.1%),19 PR (20.9%),42 SD(46.2%) and 19 had PD(20.9%). When considered CR and PR as good response,30 patients (33.0%) received good response to RAI. The ratio were significantly different between F+ and F- groups (p=0.019). Univariate analysis showed only gender was significant in changes in CT image after therapy (P values 0.022). **Conslusions:** This retrospective study indicated that most of the FDG avid pulmonary metastases from DTC were older at first diagnosed age and bigger size on CT images. The lack of uptake FDG, without statistical results, may the good predictive factors for RAI.The lower initial s-Tg and the 131I-avid lung metastasis may achieve a good response to RAI according to s-Tg. Only gender was significant in changes in CT image after therapy.

EP-0835

Efficacy And Dosimetry Analysis In Low Risk Thyroid Carcinoma Patients Treated With Low Doses Of 131-I

M. Guiote Moreno, A. Santos Bueno, L. Mena Bares, F. Maza Muret, E. Carmona Asenjo, M. Albalá González, E. Ortega Moreno, E. Rodriguez Cáceres, J. Vallejo Casas; Hospital Universitario Reina Sofia, IMIBIC, Córdoba, SPAIN.

Aim: To evaluate the dosimetry of patients with differentiated thyroid cancer, who were treated with low doses of 131-I . Mate-

rials and methods: A retrospective observational analysis of 113 patients (98 females and 15 males) between the ages of 18 and 81 (mean 48.15 years) was performed in the 2009-2016 period. Histologically, there were 93 papillaries, 14 multiple micropapillaries, 1 mixed pattern and 5 follicular. 90% of the patients had a Stage I and the remaining 10% had Stage II. Dosimetry was measured postherapy at 50 cm of the mediastinum, in mSv/h. And also, the treatment results were evaluated at 12 months by determination of stimulated thyroglobulin, antithyroglobulin antibodies and whole bodyscan after rhTSH stimulation and dose f 4 mCi (148 MBq) of 131-I. **Results:** Mean stay during treatment was 5.31 hours, after determining dosimetry below 60 mSv / h at 50 cm. In postherapy screening, 99.1% of the patients showed only remains in the thyroid bed (1 patient with cervical lymphadenopathy). 88.5% of the patients showed undetectable stimulated thyroglobulin. In the annual evaluation, a complete response was considered, with no need for new treatment in 96 patients (negative or minimal intensity screening and undetectable thyroglobulin with negative antithyroglobulin antibodies). In 17 cases a second dose of 30 mCi (1110 MBq) of 131-I was administered. A case of dedifferentiation with structural and biochemical progression was observed. **Conclusion:** Dosimetry after treating differentiated thyroid cancer with low doses of 131-I, was determinated always below 60 mSv/h, very low compared with treatment with higher doses of 131I, allowing to discharge from the hospital sooner, and having really positive results after a year of treatment. This procedure is cost-effectiveness in the treatment of low risk patients with differenciated thyroid carcinoma.

EP-0836

Is F-18 Fluorodeoxyglucose PET/CT Useful In The Management Of TENIS?

A. Bhattacharya, D. Singh, A. Jois, A. Sood, B. R. Mittal;
Postgraduate Institute of Medical education and Research, Chandigarh, INDIA.

Introduction: This study was conducted to evaluate the role of F-18 fluorodeoxyglucose positron emission tomography / computed tomography (FDG PET/CT) in detection of residual/ recurrent disease in patients of differentiated thyroid carcinoma (DTC) with elevated serum thyroglobulin (Tg) and negative diagnostic Iodine-131 (I-131) scan (TENIS). We also evaluated the management and long-term survival of these patients. **Subjects and Methods**: We retrospectively evaluated 1021 patients of DTC who underwent I-131 scan following total thyroidectomy between December 2010 and March 2017; 146 patients (14.3%) were diagnosed as TENIS, and 83/146 (29M, 54F) aged 17-77 (44±15) years underwent FDG PET/CT scan. Patients were followed up with stimulated Tg assay, treated with empirical I-131 therapy and/or underwent re-surgery / FNAC / biopsy. **Results**: Initial mean stimulated Tg was 185.8 ± 366.3 ng/ml (2.5-3000). FDG PET/CT was normal in 19/83 patients; while no further treatment was given in 8 patients, 11 were empirically treated with 53-517 (133.9 ± 129.9) mCi I-131 therapy. All 19 patients are doing well on follow-up. In the re-

maining 64 patients, FDG PET/CT showed only remnant tissue in 10, remnant with regional lymph nodes in 9, regional lymph nodes in 25 and metastatic disease with/without regional disease in 20, with mean SUVmax 10.7 ± 7.3 (2.2-40.2). No correlation was found between Tg and SUVmax (*p*=0.476). ROC analysis identified highest diagnostic accuracy of PET/CT to localize disease with sensitivity 70.3% and specificity 73.7% at cutoff Tg 38.6 ng/ml. I-131 therapy [50-525 (164.5 ± 102.6) mCi] was empirically given in 38/64 patients, with post-therapy radioiodine scan positive in 16 and negative in 22 patients. Thirteen of 64 patients were subjected to re-surgery and histopathology/ FNAC directed by PET/CT findings, followed by I-131 therapy in 8/13 patients. No treatment was given in the remaining 13/64 patients with abnormal PET/CT findings. Mean Tg after radioiodine therapy was 93.1 ± 128.37 ng/ml (0.2-500) with statistically significant decrease of 42.6 ng/ml (*p*=0.03). Median follow-up was 28 (6-76) months. Mean survival by Kaplan- Meier analysis was 35 months in treated and 31 months in non-treated patients. Log rank test for survival distribution showed no significant statistical difference in treated vs. non-treated patients, $\chi^2(2)$=1.005, *p*=0.316. **Conclusion**: FDG PET/CT is useful to localize disease and guide further management with empirical I-131 / surgical resection in patients of TENIS with Tg > 39 ng/ ml. However there is no significant difference in long-term survival in treated compared to non-treated patients.

EP-0837

Clinical outcome of radioiodine therapy in Graves' disease related to patient specific thyroid absorbed dose calculations- 3 years of experience in Nuclear Medicine Department of "Theagenio" Anticancer Hospital of Thessaloniki

M. Kotzasarlidou[1], K. Gianopoulou[2], P. Exadaktilou[1], V. Mamouga[1];
[1]"Theagenio" Anticancer Hospital, Thessaloniki, GREECE,
[2]Aristotelion University of Thessaloniki, Thessaloniki, GREECE.

Introduction: According to literature, in radioiodine(RAI) therapy for Graves' disease(GD), treatment outcome is related to thyroid absorbed dose,D, although its target value for successful treatment is still under dispute. **Aim:** This study aims to present efficacy of RAI therapy within 1 year after treatment among patients who received a wide range of thyroid absorbed doses. **Materials and Methods:** Pretherapeutic patient-specific dosimetry, as per EANM Dosimetry Committee's guidelines, was performed to 17 patients with GD, referred to our department, since mid 2014. Volume and weight,w[g], of each patient's thyroid gland was estimated by ultrasound and computed tomography. Four measurements of I-131 thyroid uptake, U[%] were obtained 4,24,48,92-168h after oral administration of tracer activity, 140±30μCi [5.18±11kBq], using CAPTUS 3000 thyroid uptake system. LABfit software was used for time activity curve-fitting and integral calculation in order to determine residence time τ_r[d] of I-131 in thyroid gland. Thyroid absorbed dose per unit administered activity,D/A_a, was by applying the following equation: D/A_a[Gy/MBq]-E* τ_r/w, whereas E=2.8 Gy.g/ MBq.d Physicians determined the amount of therapeutic radio-

iodine dose,A_a, based on the modified Marinelli-Quimby formula. Applying the equation shown above, thyroid absorbed dose was calculated. During patient's clinical follow-up, therapy outcome was classified as successful, if clinical symptoms of hypothyroidism were developed and/or serum TSH was elevated to normal or above normal levels. Mean follow-up period was 1 year. Relation between treatment's success rate and gland's volume, thyroid absorbed dose, patient's age and sex, pretherapy serum TSH values was analysed. Results: Thyroid volume ranged from 10 to 75.8ml and glandular absorbed dose per unit administered activity,D/A_a varied from 0.14 to 2.82 Gy/MBq. Therapeutic radioiodine administered activity,A_a, ranged from 296 to 444MBq whereas mean thyroid absorbed dose was 371Gy with a standard deviation of 230Gy. 16 patients had successful outcome after one therapeutic dose of I-131, whereas 1 patient remained hyperthyroid. Success of therapy was not related to age or sex of patients, or TSH values before therapy. Conclusions: Mean thyroid absorbed dose of 370 Gy could be considered as a target therapeutic dose in GD therapy planning, since administered radioiodine activities delivering higher absorbed dose, don't increase the success rate. In addition, based on our experience, pretherapy patient-specific thyroid dosimetry, as per EANM guidelines, is an easily applicable procedure, which definitely improves the quality of radioiodine therapy.

EP-0838

Is serum Thyroglobulin level an indication of distant metastasis location?

F. Norton Brandão, M. Silvestre, M. Rio Carvalho, I. Patrocínio Carvalho, R. Sousa, P. Ratão, T. C. Ferreira, L. Salgado; Instituto Português de Oncologia Lisboa Francisco Gentil E.P.E., Lisboa, PORTUGAL.

Introduction: Regarding differentiated thyroid carcinoma, serum thyroglobulin (Tg) is a tumor marker that can be used to assess the presence of thyroid tissue after the initial treatment and rising Tg values over time are suspicious for growing thyroid tissue or cancer. The aim of this study was to assess the relation between Tg levels and the location of metastasis. **Methods & Materials:** We retrospectively reviewed all 1389 patients that performed a therapeutic procedure with Iodine-131 from January 1st 2014 to March 31st 2017 in our Nuclear Medicine department. All patients performed a WBS after therapeutic Iodine-131 administration. Only patients that had distant iodine-avid metastasis, exclusively well differentiated histology and negative anti-thyroglobulin antibodies (ATAs) were included. Values of serum thyroglobulin, both nonstimulated and stimulated, were collected, and stimulated Tg levels in patients with thyroid-stimulating hormone (TSH) inferior to 20 μUI/mL were disregarded. These patients were further divided into two sub-groups: patients exclusively with lung metastases (n = 13); patients exclusively with bone metastases (n = 11). The selected patients' Tg levels were then compared between sub-groups and their difference tested through a Student's t-Test. **Results:** Three percent of all 1389 patients had detectable distant metastasis in

WBS. For the group with exclusively lung metastasis, nonstimulated Tg levels ranged from 6.6 ng/mL to 18064 ng/mL (median 75.5 ng/mL) and stimulated Tg levels ranged from 64.2 ng/mL to 18731 ng/mL (median 885.0 ng/mL). For the group with exclusively bone metastasis, nonstimulated Tg levels ranged from 0.6 ng/mL to 8189.0 ng/mL (median 171.05 ng/mL) and stimulated Tg levels ranged from 4.6 ng/mL to 16884.0 ng/mL (median 367.5 ng/mL). There was no statistically significant difference between the two sub-groups for both nonstimulated Tg (p-value 0.80) and stimulated Tg (p-value 0.83). **Conclusion:** Both nonstimulated and stimulated serum Tg levels highly overlap between the two sub-groups, with no statistically significant difference. These findings suggest that no practical information about the metastases locations can be withdrawn from them. The lower limit for Tg values in the bone metastases sub-group shows that Tg alone may not predict the presence of metastases, emphasizing the need for additional data, such as clinical observation, Tg trend over time and, if needed, imaging for structural evidence of disease. The authors recognize the small sample size, which can be a limitation in the inferences made.

EP-0839

Thyroid ablation with 1.1GBq (30mCi) iodine-131 with patients with papillary thyroid carcinoma at intermediate risk for recurrence

I. El Bez, M. Somai, S. Bennour, I. Slim, M. Ben Slimene; institut Salah Azaiez, Tunis, TUNISIA.

Introduction: Little is known about the medium- and long-term outcomes of thyroid ablation with 1.1 GBq (30 mCi) [131]I in patients with papillary thyroid carcinoma who have a tumor>4 cm or accompanied by extra thyroid invasion or clinically detected lymph node metastases (cN1). The objective of this study was to evaluate the efficacy of ablation with 30 mCi ^{131}I in this subgroup of patients and to report the medium-term outcomes. **Methods:** We studied 152 patients with papillary thyroid carcinoma submitted to total thyroidectomy with apparently complete tumor resection, who had a tumor>4 cm or 2-4 cm accompanied by extra thyroid invasion or lymph node metastases, or ≤2 cm accompanied by both extra thyroid invasion and lymph node metastases. Patients with extensive extra thyroid invasion by the primary tumor were excluded. Lymph node involvement was detected by ultrasonography or palpation (cN1). **Results:** Forty-two patients were prepared by administration of recombinant human thyrotropin and 110 by levothyroxine withdrawal. Post therapy whole-body scanning revealed unequivocal ectopic uptake in three patients. When evaluated 9-12 months after ablation, 123 patients had achieved complete ablation (stimulated thyroglobulin [Tg] <1 ng/mL, negative anti-Tg antibodies, and neck ultrasonography); a new post therapy whole-body scanning revealed persistent disease in 2 patients whose initial post therapy whole-body scanning (obtained at the time of ablation) had already shown ectopic uptake; 12 patients presented with a Tg >1 ng/mL and 14 had positive anti-Tg antibodies without apparent metastases; 1 patient had metastases not detected at the time of ablation. Recurrence was observed in an additional 6 patients during

follow-up (median 76 months). There was no case of death related to the disease. Therefore, an activity of 30 mCi failed in only 9 (6%) patients with persistent disease or recurrence after ablation. None of the variables analyzed (sex, age, tumor size, multi centricity, extra thyroid invasion, lymph node metastases, preparation [recombinant human thyrotropin or levothyroxine withdrawal]) was a predictor of ablation failure. **Conclusion:** An activity of 30 mCi ^{131}I is effective in thyroid ablation in patients with stage T3 and/or N1 papillary thyroid carcinoma.

EP-0840

Efficacy of Radiolodine Therapy For Graves' Disease: Standardized Vs Calculated Activity

I. Slim, N. Sahli, T. Ben Ghachem, I. El Bez, I. Meddeb, K. Limam, A. Mhiri, I. Yeddes, M. F. Ben Slimene; *Department of Nuclear Medicine, Salah Azaiez Institut, Faculty of Medicine of Tunis, University of Tunis El Manar, Tunis, TUNISIA.*

Introduction: Despite the long experience with radioiodine (I131) for hyperthyroidism. The optimal method for determining I131 treatment activity for Graves' disease (GD) remains controversial. Various techniques suggest either fixed doses or dosimetric calculation based on gland size and iodine uptake. The aim of the study was to compare the effectiveness of these two methods for treatment of Graves' thyrotoxicosis. **Subjects and Methods:** We retrospectively analyzed 126 patients with GD who had not been previously treated with I131. Group I (n=63, 23 M, 40 F, mean age: 42 years) included patients who were treated with a standardized activity of 555 MBq of I131. Group II included 63 patients (25 M, 38 F, mean age: 51 years) who were given 37 MBq/10 g of the thyroid weight adjusted for 24 h radioiodine uptake. Therapeutic success was defined as the elimination of hyperthyroidism 6 months after I131 application. **Results:** In Group I, 17 patients (27%) became euthyroid and 41 (65%) hypothyroid (an overall response of 92%), while 5 (8%) remained hyperthyroid by the end of the follow-up period. In Group II, 10 patients (16%) became euthyroid and 23 (36%) hypothyroid, an overall response of 52%. Non responders were 30 patients (48%). The success of therapy was significantly higher in Group I than in Group II (p<0.001). The incidence of hypothyroidism was less in Group II than in Group I. No difference was noted between the outcome of treatment and age, sex, size of the thyroid in each Group of patients. **Conclusion:** Adding to simplicity and time-saving, fixed activity (555 MBq) of I131 is more useful and effective for the treatment of GD as compared to calculated procedure.

EP-0841

The Relationship BetweenDisease Perception, Anxiety, Depression And Life QualityIn Thyroid Cancer Patients

U. Elboga, G. Akyıldız, Y. Celen; *Gaziantep University, Gaziantep, TURKEY.*

Introduction: We evaluated disease susceptibility, anxiety, depression and quality of life in well differentiated thyroid cancer patients who had received radioactive iodine 131 treatment after total thyroidectomy. **Methods:** We were researched whether patients, who were in the process of new diagnosis and treatment, whose treatment was completed and the whole body scan was performed with iodine-131 for 6 months were controlled by TSH, triggered symptoms of anxiety and depression and adversely affected quality of life. Sickness Perception Scale (SFI), SF-36 Quality of Life Scale, Beck Depression Scale, Beck Anxiety Scale and socio-demographic form prepared by the researcher were applied when all diseases were evaluated. **Results:** The mean age of the participants was 40.62 ± 10,28 years. There were 84 (84.0%) female and 16 (16.0%) male cases. 72 reported that they had lost power, and 60% of them attributed this symptom to the disease. 60 patients stated that they had difficulty in breathing, and 48 percent of them said it was related to the disease. The symptom of pain remained at 40%, the result is that the symptoms of pain in the cases of differentiated thyroid cancer are not a defining symptom of the disease. The symptoms of weight loss were the least number of symptoms associated with the disease, the actual complaint of most women was 'weight gain. **Conclusion:** There was a noticeable decrease in the patient's ability to understand the disease. The scores on the quality of life scale were slightly lower. However, significantly higher fatigue and power anxiety, lower quality of life, emotional role strength and physical role weakness were found in our cases.

EP-0842

Over-time Titers Evolution of Positive Thyroglobulin Antibodies at Radio Iodine Ablation Treatment

P. Soeiro[1], R. Silva[1,2], G. Costa[1,3], P. Gil[1], J. Pedroso de Lima[1,2,3]; [1]Serviço de Medicina Nuclear do Centro Hospitalar e Universitário de Coimbra, Coimbra, PORTUGAL, [2]Instituto das Ciências Nucleares Aplicadas à Saúde, Coimbra, PORTUGAL, [3]Faculdade de Medicina da Universidade de Coimbra, Coimbra, PORTUGAL.

Purpose/Introduction: Thyroglobulin antibodies (TgAb) occurs in approximately 25% of well-differentiated thyroid cancer (WDTC) patients and are present in 10% of the general population. They can be used after radioiodine ablation treatment (RIAT) as a surrogate tumor marker. We aimed to evaluate the clinical significance and the titers evolution over time of the positive TgAb at RIAT. The clinical significance of other variables, in this context, was also assessed. **Subject & Methods:** All patients with positive TgAb(>20IU/mL) submitted to RIAT between 27-12-1995 and 28-03-2016 were selected. All relevant data was recorded, including demographic variables, histopathologic findings and diagnosis of recurrence/persistence disease in the follow-up. TgAb and thyroglobulin (Tg) evolution over time was also recorded. Statistical analysis was performed using SPSS 22. **Results:** A total of 1039 RIAT were performed during the selected period of time. Positive TgAb were detected in 43(4.1%) patients (38 women,5 men; average age:50.1±16.0 years). Average TgAb at RIAT:188.1±253.1IU/mL(range:40-1466). All patients had papillary carcinoma (aggressive histologic subtypes were found in 23 patients) and were either AJCC stage

I(n=36) or II(n=7). Positive Tg were detected in 14 patients (7.3±15.1ng/mL;range:0.1-53). Disease recurrence/persistence was diagnosed in 7 patients. All patients without evidence of disease recurrence/persistence presented progressive decrease in TgAb titers until they became negative (average TgAb half-life:314±18days; average time to negativation:439±21days). Patients with recurrent disease maintained persistently elevated or increasing TgAb and/or Tg values. No statistical significant difference was found between TgAb titers at RIAT in patients with and without disease recurrence/persistence (Mann-Whitney U, p=0.84). However, disease recurrence/persistence was statistically more frequent in patients with high risk histologies (Pearson Chi-square, p=0.071) and AJCC stage II patients (Pearson Chi-square, p=0.037). A statistical significant difference was found between Tg values in patients with and without disease recurrence/persistence (Mann-Whitney U, p=0.016). In multivariable analysis, only the Tg values at RIAT remained as statistically significant (binary logistic, p<0.05). **Discussion/Conclusion:** In our sample, patients rendered free of disease after RIAT showed a slow, but progressive, decline in TgAb titers until they become unmeasurable (in average after 439±21days). Non-decreasing or rising TgAb titers were associated with disease recurrence/persistence. These findings confirm the role of TgAb as a surrogate tumor marker. No statistical significant difference was found between TgAb titers at RIAT and disease recurrence/persistence. Several variables were statistically associated with disease recurrence/persistence, however in multivariable analysis only Tg remained as statistically significant. However, due to the small sample size and retrospective nature, more studies are warranted.

EP-0843

Detecting dedifferentiation in differentiated thyroid carcinoma - our experience

F. N. Brandão, M. Silvestre, M. Rio Carvalho, I. Patrocínio Carvalho, R. Sousa, P. Ratão, T. C. Ferreira, L. Salgado; Instituto Português de Oncologia Lisboa Francisco Gentil E.P.E., Lisboa, PORTUGAL.

Introduction: Most thyroid carcinomas have an excellent prognosis when properly treated. However, 10% to 15% exhibit aggressive behavior, with metastases occurring in 10% of patients at initial staging. The detection of lesions by ^{18}F-FDG-PET-CT (PET) correlates with prognosis, as high glucose metabolism signifies poor tumor differentiation and, consequently, poor prognosis. Dedifferentiation occurs in about 30% of patients with persistent or recurrent thyroid cancer. The aim of this work is to evaluate the patients with differentiated thyroid carcinoma (DTC) referred to our Nuclear Medicine department in terms of dedifferentiated disease, comparing the findings of PET and Iodine-131 whole-body scans (WBS). **Methods & Materials:** We retrospectively reviewed all 1389 patients with thyroid carcinoma treated with Iodine-131 from January 1st 2014 to March 31st 2017. All patients performed a WBS after therapeutic Iodine-131. Data including histology, date of diagnosis, follow-up time, justification for PET, serum thyroglobulin (Tg), thyroid-stimulating hormone (TSH) and anti-thyroglobulin an-

tibodies (ATAs) was collected for patients with exclusively differentiated disease in histology and who had distant iodine-avid or FDG-avid metastases. WBS and PET were reviewed and Iodine and FDG avidities were compared. Metastatic patients that performed both WBS and PET were selected; two were excluded due to a large time gap between WBS and PET (n = 24). **Results:** Four percent of the 1389 patients had detectable distant metastasis along the course of their disease (follow-up time 2-307 months, median 37 months) with 43% developing at least one FDG-avid lesion along the course of their disease, revealing dedifferentiation (time to dedifferentiation 0 to 23 years, median 34 months). The most frequent reason for performing PET was increasing biochemical evidence of disease (Tg or ATAs). In the selected patients: 8 showed exclusively FDG-avid lesions; 5 showed exclusively Iodine-avid lesions; 1 showed lesions that were exclusively Iodine-avid or FDG-avid; 5 showed lesions avid for both FDG and Iodine; 3 showed Iodine-avid lesions that also became FDG-avid in the course of disease; 2 showed Iodine-avid lesions that became FDG-avid, but lost Iodine avidity in the course of disease. **Conclusion:** In our sample, the rate of patients with metastasis from DTC is in accordance with what's described in the literature. A high rate of patients had uptake in both PET and WBS, not showing the flip-flop phenomenon. This data strengthens the role of PET scans in monitoring aggressive disease in thyroid differentiated carcinoma, especially when dedifferentiation is suspected or needs to be excluded.

EP-0844

The efficacy of radioiodine therapy in patients with non-toxic multinodular goiter with large cold nodules

S. S. Abdelrazek, P. Szumowski, A. Polak, M. Mojsak, P. Lisiewicz, A. Konopka, J. Mysliwiec; Department of Nuclear Medicine Medical University of Bialystok, Bialystok, POLAND.

The clinical presentation of a patient with multinodular goiter (MNG) varies from a completely asymptomatic goiter to a life-threatening disease due to upper airway compression. Surgery is the treatment of choice in patients with cold nodule and low radioactive iodine uptake (RAIU), presence of symptoms or signs of compression within the neck. Total thyroidectomy is associated with the risk of surgical complications and is often refused by the patient. Radioactive iodine therapy 131I (RAIT) is an alternative to thyroid surgery to reduce the size of benign MNG. Studies have demonstrated that 131I is safe and effective, leading to significant thyroid volume (TV) reduction. The therapeutic efficacy of 131I in patients with MNG depends to some extent on the RAIU. The aim of our study was to evaluate the efficacy of radioiodine therapy to reduce thyroid volume in patients with cold nodule by the use of two doses of radioiodine 131I. **Methods**: We treated 90 patients with non-toxic MNG with large cold nodule, aged 18 and 68 years; initial 24h RAIU was ranged between 18-45%, and TV ranged between 48 and 120 ml, effective half-life was more than 3 days at the time of treatment. Malignant changes were excluded in all nodules by fine needle aspiration biopsy. The activity dose was calcu-

lated by the use of Marinelli's formula and ranged between 280 and 800 MBq. Thyroid ultrasonography, and thyroid scan with RAIU at 24 was done before and after 6 and 12 months of RAIT. Follow up control was done every 6 weeks. **Results**: After 6 months of first radioiodine dose, the cold nodules changes to hot nodules in all the patients. In 22 patients the size of the thyroid gland decrease to 48%, and no need for the second dose of radioiodine therapy. 68 patients received second dose of RAIT to decrease the nodule which was cold and turned to hot after the first dose. After 12 months of the second dose of radioiodine a mean TV reduction of 56% was achieved. After 12 months of RAIT euthyroidism persist in 53% of patients, and hypothyroidism develop in 47% of patients. **Conclusions**: Radioiodine is non-invasive, safe and cost effective method of therapy for reduction of large non-toxic goitre even with cold nodule. The reduction of the cold nodule and the thyroid volume, were due to well accurate measurement of administered activity, relatively high effective half-life and well-organised follow up.

EP-0845

Effect of radioiodine ablation in Graves' ophthalmopathy

P. K. Pradhan, N. Yadav, A. Arya, S. Yadav, V. Kanojia; SGPGIMS, Lucknow, INDIA.

Introduction: Graves' disease is characterized by hyperthyroidism, ophthalmopathy and rarely dermopathy. Thyroid associated ophthalmopathy may precede, coincide or follow the systemic complications of dysthyroidism. Present treatment options for Graves' disease are ATDs, radioactive iodine ablation and surgery.Its thought in traditional practice that radioiodine cause worsening in ophthalmopathy. **Objective:** To determine effect of radioiodine ablation on course of Graves' ophthalmopathy. **Subjects and Methods:** 60 patients of Graves' disease with or without opthalmopathy were included in this study and alloted to two groups, both having 30 patients each. Group 1 Graves' disease without ophthalmopathy and Group 2 with ophthalmopathy. They were evaluated for duration of symptoms, treatment received, clinical activity score (CAS) ophthalmological consultation and thyroid hormones, scan and followed up at 3 and 6 months interval following radioiodine ablation with thyroid hormones, CAS and ophthalmic evaluation as acuity of vision, exophthalmometry and perimetry. **Results:** Mean CAS of Group 1 and Group 2 were 0.0 and 1.2±0.52 at baseline and 0.16±0.46 and 0.96±0.76 at 6 months respectively. Mean duration of ATD treatment before RAI ablation was 4.6±5.04 months for group 1 and 8.3±8.5 months for group 2. In group 1, 4 out of 30 patient shows new ophthalmopathy and 7 out of 30 patients shows progression of ophthalmopathy in Group 2 at 6 months. 4 patients which showed progression of ophthalmopathy in Group 1, 2 patients showed increase in proptosis ≥ 2mm, 1 patient had redness of conjunctiva and spontaneous orbital pain and 1 , had only spontaneous orbital pain at 6 months . In group 2, out of 7 patients which showed progression of ophthalmopathy , 3 out of 7 had increase in proptosis ≥ 2mm and spontaneous orbital pain, 1 patient had only increase in proptosis ≥ 2mm and 3 patients had redness of conjunctiva and spontaneous orbital pain at 6 months follow up.However,none required any clinical intervention except regular follow up. **Conclusion:** There is increase in proptosis in patients by exophthalmometry and that too small in number and rest of the patients has only transient symptoms of redness of eye and retro orbital pain. However, none required any steroid or any other intervention implying nonsignificant clinical course of ophthalmopathy following radioiodine ablation and this treatment can be done safely in patients of Graves' ophthalmopathy.

EP-0846

Low Iodine Diet In Patients With Differentiated Thyroid Cancer

M. Dobrenic; Clinical Hospital Centre Zagreb, Zagreb, CROATIA.

Introduction: Low iodine diet, or restricted intake of iodine-rich food is recommended to all patients with differentiated thyroid cancer prior to I-131 administration. The majority of guidelines recommend low iodine diet prior to I-131 application, but its duration and effectiveness, as well as target urinary iodine concentration are not established. The aim of this study is to evaluate the influence of low iodine diet on total body iodine content and on radioiodine avidity of tumor cells in patients with differentiated thyroid cancer and biochemically persistent disease. **Materials and Methods:** A total of 77 patients with differentiated thyroid cancer, thyroglobulin &gt 2 ng/mL, and negative I-131 whole body scan underwent low iodine diet. Each patient underwent a two-week low iodine diet, with the aim to achieve moderate iodine deficiency. Those who accomplished only mild iodine deficiency after a two-week low iodine diet received a recommendation to follow the diet for a further week (three-week diet) before the next I-131 administration.To evaluate the effectiveness of low iodine diet, iodine concentration in morning urine samples was measured in each patient, a day before starting the diet and on the 15th (21st) day after starting it.For the impact assessment of low iodine diet on radioiodine tissue avidity, whole body radioiodine scans before and after low iodine diet were visually compared. **Results:** Following self-managed low iodine diet, all patients were able to significantly reduce their total body iodine content by 50% (range 18-64%). A total of 68 patients (88%) accomplished mild iodine deficiency and 9 patients (12%) achieved the targeted moderate iodine deficiency state. There was no significant difference in the reduction of total body iodine content between groups that underwent two and three-week iodine diets. Furthermore, there was no significant impact of reduced total body iodine content on radioiodine avidity of tumor cells in patients who underwent low iodine diet. **Discussion:** Low iodine diet is an effective way to reduce total body iodine content in patients with differentiated thyroid cancer prior to I-131 administration. However, in patients with biochemically persistent malignant disease, neither mild nor moderate iodine deficiency had an effect on radioiodine avidity of tumor cells.

Radionuclide Therapy & Dosimetry: Bone Metastases - Pain Palliation

EP-0847

Role of tALP and ECOG Performance Status in predicting survival in mCRPC patients receiving 223Ra-dichloride

G. A. Follacchio[1], V. Frantellizzi[1], S. Sollaku[1], M. S. De Feo[1], F. Monteleone[1], M. Liberatore[1], A. Farcomeni[1], M. Pacilio[2], G. De Vincentis[1]; [1]Sapienza University of Rome, ROME, ITALY, ITALY, [2]Policlinico Umberto I, ROME, ITALY, ITALY.

Introduction: In mCRPC patients treated with [223]Ra, several baseline prognostic markers have been identified, whilst only tALP is under evaluation as predictive factor for survival. Aim of this single-center analysis was to assess the predictive role of baseline clinical variables in patients receiving [223]Ra treatment. **Subjects and Methods:** Patients receiving [223]Ra in our Nuclear Medicine Unit were evaluated. Baseline clinical data were retrospectively collected including age, weight, Gleason Score, ECOG Performance Status (PS), number of systemic treatments prior [223]Ra, Hemoglobin (Hb), Prostate-Specific Antigen (PSA) and total Alkaline Phosphatase (tALP). OS was established from first [223]Ra administration until date of death from any cause. To evaluate baseline tALP as predictive marker for survival, median baseline value was used as cut-point to stratify patients into two subgroups and ROC curve analysis was performed. **Results:** 390 [223]Ra cycles were delivered to 92 pts (mean age 73y, mean Gleason Score 8, mean ECOG PS 1.1). Median follow-up from first [223]Ra administration was 6 months (range 1-31 months). Median OS was 10 months (95%CI 7-16 months). Baseline patients' weight, ECOG PS, Hb and tALP were significantly associated with OS. On multivariable analysis, only baseline Hb and ECOG PS were correlated with OS (p<0.001). Median baseline tALP was 226 U/l. For patients with baseline tALP<226 U/l (46 pts) median OS was 14 months (95%CI 11 months-NE), for baseline tALP≥226 U/l (46 pts) median OS was 7 months (95%CI 6-11 months). tALP stratification showed HR=2.291 (95%CI 1.237-4.241, p=0.008). ROC curve analysis built to assess the power of this biomarker as a baseline predictor for survival showed an AUC of 74%. A Predictive Score (PrS) was produced by combining baseline tALP and ECOG PS. One point was assigned for tALP value ≥226 mg/dl and one point was added for every ECOG PS score going from 1 to 3. This resulted in a PrS ranging from 0 to 4. OS for the five subgroups resulted: PrS=0 (10 pts) OS>16 months, PrS=1 (34 pts) OS=16 months, PrS=2 (31 pts) OS=7 months, PrS=3 (14 pts) OS=5 months, PrS=4 (3 pts) OS=3 months. p-value was 0.00121. ROC curve analysis for PrS showed an AUC of 73.2%. **Conclusions:** Baseline tALP was a reliable predictive factor for 6-months survival in mCRPC patients receiving [223]Ra treatment. The Predictive Score composed by baseline tALP level and ECOG PS allowed to identify patients who were more likely to complete [223]Ra treatment thus obtaining the best therapeutic benefit.

EP-0848

Definition of a Predictive Score to guide therapeutic management in metastatic CRPC patients eligible to 223Ra-dichloride treatment

G. A. Follacchio[1], V. Frantellizzi[1], M. Pontico[1], M. S. De Feo[1], F. Monteleone[1], M. Liberatore[1], A. Farcomeni[1], M. Pacilio[2], G. De Vincentis[1]; [1]Sapienza University of Rome, Rome, Italy, ITALY, [2]Policlinico Umberto I, Rome, Italy, ITALY.

Introduction: Despite the increasing clinical experience involving [223]Ra-dichloride use in mCRPC patients, variables that may predict response to [223]Ra treatment are still hard to identify. Aim of this single-center retrospective analysis was to define a Predictive Score based on baseline clinical variables to guide the clinical use of [223]Ra in mCRPC patients. **Subjects and Methods:** Patients treated with [223]Ra in our Nuclear Medicine Unit were evaluated. Baseline clinical data relevant to the survival analysis were retrospectively collected including age, BMI, Gleason Score, ECOG Performance Status (PS), number of systemic treatments prior [223]Ra, Hemoglobin (Hb), Prostate-Specific Antigen (PSA) and total Alkaline Phosphatase (tALP). Due to the heavily skewed distribution of PSA values, a logarithmic transformation was applied for regression analysis. OS was established from first [223]Ra administration until date of death from any cause. A Predictive Score (PrScore) was obtained combining baseline ECOG PS, tALP and PSA. One point was assigned for tALP≥226 U/l, 1 point for PSA≥20 ng/ml and 1 point was added for every ECOG PS score going from 1 to 3. **Results:** 390 [223]Ra cycles were delivered to 92 pts (mean age 73y, mean BMI 25, mean Gleason Score 8, mean ECOG PS 1.1). Median follow-up time from first [223]Ra administration was 6 months (range 1-31 months). Median OS was 10 months (95%CI 7-16 months). Baseline patients' weight, ECOG PS, Hb and tALP were significantly associated with OS. Only baseline Hb and ECOG PS remained correlated with OS (p<0.001) at multivariable analysis. Baseline logPSA resulted significantly associated to OS (HR=1.20, 95%CI 1.02-1.43, p=0.033). PrScore ranged from 0 to 5. Estimated OS for the six subgroups resulted as: PrScore=0-1 (23 pts) OS>11 months, PrScore=2 (24 pts) OS=11 months, PrScore=3 (29 pts) OS=8 months, PrScore=4 (14 pts) OS=5 months, PrScore=5 (2 pts) OS=3 months. p-value was 0.000117. ROC curve analysis for PrScore showed an AUC of 76%. **Conclusions:** The PrScore shows how patients with baseline PSA<20 ng/ml, tALP<226 U/l and ECOG PS≤1 are more likely to complete [223]Ra administrations, thus receiving the best therapeutic benefit from this treatment. The application of the PrScore would allow to simplify the clinical management of mCRPC patients eligible to [223]Ra treatment.

EP-0849

Prediction of the response to the pain palliation radionuclide therapy for metastatic bone pain: the role of 188Re-HEDP SPECT/CT

C. Liu, Y. Zhang, B. Zhu, Q. Yue; Fudan University Shanghai Cancer Center, Shanghai, CHINA.

Purpose: The authors prospectively evaluated the correlation between rhenium-188 hydroxyethylidenediphosphonate (188Re-HEDP) accumulation in tumors and response to the pain palliation therapy in patients with metastatic bone pain. **Methods:** Thirty-six patients (prostate cancer, n=13; breast cancer, n=10, lung cancer, n=13) with bony metastases were enrolled. Analgesic therapies randomly conducted with 30MBq/kg (n = 13), 40MBq/kg (n = 14), 50MBq/kg (n = 9) 188Re-HEDP were evaluated. Anterior and posterior whole-body imagines were obtained using identical acquisition parameters 4 hours after the treatment. 188Re-HEDP tumor uptake ratio(TUR) was calculated. After therapy, patients were followed-up by assessment of pain palliation and clinical outcome for at least twelve weeks. Then according to the efficacy, 36 patients were divided into effective group and void group. The correlation between TUR and therapeutic effect was examined. **Results:** Overall, medium and high degree of pain palliation was achieved in 24 patients (effective group). The EUR of 188Re-HEDP (3.72±0.97) in the effective group was significantly higher (p<0.001) compared with that (1.67±0.26) in the void group. In the 24 responding patients, the mean (±SD) NRS (numerical rating scale) value decreased from 6.5 (±1.7) to 3.8 (±1.2, p<0.001). The difference of the EUR between the long-term (4.22±0.58) and short-term (1.98±0.62) pain palliation was also statistically significant (p=0.003). In all patients, toxicity was low, with moderate thrombopenia and leukopenia (maximum common toxicity criteria grade of 2). The radioactive count of soft tissues background (49.34±0.57) in the myelosuppressive group was significantly higher (p<0.001) compared with that (21.07±0.26) in the no myelosuppressive group. **Conclusions:** 188Re-HEDP is an effective radionuclide used in the palliative treatment of metastatic bone pain. The early uptake ratios of 188Re-HEDP calculated with SPECT/CT may have predictive value for identifying the response. These results will play an important role for clinical individualized medication in the next phase of study.

EP-0850

^{18}DFG PET is predictive of patient outcome in Xofigo therapy

*A. Tofani[1], R. Pirisino[1], P. Pizzichini[1], **F. Scopinaro**[2]; [1]Azienda Ospedaliera Sant'Andrea, Roma, ITALY, [2]Sapienza Università di Roma, Roma, ITALY.*

Introduction: ^{223}Ra Cl$_2$ shows significant advantages in terms of overall survival of patients with castration resistant prostate cancer (CRPC). Ecog status, imaging, blood tests are generally evaluated to select eligible patients; ^{18}F DFG PET is poorly used, altough it is able to indicate the aggressiveness of metastases. **Aim:** To verify if ^{18}F DFG PET is a valuable method to optimize the selection and to predict the outcome of patients for ^{223}Ra Cl$_2$ therapy. Methods. 25 patients were submitted to ^{18}F DFG PET before starting ^{223}Ra Cl$_2$ therapy and divided in two groups by SUV max of the hottest lesion, according with Meirelles et al, 2010: group 1 of 9 patients with SUVmax > 6 and group 2 of 16 patients with SUVmax < 6. **Results:** The two groups resulted matched for ECOG score, bone scan index, Hemoglobin, platelets, PSA. Actually ECOG score was 1.43± 072 in Group 1 versus

1.44± 0.95 in Group 2; bone scan index was 2.6± 0.7 in Group 1 versus 2.4± 0.6 in Group 2, Hb was 12.11± 1.4 g/dl versus 11.92± 1.3, platelets 227000± 108000 vs. 292000± 95000, PSA was 131± 158 ng/ml versus 108 ± 292. Three patients belonging to group 1 died before completing the six month ^{223}Ra Cl$_2$ therapy and only one of them survived more than 1 y. The therapy was completed in all the patients of group 2. All but one patient of group 2 survived more than 1 y. Survival at 1 y from onset of the ^{223}Ra Cl$_2$ therapy showed highly significant difference between the 2 groups (Fisher exact test: P< 0.01). The group 1 showed median survival of 6 months, group 2 of 15 months. At the moment 12 patients of group 2 are still in follow up. The kaplan-Meier curve showed significant difference between groups (Mantel test P < 0.01). HR was 10.59 (95% CI = 2.2 to 51.4). No other imaging or non-imaging method including bone scan, MRI, CT, PSA, ALP, CGA or HB, ECOG score was able to differentiate patients with good from poor life expectancy after Xofigo therapy. **Conclusions:** Our study is in progress, it obviously needs larger cohorts; however it achieved some significant results, though with the present small number. ^{18}F DFG PET discriminates CRPC patients with long to short life expectancy. It can be used when scheduling the patients for Xofigo therapy to improve their prognosis.

EP-0851

Baseline 18F-FDG PET/CT and bone scintigraphy in the prediction of response and prognosis of patients treated with 223-Ra

A. García Vicente[1], F. Pena Pardo[1], W. Martinez Bravo[1], M. Amo-Salas[2], B. Gonzalez Garcia[1], I. Garcia Carbonero[3], J. Villa Guzman[1], B. Sanchez Gil[4], N. Mohedano Mohedano[5], J. Gomez-Aldaravi Gutierrez[6], L. Martinez Dhier[7], A. Soriano Castrejon[1]; [1]General Hospital of Ciudad Real, Ciudad Real, SPAIN, [2]Universidad de Castilla La Mancha, Ciudad Real, SPAIN, [3]Complejo Hospitalario de Toledo, Toledo, SPAIN, [4]Hospital La Mancha Centro, Alcazar. Ciudad Real, SPAIN, [5]Hospital General de Guadalajara, Guadalajara, SPAIN, [6]General Hospital of Albacete, Albacete, SPAIN, [7]Hospital de las Tres Culturas, Toledo, SPAIN.

Purpose: To establish the utility of basal ^{18}F-Fluorocholine PET/CT and bone scintigraphy (BS) in the prediction of treatment response and prognosis in patients with castration-resistant prostate cancer and bone metastases (CRPC-BM) treated with ^{223}Ra. **Subjects & Methods:** Prospective, multicenter and non-randomized study (ChoPET-Rad study). ^{18}F-Fluorocholine PET/CT and BS were performed before the initiation of ^{223}Ra (basal PET/CT and BS). Bone disease was classified attending the number of lesions in basal BS and PET/CT: oligometastatic or multimetastatic disease. The extension of BM was classified in grades (from Grade I: single or oligometastastatic disease to Grade IV: superscan). PET/CT was semiquantitatively evaluated to obtain the SUVmax in the 5 bone lesions with the highest metabolism, and the average SUVmax. The density of BM was classified in predominantly osteoblastic (>50% of blastic lesions), osteolytic (>50% lytic lesions) or mixed. The clinical variables evaluated were: Gleason, baseline levels of prostate specific antigen (PSA), alkaline phosphatase (AP) and lactate dehydrogenase (LDH),

time of evolution of prostate cancer, time of evolution of BM and [223]Ra line. Each patient was clinically and biochemically monitored. Progression free survival (PFS) and overall survival (OS) since the onset of [223]Ra was calculated. Relations between clinical and imaging variables with PFS and OS were evaluated by Pearson, Mann-Whitney tests and Kapplan-Meier analysis. The association of SUVmax, average SUVmax and basal PSA with the prognosis was studied with ROC analysis. **Results:** Of the 28 patients enrolled, multimetastatic disease was found in 85.7% and 68.4% in basal BS and PET/TC respectively. The osteoblastic pattern was the most prevalent (68.4%). The mean±SD of PFS and OS were 6.2±2.7 and 11.6±7.3 months respectively. 6 patients dead and 27 patients progressed during the follow-up. The extension of the bone disease by PET/TC (p=0.031, χ^2= 8.69), AP (p=0.080, χ^2=3.07) and density of BM (p=0.073, χ^2=5.24) showed association with OS. No association was found for the PFS. ROC analysis revealed no significant association of SUVmax, average SUVmax and basal PSA with survival. **Conclusion:** The extension of bone metastases defined by ^{18}F-Fluorocholine PET/CT had prognostic aim in the prediction of OS. None clinical or imaging variable was able to predict the treatment response.

EP-0852

The Effects of prior Docetaxel administration on the result of Ra223 therapy

Z. Képes[1], M. Ilyés[2], Á. Deák[3], A. Vánczku[2], A. Káplár[2], O. Sántha[4], I. Garai[2]; [1]Department of Medical Imaging, University of Debrecen, Debrecen, HUNGARY, [2]ScanoMed Ltd, University of Debrecen, Debrecen, HUNGARY, [3]Medical School of University of Debrecen, Debrecen, HUNGARY, [4]Hospital of the County of Borsod-Abaúj-Zemplén and the Teaching Hospital of the University of Debrecen, Diagnostic and Therapeutic Department of Nuclear Medicine, Miskolc, HUNGARY.

Background: Ra-223 dichloride is approved for the treatment of patients with castration-resistant prostate cancer suffering from symptomatic bone metastases and no evidence of visceral metastatic disease. Ra-223 dichloride is the first alpha-particle emitting radiotherapeutic drug for systemic use. As calcium analogue, it forms complexes with hydroxyapatit crystals especially in the areas of increased bone turnover. In our study we analysed efficacy of the therapy on bone pain and on the survival of the patients treated with Ra-223 dichloride. **Methods:** We treated 51 patients (mean age 68,51 year, 44-89 y) with 271 cycles of Ra-223 dichloride therapy matching the approved inclusion criteria for the treatment. The mean follow-up period was 15 months (6-29 months). The time from the diagnosis of bone metastases to the therapy was mean 3,3 years (1-16y). Every patient had at least 3 bone metastases especially in the axial skeleton. 50 kBq/kg Ra223 dichloride was administered iv. in 6 cycles, with 4-week intervals. During the follow-up we controlled the hematological status with lab tests and the intensity of the pain using 10-point visual scale. 22 patients got chemotherapy (Docetaxel) before Ra-223 therapy. All statistical calculations were carried out by IBM SPSS statistics software. **Results:** 36/51 patients completed 6 cycles of radioisotope therapy. We had to

discontinue the treatment in 15 cases. The median overall survival after Ra-223 therapy was 11 months. Kaplan-Meier analysis proved that there is no significant difference in survival time between patients who underwent chemotherapy prior to Ra-223 therapy or did not (12 months vs. 11 months). The significance was calculated by Breslow (Generalized Wilcoxon) test, p=0,506. We could not find significant changes in laboratory parameters (Mann-Whitney test) during the therapy. Jonckheere-Terpstra test was applied to examine trends in pain response during the treatment. The p=0.000 indicated the differences in pain (the median of pain value changed from score 6 to score 2). **Conclusion:** Radium-223 dichloride is the first systematic α-emitter therapeutic agent that has shown significant benefits to soothe bone pain in prostatic cancer patients having bone metastases.

EP-0853

Semiquantitative evaluation of 223Radium-dichloride uptake in bone metastases during radiometabolic therapy in castration-resistant prostate cancer

A. Cimino, A. Niccoli Asabella, C. Ferrari, V. Lavelli, C. Altini, N. Addante, M. Fanelli, G. Rubini; *Nuclear Medicine Unit, AOU Policlinic of Bari, University of Bari, bari, ITALY.*

Aim: The aim of the study was to set up a reliable method for a semiquantitative evaluation of 223Radium-dichloride (223Ra) uptake in bone metastases (MTX) and to correlate it with serum alkaline phosphatase (ALP), prostatic specific antigen (PSA) levels and pain during radiometabolic therapy (223Ra-Th) in patients with castration-resistant prostate cancer (CRPC). **Methods**: Eight patients with symptomatic multiple bone metastases from CRPC underwent 223Ra-Th, consisting of 6 administrations of 55 kBq/kg iv every 28 days. A planar whole-body scan (RaS) 4 hours after each 223Ra dose (GE Infinia, high-energy collimators, energy peaks: 82, 154 and 270 KeV) was performed. Semiquantitative evaluation was based on drawing ROIs on the 3 most evident MTX identified in pre-therapy 99mTc-MDP whole-body scan. Another ROI was drawn on healthy bone, taken as a reference. The same ROIs were copied on RaS images and mean counts for each MTX were normalized according to the formula: MTX ROI mean counts/healty bone ROI mean counts. ALP, PSA and pain (by the 10-points scale "Brief Pain Inventory-Short Form") were evaluated after every dose of 223Ra. **Results:** 24 MTX were monitored in 8 patients: 9/24 (37.5%) MTX of 3 patients who completed all 6 223Ra doses, 6/24 (25%) of 2 patients underwent 4 doses and 9/24 (37.5%) of 3 patients who received 3 doses. From the first to the third dose an increased 223Ra uptake was evidenced in all MTX. After the fourth administration, among 15/24 MTX, 4/15 MTX (27%) showed an increased 223Ra uptake, 7/15 (46%) a stationary level and 4/15 (27%) a decrease. After the sixth dose, among 9/24 MTX, there was an increased 223Ra uptake in 1/9 (11%), a stationary result in 2/9 (22%) and a decrease in 6/9 (67%). ALP values showed a decrease after each 223Ra administration in all patients, while PSA level demonstrated a variable course; both parameters moved independently from 223Ra uptake trend. After the last 223Ra dose, pain resulted improved in 5/8 (63%) patients, stationary in 1/8 (12%) and worse in 2/8 (25%). **Conclusion:** Our

results showed the RaS semiquantitative analysis reflected the trend of treatment response and, after the fourth administration, MTX uptake reduction could be predictive of 223Ra-Th success. The method we propose has the advantage to be easily reproducible and based on already available data which can integrate ALP biomarker role, obtaining clinically relevant information.

EP-0854

Description of the first 51 patient trated with Radium 223 dichloride in Argentina

M. J. Bastianello[1,2,3]; [1]Instituto Universitario CEMIC, Ciudad de Buenos Aires, ARGENTINA, [2]Instituto Alexander Fleming, Ciudad de Buenos Aires, ARGENTINA, [3]Clinica Reina Fabiola, Cordoba, ARGENTINA.

Objective: Here we describe the experience with Radium-223 dichloride in Argentina, prior to the start of its commercialization. **Methods:** 51 patients received Radium-223 between Aug-2014 and Nov-2016. Treatment scheme was: 50kBq/kg once every 4 weeks, for 6 total injections. For the purpose of this description, we retrospectively collected age and ECOG-PS for all 51 patients. Also; we collected the following blood parameters: Hb, ANC, platelets count, ALP, PSA; along with prior systemic treatment lines for metastatic disease, for 30 patients. All the patients had bone scan with two or more bone metastases and not known visceral metastases. As describe by other authors, it seems that benefit from Radium-223 is maximized receiving full treatment scheme. Because of that, we also described this experience splitting the group in: patients receiving 1 to 4 doses and patients receiving 5 or 6 doses. **Results:** among all 51 patients, median age was 72yo; and median dose received was 6. When splitting, group of doses 1-4 median age was 73yo, median dose received was 2. 16 patients were ECOG 2; 5 patients ECOG 1, 1 patient was ECOG 0 and 1 patient was ECOG 3. 10 patients received Radium-223 in 3rd line treatment, 3 in 2nd line, and 1 in 4th and 5th line. Media of lab works were: Hb 10.9mg/dl; ANC 4402; platelets count 216000; ALP 391 UI/L; and PSA 317 ng/ml. Group of doses 5-6 median age was 72yo, median dose received was 6. 12 Patients were ECOG 0; 9 patients ECOG 1; 6 patients ECOG 2; and 1 patient ECOG 3. 5 patients received Radium-223 in 3rd line of treatment; 4 patients in 2nd line; and 2 patients in 1st, 4th and 5th line. Media of lab works were: Hb 11.35mg/dl; ANC 4128; platelets count 184000; ALP 759 UI/L; and PSA 303 mg/ml. **Conclusions:** Radium-223 dichloride is a novel therapeutic agent for mCRPC, many aspects are still to be defined. It is important to note that patients receiving 5-6 doses have much better overall survival outcome. From this dataset, no strong conclusions can be made, due to the short number of patients included and the method in which data was obtained. However, it seems that some parameters could be better candidates for deeper analysis for treatment completion prediction. Clinical condition could perhaps be of value, despite of subjectivity of ECOG PS.

EP-0855

Dosimetry of Targeted Ra-223 Treatment for Metastatic Castration-Resistent Prostate Cancer

S. Matsuo[1], S. Kinuya[1], A. Mizokami[1], K. Nakajima[1], H. Wakabayashi[1], T. Kudo[2]; [1]Kanazawa University, Kanazawa, JAPAN, [2]Nagasaki University, Nagasaki, JAPAN.

223Ra selectively targets bone metastases with alpha particle. 223Ra also releases gamma rays accompanying alpha or beta rays. However, the therapeutic effect and its radiation dose assessment have not yet been adequately studied. We investigated the side effects and therapeutic effects of 223Ra radiation therapy by using radiation dosimetry for patients with castration - resistant prostate cancer. The study subjects were 17 male patients with castration-resistant prostate cancer who underwent radiotherapy at our hospital from June 2016. Bone scintigraphy was performed before and after the therapy in all subjects, as well as the measurement of PSA. Bone scan index (BSI), artificial neural network (ANN) value and hotspot number (HSn) were analyzed by a computer-assisted diagnosis system using BONENAVI system (EXNI /FUJIfilm RI farma). Firstly we performed the investigation of phantom study using four types of collimators including low-energy general purpose, extendent low energy general purpose, middle energy general purpose and high energy general purpose type. We observed that middle energy general purpose image was more efficient than a dedicated alpha detector which showed remarkably decreasing counting rates. We therefore constructed procedures and standards for handling 223Ra in clinical practice. For evaluation of whole body distribution of 223Ra, planar images and SPECT• CT imaging were carried out in three cases using SPECT• CT apparatus. Our preliminary findings obtained in our institution was that bone scan index was useful in monitoring the patients regarding pre- and post-treatment. It could be a future prognostic indicator for 223Ra treatment when alpha treatment can be monitored with bone scan index of boneNAVI. Detailed information on a lesion of bone metastasis and non-metastasis accumulation and irradiation dose evaluation was obtained with radiation dosimetry. The accumulation of normal tissue was found to be low in relation to targeted tumor cell. We also observed symptom regarded as side effects in half of the subjects. The symptom after the injection included the increase of bone pain as well as bone pain loss, exacerbation, loss of appetite and so on during the treatment. There was a significant relationship between the site of 223Ra accumulation and the symptom of side effects by the treatment. The evaluation of radiation exposure dose in the non-target organ including intestine, bone, urinary bladder could be recognized with 223Ra imaging. **Conclusion:** Alpha treatment can be monitored by nuclear medicine detectors under optimization of measurements. Side effect might be predicted with imaging of 223Ra.

EP-0856

Safety, effectiveness and haematological toxicity of 223Ra-dichloride: a single Centre experience

R. Laudicella, F. Minutoli, A. Sindoni, F. E. M. Quattrocchi, L. Sturiale, S. A. Pignata, B. Pagano, S. Baldari; Unit of Nuclear Medicine, Department of Biomedical and Dental Sciences and of Morphofunctional Imaging; University of Messina, Messina, ITALY.

Aim: ^{223}Ra-dichloride is an alpha-emitting radiopharmaceutical approved for treatment of adults with castration-resistant prostate cancer (CRPC), symptomatic bone metastases and no visceral metastases. The aim of this study is to describe our experience in this set of patients, evaluating safety, effectiveness and haematological toxicity of ^{223}Ra-dichloride treatment. **Materials and Methods:** We retrospectively evaluated forty-six patients (mean age 73.2 ± 7.3 years, range 57 - 89) treated in our centre. CT scan and bone scan were performed at enrolment. Pain scores, complete blood counts, serum Alkaline phosphatase (sALP) and prostatic specific antigen (sPSA) were evaluated at baseline and before each ^{223}Ra administration. ^{223}Ra-dichloride was administered at the therapeutic activity of 50 or 55 kBq/kg i.v. every 28 days for a maximum of 6 cycles (median 3.5, range 1-6). 30/46 patients were previously treated with docetaxel. 24/46 patients underwent 4 or more treatments (12/46 underwent six cycles of treatment). **Results:** Overall, 172 administrations were performed in 46 pts. Mean sPSA at enrolment was 616.1 ng/ml). Baseline pain score, haemoglobin, white blood cells and platelets counts were 2.67 ± 2.68, 12 ± 1.41 g/dl, 7423.41 ± 2306.17/mmc and 262146.34 ± 105672.98/mmc, respectively. 23/46 patients experienced a condition of pain relief/stabilization and reduced pain drugs intake, whereas 23/46 had mildly worsening pain. Percentage of patients showing reduction in sPSA values increased linearly with the number of radiopharmaceutical administrations (R^2=0.9975, P=0.0319). ALP values dropped more significantly in patients receiving more administrations (79% after 4, 63% after 5 and 71% after 6 cycles). None suffered from anorexia; delay in treatment for toxicity occurred only in 1 patient. Cholecystitis occurred in one and diarrhoea in 10/46 (21.7%) cases. After last treatment, 39 patients had mild-moderate anaemia whereas only one patient had severe (i.e. between 6.5 and 7.9 g/dl) haemoglobin reduction; 11/15 patients with moderate-severe anaemia were previously treated with docetaxel (mean haemoglobin levels at baseline and after last administration were 11.73±1.38 g/dl and 10.54±1.96 g/dl, P<0.001). Mild-moderate thrombocytopenia occurred in 9 patients. **Conclusion:** ^{223}Ra-dichloride can be safely used, leading mainly to mild/moderate haematological toxicity (more frequently in patients previously treated with docetaxel). This approach allowed to reach significant pain relief with reduction of pain drug consumption and biomarkers decrease in the majority of patients with a favourable hematologic toxicity profile; in particular, in our experience ALP values decreased earlier than PSA values.

EP-0857

Co-existing lymph node and bone metastases may be negative predictive marker of survival in patients with CRPC treated with 223Ra-dichloride

S. Dizdarevic, M. Jessop, P. Begley, A. Robinson; Brighton and Sussex University Hospitals NHS Trust, Brighton, UNITED KINGDOM.

Aim: Aim of this study was to investigate a prevalence of co-existing bone and lymph node metastases in patients treated with 223Ra-dichloride in relation to bone disease burden as assessed by bone scintigraphy and the overall survival outcome in routine clinical practice. **Methods:** All patients treated in period March 2014 to March 2016 were included. Extent of bone disease (EOBD) was categorised from a pre-treatment bone scan: EOBD1< than 6 metastases, EOBD2 = 6-20, EOBD3 >20, EOBD4 = 'superscan'. Overall survival was assessed for following groups: Group 1- baseline lymph node metastasis; Group1a-lymph node progression; Group 2-no lymphadenopathy at any stage. Two patients developed new lymph node disease during the course of treatment-Group 3. Overall survival was defined as the time from first dose to the date of death, regardless of cause. A log-rank test was applied to Kaplan-Meier survival analysis. EOBD was correlated with lymph node disease. **Results:** Forty-four of 57 patients with recent cross-sectional imaging within 3 months were assessed for lymph node involvement: 12/44 (Group 1; 27.3%), all had small volume lymph nodes, of which 5/12 (Group 1a; 41.7%) progressed during the treatment; 32/44 (71%) did not have lymph nodes at baseline and 30/44 (Group 2; 68%) did not have lymph nodes at any stage, as 2/44 developed new lymph nodes during the treatment (Group 3;4.5%, small size sample). Group 1 (median survival 201days; IQR 111.75-268.5) and 1a (median survival 201days; IQR 160.5-302.75) have statistically shorter survival times (p < 0.01) than Group 2 (median survival 277days; IQR 111.5-374.5). Four/12 (33.3%) patients with lymph node disease had EOBD 4; 4/12 (33.3%) had EOBD3; 2/12 (16.7%) had EOBD 2 and 2/12 (16.7%) had EOBD 1. In-group 1a, 1/5 (20%) patient had EOBD1, 2/5 (40%) patients had EOBD3 and 2/5 (40%) had EOBD4. **Conclusion:** More than a quarter of patients had co-existing lymph node disease prior to 223Ra-dichloride in this study, with significantly poorer survival than those with no lymph nodes. Co-existent lymph node disease or its progression during the treatment may be negative predictive markers of survival. This preliminary data also suggests that the co-existent lymph node disease seems to correlate with bone disease burden, although it may be present regardless of EOBD. Patients with co-existing bone and lymph node metastases should be considered for combined treatment at an earlier stage and larger prospective studies should be undertaken to assess their outcomes in relation to treatment prescribed.

EP-0858

Experiences with Xofigo (^{223}RaCl$_2$) Therapy

R. Német[1], Z. Besenyi[1], L. Pávics[1], A. Maráz[2]; [1]Department of Nuclear Medicine, University of Szeged, Szeged, HUNGARY, [2]Department of Oncotherapy, University of Szeged, Szeged, HUNGARY.

Introduction: Prostate cancer is one of the most common malignant tumor in men. The disease prognosis is poor, metastases are common, 85-90% in the bones. The treatment with Ca analog ^{223}RaCl$_2$ (Xofigo) is the first alpha emitting product not only relieves bone pain, but also improves the overall survival of the patients. **Methods:** 30 patients were involved in the sudy treated with Xofigo. 141 treatment with ^{223}RaCl$_2$ were performed (mean activity was: 4.37 (± 1.3) MBq) Haematological parameters of the patients were tested before each treatment. For

the first treatment they arrived with medical referral and bone scintigraphy result. The pain intensity changes were measured by Visual Analog Pain Scale (Pain Assasment Scales, NIPCTM). Bone scintigraphy was performed within 3 months before and after therapy. **Results:** According to the hematological parameters there were no significant changes in red blood cell, hemoglobin and platelet counts. In red blood cell 0.7 (±0.18), T/L, in hemoglobin 10 (±4.56) g/L, and in platelet 90 (±17.37) g /l average decrease was only observed. Higher decrease was found in white blood cell and neutrophil granulocyte count, in white blood cell 3 (±1.031) g/L, and in neutrophil count 1.8 (±0.6) g/l. 16 patient got the full six cycle treatment. The therapy was suspended in 3 cases due to major haematological changes. In those cases when patient received less than 6 cycle of treatment, the treatment was terminated due to other reasons, undependently from the Xofigo therapy (predominantly visceral progression). The bone pain intensity of the patients were gradually decreased during the treatment. In most cases after the fourth cycle the bone pains were almost completely gone. Based on the numeric pain scale, the pre-treatment mean value 6.4 (±2) was decresed to 1.2 (±1) post-treatment. Comparing the pre and post therapy bone scintigraphy images, in most cases the number and/or the intensity of the bone metastatic lesions were reduced. **Conclusion:** The alpha-emitting ^{223}RaCl$_2$ is safely used for the treatment of castration-resistant prostate cancer with bone metastasis. Compliance with the general rules of radiation safety, increased background radiation was not observed. The condition of the patients usually were improved, their bone pains were decreased, almost in every cases completely disappeared. Bone scintigraphy is suitable to follow-up the treatment effectiveness.

EP-0859

Samarium-153-EDTMP For Bone Pain Relief in Patients With Metastatic Superscan

I. Slim, I. El Bez, I. Meddeb, M. Somai, T. Ben Ghachem, A. Mhiri, I. Yeddes, M. F. Ben Slimene; Department of Nuclear Medicine, Salah Azaiez Institut, Faculty of Medicine of Tunis, University of Tunis El Manar, Tunis, TUNISIA.

Introduction: Bone metastasis are a major complication of several different cancers and can lead to severe pain. Bone-seeking radiopharmaceuticals are one of the available therapeutic tools for palliation of bone pain. It may be preferable in the case of diffuse metastatic bone involvement. Aim: the aim of our study was to assess the effectiveness of Samarium-153- EDTMP for palliation of metastatics bone pain in patients with superscan appearance on bone scintigraphy. **Subjects and Methods:** between January 2004 and December 2015, we treated 165 patients with Samarium-153- EDTMP (1mCi/kg) for painful bone metastasis. In 22 from them (20 male, 2 female), a metastatic superscan appearance was faound in bone scintigraphy with various cancers (17 prostate, 2 bladder, 2 breast, 1 nasopharynx). All of this 22 patients had blood cell count within certain limits (leukocyte > 2.5 x 10^9/L and thrombocyte >100 x 10^9/L). Seventy two percent of them were taking opioid analgesics

(16/22). After Radionuclide therapy, patients were followed-up by assessment of pain palliation and hematologic tests every 2 weeks until 2 monthes. **Results:** pain palliation was achieved in 55% of patients (12/22), without change of the opioid analgesics consumption. In the 12 responding patients, the mean VAS (visual analogue scale) value decreased from 6.5 (±1.51) to 3 (±1.1; p<0.05) and the mean Karnofsky value increased from 53% to 69% (p<0.05). The pain relief was complete in only three patients. Hematologic toxicity was observed in 63% of patients (14/22). Grade 2 or less toxicity was observed in 72%. Grade 3 anemia was noted in 4 patients. Thrombopenia and leukopenia were reversible in all patients except one with rapid progression of disease. **Conclusion:** Samarium-153- EDTMP treatment is safety in painful bone metastasis in patients with superscan. However, it seems to be less effective than in patients with focal bone metastasis. Nevertheless, in responder subjects, a significant improvement in quality of life was achieved.

EP-0860

Objective response evaluation to therapy with 223Ra-dichloride by absolute quantification of 99mTc-MDP uptake and dose-response relationship evaluation: preliminary results

C. Tranfaglia[1], C. P. L. Fulcheri[2], V. Reggioli[2], R. Tarducci[2], M. E. Dottorini[1]; [1]Nuclear Medicine Department, Hospital Santa Maria della Misericordia, Perugia, ITALY, [2]Medical Physics Department, Hospital Santa Maria della Misericordia, Perugia, ITALY.

Aim: Collecting data for response biomarkers development and dosimetry evaluation may be useful in tailoring and optimizing in the future ^{223}Radium-dichloride treatment. In this study, imaging biomarkers from quantitative ^{99m}Tc-MDP SPECT were evaluated to assess the therapy response and lesion dosimetry was done to gain additional insights into the dose-response relationship. **Subjects & Methods:** A 71-years-old male with symptomatic bone metastases treated with ^{223}Ra-dichloride underwent a ^{99m}Tc-MDP WB scan with quantitative xSPECT/CT study before cycle n.1 and n.4. A SIEMENS Symbia Intevo SPECT/CT was used for acquisitions and quantification was performed by xSPECT-Bone reconstruction. Five lesions were chosen based on prominent symptomatology and/or marked uptake on WB scan. Their contours were delineated by an experienced physician independently on CT and xSPECT images. For uptake volume contouring a 25% threshold in the concentration activity, corresponding to 164 kBq/ml, was applied. Lesions macrodosimetry was performed according to the Italian Multicentre Dosimetric Protocol [Pacilio]. **Results:** During treatment period (5 cycles completed) the patient referred good clinical conditions and stable pain reduction. As side effect only episodic slight nausea occurred. Alkhaline Phosphatase (ALP) reduction was observed (277 UI/L at beginning, 187 UI/L, 187 UI/L and 172 UI/L after the 2nd-3rd and 4th administration of Ra-223 respectively), but no stable reduction of PSA (52.74 ng/ml at beginning and 30.36 ng/ml , 45.46 ng/ml, 48.41 ng/ml after cycle 2-3 and 4 respectively). After completion of the 3rd cycle, a 14% reduction in the metabolically active volume of ^{99m}Tc-MDP was found.

Doses to the lesions studied, considering all treatments, ranges from 4.0 to 8.6 Gy (average 5.9±1.4Gy), tending to reduce in the last cycle (not exceeding 5.8 Gy) **Discussion:** In this patient the absolute quantification of ^{99m}Tc-MDP uptake permitted to objective evaluate osteoblastic activity as a possible marker of response to ^{223}Ra-dichloride treatment. Reduction of bone lesions uptake corresponded to reduction of ALP, DRBE (at last cycle) and pain. Our first results suggest that absolute scintigraphic uptake quantification can be useful for therapy response evaluation, but also for eventual previsional dosimetric evaluations. Although these preliminary data need to be prospectively statistically validated in a large sample of patients and lesions. As found in other studies, one limit of this research was that the image-based macrodosimetry could only approximately reflect real tumor doses. Further xSPECT/CT acquisitions and a more comprehensive dose evaluation will be done at the end of n.6 cycle of this patients and in other patients.

EP-0861

Optimal selection of patients for Xofigo treatment and case report on our first patient with re-treatment

R. P. Jóba, S. Czibor, I. Szilvási; Medical Center, Hungarian Defence Forces, Budapest, HUNGARY.

Aim: In our prospective study, we evaluated various clinical data before, during and after Xofigo treatment (XT) for optimal selection of patients in the post-ALSYMPCA era with novel treatment possibilities. We also report on our first patient with re-treatment. **Materials-Methods:** In the last 32 months 28 patients with mCRPC were treated, and one patient re-treated with Xofigo in our department. The median follow-up period was 16,9±7,1 months. Whole body bone scan (BS) was performed 1 month before the first and 2 months after the last dose. BS was evaluated semi-quantitatively. The serum levels of PSA and ALP were measured before and every eight weeks; hemoglobin, the absolute number of granule- and thrombocytes were measured before XT and every 2nd week. Bone pain was monitored by the NRS-11-scale. One patient after an effective 6 doses XT with no evidence of progression, later had again documented progression in bone. We started a second course of XT with the same protocol. **Results:** 22 patients had a full course of XT. In 6 patients it was discontinued after 1-3 injections, in 4 of them due to severe (grade III-IV) granule- and/or thrombocytopenia. Initial thrombocytopenia, high ALP and tumor burden to the bone on BS correlated with discontinuation of XT. Increase of serum PSA level was more expressed in patients with low initial number of granule- and thrombocytes. In 2 patients serum PSA decreased during XT, both patients had a normal initial number of granule- and thrombocytes and normal ALP level. ALP decreased continuously during XT, however, it started to rise again in the follow-up period. The number and intensity of focal lesions on BS decreased significantly in half of the patients, but the bone pain decreased in 27 out of 28 patients significantly, independently from the initial laboratory parameters. No patient had symptomatic skeletal event. In the re-treated patients after the 3rd injection bone pain improved and ALP reduced without any serious adverse events.

Conclusions: based on our preliminary study XT is very effective in pain relief, but it is better tolerated in patients with a moderate tumor burden to the bone (reflected by the number of granule- and thrombocytes, serum ALP level and number of osteoblastic lesions on BS). This speaks for early access to XT. In well-selected patients re-treatment with Xofigo seems to be promising. Further studies are needed to define biomarkers for selection of patients with increased overall survival after XT.

EP-0862

Evolutionary assesssment with 18F-Fluoride PET / CT in patients with castration-resistant metastatic prostate cancer treated with Ra-223

J. S. Blanco Cano, Sr., A. Garcia Burillo, D. Villasboas Rosciolesi, E. Carrillo Villamizar, J. Castell Conesa; Hospital Universitari Vall d´Hebron, Barcelona, SPAIN.

Objective: Qualitative and evolutionary assessment of skeletal tumor burden in patients with castration-resistant metastatic prostate cancer treated with Ra-223 and its possible correlation with clinical and biochemical parameters. **Population and Method:** Descriptive study including 13 patients (age 76.99 ± 1.41) from February 2016 to February 2017, with castration-resistant metastatic prostate cancer (CRPC) treated with Ra-223, to which PET / CT (Biograph mCT 64s Siemens) with 18F-Fluoride was permormed (5 MBq/kg at 60 min) for evaluation of skeletal metastatic disease. Four patients were treated with 6 doses of Ra-223 were completed and 3 PET-CTs sessions (PreTto/Interim/PostTto) were performed. The rest of them were only treated with 2 PET-CT (PreTto / Interim) sessions. The pattern of metastatic dissemination and its subsequent evolution after the therapeutic doses of Ra-223, the evolution of pain according to the EVA scale and levels of alkaline phosphatase have been qualitatively evaluated. **Results:** We observed different metastatic patterns, 9 of the patients had increased global skeletal diffuse uptake, 3 had multiple poits focal and 1 with presented predominantly monostotic involvement. 2 out of 11 patients were excluded, one due to progression criterion according to medical profesional after the first 3 cycles of Ra-223 and another due to pancytopenia as a side effect after the second dose of Ra-223. In 10 patients the skeletal tumor burden decreased. In 1 patient there was a transient increase in intensity which was interpreted with a flaire effect. 7/11 (63.63%) completed 6 cycles; of them, 4 were exitus at 6 months of the last dose and 3 of them have survived at the present time. 2/11 (18,18%) did not complete the treatment because they were exitus, 1 at 3 months of the third dose and one at month of the fifth cycle. 3/11 (27,27%) are pending completion of the treatment at the time of writing the abstract. The pre-treatment pain obtained an average score of 6.5 points (5-8), after the third cycle this average was reduced to 3.7 points (1-6) and after the sixth cycle the mean was reduced to 1, 6 points (0-4), decreasing analgesic requirements in all patients. In 8 of 11 (72,72%) there was a decrease in alkaline phosphatase values. **Conclusions:** The qualitative evaluation of skeletal tumor burden with 18F-fluoride PET / CT seems to be related to the progressive improvement of alkaline phosphatase values, symptomatology and significant reduction of analgesic needs.

Radionuclide Therapy & Dosimetry: Local Radionuclide Treatment

EP-0863

Yttrium-90 resin microspheres radioembolization (SIRT) of primtive and secondary liver tumors : survival and safety study

V. Frusciante, Sr., G. Castriotta, F. Florio, M. C. D' Arienzo, M. Scarale, A. Ippolito, A. M. Varraso; Casa Sollievo della Sofferenza, San Giovanni Rotondo (FG, ITALY.

Aim: To assess the overall survival and safety of radioembolization in Hepatocarcinomas (HCC), Intrahepatic Cholangiocarcinomas (ICC) and liver metastases (LM). **Methods**: Patients with unresectable HCC or ICC and pts already treated with a first line or second line chemiotherapy for metastases were enrolled. Survival was calculated from the date of first ^{90}Y procedure. National Cancer Institute Common Terminology Criteria (NCI CT-CAE) were used for complications. 24 HCC underwent a total of 26 ^{90}Y microspheres treatments. 4 ICC underwent a total 5 ^{90}Y treatments. 9 pts with liver metastases (8 from colorectal cancer and 1 from pancreatic cancer) were enrolled. Dose administered was calculated from surface area and percentage of neoplastic involved liver. **Results**: Median Survival was 9.61 months for HCC, 19.1 months for ICC, 16,1 months for metastases. As to HCC group we compared by rank sum test PS 0 pts vs PS 1 pts and Child A group vs Child B group; survival was longer in Child A and PS 0 groups but no statistical significant difference was found. A complete response was observed in 5 HCC, 1 ICC and 3 LM; a partial response or stable disease was evident in 17 HCC, 3 ICC and 5 LM. In 20 % of pts we observed fatigue and in 26 % transient abdominal pain. One patient developed grade 3 trombocytopenia. **Conclusion**: SIRT is an effective tool in treatment of HCC (score B or C of BCLC) , in chemorefractory ICC and liver metastases. SIRT is quite safe and effective also in patients with portal invasion.

EP-0864

Clinical Outcome Of "Real Life" HCC Patients Treated With ^{90}Y MicrospheresRadioembolization: A Single Center Experience

M. FINESSI, F. CHECCHI, R. PASSERA, M. BELLO,' G. BISI, D. DEANDREIS; Nuclear Medicine, AOU Città della Salute e della Scienza di Torino, Torino, ITALY.

Introduction: Several phase-2 clinical trials demonstrated that in intermediate and advanced HCC, transarterial radioembolization with ^{90}Y-microspheres (TARE) is well tolerated with impact on overall survival (OS) and time to progression (TTP), in particular in patient with portal vein thrombosis (PVT). Nevertheless guidelines not recommend TARE in clinical management of non-resectable HCC, so in "real-life" patients, TARE is often proposed as palliative cure after multiple treatments. The aim of this study is to investigate OS and TTP in "real life" patients. **Subjects & Methods:** A total of 18 cirrhotic patients (17 male and 1 female) median age 61y (range 52-66) with intermediate to advanced HCC were treated using glass microspheres (Therasphere®). Four patients had bilobar, 14 lobar disease with multiple lesions (median maximum size was 46 mm, range 10-86). Child-Pugh classification was: A5 (n=12), A6 (n=5) and B7 (n=1). Barcelona-Clinic Liver Cancer (BCLC) classification was: B (n=5) and C (n=13). PVT was present in 7 patients. In 10 patients TARE was used ad first line of therapy (naïve), while 8 patients underwent prior several loco-regional treatment such as TACE or radioablation. Prescribed activity was chosen according to standard indications (120 Gy to lobe). TTP and OS were calculated from TARE to the first radiological progression at any site and death from any cause respectively. **Results:** Median administered activity was 2,4 GBq (1,6-2,6). Median follow-up was 3,9 months (2-13,7) after treatment. Objective response was observed in 7 patients. Median TTP and OS for all patients was 5,9 months (2,1-8,4) and 7,4 months (2,0-20,6) respectively. Median TTP for BCLC B and BCLC C was 8,3 months (6,5-20,7) and 2.8 months (2-6) respectively (p= 0.1). Median OS for BCLC C was 6 months (4-not reached)(p=0.079) while all BCLC B patients are alive at the end of follow-up. Statistical analysis found no substantial differences in TTP for different Child score (p = 0.559), PVT (p= 0.312) and previous treatment/naïve (p=0.348) **Discussion:** Compared to clinical trial results, our little cohort demonstrated poor TTP and OS. An explanation could be different patient selection: in phase-2 trials patient are included by strict selection criteria, while in clinical practice often is not possible. Furthermore in our cohort patients BCLC C that have an expected median OS of 6 months were the majority. In conclusion, is mandatory a better selection of "real life" patients to obtain better results in clinical routine. Our hypothesis must be confirmed using a larger patients dataset.

EP-0865

Is the Technetium-^{99m} Macroaggregated Albumin Scintigraphy a Certain Surrogate of ^{90}Y-loaded Microspheres In the Treatment of Primary and Secondary Liver Cancer?

R. De Teresa Herrera, I. Plaza De Las Heras, C. Field Galan, S. Seijas Marcos, B. Rodriguez Alfonso, J. Cardona Arbories, S. Mendez Alonso, M. Mitjavila Casanovas; Hospital Universitario Puerta De Hierro, Majadahonda, MA, SPAIN.

Introduction: The technetium ^{99m} macroaggregated albumin (^{99m}Tc-MAA) single photon emission CT(SPECT) /CT pre-treatment study has been suggested as an useful surrogate in order to plan the treatment of primary or metastatic liver malignancies with ^{90}Y-loaded microspheres. **Subjects and Methods:** A retrospective analysis of patients with liver lesions from either primary or metastatic tumors as a part of the procedure with selective internal radiation therapy (SIRT) studied with ^{99m}Tc-MAA SPECT/CT and ^{90}Y SPECT/CT between 03/2015 and 04/2017 was carried out. We compared the distribution of MAA and ^{90}Y radiolabeled glass or resin particles inside the treatment target lobe in the

cross sectional images of the SPECT/CT and then classified them as consistent (C), when it was similar between both radiotracers, or not consistent (NC), and the relationship between tumor to non tumor uptake ratios (T/NT) was calculated. The C pattern was related with the therapeutic response according to clinical criteria and tumoral viability (EASL, modified RECIST 1.1 criteria) (European Association for Study of the Liver, modified Response Evaluation Criteria in Solid Tumors). Of 38 patients preselected, 6 were excluded because they didn't met the requirements (shunt > 20%, liver failure risk, clinical criteria for progression). We treated 32 patients, 8/32 with metastatic colorectal carcinoma (CRC), 20/32 with hepatocellular carcinoma (HCC) and 4/32 with other tumors (neuroendocrine, GIST, cystic adenoid). **Results:** We treated 32 patients and 42 hepatic lobes. In 26/42 lobes and in 18/32 patients we found a C pattern between MAA simulation and ^{90}Y radiolabeled microspheres therapy. The C pattern was observed more often in patients with primary liver disease (13/32). A better T/NT relationship was found in 22/42 lobes with MAA compared to ^{90}Y. 12/32 patients have a parcial therapeutic response and 20/32 showed progression of the disease. The C pattern was observed in 10/12 patients who responded (83,3%) vs 8/20 unresponsive (40%). **Conclusion:** MAA are a good surrogate for ^{90}Y microspheres. In some patients, the MAA underestimate the distribution of ^{90}Y into healthy liver tissue, thus the pretreatment estimation should be done in a more conservative way. A ^{90}Y post-therapy image should always be perfomed in order to estimate the dose received in both tumor and healthy liver tissue. These data suggest that a C pattern may predict a positive response to treatment although further investigation in needed.

EP-0866

Monte Carlo Based Dose Assessment for ^{90}Y Radioemboliation, a Comparison Between ^{99m}Tc-MAA SPECT/CT and ^{90}Y-TheraSpheres PET/CT

S. Rijnsdorp[1], A. L. Wolf[2], D. E. Oprea-Lager[3], J. J. J. de Vries[3], A. van Lingen[3]; [1]Catharina Hospital, Eindhoven, NETHERLANDS, [2]Netherlands Cancer Institute, Amsterdam, NETHERLANDS, [3]VU Medical Center, Amsterdam, NETHERLANDS.

Aim: Radioembolization of the liver using ^{90}Y-microspheres (TheraSpheres) is a form of selective internal radiotherapy (SIRT) for patients suffering from Hepatocellular Carcinoma (HCC). Eligible patients undergo a SPECT/CT after administration of ^{99m}Tc Micro Aggregated Albumin (^{99m}Tc-MAA) to estimate the distribution of ^{90}Y-microsheres and to determine relevant parameters such as lung shunt fraction (LSF). If the targeting of the tumor(s) is optimal and the radiation dose to the lungs is acceptable, ^{90}Y-microspheres are administered and a PET/CT scan is thereafter performed for control. The activity (GBq) of ^{90}Y-microspheres needed to reach the desired radiation dose (Gy) is determined using the liver volume, calculated from a diagnostic CT scan. This approximation, however, suggests a homogeneous dose distribution. Aim of this research is to assess the agreement between the distribution of ^{99m}Tc-MAA and ^{90}Y-microspheres, as well as the agreement between the desired dose and the true dose in the target area. **Method:** The relative distribution of ^{90}Y-microspheres was estimated in 5 patients, using the activity distributions from ^{99m}Tc-MAA SPECT/CT and ^{90}Y-PET/CT imaging. For the SPECT/CT scan, the assumption was made that the location of the ^{99m}Tc-MAA coincides with the location of the ^{90}Y-microspheres. The CT scans were transformed to 3D matrices containing atomic densities using the conversion from Hounsfield Units to materials. A Monte Carlo simulation using the relative activity distributions was used to calculate the liver dose. β^{-}-particles are emitted isotropically, with an energy specified using a probability distribution. Subsequently, the true dose was calculated by multiplying it with the ratio between the total number of decays in the patient and the number of simulated decays. **Results:** A large difference in radiation dose was found when comparing ^{99m}Tc-MAA and ^{90}Y-microspheres distributions. In addition, the ^{90}Y-microspheres distribution obtained from the PET images in the liver was highly inhomogeneous: up to about 10% of the target volume delineated by the radiologist received a higher dose than the desired dose of 80 - 120 Gy, while large parts of the target volume were underdosed. Improving ^{90}Y-microspheres PET acquisition may lead to less noisy imaging and therefore more accurate calculated dose distributions. **Conclusion:** Relative ^{99m}Tc-MAA distribution does not necessarily comply with the distribution of ^{90}Y-microspheres. Therefore, ^{99m}Tc-MAA scans cannot directly be used for prospective radiation dose assessment. Due to the inhomogeneity of the distribution of ^{90}Y-microspheres, the estimated radiation dose in large parts of the targeted lobe(s) is smaller than the desired dose.

EP-0867

Uncertainties in geometric-mean based lung shunt fraction for 90Y radioembolization

S. C. Kappadath, A. Balagopal, A. Mahvash; UT MD Anderson Cancer Center, Houston, TX, UNITED STATES OF AMERICA.

Purpose: 90Y-radioembolization treatment planning includes determination of the lung shunt fraction (LSF) to maintain mean absorbed dose to lung below 25-30Gy. Geometric-mean (GM) images of the lung and liver following administration of 99mTc-MAA is used most commonly to calculate LSF. The objective of this work is to investigate the sensitivity of GM-based LSF calculations on (1) the relative distribution of 99mTc-MAA within the liver, and (2) the shine through of liver signal in the right lung region. **Materials and Methods:** A retrospective study was conducted on 51 consecutive HCC patients assessed for 90Y-radioembolization at our institution from 2015-2016. Liver and Lung ROI counts from Anterior (ANT) and Posterior (POST) views were extracted for calculating LSF using the following 3 approaches: GM images (LSF_GM), Anterior images only (LSF_ANT), Posterior images only (LSF_POST). The null hypothesis of LSF_GM = LSF_ANT = LSF_POST is true when ANT counts are equal to POST counts for lungs and liver ROIs. If liver MAA distribution is displaced ANT or POST then LSF_ANT or LSF_POST, respectively, will yield the appropriate LSF. Case fractions where (LSF_ANT minus LSF_POST) was substantially different than zero were computed and correlated with liver ANT/POST count

ratios. Lung volumes were extracted via region-growing from diagnostic CT images for 48 patients to calculate the ratio of right/left lung counts/ml. The nominal ratio of right/left lung volume is 1.15. Case fractions were computed for substantially larger right/left lung count/ml ratios, indicative of liver signal shine through into the right lung ROI. **Results:** The mean (range) for (LSF_ANT minus LSF_POST) was 5.5% (0.02%-24.2%), and its magnitude was >2%, >5%, and >10% for 67%, 43%, and 18% of the cases. The mean (range) for liver ANT/POST counts was 2.4 (0.5-17.8). (LSF_ANT minus LSF_POST) correlated (r=0.41; p<0.005) with the ratio of liver ANT/POST counts. The appropriate LSF (either LSF_ANT or LSF_POST) was lower than LSF_GM by >2% and >5% in 39% and 12% of cases. The average (range) ratio of right/left lung counts/ml was 1.45 (0.6-4.4), and its magnitude was >1.3, >1.5, and >2.0 in 54%, 29%, and 13% of the cases. **Conclusions:** Over 67% of radioembolization cases had errors in LSF when using GM_LSF. Clinician review is recommended when (1) absolute(LSF_ANT minus LSF_POST)>2% to select the appropriate view for LSF calculation, and (2) right/left lung counts/ml is >1.3 to assess for liver shine through and redrawn or the right lung contour.

EP-0868

Hepatic Radioembolization With ⁹⁰Y Glass Microspheres: Our Experience

M. L. Dominguez[1], C. Vigil[1], J. E. Rodriguez[2], B. Fernandez[1], A. M. Alvarez[1], N. Martin[1], N. A. Perez[1], C. Salvat[1], F. M. Gonzalez[1]; [1]Nuclear Medicine Department. Central University Hospital of Asturias, Oviedo, SPAIN, [2]Radiology Department. Central University Hospital of Asturias, Oviedo, SPAIN.

Purpose: To follow-up clinically patients with unresectable malignant/metastatic liver lesions treated with ⁹⁰Y glass microspheres (Therasphere©) using intraarterial hepatic radioembolization, and *c*omparison Bremsstrahlung SPECT/CT with PET/CT in treatment verification and detection of extrahepatic uptake. **Subjects & Methods:** Between December 2014 and February 2017, 25 patients eligible for radioembolization were included in this retrospective single-center study. Medium age was 68 years (range 44-82)(88% men). All patients had pre-treatment planning ⁹⁹ᵐTc-MAA planar images in order to assess the lung shunt and SPECT/CT to detect possible shunting into gastrointestinal vasculature and to simulate the liver distribution of the microspheres. Post-procedural imaging (Bremsstrahlung -planar images and SPECT/CT- and PET/CT) confirmed the correct localization of the microspheres in the hepatic tumoral lesions. Therapy responses were determined based on RECIST (Response Evaluation Criteria In Solid Tumors) criteria. Average follow-up was 12.3 months (range 2-28). **Results:** Selection: 3 patients were excluded for the radioembolization: absence of ⁹⁹ᵐTc-MAA in the tumor (2) and pulmonary shunt >20% (1). 22 patients were referred for radioembolization due to hepatocellular carcinoma (15), colorectal tumours (3), neuroendocrine tumor (3) and cholangiocarcinoma (1). Median pulmonary shunt was 8.15%. Treatment: 23 treatments were performed (1 patient was submitted twice with an interval > 2months) to the two lobes (12) or to

one lobe (11). Medium dose administered was 3.2 and 2.9GBq for the two and one lobe respectively. No significant side effects and treatment related complications were observed. Posttreatment images: Bremsstrahlungs-SPECT/CT and ⁹⁰Y PET/CT were similar in treatment verification. SPECT/CT detected extrahepatic uptake in 5 patients: gallblader wall (3), falciform artery (1) and prophylactic cystic artery occlusion (1), and ⁹⁰Y PET/CT detected additional uptake in 2 patients: falciform and origin of gastroduodenal artery. Treatment response: Response assessment was performed and showed complete remission in one patient, stable disease or partial response in 11 patients, and progressive disease was observed in 5 patients, with median progression-free survival time of 7.6 months. Six patients died with a median survival of 7 months (range 5-19): 3 patients without hepatic progression, and 1 with disease progression died because of an encephalitis due to *Listeria*. **Conclusion:** Hepatic selective internal radiation therapy using glass 90Y microspheres is a complex but feasible and safe technique. At our institution, 88% of patients with clinical indication were candidate for treatment, and local control of the hepatic disease was reached in 65% of the treated patients. Y90 PET/CT was superior to Bremsstrahlungs-SPECT/CT detecting extrahepatic uptake.

EP-0869

Comparison of Therapy Response Between PERCIST and RECIST Criteria After Yttrium-90 Therapy in HCC Patients

S. Sager, Sr., E. Akgün, L. Uslu, S. Asa, O. E. Sahin, B. Akovalı, F. Gülsen, M. Abuqbeitah, M. Demir, H. B. Sayman, K. Sönmezoglu; Istanbul University, Cerrahpasa Medical School, Istanbul, TURKEY.

Objective: Y90 microsphere therapy has been increasingly used for treatment hepatocellular carcinoma (HCC) and metastatic colorectal cancer (mCRC). This study aims to compare two different criterias (metabolic based PERCIST and anatomical based RECIST) for evaluating post-therapeutic response within same group of patients. **Material and Methods:** This study comprised of 21 HCC patients with 36 lesions respectively. The lesions were evaluated before and after therapy by CT\MRI or F18-FDG PET/CT as well as lung shunt was priorly demonstrated and hepatic angiography or Tc-99 MAA scintigraphy. Several parameters were analyzed including SUVmax, SUVmean, MTV (metabolic tumor volume) and TLG (total lesion glycolysis). The volume was determined using CT or MRI images for all lesions and the applied activity estimated to impart 120 120±20 Gy for the treated lobe. Following six weeks F18-FDG PET\CT scan was performed to evaluate the metabolic response (PERCIST) and the changes in the volume of each lesion for RECIST evaluation. Upon to that, the overall survival was determined in order to compare the superior criteria for therapy response evaluation. **Results:** There was no major complication noted during course of therapy and 36 lesions were successfully treated. The mean tumor volume of HCC patients before therapy was 70.29 cm³ and similarly calculated as 70.03 cm³ after therapy. The average MTV of the same lesions was calculated 81,29 cm³ before therapy and 60,78 cm³ after therapy using PET images. The consequent evaluation illustrated mismatch between RECIST and PERCIST in

13\36 HCC. The mean overall survival (OS) was calculated 12,2 months. **Conclusion**: Y-90 microsphere therapy seems effective treatment tool for hepatocellular carcinoma HCC. The anatomic method for HCC response evaluation is relatively more accurate while the MTV using PET scan showed great importance in evaluating response of therapy.

EP-0870

Incidence of Kidney Injury Post Y-90 Radioembolization: A Single Centre Experience

W. Peh, Y. Khor; Singapore General Hospital, Singapore, SINGAPORE.

Aim: Up to 85% of hepatocellular carcinoma is inoperable at the time of diagnosis. Selective Internal Radiation Therapy using Yttrium-90 microspheres has emerged as an efficacious locoregional palliative treatment option for these patients as well as for treatment of hepatic metastases from other cancers. While the treatment procedure has a good safety profile with relatively few side effects, contrast-induced nephropathy is a potential complication due to the use of iodinated contrast medium during the hepatic angiography procedures, particularly in patients with existing chronic kidney disease, which is a relative contraindication to the procedure. This study investigates the incidence and risk factors of kidney injury following Y-90 radioembolization. **Materials and Methods:** 171 patients undergoing a total of 180 Y-90 radioembolization treatments from 1 September 2014 and 31 August 2016 were enrolled. Patients were classified into KDOQI stages of kidney disease, with worsening of renal function defined as a progression in stage. The incidence and risk factors of long-term kidney injury were examined. **Results:** The study is ongoing. At baseline, 32 patients (18.7%) were KDOQI stage 2 and below, while 13 patients (7.6%) were stage 3 and below. Within the study population, 7 patients (4.1%) developed transient worsening of renal function which subsequently resolved and returned to baseline, while 7 patients (4.1%) developed permanent worsening of renal function. Associations between higher baseline serum total bilirubin (OR 1.07, p = 0.10), lower serum albumin (OR 0.86, p=0.06) and presence of diabetes mellitus (OR = 1.73, p=0.39) were found with subsequent worsening of renal function, although they did not reach statistical significance. Total amount of IV contrast used during the two hepatic angiography procedures, total administered Y-90 activity, baseline renal insufficiency, prior TACE/chemotherapy and Child-Pugh Score at baseline were not found to be significant risk factors. **Conclusion:** Y-90 radioembolization is associated with a low incidence of long-term renal injury and may be considered as a treatment option even in patients with existing renal impairment.

EP-0871

Autoradiography of a resected hepatocellular carcinoma treated with 90Y radioembolization illustrates uptake differences between viable and infarcted areas

J. Hemmingsson[1], J. Mölne[2], J. Högberg[3], J. Svensson[1], M. Rizell[1], P. Bernhardt[1]; [1]Clinical Sciences, Gothenburg, SWEDEN, [2]Biomedicine, Gothenburg, SWEDEN, [3]Medical Physics, Linköping, SWEDEN.

Introduction: The efficacy of radioembolization (RE) is dependent on a higher concentration of microspheres in tumor tissue compared to normal tissue. In this study the microsphere distribution in differing tissue regions of a resected hepatocellular carcinoma (HCC) has been analysed by autoradiography. **Subjects & Methods:** A 63-year-old man with HCC received a right lobar injection of 2.0 GBq ^{90}Y resin microspheres (SIRTEX®) as neo-adjuvant treatment to lower the risk of recurrence in the resection boundaries. The right lobe consisted of 730 g normal tissue and 270 g of HCC tumor tissue. Resection was made 10 days post-therapy; the tissue was fixated in buffered formaldehyde for 48 hours and sectioned in 2 mm thick slices before being placed between two sheets of autoradiographic film. Images of the slices were fused with the corresponding autoradiography to delineate 4 different regions: normal tissue, viable tumor tissue with and without infarcted areas and tumor/infarction areas with organized haemorrhage (macrophages containing hemosiderin). To enable activity quantification and tissue characterisation, each slice was also punched for biopsies (0.2-0.4 cm^2), fixated and measured in an automatic gamma well counter calibrated for ^{90}Y activity measurements. Each biopsy was sectioned for light-microscopic analysis. **Results:** Compared to normal tissue, the biopsy measurements resulted in activity concentrations roughly 10 times higher for viable tumor and infarcted areas respectively while it was found to be similar for the tumor/infarction area with organized haemorrhage. **Conclusion:** A desirable difference in activity concentration was found between the viable tumor regions and normal tissue.

EP-0872

Multi-modal image analysis for optimized treatment safety and effectiveness of radioembolization of liver tumors

E. Jafargholi Rangraz, K. Baete, M. Koole, G. Maleux, C. Deroose, J. Nuyts; KU Leuven, Leuven, BELGIUM.

Aim: Radioembolization (RE) therapy consists of the intrahepatic administration of beta-emitting spheres (e.g. containing yttrium-90; ^{90}Y-μs) via the different branches of the hepatic artery, feeding different liver lobes or segments. The spheres accumulate at a higher concentration in tumoral tissue than in non-tumoral liver tissue. Dosimetric methods for determination of the injected activity (IA) can optimize treatment safety (healthy liver absorbed dose as predictor of liver toxicity) and effectiveness (tumor absorbed dose as predictor of tumor response). We present a multi-modal image analysis approach, in which a voxelized, personalized absorbed dose map is derived from various pre-treatment image modalities, that can guide the IA calculation. **Material and Methods:** Before treatment, quantitative ^{99m}Tc-MAA-SPECT/CT is performed as a RE simulation, predicting voxel-level fractional uptake (FU) of ^{90}Y-μs. During the angiographic work-up, contrast-enhanced cone beam CTs (cbCT) are acquired in the arterial and venous phase, outlining the perfusion territories of the hepatic artery branches. For patients with FDG-avid tumors, an ^{18}F-FDG-PET/CT is performed to provide tumor metabolic data. After registering all cbCTs rigidly

to an identical space, a so-called meta-cbCT is created by averaging. Subsequently, a non-rigid registration is applied to align this meta-cbCT and the ^{18}F-FDG-PET/CT with the ^{99m}Tc-MAA-SPECT/CT. The whole liver is segmented by a region-growing method, using both CT and ^{18}F-FDG-PET information and tumor lesions are delineated by thresholding the ^{18}F-FDG-PET data while delineation of liver perfusion territories is performed on the cbCT datasets. FU is converted to voxel-level dose maps by using the local energy deposition method for different amounts of IAs. Finally, dose volume histograms and iso-dose contours are generated. This methodology has been tuned on a set of 9 patient studies. Another set of 10 patient studies were used for independent evaluation. **Results:** Image registrations were successful for all test cases. Liver segmentation needed small manual adjustments for 7 cases and significant adjustments for 3 cases. Liver perfusion territories were delineated without any manual adjustment for all the cases. Personalized voxel-level dosimetry were estimated and the IA as obtained with this method were compared with non-dosimetric methods. **Conclusion:** A multi-modal image analysis approach was developed to obtain a personalized liver map (liver, perfusion territories and tumor segmentation) from the pre-treatment ^{99m}Tc-SPECT/CT, ^{18}F-FDG-PET/CT and cbCT images. This procedure provide semi-automatic voxel-level FU predictions based on the ^{99m}Tc-SPECT/CT. By using this workflow, various dosimetry reports can be computed which can be used to evaluate/improve RE treatment safety and effectiveness.

EP-0873

Effectiveness and safety of transarterial Y-90 radioembolization for unresectable intrahepatic cholangiocarcinoma

G. Boni[1], T. Depalo[1], I. Bargellini[2], C. Vivaldi[3], S. Mazzarri[1], F. Guidoccio[1], E. Bozzi[2], L. Caponi[1], C. Traino[4], G. Manca[1], G. Masi[3], R. Cioni[2], D. Volterrani[1]; [1]Regional Center of Nuclear Medicine, University Hospital of Pisa, Pisa, ITALY, [2]Department of Radiology, Vascular and Interventional Radiology, University Hospital of Pisa, Pisa, ITALY, [3]Division of Oncology, Hospital of Pisa, Pisa, ITALY, [4]Health Physics Unit, Section of Medical Physics, University Hospital of Pisa, Pisa, ITALY.

Aim: Preliminary experience to assess the safety, feasibility and clinical efficacy of the single and/or multiple transarterial radioembolization (TARE) with yttrium-90 (Y-90) microspheres in patients with unresectable intrahepatic cholangiocarcinoma (ICC). **Material and Methods:** Since 2012 up to now, all consecutive patients with unresectable ICC, who referred to our center for treatment with Y-90 TARE, were included for this study. All patients previously selected by MRI or CT scans had pre-TARE planning angiography and Tc-99m-MAA SPECT/CT in order to detect possible anatomical variants of the gastrointestinal vasculature, to assess the lung shunt and to simulate the hepatic distribution of the activity. TARE with Y-90 resin microspheres was performed 7-14 days later followed by PET/CT imaging within 24 hours. The estimated activity was determined using the BSA method and voxel dosimetry in selected cases. Response to TARE was evaluated with mRECIST criteria at 4-6 weeks and then every 3 months on CT or MRI scan. **Results:** Twenty patients (13 males and 7 females), mean age of 60±11 years at the time of diagnosis of ICC, were recruited and considered fit for TARE treatment after assessment by angiography and Tc-99m-MAA SPECT/CT. Fifteen patients (75%) received previous treatment with chemotherapeutic agents and surgical partial liver resection in 5 of them. A total of 29 TARE were performed (including dual-lobe treatments in 6 patients and retreatments in the same lobe in 3 patients because of local relapse). The mean injected activity, with single (72%), double (24%) or triple (3%) administration of Y-90 resin microspheres was 0.97±0.33 GBq. TARE procedure was well tolerated; no adverse events were reported, even in patients undergoing multiple treatments. We observed an overall response in 15 out of 20 patients (75%; 3 PR and 12 SD) at 3 months after TARE. In addition, the median time to progression was 7.3 months (95% CI: 5.1-9) in 10/15 responders evaluated during the subsequent follow-up. In the 3 patients re-treated with TARE after local relapse in the same hepatic lobe, 2 patients had SD lasting 5 and 16.4 months; while the third patient had PD one month after TARE. The overall 6, 12 and 18 months survival rate was 95%, 75% and 65% respectively. **Conclusions:** In our experience, Y-90 TARE is a feasible and safe procedure to treat unresectable ICC in the contest of tailored multimodal oncological therapy, useful to provide patients' optimal outcomes.

EP-0874

Radioactive Synoviorthesis on Hemophilic Arthropathy : Tunisian First Cases

I. Slim[1], I. Meddeb[1], I. El Bez[1], T. Ben Ghachem[1], S. Bennour[1], A. Mhiri[1], W. Saied[2], I. Yeddes[1], M. F. Ben Slimene[1]; [1]Department of Nuclear Medicine, Salah Azaiez Institut, Faculty of Medicine of Tunis, University of Tunis El Manar, Tunis, TUNISIA, [2]Department of orthopaedic surgery, Children hospital of Tunis, Tunis, TUNISIA.

Introduction: Radioactive synoviorthesis (RS) has been used to treat chronically inflamed joints refractory to treatment using conventional agents and it has been known as a successful alternative treatment to invasive surgical synovectomy. Aim: we report our first results concerning Radionuclide Synovectomy on hemophilic arthrophaty. **Subjects & Methods**: It concern 20 children aged from 7 to 15 years, with chronic hypertrophic hemophilic synovitis of the elbow (10 joints) and/or the knee (16 joints). We used the Yttrium 90 (Y90) for the Knees and the Rhenium 186 (Re186) for the elbows. Prophylactic coagulation factor infusion was done before the radioisotopes injection witch was performed under surgical conditions. The injections are done under fluoroscopic control (for the elbows) to ovoid extravasation of the isotope. Treated joints was immobilized for 2 days. The scintigraphic control showed homogeneous distribution of the radiopharmaceutics without articular escape. In the follow up until 6 months, excellent response (no bleeding) were observed in 84% for elbows and in 92% for knees. Improvement of the articular range of motion were observed in all children. No adverse events such as radioisotope leakage, local inflammatory reactions were observed during and after RS. **Conclusion:**

We believe that RS should be performed as soon as possible to minimize the degree of articular cartilage damage, which is irreversible, when radioactive materials are available. It is easy to perform and not an expensive procedure. Surgical synovectomy (open or by arthroscopy) should be considered only when consecutive synoviorthesis failed to halt synovitis.

EP-0875
Experience with 223-Radium in the Czech Republic

A. Chodacki; Masaryk Hospital, Usti n. L., KZ a.s., Usti nad Labem, CZECH REPUBLIC.

Xofigo (223-Radium dichloride) is a radionuclide for the treatment of adult men with castration-resistant prostate cancer, symptomatic bone metastases and no known visceral metastases. The State Institute for Drug Control has defined the prescription limitations in Czech Republic. Patients should be treated with docetaxel or be unsuitable for docetaxel prior to administration of Xofigo. Oncologists from Complex Oncological Centers (CCCs) in collaboration with urologists and nuclear medicine physicians are the only ones who can initiate 223-Radium therapy. There are 19 CCCs in Czech Republic, so coverage is optimal. Their 223-Radium application partners are the Departments of Nuclear Medicine. The Czech Nuclear Medicine Society and The Czech Society for Oncology have defined 18 Nuclear Medicine Centers as partners for 19 CCCs. Since January 2017, only 15 hospitals have been contracted with insurance companies. This is why 4 CCCs still have trouble initiating 223-Radium treatment because they should send patients to another CCC that has these contracts. From September 2014, 223-Radium therapy was initiated in 110 patients in all 19 CCCs and 223-Radium was administered in 16 Nuclear Medicine Centers that performed the calibration. Eighty-four patients completed treatment with Xofigo with an average number of 4,8 out of 6 applications. We identified a group of patients after docetaxel (82%) and a docetaxel-free group who were not eligible for docetaxel (18%). 223-Radium is most commonly used as the second line (after docetaxel) or as the third line of treatment (after abiraterone and docetaxel). During three workshops where we met oncologists from all 19 CCCs, we discussed the key success factors of 223-Radium treatment (post-chemo vs. pre-chemo, treatment line of mCRPC, PSA, ALP, etc.). In conclusion, Xofigo is a very safe therapy that can be used after and prior to chemotherapy. Also, the third line of mCRPC treatment does not cause troubles when the patient is in good condition. Elevated PSA should not be the reason to discontinue treatment with 223-Radium. For our patients, we see a good opportunity in 223-Radium therapy in combination with abiraterone, enzalutamide or docetaxel.

EP-0876
Re-188 Patch Radionuclide Therapy for Keloids: A 3 year follow up study

P. Gupta, K. K. Verma, R. Kumar, P. Kumar, A. Malhotra, G. P. Bandopadhyaya, C. S. Bal; All India Institute of Medical Sciences, New Delhi, INDIA.

Background: Keloids are irregularly shaped scars composed of mainly either type III (early) or type I (late) collagen which tend to enlarge progressively. No treatment is 100% effective and invasive methods like surgery lead to recurrence & increase in size. Purpose: The aim of the study was to determine the efficacy of Re-188 radioactive skin patches for treatment of keloids and to determine the long term effects of the patch radionuclide therapy. **Methods**: Eleven patients (2 males and 9 females) aged between 22-62 years with 33 lesions were included in the study. All patients had clinically diagnosed keloids. Fifteen lesions were on chest, 6 on arms, 4 on shoulder, 3 on pubis, 2 each on earlobes and abdomen and one lesion was on neck. All the patients complained of pruritus and pain over the lesions. None had infection or exudations from the lesion. Sealed patches incorporating Re-188 were custom made according to size and shape of the lesions and applied locally on the lesion site. The patches were reapplied on alternate days so as to deliver approximately 50 Gy of radiation dose superficially in total 3 fractions. Patients were followed up initially at 2 weeks, 4 weeks, 8 weeks and 12 weeks. Post 3 month follow up, patients were followed up 6 monthly to determine any recurrence or any long term effects. **Results:** Excellent response with almost complete disappearance of lesion was seen in 14 (43%) lesions. Eight lesions (24%) showed good response and the remaining 11 lesions (33%) demonstrated partial response respectively. There was a greater than 50% decrease in lesion size in 22 (67%) lesions. Spectrum of radiation dermatitis ranging from pain, itching, erythma, crusting and desquamation was observed as side effects in all lesions post therapy which gradually healed by 8 weeks. Routine haematological and biochemical examinations at the follow ups did not reveal any toxicity. None of the lesions had any recurrence upto 3 years post therapy. **Conclusion:** Re-188 Patch Radionuclide Therapy is an effective and safe therapeutic option for treatment of keloids.

EP-0877
Radioactive Synoviorthesis In Chronic Sinovitis. Is It A Good Choice? A Review Of Cases

I. Javato Moreno[1], **B. Perez Lopez**[2], M. E. Martin Gomez[2], P. Garcia-Talavera San Miguel[2], C. Montilla Morales[3], E. Martin Gomez[2], F. Gomez-Caminero Lopez[2], C. A. Achury Murcia[2], M. P. Tamayo Alonso[2]; [1]University of Salamanca, Salamanca, SPAIN, [2]Nuclear Medicine Department. University Hospital of Salamanca, Salamanca, SPAIN, [3]Rheumatology Department. University Hospital of Salamanca, Salamanca, SPAIN.

Aim: Chronic synovitis is a very incapacitating pathology that mainly occurs as a part of a rheumatological disease. It produces destruction of the joints, leading to a significant morbidity in these patients. Local treatment by intra-articular anti-inflammatory drugs or steroids injection attempts to control inflammation and pain to improve quality of life. But it is not effective in many patients, who require surgical ablation of the synovial membrane, manly performed by arthroscopic. Radioactive synoviorthesis (RSO) with yttrium-90 colloid (Y-90) and Rhenio-186 (Re-186) offers a local and minimally invasive

therapy to treat chronic synovitis. RSO has been known as a safe and successful alternative treatment to invasive surgical synovectomy with good results of effectiveness. Our aim is to evaluate the efficacy of RSO with Y-90 and Re-186 in patients with chronic synovitis in our health area. **Methods:** We reviewed retrospectively all patients with chronic synovistis derived from Reumathology Department from January 2011 to December 2016. 36 patients were included, aged from 21 to 83 years old , with hypertrophic and exudative synovitis as a part of rheumatic diseases such as rheumatoid arthritis, psoriatic arthritis and spondyloarthropathies. Radioactive synoviorthesis was performed by an intra-articular injection of 185-222 MBq of radiopharmaceutical colloid of Y-90 and 74 MBq in case of using Re-186. After the administration, treated joint was immobilized for 48 h. Response to RSO was evaluated 6 months post-treatment by measuring changes in intensity of arthralgia according to the visual analog scale (VAS), joint effusion, and range of motion. **Results:** 27 patients were treated with 90-Y, mainly in the knee and 9 were treated with Re-186 in smaller joints. 19 patients of the 27 (70%) treated with Y-90 colloid showed a significant improvement. Clinical parameters such as pain, limitation of movement and effusion decreased in all of them. In 14 patients (52%) of them, there was a total disappearance of the symptoms (complete response) and in 5 (18.5%) a partial reduction of them was revealed. Regarding patients treated with Re-186, there was complete response in the 22% while the 70% showed a partial response. **Conclusion:** Radiosynovectomy has proved to be a safe and well tolerated therapeutic option in the management of chronic synovitis associated to different kinds of arthritis. It should be considered in patients when other therapies (including locally injected steroids) have failed, as an alternative to the surgical synovectomy.

EP-0878

The Relation Between Tumor Metabolic Parameters on F-18 FDG PET/CT, Hepatic Artery Perfusion Scan and Therapy Response in Cholangiocellular Carcinoma Treated with Y-90 Microspheres

M. Bozkurt, B. Volkan Salanci, U. B. Bozkulut, G. Eldem, M. F. Bozkurt, S. Kilickap, B. Peynircioglu, B. Cil, O. Ugur; Hacettepe University Faculty of Medicine, Ankara, TURKEY.

Introduction: For the patients with unresectable intrahepatic cholangiocellular carcinoma (CSC), selective intraarterial Y-90 microsphere therapy (SIRT) is a treatment of choice. In this study, the therapy response after SIRT was evaluated by F-18 FDG PET/CT and CT images in CSC patients and its relation with hepatic artery perfusion scan (HAP) images were assessed retrospectively. **Methods:** We recruited 18 CSC patients (Mean age:54 years±8.9) treated with SIRT between January 2008- November 2016 [Male/Female:15/ 3 (%16,6)]. The relation between HAP, metabolic tumor volume (MTV), total lesion glycolysis (TLG) on F-18 FDG PET-CT images (n:6) both before and after SIRT and pre- and post-treatment abdominal CT (n=10) were determined. The therapy response was evaluated using PERCIST and RECIST criteria. **Results:** Before SIRT, 9 patients had chemother-

apy (%50), 1 patient had radiotherapy (%5.5), 6 patients had a surgical procedure (%33.3), 1 patient had gone through transarterial chemoembolization(TACE) (%5.5) and 7 patients had SIRT as the first line (%38.8) therapy. SIRT was applied in a total number of 20 [glass:13 (%65); resin: 7 (%35), right lobe (n:11), left lobe (n:5) and both lobes (n:4)]. The mean follow-up was 17.7±2.7 months. 13 patients died at follow-up (Overall survival (OS): 11.7 months ± 4.8), 5 patients are still alive during the analysis. The radiation dose applied to right lobe was significantly higher in patients treated with glass microspheres (p:0.001). Microsphere type and OS were not correlated [Resin: 8.7months±2.3, Glass: 9.7months±2.7(p=0.703)]. There were no significant difference between whole blood count, serum markers of liver functions and kidney functions at baseline, 15 days and 4-8 weeks after SIRT. F-18 FDG PET/CT was performed after an average of 1.8 months±0.8 [1-2.9]. Of the 6 patients evaluated, one had stable disease and 5 patients had partial metabolic response. Mean MTV was 301.8 cm3±191.2 and mean TLG was 1783.5g ±1474.9 in baseline FDG PET/CT (mean follow-up: 451.5 days ±273.4). There was no significant correlation between follow-up period and baseline MTV or TLG of these patients (p=0.397 and p=0.208, respectively). **Conclusion:** According to lesion based evaluation, areas of partial treatment response were similar to MAA distribution pattern in HAP scan images, and this distribution pattern might be used to estimate recurrence location.

EP-65   **during congress opening hours, e-Poster Area**

Radionuclide Therapy & Dosimetry: Data Collection Methods & Pharmacokinetics

EP-0879

Quantification of the Fat Fraction in Bone Marrow using Fat-Water Magnetic Resonance Imaging

M. Salas-Ramirez[1], J. Tran-Gia[1], C. Kesenheimer[1], A. M. Weng[2], H. Köstler[2], M. Lassmann[1]; [1]Department of Nuclear Medicine, University of Würzburg, Würzburg, GERMANY, [2]Department of Diagnostic and Interventional Radiology, University of Würzburg, Würzburg, GERMANY.

Aim: In molecular radiotherapies, the assessment of the absorbed dose to the active bone marrow is of high importance, as it is one of the most radiosensitive tissues. Clinically, active bone marrow can be defined as the fraction of bone marrow not occupied by adipose tissue. In the last decade, a growing number of magnetic resonance imaging (MRI) techniques have been developed for non-invasively quantifying the fat-water fraction in human tissues. The aim of this study was to validate a clinically available MRI sequence for quantification of the fat fraction in bone marrow to sound out its potential for patient-specific absorbed dose calculations. **Materials and Methods:** All measurements were performed using a clinical 3T MRI system (MAGNETOM Prisma, Siemens Healthcare). In vitro validation of the MRI sequence was performed with a fat-water phantom consisting of eleven vials with different fat concentrations in

water (between 0% and 100%). The fat fractions in all vials were first measured using CAIPIRINHA DIXON - Volume interpolated breathhold examination (CD-VIBE) sequence (TR: 5.36ms, TE: 2.46ms, flip angle: 9°, total acquisition time: 20.1s, voxel size: 1.25×1.25×2mm³, imaging volume: 325×400×240mm³). Subsequently, magnetic resonance spectroscopy (MRS) acquisitions - the fold standard for MR-based water-fat separation - were performed separately in each vial (volume: 15x15x15mm³, TR: 5000ms, TE: 33ms, 10 averages, flip angle: 90°, no water suppression, bandwidth: 1200Hz). Subsequently, in vivo validation was performed in five vertebrae of three healthy volunteers (volunteer 1: 60y male, volunteer 2: 31y male, volunteer 3: 28y female) using the same sequences (MRI: one abdominal acquisition, MRS: one acquisition per vertebra). **Results:** The MRI-based fat fraction values showed a good correlation with both the nominal values (r = 0.993, p = 0.000) and the MRS-based values (r = 0.992, p = 0.000). An additional Bland-Altman analysis showed a maximum difference of 9.8% between MRI-based and nominal fat fractions and 8.7% between MRI-based and MRS-based fat fractions. The volunteer measurements showed a non-significant difference (p = 0.19) between MRI-based and MRS-based values. **Conclusion:** Our study shows that state-of-the-art MRI imaging (more specifically: the CD-VIBE sequence) holds the potential for fast (acquisition time ≈ 20s for the entire abdomen) and highly-resolved (<2mm isotropic) quantification of the cellularity in bone marrow. By applying such techniques, patient-specific quantification of the bone marrow cellularity could be non-invasively and time-effectively performed to improve internal radiation dosimetry.

EP-0880

A method for ^{177}Lu-PRRT tumour dosimetry based on hybrid planar-SPECT/CT images and semi-automatic segmentation

D. Roth[1], J. Gustafsson[1], A. Sundlöv[2,3], K. Sjögreen-Gleisner[1]; [1]Medical Radiation Physics, Clinical Sciences Lund, Lund University, Lund, SWEDEN, [2]Oncology and Pathology, Clinical Sciences Lund, Lund University, Lund, SWEDEN, [3]Department of Oncology, Skåne University Hospital, Lund, SWEDEN.

Aim: As part of an ongoing ^{177}Lu-Dotatate clinical trial (www.clinicaltrials.gov, NCT01456078) patient image acquisitions are performed for each cycle, and consist of a combination of anterior-posterior whole-body scans at four time points and one SPECT/CT. Image-based activity quantification is made as part of this clinical trial and methods have been presented previously. The aim of this work is to develop and evaluate a hybrid planar/SPECT-based method for tumour dosimetry. **Materials and Methods**: An active ray-based segmentation method is developed and used for tumour delineation in the planar images. SPECT image segmentation is performed using a method based on deformable surfaces. Hybrid planar-SPECT/CT time-activity concentration curves (TACCs) are calculated, where the curve shape is derived from the planar images and is then scaled to the activity concentration estimated from the SPECT image. Evaluation is performed in five patients for whom parallel acqui-

sitions of 4 whole-body scans and 4 SPECT/CT have been made. In addition, Monte Carlo simulated images are used, emulating ^{177}Lu-Dotatate pharmacokinetics and the imaging protocol employed. The hybrid method is evaluated in terms of effective half-lives, time-integrated activity concentration coefficients and mean tumour absorbed doses, using as reference either the SPECT-derived TACCs for patients, or the reference values for the simulated images. The operator dependency in the planar segmentation is also evaluated by comparing regions of interest and effective half-lives obtained from delineation by two operators. **Results and discussion**: In the patient material, the 10th, 50th and 90th percentiles for differences in estimated absorbed doses using the hybrid method and the SPECT-only method are -17 %, -7 % and 6 %, respectively. In the simulated images, it is seen that small tumours are unsuitable for evaluation due to a greater sensitivity to volume inaccuracies and partial volume effects, causing activity concentration underestimations. Tumours located in a surrounding with high peritumoral activity in the anterior-posterior direction might be unsuitable for evaluation since the TACC shape and effective half-life can be affected by the peritumoral pharmacokinetics. The operators' results generally agree well, with a median Dice similarity coefficient of 0.97 and a mean absolute half-life difference of 2 %. **Conclusions** The hybrid planar-SPECT/CT tumour dosimetry method performs well in relatively large tumours not surrounded by high-activity uptakes in the anterior-posterior direction. The planar semi-automatic segmentation offers less time-consuming delineations compared to manual segmentation with little operator dependency.

EP-0881

Radiation self-monitoring data of patients receiving ^{177}Lu-DOTATATE peptide receptor radiotherapy for dosimetry informed radiation protection

L. Livieratos[1,2], T. Brothwood[1], D. Aniceto[1], R. Fernandez[1], C. Sibley-Allen[1], K. Adamson[1], S. Allen[1], V. Lewington[1,2]; [1]Guy's and St Thomas' Hospitals, London, UNITED KINGDOM, [2]King's College, London, UNITED KINGDOM.

Background: Following ^{177}Lu-DOTATATE therapy for metastatic neuroendocrine tumours, radiation protection advice is provided to patients based on short-term whole-body retention measurements undertaken during their hospital admission. Measurements beyond 24 hours would provide evidence to review current practice with accurate, personalised data. This study aims to extend a previous pilot audit and to collate self-monitoring data post-treatment. **Methods:** After demonstration and testing of the measurement procedure during their inpatient stay, patients were given a portable energy-compensated GM monitor to record twice-daily external dose rates at arm's length as fixed detection geometry. These data were cross-calibrated against standard dose rate measurements at 2m. **Results:** Data were collected following 1-4 cycles of ^{177}Lu-DOTATATE therapy from 40 patients living up to 517km from our centre. Over 80 monitoring data sets were acquired. Compliance was excellent with each patient recording data for 14-28 days. A key

motivation appears to be the ability of such measurements to familiarise patients with the concept of radioactivity retention. Effective half-life (slow component) varied from 2.3-4.3 days non decay-corrected. Radiation exposure at arm's length 14 days post-administration varied from 0.9 - 11.0 µSv/hr while maximum (minimum) exposure 20 days post-therapy was 9 (0.39) µSv/hr. Whole-body retention at 14 days varied from <1 to 2.3% of injected activity. MIRD-based whole-body absorbed dose was within the range of values (0.2-0.4Gy) calculated by imaging in similar cohort. **Conclusion:** Self-performed dose rate measurements at home are feasible and realistic for robust data collection for radiation protection, personalised whole-body retention and dosimetry. For the first time, this initiative allows dose rate monitoring and patient participation whilst avoiding geographic and fixed-site equipment constraints. We feel this could have a significant positive impact upon patient care and the safety advice given to patients and their families after radio-peptide treatment.

EP-0882

OpenDose: Generating reference data for Nuclear Medicine dosimetry

M. Chauvin[1], D. Borys[2], F. Botta[3], P. Bzowski[2], M. A. Coca Perez[4], M. Cremonesi[3], J. Dabin[5], A. M. Denis-Bacelar[6], A. Desbree[7], Z. El Bitar[8], N. Falzone[9], L. Ferrer[10], D. Franck[7], N. Lanconelli[11], A. Mairani[12], A. Malaroda[13], K. Matusik[2], E. Mckay[14], M. Pacilio[15], J. Pieter[2], J. L. Rodriguez[16], L. Struelens[5], L. A. Torres Aroches[17], A. Vergara Gil[17], M. Bardies[1]; [1]Centre de Recherches en Cancérologie de Toulouse, Toulouse, FRANCE, [2]Silesian University of Technology, Gliwice, POLAND, [3]Istituto Europeo di Oncologia, Milano, ITALY, [4]MEDSCAN Nuclear Medicine and PET/CT Centre, Concepción, CHILE, [5]Belgian Nuclear Research Centre, Mol, BELGIUM, [6]National Physical Laboratory, Teddington, UNITED KINGDOM, [7]Institut de Radioprotection et de Sûreté Nucléaire, Fontenay-aux-Roses, FRANCE, [8]Institut Pluridisciplinaire Hubert Curien, Strasbourg, FRANCE, [9]Oxford Institute for Radiation Oncology, Oxford, UNITED KINGDOM, [10]Institut de Cancérologie de l'Ouest, St Herblain, FRANCE, [11]University of Bologna, Bologna, ITALY, [12]Centro Nazionale di Adroterapia Oncologica, Pavia, ITALY, [13]University of Wollongong, Wollongong, AUSTRALIA, [14]Saint George Hospital, Sydney, AUSTRALIA, [15]Azienda Ospedaliera Universitaria Policlinico Umberto I, Roma, ITALY, [16]Clínica Las Condes, Santiago de Chile, CHILE, [17]Centro de Isótopos (CENTIS), La Habana, CUBA.

Aim: Radiopharmaceutical dosimetry relies on the location in space and time of radioactive sources, and how emitted radiation propagates and deposits energy in tissues. The latter can be expressed by S-values, which represents the mean absorbed dose (Gy.Bq^{-1}.s^{-1}) in a given target from a single decay in the source. For decades, the only reference data available were S-values generated from mathematical models. The transition from mathematical to voxel-based models requires new reference data, which currently are not freely available. *The Open-Dose project brings together resources and expertise through an international collaboration to generate, validate and disseminate reference dosimetric data to the Nuclear Medicine commu-nity.* **Material and methods:** The ICRP 110 adult female model was selected for a feasibility study. This computational model has 140 segmented tissues-organs (more than 19,000 different source-target combinations). As a preliminary assessment, Specific Absorbed Fractions (SAFs) are being computed, for a compact (liver) and an extended (blood vessels) sources, using 10^8 particles for 7 energy and 2 particle type (photons, electrons). To achieve a suitable energy sampling, 91 monoenergetic emissions will be simulated over the energy range [5 keV - 10 MeV] for both particle type. The reference emission values will be extracted from the MIRD reference book (Eckerman and Endo 2009). **Results:** At the time of writing, 12 partners joined the Open-Dose collaboration, representing most of the major codes used in radiopharmaceutical dosimetry (GATE, Fluka, EGSnrc, MCNP/MCNPX, Penelope). A 3D SAF map (1 source and 140 targets for a single particle energy) represents a 55 MB dataset. For GATE, this required ~1 day for a single energy and 10^8 primary particles on a single CPU. Next steps include: Appraisal and analysis of variations between codes, Integration of SAF results over radio-isotope emission spectra to provide reference S-values, Development of an open database, in a format that allows Nuclear Medicine centres to perform dosimetry and/or benchmark their results against verified reference data. **Conclusion:** The objective is to set up a long-term international collaboration to generate a freely accessible database for use in radiopharmaceutical dosimetry. We demonstrated the feasibility and relevance of the concept, in a structured way that allows further partner integration and generation of reference dosimetric data for new models and computing codes. The computation of SAFs is feasible within a reasonable timeframe that will be further reduced by accessing to various academic computing resources.

EP-0883

Compartmental model for ^{223}Ra-Dichloride in Patients with metastatic bone disease from castration-resistant prostate cancer

J. Taprogge[1], I. Murray[2], G. Flux[2]; [1]St George's University Hospitals NHS Foundation Trust, London, UNITED KINGDOM, [2]Joint Department of Physics, Royal Marsden NHS Hospital, Sutton, UK & the Institute of Cancer Research, London, UNITED KINGDOM.

Aim: In publication 67 the ICRP introduced a generic compartmental model for calcium-like radionuclides, including radium [1]. The aim of this work was to develop a compartmental model for ^{223}Ra-Dichloride in patients with metastatic bone disease from castration-resistant prostate cancer to determine the inter- and intra-patient ranges of rate constants. **Materials and Methods:** Activity retention data were obtained for the whole body and for individual organs of six patients treated twice as part of a "Phase 1, Open-Label Study of the Biodistribution, Pharmacokinetics, and Dosimetry of ^{223}Ra-Dichloride" [2]. A compartmental model was developed by simplification of the ICRP model and adaptation to the available dataset. Compartmental analysis was performed using SAAM II v2.3. The model was populated with activity retention data for plasma, bone surfaces, small intestines, upper large intestines, lower large intestine and ex-

cretion data (faeces and urine) to determine the rate constants. **Results:** Rate constants were determined for 4 patients receiving 2 treatments. The median rate constant from the plasma compartment to the skeleton compartment was determined as 2.5 h^{-1} (range 2.0 - 4.3 h^{-1}) while the median rate constant for the transport from skeleton to plasma is 0.01 h^{-1} (range 0.004 - 0.2 h^{-1}). Excretion occurs mainly via the faeces with a median rate constant of 2.4 h^{-1} (range 1.7-4.0 h^{-1}) from plasma to small intestines (SI). Median rate constants from SI to upper large intestines (ULI) and ULI to lower large intestines (LLI) are 0.05 h^{-1} (range 0.03-0.34 h^{-1}) and 0.03 h^{-1} (range 0.01 - 0.05 h^{-1}), respectively. For each patient the values for the second treatment correlated closely with those of the first. **Conclusions:** A compartmental has been developed specifically for Ra-223 treatment of bone metastases from CRPC. This may be developed to aid understanting of the biokinetics and to facilitate patient-specific treatment planning. References [1] ICRP. Age-dependent Doses to Members of the Public from Intake of Radionuclides - Part 2 Ingestion Dose Coefficients. ICRP Publication 67. Ann. ICRP. 1993; 23:3-4. [2] Chittenden SJ, et al. A Phase 1, Open-Label Study of the Biodistribution, Pharmacokinetics, and Dosimetry of 223Ra-Dichloride in Patients with Hormone-Refractory Prostate Cancer and Skeletal Metastases. J Nucl Med. 2015;56:1304-9.

EP-0884

A method to objectively determine the internalization rate of radiolabelled ligands using mathematical modelling

*A. Vogt[1], **G. Winter**[1], N. J. Begum[2], C. Solbach[1], A. J. Beer[1], G. Glatting[2], P. Kletting[2]; [1]Department of Nuclear Medicine, Ulm University, Ulm, GERMANY, [2]Medical Radiation Physics, Department of Nuclear Medicine, Ulm University, Ulm, GERMANY.*

Introduction and Aim: Individualized molecular radiotherapy is targeting the specific tumour characteristics of each patient for optimized treatment. For this individual treatment planning, physiologically-based pharmacokinetic (PBPK) models show higher prediction accuracy than simpler models but require accurately determined physiological parameters such as the binding kinetics. Substance and cell specific parameters like association rate k_{on} and dissociation rate k_{off} as well as the internalization rate parameter could and should however be determined *in vitro* to reduce the number of undefined parameters in the PBPK model. In this work, a method to objectively determine these parameters is demonstrated for the PSMA-specific peptides PSMA-11 and PSMA-617. **Material and Methods:** The association rate (k_{on}) or dissociation rate (k_{off}) were determined using surface plasmon resonance (SPR) spectroscopy. For internalization experiments the prostate cancer cell lines LNCaP C4-2 and PC-3 were seeded to 12-well plates and specific internalization was obtained by adding the inhibitor 2-PMPA. The experiments were performed for concentrations of 0.09 nM, 0.9 nM, 8.8 nM and 77 nM at 37°C for the following time points: 10 min, 60 min, 120 min and 180 min. Following the washing procedure, the surface bound and the internalized activity were detected separately using a gamma counter (COBRA II, Perkin Elmer). The internalization rate was fitted to the experimental

data using a fixed recycling rate of and a herein developed compartment model employing SAAM II software (The Epsilon Group, USA, ver. 2.2). **Results:** The measured k_{on} ($2.8\pm2.0 \times 10^6$) $(Ms)^{-1}$ and k_{off} ($17\pm9.8 \times10^{-5}$) s^{-1} for PSMA-11 and k_{on} ($3.9\pm2.7 \times 10^6$) $(Ms)^{-1}$ and k_{off} ($5.4\pm4.7 \times10^{-5}$) s^{-1} for PSMA-617, respectively, were implemented in the model and the internalization rate was estimated to be ((0.025 ± 0.0016) min^{-1}). The rate of recycling kr was fixed to 0.04 min^1. **Conclusion:** A method to accurately and objectively determine important parameters in vitro was developed. For the observed substances, the internalization rate seems to be concentration independent. These parameters can be used in patient specific PBPK models to reduce the number of unknown parameters.

EP-0885

A Full Reference Tissue Model with Non-Vanishing Blood Volume Fractions for Kinetic Analysis of Dynamic FDG-PET Data

M. Scussolini[1], S. Garbarino[2], G. Sambuceti[3], M. Piana[1], A. Buschiazzo[3], M. Bauckneht[3], C. Marini[4], G. Caviglia[1]; [1]Department of Mathematics, University of Genova, Genova, ITALY, [2]Centre for Medical Image Computing, Department of Computer Science, University College London, London, UNITED KINGDOM, [3]Nuclear Medicine Unit, Department of Health Sciences, University of Genova and IRCCS AOU San Martino-IST, Genova, ITALY, [4]CNR Institute of Bioimages and Molecular Physiology, Section of Genova, Genova, ITALY.

Purpose: Compartmental models are a basic tool for radiotracer kinetic analysis of PET data and require the Time Activity Curves (TACs) of tracer concentrations in the Target Tissue (TT) and arterial blood, the latter playing the role of Input Function (IF). The determination of the IF is subject to systematic errors and may depend upon a whole-body acquisition. We propose a novel Reference Tissue Model (RTM) for FDG-PET data capable of determining the kinetic parameters of tracer flow in the TT exploiting the TAC of a suitably chosen Reference Tissue (RT) and avoiding the measurement of the IF. **Subjects and Methods:** FDG-PET data of murine models were obtained by means of a micro-PET system (Albira, Bruker, USA). A dose of 3-4 MBq of FDG was injected through a tail vein and the dynamic acquisition lasted 40 minutes. Animals were inoculated subcutaneously in the dorsal hip muscles with murine cancer cell lines CT26 (colon). The regions of interest (ROIs) over the cancer lesion and the resting thigh muscle supplied the TACs of the TT and RT, respectively. The RTM considered a one-compartment RT with negligible bound tracer, a two-compartment TT for free and metabolised tracer, and non-vanishing blood volume fractions for both the RT and TT. The model assumed six exchange parameters: FDG transport from blood to RT and back, from blood to TT (k_1) and back (k_2), FDG phosphorylation (k_3) and dephosphorylation (k_4). Given the measured TACs in the RT and TT, a mathematical procedure was applied providing a unique reconstruction of the kinetic parameters. The method involved the asymptotic Logan plot of the RT and a numerical optimization based on the Gauss-Newton algorithm. **Results:**

Our RTM approach estimated kinetic parameters close to the ones obtained with the full compartmental model comprising the IF (measured on the ROI around the left ventricle): FDG influx rate into the TT k_1 (0.24±0.04 vs 0.24±0.03) was lower than the efflux rate k_2 (0.43±0.06 vs 0.48±0.07); FDG phosphorylation rate k_3 (0.11±0.04 vs 0.12±0.03) was significantly higher than the dephosphorylation rate k_4 (0.04±0.01 vs 0.03±0.01). The results agreed with recent findings in literature. **Conclusion:** The proposed RTM allows the FDG kinetic analysis in the tissue of interest without explicit knowledge of the tracer concentration in the arterial blood. The method proved to be effective in the determination of the kinetic parameters in the case of mice and can be extended to application on human patients.

EP-0886

Investigation of influence of anti-thyroid drug discontinuation time on ^{131}I biokinetics in patients with benign thyroid disease

V. Topic Vucenovic[1], K. Vucicevic[2], Z. Rajkovaca[3], D. Stanimirovic[3], G. Vuleta[3], D. Jelic[4], B. Miljkovic[2]; [1]Department of Pharmacokinetics and Clinical Pharmacy, University of Banja Luka - Faculty of Medicine, Banja Luka, BOSNIA AND HERZEGOVINA, [2]Department of Pharmacokinetics and Clinical Pharmacy, University of Belgrade - Faculty of Pharmacy, Belgrade, SERBIA, [3]Institute of Nuclear Medicine and Thyroid Gland Disease, University Clinical Centre of the Republic of Srpska, Banja Luka, BOSNIA AND HERZEGOVINA, [4]Department of Physical Chemistry, University of Banja Luka - Faculty of Medicine, Banja Luka, BOSNIA AND HERZEGOVINA.

Introduction: Biokinetics of ^{131}I in the thyroid gland shows great inter-individual variability between patients. The aim of the study was to investigate and quantify the influence of anti-thyroid drugs discontinuation time prior the radioiodine uptake test (THDT) on ^{131}I biokinetics in thyroid using nonlinear mixed effect modelling approach. **Subjects and Methods:** Routine clinical radioiodine uptake test data were available from patients with benign thyroid disease. Data on anti-thyroid drugs use and THDT were retrospectively collected from the medical records. Radioiodine uptake (RIU(t)) was measured 4, 24, 48 h, and in some patients 168 h following oral administration of nominal test activity of 1.85 MBq of ^{131}I. Population analysis was performed using NONMEM® software (v7.3) and PsN® (v4.6.0). The influence of other factors such as diagnosis, fT_4 in plasma, functional thyroid volume and age on ^{131}I biokinetics was assessed as well. The two-compartment model was applied to explain ^{131}I biokinetics. FOCE with interaction was used for parameters estimation. **Results:** Data for the analysis included 899 uptake measurements obtained from 366 adult patients. In total, 194 (53%) patients were using methimazole (169 patients) or propylthiouracil (25 patients) within four months before the radioiodine uptake test. The median (range) value of THDT was 21 day (1 - 120 days). According to the developed final model, discontinuation of anti-thyroid drugs use 1 to 9 days prior the application of the radioiodine leads to an increase of the rate constant of the uptake (k_{tu}) for an average 113% (63 - 164%) compared to the non-pretreated patients. The increase

is less pronounced (65.5%), if therapy was withdrawn 10 days before uptake measurement, followed by slow decline to the baseline at rate of 4% per each additional week. Inclusion of THDT in the model (after diagnosis and fT4) decreased the inter-individual variability in k_{tu} from 61.2 to 56.9%. The eligibility of the final model was confirmed by bootstrap analysis and predictive checks. **Conclusion**: Our results show that the time of anti-thyroid therapy discontinuation has significant influence on ^{131}I biokinetics in thyroid of patients with benign thyroid disease and it explained a part of inter-individual variability in ^{131}I biokinetics.

EP-0887

SPECT/CT calibration using clinical dosimetry workstations for peptide receptor radionuclide therapy (PRRT) in patients treated with 177Lu-DOTATATE

E. Mora Ramirez[1,2,3], L. Santoro[4], D. Trauchessec[4], S. Chouaf[4], E. Deshayes[4,5], J. Pouget[5], P. Kotzki[4,5], M. Bardies[1,2]; [1]Centre de Recherche en Cancérologie de Toulouse, France, Toulouse, FRANCE, [2]UMR 1037 INSERM/Université Paul Sabatier, Toulouse, FRANCE, [3]Universidad de Costa Rica, CICANUM, Escuela de Física, San Pedro, San José, COSTA RICA, [4]Department of Nuclear Medicine, Institut du Cancer de Montpellier, Montpellier, FRANCE, [5]INSERM UMR 1194, Montpellier Cancer Research Institute, Montpellier, FRANCE.

Aim*:* Calibration is essential to insure accurate clinical ^{177}Lu dosimetry. Commercial workstations are now available, but there is no standardized calibration procedure to date. In this work we implemented different acquisition protocols to calibrate quantitative imaging for dosimetry on commercial dosimetry workstations. **Materials and Methods***:* GE Healthcare Dosimetry Toolkit (DTK) requires a calibration factor in cps/MBq obtained from planar acquisitions (assuming no sensitivity variation with distance). The HERMES Hybrid Viewer Dosimetry Module™ (HVDM) requires a calibration factor in MBq/counts obtained from SPECT acquisitions. Acquisitions were generated for several configurations: - Planar images at different source to collimator distances using a fillable sphere, - SPECT/CT of a sphere placed in the middle of cylindrical phantom, empty or filled with water, to replicate the procedure implemented in the MetroMRT European project (Wevrett *et al.* Rad Phys Chem 2017). SPECT datasets were reconstructed independently using Volumetrix™ from (GE) and HybridViewer™ 2.6 from HERMES, using OSEM for a combination of reconstructions and corrections methods. Planar sensitivity was estimated using ImageJ and Xeleris™. SPECT sensitivity was estimated using Volumetrix™ and HybridViewer™. Quantitative imaging validation was performed on SPECT/CT acquisitions of an elliptical phantom filled with water and containing a fillable bottle (500 ml) to mimic a kidney imaged at 4, 24 and 168h, by deriving the residences time (exact value should be 1.443xTphy=232h). **Results:** Best reconstruction settings were OSEM (6i, 10ss) using attenuation, collimator response, Gaussian post-filter of 0.11 cm. With HVDM, the main energy window (208keV at 20%) was used and the Hermes scatter correction (based on Monte Carlo modelling) was applied. For DTK, the double energy windows (DEW) scatter correction

was applied using a second energy window (177keV at 10%). Residence time for DTK was 192.95h (-16,16%) with a sensitivity factor (6.11 counts/MBq.s) derived from planar acquisitions. Residence time for HVDM was 219.04h (-4,83%) with a SPECT sensitivity factor of 14,13E-6 MBq/counts. **Conclusion:** The calibration procedure varies a lot according to the dosimetry software, and is far from being standardized. The consequences are that calibrating a given system is a complex process. Still, it is possible to optimize acquisition/processing so that an acceptable accuracy (on phantom) is achieved, and to grant the possibility to compare results obtained from different systems.

EP-0888

Dosimetric estimations using commercial workstations for peptide receptor radionuclide therapy (PRRT) patients treated with 177Lu-DOTATATE

E. Mora Ramirez[1,2,3], L. Santoro[4], D. Trauchessec[4], S. Chouaf[4], E. Deshayes[4,5], J. Pouget[5], P. Kotzki[4,5], **M. Bardies**[1,2]; [1]Centre de Recherches en Cancérologie de Toulouse, Toulouse, FRANCE, [2]UMR 1037 INSERM Université Paul Sabatier, Toulouse, FRANCE, [3]Universidad de Costa Rica, CICANUM, Escuela de Física, San Pedro, San José, COSTA RICA, [4]Department of Nuclear Medicine, Institut du Cancer de Montpellier, Montpellier, FRANCE, [5]INSERM UMR 1194, Montpellier Cancer Research Institute, Montpellier, FRANCE.

Aim: Optimizing peptide receptor radionuclide therapy (PRRT) can be based on the evaluation of absorbed doses delivered to critical organs. Commercial packages are arriving on the market. In this study, we compared dosimetric estimates obtained from different commercial workstations on the same patient datasets. **Materials and Methods:** Two patients (one male, one female) who benefited from PRRT with ^{177}Lu were considered in this study. Images were acquired at 4, 24, 72 and 168h using a SPECT/CT GE-Discovery NM/CT 670. Three software were used: GE Healthcare Dosimetry Toolkit (DTK), HERMES Hybrid Viewer Dosimetry Module™ (HVDM) and DOSISOFT PLANET® Dose (PDose). Projections were independently reconstructed using OSEM (6i, 10ss) with attenuation, scatter, collimator response corrections and Gaussian post-filter was set at 0.11 cm. With HVDM, the main energy window (208keV at 20%) was used and Hermes scatter correction (based on Monte Carlo modeling) was applied. For DTK, the double energy windows (DEW) scatter correction was applied using a second energy window (177keV at 10%,). PDose for systemic dosimetry is under development. Reconstructed slices (from HERMES workstation) were uploaded in PDose. Registration between sequential SPECT/CT was performed in all 3 workstations by taking the first SPECT/CT as reference. Segmentation was generated manually slice by slice. Residence times for liver, spleen, and kidneys could be estimated for both patients on the 3 different workstations. Absorbed doses were calculated with OLINDAv.1 (DTK) and OLINDAv.2 (HVDM). **Results:** Results are given for kidneys, liver and spleen. Residence times in hour (h) were respectively: For DTK: 1.38, 39.38, 0.63 for the female patient, and 1.37, 1.89, 1.17 for the male patient; For HVDM: 1.63, 42.57, 0.71 for the female patient, and 1.61, 2.92, 1.87 for the male patient; For PDose: 0.98,

33.75, 0.61 for the female patient, and 2.64, 2.99, 2.20 for the male patient. Absorbed doses in gray (Gy) were respectively: For DTK: 3.72, 17.80, 2.64 for the female patient, and 2.86, 0.63, 3.99 for the male patient; For HVDM: 3.84, 19.30, 3.44 for the female patient, and 3.27, 1.05, 7.78 for the male patient. **Conclusion:** These preliminary results demonstrate that different commercial workstations provide results in the same order of magnitude. These results will be confirmed on more patients and other software (Stratos). We will also establish the dosimetric consequences of the variability of the residence times, and address the fact that some workstations use pre-computed S values, whereas others compute the absorbed dose specifically.

EP-66   during congress opening hours, e-Poster Area

Radionuclide Therapy & Dosimetry: Preclinical and Clinical Dosimetry & Radiobiology

EP-0889

Eye lens dosimetry of workers during medical interventional procedures and surgery

G. Bera[1], G. Gellie[2], X. Michel[2]; [1]Groupe Hospitalier Pitié-Salpêtrière, Paris, FRANCE, [2]SPRA HIA PERCY, Clamart, FRANCE.

Aims: The lens of the eye is one of the most radiosensitive tissues of the human body, if exposed to ionizing radiation it can develop radiation-induced cataract at early ages. Eye lens dosimetry in interventional medical practices and surgery has been published in few clinical trials and an active debate about the causality of radiation induced cataract is still on-going. In 2007, the International Commission on Radiological Protection (ICPR) recommended a reduction in the annual dose limit for occupational exposure for the lens of the eye from 150 to 20 mSv, averaged over a period of 5 years, with the dose in a single year not exceeding 50 mSv. The compliance to this new requirement could be difficult in some workplace. The aim of this work is to assess the radiation dose to the eye lens of interventional procedures (IP) in the field of cardiology, radiology, gastroenterology and surgery in a military hospital. **Materials and Methods:** This study includes 90 medical practitioners. The measured radiation exposure represented the exposure in a normal working schedule of a random worker during 3 months and this cumulative eye lens dose is extrapolated to 1 year. The eye lens doses are measured from eye dosimeter close to the right/left eye, on the temple, according to the nearest side of the radiation source. For workers wearing lead glasses the dosimeter are placed on the glasses. **Results:** The estimated annual eye lens doses ranges from a minimum of 0.4 mSv to a maximum of 3.5 mSv with an average dose of 1.3 mSv, considering that the use of lead glasses is not taken into account. The average eye lens doses are 1.2 ± 0.5 mSv for the radiological (mainly vascular catheterization, biopsy, infiltrations, embolization), 1.5 ± 0.7 mSv for cardiological (coronarography, ablations, implantation of pacemakers or defibrillators), 0.5 ± 0.3 mSv for gastroenterological (mainly retrograde cholangiopancreatectomy) and 1.3 ±

0.4 mSv for surgical (limbs fractures, vertebroplasty) procedures. **Conclusion:**The estimated annual eye lens dose is well below the revised ICPR's limit of 20 mSv/year for interventional radiology, cardiology and surgery workers. With radiation induced cataract being explained as a possible stochastic effect, without a threshold dose, workers who regularly work in a radiological environment should remain vigilant and maintain radiation safety standards at all times. This includes adequately protective equipment, keeping distance, routine monitoring, appropriate education and for a minority the use of eye dosimeter.

EP-0890

[44Sc] Sc-PSMA-617-an alternative to [68Ga]-PSMA-617 for pre therapeutic dosimetry in metastatic castration resistant prostate carcinoma (mCRPC)?

A. Khawar[1], *E. Eppard*[1], *H. Ahmadzadehfar*[1], *S. Kürpig*[1], *M. Meisenheimer*[1], *J. P. Sinnes*[2], *F. C. Gaertner*[1], *F. Roesch*[2], *M. Essler*[1], *R. A. Bundschuh*[1]; *[1]Department of nuclear medicine, University Hospital, Bonn, GERMANY, [2]Institute for nuclear chemistry, Johannes Gutenberg-University, Mainz, GERMANY.*

Purpose: With 3.9h half life and *in vitro* and *in vivo* characteristics similar to [177Lu]Lu-PSMA-617, [44Sc]Sc-PSMA-617 is assumed to perform better for pre [177Lu]Lu-PSMA-617 therapy dosimetric assessment in mCRPC patients as compared to [68Ga]Ga-PSMA-617 ([68Ga] t½ = 1.1 h). In this study we investigated the biodistribution and evaluated radiation exposure to normal organs with [44Sc]Sc-PSMA-617 in mCRPC patients. **Subjects & Methods:** Four mCRPC patients (mean age 70yr) enrolled for [177Lu]Lu-PSMA-617 therapy were injected 40-62 MBq of [44Sc]Sc-PSMA-617 i.v. Siemens Biograph 2 PET/CT system was used to acquire initial dynamic PET data (30 min) of abdomen in list mode followed by static PET/CT data (skull to mid-thigh) at 45 min, 2 and 18 h post injection (p.i). For qualitative and quantitative analysis dynamic images were reconstructed as 6 images of 300 s. MEDISO interview fusion software was used for drawing VOIs for source organs on CT images and calculating average counts/ml from PET images. Total and % activity in source organs was also determined. Residence times for source organs were calculated using OLINDA/EXM. Sogouros blood based method was used to calculate marrow residence time. Trapezoidal method was used to measure urinary bladder contents residence times. Organ absorbed doses and effective doses were calculated using OLINDA/EXM after applying correction factor for patient weight. Results presented as mean organ absorbed doses and effective doses. **Results:** Physiological tracer uptake was seen in kidneys, liver spleen, small intestine, urinary bladder, salivary glands and pathological uptake in metastases. Total and % activity was seen to be highest in liver followed by kidneys, spleen, small intestine and salivary glands. Residence times for all source organs were found to be higher than residence times of [68Ga]Ga-PSMA-617 in literature. Kidneys received the highest radiation absorbed dose of 3.54E-01 mSv/MBq followed by urinary bladder wall (2.63E-01 mSv/MBq), spleen (1.77E-01 mSv/MBq) and liver (1.10E-01 mSv/MBq). Red marrow dose was found to be 3.28E-02 mSv/MBq. Organ absorbed doses in our study were also higher in comparison with [68Ga]Ga-PSMA-617. The mean effective dose/MBq was found to be 4.1E-02 and thus giving a total effective dose of 2.05 mSv from 50 MBq (ususal clinical dose) of [44Sc]Sc-PSMA-617 in contrast to 4.3 mSv from 203 MBq of [68Ga]Ga-PSMA-617. No adverse pharamacological effects were seen **Conclusion:** [44Sc]Sc-PSMA-617 with less effective dose and better organ absorbed dose calculations seems to be a better alternative for pre [177Lu]Lu-PSMA-617 therapeutic diosimetric assessment.

EP-0891

Assessment of Statistical Dose Uncertainty Propagation for Lu177 SPECT Imaging with an Automated Internal Dosimetry Research Tool as a result of fast SPECT Acquisition Protocols

A. Vija[1], *M. Cachovan*[2], *G. Böning*[3]; *[1]Siemens Medical Solutions USA, Inc., Molecular Imaging, Hoffman Estates, IL, UNITED STATES OF AMERICA, [2]Siemens Healthcare GmbH, Forchheim, GERMANY, [3]Klinikum der Universität München, München, GERMANY.*

Aims: The goal is to assess the statistical based dose uncertainty from SPECT scans as fast as 4 min per bed. We compute the voxelized statistical uncertainty propagation of a 4 time point Lu177 Theranostic acquisition sequence as a function of statistical noise. **Methods:** We use a fully automated dosimetry research tool (DRT). It performs all steps needed for a MIRD based dosimetry as well as voxelized dosimetry using Lu177 Monte Carlo derived dose kernels where the input requires quantitative SPECT data. We use commercially available xSPECT reconstructions (Siemens 2017) from data acquired with Symbia systems calibrated with a 3% NIST traceable Se75 reference source, which is also used to cross calibrate with the dose calibrator. We use research software with 10 realizations of binomial subsampled projection data to get an estimate for the voxelized activity variance. We use as baseline a 7.4 GBq Lu177 injection, with 15 min acquisition time per bed and subsample to 3/4, 1/2, 1/3 and 1/4 using list mode data. The analysis evaluates VOI's in the liver (l), spleen (s) and kidneys (k) as a function of dose uncertainty. **Results:** Dose uncertainty as a function of statistical noise in the reconstructed data equaled (3%, 5%, 4%) in the (l,s,k) VOI's for a 15 min acquisition. The dose uncertainty as a function of statistical noise is best expressed as 1SD per accumulated photopeak Mcounts equaling (l,s,k)=(0.18, 0.30, 0.24) %/Mcounts. With decreasing acquisition time we observed only a mild increase in dose uncertainty of about 1% for each organ for the fastest acquisition speed. This equals to a dose uncertainty of (0.98, 1.46, 1.22) %/Mcounts. Owing to the relatively large VOI of the organs the dose uncertainty for the reduced time acquisitions expressed as the standard deviation of the resulting organ dose equaled (l,s,k)=(0.5%, 2.3%, 2%). **Conclusion:** We found that the dose uncertainty (1SD) due to acquisition time reduction is within 5% for 3 patient datasets for a 4 time point Lu177 protocol using quantitative xSPECT technology. Systematic uncertainty can be controlled using a comprehensive and rigorous reconstruction and compensation scheme. Statistical uncertainty is then the largest source of error, followed by the fitting error.

Dose uncertainty errors can be limited to < 6 % using a mono exponential fit, and are driven by the early time points, implying an optimized workflow is to acquire for same total count at all time points, and subject of future research.

EP-0892

Identification of mediators in media-transferred radiation-induced bystander effect in breast cancer cells

K. L. Madsen, P. F. Høilund-Carlsen, B. B. Olsen; Odense University Hospital, Odense, DENMARK.

Aim: Radiation-induced bystander effect (RIBE) is defined as radiation-like lesions in non-irradiated cells, like those found in directly exposed cells. Current models of the biological effects of external radiation therapy are mostly based on locally absorbed radiation dose, but may be inaccurate if the bystander effect plays a significant role in vivo. RIBE is a result of signals received from nearby irradiated cells and several potential signal mediators have been suggested including nitric oxide (NO), reactive oxygen species (ROS) and recently also microRNA. However, it appears that little is known about the relative contribution of each of these factors. The aim was to investigate if these signal mediators play a role in RIBE in non-irradiated breast cancer cells. **Material and Methods:** Breast cancer cells were irradiated with 2 Gy and the irradiated cell-conditioned medium (ICCM) was transferred to non-irradiated breast cancer cells. ICCM was incubated with RNase to deplete RNA, furthermore DMSO and aminoguanidine were included, which scavenge ROS and NO, respectively. RIBE was analysed by the comet assay, which detects DNA damage within single cells and % tail DNA was calculated using the OpenComet software. **Results:** Ionizing irradiation induced DNA damage in directly irradiated cells since % tail DNA significant increased from 11.9±4.2 (0 Gy) to 24.5±9.8 (2 Gy) (P<0.0001). In bystander cells incubated with ICCM, the % tail DNA also significantly increased from 13.7±10.7 to 25.3±16.1 (P<0.0001). When the ICCM was depleted of RNA the % tail DNA significantly decreased to 15.4±6.3 (P<0.0001). A significant decrease in % tail DNA was also observed when DMSO 12.6±4.8 (P<0.0001) or aminoguanidine 16.7±7.1 (P<0.0001) were included. **Conclusion:** The mediators involved in media-transferred RIBE in breast cancer cells are several, since not only ROS and NO, but also RNA could induce DNA damage observed in bystander cells. This may have significant consequences for the choice between delivering a homogenous or heterogeneous prescription dose to a particular tumour in vivo. Further experiments are needed, in particular to identify the RNA molecules involved in RIBE.

EP-0893

The simulation of a 70% decrease in injected dose doesn't affect the measurement of left ventricular ejection fraction with radionuclide equilibrium angiography planed on the highly-sensitive DSPECT CZT-camera

H. Tissot[1], O. Morel[2], L. Imbert[1,3,4], V. Roch[1,4], M. Claudin[1], M. Perrin[1], A. Verger[1,4,5], G. Karcher[1,4,6], P. Marie[1,4,6]; [1]CHRU de Nancy, Service de Médecine Nucléaire, Nancy, FRANCE, [2]CHRU de Besançon, Hôpital Jean Minjoz, Service de Médecine Nucléaire, Besançon, FRANCE, [3]Institut de Cancérologie de Lorraine, Vandœuvre-lès-Nancy, FRANCE, [4]Plateforme d'imagerie expérimentale Nancyclotep, Nancy, FRANCE, [5]IADI, U947, Inserm, Nancy, FRANCE, [6]Université de Lorraine, Faculté de Médecine, Nancy, FRANCE.

Introduction. Radionuclide equilibrium angiography (RNA) provides a precise and reproducible measurement of the left ventricular fraction ejection (LVEF) but with a rather high body radiation (5.9 mSv for 850 MBq of Tc-99m) for serial monitoring. This study was aimed to determine whether the LVEF measurement, provided by radionuclide equilibrium angiography recorded on the highly-sensitive DSPECT CZT-camera, would be impacted by the simulation of a 70% reduction in injected doses. This level of dose reduction was already shown to be feasible with this camera, but only for myocardial perfusion SPECT exams. **Materials & Methods.** RNA was performed after the in vivo labelling of red blood cells with 850 MBq of Tc-99m in 49 patients who were referred to a conventional 2D recording on an Anger camera (Anger-2D), immediately followed by a 10-min 3D-recording by the D.SPECT camera (DSPECT-100%). The CZT recordings of all projections were subsequently shortened to 30% of their initial durations (DSPECT -30%) in order to provide a 70% reduction in recorded counts. **Results:** mean LVEF values were 62.7+/-11.1% on conv-2D and significantly higher on both DSPECT-100% (66.8+/-14.8%) and DSPECT-30% (66.3+/-15.7%). The correlation coefficients with the LVEF obtained with Anger-2D method were equivalents for DSPECT-100% (r^2=0.73) and DSPECT-30% (r^2=0.70) and with an equivalent overestimation for the highest LEVF values. Finally the DSPECT-30% measurement of LVEF was strongly linked to that provided by DSPECT-100% (r^2=0.94) with a mean difference of only 0.47 point (+/-3.86%) between the 2 measurements. **Conclusion.** A 70% reduction in injected dose is very unlikely to significantly impact the LVEF measurement provided by RNA recorded on the DSPECT camera, although the highest LVEF values appears overestimated by this tomographic technique, whatever the level of recorded counts.

EP-0894

Assessment of Dose Uncertainty Propagation using standardized Quantitative Lu177 SPECTImaging and an Automated Internal Dosimetry Research Tool

A. Vija[1], M. Cachovan[2]; [1]Siemens Medical Solutions USA, Inc., Molecular Imaging, Hoffman Estates, IL, UNITED STATES OF AMERICA, [2]Siemens Healthcare GmbH, Forchheim, GERMANY.

Aims: This study is aimed to assess the voxelized statistical and systematic uncertainty propagation of a 4 time point Lu177 Theranostic acquisition sequence based on standardized quantitative SPECT imaging.A voxelized cumulative dose error over multiple cycles is then possible. **Methods:** We use a fully automated dosimetry research tool (DRT). It performs all steps needed for avoxelized dosimetry using Lu177 Monte Carlo derived dose kernels where the input requires quantitative SPECT data. We use commercially available xSPECT reconstructions (Siemens 2017) from data acquired with Symbia systems calibrated

with a 3% NIST traceable Se75 reference source, which is also used to cross calibrate with the dose calibrator. We use research software to perturb the (cross)-calibration factors, dead time correction (live measurement in real system) as well as other key parameters to estimate systematic uncertainty, and use reconstructions with 10 bootstrap realizations for the voxelized variance estimation. 3D segmentation and labeling sequence creates a multi modal zone map yielding anatomical structure and tumor boundaries, resulting in dose histograms of VOI's. We use 4 time point sand a mono-exponential fit. A numerical phantom with known residence time is used for verifying DRT computations, while patient data was used for remainder of the work. We show work flow feasibility and accuracy from 1 cycle of 1 patient. **Results:** The cross calibration yields a dose uncertainty (1SD) of 1% per 1% deviation of incorrect injection dose(ID). The dead time correction yields a dose error of 0.32% per 1% deviation of incorrect ID. The statistical uncertainty contributes to 0.65% per GBq ID, or 0.29% per Mc in the FOV. The overall dose uncertainty ranges from 2% to 8% for the different organs. **Conclusion:** The internal dose uncertainty from incorrect injection dose measurement propagates 1%-for-1%,and demonstrated the importance for using a standardized reference source for calibrating and cross calibrating SPECT and the dose calibrator. Systematic uncertainty can be controlled using comprehensive and rigorous reconstruction and compensation scheme. Statistical uncertainty is then the largest source of error, followed by the fitting error. Voxelized dose and cumulative dose uncertainties can be computed and displayed for increased confidence. Dose uncertainty errors can be limited to < 8 % for organs such as the kidney, for a standard 4 time point using a mono exponential fit for one cycle. Next steps will expand on this work to establish statistics for a large collective of patient data sets.

EP-0895

Quantification of Gadolinium Nanoparticles Concentration with Preclinical SPECT Scanner

O. Kochebina[1], A. Halty[1], J. Taleb[2], D. Kryza[2], M. Janier[2], C. Mory[1], T. Baudier[1], D. Bar-Ness[1], S. Rit[1], D. Sarrut[1]; [1]CREATIS, Lyon, FRANCE, [2]LAGEP, Lyon, FRANCE.

Introduction: Gadolinium nanoparticles (NP) could be used for tumors radiosensitization. The quantification of NP concentration is a crucial task for radiotherapy treatment as this will define the delivered dose. Image based quantification could be done, for example, on spectral photon counting CT (SPCCT) for Gd detection or single photon emission CT (SPECT) for detection of NPs coupled with In-[111] tracer. This presentation is focused on Gd-NP quantification on phantoms with nanoSPECT/CT scanner. We compare these preliminary results to the SPCCT measurements and outline the pros and cons of each modality for quantification tasks. We will also show the very first preclinical images. **Methods:** For the image quantification we use eight 500µl tubes filled with saline solution with different concentrations of Gd-nanoparticles coupled with In-[111]. We obtain radioactivity concentration distribution with nanoSPECT/CT (Bioscan Inc., Washington D.C., USA) images calibrated with a gamma count-

er. These quantification measurements are compared to results from SPCCT (Philips Healthcare, Haifa, Israel*).* The first preclinical tests is done on the same machines. We scan 5 rats with chondrosarcomas 1h, 2h and 24h post injection. The data analysis is ongoing. **Results:** The preliminary results show that activities above 1 MBq could be observed on nanoSPECT/CT images and that the discrepancy between quantification activity measurements and gamma counter ground values is ~10-20%. Such a large disagreement could be due to several factors that has not yet been corrected: attenuation, scattering, collimator detector response, motion, kinetic of the activity distribution, partial volume effect (spill-in/spill-out) etc. We illustrate importance of the last one in the bias of quantified measurements. **Conclusions:** The quantification of Gd nanoparticles is possible with SPECT and SPCCT imaging for activities above 1 MBq. The preliminary results obtained in phantoms show the linear correspondence between the concentration of nanoparticles in SPCCT images and activity concentration in SPECT images.

EP-0896

Pre-therapy imaging for 90Y microsphere treatment demonstrates limited predictability for tumour absorbed dose

A. J. Craig[1], B. Rojas-Fisher[2], A. M. Denis-Bacelar[3], I. Murray[1], N. Khan[4], A. Maenhout[4], L. Hossen[2], G. Flux[1]; [1]Royal Marsden Hospital NHSFT, Sutton, UNITED KINGDOM, [2]Royal Brompton Hospital NHSFT, London, UNITED KINGDOM, [3]National Physical Laboratory, London, UNITED KINGDOM, [4]Chelsea & Westminster Hospital NHSFT, London, UNITED KINGDOM.

Aim: Pre-therapy imaging is used for treatment planning in 90Y-microsphere therapy. The aim of this study was to compare absorbed doses generated from pre- and post-therapy imaging to determine the predictive accuracy of dosimetry performed with pre-therapy imaging. **Material and Methods:** Retrospective analysis was performed on 11 patients who had undergone 90Y resin microsphere treatment. All patients received a pre-therapy 99mTc-MAA SPECT-CT and a post-therapy 90Y SPECT-CT. Patients were from a mixed group of primary cancers including colorectal, pancreatic and gastro-oesophageal. Patient relative calibration factors converted SPECT counts to activity; the administered 90Y activity was used in both cases. The local deposition method was used to derive pre-therapy and post-therapy absorbed dose maps. Normal and tumoural liver were manually delineated on contrast-enhanced CT scans performed prior to treatment: 109 tumours were identified with a range of volumes of 0.2 to 674cm³. Absorbed dose maps were registered to the delineated contrast-enhanced CT scans in order to determine tumoural and normal liver voxel dose values. Pre- and post-therapy normal liver mean absorbed dose and Biological Effective Dose (BED); tumour mean absorbed dose; and tumour to normal liver ratios (TNR) were compared. Wilcoxon signed ranks tests were performed alongside Bland-Altman and correlation analysis. **Results:** The normal liver mean absorbed dose range for pre-therapy was 17 to 53 Gy (mean 38 Gy, 95% CI: 30 - 45 Gy) compared to 19 to 61 Gy (mean 43 Gy, 95% CI: 35 - 52 Gy) for post-therapy. A strong correlation r=0.9307 (p<0.0001) was

found. Bland-Altman analysis demonstrated a bias of 5 Gy. A strong correlation r=0.7364 (p=0.0128), and a bias of 31 Gy was determined for Normal liver mean BED. The mean tumour absorbed doses for the pre-therapy study were 1 to 218 Gy and 15 to 135 Gy for post-therapy and the Wilcoxon signed ranks established no significant difference (p=0.6769). Moderate correlation r=0.4614 (p<0.0001) was found and a bias of 3 Gy. No significant differences in the medians of TNR (p=0.2568) with a weak correlation r=0.3648 (p<0.0001) were found. **Conclusion:** Tumour mean absorbed dose and TNR demonstrated no difference in sample medians. However there was only moderate correlation and large differences at higher values were demonstrated by Bland-Altman plots. A strong correlation was demonstrated for pre- and post-therapy normal liver mean absorbed doses and BED. Analysis will be extended to include more patients.

EP-0897

Evaluation of dose response after combined bone marrow and lesion based dosimetry

M. Abuqbeitah, M. Demir, N. Yeyin, L. Kabasakal, K. Sönmezoğlu; *Istanbul university, istanbul, TURKEY.*

Aim: Differentiated thyroid cancer (DTC) is a malignant tumor with a favorable prognosis. Despite of Radioiodine (^{131}I) has been used widely, many strategies of radioiodine administration are available at present and determination the optimum effective activity still subject to debate. **Methods and Materials**: Our study includes 3 patients (2 female and1 male) enrolled to dosimetry protocol after failure of empiric therapy with (TSH) ≥ 30 μIU/ml. The age of patients was 33±11 year, Height 1.8±0.1 m, weight 82±7 kg, and the average Tg level was 99±19 ng/ml. 74 MBq was administered for each patient followed by multiple whole body scans and blood samples up to more 96 h. bone marrow dose and lesion dose were estimated and subsequently the therapeutic activity was given after one week. The result of the therapeutic activity was evaluated after 6 months using WBSs and Tg level. **Results:** the residence time of the patients was 63, 37, and 29 h and the maximum safe dose was consequently 9.5, 21 and 26 GBq. Lesion absorbed dose was 0.01-0.15 Gy/MBq. The dose supposed to be delivered after therapy had range 83-824 Gy. After 6 months, WBSs showed disappearance of skeletal lesion with very faint uptake caused by by dose more than 700 Gy. Bone lesions did not show change after delivering doses 80-160Gy. Tg level of patient with positive responding lesions had Tg level 0.02 ng/ml. **Conclusion:** combination between bone marrow and lesion absorbed dose for therapy planning could help to maximize the effective activity to optimize lethal dose especially for bone lesions

EP-0898

Dosimetry study of 99mTc-NTP 15-5 imaging of cartilage in preclinical and clinical trials using the GATE Monte Carlo platform

G. Fois[1,2], *C. Valla*[3], *E. Jouberton*[3,4], *P. Auzeloux*[4], *N. Sas*[3], *F. Cachin*[3,4], *J. Chezal*[4], *E. Miot-Noirault*[4], *L. Maigne*[1,2]; *[1]Clermont Auvergne University, Aubiere, FRANCE, [2]UMR6533 CNRS/IN2P3, Clermont-Ferrand, FRANCE, [3]CLCC Jean Perrin, Clermont-Ferrand, FRANCE, [4]UMR1240 INSERM, Clermont-Ferrand, FRANCE.*

Introduction: Osteoarthritis is one of the most common musculoskeletal disorders, it is a slowly progressive pathology characterized by cartilage destruction leading to joint instability and painful symptoms. A sensitive imaging approach is essential to quantify osteoarthritis progression and monitor response to new therapies. In this context, INSERM/UCA-UMR1240 (Grants: ANR, A-SPECT project; ITMO-AVIESAN) developed a radiotracer called 99mTc-NTP 15-5 (world patent WO 01/00621 A1), which binds to cartilage proteoglycans whose decrease content is associated to a loss of biomedical function of cartilage. We have implemented the whole dosimetry study concerning this new radiotracer for rabbits and humans using the GATE Monte Carlo platform. **Material and Methods:** Absorbed doses to critical organs was determined using the MIRD formalism from bio-distribution data in rabbits obtained by organ sampling at different times after radiotracer injection. Bio-distribution for humans has been extrapolated from animal data using the %kg-dose/g method. Primary sources were cartilage in knees and intervertebral disks due to 99mTc-NTP 15-5 accumulation (about 80MBq.s/g cumulated activity in cartilage for an injected activity of 1MBq), other relevant sources were identified in liver and kidneys. S-factors were calculated for 4 rabbits and one human CT scan. GATE version 8.0 (using Geant4 Standard physics list option 3) has been used for the study. With this version it is now possible to manage DICOM files. This version has been modified to manage RT-struct files in the objective to directly convert segmented CT scans into voxelized volumes. Then, simulations have been performed by defining source and target volumes of interest. Source emission was managed with the split exponential Track Length Estimator (seTLE) method implemented in GATE to reduce computing time while keeping a good level of accuracy compared to a conventional Monte Carlo method. **Results:** The dosimetry performed in the rabbit model, showed self doses for organs such as liver and kidneys in the order of tens of μGy per MBq of injected activity. Doses for organ at risks for human, especially for bone marrow, bones, kidneys and liver were evaluated to be lower the limits usually recommended for diagnostic imaging in nuclear medicine. **Conclusions:** The dosimetry profile of 99mTc-NTP 15-5, in the context of preclinical trials, is of major importance in order to make sure that organs at risk will not be overexposed for diagnostic imaging. This study also shows the possibility to perform a complete internal dosimetry calculation using GATE.

EP-0899

Relative error in the Survival Fraction and the Biologically Equivalent Dose due to uncertainties on the absorbed dose estimations in Molecular Radiotherapy

A. Malaroda; University of Wollongong, Wollongong, AUSTRALIA.

Aims: In Molecular Radiotherapy, it is widely accepted that the Linear Quadratic model (LQ) can be used to describe the bio-

logical response to radiation in terms of Survival Fraction (SF) or Biologically Equivalent Dose (BED). Especially because of uncertainties on the estimation of cumulated activities, relative errors on the delivered dose can be up to 100%. This study analysed the impact of the uncertainties on the calculated absorbed dose on the SF and the BED, assuming negligible uncertainties on the radiobiological parameters α and β, and ignoring the effects of repair and repopulation. **Methods:** Propagation of errors was applied to the Linear Quadratic model in order to calculate the relative error on SF and BED as a function of the standard deviation on the absorbed dose. Clinically relevant absorbed doses ranging between 0 to 100 Gy were considered, biological response for late and early responding tissue/cancer was taken into account (α/β ratios of values between [0.5,6] Gy and [7,20] Gy, respectively). **Results:** Mathematically, the relative error on the BED is a function of the dose, the α/β ratio and the relative uncertainty on the absorbed dose, while the relative error on the SF is given by the product of the absolute uncertainty on the BED with the radiobiological parameter α. The relative error on the BED tends to a value equal to 2 times the relative uncertainty on the absorbed dose for value of the absorbed dose much greater than the α/β ratio. For doses up to 100 Gy, the relative error on the SF can be up to 30 (early responding) or 400 (late responding) times the radiobiological parameter α multiplied by the absorbed dose standard deviation. For doses in the range [40,60] Gy, the relative uncertainty of the SF varies between [4,18], early responding, and [12,240], late responding, times the radiobiological parameter α multiplied by the absorbed dose standard deviation. **Conclusion:** Ignoring the contributions of the uncertainties on the dose rate and on the radiobiological parameters, the relative error on the biological effects of Molecular Radiotherapy (SF or BED) can be significant, depending strongly on the relative error on the absorbed dose. In particular, the relative error on the BED is between 1 and 2 times the relative error on the dose. This will affect the clinical power in establishing BED- or SF-response relationships.

EP-0900

Impact of image reconstruction parameters on the dose-volume histogram for PET-based dosimetry for Y-90 radioembolization

H. Ma[1], X. Hou[1], F. Benard[2], A. Celler[1]; [1]University of British Columbia, Vancouver, BC, CANADA, [2]British Columbia Cancer Research Centre, Vancouver, BC, CANADA.

Liver radioembolization (RE) with Y-90 is a well-established method for treatment of liver tumours. For therapy planning and evaluation, it is important to determine the dose delivered both to the tumour and the healthy parenchyma. In the external beam therapy, the dose volume histogram (DVH) can be used to assist in treatment planning. A similar approach can be applied in RE using dose maps obtained from quantitative PET images. However, the quality of Y-90 PET images is extremely poor due to low intensity of positron emissions. Additionally, it is not clear how image reconstruction affects DVH. The aim of this study was to investigate how the parameters of reconstruc-tion, performed using traditional OSEM and the new Q.Clear algorithm developed by GE, impact the accuracy of the DVH curves. A phantom (IEC) with a lung insert and 6 spheres (0.5 - 26 mL) was filled with 3GBq of Y-90 (spheres concentration 2.45 MBq/mL, SBR = 7.5, 15 min scan-duration). The images were reconstructed using OSEM: (a)2it/24s/no-filter recommended for quantification (Willowson 2015), (b)3it/18s/6mm Gaussian filter recommended for visual quality (Kao 2013), and Q.Clear with β (smoothing parameter) ranging between 0-8000. The Y-90 dose kernel (created by GATEv6.1) was convolved with each reconstructed image to create a dose map. The DVHs for the entire phantom and the largest sphere (26 mL) were compared using the percent difference (PD) to the true distributions derived from the digital CT-based image. The PD for DVH derived from the OSEM reconstructed images were (a) 28% and (b) 17% for the entire phantom, and (a) 16% and (b) 13% for the largest sphere. When using Q.Clear reconstruction, PD for the entire phantom decreased with increasing value of β i.e. 52.6% (β=0), 16.4% (β=1300), 8% (β=4000) and 6.6% (β=8000). However, for the largest sphere, the PD values were 29% (β=0), 13.5% (β=1300), 16.6%(β=4000) and 21.8% (β=8000). We showed that reconstructions optimized for quantitative imaging do not result in the most accurate DVHs for medium sized lesions. Using OSEM optimized for visual quality provided more accurate DVH than that optimized for quantification. Considering entire phantom, the larger β in Q.Clear resulted in more accurate DVH. However, for a 26 mL sphere (representing the tumour or an organ at risk), the most accurate DVH was obtained by using β=1300. These phantom results underline the importance of image reconstruction in DVH evaluation and will serve as guidance in our patient studies.

EP-0901

Is there agreement between predicted ^{99m}Tc-MAA-SPECT and post-treatment ^{90}Y-PET absorbed doses in SIRT using 3D voxel dosimetry?

L. Sancho Rodriguez[1], M. Rodríguez-Fraile[1], J. Bilbao[1], M. Iñarrairaegui[1], C. Beorlegui Arteta[2], A. Benito[1], V. Moran[1], J. Martí-Climent[1], E. Guillen[1], B. Sangro[1]; [1]Clínica Universidad de Navarra, Pamplona, SPAIN, [2]Universidad de Navarra, Pamplona, SPAIN.

Aim: To study the correlation between pre-treatment predicted ^{99m}Tc-MAA-SPECT and post-treatment ^{90}Y-PET absorbed doses in the target non tumoral liver (TNTL). **Material and Methods:** Retrospective analysis of patients with primary and secondary liver tumors submitted to SIRT with ^{90}Y-resin microsphere between 2012 and 2015. The right lobe was in all cases the target hemiliver for SIRT, and included tumor and TNTL. The same interventional radiologist performed both procedures, being almost identical the catheter tip position. MIM processing software (Sureplan, MIM Software Inc, Cleveland, OH) was used for image processing and dosimetry calculation. Firstly, the volumes of interest were drawn using contrast-enhanced CT or MR to aid in anatomical delineation. Afterwards, those contours were automatically transferred to

fused ^{99m}Tc-MAA-SPECT/CT and ^{90}Y-PET/CT images, using rigid registration and manual adjustment. Finally, 3D pre-treatment (^{99m}Tc-MAA-SPECT) and post-treatment (^{90}Y-PET) voxel dosimetry was obtained by means of the local deposition method. Absorbed dose parameters studied (D_{mean}, D_{20}, D_{50}, D_{70} and D_{90}) were obtained from the TNTL dose-volume histograms (DVHs). In order to assess agreement between ^{99m}Tc-MAA-SPECT and ^{90}Y-PET absorbed dose parameters of the TNTL, the Lin concordance coefficient correlation was used. **Results:** Fourteen patients were evaluated. The majority of them had hepatocellular carcinoma (78.6%) and suffered from cirrhosis (71.4%). The median predicted absorbed dose for ^{99m}Tc-MAA was 29.7Gy, and for ^{90}Y-PET was 23.3 Gy. ^{99m}Tc-MAA and ^{90}Y-PET absorbed doses reach the maximum agreement for D_{mean} (CCC Lin = 0.823, p < 0.001), followed by D_{90} (CCC Lin = 0.730, p < 0.001), although agreement was reached for all the parameters obtained from DVHs. The lowest concordance is observed for D_{70}, with the remaining doses showing an intermediate agreement. There is no complete agreement between ^{99m}Tc-MAA and ^{90}Y-PET, but D_{mean} predicts linearly the real dose to be absorbed, with a moderate determination coefficient (linear regression, R^2=0.696, p < 0.001), despite the few data. Regarding whether ^{99m}Tc-MAA predicted absorbed doses overestimate or underestimate ^{90}Y-PET absorbed doses, it has been observed that for D_{mean}, D_{20} and D_{70}, ^{99m}Tc-MAA overestimate ^{90}Y-PET absorbed doses in 50% of the cases. However, for D_{50} absorbed doses, 57.1% of cases are overestimated and for D_{90}, 64.3% are underestimated. **Conclusion:** The agreement observed between predicted ^{99m}Tc-MAA-SPECT and post-treatment ^{90}Y-PET absorbed doses in the TNTL for all absorbed dose parameters collected from DVHs shows that predictive dosimetry with ^{99m}Tc-MAA-SPECT is feasible.

EP-0902

Absorbed kidney doses in patients retreated with Lu-177-octreotate at progression

V. Reijonen, H. Mäenpää, J. Heikkonen, M. Tenhunen; Helsinki University Hospital Comprehensive Cancer Center, Helsinki, FINLAND.

Aim: Lu-177-octreotate is an effective treatment for patients with metastatic Grade 1-2 neuroendocrine tumors with median progression free survival of more than 40 months. Some patients receive retreatment in progression. In the long term, the kidney is considered to be a dose-limiting organ, and the cumulative kidney dose can become high. We studied the kidney doses of patients who had been retreated with Lu-177-octreotate. **Materials and Methods:** 14 patients (9 females, 5 males; age 41-73 y at the time of the first cycle) with metastatic G1-2 neuroendocrine tumors treated in the Helsinki University Hospital, Finland, received Lu-177-octreotate (median activity per cycle 7.5 GBq, SD 1.6 GBq, range 3.6-8.3 GBq) in 3-4 cycles with amino acid solution to decrease renal uptake. Later in progression, these patients received retreatment (median activity per cycle 7.3 GBq, SD 1.0 GBq, range 3.7-7.7 GBq) in 2-4 cycles. The mean time to retreatment was 28 months (range 10-48 m). The absorbed

dose to the kidney was determined using the same dosimetry method based on SPECT/CT imaging of the kidney region. **Results:** The mean kidney dose divided by the administered activity was 0.45 Gy/GBq (range 0.26-0.61 Gy/GBq) in the initial treatment cycles, and 0.48 Gy/GBq (0.22-0.77 Gy/GBq) in the retreatment cycles. A paired-samples T-test indicated that there was not a significant difference in kidney dose per activity in the initial treatment cycles and the retreatment cycles; t(13)=0.957, p=0.361. The ratio of the patient's mean kidney dose per activity in the retreatment cycles and the initial treatment cycles varied from 0.69 to 1.69 (mean 1.09, SD 0.29). There was no correlation between this ratio and the patient's mean cumulative kidney dose before retreatment (mean 11.6 Gy, SD 3.4 Gy, range 7.4-18.3 Gy); Pearson's r=0.083, n=14, p=0.778. However, there was a correlation between the mean kidney dose per activity in the retreatment cycles and in the initial treatment cycles; Pearson's r=0.557, n=14, p=0.039. The mean cumulative kidney dose after retreatment was 21.3 Gy (SD 6.1 Gy, range 11.2-30.0 Gy). **Conclusion:** When compared to the initial treatment, it appears that there is no significant change in the mean absorbed dose to the kidneys per administered activity in retreatment at progression.

EP-0903

Gelofusine improves the Clinical Feasibility of Insulinoma Treatment using Radiolabeled Exendin

T. Jansen[1], M. Buitinga[1], I. van der Kroon[1], M. Boss[1], M. Béhé[2], M. Janssen[1], M. Brom[1], E. Visser[1], M. Gotthardt[1]; [1]Radboud university medical center, Nijmegen, NETHERLANDS, [2]University Hospital of Freiburg, Freiburg, GERMANY.

Introduction: Endogenous hyperinsulinemic hypoglycemia is most commonly caused by insulinomas and the only curative treatment is surgical removal. Exendin specifically binds to the glucagon-like peptide-1 (GLP-1) receptor, which is abundantly expressed in most insulinomas (>90%). Radiolabeled exendin followed by nuclear imaging is suitable for insulinoma localization and might therefore be feasible for peptide receptor radionuclide therapy (PRRT) of metastasized insulinomas. A major disadvantage is the high accumulation in the kidneys. Succinylated gelatin (Gelofusine) lowers renal retention and might lead to a considerable reduction in renal uptake of radiolabeled exendin. We studied the effect of Gelofusine (GELO) on renal uptake and explored the feasibility for insulinoma treatment using radiolabeled exendin. **Materials and Methods:** In a controlled cross-over trial (two arms) 10 healthy volunteers were included and 2 SPECT/CT scans per subject were performed, 24 h after the injection of 50 MBq ^{111}In-exendin. In the first study arm GELO was co-injected with ^{111}In-exendin and after 3 weeks this was repeated administering only saline, for the second study arm co-injections were done in reverse order. Kidney and pancreas uptake were calculated based on volumes of interest. The effect of GELO was then used as input for a previously published whole organ and pancreatic islet dosimetry model to calculate changes in therapeutic dose (^{177}Lu-exendin) for insulinomas. For this, dosimetric data of 2 insulinoma patients (one benign, one malignant) were used. Furthermore, doses to the pancreatic is-

lets and pancreas were calculated with and without the effect of GELO. In both situations a maximum tolerable absorbed kidney dose of 23 Gy was used. **Results:** GELO lowered renal uptake of ^{111}In-exendin significantly with a mean reduction of 18.1 ± 4.2% (p<0.001). Concomitantly, a significantly higher cumulative urinary excretion of ^{111}In-exendin was observed. No significant reduction in pancreatic uptake was seen. The allowable injected dose of ^{177}Lu-exendin increased from 1.5 to 1.8 GBq with the use of GELO. The absorbed doses were (without/with GELO): islets (3.3/4.0 Gy), pancreas (0.3/0.3 Gy), insulinoma (benign: 13.6/16.6 Gy, malignant: 5.8/7.0 Gy). GELO can increase the dose to both types of insulinomas with more than 20%. The higher allowable injected dose increased the islet dose while the pancreas dose remained equal. **Conclusion** Gelofusine can significantly reduce renal uptake and thereby the radiation dose to the kidneys. The observed reduction in kidney uptake using Gelofusine might allow an increase of the insulinoma dose by 20% which improves the feasibility of PRRT with radiolabeled exendin.

EP-0904

Influence of Breathing Motion on Kidney Volume Determination for Application in Targeted Radionuclide Therapy

C. Sebesta[1], J. C. Sanders[1,2], C. Schmidkonz[1], M. Beck[1], T. Kuwert[1], P. Ritt[1]; [1]University Hospital Erlangen, Erlangen, GERMANY, [2]Pattern Recognition Lab, Friedrich-Alexander-University Erlangen-Nürnberg, Erlangen, GERMANY.

Purpose: In Targeted Radionuclide Therapies (TRT), such as Lu-177-DOTATATE or Lu-177-PSMA, energy dose to the kidneys is proportional to area under the time-activity-curve (TAC) and inversely proportional to the kidneys' volume. Consequently, the accuracy of volume determination itself directly influences the accuracy of dosimetry. SPECT and CT images from multimodal SPECT/CT are often used for sampling the TAC and for determining the kidneys' mass. It is known that the kidneys are perturbed by respiratory motion. If the respective CT subsystem is not able to achieve the necessary scanning speeds for breath-hold CT, motion will be present during the scan and respiratory artifacts could result. This confounds delineation of the kidney boundary, leading to an erroneous volume determination and incorrect dosimetry. The aim of this study was to assess the differences in kidney volume determination between slow (free-breathing) and fast (breath-hold) CT acquisitions and thus shed light on the corresponding consequences for dosimetry. **Subjects & Methods:** In 8 patients, breath-hold (Siemens Biograph mCT, 40 CT detector slices or equivalent), as well as free-breathing CTs (Siemens Symbia T2, 2 detector slices) were acquired. The time difference between the two acquisitions was on average 69±42 (1-143) days. The volumes of left and right kidneys were independently determined by manual segmentation of the transaxial CT slices by one experienced reader. The breath-hold CT was considered as reference. **Results:** The average volume difference between breath-hold and free-breathing CT was 8.5±6.3% (ranging 2.4-16.3%, p<0.05), and 10.5±5.3% (2.9-16.5%, p<0.01), for left and right kidneys, re-

spectively. This corresponds to a volume difference of 15.1±13.5 (3.4-37.8) ml and 18.8±11.4 (2.6-33.2) ml. 10 and 8 datasets had higher and lower volumes, respectively, in the free-breathing versus the breath-hold acquisitions. The difference in measured volume was strongly correlated between left and right kidneys (p<0.01). **Conclusion:** Determination of liver volume based on free-breathing CT examinations results in significant volume inaccuracies when compared to breath-hold CT. These errors directly affect dosimetry, and, depending on the respiratory movement relative to the patient table motion during the CT acquisition, the volume and energy dose may be either over- or under-estimated.

EP-0905

Dose distribution in human kidneys after treatment with ^{177}Lu-DOTATATE using EUBED

K. Olde[1], J. Svensson[1], T. Rydén[2], R. Hermann[2], E. Forssell-Aronsson[2], B. Wängberg[3], P. Bernhardt[2]; [1]Department of Oncology, The Sahlgrenska Academy, Sahlgrenska University Hospital, Gothenburg, SWEDEN, [2]Department of Radiation Physics, Institute of Clinical Sciences, The Sahlgrenska Academy, Sahlgrenska University Hospital, Gothenburg, SWEDEN, [3]Department of Surgery, The Sahlgrenska Academy, Sahlgrenska University Hospital, Gothenburg, SWEDEN.

Introduction: In peptide receptor radionuclide therapy (PRRT) the kidneys are known to be one of the dose-limiting organs, and dosimetry is usually performed in each patient treated with ^{177}Lu-DOTATATE. In SPECT scan post treatment, the kidneys visually display an in-homogenous distribution pattern, making today's use of mean absorbed dose a rather coarse way of describing the dose distribution. The aim of this study was to make a first evaluation of equivalent uniform biologically effective dose [EUBED] as a method of describing the dose distribution pattern in kidneys after treatment with ^{177}Lu-DOTATATE. **Materials and Methods:** For the analysis, post treatment SPECT images from 24 patients treated with ^{177}Lu-DOTATATE at Sahlgrenska University Hospital was created by Monte Carlo based iterative reconstruction. The kidneys were marked as a volume of interest and the activity data collected. A dose-volume histogram was created and BED, EUD and EUBED were calculated using the mean absorbed dose and half-life of ^{177}Lu-DOTATATE from each individual treatment occasion. BED, EUD, EUBED and mean absorbed dose were all correlated to baseline kidney function (GFR) using linear regression. **Results:** BED was 7.9% (7.5-8.4, KI95), EUD 5.7% (5.4-6.0) and EUBED 17% (16.7-17.9) higher than the mean absorbed dose to the kidneys. Linear regression showed a weak correlation between mean absorbed dose, BED, EUD and EUBED and kidney function (GFR) (r^2=0.28-0.31). In patients where EUBED was more than 20% higher than the mean absorbed dose the dose-volume histogram had a flatter appearance. **Conclusion:** The results give an indication that the EUBED formula could contribute to a better description of the dose distribution in kidneys after treatment with ^{177}Lu-DOTATATE for advanced NET. Further studies in this field needs to be performed to draw more certain conclusions.

EP-0906

Value of personalised radiation absorbed dose calculations for the radioiodine ablation therapy in patients with low-risk well differentiated thyroid cancer

N. Yeyin[1], **N. Alan Selcuk**[2], E. Demirci[3], T. Toklu[2], R. Akyel[4], O. Sahin[1], A. Boz[5], F. Yapar[6], M. Abuqbeitah[1], L. Kabasakal[1]; [1]Department of Nuclear Medicine, Cerrahpasa Medical Faculty, Istanbul University, istanbul, TURKEY, [2]Department of Nuclear Medicine, Faculty of Medicine, Yeditepe University, istanbul, TURKEY, [3]Department of Nuclear Medicine Sisli Etfal Training and Research Hospital, Istanbul, istanbul, TURKEY, [4]Department of Nuclear Medicine Umraniye Training and Research Hospital, Istanbul, istanbul, TURKEY, [5]Department of Nuclear Medicine, School of Medicine, Akdeniz University, Antalya, TURKEY, [6]Department of Nuclear Medicine, Cukurova University Faculty of Medicine, Adana, TURKEY.

Aim: Radioiodine (RI) ablation therapy in low risk thyroid cancer patients can be performed in fixed amount of RI doses either with low (1.1GBq) or high (3.7 GBq) doses. Another approach can be the calculation of radiation doses given to the target doses. From historical calculations it has been shown that 300 Gy of radiation-absorbed doses to the remnant thyroid tissue would be sufficient for the ablation. However, it is not known which technique is better, since lower amount of effective RI would improve patient care. **Material and Methods:** A prospective randomized non-inferiority observational trial is conducted one-to-one comparing calculated amount of radiation dose to the target (G1) and fixed amount of 30 mCi RI (G2). From 4 centers in Turkey, 104 patients enrolled to the study, who had low risk thyroid cancer and planned to give RI ablation therapy. End point was ablation of remnant thyroid tissue assessed by neck US, stimulated Tg level (<2.0 ng/ml) and diagnostic RI whole body scan, 6-8 months after RI therapy. All patients had uptake measurements up to 166 h and thyroid volume is calculated from planar images and radiation-absorbed doses given to the target tissue is calculated from these parameters. **Results:** Median age was 42 years ranging from 20 to 76 years. There were 56 patients in G1 and 48 patients in G2. Ablation rate was 82% in G1 and 81% in G2 (P>0.5). The median amount of RI given to the patients was 2.3 GBq for G1 and 1.1 GBq for G2 (P<0.001). However, the radiation-absorbed dose given to the target was similar 346 vs 344 Gy for G1 and G2, respectively(P>0,5). There was not any significant difference between ablated and not ablated groups in terms of volume, amount of RI and radiation-absorbed dose in G1. However, in patients who were treated with fixed RI doses (G2) the amount of radiation dose given to the patients was significantly lower in patients who did not ablated. Radiation dose given to the ablated patients were 343 and 157 Gy (P<0.05), respectively. **Conclusion:** Although the ablation rate of RI ablation therapy using dozimetric calculations is similar to fixed RI dose therapy, it seems that radiation dose given to the target is an important factor, should be taken account. However, improved calculation methods are mandatory.

EP-0907

Prediction vs Prognosis of Ki-67 Index Expression After Combined In-111-DTPA-oc / n.c.a. Lu-177-Dotatate Intra-arterial Infusions, in GEP-NETs Treated Patients

G. S. Limouris[1], M. Paphiti[1], I. Karfis[1], E. Z. Dimitriadi[2], S. Chondroyiannis[3], V. R. Mccready[4], D. Rubello[3]; [1]Medical Faculty, National and Kapodistrian University of Athens, Athens, GREECE, [2]Institute Claudus Regaud, University of Paul Sabatier, Toulouse, FRANCE, [3]Nuclear Medicine Department, Santa Maria della Misericordia Hospital, Rovigo, ITALY, [4]Institute Cancer Research, Sutton Surrey & Royal Sussex County Hospital, Brighton, UNITED KINGDOM.

Introduction: The role of the Ki-67 tumour proliferation index, in some way to "presee-prognose" or to "predict" the efficacy of peptide receptor radionuclide therapy (PRRT) in GEP-NETs, still remains undetermined. Aiming to evaluate its impact on tumor behavior, in patients with GEP-NETs, we compared and analyzed the correlation between its expression pattern with patients' survival. **Subjects and Methods:** We retrospectively studied a consecutive cohort of 13 patients with non-functioning, unresectable liver-metastatic GEP-NETs, originated from pancreas and lungs and undergoing intra-arterial infusions, firstly with ^{111}In-DTPA-OC (12 sessions with 4.995 GBq per cycle, at standard intervals of 2 mo) and after 2 years the same group due to relapse, with non-carrier-added ^{177}Lu-DOTATATE (6 sessions each with 7.2 GBq per cycle, at standard intervals of about 2 mo, too). Patients (9, originated from pancreas and 4, from lungs) were graded as (G1/G2) and (G3) and were under long-acting somatostatin analog treatment. We classified the included patients in two groups as following: group A, with Ki-67 < 20 % and group B with Ki-67 > 20%. Response was evaluated according to RECIST criteria. Survival was analyzed according to Kaplan-Meier curve method. Cr-A was radioimmunologically measured and correlated with Ki-67 results. **Results:** The response rates regarding [117]Lu-DOTATATE in A and B group were 65.0% vs 22.0% as partial response, 14.0% vs 46.0% as stable disease and 21.0% vs 32.0% as progressive disease. As far as ^{111}In-DTPA-OC in A and B group we had 52.9% vs 18.0% as partial response, 17.7% vs 48.0% as stable disease and 29.4% vs 34.0% progressive disease. The median time of progression-free survival for [117]Lu-DOTATATE in group A was 69 and for group B, 54 mo. Regarding ^{111}In-DTPA-OC, PFS in A and B group was 56 and 41 mo, respectively. Cr-A values showed a parallel to Ki-67 values, level. **Conclusion:** Taken into account that Ki-67 may (α) change throughout the disease course, (β) differ between primary tumor and metastases, and (γ) often behaving more aggressive, progressively, it would be inappropriate to draw hints regarding its "predictive" value. Eventhough Kaplan-Meir results of this study, demonstrated a favorable match response in long-term, in cases with G1/G2 as well as with G3 GEP-NETs, patients with a Ki-67 index of greater than 20% seemed, even inconcordant, to benefit from PRRT, with a notable long-term outcome. We instead to conclude that we should be very cautious, regarding its "prediction" and not its "prognosis", in GEP-NETs.

EP-0908

Improved models of hepatic artery vasculature for improved treatment planning of radioembolization of liver cancer

N. Crookston, E. Frey; Johns Hopkins University, Baltimore, MD, UNITED STATES OF AMERICA.

Background: Current dosing approaches to radioembolization using glass microspheres are based on average dose to the treated volume, resulting in variation of dose to the normal liver and tumor across patients. The use of Tc-99m MAA to plan dosimetry has been proposed, but differences in images of the activity distribution between MAA and Y-90 microsphere images in normal tissues have been observed. In addition, the average dose to normal liver parenchyma is higher than in external beam therapy. We have developed a patient-specific model of liver vasculature to investigate the sources of these discrepancies. **Methods:** In this model, we model the large-scale vasculature of the hepatic arterial tree based on segmented scans of a patient liver. We then build a model of the vasculature tree down to the scale of capillaries using a macrocell-based model of liver tissue growth constrained by the shape of the patient's liver. The model uses hemodynamic considerations to calculate the diameter of arterioles at each branching point. Microsphere infusion is then simulated using microspheres with radii sampled from an assumed distribution of sizes. Microsphere trapping in the tree uses an asymmetric branching method similar to that proposed by Walrand, but modified to trap microspheres in vessels when the microsphere diameter is greater than or equal to the vessel diameter. Various levels of embolic effect of the trapped microspheres are modeled. Lobule doses are then calculated based on the distributions of microspheres. **Results:** The median dose to each lobule in normal tissue is significantly lower than the average dose, which indicates that the dose is heterogeneous and more sparing of tissue per unit dose than a homogeneous distribution. We have investigated differences in the distributions of particles for particle size distributions that approximate those of MAA and glass microspheres. Differences in distributions of particles in the liver were small based on the scale of imaging voxels, indicating that particle size is not a sufficient explanation for the differences in activity distributions of Tc-99m MAA and Y-90 glass microspheres in normal liver. **Conclusions:** The proposed model can be personalized with patient specific information such as imaging-based perfusion data, input and output pressures, the upper-level hepatic arterial tree, and liver shape. Models for tumor vasculature are under development. Using these, patient-specific micro-scale dosimetry simulations may be possible, allowing more accurate and individualized treatment planning in the future.

Radionuclide Therapy & Dosimetry: Miscellaneous

EP-0909

Effects of Zinc for Gastrointestinal System as a Radioprotective Agent

A. Akbulut[1], M. Sadic[1], N. Yumusak[2], F. N. Aydinbelge[1], G. Koca[1], M. Korkmaz[1]; [1]Department of Nuclear Medicine, University of Health Sciences, Ankara Training and Research Hospital, Ankara, TURKEY, [2]Department of Pathology, Harran University Faculty of Veterinary Medicine, Sanliurfa, Sanliurfa, TURKEY.

Purpose/Introduction: Radioiodine I131 (RAI) therapy is an efficient method to decrease the function of very active thyroid tissues and to ablate the remnant thyroidal tissue after surgery and its metastases in differentiated thyroid carcinomas. The radioprotective effects of zinc have been recently demonstrated and we hypothesized that if zinc would ameliorate the radiation induced histopathologic characteristics in rat gastrointestinal system. **Subjects & Methods:** We have grouped twenty female Wistar albino rats into two, as ten rats in each group. 111 Mbq/kg I131 was administrated to each rat in both groups. In group 2, zinc was started via gastric gavage two days before I131 administration and continued for five days after RAI. Twenty-four hours after the last dosage of zinc, the animals were sacrificed and the gastrointestinal tissues, including stomach, duodenum, ileum and colon were removed for histopathological examination. **Results:** Compared to only I131 given group (Group 1), all the histopathologic parameters were diminished in zinc and I131 given group (Group 2). The histopathologic differences between the groups in stomach, duodenum, ileum and colon, were statistically significant in most of the parameters ($p < 0.05$). **Conclusion:** Our results demonstrate the radioprotective effect of zinc in gastrointestinal system by histopathologic examination.

EP-0910

Review Of Our Experience In Treatment Of Liver Tumors With Y-90 SIR-Spheres

T. Pipikos[1], M. Glinos[2], F. Vlachou[1], K. Dalianis[3], G. Tsoukalos[2], M. Vogiatzis[1], E. Tsiakas[1], D. Papoutsani[1], V. Prassopoulos[1]; [1]Nuclear Medicine & PET/CT Department, Hygeia SA, Marousi, GREECE, [2]Interventional Radiology Department, Hygeia SA, Marousi, GREECE, [3]Medical Physics Department, Hygeia SA, Marousi, GREECE.

Aim: The review of our experience in treatment of liver tumors with Y-90 sir-spheres. **Materials and Methods:** Between October of 2012 and December 2016, 20 patients (mean age 65±8 years old) with unresectable liver tumors were treated in our hospital with radioembolization . Resin spheres were used. Selection of the patients for the specific treatment was made according to current recommendations. Eight (8) patients had metastases from colon cancer, four (4) patients had hepatocellular cancer (HCC), one (1) patient had metastases from holangiocarcinoma, two (2) from pancreatic cancer , two (2) from breast cancer, two (2) had metastatic NET and one (1) metastases from vaginal cancer. At the initial phase of the therapy the patients underwent angiography for identifying anatomic variations and coil embolization of hepatic artety branches that supply extra-hepatic organs (gastroduodental, right gastric etc.). Afterwards the patient underwent a Tc-99m MAA SPECT/CT for calculation of lung and gastrointestinal shunt and tumor to normal

liver calculations. If all the requisites were in corcordance with guidelines the patient proceeded within 4 weeks to therapy. In seven (7) patients the therapy was performed in one phase with subsequental administration of the microspheres through the right and left hepatic artery. In ten (10) patients the therapy was performed in two phases with 4-6 weeks interval, while in three (3) patients the therapy was performed with super selective administration (HCC cases). Patient's dose was calculated using the partition model method. **Results:** From a technical aspect the procedure was successful in all the patients. Overall patients reported an excellent tolerance to therapy with no major undesirable effects on life quality one patient 30 days after the radiopharmaceutical administration developed REILD syndrome and deceased. The specific patient had a major tumor burden and borderline bilrubin levels (1,8 mg/dl). The rest of the patients did not develop any major complication. Minor side effects like fatigue were given supportive care. Three (3) patients did not respond to the therapy with rapid disease progression, eight (8) patients had a good response with necrosis of the tumor sites; eight (8) patients had partial response with relatively stable disease for at least 9-12 months. **Conclusion:** Radioembolization when performed with the right planning is a procedure with good results and minor side effects for the patients compared with other treatments. The combination of the method with first line chemotherapy could further expand its application in earlier cancer stages.

EP-0911

Uncertainty analysis in the calibration of an emission tomography system for quantitative imaging

M. D'Arienzo[1], M. Cox[2]; [1]ENEA, National Institute of Ionizing Radiation Metrology, Rome, ITALY, [2]NPL, National Physical Laboratories, Teddington, UNITED KINGDOM.

Aim: It is generally acknowledged that calibration of the imaging system (be it a SPECT or a PET scanner) is one of the critical components associated with in-vivo activity quantification in nuclear medicine. The system calibration is generally performed through the acquisition of a source with a known amount of radioactivity. In the present study the factors contributing to the combined uncertainty associated with the system sensitivity are analyzed. **Materials and Methods:** The general formalism for the evaluation of the system calibration factor is given in the NEMA publication NU 1-2012. The decay-corrected calibration factor is the 'output' quantity in a measurement model for the process. This quantity is a function of a number of 'input' variables, including total counts in the volume of interest (VOI), radionuclide activity concentration, source volume, acquisition duration, radionuclide half-life and calibration time of the radionuclide. Uncertainties in the input variables propagate through the calculation to the 'combined' uncertainty in the output quantity. Using the general formula given in the GUM (Guide to the expression of uncertainty in measurement) for combining uncertainty components we derived a relation to assess the combined standard uncertainty for the calibration factor. **Results:** For radionuclides used in molecular radiothera-

py such as ^{90}Y, ^{177}Lu and ^{131}I the dominant sources of uncertainty in the calibration factor are the number of counts recorded in the VOI and the activity concentration of the radionuclide. The standard uncertainty associated with the former depends on a number of factors, among which the radionuclide and the image reconstruction/acquisition parameters. The standard uncertainty associated with the latter is likely to lie in the range 1%-3% when secondary or reference radionuclide calibrators are used. Finally, the relative standard uncertainty associated with the half-life of the above-mentioned radionuclide is about 0.05% and so makes negligible contribution to the combined uncertainty. Ultimately, clock offsets between the calibration time of the radionuclide and the acquisition start time introduce further uncertainty. **Conclusion:** In addition to demonstrating the need for accurate system calibration, our results show that the combined standard uncertainty achievable in the calibration factor in emission tomography systems is likely to lie in the range 5%-10%, depending on the radionuclide under investigation, and provided that account is taken of all meaningful sources of uncertainties. At a time of increasing need for accuracy in quantification studies, the proposed approach has the potential to be easily. implemented in the clinical practice.

EP-0912

A tool for treatment planning of ^{90}Y-microsphere radioembolization

*V. Raposo, D. Martínez, N. Gallardo, **F. Mañeru**, M. Ribelles, F. Caudepón, L. Bragado, N. Fuentemilla, A. Rubio, S. Miquelez, S. Pellejero; Complejo Hospitalario de Navarra, Pamplona, SPAIN.*

Aim: A simple-use tool is presented to organize and calculate treatment cases of ^{90}Y microspheres radioembolization. It incorporates a database of patient cases and treatment plans and also contains the necessary tools for estimation of activity and dosimetry, according to the most common methods available today. **Materials and Methods:** The tool consists in an Excel workbook with several worksheets. Each worksheet includes the data collection and the calculus for a step of the treatment process. Visual Basic macros have been developed in order to prevent program errors and make modifications accessible to users. Activity and dose calculations are based on international recommendations. The Medical Image Radiation Dose (MIRD) schema is used for absorbed dose estimation. Software has been tested with a database of more than 40 real cases treated in our center with resin and glass spheres. Details of workbook have been improved for five years. **Results:** From a user-friendly main menu, the user can navigate through the different subprocesses of the planification and treatment in the radioembolization procedure: -Introduction of patient data. -Estimation of lung shunt fraction and tumor-to-normal liver ratio. -Calculation of desired activity to the patient using three different methods: Body Surface Area Method, Partition Method and Mono-compartimental PTV-based Method. -Estimation of absorbed dose to organs and tumor previous to treatment according to the desired dose. -^{90}Y vial preparation -Estimation of delivered absorbed dose to organs and tumor according to the adminis-

tered activity, including a final report. The workbook contains a table with non-protected data useful for exporting all the information if needed. It also includes instructions for use for the users, who can modify or add other options easily. It is free available for Medical Physicist who need it. **Conclusion:** An excel workbook is presented for full gestion of radioembolization process. It includes planning and dosimetry tools according to present recommendations. The software is easy to use and can be edited by the user.

EP-0913
Dose-rate correlation with tumour volume in NET patients occurring Lu-177-DOTATATE therapy

S. Gnesin[1], M. Monteiro[2], N. Schaefer[2], J. O. Prior[2]; [1]Institute of Radiation Physics, Lausanne, SWITZERLAND, [2]Department of Nuclear Medicine and Molecular Imaging, Lausanne University Hospital, Lausanne, SWITZERLAND.

Aim: Lu-177-DOTATATE peptide receptor radionuclide therapy (PRRT) is a growing therapeutic option for patient occurring neuroendocrine tumours. In Europe, Lu-177-DOTATATE PPRT is usually performed during hospitalisation for radioprotection reasons. We aimed at analysing factors contributing to differences in patient dose rates and whether it is predictable. **Materials and Methods:** We collected standardized dose rate (DR) measurement for eight patients receiving therapeutic administration of Lu-177-DODATATE (range: 5.5-7.9 GBq) over 1-4 cycles (18 cycles in total: 2×1 cycle, 3×2 cycles, 2×3 cycles, 1×4 cycles) over a period of 54±14h (range 30-74h) post administration. Patient DR was measured at 1-m distance and 1-m off the floor with the same instrument (Model 6150AD4, Automess, Germany). DR values for each therapy cycle were fitted by bi-exponential time curves to derive decay and half-life constants. To study correlation with patient parameters, we used the effective half-life describing the late part of the bi-exponential curve (T1/2a). Tumour Volume (TV) was segmented on the 1-cycle Lu-177-DO-TATATE SPECT/CT post-therapy with adaptive-threshold modelling. Inter-patient and intra-cycle DR variability was assessed by ANOVA and linear regression. The time required to achieve a DR<10 μSv/h@1m was calculated from the fitted curve and correlated with tumour volume, body mass and body mass index (BMI). **Results:** Variations in elimination half-life (T1/2a) among cycles were 30 times smaller than among patients (partial sum-of-squares 43 vs. 1273). T1/2a was 32±10h (range 15-50) and did not vary significantly among cycles (p=0.8), contrariwise among patients (p=0.03). Of note, the elimination half-life was correlated to TV (p<0.0001), but not to body mass or BMI (p>0.1). Time duration to reach DR<10μSv/h@1m was 22±10h for tumour volumes above 800mL (n=8). Conversely, a DR<10μSv/h@1m was reached in less than 8h duration for tumour volumes <800mL. **Conclusion:** Elimination half-life (or DR reduction) was relatively constant among cycle for a given patient, but was highly variable among patients. It was significantly correlated with tumour volume. This helps estimating the time needed to reach a given DR threshold, and allows prediction of Lu-177-DOTATATE PRRT hospitalisation duration.

Conventional & Specialised Nuclear Medicine: Endocrinology

EP-0914
99mTc-MIBI Or 11C-Methionine PET/CT In Primary Hyperparathyroidism With Inconclusive Preoperative Work-up?

D. Maccora[1], C. Caldarella[2], A. Giordano[1], I. Bruno[3]; [1]Institute of Nuclear Medicine, Università Cattolica del S. Cuore "A. Gemelli", Rome, ITALY, [2]PET-CT Center, Policlinico "A. Gemelli", Rome, ITALY, [3]Nuclear Medicine Unit, Policlinico "A. Gemelli", Rome, ITALY.

Introduction: Accuracy of 99mTc-MIBI (MIBI) scan in detecting pathologic parathyroid glands is well-known. PET/CT using Carbon-11-Methionine (C-MET) is a promising imaging method in detecting abnormal glands. Aims of the study were: to evaluate the role of additional C-MET in patients with inconclusive standard diagnostic work-up; to demonstrate the presence of predicting elements in choosing the correct diagnostic method. **Subjects and Methods:** Patients with primary hyperparathyroidism, having performed C-MET after an inconclusive preoperative conventional work-up, were included. Histological diagnosis, postoperative normalization of serum calcium and parathyroid hormone (PTH) were the reference standard. Early and delayed MIBI images were obtained at 5 and 120 minutes after injection, respectively, followed by 99mTc-pertechnetate scan for functioning thyroid tissue definition. C-MET images of neck and mediastinum were acquired 15 minutes after injection, lasting 10 minutes. Diagnostic performances of C-MET alone and of the integration of the two techniques were compared. Analysis was based on the identification of the correct side of the neck and of each abnormal gland, including clinical-pathological data. **Results:** Twenty-seven patients were included: 22 with single parathyroid adenoma removed, 2 with double adenoma removed and 3 with negative surgery. Median serum calcium and PTH values were 11.2 mg/dl [interquartile range (IQR) 10.6-11.7] and 187.3 pg/ml (IQR 110.7-232.5), respectively. MIBI scan detected the side of the neck in 10 cases, the abnormal gland in 6; C-MET detected the side of the neck in 22 cases, the abnormal gland in 19. C-MET identified the abnormal gland in 14 cases whose MIBI scan showed false negative or false positive results; MIBI scan identified the hyperfunctioning gland in 2 cases whose C-MET showed false negative results. Sensitivity, specificity and accuracy for C-MET in detecting the correct side of the abnormal gland were 85%, 67% and 83%, respectively; in detecting each abnormal gland were 79%, 40% and 72%, respectively. The integration of MIBI and C-MET identified the side of the abnormal gland with sensitivity, specificity and accuracy of 93%, 100% and 93%, respectively, and each abnormal gland with 92%, 40% and 83%, respectively. Clinical data (serum calcium and PTH values; size/weight of excised glands) showed no significant correlation with either MIBI or C-MET results. **Conclusion:** In this population the integration of both MIBI and C-MET showed the highest accuracy in detecting hyperfunctioning glands and should be suggested

in patients with inconclusive diagnostic work-up. Clinical data could not guide in choosing which single method should be preferred.

EP-0915

Comparison of ⁹⁹ᵐTc-sestaMIBI and ¹⁸F-Fluorocholine PET/CT in localization of hyper-functioning parathyroid glands

I. Bossert[1], S. Chytiris[2], M. Hodolič[3,4], C. Vellani[1], E. Brugola[1], D. D'Ambrosio[5], G. Mariani[6], L. Chiovato[2], G. Trifirò[1]; [1]Nuclear Medicine Unit – Istituti Clinici Scientifici Maugeri SpA SB IRCCS, Pavia, ITALY, [2]Endocrinology Unit – Istituti Clinici Scientifici Maugeri SpA SB IRCCS, Pavia, ITALY, [3]Nuclear Medicine Research Department Iason, Graz, AUSTRIA, [4]University Olomouc, Olomouc, CZECH REPUBLIC, [5]Medical Physics Unit – Istituti Clinici Scientifici Maugeri SpA SB IRCCS, Pavia, ITALY, [6]Regional Center of Nuclear Medicine, University of Pisa, Pisa, ITALY.

Aim: To evaluate the diagnostic value of ¹⁸F-Fluorocholine (FCH) PET/CT in comparison to gold standard imaging modality ⁹⁹ᵐTc-sestaMIBI scintigraphy in localizing hyperfunctioning parathyroid glands. **Materials and Methods:** From February to October 2016, 46 consecutive patients (pts) with hyperparathyroidism (increased serum PTH level and/or hypercalcemia) were prospectively enrolled in our study. Pts underwent ultrasound of the neck (US) performed by an expert endocrinologist, a dual tracer ⁹⁹ᵐTc-sestaMIBI scintigraphy and FCH PET/CT. Two nuclear medicine physicians read nuclear medicine scans; disparities were resolved by consensus. **Results:** 31 females and 15 males, mean age 60.8 years (range 14-83), were included in this study. Ultrasound (US), ⁹⁹ᵐTc-sestaMIBI scintigraphy and FCH PET/CT scan were performed in all 46 pts. One pt was excluded from study because of a breast cancer diagnosis. Here we present a data from 13 out of 45 pts who had pathohistology or citology results. Mean serum levels were: PTH: 145,42 pg/ml (range 54,3 - 615,7 pg/ml); 10,2 calcium: mg/dl (range 7,8 - 11,3 mg/dl); phosphorus: 3,13 mg/dl (range 2 - 4,7 mg/dl). Three out of these 13 pts had normal serum PTH levels with isolated hypercalcemia. Pathohistology showed: 8 adenomas and 2 parathyroid hyperplasias. Three pts had a cytological confirmation of the disease: elevated PTH in washing liquid after FNAB. Twelve out of 13 pts were positive on FCH PET/CT, 4 pts were positive on ⁹⁹ᵐTc-sestaMIBI and 11 were positive on US. Among pts positive on FCH PET/CT, 11 pts were positive on US. Every pt who had positive ⁹⁹ᵐTc-sestaMIBI scan had also positive FCH PET/CT, while 1 of them was negative on US (this pt had a large goiter which prevent the parathyroid identification). There was one false negative result on all imaging techniques (intra-thymic parathyroid adenoma diagnosed at surgery) and there were no false positive scans (when positive, these 3 techniques were always concordant about the localization of the hyperfunctioning gland, and this localization was always confirmed at the cyto-hysto-pathological specimen). In this study, sensitivity to detect hyperfunctioning parathyroid gland with ⁹⁹ᵐTc-sestaMIBI scintigraphy and FCH PET/CT was 31% and 92% respectively. **Conclusion:** This study performed on a small group of pts suggests that FCH

PET/CT can be efficient imaging modality in preoperative localization of hyperfunctioning parathyroid glands. Further analyses are ongoing.

EP-0916

F18-choline PET/CT as a second line tracer for parathyroid adenoma detection in primary hyperparathyroidism

E. Quak[1], D. Blanchard[1], B. Houdu[2], Y. Le Roux[2], R. Ciappuccini[1], D. De Raucourt[1], J. Grellard[1], Y. Reznik[2], B. Clarisse[1], N. Aide[2]; [1]Francois Baclesse Cancer Centre, Caen, FRANCE, [2]University Hospital, Caen, FRANCE.

Aim: To evaluate the performance of F18-choline (FCH) PET/CT for parathyroid adenoma detection prior to surgery in patients with primary hyperparathyroidism and negative or inconclusive conventional imaging (cervical ultrasound and Tc99m-sestaMIBI SPECT/CT). **Materials and Methods:** Twenty patients were prospectively included and underwent FCH PET/CT. The result was scored positive, inconclusive or negative. The number of uptakes and their site were recorded. The FCH PET/CT result guided the surgical procedure (minimally invasive parathyroidectomy, bilateral cervical exploration, or other in case of multiple or ectopic foci). FCH PET/CT results were compared to the surgical and pathological findings and the follow-up. **Results:** Mean calcium and PTH levels prior to surgery were 2.75 ± 0.22 mmol/l and 98.1 ± 38.4 pg/ml. Seventeen (85%) FCH PET/CTs were scored positive, 2 (10%) inconclusive and 1 (5%) negative, showing 22 foci in total (21 habitual and 1 ectopic localization, mean size 13.4 mm (range (6.3-37.0)). FCH PET/CT guided surgery in 19 (95%) patients, allowing for 16 minimally invasive parathyroidectomies, 1 bilateral cervical exploration for multiple bilateral foci and 2 other surgical procedures. The 1 patient with negative FCH-PET/CT underwent bilateral cervical exploration. The per lesion and per patient analyses respectively showed 95.0% (95%CI: 75.1-99.9) and 94.4% (95%CI: 72.7-99.9) sensitivity of FCH-PET/CT for parathyroid adenoma detection, with positive predictive values of 90.5% (95%CI: 89.6-91.3) and 89.5% (95%CI: 88.4-90.5). Mean calcium levels after surgery were 2.39 ± 0.19 mmol/l. **Conclusion:** FCH PET/CT can successfully guide parathyroidectomy in the majority of patients with primary hyperparathyroidism and negative or inconclusive conventional imaging results, and should be used as such. Clinicaltrial: NCT02432599

EP-0917

An insulinoma in a critically hypoglycemic newborn identified by F18-FDOPA PET-CT

S. Salamon, H. Kvaternik, C. Gstettner, C. Hosbein, R. M. Aigner; Medical University of Graz, Department of Radiology, Division of Nuclear Medicine, Graz, AUSTRIA.

Introduction: The vast majority of congenital hyperinsulinism (CHI) cases in newborns are caused by defects in insulin regulating genes, perinatal stress, suboptimal intrauterine conditions, and maternal diabetes mellitus. About 1% of these cases

become persistent hyperinsulinemic hypoglycemia of infancy (PHHI). Either diffuse or focal disease can be present. Pancreatic tumors, including insulinoma, are exceedingly rare in children, yet a highly curable cause of focal CHI/PHHI. **Subjects and Methods:** A female newborn presented with seizures and cardiorespiratory arrest on the second day after birth. Thereafter, she required continual parenteral administration of {high percentage} glucose due to recurrent hypoglycemias, but suffered no sequelae of resuscitation. Based on low values of ketone bodies and free fatty acids in the absence of increased lactate and increased C-peptide in the serum, PHHI was suspected. Ga68 labeled somatostatin analogs were not available at that time. **Results:** A F18-FDOPA PET-CT showed a significantly increased tracer uptake in the pancreatic head, highly suggestive of insulinoma. Two weeks later, at the age of 3 months, the patient underwent a curative partial pancreatic resection. In the subsequent 5 years of regular control examinations, she has remained normoglycemic and has exhibited no developmental abnormalities. **Conclusion:** This case demonstrates that a life-threatening condition such as PHHI can be successfully cured when promptly diagnosed and treated. This prevents disease progression and ensures a normal neurodevelopmental outcome. F18-FDOPA PET-CT is a highly sensitive tool that can not only aid in locating PHHI-causing lesions but also differentiate between focal and diffuse causes and delineate the presence of ectopic foci. This enables targeted curative surgical management.

EP-0918

Determine the relationship between scintigraphic Sestamibi uptake and biological parameters of parathyroid adenomas in patients underwent surgery at our Center since 2005 to 2015

B. Nuñez, D. Ruiz, A. Renda, F. Zelaya, M. Castrillon, C. Castillo, F. Loira, J. Nogueiras, L. Campos, A. Lopez; Hospital de Meixoeiro, Vigo, SPAIN.

Aim: Determine the correlation between the sestamibi scintigraphic uptake and biological parameters (weight glandular/preoperativePTH) of parathyroid adenomas operated in our Center from 2005-2015. **Materials and Methods:** Retrospective review of medical records of the patients underwent surgically at our Centre for a period of 10 years (2005-2015) with a total of 254 cases. We consider inclusion criteria: scan planar dual-phase and double-tracer99mTc-sestamibi-99mTcO4(PDPDT)preoperative, diagnosis of parathyroid adenoma confirmed by matching reports location in pathology and scan, as well as intraoperative PTH decline <50%(10´after surgery). Standard dose was administered (740Mbq-99mTc-sestamibi+185Mbq-99TcO4), acquiring cervical images with Pin-Hole collimator the 20minutes (early) and 2-3hours(delay), then were compared with standart thyroid scan. Images were rewied by two nuclear medicines (senior physician and training). We make groups with preoperative PTH levels: PTH1:<150pg/ml, PTH2:150-300pg/ml, PTH3:>300pg/ml; weight: W1:<1g,W2:1-3gr,W3:>3gr and according to its intensity scintigraphic uptake pattern (scale of colors and raw) UpT1:low,UpT2:medium,UpT3:high. We additionally assessed the uptake within adjacent tissue and the washout in delay images (minor criteria). **Results:** 113 patients with were included, age average (59 +/-13), female 80%(90p), most frequent location was left(55%). The scintigraphic uptake according to pattern UpT1:0.9%, UpT2:17.7%, UpT3:81.4%. Weight average 1.32gr+/-1.39(range:0.001gr-7gr), the average of PTH 268,2pg/ml+/-245,7 (range:60pg/ml-1800pg/ml). The 80% of the sample presented a high intensity of uptake, in the remaining 20% (UpT1:1.73%/UpT2:17.39%) it was necessary to rely on the minor criteria. When comparing these patterns with PTH levels, we saw that in UpT2, 45% of cases had PTH1: (<150), and in UpT3 43.5% had values of PTH2(150-300). When we correlated the level of uptake with the weight we saw that in UpT2(70%) and UpT3(56%) they had a weight<1gr. After the statistical analysis of the results, no correlation was found between PTH levels, weight and intensity of uptake. UpT1 was rejected in this analysis, since only 1 case was registered. **Conclusions**: The findings of our review agree with those reported in the literature that when PDPDT is valued as a function of the uptake pattern, it has a very high performance for the diagnosis of parathyroid adenoma. In our study we have not found statistically significant correlation; between the intensity of uptake and biological parameters (weight-PTH Preoperative), this could be explained by methodological failures(non-standardised weight estimation in the sample of pathological anatomy, and PTH values seen by groups). Although there is no clear evidence in the studies similar to ours, since some of these studies, the results are even opposite

EP-0919

Our experience in the diagnosis of parathyroid adenoma with planar scintigraphy 99mTc-Sestamibi-99mTO4 during the last 10 years

B. Nuñez, D. Ruiz, A. Renda, F. Zelaya, M. Castrillon, C. Castillo, F. Loira, J. Nogueiras, L. Campos, A. Lopez; Hospital de Meixoeiro, Vigo, SPAIN.

Aim: To determine the dignosis accuracy of the planar scintigraphy dual-phase and double tracer 99mTc-sestamibi-99mTO4(P-DPDT)in the study of the parathyroid adenoma. **Materials and Methods:** Retrospective review of the medical reports of patients who subjected excision of the adenomas in our center for a period of 10 years (2005-2015), getting a total of 213 studies. Inclusion criteria: diagnosis of parathyroid adenoma confirmed by matching reports location in pathology and scan, as well as intraoperative PTH decline <50%(10´after surgery). Standard dose was administered (740Mbq-99mTc-sestamibi+185Mbq-99TcO4), acquiring cervical images with Pin-Hole collimator the 20minutes (early) and 2-3hours(delay), then were compared with standart thyroid scan. Images were rewied by two nuclear medicines(senior physician and training); by grouping them in three patterns depending on its intensity(scale of colors/raw images) UpTP1: Low, UpT2: medium, UpT3: High. We additionally assessed the uptake within adjacent tissue and the washout in delay images (minor criteria). **Results:** The total of studies (213p), we obtained a sample 114 cases (fulfilling the inclusion criteria)with a mean age 59.23 +/- 13(90p), women(78.94%), left was the most fre-

quent location (53.91%). Subsequently we classify the studies according to three patterns observing UpT1:1.73%, UpT217.39:% and UpT3:80.86%. In doubtful cases, we reviewed the delayed phase images to evaluate the washing and compare tissue adjacent to the lesion. **Conclusions:** The 80% of the sample presented a pattern Type 3, mainly determined by the intensity of uptake, in the remaining 20% (type1:1.73%/Type2 17.39%) it was necessary to rely on the minor criteria. The findings of our review are consistent with those reported in the literature; when GGPDF-DT is valued as a function of the uptake pattern, it has a very high performance for the diagnosis of parathyroid adenoma.

EP-0920

Serum Osteoprotogerin Levels in Primary Hyperparathyroidism and its Correlation with Hyperparathyroidism Markers: A Randomized Controlled Trial

B. T. Okudan[1], A. Ç. Karcı[2], M. Kılınçkaya[3], N. Coşkun[1], T. Turhan[3], D. Berker[2]; [1]Ankara Numune Hospital Nuclear Medicine Clinic, Ankara, TURKEY, [2]Ankara Numune Hospital Endocrinology Clinic, Ankara, TURKEY, [3]Ankara Numune Hospital Biochemistry Clinic, Ankara, TURKEY.

Aim: In primer parathyroidism (PHPT), secretion of parathyroid hormone (PTH) from the parathyroid glands increases autonomously and affects the bones. In bone metabolism, osteoprotogerin (OPG) is a protein expressed by osteoblasts, inhibiting osteoclastic activity. The effect of PTH on the expression of OPG remains controversial. In this prospective study, we investigated patients with PHPT who underwent parathyroid scintigraphy and ultrasonography for localization of parathyroid adenoma and we aimed to assess the correlation between serum OPG levels and hyperparathyroidism parameters. **Methods:** Forty-four patients with biochemical evidence of PHPT (PTH>65 pg/mL, serum calcium>10.5 mg/dL) scheduled for surgery (study group, 13 males, 31 females, mean age 53.04±10.01) and 38 healthy volunteers (control group, 10 males, 28 females, mean age 51.13±8.4) were included in this prospective study. Patients in the study group underwent ultrasonography, scintigraphy and SPECT/CT imaging before surgery. Serum samples of study group were also obtained preoperatively. For scintigraphy, following the injection of the activity (555 MBq Tc-99m-MIBI), planar and late SPECT/CT imaging was obtained after 20 and 180 minutes. **Results:** were considered to be positive if they showed at least one site on the MIBI scan in planar or SPECT/CT images. Preoperative imaging results, biochemical hyperparathyroidism markers and serum OPG levels were then compared with histopathological findings and the control group. **Results:** Forty-four patients with parathyroid adenoma underwent surgery for PHPT. All patients had positive results on MIBI scintigraphy and ultrasonography. There were statistically significant differences between two groups: Mean OPG (pmol/L) values were 47359 (± 28569, min: 13134, max: 163626) in the study group and 112390 (± 182021, min: 13564, max: 1033356) in the control group (p=0.02). Mean PTH (pg/mL), phosphorus (mg/dL), serum calcium (mg/dL) and urine calcium (mg/day) values

were 248.65 (± 183), 2.33 (± 0.46), 11.29 (±0.92) and 378.48 (± 178.02) for the study group and 54.77 (± 19.89), 3.18 (± 0.47), 9.39 (± 0.35), 127.04 (± 28.82) for the control group respectively. Spearman's correlation coefficient between OPG-PTH levels and OPG-Ca levels were -0.31 and -0.345, respectively (weak negative correlation, p: 0.005) Conclusion: OPG values of patients that were preoperatively confirmed to have parathyroid adenoma were compared with a control group. The results show that study group has significantly lower OPG levels compared to control group and that OPG-PTH and OPG-Ca values compared between two groups have a weak negative correlation. The influence of OPG on serum Ca and PTH metabolism itself seems uncertain and needs further investigation.

EP-0921

SPECT/CT's Superiority over Ultrasonography for Preoperative Localization of Parathyroid Adenomas in Primary Hyperparathyroidism: A Retrospective Clinical Trial

N. Coşkun, B. T. Okudan; Ankara Numune Hospital, Nuclear Medicine Clinic, Ankara, TURKEY.

Purpose: The aim of this study is to determine the accuracy of Tc99m MIBI with SPECT/CT for preoperative localization of parathyroid adenomas and to assess the correlation between SPECT/CT, ultrasonography and serum parathyroid hormone (PTH), phosphorus (P) and calcium (Ca) levels. **Methods:** Two-hundred-sixty patients who underwent pre-operative imaging with ultrasound and SPECT/CT for localization of parathyroid adenoma between January 2015 and February 2017 were screened retrospectively. Biochemical parameters of patients were measured routinely as the mean, standard deviation and median values. Normal ranges of PTH, Ca, and P were admitted as 10-65 pg/mL, 9.5-10.5 mg/dL and 2.5-4.5 mg/dL, respectively. Seventy-nine patients (15 males, 64 females, mean age: 51.46±11.2) who were operated for parathyroid adenoma were included in this study. For parathyroid scintigraphy, following an injection of 555 MBq Tc-99m-MIBI, early planar and late SPECT/CT imaging was performed after 20 and 180 minutes. SPECT/CT results were considered to be positive if they showed at least one site on the MIBI scan at planar or SPECT/CT images. The relationship between serum hyperparathyroidism markers and imaging findings was then evaluated statistically. Preoperative SPECT/CT and ultrasonography results were compared with postoperative histopathological reports as a gold standard. **Results:** Sixty-five patients were confirmed to have parathyroid adenoma with histopathological examination while 4 patients were reported as parathyroid hyperplasia. Mean PTH, Ca and P levels of these patients were found as 235,7 pg/mL (median: 175, range: 2.9-1203.6), 10.64 mg/dL (median: 10.8, range: 6-13.2) and 2.27 mg/dL (median: 2, range: 1-4.6) respectively. Based on histopathological data, sixty-three patients were preoperatively identified with scintigraphy and 37 patients with ultrasonography. Two patients (5.4%) were diagnosed with ultrasonography only and missed by SPECT/CT, while 28 patients (44.4%) were diagnosed with SPECT/CT only and missed by ultrasonography. In 26 patients

(40%), planar scintigraphy was seen as normal while SPECT/CT revealed at least one adenoma. Sensitivity and accuracy of SPECT/CT was 96.9% and 79% respectively, while sensitivity and accuracy of ultrasonography was 56.9% and 49.3% respectively. Ultrasonography and SPECT/CT combined was found to have an overall sensitivity of 100%. **Conclusion:** In this retrospective study we demonstrated that SPECT/CT has a superior value over planar scintigraphy and ultrasonography in localizing parathyroid adenomas accurately. SPECT/CT should be regarded as an indispensable step in parathyroid scintigraphy. Also an alternative management plan would be performing SPECT/CT first and proceeding to ultrasonography only in patients with a negative scintigraphy except those with thyroid nodules.

EP-0922

Contribution of SPECT/CT Imaging to 131-I NP-59 Planar Images in Patients with Hypersecretory Adrenal Syndromes and Incidentally Discovered Adrenal Masses

A. Sainz-Esteban, M. Ruiz Gómez, J. Gómez Hidalgo, A. Rodríguez Cobo, M. González Selma, C. Gamazo Laherrán, M. Alonso Rodríguez, R. Ruano Pérez; Hospital Clínico Universitario de Valladolid, VALLADOLID, SPAIN.

Purpose: To assess the contribution of SPECT/CT to planar images in hypersecretory adrenal syndromes and characterization of incidentally discovered adrenal masses investigated with radioiodinated I-6-ßiodomethyl-19-norcholesterol (NP-59) in terms of diagnostic accuracy and anatomic localization. **Subjects and Methods:** We include 23 patients (12 men, mean age: 61±12) investigated for adrenal hypersecretory syndromes, with or without adrenal nodules, (13 patients with adrenocorticotropic hormone (ACTH)-independent Cushing's disease and seven hyperaldosteronism) and for characterization of incidentally discovered adrenal masses (three patients) using NP-59 scintigraphy with SPECT/CT imaging. Sequential anterior and posterior images of the upper abdomen were acquired between 2 and 7 days following intravenous injection of 37 MBq I-131 NP-59. Saturated solution of potassium iodide was given to block free radioiodine thyroid uptake. Thirteen patients with suspected hyperaldosteronism received pharmacological adrenosuppressive preparation with dexamethasone. SPECT/CT imaging was performed on day 5 postinjection. Clinical and imaging data were reviewed to evaluate whether additional information derived from near-simultaneous anatomic localization aids study interpretation. The final diagnosis was obtained with clinical follow-up, other imaging tests and/or pathological studies when available. **Results:** Of the 13 patients with suspected Cushing's disease, six presented with hyperfunctional adrenal nodules, two with nonfunctioning adrenal nodules and five with bilateral adrenal hyperplasia. Of the seven patients with suspected hyperaldosteronism one presented with a hyperfunctional adrenal nodule, one with a nonfunctioning adrenal nodule and five with bilateral adrenal hyperplasia. Of the three patients with incidentally discovered adrenal masses, one presented a carcinoma and two with hyperfunctional adrenal nodules. SPECT/CT assisted study interpretation by localizing focal uptake in small adrenal

adenomas in three patients, and distinguishing malignant radiological pattern on the CT in one patient. In the rest of the patients SPECT/CT confirmed adrenal origin of activity increasing reader confidence but did not change the planar interpretation of the study. **Conclusion:** Utilization of SPECT/CT with NP-59 scintigraphy allows precise localization of the functional activity to anatomic structures improving diagnostic interpretation.

EP-0923

Comparison of early SPECT/CT and dual-phase planar imaging with early SPECT/CT Tc-99m Sestamibi Parathyroid Scintigraphy. Can we avoid planar imaging?

*J. Gómez Hidalgo, **A. Sainz-Esteban**, A. Cobo Rodríguez, M. González Selma, M. Ruiz Gómez, C. Gamazo Laherrán, M. Alonso Rodríguez, R. Ruano Pérez; Hospital Clínico Universitario de Valladolid, VALLADOLID, SPAIN.*

Aim: The purpose of our investigation was to directly compare diagnostic accuracies and confidences of two imaging protocols on same patients in the detection and localization of parathyroid adenomas. **Methods:** From January 2013 to December 2015 scintigraphy was performed on 487 patients with primary hyperparathyroidism. Of these, 61 had histologically proven single adenomas (54) or hyperplasias (7) and are the subject of this review. Planar imaging was performed at 15 min and 2 h after injection. Besides, SPECT/CT was performed after the early planar image. Two image sets (early SPECT/CT and dual-phase planar imaging with early SPECT/CT) were reviewed for probability of adenoma on 5-point scale (1: definitely negative, 2: probably negative, 3: equivocal, 4: probably positive, and 5: definitely positive). Besides, the two image sets were also reviewed for adenoma and hyperplasia localization at 4 possible sites (right, left, mediastinal and multiple sites). Each review was scored for location and certainty of focus by 2 reviewers. Surgical location served as the standard. **Results:** Dual-phase planar imaging with early SPECT/CT detected 53 pathological parathyroids (86.9%) and correctly localized 46 (75.4%). False negative corresponded to one hyperplasia and seven single adenomas. Early SPECT/CT detected 50 pathological parathyroids (82.0%) and correctly localized 46. False negative corresponded to two hyperplasia and nine single adenomas. Regarding the equivocal cases, early SPECT/CT presented seven equivocal cases, while dual-phase planar imaging with early SPECT/CT only five. **Conclusion:** Dual-phase planar imaging with early SPECT/CT allows more accurate detection of parathyroid adenomas than early SPECT/CT. Our experience suggests that dual phase remains particularly useful in hyperplasias and small adenomas.

EP-0924

Added Value of SPECT-CT Scintigraphy in The assessment of Patients With Hyperparathyroidism

I. Slim, I. El Bez, I. Meddeb, T. Ben Ghachem, K. Trabelsi, A. Mhiri, I. Yeddes, M. F. Ben Slimene; Department of Nuclear Medicine, Salah Azaiez Institut, Faculty of Medicine of Tunis, University of Tunis El Manar, Tunis, TUNISIA.

Introduction: Despite progress in parathyroid imaging, detection and correct localization of hyperfunctioning parathyroid glands in patients with hyperparathyroidism remains a problem. The purpose of the present study was to evaluate the incremental dignostic value of early single photon emission computed tomography with low dose CT study (SPECT-CT) in detection and localisation of abnormal parathyroid glands as compared with planar imaging alone. **Subjects and Methods:** We evaluate 60 patients with biochemical diagnosis of hyperparathyroidism : 21 patient (8 M, 24 F, age 56,5±17 years) with primary hyperparathyroidism (PHP) and 28 patients (14 M, 14 F, age 43,9±18 years) with secondary hyperparathyroidism (SHP). All patients underwent an optimized parathyroid scintigraphic protocol based on planar imaging with dual-phase, dual-tracer scintigraphy and an early SPECT-CT study. Scintigraphic imaging protocol included: thyroid exam with 50 MBq of pertechnetate and dual-phase parathyroid planar study (at 10 min and 150 min) post 99mTc-Sestamibi (740 MBq) injection. SPECT /low dose CT of the neck and chest was acquired with a Symbia T camera at early phase (30-40 min after Sestamibi injection). **Results:** Planar imaging identified hyperfunctioning parathyroid glands in 40 patients: 22 with PHP (69%) and 18 with SHP (64%), while SPECT/CT detected hyperfunctioning parathyroid glands in 48 patients: 28 with PHP (87,5%) and 20 with SHP (71%). In 6 cases ectopic glands was detected by planar imaging and SPECT/CT study provided more precise localisation. In 8 more patients, SPECT/CT localised ectopic glands while planar study was negative in 2 cases. Discordant planar - SPECT/CT information was obtained in 14 patients (24%). **Conclusion:** According to our results, preoperative SPECT/CT enhances sensitivity for parathyroid detection over planar scintigraphy and also provides incremental anatomic information wich is meaningful to the surgeon.

EP-0925

A Type of Uptake in Dual-Phase of ⁹⁹ᵐ Tc Sestamibi SPECT/CT Parathyroid Scintigraphy in Patients with Inadequately Controlled Secondary Hyperparathyroidism in Relation to Histopathology and Parathormone Level-Expierence of One Centre

M. H. Listewnik, H. Piwowarska-Bilska, K. Safranow, M. Ostrowski, J. Iwanowski, M. Chosia, M. Laszczynska, M. Kurnatowicz, B. Birkenfeld; Pomeranian Medical University in Szczecin, Szczecin, POLAND.

Introduction/Purpose: Prospectively was assessed the concordance between abnormal results of preoperative dual-phase ⁹⁹ᵐTc-Sestamibi parathyroid scintigraphy, histopathology (HP) and parathormone (PTH) in patients operated due to secondary hyperparathyroidism (sHPT) after pharmacological treatment. **Subjects & Methods:** Among 75 patients with SPECT/CT 27 (the mean age 46.3 years) had surgery. There were 75 localizations considered: n=59 abnormal in SPECT/CT removed by surgeon and sent for HP & n=10 lesions not revealed in SPECT/CT (own surgeon decision); remaining 6 with abnormal lesions in SPECT/CT were not found by surgeon (HP-). Four types of the tracer uptake were described: I=lack in an early phase (EP-) with presence in a delayed phase (DP+), Type II=EP(+)&DP(+); Type

III=EP(+)&DP(-);Type IV=EP(-)&DP(-). The latter covered lesions without abnormal uptake diagnosed in HP (HP+) The association between PTH and HP was based on 27 patients (one PTH and one HP result). In the "other" group were lymph nodes, fatty tissue and normal thyroid gland tissue. **Results:** In abnormal SPECT/CT & HP(+) group: parathyroid adenomas (n=28; 40.6%), parathyroid hyperplasias (n=12; 17.4%), NPT (n=10; 14.5%),"others" group (n=9; 13,0%); in SPECT/CT negative & HP(+) group (own surgeon decision) : parathyroid hyperplasias (n=2; 2.9%), NPT (n=2; 2.9%), "others" group (n=6, 8.7%) were found. In Type I in HP: 3 adenomas, 2 NPT and 4 "others"; Type II in HP: 25 adenomas, 12 hyperplasias, 7 NPT, 5 "others". In Type III 1 NPT and in Type IV 2 hyperplasias, 2 NPT and 6 "others" were found. Parathyroid adenoma, hyperplasia and NPT were acknowledge as true positive in HP. A significant difference between HP to I and II Type of uptake was found (p=0.027). HP of parathyroid hyperplasia and parathyroid adenoma in both Types were significantly different in relation to "others" group (p=0.045 and p=0.021 respectively). Abnormal uptake was associated with significantly (p=0.003) higher odds of detecting abnormal parathyroid gland (OR:13.3; 95%CI:2.30 - 77.19) in relation to negative SPECT/CT. Quality parameters: sensitivity -92.6%, specificity -40.0%, accuracy -81.2%, positive predictive value -84.7%, negative predictive value -60.0%. There was no significant difference between HP in relation to PTH concentration (p=0.180). **Conclusions:** ⁹⁹ᵐTc-Sestamibi SPECT/CT "wash-out" method is of critical value in detecting parathyroid pathology in patients operated on for sHPT with inadequately controlled condition. Own surgeon decisions should be limited to carefully selected lesions if not proved in SPECT/CT. This study was supported by a grant from budget resources for science in the years 2010-2015 as research project No. N N402 463339.

EP-0926

Optimization of ⁹⁹ᵐTc-sestamibi/¹²³I subtraction SPECT/CT protocol for parathyroid scintigraphy

V. Tunninen[1], T. Kauppinen[2], H. Eskola[3,4]; [1]Satakunta Central Hospital, PORI, FINLAND, [2]Helsinki University Hospital/HUS Medical Imaging Center, Helsinki, FINLAND, [3]Faculty of Biomedical Sciences and Engineering, Tampere University of Technology, Tampere, FINLAND, [4]Deparment of Radiology, Tampere University Hospital, Tampere, FINLAND.

Introduction: The aim of this study was to optimize ⁹⁹ᵐTc-sestamibi/¹²³I subtraction SPECT/CT - protocol for parathyroid scintigraphy using an anthropomorphic phantom. The effect of collimator choice, the detector configuration and the matrix size in addition to the reconstruction parameters were studied. **Subjects and Methods:** For the purpose of this study, an anthropomorphic phantom mimicking a parathyroid patient with a thyroid gland and one parathyroid adenoma (0,25 ml, 150kBq) was set up. A total of four SPECT/CT scans were performed with Low-Energy High Resolution (LEHR) and Low-Energy Ultra High Resolution (LEUHR) collimators with detectors configured in 180 degree angle (H-mode) and 90 degree angle (L-mode). All acquisitions were performed with Siemens Symbia Intevo

T2 SPECT/CT. An acquisition matrix of 256x256 was used. Projection datasets were also converted into 128x128 matrix after acquisition. All ^{99m}Tc-sestamibi and ^{123}I SPECT images (with attenuation correction) were reconstructed (FLASH 3D, 8-32 iterations, 8 subsets, Gaussian 9.00 filter, TEW+/-). Normalized ^{123}I SPECT images were subtracted from ^{99m}Tc SPECT images. All reconstructed images were subjected to visual evaluation. Images without distinct subtraction artefacts were further subjected to quantitative analysis, and contrast values were calculated for the adenoma. **Results**: The adenoma was clearly visible in all phantom images, but there was notable difference with the presences of artefacts in the images. All images acquired with detectors in L-mode were faintly blurred with more subtraction artefacts present. Images acquired with LEHR collimators and detectors in H-mode had more subtraction artefacts present compared to those acquired with LEUHR collimator. The visual appearance of the adenoma was very similar in all images acquired with LEUHR collimators in H-mode. The contrast of the adenoma was between 80% - 173%. Lowest contrast was achieved with 128×128 matrix size and 8 iterations without scatter correction. Highest contrast values were with 256×256 matrix size 32 iterations and with scatter correction applied. **Conclusion**: This study indicates that the selection of collimator and the acquisition and reconstruction parameters have a significant effect on visual appearance and adenoma contrast in parathyroid ^{99m}Tc-sestamibi/^{123}I subtraction SPECT/CT. An ultra high-resolution collimator together with 256x256 acquisition matrix yielded best results with higher number of iterations in reconstruction with some improvement with scatter correction. If ^{99m}Tc-sestamibi/^{123}I subtraction SPECT/CT protocol for parathyroid scintigraphy is used in clinical practice, all combinations of collimator and camera together with acquisition and processing parameters should be tested with known phantoms in order to optimize the protocol.

EP-69   during congress opening hours, e-Poster Area

Conventional & Specialised Nuclear Medicine: Thyroid (Benign)

EP-0927

The role of Natural killer T cells in autoimmune thyroid disease during pregnancy and postpartum

T. Bogović Crncic[1], S. Grbac Ivankovic[1], N. Girotto[1], I. Mrakovcic Sutic[2]; [1]Dept. of Nuclear medicine, Clinical Hospital Centre Rijeka, Rijeka, CROATIA, [2]Dept. of physiology and immunology, Medical faculty, University of Rijeka, Rijeka, CROATIA.

Aim: Natural killer T cells (NKT) is unique population of immunoregulatory T cells that plays an important role in immune surveillance and autoimmune disorders. The aim of our study was to investigate the changes of NKT cells in pregnant and postpartum women with autoimmune thyroid disease (AITD) and to compare the results to healthy pregnant and postpartum women. **Subjects and Methods:** The study included 185 pregnant women with no prior history of thyroid disease; 111 women in 1. half of pregnancy (6-20 weeks), 74 in 2. half of pregnancy (21-36 weeks) and 77 women in postpartum period (3 weeks-9 months after delivery). Peripheral blood and sera obtained from women were screened for thyrotropin (TSH), free thyroxine, free triiodothyronine levels, titres of thyroid peroxidase (TPO), thyroglobulin (TgAbs) antibodies and TSH receptor stimulating antibodies (TSI). According to the results women were divided into 6 groups: normal pregnant and normal postpartum women, euthyroid women with thyroid autoimmunity in pregnancy and postpartum, women with autoimmune subclinical or clinical thyroid dysfunction (hypothyroidism and hyperthyroidism) in pregnancy and postpartum and non pregnant controls. Peripheral blood mononuclear cells were separated from blood samples by gradient centrifugation. Simultaneous staining of surface antigens on lymphocyte NKT subpopulation (CD3/CD56/CD16) was performed and analysed on fluorescence-activated cell sorter (FACS). **Results:** The percentage of NKT cells was significantly higher in 1. and 2. half of healthy pregnant compared to non pregnant women. Moreover, the percentage of NKT cells was significantly higher in 1. and 2. half of pregnancy with autoimmune subclinical or clinical hypothyroidism and hyperthyroidism compared to respective pregnant and non pregnant control groups. The percentage of NKT cells was also significantly higher in postpartum women with subclinical or clinical thyroid dysfunction compared to control postpartum women. **Conclusion:** Significantly higher number of NKT cells in pregnancy and postpartum in women with autoimmune thyroid dysfunction indicates that these cells are involved in the immune regulation. These results may lead to the hypothesis that NKT cells play an important role in inducing tolerogenic mechanisms in AITD in pregnancy and postpartum.

EP-0928

Thyroid vascularisation correlates with skin microcirculation in patients with Graves' disease

K. Zaletel[1], N. Bedernjak Bajuk[1], S. Gaberšček[1,2], H. Lenasi[2]; [1]Department of Nuclear Medicine, University Medical Centre Ljubljana, Ljubljana, SLOVENIA, [2]Faculty of Medicine, University of Ljubljana, Ljubljana, SLOVENIA.

Objectives: Graves' disease (GD) is the main cause of hyperthyroidism, which is associated with a marked decrease in vascular resistance by affecting the function of vascular endothelial and smooth-muscle cells. In untreated GD, several studies indicate that thyroid blood flow is significantly increased. Less data are available on skin microcirculation which potentially reflects generalized vascular function. Our aim was to evaluate the thyroid vascularisation in untreated and treated GD and its association with skin microcirculation. **Methods:** In our prospective case-control study, we included 31 hyperthyroid GD patients (hyperthyroid GD) and 30 age- and sex-matched healthy volunteers (controls). Patients were treated with methimazole and after 5.8±0.8 months, when euthyroid state was established, 26 GD patients were re-examined (euthyroid GD). Physical examination, thyroid ultrasound including measurements of the peak systolic velocity (PSV) at the level of intrathyroid arteries

by the spectral Doppler and baseline laser Doppler flux (LDF) of skin microcirculation on the volar forearm were performed. Thyroid hormones and TSH receptor antibodies (antiTSH-R) were measured. **Results:** In hyperthyroid GD patients, PSV at the level of intrathyroid arteries was significantly higher than in the euthyroid GD group and in controls (p<0.001 and p<0.001, respectively). In euthyroid GD patients, PSV was higher than in controls (p<0.001). In all subjects, the baseline LDF on volar forearm positively correlated with PSV at the level of intrathyroid arteries (R=0.450; p<0.001) and also with antiTSH-R concentration (R=0.353; p=0.008). In the euthyroid GD group with increased levels of antiTSH-R, a significantly positive correlation of LDF and PSV with antiTSH-R concentration was established (R=0.821; p<0.05 and R=0.681; p<0.010, respectively). **Conclusions:** GD patients have significantly increased intrathyroid blood flow, which correlates with the baseline LDF on volar forearm. Intrathyroid and skin microcirculation blood flow might also be regulated by antiTSH-R, which is supported by our findings.

EP-0929

Thyroid disorders in children and teenagers with down syndrom: accidental association or cross linking?

*I. El Bez, **M. Somai**, D. Ben Sellem, M. Ben Slimene; institut Salah Azaiez, Tunis, TUNISIA.*

Introduction/Purpose: The prevalence of thyroid disease is increased in Down's syndrome. The association of Down syndrome with thyroid disorders has been recognized for decades and up to 54% of individuals with Down syndrome are reported to have thyroid disorders, mainly hypothyroidism. We studied longitudinally thyroid function in patients with Down's syndrome in Tunis, (30 patients) up to the age of 17 years. **Methods:** Observational study, based on yearly follow up in a children's clinic. Thyroid function tests were performed. A thyroid scintigraphy was performed in all patients. **Results:** Hypothyroidism was found in 16 and hyperthyroidism was found in 14 of the 30 patients. No sex difference was seen. Half of the patients with hypothyroidism acquired the condition before the age of 10 years, but only one of them displayed thyroid autoantibodies at diagnosis. Most patients who developed hypothyroidism after this age had thyroid autoantibodies. In prepubertal patients with hypothyroidism, growth velocity was lower during the year before the start of thyroxine treatment than during the year after the beginning of the treatment; it was also lower than that of sex and age matched euthyroidic children with Down's syndrome. In patients with hyperthyroidism, Graves' disease was the most frequent etiology. **Conclusion:** Thyroid dysfunction in patients with Down's syndrome is common in childhood. Consequently, annual screening is important. Autoimmune thyroid disease is uncommon in young children with Down's syndrome but is common after 10 years of age. There is an increased incidence of hyperthyroidism, specifically Graves' disease, in Down syndrome. Physicians taking care of these patients need to be aware of this association and consider a low threshold for obtaining thyroid function

Conventional & Specialised Nuclear Medicine: Pulmonology

EP-0930

The role of SPECT/CT in lymphoscintigraphy for diagnosis of chylothorax

*G. Petracca Ciavarella, Sr., M. Totaro, M. Scarale, F. Dicembrino, **V. Frusciante, Sr.**; Casa Sollievo della Sofferenza, San Giovanni Rotondo (FG, ITALY.*

Introduction: Chylothorax represents about 4% of complications after esophagectomy. CT is often used for radiological diagnosis of chylothorax though it does not fully differentiate chylothorax from other types of pleural effusion. Planar lymphoscintigraphy can identify a lymphatic leakage but does not allow a correct identification of the leakage site. Static lymphoscintigraphy associated with SPECT / CT acquisition technique could help to recognize the correct anatomical site of the lymph loss. **Case Report**: A 54 years old patient male underwent esophageal-gastric resection (Ivor-Lewis) for esophageal cancer ; after surgery he had a persistent pleural effusion associated with hypoalbuminemia. Thoracentesis revealed a triglycerides rich fluid thus supporting the clinical suspicion of chylothorax. CT scan confirmed the pleural effusion but did not allow to define its origin. Then lymphoscintigraphy was performed administering 50 MBq 99mTc-Nanocoll (human albumin nanocolloidal particles - GE) subcutaneously in each foot, the dose was injected in the first interdigital space. Thereafter (1 hour and about 2 hours after injection) planar imaging were carried out on the pelvis and chest. After about 2 hours a SPECT-CT study of the chest was performed with a double-headed Siemens Symbia camera, high resolution / low energy collimators, 32 views, 35s / view, 128 matrix, 1.0 zoom, non-circular autocontour orbit, step and shoot mode). Planar imaging on the chest showed a gross high uptake area, compatible with chest lymph effusion. The study SPECT / CT confirmed the presence of chylothorax with an accurate identification of the anatomical site of leakage (T5-T6 level). **Discussion**: The esophageal-gastric resection procedures (Ivor-Lewis) for esophageal cancer often cause a rupture of the thoracic duct. Diagnosis of chylothorax is performed with laboratory tests on pleural fluid (cholesterol and triglycerides) and imaging examinations: chest X-ray, CT scan, lymphoscintigraphy. Lymphoscintigraphy associated with SPECT / CT adds functional information to anatomic data. In the case described above esophagectomy resulted in a damage of the thoracic duct with leakage of lymph in the chest; the SPECT / CT study performed in coregistration with conventional lymphoscintigraphy was crucial in the diagnosis and localization of lymphatic leakage site. **Conclusion**: lymphoscintigraphy of the lower limbs, associated with SPECT / CT, can be a valuable diagnostic aid in cases of questionable pleural effusions. Dose somministrata Sede anatomica dello spandimento

EP-0931

The Added Value of Low-Dose CT Component of V/Q SPECT/CT: A Meta Analysis

B. Gunalp, S. Ince, A. Ayan, E. Alagoz, K. Okuyucu; Gulhane Training and Research Center, Ankara, TURKEY.

Purpose/Introduction: V/Q SPECT improved the diagnostic accuracy of planar V/Q imaging and now hybrid V/Q SPECT/CT promises further improvement by adding extra information coming from low-dose CT component. The objective of this study is to determine the added value of low-dose CT to improve the diagnostic performance of V/Q SPECT for the diagnosis of pulmonary embolism (PE) and whether it can be used in substitution for ventilation SPECT and it can provide alternative diagnoses to PE. **Subjects and Methods**: We reviewed the literature using key words: Pulmonary embolism, V/Q scintigraphy, SPECT, SPECT/CT. **Results:** The studies which are comparing V/Q SPECT/CT with V/Q SPECT and CT Pulmonary Angiography (CTPA) were found that V/Q SPECTCT has higher diagnostic value with equal to or better than V/Q SPECT and CTPA. Sensitivity, specificity, positive predictive value, negative predictive value and accuracy were found 97%, 88%, 82%, 98% for V/Q SPECT, 97%, 100%, 100%, 98%, 99% for V/Q SPECT/CT, 68%, 100%, 100%, 83%, 88% for CTPA, respectively. Specificity of V/Q SPECT/CT has been found to improve due to low dose CT findings of explanations for perfusion defects such as interlobar fissures, localized hyperinflated areas, pneumonic infiltrations, atelectasis, paraseptal emphysema and pleural fluid. In 24-27% of the patients' other important pathologies were diagnosed by CT such as infectious chronic obstructive pulmonary disease exacerbation, pneumonia, acute respiratory distress syndrome, left ventricular dysfunction, pleural/pericardial effusions, pulmonary edema, atelectasis, aneurism and tumor suspected changes. Q SPECT/CT hasn't been found sufficient for the diagnosis of PE and V SPECT can not be avoided. V SPECT improves accuracy (7-31%), reduces false positives (17-43%) and reduces the risk of overdiagnosis. **Conclusion:** It is concluded that V/Q SPECT/CT has the highest diagnostic accuracy for the diagnosis of PE when compared with V/Q SPECT and CTPA. Low dose CT interpretation of the lungs in V/Q SPECT/CT increases specificity by reducing false positive results without hampering sensitivity and improves confidence in reading and reduces inconclusive test results.

EP-0932

The role of lung perfusion scintigraphy (LPS) in evaluation of patients suspected for Pulmonary Embolism. Does CTPA have any additional clinical value in cases where LPS findings are discordant with the clinical pretest probability?

E. Papadaki[1], A. Chatzidakis[2], I. Mitrouska[3], A. Tsaroucha[1], M. Stathaki[1], O. Bourogianni[1], K. Galanopoulos[1], M. Alefantinou[1], G. Notas[4], K. Perisinakis[5], **S. Koukouraki**[1]; *[1]Department of Nuclear Medicine, University Hospital, Heraklion, Crete, GREECE, [2]Department of Radiology, University Hospital of Crete, heraklion, GREECE, [3]Department of Thoracic Medicine, University Hospital, Heraklion, Crete, GREECE, [4]Department of Experimental Endocrinology, University Hospital, Heraklion, Crete, GREECE, [5]Department of Medical Physics, University Hospital, Heraklion, Crete, GREECE.*

Aims: We evaluated the clinical value of lung perfusion scintigraphy (LPS) using the PISAPED criteria in excluding Pulmonary Embolism (PE). Moreover, we sought to identify patients who could benefit from a complementary CTPA, avoiding anticoagulant treatment. **Materials and Methods**: 1183 pts suspected for PE and high values of D dimmers underwent LPS. Clinical pretest probability was based on Wells score. CTPA was performed in selected cases with inconsistent cpp to LPS results. Planar images were acquired after i.v injection of 99mTcMAA and interpreted according to PISAPED criteria. Patients are classified in 4 groups and 8 subgroups: Group A (normal LPS): 1030/1183pts (87,06%), [A1 (977/1030; 94,85%): low cpp; A2 (53/1030; 5,14%)): intermediate/high cpp]. Group B (abnormal LPS suggestive of PE): 69/1183 pts (5,83%) [B1 (48/69; 69,56%): high cpp; B2 (21/69; 30,43%): intermediate/low cpp]. Group C (abnormal LPS non suggestive for PE): 56/1183 pts (4,73%), [C1 (36/56; 64,28%): low cpp; C2 (20/56;15,71%): intermediate cpp]. Group D (non diagnostic LPS): 28/1183 (2,36%) patients, [D1 (16/28; 57,14%) low cpp; D2 (12/28; 42,85%): intermediate cpp]. CTPA was performed in groups A2, B2, C2 and D2. **Results**: In group A2, CTPA was negative: 44/53 (83,01%) and non diagnostic: 9/53 (16,98%) patients. A significant inferiority of the CTPA to provide clinically meaningful results vs LPS (p=0.002) was shown. In group B2, CTPA exclude PE in 2/21(9,52%) and was non diagnostic for PE in 3/21 (14,28%) patients (p=0.20). In group C2, CTPA was positive in 2/20 (10%) and non diagnostic in 3/20 (15%) patients (p=0.20). In Group D2, CTPA was positive in 2/12 (16,66%) and non diagnostic in 2/12 (16,66%) patients (p=0.19). **Conclusion**: For patients where LPS findings are discordant with the clinical pretest probability, CTPA will provide definitive diagnosis of PE in 9-14% of them. However, the rate of uncertain CTPA findings is still High.

EP-0933

Influence of Attenuation Correction on Lung VQ-SPECT/CT 3D Lobar Quantification

J. Polkey, S. Gregg, E. Reyes, J. Bailey, K. Wechalekar; Royal Brompton Hospital, London, UNITED KINGDOM.

Aim: Previously we demonstrated a method for 3D lung lobar quantification with VQ SPECT/CT in assessing differential and lobar lung function [1]. We used a hybrid SPECT/CT scanner, with single slice low resolution CT (LRCT) providing attenuation correction (AC) for the SPECT data. The combined radiation dose of a SPECT/CT scan to the patient is of the order of 3 mSv of which 1 mSv is attributed to the CT, a dose that could be avoided if the impact of AC on the final results were insignificant. The aim of this study was to assess the influence of AC, during reconstruction of V/Q hybrid SPECT/CT images, on 3D lobar quantification in patients with chronic obstructive pulmonary disease (COPD). **Methods:** Twenty patients (45% males, mean age 65 years) scheduled for lung volume reduction surgery were included. SPECT/CT perfusion (^{99m}Tc-MAA) and ventilation (^{81m}Kr)

images were acquired with a general purpose dual head gamma camera (GE Infinia Hawkeye). Each patient also underwent a clinically indicated high-resolution CT, which was used for image fusion and identification of fissures. The V/Q SPECT images were reconstructed separately with and without AC. Hermes Hybrid 3D pulmonary analysis application was used to assess individual lung and lobar counts in the SPECT V and Q images and their percentage contribution to total lung function were calculated and compared between AC and Non AC reconstructed images. **Results:** There was no significant difference between AC and non-AC percentage contributions to whole lung perfusion (AC, 50.03% SD±16.09 vs. non-AC, 50.00% SD±15.42; p=0.94), and ventilation (AC, 50.00% SD±17.51 vs. non-AC, 50.00% SD±17.07; p=1.00) studies. Similar results were obtained for lobar analysis. The high standard deviation within each group is due to the wide range in severity of disease. Bland-Altman plots showed good agreement between AC and non-AC results with no systematic bias. All except two data points were within the limits of agreement for both perfusion and ventilation comparisons. Outlier results were attributed to operator variability as they corresponded to patients in whom fissure identification was challenging. **Conclusion:** AC and non-AC V/Q SPECT 3D lobar quantification produce comparable results in patients with COPD undergoing lung volume reduction surgery. This may negate the use of AC from LRCT resulting in a reduction in dose by 1mSv while reducing acquisition time by up to ten minutes, thereby improving patients' experience and scan throughput. [1] Thillainathan AV, 2013, EANM, SPRINGER, Pages:S292-S293, ISSN:1619-7070

EP-0934

Prognostic impact of deep-inspiratory breath-hold pulmonary perfusion SPECT/CT in patients with pulmonary emphysema

T. Hamana, Y. Fukushima, S. Kumita, H. Hashimoto, Y. Sugihara; Nippon Medical School Hospital, Bunkyo-ku Tokyo, JAPAN.

Objectives: Pulmonary emphysema (PE) patients with impaired pulmonary perfusion have been reported to have poor prognoses. Pulmonary perfusion SPECT/CT can evaluate the severity of pulmonary perfusion impairment for patients with PE. Pulmonary perfusion SPECT/CT, using deep-inspiratory breath-hold (DIBH) acquisition, obtains static images and estimates the severity of pulmonary perfusion defects accurately. The aims of this study were to assess the severity of pulmonary perfusion defects and to evaluate the prognostic value of DIBH pulmonary perfusion SPECT/CT in patients with PE. **Materials and Methods:** Twenty-four consecutive PE patients, who underwent DIBH pulmonary perfusion SPECT/CT, were included in this study. The DIBH method required patients to hold their breath for 10 seconds during each continuous 360-degree image acquisition. It was repeated 12 times with 10-second intervals between each acquisition. The percentage of pulmonary perfusion defect (%PPD) was calculated by dividing perfusion defect volume in SPECT images by lung volume in CT images. In order to evaluate the clinical importance of %PPD, all patients were divided into two groups based on the value of %PPD us-

ing receiver-operating-curve analysis. They were observed over three years from initial SPECT/CT for the occurrence of major adverse events (MAE), defined as all-cause mortality and hospitalization due to deterioration of respiratory failure or heart failure. **Results:** Low and high %PPD groups consisted of 11 and 13 patients, respectively. Median %PPD was 19 (9-33) in the low %PPD group and 61 (53-76) in the high %PPD group. The proportion of patients that experienced MAE was significantly higher in the high %PPD group than in the low %PPD group (8 of 13 vs. 2 of 11, p < 0.05). Multivariate logistic regression analysis demonstrated that %PPD was the sole independent prognostic factor for MAE (p < 0.05). **Conclusions:** The severity of pulmonary perfusion impairment was estimated by calculating %PPD using DIBH pulmonary perfusion SPECT/CT. DIBH pulmonary perfusion SPECT/CT may have a high prognostic value for the occurrence of MAE in patients with PE.

EP-0935

Comparison Between Ventilation-Perfusion SPECT/CT And Ventilation-Perfusion Quotient Results

*R. Maleki, T. Ones, **K. Oksuzoglu**, S. Inanir, H. T. Turoglu, T. Y. Erdil; Marmara University School of Medicine, Nuclear Medicine Department, Istanbul, TURKEY.*

Introduction: Pulmonary thromboembolic diseases are common and potentially associated with high mortality, but early diagnosis and appropriate treatment reduce mortality significantly. Ventilation-Perfusion (V/Q or lately more preferred V/P) scintigraphy is an important modality for diagnosis and follow-up of these diseases. Application of hybrid SPECT/CT systems for this purpose is becoming more and more popular. Although the interpretation of V/P SPECT findings is reported to be facilitated by using "V/P Quotient", there is not any research regarding this matter in the literature. **Aim:** To compare "V/P Quotient" method with V/P SPECT/CT results and evaluate its possible advantages/disadvantages. **Material/Method:** The study was performed retrospectively on medical records and data of 204 patients suspected for pulmonary embolism who underwent V/P SPECT/CT study between 01.12.2015 and 30.04.2016. Besides of history, clinical and laboratory data; V/P SPECT/CT and "V/P Quotient" images of patients were evaluated by two nuclear medicine specialists. **Results:** We found statistically significant (p<0.001) relation between "V/P Quotient" and V/P SPECT/CT results. By taking V/P SPECT/CT results as the reference, interpretation of "V/P Quotient" images showed false positive results in %14.5 of patients and false negative results in %3.6 of patients. Sensitivity, Specificity, Positive Predictive Value, Negative Predictive Value and Accuracy Rate calculated as %96.4, %85.5, %74.6, %98.1 and %88.8 respectively. **Conclusion:** In our study, the "V/P Quotient" and V/P SPECT/CT results have shown a statistically significant relationship, especially for known cases of CTEPH and/or cases being followed for known diagnosis of PE. Besides of high negative predictive value for diagnosis of PE; "V/P Quotient" method make a contribution to evaluation of patients suspected for PE by creating the visual contrast in PE areas. By improving the accuracy of "hot spot" detection and more effective normaliza-

tion algorithms in processing stage of V/P SPECT images by "V/P Quotient" softwares, a more acceptable level of specificity and positive predictive values also may be achievable.

EP-0936
Prevalence of Incidental Findings Identified by CTPA in Women of Reproductive Age

N. Champion, J. Flemming; Memorial University of Newfoundland, St. John's, NL, CANADA.

Introduction: There have been multiple studies evaluating the prevalence of incidental findings identified by computed tomographic pulmonary angiography (CT-PA) when performed for evaluation of PE, however not specifically in reproductive-age females in the context of a normal chest radiograph, a cohort of patients where there is a viable and oft recommended alternative, VQ scan. This was the goal of this study, as the availability of additional information on CT to explain the patient's symptoms is often provided as justification to perform a CT over VQ. We also wanted to evaluate how modern, low-dose CT scans performed, as these protocols are increasingly used in this patient population. **Methods:** All female patients between 18 and 50 years of age who had CT-PA at the Health Sciences Hospital in St. John's, Newfoundland, Canada, over a one-year period with normal chest xray were included (48 patients). Incidental findings were then stratified into three categories, as proposed by Perelas et al (2015); type I findings requiring immediate follow-up or therapy, type II findings requiring outpatient follow-up, and type III findings requiring no follow-up or were previously known. This was an initial pilot project with data acquisition ongoing. **Results:** Type I findings were present in 4.2%, type II findings in 6.3%, type III findings in 27.1%, with no incidental findings in 62.5%. Among the 48 patients, 8 were diagnosed with PE and 40 without. All type I findings were subtle changes suspicious for infection. Type II findings included nonspecific ground-glass opacities with one unexplained pleural effusion. Type III findings included mostly insignificant atelectasis. Combining type III and nil findings, 89.6% of patients with normal chest radiograph were determined to have no additional significant incidental findings. We also note that the majority of patients with type 1 findings had clinical information available which was suspicious for infection. This compares to type I findings in 15% and type II findings in 17% in all patients who were included in the study by Perelas et al.. Absorbed radiation dose to the breast ranged between 10-20 mSv in CT, with an average of 1 mSv for VQ scan. **Conclusion:** Only a small number of CTPA studies demonstrated significant incidental findings in this patient cohort, with significantly higher radiation dose to the breasts. This further strengthens the argument that VQ scan should be the first line study for evaluation of PE in this patient population.

EP-0937
V/P SPECT to measure lung function deterioration in COPD

M. Bajc[1], Y. Chen[2], W. Jun[3], J. Xu[4], C. Wang[3], H. Huang[2], X. He[5], A. Lindqvist[6]; [1]University Hospital Lund, Lund, SWEDEN, [2]Chang zheng Hospital, Shanghai, CHINA, [3]Xin qiao Hospital, Chongqing, CHINA, [4]Hua dong Hospital, Shanghai, CHINA, [5]Suzhou University Affiliated Tumor Hospital, Suzhou, CHINA, [6]Helsinki University Hospital, Helsinki, FINLAND.

Introduction: Measurement of progression of both the small airway obstruction and the parenchymal damage affecting ventilation and perfusion of the lungs in COPD is important for management of patients and for predicting their prognosis. Aim was to quantify ventilation and perfusion defects in COPD patients to assess total pulmonary function and % of emphysema. **Subjects and Methods:** Thirty Chinese patients with a confirmed diagnosis of stable COPD (GOLD criteria) were enrolled in an international study and followed-up for 12 months. Age ranged 47-83 years, smoking pack years 0-104, and post-bronchodilatation FEV1 23-74 % predicted. Ventilation and perfusion tomography (V/P SPECT) was performed and interpreted according to European Nuclear Medicine guidelines. Obstructive bronchitis was classified by penetration of Technegas™ to the periphery. Missing lung function was quantified to estimate % of the total lung volume. The extent of emphysema was assessed as % of the estimated total lung volume (E%). Total preserved lung function (TPLF%) was calculated as percentage of total lung volume. Pulmonary function by FEV1 and FVC was followed-up. **Results:** The patients experiences on the average 0.6 (range 0-2) COPD exacerbations and 2 patients died due to cardiovascular events during 12 months. E% increased (10+/-15%, range 0 to 50%, p<0.05) and was related to diminishing TPLF% (-10+/-11%, range -30% to 5%). Post-bronchodilatation FVC decreased by -16+/-14 % (range -42 to 12%). Post-bronchodilatation FEV1 (1+/-9 %, range -19 to 25%) or FEV% (5+/-10 %, range -11 to 30%) did not change significantly. **Conclusion:** The results suggest that in COPD the total lung function deterioration can be measured and patients who have a rapid destruction of lung parenchyma can be identified by V/P SPECT using Technegas™ as the functional ventilation imaging agent.

EP-71   during congress opening hours, e-Poster Area

Conventional & Specialised Nuclear Medicine: Gastroenterology

EP-0938
Myotonic Dystrophy With Nonalcoholic Fatty Liver Disease: A Possible Relationship With Intestinal Permeability?

D. Maccora[1], G. Silvestri[2], D. Di Giuda[1], D. Ripani[1], S. Rossi[2], A. Petrucci[3], V. Valenza[1]; [1]Institute of Nuclear Medicine, Università Cattolica del S. Cuore "A. Gemelli", Rome, ITALY, [2]Institute of Neurology, Università Cattolica del S. Cuore "A. Gemelli", Rome, ITALY, [3]Neuromuscular and Neurological Rare Diseases Centre - Neurology and Neurophysiology Unit, Ospedale S. Camillo Forlanini, Rome, ITALY.

Introduction: Previous studies suggest that gut-derived endotoxin may be relevant in nonalcoholic fatty liver disease (NA-

FLD); in particular, increased intestinal permeability (IP), caused by the disruption of intercellular tight junctions, may play an important role in the pathogenesis of hepatic fat deposition. Myotonic dystrophies (DM1 and DM2) are caused by abnormal expansions of polymorphic repeats, located in non-coding regions of the respective genes (DMPK in DM1, CNBP in DM2). A toxic effect of the RNA transcribed from expanded alleles is the main pathogenic mechanism in DM, leading to a characteristic multisystem involvement, also including NAFLD. However, the etiology and frequency of NAFLD in this population have never been assessed. Aim of the study was to investigate IP in DM patients as well as its possible association with NAFLD. **Subjects and Methods:** DM patients were prospectively assessed and evaluated for the presence of NAFLD: 17 DM patients (15 DM1, 2 DM2) were enrolled in the study. Control groups included 32 healthy volunteers and 20 non-DM patients with NAFLD (as a model of hepatic fat deposition associated with intestinal hyperpermeability). NAFLD was defined by abnormal liver chemistry tests with ultrasound or pathologic evidence of steatosis in absence of other liver disease. IP was assessed in all cases using the urinary excretion of ^{51}Cr-EDTA. After an overnight fast, patients were given to drink 0.37 MBq of ^{51}Cr-EDTA in 10 ml of water; the standard sample (1/50 of administered dose) and a 3-ml sample of 24-hour urine collection were measured with a gamma counter. Urine sample results were expressed as percentages of the administered dose and considered indicative of altered IP when above 3%. **Results:** Sixteen out of seventeen (94.1%) DM patients showed increased IP (M±SD: 5.79%±2.71); NAFLD was found in 13/17 (76.5%) subjects. IP resulted significantly higher in DM patients compared to healthy volunteers (M±SD: 5.79%±2.71 vs. 2.02%±0.66; *p*<0.001); however, it was not different from that measured in non-DM patients with NAFLD (M±SD: 5.79%±2.71 vs. 5.63%±2.36; *p*=0.43). **Conclusion:** According to these preliminary results, NAFLD is common in DM patients with a high frequency. This study provides evidence for a strong association between DM and increased IP. It has been established that an abnormal IP plays an important role in the hepatic fat deposition; thus, a similar pathogenetic mechanism may be hypothesized for NAFLD in DM patients. Accordingly, ^{51}Cr-EDTA study to evaluate IP should be considered in DM patient management.

EP-0939

SPECT Defaecography - a Valuable Tool in Evaluation of Patients with Hirschsprung's Disease

N. H. Hansen[1,2], S. Hvidsten[1], N. Qvist[1,2], R. G. Nielsen[1], P. F. Høilund-Carlsen[1,2], **J. A. Simonsen**[1]; [1]Odense University Hospital, Odense C, DENMARK, [2]University of Southern Denmark, Odense C, DENMARK.

Purpose/Introduction: After surgery for Hirschsprung's disease in early childhood, patients may suffer from constipation, faecal incontinence, abdominal pain, and bowel inflammation throughout life. Symptoms and bowel movements are highly variable, and functional outcome may depend on the surgical procedure applied. No standard method allows for characterization and quantification of the stool pattern. We investigated

SPECT defaecography for evaluation of peristalsis and emptying of the large intestine. **Subjects & Methods:** Non-pregnant Hirschsprung's disease-patients >15 years old with prior bowel resection and anastomosis at our institution were eligible. Healthy controls were recruited after colonoscopy showing no signs of malignancy or inflammation. All participants underwent defaecography after per rectum instillation of a paste of Tc-99m-labeled methylcellulose. Fast SPECT acquisitions of the abdomen were performed threefold at intervals of 30 min: immediately after instillation and after a first and a second defaecation. SPECT images were acquired on a Philips Skylight dual headed gamma camera using LEHR collimator, 128x128 matrix, 60 projections and 20 seconds per projection. Images were reconstructed using OSEM2D, 5 iterations, and 8 subsets. A 9.3mm Gaussian 3D filter was applied. Volumes of interest were drawn on reconstructed 3D images to read the activity in the neo-rectum; the evacuation fraction (EF) was calculated as EF1=(Y-X1)/Y and EF2=(Y-X2)/Y; Y=pre-defaecation activity, X1=activity after first defaecation, X2=activity after second defaecation. Retrograde flow was assessed visually. **Results:** Twenty-three patients (mean age 22 years, 15 male) had undergone either recto-sigmoidal resection a.m. Soave (N=11), low anterior resection (LAR, N=8), or lateral sphincterotomy (N=4). Five healthy controls had a mean age of 37 years, two were male. Mean EF1 and EF2 were 45% and 55% in patients and 80% and 89%, respectively, in controls. EFs differed somewhat between individual patients and between groups; mean EF1 was 36% (Soave), 54% (LAR), and 53% (sphincterotomy), and mean EF2 was 52%, 59%, and 56%, respectively. Eleven patients (48%) had retrograde flow (64%, 25%, and 50%), while this was the case in 40% of controls. **Discussion/Conclusion:** SPECT defaecography was applicable in patients after rectal surgery. Our method allowed comparing of functional results following different surgical procedures and quantification of large intestine emptying in patients and healthy controls. The better EF in controls than in patients and the difference in EF according to surgical procedure were consistent with clinical findings. This quantitative way of characterizing bowel movements is innovative and is now open for potential application in intestinal motility disorders.

EP-0940

Abdominal retention index of 75sehcat according to response to treatment with resincolestiramine

P. C. Notta[1], J. Suils ramón[1], L. Rubio-Alvarez[1], A. Rodriguez-Gasén[1], S. Maisterra- Santos[2], J. Guardiola-Capo[2], I. Romero-Zayas[1], J. Mora-Salvado[1], P. Saldaña-Gutierrez[3], G. Reynès-Llompart[3], L. Gràcia-Sanchez[1], J. Mestre-Martí[1], C. Gámez-Cezamo[1]; [1]Nuclear Medicine-PET Department. IDI. Hospital Universitari de Bellvitge-IDIBELL. L'Hospitalet de Llobregat, Barcelona, SPAIN, [2]Gastroenterology Department. Hospital Universitari de Bellvitge-IDIBELL. L'Hospitalet de Llobregat, Barcelona, SPAIN, [3]Medical Physics Department. ICO. L'Hospitalet de Llobregat, Barcelona, SPAIN.

Introduction: The incidence of chronic functional diarrhea in general population is high. It has been postulated that bile acid malabsorption (bam) is the cause of chronic diarrhea in about

40% of patients. Nowadays many patients are diagnosis through the improvement after treatment with resincolestiramine. aims: To evaluate: 1) the utility of 75sehcat test for the diagnosis of bam, 2) the prevalence of bam in patients with chronic functional diarrhea and 3) the abdominal retention (AR) of 75sehcat after treatment with resincolestiramine. **Methods:** We prospectively studied 92 patients with chronic functional diarrhea (60 women, aged 20-87 years). The AR was measured 7 days after oral administration of 0,37 MBq 75sehcat and the test was considered positive when the AR was lower than 10%. Patients with a positive test received resincolestiramine and were classified according to the response to treatment in 3 groups: a) complete response; b) partial response; and c) non response. All treated patients were reevaluated with a follow-up 75sehcat test after 3 months of treatment. **Results:** 75sehcat test was normal in 50 out of 92 patients (54%) founding an alternative diagnosis of chronic diarrhea in up to 90% of them. 75sehcat test was positive in 42 out of 92 patients (46%) and all of them were treated with resincolestiramine (3 - 12 grams per day). After 3 months of treatment 32 out of 42 patients (76%) obtained a complete response, 8 out of 42 patients (19%) a partial response, and 2 out of 42 patients (2%) didn't show any response. After 3 months of treatment we found AR improvement in the 75sehcat test in 17 out of 32 patients with complete response, and 5 out of 8 patients with partial response. **Conclusion:** The prevalence of bam in patients with symptoms of chronic functional diarrhea is 46%. The 75sehcat test should be positioned as one of the main diagnostic tool in the study of patients with symptoms of chronic functional diarrhea. Re-evaluation with 75sehcat test after 3 months of treatment with resincolestiramine should not be recommended because of lack of improvement in AR even in patients with complete clinical response.

EP-0941

Intra gastric distribtution in gastric emptying - Does it helps?

S. Muthu, I. Niematallah, N. Ali, R. Sajjan, M. Prescott; Central Manchester University Hospitals NHS Trust, Manchester, UNITED KINGDOM.

Introduction: Gastric emptying study is used to assess functional gastric dysfunction in the absence of anatomical disorder. As the standard method of analysis, half time of gastric emptying may not be completely sufficient to address some patient population, for eg., with functional dyspepsia who may have normal half time of emptying, we performed intra-gastric distribution analysis to assess its usefulness. **Aim:** Review of intra-gastric distribution analysis in diagnosing functional dyspepsia. **Methods:** 187 patients who had gastric emptying scintigraphy over a period of 3 years in our centre have been included. Images were acquired over a period of 90 mins following ingestion of semi-solid meal. Results of gastric emptying scintigraphy together with a minimum of six months' outpatient follow up with gastroenterologist were reviewed. Intra-gastric distribution curves are obtained by dividing the stomach into proximal and distal half and drawing a ROI over it. **Results:** Out of 187

patients, 55 had normal gastric emptying half time. 40 out of the 55 patients (72.7%) had loss of proximal accommodation, 2 patients had delayed emptying from proximal to distal stomach and the accommodation was preserved in rest of the patients. Among them 16 patients are diabetics. 25 out of the 40 patients were diagnosed with non-ulcer/ functional dyspepsia and symptomatic improvement was documented in 7 patients. Investigation of other 15 patients showed other diseases for which they received treatment. It is worth mentioning that 9 patients either did not attend their follow up appointments or were not offered one. **Conclusion:** While functional dyspepsia is usually a diagnosis of exclusion, the provision of intra-gastric distribution analysis helps in identifying this small patient population, albeit normal half time of gastric emptying.

Conventional & Specialised Nuclear Medicine: Paediatrics (Benign)

EP-0942

The role of ^{99m}Tc-DMSA scan in the investigative algorithm for children with vesicoureteral reflux - retrospective study

D. Chroustova[1], J. Langer[2], I. Urbanova[3], J. Trnka[4], J. Kubinyi[1]; [1]Department of Nuclear Medicine, General University Hospital and First Faculty of Medicine, Charles University in Prague, PRAGUE 2, CZECH REPUBLIC, [2]Clinic of Paediatrics and Adolescent Medicine, General University Hospital and First Faculty of Medicine, Charles University in Prague, PRAGUE 2, CZECH REPUBLIC, [3]Department of Paediatrics, University Hospital Bulovka, PRAGUE 9, CZECH REPUBLIC, [4]Department of Medical Physics, General University Hospital and First Faculty of Medicine, Charles University in Prague, PRAGUE 2, CZECH REPUBLIC.

Aim: The grade of VUR (vesicoureteral reflux), the child's age and the severity and frequency of acute pyelonephritis determine therapeutic procedure in children with primary VUR. An important role in this process plays ^{99m}Tc-DMSA (Dimercaptosuccinic acid) scan with assessment of the split renal function and evaluation of the renal parenchyma. In our retrospective study we reported the scintigraphic findings in children with various grade of primary VUR and their role in the choice of subsequent therapy. **Patients and Methods**: A total of 236 children (85 boys, 151 girls, aged between 6 months and 10 years, an average age of 2.1 years) with different grade of primary VUR were enrolled into the study. Static renal scintigraphy was performed 2 hours after i.v. administration ^{99m}Tc-DMSA using MB 9200 gamma camera with an assessment of split renal function with correction for kidney depth. Planar scintigrams were complemented by pinhole collimator images in young children or SPECT examination using GE Infinia gamma camera in older children. Scintigraphic findings were divided into two groups: Findings with the symmetrical kidneys of their size and function were in group I, findings with asymmetrical kidneys were in group II respectively. The presence of scars regarding the grade

of VUR was monitored in both groups with the subsequent choice of therapy. **Results**: Grade III VUR was the most common VUR in group I. In this group were 68/138(49%) children without scars on DMSA scan, and 70/138(51%) patients had scars, from them 14(20%) underwent surgery, 24(34%) endoscopic therapy, 32(46%) had conservative treatment and 7 from them underwent acute pyelonephritis relapse. Grade IV VUR was the most common VUR in group II. In this group were found 24/98(24%) children without scars and 74/98(76%) patients with scars, from them 33/74(45%) had surgery, 20/74(27%) underwent endoscopic treatment, 21/74(28%) were indicated to conservative treatment and 5 from them had acute pyelonephritis relapse. **Conclusion**: Our study confirms the well-known fact that scars are more frequent at higher grade VUR. Scarring has also been demonstrated in children with a low grade VUR. In these cases the pathogen of infection and the incidence of acute pyelonephritis play a significant role. Based on our experience in children with normal DMSA findings in early childhood and persisting VUR (especially high grade), investigation of DMSA scan should be more frequent

EP-0943

Lung Perfusion Scintigraphy in Pediatric Age: Quality and Safety in 10-Year Experience regarding Pediatric Nuclear Medicine Practice

M. Pizzoferro, D. Alabrese, M. F. Villani, E. Villanucci, S. Chiapparelli, M. C. Garganese; IRCCS Bambino Gesù Paediatric Hospital, Rome, ITALY.

Purpose: Lung perfusion scintigraphy (LPS) allows an accurate evaluation of pulmonary function and it is a useful tool in pediatric patients with congenital lung and cardiovascular malformations. Technetium-99m (^{99}Tc) macroaggregated albumin (MAA) is the radiopharmaceutical used and it is considered safe with respect to the number of administered particles (especially in neonates and infants with severe reduction of the pulmonary vascular bed). Rare are the works describe the use of LPS in large pediatric groups. The aim of this study is to review our 10-Year experience, reporting on the clinical characteristics of pediatric patients underwent LPS and assessing safety of the tracer in respect to imaging quality. **Subjects and Methods**: We retrospectively reviewed 302 consecutive pediatric patients who underwent LPS in our Institute from 2004 to 2014. LPS was performed using ^{99}Tc MAA in all patients considering EANM guidelines. For all patients we analyzed clinical (age, weight, underlying disease) and imaging (administered doses in relation to limit of radiation dose-LDR, imaging quality, side-effects, number of required examinations per year) parameters. **Results:** A high prevalence of LPS was performed on patients younger than 10 years (211/302pts; 70%). Among this group, 61/211pts (29%) had ≤1 year, reaching about 40% including patients up to 2 years of age. We observed a wide weight range (1.8 -120kg): 121/302pts (40%) had a weight ≤15Kg and 87/302pts (29%) had a weight range between 16-30kg. Considering the clinical indications for LPS by dividing population in patients with congenital respiratory disease (CRD) and congenital heart disease

(CHD), we observed that 169/302pts (56%) had CRD (83% with not-embolic disease) compared to 133/302pts (44%) with CHD. Considering LDR we registered a slight increased of delivered dose in 3 newborns due to additional dose for administration difficulties. In all LPS we obtained optimal imaging quality in absence of adverse reactions. We reported a significant decline of required LPS from 2010 (in coincidence to installation of new radiological technologies). **Conclusion:** In our experience, LPS is a safe procedure in pediatric age but requires special care and experience considering high prevalence of newborns and infants. LPS can be performed in children with a low-dose exposure and without sedation. LPS still has a role in the care of children with cardio-pulmonary disease but we risk losing this useful diagnostic tool.

EP-0944

The reliability of estimated glomerular filtration rate in South African children

J. L. Holness[1], A. Brink[2], M. R. Davids[1], J. M. Warwick[1]; [1]Stellenbosch University and Tygerberg Hospital, Cape Town, SOUTH AFRICA, [2]University of Cape Town and Red Cross Children's Hospital, Cape Town, SOUTH AFRICA.

Aim: In children with chronic kidney disease and those being treated with nephrotoxic drugs accurate measurement of kidney function is essential. Glomerular filtration rate (GFR) is widely accepted as the best test for this purpose, yet the service is offered by only a few academic hospitals in South Africa. In most instances, GFR is simply estimated from the serum creatinine concentration using an empiric equation. The Schwartz formula is most commonly used, while the Flander's metadata equation, Gao's quadratic equation, and the FAS equation have been published more recently. These equations were all developed in predominantly Caucasian paediatric populations in North America and Europe. It is hypothesized that, due to differences in both pathology and socioeconomic conditions, serum creatinine levels locally will be lower on average leading to higher GFR estimates. The aim of this study is thus to determine the reliability of estimated GFR (eGFR) in South African children. **Materials and Methods**: This is an ongoing cross-sectional study of all children referred for GFR measurement at the Red Cross Children's Hospital, Cape Town, since September 2015. With parental/guardian consent, a blood sample was taken for serum creatinine measurement at the start of the GFR study. GFR was measured (mGFR) from the plasma clearance of Cr-51 EDTA, the dose of which was scaled to body surface area (BSA). Venous blood samples were taken at 2h and 4h. Clearance was calculated using the slope-intercept method, followed by correction for BSA and correction for the missing first exponential using the Jodal Brochner Mortensen equation. GFR was estimated using the new bedside Schwartz formula, the Flander's metadata equation, Gao's quadratic equation, and the FAS equation. The bias, precision and accuracy of each equation was determined. **Results:** To date, 108 children have been included (65 female; median age 9 years; median GFR 91.7 ml/min/1.73m^2). The correlation between eGFR and mGFR was poor with r^2 = 0.40-0.45. All equations over-estimated GFR

with median biases of 16.2-28.6 ml/min/1.73m^2. The precision was also poor with RMSE values of 14.4-33.6 ml/min/1.73m^2. The accuracy, expressed as the percentage of estimated GFR values within 30% of mGFR (P$_{30}$), was 44-60%. **Conclusion**: The accuracy of eGFR in South African paediatric patients is extremely poor and it cannot replace mGFR. There is a need for development of an estimating equation from local data, as well as increased availability of GFR measurement.

EP-0945

Incidental vesicourethral reflux diagnosis on excretory renal nuclear medicine investigations

D. Ben Sellem, L. Zaabar, I. El Bez, B. Dhaouadi, B. Letaief, M. F. Ben Slimene; University of Tunis El Manar, Tunis, TUNISIA.

Introduction: Vesicourethral reflux (VUR) is the most common uropathy in children, often reaching the girl. It is classified as primary and secondary reflux. The first one is the result of a congenital intrinsic abnormality of the physiological anti-reflux system and often disappears spontaneously with age. While the second is the result of underlying disease (organic or functional obstruction) and it is associated to other urinary tract pathologies (pelvi-ureteric and vesico-ureteric junction, mega-ureter, complicated duplex kidney, valves of the posterior urethra). The VUR is found most often by a urinary tract infection but sometimes may remain asymptomatic; its discovery is so coincidental. We report cases of reflux discovered incidentally during a renal scintigraphy with ^{99m}Tc-DTPA (diethylene triamine penta acetic acid) or ^{99m}Tc-Mercaptoacetyltriglycine (^{99m}Tc-MAG3). **Subjects and Methods**: Medical records of 65 children referred for renal scintigraphy based on excretion mechanisms performed with ^{99m}Tc-DTPA or ^{99m}Tc- MAG3 were reviewed. Of these children 32 (49%) were boys and 33 (51%) were girls. Renogram curves obtained from bilateral regions of interest (ROI) over each kidney and renal backgrounds and bladder were completed. All these patients had secondary peaks on renogram curves concomitant to bladder curve depletion. After eliminating any movement of the patient using the cine mode, vesicorenal reflux was then suspected. Over these 65 patients, only 50 patients underwent other investigations (radiological cystography, isotopic cystography and ^{99m}Tc-DMSA scintigraphy) and were retained, the other 15 patients were excluded. **Results:** Vesicoureteral reflux was confirmed in 39 patients. It was bilateral in 8 of them. In 11 other children, other investigations have not revealed reflux. The positive predictive value was 78 %. In 15 cases the reflux was known. But in the remaining 24 cases, the appearance of secondary peaks on renogram curves indicating a massive retrograde ascent of activity from the bladder to the kidney was indicative of reflux. This indirect evidence has also assessed the severity of reflux which is classified at least grade 2. **Conclusion**: The appearance of secondary peaks on renogram curves, in the absence of any patient motion, during ^{99m}Tc-DTPA or ^{99m}Tc-MAG3 renal scintigraphy should alarm the physician about the possibility of vesicorenal reflux and should push him to ask for further investigations, especially as asymptomatic complications can be severe and irreversible.

EP-0946

Evaluation of the EANM Pediatric Dosage Card Regarding DMSA Schintigraphy

J. Weng[1], E. Vestergren[2], E. Wikberg[2], R. Sixt[3]; [1]Department of Radiation Physics, University of Gothenburg, Gothenburg, SWEDEN, [2]Dept of Medical Physics and Bioengineering, Sahlgrenska University Hospital, Gothenburg, SWEDEN, [3]Dept Ped Clin Physiol & Ped Nucl Medicine, The Queen Silvia Children's Hospital, Gothenburg, SWEDEN.

Aim: The objective of the EANM dosage card 2014 is to obtain weight-independent effective doses to children of all ages. However, a Minimum Recommended Activity (MRA) is introduced for the smallest patients with the intention to maintain sufficient image quality for diagnostic purposes. Equal image quality for all patients is important when interpreting the examinations. The aim is to study image quality and age dependency when applying EANM's dosage card and to compare with a Body Surface Area (BSA) dosage method. **Materials and Method:** ^{99m}Tc-DMSA routine scintigraphies have been analyzed retrospectively. 88 patients (aged 0-33 years) were selected for this study with the inclusion criteria of normal side distribution (relative uptake 45-55 %). Examinations were performed with a gamma camera. Regions of interest were used to measure kidney and background counts. The number of counts was adjusted to acquisition time 480 s. Background-subtracted count density in the kidneys (counts/cm^2) was chosen as the main image quality parameter. Count density per MBq was calculated for each patient. This value was used to calculate the count density, *CD*, that would have been obtained using the EANM's dosage card and dosage according to Body Surface Area (BSA). The minimum activity was set to 18,5 MBq for both dosage methods. The patients were divided into three age groups in order to analyze age dependency in *CD* by means of linear regression analysis. **Results:** Mean value (n=6) of CD for adults (>20 years) was 11500 counts for both dosage methods. Mean value (n=57) of CD for the group 2-20 years was 9400 counts for the EANM method and 12000 counts for the BSA method. The minimum activity of 18,5 MBq was applicable to 17 patients (infant group) with the EANM method and only 3 patients with the BSA method. Using EANM, the mean value of CD for the infant group was 8600 counts with MRA and 7000 counts without MRA. Using BSA, the mean value of CD for the infant group was 10400 counts. Including all patients (0-33 years), a significant age dependency in image quality, *CD*, was found, both with and without MRA (R^2=0,121 and R^2=0,206 respectively) when using the EANM dosage card. Using BSA dosage, no age dependency in *CD* was found (R^2=0,00009). **Conclusion:** No age dependency in image quality was found when using BSA as dosage method, whilst it was found for both with and without MRA when using EANM's dosage method.

EP-0947

Evaluation of Renal Split Function in Pediatric Patients with 99m-DMSA Scintigraphy, Comparison between Geometric Mean and Voxelbased Analysis on SPECT/ldCT

M. H. Reichkendler, *L. Borgwardt; Rigshospitalet Copenhagen University hospital, Copenhagen, DENMARK.*

Purpose: To compare assessment of renal split function (RSF) in pediatric patients of various diagnostic subgroups using 99m-Tc-Dimercaptosuccinic acid(DMSA) planar scintigraphy geometric mean(GM) and SPECT with lowdose-CT(SPECT/ldCT). **Methods and Subjects:** Two experienced physicians blinded to patient diagnosis retrospectively analyzed all pediatric patients (0-18 years) with 99m Tc-DMSA-scintigraphy and SPECT/ldCT in our department from 2011-2016. RSF was assessed from planar scintigraphy using standard GM calculation, and from the SPECT/ldCT using Phillips Extended Briliance Workspace(EBW) software voxel-based analysis for kidney segmentation. Patients were divided into 4 subgroups based on referral diagnosis: Pyelonephritis(PY), hypertension/vessel stenosis(HY), parenchymal and positional malformations(MAL) and miscellaneous(MI). 70 patients had 77 examinations with both planar anterior-posterior projections and SPECT/ldCT scans. Three patients (7 examinations) were excluded (only one kidney). Two patients were excluded due to low kidney function (RSF not possible to assess). Median age at time of scan was 7 years 2 months [range 4 months to 17 years 7 months]. Female to male ratio 4:1. Number of examinations in subgroups: PY:45, HY:12, MAL:7 and MI:4. **Results:** When examining the total dataset using a Bland-Altman plot with 95% limits of agreement, no significant difference was found between RSF using GM analysis and SPECT/ldCT analysis. Difference in absolute values (%) between GM and SPECT/ldCT was 2.15 % ± 0.20 SEM. Dividing the total dataset into 37 normal (45-55 %) and 31 abnormal RSF using GM, a tendency was seen towards larger differences in assessed RSF between GM and SPECT/ldCT in the group with abnormal RSF. In 7 of 31 examinations evaluation of RSF using SPECT/ldCT changed RSF from abnormal to normal. No change was seen in the group of normal RSF on GM when performing SPECT/ldCT. In the subgroups, a tendency towards larger differences was seen in the evaluation of RSF in MAL and PY for patients with severe malformations and larger parenchymal defects. **Discussion/Conclusion:** When examining the total dataset no difference was found when assessing RSF calculated as GM compared to SPECT/ldCT. However in 10.3 % of examinations RSF status changed from abnormal to normal when using SPECT/ldCT. This could be due to underestimation of the kidney with the lowest function by GM analysis, hypothesizing that SPECT/ldCT yields a more correct sampling of counts. Also in subgroups MAL and PY evaluation of RSF with SPECT/ldCT seems to have an importance in patients with severe parenchymal and positional malformations and patients with larger parenchymal defects. Further studies are needed.

Conventional & Specialised Nuclear Medicine: Uronephrology

EP-0948

Radio guided surgery of a renal metastasis from differentiated thyroid carcinoma (DTC): a case report

L. Martino[1], R. Falabella[2], F. Ponti[2], A. Fè[1], L. Mussolin[1], A. Vita[2], G. Vita[3], L. Landolfi[4], M. Veltri[5]; *[1]Dept. of Nuclear Medicine A.O.R. San Carlo, Potenza, ITALY, [2]Dept. of Urology A.O.R. San Carlo, Potenza, ITALY, [3]SIC Dept. of Pathology A.O.R. San Carlo - IRCCS-CROB, Potenza - Rionero in Vulture, ITALY, [4]Dept. of Internal Medicine University Hospital, Salerno, ITALY, [5]Dept. of Nuclear Medicine A.O., Cosenza, ITALY.*

Introduction: metastases to kidneys from differentiated thyroid carcinoma (DTC) are quite unusual and generally are present in patients with other distant metastases, such as lungs and bones. Solitary renal lesions are very rare and only a few cases are reported in medical literature. We report a case of solitary renal metastasis from a follicular variant of papillary thyroid cancer (FV-PTC) in a 49-year-old woman, diagnosed by radio-iodine SPECT/CT, computed tomography (CT) and FDG PET/CT and subsequently treated by radio-guided surgery (RGS). The patient was submitted to total thyroidectomy with histopathologic diagnosis of FV-PTC (TNM stage pT3, Nx, R1, ATA high risk). The post-therapy ^{131}I whole-body scan (TxWBS) performed after ablative treatment (1836 MBq of ^{131}I after rh-TSH stimulation) showed thyroid remnant and an unsuspected focal lesion in the abdomen. A SPECT/CT study localized the focal uptake in the upper pole of the left kidney. A subsequent contrast enhanced CT and a FDG PET/CT excluded other lesions and confirmed the presence of a nodular hypodense sub-capsular lesion of the left kidney. At the PET/CT scan the renal lesion was FDG negative. The case was referred for surgery and were administered 144 MBq of ^{123}I after rh-TSH stimulation to perform a RGS to better localize the lesion during surgery. After nodulectomy, the histopathological report on the surgical specimen confirmed the presence of a metastasis of FV-PTC (10 mm. Md, Tg+, CD10-). **Conclusion:** this case confirm the important contribution of ^{131}I -SPECT/CT in staging and its potential to alter the patient management. Besides, radio-guided surgery confirms to be an easy approach adaptable to several clinical situations.

EP-0949

F+30 versus F-15 Furosemide Tc99m-MAG3 Renogram Drainage Parameters in Hydronephrotic and Normal Pediatric Kidneys

S. Turpin[1], P. J. Martineau[2], D. Barrieras[1], O. Djahangirian[1], J. Franc-Guimond[1], A. M. Houle[1], R. Lambert[1]; *[1]CHU Sainte-Justine, Montreal, QC, CANADA, [2]The University of Ottawa, Ottawa, ON, CANADA.*

Introduction: We compared the drainage parameters of diuretic renography with Furosemide injection either 15-minutes pre (F-15) or 30-minutes (F+30) after Tc99m-MAG3 administration in normal and hydronephrotic pediatric kidneys. **Methods:** This was an ethics-board approved retrospective study of pediatric patients who both F+30 and F-15 for evaluation of hydronephrosis. At the time of acquisition, all patients underwent IV hydration with normal saline, injection with 2-6mCi of Tc99m-MAG3 and a Furosemide dose of 1mg/kg (max 40mg). Drainage parameters for F+30 were: WO30 = washout at 30 minutes post-MAG3, PLWO = washout at 20 minutes post Lasix,

WO50 = total washout at 50 minutes post-MAG3, WO110 = additional drainage at 110 minutes post-MAG3; and for F-15: FWO30 = washout at 30 minutes post-MAG3. Based on F+30 drainage parameters, subjects were classified as follows: Class 0= WO30 > 70%, Class 1 = WO30 < 70%, PLWO > 40%, Class 2 = WO30 < 70%, PLWO < 40%, WO110 > 50% and Class 3 = WO30 < 70%, PLWO < 40%, WO110 < 50%. **Results:** A total of 223 kidneys in 104 subjects were studies, including 65 kidneys with surgically confirmed obstructions (O). Non obstructed kidneys (NO) were followed-up. In class 0, WO50 significantly was higher than FWO30 in 100 non-hydronephrotic kidneys (92±5.6 vs 82.1±8.6%, p<0.0001) and 3 NO class 0 (94.3±4 vs 79±16.5%, p=0.27) In class 1, there was no significant difference in WO50 for 33 NO and 25 O (71.9±15.5 vs 63.6±15.3%, p = 0.12). FWO30 was significantly lower in O when compared to NO (19.7±26.8% vs 61.6±23.9%, p<0.0001) and in comparison to WO50 for NO (p=0.0061) and O (p<0.0001). In class 2, there was no significant difference in WO50 for 20 NO and 25 O (25.3±8.8 vs 26.08±12.89, p=0.82). FWO30 was significantly lower in O when compared to NO (26.9±23.2 vs 40.4±21.7% p=0.05). FWO30 was significantly higher than WO50 in NO (p=0.01) but not in O (p=0.88). In class 3, there was no significant difference between FWO30 and WO50 in 2 NO (p=1) and FWO30 was significantly lower in 15 O (8.9±12.4% vs 22.3±12.2 , p=0.0004). **Conclusion:** Higher drainage values were obtained with F+30 compared to F-15 in normal kidneys, in both class 0 and class 1 hydronephrotic kidneys. However, F-15 was better at detecting detected obstruction in the latter group. In classes 2 and 3, F-15 improved drainage in non-obstructed kidneys and helped differentiate O and NO.

EP-0950

Evaluate the effects of age and sex on glomerular filtration rate

H. M. Yassin[1], M. H. Khedr[2], M. W. Shafaa[2], M. Hagar[1]; [1]Cairo Univeristy, Cairo, EGYPT, [2]Helwan Univeristy, Cairo, EGYPT.

Background: Accurate methods for evaluating the glomerular filtration rate (GFR) are extremely important. To ensure that potential kidney donors have no renal impairment, it is extremely important to have accurate methods for evaluating the glomerular filtration rate (GFR). The standard twenty four hours urinary creatinine clearance method and gamma camera based DTPA (Diethylene-triamine- penta-acetic acid) clearance method has been used to measure GFR. The aim of present study was to evaluate the effects of age and gender on renal function and present reference data. **Materials and Methods**: Analysis of one hundred fifty healthy adults with normal kidney function data were obtained from where 88 females and 62 males with age range 18-80 years were investigated. The DTPA clearance was calculated using a camera-based technique without blood or urine sampling. The creatinine clearance was measured using the plasma creatinine and a twenty four hour urine collection. The DTPA methods were corrected for body surface area. **Results**: The average twenty four hours urinary CCr and DTPA-GFR were (90.04 ± 12.10 vs. 91.35 ± 14.99 ml/min) respectively, and we found no difference between the males and females. When

relating 24 hours urinary CCr and DTPA-GFR to age however, a significant decline was found in both methods in males, but not in females in the age range of 18-80 years. CCr fell by a mean of 10 ml/min/ and DTPA-GFR by 90 ml/min in male donors. **Conclusion**: A clear difference in the effect of age was seen between male and female. Males showed a significant decrease between 18 and 80 years of age, which was not seen in females. Females seem to be protected in the pre-menopausal period probably by estrogens.

EP-0951

Impact of furosemide on image quality of Ga-68 PSMA PET-CT in prostate cancer patients

L. W. M. van Kalmthout, A. J. A. T. Braat, M. G. E. H. Lam, B. de Keizer; University Medical Center Utrecht, Utrecht, NETHERLANDS.

Aim: Radiotracer retention of ^{68}Ga-PSMA-11 (Gallium-68 Prostate Specific Membrane Antigen) in the urinary tract might complicate detection and evaluation of prostate cancer lesions. Co-aministration of furosemide and ^{68}Ga-PSMA-11 is suggested to lower activity in the urinary tract and improve image quality. Particularly the incidence of halo artifacts, photopenic zones surrounding the bladder, might impair evaluation of the pelvic area. To date, the additional value of furosemide administration has not been determined. Aim of this study was to evaluate the impact of furosemide on image quality in prostate cancer patients. **Materials and Methods:** A retrospective analysis was performed in 90 patients referred for whole body PET/CT for (re-)staging of prostate cancer, comparing PET-CT image quality in 45 patients that received ^{68}Ga-PSMA-11 with co-administration of 20 mg furosemide with 45 patients with ^{68}Ga-PSMA-11 without co-admistration of furosemide. Radiotracer activity (SUV max, peak and mean) within the bladder, right kidney, liver and the prostate region was evaluated. Subjective image quality and incidence of halo artifacts were scored independently by two nuclear medicine physicians. Additionally, in a subset of 19 patients prepared with co-administration of furosemide and ^{68}Ga-PSMA-11 the number of times of toilet visits for voiding between administration and PET scanning was recorded. Statistical analyses were performed with SPSS Statistical Software, version 24. An independent T-test was used to compare means at baseline. To compare mean PSA level at baseline and mean tracer activity in the bladder, the Mann Whitney-U test was used. **Results:** Furosemide co-injection with ^{68}Ga-PSMA-11 resulted in a decreased maximum, mean and peak activity in the bladder, compared to the control group (23.19, 20.47 and 14.08 compared to 42.16, 35.43 and 33.50; p = 0.00). SUV values in the kidney, liver and prostate region did not significantly differ in both groups (p > 0.5). A total amount of 5 halo artifacts was observed; 4 in the furosemide ^{68}Ga-PSMA-11 co-administration group and 1 in the group without furosemide co-administration (p = 0.17). Image quality in all cases in both groups was scored 'high'. Median amount of toilet visits in the group patients prepared with co-administration of furosemide and ^{68}Ga-PSMA-11 was 3. **Conclusion:** Image quality was scored "high" in all patients. Furosemide ^{68}Ga-PSMA-11 co-administration lowers urinary SUV

values in the bladder and consequently reduces, although not significantly, the incidence of halo artifacts. Co-administration of furosemide and ^{68}Ga-PSMA-11 results in frequent toilet visits between administration and scanning.

EP-0952

Gravity Assisted Diuresis Renography in patients with Urinary Diversion

G. Tartaglione[1], N. Foschi[2], C. Gandi[2], P. F. Bassi[2]; [1]Nuclear Medicine, Cristo Re Hospital, Rome, ITALY, [2]Urology, UCSC, Policlinico A. Gemelli, Rome, ITALY.

Introduction: After radical oncologic surgery, ileal reservoir and orthotopic ileal neo bladder represent the ideal solution for bladder replacement leading to acceptable long term functional results and good quality of life. Uretero-ileal anastomotic stricture is a well known complication, affecting up to 4-10% of renal units that may compromise the renal function. Traditional imaging can give uncertain responses. We propose Gravity-Assisted-Diuresis-Renography 99mTc-MAG3, with method F+10(sp), to check renal function and drainage. **Subjects & Methods:** We studied 31 patients (9 f, 22 m; 51 yrs +/-9) having a urinary diversion (18 urostomy, 13 orthotopic bladder replacement) with a suspected obstruction in the urinary tract. The mean serum creatinine was 1.35 mg/dL (range, 0.6-3.98). Renogram was performed in seated position with method F+10(sp), according to the current italian guideline (AIMN, 03/2017). A dose of 99mTc-MAG3, 150 MBq in 0.3 mL, was injected IV and a 20-min dynamic phase was acquired, with a frame rate of 2 s/frame for the first 60 frames, and 10 s/frame for 108 frames, using a 128x128 matrix and zoom x1. At 5 min after tracer injection, the patient drank 400-500 mL of water. A dose of 20 mg of Furosemide was injected IV at 10 min during dynamic acquisition. Later post-voiding scans at 20 and 60mins were acquired. % Split renal function (nv 40-60%), Time to Peak (nv <7 mins), Diuretic half-time (nv <8 mins) and ratio 20min/peak (nv <0.25) were evaluated. **Results:** The mean Tmax was 6.8 mins (+/- 5), the mean diuretic half time was 6.8 mins (+/- 7.1), the mean ratio 20min/peak was 0.28 (+/- 0.18). 22 renal units showed a normal function and drainage (ratio 20 min/peak <0.25), 5 renal units showed a delayed drainage (ratio 20 min/peak between 0.25 and 0.30, diuretic half time <8 mins), 28 renal units showed a clear obstruction (Ratio 20min/peak >0.30 and diuretic half time >8 mins), 7 renal units were absent or showed a compromised function (split renal function <10%). **Conclusion:** Thanks to a lower dose of furosemide and a better timing, the method F+10(sp) may avoid side effects typical of traditional methods, such as diuretic-induced hypotension or bladder filling, improving patient compliance and offering a more reliable quantification of renal output in a very physiological way. This approach may reduce equivocal responses, in frequent diagnostic dilemmas in management of reconstructive urological surgery, leading towards an agreement in interpretation of the results.

EP-0953

Assessment of six different single plasma sample methods measuring glomerular filtration rate in children

S. Ha, J. Lee; Asan Medical Center, Seoul, KOREA, REPUBLIC OF.

Purpose: Among different glomerular filtration rate (GFR) measurement methods using radionuclides, two-plasma-sample method (TPSM) is preferred. Single-plasma-sample methods (SPSMs) are also used for further simplicity. The aim of this study is to assess the accuracy of SPSMs using TPSM as a reference in children. **Subjects & Methods:** We retrospectively analyzed 114 consecutive children (57 boys and 57 girls, age range 6 months to 15 years). Blood samples were taken at 120 and 240 min after intravenous injection of ^{51}Cr-ethylenediaminetetraacetic acid (EDTA). Six SPSMs involved 1) Groth & Aasted's (t=120 min), 2) Ham's (t=120 min), 3) Christensen & Groth's (t=120 and 240 min, each) and 4) Jacobsson's (t=120 and 240 min, each) equations. Reference GFR was calculated using slope-intercept technique corrected by Jodal-Brochner-Mortensen equation. Patients with reference GFR < 30 ml/min/1.73 m^2 were excluded in analysis. Pearson correlation (r), linear regression and Bland-Altman analyses were performed. Accuracy of GFR estimates was assessed by standard error of the estimate (SEE). **Results:** SPSM equations generally correlated well with TPSM corrected by Jodal-Brochner-Mortensen equation (r=0.92 (Jacobsson, t=240 min) ~ 0.99 (Christensen & Groth, t=120 min)). Groth & Aasted's equation was the most accurate (SEE: 9.37, mean difference: 7.53 (95% C.l.: -3.44, 18.50) ml/min/1.73 m^2) for all study population (n=114). For patients with GFR ≥ 90 ml/min/1.73 m^2 (n=59), Groth & Aasted's equation was the most accurate (SEE: 9.36 ml/min/1.73 m^2, mean difference: 7.33 (95% C.l.: -4.17, 18.83) ml/min/1.73 m^2). For patients with 60 ≤ GFR < 90 ml/min/1.73 m^2 (n=41), Ham's equation was the most accurate (SEE: 3.59, mean difference: 2.25 (95% C.l.: -3.31, 7.81) ml/min/1.73 m^2). All SPSMs with 120 min-sample didn't work well for patients with 30 ≤ GFR < 60 ml/min/1.73 m^2 (n=14). For patients with 30 ≤ GFR < 60 ml/min/1.73 m^2, Jacobsson's equation (t=240 min) was the most accurate (SEE = 4.15, mean difference: 2.83 (95% C.l.: -3.34, 8.99) ml/min/1.73 m^2). **Conclusion:** SPSM equations assessed in this study were generally accurate referring to TPSM. However, for patients with 30 ≤ GFR < 60 ml/min/1.73 m^2, Jacobsson's equation (t=240 min) may be the appropriate SPSM.

EP-0954

Comparision of GFR Estimation by CKD-EPİ, C&G, MDRD and GFR Measuring by Tc-99m DTPA

Z. Hasbek, S. Erturk, E. Ciftci, A. Cakmakcilar, B. Turgut; Cumhuriyet University School of Medicine, Department of Nuclear Medicine, SIVAS, TURKEY.

Aim: Aim of this study the comparision of the CKD-EPI (Chronic Kidney Disease-Epidemiology Collaboration), C&G (Cockcroft&Gault) and MDRD (Modification of Diet in Renal Disease) methods for GFR estimation and double serum sampling method for measuring the glomerular filtration rate with Tc-99m DTPA. **Materials & Methods:** Patients who were undergone with glomerular filtration rate measuring by double serum sampling with Tc-99m DTPA due to suspicion of renal insufficiency between 2011 and 2016 in our nuclear medicine deaprt-

ment were included in this study**.** Formulas; • $GFR_{[CKD-EPI]}$ = 141 * min(Scr/κ,1)^α * max(Scr/κ, 1)$^{-1.209}$ x 0.993^{Age} x 1.018 [if female] * 1.159 [ifblack], Scr is serum creatinine (mg/dL), κ is 0.7 for females and 0.9 for males, α is -0.329 for females and -0.411 for males, min indicates the minimum of Scr/κ or 1, and max indicates the maximum of Scr/κ or 1. • $GFR_{[MDRD]}$=186xserum creatinine(mg/dl) $^{-1.154}$ x age$^{-0.203}$x 0.742 [if female] • $GFR_{[C\&G]}$=[(140-age)x body weight / (72xserum creatinine(mg/dl))]x 0.85 [if female]. **Results:** Seven hundred seventy six patients were included in this study. There were 408 female and 368 male patients with a median age of 65 years (range; 17-96 years). The best correlation was seen between Tc-99mDTPA mGFR and CKD-EPI method when considering all patients. Perfect correlation was seen between Tc-99mDTPA mGFR and other three methods in patients who were under the age of 65, good correlation was seen in patients who were over the age of 65 and moderate correlation was seen in patients who were over the age of 75. Good correlation was seen between Tc-99mDTPA mGFR and other three methods in patients whose GFR values under the 60ml/dk/1.73m^2, weak correlation was seen in patients whose GFR values under the 15ml/dk/1.73m^2 . Perfect and statistically significant correalation was seen between Tc-99mDTPA mGFR and other three methods when considering gender. **Conclusion:** Correlation between Tc-99mDTPA mGFR and CKD-EPI, MDRD and C&G methods was getting lower when the age of patients getting higher. And so we think that GFR measurement in older patients must be done with Tc-99mDTPA mGFR method. And we suggest that GFR measurement in patients who suspected with chronic renal insufficiency must be done with Tc-99mDTPA mGFR method because of lower realiability of other methods in these patients. When there is no way to do Tc-99mDTPA mGFR method, we think that CKD-EPI method can be used for GFR estimation.

EP-0956

Testicular Scintigraphy - Our Experience

A. Sá Pinto, V. M. Alves, A. Oliveira, J. Pereira; Centro Hospitalar de São João, Porto, PORTUGAL.

Introduction: Testicular Scintigraphy (TestSci) is a Nuclear Medicine (NM) exam with proved utility in the setting of acute scrotal pain. It is used to distinguish between a variety of entities, namely testicular torsion, orchitis and epididymitis. In our NM Department, it is also requested at the follow-up of testicular surgery, evaluation of ectopic testicle and testicular trauma. **Aim:** To analyse the main clinical indications and diagnostic value of TestSci at our NM Department. **Methods:** We reviewed data from all patients who underwent TestSci at our Department between 2005 and 2016 (n=44). We considered the TestSci result "positive" when the results encountered the clinical suspicion and "negative" when no alterations were found. TestSci Protocol: in adults, a dose of 185 MBq of ^{99m}Tc-pertechnetate is administered by intravenous injection; in children, there is an adjustment of the dose according to the "Administration of Radioactive Substances Advisory Commite" standards. Image acquisition begins immediately, with 1 minute dynamic phase followed by planar static images (anterior projection) of the pelvis and inferior abdomen during 15 minutes. When necessary, SPECT/CT is performed. **Results:** We analyse 45 TestSci of 44 patients, with a mean age of 8.32±6.88 years old. Post-surgical evaluation was the clinical request in 22 cases, followed by ectopic testicle (n=6), gonadal inflammation (n=4), differential diagnosis of testicular torsion (n=5), post-trauma evaluation (n=3), atrophy (n=3) and retractile testis (n=2). Testicular atrophy (n=24) and viability (n=17) were the main clinical questions. TestSci was considered "negative" in 16 cases, "positive" for testicular atrophy in 14 cases and for non-viable testicle in 5 cases. Concerning ectopic testicle evaluation, in 1 case the testicle was ectopic, in 1 case it was normally positioned at the scrotum and in 1 case it was a false-positive. In the other 3 cases, the testicle was absent. In 26 cases, a Testicular Doppler Ultrasound (TDU) was also requested as a post-surgical evaluation exam (n=15), to distinguish testicular torsion from other entities (n=3), to evaluate inflammation (n=3), trauma (n=2), atrophy (n=2) and ectopic testicles (n=1). The results of TestSci matched the ones of TDU in 24 cases, with 2 false-positive results. **Conclusion:** TestSci is not a frequently requested exam, but our experience showed it may have great utility in a variety of clinical situations, specially as a post-surgical evaluation exam.

EP-0957

Our Experience With DMSA In Peadiatrics Patients With Suspected APN

A. J. Guzmán Cruz, Y. Ramirez Escalante, M. Coronado Poggio, L. García Zoghby, S. Riskallal Monzón., L. Dominguez Gadea; Hospital Universitario La Paz, Madrid, SPAIN.

Background: Urinary tract infection (UTI) is a common disease in childhood, may cause diagnostic problems, because there are no specific clinical signs or symptoms in special in infants. In younger patients the differentiation of lower from upper UTI can be difficult just based on clinical and laboratory, early detection of renal involvement is essential for intensity and duration of treatment, as acute pyelonephritis (APN) may result in irreversible renal damage, with a higher risk of hypertension and chronic renal failure. In some studies when DMSA has pathological result in acute phase, this is predictive of presence of high grade vesicoureteral reflux (VUR), with high risk of renal damage and recurrent infection. **Aim:** To assess renal involvement in DMSA in pediatrics patients with febrile syndrome with UTI and compared with renal ultrasound. **Materials and Methods:** We retrospectively reviewed 31 patients, between november 2015 and January 2016, 18 females, with an average age of 1.8 years; suspected APN. We evaluated in all patients the presence of VUR, urinal culture, blood count and acute phase reactants. All had ultrasonography (US). DMSA was performed according to the current EANM protocol. Follow-up including urinal culture and or imaging control was carried out, for at least 6 months. **RESULTS:** 31 patients (p) were analyzed, all of them had fever and 23p significant bacteriuria, 22p with positive urine culture, 16 with leukocytosis and 25 CRP elevated, 15p had vesicoureteral reflux (VUR), 6p of them bilateral and different grades of VUR. In the final diagnosis 14 patients had renal involvement, catalogued as

APN for the images, urinal cultures and follow-up. DMSA findings: 13p showed renal scarring in DMSA, 11p of them had VUR. Sensibility was 93% and specificity was 95%. US showed renal scarring in 6p, sensibility 64% and specificity 95%. 17 patients had imaging control (US, DMSA or both of them), 5p showed improvement, 8p had no change and 4p worsened. Urinary culture control was performed in 22p, was negative in 19p and 3 positive received other antibiotic scheme. **CONCLUSIONS:** 1) DMSA is more sensitive than US for the diagnosis of renal involvement in patients with febrile syndrome and UTI. 2) DMSA is a good tool to rule out renal damage in patients with VUR.

EP-0958

Relative Renal Efficiency Calculation by Scintigraphy: Tc⁹⁹ᵐ MAG-3 dynamic study Versus Tc⁹⁹ᵐ DMSA static study in Different Renal Diseases

D. E. Sharaf, H. M. Gad; Urology & Nephrology Center, Mansoura, EGYPT.

Purpose: To assess the Tc-⁹⁹ᵐ mercaptoacetyltriglycerine (MAG-3) scan as an adjunct or alternative to Tc-⁹⁹ᵐ dimercaptosuccinic acid (DMSA) scan for evaluating differential renal function (DRF) in patients with renal disease. **Patients and Methods**: Ninety-four patients with different renal diseases enrolled in this study as they underwent both MAG-3 and DMSA scans for evaluation of kidney function in between 2012 and 2014. All patients should be adequately hydrated before imaging in supine position with camera facing back. Imaging technique will be done using Philips bright view dual head machine. Demographics included patient age, gender and differential renal function percentage for each right and left kidneys found by both Tc-⁹⁹ᵐ MAG-3 and Tc-⁹⁹ᵐ DMSA scans were recorded. The primary outcome is to detect if there is significant difference in between both Tc-⁹⁹ᵐ MAG-3 and Tc-⁹⁹ᵐ DMSA scans in renal function percentage estimation. **Results**: Ninety-four patients were evaluated. Sixty one were males (64.9%) and thirty three were females (35.1%). Median of age was 8 years (min = 1, max = 76 years). Comparing renal function estimated by Tc-⁹⁹ᵐ MAG-3 and Tc-⁹⁹ᵐ DMSA scans for the left and right kidney respectively was calculated by using Wilcoxon Signed Ranks Test p= 0.44 for the left side and p=0.475 for the right side. This result confirms that there is no significant difference in between both methods for evaluation of renal function. **Conclusions:** Relative renal function calculated by Tc-⁹⁹ᵐ MAG-3 scan and Tc-⁹⁹ᵐ DMSA scan for the same patient showed insignificant difference which means that Tc-⁹⁹ᵐ MAG-3 study can be the only method of choice in some cases to reduce radiation hazards and for economic consumption.

EP-0959

Nephrolithiasis:99mTc-DMSA scintigraphy

D. BEN SELLEM, L. ZAABAR, B. DHAOUADI, I. EL BEZ, B. LETAIEF, M. F. BEN SLIMENE; University of Tunis El Manar, Tunis, TUNISIA.

Introduction: ⁹⁹ᵐTc-DMSA renal scintigraphy is used to estimate the distribution of functional mass. Nephrolithiasis is a common disease responsible for loss of functional renal parenchyma. The determination of the residual functional mass is essential before nephrectomy. The aim of this study was to evaluate the contribution of ⁹⁹ᵐTc-DMSA renal scintigraphy to the exploration of nephrolithiasis that are silent or little functional on intravenous urography (*IVU*). **Subjects and Methods:** One hundred and two patients were sent to our department for ⁹⁹ᵐTc-DMSA scintigraphy to estimate the functional renal mass. The IVU showed silent kidney or delayed contrast excretion up to 3 hours. Planar renal images were acquired 3 hours after injection of ⁹⁹ᵐTc-DMSA. Qualitative interpretation and estimation of renal activity using the geometric mean of anterior and posterior acquisitions were performed. **Results:** Patients were aged from 34 to 75 years (mean ± SD = 59.93 ± 11.70 years, median 60.5 years). The sex ratio was 1.5 (68 males and 34 females). Kidneys were non-functional in 18 patients (17.65 %). The relative uptake value was inferior to 10 % in 12 cases (11.76 %), between 10 and 20 % in 15 cases (14.71 %) and between 20 and 45 % in 39 cases (38.23 %). In the remaining 18 patients (17.65 %), the relative uptake value was normal ranging between 45 and 55 %. **Conclusion:** ⁹⁹ᵐTc-DMSA scintigraphy remains the gold standard for estimation of relative uptake. In nephrolithiasis, it palliates the limitation of IVU by evaluating the functional renal mass guiding so the surgical decision.

EP-0960

Is There a Correlation Between MAG3 Tubular Extraction Rate and Estimated Glomerular Filtration Rate in Transplanted Kidney?

A. Hrelja, S. Grbac-Ivanković, J. Simić, S. Racki, B. Vujicic; Clinical Hospital Rijeka, Rijeka, CROATIA.

The aim of study was to investigate correlation of MAG3 tubular extraction rate (TER) in patients with transplanted kidney calculated by MAG3 dynamic scintigraphy (gamma camera method without blood samples) and stage of chronic kidney disease (CKD) based on estimated glomerular filtration rate (eGFR) calculated by CKD-EPI (Chronic Kidney Disease Epidemiology Collaboration) equation. **Patients and Methods:** The prospective study was based on evaluation of 205 consecutive patients who underwent 99mTc-MAG3 dynamic scintigraphy of transplanted kidney between July 2012 and January 2017. The applied activity was 300 MBq and graft depth was determined by lateral view static imaging. MAG3 TER or clearance of MAG3 was calculated by "slope method" by Inou. Those patients who had values of TER MAG3 above 90 ml/min were selected. Finally, 84 patients, 38 men (mean age 57, range 26-76) and 46 women (mean age 59, range 35-76) were recruited in the study. In each subject, within 24 hours from scintigraphy, eGFR was calculated by CKD-EPI equation from serum creatinine level modified by demographical parameters (gender, age and race). Also all other available scintigraphic and clinical parameters were analysed with focus on the functional status of graft. **Results:** The range of TER values was 98-284 ml/min and calculated median clearance and standard deviation were 150 ml/min and 38 ml/min, respectively. One patient had eGFR >90 ml/min, TER MAG3 215 ml/min (stage 0 of CKD), eight patients had eGFR 60-89 ml/

min, average TER MAG3 204 ml/min (stage 1 of CKD), 27 patients had eGFR 45-59 ml/min, average TER MAG3 163 ml/min (stage 2 of CKD), 37 patients had eGFR 30-44 ml/min, average TER MAG3 139 ml/min (stage 3 of CKD), 11 patients had eGFR 15-29 ml/min, average TER MAG3 138 ml/min (stage 4 of CKD). **Conclusion:** In patients with transplanted kidney there is a correlation between MAG3 TER calculated by gamma camera method without blood samples and stage of CKD based on eGFR calculated by CKD-EPI. However, there is a range of MAG3 TER for each stage of CKD. Consequently, the functional status of graft can be evaluated by MAG3 scintigraphy in addition to standard analysis of perfusion, morphology and excretory function of the graft. A further prospective study in a greater number of patients should be done.

EP-0961

Prediction of permanent renal damage using dimercatpo succinic acid renal scintigraphy in children with vesicoureteral reflux and urinary tract infection

M. Radulovic, L. Jaukovic, M. Sisic, B. Ajdinovic; Military medical academy, Institute of Nuclear medicine, Belgrade, SERBIA.

Objective: Dimercapto- succinic acid (DMSA) renal scintigraphy is the referent method in detection of renal cortical scarring. We aimed to asses the relationship between vesicoureteral reflux (VUR) documented on micturating cystoureterography (MCUG) and renal scarring in children with history of urinary tract infection (UTI). Patients and methods: We analyzed 117 children (70 girls and 47 boys, aged 7 months to 7 years, median 2.4) referred for scintigraphy 6 months after acute UTI. Escherichia coli was identified as the most common causative agent of UTI (85%) followed by Klebsiella (8%), Proteus (5%) and others (2%). Statistical analysis was performed using logistic regression with odds ratio representing the effect size, and considering $p < 0.05$ statistically significant. **Results:** VUR was evaluated as grade I, II, III, IV and V in 1, 47, 35, 19 and 15 children respectively. Of the 117 patients, 41 (35.0 %) had permanent renal damage according to DMSA. Patients were divided into subgroups of low grade VUR (I, II) and high grade VUR (III-V). Univariate regression analysis with 117 cases included in model revealed sex and grade of VUR to be significant independent predictors of renal damage (p<0.05). In model of multiple logistic regressions the only significant independent predictor was grade of VUR. Odds of permanent renal damage was 8.5 folds higher among children with high grade VUR than among those with low grade VUR (OR 8.5; CI 95% 2.982-24.342; p<0.001). **Conclusion:** Our results confirmed the importance of DMSA renal scintigraphy in assessment of UTI in children with VUR, especially in presence of high grade VUR. Keywords: Urinary tract infection - Vesicoureteral reflux - Renal scintigraphy- logistic regression

EP-0962

A new quality control parameter for slope-intercept GFR measurement

J. L. Holness[1,2], J. M. Warwick[1,2]; [1] Stellenbosch University, Cape Town, SOUTH AFRICA, [2] Tygerberg Hospital, Cape Town, SOUTH AFRICA.

Introduction: For glomerular filtration rate (GFR) measurement using the three-point slope-intercept (SI) method, detection of individual sample errors relies on use of the correlation coefficient (r^2) as a quality control (QC) parameter. Previous work has found that r^2 has poor sensitivity for detecting clinically significant GFR errors. In this work a novel parameter for detection of individual sample errors, the normalised range of GFR (NRG), is presented and compared to r^2. **Subjects and Methods**: Three sample SI GFR measurements from clinical cases were used to create idealised data from which reference GFR values were generated. Errors of -20% to 20% were introduced to samples 1, 2, or 3 individually, along with realistic measurement errors to model real GFR measurements. A change relative to the reference GFR of >10% was considered significant. The ability of NRG and r^2 to predict significant GFR errors was compared using receiver operating characteristic (ROC) analysis. **Results:** Reference GFR values were generated for 786 cases. These were used to model 2358 realistic GFR measurements with sample errors, of which 257 resulted in GFR errors of >10%. The area under the curve (AUC) of NRG (0.814; 95% CI 0.798 - 0.829) was found to be greater than the AUC for r^2 (0.745; 95% CI 0.726 - 0.762), p<0.01. **Discussion and Conclusion:** The detection of individual sample errors is a challenging aspect of GFR measurement QC. In this work we present a novel QC parameter for use with the 3 sample slope-intercept method. It is proposed that this parameter may complement the role currently played by r^2 to detect GFR measurements affected by this problem.

EP-0963

Technetium-99m-dimercaptosuccinic acid renal scintigraphy in children with urinary tract infections

I. El Bez, M. Somai, K. Trabelsi, A. Mhiri, D. Ben Sellem, M. Ben Slimene; institut Salah Azaiez, Tunis, TUNISIA.

Introduction: The aim of this study was to determine the incidence of abnormal dimercaptosuccinic acid-Tc-99m ((99m)Tc-DMSA) renal scintigraphy findings in children with culture proved urinary tract infection (UTI) with or without vesicoureteral reflux (VUR). **Methods:** Both (99m)Tc-DMSA renal scintigraphy and Micturating cystoureterography (MCU) were performed in 200 children with culture documented UTI (140 girls and 60 boys) aged from two months to 15 years. MCU revealed VUR that was classed grade I, II, III, IV and V. Findings of (99m)Tc-DMSA renal scintigraphy were classified as: normal and abnormal. **Results:** MCU revealed VUR in 115 children. In 15 of the 10 children the grade of VUR was I, in 15 was II, in 35 was III, in 30 was IV and 25 children had grade V of VUR. Among all these patients, Abnormal findings were detected by (99m)Tc-DMSA renal scintigraphy in 40% (80/200). In children with UTI and VUR the incidence of abnormal findings was 55% (63/115). In children with UTI without VUR the incidence of abnormal findings was 20% (17/85). In children with VUR grade V abnormal findings were 94%. **Conclusion:** (99m)Tc-DMSA renal scintigraphy in children is known as the gold standard for determination of separate renal function and for the detection of renal scars. Our results suggest that (99m)Tc-DMSA renal scintigraphy in chil-

dren can also discriminate between grade I-II and IV-V of VUR and that in children with UTI and VUR abnormal findings in the scintigraphy were more higher than in children with UTI alone.

EP-0964

Scintigraphic Evaluation of Perconditioning Protection on Renal Ischemia/ Reperfusion Injury in Rats

Z. Sedaghat[1], H. Fatemikia[1], K. Tanha[1], M. Zahiri[1], B. Seifi[2], M. Assadi[1]; *[1]Bushehr University of Medical Sciences, Bushehr, IRAN, ISLAMIC REPUBLIC OF, [2]Tehran University of Medical Sciences, Tehran, IRAN, ISLAMIC REPUBLIC OF.*

Purpose: We determined the role of remote per-conditioning (RPeC) on renal function and histology in an animal model of unilateral renal ischemia and reperfusion (IR) injury. **Methods:** Sprague-Dawley rats were subjected to 60min of unilateral renal ischemia without right nephrectomy. RPeC protocol was the application of four cycles of 5min ischemia and reperfusion of left femoral artery during renal ischemia. Assessments of histological changes and renal function were made 24h, 1wk, or 3wk later. In each time point of reperfusion, 99mTc-DMSA scan was performed using a small-animals SPECT system. **Results:** Unilateral renal ischemia and 24h reperfusion decreased the 99mTc-DMSA uptake in the left kidney compared to the intact kidney of control animals. Rats receiving RPeC have higher uptake compared to the IR group in 24h. After 1wk and 3wk, uptakes were gradually increased in both groups. Histological studies showed severe morphological changes in the ischemic kidneys which attenuated after 1wk and 3wk. No significant morphological difference was observed in the RPeC compared with the IR group in theses time points. Moreover, no differences in creatinine and blood urea nitrogen levels between IR-treated and intact animals were observed. **Conclusion:** The results of the present study suggested that remote per-conditioning improves the ability of rat kidney to tolerate subsequent ischemic injury in the first day after reperfusion. Moreover, non-invasive 99mTc-DMSA scan revealed a suitable tool in the follow-up evaluation of recovery process in the unilateral renal IR injury models of rodents. **Keywords:** Ischemia/reperfusion injury, acute kidney injury, recovery, animal SPECT, scintigraphy, remote ischemic per-conditioning, follow-up study

EP-0965

Standardisation of F-15 renography with renal output efficiency

N. D. Assaf[1], A. A. Nawwar[1,2], I. Laurence[1], F. Zananiri[1], M. Darby[1]; [1]Southmead Hospital, Bristol, UNITED KINGDOM, [2]Clinical Oncology and Nuclear Medicine department, Faculty of Medicine, Cairo University, Cairo, EGYPT.

Purpose/Introduction: Diuresis renography is a cardinal test for assessing renal drainage in patients with suspected obstruction (clinical symptoms and/or dilatation of collecting system on other imaging). There are three techniques based on timing of Furosemide; F+20, F−15 and F+0. Assessment of drainage is achieved by reviewing sequential images, renograms and quantification data including renal output efficiency (OE); a quantitative measure of drainage independent of function. Guidelines have supported administration F-15 for suspected obstruction, because of its maximum diuretic potential, as well as OE quantification. As a tertiary urology centre, this is a common problem and since 2002 we have performed only F-15 and calculated OE accordingly. Due to paucity of literature with regards to standardised curves for F-15 and OE ranges, the aim of this project is to provide standardised curves for F-15 and to define OE ranges which relate to normal, equivocal and obstructed curves. **Subjects and Methods:** Retrospective analysis of F-15 MAG3 renography examinations of 207 patients with suspected pelviureteric junction obstruction (PUJO). Our patients were 54% female and 46% male. The average age was 49.6 (range 23-96). Demographic data, curve shape and OEs taken between 27 to 33 minutes were collected and correlated. The F-15 curves were visually divided into normal, equivocal, obstructed and flat curves and OE ranges were then derived in relation to them. The number of interrupted studies was also noted. **Results:** Curves were found to fall into four main categories -Normal curves: drainage to baseline, in 61.5%, - Equivocal curves: drainage between that of normal and obstructed, in 28.8% -Obstructed curves: plateau or rising, in 9.7 %. -Flat curves: low flat, not encountered but fourth possible shape. OE correlation with curves: -Normal curves: mean OE= 94 +/- 2.6 (84.1- 98.2%) -Obstructive curves: mean OE= 51.3 +/- 16.2 (20.8- 76.6%) -Equivocal curves: mean OE= 76.1 +/- 8% (56.1- 90.5%) 8.9% of the studies interrupted for micturition with conjoined renograms. **Discussion/Conclusion:** F-15 optimises diuretic effect at time of isotope injection. Some consider it unfavourable if urgency leads to contamination and interruption of study. This was not a problem and there were no patient recalls. Using these standardised curves with OE helps objective analysis, assisting the multi-factorial process of management of PUJO. We demonstrated OE values < 55%, 75-80% and >90% suggest clear obstruction, equivocal and normal drainage respectively. If within 55-75% and 80-90% ranges, further correlation with other parameters, imaging and clinical features will be required.

EP-0966

Activity quantification (E%) in late postmobilization images with mean parenchymal transit time MPTT in dilated and obstructed pelvis when diuretic test is contraindicated

C. Olianti[1], F. Tutino[2], A. Ciaccio[2], M. Allocca[3], E. Buti[4], M. Materassi[4], M. Antonello[5], L. Masieri[6]; [1]Nuclear Medicine Unit, Careggi University Hospital, Florence, ITALY, [2]Unuversity of Florence, Florence, ITALY, [3]University of Forence, Florence, ITALY, [4]Nephrology and Dialysis Unit, Meyer Pediatric University Hospital, Florence, ITALY, [5]Radiodiagnostic Unit, Meyer Pediatric University Hospital, Florence, ITALY, [6]Pediatric Urology, Meyer Pediatric Univeristy Hospital, Florence, ITALY.

Aim: to assess the usefulness of mean parenchymal transit time (MPTT) and E% (variation of activity 60-90 min post-mobilization images respect the activity at the end of reno-scintigraphy with

[123]I-Hippuran (^{123}I-OIH) or 99mTc-MAG3), to differentiate between obstruction and dilatation in a non-obstructed system in neonates (< 4 months) or children with abdominal pain and hydronephrosis with contraindications to perform furosemide-test. **Materials and Methods:** Twenty children(mean-age 30+/-43 months, 17 males) with sonographic diagnosis of hydronephrosis 3° or 4° stage, without VUR, and antero-posterior diameter (APD) suspected for UPJ stenosis (*ClinJAmSocNephrol* 10:20015) (postnatal confirmed) were included in this study. The analysis comprises 40 renal units: 21 with hydronephrosis, 19 contralateral kidneys for control. Of them 10 renal units were operated (Dilated Obstructed DO), on the basis of significant progression of hydronephrosis (mean+/-SD APD 20.3+/- 6.4 vs. 26 +/- 5.5; p < 0.02), and 11 out of 21 Dilated-Non-Obstructed (DNO) renal units were followed conservatively for 6-18 months through repeated sonography demonstrating reduction of DAP (mean+/-SD APD 17.1+/- 5.1 vs. 11.9 +/- 5 ; p < 0.005) and urologic evaluation. The remaining 21 contralateral Normal kidneys (NK) were used as control group. The relative (RF%) and absolute (*Cl*) renal function, MPTT, E% and variation &#916APD were measured. **Results:** No significant difference was found between DO and DNO groups for *Cl* and RF% , APD and mean age at diagnosis; significant difference was found for MPTT (mean+/-SD DNO 226.1+/- 56.1 vs. DO 388.8 +/- 133.8; *p* <0.02. DO 388.8 +/- 133.8 vs NK 135.1+/- 24.2), &#916APD (mean+/-SD -5.2+/- 4.7 vs. 4.4 +/- 4.3 ; *p*<0.001) and E% (mean+/-SD 80 +/- 17 vs. 40 +/- 20 ; *p* <0.001). No difference was found between NK and DNO *Cl*, while was found for NK and DO *Cl* (mean+/-SD 306+/- 38 vs. 251 +/- 64 ; *p* <0.05). Stepwise discriminant analysis applied to 21 hydrophrotic renal units found that E% correctly identified 10/11 DNO and 9/10 DO with a diagnostic accuracy of 91% (p <0.001) and MPTT correctly identified 10/11 DNO and 8/10 DO with a diagnostic accuracy of 86% (p <0.001), E%+MTPP correctly identify 10/11 DNO and 10/10 DO with a diagnostic accuracy of 95% (p <0.0001). **Conclusion:** MPTT+E% quantification, if confirmed on a larger cohort, seems a valid tool for UPJ obstruction even in the cases where diuretic test is contraindicated.

EP-0967

Tc99m DTPA renography owes a characteristic pattern in patients with chronic parenchymal renal disease associated with significant renal function impairment

S. M. W. Yassin[1], K. Salman[2], A. Bakhsh[2], H. Abdallah[2], Z. Khan[2]; [1]King Abdulla Medical City (KAMC), Jeddah, SAUDI ARABIA, [2]King Abdulla Medical City (KAMC), Makkah, SAUDI ARABIA.

Purpose: To verify possible presence of a characteristic renogram pattern for patients with chronic parenchymal renal disease (CPRD) associated with significantly impaired renal function **Subjects and Methods:** Patients presenting for Tc99m DTPA dynamic renal scan with diagnosis of non obstructive nephropathy together with significant renal functional impairment confirmed by laboratory data , attributed to radiologically diagnosed CPRD.The renogram pattern of these kidneys is compared to the normal renogram pattern. **Results**: 49 patients (24 females and 25 male) with age range from 19 to 91 years with CPRD and significantly impaired renal function are included, with 95 functioning kidneys (2 patients with nephrectomy and one with non functioning kidney).TC99m DTPA dynamic renal scan was performed with creation of renography for each kidney. The global GFR ranges from 13.6 to 31.4 ml/min with individual GFR ranging from 5.5 ml/min up to 26.3ml/min. with a median value of 20.4 ml/min and 14.9 ml/min respectively. All renograms have low amplitude , less than 50% of normal amplitude, lacking the normal pattern and time sequences. In 89 kidneys (93.7%) the pattern is in the form of short ascent of first vascular phase followed by slowly descending curve that has a shallow slope compared to normally expected slope of third washout phase, with neither secretory phase nor normal peaking. Out of the remaining six kidneys, four (4.2%) have similar low amplitude and short ascent of the curve followed by abrupt minimal drop then the curve exhibits slow shallow slope descent. The other two kidneys (2.1%) exhibit in addition to the low amplitude, shallow slope ascending second phase with slightly delayed peak followed by shallow slope curve descent. The former curve pattern, seen in 93.7% of kidneys, is considered characteristic for patients with CPRD and significant renal functional impairment. This figure increases to 97.9% on addition of few kidneys that exhibit same curve pattern with minimal abrupt drop prior to the slow curve descent. **Conclusion:** Patients with significantly impaired renal function due to CPRD have a characteristic renogram pattern, that has an evidently low amplitude ,short ascent of the curve followed by slow curve descent that has a shallow slope, seen in 93.7% of studied kidneys, this figure increases to 97.9% by adding renograms of few kidneys in which the slow curve descent is preceeded by abrupt minimal drop of the curve, further study on a larger number of patients is advisable to confirm our data.

EP-0968

Is normalized residual activity a good marker of renal output efficiency in hydronephrosis?

I. El Bez, M. Somai, K. Trabelsi, A. Mhiri, I. Slim, M. Ben Slimene; institut Salah Azaiez, Tunis, TUNISIA.

Introduction: Hydronephrosis is a condition where urine overfills, or backs up, into the kidney, which causes the kidney to swell. Infants with hydronephrosis may be diagnosed before (prenatal) or after (postnatal) birth. The [99m]mag3 renal scintigraphy is the method of choice in the study of the functionality of obstruction in hydronephrosis. The objective of this study is to investigate the robustness of the normalized residual activity (NORA) for the estimation of renal emptying during renography. **Methods:** Thirty-one patients (19 boys and 12 girls) with 51 dilated pelvicaliceal units had undergone a [99m]mag3 diuretic renal scintigraphy. The mean age was about 5.28 years, ranges from 3 months to 17 years old. Hydronephrosis was bilateral in 12 cases. The main causes of the Conditions of hydronephrosis were ureteropelvic junction (UPJ) obstruction in 10 cases, megaureter in 5 cases, Neurogenic bladder and uropathy malformation in 2 cases, and posterior urethral valve in one case. The normalized residual activity (NORA) was defined as the renal

activity at 30 min after micturition divided by the renal activity between 1 and 2 min. **Results:** NORA was calculated in 41 cases in wich hydronephrosis was not ameliorated by the diuretic stress test. Among them 29 were reclassified into normal renal drain (NORA<1) and 12 into obstructive origin, all of them had less contribution in total renal function. After further investigations obstructive one were divided into two groups surgical and nonsurgical. Postoperatively the most common observation was improvement in the MAG3 clearance image in 4 of 7 cases and stabilized differential renal function in 2. In nonsurgical group, 1 had improved spontaneously; no significant increase in differential renal function was noted in 4. **Conclusion:** Several methods allow the evaluation of renal drainage, the most appropriate being the diuretic renal scintigraphy. However, many tests are inconclusive. NORA is an extremely simple parameter and robust method that fits better to reclassify these patients.

EP-0969

Does Anteroposterior Pelvic Diameter Predict of the Need of Diuretic in Cases of 99mTc-MAG3 Stasis after Basal Renogram?

H. C. Martins[1], G. Costa[1], A. Moreira[1,2], R. Silva[1,2], J. Pedroso de Lima[1,2,3]; [1]Centro Hospitalar e Universitário de Coimbra, Coimbra, PORTUGAL, [2]Instituto de Ciências Nucleares Aplicadas à Saúde, Coimbra, PORTUGAL, [3]Faculdade de Medicina da Universidade de Coimbra, Coimbra, PORTUGAL.

Purpose: Dynamic renal scintigraphy with ^{99m}Tc-MAG3 is an important diagnostic tool widely used to study hydronephrotic kidney (HK) in children. When poor drainage is present at the end of the basal renogram, post-micturition images (PMI) and/or post-postural drainage images (PPDI) - image acquired after move the child to upright position- may exclude obstruction. If the drainage is still impaired, then furosemide must be given. However, when children are relaxed or even sleeping, PPDI may disturb and compromise the image quality when diuretic renogram is necessary. This work aimed to know if anteroposterior pelvic diameter (APPD) can predict the cases in whom PMI/PPDI are unnecessary because they cannot avoid the diuretic renogram. **Material and Methods:** The clinical charts of children with uni/bilateral HK submitted to ^{99m}Tc-MAG3 scintigraphy between 12-2009 and 03-2017 were retrospectively analyzed. Gender, age and APPD by ultrasound were assessed. The ^{99m}Tc-MAG3 drainage patterns divided the dilated renal pelvis into five groups: G1-normal; G2-stasis that resolves after PMI/PPDI; G3-stasis that persists after PMI/PPDI but resolves after the diuretic (F+20 protocol); G4-stasis that reduces after diuretic stimulus but have significant residual activity in the renal pelvis at the end of the study; G5-complete unresponsive stasis to diuretic. For each group the mean±sd APPD was calculated and the Kruskal-Wallis test was used to study the differences between the groups. Statistical analyzes were performed using SPSS version 23. **Results:** 191 children (70 girls, 121 boys; mean age±sd=4.3±4.5 years) having a total of 247 HK were included in the study. G1(n=48): mean±sd APPD=9.6±4.7mm; G2(n=41): mean±sd APPD=16±12.3mm; G3(n=136): mean±sd APPD=15±9.1mm; G4(n=6): mean±sd

APPD=26±9.4mm; G5(n=16): mean±sd APPD=33.1±15.2mm. A statistically significant difference was observed between APPD of G5 and G1, G2 and G3 (p=0.001, p=0.002 and p=0, respectively), as well as between G1 and G2, G3 and G5 (p=0.05, p=0 and p=0, respectively). No statistic significant difference in pelvic size was found between G2 and G3 (p=1). G4 did not showed significant differences with any of the other groups. **Conclusion:** Is not surprising that this study suggests that smaller renal pelvis tend to exhibit more appropriate radiopharmaceutical elimination patterns. However, in case of ^{99m}Tc-MAG3 stasis after basal renogram, the size of the renal pelvis does not predict of the need of diuretic.

EP-0970

Value of real-time time-activity curves when evaluating need for diuretic on dynamic renograms

P. Holdgaard[1], A. Erslev[1], N. Bebbington[2]; [1]Sygehus Lillebælt, Vejle, DENMARK, [2]Siemens Healthineers, Aarhus, DENMARK.

Aim: Diuretic can give unpleasant side effects and its administration is not necessary for renograms demonstrating adequate drainage. In routine practice, technologists decide whether to administer diuretic based on apparent drainage 10 minutes post Tc-99m-MAG3 injection, but available technology to aid decision-making differs between scanners. The aim was to assess the value of real-time time-activity curves (RT-TACs) in diuretic decision-making compared with images alone. **Materials and Methods:** Renogram data for a one-year period was audited across 4 gamma cameras: 1 Philips Precedence and 1 Nephrocam (without RT-TACs), and 2 Siemens Symbia Intevos (with RT- TACs), according to whether diuretic was administered, and a χ^2-test undertaken to significance test differences. Furthermore, 14 Technologists and 7 Physicians blind-evaluated randomized data in 25 patients for the need for diuretic, with images at 10 minutes only, images at 2 &10 minutes, and RT-TACs at 10 minutes post tracer injection. Agreement in diuretic decision-making between images and RT-TACs was compared for each reader and also with 2 expert readers (RT-TACS as gold-standard evaluation tool) using Cohen's Kappa score. Agreement between Physicians and Technologists was also examined. **Results:** Audit data for 1237 patients demonstrated that a significantly greater proportion of patients were administered diuretic on systems without RT-TACs (72%) compared with those with RT-TACs (42%) (p<0.0001), suggesting that in the absence of RT-TACs, diuretic is often administered when not clinically necessary, which is consistent with expectation. Agreement with expert readers: diuretic decision-making was excellent using RT-TACs (mean kappa score 0.80, kappa range 0.41-1.0, mean agreement 90%). However, agreement was poor using only images at 10 minutes, giving a mean kappa score 0.22, range -0.23-0.56, and mean agreement 63%. Similar results were found for images at 2&10 minutes. Half of the cases of disagreement were when diuretic was clinically necessary but not given, and half where diuretic was not necessary but was given. Agreement between datasets for a given observer: poor agreement was demonstrated between RT-TACs and images only

(10 minutes: mean kappa score 0.18, kappa range -0.183-0.49, mean agreement 60%). Agreement comparing physician and technologists were similar, with slightly higher kappa scores for technologists. **Conclusions:** This study demonstrated that RT-TACs are a highly valuable tool for decision-making with respect to the need for diuretic, and observers should be extra-cautious when making decisions in the absence of RT-TACs.

EP-0971

Infected Polycystic Kidney Disease: Role Of 18F-Fluorodeoxyglucose Positron Emission Tomography/Computed Tomography

J. Benouhoud, S. CHOUKRY, Y. SHIMI, A. GUENSI; CHU Ibn Rochd, Casablanca, MOROCCO.

Aim: We aimed to report the diagnostic performance of 18F-fluorodeoxyglucose positron emission tomography-computed tomography (18FDG PET/CT) for the diagnosis of cyst infections among two cases of autosomal dominant polycystic kidney disease (ADPKD) patients. **Materials and Methods:** PET/CT was realized in two patients with ADPKD for suspected cyst infection for the motive of persistant inflammatory syndrome. **Results:** 18FDG PET/CT had found an cyst wall hypermetabolim and were retained positive while CT in these two patients were negative. Diagnosis of cyst infection in the first case was confirmed by cyst puncture made in the hypermetabolic cyst in PET/CT and in the second case retained on an index of clinical suspicion. **Conclusion:** CT or MRI may find enhancemed thickening of cyst wall or an infiltration of the adjacent fat, but those criteria are not always found and them specificity is not high. The diagnostic performances of 18FDG PET/CT are superior to CT in cyst infections, for a comparable irradiation and without nephrotoxicity. In fact the publications showed specificity of PET/CT up to 100% for this indication. PET-CT should become the first-line imaging technique for the diagnosis of cyst infection in polycystic patients.

Conventional & Specialised Nuclear Medicine: Infection & Inflammation

EP-0972

Diagnostic performance of ^{99m}Tc-HMPAO-labeled leucocyte scan for diabetic foot osteomyelitis in relation to foot part involved and imaging technique

S. Georga[1], C. Manes[2], T. Didangelos[3], G. Arsos[1]; [1]3rd Dept of Nuclear Medicine, Aristotle University Medical School, Papageorgiou General Hospital, THESSALONIKI, GREECE, [2]Diabetes Center, Papageorgiou General Hospital, THESSALONIKI, GREECE, [3]Diabetes Center, 1st Propedeutic Dept. of Internal Medicine, Aristotle University Medical School, 'AHEPA' Hospital, THESSALONIKI, GREECE.

Background and aim: Accurate diagnosis of diabetic foot osteomyelitis (DFO) remains challenging. Coexistent pathologies such as ulcer, soft tissue infection (STI) or Charcot osteoarthropathy (COA) may obscure clinical and radiological presentation of DFO and hamper diagnosis. On the other hand, imaging technique (planar, tomographic or hybrid), can substantially affect localizing and diagnostic accuracy. The study is aiming to evaluate ^{99m}Tc-HMPAO-labeled leucocyte scintigraphy (LS) in DFO diagnosis, in relation to foot part involved and imaging technique. **Patients and Methods:** 168 consecutive patients with clinical suspicion of DFO in 207 pedal sites were investigated by planar LS. Clinically suspect sites were divided into Group-1 (137 forefoot sites, 130/137 with contiguous ulcer) and Group-2 (70 mid/hind foot sites) further subdivided into subgroups 2a including 49 sites with ulcers (23 with COA) and 2b including 21 sites without contiguous ulcers. 80 sites were further investigated by SPECT/CT. Focally persistent increased leucocyte bone uptake was considered positive for DFO. Final diagnosis was based on clinical and radiological follow-up or histopathological findings. **Results:** Among the 207 sites investigated, final diagnosis was DFO in 74 sites, acute COA in 18, STI in 96 and no infection in 19. In the forefoot sensitivity, specificity, accuracy, positive (PPV) and negative predictive value (NPV) of planar LS for diagnosing DFO were 90.9%, 91.5%, 91.2 %, 87.7% and 93.7% respectively. SPECT/CT addition improved all of the aforementioned values to 100%, 96.8%, 98.2%, 96.0% and 100%, respectively. In the mid/hindfoot planar LS sensitivity, specificity, accuracy, PPV and NPV were 88.2%, 86.8 %, 87.1%, 68.2% and 95.8% respectively. SPECT/CT addition clearly improved sensitivity to 100%, but only marginally specificity from 86.8% to 90%, due to false positive findings caused by leucocyte accumulation at sites of active bone marrow. Lowest specificity and PPV of 80% and 62.5%, respectively, were observed in subgroup-2b patients with suspected mid/hindfoot DFO without contiguous ulcers and highest acute COA prevalence. **Conclusion:** ^{99m}Tc-HMPAO-labeled leukocyte scan is a highly accurate imaging modality for diagnosing DFO. Hybrid SPECT/CT imaging can maximize the diagnostic performance of planar imaging for DFO especially in the forefoot (accuracy of 98.2%) by enabling accurate localization and discrimination of bone from soft tissue infection. Although the diagnostic accuracy of planar LS in the mid/hindfoot is also improved by SPECT/CT addition, specificity of LS may remain suboptimal in the mid/hindfoot, due to modality-independent leucocyte uptake by active bone marrow foci on sites of acute Charcot arthropathy.

EP-0973

Concordance between MRI and 99mTc-HMPAO WBCs scan in suspect osteomyelitis: results from a single centre experience

I. Grassi[1], G. Pontone[1], F. Albertini[2], C. Orzincolo[3], E. Del Giudice[1]; [1]Nuclear Medicine Unit, Ospedale degli Infermi, Faenza (Ra), ITALY, [2]Infectious Diseases Unit, Ospedale degli Infermi, Faenza (Ra), ITALY, [3]Radiology Unit, Ospedale degli Infermi, Faenza (Ra), ITALY.

Introduction. Magnetic resonance imaging (MRI) is widely considered as the gold standard in osteomyelitis diagnosis, due to its high spatial resolution, its good sensitivity in evaluating soft

tissues and its lack of ionizing radiation. Nevertheless, MRI could be affected by the presence of metal implants, by patient's soma and by the risk, even if low, of hypersensitivity to the contrast medium. Aim of the present study is to compare scintigraphy with autologous white blood cells radiolabelled with 99mTc-hexamethylpropylene amine oxime (99mTc-HMPAO WBCs scan) to MRI in pts with suspect osteomyelitis. Subjects and methods. Pts who performed both 99mTc-HMPAO WBCs scan in our Nuclear Medicine Unit and MRI in Ravenna District Hospitals between 2010 and 2015 were retrospectively considered; MRI carried out in other hospitals were not considered to obtain a better homogeneity. Autologous WBCs were labelled with 99mTc-HMPAO according to EANM Guidelines. The acquisition protocol was based on AIMN Procedural Recommendations and a SPECT was performed 4 hours after injection. 1.5 Tesla MRI scans were carried out. Results. 25 consecutive pts (16M, 9F, middle age 47 y) were finally eligible. In 15 cases MRI was performed without and with contrast medium and in 10 cases only without it, according to radiologist's opinion. Disease localizations were: tibia (9 pts, 36%), foot (7 pts, 28%), knee (2 pts, 8%), fibula (2 pts, 8%), spine (1 pt, 4%), shoulder (1 pt, 4%), humerus (1 pt, 4%), femur (1 pt, 4%) and pelvis (1 pt, 4%). MRI was positive in 15 pts, that is in 60%, thus being the percentage of agreement between the two investigations. In 1 pt (4%), MRI could not distinguish between "over-load" edema and inflammatory one. In 5 pts (20%) MRI was inconclusive because of the presence of metal implants which caused artifacts. In 4 pts (16%) MRI was negative. Conclusion. Our research suggests that, when positive, 99mTc-HMPAO WBCs scan matches with MRI in 60% of cases. This percentage is probably underestimated because conditioned by the 20% of cases of inconclusive MRI. The two different investigations should be considered as complementary in the diagnosis of osteomyelitis.

EP-0974

Does Additional Low Dose Heparin Pre-administration Improve Cardiac Glucose Metabolism Suppression in FDG PET/CT?

N. L. van der Zee; *Meander Medical Center, Amersfoort, NETHERLANDS.*

Aim: FDG PET/CT in cardiac infection and inflammation detection relies on adequate suppression of physiological cardiac glucose metabolism. Many preparatory protocols have been applied, with low-carbohydrate fat-allowed diets and prolonged fasting periods being recommended by many. Additional heparin pre-administration at higher doses (50 IU/kg) has been reported to be of additional value based on its lipolytic effects. Theoretically, low dose heparin (15 IU/kg) should also induce lipolysis, but without anticoagulant effects. We compared three preparatory protocols in our institution. **Methods:** FDG PET/CT scans were selected and grouped according to 3 preparatory protocols: 6-h fast (group 1, n=50), low-carbohydrate diet plus 12-h fast (group 2, n=50), and low-carbohydrate diet plus 12-h fast plus intravenous low dose heparin pre-administration (15 IU/kg) (group 3, n=50). FDG uptake in normal myocardium was scored according to a five-point-scale ranging from 0 (uptake less than that in left ventricle blood pool) to 4 (diffuse uptake greater than that in liver). Adequate suppression was defined as non-focal uptake less than that in liver (scores < 3). Scans were scored by one experienced physician and two technicians. Final scores were based on consensus. **Results:** Adequate suppression was achieved in 32% in group 1, 84% in group 2 and 78% in group 3. Scores in groups 2 and 3 differed significantly from group 1 (P<0.0001) but group 3 did not differ significantly from group 2 (P=0.62). **Conclusion:** Additional low dose heparin pre-administration did not improve cardiac glucose metabolism suppression over low-carbohydrate diet and prolonged fast alone.

EP-0975

An enlarged left adrenal gland is an indirect sign of sepsis in patients referred to FDG PET CT for a suspected or proven infectious disease, even in the absence of any evident infectious focus on PET images

C. Drouet[1], F. Goehringer[2], C. Besseau[2], H. Tissot[2], C. Manca[2], P. Marie[2]; [1]CHU de Besançon, Besancon, FRANCE, [2]CHU de Nancy, Nancy, FRANCE.

The timely identification of septic patients is frequently critical and difficult despite extensive workups including ^{18}F-fluorodesoxyglucose Positron Emission Tomography / Computed Tomography (FDG PET/CT). This study was aimed to determine to what extent indirect signs of sepsis, such as hypermetabolism and size of the left adrenal gland, or hypermetabolism of spleen or bone marrow, might help in the identification of septic patients. **Methods:** Predictors of sepsis were searched in a study group of 56 patients (39 men, 61±18 years) who were selected retrospectively on the basis that they had been referred to FDG PET/CT for the evaluation of a suspected or proven infectious disease and for whom presence or absence of sepsis could be ascertained by subsequent workup in 44 and 12 cases, respectively. Mean and maximal Standardized Uptake Values (SUV) were determined on left adrenal gland, spleen and bone marrow, and the size of the left adrenal gland was assessed by its maximal surface on transaxial CT slices. Two additional validation groups were prospectively constituted of 12 patients hospitalized for a severe sepsis (6 men, 51±18 years) and of 39 control patients who had no sign of infectious disease (16 men, 52±15 years). **Results:** Only the maximal surface of the left adrenal gland was a significant correlate of sepsis in the initial study group (sepsis: 2.68±1.0 cm^2 vs. no sepsis: 1.85±0.76 cm^2, p = 0.006) and this parameter was also significantly different between the two validation groups (sepsis: 2.98±0.91 cm^2 vs. controls: 1.91±0.67 cm^2, p < 0.001). The criterion of a maximal surface > 1.8 cm^2 was associated with a 2-fold increase in the infection rates: 1) in patients from the initial study group (88% vs. 42%, p= 0.002), even when only considering the 31 patients who had no evident infectious focus on PET images (76% vs. 30%, p=0.02) and also 2) in the 2 validation groups considered as a whole (92% vs. 49%, p=0.009). **Conclusion:** In patients referred to FDG-PET/CT for a suspected or proven infectious dis-

ease, an enlarged left adrenal gland constitutes an indirect sign of sepsis, as already documented in previous CT studies. This sign seems particularly helpful in the absence of any evident infectious focus on PET images.

EP-0976

The presence of elevated C-reactive protein (CRP) and fever during ^{18}F-FDG-PET/CT increases diagnostic yield in patients with fever of unknown origin

K. Mulders-Manders, I. Kouijzer, M. Janssen, A. Simon, C. Bleeker-Rovers; Radboudumc, Nijmegen, NETHERLANDS.

Introduction: ^{18}F-fluorodeoxyglucose positron emission tomography with combined computed tomography (^{18}F-FDG-PET/CT) is one of the most important diagnostic techniques in the workup of patients with fever of unknown origin (FUO) in whom targeted diagnostic procedures do not lead to a final diagnosis. The diagnostic value of ^{18}F-FDG-PET/CT is expected to be higher when more inflammation is present at the time of imaging. Clinically, this is reflected as the presence of elevated C-reactive protein (CRP) or fever at the time of the procedure. We investigated whether CRP or fever could be used to optimize the diagnostic yield of ^{18}F-FDG-PET/CT in patients with FUO. **Subjects and Methods:** All patients with FUO presenting to the Department of Internal Medicine of the Radboud university medical center, the Netherlands, between January 2005 and June 2014 in whom ^{18}F-FDG-PET/CT was performed were retrospectively included. Data on outcome of ^{18}F-FDG-PET/CT, body temperature at the day of the procedure, and CRP value within two weeks before ^{18}F-FDG-PET/CT were extracted from medical records. CRP >10mg/dL was considered elevated. **Results:** In this study, 123 ^{18}F-FDG-PET/CT scans were included. Median duration of fever until presentation was 234 days. Twenty-nine ^{18}F-FDG-PET/CT scans were performed at random. Of these scans, 31.8% contributed to the final diagnosis. When elevated CRP was present within one week before ^{18}F-FDG-PET/CT, ^{18}F-FDG-PET/CT contributed in significantly more cases to the final diagnosis (34 out of 73, 45.9%) (p=0.045). In 30 cases, fever was present on the day of ^{18}F-FDG-PET/CT and ^{18}F-FDG-PET/CT contributed in 21 cases (70.0%) to the final diagnosis, which was significantly higher than in randomly performed ^{18}F-FDG-PET/CT (p<0.001) and ^{18}F-FDG-PET/CT performed when elevated CRP was present (p=0.049). **Conclusion:** In patients with FUO, both the presence of elevated CRP within one week before ^{18}F-FDG-PET/CT and the presence of fever on the day of ^{18}F-FDG-PET/CT increases the diagnostic yield of ^{18}F-FDG-PET/CT and both can thus be used as a parameter guiding the planning of ^{18}F-FDG-PET/CT in these patients.

EP-0977

Usefulness of F-18 FDG PET/CT for Detecting Bone Involvement in Patients with Sarcoidosis

A. Georgakopoulos[1], N. Pianou[1], E. D. Manali[2], L. Kolilekas[3], S. A. Papiris[2], S. N. Chatziioannou[4,1]; [1]Biomedical Research Foundation of the Academy of Athens, Clinical and Translational Research, Nuclear Medicine Division, PET/CT section, Athens, GREECE, [2]2nd Pulmonary Medicine Department, "Attikon" University Hospital, Athens Medical School, National and Kapodistrian University of Athens, Athens, GREECE, [3]7th Pulmonary Medicine Department and Asthma Center, Sotiria Hospital for Chest Diseases, Athens, GREECE, [4]2nd Radiology Department, "Attikon" University Hospital, Athens Medical School, National and Kapodistrian University of Athens, Athens, GREECE.

Purpose/Introduction: Sarcoidosis is a systematic granulomatous disease of unknown cause. Although thorax is the most common site of disease, extrathoracic involvement occurs in 25%-50% of patients. Bone involvement is often associated with a chronic and severe course. Until today, the exact prevalence of bone involvement in sarcoidosis is unknown due to the different diagnostic methods and the studied population. The aim of this study is to determine the prevalence and distribution pattern of bone involvement in the sarcoidosis patients with 18F-flurodeoxyglucose Positron Emission Tomography / Computed Tomography (F-18 FDG PET/CT). **Subjects & Methods:** Between 2013 and 2016, all biopsy proven sarcoidosis patients, from a tertiary referral center who underwent F-18 FDG PET/CT were included in the study. 18F-FDG was injected intravenously (5.5 MBq/kgr); none of the patients had blood glucose levels >160 mg/dl. PET/CT images of the brain and from the base of the skull to the feet were obtained. PET findings were described as positive for bone involvement if focally increased tracer uptake was seen in the skeleton. Also, the CT scans were evaluated. **Results:** One hundred and eighty four patients, 51% female, mean age (±SD) of 52±12.75 years were included. Findings consistent with active extrathoracic disease were identified in 108 patients (58.6%). Almost all of these patients (98%) also demonstrated active thoracic disease. In 31 patients (17.1%) PET/CT was negative for active disease, while another 42 patients (22.8%) demonstrated only active thoracic disease. A significant percentage (35 patients, 19%) revealed active bone disease. Eleven patients (31.6%) had one bone location, 12 (34.2%) two or three locations and another 12 (34.2%) revealed multiple locations of bone disease. The distribution of bone involvement was: extremities (21 patients, 60%), pelvis (17 patients, 48.5%), vertebrae (12 patients, 34.2%), ribs (7 patients, 20%) and skull (2 patients, 5.7%). **Conclusion:** F-18 FDG PET/CT provides useful information in sarcoidosis, identifying in a significant percentage of patients unsuspected active bone disease.

EP-0978

Comparative Effectiveness Of 18F-FDG PET-CT And CT Angiography For The Evaluation Of Large-Vessel Vasculitis

M. Moragas, M. Andreu, M. Monteagudo, A. Caresia, J. Martin, A. Rodríguez, C. Diaz, J. Oliva, L. Bernà; Hospital Parc Tauli, Sabadell (Barcelona), SPAIN.

Aim: Diagnosing large-vessel vasculitis remains a challenge. Using 18F-FDG PET-CT and computed tomography angiography (CTA) can improve the accuracy of diagnosis of large-vessel vasculitis. 18F-FDG PET-CT can detect large-vessel vasculitis

through metabolic changes and CTA can detect it through mural changes due to inflammatory activity. Both approaches are sensitive. We aimed to compare the effectiveness of FDG-PET and CTA in the diagnosis and monitoring of large-vessel vasculitis. **Material and Methods:** We retrospectively studied 25 patients (July 2014-April 2017), 14 with clinically suspected large-vessel vasculitis (clinical suspicion group) and 11 with known large-vessel vasculitis in whom the response to gluco-corticoid treatment was being monitored (monitoring group). CTA was performed simultaneously with PET in 15 patients, sep-arately within < 1 month in 5, and separately within > 1 month in 5. CTA criteria for large-vessel vasculitis were aortic circumfer-ential wall thickening >2 mm in areas without adjacent ather-oma and >1 mm in aortic branches and/or wall enhancement (> 40 UH) and/or irregular thickening extending to periaortic tissue. PET criteria for large-vessel vasculitis was diffuse FDG up-take in the wall of aorta and/or its main branches. Large-vessel uptake was graded on a visual scoring index comparing uptake with liver uptake (0=no uptake, 1=less than liver uptake, 2= sim-ilar to liver uptake, 3= greater than liver uptake); scores >2 for the thoracic aorta and ≥ 2 in other vascular regions were consid-ered positive. Large-vessel vasculitis was confirmed or ruled out case-by-case through clinical work-up, inflammation markers, response to corticosteroid treatment, other imaging modalities (Doppler ultrasonography, MRI), and temporal artery biopsy. **Re-sults:** Clinical suspicion group: large-vessel vasculitis was con-firmed in 4/14 patients. PET was positive in 5/14 patients with 1 false-positive in a patient with an aortic aneurysm. CTA was negative in all patients with 4 false-negatives. Monitoring group: PET and CTA were positive in 6/11 patients. In these 6 patients with active disease, the dose of corticoids was increased and/or immunosuppressed treatment was added, leading to better clinical outcome in all cases. **Conclusion:** FDG PET-CT was more useful than CTA for the early diagnosis of large-vessel vasculitis and is the best noninvasive technique for diagnosing large-ves-sel vasculitis. Both FDG PET-CT and CTA have good performance in monitoring therapy; patients with active disease on PET can benefit from CTA, as they have risk of later vascular complica-tions.

EP-0979

Effectiveness of long-term chronic suppressive antibiotic therapy in chronic joint infection: follow-up by 99mTc-HMPAO-labeled leukocyte scan

M. Ricci, M. Pontico, G. A. Follacchio, M. De feo, F. Monteleone, G. De vincentis, G. Ceccarelli, M. Liberatore; Università di Roma "Sapienza", ROMA, ITALY.

Introduction: The treatment of prosthetic joint infections (PJI) and fixation devices-related infections (FDI) can be challeng-ing, since bacteria may persist in a biofilm-based colony or have an intracellular localization, causing local and systemic complications. The long-term chronic suppressive antibiotic therapy (CSAT) can be considered a palliative approach in case of contraindication or failure of surgery and when short-term pathogen-directed antimicrobial therapy has proven to be in-

effective. However, no clear indications nor therapy monitoring tests are recommended by specific guidelines. 99mTc-HMPAO-la-beled leukocyte scan (LS) is widely used in the diagnosis and follow-up of PJI and FDI. The aim of this study is to evaluate whether LS can have a role in monitoring the effectiveness of CSAT. **Subjects & methods:** Twenty-three patients (11 male, 12 female) affected by PJI (72%) or FDI (23%) were enrolled from 2014 to 2016. All patients underwent CSAT for contraindication to surgery or for persistence/relapse after curative antimicro-bial therapy. CSAT results were evaluated by qualitative distri-bution of labeled leucocytes at the scan and periodical clinical examination. LS was performed after 2-6 months of therapy in all patients and was repeated according to the clinical features. Being a palliative approach, therapeutic goals were stability or regression of disease assessed by LS results and by evolution of the clinical picture. **Results:** In 43% of patients. the first LS re-sulted normal and, up to now, no clinical signs of relapse or clin-ical declining are referred. In 22% of patients, initial LS showed persistence of infection, but a second scan (after 0.5-3y; mean 1,3y) and results of clinical examination, performed during the follow-up, demonstrated total regression, partial regression or stability in 13%, 4.5% and 4.5% of patients respectively. Similarly, in 8% of patients regression of disease was clinically assessed, but further LS were not performed. CSAT achieved therapeu-tic goal in 74% of patients. The remaining 26% shown a clinical relapse of disease: this was confirmed by LS in 17% of patients, while in the remaining 9% LS was normal although clinical pro-gression of infection. Overall, LS showed agreement to clinical and laboratory signs of disease in 91% of cases. **Conclusion:** CSAT can be an effective palliative treatment of JI or FDI and should be considered, especially in cases of contraindication to surgery or failure of previous curative therapy. LS is an useful tool in monitoring this palliative treatment.

EP-0980

Diagnostic value of Tc99m- Ubiquicidine in differentiation between osteomyelitis and bone tumors

K. Aryana[1,2], N. Ayati[1], M. Norouzi[1]; [1]Mashhad university of medical sciences, Mashhad, IRAN, ISLAMIC REPUBLIC OF, [2]Nuclear medicine research center, Mashhad, IRAN, ISLAMIC REPUBLIC OF.

Introduction: The differentiation of osteomyelitis from bone tumors is of great importance in clinical decision making; how-ever,the features of both osteomyelitis and bone tumors are non-contributory. 99mTc-Ubiquicidin scintigraphy is a new prom-ising method, with the ability to specifically localize the infec-tion site by bacterial cell membrane binding. This study is aimed at evaluating the ability of this radiopeptide for differentiation of these two entities. **Methods:** 30 consecutive patients (mean age=20.9 years) suspicious of either osteomyelitis or bone tu-mor were included in this prospective study. 99mTc-UBI scan was performed in both dynamic and static phases and the imag-es were assessed qualitatively and semi-quantitatively. The final diagnosis was established on the basis of surgical findings and microbiological and pathology assessments as well as any other clinical, laboratory or imaging findings during patient follow up.

Results: The final diagnosis was infectious and non-infectious processes in 19 and 10 patients respectively. Visual assessment could not distinguish between osteomyelitis and bone tumors. But, quantitative analysis of the images proved to be promising. The sensitivity, specificity, negative and positive predictive value and accuracy of Time-Activity Curve for osteomyelitis were 73.6% (54-93), 100%, 66.6% (43-91), 100% and 82% respectively. The mean±SD T/NT ratios for 30 minute images were 2.22±0.45 and 2.02±0.51 for infectious and non-infectious processes respectively (p value=0.29). Using cut off value of 0.97 for T/NT ratio, the sensitivity and specificity were calculated as 78.9%, and 50% respectively. **Conclusion:** Although Tc-99m-UBI scintigraphy in the dynamic imaging format was of great value with high accuracy in differentiation between infectious and tumoral lesions, it was not of any help to distinguish these two entities based on visual assessment or T/NT ratio measurement on static images. The study also showed high accuracy of this non invasive modality in acute osteomyelitis with low diagnostic value in chronic infectious processes.

EP-0981

99mTc-sulesomab and 99mTc-nanocolloid bone marrow imaging in prosthetic joint infection

P. Gouveia, A. Sousa, R. Sousa, R. Teixeira, R. Brito, I. Amorim, M. Oliveira, A. Silva, R. Castro; Centro Hospitalar do Porto, Porto, PORTUGAL.

Aim: Autologous-labeled leukocytes combined with sulfur colloid bone marrow scan is the current imaging modality of choice for diagnosing prosthetic joint infection (PJI). Although this technique is reliable, in-vitro leukocyte labeling raises technical difficulties that limit its widespread use and sulfur colloid is increasingly difficult to obtain. Therefore, valid alternatives are needed. The purpose of our study was to determine the clinical value of 99mTc-sulesomab combined with 99mTc-colloidal rhenium sulphide (nanocolloid) bone marrow imaging in the diagnosis of infection in painful total joint arthroplasties. **Materials and Methods:** A retrospective study was conducted on a cohort of 53 patients with painful hip or knee prostheses that underwent 99mTc-sulesomab and 99mTc-nanocolloids sequentially, between January 2008 and December 2016. The combined images were interpreted as positive for infection when there was activity on the sulesomab scan without corresponding activity on the bone marrow scan. The final diagnosis was made with microbiological findings or by clinical follow up of at least 12 months. **Results:** There were 49 total knee and 4 total hip replacements. Thirteen of 53 patients were men and 40 women, with an average age of 65 years. Infections were diagnosed in 5 patients. The overall sensitivity, specificity, positive predictive value, negative predictive value and accuracy were 100%, 95.8%, 71.4%, 100% and 96.2% respectively. **Conclusion:** 99mTc-sulesomab combined with 99mTc-nanocolloid showed to be a useful method for diagnosing prosthetic joint infections. These technically simpler and ready-to-use products may be an alternative to autologous-labeled leukocytes/sulfur colloid marrow scan, although it needs validation at a larger scale.

EP-0982

Diagnostic Accuracy of 18F-FDG PET in Evaluating Disease Activity in Patients with Chronic Inflammatory Bowel Disease: a Bivariate Meta-analysis

G. Treglia[1], R. Sadeghi[2], A. Viccaro[1], B. Muoio[3], L. Giovanella[1]; [1]Nuclear Medicine and PET/CT Center, Oncology Institute of Southern Switzerland, Bellinzona, SWITZERLAND, [2]Nuclear Medicine Research Center, Mashhad University of Medical Sciences, Mashhad, IRAN, ISLAMIC REPUBLIC OF, [3]Radiation Oncology, Oncology Institute of Southern Switzerland, Bellinzona, SWITZERLAND.

Purpose: to perform a bivariate meta-analysis of published data about the diagnostic accuracy of Fluorine-18 Fluorodeoxyglucose (18F-FDG) positron emission tomography (PET) in evaluating disease activity in patients with chronic inflammatory bowel disease (IBD). **Methods**: A comprehensive computer literature search of studies published through December 2016 regarding the role of 18F-FDG PET in patients with IBD was performed using Pubmed, Scopus and Cochrane library database. Articles about the use of 18F-FDG PET in evaluating disease activity in patients with IBD were selected and reviewed. A quantitative analysis (meta-analysis) of eligible articles was performed. Pooled sensitivity, specificity, positive and negative likelihood ratios (LR+ and LR-) and diagnostic odd ratio (DOR) of 18F-FDG PET in evaluating disease activity in patients with IBD on a per segment-based analysis were calculated, including 95% confidence interval (95%CI) values. Furthermore the summary receiver operating characteristic (sROC) curve has been evaluated. **Results**: Twenty-three studies on the use of 18F-FDG PET in evaluating disease activity in patients with IBD (including 584 patients with IBD) were selected. The quantitative analysis (meta-analysis) of nine eligible studies provided the following results on a per segment-based analysis: sensitivity 85.6% (95%CI: 76-92%), specificity 85.5% (95%CI 75-92%), LR+ 5.59 (95%CI: 3.29-9.5), LR- 0.15 (95%CI: 0.07-0.32), DOR 34.64 (95%CI: 13.03-92.08). Heterogeneity among the selected studies was found. **Conclusions**: 18F-FDG PET demonstrated good diagnostic accuracy in evaluating the disease activity in patients with IBD. Large multicenter studies and cost-effectiveness analyses are needed to confirm the role of this functional imaging method in this setting.

EP-0983

Quantitative 123I-SAP scintigraphy in the follow-up of AL Amyloidosis patients

R. W. J. van Rheenen, B. P. C. Hazenberg, R. A. J. O. Dierckx, A. W. J. M. Glaudemans; UMCG, Groningen, NETHERLANDS.

Introduction: The clinical response and haematological response often do not coincide during treatment evaluation in AL amyloidosis patients. The 123I-SAP scintigraphy (SAP-scan) has potential to monitor changes in amyloid load of the body and individual organs. Visual grading of SAP scans only helps to detect large changes in the amyloid load. The aim of this study is to use quantitative 123I-SAP scintigraphy to detect smaller changes

in amyloid load during follow-up of AL amyloidosis patients. **Subjects and Methods:** Between April 2009 and December 2015, 22 patients with AL amyloidosis underwent consecutive ^{123}I-SAP scans with SPECT/CT (n=60) to evaluate the extent and distribution of the amyloidosis. In all patients, AL amyloidosis had been biopsy-proven and typed. An earlier established ratio-based assessment enabled quantitative evaluation of all scans. These findings were compared to clinical parameters and the best haematological response, classified as complete response (CR), very good partial response (VGPR), partial response (PR), stable disease (SD), and progressive disease (PD). **Results:** All 22 patients had at least one scan after the baseline SAP-scan. Eleven patients had a second follow-up scan and five patients had a third follow-up scan. Best responses were: 7 CR, 5 VGPR, 5 PR, 4 SD and 1 indeterminate response. Often a slowly continuing decrease of SAP-binding was observed in cases with responsive disease and more than 1 follow-up SAP-scan. Almost all complete responders showed quantitative improvement. Some patients without defined organ disease could - by definition - not show an organ response, but they did show quantitative improvement of the SAP scan. When the quantitative values were compared to the clinical parameters a weak correlation was found between the liver ratio and Alkaline Phosphatase levels (r = 0.31, p=0.028) and between the kidney ratio and the eGFR (r = -0.33, p=0.014). **Discussion & Conclusion:** In this study, a quantitative SAP-scan assessment was used to evaluate the treatment response in patients with AL amyloidosis. Complete haematological responders most clearly showed quantitative improvement. The current results need to be further evaluated in a larger follow-up cohort to study the variability of the quantitative results and the minimum change that is clinically relevant.

EP-0984
Valence of F-18-FDG-PET/CT in diagnostics of inflammatory foci

L. Knappe, F. A. Verburg, M. Luster, D. Librizzi; Philipps-Universität Marburg, Marburg, GERMANY.

Aim: Patients with an inflammation of unknown origin (IUO) often pose a challenge in clinical routine. The aim of this study is to evaluate the clinical efficacy of F-18-FDG-PET/CT for detection of inflammatory foci. **Material and Methods:** The study includes 130 patients who underwent an FDG-PET/CT in our department between September 2009 and November 2015 for identification of an inflammatory focus. We collected information on the duration of the inflammation, pre-examinations, pre-existing diseases and laboratory values. The follow-up of each patient was collected until June 2016 so that the result of the PET/CT could be evaluated against the clinical results as well as post-PET/CT microbiology or pathology results. **Results:** In 76% of patients a focus of inflammation could be identified. 68% of foci were of an infectious nature, 27% were autoimmune (e.g. vasculitis) and in 5% other causes were identified. In 65% of patients the findings were true positive, in 5% however false negative. This resulted in a sensitivity of 93%, a specificity of 93%, a positive predictive value of 97%, and a negative pre-

dictive value of 86%. Higher levels of C-reactive protein (CRP) correlated with true positive findings in PET/CT (p=0,011). Furthermore a reduced Butyrylcholinesterase (BCHE) correlates both with higher SUVmax (p=0,014) and higher levels of CRP (p<0,001). **Conclusion:** FDG-PET/CT yields important additional information in patients with inflammation of unknown origin on which further treatment can be based. Although all patients in the present study already underwent extensive diagnostics with negative results before undergoing a PET/CT-scan, the PET/CT nonetheless showed a sensitivity of 93%. A patient with elevated CRP and reduced BCHE has a probability of 70% of having a true positive finding in PET/CT; these parameters may be used for preselecting patients to undergo PET/CT in IUO.

EP-0986
Multimodal imaging in cardiovascular infections: the case of the infectious complications after Bentall procedure

R. Boni[1], A. Bruno[1], E. Lazzeri[2], M. Sollini[3], R. Zanca[2], A. Marciano[2], A. De La Fuente[2], R. Doria[4], F. Menichetti[4], C. Tascini[4], M. Ferrari[5], P. Erba[2]; [1]ASST Papa Giovanni XXIII-Nuclear Medicine, Bergamo, ITALY, [2]Regional Center of Nuclear Medicine, Department of Translational Research and Advanced Technology in Medicine, University of Pisa., Pisa, ITALY, [3]Nuclear Medicine Humanitas University, Rozzano, Milan, ITALY, [4]Division of Infectious Diseases, University Hospital of Pisa, Pisa, ITALY, [5]vascular Surgery, University Hospital of Pisa, Pisa, ITALY.

Aim: A Cardiovascular infections after Bentall procedure. This procedure positions a composite aortic graft (ie, a vascular tube graft with an attached mechanical or biologic valve) to replace the proximal ascending aorta and the aortic valve. In this study we assessed the diagnostic performances of WBC SPECT/CT and [18F]FDG PET/CT in the characterization of patients with suspected infection after the Bentall procedures. **Methods:** Between 2005 and 2015, we selected 47 patients (13 women and 34 men, mean age 62.2±13.7 years). All the patients were surgically treated according to the Bentall procedure. **Results:** WBC scan was totally negative in 17/41, positive in 24/41. Overall WBC scan sensitivity was 86%, specificity 85%, NPV 81%, PPV 89%, and accuracy 85%. [18F]FDGPET/CT was totally negative in 8/27 patients, positive in 19/27 patients. Overall, sensitivity was 100%, specificity 53%, NPV 100%, PPV 63%, and accuracy 74%. SUVmax and SUV mean were significantly higher in the group of patients with positive scan and negative scan as well as in patients with IE and VPI as compared with patients without infections. No significant differences in WBC scan and [18F]FDG PET/CT diagnostic performances were found in patients referred for a diagnostic scan and for antimicrobial treatment evaluation. In the group of patients with suspected very early post-surgical infections, comparative results of [18F]FDG PET/CT and WBC scan were in agreement in 4 cases (1 negative and 3 positive) , confirming the presence of infection whereas in 2 cases the positive [18F]FDG PET/CT finding were associated to a negative WBC findings. No signs of infections were found during patient's follow-up. When incorporating results of WBC scan, [18F]FDG PET/CT findings into the Duke's criteria as recommended in the 2015

New ESC Criteria, the major change is a decrease in the patients classified as Duke possible into definite or rejected category. Similarly, a significant decrease of the number of patients in the Duke rejected category is evident. **Conclusions:** Results of this study support the use of WBC SPECT/CT and [18F]FDG PET/CT in patients with high clinical suspicion of IE and/or VPI after Bentall procedure, in order to confirm the diagnosis in doubtful cases. The diagnostic accuracy of both WBC scan and [18F]FDG PET/CT does not differ significantly for what reported in case of IE and peripheral VPI. We found a specific pattern and intensity of [18F]FDG associated with the higher likelihood to predict infection.

EP-0987

Respective Role of 18F-FDG PET/CT and 99mTc-HMPAO-WBC SPECT/CT in Patients With Suspected Prosthetic Material-Associated Cardiovascular Infections

K. Šenica[1], D. Šfiligoj Planjšek[1], A. Sočan[1], M. Logar[2], J. Kšela[3], L. Ležaić[1]; [1]Department of Nuclear Medicine, University Medical Centre Ljubljana, Ljubljana, SLOVENIA, [2]Clinic for Infectious Diseases and Febrile Illnesses, University Medical Centre Ljubljana, Ljubljana, SLOVENIA, [3]Department of Cardiovascular Surgery, University Medical Centre Ljubljana, Ljubljana, SLOVENIA.

The aim: Over the past years, the number of patients with suspected prosthetic material-associated cardiovascular infections (PMACVI) has progressively risen because of increased use of prosthetic valves (PV) and nonvalvular cardiovascular devices such as pacemakers (PM), left ventricular assist devices (LVAD) and prosthetic vascular grafts (PVG). Radionuclide imaging of infectious processes has gained an important role in management of diagnostically challenging PMACVI. The aim of our study was to directly compare two competing molecular imaging techniques - 18F-FDG PET/CT and 99mTc-HMPAO-WBC SPECT/CT. **Materials and Methods:** Between November 2015 and April 2017 patients with suspected PMACVI underwent both 18F-FDG PET/CT (1 hour after injection) and 99mTc HMPAO-WBC-SPECT/CT (4 and 20 hours after reinjection) in time span of <14 days. 11 patients had PVG, 4 patients had LVAD, 4 patients had PM and 1 patient had PV suspected infection. The results of 18F-FDG PET/CT and 99mTc HMPAO-WBC-SPECT/CT were analysed separately by experienced nuclear medicine physicians. The final diagnosis was based on a positive haemoculture, positive bacteriological culture from the site of infection and patient follow-up. **Results:** 20 patients (5 women and 15 men, mean age 64 years) were included in our prospective study. 13 of them had PMACVI. With 18F-FDG PET/CT 4 patients were correctly diagnosed as positive, 1 patient as false positive (FP), 2 patients as false negative (FN), 4 patients as true negative (TN) and 9 results were equivocal. With 99mTc- HMPAO-WBC SPECT/CT 11 patients were correctly diagnosed as positive, 1 patients as FP, 2 patients as FN and 6 patients as TN. Sensitivity, specificity, positive predictive value, negative predictive value and accuracy of each imaging modality were 85 %, 57 %, 79 %, 67 % and 75 %, respectively, for 18F-FDG PET/CT; and 85 %, 86 %, 92 %, 75 % and 85 %, respectively, for 99mTc-HMPAO-WBC SPECT/CT in patient-based analyses. **Conclusion:** It was significantly more challenging to identify PMACVI with 18F-FDG PET/CT, seeing that 9 out of 20 results were equivocal. 99mTc- HMPAO-WBC SPECT/CT offers higher specificity than 18F-FDG PET/CT, hence a sequential strategy for the diagnosis of PMACVI has been proposed and consists of performing 18F-FDG PET/CT first, following 99mTc- HMPAO-WBC SPECT/CT when results of 18F-FDG PET/CT are inconclusive. Larger studies are needed to further evaluate the diagnostic performance of both nuclear imaging techniques in suspected PMACVI.

EP-0988

Evaluation of 18-FDG PET/CT in diagnosis of large vessel vasculitis

A. Bakos[1], Z. Besenyi[1], S. Urbán[1], R. Hemelein[2], L. Kovács[2], L. Pávics[1]; [1]Department of Nuclear Medicine University of Szeged, Szeged, HUNGARY, [2]Department of Rheumatology University of Szeged, Szeged, HUNGARY.

Introduction: Large vessel vasculitis (LVV) is a group of granulomatous inflammatory diseases and includes the giant cell arteritis (GCA) and Takayasu arteritis (TA). The increased inflammatory markers (C-reactive protein, erythrocyte sedimentation rate) and the clinical signs are not specific for LVV, and not always congruent with disease activity. The early diagnosis and treatment is essential to avoid the late complications. 18-FDG accumulates in activated inflammatory cells, and has superior sensitivity for the detection of vasculitis in early stage of disease and for evaluating therapeutic response. The PET/CT method provides better anatomical localisation. The aim of this study was to diagnose vasculitis in new cases and to reveal relapses. **Materials and Methods:** 24 patients (17 females, 7 males, mean age: 61 years) were involved into the study from 2015 December. The patients were selected from the Department of Rheumatology. We included cases with increased C-reactive protein, erythrocyte sedimentation rate, non-specific clinical symptoms and suspicious clinical symptoms: headache (3/24), extremity-jaw claudication (3/24), chest-abdominal pain (5/24), visual disturbance (4/24), temporal artery tenderness (1/24), proximal myalgia(2/24), dizziness (4/24), fever of unknown(2/24). The 18-FDG PET/CT was performed to diagnose primary in 19 cases and to evaluate the relapse in 5 cases. 18-FDG PET/CT images were evaluated visually by two nuclear medicine physicians, in consensus, who were blinded to clinical and laboratory data. **Results:** 18-FDG PET/CT revealed active LVV in 6 (6/19) patients as primary diagnosis. PET/CT proved extensive LVV in one patient who had arteritis temporalis as clinical diagnosis, the 18-FDG uptake was increased in the following arteries: in the thoracic aorta and major branches, in the abdominal aorta, bilateral common iliac, bilateral external iliac and bilateral femoral arteries. We proved relapses in 2 (2/5) patients who were previously diagnosed as LVV. The mean CRP level in patients with active LVV according to FDG-PET/CT were significantly higher, than in patients with inactive disease (45,91 versus 22,6 mg/l). The clinical symptoms, the CRP level and FDG uptake decreased after therapy. **Conclusion:** 18-FDG PET/CT gives additional information in diagnosis of LVV, reveals the extension of vasculitis and is effective in monitoring response to therapy.

EP-0991
Diagnosing diabetic foot infection: efficiency of radiological methods

V. Udodov[1], M. Zorkaltsev[1], V. Zavadovskaia[1], M. Zamyshevkaia[1], E. Grigoriev[2], A. Kurazhov[1]; [1]Siberian State Medical University, Tomsk, RUSSIAN FEDERATION, [2]Tomsk National Research Medical Center of the Russian Academy of Sciences, Tomsk, RUSSIAN FEDERATION.

Purpose: to compare the diagnostic values of radiological methods for the identification of osteomyelitis (OM) in the diabetic foot (DF). **Materials and Methods**: 85 patients (41 male (48.2%), 44 female (51.8%); mean age 59.4±7.1) with suspected diabetic foot bone infections were studied. Studies were performed by using Apollo Villa Sistemi Medicali (x-ray), GE Optima CT660 (CT), Philips BrightView (SPECT-WBC) and Siemens MAGNETOM ESSENZA 1.5T (MRI). Fusions of SPECT and MRI or CT were performed in program RView 9.06 (Colin Studholme). **Results:** For X-ray and CT in detection of osteomyelitis sensitivity, specificity and accuracy were 76.3%, 44.7%, 58.8% and 81.6%, 63.8%, 71.8% respectively. False positive results (FP) in Charcot foot were the reasons of low specificity of X-ray and CT. Poor visualization of soft tissues also should be noted. Values of sensitivity, specificity and accuracy of SPECT-WBC, MRI, SPECT-WBC/CT, SPECT-WBC/MRI were 94.7%, 61.7%, 76.5%; 89.5%, 80.8%, 84.7%; 94.7%, 95.7%, 95.3% and 97.4%, 97.9%, 97.6% respectively. Difficulty in determining the localization of the pathological radiopharmaceutical accumulation due to the low resolution of the method was the main reason of FP results of scintigraphy. Decrease of the MRI specificity was caused by the complexity of the differential diagnosis of bone marrow edema and inflammatory infiltration. Identified FN results of hybrid methods were due to the complexities of toes fusion. **Conclusion:** Among the available methods of radiological diagnosis of osteomyelitis in the diabetic foot, priority is given SPECT/MRI or SPECT/CT. But SPECT-WBC/MRI has potentially advantage in the indication of soft tissue infections.

EP-0992
Qualitative and semiquantitative [18F]FDG-PET/CT analysis in patients with IE: a strategy to enhance specificity?

R. Boni[1], A. Bruno[1], E. Lazzeri[2], M. Sollini[3], R. Zanca[2], A. Marciano[2], A. De La Fuente[2], U. Conti[4], R. Doria[5], F. Menichetti[5], A. Cataldi[2], P. Erba[2]; [1]ASST Papa Giovanni XXIII-Nuclear Medicine, Bergamo, ITALY, [2]Nuclear Medicine, Department of Translational Research and New Technologies in Medicine, Pisa, ITALY, [3]Humanitas University, Milan, ITALY, [4]Cardiology Unit, University Hospital of Pisa., Pisa, ITALY, [5]Division of Infectious Diseases, University Hospital of Pisa, Pisa, ITALY.

Aim: The recent 2015 ESC Guideline for the diagnosis and management of infectious endocarditis (IE) included molecular imaging procedures such as radiolabeled leukocytes and [18F]FDG-PET/CT as major criteria to establish the diagnosis of IE. Whereas in case of radiolabeled leukocytes the criteria for defining positive and negative scan are well established, in case of [18F]FDG-PET/CT a consensus of the criteria that define a positive scan is still lacking. **Materials and Methods:** In this work we prospectively evaluated a series of 90 patients (M:F=60:30, mean age 67±16 years, median age 72 years, range 18-88) that performed [18F]FDG-PET/CT for suspected IE between January 2013 and January 2016 in our center to define which pattern of uptake and semiquantitative parameters (SUVmax, SUVmean, valve/liver, valve/lung and valve/mediastinum uptake ratio) present the highest diagnostic accuracy for IE. PET/CT results were correlated with transthoracic (TTE) or transesophageal (TEE) echocardiography, blood culture, the Duke criteria. The new ESC criteria were also evaluated. **Results:** Globally PET/CT presented sensitivity=96% and specificity=75%, NPV= 97% and PPV=68%. A focal pattern of uptake was found 17/30 patients with confirmed IE (mean SUVmax=5.29±1.8, median SUVmax=5.5) whereas whereas a diffuse pattern of uptake was found in 11 patients with confirmed IE (mean SUVmax=8.1±3.5, median SUVmax=7.6). No significant differences between the valve/liver ratio uptake and the valve/mediastinum uptake ratio were found between positive and negative patients with either focal or diffuse pattern of uptake. Interesting, in presence of diffuse valve uptake both SUVmax and the valve/lung uptake ratio were significantly higher in patients with a final diagnosis of IE, including the group of patients under antimicrobial treatment (>90%). PET/CT confirmed its ability to identify extracardiac sites of [18F]FDG uptake in presence of septic embolism (35%) and in patients with other diseases (vasculitis, vascular prosthesis infections, mediastinitis and cancer, particularly in patients with IE sustained by Streptococcus Gallolyticus). **Conclusions:** Our results suggest pattern of [18F]FDG uptake more specific for valve infection is a focal uptake or a diffuse uptake with a SUVmax>5 and a valve/lung ratio >8.

EP-0993
The role of FDG-PET/CT in tuberculosis

E. Llinares Tello[1], M. Cortés-Romera[1], J. Robles-Barba[1], M. Santin-Cerezales[2], J. Rodriguez-Rubio[1], A. Sabaté-Llobera[1], J. Vercher-Conejero[1], P. Notta[1], L. Rodríguez-Bel[1], N. Calvo-Malvar[1], C. Gámez-Cenzano[1]; [1]PET/CT Unit. Department of Nuclear medicine. IDI. Hospital U. de Bellvitge-IDIBELL., Barcelona, SPAIN, [2]Department of Infectology/Internal Medicine. Hospital U. de Bellvitge-IDIBELL. L´Hospitalet de Llobregat (Barcelona). Spain., Barcelona, SPAIN.

Aim: To assess the utility of 18F-FDG-PET/CT in tuberculosis (TB). **Material and Methods:** Twenty-two patients were included (13 men, 59%) with a mean age of 48 years (range 15-83). Patients were classified in two groups according to different clinical settings: 1) 16 patients at initial evaluation (fever of unknown origin, solitary pulmonary nodule and/ or lymph-nodes characterization or TB suspicion) and 2) 6 patients for evaluation of TB treatment response, 3 during and 3 after treatment. All patients underwent a whole body PET/CT at 60-120 minutes after intravenous administration of 3.7MBq/Kg FDG. A second PET/CT was performed in 17/22 patients (12 in the first and 5 in the second group). PET/CT was considered positive (active disease) if focal accumulation of the tracer was detected. We established different pattern of

FDG uptake according to the sites of involvement: pulmonary (lung and/or hilar-mediastinal lymph-nodes), extrapulmonary (lymph-nodes and/or organs) and disseminated (pulmonary and extrapulmonary). The results were compared with the final diagnosis based on the microbiological assays, biopsy, bronchoalveolar lavage (BAL), tuberculin skin test, interferon gamma release assay (IGRA) and BKK sputum. **Results:** Twenty-one out of 22 patients had a positive PET scan (95.4%). The average of SUVmax was 8.65(range 2.8-22.5). There are different patterns of FDG uptake: pulmonary (6), extrapulmonary (9: 6 lymphatic and 3 muscle, adrenal, retroperitoneal fibrosis and bone) and disseminated (6: lymphatic,cerebral, cavum, spleen, articular and liver). In the first group (16) PET/CT served as guide to the most appropriate site for biopsy in 10, indicates BAL in 2 and BKK sputum in 1. In 11 of them (73%) were confirmed the final diagnosis as TB and the remaining 5 patients, bacteriologically unconfirmed (4 had a positive IGRA), due to clinical suspicious and the pattern of FDG uptake were categorized as TB (disease activity disappeared after TB treatment). Follow-up after TB treatment was assessed by PET/CT in 12/16 (10 were negative and 2 had markedly reduction of activity) and by CT/X-Ray in 4/16 (reduction the size of lesions). In the second group (6) PET/CT demonstrated positive/active lesions in all patients. Mycobacterium-drug-resistant was confirmed in 2 patients. PET/CT modified the therapeutic approach in 3 patients. Two patients could not be verified TB reactivation. One patient after TB treatment had a negative PET interpreted as inactive TB lesion. **Conclusion:** FDG-PET/CT helps to assess the activity of TB lesions, guide biopsy from active sites, demonstrates the correct extension of TB and is useful for monitoring response to therapy.

EP-75   **during congress opening hours, e-Poster Area**

Conventional & Specialised Nuclear Medicine: Musculoskeletal (Benign)

EP-0994

Evaluation of Kinetic Parameters of Three-phase Bone Scintigraphy of The Hip Joints

P. Korol[1,2], M. Tkachenko[2], V. Bondar[1]; [1]Clinical City Hospital #12, Kiev, UKRAINE, [2]A.A. Bohomolets National Medical University, Kiev, UKRAINE.

Purpose: To evaluate the kinetic parameters of three-phase bone scintigraphy in degenerative-dystrophic and inflammatory lesions of the hip joints. **Subjects and Methods:** 207 patients (124 women and 83 men) aged 34 to 75 years were imaged by three-phase bone scintigraphy: I stage - angiographic phase, II stage - early static phase, III stage - delayed static phase. Intestinal uptake was observed visually 3 hours after the intravenous administration of 740 MBq ^{99m}Tc MDP. **Results:** According to the scintigraphy, areas of radiopharmaceutical fixation in joints were divided into four cohorts: 1st cohort - aseptic necrosis: 154 (26%); 2nd - deforming osteoarthritis: 197 (33,2%); 3rd - post-traumatic osteoarthritis: 125 (21,1%); 4th - rheumatoid arthritis: 116 (19,7%).

Integral perfusion was moderately increased in areas of aseptic necrosis and deforming osteoarthritis (108,65 ± 11,35 and 109,19 ± 12,67 imp × s, respectively) and significantly increased in the areas of post-traumatic osteoarthritis and rheumatoid arthritis (134,38 ± 14,72 and 165,52 ± 19,15 imp × s, respectively) compared with the control group (81,45 ± 7,87 imp × s). Integral perfusion in post-traumatic was higher compared with the control group (114,45 ± 4,54 imp × s - in post-traumatic lesions and 81,45 ± 2,87 imp × s - in the control group, p<0,05). In the analysis of areas of rheumatoid arthritis were statistically significant increase in the accumulation of radiopharmaceuticals compared with the control group (4,52 ± 0,57 cm^2 and 3,11 ± 0,23 cm^2 in early static phase; 5,41 ± 0 44 cm^2 and 2,42 ± 0,51 cm^2 delayed static phase, respectively). Kinetic of radiopharmaceuticals in the areas of rheumatoid arthritis is characterized by a predominance of retention statistically significant (p = 0,68; p<0,05) and integrated perfusion in the early static phase (r = 0,73; p <0,05) and delayed static phase (r = 0,77; p <0,05), compared to fixation of the drug in deforming, aseptic and posttraumatic arthritis, which correlates with differences destructive-reparative processes in them. **Conclusion**: Calculation of kinetic parameters of three-phase bone scintigraphy enables to determine statistically significant differences in the metabolic changes in focal lesions of articular structures of the hip joints. Thus, the increased differential diagnostic possibilities for radioactive method of examination of patients with diseases of the hip joints.

EP-0995

Heterotopic ossification in Intensive Care Unit patients imaged with bone scan

*C. Sioka, E. Konstanti, K. Papadimitropoulos, A. Papadopoulos, V. Ragos, X. Xourgia, V. Koulouras, **A. Fotopoulos**; University Hospital of Ioannina, Ioannina, GREECE.*

Introduction: Heterotopic ossification (HO) may occur in patients hospitalized in intensive care unit (ICU). In this study we examined the association of HO employing three phase bone scan (3pBS) in patients previously hospitalized in ICU. **Patients and Methods:** Patient records of the last 12 years subjected to 3pBS and diagnosed with HO were retrieved from the Department of Nuclear Medicine (2004 up to 2016) and searched for a name match from ICU records. **Results:** We found 61 patients that had positive 3pBS for HO of whom 17 patients were previously hospitalized in the ICU. Among the 17 patients, twelve fulfilled the study criteria and were included in the study. The mean age was 38 years and 92% were males. HO was unilateral in 7 and bilateral in 5 patients. Patients with unilateral HO had up to 2 joints with HO, while those with bilateral had up to 4 joints. HO was most frequently observed in lower limbs, with hip being the most common joint affected. In the upper limbs, HO occurred predominantly in bilateral joints with elbow being the most frequently involved joint. Patients with longer duration of ICU stay had more joints affected. **Conclusion:** HO is a potential complication in patients after ICU hospitalization. Since 3pBS is an imaging method for early detection of HO, patients hospitalized in ICU should be screened with 3pBS for early diagnosis and treatment.

EP-0996

The value of SPECT-CT in the evaluation of pain after total ankle arthroplasty

J. Mertens[1], T. Lootens[2], J. Vercruysse[3], B. Van Den Bossche[1], F. Temmerman[1], B. Lambert[1]; [1]Department of Nuclear Medicine, Maria Middelares Hospital, Ghent, BELGIUM, [2]Department of Orthopaedic Surgery and Traumatology, Maria Middelares Hospital, Ghent, BELGIUM, [3]Department of Radiology, Maria Middelares Hospital, Ghent, BELGIUM.

Introduction: Total ankle arthroplasty (TAA) is a surgical alternative to ankle arthrodesis in the treatment of end-stage ankle osteoarthritis with good long-term results. We investigated the use of SPECT-CT in the evaluation of pain syndromes after TAA. **Subjects & Methods:** Sixteen patients who underwent one or more bone scans with SPECT-CT between 2011 and 2016 after a unilateral or bilateral TAA were included in this study. We performed a retrospective analysis of 22 SPECT-CT scans of 24 TAA in this population. The pattern of bone tracer uptake (BTU) was correlated with CT findings to establish a SPECT-CT diagnosis. The subsequent WBC scans performed in 4 patients were also taken into account. This was compared to the findings at revision surgery or clinical follow-up. **Results:** The BTU around the arthroplasty was higher than the normal background in 43 out of 48 components (90 %). The SPECT-CT diagnosis based on the combination of BTU patterns and CT findings, correctly identified the diagnosis at revision surgery or clinical follow-up in 21 out of 24 cases (88%). The final diagnoses were medial or lateral gutter impingement (n=12), periprosthetic (stress) fracture (n=5), loosening (n=5), tarsal arthritis (n=1) and erysipelas (n=1). Gutter impingement, periprosthetic fracture and loosening were correctly identified by SPECT-CT in all cases. Three patients were falsely classified as having gutter impingement (n=1) or infection (n=2; after WBC scan), respectively. SPECT-CT had an impact on clinical management in 86 % of cases, which resulted in an improvement of the initial complaints in 83 % of patients. **Conclusion:** The SPECT-CT evaluation of TAA is hampered by the high periprosthetic BTU around almost all TAA. However, by combining BTU patterns and CT findings, SPECT-CT has an adequate accuracy in identifying the underlying pathology and has an impact on clinical management in a majority of cases.

EP-0997

Bone SPECT in lumbar facet syndrome. Assessment of a four point scale

F. Medina-Romero, *Sr., A. Diaz-Silván, T. Rodriguez-Méndez, I. Cabrera-Veloz, A. Alonso-De León, M. Gonzalez-Díaz, M. Gómez-R.Bethencourt, M. Gonzalez-Soto; Hospital Universitario de Canarias, Santa Cruz de Tenerife, SPAIN.*

Introduction and Purpose: Degenerative facet joints are a recognized cause of chronic lumbar pain. Magnetic resonance has been the imaging method of choice for lumbar pain. However, diagnosis of facet joint arthropathy continues to pose a challenge. Bone SPECT shows high sensitivity in depicting active remodelling bony lesions. The main goal of the present study was to assess the utility of a bone-SPECT four point uptake scale. **Subjects and Methods:** A retrospective study was conducted of consecutive patients from January 2014 to July 2016 who underwent bone SPECT scanning for lumbar pain suspicious of lumbar facet syndrome. The population was composed of 40 subjects. Indications for the scan, imaging reports and clinical management were reviewed. CT and MRi lumbar facet joints were graded using criteria similar to those published by Pathria et al. (from 0 to 3, being 0 normal and 3 severe degenerative disease). Bone SPECT was graded using also a four point scale, from no uptake to high uptake. We performed a descriptive statistical analysis and performed agreement for each imaging modality. **Results:** Correlation between CT and MRi was high, being principal differences between grade 0 and 1. Correlation between those and bone SPECT was low for grades 0 and 1, and good for grades 2 and 3, being disagreements very rare in such cases. Bone SPECT identified less number of degenerative facet joints with low grades. **Conclusion:** CT scans and MRI are more useful as they can identify severe degeneration of the facets (hypertrophy, arthritis, oedema) and can exclude other diseases associated primarily with the disc (discopathy/hernia). As review in literature, there is agreement between MRi and CT in the assessment of severe lumbar facet joint osteoarthritis. Our four point uptake scale showed also good correlation for higher levels. We obtained less low grades diseases, which can be very useful to avoid harmful treatments or even surgery

EP-0998

SPECT/CT Imaging in Fibrous Dysplasia

D. Muñoz[1], C. Fernández[1], K. Bayardo[1,2], A. Zamora[1], M. Musetti[1], M. Ramírez[1], R. Ferrando[1,2]; [1]Clinics Hospital, University of the Republic, Montevideo, URUGUAY, [2]Ferrari Ferrando Páez Nuclear Medicine Clinic, Montevideo, URUGUAY.

Introduction: Fibrous dysplasia is a rare benign developmental disorder typically found in young patients, in which normal medullary bone is replaced by fibroosseous tissue. It can be monostotic (75-80%), polyostotic (20%), or polyostotic related to endocrine disorders (with patches of café-au-lait skin pigmentation, precocious puberty and hyperthyroidism), configuring McCune-Albright syndrome, usually unilateral. Bone scintigraphy is a sensitive method and allows the evaluation of disease extension, but specificity is limited, potentially leading to misdiagnosis of malignant lesions. Hybrid imaging can increase specificity achieving a more precise etiological diagnosis. The aim of the study is to evaluate the utility of SPECT/CT in fibrous dysplasia. **Subjects and Methods:** A retrospective study covering all bone scans performed from 2012 to date in our institutions included 10 female patients with a final diagnosis of fibrous dysplasia reached by biopsy in 5 cases or clinical consensus and follow-up in the other 5. Bone scintigraphy with 99mTc-methyldiphosphonate included whole-body images and SPECT/CT of the area of interest using low dose CT in a GE Infinia Hawkeye 4 or a Mediso AnyScan 16 gamma camera. **Results:** Mean age was 39 years (11-67 years). Five of the 7 cases with monostotic

dysplasia showed intense uptake in craniofacial bones (malar, maxilla, mandible, sphenoid and occipital) coincident with expansive images with characteristic ground glass appearance on CT. The other 2 cases presented lesions in iliac and radius with mild to moderate irregular increase in uptake, associated with expansive hypodense images with cortical thinning. The 3 patients with polyostotic dysplasia were older than 50 years. The first had vertebral and costal lesions and the second had lesions in mandible, spine and left iliac. CT also showed expansive images in ground glass. The last patient had a diagnosis of McCune-Albright syndrome, with multiple bilateral lesions in skull, spine, ribs, tibia, humerus and carpi. The younger patients and the lesions in facial bones presented more intense uptake, whereas fibrocystic lesions had lower uptake and polyostotic cases showed lesions of different intensity. **Conclusion:** SPECT/CT images allow a more precise etiological diagnosis of fibrous dysplasia by correlating scintigraphic findings with the classic radiological appearance of the lesions. Variable degrees of uptake that may be related to the location, time of evolution and type of lesions are also described. Finally, we report an unusual case of McCune-Albright syndrome with multiple lesions that affect the skeleton bilaterally.

EP-0999
Value Of SPECT - CT With HDP 99MTC In The Diagnosis Of Bone Pathology In Feet - Ankles

C. Mena Melgar, A. Herrero Muñoz, C. Sandoval Moreno, M. Balsa Bretón, M. Garcia Alonso, L. Castillejos Rodriguez, A. Ortega Valle, C. Paniagua Correa, F. Penin Gonzalez; Hospital Universitario Getafe, Getafe, SPAIN.

Introduction: Our aim was to evaluate the role of SPECT-CT for the diagnosis of benign bone pathology in ankles and feet in comparison with the analysis of the planar images alone. **Subjects and Methods:** Over one year, we analyzed 25 bone scans (18 men, 7 women), through a retrospective study, carried out in our center. Study was carried out 10 patients only with 99mTc-HDP, 6 patients with 99mTc-HDP and gallium-67, and 9 patients with 99mTc-HDP-99mTc-HMPAO and 99mTc-colloids. We compared the scintigraphic results of the planar image with the SPECT - CT information in all the patients, based on the initial clinical suspicion. The images were interpreted by two medical assistant of the Department of Nuclear Medicine, only interpreting planar image without knowing the SPECT-CT study, which was subsequently valued in order to analyze their usefulness. **Results:** In 14 of the cases studied the SPECT-CT improved the information obtained by the planar image of the bone scintigraphy. Of these, in 8 it changed the diagnosis initially issued and in the 14 helped the accurate location of the pathology. In the 25 patients it was possible to reach a diagnosis with a greater degree of certainty, confirming this in the subsequent follow-up. In 16 patients, the only diagnostic imaging test performed was bone scintigraphy. **Conclusion:** Bone SPECT-CT is a useful tool in the study of benign bone pathology in regions of great osteo-articular complexity, such as the feet and ankles, thus avoiding other complementary tests.

EP-1000
Paget Disease and Bone Scintigraphy: an 8-Year Single-Center Experience

S. Diodato, A. Matti, R. Bonfiglioli, L. Zanoni, M. Levorato, S. Fanti; S.Orsola-Malpighi Hospital, University of Bologna, Bologna, ITALY.

Aim: Paget disease is a disorder of bone metabolism with an increased resorption and altered mineralization. Bone scan with 99Tc-DPD is useful for the assessment of extension and activity of disease, due to the peculiar distribution of radiotracer in the affected bone segment. Our aim was to analyze the frequency of findings referable to Paget disease in bone scintigraphy and describe the patient's characteristics. **Materials and Methods:** We retrospectively analyzed all bone scans reported in our Nuclear Medicine Department between January 2009 and December 2016 (overall 17390 scans) and we searched for those with one or more findings referred to Paget disease. Data referring to age, gender and bone involvement were collected. When available, we considered clinical history, previous radiological imaging and clinical/radiological follow-up. **Results:** In our experience, the frequency of Paget disease was 1.6% (282/17390 scans among 260 patients). The analysis of the sample of 260 patients showed 187 men and 73 women with a mean age of 72yo (range 45-90). Clinical indications for bone scan were staging, restaging and follow-up of oncological disease (mainly prostate cancer), prosthesis complications, bone pain of unknown origin and clinical/radiological suspect of Paget disease. Overall, 59/260 patients had previous diagnosis of Paget disease. Sites of bone involvement were pelvis (64.6% of patients), lumbar and thoracic vertebrae (20.4% and 12.3% respectively), skull (14.2%), femur (13.8%), sacrum (11.5%), tibia (11.1%), humerus (7.7%), scapula (6.2%), clavicle (4.2%). We also found further rare sites of disease: calcaneus (2.7%), sternum (2.3%), tarsus (1.5%), cervical vertebrae (1.5%), thorax (1.2%), radius (0.7%), carpus (0.4%), patella (0.4%), fibula (0.4%). Polystotic and monostotic presentations were 69.6% (181/260) and 30.4% (79/260) respectively. Sites more frequently involved in polyostotic presentations were pelvis (84%) and vertebrae (26.5%), in monostotic ones were femur (20.3%), tibia (20.3%) and skull (15.2%). **Conclusion:** The frequency of Paget disease and the characteristics of our sample of patients are concordant with literature. Thanks to whole-body examination, bone scan allows to detect unknown sites of Paget disease, including uncommon localizations such as tarsus, patella and carpus. Moreover, it is useful to better discriminate Paget's localizations from oncological lesions.

EP-1001
The value of 99m Tc bone scintigraphy in detecting a low grade infection of a total hip or knee arthroplasty

C. Schlenkhoff, Jr.[1,2], P. Mantovani[1], T. Randau[1,3], F. Gärnter[1,2], M. Essler[1,2]; [1]University Bonn, Bonn, GERMANY, [2]Nuclear medicine, University Bonn, GERMANY, [3]Orthopaedics and Trauma Surgery, University Bonn, GERMANY.

Aim: The most frequent complications of a hip- or knee-prosthesis is a septic or aseptic loosening. Different treatment meth-

ods result from these two diagnoses. Especially the value of a triple-phase technetium-99m bone scan (TPBS) to detect a septic low-grad infection of a prosthesis is discussed controversial. **Materials and Methods:** We compared the findings in 62 patients who underwent surgery in cases of suspected septic or aseptic prosthesis-loosening of a hip- (22 cases) or knee-prosthesis (40 cases). 46 patients were classified as aseptic loosening (intraoperative surgical finding). 16 patients were classified as septic loosening, either based on a positive histopathological finding (8 cases) or based on a positive microbiological finding (tissue culture, sonication, molecular tests; 12 cases). A joint aspiration (microbiological culture, leukocyte count >2000/μl, neutrophil percentage >70%) was positive in 2 cases. In all cases a TPBS was performed (mean 524 MBq) and classified as unsuspicious or suspicious for prosthesis-loosening. 40 patients underwent surgery within the first three month after the TPBS, 12 patients were operated 4-6 month after the TPBS, 10 patients were operated 7-11 month after the TPBS. **Results:** The 46 patients with aseptic loosening showed following results: The TPBS classified 22 patients as suspicious for prosthesis-loosening (sensitivity 48%), 24 patients were unsuspicious for prosthesis-loosening. 4 patients had a positive microbiological finding (specifity 91%), no patient had a positive histopathological finding (specifity 100%, although 20 patients were not examined). The 16 patients with septic loosening showed following results: In the TPBS 11 cases showed a normal perfusion phase, in 9 cases the bloodpool-phase was unsuspicious and in 4 cases even the delayed phase showed no increased uptake around the joint. Consequently 12 patients were classified as suspicious for prosthesis-loosening (sensitivity 75%). As mentioned above microbiological findings had a sensitivity of 75% (12/16 patients), the histopathology had a sensitivity of 57%, (8/14 Patients, 2 patients were not examined). **Conclusion:** Our results show that the TPBS has its value in diagnosing a septic low-grade-infection, there is no cause for this method to hide from the other diagnostic procedures. The sensitivity of the TPBS is comparable to the sensitivity of microbiological findings and better than the sensitivity of histopathological findings. The surprisingly low sensitivity in diagnosing an aseptic prosthesis-loosening might be associated with a probably very high sensitivity of the gold-standard "intraoperative surgical finding", particularly in view of the fact that no fixed prosthesis was diagnosed in 62 operations.

EP-1002

Assessment of relative uptake of mandibular condyles in a normal population

A. Fernandes[1], T. Faria[1], P. Coelho[2], A. Oliveira[1], J. Pereira[1]; [1]Hospital de São João, Porto, PORTUGAL, [2]Universidade Fernando Pessoa, Porto, PORTUGAL.

Introduction: Condylar hyperplasia (CH) of the mandible is a self-limiting disease that can lead to facial asymmetry, malocclusion, pain and articular dysfunction of the temporomandibular joint (TMJ). It is crucial to differentiate active from inactive phases, especially for patients with unilateral CH, to choose the type and timing of the corrective surgery. Bone scintigraphy (BS), particularly when performed with Single photon emission computed tomography (SPECT), gives us a more sensitive and accurate idea of condylar activity - based on the radiotracer uptake -, both in growing and non-growing patients, being effective in the calculation of condylar uptake differences which reflect the relative growth rates. Studies have demonstrated a 5%-12% difference between normal condyles. **Aim**: To validate, for our population, values currently used for condylar relative uptake. **Material/Methods:** Between December 2015 and April 2017, we performed a skull SPECT to 21 patients (11 females), with ages between 5 to 32 years (mean 16,3±7,4-years), undergoing BS (HDP-Tc-99m, 740 MBq, e.v.) for unrelated reasons, without known abnormalities of the head or facial asymmetry, and with no symptoms of the TMJ. The calculating method was the uptake comparison between condyles. Informed consent was obtained. Measurements were made in the summed transaxial images by two different researchers. ROIs were drawn around the whole condyle and total counts were registered. Relative uptake was: % uptake in the right or left condyle=[right or left counts /(left counts + right counts)]*100 This is a prospective clinical trial, approved by our Hospital Ethics Committee. **Results:** The maximum condyle uptake difference was 8,2% with Researcher-1 and 8,3% with Researcher-2; variation results were 2,79%± 2,34 and 2,77%± 2,11, respectively. Data were tested for normality; t-test and One Way Anova were used. No statistically significant differences were found between sexes and age (p >0,05). There were also no significant differences for the variations and percentages measured by researcher-1 and researcher-2. **Conclusions**: BS is widely used for the evaluation of patients with suspected CH, but there are neither standardized methods nor values. The results in our population are within the published range, with the vast majority presenting a variation <4% (lower than the most commonly used 10%). Thus, the impact and significance of the higher values require further studying. This study is still ongoing, the number of patients included is expected to increase by 25% in the next months. A larger collection of patients should increase data accuracy.

EP-1003

Technetium-99m HDP SPECT/CT evaluation of persistent and recurrent pain post lumbar spine fusion

K. Al Riyami[1,2], S. Voo[3,1], J. Bomanji[1]; [1]UCLH, London, UNITED KINGDOM, [2]SQUH, Muscat, OMAN, [3]Maastricht University, Maastricht, NETHERLANDS.

Background: The evaluation of spinal SPECT/CT in post spinal fusion surgery presenting with ongoing back pain continues to be challenging. The aim of this study is to determine the common uptake patterns seen in patients with persistent/recurrent pain post lumbar spine fusion surgery. **Methods:** A total of 119 patients (mean age 55 years, range 23- 83years; 48men) who had previously undergone lumbar spine fusion were included in this analysis. Patients were divided into early; fusion within 2 yrs (34 pts), intermediate; fusion within 2-4 yrs (38 pts) and late groups; fusion >=4 yrs (47pts) according to the most re-

cent fusion related surgery. The findings visible on the SPECT/CT were classified into osteoblastic activity within the fused segments, adjacent segments, or both. The uptake was further categorized according to site e.g. Facet joint/ posterior lateral bony consolidation (PLC), intervertebral body device, end plate, screws, sacroiliac joint (SIJ) ..etc. **Results:** 84 patients had positive uptake on SPECT/CT [28 (33%) within the fused segment, 33 (39%) at adjacent segments and 23 (27%) in both]. Of the 51 patients with positive uptake in the fused segment, 23 had uptake in the facet joints/PLC, 18 in end plates, 17 in intervertebral body device and 7 in screws. The majority of positive findings in the fused segments was in the early group (45%). Of the 56 patient with positive uptake in the adjacent segments, 32 had uptake in the facet joints, 28 in the end plates and 10 at SIJ. The majority of the positive findings in the adjacent segments were seen in the late group (42%). **Conclusion:** In patients with recurrent /persistent pain post lumbar spine fusion surgery, abnormal osteoblastic activity is commonly noted within the fused segment in the first two years' post-surgery. The commonest site in both fused and adjacent segments is seen in the facet joints (65%).

EP-1004
Review of bone scan imaging in Bertolotti syndrome

F. Medina Romero, A. Díaz-Silván, T. Rodríguez-Méndez, I. Cabrera-Veloz, A. Alonso-De León, M. González-Díaz, M. Gómez-R. Bethencourt; Hospital Universitario de Canarias, Santa Cruz de Tenerife, SPAIN.

Introduction and Purpose: Transitional lumbosacral vertebrae (TLSV) (including partially sacralized L5 vertebrae and partially lumbarized S1 vertebrae) are present in 3%-21% of the population. TLSV are characterized by an enlarged transverse process that articulates or fuses with the sacrum. It can be unilateral o bilateral. Abnormal biomechanics at the transitional level can result in stress at the vertebrosacral articulation and the intervertebral disk immediately above it. According to Castellvi classification, patients with TLSV that is pseudoarticulated to the sacrum (such as unilateral-type II and bilateral-IV) were prone to back and buttock pain. Low back pain associated with a transitional vertebra is referred as Bertolotti syndrome. Bone scintigraphy is a valuable tool for the recognition of articular diseases and a screening method for patients with low back pain, specially those with known or passed malignancies. **Subjects and Methods:** From January 2014 to February 2016 we retrospectively reviewed patients with low back pain admitted to our department for a bone scan. Three phase bone scintigraphy was performed and evaluated in conjunction with SPECT, SPECT-CT, radiographs, CT and MRi, when available. We also took into account symptoms and relevant history data, like surgery or cancer. **Results:** We found 10 patients with abnormal radiotracer uptake at the articulation between the enlarged transverse process and the sacrum. 9 were type II (6 right-sided) and 1 type IV. Pain was concordant with side in each case and central in type IV. Just two of them showed increased uptake in blood pool images. SPECT-CT and CT were helpful showing

the TLSV anatomy and demonstrating sclerosis, this finding was also present but less pronounced at radiographs. **Conclusion:** Bertolotti syndrome and other common causes of low back pain can be assessed with bone scan, specially when SPECT-CT is added, being a very useful tool to localize and establish the etiology of pain.

EP-1005
Predictive value of 18F-NaF PET/CT in the assessment of osteoporosis: comparison with Dual-energy X-ray Absorptiometry (DXA)

S. Haim[1], R. Zakavi[2], L. Imamovic[1], M. Beheshti[1], A. Rezaee[1], B. Saboury[3], A. Alavi[3], W. Langsteger[1], M. Beheshti[1]; [1]PET-CT Center Linz, St. Vincent's Hospital, Linz, AUSTRIA, [2]Nuclear Mecicine Research Center, Mashhad Unviversity of Medical Sciences, Mashhad, IRAN, ISLAMIC REPUBLIC OF, [3]Division of Nuclear Medicine, University of Pennsylvania, Philadelphia, PA, UNITED STATES OF AMERICA.

Aim: The aim of this study was to examine if semi-quantitative measurement of ^{18}F-NaF PET could predict osteoporosis in patients referred for assessment of osseous diseases from other primary and if there is any correlation between ^{18}F-NaF PET uptake and the results of DXA examination. **Material & Methods:** This study included 70 women (57±12 years; range:23-88) who underwent both DXA and ^{18}F-NaF PET/CT in the context of initial staging of breast cancer. Mean interval between ^{18}F-NaF PET/CT and DXA was 3.11 months (range: 1-238 days). The exclusion criteria were any clinical or imaging evidence of bone metastases, recent surgery, trauma or fracture in lumbar spine or femurs or an interval between ^{18}F-NaF PET/CT and DXA of greater than 6 months. Patients with recent chemo- and/or radiotherapy (less than 3 months) were excluded. Semi-quantitative analysis was performed using volume of interest (VOI) which was manually drawn on the medullary part of L1, L2, and L3 as well as left femoral neck excluding the vertebral cortex. DXA measurements in the same regions were used for comparative analysis. **Results:** SUVmean showed a significant correlation with T and Z score in L1 and L2 (P = 0.01). However, there was no significant correlation between SUVmean and BMD (g/cm^2) in L1 and L3. Using linear regression, the possibility for prediction of bone mineral deficit by means of SUVmean was very low. No significant differences were noted in the bone density of patients with or without calcium supplementation, bisphosphonates, hormonal and chemotherapy. However, patients with bisphosphonates therapy had significantly lower SUV in lumbar spine compared to patients without bisphosphonate treatment. In addition, there was no significant correlation between age and SUVmean (p > 0.6), while statistically significant negative correlation was seen between age and DXA BMD. **Conclusion:** In osteoporotic patients a significant correlation was found between semi-quantitative 18F-NaF PET/CT analysis and DXA BMD T and Z scores in the lumbar spine. However, its potential for prediction of bone mineral deficit should be evaluated in future prospective studies focusing on volume-based apparent bone mineral density assessment an approximation of the volumetric density of bone calculated on different sites.

EP-1006

Scintigraphic Assessment Of Pedicular Screw Loosening In Patients With Spinal Arthrodesis

*J. Sabater-Sancho, **A. Amr-Rey**, R. Díaz-Expósito, Sr., I. Casáns-Tormo, J. Orozco-Cortés, V. López-Prior; Servicio De Medicina Nuclear. Hospital Clínico Universitario De Valencia, Valencia, SPAIN.*

Introduction: The screw loosening is a cause of failed back surgery syndrome being described in 10-40% of patients undergoing lumbar arthrodesis. We analyze the value of bone scintigraphy with SPECT and SPECT-CT technique in patients with persistent lumbar pain and screw loosening suspicion. **Materials and Methods:** We have studied 34 patients with SPECT, and SPECT-CT fusion if possible (16/34), from January 2015 to December 2016. The patients were referred to the department due to pain and screw loosening suspicion. We consider positive loosening when the uptake was localized in the screw entry point or its path. The mean age was 57 years old (36-79) and the time interval between intervention and scintigraphic study was less than one year in 3 patients, over 10 years in 6 of them, and between 3-10 years in 25. Surgery was due to degenerative pathologies in 17 (50%) patients, listhesis in 8 (24%), and mixed etiology in 9 (26%). Surgery location was lumbo-sacral in 29 (85%), lumbar in 3 (9%), thoracic and lumbar spine in 1 (3%) and thoracic-lumbo-sacral in 1 (3%). Spinal fusion was of 3 vertebrae in 11 (32.3%) patients, 4 vertebrae in 10 (29.4%), 2 vertebrae in 7 (20.5%), and the fusion involved more than 4 vertebrae in 6 patients (17.6%). None of the patients were reintervened at the follow-up. All of them were studied with CT, Rx or MR. **Results:** The consideration of positive screw loosening was done by scintigraphy in 17/34 (50%) patients and by other imaging techniques (CT or Rx) in only 3. The SPECT was positive for screw loosening in 15 (44%), negative in 8 (24%), and the uptake was attributed to an articular overload (7) or postsurgical changes (4) in 11 (32%). SPECT-CT was positive for loosening in 12/16 (75%) cases, being the SPECT negative or suspicious in 2. Of 4 patients with negative SPECT-CT, the uptake was considered negative for loosening (SPECT and SPECT-CT) in 3 patients (18,7%), and there was no uptake in 1 (6.2%). **Conclusions:** The SPECT technique is a helpful tool that allows us to predict which patients are likely to have worse evolution after spine surgery, providing us a more comprehensive follow-up. The SPECT-CT offers us an accurate localisation of the screw loosening site as well as another pathological uptake.

EP-1007

Mandibular Condylar Hyperplasia. Diagnosis And Follow-Up By Bone SPECT And SPECT/CT

A. Amr-Rey[1], I. Casáns-Tormo[1], M. Puche-Torres[2], A. Sada-Malumbres[2], R. Díaz-Expósito[1], J. Sabater-Sancho[1], J. Orozco-Cortés[1], V. López-Prior[1]; [1]Nuclear Medicine. University Clinic Hospital, Valencia, SPAIN, [2]Maxillofacial Surgery. University Clinic Hospital, Valencia, SPAIN.

Introduction: Mandibular condylar hyperplasia (MCH) is a rare pathological condition that causes persistent bone growth, with facial asymmetry, creating functional and aesthetic problems. It is essential the evaluation of increased bone metabolic activity together with the growth phase, according to the age of the patient and the clinical consequences of the facial deformity, to establish the appropriate therapeutic guidance. **Material and Methods:** We performed 48 cranial SPECT with 99mTc-HMDP in 36 patients(p): 22 women, 22 ± 6 (11-39) y/o, referred by mandibular asymmetry with suspicion of MCH. We obtained visual assessment and quantification of condylar activity in both condyles, considering condylar index (CI) ≥ 55% as significant of active process. It was possible to perform SPECT/CT fusion in 10p. We performed 1-4 follow-up studies in 7p at 6-20 months and in 1p at 5 years, to identify suspected MCH reactivation after surgery. Two groups were established considering growing phase, according to the age of patients (25p with 11-20 y/o and 21p> 20 y/o). **Results:** The mean global CI was 55.4 ± 5.5% (50-76.7), detecting significant uptake in a condyle in 21p (CI: 60.3 ± 5.1) vs 27p without it (CI: 51.6 ± 1.2, p <0.001). MCH was diagnosed in 18p (CI: 56.4 ± 5.1) and facial asymmetry without MCH in 15p (CI: 51.7 ± 1.6, p: 0.002), performing in 13/18p orthognathic surgery and orthodontic treatment (CI: 56.1 ± 5.6) vs 21p without surgery, with orthodontics alone and /or clinical follow-up (CI: 52.9 ± 3.3, p <0.05). SPECT/CT fusion improved location of the detected anomalies. In p with 11-20 y/o, CI: 55.8 ± 6.1 and in p>20 y/o, CI: 55.1 ± 5.3(NS). In the group of p with 11-20 y/o, there were 6 operated (CI: 58 ± 4.5) and 10 non-operated (CI: 51.6 ± 1.2, p: 0.001). In p> 20 y/o, there were 7 operated (CI: 54.5 ± 6.3) vs 11 non-operated (CI: 54.2 ± 4.1), NS. **Conclusions:** The cranial SPECT provides essential information in the diagnosis and follow-up of patients with suspicion of mandibular condylar hyperplasia, improving the localization by SPECT/CT. The quantification of osteoblastic activity in mandibular condyles allows a more accurate diagnosis of the disease in active phase, showing significant differences in patients undergoing surgery and in younger patients, being an essential factor in the decision to proceed with surgery, together with the growth phase according to the age of the patient.

EP-76　　　　　　　**during congress opening hours, e-Poster Area**

Conventional & Specialised Nuclear Medicine: Imaging Guided Surgery (Benign)

EP-1008

Value of the pre-iodine ablation thyroglobulin serum levels in predicting remission in differentiated thyroid cancer

H. Boudriga[1], M. Ben Fredj[2], M. Ben Rejeb[3], A. Ezzine[2], S. Mensi[2], M. Guezguez[2]; [1]Laboratory of medical imaging, LR12ES06 Monastir university, Monastir, TUNISIA, [2]University hospital of Sahloul, Nuclear medicine department, Sousse, TUNISIA, [3]University hospital of Sahloul, department of prevention and safety of care, Sousse, TUNISIA.

Introduction: Thyroglobulin is the biological marker for monitoring patients with differentiated thyroid cancer. It is used

for the long term follow up because of its good sensitivity and specificity. Our study aimed to evaluate the importance of the baseline prognostic value of thyroglobulin in order to predict remission or recurrence during follow up. **Patients and Methods:** We retrospectively enrolled 150 patients who were followed for differentiated thyroid cancer from 2001 to 2011. The mean age was 42 ±16 at diagnosis. The mean follow up period was 41 months ±43. Thyroid serum levels were obtained after thryoid hormone withdrawl. Patients with positive Tg antibodies were excluded. The multivariate analysis was used to evaluate prognostic markers including the baseline Tg level. The ROC curve indicated the cut-off value of the stimulated Tg. **Results**: We divided our patients into three groups according to the baseline Tg level 0-2, 2.1-15 and 15-1000. The cut-off value of 7,65 ng/ml indicated a disease free population with 87% sensitivity and 75% specificity (PPV= 92%, NPV= 63%). On the multivariate analysis, second [OR=5,122 ;95% CI (1,419-18,492) p=0,013] , third [OR=14,463 ;95% CI (4,186-49,968) p<0,001)] intervals of baseline thyroglobulin levels and presence of lymph node involvement p=0,03) were predictive of persistent disease. **Conclusion**: Our study was in line with other findings concerning the cut off level of baseline Tg serum level (=7,65 ng/ml) indicating its usefulness in indicating a good prognosis in DTC.

EP-1009

Decrease of the rate of affected margins in non palpable breast lesions with I125 Radioguided Seed Localization technique

O. Ajuria Illarramendi, M. Rioja Martin, A. Santos Carreño, P. Paredes Rodriguez, A. Puerta Vicente, J. Vilar Tabanera, J. Ocaña Jimenez, J. Castro Beiras; Hospital Ramon y Cajal, madrid, SPAIN.

Purpose: To review the experience of our Hospital with radioguided Seed Localization (RSL) for non-palpable breast lesion surgery and to evaluate the decrease of the affected margins of the surgical specimen. **Subjects and Method:** 218 patients with non-palpable breast lesions that were treated with RSL technique from 2010 to 2015 were considered for the study. In 186/218(85,32%) the seed was placed using ultrasound, in 30/218 (13,76%) guided by mammography and in 2/218 (0,92%) with a combination of both. Affected margin was defined as a distance from tumour <1mm and was classified according to breast section and year of surgery. Both Craneaocaudal and lateral control mammography were performed, confirming correct location when the seed was placed in the middle of the lesion, marginal when it was placed on the margin of the lesion and failed when it was placed out of the lesion. **Results:** Ultrasound seed deposition showed the following: Correct location 168/186(90,32%), marginal location 12/186(6,45%) and failed in 6/186(3,22%); mammography resulted in: correct location 22/30(73,33%), marginal 3/30(10%) and failed in 5/30(16,67%); and with the combined technique: correct location in 2/2(100%). Margins where amplified in 54/218(24,77%) while evaluating retrospectively only in 29/218(13,30%) would have been necessary. In 6/54(11,11%) the seed was marginally located. 15/218(6,88%) underwent reintervention due to affected margins. The quadrant with most affected margins: "Inferior interquadrant" 50%(3/6), followed by "Retro-areolar" 42,86%(3/7), while the less affected ones were the "upper-inner" 17,86%(1/8) and the "lower-inner" 1/8(12,5%). The rate of affected margins in 2015 was 5/66(7,57%); 19/70(27,14%) in 2014; 2/10(20%) in 2013 and 13/43(30,23%) in 2012. In 29 cases the date of the surgery is unknown. The decrease of the affected margin rate must be highlighted in 2015, as it is 3,5 lower than in 2014. In 2015 the rate of reintervention was 4/66(6,06%), lower than de average reintervetion rate (6,88%). **Conclusion:** RSL technique offers a high rate of free margins and a low rate of second interventions due to its precision. The rate of affected margins decreases every year been in 2015 of 7,57%. The results are excellent when the technique is guided by ultrasound. Due to its simplicity, excellent results and comfort, RSL has become the elected technique in our Hospital.

EP-1010

Radiotracer-guided localization for thoracosopic resection of small and subsolid pulmonary nodules

P. K. Rehm, J. Jahjah, A. Mitqhal, L. Flors; University of Virginia Health System, Charlottesville, VA, UNITED STATES OF AMERICA.

Purpose/Introduction: The purpose of this retrospective study was to evaluate the efficacy of radiotracer-guided localization of small solid or subsolid pulmonary nodules to guide thoracoscopic excisions at a single institution. **Subjects and Methods:** Patients that underwent a radiotracer-guided localization of small or ill-defined pulmonary nodules to guide thoracoscopic excisional resection during a 57-month period at our institution were retrospectively reviewed. Using computed tomographic (CT) guidance, 0.33 mCi (12.21 MBq) of technetium-99m (Tc-99m) macroaggregated albumin (MAA) in 0.3 cc saline was injected into or adjacent to a pulmonary nodule. Gamma imaging was performed after the procedure, to prove the success of the injection. During the subsequent thoracoscopic surgery, a gamma probe was used to localize the tracer and guide the surgeon to the position of the nodule. The identified lesions were successfully resected and sent for pathologic analysis. Patient demographics, oncologic history, smoking history and presence of emphysema, nodule characteristics, procedural complications, and surgical success and complications, and histology were reviewed. **Results:** 82 patients (48 females; mean age 60.7 years, range 6-85) were included in the study, with a total of 87 nodules. 45 patients (56 %) had a history of malignancy: lung (n=13), colorectal (n=10), melanoma (n=7), pancreatic (n=2), breast (n=3). 55 patients (68 %) had smoking history and emphysema was present in 35 of them. Mean nodule size was 10 ± 4.8mm (range 3-30 mm). 54 were solid (62 %) and 33 were subsolid. 17 patients (21 %) developed pneumothorax during the procedure, one required chest tube placement. All the patients had successful gamma probe localization of their lesions. There were no surgical complications. 26 (30%) nodules were visible/palpable intraoperatively. 56 nodules (64%) were malignant: lung adenocarcinoma (n=39), colorectal carcinoma (n=6), melanoma (n=4), pancreatic adenocarcinoma (n=2), ductal breast

cancer (n=1). **Discussion/Conclusion:** Small and ill-defined pulmonary nodules are often not visualized or palpable intra-operatively, rendering the use of CT-guided radiotracer localization a valuable method for guiding thoracoscopic excision of nodules. Based on our experience, CT-guided radiotracer localization using Tc-99m MAA before surgery is a safe and effective method to aid surgical resection of small or subsolid pulmonary nodules.

EP-1011

Feasibility of portable gamma camera imaging in intraoperative radioguided parathyroid adenoma identification

Z. Koç, P. Özcan Kara, A. Dağ, M. Berkeşoğlu; Mersin University Hospital, Mersin, TURKEY.

Aim: Aim of this study is to investigate the diagnostic facility and decide feasibility of performance of additional portable gamma camera imaging in intraoperative radioguided parathyroidectomy operation. **Materials and Methods:** Intraoperative radioguided parathyroidectomy operation was performed in three patients (3F; 54±1,73 years old) with diagnosis of hyperparathyroidism. Their preoperative plasma Ca and PTH levels were 11,3±1,3 and 125,4±53 respectively. Tc-99m MIBI parathyroid scintigraphy was performed in all patients prior to the operation with additional SPECT imaging (Siemens, ECam, US). Preoperative administration of Tc-99mm MIBI was performed approximately 1 hours before the operation for radioguided surgery. **Results:** Preoperative scintigraphy did not reveal a discrete point as parathyroid adenoma due to additional thyroid nodules and close proximity of the adenoma to thyroid tissue in all three cases. SPECT imaging pointed out left lobe in one patient and right lobe in two patients. Intraoperative analysis of the operation area also did not reveal certain localization by both gamma probe (Europrobe, France) and portable gamma camera (Crystal Cam, Deutschland). The lesions of the patients were localized by the surgeon successfully by gamma probe and the operation ended due to positive frozen section analysis for parathyroid adenoma. Bilateral exploration was necessary in one of three patients. **Conclusion:** Intraoperative portable gamma camera did not reveal additional benefit than gamma probe did in patients with preoperative inconclusive parathyroid scintigraphical results who have parathyroid adenomas in close proximity to the thyroid lobes. However this modality might replace frozen section analysis or quick PTH analysis in verification of excision of parathyroid adenoma. **Key Words:** Portable Gamma Camera, Gamma Probe, Radioguided, Parathyroid.

EP-1012

Radioguided surgery for primary hyperparathyroidism by evolved protocol from SPECT and portable gamma camera to SPECT CT and hybrid portable gamma camera

J. Orozco Cortés, Sr.[1], R. Díaz-Expósito[1], S. Vidal Sicart[2], N. Sanchez Izquierdo[2], D. Fuster[2], N. Cassinello Fernandez[1], O. Vidal[2], R. Jover[1], F. Lomeña[2], I. Casans Tormo[1]; [1]Hospital Clinic Valencia, Valencia, SPAIN, [2]Hospital Clinic Barcelona, Barcelona, SPAIN.

Objective: To assess the correlation between the findings of preoperative diagnostic techniques and the surgical detection with intraoperative (IO) scans in primary hyperparathyroidism (PH). To describe pre- and intrasurgical protocols optimized for radioguided surgery. **Materials and Methods:** Prospective study. Thirty three patients diagnosed with PH were included in two centers. Center A (25) and Center B (8). Protocols were based on the combination of SPECT and SPECT/ CT images with a final intraoperative image with portable gamma camera (PG) were applied. Center A performed preoperative parathyroid scintigraphy (PPS), SPECT, ultrasound and/or CT, as well as pre- and post-operative imaging with a PG. After surgery, delayed anatomopathological study of the samples and clinical and analytical follow-up were done. Center B added pre-operative planar images with pin-hole collimator, SPECT/CT and imaging with a hybrid PG (with an optical component). **Results:** Group A: 21 women (84%) and 4 men (6%), mean age 60 years (range 25-87). 6 (24%) with negative PPS, 4 (16%) doubtful PPS and 15 (60%) with positive PPS. SPECT localized pathologic tissue in 92% of cases. The final concordant PPS / localization was 16 (64%) and non-concordant in 9 (36%). The agreement between intraoperative imaging and final parathyroid tissue location was 88% (22). Mean value of pre-excision PTH was 216 pg / mL; Post-excision: 58.5 pg / mL. Pathological assessment demonstrated 22 parathyroid adenoma (88%), 2 hyperplasia (8%) and 1 thyroid nodule (4%). Group B: 4 males and 4 females, mean age 60 (range 49-71). SPECT / CT improved preoperative localization in all cases. The agreement with the IO was 87.5%. The activity / optical component concordance of 8/8. Mean PTH pre-excision: 232 pg / mL; Post-excision: 49.9 pg / mL. PA: 6 cases of parathyroid adenoma and 2 hyperplasia **Conclusion:** The preoperative SPECT/CT study allows more precise localization of hyperfunctioning parathyroid tissue. SPECT is a suitable alternative in centers without SPECT/CT. The intraoperative image increases the accuracy in the localization and improves the safety in the resection of the target tissue. An optimized protocol can be adjusted to each center according to available technology.

EP-1013

Ultrasmall gold quantum clusters intrinsically labeled with ^{64}Cu for in vivo PET/NIRF imaging of lymph nodes

H. Zhang, J. Yang, A. Ahad, W. Weber, M. Kircher; Memorial Sloan-Kettering Cancer Center, New York, NY, UNITED STATES OF AMERICA.

Aim: Complete resection of tumor lesions and metastasized lymph nodes (LNs) remains the first-line therapy of cancer treatment. Exogenous non-invasive molecular imaging agents with clinically complementary positron emission tomography (PET) for preoperative surgical planning and near-infrared fluorescence (NIRF) for intraoperative delineation and resection can remarkably enhance surgical outcomes and postsurgical survivals. Here, we developed an ultrasmall (<5 nm) dual modal PET-NIRF gold quantum cluster nanoprobe, which intrinsically fluoresces and is labeled with ^{64}Cu without chelators, and evaluated the feasibility for imaging LNs with PET/CT and NIRF. **Materials and Methods:** Gold quantum clusters (AuQCs) showing an ultras-

mall core size of 2.43±0.55 nm under TEM were synthesized using α-lactalbumin (α-LA) as ligand with fluorescence peaked at 705 nm. The intrinsic labeling of AuQCs with ^{64}Cu or ^{nat}Cu was performed in PBS. After IV injection, organ distribution and excretion profile of ^{64}Cu-AuQCs were monitored with PET/CT and NIRF. Sentinel LN drainage was also imaged using PET-NIRF by both peritumoral and footpad injections. **Results:** Monodispersed ultrasmall AuQCs with α-LA ligands displayed an intrinsic NIRF emission at 705 nm with a sufficiently large Stokes shift that can minimize autofluorescence. Radio-iTLC assay showed that ^{64}Cu-AuQCs were prepared quantitatively with specific activity of > 33.0 MBq per mL (7.5 mg/mL AuQCs). ^{nat}Cu^{2+} concentration-dependent fluorescence quenching was observed and direct detection of free ^{nat}Cu^{2+} cations verified that ^{64}Cu(II) was reduced to ^{64}Cu(0) and adsorbed on AuQCs through a chelator free manner. With IV injection of 13.2 MBq of ^{64}Cu-AuQCs, PET imaging showed that ^{64}Cu-AuQCs were dominantly excreted through urinary systems. High accumulation was found in kidneys (20 h: 19.2 ± 4.5 %ID/g) with relatively low uptake in liver (20 h: 9.3 ± 4.2 %ID/g). LN mapping was achieved at 20 h post injection, which could be delineated by both PET/CT imaging (20 h: 11.4 ± 5.6 %ID/g) and NIRF imaging. Through both peritumoral and footpad injections, sentinel LN drainage was visualized by PET-NIRF dual modalities with a high contrast ratio. Quantitative analysis of PET imaging showed the uptakes in LNs (55.5, 52.7, 34.4 and 23.8 %ID/cc at 20 h p.i.) are distance-dependent from the injection site (footpad). **Conclusion:** Dual modal PET-NIRF ^{64}Cu-AuQC nanoprobe is a promising contrast agent for preoperative lymph node detection, and intraoperative guidance of lymph biopsy, which may improve cancer patient care and compliance after its transduction into clinics. **Acknowledgements:** NIH Small-Animal Imaging Research Program grant R24 CA83084 and NIH Center grant P30 CA08748.

EP-77   during congress opening hours, e-Poster Area

Conventional & Specialised Nuclear Medicine: Miscellaneous

EP-1014
The Role of SPECT/CT for diagnosis of thoracic splenosis

M. Totaro, G. Petracca Ciavarella, M. Guerra, M. Scarale, M. Mangiacotti, **V. Frusciante, Sr.**; Casa Sollievo della Sofferenza, San Giovanni Rotondo, FG, ITALY.

Introduction: Thoracic splenosis is a splenic tissue growth into chest cavity and represents an infrequent complication (18%) of traumatic injury of the spleen. Thoracic splenosis is often discovered by chance, because it is always almost asymptomatic. Sometimes splenosis is found after investigation for recurrent hemoptysis or chest pain. **Case report:** In this study we describe the case of a 56 years old man with history of previous abdominal and chest trauma for a severe car crash and subsequent traumatic rupture of the spleen. For persistent chest pain a CT scan without contrast of the chest was performed, showing multiple nodular lesions of uncertain origin (mesothelioma? splenosis? other?). The patient, therefore, has completed the CT scan with contrast medium, which was taken up by pleural nodular formations. Patient underwent scintigraphy in our department with denatured erythrocytes radio-labeled with technetium-99m in order to reach a differential diagnosis between pleural cancer and splenosis. Scintigraphic study was performed after intravenous administration of 99m-TC Angiocis- denatured erythrocytes (555); 1 h after injection, planar views of the chest were performed. After 2 hours a SPECT-CT study on the chest was performed with a double-headed Siemens Symbia camera (high resolution / low energy collimators, 32 views , 35s / view, 128 matrix, 1.0 zoom, non-circular autocontour orbit ,step and shoot mode). Planar views of the chest showed some high-uptake areas in the left hemithorax, compatible with splenic nodules. The SPECT / CT study confirmed the presence of splenic nodules and precisely defined their number and anatomical site . **Discussion:** Chest splenosis is a sporadic complication of a spleen trauma. The diagnosis is often casual and results in several diagnostic tests and unnecessary procedures (CT without and with contrast, biopsy, thoracoscopy, thoracotomy). Scintigraphy with radio-labeled denatured erythrocytes associated with SPECT / CT allows a fast and economic diagnosis of splenosis and allows a coregistration of functional information with anatomical data. Normally there is no need to remove thoracic splenosis because the splenic tissue is slow-growing, non-invasive and benign. **Conclusions:** scintigraphy with radio-labeled denatured erythrocytes associated with SPECT / CT study may be a useful diagnostic aid in cases of thoracic nodules and should always be considered in patients with a history of traumatic rupture of the spleen.

EP-1015
The IAEA Quality Management Audit of Nuclear Medicine Facilities: Analysis of Results

R. Núñez Miller[1], M. Dondi[1], L. Torres[2], M. Marengo[3], T. Masardo[4], E. Mishani[5], A. Van Zyl Ellmann[6], K. Solanki[7], A. Bishoff-Delaloye[8], E. Estrada Lobato[1], F. Giammarile[1], F. Barajas Ordonez[1], D. Paez[1]; [1]Division of Human Health - IAEA, Vienna, AUSTRIA, [2]Centro de Investigaciones Clinicas, La Habana, CUBA, [3]Azienda Ospedaliera S. Orsola-Malpighi, Bologna, ITALY, [4]Hospital Clinico Universidad de Chile, Santiago, CHILE, [5]Cyclotron Unit/Nuclear Medicine Department, Hadassah Univeristy Hospital, Jerusalem, ISRAEL, [6]Tigerberg Hospital, Western Cape, SOUTH AFRICA, [7]Addenbrooke's Hospital/ Cambridge University Hospitals, Cambridge, UNITED KINGDOM, [8]CHUV Lausanne, Lausanne, SWITZERLAND.

Purpose/Introduction: The IAEA has a program (QUANUM) for quality management audits of Nuclear Medicine facilities worldwide. QUANUM is composed of a series of comprehensive guideline based checklists covering all thematic areas of a Nuclear Medicine department. The response to the multiple questions available in the 17 checklists can be scored from 0 (absent) to 4 (full conformance), according to the level of adherence with international and/or IAEA guidelines and standards. For each audited centre the level of adherence to standards (Level of conformance, LoC) is compared to the total achievable score.

Scores of 0, 1 and 2 are considered non-conformance (NC). The NC can be further classified as critical, major and minor, depending on issues of safety for staff, patients or environment (critical), the capacity to properly perform its activities (major) or possible optimization of processes (minor). The program provides a score for each checklist as well as an overall score (a level of 75% or more is considered a good level of practice). Our aim was to analyse the results from the reports of 38 QUANUM missions. **Subjects and Methods:** Data available of 38 reports were retrospectively analyzed. Almost all checklists were found to be applicable in the audited centres. **Results:** Overall, the audited centres showed a LoC of 73.9±8.3% (mean±1SD), ranging between 56.6% and 87.9%. Clinical requirements checklists had the highest LoC, with 83.7% for diagnostic procedures and 87.9% for therapy. Conversely, radiopharmacy level 2, computer systems and data handling and QA/QC systems, showed the lowest LoC (56.6%; 67.2% and 68%, respectively). The data deviation from each independent checklist ranged between 10.6% and 34.3%, reflecting a great variability among audited services. A total of 880 recommendations covering both critical (31.4%) and major (68.6%) NC was reported. The average of critical and major non conformities per audit was 6 (range 1 to 25) and 16 (range 1-25), respectively. The greatest proportion of recommendations was found in the managerial, organization and documentation areas. By contrast, the lowest number of recommendations was found in relation to human resources and clinical quality of diagnostic and therapeutic procedures. **Conclusion:** The IAEA QUANUM program could be implemented in a wide range of Nuclear Medicine departments worldwide. The clinical services demonstrated the highest LoC. Conversely, radiopharmacy level 2, computer systems and data handling and QA/QC were found to be more frequent areas of NC.

EP-1016

Kinetic analysis using asialoglycoprotein receptor scintigraphy with Tc-99m GSA dynamic SPECT/CT for assessment of hepatic function

Y. Fukuda[1], T. Sanomura[1], H. Okuda[1], Y. Yamamoto[1], K. Okano[2], N. Kudomi[1], Y. Nishiyama[1]; [1]Kagawa University, Kita-gun Kagawa, JAPAN, [2]Kagawa University Department of Gastrointestinal Surgery, Kita-gun Kagawa, JAPAN.

Objective: Kinetic modeling of Tc-99m diethylenetri-amine-penta-acetic acid-galactosyl human serum albumin (Tc-99m GSA) measures the total amount of asialoglycoprotein receptor within a subject's liver. The purpose of this study was to evaluate the usefulness of kinetic analysis using asialoglycoprotein receptor scintigraphy with Tc-99m GSA dynamic SPECT/CT for assessment of hepatic function. **Materials and Methods:** Seventy-four studies in 63 patients with malignant hepatic tumor were examined. Dynamic SPECT data were acquired for 20 min immediately following injection of Tc-99m GSA. CT-based attenuation-corrected SPECT images were reconstructed. The blood time-activity curve in the left ventricle was used as an input function. Applying a two-compartment three-parameter model K1, k2 and k3 were obtained. Correlations were deter-

mined between these kinetic parameters and the results of established parameters of Tc-99m GSA liver uptake ratio (LHL15), and blood pool clearance ratio (HH15), and of biochemical liver function tests which include indocyanine green retention rate at 15 min (ICGR15), serum bilirubin, serum albumin, cholinesterase, prothrombin time, and platelet. **Results:** The K1 and k3 values correlated with LHL15, HH15, ICGR15, serum albumin and cholinesterase. The k2 value correlated with LHL15, HH15, ICGR15, serum albumin, cholinesterase and platelet. **Conclusions:** Kinetic analysis using asialoglycoprotein receptor scintigraphy with Tc-99m GSA dynamic SPECT/CT might be useful for assessment of hepatic function.

EP-1017

The Value of Clinical Audit Beyond Measuring Performance: Evidence from the National NHS England PET-CT Clinical Audit Programme

P. Ross[1], J. Armstrong[2], S. Albon[2], W. Wong[3]; [1]Birkbeck University of London, London, UNITED KINGDOM, [2]Alliance Medical Limited, London, UNITED KINGDOM, [3]Mount Vernon hospital, Northwood, UNITED KINGDOM.

Purpose: to identify and evaluate the value of the National NHS England PET-CT Clinical Audit Programme from the perspective of doctors on the programme. **Methods:** A single embedded case study centred around the ninety consultant doctors currently reporting on the National NHS England Clinical Audit Programme. A mixed methods sequential approach with thirteen explorative interviews and follow-up surveys. Directed thematic analysis whereby themes derived from interviews informed the on-line survey. The survey was comprised of thirty, five point Likert scale questions and three open response questions. Exploratory factor analysis and descriptive statistical methods were applied to summarise the survey data. Data triangulation techniques to corroborate and validate findings across the different methodological techniques. **Results:** Online survey (November 2016) 62/90 doctors responded (69%) 1] **Participation in clinical audit was reassuring for doctors**: 62% agreed or strongly agreed audit was reassuring; 34% agreed or strongly agreed that audit felt threatening; 67% agreed or strongly agreed that they would wish to continue to participate in the audit programme even if it was not mandatory 2] **Clinical audit provided a potential platform for collective learning**: 67% agreed or strongly agreed that participation in audit improved their reporting skills; 68% agreed or strongly agreed that audit was a collaborative process between auditors, managers and reporters 3] **Effective clinical audit involved doctors in a process of continuous quality improvement so that standards of diagnostic reporting and patient safety were improved**: 52% agreed or strongly agreed that the audit process had improved patient safety;76% agreed or strongly agreed that participation in the audit programme helped validate their professional competence; 95% agreed or strongly agreed that audit had an important governance role. **Conclusion**: The results support the view that clinical audit does more than monitor performance. Doctors surveyed were of the view that it had the

potential to provide an arena for team learning where doctors were able to discuss diagnostic reports within an open blame free culture. However, to facilitate continuous quality improvement, clinical audit needs to foster high levels of communication and the sharing of anonymised audit feedback so that individual mistakes can be stored in the collective memory of the community of practice.

EP-1018

Optimized Lymphoscintigraphy in Grading of Lymphedema of the Lower Extremities: An Attempt to Clinicoscintigraphic Staging

M. A. A. Mostafa; Prince Mohamed Bin Abdelaziz Hospital, Riyadh, SAUDI ARABIA.

Background: An important challenge, facing the diagnosis of lower extremity (LE) lymphedema, is the proper clinicoscintigraphic staging to assess its severity. To the best of our knowledge, few attempts of such clinicoscintigraphic staging criteria were tried in the literature. Objective: To create relatively proper clinicoscintigraphic staging criteria for assessing the severity of lymphedema of the LE**. Material and Methods:** This is a retrospective study entailing reviewing of 21 cases, with unilateral or bilateral lymphedema of the LE, referred to Nuclear Medicine Division, Prince Mohamed bin Abdelaziz Hospital, Riyadh, KSA. All such cases were subjected to optimized (qualitative and semi-quantitative) lymphoscintigraphy of bilateral LEs. The acquisition of all cases comprised 3 points, 1 minute count, spot images for the site of injection (at 0, 45 and 90 minutes) to calculate the migration indices (MGI), sequential inguinofemoral dynamic imaging for the lymphogram, and 2 points sweep images for visualizing the lymphatic trunks, the lymphatic collaterals, and inguinofemoral lymph nodes, dermal backflow and popliteal lymph nodes. The 90 minute's count spot and the second 91 minutes' sweep images were performed after 30 minutes of interrupted walking (with last 10 minutes continuous walking phase just prior to scanning). Pre-analysis independent grading criteria, using clinical and scintigraphic parameters to assess the severity of lymphedema of the LE, were modified from literature (from 1 through 3) and approved by a panel of experienced vascular surgeons and nuclear medicine physicians. The data were categorized into two groups of normal LEs (A) and LEs with lymphedema (B) and verified statistically. **Results:** Twenty one cases (aged 45.68 ± 12.52 SD years; 18 females) had lymphedema of 24 LEs and 18 normal LEs. The post-exercise migration index (MGI) showed the relative highest significant difference among the two groups of normal LEs and the group with lymphedema of the LEs, respectively (p = 0.038). MGI showed the highest significant inverse correlation with the lymphogram curve grading (r = -0.93, P < 0.05) and the skin changes grading (r = -0.77, p < 0.05). Accordingly, stage I (14 LEs), stage II (3 LEs), and stage III (7 LEs) were categorized. **Conclusion:** The post-exercise MGI may represent the most significant parameter, on lymphoscintigraphy, to grade lympedema of the lower extremity. In addition, the lymphogram curve grading, and skin changes may constitute the pillars for staging of lymphedema of LEs

into three categories (mild, moderate and severe).

EP-1019

Intraperitoneal Scintigraphy in the Diagnosis of Pleural Effusion in Peritoneal Dialysis

I. Latorre Agraz, B. Cueto Cañadas, D. Balaguer Muñoz, P. Abreu Sánchez, M. D. Reyes Ojeda, T. Mut Dólera, M. C. Plancha Mansanet, E. Caballero Calabuig, M. B. Vizcaíno Castillo; Hospital Dr. Peset, Valencia, SPAIN.

Introduction: Hydrothorax is a common complication in peritoneal dialysis (PD). However, it is more unfrequent in those cases which are secondary to pleuroperitoneal shunt, due to congenital or acquired diaphragmatic defects. It is important to establish a correct differential diagnosis of its etiology to achieve an optimal therapeutic management. The intraperitoneal scintigraphy seems to be a valid diagnostic technique, but still lacks a clearly established methodology. **Purpose:** The aim is to detect an abnormal pleuroperitoneal communication in hydrothorax occuring during peritoneal dialysis by using 99mTc-DTPA scintigraphy. **Subjects and Methods:** Three patients, two men and one woman, in PD (time span in dialysis ranged from 2 months to 4 years), who presented pleural effusion without etiologic diagnosis by chest x-ray, CT scan or thoracentesis, were studied by intraperitoneal scintigraphy. 3 mCi (111MBq) of 99mTc-DTPA were administered in combination with the dialyzer liquid. We performed an early dynamic study in supine position (30 seconds per image using a 64 x 64 matrix) and late images of the thorax and abdomen up to 120 minutes after the radiotracer administration (5 minutes per image using a 128 x 128 matrix). **Results:** In the dynamic phase, we observed the presence of the radiotracer in pulmonary topography (sign of pleuroperitoneal shunt) in both patients with right pleural effusion (one had transudate characteristiques, the other revealed undeterminate). The patient with a left hydrothorax showed radiopharmaceutical retention in the peritoneal cavity, shunt was discarded, being finally diagnosed of chronic fibrinous pleuritis. Positive cases (pleuroperitoneal shunt) in scintigraphy were resolved after PD interruption, being replaced by hemodialysis. **Conclusion:** The 99mTc-DTPA scintigraphy is an effective, rapid and noninvasive diagnostic technique to demonstrate the pleuroperitoneal shunt in dialysed patients, having an important role in therapeutic management. Nevertheless, it would be convenient to agree on a standard methodology in terms of radiopharmaceutical, activity and image protocols.

EP-1020
Lymphoscintigraphic findings in patients with lipedema

P. Olivan-Sasot, C. Ruiz-Llorca, I. Forner-Cordero, J. Muñoz-Langa, A. Yepes-Agudelo, V. Vera-Pinto, L. Agudelo-Cifuentes, B. Martínez-Sanchís, P. Bello-Arques; Hospital Universitario y Politécnico La Fe, Valencia, SPAIN.

Background: Lipedema is characterized by bilateral enlargement of the lower limbs due to abnormal depositions of

subcutaneous fat, painful associated with bruising. Diagnostic criteria are not established yet. **Aim:** to describe lymphoscintigraphic findings in patients with lipedema. **Material and methods:** Prospective cohort study in patients with clinical criteria of lipedema. Lymphoscintigraphy was performed to complete the study. The clinical stages of lipedema were distributed between stages I-III (I: low grade) To perform lymphoscintigraphy, 22.2Mbq ^{99m}Tc-Nanocolloids of albumin were injected into the 1st and 3rd interdigital space in both feet, to detect subclinical abnormalities. A whole-body scan was made 15 and 180 minutes after injection was performed. Slight muscular exercise is needed in first 10 minutes for lymphatic drainage activation. One expert independent examiner described the findings in lymphoscintigraphy and classified them in different grades: - 0: Normal - 1: Low grade: Delay or slight asymmetry - 2: Low-moderate: Mild lymphatic hypoplasia - 3: Moderate: Severe hypoplasia or dysfunction - 4: Moderate-severe - 5: Severe: Aplasia +1 if there is dermal backflow or popliteal lymph nodes **Results:** From September-2012 to December-2016, 110 patients were included in the study, in 83 cases, lymphoscintigraphy was performed. The median age was 49.8 years (range 18-80.7). Body mass Index (BMI) was 30.5 (95%CI: 29.1-31.8). All the patients had bilateral and symmetrical involvement; 91.7% spare feet; 92.7% pain; 89% bruising; 84.4% absence of Stemmer sign. The most frequent type of lipedema was type III, from hip-to-ankles (67%). The stages of lipedema were well distributed between stages I to III (I: 39.8%; II: 29.6; III: 25%). Lymphoscintigraphic abnormalities were present in 47% of the patients, most of them were mild (84.6%) (Low grade: 35.9%; Low-moderate: 48.7%; Moderate: 15.4%) No differences were found in these findings related to the age (p=0.674); the presence of Stemmer Sign (p=0.572); neither de stage of lipedema. Regarding the stage of lipedema, no relation was found neither with the presence of lymphosintigraphic findings (p=0.114) neither with the grade of these findings (p=0.142). **Conclusions:** Although lymphoscintigraphic abnormalities are typically associated to the diagnosis of lymphedema, and have been used traditionally to differentiate lipedema and lymphedema, they are present also in lipedema patients. Patologic lymphoscintigraphy is not just pathognomonic of lymphedema, lipedema can't be discarted. The lymphoscintigraphic findings make us wonder if some patients can suffer both syndromes at the same time, or is any lymphatic dysfunction underlying in some lipedema patients.

EP-1021

Possible substitutes for stable iodine tablet in aim of suppression of radioactive iodine uptake

T. Hongyo, Sr., M. Namise, Y. Sawai, K. Yanamoto; *Osaka University, Suita, JAPAN.*

Aim: In the Fukushima nuclear power plant accident which took place in March 2011, a large amount of iodine-131s were radiated. Oral intake of stable iodine tablet was considered necessary for some residents, but the tablet was available to only a part of them. In case another nuclear accident happens, and the amount of stable iodine tablet is insufficient, it is important to look for substitutes for stable iodine tablet. **Materials and Methods:** Besides stable iodine tablet (potassium-iodide, 2μg/g BW), we used two different types of iodine inclusion to examine their suppression effect of the I-131 uptake: dried seaweed (5, 25, 50μg/g BW) and diluted iodine gargle (The 30 times or 100 times diluted; The iodine content was 2.33 or 0.7μg/g BW respectively). Each iodine inclusion was given to 4-week-old ICR mice through a feeding tube, and I-131 (74kBq/mouse) was given 6 hours after the iodine inclusions. The number of the mice ranged from six to 12 in each experiment. The mice were dissected 24 hours later, and the suppression effect of the I-131 uptake by iodine inclusions were examined with use of gamma scintillation-counter. The percentage of I-131 taken into the thyroid was evaluated with each iodine inclusion. We also gave iodine inclusions and I-131 to the mothers of the newborn baby mice, and the thyroid uptake suppression-effect of I-131 through breast milk was examined. Moreover, we searched for materials without iodine which can possibly be a substitute for stable iodine tablet when iodine inclusions cannot be used. **Results and Conclusion:** When dried seaweed and diluted iodine gargle were given, the thyroid uptake of I-131 was suppressed to the same degree as when stable iodine tablets were given. Dried seaweed and diluted iodine gargle may possibly be a substitute for stable iodine tablets. When the mother was given the iodine inclusions, thyroid uptake of I-131 of the baby was significantly suppressed. However, the younger the baby was, the weaker the degree of suppression was. Potassium perchlorate (6.78, 22.3μg/g BW) was shown to suppress the uptake of I-131 to the same degree as stable iodine tablets, suggesting that it can be used instead of stable iodine tablets in case the person has iodine allergy.

Technologist e-Poster Walks

Technologist e-Poster Session 1

E-TPW01

Effects of ROI definition and reconstruction method on Standardized Uptake Value

K. Škalič, D. Bogović, S. Škalič, N. Kusturič, S. Dražumerič; Institut of Oncology, Ljubljana, SLOVENIA.

Objectives: We compared the mean standard uptake values (SUVs) measured from PET images reconstructed with FBP, OSEM and TrueX with point spread function (PSF) modeling, with or without TOF correction, using phantom data. **Methods:** A Jaszczak phantom with 4 small cylinders (8 mm, 12 mm, 16 mm and 25 mm) and the body of the phantom were filled with a radioactive solution with different cylinder-to-background activity concentrations of 2,5:1 (12,95MBq/l: 5,18mBq/l). The scan was performed on Biograph mCT PET/CT scanner, manufactured by Siemens. Scanner combines a 40-slice CT and (LSO) PET system for whole body imaging with included TOF technique. We performed a scan with 15 minutes scan time and with different image reconstruction algorithms - analytical filtered back projection (FBP), iterative OSEM (4.24) and iterative True-X with PSF correction (4.21). TOF information was alternately incorporated in each reconstruction algorithm. A circular region of interest (ROI) was drawn manually at the center of each sphere in the transaxial slice on PET CT image. **Results:** The iterative algorithm True-X with TOF correction displayed the highest SUV value. Slightly lower measurements of SUV value were shown with analytical FBP, followed closely by iterative OSEM (4.24). Algorithms with incorporated TOF correction displayed higher SUV values as their non TOF variant, except in a smallest ROI. Algorithms with TOF correction showed large-scale reduction in SUV at the background measurements regardless of the reconstructive method. **Conclusions:** Mean SUV measured from FBP, OSEM and TrueX images were slightly higher when TOF correction was used in hot areas and much less lover at the background areas. On this cognition we can conclude that the TOF correction consequently increase the image contrast.

E-TPW02

The Effects of Different Reconstruction Algorithms on 18F-FDG PET/CT Images

Y. Parlak, D. Goksoy, G. Mutevelizade, G. Gumuser, E. Sayit; Celal Bayar University, Manisa, TURKEY.

Aim: F18-fluorodeoxyglucose positron-emission tomography (FDG-PET) reconstruction algorithms can have substantial influence on quantitative image data used, e.g., for therapy planning or monitoring in oncology. Reconstruction protocols in PET/CT procedure contain two modifiable parameters: Smooth/Sharp and Speed. We analyzed all the possible combinations of these two parameters and the values defined internally for Relaxation, Iteration and Kernal Width parameters in these combinations. The purpose of this study was to evaluate the activity concentrations of different reconstructed FDG-PET images and to determine the influence of varying activity concentration in distribution, signal background rate (SBR) and quantification (standardized uptake value [SUV]. **Materials and Methods:** A nonuniform "body phantom" was prepared with 6 lesions (distance; 10mm to 35mm) and filled with 207MBq 18F-FDG-water. The phantom was scanned by positioning in the center of the PET/CT (Philips, TruFlight Select, 16 slices) gantry. PET images acquired with the nonuniform phantom simulating a "body" were reconstructed by using nine different reconstruction combinations. For all combinations, data analyses were carried out using SPSS 11.0. Reconstruction algorithms, sphere diameters, SBR of the reconstructed PET data were used to analyze the association between these factors. **Results:** When quantitative images were studied, small differences between reconstruction algorithms were found. The most effective combination with better count statistics and the highest magnitude SUVmax have 3 iterations (33 subsets) and kernel width of 18.7 cm. **Conclusion:** Especially patients with head and neck malignancies, we suggest that the reconstruction protocol, combination of 3 iterations and kernel width of 18.7 cm, should be used. **Key Words:** Reconstruction, PET/CT

E-TPW03

Role of Post reconstruction Gaussian filter in PET scan

S. Tayal, A. Gandhi; Kailash Cancer Hospital & Research Centre, Vadodara, India.

Purpose: To study the effect of Gaussian filter on image quality and study the change in mean SUV value of a photopenic lesion in a background of high FDG uptake. **Methods:** Fusion PET/CT imaging of brain was performed on GE's Discovery STE model on a patient with history of metastatic carcinoma of the left breast. Images were acquired 60 mins after IV administration of 8.41 mCi of F-18 fluorodeoxyglucose (FDG). CT was performed for the purpose of attenuation correction and anatomical correlation. Blood glucose level was 119 mg/dl prior to scan. Informed consent was obtained before performing the PET scan. The data was acquired in word mode for 10 minutes in a single bed position in 128 X 128 matrix. The images of the study were reconstructed with OSEM (Ordered subset expectation maximization) algorithm with 2 iterations and 28 subsets. A Large photopenic area was noted in right parietal lobe of the patient. Post reconstruction Gaussian filter of 2,4,6,8 and 10 mm in full width at half maximum (FWHM) was applied retrospectively to the acquired data. The mean SUV value in g/ml of the photopenic lesion was measured in respective images of varying FWHM Gaussian filter and subsequently mean SUV value of a second region of interest (ROI) ,drawn over the adjacent comparative hot area was evaluated to compare the effect of smoothing with increasing width of Gaussian filter. **Result:** The image ap-

plied with 6 mm FWHM Gaussian filter showed an image, with a balance of sharpness of the edge and smoothening effect. Images reconstructed with less than 6 mm FWHM of Gaussian filter were comparatively grainy and lacked the proper defined edges whereas the images reconstructed with greater than 6 mm resulted in over smoothing and hence gradual increase of mean SUV in the photopenic lesion and vice versa in adjacent hot area. **Conclusion:** The Gaussian filter used in PET scan to blur images and remove noise, should be used optimally when studying a photopenic lesion in a background of high FDG uptake, in order to get useful clinical images

E-TPW04

Discovery IQ 4R- Otimization of parameters of acquisition and reconstruction in clinical 18F-FDG PET-CT studies

H. Paninho[1], D. Faria[1,2,3], S. Francesco[1], J. Fernandes[2,3], J. Oliveira[2,3]; [1]ESSUA-Health School of University of Aveiro, Aveiro, PORTUGAL, [2]HPP-Medicina Molecular, SA, Porto, PORTUGAL, [3]Lenitudes Medical Center & Research, SGPS, SA, Santa Maria da Feira, PORTUGAL.

Introduction: The latest innovation from GE Healthcare, PET-CT Discovery IQ scanner, provides the highest sensitivity due to the Light Burst detector with 6,3mm x 6,3mm x 6,3mm BGO crystals, the largest field of view (FOV) of the industry and the dual energy acquisition channel technology. In addition, the Bayesian penalized-likelihood reconstruction algorithm, Q.Clear, controls the noise through the use of a penalization factor (beta), that allows an effective convergence and provides measurements of Standardized Uptake Values (SUV) more consistent. **Aim:** The aim of this work is to determine the optimum penalization factor β of Q.Clear and ideal acquisition parameters for clinical settings. **Methods:** A NEMA IEC Body Phantom, filled with a background activity of 6,6 kBq/mL and spheres with 34,3 kBq/mL was acquired on a PET-CT Discovery IQ 4R with varying acquisition times and recovery coefficient (RC) and contrast recovery coefficient (CRC) were determined for images reconstructed using VUE Point HD (4 iterations, 12 subsets, 6,4 mm filter) and Q.Clear using β values from 150 - 500. Sixty patients performing 18F-FDG PET-CT were divided in 3 groups according to administered dose (2, 3 and 4 MBq/Kg) and an additional thoracic FOV was acquired with different acquisition times (30, 60, 90 and 120 seconds), reconstructed using VUE Point HD (4 iterations, 12 subsets, 6,4 mm filter) and Q.Clear using β values of 150 - 500, with a progressive increment of 50. These were evaluated for lesions SUVmax and lesion/background ratios and qualitatively by 5 experienced observers for overall image quality, noise level and contrast. **Results:** RC and CRC are higher for Q.Clear, especially for smaller structures when lower β values are used; for bigger structures, β value impact is less significant. For all different acquisition times, SUVmax values decrease as the β value increases, as well as injected activity increases, with no statistical significant difference. Lesion contrast ratios are higher with Q. Clear and β=350 when compared with VUE Point HD, but with no statistical significant difference for all image reconstruction sets. Qualitative evaluation shows better scores for images obtained with higher doses for, even if lower β values are used.

Conclusion: Study is still ongoing and preliminary results show that Q.Clear has a significant impact in lesion contrast and quantification. The optimum penalization factor of Q. Clear needs to adjusted according to the type of structure being studied, β values have more impact on small structures detectability and quantification.

E-TPW05

Studies on Scattered Radiation out of Field of View and Effect of Scatter Correction in 3D brain PET

M. Honda[1], Y. Sakuragi[2], S. Abe[2], N. Fujita[2], K. Kunimoto[1], T. Odagawa[1], K. Kato[1]; [1]Department of Radiological and Medical Laboratory Sciences, Nagoya University Graduate School of Medicine, Nagoya, JAPAN, [2]Department of Radiological Technology, Nagoya University Hospital, Nagoya, Japan, Nagoya, JAPAN.

Background and Purpose: It is known that scattered radiation out of field of view (FOV) increases random and scatter coincidence events which cause lowering of quantitativity and quality of images. In brain PET, distribution of radiopharmaceuticals in the body differs from each other and it may accumulate strongly in the trunk besides the brain. Therefore, when much higher radioactivity exists in the trunk compared to the brain, there is a possibility that scattered radiation out of FOV affects the image quality and the quantitative accuracy of PET images. In this study, we determined the influence of scattered radiation out of FOV at the detector which was located at various distances from the cylindrical phantom which mimicked the trunk on coincidence events and the standardized uptake value (SUV). In addition, we examined whether the effect of scattered radiation out of FOV was reduced by using the lead-made neck shield and scatter correction. **Materials and Methods:** We defined the radioactivity ratio of the brain phantom to the cylindrical phantom which mimicked the trunk as 1:24 and enclosed a solution of 18F into them. Distances between the brain phantom and the cylindrical phantom examined were 0, 10, 20, and 30 cm with or without a neck shield. PET data were reconstructed under the same conditions as used in a clinical setting with or without scatter correction. Square region of interest were drawn on the axial images and the average PET values were measured. Prompt coincidence and random coincidence for each acquisition condition were measured, and the ratio of random coincidence to prompt coincidence (%R) was calculated. In addition, SUV was calculated from measured PET values. **Results:** The maximum %R was 38.5%. By using the neck shield, %R improved by up to 15%. When the distance between the brain phantom and the cylindrical phantom was within 10 cm, SUV increased. Using the neck shield and scatter correction reduced SUV rise. **Conclusion:** When the cylindrical phantom was located out of FOV, there was the influence of scattered radiation out of FOV on coincidence events. When the distance between the cylindrical phantom and the detector was within 10 cm, there was the influence of scattered radiation out of FOV on SUV. Effect of scattered radiation out of FOV was reduced by using the lead-made neck shield and scatter correction.

E-TPW06

The measurement accuracy of analyzing software for PET/CT

S. Matsuzawa[1], S. Abe[2], Y. Sakuragi[2], N. Fujita[2], M. Honda[1], K. Kunimoto[1], R. Mukumoto[1], T. Odagawa[1], K. Kato[1]; [1]Nagoya University Graduate School of Medicine, Nagoya, JAPAN, [2]Nagoya University Hospital, Nagoya, JAPAN.

Purpose/Introduction: For positron emission tomography with 2-deoxy-2-[fluorine-18]fluoro-D-glucose integrated with computed tomography (^{18}F-FDG PET/CT), indices such as the standardized uptake value (SUV), metabolic tumor volume (MTV), and the total lesion glycolysis (TLG) are used to evaluate tracer accumulation. The indices are also used to evaluate the treatment response of malignant tumors. Differences in these indices may occur even with the use of the same PET scanner due to the different algorithms in the analyzing software programs. In this study, we examined the causes of these differences among four analyzing software programs. **Subjects & Methods:** Using a digital phantom, we measured SUV_{max}, SUV_{peak}, SUV_{mean}, MTV, and TLG of each intense accumulation were obtained with four different software programs such as syngo.via (Siemens), GI-PET (AZE), Metavol (Hokkaido University), and VOX-BASE II (J-MAC SYSTEM). The indices obtained with these four different software programs were compared. **Result:** About the same values for SUV_{max} were obtained with syngo.via, Metavol and Vox-BASEII. The SUV_{max} obtained with GI-PET was 3% lower than those obtained with the other three software programs. A thick slice is made by piling slices to make cubic voxels for GI-PET. Therefore, SUVmax is lowered compared with that obtained with the other three software programs because voxel values are averaged. Similar values for SUV_{peak} were obtained with syngo.via, metavol and Vox-BASEII. Differences in SUV_{mean}, MTV, and TLG were evident between GI-PET, syngo.via and the other software programs. Differences of volume data among software programs seem to occur due to the difference in the voxel size and the boundary of tumors. **Discussion/Conclusion:** The differences in the indices obtained with four software programs are attributable to varied handling of PET slice thicknesses, voxel size, and boundary of tumors. It is necessary to understand the characteristics of the software program prior to examination. The same software program has to be used for the follow up examinations of the same patients.

E-TPW07

Influence of Reconstruction Parameters on ^{18}F-FDG PET Activity Quantification in Small Objects: a Phantom Study

X. Liang[1], S. Han[1], X. Hu[1], L. Wan[2], P. Xiao[1], Q. Xie[1]; [1]Huazhong University of Science and Technology, WuHan, CHINA, [2]Raydata Technology Co., Ltd., Ezhou, CHINA.

Aim: The PET activity quantification is affected by the reconstruction parameters. The performance of parameter modification of different sizes of objects affects the use of quantitative in diagnosis and follow-up response to therapy. The aim of the study is to evaluate the influence of reconstruction method, smooth and iterations on activity quantification in objects of different sizes. **Methods:** All measurements were performed on six bar phantoms with inner dimensions of 0.5, 1, 2, 3, 4 and 10 mm in the image plane. The phantoms were filled with identical concentrations of ^{18}F-FDG solution. All data were obtained with a small animal PET system (Trans-PET BioCaliburn LH, from Raycan Technology Co., Ltd.). The data were collected with typical imaging protocol that is normally used for animal studies. Images were reconstructed using the standard parameters of 3D-OSEM method, 2 iterations with 12 subsets, Gaussian filter. Reconstruction was also performed using FBP and 3D-OSEM with 12 subsets and 1 to 20 iterations, with or without Gaussian filter. For each bar phantom, the maximum and average standardized uptake values (SUVs) were measured. The data analysis was also performed to values of resolution recovery coefficients (RC). **Results and conclusion:** With iteration increase, the maximum SUVs and RC values increased and tend to be gentle. The growth rate of these values of different object size were not consistent with the increased iteration. The smaller objects need more iteration. The maximum SUVs and RC values measured from data with Gaussian filter were lower than the without ones. The results of FBP and 3D-OSEM reconstruction method also existed differences.

E-TPW08

Activity Quantification of ^{18}F-FDG in the Presence of an Iodinated Contrast Medium

A. Svensson[1], B. Olsson[1], J. Oddstig[2], C. Hindorf[2], L. Jönsson[2,3]; [1]Clinical Physiology and Nuclear Medicine, Skåne University Hospital, Lund, SWEDEN, [2]Radiation Physics, Skåne University Hospital, Lund, SWEDEN, [3]Department of Medical Radiation Physics, Lund University, Lund, SWEDEN.

Introduction: The presence of an iodinated contrast medium could affect the attenuation correction of the PET image which would lead to an inaccurate quantification of the activity concentration and the SUV (standardized uptake value) within the volume. This would cause a problem after an extravasation of both an iodinated contrast medium and a radiopharmaceutical. The aim of the study was to investigate the influence on the activity quantification of ^{18}F-FDG in the presence of different concentrations of an iodinated contrast medium, with and without contrast compensation applied during the image reconstruction. **Subjects & methods:** Four different concentrations (0, 7, 35 and 70 mg iodine/mL) of an iodinated contrast medium (Omnipaque) diluted in water, were added into four 500 mL bottles with 20 MBq ^{18}F-FDG in each bottle. The image acquisition, with one bottle within the camera field-of-view at the time, was performed on a PET/CT (GE Discovery PET/CT 690), using a clinical low dose acquisition protocol (120 kV, 30-160 mA for the CT and 2 min/bedposition for the PET). The images were reconstructed with and without contrast compensation. The activity concentration of ^{18}F-FDG was deter-

mined from a centrally placed ROI in each of the images of the bottles. The quantified activity concentrations were corrected for decay and compared to the known activity concentrations. **Results**: The presence of the higher concentrations (35 and 70 mg iodine/mL) of iodinated contrast medium resulted in an overestimation of the activity concentration of ^{18}F-FDG by 35% and 50% respectively, when no contrast compensation was applied. When the contrast compensation was applied, the overestimation of the activity concentration decreased to about 10%. The lowest concentration of iodinated contrast medium (7 mg iodine/mL) did not affect the activity quantification significantly. **Conclusion**: This study shows that contrast compensation should be applied in the image reconstruction when a high concentration in large volumes of an iodinated contrast medium is present.

E-TPW09
Clinical Trial of PET VCAR and ROVER

N. G. Wolff[1], S. Parameswaran[2]; [1]Sydvestjysk Sygehus - Department of Radiology and Nuclear Medicine, Esbjerg, DENMARK, [2]Odense Universitetshospital - Department of Nuclear Medicine, Odense, DENMARK.

Purpose: The aim of this study is to investigate whether ROVER's PVEC is more beneficial for volume analysis in mm^3 and for FDG-uptake through SUV$_{mean}$ measurements in semiautomatic plotted 3D ROIs on local recurrence Cancer Mammae (C. mammae), than commercially recognized PET VCAR provided by GE Advanced Workstation. **Method:** The empirical data were divided into two parts in order to investigate the hypothesis on a NEMA-phantom and a retroperspective study including six spheres and 20 selected lesions. It applied for the selected lesions, that they had to be located in upper thorax and/or in the axillae. Furthermore the lesions were detected and visualized on both the image-materials from CT and PET. Both the patients and the NEMA-phantom were scanned on a GE Discovery STE (NEMA PET 2) and GE Discovery RX (NEMA PET 3). In the parametre-setting of the NEMA-phantom scanprotocols, dose modulation was deselected and the mA was set to 185, while the kV was set to 140. For analyzing the image materials, two softwares were used; PET VCAR and ROVER with and without a PVEC-algorithm. The software can from a semiautomatic plotted 3D ROI provide both volumemeasurements in mm^3 and SUV$_{mean}$-measurements. **Results:** The results from the volumemeasurements of the NEMA-phantom-scans, showed that the p-value between PET VCAR and ROVER$_{PVEC}$ was calculated to p=0,614 for NEMA PET 2 and p=0,219 for NEMA PET 3. For lesionbased analysis the p-value was p=0,300 between PET VCAR and ROVER$_{PVEC}$. The evaluation of the volumemeasurements showed, that there occurred no significant differences between a comparison of PET VCAR and ROVERPVEC in the volume quantification. In the SUV$_{mean}$-measurements the p-values were calculated to p=0,011 for NEMA PET 2 and p=0,024 for NEMA PET 3. The p-value for the lesions were p=0,000000247. In the analyses for the FDG-uptake, there was a significant difference in the comparison of PET VCAR and ROVER$_{PVEC}$. **Conclusion:** Our study reveals that ROVER$_{PVEC}$, was no more beneficial at quantifying the volume in mm^3 after a PVEC, than PET VCAR. However, significant difference was shown between PET VCAR and ROVER in regards to SUV$_{mean}$ measurements thus suggesting ROVER$_{PVEC}$ to be superior to PET VCAR in regards to these measurements. ROVER$_{PVEC}$ definitely has a potential in clinical use for analyzing the FDG-uptake through SUV$_{mean}$-measurements, because of the correction of PVE in the local recurrence C. mammae lesions. Therefore ROVER$_{PVEC}$ is more beneficial than PET VCAR for SUV$_{mean}$-measurements.

E-TPW10
Studies on the crosstalk rate in simultaneous myocardial imaging with dual radionuclides using cardiac focusing collimator

K. Kunimoto[1], S. Abe[2], N. Fujita[2], M. Honda[1], S. Matsuzawa[1], R. Mukumoto[1], T. Odagawa[1], K. Kato[1]; [1]Department of Radiological and Medical Laboratory Sciences, Nagoya University Graduate School of Medicine, Nagoya, JAPAN, [2]Department of Radiological Technology,Nagoya University Hospital, Nagoya, JAPAN.

Purpose: Recently, a cardiac focusing collimator (CF; variable-focus collimator) designed for myocardial imaging with ^{201}Tl has been developed and enables to acquire the SPECT data faster than conventional SPECT studies. Currently, in the simultaneous myocardial imaging with ^{123}I and ^{201}Tl, the conventional parallel-hole collimator has been generally used instead of CF. In the simultaneous myocardial imaging with ^{123}I and ^{201}Tl, there is an advantage that examination using two different kinds of nuclides can be simultaneously performed. But there is a disadvantage that scattering rays from one nuclide may be mixed into the energy window of the other nuclide, which may degrade the image quality by the nuclides. In this study, we investigated the crosstalk rate of CF in the simultaneous myocardial imaging with the dual nuclides in the phantom experiment. **Methods:** ^{123}I and ^{201}Tl were enclosed into the separate cylindrical phantoms. The SPECT data were acquired using low medium energy general purpose collimator (LMEGP) and CF. The regions of interest were taken on the short axis images. The total count was obtained by adding up the images of each slice, and the crosstalk ratio was calculated by comparing the total counts in the regions of each image. The crosstalk ratios were compared between before and after scatter and attenuation corrections. **Results:** The crosstalk ratio from ^{201}Tl to the energy window of ^{123}I is about 12% for both LMEGP and CF before attenuation and scatter corrections. After attenuation and scatter corrections, the crosstalk ratio was improved to 10.5% for LMEGP and to 7~9% for CF. The crosstalk ratio from ^{123}I to the energy window of ^{201}Tl was about 20.6% for LMEGP and 18~20% for CF. After attenuation and scatter corrections, the crosstalk ratio was improved to 9% for LMEGP and to 5~7% for CF. **Conclusion:** Without attenuation and scatter corrections, the crosstalk ratio from ^{123}I to ^{201}Tl was large and the influence of scattering rays from ^{123}I was larger than that from ^{201}Tl. However, the influence could be removed by attenuation and scatter corrections.

E-TPW11

NaI(Tl) and CZT-camera based detectors: comparison of image parameters

M. J. F. Sousa[1], D. Vieira[1], C. Alves[2], L. Santos[2], L. Olo[2], P. Oliveira[2], A. Nunes[2], F. Godinho[3,4], G. Cantinho[3,4], L. F. Metello[1,5]; [1]ESS-IPP, Nuclear Medicine Dept, Porto, PORTUGAL, [2]DCC – Dr. Campos Costa, Nuclear Medicine Dept, iCUF Institute, Porto, PORTUGAL, [3]Atomedical, Nuclear Medicine Dept., Lisbon, PORTUGAL, [4]Univ. Hosp. of Santa Maria, Nuclear Medicine Dept. – University of Lisbon, Lisbon, PORTUGAL, [5]IsoPor–Azores, Nuclear Medicine Dept., Angra do Heroismo, Azores, PORTUGAL.

Background: Since its invention by Hall Anger in 1952, the sodium iodine [NaI(Tl)] scintillator crystal coupled to an array of photomultiplier tubes, has been the dominant detector system for Nuclear Medicine Imaging. In order to overcome some of the intrinsic limitations of this kind of detectors, improve the diagnostic accuracy and reduce imaging acquisition times, new solutions based on semiconductor technology have emerged over the last decades. With the dramatic increase of computational power actually available, the application of advanced image processing algorithms became possible and it allowed to take the best advantage of the information contained in the detector signals acquired. The introduction of cadmium zinc telluride (CZT) detectors in the clinical setting has brought serious improvements to Nuclear Imaging including better spatial and energy resolution, together with higher sensitivity. **Aim:** To compare several aspects of systems performance, such as spatial and energy resolution, planar and tomographic sensitivity, image contrast and camera uniformity in cameras-based on CZT and NaI(Tl) detectors. **Methods:** Four different GE gamma cameras [one dedicated cardiac CZT system and three all purpose NaI(Tl) systems aging from 2 to 20 years old] were evaluated. Camera performance was assessed based on parameters such as energy resolution, planar uniformity, spatial resolution, system sensitivity and image contrast. The Guidelines on Quality Control for Nuclear Medicine Instrumentation (EANM, 2007) as well as manufacturer protocols had been used. All the tests were done using Tc-99m and have been repeated a minimum of three times. **Results and Conclusions:** Although the study is still ongoing, based on our preliminary results it has been observed improved performance for CZT detectors, comparing to NaI(Tl), particularly for energy resolution (one and a half fold increase, to approximately 5,70%), sensitivity (nearly eight fold increase) and spatial resolution (almost two fold increase, to about 5mm in clinical conditions). For the moment, the major drawbacks of the CZT detectors are related to its inherently high cost and its suboptimal performance when using medium and high energy gamma rays. The overall improved performance of CZT detectors for low energy radionuclides such as ^{99m}Tc, gives access to more accurate quantification and might either allows to lowering the exposition dose and/or shorter image acquisition times - one, other or both aspects, depending on the specific strategy being used, introducing new options for the optimization/personalization of the procedures being performed and increasing overall Diagnostic Quality, always for the best interest of the clinicians/patients involved.

E-TPW12

Impact of segmentation-based enhancement on conjugated gradient reconstruction system in bone SPECT imaging

K. Okuda, S. Fujii, S. Sakimoto, T. Ida, S. Moriyama; Tottori University Hospital, Tottori, JAPAN.

Purpose: A single-photon emission computed tomography (SPECT) reconstruction system based on ordered-subset conjugated gradient minimization (OSCGM) method, xSPECT Bone (Siemens Healthcare) features a novel algorithm using computed-tomography (CT) information as a zone-map, which segments into different tissue classes adapted for ^{99m}Tc diphosphonate bone SPECT. Although this technology has changed the concept of SPECT image innovatively, the physical characteristics of reconstructed images using zone-map enhanced OSCGM (OSCGMz), have not been evaluated yet. The aim of this study was to evaluate the effect of zone-map enhancement on SPECT images. **Methods:** Dipotassium hydrogenphosphate (K_2HPO_4) solution was used to simulate the zonal mapping and absorption by bone tissue. A compartment phantom, consisting of a non-radioactive water section, and 3 other radioactive sections supplemented with 80.4 kBq/ml of ^{99m}Tc solution containing different concentrations of K_2HPO_4 or pure water, was scanned. The SPECT data were reconstructed at varying updates from 1 to 90 using two methods: zone-map enhanced and non-enhanced OSCGM. We compared the performances of two reconstruction methods using percentage error (%error), coefficient of variation (%CV), normalized mean squared error (NMSE), and profile curves. **Results:** In the bone equivalent compartments, the %error and profile curves of OSCGMz tended to converge to the same values at lower updates compared with that of OSCGM. This tendency was noticeable in the compartment with higher concentration of K_2HPO_4: the convergence of %error for OSCGMz was obtained with very few updates, while that for OSCGM necessitated over 10 updates. OSCGMz and OSCGM both yielded low NMSE values at updates of 20 and 30, respectively. The %CV in the water equivalent compartment for OSCGMz (20 updates) was 14.90 %, and the corresponding value for OSCGM (30 updates) was 18.63 %. The edge artifacts, which were observed in OSCGM with increasing update number, were mitigated in OSCGMz. **Conclusions:** The enhancement with zone-mapping contributes to SPECT reconstruction for reproducing the radioactive concentration of bone tissues, with a lower number of OSCGM updates. Moreover, the enhancement has the effect of mitigating the degradation of uniformity and reduces the occurrence of edge artifacts on SPECT images.

E-TPW13

Scintigraphy of the nasal cavity and maxillart sinuses

M. M. Joergensen; Rigshospitalet, Copenhagen, DENMARK.

Aim: Patients with cystic fibrosis (CF) have reduced mucociliary clearance which predisposes for chronic sinusitis often with *Pseudomonas aeruginosa* infection. Some patients are treated

with nasal irrigation of antibiotics, however, it is not known if the drug distributes to the inflamed sinuses. The aim of this study was to develop a scintigraphy method that assesses whether during nasal irrigation there is penetration to the maxillary sinuses. **Materials and Methods:** 15 adult CF patients (6 females) were referred for the study that was performed after training the nasal irrigation procedure. A 2 min static image of a Co-57 marker placed outside each temporal bone was obtained. Nasal irrigation was performed sequentially through both nostrils of 200 MBq 99mTc-albumen colloid (Venticoll) in 240 ml isotonic saline with Sinus Rinse kit. Then the patient was placed on the gamma camera couch with the head fixed with a vacuum sac. Dynamic SPECT/CT was performed (one 50 mAs low dose CT and 4 sequential continuous mode SPECT each as 2*64, 8 sec projections in a 128 *128 matrix, with LEHR-collimators and 140 keV (20% width) energy windows. Attenuation and scatter correction was performed together with Astonish reconstruction (4 iterations, 16 subsets). After imaging a final nose irrigation with saline was performed before the patient left the department. **Results:** 13 patients (5 females) were examined, while two were excluded. One did not show up for the examination, while one patient had severe motion artefacts during the SPECT, so both SPECT reconstruction and alignment with CT was suboptimal. SPECT showed retention of radioactivity in the nasal cavity in all 13 patients. Eleven had penetration to the maxillary sinuses, while in two patients no retention was seen in either sinus maxillaris. **Conclusion:** The scintigraphy technique was feasible in almost all CF patients trained with the irrigation technique. Most but not all patients had drug penetration to the maxillary sinuses after nasal irrigation.

E-TPW14

A novel automatic gamma function fitting program of the time activity curve for the input function determination in the ^{99m}Tc-ECD non-invasive quantification method

Y. Tanaka[1], Y. Uchiyama[2], A. Takaki[3], S. Ito[2]; [1]Graduate School of Health Sciences, Kumamoto University, Kumamoto, JAPAN, [2]Faculty of Life Sciences, Kumamoto University, Kumamoto, JAPAN, [3]Teikyo University, Omuta, JAPAN.

Purpose: A new non-invasive semi-automatic quantitative measurement method, the improved brain uptake ratio (IBUR) method using ^{99m}Tc-ECD single photon emission computed tomography (SPECT), was recently reported. Additionally, an automatic region of interest (ROI) setting algorithm was developed to determine the input function for the ^{99m}Tc-ECD IBUR method. If an automatic gamma function fitting algorithm of a time activity curve (TAC) analysis for the ^{99m}Tc-ECD IBUR method can be developed to determine the input function, then the analysis of regional cerebral blood flow (rCBF) can be completed within a few seconds by using a fully automatic rCBF analysis program without requiring complex techniques. The purpose of this study was to develop the automatic gamma function fitting program for the ^{99m}Tc-ECD IBUR method, and to confirm the feasibility of use of this program. **Materials and Methods:** The gamma function fitting program for determina-

tion of the input function owing to mixed gamma distributions was developed by an expectation-maximization algorithm that analyzed a time activity curve of a chest radio isotope (RI) angiogram. The program was validated by using patient images obtained by different two SPECT scanners. The images of 15 consecutive patients who underwent both ^{99m}Tc-ECD chest RI angiography and SPECT examinations were used to develop an automatic arterial input function program. The images of 55 consecutive patients were used to validate the program. **Results:** The coincidence ratio between the automatic method and the manual setting method was approximately 98%. Individual integrated values of the TAC obtained using these independent techniques were reasonably well correlated (r = 0.99, p < 0.0001). Individual rCBF values obtained using these independent techniques were also reasonably well correlated (r = 0.95, p < 0.0001). The mean difference of the input function value was ±5.8%. Individual rCBF values obtained using these independent techniques were also reasonably well correlated (r = 0.94). Repeatability and reproducibility of the input function determination operations was completely improved by using the automatic program. The time for the fitting analysis using the automatic method is 2-3 s as compared to 5 min for the current analysis method. The total time for the IBUR analysis using the automatic method is 20-30 s as compared to 5-6 min for the current analysis method. **Conclusion:** The high repeatability and reproducibility of the automatic program can contribute to facilitation of the objective input function analysis for the ^{99m}Tc-ECD IBUR method.

E-TPW15

Examination of quantitative bone SPECT images by digital phantom using the anatomical normalization template

A. Kikuchi[1], G. Okuyama[1], S. Kumazawa[1], M. Kitama[1], K. Miwa[2], K. Kawakami[3]; [1]Hokkaido, Sapporo, JAPAN, [2]Tochigi, Ootawara, JAPAN, [3]Tokyo, Cyuouku, JAPAN.

Purpose: Various methods for quantification have been developed using bone SPECT data. In the quantitative method we are currently developing, anatomical normalization using the bone SPECT template and calculate the quantitative value. Therefore, the purpose of this study is to examine the change of simulated tumor lesion size by anatomical normalization in bone SPECT image. **Subjects Methods:** We used a digital phantom (XCAT) which can obtain known quantitative data. We created a skeleton digital phantom of normal accumulation assuming 99mTc-MDP SPECT / CT with three mm pixel size. In addition, we created a template of bone SPECT and normalized the digital phantom to apply it to that template. The bone SPECT template was prepared by three mm digital skeleton phantom CT dataset that was registered. In order to make a comparative study, we set simulated tumor lesions as digital phantoms. We examined whether the size of the lesion differed pre- and post- registration. The validate to be examined were lesion size and location with abnormal accumulation. We examined was as follows, the focal lesion that size was 10 mm, 15 mm and 20 mm. and the location of abnormal focal

lesion set on L4 and pelvis. For co-registered and normalized of these data's, our material used statistical parametric mapping 8 (SPM8) software. For acquisition simulation software, we used SIMIND software. The acquisition condition setting were 128 x 128 matrix, 90 view, 144 counts / pixel and 3mm/pixel. **Results:** The tumor size pre- and post- anatomical normalization showed a good correlation (R = 0.93 p <0.05) Furthermore, similar results were shown i n the difference position of tumor. **Conclusion:** In this study, changes in simulated lesion due to registered were not affected and it was shown that there was no problem in quantitative value for calculate.

E-TPW16
An exploation of the time range selection for SPECT to calculate the GFR value

Y. Wang, M. Liu; *Department of nuclear medicine Fudan University, Shanghai, CHINA.*

Objective: In the Gates process of calculating the GFR value, the radiation data of 2 to 3 minutes after injection is used to calculate the final GFR value. A retrospective analysis was carried out to verify the effectiveness of 2 to 3 minutes. The peak of GFR can represent the peak of glomerular filtration, which indirectly reflecting the renal function. It is necessary to explore a more appropriate point in time. **Methods:** Siemens SPECT/CT Symbian T16 data were retrospectively analyzed from January 2015 to March 2017 using ^{99m}Tc-DTPA 5mCi, and GFR data was processed by a single technician. Take the GFR value greater than 90ml/min data as the representative of the normal renal function into the analysis. All GFR value of Group A was greater than or equal to 100ml/min, and the value of Group B was between 90 ml/min to 100ml/min. The peak value of these two groups were analyzed. The data was chosen to take 30 seconds before and after peak time or 0 to 1 minute data to do the analysis (if the peak appears in 30 seconds). The original data was automatically analyzed of the area of interest, no manual intervention. **Results:** A total of 94 data were eligible, including 63 patients (aged 42.43±7.94 years old) in Group A and 31 patients in Group B (age 37.83±11.54 years old). Peak of Group A occurred before 30 seconds (including 30 seconds) in 11 cases, and the peak time of other 52 cases were 2.24±0.34 seconds. Group B peak appeared in 30 seconds (including 30 seconds) was 7 cases, and the remaining 24 cases peak time was 2.64±0.59 seconds. Both GFR value were recalculated and line paired t test was performed. Group A GFR value peaked within 30 seconds (t=-0.942 P=0.368), the remaining (t=0.962 P=0.340). Group B GFR value peaked within 30 seconds (t=-0.588 P=0.578), the remaining (t=0.606 P=0.550). There were 19 cases more than 20% deviation in Group A with the original GFR value, 14 cases in Group B. **Conclusion:** Due to GFR acquisition conditions, the GFR peak in some data will appear within 30 seconds. From the study, most people with normal renal function GFR peak in 2 to 3 minutes, part of the data before and after taking the peak 30 seconds to calculate the GFR value will have more than 20% impact on the GFR. The next step is to study the data of abnormal renal function.

E-TPW17
Evaluation of SPECT/CT Image Applying to Three-Dimensional Printing Phantom

J. Lee[1], H. Park[2]; [1]Songho College, Gangwon-do, KOREA, REPUBLIC OF, [2]Shingu College, Seongnam, KOREA, REPUBLIC OF.

3D printing technology is a manufacturing technology which processes digital data acquired through 3 dimensional modeling [1]. It allows various use in the field of medicine, but the use of it in nuclear medicine is inactive. We will utilize quality control phantom through 3D printing technology in nuclear medicine. By manufacturing PMMA and ABS phantoms, compared between existing phantom and 3D printing phantom through quantitative analysis. Therefore, this study evaluates the utility as phantom in medical field of nuclear medicine using 3D printers. To measure the change of radiation transmittance according to the quality of the material, PMMA phantom and ABS phantom were manufactured according to the actual size of Aluminum wedge step. We used SPECT/CT BrightView XCT, and acquired SPECT image by conditioning 128x128 matrix, 60 minutes acquisition time, Astonish reconstruction method. We used ^{99m}TcO$_4$ cylinder phantom with 0.5 Bq/ml specific activity and inserted each wedge step phantom. Results of analysis of Aluminum, PMMA and ABS phantom in planar gamma image, as the step thickness increased, the mean counts deceased. When comparing the radiation transmittance of ABS and PMMA phantom, it shows a small difference. Analysis of Aluminum, PMMA and ABS phantom in SPECT/CT image, overall Computed Tomography Attenuation Correction(CTAC) data was measured higher counts for Region of interest(ROI) of phantoms and background counts than Non Attenuation Correction(NAC). And as the step thickness increased, the ROI mean counts of phantom decreased until the 4th step. On the other hand, it showed a linear trend from the 5th step. In this study, we analyzed material characters with 3D printing technology for active quality control of nuclear medicine.

E-TPW18
Quality control on DIGIRAD Solid state X-ACT camera: the role of the technologist

S. Sustar, S. Rep, B. Trebec, B. Simonic, I. Slodnjak, L. Lezaic; *Department of Nuclear Medicine, Ljubljana, SLOVENIA.*

Intriduction: Solid state cameras use an array of individual detection elements each of which could change in sensitivity. Such local changes can result in a differential uniformity problem. However, once uniformity is calibrated, the integral uniformity of solid state detectors is typically very stable. In routine work it is necessary to perform the following QA procedures: Daily Uniformity QC, Weekly COR QC, Weekly co-registration QC of emission and tranmission scan, Daily blackscan. **Aim:** The purpose of our presentation is to describe and explain the results of the analysis of QC on DIGIRAD Solid state X-ACT camera. **Material and Methods:** From the beginning of the use the X-ACT camera, technologists were responsible to perform QC.

The Daily Uniformity QC floods are typically done with Co57 or Tc-99m and 3M counts are acquired on each detector head. A bed uniformity will show bad pixels or modules in the raw projections or sinogram. Acceptance criteria are Integral uniformity (IU) of <6% and differential uniformity (DU) <4%. A weekly COR study is performed by using Tc-99m point sorce and acquring a 64 projections, 180-degree study. A visual analysis is done of the sinogram and the reconstruction data. Any discontinuities in the sinogram or a y-shaped reconstructed COR image is an indication of an incorrect COR. Weekly co-registration QC of emission and transmission scan requires Tc-99m source in three syringes with equal activity (5-35mCi) in a volume of at least 1mm3. The three syringes are placed in the co-registration and emission and transmission phantom data are acquired. The QC will pass if the difference between the saved and calculated values is <3 mm for X and Y axis and <3 mm for Z axis. **Results:** The median IU and DU for detector-1 was 3.33 (min 2.96 max 8.52) and 2.49 (min 2.2, max 6.37), detector-2; 3.69 (min 3.06, max 9.01) and 2.81 (min 2.36, max 7.33) and for detector-3; 2.49 (min 3.34, max 12.31) and 2.93 (min2.57, max 7.67). The uniformity tests were below acceptability when we used 99mTc-MIBI instead of 99mTc-pertechnetate and a non-uniform distribution ocurred. The weekly co-registration QC tests and the visual analysis of weekly COR study confirmed normal results. **Conclusion:** In our experience solid state detectors are typically very stable. For quality examinations it is necessary to carry out the recommended QC tests.

E-TPW19

SeHCAT measurents of bile acid retention using a collimated gamma camera

M. Lorentzson, P. Fransson, A. Larsson; Umeå University, Umeå, SWEDEN.

Introduction: At Umeå University Hospital, [75]SeHCAT retention is measured using a fixed setup, with one anterior and one posterior 3-inch NaI-detector, connected to a single channel analyser system. The method needs however to be revised, preferably using a gamma camera. At many sites, SeHCAT retention is measured with an uncollimated gamma camera, but such a setup is very sensitive to a varying background. Our department includes a PET facility, and using collimators would therefore be advantageous. A few published studies have compared uncollimated and collimated cameras for SeHCAT, but to our knowledge, a comparison of stationary detectors and collimated cameras has not been performed. The aim of this study is to investigate the possibility of replacing the current method and machinery with a collimated alternative. **Material and Methods:** First, energy settings for the gamma camera, GE Infinia Hawkeye 4, were optimised and the spatial variations in sensitivity of both systems were investigated. Then SeHCAT patients were included in the study. Five have agreed to participate so far, and at least five more are planned. At Umeå University Hospital, the routine is to administer the SeHCAT capsule (370 kBq), and perform measurements over the umbicilus at 24, 48 and 72 hours post-administration. The geometric mean values of the anterior and posterior background corrected measures are then fitted to an exponential, to estimate the biological half life. The gamma camera was equipped with LEGP collimators and measurements were performed for 10 minutes. For each patient, the results from the two systems were compared. **Results:** The overall sensitivity for the detector system is higher than for the collimated gamma camera, but is as expected much more spatially varying. For the patients considered as pathological (2 of 5), the differences in half-lives were small (33 vs 36 and 14 vs 16 h) showing the detector results first. The corresponding results for the patients considered normal were more varying (202 vs 170, 88 vs 87 and 324 vs 150 h). Correlation coefficients were higher using the new method and no patient was diagnosed differently. **Conclusion:** The differences may be attributed to the difference in field of view, and spatial variations in sensitivity. The collimated gamma camera is less sensitive, but shows a better correlation to the fitted exponential. We think that the new method shows potential, but further comparisons are required and more patients will be included in the study.

E-TPW20

Comparison of different Attenuation Correction methods in DaTscan examination

*F. H. Gomes[1], **M. F. Soares[1]**, F. Brolund[2], A. Danielsson[3], L. Vieira[1]; [1]Lisbon School of Health Technology, Lisbon, PORTUGAL, [2]Karolinska Institutet, STOCKHOLM, SWEDEN, [3]Karolinska Universitetssjukhuset Solna, STOCKHOLM, SWEDEN.*

Aim: This project was developed in order to understand if there are differences in DaTscan appraisal (visual and quantitative assessments) using two different methods of attenuation correction (AC): Uniform (Chang method) and non-uniform (Computed Tomography (CT)). The blinded study compromises of two operators being clinically inexperienced Nuclear Medicine (NM) students. Furthermore, it was verified if there is any significant difference inter-operators' assessments and then, the visual assessment between the operators and doctor's report was compared. **Introduction:** The idiopathic Parkinson's disease is a neurodegenerative disease in which the dopaminergic transporters (DAT) are degenerated. DaTSCAN™ allows localizing and measuring DAT´s concentration. The attenuation phenomenon can cause artefacts in the acquired images leading to several misinterpretations. The Chang method considers the brain as a linear volume. Whereas, the CT method obtains an attenuation coefficient map. The increased use of hybrid gamma cameras (SPECT/CT) has replaced the use of the Chang method by getting a CT map. However, as the brain is a linear volume, the Chang method is still sustained in performing the examination without an extra radiation dose for the patient. **Methods:** A retrospective cohort of 15 patients (mean age 64.7) were included in this study. These patients underwent a diagnostic DaTSCAN™ examination (SPECT/CT). For each patient, the SPECT images were reconstructed with standard OSEM with CT based AC and Chang. The two sets of reconstructed images were then transferred to HERMES work station and analyzed using the quantitative BRASS software

where volume of interest were draw. The quantification of the DAT was calculated through the specific binding ratio (SBR) of the radiopharmaceutical. The visual assessment was based on two different criteria "normal" or "abnormal". **Results:** Regardless to the quantitative assessments, the operator 1 found significant differences between the methods and the operator 2 found no significant differences (p>0,05). In the quantitative assessment, the only significant difference inter-operator was with Chang's method in the left basal ganglia (p=0,039). In the Kappa analysis, there is an almost perfect agreement on the visual assessment between inter-operators and with doctor's report. **Conclusion:** The attenuation effect must be considered and properly minimized in order to get an accurate assessment. It is not possible to conclude if both methods are reliable to do a correct quantitative assessment. A database with reference values would further help to make a solid conclusion about the veracity of the obtained results. However the results obtained with the visual assessment are optimist.

Technologist e-Poster Session 2

E-TPW21

Accuracy of the F-18 Calibration Factor in a Capintec Calibrator

S. Taştan[1], S. Tanriverdi[1], E. Ozdogan[1], N. O. Kucuk[2]; [1]eczacibasi Monrol Nuclear Products, Ankara, TURKEY, [2]Ankara University, Ankara, TURKEY.

Introduction: A dose calibrator is one of the most important instruments in a radioisotope production and imaging center since it is crucial to give the right amonut of activity to the patient. The calibrator is well-type ionization chamber, which has long term stabillity and can measure activity to the desired level of accuracy. However, it is sensitive to even small changes in geometry, container type, density and volume of samples. **Method:** We used a (68)Ge/(68)Ga reference standard source (RADQUAL) to determine correction factors in Capintec CRC55rPet. Reference standard is the only direct NIST (National Institute of Standards and Technology) traceable dose calibrator standard for Ga-68 and F-18 available to relate the measurements of the Ge-68 reference standard in the activity calibrators to a measurement of F-18 solution in the same geometry. In our study; Ge-68 and F-18 were calibrated with RADQUAL Ge-68 solution. Routine F-18 dispending vial was used in calibration. (Type I with 1.0 mm wall thickness). During the transfer to vial, necessary amount of carrier solution was added to bring the final solution to original mass in syringe. **Results:** Calibration factors were 0.7301, 1.0058 and 1.0051 respectively for reference standard solution (Ge68), reference standard solution and for F-18 and routine vial. GUM (ISO Guide to the Expression of Uncertainty in Measurement) was used to analyse all uncertainty components. Readout activity which is obtained from dose calibrator must be multiplied by a correction factor in order to reach the correct activity. **Conclusion:** This study demonstrated firstly that: it was incorrect to use the manufacturing preset nuclide values in assaying Ga-68 and F-18 on the ion chamber. Secondly; dose calibrator measurements are sensitive to small changes in container type and geometry although total mass is the same.

E-TPW22

Resurrection and return to the technological cycle of enriched Molybdenum-98 from liquid waste produced by technetium-99m generators

A. Rogov, E. Stasyuk, E. Nesterov, E. Ilina, V. Sadkin, L. Larionova; National Research Tomsk Polytechnic University, Tomsk, RUSSIAN FEDERATION.

Introduction: In the production of sorption generators of technetium-99, highly enriched molybdenum-98 was used, which partly goes to liquid waste. The average market price of 1mg of molybdenum-98 enriched to 98.6% was $2.5 - 4 in 2014-2015. The activation of molybdenum-98 occurs in nuclear reactors according to the radiation capture reaction (n,γ). The radionuclide molybdenum-99 used for the production of diagnostic radionuclide technetium-99m is formed at the process of neutron irradiation of molybdenum-98 target. To produce molybdenum-99 it is consumed less than $2 \cdot 10^{-3}$% of the total mass of molybdenum-98 located in the irradiated target. The other part of expensive molybdenum-98 goes to liquid waste. For the production of technetium-99m generator, with the specific power activity 19 Gbq, 120-130 mg of activated molybdenum-98 is used. **Aim:** To reduce prime costs of technetium-99m generators produced by the technology of sorption concentration it is necessary to develop technology of molybdenum-98 extraction from liquid waste. **Methods:** To extract molybdenum-98 we studied different procedures of molybdenum-98 concentration and attempts of its precipitation as salt. The sulfide procedure of molybdenum-98 deposition was more successful. The extraction procedure includes the stages of the regenerant solution formation, the MoS_3 obtaining by means of thiosalt intermediate compounds and further heat treatment up to trioxide molybdenum-98 formation. **Results:** The conducted set of studies allowed to find the sequence of waste processing stages. We found the optimal concentration of molybdenum-98 alkaline solution, which allows to obtain molybdenum-98 thiosalt with the maximum substitution of oxygen by sulfur atoms. Further the thiosalt saturation by hydrogen sulfide excess and the subsequent acidification of the solution by hydrochloric acid allows to achieve molybdenum-98 extraction at the rate of 98%. The solution purification from the precipitated impurities of other metals occurs at the conducting of intermediate stage. The molybdenum trisulfide formed at solution processing is extracted from the solution by the filtration using filters with pore diameter of no more than 5 mkm. At final stage of molybdenum-98 extraction we carried out the stepwise heating of molybdenum trisulfide to 600°C which allows to obtain the final product as molybdenum-98 trisulfide. **Conclusions:** The developed pro-

cedure of the molybdenum extraction from liquid radioactive waste can be used to increase production profitability and to reduce the prime cost of technetium-99m generators. The molybdenum-98 extraction procedure can be applied for extraction of other isotopes molybdenum, for example ^{100}Mo used for obtaining ^{99m}Tc at the cyclotron.

E-TPW23

Determination of radioquimic purity (RCP) of 99mtc-Tektrotyd with an alternative chromatographic method

E. López Martínez, J. L. Gómez Perales, E. Ariza Cabrera, F. Martín Estrada; SAS, Algeciras, SPAIN.

Aim: To verify the validity of a new chromatographic system for the determination of the 99m-Tc-Tektrotyd radiochemical purity measurement (RCP) taking as reference the standard method. **Material/Methods**: Thirty vials of Tektrotyd were prepared according to the instructions in the technical data sheet. Alternative method proposed: stationary phase: paper chromatography (Whatman 17) and mobile phase: methyl-ethyl ketone (MEK) and Methanol: Water (1:1). Thirty different batches were used and three quality controls were made to each sample: the first at the beginning of the marking, at 3 hours later and at 6 hours after marking. **Results:** The values obtained are expressed in % RCP ± standard deviation (SD). Stationary phases: ITLC-SG / MEK: t = 0: 98.75 ± 0.26; T = 3h: 98.49 ± 0.12; T = 6h: 97.05 ± 0.06; W17 / MEK: t = 0h: 98.47 ± 0.32; T = 3h: 97.62 ± 0.77; T = 6h: 97.1 ± 0.22. Mobile Phases: ITLC-SG / ACNW: t = 0: 99.08 ± 0.66; T = 3h: 98.58 ± 0.62; T = 6h: 98.32 ± 0.10; W17 / MEK: t = 0h: 99.07 ± 0.47; T = 3h: 99.35 ± 0.33; T = 6h: 98.27 ± 0.33. **Conclusion:** The results obtained reflect an alternative to the method established in the datasheet for its similarity in values and can be established as a routine method in our unit, to offering the advantages of paper chromatography and the use of less toxic solvents.

E-TPW24

Comparison between two different methods for radionuclide purity determination in the first eluate of a 99MO/99mTc generator

A. Bassan, M. C. Marzola, C. Secchiero, A. Patrian, S. Cittadin, T. Tinazzo, A. Ferretti, A. Massaro, S. Chondrogiannis, D. Rubello; Nuclear Medicine - PET/CT centre, Santa Maria della Misericordia Hospital of Rovigo, Rovigo, ITALY.

Introduction-Aim: The radionuclide purity quality assurance must be performed on the first eluate coming from 99Mo/99mTc generator and, according with the Italian Quality Assurance System (Norme di Buona Preparazione dei radiofarmaci, NBP), the percentage of the 99Mo impurities must be less than 0.1%. Two methods are currently available for this quality control: gamma spectrometry (method A) and measure with dose calibrator (method B), differing in terms of times and technical approach. The aim of our work was to evaluate and compare the results of the two methods, applying they both to a series of consecutive "first eluates" and including "qualita-

tive" and "quantitative" parameters. **Materials and Methods:** From January to September 2016, all the 63 eluates obtained from 99Mo/99mTc generator underwent to a double quality assurance, with both gamma spectrometry and dose calibrator methods. The two methods have been compared in terms of times at which the control have been made (just after the eluition, or later) modalities of execution, technical involvement and radioprotection issues. Moreover, the results obtained with the two methods were quantitatively compared with the cut-off value proposed by the Quality Assurance System (less than 0.1% of 99Mo impurities). **Results:** Both methods have been considered simple to perform, by the technicians. Method A was performed 30-36 hours after the eluition (after 3-4 99mTc, trying to reduce the Tc interference in the gamma-count of 99Mo decay, but also after radiopharmaceutical labeling), while method B was performed just after the eluition (thus, before labeling, according to the NBP), but technician has to manipulate a relatively high activity (35000-40000 MBq). In all cases, the 99Mo percentage measured in the eluate was lower than the cut-off value (0.1 %), with small, not significant differences. **Conclusions:** The two analyzed methods, even if relatively different by a technical and practical view, can be both considered useful in the clinical practice. Moreover, with method B the radionuclide quality assurance can be performed before labeling, according to the NBP, allowing a high safety for the patient. Nevertheless, method A has been demonstrated reliable enough and it can replace the other one, if it couldn't be used, for different reasons.

E-TPW26

Action protocol in breaking the cold chain in cold kits thermolabile

E. López Martínez, E. Ariza Cabrera, M. Cardoso Rodríguez; SAS, Algeciras, SPAIN.

Aim: to development and to implementation an operating standard procedure in case of breaking the cold chain in the conservation of thermolabile cold kits.**Material/Methods:** Cold kits thermolabile are included in the pharmacotherapeutic guide Unit Radiofarmacia, they were selected and data sheets as well as the information provided by a different pharmaceutical laboratories where the term of validity are collected at room temperature that allowed us to classify them into categories and they are reviewed an action protocol in each case. **Results:** The protocol was to establish a monitoring system of the products concerned and to discard or to return to the laboratory if exceeded the limit of time or temperature in each category. The steps were:1.To calculate the number of hours during which they have remained outside the set range and the temperature at which they have been exposed since the last reading recorded: A) If the fault has been <10hour and the refrigerator door has been closed and have been preserved inside bottles of saline: the kits can be used (refrigerators are trained to maintain internal tempera) .B) If the failure was> 10hour or have obtained records out of range, you should check involvement of medication depending on the temperature reached and the exposure

time.2. Conduct an inventory of the kits with their respective lots.3. To check the list of stability thermolabile kits: They were classified into the following categories: A (stable ≥ 28days at 25 ° C): LyoMAA, Pulmocis, Macrotec, Vasculocis, DMSA, Osteomicis, Stamicis, Pentacis, Phytacis, Nanocoll, Macrotec, Nephromag; B (stable ≥ 7 days a week at 25 ° C): Technegas HDP, Technegas PYP, Technegas MAG3; C (stable ≥ 48 hours at 25 ° C): Renocis, Scintimun, Angiocis, Nanocis, Myovieu, Zevalin.4. Record in the event log and discard those that can not be used and label those that can cause problems. **Conclusion**: With this protocol we have managed to establish recommendations to follow in case of breaking of the cold chain and facilitate a rapid action in this type of situation.

E-TPW27

Creation of a labeled technetium-99m colloid drug for the detection of guarding lymph nodes

A. Rogov[1], *E. Stasyuk*[1], *E. Nesterov*[1], *E. Ilina*[1], *V. Sadkin*[1], *L. Larionova*[1], *V. Chernov*[2,3]; [1]*National Research Tomsk Polytechnic University, Tomsk, RUSSIAN FEDERATION,* [2]*Tomsk Cancer Research Institute, Tomsk, RUSSIAN FEDERATION,* [3]*National Research Tomsk Polytechnic University, Tomsk, AUSTRIA.*

Introduction: Lately the interest to use of radioactive colloidal nanomaterials in medicine has been grown. They found their application for labeling autoleucocytes, to carry out lymphoscintigraphy and to identify "sentinel" lymph nodes. The most suitable radionuclide for labeling nanoparticles is short-lived technetium-99m, which is today used for diagnosis in almost all areas of medicine. Preliminary studies have shown that stable colloidal compounds can be obtained by a simple way by means of adsorption of reduced technetium-99m on gamma-aluminum oxide. Selection for the use of aluminum oxide as a carrier of technetium-99m is its low toxicity and good adsorptive properties, availability, and low cost. At the same time, a crucial factor for success is not their chemical composition, but the size of nanoparticles. **Aim:** Obtaining suitable for tagging with technetium-99m aluminum nanopowder with particle size in the range of 50-100 nm. **Methods:** As the object of study the was used nanopowder gamma-oxide Al_2O_3. It prepared from nanopowder of aluminum hydroxide by its was gradually heating to 400°C for 2 hours. The particle size was determined using electron microscope Philips SEM515. The average particle size is in the range of 100-200 nm. Before the adsorption technetium-99m on oxide Al_2O_3 it was carried out acidizing. In this regard, were found the optimal conditions of oxides acidizing which maximum adsorption of ^{99m}Tc. The maximum of radionuclide adsorption is observed on oxide treated with HCl in an amount of $2 \cdot 10^{-4}$ mol/g. Technetium-99m presenting in the original eluate in the highest degree of oxidation (+7) and does not have a sorption capacity. Therefore, research was made to of reduced technetium-99m in lower degrees of oxidation (+5) and it is more chemically active. To of reduced technetium-99m we used Tin(II) chloride dihydrate ($SnCl_2 \cdot 2H_2O$). When carrying out the synthesis of the drug used ultrasonic and vial with preparation was heated in a water bath (70-80°C) for 30 min. In a finished pharmaceutical the particle size was determined by photons cross-correlation spectroscopy using analyzer of particle size Nanophox produced by company «Sympatec GmbH» **Conclusions:** The measurement showed that 85% of the particles are in the range of 95-150 nm. These figures confirm suitability of the drug and the feasibility of conducting trials of the drug on laboratory animals in accordance with the European Convention for the Protection of Vertebrate Animals used for Experimental and other Scientific Purposes.

E-TPW28

A method of DOTA-SP90 with ^{111}In labeling, has stability and potential for breast cancer imaging

S. Lee, *S. Lo, Y. Huang, M. Chen, M. Li, C. Chang; Institute of Nuclear Energy Research, Taoyuan, TAIWAN.*

Background: A new targeting peptide SP90, was identified by phage display, and has improved can binding the cell surface of breast cancer. We use SP90 peptide linked with 1,4,7,10-tetraazacyclododecane-N,N′,N″,N‴-tetraacetic acid (DOTA) as an new precursor. This precursor can be radiolabel with different kind of radionuclide for diagnosis or therapy purpose. The aim of this study was to find an111In labeling method of DOTA-SP90, and has good stability for breast cancer animal model imaging. **Method(s):** Quality control of DOTA-SP90 precursor were >90% by High-performance liquid chromatography (HPLC). DOTA-SP90 precursors were dissolved in 1M Sodium acetate pH6. $^{111}InCl_3$ in 0.01N HCl was from Institute of Nuclear Energy Research. The reaction mixture were performed in 300μL volumes, heating at 95℃. The labeling yields of >95% were achieved within 10min. The stability of ^{111}In-DOTA-SP90 product in normal saline and rat plasma were analyzed at 0hr, 1hr, 2hr, 4hr, and 24hr. The radiochemical purities of ^{111}In-DOTA-SP90 in normal saline were analyzed by radio-HPLC, in rat plasma were analyzed by radio instant thin-layer chromatography (ITLC). **Result(s):** The radiochemical purities of ^{111}In-DOTA-SP90 in normal saline after 0hr, 1hr, 2hr and 4hr were 98.5%, 98.4%, 97.7% and 95.6%. The radiochemical purities of ^{111}In-DOTA-SP90 in rat plasma after 0hr, 1hr, 2hr, 4hr were all >95%.No matter in normal saline or in rat plasma after 24hr, the radiochemical purities all reduced to 70%. ^{111}In-DOTA-SP90 has stability in plasma after 4hr, this time can be used for breast cancer animal model imaging timing and enough to complete the cancer binding imaging. **Conclusion:** We demonstrated that ^{111}In-DOTA-SP90 has good stability in normal saline and rat serum. ^{111}In-DOTA-SP90 show specific binding ability of cancer cell in several breast cancer animal models. ^{111}In-DOTA-SP90 has potential to become a new radiopharmaceutical for breast cancer imaging.

E-TPW29

Dynamic in vivo molecular imaging of ^{18}F-INER1577 in transgenic mice

M. Li[1], *C. Shiue*[2], *C. Feng*[1], *H. Chang*[1]; [1]*Institute of Nuclear Energy Research, Atomic Energy Council, Taoyuan City, TAIWAN,* [2]*PET Center, National Taiwan University Hospital, Taipei, TAIWAN.*

Epigenetic mechanisms mediated by histone deacetylases (HDACs) is involve in many diseases, including various neurodegenerative disorders and may offer new therapeutic opportunities. This is the reason why HDAC inhibitors (HDACIs) have been studied and shown in many research and treatment of neurodegenerative diseases. Because of many illustrate potentials of HDACis in diagnostic various neurodegenerative diseases, we assessed a novel inhibitor,[18]F-INER1577, which can permeate blood-brain barrier(BBB) highly. ^{18}F-INER1577 is a radiolabeled derivative of benzamide (4-((dimethylamino) methyl)-N-(4-((2-fluoroethyl)amino)-[1,1'-biphenyl]-3-yl)benzamide), as a PET imaging agent for estimating HDAC activity in SAMP8/SAMR1(five months age) transgenic mice model of Alzheimer's disease(AD) and SD (Sprague Dawley) rat. At first, we use ^{18}F-INER1577 to do the permeability test of the blood-brain barrier (BBB) in the SD rats. The senescence-accelerated prone SAMP8 mouse (in comparison with aged SAMR1 mouse) is a model of age-related cognitive go down with relevancy to variation of the gene expression and protein abnormalities in AD. ^{18}F-INER1577 has been synthesized in ~3 % yield (EOS) in a synthesis time of 60 min from EOB. Despite the moderate radio chemical yield, final radioactivity and radioactivity concentration values (1.870.3GBq and 180MBq/ml, respectively) should be sufficient for putative in the SAMP8/ SAMR1 transgenic mice. *In vitro* studies showed that ^{18}F-INER1577 inhibited not only HDAC 1,2,3,6,8 enzymes but inhibited growth of MCF-5 and 4T1 which are breast cancer cell line. In our research, ^{18}F-INER1577 has successfully passed the BBB in SD rat. Then we use PET-CT to find that regional INER-1577 uptake differences between the neocortex and hippocampus (0.45%ID/g in whole brain, 0.52%ID/g in neocortex and 0.54%ID/g in hippocampus at 20 min after drug injected, n=3, %ID/g means radioactivity per injected dose per body weight). For regional differences in HDAC distribution, the most striking observation in SAMP8/SAMR1 transgenic mice model show that high bio-distribution ranging from SAMP8/ SAMR1 transgenic mice than SD rat model. we synthesized a novel inhibitor ^{18}F-INER1577 which may be a HDACs imaging agent. we can assess radiotracer accumulation and density of HDAC in the SAMP8/ SAMR1 transgenic mice which displays selectivity for HDAC1,2,3,6,8 enzymes. It is the first time to use this tool to measure density of HDAC I which target isoforms 1, 2, 3, 6 and 8. Moreover, PET imaging with ^{18}F-INER1577 may help the understanding of HDACs mediated epigenetic mechanism of normal and neurodegenerative pathological processes. **Keywords:** Epigenetic mechanism; PET; histone deacetylases; neurodegenerative diseases

E-TPW30

The Effectiveness of Heat-Denatured Red Blood Cell (RBC) SPECT/CT Study for Patient Management When the Pathology is Unclear: A Pictorial Case Series

M. Carmody, M. A. Vartzokas, S. Yusuf, W. Svensson; Imperial College and Healthcare NHS Trust, London, UNITED KINGDOM.

Introduction: This case series looks at four patient cases which were performed in the Nuclear Medicine department over a six month period. Each presented with different underlying clinical histories which led to the detection of small lesions (<20mm) in the abdomen identified on diagnostic CT and Ultrasound scans. The pathology of the lesions could not be determined on anatomical imaging due to the similar appearance of neoplastic, lymphadenopathy and splenic tissue. Characterisation of these indeterminate lesions would direct patient management. All four cases were referred to Nuclear Medicine to confirm the diagnosis of suspected splenunculus (accessory splenic tissue). ^{99m}Tc-Heat-denatured Red Blood Cells are sequestrated by normal splenic tissue resulting in accumulation of tracer. Planar imaging has reduced sensitivity for small lesions due to its poor spatial resolution. The addition of SPECT/CT for these studies results in a highly sensitive and specific modality for confirming accessory splenic tissue. **Aim:** To determine if small indeterminate lesions identified on diagnostic imaging are accessory splenic tissue. **Method:** Five indeterminate lesions were assessed in four patients using In-vitro labelling of autologous heat-denatured RBC with pertechnetate. Each patient was administered with 100MBq of [99m]Tc- heat-denatured RBC. Immediate 30 minute dynamic, followed by planar and SPECT/CT imaging of the abdomen was performed as per department protocol. **Results:** SPECT/CT identified uptake of denatured RBC within four of the indeterminate lesions as splenunculi. One lesion did not demonstrate uptake, suggesting a recurrence of malignant disease. **Conclusion:** This case series shows the role of an underused functional imaging technique for characterization of indeterminate lesions, to rule out malignancy and confirm possible accessory splenic tissue which could not be confirmed on standard anatomical imaging. Heat-denatured RBC spleen study with cross-sectional hybrid imaging remains the most accurate method of identifying the presence and location of accessory splenic tissue under investigation. This simple, non-invasive and accurate test with a low radiation burden provides unique information that has a significant impact on the treatment pathway for the patients, preventing otherwise invasive investigations, unnecessary follow up scans and further emotional stress.

E-TPW31

Methods of time efficiency improvement following relocation to a new department

W. Heegaard[1], B. Hoyer Mathiasen[2], P. Holdgaard[1]; [1]Department of Nuclear Medicine,Vejle Hospital, Vejle, DENMARK, [2]Department of Procurement & Clinical Engineering, Central Denmark Region, Aarhus, DENMARK.

Aims: The aim was to investigate how to reduce non-productive time in the gamma camera rooms on relocating to a new department, due to an ongoing demand for increased efficiency and a requirement to comply with short waiting times. **Materials and Methods:** Fifteen points of contact were identified between the technologist and patient (or their examination) during each patient's visit. It was analysed as to whether tasks could be moved out of the camera room or could be delegated to other staff outside of the camera room, so the technologist's

productivity within the camera room could be increased. Time measurements were made for several tasks during the patient's visit, both before and after moving department and implementing changes. Means of times spent on the measured tasks were compared with t-tests. The changes implemented included better use of technology (e.g. gamma camera auto-contouring), delegating responsibility for checking images from physicians to technologists, and use of colour-coded areas in the department to direct patients instead of personally guiding them. **Results:** Measurements were made on 31 bone scintigraphy and 26 renography patients prior to moving department, and 30 bone and 23 renography patients after moving. For both examinations, time the technologist spent on each patient exam was significantly reduced from 29.2 minutes to 25.7 minutes (-3.5 minutes, p<0.001) for bone and from 37.6 to 31.0 minutes (-6.6 minutes, p<0.001) for renography. For both examinations, the colour-coded areas outside the camera room were particularly effective in saving technologist's time, as the patient could be left unsupervised to use toilet and then sit outside camera room (saving 3.7 minutes per patient for renography). The time the patient spent in the camera room was also reduced: for renography mainly by cannulating patients before entering the camera room (time in room:-2.8 minutes, p=0.02); and for bone, mainly due to new cameras having on-the-fly auto contouring (time in room:-2.6 minutes, p=0.01). Overall, the time the technologist spent on each patient, where the camera was not scanning, was reduced by 28 % for bone and 40 % for renography studies. Other methods of improving efficiency were also utilised and will be presented. **Conclusions:** All steps involved in a patient study were evaluated and several areas with time saving possibilities were identified. Following implementation, time efficiency was notably improved and would allow a greater throughput.

E-TPW32

Will the new PET radiopharmaceuticals overtake Myocardial Perfusion Imaging in the diagnosis of CAD?

R. F. S. Moreira, A. I. P. Queiroz, G. Paixao, C. Soares; Queen Elizabeth Hospital Birmingham, UK, Birmingham, UNITED KINGDOM.

Introduction: Coronary Artery Disease (CAD) affects half of the European population over the age of 65years, therefore it is essential to invest in the development of diagnostic tools for this pathology. Conventional protocols, are time consuming, can be inefficient and lead to ambiguous results. Research into new PET radiopharmaceuticals for cardiac imaging has exponentially increased, leading to growing evidence of the advantages of cardiac PET against Single Photon Emission Computed Tomography (SPECT) imaging and gamma emitting radiopharmaceuticals. **Purpose**: To describe the evolution of radiopharmaceuticals for PET, comparing their characteristics against each other and against radiopharmaceuticals used for SPECT imaging of CAD. Benefits and drawbacks of the use of positron emission radiopharmaceuticals as opposed to gamma emitters' radiopharmaceuticals are identified and the technical considerations of their use in clinical practice is evaluated. **Methodology**: With

access of two databases, I reviewed articles published after 2000, with aims in the Nuclear Cardiology field. A total of 150 articles were analysed, 94 of these were selected according to the aim of this project **Conclusion**: Currently, SPECT protocols remain dominant in myocardial perfusion imaging, but there are already attractive and reliable PET alternatives. Despite the inclusion of these alternatives in the CAD care guidelines, financial constraints limit their use for CAD imaging therefore hampering evaluation of their efficacy and reliability in clinical use. PET radiopharmaceuticals offer higher quality images, due to improved resolution, higher contrast and better attenuation correction associated with this imaging technique. Patients are less exposed to radiation and PET protocols are faster and simpler. PET leads in terms of diagnostic values such as sensibility, specificity and accuracy, which makes them a valid choice in a near future.

E-TPW33

Planning of multi-tracer session for clinical and research activity in a PET center

M. Scarlattei, Sr., S. Migliari, A. Sammartano, G. Baldari, C. Cidda, G. Serreli, C. Ghetti, O. Ortenzia, L. Ruffini; AOU Pr, Parma, ITALY.

Development and availability of new radiopharmaceuticals for specific diseases is one of the driving forces expanding clinical PET. However, in recent years economic viability of healthcare system is decreasing in term of personnel and technology improvement. The challenge is to pursue excellence in developing molecular probes although reduced resources. Our PET Center is a small-size facility composed of very few but highly skilled people, 1 PET/CT tomograph (Discovery IQ, GE Healthcare) and the Radiopharmaceutical Laboratory in which we synthesize and develop new different radiolabelled molecules for clinic and research. In this work we show optimized flow-chart to guarantee maximum flexibility and accessibility for patients also assuring reasearch tasks. We train every year the scientific team to work with a plethora of molecules labeled with the most used PET radionuclides F-18 ($T_{1/2}$ 109.6 min) and Ga-68 ($T_{1/2}$ 68 min). Moreover, team is trained to manage different acquisition methods depending on radiopharmaceutical and disease biology: whole body and dynamic imaging, brain 3D (18F-DOPA, 18F-FET, amyloid PET, 18F-FDG), gated cardiac PET (18F-FDG), 4D-PET, radiotherapy planning, head-to-toe scan, etc. Quantitative tools are daily used for images analysis (SPM5, SPM8, CortexID Suite, PMOD, PET VCAR). Personnel turnover is managed by highly intensive and 1-to-1 training with final validation to assure rapid and efficient results: re-training is periodically performed or planned when innovation is implemented. Results: our PET Center, started on September 2008, actually scan over 16 PET with different radiopharmaceuticals per day, starting with dynamic imaging (prostate cancer, brain, etc.). 68Ga-tracers are planned at session end when generator is fully potent (1.11GBq) then one at session beginning and 1 as the last PET study to not reduce availability. PET/CT scans increase over time (1200 exams in 2009, 3160 in 2016) enlarging spec-

trum of studied diseases although only 1 tomograph and a small staff. We are continuously expanding our radiopharmaceutical production capabilities adapting new protocols to our equipment (18F-choline in 2010, 18F-DOPA in 2012, 68Ga-DOTATOC in 2014, 18F-florbetaben in 2015, 68Ga-PSMA and 18F-flutemetamol in 2016). We are involved in clinical trials for oncology, neurodegenerative diseases and frailty, requiring tomograph qualification and images transfer to core labs (WIDEN, Hermes, ICON, Bioclinica, etc.). In conclusion, highly skilled (even if small size) staff, rigorous training and standardization of imaging protocols are essential to delivery appropriate, excellent and high quality services in Molecular Imaging facility.

E-TPW34

Impact of different acquisition and reconstruction protocols on image quality in [68Ga]PSMA PET/MRI

S. Milachowski[1], *A. Kanzog*[2], *F. Büther*[2], *T. Allkemper*[1], *L. Stegger*[2]; [1]*Institute of Clinical Radiology, University Hospital Muenster, Muenster, GERMANY,* [2]*Department of Nuclear Medicine, University Hospital Muenster, Muenster, GERMANY.*

Introduction: [68Ga]PSMA PET/MRI is a valuable tool in diagnosis of prostate cancer. Some questions about the best acquisition and reconstruction remain to be answered, specifically in current PET/MRI systems where halo artefacts around hot structures caused by inaccurate scatter correction often degrade image quality. We analysed the occurrence of these artefacts in a clinical study with different acquisition parameters. **Methods:** 15 patients were scanned 1 h p.i. of 2 MBq/kg [68Ga]PSMA-11 on a Siemens mMR system with voided bladder. PET/MRI comprised 5-7 bed positions (bp; 3 min per bp) with arms beside the body. 2.5 h p.i. and after additional bladder voiding, the patients were scanned again for 2 bp centered on the bladder (5 min per bp) with arms up. This was followed by a scan with arms beside the body in 8 patients. DIXON scans with MLAA-based extension of the field-of-view were performed to calculate attenuation maps. Scatter correction was done using both relative and absolute scaling. Early whole-body images and late images were assessed for mean bladder SUV and halo artefact around the bladder (0: no artefact, 1: slight artefact, 2: clear artefact, 3: severe artefact). **Results:** A clear correlation between bladder SUV and halo score for the whole-body images using absolute scaling was seen. This was less pronounced using relative scaling. No significant difference was seen between halo scores of early whole-body scans and late scans with arms up. In 8 patients with additional late scan with arms down, halo scores of the images with arms up demonstrated significantly smaller values than with arms down in either scatter correction. **Conclusion:** Halo artifact occurrence is correlated with higher levels of radioactivity inside the bladder. Imperfect attenuation maps caused by the presence of arms in the field of view and used within the scatter correction contribute to the presence of halo artefacts. Late scans (2.5 h p.i.) do not seem to be superior to early scans (1 h p.i.) in terms of artefacts.

E-TPW35

Assessment Ga-68 PSMA progress in patient with prostate cancer

R. R. Farshbaf Aghaenejad; *University Tehran, Tehran, IRAN, ISLAMIC REPUBLIC OF.*

Aim: In the current report we presented intense uptake in Ga-68 prostate specific membrane antigen (PSMA), (PET/CT) in early and late monitoring of 74 years old male patient with prostate carcinoma diagnoses. **Material & Method:** The patient underwent Ga-68 PSMA-HBED-CC PET/CT for restaging of prostate carcinoma. He had diagnosed as prostate adenocarcinoma in 2016 and been followed up in 2017 using Ga-68 PSMA-11. Additionally chemoradiation therapy using taxotere following partial cystectomy had been applied for high grade invasive prostate carcinoma. After chemotherapy and hormone therapy (Zometa), patient underwent Ga-68 PSMA PET/CT for elevation of serum prostate specific antigen levels (early scan). In the early PET/CTscan patient had PSA=11. For this procedure 60 MBq of Ga-68 PSMA-11 was administered intravenously via the left antecubital vein. for distribution and uptake of radiotracer, was allowed to rest quietly for 60 minutes . Imaging was an integrated 6-slice PET/CT scanner, with wholbody scaning without contrast material. **Result & Conclusion:** In maximum intensity projection and fused imags, multiple medistinal lymph node involvement in supraclavicular, restrosternal, lower paratracheal and left internal mammary stations high uptake were detected . In addition, lymph node involvement in the para-aortic area (3-4 small sizes), right iliac wing and T9 and 11th left ribs were reported. After following the patient who underwent hormone therapy each three months, PSA level rose up from 11 to 36 ng/ml and chemotherapy with no change in PSA levels was regarded. Therefore, Ga-68 PSMA PET/CT has been performed again for imaging of recurrent prostate carcinoma progression . For achieving this goal the same PET/CT protocol was done. After interpretation of these results, we found same scan patterns like pervious study in the bilateral supaclavicular lymph nodes, 9mm lymph node in the paratracheal , 15mm lymph node in the retrosternal area. Furthermore, 2-3 another lymph nodes in the lower paratracheal and retrosternal stations with increased uptake were noted. Lymph node in AP window which was 8mm with SUV max=10 now became 20 mm with SUV max=17.3. Finally, new lymphatic involvements in the left retrocrural, AP window in addition to the previously noted multiple medistinal lymph node involvement in supraclavicular, retrosternal, lower paratracheal and left internal mammary stations were diagnosed. Moreover, lymph node involvement in the para-aortic area and new bone lesions in the sternum, left scapula, multiple ribs, T5, multiple lower thoracic and lumbar vertebrae and iliac wings were seen.

E-TPW36

Gallium-67 Delayed Imaging in the Evaluation of Sarcoidosis: Is It Really Necessary?

J. Patrina[1,2], *D. B. Faria*[1,2,3], *T. S. Vieira*[1,2], *D. Sousa*[1,2], *F. A. Silva*[1,2], *J. M. P. Oliveira*[1,2]; [1]*HPP - Medicina Molecular SA, Porto, PORTUGAL,*

²Lenitudes Medical Center & Research, Santa Maria da Feira, PORTUGAL, ³School Of Health Sciences - University of Aveiro, Aveiro, PORTUGAL.

Gallium-67 scintigraphy is still an important imaging modality used for the diagnosis of sarcoidosis and evaluation of disease activity. Guidelines suggest that a dual time point acquisition protocol may be important to improve the quality of the clinical interpretation of the exam, since delayed imaging is potentially helpful when unspecific radiopharmaceutical uptake is visualized in the early time point scan. However, delayed image acquisition has implications in Nuclear Medicine Department workflow, especially in a busy department, as well as in patient's life and in the society. **The aim** of this study is to analyze the impact on image interpretation of an early single time point acquisition protocol while performing Galium-67 scintigraphy for the evaluation of sarcoidosis. **Methods:** A retrospective evaluation was performed on a total of 43 patients, 18 females and 25 males, with ages between 25 and 75 years-old, referred for the evaluation of sarcoidosis by Gallium-67 scintigraphy in the last 12 months. A dual time point acquisition protocol was conducted. Three experienced Nuclear Medicine Physicians (A, B and C) classified early and delayed images as positive or negative for sarcoidosis. Early and delayed images were interpreted separately with a 3 weeks' interval. An interrater reliability analysis using the Kappa statistic was performed to determine consistency intraraters (Cohen's Kappa) and among raters (Fleiss' kappa). **Results:** The interpretation of observer A was concordant on early and delayed images in 42 patients, of observer B in 37 patients and of observer C in 38 patients. The intraobserver reliability for observers A, B and C was found to be Kappa = 0.937, Kappa = 0.606, and Kappa = 0.672, (p <0.001) 95% CI (0.504, 0.848), respectively. All observers agreed in the evaluation of 33 patients relying on the early images, and in 38 patients regarding the delayed study. The interobserver reliability was found to be Kappa = 0.638 (p <0.001), 95% CI (0.465, 0.810) for early images, and Kappa = 0.792 (p <0.001), 95% CI (0.620, 0.965) for delayed images. **Conclusion:** Single early time point imaging acquisition is not feasible for clinical practice. Levels of intraobserver and interobserver agreement suggest that Ga-67 delayed imaging is really necessary for the scintigraphic evaluation of sarcoidosis.

E-TPW37
Copper-64 and its role in Theranostics and Nuclear Medicine

M. J. Correia¹, P. Costa¹, S. Sequeira², A. Nunes³, L. Olo³, C. Alves³, L. F. Metello¹,⁴; ¹Nuclear Medicine Department, ESS-P.Porto, Porto, PORTUGAL, ²Nuclear Medicine Department, IPOFG, Porto, PORTUGAL, ³Nuclear Medicine Department, DCC – Dr. Campos Costa – iCUF, Matosinhos, Porto, PORTUGAL, ⁴Nuclear Medicine Department, IsoPor – Azores, Angra do Heroísmo, PORTUGAL.

Introduction: Modern medicine is getting more personalized and the adequate prediction and evaluation of therapeutic efficiency is becoming of greater value. Molecular Imaging, and in particular, Nuclear Medicine, are increasing their capacity of fulfilling these needs through the development of new tracers that can gather data on every biological system, allowing imaging and radiometabolic therapy of an increasing number of pathological conditions. Between them, Copper-64 (^{64}Cu) is promising due to a favourable inorganic chemistry that entrusts this element with a unique labelling versatility, as well as singular physical properties that allow this radioisotope to be able to be produced in low/medium energy cyclotrons and easily distributed to be used as both PET imaging and therapeutic agent. **Aim:** Assuming its high potential, the aim of this paper is to review the current theranostic applications of ^{64}Cu based radiopharmaceuticals, and to approach future trends as imaging and/or therapy agent. **Methodology:** The review was done through the selection of articles mainly found in PubMed database, being prioritized the selection of articles published after 2005. The main selective filter was the radionuclide, by itself, and its potential theranostic applications. The keywords list was (not exclusively): "Nuclear Medicine"; "Theranostic applications"; "Copper-64"; "^{64}Cu imaging"; "^{64}Cu-DOTATATE"; "^{64}Cu-thiosemicarbazones" and "^{64}Cu-mAbs". **Results:** According with the results obtained after the analysis of 107 articles, ^{64}Cu based radiopharmaceuticals (including ^{64}Cu-ATSM, ^{64}Cu-monoclonal antibodies, ^{64}Cu-DOTATE, ^{64}Cu-nanoparticles and ^{64}Cu-CuCl$_2$) are highly interesting potential tools for theranostic use, with further work to be done in order to optimize the whole process and to allow its introduction in clinical practice in the management of oncological conditions, especially on situations of neuroendocrine tumours and hypoxia related lesions, between other oncological cases (lymphomas, prostate cancer, cervix cancer). Some cons related with reliability of production sites and *in vivo* instability due to unsatisfactory chelating agents performance (particularly DOTA, due to demetallation) were found and will be commented, as well as the respective ways to overcome them, with new chelating agents being explored (namely TETA, T2TE, NOTA and sarcophagine). **Conclusion:** ^{64}Cu capacity of labelling a wide variety of distinct molecules, as well as the favourable physical properties for imaging and therapy, makes this radioisotope a high-potential theranostic agent. Optimization of all technical steps from the radioisotope production to the development of efficient chelating agents may be considered critical confirming the huge potential for the ^{64}Cu based radiopharmaceuticals widespread use in a nearby future. **Keywords:** Theranostic; Nuclear Medicine; PET; Therapy; Copper-64.

E-TPW38
Optimal collimation for ²²³Ra planar imaging

T. Otani¹, Y. Kunikane², S. Takashi², R. Bando², A. Fujita², M. Amano², Y. Fukunaga¹, H. Otsuka¹, H. Miyoshi¹; ¹Tokushima University, Tokushima, JAPAN, ²Tokushima University Hospital, Tokushima, JAPAN.

Purpose: Available since 2016 in Japan, ^{223}Ra-Dichloride (^{223}Ra) is a bone-seeking alpha-emitter that prolongs survival in patients with castration-resistant metastatic prostate cancer. Because ^{223}Ra emits useful photons for imaging, mainly 82, 154, 269, 351, and 402 keV, it has the potential to be imaged with a gamma camera. Optimal image acquisition protocols have

yet to be developed. We performed this study to decide the optimal collimation of ^{223}Ra-chloride. **Methods:** Thirty-minute planar static images of a 6.6 mm point source phantom filled with 150 kBq (500 kBq/mL) ^{223}Ra were acquired using a Siemens gamma camera (Symbia T16). We calculated the sensitivity (cps/MBq), contrast-to-background noise ratio (CNR), the coefficient of variation (CV), and the spatial resolution as the full width at half maximum (FWHM). The point source phantom was imaged with three collimators; a low-energy collimator (LE), a low-medium energy collimator (LME), and a high-energy collimator (HE). The LE and LME collimators were each used with the energy windows set at two patterns: 82, 154, 270, 350 and 400 keV, and 82 and 154 keV. The HE collimator was used with the energy window set at 82, 154, 270, 351 and 402 keV. **Results:** Using the five energy windows with the LE and LME collimators, CNR was 70 and 84, respectively. The best sensitivity was acquired with the LE collimator (LE: 8740 cps/MBq, LME: 2030 cps/MBq, and HE: 993 cps/MBq). CNR and CV were better with the LME collimator (CNR: 358, CV: 19.0 %) than LE collimator (CNR: 305, CV: 26.0 %). CNR and CV with the HE collimator were 440 and 29.7 %, respectively. The best FWHM was delivered by the LE collimator (LE: 10.3 mm, LME: 13.8 mm, HE: 16.4 mm). **Conclusion:** Using LE or LME collimators, the energy windows should be set at 82 and 152 keV. Peaks > 270 keV were associated with scatter and penetration. The better total performance was acquired with an LME collimator. A HE collimator might be impractical because image quality was poor due to a low count rate.

E-TPW39

Radium-223 In The Treatment Of Metastatic Castration-Resistant Prostate Cancer

C. Vazzana[1], S. Morano[2], A. Di Lascio[3], C. Grana[4], M. Chinol[4]; [1]Veneto Oncology Institute - IOV IRCCS, Padova, ITALY, [2]Hospital Bianchi Melacrino Morelli, Reggio Calabria, ITALY, [3]Hospital A. Cardarelli, Napoli, ITALY, [4]European Institute of Oncology, Milano, ITALY.

Introduction: In the past years, the only drugs approved to relieve bone pain originating from metastatic prostate and breast cancers were β-emitting radiopharmaceuticals. These drugs did not prove to prolong survival when used as single agent and resulted associated with important adverse events. This situation has changed with the advent of radium-223 due to the good safety profile and evidence of improved survival. Cooperation between nuclear medicine physicians and other specialists involved in cancer management involved the combination of radium-223 with recently approved drugs in mCRPC patients. **Subjects & Methods:** Two recently approved drugs for the treatment of advanced prostate cancer—radium-223 (Xofigo) and abiraterone acetate (Zytiga)—will be studied in combination in a phase III clinical trial. The trial of abiraterone with or without radium- 223 has begun enrolling patients with castration-resistant prostate cancer that has spread to bone, not yet been treated with chemotherapy, and is causing no or mild symptoms. The endpoint of the randomized, double-blind, placebo-controlled study will be symptomatic, skeletal, event-free survival at 3 years, or, more specifically, whether the addition of radium-223 to standard abiraterone will prolong life and delay the time to skeletal-related events such as painful fractures or bone pain. Secondary endpoints include overall survival, time to opiate use for cancer pain, time to pain progression, time to cytotoxic chemotherapy, radiological progression-free survival, and number of participants experiencing adverse events. **Results:** Previous studies showed that all main secondary efficacy end points were achieved in radium-233 treated patients compared with placebo. Moreover, radium-223 was associated with low myelosuppression rates and fewer adverse events. **Discussion/Conclusion:** Radium-223 has been shown to delay the time to a patient's first skeletal-related event, as well as to prolong survival, in patients with mCRPC, symptomatic bone metastases, and no known visceral metastatic disease. These ongoing trials may help the oncologists to understand the best way to combine new therapies for advanced prostate cancer with radium-223.

E-TPW40

Half-Time SPECT/CT Acquisition for Post Therapy [177Lu--DOTA, Tyr3] Octreotate Imaging

T. De Sousa, S. Johnson, A. Nunes, A. Eccles, H. Ahmed, V. Lewington; Guy's and St. Thomas' NHS Foundation Trust, London, UNITED KINGDOM.

Introduction: Peptide receptor radionuclide therapy (PRRT) targets somatostain receptors overexpressed on neuroendocrine tumours (NETs). PRRT inhibits tumour growth and reduces hypersecretory symptoms. Our department PRRT protocol delivers four cycles of 7400Mbq [^{177}Lu--DOTA, Tyr^3]Octreotate by intravenous infusion at 8 - 10 weeks intervals. All patients undergo whole body and SPECT/CT imaging 24 hours post therapy. To manage rising demand and match service expansion to gamma camera capacity, we undertook a prospective review of our current imaging protocols. **Purpose:** Evaluate the reliability and clinical accuracy of the half-time acquisition SPECT/CT (10 seconds per frame) instead of 20 seconds per frame for [^{177}Lu--DOTA, Tyr^3]Octreotate post therapy scan as per published recommendations. **Method:** Eligible patients underwent imaging on a *Philips Precedence 16 Slice SPECT/CT 24 hours after 7.4 GBq* [^{177}Lu--DOTA, Tyr^3]Octreotate therapy. A sample of 20 unselected SPECT/CT scans were reconstructed and processed, using an iterative algorithm, for full time (20 seconds per frame) and half-time (10 seconds per frame) acquisitions. The SPECT/CT scans were then anonymised as to which sub-set they originated from and were reported by three Nuclear Medicine Consultants individually. **Results:** The scans were compared for visual differences and confidence level on reporting. Image quality were scored on a 1 to 5 scale. Results suggest that confidence level on reporting and general scan quality remain unaffected for half-time acquisition. **Conclusion:** The results of this study indicate that half-time acquisition for [^{177}Lu--DOTA, Tyr^3]Octreotate post therapy scanning could replace existing SPECT/CT protocols without compromising image quality or reporting confidence. This initiative would have a positive impact upon department workflow and patient experience.

Technologist e-Poster Session 3

E-TPW42

Radiation Exposure of Patients During Parathyroid Imaging: Comparison between Dual-Phase 18F-fluorocholine PET/CT, Dual-Phase 99mTc-MIBI SPECT/CT and Planar Subtraction Scintigraphy

S. Rep[1], M. Mocevar[2], J. Vaupotoc[3], U. Zdesar[4], K. Zaletel[1], L. Lezaic[1]; [1]Department of Nuclear Medicine, Ljubljana, SLOVENIA, [2]Oncological Surgery, Oncology Institute, Ljubljana, SLOVENIA, [3]Jozef Stefan Institute, Ljubljana, SLOVENIA, [4]Institute of Occupational Safety, Ljubljana, SLOVENIA.

Introduction: Tc99m-sestaMIBI (MIBI) is the most commonly used radiopharmaceutical for parathyroid scintigraphy. It can be performed in combination with Tc99m-pertechnetate for subtraction scintigraphy (MIBI- Tc99m-pertechnetate) or increasingly as hybrid SPECT/CT imaging after administration of MIBI in an early and delayed phase. Recently, F18-fluorocholine (FCH) PET/CT was introduced for second-line imaging and even as an alternative primary investigation for the purpose of localization of hyperfunctioning parathyroid glands (HPG). To date, no studies have specifically examined the effective dose (ED) and the organ doses from conventional subtraction scintigraphy, dual-phase MIBI SPECT/CT and FCH PET/CT in the localization of HPG. **Aim:** To measure the ED and organ doses for conventional subtraction scintigraphy, dual-phase MIBI SPECT/CT and FCH dual-phase PET/CT as potential future imaging method of choice for localization of HPG. **Materials and Methods:** Twenty patients with primary hyperparathyroidism referred for parathyroid imaging underwent parathyroid subtraction scintigraphy and dual-phase SPECT/CT imaging with the addition of FCH PET/CT. Radiation exposure was calculated for administered activities of radiopharmaceuticals using ICRP weighting factors and for CT exposure at hybrid imaging using dose-length products and ImPACT CT Patient Dosimetry Calculator. **Results:** The highest radiation exposure was caused by conventional parathyroid subtraction scintigraphy (7.25 mSv), followed by dual-phase MIBI SPECT/CT (6.75 mSv). The radiation exposure was lowest for dual-phase FCH PET/CT imaging (2.85 mSv). The added CT imaging for both hybrid approaches did not cause significant additional radiation exposure (1.43 mSv for MIBI SPECT/CT, additional 26.01 % to overall exposure; 0.85 mSv for FCH PET/CT, additional 44.11 % to overall exposure). **Conclusion:** In comparison to conventional scintigraphic imaging for HPG, emerging FCH PET/CT imaging technique causes lower radiation exposure to patients.

E-TPW43

The viability of the attenuation CT for calcium scoring

M. Louwe; Westfriesgasthuis, Hoorn, NETHERLANDS.

Preface: At the department of Nuclear Medicine at the Westfriesgasthuis Hoorn it's standard practice to perform a non-gated attenuation-CT(At-CT) with a myocardial perfusion SPECT. In order to assess the calcification of coronary arteries an ECG-triggered calcium score-CT(Ca-CT) is constructed. Determining the calcification of the coronary arteries contributes to predicting myocardial infarction or cardiovascular death. The extent of calcification in coronary arteries can be determined using the Agatston-score. In this study Agatston-scores of different reconstructions of the At-CT are compared to Agatston-scores of the Ca-CT to determine the viability of the At-CT. The following research question has been formulated: *'To what degree can the low dose attenuation-CT, which is performed alongside the myocardial perfusion scintigram at the Westfriesgasthuis, be used to determine a calcium scoring?'* **Methods:** 34 patients underwent an At-CT as well as a Ca-CT. Of each At-CT three reconstructions were made: At-CT with Filtered Back Projection(FB), At-CT with 50% Adaptive Statistical Iterative Reconstruction(A-SiR) and an At-CT with 100% ASiR. Images were quantified by a Nuclear Medic. For every reconstruction an Agatston-score has been determined per coronary artery and also for all coronary arteries combined. The Agatston-scores were compared to that of the Ca-CT. Afterwards the Agatston-score was categorized using following categories: low-risk(1 - 10), average-risk(11-100), high-risk(101-400) and very high-risk(>400). A categorized Agatston-score was determined for every coronary artery per reconstruction. Then a total categorized Agatston-score was determined. The categorized Agatston-scores of the reconstructions from the At-CT were compared to those of the Ca-CT. Data was analyzed with SPSS Statistics. **Results:** There is a high correlation between Agatston-scores of the coronary arteries on the reconstructions of the At-CT and Agatston-scores of the coronary arteries of the Ca-CT, with exception of the Left Main. The Right Coronary Artery scores a low p-value in the Wilcoxon signed-rank test. The total Agatston-score of the At-CT with FB is the most similar to that of the Ca-CT(73.53%). The difference with the Agatston-scores of the Ca-CT is in many cases just one category. With a margin of one category, the similarity between the total Agatston-scores of the At-CT with FB and the Ca-CT is 94.12%. **Discussion:** Many patients fell into the 0 and >400 categories. Therefore the results might suggest that the Agatston-score on the reconstructions were mostly similar to the Ca-CT Agatston-scores in the category Agatston-score 0 and Agatston-score >400. **Conclusion:** The At-CT can be used for calcium scoring based on this study's results.

E-TPW44

Implication of using cardiac MAR algorithm with regards to the interpretation of infected PM- and ICD wires

J. Ellingsen, E. Andersen, H. Stokmo; Oslo University Hospital, Oslo, NORWAY.

Introduction: ^{18}F-FDG-PET/CT is a valuable complementary tool for differentiating between post-operative inflammation and an actual infection around electrical heart implants (1, 2). The challenge is that high density materials in PMs and ICDs results in known artefacts (3). Metal implants can lead to attenuation-related artefacts in the attenuation-corrected PET images that lead

to both under- and over estimation of standard uptake value (SUV). The department's Siemens Biograph mCT utilize an image-based metal artefact reduction (MAR) algorithm to reduce attenuation artefacts due to the presence of wires from PMs and ICDs (4). Early studies show that attenuation artefacts can affect both qualitative- and quantitative interpretation of pathology (5, 6), however this is for larger metallic implants. More recent studies indicate that it is not PM wires that lead to artefacts (3, 7), but it is ICD wires. This again may affect clinical interpretation (3). A study by DiFilippo and Brunken (7) demonstrate that the MAR algorithm does not have great impact on reconstruction, but the study does not discuss whether newer PET/CT technology has deemed specialized MAR algorithms for cardiac investigations unnecessary. The objective of this pilot quality assurance study, is to assess whether the implemented MAR algorithm has a significant effect on the clinical interpretation of cardiac investigations performed with 4D-PET/CT for diagnosing infection in PM- or ICD wires. **Method:** All four patients were examined at a dedicated Siemens Syngo.via client workstation. 4D-PET/CT in expiratory phase, with and without MAR reconstructed PET WB, were examined side by side and were correctly co-registered in a 2-time point view. A region of interest (ROI) was placed in an area of the axial CT where the PM/ICD wires were lodged in the heart muscle. The density in HU was measured to ensure that it exceeded 900HU so that the MAR algorithm was applied to the reconstruction. Then, the same ROI was copied to the axial PET examination to ensure the same ROI location as on the CT. The SUV was then measured in this area on both PET reconstructions. Due to the small number of patients, descriptive statistics only have been used. **Result:** The difference between PET images reconstructed with and without MAR had minimal impact on the SUV value. **Conclusion:** PET images reconstructed with MAR do not significantly change the SUV value and thus have no effect on image interpretation.

E-TPW45
DDSA-A, microDDS-A and KARl100, what else

M. Budinsky, S. Kozakova; Masaryk Memorial Cancer Institute, Brno, CZECH REPUBLIC.

Purpose: The purpose of our study i to evaluate the effect of instrumental methods in radiopharmacy to the radiation exposure to the staff preparing radiopharmaceuticals. **Subject and Methods**: Since 2004 instrumental methods in radiopharmacy are used as a tool of radiation protection optimization for the pharmacists after PET introduction to the departments of nuclear medicine of MMCI in 2003. Different equipment for instrumental preparing of radiopharmaceuticals DDSA-A, microDDS-A and KARl100 (all Tema sinergie, Italy) during fourteen years of PET working process were used. The increase in a number of instrumental equipment - two microDDS-A and one KARl100, allows preparing three different radiopharmaceutical for PET (18F-FDG, 18F-FLT, 18F-NaF, 18F-choline, 18F-Vizamyl, 11C-methionine) in one day. The radiation exposure to the radiopharmacists was evaluated from ring dosimeters. **Results:** The introduction of PET in 2003 led to increasing of the radiation dose over legis-

lation limits to the radiopharmacists with personal maximum 814,4mSv/year for hands. As a tool of optimization, instrumental preparing radiopharmaceuticals for PET using DDS-A was introduced. In 2004 rapid reduction of radiation dose was restored to personal maximum 106,97mSv/year for hands. The increase of number and specter of PET radiopharmaceuticals during one day required the upgrade in a new equipment and increase of its number. In 2009 former DDS-A was replaced by two microDDS-A. Another equipment, KARl100 was installed in 2016. This event led to another significant reduction of radiation dose to personal maximum of 24,91mSv/year for hands. **Conclusion:** Introduction of PET and increase of radiopharmaceutical specter influence the radiation exposure to the radiopharmacists by elevation of radiation exposure dose. Instrumental methods in radiopharmacy is a possible to consider as a tool for radiation protection optimization. In conclusion, it is the possible to state that instrumental methods in radiopharmacy have a significant effect on the radiation protection to the radiopharmacists.

E-TPW46
Skin Contamination of Nuclear Medicine Staff in NM Departments: preliminary results

N. Fernandes[1], D. Neves[2,1], A. Ferrer[2], M. F. Joao[2], A. Araujo[3], J. Pereira[3], L. Metello[1,4]; [1]ESS – IPP, ATC & Curso Med. Nuclear, Porto, PORTUGAL, [2]Diaton S.A. – Leiria, Dept. de Med. Nuclear, Leiria, PORTUGAL, [3]Serviço de Med. Nuclear – Hospital de S. Joao, Porto, PORTUGAL, [4]IsoPor-Azores, Dept. de Med. Nuclear e Imagiologia Molecular, Angra do Heroismo, I. Terceira – Azores, PORTUGAL.

Aim: Skin contamination of Nuclear Medicine (NM) staff may occur rather frequently, essentially when dealing with liquid radioactive sources. The aim of this study is to analyze parameters as frequency, sources and professional profiles involved on skin contamination occurring in NM daily practice. **Material and Methods**: During 2 months, 226 inspections were held on the hands of NM technologists (84), nurses (57), and NM technologists trainees (85), after a work shift with a minimal duration of 4 hours. For contamination detection and localization, the same Geiger-Müller detector was used, being attached with a lead collimator with a $1cm^2$ circular hole when used for localization. The contamination threshold was established at a dose rate $\geq 1\mu Sv/h$. All the identified contaminations were confirmed by another detector (either a camera-gamma or a proportional counter). **Results**: Hand inspections were carried out in two distinct NM Departments (D1 = 132, D2= 94). Hand contaminations were found in 24 cases (10.6%), 16 cases (7.1%) in D1 and 8 cases (3.5%) in D2. In 75% of the detected contaminations, the worker was unaware of it. Dose rates ranged from 1 to 150 μSv/h (average = 17.07 μSv/h). The vast majority of the detected contaminations were focal (23 cases, 95.8%). Five main contamination sources were identified: radiopharmacy procedures (37.5%), radiopharmaceutical administration (37.5%), cross-contaminations (8.3%), direct contact with the patient (4.2%) and unknown origin (12.5%). The most frequent contamination sites were the tip of the index and ring finger of the non-dominant hand, corresponding its sum to 29.0% of the cases. Contamination was

found in all professional profiles: 14.0% (8 out of 57) in nurses, 11.9% (10 out of 84) in NM technologists and 7.1% (6 out of 85) in technologist trainees. **Conclusion**: The preliminary results obtained revealed that skin contamination in hands may occur with non-negligible frequency (10.6%), reaching dose rates as high as 150 μSv/h. Relevantly, in most of the cases, the worker was not aware of contamination, which occurs mainly during radiopharmaceuticals preparation and administration phases. This data suggests that a hand/skin contamination monitoring program should be considered on the daily practice on Nuclear Medicine. Further studies correlating the assessment of work practices, the frequency and magnitude of skin contamination and its contribution to extremities effective dose, are needed in order to better access the real situation and to sustain eventual improvement measures in conventional NM Departments daily practice.

E-TPW47

Development and Validation of Simple Methods to Reduce Radiation Exposure to Public from FDG PET/CT Patients

*E. Koester, S. Frye, R. Muzaffar, **M. M. Osman**; Saint Louis University, St. Louis, MO, UNITED STATES OF AMERICA.*

Objectives: Limited guidelines address the release of patients undergoing nuclear medicine exams. Nevertheless, facilities are under scrutiny to reduce radiation exposure. While patients have multiple tests and appointments in a single visit, it is important to consider the timeframe after a scan. Our study explores the frequency of elevated radiation exposure upon discharge and techniques to reduce it when undergoing an FDG PET/CT exam. We sought the least impact/inconvenience to the patient and department while reducing the radiation dose to < 2 mR/hr at 1m. Renal function was also evaluated as a potential variable. **Methods:** 44 patients undergoing standard of care PET/CT exams were willing to be enrolled in the study. An Ionization Survey meter measured radiation exposure rates at 1 meter after the exam. Patients received a weight based FDG dose (range: 6.3-15.3 mCi, mean: 11.6) followed by a 60 min uptake and whole body acquisition (total time range: 73-124 mins, mean: 88). Patients were randomly divided into 3 groups based on availability after the exam. Group 1 (n=31) exposures measured immediately after the scan, instructed to void and re-measured. Group 2 (n=13) exposures measured immediately after the scan then 30 minutes later. Group 3 (n=13) exposures measured immediately after the scan, voided after 30 mins and re-measured. To assess renal function, 32/44 had eGFR values available. **Results:** 34/44 patients (77%) exceeded 2mR/hr at 1m immediately after their scan. Group 1: 7/31 (22 %) at/above 2mR/hr with a mean exposure decrease of 19.7% (0.43mR/hr). Group 2: 2/13 (15%) at/above 2mR/hr with a mean exposure decrease of 22.4% (0.51 mR/hr). Group 3: 13/13 (100%) below 2mR/hr with a mean exposure decrease of 36.1% (0.83 mR/hr). Of the 32 patients with renal function data, 5/32 had reduced function (eGFRs <60). Of these, 4/5 (80%) were above the 2 mR/hr immediately after the scan, whereas 25/27 (93%) of normal eGFR patients were above 2mR/hr after the scan. **Conclusions:** We

continue to accrue data but our initial analysis shows >75% of patients undergoing an FDG PET/CT exam are exceeding 2mR/hr when leaving. The most effective method to reduce radiation exposure to under 2mR/hr was voiding after a 30 minute wait. This simple technique is especially important when patients have additional appointments and in close contact with others. In addition, we found impaired renal function has no effect on radiation exposure, however, further tests need to be done given the small sample size.

E-TPW48

Quantification of technegas contimination

K. S. Rømer, N. S. Larsen, M. N. Lonsdale, L. D. L. Duchstein; Bispebjerg Hospital, Copenhagen, DENMARK.

Aim: Through preliminary studies, the department of clinical physiology and nuclear medicine (KFNM) Bispebjerg, has confirmed that there is a measurable amount of radioactive contamination of the room and personal during lung ventilation examinations with technegas (dispersion of 99mTc labelled carbon). The aim of this study is to quantify the measured contamination by developing specific calibration curves for the Captus 2000 (Capintec inc.) gamma counter present in the department, and thereby establishing ground for further testing of countermeasures, such as mouth covers and a fume extraction unit. **Materials and Methods:** 7 samples of pertechnetat (^{99m}Tc) were prepared in syringes with activities varying from 114-327kBq. Background readings were made and the samples were applied one at a time on a marked area on a t-shirt, which was then folded. Measurements were made as duplicates with a 2min acquisition time and a 25cm distance between the sample and the probe. One measurement was discarded due to improper folding of the t-shirt. The data was analyzed in Microsoft Excel, where also the linearregression was calculated. The calculations were then used to quantify contamination of the mouth covers used by the technologist during the examination. **Results:** Results from the sample measurements show a linear regression with r^2 = 0,99. Contamination of mouth covers was calculated to activities ranging from 11,29kBq to 57,16kBq. **Conclusion:** Results show a strong linear regression, but more data needs to be collected. Preliminary measurements have resulted in an investment in a mobile fume extraction unit, which will be tested and compared to the initial results.

E-TPW49

Evaluation of Radiation Exposure to Nurse on Nuclear Medicine examination by Use Radioisotope

J. Jeong, C. Lee, Y. Seo, H. Choi, Y. Kim, Y. Kim, W. Won; National Cancer Center, Goyang-si, KOREA, REPUBLIC OF.

Purpose: The present study aimed to estimate the exact total exposure of the nurse in a general ward by close contact with the patient undergoing nuclear medicine examinations. **Material and Methods:** Radiation exposure rate was determined by using thermoluminescent dosimeter (TLD) and optical simulat-

ed luminescence (OSL) in 14 nurses in a general ward from October 2015 to June 2016. External radiation rate was measured immediately after injection and examination at skin surface, and 50 cm and 1 m distance from 50 patients (PET/CT 20 pts; Bone scan 20 pts; Myocardial SPECT 10 pts). After measurement, effective half-life, and total radiation exposure expected in nurses were calculated. Then, expected total exposure was compared with total exposures actually measured in nurses by TLD and OSL. **Results:** Mean and maximum amount of radiation exposure of 14 nurses in a general ward were 0.01 and 0.02 mSv, respectively in each measuring period. External radiation rate after injection at skin surface, 0.5 m and 1 m distance from patients was as following; 376.0±25.2, 88.1±8.2 and 29.0±5.8 μSv/hr, respectively in PET/CT; 206.7±56.6, 23.1±4.4 and 10.1±1.4 μSv/hr, respectively in bone scan; 22.5±2.6, 2.4±0.7 and 0.9±0.2 μSv/hr, respectively in myocardial SPECT. After examination, external radiation rate at skin surface, 0.5 m and 1 m distance from patients was decreased as following; 165.3±22.1, 38.7±5.9 and 12.4±2.5 μSv/hr, respectively in PET/CT; 32.1±8.7, 6.2±1.1, 2.8±0.6, respectively in bone scan; 14.0±1.2, 2.1±0.3, 0.8±0.2 μSv/hr, respectively in myocardial SPECT. Based upon the results an effective half-life was calculated, and at 30 minutes after examination the time to reach normal dose limit in 'Nuclear Safety Act' was calculated conservatively without considering a half-life. In oder of distance (at skin surface, 0.5 m and 1 m distance from patients), it was 7.9, 34.1 and 106.8 hr, respectively in PET/CT; 40.4, 199.5 and 451.1 hr, respectively in bone scan; 62.5, 519.3 and 1313.6 hr, respectively in myocardial SPECT. **Conclusion:** Our results clearly showed that total amount of radiation exposure caused by residual radioactive isotope in the patient body was neglectable, even comparing with the natural radiation exposure. In conclusion, nurses in a general ward were much less exposed than the normal dose limit, and the effects of exposure by contacting patients undergoing nuclear medicine examination was ignorable.

E-TPW50

Dose Rates from the Patient in Conventional Nuclear Medicine: "To Void or Not to Void", that is the Question!

A. Cunha[1], D. Neves[1,2], R. Oliveira[3], A. Nunes[4], C. Alves[4], L. Santos[4], L. F. Metello[1,5]; [1]ESS – IPP, ATC&CMN, Rua Dr. Antonio Bernardino de Almeida, 400, 4200 – 072, Porto, PORTUGAL, [2]DIATON S.A. – Leiria, Dept. de Med. Nuclear, Rua de Olhalvas, Pousos, 2410-197, Leiria, PORTUGAL, [3]FEUP – UP, Dept de Estatistica, Rua Dr. Roberto Frias, 4200 – 465, Porto, PORTUGAL, [4]DCC – Dr. Campos Costa, Dept. de Med. Nuclear, Instituto CUF, Rua Fonte das Sete Bicas, 170, 4460 – 188, Matosinhos, PORTUGAL, [5]IsoPor-Azores, Dept de Med. Nuclear e Imagiologia Molecular, Angra do Heroismo, I. Terceira, Azores, PORTUGAL.

Introduction: Patients subjected to Nuclear Medicine procedures emit radiation isotropically, exposing themselves, professional staff and public. Agents used in Nuclear Medicine are mostly excreted by the urinary system. However, when bladder emptying doesn't have image/diagnostic predictable impact, requesting patients to void before positioning is not always a common practice. Theoretically, this fact can influence patient dose rate, and therefore, occupational exposure. **Aim:** Firstly to evaluate the voiding factor impact on emitted patient dose rate in common scintigraphy procedures, in distinct anatomic areas and at different distances, and secondly to compare the results on dose rate to investigate relevancy on asking patients to void before procedures. **Material and Methods:** 85 patients/procedures where evaluated until now: 30 bone scintigraphy, 15 thyroid scintigraphy and 40 myocardial perfusion scans (20 in rest and 20 under stress conditions). Dose rates were measured before and after voiding at different anatomic areas (head-vertex, head lateral, pelvis and feet) and for different distances (0, 0.5 and 1 m). Geiger-Muller detectors were used in all situations. **Results:** The higher patient dose rates were observed at the pelvis. Before voiding, at 0, 0.5 and 1m, the mean values for emitted patient dose rates were 797 (±174,43), 121 (±19,46) and 36 (±7,47) μSv/h respectively. After voiding, obtained values were 721 (±181,36), 102 (±21,00) and 29 (±5,60)μSv/h. Lower patient dose rates were measured at the feet. Before voiding obtained values were 11 (±2,78), 4 (±3,32) and 1 (±0,68) μSv/h. After voiding, the values obtained were 8 (±2,29), 2 (±0,57) and 1 (±0,34) μSv/h. At 0m, the major reduction on dose rate was observed at the pelvis position for bone and thyroid scintigraphy (23%) cases; the minor reduction was achieved at the head-lateral in myocardial stress perfusion scans (7%). At 0.5m distance, the higher difference was observed at the feet position, for thyroid scintigraphy (36%); while the smaller reduction was achieved at the head-vertex, for myocardial stress perfusion scans (8%). At 1m distance, the major reduction was observed at the feet for thyroid scintigraphy (44%); the minor reduction was observed at the head-lateral position, also in thyroid scintigraphy, with the same value observed at the pelvis position for myocardial stress studies (18%).**Conclusion:** Strategies for emitted patient dose rate reduction are crucial for radioprotection matters. Our (preliminary) results seems to point that patients should be always encouraged to void before image acquisition in order to allow reducing exposition for all involved parts.

E-TPW51

Optimization of the exposure to the extremities of the technologists in nuclear medicine based on daily routine workflow

L. Vojo, K. Zeimpekis; University Hospital Zurich, Zurich, SWITZERLAND.

Purpose: Due to the increasing number of nuclear medicine exams in Switzerland, the exposure to the operators becomes a prominent issue. The exposure burden to the extremities of the technologists inside the same nuclear medicine department exhibits a significant variation. The exposure depends mainly on the area where the operator is working (e.g. SPECT or PET) and the radiotracers that he is handling during preparation as well as during administration. If we consider the same working area and the same type of radiotracers, then the difference of the exposure distribution along the operators comes solely from the way the operator handles the activity, his overall be-

haviour with patients (e.g. time for instructions & distance) and how much time does he or she needs. In order to achieve more normalised exposure distribution through minimizing this dose variation, we used a questionnaire with enough questions that span the entire daily routine and go step by step in the workflow in the nuclear medicine center. **Methods:** The radiation protection expert, after making a yearly dose statistics, identified the dose difference and took the lowest dose as the reference for our optimization goal. The questionnaire was made up of three parts each one associated with one specific task. The first was the „Activity Preparation (Hot Lab)" with the highest exposure risk to the extremities. The second part involved the „Administration-Injection" (operating with activity outside the lab), and the last part considered how the operator works around the injected patient. Every questionnaire was scored and in order to optimize the overall performance the operator was given the correct way to work. During the first three months, the so-called monitoring period, the monthly finger exposures were summed up and percentage differences were calculated. **Results:** Even after the first month, the operators, especially the ones with the higher finger doses, had a massive reduction of the exposure and the dose distribution more uniform. Significant reductions, in some cases more than half, were noted. **Conclusion:** The use of the questionnaire proved to be extremely helpful, since the operators considered every step of the process, as discussed in the Methods, more carefully and that led to lower extremity doses. More importantly the dose reduction was evident already after the first month. Therefore we recommend the use of the questionnaire to other nuclear medicine institutions as well, for a better dose management to the operators.

E-TPW52

The predicting value of ^{18}F-FDG PET/CT imaging of radioactive iodine treatment efficacy in patients with bone metastasis from differentiated thyroid cancer

D. Wang, *C. Ma; Affiliated Xinhua Hospital of Shanghai Jiaotong University School of Medicine, Shanghai, CHINA.*

Objective: Our study aimed to investigate the value of ^{18}F-FDG PET/CT for prognostic prediction and response assessment in patients with bone metastases originated from DTC. **Methods:** The ^{18}F-FDG PET/CT scans from 30 differentiated thyroid cancer (DTC) patients with bone metastases treated with radioactive iodine at Xinhua Hospital between 2004 January and 2017 March were retrospectively analyzed. Therapeutic response assessment was based on serum thyroglobulin (Tg) levels and anatomical imaging changes. Relationships between ^{18}F-FDG uptake and factors reflecting therapeutic response were compared using univariate analysis. **Results:** Among the 30 patients included in the study, 19 (63%) patients were ^{18}F-FDG+/[131]I+, 6 (20%) were ^{18}F-FDG+/[131]I- and 5 (17%) were ^{18}F-FDG-/[131]I +. Univariate analyses showed that ^{18}F-FDG and ^{131}I uptake pattern and the number of ^{18}F-FDG-avid lesions significantly influenced the response rate based on anatomical imaging changes (p=0.018 and 0.004). While changes in serum Tg were only related to ^{18}F-FDG and ^{131}I uptake pattern (p=0.010). **Conclusions:** ^{18}F-FDG and ^{131}I uptake pattern is significantly correlated with the therapeutic response of DTC patients with bone metastases after ^{131}I therapy. ^{18}F-FDG PET/CT scan is a useful tool for predicting the efficacy of radioactive iodine treatment in DTC patients with bone metastases.

E-TPW53

Use of 4D-PET/CT in the Radiotherapy Treatment Planning of the Retroperitoneal Lesions Near the Diaphragm

L. Pavanello, *F. Sciumè, M. Zuffante, M. Cucca, D. Grigolato, L. Locantore, M. Ferdeghini; AOUI Verona, Verona, ITALY.*

Introduction and Purpose: This study shows how a 4D-PET/CT can improve the radiotherapy treatment planning of the retroperitoneal lesions near the diaphragm, facilitating a correct target delineation and allowing a correction of the target motion due to the breath. **Materials and Methods:** At the Nuclear Medicine Unit of Verona University Hospital, 4D imaging is obtained using a PET/CT Gemini Big Bore system (with TOF reconstruction) and a respiratory synchronization system Varian Real time Position Management (RPM) interfaced with linear accelerator for radiotherapy treatment. The protocol foresees a Total Body acquisition at 60 minutes after administration of the 18F-FDG, followed by 4D-PET/CT study of the region of interest. The patient is supine in radiotherapy position on the flat radiotherapy bed. The CT parameters used for TB acquisition are: 120 KV, mAs modulated, pitch 0.813, 16x1.5mm collimation, slice thickness 3, FOV 600. The PET parameters are: 1.3 min bed position, FOV 576mm, 2.5 MBq/Kg of 18F-FDG. Varian RPM 4D-PET/CT study needs the technician to evaluate and monitor the respiratory cycles; the acquisition starts once the planned amplitude and regularity respiration are achieved. Pitch is adapted to the number of breaths per minute before acquiring a CT scan of the region of interest while PET parameters are set with a nominal phase of 20%, two minutes for phase. Retrospective reconstruction is used for each respiratory cycle phase. The breath curve is analyzed considering the respiratory cycle amplitude. **Results:** Retroperitoneal lesions are more effectively visualized with 4D-PET/CT, and the same images can be used to outline the Biological Target Volume (BTV) in radiotherapy patients. 4D-PET/CT images show a clearer pathological uptake in tumor lesions and an increase of SUV compared to a standard free-breathing PET/CT scan, where the hypermetabolic areas appear bigger and blurred. This allows better spatial delineation compared to the surrounding organs. Sometimes, the Total Body acquisition detects unrecognized repetitive lesions, causing a change in treatment management. **Conclusion:** The use of gating improves the detection and quantification of time-space movements of tumor lesions and surrounding organs. 4D-PET/CT allows a compensation of images degradation induced by respiratory movements, upgrades both diagnosis and RT treatment planning and provides information on target motion, which can be used to personalize RT treatment planning. The Total Body acquisition allows an accurate staging of the patient with possible change of treatment.

E-TPW54

Developing an Educational Strategy for Hybrid Imaging Practitioners: A Tailored Approach

R. Menezes; Oxford University Hospitals NHS Foundation Trust, Headington, Oxford, UNITED KINGDOM.

Purpose/Introduction: This research looks at the challenges of Hybrid Imaging and focuses on understanding the training needs across a Nuclear Medicine and PET/CT department. The author's core objectives are discussing the challenges of Hybrid Imaging, developing a training and education framework for practitioners and analysing the cultural changes resultant from its implementation. The author proposes the creation of tailored training frameworks dependent on practitioners' qualifications, clinical experience and self-confidence to overcome the lack of formal educational guidelines and career support mechanisms in Hybrid Imaging. The implementation of new Hybrid Imaging profiles requires careful planning and collaboration, since it implies changes in the service dynamics and in working culture. Professional diversity within the workplace can make the development of an adequate Hybrid Imaging training framework to promote a qualified and competent workforce difficult to achieve. **Subjects/Methods:** To facilitate this, the required professional knowledge and competency skills for the optimal use of Hybrid Imaging equipment were investigated through literature review. Furthermore, the author has gathered the opinions of the Hybrid Imaging Practitioners working in Nuclear Medicine and PET/CT department. This was achieved by developing a questionnaire and holding informal discussions about the emerging role of the Hybrid Imaging Practitioner. Data generated from the questionnaire was analysed with pie charts, graphs and tables to demonstrate the results. Poorly scoring areas were analysed further, and methodologies to improve these results were investigated. The results of the questionnaire were studied in relation to the notes taken during the informal discussions and meetings to comprehend the working culture of the Hybrid Imaging department and identify training needs. **Results:** Results and findings were utilised to revise core competencies and training requirements for Hybrid Imaging Practitioners, either Nuclear Medicine Technologists or Radiographers. This has encouraged the development of an educational strategy and training framework. In particular, the author proposes three educational algorithms to help identify individual training needs and ensure that both professional groups are confident and autonomous in their work. **Discussion/Conclusion:** The author concluded that appropriate clinical experience, qualifications and specific Hybrid Imaging training are key among a Hybrid Imaging team, and influence service provision. Depending on educational background and previous clinical experience, the required additional Hybrid Imaging training for each member of staff will differ. Hence, a tailored approach is necessary and paramount for success.

E-TPW55

In Search of Minimum Time-Interval Between the Two Continuous FDG-PET Scans of The Same Subjects

S. Han[1], X. Liang[1], X. Hu[1], L. Wan[2], P. Xiao[1], Q. Xie[1]; [1]Huazhong University of Science and Technology, Wuhan, CHINA, [2]Raydata Technology Co.,Ltd, Ezhou, CHINA.

Aim: In multiple FDG-PET experiments of the same subjects, the results are interfered by fast and anesthesia and other factors of the previous FDG-PET. In order to eliminate the interference, it needs enough time interval between the two continuous FDG-PET scans. The aim of this study was to evaluate the minimum time-interval between the two continuous FDG-PET scans of the same subjects. **Methods:** Thirty-five adult mice were scanned with ^{18}F-FDG. All the mice were randomly divided into seven group according to the time-interval of the two continuous experiments from 0-6 day respectively. Day 0 means the interval of the twice experiments was 24h. Day1 was 48h and so on. Mice were scanned 10 min after a 60-min uptake period. Data were acquired from the Trans-PET ® BioCaliburn ® 700 (Raycan Technology Co., Ltd, Suzhou, China) and reconstructed using the 3D OSEM algorithm. The software AMIDE was used to quantify the mean standard uptake value (SUVmean) of the whole brain. The ratio of the SUVmean of the same mouse in two different experiments was calculated to analyses the deviation of the FDG uptake of the whole brain. **Results and Conclusion**: The deviation of the FDG uptake of mouse brain which interval of 0 day is greater than 10%, reaches to 12%. The other groups are less than 10%. These preliminary findings indicate that it needs at least waiting for one day to do the second time FDG-PET scan for the same subject.

E-TPW56

Laser Scanning And Computed Tomography 3D: Application In The Skin Surface Modelling Of PIXI Phantom Head

E. Sousa[1], L. Vieira[1], D. Costa[2], D. C. Costa[3], R. Parafita[3], R. Parafita[3], M. A. R. Loja[2]; [1]Escola Superior de Tecnologia da Saúde de Lisboa, Instituto Politécnico de Lisboa, Lisboa, PORTUGAL, [2]Instituto Superior de Engenharia de Lisboa, Instituto Politécnico de Lisboa, Lisboa, PORTUGAL, [3]Fundação Champalimaud, Lisboa, PORTUGAL.

Aim: To evaluate the influence in the Modelling of 3D skin surface caused by different acquisition and reconstruction methods. **Methods**: PIXI head phantom images were acquired by Computed Tomography (CT) with 1 and 2 mm slices, and with a 3D laser scanning (3DLS). For CT acquisitions PIXI phantom was scanned on the Philips Gemini TF 16 with two different thickness of slices (1 mm and 2mm) while keeping other acquisition parameters constant: 20 mAs, 120kVp, pitch of 0.938, 512x512 pixel matrix, rotation speed of 0.5s per rotation, both studies were reconstructed in 3D imaging with ImageJ and Osyrix software. To perform the 3D laser scanning of the phantom head, was used a NextEngine system, with a medium range acquisition and a number of ten sectors with a density of 850 points per square inch. The system precision is 0.005 inch. With the 3D point cloud acquired, a subsequent mesh was generate to yield the surface reconstruction, it was carried out automatically by the same system. In order to assess the differences between

acquisition and reconstructed methods were calculated measurements between several anatomic references of PIXI phantom. For statistical evaluation it was used the Friedman test for non-parametrical pared samples. **Results:** After the comparison of all the reconstructed images measurements, there were not found any statistically significant differences, in the together comparison of the methods, (p=0.414. When maintaining the thickness of the slices and comparing the CT with laser there were not verified statistically significant differences, neither for the comparison of CT slices acquired with 1 mm neither in the comparison between CTImg1, CTOsx1 and 3DLS (p=0.981); neither in the comparison of CTImg2, CTOsx2 and 3DLS (p=0.232). Despite the non-existence of statically significant differences the results show a greater concordance between laser and the both reconstruction methods when the CT was acquired with 1 mm slices. **Conclusion:** The evaluation of spatial resolution of the applied imaging systems is essential for accurate and precise measurements. The advent of more complex imaging systems has posed an increasing challenge in our ability to assess their performance, including spatial resolution. Although there were not found statistically significant differences and all the techniques used can be applied for 3D surface modeling, there are differences that can cause inaccuracies in some applications of the 3D modeling surface, further research is needed.

E-TPW57

Optimization of parameters for SPECT/CT studies: The impact of aquisition parameters on data quality using quantitative SPECT reconstruction

B. Mirocha, M. Benke, D. Dokudowiec, A. Sackiewicz, M. Wojewódzka, M. Dedecjus; Maria Skłodowska Curie Memorial Cancer Centre and Institute, Warsaw, POLAND.

Introduction: The aim of this study was to investigate whether duration of Single Photon Emission Tomography (SPECT) imaging affects the quality of acquired data by performing quantitative measurements of 99mTc uptake based on the Standardized Uptake Value (SUV). Recently, a scanner combining SPECT and Computed Tomography (CT) has gained widespread acceptance. The addition of SPECT/CT to conventional planar scintigraphy brings significant improvement in its diagnostic accuracy. SPECT/CT devices deliver metabolic and detailed anatomical information. However, due to prolonged aquisition time SPECT/CT fused imaging is not in routine clinical practice as became PET/CT. **Materials and Methods:** The study was performed using GE Healthcare Hybrid Gamma-Camera Discovery NM/CT 670. Quality 01P Phantom filled with 34 MBq of 99mTc was chosen for SPECT/CT data obtaining. We acquired data for SPECT images depending on different gantry rotation time. Eight different SPECT parameters were defined: 90, 45, 30, 18, 15, 10, 9 and 6 views over 180°. Other conditions applied in all SPECT scans were the same: acquisition times per view 10 sec, matrix 128 x 128, 3,6 mm per pixel, rotation of detectors by 180° in noncircular orbit and step and shoot mode. Low-dose CT for attenuation correction was performed using standard parameters for each SPECT subset separately. The effective ac-

quisition time was reduced from 900 to 60 sec. Delineation of five different spherical VOIs per each phantom was performed (three VOIs over three different isotope filled compartments: VS1, VS2, VS3 and two control VOIs over blanks: VC1, VC2). The final body weight based SUVmin, SUVmean and SUVmax assessment was made using Q. Metrix segmentation tools. **Results:** Preliminary results showed that reduction of SPECT/CT acquisition time has no significant impact on quality of data in defined experimental environment. **Conclusion:** Impact of this finding on clinical practice needs to be evaluated. Statistical significance assessment of standard deviation (SD) of acquired SUV values will be implemented.

E-TPW58

Optimal timing of Furosemide administration for ¹⁸FFDG PETCT Acquisition of pelvic tumors

G. van der Ven, E. Leautaud, H. Pijpers; Instituut Verbeeten, Tilburg, NETHERLANDS.

Aim: In order to differentiate tumor uptake from urinary excretion in ^{18}F-FDG PET-CT examinations for pelvic tumors, furosemide is injected just before FDG. This method often didn't improve image quality. The aim of this study is to determine the optimal timing of Furosemide administration during PET-CT examination. **Method:** Thirty-four patients with a pelvic malignancy participated in this study. All patients were asked to drink 500 ml water within 2 hours prior to FDG. During FDG uptake period of 60 minutes 500 ml natriumchloride was administrated. Previous to the whole body scan we asked the patient to void their bladder. The scan direction was caudo-cranial to minimize bladder activity. We compared two different dosing times of furosemide administration, before FDG and directly after the whole body scan. All patients were devided in two groups. Group l (9 patients) received furosemide before FDG. The delayed pelvic scan was obtained thirty minutes after the whole body scan. Group ll (25 patients) received furosemide directly after the whole body scan. The delayed pelvic scan was obtained thirty minutes after furosemide. The iv-catheter was kept in situ for the furosemide. The delayed pelvic scans were visual classified as useful or not useful. **Results:** Furosemide administration before FDG did not improve (=decrease of) bladder activity in the delayed pelvic scan compared to the whole body scan in 8/9 exams (89%). Only one delayed pelvic scan showed improvement. Furosemide administration after whole body scan showed significant visual improvement in the pelvic area in 19/25 exams (76%). Six exams in this group showed no improvement (24%). The first group of patients showed many unwanted interruptions of pre-scan resting, due to the forced diuresis. **Conclusion:** Furosemide administration directly after the whole body scan proves to be the optimal timing for differentiating tumor uptake from urinary excretion in the pelvic area. The scans show significant decreased bladder activity and better visual tumor to background ratio's. Late furosemide administration is more patient friendly, it prevents unwanted interruptions of pre-scan resting and the whole body scan due to an urgency to void. Unnecessary furosemide administration.

An additional benefit of late furosemide administration may be lower radiation exposure for the technologist. Further research is recommended.

E-TPW59
FDG PET/CT artifacts - daily practice aspects related to a technologist perspective

M. I. Larg, C. Pestean, M. Crisan, E. Barbus, D. Piciu; "Ion Chiricuta" Institute of Oncology, Cluj-Napoca, ROMANIA.

Aim: Diagnostic accuracy is fundamental in management of oncological patients and can directly influence therapeutic decisions. By combining the positron emission tomography (PET) with computed tomography (CT) in a single scanner - positron emission tomography/computed tomography (PET-CT) represents an important achievement. 18F - fluorodeoxiglucose (FDG) is the most widely used radio-pharmaceutical in PET/CT, being a marker of glucose metabolism indicator. Besides the advantages of FDG PET/CT imaging, it may produce several artifacts. As a nuclear medicine technologist it is important to be aware of all of these aspects in order to avoid possible artifacts. **Material and Methods:** We performed a retrospective study over a one-year period during which we have made 893 FDG PET/CT scans. The images were acquired on a GE Optima 560 PET/CT (BGO detector/16 slices). CT parameters used were 100-120Kv, 50-100mA auto, and noise index 20%, slice thickness 3.75mm. PET/CT data were acquired with 3 minutes/bed, using iterative techniques (OSEM - 2 iterations/ 16 subsets) with an uptake time of 50-60minutes. **Results**: The artifacts were distributed as follow: respiratory motion 28,11% (251 cases), bladder artifacts 25,19% (225 cases), CT artifacts (CT beam hardening an CT ultra-low dose) 19,59% (175 cases), metal artifacts 15,22% (136 cases), patient motion 3,58% (32 cases), fasting conditions 14,11% (126 cases), truncation 3,02% (27cases), brown fat 1,67% (15 cases), hypoglycemia interference 0,55% (5 cases), hyperglycemia 0,55% (5 cases), noise in the PET images 0,55% (5 cases), subcutaneous tracer infiltration 0,22% (2 cases). In 0.55% of the cases it was necessary to repeat the examination in order to assess a correct image interpretation. **Discussions:** Patient size is one of the most important determinants in image quality, that is why the CT acquisition parameters should be adjusted and the injected dose should be calculated accordingly to the patient's weight. Arm positioning requires special attention in those situations where the scan is performed with arms down, to avoid beam hardening artifact. **Conclusions:** Respiratory motion and bladder artifacts were the most encountered artifacts but with a proper patient preparation and special explanations to the patient, these artifacts can be avoided. According to the job profile and daily responsibilities as a nuclear medicine technologist it is important to recognize these artifacts, to be aware of the potential causes in order to ensure the image quality and to avoid any bias in diagnostic information.

E-TPW60
Design and Evaluation of the reconstruction for a dedicated breast PET<MAMMI>

M. Sun, Y. ZHANG, L. Pan; FuDan University ShangHai cancer center, shanghai, CHINA.

Purpose: The aim of this study was to investigate the diagnostic performance of the reconstruction process with different iterations used on a dedicated breast PET. **Patients and Methods:** A scan taken with a dedicated high-resolution breast PET - MAMmography with Molecular Imaging <MAMMI>was performed 60 min after administration of 180-240MBq of ^{18}F-FDG in patients with known or suspected breast cancer. The procedure was performed with the patients in the prone position for the breast of the patient as far as possible in the field of vision. Every patient's raw data were reconstructed with 1-20 iterations. **Results:** 50 patients with total 73 breast lesions in patients with mammography were enrolled. When the reconstruction with 8 iterations the lesion-based sensitivity was 89% <65/73>; with 12 iterations the lesion-based sensitivity was 95% <70/73>; with 16 iterations the lesion-based sensitivity was 97%<71/73>; with 20 iterations the lesion-based sensitivity was 93%<68/73>.For the density of the breasts were different, 2 special lesions were considered positive in 12 iterations but cannot be found in others iteration; and other 3 special lesions were found in 16 iterations. **Conclusion:** Our preliminary study indicates that in MAMMI breast PET the number of iterations should be controlled in 12-16. We will lose part of lesions when the number of iterations is less than 12 or more than 16.And one patient's raw data should be reconstructed with both 12 iterations and 16 iterations to gain more detailed information.

Technologist e-Poster Session 4

E-TPW61
Residual Activity Correction Successfully Adjusts Myocardial Blood Flow Measurements in Time-efficient ^{13}N-ammonia Myocardial Perfusion PET/CT

P. A. Doodeman, S. V. Lazarenko, F. M. van der Zant, M. Wondergem, R. J. J. Knol; Northwest Clinics Alkmaar, Alkmaar, NETHERLANDS.

Purpose: In time-efficient ^{13}N-ammonia myocardial perfusion PET/CT, successive rest and stress acquisitions are performed within a time frame of 25 minutes. A residual activity correction (RAC) algorithm is used to account for residual activity left from the rest study in the myocardium, when initiating the stress acquisition. This study aimed to assess the effects of RAC on myocardial blood flow (MBF) analysis. **Subjects & Methods**: A total of 69 patients were included in the study, of which 33 had no history of coronary disease or cardiac events during follow up, and displayed normal MBF values. The other group of 36 patients was previously diagnosed with very low MBF values, due to proven three-vessel disease. MBF measurements were performed for both groups with and without RAC of the dynamic stress datasets. **Results**: Mean global MBF at stress was

3.15±0.40 mL/min/g without RAC and 2.73±0.42 mL/min/g with RAC (p<0.001) for the normal group. For the group of patients with known reduced MBF, mean global MBF at stress was 1.64±0.46 mL/min/g without RAC and 1.34±0.42 mL/min/g when the RAC algorithm was used (p<0.001). The amount of the stress flow overestimation without RAC correlated with the rest MBF. The mean difference between RAC and non-RAC adjusted dynamic datasets was 0.42±0.13 mL/min/g (15±5%) for the normal group versus 0.30±0.12 mL/min/g (22±9%) for the group of patients with proven three-vessel disease (p=0.484). Although not statistically significant, the latter group demonstrated a relatively higher overestimation compared to the normal group. Similar results and statistical outcomes were obtained for each of the separate LAD, LCX and RCA territories. **Conclusion**: RAC successfully adjusts dynamic stress acquisitions in both patients with normal MBF and patients with reduced MBF. RAC of stress images avoids overestimation of stress MBF in time-efficient ^{13}N-ammonia myocardial perfusion PET/CT studies.

E-TPW62

Left ventricular volumes and EF measered with ^{13}N-ammonia PET/CT varies substantially with the software package used for analysis

V. S. Barten-Bruin[1,2], S. V. Lazarenko[1,2], L. C. D. Zaat[1], F. M. van der Zant[1,2], M. Wondergem[1,2], R. J. J. Knol[1,2]; [1]Department of Nuclear Medicine, Northwest Clinics, Alkmaar, NETHERLANDS, [2]Cardiac Imaging Division Alkmaar, Alkmaar, NETHERLANDS.

Aim: Left ventricular volume measurements in myocardial perfusion studies are generally known to be imprecise and different software packages produce different measurements. In the present study, head-to-head comparisons were performed between end-diastolic volumes (EDV), end-systolic volumes (ESV) and left ventricular ejection fraction (LVEF) measured using two different software packages in patients referred for ^{13}N-ammonia PET/CT, and EDV measurements were related to a reference standard. **Materials and Methods:** A cohort of 70 patients with normal ^{13}N-ammonia PET/CTs, without history of coronary disease or subsequent cardiac events, was studied. Gated rest and stress datasets were analyzed using both Invia Corridor 4DM (Mirada Medical, USA) and Cedars QGS (Cedars Sinai, USA) and EDV, ESV and LVEF measurements were compared. A second cohort of 31 patients with proven three-vessel disease was analyzed similarly. A third cohort of 32 patients had also undergone coronary computed tomography angiography (CCTA) within 1 year before or after ^{13}N-ammonia PET/CT. Of the latter, EDV was measured in both software packages and additionally the CCTA was processed in the Cardiac Function module in Syngo. via VB10B (Siemens Medical Systems, Germany) to obtain EDV, which served as the reference standard. SPSS 22.0.0 (IBM, USA) was used for comparison between measurements using student t-tests or Wilcoxon signed-rank tests, where appropriate. **Results:** In both the normal group and the group known with three-vessel disease, significant differences (p<0.001) were detected between the analyses performed by Corridor 4DM and Cedars QGS for all EDV, ESV and LVEF measurements. In the nor-

mal group, average EDV was 11.5% (rest) and 9.5% (stress) higher in Corridor 4DM as opposed to Cedars QGS, whereas for ESV this was 27.9% and 25.4%, respectively. In the group with proven three-vessel disease, EDV was 15.3% (rest) and 16.5% (stress) higher in Corridor 4DM, whereas ESV were 25.7% and 27.8% higher, respectively. The LVEF was 10.3% (rest) and 9.0% (stress) lower in Corridor 4DM in both the normal group and 13.5% (rest) and 16.4% (stress) in the group with proven three-vessel disease. Compared to EDV measured by CCTA (129.2±30.2 mL), Cedars QGS' EDV (110.4±31.0 mL) was significantly lower (p<0.001) whereas Corridor 4DM's EDV (126.3±36.2 mL) did not differ (p=0.210). **Conclusions:** The choice of software package used for left ventricular volume measurements significantly affected the outcome in the studied cohorts. Of the studied software packages, volume measurements obtained with Invia Corridor 4DM appeared to be more consistent with measurements obtained with CCTA.

E-TPW63

Comparison of MPI SPECT/CT scans acquired with LEHR collimator and reduced time IQ•SPECT system

S. Ferreira[1], P. Begley[2], M. Jessop[2], A. Aldous[3], N. Eftychiou[2], N. Singh[2], S. Dizdarevic[2], E. Sousa[1]; [1]Lisbon School of Health Technology, Polytechnic Institute of Lisbon, Lisbon, PORTUGAL, [2]Brighton and Sussex University Hospitals, Brighton, UNITED KINGDOM, [3]North Cumbria University Hospitals, Cumbria, UNITED KINGDOM.

Aim: Compare characteristics of SPECT/CT stress images acquired using both low energy high resolution (LEHR) collimator and reduced time IQ•SPECT methodology, regarding image quality, perfusion and left ventricle ejection fraction (LVEF). **Methods:** Study of 7 male patients who underwent ^{99m}Tc-tetrofosmin regadenoson gated myocardial perfusion stress imaging using two consecutive acquisitions, LEHR and IQ•SPECT. A low-dose CT was performed after the LEHR acquisition for attenuation correction of both studies. Images were acquired with a 208º scan arc and 34 frames of 8 seconds (6.1º angular step) for IQ•SPECT and with a 180º scan arc and 128 frames of 30 seconds (2.8º angular step) for LEHR acquisition. Twenty eight sets of images (7 LEHR-NAC, 7 LEHR-AC, 7 IQ•SPECT-NAC and 7 IQ•SPECT-AC) were analysed. For image quality, endocardial edge definition, perfusion defect delineation, and image noise were visually assessed by consensus report from two experienced physicians. Perfusion defect scores for each coronary territory were semi-quantitatively determined using a 5-point scoring system. LVEF, end-diastolic (EDV) and end-systolic (ESV) volumes were automatically analysed using Cedars Sinai QGS/QPS. Results were analysed using Bland-Altman and paired t student test. **Results:** IQ•SPECT-AC showed a significant (p<0.05) improvement on endocardial edge definition, however LEHR demonstrated a better perfusion defect delineation, though not statistically significant (p=0.08). Regarding image noise, no differences were seen (p=0.36). In all coronary territories, QPS showed higher perfusion percentages for LEHR-AC than IQ•SPECT-AC (mean difference = -1.0; -5.0; -3.1, for left anterior descending (LAD), left circumflex (LCX) and right coronary artery (RCA), respectively)

and Bland-Altman analysis showed minimal bias and fair-good agreement. When comparing physician's perfusion defect visual scores, no significant differences were seen (mean difference = -0.3; +0.1; +0.3, for LAD, LCX and RCA, respectively). Regarding QPS' summed stress scores (SSS), the biggest divergence was 7, though a bias was not seen towards a specific technique. When evaluating LVEF on QGS some bias and fair agreement could be seen and there was EDV disagreement, with a tendency for a higher value for LEHR. **Conclusion:** In comparison with LEHR, ultra-fast IQ•SPECT resulted in similar image quality, demonstrated a better endocardial edge definition, but a tendency to underestimate perfusion percentage, perfusion defect delineation and EDV in this study. Larger prospective studies, including comparison with rest data, are suggested to investigate the impact of these variations on the clinical report and subsequent patients' risk assessment and management.

E-TPW64

Motion reduction activities in patients undergoing myocardial perfusion SPECT with the Discovery NM 530c(D530c)

D. Lee, W. Choi, W. Jung; Asan Medical Center, Seoul, KOREA, REPUBLIC OF.

Purpose: The D530c have cadmium zinc telluride(CZT) detectors that are arranged focus on the heart. This structural characteristic allows for quicker imaging without rotation, but this is sensitive to patient movement and can affect the test results. The aim of this study is to optimize the image quality by reducing patient movement during the examination. **Subjects and Methods:** We analyzed the patients' movements, and performed various activities such as provided patient education about correct breathing techniques and avoiding patient movements, and created breathing correction tools to minimize patient movement during exam. The 70 patients who underwent myocardial perfusion SPECT with D530c in November 2016 were categorized as the group before the corrective steps. Another 70 patients who underwent the procedure with D530c from February 14, 2017 to February 21, 2017 were categorized as the improvement group. Images acquired during stress and at rest were compared and analyzed by measuring the durations of heart movements over certain distances (4 mm, 8 mm, 12 mm, or more) noted on the x-, y-, and z- axes. **Results:** After the activities, the durations of heart movements decreased in the images acquired both under stress and at rest. In particular, there were no large motions greater than 12 mm recorded in the stress images after the improvement. There was a significant difference ($p<0.005$) in the 4-mm and 8-mm fluctuations on the X-axis and the 8-mm fluctuations on the Z axis in the stress images, but there was no significant difference ($p>0.005$) in the other stress and rest intervals. **Conclusion:** The decrease in the time of motion occurrence due to the 4mm fluctuation distance that can occur through breathing can be understood as a result of the breathing being corrected through training and motion prevention tools. It is expected that the image quality will be improved by reducing the occurrence time according

to the variation distance of 8mm or 12mm, which is expected as the actual movement of the patient other than the breathing.

E-TPW65

The washout rate and the heart to mediastinum ratio of 123I-beta-methyl-iodophenyl pentadecanoic acid can reflect the severity of myocardial damage

T. Iimori[1], H. Miyauchi[2], K. Sawada[1], T. Umezawa[1], T. Sada[1], Y. Masuda[1], Y. Kuwabara[2], T. Uno[3], Y. Kobayashi[2]; [1]Department of Radiology, Chiba University Hospital, Chiba, JAPAN, [2]Department of Cardiovascular Medicine, Chiba University Graduate School of Medicine, Chiba, JAPAN, [3]Department of Diagnostic Radiology and Radiation Oncology, Chiba University Graduate School of Medicine, Chiba, JAPAN.

Background and Purpose: 123I-beta-methyl-iodophenyl pentadecanoic acid (123I-BMIPP) scintigraphy images myocardial fatty acid metabolism. 123I-BMIPP myocardial imaging has been reported to be highly useful for the detection of ischemic myocardium and early myocardial damage, the evaluation of myocardial viability, and the diagnosis of cardiomyopathy. The aim of this study is to investigate the relations of the washout rate (WOR) to the myocardial damage, and the heart to mediastinum (H/M) ratio to the myocardial damage in 123I-BMIPP scintigraphy. **Subjects and Methods:** We conducted a retrospective survey of twenty participants (58.5±12.8 years, 12 men and 68.3±10.9 years, 8 women) who had undergone 123I-BMIPP scintigraphy. We calculated the early H/M ratio, the late H/M ratio, and the WOR of 123I-BMIPP. We also calculated the defect scores (DS) using the 17-segment model with a five-point scoring system and assessed the relations between the WOR and the DS, and the H/M and the DS. **Results:** The early H/M ratio was significantly correlated with the DS (r=0.69), and the WOR was also significantly correlated with the DS (r=0.72). **Conclusion:** The WOR and the early H/M ratio of 123I-BMIPP have been useful to assess the severity of myocardial damage.

E-TPW66

A cost effective protocol for increasing patient throughput using a combination of half time imaging with 99mTc Tetrofosmin and Regadenoson in Stress Myocardial Perfusion Imaging

P. J. Turner, T. Watts, F. Whittingham; The Royal Wolverhampton NHS Trust, Wolverhampton, UNITED KINGDOM.

Aims: In our centre by 2012 referral rates for MPS were exceeding availability resulting in excessive waiting times for the patients and fines for the Trust. As a single camera department we needed to change the way we worked in order to increase our throughput but had limited resources. The aim of this project was to optimise MPS using the Philips BrightView X-CT gamma camera and the Astonish reconstruction algorithm in conjunction with Regadenoson for stressing. The primary objective was, using the standard prescribed injected activity, to reduce the stressing and scanning time of each patient to a minimum, whilst maintaining

image quality. **Method:** Half Time imaging was evaluated using a combination of jaszczak (preliminary work) and cardiac phantom studies. Image quality was assessed on the cardiac phantom by measuring contrast and the FWHM of the phantom wall Comparison of Regadenson and Adenosine stressing was made with a view to ease of use, side effects, time and cost. **Results:** Cardiac phantom imaging demonstrated that reducing the scan time to 15 seconds per view had no statistically significant effect on the image quality. Further comparison of segmental polar maps also demonstrated little difference between original acquisition parameters and the half time scan. Stressing agent comparison demonstrated a 60% reduction in time to complete stress protocol by switching to Regadenoson. We also found that the incidences of side effects were approximately the same between both agents but the effects were on average shorter with Regadenoson. The Regadenoson protocol was simpler to perform and there was a lower likelihood of errors due to no weight dependent dosage. Cost comparison put Regadenson at ~50% more for our average patient than Adenosine, but it was offset by a reduction in the fines to the hospital and the Cardiologist's time. The combined protocol increased patient slots by 50% per cardiac session. **Conclusion:** Regadenson combined with half time imaging is a cost effective way to increase your MPS throughput while maintain diagnostic image quality. Following implementation of the new MPS protocol we reduced our waiting list over the next 24 months from 6 months to less than 6 weeks improving the patients experience and reducing fines imposed on the trust for patients breaching waiting targets.

E-TPW67
Role of F18 Choline PET/CT in Brain Tumors

*L. Reiser[1], **A. Haroon**[2], Y. Bouchareb[2], G. Testanara[2], C. Copland[2], E. Mckintosh[2], N. Hartman[2]; [1]Purdue University College of Pharmacy, West Lafayette, IN, UNITED STATES OF AMERICA, [2]Barts Health NHS Trust, St Bartholomew's Hospital, London, UNITED KINGDOM.*

Purpose: The aim of our study is to evaluate the role of ^{18}F-Choline PET/CT in detection of intracranial lesions. **Subjects and Methods:** We analysed intracranial lesions in 6 patients 3 male; 3 female; age range was 32-47 years. All patients had MRI prior to ^{18}F Choline PET/CT (except one due to metal work) with a gap of 10-78 days (mean 30 days). The patients were injected with approximately 300 MBq of ^{18}F Choline (Effective dose about 12 mSv). The PET/CT images were acquired on a Philips Gemini TF TOF 64 slice PET/CT scanner (Philips Healthcare, Cleveland, Ohio) at a single site. Scans consisted of a low dose skull CT followed by a 20 minutes brain dynamic scan (10 x 1min frames; 5 x 2min frames) starting at time 0 after IV injection. PET images were reconstructed using spherical functions-based iterative reconstruction technique using a 14.3mm width TOF kernel. Dynamic scans were analysed on Hermes workstation and were read by a Radionuclide Radiologist. SUVmax was measured in a Volume-of-Interest (VOI) and used to evaluate the tracer uptake within the brain tissue. **Results:** A total of 19 lesions in different areas of the brain were identified. All avid lesions were seen in the cerebrum. No midbrain lesion was identified. The SUVmax

range was 1.1 - 4.28 (mean 2.0). On lesion-by-lesion analysis MRI detected 17/19 intracranial lesions. One of the lesions identified on MRI in the occipital horn of right periventricular lesion was not seen on ^{18}F Choline PET. This resolved on follow-up MRI imaging and hence was thought to be due to inflammatory aetiology. **Conclusions:** ^{18}F Choline PET/CT is useful in detection of intracranial lesions. There is additional value in differentiating progression from pseudo-progression, monitoring of treatment effect. Patients with contra-indications to MRI (metal work, claustrophobia, pace-maker) can be evaluated with ^{18}F Choline PET/CT. ^{18}F-FCH is an interesting tracer and could be a useful PET/CT tracer not only for prostate cancer imaging but also for oncological brain assessment.

E-TPW68
Development of reference values for DaTSCAN semi-quantitative analysis

*A. Neves[1], B. Ribeiro[1], **M. Correia**[1], V. Lameiras[1], E. Pereira[2,3], L. Oliveira[2], E. Carolino[4], L. Vieira[5,6]; [1]Nuclear Medicine Degree, Escola Superior de Tecnologia da Saúde de Lisboa/Instituto Politécnico de Lisboa, Lisbon, PORTUGAL, [2]NuclearMed, Almada, PORTUGAL, [3]Scientific Area of Nuclear Medicine, Escola Superior de Tecnologia da Saúde de Lisboa/Instituto Politécnico de Lisboa, Lisbon, PORTUGAL, [4]Scientific Area of Mathematics, Escola Superior de Tecnologia da Saúde de Lisboa/Instituto Politécnico de Lisboa, Lisbon, PORTUGAL, [5]GIReS, Escola Superior de Tecnologia da Saúde de Lisboa/Instituto Politécnico de Lisboa, Lisbon, PORTUGAL, [6]Instituto de Biofísica e Engenharia Biomédica, Faculdade de Ciências, Universidade de Lisboa, Lisbon, PORTUGAL.*

Introduction: ^{123}I-Ioflupane SPECT (DaTSCAN) is a powerful diagnosis assistance tool for Parkinson Disease **Vs** Parkinsonian syndromes. Image analysis is mainly qualitative, which may be related to some operator dependency. Although quantitative analysis could probably promote accuracy on diagnosis, reference databases are not available for all Nuclear Medicine departments. **Aim:** To contribute to creating reference values for DaTSCAN quantitative analysis at a Nuclear Medicine department. **Methodology:** A retrospective analysis of 39 ^{123}I-Ioflupane SPECT unequivocally non pathologic studies was considered. Clinical relevance of all scans was evaluated and data was collected between January 2015 and March 2017. All SPECT scans were acquired with the same technical conditions, according to the department's protocol. All images were processed by the same operator. Previously designed standard ROI's were positioned on occipital cortex (Occ), as background, and on each striatum (S) structures: left and right striatum (LS and RS) were divided on left and right putamen (LP and RP) and left and right caudate nucleus (LC and RC). Ratios were automatically displayed: S/Occ, LS/Occ, RS/Occ, LP/Occ, RP/Occ, LC/Occ, RC/Occ and Putamen/Caudate. Descriptive statistics was used to quantitative data analysis, in order to obtain reference values (average ± standard deviation). Qualitative data was studied by frequency analysis. We also evaluated age and gender impact on quantitative data, trough multiple linear regression. All the statistical analysis considered 5% significance level. **Results:** A

significant influence of age was observed on most calculated ratios: S/Occ (*p*=0.025), LS/Occ (*p*=0.025), RS/Occ (*p*=0.031), LP/Occ (*p*=0.029) and RC/Occ(*p*=0.016). We found a linear negative effect between 0.013 and 0.015 for each additional year at the patient age. There was no significant differences related to patients gender (*p*=0.067). We were able to obtain the following reference values for DaTSCAN quantitative analysis for non pathologic diagnosis: S/Occ (3.5±0.39), LS/Occ (3.53±0.41), RS/Occ (3.48±0.39), LC/Occ (3.67±0.48), RC/Occ (3.64±0.44), LP/Occ (3.38±0.39), RP/Occ (3.31±0.39) and Putamen/Caudate (0.92±0.06). **Conclusion:** This study allowed us to obtain reference values for DaTSCAN quantitative analysis, assisting accurate diagnosis for non pathologic scans. We also conclude that, as expected, age has relevant impact on the striatum uptake ratios decrease. *Key words: DaTSCAN; Ratios; Quantification; Reference Values; Age; Gender.*

E-TPW69

Feasibility of an automatic ^{123}I-IMP non-invasive quantitative measurement method for evaluation of regional cerebrovascular reactivity

T. Tomimatsu[1], D. Koreeda[1], A. Ofuji[1], H. Ohura[2], A. Takaki[3], S. Ito[4]; [1]Graduate School of Health Sciences, Kumamoto University, Kumamoto, JAPAN, [2]National Organization Saga Hospital, Saga, JAPAN, [3]Teikyo University, Omta, JAPAN, [4]Faculty of Life Sciences, Kumamoto University, Kumamoto, JAPAN.

Purpose: Evaluation of the regional cerebrovascular reactivity (rCVR) to a cerebral vasodilatory stimulus after acetazolamide (ACZ) loading by a brain blood flow single photon emission computed tomography (SPECT) is important in the investigation of patients with ischemic cerebrovascular disease. We developed the simple non-invasive I-123-N-isopropyl-p-iodoamphetamine (^{123}I-IMP) autoradiography method by analyzing chest RI-angiography and single photon emission computed tomography (SPECT) images based 2-compartment model (SIARG method). A good correlation of the regional cerebral blood flow (rCBF) values between the SIARG and the one-point arterial blood sampling autoradiography (ARG) methods was obtained while the subjects were in the resting state. However, the feasibility of the SIARG method in the high flow range after ACZ loading is not clarified. The purpose of this study is to confirm the feasibility of use of the SIARG method for determinations in the high flow range after ACZ loading. **Materials and Methods**: The rCVR values were obtained by the split dose method of microsphere model in 30 patients. The SIARG and ARG examinations were simultaneously performed in each patient. The rCVR values of the SIARG method were compared with those of the ARG method. All SPECT images were analyzed using a 3-dimensional stereotaxic ROI template (3DSRT) on anatomically standardized CBF SPECT images to objectively estimate the rCBF. The 3DSRT was composed of 24 segments. The 12 segments located in brain surface were selected in this study. The rCBF values were defined as mean values of each segment. rCVR to ACZ was calculated as follows: rCVR(%)= ((ACZ rCBF - resting rCBF)/ resting rCBF)×100. Both rest and ACZ studies were performed within one week.

Each patient's condition did not change in this period. **Results**: The rCVR values obtained by the SIARG method increased linearly as those obtained by the ARG method increased. Values obtained by the SIARG method were approximately equal to the ARG method. A good correlation was observed between the rCVR values obtained by the SIARG method and those obtained by the ARG method (r=0.88, p<0.001). This finding indicates the potential clinical usefulness of the SIARG method for evaluation of rCVR. **Conclusion**: The SIARG method is useful for study in the high flow range after ACZ loading.

E-TPW70

Fully automatic striatal region of interest setting program using magnetic resonance images for a new 123I-FP-CIT quantification method

S. Ota[1], Y. Uchiyama[2], A. Takaki[3], S. Ito[2]; [1]Graduate School of Health Sciences, Kumamoto University, Kumamoto, JAPAN, [2]*Facuty of Life Sciences, Kumamoto University, Kumamoto, JAPAN, [3]Teikyo University, Omuta, JAPAN.*

Purpose: Specific binding ratio (SBR) is an assessment method for ^{123}I-FP-CIT single photon emission computed tomography (SPECT). However, the accuracy of SBR decreases because the count in the reference region of interest (ROI) is easy to vary. In order to improve upon this problem, we demonstrated an^{123}I-FP-CIT striatal quantification method with partial volume effect (PVE) correction at the European Association of Nuclear Medicine 2015 annual meeting. This method consists of the following five steps: 1) image fusion of SPECT/ computed tomography (CT) and magnetic resonance (MR), 2) striatal ROIs setting on the MR images, 3) PVE correction of the SPECT counts in these ROIs, 4) counts-activity conversion, and 5) calculation of SBR and striatal uptake values. An original image fusion program was developed in a previous report. However, the striatal ROI setting of this method was performed manually after SPECT/CT/MR image fusion. These procedures require cumbersome work and a long analysis time. If an automatic striatal ROI setting algorithm can be developed for our quantification method, the analysis of striatal activities can be completed within a few seconds without requiring manual input. Although several striatal ROI setting programs have been reported, the ROI setting method for an individual patient is important to obtain other correct diagnostic information from MR images. The purpose of this study was to develop an automatic striatal ROI setting program using MR images, and to confirm the program's feasibility of use. **Materials and Methods:** We developed a striatal ROI setting program for MR images after SPECT/CT and MR image fusion by using new image recognition techniques based on the level set method. The MR images were obtained by two sequences of the phase-sensitive inversion recovery (PSIR) and dual inversion recovery (DIR) methods. The accuracy of our program was evaluated by using 15 patient images. The striatal counts on the SPECT images obtained by the program were compared with those counts by the manual ROIs. **Results**: The ROIs were set in a few seconds by using the automatic program. The ROIs by the automatic program visually coincided with the manual ROIs.

The ROIs of the PSIR images were approximately equal to those of the DIR images. The difference of the striatal counts on the SPECT images between the automatic program and manual method was less than ±3%. **Conclusion:** Striatal ROIs obtained by the automatic program using MR image analysis were adaptable for the quantification in ^{123}I-FP-CIT SPECT.

E-TPW71

Clinical Usefulness of [^{18}F]FC119S PET as an Auxiliary Diagnostic Methods for Dementia

B. Byun[1], S. Lim[1], K. Lee[1], J. Choi[1], J. Ha[1], S. Park[1], D. Chi[2]; [1]Korea Institute of Radiological and Medical Sciences, Seoul, KOREA, REPUBLIC OF, [2]Research Institute of Labeling, Futurechem Co., Ltd, Seoul, KOREA, REPUBLIC OF.

Purpose: The newly developed ^{18}F-labeled amyloid tracer, 2-[2-(N-monomethyl)aminopyridine-6-yl]-6-[(S)-3-[18F]fluoro-2-hydroxypropoxy]benzothiazole ([^{18}F]FC119S, Future-Chem in South Korea) was recently introduced. We assessed the usefulness of [^{18}F]FC119S PET as an auxiliary diagnostic methods for dementia. **Methods:** 1) For the comparison of [^{11}C]PiB PET and [^{18}F]FC119S PET, a total of 48 subjects-clinically diagnosed Alzheimer's disease (AD) in 50, mild cognitive impairment (MCI) in 10, and congnitive normal subjects (CN) in 28-underwent both [^{11}C]PiB PET and [^{18}F]FC119S PET. 2) To assess the diagnostic performance of [^{18}F]FC119S, a total of 100 subjects-AD in 50, non-Alzheimer's dementia (NAD) in 15, and CN in 35-underwent brain [^{18}F]FC119S PET. For visual analysis, positive scan was defined as the PET scan with any cortical tracer uptake equal to or higher than the uptake of white matter. For semi-quantitative analysis, standardized uptake value ratio (SUVR)-the ratio of cerebral cortical SUV to the cerebellar SUV-was measured on each PET dataset. All adverse effects during the clinical trial periods were collected. **Results:** 1) The concordance rate of visual analysis of [^{11}C]PiB PET and [^{18}F]FC119S PET was 98% (44 of 45 cases) and the SUVR of [^{11}C]PiB PET and [^{18}F]FC119S PET significantly correlated (r = 0.844, p < 0.001). 2) Based on visual analysis, 46 of 50 cases with Alzheimer's disease (92%), 5 of 15 cases (40%) with non-Alzheimer's dementia (33%), and 3 of 35 normal cases (9%) were read as positive scans, respectively. Therefore, visual assessment of [^{18}F]FC119S PET yielded a sensitivity of 92% and a specificity of 84%. The mean values of SUVR were 1.22±0.16 in Alzheimer's disease, 1.05±0.06 in non-Alzheimer's dementia, and 1.02±0.06 in cognitive normal subjects, respectively. SUVR yielded a sensitivity of 84% and specificity of 84% at the criterion of SUVR > 1.07. There were no clinically significant adverse effects during trial periods. **Conclusion:** [^{18}F]FC119S PET yields high sensitivity and specificity for identifying Alzheimer's disease and therefore may be an auxiliary diagnostic methods for dementia, especially to exclude Alzheimer's disease.

E-TPW72

A Case Study Detailing the Development of a Protocol for the Detection, Diagnosis and Analysis of a Cerebral Spinal Fluid Leak Study

E. Seal; Queen Elizabeth Hospital Birmingham, Birmingham, UNITED KINGDOM.

Introduction: Nuclear Medicine is a widely used imaging modality that involves administration of a radiopharmaceutical to diagnose and in some cases treat a variety of diseases. Certain nuclear medicine procedures are more commonly performed than others; in the last 10 years our centre has only performed one Cerebral Spinal Fluid (CSF) Leak Study. CSF Leak Studies are used to establish how the CSF circulates to detect disorders or leaks of CSF. Pledgets can also be used during the study to assist in detecting leaks. The pledget counts are corrected for weight of sample and then counts per gram are compared to relevant plasma levels for that time. **Subject:** A CSF leak referral was received for a 60 year old female from Neurosurgery after an accident last year that had resulted in 25 operations to her Skull. She had previously undergone multiple imaging investigations including CT and MR but the location of the leak had not been identified. She was suffering with a long-standing discharge from a right parietal craniotomy wound with a titanium pate cranioplasty. After developing a protocol nuclear medicine performed a CSF Leak study which showed no evidence of a CSF Leak. 8 Weeks later the same patient was referred again after having had the cranioplasty plate removed and had been discharged to home. The patient was complaining of a possible CSF Leak through her nose and skin as witnessed by herself and her husband. Neurosurgery requested the protocol be adapted to change the imaging parameters and timeframe to establish if a CSF Leak is present. **Summary:** This case report demonstrates the development of a new protocol and involvement of multiple specialties to establish the CSF leak Study procedure. It will present how the imaging protocol was developed between Nuclear Medicine, Medical Physics, Radiology and Neurology. How the study was performed, the imaging parameters used and how it affected the patient management. It also shows the need to review and adapt imaging procedures to suit the individual patient and referral to aid in confirmation of a diagnosis.

E-TPW73

Comparison of Imaging Techniques spect and petct in the pre surgical evaluation of refractory epilepsy

G. Paixao, A. Queiroz, R. Moreira, C. Soares; Queen Elizabeth Hospital, Birmingham, UNITED KINGDOM.

Introduction: The introduction of radionuclide neuroimaging methods as Single Photon Emission Computed Tomography (SPECT) and Positron Emission Tomography (PET), has improved the efficiency of pre surgical epilepsy evaluation particularly in cases where no lesion is evident on Magnetic Resonance Imaging (MRI). The main purpose of this study is to establish the role of Nuclear Medicine neuroimaging techniques in multimodality evaluation of epileptogenic zones and determine its possible added value when MRI shows no evidence of the pathology. **Material and Methods:** Twenty patients aged between 12 and 57 (37.5±11.0) years, which suffer from medical refractory epilepsy, underwent video electroencephalogram (vEEG), MRI, ^{99m}Tc-HM-

PAO ictal and interictal SPECT, and interictal ^{18}F-FDG PET. A scale of concordance was established to evaluate the agreement between imaging results, in which ictal vEEG was considered to be the gold standard method. The number of localizing, non-localizing, discordant lobe/hemisphere lateralizing and no correlation studies were calculated. In addition to these, the percentage of cases in which radionuclide image techniques detected the pathology, despite the normal MRI, was calculated. **Results:** Ictal SPECT was the imaging technique that obtained a larger number of localizing studies (14/20) and therefore a higher rate of concordance with ictal vEEG results, followed by interictal PET (11/20). Interictal SPECT (10/20) and MRI (8/20) both showed to be less concordant with ictal vEEG results. In the 9 normal MRI cases, 7 proved to be localizing studies with ictal SPECT. **Discussion/Conclusion:** The results revealed that ictal SPECT is the most adequate imaging technique to be applied for pre surgical localization of the epileptogenic zone. Interictal SPECT and PET proved to be complementary imaging modalities to ictal SPECT. Non-invasive nuclear neuroimaging techniques play an important role in medical refractory epilepsy, especially in the case of normal MRI. **Keywords:** Refractory Epilepsy; Ictal SPECT; Interictal SPECT; Interictal PET; MRI; Epilepsy Surgery.

E-TPW74

Spleen Uptake on Bone Scan after Liver Transplantations

Y. LIM; Pusan National University Yangsan Hospital, YANG SAN, KOREA, REPUBLIC OF.

A 47-year-old female, alcoholic liver cirrhosis and splenomegaly patient who received liver transplantation, was performed to ^{99m}Tc-DPD bone scan for a evaluation of generalized bone pain and to distinguish compression fractures. Bone scan showed diffuse splenic uptake of ^{99m}Tc-DPD resembling nuclear medicine spleen scan. Furthermore, bone uptake of ^{99m}Tc-DPD was T4, T12, L2 level (compression fractures) and left proximal tibia(suggestive traumatic bone lesion). The patient had received liver transplantation for managing of symptoms related to liver cirrhosis. And also the patient has received splenic artery embolization for managing of symptoms of splenomegaly related to portal vein hypertension. The patient performed contrast enhanced computed tomography(CT) to evaluate the complications after liver transplantation and splenic arterial embolization. The contrast enhanced CT showed multiple poorly marginated hypo-enhancing splenic lesions corresponding to the infarction in the arterial and portal venous phase. Spleen uptake of ^{99m}Tc-DPD caused by spleen infarction may explain our findings.

E-TPW75

Static Bone Scintigraphy Images of Hands and Feet - How low can we go?

M. Tayyab, H. Mikkelsen, B. Haddock, U. B. Andersen, C. Suetta, P. Hovind; Rigshospitalet, Glostrup, DENMARK.

Introduction: The aim of the present study was to improve image quality on regional static acquisitions of hands and feet. The current protocol at our clinic on static acquisitions of hands and feet is a fixed 5 minutes recording time. With the present project we wanted to investigate if a longer recording time and/or increasing number of counts would increase image quality. **Materials and Methods**: After injecting a median dose of 507 MBq ^{99m}Tc-HDP in 13 patients, 23 dynamics acquisitions of hands and feet were obtained (20 frames of 30 sec, 128x128 matrix, LEHR collimator). The images were processed in Xeleris to create 4 sets of sum images of 2, 5, 7 and 10 minutes and the total counts in each image were registered. All acquisitions were blinded and evaluated by three experienced nuclear medicine experts, and categorized as either of poor, acceptable or good quality. **Results:** A total of 276 reconstructed images were evaluated. Of these, 144 images were judged as poor, 84 as acceptable and 48 as good quality. Images considered 'good' had a mean of 209 +/- 82 kCounts whereas 'acceptable' had 167 +/- 96 kCounts and 'poor' images had 114 +/- 83 kCounts. There was a significant relationship (p<0.001) between total counts and image rating for both hands and feet images. Images rated as 'good' had an acquisition time ranging between 5-10 minutes whereas those rated 'acceptable' and 'poor' ranged from 2-10 minutes. Identification of hot spots (areas with focally increased uptake) in the carpal and tarsal bones did not improve after 7 minutes, but in the metacarpal, metatarsal and digital bones increasing the scanning time to 7 or 10 minutes was beneficial. **Conclusion:** The study clearly demonstrated that an extended scan time with higher count total improves image quality. From the results we can conclude that the recording time should be at least 7 minutes or over 200 kCounts. There was a tendency towards an improved quality of static images of the hands by extending recording time up to 10 minutes.

E-TPW76

SPECT-MR of Spine for Patients with Back Pain: First UK Experience

*N. Musa, R. Victoria, H. Jan, M. Ahmed, J. Bull, G. Testanara, **A. Haroon**; Barts Health NHS Trust, St Bartholomew's Hospital, London, UNITED KINGDOM.*

Purpose: MR images suffer from susceptibility artifacts and low dose SPECT/CT has poor anatomical resolution for soft tissues. We evaluated the incremental value of fusion of SPECT-MR images in patients with symptoms of back pain. **Subjects and Methods:** This pilot work consisted of 10 patients; 6 females and 4 males; age range 30-80 years. These patients were investigated for symptoms of back pain and had MRI to evaluate anatomical abnormality and SPECT/CT to identify the site of osteoblastic activity as pain generator. The MRI protocol included sagittal T1 and T2, axial T1 and T2 weighted images. Sagittal T1 and T2 reformatted multiplanar images were fused with the sagittal SPECT images. MR, SPECT/CT and SPECT-MR images were read by a Radionuclide Radiologist. Lesions detected by individual modalities and discordant functional abnormalities were also noted. **Results:** This study included 117 lesions identified by SPECT/MR. Out of these 28.2% of the abnormalities were detected by SPECT/CT and 71.8% by MRI alone. A total of 33

functional abnormalities were identified with the **SPECT/CT**. These included osteoblastic foci at 24 facet joint, 2 pars defects, 2 vertebral bodies, 2 inter-vertebral discs, 1 trans-pedicular srew, 1 sacroiliac joint and incidental thickening of 1 nerve root. **MRI** detected a total of 84 anatomical abnormalities. These included facet joint arthropathy 25, disc abnormality 17, nerve root compression 9, recess narrowing 8, vertebral foraminal narrowing 8, altered morphology of the cord 6 (intradural lipoma, dysraphism, dural lesion, cord tethering, cord compression and caudal regression), vertebral marrow abnormality 4, spinal canal narrowing 3, altered morphology of the vertebra 3 (transitional vertebra, pseudoluxation and spina bifida) and ligamentum flavum hypertrophy 1. **SPECT to MR** discordant findings included 22 lesions: Osteoblastic activity at the discs 2, Facet joint 16, sacro-iliac joint 1, pars defects 2 and abnormality of the transpedicular screw in 1 patient. There were two patients in which the SPECT and MR findings were concordant. **Conclusion:** Fusion of SPECT and MR is feasible and has incremental value in detection of osteoblastic activity and altered morphology simultaneously. Anatomical and functional discordance exists and can present in varying forms. Combination of anatomical and functional imaging in the form of SPECT-MR is superior than any of the modality alone for the evaluation of back pain.

E-TPW77

Evaluation of Renal Scarring Using Ultrasound and Renal Scintigraphy

A. B. Ahmed, IV[1], A. Abdullah[2]; [1]Ministry of Health, Fujairah, UNITED ARAB EMIRATES, [2]Sudan University for science and Technology, Khartoum, SUDAN.

The aim of this study was to compare the value of renal ultrasonography and cortical scintigraphy with technetium-99m dimercaptosuccinic acid (DMSA) in detecting renal cortical scars in urinary tract infection (UTI) patients. **Materials and Methods:** Renal Scintigraphy (Tc99m - DMSA scan) and Ultrasonography studies were done in 60 children who were referred to the nuclear medicine department in Fujairah hospital between Jun 2014 and May 2015 because of documented urinary tract infection (UTI). Outcomes of both modalities were compared, with focus on renal scarring. Renal scarring detection rates of Tc-DMSA scan and Ultrasonography were compared. **Results:** In total, 60 patients with urinary tract infection (UTI) underwent both renal DMSA scintigraphy and ultrasonography. According to this study; among this 60patients 80% were female (48) and 20% were male (12), table (4-1). The mean age of our patients was 2years. DMSA scan results were normal in 45% (27 patients) and abnormal in 55% (33patients) (showing decreased cortical uptake), table (2).Renal ultrasonography's were reported as normal(no scar) in 85% (51 patients) and abnormal in 15% (9 patients) (showing scar formation or decreased cortical thickness). Both statistical and experimental analysis was used. **Conclusion:** In children with urinary tract infection (UTI), ultrasonography compared with DMSA scintigraphy, renal scars are often missed, especially when the ultrasound is difficult to interpret. In this study, Tc-DMSA scan detected scars in 30% of kidneys reported to be normal on ultrasound. Ultrasonography was found to be an inappropriate study in the detection of renal parenchymal scars.

E-TPW78

Interest of the estimation of the GFR with technetium 99m-DTPA in the comparasion of the analysis of three methods of creatinine clearance estimation after kidney transplantation

A. Sellem, K. Limam, W. Elajmi; Military Hospital, Tunis, TUNISIA.

Introduction: Surveillance of glomerular filtration rate (GFR) is essential for the management of kidney transplant recipients. **Subjects & Methods :** We compared the performance of estimation equations with 99mTechnetium 99mTc-DTPA clearance (TcGFR) in 32 of our patients, using the Modification of Diet in Renal Diseases (MDRD), Nankivell (NK), and Cockcroft-Gault (CG) formulas. All patients were adequately hydrated before study. 99mTc-DTPA was injected intravenously (maximal dose = 37 MBq). A second syringe was prepared for an aliquot of the study. Blood was sampled at 120 and 240 minutes in various sites. After centrifugation, 1.0 mL plasma was transferred into a counting vial. Both the samples and the "standard" were measured in a well counter. The mean time from transplantation to TcGFR was 47.9 months (range, 4-143 months). **Results:** The mean serum creatinine level was 124 micromol/L (range, 70-371 micromol/L). The mean TcGFR was 58.6 mL/min/1.73 m(2) (range, 14-100 mL/min/1.73 m(2)). The MDRD equation showed a median difference of 1.4 mL/min/1.73 m(2) with 81.2% of estimated GFR within 20% of TcGFR. Median differences were 8.94 and 11.47 mL/min/1.73 m(2) for NK and CG formulas, respectively. The precision of the NK and CG was such that only 56.25% and 62.5% of estimations, respectively, fell within 20% of TcGFR. **Conclusion:** In this study, the MDRD equation demonstrated the best overall performance among the 3 tested methods. It should be sufficient for routine clinical practice in kidney transplantation.

E-TPW79

Interest of 99mTc-DTPA dynamic renal scintigraphy with furosemid test in the exploration of ureteropelvic junction syndrome: Report of 37 cases

S. Touil[1,2], Y. Shimi[1,2], A. Koumba[1,2], H. Aschawa[1,2], A. Guensi[1,2]; [1]Faculty of medicine and pharmacy of Casablanca, Casablanca, MOROCCO, [2]Nuclear medicine service, Ibn Rochd University Hospital, Casablanca, MOROCCO.

Renal dynamic scintigraphy (RDS) using 99mTc-DTPA with diuresis test is a non-invasive isotopic exploration that is of appreciable interest in the exploration of the excrectrices urinary tract. In the ureteropelvic junction syndrome, it shows the functional abnormality and alteration of drainage to guide the therapeutic management. We report, through this work, a retrospective descriptive study including observation of 37 patients referred to the nuclear medicine department for their ureteropelvic junc-

tion syndrome (UPJS) exploration between January 2011 and September 2013. The RDS with exploration with 99mTc-DTPA and diuresis test of furosemide F + 20 protocol was performed in all patients, supplemented by static acquisitions post-micturition and verticalisation. Our study focused on the analysis of ureteropelvic permeability taking into account the semi quantitative parameters of the isotopic nephrogram (IN) obtained after digital reconstruction of sequential images recorded after dynamic digital processing sequential images. Of the 37 cases studied (14 F/23 M), the average age was 4,8 years with extremes spanning from 2 months to 17 years. Data from the scintigraphic exploration with 99mTc-DTPA allowed to classify our patients into three groups. Group I: absence of drainage alteration 13,5% (5 patients), with preserved function (group Ia) in 20% (one patient) and without preserved function (group Ib) in 80% of patients (4 patients). Group II: presence of altered drainage 59,5% (22 patients), with functional conservation (group IIa in 18% (4 patients) and without functional conservation (group IIb in 82% (18 patients)) . Group III: represented by an equivocal response in 27% (10 patients). Through our study, 99mTc-DTPA RDS with furosemid test allowed, it possible to make the right therapeutic indication for the patients who had functional abnormality and alteration of drainage, the patients with the equivocal response need subsequent monitoring scintigraphy.

E-TPW80

Evaluation of factors that may contribute to the hepatobiliary excretion of ^{99m}Tc-MAG3

B. Bento, C. Amorim, D. Costa, P. Santos, S. Chin, M. R. Victor, M. Filipe, A. I. Santos; *Serviço de Medicina Nuclear - Hospital Garcia de Orta, Almada, PORTUGAL.*

Introduction: Technetium-99m-mercaptoacetyltriglycine (^{99m}Tc-MAG3) is a renal tubular radiopharmaceutical, with high renal extraction but with hepatobiliary excretion. **Aim:** The purpose of this study is to evaluate factors contributing to hepatobiliary excretion of ^{99m}Tc-MAG3. **Methods:** A prospective study was performed in 49 patients (19 children and 30 adult patients) referred for dynamic renal scintigraphy. Radiochemistry quality control was performed each time a syringe was prepared. The dynamic study was acquired in anterior and posterior projections, followed by a static post-void and right lateral image of the abdominal region, between 50 and 65 minutes' post-administration of the radiopharmaceutical. The lateral projection aimed at confirming the presence and location of gallbladder. The following parameters were also evaluated: group age; time between last meal and administration of the radiopharmaceutical; and time between radiopharmaceutical preparation and the administration. Statistical analysis was performed with IBM SPSS Statistics for Macintosh, Version 24.0, using chi-square for categorical variables and Mann-Whitney test for continuous variables. **Results:** Gallbladder was only visualised in post-void images, and hepatobiliary excretion was present in 80% of adult patients and in 58% of those of paediatric age. In 3 of the 35 patients with gallbladder visualisation, there was image suspicion of low renal failure. There was no association between the pres-

ence of hepatobiliary excretion and age group (p-value=0.116). Regarding studies with and without evidence of hepatobiliary excretion, there was no statistically significant differences for: 1) time between last meal and moment of administration of the radiopharmaceutical (p-value=0.49); 2) time from radiolabelling and administration of the radiopharmaceutical (p-value=0.903); 3) radiochemistry quality control results, concerning labelling efficiency (p-value=0.807) and presence of hydrolysed technetium (p-value=0.4). In 60% of the cases with visualisation of gallbladder, the vesicle overlapped the right kidney. **Conclusions:** No association was found between the presence of hepatobiliary excretion and any of the parameters evaluated, and thus, is does not seem possible to try to reduce it through protocol optimization. Moreover, the overlap of the gallbladder with the right kidney, in post-micturition images, suggests interference with drainage quantification.

E-TPW81

Influence of the geometry and positioning of the regions of interest in the transplanted renogram

J. F. V. Rodrigues[1], J. Rayo[2], J. Vicente[2], E. Carolino[3], S. Figueiredo[4,5], L. Vieira[4,5]; [1]Escola Superior de Tecnologia da Saúde de Lisboa, Lisboa, PORTUGAL, [2]Department of Nuclear Medicine at the Hospital Infanta Cristina, Badajoz, SPAIN, [3]Scientific Area of Mathematics, Escola Superior de Tecnologia da Saúde de Lisboa/ Instituto Politécnico de Lisboa, Lisboa, PORTUGAL, [4]Scientific Area of Nuclear Medicine, Escola Superior de Tecnologia da Saúde de Lisboa/Instituto Politécnico de Lisboa, Lisboa, PORTUGAL, [5]GMOSM – Instituto Superior de Engenharia de Lisboa/Instituto Politécnico de Lisboa, Lisboa, PORTUGAL.

Aim: Assess whether there are differences in the estimation of the time to half-peak (THP) parameter, and in the computation of Hilson perfusion index (HPI), by modifying both the geometry of background's region of interest (ROI) and positioning of perfusion's ROI, in the transplanted renogram. **Materials and Methods:** 45 transplanted renogram scans were retrospectively random selected at the Department of Nuclear Medicine at the Hospital Infanta Cristina, Badajoz: 13 women and 32 men, mean age: 57.6±11.8 years old. An activity of 185MBq of mercaptoacetyltriglycerin labeled with technetium-99 metastable (^{99m}Tc-MAG3) was administered in bolus per patient. A dual phase dynamic study (1st: 30 frames, 2 sec/frame; 2nd: 76 frames, 15 sec/frame) was acquired in anterior view, with *foccus* on iliac fossa, using a General Electric Millenium VG Hawkeye™ dual head system and a Siemens T-Series™ SPECT/CT dual head gamma-camera. The 45 studies were analysed and processed with *Renal Analysis*™ software from Xeleris™ 2.0 General Electric Healthcare Workstation to obtain the THP and the HPI. The transplanted renogram studies were processed twice, per exam, by the same operator, modifying the geometry of the background ROI from automatic to manual drawing mode and varying the perfusion ROI of the iliac artery from ipsilateral to contralateral position. The Wilcoxon test was applied to compare the background's ROI geometry and the positioning of the perfusion ROI. **Results:** Wilcoxon's test indicated that there were statistically significant

differences in the background ROI geometry for the computation of the THP parameter, comparing between the automatic and the manual mode (z = -4.641, p = 0.000). There were not found statistically significant differences in the HPI, based on the positioning of the perfusion ROI, at this phase of the study (z = -0.412, p = 0.680). **Conclusions:** Based on the THP, the geometry of the background ROI that allows an accurate correction of activity's background is the one obtained by manual mode, instead of the full automatic implementation. The change of the perfusion ROI from ipsilateral to contralateral position on the iliac artery seems not affect the HPI, but this may be apparently inconclusive at this phase of the study so that further analysis needs to be undertaken, additionally using other methods for the computation of perfusion index.

E-TPW82
Tailoring gastric emptying studies to patients needs: a requirement for best practice

S. Johnson, C. Sibley-Allen, A. Nunes; Guy's and St. Thomas' NHS Foundation Trust, London, UNITED KINGDOM.

Background: Gastric emptying studies are considered a routine nuclear medicine procedure. In our department, we have had an increase of patients being referred, particularly patients with intolerances to certain elements of the meal, which makes our current standard meal unsuitable. The aim of the study is to assess the current service that we provide and look at ways to improve the service and make adjustments to suit all patients undergoing gastric emptying studies. **Methods:** A literature review was performed to assess the current recommended gastric emptying protocols internationally and how the standard meal could be adapted for patients with ingredients intolerances. We've retrospectively looked at patients referred over one year (July 2015-July 2016) looking at meal completion rate, reported results and the clinical question the referrer wanted answered. Consecutively, a departmental survey was carried out to assess the breath of knowledge of all professional groups involved in gastric emptying studies from bookings to reporting. The most important inconsistencies were highlighted and approached as areas for improvement; specific corrective measures were implemented to address the shortages and improve our current service. We looked at the standard meal we provide and compared it to others referenced in national and international literature such as the SNM guidelines. We then looked at ways to improve the service that did not include the standard meal which comprised our current imaging techniques and what our current normality ranges for reporting are. New implementations were put in place which included new patient assessment guidelines prior to the study. This enabled us to cater for those with intolerances. A new backing sheet to track all meal and scanning adjustments and more technologist involvement in processing with new software contributed for improved communication and pathways; the analysis of the impact of using alternative data for processing was initiated and is ongoing. **Conclusion:** With successful implementation of new meal assessment guidelines, backing sheets and new processing software, our department is now able to provide a more streamlined service to cater for all the needs of the current referred gastric emptying patients

Authors Index

Springer

Efetürk, H. — EP-0403
Eftekhari, M. — EP-0785
Eftychiou, N. — E-TPW63, **EP-0671**
Eftymiadou, R. — EP-0043, EP-0045
Egea, I. — EP-0750
Ege Aktas, G. — **EP-0110**, **EP-0546**
Egeler, B. — EP-0749
Eggert, A. — EP-0801
Eiber, M. — OP-126, OP-243, OP-430
Eich, H. T. — OP-543
Eidelberg, D. — EP-0425
Eikenes, L. — OP-498
Eilles, E. — EP-0440, EP-0458
Einhellig, H. — EP-0740
Einspieler, I. — E-PW007, EP-0356
Eisel, U. L. M. — OP-555, EP-0407
Ekaeva, I. V. — OP-506
Ekmahachai, M. — E-PW023
Ekoume, F. P. — **EP-0272**
Elajmi, W. — E-TPW78
El Bez, I. — EP-0446, EP-0839, EP-0840, EP-0859,
EP-0874, EP-0924, EP-0929, EP-0945
EP-0959, EP-0963, EP-0968

El Bitar, Z. — EP-0882
Elboga, U. — **EP-0841**
Eldem, G. — EP-0878
Eleftheriou, C. — EP-0377
Elekonawo, F. M. K. — **EP-0483**
Elf, A.-K. — EP-0805
El Fahimi, B. — EP-0650
El Farsaoui, K. — OP-562
Elgazzar, A. — EP-0088, EP-0664
Elhan, A. H. — EP-0824
Elia, C. — OP-194
Elisei, F. — OP-195, OP-247
Elisei, R. — E-PW040
Elizalde, A. — EP-0548
Elkholy, E. — **EP-0742**, **EP-0743**
El-Kilini, N. — EP-0742
El-Kolaly, M. T. H. — EP-0293
Ellert, E. — OP-123
Ellingsen, J. — **E-TPW44**
Ellis, J. — EP-0471
Ellis, S. — EP-0475
Ellmann, A. — EP-0020
Elmorsy, S. — EP-0819
ElNadi, E. — EP-0742
El-Nagdy, M. S. — EP-0054
El-Sabbagh, A. M. — **EP-0505**
Elsinga, P. H. — OP-639, OP-696, OP-078
E-PW072, E-PW074, EP-0230, EP-0609
Emami, A. — **EP-0003**
Emami-Ardekani, A. — EP-0785
Emdin, M. — OP-357
Emer, O. — EP-0324, EP-0511
Emi, M. — EP-0618
Emiomite, L. — OP-553
Emionite, L. — OP-176, EP-0373, EP-0377
Endepols, H. — E-PW015
Endo, K. — EP-0015
Engert, A. — OP-349, OP-543
England, C. G. — OP-067
Engler, H. — EP-0301, OP-442
Enilorac, B. — **EP-0695**
Enomoto, R. — EP-0096
Enqvist, O. — OP-657, EP-0116, EP-0641, EP-0642, EP-0770, EP-0771
Entok, E. — EP-0355, EP-0529
Epelbaum, S. — OP-128
Eppard, E. — OP-218, OP-219, EP-0605, OP-637, OP-670, EP-0890

Erba, P. A. — OP-386, EP-0678, EP-0986, EP-0992
Erdil, T. Y. — EP-0667, EP-0935
Erfanian, Y. — OP-299
Ergül, N. — OP-701
Erhardt, S. — EP-0218
Eriksson, B. — E-PW061, OP-104
Eriksson, O. — OP-107
Eriksson, T. — OP-439
Eriksson Karlström, A. — OP-062, EP-0282, EP-0306
Erkasap, S. M. — EP-0529
Erkoyun, E. — EP-0085
Ermert, J. — OP-642
Ermoschkin, L. — E-PW103, OP-429
Ernst, S. — OP-408
Erslev, A. — EP-0970
Ertl, G. — EP-0108, OP-356
Erturk, S. — EP-0474, EP-0680, EP-0820,EP-0954
Ertuğrul, C. — EP-0594
Esa Kauppila, K. E. — **EP-0661**
Eskola, H. — EP-0926
Eskola, O. — EP-0469
Eslava, A. — EP-0750
Eslick, E. — OP-428
Esmaeili, M. — OP-498
Esmail, A. — OP-655
Espallargas, I. — EP-0759
Espejo, P. — EP-0750
Espejo Niño, J. — **EP-0748**, EP-0773
Esposito, J. — EP-0285
Esposito, L. — OP-124, EP-0162
Esquinas, P. L. — E-PW035
Essamet, W. — E-PW017
Esser, J. P. — EP-0647
Essler, M. — OP-122, OP-218, OP-219, OP-237, OP-452
OP-637,OP-670, EP-0513, OP-583
EP-0605,EP-0800, EP-0890, EP-1001
Esteban Figueruelo, A. — EP-0748, EP-0773
Estellat, C. — OP-663
Estrada Lobato, E. — EP-1015
Eugenio, B. — EP-0646
Eunsun, C. — OP-211
Evangelista, L. — **OP-549**, OP-604, E-PW085, EP-0634
EP-0635, **EP-0646**, EP-0769
Evans, G. — EP-0166
Evans, M. — OP-206
Exadaktilou, P. — EP-0837
Expósito Rodríguez, A. — OP-393
Ezziddin, S. — OP-237
Ezzine, A. — EP-1008

Fabregat Pous, J. — EP-0591
Faccini, R. — EP-0304, EP-0481
Fadhel, G. — EP-0160
Fafard-Couture, L. — OP-395
Fagart, A. — OP-245
Fahmi, R. — OP-560, **EP-0427**, EP-0433
Fakirova, A. — EP-0512
Falabella, R. — EP-0948
Falch, K. — EP-0540
Falchi, A. — EP-0148
Falk, R. — EP-0292
Fallahi, B. — EP-0785
Fallanca, F. — OP-300, EP-0562
FALZONE, N. — EP-0882
Fan, A. P. — EP-0170, EP-0185
Fan, X. — OP-074
Fan, Y. — EP-0378, EP-0437, EP-0700, EP-0701
Fancourt, T. — EP-0576
Fanelli, M. — OP-136, OP-447, EP-0100, EP-0623, EP-0853

Kamiya, T.	EP-0249
Kamphuisen, P. W.	EP-0098
Kan, N.	EP-0153, EP-0789, EP-0818
Kanaev, S.	OP-246, EP-0154, EP-0525
Kanai, Y.	EP-0214, **EP-0216**, EP-0219, **EP-0249**
Kanazawa, S.	EP-0721
Kandeel, A. A.	OP-259
Kandolf-Sekulovic, L.	EP-0754
Kanenawa, T.	**OP-471**
Kang, D.-Y.	EP-0386
Kang, H.	EP-0813
Kang, J.	EP-0033, EP-0215, EP-0295
Kang, K.	EP-0545, EP-0694
Kang, K.-W.	E-TPW25
Kang, L.	**EP-0264**, EP-0701
Kang, S.	**E-PW026**, **EP-0545**, **EP-0583**
Kang, Y.-K.	**EP-0575**
Kang, Y.	**OP-190**
Kannor, C.	E-PW068
Kano, D.	**EP-0096**
Kanojia, V.	EP-0845
Kanou, M.	EP-0334
Kanoun, S.	EP-0075, OP-588
Kantz, S.	OP-122
Kanzog, A.	E-TPW34
Káplár, A.	EP-0852
Kapoor, R.	OP-113
Kappadath, S. C.	**OP-455**, **EP-0537**, **EP-0867**
Karaali, K.	EP-0508
Karabacak, N. I.	OP-191
Karacalioglu, A. O.	EP-0324, EP-0511
Karachaliou, C.-E.	EP-0200
Karadeniz, C.	OP-191
Karageorgou, M.	OP-537
Karaman, A.	EP-0618
Karanikas, G.	OP-502, E-PW088, EP-0589
Karayel, E.	OP-083, OP-216, OP-315, OP-564, EP-0677, OP-704
Karcı, A. Ç.	EP-0920
Karcher, G.	E-PW033, EP-0236, EP-0336, EP-0362, EP-0489, EP-0893
Karci, E.	EP-0620
Karczmarczyk, U.	EP-0266
Karfis, I.	OP-106, EP-0907
Kargı, A.	EP-0786
Kári, B.	EP-0016
Karimi, Z.	OP-340
Karlberg, A.	**OP-498**
Karnes, J. R.	EP-0635
Karp, J. S.	OP-517
Karpov, E. N.	OP-608
Karpov, R.	OP-409
Karpov, R. S.	EP-0326
Kartiosuo, N.	OP-505
Kas, A.	EP-0182, EP-0430, OP-617
Kashiwa, K.	**EP-0258**
Kaspiri, A.	EP-0342
Kataeva, G.	EP-0391
Katagiri, T.	EP-0828
Kato, H.	EP-0219, EP-0690
Kato, K.	E-TPW05, E-TPW06, E-TPW10, **EP-0737**
Kato, M.	EP-0451, EP-0454, EP-0460
Katsampoukas, D.	OP-140, EP-0443, EP-0829
Katsikavelas, I.	EP-0515
Katunina, T.	E-PW021, EP-0630
Katz, L. B.	OP-277
Kaufmann, J.	OP-427
Kaul, A.	EP-0265
Kaul, F.	OP-391
Kaul, U.	EP-0195
Kauppinen, T.	EP-0926
Kaviani, S.	EP-0005
Kawahara, A.	EP-0556
Kawahara, M.	EP-0254
Kawai, Y.	EP-0365
Kawakami, K.	E-TPW15
Kawano, N.	**EP-0565**
Kawashiri, S.	OP-253
Kaya, E.	**EP-0618**
Kaymak Akgun, E.	OP-083, OP-564, EP-0677
Kazama, A.	E-PW014
K. Buck, A.	EP-0042
Kedzierawski, P.	EP-0660
Keenliside, L.	EP-0180
Keijsers, R.	EP-0112
Kšela, J.	EP-0987
Kellner, M.	OP-114
Kelly, J. M.	**OP-165,** OP-435, E-PW011
Kelten Talu, E.	EP-0543, EP-0544
Kemppainen, J.	OP-120
Kenny, L.	E-PW010
Képes, Z.	**EP-0852**
Keramida, G.	OP-650, **EP-0092**, **EP-0586**
Keresztes, S.	EP-0281
Kerimel, I.	OP-196, EP-0746, EP-0747
Kero, T.	OP-510
Kerrou, K.	EP-0705
Kerschensteiner, M.	E-PW103
Kertész, I.	EP-0464, EP-0466, EP-0467, EP-0468
Kesch, C.	OP-123, OP-243
Kesenheimer, C.	OP-189, EP-0879
Keshavarz, A.	EP-0366
Kesner, A.	OP-284
Kessler, H.	OP-111
Kessler, M.	OP-694, **EP-0374**, **EP-0448**
Ketabi, A.	EP-0768, **EP-0775**
Khachirova, E.	**EP-0330**
Khader, J.	EP-0659
Khalaj, A.	EP-0299
Khalid, E.	EP-0742
Khalifé, M.	EP-0182, EP-0430, OP-617
Khalighi, M.	EP-0170
Khalil, M.	**OP-259**
Khalizadeh, M.	EP-0744
Khan, A. I.	EP-0151
Khan, N.	EP-0896
Khan, Z.	EP-0819, EP-0967
Kharina, D. S.	EP-0426
Khawar, A.	**OP-670**, **EP-0890**
Khedr, M. H.	EP-0950
Khomenko, J.	**EP-0391**
Khor, L.	EP-0582
Khor, Y.	EP-0870
Khubutia, B.	EP-0137
Khurshid, Z.	**OP-452**
Khzouz, J.	EP-0659
Kidd, M.	E-PW062, EP-0161, OP-474, EP-0807
Kido, A.	EP-0681
Kikuchi, A.	**E-TPW15**
Kikuchi, F.	EP-0553
Kil, H.	EP-0229
Kilian, K.	**EP-0247**
Kilickap, S.	EP-0878
Kim, B.	EP-0033, EP-0229, EP-0535, EP-0813
Kim, C.	**OP-714**
Kim, D.	E-PW011, OP-165, OP-435
Kim, G.	EP-0211, **EP-0238**, EP-0239
Kim, H.-S.	EP-0295
Kim, H.	EP-0577

Santoro, E.	OP-212
Santoro, L.	EP-0887, EP-0888
Santos, A. I.	OP-482, E-TPW80, EP-0050
Santos, A. C.	EP-0451, EP-0454
Santos, E. B.	OP-239
Santos, L.	E-TPW11, E-TPW50
Santos, M. V.	EP-0451
Santos, P.	E-TPW80
Santos Bueno, A. M.	OP-472, **EP-0625,** EP-0835
Santos Carreño, A.	EP-1009
Santos Mateo, J.	E-PW091, E-PW093
Santos Montero, B.	EP-0268
Sanz-Ceballos, L.	EP-0273
Sanz LLorens, R.	EP-0688
Sanz-Viedma, S.	**EP-0750, EP-0764**
Sá Pinto, A.	**EP-0346, EP-0347, EP-0956**
Sara, R.	OP-182, OP-369, OP-413, E-PW109, EP-0445
Sarabhai, T.	**OP-299,** OP-546
Sarai, M.	OP-611
Sarikaya, A.	EP-0088
Sarikaya, I.	**EP-0088, EP-0664**
Sarkar, S.	EP-0005
Sarıkaya, A.	EP-0546
Sarnelli, A.	OP-707
Sarnyai, Z.	**EP-0008**
Sarrhini, O.	OP-557, E-PW075
Sarrut, D.	OP-014, **OP-058,** EP-0895
Sas, N.	EP-0898
Sasamori, H.	EP-0534
Sasikumar, A.	**EP-0632**
Sathekge, M. M.	OP-372
Sato, H.	EP-0789
Sauerbeck, J.	OP-131
Saunavaara, V.	OP-238, EP-0172
Saushkin, V.	OP-409, **EP-0143**
Saushkina, Y.	**OP-409**
Savintseva, Z.	EP-0487
Savio, E.	EP-0301, OP-442
Savitcheva, I.	OP-367
Sawada, K.	E-TPW65
Sawai, Y.	EP-1021
Sawan, P.	EP-0289
Sawicki, L.	OP-118, OP-703, E-PW062
Sawyer, M. B.	OP-100
Sayit, E.	E-TPW02, EP-0833
Sayman, H. B.	EP-0869
Sazonova, S.	**EP-0328,** EP-0364
Scala, D.	EP-0601
Scalone, F.	EP-0388
Scalorbi, F.	OP-252, **EP-0499**
Scarale, M.	EP-0863, EP-0930, EP-1014
Scaringi, C.	OP-501
Scarlattei, M.	OP-473, **E-TPW33**
Scarpa, L.	OP-386
Scarpi, E.	OP-099, OP-102
Scavuzzo, F.	EP-0601
Schaal, K.	E-PW064
Schaarschmidt, B.	OP-546
Schaart, D. R.	OP-517
Schaefer, N.	OP-023, OP-073, OP-154, OP-355, EP-0433, EP-0477, OP-504, OP-656, EP-0913
Schaefers, K.	OP-687
Schäfer, D.	E-PW015
Schäfer, M.	OP-123, EP-0217, OP-310, OP-440, OP-491
Schäfers, K.	OP-688
Schäfers, M.	OP-105
Schaffer, P.	E-PW077, EP-0317, OP-438, OP-640, OP-644
Schaitel, B. A.	OP-100
Schatka, I.	OP-583

Schatteman, J.	**E-PW084**
Scheidhauer, K.	**OP-013,** OP-172, OP-584
Scheins, J.	EP-0021, EP-0178
Scheiwein, F.	OP-131
Scheltens, P.	OP-363
Scheper, H.	OP-373
Schepers, A.	E-PW044
Scherer, P.	OP-341
Scherr, D. S.	OP-492
Scherthan, H.	OP-053, E-PW050
Scheuba, C.	EP-0522
Schiariti, M.	EP-0481
Schiavina, R.	OP-117, OP-124, EP-0635
Schiazza, A.	EP-0494, EP-0521
Schibli, R.	OP-160, OP-391, OP-490
Schichor, C.	OP-500
Schick, U.	OP-598, OP-599
Schieferstein, H.	OP-366, OP-669
Schierholz, I.	EP-0448
Schildan, A.	OP-129
Schillaci, O.	E-PW108, EP-0388, EP-0402, EP-0442, EP-0602, OP-604
Schirbel, A.	EP-0108, **OP-547**
Schlegel, J.	EP-0497, OP-503
Schlemmer, H. P.	OP-123, OP-243
Schlenkhoff, C.	OP-218, **EP-1001**
Schlitter, A. M.	OP-172
Schlumberger, M.	OP-084, OP-562, OP-566
Schlyer, D.	OP-190
Schmaderer, C.	OP-584
Schmidbauer, V.	EP-0486
Schmidkonz, C.	**OP-119, OP-127,** EP-0904
Schmidt, D.	OP-119, OP-127
Schmidt, D.	EP-0665
Schmidt, J.	OP-310
Schmidt, K.	OP-190, OP-217
Schmidt, M. C.	**EP-0751, EP-0801**
Schmidt, R.	OP-134
Schmidt-Kreppel, B.	**EP-0605**
Schmitl, S.	EP-0246
Schmitt, V.	EP-0294
Schmitto, J. D.	EP-0118
Schmuck, S.	**E-PW069**
Schnabel, J.	OP-129
Schnettler, R.	EP-0111
Schöde, A.	EP-0118
Schöder, H.	EP-0289, EP-0732
Schoemaker, R. G.	OP-555
Scholtens, A. M.	**OP-662**
Scholz -Gutierrez, V.	EP-0764
Schönecker, S.	OP-129
Schoots, I.	OP-075
Schöppe, F.	E-PW052
Schottelius, M.	**OP-229**
Schou, M.	EP-0218
Schrader, L. D.	OP-100
Schramm, G.	EP-0424
Schramm, N.	**E-PW009**
Schreuder, H. W. B.	EP-0722
Schreuder, N.	EP-0060
Schreuder, R. S. B. H.	E-PW072, **EP-0609**
Schröder, C. P.	OP-303, EP-0532
Schubert, L.	OP-121
Schuchardt, C.	**OP-215,** OP-220, EP-0803
Schuck, P. N.	**EP-0038**
Schuit, R. C.	OP-363
Schuller, K.	EP-0068
Schultze-Seemann, W.	E-PW064
Schulze, O.	EP-0187
Schulze-Koops, H.	E-PW009

ESMIT

European School of Multimodality Imaging and Therapy

The **ESMIT initiative** represents EANM's response to huge changes in the educational needs of the nuclear medicine community and the rising demand for greater multimodality content. The EANM is convinced that the community needs not only to be educated on all modalities that are used in imaging, but also to be well prepared in the therapeutic applications of our discipline.

eanm.org/esmit

Level 3

Interactive Course on
Radiopharmacy GMP

November 9 – 10, 2017
Vienna/AT

Level 3

Advanced Course on
Imaging in Infection & White Blood Cell Labelling

December 4 – 6, 2017
Rome/IT

Level 2

Winter School

February 23 – 25, 2018
Bergamo/IT

Level 2

Spring School

May 4 – 6, 2018
Ghent/BE

Level 2

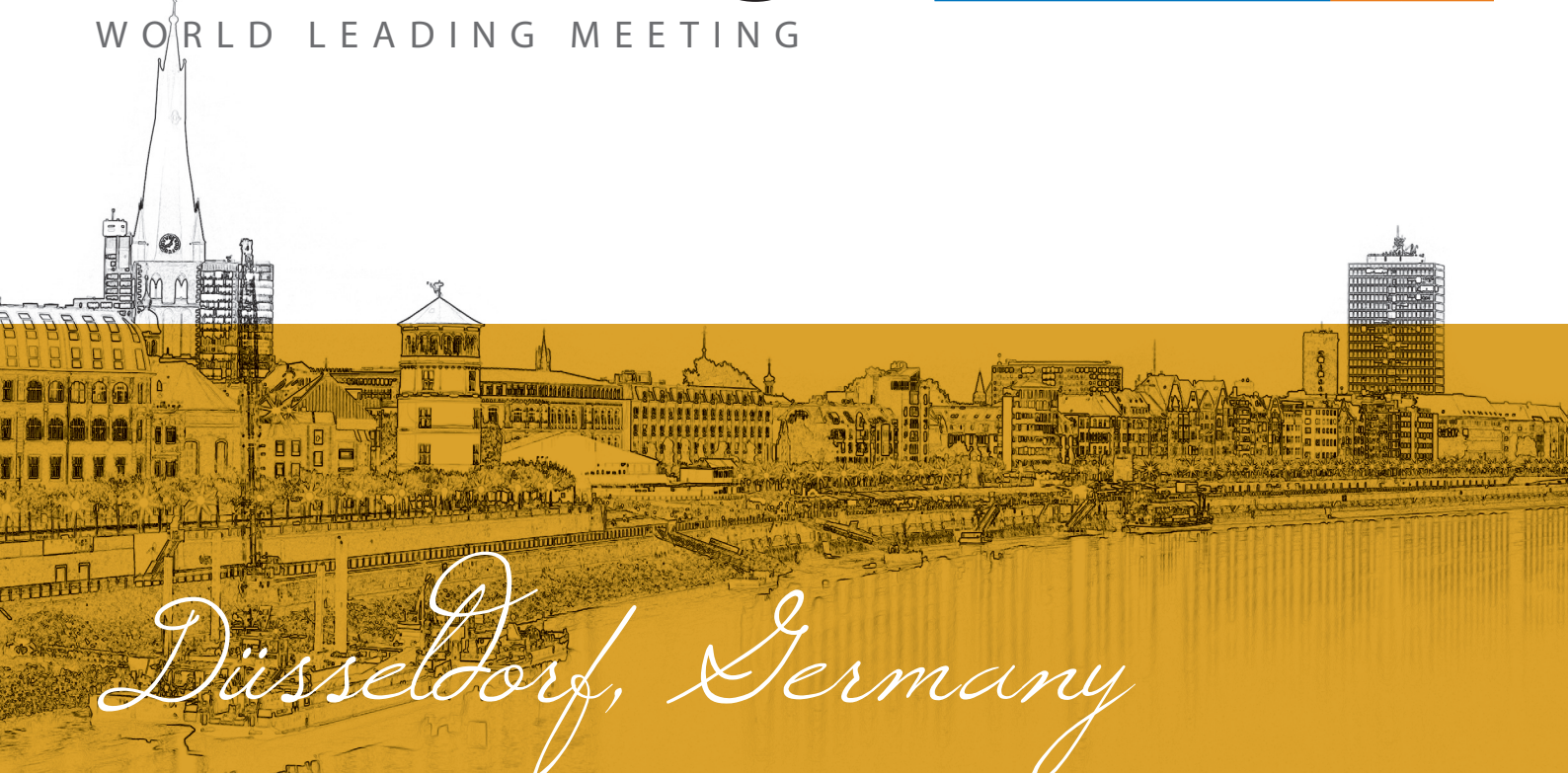## Autumn School

September 7 – 9, 2018
Belgrade/RS

EANM´18

WORLD LEADING MEETING

EANM®
European Association of Nuclear Medicine

BIOMEDICAL
IMAGING AND
THERAPY FOR
PERSONALIZED
HEALTHCARE

Düsseldorf, Germany

Annual Congress of the
European Association of Nuclear Medicine

October 13 – 17, 2018
Düsseldorf, Germany

eanm18.eanm.org

Visit us on
.com/officialEANM